HONI SOIT QUI MAL Y PENSE
DIEU ET MON DROIT

AGRICULTURAL RESEARCH INSTITUTE

PUSA

Books Received . . . 1385
Subject Index . . . 1386
Author Index . . . 1392
Index to New Books . . . 1398

REVERSIBLE POLYMERIZATION AND MOLECULAR AGGREGATION[1]

L. MICHAELIS

The Laboratories of The Rockefeller Institute for Medical Research, New York, New York

Received August 22, 1949

In addition to the irreversible polymerizations encountered in the field of rubber and plastics chemistry, reversible polymerizations have been known for a long time. Special emphasis will be put upon those cases where the forces of molecular aggregations are obviously not of the nature of a regular covalent bond. From the large field of "molecular compounds," a few will be discussed here in the form of a review of several previous papers (1 to 8) augmented by additional recent unpublished material. This paper should be considered as a contribution to the problem rather than as an exhaustive review of it.

I. THE REVERSIBLE MOLECULAR AGGREGATION OF DYESTUFFS

It has been known for a long time (10, 15, 16, 17) that the absorption spectra of the majority of organic dyestuffs in aqueous solution do not obey Beer's law; rather does the molar absorption curve in most cases depend on the concentration. This is the case in aqueous solution, whereas in alcoholic solution (not necessarily quite water-free) Beer's law is obeyed. In some cases Beer's law is valid even in aqueous solution: namely, (*1*) for such dyes as phenosafranine and related ones; the acridine dyes; several dyestuffs of the indamine and indophenol group, e.g., Bindschedler's Green; (*2*) even for those cationic dyes which, in the form of their ordinary, singly charged cation, strongly deviate from Beer's law (such as the thiazines, the oxazines, triphenylmethane dyes, etc.), Beer's law is strictly obeyed for the doubly charged cations which exist in sufficiently acid solutions; (*3*) methyl green, which is a doubly charged cation even in approximately neutral solution (pH 7 to 5, say), also obeys Beer's law in aqueous solution. The deviation from Beer's law is accounted for by the hypothesis of a reversible dimerization and polymerization. The energy of the bond is of the order of the thermal energy at room temperature, since the effect of concentration on the deviation from Beer's law depends strongly and reversibly on temperature. This bonding energy in the dissolved state is in fact the difference between the affinities of the dye molecule for another molecule of its kind and for water.

It is understandable that a doubly charged cation should resist polymerization for electrostatic reasons. However, no clear understanding has been reached as yet as to the manner in which the structure of a single charged dye ion is correlated with its tendency toward molecular association. One remarkable example is this. Whereas thionine in aqueous solution shows very strong association, oxonine (which differs from it only by having an oxygen bridge instead of a sulfur bridge) deviates from Beer's law only very slightly.

---

[1] Presented at the Twenty-third National Colloid Symposium, which was held under the auspices of the Division of Colloid Chemistry of the American Chemical Society at Minneapolis, Minnesota, June 6–8, 1949.

The evidence for polymerization in aqueous solution is derived from the absorption spectrum. Taking methylene blue as an example (figure 1) the absorption spectrum in *alcoholic* solution shows a sharp and high maximum at 650 mμ,

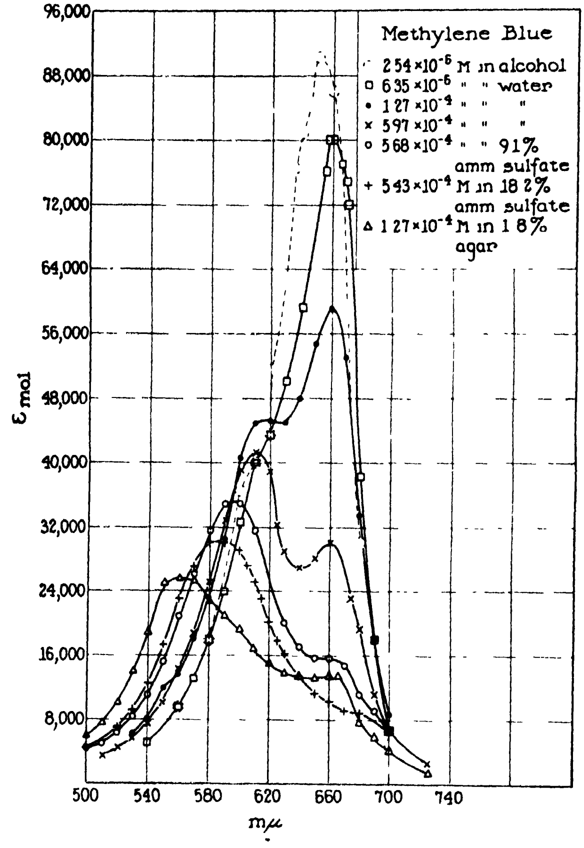

FIG. 1

which will be referred to as the α-band, and a very slight secondary hump at 590 mμ, which will be referred to as the β-band. There is, furthermore, a rather high band in the ultraviolet at 295 mμ and a smaller one at 250 mμ. First of all it should be stated that modifications of this spectrum to be discussed in what follows are concerned only with the bands in the visible spectrum. The ultraviolet bands are, for all practical purposes, unaffected by all those circumstances which so strongly influence the absorption in the visible spectrum (6). In *aqueous* solution of high dilution (10^{-7} to 10^{-6} *M*) the absorption spectrum resembles very much that in alcohol, although the peak is slightly displaced (660 mμ instead of 650). As the concentration increases in aqueous solution, the α-band decreases and the β-band increases considerably, at the expense of the α-band, soon to such a degree that the β-band almost suppresses the α-band. This effect is reversibly abolished by raising the temperature.

The following interpretation has been suggested: The α-band is characteristic of the monomeric cation and corresponds to an electric oscillator along the x-axis of the molecule (the long axis). The β-band, whenever it increases in height beyond that prevailing in alcohol, is characteristic of the dimer. It has been interpreted as due to an oscillator in the y-direction (the shorter axis in the plane of the molecule). An alternate explanation is that it is due to higher vibrational energy levels of the dye. When the dye solution of low concentration is mixed with a neutral salt, there may be, previous to distinct crystallization of the dye, a transitional colloidal or quasi-colloidal state, an "incipient salting-out" effect, which shows a molar absorption spectrum resembling that for a much higher dye concentration without salt. This fact is fair evidence that the change of spectrum with concentration is correlated with molecular aggregation. In the presence of very much ammonium sulfate in very dilute methylene blue solution (figure 1) the β-band is not only very high but even slightly displaced toward still shorter wave lengths.

When the dye is adsorbed on a stainable substrate the absorption spectrum may depend both on the relative amount of dye with respect to that of the substrate and on the chemical nature of the stainable substrate. The behavior of various stainable substrates varies between two extremes, with all transitions occurring. I may restrict myself essentially to two substrates of extremely different behavior and discuss later on, more briefly, some substrates of intermediate behavior. Those two extreme types are represented by solutions of nucleic acid (of pH about 4 to 7) (usually using yeast nucleic acid, which in this respect does not differ essentially from thymonucleic acid), and on the other hand agar (a half-ester of sulfuric acid with high-polymeric hexosan). All experiments with those two substrates can be carried out in a macrohomogeneous system and lend themselves readily to quantitative spectrophotometry in transmitted light.

The characteristic of nucleic acid is this: When a dye showing no deviation from Beer's law, such as phenosafranine, is adsorbed by nucleic acid, the peak of absorption is usually slightly shifted toward longer wave lengths. Nothing else happens. On the other hand, when a dyestuff capable of polymerization is adsorbed by nucleic acid, the situation is very different. There may be a slight displacement of the peak of the α-band too, but what is much more striking is the following phenomenon: When a solution of nucleic acid is mixed with the dye of such a concentration that in aqueous solution there would be a strong β-band and a distinctly depressed α-band, nucleic acid makes the β-band disappear and causes the α-band to increase (see figure 2). With the unaided eye, toluidine blue, for instance, at a concentration at which it appears blue-violet

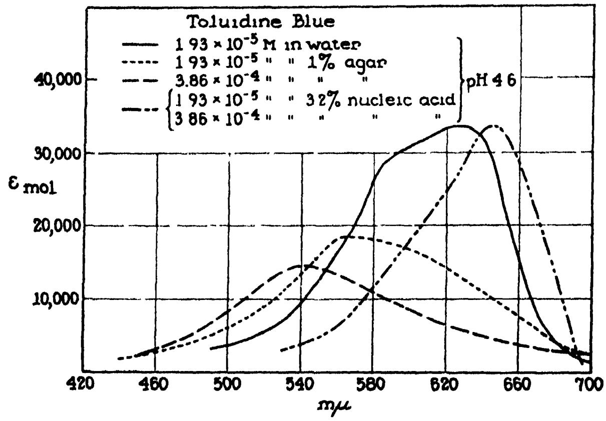

FIG. 2

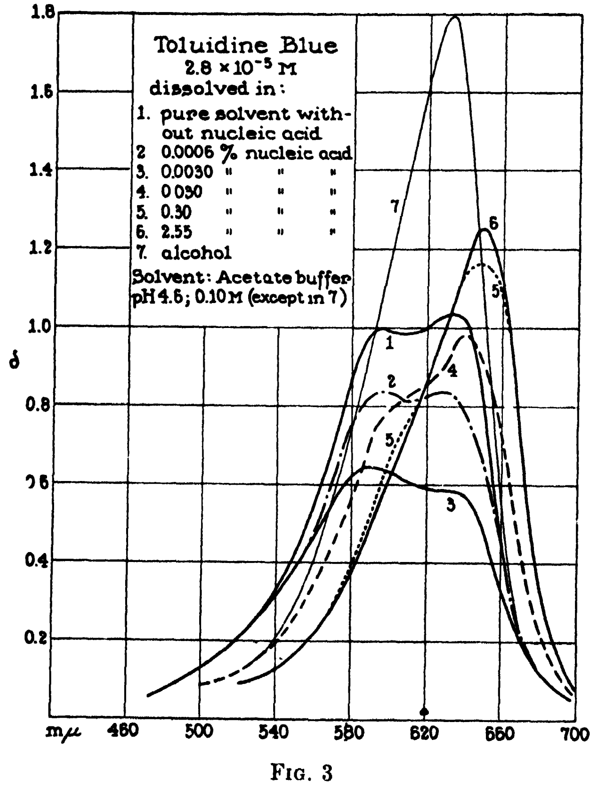

FIG. 3

in water, shows a pure blue even with greenish tint in nucleic acid. The effect of nucleic acid is as though it had "depolymerized" the dye. This interpretation is compatible with the following picture: The negatively charged groups of nucleic acid (phosphate side chains) are present in large excess over the dye cations, so the dye cations will be singly distributed over the phosphate groups of nucleic acid, and the β-band characteristic of the dimer will disappear at the expense of the increased α-band.

When nucleic acid solution of much lower concentration (figure 3) is mixed with the same amount of dye, a β-band may reappear. However, never does any other band at still shorter wave length appear, in contrast to what will be shown presently. An especially interesting phenomenon is this: When a fixed tissue slice (say of liver) is stained with a solution of such a dye (methylene blue, toluidine blue, crystal violet), the over-stained slice may be washed first with water and then with alcohol to such an extent that the dye can no longer be extracted. We may consider that all the dye permanently adsorbed is adsorbed by some cationic ion exchange: some cations previously held by the phosphate groups of nucleic acid (alkali ions, or even anions of proteins) have been replaced by dyestuff cations. Such a stained section, when viewed in the microscope, embedded in water, shows always a distinct β-band and some α-band. The same slice, viewed in alcohol, shows only a very strong α-band and no β-band. This change of spectrum, on changing from water to alcohol, is perfectly reversible and can be, in fact, reversed any number of times. The spectrum as it appears in alcohol is not essentially changed on following the customary procedure of histologic technic, passing from alcohol through xylene to balsam.

The other extreme representative of a stainable substrate is agar. Many other sulfuric esters, provided they are derived from highly colloidal carbohydrates, show the same behavior, as Lison (12, 13) first emphasized, such as mucin, chondroitinsulfuric acid, heparin, and others. Agar is the most convenient one and besides shows the specific effect to an especially high degree. The staining of substrates of this type with certain basic dyestuffs is characterized by the fact that the color of the adsorbed dye is quite different from the color of the dye solution itself, even as seen with the unaided eye. This effect has been known under the name of metachromasy (Paul Ehrlich). Good examples of metachromatic dyes are thionine and toluidine blue, which stain most stainable substrates blue, especially cellular nuclei, whereas agar is stained pink to purple. All those dyestuffs which exhibit polymerization in aqueous solution show the metachromatic effect, as has been pointed out by Kelley (11) and the speaker (6, 7). The absorption spectrum of the metachromatically adsorbed dye shows a very characteristic property: The α- and β-bands are almost or even entirely annihilated, and a new band at longer wave length appears, which is rather diffuse; e.g., in toluidine blue where the α- and β-bands are at 630 and 590 mμ, respectively, this new band has its peak at 540 mμ, varying slightly according to conditions (figures 4 and 5). The diffuseness and variability of the peak of the band obviously indicate that the curve is just the envelope of a series of overlapping bands. This complex band will be referred to as the metachromatic or μ-band. (The name "γ-band" will be reserved for something else to be discussed presently.) The absorption spectrum is reversibly shifted to the ordinary one, with α- and β-bands, in a perfectly reversible manner by warming (figure 5).

This phenomenon will become especially clear in some polymethine dyes; e.g., it has been known that pinacyanol shows a high α-band and, even in alcohol, a very distinct, although lower β-band (figures 6 and 7). In aqueous solution with increasing dye concentration the α-band is lowered and the β-band increased. At still higher concentration, another "γ-band" at still shorter wave length appears. (Furthermore, in very highly concentrated solution, where the solution becomes very viscous and shows the property of a liquid crystal, a new, very sharp band (at the red end of the spectrum) and resonance fluorescence appear, as first shown by Scheibe (16). (This interesting band is no concern of ours for the present problem.[2]) The dye is adsorbed by nucleic acid again in such a way that the β-band almost disappears and the α-band strongly increases, the absorption spectrum approaching that in alcohol solution; the dye is seemingly depolymerized by nucleic acid. In agar, however, a new very diffuse band appears, the peak of which lies at very much shorter wave length than the γ-band previously described by other authors. It will be referred to as the μ-band or metachromatic band. The color of the dyestuff is blue with nucleic acid but pink with agar.

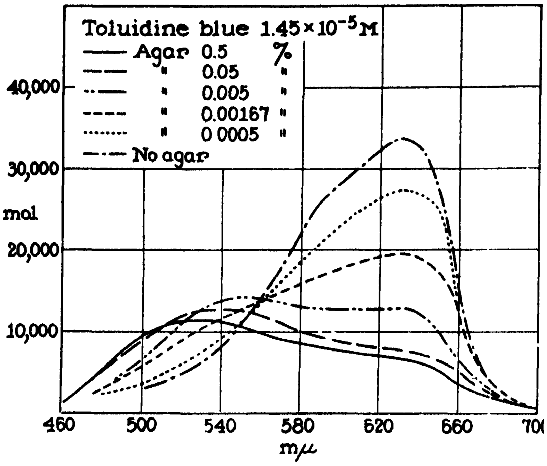

FIG 4

My previous interpretation of the μ-band was to the effect that it represents a state of high molecular aggregation of the dye. This interpretation was favored by two facts: (*1*) the metachromatic color returns to the normal color at higher temperature (70–80° C.), in a perfectly reversible manner, seemingly indicating a reversible dissociation of the polymer, the bond energy being of the same order as the thermal energy around room temperature; (*2*) the μ-band arises also when

---

[2] However, it is worth while mentioning that the little hump at about 640 mμ in the "metachromatic" band of very dilute pinacyanol shown in figures 6 and 7, as obtained in agar, appears at the same wave length as the band which in a pure aqueous solution of the dye is established only in very concentrated solutions.

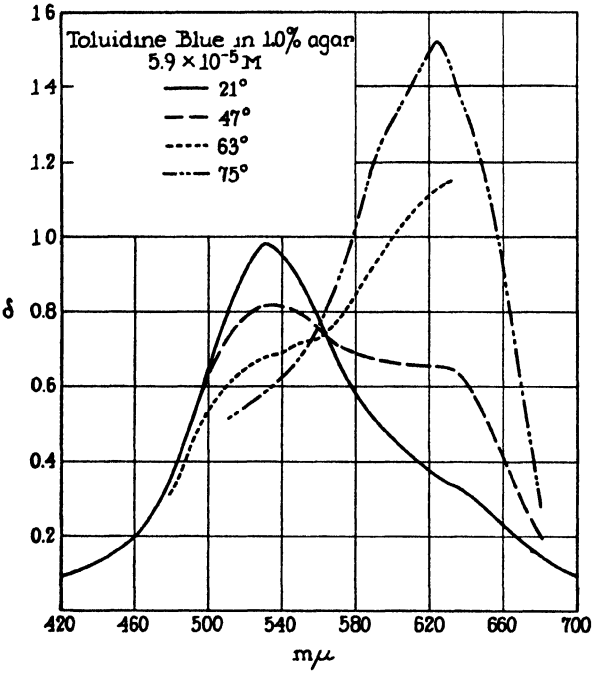
Toluidine Blue in 1.0% agar
5.9 × 10⁻⁵ M
21°
47°
63°
75°
δ
1.6
1.4
1.2
1.0
0.8
0.6
0.4
0.2
420
460
500
540
580
620
660
700
mμ

Fig. 5

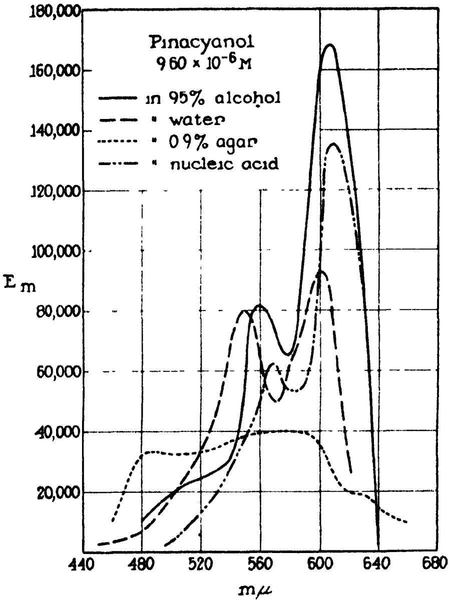
Pinacyanol
9.60 × 10⁻⁶ M
in 95% alcohol
" water
" 0.9% agar
" nucleic acid
E m
180,000
160,000
140,000
120,000
100,000
80,000
60,000
40,000
20,000
440
480
520
560
600
640
680
mμ

Fig. 6

a suitable dyestuff at a very low concentration in aqueous solution is being salted out, as with ammonium sulfate, in such a way that as a primary reaction a colloidal solution arises which only gradually undergoes distinct crystallization. It must be added, however, that the α- and β-bands lie each at a very definite wave length, which may depend slightly on the solvent (water or alcohol). Only in extremely high concentrations of the dye is the β-band perhaps slightly displaced toward shorter wave length, as can be seen from spectrophotometric graphs of methylene blue (figure 1). In contrast, the μ-band may have its peak within a certain, larger range of wave lengths, according to conditions. So, in toluidine blue, the peak of the μ-band in agar may vary from 560 to 540 mμ with increasing dye concentration.

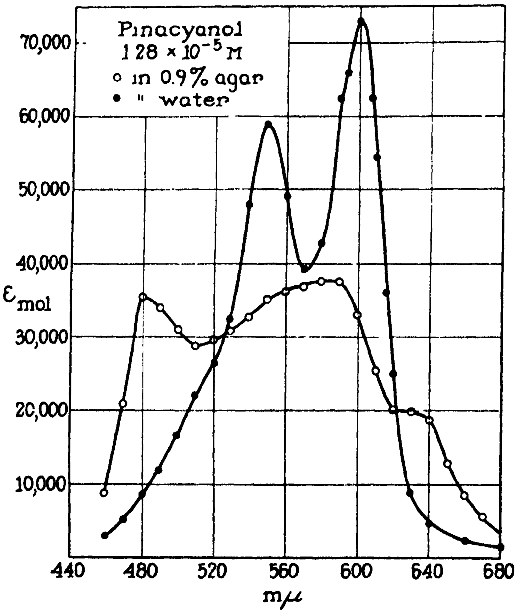

FIG. 7

However, the interpretation of the μ-band as that of a high, reversible polymer of the dye has become doubtful as to its generality. No doubt a band resembling the μ-band can be produced by incipient salting out of the dye. In this case it is certainly the polymolecular micelle which exhibits the μ-band. However, when a 1–3 per cent agar gel is stained with pinacyanol or toluidine blue, at such a low concentration of the dye that the color is distinct only on looking through the whole length of a test tube, the color is still at room temperature very decidedly the pink, metachromatic color, showing the μ-band only. In this case it is unlikely that the dye should have been adsorbed in the form of polymolecular dye micelles, rather is a monomolecular distribution of the dye over the negatively charged sites of the colloid the only reasonable assumption.

If so, the result is this: The "metachromatic" dyes are characterized by the fact that their absorption spectra, especially the number of different absorption maxima and their relative height, are very sensitive to external fields. Di- and polymerization are just two of the factors influencing the type of spectrum; the nature of the substrate by which they may be adsorbed is another factor. The two extreme types of stainable substrates in this respect are represented by nucleic acid, which influences the spectrum in the direction as though it were depolymerized, and agar, which influences the spectrum always in the direction as though it were highly polymerized. Among other stainable substrates there are some high-molecular-weight metaphosphates encountered in living cells (18) and some silicates (14) which approach the staining qualities of agar.

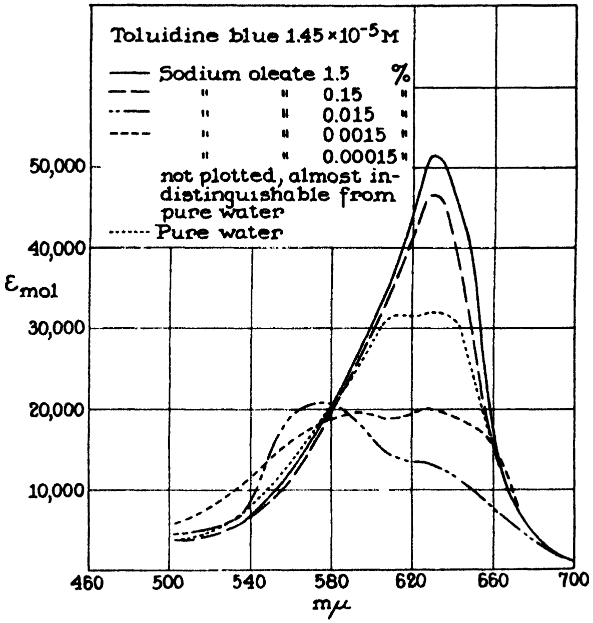

Fig. 8

We shall now discuss a few examples of stainable substrates with an intermediate behavior. Many of the long-carbon-chain "detergents" belong here. The simplest example is sodium oleate. When the concentration of the soap is very high, soap behaves as nucleic acid. It seemingly depolymerizes the dye, and only the α-band is developed. As the concentration becomes lower (figure 8) the α-band decreases and a β-band develops; on further increase a μ-band develops. Thus, toluidine blue in a soap solution may appear blue, violet, or pink according to the concentration of the soap. Other detergents behave similarly. Figure 9 shows Aerosol 22 as one example of many. Here, according to the concentration of the colloid, we have for toluidine blue either a strong α-band almost exclusively, or a strong β-band, or even a μ-band.

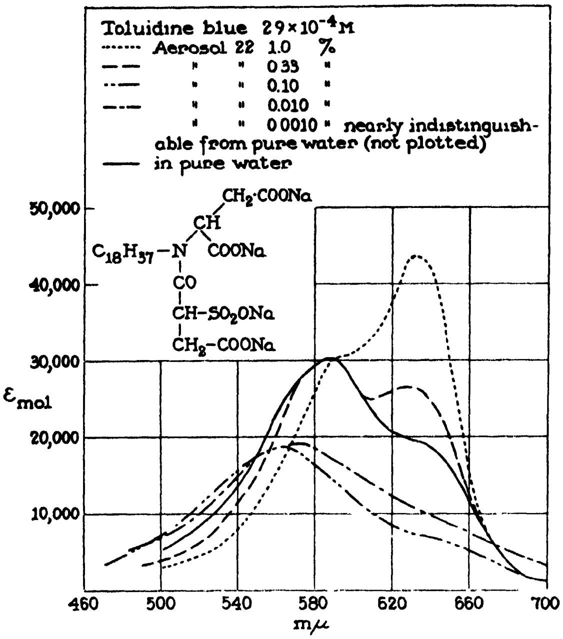
Toluidine blue 2.9×10⁻⁴M
······ Aerosol 22 1.0 %
— — " " 0.33 "
··— " " 0.10 "
—·— " " 0.010 "
" " 0.0010 " nearly indistinguishable from pure water (not plotted)
—— in pure water
CH₂·COONa
CH
C₁₈H₃₇–N COONa
CO
CH–SO₂ONa
CH₂–COONa
50,000
40,000
30,000
20,000
10,000
εmol
460
500
540
580
620
660
700
mμ

FIG. 9

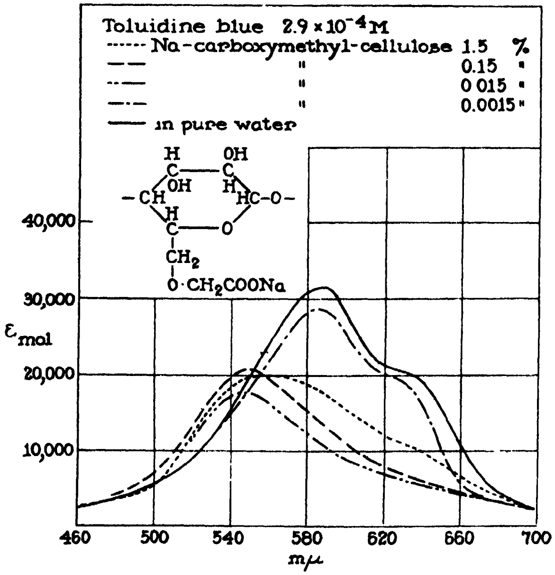
Toluidine blue 2.9×10⁻⁴M
······ Na–carboxymethyl–cellulose 1.5 %
— — " 0.15 "
··— " 0.015 "
—·— " 0.0015 "
—— in pure water
H OH
C C
–CH OH H HC–O–
H
C O
CH₂
O·CH₂COONa
40,000
30,000
20,000
10,000
εmol
460
500
540
580
620
660
700
mμ

FIG. 10

The behavior of cellulose esters is somewhat different, approaching that characteristic of agar in some degree. So, sodium carboxymethylcellulose, stained with toluidine blue, never shows a strong α-band. With increasing dye concentration it develops a μ-band, like agar.

Corrin and Harkins (9) claim that the change in the color of pinacyanol in soap solutions, from blue to pink, occurs at a very definite concentration of the soap and is indicative of the "critical concentration" of the soap solution when a true molecular dispersion begins to form molecular aggregates or micelles. The final interpretation of the color change is still open to discussion. It seems that the sensitivity of the absorption spectrum of some dyestuffs with respect to the nature of the substrate by which they are adsorbed may serve as a powerful tool for the elucidation of the structure and the chemical nature of the colloidal micelle. The final solution of the problem, however, is still far remote. I wish not to enter into a premature speculation but merely to draw your attention to an as yet unexhausted source of future information about the structure of colloidal micelles.

II. QUINHYDRONE-LIKE MOLECULAR COMPOUNDS

The molecular compounds of the quinhydrone type may be considered as dimers composed of two molecular species of the same kind, just as the dimers discussed before. To wit, quinhydrones may be considered as dimerized semiquinone radicals. On the other hand, a quinhydrone may also be conceived of as a molecular compound of a quinone and a hydroquinone, that is to say, as a compound of two molecules of different though related structures differing in their level of oxidation. Thus, quinhydrones represent a transition of the cases of the reversible polymers (to be discussed later on) which are composed of two essentially different molecular species.

The quinhydrone-like compounds may be divided into two classes, each with a somewhat different behavior: quinhydrones formed from a hydroquinone and a quinone, and quinhydrones formed from an aromatic *p*-diamine and a corresponding diimine. They all are quite stable in the crystalline solid state and dissociate very strongly in the dissolved state, the dissociation depending strongly and reversibly on temperature. They are all strongly colored compounds, very much more so than the corresponding quinones. The justification for considering them as dimers of the semiquinone radical is based on the following consideration. If Q designates the compound of quinonoid structure, B that of the corresponding benzenoid structure, S the free, paramagnetic semiquinone radical, and D the dimeric, diamagnetic, quinhydrone-like compound, the following equilibria must be considered, each characterized by an equilibrium constant K:

$$\mathrm{Q} + \mathrm{B} \overset{K_1}{\rightleftharpoons} 2\mathrm{S} \qquad 1)$$

$$2\mathrm{S} \overset{K_2}{\rightleftharpoons} \mathrm{D} \tag{2}$$

$$\mathrm{Q} + \mathrm{B} \overset{K_3}{\rightleftharpoons} \mathrm{D} \tag{3}$$

with

$$K_3 = K_1 \times K_2$$

Let us consider especially K_2, the constant involved in the dimerization of the free radical. Two general rules can be stated concerning this constant:

(*1*) If the resonance energy of the free radical is strong, the radical may be so stable a compound as to counteract dimerization. For instance, in duroquinone in alkaline solution the two limiting structures of the semiquinone may be in some loose way symbolized as in formula I. These two structures are perfectly equivalent and so bring about strong resonance and high stability, strongly counteracting dimerization. In fact, until recently it has been assumed that no real diamagnetic quinhydrone could be obtained from duroquinone. Recently its existence— at least in the solid crystalline state—has been shown (4). It is, practically speaking, completely dissociated in the dissolved state. In the same manner, phenanthrenequinonesulfonate (II) can be reduced to a semiquinone which, in alkaline solution, can be symbolized as in formula III, with two equiv-

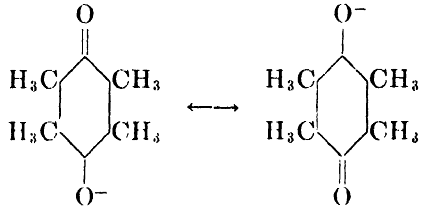

I

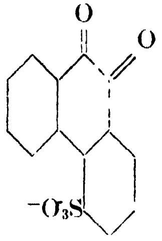

II

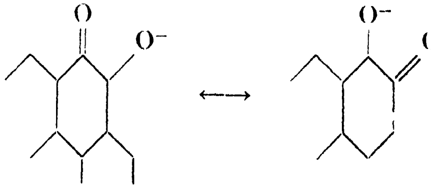

III

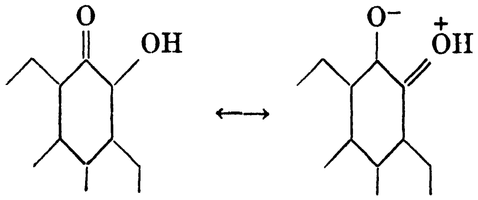

IVa IVb

alent resonating limiting structures, bringing about high stability, with little, although not entirely lacking, tendency of the free radical toward dimerization; whereas in acid solution the structure may be represented as in formulas IVa and IVb, IVb being much more improbable than IVa. Here the resonance energy is small, the stability is low, and the tendency toward dimerization is high. In fact, with this compound, in alkaline solution, a large amount of the paramagnetic free radical is formed, together with a small amount of the dimer, the diamagnetic quinhydrone, whereas in acid solution only the diamagnetic quinhydrone can be observed.

(*2*) Another factor, important for the formation of the dimer of the free radical, is the nature of the solvent. In several cases (duroquinone and phenanthrenequinonesulfonate) the dimerization of the free radical takes place only in aqueous solution. In alcohol and pyridine (even in the presence of relatively large amounts of water) the dimerization of the free radical is entirely prevented. No satisfactory explanation for this remarkable fact can be presented. It recalls vividly the fact that also the polymerization of organic dyestuffs takes place only in aqueous solution. It does not seem likely that the dielectric constant of the solvent should be the essential factor responsible for this difference.

The difference between the quinhydrones proper and the analogous compounds derived from aromatic diamines is as follows (3, 4): Benzoquinone and hydroquinone, when mixed in solution, form immediately the sparingly soluble, dark-colored, crystalline, diamagnetic quinhydrone, which in solution strongly, although not entirely, dissociates into its components. The affinity for the formation of the quinhydrone is diminished to an enormous extent if the four hydrogen atoms of the ring are methylated. As said before, the quinhydrone of duroquinone is much more difficult to obtain than ordinary quinhydrone, although the free monomeric semiquinone of duroquinone can be obtained with great ease in an alkaline solution. The methyl groups of duroquinone obviously represent steric hindrance for the formation of the dimeric quinhydrone. It may be inferred therefrom that the dimerization takes place by packing the two rings upon each other. In contrast, the dimerization of the free radical derived from *p*-phenylenediamine is not at all inhibited, rather even a little favored, by methyl groups in the aromatic ring. On the other hand, if all hydrogen atoms of the *amino* groups of the diamine are methylated, the formation of the diamagnetic quinhydrone is entirely prevented, and this is the case even in the solid crystalline state; the crystals are paramagnetic, with a permanent dipole moment corresponding precisely to one unpaired electron. (4) This compound (the univalent oxidation product of N,N'-tetramethyl-p-phenylenediamine, or "Wurster's blue," as a perchlorate) is perhaps the free radical easiest to prepare in the crystalline state and perhaps the most stable solid radical. If *not all* of the amino groups of the diamine are methylated, the crystalline compound is always entirely represented by the diamagnetic quinhydrone-like compounds which in the solid state may be considered as high polymers, although in solution they are certainly dimers to the extent to which they do exist at all in the dissolved state. These facts are compatible only with the assumption that in this case the two rings of the quinhydrone are not stacked upon each other but lie in one plane, and for this reason the substitution of all the amino hydrogen atoms prevents steric hindrance for dimerization (4).

As regards the nature of the bond which holds together the two moieties of a quinhydrone-like dimer, it may be considered first of all as a double hydrogen bond, as symbolized in formula V. However, in addition, there is a perfectly equivalent resonance. Formula V is one limiting structure, and its mirror image is the other. It is uncertain which of the two moieties has the quinonoid structure and which has the benzenoid structure. The unsubstituted hydrogen atom is necessary for the structure. This fact, although appearing self-evident, is emphasized here in contrast to a phenomenon to be described in the following section.

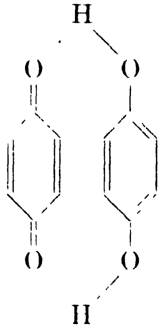

V

III. MOLECULAR COMPOUNDS COMPOSED OF TWO DIFFERENT MOLECULAR SPECIES

There are a great number of molecular compounds which resemble quinhydrone in so far as the one component is on a higher oxidation level than the other, but differ from true quinhydrones in so far as the two components are not components of one single redox system. The component of "higher oxidation level" may be a quinone or a nitro compound; the component of lower oxidation level may be a phenol, or an aromatic amine, or even an aromatic hydrocarbon. Among such compounds I wish to mention only a few typical representatives which show the various kinds of behavior. It is important to emphasize that such compounds must be dealt with on a different footing according to whether they are in the crystalline, the dissolved, or the melted state (5). To begin with the solid state, typical representatives are the strongly colored molecular compounds of quinone with phenols. Designating the quinonoid component as Q and the other component (of benzenoid structure) as B, the molecular compound may have, according to the particular compound, the composition QB, or QB_2, or in rare cases also Q_2B. However, from each given pair of components, always only *one* of the three possibilities is materialized. Thus, the intensely blue compound of chloranil with hexamethylbenzene is QB; the compound of quinone and phenol is always QB_2, independent of the ratio in which Q and B may be mixed when the compound is being prepared. Some compounds of the type Q_2B have been reported, but most of them are doubtful because of their instability. The only case (not previously described and rather unexpected) in which a compound of the composition Q_2B and sufficiently stable for a reliable analysis can be prepared is a compound of quinone and phloroglucinol. The case of quinone plus two phenols is understandable from the following picture (formula VI), with the suggestion that this structure is in resonance with another, in which the hydrogen atoms are

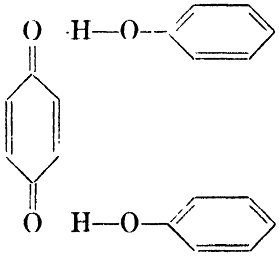

VI

covalently bound to the left-hand moiety, i. e., now hydroquinone, and bound by hydrogen bonds to two phenol radicals (phenol minus hydrogen). The same situation prevails for the compound of phenol with hydroquinone monomethyl ether.

After this very brief review of the solid compounds we should discuss those compounds in the dissolved state. First of all, they are all very strongly dissociated into their components in any solvent; secondly, a remarkable feature is the fact that in any compound in the dissolved state there could be shown to exist only a compound of the composition QB, even in those cases where in the solid state the composition is QB_2 or Q_2B. Furthermore, whereas solid compounds are formed only if hydrogen atoms are present to form hydrogen bonds, compounds of the composition QB are formed in solution and also in the melted state, even if all hydrogen atoms of the hydroxyl groups are substituted by methyl. For instance, quinone and hydroquinone dimethyl ether when melted together form an intesnsely red compound of composition QB, which exists also, to a small extent, in alcoholic solution. Hydrogen bonds are obviously not necessary for the formation of such compounds. A most interesting phenomenon can be observed in the latter case: When the melted, red compound is cooled and crystallization sets in, the color fades and separate crystals of the colorless hydroquinone dimethyl ether and of the pale yellow quinone are formed. The crystal-lattice energy of each is greater than the affinity for the two for the formation of the compound. The formation of the polymer and its complete dissociation according to the change of the solid and melted states is perfectly reversible.

The analysis of the composition of those compounds in the dissolved state can be carried out by spectrophotometry, owing to the intense color of the compound. The concentration of the compound is assumed to be proportional to its extinction coefficient at a suitable wave length. Then, a variation of the concentration of any one component showed that the extinction is proportional to the concentration of each component, and never to its square or to its square root. An example of such an experiment is shown in figure 11.

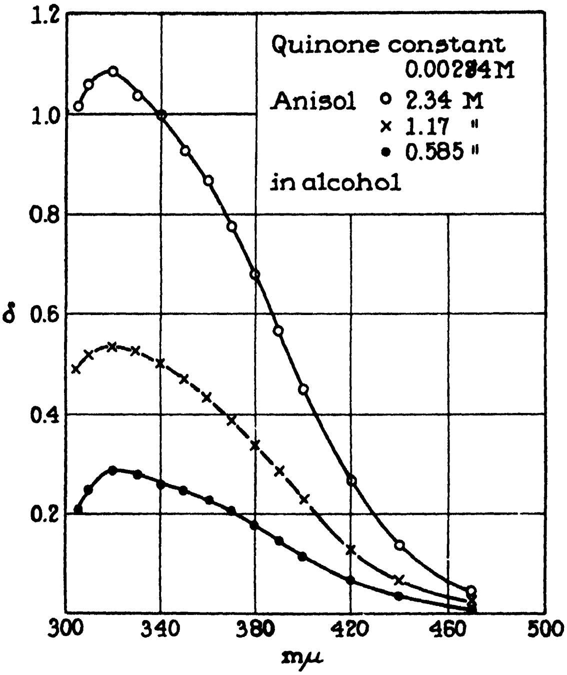

FIG. 11

It is thus shown that a molecular compound formed of two molecular species may be of quite different nature in the solid state from that formed in solution. In the solid state the composition may vary according to the individual compound between QB, QB_2, and Q_2B, but it cannot be varied for one given pair of Q and B. No solid compound is formed when the hydrogen of the phenolic hydroxyl group, or all hydrogen atoms of a polyphenol, are alkylated. Obviously hydrogen bonds are necessary. In the dissolved state, however, only compounds of the composition QB exist, even if the composition of the crystals is QB_2 or Q_2B, and molecular compounds exist even with alkylated phenols, in which case no hydrogen bonds can be formed. In the melted state a molecular compound may be formed, which, on crystallization, entirely dissociates into its components.

REFERENCES

Papers from the author's laboratory, arranged in chronological order

(1) Michaelis, L., and Fetcher, B. S.· J. Am. Chem. Soc. **59,** 2460 (1937).
(2) Michaelis, L., Boeker, G. F., and Reber, R. K.: J. Am. Chem. Soc. **60,** 202 (1938); **60,** 214 (1938).
(3) Michaelis, L., Schubert, M. P., and Granick, S.: J. Am. Chem. Soc. **61,** 1987 (1939).
(4) Michaelis, L., and Granick, S.· J. Am. Chem. Soc. **65,** 1747 (1943).
(5) Michaelis, L., and Granick, S.: J. Am. Chem. Soc. **66,** 1023 (1944).
(6) Michaelis, L., and Granick, S.. J. Am. Chem. Soc. **67,** 1212 (1945).
(7) Michaelis, L.: Cold Spring Harbor Symposia Quant. Biol. **12,** 131–42 (1947).
(8) Michaelis, L., and Granick, S . J. Am. Chem. Soc. **70,** 624 (1948).

General references

(9) Corrin, M. L., and Harkins, W. D.. J. Am. Chem. Soc. **60,** 679–83 (1947).
(10) Holmes, W. C. Ind. Eng Chem. **16,** 35 (1924).
(11) Kelley, E G., and Miller, E G., Jr. J. Biol. Chem. **110,** 113, 119 (1935).
(12) Lison, L.· *Histochimie animale*. Gauthier, Paris (1936).
(13) Lison, L.. Arch. biol. **46,** 599–606 (1935).
(14) Merrill, R. C., and Spencer, R. W.: J. Am. Chem. Soc. **70,** 3683–9 (1948).
(15) Rabinowitsch, E., and Epstein, L. F.: J. Am. Chem. Soc. **63,** 69–78 (1941).
(16) Scheibe, G.: Kolloid-Z. **82,** 1–14 (1938).
(17) Sheppard, S. E.. Rev. Modern Phys. **14,** 303–40 (1942).
(18) Wiame, J. M.· J. Am. Chem. Soc. **69,** 3146 (1947).

SPECTRA OF COPPER COMPLEXES WITH SOME PROTEINS, AMINO ACIDS, AND RELATED SUBSTANCES[1, 2]

IRVING M. KLOTZ, I. LUCILLE FALLER, AND JEAN M. URQUHART

Department of Chemistry, Northwestern University, Evanston, Illinois

Received August 22, 1949

I. INTRODUCTION

Copper complexes with proteins occur in many tissues in both animal and plant species and have been studied extensively for over a century (8). Of particular interest have been hemocyanin, the respiratory pigment of certain invertebrates, and the copper-containing enzymes, such as tyrosinase. Despite the effort expended on the problem, however, there is as yet no clear-cut indication of the nature of the bonds between the metal and any specific protein. In an attempt to contribute to the solution of this problem, an investigation has been made of the spectra of several "artificial" complexes prepared by the addition of cupric ion to crystallized proteins. The optical properties of these complexes, in turn, can be understood best by comparison with those between cupric ion and simple low-molecular-weight substances.

II. EXPERIMENTAL

The cupric ion used in the spectra described came from a reagent grade sample of $CuCl_2 \cdot 2H_2O$. The sodium acetate, acetic acid, and citric acid were also of reagent grade. The betaine hydrochloride, glycolic acid, hippuric acid, and glycine were commercial samples of C.P. or "highest purity" grade. The glycine ethyl ester was prepared by Dr. L. C. King and the glycylglycine by Mr. S. Preis of this laboratory. The glycylglycine was obtained as the hydrochloride monohydrate by following the procedure of Schott, Larkin, Rockland, and Dunn (18).

The peptides—triglycine, tetraglycine, pentaglycine, and hexaglycine—were the gift of Dr. E. F. Mellon of the Eastern Regional Research Laboratory. The samples of β-lactoglobulin and β-casein were also obtained from the Eastern Regional Research Laboratory through the kindness of Dr. T. L. McMeekin.

The bovine serum albumin and γ-globulin were crystallized samples from Armour and Company. The albumin was methylated by exposure to acidified methyl alcohol for 3 days at room temperature, according to the directions of Fraenkel-Conrat and Olcott (9).

Hemocyanin was examined in the form of the serum of the horseshoe crab,

---

[1] Presented at the Twenty-third National Colloid Symposium, which was held under the auspices of the Division of Colloid Chemistry of the American Chemical Society at Minneapolis, Minnesota, June 6–8, 1949.

[2] This investigation was supported in part by grants from the Office of Naval Research (Project No. NR 135054) and from the Carnation Company.

Limulus polyphemus. The serum was obtained by methods described previously (15). The spectrum was obtained on a sample which had been diluted fivefold.[3]

Absorption spectra were obtained with a Beckman spectrophotometer, using cells of 1 cm. depth, d. Molecular extinction coefficients, ϵ, were calculated from the usual expression, $\log_{10} I_0/I = \epsilon c d$, where c is expressed in moles per liter.

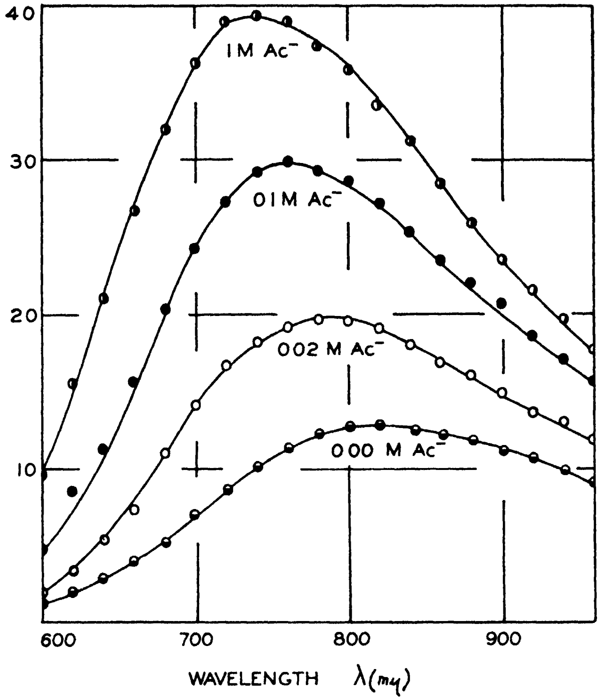

FIG. 1. Spectra of 0.01 *M* cupric ion in acetate solutions of various concentrations. The pH's were 4.49 for the three lowest concentrations and 4.83 for the 1 *M* solution.

III. RESULTS AND DISCUSSION

A. *Copper complexes with carboxylic acids*

Among the simplest of copper complexes with carboxylate ions are those with acetate ion. These complexes have been studied quantitatively by Pedersen (17), who calculated association constants, k^0, for the reactions:

$$Cu^{++} + CH_3COO^- = [Cu(CH_3COO^-)]^+ \qquad k_1^0 = 146 \quad (1)$$

$$[Cu^{++}(CH_3COO^-)]^+ + CH_3COO^- = [Cu(CH_3COO^-)_2] \qquad k_2^0 = 11 \quad (2)$$

The spectra of cupric ion in acetate solutions of various concentrations are illustrated in figure 1. In solutions of 0.02 *M* acetate ion, the position of the peak is at 790 mμ. At this concentration approximately two-thirds of the cupric ion is bound in the monoacetate complex, and perhaps one-tenth is in the form of the diacetate complex, if one may judge from Pedersen's results (17). On the other hand, in the 1 *M* solution, with an absorption maximum at 740 mμ, the cupric ion is found to be about 45 per cent in the form of the diacetate, 45 per cent as triacetate, and about 10 per cent as monoacetate complex.

---

[3] Experiments with hemocyanin were carried out at the Marine Biological Laboratory, Woods Hole, Massachusetts.

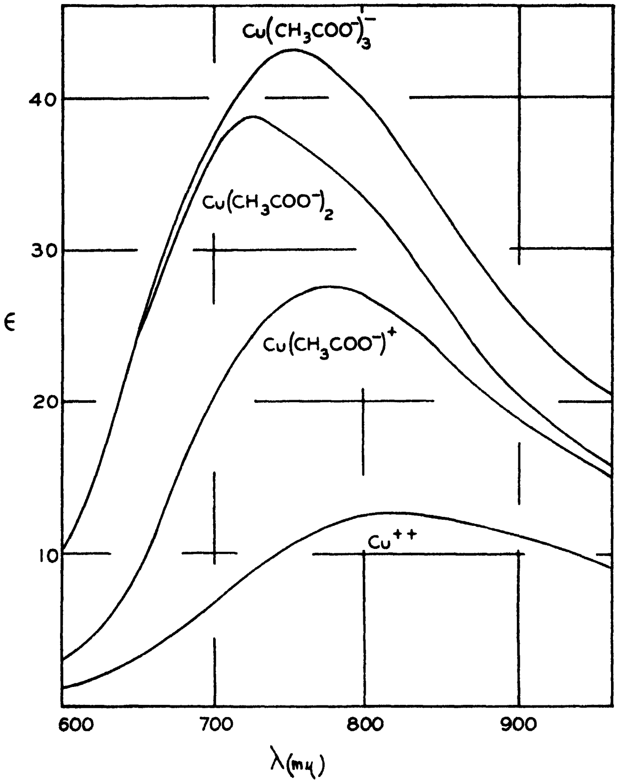

FIG. 2. Calculated absorption curves for three species of cupric-acetate complex near pH 4.5.

From these data on spectra, combined with Pedersen's (17) equilibrium studies, it is possible to calculate approximately the absorption curves which may be attributed to the individual species, $Cu(CH_3COO^-)^+$, $Cu(CH_3COO^-)_2$, and $Cu(CH_3COO^-)_3^-$, respectively. The curves obtained are illustrated in figure 2. Those for the higher complexes are less reliable than that for $Cu(CH_3COO^-)^+$, since they are based on the extrapolated portions of Pedersen's (17) measurements. Nevertheless, it is evident that cupric ion in complexes with carboxyl groups in acetate ions does not have an absorption peak below about 720 mμ even at very high anion concentrations.

In preparation for the interpretation of copper–glycine spectra, an effort was made to evaluate the influence of the positive charge on the substituent attached to the α-carbon atom. For this purpose the spectrum of cupric ion in aqueous betaine solutions was examined. Betaine, $(CH_3)_3\overset{+}{N}CH_2COO^-$, was chosen, since it contains a cationic substituent on the α-carbon atom and yet cannot ionize off a hydrogen ion.

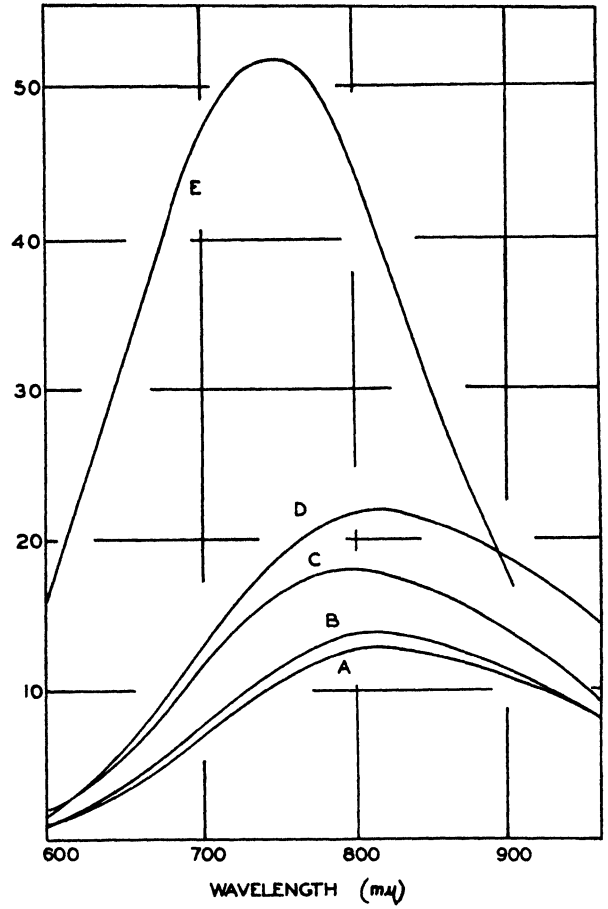

FIG. 3. Absorption spectra of 0.01 *M* cupric ion in solutions of various α-substituted carboxylate-containing organic ions: A, no added organic ion, pH 4.0; B, 0.015 *M* betaine, pH 4.0; C, 0.018 *M* hippurate, pH 4.8; D, 0.017 *M* glycolate, pH 4.8; E, 0.01 *M* citrate, pH 6.6.

The spectrum of cupric ion in 0.015 *M* betaine is illustrated in figure 3. It is apparent from the practically negligible increase in absorption over that of cupric chloride that very little cupric ion has formed a complex with the betaine. The repulsion of the positively charged substituent for the cupric cation evidently is enough to overcome the intrinsic affinity of the carboxyl group.

It is of interest in the case of these betaine complexes of cupric ion to calculate the association constant which might be predicted from theoretical considerations of electrostatic effects. In this treatment we shall neglect any effects of the $(CH_3)_3\overset{+}{N}$— substituent other than that due to the charge. On this basis the difference in the association constants of cupric ion with betaine and with acetate, respectively, may be attributed to the additional electrical work necessary to bring up the metallic cation to the betaine. Following Bjerrum (3), Neuberger (16), and others, we may obtain this electrical work, W_e, from the equation

$$W_e = -2e\psi \tag{3}$$

where ψ is the potential produced by the positively charged trimethylammonium substituent at the distance r from the carboxyl group, and e is the electronic unit of charge. The coefficient 2 arises from the divalency of the cupric ion, and the negative sign from the fact that electrical work must be done on the system in the reaction

$$Cu^{++} + (CH_3)_3\overset{+}{N}CH_2COO^- \rightleftharpoons Cu[(CH_3)_3\overset{+}{N}CH_2COO^-]^{++} \tag{4}$$

if we consider only the electrostatic effect of the $(CH_3)_3\overset{+}{N}$— group. For the present calculation, the potential ψ will be taken as

$$\psi = \frac{e}{Dr} \tag{5}$$

where D is the dielectric constant of the solvent. In view of the approximate nature of the calculation, no attempt will be made to introduce an "effective dielectric constant," such as has been suggested by Kirkwood and Westheimer (13), to take into account the cavity of low dielectric constant formed by the molecule itself. The electrical work becomes, therefore,

$$W_e = -\frac{2e^2}{Dr} \tag{6}$$

The differences in free energy of formation of the cupric complex with betaine and acetate, respectively, may be expressed, therefore, by the equation:

$$\Delta F_{\text{Cu-betaine}} - \Delta F_{\text{Cu-acetate}} = +\frac{2e^2N}{Dr} \tag{7}$$

where the introduction of N, Avogadro's number, converts the electrical work to a mole basis. If a value of 1.25 Å. is used for r, since such a value in acidity calculations (16) compensates for the use of the dielectric constant of the solvent for D, we find that the first association constant for the copper–betaine complex, k_1^0, should be

$$k_1^0 = 1.8 \times 10^{-3} \tag{8}$$

Such a value for an *association* constant is exceedingly small and implies that practically no cupric ion would be united in a complex with betaine. The observed behavior thus is qualitatively in agreement with this prediction. More detailed experiments would be necessary before quantitative agreement can be checked.

The absorption spectrum of cupric ion in solution of 0.018 *M* hippurate ion, $C_6H_5CONHCH_2COO^-$, has also been examined. In this case the positive charge of the glycine nitrogen has been eliminated but the $-\overset{\mathrm{H}}{\underset{\cdot\cdot}{\mathrm{N}}}-$ group has been retained. The absorption curve (figure 3) is below that of cupric ion in an acetate solution of roughly equal concentration (0.02 *M*). Evidently the substituent on the α-carbon atom contributes no specific affinity for the metal cation. As a result, only the polarity of the group manifests itself. The polar substituent in the α-position should reduce the affinity of the carboxyl group for cupric ion, if electrostatic considerations (3, 13, 16) alone are applicable.

In glycolic acid, in contrast to hippuric, the hydroxyl substituent on the α-carbon atom does seem to contribute to the stability of the copper complex. From polar considerations alone one would expect a decrease in affinity. Actually, the absorption of cupric ion in 0.017 *M* glycolate solution (figure 3) is somewhat more intense than that in 0.02 *M* acetate solution. Evidently the hydroxyl group stabilizes the Cu^{++} carboxyl bond, perhaps by entering itself into a bond with the cation. An enhancement of cation binding by α-hydroxy groups in organic carboylic acids has been observed also with the alkali metal ions (6).

A marked increase in the formation of complexes of cupric ion is observed with citrate ion (figure 3), in which a molecular extinction coefficient of over 50 is reached in a 0.01 *M* solution. In this case, the added affinity comes not only from electrostatic attraction of the negatively charged substituents but also from the statistical effect of having three carboxylate groups available to the cation.

It is of interest to note that the wave length of maximum absorption of copper citrate is at 7400 Å., just as it is in the case of 1 *M* acetate complexes, but that the intensity of absorption is higher. Since the cupric ion in the 1 *M* acetate solution is roughly equally divided between the di- and tri-acetate complexes, it seems reasonable to surmise that in the citrate complex all three carboxyl groups are linked to the copper. It is then apparent that even a triple complex of cupric ions and carboxyl groups does not show an absorption peak below about 7400 Å.

B. Copper complexes with glycine

The spectrum of cupric ion in aqueous glycine solutions is highly sensitive to pH, as has been clearly demonstrated previously by Borsook and Thimann (4). Typical data over the pH region of 3 to 8 are illustrated in figure 4. In the most acid solution investigated, at pH 3.09, the spectrum is quite similar to that of an acetate complex both in the height and in the wave length of the peak. Nevertheless, it seems unlikely that the cupric ion linkage is through the carboxyl group, for the electrostatic effect of the cationic $-\overset{+}{\mathrm{N}}\mathrm{H}_3$ substituent should be about the same as in betaine,[4] and hence practically no cupric ion should be in the complex at a glycine concentration of 0.02 *M*.

---

[4] The approximate equality in electrostatic effect of $-\overset{+}{\mathrm{N}}\mathrm{H}_3$ and $-\overset{+}{\mathrm{N}}(\mathrm{CH}_3)_3$ is seen from a comparison of the change in pK of the carboxyl group of the corresponding substituted acetic acids. In glycine pK_a is 2.34 (7) and in betaine it is 1.82 (10), as compared to 4.756 (11) for the parent acetic acid. ΔpK thus is 2.42 and 2.94, respectively.

As the pH is raised, the spectra of Cu^{++}–glycine complexes shift to shorter wave lengths and to higher extinction coefficients and approach a limit of 6250 Å. for λ_{max} and about 47 for ϵ_{max}. This shift parallels the ease of removal of a hydrogen ion from $-\overset{+}{N}H_3$ as the pH is increased. It seems likely, therefore, that the cupric ion is bound in a complex at least in part through the amine group. Once an $-NH_2 \cdots Cu^{++}$ bond is formed, complex formation with the carboxyl group would be facilitated, since the anionic carboxyl would be attracted to the cationic metal.

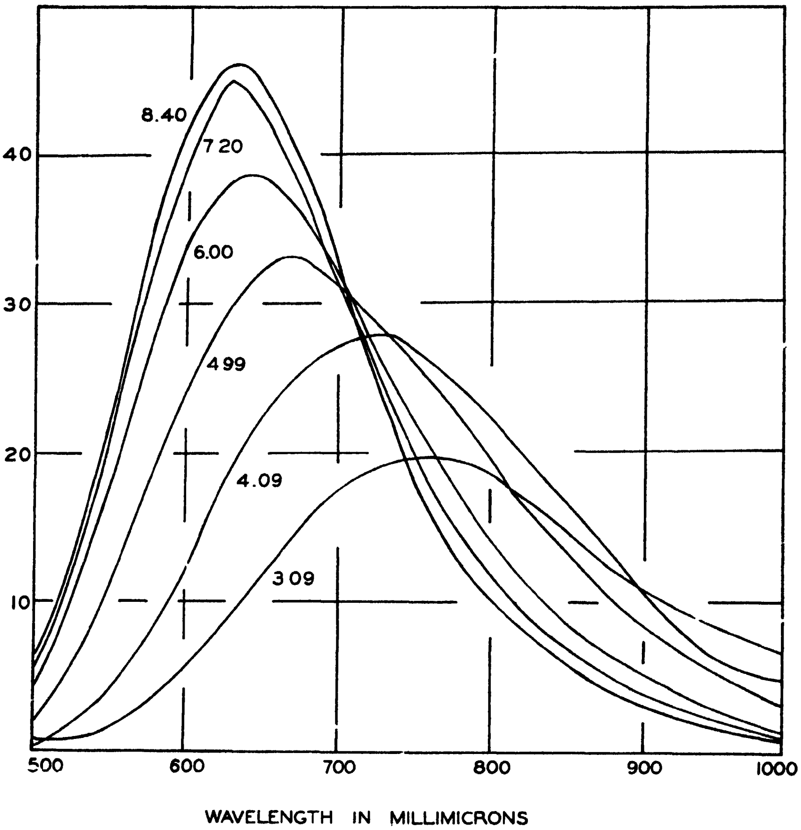

FIG. 4. Dependence of spectrum of copper–glycine complex on pH. The glycine:Cu^{++} ratio is 2. The numbers shown are the pH's as measured by a glass electrode.

The importance of the anionic COO^- group in glycine in stabilizing the cupric ion complex is seen clearly by comparison of the spectrum in the amino acid solution (figure 4) with that in a solution of glycine ethyl ester at pH 4.50 (figure 5). In the latter case practically no cupric ion is bound in a complex, despite the fact that the pK of the $-\overset{+}{N}H_3$ group is lower than that in glycine (7) and hence more favorable for the displacement of a hydrogen ion by a cupric ion. The entirely different behavior in glycine indicates clearly that the carboxyl group provides the added attraction necessary to bind the cupric ion.

The displacement of a hydrogen ion from the —$\overset{+}{N}H_3$ group in the binding of cupric ion by glycine is also indicated by the much less intense spectrum of cupric ions in hippurate solution, where the substituted nitrogen does not have much tendency to be an electron donor.

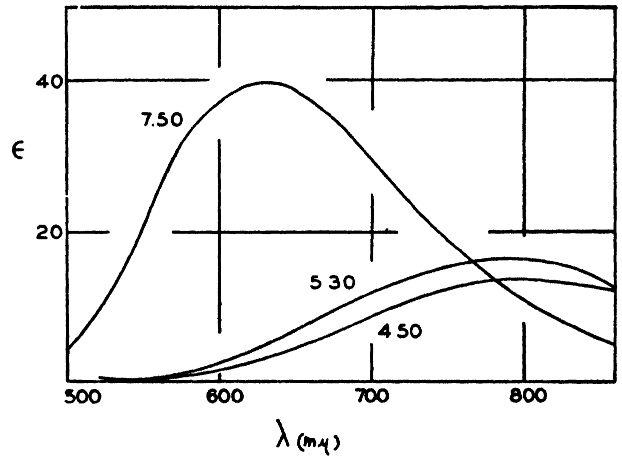

FIG. 5. Absorption spectra of cupric ion complex with glycine ethyl ester at various pH's. The glycine ester Cu^{++} ratio is 2 and the cupric-ion concentration near 0.01 *M*. The numbers shown are the pH's as measured by a glass electrode.

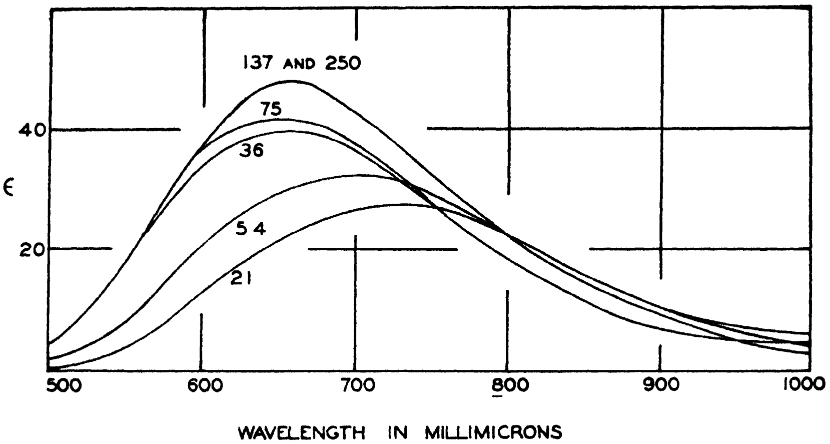

FIG. 6. Dependence of spectrum of copper–glycine complex on concentration of the amino acid. The numbers shown are the ratio of glycine : Cu^{++}. The cupric-ion concentration was 0.01 *M* and the pH 4.0 in all cases.

The effect of increasing glycine concentration at an acid pH, illustrated in figure 6, is very similar to that of increasing the pH. The absorption maximum approaches 6500 Å. and an ε of 47 as the glycine concentration is increased to 2.5 *M*. It would seem, therefore, that the nature of the bonds in copper–glycine complexes is the same at pH 4 as at 8, but that there is a lower ratio of glycine: cupric ion at the lower pH, at equivalent glycine concentrations.

C. Copper complexes with polypeptides

The spectra at pH 7.5 of copper complexes with a series of polyglycines, varying from diglycine to hexaglycine, have been compared with each other and with glycine in figure 7. It is of interest to note that all of the polyglycines show more intense absorption and have peaks at lower wave lengths than does glycine. In the latter complex it is generally assumed that the molecule forms a chelate ring with cupric ion, as illustrated by formula I.

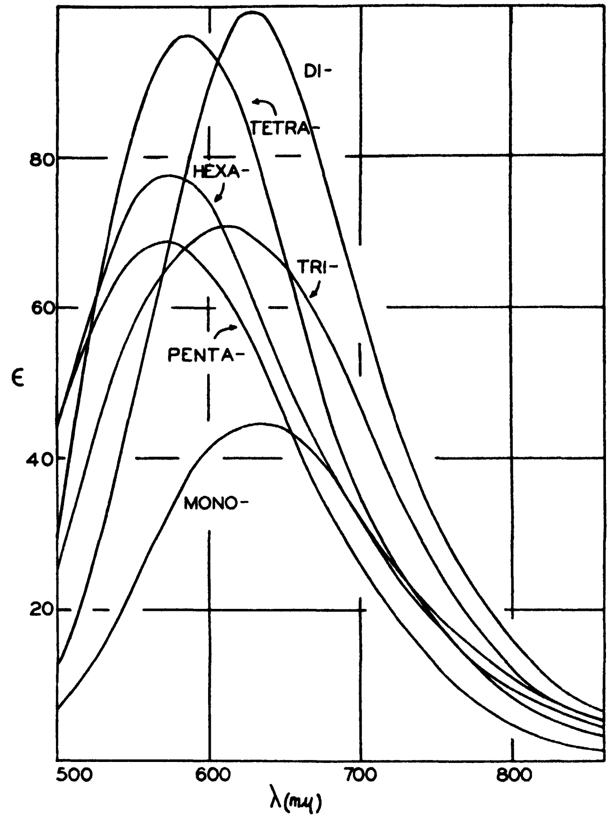

FIG. 7. Spectra of cupric-ion complexes with glycine and with polyglycines (di- to hexaglycine) at pH 7.5 The zwitterion: Cu^{++} ratio was approximately 2.1 in each case, except in the case of pentaglycine where it was 2.7 and hexaglycine where it was 2.4. The cupric-ion concentration was near 0 01 M in each case.

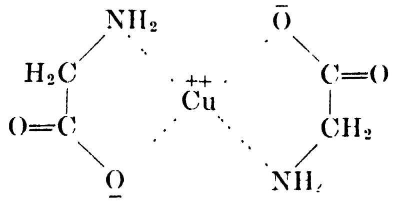

I

Such chelate ring formation is unlikely with the larger molecules, since the large rings formed would be strained and relatively unstable. Nevertheless, it is apparent from the intensity and position of the Cu^{++}–polyglycine spectra that the extent of coördination of the cation is at least as great as in the monoglycine. In fact, the spectra of the polyglycine complexes are very close to those of tetracoördinated amine complexes of copper (2).

A tetracoördinated copper complex with a polyglycine, involving combined carboxyl and amine interaction, would be possible with a structure such as II,

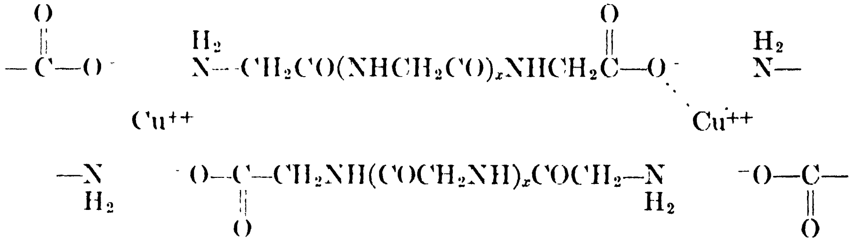

$$\begin{array}{ccc} -\overset{\overset{O}{\|}}{C}-O^- & \overset{H_2}{N}-CH_2CO(NHCH_2CO)_xNHCH_2\overset{\overset{O}{\|}}{C}-O^- & \overset{H_2}{N}- \\ & Cu^{++} \qquad\qquad\qquad\qquad\qquad\qquad Cu^{++} & \\ \underset{H_2}{-N} & {}^-O-\underset{\underset{O}{\|}}{C}-CH_2NH(COCH_2NH)_xCOCH_2-\underset{H_2}{N} & {}^-O-\underset{\underset{O}{\|}}{C}- \end{array}$$

II

suggested to us by Professor F. Basolo (1). No ring strain would be encountered in this type of structure, yet the extent of coördination of the central cupric ion would be as great in these peptides as in glycine. With the peptides, furthermore, the smaller pK of the $-\overset{+}{N}H_3$ group would make it easier to displace a hydrogen ion by a cupric ion; hence a greater degree of complex formation would be possible at comparable concentrations. The increase in complex formation would account for the higher optical absorption of the cupric ion in peptide solutions.

D. Copper complexes with proteins

Preceding investigations (14) have demonstrated that cupric ion combines extensively with crystallized bovine serum albumin at pH's between 4 and 5. Preliminary and incomplete spectra indicated that the carboxyl groups on the protein were involved in the linkage with cupric ions. A more detailed spectral examination has seemed desirable, however, particularly in view of the more extensive background data described in this paper. For this purpose, therefore, the absorption spectra of Cu^{++}–albumin complexes were examined in solutions of varying concentration of protein.

The results with a 2 per cent albumin solution at pH 4.5 are illustrated in figure 8. The shape of the curve is very similar to that of copper–acetate complexes (figure 1). It is of interest, therefore, to compare the observed molecular extinction coefficient with the value which might be expected from the number of free $-COO^-$ groups from glutamate and aspartate residues in the protein. A 2 per cent solution of albumin (whose molecular weight is 70,000) corresponds to a 0.0003 M solution. Since there are 93 free COO^- groups per mole of albumin (5), the carboxyl-ion concentration is approximately 0.03 M. The observed molecular extinction coefficient of 25 is quite close to the value one would expect for a 0.03 *M* solution of acetate ions, as estimated from the data in figure 1.

Further evidence of the participation of carboxyl residues on the protein in the binding of copper below pH 5 is available from studies with chemically modified albumins. Thus the spectrum (figure 8) of cupric ion in a 2 per cent solution of an albumin sample whose COO^- groups have been partially converted to $—COOCH_3$ groups is distinctly lower than that of the parent protein. On the other hand, an albumin in which the amino groups of the lysine residues had been acetylated showed no evidence of loss of ability to interact with cupric ion. In this case a spectrum could not be taken, however, for the acetylamino-bovine albumin precipitated immediately upon the addition of cupric ions.

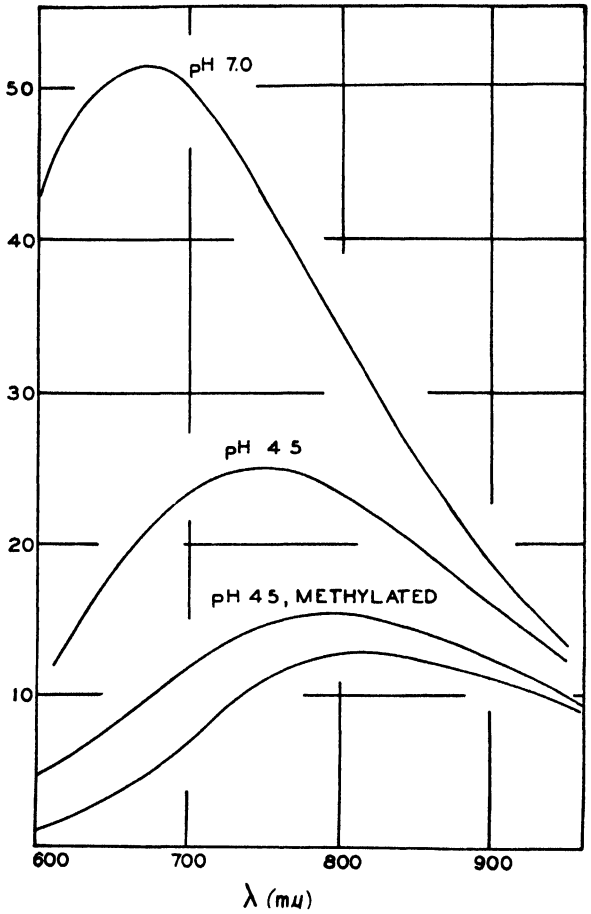

FIG. 8. Spectra of 0.01 *M* cupric-ion complexes with bovine serum albumin, parent and methylated, respectively. The spectra at pH 4.5 were with 2 per cent albumin solutions, that at pH 7 with a 9.8 per cent protein concentration. The lowest curve is that for 0.01 *M* cupric ion alone at pH 4.5.

The behavior was very similar to that of polyglutamic acid in the presence of cupric ions. In both cases, apparently, complex formation between cupric ion and the free COO^- groups removes the last polar residues in the macromolecule and hence insolubilizes the complex.

In a solution of pH 7 the effect of bovine albumin is distinctly different from that at pH 4–5. The absorption maximum of cupric ions (figure 8) is moved to 670 mμ, i.e., toward the region for amine-type bonding. It would seem, therefore, that at the higher pH, $Cu \cdots NH_2$— linkages become possible in this protein, just as they are favored in the simpler molecules discussed earlier. Spectra at higher pH's have not been investigated as yet, but they would be expected to be moved toward even shorter wave lengths.

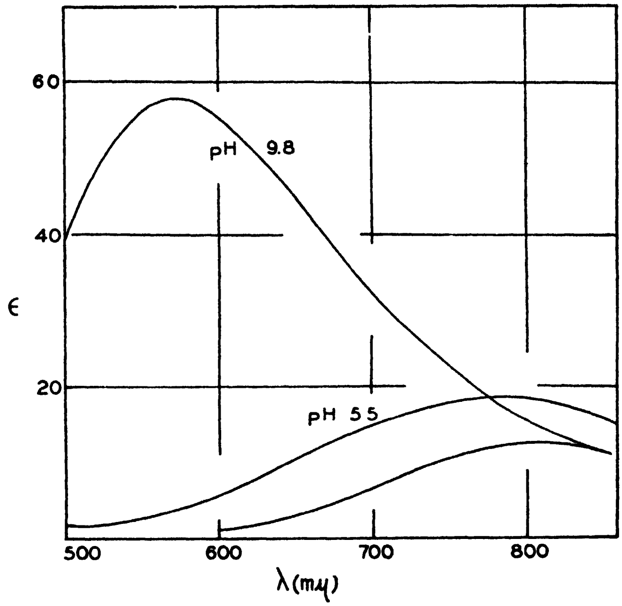

FIG. 9. Spectra of 0.01 *M* cupric-ion complexes with β-lactoglobulin (0.7 per cent) at the pH's indicated. The lowest curve is that for 0.01 *M* cupric ion alone at pH 4.5.

At a pH near 5, β-lactoglobulin (figure 9) and bovine serum γ-globulin (figure 10) also produce changes in the spectrum of cupric ion which by their appearance are consistent with a copper-carboxyl type of linkage. The γ-globulin has the smallest effect of the three natural proteins examined. It is of interest to note in this connection that the content of free COO^- residues is also lowest, per unit weight, in this protein (5).

The spectrum of copper–β-lactoglobulin complexes has been examined also at a higher pH, 9.8. The shift in wave length of the maximum (figure 9) is quite pronounced, and its position at 580 mμ and molecular extinction coefficient of nearly 60 are quite characteristic of the results obtained with copper complexes with simple amines and with polypeptides. There is thus very strong evidence that at pH's which are sufficiently high for the $—\overset{+}{N}H_3$ groups to lose their positive charge, cupric ion will form a complex with amine groups on the protein.

Similar results have been observed at pH's near 10 with β-casein (figure 10). Again the absorption maximum is in a region characteristic of the copper–amine type of linkage. The result with casein is particularly interesting, since this protein has a very low cysteine (or cystine) content, and hence practically no available sulfhydryl groups. It is apparent, therefore, that extensive copper binding can occur with proteins with linkages that do not involve —SH groups.

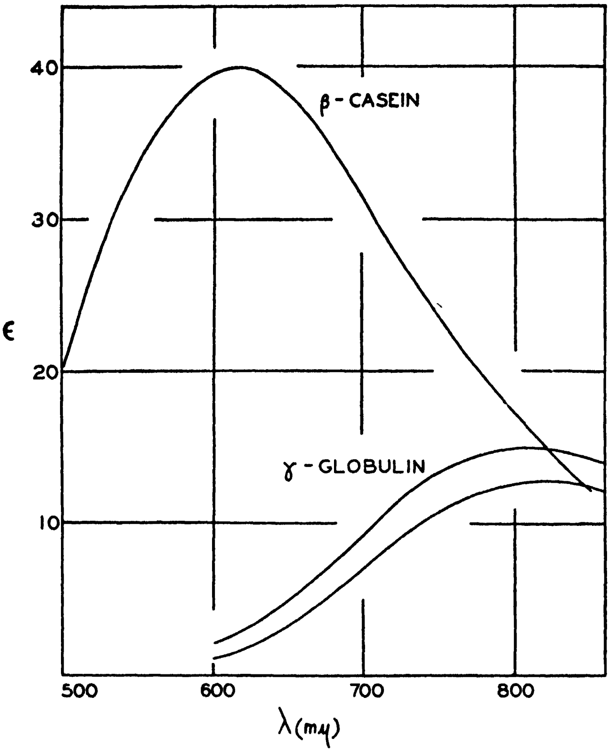

FIG. 10. Spectra of 0.01 *M* cupric-ion complexes with bovine serum γ-globulin (1 per cent, pH 4.5) and with β-casein (0.2 per cent, pH 9.9). The lowest curve is that for 0.01 *M* cupric ion alone at pH 4.5.

With this backlog of spectroscopic information it is of interest to examine a few of the naturally occurring copper proteins. The spectrum of hemocyanin, in the serum of the horseshoe crab, is illustrated in figure 11. The high molecular weight of this protein leads to much scattering at shorter wave lengths, and hence a steep rise in absorption is observed near 400 mμ. There is no doubt, however, that the cupric ion absorption peak occurs at 580 mμ. Similarly, in the copper-containing serum protein described by Holmberg and Laurell (12), the absorption peak occurs at 605 mμ. In both cases the position of the maximum is in the region of tetracoördinated copper complexes such as those illustrated in several of the figures in this paper. In hemocyanin, indirect evidence has been cited (8) that the copper is in the univalent state. In view of the similarity in spectrum of this copper protein with others described in this paper, it may be worthwhile to reëxamine the question of the valence of copper in oxyhemocyanin.

From the data presented it is apparent that the absorption peak of cupric ion in complexes shifts toward shorter wave lengths as the coördination number is increased. Tetracoördinated copper, even if two of the ligands are carboxyl groups, exhibits a spectrum in the neighborhood of 6000 Å. Both naturally occurring and artificially constructed copper proteins also absorb in the region of 6000 Å., if the pH of the solution is above 7. It seems likely, therefore, that in both types of protein the cupric ion is tetracoördinated, and that at least two of the bonds are to amine groups in the protein molecule.

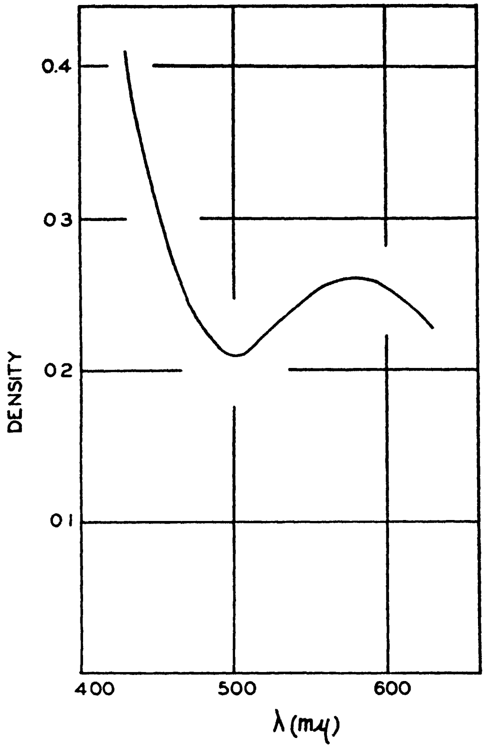

FIG. 11. Spectrum of serum of *Limulus polyphemus*, diluted 1:5, at pH 7.7

IV. CONCLUSIONS

The specificity of copper proteins may then arise from at least two configurational factors. In the metal enzymes, the type of substrate which is susceptible to the metalloprotein may be determined by the arrangement of residues in the neighborhood of bound cupric ion. The specific arrangement of these groups would determine whether the substrate could be bound by the protein at a position adjacent to the cation. Another configurational factor, which may be particularly important in hemocyanin, may lie in the relative positions of bound copper atoms. It has been well established (8) that in oxyhemocyanin the unit weight of protein which combines with one molecule of oxygen contains two copper atoms. It seems quite possible, therefore, that the oxygen molecule may act as a bridge between two copper ions, if the distance between the metals is properly fixed. Since cupric ion can have a coördination number of five, the linkage to the oxygen may supply the fifth bond. At present, however, such a structural picture lies largely in the realm of speculation.

V. SUMMARY

Optical absorptions in the region of 400–1000 mμ have been measured for cupric ion complexes with several simple, substituted carboxylate ions, including acetate, glycolate, citrate, hippurate, and betaine. These have been used to evaluate the effects which various substituents on the α-carbon atom have on the stability of the copper–carboxyl bond. Spectra of cupric ion complexes with glycine ethyl ester have also been obtained as an example of an amine-type combination.

The effects of glycine, diglycine, triglycine, tetraglycine, pentaglycine, and hexaglycine, respectively, on the absorption of cupric ions have also been measured. These have been used as a basis for the interpretation of the observed spectra of copper complexes with serum albumin, serum γ-globulin, β-lactoglobulin, and β-casein, respectively, and of hemocyanin. All copper proteins at pH's above 7 have been found to absorb light in the region of 600 mμ, a behavior which indicates that the copper is tetracoördinated and that at least two bonds are of the amine type.

REFERENCES

(1) Basolo, F.: Private communication.
(2) Bjerrum, J., and Nielsen, E. J.: Acta Chem. Scand. **2,** 297 (1948).
(3) Bjerrum, N.: Z. physik. Chem. **106,** 219 (1923).
(4) Borsook, H., and Thimann, K. V.: J. Biol. Chem. **98,** 671 (1932).
(5) Brand, E.: Ann. N. Y. Acad. Sci. **47,** 187 (1946).
(6) Cannan, R. K., and Kibrick, A.: J. Am. Chem. Soc. **60,** 2314 (1948).
(7) Cohn, E. J., and Edsall, J. T.: *Proteins, Amino Acids and Peptides*, pp. 84, 99. Reinhold Publishing Corporation, New York (1943).
(8) Dawson, C. R., and Mallette, M. F.: Advances in Protein Chem. **2,** 179 (1945).
(9) Fraenkel-Conrat, H., and Olcott, H. S.: J. Biol. Chem. **161,** 259 (1945).
(10) Gustafson, C.: Ber. **77B,** 66 (1944).
(11) Harned, H. S., and Ehlers, R. W.: J. Am. Chem. Soc. **55,** 652 (1933).
(12) Holmberg, C. G., and Laurell, C. B.: Acta Chem. Scand. **2,** 550 (1948).
(13) Kirkwood, J. G., and Westheimer, F. H.: J. Chem. Phys. **6,** 506 (1938).
(14) Klotz, I. M., and Curme, H. G.: J. Am. Chem. Soc. **70,** 939 (1948).
(15) Klotz, I. M., Schlesinger, A. H., and Tietze, F.: Biol. Bull. **94,** 40 (1948).
(16) Neuberger, A.: Proc. Roy. Soc. (London) **A158,** 68 (1937).
(17) Pedersen, K. J.: Kgl. Danske Videnskab. Selskab, Mat.-fys. Medd. **22,** No. 12 (1945).
(18) Schott, H. F., Larkin, J. B., Rockland, L. B., and Dunn, M. S.: J. Org. Chem. **12,** 490 (1947).

ELECTROPHORETIC ANALYSIS OF PROTEIN INTERACTION. I

The Interaction of Bovine Serum Albumin and Methyl Orange[1, 2]

ROBERT F. SMITH AND D. R. BRIGGS

Division of Agricultural Biochemistry, University of Minnesota, St. Paul 1, Minnesota

Received August 22, 1949

During the last few years the investigation of the interaction of proteins with other substances in solution has shown great promise of giving new information on the physical structure of proteins and the mechanism of their action in living systems. Any method which can yield information about the nature of such complexes is therefore worthy of consideration in the light of this fundamental objective. A number of papers have appeared in which it has been demonstrated that for a mixture of components where interaction occurs, the configuration of the Tiselius electrophoresis pattern obtained with the system reflects such interaction when one or more of the interacting components migrates in the electric field. Complex formation of proteins with proteins (8, 14), of proteins with nucleic acid (5, 10, 16), of proteins with polysaccharides (4, 15), and of proteins with lower-molecular-weight ionogenic substances (3, 9, 11, 13) have been indicated from the electrophoretic analyses of such mixtures.

In searching for an interpretation of the behavior of such systems in terms of the interaction constants involved it would appear advisable to start with as simple a system as possible. The equilibrium involved in the formation of the complex should be one which is established rapidly in relation to the rate of separation of the components by electrophoresis, the interaction should be strong enough to be readily detectable at low concentrations of the non-protein interactant, and the equilibrium constants should be determinable by independent methods. The reaction of serum albumin with non-aggregating monovalent dyes seems to fulfill these requirements. In our experiments, therefore, we have used bovine serum albumin with methyl orange as the interacting anion—mainly because of the extensive investigations which have already been carried out by Klotz (7) and coworkers with this mixture. They have shown that the interaction obeys the law of mass action and can be described by the Langmuir adsorption isotherm in the form:

$$\frac{1}{r} = \frac{K}{n \cdot [\mathrm{A}]} + \frac{1}{n} \tag{1}$$

where r = moles of bound dye anion per mole protein = $([\mathrm{A}_0] - [\mathrm{A}])/[\mathrm{P}_0]$

---

[1] Presented at the Twenty-third National Colloid Symposium, which was held under the auspices of the Division of Colloid Chemistry of the American Chemical Society at Minneapolis, Minnesota, June 6–8, 1949.

[2] Paper No. 2499, Scientific Journal Series, Minnesota Agricultural Experiment Station. The contents of this paper constitute a part of the thesis to be submitted by R. F. Smith to the Graduate School of the University of Minnesota in partial fulfillment of the requirements for the degree of Doctor of Philosophy.

n = the limiting value of this ratio as $[A] \rightarrow \infty$, or the maximum number of binding sites,
K = a dissociation constant,
$[A_0]$ = the total molar concentration of the dye,
$[A]$ = the molar concentration of free dye anions, and
$[P_0]$ = the molar concentration of the protein.

The constants n and K are obtained by plotting $[P_0]/([A_0] - [A])$ against $1/[A]$. Our studies have shown that, when $[A_0]$ and $[P_0]$ are known, the values of $[A]$ in the original solutions may be calculated from the boundary patterns obtained after the protein–dye mixture has been subjected to electrophoresis. A series of experiments made at varying ratios of $[A_0]$ to $[P_0]$ will yield the data required for the plot of $1/r$ *versus* $1/[A]$ and hence the interaction constants, n and K, of the reaction.

Two groups of electrophoresis experiments, which are important to our present discussion, were set up as follows: These groups of experiments will be referred to as group 1 and group 2. In both groups the buffer employed was acetate buffer, pH 5.5 (25°C.), ionic strength 0.05. The protein used was crystallized bovine serum albumin (Armour) and the dye employed was twice recrystallized sodium *p*-dimethylaminoazobenzene-*p*′-sulfonate (the sodium salt of methyl orange). Standard protein, dyestuff, and buffer solutions were made up such that when measured volumes of each were employed and diluted to a proper volume with water the required final solutions would be obtained. In the calculations, the molecular weight of 67,000 was used for this protein.

In experiments of group 1 a known amount of protein in a known volume of buffer was placed in a cellophane sac and allowed to dialyze to equilibrium without volume change at 4°C. against a known volume of buffer containing a known amount of dye. In the manner already described by Klotz *et al.* (7) the equilibrium values of $[A]$, $[A_0]$, and $[P_0]$ were obtained. From the series of experiments with varying ratios of $[P_0]$ to $[A_0]$ the plot of $1/r$ *versus* $1/[A]$ yields values of $n = 22.6$ and $K = 3.12 \times 10^{-4}$, which were in fair agreement with those reported by Klotz *et al.* for this system ($n = 22.4$ and $K = 4.48 \times 10^{-4}$).[3]

Figure 1 shows the data from these experiments plotted by the alternate linear form of equation 1, i.e., $[A]/r$ *versus* $[A]$. It is to be noted that for values of $[A]$ below about 2×10^{-4} molar the curve is linear and the values of K and n are those given above, but at higher concentrations of $[A]$ (greater than 6×10^{-4} molar) the resultant value of n increases and that of K decreases. This may mean that a second group of sites for interaction becomes important at high equilibrium dye concentrations. This possibility will be alluded to in the latter part of this paper in relation to the characteristics of the Tiselius patterns as obtained at these higher equilibrium concentrations of the dye.

For each system, so equilibrated, electrophoresis experiments were carried out at 4°C. in which the protein–dye mixture (inside the sac) was used as the lower solution in the U-tube and the equilibrium buffer–dye solution (outside the sac) was the overlying solution. Under these circumstances only one boundary migrated in each leg of the cell. (At higher dyestuff concentrations (greater than 10^{-3} molar) boundary splitting on the descending side is observed.) Figure 2

---

[3] The experiments of Klotz *et al.* were done in 0.1 M phosphate buffer, pH 5.67.

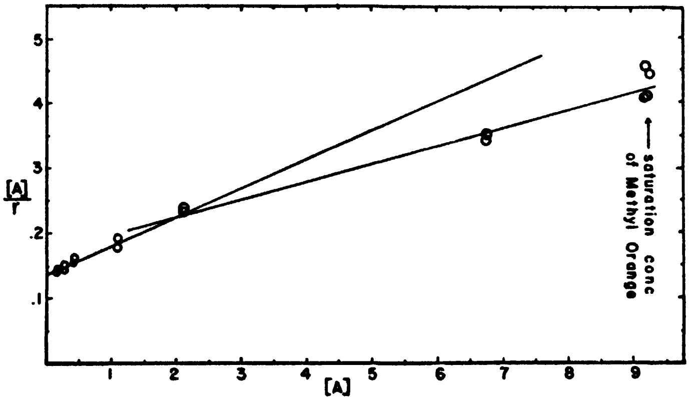

FIG. 1. Dialysis equilibrium data on bovine serum albumin and methyl orange. [A]/r (moles per liter × 10^4) *versus* [A] (moles per liter × 10^4).

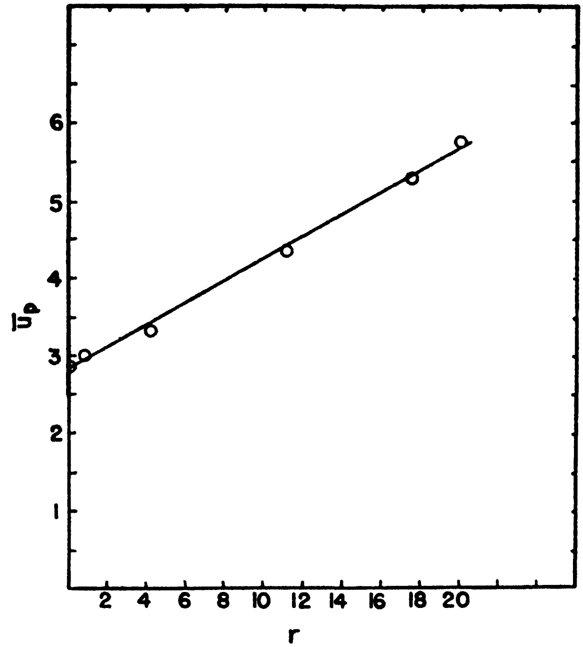

FIG. 2. Constituent mobility of the protein, $\bar{u}_P$ (cm.^{2} v.$^{-1}$ sec.$^{-1}$ × 10^5) *versus* r

shows the results obtained where the mobility found for the descending moving boundary in each experiment is plotted against the corresponding value of ([A_0] − [A])/[P_0]. It will be noted from the linear relationship shown that a unit increase in the moles of bound anion per mole of protein is accompanied by an increase in the constituent mobility of the protein (i.e., the mobility of the boundary in which the protein disappears in presence of the dye (17, 18)) equal to 0.13×10^{-5} cm.^{2} v.$^{-1}$ sec.$^{-1}$ This is about 0.33 the mobility increment due to one added electronic charge as indicated from titration data and is in qualitative agreement with the results of Longsworth and Jacobsen (9), who found that a bound methyl orange anion increased the albumin mobility about 0.4 as much as did one electronic charge.[4]

In the experiments of group 2 the protein–dye mixtures to be used as the underlying solution in the U-tube were prepared by combining measured volumes of the standard protein, standard dye, and standard acetate buffer solutions with an amount of water needed to yield a final solution of the desired pH, ionic strength, and protein and dye concentrations. As the overlying solution, buffer of the same pH and ionic strength as that of the protein–dye solution was used. Under these circumstances no dye was present in the overlying solution and, upon electrophoresis, patterns characterized by asymmetries which have been described by Longsworth and MacInnes (10) were obtained. Figures 5a, 5b, and 5c are tracings of typical scanned patterns obtained with such serum albumin–methyl orange mixtures (where the equilibrium value for [A] was less than 2×10^{-4} molar). Patterns are entirely reproducible and the areas and mobilities of the peaks are independent of the time of electrophoresis. The δ- and ϵ-boundaries are not appreciably different in magnitude from those obtained when the protein solution is dialyzed against the overlying buffer. The slow peak on the descending side migrates with the mobility of free protein and the fast peak on the ascending side (when detectable) migrates with the mobility of free dye, but the relative areas under the migrating peaks, the mobility of the leading peak on the descending side, and the mobility of the slower boundary on the rising side all vary with the relative (and absolute) concentrations of the interacting components.

The solutions in the Tiselius cell at the beginning of an experiment (group 2) are represented in figure 3a. ΣPA_i represents a series of complexes from $i = 0$ to $i = n$ existing in different concentrations in equilibrium with each other. A^- represents free dye anion. Protein, dye, and their complexes are all negatively charged at pH 5.5. In these experiments $u_A > \bar{u}_A > \bar{u}_P > u_P$ (see below for meanings of these mobility symbols). Figures 3b and 3c represent the situation in the rising and descending boundaries as developed after electrophoresis.

Before attempting to describe the behavior of this system in an electric field we must know something about the influence of the interaction upon the mobilities of each of the components as it migrates in the presence of the other. Tiselius (18) has given an equation for the constituent mobility of a component which exists in a number of forms in equilibrium with one another when the equilibrium is established rapidly as compared to the rate of electrophoretic separation:

$$\bar{u}_x = a_1 u_{x_1} + a_2 u_{x_2} + \cdots + a_n u_{x_n} \tag{2}$$

---

[4] The result of Longsworth and Jacobsen was obtained in buffers of somewhat higher ionic strength.

where $\bar{u}_x$ is the constituent mobility of the component x, or the resultant mobility of any molecule of x taken on a time average, a_i is the fraction of total x in the i^{th} form, and u_{x_i} is the mobility of the i^{th} form. Let us represent total molar concentration of protein and of dye by $[P_0]$ and $[A_0]$, respectively, moles per liter of free protein and free dye by [P] and [A], moles per liter of the i^{th} complex by $[PA_i]$, moles per liter of bound dye by $[A_0] - [A]$, the constituent mobilities of protein and dye by $\bar{u}_P$ and $\bar{u}_A$, and the mobilities of free protein and free dye by u_P and u_A.

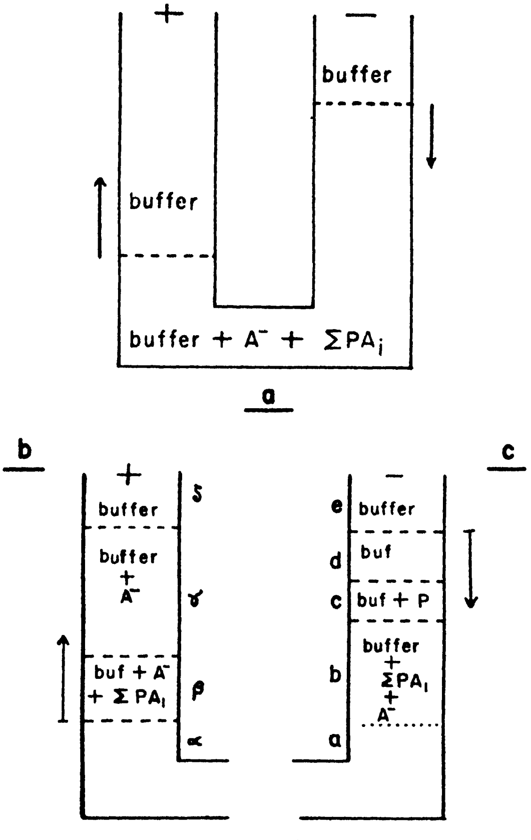

FIG. 3. Diagrammatic representation of the Tiselius cell before and after the development of the boundaries, showing the composition of the solutions in different parts of the cell and the designations used for the different regions.

The constituent mobility of the protein is:

$$\bar{u}_P = \frac{[P]}{[P_0]} u_P + \frac{[PA]}{[P_0]} u_{PA} + \frac{[PA_2]}{[P_0]} u_{PA_2} + \cdots + \frac{[PA_n]}{[P_0]} u_{PA_n}$$

$$= \frac{1}{[P_0]} \sum_{i=0}^{n} [PA_i] u_{PA_i}$$

If we assume that each anion bound increases the mobility of its complex by the same amount ($=w$), then $u_{\mathrm{PA}_i} = u_{\mathrm{P}} + iw$ and

$$\bar{u}_{\mathrm{P}} = \frac{1}{[\mathrm{P}_0]} \sum_{i=0}^{n} (u_{\mathrm{P}}[\mathrm{PA}_i] + iw[\mathrm{PA}_i]) = \frac{u_{\mathrm{P}}}{[\mathrm{P}_0]} \sum_{i=0}^{n} [\mathrm{PA}_i] + \frac{w}{[\mathrm{P}_0]} \sum_{i=0}^{n} i[\mathrm{PA}_i]$$

But

$$\sum_{i=0}^{n} [\mathrm{PA}_i] = [\mathrm{P}_0]$$

and

$$\sum_{i=0}^{n} i[\mathrm{PA}_i] = [\mathrm{A}_0] - [\mathrm{A}]$$

so

$$\bar{u}_{\mathrm{P}} = \frac{[\mathrm{P}_0]}{[\mathrm{P}_0]} u_{\mathrm{P}} + \frac{[\mathrm{A}_0] - [\mathrm{A}]}{[\mathrm{P}_0]} \cdot w = u_{\mathrm{P}} + r \cdot w \tag{3}$$

This means that if the mobility increment per anion bound is constant, the protein in the presence of constant dye concentration should move *as though* it were all in the form of a single complex of hypothetical composition PA_r independent of the nature of the interaction constants describing the formation of the complex so long as equilibrium is established quickly. The results of the experiments of group 1 (figure 2) show agreement with equation 3 up to at least $r = 20$.

The constituent mobility of dye in the presence of protein is·

$$\bar{u}_{\mathrm{A}} = \frac{1}{[\mathrm{A}_0]} \left[[\mathrm{A}]u_{\mathrm{A}} + \sum_{i=0}^{n} i[\mathrm{PA}_i] \cdot (u_{\mathrm{P}} + iw) \right]$$

The second term in brackets can be separated into two series and the constant factors taken out to give

$$\sum_{i=0}^{n} i[\mathrm{PA}_i](u_{\mathrm{P}} + iw) = ([\mathrm{A}_0] - [\mathrm{A}])u_{\mathrm{P}} + w \sum_{i=0}^{n} i^2[\mathrm{PA}_i]$$

but the series cannot be eliminated completely without the introduction of a further assumption concerning the nature of the binding constants involved. In the present system it may be assumed that the binding obeys the Langmuir adsorption isotherm (figure 1). The derivation of equation 1 depends on the assumptions that all binding sites are equivalent and that there is no interaction between bound anions. It has been shown (6, 12) that when this is the case the binding constant for the i^{th} anion is:

$$k_i = \frac{[\mathrm{PA}_i]}{[\mathrm{PA}_{i-1}] \cdot [\mathrm{A}]} = \frac{n - (i - 1)}{i \cdot K}$$

Introduction of this relationship leads to the solution that

$$\sum_{i=0}^{n} i^2[\mathrm{PA}_i] = ([\mathrm{A}_0] - [\mathrm{A}]) \left(1 + (n - 1) \frac{[\mathrm{A}]}{K + [\mathrm{A}]} \right)$$

and since from equation 1 $[\mathrm{A}]/(K + [\mathrm{A}]) = r/n$,

$$\sum_{i=0}^{n} i^2[\mathrm{PA}_i] = ([\mathrm{A}_0] - [\mathrm{A}])\left(1 + \frac{n-1}{n} r\right)$$

and

$$\bar{u}_\mathrm{A} = \frac{1}{[A_0]}\left\{[\mathrm{A}]u_\mathrm{A} + ([\mathrm{A}_0] - [\mathrm{A}])\left[u_\mathrm{P} + w\left(1 + \frac{n-1}{n} r\right)\right]\right\}$$

or

$$\bar{u}_\mathrm{A} = \frac{1}{[A_0]}\left[[\mathrm{A}]u_\mathrm{A} + ([\mathrm{A}_0] - [\mathrm{A}])\left(\bar{u}_\mathrm{P} + w\frac{n-r}{n}\right)\right] \tag{4}$$

Alberty and Marvin (1) derived this equation simultaneously with the authors of this paper.

Apparently the dye can be treated *as though* it moves in two forms only—one with the mobility of free dye and the other with the mobility of a hypothetical complex $\mathrm{PA}_{(1+r-r/n)}$.

If only one complex were formed, as would be the case if the free dye concentration were infinitely high ($r \rightarrow n$ and $[\mathrm{PA}_r] \rightarrow [\mathrm{P}_0]$), then the bound dye would exhibit a mobility equal to the constituent mobility of the protein. When $n > 1$ and $r < n$ the expression for mobility of the dye will contain the unknown constant n. And when the binding constants are to be determined from electrophoretic mobilities a series of approximations will have to be carried out to obtain accurate values of n and K.

RISING BOUNDARY

In the group 2 experiments we may picture the process occurring at the rising boundary as follows: When the current starts to flow through the cell the free dye in the ascending leg moves out ahead of the slower moving complexes and travels up the tube with a characteristic mobility. Referring to figure 3b, a decrease in concentration of all components will occur at the stationary boundary $\alpha\beta$. A small change in pH also occurs across this boundary, which will result in an indeterminate change in u_P and $\bar{u}_\mathrm{P}$. In addition, in the case of interacting systems, there will occur a shift in the equilibrium across this boundary resulting from the dilution of the interacting components beyond the boundary. Because of these changes at the $\alpha\beta$ boundary some error will be introduced by estimation of $\bar{u}_\mathrm{P}^\alpha$ from the observed displacement of the $\beta\gamma$ boundary and the calculated (or measured) value of κ^β. In many cases these errors will be negligible.

However, from the known values of $[\mathrm{P}_0]$ and $[\mathrm{A}_0]$ in the α solution and the dilution factor for the $\alpha\beta$ boundary, the values of $[\mathrm{P}_0]$ and $[\mathrm{A}_0]$ in the β solution can be safely calculated. If by any method we could determine $[\mathrm{A}]^\beta$, then the values of r^β and $[\mathrm{A}]^\beta$ could be used in the graphical determination of n and K, since the equilibrium in region β is as real as in region α.

$[\mathrm{A}]^\beta$ can, theoretically, be derived from $[\mathrm{A}]^\gamma$ by use of the moving boundary equation for weak electrolytes given by Svensson (17) and by Alberty and Nichol (2):

$$(v^\beta\kappa^\beta - \bar{u}_\mathrm{A}^\beta)[\mathrm{A}_0]^\beta = (v^\beta\kappa^\gamma - u_\mathrm{A}^\gamma)[\mathrm{A}]^\gamma \frac{\kappa^\beta}{\kappa^\gamma} \tag{5}$$

where v^{β} is the velocity of the $\beta\gamma$ boundary in cm.^{3} per coulomb and κ^{β} and κ^{γ} are the specific conductivities of the solutions in regions β and γ. Since the protein disappears in the $\beta\gamma$ boundary, the constituent mobility of the protein in β is

$$\bar{u}_{\mathrm{P}}^{\beta} = v^{\beta}\kappa^{\beta} \tag{6}$$

From equations 5 and 6 and the elimination of $\bar{u}_{\mathrm{A}}^{\beta}$ by substitution from equation 4, we can solve for $[\mathrm{A}]^{\beta}$ to obtain

$$[\mathrm{A}]^{\beta} = \frac{[\mathrm{A}]^{\gamma}\left(u_{\mathrm{A}}^{\gamma}\dfrac{\kappa^{\beta}}{\kappa^{\gamma}} - \bar{u}_{\mathrm{P}}^{\beta}\right) - [\mathrm{A}_0]^{\beta} w \dfrac{n - r}{n}}{u_{\mathrm{A}}^{\gamma} - \bar{u}_{\mathrm{P}}^{\beta} - w\dfrac{n - r}{n}} \tag{7}$$

where $\bar{u}_{\mathrm{P}}$ and u_{A} are obtained directly from the rising boundary pattern as the mobilities of the $\beta\gamma$ and $\gamma\xi$ boundaries, and $[\mathrm{A}]^{\gamma}$ from the concentration change occurring at the $\gamma\xi$ boundary.

In our experiments it was not possible to measure the $[\mathrm{A}]^{\gamma}$ value because the dye concentrations were usually too low to give a stable boundary at the $\gamma\xi$ boundary. Even when the anion is in higher concentration or possesses a higher equivalent weight, as, for example, nucleic acid (Longsworth and MacInnes (10)) which gives a large stable peak, the calculation of $[\mathrm{A}]^{\beta}$ by equation 7 cannot yield dependable values since w, n, r, κ^{γ}, and κ^{β} are unknown. When $\kappa^{\gamma} \cong \kappa^{\beta}$ and $r \cong n$, $[\mathrm{A}]^{\beta} \cong [\mathrm{A}]^{\gamma}$.

Because of these uncertainties, it appears that the rising boundary pattern is not very useful in any attempt to obtain n and K from electrophoresis data.

DESCENDING BOUNDARY

In order to devise an equation to describe the relationship between the values of $[\mathrm{P}_0]$, $[\mathrm{A}]$, and $[\mathrm{A}_0] - [\mathrm{A}]$ in the original protein–dye mixture (in group 2 experiments) and the pattern of the descending boundary after electrophoresis we have pictured the process at the descending boundary as follows (see figure 3c). Free anion moves down into the protein solution, the complexes left behind dissociate to restore the equilibrium, and the anions set free by dissociation follow those which were initially free. Eventually all the dye moves out of the upper part of the protein solution (c) and free protein is left migrating with its characteristic mobility. The dye disappears through the boundary bc. There is no change in concentration of any component at ab—the theoretical free dye boundary.

If it is pictured that all of the free dye originally present in b, c, and d has passed the point ab, then all the *free* dye now present in b must originally have been bound. The complexes in b have their original composition, so the free dye in b must have been bound by the protein in c. The amount of dye originally bound by this protein is $r[\mathrm{P}]^{c}$ times the volume of the cell occupied by c, $[\mathrm{P}]^{c}$ being the concentration of protein in c, and r being the original ratio of bound dye to total protein.

The amount of free dye in b is $[\mathrm{A}]$ times the volume of b. Since the cell is of uniform cross section, these volumes are proportional to the distances moved by the boundaries or, since all boundaries move with constant velocities, to the mobilities of the boundaries.

The mobility of boundary *bc* is the constituent mobility of the dye, $\bar{u}_A$, and that of boundary *cd* is the apparent mobility of the free protein $u_{P'}$, which differs from the true mobility of the protein, u_P, by the factor κ^b/κ^c. If $\kappa^b \cong \kappa^c$, then the mobility of boundary $cd = u_P$. The mobility of the hypothetical boundary *ab* is that of the free dye u_A, which may be determined by separate experiment in the same buffer if it is assumed that the presence of protein has negligible effect upon the free dye mobility.

Equating the amount of free dye in volume *b* to the bound dye which has been set free from the protein in volume *c*, we get

$$[A](u_A - \bar{u}_A) = ([A_0] - [A]) \frac{[P]^c}{[P_0]} (\bar{u}_A - u_{P'})$$

and

$$[A] = [A_0] \frac{\bar{u}_A - u_{P'}}{\frac{[P_0]}{[P]^c}(u_A - \bar{u}_A) + (\bar{u}_A - \bar{u}_{P'})} \tag{8}$$

where $[A_0]$ and $[P_0]$ are the original concentrations of dye and protein, $\bar{u}_A$ and $u_{P'}$ may be determined from measurements on the scanned pattern, and u_A is the known mobility of the anion.

The ratio $[P]^c/[P_0]$ can be approximated closely from areas of the descending pattern by the equation:

$$\frac{[P]^c}{[P_0]} = \frac{I_{cd}\left(1 + \frac{I_{de}}{I_{cd} + I_{bc}}\right)}{I_{cd} + I_{bc} + I_{de} - I_{A_0}} = \theta$$

where I_{cd} = area of the *cd* peak,
I_{bc} = area of the *bc* peak,
I_{de} = area of the ϵ-boundary, and
I_{A_0} = area due to total dye obtained from known value of $[A_0]$ and the refractive increment of dye in terms of the units of area measured.

Alberty and Marvin (1) have shown that the concentration of protein in *c* may be calculated from mobilities in the rising and descending legs of the tube without making *any* area measurements. Their equation is:

$$\theta = \frac{\bar{u}_P^\alpha - \bar{u}_A^b}{\frac{\kappa^b}{\kappa^c} u_P - \bar{u}_A^b} \tag{9}$$

$\bar{u}_P^\alpha$ being approximated from the mobility of the $\beta\gamma$ boundary and the dilution factor correcting for the dilution which occurs at the $\alpha\beta$ boundary. For reasons already given under the discussion of the rising boundary, the value of $\bar{u}_P^\alpha$ may better be obtained as the mobility of the moving boundary on the descending side in a separate experiment of the type described in group 1 above. Solved for $\bar{u}_P^\alpha$ this equation is:

$$\bar{u}_P^\alpha = \bar{u}_A^b(1 - \theta) + \frac{\kappa^b}{\kappa^c} u_P\theta \tag{9a}$$

Combining equations 8 and 9 and assuming that $\kappa^b \cong \kappa^c$ they get:

$$[A] = [A_0] \frac{\bar{u}_A - \bar{u}_P}{u_A - \bar{u}_P} \tag{10}$$

They have also shown that equation 10 can be derived from the definitions of $\bar{u}_A$ and $\bar{u}_P$ (equation 2) without any reference to the mechanism of the process at the descending boundary by assuming (*1*) that only one complex is formed, and (*2*) that all the protein is combined with dye, or (*3*) that the average mobility of bound anion is the same as the constituent mobility of the protein. Equation 3 above indicates that in calculating the constituent mobility of the protein assumptions (*1*) and (*2*) are allowable. Equation 4 indicates that assumption (*3*) is not strictly allowable if $n > 1$ or $r < n$. Values of [A] and $[A_0] - [A]$ calculated from the data of table 1 by equations 8 and 10 (both of which include assumption (*3*)) agree within 2 per cent (on the basis of r). Deviations are greatest, as illustrated in figure 4, in those experiments where the values of [A] are lowest. This is the condition (see above) under which the true value of $\bar{u}_P^\alpha$ will be expected to deviate most from $\bar{u}_P^\beta$. This observation exmphasizes the desirability of determining $\bar{u}_P$ by separate experiment of the group 1 type.

If it is not assumed that $\bar{u}_P$ is the same as the average mobility of bound anion we obtain from equations 3, 4, and the relationship that $r = ([A_0] - [A])/[P_0]$,

$$[A] = \frac{[A_0]\left[\bar{u}_A - \bar{u}_P + \frac{1}{n}(\bar{u}_P - u_P)\right] - [P_0](\bar{u}_P - u_P)}{u_A - \bar{u}_P + \frac{1}{n}(\bar{u}_P - u_P)} \tag{11}$$

or, eliminating $\bar{u}_P$ by equation 9a and assuming $\kappa^b \cong \kappa^c$,

$$[A] = \frac{[A_0](\bar{u}_A - u_P)\left(\frac{n-1}{n}\theta + \frac{1}{n}\right) - [P_0](1 - \theta)(\bar{u}_A - u_P)}{(\bar{u}_A - u_P)\left(\frac{n-1}{n}\theta + \frac{1}{n}\right) + u_A - \bar{u}_A} \tag{12}$$

In figure 4, the values of $1/r$ *versus* $1/[A]$, as obtained from the experimental data presented in table 1 with the aid of equation 8 (or equation 10) on the one hand and with the aid of equation 12 on the other, are plotted for comparison. Values of n obtained from these graphs for the two cases are $n = 22.0$ and 25.2, respectively. Values of K are found to be nearly the same (2.83×10^{-4} and 2.92×10^{-4}, respectively). These values of n and K as obtained from electrophoresis data are in fair agreement with those obtained from dialysis experiments (*vide supra*) ($n = 22.6$ and $K = 3.12 \times 10^{-4}$) at equilibrium values of [A] less than 2×10^{-4} molar.

TABLE 1

I	II	III	IV	V	VI
EXPERIMENT NO.	PROTEIN CONCENTRATION	PROTEIN CONCENTRATION	METHYL ORANGE CONCENTRATION	FIELD STRENGTH IN a	TIME OF RUN
	per cent	*moles/liter* × 10^4	*moles/liter* × 10^4	*volts/cm.*	*seconds*
1.	0.765	1.14	1.5	6.59	12,000
7.	0.765	1.14	1.5	6.94	14,000
8.	0.765	1.14	2.25	6.88	14,000
9.	0.765	1.14	3.0	6.92	14,000
2.	0.765	1.14	3.0	6.66	12,300
3.	0.765	1.14	5.0	6.70	10,000
4.	0.765	1.14	10.0	6.53	10,000
5.	0.510	0.762	5.0	6.99	7,000
6.	1.02	1.52	10.0	6.63	12,000

Mobilities of boundaries

I	VII	VIII	IX
EXPERIMENT NO.	u_P	$\bar{u}_A$	$\bar{u}_P$
	$cm^2\ v.^{-1}\ sec^{-1} \times 10^5$*	$cm.^2\ v.^{-1}\ sec.^{-1} \times 10^5$	$cm.^2\ v.^{-1}\ sec.^{-1} \times 10^5$
1.	2.74	3.82	2.90
7.	2.76	3.72	2.85
8.	2.76	3.76	2.80
9.	2.75	3.85	2.90
2.	2.64	3.72	2.85
3	2.70	3.98	2.95
4.	2.59	4.23	3.34
5.	2.75	4.29	3.00
6	2.60	3.95	3.23

Areas of peaks in the Tiselius patterns (planimeter units)

I	X	XI	XII	XIII	XIV
EXPERIMENT NO.	TOTAL-RISING	TOTAL—DESCENDING	*de*	$\alpha\beta$	*cd*
1.	1.88	1.86	0.02	0.15	1.43
7.	1.84	1.84	0.02	0.12	1.58
8.	1.98	1.94	0.02	0.16	1.55
9.	2.06	2.06	0.03	0.15	1.58
2.	1.89	1.86	0.06	0.13	1.42
3.	1.96	1.91	0.04	0.14_5	1.29
4.	2.00	2.03	0.04	0.14	1.03
5.	1.28	1.29	0.03	0.07	0.98
6.	2.76	2.66	0.09	0.30_5	1.33

* Calculated from distance moved by the *cd* boundary and κ^b.

† Calculated from distance moved by the $\beta\gamma$ boundary and κ^a times the dilution factor at the $\alpha\beta$ boundary.

Mobility of methyl orange taken as 10.50×10^{-5} cm.² v.⁻¹ sec.⁻¹

Refractive index increment of methyl orange in planimeter units = 164 per mole.

It is of interest to note that, in the bovine serum albumin–methyl orange systems, when the equilibrium concentration of free dye [A] in the mixture exceeds a value of about 2×10^{-4} molar (corresponding in our experiments to a $[A_0]$ of approximately 1.5×10^{-3} *M*) there appears a double peak in the *bc* boundary (the boundary in which dye disappears) in the descending pattern. The faster segment of this double peak increases in relative area as the dye concentration is increased (relative to the protein), as is illustrated by the series of descending boundary patterns shown in figure 5. The analysis of the patterns to yield values of *n* and *K* through the use of equations 8, 10, 11, and 12 is applicable only to patterns from mixtures containing dyestuff concentrations so low that the second peak does not occur. The occurrence of this second peak, when higher dye concentrations are present, may mean that a second group of sites of interaction is present, and that the *K*-value involved is such as to indicate a much weaker binding at these sites than is characteristic of those sites upon which the initial binding of the dye occurs. The *n*-value for these second sites would appear to be greater than that for the initial interaction. This phenomenon is being further studied at the present time.

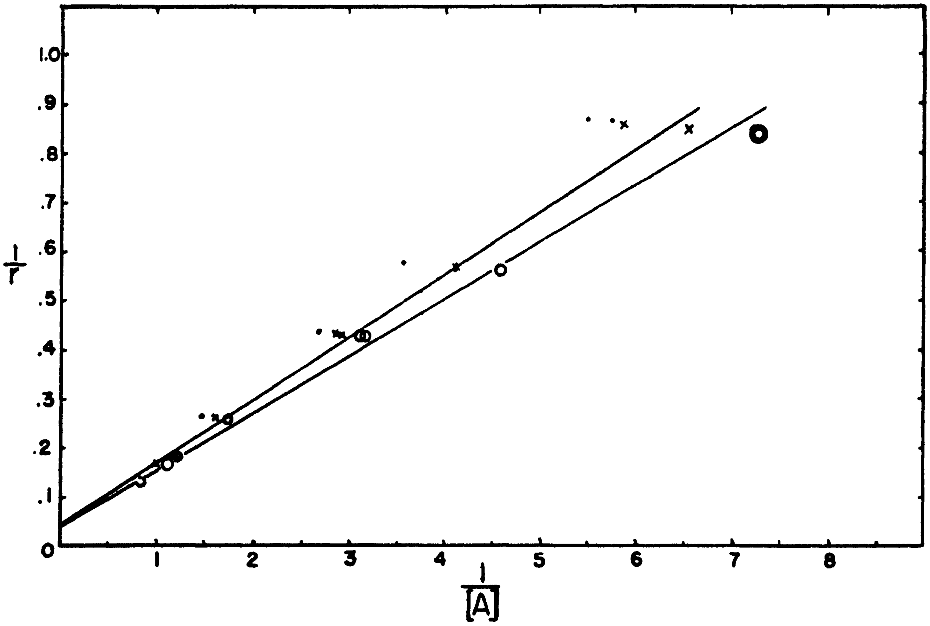

FIG. 4. $1/r$ *versus* $1/[A]$ ($\times 10^{-4}$) from electrophoresis data. Points marked × were calculated by means of equation 8, points marked ● by equation 10, and points marked ○ by equation 12 (using a value of $n = 25$ in the calculations involving equation 12).

The data contained in the paper by Longsworth and MacInnes (10) on the interaction of ovalbumin and yeast nucleic acid upon treatment according to equation 8 yielded values of $[P_0]/([N_0] - [N])$ and $1/[N]$ which are plotted in figure 6. The points fall close to a linear relationship which indicates an *n*-value

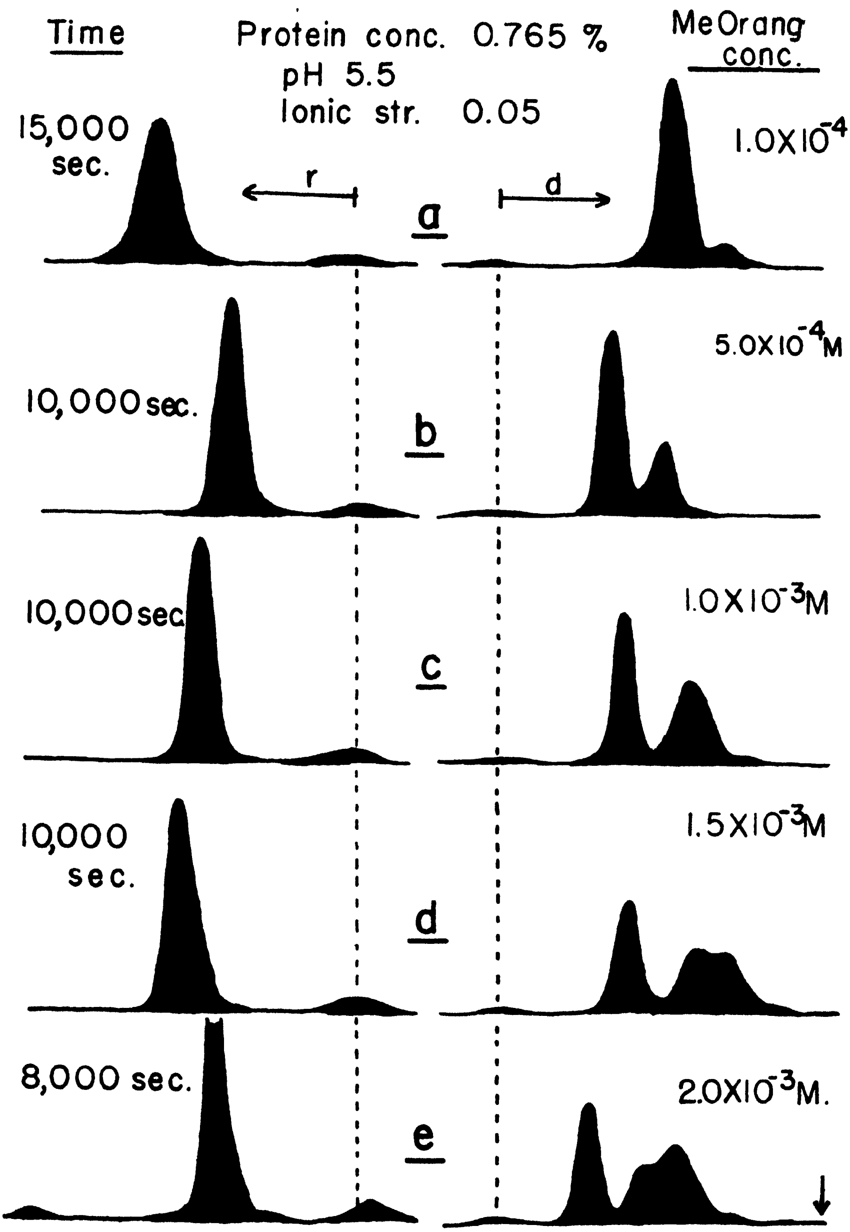

FIG. 5. Tracings of scanned pictures of Tiselius patterns obtained in experiments of group 2 with 0.765 per cent serum albumin and varying amounts of methyl orange.

of 1.1 (grams of nucleic acid per gram of protein) and a *K*-value of 2.0 (grams per liter).

It seems likely that the study of interaction by electrophoresis techniques offers wide possibilities and, in some cases, distinct advantages over other methods of such investigation.

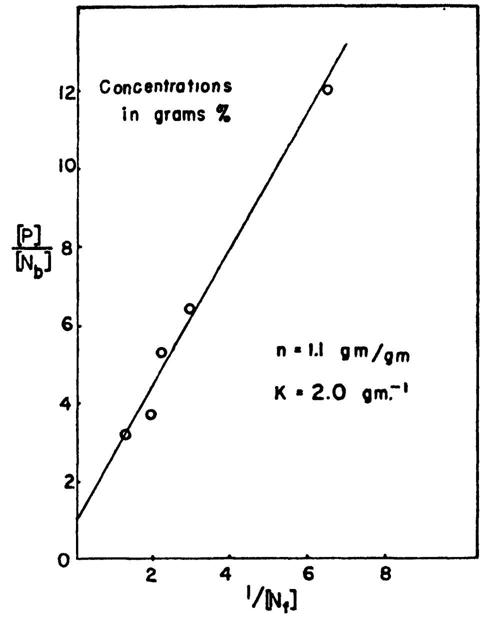

FIG. 6. $\frac{\text{Concentration of ovalbumin (in grams per cent)}}{\text{Concentration of bound nucleic acid (in grams per cent)}}$ *versus* the reciprocal of the concentration of free nucleic acid (in grams per cent) Calculated from the data of Longsworth and MacInnes (10) by equation 8.

SUMMARY

The interaction of bovine serum albumin and methyl orange in solution at pH 5.5 in acetate buffer of 0.05 ionic strength has been studied by the Tiselius electrophoresis technique and methods have been devised by which the constants of the interaction may be calculated from the boundary patterns obtained after electrophoresis of the solution. Constants thus obtained from electrophoresis data are found to agree quite satisfactorily with those obtained from dialysis equilibrium experiments on the same system. The relationships which are demonstrated to apply between the electrophoresis patterns and the interaction constants may be expected to be utilizable in the study of interaction in any system in which the formation of complexes between components follows the mass action law describable in the form of the Langmuir-type adsorption isotherm, where the rate of attainment of equilibrium is fast compared to the time required for development of the electrophoresis pattern and where at least one of the interacting components bears an electric charge under the conditions of the experiment.

The authors wish to thank the National Institutes of Health for a Public Health Service Research Grant under which the studies reported in this paper were carried out. They are pleased to acknowledge the very stimulating discussions and interchange of ideas which they have had with Dr. R. A. Alberty of the University of Wisconsin during the preparation of this paper.

REFERENCES

(1) Alberty, R. A., and Marvin, H. H.: J. Phys. & Colloid Chem. **54,** 47 (1950).
(2) Alberty, R. A., and Nichol, J. C.: J. Am. Chem. Soc. **70,** 2297 (1948).
(3) Boyer, P. D., Ballou, G. A , and Luck, J. M.: J. Biol. Chem. **167,** 407 (1947).
(4) Chargaff, E., Ziff, M., and Moore, D. H.: J. Biol. Chem. **139,** 383 (1941).
(5) Goldwasser, E., and Putnam, F. W.. J. Phys. & Colloid Chem. **54,** 79 (1950).
(6) Klotz, I. M.: Arch. Biochem. **9,** 109 (1946).
(7) Klotz, I. M., Walker, F. M., and Pivan, R. B.: J. Am. Chem. Soc. **68,** 1486 (1946).
(8) Longsworth, L. G., Cannan, R. K., and MacInnes, D. A.: J. Am. Chem. Soc. **62,** 2580 (1940).
(9) Longsworth, L. G., and Jacobsen, C. F.: J. Phys. & Colloid Chem. **53,** 126 (1949).
(10) Longsworth, L. G., and MacInnes, D. A.: J. Gen. Physiol. **25,** 507 (1942).
(11) Lundgren, H. P., Elam, D. M., and O'Connell, R. A.: J. Biol. Chem. **149,** 183 (1943).
(12) Muralt, A. L. von. J. Am. Chem. Soc. **52,** 3518 (1930).
(13) Putnam, F. W , and Neurath, H.: J. Biol. Chem. **159,** 195 (1945).
(14) Schwert, G W., Putnam, F. W., and Briggs, D. R.: Arch Biochem. **4,** 371 (1944).
(15) Seibert, F. B , and Watson, D. W. J. Biol. Chem. **140,** 55 (1941).
(16) Stenhagen, E., and Teorell, T.: Trans. Faraday Soc. **35,** 743 (1939).
(17) Svensson, H.: Acta Chem. Scand. **2,** 841 (1948).
(18) Tiselius, A.: Nova Acta Regiae Soc. Sci. Upsaliensis [4] **7,** No. 4 (1930).

STUDY OF PROTEIN–ION INTERACTION BY THE MOVING BOUNDARY METHOD

Theory of the Method[1]

ROBERT A. ALBERTY and HENRY H. MARVIN, Jr.[2]

Department of Chemistry, University of Wisconsin, Madison, Wisconsin

Received August 22, 1949

INTRODUCTION

A number of investigators have cited electrophoresis experiments as qualitative evidence of protein–ion interactions. In the preceding article Smith and Briggs (11) have shown that the same quantitative information concerning the interaction of bovine serum albumin with methyl orange may be obtained by the moving boundary method as by the dialysis method of Klotz (5). The moving boundary method for the study of protein–ion interactions is of interest because it may be applied to the study of the interactions of proteins with other proteins (e.g., the antigen–antibody reaction), polysaccharides, or nucleic acids. Since the dialysis method is not applicable to the study of the interactions of these large ions, we have undertaken the development of methods for the interpretation of such electrophoresis experiments.

---

[1] This paper was not presented at the Twenty-third National Colloid Symposium but was an outgrowth of discussions and correspondence with R. F. Smith and D. R. Briggs concerning their studies of the binding of methyl orange by bovine serum albumin (11).

[2] United States Rubber Company Fellow, 1949–50.

The foundations for the interpretation of electrophoresis experiments with interacting systems were laid by Longsworth and MacInnes (7) in their study of the interaction of ovalbumin and yeast nucleic acid. They pointed out that the nature of the electrophoretic pattern for such a mixture depends upon the rates of formation and dissociation of the complexes. Of the five general cases which they discussed qualitatively, we shall consider only the case in which the rates of complex formation and dissociation are fast compared to the duration of the electrophoresis experiment. With this reservation, moving boundary experiments with protein solutions containing other ions which interact strongly with the protein are analogous to moving boundary experiments with solutions of weak acids and bases (2, 3, 8, 12).

THEORY

In the case of protein–ion interactions a number of complexes, PA, PA_2, $\cdots$ PA_n, are in equilibrium. Our considerations will be limited to the equilibria which may be represented by the following equations (5, 10):

$$\begin{aligned} &P + A \rightleftharpoons PA && k_1 = [PA]/[P][A] \\ &PA + A \rightleftharpoons PA_2 && k_2 = [PA_2]/[PA][A] \qquad (1) \\ &\cdots && \cdots \\ &PA_{n-1} + A \rightleftharpoons PA_n && k_n = [PA_n]/[PA_{n-1}][A] \end{aligned}$$

where A is an anion or cation and the concentrations are in gram-formula weights per liter.

The fundamental relation of moving boundary systems formed by weak electrolytes is a statement of the law of conservation of mass in terms of the mobility and concentration of the constituent on either side of a boundary. The moving boundary equation for the i^{th} constituent at the moving boundary which separates the α solution from the β solution is (3, 12):

$$\frac{\bar{u}_i^\alpha \bar{c}_i^\alpha}{\kappa^\alpha} \quad \frac{\bar{u}_i^\beta \bar{c}_i^\beta}{\kappa^\beta} = v^{\alpha\beta}(\bar{c}_i^\alpha - \bar{c}_i^\beta) \qquad (2)$$

The specific conductances of these solutions are represented by κ^α and κ^β, the displacement of the boundary between the α and β solution in cm.^{3} per coulomb is represented by $v^{\alpha\beta}$, and the constituent concentration and constituent mobility of i by $\bar{c}_i$ and $\bar{u}_i$. The last three quantities are given signs; $v^{\alpha\beta}$ is positive if the boundary moves in the direction of the positive current and negative if it moves in the opposite direction, and $\bar{c}_i$ and $\bar{u}_i$ are given the sign of the ions which are in equilibrium. The constituent concentration is the total concentration, in gram-formula weights per liter, of all forms of a constituent of a solution, and in the case of the system represented by equations 1 the constituent concentrations of protein, $[\bar{P}]$, and interacting ion $[\bar{A}]$, are

$$[\bar{P}] = [P] + [PA] + [PA_2] + \cdots + [PA_n] \tag{3}$$

$$[\bar{A}] = [A] + [PA] + 2[PA_2] + \cdots + n[PA_n] \tag{4}$$

The constituent mobility is $\bar{u} = \sum_{i=1}^{n} \alpha_i u_i$, an expression first used by Tiselius (14), where α_i is the fraction of the time the molecules of the constituent exist in the form of the complex with mobility u_i. Since $[PA_i]/[\bar{P}]$ is the fraction of the time the protein constituent exists in the form PA_i, the constituent mobility of the protein is

$$\bar{u}_P = \frac{1}{[\bar{P}]}\{[P]u_P + [PA]u_{PA} + [PA_2]u_{PA_2} + \cdots + [PA_n]u_{PA_n}\} \tag{5}$$

where the mobilities u_P, u_{PA}, $\cdots$, u_{PA_n} are the mobilities of the corresponding ions in the solution containing the equilibrium mixture. Since $i[PA_i]/[\bar{A}]$ is the fraction of the time the interacting ion exists in the form PA_i, the constituent mobility of the anion in the equilibrium mixture is

$$\bar{u}_A = \frac{1}{[\bar{A}]}\{[A]u_A + [PA]u_{PA} + 2[PA_2]u_{PA_2} + \cdots + n[PA_n]u_{PA_n}\} \tag{6}$$

It may be seen by reference to equation 2 that the mobility of a constituent can be measured directly if this constituent exists only on one side of a moving boundary. The arrangement of experiments so that the desired constituent disappears across a boundary moving into the original protein solution is discussed in the following section.

Moving boundary systems for the study of interactions

Longsworth and MacInnes (7) studied the interaction of yeast nucleic acid and ovalbumin by means of electrophoresis and found that two moving boundaries were obtained in each limb of the U-tube. They showed that the mobility calculated from the velocity of the slower boundary in the descending limb corresponded to that of the protein, while the mobility calculated from the velocity of the faster ascending peak corresponded to that of the nucleic acid. The mobilities of the other two boundaries did not correspond to the mobilities of protein, nucleic acid, or complex. The moving boundary systems obtained in such an experiment are shown in figure 1, (a) and (b). For the purpose of the diagrams it is assumed that $|u_A| > |u_P|$ and $|u_{PA_i}| > |u_P|$.

In figure 1(a) it is seen that the A constituent disappears across the $\alpha\beta$ boundary. The constituent mobility for A represented by equation 6 may be obtained by application of the moving boundary equation:

$$\bar{u}_A^{\alpha} = v^{\alpha\beta}\kappa^{\alpha} \tag{7}$$

Similarly, the $\beta\gamma$ boundary in the ascending system (figure 1(b)) yields the constituent mobility of the protein represented by equation 5.

$$\bar{u}_P^{\beta} = v^{\beta\gamma}\kappa^{\beta} \tag{8}$$

However, the ascending moving boundary system has the disadvantage that the concentrations of the reactants in the solution in which the mobility is obtained (β) cannot be chosen before the experiment because of the dilution at the stationary boundary. Also the required specific conductivity, κ^β, is difficult to obtain.

Two alternatives are available for the determination of the constituent mobility of the protein in the original protein solution: (*1*) the application of the moving boundary equation and (*2*) the use of a different moving boundary system.

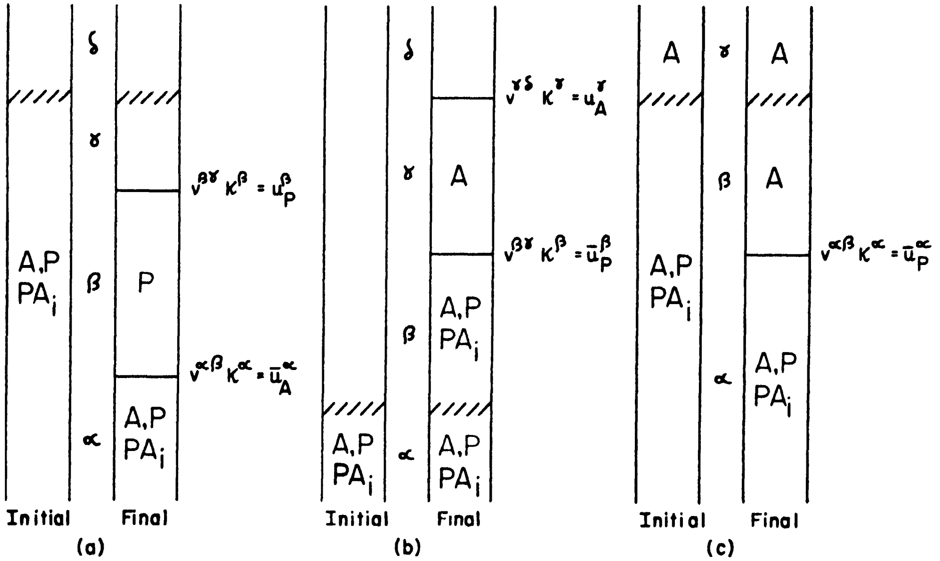
ζ
γ
β
α
A,P PA$_i$
P
A,P PA$_i$
$v^{\beta\gamma}\kappa^\beta = u_P^\beta$
$v^{\alpha\beta}\kappa^\alpha = \bar u_A^\alpha$
Initial
Final
(a)
δ
γ
β
α
A
A,P PA$_i$
A,P PA$_i$
$v^{\gamma\delta}\kappa^\gamma = u_A^\gamma$
$v^{\beta\gamma}\kappa^\beta = \bar u_P^\beta$
Initial
Final
(b)
A
γ
β
α
A,P PA$_i$
A
A
A,P PA$_i$
$v^{\alpha\beta}\kappa^\alpha = \bar u_P^\alpha$
Initial
Final
(c)

FIG. 1. Moving boundary systems involving interaction. (a), descending boundary system; (b), ascending boundary system; (c), boundary system yielding $\bar u_P$ from a descending boundary. The initial or concentration boundary is represented by //// and moving boundaries by —. (The ions of the buffer exist throughout the moving boundary system and are not indicated.)

Equation 2 for protein at the $\alpha\beta$ boundary of figure 1(a) may be written

$$\bar u_P^\alpha = \bar u_A^\alpha(1 - \theta) + \frac{\kappa^\alpha}{\kappa^\beta} u_P^\beta \theta \tag{9}$$

where $\theta = \bar c_P^\beta/\bar c_P^\alpha$ may be calculated from the refractive index changes across the $\alpha\beta$ and $\beta\gamma$ boundaries measured with the schlieren optical system, provided that the contribution of A to the refractive index of the α solution is negligible. For dilute solutions of P and A, $\kappa^\alpha/\kappa^\beta$ may be taken as unity.

A more accurate method for the determination of the quantity $\bar u_P^\alpha$ makes use of the descending boundary in the system illustrated in figure 1(c) for which

$$\bar u_P^\alpha = v^{\alpha\beta}\kappa^\alpha \tag{10}$$

The use of the moving boundary system (c), in which A is present throughout the system, for the determination of $\bar u_P$ is preferable to the use of system (b), because (*1*) the specific conductance required is simply that of the original solution and (*2*) the constituent mobility of the protein is that in the original solution rather than in the solution formed by dilution across the concentration boundary in the ascending limb.

The concentration of A in the γ solution should be somewhat less than its concentration in the β solution, which is determined by the mobilities and concentrations of the various ions in the α solution. Thus a preliminary experiment or two may be required to determine the correct concentration of the A solution to be used for the γ solution. Since three ion species are present in both initial solutions, a false moving boundary as obtained by Svensson (13) may be obtained.

It may be seen from figure 1, (a) and (b), that the moving boundary corresponding to the disappearance of a dye or pigment will in general move more rapidly than that of the protein with which it interacts. Thus in a protein mixture the specific protein responsible for interaction cannot be identified by simply noting the mobility of the dye boundary.

Equations for the study of protein–ion interaction[3]

Measured values of the quantities $\bar{u}_P$ and $\bar{u}_A$ together with equations 5 and 6 cannot be used to determine the extent of interaction without the introduction of certain assumptions. The simplest assumption is that only one complex is formed and that the concentration of the protein which is not involved in this complex is negligible. This assumption leads to the equations given in section I, which make it possible to calculate the fraction of free A from the constituent mobilities of A and P and the mobility of free A. Since Klotz (5) has shown that the binding of small ions by proteins may be represented by the Langmuir adsorption isotherm, a better approximation may be made by assuming the concentrations of the complexes to follow a statistical distribution. This method is discussed in section II. In the case of the interaction of ions of more nearly equal size the number of A ions bound will be small and cannot be represented adequately by the Langmuir adsorption isotherm. Such interactions may be treated in terms of the equilibrium between free protein and complex as discussed in section III.

I. If it is assumed that there is a single complex and no free protein, equations 5 and 6 become

$$\bar{u}_P = u_{PA_i} \tag{11}$$

since $[\bar{P}] = [PA_i]$, and

$$\bar{u}_A = \frac{1}{[\bar{A}]}\{[A]u_A + ([\bar{A}] - [A])u_{PA_i}\} \tag{12}$$

since $i[PA_i] = [\bar{A}] - [A]$. Elimination of u_{PA_i} between these equations yields:

$$[A] = [\bar{A}]\left(\frac{\bar{u}_A - \bar{u}_P}{u_A - \bar{u}_P}\right) \tag{13}$$

---

[3] Since the methods for the determination of the constituent mobilities of protein and interacting ion have been described in the preceding section, these quantities will be given without Greek superscripts in what follows.

Thus the concentration of bound interacting ion may be calculated from $\bar{u}_P$ and $\bar{u}_A$ and the mobility of the interacting ion in the same buffer determined in a separate experiment.[4] In the case of concentrated or viscous solutions an error is introduced by the fact that u_A represents the mobility of free A in the α solution, which may be somewhat less than its mobility in solutions containing only A, as determined in a separate experiment.

If $\bar{u}_P$ is eliminated by means of equation 9, assuming $\kappa^\alpha/\kappa^\beta = 1$,

$$[\bar{A}] - [A] = \frac{[\bar{A}](u_A - \bar{u}_A)}{(u_A - \bar{u}_A) + \theta(\bar{u}_A - u_P)} \tag{14}$$

which is identical with the equation derived by Smith and Briggs (11) by a different method involving assumptions as to the mechanism of separation of the boundaries. Although the above derivation of equation 14 does not involve any assumptions as to this mechanism, the two assumptions mentioned above are involved.

II. If the adsorption follows the Langmuir isotherm, the concentrations of the various complexes are found by taking the equilibrium constants (5) as

$$k_i = \frac{n - (i - 1)}{i} \cdot \frac{1}{K} \tag{15}$$

where n is the maximum number of A ions bound per P ion and K is the intrinsic equilibrium constant for the interaction. Introduction of the equilibrium constants of equations 1 into equation 6 leads to:

$$\bar{u}_A[\bar{A}] - u_A[A] = k_1[P][A]u_{PA} + 2k_1k_2[P][A]^2u_{PA_2} + \cdots + nk_1k_2 \cdots k_n[P][A]^n u_{PA_n} \tag{16}$$

The series obtained by the introduction of equation 15 into equation 16 yields

$$\bar{u}_A = \frac{[A]}{[\bar{A}]} u_A + \frac{[P]}{[\bar{A}]} \sum_{i=1}^{n} \left\{ \left(\frac{[A]}{K}\right)^i \frac{n(n - 1) \cdots (n - i + 1)}{(i - 1)!} \right\} u_{PA_i} \tag{17}$$

which cannot be simplified without information about u_{PA_i}. Smith and Briggs (11) have shown that if the mobilities of the various complexes are related to the mobility of the free protein by the following equation

$$u_{PA_i} = u_P + iw \tag{18}$$

where w is an empirical constant, the constituent mobility of the protein in the mixture is

$$\bar{u}_P = u_P + rw \tag{19}$$

where r is the ratio of the number of moles of bound ion A to the total moles of protein (5). Since

$$r = \frac{[\bar{A}] - [A]}{[\bar{P}]} = \frac{n}{\left(1 + \frac{K}{[A]}\right)} \tag{20}$$

---

[4] Information concerning the molecular weights of A and P is not required, and so calculations may be carried out on a gram basis.

equation 17 may be simplified after the introduction of equations 18 and 20 to give:

$$\bar{u}_A = \frac{1}{[\bar{A}]}\left\{[A]u_A + [\bar{P}]r\left[u_P + w\left(1 + \frac{(n-1)}{n}r\right)\right]\right\} \tag{21}$$

The elimination of w between equations 19 and 21 yields

$$[A] = \frac{[\bar{A}](\bar{u}_A - \bar{u}_P) - [\bar{P}](\bar{u}_P - u_P)}{(u_A - u_P)} \tag{22}$$

if $(n - 1)/n$ is sufficiently close to unity. If $(n - 1)/n$ is not sufficiently close to unity, a series of approximations could be made. It is noted that if the second term in the numerator of equation 22 is negligible, this equation reduces to equation 13.

III. For low values of n, it is likely that some protein may exist in the free form. If it is assumed that PA_i is the only complex formed, $[PA_i]u_{PA_i}$ may be eliminated between equations 5 and 6 to obtain:

$$\bar{u}_P[\bar{P}] - (P)u_P = \frac{1}{i}\{\bar{u}_A[A] - [A]u_A\} \tag{23}$$

The concentrations of free protein and free ion A are related by the equations

$$\left.\begin{aligned}[A] &= [\bar{A}] - i[PA_i]\\ [P] &= [\bar{P}] - [PA_i]\end{aligned}\right\} \tag{24}$$

and so [P] may be eliminated from equation 23, which may be rearranged to yield:

$$[A] = \frac{[\bar{A}](\bar{u}_A - u_P) - i[\bar{P}](\bar{u}_P - u_P)}{(u_A - u_P)} \tag{25}$$

This expression reduces to equation 13 if the concentration of free protein is negligible. The quantities on the right side of this equation are all determinable experimentally except for i. To determine whether this type of treatment is applicable to a given protein–ion interaction, [A] may be calculated from equation 25 by assuming $i = 1, 2, 3 \cdots$. The corresponding concentrations $[PA_i]$ and [P] may be calculated from equation 24 and substituted into the equilibrium expression

$$K_i = \frac{[PA_i]}{[P][A]^i} \tag{26}$$

to determine the value of i for which a constant value of K_i is obtained over a range of concentration of the protein and interacting ion.

DISCUSSION

Calculations with the equations of sections I, II, and III may be somewhat more accurate than the absolute accuracy of the mobility determinations, since only ratios of mobilities are involved. Errors in the magnification factor of the schlieren camera and in the cross-sectional area of the Tiselius cell cancel if the same limb of the same cell is used for all experiments.

In the case of both bovine serum albumin and β-lactoglobulin the rising and descending boundaries differ markedly from being mirror images of each other at pH values below the isoelectric point (1, 6, 9). Longsworth has pointed out that since these deviations from enantiography are observed at protein concentrations of 0.4–0.8 per cent in 0.1 ionic strength buffers, the patterns are not those of a simple mixture of two proteins, and he suggests that equilibria prevailing in the body of the protein solution are being continually adjusted in the boundary layers as electrophoretic separation occurs. One of the most striking features of these patterns is that the descending moving boundary has a higher velocity than the fastest ascending boundary, whereas deviations from ideality as predicted by Dole's theory (4) would cause the ascending boundary to move more rapidly. The rapidly moving descending boundary must correspond to a complex which dissociates in the ascending boundary system when it migrates out of the protein solution and into the buffer. This would explain the absence of the fast boundary in the ascending system and is in line with the fact that the complex would be expected to have a higher ratio of charge to frictional coefficient than the single albumin molecules, and therefore a higher mobility. The formation of albumin dimers or other polymers made up of identical albumin molecules would not explain the experimental results, because the unassociated albumin molecules remaining in a region from which the dimers had migrated would associate and as a result a single moving boundary would be obtained. Therefore, there must be at least two types of albumin molecules, A and B, which form a complex AB. If $| u_A | > | u_B |$, the faster descending boundary would yield the constituent mobility of A, which is

$$\bar{u}_A = \frac{u_A c_A + u_{AB} c_{AB}}{c_A + c_{AB}} \tag{27}$$

In the ascending limb the faster boundary yields the mobility of free A ions, while the slower ascending boundary yields the constituent mobility of B in the albumin solution:

$$\bar{u}_B = \frac{u_B c_B + u_{AB} c_{AB}}{c_B + c_{AB}} \tag{28}$$

The partial resolution of two such boundaries in the ascending pattern is shown by Longworth's schlieren patterns for bovine serum albumin in 0.1 N sodium acetate buffer at pH 4.63. In addition there appears to be a component which is isoelectric at this pH and which is not involved in the formation of complexes, since the stationary boundaries in both limbs are larger than would be expected for the buffer and protein concentration boundaries.

The binding of smaller ions, such as chloride ions, may also be studied by the moving boundary method. In this case the variation of the mobilities of the free protein and of the various complexes with ionic strength must be considered. Also higher protein concentrations are generally required, since the binding is weaker. In more concentrated protein solutions the effect of the microscopic viscosity of the protein solution on the mobility of the free interacting ion must be taken into consideration. Methods have been devised for such studies and will be the subject of a future publication.

SUMMARY

The moving boundary method offers a means for studying the interaction of ions of high molecular weight. If complexes of the type PA, PA_2, $PA_3 \cdots PA_n$ are in equilibrium and the rates of formation and dissociation of these ions are fast compared to the duration of an electrophoresis experiment, the system may be treated by the theory developed for solutions of weak electrolytes. If $|u_A| > |u_P|$, the faster descending boundary yields the constituent mobility of A, $\bar{u}_A$, and the slower ascending boundary yields the constituent mobility of P, $\bar{u}_P$. A better method for the determination of $\bar{u}_P$ which makes use of a descending boundary is described. Quantitative information concerning the interaction may be calculated from $\bar{u}_A$, $\bar{u}_P$, and the mobilities of free A and P if one of several conditions is satisfied. The conditions discussed are: (*1*) one complex is formed and the concentration of free P is negligible; (*2*) a Langmuir distribution of complexes with mobilities $u_{PA_i} = u_P + iw$ are formed; and (*3*) a single complex is in equilibrium with both free P and A.

This work was supported by the Research Committee of the Graduate School of the University of Wisconsin from funds supplied by the Wisconsin Alumni Research Foundation.

REFERENCES

(1) ALBERTY, R. A.: J. Phys. & Colloid Chem. **53**, 114 (1949).
(2) ALBERTY, R. A : J. Am. Chem. Soc., in press.
(3) ALBERTY, R A., AND NICHOL, J. C.: J. Am. Chem. Soc. **70**, 2297 (1948).
(4) DOLE, V P.. J. Am. Chem. Soc. **67**, 1119 (1945).
(5) KLOTZ, I. M., WALKER, F. M., AND PIVAN, R. B.: J. Am. Chem Soc. **68**, 1486 (1946).
(6) LONGSWORTH, L. G., AND JACOBSEN, C. F.: J. Phys. & Colloid Chem. **53**, 126 (1949).
(7) LONGSWORTH, L. G., AND MACINNES, D. A. J. Gen Physiol. **25**, 507 (1942).
(8) NICHOL, J. C.: J. Am. Chem. Soc., in press.
(9) SHARP, D. G., COOPER, G. R., ERICKSON, J. O., AND NEURATH, H.: J. Biol. Chem. **144**, 139 (1942).
(10) SIMMS, H S.· J. Am. Chem. Soc. **48**, 1239 (1926).
(11) SMITH, R. F., AND BRIGGS, D. R.: J. Phys. Colloid Chem **54**, 33 (1950).
(12) SVENSSON, H : Acta Chem. Scand. **2**, 855 (1948).
(13) SVENSSON, H. Arkiv Kemi, Mineral. Geol. **22A**, No. 10 (1946)
(14) TISELIUS, A.: Nova Acta Regiae Soc. Sci. Upsaliensis [4] **7**, No. 4 (1930).

ELECTROPHORETIC ANALYSIS OF PEANUT AND COTTONSEED MEALS AND PROTEINS[1]

M. L. KARON, MABELLE E. ADAMS, AND A. M. ALTSCHUL

Southern Regional Research Laboratory,[2] New Orleans 19, Louisiana

Received August 22, 1949

INTRODUCTION

The investigations of Johns and Jones (7) have indicated that the total protein of the peanut consists of globulins and a very small amount of heat-coagulable albumin. They found that it was possible, by means of ammonium sulfate fractionation of a sodium chloride extract of peanut meal, to separate the globulins into two fractions, arachin and conarachin, which differed in optical rotation and in content of sulfur, basic nitrogen, lysine, methionine, cystine, threonine, tryptophan, and tyrosine (2, 7, 10). Later, Jones and Horn (11) stated that arachin could be precipitated from the 10 per cent sodium chloride extract by dilution until the extract became cloudy followed by saturation with carbon dioxide, or by the addition of 1 volume of saturated ammonium sulfate to 1.5 volumes of the extract. Conarachin, which was the more soluble fraction, could not be isolated by dilution, but could be precipitated from the filtrates after precipitation of the arachin fraction by dialysis or complete saturation with ammonium sulfate.

The fractional precipitation of protein mixtures had been shown to be an arbitrary procedure (4) and it was not possible to decide whether the arachin and conarachin were single proteins or mixtures in more or less constant proportions. In order to determine whether these protein fractions were homogeneous, Irving, Fontaine, and Warner (6) conducted electrophoretic analyses on peanut meal, arachin, and conarachin. Their results indicated that peanut meal contained at least three and probably four components and that the arachin and conarachin fractions each consisted of mixtures of at least two components.

Johnson (8) investigated the peanut protein fractions by use of the ultracentrifuge. It appeared that the arachin fraction obtained by dilution and addition of carbon dioxide consisted of at least two differently sedimenting species of protein molecules, while the fraction obtained by ammonium sulfate fractionation had only one major constituent. The conarachin fractions consisted of two differently sedimenting species. Arachin, prepared by dilution and acidification and analyzed electrophoretically in phosphate buffer, appeared to consist of two components. Later, it was possible to obtain by salt fractionation a peanut protein fraction which appeared to be homogeneous with respect to molecular size as determined by the ultracentrifuge method, but was not homogeneous when analyzed electrophoretically.

---

[1] Presented at the Twenty-third National Colloid Symposium, which was held under the auspices of the Division of Colloid Chemistry of the American Chemical Society at Minneapolis, Minnesota, June 6–8, 1949.

[2] One of the laboratories of the Bureau of Agricultural and Industrial Chemistry, Agricultural Research Administration, U. S. Department of Agriculture.

Jones and Csonka (9) made the first extensive investigations of the proteins of cottonseed, in which they determined the solubility of the nitrogenous constituents of solvent-extracted cottonseed using successive exhaustive extractions, first with 10 per cent sodium chloride solution, then with 70 per cent ethanol, and finally with 0.5 per cent sodium hydroxide solution. Because 70 per cent ethanol did not extract any nitrogen, they concluded that a prolamine type of protein was absent. According to the fractionation scheme of these authors, the protein from cottonseed meal could be divided into the following fractions: High-ash-yielding fractions I and II, a pentose protein, a glutelin, and an α- and β-globulin. They believed the high-ash fractions to be phosphoproteins. More recent work by Fontaine, Pons, and Irving (5), however, suggested that these fractions were probably impure phytin rather than phosphoproteins. Subsequent to the work of Jones and Csonka, there has been no concerted effort to differentiate the nitrogenous constituents of cottonseed by use of the new tools of protein chemistry.

The present report is concerned with an investigation of peanut and cottonseed meals and derived crude proteins by means of the moving boundary electrophoresis method, with particular reference to the effect of the buffers used as protein solvents and the pH of the buffer on the electrophoretic patterns. Fractionation by means of saline solutions was successful in effecting separation of the two major components of cottonseed protein extracts, whereas similar procedures did not result in separation of peanut protein extracts.

EXPERIMENTAL

Although the proteins of cottonseed and peanut consist primarily of globulins, their solubility in 0.1 molar salt solutions at 0°C. is too small for electrophoretic analysis in neutral buffers; consequently alkaline buffer solutions were used as solvents in these investigations.

Longsworth (12) had shown that the best separation of the components of blood serum could be effected if 0.10 ionic strength veronal (diethylbarbituric acid) buffer at pH 8.6 was used as the solvent. The slow-moving veronal anion aids in the separation of the components of blood serum during the electrophoresis. This buffer system appears to be inapplicable to the cottonseed and peanut proteins, because slight precipitation of the protein occurs in veronal solution during the electrophoresis and it was very difficult to photograph the boundaries at the conclusion of an experiment; therefore other buffers were investigated to determine their effectiveness for use in the analysis of these proteins.

Borate and glycine buffers were prepared according to Clarke (3), veronal buffer was prepared according to Longsworth (12), and an ammonia buffer was prepared by addding 0.2 molar ammonia to 0.1 molar hydrochloric acid solution. While these buffers were satisfactory solvents for peanut meal and protein, only the glycine buffer was satisfactory as a solvent for cottonseed meal.

The proteins in cottonseed meal are less soluble than those of the peanut under the same extraction conditions and more alkaline solutions are required to solubilize the former. Even in glycine buffer below pH 10, the solubility of cottonseed protein was not sufficient to enable accurate determinations of either mobility or percentage composition. A buffer composed of 0.2 mole of ethylamine and 0.1 mole of veronal in a liter of solution having a pH of 10.7 had the most desirable characteristics.

The protein solutions were prepared by mixing 5 g. of the defatted meal with 100 ml. of the different buffers at 0°C. and allowing them to equilibrate for 3 hr. The residual meal was separated from the solution by centrifugation and the protein solution dialyzed against 2 liters of the same buffer for 20 hr. on a rocking-type dialyzer. At the conclusion of the dialysis the solution was clarified by centrifugation and placed in the electrophoresis cell. At no time was the temperature allowed to rise above 5°C.

The apparatus described by Longsworth (12) for analyzing proteins by the Tiselius moving boundary method was used in the investigation. The duration of an experiment was usually 180 min. at field strengths from 4.6 to 7.3 volts/cm. The photographic records of refractive index gradients in the boundaries were made by the schlieren scanning method and at a temperature of 0°C.

The apparent concentration of the components of either cottonseed or peanut was determined by finding the ratio in each case of the component area to the total area exclusive of the δ-boundary. The areas were measured on projected tracings of the electrophoretic pattern of the descending boundary with a planimeter, division into components being carried out by the method of Pedersen (13). Mobilities were determined from the center of the δ-boundary.

RESULTS

Peanut meal and protein

Effect of buffer and pH: The effect of the use of different buffers as the protein solvent on the electrophoretic pattern of deskinned, hexane-extracted Spanish peanuts is shown in table 1.

The data in table 1 indicate that the same electrophoretic pattern is obtained over a pH range from 8.3 to 10.2 and with a variety of buffers. Glycine buffer solutions, exhibiting sharper boundaries and allowing greater protein solubility than the other buffer solutions tested, were used in the routine electrophoretic examination of peanut protein solutions. The influence of the pH of a glycine buffer extract of peanut meal on the electrophoretic analysis of the solution was investigated over a range of pH from 8.7 to 11.4 and the results which were obtained are presented in table 2.

The data in table 2 indicate that there is no significant difference in the relative percentage of each component in the region of pH 8.7–10.2. In more alkaline pH solutions there is a significant increase in the amount of components B and C at the expense of component A. As the alkalinity of the buffer is increased above pH 11, an increasing amount of the protein components appears to become transformed into a single diffuse component which has a mobility between those of components B and C. The exact nature of the effect of alkali is not known, but the process appears to be reversible in solutions less alkaline than pH 11. As shown in table 3, a protein solution prepared in a buffer at pH 11 and reëquilibrated in buffer of pH 9 had an electrophoretic pattern characteristic of a protein solution originally prepared at pH 9.

TABLE 1

Electrophoretic analysis of different buffer extracts of peanut meal

BUFFER[*]	pH[†]	PROTEIN COMPONENT							
		A		B		C		D	
		Mobility[‡]	Per cent[§]	Mobility[‡]	Per cent[§]	Mobility[‡]	Per cent[§]	Mobility[†][‡]	Per cent[§]
Borate	8.36	−7.0	80	−5.7	7	−4.7	4	−2.5	9
Veronal	8.49	−6.7	79	−5.6	12			−3.6	9
Ammonia	8.70	−7.9	86	−5.3	6			−3.5	8
Ammonia[¶]	9.26	−6.3	76	−5.1	11			−3.7	13
Glycine	9.20	−6.9	84	−5.7	7	−4.0	5	−2.9	4
Glycine	10.21	−7.1	81	−5.4	9	−4.5	6	−3.3	4

[*] All buffers were of 0.10 ionic strength.

[†] pH determined at 25°C., using a glass electrode.

[‡] Mobility in cm.^{2}/volt/sec. × 10^5.

[§] Percentage of the total area exclusive of the δ-boundary occupied by the area of component.

[¶] Data of Irving, Fontaine, and Warner (6).

TABLE 2

Effect of pH of glycine buffer extracts of peanut meal on the electrophoretic analysis[*]

pH[†]	PROTEIN COMPONENTS							
	A		B		C		D	
	Mobility[‡]	Per cent[§]	Mobility[‡]	Per cent[§]	Mobility[‡]	Per cent[§]	Mobility[‡]	Per cent[§]
8.73	−6.2	84	−5.3	6	−3.4	6	−2.4	4
9.20	−6.9	84	−5.7	7	−4.0	5	−2.9	4
9.51	−7.2	84	−5.6	7	−4.8	6	−3.9	3
9.66	−7.4	83	−6.4	6	−4.9	7	−3.8	4
10.21	−7.1	81	−5.4	9	−4.5	6	−3.3	4
10.77	−7.7	65	−6.4	13	−5.4	16	−4.0	6
10.95	−8.0	63	−6.4	17	−5.5	17	−4.1	6
11.15	−7.7	33	−6.2	40	−5.2	10	−4.1	11
11.40	−8.3	12	−6.8	46	−5.2	29	−3.8	7

[*] Ionic strength of buffer maintained at 0.1; field strength approximately 5.0 volts/cm.; protein concentration approximately 1.0 per cent.

[†] pH determined at 25°C. with a glass electrode.

[‡] Mobility expressed as cm.^{2}/volt/sec. × 10^5.

[§] Percentage of the total area exclusive of the δ-boundary occupied by the area of component.

Effect of method of extraction and precipitation of protein: Samples of peanut meal were extracted as previously described, using 0.1 *N* solutions of sodium chloride, sodium sulfite, sodium trichloroacetate, and sodium hydroxide adjusted to pH 8.0. After equilibration for 3 hr., the residual meals were separated by centrifugation and the protein liquor was dialyzed against the glycine buffer of pH 10.5 until equilibrium was obtained. The electrophoretic analysis indicated that the extracts had identical composition irrespective of the solvent used for extracting the protein. If, however, one part of peanut meal was washed with 10 volumes of water adjusted to pH 5.0 prior to the extraction of the protein, appreciable soluble sugars and phytin were removed and the protein isolated from the washed meal had an electrophoretic pattern which was different from that of the usual salt- or alkali-extracted protein.

TABLE 3

Reversible pH effect of glycine buffer extracts of peanut meal on the electophoretic analysis

pH	LENGTH OF EQUILIBRATION	PROTEIN COMPONENT							
		A		B		C		D	
		Mobility*	Per cent†	Mobility*	Per cent†	Mobility*	Per cent†	Mobility*	Per cent
	hours								
9.20	20	−6.9	84	−5.7	7	−4.0	5	−2.9	4
9.17	188	−6.8	86	−5.3	4	−4.2	5	−3.1	5
10.95	20	−8.0	63	−6.4	17	−5.5	17	−4.1	6
10.95	96	−8.0	55	−6.3	20	−5.1	21	−3.7	4
10.95–9.17	96‡	−7.3	83	−6.2	7	−3.5	6	−2.1	4

* Mobility expressed as $cm.^2/volt/sec. \times 10^5$.

† Percentage of the total area exclusive of the δ-boundary occupied by the area of component.

‡ Equilibrated for 24 hr. at pH 10.95 and then reequilibrated for 72 hr. at pH 9.17.

In most electrophoretic analyses of peanut protein, component A appeared to be present to the extent of 83 per cent of the entire protein concentration. In the protein isolated from the washed meal, however, component A was no longer present, but appeared to be replaced by two components, A_1 and A_2, which were present to the extent of 45 and 37 per cent, respectively. This effect of washing the meal is clearly shown in figure 1.

Protein concentrates were prepared from fat-free peanut meal by first extracting the meal with either salt solution or mild alkali solution adjusted to pH 7.5, then clarifying the extract by centrifugation and precipitating the protein by acidifying the clarified extract to pH 4.5 and drying the wet curd. Protein prepared in this manner had a distribution of components as determined in the electrophoresis apparatus similar to that of extracts of unwashed peanut meal. If, however, the protein concentrate was prepared from pre-washed meal or if the crude protein curd was washed with water prior to the other prepurification operations, two components, A_1 and A_2, were obtained just as in the case of protein extracts of pre-washed meal.

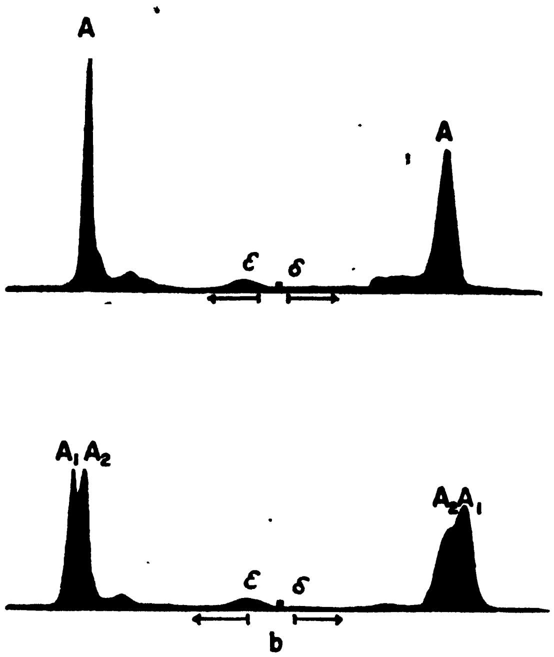

FIG. 1. (a) Normal pattern of a glycine buffer extract of peanut protein after electrophoresis for 180 min. in glycine buffer at pH 9.50. (b) Pattern of a glycine buffer extract of peanut protein isolated from washed peanut meal after electrophoresis for 180 min. at pH 9.50.

TABLE 4

Effect of pH of glycine buffer on the electrophoretic pattern of cottonseed meal extracts*

pH†	PROTEIN COMPONENTS							
	A		B		C		D	
	Mobility‡	Per cent§	Mobility‡	Per cent§	Mobility‡	Per cent§	Mobility‡	Per cent§
10.25	−6.8	10	−5.4	32	−3.7	50	−2.1	3
10.40	−6.8	14	−5.5	35	−4.2	39	−2.5	6
10.65			−5.8	95				
10.75			−6.4	91				
10.85			−5.7	95				
11.03			−5.6	92				

* Buffer of 0.1 ionic strength; protein concentration, 1.2 per cent.

† pH determined at 25°C. with a glass electrode.

‡ Mobility expressed as cm.^{2}/volt/sec. × 10^5.

¶ Percentage of the total area exclusive of the δ-boundary occupied by the area of component.

Cottonseed meal and protein

Effect of buffer and pH: The low solubility of cottonseed proteins in buffer solutions less alkaline than pH 9 limited the number of buffers available for use in electrophoretic investigations of these proteins. A comparison of electrophoretic analyses of cottonseed protein solutions in glycine and ethylamine–veronal buffers is given in tables 4 and 5. The data indicate that glycine buffer is suitable for electrophoresis analysis of cottonseed proteins only over a very limited range of pH. Ethylamine-veronal buffer, however, can be used in the electrophoretic analysis of cottonseed proteins over a much wider range of pH.

TABLE 5

Effect of pH of ethylamine-veronal buffer on the electrophoretic pattern of cottonseed meal extracts*

pH†	PROTEIN COMPONENTS							
	A		B		C		D	
	Mobility‡	Per cent§	Mobility‡	Per cent§	Mobility‡	Per cent§	Mobility‡	Per cent§
9.16	−5.6	25	−4.1	54	−1.8	10	−1.0	11
9.71	−5.7	35	−3.9	51	−2.0	8	−0.8	6
10.16	−6.5	36	−4.7	56	−2.9	6	−1.5	2
10.54	−6.7	49	−5.0	42	−4.0	7	−1.9	2
10.62	−6.8	35	−5.1	58	−3.6	5	−2.2	2
10.72	−6.4	27	−5.1	64	−3.7	6	−1.9	3

* Buffer is of 0.1 ionic strength; protein concentration is 1.2 per cent.

† pH determined at 25°C. with a glass electrode.

‡ Mobility expressed as cm.^{2}/volt/sec. $\times 10^5$.

§ Percentage of the total area exclusive of the δ-boundary occupied by the area of component.

TABLE 6

Effect of protein extractant on the electrophoretic analysis of cottonseed meal extracts in ethylamine–veronal buffer at pH 10.7

EXTRACTING SOLUTION	PROTEIN COMPONENTS							
	A		B		C		D	
	Mobility*	Per cent†	Mobility*	Per cent†	Mobility*	Per cent†	Mobility*	Per cent†
0.2 *N* Na_2SO_3	−6.2	16	−4.8	57	−3.5	16	−1.9	11
0.2 *N* NaCl..	−6.6	44	−5.7	46	−3.5	5	−1.7	5
0.2 *N* $NaOOCCCl_3$ (trichloroacetate)	−6.3	17	−5.0	56	−3.6	16	−2.0	11
NaOH to pH 10.0	−6.8	35	−5.1	58	−3.6	5	−2.1	2

* Mobility expressed as cm.^{2}/volt/sec. $\times 10^5$.

† Percentage of the total area exclusive of the δ-boundary occupied by the area of component.

Effect of method of extraction of protein: A series of experiments were conducted in which 0.2 *N* sodium sulfite, sodium trichloroacetate, sodium chloride, and sodium hydroxide solutions which had been adjusted to pH 10.0 were each used to extract the protein from samples of cottonseed meal. The protein liquors were equilibrated against ethylamine–veronal buffer and analyzed in the electrophoresis apparatus. The results are given in table 6.

TABLE 7

Electrophoretic analysis of major components of sodium chloride extracts of cottonseed meal in ethylamine–veronal buffer at pH 10.62

NORMALITY OF NaCl SOLUTION YIELDING EACH FRACTION	PER CENT OF TOTAL EXTRACTED NITROGEN	PROTEIN COMPONENTS							
		A		B		C		D	
		Mobility*	Per cent†	Mobility*	Per cent†	Mobility*	Per cent†	Mobility*	Per cent†
1.0–0.0	100	−6.7	49	−5.0	42	−4.0	7	−1.9	2
1.0–0.9	17.0	−6.0	63	−5.1	18	−4.2	16		
0.9–0.8	11.3	−6.0	81	−4.6	17	−3.4	2		
0.8–0.7	11.4	−7.0	73	−5.3	25			−2.0	2
0.7–0.6	12.7	−6.7	63	−5.5	37				
0.6–0.5	1.2	−7.0	55	−4.7	45				
0.5–0.4	12.8		20		80				
0.4–0.3	5.0	−6.5	8	−5.2	92				
0.3–0.2	4.0	−6.6	3	−5.1	97				
0.2–0.1	6.8	−6.3	12	−4.6	88				
Remaining in 0.1 solution	17.8								

* Mobility expressed as cm.^{2}/volt/sec. × 10^5.

† Percentage of the total area exclusive of the δ-boundary occupied by the area of component.

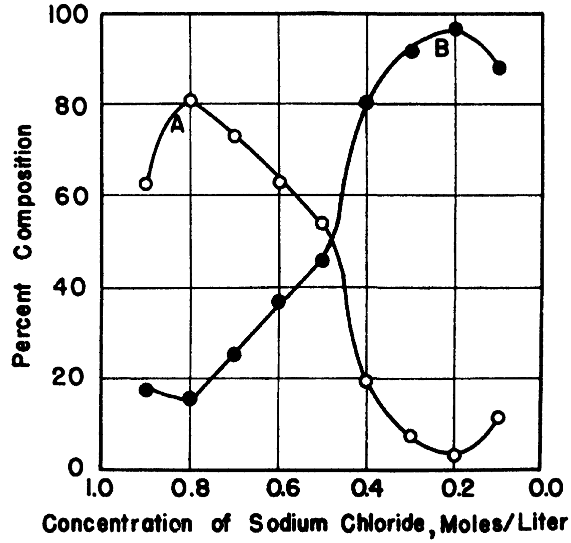

FIG. 2. Distribution of the major components, A and B, in the precipitates removed after equilibrium was reached at each final concentration of sodium chloride solution used.

Unlike the behavior of peanut proteins, the type of anion used in the extractant had a marked effect upon the distribution of protein components in the cottonseed meal extract. The greatest difference was observed in the distribution of components A, C, and D. Component B was equally well extracted by all protein extractants. In a previous publication (1) it was shown that extraction of proteins with sodium sulfite yields a protein product which can more easily be spun into a fiber than one extracted with alkali. It is entirely possible that the properties of a protein concentrate which determine its usefulness in industrial applications are dependent upon the nature of the distribution of the various protein components.

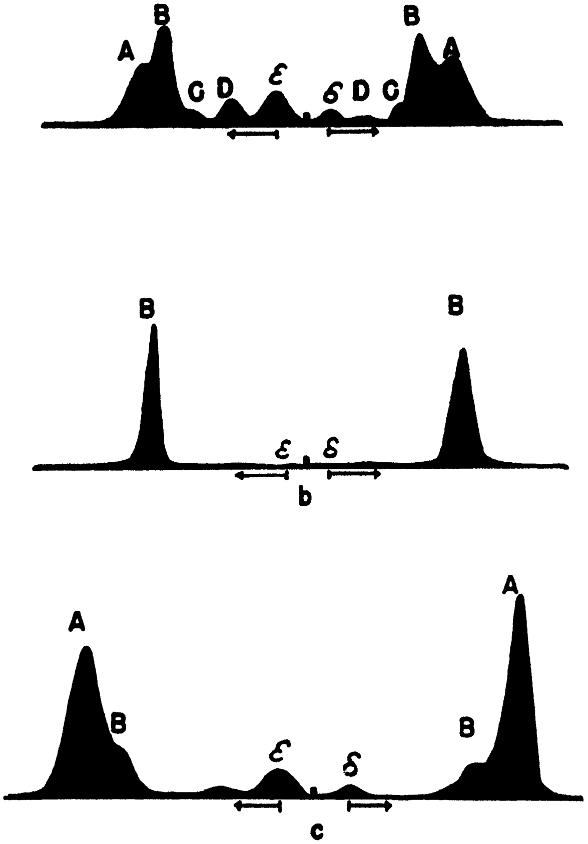

FIG. 3. Effect of fractional dialysis of a sodium chloride extract of cottonseed meal on the electrophoretic pattern of purified fractions. (a) Whole cottonseed meal in ethylamine-veronal buffer pH 10.5, 120 min. at a field strength of 7.0 volts/cm. (b) Cottonseed protein fraction precipitated from 0.4 to 0.3 N sodium chloride in ethylamine-veronal buffer pH 10.5, 160 min. at a field strength of 7.0 volts/cm. (c) Cottonseed protein fraction precipitated from 0.9 to 0.8 N sodium chloride in ethylamine-veronal buffer pH 10.5, 180 min. at a field strength of 7.0 volts/cm.

Fractionation of protein components: The partial fractionation achieved simply by difference in type of extraction anion (table 6) suggested that it might be possible to obtain pure protein components from cottonseed by relatively simple means. Cottonseed meal (50 g.) was reëxtracted eight times with 200-ml. portions of normal sodium chloride and the extract solutions combined. The combined solution was analyzed in the electrophoresis apparatus and then was dialyzed against an equal volume of 0.8 *N* sodium chloride solution. After equilibrium was attained, the resulting cloudy mixture was centrifuged, the precipitate collected, and the supernatant dialyzed against 0.7 *N* sodium chloride solution. This process was repeated using lower and lower normalities of sodium chloride solution as the dialyzing medium. The precipitates obtained after each dialysis operation were analyzed in the electrophoresis apparatus with the results given in table 7.

The distribution of the major components, A and B, in the precipitates removed after equilibrium was reached at each final concentration of sodium chloride solution used, is plotted in figure 2. It can be seen that the precipitate obtained by lowering the concentration of sodium chloride solution from 0.9 to 0.8 *N* had a high concentration of component A and that the precipitate formed by reducing the concentration from 0.3 to 0.2 *N* sodium chloride was almost pure component B. Electrophoretic patterns of extract of cottonseed meal and of the purified fractions obtained by stepwise dialysis with sodium chloride solution are shown in figure 3.

DISCUSSION

Although peanut and cottonseed have little in common, it is interesting to compare the properties of their proteins as determined by electrophoretic measurements. In both cases the protein nitrogen is distributed over two major and several minor components. Peanut proteins resist fractionation and seem to be bound together by complex-forming agents. The fact that component A can be separated into two components by pre-washing the meal or washing the wet protein curd suggests that the binding agents may be carbohydrate and phytin components in the meal. There is considerable asymmetry between the patterns of the ascending and descending boundaries of peanut protein solutions and probably considerable protein–protein interaction. More evidence for the close relationship between the protein components of the peanut is the reversible interconversion from one component to the other which takes place in alkaline buffer solutions.

Cottonseed proteins do not seem to be as closely bound as peanut proteins. There is less asymmetry in the patterns of the two boundaries, no marked effect of alkalinity on the relative abundance of the protein components, and a much greater ease in separation of the individual components by methods of extraction and salt fractionation.

SUMMARY

Cottonseed and peanut meals have been analyzed electrophoretically. The factors investigated were (*1*) the effect of buffer used in the electrophoretic analysis, (*2*) the pH of the buffer, and (*3*) the effect of the solvent used to extract the protein from the meal.

Peanut protein has been found to consist of two major and several minor components. The major components migrate as a single entity under most

conditions; however, if the protein was separated from a meal which had been washed with water adjusted to pH 5 to remove soluble sugars and phytin, the major components separated into two almost equal fractions.

Cottonseed meal protein has two major and two minor components. By fractional precipitation involving a change of ionic strength of the sodium chloride solution which was the solvent, purified fractions of the major components could be obtained.

REFERENCES

(1) Arthur, Jett C., Jr., and Karon, Melvin L.: J. Am. Oil Chemists' Soc. **25,** 99–102 (1948).

(2) Brown, W. L.: J. Biol. Chem. **142,** 299 (1942); **154,** 57 (1944).

(3) Clark, W. M.: *The Determination of Hydrogen Ions*, 3rd edition, p. 206. The Williams & Wilkins Company, Baltimore, Maryland (1928).

(4) Cohn, E. J., McMeekin, T. L., Oncley, J. L., Newell, J. M., and Hughes, W. L.: J. Am. Chem. Soc. **62,** 3386 (1940).

(5) Fontaine, T. D., Pons, W. A., Jr., and Irving, G. W., Jr.: J. Biol. Chem. **164,** 487–507 (1946).

(6) Irving, G. W., Jr., Fontaine, T. D., and Warner, R. C.: Arch. Biochem. **7,** 475–89 (1945).

(7) Johns, C. O., and Jones, D. B.: J. Biol. Chem. **28,** 77 (1916); **30,** 33 (1917).

(8) Johnson, P.: Trans. Faraday Soc. **42,** 28–45 (1946).

(9) Jones, D. B., and Csonka, F. A.: J. Biol. Chem. **64,** 673–83 (1925).

(10) Jones, D. B., Gersdorff, C. E. F., and Moeller, O.: J. Biol. Chem. **62,** 183 (1924–25)

(11) Jones, D. B., and Horn, M. J.: J. Agr. Research **40,** 673 (1930).

(12) Longsworth, L. G.: Chem. Revs. **30,** 423 (1942); Ind. Eng. Chem., Anal. Ed. **18,** 219 (1946).

(13) Svedberg, T., and Pedersen, K. O.: *The Ultracentrifuge*, p. 296. Oxford University Press, London (1940).

THE CONVERSION OF FIBRINOGEN TO FIBRIN. II

Influence of pH and Ionic Strength on Clotting Time and Clot Opacity[1]

SIDNEY SHULMAN and JOHN D. FERRY

Department of Chemistry, University of Wisconsin, Madison, Wisconsin

Received August 22, 1949

The time required for the clotting of fibrinogen by thrombin is prolonged by a variety of hydroxyl compounds, as described in the first paper of this series (8), by increasing concentration of electrolyte (1, 7, 9), and by shift of the pH either above or below the neutral zone, as noted by a number of investigators (1, 7, 16, 23). Under all these circumstances except decreased pH, the prolongation of clotting time is accompanied by a lowering of clot opacity, indicating a decrease in coarseness of structure (7, 8). This would be expected if the slowing of the reaction is due to a diminished probability of association (especially lateral association) of fibrinogen molecules, caused by steric hindrance of lightly adsorbed reagent molecules in the case of the hydroxyl compounds, by diminished dipole and multipole electrical attractions in the case of electrolytes, and by increased coulombic repulsion in the case of high pH. The above correlation fails, however, for the prolongation of clotting time when the pH is decreased toward the isoelectric point of fibrinogen. Here there is a progressive *increase* in opacity, demonstrating the coarsening of structure which would indeed be expected to accompany decreasing coulombic repulsion. Accordingly, the slowing of the reaction at low pH must have some quite different cause.

---

[1] Presented at the Twenty-third National Colloid Symposium, which was held under the auspices of the Division of Colloid Chemistry of the American Chemical Society at Minneapolis, Minnesota, June 6–8, 1949.

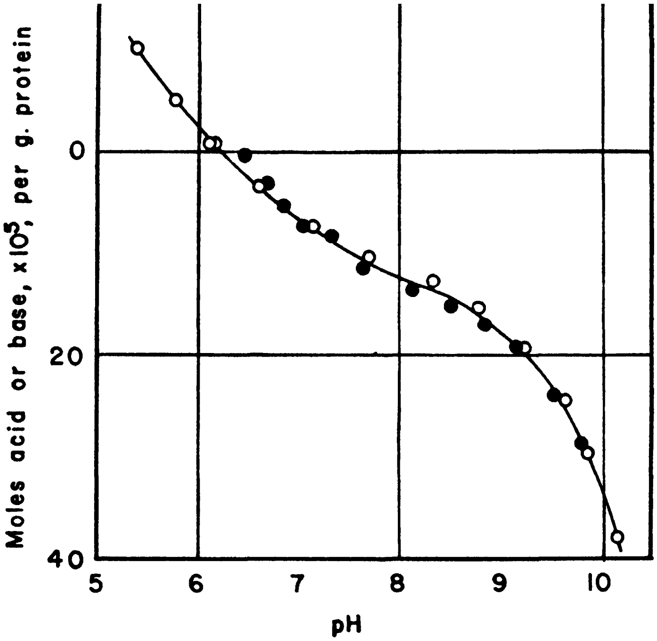

FIG. 1. Titration curve for fibrinogen at ionic strength 0.15 Open circles, 90 per cent clottable protein; filled circles, 87 per cent clottable protein.

In the present study, the dependence of clotting time and clot opacity on pH and ionic strength has been determined over a wider range of these variables than has previously been reported in a single investigation. The observed phenomena may be explained in part by the operation of electrostatic forces and in part by the presence of a dissociable group which is essential for the clotting reaction.

MATERIALS AND METHODS

Bovine fibrinogen (Fraction I, Preparation C–739) and thrombin (Preparation C–173B) were furnished through the kindness of Drs. J. D. Porsche and J. B.

Lesh of Armour and Company, to whom we are deeply indebted for the gift of these materials. In the Fraction I the protein was 65 per cent clottable, as determined by the assay method of Morrison (17); the thrombin had an activity of 4.7 units per milligram (8, 17).

Fibrinogen and thrombin solutions were prepared as previously described (8). The dialyzed fibrinogen solutions contained no buffer, the only electrolyte present being sodium chloride. The pH was adjusted by dilute sodium hydroxide or hydrochloric acid (made up in sodium chloride of the same concentration) and measured with a Beckman glass electrode. Measurements of clotting time and clot opacity (at a wave length of 6000 Å.) were carried out as previously described (8). The thrombin concentration in the clotting mixture was always 1 unit/cc. Above pH 9 the samples were covered with paraffin oil immediately after the introduction of thrombin, to avoid subsequent absorption of atmospheric carbon dioxide; development of rigidity at the clotting time was gauged by moving a stirring rod left immersed in the solution. In the case of very long clotting times

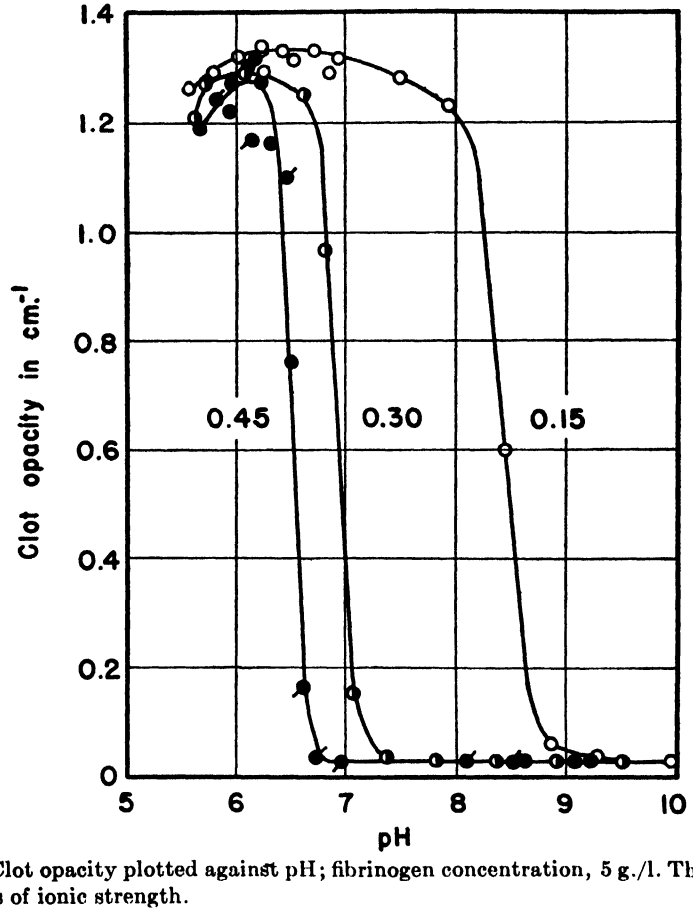

Fig. 2. Clot opacity plotted against pH; fibrinogen concentration, 5 g./l. The figures denote values of ionic strength.

both above pH 9 and below pH 6, tests on control samples containing no thrombin showed that the pH had not changed significantly while standing. All experiments were made at room temperature (25°C. ± 2°).

To obtain an estimate of the valence of fibrinogen as a function of pH, titrations with sodium hydroxide and hydrochloric acid were carried out in 0.15 *M* sodium chloride on two samples of bovine fibrinogen which had been fractionated in collaboration with Professor P. R. Morrison (18), containing 90 per cent and 87 per cent, respectively, of clottable protein. The proportion of bound acid or base was calculated following conventional procedures (3). In correcting for free hydroxyl in the more alkaline systems, the activity coefficient was taken as 0.70. The results are shown in figure 1. Titration curves were also determined in 0.15, 0.30, and 0.45 *M* sodium chloride on another sample of 82 per cent purity; these were almost identical and agreed with the data of figure 1 within about 10 per cent. For the purposes of the calculations to be described below, figure 1 was assumed to represent the acid- and base-binding capacity of pure fibrinogen.

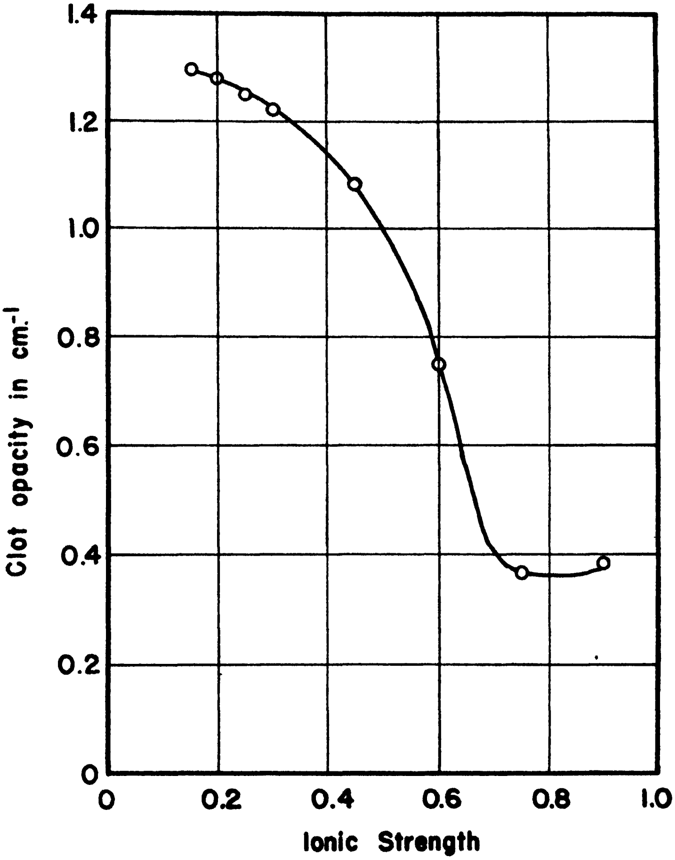

FIG. 3. Clot opacity plotted against ionic strength at pH 6.3 and a fibrinogen concentration of 5 g./l.

RESULTS

The clot opacity, or extinction coefficient, is plotted against pH in figure 2 at three different values of the ionic strength, the fibrinogen concentration being 5 g./l. Below pH 6 the opacity is above 1.0, representing milky-white turbidity, and above pH 9 it is 0.03 or less, representing near transparency. The drop in opacity occurs rather abruptly at about pH 6.3, 6.9, and 8.4, respectively, for ionic strengths of 0.45, 0.30, and 0.15. The results are qualitatively similar to earlier, less detailed measurements on human fibrinogen and thrombin (7), except that the transitions appear to be sharper, and they occur at higher pH values in the bovine system.

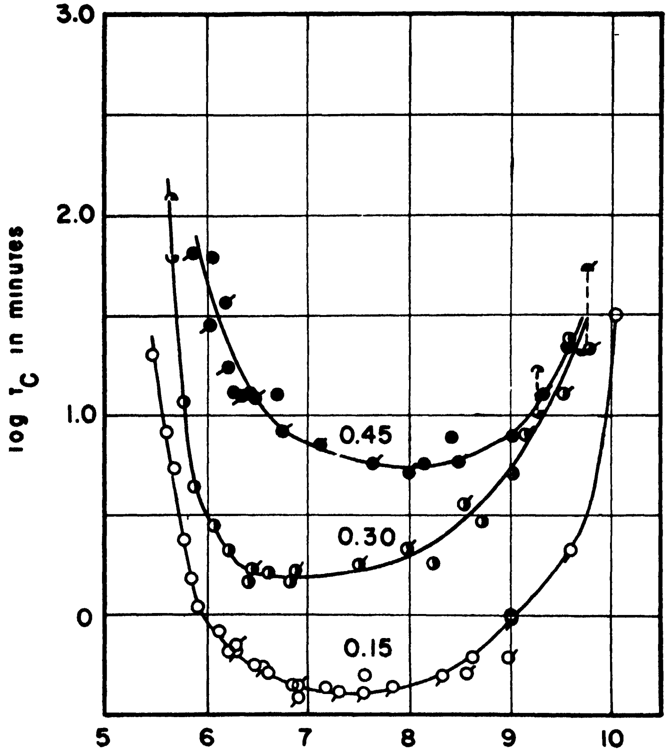

FIG. 4. Logarithm of clotting time plotted against pH; fibrinogen concentration, 1 g./l. The figures denote values of ionic strength.

In figure 3 the opacity is plotted against ionic strength at pH 6.3; it decreases with increasing ionic strength up to 0.8.

The logarithm of the clotting time is plotted against the pH for three values of the ionic strength at a fibrinogen concentration of 1 g./l. in figure 4, and at a fibrinogen concentration of 5 g./l. in figure 5. In each case a minimum is observed. The longest measured clotting times, near pH 5.5 and 10, are forty to one hundred times greater than the minimum times. The higher the ionic strength, the higher the pH at which the minimum clotting time appears. The behavior depends very

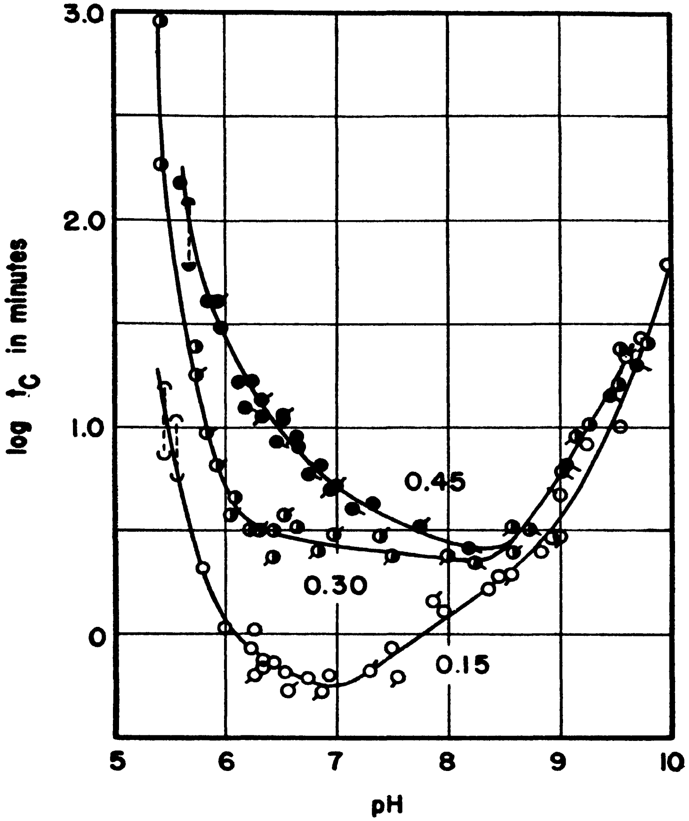

FIG. 5. Logarithm of clotting time plotted against pH; fibrinogen concentration, 5 g./l. The figures denote values of ionic strength.

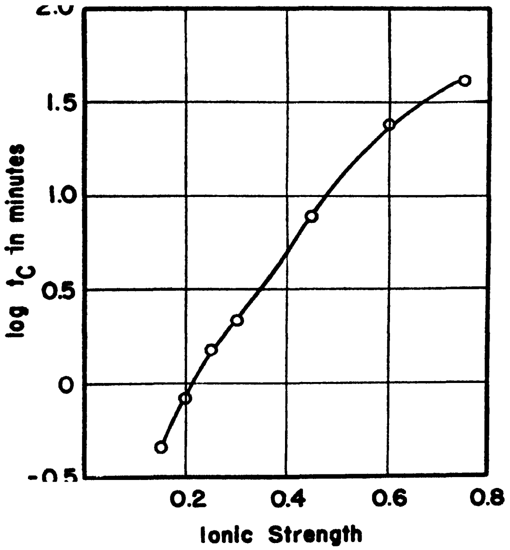

FIG. 6. Logarithm of clotting time plotted against ionic strength at pH 6.3 and a fibrinogen concentration of 5 g./l.

little on fibrinogen concentration, although at 1 g./l. the minima are shallower and the dependence on ionic strength is more marked.

In figure 6 the logarithm of the clotting time is plotted against ionic strength at pH 6.3 and a fibrinogen concentration of 5 g./l. A monotonic increase up to ionic strength 0.9 is observed.

The outer limits of the pH range within which clotting occurs are defined by the data of table 1. Below pH 5.3 and above pH 10, clotting was prolonged at least 24 hr.; in some cases samples remained unclotted as long as two weeks. Although it might at first be suspected that denaturation had occurred at these extreme values, control experiments with the individual proteins showed that the inhibition was not primarily due to destruction of either fibrinogen or thrombin (table 2). Solutions of fibrinogen or thrombin were adjusted to pH values near the outer limits defined by table 1, kept for periods up to 3 hr., and then brought back to a pH between 6 and 7 and used to form clots with fresh thrombin or fibrinogen, respectively. Clots with about the normal clotting time and clot

TABLE 1

Inhibition of clotting at low and high pH

Fibrinogen, 5 g./l.; thrombin, 1 unit/cc.

IONIC STRENGTH	EXPT. NO.	pH	REMARKS
0.30	3	5.30	Clotting time 24 hr.
		5.23	No clot in 48 hr.
	6	5.29	Clotting time < 17 hr.
		5.21	No clot in 41 hr.
0.45	1	5.51	Clotting time < 15 hr.
		5.38	No clot in 40 hr.
	5	5.50	Clotting time < 14 hr.
		5.37	Reticulum in 41 hr.
		5.25	Reticulum in 88 hr.
		5.10	No clot in 88 hr.
	10*	5.70	Clotting time < 21 hr.
		5.52	Reticulum in 21 hr.
		5.33	No clot in 48 hr.
0.15	8	9.75	Clotting time 0.4 hr.
		10.39	No clot in 71 hr.
0.30	8	9.80	Clotting time 0.4 hr.
		10.10	No clot in 70 hr.
0.45	9	9.70	Clotting time 0.3 hr.
		10.27	No clot in 40 hr.

* Fibrinogen concentration, 1 g./l.

opacity were obtained. Thus prolongations of the clotting time up to several hours cannot be attributed to irreversible changes in either protein. Of course, such changes may have occurred in samples kept for many days.

Qualitative observations of the progress of clotting just inside the inhibition limits indicate that the prolongations of clotting on the acid side and on the alkaline side do arise from quite different causes, as inferred above. For ionic strength 0.45 and fibrin concentration 5 g./l., for example, the clot is very opaque and visibly homogeneous at pH 6.1. The high opacity implies that the fibrin network is relatively coarse compared with that present in a transparent clot (7), although the strands are not visible to the eye. At pH 6.1–5.6 the clotting mixture first forms a two-dimensional network around the periphery (solution–glass and solution–air interfaces) which is coarse enough so that individual strands are visible; this is later filled in by a homogeneous opaque clot. At pH 5.6–5.4 the clot is not homogeneous at all; it is a reticulum, with visible strands and large interstices, which pervades the system (*cf.* table 1). The lower the pH, the larger the interstices, until below pH 5.3 clotting is completely inhibited. On the alka-

TABLE 2

Reversibility of inhibition

PROTEIN ADJUSTED	IONIC STRENGTH	EXTREME pH	TIME ELAPSED	RETURN pH	CLOTTING TIME	NORMAL CLOTTING TIME*	OPACITY τ	NORMAL OPACITY*
			hours		*min.*	*min.*	$cm.^{-1}$	$cm.^{-1}$
Fibrinogen (5g /l.)	0.15	5.47	0.5	6.35	0.75	0.76	1.35	1.34
	0.30	5.17	0.5	7.20	1.8	2.6	0.07	0.09
		5.10†	0.3	6.18	2.2	2.2	0.51	0.49
	0.45	5.00	0.5	6.57	11.7	8.5	0.39	0.42
		5.38	0.5	6.28	20.0	14.5	1.14	1.33
	0.15	10.83	0.5	6.25	1.07	0.83	1.28	1.33
	0.30	10.85	0.5	7.62	2.17	2.45	0.24	0.03
	0.45	10.58	0.5	6.37	13.3	12.0	0.84	1.12
		10.00	3	6.13	14.2	18.5		
Thrombin (20 units/cc.)	0.30	5.38	3	6.00‡	3.2	3.3		
		5.80	3	6.16‡	3.3	3.3		
		8.10	3	6.33‡	3.3	3.3		
		9.20	3	6.33‡	3.2	3.3		
		10.38	3	6.40‡	3.3	3.3		

* Interpolated from figures 2, 4, and 5, and normal opacity data at 1 g. of fibrinogen per liter (unpublished).

† Fibrinogen concentration, 1 g./l.

‡ Clotting test made with a fibrinogen concentration of 5 g./l., at pH 6.23, at ionic strength 0.30, and with a thrombin concentration of 1 unit/cc.

line side, on the other hand, no structural changes can be observed; at pH 10 clotting is preceded by a very slow and gradual increase in viscosity, with practically no change in opacity; above pH 10.3 clotting does not occur. The behavior may be described by the statement that on the acid side inhibition is the culmination of a progressive coarsening of structure, while on the alkaline side it is the culmination of a progressive attentuation of structure.

DISCUSSION

Previous studies of the conversion of fibrinogen to fibrin (7, 8) have been interpreted by the hypothesis that the fibrin network strands are built up by end-to-end junction of the fibrinogen rodlets, accompanied by varying degrees of lateral association; the more lateral association, the coarser the strands. An alternative and almost equivalent hypothesis (19) is that the rods join side by side with varying degrees of overlapping; the greater the average extent of overlapping, the coarser the strands. Although some recent notes (10, 13) suggest that these concepts are oversimplified, they will serve nevertheless for interpreting the present study until a more complicated mechanism is definitely established.

PROLONGATION OF CLOTTING AT HIGH pH

Regardless of the details of the conversion process, and whether, for example, the rate-determining step involves a reaction between fibrinogen and thrombin or between two fibrinogen molecules, it would be expected qualitatively that increasing the pH above the neutral zone would increase the net charge of both proteins and hence, owing to electrical repulsion, decrease the rate of conversion in the manner observed. The increase in clotting time with pH is probably primarily due to this electrostatic effect; in fact, it agrees semiquantitatively with theoretical calculations of the effect of repulsion between two fibrinogen molecules, as follows:

It is assumed that the rate-determining step is the junction of two fibrinogen molecules end to end. The progressive attenuation of network strands with pH indicates that at the upper end of the pH range, at least, any side-by-side overlapping is relatively slight. Although at least one of the fibrinogen molecules is presumably activated by thrombin, they are considered to be identical from an electrostatic standpoint and represented by infinitely thin rods of length L and a uniformly distributed charge per unit length σ. The rate constant is written as $k_1 = k_0 f_e f_s$, where f_e is a factor less than unity representing the effect of electrostatic repulsion in the absence of salt, and f_s is a factor greater than unity due to interaction with electrolyte.

As in the theory for ordinary ions (15), $\ln f_e$ is taken as $-E/kT$, where E is the mutual electrostatic energy of the two molecules in the dimeric configuration; for two rods end to end,

$$\ln f_e = -(\sigma^2/DkT)2L \ln 2$$

where D is the dielectric constant, k is Boltzmann's constant, and T is the absolute temperature. The factor f_s is calculated from the activity coefficient, γ, of a charged rod in salt solution, using the method of Brønsted (2) and Scatchard (20). Kirkwood (12) has derived the following equation for the activity coefficient of an infinitely thin rod:

$$\ln \gamma = -(\sigma^2 L/DkT)\,\{C + \ln \kappa L - \mathrm{Ei}(-\kappa L) + (1 - e^{-\kappa L})/\kappa L - 1\} \qquad (1)$$

Here C is Euler's constant, Ei is the exponential integral function, and κ is the Debye–Hückel parameter, $(8\pi N\epsilon^2/1000DkT)^{1/2}(\Gamma/2)^{1/2}$, where N is Avogadro's number, ϵ is the electronic charge, and $\Gamma/2$ is the ionic strength. For fibrinogen $L = 700$ Å. (6), and in our ionic strength range κL is of the order of 100; under

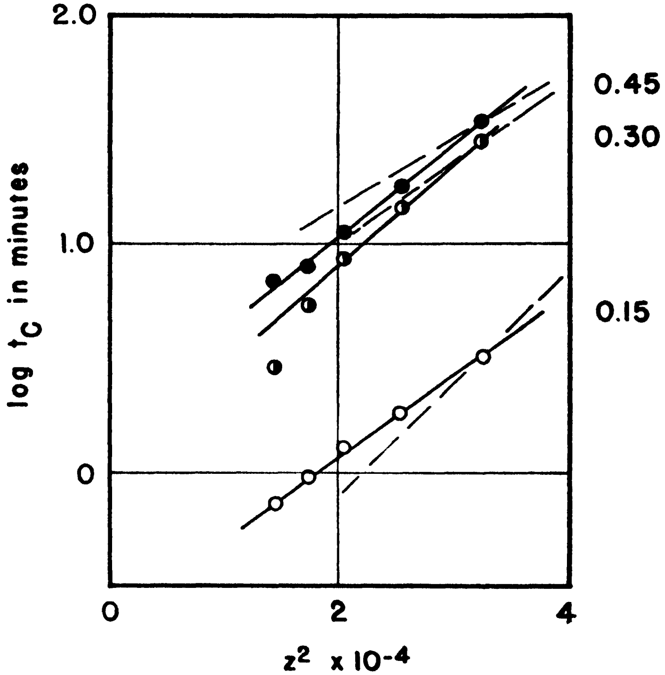

FIG. 7. Logarithm of clotting time at fibrinogen concentration of 1 g./l., plotted against square of fibrinogen valence. The dashed lines represent the theoretical slopes calculated from equation 2. The figures denote values of ionic strength.

these conditions the exponential and exponential integral terms are extremely small, and equation 1 is closely approximated by

$$\ln \gamma = -(\sigma^2 L/DkT)(C + \ln \kappa L + 1/\kappa L - 1)$$

When two molecules form an end-to-end dimer, L is doubled and σ is unchanged. It follows that

$$\ln f_s = (\sigma^2/DkT)(2L \ln 2 - 1/\kappa)$$

Noting that $\sigma = z\epsilon/L$, where z is the fibrinogen net charge, and combining the values for f_r and f_s, we obtain

$$\ln k_1 = \ln k_0 - z^2\epsilon^2/L^2\kappa DkT \qquad (2)$$

so the logarithm of the rate constant should be a linear function of the square of the fibrinogen net charge.

For comparison with experiment, two more assumptions must be made: that the clotting time is inversely proportional to the rate constant, and that the net charge is equal to the valence of fibrinogen as determined from a titration curve. The first probably holds approximately if we avoid the pH region where a sharp transition in structure occurs, as evidenced by change in opacity; this restricts the discussion, at least at ionic strength 0.15, to pH values above 8.7. The second assumption is probably quite adequate for the present treatment; the net charge and the valence would differ only through unequal binding of sodium and chloride ions, and this should be small compared with the charge arising from dissociable groups above pH 8.7. Accordingly, we should find

$$\mathrm{d}\log_{10} t_c/\mathrm{d}(z^2) = (1/2.303)(\epsilon^2/L^2\kappa DkT)$$

where z is taken as the valence. The value of this quantity, with L = 700 Å. (6), in water at 25°C., is 5.0×10^{-5} at $\Gamma/2 = 0.15$ and 2.9×10^{-5} at $\Gamma/2 = 0.45$.

In figure 7 $\log_{10} t_c$ is plotted against z^2, the values of z having been taken from figure 1, assuming that the isoelectric point of fibrinogen is 5.5 (22) and that its molecular weight is 500,000. With the exception of two points at ionic strength 0.3, the data are well fitted by straight lines whose slopes are all about 4×10^{-5}. The theoretical slopes are represented by dashed lines. Although the experimental slopes appear to be independent of the ionic strength instead of inversely proportional to its square root as predicted, their agreement in magnitude with the theoretical values is surprisingly good in view of the many simplifying assumptions. The results are thus consistent with the calculated effect of electrostatic repulsion.

EFFECT OF IONIC STRENGTH

The increase of clotting time with ionic strength can also be interpreted qualitatively in terms of electrostatic forces, by analogy with equations developed by Kirkwood for spherical molecules (11). Besides the contribution to the activity coefficient of a protein molecule in electrolyte due to net charge alone, as described in the preceding section, there is a large contribution from the interaction of electrolyte with dipole and multipole moments arising from the detailed charge configuration of the protein (5). Other things being equal, small molecules interact more strongly than large, and the magnitude of the interaction increases with ionic strength, so the Brønsted treatment implies a decrease in rate constant for dimerization with increasing ionic strength.

PROLONGATION OF CLOTTING AT LOW pH

On the basis of electrostatic forces the clotting time should decrease monotonically as the pH is decreased until both proteins become positively charged; since the isoelectric point of thrombin is between 4.2 and 4.8 (21), the latter condition is not attained in our experimental pH range. To explain the increase which actually occurs below pH 7, the most attractive hypothesis is that combination of protons with some dissociable group interferes with some stage of the clotting reaction. The only amino acid side chain which dissociates in this region is the imidazole group of histidine; it is postulated, therefore, that imidazole must be uncharged to permit the reaction to occur. Either an uncharged imidazole (on fibrinogen or thrombin) participates in the reaction, or else a charged imidazole is in a position to block the reaction.

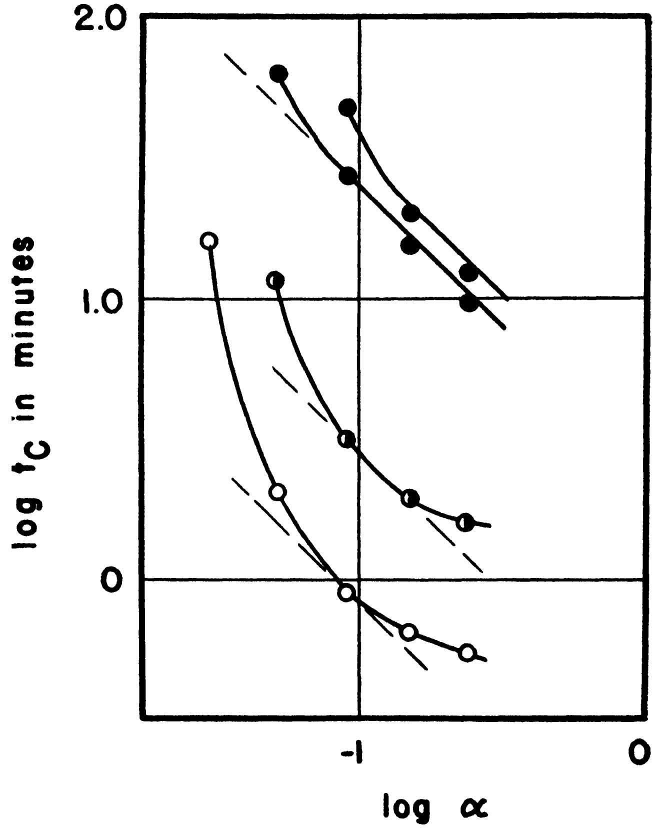

FIG. 8. Logarithm of clotting time plotted against the calculated fraction dissociated of imidazole. The dashed lines represent the theoretical slope. The curves refer to the following fibrinogen concentrations and ionic strengths, in descending order: 1 g./l., 0.45; 5 g./l., 0.45; 1 g./l., 0.30; 1 g./l., 0.15.

In this case, if one group is involved, the rate constant should be proportional to the fraction of imidazole groups dissociated, α, and the clotting time, if again assumed inversely proportional to the rate constant, should be inversely proportional to α. Comparison with experiment is restricted to pH values below the opacity transition, i.e., about 6.5. Here the valence is small enough so that the effect of electrostatic repulsion can be ignored. The imidazole group has a pK of 6.7 in egg albumin and 6.8 in β-lactoglobulin (4). To calculate α, we have taken pK = 7.0, independent of ionic strength. In figure 8 log t_c is plotted against log

α. While the plots show curvature, their slopes are of the order of the expected value of -1. Thus the data are roughly consistent with the hypothesis of the role of a dissociable group.

A far better test of the kinetic interpretations which have been given here could be provided by experimental studies of the early stages of fibrinogen polymerization by such methods as viscosity and light scattering, rather than by measurements of clotting times. It is hoped that such studies will be forthcoming in the future.

SUMMARY

1. The clotting time of bovine fibrinogen by thrombin, and the opacity of the resulting clot, have been studied as functions of pH and ionic strength in sodium chloride solution.

2. With increasing pH the clotting time goes through a minimum, which lies between pH 7.0 and 8.5 depending on the ionic strength and fibrinogen concentration. Below pH 5.3 and above pH 10 clotting does not occur. The inhibition is not primarily due to destruction of either fibrinogen or thrombin. At constant pH the clotting time increases with ionic strength.

3. With increasing pH the clot opacity falls rather sharply at a value which increases with decreasing ionic strength. At constant pH the opacity decreases with increasing ionic strength and passes through a minimum.

4. The prolongation of clotting at high pH is ascribed to the effect of electrostatic repulsion, probably between two fibrinogen molecules in end-to-end union; the prolongation at low pH is ascribed to the combination of protons with the imidazole group of histidine.

This investigation was supported in part by a research grant from the Division of Research Grants and Fellowships of the National Institute of Health, U. S. Public Health Service, and in part by the Research Committee of the Graduate School of the University of Wisconsin from funds supplied by the Wisconsin Alumni Research Foundation. The authors are indebted to Professor J. W. Williams for the use of a Beckman spectrophotometer, to Professor J. G. Kirkwood for permission to quote equation 1, to Professor F. T. Adler for suggestions regarding theoretical calculations, and to Mr. M. Miller for help in some of the experiments.

REFERENCES

(1) ASTRUP, T.: Acta Physiol. Scand. **7**, Suppl. xxi (1944).
(2) BRØNSTED, J. N.: Z. physik. Chem. **102**, 169 (1922).
(3) COHN, E. J., AND EDSALL, J. T.: *Proteins, Amino Acids, and Peptides*, p. 457. Reinhold Publishing Corporation, New York (1943).
(4) Reference 3, p. 477.
(5) Reference 3, p. 611.
(6) EDSALL, J. T., FOSTER, J. F., AND SCHEINBERG, H.: J. Am. Chem. Soc. **69**, 2731 (1947).
(7) FERRY, J. D., AND MORRISON, P. R.: J. Am. Chem. Soc. **69**, 388 (1947).
(8) FERRY, J. D., AND SHULMAN, S.: J. Am. Chem. Soc. **71**, 3198 (1949).

(9) Glazko, A. J., and Ferguson, J. H.: J. Gen. Physiol. **24**, 169 (1940); Am. J. Physiol. **134**, 54 (1941).
(10) Hall, C. E.: J. Biol. Chem. **179**, 857 (1949).
(11) Kirkwood, J. G.: J. Chem. Phys. **2**, 351 (1934).
(12) Kirkwood, J. G.: Private communication.
(13) Laki, K.: Federation Proc. **8**, 90 (1949).
(14) Laki, K. L., and Mommaerts, W. H. F. M.: Nature **156**, 664 (1946).
(15) Moelwyn-Hughes, E. A.: *The Kinetics of Reactions in Solution*, 2nd edition, p. 92. Oxford University Press, London (1947).
(16) Mommaerts, W. H. F. M.: J. Gen. Physiol. **29**, 103, 113 (1946).
(17) Morrison, P. R.: J. Am. Chem. Soc. **69**, 2723 (1947).
(18) Morrison, P. R , Edsall, J. T., and Miller, S. G.: J. Am. Chem. Soc. **70**, 3103 (1948).
(19) Nanninga, L. B.: Thesis, Amsterdam, 1947.
(20) Scatchard, G.: Chem. Revs. **1**, 229 (1932).
(21) Seegers, W. H.: Private communication.
(22) Seegers, W. H., Nieft, M. L., and Vandenbelt, J. M.: Arch. Biochem. **7**, 15 (1945).
(23) Seegers, W. H , and Smith, H. P.: Am. J. Physiol. **137**, 348 (1947).

ELECTROPHORETIC STUDY OF THE INTERACTION OF SERUM ALBUMIN AND THYMUS NUCLEIC ACID[1]

EUGENE GOLDWASSER and FRANK W. PUTNAM

Department of Biochemistry, University of Chicago, Chicago, Illinois

Received August 22, 1949

The interaction of purified proteins with inorganic anions, monomeric dyes, and the synthetic detergents has frequently been demonstrated by several methods (14, 17, 18, 19, 21). The application of the law of mass action to the binding of small organic or inorganic ions has allowed the evaluation of binding energies and study of the molecular nature of the protein–anion complex (2, 14, 15). However, little investigation has been made of the interaction of proteins with biologically important polymers such as the nucleic acids or other highly charged substances which occur naturally in association with proteins. The size, asymmetry, and polyvalence of the nucleic acids impose stereochemical difficulties for stoichiometric combination with globular proteins and preclude study by the equilibrium dialysis method. However, electrophoretic analysis has been shown to be applicable to the quantitative evaluation of protein–anion interaction (16, 17, 18, 20), and, accordingly, such an investigation of nucleic acid–protein complex formation was undertaken in a model system containing purified thymus nucleic acid and crystalline serum albumin.

---

[1] Presented at the Twenty-third National Colloid Symposium, which was held under the auspices of the Division of Colloid Chemistry of the American Chemical Society at Minneapolis, Minnesota, June 6–8, 1949.

The work was aided in part by a grant from the Dr. Wallace C. and Clara A. Abbott Memorial Fund.

Some evidence already exists for the interaction of nucleic acids with proteins, and for the physiological significance of this phenomenon. Thus, physical-chemical studies have demonstrated that thymus desoxyribonucleoproteins are largely dissociated in molar sodium chloride (29, 30). Electrophoresis of tissue extracts (24) or of other naturally occurring mixtures of proteins with nucleic acids (22) has revealed that interaction occurs even on the alkaline side of the isoelectric point, where both components are similarly charged. Greenstein (6, 7) has reported that serum albumin diminishes the viscosity of thymus nucleic acid and also renders it osmotically ineffective, and has summarized other evidence that the physical properties of sodium thymus nucleate are affected by the presence of native proteins (8). In an electrophoretic study of the properties of thymonucleic acid Stenhagen and Teorell (28) observed that in mixtures of serum albumin and this nucleic acid the mobilities of the components were modified by their mutual presence. However, the lack of a modern optical system prevented these authors from making a quantitative analysis of the electrophoretic patterns. More recently, Longsworth and MacInnes (16) in a classical investigation studied the interaction of yeast nucleic acid and egg albumin and established the principles for evaluation of the effect of electrophoresis on the interaction equilibrium.

EXPERIMENTAL

Materials and methods

The crystalline bovine serum albumin (Lot 20) was obtained from the Armour Laboratories, Chicago, Illinois. It yields a single boundary upon electrophoresis at 0.1 ionic strength at pH 3.0–3.9 and pH 5.5–8.6, but in the isoelectric region gives the asymmetric patterns reported by other authors (1, 17). The latter anomaly is not related to ultracentrifugal homogeneity, for the sedimentation diagrams were unaltered from pH 3.6 to pH 7.0.

The thymus nucleic acid (desoxyribonucleic acid, DNA) was prepared from calf thymus by the method of Hammarsten (10) and was precipitated four times. It was biuret-negative and had a N/P ratio of 1.82 but contained some dialyzable phosphorus. Since the molecular homogeneity of thymus nucleic acid is often questionable (8, 12) and is important in the interpretation of its combination with proteins, dialyzed solutions of the desoxyribonucleic acid were examined in the analytical ultracentrifuge. The ultracentrifuge diagrams in figure 1 show that the dialyzed nucleic acid sediments with a single sharp slightly asymmetric boundary, which had a sedimentation constant of 5.1 S. This value is in good agreement with the figure reported by Kahler (12) at the same nucleic acid concentration. However, on extrapolation to infinite dilution, the latter author obtained a sedimentation constant of 12.5 S. From combined sedimentation and diffusion data Kahler calculated that his preparation of desoxyribonucleic acid had a frictional ratio of 6.8 and a molecular weight of 1.5×10^6. Since the apparent frictional ratio of the desoxyribonucleic acid used in this investigation was somewhat lower (4.35 as calculated from viscosity data and assuming a rod-like shape and the validity of the Simha equation (25)), the molecular weight of our preparation is probably in the range of 5×10^5 to 1×10^6 reported by other authors (see 8).

The solutions for electrophoretic analysis were made up by weight in the desired buffer and equilibrated by dialysis. The desoxyribonucleic acid content of the dialyzed mixtures was determined by phosphorus analysis, using a modified Gomori method (5), and the protein content was estimated by measurement of the refractive increment, correction being made for the increment due to desoxyribonucleic acid. Since Stenhagen and Teorell (28) state that the mobility of thymus nucleic acid depends on the voltage gradient, analyses were routinely done at approximately the same electrical field strength. Because of the skewness of some of the curves, all mobilities were calculated from the displacement of the centroidal ordinates. Relative areas were determined planimetrically from the enlarged patterns by arbitrarily drawing an ordinate between two adjacent peaks.

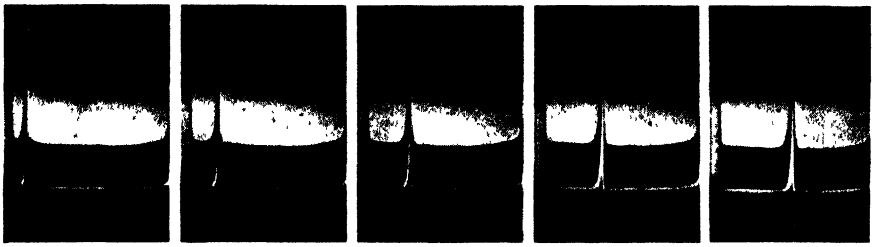

FIG. 1. Ultracentrifuge diagrams of purified calf thymus nucleic acid. Photographs were taken with a bar angle of 60° at intervals of 16 min. and at a speed of 59,780 R.P.M. The solution contained 0.5 per cent nucleic acid in a 0.2 M sodium acetate buffer, pH 5.5. In the first exposures the boundary is so sharp that part of the entering light beam is completely deflected below the camera lens, as is indicated by the vertical line below the base line.

The electrophoresis apparatus used was a commercial model equipped with the schlieren scanning camera. An electrically driven analytical ultracentrifuge[2] was employed for sedimentation velocity analysis. Viscosities were measured at 25°C. in Ostwald viscometers.

Electrophoretic analysis

Preliminary investigation of the interaction of serum albumin and desoxyribonucleic acid revealed that precipitation takes place on the acid side of the isoelectric point and that mixtures of the two substances are very turbid up to pH 5.2. For this reason all electrophoretic analyses were made at pH 5.5 or higher. In the electrophoretic investigation a systematic study was made of the effect of pH, ionic strength, and protein/nucleic acid concentration ratio on the interaction of serum albumin and desoxyribonucleic acid.

---

[2] This ultracentrifuge was designed by Dr. E. G. Pickels and is available from the Specialized Instruments Corporation, Belmont, California.

Effect of pH

The influence of pH on the electrophoretic patterns of mixtures of desoxyribonucleic acid and serum albumin was studied at pH 5.5, 6.4, and 7.6. In this region desoxyribonucleic acid has a high anodic mobility essentially independent of pH, and the separate components migrate with a single boundary except that at pH 6.4 the nucleic acid has a small amount of a component that moves somewhat more slowly than the major boundary.

In mixtures of the protein and nucleic acid at pH 6.4 and 7.6 the electrophoretic patterns were essentially the sum of those obtained for the separate components. Although the descending boundaries were skewed, both patterns contained only two major components. The areas were closely proportional to the concentrations of the components (after allowance was made for the difference in refractive increments of protein and desoxyribonucleic acid), and the mobilities of the descending fast and slow boundaries corresponded to those obtained for pure nucleic acid or serum albumin, respectively. However, at pH 5.5 the patterns were not even qualitatively symmetrical with regard to the number of boundaries found on the two sides of the cell. In addition to the two expected boundaries, a complex of intermediate mobility and varying proportion appeared in the ascending limb, while on the descending side, where only two peaks were visible, the area of the fast component exceeded that attributable to the desoxyribonucleic acid content of the mixture. Such asymmetry has been ascribed to the formation of reversibly dissociable complexes (16), and the effect of pH on the electrophoretic patterns suggests that the nature of the interaction is electrostatic.

Effect of ionic strength

The influence of ionic strength on mixtures of desoxyribonucleic acid and serum albumin was studied at pH 5.5 at a concentration ratio of protein to nucleic acid approaching unity. The ionic strength was varied over a tenfold range—from 0.02 to 0.2—using sodium acetate-acetic acid buffers. The striking change which occurred in the electrophoretic patterns is illustrated in figure 2. At low ionic strength, i.e., from 0.02 to 0.05 (figures 2A–2C) the patterns in the two limbs of the cell were more or less enantiographic, but were not related to the concentrations or the number of the components of the mixtures. However, at higher ionic strengths qualitative agreement of the electrophoretic patterns with the composition of the mixtures obtained: that is, when the ionic strength reached 0.1 (figure 2D) although the rising pattern was still asymmetric, there were only two descending peaks; and, finally, at ionic strength 0.2 (figure 2F) the patterns approached enantiography.

In this series of experiments the mobilities of the pure constituents, as well as of the components of the mixtures, were determined at each ionic strength. The ascending fast component had the mobility of desoxyribonucleic acid; the descending slow component the mobility of serum albumin. However, except at ionic strength 0.2, the mobilities of the descending fast peak and the ascending

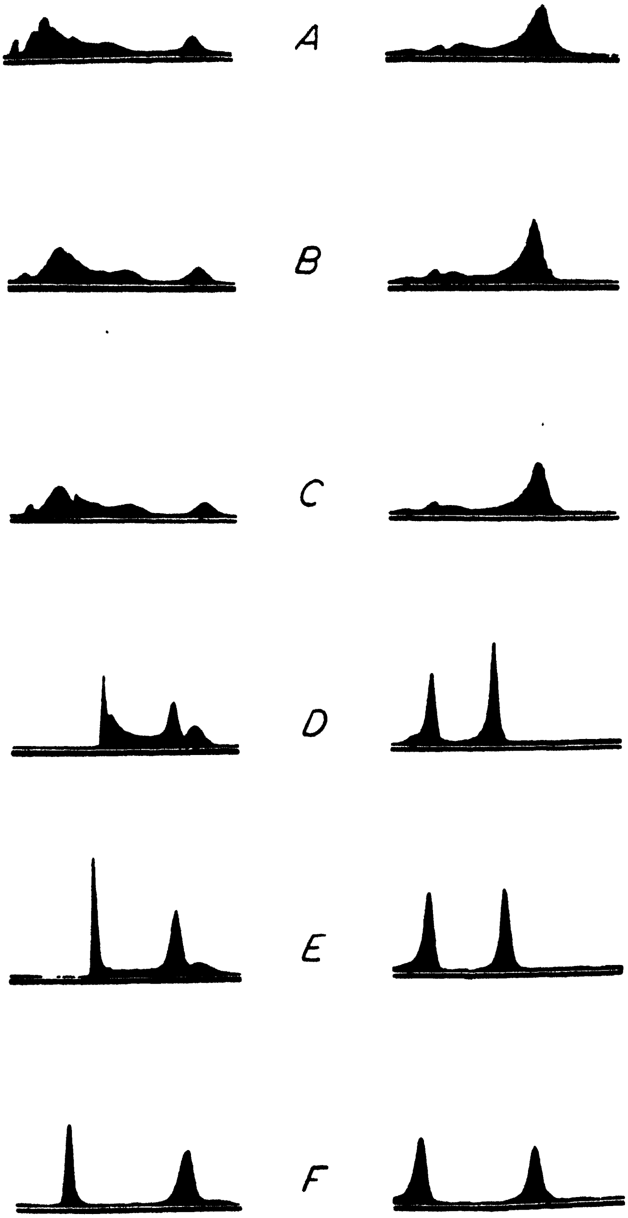

FIG. 2. Influence of ionic strength on the electrophoretic patterns of mixtures containing approximately 0.5 mg. per milliliter each of bovine serum albumin and purified thymus nucleic acid. The starting boundary is superimposed on the patterns: left, ascending; right, descending. Reading from top to bottom the ionic strength was: 0.02 (A); 0.04 (B); 0.05 (C); 0.10 (D); 0.15 (E); and 0.20 (F). Only at 0.2 ionic strength are the patterns nearly enantiographic and quantitatively related to the number and concentrations of the components of the mixture.

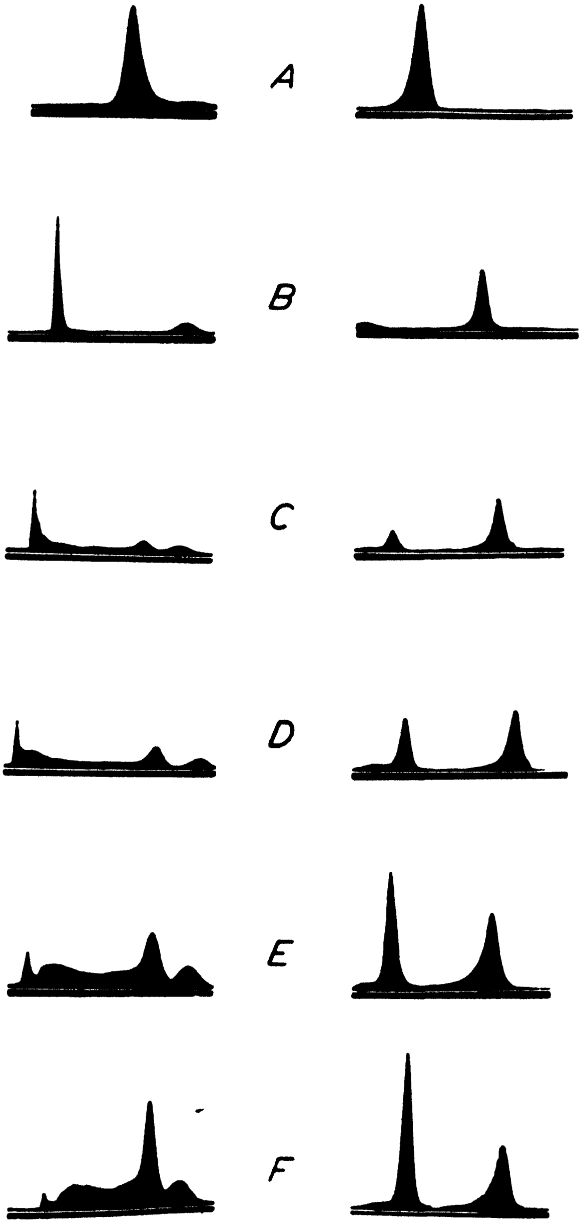

FIG. 3. Influence of the protein/nucleic acid concentration ratio on the electrophoretic patterns of mixtures of bovine serum albumin and purified thymus nucleic acid at pH 5.5 in 0.1 ionic strength acetate buffer solutions. The starting boundary is superimposed on the patterns: ascending, left; descending, right. A represents the crystalline protein, B the nucleic acid, and all others refer to mixtures of the two components. The protein/nucleic acid concentration ratio increases in going from C to F. The concentrations of protein and nucleic acid, the mobilities of the boundaries, and the area distribution are given in table 1.

slow peak did not correspond to the values obtained for pure desoxyribonucleic acid and protein, respectively. Only at the highest ionic strength studied, i.e., 0.2, did the patterns of the mixtures and the mobilities of the boundaries correspond both qualitatively and quantitatively to the expected values. Moreover, at that ionic strength electrophoretic separation of the ascending fast component followed by chemical analysis revealed it to contain only desoxyribonucleic acid. Similarly, the descending slow component was found to be pure protein. Since complex formation was inhibited by increasing the ionic strength, the interaction was considered electrostatic. It is to be noted that there is likewise a strong influence of pH and ionic strength on the precipitation of ovalbumin by desoxyribonucleic acid (11).

TABLE 1

Electrophoretic analysis of mixtures of serum albumin and thymus nucleic acid in 0.1 N sodium acetate buffer at pH 5.5 and 2°C.

EXPT. NO.*	COMPOSITION		ELECTROPHORETIC MOBILITY				RELATIVE AREA				
	Albumin	DNA†	Ascending		Descending		Ascending‡			Descending	
			Fast	Slow	Fast	Slow	Fast	Intermediate	Slow	Fast	Slow
	mg. per ml		*10^{-5} cm.^{2} sec.$^{-1}$ volt^{-1}*				*per cent total area*				
A	7.3			3.42		2.73			100		100
B		3.9	18.9		16.6		100			100	
C	2.5	3.1	18.7	4.88	16.8	2.78	26.4	52.0	21.6	74.8	25.2
D	5.0	4.7	18.9	4.56	15.0	2.90	15.6	56.6	27.8	63.8	36.2
D′	5.0	3.6	18.3	4.40	16.0	2.90	21.5	51.3	27.2	65.6	34.4
E	10.0	3.7	18.9	4.87	14.6	3.19	10.6	35.8	53.6	51.4	48.6
F	15.0	3.1	18.4	4.13	12.2	2.54	2.8	48.5	48.7	44.0	56.0
G	10.5	1.87	18.6	3.95	12.4	2.88	2.0	42.5	55.5	39.0	61.0
H	10.7	1.49	18.3	3.45	11.3	2.79	1.0	30.2	68.6	36.0	64.0

* Experiment numbers correspond to diagrams of figure 3. Field strength varied from 4.74 to 5.33 volts cm.$^{-1}$

† DNA = desoxyribonucleic acid.

‡ Ascending mobilities uncorrected for δ anomaly.

Influence of protein/nucleic acid ratio

An ionic strength of 0.1 and a pH of 5.5 was chosen for study of the influence of the protein to nucleic acid concentration ratio on the electrophoretic patterns of mixtures of the two substances. As shown in figure 3A, serum albumin by itself gives a single symmetrical boundary under these conditions, as does desoxyribonucleic acid (figure 3B). The mobility of desoxyribonucleic acid is -16.6×10^{-5} cm.^{2} sec.$^{-1}$ volt^{-1}, while that of the protein is -2.73×10^{-5} cm.^{2} sec.$^{-1}$ volt^{-1}. Under the conditions of study the descending patterns of mixtures always contain only two moving boundaries.[3]

---

[3] If the potential gradient is changed from 2 volts per centimeter to 16 volts per centimeter, other conditions being kept constant, the electrophoretic patterns show no appreciable change. Nor is the distribution of the patterns significantly altered with time of electrophoresis at constant potential gradient.

The concentration ratio was varied over about a tenfold range and some representative patterns are presented in figure 3. The composition of the mixtures and the mobilities and relative areas of the several boundaries are given in table 1. The ascending fast component, which is greatly diminished in area at high protein/desoxyribonucleic acid ratios, has the mobility of free desoxyribonucleic acid; the descending slow boundary, though variable in mobility, migrates at a rate similar to free albumin. Moreover, chemical analysis of the electrophoretically isolated slow component showed it to be essentially pure serum albumin; thus, in one case, the isolated material contained 2.96 mg. protein per milliter and only 0.032 mg. desoxyribonucleic acid per milliliter. However, at high ratios of protein to nucleic acid the mobility of the descending fast component was significantly less than that of the free nucleic acid, and the area of this boundary in all instances exceeded that attributable to the desoxyribonucleic acid content of the mixture. For example, in experiment H of table 1, where the desoxyribonucleic acid comprised 12.2 per cent of the mixture by weight, the fast boundary represented 36 per cent of the area. Since the refractive increment of the protein exceeds that of the nucleic acid, the lack of correlation of the desoxyribonucleic acid content of the mixture and the electrophoretic concentration of the descending fast component is even more marked than is indicated by the relative area figures. The conclusions reached from study of the mobility and area data for the descending patterns are that the slow boundary represents essentially pure serum albumin and the fast boundary a complex of nucleic acid and the protein. On the ascending side the fast component appears to be free desoxyribonucleic acid; the intermediate boundary seems to represent a complex of changing composition; and the slow boundary is largely due to serum albumin, which, however, is migrating to a viscous medium containing nucleic acid.

DISCUSSION

The electrophoretic analysis of mixtures in which interaction occurs may lead to pattern asymmetries such as those observed in this investigation.[4] Longsworth and MacInnes (16) have attributed these asymmetries to a disturbance of the equilibrium caused by the tendency of the components to separate, owing to their mobility differences.[5] They pointed out that the extent to which the equilibrium will shift depends on the magnitudes of the reaction velocity constants in comparison with the rate of electrophoretic separation, and they distinguished five cases. Since dissociation occurs only at a concentration gradient, and not in the body of the solution, the composition and mobility of the complex are not given by any boundary, and, accordingly, the equilibrium constant can not be calculated. However, the migration of the faster anion into solvent on the anode side but into solution on the cathode side, in general, results in the separation of pure anion as the leading boundary and of pure protein as the trailing boundary.

---

[4] It is to be noted that patterns which are enantiographic except for δ- and ϵ-effects have been obtained in some instances of component interaction; for example, in the electrophoretic analysis of mixtures of serum albumin and sodium dodecyl sulfate (20).

[5] Recently, Smith and Briggs (26) have developed a method for the analysis of electrophoretic patterns of protein–anion complexes which rests on the assumption that the electrical field does *not* cause dissociation of the complex in the ascending limb or in the body of the solution, but merely removes excess free anion on the descending side, thereby allowing the separation of free protein and of a boundary representing complex of altered composition. While their electrophoretic analysis of the combination of methyl orange with bovine serum albumin at pH 5.5 has yielded binding constants, similar to those found by Klotz *et al.* (13) using the equilibrium dialysis method, application to our data has been unsuccessful. Moreover, the asymmetry of patterns obtained with mixtures of desoxyribonucleic acid and serum albumin precludes calculation by another suggested method which requires that only two moving boundaries (exclusive of δ- or ϵ-effects) are formed in each

Although the patterns obtained in this investigation do not conform clearly to any of the five cases listed by Longsworth and MacInnes (16), they may result from the fourth case in which the rate of adjustment of the equilibrium is comparable to the rate of electrophoretic separation. These authors mention unpublished experiments with ovomucoid and nucleic acid in which three moving boundaries were observed in one channel and only two in the other. Similar results have been obtained in electrophoretic studies of mixtures of serum albumin and heparin (4). Although asymmetries of this type have not been satisfactorily explained, they are not encountered in the interaction of serum albumin with dodecyl sulfate (20) or methyl orange (26), and hence are apparently unrelated to the known electrophoretic complexity of this protein. It is to be noted that whereas Stenhagen and Teorell (28) observed only two distinct boundaries in each channel in an electrophoretic analysis of mixtures of human serum albumin and thymus nucleic acid, these authors utilized an early optical system incapable of giving the resolution obtained in this study and, moreover, employed only a limited set of conditions.

Much recent work has supported the suggestion of Steinhardt (27) and of Putnam and Neurath (19–21) that proteins combine stoichiometrically with anions by electrostatic interaction with positively charged groups of the protein, only some of which are ordinarily available for combination. Although the effect of increasing pH and ionic strength on the abolition of the interaction of serum albumin and thymus nucleic acid establishes the electrostatic nature of the phenomenon, no evidence has been obtained for the formation of protein-nucleate complexes of definite composition. Indeed, the distribution of the electrophoretic patterns, though duplicable under identical conditions, varies continuously with increasing protein/nucleic acid concentration ratio.

With small univalent ions, the number of anions bound per molecule of serum albumin has ranged up to one hundred or more for anions of high affinity (21, 23), one equivalent apparently reacting with each basic group of the protein. However, a different situation must prevail for a polyvalent asymmetric anion of high molecular weight such as thymus nucleate. Titration and analytical data

---

limb of the U-tube (private communication from R. A. Alberty). In addition, it should be noted that the statistical treatment of protein-anion combination developed by Klotz (13–15) neglects electrostatic repulsions of neighboring groups. Though this effect may be small for univalent ions, it becomes appreciable for trivalent ions, and must be important for a polyvalent ion such as desoxyribonucleic acid.

show that there is one primary phosphoryl group in a free titratable state per phosphorus atom of desoxyribonucleic acid (9). This corresponds to a maximum negative charge of about 300 per 10^5 g. of desoxyribonucleic acid, which, on a weight basis, is more than double the maximum acid-binding capacity of serum albumin (143 moles per 10^5 g. (3)). Consideration of the relative molecular weights and axial ratios of the protein and the nucleic acid makes clear that stereochemical restrictions limit the stoichiometric combination of an asymmetric polyvalent anion such as desoxyribonucleic acid with a globular protein such as serum albumin. While viscosity measurements (6) indicate that the high degree of asymmetry of thymus nucleic acid is lost upon combination with proteins, and the data presented here demonstrate the electrostatic nature of the binding, no information is yet available on the fine structure of the complex. However, Greenstein (8) has considered the problem of fitting the much more asymmetric thymus nucleic acid particles into the nucleohistone molecules from which they are derived, and Stern (29) has discussed the possible biological significance of the reversible shape changes which nucleoproteins undergo as a function of the ionic environment.

SUMMARY

Electrophoretic analysis of mixtures of crystalline bovine serum albumin and purified thymus nucleic acid has revealed the formation of reversibly dissociable protein–nucleate complexes under conditions where both components are negatively charged. Interaction occurs in acetate buffers at pH 5.5 and ionic strength below 0.2, and the electrophcretic patterns do not conform to the composition of the mixtures. The ascending and descending patterns are not enantiographic, differing both in the number of boundaries and in the distribution of the apparent components. While only two distinct boundaries are obtained in the descending arm, the ascending patterns contain intermediate complexes, the distribution of which depends on the concentration ratio of protein and nucleic acid. However, at pH 5.5 the asymmetries diminish with increasing ionic strength, vanishing at 0.2 ionic strength. Likewise at higher pH the protein and nucleic acid migrate independently. The dependence of electrophoretic behavior on pH, ionic strength, and the composition of the mixture indicates that the nature of the interaction is electrostatic.

The authors are grateful to Dr. E. S. G. Barron for making available the electrophoretic apparatus and the ultracentrifuge used in this investigation.

REFERENCES

(1) Alberty, R. A.: J. Phys. & Colloid Chem. **53**, 114 (1949).
(2) Boyer, P. D., Ballou, G. A., and Luck, J. M.: J. Biol. Chem. **167**, 407 (1947).
(3) Brand, E.: Ann. N. Y. Acad. Sci. **47**, 187 (1946).
(4) Chargaff, E., Ziff, M., and Moore, D. H.: J. Biol. Chem. **139**, 383 (1941).
(5) Gomori, G.: J. Lab. Clin. Med. **27**, 955 (1942).
(6) Greenstein, J. P., and Jenrette, W. V.: Cold Spring Harbor Symposia Quant. Biol. **9**, 236 (1941).

(7) Greenstein, J. P.: J. Biol. Chem. **150**, 107 (1943).
(8) Greenstein, J. P.: Advances in Protein Chem. **1**, 209 (1944).
(9) Gulland, J. M.: Cold Spring Harbor Symposia Quant. Biol. **12**, 95 (1947).
(10) Hammarsten, E.: Biochem. Z. **144**, 383 (1924).
(11) Hammarsten, E., and Hammarsten, G.: Acta Med. Scand. **68**, 199 (1928).
(12) Kahler, H.: J. Phys. & Colloid Chem. **52**, 676 (1948).
(13) Klotz, I. M., Walker, F. M., and Pivan, R. B.: J. Am. Chem. Soc. **68**, 1486 (1946).
(14) Klotz, I. M., Triwush, H., and Walker, F. M.: J. Am. Chem. Soc. **70**, 2935 (1948).
(15) Klotz, I. M., and Urquhart, J. M.: J. Phys. & Colloid Chem. **53**, 100 (1949).
(16) Longsworth, L. G., and MacInnes, D. A.: J. Gen. Physiol. **25**, 507 (1942).
(17) Longsworth, L. G., and Jacobsen, C. F.: J. Phys. & Colloid Chem. **53**, 126 (1949).
(18) Lundgren, H. P., Elam, D. W., and O'Connell, R. A.: J. Biol. Chem. **149**, 183 (1943).
(19) Putnam, F. W., and Neurath, H.: J. Am. Chem. Soc. **66**, 692 (1944).
(20) Putnam, F. W., and Neurath, H.: J. Biol. Chem. **159**, 195 (1945).
(21) Putnam, F. W.: Advances in Protein Chem. **4**, 79 (1948).
(22) Putnam, F. W., Kozloff, L. M., and Neil, J. C.: J. Biol. Chem. **179**, 303 (1949).
(23) Scatchard, G., and Black, E. S.: J. Phys. & Colloid Chem. **53**, 88 (1949).
(24) Seibert, F. B.: J. Biol. Chem. **133**, 593 (1940).
(25) Simha, R.: J. Phys. Chem. **44**, 25 (1940).
(26) Smith, R. F., and Briggs, D. R.: J. Phys. & Colloid Chem. **54**, 000 (1950).
(27) Steinhardt, J.: Ann. N. Y. Acad. Sci. **41**, 287 (1941).
(28) Stenhagen, E. and Teorell, T.: Trans. Faraday Soc. **35**, 743 (1939).
(29) Stern, K. G.: Scientia **82**, 74 (1947).
(30) Van Winkle, Q., and France, W. G.: J. Phys. & Colloid. Chem. **52**, 207 (1948).

THE ACTION OF PHOSPHATES ON KAOLIN SUSPENSIONS[1]

JOHN R. VAN WAZER[2] AND EVELYN BESMERTNUK

Research Department, Rumford Division, Heyden Chemical Corporation,
Rumford, Rhode Island

Received August 22, 1949

The ability of some sodium phosphates to deflocculate and liquefy plastic masses is most interesting and impressive. For example, if a mere pinch of a powdered sodium phosphate glass is added to a firm ball of clay about the size of a baseball, the entire mass of clay will be reduced to the consistency of soup when the phosphate is thoroughly worked into the clay. This deflocculating action of the vitreous phosphates has found extensive application in industry. In the drilling of oil wells (1, 4, 11, 13, and 20), the coating of paper (2, 10), and the purification of clay the use of phosphates is well known; additional commercial applications are constantly being found.

---

[1] Presented at the Twenty-third National Colloid Symposium, which was held under the auspices of the Division of Colloid Chemistry of the American Chemical Society at Minneapolis, Minnesota, June 6–8, 1949.

[2] Present address: Research Laboratory, Great Lakes Carbon Corporation, Morton Grove, Illinois.

It is the purpose of this paper to report rheological data on some of the various kaolin–phosphate–water systems, and to interpret the observations in terms of what is now known about the structure of phosphates and of clays. The experiments reported here are also useful in attempting to explain the mechanism of the plasticity observed in clay–water systems.

PREPARATION OF THE KAOLIN (17)

Since natural clay may contain many different exchangeable cations, it seemed desirable to prepare clay in which only a single cation is present. Then the action of the phosphate anions would not be complicated, or overshadowed, by the effects due to exchange of one clay cation for another. The various prepared forms of kaolin were made according to the following procedure.

Kaolin of N. F. grade obtained from Eimer and Amend was washed about six times with 10 per cent hydrochloric acid. Each time the clay was stirred up with the acid and allowed to settle overnight, after which the acid was decanted and fresh acid added. The first two portions of decanted acid were green, but the remaining portions of acid were colorless. After treatment with acid, the clay was washed several times with distilled water and filtered dry. It was then electrodialyzed for about 48 hr. at a current density of *ca.* 400 ma. Electrodialysis was stopped when the resistance approached that observed for the cell containing distilled water. The clay was filtered once again and neutralized with the appropriate base. In some cases the water was removed from the clays by drying in an oven for several days at 110°C. The clay concentrations reported in this paper are based on clay dried to constant weight at 110°C.

THE PHOSPHATES

It has been shown that all phosphate anions are made up of PO_4 groups in which a central phosphorus atom is surrounded by a tetrahedral arrangement of oxygen atoms. These PO_4 tetrahedra can be joined together, or polymerized, by the sharing of oxygen atoms to form polyphosphate chains and metaphosphate rings (28). The various polymers are very stable in aqueous solution and, unlike many inorganic polyanions, are not converted back and forth, one to another, by pH or concentration changes. They do, however, undergo a slow hydrolytic depolymerization which is of no importance to the work reported here. All of the phosphates used in this work dissolve to give completely clear solutions exhibiting no Tyndall effect. A list of the phosphate anions tested is given in table 1. These anions make an interesting lyotropic series in which the members are related not only by their colloidal activities but by the fact that they also belong to a single chemical family, similar to the homologous series of organic compounds.

It is known that the chain phosphate anions form complexes with the common metal ions, including sodium (28). However, no complexes are formed with tetramethylammonium ions. Therefore, in order to determine how much of the observed deflocculating action is due to complex formation with exchangeable ions of the clay, it seemed desirable to prepare a tetramethylammonium polyphosphate which could be added to a tetramethylammonium clay. The tetramethylammonium phosphate was made by exchanging sodium ions for hydrogen, using Dowex cation-exchange resin. The resin was also used in making an acid sodium tripolyphosphate so that the pH of the sodium clay–sodium tripolyphosphate mixture could be adjusted.

RHEOLOGICAL CHARACTERISTICS

Since the various flow anomalies (e.g., 5) are not always observable when rheological measurements are carried out in a single apparatus, we used one viscosimeter in which the rate of shearing strain could be adjusted and the resulting shearing stress read, and another in which the stress was adjusted and the resulting shear rate observed. The instrument having an adjustable shear rate was a MacMichael viscosimeter with an added lever arm which permitted the range of measurable torque to be extended far above that obtainable with the largest torsion wire. A full selection of inner and outer cylinders was used, and one of the outer cylinders was arranged so that the temperature could be controlled by circulating water from a thermostat. A ruggedly constructed Stormer viscosimeter allowed the shearing stress to be adjusted. This instrument was also fitted with a removable lever arm that could be attached to the shaft holding the rotating cylinder. The lever arm extended the range in which yield values could be obtained to very much higher values than the instrument was normally capable of measuring. Two close-fitting concentric cylinders were made for the Stormer with grooves cut in their walls to avoid slippage, as described by Green (14).

The sodium kaolin, adjusted to pH 7, appeared to be a plastic solid obeying the Bingham law of flow. When the undeflocculated sodium clay was sheared between relatively close-fitting concentric cylinders, it was found to give the type of consistency curve observed by Volarovitch and Tolstoy (29), and the yield value computed from the equation of Reiner and Rivlin (26) agreed with the yield value calculated from the torque just necessary to rotate the inner cylinder. Also, when a large outer cylinder was used with a small inner cylinder and a radial line was marked on the surface of the clay with ink, it was found that the point at which the line started to curve after many rotations could be used to calculate a yield value which corresponded, within experimental error, to the yield values measured as described above. In figure 1 the yield value and plastic viscosity (14) are given as a function of concentration of the sodium kaolin in water at pH = 7. The sodium kaolin appeared to exhibit little, if any, thixotropy, although, of course, the resistance to shear would increase greatly, especially at the lower concentrations, if the clay were allowed to settle out and form a tightly packed mass at the bottom.

The calcium kaolin at pH 7 was also a plastic solid which, however, did not obey Bingham's law, since the yield value calculated from the upper part of the consistency curve was about twice as large as the yield value measured directly. As might be expected, the yield value obtained by marking a line on the surface of the clay, and that obtained by measuring the torque just necessary to rotate the inner cylinder, were the same within experimental error. The plastic viscosity,

TABLE 1

A list of the phosphates used as deflocculants

NAME OR DESCRIPTION	CLASSICAL VALENCE FORMULA OF ANION AT A pH OF 7	TYPE OF ANION	AVERAGE ANIONIC CHARGE AT pH 7	REMARKS ABOUT SODIUM SALT
Orthophosphate	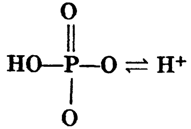 $\mathrm{HO{-}\underset{\underset{O}{\mid}}{\overset{\overset{O}{\|}}{P}}{-}O \rightleftharpoons H^+}$	Monomer	1.5	Crystalline
Pyrophosphate	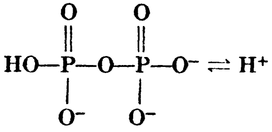 $\mathrm{HO{-}\underset{\underset{O^-}{\mid}}{\overset{\overset{O}{\|}}{P}}{-}O{-}\underset{\underset{O^-}{\mid}}{\overset{\overset{O}{\|}}{P}}{-}O^- \rightleftharpoons H^+}$	Dimer chain	2.5	Crystalline
Tripolyphosphate	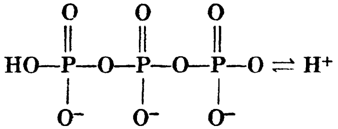 $\mathrm{HO{-}\underset{\underset{O^-}{\mid}}{\overset{\overset{O}{\|}}{P}}{-}O{-}\underset{\underset{O^-}{\mid}}{\overset{\overset{O}{\|}}{P}}{-}O{-}\underset{\underset{O^-}{\mid}}{\overset{\overset{O}{\|}}{P}}{-}O \rightleftharpoons H^+}$	Chain	3.5	Crystalline
Distribution of polyphosphates with a number average of 5.0 phosphorus atoms per chain	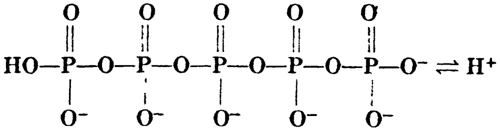 $\mathrm{HO{-}\underset{\underset{O^-}{\mid}}{\overset{\overset{O}{\|}}{P}}{-}O{-}\underset{\underset{O^-}{\mid}}{\overset{\overset{O}{\|}}{P}}{-}O{-}\underset{\underset{O^-}{\mid}}{\overset{\overset{O}{\|}}{P}}{-}O{-}\underset{\underset{O^-}{\mid}}{\overset{\overset{O}{\|}}{P}}{-}O{-}\underset{\underset{O^-}{\mid}}{\overset{\overset{O}{\|}}{P}}{-}O^- \rightleftharpoons H^+}$	Chain	5.5	Commercial sodium phosphate glass called Quadrafos (registered trademark, Rumford Division of Heyden Chemical Corporation)
Distribution of polyphosphates with a number average of 200 phosphorus atoms per chain	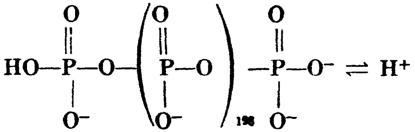 $\mathrm{HO{-}\underset{\underset{O^-}{\mid}}{\overset{\overset{O}{\|}}{P}}{-}O{-}\left(\underset{\underset{O^-}{\mid}}{\overset{\overset{O}{\|}}{P}}{-}O\right)_{198}{-}\underset{\underset{O^-}{\mid}}{\overset{\overset{O}{\|}}{P}}{-}O^- \rightleftharpoons H^+}$	Long chain	*ca.* 200	Vitreous sodium metaphosphate that is extensively dehydrated; often called Graham's salt

Trimetaphosphate	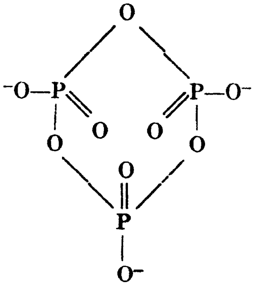	Ring	3	Crystalline ($NaPO_3$-I)

the yield value observed by measuring the torque just necessary to rotate the inner cylinder, and the yield value extrapolated from the upper portion of the consistency curve by the equation of Reiner and Rivlin are presented in figure 1 for various concentrations of the calcium clay in water.

At high solids concentration the clays containing an adequate amount of chain phosphate anions appeared to be dilatant, as shown in figure 7. These mixtures were dilatant in every sense of the word; i. e., they not only had a dilatant type of consistency curve, but they also exhibited a smooth, shiny surface which became dry and granular on being disturbed. Furthermore, when stirred with a spatula, the mass strongly resisted fast motions; and if a piece of the material were quickly lifted out on the spatula, the piece would have sharp edges and rough surfaces that soon melted away so that the material dripped freely. Such dilatancy has been reported by Daugherty (8) for a suspension of calcium carbonate in water containing a sodium phosphate glass with about seven phosphorus atoms per chain. We have also carried out a number of experiments in which sodium polyphosphates were used to deflocculate inorganic pigments and have found that whenever the solid content was so high that the material was quite firm, dilatancy could be observed. This dilatant behavior has little significance in the usual commercial applications of phosphates as deflocculants, since the effect is only observable over a very restricted range of solids concentration. We believe that all colloidal systems that are treated with good deflocculants at high solids concentrations will necessarily be dilatant.

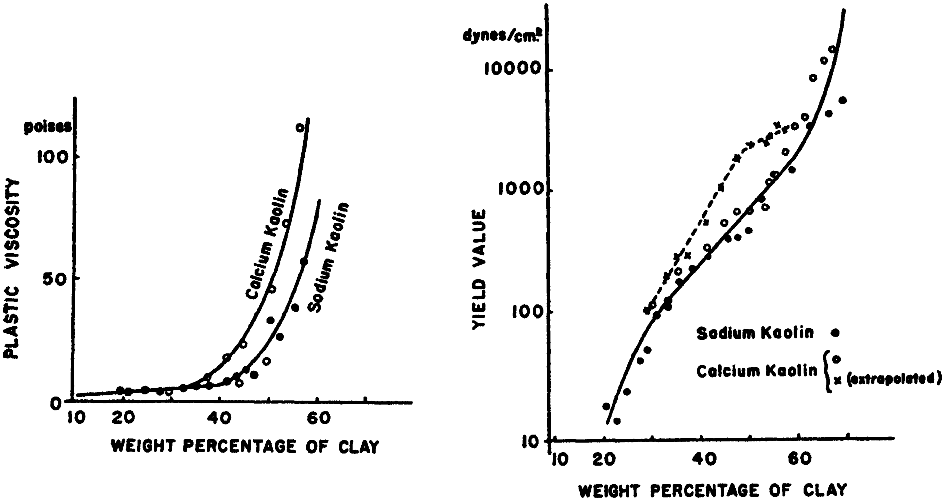

FIG. 1. The rheological constants of slurries of sodium and calcium kaolins as a function of the amount of clay in the slurries.

In the presence of enough polyphosphate to deflocculate the clay adequately and also enough water to make the colloidal suspension quite fluid, a hitherto neglected flow anomaly is found. When such a material is contained in a viscosimeter in which the shearing rate is adjustable, and the resulting shearing force is measured, it is found that upon the application of a fast rate of shear to the material, the resulting torque rises sharply and then slowly decreases from a high value to a constant value. If the shearing rate is suddenly lowered, the shearing force quickly falls away and then slowly increases again to practically the same constant value. When the speed remains constant, the shearing force reaches a given value which appears to be practically independent of shearing rate. This anomaly, which is similar to or identical with the one reported by Rossi (27), is apparent only when the rate of flow is accelerated or decelerated, as is shown in figure 2. If one wished to apply a Greek sobriquet to this effect, it could be called "tachypyknosis".[3]

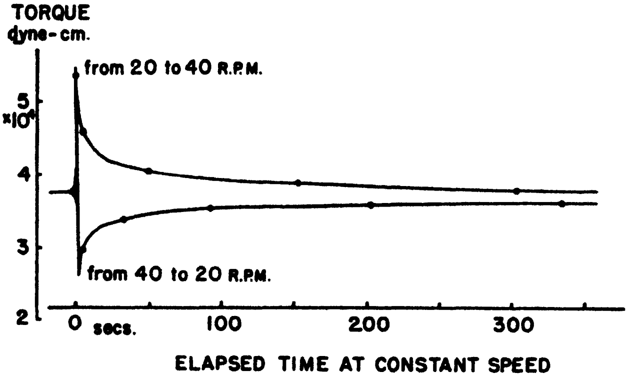

FIG. 2. An example of tachypyknosis. A 50 per cent tetramethylammonium kaolin with 3 milligram atomic weights of phosphorus per 100 g. of dry clay, the phosphate being present as a tetramethylammonium polyphosphate with five phosphorus atoms per chain. Viscosimeter inner cylinder radius = 2 cm.; outer cylinder radius = 3.4 cm. Natural period of vibration of suspended system = 1.5 sec.

The reason for this peculiar effect is not at all clear. Since the natural period of vibration of the suspended system was always many times smaller than the time in which the shearing force achieved its equilibrium value, the effect is not due to the mechanics of the viscosimeter. As the suspensions exhibit a yield value, one might imagine that there was a layer of immobile slurry at the outer cylinder wall which would change thickness very slowly after the rate of flow was altered. Thus, when the flow rate was increased, the layer would wear away gradually so that the measured shearing force would decrease with time. After decreasing the flow rate, the layer would presumably slowly build up in thickness. This idea seems quite satisfactory, except for the fact that the observed variation in shearing force with time was always much greater than would be expected from the observed thickness and change in thickness of the immobile layer. Therefore, it would seem that the material itself thickens and softens in such a maner that the stress is a function of the *second* derivative of the strain with respect to time. Further investigation of this phenomenon with an instrument designed for this type of study (6) would be desirable.

---

[3] This term was kindly furnished by Professor C. A. Lynch of the Department of Classics in Brown University.

Experiments carried out at high solids concentration in the range where the material is dilatant indicate that tachypyknosis is also at work here, but that the rate of change in consistency is very much slower than that observed at lower concentrations of solids. Naturally, the part of the above process in which the shearing force decreases with time at a constant rate of shear can be easily confused with thixotropy or work-softening; and the part of the process in which the shearing force increases with time can be confused with false body or work-hardening. At high solids concentration, the "thixotropic" part of the tachypyknotic process is most apparent; while at any concentration of solids, the thixotropic part of the process is most readily observed when a Stormer or other adjustable torque viscosimeter is used.

When the pure kaolin or kaolin–phosphate slurries have high enough solids concentrations so as to be quite firm, elasticity is always present as indicated by a distinct rebound when the shearing torque is removed. A previous report (20) that polyphosphates destroy elasticity was based on measurements at relatively low solids concentration and is not valid when the material is firm.

We believe that the dilatancy, tachypyknosis, possible thixotropy, elasticity, etc. exhibited by colloidal suspensions deflocculated with polyphosphates are all aspects of a single flow anomaly which we are unable to describe properly or even to comprehend at the present time. This work is but another of the many examples which show that many everyday rheological phenomena are extremely complex—so complex, in fact, that at present it is not worthwhile to theorize extensively about the mechanism of flow, since the ideal body postulated may not be even similar to any real material when considered as a whole.

EFFECT OF CATIONS

A study of the efficacy of a given phosphate in reducing the consistency of a clay in the presence of tetramethylammonium ion as compared with the efficacy in the presence of, let us say, sodium ion affords a measure of the contribution to the overall reduction in consistency of an interaction between the phosphate and the exchangeable cations. In figure 3 a plot of the measured variation of yield value with phosphate concentration is given for the systems tetramethylammonium polyphosphate–tetramethylammonium kaolin, and sodium polyphosphate–sodium kaolin, at pH 7 in both cases. The same distribution of polyphosphate anions, corresponding to an average number of 5.0 phosphorus atoms per chain, was used in both systems. Since approximately identical effects were noted in the presence of either sodium or tetramethylammonium ions, it seems that the mechanism of the softening process is not primarily dependent on the ability of the phosphate to form soluble complexes with the exchangeable cations.

COMPARISON OF THE PHOSPHATES

The rheological data reported in this section were obtained with the MacMichael viscosimeter, using a small inner cylinder and a large outer cylinder. Since the phosphate concentration range was large and the flow was therefore very anomalous, it seemed desirable to report the results in terms of an empirical equation which would fit the data and yet avoid the implication that the flow behavior was of a theoretically recognized type. The logarithmic equation introduced by Ostwald (24) appeared to fulfill these requirements and was used in the following form:

$$S = k\Omega^A$$

where S is the shearing stress in dynes per square centimeter at the inner cylinder wall (radius = 1 cm., length = 5 cm.), Ω is the rate in radians per second at which the outer cylinder (radius = 5 cm.) revolved, and k and A are constants.

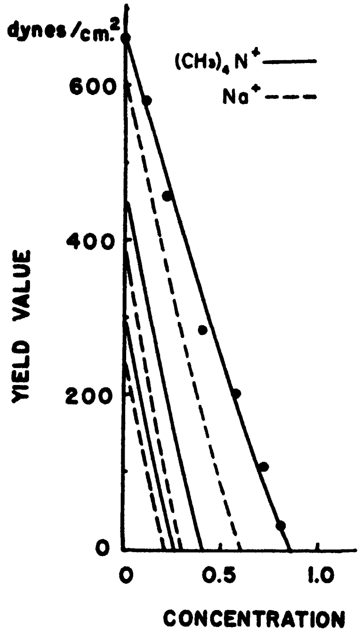

FIG. 3. Variation of yield value with amount of added polyphosphate. Two highest curves for 50 per cent clay slurries, next two for 45 per cent, and two lowest for 40 per cent slurries. Concentration given in terms of milligram atomic weights of phosphorus per 100 g. of dry clay.

The sodium phosphate was added to the sodium kaolin in such a way as to keep the pH constant at 7. This means, of course, that the amount of sodium ion in the solution could not be directly controlled, as it was a dependent variable. However, since the addition of sodium chloride had such a slight effect on the viscosity of the clay, it would seem that differences ranging between 1 and 1.5 in the ratio of sodium to phosphorus should be of negligible importance for comparisons made at a given concentration of phosphorus atoms.

The constants k and A are plotted in figure 4 as a function of the phosphate concentration. In figure 4A it is seen that the initial lowering of the constant k (which gives a better measure of the ease with which the slurry can flow than either the constant A or the yield value) is proportional to the number of P—O—P connections present, regardless of ion size and configuration. All of the phosphates tested have P—O—P connections except the orthophosphate monomer. Figure 4B demonstrates that the process whereby the slurry thickens is dependent on molecular size and configuration, and figure 4C shows that addition of phosphorus atoms in any phosphate ion causes the constant A to decrease rapidly at first and then gradually increase in the same manner as it does upon the addition of sodium chloride. Figure 5 is a plot of the yield values calculated

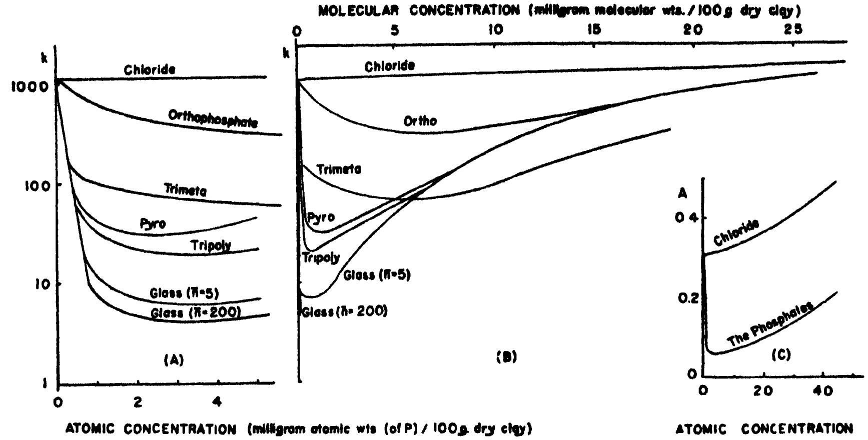

FIG. 4. Empirical constants k and A as a function of the amount of sodium phosphate added to a 42.8 per cent sodium kaolin.

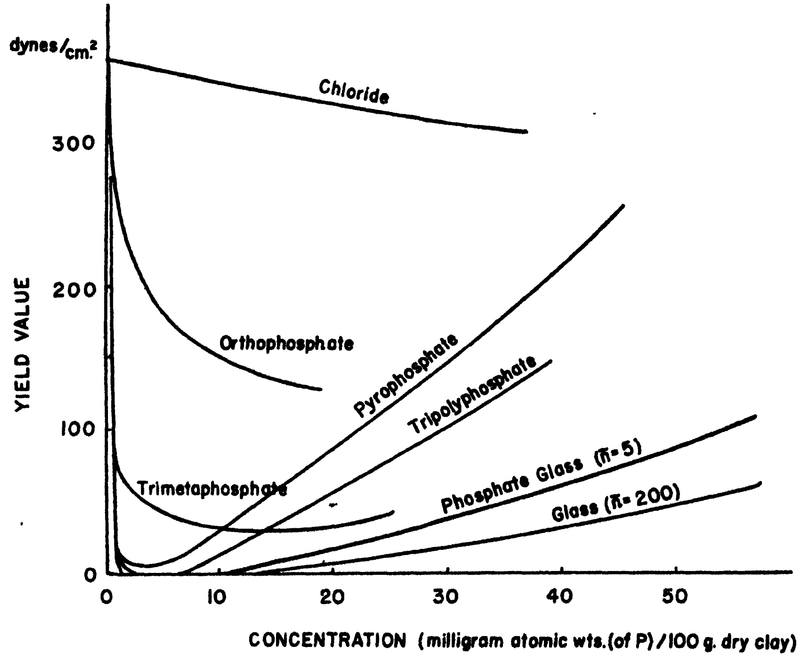

FIG. 5. Reduction in yield value upon adding various sodium phosphates to a 42.8 per cent slurry of sodium kaolin.

from the torque just necessary to cause flow. It should be noticed that the increase in yield value upon addition of excess polyphosphate is a function of ionic concentration; i. e., when the yield values are plotted against ionic concentration, the points for the chain phosphates lie approximately on a single line.

From figures 4A, 4B, and 5 it is apparent that the chain phosphates make up a lyotropic series in which the ability to soften clay slurries is in the order of increasing ionic weight. If we consider that the deflocculating ability of the chain phosphates is measured by the minimum value of k, it is seen that this ability increases very greatly when going from the monomer to the dimer, much less markedly when going from the dimer to the trimer, and even less when going from the five-membered to the 200-membered chain. This seems to indicate that the effect of increasing charge on the anions is very important for small values of the charge, and hardly counts as the charge becomes very large. Since the polarographic data on complex formation show that the dimer is as good a complex-forming agent as the polymers with very long chains (28), one might think that the ability to deflocculate is related to anionic charge alone and that complex formation is insignificant here. This conclusion, however, would be faulty, as can be seen when the ring polymer, trimetaphosphate, is compared with the pyro- and tri-polyphosphate chains: Although the charge on the pyro ion at pH 7 is equal to that on the trimeta ion, and the trimeta ring on cleavage turns into the tripoly chain, the trimeta ring is seen to be the least effective in reducing consistency. Therefore, we must conclude that part of the liquefying ability exhibited by the phosphates is due to the large anionic charge and part to the ability to form complexes with the surface ions in the crystal lattice of the clay particles.

EFFECT OF SOLIDS CONCENTRATION

In a very interesting series of experiments dry clay was mixed with dry phosphate and successive portions of water were added to the mixture. This operation was carried out on the sodium and calcium clays mixed with either sodium pyrophosphate or the sodium phosphate glass corresponding to a distribution of chains with a number average of 5.0 phosphorus atoms per chain. In all cases 5 mg. atomic weights of phosphorus per 100 g. of clay was used, since this concentration was found to thin down the clay most effectively (see figures 4 and 5). When the first portions of water were added to the clay–phosphate mixture, the mass was worked by pressing it together and crumbling up the lumps by hand. When almost enough water had been added to make the mass coherent and plastic, the material was seen to remain in lumps which could be easily broken apart. From this point on the water was added very carefully and during the working of the clay the lumps were pressed together and rubbed with the thumb. When the rubbed surface appeared perfectly smooth with no cracks or rough spots, the mass was said to be plastic. In all cases, whether or not the clay was treated with phosphate, this upper limit of plasticity occurred at 77 ± 0.5 per cent of kaolin by weight, which corresponds to a volume concentration of 56 per cent. For an assemblage of equal-sized spheres in open pack the volume concentration of solids equals 52 per cent. Therefore, it seems reasonable that the upper limit of plasticity corresponds to the point where the voids between the clay particles are just filled with water and each particle is touching the ones immediately adjacent to it.

After the upper limit of plasticity was passed, additional portions of water were added and rheograms were taken between additions. For the untreated clay the flow curves had the shape expected for a plastic material (Bingham body) as is shown in figure 6. The phosphate-treated clays, however, exhibited dilatant flow curves, examples of which are given in figure 7. Although the shapes of the consistency curves are quite different for pure clay and phosphate-treated clay, it should be noted that the phosphate-treated clay becomes very fluid upon the addition of only a small percentage of water beyond that necessary to make the clay plastic. Since there is no method known at present for comparing curves for dilatant and plastic flow, the yield value, as measured by the torque necessary to initiate flow, is plotted in figures 8 and 9 as a function of solids concentration. For all the clays the yield value tends to infinity as the plastic limit is approached. The untreated clays exhibit a wide range of concentration within which the yield value decreases relatively slowly; but, for the clays containing phosphates, the yield value diminishes rapidly with decreasing solids concentration.

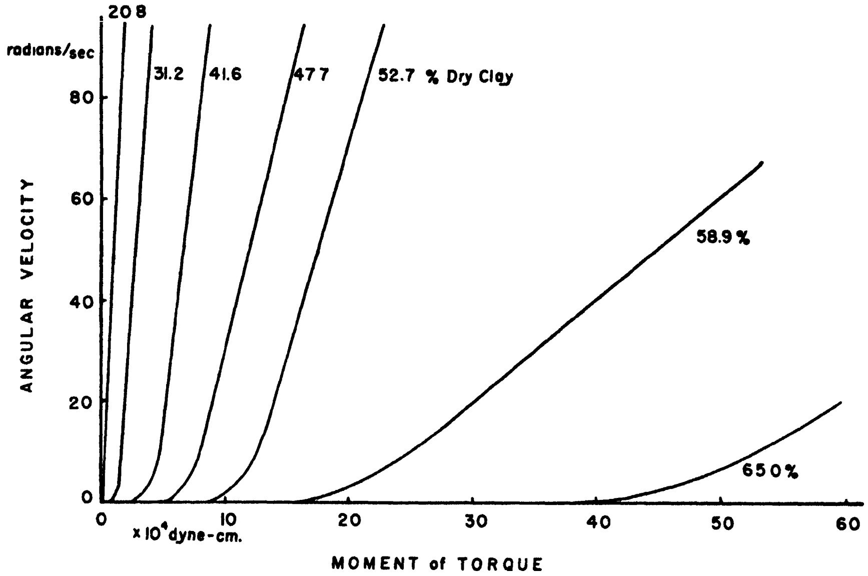

FIG. 6. Rheograms or consistency curves of untreated sodium kaolin slurries containing various amounts of dry clay. Viscosimeter inner cylinder length = 4.8 cm., radius = 1.92 cm.; outer cylinder radius = 2.35 cm.

CATAPHORESIS

Since the electrical charge on colloidal particles determines many of their bulk properties, it seemed desirable to obtain a qualitative measure of the change in

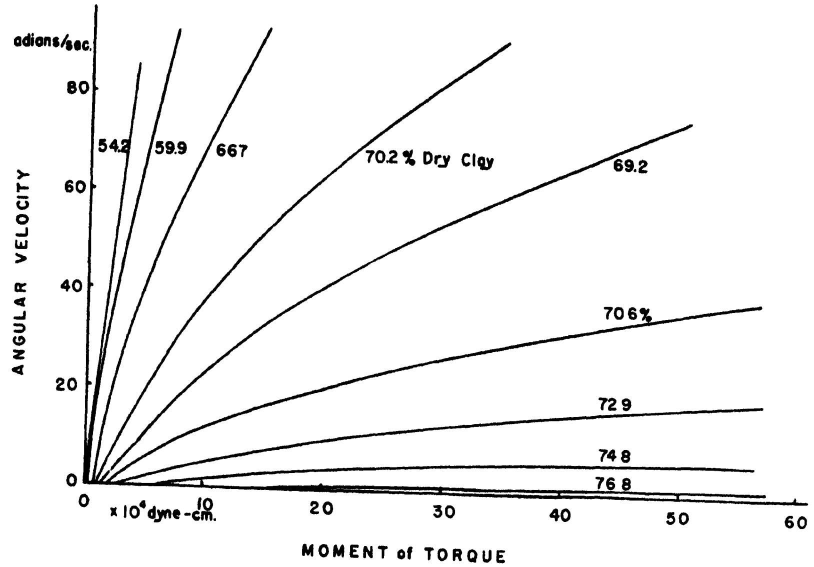

FIG. 7. Rheograms or consistency curves of sodium kaolin slurries treated with 5 milligram atomic weights of phosphorus per 100 g. of dry clay, the phosphorus being present as a polyphosphate with five phosphorus atoms per chain. Same cylinders as in figure 6.

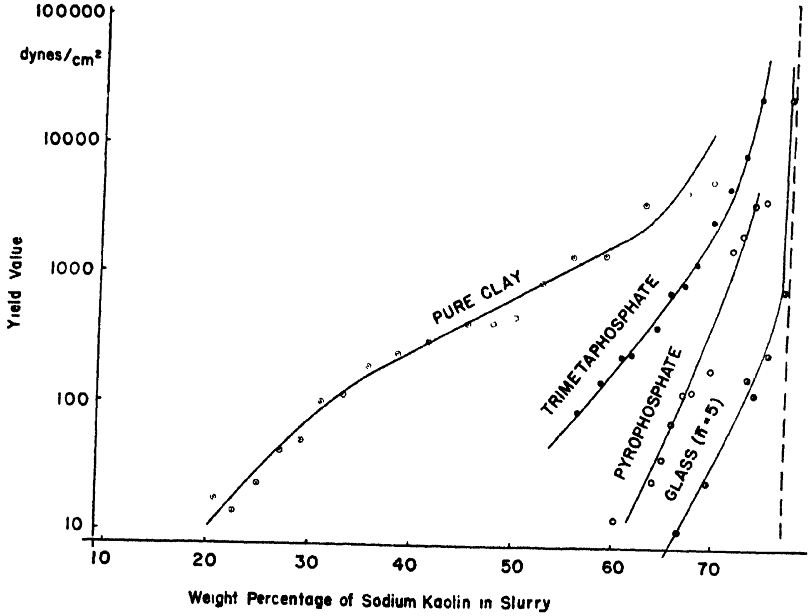

FIG. 8. Variation of yield value with amount of clay in slurry. Sodium kaolin treated with 5 milligram atomic weights of phosphorus per 100 g. of dry clay, the phosphorus being present as the sodium phosphates noted. Upper limit of plasticity at dotted line.

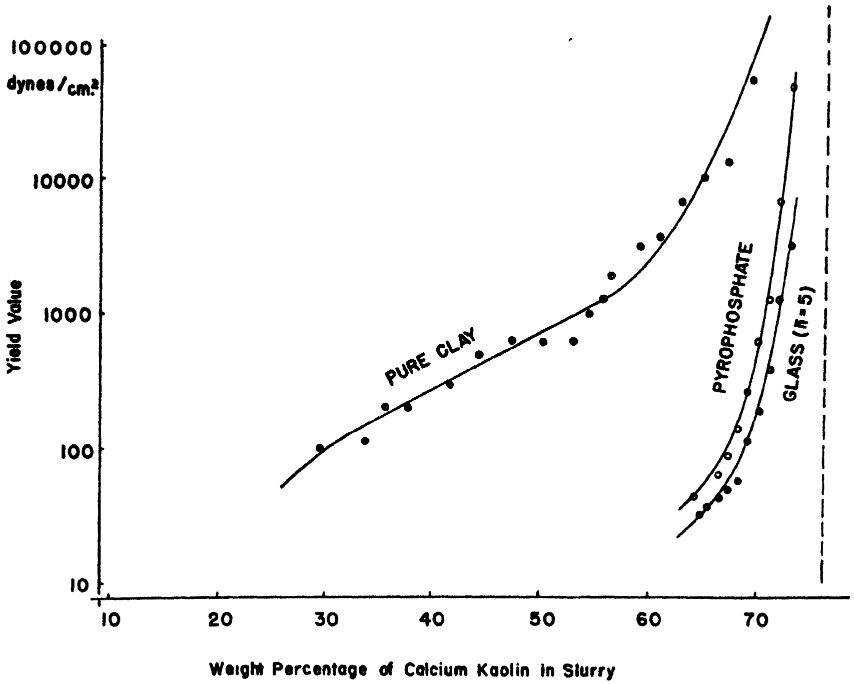

FIG. 9. Variation of yield value with amount of clay in slurry. Calcium kaolin treated with 5 milligram atomic weights of phosphorus per 100 g. of dry clay, the phosphorus being present as the various sodium phosphates noted. Upper limit of plasticity at dotted line.

TABLE 2

Data from cataphoresis studies on clays suspended in liquors obtained from centrifuging 45 per cent clay slurries

Deflocculants present in slurry to extent of 5.0 milliatomic weights (of phosphorus) per 100 g. of dry clay

DEFLOCCULANT ADDED	CATAPHORETIC VELOCITY	CALCULATED ZETA POTENTIAL	APPEARANCE OF CLAY IN MICROSCOPE (MAGNIFICATION 120×)
Clay: sodium kaolin, pH = 7.0			
	μ/sec. at 1 volt/cm.	*millivolts*	
None	−5.0	−71	Flocs in clear liquid
Sodium chloride	−5.1	−72	As above
Sodium orthophosphate	−7.7	−109	Some small flocs
Sodium trimetaphosphate	−6.6	−93	Many very small flocs
Sodium pyrophosphate	−8.1	−114	Some very fine flocs
Glass: $7Na_2O \cdot 5P_2O_5$ ($\bar{n} = 5.0$)	−9.2	−130	Unresolved milky liquid
Glass: $Na_2O \cdot P_2O_5$ ($\bar{n} = 200$)	−9.6	−135	As preceding sample
Clay: calcium kaolin, pH = 7.0			
None	−2.4	−34	Very large flocs
Sodium chloride	−3.7	−52	Large flocs
Glass: $7Na_2O \cdot 5P_2O_5$ ($\bar{n} = 5.0$)	−9.4	−133	Unresolved milky liquid

the zeta potential of the clay on addition of a sodium phosphate glass. The apparatus described by Mattson (21) was used to measure the cataphoretic velocity of the clay particles. Since this type of measurement can only be made when there are relatively few suspended particles in a large amount of solution, i. e., at extremely low solids concentration, it was necessary to dilute the suspensions used in the rheological measurements. This dilution was carried out by centrifuging large portions of a 45 per cent sodium kaolin slurry containing 5.0 milliatomic weights of the various phosphates per 100 g. of clay in order to obtain some of the clay-free liquid, to which was added one drop of the original slurry. In making the measurement, the recommendations of Mattson were followed. Table 2 gives the cataphoretic velocity and the resulting zeta potential calculated according to the simple equation assuming spherical particles (9).

It is evident from table 2 that all of the salts tested caused the zeta potential to become more negative. By examining only the results obtained from cataphoretic measurements, a person unfamiliar with the effect of phosphates on colloids would be unable to predict that some of the suspensions would be very thick, while others would be very thin and soupy. In other words, it seems that there are forces other than the zeta potential which determine the consistency of the slurry.

GENERAL DISCUSSION

A rather thorough review of the ideas suggested by various authors to explain the deflocculation and liquefaction of clay slurries has been given by Johnson and Norton (19). Some early workers thought that there was a large amount of "bound" water rigidly held on the clay particles, and that the addition of a deflocculating agent reduced the amount of water held. This theory is said to be untenable because (*1*) the partial pressure of water over a clay slurry is the same as that over pure water, (*2*) suspensions of bentonite containing only a few per cent of solid material have shown measurable yield values, and hence must contain unbelievably large portions of the water in "bound" form, and (*3*) microscopic observations of clay slurries indicate that a large amount of the "bound" water is free to move.

Theories other than the "bound" water theory are best discussed in terms of the experiments described in this paper. Since tetramethylammonium clays are deflocculated and made soupy by small amounts of tetramethylammonium polyphosphate at a neutral pH, we can conclude that the effect is not attributable to the exchangeable cations associated with the clay particles. It is also seen that the presence of free hydroxyl ions is unnecessary. Our experiments on comparing the viscosity-reducing effect of the various phosphates show that an increase in anionic charge increases the effectiveness of the deflocculant in liquefying clay slurries, and that the surface complex formation is probably even more important. Experiments (e. g., 3, 16, and 22) have shown that the two most effective deflocculants, the phosphate and hydroxyl anions, are strongly sorbed on the clay particles. Although the complex-forming ability of the hydroxyl ion is not often discussed *per se*, hydration of cations and formation of such anions as the aluminates and complex silicates can be interpreted in terms of hydroxyl complexes. Therefore, it would appear that chemisorption of the deflocculating anion through formation of complexes with some of the surface silicon and aluminum atoms on the clay particles is necessary in order to have deflocculation and liquefaction (7). Such sorption, by the way, would always lead to a negative increase of the zeta potential.

In order to visualize the forces that are at work in the clay slurries, it seems desirable to discuss two hypothetical systems: If we have an assembly of small suspended particles that repel each other, the particles will be in equilibrium when they are equally spaced and separated from each other as far as possible. Such a system, when viewed under the microscope, would appear to be deflocculated. It would also resist any rapid distortion or change in the rate of distortion, since such action would cause the particles to approach each other. If the concentration were low enough so that the particles would not interfere mechanically, there could be no yield value. The properties of this ideal system appear to be very similar to the properties of the phosphate-treated clays. It should be noted that the general term "repulsive force" used above includes electrical forces, such as would be found between negatively charged particles suspended in a continuous medium having a net positive charge equal to the sum of the negative charges on all the particles.

The other hypothetical system is one in which the particles attract each other. In this system the particles will clump together or flocculate. Instead of drawing together into one closely packed mass, it is more probable that an assembly of mutually attracting particles of different shapes and sizes would aggregate in such a way as to leave many large spaces between them. Such a system would undoubtedly exhibit a yield value. Furthermore, if the rate of distortion were great enough to break down the static structure, a slight increase in the distorting force should result in a relatively large increase in the rate of flow. This ideal system seems to have properties that are very similar to the untreated clay slurries.

From these ideal systems it appears that there is a long-range attractive force between particles which is counteracted by a repulsive force due to the zeta potential. Probably the long-range attractive force can be attributed to the additive properties of van der Waals forces (12, 15), although it may be possible to attribute the attraction entirely to coulombic forces (18).

When the polyphosphates were introduced into clay technology, they were found to be superior in many cases to deflocculants previously used, and so the question rose as to whether there might not be a hitherto untried deflocculant that would be greatly superior as a liquefying agent to those now known. We believe that this rheological study provides a negative answer to this question, for the following reasons: It was observed that the upper limit of plasticity was virtually unaffected by the addition of the deflocculant. Furthermore, this upper limit occurred at a volume concentration corresponding to open-packed spheres of equal size—a state of affairs that seems reasonable, since the clay had been washed many times so that only the larger particles would be probably left to form a relatively monodisperse system. Thus the upper limit of plasticity is attributable to simple mechanical interference between the particles—an interference which cannot be reduced without destroying the particles themselves. This means that the deflocculant can only act so as to cause a rapid reduction in consistency when more water than that corresponding to the plastic limit is introduced. As shown in figure 8, only a slight improvement over the behavior of the sodium phosphate glasses is conceivable in this respect.

THE PLASTICITY OF CLAY

Since early times man has used plastic mixtures of clay and water for molding pottery and for other uses. However, we believe that so far a clear picture has been lacking to explain why clay–water mixtures are plastic over the observed wide range of concentration. In a recent paper by Norton (23) it is suggested that the surface tension of the water held in the capillaries and interstices between the clay particles accounts for the plasticity and acts like a strong membrane holding the mass of clay together. Undoubtedly this mechanism explains the plasticity of clay when there is just enough, or only slightly more than enough, water present to fill the interstitial spaces. Since we found that the amount of water just necessary to make the mass plastic (i. e., barely to fill the interstices) did not depend on the presence or amount of deflocculating agent, our work supports Norton's theory for the case where the interstices are barely filled. But Norton's theory, as presented, only covers mechanical interference and cannot explain the plasticity of mixtures containing as much as 50 per cent of water by weight, especially in view of the fact that the addition of a small amount of phosphate to this 50 per cent mixture causes the mass to become completely fluid without appreciably affecting the surface tension. The polyphosphates are only slightly surface active; in fact, solutions of phosphates in water show approximately the same surface tensions as solutions of other salts at equivalent concentrations.

In view of the work on deflocculation we should like to modify Norton's theory as follows: When barely enough water has been mixed with the clay to make the mass plastic, the compressive effect of the surface tension of the water acts against the mechanical interference of the particles to result in a yield value. As more water is added to the clay, large spaces are formed because the particles attract each other and clump together in an irregular manner. When a deflocculant is added to the clay mass having large spaces, the attractive force between the clay particles is destroyed, and the fluid contained in the spaces distributes itself evenly between the particles; i. e., instead of having the particles touch one another to form an irregular network interspersed with large pockets of liquid, the liquid becomes evenly distributed and the individual particles no longer touch. We believe that the compressing action of the capillary force and mechanical interference between particles must be supplemented by an interparticle attraction in order to have a theory of plasticity that covers the large concentration range observed for plastic clay masses.

The authors wish to thank Professor Ernst Hauser of the Massachusetts Institute of Technology for his helpful criticism and advice. Their deep appreciation is also due to Mr. Albert E. Marshall for his kind interest in this work and to Mr. Theophil Laanes for reading the manuscript.

REFERENCES

(1) American Cyanamid and Chemical Corporation (New York): Pamphlet entitled *Chemical Treatment of Drilling Muds.*
(2) Arnold, K. A.: Doctoral thesis entitled "Flow Properties of Coating Clays at High Rates of Shear," Lawrence College, Appleton, Wisconsin, May, 1942.
(3) Barbier, G., Charbannes, J., and Miallet, P.: Ann. agron. **16**, 7–33 (1946).
(4) Bonnet, C. F., and Howell, B. N.: Oil Gas J. **39**, No. 23, 58, 61 (1940).
(5) British Rheologists' Club: Nature **149**, 197, 702 (1942).
(6) Carver, E. K., and Van Wazer, J. R.: J. Phys. & Colloid Chem. **51**, 751–62 (1947).
(7) Chwala, A.: In *Colloid Chemistry, Theoretical and Applied*, edited by Jerome Alexander, Vol. 3, pp. 179–88. The Chemical Catalog Company, Inc., New York (1931).
(8) Daugherty, T. H.: J. Chem. Education **25**, 482–8 (1948).
(9) Debye, P., and Hückel, E.: Physik. Z. **25** (3), 49–52 (1924).
(10) Erbring, H., Broese, S., and Bauer, H.: Kolloid-Beihefte **54**, 365–434 (1943).
(11) Fancher, G., and Whiting, R. L.: Petroleum Technol., T.P. 1589 (March, 1943).
(12) Freundlich, H.: *Thixotropy.* Hermann et Cie., Paris (1935).
(13) Garrison, A. D., and Ten Brink, K. C.: Petroleum Technol., T.P. 1124 (November, 1939).
(14) Green, H.: Ind. Eng. Chem., Anal. Ed. **14**, 576–85 (1942).
(15) Hamaker, H. C.: Rec. trav. chim. **55**, 1015–26 (1936).
(16) Hatch, G. B., and Rice, O.: Ind. Eng. Chem. **31**, 51–7 (1939).
(17) Hauser, E. A.: Chem. Revs. **37**, 287–321 (1945).
(18) Hauser, E. A., and Hirshon, S.: J. Phys. Chem. **43**, 1015–36 (1939).
(19) Johnson, A. L., and Norton, F. H.: J. Am. Ceram. Soc. **24**, 189–203 (1941).
(20) Loomis, A. G., Ford, T. F., and Fidiam, J. F.: Petroleum Technol., T.P. 1201 (May, 1940).
(21) Mattson, S.: J. Phys. Chem. **32**, 1532–52 (1928).
(22) Mattson, S.: Proc. 1st Intern. Congr. Soil Sci. **2**, 199–211 (1927).
(23) Norton, F. H.: J. Am. Ceram. Soc. **31**, 236–40 (1948).
(24) Ostwald, W.: Kolloid-Z. **36**, 99 (1925).
(25) Reid, A., and Sen Gupta, N. C.: Nature **159**, 336–7 (1947).
(26) Reiner, M., and Rivilin: Kolloid-Z. **43**, 72 (1927).
Reiner, M.: J. Rheol. **1**, 1–10 (1929).
(27) Rossi, C.: Gazz. chim. ital. **67**, 751 (1937).
(28) Van Wazer, J. R.: J. Am. Chem. Soc., four papers now in press.
(29) Volarovitch, M. P., and Tolstoy, D. M.: Kolloid-Z. **70**, 165–74 (1935).

THE ACTIVITY COEFFICIENT OF SURFACE-ACTIVE MATERIALS IN AQUEOUS SOLUTIONS[1]

HAROLD M. SCHOLBERG

Central Research Department, Minnesota Mining & Manufacturing Company, St. Paul, Minnesota

Received August 22, 1949

Because, up to the present time, no satisfactory method has been available for estimating the activity coefficient of surface-active substances in aqueous solutions, the far too common practice has been to ignore the question. The standard methods for the determination of the activity of a solute, such as change in vapor pressure or osmotic pressure of the solvent, are of questionable value because the presence of micelles raises the effective molecular weight of the solute to too high a value to allow any degree of precision. The experiments outlined in this paper are an attempt to show that surface tension measurements can be used to determine the activity coefficients of surface-active materials. The method allows a considerable increase in accuracy, for it is in the very dilute regions that surface tension measurements show the greatest changes. It is believed that the arguments in this paper lead, in addition, to a clearer understanding of the Gibbs adsorption equation.

Many attempts have been made to verify the Gibbs adsorption equation. Donnan and Barker (2), Harkins and Gans (4), and McLewis and Patrick (9) reported fairly good agreement, although in all these tests the experimental value of the amount adsorbed tended to be larger than the theoretical value. McBain and his coworkers (8) stated that, with the exception of nonylic acid, the amounts adsorbed in all cases greatly exceeded those calculated with the aid of the Gibbs equation.

Lately much work has been reported on the determination of the point, or concentration, corresponding to the beginning of micelle formation. The change in the absorption spectrum of a cyanine dye, as developed by Harkins and his coworkers (1), gives good results. Surface pressure measurements are here shown to provide a good method for the determination of the critical point.

EXPERIMENTAL

Figures 1 and 2 show typical curves obtained for Duponol OS, Triton NE, Duponol 80, Tergitol No. 7, Tergitol No. 4, and Tergitol No. 8. Figure 3 shows the data on sodium cetyl sulfate taken from the paper by Nutting and Long (10) and also the curve for hexanolamine oleate.

The surface pressure of solutions of wetting agents was determined as a function of the logarithm of the concentration.

The solution whose surface pressure was to be determined was sealed into a test tube. The distance from the bottom of the meniscus to where it came in

---

[1] Presented at the Twenty-third National Colloid Symposium, which was held under the auspices of the Division of Colloid Chemistry of the American Chemical Society at Minneapolis, Minnesota, June 6–8, 1949.

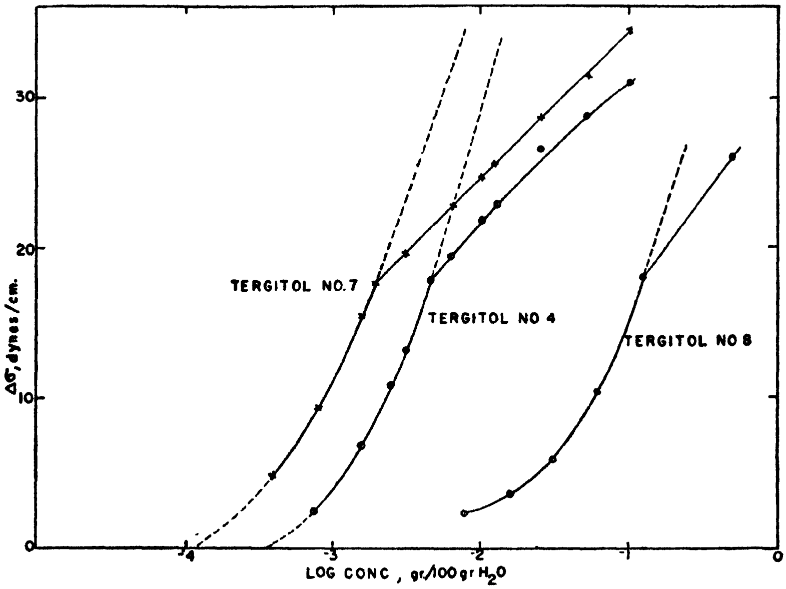

FIG. 1. Surface tension measurements on Tergitol No. 4, Tergitol No. 7, and Tergitol No. 8

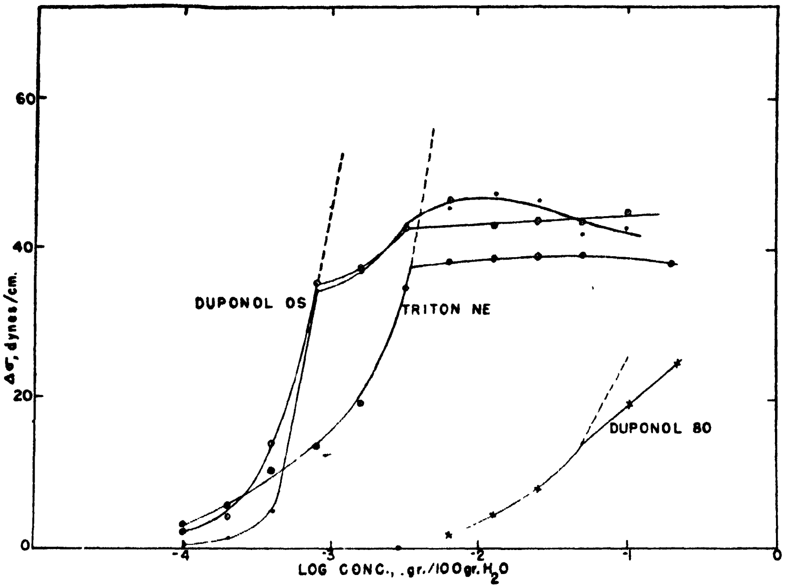

FIG. 2. Surface tension measurements on Duponol OS, Triton NE, and Duponol 80. On the Duponol OS curves · represents fresh solutions run on December 12, 1946 and ⊙ represents the same solutions run on January 31, 1947.

contact with the wall of the test tube was measured with a traveling microscope. The value of the capillary constant, $a^2 = 2\sigma/\rho g$, was read from a calibration curve of a^2 against h, the height of the meniscus, prepared from a series of pure liquids. From these data, the density, and the surface tension of pure water, the surface pressure was calculated, the surface pressure being defined as the surface tension of the solvent minus that of the solution. All determinations were made at room temperature. It is estimated that the values of $\Delta\sigma$, the surface pressure, are probably correct to 1 per cent.

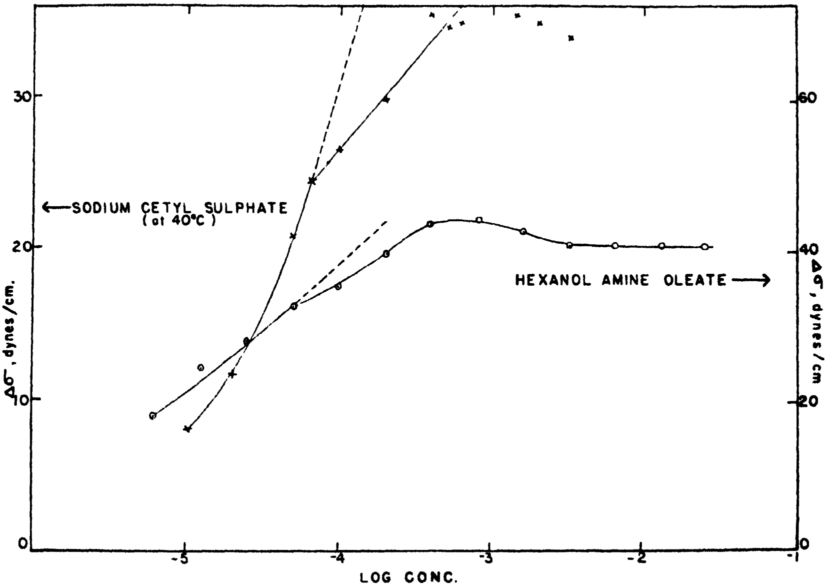

FIG. 3. Surface tension measurements on sodium cetyl sulfate (concentration expressed in moles per liter) and on hexanolamine oleate (concentration expressed in moles per liter).

DISCUSSION

The break in the surface pressure curves is contrary to what the Gibbs equation would lead us to expect, for this discontinuity says that as the film pressure is increased the area per molecule increases, and this can hardly be allowed. It can be reconciled, however, if we call the part of the curve below the critical break point and its extrapolation above that point, as shown by the dotted lines, the activity curve. The difference between the two curves at a given surface pressure is then the logarithm of the activity coefficient. The justification for this is given below.

Let us suppose that two different wetting agents are dissolved in water and that at the same activity of the solute, the drop in surface tension is the same in both solutions. Let us further suppose that wetting agent A gives a surface film that obeys the simple gas law; that B gives a solid film, as, for instance, stearic acid spread on dilute hydrochloric acid. For simplification we also set the condition that the solutions are sufficiently dilute so that the amount of wetting agent at the solution–air interface due to adsorption at the interface is much greater than the amount which would be at the interface if there were no adsorption.

Gibbs's equation may be written as: (1)

$$\frac{10^{-16}}{2.303kT}\,\frac{d\Delta\sigma}{d\log a_2} = \Gamma$$

This may be integrated thus: (2)

$$\frac{10^{-16}}{2.303kT}\int\frac{d\Delta\sigma}{\Gamma} = \int d\log a_2$$

Under the conditions above

$$\Gamma = \frac{1}{A}$$

and equation 2 may be written

$$\frac{10^{-16}}{2.303kT}\int A\,d\Delta\sigma = \int d\log a_2 \tag{3}$$

where k = the gas constant per molecule,
T = the absolute temperature,
$\Delta\sigma$ = the surface pressure of the solute,
a_2 = the activity of the solute,
Γ = the molecules per square Ångström adsorbed at the interface, and
A = the area per molecule in square Ångströms.

Equation 3 was integrated for the two solutions mentioned above, assuming a surface tension lowering of 20 dynes per centimeter and $\log a_2 = -2$ as the starting point. In figure 4 curve A is for the gaseous film ($\Delta\sigma A = kT$), and curve B is for the stearic acid, solid-type film. The point of this example is to show that the two *extreme* types of surface films give curves which, to a rather high degree of accuracy, will extrapolate above 20 dynes substantially the same and almost in a straight line when the variables are $\log a_2$ and $\Delta\sigma$. By the nature of Gibbs's law, the slope of these curves must always increase as the surface pressure increases. This last statement may be amplified as follows: Suppose the surface pressure continued to increase but the slope of the curve became less positive. This would mean that the amount adsorbed at the interface was decreasing, which is the same as saying that the area per molecule in the surface film becomes greater as the film pressure rises. Also as long as the film pressure is increasing with increasing concentration, the activity must increase for, if it did not, the area per molecule would become either zero or negative. None of these later possibilities are possible and we may consider ourselves justified in extrapolating these curves smoothly as long as the surface pressure is increasing.

We now make the assumption that below the discontinuity in the surface pressure–log concentration curves the concentration is substantially equal to the activity. This assumption is justified by the fact that the concentrations of wetting agents are, in all cases, very low. Furthermore, if the activity were considerably less than the concentration in this region, the calculated values of the area per molecule at close packing at the interface, using the value of the slope at the break point taken from the concentration curve, would be low. These values of area (see table 1) are in all cases consistent with similar values obtained from film balance data.

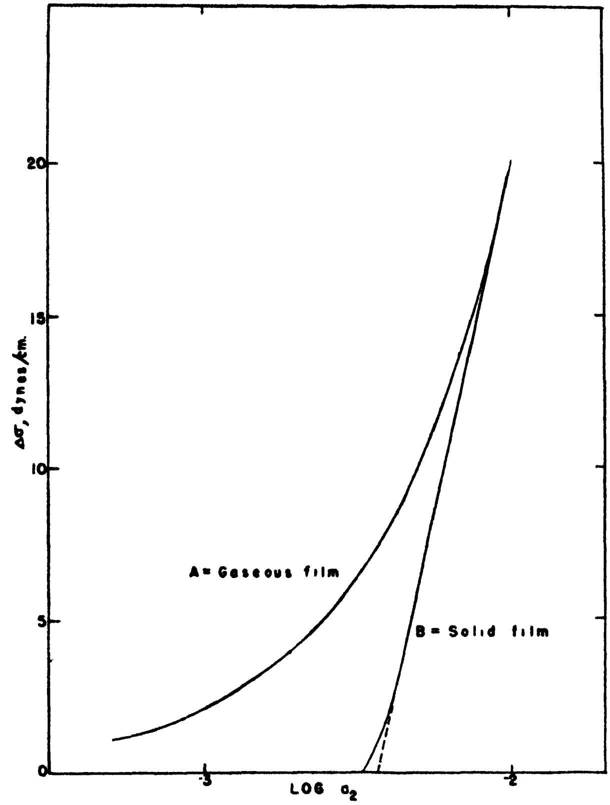

FIG. 4. Curves obtained with two extreme types of surface films

TABLE 1

Area per molecule at the point of discontinuity

WETTING AGENT	CALCULATED AREA PER MOLECULE
	Å.²
Tergitol No. 7	36.2
Tergitol No. 4	26.0
Tergitol No. 8	30.5
Duponol OS	12.8
Triton NE	15.5
Duponol 80	32.2
Hexanolamine oleate	46.7
Sodium cetyl sulfate	21.9

The log activity coefficient is obtained by subtracting the log concentration from log activity at any given surface pressure. The discontinuity in the surface pressure–log concentration curve probably corresponds to the beginning of micelle formation, while the maximum in the curve corresponds to the end of micelle formation.

Duponol OS and hexanolamine oleate both show a maximum in the surface pressure curve. It may be that this represents a region of unstable equilibrium and that measurements on old solutions would not show a maximum. Measurements of the solutions of Duponol OS after standing about two months seemed to indicate that this was so (see figure 2).

An illustration of this procedure is the case of hexanolamine oleate. The activity coefficients, calculated from the surface pressure curve in figure 3, are shown in figure 5, together with the activity coefficients calculated from the data of McBain (3), which are based on the lowering of the freezing point. The agreement between the two methods is rather striking, particularly in view of the fact that the work was done in different laboratories on different samples of soap. The point *A* in figure 3 is the critical point for micelle formation, according to McBain (3).

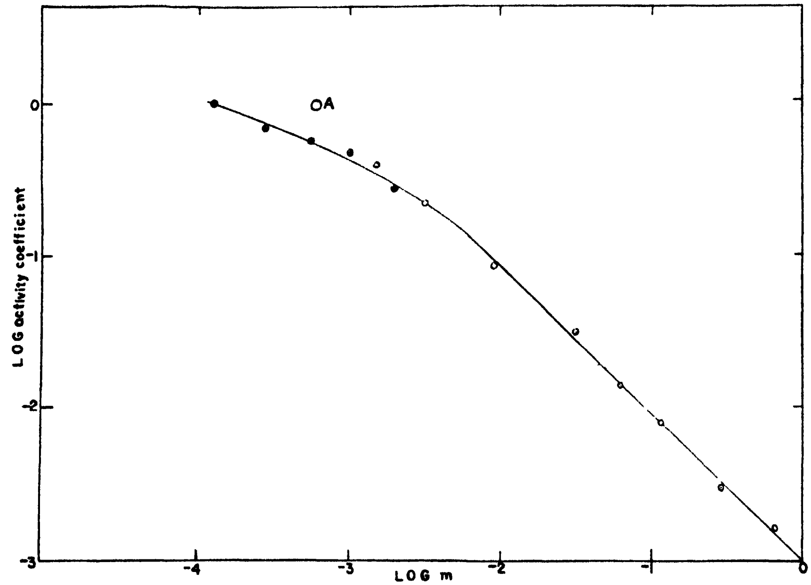

FIG. 5. Activity coefficients for hexanolamine oleate: ⊙, data on freezing-point lowering; ⊕, surface tension data.

The data from surface pressure measurements have been used in plotting figure 5 only up to the maximum of the surface pressure curve, since beyond the maximum, in the regions of higher concentration, we do not know what the activity is. However, a slope of −1 would mean that the activity is a constant in that region, and this is a probable conclusion from the surface tension data. It is possible that the ideas given here may help to explain the maxima which are found in the surface pressure curves of many substances.

Because it was thought that the observed break in the surface pressure curve might be due to impurities in the sample, a search was made of the literature to find a material which exhibited the break point, which was very probably pure, and for which activity coefficient data existed. Figure 6 shows the data for ethyl alcohol taken from the *International Critical Tables*. Curve A shows the curve of surface pressure (6) *vs.* logarithm of the mole fraction; curve B shows the partial pressure (5) of alcohol vapor *vs.* the logarithm of the mole fraction. Activity coefficients for alcohol cannot be calculated by this method, for the coefficient deviates from 1 in the low-concentration region. The coincidence of the break points offers confirmation of the method developed here. It also indicates that the method has rather wide applicability.

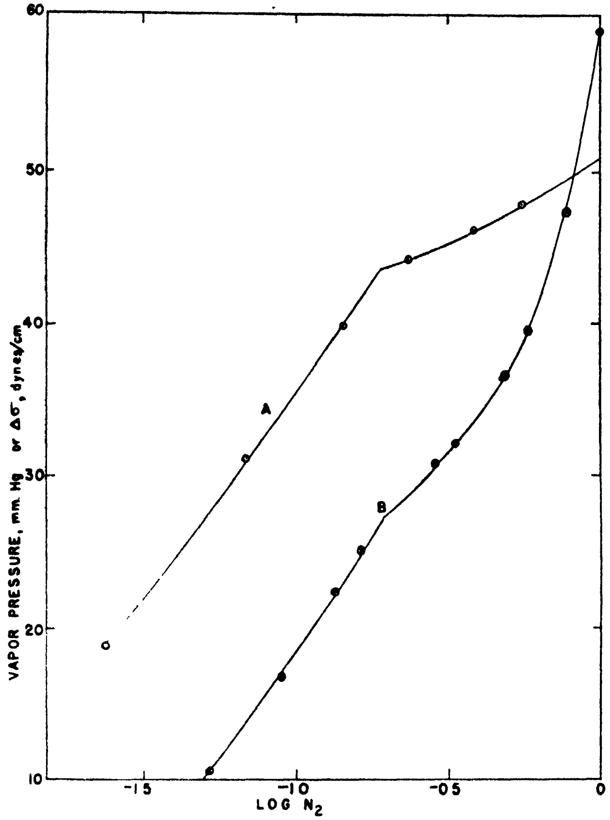

FIG. 6. Ethyl alcohol-water solutions. Curve A, curve of surface pressure *vs.* logarithm of the mole fraction; curve B, curve of partial pressure of alcohol vapor *vs.* the logarithm of the mole fraction.

Since ethyl alcohol-water mixtures show a maximum in the viscosity-concentration curve at the critical concentration (7), it is tempting to interpret the break point as micelle formation. However, if such a micelle did exist, it would be extremely dilute.

These data show why the attempts to verify the Gibbs absorption equation have given high values except in the case of nonylic acid, where extremely dilute solutions were used. Presumably the measurements in this case were made at concentrations below the critical.

SUMMARY

1. A method has been suggested for the determination of the activity coefficient of surface-active materials at low concentrations in water solutions.

2. Data are presented to show that the method has wide applicability.

3. The apparent lack of applicability of the Gibbs adsorption equation to such systems is shown to be due to large variations in the activity coefficient of dissolved surface-active material.

REFERENCES

(1) Corbin, M. L., Klevens, H. B., and Harkins, W. D.: J. Chem. Phys. **14**, 216 (1946).
(2) Donnan, F. G., and Barker, J. T.: Proc. Roy. Soc. (London) **A85**, 557 (1911).
(3) Gonick, E., and McBain, J. W.: J. Colloid Sci. **1**, 127 (1946).
(4) Harkins, W. D., and Gans, D. M.: Colloid Symposium Monograph **5**, 40 (1927); **6**, 36 (1928).
(5) *International Critical Tables*, Vol. III, p. 290. McGraw-Hill Publishing Company, New York (1928).
(6) *International Critical Tables*, Vol. IV, p. 467. McGraw-Hill Publishing Company, New York (1928).
(7) *International Critical Tables*, Vol. V, p. 22. McGraw-Hill Publishing Company, New York (1929).
(8) McBain, J. W., and Davies, G. P.: J. Am. Chem. Soc. **49**, 2230 (1927).
(9) McLewis and Patrick, W. A.: Phil. Mag. 1908 and 1909
(10) Nutting, G. C., Long, F. A., and Harkins, W. D.: J. Am. Chem. Soc. **62**, 1496 (1940).

SURFACE AREAS OF CRYSTALLINE CARBON AND CARBIDE POWDERS AS MEASURED BY THE ADSORPTION OF NITROGEN[1, 2]

F. E. BARTELL AND CHARLES G. DODD[3]

Department of Chemistry, University of Michigan, Ann Arbor, Michigan

Received August 22, 1949

The problem of measuring specific surface areas of finely divided solids has been attacked quite successfully in recent years by methods involving treatments

---

[1] Presented at the Twenty-third National Colloid Symposium, which was held under the auspices of the Division of Colloid Chemistry of the American Chemical Society at Minneapolis, Minnesota, June 6–8, 1949.

[2] The data presented in this paper are from a dissertation submitted by Charles G. Dodd to the Horace H. Rackham School of Graduate Studies of the University of Michigan in partial fulfillment of the requirements for the degree of Doctor of Philosophy, 1948.

[3] Present Address: Petroleum Experiment Station, U. S. Bureau of Mines, Bartlesville, Oklahoma.

of low-temperature gas adsorption data. Notable among these methods have been those of Brunauer, Emmett, and Teller (4) and of Harkins and Jura (10). At the time the investigations described herein were made, other workers in this laboratory were studying the adsorption of aliphatic acids and alcohols from aqueous solution on various carbon powders (8). The gas adsorption experiments were intended to complement the adsorption work from aqueous solutions. In selecting the adsorbents to be used in this investigation, major emphasis was put on elemental carbon in its various forms. These forms included crystalline graphite powders, a carbon black of moderate specific surface area, a finely divided diamond dust, and, for comparison, a finely divided silicon carbide powder. The latter was included because it has the same crystal structure as diamond with half of the carbon atoms replaced by silicon. All of the adsorbents but the carbon black were believed to be made up of crystalline grains possessing essentially plane crystal surfaces, and all were considered to be nonporous to the adsorption of nitrogen.

Nitrogen was used as the adsorbate gas in all the experiments because there is much information in the literature concerning the adsorption of this gas on solids at temperatures near its boiling point. The estimated cross-sectional area of the adsorbed nitrogen molecule is generally believed to be more accurate than the areas of other gases which might have been employed as adsorbates.

The multilayer theory of the physical adsorption of gases as developed by Brunauer, Emmett, and Teller (4), often referred to as the B.E.T. theory, has stimulated the development of adsorption theory and led to a generally accepted method for measuring specific surface area. Using the notation of Brunauer (3), the complete B.E.T. isotherm equation is expressed as:

$$V = \frac{V_m Cx}{1 - x} \frac{1 - (n + 1)x^n + nx^{n+1}}{1 + (C - 1)x - Cx^{n+1}} \tag{1}$$

The parameter n, according to the B.E.T. model, is considered to represent the number of adsorbed molecular layers. The term x is shown to be equivalent to P/P_0, the relative pressure. C is another parameter which is considered to involve the heats of adsorption and liquefaction. For cases where a large number of adsorbed layers are formed on the surface of the adsorbent it is assumed that n is infinite, and the integration involved in the derivation of equation 1 is thereby simplified. The resulting equation is expressed as:

$$V = \frac{V_m Cx}{(1 - x)(1 - x + cx)} \tag{2}$$

For purposes of plotting data, equation 2 may be rearranged as follows:

$$\frac{P}{V(P_0 - P)} = \frac{1}{V_m C} + \frac{C - 1}{V_m C} \frac{P}{P_0} \tag{3}$$

Equations 2 and 3 are often referred to as forms of the "simple" or "infinity" B.E.T. adsorption equation to distinguish them from the "complete" form of the equation (equation 1).

The two unknowns in equation 3 may be determined from the slope and intercept of the straight-line plot. Equation 1, on the other hand, involves a third unknown, n, and requires a longer trial-and-error procedure before the three unknowns V_m, C, and n can be determined. For this reason the majority of published applications of adsorption data to surface area determinations have employed the simple B.E.T. equation.

Recently Joyner, Weinberger, and Montgomery (11), following earlier work by Dietz and Gleysteen (5), have described a method whereby equation 1 may be reduced to the form of a linear equation:

$$\frac{\Phi(n, x)}{V} = \frac{1}{V_m C} + \frac{\theta(n, x)}{V_m} \tag{4}$$

where

$$\Phi(n, x) = \sum_{i=1}^{n} i x^i = \frac{x - (n + 1)x^{n+1} + nx^{n+2}}{(1 - x)^2} \tag{5}$$

and

$$\theta(n, x) = \sum_{i=1}^{n} x^i = \frac{x - x^{n+1}}{1 - x} \tag{6}$$

Joyner and coworkers have prepared tables giving numerical values of the functions expressed in equations 5 and 6 for various assumed values of n ranging from 1.05 to 9.0 and for values of x from 0.10 to 0.60. The authors kindly made these tables available, and they were used for calculations described in this paper.

Harkins and Jura (10) have presented a new method for calculating specific surface areas from gas adsorption data which has enjoyed wide acceptance and which has been shown by various investigators to give results comparable to those obtained by the B.E.T. equations. The Harkins and Jura theory is based on the assumption of an equation of state for adsorbed films on solids analogous to those developed for condensed films of insoluble substances on aqueous substrates (1). In the derivation of the Harkins and Jura isotherm equation this empirical equation of state is combined with a form of the Gibbs adsorption equation to give:

$$\log P/P_0 = B - A/V^2 \tag{7}$$

In this equation A and B are constants. The quantity $\log P/P_0$ is plotted against $1/V^2$ and the slope, A, of the straight line measured. The surface area is then obtained from the equation:

$$\text{Surface area} = k(A)^{1/2} \tag{8}$$

where the empirical constant k has been independently determined by a calorimetric procedure for measuring specific surface (9).

EXPERIMENTAL

Powders

All of the powders used, with the exception of graphite B which had a low ash content as received, were purified carefully to eliminate impurities present in the commercially obtainable material. In the case of the graphite and silicon carbide powders the major impurity was iron, which was introduced into the powder during the commercial grinding process. With all the powders except diamond and graphite B the last stage of purification before storing was a heat treatment in a high vacuum to remove, insofar as possible, all tenaciously held chemisorbed surface contaminants. The purification procedure for each powder is described below and summarized in table 1, together with the source of each and the residual ash.

Graphite: All graphite powders were carefully purified by repeated treatment with hydrochloric acid, with hydrofluoric acid, and finally with distilled water.

TABLE 1

Purification of powders

POWDER	SOURCE	TREATMENT WITH				HEAT TREATMENT IN HIGH VACUUM	FINAL PER CENT ASH
		HCl	Chromic acid	HF	Organic solvents		
Graphite B	Acheson Colloids Corporation	No	No	No	No	No	0.38
Graphite C	Acheson Colloids Corporation	Yes	No	Yes	No	850°C.	0.034
Graphite D	National Carbon Company	Yes	No	Yes	No	1000°C.	0.18
Graphite E	National Carbon Company	Yes	No	Yes	No	1000°C.	0.023
Furnace black	*	No	No	No	No	1000°C.	0.078
Silicon carbide	Norton Company	Yes	No	No	Yes	1000°C.	
Diamond dust	United States Industrial Diamond Corporation	No	Yes	Yes	No	No	0.1

* The semi-reinforcing furnace black was believed to be a sample of standard Gastex carbon black.

They were given a final heat treatment at 850–1000°C. in a high vacuum for 24–48 hr.

Spectrographic analyses were made on several of the purified graphite powders to detect inorganic impurities. No difference could be detected between the arc emission spectra of the purified graphite powders and that of "spectroscopically pure carbon." X-ray diffraction powder diagrams were made on all the graphite powders to confirm the graphite crystal structure. All the diffraction diagrams were identical, regardless of whether the samples were taken before or after purification.

Furnace black: The carbon black sample used in the work was a semi-reinforcing furnace black of moderate surface area previously used by other workers in this laboratory and was designated as "standard Gastex" carbon black. It had been subjected to a heat treatment at 1000°C. for 24 hr. in a high vacuum.

Diamond: The diamond powder consisted of industrial diamond dust graded to include particles not over 2 microns in diameter. The entire batch of this material (10 g.) was rigorously purified with 150 ml. of hot cleaning solution prepared with reagent grade sulfuric acid and potassium bichromate. The powder was separated from the solution by centrifuging, washed several times with distilled water, transferred to a platinum dish, and evaporated almost to dryness on a steam cone. Five milliliters of 1:1 sulfuric acid and 40 ml. of hydrofluoric acid were added and the evaporation to fumes on a steam cone repeated. Finally the dish was heated over a low flame to expel all fumes of sulfur trioxide.

After completion of the purification with acids the powder was washed with distilled water and finally with redistilled reagent acetone, again using a centrifuge for all separations. The acetone-wet powder was dried in an oven at 110°C. and stored in a desiccator over anhydrous calcium sulfate. The final drying from acetone was intended to prevent the caking which occurred when the water-wet powder was dried. It proved to be effective for this purpose. X-ray diffraction powder diagrams confirmed the diamond crystal structure.

Silicon carbide: The silicon carbide powder had been ground very fine. It was purified by treatment with hydrochloric acid and washed in the same manner as the graphite. Further purification consisted of extraction in a Soxhlet extractor with reagent grade carbon tetrachloride, acetone, and then distilled water in succession. The powder was washed with acetone and then ether. The ether-wet powder was dried at 110°C. in a high vacuum. As judged by its wetting properties it seems probable that the surface of this powder was at least partially oxidized to silica. X-ray diffraction powder diagrams confirmed the identity of the powder.

Gas adsorption apparatus

The apparatus used to determine the low-temperature nitrogen adsorption isotherms on the powders was similar to the standard design described by Emmett (7). The important changes in and additions to the apparatus will be described briefly.

Systems for purification of the helium and nitrogen gases used were included in the apparatus. The helium purification system consisted simply of a trap containing activated charcoal, which was immersed in liquid nitrogen when in use. Nitrogen for use as the adsorbate in the determination of the actual adsorption isotherm was obtained from a cylinder of water-pumped nitrogen of approximately 99.8 per cent purity. The gas was dried by passing it through a tube of anhydrous calcium chloride and then through a purification system for the removal of oxygen which was similar to that described by Meyer and Ronge (13). The oxygen-free nitrogen was passed successively through tubes of Drierite and a liquid-air trap before going to the gas reservoir.

The thermostat bath used for controlling the sample temperature during adsorption runs consisted of an unsilvered Dewar flask filled with commercial liquid nitrogen through which a stream of nitrogen gas was bubbled to stir the liquid. The temperature of the thermostat bath was measured by a five-junction copper–constantan thermocouple in conjunction with a White potentiometer.

For the calibration of the thermocouple at low temperatures the table of Scott (15) was selected as that of a "standard" copper–constantan couple, together with the nitrogen vapor-pressure tables of Dodge and Davis (6). In later experiments a more convenient nitrogen vapor-pressure thermometer was used to measure the temperature of the liquid-nitrogen bath. The temperature as measured by the thermocouple agreed with that determined by the vapor-pressure thermometer to within 0.1°K.

Before each adsorption run the bulb containing the sample was surrounded by a furnace at from 150° to 250°C. and evacuated overnight with the mercury diffusion pump on. In order to facilitate the more efficient use of the gas adsorption apparatus a multiple-sample attachment was sealed on for simultaneous heating and evacuation of three powder samples. The helium dead-space determinations were made on the three samples successively, the helium evacuated, and the nitrogen adsorption isotherms made in the usual manner.

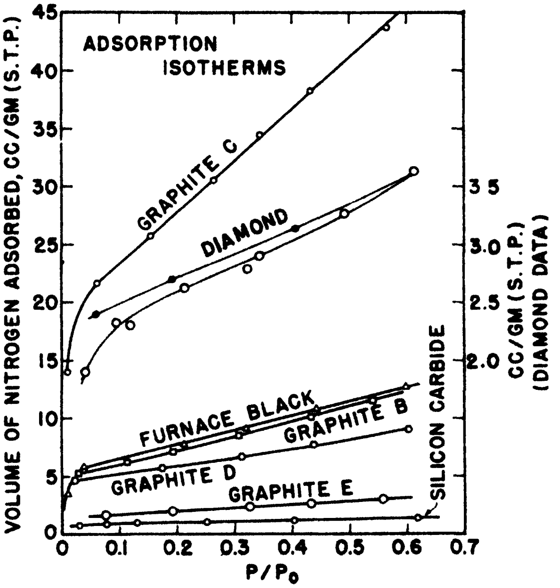

Fig. 1. Isotherms for adsorption of nitrogen on the nonporous solids

The total volume of the capillaries from the gas buret to the manometer, to the stopcock leading to the vacuum manifold, and to the stopcock above the sample tubes was calculated to be 6.5 ml. This was checked by a determination varying the volume in the gas buret and applying the simple gas laws.

During the adsorption and desorption runs an equilibration period of from 3 to 15 min. was allowed to elapse after each addition or removal of adsorbate gas in order for the final pressure reading to become constant.

RESULTS AND DISCUSSION

The adsorption isotherms for all the powders are presented in figure 1. It should be noted that the scale of the ordinate, *V*, for the diamond adsorption data is presented on the right-hand side of the figure. No effort was made to extend the isotherms to a relative pressure of 1.0, because the principal purpose was merely to obtain adequate data for the calculation of specific surface areas. The adsorption isotherms were followed up to relative pressures of about 0.6, approximately 450–500 mm. of mercury pressure. Also, since the tables of Joyner, Weinberger, and Montgomery (11) include only the relative pressure range from 0.1 to 0.6, it would have been necessary to extend these tables before higher relative pressure data could have been plotted by their method. The temperature at which each isotherm was determined is indicated in table 2.

In the case of the diamond isotherm three desorption points were determined. These data are indicated by solid points on figure 1. No desorption points were determined for the graphites or furnace black at liquid-nitrogen temperatures, because previous work at liquid-oxygen temperatures had indicated complete reversibility for nitrogen adsorption with these powders. The diamond desorption curve shows a slight amount of hysteresis which is somewhat greater than the estimated experimental error. Hysteresis of this type could not be attributed to capillary condensation, because diamond crystals cannot be considered to possess capillary pores.

TABLE 2

Comparison of constants and specific surface areas obtained by the simple B.E.T. equation, the equation of Harkins and Jura, and the complete B.E.T. equation

POWDER	ADSORPTION TEMPERATURE	SIMPLE B.E.T. EQUATION		HARKINS AND JURA EQUATION AREA	COMPLETE B.E.T. EQUATION		
		C	Area*		n	C	Area*
	°K.		m.^{2}/gram	m.^{2}/gram			m.^{2}/gram
Graphite B	78.1	70	27	24	5.0	83	26
Graphite C	78.0	123	100	105	3.4	35	111
Graphite D	77.7	100	21	21	3.6	26	21
Graphite E	77.6	58	8.3	7.8	4.0	34	9.1
Furnace black	77.9	160	27	26	4.5	86	28
Silicon carbide	77.5	110	4.0	3.8 and 4.3	4.0	140	3.8
Diamond dust	77.3	80	9.1	9.2 and 11.5	3.0	240	9.2

* A cross-sectional area of 16.2 Å.^{2} has been assumed for the adsorbed nitrogen molecule.

The adsorption of nitrogen on diamond at 77°K. has been shown to combine several interesting features seldom observed in the physical adsorption of gases. The desorption hysteresis shown in figure 1 is so small that its existence should be verified by further experiment, but the unusually low B.E.T. n-value of 3.0 which was obtained for this nonporous adsorbent together with the apparent hysteresis raises the question of the existence of some type of activated adsorption or chemisorption. A further adsorption study of the diamond–nitrogen system at various temperatures using a more sensitive apparatus is needed to clarify this point.

Reference to the diamond isotherm indicates that the precision of the experimental points is somewhat lower than that of the other isotherms, but it should be noted that the ordinate was plotted on an expanded scale. Difficulties were encountered in evacuating the samples of diamond dust preparatory to measuring the adsorption. Adsorbed gases on the surface of the powder were removed with difficulty. Furthermore, equilibration was slow following each addition of adsorbate gas. These factors, which are sometimes characteristic of activated adsorption, probably accounted for the somewhat poorer reproducibility of the diamond experimental results.

Figures 2 and 3 show the adsorption data plotted according to the simple or infinity B.E.T. equation (3). The data shown in figure 2 for the graphites and the furnace black are fitted well by the simple B.E.T. equation. In no case is there any difficulty in determining a good straight line passing through the experimental points up to relative pressures of about 0.35, the usual range of applicability of the simple B.E.T. equation.

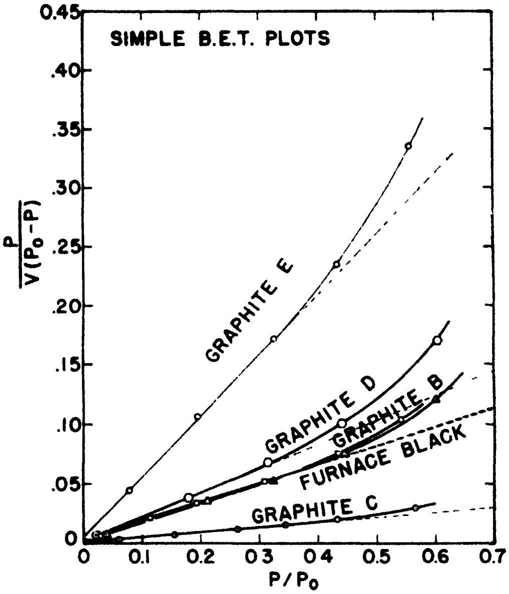

Fig. 2. Simple B.E.T. plots for adsorption of nitrogen on graphites B, C, D, and E and on furnace black carbon.

The simple B.E.T. plots of the diamond and silicon carbide data shown on figure 3 are less satisfactory because the experimental points leave the B.E.T. straight lines at relative pressures of about 0.25. This deviation is in such a direction as to indicate less adsorption than is called for by the simple B.E.T. theory. However, the specific surface areas calculated from these plots are consistent.

On most of the simple B.E.T. plots the intercept could not be determined precisely. A consequence of this was a corresponding uncertainty in the calculated value of the B.E.T. constant, C, because the intercept is equal to $1/V_mC$, but the precision of the calculation of the specific surface area was scarcely affected. The reason for this apparent discrepancy is seen when it is considered that the slope of the straight line plotted according to equation 3 is $(C - 1)/V_mC$. Unless the value of C for the system is close to unity the slope of the line is very insensitive to C, but the intercept is difficult to determine only when the value of C is high. Thus it is always possible to determine a good value of specific surface area from the slope, although the intercept, and consequently C, may be difficult to measure. Specific surface areas and values of C calculated from the simple B.E.T. straight lines are shown in table 2, but the C-values obtained by the use of the complete B.E.T. equation are considered the most reliable of those shown in table 2. The area calculations for all the B.E.T. plots were made assuming a value of 16.2 Å.^{2} for the cross-sectional area of the adsorbed nitrogen molecule at 77°K. In connection with the areas shown for the furnace black it may be pointed out that Amon, Smith, and Thornhill (2) found standard Gastex carbon black to have an area of 26 sq. m./g., a value seen to be in agreement with the calculated areas for the furnace black.

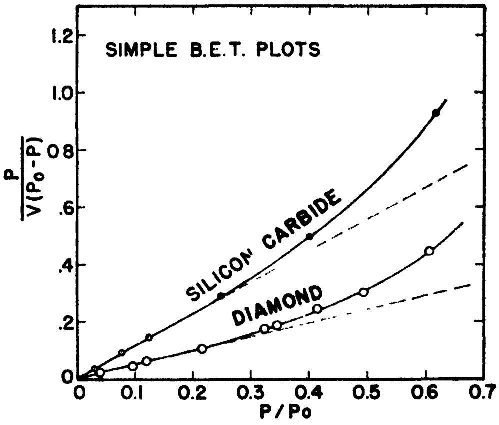

Fig. 3. Simple B. E. T. plots for adsorption of nitrogen on silicon carbide and on diamond powders.

Figures 4, 5, and 6 show the data plotted according to the Harkins and Jura isotherm, equation 7. Figure 4 shows the satisfactory type of correlation obtained with the graphites and the furnace black. On figure 4 the scale used for the abscissas should be multiplied by the factor shown in parentheses along each straight line.

The silicon carbide adsorption data shown plotted in figure 5 according to the Harkins and Jura equation generate a smooth curve from which two linear portions may be selected with corresponding specific surface areas of 3.8 and 4.3 sq. m./g., the mean of which agrees well with the calculated B.E.T. areas. The diamond data shown in figure 6 are more erratic, with two linear portions from which specific surface areas of 9.2 and 11.5 sq. m./g. may be calculated.

It will be noted, if figures 4, 5, and 6 are compared with figure 1, that the points used to determine the Harkins and Jura plots are not necessarily the experimental points. When the experimental points were originally used for these plots the resulting patterns were too scattered in some cases to permit the establishment of a linear portion of the plot. In some cases the difficulty was lessened by the transformation of coördinates of points on the simple B.E.T. straight line to the Harkins and Jura plot, but this was considered an unwarranted procedure.

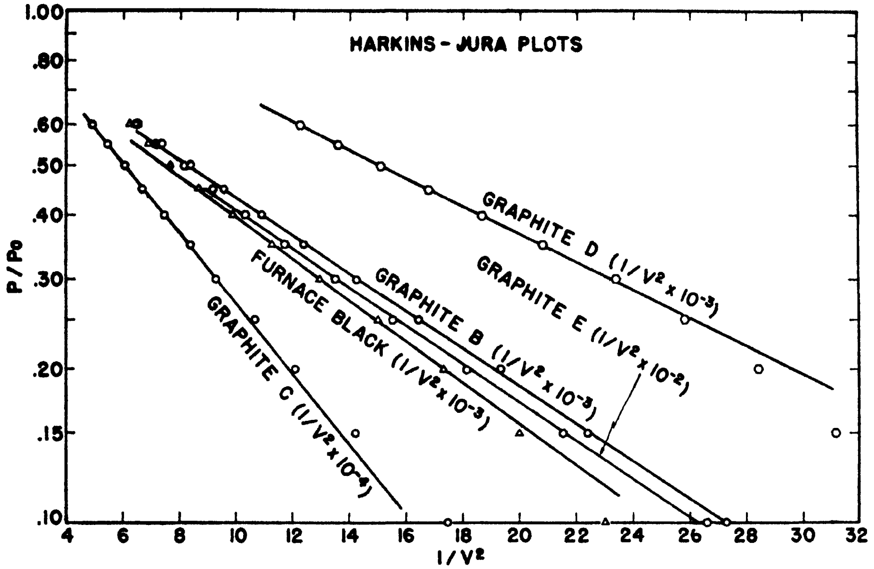

Fig. 4. Harkins–Jura plots for adsorption of nitrogen on graphites B, C, D, and E and on furnace black carbon.

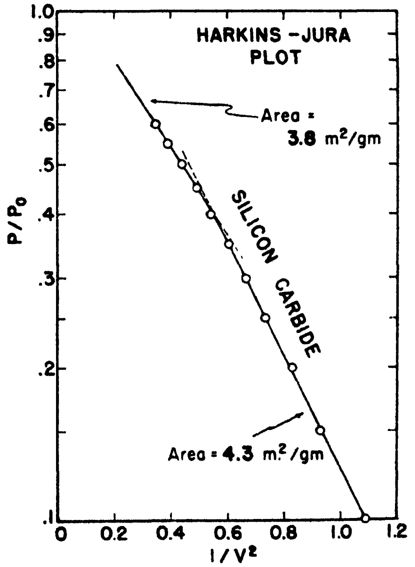

Fig. 5. Harkins–Jura plot for adsorption of nitrogen on silicon carbide

The best results were finally obtained by selecting a number of evenly spaced points from the isotherms (also used for the complete B.E.T. plots) and plotting them according to the Harkins and Jura equation. This has been done on figures 4, 5, and 6. An examination of figure 4 shows that well-defined linear portions were obtained for the graphite and furnace black adsorption data. The calculated specific surface areas are shown in table 2.

The Harkins and Jura plot involves the use of $1/V^2$ as the abscissa. Where the experimental data are slightly in error (usually resulting from inaccurate dead-space corrections with powders of low specific surface area), the errors in the abscissas are squared. On the B.E.T. plot V is involved only to the first power. This factor was probably responsible for some of the difficulties involved in using the experimental points on the Harkins and Jura plots, but it serves to emphasize one advantage of the B.E.T. plot. In addition it will be noted that the B.E.T. plot uses data at low relative pressures, where the dead-space corrections are of little consequence. The linear portions of the Harkins and Jura plot, on the other hand, occur at higher relative pressures where the dead-space corrections become quite appreciable.

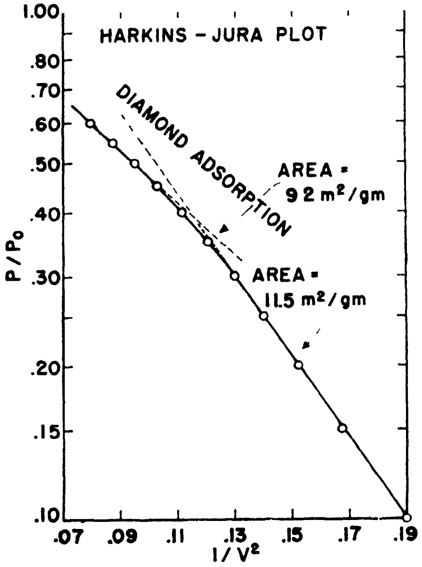

Fig. 6. Harkins–Jura plot for adsorption of nitrogen on diamond

Reference to the results in table 2 shows generally good agreement between specific surface areas calculated from experimental data by the simple and complete B.E.T. equations and the equation of Harkins and Jura for the four graphites and the furnace black. For all five adsorbents the extreme variations in the surface areas determined by both B.E.T. isotherms and the Harkins and Jura isotherm is good, i.e., within about 10 per cent.

The Harkins and Jura specific surface areas as determined for the silicon carbide and diamond are, on the other hand, somewhat ambiguous, unless one has some way of knowing *a priori* which portion of the plot should be used. For both the silicon carbide and the diamond the slope of the linear plot between relative pressures of about 0.5 and 0.6 gives a specific surface area which closely checks the area determined from the complete B.E.T. plot If the area determined by the complete B.E.T. plot is assumed to be correct, however, the area determined from the lower pressure linear portion of the Harkins and Jura plot is too high by 13 per cent for the silicon carbide and too high by 25 per cent for the diamond dust. This difficulty is not serious in the case of the silicon carbide, for which the B.E.T. parameter n was calculated to be about 4.0, because the deviation of the mean from the extremes is relatively low and an average value may well be employed. In the case of the diamond isotherm the deviation of the extremes is significantly large.

The applicability of the Harkins and Jura isotherm to the measurement of specific surface depends on a knowledge of the range of relative pressure within which the two-dimensional state of aggregation of the adsorbed film is expressed by the same empirical equation of state which is applied to condensed films of insoluble monolayers on aqueous substrates. Ries, Van Nordstrand, and Kreger (14) have stated that Dr. Jura informed them in a private communication that "the best straight line is drawn through the points in the relative pressure range 0.1 to 0.4 . . .," when nitrogen is used as the adsorbate at 77°K. Reference to figure 4 reveals that even with adsorbents which gave sufficiently long linear plots according to the Harkins and Jura isotherm it is necessary to use different portions of the relative pressure range for calculations with the different powders. For three of the five isotherms shown on figure 4 the linear plot does not extend appreciably below relative pressures of 0.2.

Smith and Bell (16) have recently discussed the importance of the B.E.T. parameter n as a criterion for agreement between the Harkins and Jura equation and the complete B.E.T. equation. In common with Joyner, Weinberger, and Montgomery (11), Smith and Bell found that their Harkins and Jura plots of adsorption experiments on highly porous amorphous carbons were invariably curved. In order to explain this behavior they extended the earlier treatment of Livingston (12), who had attempted to relate the infinity B.E.T. equation and the Harkins and Jura equation by application of the Gibbs adsorption isotherm to solid surfaces. For an assumed B.E.T. C of 50 and a P_0 of 800 they showed that the Harkins and Jura plot should not be expected to be linear when the B.E.T. n is appreciably less than 5. The data obtained in the present investigation are considered experimental verification of this conclusion for nonporous carbon adsorbents. The value of 3.0 for the constant n as determined for the diamond isotherm is, we believe, the lowest such figure so far reported in the literature for nonporous adsorbents. Practically it is seen that the curvature of the Harkins and Jura plot does not become too troublesome until the value of n drops to about 3.0. As a matter of interest it is noted that the adsorption of nitrogen on the anatase powder used by Harkins and Jura (9) to determine the empirical constant k in equation 8 was found by Joyner, Weinberger, and Montgomery (11) to have an n-value of 3.47.

Since there is no way of knowing in advance within what range of relative pressure the Harkins and Jura equation will give a linear plot, it is always necessary to determine a large number of points on the isotherm. On the other hand, the simple B.E.T. method requires a minimum of only one experimental point at about 0.3 relative pressure because the line also passes close enough to the origin to give a specific surface within 10 per cent of that obtained by the use of more points (7). The simple B.E.T. equation is thus considered to possess a distinct advantage of convenience for the routine determination of specific surface area by the low-temperature adsorption of nitrogen. Reference to table 2 shows good agreement in areas determined by both B.E.T. equations. In all cases the agreement is within about 11 per cent or better. A comparison of the values of C determined by both B.E.T. equations shows much greater discrepancies.

For the relatively few adsorbents, such as diamond, which are characterized by n-values of about 3.0 or less, the complete B.E.T. equation is the only one which gives an extensive linear plot.

In their original publication Harkins and Jura recognized this difficulty in applying their isotherm to the measurement of surface area when the plot of $\log P/P_0$ *vs* $1/V^2$ was curved. They stated, "If the linear region is not sufficiently extensive, the method should not be used." (10)

On figure 7 are presented complete B.E.T. plots for all the powders used. The data were calculated according to the method of Joyner, Weinberger, and Montgomery (11) and plotted according to their equation 4. The procedure employed to determine the straight lines shown in figure 7 was the same as that described by Joyner and coworkers, except that it was not considered necessary to use the method of least squares. For each powder different series of values for n were assumed until the resulting plot gave a good straight line over the entire relative pressure range from 0 to 0.6. The adsorption data used in the calculations were taken from the isotherms at selected points from relative pressures of 0.10 to 0.60 in increments of 0.05 so that the tables of Joyner *et al.* could be employed for the calculations. It should be emphasized that the lines shown on figure 7 are only those finally selected as the best linear plots of the data. On each line on figure 7 is shown the corresponding value of n which was assumed for the calculation of the points on the line. The points shown on each linear plot in figure 7 correspond to the range of relative pressure from 0.10 to 0.60. Calculated data based on these plots are shown in table 2.

An examination of figure 7 shows that the complete B.E.T. equation gives good correlation with all the data obtained in this investigation once the proper value of n is determined. No ambiguity remains in the calculation of the specific surface area of each powder aside from the necessary assumption for the cross-sectional area of the adsorbed nitrogen molecule. The correlation is generally more satisfactory than that obtained with either the Harkins and Jura or the simple B.E.T. equation.

It may be concluded on the basis of the data presented in table 2 that either the method based on the simple B.E.T. equation or the less convenient Harkins and Jura method may be applied to nitrogen adsorption data on nonporous carbon powders when the B.E.T. parameter *n* is greater than about 3 and the value of the B.E.T. constant *C* is low, i.e., less than about 200. When the value of *n* is less than about 3 and that of *C* greater than about 200 only the complete B.E.T. equation represents the data well, although the simple B.E.T. equation may be used for approximate measurements of specific surface. The Harkins and Jura equation does not give a unique value of specific surface when *n* is less than about 3. These conclusions are, in general, the same as those of Joyner, Weinberger, and Montgomery (11) and of Smith and Bell (16), except that in the present work systems have been investigated which are believed to be crystalline and nonporous; thus the low values of *n* are not thought to be the result of adsorption in capillary pores.

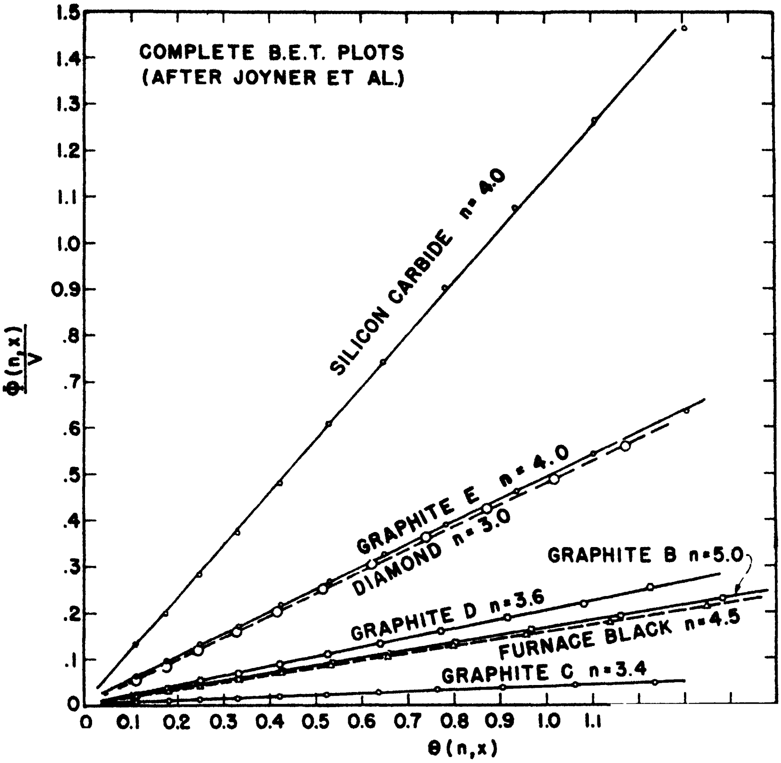

Fig. 7. Complete B.E.T. plots for adsorption of nitrogen on graphites B, C, D, and E, on furnace black carbon, on silicon carbide, and on diamond (data calculated according to the method of Joyner, Weinberger, and Montgomery).

The authors wish to acknowledge the assistance of Dr. S. S. Kistler of the Norton Company, who supplied them with the specially ground sample of silicon carbide, that of the Acheson Colloids Corporation and the National Carbon Company, which supplied the graphite, and that of the United States Industrial Diamond Corporation, which loaned them the specially graded sample of diamond dust. Further, the authors wish to thank Dr. Ying Fu of this laboratory for valuable suggestions relating to this work.

REFERENCES

(1) **Adam**: *The Physics and Chemistry of Surfaces*, 3rd edition, pp. 17–105. Oxford University Press, London (1941).

(2) **Amon, Smith, and Thornhill**: Ind. Eng. Chem., Anal. Ed. **15**, 257 (1943).

(3) **Brunauer**: *The Adsorption of Gases and Vapors. Vol. I. Physical Adsorption*, pp. 151–5. Princeton University Press, Princeton (1943).

(4) **Brunauer, Emmett, and Teller**: J. Am. Chem. Soc. **60**, 309 (1938).

(5) **Deitz and Gleysteen**: J. Research Natl. Bur. Standards **29**, 191 (1942).

(6) **Dodge and Davis**: J. Am. Chem. Soc. **49**, 610 (1927).

(7) **Emmett**: *Advances in Colloid Science*, edited by E. O. Kraemer, pp. 1–36. Interscience Publishers, Inc., New York (1942).

(8) **Fu, Hansen, and Bartell**: J. Phys. & Colloid Chem. **52**, 374 (1948).

(9) **Harkins and Jura**: J. Am. Chem. Soc. **66**, 1362 (1944).

(10) **Harkins and Jura**: J. Am. Chem. Soc. **66**, 1366 (1944).

(11) **Joyner, Weinberger, and Montgomery**: J. Am Chem. Soc. **67**, 2182 (1945).

(12) **Livingston**: J. Chem. Phys. **15**, 617 (1947).

(13) **Meyer and Ronge**: Angew. Chem. **52**, 637–8 (1939).

(14) **Ries, Nordstrand, and Kreger**: J. Am. Chem. Soc. **69**, 39 (1947).

(15) **Scott**: "The Calibration of Thermocouples at Low Temperatures" in *Temperature, Its Measurement and Control in Science and Industry*, American Institute of Physics, pp. 210–11. Reinhold Publishing Corporation, New York (1941).

(16) **Smith and Bell**: Nature **162**, 109 (1948).

COLLOIDAL DIHYDROXY DIHYDROGEN PHOSPHATES OF ALUMINUM AND IRON WITH CRYSTALLINE CHARACTER ESTABLISHED BY ELECTRON AND X-RAY DIFFRACTION[1, 2]

C. V. COLE AND M. L. JACKSON

Department of Soils, University of Wisconsin, Madison, Wisconsin

Received August 22, 1949

Soluble phosphate fertilizers, when applied to acid soils high in minerals of advanced weathering stages (6), become fixed in much less soluble forms which are only slowly available to plants. The nature and properties of the aluminum and iron phosphates formed have been the object of considerable investigation in attempts to develop reliable tests of phosphate fertility and fixing capacity of soils and to form the basis of more efficient agronomic practices. The demands for a better understanding of the processes of phosphate fixation have been

---

[1] Presented at the Twenty-third National Colloid Symposium, which was held under the auspices of the Division of Colloid Chemistry of the American Chemical Society at Minneapolis, Minnesota, June 6–8, 1949.

[2] This work was supported in part by the Graduate Research Committee through a grant from the Wisconsin Alumni Research Foundation.

intensified by the need for phosphate fertilization of such soils in this country and in tropical areas being developed for food production or being considered for development. Full interpretation of the results of recent experiments on phosphate fertilizer uptake using radioactive phosphorus has been severely hampered by a lack of knowledge of the forms in which phosphate is present in the soil system and the properties of the various phosphate compounds in soils.

Because of the extreme complexity of the soil system, many different concepts of the chemical mechanism of phosphate fixation have been advanced. A number of investigations (1, 5, 7, 8, 9, 11) support the view that precipitation of colloidal iron and aluminum hydroxy phosphates is the cause of fixation by highly weathered acid soils. Swenson, Cole, and Sieling (10) determined the pH values of series of solutions of iron and aluminum chloride, each containing a known excess of hydrochloric acid and a known amount of phosphate, after addition of increments of standard sodium hydroxide solution and digestion of the suspensions for 1 hr. at 100°C. The inflection points of the resulting titration curves corresponded to the points of maximum precipitation of phosphate, pH 3–3.4 for the iron phosphate and pH 3.8–4.0 for the aluminum phosphate (10). It was found that the sum of the milliequivalents of hydroxyl ion added to reach the isoelectric point (after the neutralization of excess free hydrochloric acid) and the milliequivalents of phosphate chemically combined as $H_2PO_4^-$ exactly equaled the milliequivalents of iron or aluminum in the original solutions, indicating that the precipitates were dihydroxy dihydrogen phosphates. The isoelectric point of the aluminum compound as determined by the inflection in the titration curve and the pH value of maximum phosphate precipitation was confirmed by observation of the migration of the precipitates in a microcataphoresis cell. They concluded that, at the isoelectric pH values, aluminum and iron dihydroxy dihydrogen phosphates, $Al(OH)_2H_2PO_4$ and $Fe(OH)_2H_2PO_4$, were precipitated rather than the normal phosphates. The coördinated water given in their formulas (10) does not occur in the crystals and is therefore omitted as cited here. Precipitates formed under these conditions were further examined in the present study.

Ensminger (3) has recently reported a study of the compounds formed as the result of the precipitation of aluminum from solution by addition of ammonium phosphate and phosphating aluminum oxide, kaolinite, and soil colloids. He concluded that the valence of the phosphate ion in the precipitate increased from one to two or three on increasing the pH value of the phosphating solution. He reported x-ray diffraction patterns of crystalline preparations of aluminum phosphate which were described as being different from $AlPO_4$.

The objectives of the present study were (*a*) to determine whether the species of aluminum phosphate formed from solution are the same as those formed upon phosphating aluminum-containing minerals and (*b*) to determine whether these species formed by prolonged digestion at steam hotplate temperatures are the same as the colloidal aluminum and iron phosphates which precipitate at room temperature, such as would occur under soil conditions. The crystalline character of the phosphates prepared from solution was investigated by means of x-ray diffraction, electron diffraction, and the electron microscope. The stoichiometric relations were studied by chemical and thermal analyses.

INSTRUMENTAL TECHNIQUES

X-ray diffraction patterns were obtained by means of the General Electric X-ray Diffraction Apparatus, unfiltered iron radiation being used for the film type (XRD-1) and nickel-filtered copper radiation being used for the General Electric Geiger counter type (XRD-3). Electron microscope photographs of the precipitates were made with the RCA electron microscope (EMU-1), equipped with a high-intensity "biased" electron gun. Electron microscope slides were prepared by placing a drop of a barely opalescent suspension of the colloid on a 200-mesh screen previously covered with a thin film of Formvar, and then drying it in a desiccator. The electron diffraction patterns were made with the electron diffraction adapter of the same instrument. The electron beam was accelerated with a fixed potential of 50 kv. corresponding to a wave length of about 0.05 Å. Transmission patterns were obtained by supporting the sample on a 200-mesh wire screen covered with a thin film of Formvar. Slides were prepared by drying down a sufficient amount of an aqueous suspension of the precipitate on the Formvar so that the film of precipitate was almost opaque to light.

PREPARATION OF THE PHOSPHATE PRECIPITATES

The iron and aluminum phosphates studied were prepared by adding, with stirring, approximately 0.1 *N* sodium hydroxide to slightly acid solutions of aluminum or iron chloride containing a 2:1 excess of phosphate (as KH_2PO_4 or NaH_2PO_4) until the desired pH value was obtained. These phosphates were prepared at pH values ranging from 2 to 8 to observe the effects of pH on the type of compound formed. After the addition of sodium hydroxide, the sample of suspension was placed on a steam-pressure hotplate, where it reached a temperature of 90°C. After digestion on the hotplate for varying periods of time the precipitate was filtered on a Büchner funnel, redispersed, and washed three times in hot 1 per cent sodium chloride solution to remove the sorbed or saloid-bound phosphate. The precipitate was then washed with hot distilled water until the filtrate was chloride-free. Portions of the still wet precipitate were redispersed for preparation of electron microscope and electron diffraction slides and the bulk of the sample was air-dried, lightly crushed to pass a 160-mesh sieve, and stored for x-ray diffraction analysis, chemical analysis, and thermal weight-loss studies.

CRYSTAL SPECIES OF PRECIPITATED ALUMINUM AND IRON PHOSPHATES

Freshly precipitated aluminum and iron phosphates were found to be x-amorphous,[3] producing no diffraction patterns with iron x-radiation (1.93 Å. wave length). These precipitates were found to consist of extremely minute crystals which did produce electron diffraction patterns. Larger crystals were produced when the colloidal suspensions were digested at temperatures of 70–100°C. The larger crystals formed in this way gave x-ray diffraction patterns with increasing sharpness of lines as the crystal size increased. The nature and relationships of the different crystal sizes are similar to those of oxide and hydroxide crystals as reported by Weiser and Milligan (12).

---

[3] The term x-amorphous is employed to refer to a material which does not give a powder x-ray diffraction pattern. An x-amorphous material may or may not be crystalline enough to give electron diffraction patterns, and may give a broad diffuse x-ray diffraction band typical of amorphous materials.

Electron microscopic observations

Crystals of different sizes were observed under the electron microscope in precipitates which had been digested for increasing periods of time. Electron micrographs of the freshly precipitated phosphates of aluminum and iron (figures 1 and 4, respectively) showed minute crystals. In the next stages of growth, after digestion at 90°C. from 8 hr. to 2 days depending on the method of initial precipitation, the precipitates consisted of minute well-defined single hexagonal crystals (figure 2) or aggregates. These aggregates of fine crystals frequently formed hexagonal networks. Precipitates which had been digested for longer periods of time contained well-defined hexagonal crystals, approximately 1–5 microns in diameter and 0.5–1 micron in thickness. These crystals were opaque to the electron beam (figures 3, 5, and 6). Rupturing and curling of the supporting film occurred with an intense electron beam, and the crystals were thus rotated in the microscopic field and seen to consist of thin hexagonal plates.

The hexagonal aggregates of the finer crystals of precipitates in earlier stages of growth provide evidence that the mechanism of crystal growth in these precipitates is not only the usual process of the dissolution of the finer crystals and the deposition on single larger crystals. The mechanism of crystal growth includes also a process in which the smaller crystals aggregate to form the framework of a much larger crystal which is gradually filled in by crystallographically oriented finer crystals, the whole being cemented together by the usual solution and deposition process. The occurrence of this phenomenon is probably indicative of the extreme insolubility of the crystal species involved. The growth of crystals to appreciable size by digestion at hotplate temperature is extremely slow, requiring days or weeks to convert the finest crystals (figure 1) to the 1–5 micron range.

The crystal size found in fresh precipitates was determined by the usually dominant factor—namely, rate of precipitation—as determined by the temperature, the concentrations of the solutions, and rate at which they were mixed. The formation of relatively large crystals through control of the processes of precipitation is more effective than the growth of extremely small crystals to larger sizes, a fact indicative of the extreme insolubility of the crystal species involved.

It was also observed that under the most intense electron beam (biased gun), crystals of both the iron and the aluminum phosphates soften and fuse into droplets. The fusion has also been observed in the finer material, which under a moderately intense beam softens and takes on regular hexagonal shape before fusing into droplets. Hexagonal aggregates of smaller crystals have been observed to fuse into single crystals under this heating effect of the electron beam. During

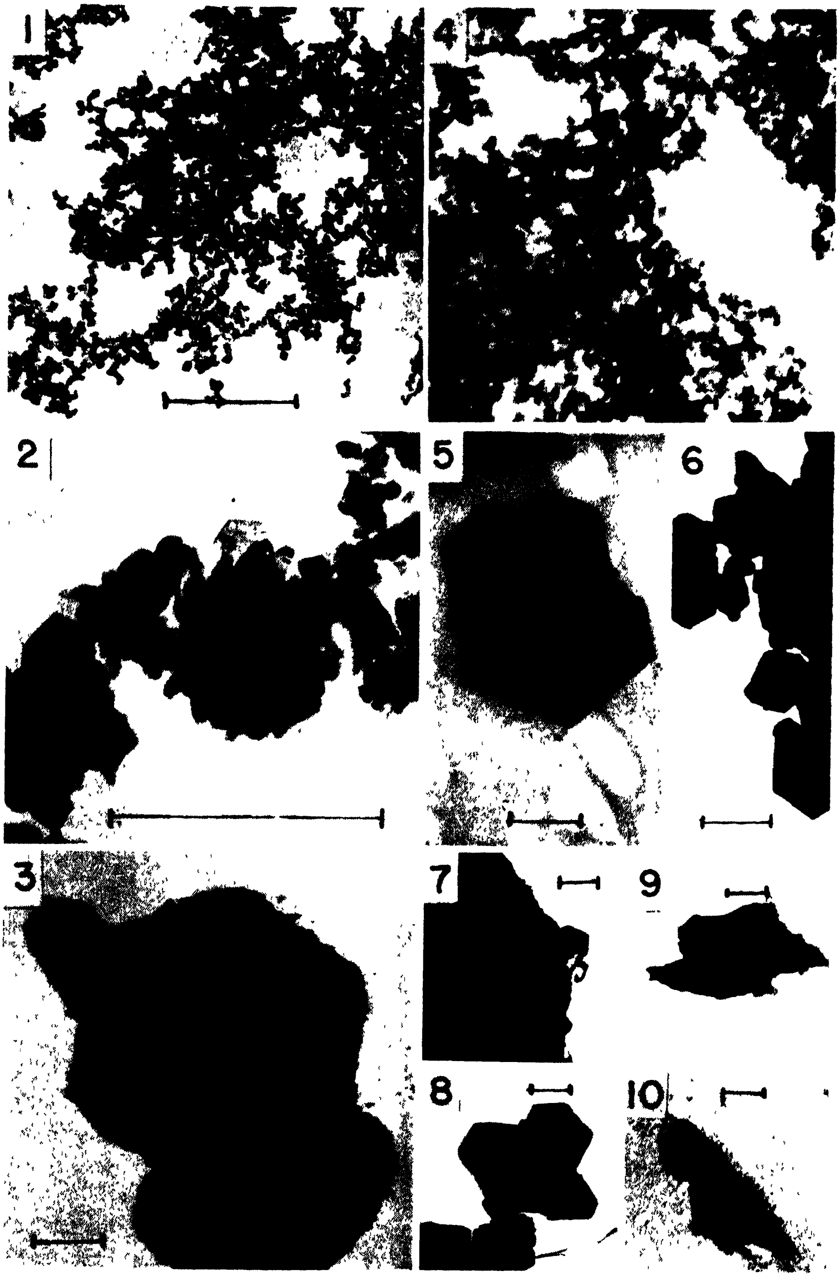

Figs. 1, 2, and 3. Aluminum dihydroxy dihydrogen phosphates: 1, freshly precipitated; 2, after moderate digestion; 3, after extensive digestion.

Figs. 4, 5, and 6. Ferric dihydroxy dihydrogen phosphates; 4, freshly precipitated; 5 and 6, after extensive digestion.

Figs. 7 and 8. Crystals of precipitated aluminum hydroxide

Figs. 9 and 10. Crystals of precipitated ferric hydroxy oxide the other observations, the electron beam intensity was kept far below that necessary to cause fusion of the crystals.

Hexagonal crystals very similar to those of the aluminum and iron phosphates have been observed in precipitates of both the aluminum and iron hydroxy oxides (figures 7, 8, 9, and 10). These crystals, in contrast to those of the phosphates, did not fuse under the most intense electron beam. The presence or absence of these oxides in prepared precipitates may also be determined readily by both electron and x-ray diffraction techniques.

X-ray diffraction data

The aluminum phosphate preparations were classified, by comparison of their x-ray diffraction patterns (table 1), into three types, termed for convenience A, B, and C. The preparations of type A were formed by precipitation at a pH value of 3.8 (the isoelectric pH) and digestion of the colloidal suspensions at 90°C. The x-ray diffraction data (table 1) of preparation A showed it to consist mostly of the crystal species variscite,[4] an aluminum dihydroxy dihydrogen phosphate mineral, $Al(OH)_2H_2PO_4$. Variscite is given the formula $AlPO_4 \cdot 2H_2O$ by Winchell (13), a formula which is equivalent to $Al(OH)_2H_2PO_4$, the latter being more appropriate terminology according to its chemical properties and dehydration data considered below. Preparation A also contained a small amount of the crystal species sterrettite.[5]

The aluminum phosphates of type B were obtained by precipitation at a pH value of 5.5 and digestion of the colloidal suspensions at 90°C. These precipitates consisted mainly of the crystal species sterrettite,[1] an aluminum dihydroxy monohydrogen dihydrogen phosphate, $[Al(OH)_2]_3HPO_4H_2PO_4$. This precipitate also contained a small amount of the crystal species variscite. It is significant that sterrettite was also prepared by digesting a suspension of aged aluminum hydroxide, $Al(OH)_3$, in a phosphate solution at 90°C.

X-ray diffraction patterns of the Geiger counter type obtained from the aluminum preparation B are shown in figure 11. Curve *a* represents the x-ray crystalline precipitate prepared by extensive digestion at 90°C. Curve *b* represents the x-amorphous precipitate prepared by digestion for only a short time. The correspondence of position and intensity of the peaks in the x-amorphous preparation (curve *b*) to the peaks of the more highly crystalline preparation (curve *a*) suggests that the two precipitates might consist of the same crystal species—namely, sterrettite. The arrows in figure 11 indicate the position of electron diffraction maxima of the x-amorphous preparation. These maxima correspond to those of variscite and sterrettite (table 1).

Preparation C was formed when a suspension of colloidal aluminum phosphate was taken to dryness on the hotplate at approximately 105°C. The crystal species of this preparation has not as yet been identified. The species does not correspond to the aluminum hydroxy phosphate minerals wavellite or vashegyite. This

---

[4] Mineral specimen obtained from Ward's Natural Sciences Establishment, Rochester, New York.

[5] American Society for Testing Materials X-ray Diffraction Card File No. II 338.

TABLE 1

Diffraction spacings and identification of various aluminum and iron phosphates

ALUMINUM PHOSPHATES																	IRON PHOSPHATES									
X-ray diffraction												Electron diffraction			X-ray diffraction		X-ray diffraction						Electron diffraction		X-ray diffraction	
Preparation A				Variscite		Sterrettite A.S.T.M. file card No. II 338		Preparation B				Aged preci-pitate		Fresh preci-pitate	Prepara-tion C		Strengite A.S T.M. file card No. II 515		Preparation P				Aged precipi-tate	Fresh precipi-tate	Preparation Q	
XRD* 103		XRD 3478		XRD 3441				XRD 3146		XRD* 101					XRD 3143				XRD 3211		XRD* 202				XRD 3138	
Å.	*I*	Å.	*I*	Å.	*I*	Å.	*I*	Å.	*I*	Å.	*I*	Å.	*I*	Å.	Å.	*I*	Å.	*I*	Å.	*I*	Å.	*I*	Å.	Å.	Å.	*I*
		10.7	W	11.0	W										11.08	S										
9.82	M																								8.83	VS
7.90	W							7.58	W												7.32	S				
		6.91	W			6.94		6.87	VS	6.97	VS															
6.61	M			6.43	W					6.71	S								6.50	W						
6.24	S	6.29	S														6.1	M								
				5.94	W																					
5.57	VS			5.39	S			5.46	S	5.54	VS				5.59	S	5.5	S	5.54	W						
5.22	W	5.29	W			5.25	W												5.17	W						
		4.97	M	4.85	M	4.88	VS	4.84	S	4.93	S	4.88		4.88			4.90	S	4.85	S			4.85			
		4.79	M	4.72	W																					
		4.54	S			4.51	S	4.53	S	4.62	W								4.65	M	4.67	M	4.65	4.65		
4.44	S	4.41	VW	4.44	M										4.43	W	4.36	VS	4.39	VS	4.40	S				
		4.21	VS	4.29	VS			4 26	W	4.31	M															
								4.12	M	4.19	S				4.03	M	4.00	S	4.02							
4.00	W	4.00	VW	3.92	M			3.91	M	3.97	M															
		3.85	M																							
3.75	VW			3.75	VW	3.79	M			3.83	W						3.70	M							3.76	VS
3.69	VW			3.66	VW																					
															3.61	W			3.62	M	3.62	M				
								3.53	W																	
3.49	W	3.49	S	3.45	M										3.44	W										
																	3.43	M								
				3.35	W			3.30	W	3.35	M						3.29	M					3.32			
		3.22	W	3.20	W			3.20	S	3.24	VS				3.23	S							3.20			
3.19	VS									3.18	S															
								3.14	M	3.12	M						3.12	S	3.11	M						
		3.09	W					3.07	W						3.09	W										
3.01	W			3.04	S																				3.00	S

		2.97	M	2.99	VW											2.99	S								
2.90	M			2.93	VW	2.90	S	2.90	S	2.92	S			2.92	M							2.92			
				2.88	W					2.81	S			2.81	W	2.86	S	2.81	S	2.82	S				
2.77	M	2.70	VS	2.74	M	2.76	M	2.77	M			2.77				2.79	W								
				2.69	S	2.66										2.69	W								
2.62	M									2.61	S					2.62	W								
2.49	M	2.57	M	2.57	W			2.58	S	2.56	S					2.54	S	2.55		2.53	W				
2.45		2.49	W	2.47	M	2.44		2.43	M	2.46	M	2.40	2.40	2.47	W	2.43	M							2.41	W
		2.42	VW	2.39	W											2.36	M	2.37		2.37	W				
2.32	M	2.38	VW	2.31	W	2.33		2.31		2.33	W					2.28	W							2.33	W
2.26	W	2.28	M	2.20	W	2.24		2.28	M	2.31	M														
2.19	S	2.20	M	2.13	M			2.21	W	2.24	M					2.13	M	2.19				2.20	2.20		
2.06	W	2.15	M	2.09	W	2.07	M	2.08	S	2.10	S					2.09	W								
		2.05	M	2.02	W			2.01	W	2.03	W					2.06	M								
		2.00	W	2.00	W			1.95	W	1.97	W					2.00	M	2.01	M	1.99	M	2.04		2.03	M
1.95	W	1.95	S	1.95	M			1.93	W	1.96	W	1.94				1.96	M							1.92	W
1.88	M	1.93	VW	1.90	W			1.86	M	1.88	W							1.87							
1.82	W	1.85	VW	1.84	VW	1.83		1.83	M	1.84	M					1.80	M	1.81				1.80		1.83	W
1.77	W	1.78	VW	1.77	W	1.77		1.77	M	1.77	M					1.76	M	1.73							
		1.76	VW	1.74	VW			1.76		1.72	VW					1.72	M								
1.72	W	1.71	M	1.72	W	1.71	M	1.71	S	1.70	W														
		1.69	W	1.68	M			1.68	W	1.67	VW					1.69	M	1.68							
1.64	VW	1.66	M	1.65	W			1.64	W	1.65	VW			1.66	W	1.65	M	1.65	M			1.65			
1.61	W	1.619	W	1.61	M	1.61		1.61	S	1.626	S					1.61	S	1.59						1.58	M
1.58	VW	1.580	W	1.59	W	1.54				1.595	VW			1.58	W	1.54	M	1.54	W						
1.508	VW	1.507	VW	1.502	VW	1.49		1.58	M	1.580	M					1.48	S	1.50							
1.441	VW	1.481	M	1.462	W	1.43		1.52	S	1.528	M			1.42	W	1.44	M	1.43						1.46	W
1.431	VW			1.427	W	1.37		1.37	M	1.384	W					1.42	M								
1.379	VW	1.399	W	1.388	W	1.35		1.32	W	1.334	VW					1.41	M								
1.337	VW	1.310	VW	1.300	W	1.31		1.31	M	1.320	W							1.38						1.39	W
		1.290	W					1.290	W	1.299	W							1.34						1.33	W
		1.279	W					1.275		1.284	VW							1.30							
				1.262	VW			1.264	W																
		1.252	W					1.248	W									1.24							
				1.238	VW			1.231	W																
				1.223	VW			1.217	W			1.22	1.22					1.20				1.25	1.25	1.23	W
				1.213	VW			1.196	W																
				1.184	VW			1.173	W																
				1.175	VW			1.158	W																

---

* XRD-3 Geiger counter technique.

species is considered unlikely to form in soils because of the high temperature involved in its preparation.

The iron phosphate preparations were differentiated, by comparison of their x-ray diffraction patterns, into two types termed for convenience P and Q. The preparations of type P were formed by precipitation at pH values ranging from 2 to 5 and digestion at 90°C. The crystal species formed was found to be strengite,[6] a ferric dihydroxy dihydrogen phosphate, $Fe(OH)_2H_2PO_4$. Strengite is given the formula $FePO_4 \cdot 2H_2O$ by Winchell (13), but the dihydroxy dihydrogen terminology is more correct according to the chemical properties and dehydration data considered below. The two minerals variscite and strengite are end members of a dihydroxy dihydrogen phosphate series, $(Al,Fe)(OH)_2H_2PO_4$, of which barrandite[7] is an intermediate member (13, p. 138). The aluminum and iron apparently may replace each other in all proportions. The x-ray diffraction film patterns of variscite and strengite (figure 12) illustrate the similarity of the two crystal species and the clear definition of the x-ray diffraction lines of these phosphate preparations. Further study of the longer spacings in the strengite lattices (table 1) is needed to relate the presence or absence of lower order (*hkl*) spacings to crystal habit and conditions of preparation.

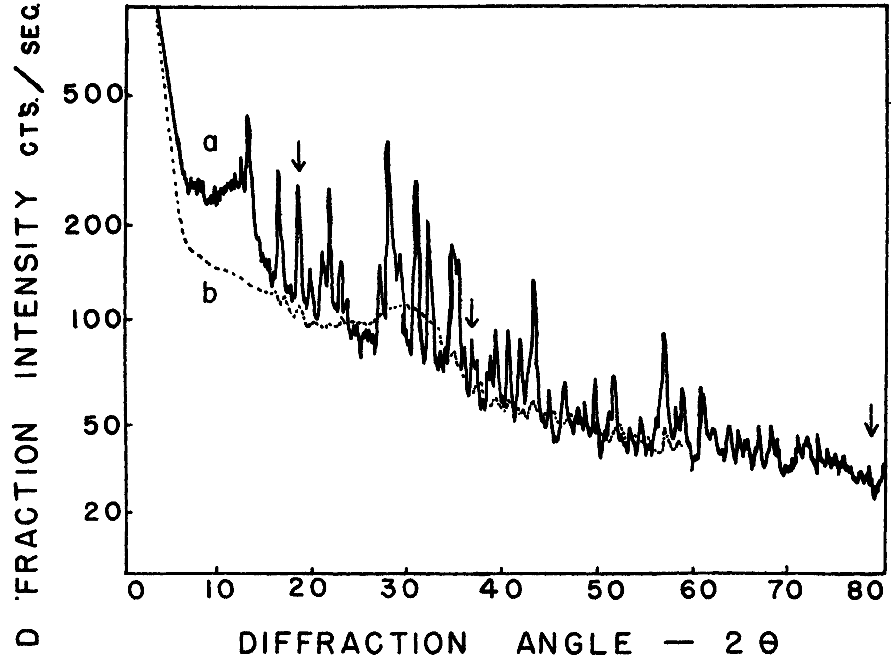

FIG. 11. Geiger counter x-ray spectrometer patterns of the precipitated aluminum dihydroxy (mono, di)-hydrogen dihydrogen phosphate, sterrettite, $[Al(OH)_2]_3HPO_4H_2PO_4$. Curve *a*, x-ray crystalline pattern after extensive digestion of the precipitate; curve *b*, amorphous band, after slight digestion of the precipitate.

---

[6] American Society for Testing Materials X-ray Diffraction Card File No. II 515.

[7] American Society for Testing Materials X-ray Diffraction Card File No. II 275.

The crystal species of preparation Q was formed when a colloidal iron phosphate suspension was taken to dryness on the hotplate at approximately 105°C. This species, as yet not identified, does not correspond to the iron hydroxy phosphate mineral dufrenite. A considerable number of other species of aluminum and iron phosphates are known to be formed under various conditions of precipitation and heating, which are not likely to occur in soils, and therefore such preparations were not characterized in the present study.

Electron diffraction data

Electron diffraction by the freshly precipitated x-amorphous phosphate precipitates established that these precipitates were actually crystalline. The crystals were evidently too fine to show diffraction with x-rays. *The fresh precipitates formed from solutions at room temperature gave the same electron diffraction patterns as those formed from hot solutions or digested at hotplate temperatures of 70° to 100°C.* The electron diffraction patterns of both the freshly precipitated aluminum and iron phosphates consisted of three well-defined broadened electron diffraction lines (table 1). Precipitates which had been digested for 3 hr. or longer, though still x-amorphous, produced sharp electron diffraction patterns. The spacings of the broadened-line and of the sharp-line electron diffraction patterns of the aluminum and iron compounds corresponded to the x-ray diffraction spacings of variscite, sterrettite, and strengite, the crystal size of which had been increased by more extensive digestion of the precipitates (table 1).

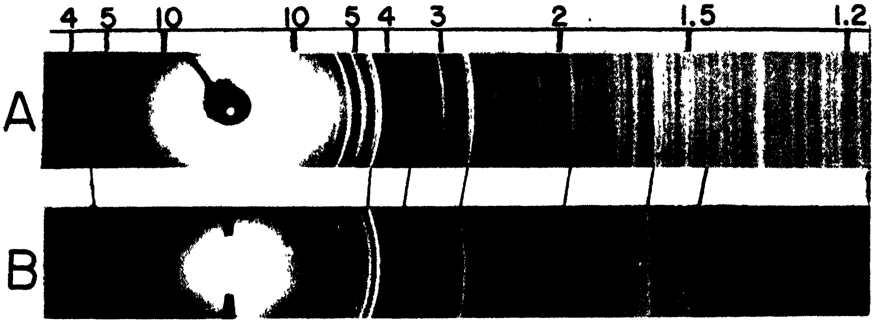

FIG. 12. X-ray diffraction film patterns of variscite and strengite. A, the mineral variscite, $Al(OH)_2H_2PO_4$ B, "precipitated" strengite, $Fe(OH)_2H_2PO_4$. The scale shown is in Ångström units.

The presence of only three diffraction maxima in the electron diffraction patterns of the fresh precipitates evidently reflects a crystallographic orientation of the crystals in the specimens. The oriented crystals give diffraction maxima corresponding to only one set of (*hkl*) spacings. Thus in table 1, the fresh aluminum dihydroxy dihydrogen phosphate precipitate gives electron diffraction spacings of 4.88, 2.40, and 1.22 Å. (arrows in figure 11) which correspond to first, second, and fourth, or second, fourth, and eighth orders of the one fundamental spacing. These correspond to spacings found in the powder x-ray diffraction pattern (XRD 3146, table 1) at 4.84, 2.43, and 1.217 Å., identified as that of sterrettite. But the powder diffraction pattern shows a large number of other (*hkl*) spacings, a fact which suggests that the electron diffraction specimen was highly oriented with respect to one (*hkl*) index of the crystals. The electron micrographs (figures 1 to 6) show the crystals to be flat and hexagonal, and the flat crystals to be mainly oriented with their flat surface normal to the electron beam. It is likely therefore that the diffraction pattern represents the (0001) indices of the hexagonal crystals. It is interesting to note the hexagonal crystal habit observed as contrasted to the orthorhombic crystallographic system listed in the literature (table 2).

A further explanation of the limited number of electron diffraction lines can be formulated on the basis of the platy crystal habit observed in the electron microscope. One dimension may exceed the critical size range for an electron diffraction pattern by the transmission method. If the long axis is opaque to the electron beam, no spacings may correspond to this axis, since the entire electron beam may be absorbed or deflected. However, if the crystals are thin enough so that the electron beam easily passes through, the diffraction spacings may represent the indices along the short (*c*) axis. When the sample for electron diffraction was digested to increase crystal size and the specimen on the formvar film was stirred up to give random instead of oriented crystals, various other electron diffraction spacings were obtained (table 1). Under these circumstances, reflection patterns could be produced by the random crystals without the necessity of penetration through the thick crystals. A crystallographic analysis of the diffraction spacings in terms of (*hkl*) indices is needed.

COMPOSITION AND MOLAR RATIOS OF THE PRECIPITATED PHOSPHATES AND THE CORRESPONDING MINERAL PHOSPHATES

The chemical composition of the precipitated phosphates compares closely with that of the corresponding mineral phosphates (table 2). The chemical formulas presented in the table correspond more closely to the properties of the compounds than do the formulas given in earlier literature, for example, $AlPO_4 \cdot 2H_2O$ (13). In this regard, it is significant that the ignition losses occur gradually over a temperature range considerably above 105°C. in much the same way that water is lost from gibbsite, $Al(OH)_3$. The ignition loss represents in both cases OH^- of the lattice rather than molecular H_2O.

The isomorphous series variscite–barrandite–strengite, $(Al,Fe)(OH)_2H_2PO_4$ (table 2), is a dihydroxy dihydrogen phosphate series in which aluminum and iron are isomorphously substituted. The ignition losses at 105–800°C. by the precipitated phosphates variscite and strengite show good agreement with the theoretical values (table 2). The x-ray diffraction patterns of variscite (Al) and strengite (Fe) are very similar (table 1), with the strengite pattern having slightly greater spacings due to the larger size of the ferric ion as compared with the aluminum ion. The barrandite spacings[7] are intermediate between those of variscite and strengite.

For sterrettite, the ratio of aluminum to phosphate and the chemical char-

TABLE

Chemical and crystallographic constitution of hydroxy phosphates of aluminum and iron

MINERAL OR CRYSTAL SPECIES	FORMULA	IGNITION LOSS AT 105–800°C.	MOLAR RATIOS		CRYSTAL SYSTEM	AXIAL RATIOS	CRYSTAL HABIT
			M^{3+}/P	Oxides			
		per cent					
Variscite (13).....	$Al(OH)_2H_2PO_4$	22.8	1:1	$Al_2O_3:P_2O_5:4H_2O$	Orthorhombic	0.873:1:0.979	Pyramidal fibrous
Metavariscite (13).	$Al(OH)_2H_2PO_4$		1:1	$Al_2O_3:P_2O_5:4H_2O$	Orthorhombic	0.894:1:1.092	Prismatic laths
Preparation A....	$Al(OH)_2H_2PO_4$	21.7	1:1	$Al_2O_3:P_2O_5:4H_2O$			Micro hexagonal plates
Barrandite (13)...	$(Al, Fe)(OH)_2H_2PO_4$		1:1	$(Al, Fe)_2O_3:P_2O_5:4H_2O$	Orthorhombic		Fibrous
Strengite (13).....	$Fe(OH)_2H_2PO_4$	19.3	1:1	$Fe_2O_3:P_2O_5:4H_2O$	Orthorhombic	0.866:1:0.978	Pyramidal
Preparation P.....	$Fe(OH)_2H_2PO_4$	20.7	1:1	$Fe_2O_3:P_2O_5:4H_2O$			Micro hexagonal plates
Sterrettite (13)....	$[Al(OH)_2]_3HPO_4H_2PO_4$	21.6	3:2	$3Al_2O_3:2P_2O_5:9H_2O$			
Preparation B.....		14.2					Micro hexagonal plates
Wavellite (13).....	$Al_3(OH)_3P_2O_8\cdot 5H_2O$	21.9	3:2		Orthorhombic	0.564:1:0.408	Fibrous, radiated
Dufrenite (13)....	$Fe_2(OH)_3PO_4$	20.3	2:1		Monoclinic		Fibrous
Vashegyite (13)...		38.6	4:3	$4Al_2O_3:3P_2O_5:30H_2O$			Fibrous
Palmerite (ASTM II 7).		24.3	2:3	$2Al_2O_3:2K_2O:3P_2O_5:15H_2O$			

acteristics of the aluminum phosphate precipitates support the formula $[Al(OH)_2]_3HPO_4H_2PO_4$ (table 2). Only consideration of the crystal structure of this species will finally establish the formula. The ignition losses of the sterrettite precipitates did not show good agreement with the theoretical values according to the above formula for the mineral sterrettite (table 2). Because of the small particle size of the precipitated sterrettite, lattice OH^- ions may be lost at temperatures lower than 105°C. Similar loss of water derived from lattice OH^- ions is observed in precipitated gibbsite and various hydroxy oxides. The formulas of other mineral phosphates—wavellite, dufrenite, vashegyite, and palmerite—are also listed in table 2 for comparison.

The process of precipitation of aluminum and iron dihydroxy phosphates is pictured as the polymerization of Werner-type complexes $Al(OH)(H_2O)_4H_2PO_4^+$ and $Fe(OH)(H_2O)_4H_2PO_4^+$ from solution. The tendency for ions of aluminum and iron to form complexes with various anions such as phosphate is well known (4, p. 820). During precipitation of the phosphate crystals, water is visualized as being replaced from the complex ion by shared crystal lattice OH^- ions forming, for example, the sterrettite or variscite lattices, depending upon the conditions of precipitation.

In the present investigation, rapid precipitation and digestion at pH values of 5 to 6 favored the formation of sterrettite containing both $H_2PO_4^-$ and HPO_4^{--} ions, in 1:1 ratio. Slower precipitation and digestion at lower pH values (2.3–4), on the other hand, favored the formation of variscite containing phosphate as the $H_2PO_4^-$ ion only. Swenson *et al.* reported (10) that precipitated aluminum phosphate contains a higher aluminum to phosphate ratio than 1:1 when freshly precipitated, but that this ratio approaches 1:1 as the precipitate is digested. Increases of the phosphate concentration in solution also favored the approach to this ratio. This equilibrium type of reaction is interpreted, in view of the present identification of the crystal species formed, to represent the conversion of the sterrettite component of the precipitate, with an aluminum to phosphate ratio of 3:2 (table 2), to variscite with an aluminum to phosphate ratio of 1:1. In the work of Swenson *et al.* (10), the mole ratio of phosphate to aluminum or iron did not exceed 1:1 in the precipitate, even in the presence of a ninefold excess of phosphate in solution, when sorption of saloid-bound phosphate was prevented by the presence of a high concentration of sodium chloride. Digestion of the precipitates in solutions of high phosphate concentration is readily seen to favor formation of the crystal species with the maximum phosphate content (minimum phosphate valence $H_2PO_4^-$)—namely, variscite.

The fact that the precipitates prepared at room temperature are crystalline (to electron diffraction) and are the same species as the precipitates made x-ray crystalline by digestion at hotplate temperatures is important new information relative to the interpretation of phosphate precipitation ("fixation") in soils. Dean and Rubins (2, p. 378) had visualized phosphate fixation as replacement by $H_2PO_4^-$ of OH^- from the crystal lattices of soil minerals. Sieling (9) had concluded that the mechanism of phosphate precipitation by ground or alkali-activated kaolinite involved reaction with "free (hydroxy) alumina" rather than with the kaolinite lattice. Low and Black (8) similarly had concluded that phosphate precipitation by kaolinite was through reaction with alumina released from the kaolinite lattice, and they showed a simultaneous release of silica from the kaolinite lattice as alumina was lost. Ensminger (3) had established that x-ray crystalline aluminum ammonium phosphates are produced by the reaction of ammonium phosphates with kaolinite, aluminum oxides, and soil colloids. Aluminum and iron hydroxy phosphates are so extremely insoluble that they do not at room temperature form crystals of large enough size to be x-ray crystalline. The identification by electron diffraction *of the crystal species formed at room temperature* (*cf.* soil temperatures) constitutes the first direct evidence of the particular crystal species of aluminum and iron phosphates which probably precipitate during phosphate fixation under acid soil conditions: namely, members of the variscite–barrandite–strengite isomorphous series, (Al,Fe) dihydroxy dihydrogen phosphate, and sterrettite, aluminum dihydroxy (mono, di)-hydrogen phosphate.

SUMMARY

Aluminum and iron phosphates precipitated from slightly acid solutions have been investigated to identify the crystalline species formed after treatment to increase the crystal size. The objective was also to determine whether these crystal species are the same as those formed immediately upon precipitation from solutions at room temperature and thus probably formed under acid soil conditions. The results of the investigation may be summarized as follows:

1. Electron micrographs of precipitated phosphates of aluminum and iron which had been digested for several hours at 90°C. showed the presence of minute, but well-defined, hexagonal crystals occurring singly and in aggregates. Precipitates which had been digested for several days contained well-defined hexagonal crystals approximately 1–5 microns in diameter and 0.5–1 micron in thickness.

2. Extended digestion at 90°C. of the freshly precipitated dihydroxy dihydrogen phosphates which were x-amorphous (amorphous to x-rays) produced precipitates which gave sharp line x-ray diffraction patterns. Intermediate digestion periods resulted in precipitates which gave amorphous-type, broad-line x-ray diffraction patterns.

3. The crystal species variscite and sterrettite were identified in the aluminum phosphate precipitates by means of their diffraction spacings. Precipitate A, precipitated and digested at pH 3.8, consisted mostly of variscite, $Al(OH)_2H_2PO_4$, with some sterrettite. Preparation B, digested at pH 5.5, consisted mostly of sterrettite, $[Al(OH)_2]_3HPO_4H_2PO_4$, with some variscite.

4. The iron phosphate precipitate was identified as the strengite crystal species, $Fe(OH)_2H_2PO_4$, by means of its x-ray diffraction spacings. This preparation was found in precipitates formed at pH values ranging from 2 to 5.

5. Electron diffraction patterns showed that the dihydroxy dihydrogen phosphates freshly precipitated from solutions at room temperature or at 90°C. consisted of minute crystals which were of the same species as those made x-ray crystalline by digestion of the suspensions at 90°C. for several hours or days.

The fact that the precipitates prepared at room temperature are crystalline (to electron diffraction) and are the same species as are formed by digestion at hotplate temperatures is important new information relative to the interpretation of phosphate precipitation ("fixation") in soils. This relationship constitutes the first direct evidence of the particular crystal species of aluminum and iron phosphates which are probably precipitated under acid soil conditions: namely, members of the variscite–barrandite–strengite isomorphous series, (Al,Fe) dihydroxy dihydrogen phosphates, and sterrettite, aluminum dihydroxy (mono, di)-hydrogen phosphate.

REFERENCES

(1) Coleman, R.: Soil Sci. Soc. Am. Proc. (1944) **9,** 71 (1945).
(2) Dean, L. A., and Rubins, E. J.: Soil Sci. **63,** 377 (1947).
(3) Ensminger, L. E.: Soil Sci. Soc. Am. Proc. (1948) **13,** in press (1949).
(4) Graham, R. P., and Thomas, A. W.: J. Am. Chem. Soc. **69,** 816 (1947).
(5) Heck, A. F.: Soil Sci. **37,** 343 (1934).
(6) Jackson, M. L., *et al.*: J. Phys. & Colloid Chem. **52,** 1237 (1948).
(7) Kelley, J. P., and Midgley, A. R.: Soil Sci. **55,** 167 (1943).
(8) Low, P. F., and Black, C. A.: Soil Sci. Soc. Am. Proc. (1947) **12,** 180 (1948).
(9) Sieling, D. H.: Soil Sci. Soc. Am. Proc. (1946) **11,** 161 (1947).
(10) Swenson, R. M., Cole, C. V., and Sieling, D. H.: Soil Sci. **67,** 3 (1949).
(11) Truog, E.: J. Am. Soc. Agron. **22,** 874 (1930).
(12) Weiser, H. B., and Milligan, W. O.: J. Phys. Chem. **44,** 1081 (1940).
(13) Winchell, A. N.: *Elements of Optical Mineralogy. II. Descriptions of Minerals,* 2nd Edition. John Wiley and Sons, Inc., New York (1927).

BEHAVIOR OF THE ALUMINA-WATER SYSTEM[1]

W. E. HAUTH, JR.[2]

Iowa Engineering Experiment Station and Ceramic Engineering Department, Iowa State College, Ames, Iowa

Received August 22, 1949

INTRODUCTION

This work was initiated for the purpose of investigating and improving the slip casting method for the formation of articles from non-plastic, pure refractory oxides, aluminum oxide being the specific material used. In conjunction with this, a theoretical basis was offered for this process. The theory is based upon the principles of colloid chemistry, since the system studied exhibits many of the phenomena so familiar to the colloid chemist. It should be noted, however, that the suspensions employed are highly concentrated and, as such, are able to be treated only qualitatively or, at best, semiquantitatively. Although only the alumina–water system was thoroughly investigated, it is the author's belief that the theories presented apply, with some modification, to any similar system of "non-plastic" and water.

---

[1] Presented at the Twenty-third National Colloid Symposium, which was held under the auspices of the Division of Colloid Chemistry of the American Chemical Society at Minneapolis, Minnesota, June 6–8, 1949.

[2] This paper is based on material submitted by W. E. Hauth, Jr., as a thesis in partial fulfillment of the requirements for the degree of Doctor of Science at the Massachusetts Institute of Technology.

REVIEW OF THE LITERATURE

The earliest reference found pertaining to the development of plasticity in non-plastic materials was the work of Schwerin (5) in Germany in 1910. He reported the treatment of alumina by grinding in acid to form colloidal particles and thus producing a mix exhibiting plastic properties.

In 1924 Ruff (4) published an account of his work on non-plastic materials. He stated that a certain degree of plasticity could be induced in such materials by the proper degree of grinding and subsequent treatment by dilute hydrochloric or nitric acid.

Since these early experiments a number of investigations have utilized this treatment for the fabrication of refractory shapes; however, none have offered a theoretical explanation of the principles involved.

PREPARATION OF SUSPENSION

The procedure used for the preparation of the alumina–water suspension is, in general, the same as that presented in the reports on previous work. The alumina is milled in a steel ball mill and then treated with hydrochloric acid to dissolve the iron introduced, the resulting suspension being washed with dilute hydrochloric acid to remove the ferrous salts.

Two grinding methods and times were used to study the effect of particle-size distribution on the properties of the suspension. Distribution curve 1, shown in figure 1, was obtained by grinding 1000 g. of alumina for 32 hr. in the dry state. Reference will be made to this material throughout this presentation as dry-ground alumina. Distribution curve II, figure 1, was obtained by grinding 500 g. of alumina with 500 ml. of distilled water for 16 hr. This material will be referred to as wet-ground alumina. Table 1 is a detailed flow sheet depicting the preparation of the dry-ground alumina and its subsequent treatment; table 2 is the flow sheet dealing with the wet-ground alumina.

It is interesting to note in connection with tables 1 and 2 that a suspension of alumina in water may be formed in either an acid or a basic medium.

PROPOSED THEORY

The proposed theory relating to the formation of alumina suspensions is based upon a correlation of fundamental colloidal theory and the results of the experiments discussed below. Since the basic prerequisite for the occurrence of colloidal behavior in a suspension is the presence of particles in a fine state of subdivision, the development of a degree of plasticity in non-plastics by grinding and acid treatment may be attributed primarily to the formation of particles having dimensions in the colloidal range. A consideration of figure 1 shows that

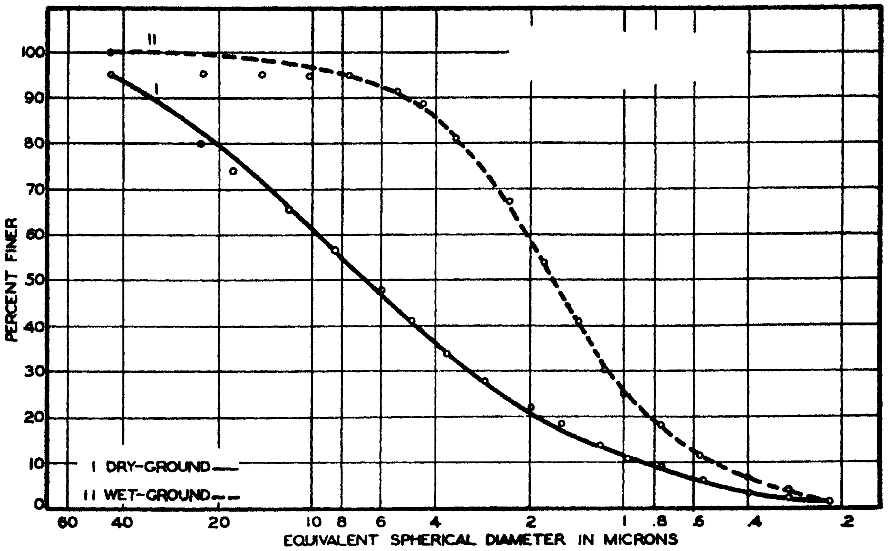

FIG. 1. Particle-size distribution

TABLE 1

Flow sheet for the dry-ground process

RAW MATERIAL	#38 Alundum, 220 mesh
GROUND 32 HR.	1 gal. steel ball mill, 125 R.P.M. 10 kg. steel balls 1 kg. Al_2O_3
MAGNETIC SEPARATION	add 2 liters of water pass twenty-five times
ACID TREATMENT	200 ml. of concentrated HCl agitated for 8 hr.
SETTLED AND SIPHONED	
WASHED AND SETTLED	1.5 liters of 5 per cent by volume HCl three to four times, agitated for 4 hr.
FLOCCULATED	increase pH to 8.0 with NaOH
FILTERED	
WASHED AND FILTERED	blunge with 1 liter of water three times
DEFLOCCULATED	hydrochloric acid or tetramethylammonium hydroxide

the particles present in the suspensions employed in this investigation may be divided into two classes: those particles having colloidal dimensions which are responsible for the formation of the suspension and for its behavior upon addition of electrolytes, and those particles larger than colloidal size which are inert and act as a filler in the suspension. The exact percentage of each class of particles cannot be stated, because of the arbitrary value of the upper limit of the colloidal range. However, it may be seen from figure 1 that the wet-ground alumina contains the larger percentage of colloidal particles and would be expected to exhibit different properties from the dry-ground.

TABLE 2

Flow sheet for the wet-ground process

RAW MATERIAL	#38 Alundum, 220 mesh
GROUND 16 HOURS	1 gal. steel ball mill, 125 R.P.M. 10 kg. steel balls 500 g. Al_2O_3 + 500 ml. water
ACID TREATMENT	400 ml. concentrated HCl + 1.5 liters water, agitated for 8 hr.
SETTLED AND SIPHONED	
WASHED AND SETTLED	1.5 liters of 5 per cent by volume HCl three to four times, agitated for 4 hr.
FLOCCULATED	increase pH to 8.0 with NaOH
FILTERED	
WASHED AND FILTERED	blunge with 1 liter of water three times
DEFLOCCULATED	hydrochloric acid or tetramethylammonium hydroxide

By consideration of the principles stated it is possible to present a picture of the alumina–water system and, further, to explain its behavior upon the addition of various amounts and types of electrolyte. The fact that the colloidal alumina particle in an acid medium possesses a net positive charge is well known and can be easily demonstrated by subjecting such a suspension to a potential gradient. It is difficult to conceive that this charge could be caused by surface dissociation because of the structural configuration of alumina, the bonds being strong ionic aluminum-to-oxygen bonds. Further, it has been shown that colloidal alumina possesses a strong preferential adsorption tendency toward the hydrogen ion. Weiser (7) offers the following evidence of this fact: "The equilibrium in a solution between dichromate and chromate ions may be represented by the equation:

$$Cr_2O_7^{--} + H_2O \rightleftharpoons 2H^+ + 2CrO_4^{--}$$

Alumina shows such a strong preferential adsorption for hydrogen ions that the presence of the oxide in a finely divided condition shifts the equilibrium to the right with the formation of chromate ion at the expense of the dichromate. Colloidal alumina stabilized by preferential adsorption of hydrogen ion has a comparatively slight effect on the equilibrium."

Returning to the suspensions obtained in this work, the cations present in the solution after the final washing are predominantly hydrogen ions, with a small amount of aluminum ions produced by the leaching action of the acid. Thus, ruling out surface dissociation, the adsorbed cations are most probably hydrogen ions with a possibility of some aluminum ions being present. These cations form a monomolecular layer on the surface of the particle, being held to the oxygens of the alumina by forces which can be attributed to broken surface bonds.

The anions present in the suspension are chloride ions from the acid and hydroxyl ions at such a concentration as would be given by the dissociation of the water at a pH of approximately 2.0. Since the concentration of hydroxyl ions is negligible compared to the chloride-ion concentration, it may be assumed that the anions present in the counter ion positions are chloride ions. Figure 2 gives a schematic picture of the particle surface and the adjacent liquid medium at this stage.

To prepare the final suspensions from the system as represented by figure 2, sodium hydroxide was added to bring about flocculation, the replacement of the chloride counter ions by hydroxyl ions resulting in a flocculated system. This may then be filtered and the concentration of sodium and chloride ions greatly reduced by washing.

Upon the addition of hydrochloric acid to the filter cake, any free hydroxyl ions will tend to combine with the hydrogen ions to form water. In addition, the chloride ions will tend to replace hydroxyl ions as the counter ions to a very limited extent because of the mass action effect of concentration. Any hydroxyl ions so freed can then combine with free hydrogen ions and the reaction will tend toward complete replacement of the hydroxyl ions by the chloride ions. Therefore, in a deflocculated system in an acid medium, the state of the system is represented as shown in figure 2.

Before consideration of the formation of a deflocculated system in a basic medium, it is necessary to inspect in greater detail the phenomenon of charge reversal which involves a change in the sign of the zeta potential. This change may be substantiated by subjecting the suspension to a potential gradient. The particles in the acid medium flow toward the cathode, whereas the particles in a basic medium tend to migrate to the anode, indicating a positive zeta potential in the first case and a negative zeta potential in the second. This has been attributed either to the neutralization of the original charge on the particle plus the formation of a new diffuse double layer or to the decrease of the thickness of the double layer to such an extent that it collapses and re-forms with the charges reversed. Considering alumina suspension, it seems that the choice is merely one of definition in that, upon complete neutralization, the surface consists of a

FIG. 2. Acid-deflocculated alumina suspension (schematic)

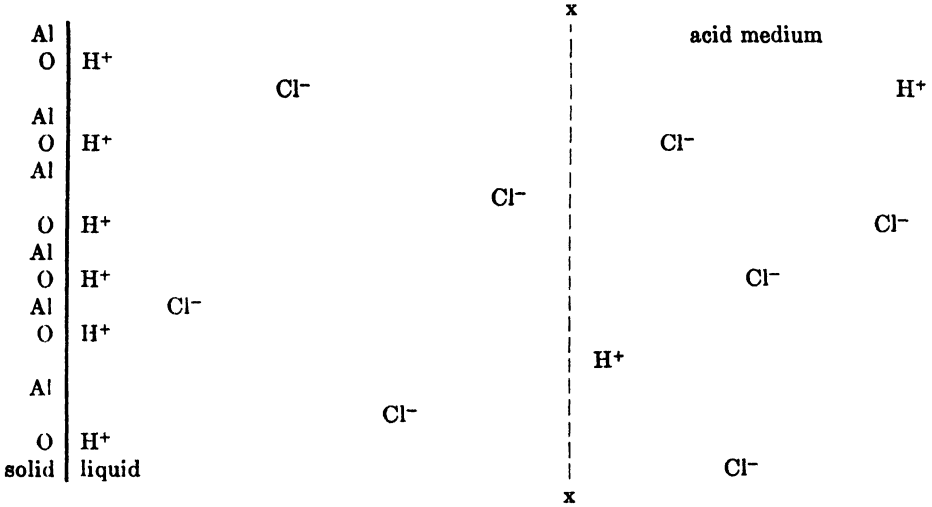

x— —x, edge of the attached water layer.

FIG. 3. Base-deflocculated alumina suspension (schematic)

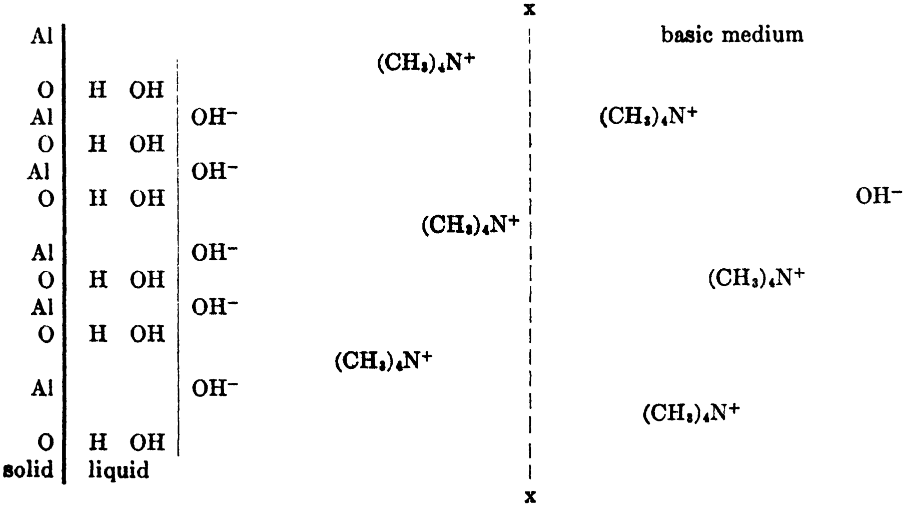

x— —x, edge of the attached water layer.

monomolecular layer of hydrogen ions surrounded by an essentially monomolecular layer of hydroxyl ions. If this may be considered to be complete collapse of the double layer, there is little to choose between the two theories. Therefore, it is postulated that upon addition of the base, tetramethylammonium hydroxide, to the flocculated system, the hydroxyl ions will tend to be adsorbed to the unsatisfied surface bonds. This gives the particle a negative surface charge which is satisfied by the formation of a diffuse cloud of tetramethylammonium ions in the fixed and movable medium, the free medium containing an excess of hydroxyl ions. The idealized system may be represented as shown in figure 3.

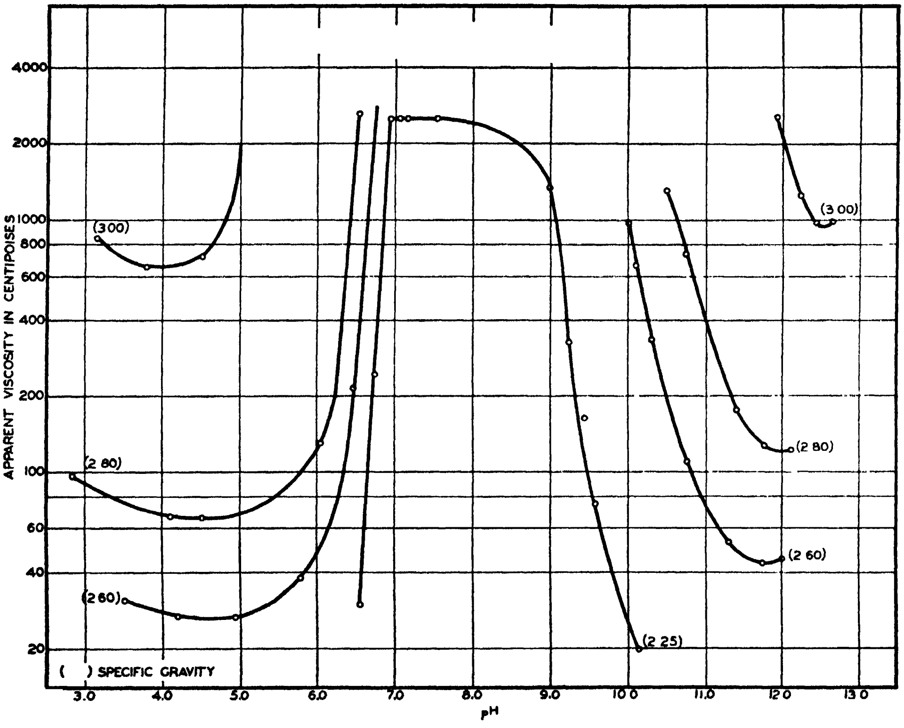

Fig. 4. Viscosity for dry-ground alumina

FLOW PROPERTIES

Viscosity

The curves presented in figure 4 show a plot of apparent viscosity in centipoises *versus* pH for suspensions produced from dry-ground alumina, the data being obtained on a modified MacMichael viscosimeter as described by Johnson and Norton (3). It may be seen that the viscosity is dependent chiefly upon two factors: the pH, and the specific gravity of the suspension, or more correctly, the ratio of the mass of the particles to the amount of freely movable liquid in the system. With an increase in this ratio, the effective separation of the particles is reduced and increased interference between particles causes an increase in the apparent viscosity. The pH, as governed by the concentration of electrolyte, determines the zeta potential. At low concentrations of electrolyte, or in a neutral medium, attraction forces predominate at the edge of the solvated hull and the system is flocculated, as is indicated by the high value of apparent viscosity. Upon the addition of hydrochloric acid, the chloride ions replace the hydroxyl ions as the counter ions and, being less tightly held to the particle, are able to assume larger equilibrium distances from the surface of the particle, thereby increasing the repulsion forces between particles. This increase causes a rapid decrease in viscosity of the system, as shown in figure 4. Continued addition of electrolyte further increases these repulsion forces by decreasing the dielectric constant of the medium and increasing the equilibrium distances of the ions. This permits a lower concentration of counter ions in the bound water layer about the particle and thus increases the zeta potential. Beyond the point of maximum deflocculation, more counter ions are forced into the bound water layer by the increasing concentration of electrolyte and the viscosity increases.

The mechanism for deflocculation by the addition of tetramethylammonium hydroxide is essentially the same as for hydrochloric acid. However, sufficient base must be added to neutralize completely the adsorbed hydrogen ions plus that which is, in turn, adsorbed to build up a negative surface charge on the particle. This is believed to explain the slow initial decrease in viscosity observed upon the first additions of the base to the flocculated suspension. It is interesting to note the almost uniform decrease to minimum viscosity for the basic suspensions as compared to the acid suspensions. An explanation for this difference may be the fact that the acid suspensions already have practically all the positions for preferentially adsorbing hydrogen ions filled before deflocculation, whereas the hydroxyl layer responsible for the negative surface charge in the basic slips may continue to be filled as the concentration of base is increased. This would tend to give a buffer action against any rapid decrease in viscosity in that the interference effects arising from less complete deflocculation, due to a lower zeta potential, would tend to balance rapid increases in the zeta potential. This same effect is believed to explain the presence of the narrow range of pH in which minimum viscosity is obtained for the basic suspensions.

Figures 5 and 6 show a comparison of the apparent viscosity curves obtained on the wet-ground and dry-ground alumina in acid and basic media, respectively. A comparison of the curves for a specific gravity of 2.60 indicates that, at maximum deflocculation, the wet-ground suspensions have a considerably higher viscosity. This may be explained by considering the fact that each particle in the colloidal range is coated with a fixed film of water which tends to act as an integral part of the particle. Because of a larger percentage of colloidal material in the wet-ground alumina, more of the water present would be attached to particles and, for a given solid-to-liquid ratio, the effective separation of the particles would be decreased. This increases the interference effects between particles and causes the observed increase in the apparent viscosity. Increased interferences between particles may also be caused by the increase in the total number and surface area of the particles in the wet-ground alumina as compared to the dry-ground alumina.

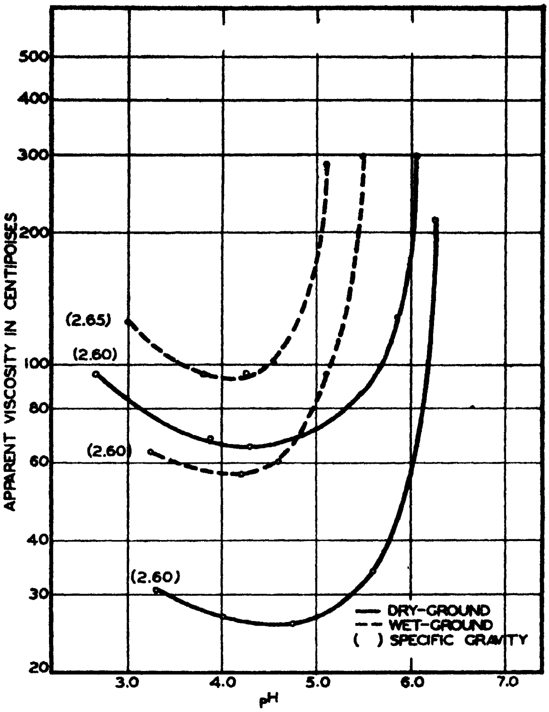

FIG. 5. Viscosity for acid suspensions

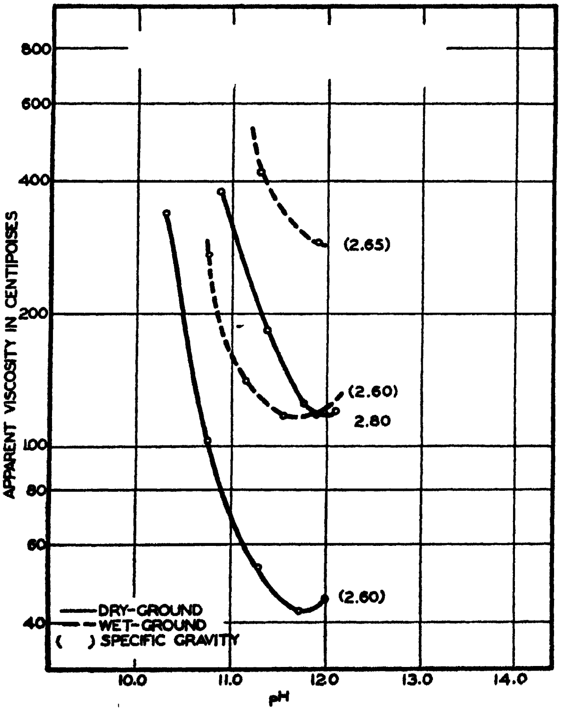

FIG. 6. Viscosity for basic suspensions

There exists an alternate explanation which might possibly account for the observed increase in viscosity with an increase in the fraction of colloidal particles. That is, if the individual particles have a lower zeta potential, the viscosity would increase. However, in work on clays Coughanour and Utter (1) determined that the zeta potential depends on particle size and solids concentration at maximum deflocculation. Since, in the case under discussion, the solids concentration is constant and, from figure 1, the particle sizes in the wet-ground material are the same as for the dry-ground, the zeta potentials should be essentially equal.

Finally, figure 4 shows that the minimum viscosity obtainable at a given specific gravity is lower for the acid slips than for the basic. This is believed to be caused by the presence of a higher zeta potential on the particles in the acid medium. Another possible cause could be the existence of a thicker attached water layer on the particles in the basic suspension. No direct proof may be given to substantiate either theory, but results obtained on the measurement of yield values indicate that a higher degree of attraction, or a lesser repulsion force, exists between the particles for basic suspensions, indicating a lower zeta potential on the particle in a basic medium. Further consideration of this question will be given in the following discussion.

Dilatancy

It may be noted that viscosity measurements on the wet-ground alumina were not made for specific gravities higher than 2.65. This is due to the highly dilatant nature of the slip at higher specific gravities. At a value of 2.68, the slip becomes so dilatant that viscosity measurements are not possible at 100 R.P.M. and at 2.70 a homogeneous suspension cannot be obtained because of the difficulty encountered in mixing. However, viscosity determinations were possible on suspensions produced from the dry-ground material for specific gravities up to 3.05.

According to the modern theory, the phenomenon of dilatancy may be attributed to the ability of the particles to form a close-packed system when subjected to a given rate of shear stress, thereby causing a greatly increased resistance to flow at the point of shear. In order for the particles to assume these close-packed positions the particles must exist as individuals and be able to move freely one over the other. Also, such a system should be assumed more easily the smaller the separation distance of the particles. Applying this reasoning to the alumina–water system, experimental results in this investigation show that, with a given suspension, the dilatant properties increase rapidly with increasing specific gravities above a certain value of solids concentration and decrease somewhat with decreasing degree of deflocculation. Since the specific gravities at which dilatancy appears in the dry-ground and wet-ground suspensions differ greatly, the cause of this difference must be due to a decreased particle-to-particle separation distance in the wet-ground suspension, this being analogous to increasing the effective solids concentration. Similarly, since no readily discernible variation in the lower limit of dilatancy was found in comparing acid and basic suspensions, the cause of other variations observed, such as viscosity, yield value, etc., must be attributed to the presence of a difference in the zeta potential of the particles in the two suspensions.

Yield value

The values of the yield point at zero rate of shear strain for the suspensions investigated were determined on the MacMichael viscosimeter and are given in table 3. These values, with the exception of those obtained for the highest specific gravities, are as would be expected, the yield point decreasing in value as the degree of deflocculation is increased. This is attributed to the increasing zeta potential which increases the repulsion forces between particles and thereby reduces the tendency to form a rigid structure capable of giving a yield value. Also increased specific gravity, excepting the highest specific gravities, again increases the value of the yield point. This is probably caused by the decreased distance of particle separation, which increases the ease of formation of the required network. However, the relative effect of each of these factors is not equal. Consideration of the data presented in table 3 shows that changes in pH, corresponding to changes in zeta potential, have a much greater influence on the yield value than changes in specific gravity. Thus the order of magnitude of differences between the suspensions should indicate the cause of the variation.

The basic suspensions exhibit a relatively higher yield value than the acid suspensions and, as has been discussed concerning viscosity and dilatancy, the primary difference arises from a lower zeta potential on the particle in the basic medium. As may be seen from the data on wet-ground alumina suspensions of specific gravity 2.60, a very high value for the yield point exists in basic suspensions as compared to acid suspensions at maximum deflocculation. Because of the proximity of this concentration to the lower limit of dilatancy, the increase in bound water thickness in the basic system of such an extent as to cause the observed increase in yield point would bring about dilatant properties. However, as this is not observed, it seems logical to attribute this effect to a lower value of zeta potential and decreased repulsion forces between particles. Or, stated in another manner, the observed difference for these particular suspensions seems to be more of the order of magnitude for changes observed in the degree of deflocculation than for changes caused by decreasing particle-to-particle distance. The difference is most pronounced in the suspension containing the larger fraction of colloidal particles, since the change in zeta potential affects this suspension to the greater extent.

Perhaps the most interesting feature of the yield point data is the value of zero obtained for all suspensions of highest specific gravity. As has been already discussed, these suspensions possess the property of dilatancy, and it is this dilatant nature which causes the deviation from the expected behavior. In determining the value of the yield point, the inner cylinder of the viscosimeter is rotated a given amount, thereby applying a stress to the sample. For dilatant suspensions, this stress causes local packing of the particles. Upon release of the stress, the particles tend to assume their equilibrium positions and this is most easily done by refilling the voids caused by the stressing. This produces an elastic effect, for momentarily applied stresses, and causes the cylinder to return to its original position, as may be seen in its rapid return for the dilatant suspensions as contrasted to the slow return for those not exhibiting dilatancy.

TABLE 3

Yield point values

DRY-GROUND ALUMINA			WET-GROUND ALUMINA		
Specific gravity	pH	Yield point	Specific gravity	pH	Yield point
		dynes/cm.^{2}			*dynes/cm.^{2}*
2.60	6.45	38	2.60	5.70	19.5
	5.80	1.50		5.30	1.13
	4.95	0.40		4.80	2.60
	4.20	0.00		4.40	1.60
	3.50	1.07		3.95	2.19
2.80	6.50	*	2.65	5.50	0.00†
	6.05	78		4.75	0.00†
	5.10	1.88		4.45	0.00†
	4.50	1.12		4.00	0.00†
	4.10	1.50		3.20	0.00†
	2.85	1.95			
			2.60	10.40	265
3.00	4.50	0.00†		10.75	45
	3.80	0.00†		11.15	23.5
	3.20	0.00†		11.55	19.0
				11.90	15.0
2.60	10.00	203			
	10.30	89	2.65	10.95	0.00†
	10.75	20		11.30	0.00†
	11.30	1.5		11.90	0.00†
	11.75	1.3			
	12.00	1.3			
2.80	10.50	123			
	10.75	86			
	11.40	15.8			
	11.75	5.8			
	12.10	5.8			
3.00	11.90	0.00†			
	12.20	0.00†			
	12.40	0.00†			
	12.60	0.00†			

* Value too high to be measured.

† See discussion of results.

Sedimentation volume

Hauser (2) discusses the factors influencing the sedimentation volume of anisodimensional particles. Although the alumina particles are isodimensional, the experimental data given in table 4 indicate that similar considerations apply to the systems tested. This is believed to be caused by the presence of a wide range of particle sizes, which permits a fairly close-packed system under the proper conditions.

Therefore, it would be expected that the sedimentation volume would decrease with increasing degree of deflocculation, as is shown in table 4. This may be attributed to the increasing repulsion forces between the particles, which permit them to orient themselves on settling in a close-packed system. The solvated water hull acts as a lubricant and allows the particles to slide over one another until they have attained minimum free energy positions, in this way attaining small sedimentation volumes. If the particles are settled when the repulsion forces are very small, or attraction forces predominate, they will tend to remain in their initial settled positions, resulting in a comparatively loose packing and a large volume of sedimentation.

TABLE 4

Sedimentation volume

Settled volume from 15 ml. of suspension

DRY-GROUND ALUMINA			WET-GROUND ALUMINA		
Specific gravity	pH	Volume	Specific gravity	pH	Volume
		ml.			*ml.*
2.60	6.15	13.6	2.60	4.30	12.5
2.60	5.80	12.6	2.65	4.20	12.9
2.60	4.70	11.8			
2.60	3.60	12.1	2.60	11.5	13.1
			2.65	12.0	12.5
2.60	4.70	11.8			
2.65	4.50	12.2			
2.80	4.60	12.9			
3.00	3.90	13.3			
2.60	11.70	12.4			
2.65	11.80	12.7			
2.80	12.00	13.2			
3.00	12.40	13.6			

From table 4 it may be seen that wet-ground alumina suspensions give a greater volume than dry-ground for both basic and acid suspensions at the same specific gravity. The increase in volume of approximately 0.7 ml. is caused by an increased percentage of colloidal particles and, consequently, an increased number of water films. Since these water films are firmly attached to the particles, they are not lost in settling, although the solvated layers of the first particles to settle may be distorted by the pressure exerted on them by the following sedimentation. Therefore, the volume of these water hulls contributes significantly to the total volume. The difference in particle-size distribution in the slips may also contribute to this difference, since the larger range of particle sizes in the dry-ground alumina might tend to produce a smaller volume by more efficient packing. However, this is not believed sufficient to account for all of the observed difference in volume.

The basic suspensions exhibit a slightly higher sedimentation volume than the acid at minimum viscosity and, as has been noted for yield value and viscosity, this difference could be caused by a lower zeta potential. An alternate cause could be the presence of a thicker water hull on the particles in the basic medium. However, if the zeta potential were to have a value equivalent to that in the acid slips and the increase in sedimentation volume were caused by a larger solvated hull, as has been shown to be the case in wet-ground alumina suspensions, dilatancy could be expected at a sedimentation volume of approximately 13.0 ml. This follows from the volume of 12.9 ml. obtained for acid wet-ground suspensions of specific gravity 2.65. Therefore, a basic dry-ground suspension should be dilatant at a specific gravity of 2.80. Similarly, basic wet-ground alumina suspensions of specific gravity 2.60 should possess dilatant properties, which were not observed. Thus, the sedimentation volume data tend to strengthen the belief that the primary difference in behavior between acid and basic suspensions is caused by a difference in zeta potential, whereas the difference between dry-ground and wet-ground alumina suspensions is attributed to the presence of an increased number of colloidal particles in the wet-ground alumina.

CONCLUSIONS

The purpose of this investigation was to determine and rationalize the behavior of the alumina-water suspensions. From the results obtained it may be concluded that:

1. Fused aluminum oxide may be suspended in water by grinding and acid treatment.
2. A deflocculated system may be obtained in either an acid or a basic medium.
3. The action of electrolytes on these suspensions may be explained by assuming the formation of a diffuse double layer about particles having colloidal dimensions.
4. The effect of variation in particle size on the behavior of the suspension may be attributed to an increased number of particles of colloidal size.
5. The difference in properties of acid and basic suspensions is caused by a lower zeta potential of the particles in the basic medium.

Further, other workers (6) have shown that this method of treatment may be applied to other non-plastic materials than that used in this investigation. This is to be expected, since the fundamental basis of the process is the development of colloidal properties in the material used. Therefore, it is the opinion of the author that the theory presented will apply to other non-plastic-water systems, with certain modifications as necessitated by the chemical nature of the raw material.

REFERENCES

(1) Coughanour, W. L., and Utter, J. L.: J. Am. Ceram. Soc. 27, 116 (1944).

(2) Hauser, E. A.: *Colloidal Phenomena*. McGraw-Hill Book Company, Inc., New York (1939).

(3) JOHNSON, A. L., AND NORTON, F. H.: J. Am. Ceram. Soc. **24,** 64 (1941).

(4) RUFF, O.: Z. org. Chem. **133,** 193 (1924).

(5) SCHWERIN, GORAF B.: German patents 274,039 and 276,244 (1910).

(6) THOMPSON, J. C., AND MALLET, M. W.: "Preparation of Crucibles from Special Refractories by Slip Casting," Bureau of Standards Research Paper No. 1236, 9 pp.

(7) WEISER, H. B.: *Inorganic Colloidal Chemistry*, Vol. II. John Wiley and Sons, Inc., New York (1935).

A QUANTITATIVE ELECTROCHEMICAL THEORY OF THE ELECTROLYTE PERMEABILITY OF MOSAIC MEMBRANES COMPOSED OF SELECTIVELY ANION-PERMEABLE AND SELECTIVELY CATION-PERMEABLE PARTS AND ITS EXPERIMENTAL VERIFICATION. I[1]

AN OUTLINE OF THE THEORY AND ITS QUANTITATIVE TEST IN MODEL SYSTEMS WITH AUXILIARY ELECTRODES

REX NEIHOF[2] AND KARL SOLLNER[2]

Department of Physiological Chemistry, The Medical School, University of Minnesota, Minneapolis 14, Minnesota; and Laboratory of Physical Biology, Experimental Biology and Medicine Institute, National Institutes of Health, Bethesda 14, Maryland

Received August 22, 1949

I

The complex nature of the majority of the biologically important membranes is generally recognized today. Many of the involved *in vivo* functions of living membranes are attributed to the intricacies of their physicochemical structure (9). Thus, the elucidation of the fundamental physical chemistry of membranes of complex structure arises as a problem challenging to the physical chemist interested in biology.

Complex membrane structures, aside from still more involved cases, might be either "layered" membranes composed of several layers of different properties, or the membranes may have a "mosaic" structure consisting of parts of different properties in juxtaposition. One special case of this latter nature will be investigated here.

With membranes of porous character the simplest case of a mosaic-like structure consists of membrane heteroporosity. The characteristic permeability and osmotic properties of these membranes can be explained only on this basis (3, 8, 10, 11, 18, 19).

Another possible mosaic structure among the membranes of porous character consists of a membrane which is composed of selectively anion-permeable and selectively cation-permeable parts. The simplest case of a mosaic membrane of this general type obviously consists of a membrane which is composed both of *ideally* anion-selective and *ideally* cation-selective parts.

A quantitative theory of the electrolyte permeability of mosaic membranes of this latter type was outlined some time ago by one of the present writers (12). At that time it could not be tested experimentally, as suitable membranes were lacking. Now, however, this test has become an experimental possibility, owing to the availability of the recently developed permselective collodion and protamine collodion membranes (1, 2, 6, 7, 14, 15, 16). This test is the main topic of the present investigation.

---

[1] Presented at the Twenty-third National Colloid Symposium, which was held under the auspices of the Division of Colloid Chemistry of the American Chemical Society at Minneapolis, Minnesota, June 6–8, 1949.

[2] Present address: Laboratory of Physical Biology, Experimental Biology and Medicine Institute, National Institutes of Health, Bethesda 14, Maryland.

The theory of the electrolyte permeability of mosaic membranes which are composed of ideally anion-permeable and of ideally cation-permeable parts is most easily developed by reference to a sequence of line drawings.

Figure 1 illustrates schematically a system in which a mosaic membrane of this type separates a lower compartment (of invariable volume) from an upper compartment, the striated structure in the figure indicating the membrane itself. The electronegative, cation-permeable (anion-impermeable) parts of the membrane are indicated by minus signs, and the electropositive, anion-permeable (cation-impermeable) parts by plus signs. The lower compartment is assumed to be filled with 0.1 N potassium chloride solution and the upper compartment with 0.01 N solution of the same electrolyte.

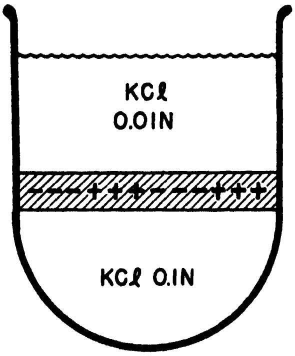

FIG. 1

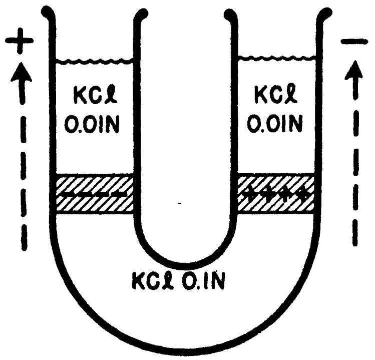

FIG. 2

Contrary to certain ideas which are reviewed in Höber's book (9), quoted above, it was postulated that such membranes must permit the penetration of electrolytes from the lower compartment to the upper one (12). Cations move through the electronegative parts of the membrane and anions through the electropositive parts, neutralizing each other electrically. Thus a continuous movement of the electrolyte occurs across the membrane which does not cease until equilibrium between the two compartments is established.

In formulating this qualitative concept in a manner which is susceptible to a critical, preferentially to a quantitative, test it is necessary to consider a system in which the cation-permeable and anion-permeable parts are separated from each other. Figure 2 shows a U-tube containing in its left arm an electronegative (cation-permeable) and in its right arm an electropositive (anion-permeable) membrane, both membranes being assumed to be of an ideal degree of ionic selectivity. The lower part of the system (having an invariable volume) is filled with 0.1 N potassium chloride solution, while the two separate compartments above the membranes contain 0.01 N solution of the same electrolyte. The only processes, according to the premises, which can occur in this system consist of the establishment of static membrane potentials (concentration potentials) across the two membranes, and the establishment of a hydrostatic pressure in the lower compartment, due to the difference in water activity between the concentrated and the dilute solution.

The magnitude of each of the two membrane potentials in the system of figure 2 is numerically defined by the Nernst equation:

$$\epsilon = RT \ln \frac{a_1}{a_2} \tag{1}$$

where ϵ is the electromotive force and a_1 and a_2 are the molar activities of the electromotively active ion. The direction of the two electromotive forces is obvious from the mechanism of their origin; it is indicated in figure 2 by broken-line arrows pointing at a plus and a minus sign, respectively. The numerical value of ϵ amounts to +55.1 mv. and −55.1 mv. for the pair of solutions indicated in the figures. As is evident from figure 2, the dilute solution in the upper left-hand compartment, according to the premises, will have a potential difference of +110.2 mv. against the solution in the upper right-hand compartment.

In order to reëstablish in figure 2 the essential features of the situation represented in figure 1, it would be necessary to connect the two compartments containing dilute solution by a liquid conduit filled with 0.01 N potassium chloride solution, as shown in figure 3.

Figure 3 can be considered from two different viewpoints. On the one hand, it represents in a slightly more elaborate manner the essential situation of figure 1: potassium ions will migrate to the dilute solution through the cation-permeable membrane and chloride ions through the anion-permeable membrane, the broken-line arrows in figure 3 indicating the direction of the movement of the cations and anions, respectively.

On the other hand, the system of figure 3 may also be considered as a "Flüssigkeitsring," an "all-liquid electrical circuit" or, better, an "all-electrolytic electrical circuit" in the sense of Dolezalek and Krüger (4),[3] a (positive) electric current flowing in a clockwise direction through the system, as is indicated by the solid arrows in figure 3. The total E.M.F. in the system, E, as stated above, is 110.2 mv. The strength of the current, I, is defined by Ohm's law,

$$I = \frac{E}{R} \tag{2}$$

where R is the total resistance of the system. The current which flows in a clockwise direction in the system of figure 3 is transported through the negative membrane in the left arm of the system exclusively by cations which move clockwise, in the direction of the broken-line arrow; through the positive membrane in the right arm the electricity is transported exclusively by an equivalent quantity of anions which move in a counterclockwise direction, as indicated by a broken-line arrow.

---

[3] Dolezalek and Krüger deduced from Nernst's theory of the liquid-junction potential that an electric current must of necessity flow in a closed ring filled with nothing but a sequence of electrolyte solutions, provided any asymmetry of an electrical nature arises in the system. They proved this point by demonstrating the deflection of a magnetic needle placed in the center of an all-electrolytic ring system made up of a sequence of properly selected electrolyte solutions (4).

Accordingly, the quantity of electrolyte (in equivalents) which moves in a given time in the mosaic system of figure 3 from the concentrated to the dilute solution must be numerically identical with the number of electrochemical equivalents of current (faradays) which flow in the system during the same period.

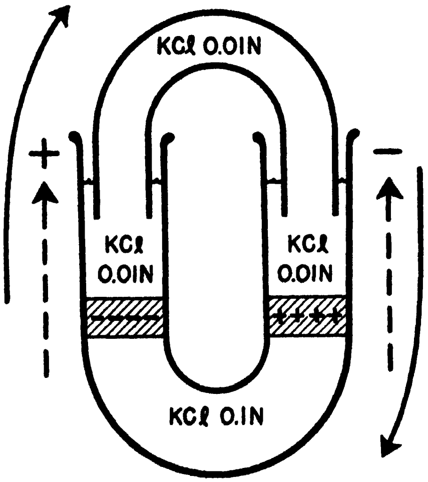

FIG. 3

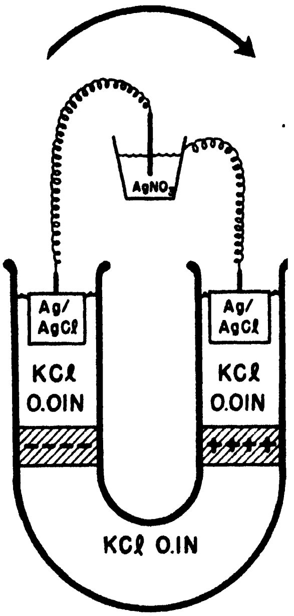

FIG. 4

II

The ultimate goal of the experimental test of the outlined theory of the electrolyte permeability of mosaic membranes obviously is its quantitative verification in model systems identical in all essential features with the all-electrolytic ring system of figure 3.

The general approach toward this end—in principle, at least—is exceedingly simple. It aims at the comparison of the number of equivalents of electrolyte which traverse the membranes in a given time and the number of faradays which flow in the system during the same period, the theory predicting numerical identity of these two magnitudes.

From the experimental point of view, however, the situation is not quite as favorable as might be supposed at first sight.

While the quantity of electrolyte which moves in a given period from the more concentrated to the more dilute solution can readily be determined conductometrically or by chemical-analytical methods, a model system of the type shown in figure 3 does not lend itself readily to a quantitative determination of the strength of the electric current which flows in it. The deflection of a magnetic needle, e.g., as used by Dolezalek and Krüger (4), under the most favorable conditions, can demonstrate the existence of an electric current in an all-electrolytic circuit, but an arrangement of this nature is not suitable for the quantitative determination of current intensities.

The main difficulty one is confronted with, therefore, consists in the exact determination of the number of coulombs which flow in an all-electrolytic ring system during a measured period.

The seemingly most straightforward way of circumventing this difficulty consists in calculating the number of coulombs flowing in the system during a given period from the readily measured E.M.F. of the system, its total ohmic resistance, and the duration of the experiment

The E.M.F. of the system and its resistance, however, are not constant over any experimentally useful period. A system like that of figure 3 is nothing but a working and, thereby, degradating all-electrolytic galvanic cell. The unavoidable degradation of the system during the experimental period results in a decrease in its E.M.F.; likewise, the resistance of the system does not remain constant. The conductance of its component parts, of the solutions and of the membranes alike, varies as the electrolyte concentration of the solutions in the two compartments changes. In addition, membrane polarization might arise as a further complication, since concentration polarization occurs at membrane | solution interfaces in the same manner as at metallic electrodes. This effect cannot be ignored or ruled out *a priori*; it must be tested for in the working model systems.

The exact calculation from E.M.F., resistance, and time measurements of the number of coulombs which flow in an all-electrolytic circuit in a given time is, therefore, a problem which can be solved in a satisfactory manner, if at all, only after considerable exploratory work. Thus, it becomes necessary to look for some other exact method of current measurement.

The obvious approach to this problem consists in some alteration in the simple theoretical model of figure 3 which will permit the current in the system to flow through some measuring instrument.

The practical way of doing this is to cut the system at some suitable point and attach to the two open ends of the interrupted circuit two symmetrical electrodes which can reversibly take the current from and return it to the system. The two electrodes in turn are connected to each other by some conventional current-measuring instrument and a closed circuit is thus reëstablished. The electrodes must be chosen so that they do not bring about any significant change in the original system which would not occur on closed circuit in their absence.

The system shown in figure 4 illustrates schematically one possible arrangement of this nature which makes use of silver | silver chloride electrodes in chloride solutions.[4] It may be represented as a galvanic cell in the conventional way, double vertical lines representing the negative and the positive membranes, respectively:

$$\mathrm{Ag} \underset{\epsilon_1}{|} \mathrm{AgCl} \underset{\epsilon_2}{|} \mathrm{KCl}\ c_1 \underset{\epsilon_3}{\overset{-}{||}} \mathrm{KCl}\ c_2 \underset{\epsilon_4}{\overset{+}{||}} \mathrm{KCl}\ c_1 \underset{\epsilon_2'}{|} \mathrm{AgCl} \underset{\epsilon_1'}{|} \mathrm{Ag}$$

In this chain the electromotive forces ϵ_1 and ϵ_1', and ϵ_2 and ϵ_2', are equal but opposite in direction; they cancel out and do not contribute to the total (effective) E.M.F. of the cell.

The introduction of reversible and symmetrical electrodes in a mosaic model system makes it, therefore, possible to determine directly and accurately the number of faradays which flow in it during the period for which the circuit is closed.

Thus, by the use of systems involving auxiliary electrodes, one should be able to compare accurately in the modified mosaic system of figure 4 the number of faradays which flow and the number of equivalents of electrolyte which are found analytically as having been transferred during the same period. If the ratio of these two magnitudes is found to be 1:1, within the limits of the experimental error, the outlined theory of mosaic membranes would be proven to be correct, at least for the type of model systems in which a pair of reversible electrodes has been introduced. This would mean that one is able for the first time to calculate from purely electrical data the rate of electrolyte permeation in a complex membrane system.

III

The experimental plan to be pursued towards this end must be introduced with some considerations of a general nature:

The geometry of the experimental system, that is, the size and shape of its component parts, is inconsequential from the point of view of the theory, provided the essential electrical features of the model are not altered. Likewise, the electrolyte used, the resistance of the membranes, the absolute concentration of the two electrolyte solutions, and also their concentration ratio may be freely selected as required by the experiment. Here, the only restricting condition is that the ionic selectivity of the membranes must be so high that the "leak" of noncritical ions does not blur the essential features of the model system.[5]

---

[4] The electrode reaction on the right-hand side of figure 4 consists in the formation of solid silver chloride from the silver of the electrode and chloride ions identical in number with those which have traversed the positive membrane. The electrode reaction on the left-hand side of the system is the formation of metallic silver from the solid silver chloride of the electrode and the release into the solution of an equivalent number of chloride ions. The net process in the cell of figure 4 is thus the same as that in the model without electrodes of figure 3: namely, the transfer of electrolyte.

[5] The imperfection in the ionic selectivity of a membrane which results in the movement of ions of the "noncritical" species across it (of anions in the case of the negative membranes, and of cations in the case of the positive membranes) can be calculated conven-

This freedom in the choice of the experimental details of the model studies is of considerable importance in view of the fact that even the best available membranes, the permselective membranes, generally speaking are not of ideal ionic selectivity. With such nonideal membranes it is necessary to balance carefully the several variable factors of the system with one another in such a manner as to establish the approximate optimum conditions.

It is advisable to reduce the experimental periods as much as practical (since the absolute "leak" of ions across a given membrane is proportionate to the duration of the experimental period) and to increase the current intensity in order that the effect of the "leak" may become small or, better still, insignificant.

One of the most important steps in the direction of decreasing the resistance of the experimental model systems consists in the selection of a suitable geometric arrangement. It will be helpful to increase the cross-sectional dimensions of all the component parts of the system and to make all dimensions in the direction of the flow of the current as small as possible. This is particularly true of the dilute solution.

One also might increase the absolute concentration of the solutions in order to decrease the resistance of the system. The full exploitation of this possibility is limited by the fact that the "leak" of the membranes increases considerably as the absolute concentration of the two solutions is raised (5, 6).

Another possibility of increasing the current lies in the choice of a high concentration ratio, which would result in an increase in the E.M.F. of the system. The usefulness of this possibility is also limited. Too high a concentration of the concentrated solution increases the "leak," and too low a concentration of the dilute solution unduly increases the resistance of the system.

The resistance of the membranes can be varied (5, 6, 7), but it cannot be lowered too much without adversely affecting their ionic selectivity; this means without increasing the "leak" of noncritical ions.

---

iently from membrane concentration potential and expressed in terms of per cent "leak" (1, 2).

The Nernst equation for the diffusion potential may be applied to the case on hand. For a uni-univalent electrolyte it assumes the following form:

$$E = \frac{\tau_- - \tau_+}{\tau_- + \tau_+} RT \ln \frac{a_1}{a_2} \tag{3}$$

where τ_- and τ_+ are the relative contributions of anions and cations, respectively, to the virtual transport of electricity across a (positive) membrane, and a_1 and a_2 the activities of the electrolyte in the two solutions.

The value of $RT \ln a_1/a_2$ for 0.1 N/0.01 N potassium chloride solution, e.g., is −55.1 mv. at 25.0°C. If a concentration potential, E, of −53.0 mv. is measured for this case the leak of cations can be calculated as follows:

$$-53.0 = \frac{\tau_- - \tau_+}{\tau_- + \tau_+} (-55.1) \tag{4}$$

therefore,

$$\frac{\tau_+}{\tau_-} = \frac{2.1}{108.1}. \tag{5}$$

This corresponds to a cation leak of about 2 per cent.

The choice of the electrolyte to be used does not represent any difficulty. Any readily available strong, neutral, uni-univalent electrolyte can be expected to be suitable with only minor differences between different salts (15, 16). With other electrolytes, e.g., uni-bivalent salts, the membranes must be selected with special care; otherwise the "leak" may become a very disturbing factor.

The nature of the electrodes to be used, in essence, is immaterial provided they are strictly reversible, not polarized too much by the current intensities likely to be encountered, and of low resistance, the two latter factors being influenced favorably by large cross-sectional dimensions.

The problem of concentration polarization at the four membrane | solution interfaces is not a serious one in models with auxiliary electrodes, since the number of coulombs flowing in the system is measured directly.

Stirring would be helpful in reducing any polarization which may arise in the systems on closed circuit. It will be helpful also in maintaining homogeneous the composition of the individual solutions and in keeping the full concentration difference active across the membrane itself.

The possibility must also be considered of a disturbing osmotic movement of liquid across the membranes which might occur, owing to the difference in the concentration of the two solutions. However, if permselective membranes are used there is no such difficulty, since the osmotic water movement which occurs across these membranes with concentration differences of a magnitude which is of interest here is insignificantly small, of the order of magnitude of 0.01 ml. per 100 cm.^{2} per hour (1).

IV

This section describes the special geometrical arrangement of the actually constructed and studied model systems with auxiliary electrodes; the individual component parts of these models; certain auxiliary procedures, including an appropriate method of correcting the raw experimental data for the "leak" of the membranes; and the calculation of the results and the method of their evaluation.

A suitable *geometrical arrangement* consists of two test tube-shaped membranes, the annular space between the two membranes being filled with the dilute solution. The smaller membrane throughout its length is provided with a concentric electrode and filled with concentrated solution. The larger membrane is surrounded by a cylindrical electrode, and is immersed in a container also filled with concentrated solution. The two electrodes are thus electrochemically symmetrical (though they are not identical in size or shape). This arrangement embodies large membrane (and electrode) areas with a short distance for the current to travel through the more dilute solution. It has the additional practical advantage that it does not require a tight sealing of membranes between flanges, a likely source of experimental errors when flat membranes are used.

Figure 5 shows the actual experimental model system of this type with specific (Ag | AgCl) electrodes. The elements of this system bear the same essential relationship to one another as in the corresponding theoretical model of figure 4.

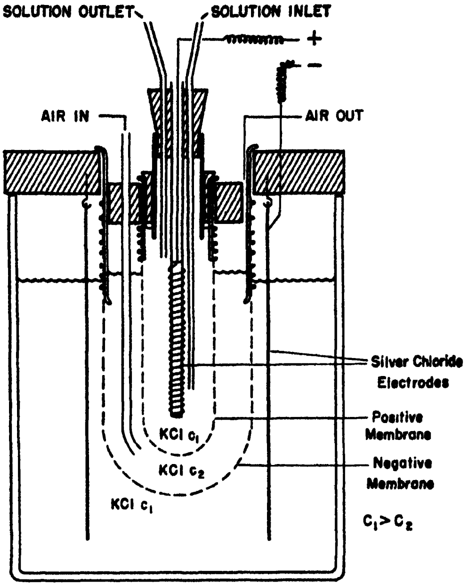
SOLUTION OUTLET
SOLUTION INLET
+
−
AIR IN
AIR OUT
Silver Chloride Electrodes
Positive Membrane
Negative Membrane
KCl c_1
KCl c_2
KCl c_1
$c_1 > c_2$

FIG. 5

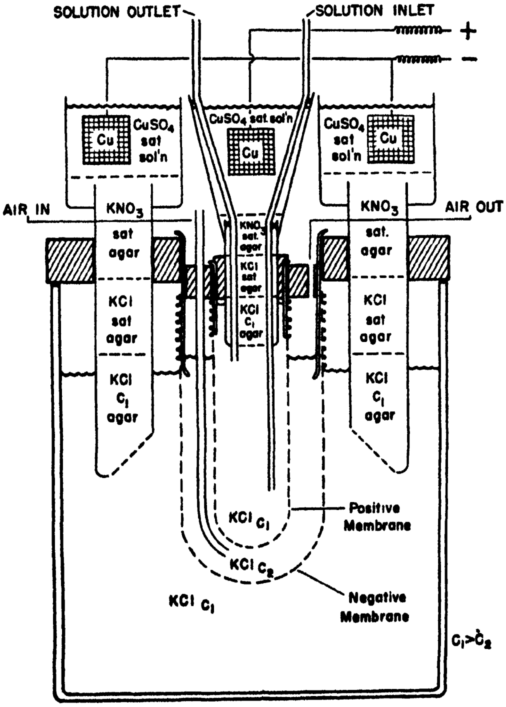
SOLUTION OUTLET
SOLUTION INLET
+
−
Cu
$CuSO_4$ sat sol'n
$CuSO_4$ sat. sol'n
Cu
$CuSO_4$ sat sol'n
Cu
AIR IN
AIR OUT
KNO_3 sat agar
KCl sat agar
KCl c_1 agar
KNO_3 sat. agar
KCl sat agar
KCl c_1 agar
KNO_3 sat. agar
KCl sat agar
KCl c_1 agar
KCl c_1
KCl c_2
KCl c_1
Positive Membrane
Negative Membrane
$c_1 > c_2$

FIG. 6

The singly existing, minor difference is that the dilute solution is contained in a single compartment, while the concentrated solution is separated into two parts.

The analogous model system with nonspecific electrodes is shown in figure 6.

In the models shown in figures 5 and 6, several precautions were taken to assure that the experimental conditions were maintained as closely as possible to those assumed in the theoretical model.

The concentration of the solution inside the positive membrane was maintained constant during the experiment by a stream of fresh solution (500 ml. per hour) coming under low pressure by gravity from a large storage bottle. Entering near the bottom of the membrane through a small glass tube, as shown in figures 5 and 6, the solution left through another tube at the top of the membrane and was discarded. This also provided an adequate intensity of *stirring*.

The dilute solution was stirred by means of a current of air bubbles, about two per second, issuing from a small glass tube in the lower part of the space between the two membranes. It escaped from the system through a small groove in the stopper supporting the glass ring of the positive membrane. The concentrated solution outside the negative membrane was neither changed nor stirred, since preliminary experiments had shown that these precautions were without detectable influence.

No accurate *control of the temperature* is necessary in the study of model systems with auxiliary electrodes. Fluctuations in the temperature are entirely immaterial if the number of coulombs flowing in the system are measured directly. They are of minor significance only if an ammeter is used, provided an adequate number of readings are taken at appropriate intervals. All experiments reported here were carried out at room temperature, the variation in temperature during any single experiment being rarely as much as 2.0°C.

The *membranes* used in the model experiments were permselective collodion and protamine collodion membranes prepared according to the method described by Carr, Gregor, and Sollner (1, 5, 6, 7). The inside (smaller) membranes were cast on 25 mm. glass mandrels; the outer (larger) membranes on similar 45 mm. test tubes which, for the casting, were rotated at the same peripheral speed as the 25 mm. mandrels. The membranes were attached to glass rings, as previously described (1, 6, 7). As a special precaution their top edges were sealed to the glass rings with paraffin to insure against any possible leakage by capillarity of the solutions between membrane and ring.

The suitability of the various membranes for use in the model systems was appraised in a preliminary manner on the basis of their characteristic concentration potential (abbreviated C.Co.P.) and their ohmic resistance in 0.1 N potassium chloride, $\rho_{0.1\text{ N KCl}}$.

The C.Co.P., that is, the potential of the concentration chain,

$$0.1\text{ N KCl} \mid \text{membrane} \mid 0.01\text{ N KCl}$$

of the various membranes was measured with a probable error of ± 0.1 mv. An experimental C.Co.P. less than the theoretically possible maximum (+55.1 and −55.1 mv., respectively) indicates a "leak" of the noncritical ion species which may be calculated as discussed in footnote 5. Negative membranes with a C.Co.P. of less than +54.9 mv. were not considered potentially useful in the model system; positive membranes with a C.Co.P. more than 2.0 mv. below the maximum were not used.[6]

The ohmic resistance of the positive membranes was measured by the method and with the equipment described by Gregor and Sollner (6). The resistance of the larger, negative membranes was obtained in a similar manner, but instead of platinum foil electrodes a platinized platinum wire cage about 60 mm. wide and 120 mm. high was used as the outside electrode and a helical coil 5 mm. in diameter and 80 mm. in length of platinized platinum wire wound round a glass rod as the inside electrode. The resistance data, recorded in the tables, are given in ohms per membrane, $\rho_{0.1\ \mathrm{N\ KCl}}$.[7]

The *electrolytes* chosen for the experiments reported below were potassium chloride, lithium chloride, and potassium sulfate.

The range of the *absolute concentration of the* two *electrolyte solutions* and the *ratio of the concentrations* of the concentrated and the dilute solutions were explored in a series of preliminary experiments; a fairly broad range of useful concentration was found to exist. Half of the final experiments were carried out with pairs of solutions 0.05 N/0.0015 N, other combinations used being 0.05 N/0.005 N and 0.1 N/0.01 N.

Two different types of *electrode systems* were employed, silver | silver chloride electrodes as specific electrodes with chloride solutions, and Cu | $CuSO_4$ | agar bridge electrodes as nonspecific electrodes which may be used with any electrolyte solution.

The larger one of the *silver | silver chloride electrodes*, which acts as the negative pole of the model system of figure 5, was a cylinder 125 mm. high and 61 mm. in diameter shaped from a piece of chemically pure sheet silver 0.25 mm. in thickness. The inside electrode was a spiral of chemically pure silver wire closely wound around a glass rod 10 mm. in diameter and about 80 mm. in length. These electrodes were covered electrolytically in the conventional manner with a layer of silver chloride. Whenever they became asymmetrical in use by more than 2 mv. they were renewed. The polarization of the electrodes on closed circuit seems to be small,—in the majority of instances not more than 2 or 3 mv. This is insignificant compared with the sum of the electromotive forces of the model systems used (110–160 mv. in the majority of instances).

For *nonspecific electrodes* any reversible electrodes may be used which are connected to the solutions by means of a sequence of suitable electrolyte solutions or electrolyte solutions immobilized in agar gels. A suitable arrangement with nonspecific electrode assemblies is shown in figure 6. It represents a chain, which in the conventional manner may be written as follows, the double vertical lines representing the membranes:

---

[6] Some of the permselective protamine collodion membranes which were used in the experiments described later in this paper were prepared with protamine which had been modified by (partial) esterification of the free carboxyl groups which exist, probably as end groups, in the native protamine molecule. The ionic selectivity of the improved membrane is significantly greater than that of the previously described protamine membranes, their C.Co.P. being increased up to −54.1 ± 0.1 mv. against the heretofore reached optimum of about −53.2 ± 0.1 mv.

[7] The membrane resistance $\rho_{0.1\ \mathrm{N\ KCl}}$ does not give the resistance which the membranes show in the mosaic model, since membrane resistance is a function of the electrolyte used and of the concentration of the adjacent solutions (5, 17).

$$\begin{array}{c|c|c|c|c|c||c||c|c|c|c|c|c}
 & & & & & & - \quad\quad + & & & & & & \\
 & & \text{c} & \text{b} & \text{a} & & & & \text{a} & \text{b} & \text{c} & & \\
\text{Cu} & \begin{matrix}\text{CuSO}_4\\ \text{satd.}\end{matrix} & \begin{matrix}\text{KNO}_3\\ \text{satd.}\\ \text{agar}\end{matrix} & \begin{matrix}\text{KCl}\\ \text{satd.}\\ \text{agar}\end{matrix} & \begin{matrix}\text{KCl}\\ c_1\\ \text{agar}\end{matrix} & \begin{matrix}\text{KCl}\\ c_1\end{matrix} & \begin{matrix}\text{KCl}\\ c_2\end{matrix} & \begin{matrix}\text{KCl}\\ c_1\end{matrix} & \begin{matrix}\text{KCl}\\ c_1\\ \text{agar}\end{matrix} & \begin{matrix}\text{KCl}\\ \text{satd.}\\ \text{agar}\end{matrix} & \begin{matrix}\text{KNO}_3\\ \text{satd.}\\ \text{agar}\end{matrix} & \begin{matrix}\text{CuSO}_4\\ \text{satd.}\end{matrix} & \text{Cu}
\end{array}$$

$$\epsilon_1 \quad \epsilon_2 \quad \epsilon_3 \quad \epsilon_4 \quad \epsilon_5 \quad \epsilon_6 \quad \epsilon_7 \quad \epsilon_5' \quad \epsilon_4' \quad \epsilon_3' \quad \epsilon_2' \quad \epsilon_1'$$

The only nonsymmetrical and therefore active electromotive forces in this system are ϵ_6 and ϵ_7, the two membrane potentials.[8] The situation is identical with that arising in systems with specific electrodes.

Four electrode assemblies connected in parallel were dipped into the outside solution and constituted the negative pole of the model systems; one assembly was used inside the positive membrane as the positive pole. The five electrode assemblies to be used simultaneously in one model system were prepared at the same time with the same solutions to assure electrode symmetry. The potential difference between the two poles of the model systems (when they were immersed in the same solution before the experiment) was never more than 2 mv. After an experimental run the asymmetry of the nonspecific electrodes usually had shifted somewhat from the initial value, but it never amounted to over 5 mv.

The *quantity of electricity flowing in the model systems* was measured directly with a semi-micro silver coulometer or calculated from the area under a current–time curve. The maximum error in weight of the deposited silver was about ±0.00004 g.

The *quantity of electricity in faradays* calculated *from* these *coulometric data*, N_{coul}, is

$$N_{\text{coul}} = \frac{W_t - W_0}{107.88} \tag{6}$$

where W_0 and W_t are the initial and final weights of the coulometer crucible in grams. The accuracy of the N_{coul} data reported later in this paper can be estimated to vary from 0.5 per cent up to 2.0 per cent, according to the different weights of the silver deposited in the several experimental cases.

---

[8] The agar plugs, **a**, in this chain contain the same electrolyte at the same concentration as the solutions in which they dip in order to prevent any disturbing concentration changes in these solutions. The next agar plugs, **b**, are made of a saturated solution of the same electrolyte so as to keep the resistance of the electrodes low, while increasing the distance between the plugs **c** and the solutions. This third set of agar plugs, **c**, which contact the copper sulfate compartments, are saturated with potassium nitrate. They serve to separate the agar plug saturated with the electrolyte used in the model from the copper sulfate solution, thus preventing possible reactions there which would adversely affect the electrodes.

For determining the number of *coulombs* moved *from current–time curves* two (factory new) Weston ammeters were available: one with an internal resistance of 55 ohms and a range of 0–500 microamp. and the other with an internal resistance of 5.7 ohms and a range of 0–5 milliamp. The probable error of the individual current readings was not more than ±0.5 per cent of the full scale value. The *time* was measured with an electric timer.

Since the intensity of the current diminished in the course of an experiment, decreasing very considerably in some instances, an appropriate number of current–time readings were noted in each case. These data gave the ampere-minutes of current which had flowed *in toto* through the model system while the circuit was closed.

The *quantity of electricity* moved, *expressed in faradays*, as *calculated from the current-time data*, N_{amp}, is

$$N_{\text{amp}} = \frac{\Sigma \text{ ampere-minutes} \times 60}{96{,}494} \tag{7}$$

The accuracy of the experimental N_{amp} values varies from less than ±1.0 per cent to ±2.0 per cent, according to the strength of the current measured in the different experiments.

The *quantity of electrolyte which penetrates* across the membranes from the concentrated *to the dilute solution* in a given time, either on open or on closed circuit, can be calculated from the known volume of the dilute solution and the increase of its concentration during the period under consideration.

All *concentration determinations* were made conductometrically ($T = 25.00°\text{C.} \pm 0.05°$). For the measurements the conductivity cell was rinsed at least three times with a solution of approximately the same concentration of the same electrolyte as the unknown. The last rinse solution was removed as completely as possible from the cell, with only an insignificant quantity of adhering solution remaining in it. About 5 ml. of the unknown solution was then transferred with a pipet from the model system to the conductivity cell, withdrawn from it, and returned to the model. Thereafter another 5-ml. sample of the unknown was transferred to the conductivity cell for the actual resistance measurement after which the solution, as before, was returned to the model. These concentration determinations were accurate to about 0.2 per cent.

The *quantity of electrolyte moved on closed circuit* in a mosaic model system with nonideal, leaky membranes is obviously composed of three parts: the electrolyte, the movement of which is physically identical with the flow of current; some electrolyte which might leak across the negative membrane; and some electrolyte which leaks across the positive membrane.

The translocation of electrolyte due to leak of the membranes, if of sufficient magnitude, would falsify the experimental results. Therefore, the *leak of electrolyte* of the model systems, the sum of the two possible separate leaks, must be measured and appropriate corrections must be applied to the raw experimental data.

The obvious way of making these corrections consists in determining the rate of the leak on open circuit before and after the experiment and in applying a proportionate correction to the conductometrically determined quantity of electrolyte which on closed circuit is transferred to the dilute solution. Since the leak is small in comparison with the looked-for effect, the correction for the leak of electrolyte across the membranes, which corresponds to the closed-circuit period of each experiment, was made by straight-line extrapolation either graphically or by an equivalent calculation.[9]

The *number of electrochemical equivalents of electrolyte moved on closed circuit corrected for leak*, $N_{\Delta\text{conc}}$, was calculated from the equation

$$N_{\Delta\text{conc}} = \frac{(C_t - C_0 - \Delta_{\min} \times t)v}{1000} \tag{8}$$

In this equation C_0 and C_t are the concentrations in equivalents per liter of the dilute solution in the middle compartment of the model system at the beginning and at the end of the closed circuit period; $\Delta_{\min}$ is the concentration change per minute of the dilute solution in equivalents per liter which is due to the leak of electrolyte (as determined on open circuit); t is the duration of the closed circuit period in minutes; and v is the volume of the dilute solution in milliliters. The accuracy of the $N_{\Delta\text{conc}}$ data reported later can be estimated to vary from 1.5 per cent to 2.5 per cent, depending on the magnitude of the relative increase in the concentration of the dilute solution.

The *evaluation of the experimental data* consists in the comparison of the (corrected) number of electrochemical equivalents of electrolyte, $N_{\Delta\text{conc}}$, which have moved into the compartment of the dilute solution and the number of faradays which have flowed in the systems, N_{coul} or N_{amp}, as the case may be. The theory predicting identity of these two sets of figures, their *per cent deviation* from this prediction, Δ per cent, can be calculated readily, e.g., according to equations 9 and 9a, which define $N_{\Delta\text{conc}}$ as the reference unit:

$$\Delta \text{ per cent} = \frac{(N_{\text{coul}} - N_{\Delta\text{conc}}) \times 100}{N_{\Delta\text{conc}}} \tag{9}$$

and

$$\Delta \text{ per cent} = \frac{(N_{\text{amp}} - N_{\Delta\text{conc}}) \times 100}{N_{\Delta\text{conc}}} \tag{9a}$$

The deviation of Δ per cent from zero which results alone from the random combination of the above-discussed errors in N_{coul}, N_{amp}, and $N_{\Delta\text{conc}}$ can be expected to amount in the average to ±2.0 per cent or 2.5 per cent. In rare instances it might be up to about 5 per cent.

V

This section presents a description of the experimental procedures employed in running the actual test experiments and representative experimental data.

---

[9] In some instances it was ascertained by separate tests that the membranes had a negligible leak of electrolyte under the conditions of the experiments. In such cases the described experimental procedure could be omitted when carrying out an actual experiment.

A typical experiment with a model with silver | silver chloride electrodes (figure 5) proceeded as follows: A positive and a negative membrane of the desired characteristics, mounted by means of their glass rings, were hung concentrically in the middle of the rubber plate which also carried the large outside silver | silver chloride electrode. The positive membrane was filled with the more concentrated solution and its glass ring was tightly closed with a rubber stopper

TABLE 1

Model experiment with specific electrodes

Negative membrane: C.Co.P. = +55.0 mv.; $\rho_{0.1\text{ N KCl}}$ = 2.0 Ω
Positive membrane: C.Co.P. = −54.0 mv.; $\rho_{0.1\text{ N KCl}}$ = 18.0 Ω
Electrolyte: KCl
Concentration of concentrated solution = 0.050 N
Volume of dilute solution, v, = 70.0 ml.

t	DURATION OF INTERVAL	CURRENT I	AVERAGE I IN INTERVAL	ELECTRICITY MOVED	CONCENTRATION OF DILUTE SOLUTION	LEAK PER MINUTE $\Lambda_{\text{min.}}$
min.	*min.*	*amp.* × 10^{-3}	*amp.* × 10^{-3}	*amp.-min.* × 10^{-3}	*equiv./l*	*equiv./l.*
0		--			0.00528	
	600		—	—		0.00000025
600*		1.18			0.00543	
	20		1.15	23.00		
620		1.12			—	
	15		1.11	16.65		
635		1.10			—	
	15		1.09	16.35		
650		1.08			—	
	60		1.06	63.60		
710		1.03			—	
	15		1.03	15.45		
725		1.03			—	
	15		1.02	15.30		
740		1 02			—	
	20		1.02	20.40		
760		1.02			—	
	70		1.00	70.00		
830		0.98			0.00757	
	230			240.75		

↑
(600th to 830th)

* Circuit closed at t = 600 min.

$$N_{\text{amp}} = \frac{240.75 \times 10^{-3} \times 60}{96{,}494} = 149.7 \times 10^{-6}\text{ faradays}$$

$$N_{\Delta\text{conc}} = \frac{(0.00757 - 0.00543 - 0.00000025 \times 230) \times 70}{1000} = 145.6 \times 10^{-6}\text{ equivalents}$$

$$\Delta\text{ per cent} = \frac{149.7 \times 10^{-6} - 145.6 \times 10^{-6}}{145.6 \times 10^{-6}} = +2.8\text{ per cent}$$

which carried the smaller of the above-described silver | silver chloride electrodes and the two glass tubes for flowing solution through the innermost compartment of the system. Next, a measured volume of dilute solution was pipetted into the space between the two membranes. The assembly prepared in this manner was lowered into the glass vessel containing a large volume (about 1000 ml.) of the concentrated solution and the level of this outside solution was adjusted to coincide approximately with that of the dilute solution between the membranes. The flow of solution through the innermost compartment and the stirring by air of the dilute solution were started.

TABLE 2

Model experiment with nonspecific electrodes

Negative membrane: C.Co.P. = +54.9 mv.; $\rho_{0.1\,\mathrm{N\,KCl}}$ = 115 Ω
Positive membrane: C.Co.P. = −53.5 mv.; $\rho_{0.1\,\mathrm{N\,KCl}}$ = 50 Ω
Electrolyte: KCl
Concentration of concentrated solution: 0.050 N
Volume of dilute solution, v, = 80.0 ml.

t	WEIGHT OF COULOMETER	CONCENTRATION OF DILUTE SOLUTION	LEAK PER MINUTE
min.	*grams*	*equiv./liter*	*equiv./liter*
0*	16.84855	0.001510	Insignificant
360	16.85150	0.001860	

* Circuit closed at t = 0.

$$N_{\mathrm{coul}} = \frac{16.84855 - 16.85150}{107.88} = 27.3 \times 10^{-6} \text{ faradays}$$

$$N_{\Delta\mathrm{conc}} = \frac{(0.001860 - 0.001510) \times 80}{1000} = 28.0 \times 10^{-6} \text{ equivalents}$$

$$\Delta \text{ per cent} = \frac{27.3 - 28.0}{28.0} = -2.5 \text{ per cent}$$

In this system the concentration of the dilute solution was measured repeatedly on open circuit during a period usually ranging from 2 to 18 hr. Immediately after the last of these concentration measurements and without making any other changes in the system, the circuit was closed with the current flowing through the silver coulometer or one of the ammeters. When an ammeter was used a series of readings was made of the current intensity and of the time elapsed since the moment of closing the circuit. After the current had flowed for a period ranging from 1 to 6 hr. the circuit was interrupted and the final concentration of the dilute solution was determined. This concluded the experiment, except for some additional determinations of the leak which were added in many instances.[10]

The experimental procedure in the case of the model systems with nonspecific Cu | $CuSO_4$ | agar gel electrodes (figure 6) was essentially the same as with the

---

[10] The leak after the closed-circuit period was found to be practically the same as initially; it, therefore, was not measured in many of our later experiments.

TABLE 3

Several model experiments in which the quantity of electricity transferred was determined coulometrically

EXPT. NO.	NEGATIVE MEMBRANE		POSITIVE MEMBRANE		ELECTROLYTE SOLUTIONS		ELECTRODES	VOLUME OF DILUTE SOLUTION	INCREASE IN CONCENTRATION OF DILUTE SOLUTION	CORRECTION FOR LEAK	$N_{\Delta cond}$	WEIGHT OF SILVER DEPOSITED	N coul	Δ PER CENT
	C.Co.P.	$\rho_{0.1\ N\ KCl}$	C.Co.P.	$\rho_{0.1\ N\ KCl}$	Electrolyte used	Concentration on closing of circuit		v	$C_t - C_0$	$A_{min} \times t$		$W_t - W_0$		
	mv.	Ω	mv.	Ω		equiv./liter		ml.	equiv./liter	equiv./liter	equiv. $\times 10^{-6}$	grams	F $\times 10^{-6}$	per cent
1*	+54.9	115	−53.5	50	KCl	0.050/0.001510	Cu|CuSO$_4$|agar	80.0	0.000350	None	28.0	0.00295	27.3	−2.5
2	+55.0	2.0	−54.0	18	KCl	0.050/0.00516	Ag|AgCl	70.0	0.00216	None	151.2	0.01697	157.3	+4.0
3	+55.0	10.0	−54.1	18	KCl	0.050/0.00521	Ag|AgCl	70.0	0.00116	None	81.2	0.00887	82.2	+1.2
4	+54.9	2.0	−53.5	4.0	K$_2$SO$_4$	0.050/0.001591	Cu|CuSO$_4$|agar	74.0	0.000609	0.000117	36.4	0.00368	34.1	−6.3
5	+55.0	2.0	−53.2	16	K$_2$SO$_4$	0.050/0.001681	Cu|CuSO$_4$|agar	74.0	0.000417	0.000064	26.1	0.00277	25.7	−1.5

* See table 2.

TABLE 4

Several model experiments in which the quantity of electricity transferred was calculated from current and time data

EXPT. NO.	NEGATIVE MEMBRANE		POSITIVE MEMBRANE		ELECTROLYTE SOLUTIONS		ELECTRODES	VOLUME OF DILUTE SOLUTION	INCREASE IN CONCENTRATION OF DILUTE SOLUTION	CORRECTION FOR LEAK	$N_{\Delta cond}$	ELECTRICITY MOVED	N_{amp}	Δ PER CENT
	C.Co.P.	$\rho_{0.1\ N\ KCl}$	C.Co.P.	$\rho_{0.1\ N\ KCl}$	Electrolyte used	Concentration on closing of circuit		v	$C_t - C_0$	$A_{min} \times t$				
	mv.	Ω	mv.	Ω		equiv./liter		ml	equiv./liter	equiv./liter	equiv. $\times 10^{-6}$	amp.-min. $\times 10^{-3}$	F $\times 10^{-6}$	per cent
6*	+55.0	2.0	−54.0	18	KCl	0.050/0.00543	Ag|AgCl	70.0	0.00214	0.00006	145.6	240.8	149.7	+2.8
7	+55.0	10.0	−54.0	18	KCl	0.050/0.00548	Ag|AgCl	70.0	0.000740	0.000030	49.7	80.19	49.9	+0.4
8	+55.0	15	−54.0	18	KCl	0.100/0.01050	Ag|AgCl	65.0	0.00105	0.00008	63.1	99.42	61.8	−2.1
9	+55.1	22	−53.3	11	LiCl	0.050/0.001505	Ag|AgCl	70.0	0.000465	None	32.6	51.67	32.1†	−1.5
10	+54.9	115	−53.5	50	KCl	0.050/0.001500	Cu|CuSO$_4$|agar	80.0	0.000420	None	33.6	53.94	33.5	−0.3

* See table 1.

† 32.4 × 10^{-6} faradays from simultaneously obtained coulometric data.

systems with silver | silver chloride electrodes. However, where an initial run on open circuit of considerable length was indicated the electrodes were not inserted from the beginning but added later when the circuit was to be closed. This procedure prevented contamination of the solutions into which the electrodes dipped and, equally important, the electrodes could be prepared just prior to the critical, closed-circuit part of the experiments.

Table 1 shows as an example the detailed experimental data pertaining to a model with specific auxiliary electrodes, silver | silver chloride in potassium chloride solutions, and membranes of fairly low resistance. The number of coulombs moved in this experiment is obtained from current and time readings. The quantity of electrolyte transferred is duly corrected for the "leak" of the system.

Table 2 shows the analogous data for a system with non-specific electrodes and membranes of fairly high resistance, the "leak" of the membranes in this case being insignificantly small. The number of coulombs moved here is measured with a coulometer.

Table 3 summarizes, in an abbreviated form, several more experiments with models in which the quantity of electricity transferred was determined coulometrically. Table 4 does the same for several systems in which current and time readings were taken.

VI

The experimental data summarized in tables 1 to 4 do not require extensive comment.

The number of faradays moved, N_{coul} and N_{amp}, and the number of equivalents of electrolyte transported, $N_{\Delta\mathrm{conc}}$, agree satisfactorily. The per cent deviations of their ratios from the theoretically predicted 1:1 ratio, Δ per cent, given in the last column of the summarizing tables 3 and 4, are of the magnitude which must be expected in view of the previously discussed limits of the accuracy of the measurements, the mean deviation being less than ± 2.5 per cent. The theory of the electrolyte permeability of mosaic membranes outlined in this paper must, therefore, be considered to be verified by the experiment. One is now able to calculate solely from the electrical characteristics of a mosaic system the quantity of electrolyte permeating to the dilute solution per unit of time.

The verification of the theory of the electrolyte permeability of mosaic membranes in systems *with* auxiliary electrodes is conclusive and adequate from the strictly physicochemical point of view. The demonstration of the applicability of the theory in model systems *without* electrodes remains, however, desirable in order to show directly that all-electrolytic systems can not only be discussed adequately from the theoretical viewpoint, but can also be investigated quantitatively without any auxiliary devices.

We expect to report shortly, in Part II of this paper, on the promising experiments which are currently being carried out on mosaic model systems without auxiliary electrodes.

SUMMARY

1. The electrolyte permeability of mosaic membranes which are composed of ideally anion-selective parts and ideally cation-selective parts in juxtaposition is investigated theoretically by the consideration of model systems in which the anion-selective and the cation-selective parts of the membrane are separated from each other. A ring system is discussed quantitatively which consists of the cyclic arrangement of four component parts: | dilute solution | anion-selective membrane | concentrated solution | cation-selective membrane | .

2. In the ring systems described in paragraph 1 cations move from the concentrated to the dilute solution across the cation-selective membrane in the one arm of the model, and an equivalent number of anions through the anion-permeable membrane in the other arm, their electrical charges neutralizing each other. The system is also an "all-electrolytic electrical circuit" in the sense of Dolezalek and Krüger. The intensity of the current flowing in it at any given moment is determined by the total E.M.F. of the system, the sum of the two membrane potentials, and its total resistance. The movement of ions and the flow of current being only two different aspects of the same physical process, the number of electrochemical equivalents of electrolyte which penetrate across the membranes in a model system must be identical with the number of faradays which flow during the same period in it.

3. The general electrochemical considerations are presented which form the basis for an experimental test of the theory of the electrolyte permeability of mosaic membranes by means of model systems which involve the use of auxiliary electrodes. The limitations in the choice of the geometry of the model systems and in the conditions of their operation which stem from the lack of an ideal degree of ionic selectivity of the available membranes are evaluated.

4. Model systems are constructed consisting of a pair of coaxially arranged, test tube-shaped membranes (one being anion-selective and the other cation-selective), and two auxiliary electrodes, either specific Ag | AgCl electrodes in chloride solutions or non-specific electrodes of the Cu | $CuSO_4$ | agar bridge type. The annular space between the two membranes is filled with a known volume of the dilute solution of some (preferentially) uni-univalent electrolyte. The inside of the smaller membrane is filled with a more concentrated solution of the same electrolyte, and the larger membrane is placed in a container filled with identical solution. Symmetrical electrodes are immersed in the latter two compartments. The number of faradays moved and the number of electrochemical equivalents of electrolyte translocated on closed circuit in such systems show a 1:1 ratio, with a mean deviation of less than ±2.5 per cent. The predictions of the theory, therefore, must be considered as proven quantitatively, well within the limits of the experimental error.

The thanks of the authors are due to Dr. Charles W. Carr for valuable suggestions and active help in the course of the experimental work presented here.

REFERENCES

(1) Carr, C. W., and Sollner, K.: J. Gen. Physiol. **28**, 119 (1944).
(2) Carr, C. W., Gregor, H. P., and Sollner, K.: J. Gen. Physiol. **28**, 179 (1945).
(3) Collander, R.: Kolloidchem. Beihefte **19**, 72 (1924); Soc. Sci. Fennica, Commentationes Biol. **2**, 6 (1926).
(4) Dolezalek, F., and Krüger, F.: Z. Elektrochem. **12**, 669 (1906).
(5) Gregor, H. P.: Ph. D. Thesis, University of Minnesota, 1945.
(6) Gregor, H. P., and Sollner, K.: J. Phys. Chem. **50**, 53 (1946).
(7) Gregor, H. P., and Sollner, K.: J. Phys. Chem. **50**, 88 (1946).
(8) Grollman, A., and Sollner, K.: Trans. Electrochem. Soc. **61**, 487 (1932).
(9) Höber, Rudolf: *Physical Chemistry of Cells and Tissues*. The Blakiston Company, Philadelphia (1945).
(10) Michaelis, L.: Bull. Natl. Research Council (U. S.) **No. 69**, 119 (1929).
(11) Sollner, K.: Z. Elektrochem. **36**, 36, 234 (1930); Kolloid-Z. **62**, 31 (1933).
(12) Sollner, K.: Biochem. Z. **244**, 370 (1932).
(13) Sollner, K., and Gregor, H. P.: J. Am. Chem. Soc. **67**, 346 (1945).
(14) Sollner, K., and Gregor, H. P.: J. Phys. Chem. **50**, 470 (1946).
(15) Sollner, K., and Gregor, H. P.: J. Phys. Chem. **51**, 299 (1947).
(16) Sollner, K., and Gregor, H. P.: J. Phys. & Colloid Chem. **54** (March, 1950).
(17) Sollner, K., and Gregor, H. P.: In preparation.
(18) Sollner, K., and Grollman, A.: Z. Elektrochem. **38**, 274 (1932).
(19) Weech, A. A., and Michaelis, L.: J. Gen. Physiol. **12**, 55 (1928).

THE DETERMINATION OF SODIUM-ION AND CHLORIDE-ION ACTIVITIES IN PROTEIN SOLUTIONS BY MEANS OF PERMSELECTIVE MEMBRANES[1]

CHARLES W. CARR

Department of Physiological Chemistry, The Medical School, University of Minnesota, Minneapolis 14, Minnesota

AND

LEO TOPOL

Division of Physical Chemistry, School of Chemistry, Institute of Technology, University of Minnesota, Minneapolis 14, Minnesota

Received August 22, 1949

The study of the interaction of various ions with proteins in solution has been of considerable interest for many years. It is now well known that the activity of many ionic substances is markedly influenced by the presence of proteins, the most familiar case being that of the binding of acids and bases. Through the use of various experimental techniques, it has also been shown that the activity of many organic ions, heavy metal cations, and alkaline earth cations is decreased considerably in protein solutions, owing to combination with the proteins. Recently it has been found that many of the common anions, including chloride, are bound to a certain extent to proteins (10, 13, 24, 27, 28). There are some indications that the alkali metal cations may also interact with some proteins, but this problem has not been completely elucidated (4, 8, 11, 22).

---

[1] Presented at the Twenty-third National Colloid Symposium, which was held under the auspices of the Division of Colloid Chemistry of the American Chemical Society at Minneapolis, Minnesota, June 6–8, 1949.

It is the intention of the present paper to show how membrane electrodes might be applied to the study of the interaction of the alkali metal cations and halogen anions with proteins. With the use of such electrodes it is possible to measure directly the activity of certain ions. In experiments of this nature any decrease in activity of a given species of ions in a protein solution below that which it shows in a solution of the same ionic concentration without protein can be taken as an indication of some type of interaction between the ions and the proteins.

Specific electrodes for the determination of the activities of sodium and chloride ions in protein solutions have occasionally been used in the past. Several workers have used the sodium amalgam electrode to study the sodium-ion activity in blood serum (19, 20, 23). Although the presence of proteins increases considerably the error involved in the use of this electrode, it has been the general conclusion that the sodium-ion activity in serum is unaffected by the presence of the proteins. Kirk and Schmidt (9) have used this electrode in solutions of sodium caseinate. Their results showed that the casein also had no detectable effect on the activity of sodium ions. Because of the extreme care necessary for their preparation and use and the error introduced by the presence of protein, the amalgam electrodes are limited in their usefulness for such studies.

Hitchcock (7) has used the silver–silver chloride electrode to measure the chloride-ion activity in gelatin solutions. He worked at relatively low pH's (1–2) and found that a small amount of chloride (2×10^{-4} equivalents per gram) was bound to the gelatin. Northrop and Kunitz (21) also used this electrode in solutions of gelatin and found that at a higher pH (4.7) no detectable chloride was bound in a 1 per cent solution of gelatin. At higher concentrations (6–15 per cent) they found the chloride-ion activity to decrease slightly below that found in salt solution without protein.

Membrane electrodes for the determination of ion activities other than hydrogen have just recently been developed. Sollner (26) and Gregor (5) have shown that specially prepared permselective collodion membranes may be used for the determination of some of the more common cations, including sodium, potassium, ammonium, and magnesium. Similarly, permselective protamine collodion membranes may be used for the determination of the anions chloride, bromide, nitrate, acetate, and several others. Marshall and his collaborators (14, 15, 16, 17, 18) have used clay membranes successfully for the activity determinations of sodium, potassium, ammonium, magnesium, and calcium ions. Wyllie and Patnode (29) very recently have prepared an artificial membrane by bonding a cation-exchange resin in an inert plastic. Their membranes have been found to give good results for the determination of sodium-ion activities in solutions as concentrated as 4 molal sodium chloride.

The membranes used in the present work are the collodion and protamine collodion membranes, and the ion activities are determined by the titration procedure of Sollner (26). The proteins used are gelatin and casein, and the electrolyte used is sodium chloride.

II

The determinations of ion activity are made by carrying out a potentiometric titration. The solution of unknown activity is placed on one side of the membrane and a known volume of water on the other side. A strong solution of known concentration of an electrolyte which has the same ion as the one being determined is added to the water from a buret. After each addition of electrolyte the membrane potential is measured, and the addition of electrolyte is continued until the potential changes in sign. At the point of zero potential the activity of the ion under consideration is equal to that of the same ion in the outside solution. From the volume and concentration of strong electrolyte added to a given volume of water, the concentration of this electrolyte at the zero potential is calculated, and from this concentration the activity of the ion under investigation is estimated.

The exact procedure for carrying out the titrations was similar to that described previously (2). The membranes which were used were prepared as described by Sollner and coworkers (1, 3, 6). They are bag-shaped, being formed over 25 x 100 mm. test tubes, and hold about 30 ml. of solution. For the determination of cation activity the oxidized collodion membranes are used. These membranes are negatively charged with respect to the solutions in which they are immersed. For the determination of anion activity the positively charged protamine collodion membranes are used.

A known volume of water is added to a beaker of such size that the beaker is about one-half to two-thirds filled. Next, the membrane is filled with the solution to be investigated. About two-thirds of its length is immersed in the beaker containing the water, and the membrane is then clamped in position. For a clamp a wooden test tube holder held to a ringstand with a right-angle clamp is convenient.

The temperature is measured and titration is started. The electrolyte solution used as titrant should be at least ten times as concentrated as the solution being titrated to avoid the addition of excessively large volumes which would be needed to reach the end point. After each addition the E.M.F. of the system is determined:

$$\mathrm{Hg}|\mathrm{Hg_2Cl_2(s)}\ \mathrm{KCl(satd.)}\left|\begin{array}{c}\text{outside}\\ \text{solution}\\ c_1\end{array}\right|\text{membrane}\left|\begin{array}{c}\text{inside}\\ \text{solution}\\ c_2\end{array}\right|\mathrm{KCl(satd.)}\ \mathrm{Hg_2Cl_2(s)}|\mathrm{Hg}$$

The saturated calomel electrodes are connected with the two solutions by means of specially constructed agar bridges saturated with potassium chloride. These bridges are made with 3-mm. glass tubing, and the tips which make contact with the solutions are about 1 mm. in diameter. The small contact area is necessary to minimize the diffusion of potassium chloride into either solution. To minimize this diffusion still further, the bridges are removed from the two solutions after each measurement of the potential and placed in saturated potassium chloride solution. Just before use they are wiped dry and placed in the solutions being measured.

In making the potential measurements, two readings were always taken. After the first reading the agar–potassium chloride bridges were changed around so that the solutions with which they were in contact became reversed. A second reading was then taken, which usually varied from the first by a few tenths of a millivolt. The average of the two readings was taken to be the observed potential. This potential was plotted on the linear axis of semilogarithmic graph paper, and the concentration of the outside solution was plotted on the logarithmic axis. A straight line with nearly the theoretical slope was always obtained. The intersection of this line with the line of zero potential thus gives the concentration in the outside solution which corresponds to the zero potential. This concentration at which the zero potential is obtained will hereafter be referred to as the end point of the titration. For known solutions in the range of concentration of 0.005 *M* to 0.2 *M*, the correct end point can be reproduced with an accuracy of about ±1–2 per cent.

Since the protein solutions which we intended to study vary considerably in pH, we have determined the pH range in which the membranes can be used without introducing serious error.

Sodium chloride solutions (0.100 *N*) were prepared, and the pH of these solutions was varied by addition of small amounts of hydrochloric acid or sodium hydroxide. Although the pH values of these unbuffered solutions were not known very accurately, they were known with sufficient accuracy to determine in which range of pH the membranes would be useful. The solutions were titrated immediately after preparation with the use of a neutral solution of 1 *N* sodium chloride as the titrant. It was found that when 0.1 *N* sodium chloride was placed in a negative membrane, the end point was reached after the correct amount of titrant was added only when the pH was greater than 4.5. As the pH decreased below 4.5, it required more than the correct amount of 1 *N* sodium chloride to reach the end point. The correct end point was also reached when the pH was as high as 10.0. It was concluded that the negative membranes could be used successfully for the determination of sodium ion over a pH range of 4.5–10.0.

When the 0.1 *N* sodium chloride was placed in a positive membrane, the correct end point was reached at a pH of 9.5 but not at 10.0. The correct end point was also reached at a pH as low as 3.0. It appears that the positive membranes can be used successfully for the determination of chloride ion over a pH range of 3.0–9.5.

The proteins used in these experiments were commercial preparations which were purified further to make sure that the electrolyte content was negligible.

The gelatin was purified by a method outlined by Schmidt (25). It was washed with dilute acetic acid at 5°C., washed with water at the same temperature, and electrodialyzed. It was then washed with ethanol and ether and finally dried. A

2 per cent stock solution of the gelatin and a 0.300 *N* stock solution of sodium chloride were prepared. Known volumes of the two solutions were mixed so that when the final dilution was made, the concentration of gelatin was 1.0 per cent and the concentration of sodium chloride was 0.100 *N*. Just before the final dilution was made the pH was adjusted to approximately the desired value by the addition of a small amount of either standard hydrochloric acid or standard sodium hydroxide. Thus, except in one instance the final sodium-ion concentration was not exactly equal to the chloride-ion concentration. In all cases the pH of the solution as it was finally prepared was measured with a pH meter. The pH of these solutions was varied from 4.0 to 8.2.

A second series of 1.0 per cent gelatin solutions was also prepared in which the final concentration of sodium chloride was 0.0100 *N* and in which the pH varied from 3.9 to 9.1.

The casein was precipitated at its isoelectric point by the addition of acid to an alkaline solution of casein. The precipitate was then thoroughly washed and finally extracted with methanol and dried. Solutions were prepared by adding a known amount of standard sodium hydroxide to weighed amounts of casein, and the solutions were then brought to approximately the desired pH by the addition of standard hydrochloric acid. Distilled water was then added so that the final casein concentration was always 1.0 per cent. The amount of standard base was chosen so that the final concentration of sodium was 0.100 *N* in one series and 0.0100 *N* in the other series. The chloride concentration varied from these figures, depending on the amount of standard acid needed to reach the desired pH. For the solution on the acid side of the isoelectric point, it was necessary to dissolve the casein in 0.0100 *N* hydrochloric acid and adjust the pH by the addition of standard sodium hydroxide. In all cases the pH of each solution was measured after the final dilution. The variation in pH was over the range 3.9–9.1.

III

We turn now to the measurement of the sodium chloride solutions containing 1 per cent gelatin and 1 per cent casein, respectively, the results of these determinations being given in tables 1–4. The first column in each table shows the pH of the solutions as measured with the pH meter. The second column gives the known concentration of the ion being studied that was added to the protein solution. In the third column is the activity of that ion calculated on the basis that it behaves as a completely dissociated ion in a solution of a uni-univalent electrolyte of the concentration given in column 2. To make this calculation, we have used the single ion activity coefficients as given by Lewis and Randall (12). Thus the figures in column 3 of the tables are obtained by multiplying the known concentration given in column 2 by the activity coefficient at that concentration.

In the fourth column is the measured activity of the ion being determined in the protein solutions. These values are obtained by multiplying the end point concentration of sodium chloride in the solution containing no protein by the activity coefficient for the ion in question. The ionic activity coefficients used here are the same as those used for the figures in column 3.

TABLE 1

Determination of the chloride-ion activities in 1 per cent gelatin solutions containing known concentrations of sodium chloride

(1) pH	(2) CONCENTRATION OF ADDED CHLORIDE ION	(3) CALCULATED ACTIVITY OF CHLORIDE ION	(4) MEASURED ACTIVITY OF CHLORIDE ION	(5) RELATIVE CHLORIDE-ION ACTIVITY: MEASURED ACTIVITY/CALCULATED ACTIVITY
8.2	0.100	0.079	0.080	1.01
6.0	0.100	0.079	0.080	1.01
5.0	0.102	0.080	0.079	0.99
4.0	0.103	0.081	0.081	1.00
8.1	0.0100	0.0092	0.0093	1.01
6.7	0.0100	0.0092	0.0094	1.02
4.5	0.0118	0.0107	0.0108	1.01
3.9	0.0128	0.0116	0.0116	1.00

TABLE 2

Determination of the sodium-ion activities in 1 per cent gelatin solutions containing known concentrations of sodium chloride

(1) pH	(2) CONCENTRATION OF ADDED SODIUM ION	(3) CALCULATED ACTIVITY OF SODIUM ION	(4) MEASURED ACTIVITY OF SODIUM ION	(5) RELATIVE SODIUM-ION ACTIVITY: MEASURED ACTIVITY/CALCULATED ACTIVITY
8.2	0.101	0.081	0.083	1.02
6.0	0.100	0.080	0.080	1.00
5.0	0.100	0.080	0.080	1.00
9.1	0.0115	0.0105	0.0107	1.02
8.1	0.0108	0.0099	0.0101	1.02
6.7	0.0100	0.0092	0.0093	1.01
4.5	0.0100	0.0092	0.0094	1.02

TABLE 3

Determination of the chloride-ion activities in 1 per cent casein solutions containing known concentrations of sodium chloride

(1) pH	(2) CONCENTRATION OF ADDED CHLORIDE ION	(3) CALCULATED ACTIVITY OF CHLORIDE ION	(4) MEASURED ACTIVITY OF CHLORIDE ION	(5) RELATIVE CHLORIDE-ION ACTIVITY: MEASURED ACTIVITY/CALCULATED ACTIVITY
9.0	0.087	0.069	0.070	1.01
7.6	0.091	0.073	0.074	1.01
5.9	0.095	0.075	0.074	0.99
5.2	0.0074	0.0069	0.0068	0.99
3.9	0.0100	0.0092	0.0094	1.02

Finally, in column 5 we have the ratio of the figures in columns 4 and 3, measured ion activity/calculated ion activity; this ratio is called the relative ion activity. If the relative activity is 1.00 ± 0.02, then we can conclude that the presence of the protein in the sodium chloride solution has not significantly changed the ionic activity. A value of less than 1.0 for this ratio indicates some kind of effect on the activity of the ion in question.

It should be pointed out here that any error in the single ion activity coefficients which we have used will cause no significant change in the ratios of column 5. These activity coefficients, based on extrathermodynamic assumptions, are used for both values in the ratio, and any error would cancel out. In other words, the results which we obtain are not necessarily the absolute ion activities but are only relative to sodium chloride solutions of known concentration.

TABLE 4

Determination of the sodium-ion activities in 1 per cent casein solutions containing known concentrations of sodium chloride

(1) PH	(2) CONCENTRATION OF ADDED SODIUM ION	(3) CALCULATED ACTIVITY OF SODIUM ION	(4) MEASURED ACTIVITY OF SODIUM ION	(5) RELATIVE SODIUM-ION ACTIVITY: MEASURED ACTIVITY/CALCULATED ACTIVITY
9.0	0.098	0.078	0.076	0.97
7.6	0.088	0.071	0.069	0.97
5.9	0.100	0.080	0.080	1.00
8.7	0.0100	0.0092	0.0069	0.75
8.0	0.0100	0.0092	0.0072	0.78
7.0	0.0100	0.0092	0.0082	0.89
5.2	0.0100	0.0092	0.0093	1.01

IV

The data of tables 1 and 2 show quite clearly that for every solution tested the activities of both chloride ion and sodium ion are unchanged by the presence of the gelatin. Even in the 0.0100 *N* solutions, the measured ion activities are the same as the calculated ion activities over a pH range of 4–9.

The results in table 3 show also that there is no measurable effect of casein on the activity of chloride ions in solution. Over a pH range of 3.9–9.0 and in 0.1 *N* and 0.01 *N* solutions the activity of the chloride ion is the same as in known sodium chloride solutions containing no casein.

With regard to the sodium ion in casein solutions, a different situation appears to exist. In solutions 0.1 *N* in sodium, at a pH above 7, there may be some interaction. The decrease in the values of the relative activities is just on the border line of being significantly lower than 1.0. In the more dilute solutions, however, it is quite evident that some kind of an effect exists at a pH of 7 and above. At a pH of 5.2 the relative activity is 1.01. As the pH increases the ratio becomes smaller and smaller. At pH 7 the activity of sodium ion in the outside solution at the end point of the titration is 11 per cent lower than the calculated activity of sodium ion in the casein solution. At pH 8.7 this difference has increased to 25 per cent.

Further experiments to confirm this effect for casein solutions have indicated that this decrease in sodium-ion activity is directly proportional to the amount of casein present. For example, at pH 7.5 and 0.02 *N* sodium concentration, the difference between the measured sodium-ion activity and the calculated sodium-ion activity in a 1 per cent casein solution is equivalent to 0.18 milliequivalent of sodium per gram of casein. In a 2 per cent casein solution of the same pH and sodium concentration this figure is 0.21 milliequivalent per gram, and in a 4 per cent casein solution it is 0.20 milliequivalent per gram. These three values are the same within the limits of error of the experiments.

Kirk and Schmidt (9) in their work measured the sodium-ion activity in casein solutions only at a pH of about 5.5. Their results also showed that in this pH range the casein has no detectable effect on the activity of sodium ions. They did not, however, make any measurements at higher pH's.

From our results it appears that in casein solutions which are slightly alkaline, the activity of sodium ions is appreciably depressed. However, further experiments will be necessary to confirm this point. For all the other cases studied the presence of either gelatin or casein does not affect the activity of either the sodium or the chloride ions.

These experiments indicate that the method offers a relatively simple technique for studying the problem of the interaction of proteins with small ions. For example, it would be of interest to confirm the binding of chloride and other small ions to serum albumin (24) by the use of this method. Another problem which can be attacked is the determination of the effect of the muscle proteins on the activity of potassium ion (4, 11, 22). Similarly, one could study the activity of ions in solutions of purified enzymes, especially those enzymes which are activated by the presence of such ions as magnesium, calcium, or chloride. Therefore we hope to continue this work along these lines.

SUMMARY

Specially prepared collodion membranes have been used as electrodes for the determination of sodium-ion activity in protein solutions. Similarly, protamine collodion membranes have been used for the determination of chloride-ion activity.

In 1 per cent solutions of gelatin containing known concentrations of sodium chloride, the activity of both the sodium and the chloride ions was found to be the same as in solutions of sodium chloride of the same concentration containing no protein. The concentrations of sodium chloride used were 0.1 *N* and 0.01 *N*; the pH of the solutions was varied from 3.9 to 9.1.

In 1 per cent solutions of casein containing known concentrations of sodium chloride, the activity of the chloride ions was found to be unaffected by the presence of the protein. The variation in salt concentration and pH was the same as for the gelatin experiments. The sodium-ion activity was the same as in

protein-free sodium chloride solutions at pH 5.2. At pH 7 and in 0.01 *N* sodium chloride solutions, however, the sodium-ion activity was found to be 11 per cent lower and at pH 8.7 was 25 per cent lower than in sodium chloride containing no casein.

The results indicate that the method will be applicable to the determination of the activity of many small ions in the presence of any water-soluble protein.

The authors wish to thank Dr. Karl Sollner for his helpful suggestions and criticisms in the preparation of the manuscript.

REFERENCES

(1) Carr, C. W., Gregor, H. P., and Sollner, K.: J. Gen. Physiol. **28,** 179 (1945).

(2) Carr, C. W., Johnson, W. F., and Kolthoff, I. M.: J. Phys. & Colloid Chem. **51,** 636 (1947).

(3) Carr, C. W., and Sollner, K.: J. Gen. Physiol. **28,** 119 (1944).

(4) Fenn, W. O.: Physiol. Rev. **16,** 450 (1936).

(5) Gregor, H. P.: Ph.D. Thesis, University of Minnesota, 1945.

(6) Gregor, H. P., and Sollner, K.: J. Phys. Chem. **50,** 53, 88 (1946).

(7) Hitchcock, D. I.: J. Gen. Physiol. **12,** 495 (1928).

(8) Ingraham, R. C., Lombard, C., and Visscher, M. B.: J. Gen. Physiol. **16,** 637 (1932–33).

(9) Kirk, P. L., and Schmidt, C. L. A.: J. Biol. Chem. **76,** 115 (1928).

(10) Klotz, I. M., and Urquhart, J. M.: J. Phys. & Colloid Chem. **53,** 100 (1949).

(11) Kometiani, P. A.: Biokhimiya **13,** 137 (1948).

(12) Lewis, G. N., and Randall, M.: *Thermodynamics*, p. 382. McGraw-Hill Book Company, Inc., New York (1923).

(13) Longsworth, L. G., and Jacobsen, C. F.: J. Phys. & Colloid Chem. **53,** 126 (1949).

(14) Marshall, C. E., and Ayers, A. D., J. Am. Chem. Soc. **70,** 1297 (1948).

(15) Marshall, C. E., and Bergman, W. E.: J. Am. Chem. Soc. **63,** 1911 (1941).

(16) Marshall, C. E., and Bergman, W. E.: J. Phys. Chem. **46,** 325 (1942).

(17) Marshall, C. E., and Eime, L. O.: J. Am. Chem. Soc. **70,** 1302 (1948).

(18) Marshall, C. E., and Krinbill, C. A.: J. Am. Chem. Soc. **64,** 1814 (1942).

(19) Michaelis, L., and Kawai, S.: Biochem. Z. **163,** 1 (1925).

(20) Neuhausen, B. S., and Marshall, E. K., Jr.: J. Biol. Chem. **53,** 365 (1922).

(21) Northrop, J. H., and Kunitz, M.: J. Gen. Physiol. **7,** 25 (1924–25).

(22) Peters, J. P.: Physiol. Rev. **24,** 491 (1944).

(23) Ringer, W. E.: Z. physiol. Chem. **130,** 270 (1923).

(24) Scatchard, G., and Black, E. S.: J. Phys. & Colloid Chem. **53,** 88 (1949).

(25) Schmidt, C. L. A.: *Chemistry of the Amino Acids and Proteins*, p. 174. Charles C. Thomas, Baltimore (1944).

(26) Sollner, K.: J. Am. Chem. Soc. **65,** 2260 (1943).

(27) Steinhardt, J.: Ann. N. Y. Acad. Sci. **41,** 287 (1941).

(28) Velick, S. F.: J. Phys. & Colloid Chem. **53,** 135 (1949).

(29) Wyllie, M. J. R., and Patnode, H. W.: J. Phys. & Colloid Chem. **54,** 204 (1950).

THE MECHANISM OF DIFFUSION OF IONS ACROSS A PHASE BOUNDARY AND THROUGH CELL WALLS[1]

J. T. DAVIES[2, 3]

Department of Chemistry, Stanford University, California

Received August 22, 1949

INTRODUCTION

Although the problem of the diffusion of material across the plasma membrane of a living cell has been studied for many years, there is still considerable controversy over the cause of the widely differing diffusion rates and correlation of these with a picture of the structure of the cell wall. Since the diffusion of *ions* is known to proceed often against concentration gradients and is frequently much slower than that of *nonelectrolytes*, it is perhaps inevitable that more progress has been made in interpreting the permeability figures of the latter in terms of oil–water partition coefficients, molecular size, molecular weight, polarity, temperature, and, in some cases, also the pore diameter of the cell wall. The work of Collander and of Overton must be specially noted in this connection (16, 19, 22, 46, 50, 55). Even under the most favorable conditions for diffusion, when we consider a nonionic solute (e.g., triethyl citrate (16)), equally soluble in the oil and in the aqueous phases, the diffusion constant is about 100,000 times smaller than that in water. Most diffusing electrolytes and nonelectrolytes have still lower diffusion rates across the cell wall.

These figures have been previously explained partly in terms of a high viscosity in the cell membrane, but recourse must also be had to an arbitrary "probability" factor (22). The present work is an attempt to understand the physical diffusion process occurring at the phase boundaries.

Although recent optical (51) and electron microscopic (54) examinations of the erythrocyte membrane and the use of radioactive tracers have advanced our understanding of the penetration of *ions* into cells, up until the present time the concept of charged pores in the cell membrane has largely dominated ideas of the nature of the process.

Wolpers (54) found that the electron microscope showed the membrane of the erythrocyte to be made of a framework of protein in a lipid phase, a conclusion previously suggested from examinations with the polarizing microscope (51); on the basis of these findings the correlation of the oil solubility and rate of transfer of material has been extended in the present paper from nonelectrolytes to salts of physiological importance, using a model interface between water and nitrobenzene.

It has been previously suggested (22) that orientation of the lipids at the surface is often of great importance in the diffusion process, but investigation of the transmission of ions through a water–oil interface has not, in this work or that of Sjölin (52), given any indication that films of lipids or proteins can influence the diffusion rate. In the case of the diffusion of the lower aliphatic alcohols, however, Hutchinson (31) found that a detergent film retarded considerably the diffusion from water to benzene.

---

[1] Presented in part at the Twenty-third National Colloid Symposium, which was held under the auspices of the Division of Colloid Chemistry of the American Chemical Society at Minneapolis, Minnesota, June 6–8, 1949.

[2] Bristol Myers Company Postdoctorate Fellow and Research Associate in Chemistry.

[3] Present address: Royal Institution, 21 Albemarle Street, London W. 1, England.

The thickness of the erythrocyte membrane has been found to be greater than some investigators formerly believed, and is probably between 120 and 250 Å. (53, 54), so that the membrane may with more justification be considered a separate phase, with the relatively high value of between 12 and 25 for its dielectric constant (15). It may be noted that salts are slightly soluble in oils of dielectric constants of this order. In the past much work has been carried out in investigation of the potentials at oil–water interfaces. Phenol, cresol, and nitrobenzene have been found to be convenient oils in such studies. Special mention must be made of the careful work of Nernst (41, 42), Beutner (6), and Osterhout (43). Although relative mobilities of anions and cations may be obtained from such measurements, electrical potentials alone cannot give actual ionic speeds, but only their ratios. The suggestion has repeatedly been made that the rate of transfer of a solute across a phase boundary is a very slow process, even with a clean surface and liquids of low viscosity. Although Lewis and Whitman (37), as long ago as 1924, realized that transfer from one phase to another was a slow process, the experiments of Irwin (34) and Sjölin (52) placed this idea on a firmer basis. It is proposed here to put forward a physical theory of this rate process for the particular case of the diffusion of ions across the nitrobenzene–water interface.

EXPERIMENTAL

Procedure

The diffusion cell, somewhat similar to that of Sjölin (52), was constructed of Pyrex glass and is shown diagrammatically in figure 1. In the lower portion of the cell and covering the electrodes was pure nitrobenzene, previously equilibrated with conductivity water in a thermostat at the temperature at which the diffusion was to be measured. On top of this was the solution of electrolyte in conductivity water, which had previously been equilibrated with nitrobenzene.

The rates of diffusion were obtained from the decrease in resistance of the nitrobenzene with time, as the salt diffused into it. The resistance was measured with a Leeds & Northrup bridge with a Wagner ground, using A.C. at about 0.1 v. A narrow band amplifier in connection with a cathode ray oscilloscope was used to determine the balance point. A frequency of 500 cycles per second was found satisfactory in most runs, but where the salt concentration in the nitrobenzene was high, it was necessary to use 2000 cycles per second to avoid polarization. In the absence of polarization, resistances at the two frequencies were very close.

Constant temperature in the diffusion cell was maintained by circulating water through the outer glass vessel.

The platinum electrodes were each 4 x 1 cm. and were placed about 2 mm. apart. Copper wires leading from them terminated in mercury cups. Initially, bright platinum was tried, but polarization occurred even in the very dilute solutions of salts in nitrobenzene, so a light coat of platinum black was deposited. With this separation of the electrodes, the resistance of nitrobenzene in equilibrium with aqueous potassium iodide was about 3000 ohms.

During the diffusion run, the nitrobenzene was stirred steadily at 100 R.P.M. with a stirrer consisting of two small fins attached to a glass rod, ground to fit into a depression in the bottom of the vessel. A stationary glass tube enclosed the stirring rod where it passed through the interface. Slight undulations of the surface due to the stirring were inevitable, since the density of the aqueous salt solutions was but slightly less than that of the nitrobenzene. Extrapolation to zero rate of stirring, as explained below, minimized the errors from this cause. Partition coefficients were measured by allowing the diffusion to proceed for 24 hr. and measuring the conductivity of the oil phase or by finding the value from which the observed conductivities must be subtracted to obtain a linear logarithmic plot against time. Where both methods were employed the agreement was good, but because of slow decomposition of the iodides, the second method was generally used.

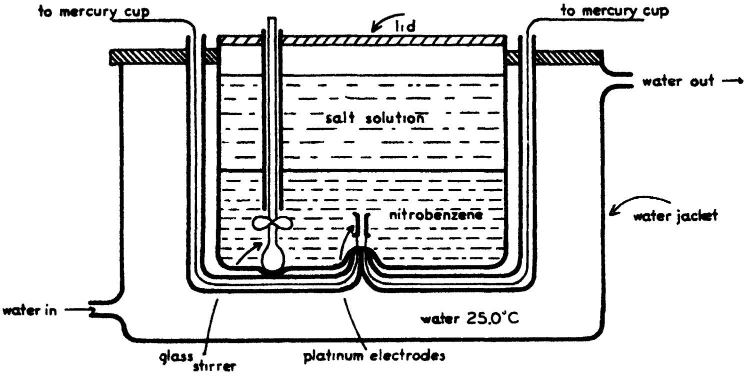

FIG. 1. Diagram of the diffusion cell

Films were spread from a micrometer syringe into the interface. The film pressures were measured by means of a Wilhelmy surface balance by the method of Cheesman (11). The upper rim of the cell was ground so that a flat lid, with holes for the stirrer and hanging plate, minimized evaporation of water. At the beginning of each run, the interface was sucked clean with a capillary attached to a water pump.

Preparation of materials

Water was obtained from an all-glass conductivity still.

Eastman nitrobenzene was redistilled in an all-Pyrex apparatus to remove surface-active materials. Between runs the nitrobenzene was cleaned either by re-distillation or by shaking it for 10 min. with water, and allowing it to stand in contact with water for 48 hr. These treatments were found to remove all traces of dissolved salt.

The salts potassium chloride, potassium bromide, potassium iodide, sodium iodide (all C.P.) and tetraethylammonium iodide (Kahlbaum) were used without further purification.

Lithium iodide (Kahlbaum), rubidium iodide (de Haën), and tetra-*n*-butylammonium iodide (Eastman) were purified by shaking the aqueous solutions with Florisil.

Lecithin *ex ovo* (Pfanstiehl) was purified by the method of Bungenberg de Jong *et al.* (10). Lecithin and cephalin were spread from solutions in redistilled *n*-propyl alcohol. Gliadin was spread from 60 per cent ethanol solution.

Before each run the cell was cleaned with hot chromic acid. To remove any adsorbed chromate ions, the cell was washed several times with hot tap water, followed by a wash with syrupy phosphoric acid. After further rinsing with hot tap water, the cell was washed three times with conductivity water and then dried in an air oven.

The cell was calibrated with nitrobenzene in equilibrium at 25°C. with 1 N aqueous potassium iodide. Then the concentration of potassium iodide in the oil was 1/[5450 ± 100] (33) and the resistance was 3350 ohms.

RESULTS

The diffusion of potassium iodide and the other inorganic salts from water to nitrobenzene was found to obey the equation:

$$\frac{1}{A} \cdot \frac{dn}{dt} = kc_1 - k_r c_2 \qquad (1)$$

where c_1 = the concentration of salt in the aqueous phase,
c_2 = the concentration of salt in the oil phase,
A = the area through which diffusion occurs,
$\frac{dn}{dt}$ = the diffusion rate (in moles sec.$^{-1}$), and

k and k_r are expressed in cm. sec.$^{-1}$ and are the forward and reverse permeability constants for a given electrolyte at constant temperature. Concentrations at equilibrium will be denoted by the subscript e.

Under the experimental conditions the volumes of aqueous solution and nitrobenzene (320 ml.) were about equal, so c_1 was practically unaltered during the diffusion, since c_2 is at all times small. Potassium chloride is known to be very insoluble in nitrobenzene, so in this case c_1 was 2.69 N. For all other salts used, however, c_1 was 1 N, except that, because of its low partition coefficient, tetra-*n*-butylammonium iodide was made up to be 0.06 N to prevent the concentration in the oil from becoming so high as to cause extensive association into "ion pairs." In this case and in that of tetra-*n*-butylammonium iodide, equation 1 was modified for variations of c_1 with time.

In all cases initially $c_2 = 0$, and the equation

$$\frac{1}{A} \cdot \frac{dn}{dt} = kc_1$$

is obeyed when t is small. dn/dt is proportional to the rate of change of conductance, and since k and c_1 are constant, the plot of conductance against time should be linear at first. This is what was indeed observed (figure 2), and k can be calculated approximately from the slope of the line. A in all cases is 71.5 cm.[2]

TABLE 1

SALT	B (WATER/$C_6H_5NO_2$) (25.0°C.)	k (25.0°C.)	k_r (25.0°C.)	D IN H_2O (13°C.)	D^* IN $C_6H_5NO_2$ (20) (25°C.)
		cm. sec.$^{-1}$	*cm. sec.*$^{-1}$	*cm.*^{2} *sec.*$^{-1}$	*cm.*^{2} *sec.*$^{-1}$
LiI	1.0×10^5	9.5×10^{-10}	1.0×10^{-4}	0.9×10^{-5}	4.4×10^{-6}
NaI	3.9×10^4	3.9×10^{-9}	1.5×10^{-4}	1.1×10^{-5}	5.0×10^{-6}
KI	5.5×10^3	2.7×10^{-8}	1.5×10^{-4}	1.4×10^{-5}	5.3×10^{-6}
RbI	4.0×10^3	6.2×10^{-8}	2.5×10^{-4}	1.4×10^{-5}*	5.5×10^{-6}
$(C_2H_5)_4NI$	4.5×10^1	3.9×10^{-6}	1.8×10^{-4}	0.8×10^{-5}*	5.0×10^{-6}
n-$(C_4H_9)_4NI$	8.6×10^{-1}	1.4×10^{-4}	1.2×10^{-4}	0.6×10^{-5}*	4.3×10^{-6}
KCl	2.3×10^5	1.4×10^{-10}	0.33×10^{-4}	1.4×10^{-5}	4.9×10^{-6}
KBr	1.1×10^5	1.5×10^{-9}	1.6×10^{-4}	1.4×10^{-5}	5.2×10^{-6}
KI	5.5×10^3	2.7×10^{-8}	1.5×10^{-4}	1.4×10^{-5}	5.3×10^{-6}

* Calculated from ionic mobility data.

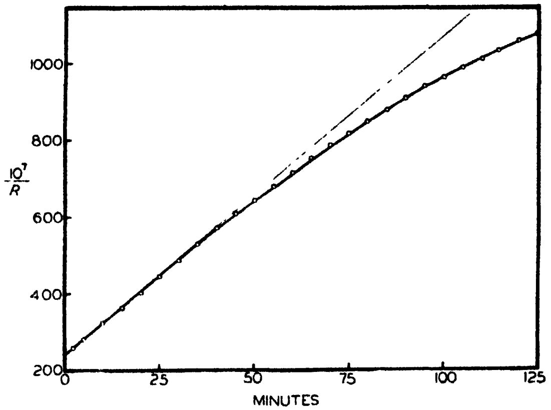

FIG. 2. Variation of conductance (× 10^7) of nitrobenzene phase with time, in the initial state of the diffusion process. 1 N potassium iodide in aqueous phase; temperature, 25°C.; stirrer, 100 R.P.M.

When equation 1 is integrated, it is seen that the plot of log $((c_2)_e - c_2)$ against t gives a constant slope of $Ak_r/V \times 2.303$, where V is the volume of nitrobenzene (figure 3). Values of k_r thus calculated and corrected as described below are given in table 1. From k_r and the partition coefficient B can be obtained the exact value of k, since $Bk = k_r$. B was obtained directly from $(c_2)_e$.

It is known (24, 48) that salts in solvents of dielectric constant as high as that of nitrobenzene (36.1 at 20°C.) are about 98–99 per cent dissociated in 10^{-4} N solution, and about 93 per cent in 10^{-3} N solution, so that no correction was applied for incomplete dissociation except in the runs using tetraethyl- and tetra-*n*-butylammonium iodides, when the equation

$$v^{1/3} = \frac{\text{constant}}{1 - \alpha}$$

where v is the dilution and α the degree of dissociation (24), was used in the conversion of conductances into concentrations. Correction was also made for the specific conductances (20) of the different salts in nitrobenzene relative to that of potassium iodide. No allowance was made for small quantities of water present in the oil, but since relative mobility figures were used, this omission will not be important.

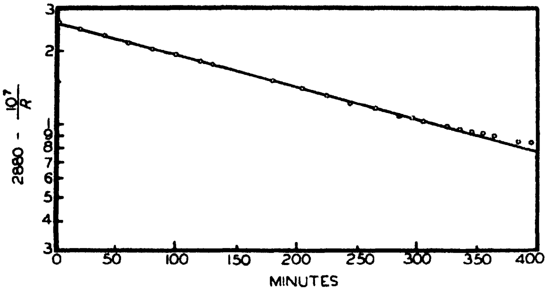

FIG. 3. Logarithmic plot of difference of conductances of the nitrobenzene phase at equilibrium and at various times *vs*. time in minutes. 1 N potassium iodide in aqueous phase; temperature, 25°C.; stirrer, 100 R.P.M.

It was also necessary to make a correction for the rate of stirring. It was found that increasing the rate of stirring accelerated the diffusion, as found by Sjölin (52). The rate figures were therefore corrected to zero rate of stirring by multiplying by a factor of 0.58, found by comparing the rates when stirring was carried out immediately before taking a reading (to circulate the oil solution between the electrodes) and when the stirrer rotated at the usual speed of 100 R.P.M.

All the values quoted have been corrected for mobility and stirring errors, and those for tetraethylammonium iodide and tetra-*n*-butylammonium iodide are corrected for incomplete ionization. The permeability constants k and k_r may be compared with values of the diffusion constants in water and in nitrobenzene (20) (table 1).

The specific resistance of the water-saturated nitrobenzene was initially about 8×10^6 ohms, and this was always measured and allowed for in the calculation of B. In the case of equilibrium with 2.69 N aqueous potassium chloride, the specific resistance of the oil decreases to about 9×10^5 ohms. These small changes have previously made measurements of partition coefficients of such sparingly soluble materials too difficult (43).

Films of lecithin, cephalin, and gliadin (up to 16 dynes cm.$^{-1}$) were without effect on the rate of transmission of potassium iodide through the water–nitrobenzene interface. Films of lecithin and cephalin were stable only when calcium ion ($N/200$) was present, an observation previously made for cephalin at the benzene–water interface (2). Even in the presence of 10^{-3} M copper ion and with pH values of the aqueous phase between 2 and 11 (the usual value was 5.5) the diffusion rate was unaffected.

DISCUSSION

It has long been realized that partition coefficients play an important part in diffusion rates of nonelectrolytes from one phase to another (16, 19, 44, 45, 46, 49). The rates of penetration of many undissociated molecules from water to oils and through plant cell walls are approximately inversely proportional to the partition coefficient of the solute between water and oil. So far, however, only a few incomplete observations have been made on the diffusion kinetics of ions across such interfaces (41, 43, 52), and the mechanism and theory of such processes have not been elucidated. Recently Barrer (3, 4) has pointed out that diffusion may occur with, as well as against, a concentration gradient in a three-component system at a rate proportional to the product of the chemical potential gradient and the concentration. His equation can be used to derive a diffusion equation similar to that in the present work, as can also the general empirical diffusion equation developed by Daniel (18) in connection with ternary alloys. However, these equations were developed for neutral molecules.

The equation used in the present work applies to completely ionized electrolytes and may be derived from first principles as follows:

u and v are the velocities under unit potential gradient of cations and anions, respectively, in the diffusion process across the interface. E is the electrical diffusion potential at the interface. x is the coördinate perpendicular to the plane of the surface, of area A. μ^0_+ and μ^0_- are the standard chemical potentials of the cations and anions, respectively. F is the Faraday unit. $B = (c_1/c_2)_e$ is the partition coefficient. Subscript e refers to equilibrium conditions, when $t \to \infty$.

Generalizing by the addition of a term for the chemical potential gradient the equation of Nernst (42), we may write for diffusion from water to oil ($B \gtrless 1$),

$$\text{Velocity of cations} = -\frac{u\,\mathrm{d}E}{\mathrm{d}x} - \frac{uRT}{c_1F}\frac{\mathrm{d}c}{\mathrm{d}x} - \frac{u}{F}\frac{\mathrm{d}\mu^0_+}{\mathrm{d}x} \tag{2}$$

$$\text{Velocity of anions} = +v\frac{\mathrm{d}E}{\mathrm{d}x} - \frac{uRT}{c_1F}\frac{\mathrm{d}c}{\mathrm{d}x} - \frac{v}{F}\frac{\mathrm{d}\mu^0_-}{\mathrm{d}x} \tag{3}$$

$$\begin{aligned}\frac{\mathrm{d}n}{\mathrm{d}t} &= -uA\left(\frac{c_1\,\mathrm{d}E}{\mathrm{d}x} + \frac{RT}{F}\frac{\mathrm{d}c}{\mathrm{d}x} + \frac{c_1}{F}\frac{\mathrm{d}\mu^0_+}{\mathrm{d}x}\right)\\ &= +vA\left(\frac{c_1\,\mathrm{d}E}{\mathrm{d}x} - \frac{RT}{F}\frac{\mathrm{d}c}{\mathrm{d}x} - \frac{c_1}{F}\frac{\mathrm{d}\mu^0_-}{\mathrm{d}x}\right)\end{aligned} \tag{4}$$

Solving for $\frac{dE}{dx}$,

$$\frac{dE}{dx} = -\frac{(u-v)}{(u+v)}\frac{RT}{c_1 F}\frac{dc}{dx} - \frac{1}{F(u+v)}\left(\frac{u\,d\mu_+^0}{dx} - \frac{v\,d\mu_-^0}{dx}\right) \tag{5}$$

This expression reduces to that of Nernst (42) if the medium is homogeneous, since in this case $d\mu_+^0 = 0 = d\mu_-^0$.

If the value of dE/dx from equation 5 is substituted into equation 4, it follows that

$$\frac{1}{A}\frac{dn}{dt} = -\frac{2RT}{F}\left(\frac{uv}{u+v}\right)\frac{dc}{dx} - \frac{c_1}{F}\left(\frac{uv}{u+v}\right)\left(\frac{d\mu_+^0 + d\mu_-^0}{dx}\right) \tag{6}$$

Now, at equilibrium, the chemical potential μ of the salt must be the same everywhere in the system, so that $d\mu = 0$. But since

$$\mu_+ = \mu_+^0 + RT \ln (c)_e \quad \text{and} \quad \mu_-^0 = \mu_-^0 + RT \ln (c)_e$$

$$0 = d\mu_+^0 + d\mu_-^0 + d(2RT \ln (c)_e) \tag{7}$$

Hence

$$d\mu_+^0 + d\mu_-^0 = \frac{-2RT}{(c_1)_e}\, d(c)_e$$

therefore

$$\frac{1}{A}\frac{dn}{dt} = -\frac{2RT}{F}\left(\frac{uv}{u+v}\right)\left(\frac{dc}{dx} - \frac{c_1}{(c_1)_e}\frac{d(c)_e}{dx}\right) \tag{8}$$

Under the conditions obtaining experimentally

$$c_1 = (c_1)_e = \text{constant} \tag{9}$$

therefore

$$\frac{1}{A}\frac{dn}{dt} = -\frac{2RT}{F}\left(\frac{uv}{u+v}\right)\left(\frac{dc}{dx} - \frac{d(c)_e}{dx}\right) \tag{10}$$

Assuming that the concentration gradient is uniform across the interface,

$$\frac{1}{A}\frac{dn}{dt} = -\frac{2RT}{F}\left(\frac{uv}{u+v}\right)\left(\frac{\Delta c}{\Delta x} - \frac{\Delta(c)_e}{\Delta x}\right) \tag{11}$$

$$= -\frac{2RT}{F}\left(\frac{uv}{u+v}\right)\left[\frac{(c_2 - c_1) - (c_2 - c_1)_e}{\Delta x}\right] \tag{12}$$

or, by equation 9,

$$\frac{1}{A}\frac{dn}{dt} = -\frac{2RT}{F}\left(\frac{uv}{u+v}\right)\left(\frac{c_2 - (c_2)_e}{\Delta x}\right) \tag{13}$$

But

$$B = \frac{(c_1)_e}{(c_2)_e} \doteq \frac{c_1}{(c_2)_e} \tag{14}$$

Hence

$$\frac{1}{A}\frac{dn}{dt} = \frac{2RT}{F\Delta x}\left(\frac{uv}{u+v}\right)\left(\frac{c_1}{B} - c_2\right) \tag{15}$$

In the experimental work described here, the expression

$$\frac{1}{A}\frac{dn}{dt} = kc_1 - k_r c_2 \tag{1}$$

has been used, where k and k_r are the forward and reverse rate constants (expressed in cm. sec.$^{-1}$) for the diffusion of salt from water to nitrobenzene.

Although it is clear from equilibrium considerations for any substance that

$$\frac{k_r}{k} = B$$

the values of k and k_r for *different diffusing electrolytes* can only be interpreted by comparing equations 1 and 15, when it is seen that

$$k = \frac{2RT}{F\Delta x}\frac{1}{B}\left(\frac{uv}{u+v}\right) \tag{16}$$

$$k_r = \frac{2RT}{F\Delta x}\left(\frac{uv}{u+v}\right) \tag{17}$$

The same result may be derived from the empirical equation for the diffusion of copper in alloys advanced by Daniel (18).

$$\frac{\partial(c_e - c)}{\partial t} = D\frac{\partial^2(c_e - c)}{\partial x^2} \tag{18}$$

Integrating,

$$\frac{\partial(n - (n)_e)}{A\cdot\partial t} = D\frac{\partial(c_e - c)}{\partial x} \tag{19}$$

where, as before, $\partial n/\partial t$ is the rate of passage of material into the oil. Hence,

$$\frac{1}{A}\frac{\partial n}{\partial t} = D\left(\frac{\partial(c)_e}{\partial x} - \frac{\partial c}{\partial x}\right) \tag{20}$$

Assuming again a linear concentration gradient at the interface,

$$\begin{aligned}\frac{1}{A}\frac{\partial n}{\partial t} &= D\left(\frac{(c_2)_e - (c_1)_e - (c_2 - c_1)}{\Delta x}\right)\\ &= D\left[\frac{(c_2)_e - c_2}{\Delta x}\right]\\ &= \frac{D}{\Delta x}\left(\frac{c_1}{B} - c_2\right)\end{aligned} \tag{21}$$

Equation 21 becomes identical with equation 15 if

$$D = \frac{2RT}{F}\left(\frac{uv}{u+v}\right) \tag{22}$$

Barrer (4) pointed out that diffusion occurs under the influence of the chemical potential gradient, $\partial\mu/\partial x$, which represents the force on *each* particle, so on all the particles the driving force is proportional to $c\partial\mu/\partial x$. The diffusion equation then becomes

$$\frac{\partial c}{\partial t} = \frac{\partial}{\partial x}\left(Dc\frac{\partial\mu}{\partial x}\right) \tag{23}$$

Barrer (4) uses the activity, a, of the solute, substituting

$$\partial\mu = RT\,\partial \ln a$$

This can be shown to give an equation of the type derived from Daniel's formula when similar assumptions are made. It is of interest to note that if $B \leqslant 1$ and c_2 is constant, equation 11 gives

$$\frac{1}{A}\frac{\mathrm{d}n}{\mathrm{d}t} = -\frac{2RT}{F\Delta x}\left(\frac{uv}{u+v}\right)(-c_1 + B(c_2)_e) \tag{24}$$

which in the case of diffusion from water to oil corresponds to

$$\frac{1}{A}\frac{\mathrm{d}n}{\mathrm{d}t} = kc_1 - k_rc_2 \tag{25}$$

where

$$k = \frac{2RT}{F\Delta x}\left(\frac{uv}{u+v}\right) \tag{26}$$

and

$$k_r = \frac{2RT}{F\Delta x}B\left(\frac{uv}{u+v}\right) \tag{27}$$

so that $k_r \ll k$, while k is now independent of B and k_r varies directly as B.

The various types of system may be easily understood by reference to the free energy diagram (figure 4) showing the energy hill over which the ions must pass to diffuse from water to oil. When $B > 1$, as is usually the case, the barrier to diffusion from water to oil includes the partition coefficient energy hill, so that this process is retarded. The reverse process can be seen not to depend kinetically on the partition coefficient. When a solute is very soluble in oil, and $B < 1$, then k_r is correspondingly decreased, since the ion in passing out of the oil has now to surmount the partition coefficient energy hill as well as that of the simple diffusion process. Under these conditions, however, the rate of transmission from water to oil is independent of B.

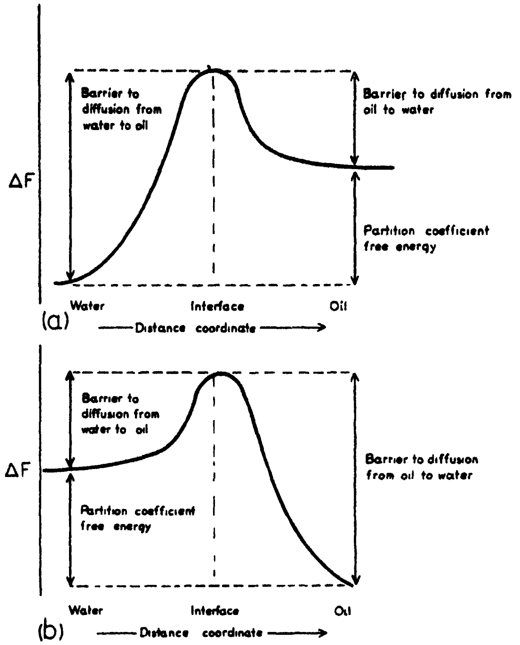
ΔF
Barrier to diffusion from water to oil
Barrier to diffusion from oil to water
Partition coefficient free energy
Water
Interface
Oil
(a)
Distance coordinate
ΔF
Barrier to diffusion from water to oil
Partition coefficient free energy
Barrier to diffusion from oil to water
Water
Interface
Oil
(b)
Distance coordinate

FIG. 4. Free energy barriers at the interface between water and oil. (a) Energy barrier between water and oil, $B > 1$; (b) energy barrier between water and oil, $B < 1$.

In the investigation described in this paper, $B \gg 1$, so equation 15 is applicable. Use is then made of the logarithmic form of equation 16.

$$\log k = \log\left(\frac{2RT}{F\Delta x}\right) - \log B + \log\left(\frac{uv}{u+v}\right)$$

which reduces to

$$\log k = \text{constant} - \log B + \log\left(\frac{uv}{u+v}\right) \tag{28}$$

if Δx, the length of the diffusion path, is constant.

Deviations from proportionality between k and $1/B$ are then due to variations in ionic mobilities. If, as a first approximation, we consider $uv/(u + v)$ constant for different electrolytes, then the plot of $-\log k$ against $\log B$ should be a straight line of slope +1. That this is true is confirmed from figure 5. Slight deviations from linearity in these diffusion results at the water–nitrobenzene interface indicate that there are small variations in u and v for the different ions, as is to be expected by analogy with bulk diffusion results. The results of Hutchinson (31, 32) for the diffusion of alcohols across the water–benzene interface, recalculated to absolute units, also lie on a straight line of slope +1, but it is seen that the mobility of the alcohol molecules is about 32 times greater than that of the ions at equal values of the partition coefficient.

For the ions, u and v are of the order of 10^6 times less than in homogeneous systems if the thickness of the interface be taken as 10 Å. The partition coefficient of potassium iodide being about 10^3, the diffusion constant from water to nitrobenzene is smaller than in bulk diffusion by a factor of 10^9.

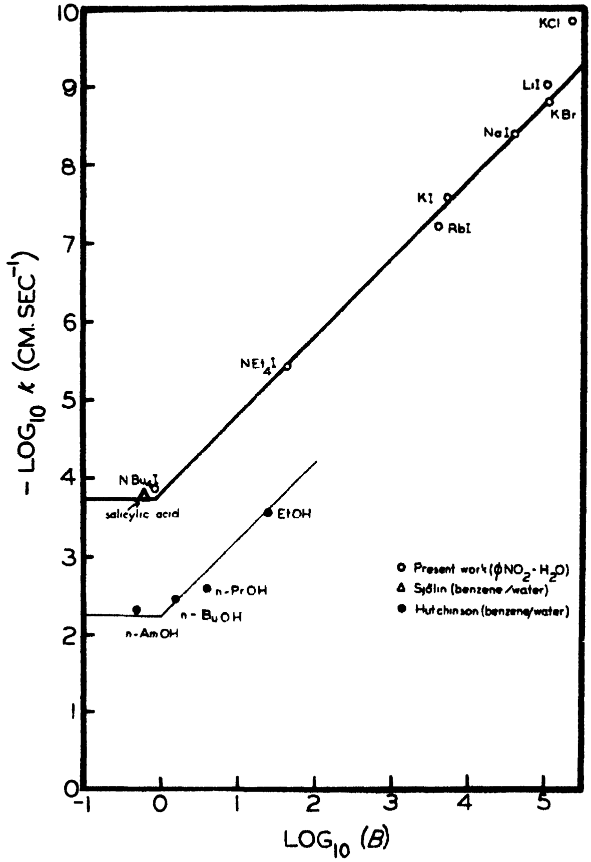

FIG. 5. log $(1/k)$ *vs.* logarithm of partition coefficients. Diffusion of different salts into nitrobenzene at 25°C. Included also are the recalculated results of Hutchinson and Sjölin. The straight lines passing through points for which log $B > 0$ are of slope +1.

THERMODYNAMICS OF INTERFACIAL DIFFUSION

The rate of passage of ions across the water–oil interface from water into oil depends on the rate at which ions strike the surface and on the probability of an ion possessing sufficient free energy to cross the energy barrier (figure 4). The collision rate is given (1) by $c_1 A \left(\frac{RT}{2\pi m}\right)^{1/2}$, where $R = 8.32 \times 10^7$ dynes cm.; T is the absolute temperature, and m is the mass of the ion. The probability factor is given by $e^{-\Delta F^*/RT}$, ΔF^* being the height of the free energy hill in the transition state. The observed rate is given by c_1Ak, so that

$$c_1Ak = c_1A\left(\frac{RT}{2\pi m}\right)^{1/2} e^{-\Delta F^*/RT}$$

or

$$e^{\Delta F^*/RT} = \frac{1}{k}\left(\frac{RT}{2\pi m}\right)^{1/2}$$

$m^{1/2}$ here denotes the quantity $\frac{\sqrt{m_+} + \sqrt{m_-}}{2}$, where m_+ and m_- are the gram-molecular weights of anion and cation.

In the case of potassium iodide at 25.0°C. at the water–nitrobenzene interface, $k = 2.7 \times 10^{-8}$ cm. sec.$^{-1}$, $m^{1/2} = 8.76$, $T = 298.1$, so that

$$e^{\Delta F^*/RT} = 2.66 \times 10^{11}$$

or

$$\Delta F^* = 15{,}700 \text{ cal. mole}^{-1}$$

For the reverse process under the same conditions,

$$\Delta F_r^* = 10{,}600 \text{ cal. mole}^{-1}$$

the difference of 5100 cal. mole^{-1} being equal to the equilibrium partition coefficient standard free energy change, calculated from $e^{\Delta F/RT} = B$ (figure 4).

The process of diffusion of an ion across the interface from nitrobenzene to water thus requires *free energy* to the extent of 10,600 cal. mole^{-1}, a value much greater than the 3000 cal. mole^{-1} (approximately) for the activation free energy in bulk diffusion (27).

TABLE 2

Diffusion of potassium iodide from nitrobenzene to water at different temperatures

T	k_r
°C.	*cm. sec.*$^{-1}$
25.0	1.5×10^{-4}
44.3	2.4×10^{-4}
61.3	2.9×10^{-4}
66.5	3.9×10^{-4}

The effect of temperature (table 2) gives the ΔH_r^* value, connected with ΔF_r^* by the identity:

$$\Delta F_r^* = \Delta H_r^* - T\Delta S_r^*$$

where ΔS_r^* is the entropy of diffusion.

Substituting $\Delta H_r^* = 4600$; $\Delta F_r^* = 10{,}600$

$$T\Delta S_r^* = -6000$$

$$\therefore \Delta S_r^* = -20 \text{ E.U.}$$

A very large negative entropy of activation is unusual in diffusion processes, most substances diffusing with a very small ΔS^*, or sometimes with a positive value of a few units (27).

The mechanism of the diffusion process at the interface probably consists in the progressive diffusion of solvate molecules away from the solute molecule or ion, so that the large negative entropy of diffusion is related to the removal, in a selective order, of many such solvate molecules, one by one, in the process of replacing them all by the new solvate. The energy hill for simultaneous removal of all the nitrobenzene molecules held by ion–dipole forces around the ions would be impossibly high ($\backsim$40,000 cal. mole^{-1}), so that the ion cannot pass the boundary into the aqueous phase until vigorous solvent collisions have given each coördinated nitrobenzene molecule enough energy to break away. Thus the negative entropy means that the probability of a solvated ion passing across the interface is low, and that the solvate molecules must be exchanged in a selective manner.

The ΔH_r^* value for each solvate molecule is made up of two components:

(*1*) The mean activation energy of diffusion of one solvate molecule away from the vicinity of the ion, essentially a process of self-diffusion of the molecules.

(*2*) The electrical work done in removing the dipole of the solvent molecule away from the ion.

For the first component, a value of 3000 cal. mole^{-1} is probably a good approximation (27). The second may be obtained from the relative rates of interfacial diffusion of ionic and nonionic solutes, when B and T are constant. The data of Hutchinson (31, 32) for the diffusion of alcohols at the water-benzene interface show that k_r is greater than for the diffusion of ions by a factor of 32, which corresponds to a free energy decrease of 2000 cal. mole^{-1}. Assuming the entropy of activation of the process has not changed, this is also the increment in ΔH_r^*.

The agreement of the values ΔF_r^* found above, and that calculated from

$$\Delta F_r{}^* = \Delta H_r{}^* - T\Delta S_r{}^*$$

can now be checked, since $\Delta H_r^* = 5000$, and $T\Delta S_r^* = -6000$. So $\Delta F_r^* =$ 11,000 cal. mole^{-1}, in good agreement with the value 10,600 cal. mole^{-1}, obtained above.

The electrical field around a small ion is more intense than that near a large ion, so that the 2000 cal. mole^{-1} contribution to ΔH_r^* will decrease as the size of the ion increases, so that, comparing values of k_r, we should find

$$\mathrm{Rb}^+ > \mathrm{K}^+ > \mathrm{Na}^+ > \mathrm{Li}^+$$

The observed order (table 1) is

$$\mathrm{Rb}^+ > \mathrm{K}^+ = \mathrm{Na}^+ > \mathrm{Li}^+$$

The anions, being larger than the inorganic cations, will probably have slightly greater mobilities than the former. The predicted order, based on ionic radii, is

$$\mathrm{I}^- > \mathrm{Br}^- > \mathrm{Cl}^-$$

and that found (table 1) is

$$I^- \sim Br^- > Cl^-$$

The result of Sjölin (52) for the diffusion of salicylic acid at the water–benzene interface, recalculated from his paper (and arbitrarily divided by 2 to correct for his stirring factor), is seen from figure 5 to lie close to the curve for electrolytes. Salicylic acid is ionized in water, but not in benzene, and evidently the readjustment of the molecule at the interface causes k_r to be as small as in the case of salts fully ionized in the oil phase.

COMPARISON WITH BIOLOGICAL DATA

A. Diffusion rates

If it be imagined that a thin layer of nitrobenzene separates two aqueous phases, in which the concentrations of salt are c_1 and c_3, the diffusion rates at each interface will be given by

$$\frac{1}{A}\frac{dn}{dt} = kc_1 - k_r c_2$$

$$\frac{1}{A}\frac{dn}{dt} = k_r c_2 - kc_3$$

When a steady state of diffusion has been set up these rates are equal, so that if the rate of diffusion across the interface is much less than that inside the interface

$$\frac{1}{A}\frac{dn}{dt} = \frac{kc_1}{2} - \frac{kc_3}{2} = \frac{k}{2}(c_1 - c_3)$$

Accordingly, values of $k/2$ may be compared with recalculated figures of permeability in biological systems (table 3). The orders of magnitude are in reasonable agreement, although the apparently rather high potassium-ion mobility *in vivo* may be connected with active penetration of this ion. Since spread films have no effect in the model system, the change of phase would seem to be the rate-controlling factor. Thus, in the biological as well as the model process, the diffusion rate will be determined by the partition coefficient *free energy* (rather than the heat of diffusion), and by the standard mobilities of the individual ions across the interfaces. The penetration rate is a function of the dielectric constant of the cell membrane, itself a function of the orientation of the lipids and proteins constituting it (15). As dipolar ions, the phospholipid molecules comprising the membrane would be expected to have a fairly high dielectric constant. It is established that aqueous proteins also have very high dielectric constants (25, 26). Since the solubility of ions varies exponentially with the negative reciprocal of the dielectric constant of the solvent, the partition coefficient is less, and therefore $k/2$ is greater, in polar solvents. Since the rates of penetration are rather greater in biological systems, it seems probable, especially when it is remembered that all the cell surface may not be permeable to ions, that the part of the cell surface responsible for ionic diffusion is more highly polar than nitrobenzene (dielectric constant = 36.1). Since anions are known to exchange across the erythrocyte membrane at least 1000 times as rapidly as cations, there must be a much greater solubility of the anions in the membrane, probably caused by positive charges in the vicinity of the points of penetration. It is seen that this solubility theory and that of a charged porous membrane, as developed by Sollner, overlap here. In both theories the coördinating power of the ion is important, and

$$u_{\mathrm{Rb}^+} > u_{\mathrm{K}^+} > u_{\mathrm{Na}^+} > u_{\mathrm{Li}^+}$$

Thus it seems that a penetrating ion becomes solvated with phospholipid at the cell surface, and, because there will be kinetic equilibrium between the interior and the exterior of the membrane, the ion is able to be carried across the nonaqueous layers.

TABLE 3

SALTS	$k/2$* AT WATER-NITROBENZENE INTERFACE AT 25.0°C FOR DIFFERENT SALTS	BIOLOGICAL PERMEABILITIES	REFERENCE
KCl	0.7×10^{-10}	K^+ into erythrocyte of	
KBr	7.5×10^{-10}	(a) man. 5×10^{-8}	
KI	1.4×10^{-8}	(b) dog 1×10^{-8}	(39)
		(c) rat 10×10^{-8}	
		K^+ into chick embryo 2×10^{-7}	(12)
NaI	0.2×10^{-8}	Na^+ into erythrocyte of	
		(a) rabbit 3×10^{-8}	
		(b) dog 0.5×10^{-8}	(36)
		Na^+ through excised	
		frog skin 5×10^{-8}	(35)
		Na^+ into *Halicystis* 1×10^{-8}	(17)
RbI	3.1×10^{-8}	Rb^+ into *Valonia* 5×10^{-6}	(9)
		Rb^+ through excised	
		frog skin 1.3×10^{-6}	(35)

* All permeabilities in this table have been converted into cm. sec.$^{-1}$ units.

Although the entropy, free energy, and heat terms for the diffusion of ions at the lipid–water interface are not yet known, they are probably not far from those for the diffusion at the nitrobenzene–water surface, but more detailed work must still be carried out.

B. Electrical resistance

This is known to be very high across cell membranes, the squid axon having a resistance as great as that of glass if it is due to a uniform effect across a film 100 Å. thick (29). It seems likely from the present study, however, that the transfer of an ion across the oil–water *interface* is the slow process, while the mobilities of the ions, once these are inside the oil, are relatively great. On this assumption, if the thickness of the *interfacial* diffusion path is 10^{-7} cm., the diffusion constant is about $\frac{2 \times 10^{-11}}{B}$ cm.^{2} sec.$^{-1}$, smaller by the factor $10^{-6}/B$ than that in bulk aqueous solution. Since the diffusion constant varies dimensionally as the first power of the ionic mobility (equation 16), it is clear that the interfacial electrical resistance must be higher than that in bulk phases by a factor $B \times 10^6$. Taking the resistance of an $N/6$ aqueous solution of potassium chloride 1 cm.^{2} in area and 10^{-7} cm. thick as 100×10^{-7} ω, the surface resistance of a membrane will be

$$B \times 10^6 \times 100 \times 10^{-7} = 10B\omega$$

Table 3 shows that the penetration rates *in vivo* are generally about 10^{-7} to 10^{-8} cm. sec.$^{-1}$, so that taking $k_r/2$ as 10^{-4} cm. sec.$^{-1}$, B is 10^3 to 10^4. Thus the calculated surface resistance of the cell surface is about 10,000 to 100,000 ω cm.$^{-2}$, a value in comparison with which the resistance inside the membrane may be neglected.

Observed resistances are found to be:

Squid nerve	1,000 ω cm.$^{-2}$	(14)
Nitella	100,000 ω cm.$^{-2}$	(13)
Valonia	5,000 ω cm.$^{-2}$	(7)

These values are in reasonable agreement with those calculated. On stimulation the resistances of the cell walls decrease to the following values:

Squid nerve	28 ω cm.$^{-2}$
Nitella	500 ω cm.$^{-2}$

This means that B must also decrease to about 2 and 50, respectively, while in the resting cells the values are 10^2 and 10^4. This may well be caused by a change in orientation in the membrane surface, due to the presence of a surface-active material which penetrates or breaks down the films (5, 40), allowing a freer orientation of the dipoles around the entering ion, increasing the ionic solubility, and decreasing B. Alternatively, aqueous channels may form momentarily.

Lipoprotein links may also be broken by the loss of calcium ion on stimulation (38), which would again increase the polarity of the membrane, since the calcium ion neutralizes and binds together the polar groups.

C. *Temperature effects*

The value of Q_{10} for cations passing the erythrocyte boundary is about 2 (21, 23), though for anions the value is between 2 and 3 (28, 47). The Q_{10} for the diffusion at the water–nitrobenzene interface is 1.30, and B is found to be independent of temperature, but if the salt is relatively more soluble in the oil phase as the temperature is increased, Q_{10} would exceed this value. Thus in the case of erythrocytes it seems likely that B for potassium ion and chloride ion is slightly less at higher temperatures. The Q_{10} for the membrane potential in *Halicystis* (8) is also 1.2.

D. Comparison with nonionic penetrants

Comparing the rates of transmission of alcohols through cell membranes with the results of Hutchinson (31) for the water–benzene interface, it is found that propyl alcohol penetrates ox erythrocytes with a permeability constant of 1.0×10^{-4} cm. sec.$^{-1}$ (22), while the $k/2$ value, calculated from Hutchinson's data, using a value of 1.5 cm. for the diameter of the diffusion surface (32), is 13×10^{-4} ($B = 4.3$, between water and benzene). Since the cell wall is relatively polar, B for this case is certainly less than unity, so that the rate will vary directly with B (equation 27). $k_r/2$ is about 3×10^{-3} for the alcohols, giving from $B \cdot k_r/2 = 1 \times 10^{-4}$, $B = 0.03$.

This ratio of the B-values of about 100 shows that the polarity of the cell wall is greater than that of benzene, because polar compounds are found to be more soluble (i.e., B is smaller) in polar solvents. Many of the substances studied in penetration experiments have B 5 to 100 times less for ether (D.C. = 4.3) than for benzene (D.C. = 2.3) or olive oil (D.C. = 3.1). Further, Irwin (34) noted that the net diffusion rate of dyes from water across the interfaces of a stirred layer of chloroform (D.C. = 5.2) into *Nitella* or *Valonia* sap was close to that in the cell wall.

Summarizing, it seems that the inorganic ions diffuse through cell walls by dissolving in the membrane at highly polar points, associated with lipoprotein and charged groups. The rate-determining step would be expected to be the passage across the phase boundary involving a change of solvate. This step will be very slow, especially if B is large. If the dielectric constant increases on excitation, the reduction in membrane resistance is a simple corollary of the ideas presented here.

The points in the cell wall through which nonionic substances pass seem to be more polar than triolein or cholesterol (dielectric constant about 3) but are not necessarily of as high a polarity as those at which inorganic ions diffuse.

SUMMARY

The rates of diffusion of various salts through the water–nitrobenzene interface have been measured. It is found that they are inversely proportional to the water–oil partition coefficient, while the reverse rates are nearly constant, in agreement with a generalized theory of diffusion. In all cases it has been found that the ionic mobility at the phase boundary is about a million times slower than in homogeneous systems, and this has been explained, in conjunction with the highly negative entropy of diffusion, as a result of the process of diffusion across an interface involving a selective redistribution of many solvate molecules. Monolayers of lipid and protein at the interface have no effect on the rate of diffusion.

The rates of diffusion of salts at the water–nitrobenzene interface are compared with those in biological systems, and it appears that if *interfacial* diffusion is the rate-controlling factor in the passage of salts through the plasma membrane, the latter must be highly polar.

The author wishes to thank Professor J. W. McBain for his constant encouragement during the course of this work.

REFERENCES

(1) Adam, N. K.: *The Physics and Chemistry of Surfaces*, 3rd edition. The Clarendon Press, Oxford (1941).

(2) Alexander, A. E., Teorell, T., and Aborg, C. G.: Trans. Faraday Soc. **35**, 1200 (1939).

(3) Barrer, R. M.: J. Soc. Dyers Colourists (Symposium on Fibrous Proteins), p. 108 (1946).

(4) Barrer, R. M.: Discussions of the Faraday Society **4**, 68 (1948).

(5) Belfanti, S., and Arnaudi, C.: Bull. Soc. Intern. Microbiol. **4**, 399 (1932).

(6) Beutner, R.: *Die Entstehung elektrischer Ströme in lebenden Geweben*. Enke, Stuttgart (1920).

(7) Blinks, L. R.: J. Gen. Physiol. **13**, 361 (1929).

(8) Blinks, L. R.: Cold Spring Harbor Symposia Quant. Biol. **8**, 204 (1940).

(9) Brooks, S. C.: J. Cellular Comp. Physiol. **6**, 169 (1935).

(10) Bungenberg de Jong, H. G., Verberg, G., and Westerkamp, R. F.: Kolloid-Z. **71**, 184 (1935).

(11) Cheesman, D F Arkiv. Kemi, Mineral. Geol. **22B**, [1] (1946).

(12) Cohn, W. E., and Brues, A M. J. Gen. Physiol. **28**, 449 (1945).

(13) Cole, K. S , and Curtis, H. J · J Gen. Physiol. **22**, 37 (1938).

(14) Cole, K. S , and Curtis, H. J : J. Gen. Physiol. **22**, 649 (1939).

(15) Cole, K. S. Cold Spring Harbor Symposia Quant. Biol. **8**, 110 (1940)

(16) Collander, R.. Trans. Faraday Soc. **33**, 985 (1937)

(17) Cooper, W C., Dorcas, M. J., and Osterhout, W. J. V.· J. Gen. Physiol. **12**, 427 (1928).

(18) Daniel, V.. Proc Roy. Soc. (London) **A192**, 575 (1948).

(19) Danielli, J F.· Trans Faraday Soc. **37**, 121 (1941).

(20) D'Ans, J., and Lax, E.· *Taschenbuch fur Chemiker und Physiker*, p. 1241. Berlin (1943).

(21) Davson, H.. J. Cellular Comp. Physiol. **10**, 247 (1937).

(22) Davson, H., and Danielli, J. F.. *The Permeability of Natural Membranes*. The Macmillan Company, New York (1943)

(23) Dean, R. B.· Cold Spring Harbor Symposia Quant. Biol. **8**, 266 (1940).

(24) Falkenhagen, H.: *Elektrolyte*. S. Hirzel, Leipzig (1932).

(25) Fricke, H., and Jacobson, L E : J. Phys. Chem. **43**, 781 (1931).

(26) Fricke, H., and Parker, E . J. Phys. Chem. **44**, 716 (1939).

(27) Glasstone, S., Laidler, K. J., and Eyring, H.: *The Theory of Rate Processes*, 1st edition. McGraw-Hill Book Company, Inc., New York (1941).

(28) Hahn, L., and Hevesy, G.: Acta Physiol. Scand. **3**, 193 (1942).

(29) Hober, R.: *The Physical Chemistry of Cells and Tissues*, p. 347 The Blakiston Company, Philadelphia (1945).

(30) Höber, R.. Reference 29, p. 280.

(31) Hutchinson, E.: J. Phys. & Colloid Chem. **52**, 897 (1948).

(32) Hutchinson, E.: Private communication.

(33) *International Critical Tables*, Vol. III, p. 422. McGraw-Hill Book Company, Inc., New York (1928).

(34) Irwin, M.: Proc. Soc. Exptl. Biol. Med. **26**, 125 (1928).

(35) Katzin, L. J.: Biol. Bull. **77**, 302 (1939).

(36) Krogh, A.: Proc. Roy. Soc. (London) **B133**, 140 (1946).

(37) Lewis, W. K., and Whitman, W. G.: Ind. Eng. Chem. **16**, 1, 215 (1924).

(38) Monné, L.: Advances in Enzymol. **8**, 1 (1948).

(39) Mullins, L. J., *et al.*: Am. J. Physiol. **135**, 93 (1941).

(40) Nachmansohn, D.: In *Currents in Biochemical Research*, edited by D. E. Green. Interscience Publishers, Inc., New York (1946).

(41) Nernst, W.: Z. physik. Chem. **9**, 140 (1892).
(42) Nernst, W.: Z. physik. Chem. **2**, 613 (1888).
(43) Osterhout, W. J. V.: Cold Spring Harbor Symposia Quant. Biol. **8**, 51 (1940).
(44) Osterhout, W. J. V.: J Gen. Physiol. **16**, 529 (1932).
(45) Osterhout, W. J. V., Kamerling, S. E., and Stanley, W. M.: J. Gen. Physiol. **17**, 445 (1934).
(46) Overton, E.: Jahrb. wiss. Botan. **34**, 669 (1900).
(47) Parpart, A. K.: Cold Spring Harbor Symposia Quant. Biol. **8**, 25 (1940).
(48) Philip, J. C., and Oakley, H. B.: J. Chem. Soc. **125**, 1189 (1924).
(49) Rashevsky, N., and Landahl, H. D.: Cold Spring Harbor Symposia Quant. Biol. **8**, 151 (1940).
(50) Ruhland, W., and Hoffmann, C.: Planta **1**, 1 (1925).
(51) Schmitt, F. O., Bear, R. S., and Ponder, E.: J. Cellular Comp. Physiol. **9**, 89 (1936).
(52) Sjölin, S.: Acta Physiol. Scand. **4**, 365 (1942).
(53) Waugh, D. F., and Schmidt, F. O.: Cold Spring Harbor Symposia Quant. Biol. **8**, 233 (1940).
(54) Wolpers, C.: Naturwissenschaften **29**, 416 (1941).
(55) Yonge, C. M.: Proc. Roy. Soc. (London) **B120**, 15 (1936).

THE DEVELOPMENT OF MEMBRANES PREPARED FROM ARTIFICIAL CATION-EXCHANGE MATERIALS WITH PARTICULAR REFERENCE TO THE DETERMINATION OF SODIUM-ION ACTIVITIES[1]

M. R. J. WYLLIE and H. W. PATNODE

Gulf Research & Development Company, Pittsburgh, Pennsylvania

Received August 22, 1949

INTRODUCTION

The classical early work of Michaelis and his collaborators on the membrane potentials (concentration potentials) of dried collodion membranes has been reviewed by Sollner (13–15). Sollner in the same papers summarized his own data on collodion membranes of all types and in addition critically reviewed the current theories of membrane action. In particular (14) he reviewed the well-known Meyer and Sievers (10) and Teorell (17) theories of membrane potentials and concluded that the essential weakness of these theories was the neglect of the structural factors inherent in any real membrane. Thus the Meyer and Sievers and Teorell theory postulates a selectivity constant, A, which may be defined as the charge on the membrane expressed as an ionic activity. This constant may be determined from measurements of the potential across a membrane for solutions of the symmetrical valence type when the concentration of one of the solutions is progressively increased, the ratio of the cationic[2] activities of the two solutions being kept constant. Sollner showed for collodion membranes that while the Meyer and Sievers and Teorell theory predicted in a semiquantitative way the shape of the potential–concentration curve, the value of the selectivity constant derived from the potential measurements was very different from that determined by cation-exchange methods. He concluded that the pore systems of real membranes could be visualized as consisting of narrow channels and wider cavities which, interconnected at random, traversed the membrane. The electrical behavior of these pore systems was governed by two factors: the ability or inability of ions of an electrolyte to enter purely on a basis of size, and an electrical factor, the repelling forces emanating from fixed dissociable groups on the pore walls. If the combination of structural and electrical factors was perfect and one ion of a binary electrolyte was wholly excluded, the membrane action would be perfect and the membrane would behave as an electrode reversible with respect to the other ion. If the membrane was not perfect, there would be an ionic leak and the membrane would not function as a reversible electrode. In the case of certain collodion membranes it appears from the work of Sollner and Carr (16) that the almost perfect membrane action with potassium chloride solutions is lost when the concentration of one of the potassium chloride solutions exceeds 0.1 molal. For concentrations in excess of 0.1 molal, potentials become progressively less than the theoretical values. Similar results were obtained by Marshall and his coworkers (5–8), using membranes made from colloidal clays. The maximum concentration to which almost perfect membrane action was attained never exceeded about 0.1 molal in the case of mono-monovalent salts, while the upper concentration found for cations of higher valency was less than 0.1 molal.

---

[1] Presented at the Twenty-third National Colloid Symposium, which was held under the auspices of the Division of Colloid Chemistry of the American Chemical Society at Minneapolis, Minnesota, June 6–8, 1949.

It thus appeared that the production of membranes which would respond to the activities of monovalent cations of solute concentrations greater than 0.1 molal, while theoretically feasible, was a practical problem of some difficulty. Recent work with membranes made from small portions of natural shales (18) has shown, however, that in the case of a Woodford carbonaceous shale, potentials may be obtained with sodium chloride solutions which apparently closely approximate those demanded by the Nernst equation. Using as assumptions in the calculation of sodium-ion activities (*a*) that in potassium chloride solutions the activity of K^+ is equal to that of Cl^-, and (*b*) that in solutions of other chlorides the activity of the chloride ion is the same as that of the chloride ion in a solution of potassium chloride of the same ionic strength, it was shown that the Nernst equation was closely followed up to a sodium chloride concentration of 1.0 molal. At sodium chloride concentrations in excess of 1.0 molal the potentials obtained were still considerable, although smaller than those computed when using the sodium-ion activities derived with the aid of the assumptions given.

The uncertainties in the computation of sodium-ion activities using these assumptions have been discussed by Marshall (4) in the case of dilute solutions and the problem will be given further consideration below.

---

[2] The case of fixed negative charges on the membrane will be considered specifically in this paper. For fixed positive charges, the principles discussed remain unchanged.

It was considered, however, that the potential deficiencies relative to the computed values obtained at sodium chloride concentrations in excess of 1.0 molal were probably due in a larger measure to the effects of anionic leaks across the membranes than to errors in the computed sodium-ion activities. This view seemed to derive some support from the fact that a statistical analysis made from electrical logs (19) of the electrochemical action of shales *in situ* shows that potentials very similar to those computed are obtained for total concentrations up to 170,000 p.p.m. of saline solids in underground formation waters (about 3.0 molal in terms of sodium chloride). The electrochemical cells in the earth involve very large volumes of well-compacted shale, and it seems possible that both a thickness effect and a comparative absence of physical imperfections such as cracks in these thick shale bodies contribute to their apparently excellent electrochemical behavior. The effect of cracks in laboratory shale samples is to decrease very markedly observed potentials at all concentrations of sodium chloride used (18). No thickness effect was apparent in the laboratory studies, but the range of thicknesses which it was practicable to investigate without using cracked shale samples was limited.

The effects of cracked or faulty laboratory shale specimens, even if the cracks are microscopic, will be to give rise to anionic leaks between the two solutions separated by the shale membrane and thus impair the electrochemical performance. A similar effect is possible in a shale if the electrically conducting paths through the membrane do not all involve passage through materials which possess the necessary structural and electrical factors to reduce to zero the transport number of the anion of the solutions separated by the membrane. If it is assumed that the materials in shales which possess the necessary fixed dissociable groups to repel anions are the clay minerals which exhibit cation exchange, then the overall electrochemical efficiency of a shale membrane may be affected both by the chemical structure of the clay minerals it contains and the distribution of the clay particles, and by the nature and arrangement of the electrochemically inactive materials which comprise what may be termed the matrix of the shale. If this shale matrix possesses some electrical permeability to anions whereas the clay minerals imbedded in it possess none, the shale might be expected to show improved electrochemical performance with increase in thickness. This case is in fact analogous to one considered by Sollner (14) and involves the conclusion that all shales would tend to give the theoretical reversible electrode potentials if sufficiently thick. It is probable that this view is an oversimplification, since it appears unlikely that the clay minerals present in the shales have the perfect structural and electrical factors necessary to prevent completely any anion conduction. However, even if the clay minerals are not electrochemically perfect in the sense described, the conclusion that a sufficiently thick shale sample would tend to give the theoretical potential would still be valid. This conclusion seems to be supported by observations of shale potentials in the earth (19, 20).

It is evident from this discussion that if the matrix of the shale could be rendered electrically insulating and if any physical imperfections such as cracking in the shale could be prevented, an improved electrochemical performance in the laboratory would be anticipated. Experiments carried out to this end have tended to confirm this view and have led to the development of artificial membrane electrodes based on the assumed electrochemical structure of shales. These artificial membranes appear to have excellent reversible electrode characteristics.

THE DEVELOPMENT OF ARTIFICIAL SHALE MEMBRANES

Initial experiments had as their object the modification of a natural shale matrix in such a manner as to eliminate minute cracks in the shale. A secondary object was to decrease, if possible, electrical conduction through the electrochemically inactive shale constituents. To achieve this, a sample of Woodford shale which had previously been found rather satisfactory as a membrane was ground in a disc mill. The powder passing a 120-mesh U.S. standard screen was intimately mixed with granular methyl methacrylate resin in the proportion of 4 g. of powdered shale to 1 g. of resin. The mixture was moulded in a conventional hydraulic press used for mounting metallurgical specimens to yield a disc 2.5 cm. in diameter and 5 mm. thick. This disc was sealed to the base of a 22 mm. internal diameter glass tube with optical pitch in such a manner that the pitch covered only the sides of the disc, the two faces of the disc being left exposed. The inside of the tube was filled with sodium chloride solution of one concentration and the tube was then immersed in a beaker containing a sodium chloride solution of different concentration. Electrical contact with the two solutions was made with saturated potassium chloride bridges connected to saturated calomel electrodes and the potential across the membrane measured. The total resistance of this membrane was about 800 ohms and with 0.4 molal and 0.04 molal sodium chloride solutions, a potential of 7.7 mv. was recorded, the dilute solution being positive. The disc soon disintegrated and it was clear that there was insufficient of the plastic to bond the shale particles adequately. The ratio of resin to shale was then progressively increased and although it was found that the overall resistance of the membranes increased with increase in the quantity of bonding resin used, it was nevertheless quite feasible to reduce the weight of shale to 5–10 per cent of that of the resin without causing the membrane resistance to become prohibitively high for E.M.F. measurements. Membranes of such high resin content seemed unaffected by wetting over prolonged periods and were generally very superior mechanically to those membranes which were prepared with an amount of resin closer to that theoretically necessary to bond the shale particles together.

The membranes prepared from the mixtures of inert insulating bonding resin and powdered shales gave E.M.F. values with sodium chloride solutions which were very close to the calculated Nernst equation potentials. The best results in this respect were achieved with a weight of shale about 30 per cent of the weight of the methyl methacrylate bonding resin used. It was, however, not found possible to obtain potentials with the resin–shale mixture for high sodium chloride concentrations which were notably larger than those obtained in the laboratory with an uncracked natural shale specimen.

The fact that moulded resin–shale mixtures could be made in this manner which were electrically conducting, were robust mechanically, and were apparently unaffected by prolonged immersion in water suggested that better membranes could be made if the shale powder were replaced by clay of reasonable purity. It was felt that the substitution of clay for shale would eliminate to a large extent the effects of the electrochemically inactive constituents of the shale. If, as was believed, the clays in the shale were principally responsible for the existence of the observed potentials, it was felt reasonable to assume that a clay–resin membrane would tend to be more efficient than a similar shale–resin membrane, since the number of conducting paths through the membrane unguarded by the fixed dissociable groups of the clays would be reduced by the absence of electrochemically inert shale constituents.

The powdered shale was accordingly replaced in the production of a number of membranes by Wyoming bentonite, a specimen of illite from Fithian, Illinois, and fuller's earth. It was found that all three substances gave rise to electrically conductive membranes which showed potentials of a polarity opposite to that of an ordinary boundary potential when they were used to separate sodium chloride solutions of different concentrations. Of the three types of membranes made, those in which bentonite was incorporated in the methyl methacrylate resin appeared best, inasmuch as they gave potentials which closely approximated the potentials computed by the Nernst equation over a range of sodium chloride concentrations which extended as high as 2.0 molal. Membranes made from the clay sample from Fithian, Illinois, were less efficient, the potential registered being only about 80 per cent of the Nernst equation potential in the case of 0.4 molal–0.04 molal sodium chloride concentrations. The fuller's earth membranes gave very poor results in all cases, potentials only 25 per cent of the theoretical being obtained even at low sodium chloride concentrations.

✓ The principal difficulty associated with the use of the bentonite–resin membrane electrodes was the necessity for permitting the electrodes to stand in contact with the test solutions for a considerable period before equilibrium was attained. During this period absorption of water by bentonite took place, this absorption resulting in the marked swelling of the clay particles which is so characteristic a feature of sodium montmorillonite. The swelling of the clay particles frequently sufficed to cause rupture of the bonding resin and the consequent production of electrical leaks across the membrane. The substitution of other resins such as phenol–formaldehyde for the methyl methacrylate and the use of bentonite in the moulding mixture, which had been partially preswelled by soaking in water, did not serve to produce a consistent improvement in the quality of the membranes made. It should be remarked that none of the powdered shale membrane electrodes failed by cracking caused in this manner, a fact which may indicate that the electrochemically active clay constituent of the shales used is not of the swelling montmorillonite type.

The best results were obtained with methyl methacrylate–bentonite membranes in which the amount of bentonite was kept at a minimum and the moulding of 11 per cent by weight of air-dried bentonite in granular resin proved moderately satisfactory. Such electrodes when 2–3 mm. thick had an initial resistance too high to permit potential readings being made with a potentiometer and thermionic amplifier. The initial resistance in many cases exceeded 30 megohms. After some days of soaking in a sodium chloride solution the resistance dropped to a value sufficient to allow potential measurements to be made, and at this stage the potentials tended very closely to those computed from the Nernst equation. With increased time the resistivity decreased further, and in many cases the electrode action became poorer as cracking of the resin occurred. In certain cases, however, full electrode function was retained for periods up to 4 weeks, the membranes being kept immersed in the solutions throughout this period. Experiments tended to show that better results were obtainable when the bentonite was finely divided than when coarse or unsorted, but the inconsistencies caused by the swelling of the particles and cracking of the plastic made exact observations unreliable.

It was established, however, that membranes made of moulded bentonite and plastic gave potentials with sodium chloride solutions which tended to the computed Nernst equation potentials to much higher concentration of sodium chloride than was found by Marshall and Krinbill (8) when using the same solutions and membranes made from colloidal bentonite. This observation points to the fact that the electrochemical performance of a membrane material is largely controlled by its physical nature. This view would be in general accord with the ideas of Sollner previously considered.

THE DEVELOPMENT OF SYNTHETIC MEMBRANES

The requirements for good membrane electrodes

It is clear from the preceding discussion that a perfect membrane electrode which would be reversible with respect to the cations in a simple salt solution would be one which possessed the necessary structural and electrical factors to prevent entirely the movement of anions through it. This implies that all electrically continuous paths through the membrane, which must be paths available for electrolytic conduction, will be open only to the movement of cations. The best information available appears to indicate that the movement of anions through small pores in a membrane can be prevented if each pore contains negative charges which are normally electrically balanced by the appropriate number of dissociable cations. The fact that the collodion membranes of Sollner and the colloidal clay membranes of Marshall both appear to possess almost perfect membrane properties, provided the concentration of the solutions in contact with them does not exceed about 0.1 molal, indicates also that with higher anion concentration previously barred pores may become anion permeable. If this is so, it seems reasonable to believe that the ability of a membrane to retain good electrochemical action to high concentrations would be increased if the number of dissociable groups along any conducting path through the membrane were a maximum. This implies, as has been pointed out by Sollner

(14), that the dissociable groups must be suitably arranged to prevent anionic movement, i.e., that the width of the conducting path must not greatly exceed the effective repulsion volume of a dissociable group. On this basis, a material possessing a larger number of dissociable groups might be expected to have good membrane potentialities. Since the number of dissociable groups in this sense is fundamentally similar to the cation-exchange capacity of the material, a material with a high cation-exchange capacity would be an obvious choice for a membrane. Marshall and Bergman (6) chose bentonite on this basis and prepared membranes 0.1–0.5 mm. thick by evaporating a colloidal dispersion of the material. The membranes of Marshall and Bergman were successful up to a concentration of 0.1 molal but failed at higher concentrations. This may be partly due to the fact that their membranes had to be baked at temperatures up to 490°C., conditions which may have destroyed some of the cation-exchange capacity of the bentonite. On the other hand, as Sollner (14) has pointed out for the case of collodion membranes, high electrochemical activity is always associated with high cation-exchange capacity, but medium and low cation-exchange capacity occurs with electrochemically active as well as inactive preparations. The structural factors are thus also important and it seems probable that the relatively poor performance of Marshall's membranes at high concentrations is largely caused by their thinness and the geometry of the constituent particles.

The technique of setting a high cation-exchange material, such as bentonite, in resin appears to improve greatly the structural factors involved, probably owing to the fact that relatively little conduction around and between clay particles can occur, whereas with Marshall's unbonded clay membranes there may have been interstices which were either rather large or which possessed too few dissociable groups to prevent anionic leakage at the higher anion concentrations. The structure of montmorillonite (3) appears to lend some support to this conception, since the outside of the small plates of the crystals probably exhibit little cation exchange. Hence, if electrical conduction around the plates can be prevented, the membrane efficiency will tend toward a maximum.

The bonding technique makes it feasible to use any cation-exchange material to prepare a membrane, although it is apparently undesirable, if not entirely impossible, to use a material in which the cation-exchange groups exist only on the surface. However, most of the common synthetic cation-exchange materials have a porous structure and thus possess internal channels and passages in which dissociable groups exist. Thus, they appear to possess the necessary structural and electrical factors to repress anion conduction, but the overall efficacy of these factors can only be determined experimentally. In addition, many of the newer synthetic cation-exchange materials have a very high cation-exchange capacity, and since their tendency to swell on contact with water is less marked than in the case of sodium montmorillonite, it was decided to test the electrochemical efficacy of certain of these materials when bonded with thermoplastic resins to form membranes.

Preparation of membranes

Initial experiments were carried out with two commercial synthetic cation-exchange materials. The first was a phenol–formaldehyde type cation-exchange resin made by the Rohm and Hass Company of Philadelphia. Two kinds were available, an early variety designated Amberlite IR-1 and a later one, Amberlite IR-100. The Amberlite IR-100 was obtained in the analytical grade in the hydrogen form and was converted to the sodium form by treatment with a large excess of a 5 per cent solution of analytical grade sodium chloride, followed by washing with neutral distilled water until the filtrate gave no test for chloride ion. The second cation-exchange material was a sodium Zeokarb made by the Permutit Company of New Jersey and was supplied in the sodium form.

Both synthetic cation-exchange materials were air-dried and then ground in a mortar to pass an 80-mesh U. S. standard screen. The screened powder was then intimately mixed by grinding with different percentages by weight of P4942, commercial granular methyl methacrylate bonding resin, made by the Eastman Kodak Company, and moulded at 3000 lb./sq. in. pressure and a maximum indicated temperature of 150°C. in a Buehler 1315 hydraulic specimen mounting press. Discs 2.5 cm. in diameter were obtained in which the particles of the cation-exchange material could be clearly discerned scattered throughout the transparent plastic matrix. Some of the particles were exposed and were in a position to absorb moisture. Discs in which the plastic faces showed no particles were, of course, nonconducting and were rejected.

TABLE 1

Potentials obtained with 1.0 m and 0.1 m sodium chloride solutions

CATION-EXCHANGE MATERIAL	BONDING PLASTIC	MEMBRANE THICKNESS	E.M.F	TEMPERATURE
	weight per cent	*mm*	*mv.*	*°C.*
Amberlite IR-1	75	2.5	55.1	26.8
Na Zeokarb	75	4.0	53.7	26.8
Na Zeokarb	75	2.0	54.6	27.3
Na Zeokarb	85	6.0	53.1	26.8
Na Zeokarb	85	2.0	51.3	26.8
Amberlite IR-100-Na	66	6.5	55.6	26.3
Amberlite IR-100-Na	66	5.0	53.9	26.3

Table 1 gives the early results obtained with the membrane discs made in this manner and mounted with optical pitch on the ends of 22 mm. diameter glass tubes. The test solutions used were 1.0 molal and 0.1 molal sodium chloride, and E.M.F. measurements were made with saturated calomel electrodes and saturated potassium chloride bridges. A Leeds & Northrup Type K potentiometer with a Leeds & Northrup thermionic amplifier adjusted to a control current less than 10^{-14} amp. was used. On the basis of the assumptions given above the Nernst equation potential at 26°C. would be 56.9 mv. if the mean activity coefficients for sodium chloride and potassium chloride given by Robinson and Harned (12) are used.

The Amberlite IR-100 appeared from these experiments to be superior to the sodium Zeokarb for two reasons: (*1*) because more stable potentials were obtainable (the sodium Zeokarb membrane potentials tended to drift slightly during the course of an E.M.F. reading) and (*2*) because it appears (9) that the cation-exchange capacity of the Amberlite is superior to that of many other commercial types. Experiments were therefore continued, using the Amberlite IR-100-H cation-exchange material as starting material.

It was apparent that the early method of mixing Amberlite passing an 80-mesh screen with methyl methacrylate of a larger grain size was unsatisfactory, since it was difficult to attain uniformity of dispersion of the Amberlite in the plastic matrix. It was found that this condition could be improved considerably if both the Amberlite and the methyl methacrylate powders used passed the same sieve size and were ground together in a mortar before being moulded. Accordingly, twelve membranes were made from powders passing an 80-mesh U.S. standard screen. Six of these membranes incorporated air-dried Amberlite in the sodium form[3] and six incorporated air-dried Amberlite in the hydrogen form. The percentage of Amberlite by weight in these membranes is given in tables 2 and 3. Moulding took place at 3000 lb./sq. in. and a maximum indicated temperature of 150°C.

The membranes prepared were mounted on the ends of glass tubes, and the potentials obtained in sodium chloride and hydrochloric acid solutions were measured in the same manner as previously described. Certain of the electrodes showed initially a resistance too high to permit E.M.F. measurements, but all proved satisfactory in this respect after 24 hr. soaking in the solutions. It was found that all the membranes took about 3 days to attain stable equilibrium potentials. Final potentials were obtained in all cases only after changing the solutions two or more times until a reproducible potential was achieved. The solutions were then reversed and the procedure of changing solutions followed until stable reproducible potentials were again obtained. Tables 2 and 3 give for each membrane the arithmetical mean of these two potentials.

It was noted that the membranes containing Amberlite in the sodium form gave potentials in hydrochloric acid which were initially about 30 mv. lower than the final equilibrium values while, conversely, membranes with Amberlite in the hydrogen form in sodium chloride solutions yielded potentials which were initially about 30 mv. too high but which fell off in the course of 2 or 3 days to an equilibrium value. If, as is believed, these nonequilibrium potentials are the result of cation exchange between sodium and hydrogen ions in Amberlite particles within the membranes, it would indicate that the rate of diffusion of ions from these Amberlite particles into the bulk of the solutions is extremely slow. The final equilibrium potentials do not seem to be affected by the ion initially present on the Amberlite.

In table 2 the observed E.M.F. values are compared with theoretical potentials computed by the Nernst equation, using the assumptions already given to estimate the sodium-ion activities of the solutions. It will be seen that for the 1.000 *m* and 0.1094 *m* sodium chloride solutions the agreement between observed and computed potentials is only fair and there is considerable variation between the potentials given by individual membranes. With 3.000 *m* and 0.462 *m* sodium chloride solutions the observed potentials are consistently much lower than those calculated.

---

[3] The percentage water in the air-dried sodium Amberlite used in this work was found to be 20–30 per cent of the oven-dried weight of Amberlite.

In table 3 the observed potentials have been compared with the difference between the potentials measured first in one hydrochloric acid solution and then in the other with a Beckman glass electrode and saturated calomel reference electrode. The measuring circuit used was as before a potentiometer and thermionic amplifier. The glass electrode potential thus obtained may not possess the highest accuracy, but comparison with it of the potentials observed when using the Amberlite membrane electrodes certainly shows that the response of these electrodes to hydrogen ions is very similar to that of a glass membrane. It may be noted that the equilibrium potentials in table 3 indicate that the response of Amberlite membranes of this type to hydrogen ions is somewhat more consistent than that shown for sodium ions in table 2. The pH values of the hydrochloric acid solutions used were determined on a standard Beckman pH meter and found to be 0 and 1.1.

TABLE 2

Potentials obtained at 22°C. using bonded Amberlite IR-100 and methyl methacrylate plastic resin membranes separating sodium chloride solutions

ELECTRODE NUMBER	COMPOSITION OF MEMBRANE BY WEIGHT PERCENTAGES	THICKNESS OF MEMBRANE	1.000 *m* NaCl *vs.* 0.1094 *m* NaCl		3.000 *m* NaCl *vs.* 0.462 *m* NaCl	
			Mean E.M.F. observed (±0.1 mv.)	Theoretical E.M.F.	Mean E.M.F. observed (±0.1 mv.)	Theoretical E.M.F.
		mm.	*mv.*	*mv.*	*mv.*	*mv.*
Na 1	20 Na Amberlite 75 plastic	4.0	52.4	53.8	35.1	54.1
Na 2	25 Na Amberlite 75 plastic	3.0	53.3	53.8	38.1	54.1
Na 3	25 Na Amberlite 75 Plastic	3.0	52.5	53.8	35.8	54.1
H 4	20 H Amberlite 80 Plastic	2.0	50.5	53.8	33.6	54.1
H 5	20 H Amberlite 80 Plastic	2.5	56.1	53.8	45.0	54.1
H 6	20 H Amberlite 80 Plastic	2.0	50.7	53.8	34.1	54.1

These preliminary results seemed to show that it was possible to make membranes possessing reasonably good sodium electrode functions in sodium chloride solutions as strong as 1.0 molal. On the other hand, the potentials obtained in

3.0 molal solutions were probably too low. The apparent breakdown in theoretical sodium electrode function of the membranes in the 3.0 molal sodium chloride solution was considered to have three possible explanations: (*1*) the sodium-ion activities computed and used to determine the Nernst equation E.M.F. in sodium chloride solutions more concentrated than 1.0 *m* were quite erroneous; (*2*) Amberlite does not possess the necessary structural and electrical factors to prevent anionic conduction when in contact with sodium chloride solutions as concentrated as 3.0 *m*; and (*3*) an optimum geometrical arrangement of the Amberlite particles and bonding of the particles in the plastic matrix in such a way as to prevent anionic conduction leakages through the membranes had not yet been achieved.

TABLE 3

Potentials obtained at 22°C. using bonded Amberlite IR-100 and methyl methacrylate plastic and hydrochloric acid solutions of pH approximately 0.0 and 1.1

ELECTRODE NUMBER	COMPOSITION OF MEMBRANE BY WEIGHT PERCENTAGES	THICKNESS OF MEMBRANE	MEAN E M F OBSERVED (±0.1 MV.)	E M F OBSERVED WITH GLASS ELECTRODE
		mm	*mv*	*mv*
H 1	20 H Amberlite 80 Plastic	2.0	65.3	64.3
H 2.	20 H Amberlite 80 Plastic	2.0	65.4	64.3
H 3.	20 H Amberlite 80 Plastic	2.0	63.9	64.3
Na 4	25 Na Amberlite 75 Plastic	3.5	65.4	64.3
Na 5	25 Na Amberlite 75 Plastic	2.5	65.4	64.3
Na 6	25 Na Amberlite 75 Plastic	3.0	64.7	64.3

Field observations made from electrical logs of the potentials given by shale beds in contact with saline solutions as concentrated as 3.0 *m* sodium chloride (19), as well as the preliminary results with bonded clay electrodes, indicated that an error in the computed sodium-ion activities sufficiently large to explain the potential discrepancies noted in table 2 was improbable. Attention was therefore directed to improved methods of bonding the Amberlite in the plastic matrix.

MEMBRANES CONTAINING FINELY DIVIDED AMBERLITE

Methyl methacrylate bonding plastic

Experiments in which the amount of bonding plastic was reduced to quantities which more closely approximated the theoretical intergranular porosity of the

Amberlite particles showed that the electrochemical performance of membranes moulded from methyl methacrylate plastic and Amberlite powders was seriously impaired. This phenomenon appeared to be general when using methyl methacrylate plastic as the bonding medium and seemed independent of the particle size of the Amberlite and methyl methacrylate powders used. In general, it was found that although the exact percentage by weight of Amberlite moulded was not critical, it was preferable to maintain it at about 20–30 per cent. This conclusion meant that it was not possible to decrease significantly the overall resistances of the membranes by increasing the percentage of the Amberlite in the methyl methacrylate plastic matrix to 60 or 70 per cent.

Variation in the particle size of the Amberlite and methyl methacrylate resin moulded proved, for low Amberlite concentrations, to be of considerable importance. Experiments were conducted with Amberlite in the sodium form and methyl methacrylate plastic, both materials being separately ground in a ball mill using agate balls. The ground materials were sieved and the fractions of each passing 120-mesh and 250-mesh U.S. standard screens were collected.

Membranes were then moulded from intimately ground mixtures of Amberlite and methyl methacrylate plastic, both powders in the mixtures passing either the 120-mesh or 250-mesh screens. In all cases a moulding pressure of 3000 lb./sq. in. and a maximum indicated temperature of 150°C. were found most satisfactory.

The membranes moulded from the $<$ 250 mesh powders showed very high resistances, even after prolonged soaking in sodium chloride solutions, unless the Amberlite content of the mixture moulded was about 50 per cent or more. Those membranes moulded from a mixture containing 20 per cent and 25 per cent by weight of Amberlite showed a resistance too high to permit a potential measurement after soaking for 5 weeks in a solution of sodium chloride, while the resistance after prolonged soaking of membranes moulded from a 33 per cent Amberlite mixture was of the order of 10 megohms. The potentials given by 33 per cent Amberlite membranes were, however, fairly satisfactory and comparable to those values given in table 4.

Membranes moulded from 50 per cent by weight of the Amberlite had a resistance of the order of 100 ohms after a month of soaking in a sodium chloride solution, but gave potentials at high sodium chloride concentrations which appeared to be only about 60 per cent of the theoretical. The percentage weight increase of these discs after soaking averaged about 40 per cent.

Similar results were obtained with membranes moulded with $<$ 120 mesh Amberlite and methyl methacrylate powders, except that the membrane resistances were in general lower than in the case of the $<$ 250 mesh powders and an optimum weight percentage of Amberlite of about 25 per cent was found to give membranes with good electrochemical performance allied to relatively low resistance.

Six disc membranes were prepared from air-dried Amberlite in the sodium form and methyl methacrylate resin, both powders being $<$ 120 mesh. The discs were prepared in two batches of three by using four flat dies in the moulding cylinder of the hydraulic press. Three of the discs were moulded from a mixture containing 25 per cent by weight of air-dried Amberlite and three from a 22.5 per cent mixture. The thicknesses of the discs are shown in table 4.

The six discs so prepared were weighed and allowed to soak in 3.000 *m* sodium chloride solution. The discs were removed daily from the solution, wiped dry, and re-weighed, and the soaking was continued until a constant weight was attained for each disc. The soaking period necessary was found to vary from 8 to 24 days, depending upon the thicknesses of the discs. The weight increases which occurred were:

TABLE 4

Potentials obtained at 22°C. with bonded <120 mesh Amberlite IR-100-Na and methyl methacrylate plastic membranes separating sodium chloride solutions

ELECTRODE NUMBER	COMPOSITION OF MEMBRANES BY WEIGHT PERCENTAGES OF NA AMBERLITE	THICKNESS OF MEMBRANE	TOTAL RESISTANCE OF MEMBRANE	ASYMMETRY POTENTIAL IN 3.000 *m* NaCl (±0.1 mv.)	3.000 *m* NaCl AND 0.462 *m* NaCl: Mean E.M.F. observed (±0.1 mv.)	3.000 *m* NaCl AND 0.462 *m* NaCl: Theoretical E.M.F.	3.000 *m* NaCl AND 0.462 *m* NaCl: Computed asymmetry potential (±0.1 mv.)	4.000 *m* NaCl AND 0.700 *m* NaCl: Mean observed E.M.F. (±0.1 mv.)	4.000 *m* NaCl AND 0.700 *m* NaCl: Theoretical E.M.F.	4.000 *m* NaCl AND 0.700 *m* NaCl: Computed asymmetry potential (±0.1 mv.)
		mm	*ohms*	*mv*	*mv*	*mv*	*mv*	*mv*	*mv*	*mv*
Na 20	25	1.3	370,000	+1.5	54.1	54.1	+1.6	52.7	54.8	+2.5
Na 21	25	2.3	142,000	-1.3	53.5	54.1	-1.1	51.0	54.8	0.7
Na 22	25	1.9	180,000	-0.4	53.7	54.1	-0.2	51.8	54.8	-1.9
Na 23	22.5	1.8	250,000	-2.3	52.6	54.1	-1.9	53.7	54.8	-1.5
Na 24	22.5	2.6	24,000	-1.7	53.4	54.1	-1.3	53.2	54.8	-0.9
Na 25	22.5	3.5	36,000	+0.6	53.7	54.1	+0.8	53.3	54.8	+0.5

MEMBRANE	WEIGHT INCREASE	MEMBRANE	WEIGHT INCREASE
	per cent		*per cent*
Na 20	16.0	Na 23	14.9
Na 21	13.6	Na 24	14.2
Na 22	12.3	Na 25	15.0

The percentages were calculated on the weight of air-dried Amberlite in each disc, assuming uniform distribution of the Amberlite powder in the plastic matrices.

After the discs had attained constant weight they were cemented with optical pitch to the ends of 22 mm. internal diameter glass tubes and the net asymmetry potential across them in 3.000 *m* sodium chloride solution measured using calomel electrodes. The data so obtained are given in table 4, plus signs indicating that the outside faces of the membrane discs were found positive.

The total resistances of the mounted membranes in 3.000 *m* sodium chloride solution were determined by measuring the resistances between two platinized platinum electrodes 20 mm. in diameter, one electrode being held close to the membrane within the glass tube and the other adjacent to the outside face of the disc. A Kohlrausch 1000-cycle bridge was used for the measurements. The resistances so obtained must be considered approximate, since the areas of membrane exposed to the solutions varied somewhat with the amount and distribution of the optical pitch used for sealing them to the ends of the glass tubes.

All six discs prepared in this manner appeared to be very homogeneous and had the dull reddish appearance of ground Amberlite. Both faces of the discs were slightly rough, and it was apparent that numerous fine Amberlite particles were penetrating through the methyl methacrylate matrix. There was no indication in these membranes of areas of segregation between Amberlite and bonding plastic. After periods of two months' continuous immersion in sodium chloride solutions these membranes appeared to be undamaged physically and gave unimpaired electrochemical performances. During this period the total resistances of the membranes remained nearly constant. A sudden change in the potential given by a membrane was generally found to mean that a minute leak had developed in the optical pitch used for cementing the membranes to the tubes. This condition could be satisfactorily remedied by scraping the pitch from the membranes with a sharp knife and recementing.

Table 4 gives the thicknesses, resistances, and mean potentials obtained using the six membranes. The mean potentials, as before, are the arithmetical mean of the equilibrium potentials obtained when the solutions are reversed. The computed asymmetry potential is then half the difference between the two equilibrium potentials, and its sign has been arbitrarily chosen positive if the outside of the membrane is apparently positive with respect to the inside. In all cases before the solutions were reversed or changed in concentration the membrane and tubes were washed thoroughly with distilled water and dried with an absorbent cloth.

It was found that, on the average, when the solutions were reversed it took 24 hr. to reach a potential of 90 per cent of the equilibrium value and 2–3 days to attain the final equilibrium potential. When the solution on only one side of the membrane was changed, a new equilibrium was reached very much more rapidly and a value within 5 per cent of the equilibrium potential could be obtained in less than 30 min. and the equilibrium potential itself within 24 hr. This time applies to concentration changes from 4.0 *m* to 0.02 *m* and is less the smaller the concentration change made.

The data in table 4 show that there is no obvious connection between membrane resistance and thickness or between resistance and percentage of Amberlite in the membrane. It is not believed that the effect of the optical pitch cement on the area of membrane exposed to the solutions significantly affects this statement. The results seem to indicate the the mixing of the two powders and the effect of the moulding conditions on the overall conductivity of the Amberlite grains were inconsistent. In all cases the resistances are too high to enable accurate potential measurements to be made with a potentiometer alone, but the resistances are nevertheless very much more readily manageable than those associated with glass membrane electrodes.

The potential data show that the electrochemical efficiency of the membranes is largely independent of their resistances. The same is true for membrane thickness within the thickness range covered by the six membranes.

The agreement between the mean potentials given by the membranes both with one another and with the potential computed using the Nernst equation may be considered reasonably satisfactory in the case of the 3.000 *m* and 0.462 *m* sodium chloride solutions and fair in the case of the 4.000 *m* and 0.700 *m* sodium chloride solutions.

The computed asymmetry potentials in the case of the 3.000 *m* and 0.462 *m* tests agree reasonably well with those measured initially in 3.000 *m* sodium chloride, but the computed asymmetry potentials in the more concentrated solutions differ markedly from these values, although the sign of the asymmetry potential remains unchanged in each case. The effect of concentration on the computed asymmetry potential over a wider concentration range will be shown again in table 5.

TABLE 5

Potentials obtained at 22°C. with bonded <250 mesh Amberlite IR-100-Na and polystyrene resin membranes separating sodium chloride solutions

COMPOSITION OF MEMBRANE IN WEIGHT PERCENTAGES OF NA AMBERLITE	THICKNESS OF MEMBRANE	TOTAL RESISTANCE OF MEMBRANE	4.000 *m* NaCl AND 0.700 *m* NaCl			2.000 *m* NaCl AND 0.250 *m* NaCl			1.000 *m* NaCl AND 0.107 *m* NaCl			0.100 *m* NaCl AND 0.010 *m* NaCl		
			Mean E M F observed (±0.1 mv.)	Theoretical E M F	Computed asymmetry potential	Mean E M F observed (±0.1 mv.)	Theoretical E M F	Computed asymmetry potential	Mean E M F observed (±0.1 mv.)	Theoretical E M F	Computed asymmetry potential	Mean E M F observed (±0.1 mv.)	Theoretical E M F	Computed asymmetry potential
	mm	*ohms*	*mv*	*mv.*	*mv*	*mv*	*mv*	*mv*	*mv*	*mv*	*mv*	*mv*	*mv*	*mv*
50	0.5	1,200,000	51.8	54.8	+1.8	53.7	53.1	−0.3	59.2	58.2	+1.6	54.5	55.0	+1.9
60	1.1	230,000	51.7	54.8	−0.4	53.7	53.1	−2.1	58.8	58.2	−1.9	55.5	55.0	−1.5
60	1.2	220,000	52.4	54.8	−1.4	53.8	53.1	−4.5	59.3	58.2	−2.4	56.0	55.0	0
70	1.3	3,600	53.2	54.8	−1.2	53.3	53.1	−1.3	58.5	58.2	+1.6	55.8	55.0	+3.5
70	1.6	6,000	53.0	54.8	−1.9	54.0	53.1	−2.0	58.9	58.2	+1.3	55.6	55.0	+3.3
70	4.2	1,340	53.3	54.8	+0.6	53.3	53.1	+0.7	59.0	58.2	+1.5	55.1	55.0	+3.2
70	1.8	5,600	53.5	54.8	+0.9	55.0	53.1	+1.2	60.3	58.2	+2.5	55.2	55.0	+4.0

Polystyrene bonding plastic

Although the methyl methacrylate plastic–Amberlite membranes appeared to have excellent electrochemical properties and were easily made, they suffered from the disadvantage that the optimum Amberlite percentage was small. This low Amberlite content, much smaller than the theoretical value for the ideal case where the plastic content is only sufficient to fill the interstices between the Amberlite granules, introduces two major difficulties. Firstly, it is not easy to ensure uniform and optimum dissemination of the Amberlite granules in the relatively large volume of bonding plastic when using the rather crude moulding technique employed, and secondly, the area of Amberlite available for current conduction remains so small that the membrane resistances cannot be reduced sufficiently to enable a potentiometer alone to be used for potential measurements.

It was, therefore, decided to substitute another resin for the methyl methacrylate in an attempt to make good membranes of higher Amberlite content. Polystyrene was chosen, since it has a higher resistivity than methyl methacrylate as well as a lower water absorption, and thus appears very suitable electrically. The polystyrene powder used was listed as P 8 fines and was made by the Koppers Company. It was reduced to the appropriate size ranges by reduction in a ball mill, using agate balls. The moulding conditions finally adopted consisted in all cases in maintaining the mixed polystyrene and Amberlite powders at 1000 lb./sq. in. in the hydraulic press until a temperature of 120°C. was indicated. At this point the pressure was increased to 5200 lb./sq. in. and heating continued to a maximum indicated temperature of 205°C. The mould was then allowed to cool to atmospheric temperature with the heating element in place and the pressure maintained. Using this technique, the membranes made could be fairly readily removed from the mould and were not excessively brittle. In general, however, the mechanical properties of polystyrene–Amberlite electrodes are less satisfactory than those made with methyl methacrylate moulding plastic.

Experiments showed that the beneficial effects of reducing the particle size of the Amberlite and polystyrene powders in the mixture used for moulding were similar to those observed with methyl methacrylate and Amberlite, except that the optimum mixture appeared to consist of < 250 mesh U.S. standard screen powders. Membranes were moulded from < 250 mesh Amberlite in the sodium form and < 250 mesh polystyrene in the proportions 20, 50, 60, 70, and 80 per cent by weight of air-dried Amberlite. It was found that 80 per cent of Amberlite in these mixtures represented a proportion which was definitely too high for satisfactory mechanical properties, the majority of the membranes moulded fracturing on removal from the mould. With great care, however, a proportion of satisfactory membranes could be made from this high-Amberlite mixture. Mixtures containing 70, 60, 50, and 20 per cent of Amberlite gave mechanically satisfactory membranes, although all were more brittle than those made with methyl methacrylate moulding plastic.

It was found that those membranes which were moulded from powder mixtures containing 20 per cent of the Amberlite were unusable, since soaking for more than a month in a sodium chloride solution did not suffice to make them conductive. Membranes prepared from mixtures containing 50 per cent of Amberlite were conductive after about 20 min. soaking in a sodium chloride solution, whereas those containing upwards of 60 per cent Amberlite gave immediate potential readings when used to separate two sodium chloride solutions. These immediate readings, even in the case of 4.000 *m* and 0.700 *m* sodium chloride solutions, were generally within 1 mv. of the final equilibrium potential obtained. The resistances measured across the mounted membranes after they had soaked for some time and had reached a stable value were found to vary very markedly with the percentage of Amberlite in the original mixtures moulded. Some of the resistance data obtained on typical unselected membranes are shown in table 5, but in general it was found that for 50 per cent Amberlite in the original mixture the total membrane resistance was about 10^6 ohms, for 60 per cent 10^5 ohms, for 70 per cent 10^3 ohms, and for 80 per cent 10^2 ohms. Satisfactory potential readings at the highest concentrations of sodium chloride were obtained with 80 per cent Amberlite membranes having a resistance of 300 ohms, but these membranes were so poor mechanically that in all cases they failed by cracking after a relatively short period of use. The optimum Amberlite percentage in the moulding mixture, to give membranes with both reasonably good mechanical properties and resistances sufficiently low to permit satisfactory potential measurements with a potentiometer alone, appears to be about 70 per cent. The percentage weight increase of 70 per cent membrane discs after prolonged soaking was found to average about 19 per cent.

Seven membranes were made and without any selection were used to give the data shown in table 5. The readings were started in the 4.000 *m* and 0.700 *m* solutions and continued with the 2.000 *m*, 1.000 *m*, and 0.100 *m* pairs.

The usual technique of changing solutions until an equilibrium potential was obtained and then washing the membranes and reversing the solutions was followed for each of the four pairs of solutions. The asymmetry potentials are, as before, half the difference between the two potentials so obtained for each pair of solutions used. It was found that the rate of attainment of an equilibrium potential increased with the Amberlite content of the membranes. In the case of membranes containing 70 per cent of Amberlite in the original mixture moulded, only 4 min. was needed to reach the equilibrium potential after reversal of the 4.000 *m* and 0.700 *m* sodium chloride solutions, and the same was true of changing to another pair of solutions of different sodium chloride concentrations.

In all cases the theoretical potential has been calculated from the Nernst equation, using the mean activity coefficient data for sodium chloride and potassium chloride given by Robinson and Harned.

It will be seen that the agreement between the potentials given in each pair of solutions by the seven electrodes is fairly good, the difference between the maximum and minimum values never exceeding 1.8 mv. or about 3 per cent of the total potentials recorded. This agreement is, of course, extremely poor as judged by the standards of reversible electrochemical cells, but is encouraging inasmuch as it indicates that reasonably reproducible potentials can be obtained with electrodes of low resistance in solutions with high sodium chloride concentrations. The agreement between the observed potentials and those computed from the Nernst equation is within about 1 mv., except in the case of the 4.000 *m* and 0.700 *m* sodium chloride solutions. At the lowest sodium chloride concentrations used the agreement seems to be about the same as that found by Marshall and Bergman (6), using clay membrane electrodes and solutions of similar concentration. As stated in more detail below, however, the reproducibility of the potentials given by the electrodes must be considered of more significance than any close agreement between the observed and Nernst equation potentials. This is particularly so in the case of the solution pairs containing high concentrations of sodium chloride.

Table 5 shows that the computed asymmetry potentials of the membranes can be both large and very variable; in certain cases even the sign of the asymmetry potential is inconstant. It appears that the asymmetry potential changes unpredictably with aging of an electrode but is, nevertheless, reasonably constant over the time necessary to obtain the equilibrium potentials in a pair of solutions. Variation in asymmetry potentials is, however, almost certainly one of the factors leading to the differences noted between the mean potentials given by the seven membranes when separating a particular pair of solutions.

Effect of membrane thickness on potential

Observations on the effect of the thickness of membranes of a particular composition on the potentials observed are complicated by the difficulties encountered in making mechanically satisfactory membranes thinner than about 0.5 mm. It has been found that for membrane thicknesses from 0.5 mm. to 5 mm. there is no clear connection between thickness and potential, and it appears that all membranes in this range of thicknesses which are structurally sound tend to give the same potential. Membranes with thicknesses of 0.1 and 0.2 mm. have always been found to give lower potentials than those of greater thickness than 0.5 mm., and the differences appear to be larger the higher the concentration of one of the solutions of the pair separated by the membranes. The results are, however, extremely erratic and it has not yet been possible to distinguish a genuine electrochemical effect due to thickness, of the type observed by Sollner (14) with collodion membranes, from spurious effects resulting from mechanical imperfections in very thin membranes.

DISCUSSION

Calculation of sodium-ion activities

It seems generally conceded that there is at present no thermodynamical method of computing single ion activities, and in fact it has been stated by Guggenheim (2) that no experimental method can ever be found for a quantity which physically does not exist. From a strictly thermodynamical approach to the problem this view is not disputed. However, an analogous situation exists in the measurement of pH with the glass electrode and the relationship between the activities of hydrogen ions computed from the pH measurements and true hydrogen-ion activities. All pH measurements involve liquid junctions in the cells set up and thus any activities computed from E.M.F. measurements of the cells must be for this reason alone in error to an indeterminate extent. However, the glass electrode potential may be compared directly with the potential of a hydrogen electrode and it may be shown that under the same conditions in the appropriate range of acidity the potentials obtained are sensibly identical. The glass electrode thus fulfils its major present role as a convenient device which can be substituted for the clumsy and less manageable hydrogen electrode, and the pH values determined with the glass electrode may be interpreted in terms of the hydrogen electrode. Results so obtained, although they may be in a strictly thermodynamical sense empirical and comparative, are nonetheless of great value.

The problem of developing an artificial electrode which will give in neutral solutions of sodium salts of strong electrolytes the same potential as that of a perfect sodium electrode is complicated by the fact that it is not possible to make a sodium electrode which will function over the concentration range desired. Thus, it is not feasible to make the same direct comparison between the potentials obtained with the artificial electrode and the sodium electrode as is possible with the glass and hydrogen electrodes. Since a direct criterion of the electrochemical efficiency of a membrane for sodium ions is not available (and the same is true for other alkaline earth cations), it becomes necessary to estimate the sodium-ion activities of sodium chloride solutions of different molalities and to use these quantities in the Nernst equation to compute the sodium electrode potential. Such a course clearly involves nonthermodynamic assumptions and may give potentials which are very seriously in error, particularly at high sodium chloride concentrations. Marshall (4) faced the same difficulty when using clay membrane electrodes, but his problem was simplified to the extent that he was not using solutions with molalities exceeding 0.1 *m*. In the range of molalities up to 0.1 *m* sodium chloride Marshall computed sodium-ion activities on the basis of the equality of the activities of the potassium and chloride ions in solutions of potassium chloride and assumed, following the empirical findings of Lewis and Randall. that the activity of the chloride ion is identical in all chloride solutions of the same ionic strength.

The overall accuracy of these assumptions is unknown, but Marshall found excellent agreement between potentials computed on these assumptions and those measured by use of his clay electrodes. Wyllie (18) has found that the same assumptions gave a potential in good agreement with that measured with a natural shale membrane when using 1.0 *m* and 0.4 *m*. sodium chloride solutions. The difference between the observed and computed potentials was 0.3 mv., which is, of course, poor if compared with observations on cells not involving liquid junctions. Nevertheless, it appears that at least to a first approximation Marshall's assumptions may give potentials which agree with those of a true sodium electrode. The theoretical sodium electrode potentials for sodium chloride concentrations up to 4.0 *m* have been computed from the mean activity coefficients of potassium chloride and sodium chloride and used in this work as a basis of comparison for the performance of the membranes at the appropriate concentrations.

It was realized that the reproducibility and consistency of the potentials obtained with the membranes at any concentration differential was of far greater importance than any exact agreement with the corresponding theoretical potentials. Nevertheless, it was also felt that if reproducible potentials in reasonably good agreement with those computed were obtained, the efficiency of the membranes could justifiably be considered as high. The relatively good agreement noted in table 3 between the potentials obtained with the membrane and glass electrodes may be taken as independent evidence that in hydrochloric acid of a pH of 0.0 the permeability of the membranes to chloride ions is essentially zero. Similar impermeability to the chloride ion of sodium chloride solutions up to 4.0 *m* concentration is thus feasible and may well have been attained with those electrodes incorporating fine-grained Amberlite membranes. Nevertheless, this cannot be proved.

If it is, in fact, assumed that the electrodes giving the highest potentials are acting as almost perfect sodium electrodes, it follows that the empirical assumptions of Marshall and of Lewis and Randall may be used to compute sodium-ion activities over a wide concentration range with a degree of accuracy which may be of considerable value to the geologist (20). On the other hand, the uncertainties involved in comparing the measured and computed potentials may be considered too large to justify interpretation of the measured potentials as identical with those of a true sodium electrode. It still seems feasible, however, in view of the consistency of the results obtained, to calibrate the electrodes in terms of the assumed sodium-ion activities of known sodium chloride solutions and to use them in a manner analogous to the glass electrode for the reproducible pNa measurement of appropriate colloidal or physiological solutions containing sodium ions. A disadvantage is the lack of specificity of the membranes, since it has been shown here that they respond to both sodium and hydrogen ions, and a few tests not described have indicated that the same is certainly true for potassium and calcium ions. If, however, the mobility ratio of sodium to hydrogen is determined for a membrane in the manner set forth by Marshall (4), it is still possible in many cases to find the apparent sodium-ion activity of a solution containing both sodium and hydrogen ions. Thus, if U_H/U_{Na} is the measured mobility ratio of hydrogen to sodium ions for a given membrane and a_H is the hydrogen-ion activity derived from a glass electrode measurement in the mixed solution,

$$E = \frac{RT}{F} \ln \frac{a'_{Na}}{a''_{Na} + U_H/U_{Na} \cdot a_H}.$$

where E = observed E.M.F.,
a'_{Na} = sodium-ion activity used as calibration standard, and
a''_{Na} = sodium-ion activity in the solution containing both sodium and hydrogen ions.

The structure of bonded Amberlite–resin membrane electrodes

It seems possible to give at this stage a general picture of the probable structure of the bonded Amberlite–resin membranes. It has been stated by Myers, Eastes, and Myers (9) that the structure of the Amberlite IR resins may be visualized as a very porous open "lattice" or gel structure. A similar picture is drawn by Nachod (11) on the basis of reaction velocities of ion exchange. Nachod states that his data fit a gel structure which may be visualized as an anionic sponge filled with cations, these cations being replaceable by a mechanism similar to musical chairs. An essentially similar structure for the organic cation-exchange resin Dowex 50 is postulated by Bauman and Eichhorn (1), the cations being considered completely dissociated from the fixed negative groups on the skeleton of the gel. Myers, Eastes, and Myer state further that the gel structure of the resin combines a large inner surface and high reactivity with considerable mechanical strength. The resin shows also little variation of cation-exchange capacity with developed surface, a fact which points to the absence in the resin granules of cavities which have no connection with the exterior of the granules.

Each individual granule of Amberlite IR-100 thus possesses the two fundamental requirements postulated by Sollner for good membrane performance, *viz.*, small pores penetrating through the granule and numerous dissociable groups existing along each pore. Since the rigid structure of the homogeneous gel may be considered inert in the presence of aqueous solutions of simple salts, any conduction across a granule of Amberlite IR-100 must occur by ionic movement within its pores. In a closely packed assembly of such granules the same is true, provided that all intergranular interstices are entirely filled with a substance which is effectively an insulator. The conducting structure of an ideal Amberlite–insulating plastic resin membrane may thus be visualized as a complex network of pores within the Amberlite granules, the conduction from granule to granule being made possible by intimate contacts existing between the granules as a result of the high moulding pressures employed.

If a membrane possessing such a structure is to function as a perfect sodium electrode when used to separate two sodium chloride solutions, it follows that all current carried across the interface between the solutions and some neutral zone within the membrane must be carried by sodium ions alone. It is suggested that this actually occurs in practice as a result of the repulsive effect on anions of the fixed negative charges situated along the surface of the pores within the Amberlite granules. It is not suggested that the penetration of anions into the pores in the Amberlite granules is negligible, but rather that the movement of an anion along a pore network suffers a retardation in the zone of repulsion surrounding each fixed negative charge encountered. The summation of these retardations within the pore network may be considered to reduce to zero the transport number of the anions in a small but finite distance, this distance varying with the size of the pores entered by the anions, the anion concentration, and the number and location of the fixed negative charges within the pores. On this basis, a minimum membrane thickness for perfect electrochemical action must be inferred, and this minimum should be to some extent dependent on the anion concentrations in contact with the membrane. As explained above, no conclusive experimental verification of this minimum membrane thickness concept has been achieved. It is probable that in ideal membranes the conduction of current is by sodium ions which move from an equilibrium position in the region of one fixed negative charge to a similar equilibrium position in the region of the next such charge along a pore. It may be pointed out that since these sodium ions are presumably to a greater or lesser extent hydrated, there will be an effective transfer of water across the membrane. If this is so, the potential of even a perfect membrane electrode must differ from that of the ideal sodium electrode by an amount equal to the difference between the activities of water in the two sodium chloride solutions separated.

Perfect membrane action would only be achieved with this mechanism in the absence of any form of leak across the membrane which would be permeable to anions. Such an anionic leak could result mechanically if the adhesion of the interstitial plastic bonding resin to the surfaces of the Amberlite granules were imperfect, if the membrane were cracked, or if the bonding resin itself possessed some measure of conductivity. A leak could also occur through the granules of Amberlite if the continuous pore systems within the granules connecting the two solutions either possessed insufficient negative charges to reduce to zero the transport number of the anion or were so large in diameter with respect to the zone of repulsion of the fixed netative charges that the effective anionic retardation effected by each group was very small.

It would seem that a second function of the plastic matrix, in addition to its role as an interstitial bonding and insulating medium, may be to prevent undue swelling of the Amberlite granules after the membranes have been soaked in the aqueous solutions, and thus forcibly to prevent enlargement of the conducting pores.

In this connection it is of interest to note that satisfactory Amberlite–methyl methacrylate and Amberlite–polystyrene membranes appeared to increase in weight to the extent of 15–20 per cent of the weight of the air-dried Amberlite originally moulded, whereas electrochemically unsatisfactory membranes moulded with methyl methacrylate showed about a 40 per cent weight increase under the same conditions of measurement. The higher take-up of water is apparently associated in the methyl methacrylate membranes with high Amberlite contents, but it is not possible to say whether the higher water content involves larger pore sizes in the Amberlite granules or merely interstices between the granules where the Amberlite–methyl methacrylate bonding has been inefficient. Both possibilities could account for the observed poor electrochemical performance and low resistance of these membranes. On the whole, it seems more probable that the difficulties experienced in making satisfactory methyl methacrylate membranes with high Amberlite content lies in the poorer adhesion of this material to the Amberlite granules as compared with polystyrene.

The results obtained generally confirm the theoretical view that the potentials given by well-bonded Amberlite membranes are independent of the quantity of Amberlite in the plastic matrix. In the case of polystyrene–Amberlite membranes, it has been shown that the overall resistance of membranes is very sensitive to the amount of Amberlite moulded. It seems feasible to believe that refinement in moulding technique and the use of other plastic bonding agents and cation-exchange materials may yield electrodes with resistances of the order of 10^2 ohms possessing excellent reversible electrode characteristics over a wide range of electrolyte concentrations. It may also be possible to produce membranes without the inconveniently large and variable asymmetry potentials recorded in this work. Another possibility which may result from the use of artificial cation-exchange materials other than Amberlite IR-100 is that of producing membranes responsive only to particular ions or ions of particular valence. This aspect of the problem is under investigation.

The results reported involving the use of shale and clays set in a methyl methacrylate plastic matrix taken with those involving artificial cation-exchange materials set in a similar matrix seem to substantiate the theory set out in the introduction regarding the mechanism of the electrochemical properties of natural shales. It would appear that in a broad sense the constituents of a shale which do not possess cation-exchange properties act electrochemically merely as an inert matrix analogous to the inert plastic of the artificial membrane electrodes. The main components of shales showing cation-exchange properties are probably certain clay minerals, although organic materials may also contribute. The fact that the total quantity of cation-exchange material in a membrane has been shown to have no effect on its electrochemical properties probably accounts for the observed similarity (19) of the electrochemical properties of many shales which undoubtedly vary greatly in cation-exchange capacity. The thickness of shale in which anion mobility is effectively reduced to zero may be, however, many orders of magnitude greater than that existing in Amberlite-plastic membranes.

SUMMARY

Membranes have been prepared by bonding together intimately powdered mixtures of thermoplastic resins and artificial cation-exchange materials. Membranes so formed when used to separate two sodium chloride solutions give rise to potentials which appear to follow those computed for the sodium electrode using the Nernst equation.

It is suggested that the similar electrochemical properties of natural shales result from the similarity of their structure to that of the artificially prepared membranes, the cation-exchange material in the shale consisting primarily of clay minerals and the plastic bonding material being replaced by the electrochemically inert constituents of the shale.

The authors wish to thank Dr. Paul D. Foote, Executive Vice President, Gulf Research & Development Company, for permission to publish this paper and Mr. Ben B. Cox, Director, Geology Division, for his help and encouragement in carrying out this work.

REFERENCES

(1) Bauman, W. C., and Eichhorn, J.: J. Am. Chem. Soc. **69**, 2830 (1947).
(2) Guggenheim, E. A.: J. Phys. Chem **33**, 842 (1929).
(3) Kelley, W. P.: *Cation Exchange in Soils*. Reinhold Publishing Corporation, New York (1948).
(4) Marshall, C. E.: J. Phys. Chem. **48**, 67 (1944).
(5) Marshall, C. E., and Ayers, A. D.: J. Am. Chem. Soc. **70**, 1297 (1948).
(6) Marshall, C. E., and Bergman, W. E.: J. Am. Chem. Soc. **63**, 1911 (1941).
(7) Marshall, C. E., and Eime, L. O.: J. Am. Chem. Soc. **70**, 1302 (1948).
(8) Marshall, C. E., and Krinbill, C. A.: J. Am. Chem. Soc. **64**, 1814 (1942).
(9) Myers, R. J., Eastes, J. W., and Myers, F. J.: Ind. Eng. Chem. **33**, 697 (1941).

(10) Meyer, K. H., and Sievers, J. F.: Helv. Chim. Acta **19**, 649 (1936).
(11) Nachod, F. C., and Wood, W.: J. Am. Chem. Soc. **66**, 1380 (1944).
(12) Robinson, R. A., and Harned, H. S.: Chem. Revs. **28**, 419 (1941).
(13) Sollner, Karl: J. Phys. Chem. **49**, 47 (1945).
(14) Sollner, Karl: J. Phys. Chem. **49**, 171 (1945).
(15) Sollner, Karl: J. Phys. Chem. **49**, 265 (1945).
(16) Sollner, Karl, and Carr, C. W.: J. Gen. Physiol. **28**, 1 (1944).
(17) Teorell, T.: Proc. Soc. Exptl. Biol. Med. **33**, 282 (1935); Proc. Natl. Acad. Sci. (U. S.) **21**, 152 (1935).
(18) Wyllie, M. R. J.: Science **108**, 684 (1948).
(19) Wyllie, M. R. J.: Bull. Am. Assoc. Petroleum Geol. **33**, 1892 (1949).
(20) Wyllie, M. R. J.: Am. Inst. Mining Met. Engrs., Tech. Pub. No. **2511**, J. Petroleum Technol. **1**, 17 (1949).

THE NATURE OF CARBON BLACK SURFACES AS REVEALED BY ADSORPTION STUDIES[1]

W. D. SCHAEFFER, M. H. POLLEY, and W. R. SMITH

Research and Development Laboratory, Godfrey L. Cabot, Inc., Boston, Massachusetts

Received August 22, 1949

A rubber-reinforcing agent has been defined as a material which imparts, to rubber, strength and serviceability far beyond that possessed by the rubber alone (19). Carbon black is the principal reinforcing agent in use today, and its unparalleled ability to improve the serviceability of rubber is most strikingly demonstrated in the 20,000–30,000 miles of roadwear inherent in the modern rubber tire.

The superiority of carbon black over other materials as a reinforcing agent has been associated with its suspected fine degree of subdivision for many years (19). However, it remained for the electron microscope to substantiate this view by demonstrating that reinforcing carbon blacks lie in the 100–500 Å. particle size range—a degree of subdivision equalled by few other commercially available pigments. A considerable volume of literature (17) is available in which physical properties of rubber stocks loaded with carbon black have been catalogued in terms of particle size of the black. Thus it has been found that hardness, tensile strength, hysteresis properties, and to a certain degree resistance to abrasive wear do increase quite regularly with decreasing particle size of the carbon black. Since carbon black remains as a discrete phase in all its applications, the properties of the systems in which it is incorporated must be controlled by the extent and nature of the carbon interface. While adequate data on particle diameters and total surface area are now available (2, 10, 12, 16, 21, 27), information regarding the specific surface nature or activity of various carbon blacks has been extremely scanty. Consequently, the question as to whether rubber reinforcement is solely a function of particle size and would be displayed in equal degree by all solids if of comparable fineness, or whether there is a specificity associated with carbon black surfaces, has so far remained unanswered. To provide information on this latter point, we have measured the heats of adsorption of a number of hydrocarbons on a variety of carbon blacks in the belief that such measurements would reflect the magnitude of the binding forces operative at carbon black surfaces and might also reveal their nature. In previous publications (4, 5) we have described results obtained when nitrogen, oxygen, and argon, and a series of hydrocarbons up to C_5 were adsorbed on a number of carbon blacks at −195° and 0°C., respectively. Under these conditions the adsorption was entirely of the van der Waals type.

---

[1] Presented at the Twenty-third National Colloid Symposium, which was held under the auspices of the Division of Colloid Chemistry of the American Chemical Society at Minneapolis, Minnesota, June 6–8, 1949.

In the present paper heat of adsorption data for *n*-decane and dihydromyrcene on a fully reinforcing carbon black, Spheron 6, are described. The adsorption was carried out at 100°C. Dihydromyrcene was included in the study as it is the simplest diolefin possessing the same unsaturation pattern present in natural rubber. If this hydrocarbon were to undergo a chemisorption, this fact should be more evident at 100°C. than at the lower temperature, 0°C., employed in our earlier work (5).

MATERIALS AND PROCEDURES

The dihydromyrcene used in the present work was prepared by the reduction of geraniol with sodium and ethyl alcohol in liquid ammonia as described by Chablay (8). We are indebted to Dr. Koch of the British Rubber Growers' Research Laboratories at Welwyn for a sample of dihydromyrcene similarly prepared in their laboratory. The physical data collected on these two samples are as follows:

	G. L. CABOT PREPARATION	B. R. G. R. L. PREPARATION
Refractive index, $n_D^{20°}$	1.4489	1.4479
Boiling point (20 mm.)	67°C.	67°C.

The *n*-decane was obtained from Humphrey-Wilkinson, Inc., New Haven, Connecticut. It was stated to be of at least 95 mole per cent purity. The refractive index, $n_D^{20°}$, was 1.4121 compared with the value of 1.4119 quoted in A.P.I. Project 44 (1). The *n*-decane was used without further purification.

The carbon black used as the adsorbent was a fully reinforcing grade of medium processing channel black, Spheron 6, produced by Godfrey L. Cabot, Inc.

All particle size data were obtained with the RCA-EMU electron microscope. In mounting, the "dry" technique was employed. Polyvinylformal was used for the supporting film and the blacks were dusted on the film by means of the discharge from a high-frequency Tesla coil. The plates were taken at 8000 diameters magnification and enlarged to 50,000 or 100,000 diameters for counting.

In counting, only particles with at least a half perimeter visible were measured. Measurements were made to the nearest 0.25 mm.

Surface area values were also evaluated from the low-temperature nitrogen isotherms (11). In all instances the isotherms were sigmoid (B.E.T. type II) (14), and the monolayer volume (V_m) was in satisfactory agreement when obtained from either the *B* point (11) or the standard B.E.T. plots (7). In computing surface areas 16.2 sq. Å. was employed as the cross-sectional area of the nitrogen molecule.

The bound rubber data were obtained by the procedure described by Fuller (15). A 0.3-g. sample of the rubber stocks was cut into twenty equal sections and distributed, two to each screen. The cell was then filled with 100 ml. of benzene, and allowed to stand in the dark at 25–30°C. for 24 hr. The benzene was then drawn off, 50 ml. evaporated, and the extracted rubber content determined by weighing.

The adiabatic calorimeters used in the present work have been described in our previous publications (4, 5). The adsorption "line" external to the constant-temperature bath used in the 100°C. measurements on the C_{10} hydrocarbons was wrapped with chromel heater ribbon to prevent condensation. The current through these circuits was controlled manually, the temperature remaining at 120°C. ± 1°. The gas burets and calorimeter were entirely immersed in an oil bath maintained at 100°C. ± 0.015°C. Pressure measurements in the gas buret and in the calorimeter were made by using quartz Bodenstein gauges as null point instruments. These gauges, being external to the bath, were also wrapped with chromel heater ribbon. The pressure was read from mercury manometers in conjunction with the Bodenstein gauges. Pressure readings in this system were reproducible to ±0.15 mm. The main experimental difficulty encountered was associated with the stopcock lubricants. It was necessary to use stopcocks, since the use of mercury "cutoffs" was excluded by the high temperature and metal valves proved unsatisfactory. While Silicone grease proves satisfactory from the point of view of vacuum tightness, at 100°C. sufficient sorption of hydrocarbons occurred to complicate the procedure. A satisfactory lubricant, both with regard to vacuum "tightness" and insignificant hydrocarbon sorption, was finally found in the cellulose acetate polyethylene glycol lubricant described by Pearlson (18). This lubricant was used in all experiments described in the present paper.

Radiation losses from the calorimeter at 100°C. were, of course, greater than those encountered in our previous work (4, 5), performed at −195°C. and 0°C. Consequently, the calorimeter did not operate as adiabatically as at the lower temperatures. In extrapolating the time–temperature tracings back to the initial heat value for a given increment of gas adsorbed, no correction was made for the radiation losses, since reconstruction of both calibration and experimental curves proved that the heat losses were identical when adsorption was rapid. In some runs involving dihydromyrcene, to be described below, the heat was evolved over a period of some 15 min. in contrast to the nearly instantaneous evolution noted when purely physical adsorption was being studied. In these instances the data were corrected for cooling losses (23). This was accomplished by applying Newton's expression

$$dT/dt = K(T_j - T)$$

where T_j is the temperature of the jacket and T is the temperature of the calorimeter. K, the leakage modulus, was evaluated from the electrical calibration curves. Orienting experiments demonstrated that no significant differences could be noted in the heat value after 15 min. of equilibration of each increment of adsorbate. Accordingly, the heat evolved in this period was accepted as the final value. Owing to these factors, there is an uncertainty in the absolute value of these differential heats of perhaps 10 per cent, in spite of the fact that the reproducibility in all experiments was generally better than 5 per cent.

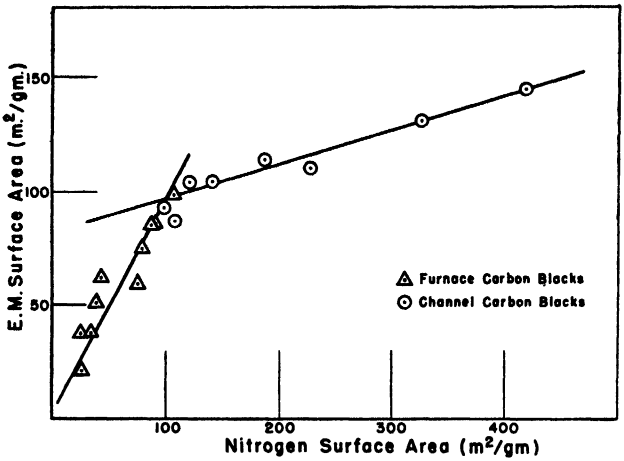

FIG. 1. Surface areas of furnace and channel blacks calculated from nitrogen adsorption and electronmicrographs.

EXPERIMENTAL RESULTS AND DISCUSSION

The surface area and particle size of the carbon black will, of course, determine the maximum extent of carbon–rubber interface in a carbon–rubber system. In this regard it is of interest to compare the specific surface areas of various carbon blacks as determined both from the surface average diameters computed from size distribution curves obtained from electron microscope data and from the B.E.T. (7) plots of low-temperature nitrogen adsorption data. These two areas are plotted in figure 1 for a variety of carbon blacks used in the rubber industry, ranging from semi-reinforcing furnace blacks (22) to the most finely divided rubber grades of channel blacks. The furnace blacks fill the nitrogen surface area range from 26 to 110 sq.m. per gram, while the channel grades extend from 100 to 420 sq.m. per gram. In the case of the furnace blacks, both the electron microscope and the nitrogen surface area values are in good agreement. For the channel grades of blacks, however, the slope changes sharply and the adsorption method gives higher areas. This, we feel, reflects a considerable degree of porosity which would not, of course, be revealed by the electron microscope. When the method of manufacture (22). of the furnace and channel blacks is considered, this conclusion seems logical. Furnace blacks are produced in a closed system in a considerable deficiency of oxygen. Their "volatile content," which is essentially chemisorbed oxygen, is extremely low, seldom exceeding 0.8 per cent. The channel blacks, produced by impingement of a freely burning flame, have opportunity to chemisorb much larger quantities of oxygen as reflected in the 3–5 per cent "volatile content" normally present on channel blacks. Chemisorption of oxygen by carbon black at elevated temperatures is accompanied by evolution of carbon monoxide and an increase in nitrogen surface area without significant alteration in the diameter of the particles as observed under the electron microscope (2, 21).

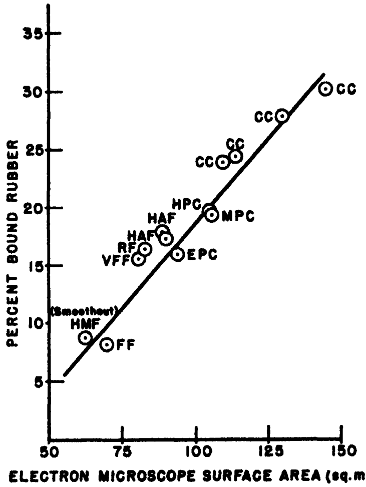

FIG. 2. Bound rubber and external surface area

This "etching" effect of oxygen is doubtless associated with a preferential oxidation of the surface.

The data presented in figure 2, relating the per cent of "bound" rubber (3, 14) to the electron microscope surface areas, indicate that only the "external" surface of carbon black is available to the rubber molecules. While these data demonstrate the role of particle size in rubber reinforcement with carbon black, they do not answer the question as to the nature of the association nor the vigor of binding of rubber to the carbon surface.

Figure 3 summarizes the differential heats of adsorption of ethane, propane, *n*-butane, and *n*-pentane at 0°C. on the reinforcing channel black, Spheron 6. The general shape of the curves is similar in each case. When surface coverage, (V/V_m), is low, high heat values are found which decrease regularly with increasing coverage, approaching the heat of liquefaction of each hydrocarbon beyond the first molecular layer. This variation of binding energy with surface coverage may be interpreted as a distribution of energy sites of varying intensity over the carbon surface. As reported previously (5), these high initial heat values can be considerably reduced by partial graphitization of the black. The differential heats of adsorption of *n*-decane on Spheron 6 at 100°C. are presented in

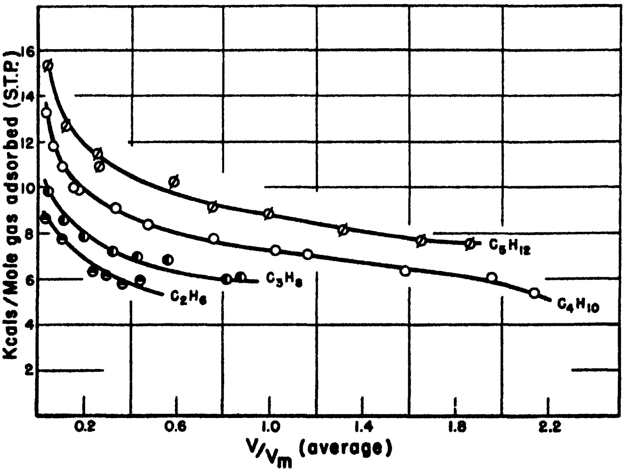

FIG. 3. Differential heats of adsorption of the normal paraffins C_2 to C_5 on Spheron 6 at 0°C.

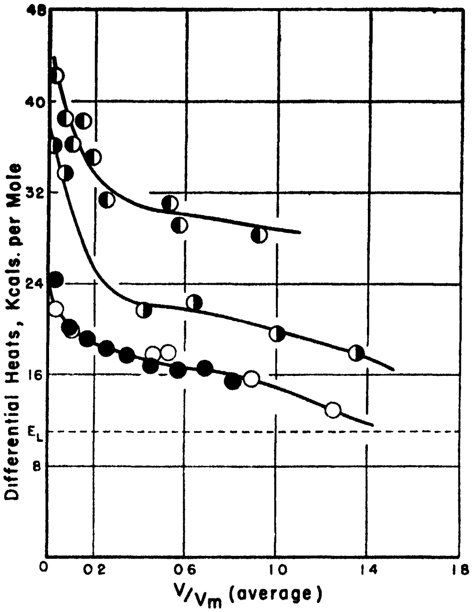

FIG. 4. Differential heats of adsorption of *n*-decane and dihydromyrcene on Spheron 6 at 100°C. *n*-Decane: ○, run 77B; ●, run 78B. Dihydromyrcene: ◐, run 79B; ◑, run 80B.

figure 4. The heats of adsorption for the saturated hydrocarbons at low surface coverage (0.05 V/V_m) are replotted in figure 5 as a function of the number of carbon atoms in the hydrocarbon chain. The 100°C. data for *n*-decane are also included. The heats of adsorption increase quite regularly with chain length, and, as expected, do not vary greatly over the temperature range 0° to 100°C. The fact that these heats of adsorption increase with increasing molecular weight at about the same rate as the heat of liquefaction suggests strongly that forces involved in the adsorption of saturated hydrocarbons on carbon black are primarily van der Waals in nature. The magnitude of these forces, particularly in the case of the higher hydrocarbons, appears quite sufficient to impose a considerable degree of restriction on the adsorbed molecule. van der Waals adsorption is commonly described as essentially nonspecific with regard to the surface nature of the adsorbent. While it is true that the effect is probably much less pronounced than in chemisorption, the adsorption data we have so far collected regarding the variation of the heats of adsorption with surface coverage and the marked changes brought about by partial graphitization of the carbon black (Graphon) (4) suggest a considerable degree of specificity in van der Waals adsorption.

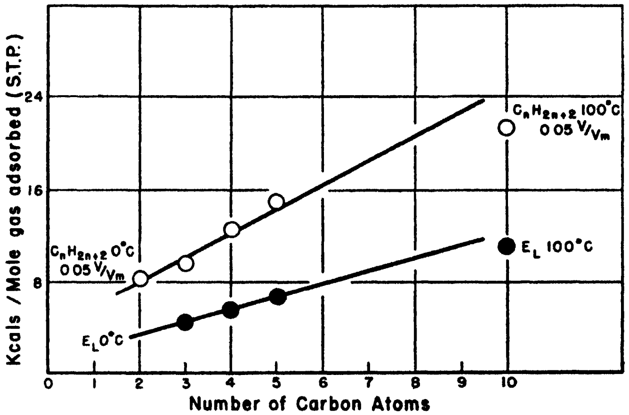

FIG. 5. Heats of adsorption of the normal paraffin hydrocarbons as a function of chain length.

The hydrocarbons so far discussed are saturated, while rubbers—both natural and synthetic—possess some degree of unsaturation. The work of Farmer (13) has shown that in natural rubber, chemical activity, such as vulcanization, oxidation, etc., is associated with the doubly interrupted pattern of unsaturation present in the elastomer. Accordingly, the question as to whether or not anything other than physical associations involved in rubber reinforcement cannot be answered until adsorption data on hydrocarbons possessing this same unsaturation pattern are considered. Dihydromyrcene ($C_{10}H_{18}$) is the simplest analog of natural rubber and, accordingly, was selected for study. Earlier work on the adsorption of C_4 olefins on carbon black at 0°C. revealed no essential difference between their adsorption and that of *n*-butane (5). The C_4 olefins, however, do not possess the same unsaturation pattern as in rubber and, further, if chemisorption were involved, it is quite possible that it would not be evident at 0°C. For this reason the adsorption data on dihydromyrcene were collected at 100°C., a temperature which approaches that encountered during the compounding of rubber and carbon black. Adsorption isotherms for dihydromyrcene and *n*-decane on Spheron 6 are presented in figure 6, and the corresponding B.E.T. plots in figure 7.

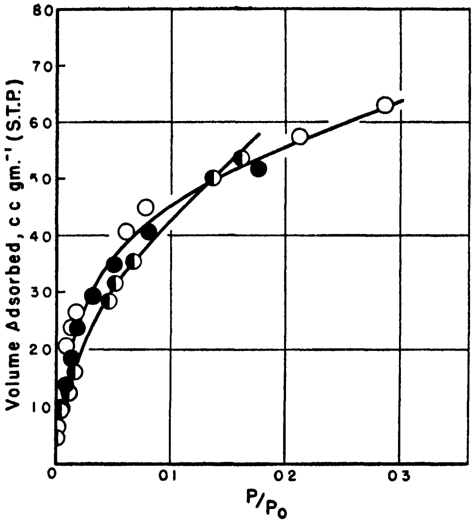

FIG. 6. Adsorption iotherms on Spheron 6 at 100°C. *n*-Decane: ○, run 77B; ●, run 78B. Dihydromyrcene: ◐, run 79B.

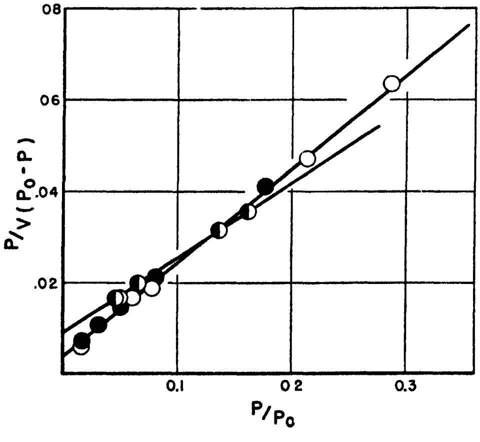

FIG. 7. B.E.T plots for the C_{10} hydrocarbons on Spheron 6. *n*-Decane: ○, run 77B; ● run 78B. Dihydromyrcene: ◐, run 79B.

From figure 4 it is quite evident that the initial heats of adsorption for dihydromyrcene are some 20 kcal. higher than those obtained with *n*-decane. Since the heat of liquefaction of dihydromyrcene closely approximates that of *n*-decane, 11 kcal. per mole, the implication is that the adsorption of dihydromyrcene involves something other than physical adsorption. The difference in the nature of the adsorption of these two hydrocarbons is evidenced in other ways. For example, subsequent runs on the same sample of carbon black with dihydromyrcene, even after evacuation at 250°C., generally produced lower heat values as depicted in the middle curve in figure 4. Another difference is noted in the nature of the time–temperature cooling curves. With *n*-decane adsorption, the heat is evolved rapidly and the temperature falls off (due to lack of adiabaticity at 100°C.) quite smoothly in the same fashion as the electrical calibration curves. With dihydromyrcene, however, the initial heat evolution is followed by a fairly steady evolution of heat. If this effect were due to slow diffusion, or other experimental features, it should also have been noted in the *n*-decane runs. Since such is not the case, we are of the opinion that in the adsorption of dihydromyrcene a rate process is involved. This process could presumably be either chemisorption, polymerization, or cyclization. As far as polymerization is concerned, the saturation pressure of the dihydromyrcene remaining in the buret at 100°C. during each run showed no change. Farmer (13) has stated that dihydromyrcene has a strong tendency to undergo cyclization in the presence of acids. Since the acidity of water slurries of channel blacks is well substantiated (9, 24,26) it seems permissible to consider carbon blacks with their partially oxidized surface as solid acids. Consequently, the cyclization of the adsorbed dihydromyrcene may explain the high energy adsorption. The effects of removing the surface oxygen complexes from the black were next investigated, for this procedure causes a greatly increased pH of carbon black–water slurries (26).

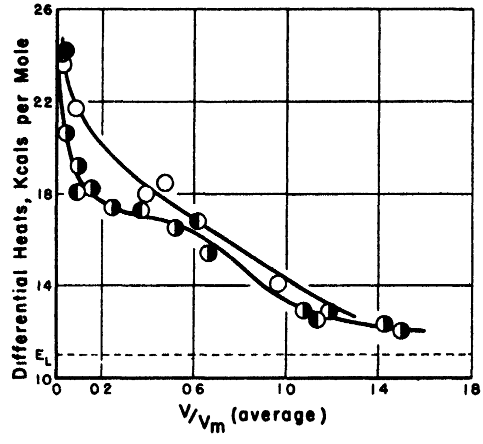

FIG. 8. Differential heats of adsorption on devolatilized Spheron 6 at 100°C. *n*-Decane: ○, run 71B; ●, run 72B. Dihydromyrcene: ◑, run 73B; ◐, run 74B.

Spheron 6 was devolatilized at 925°C. in vacuum over a 3.5-hr. period. The lower differential heat curve in figure 8 was obtained for the adsorption of dihydromyrcene on this "devolatilized" carbon black. For equivalent surface coverages, this curve is approximately 20 kcal. per mole lower than the data for dihydromyrcene on standard Spheron 6. Moreover, all evidence of irreversibility disappeared and successive runs showed good reproducibility of both isotherms and heat curves when the devolatilized Spheron 6 was used as the adsorbent.

The responsibility of the volatile matter for the high energy dihydromyrcene adsorption having been affirmed, the precise mechanism of the "chemisorption" remains unsolved. Whether the heat of cyclization of dihydromyrcene is as large as 20 kcal. per mole, the difference observed between the heats of physical and chemisorption must await independent experimental verification.

The mechanism of chemisorption deserves consideration. Qualitative analyses of the oxygen complexes on carbon black surfaces have been determined by their reaction with Grignard reagent (25) and by their emission spectra (20). These independent techniques have identified the oxygen-containing groups OH, CO, —O—, and OH, CO, CO$^+$, COO$^+$, and CHO, respectively. The possibility of these surface oxygen complexes participating in a structure similar to the diperoxide formation on oxidation of dihydromyrcene, as proposed by Bolland and Ten Have (6), should be considered. Certainly the presence of molecular oxygen derived from decomposition of the surface oxides is thermodynamically improbable. However, if the packing of the surface oxides were such as to favor sterically the formation of an intermolecular structure, the formation of a stable six-membered cyclic product on the carbon black surface might be admitted. Admitting this possibility, then at fairly low surface coverage ($V/V_m = 0.25$ -0.5) the "chemisorption" heat curves should approach the van der Waals heat curve as the sterically favorable sites are filled. Experimentally this has not been realized; instead, the chemisorption curve levels off at 30–31 kcal. per mole at 0.3 V/V_m. This hypothesis will be further tested as more carbon blacks are studied. The furnace blacks with their low volatile concentration, usually less than 1 per cent by weight, should be of special interest. One preliminary experiment was attempted in which 0.03 millimole of oxygen was chemisorbed per

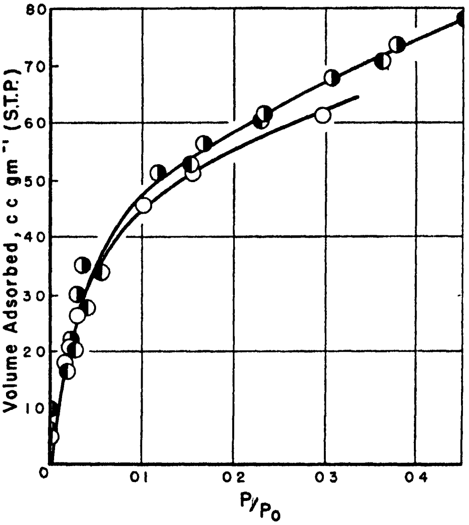

FIG. 9. Adsorption isotherms on devolatilized Spheron 6 at 100°C. n-Decane: ○, run 71B. Dihydromyrcene: ◑, run 73B; ◐, run 74B.

gram at 100°C. on previously devolatilized Spheron 6. The heat evolved for the first increment of oxygen chemisorbed was about 95 kcal. per mole. The dihydromyrcene heats of adsorption and area per molecule on the "reoxidized" sample were identical with those determined previously on the "bare" carbon surface. Thus, either the chemical identities of the oxygen complexes formed on the reoxidation were different from the 1.4 millimoles normally present on Spheron 6, or the chemisorption of dihydromyrcene was hindered sterically by the much sparser population of surface oxides.

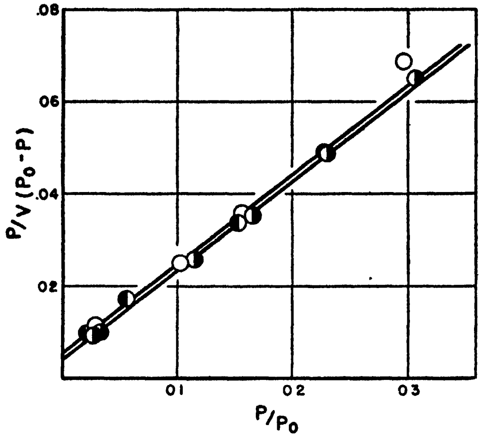

FIG. 10. B.E.T. plots for the C_{10} hydrocarbons on devolatilized Spheron 6. *n*-Decane: ○, run 71B. Dihydromyrcene: ◑, run 73B; ◐, run 74B.

TABLE 1

RUN NO.	ADSORBENT	ADSORBATE	V_m	c	$E_1 - E_L$	Σ*	σ†
			ml. at S.T.P.		*kcal. per mole*	*sq. m. per gram*	*Å.²*
78B. . .	Spheron 6	$C_{10}H_{22}$	4.6^8	49	2.9	121	96
79B . .	Spheron 6	$C_{10}H_{18}$	5.6^6	20	2.2	121	80
71B .	Spheron 6 (devolatilized)	$C_{10}H_{22}$	4.8^7	35	2.6	112	86
73B . . .	Spheron 6 (devolatilized)	$C_{10}H_{18}$	4.9^7	61	3.1	112	84

* Surface area determined by nitrogen adsorption.

† Area per molecule calculated from the 16.2 sq. Å. molecular area of nitrogen.

The differential heats of adsorption for *n*-decane on the devolatilized carbon black are also included in figure 8. Comparison of these data with that for *n*-decane adsorption on standard Spheron 6 contained in figure 4 shows that the adsorption of *n*-decane is not influenced by surface oxygen complexes. Similar results were noted in our earlier work at 0°C., where all adsorption studied was of the van der Waals type.

Table 1 summarizes the data from the isotherms and B.E.T. plots in figures 6, 7, 9, and 10. The most striking feature is the apparent 24 Å.² contraction of the dihydromyrcene molecule when chemisorbed as compared to that when bound to the surface by van der Waals forces. Actually the 104 Å.^{2} molecular area for dihydromyrcene is probably too large, for the 18 sq.m. increase in the nitrogen area on devolatilization of Spheron 6 is not entirely available to the much larger dihydromyrcene molecule. Considering the 96 Å.^{2} molecular area of *n*-decane to be the lower limiting value of the physically adsorbed dihydromyrcene area, then a contraction of approximately 17 per cent occurs on chemisorption.

While the present data are limited with respect to the number of carbon blacks studied, they are sufficient to indicate that the nature of association between rubber and carbon may involve the unsaturation of the elastomer and the volatile matter normally present on the carbon black. While the function of the rubber and the extent of carbon surface involved may be small, and hence detection difficult, it may be that a few points of exceptionally strong cross linkage may play an important role in reinforcement, and that the small fractions of the carbon surface involved may be highly specific.

SUMMARY

The maximum extent of the carbon–rubber interface is determined by the external particle surface of carbon blacks, rather than the total surface as revealed by nitrogen adsorption.

Heats of adsorption of *n*-decane and dihydromyrcene on Spheron 6 and devolatilized Spheron 6 reveal a high degree of specificity with regard to the unsaturation of the adsorbate, and either the concentration or the identity of the oxygen complexes on the carbon black surface.

We wish to express our appreciation to Miss Mary Martin for the electron microscope data, to Mr. C. B. Wendell, Jr., for the construction and maintenance of the apparatus used in measuring the heats of adsorption, and to Mr. Joseph Cavanagh for the data on bound rubber.

REFERENCES

(1) American Petroleum Institute Research Project 44 at the National Bureau of Standards: Selected Values of Properties of Hydrocarbons, Table 20a, Boiling Point, Refractive Index, Density and Freezing Point, June 30, 1948.

(2) Anderson, R. B., and Emmett, P. H.: J. Applied Phys. **19**, 367 (1949).

(3) Baker, W. O., Walker, R. W., and Pape, N. R.: Report CR-352, June 16, 1944.

(4) Beebe, R. A., Biscoe, J., Smith, W. R., and Wendell, C. B.: J. Am. Chem. Soc. **69**, 95 (1947).

(5) Beebe, R. A., Polley, M. H., Smith, W. R., and Wendell, C. B.: J. Am. Chem. Soc. **69**, 2294 (1947).

(6) Bolland, J. L., and Ten Have, P.: Trans. Faraday Soc. **45**, 99 (1949).

(7) Brunauer, S., Emmett, P. H., and Teller, E.: J. Am. Chem. Soc. **60**, 309 (1938).

(8) Chablay, E.: Ann. chim. **8**, 145 (1917).

(9) Cohan, L. H.: Chem. Eng. News **23**, 2082 (1945).

(10) Dannenberg, E. M., and Collyer, H. J.: Ind. Eng. Chem. **41**, 1607 (1949).

(11) Emmett, P. H., and Brunauer, S.: J. Am. Chem. Soc. **59**, 1553 (1937).

(12) Emmett, P. H., and De Witt, T.: Ind. Eng. Chem., Anal. Ed. **13**, 28 (1941).

(13) Farmer, E. H.: *Advances in Colloid Science*, edited by H. Mark and G. S. Whitby Vol. II. Interscience Publishers, Inc., New York (1946).

(14) Fielding, J. H.: Ind. Eng. Chem. **29**, 884 (1937).
(15) Fuller, C. S.: Bell System Tech. J. **25**, 374 (1946).
(16) Martin, M., and Smith, W. R.: "Particle Size and Surface Area of Several Types of Commercial Carbon Blacks." Godfrey L. Cabot, Inc., Boston (1949).
(17) Parkinson, D.: *Advances in Colloid Science*, edited by H. Mark and G. S. Whitby, Vol. II, p. 389. Interscience Publishers, Inc., New York (1946).
(18) Pearlson, W. H.: Ind. Eng. Chem., Anal. Ed. **16**, 415 (1944).
(19) Shepard, N. A., Street, J. N., and Park, C. R.: In *The Chemistry and Technology of Rubber*, edited by C. C. Davis and J. T. Blake. Reinhold Publishing Corporation, New York (1937).
(20) Smith, W. R., and Schaeffer, W. D.: Proceedings of the Rubber Technology Conference (London) **1948**, in press.
(21) Smith, W. R., Thornhill, F. S., and Bray, R. I.: Ind. Eng. Chem. **33**, 1303 (1941).
(22) Smith, W. R., and Wilkes, B. A.: India Rubber World **116**, 361 (1947).
(23) Sturtevant, J. M.: *Physical Methods of Organic Chemistry*, edited by A. Weissberger, Vol. I, p. 336. Interscience Publishers, Inc., New York (1945).
(24) Villars, D. S.: J. Am. Chem. Soc. **69**, 214 (1947).
(25) Villars, D. S.: J. Am. Chem. Soc. **70**, 3655 (1948).
(26) Wiegand, W. B.: Ind. Eng. Chem. **29**, 953 (1937).
(27) Wiegand, W. B., and Ladd, W. A.: Rubber Age **50**, No. 6, 431 (1942).

THIXOTROPIC BEHAVIOR OF CARBON BLACK IN RUBBER[1]

L. MULLINS

Research Association of British Rubber Manufacturers, 105 Lansdowne Road, Croydon, Surrey, England

Received August 22, 1949

I. INTRODUCTION

Solid fillers were first incorporated into rubber as diluents to cheapen the finished rubber products, but it was soon found that some fillers gave improved strength and serviceability as compared with pure rubber, and to these fillers the term "reinforcing agents" has been applied. It is now possible by a suitable choice of fillers and other compounding ingredients to produce rubbers with a whole range of desired physical properties. Carbon blacks are by far the most important fillers used in the rubber industry, and are the only ones capable of giving the highest degree of "reinforcement"; the carbon blacks used are of extremely fine particle size and range from the coarser lampblacks with average particle diameters of about 2000 Å. to very fine colloidal blacks with average particle diameters as small as 200 Å. Relatively large concentrations of black are often employed, and concentrations of 20 per cent by volume are usual.

Investigations into the behavior of concentrated dispersions of colloidal carbon black in oil or water have shown that it is complex; often they possess thixotropic properties—if allowed to stand they may progressively increase in consistency only to become more mobile during working (1, 2, 20). Similar time-dependent thixotropic properties are observed in other systems, and it is almost invariably found that these systems possess some kind of internal structure, this structure being formed by interactions between the dispersed particles which lead to flocculated aggregates. Breakdown and subsequent re-formation of this structure are responsible for the thixotropic behavior of the system.

---

[1] Presented at the Twenty-third National Colloid Symposium, which was held under the auspices of the Division of Colloid Chemistry of the American Chemical Society at Minneapolis, Minnesota, June 6–8, 1949.

It has not been generally recognized that many of the physical properties of rubbers containing carbon black or other fine-particle fillers show evidence of similar thixotropic behavior, and in this paper we shall describe the influence of these effects on the properties of both vulcanized and unvulcanized rubbers and discuss their bearing on theories of the reinforcement of rubber by fillers.

II. EXPERIMENTAL INVESTIGATIONS

A. Unvulcanized rubber

Before vulcanization rubber is a plastic material capable of being shaped and moulded, and in this state it is its flow properties—viscosity or plasticity—which are of importance. A series of experiments on the effect of carbon blacks on the plasticity of rubber stocks, to be reported in detail elsewhere, has recently been carried out by Mullins and Whorlow (13). Work was confined to rubber stocks without vulcanizing ingredients to avoid complications due to vulcanization occurring during plasticity measurements. The measurements were made on the modified Mooney shearing disc plastimeter described by Piper and Scott (16); this uses a biconical rotor to give a substantially uniform rate of shear throughout the rubber. Measurements were made of the torque required to shear rubber stocks, held at 100°C., at various rates of shear. The torque readings are given in arbitrary units; as a rough guide 200 of these units correspond to a shear stress of 10^6 dynes/sq.cm.

Preliminary experiments showed that the rheological properties of the rubber stocks depended upon the past history of the material; for example, their properties were changed continuously on the one hand by shearing and on the other hand by standing. Indeed, a wide range of values for the "plasticity" could be obtained, depending on this history and the conditions of test. Thus to obtain reproducible measurements at any chosen shear rate it was found necessary first to shear continuously for a relatively long period at a much higher rate of shear; this conditioning treatment brought the rubber stocks to a reproducible level where the behavior was substantially independent of differences in past history, and was adopted throughout the investigations.

It was found that during standing at an elevated temperature (e.g., 100°C.) the rubber stocks grew progressively stiffer. Figure 1 shows typical families of torque–time curves determined during the continuous shearing of two rubber stocks, a masticated smoked sheet (Mix A) and a carbon black stock containing 22 volumes of an M.P.C. carbon black to 100 volumes of rubber (Mix B). The stocks had been previously brought to a reproducible level by shearing for 20 min. at a shear rate of 10 sec.$^{-1}$, and measurements were subsequently made, after various periods of standing, at a shear rate of 1 sec.$^{-1}$ These curves show clearly the progressive increase in stiffness which occurs on standing; they also show a softening occurring during the continuous shearing of the stocks. This softening occurs rapidly at first and then more slowly until an approximately steady value of the torque is attained.

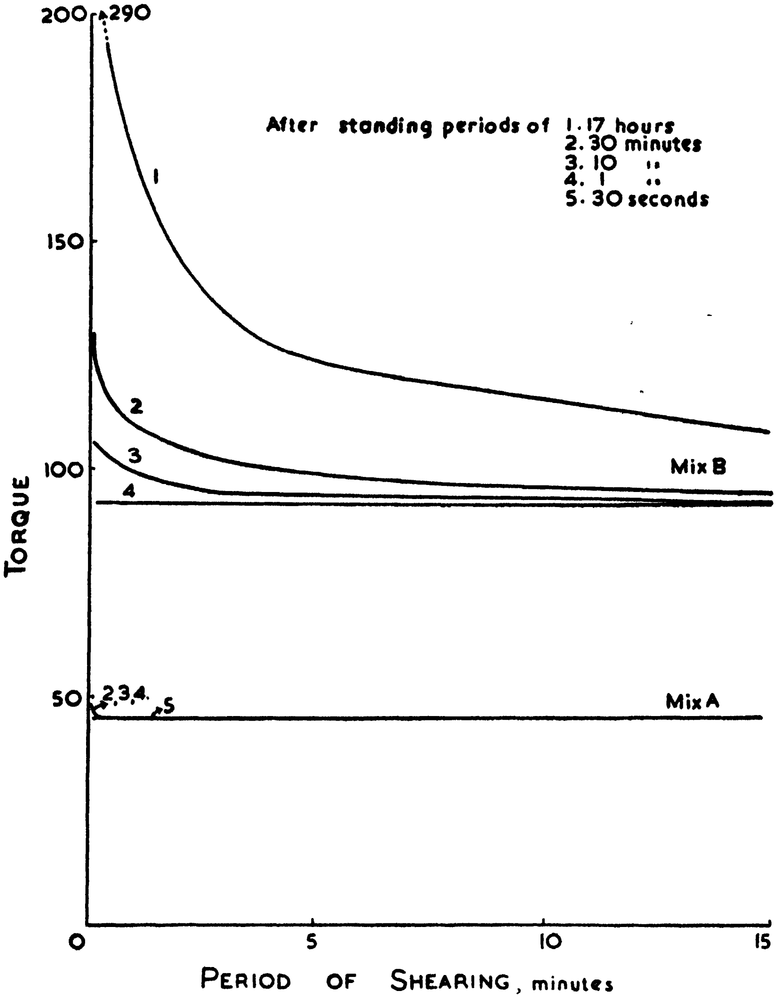

FIG. 1. Typical families of torque–time curves determined during the continuous shearing of two rubber stocks.

It appears that at least two processes are taking place during the continuous shearing of rubber stocks: firstly, a growth in structure which leads to an increase in the torque required to shear the material, and secondly a breakdown in structure which causes a decrease in torque. The steady value of the torque is reached when the rate of growth equals the rate of breakdown, and it can be considered to be a state of dynamic equilibrium, less structure being present at equilibrium during shearing at higher rates, as at these rates the breakdown is more rapid.

Both the masticated smoked sheet and the black-loaded stocks show evidence of internal structure that can be either broken down or built up. The changes occurring in the smoked sheet are very small compared with those in stocks containing carbon black; in smoked sheet the structure is weak, is readily broken down, and quickly re-forms; on the other hand, the structure in black-loaded stocks is much stronger, is only slowly broken down by shearing, re-forms continuously on standing, and may produce a manifold increase in stiffness. It appears that all important structural changes are due to the presence of fillers.

In cases where considerable structure was present, it was found that for short periods of shearing the amount of thixotropic breakdown occurring in loaded stocks was a function of the work done on the stock; that is, if the total work done on the stock was the same, the amount of breakdown was independent of how the work was applied (e.g., rapid shearing for a short time or slow shearing for a long time). A simple relationship of this type no longer held if shearing took place at a very low rate, i.e., over a very extended period, but this was not unexpected because standing at elevated temperatures besides producing a growth of structure also lessened the ability of the material to form structure subsequently. The approximately steady state to which reference has already been made is thus not a true equilibrium.

The growth of structure during standing can conveniently be represented by the change in torque required to shear the material after various periods of standing. Figure 2 shows the change in the torque (read after shearing for 1 min.) with period of standing at 100°C.; the results were obtained on stocks which contained the same volume loading of a number of carbon blacks, together with a result obtained on masticated smoked sheet. All of the stocks had been mechanically conditioned, as described above, before the commencement of the period of standing. The steady value of torque after conditioning but before standing is greatest for Shawinigan and smallest for M.T. black, among the carbon blacks studied. Differences in this steady value of torque correspond to filler structure which has not been broken down by previous shearing (conditioning) at 10 sec.$^{-1}$, the Shawinigan black showing the greatest amount of this "permanent" structure. The shapes of the curves also show pronounced differences; both the Shawinigan and the M.T. black show little growth of structure during standing. It thus appears that the Shawinigan black has a strong structure which is not easily broken down by shearing and which shows little growth on standing; the M.T. black shows little structure at all. On the other hand, the M.P.C. and U.F. blacks have a structure which is broken down by shearing and re-forms on standing; indeed, after long periods of standing the structure in these stocks exceeds that in the Shawinigan black stocks.

The ability of the stocks to form structure is decreased by storage at elevated temperatures before the commencement of the mechanical conditioning treatment and subsequent standing; it may also be profoundly influenced by the addition of small quantities of surface-active materials.

B. Vulcanized rubber

Similar thixotropic behavior is observed in vulcanized rubber. Probably the most popular physical test on vulcanized rubber is a tensile stress–strain test.

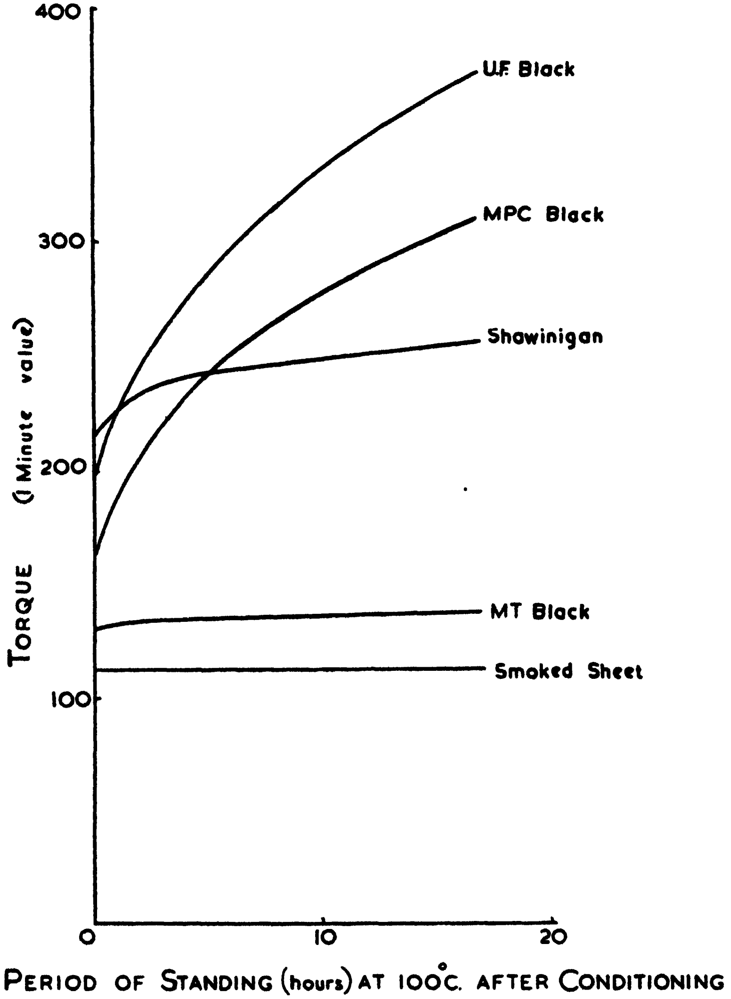

FIG. 2. Change in torque with period of standing at 100°C.

Results showing the effect of previous stretching on the tensile properties of rubber have been discussed by the author elsewhere (11); here it was shown that the shapes of stress–strain curves are not reproducible but change with each successive deformation. "Pure gum" vulcanisates without fillers are only slightly affected by previous stretching. On the other hand, vulcanisates containing fillers (such as carbon black) which stiffen the rubber may be considerably softer on second stretching, the original increase in stiffness produced by these fillers being largely destroyed at elongations less than the maximum elongation of previous stretch. Figure 3 shows typical results obtained on a natural rubber vulcanisate containing 28 volumes of M.P.C. black to 100 volumes of rubber; it gives stress–strain curves for samples which had been (*1*) not previously stretched, (*2*) previously stretched to 280 per cent, and (*3*) previously stretched to the breaking elongation. A pure gum vulcanisate (without fillers) is given for comparison.

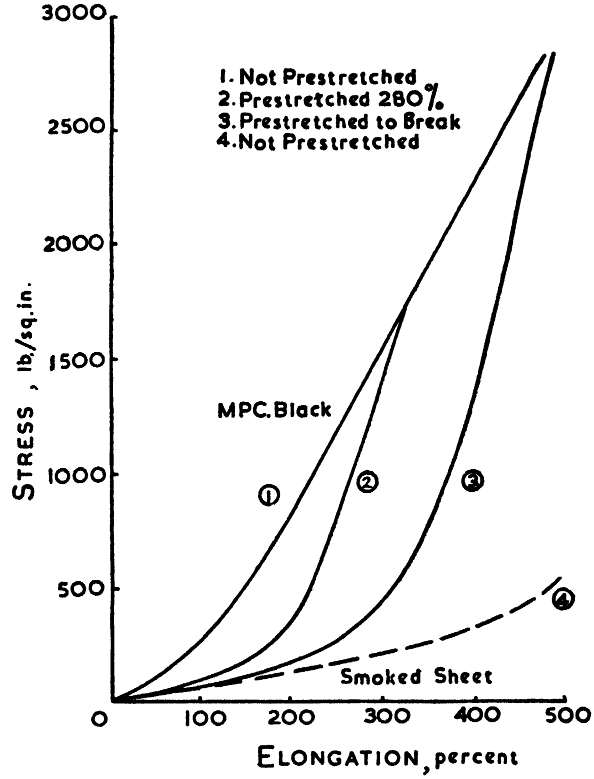

FIG. 3. Typical results obtained on a natural rubber vulcanisate containing 28 volumes of M.P.C. black to 100 volumes of rubber.

This softening is attributed to a breakdown of filler structure, and the degree of breakdown is greater the greater the stiffening effect of the filler. The major portion of the relaxation of stress which occurs in strongly reinforced vulcanisates held at constant strain at normal temperature was also shown to be due to a breakdown of filler structure. Although stretching produces a softening in all directions throughout the rubber, the degree of softening is not the same in all directions, being greatest in the direction of stretch, so that anisotropic stress–strain properties result from previous stretching. After breakdown the structure tends to re-form, but for most practical purposes the softening can be considered permanent, as the regrowth of structure is slow at normal temperatures, and although it is more rapid at high temperatures it appears that once a loaded vulcanisate has been used it will probably never completely return to its initial state.

These results immediately raised questions about the effect of such treatment on other physical properties of vulcanized rubber.

In just the same way that the modulus of rubbers is affected by stretching, the hardness is also sensitive to previous history. The hardness of both the pure gum and the M.P.C. black vulcanisate before and after previous stretching to their breaking elongation is given below. Here the hardness is quoted as the indentation in hundredths of a millimeter (B.S. hardness number, B.S. 903–1940, p. 47).

	BEFORE STRETCHING	AFTER STRETCHING
M.P.C. black-loaded vulcanisate	36	66
Pure gum vulcanisate	143	154

These results clearly show that previous stretching leads to a considerable softening of the black vulcanisate and a slight softening of the unloaded vulcanisate, and so demonstrate the breakdown of some of the increased stiffness which results from the inclusion of carbon black. It is of interest to note that even after previous stretching the loaded vulcanisate is still considerably harder than the unloaded one; this should be contrasted with a substantially complete breakdown of this increased stiffness in the direction of stretch which was shown in the tensile stress–strain test. A possible source of this difference is the anisotropic nature of the stiffness after previous stretching.

Tests on the effect of previous stretching on tear resistance also show evidence of the anisotropic properties which result. The resistance to the propagation of a tear at right angles to the direction of previous stretch may actually be increased, owing to the orientation of anisotropic filler particles or particle chains in the direction of stretch. The results for the two vulcanisates which are being used to illustrate this section of the investigation are given below. Measurements were made on 0.1 in. thick, crescent-shaped test pieces (ASTM Designation D 624–41 T, die B) which had been given a single nick of depth 0.02 in. at the center of the concave inner edge of the test piece; results are quoted as the load (per inch thickness) required to tear the test piece.

	LOAD IN POUNDS	
	M.P C. black	Pure gum
Without previous stretching	550 (15)*	250 (16)*
After stretching (parallel to the direction of stretch)	790 (40)	280 (18)
After stretching (perpendicular to the direction of stretch)	570 (15)	260 (16)

* Figures for the standard error are given in parentheses.

Tearing is strongly structure-sensitive, and inclusions lying perpendicular to the direction of propagation of tear can increase the resistance to tearing.

The anisotropic arrangement of filler structure which results from stretching has also been shown to be the cause of most of the "permanent set" in all but grossly undercured vulcanisates (12). This residual extension which remains after previous stretching is due to the incomplete recovery of anisotropic filler particles or particle chains which have been oriented in the direction of stretch. Fillers which have anisotropic particles or which readily form chains of particles show greater set than fillers with spherical particles.

Hysteresis properties of rubber vulcanisates are also affected by previous history, and with rubbers containing fillers a considerable amount of energy may have to be expended to break down filler structure during a cycle of deformation. The "resilient energy" or work required to rupture a sample of rubber in a simple tensile test has been widely used as an index of the quality of the rubber; and the difference between the resilient energies of loaded and unloaded vulcanisates, the ΔA function of Wiegand (22), is used as a criterion of the reinforcement produced by the filler. It has been usual to determine resilient energies from initial stress-strain curves, but it is now obvious that the values obtained in this way may vary considerably with the mechanical and thermal history of the material. The results in table 1, determined before and after previous stretching to the breaking elongation, show that whereas previous stretching has only a small effect on the resilient energy of the pure gum vulcanisate, the increase in resilient energy produced by the incorporation of M.P.C. black is substantially destroyed by previous stretching. Thus the use of this property as an index of reinforcement is not recommended, as it may be quite misleading.

TABLE 1

	RESILIENT ENERGY	ΔA
	lb./in^3	*lb./in*^{3}
M.P.C. black-loaded vulcanisate:		
Without previous stretching	5780	3030
After previous stretching	3020	370
Pure gum vulcanisate:		
Without previous stretching	2750	
After previous stretching	2650	

On the other hand, tests on the effect of previous stretching on tensile strength and abrasion resistance show that neither of these properties is significantly altered. Typical results are given below; those for abrasion resistance were ob-

M.P.C. BLACK-LOADED VULCANISATE	TENSILE STRENGTH	VOLUME LOSS PER HOUR
	lb./sq. in.	*ml.*
Without previous stretching	2820 (53)*	6.5 (0.4)
After previous stretching	2880 (57)	6.9 (0.4)

* Figures for the standard error are given in parentheses.

tained on a Du Pont machine, using built-up samples, the abraded surface being that of a 2 cm. square cut from a 0.1 in. thick sheet. After completion of a running-in period the volume loss during a 1-min. test run was determined.

There have been a number of investigations which record thixotropic effects shown by the electrical properties of rubbers loaded with carbon black (3, 11, 21). There it has been recognized that previous thermal or mechanical treatment may profoundly affect such properties as conductivity, permittivity, and power factor. These results are of particular interest, as they show the existence of coherent contacting chains of carbon particles, these chains being disrupted by both mechanical and thermal changes and re-forming again on standing.

The results quoted here to illustrate the behavior of vulcanized rubbers were obtained on two vulcanisates, one a pure gum and the other a M.P.C. black vulcanisate; in all cases when other vulcanisates containing various furnace, channel, and thermal blacks were investigated, the differences observed were only ones of detail. Fine channel and furnace blacks showed large thixotropic structural effects, while thermal blacks with relatively large particles showed little evidence of this type of structure.

III. DISCUSSION OF RESULTS

The results that have been described show clearly that in all rubbers, whether vulcanized or unvulcanized, there is some kind of internal structure which can be broken down by mechanical treatment and which forms again on standing. In rubber free from fillers this structure breakdown is relatively small and can be accounted for by a disentanglement and orientation of the long-chain rubber molecules; these readjustments result in a softening, and on standing thermal motion of the molecules allows them to return to the more probable entangled configuration. In rubbers containing fillers the softening and stiffening due to structural changes may be much more pronounced, the amount of structure which can be built up or broken down in this way depending on the nature of the fillers. In this case an additional process involving the formation or breakdown of interactions between neighboring filler particles or between filler particles and rubber is responsible for this behavior.

As yet there is a serious lack of data on the exact nature of this structure, and no clear theoretical basis for relating internal structure with mechanical properties. Any theory which attempts to describe the effect of fillers on the physical properties of rubber must take into account these thixotropic phenomena. Here the main problem is to predict the behavior of the material from a knowledge of its past history. It will be recognized that this task is difficult even in the simplest case when all the structural changes are completely reversible, and that with loaded rubbers where some irreversible structural changes also take place the task is extremely complex.

There are obvious difficulties in the measurement of the physical properties of any thixotropic system. The measured values depend upon the past history of the system, upon both the magnitude and the duration of stresses which have been previously applied, and upon the time of recovery which has elapsed since their removal; in addition, they are sensitive to temperature. In general, the properties of such systems are also altered by the act of measurement; thus any of a wide range of values can be obtained depending upon the history of the material and conditions of test. These difficulties may be overcome by using a standard instrument operating under closely controlled conditions, the usefulness of the results being determined by how well these conditions line up with working conditions, but before any data can be put to practical use the first essential is that they should be reproducible. The implications of the thixotropic behavior of rubber stocks and vulcanisates have not yet been fully recognized in the rubber industry and it is clear that ideas on a number of popular tests require drastic revision,—in particular, tests of plasticity, stiffness, and hardness.

There are a number of suggested modifications which can usefully be put forward at this stage. Probably the most important practical consequence in the measurement of any property which is sensitive to previous history is that it is important that either the complete history of the rubber should be closely controlled, or the rubber should be conditioned before measurement so that its properties are substantially independent of differences in previous history. This latter course may not always be possible if samples differ considerably in history. If neither of these two conditions is satisfied, then the results obtained may be completely misleading and certainly not capable of providing maximum information. The relative merits of these alternative methods of ensuring reproducibility will depend upon the use to which the results are to be put, and careful consideration will have to be given to details of any conditioning treatment adopted.

It will be recognized that conditioning only brings the material to an arbitrary reference level and that, although comparative results will be obtained on samples of different materials which have had similar conditioning treatments, the ratings of the materials may be very different for different types of conditioning. An example of this has already been mentioned during consideration of the results of plasticity measurements. If both the conditioning and the measurement involve little breakdown of structure, then the results will be of little use in forecasting the likely behavior of the material under conditions which involve more severe deformations. If results are to be useful for design purposes, then it is obviously essential that the material should have been previously deformed at least as severely as it is likely to be in service.

IV. THEORIES OF REINFORCEMENT

We can now review current theories of the reinforcement of rubber produced by fillers. The term "reinforcement" has been applied to the improvement of almost any mechanical property which results from the addition of fillers, but it is now generally accepted that the improvement of any one property such as stiffness, tensile strength, tear strength, abrasion resistance, etc. does not mean that the rubber has been reinforced. Parkinson (14), for example, has suggested that a filler should not be classed as reinforcing unless it substantially improves both abrasion and tear resistance.

As the tensile stress–strain test has been the most popular physical test on vulcanized rubbers it is not unnatural that results of tensile tests should have been widely used to give comparisons of the reinforcing ability of different fillers, and all of the so-called theories of reinforcement have been theories of the stiffening action of fillers. Here the possibility of using theories which have been developed to account for the viscosity of suspensions has attracted considerable attention. The basic theory developed by Einstein (6) describes the behavior of hard, spherical, noninteracting particles in a liquid which wets them completely and considers only small volume concentrations. This theory has been extended to allow for higher concentrations, where interactions occur between neighboring particles and also to allow for nonspherical particles (7, 10). Guth and Gold have shown fair agreement between their modification of Einstein's theory and experiment up to volume concentrations as high as 25 per cent; for spherical particles they show that the viscosity η and the volume concentration c are related by the equation

$$\eta = (1 + 2.5c + 14.1c^2)$$

while for rod-shaped particles the relationship is modified to

$$\eta = \eta_0 (1 + 0.67fc + 1.62fc^2)$$

where the form factor f is the ratio of the length and breadth of the particles. Vand (19) has obtained an alternative formula which he shows is in good agreement with experimental results.

Smallwood (18), Rehner (17), and Guth (8, 9) have all employed equations of this type to account for the increase in stiffness or change in flow properties which result from the incorporation of fillers into rubber, and more recently Cohan (4, 5) has provided much experimental data which he claims supports the use of these equations. Smallwood recognized the need to condition his samples mechanically by previous stretching to high elongations to get reproducible results, and Guth in his earlier work describes a conditioning procedure; however, more recently Guth (9) and Cohan (5) have reported experimental work which does not fully appreciate the need to condition samples, and the very large thixotropic effects which we have shown are present in many measurements on both vulcanized and unvulcanized rubbers. Thus it appears that the reported agreement between theory and experiment must in some cases be fortuitous. Furthermore, changes in the shape of assemblies of filler particles which result from thermal or mechanical treatment of the rubber are presumably considerable, and thus a single valued form factor to describe the shape of assemblies of filler particles will not usually be justified. In addition it must not be forgotten that the conditions existing in the rubber–filler system and those assumed in the theory may be quite different, and thus the validity of the formulae that have been put forward should be checked and their limitations recognized before any further endeavor is made to use them to account for the behavior in our complex rubber–filler system.[2] It appears that the increase in stiffness which results from

[2] The author has recently had the opportunity of seeing an as yet unpublished paper by Professor Stacey G. Ward and Mr. H. L. Whitmore of Birmingham University; they have shown that, even over a very limited range, particle-size distribution may have a considerable effect on the viscosity of fairly concentrated dispersions of spherical particles.

the incorporation of fillers will often be merely an indication of the ability of the filler to form a thixotropic internal structure, and as this structure is sensitive to previous history it cannot be recommended as a suitable index to characterize the increased quality ("reinforcement") of rubbers which results from incorporation of fillers.

There have been numerous discussions on the important features of fillers which govern their effect on the physical properties of rubber (see, for example, 4 and 14). The size and shape of the filler particles, the chemical nature and structure of their particles, and particle surfaces have all been shown to be important. However, it appears that particle size is the primary factor influencing the reinforcing action of a filler, the finer particle fillers showing greater reinforcement. Of all the available fillers carbon blacks have the finest particle size, and this probably accounts for much of their importance as reinforcing fillers for rubber. Electron-microscope studies show that the carbon blacks of finer particle size form strong primary aggregates which are difficult to break down by mechanical means, and this investigation shows that when fine particle blacks are compounded with rubber they form a structure which can readily be broken down or built up, and which is associated with the formation of weak secondary aggregates of the filler particles or of those primary aggregates which have not been broken down by milling. It is interesting to note that properties which are now normally associated with reinforcement—such as tensile strength, tear resistance, and abrasion resistance—are unaffected by previous deformation, and thus the presence of secondary aggregates is not essential for reinforcement.

V. SUMMARY

The addition of carbon black may cause considerable changes in the physical properties of rubber. Often rubbers compounded with carbon black or other fillers show evidence of thixotropic behavior—their properties depend upon the past history of the rubber and may be changed on the one hand by continuous standing and on the other hand by working. This paper describes investigations into the behavior of both unvulcanized and vulcanized rubbers, and discusses the thixotropic build-up and breakdown of colloidal carbon black structures which are shown to exist in the rubber. The importance of this build-up and breakdown of structure has not been adequately appreciated in many measurements on compounded rubbers; for example, the terms viscosity, plasticity, and stiffness (modulus) can only be defined when complications due to thixotropy are carefully controlled before and during the actual measurement. A knowledge and understanding of this behavior enables the significance of the results of various tests on these materials to be more correctly assessed and accounts for behavior which has previously appeared to be anomalous. The deficiencies of earlier theories of the reinforcement of rubber produced by carbon black are indicated, and modifications making allowance for thixotropic filler structure are proposed.

REFERENCES

(1) **Arnold, J. E.**: J. Oil & Colour Chemists' Assoc. **31**, 237 (1948).
(2) **Arnold, J. E., and Goodeve, C.**: J. Phys. Chem. **44**, 652 (1940).
(3) **Bulgin, D.**: Trans. Inst. Rubber Ind. **20**, 24 (1944).
(4) **Cohan, L. H.**: India Rubber World **117**, 343 (1947).
(5) **Cohan, L. H.**: Proceedings of the Second Rubber Technology Conference (London) **1948**, p. 365.
(6) **Einstein, A.**: Ann. Physik **19**, 289 (1906); **34**, 591 (1911).
(7) **Eirich, F. R.**: Repts. on Progress Phys. **7**, 329 (1940).
(8) **Guth, E.**: J. Applied Phys. **16**, 20 (1945).
(9) **Guth, E.**: Proceedings of the Second Rubber Technology Conference (London) **1948**, p. 353.
(10) **Guth, E., and Gold, C. O.**: Phys. Rev. **53**, 322 (1938).
(11) **Mullins, L.**: J. Rubber Research **16**, 275 (1947).
(12) **Mullins, L.**: Proceedings of the Second Rubber Technology Conference (London) **1948**, p. 179.
(13) **Mullins, L., and Whorlow, R. W.**: In press.
(14) **Parkinson, D.**: Advances in Colloid Sci. **2**, 389 (1946).
(15) **Parkinson, D., and Blanchard, A. F.**: Proceedings of the Second Rubber Technology Conference (London) **1948**, p. 414.
(16) **Piper, G. H., and Scott, J. R.**: J. Sci. Instruments **22**, 206 (1945).
(17) **Rehner, J.**: J. Applied Phys. **14**, 638 (1943).
(18) **Smallwood, H. M.**: J. Applied Phys. **15**, 758 (1944).
(19) **Vand, V.**: J. Phys. & Colloid Chem. **52**, 277 (1948).
(20) **Voet, A.**: J. Phys. & Colloid Chem. **51**, 1037 (1947).
(21) **Wack, P. E., Anthony, R. L., and Guth, E.**: J. Applied Phys. **18**, 456 (1947).
(22) **Wiegand, W. B**: Ind. Eng. Chem. **17**, 939 (1925).

THE SORPTION OF GR-S TYPE RUBBER BY CARBON BLACK. I[1,2]

Sorption from Benzene Solution by Graphon

I. M. KOLTHOFF AND ALLAN KAHN

School of Chemistry, University of Minnesota, Minneapolis 14, Minnesota

Received August 22, 1949

INTRODUCTION

The reinforcement of natural rubber by carbon black first became known about 1910. Since that time there have been many studies attempting to correlate the properties of a given carbon black with the ultimate physical properties of

---

[1] Presented at the Twenty-third National Colloid Symposium, which was held under the auspices of the Division of Colloid Chemistry of the American Chemical Society at Minneapolis, Minnesota, June 6–8, 1949.

[2] This investigation was carried out under the sponsorship of the Reconstruction Finance Corporation, Office of Rubber Reserve, in connection with the synthetic rubber program of the United States Government.

the rubber into which it is incorporated. These studies have been intensified since the development of synthetic rubbers in which carbon black reinforcement is more marked than in natural rubber.

Previous work on the evaluation of carbon blacks has consisted of studies of such properties as iodine and diphenylguanidine adsorption; the determination of volatile matter and extractable matter, etc. (4); and more recently the determination of surface area, pH, and structure (6). The sorption of rubber from solution (5) had been considered also, but until the recent work of Baker (1) there had been no systematic investigation of this phenomenon.

The present study deals with the sorption of GR-S type rubber from solution by various kinds of carbon black. With a certain type of black (Graphon) it was found that the sol part of the rubber could be sorbed completely, whereas the microgel[3] part was not or was hardly sorbed.

TABLE 1

The variation of the amount of rubber sorbed on Graphon with time of shaking

4 g. of Graphon and 100 ml. of rubber solution; initial concentration = 0.25 g./100 ml.

TIME OF SHAKING	57 PER CENT CONVERSION		61 PER CENT CONVERSION		77 PER CENT CONVERSION	
	Amount sorbed	Intrinsic viscosity	Amount sorbed	Intrinsic viscosity	Amount sorbed	Intrinsic viscosity
hours	*grams*		*grams*		*grams*	
0.00	0.000	1.29	0.000	1.20	0.000	2.50
0.25	0.122	1.45			0.078	3.26
0.50	0.129	1.32			0.094	3.53
0.75	0.133	1.28			0.100	3.61
1.00	0.131	1.19	0.133	1.61	0.102	3.61
2			0.130	1.83		
4	0.136	0.96	0.137	1.36	0.114	3.76
8			0.135	1.14		
16			0.137	1.07		
24	0.136	0.64	0.140	1.00	0.120	
48	0.136	0.67	0.139	0.85	0.122	3.68
120	0.138	0.63	0.141	0.83	0.125	

EXPERIMENTAL

Materials

Various samples of GR-S type rubber coagulated from latex of between 38 per cent and 90 per cent conversion and containing a small amount of antioxidant were used. All the latices were prepared by the so-called Mutual recipe at 50°C.

Mallinckrodt reagent grade benzene was used as a solvent.

Seven commercial samples of carbon black were obtained from Godfrey S. Cabot Inc., Boston, Massachusetts. It was found that when shaken with benzene solutions of rubber all except one (Graphon) gave very dark suspensions of carbon black which would not settle out even on prolonged centrifuging.[4] Therefore, Graphon was used exclusively in this study.

---

[3] For a comprehensive study of microgel see reference 1.

TABLE 2

Sorption of rubber from solution in benzene by Graphon at 30°C. and 50°C.

100 ml. of solution; initial concentration = 0.279 g./100 ml.

AMOUNT OF GRAPHON	AMOUNT SORBED			
	67 per cent conversion		90 per cent conversion	
	30°C.	50°C.	30°C.	50°C.
grams	*grams*	*grams*	*grams*	*grams*
1.5			0.052	0.049
2	0.077	0.076		
4	0.144	0.144		
6	0.203	0.201		

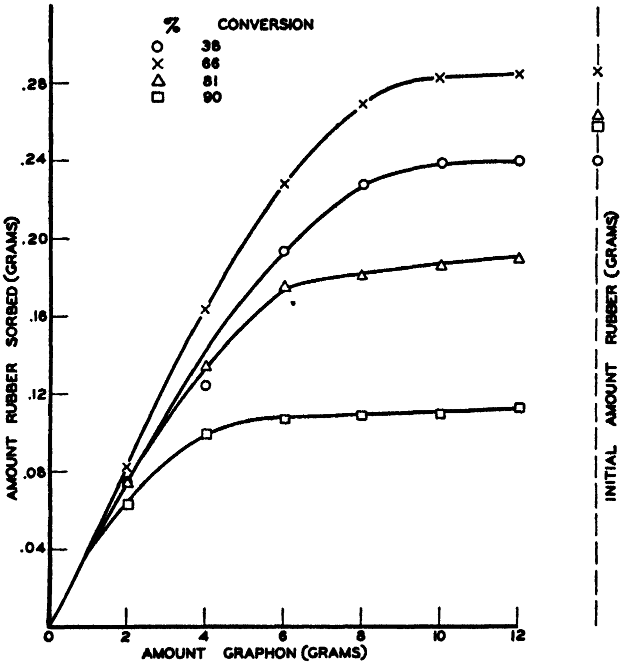

FIG. 1. Amount of rubber sorbed from solution in benzene by various amounts of Graphon.

Method

In general, from 2 to 12 g. of Graphon was added to a bottle containing 100 ml. of a 0.25 per cent rubber solution in benzene. The bottle was then clipped to the outside of a cylinder 18 in. in diameter which was rotated at 32 R.P.M. in a water bath at 30°C. After 48 hr. (unless otherwise noted) the bottles were centrifuged to settle out the carbon black. Aliquots (25 ml.) of the supernatant liquid were evaporated to determine the amounts of residual rubber. On many samples the relative viscosity at 30°C. of the supernatant liquid was also determined.

---

[4] Later it was found that clear solutions could be obtained with many of the carbon black samples when the sorption was determined in chloroform solutions of rubber.

RESULTS

Effect of time of shaking

Samples (100 ml.) of rubber of 57, 61, and 77 per cent conversion were shaken with 4 g. of Graphon for various periods of time. The results are given in table 1.

Effect of temperature

Sorption data for two different samples of rubber were obtained at 30°C. and 50°C. The results are given in table 2. The data show that the amount of rubber sorbed from a solution in benzene by Graphon is hardly dependent on the temperature between 30° and 50°C.

TABLE 3

Microgel content of rubber samples of various conversions

CONVERSION	MICROGEL	RUBBER NOT SORBED BY GRAPHON*
per cent	*per cent*	*per cent*
38	0	0
66	0	0
72	5	14
77	25	25
81	33	28
82	46	40
86	58	50
87	58	51
90	69	56

* 12 g. of Graphon shaken with benzene solution containing 0.25 g. of rubber.

Sorption data for rubber samples of various degrees of conversion

The amount of rubber sorbed from solution in benzene by various amounts of Graphon is plotted in figure 1 for four samples of rubber of different conversions.

All of the rubber in the samples of 38 per cent and 66 per cent conversion was sorbed by 12 g. of Graphon. However, with the samples of 81 per cent and 90 per cent conversion, although the initial sorption was comparable to that with the other samples, only a fraction of the rubber could be sorbed, even with large amounts of Graphon.

It was thought that there might be some connection between the amount of rubber not sorbed by Graphon and the amount of microgel in the samples. Therefore the microgel content of a number of rubber samples was determined by the method of Medalia and Kolthoff (3). The amount of rubber not sorbed on 12 g. of Graphon from 100 ml. of benzene solution containing 0.25 g. of rubber was also determined. The results are given in table 3.

DISCUSSION

The results of the effect of time of shaking on the sorption of rubber show that the sorption takes place very rapidly. Especially with low conversion samples there was very little change in the amount of rubber sorbed after 1 hr. With the samples of 57 per cent and 61 per cent conversion the intrinsic viscosity[5] of the supernatant liquid from each sample increased initially and then decreased. The results for the rubber of 77 per cent conversion are complicated by the presence of microgel in the sample. Separate tests showed that the intrinsic viscosity of the solutions remained unchanged when they were shaken for 120 hr. without carbon black. Therefore it seems probable that the lower-molecular-weight fractions are sorbed faster than the higher-molecular-weight fractions, but that the former are replaced by the latter upon longer periods of shaking. Thus when dealing with a heteromolecular solution of rubber, true sorption equilibrium is not reached until after a long period of shaking. As demonstrated by the results in table 1, the *amount* of rubber sorbed remains constant after a few hours of shaking, but the molecular weight of the sorbed rubber increased with time of shaking (up to about 48 hr.).

The relatively negligible dependence on temperature of the amount of sorption, as shown in table 2, is generally found in sorption from liquids (2).

The results plotted in figure 1 are representative of those obtained with a larger number of samples. It was found that below about 70 per cent conversion all the rubber from 100 ml. of a 0.25 per cent solution in benzene could be sorbed by 12 g. of Graphon. However, above 70 per cent conversion the sorption curves are seen to be flattened before all the rubber is removed, indicating the presence of a fraction which is sorbed to only a small extent, if any, by Graphon. The results of table 3 definitely show that it is the microgel fraction of the rubber which is not or hardly sorbed on Graphon. This difference of sorption can thus be used to differentiate between sol and microgel solutions of rubber. The agreement between the amount of microgel determined by a conventional method (3) and that indicated by the results of the sorption experiments is satisfactory.

SUMMARY

The sorption of GR-S type rubber from solution in benzene by Graphon carbon black has been investigated, and it has been found that:

1. The amount of rubber sorbed remains unchanged after several hours of shaking, but the intrinsic viscosity of the remaining solution changes slowly with continued shaking (up to about 48 hr.). It seems probable that the lower-molecular-weight fractions are sorbed faster than the higher-molecular-weight fractions but that the former are replaced by the latter upon longer periods of shaking.

---

[5] Actually, $\ln \eta_r/c$ was determined, where η_r is the relative viscosity and c is concentration in grams per 100 ml. However, at the concentrations used this is a close approximation to the intrinsic viscosity:

$$\lim_{c \to 0} \frac{\ln \eta_r}{c}$$

2. The amount of sorption at 50°C. is not appreciably different from that at 30°C.

3. The microgel fraction in rubber is not or is hardly sorbed by Graphon; the sol fraction is sorbed completely.

REFERENCES

(1) Baker, W. O.: Ind. Eng. Chem. **41**, 511 (1949).
(2) Freundlich, H.: *Colloid and Capillary Chemistry*, p. 224. Methuen and Co. Ltd., London (1926).
(3) Medalia, A. I., and Kolthoff, I. M.: Unpublished work from this laboratory.
(4) Shepard, N. A.: "Carbon Black in the Rubber Industry," in *Colloid Chemistry*, edited by Jerome Alexander, Vol. IV. The Chemical Catalog Company, Inc., New York (1932).
(5) Stamberger, P.: Kautschuk **7**, 182 (1931).
(6) Wiegand, W. B.: Can. Chem. Process Ind. **28**, 151 (1944).

STRUCTURE OF LYOGELS. V[1]

A Study of Polymer Fractions Prepared from Smoked Sheet, Standard GR-S, Low-Temperature GR-S (X-435), and Neoprene 10

E. A. HAUSER

Department of Chemical Engineering, Massachusetts Institute of Technology, Cambridge, Massachusetts, and Department of Chemistry and Chemical Engineering, Worcester Polytechnic Institute, Worcester, Massachusetts

AND

D. S. le BEAU

Midwest Rubber Reclaiming Company, East St. Louis, Illinois

Received August 22, 1949

Previous experiments had shown that the structure of the polymer film as observed in the ultramicroscope using incident light depended on the molecular weight of the polymer (molecular weight distribution) and on the physical structure of its chains. The effect of time and temperature on the structure of natural isoprene polymer films had been correlated with the folding and the internal structure of the natural polymer chains (6, 7). The effect of the molecular weight on the flow of isobutylene polymers had also been studied (8). Because flow can be considered a phenomenon closely related to molecular weight and its distribution as well as to the physical and chemical nature of the polymer, it was felt that it deserved more attention.

Therefore smoked sheet, standard GR-S, low-temperature GR-S, and Neoprene were studied in greater detail by subjecting each polymer to fractionation by precipitation. The viscosity of each of the various fractions was determined. Polymer film preparations of each of the fractions for observation in the incident light microscope were made and studied at various temperatures and over a period of time. Some of the fractions were also subjected to infrared spectroscopic studies for the purpose of evaluating the differences in molecular configuration of the high polymer.

---

[1] Presented at the Twenty-third National Colloid Symposium, which was held under the auspices of the Division of Colloid Chemistry of the American Chemical Society at Minneapolis, Minnesota, June 6–8, 1949.

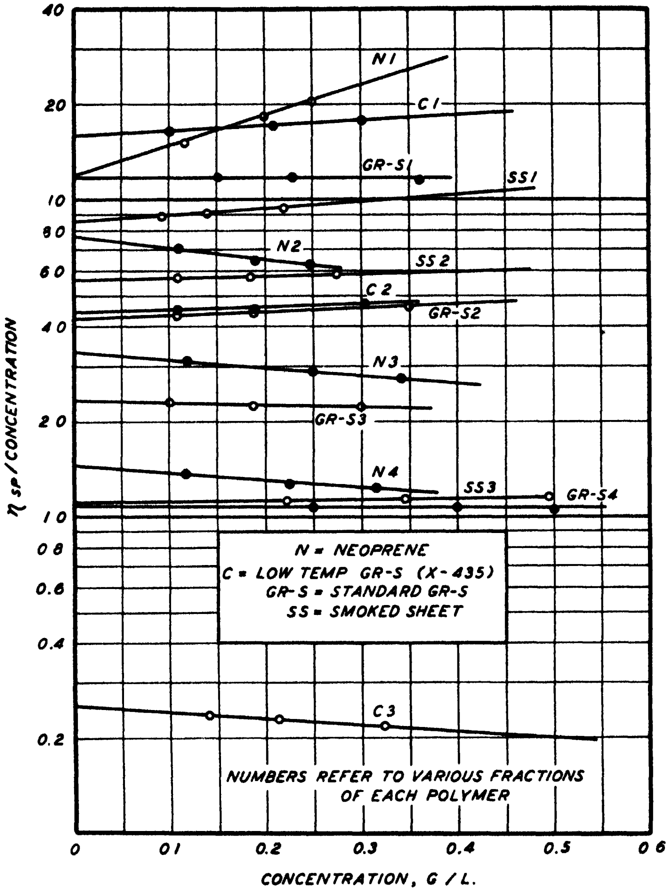

FIG. 1. Plot of η_{sp}/concentration *versus* concentration for the various fractions of each polymer.

FRACTIONATION

The polymer was first subjected to either acetone or ethyl alcohol extraction to remove nonrubber constituents. Acetone was used for this purpose for smoked sheet; ethyl alcohol was used for the synthetic high polymers. To eliminate any differences in the microscopic structure of these films which might possibly be ascribed to the use of different solvents it was decided to use the same solvent for all microscopic preparations and fractionations. Benzene was used to dissolve the polymers and only that part of the polymer which was soluble in benzene was considered for further study. Fractionation was carried out at 25°C., using acetone as precipitant. The precipitated sample was stored overnight to obtain better separation. The supernatant liquid was decanted and each fraction was redissolved in benzene and again precipitated. This procedure proved adequate for the high-molecular-weight fraction but became more and more difficult as the polymer size decreased. The precipitate became of colloidal size and settling of it by such means as freezing out or even centrifuging (up to 10,000 R.P.M.) was not successful. The first fractions of each of the polymers were tough and elastic upon drying. The toughness of the fractionated polymer decreased as its molecular size decreased until the fractions of very low molecular weight resembled highly viscous liquids. Each fraction was dried in vacuum to weight constancy before viscosity measurements or microscopic studies were attempted.

VISCOSITY

Each of the fractions was dissolved in benzene and the viscosity was determined by means of an Ostwald viscosimeter at 25°C. Figure 1 shows the relationship between η_{sp}/concentration (in grams per liter $\times 10^{-1}$) and concentration (in grams per liter $\times 10^{-1}$). Except for Neoprene it can be seen that this relationship was found to be quite constant. In the case of Neoprene the greatest deviation from constancy was observed for the fraction of highest molecular weight.

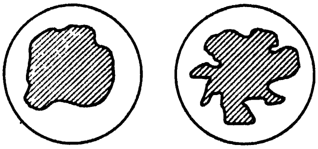

FIG. 2. Film spread from high-molecular-weight fractions of elastomers: (a) Hevea rubber; (b) cold butadiene–styrene copolymer.

FILM-FORMING PROPERTIES

The special technique developed for the preparation of microscopic film specimens from high-polymer solutions has been described in full detail (3). To study the macroscopic film formation of each high-polymer fraction a drop of a 0.5 per cent benzene solution of each of the fractions was placed on a clean water surface preparatory to microscopic manipulations and was observed for its film-forming characteristics. All smoked sheet fractions gave smooth, round, soft, and pliable films (figure 2a). Microscopic observation as usual showed a greater amount of netting for the fractions of higher molecular weight than for those of lower molecular weight (figure 3a, b, c).

The macroscopic appearance of films prepared from the various fractions of X-435 and standard GR-S varied considerably with the molecular weight of these fractions. The very low-molecular-weight, viscous fractions of X-435 as well as of standard GR-S form very soft and weak films on water. It was difficult to obtain any microscopic specimen from these fractions; thread formation did not occur and the films broke in the manner characteristic for viscous liquids (figure 4d). As the viscosity of the fractions of X-435 increased, the films became stronger and single threads appeared in the microscopic preparations (figure 4c). Higher-molecular-weight fractions of X-435 gave films which lost the smooth round contours and pliability and appeared to possess a certain amount of rigidity (figure 2b). Microscopic observation of these fractions showed netting; however, threads which had broken appeared stiff (figure 4b). Netting increased progressively with increasing molecular weight of these fractions (figure 4a). Also, a contraction of the spread film upon solvent evaporation could be noticed.

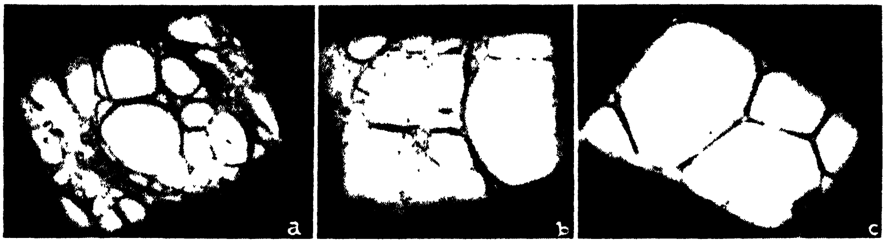

FIG 3. Smoked sheet: (a) fraction 1; (b) fraction 2; (c) fraction 3

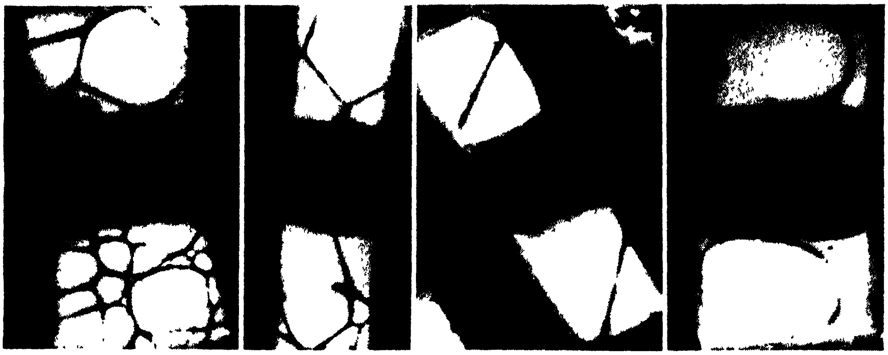

FIG. 4. Low-temperature GR-S (X-435): (a) fraction 1; (b) fraction 2; (c) fraction 3; (d) fraction 4.

The low-molecular-weight fractions of standard GR-S behaved very similarly to those of X-435 (figure 5d). However, films prepared from the fractions of standard GR-S of middle and higher molecular weight do not compare in appearance with those obtained from X-435. They appear stiff, show very ragged contours, and fall completely apart into small feathery pieces. This phenomenon becomes more pronounced the higher the molecular weight of the fractions (figure 6a).

Microscopic preparations were difficult to obtain from these feathery film pieces, and observations show that netting again increases as the molecular weight of the fraction increases.

If solutions (4 per cent) of either standard GR-S or X-435 are heated to 75°C.

for 1.5 hr. and films prepared from these solutions are then subjected to microscopic observation no change can be observed in their structure. This is interesting to note, since it had been found previously that, contrary to this behavior, smoked sheet would break down in its film structure when subjected even to lower temperatures (9). Also, if film preparations of the highest fractions of either standard GR-S or X-435 are heated to 60°C. while under microscopic observation flow does not appear to occur and the microscopic preparations do not change during an observation period of as long as 2 hr. at that temperature. The same holds true for the standard GR-S fraction when heated to 75°C. In contrast thereto it was found that the X-435 fraction will show flow under these conditions within half an hour.

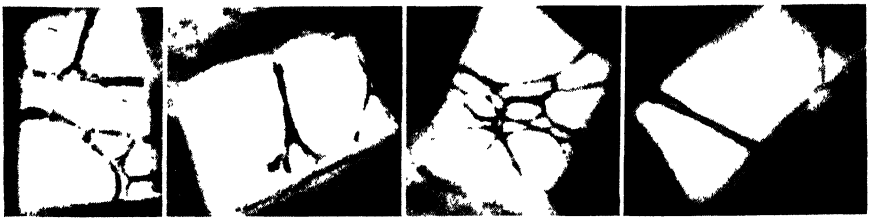

FIG. 5. Standard GR-S: (a) fraction 1; (b) fraction 2; (c) fraction 3, (d) fraction 4

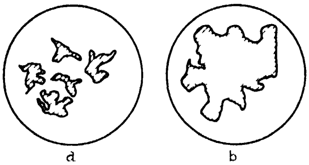

FIG. 6. Film spread from high-molecular-weight fractions of elastomers· (a) standard butadiene–styrene copolymer, (b) Neoprene

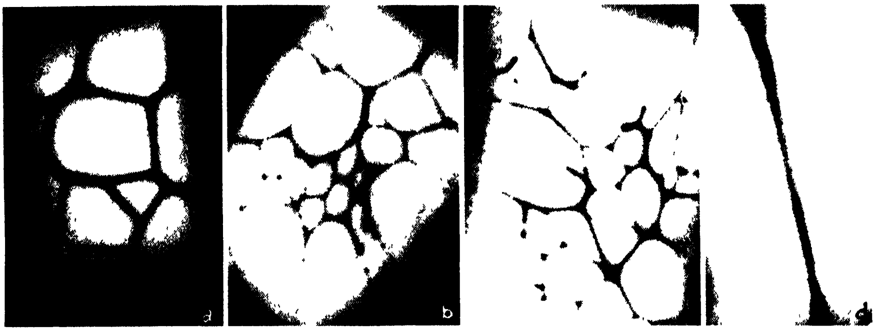

FIG. 7. Neoprene: (a) fraction 1; (b) fraction 2; (c) fraction 3; (d) fraction 4

If Neoprene 10 is fractionated and the fractions are subjected to microscopic observations, the same general trend in the structure of the films prepared from these fractions can be seen. The fraction of lowest molecular weight shows the formation of single threads only (figure 7d). More and more net formation can be noticed as the molecular weight of the fractions increases (figure 7c and 7b). However, figure 7c also shows the occurrence of flow at room temperature. The fraction of highest molecular weight exhibits netting of fairly coarse bands; flow is no more apparent (figure 7a).

Macroscopically, the films obtained on water from Neoprene 10 fractions (figure 6b) are smoother than those obtained from standard GR-S fractions and fairly pliable, comparing rather favorably in these properties with films which had been previously obtained by spreading balata on warm water.

Since flow seemed to be absent in the highest-molecular-weight fraction of Neoprene 10, it was decided to study the time–temperature factor of flow on this fraction in greater detail. A microscopic preparation of this fraction was stored for 24 hr. at room temperature (26°C.) (figures 8a and 8b). No change could be observed. However, if a preparation of this fraction was heated to 40°C., indications of flow were visible after 1 hr. Photomicrographs of such a preparation taken at time intervals up to 5 hr. reveal the change of the preparation due to the progress of flow (figure 9 a–f). A similar experiment carried out at 70°C. shows the increase in the rate of flow with increasing temperature (figure 10 a–d).

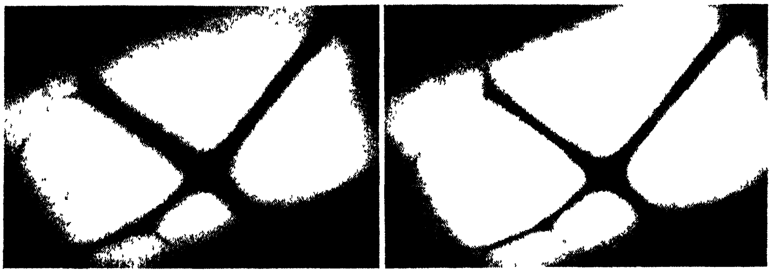

FIG. 8. Neoprene 10, fraction 1 at 26°C.: (a) immediately; (b) after 24 hr

Time–flow studies carried out with a low-molecular-weight fraction of Neoprene 10 show that some flow occurs at 40°C. immediately and that after 25 min. of heating to 40°C. part of the preparation has disappeared, owing to flow (figure 11 a–c). At 70°C. flow of this lower-molecular-weight fraction is so great that the photographic picture appears slightly blurred. (Exposure times for such photomicrographic Kodachrome pictures range between 10 and 30 sec.) After 4 min. of heating, however, most of the flow has occurred and the photomicrographic picture appears clear again (figures 12a and 12b).

INFRARED SPECTROGRAPHIC STUDIES

In view of the differences encountered in the macroscopic film formation between the higher-molecular-weight fractions of standard GR-S and those of X-435 and the differences between these fractions in flow at increased temperatures such as observed in the ultramicroscope, it was originally suspected that these fractions differed in their chemical and physical makeup. For this purpose infrared spectrograms were made of each of the two fractions of highest molecular weight obtained from standard GR-S and X-435 to determine whether a difference in the styrene content or in the amount of 1,2 addition of butadiene had occurred which could well explain the difference in rigidity and fragility of films prepared from these fractions.

The fractions were dissolved in carbon tetrachloride and spread onto a rock salt plate (1). The amount of polymer deposited on these plates was in each case determined. After drying, the polymers were subjected to infrared analysis.

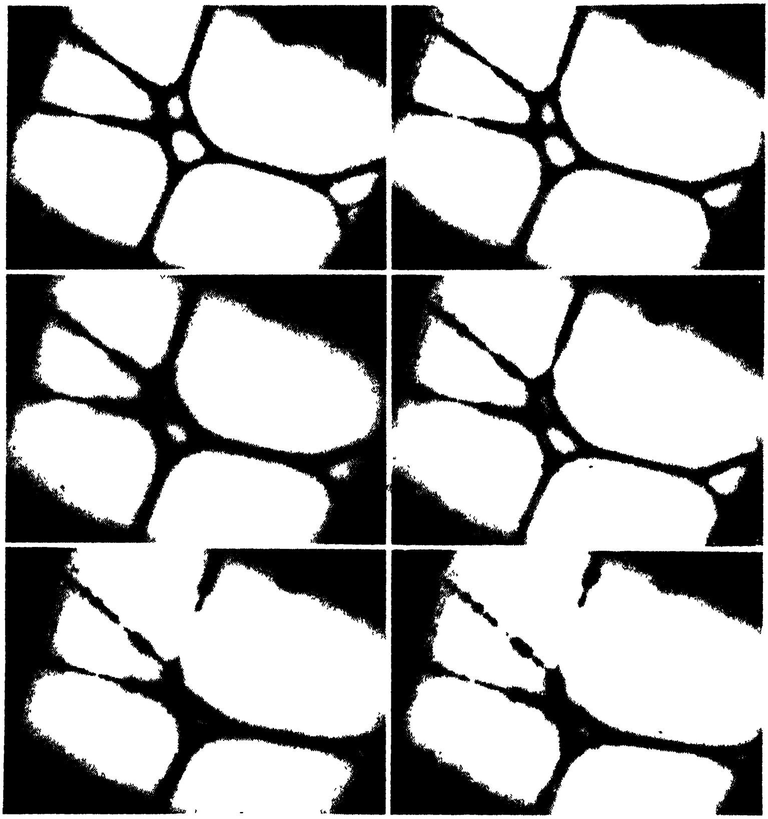

FIG. 9. Neoprene 10, fraction 1 at 40°C.: (a) immediately; (b) after 1 hr.; (c) after 2 hr.; (d) after 2.5 hr.; (e) after 4 hr.; (f) after 5 hr.

One fraction each of the standard GR-S and X-435 was studied over the whole region of 650 cm.$^{-1}$ to 3500 cm.$^{-1}$ without detecting any obvious differences between them. The relative amounts of 1,2 and 1,4 addition were studied by determining the ratio of the extinction coefficients ($K = \ln 1/T$, T being the per cent transmission) of the band representing terminal double bonds (912 cm.$^{-1}$) to the band representing internal double bonds (966 cm.$^{-1}$). No difference in this ratio could be found between any of the high-molecular-weight fractions of standard GR-S and X-435.

The relative amount of styrene present in the highest-molecular-weight fraction of each of the two polymers was determined by comparing the ratios of the extinction coefficients of the 911 cm.$^{-1}$ band characteristic for butadiene with that of the 701 cm.$^{-1}$ band characteristic for styrene. Also the ratios of the extinction coefficients at the 1488 cm.$^{-1}$ band (aliphatic CH bonding) and that at the 1446 cm.$^{-1}$ band (phenyl CH bonding) were determined.

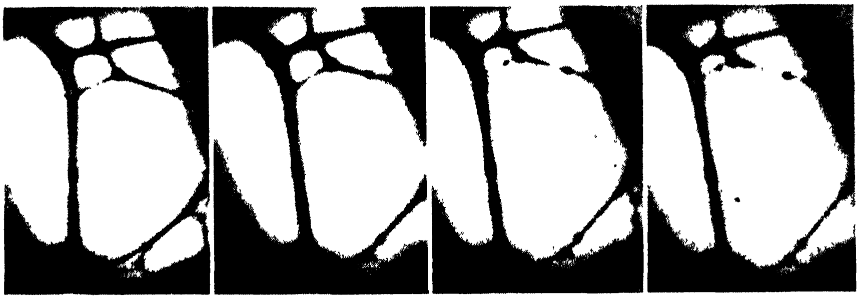

FIG. 10. Neoprene 10, fraction 1 at 70°C.: (a) immediately, (b) after 15 min., (c) after 30 min.; (d) after 1 hr.

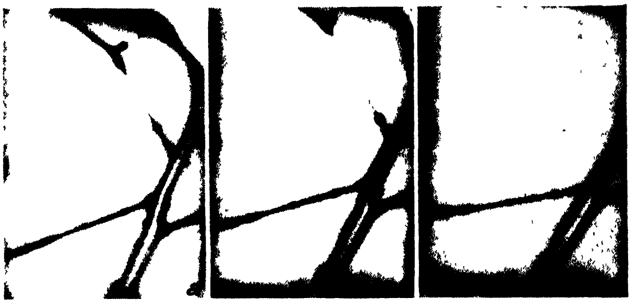

FIG. 11. Neoprene 10, fraction 3 at 40°C.: (a) immediately; (b) after 15 min.; (c) after 25 min.

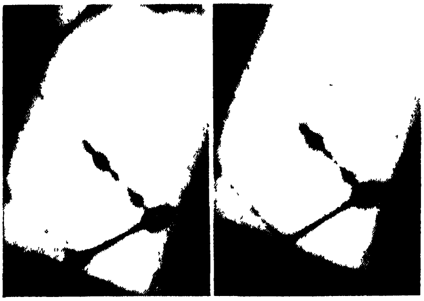

FIG. 12. Neoprene 10, fraction 3 at 70°C.: (a) after 2 min.; (b) after 4 min.

These ratios were alike within experimental error for each fraction and for both polymers. Minor differences in the amount of 1,2 addition between net fractionated standard GR-S and low-temperature GR-S polymers have been reported (5). However, the major change so far reported in the structure of the low-temperature GR-S polymers has been an increase in the amount of *trans* polymer (4). Ultramicroscopic observations on natural isoprene polymers have shown that balata, the *trans*-isoprene polymer, will give less smooth and somewhat stiffer films than natural rubber, which corresponds to the *cis* structure. If the *trans* configuration of the GR-S polymer were responsible for the film behavior, we should expect greater film rigidity from the low-temperature GR-S polymers. This, however, was not apparent. Yet the sharp break in the flow behavior of X-435 at a definite temperature as observed under the microscope indicates changes in the melting point which should occur as the *trans* component of the polymer increases. Therefore no explanation for the peculiar film deficiency of the high-molecular-weight fractions of standard GR-S can be offered. However, it should be remembered that a very small amount of netting (2) could change the physical configuration of the polymer chains enough to account for the differences observed in film formation without necessarily changing the results obtained from infrared spectrography.

SUMMARY AND CONCLUSIONS

Smoked sheet, standard GR-S, low-temperature GR-S (X-435), and Neoprene 10 were subjected to fractionation. The ratios of η_{sp}/concentration (in grams per liter $\times$ 10^{-1}) were determined over a range of concentrations. The fractions were submitted to microscopic observation by incident light. On the basis of this and previous work, it can be concluded that the structure of the polymer fractions as observed in the microscope and previously observed in the electron microscope does not depend on the chemical composition but must be considered to be dependent on the physical structure of the polymer molecules, including their length and size distribution, as well as on their configuration.

Net-like structures can result from an increase in the forces acting between the chains as well as from an increase in actual chemical bonds between them.

In polymers of very low molecular weight, be they synthetic or natural, surface forces predominate during film formation and film breaking; hence the microscopic structures of such polymers show the characteristics of viscous liquids.

REFERENCES

(1) Dinsmore, H. L., and Smith, D. C.: Anal. Chem. **20,** 11 (1948).
(2) Flory, P. J.: J. Am. Chem. Soc. **69,** 2893 (1947).
(3) Hall, E., *et al.*: Ind. Eng. Chem. **36,** 634 (1944).
(4) Hampton, R. R.: Paper presented before the Division of Rubber Chemistry of the American Chemical Society at a meeting held in Boston, Massachusetts, May 23–25, 1949.
(5) Hart, E. J., and Meyer, A. W.: Paper presented before the Division of Rubber Chemistry of the American Chemical Society at a meeting held in Detroit, Michigan, November 8–10, 1948.
(6) Hauser, E. A., and le Beau, D. S.: India-Rubber J. **111,** 453 (1946).
(7) Hauser, E. A., and le Beau, D. S.: J. Phys. & Colloid Chem. **51,** 278 (1947).
(8) Hauser, E. A., and le Beau, D. S.: J. Phys. & Colloid Chem. **52,** 27 (1948).
(9) Hauser, E. A., and le Beau, D. S.: J. Phys. & Colloid Chem. **53,** 274 (1949).

THE DISAPPEARANCE OF UNADSORBED SOAP DURING THE EMULSION POLYMERIZATION OF STYRENE[1,2]

M. L. CORRIN

Department of Chemistry, The University of Chicago, Chicago 37, Illinois

Received August 22, 1949

INTRODUCTION

It has been postulated by Harkins (3) that the principal locus for the initiation of polymer in emulsion polymerization is the soap micelle containing solubilized monomer; the polymer particles thus initiated dissolve monomer to form a polymer–monomer particle. Since the size of these polymer–monomer particles is much smaller than that of the monomer emulsion droplets initially present, the total interfacial area existing between the hydrocarbon and aqueous phases increases rapidly with the yield of polymer. It is thus apparent that the amount of soap adsorbed at this interface should increase with yield until the concentration of soap in the aqueous phase falls below the critical concentration for the formation of micelles. According to Harkins' theory the rate of polymer particle initiation is a function of the micelle concentration and should thus also decrease with yield.

Data for the variation in concentration of unadsorbed potassium laurate and potassium myristate as a function of polymer yield have been previously reported (4). These values were calculated on the basis of the assumption that the area of the adsorbed soap molecule becomes constant at equilibrium soap concentrations exceeding the critical concentration. This assumption is now known to be false (2). This paper presents the variation in unadsorbed soap concentration as a function of yield as calculated on the basis of the observed soap adsorption isotherms.

EXPERIMENTAL

Preparation and analysis of latices

Polystyrene latices of varying polymer conversion were prepared according to the Mutual recipe, and the yields and monomer–polymer ratios were determined by the method reported by Herzfeld, Roginsky, Corrin, and Harkins (5). Centrifuged samples were employed in the determination of the concentration of unadsorbed soap.

Dye titrations

The latices were titrated in the presence of one of two dyes, Rhodamine 6G and acriflavine, which have been shown to be suitable for the determination of

---

[1] Presented at the Twenty-third National Colloid Symposium, which was held under the auspices of the Division of Colloid Chemistry of the American Chemical Society at Minneapolis, Minnesota, June 6–8, 1949.

[2] This investigation was carried out under the sponsorship of the Reconstruction Finance Corporation, Office of Rubber Reserve, in connection with the synthetic rubber program of the United States Government.

critical concentrations (1). Owing to the high scattering power of the latex, which tends to mask color changes, it is necessary in the titration of latices to employ a dye which gives a fluorometric end point. Titrations in polystyrene latex are far less satisfactory than those in water, since in latex the quenching of fluorescence in the absence of micellar soap is much less pronounced than in water.

After considerable experimentation the following procedure was adopted as the most satisfactory: A weighed sample of latex was made up to 0.04 per cent in dye and 1.5 per cent in catechol; the latter serves to quench partially the fluorescence below the critical concentration. This sample was titrated with an aqueous solution of dye and quencher of the same composition as that of the sample. Quartz containers were employed and a General Electric B-H4 lamp served as the ultraviolet source. A sample of latex made up to the same dye and catechol concentration was used as a blank. In order to maintain the polystyrene concentration equal in the unknown and the blank the latter was titrated along with the unknown with a solution of dye and quencher containing sufficient soap to maintain the soap concentration in the blank above the critical concentration. The first *marked* departure in fluorescence of the unknown sample from that of the blank was taken as the end point. This procedure is undoubtedly less precise than that used in the determination of the critical concentrations of soap in the absence of latex particles.

CALCULATIONS

Amount of soap adsorbed at the critical concentration

The amount of soap adsorbed at the end point in the titration, i.e., at an equilibrium concentration equal to the critical concentration, is given by

$$W_{S(A)} = W_L\ (W_{S(I)}/W_A) - M_S\,[(180W_L/W_A) + W_T]C_\mu/1000$$

in which $W_{S(A)}$ is the weight in grams of adsorbed soap, W_L is the weight of the sample titrated, $W_{S(I)}$ is the weight of soap in the titrated sample originating from the initial charge, W_A is the weight of the aqueous phase (the total weight minus that of the monomer which can be centrifuged out) at the given polymer yield, M_S is the molecular weight of the soap, W_T is the weight of water added in the titration, and C_μ is the critical concentration of the soap expressed as moles of soap per 1000 g. of water. Values of W_A as a function of yield were taken from the paper of Herzfeld, Roginsky, Corrin, and Harkins (5) and of C_μ from that of Corrin and Harkins (1).

Average particle diameter and particle number

The surface average particle diameter may be calculated from $W_{S(A)}$ by the equation

$$d_{\bar{s}} = \frac{6PM_S}{W_{S(A)}N_0\sigma_S\rho}$$

in which $d_{\bar{s}}$ is the surface average particle diameter, P is the total weight of polymer and dissolved monomer in the sample titrated, N_0 is Avogadro's number, σ_S is the area occupied per soap molecule on the surface of the polymer–monomer particle at an equilibrium soap concentration equal to the critical concentration, and ρ is the density of the polymer–monomer particle. A value of 0.9 g./ml. was assumed for ρ and values of σ_S were taken from the paper of Corrin, Lind, Roginsky, and Harkins (2).

The number of particles per 100 g. of monomer initially used may be approximated in a somewhat uncertain manner from the surface average particle diameters as

$$N = \frac{6Y(R+1)}{\pi d_S^3 \rho}$$

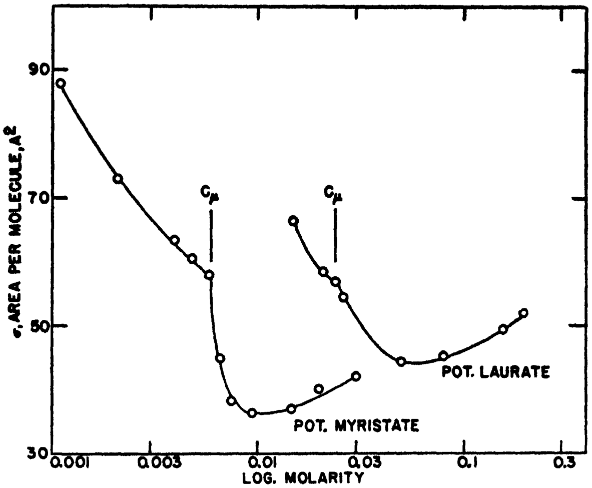

FIG. 1. Adsorption isotherms of potassium laurate and potassium myristate on ash-free graphite.

in which N is the number of particles, Y is the yield of polymer in grams, and R is the monomer–polymer ratio. It is obvious that numbers so calculated differ from the true values in a manner dependent upon the nature of the particle-size distribution curve.

Concentration of unadsorbed soap

The adsorption isotherms of potassium laurate and potassium myristate on ash-free graphite of known surface area have been measured (2). The area occupied per molecule of adsorbed soap on this adsorbent is shown in figure 1; a logarithmic concentration scale is used in order that the myristate and laurate data may be plotted on the same graph. It is obvious from this figure that the amount of adsorbed soap is not constant at concentrations exceeding the critical concentration. Whether the area values plotted in figure 1 are valid for adsorption on the polymer–monomer particle is a matter of conjecture. It has been found, however, by Willson, Miller, and Rowe (6) on the basis of soap titration and electron microscope measurements that σ_S for potassium myristate at the critical concentration is 59 Å.^{2}, while the value of σ_S as determined by adsorption on graphite is 56 Å.^{2} The general form of the area relationships observed on graphite has, moreover, been found to be true for polystyrene (2).

The amount of soap adsorbed at any given equilibrium concentration may be calculated from the amount adsorbed at the critical concentration, $W_{S(A)}$, by a method of successive approximations. The first approximation gives

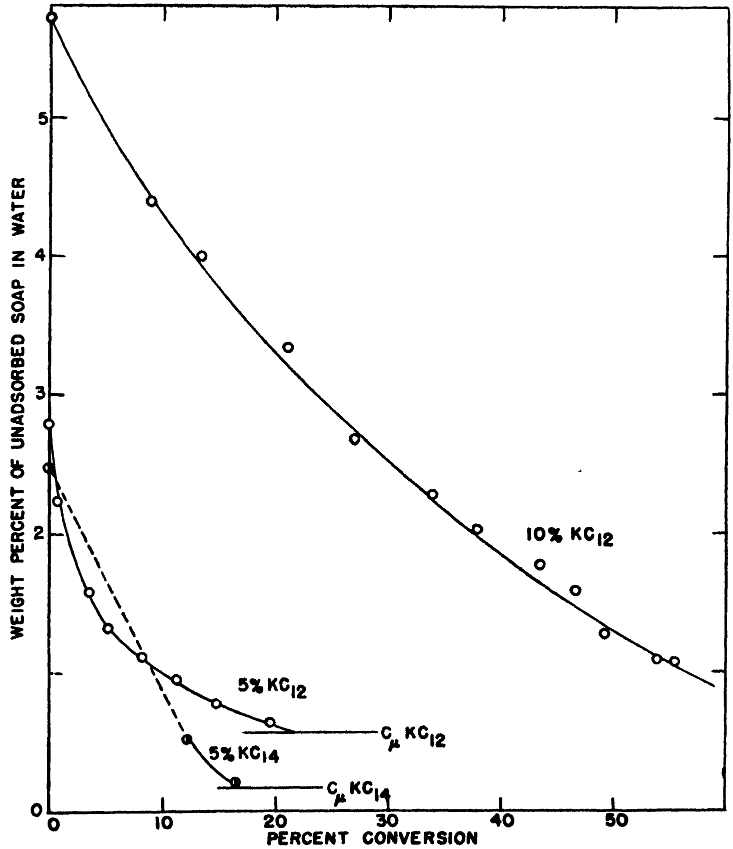

FIG. 2. Concentration of unadsorbed potassium laurate and potassium myristate as a function of polymer yield for systems containing initially 5 and 10 per cent potassium laurate and 5 per cent potassium myristate.

$$C_{S(E)} = \frac{(180W_L/W_A + W_T)C_\mu}{180{,}000W_L/M_A}$$

in which $C_{S(E)}$ is the equilibrium concentration of soap. The amount of soap adsorbed at this concentration is then given by

$$W_{S(A)_E} = W_{S(A)} \frac{\sigma_{C_\mu}}{\sigma_{C_E}}$$

in which $W_{S(A)_E}$ is the amount of soap adsorbed at the equilibrium soap concentration in the latex before titration; σ_{C_μ} is the area per adsorbed molecule at the critical concentration, and σ_{C_E} is the area occupied per adsorbed molecule at the equilibrium concentration $C_{S(E)}$.

A second approximation may the be made for $C_{S(E)}$ and the process repeated until no significant changes are produced in $C_{S(E)}$. For a 1 per cent constancy in $C_{S(E)}$ two approximations are usually sufficient except in the neighborhood of the minimum in the specific area curve; in this region, six or seven approximations are required.

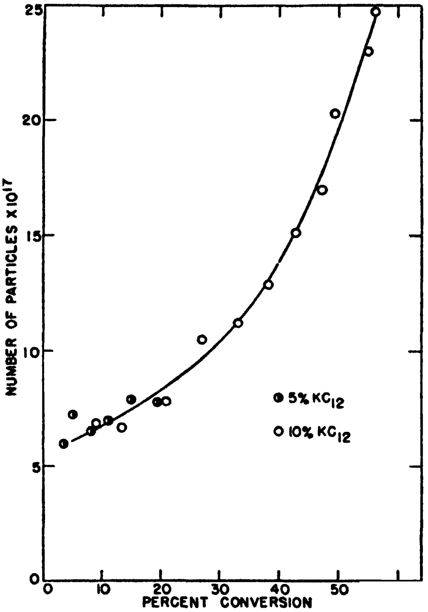

FIG. 3. Number of particles for initial potassium laurate concentrations of 5 and 10 per cent plotted as a function of the yield.

RESULTS AND DISCUSSION

The concentration of unadsorbed potassium laurate and potassium myristate as a function of polymer yield is shown in figure 2 for systems containing initially 5 and 10 per cent potassium laurate and 5 per cent potassium myristate; these percentages are based on monomer. The concentrations are given in terms of weight per cent of soap in water. No data are given for potassium myristate at low yields, since the adsorption isotherm of this soap at these relatively high equilibrium concentrations has not been measured. The critical concentrations of potassium laurate and myristate are indicated in the plots. It is seen that with an initial concentration of 10 per cent potassium laurate micellar soap is still present at polymer yields in excess of 50 per cent. With an initial concentration of 5 per cent potassium laurate the micellar soap disappears at a polymer yield of approximately 20 per cent, while with an initial concentration of 5 per cent potassium myristate the micellar soap disappears at a polymer yield of approximately 17 per cent.

The number of particles for initial potassium laurate concentrations of 5 and 10 per cent is plotted as a function of the yield in figure 3. Insofar as these data are of any validity the number of particles produced at any given yield below 20 per cent is the same for the two initial soap concentrations. Since the rate of polymerization is considerably greater in the case of the 10 per cent soap system, this would indicate that the rate of polymer particle initiation with respect to time increases with initial soap concentration. This is in agreement with previous observations.

SUMMARY

The concentration of unadsorbed soap as a function of polymer yield has been determined for two initial concentrations of potassium laurate and one initial concentration of potassium myristate in the emulsion polymerization of styrene. These results are based on the fluorometric dye technic; calculations involve the monomer–polymer ratio and the adsorption isotherms of the soaps. The experimental details and the calculations are presented in detail.

For initial concentrations of 5 per cent potassium laurate and 5 per cent potassium myristate based on monomer the micellar soap disappears at polymer yields of approximately 20 per cent. For an initial concentration of 10 per cent potassium laurate micellar soap is still present at polymer yields in excess of 50 per cent.

It is possible to obtain a rough measure of the number of polymer particles as a function of yield from the surface average particle diameters calculated from the adsorption data. As calculated in this way the number of particles at any given polymer yield below 20 per cent is essentially identical for systems containing initially 5 and 10 per cent potassium laurate.

REFERENCES

(1) Corrin, M. L., and Harkins, W. D.: J. Am. Chem. Soc. **69**, 679 (1947).

(2) Corrin, M. L., Lind, E. L., Roginsky, A., and Harkins, W. D.: J. Colloid. Sci. **4**, 485 (1949).

(3) Harkins, W. D.: J. Chem. Phys. **13**, 381 (1945); **14**, 47 (1946).

(4) Harkins, W. D.: J. Am. Chem. Soc. **69**, 1428 (1947).

(5) Herzfeld, S. H., Roginsky, A., Corrin, M. L., and Harkins, W. D.: J. Polymer Sci., in press.

(6) Willson, E. A., Miller, J. R., and Rowe, E. H.: J. Phys. & Colloid. Chem. **53**, 357 (1949).

THE EFFECT OF ALCOHOLS AND OF ALCOHOLS AND SALTS ON THE CRITICAL MICELLE CONCENTRATION OF DODECYLAMMONIUM CHLORIDE[1,2]

S. H. HERZFELD,[3] M. L. CORRIN, AND WILLIAM D. HARKINS

Department of Chemistry, University of Chicago, Chicago 37, Illinois

Received August 22, 1949

The nature of the effects produced by alcohols upon the critical concentration for the formation of micelles in solutions of long-chain electrolytes is a matter of some dispute. Thus Ward (12) found that the critical concentration of sodium dodecyl sulfate passes through a minimum on the addition of ethanol. In solutions of high alcohol concentration no critical concentration was observed. The effect of ethanol on the critical concentration of dodecylammonium chloride has been discussed in general terms by Ralston and Hoerr (10); these same authors found that no depression of the critical concentration resulted from the addition of ethanol (11). At alcohol concentrations exceeding approximately 15 mole per cent the critical concentration increased rapidly with increasing alcohol concentration. Corrin and Harkins (3) measured the critical concentration of decyltrimethylammonium bromide and dodecylammonium chloride in the presence of methanol, ethanol, 1-propanol, 2-propanol, and 1-butanol. The critical concentration of the quaternary salt was shown to pass through a minimum with increasing concentration of methanol and ethanol. With the other monohydric alcohols studied the critical concentration was still decreasing at the highest alcohol concentrations investigated.

It has been reported by Ralston and Eggenberger (9) that the critical concentration of dodecylammonium chloride is markedly depressed in saturated aqueous solutions of 1-hexanol, 1-octanol, 1-dodecanol, and 1-octadecanol. The effect of methanol on the critical concentration (conductivity "break-point") of several long-chain quaternary ammonium salts has been studied by Evers and Kraus (6) and by Grieger and Kraus (7). No minimum in the critical concentration was noted in the range of alcohol concentration investigated; in all cases the critical concentration in the presence of the alcohol was greater than that in water. It is pointed out by these authors, however, that it is possible that small amounts of methanol might cause a depression of the critical concentration. The importance of the gegen-ion with respect to the position of the "break-point" is stressed by these investigators. The effect of methanol, 2-propanol, and 2-methyl-2-propanol (*tert*-butyl alcohol) on the critical concentration of dodecylammonium chloride and several quaternary salts has been studied by Brown, Grieger, and Kraus (1).

---

[1] Presented at the Twenty-third National Colloid Symposium, which was held under the auspices of the Division of Colloid Chemistry of the American Chemical Society at Minneapolis, Minnesota, June 6–8, 1949.

[2] This investigation was carried out under the sponsorship of the Reconstruction Finance Corporation, Office of Rubber Reserve, in connection with the synthetic rubber program of the United States Government.

[3] Present address: Velsicol Corporation, Chicago, Illinois.

The critical concentration of the amine hydrochloride passes through a minimum with increasing concentration of 2-propanol; it was still decreasing at the highest concentration of 2-methyl-2-propanol employed. The effect of the 2-methyl-2-propanol on the quaternary salts was similar in that the critical concentration was still decreasing in a 7.9 per cent solution of the alcohol. The addition of 1-dodecanol to a methanol-water solution of dodecylammonium chloride was found to result in a marked decrease in critical concentration; the critical concentration decreased with increasing alcohol concentration.

Little attention has been paid to the variation in critical concentration of a long-chain electrolyte with respect to the concentration of alcohol; this is especially true for the long-chain alcohols. The study of the relation between critical concentration and alcohol concentration is one of the primary objects of this investigation.

The addition of salts is known to depress the critical concentration for the formation of micelles in solutions of long-chain electrolytes; the addition of long-chain alcohols produces the same effect. The salt effect has been interpreted in two ways.

(*1*) The decrease in critical concentration in the presence of added salt is due to a decrease in repulsive forces between the polar head-groups of the molecules in the micelle as the counter-ion concentration in the ionic double layer is increased. This interpretation, advanced by Debye and Anacker (5), leads to the postulate that the number of long-chain molecules in the micelle increases with the concentration of added salt.

(*2*) The decrease in critical concentration in the presence of added salt is due essentially to a common-ion effect on the assumption that the number of long-chain molecules in the micelle remains constant. A treatment of this sort has been discussed by Corrin (2).

The mechanism by which long-chain alcohols depress the critical concentration is unknown. It has been definitely established, however, that the molecules of the long-chain alcohol enter into the oriented structure of the micelle (8). It is thus possible to attempt an explanation of the alcohol effect based on the concept of a decreased head-group repulsion in the micelle; this is brought about by introduction of the alcohol molecules between the ions (or molecules) of the long-chain electrolyte. It is possible that dielectric effects may play a role in the case of the shorter chain alcohols (12).

It is thus of considerable interest to study the mutual effect of long-chain alcohols and salts on the critical concentration. This paper gives the results of such an investigation. The long-chain electrolyte was dodecylammonium chloride; the long-chain alcohols were 1-hexanol and 1-decanol; the salt was potassium chloride.

EXPERIMENTAL

Materials

The dodecylammonium chloride was of a lot obtained from Armour and Company. It had been prepared from dodecylamine, whose freezing point was given as 28.21°C.

The ethanol was commercial absolute material. 1-Propanol, 2-propanol, and 1-butanol had been purified by distillation through a 5-ft. glass-packed column; only the middle portion was collected. 1-Hexanol was distilled through a 10-in. Vigreaux column and the middle third collected. The 1-heptanol was East-

TABLE 1

The effect of alcohols on the critical micelle concentration of dodecylammonium chloride (25°C.)

C_a (MOLARITY OF ALCOHOL)	C_μ (CRITICAL CONCENTRATION)
Ethanol	
	moles/liter
0	0.0131
0.569	0.0126
0.868	0.0120
1.918	0.0106
2.627	0.00973
3.163	0.00875
1-Propanol	
0	0.0131
0.385	0.0109
0.631	0.00899
0.988	0.00703
1-Butanol	
0	0.0129
0.155	0.00903
0.342	0.00596
0.464	0.00406
1-Hexanol	
0	0.0127
0.50×10^{-2}	0.0117
0.66	0.0113
0.82	0.0106
1.18	0.0101
1.46	0.0095
1.64	0.0094
1.68	0.0091
1.96	0.0084
1-Heptanol	
0	0.0127
1.90×10^{-3}	0.0115
2.74	0.0111
3.59	0.0109
4.94	0.00997
1-Heptanol—*Contd.*	
	moles/liter
5.96	0.00902
6.43	0.00865
7.07	0.00855
7.73	0.00780
1-Decanol	
0	0.0126
0.902×10^{-4}	0.0109
1.43	0.00943
1.88	0.00827
2.00	0.00791
2.31	0.00761
1-Undecanol	
0	0.0125
0.484×10^{-4}	0.0106
0.639	0.00943
0.831	0.00919
1.01	0.00747
1.28	0.00707
2-Propanol	
0	0.0130
0.654	0.00953
1.046	0.00762
Triethylcarbinol	
0	0.0124
0.639×10^{-2}	0.0118
1.22	0.0111
2.22	0.0101
3.08	0.00932
3.72	0.00844
4.27	0.00776
4.80	0.00727

man white label material. Both the 1-decanol and the 1-undecanol were samples of high purity and had been used previously in this laboratory in the study of surface films.

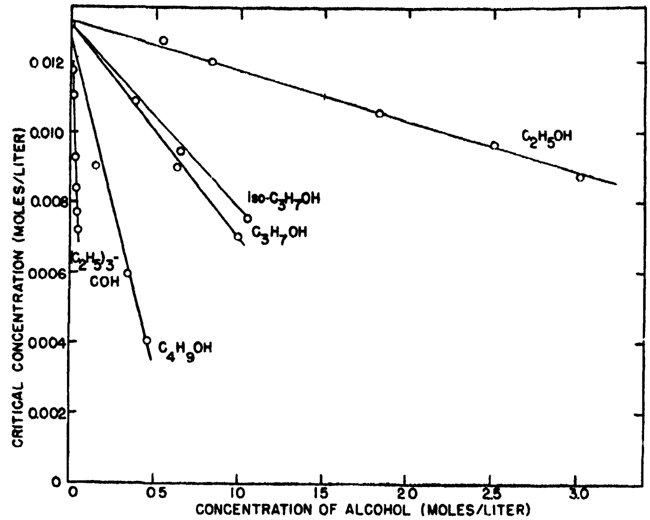

Fig. 1. The effect of the concentration of ethanol, 2-propanol, 1-propanol, 1-butanol, and triethylcarbinol on the critical micelle concentration of dodecylammonium chloride at 25°C.

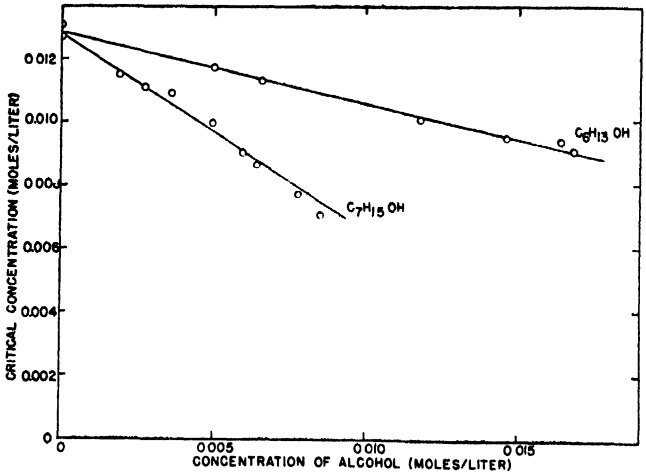

Fig. 2. The effect of the concentration of 1-hexanol and 1-heptanol on the critical micelle concentration of dodecylammonium chloride at 25°C.

The potassium chloride was of reagent grade.

The 2,6-dichlorophenol-indophenol was a commercial preparation and was used without further purification.

Determination of critical concentrations

Critical concentrations were determined by the visual dye method (4). The indicator used was 2,6-dichlorophenol-indophenol (1×10^{-4} molar) in hydrochloric acid solution (initially 3×10^{-4} molar). Both the critical concentration and the concentration of alcohol at the critical concentration are calculated from the titration end point and are hence subject to titration error. This error is on the order of 5 per cent. The measurements were made at 25°C. ± 0.5°, and the end point was taken as the point of maximum color change from blue to red. When salts were used, the salt concentration was maintained constant.

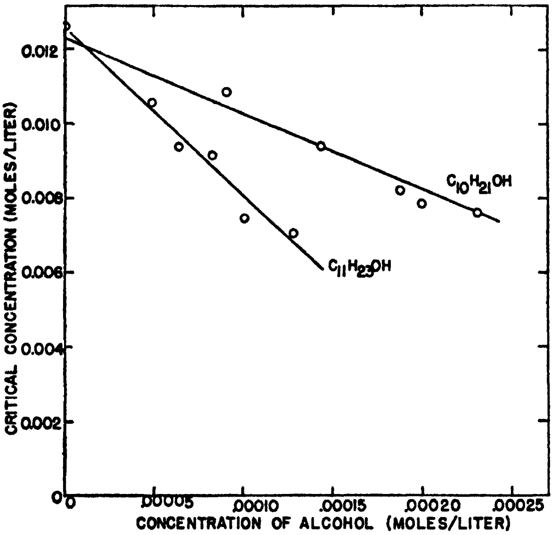

FIG. 3. The effect of the concentration of 1-decanol and 1-undecanol on the critical micelle concentration of dodecylammonium chloride at 25°C.

TABLE 2

The rate of change of critical concentration of dodecylammonium chloride at 25°C. with concentration of alcohol

ALCOHOL	dC_μ/dC_a
Ethanol	0.00145
Propanol	0.00624
2-Propanol	0.00516
1-Butanol	0.0192
1-Hexanol	0.213
1-Heptanol	0.623
Triethylcarbinol	0.108
1-Decanol	20.2
1-Undecanol	44.5

RESULTS

Values of the critical concentration of dodecylammonium chloride, C_μ, as a function of the initial alcohol concentration, C_a, are listed in table 1 and plotted in figures 1, 2, and 3. The data for ethanol, 1-propanol, 2-propanol, and 1-butanol have been recalculated from the earlier work of Corrin and Harkins (3). Within the error of the determinations, which is on the order of 5 per cent for both the critical concentrations and the alcohol concentrations, the critical concentration is a linear function of the alcohol concentration. This relation may be put in the form

$$C_\mu = -(\mathrm{d}C_\mu/\mathrm{d}C_a)C_a + C_\mu^0 \qquad (1)$$

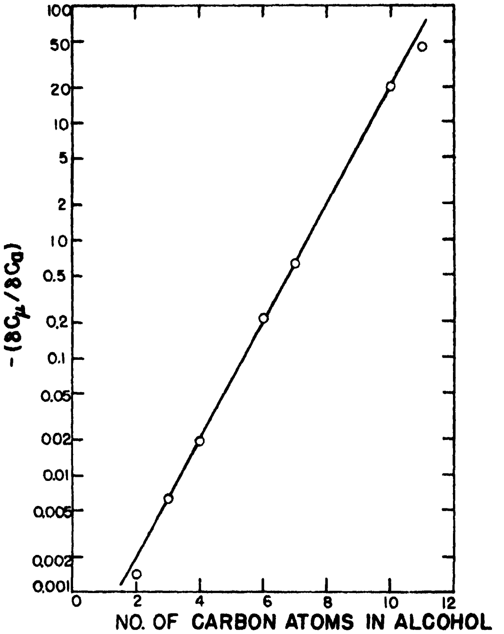

FIG. 4. Plot illustrating the logarithmic relation between the rate of change of critical concentration with alcohol concentration and the chain length of the alcohol.

in which C_μ^0 is the critical concentration in the absence of alcohol. The rate of change of critical concentration with alcohol concentration, $\mathrm{d}C_\mu/\mathrm{d}C_a$, is a constant for a given alcohol but varies with the alcohol employed. Values of $\mathrm{d}C_\mu/\mathrm{d}C_a$ for the various alcohols investigated are collected in table 2; these values were calculated by least squares.

It will be noted that for 2-propanol and triethylcarbinol $\mathrm{d}C_\mu/\mathrm{d}C_a$ is smaller for the branched-chain alcohol than for the straight-chain compound with the same number of carbon atoms. This presumably indicates some difficulty in fitting the branched-chain alcohols into the micelle.

It should be further emphasized that the relationship between critical concentration and alcohol concentration is linear only within a rather large experimental error; additional more refined experiments may indicate that the linearity is fortuitous.

TABLE 3

The effect of 1-hexanol and potassium chloride on the critical micelle concentration of dodecylammonium chloride at 25°C.

C_s (CONCENTRATION OF KCl)	C_a (CONCENTRATION OF 1-HEXANOL)	C_μ (CRITICAL CONCENTRATION)
moles/liter	*moles/liter*	*moles/liter*
0	0	0.0127
0.0075	0	0.0100
0.0075	0.403×10^{-2}	0.00941
0.0075	0.820	0.00870
0.0075	1.20	0.00761
0.0075	1.60	0.00679
0.0075	1.93	0.00613
0.0075	2.23	0.00569
0.0075	2.54	0.00539
0.0150	0	0.00800
0.0150	0.346×10^{-2}	0.00779
0.0150	0.979	0.00602
0.0150	1.37	0.00562
0.0150	1.65	0.00508
0.0150	1.91	0.00471
0.0300	0	0.00650
0.0300	0.488×10^{-2}	0.00570
0.0300	0.788	0.00461
0.0300	1.10	0.00430
0.0300	1.36	0.00397
0.0300	1.44	0.00338
0.0300	1.69	0.00329
0.0600	0	0.00450
0.0600	0.478×10^{-2}	0.00386
0.0600	0.754	0.00305
0.0600	0.996	0.00268
0.0600	1.17	0.00236
0.0600	1.29	0.00209
0.0600	1.41	0.00190

For alcohol chain lengths of from three to ten carbon atoms the following empirical relation has been observed:

$$\log_{10} (dC_\mu/dC_a) = 0.5017N_C - 3.7024 \qquad (2)$$

in which N_C is the number of carbon atoms in the alcohol molecule. This relation is shown in figure 4. The deviation of dC_μ/dC_a from the logarithmic relation for ethanol and 1-undecanol is greater than would be expected from the experimental error of the measurements; the maximum deviation of dC_μ/dC_a from the empirical equation for the other alcohols is 3.5 per cent.

Any theoretical analysis of the alcohol effect on the critical concentration must take into account a rather large number of possible contributing factors. Probably the most important of these is the established fact that alcohol molecules enter into the structure of the micelle (8).

TABLE 4

The effect of 1-decanol and potassium chloride on the critical micelle concentration of dodecylammonium chloride at 25°C.

C_s (CONCENTRATION OF KCl)	C_a (CONCENTRATION OF 1-DECANOL)	C_μ (CRITICAL CONCENTRATION)
moles/liter	*moles/liter*	*moles/liter*
0	0	0.0126
0.0075	0	0.0100
0.0075	0.681×10^{-4}	0.00863
0.0075	1.10	0.00695
0.0075	1.56	0.00657
0.0075	1.97	0.00623
0.0075	2.18	0.00553
0.0075	2.44	0.00515
0.0150	0	0.00810
0.0150	0.552×10^{-4}	0.00673
0.0150	0.942	0.00574
0.0150	1.51	0.00461
0.0150	1.71	0.00417
0.0150	1.86	0.00379
0.0300	0	0.00670
0.0300	0.496×10^{-4}	0.00600
0.0300	0.823	0.00498
0.0300	1.03	0.00414
0.0300	1.26	0.00382
0.0300	1.44	0.00348
0.0300	1.63	0.00321
0.0600	0	0.00481
0.0600	0.252×10^{-4}	0.00443
0.0600	0.453	0.00398
0.0600	0.632	0.00370
0.0600	0.805	0.00353
0.0600	0.886	0.00311
0.0600	1.01	0.00295

The critical concentrations of dodecylammonium chloride in the presence of 1-hexanol and potassium chloride are listed in table 3 and are plotted as a function of alcohol concentration at constant salt concentration in figure 4. Similar data for 1-decanol and potassium chloride are listed in table 4 and plotted in figure 5.

To a first approximation and within experimental error the critical concentration of dodecylammonium chloride at constant salt concentration is a linear function of the alcohol concentration; i.e.,

$$C_\mu = -(dC_\mu/dC_a)_{C_s}C_a + (C^0_\mu)_{C_s} \tag{3}$$

in which $C_{C\mu}$ is the critical concentration; $(dC_\mu/dC_a)_{C_s}$ is the rate of change of critical concentration with alcohol concentration at constant salt concentration,

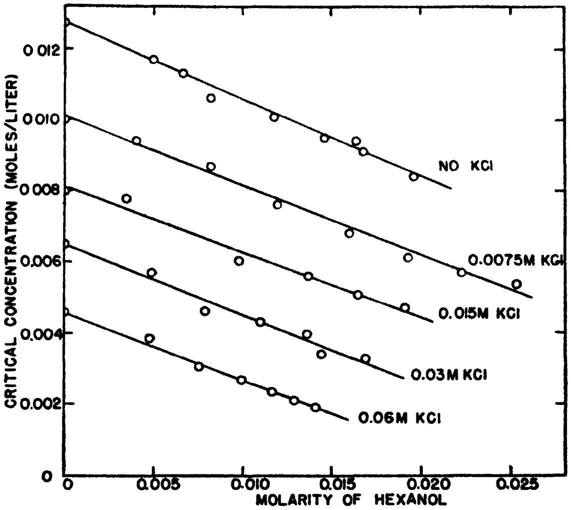

Fig. 5. The effect of 1-hexanol and potassium chloride on the critical concentration of dodecylammonium chloride at 25°C.

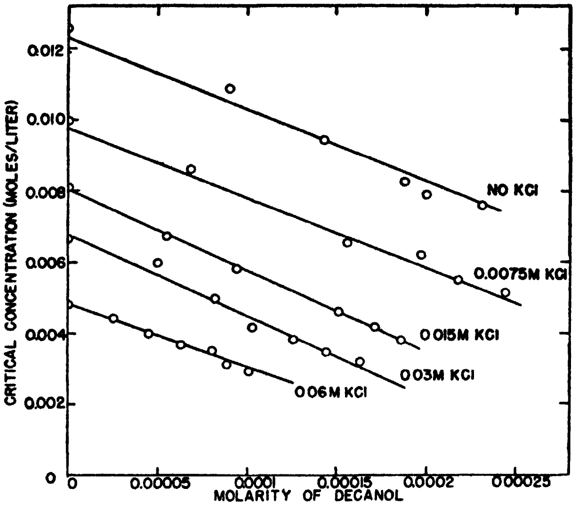

Fig. 6. The effect of 1-decanol and potassium chloride on the critical concentration of dodecylammonium chloride at 25°C.

C_s; C_a is the concentration of alcohol; and $(C_\mu^0)_{C_s}$ is the critical concentration in the absence of alcohol at constant salt concentration, C_s. The parameters in equation 3 calculated by least squares are listed in table 5 for 1-hexanol and in table 6 for 1-decanol. The mean value of $(dC_\mu/dC_a)_{C_s}$ for 1-hexanol is 0.1970 and the maximum deviation from the mean is 8 per cent; the mean value for 1-decanol is 20.78 and the maximum deviation from the mean is 11 per cent. No systematic trend of $(dC_\mu/dC_a)_{C_s}$ with salt concentration is apparent. In view of the experimental error of approximately 5 per cent in C_μ and C_a it must thus be concluded on the basis of the present results that $(dC_\mu/dC_a)_{C_s}$ for a given alcohol is independent of salt concentration.

TABLE 5

Constants in the linear least-squares equations for the variation in critical concentration of dodecylammonium chloride as a function of concentration of 1-hexanol at constant concentration of potassium chloride

C_s (CONCENTRATION OF KCl)	$(C_\mu^0)_{C_s}$ (CRITICAL CONCENTRATION IN ABSENCE OF ALCOHOL IN SALT CONCENTRATION, C_s)	$(dC_\mu/dC_a)_{C_s}$
moles/liter	*moles/liter*	
0	0.0127	0.2130
0.0075	0.0101	0.1945
0.0150	0.00811	0.1831
0.0300	0.00647	0.1983
0.0600	0.00464	0.1959

TABLE 6

Constants in the linear least-squares equations for the variation in critical concentration of dodecylammonium chloride as a function of concentration of 1-decanol at constant concentration of potassium chloride

C_s (CONCENTRATION OF KCl)	$(C_\mu^0)_{C_s}$ (CRITICAL CONCENTRATION IN ABSENCE OF ALCOHOL IN SALT CONCENTRATION, C_s)	$(dC_\mu/dC_a)_{C_s}$
moles/liter	*moles/liter*	
0	0.0123	20.23
0.0075	0.00976	19.41
0.0150	0.00802	22.79
0.0300	0.00682	23.07
0.0600	0.00484	18.43

Cross plots for the critical concentration as a function of salt concentration at constant alcohol concentration as calculated from the data in tables 2 and 3 show a family of curves with constant displacement along the C_μ-axis as the alcohol concentration is increased.

DISCUSSION

In the absence of additives and in solution sufficiently dilute so that intermicellar interactions are negligible the micelle can be considered to a fairly good approximation as a stoichiometric entity. This is equivalent to the concept that the size of all micelles in a given solution can vary only between narrow limits, i.e., the size distribution of micelles is essentially monodisperse. This matter has been treated by Debye and Anacker (5).

In the process of micellization two energy terms are of major importance. A decrease in free energy is brought about by removal of the nonpolar portion of the long-chain ion from its aqueous environment into the interior of the micelle (environmental energy); this decrease in free energy will be maximal when the removal of the nonpolar chain from the water is as complete as possible. As the molecules are brought together in the micelle, short-range repulsive forces between the polar head-groups come into play and a corresponding free energy increase (repulsive energy) must be taken into account.

On the basis of the environmental free energy term the most stable micelle would be one containing the largest number of long-chain ions compatible with the geometric restrictions involved in fitting the ions into the micellar structure. On the basis of both environmental and repulsive terms the most stable micelle would contain fewer ions than the limit set by steric factors. A decrease in the number of ions per micelle would bring water into contact with the nonpolar portion of the long-chain ions in the micelle; any increase in number becomes energetically unlikely, owing to the short-range nature of the repulsive forces. Hence the number of ions in the micelle of any given long-chain electrolyte can vary only between narrow limits.

These considerations deal with the micelle in the absence of any additive. In the presence of an additive the following questions arise: (*1*) Does the micelle size increase in the presence of added salt? (*2*) Does the micelle size increase in the presence of added alcohol?

No clear-cut answer can be given to the first question. If the experimental results of Debye and Anacker are correct (5), the number of ions in the micelle increases rapidly with the concentration of added salt. On the basis of the assumption that the micelle size remains constant it has been possible to derive an expression which satisfactorily relates the critical concentration and the concentration of added salt (2).

The answer to the second question is to some extent more definite. A micelle formed in the presence of a long-chain alcohol undoubtedly contains alcohol molecules in its oriented structure (8). Two additional questions now suggest themselves. (*3*) What is the relation between the number of alcohol molecules in the micelle and the concentration of alcohol in the surrounding solvent? (*4*) In what manner is the number of long-chain ions in the micelle affected by the inclusion of alcohol molecules in the micelle?

Answers to questions 3 and 4 are not known. It would be reasonable to expect that the number of alcohol molecules entering into the micelle would be some function of the alcohol concentration; the form of this function is, however, a matter of mere speculation. It is also reasonable to expect that the repulsive potential between the polar head-groups in the micelle would be altered in the presence of alcohol; this would lead to a variation in the number of long-chain ions per micelle as some unknown function of the alcohol concentration. We may rephrase questions 3 and 4 to include the mutual effect of both alcohol and salt; again the answers are not known.

The interpretation of the effect of added salts and alcohols on the critical concentration for micelle formation can proceed along two lines. If the micelle represents a stoichiometric unit independent of salt concentration but variable with alcohol concentration then a straightforward analysis based on a simple form of the law of mass action is possible. Such an analysis would require knowledge of the following facts: (*A*) The relation between the number of alcohol molecules in the micelle and the concentration of the alcohol both in the presence and the absence of added salt; (*B*) the relation between the number of long-chain ions in the micelle and the concentration of alcohol in the presence and absence of added salt; (*C*) the relation between the degree of ionization of the long-chain ions in the micelle and the concentration of alcohol; (*D*) the relation between the equilibrium constant for micellization and the concentration of alcohol. It is obvious that if some of these relations are known the others may be worked out experimentally.

If the micelle represents a stoichiometric unit variable with both salt and alcohol concentration, then an analysis of the salt and alcohol effects becomes exceedingly complicated. It should be noted for a complete analysis that the effect of alcohol chain length must be considered.

SUMMARY

It is shown that within an experimental error of 5 per cent the critical concentration of dodecylammonium chloride is a linear function of alcohol concentration for alcohols ranging from two to eleven carbon atoms in chain length. The rate of change of critical concentration with alcohol concentration is smaller for branched-chain alcohols than for straight-chain compounds with the same number of carbon atoms. The logarithm of the derivative of the critical concentration with respect to the alcohol concentration is a linear function of the chain length of the alcohol for alcohols of from three to ten carbon atoms.

The critical concentration of dodecylammonium chloride has been measured as a function of the concentration of both added long-chain alcohols and of potassium chloride. The long-chain alcohols investigated were 1-hexanol and 1-decanol.

The effect of alcohol and the effect of salts are essentially additive.

The general attack required for theoretical analysis of the alcohol and salt effect is outlined in general terms.

REFERENCES

(1) Brown, G. L., Grieger, P. F., and Kraus, C. A.: J. Am. Chem. Soc. **71,** 95 (1949).

(2) Corrin, M. L.: J. Colloid Sci. **3,** 333 (1948).

(3) Corrin, M. L., and Harkins, W. D.: J. Chem. Phys. **14,** 640 (1946).

(4) Corrin, M. L., and Harkins, W. D.: J. Am. Chem. Soc. **69,** 679 (1947).

(5) Debye, P., and Anacker, E. W.: Private communication.

(6) Evers, E. C., and Kraus, C. A.: J. Am. Chem. Soc. **70,** 3049 (1948).

(7) Grieger, P. F., and Kraus, C. A.: J. Am. Chem. Soc. **70,** 3803 (1948).

(8) HARKINS, W. D., MATTOON, R. W., AND MITTELMANN, R.: J. Chem. Phys. **15**, 763 (1947).
(9) RALSTON, A. W., AND EGGENBERGER, D. N.: J. Am. Chem. Soc. **70**, 983 (1948).
(10) RALSTON, A. W., AND HOERR, C. W.: J. Am. Chem. Soc. **68**, 851 (1946).
(11) RALSTON, A. W., AND HOERR, C. W.: J. Am. Chem. Soc. **68**, 2460 (1946).
(12) WARD, A. F. H.: Proc. Roy. Soc. (London) **A176**, 412 (1940).

SOLUBILIZATION OF POLYCYCLIC HYDROCARBONS[1,2]

H. B. KLEVENS

Division of Agricultural Biochemistry, University of Minnesota, St. Paul, Minnesota

Received August 22, 1949

In the course of a study of a possible mechanism of transport of carcinogenic polycyclic hydrocarbons in the body, it was of some interest to determine their solubility in various media. Data are presented here concerning the solubility of various hydrocarbons in water and their solubilization in potassium laurate solutions. Systems in which salts of bile acids and mixtures of these salts with fatty acid soaps act as solubilizers will be described in a later report. These latter data indicate that the "choleic" acid principle also plays a part in solubilization.

It has been reported previously (15) that there are apparently at least two types of solubilization: one involving hydrocarbons such as *n*-heptane and ethylbenzene in which there is a constant increase in the number of moles of compound solubilized with increase in soap concentration (MR) (7), and the other in which there is a constant MR or one which decreases slightly with increase in soap concentration. Examples of the latter are typical water-insoluble dyes, such as Orange OT (*o*-tolylazo-β-naphthol) and Yellow AB (phenylazo-β-naphthylamine) (18) and long-chain alcohols and amines (5). Data illustrative of these effects are seen in figure 1.

Extensive x-ray studies on soap–hydrocarbon systems indicate that solubilization involves incorporation of the hydrocarbon in the region of the micelle center (18), as seen by an increase in x-ray spacing. Solubilization of long-chain alcohols involving palisade formation has recently been shown to cause no swelling of the micelle (6). Further, recent results indicate definitely two different loci of solubilization in the soap micelle, for the solubility of *n*-heptane and of 1-heptanol is shown not to be additive but, rather, the presence of long-chain alcohols greatly increases the solubilizing power of a soap solution for a hydrocarbon (16).

The data presented below attempt to bridge, in part, the gap between the above phenomena. The importance of many of the compounds studied here and their derivatives as carcinogenic agents has been well established (4).

---

[1] Presented at the Twenty-third National Colloid Symposium, which was held under the auspices of the Division of Colloid Chemistry of the American Chemical Society at Minneapolis, Minnesota, June 6–8, 1949.

[2] Paper No. 2533, Scientific Journal Series, Minnesota Agricultural Experiment Station.

EXPERIMENTAL

Two experimental methods may be employed for the determination of the solubilization of polycyclic hydrocarbons. The first involves adding a known amount of an acetone or alcohol solution of the polycyclic hydrocarbon to a soap solution, agitating this mixture, and then evaporating off the organic solvent. A certain amount of water will be lost in this manner but this can easily be corrected for in subsequent calculations. Saturation of the soap solution by hydrocarbon can be determined by turbidity. In the second method, sealed ampules containing soap solution and solid polycyclics are shaken for periods up to three months, or until equilibrium results are obtained, at 25°C. ± 2°. The ampules are then allowed to stand at room temperatures for a few days, and centrifuged at about 3000 g to insure settling out of residual polycyclic material. Samples are withdrawn through a plug in order to hold back any solid polycyclics, diluted in alcohol or some other suitable solvent, and the spectra determined in the region of the most intense band. In the *cata*-condensed polycyclics, this is the ${}^1A$—${}^1B_b$ transition (that associated with polarization along the long axis of the molecule), which is 100–500 times more intense than those of the weak, forbidden, long wave length ${}^1A$—${}^1L_a$ and ${}^1A$—${}^1L_b$ transitions (13). This second method was found to be more satisfactory and was used for most of the data reported here.[3]

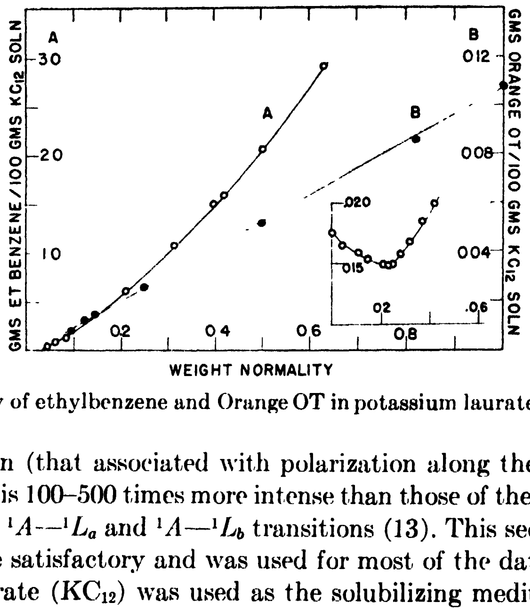

FIG. 1. Solubility of ethylbenzene and Orange OT in potassium laurate solutions (25°C.)

Potassium laurate (KC_{12}) was used as the solubilizing medium and was prepared by saponification of the methyl ester which had previously been fractionally distilled. The soap was recrystallized a number of times from ethanol and acetone and then dried *in vacuo*.

The polycyclics were, for the most part, those obtained from Dr. R. N. Jones and were purified by formation of the picrate complex followed by chromatog-

[3] Recently Ekwall and Setala (Acta Chem. Scand. **2**, 733 (1948)) have determined the approximate solubility values of three polycyclic hydrocarbons, 1,2,5,6-dibenzanthracene, 20-methylcholanthrene, and 9,10-dimethyl-1,2-benzanthracene, by the measurement of their fluorescent intensities. This method of measurement is complicated by the quenching of fluorescence by the soap and other substances (e.g., oxygen) as well as by self-quenching.

raphy. The spectra of these compounds have been reported by Jones (10) and others (13) and these data were used in the calculations of concentrations in those solubilization studies.

SOLUBILITY IN WATER

The solubility of various polycyclics in water was determined by shaking crystals of each compound in 1 liter of water for as long as three months. Aliquots were removed and concentrations determined by spectra. For the sparingly soluble polycyclics, a special 1-meter cell with lenses as windows was used for the spectral analysis. The results obtained in this manner are collected in table 1. In the alkylbenzene series, the decrease in log S (solubility) or V (volume oil) is roughly linear with molar volume. Similar results as to log S are obtained if only the linear polyacenes (benzene, naphthalene, anthracene, etc.) are considered. However, the nonlinear polycyclics do not follow this relationship.

TABLE 1

Solubility (S) of various hydrocarbons in water (25°C.)

COMPOUND	S	S_M	LOG S_M	MOLAR VOLUME	LENGTH	VOLUME OF OIL (V)	LOG V
	µ grams/liter	*moles/liter* $\times 10^6$			Å.	*ml./liter*	
Benzene	1,860,000	23,900	−1.62	89	5.5	2.12	0.32
Toluene	500,000	5,430	−2.27	106	7.0	0.575	−0.24
Ethylbenzene	175,000	1,640	−2.76	123	(8.25)	0.205	−0.69
n-Propylbenzene	120,000	1,000	−3.00	145	(9.0–9.5)	0.145	−0.85
n-Butylbenzene	50,000	370	−3.43	156	(9.8–10.8)	0.058	−1.24
Naphthalene	12,500	97.5	−4.01	112	8.0	0.0109	−1.96
Phenanthrene	1,600	9.0	−5.05	151	9.5	0.00137	−2.86
Anthracene	75	0.447	−6.34	142.6	10.5	0.00006	−4.22
Triphenylene	43	0.188	−6.73		9.5		
Pyrene	175	0.77	−6.12	159	9.5	0.00014	−3.86
Chrysene	6	0.0276	−7.45	178	11.8	0.0000031	−5.52
1,2-Benzanthracene	10	0.0431	−7.27	182	11.8	0.0000089	−5.08
Naphthacene	(1.5)*	0.0066	−8.18		13.0		
1,2,5,6-Dibenzanthracene	(0.6)*	0.00215	−8.67		13.5		
Fluoranthrene	265	1.32	−5.88	163	9.4	0.0002	−3.68

* Approximate values.

Complete density and molar volume data are not available for all the nonlinear polyacenes, so that a complete comparison of molar volume and solubility could not be obtained. However, by use of tables of bond distances and bond angles (21), it is possible to obtain the length of the various molecules along their major axis. The change in log S with length in Å. is seen to follow a linear relationship in figure 2. A few of the points, those for the highly condensed pyrene and triphenylene, do not coincide with the curve, a result which indicates that this linear relationship may be valid only for the linear or near-linear polycyclics. In addition, 3,4-benzopyrene and perylene fall about as much below the curve as does pyrene; picene, cholanthrene, and methylcholanthrene, all somewhat less condensed than pyrene and perylene, fall on this curve (2). The naphthacene value is an approximate one because of the instability of this compound in solution.

SOLUBILITY IN POTASSIUM LAURATE SOLUTIONS

Data for the solubilization of benzene and various polycyclic hydrocarbons in various concentrations of potassium laurate solutions are collected in table 2 and some of these data are plotted in figures 3 to 5. When all data are corrected for solubility of the hydrocarbons in water, the curves intercept the concentration axis at about 0.25 M potassium laurate. This is the concentration at which micelles form and can be compared with a value of 0.255 M found by refraction (12) and one of 0.23 M found by the dye–spectral method (1) for the same preparation of potassium laurate.

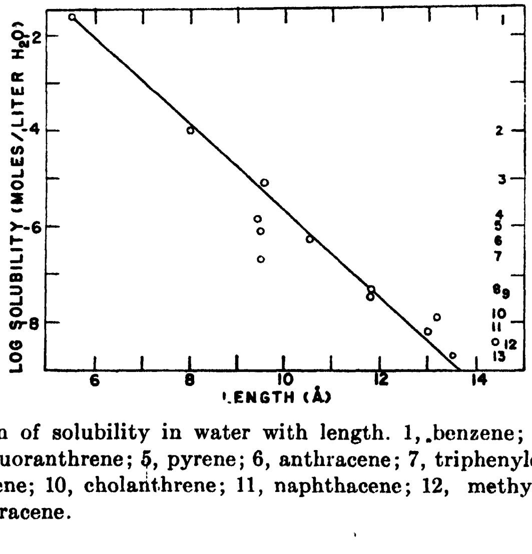

FIG. 2. Variation of solubility in water with length. 1, benzene; 2, naphthalene; 3, phenanthrene; 4, fluoranthrene; 5, pyrene; 6, anthracene; 7, triphenylene; 8, 1,2-benzanthracene; 9, chrysene; 10, cholanthrene; 11, naphthacene; 12, methylcholanthrene; 13, 1,2,5,6-dibenzanthracene.

The data in column 5 of table 2, molecules of oil per micelle, are based on a value of 150 molecules of potassium laurate per hydrocarbon-swollen soap micelle. This is an approximately average value of a number of different calculations for a soap of this chain length: (*1*) a value of 140 as calculated from x-ray evidence of swollen micelles (19), in which it is indicated that swollen micelles have about twice the number of soap molecules as the hydrocarbon-free micelles; (*2*) one of 130 calculated from equations describing the size of swollen micelles (14), using as a basis of the molecular weight values of nonswollen micelles as de-

TABLE 2

Solubility of various hydrocarbons in potassium laurate (KC_{12}) *solutions* (*25°C.*)

(Corrected for solubility in water)

KC_{12} IN MOLES PER LITER	GRAMS OF OIL PER LITER OF SOAP SOLUTION	MOLES OF OIL PER LITER OF SOAP SOLUTION ($\times 10^3$)	MOLES OF OIL PER MOLE OF SOAP ($\times 10^3$)	MOLECULES OF OIL PER MICELLE	MOLECULES OF OIL PER MICELLE (CORRECTED)	VOLUME OF OIL (ML. PER LITER OF SOAP SOLUTION)
Benzene						
0.50	30.6	391	782	118	123	34.3
0.42	24.08	309	737	111	119	26.9
0.30	15.45	198	660	99	108	17.3
0.21	9.90	127	605	90	103	11.1
0.105	3.60	46.1	438	66	97	4.02
0.060	1.55	19.9	331	50	83	1.73
Naphthalene						
0.63	5.38	42.0	66.7	10.0	10.5	4.70
0.50	4.26	33.3	66.6	10.0	10.4	3.72
0.42	3.51	27.4	65.4	9.8	10.4	3.05
0.30	2.46	19.2	64.0	9.6	10.4	2.15
0.21	1.60	12.5	59.5	9.0	11.0	1.40
0.145	1.13	8.91	61.6	9.1	11.1	0.99
0.073	0.448	3.50	47.8	7.2	11.0	0.39
0.036	0.103	0.81	22.1	3.3	10.9	0.09
Acenaphthene						
0.650	1.31	8.50	13.1	2.0	2.1	1.28
0.530	1.06	6.91	13.0	2.0	2.1	1.04
0.370	0.708	4.60	12.4	1.9	2.0	0.692
0.300	0.581	3.75	12.5	1.9	2.0	0.567
0.159	0.301	1.95	12.3	1.8	2.2	0.294
0.079	0.124	0.81	10.3	1.6	2.2	0.121
Fluorene						
0.650	0.956	5.76	8.88	1.3	1.4	
0.530	0.790	4.75	8.97	1.3	1.4	
0.370	0.533	3.20	8.68	1.3	1.4	
0.300	0.424	2.55	8.50	1.2	1.4	
0.159	0.219	1.32	8.28	1.2	1.5	
0.079	0.0897	0.54	6.83	1.0	1.5	
Phenanthrene						
0.63	1.55	8.53	13.5	2.0	2.1	1.22
0.50	1.21	6.65	13.3	2.0	2.1	1.03
0.42	1.02	5.60	13.3	2.0	2.1	0.865
0.30	0.70	3.83	12.8	1.9	2.1	0.593
0.21	0.48	2.64	12.6	1.9	2.1	0.408
0.145	0.335	1.84	12.7	1.9	2.3	0.285
0.073	0.148	0.82	11.4	1.7	2.5	0.126
0.036	0.050	0.275	7.7	1.1	3.7	0.0424

TABLE 2—*Continued*

KC_{12} IN MOLES PER LITER	GRAMS OF OIL PER LITER OF SOAP SOLUTION	MOLES OF OIL PER LITER OF SOAP SOLUTION ($\times 10^3$)	MOLES OF OIL PER MOLE OF SOAP ($\times 10^3$)	MOLECULES OF OIL PER MICELLE	MOLECULES OF OIL PER MICELLE (CORRECTED)	VOLUME OF OIL (ML. PER LITER OF SOAP SOLUTION)
			Anthracene			
0.63	0.197	1.08	1.71	0.26	0.27	0.157
0.50	0.155	0.85	1.70	0.26	0.27	0.123
0.42	0.130	0.715	1.71	0.26	0.27	0.103
0.30	0.090	0.495	1.65	0.25	0.27	0.0715
0.21	0.063	0.346	1.65	0.25	0.28	0.0502
0.145	0.039	0.215	1.48	0.22	0.27	0.0311
0.073	0.0155	0.085	1.16	0.17	0.27	0.0123
			Fluoranthrene			
0.65	0.768	3.81	5.86	0.88	0.91	0.614
0.50	0.578	2.86	5.72	0.86	0.90	0.469
0.37	0.428	2.12	5.73	0.86	0.91	0.355
0.30	0.335	1.66	5.53	0.83	0.90	0.272
0.159	0.153	0.76	4.77	0.72	0.84	0.124
0.079	0.062	0.307	3.88	0.59	0.84	0.0502
			Pyrene			
0.65	0.601	2.98	4.58	0.68	0.71	0.472
0.53	0.484	2.40	4 53	0.68	0.71	0.381
0.37	0.325	1.61	4.36	0.66	0.70	0.256
0.30	0.260	1.29	4.30	0.65	0.70	0.204
0.159	0.126	0.623	3.93	0.58	0.70	0.099
0.079	0.048	0.238	3.02	0.45	0.67	0.0378
			Chrysene			
0.597	0.172	0.755	1.27	0.19	0.20	0.135
0.50	0.143	0.627	1.25	0.19	0.20	0.102
0.418	0.121	0.530	1.27	0.19	0.20	0.0952
0.299	0.0836	0.369	1.24	0.19	0.20	0.0734
0.119	0.0308	0.136	1.14	0.17	0.21	0.0242
			1,2-Benzanthracene			
0.597	0.170	0.746	1.25	0.19	0.20	0.137
0.50	0.145	0.635	1.27	0.19	0.20	0.117
0.418	0.119	0.525	1.26	0.19	0.20	0.0956
0.299	0.0810	0.356	1.19	0.18	0.20	0.0650
0.119	0.0288	0.127	1.06	0.16	0.20	0.0232
			Triphenylene			
0.56	0.088	0.387	0.693	0.10	0.11	
0.50	0.0765	0.336	0.672	0.10	0.11	
0.35	0.0526	0.231	0.660	0.10	0.11	
0.28	0.0421	0.186	0.665	0.10	0.11	
0.112	0.0147	0.0645	0.577	0.09	0.11	

TABLE 2—*Concluded*

KC_{12} IN MOLES PER LITER	GRAMS OF OIL PER LITER OF SOAP SOLUTION	MOLES OF OIL PER LITER OF SOAP SOLUTION ($\times 10^3$)	MOLES OF OIL PER MOLE OF SOAP ($\times 10^3$)	MOLECULES OF OIL PER MICELLE	MOLECULES OF OIL PER MICELLE (CORRECTED)	VOLUME OF OIL (ML. PER LITER OF SOAP SOLUTION)
		Methylcholanthrene				
0.597	0.105	0.377	0.632	0.095	0.10	
0.50	0.087	0.323	0.646	0.097	0.10	
0.418	0.0725	0.270	0.645	0.097	0.10	
0.299	0.0520	0.193	0.645	0.097	0.11	
0.119	0.0153	0.055	0.460	0.069	0.09	
		1,2,5,6-Dibenzanthracene				
0.63	0.030	0.108	0.171	0.026	0.027	
0.50	0.024	0.0862	0.172	0.026	0.027	
0.42	0.0196	0.0702	0.168	0.025	0.027	
0.21	0.00852	0.0308	0.148	0.022	0.025	
0.145	0.0061	0.0221	0.152	0.023	0.027	
0.073	0.0025	0.0090	0.124	0.019	0.034	
0.036	0.0012	0.0043	0.120	0.018	0.058	

termined by light scattering (3); and (*3*) one of 140–160 as obtained from preliminary light-scattering measurements on hydrocarbon-swollen micelles (17). The corrected value of molecules of oil per micelle is based on the assumption that 0.025 *M* KC_{12} exists in all systems as nonmicellar (free) soap, and thus this amount does not play a part in solubilization. By use of this correction of "free" (nonmicellar) soap, it is possible to obtain a more accurate mole ratio of hydrocarbon to micellar soap (the only soap which plays a role in solubilization). Plots of molecules per micelle, in the case of benzene, as a function of total soap concentration result in two fairly straight lines with the curve of the corrected values lying above and with a somewhat smaller slope than the other curve. These will, of course, approach each other at higher soap concentrations, where the amount of "free" soap is negligible compared with the total soap present. Further, the use of the corrected data shows that the micelle has undergone its greatest change in solubilizing power per unit change in concentration up to a concentration of about 0.1 *M*. Above this concentration, the rate of change is constant, a small positive value in the case of the normal paraffins and the alkylbenzene series, and a value of essentially zero for the more complex polycyclics. Without consideration of this "free" soap, this concentration of maximum change in solubilization would appear to occur at about 0.2 *M*. A number of points regarding the data in table 2 and the corresponding figures 3 to 5 will be considered below.

Curvature of solubility curves

The slope of solubility curves of simple aliphatic hydrocarbons, such as propene, *n*-hexane, *n*-heptane, etc., and of benzene and the alkylbenzenes, such as toluene, ethylbenzene, *n*-butylbenzene, etc., increases with increasing soap

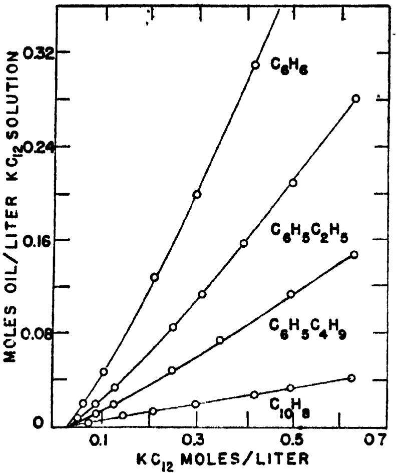

FIG. 3

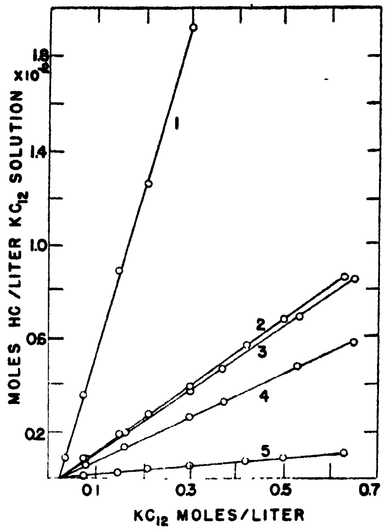

FIG. 4

FIG. 3. Solubility of various polycyclic hydrocarbons in potassium laurate solutions

FIG. 4. Solubility of various polycyclics in potassium laurate solutions. 1, naphthalene; 2, acenaphthene, 3, fluorene; 4, phenanthrene, 5, anthracene.

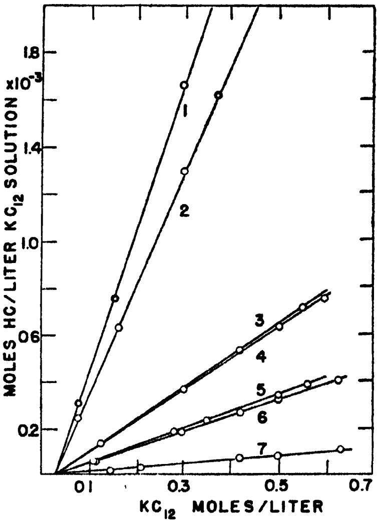

FIG. 5

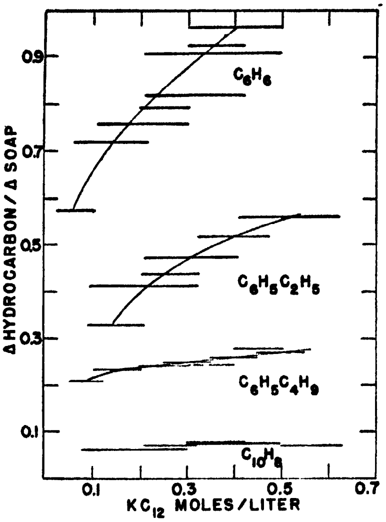

FIG. 6

FIG. 5. Solubility of various polycyclics in potassium laurate solutions. 1, fluoranthrene; 2, pyrene; 3, chrysene; 4, 1,2-benzanthracene; 5, triphenylene; 6, methylcholanthrene; 7, 1,2,5,6-dibenzanthracene.

FIG. 6. Chord plots of the data in figure 3 indicating the change, with soap concentration, of the increment in the number of molecules of hydrocarbon solubilized per increment in soap concentration.

concentration. This would indicate that the expansion and probable increase in size of the hydrocarbon-swollen micelle are accompanied by an enhancement of the solubilizing power per soap molecule. This increase in slope with soap concentration observed in solubilization of the simpler hydrocarbons is accompanied by incorporation in the micelle at 0.63 *N* KC_{12} of about 20–125 molecules of hydrocarbon per micelle, as can be seen in table 3. Similar amounts of long-chain alcohols are incorporated per soap micelle, but in this case there is a decrease in slope (5).

TABLE 3

Effect of unsaturation and cyclization on solubilization in 0.63 N KC_{12}

COMPOUND	GRAMS PER LITER OF SOAP SOLUTION	MOLES PER LITER OF SOAP SOLUTION	MOLECULES OF HYDROCARBON PER MICELLE	$\frac{\Delta \text{ SLOPE}}{\Delta \text{ SOAP CONCENTRATION}}$
n-Hexane	15.3	0.178	42	+
Hexatriene	33.8	0.425	99	+
Benzene	41.5	0.533	126	+
Cyclohexane	36.0	0.430	102	+
n-Heptane	12.5	0.125	30	+
Toluene	37.5	0.403	96	+
n-Octane	12.0	0.105	24	+
Ethylbenzene	29.5	0.28	66	+
Styrene	34.5	0.332	78	+
n-Decane*	8.5	0.058	14	
n-Butylbenzene	18.7	0.147	35	+
Naphthalene	5.38	0.042	10	0
Phenanthrene	1.55	0.0085	2.0	0
Fluorene	0.92	0.0056	1.3	0
Anthracene	0.197	0.00108	0.26	0
o-Tolylazo-β-naphthol†	0.61	0.0025	0.60	0
Dinitrodiphenylamine*	15.0	0.058	14	0

* See reference 23.

† See reference 18.

As the size of the molecule is increased to a system of two or more rings—either in the planar form, of which naphthalene is the simplest, or to a substituted biphenyl, as dinitrophenylamine (23)—the number of molecules per micelle decreases markedly and the change in slope becomes zero. This is found to occur in the case of solubilization of the various polycyclics studied here.

This is further exemplified by consideration of the chord plots in figure 6, which show the changes, with soap concentration, of the increment in the number of molecules of hydrocarbon solubilized per increment in soap concentration. There is some indication of a lessening in the increase in slope with increase in the length of the side chain on the benzene nucleus (H → C_2H_5 → C_4H_9) and an approach to a zero slope increment with the simplest polycyclic, naphthalene. All higher-order polycyclics show no change in slope with soap concentration, as can be seen in table 3. No evidence is as yet available to indicate that the slope increment would approach or become equal to zero as the alkyl group on the benzene is increased in length to C_8, C_{10}, or C_{12}. On the basis of published x-ray evidence on hydrocarbon-swollen micelles (8), it is to be expected that a certain number of molecules or portions of these long alkylated molecules would extend into the region between adjacent soap molecules in the micelle (the palisade of soap molecules). It seems well established that this occurs in the solubilization of long-chain alcohols (6). Charged dye molecules, after binding with individual soap molecules, are probably solubilized also by inclusion in the palisade. As mentioned previously, these compounds upon solubilization show a zero or a negative change in slope. The lack of change in slope with concentration in the polycyclics does not necessarily indicate that the polynuclear hydrocarbon forms a part of the palisade of soap molecules in the micelle, but it may be explained on the basis that little or no energy is contributed by the solubilized polycyclic as to van der Waals attraction to enhance the energy necessary for micelle formation. The increase in slope in solubilization of simpler hydrocarbons must be due, in part at least, to this enhancement of van der Waals attractive forces, owing to the presence of the hydrocarbons in the region of the soap hydrocarbon tails.

Effect of unsaturation and cyclization on solubilization

A comparison of the various groups of compounds in table 3 indicates that there is an enhanced solubilization upon unsaturation, as can be seen by a comparison of benzene and cyclohexane, hexatriene and *n*-hexane, and styrene and ethylbenzene. Further, one unsaturated ring in the compound increases its solubility when compared to an alkane of the same number of carbon atoms. Thus, benzene, toluene, etc. are almost three times as soluble in 0.63 *N* KC_{12} as *n*-hexane, *n*-heptane, etc.

However, the presence of a second ring, as in the substituted biphenyl, or, more particularly, in the polycyclic, naphthalene, causes a change in the opposite direction so that these compounds are even less soluble than the normal paraffin of about the same molecular weight. Thus, naphthalene is much less soluble in KC_{12} solutions than either *n*-decane or *n*-butylbenzene. Preliminary studies on tetralin and decalin indicate that both are more soluble than naphthalene, with decalin slightly more soluble than the two other compounds (17).

Although cyclohexane is less soluble than benzene, owing probably to the more polar, partial double bonds in the latter compound (also possibly owing to the smaller size of the benzene molecule), it is much more soluble than the linear *n*-hexane.

Effect of length and molar volume of molecule on solubility

No simple linear relationship as indicated between volume of oil solubilized and the molar volume for the alkylbenzene and normal paraffin series (23) can be obtained in the case of solubilization of the polycyclics. However, as can be seen in figure 7, a plot of the log solubility of various polycyclics as a function of length of the molecule along its major axis yields a fairly straight line.

Deviations from linearity are most marked in the case of the more highly condensed polycyclics, for the lengths of these molecules are about equal to their more nearly linear "parent" polyacenes. Thus, the solubility per liter of 0.5 N KC_{12} of acenaphthene is 6.48×10^{-3} and of naphthalene 33.3×10^{-3} moles; that of pyrene 2.24×10^{-3} and that of triphenylene 0.336×10^{-3}, as compared with the solubility of phenanthrene of 6.65×10^{-3} moles. The two compounds which are structurally very similar and also of the same length, chrysene and 1,2-benzanthracene, are seen to have essentially the same solubility values.

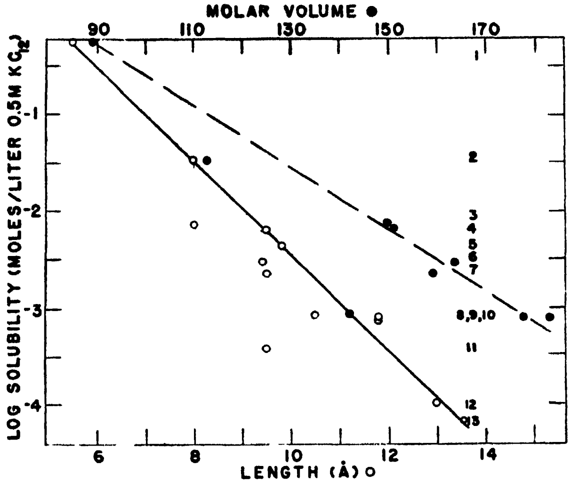

FIG. 7. Variation of solubility in potassium laurate solutions with molar volume and length. 1, benzene; 2, naphthalene; 3, acenaphthene; 4, phenanthrene; 5, fluorene, 6, fluoranthrene; 7, pyrene; 8, anthracene; 9, chrysene; 10, 1,2-benzanthracene; 11, triphenylene; 12, naphthacene; 13, 1,2,5,6-dibenzanthracene.

There are two curves which may be drawn through the solubility–molar volume data, one for the linear polyacenes, benzene, naphthalene, anthracene, which will coincide essentially with the log S–length curve, and the other for the nonlinear *cata-* and the *peri*-polycyclics. Variations from these two curves are less than those of the highly condensed *peri* compounds from the log S–length curve. It should be noted that essentially the same division into two curves is required in the case of plots obtained from log S–molar volume data of the solubility of the polycyclics in water.

A linear increase in expansion in Å. per mole of hydrocarbon per mole of soap with molar volume of normal paraffins and another with the alkylbenzenes has been noted from the extensive x-ray studies on the increase in long spacing with added hydrocarbon of Hughes, Sawyer, and Vinograd (8). A similar attempt to treat solubilization data (volume of hydrocarbon per unit soap concentration as a function of molar volume) resulted in considerable scatter of points about the linear plot (23). The volume of hydrocarbon solubilized in the polycyclic series falls rapidly with increase in number of rings in the compound, as seen in table 4, and no linear relationship can be observed. Attempts to find some linear dependence of log volume as a function of length or molar volume of the polycyclic resulted in much more scattering of points about the best line drawn through these data than that observed in a similar plot of solubility.

No correlation of solubility could be found with area or volume occupied per polycyclic molecule, assuming that the area or volume had for its major axis the distance equivalent to the length along the major axis.

TABLE 4

Solubility of various hydrocarbons in 0.5 M KC_{12} *(25°C.)*

(Corrected for water solubility)

COMPOUND	GRAMS OF OIL PER LITER OF SOAP SOLUTION	S MOLES OF OIL PER LITER OF SOAP SOLUTION ($\times 10^3$)	LOG S	MOLECULES OF OIL PER MICELLE	MOLECULFS OF OIL PER MICELLE (CORRECTED)	VOLUME OF OIL (ML. PER LITER OF SOAP SOLUTION)
Benzene	30.6	391	−0.41	118	123	34.3
Ethylbenzene	22.0	208	−0.68	63	66	25.6
n-Butylbenzene	14.9	112	−0.95	33	36	17.3
Naphthalene	4.26	33.3	−1.48	10	10.4	3.72
Acenaphthene	1.00	6.48	−2.19	2.0	2.1	0.975
Fluorene	0.728	4 38	−2.36	1.3	1.4	
Phenanthrene	1.21	6.65	−2.18	2.0	2.1	1.03
Anthracene	0.155	0.85	−3.07	0.26	0.27	0.123
Fluoranthrene	0.578	2.86	−2.54	0.86	0.90	0.469
Pyrene	0.453	2.24	−2.65	0.68	0.71	0.345
Chrysene	0.143	0.627	−3.20	0.19	0.20	0.102
1,2-Benzanthracene	0.145	0.635	−3.20	0.19	0.20	0.117
Triphenylene	0.0765	0.336	−3.47	0.10	0.11	
Naphthacene ..	(0.023)*	(0.10)*	(−4.0)*	0.030	0.032	
Methylcholanthrene	0.087	0.323	−3.49	0.10	0.10	
1,2,5,6-Dibenzanthracene.	0.024	0.0862	−4.06	0.026	0.027	

* Approximate value.

DISCUSSION

The low concentrations of the polycyclic hydrocarbons with $n \geqq 4$ (n = number of rings) solubilized even at soap concentrations of 0.5–0.6 *M* indicate that at the concentrations of materials (about 1 per cent) in the blood capable of acting as solubilizing agents (sterols, fatty acids, lipoproteins, etc.), there is only a minute amount of the polycyclic carried from point of primary injection by these agents to the region of the body where cancerous growth is noted. This concentration solubilized is probably somewhat larger than the amount soluble in the fatty acid soaps, for the solubility of 1,2-benzanthracene, for example, is about doubled when sodium taurocholate is used in place of potassium laurate. Further, it has been found that the "choleic" acid principle holds in the solubilization of the polycyclics, for certain mixtures of bile salts and fatty acid soaps are more active as solubilizers than either of the individual components (17).

Extremely minute amounts of carcinogenic agents have been "dissolved" and then utilized to bring about tumor formation in the brain cavity even when the polycyclic hydrocarbons in the form of minute crystals have been injected through the skull and laid on the meninges (membrane covering the brain), a region of very high phospholipid concentration (20). This further indicates that very few carcinogenic hydrocarbons are necessary for collision and possible binding with that portion of the cell concerned with control of the kinetics of cell division and reproduction.

The fact that the number of molecules of oil solubilized per micelle is constant in the case of the polycyclics and that there is a continuous decrease in this constant value with increase in size of the hydrocarbon through phenanthrene indicates that micelles of about 150 soap molecules play a role in the solubilization of these polyacenes. The fact, as seen in tables 2 and 4, that for anthracene and for those polycyclics with $n \geq 4$ only a fraction of a hydrocarbon molecule can be solubilized per 150-molecule micelle, indicates that there must be present, in these systems, micelles of larger size. The number of these larger micelles would be extremely small and probably would be found only when insoluble compounds as the $n \geq 4$ polycyclics are present.

TABLE 5

Probable size of micelle necessary for solubilization of polycyclic hydrocarbons

(N = number of soap molecules per micelle)

COMPOUND	MOLECULES OF OIL PER MICELLE (150 MOLECULES)	N	D
			Å.
Benzene	118	150	60
Naphthalene	10	150	60
Acenaphthene	2.0	150	60
Phenanthrene	2.0	150	60
Anthracene	0.26	600	120
Fluoranthrene	0.86	175	65
Pyrene	0.68	220	73
Chrysene	0.19	790	138
1,2-Benzanthracene	0.19	790	138
Triphenylene	0.10	1500	190
Naphthacene	0.030	5000	360
Methylcholanthrene	0.10	1500	190
1,2,5,6-Dibenzanthracene	0.026	6000	390

The number of soap molecules per micelle, N, necessary to account for the solubilization of these polycyclics are seen in table 5. On the basis that each soap molecule occupies about 30 Å.^{2} and that the soap micelle is a cylinder composed of two layers of soap molecules, the diameters, D (Å.), of these probable aggregates have been calculated and collected in table 5. The presence of any appreciable amount of particles of diameters of 300–400 Å. would result in a turbid system if the refractive indices of the large micelles were sufficiently different from those of the balance of the system (water, free soap, smaller micelles). These systems, at equilibrium, were quite transparent, owing probably to a negligible refractive index increment. It has been found, for example, that the refractive index of "free" potassium laurate is about 1.495, whereas that of the fully formed micelle (above about 0.15 *M*) is constant and equal to about 1.490 (11). If a molecule of polycyclic hydrocarbon were solubilized in this very large aggregate, the total refractive index of this latter particle would not be sufficiently different from the refractive index of the medium (water, "free" soap, normal micelles) to result in any apparent opacity.

An attempt has been made to extend these measurements to include the *peri*-polycyclics, anthanthrene ($n = 6$) and coronene ($n = 7$), but after shaking intermittently for 6 to 8 months, no consistent results have as yet been obtained. The solubility of these compounds in water was too small to determine by the present methods and this might be one of the factors complicating the determination of solubilization of these polycyclics.

That there is no definite layering and orientation of polycyclic hydrocarbons such as naphthalene or benzene within the micelle can be assumed, for no observable differences in spectra could be found between naphthalene in a nonpolar solvent and in the micelle. Any observed spectral changes would be due to electronic resonance between molecules such as is observed in various cyanine dyes (9, 22) or in the starch–iodine complex (24). The complete absence of this type of spectral change would indicate that the density of the polycyclics in the micelle is equal to or less than their bulk density.

The possibility of micelles of about 5000 soap molecules which would be capable of solubilizing a molecule of dibenzanthracene is not difficult to accept, for Professor Debye (private communication) has mentioned alkylamine hydrochloride systems containing an added electrolyte which show a blue Tyndall effect. This would indicate particles of the order of magnitude of 200–500 Å. It is, of course, not known whether these systems are aggregates of micelles, not capable of acting like a single large micelle, which must be present just before salting-out occurs.

No quantitative data are available at the present time regarding the solubility of the $n \geq 4$ polycyclics in hydrocarbons such as *n*-hexane, which might present an atmosphere similar to that which occurs in the micelle. It is known, however, that the solubility of these polyacenes is extremely low in these solvents, but the order of magnitude is not known.

It does not seem necessary to look for another type of mechanism of solubilization to explain the apparently large micelles calculated here. Rather, it should be sufficient to recognize the fact that each molecule of dibenzanthracene, for example, requires a certain critical volume of hydrocarbon atmosphere for its solubility. This atmosphere can only be supplied by a large aggregate of soap molecules. The smaller aromatics, such as benzene and naphthalene, need a much smaller volume of hydrocarbon per solubilized molecule and thus many more can fit into a single swollen micelle.

SUMMARY

The log of the solubility (S) in water of the condensed polycyclic hydrocarbons from $n = 1$ to $n = 5$ (n = number of rings) decreases linearly with the length (L) of the molecule. In contrast to the alkylbenzene series, where the volume of oil solubilized at one particular soap concentration decreases approximately linearly with L or the molar volume, a linear decrease for the condensed ring systems is obtained only with a log S *vs.* L curve. Two curves are necessary to obtain linearity of log S *vs.* molar volume, one for the linear polyacenes, benzene, naphthalene, anthracene, ..., and the other for the nonlinear polycyclics. The differential change in the slope of S as a function of concentration curves is seen to be largest with benzene, decreasing with increase in substitution through toluene, ethylbenzene, and *n*-butylbenzene and becoming equal to zero for the condensed-ring polycyclics, similar to the results obtained in the case of dye solubilization. Solubilization data of the alkylbenzenes, naphthalene, phenanthrene, and dimethylaminoazobenzene are in accord with the concept of the expanded hydrocarbon-containing micelle (as advanced by x-ray measurements), for one or more molecules of hydrocarbon can be solubilized per micelle. However, for polycyclics such as anthracene and those with $n \geq 4$, a larger micelle than that of the above size would be required for solubilization per polycyclic molecule.

REFERENCES

(1) Corrin, M. L., Klevens, H. B., and Harkins, W. D.: J. Chem. Phys. **14**, 480 (1946).

(2) Davis, W. W., Krahl, M. E., and Clowes, G. H. A.: J. Am. Chem. Soc. **64**, 108 (1942).

(3) Debye, P.: J. Colloid Sci. **3**, 407 (1948); J. Phys. & Colloid Chem. **53**, 1 (1949).

(4) For recent review, see Haddow, A.: Brit. Med. Bull. **4**, 331 (1947)

(5) Harkins, W. D., and Oppenheimer, H.: J. Am. Chem. Soc. **71**, 808 (1949).

(6) Harkins, W. D., and Mittelmann, R.: J. Colloid Sci. **4**, 367 (1949).

(7) Heller, W., and Klevens, H. B.. J. Chem. Phys. **14**, 567 (1946).

(8) Hughes, E. W., Sawyer, W. M., and Vinograd, J. R.: J. Chem. Phys. **13**, 131 (1945).

(9) Jelley, E. E.: Nature **139**, 631 (1937).

(10) Jones, R. N.: Chem. Revs. **32**, 1 (1943).

(11) Klevens, H. B.: J. Chem. Phys. **14**, 567 (1946).

(12) Klevens, H. B.: J. Phys. & Colloid Chem. **52**, 130 (1948).

(13) Klevens, H. B., and Platt, J. R.: J. Chem. Phys. **17**, 470 (1949).

(14) Klevens, H. B.: Paper presented at the Twenty-second National Colloid Symposium, which was held under the auspices of the Division of Colloid Chemistry of the American Chemical Society at Cambridge, Massachusetts, June, 1948.

(15) Klevens, H. B.: Paper presented at the 112th meeting of the American Chemical Society, which was held in New York City, September 15–19, 1947; J. Am. Oil Chemists' Soc. **26**, 456 (1949).

(16) Klevens, H. B.: J. Chem. Phys. **17**, 1004 (1949).

(17) Klevens, H. B.: Unpublished data.

(18) McBain, J. W.: *Advances in Colloid Science*, Vol. I. Interscience Publishers, Inc., New York (1942).

(19) MATTOON, R. W., STEARNS, R. S., AND HARKINS, W. D.: J. Chem. Phys. **16**, 644 (1948).
(20) MOORE, G. E.: Science **106**, 130 (1947); also private communication.
(21) PAULING, L. S.: *The Nature of the Chemical Bond*, 2nd edition. Cornell University Press, Ithaca, New York (1940).
(22) SCHEIBE, G.: Angew. Chem. **52**, 631 (1939).
(23) STEARNS, R. S., OPPENHEIMER, H., SIMON, E., AND HARKINS, W. D.: J. Chem. Phys. **15**, 496 (1947).
(24) STEIN, R. S., AND RUNDLE, R. E.: J. Chem. Phys. **16**, 195 (1948).

THE SYSTEM Na_2O–SiO_2–H_2O: ISOTHERMS AT 10° AND 31°C.

C. L. BAKER

Philadelphia Quartz Company, Public Ledger Building, Philadelphia 6, Pennsylvania

AND

L. R. JUE

Philadelphia Quartz Company of California, Berkeley, California

Received March 7, 1949

INTRODUCTION

A number of papers have been published, since Harman's (3) work in 1927, showing isotherms for the Na_2O–SiO_2–H_2O system from 14° to 25°C. The latest and perhaps the best of these is that by Lange (4).

Data for isotherms at 10°C. and 31°C. are presented here. The extrapolations show definitely the salts $Na_2SiO_3 \cdot 9H_2O$, $Na_2SiO_3 \cdot 6H_2O$, $Na_2SiO_3 \cdot 5H_2O$, and $Na_3HSiO_4 \cdot 5H_2O$. In addition a very short region of existence of $Na_2SiO_3 \cdot 8H_2O$ is shown. The stable phases found have been described minutely by Baker, Woodward, and Pabst (2).

MATERIALS AND PROCEDURE

The materials and procedure used have been described by Baker and Jue (1). In addition to the materials described by them, sodium hydroxide carefully freed from carbonate by precipitation with lime was used as a source of sodium oxide in the more alkaline regions. Where the concentration of sodium oxide was high, the sodium hydroxide was recrystallized twice in the form of $NaOH \cdot H_2O$ and centrifuged inside a tight cellophane bag so as to prevent the absorption of carbon dioxide.

For points on the curve more siliceous than the sodium metasilicate, small amounts of clarified commercial sodium silicate solutions were used.

During the course of this work the microscope was used continuously to check the habit of the crystals in the solid phase. We were thus able to keep continuous check on the identity of the crystals present.

As indicated in our previous paper we were careful to repeat analyses at intervals of at least 1 week until two and preferably more analyses indicated that the system had come to equilibrium. When we were fairly certain of equilibrium from supersaturation, two or more samples of undersaturated solution containing an excess of crystals were usually prepared to check the point from undersaturation. A period of from 6 to 10 weeks was usually required to establish the true solubility, and even longer periods were necessary in the more siliceous regions. Analyses were usually made in duplicate.

Particular care was taken to determine transition points accurately. Usually, metastable points beyond the transition point were obtained in order to determine the intersection of the curves by interpolation. Then systems containing

TABLE 1

The system Na_2O–SiO_2–H_2O *at 10°C.*

STABLE SOLID PHASE	COMPOSITION OF SOLUTION		COMPOSITION OF RESIDUE	
	Na_2O	SiO_2	Na_2O	SiO_2
	per cent	*per cent*	*per cent*	*per cent*
$NaOH\cdot H_2O$	38.45 ± 0.1		52.0 ± 0.1	
Pickering's value	40.7			
$NaOH\cdot H_2O$ $Na_3HSiO_4\cdot 5H_2O$	38.3 ± 0.1		45.0	8.8
$Na_3HSiO_4\cdot 5H_2O$	38.0 ± 0.05	0.13 ± 0.02	37.07 ± 0.07	18.85 ± 0.05
	36.58	0.13	36.80	18.40
	34.20	0.14	36.50	21.61
	32.8	0.12	36.05	20.05
	29.95	0.28	36.32	22.07
	29.05	0.30	36.87	23.80
	27.74	0.66	35.93	21.57
	26.85	0.935	36.52	23.78
	26.45	1.09	36.4	23.0
$Na_3HSiO_4\cdot 5H_2O$ $Na_2SiO_3\cdot 5H_2O$ (transition point)	26.43 ± 0.05	1.04 ± 0.02		
$Na_2SiO_3\cdot 5H_2O$	27.15 ± 0.05	1.04 ± 0.02	29.12 ± 0.05	27.52 ± 0.05
Metastable	26.72 ± 0.05	1.06 ± 0.04	29.08	27.50
	25.92 ± 0.05	1.02 ± 0.02	28.8	26.55
	25.22	1.04	29.15	27.7
	24.65	1.06	28.85	26.55
Metastable	24.28	1.07	29.03	27.22
$Na_2SiO_3\cdot 5H_2O$ $Na_2SiO_3\cdot 6H_2O$ (transition point)	24.65 ± 0.05	1.05 ± 0.02		
$Na_2SiO_3\cdot 6H_2O$ Metastable	24.82 ± 0.05	1.06 ± 0.02	26.85 ± 0.05	25.47 ± 0.05
Metastable	24.72	1.05	26.80	24.4
	24.05	1.01	26.65	24.68
	23.52	1.05	26.60	24.7
Metastable	22.78	1.03	26.5	24.32
$Na_2SiO_3\cdot 6H_2O$ $Na_2SiO_3\cdot 9H_2O$ (transition point)	23.46 ± 0.05	1.05 ± 0.02		
$Na_2SiO_3\cdot 9H_2O$	23.5 ± 0.07	1.05 ± 0.03	21.75 ± 0.05	20.1 ± 0.05
	22.47	0.80	21.80	19.97
	21.40	0.64	21.68	19.93
	18.00	0.44	21.4	19.15

TABLE 1—*Concluded*

STABLE SOLID PHASE	COMPOSITION OF SOLUTION		COMPOSITION OF RESIDUE	
	Na_2O	SiO_2	Na_2O	SiO_2
	per cent	*per cent*	*per cent*	*per cent*
$Na_2SiO_3 \cdot 9H_2O$	16.32	0.38		
	14.77	0.37	21.08	18.85
	13.25	0.43	20.82	18.92
	7.88	0.67	20.82	19.55
	5.32	1.17	21.20	20.35
	4.46	1.92	21.30	20.60
	4.64	3.50		
	5.29 ± 0.10	5.11 ± 0.07	21.52	20.68
	6.63	8.69	21.72	21.22
	8.70	13.3	21.50	20.75
	9.57	15.1	21.08	20.68
	10.85 ± 0.10	18.45 ± 0.10		
	12.33 ± 0.15	21.55 ± 0.15	21.47 ± 0.1	21.10 ± 0.08
	14.75 ± 0.15	26.72 ± 0.15	21.8 ± 0.1	21.28 ± 0.10
	18.55 ± 0.2	32.18 ± 0.2	21.5 ± 0.1	23.05 ± 0.10

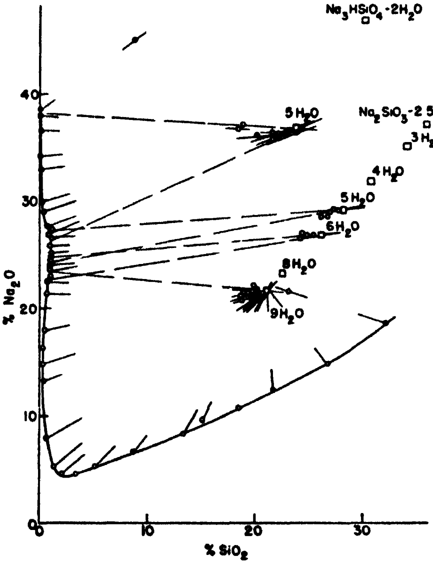

FIG. 1. The isotherm at 10°C.

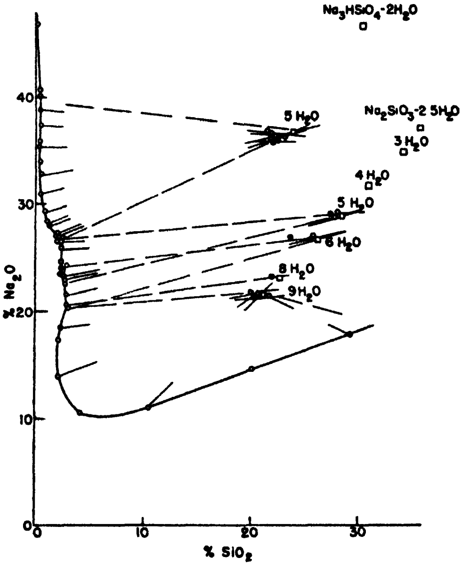

FIG. 2. The isotherm at 31°C.

both salts at the transition point were very carefully prepared and studied until it was certain that the crystals were truly in equilibrium.

DATA

The data obtained are given in table 1 and table 2 and shown in the corresponding figures 1 and 2. Compositions are given in per cent by weight. The

TABLE 2

The system Na_2O–SiO_2–H_2O *at 31°C.*

SOLID PHASE	RESIDUE		SOLUTION	
	Na_2O	SiO_2	Na_2O	SiO_2
	per cent	*per cent*	*per cent*	*per cent*
$Na_2SiO_3\cdot 9H_2O$	21.65	21.47	18.12	29.2
	21.65	21.47	18.12	29.20
	21.57		14.58	20.02
	21.70	20.90	11.14	10.48
	21.72		10.50	4.10
	21.72	20.60	13.87	2.12
	21.75		17.28	2.16
	21.78	19.91	18.48	2.27
	21.41	20.00	20.37	2.97
$Na_2SiO_2\cdot 9H_2O$ $Na_2SiO_3\cdot 6H_2O$			20.35	2.95
$Na_2SiO_3\cdot 8H_2O$	23.20	21.77	20.58	2.93
$Na_2SiO_3\cdot 6H_2O$	26.92	25.90	20.32	2.93
	26.87	25.53	21.50	2.72
	26.95		21.68	2.78
	26.92		22.40	2.73
	26.90		22.53	2.63
	27.05	25.70	23.15	2.59
	26.82	23.51	24.32	2.81
$Na_2SiO_3\cdot 6H_2O$ $Na_2SiO_3\cdot 5H_2O$			22.95	2.63
$Na_2SiO_3\cdot 5H_2O$	29.23		22.76	2.68
			22.97	2.57
	29.05	27.44	23.18	2.50
	29.25		23.42	2.33
	29.10		24.16	2.40
	29.00		24.60	2.31
	29.05		24.73	2.31
	29.10		25.91	2.23
	29.21	27.81	26.54	2.27
	29.05	27.66	25.67	2.28
$Na_2SiO_3\cdot 5H_2O$ $Na_3HSiO_4\cdot 5H_2O$			26.72	2.28
$Na_3HSiO_4\cdot 5H_2O$	36.35	22.64	26.72	2.14
	36.08	22.33	26.98	2.13
	36.41	23.00	27.21	1.82
	36.01	22.35	27.98	1.20
	36.10	21.68	28.10	1.00
	36.31	22.10	29.20	0.73

TABLE 2—*Concluded*

SOLID PHASE	RESIDUE		SOLUTION	
	Na_2O	SiO_2	Na_2O	SiO_2
	per cent	*per cent*	*per cent*	*per cent*
$Na_3HSiO_4\cdot 5H_2O$	36.27	22.00	31.07	0.43
	36.13	21.71	32.73	0.41
	36.52		33.95	0.39
	35.90	22.13	35.41	0.34
	36.20		35.72	0.37
	36.61	21.85	37.50	0.37
	36.90	21.42	38.88	0.37
$NaOH\cdot H_2O$		0.07		
	51.25	0.07	40.10	0.30
	51.41	0.08	40.60	0.26
	52.17	0.00	40.85	0.00

temperature was controlled at about 31°C. ± 0.05° and at 10°C. ± 0.2°. It is important to note how closely the extrapolated lines intersect at the composition of the solid phase. Similar work published by other authors has frequently been equivocal.

The crystals of $Na_2SiO_3\cdot 9H_2O$ grown at 10°C. changed their habit according to whether they were grown in solutions more or less alkaline at about the $3Na_2O:2SiO_2$ ratio. In the more alkaline range they appeared as flat plates, while they seemed equidimensional in the more siliceous range.

The solubility of $NaOH\cdot H_2O$ was found to be lower than that given by Pickering (5).

Particularly noteworthy is the short region of stability of the $Na_2SiO_3\cdot 8H_2O$ described by Baker *et al.*

DISCUSSION

We have tried repeatedly but without success to duplicate the appearance of the hydrated disilicate indicated by Harman. We did not find evidence at either 10°C. or 31°C. of the crystal $Na_3HSiO_2\cdot 2H_2O$ found by Sprauer and by Leidenroth at 25°C. and 20°C., respectively.

Our isotherm at 31°C. does not indicate the complexity found by Lange *et al.* at 25°C. It is difficult to judge how much the temperature has affected the condition of the nonahydrate curve. His metastable hexahydrate curve could well be an extension of a hexahydrate curve corresponding to ours.

CONCLUSIONS

Isotherms at 10°C. and 31°C. for the system Na_2O–SiO_2–H_2O have been presented. The following salts have been found as solid phases: $Na_2SiO_3\cdot 9H_2O$, $Na_2SiO_3\cdot 8H_2O$, $Na_2SiO_3\cdot 6H_2O$, $Na_2SiO_3\cdot 5H_2O$, and $Na_3HSiO_4\cdot 5H_2O$.

REFERENCES

(1) **Baker, C. L., and Jue, L. R.**: J. Phys. Chem. **42**, 165–9 (1938).
(2) **Baker, C. L., Woodward, H. T., and Pabst, A.**: Am. Mineral. **18**, 206–15 (1933).
(3) **Harman, R. W.**: J. Phys. Chem. **31**, 511–18 (1927).
(4) **Lange, H., and von Stackelberg, M.**: Z. anorg. Chem. **256**, 273–84 (1948).
(5) **Pickering, S. U.**: J. Chem. Soc. **63**, 890 (1893).

A REVIEW OF THE SYSTEM Na_2O–SiO_2–H_2O

J. H. WILLS

Philadelphia Quartz Company, Public Ledger Building, Philadelphia 6, Pennsylvania

Received March 7, 1949

INTRODUCTION

When Harman (5) published his study on the stability of sodium silicate solutions in 1927 no other work was available save that on isolated solutions such as those mentioned by Erdenbrecher (4), from which crystals had been separated. There was no evidence that equilibrium had been reached and it was impossible to use such data for determining the composition of the crystals indirectly. Sprauer (8) has since published some results at 25°C. and Lange *et al.* (6) have done careful work at 14°C. and 25°C. Leidenroth (7) has published results at 20°C. which correlate well with the data of others. He also includes some data at 60°C. and 100°C. The preceding paper by Baker and Jue (2) reports isotherms at 10°C. and 31°C.

DISCUSSION

The system is not an easy one to work out. It frequently allows the determination of metastable curves. In the siliceous ranges crystallization may be very slow and many weeks may be required to reach equilibrium. In the same range viscosities are likely to be high and separation of the liquid phase is difficult. In the alkaline range the crystals may change their habit without changing composition. Residual alkali is difficult to remove from the solid phase and may cause difficulty in analysis.

All investigators have used some form of suction to remove samples. It is important to recognize that this raises the question of evaporation losses when filtration is difficult. Baker and Jue (1, 2) did use a high-speed centrifuge on a sample enclosed against evaporation losses and contact with carbon dioxide where a thick magma or high viscosity was encountered.

Of the group who have prepared solubility curves only Harman (5) and Baker and Jue have worked on the siliceous side of the metasilicate ratio. While Harman's data on $Na_2SiO_3 \cdot 9H_2O$ appear to be satisfactory, no one else has been able to observe any indication of the hydrated disilicate. Unpublished work indicates that the so-called sodium tetrasilicate (9) is stable in this area of exceedingly viscous systems. Harman's analysis depends on three extrapolations which do not meet in a point and his method of analysis in this region is admittedly open to question.

Recently, a solution containing 19.52 per cent Na_2O and 31.62 per cent SiO_2 was analyzed after over ten years' contact at room temperature with anhydrous sodium disilicate crystals in a can lined with alkali-resistant paint. The sodium oxide content had risen to 20.06 per cent, but even this slight change may have been caused by difficulty in sampling rather than slow solution of the solid phase. This point is about on the $Na_2SiO_3 \cdot 9H_2O$ equilibrium line at 25°C.

Two other solutions were left in contact with sodium tetrasilicate (9) over the same period. Some crystal growth occurred but the change in concentration can only be accounted for by slight evaporation. One solution which gave an analysis of 13.3 per cent Na_2O and 28.7 per cent SiO_2 may be close to equilibrium, but the other at 2.84 per cent Na_2O and 10.97 per cent SiO_2 is probably still far from equilibrium. Both original solutions were prepared relatively close to the expected equilibrium line.

When plotted carefully, one of Harman's points on the $Na_2SiO_3 \cdot 6H_2O$ curve appears to be for $Na_2SiO_3 \cdot 5H_2O$ and its solubility indicates that his hexahydrate may be metastable. His $Na_3HSiO_4 \cdot 5H_2O$ curve, which he thought was $Na_2SiO_3 \cdot 2.5H_2O$, seems entirely wrong but the less hydrated $Na_3HSiO_4 \cdot 2H_2O$ curve, which Harman thought might be anhydrous metasilicate, may be about correct. Both Sprauer (8) and Leidenroth (7) have found this solid phase and it is probably stable in the region of highest alkalinity.

Sprauer did not find that $Na_2SiO_3 \cdot 9H_2O$ carried its solubility curve to as high an alkalinity but found instead a hexahydrate. This hexahydrate occurs in about the same position as the lower portion of Harman's curve. It is in fair agreement with the curve found by Leidenroth at 20°C., with the curve of Baker and Jue (2) at 10°C., and with Lange's (6) metastable curve at 14°C. Lange declares, however, that the pictures show it to be a different form of hexahydrate than that shown by Baker *et al.* (3), Erdenbrecher (4), and Lange. He intimates that Sprauer's picture may really show the nonahydrate. However, it seems likely that a continuous curve exists, combining Lange's more alkaline portion with the others. From experience with the system it is judged that Sprauer's illustration 1B was probably mainly pentahydrate.

Sprauer found evidence of the existence of $Na_2SiO_3 \cdot 5H_2O$ but he obtained no curve. His curve for $Na_3HSiO_4 \cdot 5H_2O$ is quite comparable to those of others. Sprauer may have been misled in some cases by his failure to check equilibria closer than 1 per cent sodium oxide. He was the only investigator to determine sodium by precipitation.

Lange carried out good and careful work which showed the existence of a long metastable section of the nonahydrate curve. Two points are of particular interest because, although Lange includes them in his nonahydrate curve, they appear to be part of a curve for a salt of slightly lower solubility and the wet residue extrapolations indicate that they may have been made by the octahydrate found by Baker and Jue at 31°C.

Lange's results are interesting for the long, partly metastable $Na_2SiO_3 \cdot 5H_2O$ curve and a metastable $Na_2SiO_3 \cdot 6H_2O$ curve, which is in a position different from the experience of others but similar to Harman's and may be considered a metastable extension of other data.

TABLE 1

Leidenroth's data at 20°C. as recalculated by T. R. Foltz

SOLUTION NO	NaOH	SiO_2	SPECIFIC GRAVITY	Na_2O	SiO_2	SOLID PHASE
	N	*M*		*per cent*	*per cent*	
1.	3.0	1.44	1.037	7.0	8.3	$Na_2SiO_3 \cdot 9H_2O$
2	2.7	1.06	1.035	6.3	6.1	
3	2.6	0.94	1.036	6.0	5.4	
4	2.5	0.57	1.036	5.3	3.3	
5.	2.8	0.36	1.036	6.5	2.1	
6	2.9	0.32	1.036	6.7	1.9	
7	4.1	0.21	1.036	9.5	1.2	
8	6.4	0.18	1.036	14.8	1.0	
9	8.6	0.26	1.039	19.9	1.5	
10	9.0	0.29	1.039	20.8	1.5	$Na_2SiO_3 \cdot 6H_2O$
11	9.5	0.35	1.040	22.0	2.0	
12	9.5	0.34	1.040	22.0	2.0	
13	9.7	0.37	1.040	22.4	2.1	
14	10.2	0.35	1.040	23.6	2 0	
15	10.5	0.35	1.040	24.2	2.0	
16	10.8	0.37	1.040	24.9	2.1	
17	11.0	0.36	1.041	25.4	2.1	
18	11.4	0.38	1.041	26.3	2 2	
19	11.7	0.43	1.041	27.0	2.5	
20.	12.1	0.28	1.042	27.9	1.6	$3Na_2O \cdot 2SiO_2 \cdot 12H_2O$
21.	12.4	0.22	1.041	28.6	1.3	
22	14.7	0.07	1.043	33.8	0.4	
23	15.0	0.06	0.043	34.5	0.3	
24.	17.0	0 06	0.044	39.1	0.3	
25	17.7	0.06	0.044	40.7	0.3	
26.	18.3	0.05	0.045	42.0	0.3	
27	18.6	0.06	0.045	42.7	0.3	
28	18.6	0.06	0.045	42.7	0.3	
29	19.7	0.05	0.046	45.2	0.3	$NaOH \cdot H_2O$

Leidenroth did his work at 20°C. ±0.1°. He made check analyses from time to time until equilibrium was reached. Two analyses appear to have been obtained with a $Na_2SiO_3 \cdot 5H_2O$ solid phase and these would indicate that the hexahydrate is metastable with respect to the pentahydrate. He also carried out a number of determinations at approximately 20°C. but without determining the equilibrium composition. These indicate the existence of $Na_2SiO_3 \cdot 5H_2O$ and

$Na_2SiO_3 \cdot 6H_2O$ in about the same positions as found by Baker and Jue. He also found the existence of two hydrates of sodium sesquisilicate which he believed to be slightly more hydrous than our analyses indicate.

Leidenroth erroneously concluded that it was not possible to use colloidal waterglass to make up solutions for use in investigation of solubility relations. While there is no conclusive evidence to present, it is believed that the use of solutions prepared from the colloidal liquids may tend to produce different crystal phases than those which would appear when the solutions are prepared from the usual $Na_2SiO_3 \cdot 9H_2O$, for instance. However, we believe that when seeds are used to initiate crystallization, there is no substantial variation in results.

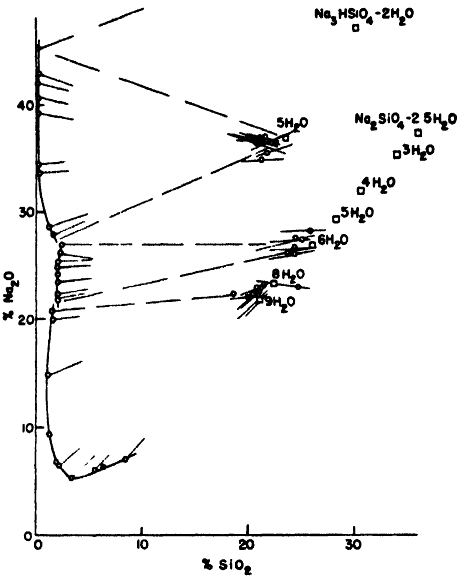

FIG. 1

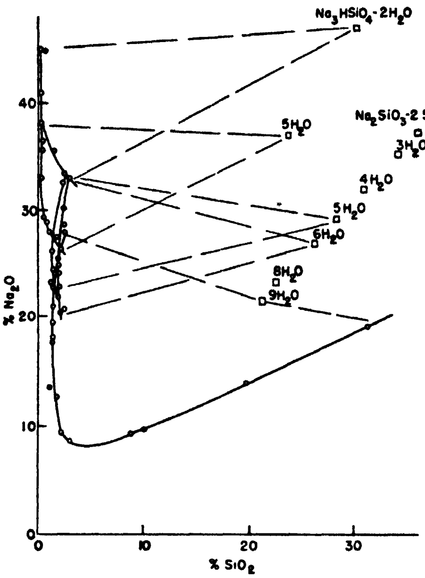

FIG. 2

FIG. 1. Leidenroth's data for the isotherm at 20°C. as recalculated on a weight per cent basis by T. R. Foltz.

FIG. 2. A composite curve for the isotherm at 25°C.

Leidenroth expressed his results in normalities. We are indebted to T. R. Foltz for his calculation of the most probable specific gravities of the equilibrium solutions obtained by Leidenroth and for his recalculation of the results on the percentage basis used by other investigators (table 1). For convenience, these have been plotted in figure 1.

The isotherm at 14°C. obtained by Lange seems to be essentially correct as far as it goes and comparable to curves established by the other references. Lange pointed out that Harman's $Na_2SiO_3 \cdot 2.5H_2O$ and Erdenbrecher's $Na_2SiO_3 \cdot 4H_2O$ are undoubtedly $Na_3HSiO_4 \cdot 5H_2O$. Pictures by Sprauer, Erdenbrecher, and Lange support this finding. Leidenroth actually repeated Erdenbrecher's experiment and obtained $Na_3HSiO_4 \cdot 5H_2O$ rather than $Na_2SiO_3 \cdot 4H_2O$.

TABLE 2

Composite 25°C. isotherm

PER CENT BY WEIGHT		SOLID PHASE	SOURCE
Na_2O	SiO_2		
19.32	31.33	$Na_2SiO_3 \cdot 9H_2O$	Harman
14.11	19.65	$Na_2SiO_3 \cdot 9H_2O$	Harman
9.65	10.1	$Na_2SiO_3 \cdot 9H_2O$	Sprauer
9.37	8.74	$Na_2SiO_3 \cdot 9H_2O$	Harman
8.69	2.93	$Na_2SiO_3 \cdot 9H_2O$	Sprauer
9.45	2.22	$Na_2SiO_3 \cdot 9H_2O$	Harman
12.7	1.82	$Na_2SiO_3 \cdot 9H_2O$	Lange
17.8	1.46	$Na_2SiO_3 \cdot 9H_2O$	Sprauer
18.2	1.42	$Na_2SiO_3 \cdot 9H_2O$	Lange
19.5	1.45	$Na_2SiO_3 \cdot 9H_2O$	Lange
21.1	1.50	$Na_2SiO_3 \cdot 9H_2O$	Lange
22.9	1.64	$Na_2SiO_3 \cdot 9H_2O$	Lange
24.9	1.88	$Na_2SiO_3 \cdot 9H_2O$	Lange
26.5	2.14	$Na_2SiO_3 \cdot 9H_2O$	Lange
27.9	2.59	$Na_2SiO_3 \cdot 9H_2O$	Lange
23.0	1.6	$Na_2SiO_3 \cdot 9H_2O$ and $Na_2SiO_3 \cdot 5H_2O$	
25.5	2.0	$Na_2SiO_3 \cdot 9H_2O$ and $Na_2SiO_3 \cdot 6H_2O$	
20.6	2.18	$Na_2SiO_3 \cdot 6H_2O$	Sprauer
20.7	2.39	$Na_2SiO_3 \cdot 6H_2O$	Sprauer
21.8	1.97	$Na_2SiO_3 \cdot 6H_2O$	Sprauer
22.9	1.98	$Na_2SiO_3 \cdot 6H_2O$	Sprauer
24.2	2.04	$Na_2SiO_3 \cdot 6H_2O$	Sprauer
27.52	1.84	$Na_2SiO_3 \cdot 6H_2O$	Harman
28.8	2.49	$Na_2SiO_3 \cdot 6H_2O$	Lange
30.3	2.50	$Na_2SiO_3 \cdot 6H_2O$	Lange
33.02	2.92	$Na_2SiO_3 \cdot 6H_2O$	Harman
22	2.0	$Na_2SiO_3 \cdot 6H_2O$ and $Na_2SiO_3 \cdot 5H_2O$	
23.3	1.59	$Na_2SiO_3 \cdot 5H_2O$	Lange
24.6	1.51	$Na_2SiO_3 \cdot 5H_2O$	Lange
26.2	1.39	$Na_2SiO_3 \cdot 5H_2O$	Lange
27.3	1.54	$Na_2SiO_3 \cdot 5H_2O$	Lange
32.4	2.43	$Na_2SiO_3 \cdot 5H_2O$	Lange
26.5	1.9	$Na_2SiO_3 \cdot 6H_2O$ and $Na_3HSiO_4 \cdot 5H_2O$	
27.7	1.4	$Na_2SiO_3 \cdot 5H_2O$ and $Na_3HSiO_4 \cdot 5H_2O$	
26.4	2.07	$Na_3HSiO_4 \cdot 5H_2O$	Sprauer
27.2	1.55	$Na_3HSiO_4 \cdot 5H_2O$	Sprauer
27.8	0.76	$Na_3HSiO_4 \cdot 5H_2O$	Lange

TABLE 2.—*Concluded*

PER CENT BY WEIGHT		SOLID PHASE	SOURCE
Na_2O	SiO_2		
27.9	1.01	$Na_3HSiO_4 \cdot 5H_2O$	Sprauer
28.9	0.75	$Na_3HSiO_4 \cdot 5H_2O$	Sprauer
29.2	0.47	$Na_3HSiO_4 \cdot 5H_2O$	Lange
33.0	0.34	$Na_3HSiO_4 \cdot 5H_2O$	Sprauer
36.7	0.30	$Na_3HSiO_4 \cdot 5H_2O$	Sprauer
37.1	0.38	$Na_3HSiO_4 \cdot 5H_2O$	Sprauer
38	0.6	$Na_3HSiO_4 \cdot 5H_2O$ and $Na_3HSiO_4 \cdot 2H_2O$	
35.4	1.6	$Na_3HSiO_4 \cdot 2H_2O$	Sprauer
41.0	0.34	$Na_3HSiO_4 \cdot 2H_2O$	Sprauer
44.78	0.85	$Na_3HSiO_4 \cdot 2H_2O$	Harman

THE MOST PROBABLE CURVE AT 25°C.

Only Lange and Harman determined the $Na_2SiO_3 \cdot 9H_2O$ curves from undersaturation and they agree quite well on the intersection of the $Na_2SiO_3 \cdot 9H_2O$ curve with that for $Na_2SiO_3 \cdot 6H_2O$. Apparently Lange determined some points on his curves from both under- and over-saturation. Baker and Jue also checked their equilibria carefully in this way. The other investigators apparently determined all points from supersaturation. The points of intersection for the $Na_2SiO_3 \cdot 9H_2O$ curve with that of $Na_2SiO_3 \cdot 6H_2O$ follow a smooth line on the stability diagram except for the results of Lange. However, the temperature shift of the solubility curves of $Na_2SiO_3 \cdot 6H_2O$ and $Na_2SiO_3 \cdot 5H_2O$ is such as to suggest that the line separating the fields for $Na_2SiO_3 \cdot 9H_2O$ and $Na_2SiO_3 \cdot 6H_2O$ may not be a smooth curve and that the composite curves as shown in figure 2 are correct.

These composite curves at 25°C. were made up from the data shown in table 2. The $Na_2SiO_3 \cdot 5H_2O$ curve was found not to cross the $Na_2SiO_3 \cdot 6H_2O$ curve, at least above 22 per cent Na_2O and 2 per cent SiO_2. Sprauer's $Na_2SiO_3 \cdot 6H_2O$ curve appears to be a metastable extension of that of Lange and Harman. The actual intersection of the curve for $Na_2SiO_3 \cdot 9H_2O$ with that for $Na_2SiO_3 \cdot 6H_2O$ should be studied from over- and under-saturation.

The stability fields from 0°C. to 31°C. were plotted on the basis of sodium oxide. This plot demonstrated clearly that additional work is needed to complete this system from a theoretical point of view. In the most highly alkaline ranges the data are very sketchy. Only the lines separating the fields of $Na_2SiO_3 \cdot 9H_2O$ and $Na_2SiO_3 \cdot 6H_2O$, $Na_2SiO_3 \cdot 5H_2O$ and $Na_3HSiO_4 \cdot 5H_2O$, $Na_2SiO_3 \cdot 6H_2O$ and $Na_3HSiO_4 \cdot 5H_2O$, and $Na_2SiO_3 \cdot 6H_2O$ and $Na_2SiO_3 \cdot 5H_2O$ have more than two points and the points at 25°C. for lines separating $Na_2SiO_3 \cdot 5H_2O$ from $Na_3HSiO_4 \cdot 5H_2O$ and $Na_2SiO_3 \cdot 9H_2O$ from $Na_2SiO_3 \cdot 6H_2O$ are questionable in view of the composite curve determined. A plot has not been included because the lines are so uncertain.

CONCLUSIONS

1. A composite isotherm at 25°C. has been prepared to correlate previous work.
2. Data for Leidenroth's isotherm at 20°C. have been recalculated and plotted for comparison with the work of others.
3. The system from 10°C. to 31°C. has been surveyed critically and it is concluded that the following salt phases are stable under some conditions: $Na_2SiO_3 \cdot 9H_2O$, $Na_2SiO_3 \cdot 8H_2O$, $Na_2SiO_3 \cdot 6H_2O$, $Na_2SiO_3 \cdot 5H_2O$, $Na_3HSiO_4 \cdot 5H_2O$, $Na_3HSiO_4 \cdot 2H_2O$.

REFERENCES

(1) Baker, C. L., and Jue, L. R.. J. Phys. Chem. **42**, 165-9 (1938).
(2) Baker, C. L., and Jue, L. R : J. Phys. & Colloid Chem. **54**, 299 (1950).
(3) Baker, C. L., Woodward, H. T., and Pabst, A.: Am. Mineral. **18**, 206-15 (1933).
(4) Erdenbrecher, A. H.: Z. anorg. allgem. Chem. **124**, 339-54 (1922).
(5) Harman, R. W : J. Phys. Chem. **31**, 511-18 (1927).
(6) Lange, H., and von Stackelberg, M.: Z. anorg. Chem. **256**, 273-84 (1948).
(7) Leidenroth, K.: "Ein Beitrag zur Kenntnis der Natrium Silikate," Inaugural Dissertation, Martin Luther University, Halle-Wittenberg, June 29, 1939.
(8) Sprauer, J. W., and Pearce, D. W.: J. Phys. Chem. **44**, 909-16 (1940).
(9) Wegst, W. F., and Wills, J. H.: U. S. patent 2,179,806 (1939); U. S. reissue 23,043 (1948).

THE ACTIVITY COEFFICIENTS OF THE UNDISSOCIATED PART OF WEAK ACIDS. III

Orthophosphoric Acid

W. D. LARSON

Department of Chemistry, College of St. Thomas, St. Paul, Minnesota

Received April 11, 1949

Measurements of the E.M.F. of the cells

$$H_2 \mid H_3PO_4(m), Hg_2HPO_4(s) \mid Hg \qquad (I)$$

have been made over a concentration range of 0.01 to 4.0 molal in the acid. From these results the standard E.M.F. of the electrode $Hg \mid Hg_2HPO_4(s), H_2PO_4^-$ has been evaluated, as well as the activity of the undissociated part of the acid over the concentration range covered in the experiments. Elmore, Mason, and Christensen (2) have made vapor pressure measurements by the isopiestic method on phosphoric acid, from which they computed the activity of the undissociated acid over a very wide range of concentrations. Mason and Blum (8) measured the cells

$$Pb(\text{two-phase amalgam}) \mid PbHPO_4(s), H_3PO_4(m) \mid H_2 \qquad (II)$$

and calculated the standard E.M.F. of the electrode Pb | $PbHPO_4(s)$, $H_2PO_4^-$ and the activity of the undissociated molecules of phosphoric acid. De Vries and Cohen (1) have made a study of cell I over a concentration range of 0.001 to 0.2 molal. These workers did not obtain good reproducibility of cell E.M.F.'s in their study.

EXPERIMENTAL

Phosphoric acid from Mallinckrodt was used without further purification. It was shown to be free from reducing substances. The mercury and water used were redistilled. Electrolytic hydrogen from a commercial cylinder was passed through a quartz tube at 500°C. The tube was packed with degreased copper turnings. The gas was then saturated at the temperature of the thermostat with the vapor of the solution being studied.

Mercurous phosphate was prepared by adding 0.05 *M* mercurous nitrate solution to an equal volume of well-stirred 0.5 *M* phosphoric acid solution. The white precipitate was washed several times with water, and finally with the phosphoric acid solution being studied. From the statements made by Mellor (9), it was assumed that the white precipitate might be Hg_3PO_4. To determine the composition of the product, it was analyzed essentially according to the directions given by Treadwell and Hall (11), using platinum crucibles as cathodes. Four concordant analyses gave 80.62 per cent Hg. The compound Hg_3PO_4 contains 86.36 per cent Hg, but Hg_2HPO_4 contains 80.69 per cent Hg. These results are in agreement with those of De Vries and Cohen (1), and are taken as sufficient evidence that the white precipitate is Hg_2HPO_4.

The equipment for the E.M.F. measurements was that used previously (5); the Eppley standard cell had been recertified by its makers, and was compared with an unsaturated cadmium cell of the same type made and certified by the Weston Laboratories.

The temperature was 25.00°C. ± 0.05° as read from a mercury-in-glass thermometer which had been compared with a similar one certified by the National Bureau of Standards. The temperature was controlled to within 0.03°C.

The Pyrex cell vessels were of the H type; there was a stopcock in the horizontal member. It was kept closed except during the actual voltage measurements. Two platinized hydrogen electrodes were used in each cell. They were cleaned and replatinized between runs. If the two electrodes did not agree within 0.05 mv., they were cleaned and replated until such agreement was found. A fresh batch of Hg_2HPO_4 was prepared for each cell. It was washed several times with the acid solution being studied, and allowed to stand in contact with this solution and some mercury for several days before being introduced into the cell. It was found unnecessary to exclude oxygen from the cells. Cells were measured at least in duplicate, and agreed to within 0.2 mv. except at the lowest concentration (0.01 *m*) studied, where four cells were measured. The maximum difference in the E.M.F. of these four cells was a little less than 1 mv. The value of RT/F was taken from Manov, Bates, Hamer, and Acree (7).

The acid solutions were analyzed by titration with standard sodium hydroxide solution, using bromcresol green indicator (3). The titration became quite accurate when a reference solution of potassium dihydrogen phosphate was used. The volumes of reference solution and solution being titrated were made equal at the end-point. The same amount of indicator was present in each of the solutions. A precision of 0.2 per cent was attained in this way. The concentrations of several solutions were checked by gravimetric determination as $Mg_2P_2O_7$. Good agreement was obtained.

STANDARD E.M.F. OF THE MERCUROUS PHOSPHATE ELECTRODE

The electromotive force of cell I is given by

$$E = E^0 - RT/2F \ln a_{H^+}a_{H_2PO_4^-} \tag{1}$$

where the symbols have their usual significance. This equation was derived on the basis that orthophosphoric acid may be treated as a uni-univalent electrolyte at finite concentrations. The values of K_1 and K_2 (7.516×10^{-3} and 6.226×10^{-8}, respectively) show that the ratio of $H_2PO_4^-$ ion to HPO_4^{--} ion will be about 10^6, so that for our purpose the concentrations of H^+ and $H_2PO_4^-$ ions will be equal. If K_1 is the first ionization constant of the acid and a_u is the activity of the molecules, then equation 1 becomes

TABLE 1

Standard E.M.F. of the mercurous phosphate electrode

m	E_{760}	α	$RT/2F \ln K_1m(1 - \alpha)$	E^0
0.01035	0.77010	0.5989	0.12372	0.64638
0.02173	0.75652	0.4844	0.12050	0.63602
0.03050	0.75087	0.4340	0.11494	0.63593
0.05149	0.74259	0.3656	0.10675	0.63584
0.07845	0.73654	0.3184	0.10052	0.63602
0.09703	0.73310	0.2968	0.09729	0.63581

$$E = E^0 - RT/2F \ln K_1a_u \tag{2}$$

Now a_u may be set equal to $m(1 - \alpha)\gamma_u$, where m is the molality of the acid, α is the fraction ionized (for the first step), and γ_u is the activity coefficient of the undissociated part of the acid. Then equation 2 may be written

$$E = E^0 - RT/2F \ln K_1m(1 - \alpha)\gamma_u \tag{3}$$

Values of α were taken from Elmore, Mason, and Christensen (2). They were computed from conductance data, and extend only from 0.01 to 0.10 m. In line with our previous methods, γ_u has been assigned a value of 1 (4, 5, 6). This is of course arbitrary (12). The values of E^0 thus obtained are tabulated in table 1. It may be seen that (except for the most dilute solution) the E^0 values are sensibly constant. Our assumption concerning γ_u, while not necessarily correct, gives constant E^0 values; this means that γ_u does not vary over the concentration range covered here.

Attempts were made to compute the standard E.M.F. from equation 1, setting the activities of H^+ and $H_2PO_4^-$ equal to each other. The ionic strength was taken as αm (the use of molalities at low ionic strengths instead of molarities will not introduce a large error), and ionic activity coefficients were computed from the Debye–Hückel limiting law. The values of E^0 thus obtained varied systematically from 0.6344 v. at 0.02 m to 0.6372 v. at 0.10 m.

Similarly, when the a_u values of Elmore, Mason, and Christensen (2) were substituted into equation 2, unsatisfactory E^0 values were obtained.

TABLE 2

Activity of orthophosphoric acid

m	E	a_u (THIS WORK)	a_u*	a_u†
0.02	0.7568	0.01154	0.01045	0.01031
0.03	0.7509	0.01771	0.01758	0.01738
0.05	0.7429	0.03200	0.03331	0.03291
0.08	0.7359	0.05521	0.05913	0.05851
0.10	0.7329	0.06973	0.07779	0.07688
0.20	0.7228	0.1530	0.1708	0.1605
0.30	0.7171	0.2386	0.2675	0.2493
0.40	0.7128	0.3336	0.3666	0.3417
0.60	0.7071	0.5199	0.5809	0.5360
0.80	0.7029	0.7211	0.8132	0.7425
1.0	0.6999	0.9108	1.060	0.9615
2.0	0.6900	1.965	2.585	2.275
4.0	0.6802	4.223	7.600	6.461

* Mason and Blum (8).

† Elmore, Mason, and Christensen (2).

Thus, the value 0.6359 v. has been selected as the standard E.M.F. of cell I, from the results reported in table 1.

ACTIVITY AND ACTIVITY COEFFICIENTS OF THE UNDISSOCIATED PART OF THE ACID

On account of the method used for computing E^0, the γ_u values computed from the results up to 0.10 m will be 1. Above 0.1 m there cannot be computed values of γ_u, since accurate values of α are known only up to 0.1 m. Accordingly, following the lead of Mason and coworkers, values of a_u are presented in table 2. They were computed using equation 2 and $E^0 = 0.6359$ v. with Nims' value for K_1 (10). The last two columns contain data from E.M.F. and from vapor pressure measurements, respectively, of Mason *et al.* (2, 8). The values of E, the electromotive force of the cells at round concentrations, were taken from a plot of E against the logarithm of the molality. This plot was linear, except for the most dilute solution used (0.01 m).

DISCUSSION

Whether the value assigned to the standard E.M.F. of cell I in this paper is the correct value depends upon our hypothesis about the activity coefficient of the undissociated part of the weak acid. It seems from the results presented in table 1 that this quantity does not change enough to be evident from E.M.F. measurements over the concentration range from 0.02 to 0.1 m. There does not seem to be any way to determine the true value of the activity coefficient without reference to some hypothesis. Among these hypotheses the simplest one has been chosen: namely, that γ_u will have a value of 1 at low ionic strengths.

No claim is made that the values of a_u reported in this paper are better than those given by Elmore, Mason, and Christensen (2). They are presented only for comparison. The values resulting from the measurements reported in this paper do not depend upon the limiting law of Debye and Hückel. Those of Mason (2, 8) appear to depend upon an ionic activity coefficient for 0.1 m phosphoric acid. The ionic strength of this solution is about 0.03. It is not certain that the limiting law may be applied to ions in solutions as concentrated as this.

Corrections for the solubility of the mercurous phosphate were not made, since no data are available for this purpose. If it be granted that the salt is a slightly soluble one, then a treatment (assuming that the degree of ionization of the acid is not affected by it) similar to that given by Larson and MacDougall (4) shows that no error is introduced by this slight solubility, and therefore no corrections for it are needed.

It seems likely that the reason for the discrepancy in the E-value for the most dilute solution in table 1 may be that a basic mercurous phosphate begins to form at low acid concentrations.

SUMMARY

1. When a mercurous nitrate solution is added to one of orthophosphoric acid, the white precipitate formed has a percentage ot mercury which corresponds to the formula Hg_2HPO_4.

2. The standard E.M.F. of the $Hg \mid Hg_2HPO_4(s), H_2PO_4^-$ electrode is -0.6359 v. at 25°C.

3. The activity coefficient of the undissociated part of the orthophosphoric acid does not change from 0.02 to 0.1 m.

4. The activity of the undissociated part of orthophosphoric acid has been computed from E.M.F. measurements from 0.02 to 4 m.

REFERENCES

(1) De Vries and Cohen: J. Am. Chem. Soc. **71,** 114 (1949).
(2) Elmore, Mason, and Christensen: J. Am. Chem. Soc. **68,** 2530 (1946).
(3) Kolthoff and Sandell: *Textbook of Quantitative Inorganic Analysis*, p. 532. The MacMillan Company, New York (1936).
(4) Larson and MacDougall: J. Phys. Chem. **41,** 493 (1937).
(5) Larson and Tomsicek: J. Am. Chem. Soc. **63,** 3329 (1941).
(6) Larson and Tomsicek: J. Am. Chem. Soc. **61,** 65 (1939).
(7) Manov, Bates, Hamer, and Acree: J. Am. Chem. Soc. **65,** 1765 (1943).

(8) Mason and Blum: J. Am. Chem. Soc. **69**, 1246 (1947).

(9) Mellor: *Comprehensive Treatise on Inorganic Chemistry*, Vol. IV, p. 1002. Longmans, Green and Company, London (1929).

(10) Nims: J. Am. Chem. Soc. **55**, 1946 (1933); **56**, 1110 (1934).

(11) Treadwell and Hall: *Analytical Chemistry*, Vol. II, p. 175. John Wiley and Sons, Inc., New York (1924).

(12) Van Rysselberghe: J. Phys. Chem. **39**, 418 (1935).

OBSERVATIONS ON THE RARE EARTHS. LVI[1]

Spectrophotometric Studies on Colloidal "Lanthanum Blue"

THERALD MOELLER and GLADYS HELEN QUINTY

Noyes Chemical Laboratory, University of Illinois, Urbana, Illinois

Received April 14, 1949

INTRODUCTION

The development of an intense blue color as a result of adding iodine to hydrous lanthanum hydroxide precipitated from acetate-containing solutions was first reported by Damour (2, 3, 4). Biltz (1) obtained the same blue precipitate by treating either lanthanum acetate solutions or lanthanum nitrate solutions containing acetic acid with iodine dissolved in potassium iodide, adding ammonia just short of destruction of the yellow color, and warming. At lower concentrations, however, only clear blue "solutions" resulted. Similar blues have been obtained in the presence of the propionate ion (5) but not in the presence of a large number of other organic anions (5, 6). The behavior of the other lanthanides is somewhat obscured by controversial literature statements, but it appears that only the most basic members of the series yield corresponding blues (5, 15), ions less basic than tripositive samarium being without effect.

The conditions for the formation of blue precipitates and the properties of such materials have been investigated extensively. However, the blue "solutions" (better "sols") of Biltz have received little or no attention. While the exact natures of the precipitated blues have not been determined, their characteristics are those of colloidal gels containing adsorbed iodine. This view is supported by the extensive adsorption studies of Biltz (1) and Lottermoser (11), but it is not apparent how the combined presence of hydrous hydroxide, iodine, and acetate or propionate result in blue colorations. Such analogies as have been drawn between these systems and the starch–iodine system are no more than qualitative in nature.

Any experimental condition which favors the production of a precipitate with a highly active and well-developed surface appears to favor the formation of the insoluble blues. Thus, for best results, acetate or propionate should be present prior to precipitation (1, 5), the precipitate should be formed as a slimy and gelatinous mass (1, 5) and not be allowed to age (11), excessive heating of the suspended material should be avoided (11), and flocculating or precipitating anions (e.g., sulfate, fluoride, phosphate, etc.) should not be present (6). Optimum conditions embrace the use of lanthanum nitrate solutions containing acetate or propionate and iodine and the addition of somewhat less than an excess of ammonia with no more than gentle warming.

---

[1] For the preceding communication in this series see Moeller, T.: J. Phys. Chem. **50**, 242 (1946).

The utility of the lanthanum blue reaction as a qualitative test for iodine, acetate, or propionate (5, 6, 7, 8, 9, 10, 14, 16) plus the reported sensitivity of some 0.05 mg. for the detection of either of the two organic acids (9) suggest that the reaction may be of some quantitative significance. An obvious, but apparently unreported, approach to such a phase of the problem would involve quantitative colorimetric measurements. The precipitated blues would not lend themselves readily to such an investigation, but the blue sols of Biltz (1) would appear well adapted. The present paper summarizes spectrophotometric data obtained for such sols and sheds further light both on the sensitivity of the reaction and on the reproducibilities of such systems so necessary to analytical practice. Incidental to spectrophotometric studies on lanthanum blue sols containing acetate and propionate, evaluation of the conditions essential for the preparation of the systems, the effects of other anions, and the behavior of other lanthanides and yttrium were also investigated.

EXPERIMENTAL

A. Materials and apparatus

The yttrium and rare earth materials used were from the stocks accumulated at the University of Illinois. The yttrium sample had an average atomic weight of 91–93, and the lanthanum material contained a trace of praseodymium. Neodymium and samarium materials were of atomic weight purity. Tenth-molar nitrate solutions were prepared by dissolving the calculated weights of the freshly ignited oxides in dilute nitric acid, evaporating to dryness on the steam bath, taking up the residues in distilled water, and diluting to volume. Final standardization was effected by oxalate precipitation and ignition to weighable oxides.

Other chemicals were of analytical reagent quality. Approximately 0.1 M aqueous ammonia, acetic acid, and propionic acid solutions were prepared by diluting the stock reagents. These solutions were standardized by the usual procedures. Tenth-molar solutions of other organic acids were prepared by diluting weighed quantities of the pure acids with water. An approximately 0.05 M stock solution of iodine in potassium iodide was prepared in the usual manner and standardized frequently against arsenious acid. This was diluted to 0.001 M before being used. To obviate carbon dioxide absorption, which is so characteristic of hydrous lanthanum hydroxide sols (12, 13) and which effects their flocculation and destruction, all solutions were prepared with carbon dioxide-free water and were protected from the carbon dioxide of the atmosphere.

All spectrophotometric measurements were made with a Beckman Model DU

Spectrophotometer using 1 cm. cells. In the studies reported, only the visible region (400–700 mμ) of the spectrum was investigated.

B. Procedure

Conditions essential to the reproducible formation of blue sols were determined for both acetate and propionate systems by varying the lanthanum, acid, ammonia, and iodine concentrations individually in regular series while maintaining the others constant. Similar studies were also carried out for lanthanum systems containing formic, butyric, monochloroacetic, and trichloroacetic acids and for systems containing acetic or propionic acid and yttrium, neodymium, or samarium ions.

Spectrophotometric studies were carried out on the blue sols in the usual fashion, measurements being made only at 5–10 mμ intervals because of the absence of sharp absorption bands. Because the colors of the sols reached maximum intensities only after at least 30 min., measurements were made not less than 1 hr. after preparation of the samples. After preparation, the sols were stored in tightly stoppered containers to eliminate carbon dioxide absorption.

RESULTS AND DISCUSSION

The blue "solutions" reported by Biltz (1) have all of the characteristics of colloidal sols made up of aggregates containing hydrous lanthanum hydroxide, acetate (or propionate), and iodine. They are readily flocculated to blue precipitates by electrolytes, among them lanthanum salts and acetates or propionates when present in excessive quantities. Because of the high basicity of lanthanum hydroxide (12, 13), they absorb atmospheric carbon dioxide readily and are thereby destroyed.

Studies involving combinations of varying quantities of reagents show the close dependence of sol formation on reagent concentrations. Thus, suitable combinations for the production of stable, clear blue sols amounted to 2.5 ml. of 0.1 *M* lanthanum nitrate solution, 0.4–0.5 ml. of 0.001 *M* iodine solution, 0.5–3.5 ml. of 0.1 *M* acetic acid solution, and twice the volume of 0.1 *M* aqueous ammonia as the volume of acetic acid used. When the reagents were mixed in these quantities and shaken, reproducible blue sols developed rapidly and increased slowly in color intensity for some 30 min. Larger quantities of iodine gave brownish colors, while excessive amounts of aqueous ammonia destroyed the blue colors, probably because of reaction with the iodine. With the propionate system, only sols prepared from 2.5 ml. of 0.1 *M* lanthanum nitrate solution, 0.1–1.0 ml. of 0.001 *M* iodine solution, 2.5 ml. of 0.1 *M* propionic acid solution, and 5.0 ml. of 0.1 *M* aqueous ammonia were stable with respect to flocculation. No blue sols were obtained in any combination containing formic, monochloroacetic, trichloroacetic, or butyric acid.

Spectrophotometric studies on the acetate-containing blue sols showed them to be characterized by a single broad absorption band centering at approximately 580 mμ. Absorption spectra of the propionate-containing sols were similar except that the absorption band centered at roughly 600 mμ.

Early expectations that the intensity of absorption at these wave lengths might be dependent upon the acetate- or propionate-ion concentration in the system were not realized. On the contrary, it was found that the intensity of absorption actually decreased from a peak value as the anion concentration was increased beyond a certain limit. For the acetate-containing systems this limit amounted to approximately 0.025 mole per liter. A corresponding value was not obtained for the propionate systems, although the same general behavior was noted. It appears that for a given quantity of lanthanum ion, a certain liminal concentration of acetate (or propionate) is essential for sol formation. The colloidal systems are able to tolerate limited excesses of anions beyond these liminal values but undergo partial or complete flocculation, with attendant decrease in absorption, as the quantities added become still larger.

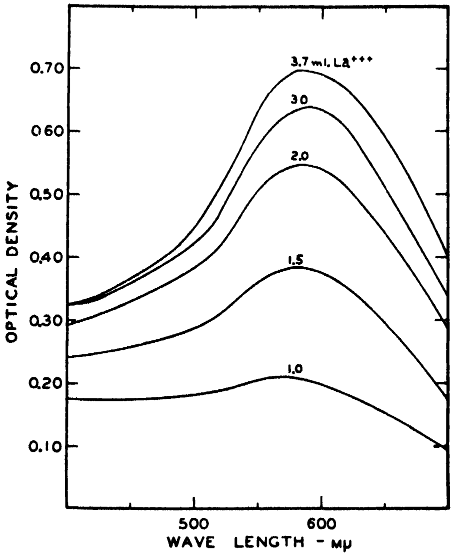

FIG. 1

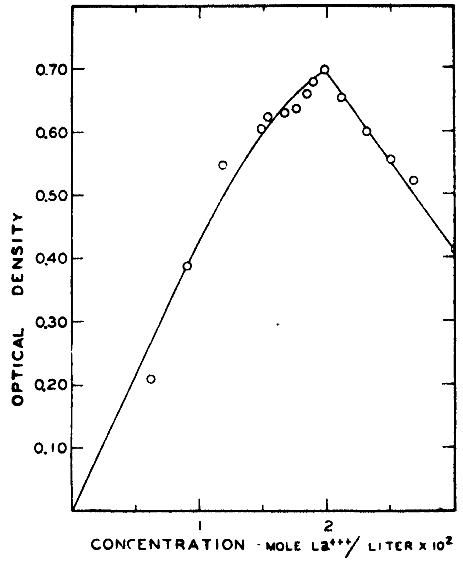

FIG. 2

FIG. 1. Effect of lanthanum ion on absorption in acetate systems

FIG. 2. Relation of absorption in acetate systems to lanthanum-ion concentration at 580 mμ

Dependence of absorption intensity upon the quantity of lanthanum ion added in systems containing acetate is shown in part in figure 1. Data plotted in this figure are from those obtained for a series in which 1.0–6.5 ml. portions of 0.1 *M* lanthanum nitrate solution were combined with 0.5 ml. of 0.001 *M* iodine solution, 5.0 ml. of 0.1 *M* acetic acid solution, and 10.0 ml. of 0.1 *M* aqueous ammonia, each combination being diluted to 25 ml. before being measured. Although absorption increases regularly with lanthanum concentration for the combinations summarized in figure 1, regular decreases in amount of absorption occurred with volumes of lanthanum nitrate solution in excess of 3.7 ml. All these variations are indicated in the Beer's law plot given in figure 2 for the range of concentrations studied at the wave length of maximum absorption, 580 mμ. It appears probable that complete iodine adsorption is reached at the maximum point and that flocculation effects beyond this point decrease the amount of light absorption. Adherence to Beer's relation is far from rigid at the lower lanthanum-ion concentrations, although the experimental points do approach this limiting law up to a lanthanum-ion concentration of about 0.02 *M*.

Light absorption by the blue sols is more sensitive to their iodine content. Results of quantitative spectrophotometric studies on sols containing in a total volume of 25 ml. 2.5 ml. of 0.1 *M* lanthanum nitrate solution, 5 ml. of 0.1 *M* acetic acid solution, 10 ml. of 0.1 *M* aqueous ammonia, and varying volumes of 0.001 *M* iodine solution are summarized in figure 3. Corresponding data for sols containing 2.5 ml. of 0.1 *M* lanthanum nitrate solution, 2.5 ml. of 0.1 *M* propionic acid solution, 5 ml. of 0.1 *M* aqueous ammonia, and varying volumes of 0.001 *M* iodine solution, all in total volumes of 15 ml., are given in figure 4. Regularities characterizing these sets of data are more apparent in the plot of optical density at the wave length of maximum absorption against iodine concentration given in figure 5. Adherence to Beer's law is reasonably good for both acetate and propionate systems up to some 5 × 10^{-5} moles of iodine per liter, and in this range data for the two systems are nearly identical even though the wave lengths of maximum absorption differ by 20 mμ. It is apparent that development of a colorimetric method for the estimation of trace amounts of iodine based upon light absorption by lanthanum blue sols is very possible, sensitivities to about 1 × 10^{-5} mole per liter being indicated.

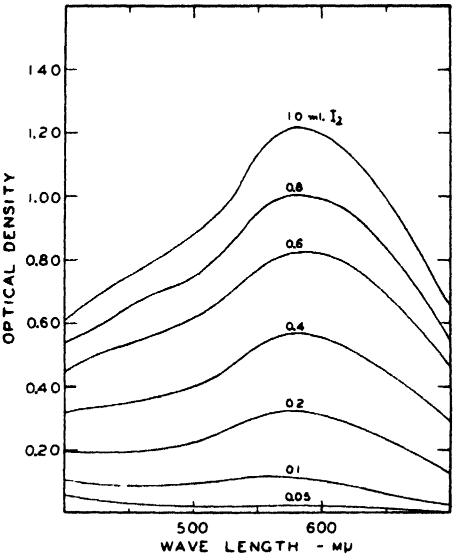

FIG. 3

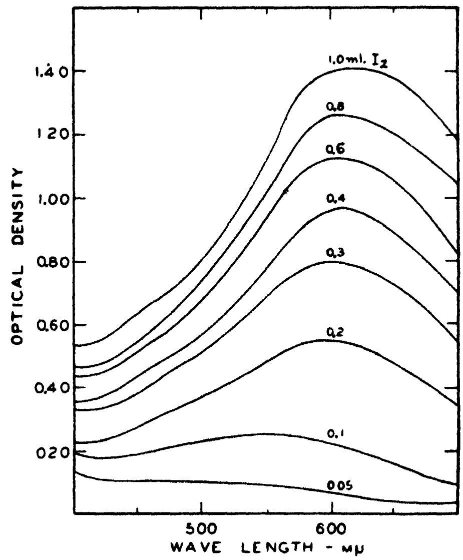

FIG. 4

FIG. 3. Effect of iodine on absorption in acetate systems
FIG. 4. Effect of iodine on absorption in propionate systems

Qualitative studies involving yttrium, neodymium, and samarium ions in combination with formic, acetic, propionic, and butyric acids showed that only those systems containing neodymium and acetate or propionate ions yielded blue sols analogous to the lanthanum blues. Iodine adsorption appeared to take place more slowly with the neodymium systems than with those containing the lanthanum ion. As with the lanthanum systems, the propionate sols flocculated more readily than the acetate sols. Under a given set of concentration conditions, propionate sols appeared to have deeper colors than those containing acetate. Absorption spectrum data for three representative sols prepared by combining 2 ml. of 0.1 *M* neodymium nitrate solution, 5 ml. of 0.1 *M* acetic acid solution, 10 ml. of 0.1 *M* aqueous ammonia, and 0.3–0.5 ml. of 0.001 *M* iodine solution are plotted in figure 6. The nature of the absorption appears to be very much the same as that shown by the acetate lanthanum blue sols, the wave length of maximum absorption being 580 mμ in both cases. Absorption intensity appears to be slightly greater for neodymium blues than for lanthanum blues. It is noteworthy that none of the characteristic absorption bands of the neodymium ion appear in the spectra plotted in figure 6. This lends further support to the view that conversion of the lanthanide ion into insoluble (though colloidally dispersed) hydrous hydroxide is essential to blue formation.

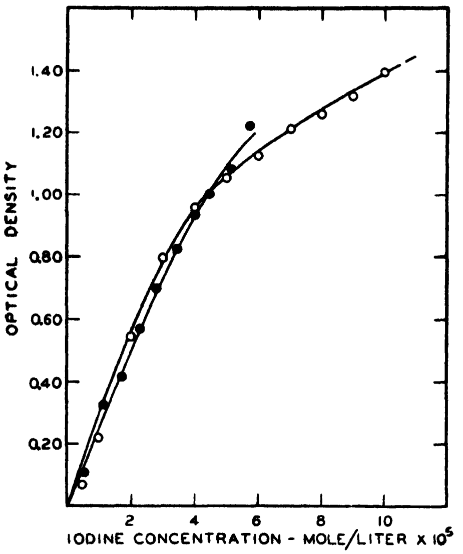

FIG. 5

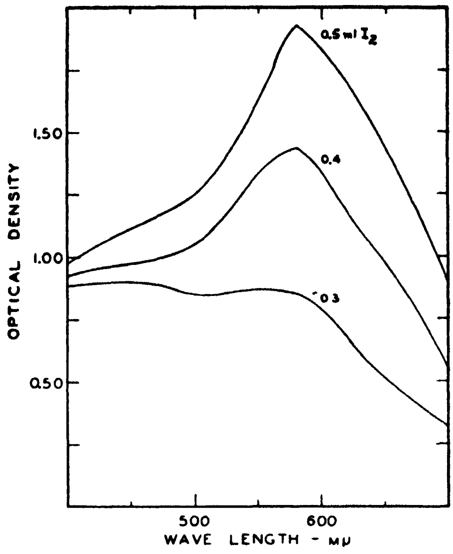

FIG. 6

FIG. 5. Relation of absorption to iodine concentration in acetate and propionate systems. ●, acetate, 580 mμ; ○, propionate, 600 mμ.

FIG. 6. Absorption spectra of acetate-containing neodymium blues

SUMMARY

1. The conditions necessary for the reproducible preparation of stable lanthanum blue sols containing acetate or propionate have been determined.
2. The absorption spectra of such sols have been measured over the spectral range 400–700 mμ as functions of the lanthanum, iodine, and organic anion

contents and have been found to be characterized by single broad absorption bands centering at 580 mμ and 600 mμ, respectively, for acetate and propionate systems.

3. For both acetate and propionate systems, absorption at these wave lengths has been related to iodine content by Beer's law up to 5×10^{-5} moles of iodine per liter. Beer's law has been found to apply only roughly in the acetate sols as the lanthanum content increases to 0.02 mole per liter. Intensity of absorption has been shown to be unrelated to organic anion concentration when the latter is insufficient to effect flocculation of the sols.

4. Use of lanthanum blue sols has been proposed for the colorimetric estimation of iodine in small quantities.

5. Of the tripositive ions yttrium, samarium, and neodymium, only the last has been found to yield blue sols in the presence of iodine, alkali, and acetate or propionate. Absorption spectra of such sols have been found to be comparable with those for the lanthanum blues.

REFERENCES

(1) BILTZ: Ber. **37,** 719 (1904).
(2) DAMOUR: Compt. rend. **43,** 976 (1856).
(3) DAMOUR: Ann. **101,** 365 (1857).
(4) DAMOUR: J. prakt. Chem. [2] **71,** 305 (1857).
(5) KRÜGER AND TSCHIRCH: Ber. **62B,** 2776 (1929).
(6) KRÜGER AND TSCHIRCH: Ber. **63B,** 826 (1930).
(7) KRÜGER AND TSCHIRCH: Pharm. Zentralhalle **71,** 145 (1930).
(8) KRÜGER AND TSCHIRCH: Pharm. Acta Helv. **5,** 25 (1930).
(9) KRÜGER AND TSCHIRCH: Mikrochemie **2,** 337 (1930).
(10) KRÜGER AND TSCHIRCH: Dyestuffs **32,** 91 (1931).
(11) LOTTERMOSER: Kolloid-Z. **33,** 271 (1923).
(12) MOELLER AND KRAUSKOPF: J. Am. Chem. Soc. **60,** 726 (1938).
(13) MOELLER AND KRAUSKOPF: J. Phys. Chem. **43,** 363 (1939).
(14) NEELAKANTAM AND ROW: Proc. Indian Acad. Sci. **13A,** 194 (1941).
(15) ORLOV: Chem. Ztg. **31,** 45 (1907).
(16) TSCHIRCH: Oesterr. Chem. Ztg. **34,** 38 (1931).

THE RELATIVE PHASE POTENTIAL WITHIN A HALF-CELL

CARL L. CARLSON, EARL W. MALMBERG, AND D. J. BROWN
Avery Laboratory, University of Nebraska, Lincoln 8, Nebraska

Received March 16, 1949

Cells in different solvents may have different observed values for the electromotive force when the chemical potentials of the components are the same (1, 2). This may be interpreted as due to the effect of the interface within each half-cell. The work here reported was undertaken to determine experimentally the relation of this potential in a second solvent to that in water when the reactants in the cell are at the same chemical potential.

In any solvent when

$$\mathrm{Pb(s)} + \mathrm{Hg_2Cl_2(s)} = 2\mathrm{Hg(l)} + \mathrm{PbCl_2(s)}$$

represents the cell reaction, the change of free energy of the reaction is the same independent of the solvent. Since the chemical potentials of the solutes are the same in both solvents, the liquid-junction potential due to the solutes is zero. As in the calculation of "liquid-junction potentials," the value due to diffusion of solvents is considered negligible.

In a preliminary study it was found that neither lead chloride, mercurous chloride, nor potassium chloride was solvated by methyl alcohol, which was selected as the second solvent.

The reagents met the A.C.S. specifications. Since the cells in water as a solvent gave sufficiently consistent results, these reagents were considered satisfactory.

Since very small amounts of water may have relatively large effects on the potential of the half-cell in nonaqueous solvents (2), the methyl alcohol was treated with quicklime and distilled. The water was redistilled after treatment with alkaline permanganate. Each solvent was saturated with lead and potassium chlorides at a slightly higher temperature and allowed to cool slowly to 25°C. After each half-cell was prepared a crystal of potassium chloride was added.

In the preparation of a mercury–mercurous chloride half-cell a paste of the two was prepared, using the appropriate solution as prepared above, and placed on the mercury.

In the case of the lead–lead chloride half-cell lead foil was immersed for at least 2 days in 6 *N* hydrochloric acid at 25°C. The lead was not at the "standard state," which is an unstrained crystalline form, but the results in the water solution show that the data were reproducible within the requisite limits. The treated lead was dried at 110°C., kept in a desiccator, and immersed in the appropriate solvent for the half-cell.

A Leeds & Northrup Type K potentiometer and Type R galvanometer were used. The reference cell was calibrated against a Bureau of Standards cell. The cells and solutions were kept in an air bath at 25°C.

The following set-up, in which E represents each half-cell and π the junction of the two solutions, was used:

$$
\begin{array}{lcr}
E_1 & & E_2 \\
Pb(s)\,| & PbCl_2(s),\ KCl(s)\ \text{in}\ H_2O,\ Hg_2Cl_2(s) & |\,Hg(l) \\
 & \pi & \\
Pb(s)\,| & PbCl_2(s),\ KCl(s)\ \text{in}\ CH_3OH,\ Hg_2Cl_2(s) & |\,Hg(l) \\
E_3 & & E_4
\end{array}
$$

A stopcock with a 0.6 cm. bore was used to make a junction of the solutions. It was filled with the solution which had the higher specific conductance. The solution of higher conductance was placed below. To prevent flow within the stopcock the higher level of the second solution was "compensated" by a safety tube to the first solution filled to the appropriate level.

TABLE 1

A series of potential differences for four half-cells as indicated

TIME	ΔE_{12}	ΔE_{34}	$\Delta E_{1\pi 4}$	$\Delta E_{3\pi 2}$	$\Delta E_{1\pi 3}$	$\Delta E_{2\pi 4}$
min.						
0	+0.5304	+0.5075	+0.4977	+0.5319	−0.0024	−0.0317
10	0.5304	0.5017	0.4991	0.5326	0.0040	0.0309
20	0.5339	0.5036	0.5020	0.5339	0.0019	0.0313
40	0.5365	0.5023	0.5027	0.5359	+0.0006	0 0318
120	0.5360	0.5052	0.5052	0.5323	−0.0013	0.0300
240	0.5361	0.5040	0.5059	0.5343	0.0034	0.0277
Average	+0.5356	+0.5038	+0.5040	+0.5341	−0.0015	−0.0302

As recorded in the tables ΔE_{12} represents the observed electromotive force of the cell in water in direct relation to the chemical equation above. ΔE_{34} likewise represents observed values with methyl alcohol as the solvent. $\Delta E_{1\pi 4}$ and $\Delta E_{3\pi 2}$ in each case represent the same cell, but each half-cell is in a different solvent. $\Delta E_{1\pi 3}$ and $\Delta E_{2\pi 4}$ in each case represents the same half-cell, but each is in a different solvent.

Table 1 gives an example of a series of observations using a "nest" indicated above, with the calculated averages omitting the initial and the 10-min. observations. These averages are the first series in table 2.

Table 2 gives such averages for seven consecutive series and their average, asterisks being used to indicate values not included in the final averages.

Let E_F represent the potential of the half-cell in accord with its true free energy, and ϵ the effect on the electromotive force due to the phase boundary between the metal and the solution. Then when E is the observed potential, $E = E_F + \epsilon$. As previously stated, ϵ_π, the potential due to the diffusion of the solvents, may be considered zero (see table 3).

The first column represents the determinations as represented in tables 1 and

2. The second is the relation of the potential to the possibilities. Using these, the values could not be calculated. The third column represents the equation used to calculate the relation of the effect of the phase boundary to that in water, ϵ'. The last column gives the numerical averages from table 2.

The fifth series above is anomalous. On study of the variant half-cell, E_4, no reason could be found. If small amounts of water affect a nonaqueous half-cell (3), infinitesimal amounts of other substances may have a similar effect. No observed value including this series varied as much as 10 mv. from any final average in table 2.

TABLE 2

Representative averages as in table 1

ΔE_{12}	ΔE_{34}	$\Delta E_{1\pi 4}$	$\Delta E_{3\pi 2}$	$\Delta E_{1\pi 3}$	$\Delta E_{2\pi 4}$
+0.5356	+0.5038	+0.5040	+0.5341	−0.0015	−0.0302
0.5356	0.5039	0.5040	0.5334	0.0020	0.0291
0.5339	0.5041	0.5030	0.5328	0.0021	0.0297
0.5334	0.5056	0.5085	0.5330	0.0000	0.0275
0.5344	0.4960*	0.4975*	0.5336	0.0010	0.0371*
0.5353	0.5039	0.5048	0.5330	0.0017	0.0291
0.5336	0.5050	0.5006	0.5364	0.0031	0.0312
+0.5345	+0.5044	+0.5042	+0.5337	−0.0016	−0.0295

TABLE 3

Relation of observed values to possible potential differences

$$\begin{aligned}
\Delta E_{12} &= \Delta E_{F} + \epsilon_2 - \epsilon_1 & &= +0.5345 \\
\Delta E_{34} &= \Delta E_{F} + \epsilon_4 - \epsilon_3 &= \Delta E_{12} + \epsilon_4 - \epsilon_3 &= +0.5044 \\
\\
\Delta E_{1\pi 2} &= \Delta E_{F} + \epsilon_4 + \epsilon_\pi - \epsilon_1 &= \Delta E_{12} + \epsilon_4' &= +0.5042 \\
\Delta E_{3\pi 2} &= \Delta E_{F} + \epsilon_2 - (\epsilon_3 + \epsilon_\pi) &= \Delta E_{12} + \epsilon_3' &= +0.5337 \\
\Delta E_{1\pi 3} &= 0 + \epsilon_3 + \epsilon_\pi - \epsilon_1 &= \epsilon_3' &= -0.0016 \\
\Delta E_{2\pi 4} &= 0 + \epsilon_4 + \epsilon_\pi - \epsilon_2 &= \epsilon_4' &= -0.0295
\end{aligned}$$

Using the value of the "saturated calomel" half-cell in water as the unit of comparison and the relative potential for the interface in methyl alcohol, the calculated value in methyl alcohol is:

$$Hg_2Cl_2(s) + 2e = 2Hg(l) + 2Cl^-(KCl) \quad E^0 = +0.2466 - 0.0295 = +0.2171$$

$$PbCl_2(s) + 2e = Pb(s) + 2Cl^-(KCl) \quad E^0 = +0.2171 - 0.5044 = -0.2873$$

When the determinants of the electromotive force of a cell in two different solvents are at the same chemical potential, the observed values of the electromotive force may be different. The effect of the solvent may be different for different half-cells. This is due to the effect of the interface within each half-cell. The relative values of this effect have been studied in water and methyl alcohol.

REFERENCES

(1) HARNED AND OWEN: *The Physical Chemistry of Electrolytic Solutions*, pp. 314–16. Reinhold Publishing Corporation, New York (1943).

(2) HARTLEY AND MACFARLANE: Phil. Mag. **20**, 611 (1935).

(3) NONHEBEL AND HARTLEY: Phil. Mag. **50**, 734 (1925).

THE ELECTROCHEMISTRY OF PERMSELECTIVE PROTAMINE COLLODION MEMBRANES. I

RATE STUDIES ON THE ESTABLISHMENT OF THE CONCENTRATION POTENTIAL ACROSS VARIOUS TYPES OF PERMSELECTIVE PROTAMINE COLLODION MEMBRANES

KARL SOLLNER[1] AND HARRY P. GREGOR[2]

Department of Physiology, University of Minnesota, Minneapolis 14, Minnesota, and the Laboratory of Physical Biology, Experimental Biology and Medicine Institute, National Institutes of Health, Bethesda 14, Maryland

Received April 11, 1949

In two preceding papers (2, 3) improved and reproducible methods of preparation of various types of permselective (electronegative) collodion and (electropositive) protamine collodion membranes were described. In addition to data on their water content these membranes were characterized by (*a*) the "characteristic concentration potential," i.e., the potential of the chain 0.1 N potassium chloride | membrane | 0.01 N potassium chloride; (*b*) the "bi-ionic potential" (B.I.P.) of the chains 0.1 N potassium chloride | membrane | 0.1 N lithium chloride and 0.1 N potassium chloride | membrane | 0.1 N potassium acetate, respectively; and (*c*) the electrical resistance of the membranes in contact with 0.1 N potassium chloride solution. In addition, certain data on the rate of ion exchange across a few of the membranes were presented. In subsequent publications a study was made of the rates at which final, stable concentration potentials with various electrolytes are established across several types of permselective *collodion* membranes (8) and of the final concentration potentials established by various electrolytes at different concentrations across these membranes (9). The present communication and the subsequent paper present analogous experimental studies with *protamine collodion membranes*.[3]

---

[1] Present address: Laboratory of Physical Biology, Experimental Biology and Medicine Institute, National Institutes of Health, Bethesda 14, Maryland.

[2] Present address: Polytechnic Institute of Brooklyn, Brooklyn 2, New York.

[3] The authors wish to express their thanks to Eli Lilly and Company for the donation of the several samples of protamine sulfate which were used in these investigations.

In considering the rate of the establishment of final, stable concentration potentials across these membranes, two fundamentally different possibilities must be distinguished. The first arises when a membrane saturated with critical ions of one species is brought into contact with the solution of an electrolyte having some other critical ion. Here, ion exchange—anion exchange in the case of electropositive membranes—must take place throughout the pore system of the membranes before final potentials can be obtained. In the other case the membrane has already undergone ion exchange previously; with electropositive membranes the cationic (basic) wall groups are already compensated for by anions of the same species as the anions in solution. Here, an exchange of critical ions between the solutions and the membrane does not occur; only equilibration between the external solutions and the electrolyte in the wider parts of the pores of the membrane must take place. For reasons outlined previously (8) the former case involving ion exchange will be emphasized.

The determination of the concentration potential was carried out with the conventional technique employing saturated calomel electrodes and saturated potassium chloride–agar bridges.[4] To minimize the contamination of the solutions by potassium chloride diffusing from the potassium chloride–agar bridges, the latter were dipped in the electrolyte solutions only for the duration of the actual measurements.

The permselective protamine collodion membranes not being of ideal ionic selectivity, a significant leak of electrolyte across the membranes is likely to occur even at low concentrations during the period in which the system reaches the final state. To avoid errors due to this factor or to contamination of the solutions with potassium chloride from the agar bridges, the two solutions separated by the membrane were renewed periodically.

For the rate studies three types of membranes were selected from the large number of different varieties which were prepared. The system of designation of the membranes follows the previously established convention (3). A membrane designated as Hum 58—Shr 58 is one which was dried on its mandrel at 58 per cent relative humidity until equilibrium had been established, removed from the mandrel and dried once more without support of a mandrel (i.e., "shrunk") at a relative humidity of 58 per cent.

The membranes (after being aged by at least 3 days' immersion in 0.1 N potassium chloride solution) were equilibrated for at least 24 hr. with repeatedly changed distilled water, in order to remove ions of the critical species under investigation.[5] They were always returned to this state before use with a solution of different concentration of the same electrolyte or the solution of another electrolyte (8). In order that relatively small differences in the behavior of different electrolytes would not be overshadowed by minor differences between different membrane specimens of the same type, all experiments on the time effect reported for one type of membrane were performed with a single membrane specimen.

---

[4] The water permeability of these membranes is so low that the stable potential is established before a detectable movement of water occurs (6).

[5] For the case of the protamine collodion membrane it has as yet not been established which species of ions is present in the membranes as counter ions of the fixed wall groups after prolonged washing with distilled water. In the case of the (acidic) collodion membrane hydrogen ions were shown to be present (4, 5, 7); with the protamine collodion membrane hydroxyl, bicarbonate (from the distilled water), and nitrate ions may be present, the latter originating from the unavoidable, though very slow, hydrolysis of the cellulose nitrate (which is likely to be accelerated by the presence of the fairly strongly basic protamine).

Only electrolytes with univalent critical ions (anions) are discussed here. Preliminary experiments have shown that it is difficult to obtain meaningful data with electrolytes having bivalent anions; a separate investigation will be necessary for the adequate treatment of this problem.

Figure 1 shows the rate of establishment of the concentration potential (at 25.00°C. ± 0.05°) for three different membranes with potassium chloride, potassium iodate, and magnesium sulfate for two concentration ratios, 0.01 N/0.001 N and 0.1 N/0.01 N. These data are given as measured, without correction for the asymmetry in the two liquid-junction potentials which arise between the potassium chloride–agar bridges and the two solutions of different concentration. The figures are accurate to about 0.10 mv. for the values in the final state.

III

Figure 1 shows that the rate at which stable potentials are established across the various permselective protamine membranes depends on the nature of the electrolyte and the nature of the membrane, and also upon the absolute concentration of the solutions used. In some instances stable potentials are reached within less than 1 hr.; in other instances several hours may be required. A comparison with previously published rate studies on permselective collodion membranes[6] (8) shows that the stable state with the permselective protamine collodion membranes is reached more slowly than in the former case.[7]

The experimental data presented in figure 1 show specifically that the denser the membranes the more slowly are the final, steady potentials established. The difference between membrane Hum 20—Shr 20 and membrane Hum 58—Shr 58 at the higher concentration level is small, in agreement with the close similarity of action of these membranes with respect to the final, stable concentration potential (3, 10). With potassium iodate, that is, with an electrolyte having a large anion, the stable state (with one doubtful exception) is reached much more slowly than with potassium chloride, which has an anion of smaller hydrated size. The rate at which the stable potential is established with potassium chloride and magnesium chloride is identical within the limits of significance of the experimental data. In other words, the rate at which the final, stable concentration

---

For the reasons outlined it does not seem promising to make quantitative anion-exchange studies with protamine collodion membranes, analogous to the cation-exchange experiments which have been carried out with collodion membranes (4, 5, 7).

[6] The scale on the time axis of figure 1 is one-half of the scale used in an analogous figure in the paper on the rate effect with permselective collodion membranes (8).

[7] The probable cause of this difference between the permselective collodion and the permselective protamine collodion membranes will be discussed at a later date, when the ohmic resistance of these membranes will be considered.

potentials are reached seems to be practically independent of the nature (size and valency) of the noncritical ion. With more dilute solutions (0.01 N/0.001 N) equilibrium is reached somewhat faster than with more concentrated (0.1 N/0.01 N) ones.

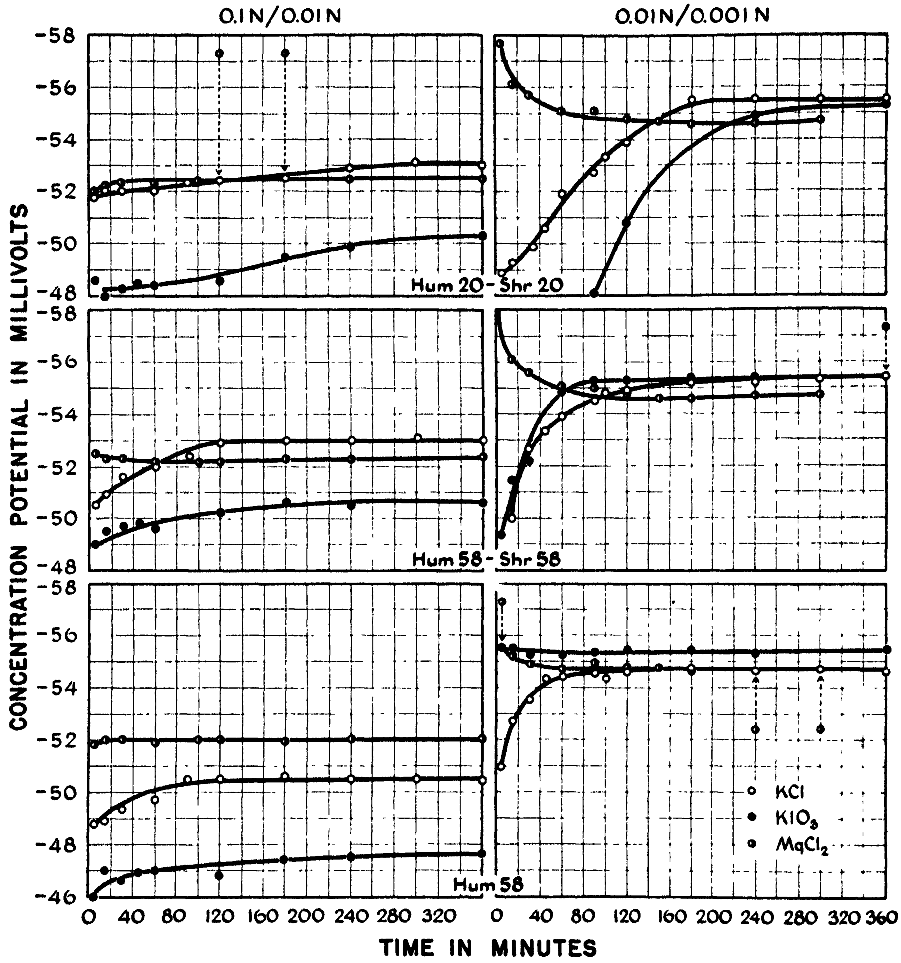

FIG. 1. The rate of establishment of steady concentration potentials $c_2:c_1 = 10:1$ of several electrolytes across various permselective protamine collodion membranes.

These results are strictly parallel with those obtained for the permselective collodion membranes. The observation is confirmed that the nature and valency of the noncritical ion do not play an important role with regard to the rate at which the final, stable concentration potentials are established. The possible significance of these results for the broader problem of the geometrical and electrical structures of membranes of porous character was indicated previously (8).

With respect to the rate of establishment of the concentration potential across membranes which are already saturated with the critical ion species by prior ion exchange, it might be reported that these rates are much higher and less characteristic for the different ions, in agreement with the results obtained with the electronegative collodion membranes. From the practical point of view, however, it is interesting to note that with such membranes final, stable potential readings can frequently be made almost instantaneously, in most instances within 2 min.; adaptation periods of more than 10 min. are rare.

SUMMARY

1. A study was made of the rates at which final, stable concentration potentials are established with three electrolytes—potassium chloride, potassium iodate, and magnesium chloride—across three types of permselective protamine collodion membranes which had been carefully freed of ions of the critical species, that is, the anions of the electrolytes in the external solutions.

2. The rates at which stable concentration potentials across these membranes are established depend on the nature of the membrane, the nature of the electrolyte, and the absolute concentrations of the adjacent solutions. The time required for the establishment of final stable potentials varies from less than 1 hr. up to several hours. Specifically, it was found that: (*a*) the denser the membranes the more slowly are the final steady concentration potentials established; (*b*) with potassium iodate, i.e., with an electrolyte having a large critical ion, equilibrium is reached much more slowly than with potassium chloride, an electrolyte having a critical ion of smaller hydrated size; (*c*) the rates at which equilibrium is established with potassium chloride and magnesium chloride are identical within the limits of the significance of the experimental data; in other words, the rate at which the final, stable concentration potentials are reached seems to be practically independent of the nature (size and valency) of the noncritical ion (the cation); (*d*) with more dilute solutions (0.01 N/0.001 N) equilibrium is reached somewhat faster than with more concentrated (0.1 N/0.01 N) ones.

3. The establishment of stable concentration potentials across membranes which are already saturated with the critical ion species by prior ion exchange occurs much faster than in the cases where ion exchange must occur; stable potentials are frequently obtained nearly instantaneously, adaptation periods of more than 10 min. being rare in this case.

4. The experimental results obtained with the (electropositive) permselective protamine collodion membranes and the conclusions which can be derived from these data are strictly parallel to those obtained previously with (electronegative) permselective collodion membranes.

REFERENCES

(1) Gregor, H. P.: Ph.D. Thesis, University of Minnesota, 1945.
(2) Gregor, H. P., and Sollner, K.: J. Phys. Chem. **50**, 53 (1946).
(3) Gregor, H. P., and Sollner, K.: J. Phys. Chem. **50**, 88 (1946).
(4) Sollner, K.: J. Phys. Chem. **49**, 47, 171 (1945).
(5) Sollner, K., and Anderman, J.: J. Gen. Physiol. **27**, 433 (1944).
(6) Sollner, K., and Carr, Ch. W.: J. Gen. Physiol. **28**, 119 (1944).
(7) Sollner, K., Carr, Ch. W., and Abrams, I.: J. Gen. Physiol. **25**, 411 (1944).

(8) Sollner, K., and Gregor, H. P.: J. Phys. Chem. **50**, 470 (1946).
(9) Sollner, K., and Gregor, H. P.: J. Phys. & Colloid Chem. **51**, 299 (1947).
(10) Sollner, K., and Gregor, H. P.: J. Phys. & Colloid Chem. **54**, 330 (1950).

THE ELECTROCHEMISTRY OF PERMSELECTIVE PROTAMINE COLLODION MEMBRANES. II

Experimental Studies on the Concentration Potential across Various Types of Permselective Protamine Collodion Membranes with Solutions of Several Electrolytes

KARL SOLLNER[1] and HARRY P. GREGOR[2]

Department of Physiology, University of Minnesota, Minneapolis 14, Minnesota, and the Laboratory of Physical Biology, Experimental Biology and Medicine Institute, National Institutes of Health, Bethesda 14, Maryland

Received April 11, 1949

I

The preceding paper (19) presents data concerning the rates at which final, stable concentration potentials with various electrolytes are established across several types of permselective protamine collodion membranes. The present paper is a further contribution to the systematic investigation of the permselective membranes and presents an experimental study of the final, stable concentration potentials established by various electrolytes at different concentrations across several types of permselective *protamine* collodion membranes. Not only are such studies necessary to enhance an understanding of the fundamental physical chemistry of membranes of porous character, but they are also desirable in view of the usefulness of these membranes in such investigations as, e.g., the study of Gibbs–Donnan membrane equilibria (5, 13, 14, 16) and in the electrometric determination of ion activities (3, 5, 12).

The present investigation is parallel in plan, theoretical background, and technique to an earlier study on the concentration potentials arising across (electronegative) permselective collodion membranes (18). Certain details which are treated briefly here are described in greater length in this previous paper.

II

The physical meaning of experimental concentration potentials measured across ion-selective membranes can be visualized best by reference to the theoretical limits of the possible electromotive properties of real membranes. With membranes of high ionic selectivity the more important of these limits are the

---

[1] Present address: Laboratory of Physical Biology, Experimental Biology and Medicine Institute, National Institutes of Health, Bethesda 14, Maryland.

[2] Present address: Polytechnic Institute of Brooklyn, Brooklyn 2, New York.

(calculated) potentials, E_{max}, which would arise if the membrane would permit the reversible transfer of a single, the "critical," ion species, thus acting as reversible "membrane electrode" (3, 5, 12). The "critical" ion in the case of electropositive membranes, such as protamine collodion membranes, is the anion. The other, lower, limit of the possible electromotive properties of real membranes is the potential which would arise across a membrane which does not show any ion selectivity of its own; it is identical with the liquid junction potential E_l which arises on free diffusion in solution.

The theoretically possible maximum values of the concentration potential, E_{max}, across a positive membrane in the chain: saturated calomel electrode | solution 1 | membrane | solution 2 | saturated calomel electrode, is defined by the general equation

$$E_{max} = -\frac{RT}{z_-F} \ln \frac{a_-^{(1)}}{a_-^{(2)}} \tag{1}$$

where z_- is the valency of the critical anion (considered as a positive quantity) and $a_-^{(1)}$ and $a_-^{(2)}$ are its activities $c_-^{(1)} \cdot \gamma_-^{(1)}$ and $c_-^{(2)} \cdot \gamma_-^{(2)}$ in the two solutions.[3]

The majority of the numerical values necessary for these and the subsequent calculations were taken preferentially from Harned and Owen (7), MacInnes (9), and the *International Critical Tables* (8), intermediate data being interpolated graphically. The probable errors in the calculated E_{max} values are probably small compared with the accuracy and reproducibility of our experimental data.

The potential arising from diffusion in free solution, that is, the liquid-junction potential c_2/c_1, was calculated from the equation

$$E_{l(\text{calc})} = \frac{t_+}{z_+}\frac{RT}{F} \ln \frac{a_+^{(2)}}{a_+^{(1)}} - \frac{t_-}{z_-}\frac{RT}{F} \ln \frac{a_-^{(2)}}{a_-^{(1)}} \tag{2}$$

where $E_{l(\text{calc})}$ is the liquid-junction potential, and where t and a refer to transference numbers and single ion activities in the respective solution.[4] With electrolytes other than potassium chloride, systematic errors of at least 0.10 mv. may occur in the calculated values of $E_{l(\text{calc})}$.

III

The technique used for the measurement of the concentration potential across the membranes was the same as that described in the preceding paper: saturated calomel electrode | saturated potassium chloride | saturated potassium chloride–

---

[3] In the case of uni-univalent electrolytes, mean activities ($a_- = a_\pm$) were used. With the bi-univalent electrolyte magnesium chloride the activity coefficient for the critical ion, the chloride ion, is calculated assuming that the activity coefficient of a given ion is a function only of the ionic strength of the solution. Then the activity coefficient γ_{Cl^-} in a solution of magnesium chloride is the same as γ_{Cl^-} in a potassium chloride solution having the same ionic strength, assuming that $\gamma_{Cl^-} = \gamma_{K^+}$ in a solution of potassium chloride alone.

[4] In a previous paper (18) the transference numbers were referred to as being "within the membrane" (J. Phys. & Colloid Chem. **51**, 300 (1947), line 7 from the bottom) when their values in free solution were meant, and referred to as such further below in the text.

agar bridge | electrolyte c_2 | membrane | electrolyte c_1 | saturated potassium chloride–agar bridge | saturated potassium chloride | saturated calomel electrode. In all instances the final, stable concentration potentials ϵ were determined with all the precautions discussed in preceding papers (17, 18, 19).

The electrolytes used were potassium chloride, potassium iodate, lithium chloride, and magnesium chloride. The concentrations investigated ranged from 0.002 N/0.001 N to 0.4 N/0.2 N. Three types of membranes, Hum 20—Shr 20, Hum 58—Shr 58, and Hum 58, were studied. All measurements reported in table 1 for one type of membrane were performed successively with a single membrane specimen. The reproducibility of the measurements is, in most cases, approximately ±0.10 mv.; in some instances the error may be twice as large, particularly with the most concentrated and the most dilute solutions.

The liquid-junction potential $E_{l(\mathrm{exp})}$ of the membrane-free chains: saturated calomel electrode | saturated potassium chloride | saturated potassium chloride–agar bridge | electrolyte c_2 | electrolyte c_1 | saturated potassium chloride–agar bridge | saturated potassium chloride | saturated calomel electrode were measured in a simple W-shaped tube (18). At medium and higher concentrations the measurements were reproducible within about 0.10 mv.; at the lowest concentrations the probable error is greater than 0.10 mv. in some instances.

Table 1 gives the values of the liquid-junction potential, $E_{l(\mathrm{exp})}$*, as measured, together with the corresponding calculated values, $E_{l(\mathrm{calc})}$, and their differences, Δ. The difference Δ is a correction which must be applied to the concentration potentials as measured in the experimental membrane chains in order to arrive at the true values of the concentration potential as it was discussed in a preceding paper (18). Values of Δ which are positive have to be deducted from the (negative) experimentally determined value of the concentration potential; negative Δ-values have to be added. The values of the concentration potentials ϵ given in table 1 are all corrected in this manner.

Table 1 gives the experimental and calculated data at the temperature 25.00°C. ± 0.05° for four different electrolytes. Column 1 gives the concentrations, c_2 and c_1, of the electrolyte solutions used in equivalents per liter; column 2 gives the theoretically possible, maximum value of the concentration potential E_{max} calculated as outlined in the preceding section; columns 3, 4, and 5 present the concentration potentials ϵ across three different membranes corrected as outlined above; column 6a gives the calculated liquid-junction potential $E_{l(\mathrm{calc})}$ in free solution, computed as indicated before; column 6b gives the liquid-junction potential $E_{l(\mathrm{exp})}$ as measured; column 6c gives Δ, the difference between 6a and 6b, which has been applied to the values given in columns 3, 4, and 5. Figure 1 presents these data in the form of graphs to facilitate their visualization and evaluation.[5] Following an established convention the concentration c_1

---

* See p. 333.

[5] In many instances the experimental concentration potentials obtained with different membranes and the same electrolyte coincide. In order to make the graphic representation of these points feasible, the expedient has been chosen in figure 1 of not plotting some of the points in their proper positions but of arranging them outside the curves and indicating their proper positions by arrows.

TABLE 1

Concentration potentials ($c_2:c_1 = 2:1$) of several electrolytes across various permselective protamine collodion membranes

(1)	(2)	(3)	(4)	(5)	(6a)	(6b)	(6c)
CONCENTRATION OF ELECTROLYTE SOLUTIONS	CONCENTRATION POTENTIAL				DIFFUSION POTENTIAL, E_l, IN FREE SOLUTION		
$c_2:c_1$	Theoretical maximum E_{max}	Membrane Hum 20—Shr 20 ϵ	Membrane Hum 58—Shr 58 ϵ	Membrane Hum 58 ϵ	$E_{l(calc)}$	$E_{l(exp)}$	Δ
			A. Potassium chloride				
equiv/liter	*mv.*	*mv.*	*mv.*	*mv.*	*mv.*	*mv.*	*mv.*
0.002/0.001	−17.5	−16.4	−16.5	−16.4	−0.3		Nil
0.004/0.002	−17.3	−16.5	−16.5	−16.5	−0.3		Nil
0.01/0.005	−17.1	−16.2	−16.2	−16.3	−0.3		Nil
0.02/0.01	−16.9	−16.2	−16.1	−16.0	−0.3		Nil
0.04/0.02	−16.6	−15.9	−15.9	−15.5	−0.3		Nil
0.1/0.05	−16.3	−15.2	−15.3	−14.3	−0.3		Nil
0.2/0.1	−16.1	−14.5	−14.5	−12.9	−0.3		Nil
0.4/0.2	−16.0	−13.2	−13.0	−11.0	−0.3		Nil
			B. Potassium iodate				
0.002/0.001	−17.5	−16.2	−16.2	−15.9	+5.5	+5.0	+0.5
0.004/0.002	−17.3	−16.2	−16.1	−15.8	+5.5	+5.0	+0.5
0.01/0.005	−16.9	−16.1	−16.0	−15.4	+5,4	+5.0	+0.4
0.02/0.01	−16.7	−16.0	−16.0	−15.0	+5.3	+5.1	+0.2
0.04/0.02	−16.1	−14.9	−14.9	−13.5	+5.2	+5.0	+0.2
0.1/0.05	−15.1	−12.4	−12.6	−10.2	+5.0	+4.9	+0.1
0.2/0.1	−14.1	−10.2	−10.2	−6.9	+4.8	+4.7	+0.1
0.4/0.2							
			C. Lithium chloride				
0.002/0.001	−17.5	−16.6	−16.6	−16.6	−5.8	−5.7	−0.1
0.004/0.002	−17.3	−16.5	−16.5	−16.6	−5.8	−5.7	−0.1
0.01/0.005	−17.1	−16.6	−16.6	−16.5	−5.8	−5.6	−0.2
0.02/0.01	−16.9	−16.4	−16.4	−16.1	−5.8	−5.6	−0.2
0.04/0.02	−16.7	−16.3	−16.4	−16.0	−5.9	−5.5	−0.4
0.1/0.05	−16.5	−16.2	−16.1	−15.3	−6.0	−5.4	−0.6
0.2/0.1	−17.0	−16.2	−16.0	−15.0	−6.3	−5.1	−1.2
0.4/0.2	−16.9	−16.1	−16.1	−14.2	−6.5	−4.7	−1.8
			D. Magnesium chloride				
0.002/0.001	−17.4	−17.5	−17.3	−17.1	−7.2	−6.7	−0.5
0.004/0.002	−17.1	−17.3	−17.2	−16.9	−7.1	−6.5	−0.6
0.01/0.005	−16.9	−16.7	−16.7	−16.5	−7.1	−6.7	−0.4
0.02/0.01	−16.7	−16.4	−16.3	−16.0	−7.1	−6.8	−0.3
0.04/0.02	−16.4	−16.2	−16.1	−15.8	−7.1	−6.8	−0.3
0.1/0.05	−16.1	−16.0	−16.0	−15.1	−7.2	−6.7	−0.5
0.2/0.1	−15.9	−16.0	−16.0	−15.3	−7.2	−6.4	−0.8
0.4/0.2	−15.8	−16.0	−16.0	−15.0	−7.0	−5.3	−1.7

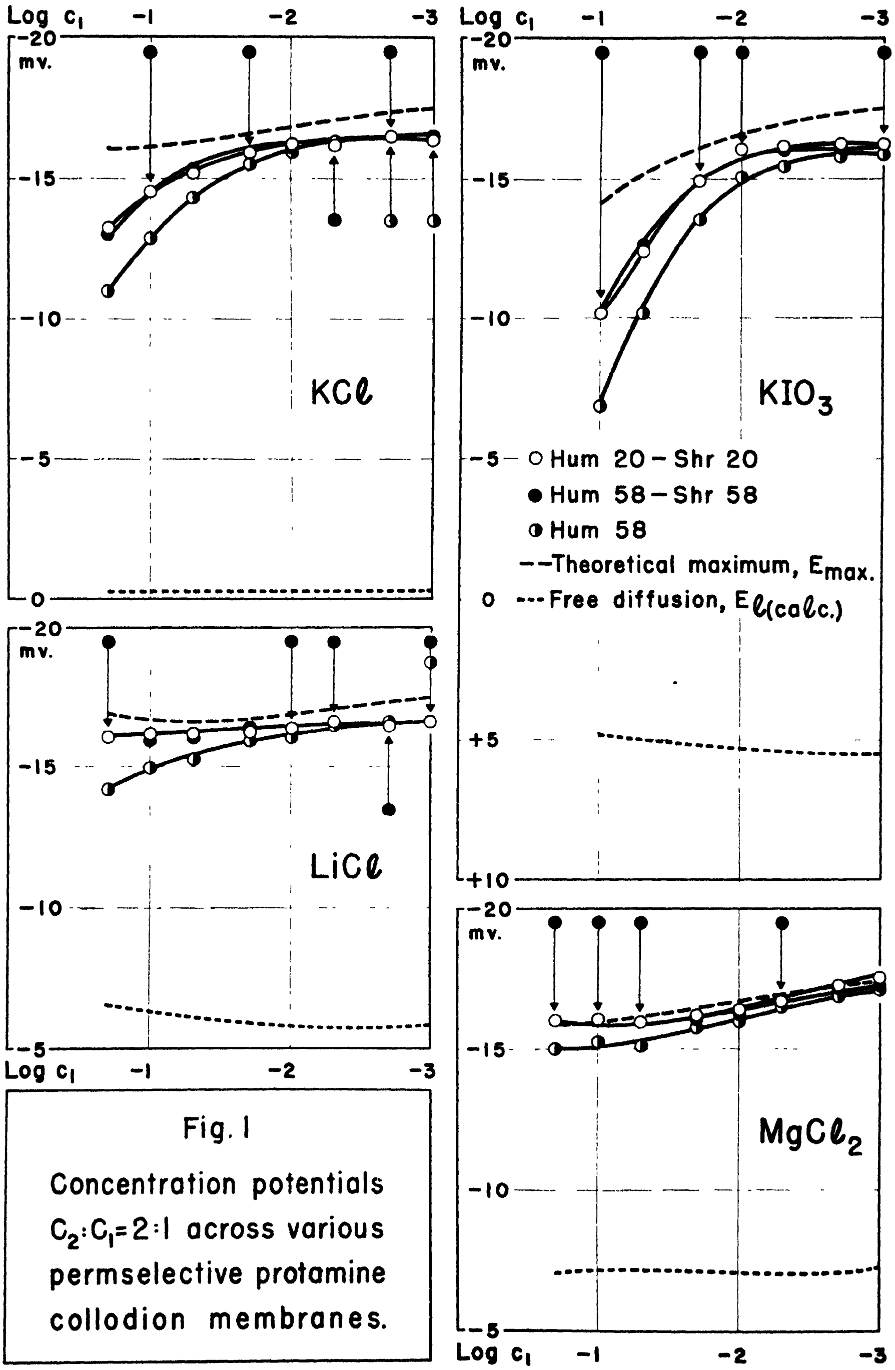

Fig. 1

Concentration potentials $C_2:C_1 = 2:1$ across various permselective protamine collodion membranes.

indicated in the graph refers to the more dilute solution; plotted in this manner the data become easily comparable to analogous data on permselective collodion membranes and numerous other data published in this literature.

IV

The data of table 1 and figure 1 show the same high degree of regularity and consistency that was previously observed in the case of the permselective collodion membrane (18). As in the former case we shall evaluate these data here merely in the conventional qualitative and semiquantitative manner, postponing to a later date the attempt at their quantitative evaluation from a more theoretical viewpoint.

The criterion for the evaluation of the data on membrane concentration potentials is the difference between the calculated theoretically possible maximum values, E_{max}, and the corresponding experimental concentration potential, ϵ. The smaller the difference between two corresponding such values, the higher is the "ionic selectivity" of a membrane under the particular conditions.

In comparing the different types of membranes, it is obvious that the membrane Hum 20—Shr 20 and the membrane Hum 58—Shr 58 used in the present study behaved in the concentration chains virtually the same; no significant differences between the two membrane specimens are evident (6). Membrane Hum 58 is of decidedly lower ionic selectivity as compared with the two other membranes (5, 6). This lower selectivity of the less dense membranes is conspicuous particularly at the higher concentrations, as is the case with the collodion membranes (18).

In the comparison of the concentration potentials which are observed with the solutions of various electrolytes it is necessary to keep in mind the limits of the accuracy of the calculated as well as of the experimental data. Any conclusions which are drawn with respect to the differences of behavior of different electrolytes should be based primarily on the trend of the curves over wide concentration ranges and on the data obtained with higher concentrations (18).

From table 1 and figure 1 it is immediately evident that the agreement between the calculated and the experimental concentration potentials is best with magnesium chloride; the ionic selectivity of the membranes is highest in this case. With magnesium chloride ideal ionic selectivity is approached closely in the case of the two denser, more highly dried membranes.

None of the membranes referred to in table 1 and figure 1 shows an ideal degree of ionic selectivity with uni-univalent electrolytes, or nearly so. Even at the lowest concentrations there exists a considerable difference between the measured and the theoretically possible maximum concentration potentials, in full agreement with previously published, less extensive data (1, 2, 5).

With the uni-univalent electrolytes the membrane selectivity is highest with lithium chloride, less with potassium chloride, and still less, to a very considerable extent, with potassium iodate.

The results are in full agreement with the concept put forward by Michaelis (10) that electrical and steric pore blocking account for the characteristic ionic selectivity of membranes of porous character, as exhibited in concentration chains. The electrical and the steric blocking reinforce one another in the case of the magnesium chloride: the magnesium ion is prevented from penetrating the membrane both on account of its large size and on account of the electric repulsion which arises between the fixed positive groups at the pore walls and its two positive charges. On account of its double charge alone the magnesium ion would be screened out much more effectively than ions which carry single charges only, such as the potassium ion.

With potassium chloride the steric factor does not play an important role, since potassium and chloride ions have very nearly the same size; here, essentially the electric factor of pore blocking alone is operative. In the case of lithium chloride the steric factor of pore blocking comes prominently into play on account of the great size of the hydrated lithium ion. Certain pathways across the membrane on a purely steric basis are inaccessible to the noncritical (lithium) ion.[6] The opposite situation prevails in the case of the potassium iodate; here the critical ion, the iodate ion, is considerably larger than the noncritical (potassium) ion[6]; the latter has a *relatively* better chance to penetrate the membrane than in the case of potassium chloride, the result being the observed, somewhat smaller, ionic selectivity in the case of the potassium iodate.

The fact that the permselective protamine collodion membranes even in fairly dilute solutions do not show a virtually ideal degree of ionic selectivity (except in cases of extreme steric hindrance of unusually large or polyvalent cations), as is found with their (electronegative) collodion counterparts, may be explained by the presence in the protamine molecule of at least one acidic (anionic) group. Accordingly, acidic groups must occupy some critical spots in the pore system of the protaminized membranes. These membranes, therefore, represent mosaics of numerous selectively anion-permeable pores and a few selectively cation-permeable pores, an electrochemical structure, which, according to all available information (15) could not result in an ideal degree (of purely electrical) ionic selectivity. The relative leak of noncritical ions can, of course, be calculated readily from the ratio of the values of the experimental concentration potential and its theoretically possible maximum (4); it is approximately 3 per cent even in dilute solutions.

It might be added here that the concentration range of usefully high ionic selectivity of these membranes, as was also the case with the permselective collodion membranes, can be expanded an appreciable extent beyond that indicated in table 1 and figure 1 by keeping the concentration at the one side of the membrane fairly low, e.g., ten or one hundred times lower than that of the more concentrated solution. With this precaution the membrane selectivity as determined by potential measurements can be fully satisfactory, e.g., for electrometric ion activity determinations (3, 5, 12) at electrolyte concentrations considerably higher than those indicated by the experimental data which employ a 2:1 concentration ratio. A probable explanation of this effect was discussed previously (18).

---

[6] The relative diffusion coefficients of the potassium, chloride, lithium, and iodate ions in solution are in the ratio of approximately 1:1:0.5:0.5.

Although the inherent shortcomings of the permselective protamine collodion membrane available at present have not prevented their successful use as physicochemical and analytical tools (3, 5, 12, 13, 14, 16) and in certain model studies (11, 20), their usefulness is such as to emphasize the desirability of further improvements in the degree of ionic selectivity of these membranes. Certain efforts in this direction are under way at present.

SUMMARY

1. Concentration potentials of potassium chloride, potassium iodate, lithium chloride, and magnesium chloride solutions across several types of permselective protamine collodion membranes were measured at several concentration levels between 0.001 N and 0.4 N, the concentration ratio being 2:1.

2. The experimentally obtained concentration potentials are compared with the calculated values of the concentration potentials which would arise with membranes of ideal ionic selectivity, in other words, with the potentials which would originate if the membrane would act as ideal reversible membrane electrodes for the critical anion.

3. Ideal ionic selectivity is not observed with uni-univalent electrolytes. An appreciable leak of noncritical ion occurs in all instances,—approximately 3 per cent, even in the most dilute solutions. With magnesium chloride, an electrolyte with a very large and bivalent noncritical ion, ideal ionic selectivity is approached closely over a wide concentration range. The correlation between the selectivity of the membranes and the nature of the electrolytes is that expected on the basis of theoretical considerations. The membrane selectivity decreases in the series magnesium chloride, lithium chloride, potassium chloride, and potassium iodate.

4. The desirability of further improvements in the ionic selectivity of the permselective protamine membranes is stressed.

REFERENCES

(1) Abrams, I., and Sollner, K.: J. Gen. Physiol. **26**, 369 (1943).
(2) Carr, Ch. W., Gregor, H. P., and Sollner, K.: J. Gen. Physiol. **28**, 179 (1945).
(3) Carr, Ch. W., Johnson, W. F., and Kolthoff, I. M.: J. Phys. & Colloid Chem. **51**, 636 (1947).
(4) Carr, Ch. W., and Sollner, K.: J. Gen. Physiol. **28**, 119 (1944).
(5) Gregor, H. P.: Ph. D. Thesis, University of Minnesota, 1945.
(6) Gregor, H. P., and Sollner, K.: J. Phys. Chem. **50**, 88 (1946).
(7) Harned, H. S., and Owen, B.: *The Physical Chemistry of Electrolyte Solutions*. Reinhold Publishing Corporation, New York (1943).
(8) *International Critical Tables*, Vol. VI. McGraw-Hill Book Company, Inc., New York (1929).
(9) MacInnes, D. A.: *The Principles of Electrochemistry*. Reinhold Publishing Corporation, New York (1943).
(10) Michaelis, L.: Bull. Natl. Research Council, No. **69**, 119 (1929); Kolloid-Z. **62**, 2 (1933).
(11) Neihof, Rex: Ph. D. Thesis, University of Minnesota, 1950 (in preparation).
(12) Sollner, K.: J. Am. Chem. Soc. **65**, 2260 (1943).
(13) Sollner, K.: J. Phys. Chem. **49**, 265 (1945).
(14) Sollner, K.: J. Am. Chem. Soc. **68**, 156 (1946).
(15) Sollner, K., and Carr, Ch. W.: J. Gen. Physiol. **26**, 309 (1943).

(16) Sollner, K., and Gregor, H. P.: J. Am. Chem. Soc. **67**, 346 (1945).
(17) Sollner, K., and Gregor, H. P.: J. Phys. Chem. **50**, 470 (1946).
(18) Sollner, K., and Gregor, H. P.: J. Phys. & Colloid Chem. **51**, 299 (1947).
(19) Sollner, K., and Gregor, H. P.: J. Phys. & Colloid Chem. **54**, 325 (1950).
(20) Sollner, K., and Neihof, R. A.: J. Phys. & Colloid Chem. **54**, 157 (1950).

SEDIMENTATION EQUILIBRIA OF POLYDISPERSE NONIDEAL SOLUTES. III

The Degradation of Polystyrene in Solution[1]

J. O. THOMPSON[2]

Department of Chemistry, University of Wisconsin, Madison, Wisconsin

Received March 28, 1949

I. INTRODUCTION

The molecular size distribution existing in polymeric systems at equilibrium may be derived by statistical thermodynamics. This has been done for vinyl-type systems by Tobolsky (12), who assumes that simultaneous polymerization and degradation may exist under certain conditions. Flory's derivation (3), specifically for condensation systems, yields a similar result, but with reference to this result he states: "Vinyl type polymerizations could be included, although these processes generally are not reversible in the thermodynamic sense."

The attainment of thermodynamic equilibrium in vinyl systems under various conditions of heat, light, and catalyst has been suggested (6, 7, 9, 11). The depolymerization reaction was assumed to proceed by way of a radical chain mechanism and to compete with the polymerization reaction. On the basis of this simultaneous polymerization and depolymerization thermodynamics is introduced to determine the equilibrium distribution of molecular sizes. This equilibrium distribution turns out to be such that it may be regarded as being the result of a random scission process on an "infinite" linear polymer. For this size distribution the ratio of the number-average, weight-average, and z average molecular weights, $\bar{M}_n:\bar{M}_w:\bar{M}_z$, approaches 1:2:3 as the fraction of parent molecules decreases (4, 8, 10).

It is the purpose of this paper to describe an investigation into the mechanism of attainment of this so-called equilibrium, and to show that the apparent approach to a steady-state relative viscosity may not be construed as indicating an approach to equilibrium conditions. Some preliminary experiments (Section III)

[1] More complete details of this work are to be found in the thesis submitted by J. O. Thompson to the Faculty of the University of Wisconsin in partial fulfillment of the requirements for the degree of Doctor of Philosophy, June, 1948.

This work was supported in part by a grant from the Wisconsin Alumni Research Foundation.

[2] Present address: The Institute of Paper Chemistry, Appleton, Wisconsin.

are described which were performed with the view to clarifying the picture as to the effectiveness of each of the factors heat, light, air, and benzoyl peroxide in the degradation of polystyrene in toluene solution. A larger number of more detailed experiments concerned with the degradation of polystyrene in solution by the action of benzoyl peroxide were also performed (Section IV). In all of the experiments to be described no monostyrene was initially present, and the main effect observed was a random degradation of the polymer (polystyrene in various solvents) regardless of initial molecular weight.

II. EXPERIMENTAL DETAILS

All polystyrenes used in this investigation were prepared in the oil phase in the presence of benzoyl peroxide as catalyst. The polymerizations were carried out in sealed tubes under nitrogen with dried vacuum-distilled styrene which had been freed of inhibitor by multiple washing with dilute sodium hydroxide. The polymer was removed from unreacted monomer by solution in benzene and triple precipitation with an excess of methanol. The final product was obtained by solution in benzene, shell-freezing, and sublimation.

Solutions for degradation study were made up in Merck reagent-grade redistilled solvents. The benzoyl peroxide used was Eastman White Label grade, m.p. 103–104°C., and contained 100 per cent benzoyl peroxide by iodometric titration.

The progress of polystyrene degradations in the preliminary experiments was followed in reversible viscometers of the type described by Mesrobian and Tobolsky (6). In these viscometers the change in relative viscosity of the polymer solutions with time could be followed without opening the vessels for the extraction of samples. The flow time for toluene at 30°C. was of the order of 35 sec. The more detailed degradation experiments were performed in sealed tubes, and the degraded polystyrenes were isolated from the reaction mixtures by precipitation with four volumes of methanol followed by solution in benzene, shell-freezing, and sublimation under vacuum. In all of the experiments where air (oxygen) was to be excluded the vessels were flushed with dry nitrogen before sealing.

Intrinsic viscosities were obtained from measurements made on benzene solutions at 30°C. by using standard extrapolation methods. The instrument used was an Ostwald-type viscometer of flow time 179 sec. for benzene. All solvent used was thiophene-free and redistilled. Viscosity-average molecular weights, $\bar{M}_v$, were obtained from a composite viscosity–molecular weight relation of Wales *et al.* (14).

Osmotic pressure measurements were made on butanone solutions of the polystyrenes with a glass osmometer of the Zimm and Myerson (15) design. Membranes were prepared from du Pont 600 P.T. nonwaterproofed cellophane by treating with 30 per cent potassium hydroxide at room temperature for 18 hr. The "period of half-life" of the osmometer for butanone at 30°C. was 1 hr. The "semi-static" method of measurement was used throughout this work.

Sedimentation equilibrium experiments were performed in butanone with a small Svedberg equilibrium ultracentrifuge with direct motor drive. The methods employed in the calculation of the various molecular weight averages have been fully described elsewhere (13, 14).

III. PRELIMINARY OBSERVATIONS

The following preliminary results were obtained from experiments with toluene solutions of polystyrene:

(*1*) In the complete absence of air (oxygen) and benzoyl peroxide, heating at 100°C. for six months results in no detectable degradation. Supplementary intrinsic viscosity measurements made on polystyrenes which had been stored in benzene solution in air at room temperature for two years showed no evidence of degradation.

(*2*) In the absence of oxygen and benzoyl peroxide, ultraviolet light ($\lambda >$ 3000 Å.), though producing a blue fluorescence, produces no detectable chain scissioning even when maintained for one month at 80°C.

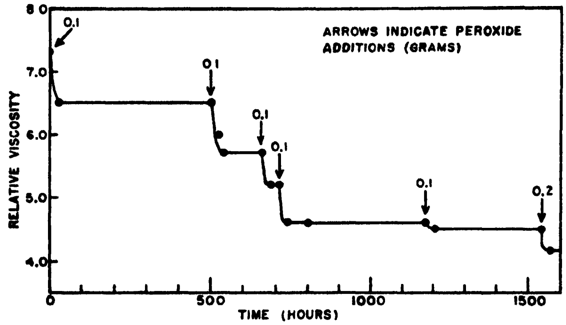

FIG. 1. Plot of relative viscosity against time for degradation experiment 3R; peroxide additions are indicated by the arrows (see table 8).

(*3*) Heating at 100°C. in the presence of oxygen or benzoyl peroxide produces degradation, as indicated by a decrease in relative viscosity. For each addition of air or peroxide the relative viscosity remains constant after approximately 24 hr.

(*4*) When repeated additions of benzoyl peroxide are made, though the decrements in relative viscosity decrease with each successive equal addition, the value of the relative viscosity has not reached a constant value even after the addition of 140 per cent by weight of peroxide has been made. One complicating factor here certainly is that the reaction mixture is continually changing as the peroxide additions are made. Initially there is present only polystyrene and toluene, but as peroxide additions are made and the degradation proceeds the decomposition products of the peroxide itself are accumulating. These latter products almost certainly interfere with the scissioning ability of subsequent peroxide additions. This behavior is shown graphically for one case in figure 1.

IV. BENZOYL PEROXIDE DEGRADATION OF POLYSTYRENE

A. General experiments

The preliminary experiments suggested that the degradation of polystyrene in solution depends on some sort of oxidation. No steady-state relative viscosity was observed in these experiments. Further investigations into the degradation of the polymer were then conducted and the data are collected in a number of tables to facilitate discussion. Some physical constants for the polystyrenes used as starting materials are contained in table 1.

TABLE 1

*Collected physical constants for original polystyrenes**

POLYSTYRENE	TEMPERATURE OF PREPARATION	$[\eta]$	$\times 10^{-3}$					BENZOYL PEROXIDE	CONVERSION
			$\overline{M}_\eta$	$\overline{M}_n$	$\overline{M}_w$	$\overline{M}_z$	$\overline{M}_{z+1}$		
	°C.							*mole per cent*	*per cent*
A	60	0.82	202	109	219	320	390	0.2	48.7
C	60	1.40	456	226	459	(833)‡		0.04	17.0
E†	60	0.97	267	144	289	464	705	0.13	18.5
2A-W		1.51	507	400					
5-W		0.75	185	155	186	230			
8-W		0.18	30						
H	100	0.88		145				0.025	33.5

* Molecular weight data were obtained by using viscosity ($\overline{M}_\eta$), osmotic pressure ($\overline{M}_n$), or sedimentation equilibrium methods.

† This sample has been previously described (14); the fractions 2A-W, 5-W, and 8-W were prepared from it.

‡ The nonideality correction was so large for this sample that the values for M_z and M_{z+1} are doubtful (14). M_z would be expected to be about 700×10^3.

TABLE 2

Reproducibility of degradation experiments

Starting material, polystyrene E, $[\eta] = 0.97$ (*cf.* table 1); 100°C. ± 0.5°; 0.5 g. polystyrene in 11 ml. toluene; 0.1 g. benzoyl peroxide added; reaction time, 48 hr. (to constant relative viscosity)

EXPERIMENT	$[\eta]$	$\times 10^{-3}$					PER CENT RECOVERY OF DEGRADED PRODUCT
		$\overline{M}_\eta$	$\overline{M}_n$	$\overline{M}_w$	$\overline{M}_z$	$\overline{M}_{z+1}$	
D-1A	0.77	190	102	201	297	362	99
D-1B	0.77	190					97
D-1C*	0.77	190					96
D-1D	0.76	187					96

* The toluene used as solvent here was washed with concentrated sulfuric acid, then with water, dried, and fractionally distilled.

First of all, it is necessary to have some idea of the reproducibility of the degradation reaction as indicated by intrinsic viscosity measurements. Data for this purpose (table 2) are seen to be entirely satisfactory.

The effects of variations in polymer and peroxide concentrations at 100°C. are illustrated by the data of table 3. The extent of degradation, as indicated by the decrease in intrinsic viscosity, depends on the concentrations of both polymer and peroxide. An increase in the concentration of either favors degradation. In comparable experiments where the respective weights of polymer and peroxide are the same, the extent of the degradation decreases as the amount of solvent is increased. These results suggest that both polymer and solvent are competing for the peroxide.

Degradation experiments were carried out with unfractionated polystyrene E to study the effects of method of peroxide addition (table 4), of temperature (table 5), and of nature of solvent (table 6) on the scission efficiency of the reactant. The data show that the amount of detectable scissioning produced by a given weight of peroxide depends upon the mode of addition of the reagent. The lower efficiency when the peroxide is added in one amount is not surprising, since the extent of peroxide "wastage" (2) increases with peroxide concentration. Temperature has only a slight effect on scissioning efficiency.

TABLE 3

Influence of reaction mixture composition on the scissioning efficiency of benzoyl peroxide at 100°C.

EXPERIMENT	VOLUME OF TOLUENE	WEIGHT OF POLYMER	WEIGHT OF PEROXIDE	[η]	$\times 10^{-3}$					RECOVERY OF DEGRADED PRODUCT
					$\bar{M}_\eta$	$\bar{M}_n$	$\bar{M}_w$	$\bar{M}_z$	$\bar{M}_{z+1}$	
A. Starting material, polystyrene E (*cf* table 1)										
	ml.	*grams*	*grams*							*per cent*
D-1A	11	0.5	0.1	0.77	190	102	201	297	362	98
D-2A	11	0.5	0.2	0.72	178	95				92
D-3A	22	0.5	0.1	0.83	220	120				95
D-4A	5.5	0.5	0.1	0.71	175	95				90
B. Starting material, polystyrene C (*cf.* table 1)										
D-9	11	0.5	0.1	1.09	309	155				100
D-10	11	0.5	0.2	0.97	270	145				96
C. Starting material, polystyrene A (*cf.* table 1)										
D-7	11	0.5	0.1	0.67	162	87				96
D-8	11	0.5	0.2	0.65	155	84				98
D-16	4.3*	0.8	0.1	0.61	140	75				98
D-17	4.3	0.8	0.1	0.70	170	90	185	288	356	99
D-18	2.17*	0.8	0.1	0.58	132					99
D-19	2.17*	0.8	0.2	0.49	102	64	172	342	500	100

* Benzene as solvent.

It will be observed that the nature of the solvent also plays a part in the degradation reaction. From the data in table 6 it can be seen that the extents of degradation in the solvents benzene and carbon tetrachloride are the same, and are greater than that which results when toluene is used as solvent. If a reversible polymerization–depolymerization process involving a radical chain mechanism were occurring, it would be expected that the molecular weights of the products would be related to the chain transfer constants of the respective solvents (5). This is clearly not the case.

To determine the influence of a readily oxidizable substance on the scissioning ability of benzoyl peroxide two degradation experiments were performed in the presence of hydroquinone. The results of these experiments are given in table 7.

TABLE 4

Influence of method of peroxide addition on the scissioning efficiency of benzoyl peroxide at 100°C.

Starting material, polystyrene E (*cf.* table 1)

EXPERIMENT	METHOD OF ADDITION*	$[\eta]$	$\times 10^{-3}$		RECOVERY OF DEGRADED PRODUCT
			$\overline{M}_\eta$	$\overline{M}_n$	*per cent*
D-2A	One addition	0.73	180	97	98
D-2B	Two additions	0.66	158	85	96

* The total amount of peroxide added was 0.2 g. In experiment D-2B the original polymer was treated with 0.1 g. of peroxide, the product isolated, and then treated with another 0.1 g. of peroxide. Concentration, 0.5 g. polymer in 11 ml. toluene.

TABLE 5

Influence of temperature on the scissioning efficiency of benzoyl peroxide

Starting material, polystyrene E (*cf.* table 1); 0.1 g. peroxide added; concentration, 0.5 g. polymer in 11 ml. toluene

EXPERIMENT	TEMPERATURE	$[\eta]$	$\times 10^{-3}$					RECOVERY OF DEGRADED PRODUCT
			$\overline{M}_\eta$	$\overline{M}_n$	$\overline{M}_w$	$\overline{M}_z$	$\overline{M}_{z+1}$	
	°C.							*per cent*
D-1A	100	0.77	190	102	201	297	362	98
D-6A	125	0.74	185	92	195	300	370	98

TABLE 6

Influence of solvent nature on the scissioning efficiency of benzoyl peroxide at 100°C.

Starting material, polystyrene E (*cf.* table 1); 0.1 g. peroxide added; concentration, 0.5 g. polymer in 11 ml. solvent

EXPERIMENT	SOLVENT	$[\eta]$	$\overline{M}_\eta \times 10^{-3}$	RECOVERY OF DEGRADED PRODUCT
				per cent
D-1A	Toluene	0.77	190	98
D-4	Benzene	0.61	140	90
D-5	Carbon tetrachloride	0.61	140	97

It is seen that the hydroquinone competes for and is preferentially attacked by the peroxide. It cannot be stated with certainty that these results in themselves rule out a chain mechanism, but at the same time they are in agreement with what would be expected on the basis of a simple oxidative mechanism.

In the attempt to obtain an equilibrium polystyrene mixture such as has been suggested elsewhere (6, 7), a number of degradation experiments were performed in which large percentages of benzoyl peroxide were added as degradation "catalyst" over an extended period of time. Both fractionated and unfractionated polystyrenes were used in these experiments. The concentration in each case was 0.5 g. polymer in 11 ml. toluene. The total amount of benzoyl peroxide added and the methods of addition were as follows:

Method (a)	5 × 0.1 g.; 1 × 0.2 g.	Total weight of peroxide = 0.7 g. Weight per cent of peroxide = 140 Reaction period = 12 days
Method (b)	5 × 0.1 g.; 5 × 0.2 g.	Total weight of peroxide = 1.5 g. Weight per cent of peroxide = 300 Reaction period = 20 days

In all cases the minimum reaction period between peroxide additions was 48 hr., and the reaction vessel was purged with dry nitrogen after each addition of peroxide and before sealing. The results of these experiments are given in table 8.

TABLE 7

Influence of added hydroquinone on the scissioning efficiency of peroxide at 100°C. in toluene

Starting material, polystyrene H (*cf.* table 1); concentration, 1.6 g. polymer in 10 ml. toluene

EXPERIMENT	MOLES HYDROQUINONE / MOLES BENZOYL PEROXIDE	$[\eta]$	$\bar{M}_n$
D-56	0	0.61	102,000
D-61*	0.3	0.76	
D-62*	0.6	0.82	

* These reaction mixtures became deep red in color as the degradation proceeded, because of the formation of the quinoid structure.

The values of the intrinsic viscosities obtained for the degradation products demonstrate that equilibrium mixtures were not obtained even after 300 per cent by weight of benzoyl peroxide had been added.

A similar experiment was performed on polystyrene of low molecular weight to test the validity of the assumption that both aggregative and disaggregative processes occur to yield the "steady-state" viscosity when polystyrene solutions are treated with benzoyl peroxide. If the assumption is to be acceptable, then it should be possible to demonstrate a net aggregative reaction by starting with a polystyrene having a viscosity well below that of the "steady-state" value, i.e., 3.0 (7). Fraction 8W with an intrinsic viscosity of 0.18 was selected as the starting material. The viscosity-average molecular weight was 30,000, and the relative viscosity at a concentration of 4 g./100 ml. was 1.8. After the reaction the intrinsic viscosity was 0.17.

Thus, the results from this group of experiments do not support the view that an equilibrium polystyrene mixture is obtained when a polystyrene solution is heated with even as much as 300 per cent of peroxide as catalyst. Indeed, the experiments suggest that the scissioning process may be caused to continue by peroxide addition until all the polymer as such has lost its identity.

Degradation experiments were performed on unfractionated polymers having $\bar{M}_n$ values between 100,000 and 250,000. Predicted and observed number-average molecular weights for degraded polystyrenes have been collected to form table 9. The results show that within the molecular range covered (at least) the scissioning ability of benzoyl peroxide is independent of the molecular weight of the original polymer.

TABLE 8

Protracted degradations of polystyrene in toluene

EXPERIMENT	PEROXIDE ADDITION	TEMPERATURE	$[\eta]$	$\times 10^{-3}$					RECOVERY OF FINAL PRODUCT
				$\bar{M}_\eta$	$\bar{M}_n$	$\bar{M}_w$	$\bar{M}_z$	$\bar{M}_{z+1}$	
		°C.							*per cent*
Polystyrene C:			1.40	456	226	459	(833)		
D-11	(a)	100	0.60	138	75				96
D-12	(b)	100	0.44	89	48	97	134	161	100
Fraction 5W:			0.75	185	155	186	230		
3R.	(a)	100	0.45	89	61	88	114		
Fraction 2A-W:			1.51	507	400				
D-14	0.1 g. added	100	1.00	280					
D-15	(b)	100	0.38	72	*	82	136	169	
Fraction 8W:			0.18	30					
8R.	(c)	111	0.17						

* M_n expected to be about 41,000. Note ratios of other moments.

(a) Concentration, 0.5 g. polymer in 11 ml. toluene. Five additions of 0.1 g. peroxide spaced at least 48 hr. apart; final addition of 0.2 g. peroxide. Weight per cent peroxide added (on polymer basis), 140 per cent. Total reaction period, 12 days.

(b) Same as (a) except that five additions of 0.2 g. peroxide were made after the five additions of 0.1 g. Total weight of peroxide added = 300 per cent of polymer weight. Reaction period, 20 days.

(c) Concentration, 0.125 g. polymer in 0.78 ml. toluene. Seven additions of 0.05 g. peroxide; two additions of 0.1 g. Total = 440 per cent. Reaction period, 18 days.

A set of data relative to the influence of temperature of polystyrene polymerization on the degradation behavior in toluene at 100°C. is given in table 10. The temperature of preparation for the polystyrenes used in all of the other experiments was 60°C. Though the limited data suggest that the scissioning efficiency of the peroxide may be somewhat greater in the case of polystyrene prepared at 60°C., the order of the difference is insufficient to indicate that different scissioning mechanisms are operative in the two cases.

B. Sedimentation equilibrium studies

Sedimentation equilibrium experiments were performed with a selected number of degraded polystyrenes. The data from these experiments were intended to show the behavior of the molecular weight distribution of the polystyrene systems at various extents of degradation, and also to permit an assessment of the extent to which the viscosity–molecular weight relationship for the original polystyrenes remains valid for the degraded products.

TABLE 9

Influence of molecular weight of original polymer on the scissioning efficiency of peroxide in toluene at 100°C.

EXPERIMENT	INITIAL $\bar{M}_n \times 10^{-3}$	PEROXIDE ADDED	FINAL $\bar{M}_n \times 10^{-3}$		CALCULATED ASSUMING PEROXIDE EFFICIENCY INDEPENDENT OF PEROXIDE CONCENTRATION	RECOVERY OF DEGRADED PRODUCT
			Calculated*	Observed		
		grams				*per cent*
D-7	108	0.1		87		96
D-1A ..	144	0.1	109	102		99
D-9 ...	226	0.1	150	155		100
D-2B..	102	0.1	83	85		96
D-8	108	0.2		85	73	98
D-2A .	144	0.2	106	100	88	96
D-10 .	226	0.2	144	145	117	97

* One experiment was selected from each series and the number of chain scissions computed from the change in $\bar{M}_n$. Then the $\bar{M}_n$ to be expected was calculated from the original value of M_n for the other experiments in the same series, assuming this same number of chain scissions to be independent of molecular weight.

TABLE 10

Influence of temperature of polymerization of polystyrene on degradation behavior at 100°C. in toluene

Concentration, 0.5 g. polymer in 11 ml. toluene

EXPERIMENT	WEIGHT OF PEROXIDE	[η]	$\bar{M}_n \times 10^{-3}$	RECOVERY OF DEGRADED PRODUCT
A. Polystyrene H, prepared at 100°C.				
	grams			*per cent*
Polystyrene H ..		0.88	145	
D-51 ...	0.1	0.71	118	98
D-52	0.2	0.66	107	98
B. Polystyrene E, prepared at 60°C.				
Polystyrene E ...		0.97	144	
D-1A	0.1	0.77	102	98
D-2A.	0.2	0.72	95	92

As previously outlined the ratios of $\bar{M}_n:\bar{M}_w:\bar{M}_z$ should tend to 1:2:3 as degradation proceeds, whether the degradation process involves an approach to an equilibrium condition by way of a radical chain mechanism or whether the degradation process is one involving simple scissioning of "infinite" chains. Thus, if the original polymer has a molecular weight distribution such that the ratios $\bar{M}_n:\bar{M}_w:\bar{M}_z$ are 1:2:3, these ratios should be maintained as degradation proceeds. For fractionated polystyrenes of sharper distribution, however, degradation should cause the distribution to broaden and the ratios should tend toward 1:2:3. If a chain radical mechanism is the correct mechanism for the degradation reaction, with the peroxide acting as chain initiator, then it would be expected that for fractionated polystyrenes a small amount of peroxide would produce a relatively large change in distribution, even though the net number of detectable scissions was small. However, if the degradation proceeds by way of a simple irreversible scissioning process, then the rate at which the distribution broadens would be more closely related to the rate at which the number of detectable scissions is produced.

A comparison of the weight- and viscosity-average molecular weights (table 1) of the unfractionated polystyrenes A, C, and E prepared in the oil phase at 60°C. shows that these two molecular weight averages do not differ by more than 8 per cent. The viscosity–molecular weight relation may be expressed in the form $[\eta] = kM^a$, where the values of the constants, k and a, depend on the temperature of polymerization (1). Thus it follows that if simultaneous polymerization–depolymerization is involved in the peroxide degradation of the polystyrene then the viscosity–molecular weight relationship, which holds well for the unfractionated polystyrenes prepared at 60°C., should fail to hold for the products obtained upon degradation at 100°C. and 125°C. If, however, the degradation process involves simple scissioning of the parent molecules, the viscosity relation would be expected to remain more nearly valid even after considerable scissioning and regardless of the temperature at which the scissioning occurs. The scissioning must, of course, occur in solutions sufficiently dilute so that cross-linking does not interfere.

The collected data for the degraded polystyrenes on which sedimentation equilibrium experiments were made are given in table 11, together with the corresponding data for the original polymers. The ratios of the molecular weights are given in the form $\bar{M}_{q+1}/\bar{M}_q$ (where q takes the values 0, 1, and 2) instead of the form $\bar{M}_n:\bar{M}_w:\bar{M}_z$, for greater flexibility in handling the data.

The values of the molecular weight ratios for experiment 3R show the broadening of the molecular weight distribution with degradation. The extent of this broadening, however, appears to be small, considering that 140 per cent by weight of peroxide had been used in the degradation. This result supports the simple scissioning hypothesis, for had a chain mechanism been involved greater spreading should have resulted. The data for experiments D-1A and D-6A in which the degradations were performed at 100°C. and 125°C., respectively, with 20 per cent by weight of peroxide, show that the molecular weight ratios are in each case essentially the same as for the original polystyrene E. The results for experiments D-12 and D-17 also show no appreciable change in molecular weight distribution from the original polystyrene A. Strong evidence for the occurrence of cross-linking when the degradation is carried out at higher polymer concentrations is provided by the data for experiment D-19, where not only are the molecular weight ratios markedly higher than expected, but also the deviation between $\bar{M}_\eta$ and $\bar{M}_w$ shows the marked failure of the viscosity–molecular weight relationship. Though complete data were not available for the degradation product from experiment D-15 nor for the original polystyrene fraction 2A, the results indicate a marked broadening of the distribution. From the sedimentation data alone for this experiment it would appear that the molecular weight distribution had broadened to the limiting function.

A comparison of the viscosity-average and weight-average molecular weights (columns 7 and 8 of table 11) shows that the viscosity–molecular weight relationship holds as well for the degradation products as for the original polystyrenes.

TABLE 11

Collected data for sedimentation equilibrium experiments on degraded polystyrenes

EXPERIMENT	CONCENTRATION OF DEGRADATION SOLUTION	WEIGHT PER CENT PEROXIDE	DEGRADATION TEMPERATURE	$[\eta]$	$\times 10^{-3}$					RATIO M_{q+1}/M_q		
			°C		$\bar{M}_n$	$\bar{M}_\eta$	$\bar{M}_w$	$\bar{M}_z$	$\bar{M}_{z+1}$	$q = 0$	$q = 1$	$q = 2$
Fraction 5W.....				0.75	155	185	186	230		1.20	1.24	
3R.. . .	0.5 g. in 11 ml. toluene	140	100	0.45	61	89	88	114		1.44	1.30	
Whole E.. ..				0.97	144	267	287	469	705	1.99	1.63	1.50
D-1A .	0.5 g. in 11 ml. toluene	20	100	0.77	102	190	201	297	362	1.97	1.48	1.22
D-6A.	0.5 g. in 11 ml. toluene	20	125	0.74	92	185	195	300	370	2.12	1.54	1.23
Whole A.				0.82	109	202	219	320	390	2.00	1.46	1.22
D-12	0.5 g. in 11 ml. toluene	300	100	0.44	48	89	97	134	161	2.02	1.38	1.20
D-17 . ..	0.8 g. in 4.3 ml. toluene	12.5	100	0.70	84	170	185	288	356	2.20	1.55	1.24
D-19..........	0.8 g. in 2.15 ml. benzene	25	100	0.49	64	102	172	342		2.70	1.99	
Fraction 2A. .				1.51	400	507				1.27		
D-15...	0.5 g. in 11 ml. toluene	300	100	0.38	*	72	82	136	169		1.60	1.24

* M_n too low for reliable osmotic measurement.

The only exception is in the data for experiment D-19, where the deviation is almost certainly the result of cross-linking, as previously mentioned. That the viscosity–molecular weight relationship holds as well for the degradation products as for the original polystyrenes is strong evidence supporting the simple scissioning hypothesis.

C. Viscometry

In the viscosity equation

$$\frac{\eta_{sp}}{c} = [\eta] + k'[\eta]^2c$$

the value of the constant k' for dilute solutions of polystyrene depends on the nature of the solvent and the temperature of preparation of the polymer (1). If a chain radical mechanism predominates in the peroxide degradation of polystyrene, the value of k' for degradation products should tend to an equilibrium value. Actually, the observed values for k' in a number of degradation systems show no trend away from those for the corresponding original polystyrenes, the deviations which exist being always within the limits of experimental accuracy. So, again the evidence supports an oxidative scissioning mechanism rather than a catalyzed chain radical mechanism.

V. GENERAL REMARKS

Since the statement has been made that " . . . polymerization catalysts—such as benzoyl peroxide—which decompose to free radicals may also catalyze degradation" (7), it is of interest to assess the efficiency of the peroxide in degradations of this type. Calculation of this efficiency from the number-average molecular weights before and after degradation shows that in all of the experiments performed more than 150 molecules of peroxide were required for each detectable scission. On this basis, therefore, benzoyl peroxide may not be regarded as a chain radical catalyst in the degradation process. It may be argued that the net number of detectable scissions is very small as compared with the actual number of scissions which would be detectable were it not for an aggregative free-radical process. That there is no appreciable rearrangement or aggregation of free-radical fragments during the degradation process is indicated by the following experimental observations:

(*1*) No aggregative reaction was detected for polymers of very low molecular weight.

(*2*) The intrinsic viscosity–molecular weight relation which holds well for the original polystyrene holds equally well for the degraded products.

(*3*) The rate at which the molecular weight distribution of a polystyrene fraction broadens with peroxide addition is very slow.

(*4*) The value of the constant k' in the reduced viscosity equation shows no marked deviation from its original value as degradation proceeds.

Hence, viscosity measurements alone and combined with the weight-average molecular weights from sedimentation equilibrium measurements provide strong support for a simple scissioning mechanism. The evidence, however, is markedly more conclusive when we consider the higher molecular weight averages determined by sedimentation equilibrium measurements. The ratios of the various average molecular weights of a polymer are functions of the molecular weight distribution of the polymer. When these ratios increase very slowly as degradation proceeds, it may be safely concluded that the molecular weight distribution also broadens very slowly.

A further point which must not be overlooked, though it does not appear to be significant from the experimental results obtained, is the possible occurrence of preferential scissioning of small segments from the ends of the polymer chains. A moderate amount of such scissioning would not be detectable by the physicochemical techniques employed; a large amount of such scissioning would be indicated by low values for "percentage recovery" in the degradation experiments. The experimental values for the recovery did not indicate any such marked preferential chain end scissioning.

From the statement " . . . catalysts of polymerization are also in general catalysts for degradation, and that in many cases steady states, or possibly equilibrium states, are reached for which the rates of polymerization and degradation become equal" (6), it is seen that the criterion which has been accepted as indicating the existence of simultaneous polymerization and degradation is the approach to a steady-state viscosity as degradation proceeds. An analysis of the validity of this criterion follows.

Consider unfractionated polystyrene prepared in the oil phase at 60°C. with benzoyl peroxide as catalyst where the ratio $\bar{M}_n:\bar{M}_w = 1:2$.[3] Assume that this polymer in solution is subjected to some random scissioning process, the exact mechanism of which is immaterial. Then the value of the ratio $\bar{M}_n:\bar{M}_w$ will remain 1:2 as the degradation proceeds. For simplicity of argument consider one polymer molecule and let it be scissioned once, i.e., one molecule becomes two molecules and $\bar{M}_n$ changes by 50 per cent. Let the scissioning process continue until the original molecule has become 100 molecules; then as a result of the next single scission the 100 molecules become 101 molecules and $\bar{M}_n$ changes by 1 per cent. Applying this same argument to the whole polymer sample and remembering that the ratio $\bar{M}_n:\bar{M}_w$ remains 1:2, we find that the change in $\bar{M}_w$ for the first cut per molecule is 50 per cent while it is but 1 per cent for the hundredth cut, and so on. Thus, if we start with k molecules of polymer of $\bar{M}_n = \bar{M}_{n_0}$, and if we distribute among them k scissions at random, and repeat the scissioning at equal time intervals (i.e., uniform rate of scissioning of k scissions per unit time), the molecule weight $\bar{M}_n$ of the product will take on the successive values $\bar{M}_{n_0}$, $\bar{M}_{n_0}/2$, $\bar{M}_{n_0}/3, \ldots$, or $\bar{M}_{n_0}/(N+1)$, where N is the number of equal time intervals completed. Since $\bar{M}_w$ is always equal to $2\bar{M}_n$, $\bar{M}_w$ takes on the successive values

$$\frac{\bar{M}_{w_0}}{N+1} \qquad \text{where } N = 0, 1, 2, \cdots$$

Thus, we may say that $\bar{M}_w$ decays "harmonically" with the number of scissions, or with time if the rate of scissioning is uniform.

Let us now consider the accompanying change in viscosity. Since the viscosity of a polymer in a given solvent at constant concentration depends on (*a*) the size of this type of polymer molecules, and (*b*) the amount of "interference" between molecules, we see that the contribution to the viscosity due to size will decrease approximately "harmonically" along with $\bar{M}_w$, or, what is almost equivalent, the intrinsic viscosity decreases "harmonically"; the "interference" factor varies approximately exponentially with particle size for constant concentration, and for uniform decrease in $\bar{M}_w$ the "interference" factor falls off roughly exponentially. From this it follows that the rate of change of relative viscosity with time—assuming a hypothetical uniform rate of scissioning—combines both the "harmonic" and exponential rates of decay; and on plotting relative viscosity against time for the hypothetical scissioning process a curve is obtained which has a sharp initial slope, and which rapidly tends to almost zero slope. We thus have what appears to be a "steady-state" viscosity even though scissioning continues at a uniform rate (figure 2).

---

[3] Even where the ratio $\bar{M}_n:\bar{M}_w$ for the original polystyrene differs from 1:2 the argument remains valid in essence, for we have shown that the rate at which this ratio changes with peroxide addition is very slow.

The important conclusion to be drawn from this argument is that ordinary viscosity measurements will appear to indicate the existence of a steady-state viscosity; and it is true that the viscosity does remain very nearly constant as peroxide addition is continued. Yet the number of scissions, i.e., the amount of degradation, produced by each 0.1 g. of peroxide in the "steady-state" portion of the curve for the hypothetical scissioning process is exactly the same as that produced by the first addition of peroxide where the viscosity changes rapidly. Very accurate intrinsic viscosity measurements would be essential for the experimental detection of this fact. If the peroxide addition were carried on long enough it is apparent that the decrease in intrinsic viscosity produced by 0.1 g. of peroxide would lie well within the limits of experimental accuracy of the usual viscosity measurements.

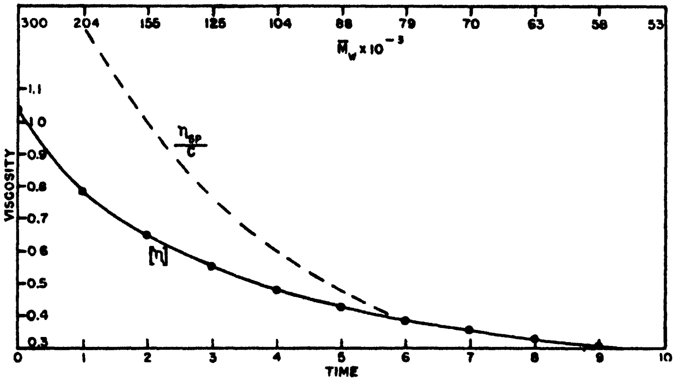

FIG. 2. Plot of viscosity against time for the degradation of polystyrene in solution showing viscosity behavior for a hypothetical uniform-rate scissioning process, and weight-average molecular weights corresponding to equal time intervals.

The above discussion has assumed that each addition of peroxide produces the same number of scissions. This has been shown to hold over the number-average molecular weight range 100,000 to 250,000 provided the degradation product is isolated after each peroxide addition. However, if the polymer is not isolated at each stage, it is clear that the degradation products of the peroxide itself will accumulate, and the detectable scissioning ability of the peroxide will fall off as the process continues, owing to the ever-increasing interference of these accumulating degradation products. Thus, in such an experiment the attainment of a "steady-state" viscosity would appear even more real than if the polymer product were isolated after each peroxide addition.

The results of the degradation experiments which showed that the scissioning ability of benzoyl peroxide varies with temperature, peroxide and polymer concentration, and nature of solvent are in accord with the recent work of several authors (2), (although temperature variation is slight, as shown in table 5). They have shown that, though the manner of decomposition of benzoyl peroxide under different conditions is not yet fully understood, the kinetics and also the stoichiometry of the decomposition in solution vary with these factors. Thus it is reasonable to expect that the scissioning ability of benzoyl peroxide on polystyrenes should also vary with temperature, peroxide concentration, and nature of solvent. The "peroxide wastage" factor of Barnett and Vaughan (2), i.e., dissipation of the catalyst without forming free radicals, appears to be related to our observation that the scissioning efficiency of the peroxide decreases as its concentration is increased. Further, since the mode of peroxide decomposition varies with the nature of the solvent, it follows that its mode of decomposition will also vary with the nature of other solutes, e.g., monostyrene, polystyrene, hydroquinone, products from its own decomposition, etc.

Reactions involving the decomposition of benzoyl peroxide are undoubtedly very complicated—some of them are known to involve free radicals and others not—hence it appears judicious at this time to reserve speculation on the exact nature of the reaction involved in polymer scissioning until more detailed information on the manner of benzoyl peroxide decomposition under simpler conditions is available. Free radicals may play a part in the degradative process, but certainly not in the same manner as they do in the polymerization of the monomer. The mechanisms of the two reactions are quite different; the polymerization reaction involves a chain radical mechanism, whereas the depolymerization reaction is probably one of simple random oxidation. Therefore the conclusion from this work must be—as stated by Flory (3) for vinyl-type polymerizations—that "these processes generally are not reversible in the thermodynamic sense."

VI. SUMMARY

The degradation of polystyrene in solution under a variety of conditions has been studied by the techniques of viscometry, osmometry, and sedimentation equilibrium. In the absence of oxygen and benzoyl peroxide at 100°C. no detectable degradation occurs within a period of six months; at room temperature and in the presence of oxygen no measurable degradation occurs within a period of two years. In the presence of oxygen or benzoyl peroxide the extent of the degradation depends on the concentration of the polymer and peroxide (or oxygen), and the nature of the solvent. There is little temperature dependence. For conditions otherwise constant the scissioning efficiency of benzoyl peroxide is independent of the molecular weight of the initial polystyrene. The scissioning efficiency of the peroxide for all of the conditions investigated was very low; each detectable scission required more than 150 molecules of peroxide. No evidence for the occurrence of an aggregative reaction in dilute solution was obtained.

Sedimentation equilibrium, viscosity, and osmotic pressure studies made on the isolated degradation products support a simple oxidative mechanism for the degradation reaction rather than a chain mechanism. The approach to a steady-state viscosity as degradation proceeds is shown to be an insufficient criterion for establishing the existence of simultaneous polymerization and depolymerization.

The author wishes to express his appreciation to Drs. M. Wales and J. W. Williams for their interest, suggestions, and encouragement.

REFERENCES

(1) ALFREY, T., BARTOVICS, A., AND MARK, H.: J. Am. Chem. Soc. **65**, 2319 (1943).

(2) BARNETT, B., AND VAUGHAN, W. E. J:. Phys. & Colloid Chem. **51**, 926 (1947); see also CASS, W. E.: J. Am. Chem. Soc. **68**, 1976 (1946); KHARASCH, M. S., JENSEN, E. V., AND URRY, W. H.: J. Org. Chem. **10**, 386 (1945); NOZAKI, K., AND BARTLETT, P. D.: J. Am. Chem. Soc. **68**, 1686 (1946).

(3) FLORY, P. J.: J. Chem. Phys. **12**, 435 (1944).

(4) KUHN, W.: Ber. **63**, 1503 (1930).

(5) MAYO, F. R.: J. Am. Chem. Soc. **65**, 2324 (1943).

(6) MESROBIAN, R. B., AND TOBOLSKY, A. V.: J. Am. Chem. Soc. **67**, 785 (1945).

(7) MESROBIAN, R. B., AND TOBOLSKY, A. V.: J. Polymer Sci. **2**, 463 (1947).

(8) SCATCHARD, G., ONCLEY, J. L., WILLIAMS, J. W., AND BROWN, A.: J. Am. Chem. Soc. **66**, 1980 (1944).

(9) SPODHEIM, H. W., BADGLEY, W. J., AND MESROBIAN, R. B.: J. Polymer Sci. **3**, 410 (1948).

(10) STOCKMAYER, W. H.: In *Advancing Fronts in Chemistry*, Vol. 1. Reinhold Publishing Corporation, New York (1945).

(11) TAYLOR, H. S., AND TOBOLSKY, A. V.: J. Am. Chem. Soc. **67**, 2063 (1945).

(12) TOBOLSKY, A. V.: J. Chem. Phys. **12**, 402 (1944).

(13) WALES, M.: J. Phys. & Colloid Chem. **52**, 235 (1948).

(14) WALES, M., WILLIAMS, J. W., THOMPSON, J. O., AND EWART, R. H.: J. Phys. & Colloid Chem. **52**, 984 (1948).

(15) ZIMM, B. H., AND MYERSON, I.: J. Am. Chem. Soc. **68**, 911 (1946).

HEATS OF ADSORPTION. III

METHANOL ON CARBON[1]

CONWAY PIERCE AND R. NELSON SMITH

Department of Chemistry, Pomona College, Claremont, California

Received May 2, 1949

Recent papers by Halsey (5) and by the writers (11) have independently given arguments supporting the view that adsorbing surfaces of solids are nonuniform in physical adsorptions. This view is not new, but it has largely been ignored in recent years because of the success of the B.E.T. equation, which is based upon the assumptions that the heat of adsorption is uniform in the first layer and that after the first layer is completed further adsorption is on a uniform and liquid-like surface. Actually, these assumptions are not needed in the basic B.E.T. concept of multimolecular adsorption in layers of varying thickness, and Joyner and Emmett (7) stress the fact that E_1 as used in the equation does not necessarily agree with direct experimental values for heat of adsorption in the first layer. There is, however, a general tendency to ignore the fact that these assumptions are simplifications needed to carry out the mathematical derivation of the B.E.T. equation and to accept them as rigorously true.

In our previous work we concluded that (*1*) surfaces have sites of varying activity, each of which can hold adsorbate at a given relative pressure; (*2*) a type II isotherm is the result of two separate processes, adsorption on a bare surface and on a previously covered surface, and these can be described by a two-term equation

$$V = \frac{ax}{1 + bx} + \frac{\alpha x}{1 - \beta x} \tag{1}$$

in which the first term gives adsorption on the bare surface and the second adsorption beyond the first layer[2]; (*3*) the net heat of adsorption does not become zero until $p = p_0$; (*4*) in layers beyond the first the net heat is related to relative pressure by the equation

$$E - E_L = K(1 - x) \tag{2}$$

We have found further evidence for our views in a new type of adsorption isotherm, that of methanol on nonporous carbon surfaces, which is described herein.

EXPERIMENTAL

Isotherms were determined for methanol on graphite NC-1, Graphon, and activated charcoal S600H.

---

[1] This is a progress report on work done under Contract N8 onr 54700 with the Office of Naval Research.

[2] Halsey (5) expresses the same idea by the relation $\theta = \theta_{c-1} + 1$ in his discussion of the B.E.T. equation.

Graphite NC-1 was obtained from the National Carbon Company.[3] It has an ash content below 0.001 per cent and is free of oxygen complex. The nitrogen area[4] is 4.0 sq. m. per gram. The sample was from the lot previously used for determination of the isotherms of ethyl chloride, ammonia, and water (11).

Graphon[5] is graphitized Spheron Grade 6 carbon black. The sample was from the same batch as that used by Beebe and associates (1) and by Joyner and Emmett (7). The nitrogen area is *ca.* 80 sq. m. per gram.

Charcoal S600H was prepared by the carbonization of Saran. Its preparation and properties have been described in a previous publication from this laboratory (8).

Isotherms were determined at temperatures of 0° and 28.9°C. when isosteric heats were desired, otherwise at 0°C. only. All isotherms were determined by a gravimetric method of removing and weighing the sample bulb after each addition of vapor. At 0°C. the vapor pressures were read by a modified McLeod gage.

The complete isotherm for NC-1 at 28.9°C. is shown in figure 1. Figure 2 shows the low pressure region for the NC-1 isotherms at 0° and 28.9°C. and a portion of the 0°C. isotherm for Graphon. The latter was extended to 167 ml. (S.T.P.) at $x = 0.98$. The 0°C. isotherm for S600H is shown in figure 6. The lower curve gives the low pressure values on expanded scale.

DISCUSSION

The isotherms of figures 1 and 2 are of a type not previously reported. In line with Brunauer's classifications, we suggest that they be designated as type VI. As shown in figures 1 and 2, these isotherms start out convex to the pressure axis, or as type III or V, then become concave and change to a type II shape. From point *B* on they are exactly like the type II ethyl chloride isotherms on the same adsorbents.

These type VI isotherms provide evidence for our postulate that adsorption in the first layer must be treated as a separate process from adsorption in layers beyond the first. For both graphite and Graphon the amount taken up at point *B* corresponds closely with the computed value of V_m, based on the known nitrogen surface areas of the samples and a computed area of 16.2 sq. Å. for the methanol molecule. NC-1 has a computed V_m value of 0.89 ml. (S.T.P.), as compared with a point *B* value of near 0.9, and Graphon has a computed V_m value of 18.7 ml., as compared with a point *B* value of about 19 ml. These isotherms, therefore, show that the first layer is essentially filled before there is appreciable multilayer adsorption, even though the first layer does not fill at the low relative pressures which are characteristic of type II isotherms (where point *B* is usually located at relative pressures below 0.1).

Isosteric heats of adsorption for methanol on graphite are shown in figure 3.

---

[3] Through the courtesy of Dr. Lester L. Winter, National Carbon Company, Cleveland, Ohio.

[4] Determined by Professor R. A. Beebe and Miss M. H. Polley of Amherst College.

[5] Furnished by Dr. Walter Smith of the Godfrey L. Cabot Company, Boston, Maasschusetts.

As might be predicted from the shapes of the isotherms, the net differential heats of adsorption are quite different from those previously reported (11) for ethyl chloride on the same adsorbent. For ethyl chloride $E - E_L$ is above 1800 cal. per mole until after completion of the first layer; then it drops rapidly to the low values characteristic of adsorption beyond the first layer. The net heat for methanol drops from 3000 cal. per mole for the first portions adsorbed to about 600 cal. per mole at about $0.5V_m$, then remains fairly constant until the first layer is completed, after which it drops to the low value for multilayer adsorption.

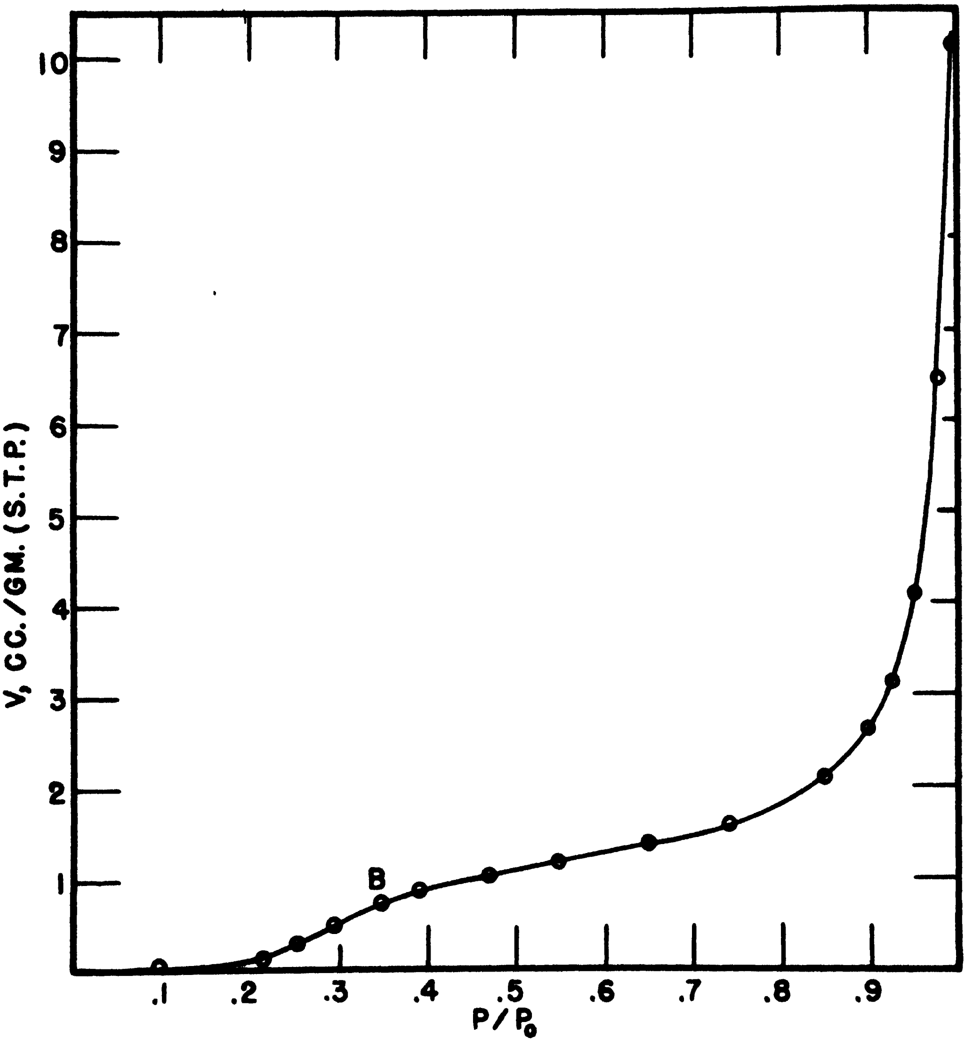

FIG. 1. Isotherm of methanol on graphite NC-1 at 28.9°C.

The shape of the methanol heat-volume curve indicates nonuniformity of the surface. Only a small fraction of sites can hold adsorbate at low relative pressure, but as pressure is increased the active fraction of the surface increases rapidly and complete coverage occurs at relative pressure near 0.3. After this occurs another type of distribution of active sites governs adsorption beyond the first layer. The similarity of the isotherm to that for ethyl chloride after point *B* is passed indicates that the same distribution of sites is effective for both ethyl chloride and methanol after the first layer is completed.

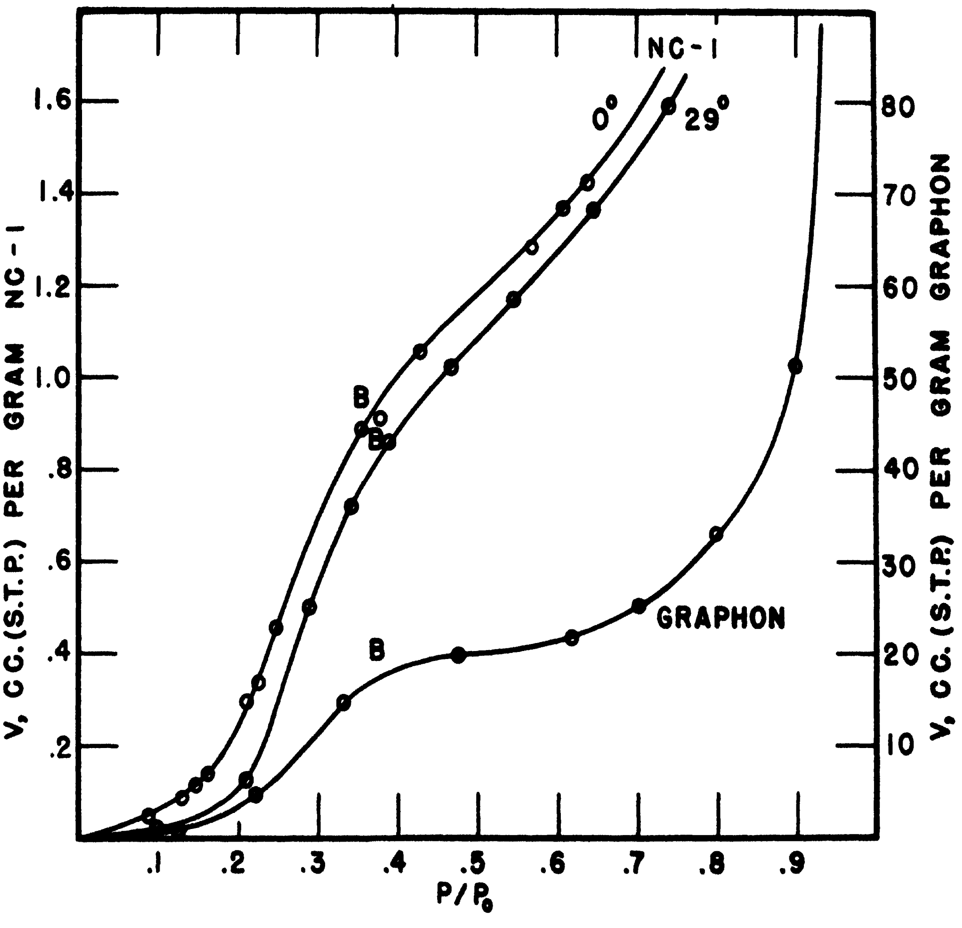

FIG. 2. Isotherms of methanol on graphite and Graphon

The flattening of the heat-volume curve in the region $0.5V_m$ to V_m may be due either to a uniform activity of the last half of the surface (after the most active sites have been covered) or to the influence of previously adsorbed molecules after the surface has become partially covered. The data do not permit one to prove either explanation to the exclusion of the other.

The discovery of type VI isotherms as intermediate between types II and III permits a generalization as to the relation between heat of adsorption and the type of isotherm that is obtained. When the heat of adsorption is high at *all* sites, the first layer is formed at low relative pressure and the isotherm is type II. When only a small fraction of sites can adsorb at low relative pressure the first layer is not completed until pressures are so high that multilayer adsorption is extensive. In this case there is no break in the isotherm at completion of the monolayer and the isotherm is type III, convex to the pressure axis at all relative pressures. Finally, when surface activity is low but all sites can adsorb a first layer before the pressure is high enough for much multilayer adsorption, a type VI isotherm is obtained.

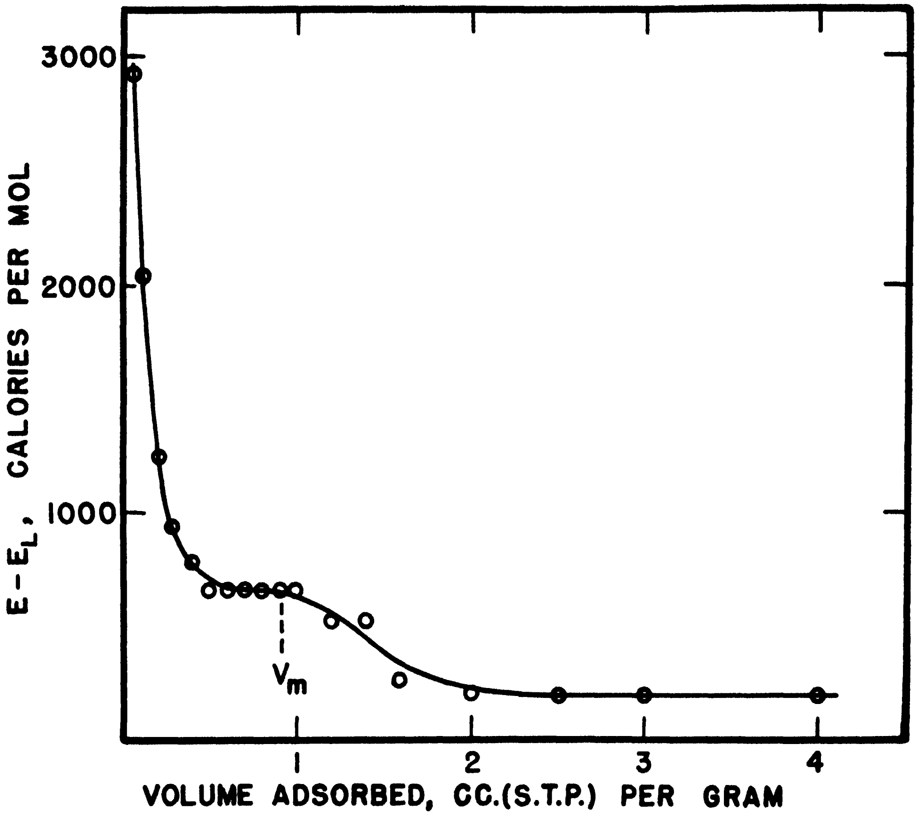

FIG. 3. Isosteric heats of adsorption for methanol on graphite

Type III isotherms are exceedingly rare; in fact, we know of but one example, water on graphite. In a previous paper (11) we listed ammonia on graphite as belonging to type III, but re-examination of the data now leads to classifying it as type VI. There is a small discontinuity near $0.5p_0$ and the points are better fitted by drawing the isotherm as type VI. Moreover, the rise occurs where the amount adsorbed is about that computed for a monolayer, as in the methanol isotherms. We were aware of this apparent break in the curve at the time the isotherms for ammonia were determined but assumed the break to be due to experimental error. That the isotherm is really type VI now seems probable.

In early applications of the B.E.T. theory Brunauer, Deming, Deming, and Teller (3) listed the isotherms of bromine and iodine on silica gel, determined by Cameron and Reyerson (4), as belonging to type III. Actually, this is not consistent with the typical type III isotherm later given by Brunauer in his book (2, page 150). The typical isotherm is a smooth convex curve extending to near p_0, while the bromine and iodine isotherms when plotted on a relative pressure basis as in figures 4 and 5 are rising too steeply to be type III. Since silica gel is known to have capillaries we believe that the bromine and iodine isotherms if continued to high relative pressures would be type V, or like the isotherms of water on charcoal.

On the basis of the B.E.T. treatment and the extension given by Brunauer, Deming, Deming, and Teller (3) it is customary to assume that when an isotherm is concave to the pressure axis $C > 1$ or $E_1 > E_L$. Conversely, it is held that a convex isotherm is indicative that $C \leq 1$ or $E_1 \leq E_L$. Our data for methanol show conclusively that these assumptions are incorrect. The methanol isotherms are initially convex where the net heat of adsorption has a high positive value and they become concave in a region where the net heat is small, some 600 cal. per mole. Our interpretation is, as stated above, that whether an isotherm is concave or convex depends upon the distribution of active sites and the manner in which the distribution changes with increase in pressure. Our data in this and the preceding papers show that for both convex and concave isotherms the net heat is positive.

We cannot agree with the interpretation given by Brunauer, Deming, Deming, and Teller for the isotherms of bromine and iodine on silica gel. The original adsorption data are replotted on a relative pressure basis in figures 4 and 5. To make these plots we used the vapor pressure data of the *International Critical Tables* for iodine and the values of Scheffer and Voogd (10) for bromine.

With the exception of a few scattered points the bromine data for temperatures of 58°, 79°, and 99.9°C. fall on one curve and the data for 117.5° and 137.7°C. on another curve which is displaced to the right or in a direction to indicate a positive net heat of adsorption. If the net heat is zero, as assumed, all points should lie on the same curve.

There is considerable spread in the iodine points and for all temperatures except 98°C. the data fall near a median curve; the 98°C. points fall to the right or in a direction to indicate a negative net heat. We feel, however, that this shift is not conclusive in view of the spread in points for all other temperatures. Our interpretation of the relative pressure plots of the isotherms is that the data do not justify a positive conclusion regarding the sign of the net heats of adsorption. They do indicate that the net heats of adsorption are small. Certainly they do not warrant the assumption made that $E_1 - E_L$ for iodine is -3500 cal. For a heat difference of such magnitude there should be a wide spread between the isotherms for the various temperatures, when these are plotted against relative pressures.

None of the existing isotherm equations will fit a type VI isotherm throughout the entire relative pressure range, nor does it appear feasible to devise a single equation which will fit. The difficulty is that the term which fits the first portion must be of such a nature as to become constant when the monolayer has been

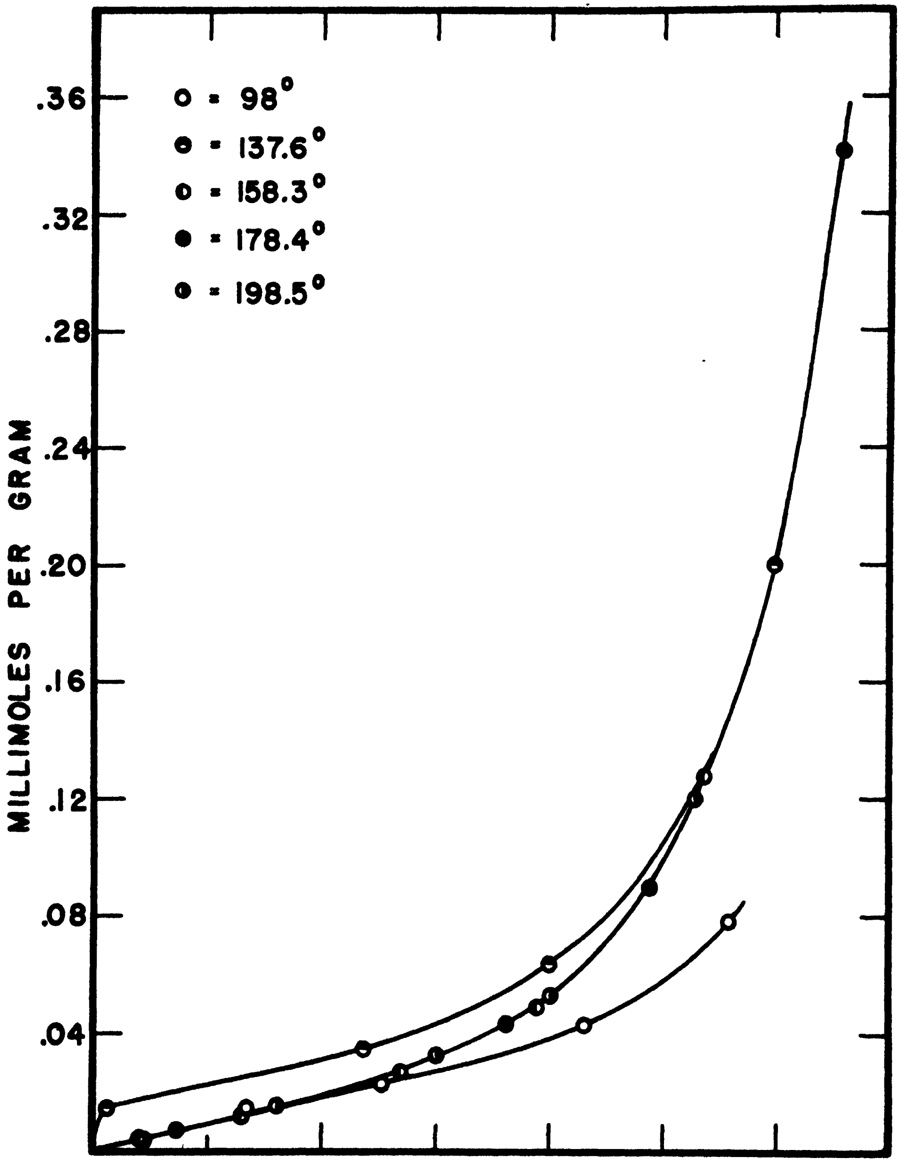

FIG. 4. Isotherms of iodine on silica gel; data of Cameron and Reyerson (4)

completed. From point *B* on, however, the isotherm can be fitted by an equation of the form

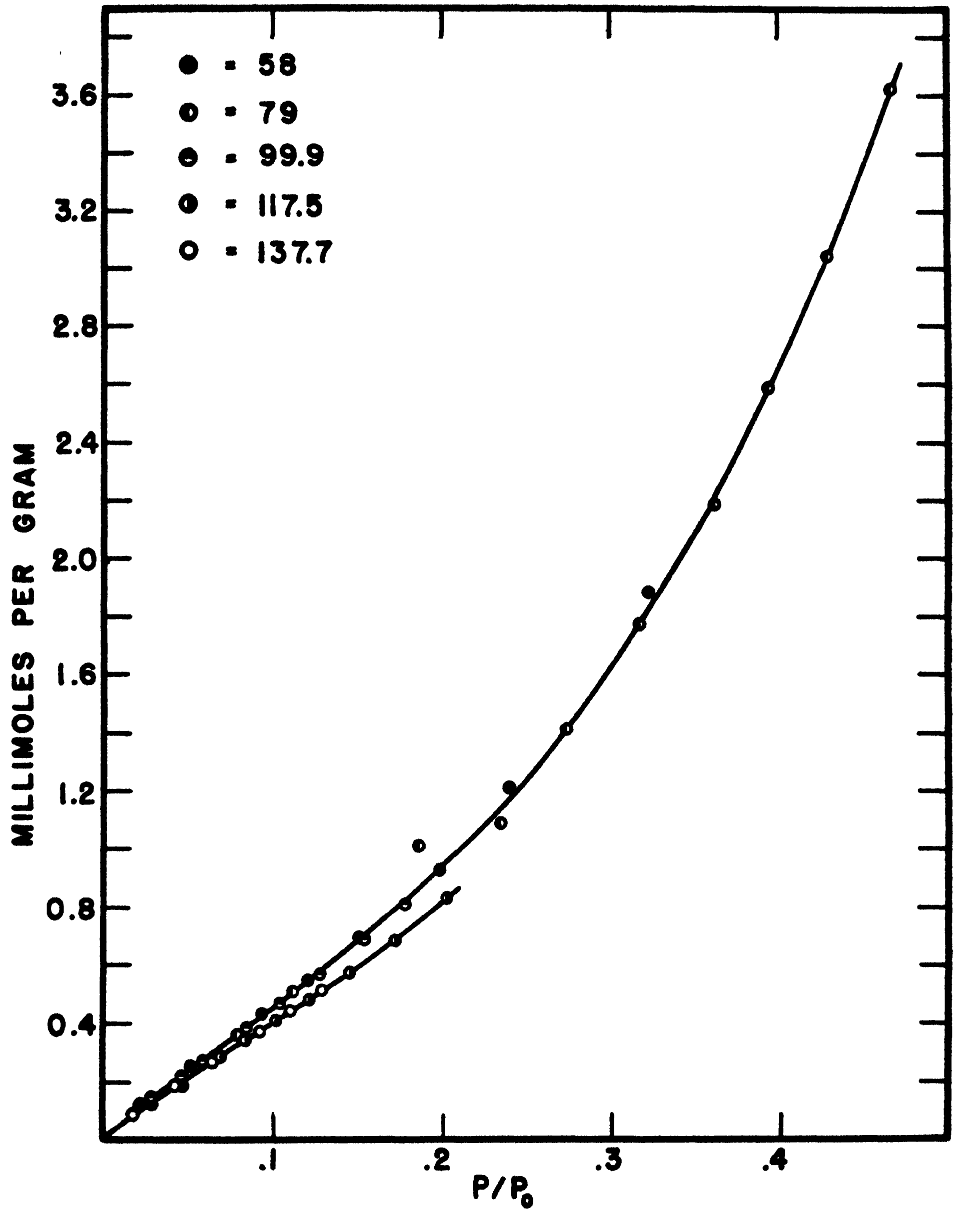

Fig. 5. Isotherms of bromine on silica gel; data of Cameron and Reyerson (4)

$$V = V_m + \frac{\alpha x}{1 - \beta x} \tag{3}$$

The second term of this gives the adsorptions beyond the first layer, as previously shown for numerous isotherms.

In a recent paper (8) we showed that activated charcoal will hold a given adsorbate much more tenaciously than will a nonporous carbon surface. We attribute the difference to the coöperative effect of opposite walls in the capillaries of charcoal. The adsorption of methanol gives a good example of this effect. The isotherm of methanol on a fine-pore charcoal, charcoal S600H, is shown in

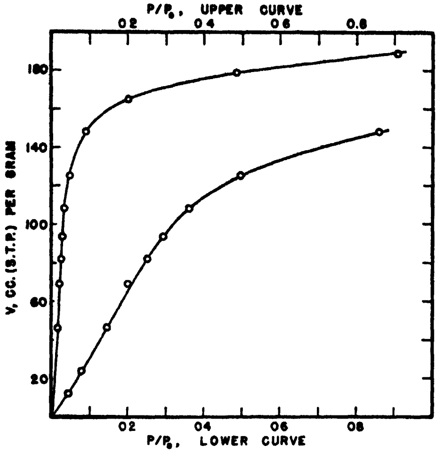

FIG. 6

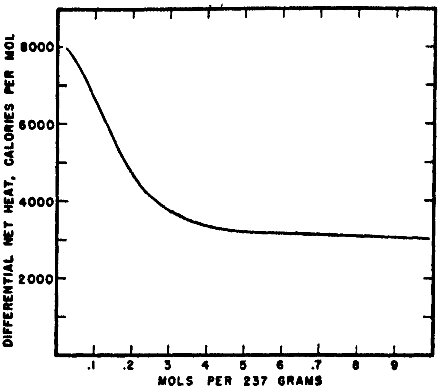

FIG. 7

FIG. 6. Isotherm of methanol on activated charcoal. The lower curve shows the low pressure region on an expanded scale.

FIG. 7. Net heat of adsorption for methanol on charcoal. Computed from Razouk's data (9) for heats of wetting.

TABLE 1

Computation of integral heat of adsorption of methanol on charcoal from heats of wetting Data of Razouk (9)

(1) p/p_0	(2) WEIGHT OF CH_3OH PER GRAM	(3) MOLES ADSORBED PER 237 G CHARCOAL	(4) HEAT OF WETTING	(5) DECREASE IN HEAT OF WETTING PER GRAM	(6) INTEGRAL HEAT OF ADSORPTION (COLUMN 5 × 237)
			cal./gram	*cal /gram*	
0.000	0.0000	0.000	17.0	0.0	0
0.002	0.0192	0.142	12.5	4.5	1065
0.008	0.0391	0.29	9.8	7.2	1710
0.017	0.0477	0.354	8.9	8.1	1920
0.040	0.0673	0.50	6.9	10.1	2390
0.079	0.0810	0.60	5.5	11.5	2720
0.173	0.0963	0.715	4.0	13.0	3080
0.273	0.1054	0.78	2.8	14.2	3360
0.372	0.1117	0.825	2.3	14.7	3480
0.521	0.1197	0.887	1.7	15.3	3620
0.621	0.1239	0.917	1.3	15.7	3720
0.760	0.1288	0.955	0.7	16.3	3860
0.884	0.1328	0.98	0.3	16.7	3950
0.972	0.1343	0.995	0.1	16.9	4000
1.000	0.1350	1.00	0.0	17.0	4030

figure 6. Comparison with figures 1 and 2 shows that the initial convex portion of the isotherm has practically disappeared in charcoal adsorption and that at a relative pressure of 0.1 the charcoal holds some 80 per cent of its saturation volume. As previously discussed, we believe that there is capillary condensation in charcoal pores at pressures even lower than those which produce a monolayer on a plane carbon surface.

With our data for graphite and the data of Razouk (9) for heats of wetting, we can compare relative heats of adsorption for methanol on charcoal and graphite. Razouk measured heats of wetting for charcoal samples previously brought to equilibrium with various partial pressures of methanol vapor. As shown by Harkins and Jura (6), integral heats of adsorption can be computed from such data, since the heat of wetting for a partially saturated sample is less than that of a dry sample by an amount equal to the heat evolved when the given amount of vapor was adsorbed. Details of the calculation from Razouk's data are shown in table 1. His original values are given in terms of 1 g. of charcoal and are converted to values per mole of alcohol adsorbed by multiplication with the factor 237, which is the weight of charcoal to adsorb 1 mole of methanol at saturation. The integral heats of adsorption so computed were plotted and the differential heats obtained from the slope of this curve. A plot of the differential heats for charcoal is shown in figure 7. Comparison with figure 3 shows that the heats of adsorption on charcoal are much greater than on graphite; the last portions adsorbed by charcoal show as high a net heat as the first portions on graphite. This great increase in heat of adsorption we attribute to the effects of neighboring walls of the capillaries.

SUMMARY

The isotherm for methanol on a nonporous carbon surface is a new type, which is designated as type VI. It starts as a type III isotherm, up to completion of a monolayer, then shows multilayer adsorption similar to a type II isotherm. The first layer is essentially completed before there is appreciable adsorption in multilayers.

Isosteric heats of adsorption were computed from isotherms at 0° and 28.9°C. They show that it is not necessary to assume zero or negative net heats of adsorption for a convex isotherm. Rather, it is shown that the shape of the isotherm depends upon the distribution of active sites that can adsorb at given pressures and the way in which this distribution varies with change in pressure.

Isotherms of methanol on nonporous and porous carbon surfaces are compared. The heat of adsorption on charcoal is much greater than on graphite.

REFERENCES

(1) Beebe, Polley, Smith, and Wendell: J. Am. Chem. Soc. **69**, 2294 (1947).
(2) Brunauer: *The Adsorption of Gases and Vapors*. Princeton University Press, Princeton, New Jersey (1943).
(3) Brunauer, Deming, Deming, and Teller: J. Am. Chem. Soc. **62**, 1723 (1940).
(4) Cameron and Reyerson: J. Phys. Chem. **39**, 169 (1935).
(5) Halsey: J. Chem. Phys. **16**, 931 (1948).
(6) Harkins and Jura: J. Am. Chem. Soc. **66**, 919 (1944).

(7) JOYNER AND EMMETT: J. Am. Chem. Soc. **70**, 2353 (1948).
(8) PIERCE, WILEY, AND SMITH: J. Phys. & Colloid Chem. **53**, 669 (1949).
(9) RAZOUK: J. Phys. Chem. **45**, 190 (1941).
(10) SCHEFFER AND VOOGD: Rec. trav. chim. **45**, 214 (1926).
(11) SMITH AND PIERCE: J. Phys. & Colloid Chem. **52**, 1115 (1948).

EXTENSION OF THE THEORY OF REVERSIBLE ELECTROPHORETIC BOUNDARY SPREADING OF PROTEINS[1]

RAYMOND A. BROWN AND JOHN R. CANN

Gates and Crellin Laboratories of Chemistry, California Institute of Technology, Pasadena, California

Received February 7, 1949

There are two criteria for the electrophoretic homogeneity of a protein. The first is that under the influence of an electric field the protein should migrate as a single boundary in buffers of various hydrogen-ion concentrations and ionic strengths. The second is that the rate of spreading of the protein boundary under conditions such that convection and anomalous electrical effects are avoided should be no greater than that due to diffusion alone. In the absence of spreading due to convection and conductivity or pH differences, boundary spreading indicates heterogeneity.

The boundary of an inhomogeneous protein is spread simultaneously by diffusion and by the differences in the mobilities of the differently charged ions. Sharp and coworkers (9) have shown that the mobility distribution may be obtained from the refractive-index gradient curves. In particular tney showed that, in the case in which spreading due to diffusion is negligible compared to electrical spreading, the standard deviation of the mobility distribution, H, may be calculated from the relation

$$H = \frac{\Delta\sigma}{\Delta t E} \tag{1}$$

where $\Delta\sigma/\Delta t$ is the time rate of change of the standard deviation of the gradient and E the electric field strength. H is called a heterogeneity constant.

Recently Alberty and coworkers (1, 2, 3) have considered the case in which diffusion of the protein is not negligible and the mobility distribution may be represented by the Gaussian probability function. Assuming that the diffusion constant, D, is the same for all protein ions, they showed that in this case the refractive-index gradient will have a Gaussian form. A heterogeneity constant, h, may be calculated from the equation

$$D^* = \frac{\sigma^2 - \sigma_0^2}{2t_E} = D + \frac{E^2h^2}{2}\, t_E \tag{2}$$

---

[1] Contribution No. 1381 from the Gates and Crellin Laboratories of Chemistry.

where σ_0 is the standard deviation of the gradient curve at the moment the field is applied, and σ is the standard deviation after electrophoresis for t_E seconds. The heterogeneity constant, h, is actually the standard deviation of the mobility distribution $q(u)$.

$$q(u) = \frac{1}{h\sqrt{2\pi}}\, e^{-u^2/2h^2} \tag{3}$$

The theory of boundary spreading as developed by Alberty and coworkers is limited in that it is applicable only to those proteins possessing a Gaussian distribution of mobilities. Furthermore, the theory yields the necessary condition that if the gradient curve is Gaussian in form then the mobility distribution is Gaussian, but fails to show that this is a sufficient condition. The purpose of this paper is to present a general theory of reversible boundary spreading applicable to both those proteins possessing Gaussian mobility distributions and those possessing distributions which deviate from the Gaussian.

In applying equation 2 to the interpretation of the results of spreading experiments Alberty and coworkers calculate the apparent diffusion constants from the half-widths at the inflection points of the gradient curves. However, this method of computation is valid only if the gradient curves are Gaussian in form. If the curves are non-Gaussian D^* calculated in this manner does not plot as a straight line *vs.* t_E. It is a consequence of the theory presented here that, no matter what form the gradient curves assume, the apparent diffusion constants calculated from the second moments of the gradient curves plot as a straight line *vs.* the time of electrophoresis. Furthermore, the standard deviation of the mobility distribution may be calculated from the slope of this line.

THEORETICAL

If the electrophoresis of a heterogeneous protein with a mobility distribution $q(u)$ is carried out under conditions such that convection and anomalous electrical effects are avoided, the refractive-index gradient, $\partial n/\partial x$, as a function of height in the electrophoresis cell, x, at time t_D after the formation of the boundary and time t_E after application of the electric field, is given by equation 4. This equation assumes that diffusion is simply superimposed on the electrophoretic migration. D is the diffusion constant which is assumed to be

$$\frac{\partial n}{\partial x} = \frac{(n_1 - n_2)}{2\sqrt{\pi D t_D}} \int_{-\infty}^{+\infty} q(u) e^{\frac{-(x - uEt_E)^2}{4Dt_D}}\, du \tag{4}$$

the same for all protein molecules. $(n_1 - n_2)$ is the difference in refractive index of the protein solution and the buffer. It is assumed that the refractive-index increment is the same for all protein molecules. u is the electrophoretic mobility and E the field strength.

Equation 4 may be transformed into the general form

$$f(x) = a \int_{-\infty}^{+\infty} q\left(\frac{u'}{Et}\right) k(x - u')\, du' \tag{5}$$

the solution of which is given by

$$q(u) = 1/2\pi a \int_{-\infty}^{+\infty} [F(s)/K(s)]e^{iu's}\, ds \tag{6}$$

$F(s)$ and $K(s)$ are the Fourier transforms of $f(x)$ and $k(x)$, respectively, and u' is equal to uEt_E.

It is convenient to represent the experimental refractive-index gradient curve in terms of its moments about the centroidal axis by means of a Gram–Charlier series (8):

$$f(x) = [(n_1 - n_2)/\sigma\sqrt{2\pi}]e^{-x^2/2\sigma^2}\left\{1 + \sum_{k=3}^{\infty} \frac{c_k}{k!} H_k\left(\frac{x}{\sigma}\right)\right\} \tag{7}$$

H_k is the k^{th} Hermite polynomial, and σ^2 is the second moment of the gradient curve, $\overline{x^2}$. The coefficients c_k are related to the higher moments of the gradient curves, e.g.,

$$C_3 = \overline{x^3}/\sigma^3, \qquad C_4 = \overline{x^4}/\sigma^4 - 3$$

Insertion of the Fourier transform of equation 7 into equation 6 and integration yields the mobility distribution[2]:

$$q(u) = (1/\beta\sqrt{2\pi})e^{-u^2/2\beta^2}\left\{1 + \sum_{k=3}^{\infty} \frac{C_k}{k!} (-i)^k\alpha^k H_k(iu\sigma/Et_E\beta^2\alpha)\right\} \tag{8}$$

$$\beta^2 = (\sigma^2 - 2Dt_D)/E^2t_E^2 = (\sigma^2 - \sigma_0^2 - 2Dt_E)/E^2t_E^2$$

$$\alpha = [1 - 2(\sigma/\beta Et_E)^2]^{1/2}$$

It will be noted that the coefficients C_k in the expression for $q(u)$ are the same as those appearing in equation 7. σ_0 is the standard deviation of the gradient curve at the moment the electric field is applied.

From equation 8 one sees immediately that the necessary and sufficient condition for a Gaussian distribution of mobilities is a Gaussian refractive-index gradient curve. In this case the standard deviation of the mobility distribution, β, is identical with the heterogeneity constant, h, of Alberty and coworkers (1, 2, 3). Deviations from a Gaussian distribution of mobilities are given by the third and higher moments of the gradient curve.

If spreading of the gradient curve due to diffusion is negligible compared to electrical spreading, β reduces to the heterogeneity constant, H, of Sharp and coworkers (9) for both Gaussian and non-Gaussian distributions. If diffusion is not negligible, H will decrease with time and approach β asymptotically according to equation 9.

---

[2] *Note added in proof:* The mathematical restrictions which must be placed upon $q(u)$ in order that equation 8 be a valid solution of the problem have not been considered in the paper. A discussion of the problem may be found in Titchmarsh's book on Fourier integrals. If $q(u)$ is a sum of delta functions, it is doubtful whether the series on the right-hand side of equation 8 converges uniformly to $q(u)$. However, it has been found that equation 10 applies even if $q(u)$ is a sum of delta functions and each species has a different diffusion constant. In this case a plot of D^* *versus* time is a straight line extrapolating back to an average diffusion constant and β calculated from the slope is the second moment of the mobility distribution.

$$H = \sqrt{\beta^2 + 2D/E^2t_E} \tag{9}$$

For both Gaussian and non-Gaussian distributions of mobilities β may be calculated from the equation:

$$D^* = \frac{\sigma - \sigma_0^2}{2t_E} = D + E^2\beta^2/2t_E \tag{10}$$

D^* is the "apparent diffusion constant" calculated from the second moment of the experimental gradient curves during the electrophoresis. It is not permissible, of course, to use the half-width at the inflection point to determine the apparent diffusion constant in the case of a non-Gaussian mobility distribution. According to equation 10 a plot of the apparent diffusion constant *vs.* the time of electrophoresis should yield a straight line, which extrapolates back to the normal diffusion constant at zero time. The standard deviation of the mobility distribution may be calculated from the slope $E^2\beta^2/2$.

EXPERIMENTAL

The optical system used in this work was the cylindrical-lens schlieren optical system described by Longsworth (6). A diagonal knife edge brought in from below the optical axis was used in the optical system. The refractive-index gradient curves were recorded photographically on Eastman Kodak Company CTC plates. The photographs were enlarged and traced.

Boundary spreading experiments were carried out with 0.5 per cent protein solution equilibrated against cacodylate buffer (0.08 N sodium chloride–0.02 N sodium cacodylate). These experiments were performed at the average isoelectric point of the protein. The power dissipation was less than 0.015 watt/cc.

The bovine γ-globulin (Fraction II of bovine plasma) used in this investigation was kindly supplied by Armour Laboratories, Armour and Company, Chicago, Illinois.

RESULTS AND DISCUSSION

If the refractive-index gradient curves of a heterogeneous protein are Gaussian in form, i.e., the protein possesses a Gaussian mobility distribution, the standard deviation of the mobility distribution, β, is identical with the heterogeneity constant, h, of Alberty and coworkers (1, 2, 3). In this case the apparent diffusion constants may be calculated either from the second moments or from the half-widths at the inflection point of the gradient curves. This is well illustrated by electrophoretic spreading experiments performed on a fraction of bovine γ-globulin designated as Fraction A.[3] Figure 1 shows that D^* plots as a straight line

---

[3] Fraction A was separated from bovine γ-globulin (Armour Fraction II) by electrophoresis-convection (5, 7). It had a mobility of -1.35×10^{-5} cm.^{2} volt^{-1} sec.$^{-1}$ in barbital buffer, pH 8.7 and ionic strength 0.1, and an isoelectric point of 7.03 in cacodylate buffer (0.08 N sodium chloride–0.02 N sodium cacodylate). Fraction A corresponds roughly to the γ_2-globulin of Hess and Deutsch (4).

vs. t_E as predicted by equation 10. The line extrapolates back to the diffusion constant observed upon reversal of the current at 240 min. for an equal period of time (2.3×10^{-7} cm.^{2} sec.$^{-1}$). The heterogeneity constant calculated from the slope of the plot is 0.62×10^{-5} cm.^{2} volt^{-1} sec.$^{-1}$. It will be noted that the apparent diffusion constants calculated from the second moments and the half-widths at the inflection point of the gradient curves are in excellent agreement.

The interpretation of the results of electrophoretic spreading experiments performed with bovine γ-globulin (Armour Fraction II) affords an illustration of the application of the general theory of reversible boundary spreading to a heterogeneous protein possessing a non-Gaussian mobility distribution. In this case it is not permissible to calculate the apparent diffusion constants from the half-widths at the inflection point of the gradient curves. Referring to figure 2, it will be noted that the plot of D^* calculated from the half-widths at the inflection point *vs.* t_E is not linear but is concave to the abscissa. A similar result was reported by Anderson and Alberty (3) for the normal γ-globulin of horse plasma. However, the apparent diffusion constants calculated from the second moments of the gradient curves plot as a straight line *vs.* the time of electrophoresis as predicted by equation 10. The standard deviation of the mobility distribution, β, calculated from the slope of the line is 0.67×10^{-5} cm.^{2} volt^{-1} sec.$^{-1}$

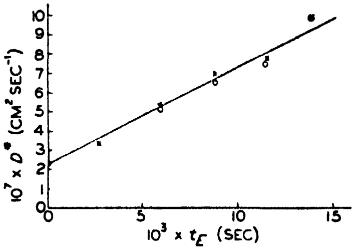

FIG. 1

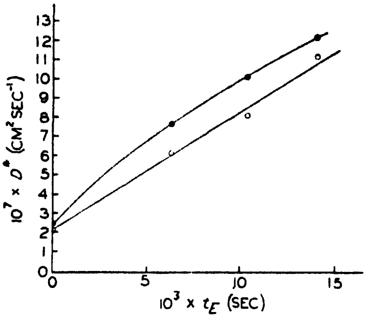

FIG. 2

FIG. 1. Apparent diffusion constant as a function of time of electrophoresis for Fraction A of bovine γ-globulin: ×, computed from half-widths at inflection point of gradient curves; ○, computed from second moments of gradient curves.

FIG. 2. Apparent diffusion constant as a function of time of electrophoresis for bovine γ-globulin: ●, computed from half-widths at inflection point of gradient curves; ○, computed from second moments of gradient curves.

The heterogeneity constant, H, of Sharp and coworkers (9) calculated from the second moments of the gradient curves using equation 1 is plotted *vs.* t_E in figure 3. H decreases with time and approaches β asymptotically because diffusion is not negligible. In figure 3 the solid curve through the experimental points was calculated from equation 9, using $\beta = 0.67 \times 10^{-5}$ and $D = 2.2 \times 10^{-7}$.

A complete representation of the mobility distribution of the protein entails, of course, the determination of the higher moments of the gradient curves. An attempt was made to compute the third and fourth moments of the gradient curves. However, the precision and accuracy involved in the computations did not warrant inclusion of those terms defining the departures from the Gaussian in the expression for the mobility distribution, equation 8. Using refined experimental techniques, e.g., sharpening of the initial boundary, it might be feasible to determine the higher moments of the gradient curves, particularly if the curves depart markedly from the Gaussian.

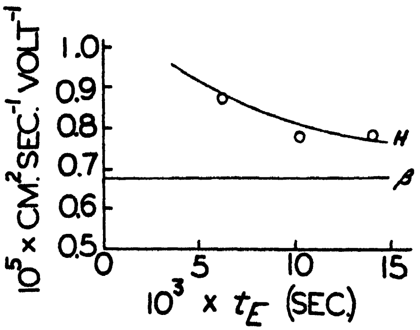

FIG. 3. Heterogeneity constant, H, as a function of time of electrophoresis

SUMMARY

A general theory of the reversible electrophoretic boundary spreading of inhomogeneous proteins has been developed. The theory has been applied to the interpretation of the results of spreading experiments performed with proteins possessing both Gaussian and non-Gaussian mobility distributions.

The authors are indebted to Dr. J. G. Kirkwood for his interest and helpful suggestions and for his review of the manuscript. They also wish to express their appreciation to Dr. Frank P. Buff for helpful suggestions.

REFERENCES

(1) ALBERTY, R. A.: J. Am. Chem. Soc. **70**, 1675 (1948).

(2) ALBERTY, R. A., ANDERSON, E. A., AND WILLIAMS, J. W.: J. Phys. & Colloid Chem. **52**, 217 (1948).

(3) ANDERSON, E. A., AND ALBERTY, R. A.: J. Phys. & Colloid Chem. **52**, 1345 (1948).

(4) HESS, E. L., AND DEUTSCH, H. F.: J. Am. Chem. Soc. **70**, 84 (1948).

(5) KIRKWOOD, J. G.: J. Chem. Phys. **9**, 878 (1941).

(6) LONGSWORTH, L. G.: Ind. Eng. Chem., Anal. Ed. **18**, 219 (1946).

(7) NIELSEN, L. E., AND KIRKWOOD, J. G.: J. Am. Chem. Soc. **68**, 181 (1946).

(8) RIETZ, H. L.: *Mathematical Statistics*, p. 65. The Open Court Publishing Company, La Salle, Illinois.

(9) SHARP, D. G., HEBB, M. H., TAYLOR, A. R., AND BEARD, J. W.: J. Biol. Chem. **142**, 217 (1942).

ELIMINATION OF CARBON MONOXIDE FROM SYNTHESIS GASES BY ABSORPTION IN CUPROUS SALT SOLUTIONS[1]

D. W. VAN KREVELEN AND C. M. E. BAANS

Central Laboratory of the Netherlands State Mines, Geleen, Holland

Received January 15, 1949

INTRODUCTION

Almost complete elimination of carbon monoxide from synthesis gas is of paramount importance for nitrogen fixation plants. Especially in factories operating on a basis of semi water gas, ammoniacal solutions of copper salts are used for the elimination of the residual quantities of carbon monoxide which remain in the gas after catalytic conversion with steam.

Many investigations on this absorption process have been performed and many valuable experimental data obtained. However, until now the quantitative laws of equilibria and the velocity of the carbon monoxide absorption process have not been described in the literature and only suppositions have been made as to the mechanism of the reaction and the constitution of the reaction complex.

In this paper we are communicating the results of a detailed investigation of the following subjects: (*1*) the composition of the reaction complex formed by the absorption of carbon monoxide in ammoniacal cuprous salt solutions, (*2*) the equilibria between carbon monoxide and cuprous salts in concentrated ammoniacal solutions, and (*3*) the rate of absorption of carbon monoxide in these solutions.

---

[1] Nomenclature:

a = specific packing surface (sq. m./cu. m.)
A = total cuprous salt concentration
B = total free ammonia concentration before carbon monoxide absorption
c = dimensionless constant
C = concentration of reaction product, $Cu(NH_3)_3CO^+$
c_i = ionic concentration
C_{eq}, C'_{eq} = apparent equilibrium constants
(Cu) = concentration of $Cu(NH_3)_2^+$
d_p = diameter of scrubber packings
D = diffusivity
g = acceleration due to gravity
H = Henry's law coefficient
I = ionic strength of the solution $(= \frac{1}{2}\sum_i c_i z_i^2)$
k = mass transfer coefficient
K, K' = real equilibrium constants
m = gram-moles of monovalent copper per gram-mole of carbon monoxide absorbed
n_A = differential rate of absorption (kg. moles/(sq. m.)(sec.)(atm.))
N_A = experimental overall rate of absorption (same dimension)
p = partial pressure
p_{CO} = partial carbon monoxide pressure in atmospheres
P_{CO} = carbon monoxide pressure in millimeters of mercury
u = superficial liquid velocity (meters per second)
v = superficial gas velocity (meters per second)

I. PREPARATION AND ANALYSIS OF THE REACTION PRODUCT IN AMMONIACAL CUPROUS SALT SOLUTIONS

Earlier investigations on the composition of the carbon monoxide–cuprous salt complex

In 1908 Manchot and Newton Friend (5) stated that in acid, neutral, and very weakly ammoniacal cuprous chloride solutions the following complex compound is formed after absorption of carbon monoxide:

$$CuCl \cdot 2H_2O \cdot CO$$

They supposed, however, that in concentrated ammoniacal solutions quite different reaction products are formed. The varying behavior of ammoniacal solutions has been neglected by other investigators.

For example, Moser and Hanika (6) assumed the existence of the complex $CuCl \cdot 2H_2O \cdot CO$ both in acid and in ammoniacal solutions of cuprous chloride (the complex $CuCl \cdot 2H_2O \cdot CO$ does exist). Brueckner and Groebner (2) supposed that in ammoniacal solutions the compound $Cu[(NH_3)_2CO]Cl$ is formed, but its existence has not been proved. As cuprous chloride also dissolves in some ammonium salts and the solution thus obtained can absorb carbon monoxide, Brueckner and Groebner assumed that in those neutral solutions compounds of the type

$$Cu[(NH_4Cl)_4CO]Cl$$

are formed.

It is obvious that, for a quantitative treatment of equilibria and reaction rate of the carbon monoxide absorption, an exact knowledge of the mechanism of the absorption reaction is necessary. As the available literature did not afford sufficient data, we decided to perform supplementary experimental work.

---

z_i = ionic valency
γ_i = activity coefficient of compound i
γ_t = overall activity coefficient
μ = viscosity
ρ = density
$\varphi = k_G(RT)/c_G$
$\psi = k_L/c_L$

General subscripts

G = gas phase
L = liquid phase
i = interface gas-liquid

Dimensionless groups

Re_G = Reynolds number of gas flow $\left(= \frac{vd_p\rho}{\mu}\right)$
Re_L = Reynolds number of liquid flow $\left(= \frac{u\rho}{a\mu}\right)$
Sc = Schmidt number $\left(= \frac{\mu}{\rho D}\right)$

Preparation of the carbon monoxide complex

An ammoniacal solution of ammonium chloride containing about 220 g. of ammonia per liter was saturated with cuprous chloride at 70°C. The solution was heated at 80°C. with finely divided copper in order to be sure of complete reduction to the cuprous salt. Then it was cooled to room temperature with continuous stirring. A crystalline precipitate was formed, consisting of colorless needles of $Cu(NH_3)_2Cl$. The mother liquid contained (in gram-moles per liter): $CuCl$, 2.77; NH_4Cl, 0.78; NH_3, 11.44. In the dry state the compound $Cu(NH_3)_2Cl$ is fairly stable.

Concentrated ammonia water was saturated with this salt at 60°C., and 50 ml. of the resulting solution was transferred to a Pyrex absorption vessel (see figure 1); immediately the absorption was started by bubbling pure carbon monoxide through the solution. This gas was saturated beforehand with ammonia by passing it through a vessel containing concentrated ammonia water.

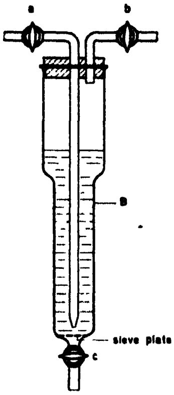

FIG. 1. Pyrex absorption vessel

As the solution cooled the compound $Cu(NH_3)_2Cl$ was precipitated, but the quantity of precipitate diminished after cooling to room temperature, owing to its reaction with carbon monoxide. Thereupon the vessel was cooled by ice water and for some hours carbon monoxide was introduced at such a rate that solution and crystals were just kept in motion. Meanwhile the solution attained a state of supersaturation and suddenly a voluminous mass of colorless, more or less cubic crystals appeared. The introduction of carbon monoxide was continued for an hour after the last needles of $Cu(NH_3)_2Cl$ had disappeared, in order to complete the reaction.

Analysis of the carbon monoxide complex

The analysis of the reaction product obtained caused great difficulties, as the compound proved to be extremely unstable. It was impossible to dry the crystals without causing considerable decomposition, and it was necessary to analyze the compound *in situ*. The following method proved to be satisfactory.

Vessel B (figure 2), filled with crystals and mother liquor, was connected to a weighed receiver (C) containing dilute sulfuric acid. A calibrated cylinder (H) was connected to C. By means of nitrogen (*via* a) a large part of the mother liquor was displaced from B into C and the carbon monoxide which was formed was collected in the cylinder H. The stopcock c was closed, the gas volume and pressure in H were measured, and C was weighed again. The copper and ammonia in the acid solution were determined. An example of an analysis of the mother liquor was as follows:

	gram-moles		*gram-moles*
Cu	0.0624	NH_3	0.2380
Cl	0.0622	CO	0.0502

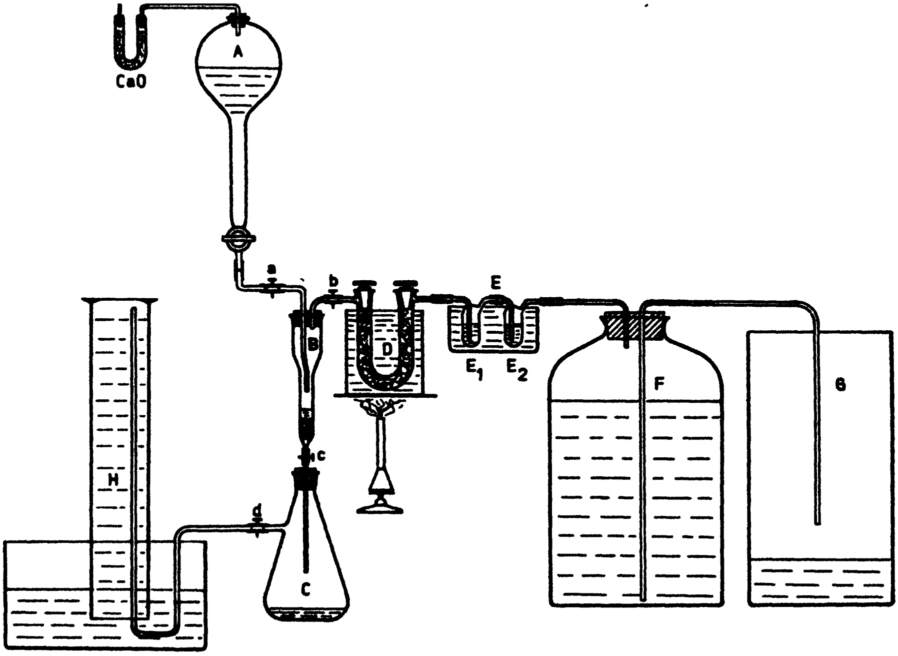

FIG. 2. Apparatus for the analysis of the copper–ammonia–carbon monoxide complex

Receiver C was emptied, connected with B, and evacuated. The crystals in B were washed three times with about 30 ml. of concentrated ethyl alcohol (from A) which had been cooled to −10°C. Thereupon vessel B was weighed rapidly and connected with the absorption vessels D and E_1 and E_2. Nitrogen was introduced into B (*via* a), and B was heated slowly. The gases formed were swept out by the nitrogen; water was absorbed in D (filled with calcium oxide and heated by boiling water); alcohol and ammonia were absorbed in vessels E_1 and E_2 (filled with concentrated sulfuric acid and cooled by ice), and the residual gases were collected in the holder F and analyzed. The residue in B was weighed and analyzed.

The results of three experiments were as follows:

	GRAM-MOLES PER GRAM-ATOM OF COPPER		
Cu	1.00	1.00	1.00
Cl	0.95	0.93	1.01
NH_3	2.83	2.95	2.98
CO	0.71	0.87	1.04
H_2O		1.27	1.05

In fact the ratio Cu:Cl must be 1.0. From quantitative absorption experiments the maximum absorption capacity of ammoniacal cuprous chloride has been proved to be 1 mole of carbon monoxide per gram-atom of copper. Considering these facts, together with the above analysis of the prepared complex, it can be stated that the formula of the copper–ammonia–carbon monoxide complex must be $Cu[(NH_3)_3CO]Cl \cdot H_2O$.

Conclusion

Since Bjerrum (1) has proved that cuprous salts in an ammoniacal medium are always present in the form $Cu(NH_3)_2^+$ as long as the free ammonia concentration is greater than 0.001, we may conclude that the mechanism of the carbon monoxide absorption in ammoniacal solutions can be represented by the equation:

$$Cu(NH_3)_2^+ + CO + NH_3 = Cu(NH_3)_3CO^+$$

In the next section we shall show that the experimental data of the absorption equilibrium can be calculated quantitatively from the proposed mechanism.

II. EQUILIBRIA BETWEEN CARBON MONOXIDE AND CUPROUS SALTS IN CONCENTRATED AMMONIACAL SOLUTIONS

Earlier investigations

Measurement of the absorption equilibrium of carbon monoxide in ammoniacal cuprous salt solutions has been the subject of several investigations. Hainsworth and Titus (3) and Larson and Teitsworth (4) measured carbon monoxide pressures of solutions of copper carbonate and copper formate.

Zhavoronkow and Reshikow (9) also investigated solutions of chlorides, acetates, and lactates, whereas Zhavoronkow and Chagunawa (10) worked with solutions containing formates as well as carbonates.

Notwithstanding the large number of valuable experimental data thus obtained, there is still a lack of fundamental knowledge correlating the influence of the operating variables (such as copper and ammonia concentration, nature of the negative ions, degree of saturation of the solution with carbon monoxide, etc.) on the partial carbon monoxide pressure of the solution. Moreover, we suspect inaccuracies in some of the data from the literature. This is the reason why the authors have performed a large number of new experimental measurements, on which their conclusions will be based. Afterwards the derived relationship will be applied to the data from the literature as an additional confirmation of its correctness.

The apparatus used for our measurements was reproduced from that of Hainsworth and Larson, so that for a description of it we may refer to the literature.

Derivation of the equilibrium equation for the carbon monoxide pressure

We have demonstrated that the mechanism of the carbon monoxide absorption is the following:

$$Cu(NH_3)_2^+ + NH_3 + CO = Cu[(NH_3)_3CO]^+$$

When equilibrium is attained the law of mass action can be applied:

$$K = \frac{[Cu\{(NH_3)_3CO\}^+]}{[Cu(NH_3)_2^+]\,[NH_3]\,[CO]} \cdot \frac{\gamma_{Cu\{(NH_3)_3CO\}^+}}{\gamma_{Cu(NH_3)_2^+} \cdot \gamma_{NH_3} \cdot \gamma_{CO}}$$

where the γ's are the activity coefficients of the individual reaction components. Writing for the factor

$$\frac{\gamma_{Cu(NH_3)_3CO^+}}{\gamma_{Cu(NH_3)_2^+}\ \gamma_{NH_3}\ \gamma_{CO}} = \gamma_t$$

and equating according to Henry's law $[CO] = Hp_{CO}$, the following equation is obtained:

$$\frac{KH}{\gamma_t} = \frac{[Cu(NH_3)_3CO^+]}{[Cu(NH_3)_2^+] \cdot [NH_3] \cdot p_{CO}} \qquad (2)$$

Now defining

A = total cuprous salt concentration
B = total free ammonia concentration before carbon monoxide absorption
$1/m$ = moles carbon monoxide absorbed per mole cuprous salt,

we get:

$$[Cu(NH_3)_3CO^+] = A/m$$

$$[Cu(NH_3)_2^+] = A - A/m = A\,\frac{m-1}{m}$$

$$NH_3 = B - A/m = \frac{mB - A}{m}$$

Substitution in equation 2 gives:

$$\frac{KH}{\gamma_t} = \frac{m}{(m-1)\,(mB - A)p_{CO}} = C_{eq} \qquad (3)$$

This equation gives the partial carbon monoxide pressure as a function of the composition of the solution. K and H are functions of temperature, γ_t will principally be a function of the ionic strength of the solution. The negative ion will only have an influence upon γ_t. From the experiments the values of C_{eq} will be determined as a function of the operating variables.

Application of equation 3 to the authors' experiments

The compositions of the solutions for which equilibrium measurements were performed are given in table 1. A survey of the experimental data can be found in table 2, where also the calculated C_{eq}-values are given. It is obvious that the C_{eq}-values at constant temperature are approximately constant; this proves the correctness of the postulated mechanism.

In figure 3 the logarithmic values of C_{eq} (for the series B_I, thus maintaining constant ionic strength) are plotted as a function of the reciprocal absolute temperature. The points lie on a straight line, from which an apparent activation energy of 11,900 cal./mole may be calculated. In figure 4 the C_{eq}-values, reduced to 293°K., are plotted on a logarithmic scale against the ionic strength ($I = \frac{1}{2}\sum c_i z_i^2$, where c_i and z_i are the concentration and the valency of the ion i) for the whole series of experimental data. In the investigated concentration range a linear relationship appears to exist. Only the C_{eq}-value for the formate solution is higher. All the data for the chlorides can be represented by the equation:

TABLE 1

Composition of the solutions in gram-moles per liter

COMPONENTS	SOLUTIONS USED								
	B1	B4	B5	B6	B7	B8	B9	B10	B11
Cu^+	0.59	1.78	1.71	1.42	1.74	1.25	0.88	0.93	0.94
Cu^{++}	0.01	0.03	0.03	0.04	0.03	0.03	0.01	0.02	0.02
Cl^-	1.71	2.56	2.44	1.32	2.34	1.69	1.12	1.71	
$HCOO^-$									1.72
NH_3 (total)	8.25	6.72	8.07	10.53	9.27	6.73	5.78	7.11	7.01
NH_3 (free + complex)	7.15	6.00	7.40	10.38	8.65	6.28	5.57	6.37	6.27
NH_3 (free)	5.93	2.30	3.84	7.40	5.17	3.77	3.77	4.42	4.31

$$\log_{10} C_{eq} = \frac{11{,}900}{2.3RT} - 0.040I - 8.790 \tag{4}$$

Table 3 gives the calculated and experimental values of C_{eq}.

Application of equation 3 to Larson's data for copper formate solutions

Our equation will now be checked with data from the literature, *viz.*, for absorption equilibria in copper formate solutions.

Table 4 shows the composition of Larson's solutions and the C_{eq}-values calculated from his equilibrium measurements. This series of C_{eq}-values can be satisfactorily correlated by the equation:

$$\log_{10} C_{eq} = \frac{13{,}500}{2.3RT} - 0.040I - 9.830 \tag{5}$$

In figures 5–8 Larson's data are plotted and are compared with the values predicted according to equation 5 (the drawn curves). The agreement proves to

TABLE 2

Experimental data

SOLUTION	TEMPERATURE °C.	NO. OF EXPERIMENT	pCO	1/m	C_{eq} (t °C.)	C_{eq} AVERAGE (t °C.)
B1	0	1	0.164	0.815	4.92	4.8
		2	0.044	0.561	5.15	
		3	0.017	0.297	4.26	
B1	10	1	0.768	0.913	2.51	2.44
		2	0.344	0.826	2.51	
		3	0.272	0.780	2.37	
		4	0.147	0.663	2.37	
		5	0.082	0.533	2.44	
B1	20	1	0.351	0.666	1.02	1.15
		2	0.203	0.563	1.13	
		3	0.096	0.403	1.22	
		4	0.090	0.392	1.24	
		5	0.051	0.250	1.12	
B1	30	1	0.738	0.712	0.61	0.58
		2	0.543	0.595	0.45	
		3	0.292	0.537	0.72	
		4	0.227	0.427	0.57	
		5	0.085	0.209	0.53	
B4	22.8	1	0.133	0.175	0.80	0.81
		2	0.101	0.152	0.87	
		3	0.111	0.154	0.81	
B5	22.3	1	0.085	0.200	0.83	0.81
		2	0.179	0.309	0.75	
		3	0.110	0.232	0.79	
B6	20.4	1	0.060	0.306	1.05	1.04
		2	0.056	0.282	1.00	
		3	0.062	0.314	1.06	
B7	23.2	1	0.113	0.286	0.76	0.75
		2	0.099	0.265	0.77	
		3	0.108	0.268	0.72	
B8	22.7	1	0.158	0.323	0.88	0.86
		2	0.183	0.351	0.86	
		3	0.116	0.247	0.84	
B9	22.7	1	0.209	0.386	0.88	0.89
		2	0.199	0.376	0.88	
		3	0.168	0.354	0.94	
B10	21.7	1	0.838	0.757	0.99	0.98
		2	0.841	0.757	0.98	
		3	0.836	0.754	0.97	
B11	22.0	1	0.853	0.784	1.18	1.16
		2	0.833	0.765	1.09	
		3	0.826	0.777	1.17	

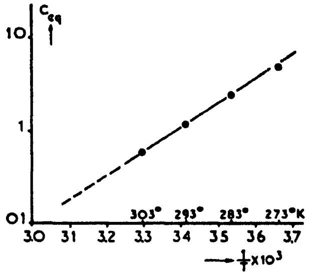

FIG. 3

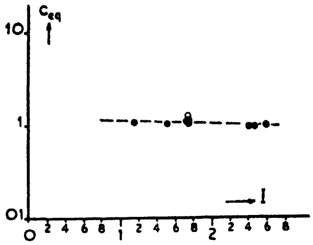

FIG. 4

FIG. 3. Plot of the logarithmic values of C_{eq} as a function of the reciprocal absolute temperature.

FIG. 4. Plot of C_{eq}-values against the ionic strength. ●, chloride solutions; ○, formate solutions.

TABLE 3

Calculated and experimental values of C_{eq}

SERIES	I	T	C_{eq} (CALCULATED)	C_{eq} (EXPERIMENTAL)
		°K.		
1	1.76	273	4.7	4.8
		283	2.2	2.4
		293	1.05	1.15
		303	0.53	0.58
4........ . .	2.59	296	0.79	0.81
5.	2.47	295	0.85	0.81
6..	1.52	293	1.06	1.04
7.....	2.41	296	0.78	0.75
8........ .. .	1.76	296	0.84	0.86
9...	1.16	296	0.88	0.89
10.......... .	1.73	295	0.92	0.98

TABLE 4

Composition of the solutions used by Larson and Teitsworth in gram-moles per liter

	L2	L3	L4	L10
Cu^+.	0.84	(0.84)	0.99	0.80
Cu^{++}.	0	0	0	0
$HCOO^-$	3.04	3.20	3.20	1.37
NH_3 (total)	6.52	7.17	5.87	4.47
NH_3 (free + complex).	4.32	(4.81)	3.66	3.90
NH_3 (free)............... . . .	2.64	(3.13)	1.68	2.30
C_{eq} (273°K.).....	7.4	7.5	6.0	7.9
C_{eq} (293°K.)......	1.31	1.17	1.17	
C_{eq} (313°K.)............	0.29	0.29	0.27	
C_{eq} (333°K.).	0.08	0.09		0.10

be very good. Another illustration of the correlation of calculated and experimental C_{eq}-values is given in table 5. (This table also contains the C_{eq}-values of our own experimental series B11 when the formate solutions were used.)

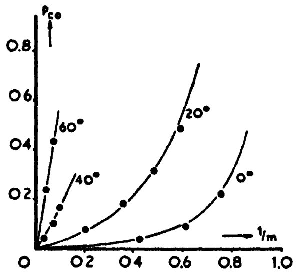

FIG. 5

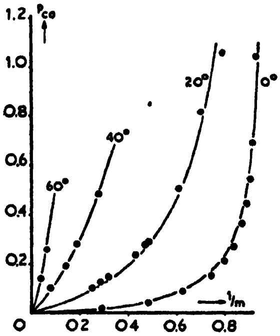

FIG. 6

FIG. 5. Cu^+, 0.84 gram-mole per liter; free NH_3, 2.64 gram-moles per liter; solution L2
FIG. 6. Cu^+, 0.84 gram-mole per liter; free NH_3, 3.13 gram-moles per liter; solution L3

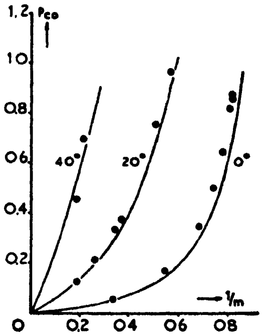

FIG. 7

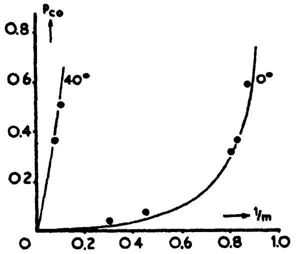

FIG. 8

FIG. 7. Cu^+, 0.99 gram-mole per liter; free NH_3, 1.68 gram-moles per liter; solution L4
FIG. 8. Cu^+, 0.80 gram-mole per liter; free NH_3, 2.30 gram-moles per liter; solution L10

Significance of the formula of Zhavoronkow and Chagunawa

Zhavoronkow and Chagunawa derived a very simple relation between the carbon monoxide pressure and the quantity of carbon monoxide which is absorbed. Their formula is:

$$\frac{1}{V_{CO}} = \frac{1}{V_m} + \frac{1}{V_m \alpha P_{CO}} \tag{6}$$

where V_{CO} = milliliters of carbon monoxide absorbed per milliliter of solution
V_m = maximum absorption, milliliters of carbon monoxide per milliliter of solution

P_{CO} = carbon monoxide pressure in millimeters of mercury
α = constant depending upon temperature.

As in our nomenclature $V_{CO} = RTA/m$ and $V_m = RTA$, substitution gives

$$m = 1 + \frac{1}{\alpha P_{CO}} \text{ or } \alpha = \frac{1}{(m-1)P_{CO}} = \frac{1}{760(m-1)p_{CO}} \qquad (7)$$

According to our formula 3 we have

$$C_{eq} = \frac{m}{(m-1)(mB-A)p_{CO}}$$

so that equation 7 can only be valid if $m/(mB - A)$ is constant. The latter is only true as long as B (free ammonia concentration) is large and A (copper concentration) is small. For these solutions the curves $1/p_{CO} = f(m)$ become straight lines. As the solution becomes saturated with carbon monoxide (small m-values) the lines will bend off to the point $1/p_{CO} = 0$; $m = 1$.

TABLE 5

Illustration of correlation of calculated and experimental C_{eq}-values

SERIES	I	T	C_{eq} (CALCULATED)	C_{eq} (EXPERIMENTAL)
		°K		
L2	3.04	273	7.3	7.4
		293	1.32	1.31
		313	0.30	0.29
		333	0.08	0.08
L3	3.20	273	7.1	7.5
		293	1.29	1.17
		313	0.29	0.29
		333	0.08	0.09
L4	3.20	273	7.1	6.0
		293	1.29	1.17
		313	0.29	0.27
L10	1.37	273	8.3	7.9
		333	0.09	0.10
B11	1.74	295	1.25	1.16

Figures 9 to 11 prove that the experimental data are in complete agreement with theory.

III. RATE OF ABSORPTION OF CARBON MONOXIDE IN CONCENTRATED AMMONIACAL CUPROUS SALT SOLUTIONS

Description of the apparatus

The absorption experiments were performed with mixtures of nitrogen and carbon monoxide. The latter was stored in a small gas holder from which it was

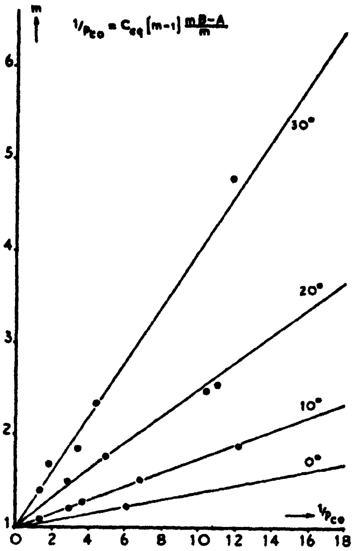

FIG. 9

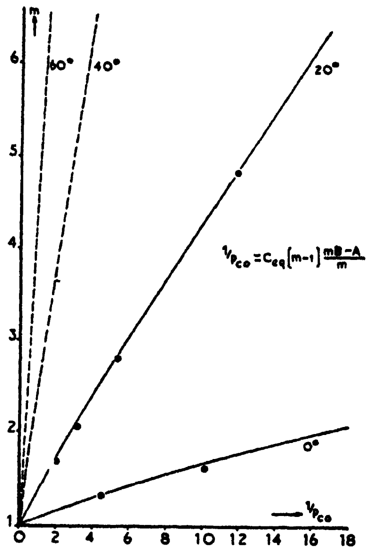

FIG. 10

FIG. 9. Cu^+, 0.59 gram-mole per liter; free NH_3, 5.93 gram-moles per liter; solution B1
FIG. 10. Cu^+, 0.84 gram-mole per liter; free NH_3, 2.64 gram-moles per liter; solution L2

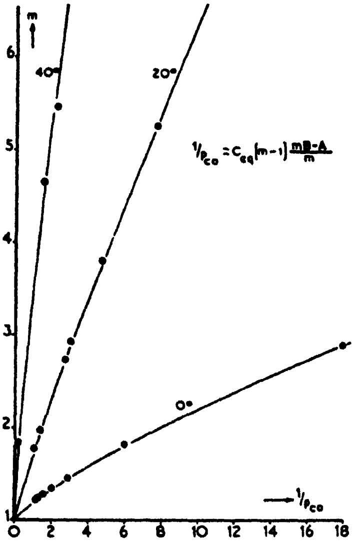

FIG. 11. Cu^+, 0.99 gram-mole per liter; free NH_3, 1.68 gram-moles per liter; solution L4

transferred to the apparatus by means of water pressure. It was thoroughly mixed with pure nitrogen. After sampling, the mixture flowed through a scrubber where it was washed by means of copper solution. The exit gases were sampled, freed from stripped ammonia, and passed through a gas meter. Gas and liquid velocities were measured in calibrated flow meters. Temperatures in the absorber were measured at three points, *viz.*, at the entrance and the exit of the liquid and somewhere in the middle of the column. Entering and exit gas and liquid were carefully analyzed.

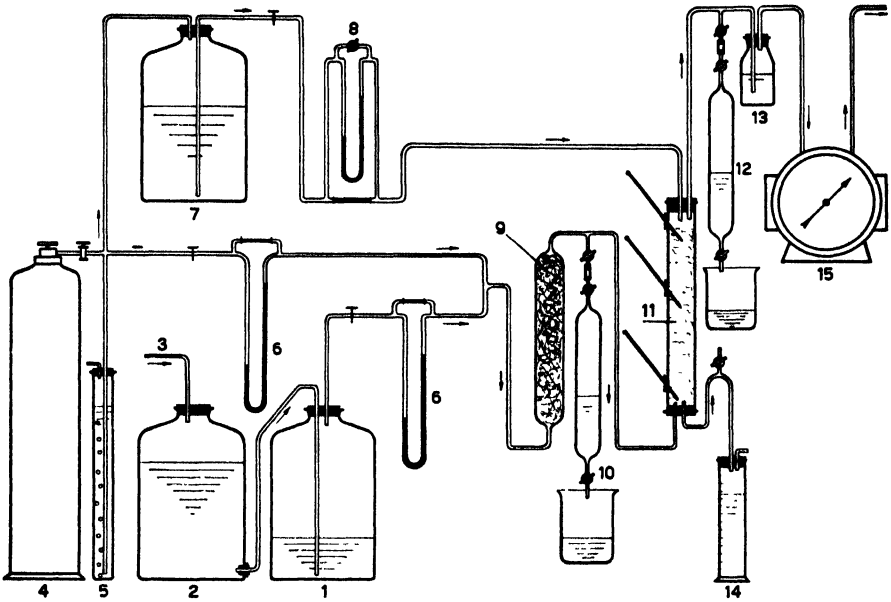

FIG. 12. Flow sheet of the apparatus for determination of the rate of absorption

1 = vessel containing carbon monoxide
2 = vessel containing alkaline water (under pressure)
3 = air or nitrogen (30 cm. of mercury overpressure)
4 = cylinder containing pure nitrogen
5 = safety
6 = flow meters for gases
7 = absorption liquid
8 = flow meter for liquid
9 = mixing column
10 = sampling flask for entering gas mixture
11 = absorption column
12 = sampling flask for exit gas
13 = bubbler containing dilute sulfuric acid (for ammonia removal)
14 = measuring cylinder
15 = gas meter

The absorber was a glass tube of height 40 cm. and 30 mm. internal diameter, filled with 5.5-mm. glass Raschig rings.

Figure 12 shows a flow sheet of the apparatus.

The composition of the solutions used is given in table 6, while table 7 shows the data of the absorption experiments.

Discussion of results

As we have demonstrated, the mechanism of the carbon monoxide absorption in these concentrated ammoniacal solutions can be formulated as follows:

$$Cu(NH_3)_2^+ + NH_3 + CO = Cu(NH_3)_3CO^+$$

It is well known that this reaction proceeds extremely fast. As the physical solubility of carbon monoxide is very small, it seems probable that the reaction zone will coincide with the phase boundary and that the rate of the absorption process will be determined by the mass transfer of reactants and reaction products.

TABLE 6

Composition of washing liquids

WASHING LIQUD NO.	COMPOSITION IN GRAM-MOLES PER LITER							DENSITY, IN KILOGRAMS PER CUBIC METER AT 20°C.	VISCOSITY (μ), IN KILOGRAMS PER METER SECOND AT 20°C.	IONIC STRENGTH, I
	Cu^+	Cu^{++}	Cl^-	CO_3^{--}	Total NH_3	Free NH_3	NH_4^+			
65	0.69	0.01	0.69	0.245	9.28	7.38	0.47	1007	1.365×10^{-3}	1.44
68	0.715	0.01	0.50	0.276	5.87	4.09	0.31	1027	1.27	1.34
71	0.45	0.00	0.42	0.078	5.02	4.00	0.13	1003	1.22	0.66
74	0.69	0.01	0.51	0.325	8.09	6.22	0.45	1016	1.34	1.50
75	0.43	0.01	0.40	0.113	7.80	6.72	0.18	986	1.27	0.75
77	0.68	0.00	0.49	0.319	8.10	6.29	0.45	1015	1.33	1.45
79	0.44	0.01	0.61	0.145	11.23	9.86	0.44	973	1.30	1.06
80	1.39	0.01	2.16	0.062	8.64	4.95	0.87	1079	1.26	2.36
87	1.435	0.01	2.13	0.120	6.22	2.40	0.91	1100	1.16	2.50
89	0.435	0.00	0 52	0.115	2.13	0.95	0.31	1028	1.04	0.86
95	0.715	0.02	1.10	0.000	15.84	13.97	0.34	977	1.51	1.12
103	0.67	0.00	0.78	0.077	4.25	2.65	0.26	1036	1.20	1.01
106	1.16	0.02	1.225	0.008	12.47	9.67	0.04	1016	1.44	1.45
111	0.70	0.00	0.69	0.180	8.15	6.40	0.35	1013	1.37	1.23
112	1.005	0.00	1.02	0.108	11.03	8.78	0.24	1014	1.49	1.35
118	1.77	0.02	2.27	0.065	11.31	7.09	0.59	1087	1.486	2.46
121	1.445	0.02	1.84	0.153	9.33	5.69	0.67	1075	1.39	2.32
125	1.42	0.03	1.30	0.153	10.72	7.62	0.13	1050	1.50	1.79
128	1.11	0.01	1.035	0.228	10.25	7.63	0.36	1034	1.46	1.73
196	0.935	0.02	(formate) 1.72	0.000	7.00	4.30	0.74	1041	1.17	1.73
198	0.935	0.01	(chloride) 1.71	0.000	7.12	4.42	0.75	1029	1.17	1.73

Taking this assumption as a working hypothesis the schedule of the absorption mechanism given in figure 13 can be made. Then for a thin cross-section of the scrubber, the rate of absorption, expressed as kilogram-moles per square meter of contact surface per second, can be written as follows:

$$n_A = k_G(p_G - p_i) = k_L(C_i - C_L) \qquad (8)^2$$

---

[2] For nomenclature see footnote 1.

TABLE 7

Survey of absorption experiments

RUN	WASHING LIQUID NO.	p_e	T_m	v_g	LIQUOR VELOCITY	N_A ($\times 10^{-7}$)	P ($\times 10^{-8}$)	Q ($\times 10^{-11}$)	R	S ($\times 10^{-8}$)	$\frac{\varphi}{RT}$ ($\times 10^{-4}$)	ψ ($\times 10^{-4}$)	c_G	c_L
		atm.	°C.	*cm./sec.*	*liters/hr.*	*kilogram-moles/sec. m.² atm.*								
1	65	0.179	20.8	3.42	4.15	6.30	1.08	0.299	0.383	2.96	9.90	2.20	0.028	0.016
2....	68	0.176	19.0	3.38	3.22	5.18	0.81	0.131	0.292	1.61	9.89	1.74	0.031	0.019
3	71	0.197	21.9	3.17	3.70	3.78	0.60	0.056	0.192	0.60	9.29	2.23	0.027	0.015
4......	74	0.179	21.1	3.18	3.65	5.38	0.88	0.173	0.333	2.00	9.44	1.97	0.028	0.016
5......		0.163	21.1	3.38	3.47	5.02	0.81	0.154	0.328	1.89	9.82	1.90	0.027	0.015
6......	75	0.196	19.7	3.31	4.09	5.22	1.05	0.214	0.314	1.53	9.70	2.13	0.031	0.017
7.....	77	0.193	19.3	3.32	3.84	6.42	1.16	0.299	0.413	2.76	9.75	1.96	0.030	0.017
8..		0.196	19.5	3.17	3.62	6.13	1.12	0.274	0.423	2.65	9.35	1.89	0.029	0.016
9. ..	79	0.184	17.9	3.52	3.22	5.13	1.25	0.337	0.440	2.39	10.21	1.67	0.031	0.019
10 ...		0.198	18.1	3.60	4.08	6.02	1.48	0.453	0.466	2.79	10.43	1.96	0.031	0.018
11......	80	0.198	20.5	2.98	3.89	7.89	1.11	0.310	0.450	5.09	8.87	2.29	0.029	0.017
12		0.177	20.5	3.41	3.33	7.38	1.04	0.266	0.445	4.63	10.05	2.07	0.029	0.016
13......	87	0.175	20.9	3.22	3.00	5.40	0.68	0.067	0.280	1.70	9.44	2.15	0.026	0.014
14.. .	89	0.176	18.3	3.22	3.92	2.12	0.25	0.0057	0.051	0.108	9.57	2.52	0.036	0.020
15......	95	0.167	18.0	4.47	3.95	6.46	1.21	0.537	0.480	5.34	12.45	1.65	0.031	0.019
16 ...	103	0.185	21.0	3.06	3.90	4.48	0.61	0.055	0.176	0.765	9.08	2.33	0.029	0.017
17. . .	106	0.178	21.0	3.56	3.35	7.41	1.17	0.480	0.525	6.81	10.22	1.72	0.031	0.019
18	111	0.157	22.0	3.22	3.03	4.43	0.69	0.114	0.291	1.75	9.44	1.72	0.029	0.016
19		0.186	22.6	3.41	2.76	5.02	0.85	0.143	0.339	1.77	9.90	1.64	0.029	0.017

20......		0.193	20.8	3.34	2.80	7.08	1.25	0.417	0.570	5.22	9.70	1.48	0.032	0.019
21......	112	0.198	20.7	3.21	3.12	7.45	1.30	0.463	0.570	5.66	9.43	1.58	0.031	0.019
22 . . .		0.188	20.8	3.05	3.20	6.78	1.14	0.383	0.540	5.14	9.10	1.60	0.030	0.018
23.. ..	118	0.236	21.5	2.62	2.95	8.56	1.29	0.473	0.730	8.89	7.98	1.64	0.030	0.018
24		0.234	21.5	2.53	2.92	8.21	1.23	0.424	0.720	8.42	7.79	1.62	0.030	0.018
25	198	0.224	20.8	2.59	3.06	5.80	0.94	0.148	0.456	2.21	7.97	2.04	0.021	0.013
26 ..	97	0.189	23.8	3.15	4.22	5.13	0.795	0.120	0.217	1.15	9.17	2.36	0.030	0.018
27 ...		0.160	23.9	3.29	4.78	4.97	0.73	0.112	0.194	1.15	9.48	2.58	0.029	0.017
28 ..		0.233	13.8	2.31	2.84	7.89	1.48	0.763	1.005	12.95	7.49	1.31	0.032	0.019
29 .. .	125	0.224	13.8	2.21	2.99	7.35	1.32	0.672	0.925	11.86	7.24	1.35	0.031	0.019
30 .		0.203	26.5	2.72	3.70	6.32	0.87	0.178	0.450	3.78	8.08	2.09	0.025	0.014
31		0.210	26.4	2.77	3.90	6.85	0.945	0.212	0.453	4.13	8.23	2.17	0.026	0.015
32 . .		0.222	13.2	2.54	3.15	7.89	1.63	0.842	0.938	10.56	8.06	1.44	0.030	0.017
33	128	0.215	13.1	2.50	2.92	7.49	1.53	0.761	0.919	10.15	7.97	1.37	0.029	0.017
34 . ..		0.193	27.0	2.82	3.44	5.78	0.81	0.150	0.354	2.64	8.32	2.00	0.027	0.015
35 . .		0.199	27.0	2.66	3.75	5.90	0.82	0.156	0.352	2.78	7.96	2.11	0.028	0.016
36 ...	196	0.215	21.1	2.48	2.60	6.15	0.97	0.188	0.392	2.55	7.72	1.83	0.029	0.017
37 .		0.230	20.9	2.53	3.24	7.24	1.15	0.269	0.402	3.11	7.80	2.15	0.030	0.018

At the interface equilibrium exists, so that

$$\frac{C_i}{(\mathrm{Cu}_i)(\mathrm{NH}_3)_i p_i} = C_{\mathrm{eq}} \tag{9}$$

Moreover, the rate of supply of free copper to the reaction zone will be equal to the rate of transfer of the carbon monoxide complex from the reaction zone, thus:

$$C_i - C_L = (\mathrm{Cu})_L - (\mathrm{Cu})_i \qquad (10)^{3}$$

From equation 8 we derive:

$$p_i = p_G - \frac{n_A}{k_G}$$

$$(\mathrm{Cu})_i = (\mathrm{Cu})_L - \frac{n_A}{k_L}$$

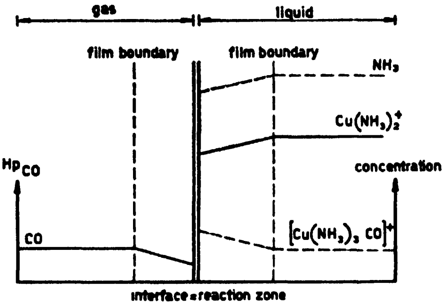

FIG. 13. Scheme for the absorption mechanism

and by combination of equations 8 and 10:

$$C_i = (\mathrm{Cu})_L + C_L - (\mathrm{Cu})_i = C_L + \frac{n_A}{k_L}$$

Substitution of these expressions in equation 9 gives:

$$\frac{C_L + \dfrac{n_A}{k_L}}{\left((\mathrm{Cu})_L - \dfrac{n_A}{k_L}\right)(\mathrm{NH}_3)_i\left(p_G - \dfrac{n_A}{k_G}\right)} = C_{\mathrm{eq}} \tag{11}$$

or

$$\frac{k_G(C_{\mathrm{eq}}(\mathrm{NH}_3)_m p_G + 1)n_A - C_{\mathrm{eq}}(\mathrm{NH}_3)_m n_A^2}{k_G[C_{\mathrm{eq}}(\mathrm{Cu})_L(\mathrm{NH}_3)_m p_G - C_L] - C_{\mathrm{eq}}(\mathrm{Cu})_L(\mathrm{NH}_3)_m n_A} \qquad (11)^{4}$$

---

[3] The diffusion coefficients (and therefore the mass transfer coefficients) of $\mathrm{Cu(NH_3)_2^+}$ and $[\mathrm{Cu(NH_3)_3CO}]^+$ are assumed to be equal, *viz.*, 1.0 × 10^{-9} sq. m./sec. (determined by the authors).

[4] As the ammonia is present in large excess, it is assumed that $(\mathrm{NH_3})_i$ equals $(\mathrm{NH_3})_m$ (the logarithmic mean $(\mathrm{NH_3})$).

In order to apply this equation to the whole scrubber we, have to use the overall value of $n_A(= N_A$, the experimentally determined rate of absorption) and average values for the other variables.

Defining:

$$(C_{eq}(\mathrm{NH_3})_m p_{Gm} + 1)N_A = P$$

$$C_{eq}(\mathrm{NH_3})_m N_A^2 = Q$$

$$C_{eq}((\mathrm{Cu})_L(\mathrm{NH_3})p_G - c_L)_m = R$$

$$C_{eq}(\mathrm{Cu})_L(\mathrm{NH_3})_m N_A = S$$

where the index m indicates the logarithmic mean value, we get by substitution:

$$k_L = \frac{P\,k_G - Q}{R\,k_G - S}$$

As k_G and k_L are functions of the superficial gas and liquid velocities, we use the dimensionless equations (see 7 and 8):

$$k_G = \frac{c_G}{RT}(Re_G)^{0.8}(Sc)^{0.33}\left(\frac{D_G}{d_p}\right) = \frac{c_G}{RT}\varphi$$

$$k_L = c_L(Re_L)^{0.67}(Sc_L)^{0.33}\left(\frac{D_L}{(\mu^2/g\rho^2)^{1/3}}\right) c_L\,\psi$$

So we get

$$c_L = \frac{c_G P' - Q'}{c_G R' - S'} \qquad (12)$$

where

$$P' = P\frac{\psi}{RT}$$

$$Q' = Q$$

$$R' = R\frac{\varphi\psi}{RT}$$

$$S' = S\,\psi$$

Equation 12 can be solved by trial and error.

In table 7 the values of c_G and c_L are given for each experiment. For the whole series of experiments they prove to be fairly constant. The average values of c_G and c_L are 0.029 and 0.017, respectively.

The correctness of our working hypothesis, *viz.*, that the rate of absorption of carbon monoxide in concentrated ammoniacal solutions is only determined by mass transfer processes, can be proved now by independent determinations constants c_G and c_L.

Independent determinations of c_G and c_L

The value of c_G has been determined in the same apparatus by experiments on water evaporation into a current of air (at 20°C.). In figure 14 the experimental data are plotted as a function of the above-mentioned dimensionless groups. From these data a c_G-value of 0.026 can be calculated. The value of c_L has been determined from experiments on carbon dioxide absorption in water at 20°C., also in the same apparatus. From the data, which are reproduced graphically in figure 15, a c_L-value of 0.014 can be calculated.

The fact that these independently determined c_G- and c_L-values are about the same as those found from the carbon monoxide absorption experiments is a proof of the correctness of our assumptions.

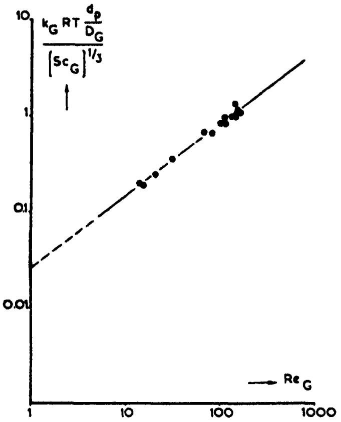

Fig. 14. Plot of experimental data as a function of the dimensionless groups.

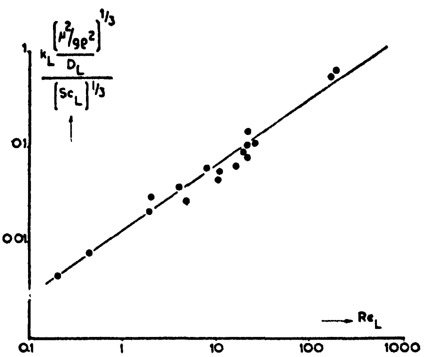

Fig. 15

SUMMARY

A method is described by which the reaction complex of cuprous chloride and carbon monoxide in ammoniacal solutions has been prepared as a crystalline product. Its composition was proved to be $Cu[(NH_3)_3CO]Cl \cdot H_2O$. This compound is very unstable in the crystalline state and decomposes at room temperature with loss of carbon monoxide and ammonia. It could be stated that the absorption mechanism is the following:

$$Cu(NH_3)_2^+ + CO + NH_3 = Cu(NH_3)_3CO^+$$

Using this equation the authors have derived formulae from which the carbon monoxide equilibrium pressure can be calculated as a function of the temperature, the copper, ammonia, and carbon monoxide content, and the ionic strength of the solution. The correlation with the authors' experimental data and with data of Larson and Teitsworth proves to be very satisfactory.

The reaction between carbon monoxide and cuprous salts in a concentrated ammoniacal solution is immeasurably rapid. The rate of mass transfer of the

reaction product (the carbon monoxide–copper complex) is controlling for the absorption velocity. The values found for the mass transfer coefficients in this complex absorption are the same as those found for simple physical absorption and desorption in the same apparatus.

The rate of absorption of carbon monoxide in neutral and weakly ammoniacal solutions proves to be much smaller than in concentrated ammoniacal solutions. In these cases the chemical reaction velocity is partly rate controlling for the absorption process.

REFERENCES

(1) Bjerrum, J.: Kgl. Danske Videnskab. Selskab, Mat.-fys. Medd. **11**(5) (1931), **11**(10) (1932), **12**(15) (1934).

(2) Brueckner, H., and Groebner, W.: Gas-u. Wasserfach **78**, 269–73 (1935).

(3) Hainsworth, W. R., and Titus, E. Y.: J. Am. Chem. Soc. **43**, 1–11 (1921).

(4) Larson, A. R., and Teitsworth, C. S.: J. Am. Chem. Soc. **44**, 2878–85 (1922).

(5) Manchot, W., and Friend, J. Newton: Ann. **359**, 100–28 (1908).

(6) Moser, L., and Hanika, F.: Z. anal. Chem. **67**, 448–56 (1925/26).

(7) Van Krevelen, D. W., and Hoftijzer, P. J.: Rec. trav. chim. **66**, 49–65 (1947).

(8) Van Krevelen, D. W., Hoftijzer, P. J., and van Hooren, C. J.: Rec. trav. chim. **66**, 513–32 (1947).

(9) Zhavoronkow, N. M., and Reshikow, P. M.: J. Chem. Ind. (U.S.S.R.) **10**, 41–9 (1933).

(10) Zhavoronkow, N. M., and Chagunawa, V. T.: J. Chem. Ind. (U.S.S.R.) **17**, 25–9 (1940).

APPENDIX

Rate of absorption of carbon monoxide in neutral and weakly ammoniacal copper solutions

Only preliminary experiments have been performed for the cases when the cuprous solution (*a*) is about neutral (not containing free ammonia) or (*b*) contains ammonia combined with carbon dioxide.

Case a: With a solution containing 1.77 gram-moles of cuprous chloride and 6.85 gram-moles of ammonium chloride per liter an overall absorption coefficient

$$K_G = \frac{N_A}{(p - p_{\mathrm{equil}})} = 1.4 \times 10^{-6} \text{ kg.-moles/(atm.) (sec.) (sq. m.)}$$

has been measured. This value is five to ten times smaller than corresponding K_G-values for ammoniacal copper solutions, so that the reaction:

$$\mathrm{CO} + \mathrm{Cu(NH_4Cl)_3^+} = \mathrm{Cu[(NH_4Cl)_3CO]^+}$$

is not of the type of immeasurably rapid reactions. From the dimensionless k_G-equation a k_G-value of 2×10^{-5} for the conditions in the experiment can be calculated, so that the gas film resistance only amounts to about 10 per cent of the total absorption resistance. The major resistance must be sought in the reaction velocity in the liquid film.

Case b: In this case the ammonia is buffered by the equilibria

$$NH_2COO^- + H_2O = NH_3 + HCO_3^-$$

$$NH_4^+ + CO_3^{--} = NH_3 + HCO_3^-$$

so that during the absorption the consumption of free ammonia by the reaction

$$Cu(NH_3)_2^+ + NH_3 + CO = Cu(NH_3)_3CO^+$$

is opposed by ammonia formation due to the above-mentioned shift reactions. Also in this case the rate of carbon monoxide absorption is considerably less than for concentrated ammoniacal solutions. For a solution containing (in gram-moles per liter):

Cu^I	Cu^{II}	$HCOO^-$	FIXED CO_2	TOTAL NH_3
1.67	0.16	2.35	1.84	8.19

we found the following absorption coefficient:

$$K_G = \frac{N_A}{(p - p_{\text{equil}})} = 2.1 \times 10^{-6} \text{ kg.-moles/(atm.)(sec.)(sq. m.)}$$

Obviously in this case also a chemical reaction velocity is the rate-controlling factor. It is possible that the velocity of the shift reactions is rather slow, so that during the reaction the liquid becomes neutral and the mechanism changes. Both case (a) and case (b) will have to be the subjects of further study.

THE SOLIDS CONDENSED FROM CARBON MONOXIDE BY ALPHA PARTICLES

JOHN H. L. WATSON

Edsel B. Ford Institute for Medical Research, Detroit 2, Michigan

MARCEL VANPEE[1]

Graduate School, University of Minnesota, Minneapolis, Minnesota

AND

S. C. LIND

Carbide and Carbon Chemicals Corporation, Oak Ridge, Tennessee

Received February 3, 1949

INTRODUCTION

When radon is mixed with carbon monoxide the action of the α-particles (3) produces one gaseous and two solid substances: carbon dioxide, carbon, and a suboxide of carbon. The overall reaction is approximately given in equation 1.

$$6CO \xrightarrow{\alpha} 2CO_2 + C + C_3O_2 \tag{1}$$

There is some evidence to suggest that the reaction occurs in several successive steps. First, ionization of carbon monoxide causes the reaction in the gas phase represented by equation 2.

$$3CO \rightarrow CO_2 + C_2O \tag{2}$$

A triple collision is not required if the CO^+ ion can collect two neutral carbon monoxide molecules before it is neutralized by a free electron. While the experimental data do not give $-M_{CO}/N_{CO}$ higher than 2, there is evidence of a reverse reaction which may well lower the yield from the required value of 3. The hypothetical gaseous suboxide would then undergo the reaction in equation 3.

$$2C_2O \rightarrow C + C_3O_2 \tag{3}$$

It is thought that the carbon condenses and falls by gravity to the bottom of the vessel and that the suboxide (C_3O_2) diffuses to the wall and polymerizes as a thin, evenly distributed film which can be removed intact (see photograph mentioned in reference 2). With some variations this picture is supported by the present work.

For some undetermined cause it has not been possible to reproduce the polymerized film of suboxide in the present experiments. Despite several attempts the carbon and the suboxide have fallen to the bottom together, with some attachment also to the neck and sides of the vessel, and no separation has been effected. However, the electron microscope has revealed two distinct solids in the mixture, and four lines of graphite in hexagonal structure have been identified by x-ray diffraction, along with lines of a new, unidentifiable solid which is presumed to be the suboxide.

---

[1] Present address: The Edsel B. Ford Institute for Medical Research, Detroit 2, Michigan.

ELECTRON MICROSCOPY

A. Sample preparation

The sample is a dark brown powder adhering to the neck, sides, and base of a glass flask of 8 cm. diameter. The carbon monoxide gas, mixed directly with radon, was irradiated for more than a month with an initial activity of about 100 millicuries of radon. After the bombardment period the carbon dioxide and residual monoxide were pumped off and the flask was immediately filled with nitrogen and sealed.

For the purposes of electron microscopy the flask was broken and samples were prepared and examined in some cases immediately by rubbing the dry material upon prepared Formvar films. Other specimens were prepared in the same manner at later dates to discover what effects exposure to air might have upon the substance.

One plate was taken at a magnification of 13,880 × to show the fine structures, but the rest were taken at 4500 ×, a magnification which showed up all pertinent detail and provided at the same time a sufficient number of particles for statistical accuracy in the counting procedures. Shadow-cast specimens, shadowed with chromium at an angle with tangent of $\frac{3}{4}$, were also micrographed at the lower magnification.

B. Qualitative observations

The material is particulate, and separate particles are recognized readily in the micrographs. The projected images have nearly the same dimensions in all directions in most cases, and shadow casting indicates that the particles are at least as high as they are wide. The edges are not smooth and from considerations of image intensity appear to have small flakes projecting from them. From these observations it is concluded that the particles are agglomerations of solid flaky material and have grown about equally in all directions.

In the electron microscope, upon the fluorescent viewing screen a considerable number of the particles are observed to be hexagonal in shape (see figures 1a and 1b at the arrows and elsewhere). When the micrographs are enlarged and reproduced in prints, and when the morphology of the ragged edges becomes visible, this hexagonal appearance is not seen so strikingly, although the impression is still given. In shadow-cast specimens many of the shadows are straight-edged and show up as from hexagonally shaped particles (figures 2a and 2b). For these reasons, a differential count was made on the particles so that the hexagonal and the nonhexagonal ones could be studied separately as well as in totality. Examples of straight-edged shadows are noted at the arrows in figure 2.

The flakes which project from the particle edges (see arrows in figure 3) are straight-edged and seem to be crystalline. In a dark field the samples exposed to very light electron bombardment in the microscope (figure 4a) show no crystal

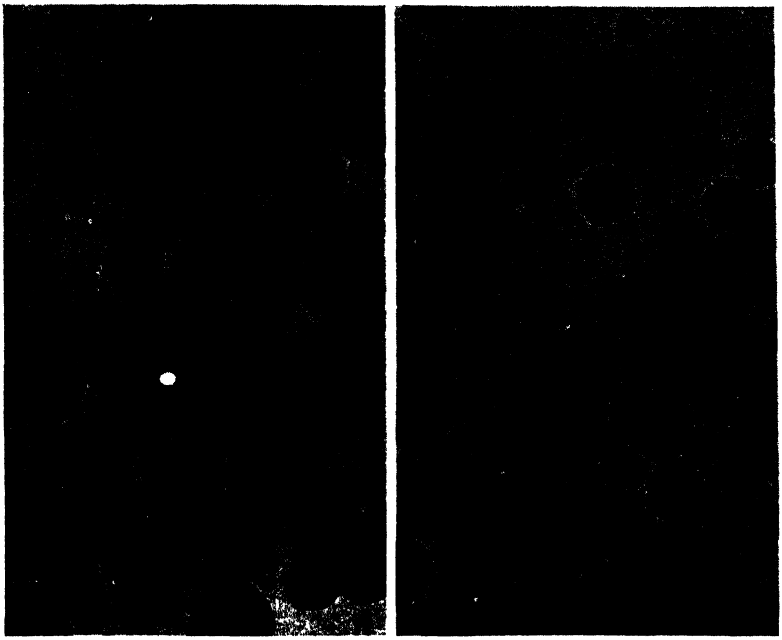

FIG 1 Electron micrographs of carbon monoxide residue in bright field Typical hexagonal images are indicated at the arrows The rough appearance of the particle edges is also visible. (a) Taken from the base of the flask (b) Taken from the neck of the flask. 15,000 ×

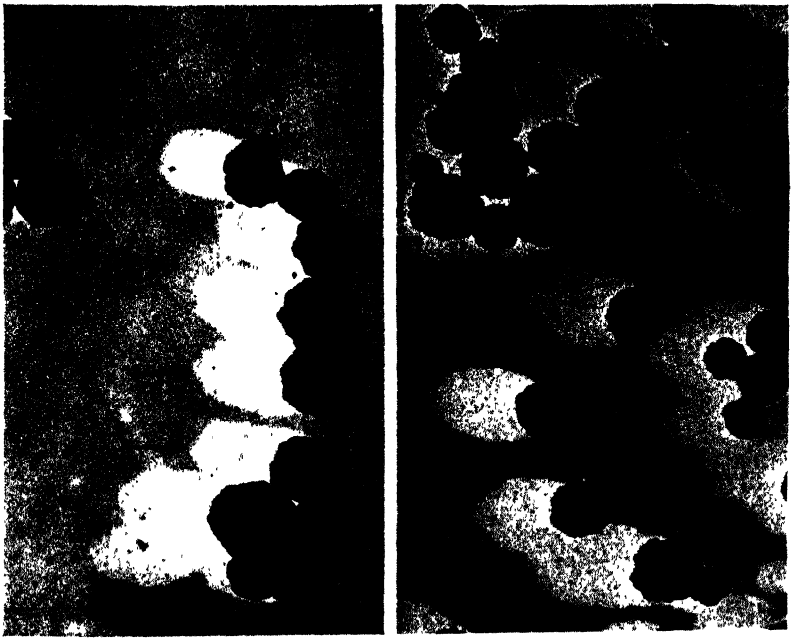

FIG 2. Electron micrographs of shadow-cast carbon monoxide residue in bright field. Typical shadows which show up as from hexagonally shaped particles are shown at the arrows. 15,000 ×.

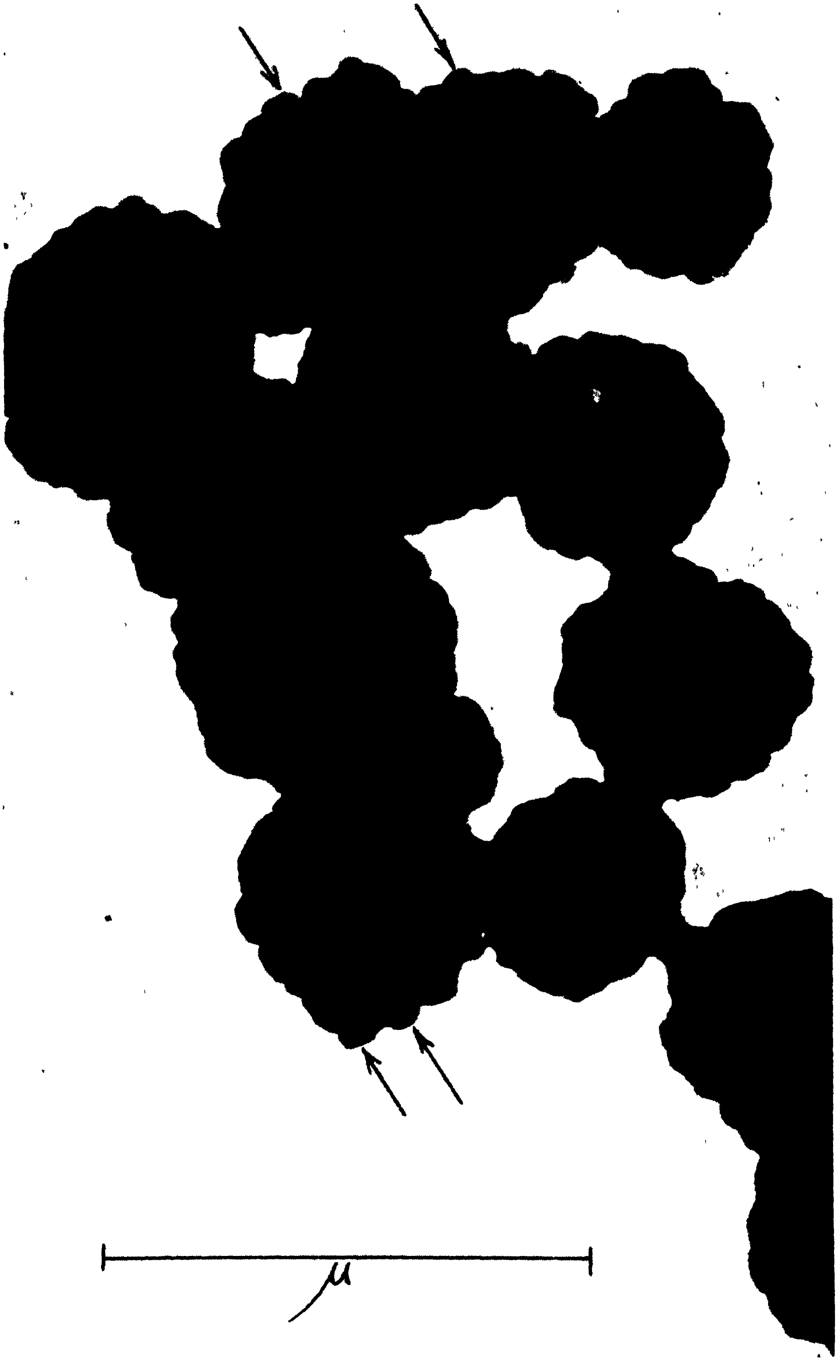

FIG 3 Electron micrograph in bright field to show the rough flaky edges and joining necks between particles, at a higher magnification 65,000 ×

reflections regardless of whether or not the focal length of the objective is varied during examination, unless some of the intensity discontinuities around the edges, which are reminiscent of those in Hall's (1) dark-field micrographs of carbon black, may be so interpreted (see figure 4b at arrows). Dark-field examination of lightly bombarded material indicates a region of high but diffuse scattering power immediately upon the surface of the particles, which suggests that they have a thin surface layer about 400 Å. thick. The major portion, however, of any bombarded particle appears to scatter and absorb electrons too effectively, and there is very little observable structure over their surfaces.

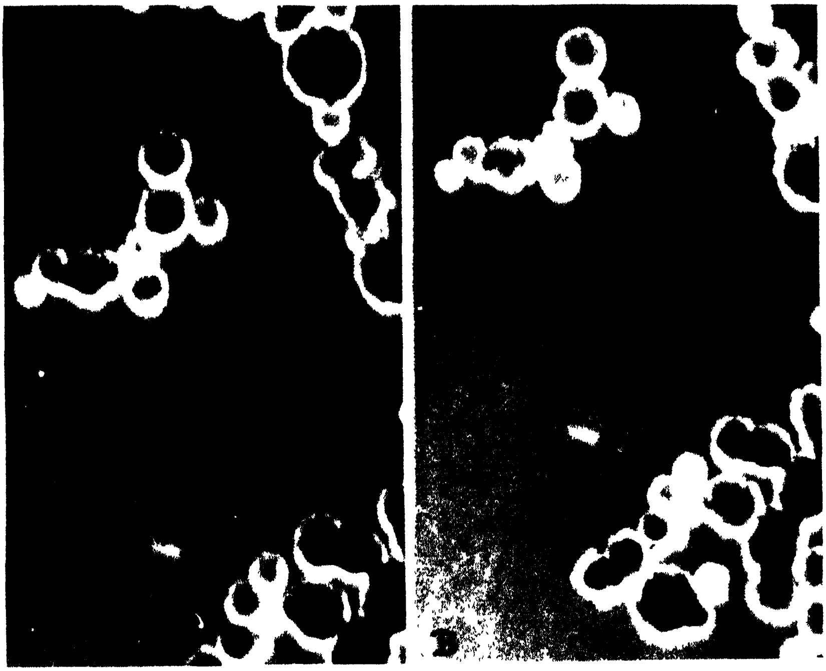

FIG 4 Electron micrographs in dark field of carbon monoxide residues (a) before and (b) after intense electron bombardment in vacuum, same field 15,000 ×

Strong Bragg reflections have been observed at several isolated locations *after* an *intense* electron bombardment. Intense bombardment causes a particle shrinkage which averages about 10 per cent and may be as high as 20 per cent on individual particles or groups. Some also develop a striated structure over their surface (see figure 4b at arrows).

The occurrence of these striations supports the earlier observation that the material is composed of particles which are themselves made up of platelets. The nonoccurrence of the striations in some particles is explainable on the assumption that unless the particle and the flakes within it are oriented suitably with respect to the beam, the reflections will not be seen in the dark-field image. The distance between striations averages about 850 and ranges anywhere from 650 to 920 Å.

Even under prolonged intense bombardment from a biased gun in a vacuum the material does not completely sublime or undergo changes any more startling than those already discussed. Electrons are less effectively scattered and absorbed by the body of the particles after bombardment (compare figures 4a and 4b), and this fact coupled with the noticeable shrinkage suggests that there are two components in the material, one of which is affected more radically than the other by the heating effect of the beam. Light-field microscopy suggests further that one of these components is a viscous liquid material which lies over the particles and probably penetrates them. In figure 3 a neck, which is more easily penetrated by electrons than the main body of the particle, is seen to be joining one particle to another. These necks can be stretched before breaking and resemble in this way the necks which join particle to particle in α-ray cuprene (6, 7, 10) (alprene[2]). The difference is that in alprene the neck and the particle are one, but here, in the radiation product from carbon monoxide, the neck is one component and the main body of the particle a second.

TABLE 1

Data from the total distribution of particles found in the radiation product from carbon monoxide bombarded by α-particles

DATE OF PREPARATION	LOCATION OF DEPOSIT IN FLASK	NUMBER OF PARTICLES	ARITHMETIC MEAN	STANDARD DEVIATION	TOTAL RANGE
			μ	μ	μ
August 5, 1948	Base	388	0.54	0.16	0.2-1.0
August 10, 1948	Top	326	0.43		0.2-0.8
August 21, 1948	Base	248	0.51	0.16	0.24-0.72
August 21, 1948	Side	144	0.42	0.11	0.32-0.56
August 21, 1948	Top	206	0.42	0.13	0.2-0.6

C. *Quantitative observations*

The particles were counted and measured by methods already published (8), and the data were used statistically to give the observations recorded in tables 1, 2, 3, and 4. Figure 5 shows typical distribution curves for the material plotted upon logarithmic probability paper.

Several observations may be made from these data. In table 1 it appears that there has been a slight decrease in particle size during a 16-day exposure to air, from a mean diameter of 0.54 micron to one of 0.51 micron, or a difference of about 5 per cent. This is within the order of accuracy claimed for the experiments, and therefore is not conclusive. However, the difference of over 16 per cent between the mean diameter of a sample taken from the base and that of one taken from the neck of the flask is significant and indicates that there is a spectrum of particle sizes over the surface of the flask with the larger and presumably heavier particles tending to deposit upon its base.

---

[2] Alprene is a polymer of acetylene formed by the bombardment of acetylene gas by α-particles from radon.

TABLE 2

Data from the distribution of the hexagonal particles alone in the radiation product from carbon monoxide bombarded by α-particles

DATE OF PREPARATION	LOCATION OF DEPOSIT IN FLASK	NUMBER OF PARTICLES	ARITHMETIC MEAN	TOTAL RANGE
			μ	μ
August 5, 1948	Base	74	0.46	0.2–1.0
August 10, 1948	Top	56	0.40	0.2–0.8
August 21, 1948	Base	25	0.46	0.24–0.72
August 21, 1948	Side	15	0.39	0.32–0.56
August 21, 1948	Top	38	0.41	0.2–0.6

TABLE 3

Comparison of the mean diameters of the hexagonal and nonhexagonal particles in the five preparations

DATE OF PREPARATION	DIFFERENCE IN DIAMETERS	PERCENTAGE DIFFERENCE
	Å.	*per cent*
August 5, 1948	620	11.5
August 10, 1948	340	8.0
August 21, 1948	280	5.5
August 21, 1948	290	7.0
August 21, 1948	270	4.0

TABLE 4

The percentage by which the hexagonal particles make up the whole distribution

DATE OF PREPARATION	NUMBER OF HEXAGONALS	TOTAL NUMBER OF PARTICLES	PERCENTAGE OF HEXAGONALS
August 5, 1948	74	388	19
August 10, 1948	56	326	17
August 21, 1948	25	248	10
August 21, 1948	15	144	10
August 21, 1948	38	206	14

In table 2 the hexagonal component follows the same trends as the total distribution does, but in table 3 there is an indication that the hexagonal particles tend to have a smaller mean size than those which appear nonhexagonal in the micrographs. Table 4 is included to show that the frequency of occurrence of hexagonal particles is appreciable and varies between 10 and 20 per cent of the count totality. Almost certainly this percentage should be even higher, since from shadow-casting experiments it is obvious that many particles which do not appear to be hexagonal in silhouette do throw shadows as from hexagonal particles.

X-RAY DIFFRACTION

X-ray diffraction analysis was made upon the sample. The experiment was repeated and the same results were achieved each time. A 114.59 mm. Norelco powder camera was used with nickel-filtered copper radiation for a 2-hr. exposure at 35 kv. and 25 ma. The specimen was scraped from the reaction flask and broken with a knife on a glass plate to as fine a powder as possible. A 0.3 mm. glass fiber was dipped into collodion and rolled in the sample until it was evenly covered. During the exposure the sample was rotated continuously.

TABLE 5

X-ray diffraction data for the residue formed by α-ray bombardment of carbon monoxide

LINE NO.	MEASURED d-VALUE	ESTIMATED I/I_0	STANDARD GRAPHITE d-VALUES*	I/I_0
	Å.		Å.	
1	5.38	0.7		
2	3.38	1.0	3.37	1.0
3	2.88	0.2		
4	2.695	0.6		
5	2.53	0.8		
6	2.21	0.8		
7	2.11	0.3	2.11	0.30
8	2.03	0.4	2.03	0.60
9			1.81	0.01
10	1.695	0.1	1.690	0.02
11	1.61	0.1		
12			1.560	0.02
13	1.52	0.6		
14	1.33	0.1		
15	1.26	0.1		
16			1.227	0.35

* Values taken from Hull: Phys. Rev. **10**, 661 (1917).

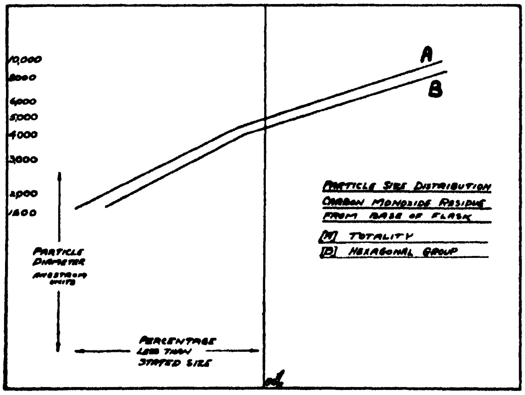

FIG. 5. Typical particle-size distribution curves for carbon monoxide residue

Data for the lines recorded are given in table 5 along with the values for a standard graphite. The evidence that the sample contains graphite is substantial, and the fact that the relative intensity of the lines agrees fairly well is added proof that graphite is present. On the other hand, lines 1, 3, 4, 5, 6, 11, 13, 14, and 15 are unidentified but prominent in the pattern. The unknown substance which gives rise to these lines may be the suboxide, the x-ray data of which are given separately in table 6.

Figure 6 shows the pattern from the residue. Little if any line broadening is present in it, and the lines are sharp and relatively strong although not spotted like those from the usual graphite standard. Qualitatively, they indicate a fairly well-developed graphite oriented at random with respect to the beam and with relatively small particle size.

The perfection of the pattern which gave the data in tables 5 and 6 and which is reproduced in figure 6 was not always reproducible and sometimes no rings at all were visible. This fact was studied extensively and all mounting media were checked for impurities, but none was found. Therefore, the variability of pattern perfection has been concluded to be a function of the mounting, not of the material. The d-values from each pattern were the same from sample to sample, but the number of lines in the patterns varied. In the same experiments samples of pure graphite from unused spectrograph sources were used to check the data from Hull's experiments. There was good agreement.

TABLE 6

Possible x-ray diffraction data for the unknown component present in the residues formed by α-ray bombardment of carbon monoxide

(Those starred are doubtful as possibly belonging to graphite)

d VALUES	ESTIMATED I/I_0	d VALUES	ESTIMATED I/I_0
Å		Å	
5.38	0.7	1.61	0.1
2.88	0.2	1.52*	0.6
2.695	0.6	1.33	0.1
2.53	0.8	1.26*	0.1
2.21	0.8		

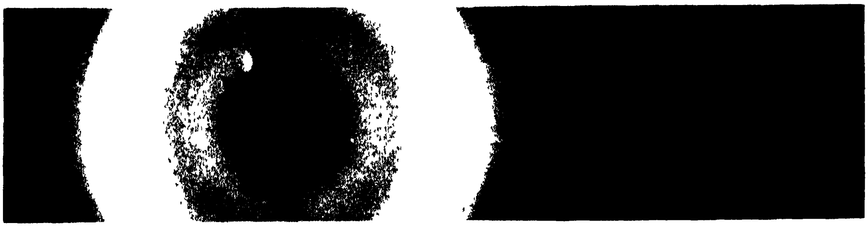

FIG. 6. X ray diffraction pattern from carbon monoxide residue

DISCUSSION

The appearance of the carbon monoxide residues in electron micrographs is different in some ways from all of the other polymerized gases studied by the same means so far (6, 7, 10). It is like alprene and the hydrogen cyanide polymer in that it has recognizable particles sometimes joined by necks, but where the particles in these two substances are completely smooth, those in the carbon monoxide residues are rough and composed of a flaky material. It is similar in appearance to the cyanogen polymer made by α-ray bombardment, in that both materials have rough particles which appear crystalline by bright-field microscopy, but necks are not demonstrable in the cyanogen polymer and the mean particle size of this polymer is about three to four times less. Comparisons of this type would be more significant, however, if they were made between samples formed under more nearly identical and controlled conditions.

There are several indications from this work that there is more than one phase present in the carbon monoxide residues. The difference in particle size between material taken from the base and the top and the double shape distribution are suggestive but not conclusive. More significant is the liquid component, which is distinguishable from the solid component that it encases. It is recognized in bright-field microscopy where it joins particle to particle and in dark-field microscopy where it gives evidence of an area of high scattering power around and between them. X-ray diffraction studies indicate that the solid component is graphitic. It is unlikely that graphite will be affected by the beam, and the shrinkage of the material under intense electron bombardment can only be explained by assuming that a second substance, presumably the polymerized suboxide, is present and is evaporated somewhat by the heating effect of the electron beam in vacuum.

Dark-field microscopy indicates diffuse rather than crystalline scattering from the unbombarded material. However, since fairly strong, sharp lines are obtained in x-ray diffraction patterns, it may be that the discontinuities or "spikes" seen along the image edges in the dark field are similar in nature to those described by Hall (1) for carbon black and that crystalline reflections do originate from the unbombarded residues. Since the substance is composed largely of graphite, it is reasonable to expect that such reflections do occur, and to conclude that the spikes are crystal reflections.

Dark-field microscopy also shows that the particles are very opaque to electrons through most of their volume, but that there is a region at the edge and between particles which scatters well and is quite thick electron optically, but which is thin enough so that wide-angle, diffuse scattering is not predominant. After bombardment the opacity of the whole particle is decreased considerably, and very wide angle scattering no longer predominates over the field.

The hexagonal nature of an appreciable number of the particles is a reproducible observation from preparation to preparation, but it is difficult to account for it. Hexagonal forms are often observed in heat-treated (4) and untreated (5, 9) carbon blacks, where it is well known that the ultimate structure is an hexagonal net.

It appears that particle growth has occurred in the gas phase, since the particles, though rough, are developed to a similar extent in all directions. This is also indicated by the fact that when the particles grow large enough they fall out under gravity so that the larger ones collect at the bottom and the smaller ones near the top, there still being a probability that some of either extreme will be found at any location within the flask. It also appears that, unlike alprene, the ultimate building units are much larger so that, instead of being round and smooth, particles are rough.

Measurements made upon the projecting flakes give a mean size of about 615 Å., a value which is the order then to which some first-forming unit grows before the secondary growth commences, whereby these unite to form the much larger particles shown here.

SUMMARY AND CONCLUSIONS

1. Carbon monoxide, when polymerized by α-rays from radon, exhibits a particulate structure. The particles have recognizable shape and have nearly the same dimensions in all directions.
2. There are two components in the residue. The first consists of solid particles which are rigid aggregates of graphitic flakes. The second is a viscous liquid material which surrounds the particles, may exist within them, and often joins them one to the other by short necks.
3. The mean diameter of the material taken from the base of the flask is about 0.5 micron and that of the material from the neck of the flask about 0.41 micron.
4. About 15 per cent of the silhouette images of the particles appear hexagonal in shape. The percentage of particles having this shape is undoubtedly even higher than this, since nonhexagonal images often are accompanied by hexagonal shadows.
5. The approximate uniformity of particle dimensions in all directions and the increase in particle size toward the base of the flask indicate that the particles are formed and grow in the gas phase, and that the larger ones fall out under gravity. Many, both large and small, also diffuse to the walls.

Shadow casting was accomplished through the kind coöperation of the Physics Instrumentation Department of the Research Laboratories Division, General Motors Corporation. In this regard the authors are indebted particularly to Mr. William L. Grube, of that company. Mr. Jonathan Parsons, of the staff of the Edsel B. Ford Institute for Medical Research, took the x-ray diffraction patterns.

REFERENCES

(1) Hall, C. E.: J. Applied Phys. **19**, 271-7 (1948).
(2) Lind, S. C.: *The Chemical Effects of Alpha Particles and Electrons*, 2nd edition, p. 153 (photograph). The Chemical Catalog Company, Inc., New York (1928).
(3) Lind, S. C., and Bardwell, D. C.: J. Am. Chem. Soc. **47**, 4682 (1925).
(4) Schoon, Th., and Koch, H. W.: Kautschuk **17**, 1 (1941).
(5) Watson, John H. L.: J. Applied Phys. **17**, 121 (1946).
(6) Watson, John H. L.: J. Phys. & Colloid Chem. **51**, 654 (1947).
(7) Watson, John H. L.: J. Phys. & Colloid Chem. **52**, 470 (1948).
(8) Watson, John H. L.: Anal. Chem. **20**, 576 (1948).
(9) Watson, John H. L.: J. Applied Phys. **20**, 747 (1949).
(10) Watson, John H. L., and Kaufmann, K.: J. Applied Phys. **17**, 996 (1946).

AN OSCILLOGRAPHIC POLAROGRAPH FOR HIGH RATES OF POTENTIAL VARIATION[1]

PAUL DELAHAY[2]

Department of Chemistry, University of Oregon, Eugene, Oregon

Received April 4, 1949

In a previous paper (1) some of the main features of oscillographic polarography have been discussed. In the course of further studies on the mechanism of polarographic reduction the need arose for an instrument generating the potential variation at rates higher than those available with the instrument previously described. Some modifications were introduced for this purpose and, at the same time, a number of improvements were added to our technique.

SHAPE OF THE VOLTAGE WAVE APPLIED TO THE POLAROGRAPHIC CELL

In the instrument described in the present paper a saw-tooth wave with a quiescent period is applied to the polarographic cell (figure 1). Electrolytic reduction is taking place at the dropping electrode during the rise of potential exactly as in the instrument previously described (1). During the quiescent period the substance which has been reduced during the preceding sweep is, in general, oxidized to a fairly large extent. The anodic current corresponding to that oxidation decreases rapidly and becomes equal to zero before the end of the quiescent period. There is thus no interference between anodic and cathodic currents. When the saw-tooth wave does not present any quiescent period, as was the case in our previous instrument (1), the oxidation of the substance reduced during the preceding sweep occurs when the next sweep starts. The early part of the oscillographic wave thus represents a combination of the anodic and capacity currents. Since the anodic current is not negligible, the oscillographic wave is distorted and the maximal peak current is affected with an error which is by no means negligible.

The previous considerations are represented in figures 2 and 3. These waves have been recorded during the last instants of the life of a mercury drop at the electrode and during the early stages of the next drop. Only the wave corresponding to the maximum area of the drop should be taken into consideration. Figure 2 shows a wave recorded with the arrangement described in the present paper. The segment *AB* corresponds to the quiescent period of the voltage wave. The segment of curve *BD* represents the charging current of the double layer. The portion *DF* is the polarographic wave itself. Figure 3 has been recorded with an instrument generating a saw-tooth wave with no quiescent time and the distortion of the left portion of the wave is apparent.

A similar distortion of the polarographic wave is observed when the frequency of the sweep generator reaches a value of about one hundred sweeps per second even when a saw-tooth wave with quiescent period is applied to the cell. At such a relatively high frequency, the quiescent period becomes too short to allow a fairly complete oxidation of the reduction product resulting from the preceding sweep. This circumstance would limit the rate of potential variation to about 100 v. per

---

[1] Presented before the Division of Physical and Inorganic Chemistry at the 115th Meeting of the American Chemical Society, which was held in San Francisco, March, 1949.

[2] Present address: Department of Chemistry, Louisiana State University, Baton Rouge 3, Louisiana.

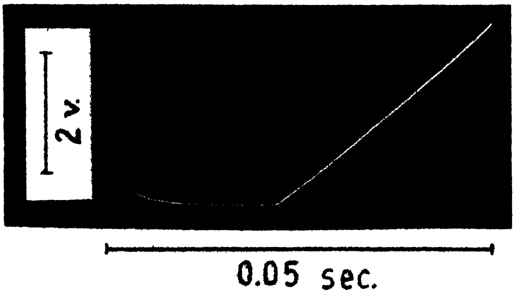

FIG. 1. Saw-tooth wave with quiescent period recorded at a frequency of 20 sweeps per second.

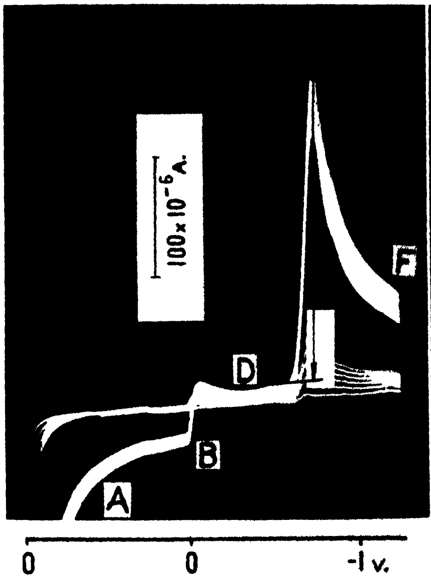

FIG. 2

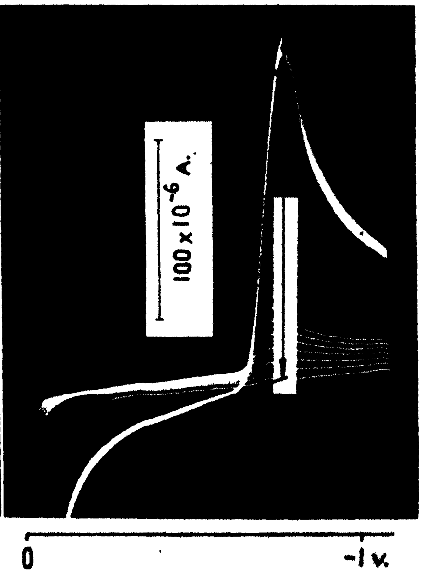

FIG. 3

FIG. 2 Example of oscillographic wave. Saw-tooth wave with a quiescent period applied to the polarographic cell. 10^{-3} M Pb^{++} solution in 0.5 N potassium nitrate solution. m = 1.41 mg./sec.; τ = 3.48 sec.; S = 20 sweeps/sec.; v = 22.0 v./sec.

FIG. 3. Example of oscillographic wave. Saw-tooth wave with no quiescent time applied to the polarographic cell. 10^{-3} M Pb^{++} solution in 0.5 N potassium nitrate solution. m = 1.41 mg./sec.; τ = 3.48 sec.; S = 20 sweeps/sec.; v = 22.0 v./sec.

second. However, this limit can be extended to about 1000 v. per second by applying to the cell a saw-tooth wave for which the rise of potential occurs within a small fraction of the total duration of one sweep. The rate of potential variation is increased consequently, although the frequency of the sweep generator does not need to be increased.

Figure 4 shows an example of a polarographic wave recorded at a high rate of potential variation.

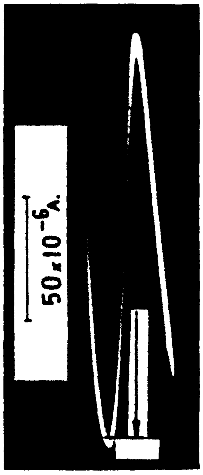

FIG. 4. Example of oscillographic wave recorded at a high rate of potential variation. 5×10^{-4} *M* potassium iodate in 1 *N* potassium chloride solution. m = 1.41 mg./sec., τ = 4.65 sec.; S = 60 sweeps/sec.; v = 1100 v./sec.

SWEEP GENERATOR AND PREAMPLIFIER

A schematic diagram of the sweep generator and preamplifier is shown in figure 5. The variations with time of the voltage on several points of the circuit are shown in figure 6. The instrument is connected in K to the plate of a thyratron of a saw-tooth wave generator, which can be, very conveniently, the time base of a commercial oscillograph. The frequency of the saw-tooth generator is standardized against the 60-cycle frequency (1). Frequency stabilization is obtained by applying a 60-cycle voltage of small amplitude to the grid of the thyratron of the time base. The arrangement for this frequency stabilization is generally incorporated in commercial oscillographs.

The voltage in point K presents a constant voltage component equal to the extinction voltage of the thyratron tube (figure 6A). When a condenser (C) is connected in K, the voltage on the other terminal (L) of this condenser follows a symmetrical wave such as that of figure 6B. This symmetrical voltage wave is applied to a special circuit having two diodes (tube T_1) connected in opposition in such a manner that the positive half-wave flows through resistance r_{NY} while the negative half-wave flows through the resistance r_1 (figures 6C, 6D). The voltage between point N of potentiometer p_1 and ground is amplified by tube T_3. The voltage applied to the polarographic cell, connected in XX, is derived from the cathode bias r_5 of tube T_2. The shape of the saw-tooth wave applied to the amplifier tube T_3 depends on the value of the ratio r_1/r_{NY}. When that ratio is equal to unity, the quiescent period and the active period are approximately of equal duration (figure 1). This shape of voltage wave is most convenient for analytical work. When the ratio r_1/r_{NY} is larger than unity, the quiescent period becomes longer compared to the active period. Voltage waves of this shape are used only when a high rate of potential change needs to be used. The value of the ratio r_1/r_{NY} is modified very simply by connecting a resistance r_2, r_3, or r_4 in parallel with potentiometer p_1 by means of switch S_1. When resistance r_1 is zero the saw-tooth wave, generated on the terminals of potentiometer p_1, presents no quiescent period any more (figure 6E).

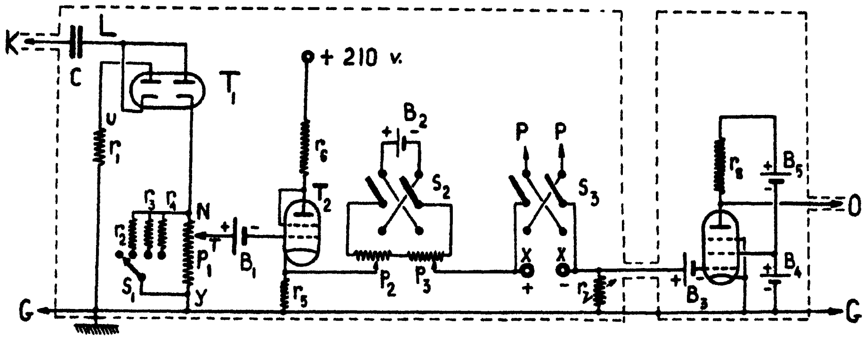

FIG. 5. Circuit diagram of the sweep generator and amplifier

r_1 = 3 megohms, 2 watts
r_2 = 200,000 ohms, 2 watts
r_3 = 100,000 ohms, 2 watts
r_4 = 50,000 ohms, 2 watts
r_5 = 300 ohms, 2 watts
r_6 = 5000 ohms, 10 watts
r_7 = 0–9999 decade resistance box
r_8 = 100,000 ohms, 2 watts
p_1 = 3 megohm potentiometer
p_2 = 6 ohm potentiometer
p_3 = 100 ohm potentiometer

C = paper condenser, 1 microfarad, 1000 v.
T_1 = twin diode 6 H 6
T_2 = tetrode 6 V 6
T_3 = pentode 6 S J 7
B_1 = C supply battery, 12 v.
B_2 = dry cell, 3 v.
B_3 = C supply battery, 3 v.
B_4, B_5 = B supply battery, 90 v.
S_1 = circuit selector
S_2, S_3 = double-throw, double-pole switch

K, connected to the plate of the thyratron tube of a conventional saw-tooth generator
G, ground connection
O, connected to the input terminal of the vertical deflection amplifier of the oscillograph
PP, connected to the voltage-measuring potentiometer
XX, connected to the polarographic cell

The constant voltage applied during the quiescent period is adjusted by means of potentiometers p_2 and p_3 (figure 5), no saw-tooth wave being applied to the amplifier tube T_3 (potentiometer p_1 set in position Y). The latitude of this adjustment extends from +0.6 to −3 v. The amplitude of the saw-tooth wave is adjusted by means of potentiometer p_1 over the range of 0–3 v. Voltage measurements are carried out by means of a potentiometer connected in PP (figure 5). The zero instrument of this potentiometer circuit is shunted by a 500-microfarad electrolytic condenser in order to eliminate the vibrations of the needle of the instrument. During the recording of a wave the potentiometric circuit is switched off (S_3) in order to prevent the appearance of a 60-c.p.s. voltage on the terminals of the polarographic cell.

The ratio of the amplitude of the saw-tooth wave to the average voltage read on the potentiometer is determined by graphical integration once and for all for the different values of r_1/r_{NY} and for the different frequencies at which measurements are usually carried out.

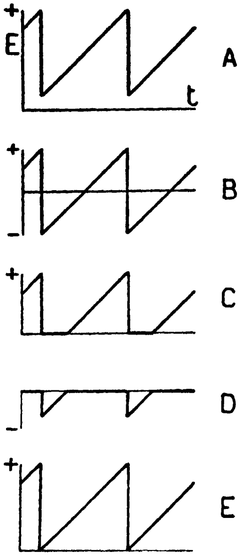

Fig. 6. Variation of voltage in different points of the circuit of the sweep generator 1A, point K and G; 1B, point L and G; 1C, point N and G; 1D, point U and G; 1E, point N and G, resistance r_1 being equal to zero.

The current flowing through the polarographic cell is measured by the drop of potential on the terminals of a decade resistance box r_7. It was found in our previous investigation (1) that a serious error affects the strength of the maximal peak current when the drop of potential in resistance r_7 exceeds 0.005 v. This voltage is too small to be applied to the vertical deflection amplifier of most commercial oscillographs. It is therefore indispensable to interpose a preamplifier between resistance r_7 and the vertical deflection amplifier of the oscillograph. The circuit of the preamplifier, shown in figure 5, is of a conventional type. It is a battery-operated one-stage D.C. amplifier. In order to eliminate vibrations, the chassis of the amplifier is loaded with 5 lb. of lead and suspended by means of four coil springs. The potentiometer controlling the gain of the vertical deflection amplifier of the oscillograph is always set in the position corresponding to the maximum sensitivity. The amplitude of the oscillographic wave is then adjusted by means of resistance box r_7.

In the case of the 208 B Du Mont oscillograph, which has been used in this investigation, two input circuits of different sensitivities are provided. However, the circuit of maximum sensitivity cannot be used in the present case. Indeed, when a fairly large resistance is connected to the input of the amplifier a parasitic 60-c.p.s. voltage is superposed to the polarographic wave. Therefore only the circuit of lower sensitivity has been used. However, with the arrangement of figure 5, the full deflection on the screen of the oscillograph corresponds to a 0.005-v. drop of potential in resistance r_7.

The device of figure 5 is supplied at 210 v. D.C. from a regulated power supply equipped with a suitable filtering circuit (1). This power supply and the oscillograph are supplied at 110 v. A.C. by means of a constant-voltage transformer. The filaments are connected to a 6-v. storage battery.

POLAROGRAPHIC CELL

In our previous work we used an unshielded polarographic cell immersed in a thermostatic bath. The electrical equipment of the bath had to be switched off during recordings because of the absence of shielding. This inconvenience has been eliminated in the shielded cell represented in figure 7. The cell, of conventional design, is placed in a shielding box made of copper sheet. Two lateral panels of the shielding box are of copper gauze in order to facilitate the circulation of water around the cell. The shielding box is attached to the edge of the water bath by means of a bracket.

The mercury reservoir is placed in a copper shielding box. The rubber tube connecting the mercury reservoir to the capillary tube is shielded by means of a flexible metallic envelope. When the cell is not in use, the rubber tube is pinched by placing a clamp over the metallic envelope. To eliminate magnetic interference, the water bath should be located at least 2 ft. from the oscillograph. To prevent any vibration of the cell, the stirrer of the water bath should be attached by means of a wall bracket.

ACCURACY AND REPRODUCIBILITY OF EXPERIMENTAL RESULTS

Method of recording

An essential condition for accurate work is that the highest wave recorded photographically, truly corresponds to the maximum area of the mercury drop. The simplest manner to observe this condition is to make an exposure for a duration corresponding to the life of several mercury drops. This method has been followed exclusively in a previous investigation (1). In some cases, however, the lower portion of the wave of maximum height is located below waves which have been recorded during earlier stages of the mercury drop. The resulting picture is not clear and the maximal peak current cannot be measured with accuracy. This difficulty is eliminated when one records only the waves occurring during the last instants of the life of one single mercury drop. The frequency of the sawtooth generator is thus selected in such a manner that a fairly large number of sweeps occur during the life of a single drop. Very satisfactory results have been obtained in this manner by recording waves at the frequency of 20 or 30 sweeps per second with a drop time of 3–4 sec. This procedure is thus recommended for analytical work.

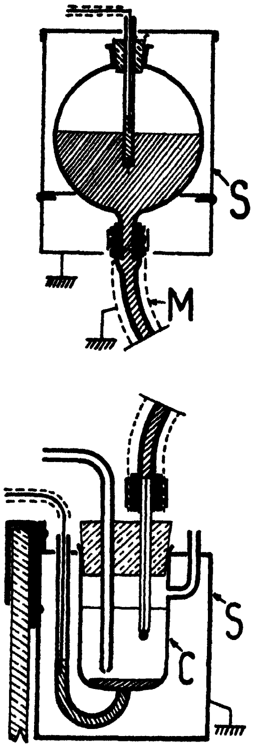

Fig. 7

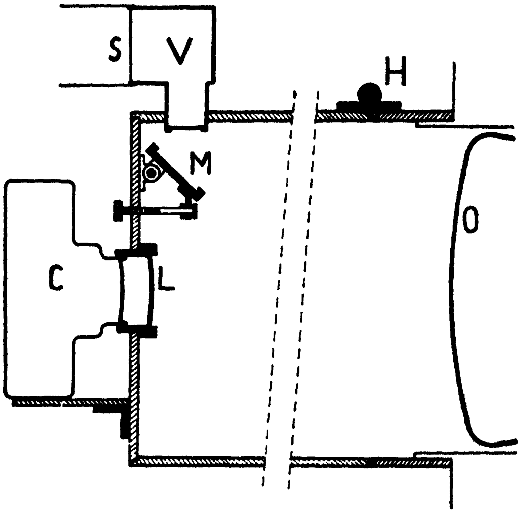

Fig. 8

Fig. 7. Shielded polarographic cell. C, polarographic cell; S, shielding box; M, flexible metallic envelope.

Fig. 8. Arrangement for the photographic recording of oscillographic waves. L, "Portra" lens + 3; C, Kodak 35 camera; V, reflex viewfinder; M, adjustable mirror; S, screen of viewfinder; H, hinge; O, screen of oscillograph.

Recordings are carried out very conveniently by means of the device shown in figure 8. With this device one observes the screen of the oscillograph in a reflex viewfinder during recordings. The recording and the determination of the wave height are carried out as previously described (1).

Experimental results

The dependence of the maximal peak current on the concentration of reducible substance has been determined in the case of zinc and cobaltous ion solutions.

Zinc ion has been selected because it is reduced reversibly at the dropping mercury electrode (2), cobalt ion because it is reduced irreversibly (3). For each concentration, five waves have been recorded. The maximal peak current has

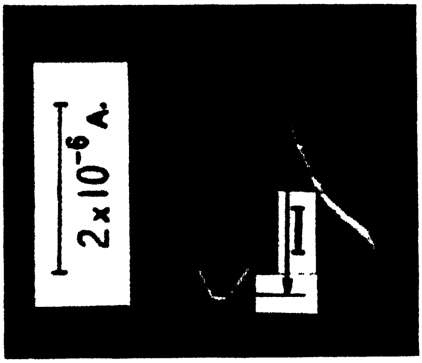

FIG. 9. Example of oscillographic wave recorded in the low concentration range 2×10^{-5} M Zn^{++} solution in 1 M potassium chloride. m = 1.41 mg./sec.; τ = 3.50 sec.; S = 20 sweeps/sec.; v = 16.5 v./sec.

TABLE 1

Variation of the maximal peak current with the concentration of reducible substance

Zinc ion in 1 M potassium chloride; m = 1.41 mg./sec.; τ = 3.20 sec.; S = 20 sweeps/sec.; v = 33.0 v./sec.

CONCENTRATION	MAXIMAL PEAK CURRENT	EXPERIMENTAL DEVIATION	AVERAGE MAXIMAL PEAK CURRENT	EXPERIMENTAL ERROR
millimoles liter	*microamp*	*per cent*	*microamp*	*per cent*
0.01	0.70	−2.0 +2.0		
0.02	2.01	−2.3 +1.9		
0.04	4.17	−0.4 +0.3		
0.06	6.80	−0.1 +0.2		
0.08	10.6	−0.4 +0.5		
0.1	13.9	−0.6 +0.4	14.0	−0.7
0.2	28.9	−0.1 +0.1	28.0	+3.3
0.4	56.1	−0.5 +0.1	56.0	+0.2
0.6	83.2	−1.0 +0.1	84.0	−0.9
0.8	111.2	−0.8 +0.8	112.0	−0.7
1	138	−0.6 +0.7	140.0	−1.4
2	270	−0.5 +0.3		
3	389	−1.0 +1.7		
4	503	−0.5 +0.6		
5	582	−0.3 +0.5		
Average		−0.8 +0.7	Average	−0.9 +1.8

been determined graphically as indicated previously (1). In the 10^{-5} to 10^{-4} molar concentration range the wave height has been measured as shown in figure 9. Although this method gives results which are too low, it is more accurate than the method in which the current is measured by superposing the maximal wave on the maximal capacity current curve. In the range of concentrations in which this empirical method has been applied, the maximal peak current is no longer exactly proportional to the concentration of the reducible substance.

In the 10^{-4} to 10^{-3} molar concentration range, the maximal peak current is exactly proportional to the concentration. The errors affecting the experimental values of the maximal peak current can thus be calculated. Tables 1 and 2 show that these errors do not exceed ±2 to 3 per cent, in general.

For concentrations larger than 10^{-3} molar, the maximal peak current being rather large, the influence of the resistance of the circuit becomes noticeable and, as a result, the strength of the experimental currents in this range is smaller than the value calculated from experimental data at lower concentrations.

TABLE 2

Variation of the maximal peak current with the concentration of reducible substance in the case of an irreversible reaction

Cobaltous ion in 1 M potassium chloride; m = 1.41 mg./sec.; τ = 2.90 sec.; S = 20 sweeps/sec.; v = 26.1 v./sec.

CONCENTRATION	MAXIMAL PEAK CURRENT	EXPERIMENTAL DEVIATION	AVERAGE MAXIMAL PEAK CURRENT	EXPERIMENTAL ERROR
millimoles/liter	*microamp*	*per cent*	*microamp*	*per cent*
0.1	3.34	−0.7 +0.7		
0.2	7.08	−0.8 +0.8	7.20	−1.7
0.4	14.75	−0.1 +0.2	14.40	+2.4
0.6	21.90	−0.7 +0.8	21.60	+1.4
0.8	28.60	−0.6 +0.8	28.80	−0.7
1	37.30	−0.6 +1.2	36.0	+3.6
2	81.0	−1.2 +0.5		
3	131.8	−1.8 +1.6		
4	185.7	−1.0 +1.2		
Average .		−0.8 +0.9	Average	−1.2 +1.5

Table 1 shows that, in the range extending from 4 × 10^{-5} to 10^{-3} molar, the reproducibility of the experimental results remains practically constant and the experimental deviations do not exceed ±1 per cent.

SUMMARY

A new method of oscillographic polarography for measurements at high rates of potential variation is described. A saw-tooth wave with a relatively long quiescent period and a steep rise is applied periodically to the polarographic cell. The instrument covers a range of rates of potential variation extending from about 5 to 1000 v. per second. For a rate of potential variation lower than about 100 v. per second, results are in general reproducible within ±1 to 2 per cent with an error not exceeding ±2 to 3 per cent.

The experimental arrangement is described in detail.

This work is part of a research project entitled "Polarographic Study of Corrosion Phenomena" carried out at the University of Oregon under contract with the Office of Naval Research. The author wishes to thank Professor Pierre Van Rysselberghe, director of the project, for his interest and advice.

REFERENCES

(1) Delahay, P.: J. Phys. & Colloid Chem. 53, 1279 (1949).
(2) Kolthoff, I. M., and Lingane, J. J.: *Polarography*, p. 271. Interscience Publishers, Inc., New York (1941).
(3) Reference 2, p. 284.

CALCULATION OF HEATS OF ADSORPTION FROM ADSORPTION ISOSTERES[1]

ROBERT S. HANSEN
Department of Chemistry, Iowa State College, Ames, Iowa

Received March 3, 1949

On the basis of an equation, arrived at by statistical reasoning, Wilkins (4) has argued that the commonly used method of calculating differential heats of adsorption from adsorption isosteres: namely,[2]

$$\left(\frac{\mathrm{d}\ln p}{\mathrm{d}T}\right)_N = \frac{q_d}{RT^2} \tag{1}$$

is incorrect, and that instead of this equation the equation

$$\left(\frac{\mathrm{d}\ln p}{\mathrm{d}T}\right)_\theta = \frac{q_d}{RT^2} \tag{2}$$

should be used. The symbol N refers to the number of moles adsorbed, and the symbol θ to the "surface concentration" N/N_m, where N_m is the limiting number of moles adsorbed. Since N_m is in general temperature dependent, the two methods are not equivalent.

Armbruster and Austin (1) have presented an argument for the equivalence of heats of adsorption calculated by the Wilkins convention and those obtained from the C constant of the Brunauer–Emmett–Teller equation. Joyner and Emmett (3) have found that certain conclusions following from Wilkins' convention are not in agreement with their experimental data.

In view of the uncertainty resulting from Wilkins' argument, it would appear worthwhile to investigate the Clapeyron equation as applied to the adsorption of gases by solids thermodynamically.[2]

---

[1] Contribution No. 44 from the Institute for Atomic Research and from the Department of Chemistry, Iowa State College, Ames, Iowa.

[2] Following common usage, the heat of adsorption is considered positive when heat is evolved during adsorption.

Consider a solid (single component) in equilibrium with a single-component gas. A volume increment V_g in the gas phase sufficiently far from the solid surface to be uninfluenced by adsorptive forces containing N_g moles of gas of entropy S_g and chemical potential μ_g must satisfy, for homogeneous equilibrium, the equation[3]:

$$0 = -S_g\mathrm{d}T + V_g\mathrm{d}p - N_g\mathrm{d}\mu_g \tag{3}$$

$$\mathrm{d}\mu_g = -\bar{S}_g\mathrm{d}T + \bar{V}_g\mathrm{d}p \tag{4}$$

Following Gibbs we treat the inhomogeneous region by the use of a mathematical surface, located in or near this region but as yet with one degree of freedom in its location. The surface excess of a quantity is then the amount of the quantity in the inhomogeneous region in excess of the amount there would be if the bulk phases remained uniform up to the mathematical surface. Let N_s' and N_s'' be the surface excesses of the components (loosely speaking, the solid and gaseous components, supposing that their mutual solubility is negligible), μ_s' and μ_s'' their chemical potentials, S_s the surface excess of entropy, A the surface area, and γ the specific free surface energy. Then[4]

$$0 = S_s\mathrm{d}T + A\mathrm{d}\gamma + N_s'\mathrm{d}\mu_s' + N_s''\mathrm{d}\mu_s'' \tag{5}$$

We now make the location of the mathematical surface precise by setting N_s', the surface excess of the "solid" component, equal to zero, and in so doing give unique significance to the remaining quantities in equation 5. We denote this unique value of S_s by S_σ, of N_s'' by N_σ, and replace $\mathrm{d}\mu_s''$ by $\mathrm{d}\mu_\sigma$ for symmetry in notation. Then

$$0 = S_\sigma\mathrm{d}T + A\mathrm{d}\gamma + N_\sigma\mathrm{d}\mu_\sigma \tag{6}$$

or

$$\mathrm{d}\mu_\sigma = -\bar{S}_\sigma\mathrm{d}T - \bar{A}\mathrm{d}\gamma \tag{7}$$

Here it should perhaps be noted that, if the solubility of the gas in the solid is negligible and the vapor pressure of the solid negligible compared to the equilibrium pressure of the gas, the mathematical surface as located by the convention chosen coincides essentially with the solid surface. Guggenheim and Adam (2) have discussed this point in detail, and their justification for thus interpreting a mathematical surface located by their "V" convention applies *a forteriori* to the great majority of gas–solid adsorption equilibria. Under these circumstances, "amounts adsorbed" obtained by the volumetric method with dead-space corrections obtained by a nonadsorbed gas are properly interpreted as surface excesses in the sense of the convention chosen.

---

[3] Equation 3 is ordinarily given as a step in the derivation of the Gibbs–Duhem equation. See, for example, W. GIBBS: *Collected Works*, Vol. I, p. 88, Eq. 97, Yale University Press, New Haven, Connecticut (1948).

[4] GIBBS, W.: *op. cit.* in footnote 3, p. 230, Eq. 503. See also pp. 219–29 for a detailed discussion of the treatment of the inhomogeneous region, construction of mathematical surfaces, and significance of surface excesses, all of which are used above in the Gibbsian sense.

We are interested in comparing intensive parameters under two different equilibrium conditions. For equilibrium to exist between substances in homogeneous and inhomogeneous regions it is necessary that

$$\mu_g = \mu_\sigma \tag{8}$$

and we are interested in comparing variation in intensive parameters under maintenance of equilibrium, so that, in addition,

$$d\mu_g = d\mu_\sigma \tag{9}$$

From equations 4 and 7 we have, by virtue of equation 9,

$$(\bar{S}_g - \bar{S}_\sigma)dT = \bar{V}_g dp + \bar{A} d\gamma \tag{10}$$

Therefore

$$\left(\frac{\partial p}{\partial T}\right)_\gamma = \frac{\bar{S}_g - \bar{S}_\sigma}{\bar{V}_g} \tag{11}$$

The quantity $N_\sigma(\bar{S}_\sigma - \bar{S}_g)$ is the total change in entropy which the system solid–gas undergoes as a result of adsorption, assuming the amount of gas to be sufficiently large so that its pressure change during the process is negligible. The quantity $(\bar{S}_g - \bar{S}_g)$ is therefore the integral change in entropy per mole surface excess due to adsorption. This result is not of particular interest, for the condition of constant free surface energy required in evaluating the derivative $\left(\frac{\partial p}{\partial T}\right)_\gamma$ cannot be realized experimentally at present. We may, however, eliminate the differential $d\gamma$ by considering γ to be (at equilibrium) a bivariant function, and choose T and $\bar{A}$ as the independent variables characterizing it.

Then

$$d\gamma = \left(\frac{\partial \gamma}{\partial T}\right)_{\bar{A}} dT + \left(\frac{\partial \gamma}{\partial \bar{A}}\right)_T d\bar{A} \tag{12}$$

and equation 10 becomes

$$\left[\bar{S}_g - \bar{S}_\sigma - \bar{A}\left(\frac{\partial \gamma}{\partial T}\right)_{\bar{A}}\right] dT = \bar{V}_g dp + \bar{A}\left(\frac{\partial \gamma}{\partial \bar{A}}\right)_T d\bar{A} \tag{13}$$

whence

$$\left(\frac{\partial p}{\partial T}\right)_{\bar{A}} = \frac{\bar{S}_g - \bar{S}_\sigma - \bar{A}\left(\frac{\partial \gamma}{\partial T}\right)_{\bar{A}}}{\bar{V}_g} \tag{14}$$

Since, in equation 7, $d\mu_\sigma$ is an exact differential we may construct the exact differential

$$d(\mu_\sigma + \bar{A}\gamma) = -\bar{S}_\sigma dT + \gamma d\bar{A} \tag{15}$$

whence, by cross-differentiation

$$-\left(\frac{\partial \bar{S}_\sigma}{\partial \bar{A}}\right)_T = \left(\frac{\partial \gamma}{\partial T}\right)_{\bar{A}}$$

Further, $\bar{A} = A/N_\sigma$, where A, the total surface area, is certainly independent of N_σ; therefore

$$\left(\frac{\partial \bar{S}_\sigma}{\partial \bar{A}}\right)_T = \left(\frac{\partial \bar{S}_\sigma}{\partial N_\sigma}\right)_T \left(\frac{\partial N_\sigma}{\partial \bar{A}}\right)_T \tag{16}$$

and so

$$\bar{A}\left(\frac{\partial \bar{S}_\sigma}{\partial \bar{A}}\right)_T = -N_\sigma \left(\frac{\partial \bar{S}_\sigma}{\partial N_\sigma}\right)_T \tag{17}$$

Hence

$$\left(\frac{\partial p}{\partial T}\right)_{\bar{A}} = \frac{\bar{S}_g - \bar{S}_\sigma - N_\sigma\left(\frac{\partial \bar{S}_\sigma}{\partial N_\sigma}\right)_T}{\bar{V}_g} \tag{18}$$

It has been shown previously that the integral change in entropy occasioned by the adsorption of N_σ moles is

$$\Delta S = N_\sigma(\bar{S}_\sigma - \bar{S}_g) \tag{19}$$

The *differential* change in entropy is therefore

$$\left(\frac{\partial \Delta S}{\partial N_\sigma}\right)_{p,T} = \bar{S}_\sigma - \bar{S}_g + N_\sigma\left(\frac{\partial \bar{S}_\sigma}{\partial N_\sigma}\right)_T \tag{20}$$

since $\bar{S}_g$ is independent of N_σ. Replacing $\left(\frac{\partial \Delta S}{\partial N_\sigma}\right)_{p,T}$ by $-q_d/T$, we have by reason of equations 18 and 20

$$\left(\frac{\partial p}{\partial T}\right)_{\bar{A}} = \frac{q_d}{T\bar{V}_g} \tag{21}$$

or within the limits of applicability of the ideal gas law

$$\left(\frac{\partial \ln p}{\partial T}\right)_{\bar{A}} = \frac{q_d}{RT^2} \tag{22}$$

where q_d is the *differential* heat of adsorption at constant pressure in heat units per mole surface excess. The latter quantity is conveniently identified with the amount adsorbed as measured experimentally.

It is believed that equation 21 has been obtained in a thermodynamically rigorous fashion. The derivative evaluated at constant $\bar{A}$ is equivalent to that evaluated at constant N_σ, provided the surface area of the solid may be considered temperature independent. It is not equivalent to the derivative evaluated at constant θ (Wilkins' convention), since even if the surface area were temperature independent the quantity N_m would in general not be. To compare equation 22 with the commonly used equation 1 rigorously, we have

$$\left(\frac{\partial \ln p}{\partial T}\right)_{N_\sigma} = \left(\frac{\partial \ln p}{\partial T}\right)_{\bar{A}} + \left(\frac{\partial \ln p}{\partial \bar{A}}\right)_T \left(\frac{\partial \bar{A}}{\partial T}\right)_{N_\sigma} \tag{23}$$

or

$$\left(\frac{\partial \ln p}{\partial T}\right)_{N_\sigma} = \left(\frac{\partial \ln p}{\partial T}\right)_{\bar{A}} - \left(\frac{\partial \ln p}{\partial \ln N_\sigma}\right)_T \cdot \frac{1}{A}\frac{dA}{dT} \tag{24}$$

To evaluate the relative orders of magnitude of the terms in this equation we note that the first term on the right is at least 10^{-2} per degree for the majority of systems at room temperature. The quantity $\frac{1}{A}\frac{dA}{dT}$ is the coefficient of area expansion and should be about 10^{-5} per degree for solids expanding uniformly. Then if $\left(\frac{\partial \ln p}{\partial \ln N_\sigma}\right)_T$ is less than 10, the second term on the right is less than 1 per cent of the first and may be neglected within the limit of experimental error. For low adsorptions this should certainly be valid, since for this case by Henry's law

$$\left(\frac{d \ln p}{d \ln N_\sigma}\right)_T = 1$$

This quantity might well exceed 10, however, in Langmuir-type adsorption isotherms toward the saturation region, causing the second term on the right in equation 24 to be a significant fraction of the first.

SUMMARY

A thermodynamic derivation of the Clapeyron equation as applied to the calculation of heats of adsorption from adsorption isosteres is given. It is concluded that the derivative dp/dT should be evaluated at constant $\bar{A}$ (total surface area of the solid divided by the number of moles surface excess). This is not equivalent to evaluation at constant N/N_m (where N_m is the number of moles adsorbed at saturation) as proposed by Wilkins. The commonly used evaluation at constant N should give values equivalent to those obtained by evaluation at constant $\bar{A}$ within experimental error except at surface excesses approaching saturation.

REFERENCES

(1) Armbruster, Marion H., and Austin, J. B.: J. Am. Chem. Soc. **66**, 159–71 (1944).
(2) Guggenheim, E. A., and Adam, N. K.: Proc. Roy. Soc. (London) **A139**, 218–36 (1933).
(3) Joyner, L. G., and Emmett, P. H.: J. Am. Chem. Soc. **70**, 2353–9 (1948).
(4) Wilkins, F. J.: Proc. Roy. Soc. (London) **A164**, 496–509 (1938).

THE ELECTRIC POTENTIAL OF WATER FILMS

OLUS J. STEWART

Department of Chemistry, University of Kentucky, Lexington, Kentucky

Received March 28, 1949

By means of an elegant and direct measurement, Haber and Moser (2) proved experimentally that the voltage of an oxidation–reduction gas cell varies logarithmically with the partial pressures of the reacting gases. This was accomplished by causing the two gaseous electrode processes, sans solvent, to proceed on opposite sides of hot platinum-coated glass. The high resistance of the glass, and the lack of sensitive potentiometers, forced these workers to maintain a cell temperature of about 500°C. But now that electronic potentiometers, and glass of relatively high conductivity, are available, the present writer conceived the idea of using this newer glass in the construction of a cell of the Haber–Moser type and of operating it at room temperature.

When this program was put into effect, employing both wet and dry gases, it soon became clear that in the temperature range 0–45°C. the observed potential had its origin, not in the partial pressures of the gases, such as carbon monoxide, carbon dioxide, oxygen, hydrogen, and gaseous water, but in a film of moisture adsorbed on the surface of the metal-coated glass. More precisely, the observed potentials appeared to represent the voltage across a condenser, comprising a double layer of charges established through the orientation of the dipoles of electrically unsymmetrical water molecules adsorbed fixedly on the glass. Attention was then directed to the measurement of the potentials of these films.

A variety of cells was constructed during this study, but only two varieties, cells 1 and 2 (figures 1 and 2), furnished the data for this paper. Cell 1 was made by blowing a thin-walled bulb, about 3 cm. in diameter, at one end of the Corning No. 015 glass tube A, as shown, and coating the bulb inside and out with gold leaf. The gold, in turn, made contact with platinum wires which led to a Coleman Model 3 D electrometer. The cell was mounted in a cork-stoppered bottle, and the latter was connected with a Nesbitt absorption bulb (not shown) filled with hydrated copper sulfate crystals, to aid in maintaining within the bottle an atmosphere of constant humidity. Cell 2 had a very thin arched diaphragm of Corning No. 015 glass fused across the bottom of tube A. This diaphragm, which was somewhat less than 1 cm. in diameter, separated the two metallic electrodes, i.e., an upper pool of mercury and a lower layer of gold leaf, both electrodes making contact with platinum wires which led to the potentiometer. Although the mercury electrode appeared to be quite insensitive to water vapor, an atmosphere of constant humidity about this electrode was provided.

In addition to the apparatus already mentioned, there was a water bath containing a submerged U-tube system with a 40 in. x 1 in. column of glass beads moistened with water, and a tall, partially submerged beaker in which the cell was located. In practice a very slow stream of air, 6–7 ml./min., humidified by passage over the moist beads, entered either cell at H and escaped at E. When the potential, E_m, had become constant, the current of moist air was replaced by one dried in a Nesbitt bulb charged with Drierite, the stream continuing until the potential E_d was constant.

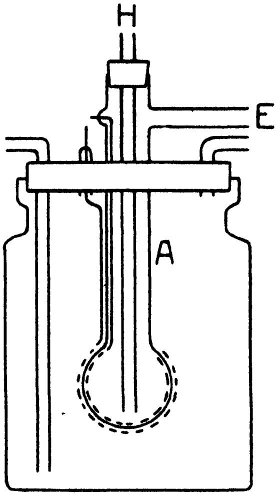

Fig. 1. Cell No. 1

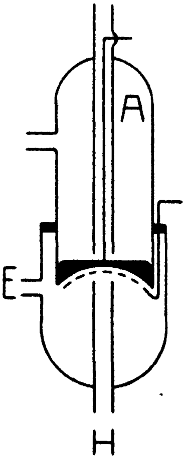

Fig. 2. Cell No. 2

TABLE 1

Data obtained with cell No. 1 in one series of observations

TIME	TEMPERATURE	CHARACTER OF AIR STREAM	E_d	E_m	$E_d - E_m$
	°C		mv.	mv.	mv.
8:18	20.6	(Start moist air through cell)			
8:25	20.6	Wet		61	
8:40	20.7	Wet		48	
8:56	20.7	Wet		38	
9:12	20.7	Wet		33	
9:18	20.7	Wet		33	
9:18		(Start dry air through cell)			
9:36	20.8	Dry	113		
9:50	20.8	Dry	121		
10:04	20.8	Dry	122		(122 − 33) = 89
10:04		(Start moist air through cell)			
10:17	20.8	Wet		42	
10:29	20.8	Wet		42	
					(122 − 42) = 80
10:29		(Start dry air through cell)			
10:40	20:8	Dry	121		(121 − 42) = 79
Mean					83

In order to make the procedure clear, the data obtained with cell No. 1 in one series of observations is given in full in table 1.

Many series of observations of this nature were made, some as consistent as that appearing in table 1, others of wider variations. In the interest of economy there are listed in table 2 the average values of about one hundred and fifty E_d and E_m values obtained at the respective temperatures. The same data also appear in the curve of figure 3, peak voltage occurring at about 21°C.

Throughout the work with the glass cell, the electrode exposed to the variable humidity was the negative electrode. Clearly then, the adsorption of water rendered this electrode more positive. This fact supports the assumption that the adsorbed water molecules were so spatially oriented that the oxygen atoms, for example, were in contact with glass, while the hydrogen atoms reached toward or touched the gold. Thus there were two layers, one positive, the other negative. The charge across this condenser, other factors remaining constant, should depend upon the number of water molecules so oriented per unit area, and the maximum charge should be that of a complete and closely packed monolayer of oriented water molecules. In addition, one can conceive of a second, third, etc., superimposed layer of water molecules corresponding to the X and Y multilayers of soap molecules studied by Blodgett and Langmuir (1).

TABLE 2

Average values of E_d and E_m

CELL NO.	TEMPERATURE	MEAN E_d	MEAN E_m	$E_d - E_m$
	°C.	mv.	mv.	mv.
2	0.9	63	54	9
2	4.7	98	29	69
2	10.5	73	29	44
2	14.3	72	29	43
2	16.5	72	28	44
2	18.7	119	46	73
2	19.3	100	17	83
2	20.8	120	21	99
1	21	118	12	106
1	21.5	116	11	105
1	22.8	111	30	81
1	23.6	135	68	67
1 and 2	24	123	26	97
1 and 2	24.4	111	27	84
2	24.8	114	39	75
2	26.6	121	46	75
2	27.5	120	46	74
2	28.4	121	57	64
1	29.6	113	43	70
2	30.5	156	89	67
2	35.1	135	78	57
2	39.5	138	95	43
2	40.1	138	93	45
2	44.9	71	52	19

Porter and Wyman (5) reported that calcium stearate X-type multilayers on a metal plate gave contact potentials of about 70 mv./layer at 26°C. In figure

3 of the present paper a voltage of about 70 mv. occurs at 17°C. and again at 27°C. That the potential of a calcium stearate film should be identical with that of a water film at these two temperatures seems to be more than a coincidence. Now, these soap films owed their orientation, at the time of formation, to the compatibility of the calcium ion, and the incompatibility of the stearate ion, for water. Thus, the top layer of water in the trough where the films were formed, and the monomolecular layer of soap oriented on the water, must have formed a more or less inseparable entity, which Porter and Wyman floated onto a metal plate for their study. If no steps, other than drainage, were taken to dry the films, the water film, or substratum, must still have been present during the measurement of the contact potential. Indeed, the adhering film of water could have been removed only by a careful drying process, as by a stream of dry air. Furthermore, had the water film been removed, the soap film probably would have lost its state of orientation. This did not occur, however, because Porter and Wyman were able to differentiate multi-*X* from multi-*Y* films by their voltages. One can hardly expect these soap films to emerge from water in a dry condition when one side is hydrophilic.

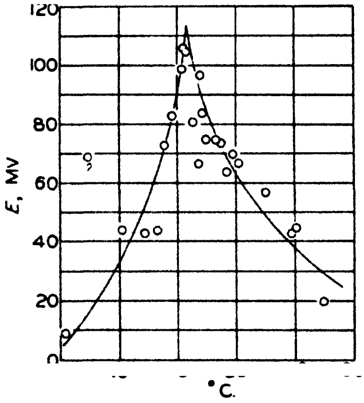

FIG. 3. CURVE 1

Porter and Wyman (4) also state that the organic end of the soap molecule was situated adjacent to the metal plate. If a water film was also present, as was suggested by the present author, it must have been separated from the plate by the soap film. In this connection, it is interesting to note that Langmuir (3) states that "the contact potentials observed by Porter and Wyman during the building up of calcium stearate multilayers of type X on alkaline solutions, seem to be due to a surface charge on the uppermost monolayer rather than to the presence of a dipole molecule within the film." Langmuir, however, showed that the charge on the outermost monolayer may have been due to adsorbed ions.

These considerations seem to force the conclusion that the most realistic interpretation of Porter and Wyman's measurements is that their readings represent the potential of a composite film of soap and water in contact with metal, rather than the potential of a soap film alone in contact with metal. However, the evidence suggests strongly that they, in reality, may have measured only the charge on a water film.

In order to ascertain if the potentials reported in this paper were by any chance those of a concentration cell, e.g., alkali from glass dissolved in the water film, a glass-less rubber cell was constructed. This cell duplicated the glass cell in design, but contained no glass that could in any way affect the voltage. The outcome of this part of the investigation was the discovery that the rubber cell responded to moisture as did the glass cell, and, while the responses of the two cells were alike in voltage, they were opposite in polarity. This difference in polarity recalls to mind the difference in electrification of glass rubbed with silk and of gutta-percha rubbed with flannel.

This essentially glass-free cell was made by stretching toy balloon rubber across the mouth of a hard plastic cup, simulating the head of a tiny drum. The cell was completed by coating the rubber diaphragm on both sides with gold leaf connected with the electrometer, and providing two glass tubes to carry the moist and dry air to and from the inclosed space. At room temperature the average $E_d - E_m$ value was 81 mv. Unfortunately, the experiment with the rubber cell did not completely solve the problem at hand, for although it eliminated the alkali of glass as the source of potential, at the same time it introduced the possibility of contaminants from the rubber. It may be of interest, in this connection, to report that even a dry hen's egg half-shell, coated inside and out with gold leaf, also exhibits an observable, but fleeting, voltage change when streams of moist and of dry air alternately play upon one side.

As stated earlier, the writer was obliged to use a potentiometer having an amplified circuit. It seemed desirable, however, to repeat some of the measurements at room temperature, employing other electronic voltage-measuring devices. To this end a Beckman pH meter, and a RCA electronic voltmeter, or "VoltOhymst," were used. The readings observed with these instruments were similar to those obtained with the Coleman electrometer, though the electronic voltmeter lacked sensitivity. It is believed therefore that the observations reported in this paper were not fortuitous, i.e., were not the result of accidental feed-back from the electronic potentiometer, because it is very improbable that three differently constructed electronic devices would yield identical feed-back voltages.

SUMMARY

Glass cells of the Haber–Moser type do not respond at ordinary temperatures to the partial pressures of gaseous reactants but to moisture, the maximum voltage occurring at about 21°C. A cell of similar design, but containing a diaphragm of rubber instead of glass, behaved in a similar fashion except for polarity.

The author acknowledges his indebtedness to Professor James I. Watters, Department of Chemistry, Ohio State University, for his interest and helpful suggestions during the writing of this paper.

REFERENCES

(1) **Blodgett and Langmuir**: Phys. Rev. **51,** 664 (1937).
(2) **Haber and Moser**: Z. Elektrochem. **11,** 593–609 (1905).
(3) **Langmuir**: J. Am. Chem. Soc. **60,** 1190 (1938).
(4) **Porter and Wyman**: J. Am. Chem. Soc. **59,** 1883 (1937).
(5) **Porter and Wyman**: J. Am. Chem. Soc. **59,** 2746 (1937).

THE EFFECT OF ADDED ELECTROLYTES UPON THE X-RAY LONG SPACING OF SOME COLLOIDAL ELECTROLYTES[1]

O. A. HOFFMAN[2]

Department of Chemistry, Stanford University, California

Received March 21, 1949

INTRODUCTION

The x-ray investigation of solutions of colloidal electrolytes shows that some give x-ray spacings while others do not (10, 11). The most familiar examples giving definite x-ray long Bragg spacings d_1 are the soaps and alkyl sulfates in concentrations above 5 or 10 per cent (5). As was pointed out and emphasized by Harkins and collaborators (3, 13), in addition to the long spacing there is an intermediate spacing called the d_M band corresponding to a double lamella such as was suggested by McBain on other grounds as early as 1923. Since the lamellae are charged, they must be surrounded by a diffuse ionic double layer. According to Hess and collaborators, this results in a parallel arrangement of the McBain micelles at the distance d_1. This parallelism has recently been queried (3, 4).

The theory of the diffuse double layer, insofar as the effects of electrostatic attraction and repulsion and the Brownian movement are concerned, has now been generally accepted (16). It has been recognized since the original work of Gouy (2) in 1910 that added salts should diminish the thickness of the diffuse double layer. A number of authors have therefore tested the effect of added salts on the long spacing (d_1).

Kiessig and Philippoff (8) reported that sodium hydroxide added to 15 per cent sodium oleate had no effect upon long spacing other than to make the pattern more diffuse. Hess, Kiessig, and Philippoff (6) report that potassium hydroxide added to 18 per cent potassium laurate causes a decrease in the long spacing. Harkins, Mattoon, and Corrin (4) have reported adding sodium chloride and potassium chloride to potassium laurate solutions and finding a definite increase in long spacing, accompanied by an increasing diffuseness of the diffraction band. However, with sodium chloride the result is complicated by metathesis. Palmer and Schmitt (14) report that total nerve lipides are made up of leaflet-shaped micelles. In water suspensions the water layers between the micelles are decreased in thickness by the addition of foreign ions, calcium ion being much more effective than potassium ion.

---

[1] A part of this study was conducted under Navy contract at Stanford University and the Stanford Research Institute under the supervision of Professor J. W. McBain.

[2] Present address: Operations Evaluation Group, CNO (Op342E), Pentagon, Washington 25, D. C.

The experiments reported here include the effects of more dilute solutions of added salts on potassium laurate and the cation-active detergent cetylpyridinium chloride. They show that dilute solutions decrease the spacing in the manner to be expected from the theory of the diffuse double layer, but that further addition reverses the effect and causes a marked increase.

TABLE 1

Effect of added potassium chloride upon long spacing of 18 per cent potassium laurate solution

KCl	d/n	KCl	d/n	KCl	d/n
m	Å.	m	Å.	m	Å.
0.000	50.3	0.134	49.4	0.385	51.4
0.013	48.4	0.210	49.4	0.540	49.7
0.034	49.4	0.156	49.7	0.683	53.6
0.066	49.0	0.270	50.4	0.770	No line
0.112	51.8				

TABLE 2

Effect of added potassium chloride upon long spacing of 20 per cent cetylpyridinium chloride solution

KCl	d/n	KCl	d/n	KCl	d/n
m	Å.	m	Å.	m	Å.
0.000	66.4	0.134	63.4	0.430	73.1
0.034	65.5	0.173	62.9	0.588	73.3
0.067	64.9	0.392	72.3	0.682	77.0

EXPERIMENTAL

The measurements were made with a General Electric Type XRD1 unit with copper target, beryllium windows, and nickel filter, using guarded pinholes 0.01 in diameter, 100 mm. apart, with a sample-to-film distance of 163–250 mm. Some of the samples were mounted in the type of capillaries described by Marsden (12) and some were mounted in a metal sample holder described by Hoffman (7).

The numerical data are presented in tables 1 to 4 and in figures 1 to 4. In every case the addition of electrolyte caused the long spacing line to become diffuse. Also, the diffraction band was much less intense in the presence of salt than without it except for the potassium laurate to which sodium chloride was added, where the long spacing line becomes both more diffuse and more intense, evidently a result of metathesis.

In all cases above about 0.2 m concentration of added salt, the pattern becomes diffuse, and at relatively high concentration it was found necessary to

TABLE 3

Effect of potassium hydroxide upon long spacing of 18 per cent potassium laurate solution

KOH	d_1/n	SOURCE	KOH	d_1/n	SOURCE
m	Å.		*m*	Å.	
0.000	50.3	Hoffman	0.382	48.1	Hoffman
0.000	50.3*	Hess (5)	0.400	48.*	Hess (5)
0.200	49.*	Hess (5)			

* These points read from a curve.

TABLE 4

Effect of sodium chloride upon long spacing of 18 per cent potassium laurate solution

NaCl	d_1/n	NaCl	d_1/n
m	Å.	*m*	Å.
0.000	50.3	0.125	49.2
0.079	49.5	0.178	51.2

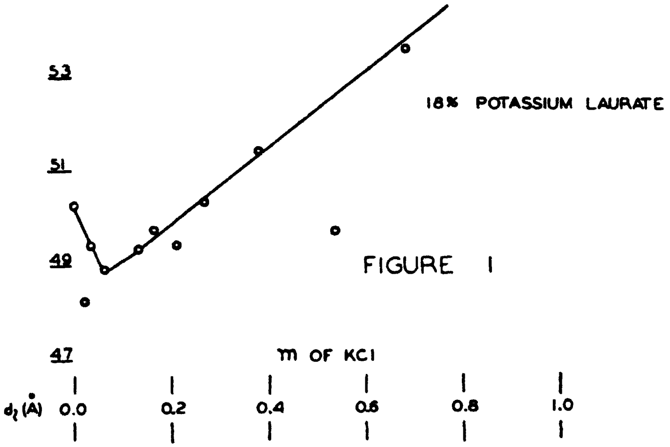

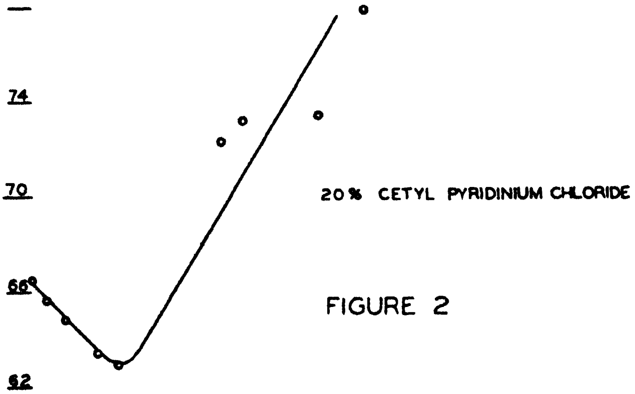

FIG. 1. The long x-ray spacing, d_1, in Ångström units, before and after potassium chloride is added to an 18 per cent solution of potassium laurate.

FIG. 2. The long spacing, d_1, of a 20 per cent solution of cetylpyridinium chloride before and after addition of potassium chloride.

make many measurements of the maximum and minimum diameters of a ring and strike an average. The precision of the measurements at salt concentrations below 0.1 *m* is generally a few tenths of an Ångström unit, but this becomes progressively less until at 1.0 *m* salt the deviation may be several Ångström units.

The d_l spacing is decreased by the first addition of electrolyte, passes through a minimum, and then increases rapidly.

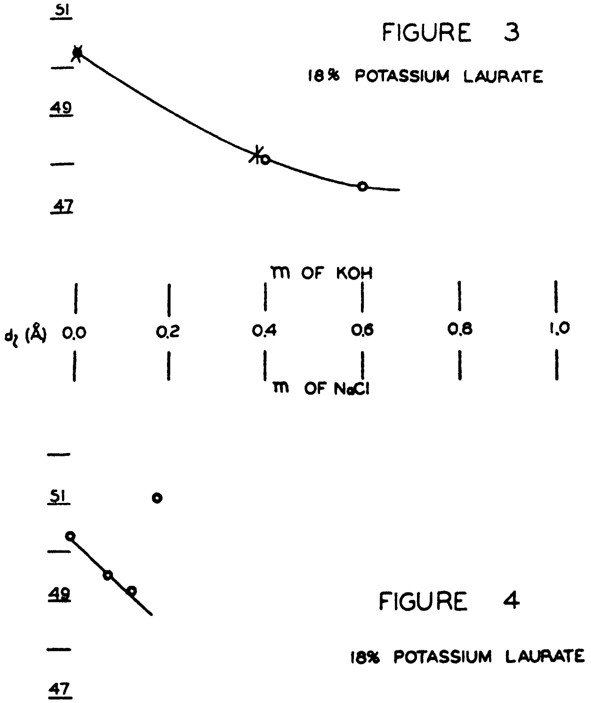

FIG. 3. Long Bragg x-ray spacings, d_l, for 18 per cent potassium laurate before and after addition of potassium hydroxide. Crosses are present data; circles are data of Hess (5).

FIG. 4. Effect of sodium chloride upon long spacings, d_l, of an 18 per cent solution of potassium laurate.

DISCUSSION

In all four systems studied, the long spacing d_l is decreased at low concentrations of added salt. It then passes through a minimum. Larger concentrations definitely increase the spacing, as was found by Harkins. The reversal appears to occur somewhat above 0.1 *N* in the case of potassium chloride, but with potassium hydroxide it is not observed up to 0.6 *N*.

It seems rather arbitrary to ascribe this to changes in the size of micelles. The present theory of the double layer is also inadequate to account for changes in opposite directions. The author inclines to the view that the d_l spacing observed arises from Hess micelles, and the diffuse character of the spacing after adding salt to repress the ionic double layer lends some support.

It is of interest that viscosity curves of soaps with added electrolytes show similar minima. At first the viscosity is reduced by added salt, whereas large additions greatly increase it. The experiments of Goldschmidt and Weissmann (1) were with potassium hydroxide and potassium chloride added to solutions of the potassium salt of the fatty acids of palm kernel oil. The concentration of alkali necessary to pass the minimum depended greatly upon the concentration of the soap, but was not much influenced by temperature.

Miss King (9) found similar results with sodium chloride added to sodium palmitate, as did Hess, Kiessig, and Philippoff (6) on adding potassium hydroxide and potassium chloride to solutions of potassium laurate. Other measurements are recorded by Philippoff (15).

SUMMARY

The x-ray long spacings, d_1, of solutions of moderately concentrated solutions of potassium laurate and cetylpyridinium chloride are first diminished by the addition of electrolytes, but excess of chloride brings about a strong change in the opposite direction. Existing theory does not account for these two effects in opposite directions.

REFERENCES

(1) Goldschmidt, F., and Weissmann, L.: Z. Elektrochem. **18**, 382 (1912).
(2) Gouy, G.: J. phys. [4] **9**, 457 (1910); Ann. phys. [9] **7**, 129 (1917).
(3) Harkins, W. D.: J. Am. Chem. Soc. **69**, 1428 (1947).
(4) Harkins, W. D., Mattoon, R. W., and Corrin, M. L.: J. Am. Chem. Soc. **68**, 220 (1946).
(5) Hess, K., and Gundermann, J.: Ber. **70**, 1800 (1937).
(6) Hess, K., Kiessig, H., and Philippoff, W.. Fette u. Seifen **48**, 377 (1941).
(7) Hoffman, O. A.: Rev. Sci. Instruments **19**, 277 (1948).
(8) Kiessig, H., and Philippoff, W.: Naturwissenschaften **27**, 593 (1939).
(9) King, Miss A. M.: J. Soc. Chem. Ind. **41**, 147 (1922).
(10) McBain, J. W., and Hoffman, O. A.: J. Phys. & Colloid Chem. **53**, 39 (1949).
(11) McBain, J. W., and Marsden, S. S.. Acta Crystallographica **1**, 270 (1948).
(12) Marsden, S. S.: Rev. Sci. Instruments **16**, 192 (1945).
(13) Mattoon, R. W., Stearns, R. S , and Harkins, W. D.: J. Chem. Phys. **15**, 209 (1946).
(14) Palmer, K. J., and Schmitt, F. O.: J. Cellular Comp. Physiol. **17**, 385–94 (1941).
(15) Philippoff, W.: *Viskosität der Kolloide*. T. Steinkopff, Dresden (1942).
(16) Verwey, E. J. W., and Overbeek, J. Th. G.: *Theory of the Stability of Lyophobic Colloids*. Elsevier Publishing Company, Inc., New York (1948).

THE FREEZING-POINT DIAGRAM OF THE SYSTEM SILVER CHLORIDE–CADMIUM CHLORIDE[1]

CARL WAGNER[2] AND PAUL HANTELMANN

Eduard Zintl Institut für Anorganische und Physikalische Chemie der Technischen Hochschule, Darmstadt, Germany

Received March 7, 1949

INTRODUCTION

According to measurements of the electrical conductivity of solid mixtures consisting of silver chloride and cadmium chloride (1), solid silver chloride dissolves considerable quantities of cadmium chloride, amounting to at least 10 mole per cent at 350°C. In figure 1 is shown a model of the lattice involving cation vacancies, which are indicated by squares. To supplement the conclusions drawn from conductivity measurements, the freezing-point diagram has been investigated with the aid of thermal analysis.

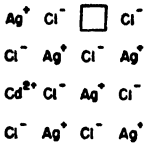

FIG. 1. Silver chloride with cadmium chloride

EXPERIMENTAL

Each sample amounted to 40 g. Temperatures were determined with a platinum and platinum–rhodium thermocouple, the thermoelectric force of which was measured with the aid of a potentiometer and a reflecting galvanometer. Results are shown in figure 2. Temperatures at the end of crystallization for mixtures up to 20 mole per cent of cadmium chloride are omitted in figure 2, because the intervals between the beginning and the end of the solidification were very narrow. A constant temperature over a longer period of time, corresponding to eutectic crystallization, was obtained only with mixtures containing 30 mole per cent or more of cadmium chloride.

CONCLUSIONS

The maximum of the liquidus curve at about 10 mole per cent is remarkable. In general, such a maximum indicates the occurrence of a compound. Here, however, the other characteristics of the occurrence of a compound, such as two different eutectic temperatures at both sides, are missing. According to Konowalow a maximum of the liquidus curve can also occur in the case of equilibrium between a liquid and a solid solution if the equilibrium composition of the liquid phase is the same as that of the solid phase. Accordingly the solidus curve is drawn in figure 2.

---

[1] GS-ORD-FT Bliss Texas No. 68.

[2] Present address: Department of Metallurgy, Massachusetts Institute of Technology, Cambridge, Masshachusetts.

From inspection of figure 2 it follows that at low concentrations of cadmium chloride the partition ratio of cadmium chloride between liquid and solid phases is less than unity, whereas at higher concentrations this ratio becomes greater than unity. This increase of the partition ratio with increasing concentration of cadmium chloride is a necessary consequence of the logical application of the law of mass action. The transition of cadmium chloride from the liquid into the solid solution may be described by the stoichiometric equation

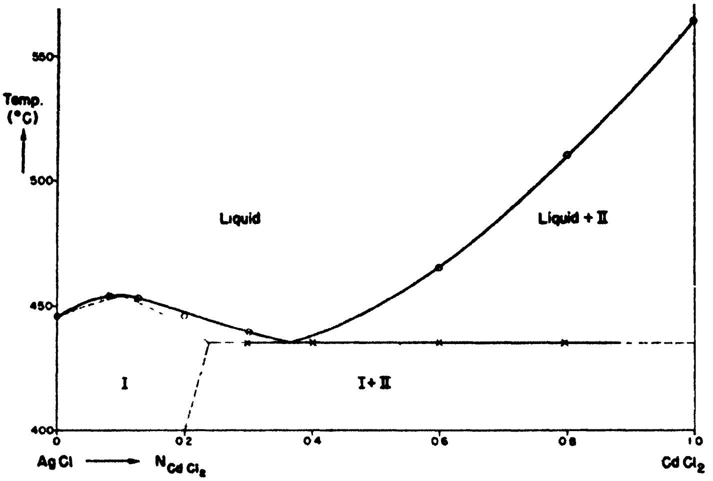

FIG. 2. Freezing-point diagram of the system silver chloride–cadmium chloride. ○, beginning of crystallization; ×, end of crystallization. I, mixed crystals of silver chloride and cadmium chloride; II, solid cadmium chloride.

$$\mathrm{Cd^{2+}(l) + 2Cl^-(l) = Cd^{2+}(cr) + h(Ag^+) + 2Cl^-(cr)} \qquad (1)$$

where the suffix (l) indicates ions in the liquid phase, h(Ag$^+$) is a cation vacancy in the solid phase, and the suffix (cr) indicates ions in normal lattice positions for cations and anions, respectively. Disregarding the concentrations of chloride ions in either phase, we have the equilibrium condition

$$N_{\mathrm{Cd^{2+}(l)}}/[N_{\mathrm{Cd^{2+}(cr)}} \times N_{\mathrm{h(Ag^+)}}] = K \qquad (2)$$

where the symbol N represents the concentration of the respective constituent in terms of mole fractions and K is a constant.

Under the conditions in question, the concentration of cadmium ions in the solid phase practically equals the concentration of cation vacanies, since one molecule of cadmium chloride contains only one cation for each two anions and interstitial cations can be disregarded. Thus, we obtain the modified form of the partition law

$$N_{\mathrm{Cd^{2+}(l)}}/N^2_{\mathrm{Cd^{2+}(cr)}} = K \qquad (3)$$

analogous to the relation for the partition of acetic acid between benzene and water according to the reaction

$$(HC_2H_3O_2)_2(\text{benzene}) = 2HC_2H_3O_2(\text{aq})$$

or the dissolution of hydrogen in palladium:

$$H_2(\text{gas}) = 2H(\text{in palladium})$$

The dissociation equilibria of the latter reactions correspond to the coupled occurrence of one cadmium ion and one cation vacancy in the solid phase. Upon transformation of equation 3, it follows that:

$$N_{Cd^{2+}(l)}/N_{Cd^{2+}(cr)} = K \times N_{Cd^{2+}(cr)} \qquad (4)$$

This equation shows that the partition ratio should increase with increasing concentration of cadmium chloride.

It must be emphasized that the introduction of the ideal law of mass action does not yield results which are quantitatively correct, for large deviations from the relations for ideal solutions occur, as shown recently by Wagner and Zimens (2). Consequently, it is not possible to draw quantitative conclusions from the concentration corresponding to the maximum of the liquidus curve.

The modified form of the partition law given in equation 3 may possibly be confirmed in other systems such as potassium chloride–strontium chloride, where the degree of disorder of the pure solvent is very low and only small concentrations of the solute occur in the solid phase. The inconstancy of the usual partition law is to be borne in mind when mixed crystals are drawn from liquid mixtures of different concentrations.

If, however, the concentration of an additive in the solid phase is small in comparison with the degree of disorder of the solvent, the concentration of cation vacancies represents a constant value and then the conventional partition law is valid.

SUMMARY

The freezing-point diagram of the system silver chloride–cadmium chloride has been investigated. At about 10 mole per cent of cadmium chloride there is a flat maximum corresponding to equal composition of the liquid and the solid solution of cadmium chloride in silver chloride.

It is shown that, according to the ideal law of mass action, the cadmium chloride concentration in the liquid phase should vary as the square of the cadmium chloride concentration in the solid phase insofar as the number of cadmium ions in the solid phase equals the number of cation vacancies.

REFERENCES

(1) Koch, E., and Wagner, C.: Z. physik. Chem. **B38**, 295 (1937).
(2) Wagner, C., and Zimens, K. E.: Acta Chem. Scand. **1**, 539 (1947).

INHIBITION OF FOAMING. II[1,2]

A MECHANISM FOR THE RUPTURE OF LIQUID FILMS BY ANTIFOAMING AGENTS

SYDNEY ROSS

Department of Chemistry, Rensselaer Polytechnic Institute, Troy, New York

Received March 2, 1949

The similarity, pointed out by Edser (4), between the spreading of a rupture in a soap bubble and the spreading of a film of oil over pure water suggested to some workers with antifoaming agents that the presence in a thin film of a substance that spreads could be considered equivalent to the existence of a rupture in the film, with the obvious exception that in the case of the spreading substance a thin film of the substance would remain, whose stability would however be so slight that it would soon vanish. Leviton and Leighton (8) thus connected in a qualitative way the spreading power of an agent with its effectiveness as an antifoam.

In a previous publication on this subject (11) the results of bulk foaming tests were shown to have a large degree of correspondence with the action of an additive on a single film. At that time a mechanical model for the rupture of single films was discussed, based on the observation that effective antifoaming agents spread on the surface of the liquid film before they cause it to rupture. This discussion was limited to *insoluble* additives but the insolubility of the additive is a widespread condition, found in more than 90 per cent of successful antifoaming agents.

A subsequent study by Robinson and Woods (10) described in some detail a mechanism of bubble coalescence. According to this picture two bubbles will coalesce "as a result of a triple coincidence, namely the practically simultaneous collision of two air bubbles with the same droplet of the dispersed foam inhibitor." It is probable, however, that this relatively rare three-body coincidence need not be invoked. The consideration of the force vectors of the various surface tensions involved shows that under the proper conditions droplets of the antifoaming agent are actually drawn by surface tension forces into the liquid film existing between bubbles. The proper conditions are that

$$\gamma_F + \gamma_{D'F'} > \gamma_D$$

where the subscript F refers to the original (foaming) liquid, D refers to the antifoaming agent, and the same letters primed refer to each liquid saturated with

---

[1] The paper now included as the first of this series (reference 11) was written in collaboration with Professor J. W. McBain in connection with an investigation sponsored and financed by the National Advisory Committee for Aeronautics. The present and succeeding studies are a continuation of this work, but have been conducted without dependence on the previous sponsorship.

[2] Presented before the Division of Colloid Chemistry at the 116th National Meeting of the American Chemical Society, which was held in Atlantic City New Jersey, September 18-23, 1949; see Abstracts of Papers, p. 12G.

the other. Robinson and Woods have defined an "entering coefficient", E, by the expression

$$E = \gamma_F + \gamma_{DF} - \gamma_D$$

For values of $E > 0$ the antifoaming agent is drawn into the liquid film and bridges the two air bubbles. For values of $E < 0$ the antifoaming agent will be ejected from the liquid film should it happen by chance to arrive near it.

It is reasonable to follow Harkins' treatment of "spreading coefficients" (5) and define three different "entering coefficients", E_{DF}, $E_{D'F}$, and $E_{D'F'}$—named, respectively, the initial, the semi-initial, and the final entering coefficients.

$$E_{DF} = \gamma_F + \gamma_{D'F'} - \gamma_D \tag{1}$$

$$E_{D'F} = \gamma_F + \gamma_{D'F'} - \gamma_{D'} \tag{2}$$

$$E_{D'F'} = \gamma_{F'} + \gamma_{D'F'} - \gamma_{D'} \tag{3}$$

The initial entering coefficient exists when the antifoaming agent has been newly added to the foaming system. The semi-initial entering coefficient exists when the droplets of the insoluble antifoaming agent have been saturated by the foaming liquid; it is probable that the numerical value of the semi-initial entering coefficient does not differ much from that of the initial entering coefficient. The final entering coefficient exists when both foamer and antifoamer are mutually saturated.

The condition for the liquid antifoam to spread on the surface of the foaming liquid is that

$$\gamma_F > \gamma_{D'F'} + \gamma_D$$

Harkins (5) has defined the initial, semi-initial, and final spreading coefficients as follows:

$$S_{DF} = \gamma_F - \gamma_{D'F'} - \gamma_D \tag{4}$$

$$S_{D'F} = \gamma_F - \gamma_{D'F'} - \gamma_{D'} \tag{5}$$

$$S_{D'F'} = \gamma_{F'} - \gamma_{D'F'} - \gamma_{D'} \tag{6}$$

The same remarks that were made to distinguish the three entering coefficients apply to the three spreading coefficients.

Harkins (5) has shown by calculation of the Gibbs free energy that a positive value of the initial spreading coefficient, S_{DF}, means that the antifoam liquid D will spread as a duplex film on the foaming liquid F. He has also demonstrated that such duplex films are unstable and after a time will gather into a liquid lens in equilibrium with a monolayer film. The time required for this transformation is that taken for the initial spreading coefficient to change to the final spreading coefficient, i.e., the time required for mutual saturation of the two liquids. The value of the final spreading coefficient is always negative.

The relation between entering and spreading coefficients is obtained by combining the previous equations:

$$E_{DF} = 2\gamma_{D'F'} + S_{DF} \tag{7}$$

$$E_{D'F} = 2\gamma_{D'F'} + S_{D'F} \tag{8}$$

$$E_{D'F'} = 2\gamma_{D'F'} + S_{D'F'} \tag{9}$$

It can be seen from these equations that it is possible for the entering coefficient to be positive and the spreading coefficient to be negative. Such cases would be associated with pairs of liquids having relatively high interfacial tensions. A different situation exists for pairs of liquids having relatively low interfacial tensions. There the entering coefficient is approximately equal to the spreading coefficient.

The mechanism proposed for the rupture of liquid films is:

(*1*) *Entering:* The entering coefficient must be positive so that a drop of the antifoaming agent is drawn into the liquid film between bubbles.

(*2*) *Spreading:* The spreading coefficient must be positive so that after the drop has made itself a part of the liquid film it will spread out as a duplex film on each side of the original film between the bubbles.

(*3*) *Rupture:* As the antifoaming agent spreads as two duplex films the original droplet of the agent thins out, drawing the two bubbles closer together and squeezing out the original liquid from the film between them. As this process continues the liquid film develops a thin spot at the place where the droplet of antifoaming agent was originally situated. At the same time the presence of the duplex film lowers the surface tension inside the bubble, as spreading could not take place at all unless $\gamma_F > \gamma_D$. This produces an increase in the radii of curvature of the bubbles, which serves further to decrease the thickness of the film between them. The total effect is the replacement in the film of a liquid capable of sustaining stable films by a liquid which does not possess that property. The film is thinnest precisely at the place where it is composed *entirely* of the antifoaming agent and it is therefore at this spot that rupture of the film can be expected to take place.

This mechanism differs from that suggested by Robinson and Woods in requiring entering *and* spreading, rather than entering alone, as a necessary preliminary to film rupture. A positive spreading coefficient, rather than a positive entering coefficient, is taken as the criterion for an effective antifoaming agent.

The following combinations of effects are possible:

Initial coefficients

(*1*) *E less than zero:* By equation 7 if the entering coefficient is negative, the spreading coefficient is also negative. In such a case the antifoaming droplet does not even enter the liquid film and the substance would not be a defoamer by this mechanism.

(*2*) *E greater than zero; S less than zero.* This could happen when the entering coefficient is not very large, or if the interfacial tension is high, though the number of agents in this category is probably not large. The material enters the liquid film but does not spread over it as a duplex film. It will remain as a drop or liquid lens in equilibrium with a monolayer of D spread on the surface of F. It does not seem that this situation would necessarily lead to a rupture of the film. Single bubbles have been examined that were formed underneath the surface of water in a trough on which an insoluble monomolecular layer was present. The bubbles carried the monomolecular film upwards as they reached the surface, so that at rest the outermost surface of the liquid film that enclosed the bubble was covered with the monomolecular layer. The stability of the single bubbles thus produced was measured as a function of the degree of compression of the monomolecular film (12, 13). The stability of the bubble is found to be low at low compressions, where the monomolecular film is gaseous and so lacks coherence. As the degree of compression of the film increases, interactions between the molecules on the surface takes place and a greater degree of cohesion of the film is reached; the stability of the single bubble correspondingly increases. At higher compressions, however, the monomolecular layer may become too coherent and show a tendency in the solid surface phase to pile up and reconstruct the three-dimensional crystal. The lack of fluidity in the surface film is accompanied by a decrease in the stability of the single bubbles. The bubble stability, therefore, has a maximum value at a degree of film compression of the appropriate fluidity, neither too vaporous to lack coherence nor too solid to lack elasticity. A similar maximum has been observed as a function of bulk concentration in solutions of ethyl alcohol (2). Calculations made by the author's students (3) have shown that, in this case also, the maximum of bubble stability occurs at a state of the adsorbed surface film of the appropriate fluidity.

These considerations apply also to a drop or liquid lens of defoamer in equilibrium with a monomolecular layer of defoamer on the surface of a liquid capable of foaming. It should be considered that a mixed monolayer is now present on the surface of any liquid film, and that this mixed monolayer may be capable of either impairing or improving the cohesion of the original film. Impairment of the stability will follow when the agent is composed of small molecules, such as relatively short chain alcohols. The molecules interact with those of the foam-producing liquid and lessen the cohesion that is required to maintain the stability of the film, or they may even entirely substitute themselves for the molecules of the foam-forming substance at the surface of a liquid film. The monolayer now lacks the coherence necessary to maintain a film and the solution is no longer able to sustain a foam (7, 14).

If the agent in the mixed monolayer has a chemical constitution such that it either does not affect or even improves the coherence of the original film, then there will be no antifoaming effect of the agent.

The gist of these considerations is that if the liquid D enters the film and does not spread, it may still act as an antifoaming agent, but it does so by a different mechanism than the one suggested as operative when the agent both enters the film and then spreads as its own duplex film.

(3) *E greater than zero; S greater than zero:* This is the situation where the liquid

D enters the film of F and then spreads as a duplex film on each side of it. By the proposed mechanism this leads to the rupture of the film.

Final coefficients

According to Harkins (5) the final spreading coefficient is always negative. Consequently only two cases are possible here, corresponding to the first two combinations of the initial coefficients. After the two liquids have become mutually saturated, the liquid D either does not enter the liquid film of F at all or, having entered it, does not spread as a duple film.

This leads to the interesting practical conclusion that a good antifoaming agent must eventually lose much of its antifoaming effectiveness. It has a positive initial spreading coefficient but after a period of contact with the foaming system its spreading coefficient becomes negative. When the interfacial tension is low, the final entering coefficient is also negative and the antifoaming agent will not even enter the film between the bubbles (case 1). If the interfacial tension is large, the agent may enter but will not spread as a duplex film (case 2).

Direct experimental testing of this prediction is complicated by the changes that have taken place in the foaming system itself by the time the final coefficients are established. The liquid F is now saturated with the liquid D and, quite apart from considerations of surface tension, may now be so altered in the structure of its surface phase that it no longer supports a foam to the extent that it did formerly. Nevertheless the observation of a loss of effectiveness of the antifoam agent after a period of use is well known to those who have experience with the practical part of the subject. This loss of effectiveness is usually accelerated by a rise in temperature, so much so that it is common to find antifoaming agents good at room temperature that are permanently impaired on raising the temperature. The widespread occurrence of these two related observations indicates a general cause rather than a series of specific causes. Not enough studies have been made of the effect of the passage of relatively long periods of time on systems containing antifoaming agents.

Another observation that is readily described by the present mechanism is the presence of a residue of fine stable bubbles on the surface of a solution to which an effective antifoaming agent has been added. The major quantity of foam is successfully broken and the small bubbles remaining in the surface are usually of no practical disadvantage. Their presence may be ascribed to some of the droplets of liquid D that have already attained their final spreading coefficient and so provided a stabilizing monolayer of D on the surface of F. The series of foaming solutions and their effective antifoaming agents that were first devised and investigated by Ross and McBain (11) provides a large number of systems suitable for further theoretical studies. A selection of some of these systems was taken by Robinson and Woods (10), to compare entering and spreading coefficients with the results of foam inhibition. They measured both surface tensions and interfacial tensions, using a Cenco-du Noüy tensiometer with a platinum–iridium ring 4.00 cm. in diameter. The surface tensions were measured on the phases separately, not mutually, saturated. The ring corrections were made by the method of Harkins and Jordan (6), which requires the measurement of the density of each liquid.

Table 1 is a comparison of initial spreading coefficients and the results of a test that measured the foam-inhibiting action of the additive on three known foaming systems. The data are compiled from the publications of Robinson and Woods (10).

In general, table 1 reveals a high degree of correspondence between a positive initial spreading coefficient and effective foam inhibition by an additive. The few instances where the initial spreading coefficient is negative and the initial entering coefficient is positive (case 2) are indicated by an asterisk. Here the additive enters the film but does not spread as a duplex film. Only four examples were discovered, and in each case the additive showed definite antifoaming action. Another observation of interest is the behavior of the well-known silicone oil defoaming agent. This material displayed the highest positive values for the initial spreading coefficients and so should have shown the most pronounced action as a foam-inhibiting agent. It is therefore surprising that in systems A and C only moderate antifoaming action is reported, while for system B no antifoaming action at all is reported. Experience with this agent has shown that foaming tests must be carried out with particular regard to the degree of dispersion of the agent in the foaming liquid. Silicone oil has an exceptionally high interfacial tension, which provides a high energy barrier to its dispersal as an emulsion. Once adequately dispersed, silicone oil has proved itself to be an exceptional defoaming agent. The lack of correlation of the data of Robinson and Woods is caused by poor dispersion of the silicone oil. Experiments by the author have demonstrated excellent defoaming action for silicone oil on systems A, B, and C when the agent is sufficiently dispersed. This outstanding exception in the results of Robinson and Woods therefore disappears.

Even with the exception noted the results display a definite agreement with the requirements of the hypothetical concept. Of thirty-five additives having positive spreading coefficients on a certain foaming system only two were found to fail as antifoaming agents; of nineteen additives having negative spreading coefficients only four were found to have antifoaming properties. Perfect correspondence between theory and experiment is prevented by uncontrolled variables, such as the rate of departure from the initial spreading coefficient to the final spreading coefficient after the additive has been added to the foaming system. Antonoff (1) has emphasized that in some cases it is a matter of some practical difficulty, requiring the passage of a surprisingly long period of time, for mutual saturation of two liquids to be completed. Such systems would retain a defoamed property for a relatively long time. They are usually characterised by a high interfacial tension. Systems with a low interfacial tension are likely to approach the condition of the final spreading coefficient more rapidly and so lose their defoamed property sooner.

Another difficulty is the impossibility (at present) of predicting the behavior of an agent of the type given by case 2, which enters the film and produces a mixed monolayer, but does not spread as a duplex film. The few data available show antifoaming action for this situation, but our discussion revealed the possibility of foam stabilizing by some agents of this type.

It is not to be supposed that the mechanism of film rupture by the formation of a duplex film of the agent is more than one among a number of different ways of reducing film stability. McBain (9) has stated that the lack of general correlations between defoaming ability and other physical properties has led to an undue insistence on the insolubility of the antifoaming agent as a *sine qua non* of its effectiveness. Although considerably less common, many examples are known of defoaming by soluble agents. They are usually described as acting by adsorption displacement of the foaming material at the surface of the film by the antifoaming agent, and so correspond to case 2 described above, where a monolayer of the additive is formed on the film. This clearly is not enough by itself to produce a defoamed system, since, if that were true, every material that lowers surface tension, and so is positively adsorbed at the surface, would be expected to act as a defoaming agent; unfortunately, defoaming agents are not come by thus readily. It is probable that in many cases of defoaming by soluble agents, specific chemical reactions are taking place at the surface, causing the chemical destruction of the foam stabilizer.

TABLE 1

Comparison of spreading coefficients and foam-inhibiting action

Initial spreading coefficients (*S*) and foam-inhibiting action (*F*) of various agents on three different foaming systems: A = 7.75 per cent Aerosol OT in triethanolamine; B = 1.5 per cent Nacconol NR in water: C = 5.5 per cent Aerosol OT in diethylene glycol

NUMBER	NAME OF ADDITIVE	SYSTEM A		SYSTEM B		SYSTEM C	
		S	*F*	*S*	*F*	*S*	*F*
1	Ethyl oleyl glycol orthophosphate	4.2	E	− 2.2*	M	1.5	E
2	Trioctyl tripolyglycol tetrapolyphosphate	10.8	E	4.9	M	9.6	M
3	Glyceryl monoricinoleate	−0.2*	E	− 4.3	N	−1.4*	E
4	2-Amino-2-methyl-1-propanol	3.4	M	− 1.0	M	1.4	M
5	Tetraoctyl pyrophosphate	3.8	E	2.0	M	3.4	E
7	Carbitol maleate	−0.1	N	− 5.4	N	−1.3	N
8	Monoöleyl dipolyglycol orthophosphate	5.7	E	1.2	M	5.4	E
9	Diethylene glycol monoöleate	4.3	E	− 0.3*	M	3.9	E
10	Diglycol dinaphthenate	3.3	E	− 1.9	N	4.0	E
11	2-Amino-2-ethyl-1,3-propanediol	−4.5	N	− 9.0	N	−5.2	N
12	Sapamine MS	6.0	E	2.0	N	5.6	E
13	Polymerized dimethyl silicone	8.8	M	6.0	N	12.2	M
15	Penetrol 60	2.7	M	− 4.0	N	3.0	M
16	Diethylene glycol	−7.8	N	−13.0	N	−9.0	N
17	Ethyl phosphate	6.1	M	− 1.5*	M	5.9	M
18	Polyoxyalkylene sorbitan monoöleate	1.5	E	− 1.5	N	1.4	E
19	*n*-Nonyl alcohol	8.1	M	1.1	E	7.6	M
22	*n*-Butyl phthalate	2.6	E	0.2	N	1.9	E

* Agent with negative initial spreading coefficient and positive entering coefficient.

SUMMARY

A combination of the concepts of the entering coefficient of Robinson and Woods and the spreading coefficients of Harkins is used to furnish a mechanical description of some observed phenomena associated with the destruction of liquid films by antifoaming agents.

REFERENCES

(1) Antonoff, G.: Arch. Biochem. **6**, 199 (1945).
(2) Clayton, W.: *The Theory of Emulsions and their Technical Treatment*, 3rd edition, p. 44, London (1935).
(3) Dauber, L.: "The Surface Structure of Alcohol-Water Solutions," B. Chem. Eng. Thesis, Rensselaer Polytechnic Institute, 1949.
(4) Edser, E.: Trans. Faraday Soc. **17**, 664 (1922).
(5) Harkins, W. D.: J. Chem. Phys. **9**, 552 (1941).
(6) Harkins, W. D., and Jordan, H. F.: J. Am. Chem. Soc. **52**, 1751 (1930).
(7) Lachampte, F., and Dervichian, D.: Bull. soc. chim. France **1946**, 495.
(8) Leviton, A., and Leighton, A.: J. Dairy Sci. **18**, 105 (1935).
(9) McBain, J. W., and coworkers: Natl. Advisory Comm. Aeronautics, Wartime Rept. ARR No. 4105 (1944).
(10) Robinson, J. W., and Woods, W. W.: Natl. Advisory Comm. Aeronautics, Tech. Note No. 1025 (1946): J. Soc. Chem. Ind. **67**, 361 (1948).
(11) Ross, S., and McBain, J. W.: Ind. Eng. Chem. **36**, 570 (1944).
(12) Talmud, D., and Suchowolskaja, S.: Z. physik. Chem. **154**, 277 (1931).
(13) Trapeznikov, A.: Acta Physicochim. U.R.S.S. **13**, 265 (1940).
(14) Trapeznikov, A., and Rebinder, P. A.: Compt. rend. acad. sci. U.R.S.S. **18**, 427 (1938).

NEW BOOKS

Physical Methods of Organic Chemistry. Vol. I, Part I. Second edition. **Arnold Weissberger**, *Editor*. 1084 pp. New York: Interscience Publishers, Inc., 1949. Price: $12.50.

Volumes I and II of the first edition of this work have been used extensively as references in this laboratory in studying the physical properties of fluorocarbons An examination of Part I of the second edition indicates that this edition is a much more useful compilation of methods for determining physical properties. Recent techniques and up-to-date data have been included in some of the old chapters as well as the new ones. The four new chapters, "Temperature Measurement," "Temperature Control," "Determination of Vapor Pressure," and "Determination with the Ultracentrifuge," broaden the scope of the book.

Each author outlines the fundamentals of the respective subjects and also presents a description of pertinent apparatus and a list of references. For example, in the chapter on calorimetry sufficient description of each type of calorimeter is given so that the reader may make a selection of a desired method, and then pursue further knowledge on the subject in the many up-to-date literature references given. In many instances, an evaluation of the limitations and usefulness of a method is given along with its description.

The chapter on the determination of vapor pressure is a definite asset to the book. This new section presents general and special methods of determining vapor pressures, as well as mathematical treatment of experimental data, including the estimation of critical constants.

Chapters on temperature measurement and control, density, boiling and condensation temperatures, solubility, and viscosity should be particularly helpful to the organic chemist in the identification of new compounds. The chapter on density contains a new section on isotope analysis. The chapter on microscopy is very complete, including the presentation of the fundamentals, techniques, and applications of the electron microscope.

This book is highly recommended as a reference work for any research or analytical laboratory.

George D. Oliver.

THE DISSOLUTION OF METALS OVER THE TEMPERATURE RANGE 25°C. TO −60°C. I[1]

THE DISSOLUTION OF MAGNESIUM IN HYDROCHLORIC ACID–METHYL ALCOHOL–WATER SOLUTIONS

A. B. GARRETT AND R. R. COOPER

Department of Chemistry, The Ohio State University, Columbus, Ohio

Received April 27, 1949

PURPOSE OF INVESTIGATION

This series of investigations is designed to show the general characteristics of the dissolution of metals in hydrochloric acid over the temperature range 25°C. to −60°C. From the data can be calculated the order of reaction, the rate of reaction at various stirring speeds and temperatures, and the temperature coefficient of the reaction rate, i.e., the activation energy of the process.

HISTORICAL

The dissolution of magnesium in acid media at room temperature has been studied by King (6, 7) and coworkers, by Kilpatrick (3, 4, 5, 8) and coworkers, by G. E. Coates (1), and by T. H. James (2). In the earlier papers by Kilpatrick (3, 4, 5) an attempt was made to show that the dissolution rate of magnesium was dependent on the acid strength in the same manner as in homogeneous acid–base catalysis, i.e., that $k_A = GK_A^x$. Subsequent work by King (6) indicated that the dissolution rate closely followed the diffusion coefficients of the acids and was therefore diffusion controlled; these findings were also substantiated by Coates (1). The diffusion characteristics of magnesium in absolute ethyl alcohol have been studied by Sclar and Kilpatrick (8). It was found to be a complicated process involving the reaction of magnesium with the acid, followed by a reaction of the magnesium with the alcohol. The dissolution characteristics of magnesium in ethyl alcohol–water mixtures have been studied by King (7) and found to be about the same as its dissolution characteristics in aqueous solutions. The findings of King can be summarized as follows: (*1*) the dissolution rate of magnesium is first order with respect to the acid concentration, (*2*) the dissolution rate of magnesium follows the diffusion coefficient of the acids very closely, (*3*) the dissolution rate is greatly affected by the rate of stirring, (*4*) the temperature coefficient of the dissolution process is much lower than that of a chemically controlled reaction, and (*5*) the dissolution rate of magnesium is not increased by the addition of a depolarizer.

EXPERIMENTAL

Apparatus

The thermostat used in this research was a triple-wall, air-bath type. Temperature control was obtained by means of DeKhotinsky thermoregulator which gave

---

[1] This work was initiated and is supported by the Battery Branch of the Signal Corps Engineering Laboratories at Fort Monmouth, New Jersey.

a temperature control of ±0.5°C. A fan was in constant operation to give complete circulation at all times. All work was done in an atmosphere of nitrogen.

The stirring mechanism used to agitate the metal plates is shown in figure 1. With this apparatus, the stirring speed of the metals could be determined.

In this investigation each metal plate was supported by two glass hooks (figure 1). This was necessary because at low temperatures (involving increased viscosity of solutions) it was found that the dissolution rate at high stirring speeds was not appreciably higher than it was at slower stirring speeds. This was found to be caused by the magnesium plates pivoting on a single glass hook upon which they were supported and swinging back, thus decreasing their effective linear speed. Similar effects were not noted in the case of zinc or cadmium, presumably because the more dense metals possessed sufficient centrifugal force to overcome the frictional drag of the solution.

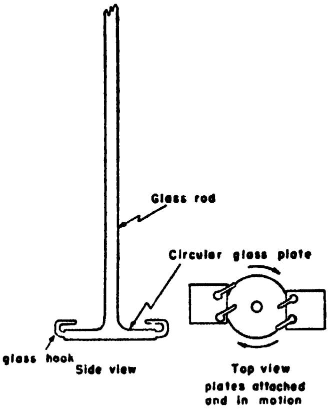

FIG. 1. Stirring mechanism

Materials

Two grades of magnesium sheet were obtained from the Dow Chemical Company for this research: one contained 0.03 per cent iron and 0.1 per cent manganese (hot and cold rolled); the other was high-purity distilled magnesium (hot and cold rolled), which contained less than 0.001 per cent iron, 0.0005 per cent aluminum, 0.01 per cent calcium, 0.001 per cent copper, 0.004 per cent manganese, 0.004 per cent nickel, 0.001 per cent lead and silicon, 0.001 per cent tin, and 0.01 per cent zinc. The magnesium sheet was cut into plates 1.50 cm. on an edge; two holes (0.24 cm. in diameter) were drilled in one end by which the sheets could be mounted on the stirrers.

The solvent for the hydrochloric acid solutions was 90 per cent methanol and 10 per cent water by weight. The concentration of the solutions used varied from 0.0075 to 0.088 *N* hydrochloric acid. Each solution was standardized with standard sodium hydroxide; phenolphthalein was used as the indicator.

The potassium nitrate used was Baker and Adamson reagent grade, and the nitroethane used was repurified by treatment with aluminum chloride, followed by distillation from boric acid.

PROCEDURE

The solution: A sufficient quantity of methanol–water–hydrochloric acid solution was measured in the reaction vessel so that at the temperature of the determination there would be 700 ml. of solution. This solution was cooled to the temperature at which the determination was to be made and was brought to thermal equilibrium with the cryostat.

The magnesium: Two procedures were used to prepare the magnesium plates. In one the plates were measured, polished with fine emery paper, washed with water, dried by absorbing the moisture on filter paper, and weighed just prior to a determination. This method was replaced later by one which gave more reproducible results; in this second one the plates were polished with fine emery paper, washed, placed on the stirrers, and immediately pre-run in hydrochloric acid solution of 90 per cent methanol for a few minutes to give an acid-etch. They were then removed from the solution, dried, weighed, and measured. After this treatment they were ready to be placed on the stirrers for a determination. Following the determination they were dried as before, reweighed, and the dimensions measured. They were then used over and over again without the necessity of re-etching for following determinations.

Many of the determinations were made in duplicate by using two stirrers driven by the same stirring motor.

Errors: The calculation of the reaction velocity constant involved measurements of area, time, temperature, volume, acid concentration, and weight loss. The area determinations, made with vernier calipers, were accurate to 0.03 sq. cm., giving an accuracy of 6.5 parts per thousand. The time measurements, made with an electric timer, were accurate to 4.2 parts per thousand for the shortest runs, but were accurate to 0.6 part per thousand or better for long runs. The volume measurements were made in a graduated cylinder and were accurate to 5.7 parts per thousand. The accuracy of the acid concentration was also 5.7 parts per thousand. The weight determinations were accurate to 0.1 mg. for these determinations. This gave an accuracy of 20 parts per thousand, but for the most part the accuracy was between 9 and 6 parts per thousand. It is obvious, then, that the values of the reaction velocity constant obtained in the investigation are accurate to 20 parts per thousand for a few determinations of small weight loss, and from 9 to 6.5 parts per thousand for others.

Other factors influencing the reproducibility are the temperature control and the rate of stirring. Temperature control was accurate to ±0.5°C. and the stirring rate was accurate to about 6 R.P.M. per thousand.

At 25°C. the values obtained for the reaction velocity constant for two determinations deviate from the mean by an average of 0.5 per cent, the maximum deviation being 2 per cent. Corresponding values at 0°, −30°, and −60°C. for average and maximum deviation from the mean are 0.5 per cent, 1.1 per cent, 1.3 per cent, and 2.6 per cent, 1.3 per cent, 3.5 per cent, respectively. The deviations from the mean for static data are much higher. It is concluded that the static data give only an order of magnitude and are not to be considered as highly accurate.

DATA

Measurements obtained

The dissolution characteristics of magnesium were evaluated by determining its dissolution rate as a function of the following variables: (*1*) *Acid concentration (other factors constant)*: The acid concentration and/or the time of reaction were varied over wide limits at 25°C. and −60°C., respectively. (*2*) *Stirring speed (other factors constant)*: Dynamic dissolution data were obtained at seven rotational speeds, varying from 344 to 2730 R.P.M. at 25°, 0°, −30°, and −60°C., respectively. The diameter of the stirrers used was about 3.2 cm. By measuring from the center of the stirrers to the center of the plates it is possible to approxi-

TABLE 1

Determination of order of the reaction of the dissolution of magnesium with hydrochloric acid

R.P.M. = 1620

ORIGINAL QUANTITY OF ACID (a IN EQUATION 1)	METAL LOST (x IN EQUATION 1)	TIME	SURFACE AREA	VOLUME OF SOLUTION	k_1
Magnesium (0.03 per cent iron; 0.1 per cent manganese); temperature, 25°C.					
milliequiv.	*milliequiv.*	*min.*	*sq. cm.*	*ml.*	
16.70	1.900	6.0	9.41	700	1.50
16.70	3.750	12.0	9.32	700	1.59
10.04	1.534	8.0	9.56	700	1.52
10.04	2.185	12.0	9.27	700	1.54
5.02	0.902	10.0	9.19	700	1.50
5.02	1.655	20.0	9.12	700	1.53
Magnesium (0.03 per cent iron; 0.1 per cent manganese); temperature, −60°C.					
66.90	0.795	20.0	8.97	750	0.0500
66.90	1.607	40.0	8.93	750	0.0510
33.50	0.812	40.0	8.90	750	0.0518
33.50	1.566	80.0	8.87	750	0.0508
16.70	0.623	60.0	9.25	750	0.0513
16.70	1.156	120.0	9.22	750	0.0485
·Magnesium (high purity); temperature, 20°C.					
58.0	4.93	4.0	10.36	695	1.49
58.0	7.15	6.0	10.22	695	1.49
58.0	9.22	8.0	10.10	695	1.49
58.0	11.31	10.0	9.97	695	1.51
Magnesium (high purity); temperature, −60°C.					
86.9	1.032	15.0	9.77	735	0.0600
86.9	2.056	30.0	9.72	735	0.0605
86.9	3.170	45.0	9.69	735	0.0628
86.9	4.100	60.0	9.66	735	0.0614

mate the linear speed. On this basis the linear speed varies from 4600 cm./min. to 35,600 cm./min.

Static data were obtained at 25°, 0°, −30°, and −60°C., but the values of the dissolution rate were not in good agreement and very low. Reaction products were noticed on the surface of the metal after the determination had been made. (*3*) *Temperature, under dynamic conditions:* The rate of dissolution of magnesium was obtained at 10° intervals over the temperature range 25°C. to −60°C. at a stirring speed of 1620 R.P.M. (*4*) *The absence or presence of a depolarizer:* Both potassium nitrate and nitroethane were added to the acid–methyl alcohol–water mixture at 25°C. in varying concentrations. The effect of nitroethane was also observed at −60°C.

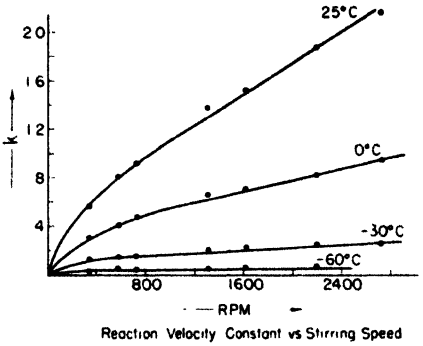

FIG. 2

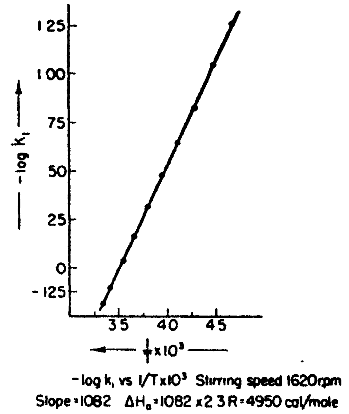

FIG. 3

FIG. 2. Dissolution of magnesium (0.03 per cent iron; 0.1 per cent manganese) in 90 per cent methyl alcohol–10 per cent water solutions containing hydrochloric acid. Reaction velocity constant plotted against stirring speed at various temperatures.

FIG. 3. Dissolution of magnesium (0.03 per cent iron; 0.1 per cent manganese) in 90 per cent methyl alcohol–10 per cent water solutions containing hydrochloric acid, $-\log k_1$ *vs.* $1/T$. Stirring speed, 1620 R.P.M. Activation energy, 4950 cal./mole.

Treatment of data

The dissolution data obtained are correlated and compared on the basis of a first-order reaction. The data in table 1 show that the dissolution of magnesium in hydrochloric acid solution of methyl alcohol–water is a first-order reaction with respect to the acid (HCl) concentration. The assumption of a first-order reaction is justified, since the first-order reaction velocity constant remained constant within experimental error over the entire range of time and acid concentration range.

The equation for a first-order reaction involving the dissolution of a metal plate in a given volume of acid of known concentration is

$$dx/dt = k_1 A(a - x)/V \tag{1}$$

where V is the volume of solution used in milliliters, A is the area of the magnesium plates in square centimeters, t is the time of the determination in minutes, a is the initial quantity of hydrochloric acid in the solution expressed in the number of equivalents, and x is the number of equivalents of magnesium reacting in time t. k_1 is then in units of centimeters per minute. When this equation is integrated between the limits 0 to t and 0 to x and solved for k_1, we have:

$$k_1 = (2.3V/At)(\log a/(a - x)) \tag{2}$$

The first-order equation was used to calculate the results of all determinations in this investigation, and table 1 shows that the first-order reaction holds in the magnesium containing 0.03 per cent iron and 0.1 per cent manganese at 25°C. and −60°C. It was assumed that there was no change in order of reaction between those temperatures.

TABLE 2

Calculation of temperature coefficients

R.P.M. = 1620

TEMPERATURE	$(k_1)_T$	$(k_1)_{T+10°}$	TEMPERATURE COEFFICIENT PER 10° INTERVAL
Magnesium (0.3 per cent iron; 0.1 per cent manganese)			
°C.			
10 to 20	0.940	1.270	1.35
0 to 10	0.685	0.940	1.37
−10 to 0	0.478	0.685	1.41
−20 to −10	0.330	0.478	1.45
−30 to −20	0.225	0.330	1.47
−40 to −30	0.148	0.225	1.52
−50 to −40	0.092	0.148	1.61
−60 to −50	0.055	0.092	1.67
Magnesium (high purity)			
10 to 20	1.160	1.500	1.29
0 to 10	0.890	1.160	1.31
−10 to 0	0.665	0.890	1.34
−20 to −10	0.480	0.665	1.39
−30 to −20	0.335	0.480	1.43
−40 to −30	0.220	0.335	1.52
−50 to −40	0.135	0.220	1.63
−60 to −50	0.072	0.135	1.88

Table 1 also shows similar data for high-purity magnesium; however, because of the large excess of acid used at −60°C., precise proof that a first-order reaction exists for high-purity magnesium over the entire temperature range was not established.

Plots of k_1 *vs.* stirring speed have been drawn to show the profound effect of stirring speed on the rate of dissolution (figure 2). Up to about 700 R.P.M. (9200 cm./min.) the velocity constant does not vary linearly with linear stirring speed, but above this speed it does. Data on the change in dissolution rate with temperature are shown in figure 2. Graphs of $-\log k_1$ *vs.* $1/T$ have been drawn for the dynamic dissolution process (nondepolarized) at a stirring speed of 1620

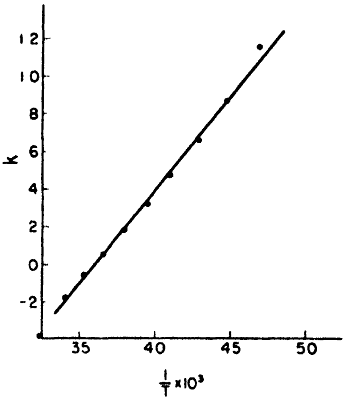

FIG. 4

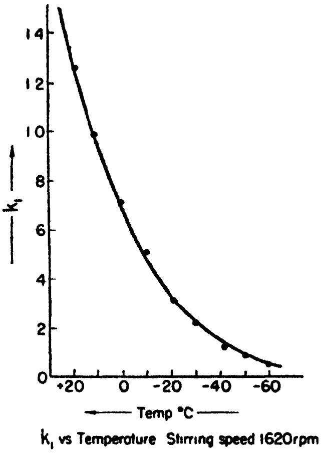

FIG. 5

FIG. 4. Dissolution of magnesium (high purity) in 90 per cent methyl alcohol-10 per cent water solutions containing hydrochloric acid, $-\log k_1$ *vs.* $1/T$. Stirring speed, 1620 R.P.M. Activation energy approximately 4500 cal./mole.

FIG. 5. Dissolution of magnesium (0.03 per cent iron; 0.1 per cent manganese) in 90 per cent methyl alcohol-10 per cent water solutions containing hydrochloric acid. Reaction velocity constant plotted against temperature. Stirring speed, 1620 R.P.M.

TABLE 3

Effect of depolarizer on dissolution rate

Magnesium containing 0.03 per cent iron and 0.1 per cent manganese; R.P.M., 1620

CONCENTRATION OF DEPOLARIZER (NITROETHANE)	ORIGINAL QUANTITY OF ACID (a IN EQUATION 1)	METAL USED (x IN EQUATION 1)	TIME	SURFACE AREA	VOLUME OF ACID	k_1
			Temperature, 20°C.			
M	*milliequiv.*	*milliequiv.*	*min.*	*sq. cm*	*ml.*	
0	10.04	3.81	20.0	9.16	700	1.25
0.015	10.04	2.14	15.0	9.39	700	1.19
0 03	10.04	2.155	15.0	9.45	700	1.22
			Temperature, −60°C.			
0	66.9	1.605	40.0	8.93	750	0.0510
0.05	66.9	0.812	20.0	9.43	750	0.0510
0.10	66.9	0.771	20.0	9.39	750	0.0493

R.P.M. in order to determine the activation energy of the dissolution process This has been done for the commercial magnesium (figure 3) and also for the chemically pure magnesium (figure 4). A simple plot of k_1 *vs.* T has also been drawn (figure 5) for general comparison. This graph was conveniently used to prepare table 2, showing the temperature coefficient per 10° interval over the temperature range covered.

DISCUSSION

The following generalizations can be made from the data obtained:

1. The dissolution process of magnesium appears to be first order with respect to the acid (HCl) concentration with or without a depolarizer present. Some question about the order of reaction of highest purity magnesium is raised by the fact that its $-\log k_1$ *vs.* $1/T$ curve is not a straight line but shows an increase in slope at the low-temperature range, indicating the influence of some new factor, perhaps a different rate-controlling mechanism.
2. The rate of stirring has a profound effect on the dissolution rate. This is an indication that diffusion is an important factor in determining the rate of reaction.
3. The energy of activation of the dynamic dissolution process is between 4000 cal./mole and 5000 cal./mole. This low energy of activation is further evidence that a mechanical process, probably diffusion, is the principal factor in determining the rate of reaction. It should be noted here again, that the activation energy curve for pure magnesium is increasing in slope in the neighborhood of -60°C. and appears to have a slope indicating an activation energy of around 6000 cal./mole at -60°C. It appears that some rate-controlling process with a higher activation energy than a diffusion process may be taking effect.
4. The dissolution rate of magnesium does not seem to be affected by the presence of a depolarizer (see table 3). This implies that magnesium has sufficient electrode potential to overbalance hydrogen overvoltage even at low temperatures.

SUMMARY

Dissolution data have been obtained for magnesium in hydrochloric acid–methyl alcohol–water solutions, with and without a depolarizer present, at various stirring speeds over the temperature range 25°C. to -60°C. A first-order reaction was found to exist over the entire temperature range. The temperature coefficient and activation energy of the reaction have been calculated. The latter is approximately 4500 cal./mole. The low activation energy and the profound effect of stirring speed on the dissolution rate have led to the conclusion that the reaction is largely diffusion controlled.

REFERENCES

(1) Coates, G. E.: J. Inst. Metals **71,** 457 (1945).
(2) James, T. H.: J. Am. Chem. Soc. **65,** 39 (1943).
(3) Kilpatrick, M.: J. Chem. Education **8,** 1567 (1931).
(4) Kilpatrick, M., and Rushton, J. H.: J. Phys. Chem. **34,** 2180 (1930).
(5) Kilpatrick, M., and Rushton, J. H.: J. Phys. Chem. **38,** 269 (1934).
(6) King, C. J., and Cathcart, W. H.: J. Am. Chem. Soc. **59,** 63 (1937).
(7) Roehl, E. J., King, C. V., and Kipness, S. J.: J. Am. Chem. Soc. **63,** 284 (1941).
(8) Sclar, M., and Kilpatrick, M.: J. Am. Chem. Soc. **59,** 584 (1937).

THEORY OF WATER-REPELLENT FILMS ON SOLIDS FORMED BY ADSORPTION FROM AQUEOUS SOLUTIONS OF HETEROPOLAR COMPOUNDS

MELVIN A. COOK AND JOHN C. NIXON[1]

Department of Metallurgical Engineering, University of Utah, Salt Lake City, Utah

Received April 28, 1949

The formation of water-repellent films on solids by treatment in aqueous solutions of heteropolar substances involves some relatively little known surface chemistry of considerable theoretical interest. The most important industrial use of the phenomenon is in the separation of minerals by flotation. Heteropolar substances useful in this application, known as "collectors," differ widely both in their solution characteristics (solubility, degree of ionization, surface activity) and in their modes of reaction at the solid surface. We believe, in fact, that water-repellent films on solids form not only by chemisorption or chemical reaction at the solid surface but also by physical adsorption, the latter type occurring commonly in the extremely capillary-active heteropolar compounds (long-chain paraffin salts, acids, and bases) (4). Water-repellent film-forming compounds may be divided into three main groups: (*a*) anionic substances, i.e., substances in which the active part of the molecule is the anion, (*b*) cationic substances, and (*c*) nonelectrolytes, listed in order of their industrial importance. The soluble nonelectrolytic collectors are also somewhat heteropolar and undoubtedly adsorb as whole molecules (examples are dixanthogen, aliphatic and aromatic sulfides and disulfides, and triphenylphosphine) (7). We shall not be interested here in water-insoluble types. Under optimum conditions for selective conditioning of solids in flotation, anionic and cationic types exist in the (bulk) solution largely as ions. Typical anionic collectors are the xanthates; these are known to be nearly completely ionized in the (generally) basic flotation circuits. Alkylamine hydrochlorides are typical cationic collectors, and these are also largely dissociated into ions in the flotation pulp. Because of the strong electrolytic properties of these substances, proposed mechanisms for the formation of hydrophobic films by type (*a*) and type (*b*) collectors have generally been ionic in character. The various mechanisms that have been suggested for the "ionic" collectors are discussed comprehensively by Wark (23).

Recently, an interesting controversy of neutral molecule adsorption *vs.* ion exchange has arisen in the theory of anion-exchange resins. Bishop (2) accounted for the "ion-exchange" properties of Amberlite IR-3 on the basis of extraction of free acids of even such strong acids as hydrochloric rather than the exchange of anions at the surface. Schwartz, Edwards, and Bourdeaux (20), in studying the removal of chloride ions from solutions by a resin prepared from a *m*-phenylenediamine–formaldehyde condensation, stated that "it appears that we are dealing with a process in which the solutes were removed as whole molecules, and that ion exchange was of very minor proportions, if it occurred at all." However, Heymann and O'Donnell (12) pointed out that neutral molecule adsorption in the "ion" exchange resins cannot yet be distinguished from anion exchange. But, if there is doubt regarding the distinction between neutral molecule adsorption and ion exchange at hydrophilic surfaces, the doubt should be even more pronounced in the cases of surfaces which end up hydrophobic. In other words, in preparing a water-repellent film by adsorption from solution, the heteropolar substances must become not only desolvated but separated from the aqueous phase entirely.

---

[1] Research Fellow, Utah Engineering Experiment Station, Salt Lake City, Utah. Now Senior Lecturer, Department of Metallurgy, University of Melbourne, Melbourne, Australia.

In this article we propose to examine briefly the various ionic mechanisms that have been proposed for collectors. Evidence will then be developed for the proposition that heteropolar substances, which form water-repellent films on solids, adsorb from aqueous solutions not as ions but as neutral molecules. It appears, as a matter of fact, that "anionic" collectors are often simply free acids, and "cationic" collectors are free bases formed in solution by hydrolysis of the corresponding "anions" and "cations," respectively (3). In the interest of brevity, the detailed mechanisms of adsorption of the neutral molecule will not be discussed here. It may be remarked, however, that sufficient experimental evidence is available in many cases to allow one to distinguish between extraction processes involving chemisorption and physical adsorption. In other words, we frequently find film-forming reactions that are strongly dependent upon temperature and time, presumably following an equation of the type

$$AB + S{-}S' \rightarrow \left(\begin{array}{c} A{-}B \\ \vdots \quad \vdots \\ S{-}S' \end{array}\right)^{\ddagger} \rightarrow \begin{array}{c} A \quad B \\ | \quad\; | \\ S{-}S' \end{array}$$

where AB represents the neutral collector molecule, SS' the adjacent surface sites, and $\left(\begin{array}{c} A{-}B \\ \vdots \quad \vdots \\ S{-}S \end{array}\right)^{\ddagger}$ a reaction complex at the top of a potential energy barrier, the height of which measures the activation energy for the chemisorption process as described by the familiar absolute reaction rate theory of Eyring. In the case of oleic acid in fluorite flotation, we believe that either physical adsorption or chemisorption occurs, depending on the temperature of conditioning (4). The physical adsorption of the collector evidently takes place at room temperature, under which conditions poor metallurgical results are obtained because both fluorite and gangue minerals tend to float. However, a selective and tenacious film forms on calcium fluoride when the ore is pretreated in oleic acid solutions at 100°C. for 5 or 10 min., due evidently to chemisorption of the collector at high temperatures. This makes possible the separation of high(acid)-grade fluorite with exceptionally high recoveries (85–95 per cent) from complex fluorite ores that otherwise could not be treated economically.

IONIC ADSORPTION MECHANISMS

Mechanisms that have been described for ionic collectors are (*1*) the direct adsorption of collector "ions," or the exchange of collector "ions" with some of the ions that initially occupied the electrical double layer at the solid–liquid interface, and (*2*) mechanisms involving metathesis in which exchange occurs between collector ions and lattice ions.

Type 1 mechanisms have been proposed by Wark (23) and Gaudin (7). They assume merely that the collector is adsorbed as ions either directly onto the solid surface or by replacement of other ions adsorbed during grinding, or at least prior to the addition of the collector to the solution phase. Ionic adsorption of type 1 should be discussed in connection with the theory of the electrical double layer of Helmholtz, Chapman, Gouy, and Stern. An interesting recent review by Grahame (9) on the structure and properties of the electrical double layer has been given. In flotation, we are dealing primarily with selective adsorption. This fact evidently limits possible adsorption of ions to positions within the compact double layer (the inner Helmholtz plane), because ions occupying the diffuse double layer are still solvated and are able to move about freely within the solution phase, the only restriction being that they are concentrated statistically toward the (dipolar) charged surface, as described by the Chapman–Gouy theory. In other words, ions in the diffuse double layer are not sufficiently localized to act as selective collectors. The problem in regard to type 1 adsorption of ions may thus be narrowed down to a discussion of the possible conditions under which collector ions adsorbed in the compact double layer are capable of rendering a surface hydrophobic.

It is generally recognized that the film producing the hydrophobic surface is composed of a heteropolar substance in which the nonpolar or hydrocarbon end is oriented approximately perpendicular to and outward from the solid. This restriction of orientation limits the type 1 ionic mechanism to one type of ionic adsorption: namely, the adsorption of the collector "ions" and their counter ions in pairs so that both types of ions occupy the compact double layer. The adsorption of a collector "ion" without its counter ion will not have the proper orientation for flotation but will be oriented with the nonpolar end toward the solid and the ionic end outward, and a hydrophilic rather than a hydrophobic surface would result. This may be shown by a simple one-dimensional treatment of the energy relations for nearest-neighbor ions, as follows:

$$\overset{-}{\cdot}\ r_1\ \overset{+}{\cdot}\ \overset{r_2}{\rule{3em}{0.4pt}}\overset{-}{\bigcirc}\ r_3\ \oplus \tag{a}$$

$$\overset{-}{\cdot}\ r_1\ \overset{+}{\cdot}\ r_4\ \overset{-}{\bigcirc}\overset{r_5}{\rule{3em}{0.4pt}}\ \oplus \tag{b}$$

The symbols are: lattice anions = $\overset{-}{\cdot}$, lattice cations = $\overset{+}{\cdot}$, heteropolar molecule ion = $\rule{3em}{0.4pt}\overset{-}{\bigcirc}$ (the line representing the hydrocarbon chain), and counter ion = $\oplus$. The various distances between sites are designated by r_1, r_2, r_3, r_4, and r_5 as illustrated. For convenience, however, we may take $r_1 = r_3 = r_4$ and $r_2 = r_5$ without destroying the essential argument. Assuming all ions to be univalent (charge = e), the configuration energies ϵ_a and ϵ_b are given as follows:

$$\epsilon_a = -e^2/r_1 + e^2/(r_1 + r_2) - e^2/(2r_1 + r_2) - e^2/r_2 + e^2/(r_2 + r_1) - e^2/r_1$$
$$\epsilon_b = -e^2/r_1 + e^2/2r_1 - e^2/(2r_1 + r_2) + e^2/(r_1 + r_2) - e^2/r_2 - e^2/r_1$$

The energy required to change the orientation from a to b is thus

$$\epsilon_a - \epsilon_b = -e^2(r_2 - r_1)/2r_1(r_1 + r_2)$$

In general, $r_2 > 6r_1$, so that $\epsilon_b - \epsilon_a > 5/14\, e^2/r_1$. Assuming a value r_1 of 2×10^{-8} cm. (or 2 Å.), the energy required to orient one mole of ions from a to b in this model would be about 50,000 cal. This would be considerably increased in the real case.

The energy difficulties of type 1 ionic adsorption (excluding adsorption in pairs) with the proper orientation for collection may be shown in another way. Since the air bubble contacts the homopolar end of the molecule (or "ion"), allowing for the sake of discussion that the proper orientation has taken place, it will actually effect a separation of the collector and its counter ions, the latter remaining in the aqueous solution. Assuming a complete or nearly complete monolayer of collector "ions" on the mineral particles, one would obtain a bulk concentrate with so much charge (if it could be formed in bulk by some mysterious nonterrestrial device) that it would explode with greater violence than an equal weight of liquid nitroglycerine! The aqueous solution left behind would likewise be explosive. In fact, a lower limit of the repulsive energy would be given by the right-hand side of the inequality

$$E_s > 6\pi A e^2/\rho a^2 = NA\epsilon^2/\tfrac{8}{3}\pi r^4 \rho N$$

where N is the number of particles of mineral per milliliter, ϵ is the charge per particle ($= 4\pi r^2 e/a$), A is a type of Madulung constant (much greater than the ordinary one for ionic crystals because all particles would have the same charge), r is the radius of the particle, and a is the area per ion.

These arguments indicate that heteropolar ions cannot adsorb as such unless the counter ions are adsorbed simultaneously and in equal amounts, i.e., so as to produce electrical neutrality in the film. The counter ions of the ion pair would be hydrogen ions and/or the cation of the original collector salt in "anionic" collectors and hydroxyl ions and/or the anion of the salt in "cationic" collectors. It is questionable that adsorption of ions in pairs would obey the same laws as neutral molecule adsorption even though the final product were the same. One may, however, be able to distinguish between ionic pair adsorption and free acid or free base by means of data on the kinetics of reaction. While adsorption of ions in pairs is a possible mechanism of "ionic" adsorption that previously has been recognized in other fields (5), no such explanation has previously been given in the literature to describe the action of "ionic" collectors.

The direct exchange of collector "ions" with lattice ions (type 2 mechanism) seems a very remote possibility for any of the known examples, except possibly in the formation of some macroscopic (perhaps visible) coatings which we shall not discuss here. For example, there seems to be no reason to expect xanthate ions to replace sulfide ions of the ionic crystal in heavy metal sulfides. Furthermore, no experimental evidence has been found for the mechanism, i.e., no evidence has been found that the adsorption of xanthate is accompanied by an increase in sulfide-ion concentration in solution.

A second metathesis mechanism involving exchange with lattice ions was suggested by Taggart and coworkers (22). This theory assumed that the mineral, or an oxidation product of it occurring on the surface, is more soluble than the salt formed by a metathesis reaction with the collector "ion." The mineral, or comparable salt, thus dissolves and undergoes metathesis with the collector ion, precipitating the less soluble (collector ion–lattice counter ion) salt onto the solid surface. Taggart considered this mechanism to apply generally to all "anionic" and "cationic" collectors. As far as the adsorption process is concerned, this is, in fact, a neutral molecule adsorption mechanism rather than an "ionic" adsorption mechanism. Wark (24), however, has demonstrated rather crucially that the Taggart mechanism is not completely general, if it occurs at all, and in many cases the "collector salt" formed in such a metathesis reaction is actually more soluble than the corresponding mineral, or the surface oxidation product. In any event, the Taggart theory is incomplete for it provided no mechanism by which the precipitate deposits selectively only on the particular mineral from which partial solution occurred, and the remarkable mobility which the theory would require for the "precipitate" to find its way to the appropriate surface.

Surely, solubility comes into consideration in determining the stability of the collector film once it has formed on the solid. Moreover, it is definitely an important factor in determining collector consumption, because soluble heavy metal salts cause the precipitation of the collector before it has a chance to form hydrophobic films on the mineral surfaces. However, solubility product probably has little, if anything, to do with the primary process of film formation.

ZETA POTENTIAL DATA

Gaudin and Sun (8) have measured the zeta potentials of various minerals both before and after treatment with collectors. The evidence from their data seems to support the above considerations that no net charge will accumulate at the surface owing to the formation of collector films. That is, the "zeta coefficients," defined by these authors as the difference in zeta potential between the untreated and the collector-coated mineral, reveal no abnormal accumulation of surface charge. Using the Müller (17) equation, we have calculated the charge for 100 per cent recovery with sodium oleate on cassiterite, from Gaudin and Sun's measurements, to be 355 E.S.U./cm.^{2}, which corresponds to 7×10^{11} univalent ions per square centimeter. Since the collector concentration for complete coverage to form a water-repellent film amounts to about 4×10^{14} collector molecules per square centimeter, the calculated charge is equivalent to 0.001–0.002 ion per collector molecule. Thus, there is no indication in this work for adsorption of ions of a given charge, since the zeta potentials obtained with minerals coated with collectors were no larger than one finds for a solid such as paraffin or palmitic acid. One may conclude, therefore, that the film is formed by the adsorption of ions either in pairs or as neutral molecules. In these interpretations we assume that zeta potential will correspond to the interface between the nonpolar film and the solution, since this is the plane where the interaction of molecules on one side with those on the other will be a minimum, i.e., this plane is automatically "lubricated."

CONTACT BUBBLE DATA ON HEAVY METAL SULFIDES

Wark and Cox (25) have carried out extensive quantitative studies of the conditions under which a stable collector film will form on the surfaces of metal sulfide minerals. They employed a type of "contact" or "captive" bubble test which consisted simply in measuring the critical pH for air bubble contact on a polished mineral surface as a function of collector concentration in solution. These data may be interpreted on the basis that the effective collectors in the "ionic" collector type are free acids ("anionic" collectors), and free bases ("cationic" collectors) formed by the hydrolysis of the collector "ions" in solution. (That the contact bubble data are an indication of floatability has been amply demonstrated by both "cylinder" flotation tests and laboratory flotation experiments.)

In interpreting the contact bubble data, we shall assume that the effective "anionic" collector (HX) forms in solution as follows: $X^- + H_2O \rightarrow HX + OH^-$. The amount of effective collector present in solution is given by the equilibrium equation

$$x = m(H^+)/(H^+ + K) \tag{1}$$

where x is the concentration of the free acid HX, m is the amount of collector salt added to the solution, and K is the free acid equilibrium constant. According to the free acid theory, there should be a critical concentration of effective collector (HX) in solution in order to obtain bubble contact. This will, therefore, be constant along the m *vs.* pH curve. Accordingly, equation 1 shows that curves of critical m *vs.* pH for bubble contact should have the general form illustrated in figure 1. Here it is tacitly assumed that m and x will not be appreciably altered by adsorption. For simplicity in evaluating experimental data we note the following conditions:

(*a*) $H^+ \gg K, m = x$. This means that the curve should become parallel to the pH axis at high hydrogen-ion concentration where the (X^-) is practically completely converted to free acid.

(*b*) For $H^+ = K$, $x = 1/2\ m$. One may therefore evaluate K by taking the intersection of the horizontal $m = 2x$ line with the curve, since the pH value of this intersection corresponds to $pK = -\log K$).

(*c*) For $K \gg H^+$, $m \gg x$. Thus, at high pH values very large concentrations of collector salt are required to produce the required x concentration for bubble contact.

For cationic collectors the free base formation is given by

$$R^+ + H_2O \rightarrow ROH + H^+$$

and

$$y = m(\mathrm{OH}^-)/(\mathrm{OH}^- + K) \tag{2}$$

where y is the critical free base (effective collector) concentration for film formation sufficient to produce bubble contact. In this case the curves become parallel to the pH axis at high pH, and go to infinity at some lower pH depending on the equilibrium constant.

In the bubble contact curves for metal sulfides, all the curves obtained by Wark and Cox have the shape required by equation 1, which indicates that x is constant along these curves as required by the free acid collector theory (except the low pH region where the collector is sometimes so unstable that it decomposes appreciably during the experiment). Figure 2 shows the case of potassium amylxanthate (m) on sphalerite. Here x was taken from the horizontal portion of the curve and K from the pH corresponding to $2x$ as explained above.

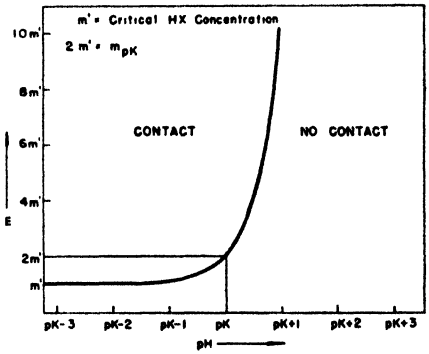

FIG. 1

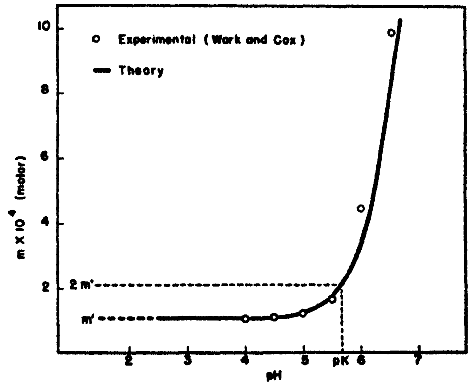

FIG. 2

FIG. 1. Theoretical m. *vs*. critical pH curve

FIG. 2. Critical pH *vs*. collector salt concentration. Potassium amylxanthate on sphalerite.

The agreement is excellent. In the case of the ethyl xanthate, all the data were taken in the region (c) where $K \gg \mathrm{H}^+$, and in this case it was, therefore, possible to evaluate only the constancy of x by means of the $(\mathrm{H}^+)(\mathrm{X}^-)$ product. Table 1 shows that the condition of constancy of HX along the contact bubble curve is indeed fulfilled. Regarding the equilibrium constant of xanthic acid, these data show only that it is much greater than 10^{-9}, the largest hydrogen-ion concentration employed in these tests. Since K is probably around 10^{-3}, according to data discussed below, these data show that the critical HX concentration for conditioning these minerals is very low (around 10^{-11} moles per liter).

The critical concentration x may be explained in some cases by solubility product; the film may be unstable unless the solution is saturated with respect to the chemisorption product. In other cases the adsorption potential, or free energy of the adsorption reaction, may be the limiting factor for x rather than solubility product. The very low critical concentration found for xanthic acid on some minerals like galena and chalcopyrite is explained simply on the basis that the adsorption potential is high and that the solubility product, the factor determining stability of the film, is very low. Cases are discussed by Wark (24) in which the solubility product clearly does not correspond to the critical concentrations observed. When the adsorption potential becomes the determining factor the critical concentration would be determined by a distribution function of the type $x^s/x = e^{\Delta F/RT}$, where ΔF is the free energy of adsorption, and x^s and x are the surface and solution concentrations (more accurately, activities) of free acid, respectively.

While we have assumed that the solubility product might frequently enter as a factor determining the stability of a collector film, some experimental evidence by Taggart and Hassialis (22) seems to prove at least that the film formation does not involve the solubility product. They found that a clean and polished sample of galena (of surface area about 60 cm.²) extracted enough xanthate from a (200 ml.) solution of concentration 5×10^{-9} M (0.0007 mg. per liter) to increase its contact angle from around 0° to 38°. (Even if all the xanthate had been extracted by the galena sample, the surface would have been covered only to the extent of about 3.6 per cent.) These investigators obtained 6.7×10^{-16} for the solubility product of lead xanthate. Hence, one requires a lead-ion (Pb^{++}) concentration of 25 M to account for any precipitation of PbX_2 in this case. This is at least 10^5 times greater than can be accounted for assuming contamination by some oxidation product of galena, such as lead sulfate! On the other hand, this evidence is striking confirmation of the extremely low critical concen-

TABLE 1

Constancy of HX *along m vs. pH curve for potassium ethyl xanthate on pyrite, galena, and chalcopyrite (data from Wark and Cox)*

MINERAL	m	H^+	K_x
	moles/liter	*moles/liter*	
Pyrite ..	3.1×10^{-5}	8×10^{-11}	2.5×10^{-15}
	1.6×10^{-4}	3.2×10^{-11}	5.0×10^{-15}
	6.2×10^{-4}	1.2×10^{-11}	7.5×10^{-15}
	3.9×10^{-3}	1.6×10^{-12}	6.2×10^{-15}
			Av. = 5×10^{-15}
Galena ..	3.1×10^{-5}	8×10^{-10}	2.4×10^{-14}
	1.6×10^{-5}	4×10^{-11}	6.0×10^{-15}
	6.2×10^{-4}	1×10^{-11}	6.0×10^{-15}
	3.9×10^{-2}	3.2×10^{-13}	1.2×10^{-15}
			Av. = 9×10^{-15}
Chalcopyrite ..	3.1×10^{-5}	3.0×10^{-12}	1.0×10^{-16}
	1.6×10^{-4}	1.6×10^{-12}	2.5×10^{-16}
	6.2×10^{-4}	5.0×10^{-13}	3.1×10^{-16}
	3.9×10^{-4}	1.0×10^{-13}	3.9×10^{-16}
			Av. = 3×10^{-16}

tration predicted by the neutral molecule theory for ethyl xanthate on galena. In fact, the theory of chemisorption of the (free acid) collector accounts for an appreciable adsorption of free acid even at such low xanthate concentrations. If we assume, for example, 25,000 cal. per mole as a reasonable adsorption potential, the relation between free energy and the equilibrium constant will account for the extraction of more than 90 per cent of the xanthate as free acid (assuming $K \sim 10^{-3}$ and that the activities are equal to the concentrations).

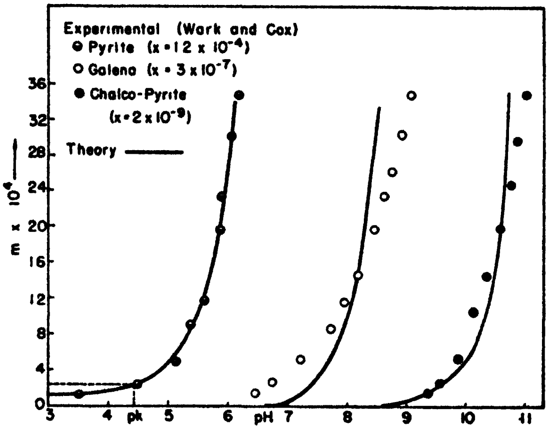

FIG. 3. Critical pH *vs.* salt concentration for sodium Aerofloat

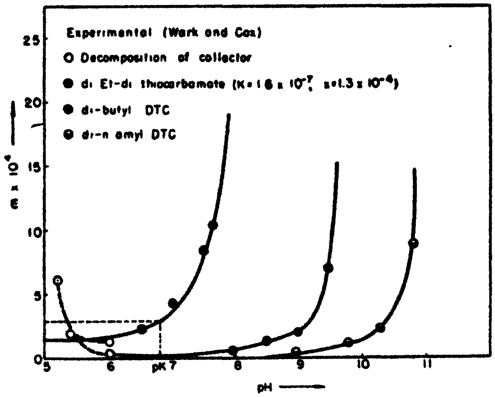

FIG. 4. Critical pH *vs.* dithiocarbamate salt concentration on sphalerite

Flotation will take place with xanthates in acid circuits, but it is much less selective than in basic circuits. The reason for this was made clear by Wark on the basis of critical concentration differences for different minerals, as illustrated in table 1 and figure 3. The fact that basic circuits are preferred to acid ones in xanthate flotation is usually regarded as evidence for ionic mechanisms. However, it is not that flotation will not occur in acid circuits (although the collector may decompose rapidly at low pH) but that selectivity is more difficult.

Figure 3 plots experimental *vs.* theoretical data for sodium diethyl dithiophosphate (Aerofloat) on pyrite, galena, and chalcopyrite. The above methods for determining x and K could be applied only to the pyrite curve. The other theoretical curves were obtained by using the value of K determined from the pyrite curve and obtaining x from a single point on the curve. Again the agreement between theory and experiment is within the experimental error claimed for the contact bubble tests. Figure 4 shows similar comparisons for various alkyl dithiocarbamates on sphalerite. Here we have plotted only the experimental data, theoretical data being difficult to determine because of excessive instability of these collectors. The shape of the curves in the region of stability of the collector is again in agreement with the theory.

Next we shall consider the accuracy of the equilibrium constants obtained from the contact bubble curves of Wark and Cox. Hantzsch and Bucirius (11) calculated a value of 0.028 for the equilibrium constant of xanthic acid from rate studies employing conductivity measurements. Halban and Hecht (10) studied the decomposition of (ethyl) xanthic acid at 0°C. in water by acidifying a solution of potassium ethylxanthate with hydrochloric acid. After certain times, sodium bicarbonate was added to stop the reaction, and the solution was titrated with iodine to evaluate the undecomposed xanthate. The dissociation constant was calculated from their rate data to be 0.030. King and Dublon (13) obtained a value of 0.031 for the constant by measuring the increase in vapor pressure over buffered xanthate solution at 25°C. These investigators all assumed that the decomposition took place according to the equation:

$$H^+ + X^- \leftrightharpoons HX \rightarrow CS_2 + C_2H_5OH$$

We have undertaken an investigation of this problem, and while our study is incomplete, we have established that several other less important decomposition reactions take place simultaneously with the above reaction. In fact, other decomposition reactions of xanthic acid are described by Klauditz (14). We followed the decomposition both by pH measurements (with a Beckmann glass glass electrode pH meter) and by iodine titrations. The two methods gave considerably different results, the iodine titration indicating sometimes as much as 10 per cent more undecomposed xanthate ($HX + X^-$) at a given time than was indicated by the amount of hydroxyl ion generated over the same period of time. We attribute this, among other reasons, to the formation of H_2S and SH^- in solution. Based on the assumption that only the above decomposition reaction is involved, however, the calculated constant K of 0.007 checked that of previous investigators within reasonable limits, but undoubtedly this is incorrect in view of the other reactions not considered in this calculation.

Simple pH titration curves for the determination of the equilibrium constants of xanthic acid (HEtX) and amylxanthic acid (H Amyl X) were also carried out. This method for K is, of course, not very reliable where decomposition is occurring at an appreciable rate at the pK point. However, measurements were made at 3°C., and acid added rapidly enough to reach the pK point in 2–3 min. total decomposition time. Under these conditions, first-order corrections from rate data indicated that the (ethyl) xanthic acid constant determined from the titration curve might be too low by a factor of 3–5, but the amylxanthate constant should be accurate within a factor of 1.2, amylxanthic acid having a decomposition rate less than one-tenth that of (ethyl) xanthic acid. The titration curves are given in figures 5 and 6. According to these curves, it seems likely that these acids are quite a bit weaker than earlier rate studies have indicated. Moreover, the titration curve gave a value of 2.5×10^{-5} for amylxanthic acid in reasonably good agreement with that obtained from the contact bubble curve: namely, 4.5×10^{-6}. Evidently, the latter value should be corrected by a factor of about 4, owing to the fact that the surface (or interfacial) concentration is roughly four times larger than the bulk concentration, according to calculations from the Gibbs adsorption theory (6). A more complete discussion of the chemistry of xanthate and related collectors will be reserved for a future paper.

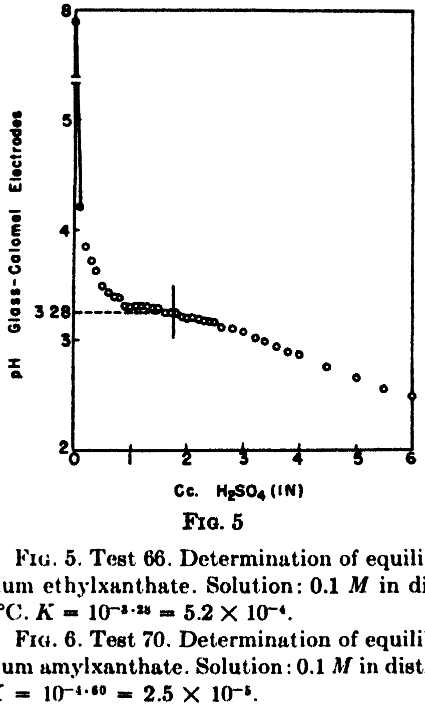

FIG. 5

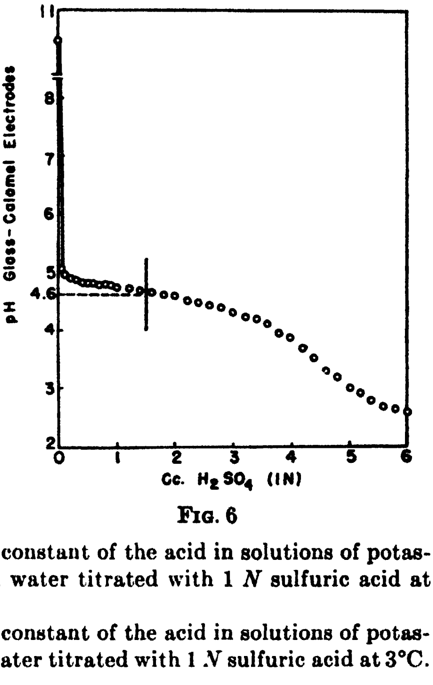

FIG. 6

FIG. 5. Test 66. Determination of equilibrium constant of the acid in solutions of potassium ethylxanthate. Solution: 0.1 *M* in distilled water titrated with 1 *N* sulfuric acid at 3°C. $K = 10^{-3.28} = 5.2 \times 10^{-4}$.

FIG. 6. Test 70. Determination of equilibrium constant of the acid in solutions of potassium amylxanthate. Solution: 0.1 *M* in distilled water titrated with 1 *N* sulfuric acid at 3°C. $K = 10^{-4.60} = 2.5 \times 10^{-5}$.

It should perhaps be mentioned that Wark (26) and Taggart (21) have offered other explanations for occasional constancy of the H^+m product (the Barsky (1) constant). In Wark's explanation, it is assumed that the collector anions and hydroxyl ions are in competition for the solid surface following the linear rule X^-/OH^- = constant. This linear competition relation is regarded by Wark as somewhat fortuitous, however. Taggart's interpretation involves the solubility product of the "precipitated" salt (K_1), the ionization constant of water K_w, and the solubility product of the metal hydroxide (K_2) and considers the Barsky constant (H^+m) to represent the product $(K_1K_w/K^2)^{1/2}$. On either theory the

Barsky constant would not be general, since no allowance is made for free acid formation. The chief argument against the Wark explanation is that a type of ionic adsorption such as that required by the theory seems to be ruled out by the energy requirements and zeta potential measurements discussed above. On the other hand, if the Taggart theory were valid, all the curves should obey the Barksy rule without the necessity for any free acid correction. The fact that the Barsky rule rarely applies without applying free acid corrections in calculating the X^- concentration is adequate proof that Taggart's explanation is incorrect. In any event, the Barsky rule (H^+m = constant) applies only to a few xanthate-type collectors, but it will be shown that the neutral molecule collector theory applies quite broadly to "anionic" collectors, a similar (ROH) constancy applying in the case of "cationic" collectors.

It is doubtful that the mechanism of adsorption of ions in pairs will account for the Barsky constant even on the basis that the counter ions are exclusively hydrogen ions (for "anionic" collectors) and hydroxyl ions (for "cationic" collectors).

DATA WITH PARAFFIN-CHAIN SALT COLLECTORS

In the case of collectors for heavy metal sulfides, we are evidently dealing with chemisorption, and the only complications encountered in the contact bubble curves are those caused by instability of the collector and sometimes extremely low critical HX values. In long-chain paraffin salt collectors, however, an additional complication arises; in addition to chemisorption, which unfortunately—as far as their utility is concerned—takes place very little under ordinary operating conditions, strong physical adsorption occurs at all surfaces and interfaces. The effect of this factor will not be discussed in the present article, and we shall only remark that the interpretation of the contact bubble curves (18, 19) is again straightforward on the neutral molecule adsorption theory. The equilibrium constants determined from the contact bubble curves, however, must be interpreted on the basis of the Gibbs adsorption theory. In other words, the concentration of collector in a surface or interface (m^s) of solutions of long-chain heteropolar molecules may be of the order of 10^5 times greater than in the bulk phase (m). (This is an estimation based on calculations by the Gibbs equation applied to the solution–air surface using observed surface tension–concentration data (6, 19).) Since the constant is calculated from the bulk concentration (m) instead of surface concentration (m^s) the constant obtained from the contact bubble curves will be only an "apparent" equilibrium constant. In view of the much greater capillary activity of the heteropolar free acid compared with its corresponding ions, one should expect that the equilibrium constant for the surface "phase" would be somewhat smaller than that applying in the bulk phase. The contact bubble curves for the long-chain heteropolar acids and bases indicate equilibrium constants of the order of 10^{-5} times those for the bulk solution. Thus, for the dilute lauric acid solutions employed in the contact bubble tests, an equilibrium constant of about 10^{-5} should be anticipated for the bulk phase. This is based on known constants for the first members of the homologous series of which this acid is a member. The contact bubble data, on the other hand, indicate a constant of about 10^{-10}. Evidently, therefore, the (apparent) equilibrium constant is about m/m^s times the real bulk phase equilibrium constant. That this is reasonable when applied to the surface phase is illustrated, for example, by the work of Long, Nutting, and Harkins (16) and Long and Nutting (15) on surface tension *vs.* pH. Figure 7 gives an example of their data, from which it appears that in the 0.005 *M* buffered solutions the laurate ion begins to show appreciable hydrolysis to free acid at a solution pH of about 10, and is largely converted to free acid at about pH = 7, as far as the surface phase is concerned. This indicates an (apparent) surface equilibrium constant of about 3×10^{-9}, in close agreement with results obtained from the contact bubble curves. It may be noted that the irregularity in the low pH region found by these investigations probably corresponds to surface supersaturation and precipitation. These authors, in fact, mention that increased turbidity of the solutions occurs in the low pH region.

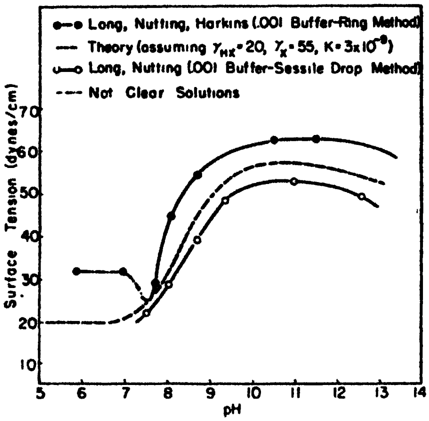

FIG. 7. Surface tension *vs.* pH; 0.005 *M* sodium laurate

A crucial verification of the theory is found in the case of phenol, since here the equilibrium constant is known accurately and Gibbs adsorption is not very large, m^s/m amounting to only about 6.0 at the solution–air interface. Rogers, Sutherland, Wark, and Wark (19) obtained data for this substance on galena leading to an (uncorrected) constant of 3×10^{-11} (the corrected constant about 1.8×10^{-10}) compared with the known value 1.3×10^{-10}. These authors also mention evidence that free palmitic and lauric acids (in acid solution) are the effective collectors in their experimental flotation of galena by the sodium and potassium salts of these acids.

SUMMARY

1. Based on arguments regarding the structure of the electrical double layer of Stern and the nature of water-repellent surfaces, the proposal is made that neutral heteropolar molecules (free acids and free bases, neutral salts, or other

neutral molecules), rather than the corresponding ions, are in general responsible for the water-repellent films that are formed on the solids that are treated with aqueous solutions of heteropolar electrolytes.

2. It is shown, in accord with the neutral molecule theory, that the free acid (HX) concentration is substantially constant along the "collector" *vs.* critical pH curves of Wark and Cox, for various xanthate, Aerofloat, and dithiocarbamate "collectors" on sphalerite, pyrite, galena, and chalcopyrite.

3. The free acid dissociation constant for hydrogen amylxanthate obtained from "captive bubble" tests is shown to be in excellent agreement with that determined by pH measurements of solutions of potassium amylxanthate.

4. The "collector" action in long-chain compounds is complicated by physical adsorption which leads to the production of double layers (with the polar end extending away from the solid surface in the second layer) with excess "collector", and generally to nonselectivity. Where chemisorption can be made to take place with these collectors, however, one obtains good selectivity, as in the high-temperature flotation of fluorite with oleic acid. Here, as in collectors for heavy metal sulfides, free acids and free bases may be shown to be the effective collectors in many cases. The equilibrium constants found for the long-chain, capillary-active hydrocarbons are consistent (*a*) with the calculated ratio of surface to bulk concentrations, which would lead one to anticipate an (apparent) surface equilibrium constant about 10^{-5} times the (real) bulk equilibrium constant, and (*b*) with surface tension *vs.* pH data which demonstrate the existence of free acid at the solution–air surface for pH ≤ 10 in solutions of long-chain fatty acids.

REFERENCES

(1) Barsky, G.: Trans. Am. Inst. Mining Met. Engrs. **112**, 236 (1934); discussion of paper by Wark and Cox.

(2) Bishop, J. S.: J. Phys. Chem. **50**, 6 (1946).

(3) Cook, M. A., "Mechanism of Collector-Mineral Attachment in Flotation" (unpublished); this paper was summarized in Eng. Min. J. **150**, No. 2, 110 (1949) and Chem. Eng. News. **27**, No. 9, 489 (1949).

(4) Cook, M. A., and Last, A. W.: "Theory of Oleic Acid Collector Action" (unpublished); see also Eng. Min. J. **150**, No. 2, 110 (1949) and Chem. Eng. News. **27**, No. 9, 589 (1949).

(5) Davis, J. T., and Rideal, E. K.: J. Colloid Sci. **3**, 313 (1948).

(6) DeWitt, C. C., Makens, K. F., and Wels, A. W.: J. Am. Chem. Soc. **57**, 796 (1935).

(7) Gaudin, A. M., Glover, H., Hansen, M. S., and Orr, C. W.: "Flotation Fundamentals. I," Utah Eng. Expt. Sta. Tech. Pub. **No. 1**, University of Utah (1928). Gaudin, A. M., and Sorensen, P. M.: "Flotation Fundamentals. II," Utah Eng. Expt. Sta. Tech. Pub. **No. 4**, pp. 7–13, University of Utah (1928).

(8) Gaudin, A. M., and Sun, S. C.: Trans. Am. Inst. Mining Met. Engrs. **169**, 347 (1946).

(9) Grahame, D. C.: Chem. Revs. **41**, 441 (1947).

(10) Halban, H. von, and Hecht, W.: Z. Elektrochem. **24**, 65 (1918).

(11) Hantzsch, A., and Bucerius, W.: Ber. **59**, 793 (1926).

(12) Heymann, E., and O'Donnell, I. J.: J. Colloid Sci. **3**, 497 (1948).

(13) King, C. V., and Dublon, E.: J. Am. Chem. Soc. **54**, 2177 (1932).

(14) Klauditz, W.: Papier-Fabr. **37**, Tech-Wiss. Tl. 251 (1939); Chem. Abstracts **33**, 8401 (1939).

(15) Long, F. A., and Nutting, G. C.: J. Am. Chem. Soc. **63**, 84 (1941).
(16) Long, F. A., Nutting, G. C., and Harkins, W. D.: J. Am. Chem. Soc. **59**, 2197 (1947).
(17) Müller, H.: Kolloidchem. Beihefte **26**, 257 (1928).
Abramson, H. A., and Müller, H.: Bull. Am. Phys. Soc. **7**, 11 (1932).
(18) Plante, E.: Mining Technol., Am. Inst. Mining Met. Engrs., Tech. Pub. **No. 2163** (July, 1947).
(19) Rogers, J., Sutherland, K. L., Wark, E. E., and Wark, I. W.: Trans. Am. Inst. Mining Met. Engrs. **169**, 287 (1946).
(20) Schwartz, M. C., Edwards, W. R., and Bourdeaux, G.: Ind. Eng. Chem. **32**, 1462 (1940).
(21) Taggart, A. F.: See reference 22 and p. 190 of reference 23.
(22) Taggart, A. F., Taylor, T. C , and Knoll, A. F.: Trans. Am. Inst. Mining Met. Engrs. **87**, 112 (1930).
Taggart, A. F., del Guidice, G. R. M., and Ziehl, O. A.: Trans. Am. Inst. Mining Met. Engrs. **112**, 348 (1934).
Taggart, A. F., and Hassialis, M. D.: Trans. Am. Mining Met. Engrs. **169**, 259 (1946).
(23) Wark, I. W.: *Principles of Flotation.* Australasian Institute of Mining and Metallurgy, Melbourne, Australia (1938).
(24) Wark, I. W., and Cox, A. B.: Trans. Am. Inst. Mining Met. Engrs. **134**, 26 (1939): **112**, 245 (1934).
(25) Wark, I. W., and Cox, A. B.: J. Phys. Chem. **41**, 673 (1937); Trans. Am. Inst Mining Engrs. **134**, 7 (1939).
(26) Wark, I. W., Reference 23, p. 189.

A NEW ACTIVITY RELATIONSHIP FOR BINARY SOLUTIONS OF NONELECTROLYTES

A. E. MARTELL

Department of Chemistry, Clark University, Worcester, Massachusetts

Received April 27, 1949

INTRODUCTION

It is the purpose of this paper to derive a simple expression for the relationship between activity and mole fraction for binary solutions of slightly associated liquids. The treatment will be limited to substances which exhibit a "continuous" type of association rather than the formation of true chemical bonds or directed forces such as hydrogen bonding, which usually lead to the formation of aggregates of a particular size and structure such as the formation of double molecules in the case of acetic acid.

In deriving a relationship of this type a balance must be struck between the number of consistent simplifying assumptions that can be made and the faithfulness with which the expression describes the behavior specified by the model employed in the derivation. Since, in this case, the expression is to be as simple and consequently as useful as possible, it will of course be necessary to make approximations and sacrifice a corresponding amount of rigor.

Such a relationship may be easily tested for solutions of volatile substances, since it would predict the partial vapor pressure of such solutions. Since the relationship derived is a simple one, it is particularly useful not only for the extension of our fundamental knowledge of such systems, but also for the derivation of a great many other relationships which depend on vapor pressure and activity. Some of these, particularly boiling-point data and relationships involving heats of mixing, will be treated in a later paper. Since the relationship derived is a general one, it is useful in the extension of our knowledge of vapor pressure to systems which have not yet been completely investigated and for the extrapolation of vapor pressure data which are incomplete.

THEORETICAL

Two theories of liquid structure have been proposed, both of which are compatible with observations. The theory favored by Prins (4), Bernal (1), and others attributes to the liquid what has been referred to as a quasi-crystalline or pseudocrystalline structure. This view supports a definite relationship for the distribution of molecules about a particular molecule at any instant. The structure differs from that of a crystal, however, because of thermal movements in the liquid. The resulting statistical average structure would be analogous to that of a solid, although the instantaneous picture is confused.

The other theory, proposed by G. W. Stewart (6), attributes a microcrystalline structure to a liquid. According to this theory, the instantaneous picture would show a large number of "cybotactic groups" in each of which a large number of molecules would be arranged in a more or less orderly manner. The regions between these groups would have a random distribution. The structural units are pictured as continually breaking up and re-forming. In this case the average of a series of instantaneous photographs would indicate a random arrangement of the molecules.

Whether the cybotactic or quasi-crystalline point of view is held, it is clear that the liquid state contains molecules which are so close together as to influence each other strongly. The molecules, therefore, are held together firmly by the strong forces of attraction that exist at such short distances. Because of thermal agitation, the pseudo-crystalline structure is continually being deformed or the microcrystalline groups are continually being broken up. The result of thermal agitation, therefore, would be to free single molecules or small groups of molecules momentarily from the force of attractions of the surrounding liquid mass. Consequently, we can conceive of a liquid as being composed of a large number of units of different sizes, continually being formed and broken up, and "single" molecules which may momentarily exist in equilibrium with such units. By "single" molecules are meant molecules upon which negligible attractive forces are operative. Such a view would seem a necessary part of the microcrystalline theory of Stewart, since the single molecules and small groups of molecules would necessarily exist as intermediates in the breaking up and re-forming of these larger groups.

In the pure state, therefore, a liquid consists of molecular aggregates of the type:

A, AA, AAA, AAAA, AAAAA . . . . whole liquid where A represents single molecules. This model of a liquid has recently been used by Redlich and Kister (4).

A pure liquid, therefore, is considered to consist of the molecular aggregations indicated above, the size of the aggregations increasing without limit.

Before a liquid can vaporize the individual molecules must be freed from their associations with the surrounding molecules. It can, therefore, be assumed that the vapor pressure of the liquid is proportional to the concentration of single molecules, A, present in the liquid. This can only be true if the substance A is present in the vapor phase exclusively as single molecules. For a pure liquid:

$$P_1^0 = C_1 X_A^0 \tag{1}$$

where the constant C_1 is a function of temperature alone, P_1^0 = vapor pressure of pure liquid, and X_A^0 = mole fraction of single molecules. Individual molecules of A are, therefore, in equilibrium with aggregates of the type A_n.

$$\begin{aligned} A + A &\rightleftharpoons A_2 \\ A_2 + A &\rightleftharpoons A_3 \\ A_3 + A &\rightleftharpoons A_4 \\ A_{n-1} + A &\rightleftharpoons A_n \end{aligned}$$

If it is assumed that the phase is ideal in the thermodynamic sense, it follows that:

$$\frac{X_{A_2}}{X_A^2} = k_1$$

Also

$$\frac{X_{A_3}}{X_A X_{A_2}} = k_1$$

$$\frac{X_{A_n}}{X_{A_{n-1}} X_A} = k_1$$

i.e., the equilibrium constant for adding one more molecule is independent of the size of the aggregate. This has been thoroughly discussed by Wilson (7) and by Mecke *et al.* (3).

Since consideration has been restricted to cases of slight association, it follows that the constant k_1 is small compared with unity. Also, since the mole fractions of dimer, trimer, ... , are given by $k_1X_A^2$, $k_1^2X_A^3$, ... , it is obvious that the mole fractions of trimer and higher aggregates are very small compared with the mole fraction of the dimer. Thus for a pure liquid, we have:

$$X_A + X_{A_2} = 1$$

Substituting in terms of the equilibrium constant k_1:

$$X_A + k_1X_A^2 = 1$$

When k_1 is very small, this expression may be replaced by:

$$X_A^0 = \frac{1}{1 + k_1} \tag{2}$$

Also, for a pure liquid consisting of molecular species B:

$$X_B^0 = \frac{1}{1 + k_2} \tag{3}$$

A liquid solution of A and B may be considered, in a similar manner, to consist of associations between like molecules and association between unlike molecules. The associations between like molecules may be considered to follow the same pattern as that outlined above for pure liquids. Since it was possible to restrict consideration to monomer and dimer for pure liquids, the same restriction will be assumed to apply for binary liquids. This leaves A_2, B_2, and AB as the only species that need be considered in a mixture of two liquids as A and B. Therefore,

$$X_A + X_{A_2} + X_B + X_{B_2} + X_{AB} = 1$$

where

$$X_{AB} = k_3 X_A X_B$$

Substituting in terms of X_A and X_B:

$$X_A + k_1 X_A^2 + X_B + k_2 X_B^2 + k_3 X_A X_B = 1$$

If k_1 and k_2 are very small compared with unity, this expression may be replaced by:

$$X_A(1 - k_1 X_A)^{-1} + X_B(1 - k_2 X_B)^{-1} + k_3 X_A X_B = 1$$

If, for the reasons noted above, terms containing constants (k_1, k_2, or k_3) of the second order or higher are neglected, the expression reduces to:

$$X_A(1 + k_1) + X_B(1 + k_2) + X_A X_B(k_3 - k_1 - k_2) = 1 \tag{4}$$

Rearranging this equation and substituting equations 2 and 3:

$$\frac{X_A}{X_A^0} + \frac{X_B}{X_B^0} + \left(\frac{X_A}{X_A^0}\right)\left(\frac{X_B}{X_B^0}\right)\left(\frac{k_3 - k_2 - k_1}{(1 + k_1)(1 + k_2)}\right) = 1 \tag{5}$$

Since the vapor pressure of A is considered to be directly proportional to the concentration of single molecules of A, X_A/X_A^0 is the ratio of the vapor pressure of A in the solution to the vapor pressure of the pure liquid. Similarly X_B/X_B^0 is the ratio of the vapor pressure of B in solution to the vapor pressure of pure B. Let P_A^0 represent the vapor pressure of pure A, assuming similar symbols for the second component, and representing the constant term in the above equation by C, we have:

$$P_A/P_A^0 + P_B/P_B^0 + C(P_A/P_A^0)(P_B/P_B^0) = 1$$

if it is assumed that the vapor behaves as an ideal gas and if the activity of the pure liquid is taken as unity; $X_A/X_A^0 = a_1$, the activity of A; and $X_B/X_B^0 = a_2$, the activity of B.

Substituting:

$$a_1 + a_2 + Ca_1a_2 = 1 \tag{6}$$

DISCUSSION

The qualitative significance of C is easily visualized. When C is equal to 0, the equation reduces to Raoult's law and the mixture behaves ideally over the whole range. When C is negative, as evaluated from experimental data, the effect of k_3 seems to be less than the effects of k_1 and k_2, positive deviation from Raoult's law develops and there is less tendency for unlike molecules to associate than exists between like molecules. For negative deviations from Raoult's law, C should be positive, indicating that the effect of k_3 is greater than the effects of k_1 and k_2, and the tendency for intercombinations would be greater than for the formation of aggregates between similar molecules. Strong negative deviations may be expected to take place with the partial formation of compounds. Since the formation of a directed bond was not considered in the derivation of the relationship, it is probable that the equation will not hold for such systems. While C is readily determined and checked from experimental data, it is impossible to calculate the k's from the equation.

TABLE 1

Mole fractions and corresponding values of C for some representative binary liquid mixtures

CARBON TETRACHLORIDE AND ETHYL IODIDE AT 50°C.		ETHYL IODIDE AND ETHYL ACETATE AT 50°C.		CARBON DISULFIDE AND BENZENE AT 30°C.		METHYL ETHYL KETONE AND ACETONE AT 20°C.		METHYL ETHYL KETONE AND ACETONE AT 30°C.	
$X_{C_2H_5I}$	C	$X_{C_2H_5I}$	C	$X_{C_6H_6}$	C	$X_{acetone}$	C	$X_{acetone}$	C
0.0364	−0.22	0.0579	−0.38	0.0800	−0.34	0.052	−0.56	0.0387	−0.72
0.0084	−0.27	0.1095	−0.37	0.2286	−0.37	0.457	−0.56	0.1327	−0.57
0.1966	−0.22	0.1918	−0.36	0.3723	−0.36	0.666	−0.55	0.496	−0.54
0.2850	−0.24	0.3718	−0.38	0.6516	−0.33	0.842	−0.53	0.651	−0.54
0.4026	−0.24	0.6349	−0.39	0.8845	−0.34	0.979	−0.36	0.838	−0.53
0.4933	−0.23	0.9093	−0.41					0.934	−0.51
								0.953	−0.53

CARBON DISULFIDE AND ACETONE AT 35.17°C.		ACETIC ACID AND TOLUENE AT 69.9°C.		CARBON DISULFIDE AND ETHER AT 20°C.		ACETONE AND WATER AT 60°C.		METHYL ALCOHOL AND WATER	
X_{CS_2}	C	X_{CH_3COOH}	C	X_{ether}	C	$X_{acetone}$	C	X_{CH_3OH}	C
0.0624	−0.86	0.0435	−0.69	0.051	−0.53	0.0333	−0.22	0.1499	+0.17
0.2761	−0.86	0.1711	−0.72	0.25	−0.56	0.0720	−0.93	0.3106	−0.20
0.6717	−0.90	0.2380	−0.71	0.65	−0.49	0.236	−0.92	0.558	−0.35
0.9620	−0.92	0.4088	−0.77	0.90	−0.44	0.554	−0.87	0.860	−0.30
		0.4651	−0.71			0.737	−0.89		
		0.5981	−0.70						
		0.8750	−0.65						

Equation 6 is probably most easily applied to vapor pressure–composition data. Such data offer an opportunity to check for the constancy of *C*. In table 1 are given a number of mole fractions and the corresponding values of *C* for some representative binary liquid mixtures. In the case of mixtures of essentially nonpolar liquids such as carbon tetrachloride–ethyl iodide, ethyl iodide–ethyl acetate, and carbon disulfide–benzene, the value of *C* is quite constant over a large intermediate range of composition. The values deviate somewhat for more highly polar liquid systems such as methyl ethyl ketone–acetone, carbon disulfide–acetone, acetic acid–toluene, carbon disulfide–ether, and acetone–water. On the other hand, the values break down completely for such polar systems as methyl alcohol–water and ethyl alcohol–water (not shown). This is not unexpected, however, since the relationship should hold only for binary mixtures of low polarity.

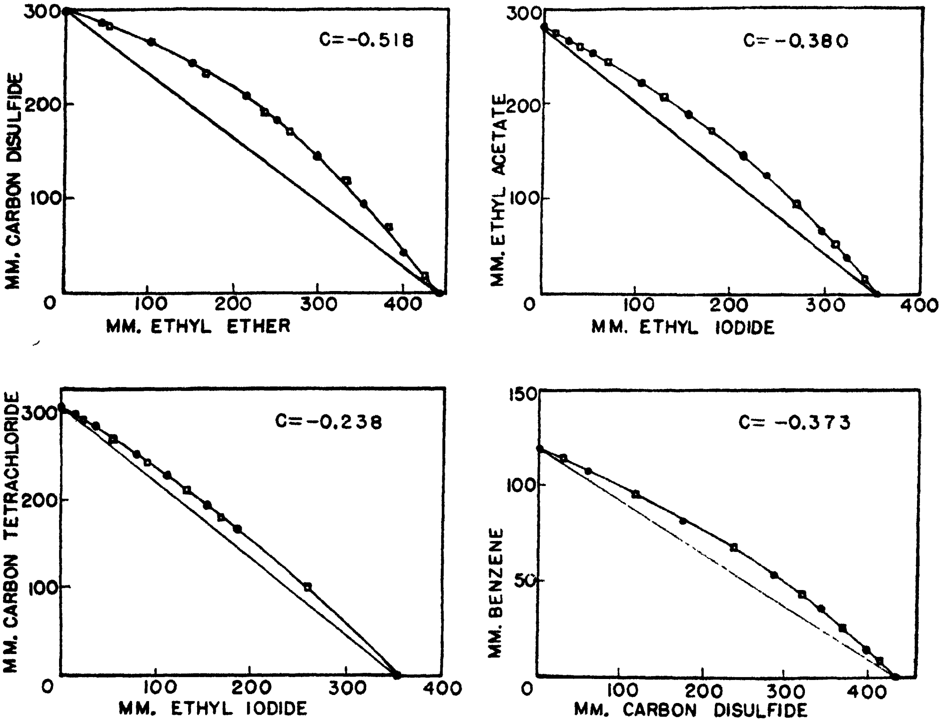

FIG. 1. Vapor pressures of binary mixtures: ●, experimental; □, calculated

It is to be noted that the values of *C* deviate greatly at the extremes of the composition range even for the slightly polar solutions. This is to be expected, since errors in most of the vapor pressure values that were used are ±0.2 mm. and, in some cases, ±1 mm. This results in errors in vapor pressure which vary ±2 per cent to as high as ± 10 per cent for low vapor pressure. Therefore, the error in *C* due to experimental error in vapor pressure alone would be at least 1 and possibly as much as 10 in the second place. The most accurate values of *C*, therefore, can be obtained near the middle of the concentration range, where the vapor pressures of both components can be measured with a fairly high degree of accuracy. For most of the systems shown, it can be seen that variation in C is not greater than the probable experimental error. The vapor pressure data used in calculating the constants in table 1 were taken from the *International Critical Tables* (2).

An important use of the relationship is the extension of activity and vapor pressure data for binary liquid systems. For example, it would be possible to obtain activity and vapor pressure values for two-component systems of low polarity over the whole range of composition if the vapor pressures of the pure components and of one mixture are known. This is all that would be needed to calculate the value of C and thus determine the desired relationship. It would be highly desirable to have a measurement of a mixture in which the vapor pressures of both components can be determined accurately in order that C be calculated with sufficient accuracy. In figure 1 are shown a number of graphs in which the activity of one component is plotted against the activity of the other. It can be seen that in most cases the experimental points (solid circles) follow the values predicted by the equation (open squares) fairly closely. In these graphs the value of C was determined from a single vapor pressure measurement at an intermediate composition at which the mole fractions of both components are nearly equal. A striking example of the usefulness of this relationship can be seen in the comparison of the experimental and calculated values for total pressure of the system carbon disulfide–acetone as shown in figure 2. Even though the deviations from Raoult's law are very great in this system, the relationship can be seen to hold fairly closely.

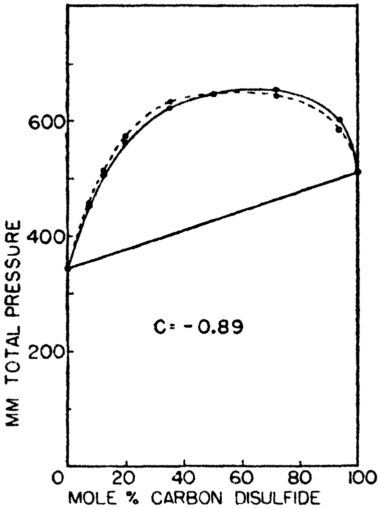

FIG. 2. Comparison of the experimental (●) and calculated (□) values for total pressure of carbon disulfide–acetone mixtures.

The derived activity relationship is an extremely useful one and may be applied to physical-chemical relationships which are related to activity. The application of this equation is being extended in a number of ways. For several systems in which vapor pressure data are available at several different temperatures, C was found to remain fairly constant. This suggests its usefulness in relationships involving the effect of temperature on vapor pressure and the possibility of deriving a relationship which will predict the temperature and composition of the constant boiling mixture. Another direction of investigation which is being pursued is the application of this activity equation to heats of mixing.

SUMMARY

A simple relationship between activity and mole fraction for binary solutions showing small positive deviations from Raoult's law is derived and discussed. The constancy of the single parameter of this equation is demonstrated at constant temperature over the whole range of composition, and the vapor pressures predicted by the equation are compared with experimental values for a number of binary systems.

The author is indebted to Dr. M. Wales and to the reviewer of this paper for valuable suggestions and criticism.

REFERENCES

(1) Bernal: Trans. Faraday Soc. **29**, 982 (1933).
Bernal and Fowler: J. Chem. Phys. **1**, 515 (1933).

(2) *International Critical Tables*, Vol. III, pp. 285–8. McGraw-Hill Book Company, Inc., New York (1926).

(3) Mecke, R., and Kempter, H.: Z. physik. Chem. **46B**, 229 (1940).
Mecke, R., and Kreuzer, J.: Z. physik. Chem. **49**, 309 (1941).

(4) Prins, J. A.: Z. Physik **56**, 617 (1929).

(5) Redlich, O., and Kister, A. T.: J. Chem. Phys. **15**, 849 (1947).

(6) Stewart, G. W.: Chem. Revs. **6**, 483 (1929); Rev. Modern Phys. **2**, 116 (1930); Trans. Faraday Soc. **29**, 982 (1933).

(7) Wilson, J. N.: Chem. Revs. **25**, 400 (1939).

THE EFFECT OF ELECTROLYTES ON THE CATHODOLUMINESCENCE OF ZINC OXIDE

SIMON LARACH

Radio Corporation of America, RCA Laboratories Division, Princeton, New Jersey

Received May 10, 1949

INTRODUCTION

It is well known that minute proportions of compounds of certain transition elements (iron, cobalt, nickel), when incorporated in most inorganic luminescent solids (phosphors) during crystallization, decrease luminescence efficiency (3). This may be termed intrinsic poisoning. In addition to this intrinsic poisoning, caused by certain incorporated inorganic impurities, investigations have shown that luminescence characteristics may be altered by extrinsically applied electrolytes acting upon the surfaces of phosphor crystals. The following experiments describe a phase of this work: namely, the effect of electrolytes on the luminescence efficiency of a zinc oxide phosphor excited by cathode rays.

EXPERIMENTAL PROCEDURE

To achieve a uniform layer of the zinc oxide phosphor, the small (1 micron, average) particles were homogeneously distributed in an aqueous solution and then the suspended particles were allowed to settle onto a glass disk substrate (2, 5).

All glass equipment was cleaned by treatment with concentrated sulfuric acid saturated with potassium nitrate, followed by successive washings with triple-distilled water. All solutions of electrolytes and suspensions of the zinc oxide phosphor were prepared with triple-distilled water.

The experimental procedure was to place an 18-mm. glass disk on the settling platform (figure 1), fill the Pyrex settling device to within a fixed distance of the top with a 0.1 *N* aqueous solution of the electrolyte undergoing test, and introduce as a 300-mg. suspension in the electrolyte medium a particular lot of zinc oxide phosphor[1] which had been partially de-aggregated[2] by ball-milling. The height of the column of liquid was 9 cm. After 10 min. of settling, at which time the settling medium was completely clear in all cases, as evidenced by absence of the Tyndall effect, the device was emptied dropwise through one of the stopcocks, and the phosphor-covered disk was removed and dried at 110°C. in air.

Two series of electrolytes were employed, one varying the cation (all as chlorides), and the other varying the anion (all as sodium compounds). The phosphor-covered disks of each series were excited under the same conditions, using a demountable-type cathode-ray tube operating at 6 kv. with a current density of approximately 3 microamp. per square centimeter. Cathodoluminescence efficiencies were obtained with a G.M. eye-corrected photocell. The electrolytes did not affect the spectral distribution of the visible emission band of the phosphor. There was no evidence throughout the course of the experiments that any appreciable amount of zinc oxide went into solution.

---

[1] Prepared by heating reagent-grade zinc oxide for 3 hr. at 1000°C. in a Vycor crucible surrounded by lampblack. Some of the luminescence characteristics of this lot of phosphor material (A-1-11-11) have been described by Shrader and Leverenz (J. Optical Soc. Am. **37**, 939 (1947)) and Nicoll (J. Optical Soc. Am. **38**, 4, 417 (1948); **38**, 9, 817 (1948)).

[2] Photomicrographs indicate that while a single zinc oxide phosphor particle averages approximately 1 micron in size, some clumping occurs and clumps of 10–15 microns are formed.

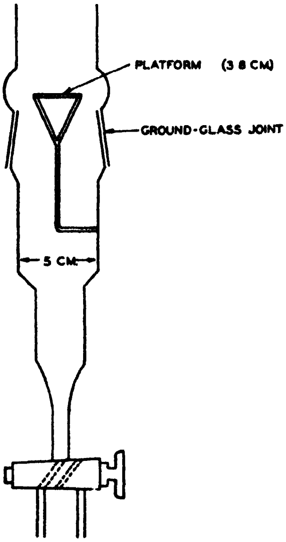

Fig. 1. Settling device

RESULTS AND DISCUSSIONS

The measured effect of electrolyte cations and anions on luminescence efficiency is shown in tables 1 and 2.

Some possible explanations for the effects shown in tables 1 and 2 are the following: (*a*) Change in optical absorption caused by adsorbed ions. Here, however, no discoloration was observed when the phosphors were viewed in reflected white light before and after settling. (*b*) Change in the secondary emission properties of the treated phosphor. This could lead to charging effects, with consequent changes of the effective accelerating potential, resulting in changes in efficiency. This has not yet been investigated, and it is not believed to be an important factor. (*c*) Change in one or more of the steps in the luminescence process of the phosphor.

It is known that cathodoluminescence is chiefly a volume effect, whereas adsorption is a surface effect. In these experiments, it is probable that adsorbed ions have a perturbing action extending some distance into the surface layers of the phosphor crystals, and this perturbation produces the observed changes in cathodoluminescence efficiency. This perturbation can affect (*a*) the luminescence centers near the surface and/or (*b*) the efficiency of the energy transfer process from the point of energy absorption to a luminescence center. The importance of the energy transfer process is demonstrated by the fact that only highly crystalline materials are efficient under cathode-ray excitation (4).

TABLE 1

Effect of cations on the cathodoluminescence efficiency of a settled zinc oxide phosphor

ELECTROLYTE CATION ADDED TO SETTLING SUSPENSION, AS CHLORIDE	RELATIVE CATHODOLUMINESCENCE EFFICIENCY*
K^+	103
Na^+	98
Ba^{++}	96
Sr^{++}	90
Li^+	90
Mg^{++}	81
Ca^{++}	69

* Screen-settled from triple-distilled water = 100.

TABLE 2

Effect of anions on the cathodoluminescence efficiency of a settled zinc oxide phosphor

ELECTROLYTE ANION ADDED TO SETTLING SUSPENSION, AS SODIUM COMPOUND	RELATIVE CATHODOLUMINESCENCE EFFICIENCY*
OH^-	111
CNS^-	109
F^-	102
Cl^-	98
Br^-	90
SO_4^{--}	90
NO_3^-	79

* Screen-settled from triple-distilled water = 100.

The penetration of a 6000-v. electron into a zinc oxide crystal may be calculated from the equation (3):

$$x = 2.5 \times 10^{-12}\,\sigma^{-1}V_0^2 \tag{1}$$

where x = penetration in centimeters,
σ = density of zinc oxide (5.6), and
V_0 = accelerating voltage (6000)

which yields a value of 16×10^{-6} cm. for x.

Electron microscope studies show the average size of a single zinc oxide phosphor crystal to be approximately 10^{-4} cm. Therefore, only about 15 per cent of an average zinc oxide crystal is penetrated by a primary 6-kv. electron. The major part of the cathode-ray energy is given up near the surface and decreases exponentially with penetration (4). The excitation density per unit volume is greatest near the crystal surface therefore, and so perturbation of the surface may produce a detectable change in cathodoluminescence efficiency when the depth of penetration of the primary electron does not greatly exceed the depth of perturbation caused by the adsorbed electrolyte ions. Long-wave ultraviolet photons have a greater probability of being absorbed directly by an activator center (4). The depth of penetration for ultraviolet photons is tremendously greater than for 6-kv. electrons. For photoluminescence, therefore, surface-layer perturbations should have little effect on efficiency. This is borne out by the fact that qualitative examination of the treated zinc oxide phosphors (tables 1 and 2), when excited by mainly 3650-Å. ultraviolet, showed no perceptible differences in luminescence efficiency.

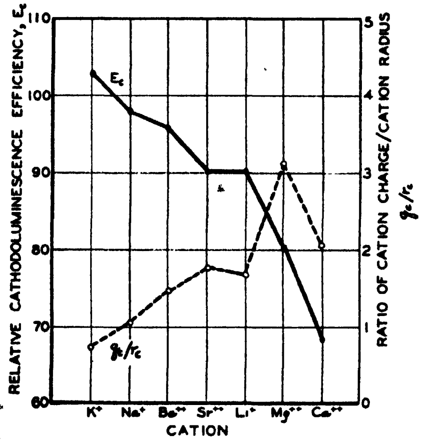

FIG. 2

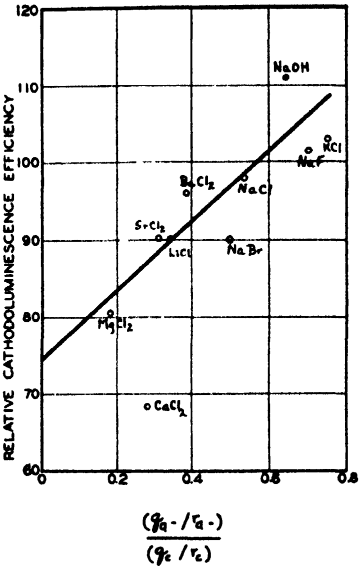

FIG 3

FIG. 2. The effect of electrolyte cations on the cathodoluminescence efficiency of a zinc oxide phosphor, in comparison with cation charge/radius ratio.

FIG. 3. Cathodoluminescence efficiency of a zinc oxide phosphor as a function of thé charge/radius ratios of electrolyte ions.

A modification of Fajans' theory of deformation (electric polarization) of adjacent ions (1) is helpful in making approximate calculations of the perturbations caused by adsorbed electrolyte ions. Assuming the deforming power of an ion to vary as the ratio of the ionic charge (q) to the ionic radius (r), we can correlate the observed changes of phosphor luminescence efficiency with the ionic properties of the electrolytes used during settling. Figure 2 is a plot of the effect of cations on efficiency (table 1) in conjunction with the charge/radius ratio (q_c/r_c) of the cations. It may be seen that an *inverse* relationship exists between cation-influenced efficiency, E_c, and cation charge/radius ratio, excepting the Ca^{++} point. Conversely, there appears to be a *direct* relationship between anion charge/radius ratio (q_a/r_a) and the resultant anion-influenced phosphor efficiency, E_a (table 2). This is readily calculated for the three halogen anions, but the radii of the other complex anions are not well enough known to allow direct comparison.

A plot of luminescence efficiency *versus* $(q_a/r_a)/(q_c/r_c)$ is shown in figure 3. It may be seen that a linear relationship is indicated, of the type

$$E = E_0 + K \frac{(q_a/r_a)}{(q_c/r_c)} \tag{2}$$

where $E_0 = 74.5$ and $K = 41$. It appears, therefore, that the surface layers of phosphor crystals are perturbed by adsorbed electrolyte ions, and this perturbation may in some cases appreciably affect luminescence efficiency. The few discrepancies observed are not surprising, considering that only first-order effects have been taken into account.

SUMMARY

The efficiency of luminescence of a zinc oxide phosphor under cathode-ray excitation can be altered by previously treating the phosphor crystals with electrolytes in aqueous solution, and subsequently drying.

A theory of perturbation of the surface layers of the phosphor crystals is proposed to account for the changes in cathodoluminescence efficiency, and an empirical expression is given which correlates efficiency with the ionic charge/ionic radius ratio of the adsorbed electrolyte ions.

The writer wishes to acknowledge the experimental assistance rendered by Dr. R. E. Shrader and the advice of Mr. H. W. Leverenz, both of the RCA Laboratories, as well as the advice of Professor J. Turkevich of Princeton University.

REFERENCES

(1) Emeléus and Anderson: *Modern Aspects of Inorganic Chemistry*, pp. 166–7. D. Van Nostrand Company, Inc., New York (1947).
(2) Leverenz: J. Optical Soc. Am. **27**, 1, 25 (1937).
(3) Leverenz: Paper PB-25481, Office of the Publication Board, Washington, D. C.; Science **109**, 183 (1949).
(4) Leverenz: Chapter in *Preparation and Characteristics of Solid Luminescent Materials*, edited by G. R. Fonda and F. Seitz. John Wiley and Sons, Inc., New York (1948).
(5) Sadowsky: J. Electrochem. Soc. **95**, 3 (1949).

OBSERVATIONS ON THE RELATION BETWEEN CATAPHORESIS, CONDUCTIVITY, AND THE PARTICLE SIZE OF SINGLE ALKALINE EARTH CARBONATES

BERNARD WOLK

Product Development Laboratories, Sylvania Electric Products, Inc., 83–30 Kew Gardens Road, Kew Gardens, New York

Received May 11, 1949

INTRODUCTION

While cataphoretic methods are used in the electron tube industry for deposition of emissive coatings on filaments and heaters, the fundamental mechanism of the coating process is not clearly understood. Problems of control and of efficient deposition may be solved more readily if some of the concepts of the cataphoretic action are clarified. The work reported here is an investigation of single alkaline earth carbonates concerning: (*1*) coating suspensions that do not utilize powders whose sizes are strictly in the colloidal range, and (*2*) nonaqueous media, an unusual technique of cataphoresis. In fact, low-water-absorption, high-dielectric materials make up the bulk of the liquid portions of the suspensions.

Properties which have significance in nonaqueous media are, primarily, viscosity and specific conductivity. The close dependence of coating behavior on these two properties is observed in actual practice.

In the past, it was felt that a more practical approach to an understanding of the electrophoretic mechanism lay in a knowledge of the conductivity of the coating suspension; as a result, such data were collected with emphasis on the obvious dependence of conductivity on the composition of both the liquid and the solid media.

The first part of this paper will carry this phase of the investigation further by presenting data relating the conductivity of dilute suspensions to the type of solid material used in the suspension. Still another section of the paper will deal with particle size and conductivity of the suspension and with conductivity as a function of precipitation impurities; the subsequent discussion will deal with a photometric analysis of the electrophoretic velocity in barium carbonate suspensions.

I. CONDUCTIVITY OF ALKALINE EARTH CARBONATES SUSPENDED IN NITROCELLULOSE LACQUERS

A. Preparation of powders

The precipitation of single alkaline earth carbonates from the nitrate solution was carried out using an excess of sodium carbonate, sodium bicarbonate, ammonium carbonate, and 1:1 combinations of these reagents, respectively. In every case, however, the other conditions were maintained constant. The temperature of precipitation was held at 60°C., while the time for the addition of precipitant was 2 min. Each sample thus prepared began with 50 g. of barium nitrate in saturated aqueous solution (pH = 5.7), while the excess weight of carbonate present in the precipitant was held constant throughout. The precipitated carbonate (pH = 11) was permitted to age 15 min., and was washed four times with hot water and twice with cold water before filtering. The powders were then dried overnight at 250°C.[1] Suspensions were prepared using these single carbonates in the following formula:

Barium, strontium, or calcium carbonate	12 g.
Amyl acetate	250 ml.
No. 3073 R & S lacquer[2]	100 ml.

These suspensions were ball milled for 15 min. in order to break up any large aggregates present and then immediately transferred to a glass container equipped with flat nickel electrodes similar to those used in actual practice for cataphoresis coating application.

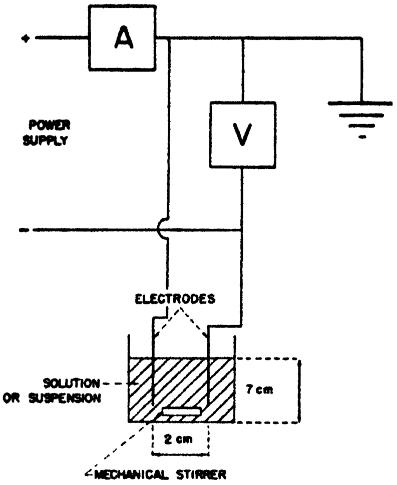

FIG. 1

B. Results

Figures 2, 3, and 4 indicate the conductivity[3] of suspensions prepared with carbonates of barium, strontium, and calcium, respectively, as determined with

---

[1] Such baking temperatures will decompose residual ammonium carbonate but will not remove any sodium carbonate residue.

[2] The composition of this lacquer is as follows:

COMPONENTS	PER CENT
60–80 min. nitrocellulose	3 (approx.)
Toluene	47
Amyl acetate	25
Ethyl acetate	25

[3] Conductivity as defined by the following equation:

$$\lambda = K \times \frac{1}{R}$$

where R = current/voltage.

the apparatus shown in figure 1. In every case the total time taken for the determination of the resistivity of the solution did not exceed 15 sec., so that sedimentation was held to a minimum.

A measurement of the conductivity of the pure nitrocellulose–amyl acetate solution in the absence of any suspended powder revealed the curve shown as a dotted line in figures 2, 3, and 4. The data were consistent each time this test was repeated, since for all the aforementioned work the source and batch of amyl acetate and No. 3073 lacquer, respectively, were the same. The double-distilled amyl acetate had a higher conductivity than when in the presence of the nitrocellulose and amyl acetate solution.

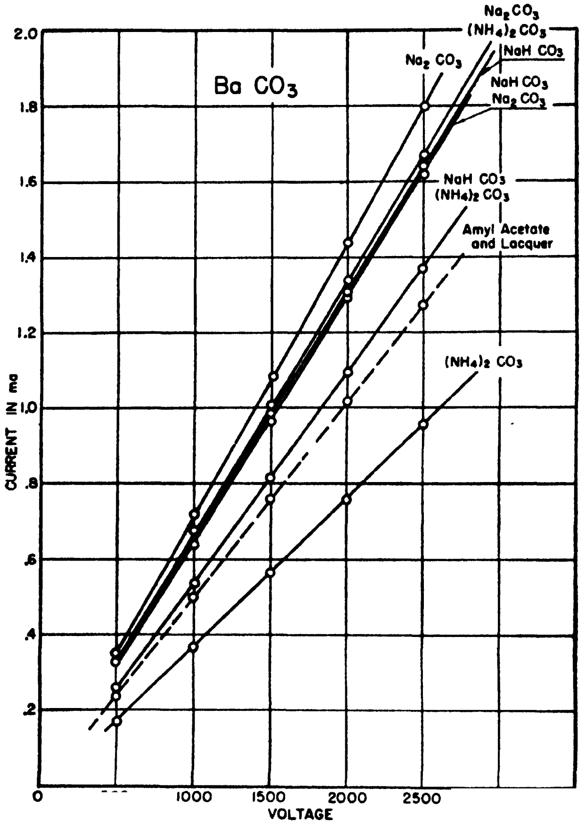

Fig. 2

A comparison of the conductivity of the dilute suspension with that of the clear liquid reveals small differences. However, the striking feature of these differences is their dependence on the previous history of the precipitating agent used. The consistently lower conductivity of barium carbonate suspensions (precipitated with ammonium carbonate) as well as the higher conductivity of another barium carbonate suspension (precipitated with sodium carbonate) have a definite interpretation which will be demonstrated in the succeeding sections.

II. PARTICLE SIZE AND CONDUCTIVITY

It was initially assumed that since the powders were prepared as mentioned above, differences in their particle size would naturally exist. Consequently, a series of measurements of average particle size were made on a Fisher subsieve sizer.[4]

The data are presented in tables 1, 2, and 3; also shown are the precipitating agents as well as the measured conductivity of the suspensions mentioned in Section I.

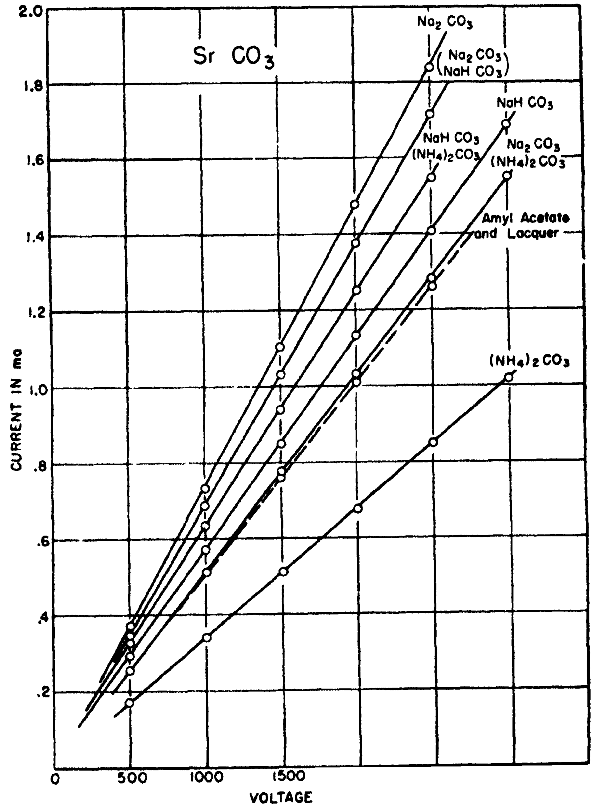

FIG. 3

The data are further illustrated in figure 5, in which we see two different systems: the barium–strontium carbonates and the calcium carbonate systems. Both curves, although differing as to slope, seem to demonstrate the inverse relationship between the particle size and the conductivity of the suspension.[5]

---

[4] Such an instrument has obvious limitations, since it is operated on the air permeability principle and the packing of a sample will depend not only on the size but also, to a lesser extent, on the shape of the individual particles.

[5] Measurements made on many double carbonates (barium and strontium) prepared in the laboratory also seem to agree generally with the curve for the barium–strontium carbonates system in figure 5.

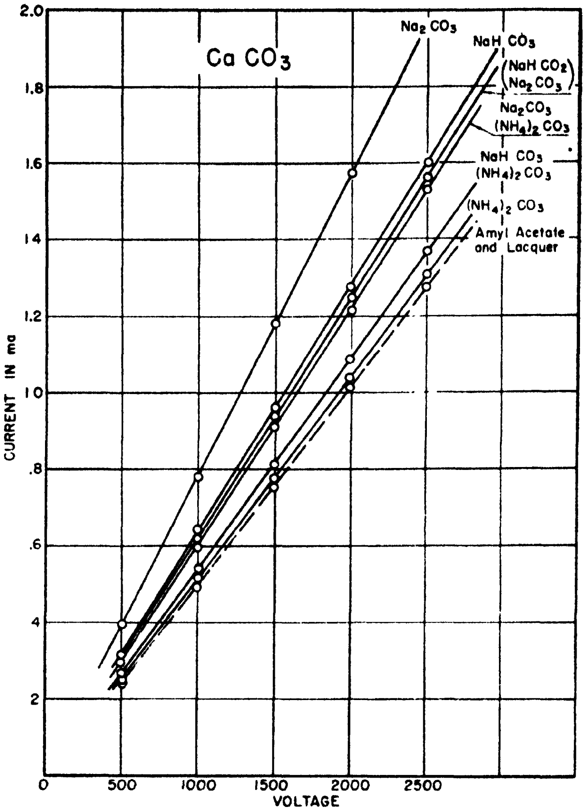

FIG. 4

TABLE 1

Particle size and conductivity of barium carbonate suspensions

SAMPLE NO.	PRECIPITANT	PARTICLE SIZE	CONDUCTIVITY
		μ	mhos
1	Na_2CO_3	1.2	7.25×10^{-7}
2	$NaHCO_3$		6.65×10^{-7}
3	$(NH_4)_2CO_3$	3.0	3.8×10^{-7}
4	$(NH_4)_2CO_3$ $NaHCO_3$	1.8	5.55×10^{-7}
5	Na_2CO_3 $NaHCO_3$	1.6	6.75×10^{-7}
6	Na_2CO_3 $(NH_4)_2CO_3$	1.5	6.8×10^{-7}

TABLE 2

Particle size and conductivity of strontium carbonate suspensions

SAMPLE NO.	PRECIPITANT	PARTICLE SIZE	CONDUCTIVITY
		μ	*mhos*
1	Na_2CO_3	1.10	7.51×10^{-7}
2	$NaHCO_3$	1.85	5.7×10^{-7}
3	$(NH_4)_2CO_3$	1.75	3.45×10^{-7}
4	$(NH_4)_2CO_3$ $NaHCO_3$	1.50	6.25×10^{-7}
5	Na_2CO_3 $NaHCO_3$	1.35	7.0×10^{-7}
6	Na_2CO_3 $(NH_4)_2CO_3$	0.95	5.25×10^{-7}

TABLE 3

Particle size and conductivity of calcium carbonate suspensions

SAMPLE NO.	PRECIPITANT	PARTICLE SIZE	CONDUCTIVITY
		μ	*mhos*
1	Na_2CO_3	1.85	7.9×10^{-7}
2	$NaHCO_3$	6.8	6.4×10^{-7}
3	$(NH_4)_2CO_3$	30.0	5.25×10^{-7}
4	$(NH_4)_2CO_3$ $NaHCO_3$	24.0	5.45×10^{-7}
5	Na_2CO_3 $NaHCO_3$	4.3	6.3×10^{-7}
6	Na_2CO_3 $(NH_4)_2CO_3$	8.5	6.15×10^{-7}

Obviously then, the particle size cannot be the *only* factor that determines the slope of the conductivity curve, else all the data would fall on one curve.

III. IMPURITIES AND CONDUCTIVITY

To prove the existence of some other factor, measurements were made on suspensions of radio mixtures 1 and 2. As described by the J. T. Baker Company, their radiochemical mixture No. 1 is an equimolecular barium and strontium carbonate which has been "washed to a predetermined alkali content," whereas the radio mixture No. 2 (also a double carbonate) was precipitated with ammonium carbonate, a procedure which resulted in a much purer product. A determination of the particle size on the subsieve sizer revealed these two mixtures to be almost identical, yet when measurements were made on standard suspensions of these two materials, the powder containing the small quantity of alkali showed a conductivity of 7.33×10^{-7} mhos, while the purer double carbonate had a value of 4.85×10^{-7} mhos.

It may be well at this point to analyze what has been found. First, that the conductivity of a standard suspension varies with the type of powder suspended. These differences, in part, can be accounted for by the differences in the particle size of the powder. Second, when the different single carbonates were precipitated and baked they were left with varying degrees of alkali impurities, the sodium carbonate giving maximum alkali residue, the sodium bicarbonate yielding less impurity, and the ammonium carbonate giving the least. There seems to be a definte relationship between the degree of such impurity and the conductivity of the suspensions. This may be inferred from figures 2, 3, and 4.

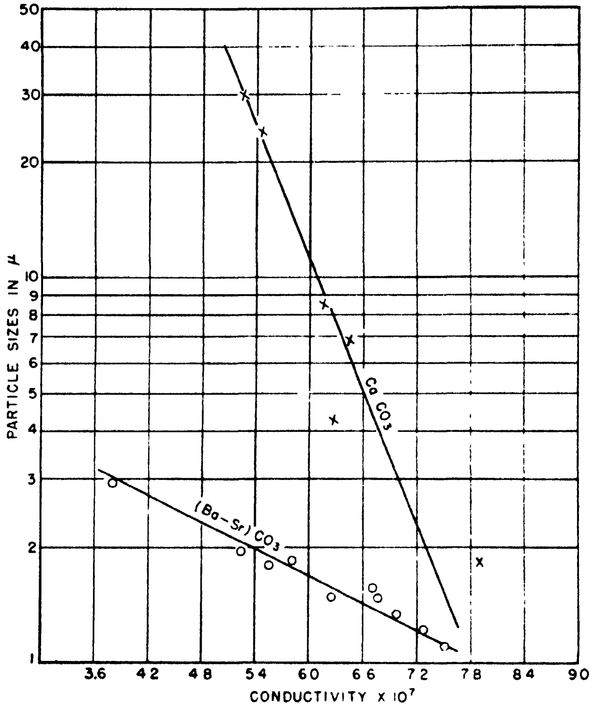

Chamot and Mason (1) state in connection with the precipitation of alkaline earth carbonates by sodium carbonate, that calcium carbonate slowly becomes crystalline if neither barium nor strontium is present, and that the carbonates of barium and strontium retain a noncrystalline appearance even on standing.

When the precipitation is carried out by ammonium carbonate they report that "... only in the case of calcium are the characteristic crystals obtained." It is perhaps for this reason that, regardless of the precipitating agent, the higher conductivity of a calcium carbonate suspension shows a distinctly different curve (figure 5). This question is outside the scope of this investigation. What is still to be done, however, is a similar analysis of carefully controlled precipitations of double and triple carbonates so that a similar correlation, if any exists, may be found between alkali impurity and the conductivity of standard dilute suspensions, such as have been used in this work. Such an analysis would be a prerequisite to any fundamental knowledge of the cataphoretic method as employed in connection with the application of radiochemicals.

IV. PHOTOMETRIC ANALYSIS OF ELECTROPHORETIC VELOCITY IN DILUTE BARIUM CARBONATE SUSPENSIONS

A. Method

The barium carbonate powders used in the following work were the same as those prepared initially, while the suspension formula (including the 15-min. milling time) was also held constant throughout. Convex slides of G-1 glass, which replaced one of the two nickel electrodes in figure 1, were first coated with a transparent, electrically conductive film of tin.[6] The intensity of the mercury-arc light beam passing through the slide was measured by a blue-sensitive photo tube whose current was indicated on a galvanometer, as shown in the circuit diagram in figure 6.

A set of eight numbered slides were thus measured for their reduction of intensity of transmitted light so that the intensity of light picked up by the photo tube was recorded as I_u.[7] These slides were then cataphoretically coated in each of the six different barium carbonate suspensions at a voltage of 1.5 kv. for 2 min. and dried. The magnitude of the light transmitted was recorded, this time as I_c.[8] As a control of such a series of tests, the slides were later wiped clean and then dipped for a 2-min. period in the same coating suspensions. During all of these tests, the suspensions were stirred. A complete set of data is presented in table 4, in which the interference of the light beam due to the coating is recorded.

B. Discussion

From our previous knowledge of the behavior of the various single carbonates discussed in this report it was felt that from results obtained with barium carbonate suspensions, certain deductions concerning the other single carbonates could be made readily. It was for this reason that this last phase of the work was limited to four barium carbonate suspensions. Although all the data are relative

---

[6] Stannic chloride vapor when in contact with hot G-1 glass deposits a film of tin with sodium chloride as a by-product.

[7] I_u = intensity of light through glass electrodes not yet coated with barium carbonate.

[8] I_c = intensity of light transmitted through glass electrodes coated with barium carbonate samples.

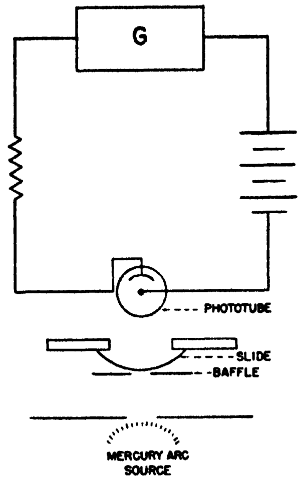

FIG. 6

TABLE 4

Interference values ($I_u - I_c$) for barium carbonate suspensions

(1) SLIDE NO	(2) CATAPHORETICALLY COATED IN Na_2CO_3-PRECIPITATED SUSPENSION	(3) CATAPHORETICALLY COATED IN $NaHCO_3$-PRECIPITATED SUSPENSION	(4) CATAPHORETICALLY COATED IN $(NH_4)_2CO_3$-PRECIPITATED SUSPENSION	(5) CATAPHORETICALLY COATED IN (Na_2CO_3 + $(NH_4)_2CO_3$)-PRECIPITATED SUSPENSION
1	36.2	28.5	20.5	29.5
2	36.3	28.9	20.6	30.6
3	37.0	27.7	20.9	29.3
4	34.0	27.6	20.1	29.6
5	39.1	29.1	20.1	31.4
6	36.9	26.8	18.0	28.3
7	36.0	28.2	20.5	29.2
8	36.4	26.7	18.2	28.0
Average value	36.3	28.0	19.9	29.4
SLIDE NO.	DIPPED IN ABOVE SUSPENSION	DIPPED IN ABOVE SUSPENSION	DIPPED IN ABOVE SUSPENSION	DIPPED IN ABOVE SUSPENSION
1	28.5	21.5	22.6	21.5
2	28.4	21.9	25.1	22.1
3	27.4	21.9	23.3	21.2
4	24.2	22.6	24.4	21.2
5	29.0	23.1	24.1	23.1
6	26.3	19.3	23.8	19.8
7	26.6	20.0	23.6	21.5
8	26.2	20.0	21.5	20.7
Average value	27.1	21.3	23.6	21.4

and depend on the particular method used, it is possible within the framework of this report to arrive at certain conclusions. The value of $I_u - I_c$ reported in the charts represents the extent to which light was obscured by the barium carbonate (column 2 of table 4 indicates a very dense coating). When originally precipitated by ammonium carbonate, the barium carbonate suspension results in a very sparsely coated slide (column 4), while an intermediate value is obtained for a barium carbonate prepared with sodium bicarbonate (column 3).

A 1:1 ratio of sodium carbonate and ammonium carbonate precipitants yielded a barium carbonate whose suspension produced a coating also having an intermediate value (column 5). Undoubtedly, there are distinct differences in the amount of light which will pass through a slide covered with different-sized particles; this is adequately demonstrated by the different values found for slides which were dipped with no potential applied to the solution. Yet the light transmitted through the slides dipped in the suspensions shows no correlation with the average particle size of the suspended powder. What appears to have greater significance, however, is the relationship between the degree of reduction of the intensity of transmitted light by the cataphoretically coated slide and the data on the conductivity of the original suspensions, as expressed graphically in figure 7.

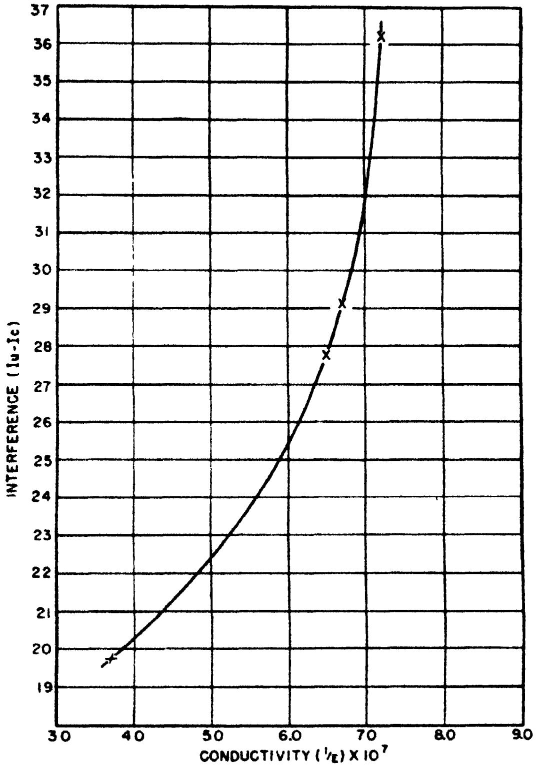

FIG. 7

Under the 1.5-kv. potential in the suspension, the slides were coated much more densely, as indicated by the greater interference value by the barium carbonate having the smallest average particle size (column 2 of table 4), while the suspension prepared from ammonium carbonate produced a coating which was less dense than even the control (column 4). The negative effect shown in this last case seems to confirm the validity of figure 2, in which the use of barium carbonate (precipitated with ammonium carbonate) decreases the conductivity of the resulting suspension.

At this point the direction for future work is indicated. A more complex but parallel study of double- and triple-carbonate suspensions should be made so that the mechanism of cataphoresis may be more adequately related to the mode of precipitation and, equally important, to the alkali impurity, while the other operative factors such as concentration, viscosity, and size and shape of electrodes are held constant.

CONCLUSIONS

The conductivity of dilute suspensions of single alkaline earth carbonates in nitrocellulose lacquer media shows a dependence on the history of the precipitation of the powders. This dependence is a function of both particle size and sodium-ion impurity. Furthermore, characteristic conductivity–particle size curves obtained for the barium, strontium, and calcium carbonate systems indicate that the conductivity of the calcium carbonate is affected by its crystalline nature in somewhat different manner than is the conductivity of the noncrystalline barium and strontium carbonate suspensions.

In the case of the barium carbonate suspensions studied, such factors as the sodium-ion impurity and particle size, which in turn determine the conductivity of their suspensions, are shown to affect the cataphoretic velocity.

REFERENCE

(1) Chamot, E. M., and Mason, C. W.: *Handbook of Chemical Microscopy*, 2nd edition, Vol. II, pp. 102–4. John Wiley and Sons, Inc., New York (1940).

SOLUBILIZATION AND COSOLVENT EFFECTS WITH SODIUM STEARATE

REYNOLD C. MERRILL

Philadelphia Quartz Company, Philadelphia, Pennsylvania

Received May 11, 1949

The ability of aqueous solutions of detergents to solubilize otherwise water-insoluble dyes and organic liquids is now well known and has been extensively studied (e.g., 3, 5, 7, 8, 15, 21, 22). Less extensive study has been given to the solubilization of high-molecular-weight soaps and detergents, such as sodium stearate, which are practically insoluble in water at ordinary room temperatures. Phase diagrams of sodium palmitate–sodium laurate mixtures (6, 13; *cf.* also 11) and of soaps from oils and fats containing mixtures of fatty acids (10) indicate that the solubility of mixtures of soaps is greater than that expected on an additivity basis, owing to solubilization of the less soluble soaps by the more soluble ones. Despite the interest in the solubilization of organic liquids by soaps, the effect of these organic liquids on the solubility and other properties of the soap itself has been studied systematically by relatively few investigators.

That such organic additives as cresol, cyclohexanol, and pine oil are soluble in soap solutions and that they increase the solubility of soaps, particularly in hard waters, has long been recognized by the soap industry. For example, Woodman (24) showed that the solubility of sodium oleate in water at 25°C. is 10.4 per cent, whereas in a 2.14 per cent phenol solution it is 12.6 per cent. Angelescu and Popescu (1) showed that the solubilization of cresols by soap solutions was accompanied by an increase and then a decrease in the viscosity, and that at the viscosity minimum the electrical conductivity was a maximum. This suggests that the micelles in the presence of cresols are smaller and less hydrated.

This paper reports the solubilization of sodium stearate by potassium stearate, sodium laurate, and several modern synthetic organic detergents. Data showing the effect of such organic additives as cresol, cyclohexanol, cyclohexylamine, and tertiary butyl alcohol on the solubility of sodium stearate are also included.

EXPERIMENTAL

The sodium stearate used in the work with the synthetic detergents was made from Eastman Kodak Company's best stearic acid after recrystallization from acetonitrile. It had an equivalent weight of 284.5, in agreement with the theoretical value. An alcoholic solution of the acid was neutralized to the phenolphthalein end point with sodium methoxide and the precipitated soap washed with alcohol and dried at 105°C. It then contained 0.05 per cent excess sodium hydroxide. The sodium stearate used in the work with organic liquids and the potassium stearate were made from another sample of the Eastman acid without recrystallization. The former contained about 4 mole per cent excess sodium hydroxide to minimize hydrolysis (*cf.* 9). The sodium laurate was prepared similarly from a recrystallized Eastman lauric acid. The acid had an equivalent weight determined by titration of 202.4 (theory, 200.3) and the soap contained 0.057 per cent excess sodium hydroxide.

The sodium lauryl sulfate was a commercial product (obtained from Eimer and Amend) which was completely soluble in alcohol. Ultrawet K is an alkyl aryl type of synthetic detergent made by the Atlantic Refining Company; it contains about 15 per cent sodium sulfate. Santomerse No. 3, produced by the Monsanto Chemical Company, is essentially sodium dodecylbenzenesulfonate and is free from inorganic salt. Rohm and Haas' Triton X-100 is a condensation product of one molecule of diisobutylphenol with about nine or ten ethylene oxide molecules (4). Renex, obtained from the Atlas Powder Company, is a condensation product of rosin and fatty acids with ethylene oxide. Their Tween 80 is described as sorbitan monoöleate.

Butyl cellosolve was obtained from the Carbide and Carbon Company, hydroabietyl alcohol from the Hercules Powder Company, and cyclohexylamine from the Monsanto Chemical Company. The cresol was a U.S.P. grade commercial product. The other organic materials were Eastman Kodak Company products.

All experimental data were obtained by the synthetic method. Weighed amounts of soap, detergent, or organic additive and water were added to narrow-neck tubes made from 13 x 100 mm. Pyrex test tubes. These were sealed to prevent changes in composition and their contents heated until they formed a homogeneous isotropic solution. On cooling to room temperature all of the systems studied contained white opaque solid crystalline soap. The solution temperature, T_c, was determined by heating slowly in a water bath until the last trace of opaque white solid had just disappeared to complete the formation of an isotropic or anisotropic solution. The T_c values are precise to ±1°C. or less. Sodium stearate systems dissolve to isotropic solution up to a concentration of about 20 per cent soap. Above this concentration the transition is from white solid to liquid crystalline (anisotropic) soap. Systems containing a synthetic detergent or an organic additive seemed to require a somewhat higher soap concentration before liquid crystal was formed, but this was not particularly studied.

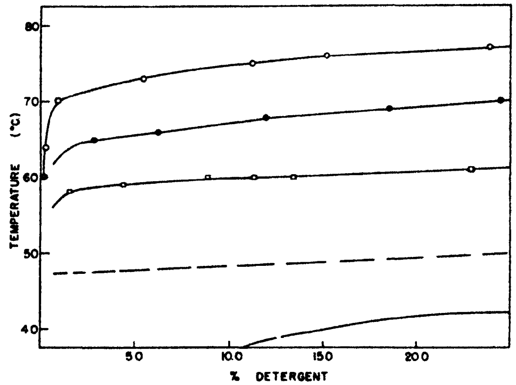

FIG. 1. Solution temperatures, T_c, for soap mixtures

○	Sodium stearate
●	50 per cent sodium stearate + 50 per cent potassium stearate
□	50 per cent sodium stearate + 50 per cent sodium laurate
— — —	Potassium stearate (data of McBain and Sierichs (9))
———	Sodium laurate (data of McBain, Brock, Vold, and Vold (14))

RESULTS

Solution temperatures for various concentrations of sodium stearate alone and mixed with equal weights of potassium stearate, sodium laurate, and four modern synthetic organic detergents are shown in figures 1 and 2. Our data on sodium stearate are in good agreement with those of McBain, Vold, and Frick (12). The solution temperatures for mixtures containing 77 per cent sodium stearate and 23 per cent Ultrawet K, Tween 80, Renex, sodium laurate, and

Triton X-100 decrease in that order at comparable concentrations, but the T_c values for even the most soluble mixture are only 4° or 5° below those of an equal weight of sodium stearate. Figure 1 shows that the solution temperatures of mixtures with the shorter chain sodium laurate are lower than those with the potassium stearate. Similarly, sodium laurate itself is more soluble than potassium stearate (9, 14). Solution temperatures for the mixtures are closer to those of the less soluble component than to those of the more soluble.

Mixtures of sodium stearate with sodium lauryl sulfate have a lower solution temperature below a concentration of 15 per cent but a higher T_c above this concentration. Santomerse No. 3, which is essentially sodium dodecylbenzenesulfonate, lowers the solution temperatures more than Ultrawet K, which also is an alkyl aryl sulfonate type of detergent but contains 15 per cent sodium sulfate. Triton X-100 lowers the solution temperatures more than the other synthetic detergents. The lowering is greater than with sodium laurate below about 7 per cent total detergent, although somewhat higher above this concentration. All of the synthetic detergents are readily soluble. For example, the solution temperature T_c for a 23.2 per cent Ultrawet K solution is 51°C.

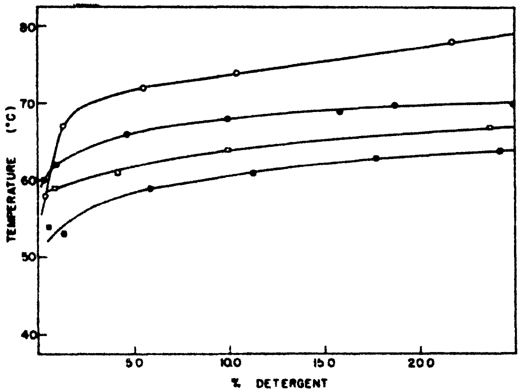

FIG. 2. T_c temperatures for sodium stearate–synthetic detergent mixtures

○	50 per cent sodium stearate + 50 per cent sodium lauryl sulfate
●	50 per cent sodium stearate + 50 per cent Ultrawet K
□	50 per cent sodium stearate + 50 per cent Santomerse No. 3
■	50 per cent sodium stearate + 50 per cent Triton X-100

Solution temperatures for various concentrations of mixtures of sodium stearate with several organic additives are given in table 1. The more extensive data with cresol, cyclohexanol, cyclohexylamine, and tertiary butyl alcohol are summarized only in figure 3. Solution temperatures for sodium stearate with butyl cellosolve, 1-octanol, and 2-ethylhexanol are lower than those for the stearate alone at concentrations from about 0.5 per cent to approximately 4, 3, and 5 per cent, respectively. At higher concentrations the solution temperatures rise rapidly to above 100°C. They appeared to consist of a milky emulsion of organic liquid in

TABLE 1

Solution temperatures, T_c, for sodium stearate–organic additive systems

ORGANIC ADDITIVE	SODIUM STEARATE*	T_c
	per cent	°C.
Butyl cellosolve	0.29	72
	0.58	65
	3.55	64
	8.30	>100
Hydroabietyl alcohol	1.13	>100
1-Octanol	0.42	56
	1.44	57
	2.05	61
	3.61	>100
2-Ethylhexanol	0.77	58
	1.72	59
	3.57	60
	4.51	61
	6.90	>100
Urea	0.27	65
	1.94	72
	4.57	76
	5.82	>100

* In all cases except for hydroabietyl alcohol the weight of the organic additive was 30 per cent of the weight of the soap. The weight of hydroabietyl alcohol was 40 per cent of the weight of the soap.

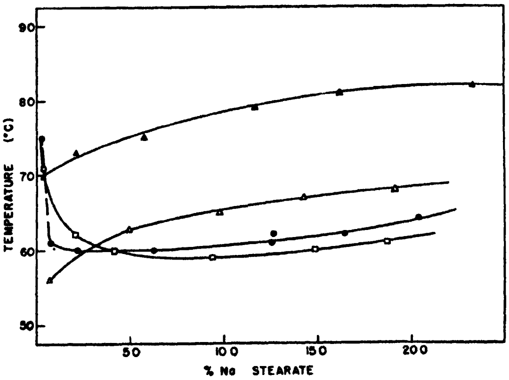

FIG. 3. Solution temperatures, T_c, for sodium stearate in aqueous solutions containing 30 per cent as much organic liquid as soap.

●	Sodium stearate + cresol
□	Sodium stearate + cyclohexanol
△	Sodium stearate + cyclohexylamine
▲	Sodium stearate + 30 per cent tertiary butyl alcohol

the soap solution. Urea increases the solution temperatures at all soap concentrations.

The lowering of the solution temperatures of sodium stearate by amounts of cyclohexylamine, cresol, and cyclohexanol corresponding to 30 per cent by weight of the soap is shown clearly in figure 3. Below a concentration of 2 per cent sodium stearate the solution temperatures increase in the presence of cresol and cyclohexanol. Unless there is about 4 mole per cent excess sodium hydroxide present a similar increase in T_c occurs for soaps alone in distilled water (9). This increase in T_c is attributable to hydrolysis and formation of the less soluble acid soaps. Hydrolysis is apparently increased by the addition of the essentially neutral cyclohexanol as well as by the acidic cresol but not by the alkaline cyclohexylamine. Similarly, Fryling and Harrington found that the pH of sodium myristate and oleate solutions decreased on the addition of acrylonitrile, styrene, methyl methacrylate, isoprene, benzene, and methyl ethyl ketone (2). Sodium stearate is less soluble in the tertiary butyl alcohol solutions than in distilled water.

DISCUSSION

Sodium palmitate and stearate, the main constituents of tallow soaps, are practically insoluble at room temperature and only become readily soluble at temperatures above 55°C. (9). It is therefore customary to add coconut oil, containing a high proportion of the shorter chain lauric acid which forms the more soluble sodium laurate, to tallow in order to obtain a mixed soap readily soluble at temperatures of practical use. Since coconut oil is more expensive and must be imported, it may be an advantage to replace the coconut oil soap with a cheaper synthetic detergent produced from petroleum or other resources in this country. Such a product was extensively used by the Army and Navy in World War II. Our data confirm their experience that a mixture of a soap from a high-titer fat such as tallow with a suitable synthetic detergent has solubility properties similar to those of tallow–coconut oil soaps.

Practical experience has indicated that it is sometimes difficult to incorporate the large amount of sodium silicate builders justified on the basis of detergent value into a tallow soap, although this is readily done with a mixed tallow–coconut oil soap. The solubility and the emulsifying and detergent (*cf.* 16) properties of mixtures of sodium stearate (a main ingredient of tallow soaps) and synthetic detergents are similar to those of sodium stearate-laurate (chief ingredient of coconut oil soaps) mixtures. It therefore seems likely that the addition of synthetic detergent to a tallow soap should aid in the incorporation of relatively large amounts of sodium silicate builders.

That the solution temperature of sodium stearate is lowered to about the same extent by 30 per cent of the cosolvents cresol, cyclohexanol, and cyclohexylamine as by 100 per cent of the solubilizing, more soluble soaps and synthetic detergents is interesting and theoretically significant. Both mechanisms probably involve the formation of smaller, less heavily hydrated micelles containing both constituents of the solution. When more experimental data are available, it seems likely that a theory of cosolvent effects for water–organic additive solutions can be developed, involving considerations of van der Waals forces, polar and dipolar forces, hydrogen bonding, resonance effects, and steric effects similar to that developed for mixtures of nonaqueous solvents (17). The effect of the three polar cyclic compounds cresol, cyclohexanol, and cyclohexylamine may be attributed to a strong tendency to combine with the carboxyl group of the stearate, thus decreasing its tendency to crystallize into the usual lattice arrangements. Another possibility is that a small amount of a sparingly soluble organic liquid may increase the extent of micelle formation, resulting in greater solubility of the soap.

Recent patents have disclosed the use of long-chain amides, nitriles, and other polar derivatives as builders for synthetic detergents (18, 19, 23). A study of their effect on solubility would be of interest, particularly in view of the recent claim (20) that dicyanodiamide increases the solubility of synthetic detergents.

SUMMARY

Solution temperatures of various concentrations of sodium stearate are decreased by potassium stearate, to a greater extent by sodium laurate and also by six modern synthetic anionic and nonionic detergents. Cresol, cyclohexanol, and cyclohexylamine also decrease the solution temperatures of sodium stearate, whereas other organic additives have variable effects.

REFERENCES

(1) Angelescu, E., and Popescu, D. M.: Kolloid-Z. **51**, 247, 336 (1930).
(2) Fryling, C. F., and Harrington, E. W.: Ind. Eng. Chem. **36**, 114 (1944).
(3) Kolthoff, I. M., and Stricks, W.: J. Phys. & Colloid Chem. **53**, 424 (1949).
(4) Marsden, S. S., Jr., and McBain, J. W.: J. Phys. & Colloid Chem. **52**, 110 (1948).
(5) McBain, J. W.: In *Advances in Colloid Science*, Vol. I, pp. 99–142. Interscience Publishers, Inc., New York (1942).
(6) McBain, J. W., and Johnston, S. A.: J. Am. Chem. Soc. **63**, 875 (1941).
(7) McBain, J. W., and Merrill, R. C.: Ind. Eng. Chem. **34**, 915 (1942).
(8) McBain, J. W., and Richards, P. H.: Ind. Eng. Chem. **38**, 642 (1946).
(9) McBain, J. W., and Sierichs, W. C.: J. Am. Oil Chemists' Soc. **25**, 221 (1948).
(10) McBain, J. W., Elford, W. J., and Vold, R. D.: J. Soc. Chem. Ind. **59**, 243 (1940).
(11) McBain, J. W., Lazarus, L. H., and Pitter, A. V.: Z. physik. Chem. **147A**, 87 (1930).
(12) McBain, J. W., Vold, R. D., and Frick, M.: J. Phys. Chem. **44**, 1013 (1940).
(13) McBain, J. W., Vold, R. D., and Jameson, W. T.: J. Am. Chem. Soc. **61**, 30 (1939).
(14) McBain, J. W., Brock, G. C., Vold, R. D., and Vold, M. J : J. Am. Chem. Soc. **60**, 1870 (1938).
(15) Merrill, R. C., and McBain, J. W.: J. Phys. Chem. **46**, 10 (1942).
(16) Morrisroe, J. J., and Newhall, R. G.: Ind. Eng. Chem. **41**, 423 (1949).
(17) Palit, S. R., and McBain, J. W.: Ind. Eng. Chem. **38**, 741 (1946).
(18) Richardson, A. S.: U. S. patent 2,383,527 (August 25, 1945).
(19) Richardson, A. S., and McAllister, W. H.: U. S. patent 2,383,738 (August 28, 1945).
(20) Shepard, N. A.: U. S. patent 2,445,975 (July 27, 1948).
(21) Smith, E. L.: J. Phys. Chem. **36**, 1401, 2455 (1932).
(22) Stearns, R. S., Oppenheimer, H., Simon, E., and Harkins, W. D.: J. Chem. Phys. **15**, 496 (1947).
(23) Tucker, N. B.: U. S. patents 2,383,525–6 (August 25, 1945); U. S. patents 2,383,739–40 (August 28, 1945).
(24) Woodman, R. M.: J. Soc. Chem. Ind. **52**, 185 (1933).

SUSPENDING ACTION OF ALKALINE ELECTROLYTES ON ILMENITE BLACK

REYNOLD C. MERRILL AND RAYMOND GETTY

Philadelphia Quartz Company, Philadelphia, Pennsylvania

Received May 9, 1949

Suspending action may be defined as the effect of added substances in decreasing the rate or amount of sedimentation of a dispersion of an insoluble solid in a liquid. The phenomenon is of theoretical interest as a part of the general problems of the stability of colloids, the nature of surfaces, the sorption of ions or molecules from solution by solids, and the interaction of particles. Suspending action in aqueous systems is of practical importance in determining particle sizes by sedimentation, purification or fractionation of insoluble solids such as clays, flotation procedures, detergent operations, and the preparation of commercially useful dispersions such as clay–silicate adhesives. In nonaqueous media suspending is important for paints, lubricating oils, printing inks, dry-cleaning solvents, and colloidal fuels.

Although relatively few comprehensive systematic investigations of suspending action have been reported in the published literature, the effect has been observed for many years. For example, Bodlander reported in 1893 that hydroxyl ions decrease the rate of settling of kaolin (2). Spring's qualitative observations in 1909 showed that soap solutions decreased the sedimentation rate of lampblack, ferric oxide, and potter's clay (16). Kohl in 1922 found that increasing amounts of sodium carbonate and sodium silicate first increased the amount of kaolin dispersed and then, after a definite maximum, clarified the suspension (9). Sodium silicate was better than sodium carbonate in small amounts and a larger amount was needed for flocculation. In 1923, Liesegang stated that barium sulfate (*blanc fixe*), which usually settled with a sharp boundary below a clear supernatant liquid, remained turbid for a long time if precipitated in an excess of barium chloride (10).

Kermack and Williamson (7) showed that sodium chloride increased the rate of sedimentation of barium sulfate suspensions in alkaline solutions but retarded it in acid, whereas potassium chloride increased it at all pH values. Disodium hydrogen phosphate, sodium citrate, and, at concentrations greater than 0.01 N in acid solutions, calcium acid phosphate stabilized the suspension. The effectiveness of salts in stabilizing the suspension decreased in the order lithium, sodium, ammonium, potassium, rubidium, and cesium. Bakh (1) observed that multivalent ions stabilized certain charcoal suspensions.

Fall (3) found that the ability to suspend manganese dioxide of soaps, sodium hydroxide, sodium carbonate, trisodium phosphates, and sodium silicates with silica-to-alkali (Na_2O) mole ratios of 1.62, 2.92, and 3.97 reached a maximum at relatively low concentrations. Qualitatively similar results have been reported with tannin and several sodium soaps (8, 17, 18). Likewise an optimum concentration of sodium hydroxide exists for stabilizing graphite (18).

In 1942 one of us (12) showed that a 0.27 per cent suspension of ilmenite black settled less rapidly in 0.0001 *M* solutions of tetrasodium pyrophosphate, trisodium and tripotassium phosphates, sodium dihydrogen phosphate, and sodium hydroxide than in distilled water. Qualitative observations indicated that all of these salts exhibited a characteristic optimum concentration for maximum suspending action which may, at great dilutions, depend on the amount of pigment to be suspended. Recently Greiner and Vold (4) found that a sodium dodecylbenzenesulfonate, *p*-toluenesulfonic acid, a complex quaternary ammonium salt, the sodium salt of dioctylsulfosuccinic acid, and sodium oleate have a sharp maximum at low concentrations in their effectiveness as suspending agents for manganese dioxide.

The present paper reports measurements on the amount of ilmenite black suspended by aqueous solutions of sodium dodecylbenzenesulfonate, sodium hydroxide, sodium carbonate, trisodium phosphate, tetrasodium pyrophosphate, and sodium silicates with silica-to-alkali (Na_2O) molecular ratios of 0.67 (sesquisilicate), 1.00 (metasilicate), 2.91, and 3.30, as well as by mixtures of the organic detergent with sodium silicates and sodium sulfate. Concentrations from $7 \times 10^{-7}M$ to $10^{-1}M$ were studied. Some observations with nonionic detergents are reported.

MATERIALS AND METHOD

The ilmenite was "Air Floated Ilmenite Black" produced by British Titan Products Co., Billingham, Stockton on Tees, England. The sodium dodecylbenzenesulfonate was Santomerse No. 3 of the Monsanto Chemical Company, which is reported to be 99+ per cent organic detergent of this type (5), although it is probably a mixture of isomers.

Triton X-100, a condensation product of diisobutylphenol with nine or ten molecules of ethylene oxide, was obtained from the Rohm and Haas Company. Renex, a condensation product of ethylene oxide with rosin and fatty acids, was obtained from the Atlas Powder Company. Igepal CA Extra, a product of the General Dyestuff Corporation, is reported to be a condensation product of ethylene oxide, probably with an alkylphenol such as diisobutylphenol.

The sodium silicates were Philadelphia Quartz Company products which contained varying amounts of water. The sodium phosphates, carbonate, sulfate, and hydroxide were Baker's analyzed reagent-grade chemicals. All data are reported in terms of molarities.

Quantitative measurements of suspending action were obtained with an apparatus similar to that described by Poliakoff (14). It consisted of a glass-stoppered 250-ml. Pyrex glass cylinder to which was attached at the 75-ml. mark an outlet tube with stopcock. Our apparatus differed from Poliakoff's in that the outlet tube was inclined *upward* at an angle of about 20° from the horizontal in order to prevent solid from settling out in it, thus giving erroneously high values.

In making measurements, 200 ml. of a 0.1 per cent suspension of ilmenite was placed in the cylinder and vigorously shaken for 1 min. After 3 hr. standing at

23°C., a 50.0-ml. sample was withdrawn through the stopcock, taking care to prevent convection in the cylinder. The sample was analyzed by measuring its light absorption in a photoelectric colorimeter and comparing this with calibration curves obtained from suspensions of known concentrations. Calibration curves for the ilmenite in different concentrations of the various dispersing agents were similar, but dispersions in good suspending agents absorbed somewhat more light than the same weight in poor dispersing agents. Likewise, the same amount of ilmenite dispersed in distilled water did not absorb as much light as when suspending agents were present. This is attributable to incomplete dispersion into primary particles and to the presence of secondary aggregates which do not absorb or scatter as much light per unit weight.

Values for the ilmenite concentration obtained by the light absorption method were checked periodically by evaporating the suspension to dryness. Only the remarkable uniformity in the particle size (of the order of 1 micron) of our material made it possible to use light absorption as a measure of concentration. Apparently the fractionation occurring in our experiments was so small that the light absorbed per unit weight of ilmenite was not much changed. Attempts to use light absorption as a measure of concentration of carbon black and raw umber suspensions failed. Considerable fractionation into different particle sizes occurred with these materials and the light absorbed or scattered per unit weight varied greatly with the dispersing agent, concentration, and time of settling.

EXPERIMENTAL RESULTS

The amounts of ilmenite suspended after 3 hr. under our experimental conditions by varying concentrations of aqueous solutions of sodium hydroxide, sodium carbonate, trisodium phosphate, and tetrasodium pyrophosphate are shown in figure 1. In general the order of decreasing effectiveness as a suspending agent is pyrophosphate, orthophosphate, carbonate, and hydroxide, although in a narrow range of concentration the hydroxide suspends more ilmenite than the carbonate. A sharp maximum in efficiency is show for the hydroxide at around $7 \times 10^{-5}M$ (*cf.* figure 2); the carbonate shows a broader maximum at about $5 \times 10^{-4}M$. A maximum for the phosphates is not evident in figure 1, although it is apparent that one must exist, since only 10 mg. per 100 ml. remains suspended after 3 hr. in distilled water. In order to show clearly the suspending action at very low electrolyte concentrations, additional data completing the range from 10^{-6} to $10^{-1}M$ are plotted on a semilogarithmic scale in figure 2. Even at a concentration of $10^{-6}M$ the pyrophosphate keeps 79 mg. of ilmenite per 100 ml. suspended. At $4.8 \times 10^{-7}M$ the amount of ilmenite suspended has decreased to 60 mg. per 100 ml.

Figure 3 shows on a linear scale the amounts of ilmenite suspended by solutions of sodium sesquisilicate, sodium metasilicate, and sodium silicates with silica-to-alkali (Na_2O) ratios of 2.91 and 3.30. In figure 4 additional data have been included and plotted on a semilogarithmic scale to bring out more clearly the effects at low concentrations. Each silicate shows a low optimum concentration for most effective suspending action. At higher concentrations the alkaline

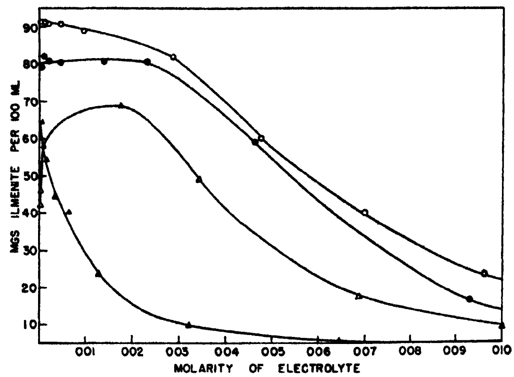

FIG. 1. Amounts of ilmenite suspended by alkaline electrolyte solutions after 3 hr. ○, $Na_4P_2O_7$; ●, Na_3PO_4; △, Na_2CO_3; ▲, NaOH.

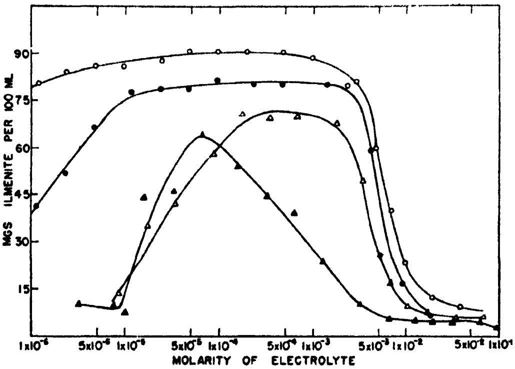

FIG. 2. Amounts of ilmenite suspended by alkaline electrolyte solutions after 3 hr. (semilogarithmic scale). ○, $Na_4P_2O_7$; ●, Na_3PO_4; △, Na_2CO_3; ▲, NaOH.

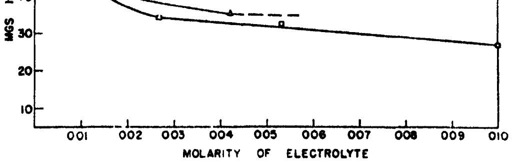

FIG. 3. Amounts of ilmenite suspended by alkaline electrolyte solutions after 3 hr.

●	Na_3HSiO_4 ($Na_2O \cdot 0.67SiO_2$)	△	$Na_2O \cdot 3.3SiO_2$
○	Na_2SiO_3	□	$Na_2O \cdot 2.8SiO_2$

silicates are the more effective suspending agents for ilmenite under these particular conditions.

Figures 5 and 6 show that sodium dodecylbenzenesulfonate has maximum suspending efficiency at concentrations around $5 \times 10^{-3}M$ and that mixtures

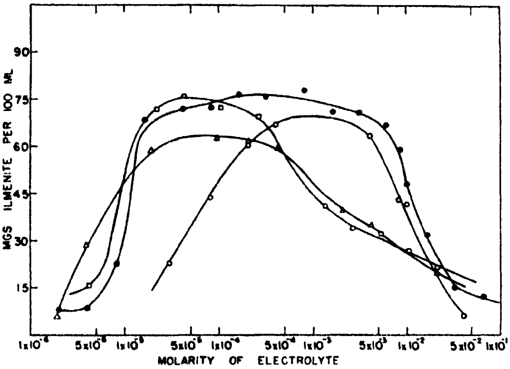

FIG. 4. Amounts of ilmenite suspended by alkaline electrolyte solutions after 3 hr. (semilogarithmic scale).

●	Na_3HSiO_4 ($Na_2O \cdot 0.67SiO_2$)	△	$Na_2O \cdot 3.3SiO_2$
○	Na_2SiO_3	□	$Na_2O \cdot 2.8SiO_2$

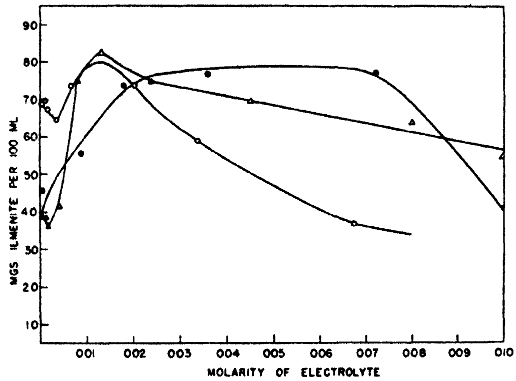

FIG. 5. Amounts of ilmenite suspended by alkaline electrolyte solutions after 3 hr.

●	Santomerse No. 3
△	60 weight per cent Santomerse + 40 weight per cent Na_2SO_4
○	60 weight per cent Santomerse + 40 weight per cent Na_2SiO_3

of the organic detergent with sodium sulfate or metasilicate exhibit two maxima in their curves of amount of ilmenite suspended as a function of concentration. The molarity used for the mixtures is the average molarity of the two salts. Each of the two components in the mixture is probably responsible for one of the maxima. However, the presence of the other electrolyte profoundly affects the suspending action, because both maxima occur at active ingredient concentrations much lower with mixtures than with single electrolytes. The second electrolyte apparently increases sorption of the first.

The amount of ilmenite remaining suspended after 3 hr. under these experimental conditions in 0.129, 0.01, 0.001, 0.0001, and 0.00001 per cent solutions of Triton X-100 was about the same as or even less than the 10 mg. per 100 ml. which remained suspended in distilled water. However, in 0.16 and 0.01 per cent Igepal CA Extra solutions the amount suspended was 19 and 17 mg. per 100 ml., respectively. The amount of ilmenite suspended in a 0.11 per cent Renex solution was 41 mg. per 100 ml. and decreased to about 14 mg. per 100 ml. at concentrations of 0.01 and 0.001 per cent. Certain nonionic detergents do therefore at particular concentrations act as suspending agents, although they are apparently considerably less effective over a wide concentration range than the silicates, ortho- or pyrophosphates, or sodium dodecylbenzenesulfonate.

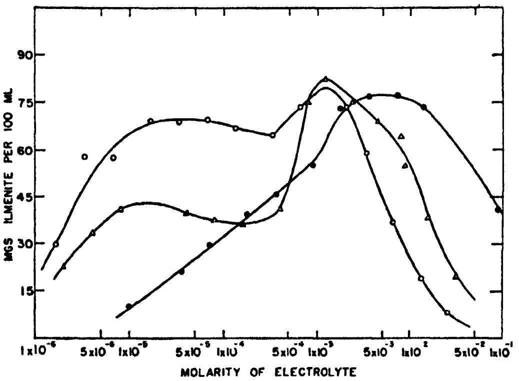

FIG. 6 Amounts of ilmenite suspended by alkaline electrolyte solutions after 3 hr. (semilogarithmic scale).

●	Santomerse No. 3
△	60 weight per cent Santomerse + 40 weight per cent Na_2SO_4
○	60 weight per cent Santomerse + 40 weight per cent Na_2SiO_3

DISCUSSION

Suspending action on insoluble powders dispersed in liquids may occur by one or all of three mechanisms. The first involves the fact that many powders do not readily disperse in a liquid to the ultimate primary particle and that the secondary aggregates or clusters of particles sediment more rapidly than a single isolated primary particle. In such cases preferential sorption of one ion of the suspending agent increases the charge or zeta potential on the particle and, owing to electrostatic repulsion, breaks up or deflocculates the secondary aggregates into primary particles (*cf.* reference 4). The decrease in suspending action at higher concentrations is attributable to discharging the particle or compressing its diffuse double layer (Gouy type) at higher concentrations. Our observation that the amount of light absorbed by a suspension of ilmenite in water is less than that absorbed by the same amount in the presence of a dispersing agent indicates that part of the suspending action on ilmenite is due to this effect.

The second mechanism involves a reduction in the rate of sedimentation of an ultimate primary particle. McBain has pointed out (11) that the electrostatic attraction of a charged particle for the small ions of opposite charge in its ionic atmosphere will slow down its rate of sedimentation. This effect is analogous to the time of relaxation effect in the Debye–Hückel theory of strong electrolytes. The maximum in the suspending power *versus* concentration curve may also be attributed to increase of charge or zeta potential on the particle with increasing concentration, owing to preferential sorption of one ion followed by discharging or compression of the double layer at high concentrations.

A third mechanism is needed to account for suspending action by nonelectrolytes, particularly that of the newer synthetic nonelectrolytic detergents. In such cases occurring in polar liquids such as water it is probable that the neutral heteropolar molecule is sorbed by the insoluble powder with its nonpolar portion towards the solid and the polar portion exposed to the solvent. The coated particle becomes more lyophilic and more heavily hydrated, and the stronger attraction between coated particle and solvent reduces the rate of sedimentation. Hydrogen bonds are frequently formed between water and hydroxyl or amino groups of the nonelectrolyte detergents coating the particles. When a powder is itself highly polar it may interact with the polar portion of the detergent, leaving a lyophobic coating on the particle, and actually increase the rate of sedimentation. This may explain the failure of an alkylated aryl polyether alcohol to suspend manganese dioxide (4).

Suspending powders by making their surface more lyophilic may be accomplished by sorption of neutral molecules or ion-pairs as well as by nonelectrolytes. For both types maximum efficiency would be expected when the surface of the particle is completely covered with a monolayer. A reduction in effectiveness would be expected above this concentration where the molecules would be adsorbed with the polar portion nearest the particle, thus leaving their nonpolar portions next to the solvent and making the particle more lyophobic.

The above mechanisms lead to the prediction that the best suspending agents would be those containing a weakly adsorbed ion with one strongly adsorbed, which will give the insoluble particle a high electrostatic charge or zeta potential and will make the surface of the particle as much like the solvent as possible. The effectiveness of the various sodium silicates in suspending a great many types of pigments or soils over a wide variety of concentrations is due to the fact that the different silicate ions and/or micelles are all sorbed to a much greater extent than sodium ions, particularly on silicious soils, as expected from the general principle of like to like. In addition it is probable that the sorbed silicates contain —OH groups which form hydrogen bonds with the water molecules and thus reduce the rate of sedimentation.

It is interesting and of both theoretical and practical importance that the silicates and phosphates are still fairly good suspending agents at concentrations as low as $10^{-5}M$. That both of these inorganic detergents suspend more ilmenite than does sodium dodecylbenzenesulfonate at concentrations below $10^{-3}M$ is of practical importance in rinsing operations. Similarly, potassium silicates with silica-to-alkali (K_2O) molecular ratios of 3.3 and 3.9 suspend more ilmenite than does a potassium coconut oil soap at concentrations below 0.1 per cent anhydrous material and are still fairly effective at 0.0003 per cent (13).

Apparently only a very small amount of a good suspending agent needs to interact with the powder to be suspended. Our preliminary experiments on sorption of the suspending agent indicated that 1 g. of ilmenite added to 100 ml. of a dilute $Na_2O \cdot 3.3SiO_2$ solution reduced the titratable alkalinity of the supernatant liquid left after centrifuging only from 0.024 per cent to 0.023 per cent sodium oxide and that the reduction in silica concentration was within the experimental uncertainty of 10 per cent. Hazel (6) found that various sodium silicates in concentrations as low as 10 p.p.m. silica were able to convert a stable, positively charged, iron oxide sol into a stable sol with a negative charge due to preferential sorption of silicate ions and/or micelles.

Powney and Noad (15) have studied the "suspending power" for ilmenite of sodium carbonate, sodium hydroxide, sodium chloride, sodium orthophosphate, sodium metasilicate, sodium "hexametaphosphate", $Na_2O \cdot 2SiO_2$, and $Na_2O \cdot 3.98SiO_2$, as well as sodium oleate and stearate, and some synthetic detergents. Actually they measured the ability of these salts to prevent the deposition of the pigment on a cotton fabric under conditions of agitation such that sedimentation under gravity was not the predominating factor. As these authors point out, their experiments deal with collision and adhesion between dirt particles and fibre surfaces rather than rate of sedimentation. However, the same mechanisms reducing sedimentation should also decrease adherence of pigments to fabrics. Their conclusions, that simple alkalies such as sodium carbonate and caustic soda increase deposition whereas sodium silicates and phosphates exert a very considerable protective action due to preferential adsorption of the anion, are, considering the differences in the experiments, at least in qualitative agreement with our results.

SUMMARY

Quantitative measurements of the suspending action on ilmenite black of solutions of sodium hydroxide, sodium carbonate, trisodium phosphate, sodium pyrophosphate, sodium sesquisilicate, sodium metasilicate, $Na_2O \cdot 2.9SiO_2$, and $Na_2O \cdot 3.3SiO_2$ show maximum efficiencies at low concentrations. Sodium dodecylbenzenesulfonate exhibits maximum efficiency at a somewhat higher concentration. Mixtures of organic and inorganic detergents show two regions of maximum efficiency, probably due to each constituent. However, the concentrations at which these occur are much lower than the corresponding concentrations for each one alone.

The mechanisms of suspending action involve separation of secondary aggregates into primary particles, decreasing the rate of sedimentation by electro-

static attraction between a charged particle and its ionic atmosphere, and increasing hydration or lyophilic nature of the particle surface.

REFERENCES

(1) Bakh, N.: Kolloid-Z. **64,** 153 (1933).

(2) Bodlander, E.: Nachricht der Göttingen Gesellschaft der Wissenschaften, **1893,** p. 267.

(3) Fall, P. H.: J. Phys. Chem. **31,** 801 (1927).

(4) Greiner, L., and Vold, R. D.: J. Phys. & Colloid Chem. **53,** 67 (1949).

(5) Harris, J. C.: Oil & Soap **23,** 101 (1946).

(6) Hazel, F.: J. Phys. Chem. **49,** 520 (1945)

(7) Kermack, W. O. and Williamson, W. T. H.: Proc. Roy. Soc. Edinburgh **45,** 59 (1925); **47,** 20E (1927).

(8) Khalapsina, E. V.: Issledovaniya Fiziko-Khim. tekh. Suspensii **1933,** 91; Chem. Abstracts **30,** 7964 (1936).

(9) Kohl, H.: Ber. Deut. Keram. Ges. **3,** 64 (1922).

(10) Liesegang, R. E.: Sprechsaal **56,** 513 (1923); Farben-Ztg. **29,** 333 (1923); Chem. Zentr. **1924, II,** 597.

(11) McBain, J. W.: In *Advances in Colloid Science*, Vol. I, p. 19. Interscience Publishers, Inc., New York (1942).

(12) Merrill, R. C.: Ph.D. Thesis, Stanford University, August, 1942.

(13) Merrill, R. C., and Getty, R.: J. Am. Oil Chemists' Soc. **26,** 5 (1949).

(14) Poliakoff, M. Z.: Anal. Chem. **19,** 140 (1947).

(15) Powney, J., and Noad, R. W.: J. Textile Inst. **30,** T157 (1939).

(16) Spring, W.: Kolloid-Z. **4,** 161 (1909); **6,** 11, 109, 169 (1909).

(17) Serb-Serbina, N. N.: J. Phys. Chem. (U.S.S.R.) **10,** 627 (1937); Chem. Abstracts **32,** 5681 (1938).

(18) Veselovskiĭ, V. S.: Issledovaniya Fiziko-Khim. tekh. Suspensii **1933,** 83; Chem. Abstracts **30,** 7964 (1936).

ORIENTATION OF A POLYFUNCTIONAL ORGANIC MOLECULE AT A STEEL SURFACE[1,2]

NORMAN HACKERMAN AND E. E. GLENN, JR.

Department of Chemistry, University of Texas, Austin, Texas

Received June 27, 1949

INTRODUCTION

The work reported here was an outgrowth of a study of corrosion inhibition by polar organic molecules. Most theories of inhibition by such substances postulate adsorption of the inhibitor molecule at the metal surface as the initial action. However, in most instances neither the rate of orientation and adsorption nor the

---

[1] Presented at the Fourth Annual Southwest Regional Meeting of the American Chemical Society, which was held at Shreveport, Louisiana, December 9–11, 1948.

[2] Based in part on a thesis submitted by E. E. Glenn, Jr., to the Graduate School of the University of Texas in partial fulfillment of the requirements for the M.A. degree, May, 1948.

nature of the sorptive forces have been given serious consideration. Some discussion of the relationship of the type of force to inhibitor effectiveness may be found in the literature (e.g., 10). In several papers (1, 2, 7, 9) the data given showed that both the adsorption rate and the firmness of attachment were involved in the overall effect. These papers, and others, have already been considered in detail elsewhere (4).

The firmness of adherence to steel of several commercial corrosion inhibitors, as well as their force–area behavior as monolayers on water, was investigated in another study (6). One of these substances showed several interesting characteristics: namely, essentially irreversible adsorption as shown by the inability of the solvent to remove all of the adsorbed material; a break in the vertical portion of the force–area curve; and efficient practical inhibition of corrosion (8). Further study of the adsorption characteristics of this material, denoted as K-115,[3] was desirable.

INSTRUMENTS

The method used here was an extension of the electron-diffraction surface-reflection technique employed earlier (5). This provided the most rapid, albeit qualitative, means of detecting adsorbed layers on the steel surfaces.

An RCA type EMU-1 electron microscope with an electron-diffraction attachment, hereafter referred to as the diffraction stage, was used. The electron beam was accelerated by a fixed potential of 50,000 v., which gave the beam a wave length of 0.05 Å. The diffraction stage, sample holders, and sample supports were as shown in a previous paper (5).

Although most of the experiments were carried out with SAE 1020 steel, in the form of 2 x 6 x 6 mm. blocks, some work was done using evaporated iron films. An RCA metal evaporater was employed for this purpose. The steel blocks were placed about 8 cm. away from a tungsten filament around which was wrapped a piece of pure iron wire. The entire assembly was enclosed in a bell jar, and the system evacuated to 10^{-4} mm. of mercury. The system was cleaned by ionization bombardment and the filament was then heated, evaporating the iron and depositing it on the metal blocks. The thickness of the film could be controlled by varying the distance of the metal blocks from the filament. It was not specifically determined whether the evaporated iron film was smoother than the polished metal itself, but the film surface was more mirror-like.

MATERIALS AND PROCEDURE

The inhibitor consisted principally of an alkylpyrrolidinedione with the length of the alkyl group unspecified, although the substance was known to have a molecular weight of about 350. The solvent used throughout was composed of a mixture of saturated hydrocarbons (*n*-hexane, 2-methylpentane, and 3-methylpentane).[4] The solvent was freed of polar impurities by percolating over activated silica gel three times. It was then stored in a dark container over dry silica gel. Solutions were made up in five weight concentrations: 0.0001, 0.001, 0.01, 0.1, and 1.0 per cent.

---

[3] Kindly supplied by the Tret-o-lite Company, St. Louis, Missouri.

[4] Skellysolve B, purchased from the Skelly Oil Company, Kansas City, Missouri.

The metal blocks were cut to size on a metal shaper, smoothed somewhat on a fine-grit belt sander, then buffed with No. 00 and finally with No. 0000 emery paper to a mirror-like surface. The blocks were then washed with the solvent, which was allowed to evaporate. A reproduction of the diffraction pattern of the metal surface so prepared is shown in figure 1.

The experiments involved placing a drop of the solution on the polished surface and immediately removing the excess by touching it with a piece of absorbent paper. Desorption was carried out simply by dipping the treated sample into pure solvent ten times.

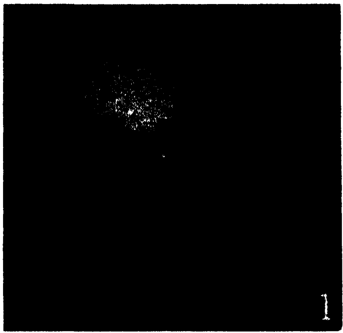

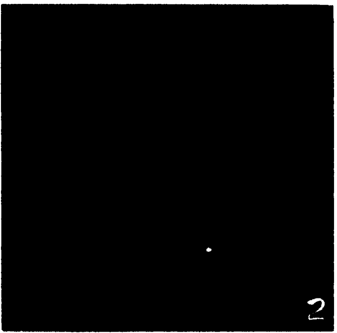

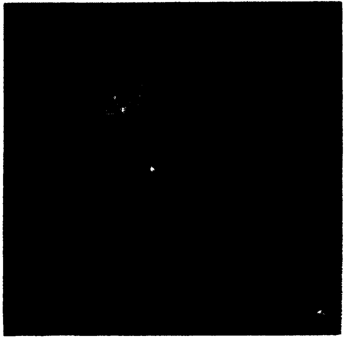

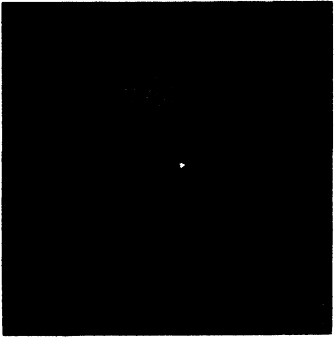

FIG. 1. Reflection pattern due to clean iron surface

FIG. 2. Reflection pattern due to 1 0, 0.1, and 0.01 per cent K-115 solutions

FIG. 3 Reflection pattern due to 0.001 and 0.0001 per cent K-115 solutions

FIG. 4. Reflection pattern due to 0 001 and 0 0001 per cent K-115 solutions after washing with solvent.

EXPERIMENTAL RESULTS

Patterns due to adsorption on the polished surface from the 1.0, 0.1, and 0.01 per cent solutions were the same (figure 2) except that the intensity of the arcs decreased with decreasing concentration. The pattern exhibited by the surfaces exposed to the 0.001 and 0.0001 per cent solutions showed only three faint, but definite, spots (figure 3). An important difference between the same concentration groups also appeared on desorption treatment. The surfaces exposed to the three most concentrated solutions appeared to be totally desorbed, since the pattern due to the original metal surface (figure 1) recurred following solvent treatment. On the other hand, although the spot pattern of the metal pieces exposed to the 0.001 and 0.0001 per cent solutions disappeared on desorption, the pattern shown in figure 4 appeared instead. It can be seen that this is not characteristic of the polished metal block. It is believed that all of the adsorbed material was not removed, but that which remained was not oriented since there was no indication of order. This led to the conclusion that the material adsorbed from more dilute solution was the more firmly adsorbed. Obviously, the systems with the more concentrated solutions had not attained equilibrium; since this effect was relatively long-lived, of the order of several hours, the possible importance in corrosion inhibition called for further study.

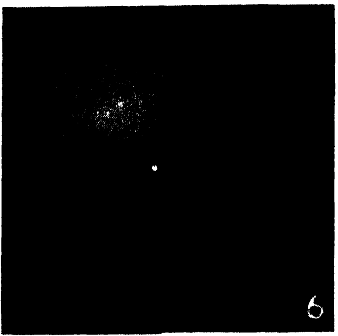

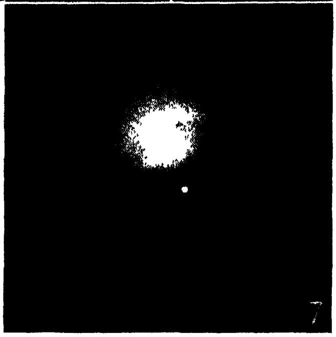

FIG. 5. Reflection pattern due to evaporated iron film

FIG 6 Reflection pattern of 0.001 and 0.0001 per cent K-115 solutions on evaporated iron film.

FIG. 7. Reflection pattern of solvent-treated sample after multiple adsorption by 0.0001 per cent followed by 1.0 per cent K-115 solutions.

Evaporated iron films

In order to obtain more decisive evidence of this effect, the experiments were repeated using evaporated iron films. The reflection pattern of the thin film of iron was much sharper and more easily recognizable than that normally obtained from the blank steel surface (figure 5). Therefore, if the inhibitor was adsorbed and did not exhibit a pattern of its own, obliteration of the strong blank pattern lines of the metal film should provide firmer evidence of adsorption than the disappearance of the relatively weaker lines of the polished blank. Further, absence of the strong pattern of the untreated block, after desorption treatment, should indicate more conclusively the firmness of adsorption.

On adsorption from the three most concentrated solutions the pattern characteristic of adsorption from this group (figure 2) was obtained. The solute molecules were essentially all desorbed by the solvent treatment, since the patterns obtained were identical with that of the evaporated iron blank.

Figure 6 is a reproduction of the pattern from the iron film after adsorption from the 0.001 and 0.0001 per cent solutions. The sharp rings due to the evaporated iron are almost completely obscured, indicating either adsorption or deposition of the solute molecules onto the surface. Upon desorption the sharp evaporated iron pattern did not reappear, indicating relatively firm adsorption. This is in accord with the observations made earlier.

Successive exposures in solutions of increasing concentration

It was reasonably certain that equilibrium had not been reached in these experiments, and the procedure described below was used to allow for easier attainment of equilibrium.

Two polished blocks were immersed in 10 ml. of the 0.0001 per cent solution, precautions being taken to prevent evaporation of the solvent. After 10 min. both were withdrawn and the adhering drops removed. A pattern was obtained of one of these blocks (A) after desorption. This block was then subjected to the desorption treatment, and then again studied in the electron microscope. The other block (B) was placed in 10 ml. of the 1.0 per cent solution for 10 min. and then subjected to the desorption treatment.

After exposure in the 0.0001 per cent solution, sample A exhibited the pattern shown in figure 3; after desorption it showed the pattern of figure 4. After the additional 10-min. exposure in the 1.0 per cent solution, block B exhibited the pattern of figure 2. Upon desorption the pattern shown in figure 7 was obtained. Thus, block A, even on longer exposure, was found to yield the same diffraction pattern as obtained in the previous experiments with 0.0001 per cent solution. Block B, after exposure to the more concentrated solution, yielded the pattern characteristic of adsorption from this solution alone. On desorption most of the arc pattern was lost. That which remained, however, was not evident on the patterns found after exposure to the 0.0001 per cent solution.

This experiment also showed that the adsorption from the more dilute solution was firmer, but that some of this difference was due to a lower orientation rate at the interface of the material adsorbed from the more concentrated solutions.

Evidence of the path of the electron beam

It was observed in the experiment described above that, upon extended exposure of the specimen to the electron beam, the arc pattern characteristic of adsorption from the more concentrated solutions gradually faded from view on the fluorescent screen. After the pattern faded the beam was interrupted for 3 min., but the pattern did not reappear. Brummage (3) found that diffraction patterns of normal paraffins and fatty acids on steel faded on extended exposure to the electron beam. However, after a 3-min. interruption of the electron beam the pattern reappeared, indicating disorientation of the molecules. It is likely that in the present work the fading was due either to volatilization or to fusion of the adsorbed molecules.

The time required for complete fading was found to depend on the concentration of the solution to which the specimen was exposed. The fading time increased from about 10 sec. for the blocks exposed to the 1.0 per cent solutions to somewhat over 2 min. for those exposed to the 0.0001 per cent solutions.

When the block was removed from the instrument after this observation, the surface with the adsorbed layer appeared unchanged from its condition before exposure to the beam. Upon desorption however, lines visible to the eye appeared on the metal surfaces exposed to the 1.0, 0.1, and 0.01 per cent solutions. The number of such lines corresponded to the number of times the pattern was allowed to fade using different positions of the specimen in the electron beam, and all the lines crossed at approximately the center of the block. It is apparent that each of these lines corresponds to the path of the beam across the block during one of the fade-out periods of the arc pattern. The lines were more intense for the surfaces exposed to the 1.0 per cent solution and decreased in intensity for the lower exposure concentrations down to 0.01 per cent. Only very faint lines appeared on the surface after desorption of the blocks treated with 0.001 per cent or 0.0001 per cent solutions.

DISCUSSION

It was found in these studies that the inhibitor was adsorbed onto the metal surface from each of the solution concentrations used. The solute molecules adsorbed from the 1.0, 0.1, and 0.01 per cent solutions gave rise to electron-diffraction patterns of diffuse arcs, which decreased in intensity with decreasing concentration. Since they were arcs and not straight lines, the molecules must have been oriented rather randomly about the surface normal. From the length of the arcs it was estimated that there was an average tilt of 20° from the surface normal. The diffuseness of the bands indicated that the molecules were not arranged in a well-defined crystal perpendicular to the metal surface. The fact that the faint spots of the patterns due to the two most dilute solutions lie on a straight line suggests that the adsorbed molecules were essentially parallel to each other and normal to the metal surface. Furthermore, the presence of spots, instead of diffuse bands, implies that the molecules were arranged in a relatively well-defined, two-dimensional cell structure.

From successive exposures in different concentrations it was found that some additional molecules were adsorbed firmly from the 1.0 per cent solution. Probably because of the relatively well-oriented structure of the molecules adsorbed from the dilute solution, the molecules subsequently adsorbed from the 1.0 per cent solution were arranged in a more orderly fashion on top of or in between the molecules already present on the steel surface.

The alkylpyrrolidinedione molecule has three possible points for attachment to the metal surface, the three adjacent polar groups. For all to be effective in adsorption the cyclic portion of the molecule must lie flat on the metal surface. If the cyclic portion of the molecule stands on edge on the metal surface, only one, or at the most, two of the polar groups may be effective in attaching the molecule to the metal. Calculations showed that the 0.0001 per cent solution had just about enough molecules present to cover the surface if the cyclic portion lay flat. However, there were enough molecules in the 0.01 per cent solution to cover the surface completely with a close-packed monolayer with the cyclic portion more or less vertical. The more firm adsorption to the metal surface from the most dilute solutions may be explained, in part at least, on the basis of the difference in orientation.

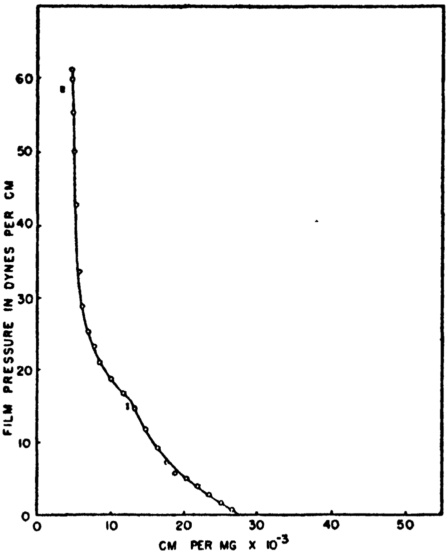

Fig. 8. Force–area curve for K-115

Figure 8 is a force–area diagram drawn from the data of Hackerman and Schmidt (6) for K-115 on a clean water surface. At low pressures, the cyclic ring may have been flat on the water surface with the alkyl chain more or less vertical to it. As the area available to the monolayer decreased to the point of the break in the curve, the ring would be forced to rise and stand on one edge. This would account for the decrease in the rise in pressure for the decreasing area at that point. Further reduction in area would pack the molecules more closely, with the ring in a vertical plane.

At point I on the curve in figure 8 the area of the film may be seen to be 1.3 × 10^3 cm.^{2}/mg., i.e., at the actual surface pressure at this point. The value at point II, on the highly compressed portion of the curve, is 0.51 × 10^3 cm.^{2}/mg.

These areas, which are proportional to the area per molecule under these pressures, yield a ratio of 2.6.

The intercept on the abscissa of the extrapolated slope from point I is 20 × 10^3 cm.^{2}/mg. and from point II, 7 × 10^3 cm.^{2}/mg. The ratio of these values is 2.8.

A calculation of the cross-sectional area of the inhibitor molecule as seen from above the block and lying flat on the surface or standing on edge yielded values of 75 Å.^{2} or 28 Å.,^{2} respectively. The ratio of these two numbers is 2.7.

The fact that these three ratios are essentially the same lends credence to the proposal that the cyclic portion of the inhibitor molecule assumes different positions on the metal surface as a function of the concentration.

It was noted earlier that the arc pattern due to the adsorbed molecules faded on extended exposure to the electron beam. Experiment showed that this was not just a disorientation effect but instead was a permanent change. The fact that the time required for complete fading was found to increase with decreasing concentration might be explained by the observation made earlier of more firm adsorption from the solutions of lowest concentration. Thus, it may be postulated that the molecules adsorbed from the more concentrated solutions were melted more quickly by the heat of the electron beam, since their attachment to the metal was less firm, and they were unable to transmit this heat to the metal block. On the other hand, molecules adsorbed from dilute solutions were more firmly adsorbed and were able to transmit some of the energy of the beam to the metal block, and therefore melted more slowly.

It was pointed out earlier that lines appeared on the metal surface after desorption, especially on blocks exposed to the more concentrated solutions. Since the lines did not appear until after the desorption treatment, it would appear that perhaps the melted area where the electron beam passed was bridged over by adjacent molecules. Upon desorption, when these molecules were removed, the bridge was lost and the path became visible.

SUMMARY

An investigation of the adsorption–desorption characteristics of a commercial corrosion inhibitor was carried out. It was found that adsorption of this inhibitor onto a steel surface was more firm from the more dilute solutions within the concentration range studied. Gradual fading of the arc pattern due to the inhibitor molecules on the steel surface was noted. Lines caused by the path of the electron beam across the inhibitor surfaced metal were observed.

A possible mechanism for the more firm adsorption from more dilute solutions and an explanation for the fading of the diffraction pattern and the lines on the metal block were presented.

The authors are pleased to acknowledge the financial support of the Corrosion Research Project Committee of the Natural Gasoline Association of America. They are also grateful to Mr. L. L. Antes, of the Department of Electrical Engineering at the University of Texas, for his valuable assistance in the use of the electron microscope.

REFERENCES

(1) **Ardagh, G. E., Roome, R. M. B., and Owens, H. H.**: Ind. Eng. Chem. **25,** 1116 (1933).
(2) **Armbruster, M. H., and Austin, J. B.**: J. Am. Chem. Soc. **61,** 1117 (1939).
(3) **Brummage, K. G.**: Proc. Roy. Soc. (London) **A191,** 243 (1947).
(4) **Hackerman, N.**: Corrosion **4,** 45 (1948).
(5) **Hackerman, N., and Schmidt, H. R.**: J. Phys. & Colloid Chem. **53,** 629 (1949).
(6) **Hackerman, N., and Schmidt, H. R.**: Corrosion **5,** 237 (1949).
(7) **Jimeno, E., Grifoll, I., and Morral, F. R.**: Trans. Electrochem. Soc. **69,** 105 (1936).
(8) **Justice, W. H., and Jones, E. N.**: NGAA Corrosion Committee Minutes **3,** 114 (1947).
(9) **Rhodes, F. H., and Kuhn, W. E.**: Ind. Eng. Chem. **21,** 1066 (1929).
(10) **Uhlig, H. H.**: Chem. Eng. News **24,** 3154 (1946).

AN ELECTRON-MICROSCOPIC STUDY OF METAL OXIDES AND METAL OXIDE CATALYSTS

JAMES T. McCARTNEY,[1] BERNARD SELIGMAN,[2] W. KEITH HALL,[2] AND ROBERT B. ANDERSON[2]

Research and Development Branch, Office of Synthetic Liquid Fuels, Bureau of Mines, Bruceton, Pennsylvania

Received July 5, 1949

This paper presents an electron-microscopic study of changes in the physical structure of precipitated cobalt and iron oxide catalysts during reduction. To obtain further information about changes occurring during reduction a number of metal oxides were also studied. A secondary purpose of this research was to determine the usefulness of the electron microscope in studies of granular catalysts.

For convenience, changes that occur during reduction may be divided into three classes: First, sintering of the unreduced material may occur at the reduction temperature, the "glowing" of oxide gels (20) being an extreme example of this phenomenon. Second, the transition from oxide to metal is usually accompanied by a decrease in volume, e.g., the volume of a mole of cobaltous oxide decreases from 13.2 ml. to 5.6 ml. on reduction to the metal. If considerable reorientation of the freshly reduced metal does not occur simultaneously with the reduction, the change in volume should make the metal-to-oxide interface accessible to the reducing gas. Third, the reduced metal reorients into a stable form.

Hüttig (8) has made extensive studies of the changes in properties of metal powders during heat treatment, a process somewhat similar to the third step postulated for reductions. He was able to correlate the observed changes in properties with α, the ratio of the absolute sintering temperature to the absolute melting point of the metal.

---

[1] Physicist, Coal Constitution and Miscellaneous Analysis Section, Bureau of Mines, Pittsburgh, Pennsylvania.

[2] Physical Chemist, Research and Development Branch, Office of Synthetic Liquid Fuels, Bureau of Mines, Bruceton, Pennsylvania.

Most reduction processes are postulated to occur at the interface between metal and metal oxide. Reductions probably occur at nuclei of reduced metal; if the rate of nuclei formation is slow (and if metal and oxide do not form a solid solution), the reduction process is autocatalytic, its rate increasing with time at the beginning of the reduction (10). The presence of a small fraction of an oxide A that is more easily reduced than oxide B will usually increase the rate of reduction of oxide B, possibly by the formation of a large number of nuclei of metal A early in the reduction. On the other hand, small fractions of an oxide C that is less easily reduced than oxide B will ordinarily decrease the rate of reduction of oxide B. The presence of oxide C will usually decrease the rate of sintering of oxide B during reductions. There are some exceptions to this, e.g., a fused magnetite catalyst with or without alumina sinters more in reduction if it contains potassium oxide (11). These phenomena are commonly utilized in catalysis. For example, with cobalt catalysts the presence of the promoters thoria and magnesia prevents excessive sintering during reduction (2), while the presence of copper oxide increases the rate of reduction (14).

Some catalysts contain carriers which are usually bulky, relatively inert materials such as kieselguhr, asbestos, infusorial earth, etc., on which the metal oxides or carbonates are precipitated to dilute the active material and to form and maintain a suitable pore structure. In some cases carriers are incorporated by merely mixing the moist precipitate with the carrier. Carriers are usually assumed to be inert, but at least with nickel–kieselguhr catalysts there is evidence of interaction between nickel oxide and kieselguhr (18, 19).

EXPERIMENTAL

A. Preparation of oxide and catalysts

Hydrous oxides were prepared by adding about the equivalent amount of sodium hydroxide solution to solutions of silver, cupric, nickelous, or ferric nitrates. Analyzed chemicals of high purity and distilled water were used in all preparations. The solutions of the metal nitrates were heated to boiling temperatures, and the sodium hydroxide solution was added with vigorous stirring. The precipitates were filtered, washed with hot water on a Büchner funnel about ten times, and dried at 100°C.

The cobaltous oxide was prepared from the nitrate by precipitation with aqueous ammonia solution as previously described (7). The preparation of the cobalt–thoria–magnesia–kieselguhr catalysts and similar preparations with one or more of the components omitted by precipitation with sodium carbonate has also been described (4). The iron–copper–potassium carbonate (100:10:0.5) catalyst was prepared by precipitation from a solution of ferric and cupric nitrates with sodium carbonate solution at about the boiling temperature. The precipitate was thoroughly washed, and while still moist was alkalinized by adding a solution of potassium carbonate and evaporating to dryness on a steam bath.

B. Reduction of oxides and catalysts

The samples were dried at 100°C. before use. They were then placed in a special adsorption tube with a four-way stopcock (1) and evaculated for 1 hr. at 100°C. The samples were reduced in an automatically controlled resistance furnace, and the weight loss on reduction and the surface area after reduction were determined. The reduced sample was transferred in a stream of carbon dioxide to a tube filled with benzene, and portions of this material wet with benzene were used in the electron-microscopic studies. Most of the hydrous oxides were in the form of powders, and these were reduced for long periods of time in slow flows of hydrogen (space velocity[3] of hydrogen of 100 or 200). The granular or pelleted cobalt catalysts were reduced under conditions normally used for reducing cobalt Fischer–Tropsch catalysts—space velocity of hydrogen of 3000 for 2 hr. at 400°C. The iron catalyst was treated with a mixture of 1 volume of hydrogen and 2 volumes of carbon monoxide at a space velocity of 100 for 24 hr. at 230°C., the usual method of induction of this tye of iron catalyst in our laboratory (16, 17).

Nitrogen adsorption isotherms were determined on the original and reduced samples by the usual volumetric methods (6), and the surface areas were estimated by the simple B.E.T. equation (5) with the cross-sectional area of the nitrogen molecule taken as 16.2 Å.^{2} The adsorption and microscopic studies of reduced catalysts were made on the same sample, but the studies of the reduced oxides were made with different portions of the oxide reduced under the same conditions.

C. Preparation of specimens for electron microscopy

Granular catalysts are not very suitable for study in the electron microscope. In the present work, the granules have been gently crushed in an effort to cause separation into ultimate particles or crystallites without altering the structure of these particles too seriously. With some amorphous, high-surface-area materials, such as gels, this does not appear possible, since the particles obtained by gentle crushing still contain considerable internal pore structure, but with other materials which do not have this structure, the method appears satisfactory.

The crushed samples were prepared for electron-microscopic examination by two methods: In the first of these, a supporting film was obtained by dipping a clean microscope slide in a 0.5 per cent solution of Parlodion in amyl acetate and allowing the solvent to evaporate. A little of the powdered sample was dusted onto the film and dispersed by exposure to a spark discharge from a high-voltage, high-frequency Tesla coil. The film was then cut into ¼-in. squares and floated off onto a water surface. A square of film was picked up, supported on a disk of 200-mesh screen, and placed in the specimen holder of the microscope. In the second method (15) the powder was mixed with two drops of a 2 per cent Parlodion solution and thoroughly dispersed on a microscope slide with a glass rod, amyl acetate being added during the dispersing process. A little of the suspension adhering to the rod was drawn out over a clean slide; after evaporation of the solvent, the film was cut and floated off as before. The latter method usually produced better dispersions.

---

[3] Volumes of hydrogen (S.T.P.) per volume of sample per hour.

EXPERIMENTAL RESULTS

Table 1 presents data for weight and surface area changes in the reduction of the various metal oxides and catalysts, together with the conditions of reduction. The surface areas in this table are given per gram of unreduced sample. For

TABLE 1

Changes in surface area upon reduction

MICROGRAPH NO.	PREPARATION	REDUCTION					SURFACE AREA(c)			
		T	α(a)	Hours	Space velocity(b)	Weight loss	Unreduced		Reduced	
							Total per gram	Complex per gram of complex(d)	Total per gram	Complex per gram of complex(d)
		°C.				*per cent*	*sq. m.*	*sq. m.*	*sq. m.*	*sq. m.*
1, 2	Ferric oxide gel	405	0.375	24	200	27.1	178.5		1.8(e)	
4, 5	Hydrous nickel oxide	250	0.303	48	200	39.6	153.0		3.6	
6, 7	Copper oxide powder	200	0.349	18	200	20.8	65.4		5.5	
8, 9	Silver oxide powder	150	0.343	46	200	7.5	1.5		0.3	
10, 11	Cobaltous oxide powder	250	0.298	24	100	30.2	67.0		3.2	
12, 13, 14	Cobalt basic carbonate	254	0.300	48	100	44.0	126.2	126.2	Not determined	
		400	0.384	2	6,000	44.2	126.2	126.2	2.5	2.5
15	Cobalt–thoria–magnesia (100:6:12) catalyst	400	0.384	2	6,000	37.7	154.8	154.8	52.8	52.8
16	Cobalt–kieselguhr (100:200) catalyst	400	0.384	2	6,000	21.1	75.6	124.7	18.3	14.2
17	Cobalt–thoria–magnesia kieselguhr (100:6:12:200) catalyst	400	0 384	2	6,000	16.7	102.9	177.5	80.2	133.2
18, 19	Ferric oxide catalyst ($Fe:Cu:K_2CO_3$ = 100:10:0.5)	230	0.278	24	100(f)	10.3	303.0		22.9	

(a) The quantity α is the quotient of the absolute temperature of reduction divided by the absolute melting point of the metal.

(b) Volumes of dry hydrogen (S.T.P.) per volume of sample per hour.

(c) Surface areas from nitrogen adsorption isotherms. All areas are based on weight of unreduced sample or complex.

(d) Complex denotes everything in cobalt catalysts except kieselguhr, and the areas of kieselguhr and complex are assumed to be additive in computing the area of the cobalt-promoter complex.

(e) The adsorption measurement was made on a sample of the same ferric oxide which was reduced for 60 hr. at 415°C.

(f) Catalyst reduced with a mixture of 1 volume of hydrogen and 2 volumes of carbon monoxide.

cobalt catalysts containing kieselguhr the surface areas are also given for the cobalt–promoter complex (that is, everything in the catalyst except the kieselguhr, assuming the areas of kieselguhr and the complex to be additive), these areas being expressed as square meters per gram of unreduced complex. The values of α as defined by Hüttig (8) corresponding to the reduction temperature are also included in table 1. Figures 1 to 19 are electron micrographs of various unreduced and reduced oxides and catalysts. Table 2 compares average particle-size measurements from electron micrographs and surface areas computed from these with average particle diameters estimated from adsorption measurements and adsorption surface areas. The average particle diameters, $\bar{d}$, from micrographs were calculated from measurements of unidirectional diameters bisecting the projected areas of the particles, averaged with the formula of Perrott and Kinney (13), $\bar{d} = \Sigma nd^3/\Sigma nd^2$. Surface areas from particle-size measurements and average particle diameters from adsorption surface areas were computed with the equation for smooth spheres (or cubes), $S = 6/\rho\bar{d}$, where S is the surface area, ρ the real density, and $\bar{d}$ the average diameter as defined above. For comparison with data from the electron micrographs the adsorption areas were corrected to square meters per gram of reduced sample.

The hydrous oxides of iron and nickel (figures 1 and 4) were composed of relatively large particles which are not consistent with their high surface area. However, the micrographs of the nickel oxide showed some fine particles, and the outlines of the particles of iron and nickel oxides appeared irregular and feathery. This probably indicates that the observed particles are aggregates of smaller ones. The particles of cobalt basic carbonate (figure 12) appeared somewhat similar to those of the iron and nickel oxides, but there was a large fraction of fine particles. The average particle diameter computed from these smaller particles agreed fairly well with that estimated from the adsorption surface area.

It is evident that to account for the high surface areas of these samples a fine structure similar to that of the cobalt basic carbonate must be postulated for each of these materials. Figure 3 illustrates how this structure may originate. This is a micrograph of a ferric oxide sol prepared in a more dilute solution than the gel in figure 1, the microscope specimen being prepared directly from the water suspension. Water was apparently held by the ferric oxide sol particles even in the vacuum of the electron microscope, but the water appears to be liberated by the heat of the electron beam, which resulted in coarsening and consolidation of the fibrous structure. Figure 3 shows an area in which the finest fibers were still preserved after slow water loss in a weak electron beam.

Although the cobaltous oxide was a very fine powder, its surface area as estimated from electron micrographs (figure 10) was only about 6 per cent of the adsorption area. The copper oxide powder (figure 6) was composed of very small, elongated, platelike crystals, and the surface area from the micrographs was about 40 per cent of the nitrogen area. The areas of the silver oxide powder estimated from the micrographs (figure 8) and adsorption measurements were about equal. Thus the oxides of copper and silver appear to have very little internal structure or porosity.

Upon reduction the surface areas of these samples decreased from 5- to 50-fold, and the areas of the reduced samples as estimated from the micrographs and from adsorption measurements were very much more nearly equal than for the unreduced samples, indicating relatively less internal area or porosity after reduction. The particles of hydrous iron oxide of 0.51 micron average diameter were converted to compact rounded particles of 0.17 micron average diameter, as shown in figure 1 and 2. The average diameter of the nickel oxide (figures 4 and 5) decreased in a similar manner on reduction. In the reduction of cobalt basic carbonate at both 250° and 400°C. the finer particles increased in size, forming large and compact ovoids (figures 12, 13, and 14). The particles of the sample reduced at 400°C. were considerably larger than those reduced at 250°C. In the reduction of cobaltous oxide (figures 10 and 11) the fine particles increased in size and formed hexagons of varying degrees of completeness, as described previously (12). It is not possible to decide whether these represent single

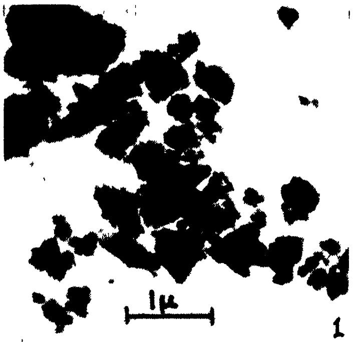

1

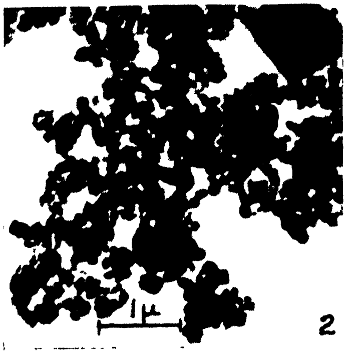

2

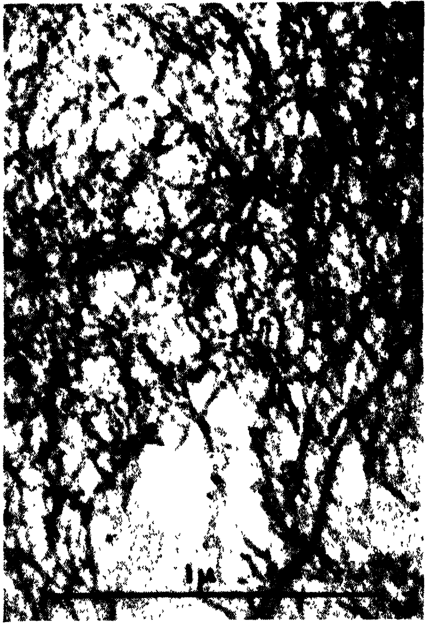

Fig. 1. Ferric oxide gel
Fig. 2. Reduced ferric oxide gel
Fig. 3. Ferric oxide sol

crystal platelets which are partly fractured by the electron beam or the method of dispersion, or merely small particles aggregated into hexagons. The formation of hexagons is not a chance phenomenon, since they have been observed in all of the several reductions of the cobaltous oxide at 250°C., nor is it related to the electron-microscopic method of examination, since the hexagons may be observed with the optical microscope. The cobalt basic carbonate reduced at 250°C. (figure 13) did not form hexagons, and the particles were considerably smaller than particles within the hexagon. It was thought that the different behavior of the cobaltous oxide and cobalt basic carbonate during reduction

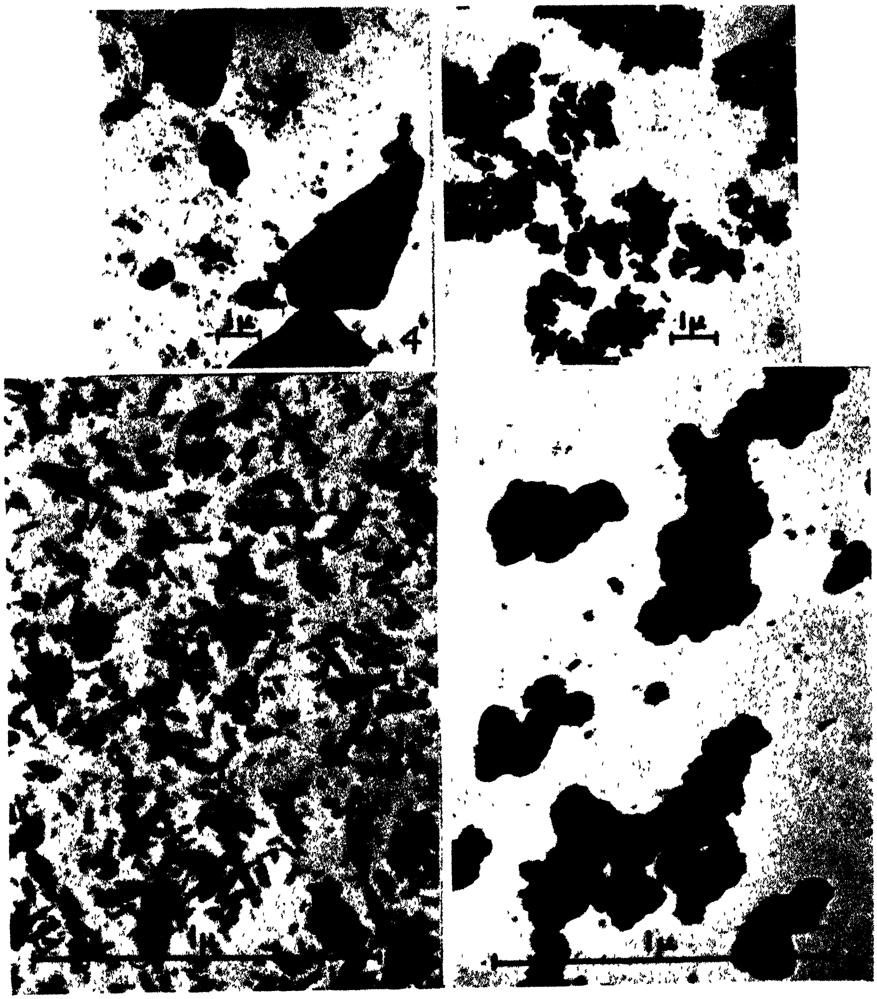

Fig. 4. Hydrous nickel oxide
Fig. 5. Reduced nickel oxide
Fig. 6 Copper oxide powder
Fig. 7. Reduced copper oxide

might be related to traces of sodium carbonate present in the basic carbonate, preventing extensive sintering and aggregation. A sample of cobaltous oxide was impregnated with sodium carbonate solution and reduced at 250°C. This

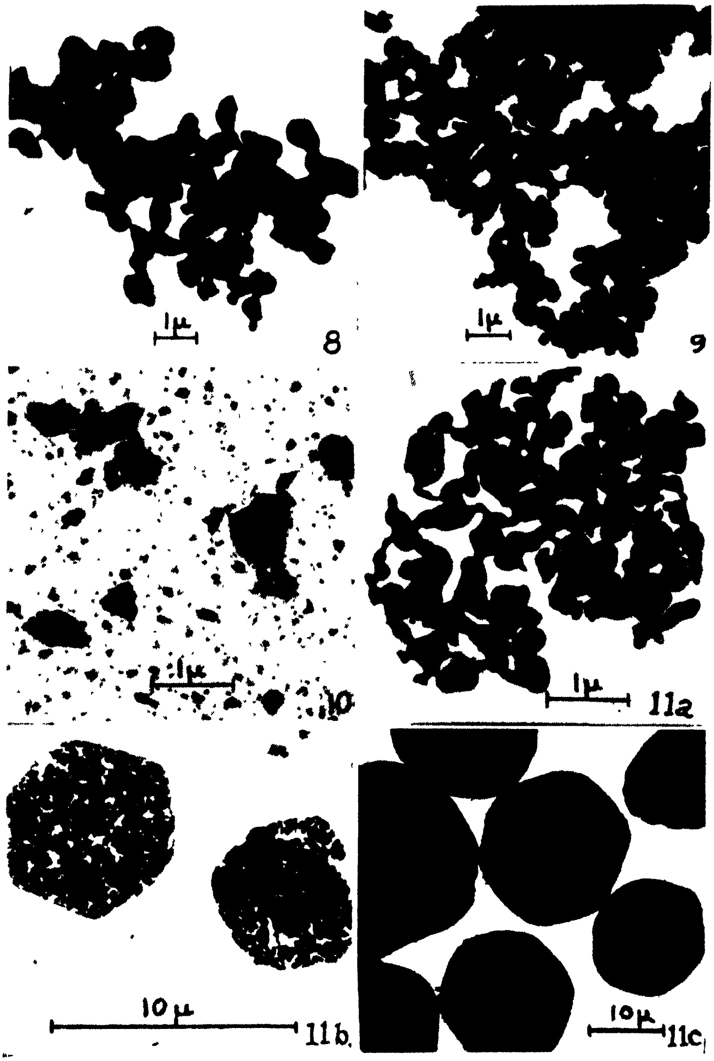

FIG. 8. Silver oxide powder
FIG. 9. Reduced silver oxide
FIG. 10. Cobaltous oxide
FIGS. 11a, b, c. Reduced cobaltous oxide in various stages of dispersion

sample also formed hexagons, and it must be concluded that sodium carbonate added in this manner did not inhibit hexagon formation.

The reduced copper oxide (figure 7) had a larger particle size than the original material (figure 6), and the reduced sample showed no geometrical forms as

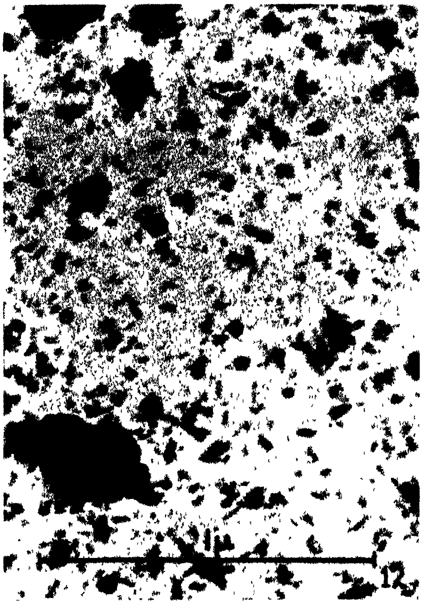

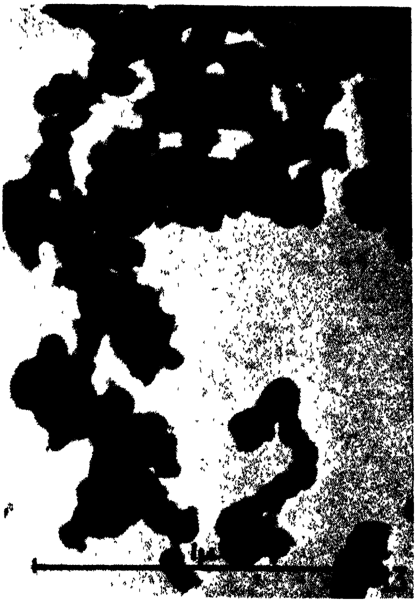

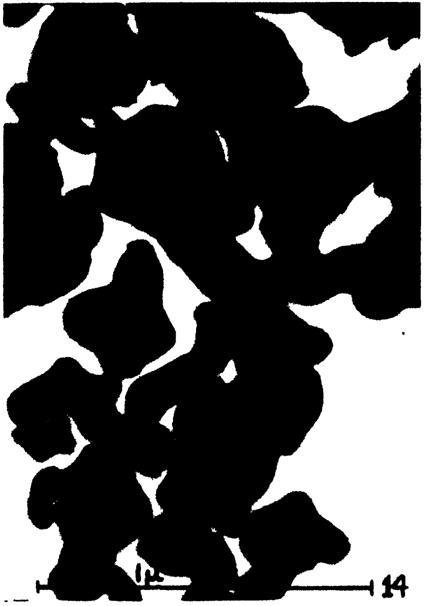

FIG. 12. Cobalt basic carbonate

FIG. 13. Reduced cobalt basic carbonate (reduced at 250°C.)

FIG. 14. Reduced cobalt basic carbonate (reduced at 400°C.)

FIG. 15. Reduced cobalt basic carbonate plus thoria and magnesia

observed in the original material. The silver oxide did not change very much in the reduction (figures 8 and 9).

Figures 14, 15, 16, and 17 show that the presence of promoters and kieselguhr decreased the sintering of cobalt basic carbonate during reduction. In table 2 the surface areas for these samples are computed for the cobalt–promoter complex per gram of complex, and the average particle diameters were determined from the fine particles, excluding the larger particles which appear to be aggregates and kieselguhr. The particles of cobalt–promoter complex were considerably smaller than those of the kieselguhr, a result which is in agreement with the nitrogen surface areas. The particles of the reduced samples containing kieselguhr and/or thoria and magnesia appear to be compact and rounded and show no tendency for the particles to grow together as observed for the reduced basic carbonate (figure 14). The kieselguhr was effective in preventing sintering, magnesia and thoria were more effective, and the combination of both promoters and carrier was the most effective as shown by both the micrographs and the adsorption surface areas. The adsorption areas of the samples containing promoters were greater than those estimated from average particle diameters, indicating the presence of some internal surface area.

The unreduced iron oxide catalyst ($Fe:Cu:K_2CO_3 = 100:10:0.5$) appears to have a gel structure similar to that of the ferric oxide gel (figures 18 and 1). In the usual induction procedure for precipitated iron Fischer-Tropsch catalysts, using a mixture of 1 volume of hydrogen and 1 volume of carbon monoxide at 230°C., the catalyst was reduced to a mixture of magnetite and iron carbide (Fe_2C) (figure 19). The adsorption area decreased from 303 to 25 m.^{2}/g. The extent of sintering was less than with a ferric oxide gel which was reduced with hydrogen, but this is probably related to the lower temperature rather than to any structural promoter action of the copper or potassium carbonate.

DISCUSSION

Some precipitated metal oxides have gel structures with fairly high mechanical strength and high surface areas. Some gels have been postulated to be "felts" of tiny filaments (9). The electron micrograph of the ferric oxide sol (figure 3) supports this postulate. The average diameter of the fibers appears to be 50–70 Å. The surface area of a long, smooth, cylindrical fiber of this diameter, computed from the equation $A = 4/d\rho$, where A is the surface area per gram, d the average diameter, and ρ the density (taken as 3.6), varies from 160 to 220 m.^{2}/g. This agrees satisfactorily with the surface area of most ferric oxide gels. However, it should be noted that coagulation and removal of water may cause either a decrease or an increase in the surface area.

The cobalt basic carbonate forms a coherent filter cake of lower mechanical strength than the iron gel and on gentle crushing breaks into particles of about the same diameter as those estimated from adsorption areas. The presence of promoters or kieselguhr decreased the amount of sintering of the cobalt basic carbonate during reduction. The promoters probably are intimately mixed with the basic carbonate, and during the reduction a matrix of relatively unchanged promoter remains. The basic carbonate decreases in volume in the reduction to metal, and groups of metal atoms probably are isolated in the matrix of the promoter, the presence of the promoter preventing the growth of

TABLE 2

Comparison of particle diameters and surface areas from electron micrographs and nitrogen adsorption measurements

MICRO-GRAPH NO	PREPARATION	SURFACE AREA[a]	WEIGHT LOSS	DENSITY	AVERAGE PARTICLE DIAMETER, d[b]		SURFACE AREAS[c]	
					From electron micrographs	From nitrogen adsorption	From electron micrographs	From nitrogen adsorption
		m.²/g.	per cent	g./ml.	microns	microns	m.²/g.	m.²/g.
1	Ferric oxide gel	178.5		3.4–3.9	0.51	0.0093	3.2	178.5
2	Ferric oxide gel, reduced	1.8	27.1	7.9	0.17	0.31[d]	4.5	2.5[d]
4	Nickel oxide	153.0		1.4	2.2	0.0089	0.6	153.0
5	Nickel oxide, reduced	3.6	39.6	8.9	0.57	0.11	1.2	6.0
6	Copper oxide	65.4		6.4	0.037	0.014	25.3	65.4
7	Copper oxide, reduced	5.5	20.8	8.9	0.13	0.10	5.2	6.9
8	Silver oxide	1.7		7.1	0.62	0.49	1.4	1.7
9	Silver oxide, reduced	0.3	7.5	10.5	0.59	1.7	1.0	0.3
10	Cobaltous oxide	67.0		5.7	0.27	0.016	3.9	67.0
11	Cobaltous oxide, reduced	3.2	30.2	8.9	0.38	0.15	1.8	4.6
12	Cobalt basic carbonate	126.2		3.8	0.010	0.013	157.9	126.2
14	Cobalt basic carbonate, reduced at 400°C.	2.5	44.2	8.9	0.22	0.150	3.1	4.5
15	Cobalt-thoria-magnesia, reduced	52.8	37.7	7.8	0.011	0.0091	69.9	84.8
16	Cobalt-kieselguhr, reduced	14.2	21.1	8.9[e]	0.028	0.027	24.1	25.6
17	Cobalt-thoria-magnesia-kieselguhr, reduced	133.2	16.7	7.8[e]	0.010	0.0038	76.9	204.9
18	Ferric oxide catalyst	303.0		5.3	1.3	0.0037	0.90	303
19	Ferric oxide catalyst, reduced	22.9	10.3	6.0	0.024	0.039	41.7	25.5

[a] Surface area per gram of unreduced catalyst.

[b] Average diameter defined by $\bar{d} = \Sigma nd^3/\Sigma nd^2$. For catalysts containing kieselguhr the average diameter is given for the cobalt–promoter complex.

[c] Surface areas per gram of unreduced or reduced material. For catalysts containing kieselguhr the area is given for cobalt–promoter complex per gram of unreduced or reduced complex.

[d] The adsorption measurement was made on a different sample of the same ferric oxide which was reduced for 60 hr. at 415°C. in hydrogen. This is very probably the reason that the area from nitrogen adsorption is less than that estimated from the electron micrographs.

[e] Density of the cobalt–promoter complex.

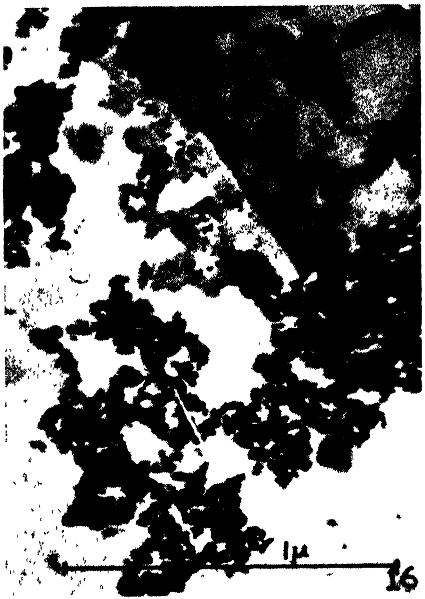

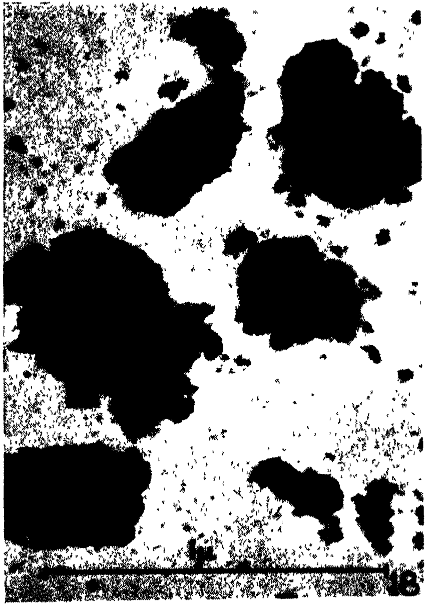

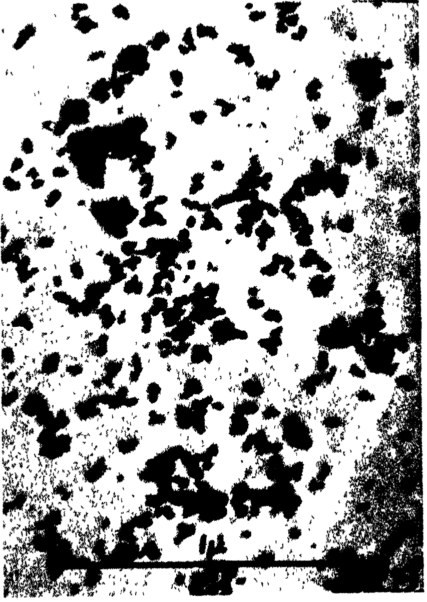

FIG. 16. Reduced cobalt basic carbonate plus kieselguhr

FIG. 17. Reduced cobalt–thoria–magnesia–kieselguhr catalyst

FIG. 18. Ferric oxide–copper oxide–potassium carbonate catalyst

FIG. 19. Ferric oxide–copper oxide–potassium carbonate catalyst treated with a mixture of hydrogen and carbon monoxide ($1H_2 + 1CO$) at 230°C.

large crystallites of metal. Kieselguhr probably prevents sintering in a similar but less intimate manner, the metal shrinking about the particles of kieselguhr.

The kieselguhr also prevents excessive decrease in the bulk volume of the catalyst. It has been postulated that the kieselguhr acts as a "brushpile" into which the other components of the catalyst are deposited; and, as the reduced metal contracts about the particles of kieselguhr, the particles of metal become separated from one another, thus preventing the growth of large particles (2). Visser and de Lange (19) and Teichner (18) have shown that there is considerable interaction between nickel oxide and kieselguhr in nickel–kieselguhr catalysts, with formation of nickel hydrosilicate bonds. Our work indicates that an interaction of this type is probably not very important in cobalt catalysts.

Fused metal oxide catalysts represent an opposite extreme to metal oxide gels. Fused catalysts [Fe_3O_4–Al_2O_3 or (MgO)–K_2O], such as are used in the ammonia synthesis, are dense solids with very little internal surface area. On reduction these catalysts form a porous structure with surface areas of 10–15 $m.^2/g.$ Anderson, Hall, and Tarn (3) have found that the external volume per gram of unreduced catalyst of particles of these catalysts as measured by displacement of mercury at atmospheric pressure does not change in the reduction.

With the precipitated oxides and catalysts reported in this paper the surface areas always decreased upon reduction. It is probable that a sizable fraction of this decrease occurred in the reduction and was not due to sintering of the unreduced material. Immediately after the removal of oxygen the metal atoms are probably in a very unstable state, and considerable reorientation and sintering occurs. There are two driving forces which can cause sintering: First, the tendency to form relatively stable crystallites or aggregates of metal atoms, and second, the decrease in surface energy by diminution of surface area. The presence of either promoters or carriers may inhibit these processes, and the rate of sintering by both processes should increase with temperature.

Hüttig (8) reported interesting changes in surface area, pore volume, and other properties of metal powders heated at various temperatures and has related these changes to α, the ratio of the absolute sintering temperature to the absolute melting point of the metal. As the temperature is increased to $\alpha = 0.23$–0.36 an increase in surface area and pore volume was observed which was attributed to activation by surface diffusion. Following this interval, from $\alpha = 0.33$ to $\alpha = 0.45$, the surface area and pore volume decreased, owing to stabilization by surface diffusion. With the onset of lattice diffusion, $\alpha = 0.37$–0.53, another activation with increases in surface area and pore volume occurred, owing to activation by lattice diffusion, followed by ($\alpha = 0.48$–0.80) decreases in area and pore volume. Another activation occurred prior to the melting point. The activations observed at the onset of surface and lattice diffusion would not be expected in a simple picture of sintering. They are probably due to a "working out" of unstable surface or lattice structures that were metastable at lower temperatures, and sufficient energy is probably liberated to exceed the increase in surface energy.

The values of α in the reduction of the samples in table 1 vary from 0.278 to 0.384 and are in the ranges of either activation or sintering due to surface diffusion; accordingly, a great part of the changes during the reduction may be attributed to surface diffusion. This is very likely a primary factor in sintering in reductions, since relatively isolated metal atoms are probably formed which may migrate to relatively stable positions in the lattice of already reduced metal. This may be considered as a type of surface diffusion. An experiment was made with carbonyl iron to determine in an approximate manner if heat treatment in hydrogen at 400°C. ($\alpha = 0.372$) for 40 hr. involved surface or lattice diffusion. In this treatment the fine powder formed into a coherent cake of considerable mechanical strength. However, examination of the sintered material with the optical microscope showed that the cake consisted of spheres of iron of about the same size as those of the original carbonyl iron but attached at the points of contact. Thus it appears that surface diffusion is the primary factor in the sintering of iron at 400°C.

We believe that electron-microscopic studies of catalysts are useful and informative, but that the micrographs are seldom simple to interpret. It is desirable to consider the micrographs together with surface areas from gas adsorption. From a comparison of particle size and shape with surface areas some estimate of the porosity of the particles may be made. The electron micrographs presented in this paper give no very direct information about pore structure. Gentle crushing of catalyst granules, at least in the case of cobalt catalysts, appears to break the sample into its ultimate particles without altering their structure very seriously. With gels of high mechanical strength the particles formed by gentle crushing usually have considerable internal surface area. It is possible that replica techniques may be used to obtain information about the pore structure of the catalyst surface, but these techniques may be quite difficult with reduced metal catalysts.

SUMMARY

Changes in metal oxides and metal oxide catalysts during reduction have been studied by electron-microscopic and adsorption methods. Metal oxides sinter considerably during reduction, but in the presence of promoters or carriers the extent of sintering is decreased. The data have been discussed with respect to Hüttig's theory of sintering, and it appears that the observed phenomena may be explained by surface diffusion of freshly formed metal.

REFERENCES

(1) Anderson: Ind. Eng. Chem., Anal. Ed. **18**, 156 (1946).
(2) Anderson, Hall, and Hofer: J. Am. Chem. Soc. **70**, 2465 (1948).
(3) Anderson, Hall, and Tarn: J. Am. Chem. Soc., to be published.
(4) Anderson, Kreig, Seligman, and O'Neill: Ind. Eng. Chem. **39**, 1548 (1947).
(5) Brunauer, Emmett, and Teller: J. Am. Chem. Soc. **60**, 309 (1938).
(6) Emmett: In *Advances in Colloid Science*, Vol. I, pp. 1–36. Interscience Publishers, New York (1942).
(7) Hofer and Peebles: J. Am. Chem. Soc. **69**, 893 (1947).
(8) Hüttig *et al.*: Kolloid-Z. **94**, 137, 258 (1941); **96**, 227 (1941); **97**, 281 (1941); **98**, 6, 263 (1942); **104**, 189 (1943); Z. anorg. Chem., **247**, 221 (1941); **249**, 134 (1942); **250**, 1 (1942); **251**, 260 (1943); **252**, 95 (1943).
(9) Kistler, Fischer, and Freeman: J. Am. Chem. Soc. **65**, 1909 (1943).
(10) Langmuir: J. Am. Chem. Soc. **38**, 2263 (1916).
(11) Love and Brunauer: J. Am. Chem. Soc. **64**, 745 (1942).
(12) McCartney and Anderson: J. Applied Phys. **18**, 902 (1947).

(13) **Perrott and Kinney**: J. Am. Ceram. Soc. **6**, 417 (1923).

(14) **Pichler**: "Synthesis of Hydrocarbons from Carbon Monoxide and Hydrogen," Bureau of Mines, Special Report.

(15) **Schuster and Fullam**: Ind. Eng. Chem., Anal. Ed. **18**, 653 (1946).

(16) **Seligman and Anderson**: To be published.

(17) **Storch** *et al.*: U. S. Bur. Mines Tech. Paper **No. 709** (1948).

(18) **Teichner**: Compt. rend. **227**, 478 (1948).

(19) **Visser and de Lange**: De Ingenieur **58**, 24 (1946).

(20) **Weiser**: *Inorganic Colloid Chemistry. Vol. II. The Hydrous Oxides and Hydroxides*, p. 22. John Wiley and Sons, Inc., New York (1935).

KINETIC LAWS IN CATALYZED SYSTEMS. I

Reactions Involving a Single Substrate

K. J. LAIDLER and IRENE M. SOCQUET[1]

Department of Chemistry, The Catholic University of America, Washington, D. C.

Received June 10, 1949

Theoretical kinetic laws for catalyzed reactions have previously been developed in an *ad hoc* manner, each of the various resulting expressions being applicable only to a limited set of experimental data. Surface catalysis, for example, is usually treated by equilibrium theory, using Langmuir isotherms; acid–base catalysis by either steady-state or equilibrium theory according to circumstances; and enzyme catalysis by a special type of treatment in which allowance is made for the amount of enzyme (but not of substrate) combined in the intermediate complex. The treatments lead to quite different types of kinetic laws in the various cases: thus the usual theory of acid–base catalysis will allow a nonlinear dependence of the rate on the catalyst concentration but a linear dependence on the substrate concentration, while the Michaelis–Menten treatment of enzyme reactions leads to a nonlinear dependence on substrate concentration and a linear dependence on catalyst concentration.

In the present paper there will be developed a more consistent set of kinetic laws which will be applicable to many types of surface, homogeneous, and enzyme catalysis involving a single substrate. The treatment will emphasize the very close resemblance between these systems and will reveal new types of relationships; some of these have been exemplified by existing experimental data, while the conditions leading to others have not yet been achieved. The work to be described was undertaken with the primary object of seeing what light can be thrown by the study of heterogeneous and acid–base catalysis on the more elusive problem of the kinetic mechanism of enzyme action.

---

[1] Present address: Sister Irene Marie, S.S.A., Anna Maria College, Marlboro, Massachusetts.

THE MECHANISM OF CATALYSIS

A catalyst diminishes the free energy of activation of a process by introducing an alternative mechanism, in most cases by forming an intermediate complex with one or more of the substrate molecules, this complex subsequently undergoing reaction. In the simplest type of catalyzed reaction, in which only one substrate is involved, the substrate and catalyst form a complex which subsequently reacts, either unimolecularly or bimolecularly, in a single stage; the overall reaction thus consists of two elementary processes,—the formation of the complex and its reaction to give the final products. Similarly, when two substrates are involved these may form with the catalyst a complex which subsequently reacts in a single step. The case of the single substrate is treated in the present paper, and that of the double one in the following paper; more complicated mechanisms, involving chain reactions and free radicals, will not be treated, as they cannot be reduced to a single scheme of elementary processes.

A kinetic mechanism to account for the mechanism of reactions involving a single substrate was put forward by K. F. Herzfeld (7), but a slightly more general mechanism, which appears to apply to most types of nonchain catalysis with only one substrate, is as follows:

$$\mathrm{C} + \mathrm{S} \underset{k_{-1}}{\overset{k_1}{\rightleftharpoons}} \mathrm{X} + \mathrm{Y} \qquad (1)$$

(2)

Here C represents the catalyst and S the substrate; X is the intermediate complex and Y some substance formed in addition to it. W is a molecule which reacts with the complex to give the product or products P with elimination of the molecule Z, which may sometimes (if W is identical with Y) be C itself. It is assumed that the reaction products are at such a low free-energy level that the reverse reaction $\mathrm{P} + \mathrm{Z} \rightarrow \mathrm{X} + \mathrm{W}$ can be neglected. The treatment to be given will apply only to initial rates of reaction; otherwise very clumsy kinetic expressions would be obtained, and the experimental data could only with difficulty be analyzed with respect to them.

In surface catalysis X is an adsorption complex and Y and W are nonexistent; k_{-1} and k_2 are in this case first-order rate constants, while k_1 is a second-order constant. The species Y and Z are also probably nonexistent in most cases of enzyme catalysis involving only one substrate. Y and Z do, however, play roles in acidic and basic catalysis in solution; thus, if C is an acid, reaction 1 involves the transfer of a proton to S, so that Y is the base conjugate to C. Similarly, in basic catalysis, Y is the acid conjugate to the base C. In acid catalysis W is a basic or amphoteric substance which accepts a proton from X and is frequently a solvent molecule; it may also, however, be a basic solute. In basic catalysis W transfers a proton to X and may be the solvent or another acidic substance present in the system.

THE INTERMEDIATE COMPLEX

The role of the intermediate complex in catalysis has been much emphasized in surface catalysis particularly by I. Langmuir (9) and C. N. Hinshelwood (8), in acid–base catalysis by J. N. Brønsted (3), N. Bjerrum (1), and H. von Euler (5), and in enzyme catalysis by L. Michaelis and M. L. Menten (10). Two extreme possibilities for the stability of the complex have been considered, and the kinetic laws obtained depend in an important manner upon what is assumed in this connection. In the first place the complex may be one which decomposes to regenerate the catalyst and the substrate at a rate which is much greater than the rate with which it undergoes reaction 2 to give the final products; under these circumstances the complex, known as an Arrhenius complex, may exist at comparatively high concentrations during the course of reaction. The rate of reaction can then be obtained by calculating the concentration of X from the equilibrium 1 above and multiplying this by k_2[W], this being the procedure, for example, with surface reactions.

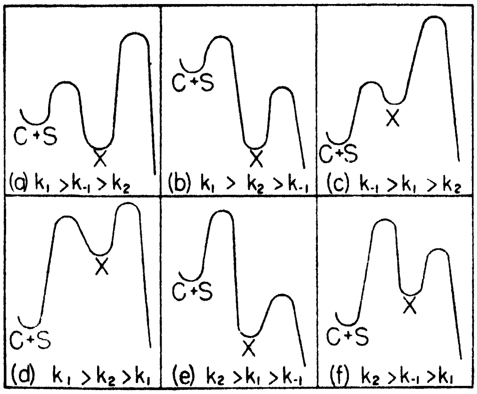

FIG. 1

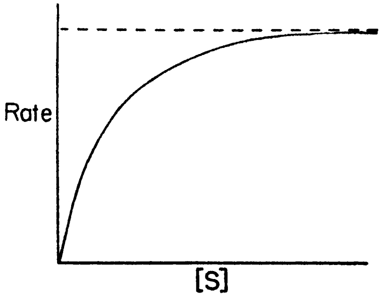

FIG. 2

FIG. 1. Schematic free-energy profiles for catalyzed systems, showing six possible cases.

FIG. 2. Relationship between rate and substrate concentration for a catalyzed reaction (equation 8) (except in acid–base catalysis, for which the relationship is always linear). A similar variation with catalyst concentration is found (equation 12).

The second possibility is that the intermediate complex is a much less stable species (a van't Hoff complex), the rate of its reaction 2 not being small compared with the reverse rate of reaction 1. It is then not permissible to calculate [X] by making use of equilibrium 1, since the rate of reaction 2 cannot be ignored. Since the concentration of X must in this case be low, the steady-state treatment may be employed.

The distinction between the two cases may be shown by means of standard free-energy diagrams. Six cases which are of special interest are illustrated in figure 1. Curve (a) corresponds to $k_1 > k_{-1} > k_2$, in which case X lies at a low free-energy level with respect to both reactants and products and is therefore a stable Arrhenius intermediate; its concentration can therefore be calculated accurately using equilibrium theory. This case is probably found in most surface reactions and in many enzyme-catalyzed reactions. The complex is also an Arrhenius one in cases (c) and (d), and equilibrium theory is therefore applicable.

In cases (b), (e), and (f), on the other hand, the steady-state treatment must be applied.

The kinetic expressions for the cases of equilibrium treatment and steady-state treatment will now be derived, and will later be applied to the various types of catalysis.

THE EQUILIBRIUM TREATMENT

In the case that the rate of reaction 2 can be neglected in calculating the concentration of X, the concentrations of X, Y, C, and S are related by

$$\frac{[X][Y]}{[C][S]} = \frac{k_1}{k_{-1}} = K_1 \tag{1}$$

where K is the equilibrium constant. If $[C]_0$ and $[S]_0$ are the initial concentrations of C and S before some of them have been used in complex formation, it follows that

$$[C] = [C]_0 - [X] \tag{2}$$

$$[S] = [S]_0 - [X] \tag{3}$$

Therefore

$$\frac{[X][Y]}{([C]_0 - [X])([S]_0 - [X])} = K \tag{4}$$

This is a quadratic in [X], and can be solved for [X]. An expression for the rate, equal to $k_2[W][X]$, can then be written down. However, it is more convenient to consider two special cases.

Case 1: If the substrate is initially present in much higher concentrations than the catalyst, i.e., if $[S]_0 \gg [C]_0$, it follows that $[S]_0 - [X]$ is very close to $[S]_0$, since [X] cannot exceed $[C]_0$; equation 4 therefore approximates to

$$\frac{[X][Y]}{([C]_0 - [X])[S]_c} = K \tag{5}$$

whence

$$[X] = \frac{K[C]_0[S]_0}{K[S]_0 + [Y]} \tag{6}$$

The rate of reaction is therefore

$$-\frac{d[S]}{dt} = k_2[X][W] \tag{7}$$

$$= \frac{k_2 K[C]_0[S]_0[W]}{K[S]_0 + [Y]} \tag{8}$$

This rate equation corresponds to a variation in rate of the type represented in figure 2; when $K[S]_0 \ll [Y]$, the rate varies linearly with $[S]_0$, while at higher substrate concentrations, when $K[S]_0 \gg [Y]$, the rate is independent of $[S]_0$. As long as the condition $[S]_0 \gg [C]_0$ holds, however, the rate varies linearly with $[C]_0$, but, as will be seen, if $[C]_0$ is increased so much that $[C]_0 \gg [S]_0$, so that case 1 no longer holds, the rate becomes independent of $[C]_0$.

This type of law (equation 8) is characteristic of most surface and enzyme reactions, for which the condition $[S]_0 \gg [C]_0$ holds in most investigations; for both of these the species Y and W are usually nonexistent and the law becomes

$$-\frac{d[S]}{dt} = \frac{k_2 K[C]_0[S]_0}{K[S]_0 + 1} \tag{9}$$

For surface reactions this corresponds to the familiar phenomenon of first-order kinetics at low concentrations and zero-order at higher ones. Equation 9 is equivalent to the Michaelis–Menten (10) law for enzyme reactions; this is usually expressed as

$$-\frac{d[S]}{dt} = \frac{k_2[C]_0[S]_0}{[S]_0 + K_m} \tag{10}$$

where K_m, the Michaelis constant, is equal to $1/K$. This law has been shown to be obeyed by a variety of enzyme-catalyzed reactions, and direct evidence has been obtained (4, 13) for the existence of the postulated enzyme–substrate complexes.

In the case of acid- and base-catalyzed reactions, which are considered in detail later, it is found that owing to the peculiar nature of the equilibria established in the solutions the condition $K[S]_0 \ll [Y]$ always holds; the rate is therefore always exactly proportional to the first power of the substrate concentration.

Case 2: If, on the other hand, $[C]_0 \gg [S]_0$, $[C]_0 - [X]$ in equation 4 can be put equal to $[C]_0$, so that

$$\frac{[X][Y]}{[C]_0([S]_0 - [X])} = K \tag{11}$$

The rate of reaction then becomes:

$$-\frac{d[S]}{dt} = \frac{k_2 K[C]_0[S]_0[W]}{K[C]_0 + [Y]} \tag{12}$$

This indicates a linear variation of the rate with $[S]_0$ (as long as the condition $[C]_0 \gg [S]_0$ holds) but a nonlinear variation with $[C]_0$, of the same type as shown in figure 2, the rate becoming independent of $[C]_0$ at sufficiently high concentrations.

Examples of the attainment of a limiting rate with increasing catalyst concentration are not easy to find, the reason being that in not many investigations does the condition $[C]_0 \gg [S]_0$ hold. In surface reactions the rate is usually found to vary linearly with the amount of surface, but at high catalyst concentrations the attainment of a limiting rate has occasionally been noted (see, for example, 11). The effect has apparently never been observed with enzyme catalysis, and this can be attributed to the fact that it is usually physically impossible to achieve the molar concentration of the enzyme that is necessary for the condition $[C] \gg [S]$ to hold. However, the analogous behavior for a two-substrate system has been found with the lactic dehydrogenase system (12, 14); this will be considered further in Part II.

In acid catalysis an example of the attainment of a limiting rate with increasing acid concentration has been found by H. von Euler and A. Olander (6) in the hydrolysis of acetamide; this is considered later.

THE STEADY-STATE TREATMENT

The steady-state expression for X is

$$\frac{d[X]}{dt} = k_1[C][S] - k_{-1}[X][Y] - k_2[X][W] = 0 \tag{13}$$

Substitution of $[C]_0 - [X]$ for [C] and of $[S]_0 - [X]$ for [S] gives

$$k_1([C]_0 - [X])([S]_0 - [X]) - k_{-1}[X][Y] - k_2[X][W] = 0 \tag{14}$$

Since [X] is small, the term in $[X]^2$ can be neglected; with this approximation equation 14 gives

$$[X] = \frac{k_1[C]_0[S]_0}{k_1[C]_0 + k_1[S]_0 + k_{-1}[Y] + k_2[W]} \tag{15}$$

and the rate of reaction is

$$-\frac{d[S]}{dt} = \frac{k_1 k_2[C]_0[S]_0[W]}{k_1[C]_0 + k_1[S]_0 + k_{-1}[Y] + k_2[W]} \tag{16}$$

This equation again indicates that at low concentrations of catalyst and of substrate the rate varies linearly with the concentration of each of these, but that at higher concentrations of either the rate will become independent of this concentration. However, since in the case of the van't Hoff intermediate either k_{-1} or k_2 or both are large compared with k_1, this behavior is only observed at higher concentrations of substrate and catalyst than are usually employed.

In catalysis by surfaces and by enzymes [W] and [Y] are generally nonexistent, and the rate law then becomes

$$-\frac{d[S]}{dt} = \frac{k_1 k_2[C]_0[S]_0}{k_1[C]_0 + k_1[S]_0 + k_{-1} + k_2} \tag{17}$$

An equation somewhat similar to this, but lacking the $k_1[C]_0$ term in the denominator, was first derived by G. E. Briggs and J. B. S. Haldane (2) for enzyme-catalyzed reactions. It is seen to predict the same type of variation of the rate with the substrate concentration as does equation 9, which is based on the equilibrium treatment, and in fact becomes equivalent to equation 9 if $k_{-1} \gg k_2$. The Michaelis constant K_m (*cf.* equation 10) is seen to be given by

$$K_m = \frac{[S]_0 + k_{-1} + k_2}{k_1} \tag{18}$$

and if from the experimental variation of the rate with the substrate concentration it is found to be much smaller than unity, it is evident that $k_1 > k_{-1}$ and $k_1 > k_2$ (cases (a) and (b), figure 1). If, on the other hand, K_m is large, it follows that either $k_1 < k_{-1}$ or $k_1 < k_2$ (or both) and the concentration of the complex is therefore small. In most of the cases that have been studied the former is the case. Similar considerations apply to surface-catalyzed reactions; the application of equation 17 to acid–base-catalyzed reactions will be considered later.

ACID–BASE CATALYSIS

The scheme of reactions 1 and 2 is applicable to most cases of acid–base catalysis, but an extension of the treatment is required to allow for the various solution equilibria that are established. The species W may be either the solvent or a species in solution, and the kinetics are in general different according to which plays the dominating role. If W is the solvent, and C is acidic, W acts as a base and Z is therefore the lyonium ion (H_3O^+ in the case of water as the solvent); similarly, if C is a basic catalyst, and W is the solvent, Z is the lyate ion (OH^- if water is the solvent). The species W may also, if C is acidic, be a basic substance present in solution, or an acidic solute if C is basic; in the former case Y is the acid conjugate to C, in the latter case Y is the base conjugate to C. These various possibilities are summarized in table 1, in which HA represents an acidic solute and B a basic one. The solvent may in general act either as an acid or as a base; it is here assumed to be water, and the application of the treatment to other solvents will be obvious. A valid mechanism corresponds to taking any pair of C and Y and combining them with any pair of W and Z, subject to the condition that if C is acting as an acid, W must act as a base, and *vice versa*; the former will be referred to as acidic catalysis and the latter, when C is basic and W acidic, as basic catalysis. It is seen that eight different possibilities exist, and the treatment is further complicated by the fact that the intermediate X may be either an Arrhenius or a van't Hoff complex. The former possibility will be considered first, and the kinetic equations will be developed in detail only for the cases of acidic catalysis; the derivation of the laws for basic catalysis proceeds in an exactly analogous manner.

TABLE 1

The nature of reacting species in acid–base catalysis

TYPE OF CATALYSIS	C	Y	W	Z
Acidic	HA	A^-	H_2O	H_3O^+
	H_2O	OH^-	B	BH^+
Basic	B	BH^+	H_2O	OH^-
	H_2O	H_3O^+	HA	A^-

THE EQUILIBRIUM TREATMENT

When the complex is stable the treatment given previously led to equations 9 and 12, but these cannot be applied directly to the case of acid–base catalysis owing to the establishment of solution equilibria, particularly those involving the solvent and the various acidic and basic species present. The equilibrium that influences the kinetics may be written as

$$C + W \rightleftharpoons Y + Z \tag{3}$$

the equilibrium constant for which is given by

$$K' = \frac{[\mathrm{Y}][\mathrm{Z}]}{[\mathrm{C}][\mathrm{W}]} \tag{19}$$

$$= \frac{[\mathrm{Y}][\mathrm{Z}]}{([\mathrm{C}]_0 - [\mathrm{X}])[\mathrm{W}]} \tag{20}$$

using equation 2. Elimination of $[\mathrm{C}]_0 - [\mathrm{X}]$ between equations 4 and 20 gives

$$\frac{[\mathrm{X}][\mathrm{W}]}{[\mathrm{Z}]([\mathrm{S}]_0 - [\mathrm{X}])} = \frac{K}{K'} \tag{21}$$

so that

$$[\mathrm{X}] = \frac{K[\mathrm{Z}][\mathrm{S}]_0}{K[\mathrm{Z}] + K'[\mathrm{W}]} \tag{22}$$

The rate of reaction is therefore equal to

$$-\frac{\mathrm{d}[\mathrm{S}]}{\mathrm{d}t} = \frac{k_2 K[\mathrm{Z}][\mathrm{S}]_0[\mathrm{W}]}{K[\mathrm{Z}] + K'[\mathrm{W}]} \tag{23}$$

The treatment has led to the result that the rate is always directly proportional to $[\mathrm{S}]_0$; this is in contrast to the situation with surface and enzyme catalysis, in which the rate becomes independent of the substrate concentration when this becomes large.

With regard to the influence of the catalyst concentration, two cases are to be distinguished.

Case 1: In the first, which will be shown later to obtain at sufficiently low catalyst concentrations, $K'[\mathrm{W}] \gg \mathrm{K}[\mathrm{Z}]$, and the rate is given by

$$-\frac{\mathrm{d}[\mathrm{S}]}{\mathrm{d}t} = k_2 \frac{K}{K'} [\mathrm{Z}][\mathrm{S}]_0 \tag{24}$$

The species Z may be either the lyonium ion (e.g., $\mathrm{H_3O^+}$) or the acidic solute species $\mathrm{BH^+}$, depending upon whether, in reaction 2, the complex gives up its proton to a solvent molecule or to a basic solute. The former corresponds to specific hydrogen-ion catalysis; the latter to general acid catalysis by the various acidic solutes present.

Case 2: If $K[\mathrm{Z}] \gg K'[\mathrm{W}]$ the rate is given by

$$-\frac{\mathrm{d}[\mathrm{S}]}{\mathrm{d}t} = k_2[\mathrm{S}]_0[\mathrm{W}] \tag{25}$$

implying that the second step, the reaction between the complex and W, is slow and rate-determining. In acid catalysis W may be either the solvent or a basic species B, and in the former case the rate is independent of the concentrations of the catalyzing species present in solution. In the latter case, since the concentration of B is proportional to the concentration of its conjugate acid $\mathrm{BH^+}$, the rate will still be proportional to the concentration of acidic species present in solution.

The fact that case 1 (equation 24) applies at low catalyst concentrations, and case 2 (equation 25) at high ones, may be shown as follows. Equations 1 and 19 combine to give

$$\frac{K'[\mathrm{W}]}{K[\mathrm{Z}]} = \frac{[\mathrm{S}]}{[\mathrm{X}]} \tag{26}$$

At low concentrations of catalyst $[\mathrm{S}] \gg [\mathrm{X}]$, since $[\mathrm{X}]$ cannot be greater than $[\mathrm{C}]_0$ which by hypothesis is small; it therefore follows from equation 26 that $K'[\mathrm{W}] \gg \mathrm{K}[\mathrm{Z}]$, so that equation 24 applies. At high catalyst concentrations, on the other hand, $[\mathrm{X}] \gg [\mathrm{S}]$, since most of the substrate is used up in forming the complex; it then follows from equation 26 that $K[\mathrm{Z}] \gg K'[\mathrm{W}]$, so that equation 25 applies.

The conclusions arrived at above may be summarized as follows, the remarks applying to the equilibrium case and to acid catalysis only:

(*1*) If the acceptor W in reaction 2 is the solvent, there is specific hydrogen-ion catalysis, the rate becoming independent of the hydrogen-ion concentration at high acid concentrations.

(*2*) If W is a solute species there is general acid catalysis, the rate varying linearly with the acid concentrations at all concentrations. The attainment of a limiting rate is therefore evidence against general acid catalysis in any particular reaction.

Whether the catalyst C is solvent or solute is seen to have no bearing on the type of catalysis.

The idea that the complex X is in equilibrium with the reactants is due to H. von Euler (6), who proposed it as a universal explanation of acid–base catalysis. Evidence for the mechanism has been obtained (6) for the acid-catalyzed hydrolysis of acetamide, the apparent catalytic constant decreasing with increasing hydrogen-ion concentration which finally has no influence on the rate. Since the attainment of a limiting rate is not obtained when the steady-state treatment is applied (see below), this result appears to indicate unequivocally that the equilibrium treatment is applicable; it also proves that the catalysis is specific, i.e., that the water is the acceptor W. In no other case, however, has good evidence been obtained for the attainment of a limiting rate, and the steady-state treatment is probably more generally applicable.

THE STEADY-STATE TREATMENT

The alternative hypothesis that the second step is not slow was proposed by J. N. Brønsted (3) and the rate equations may be formulated as follows: The general steady-state expression for the rate of a catalyzed reaction is equation 16, and since by hypothesis the rate of formation of the complex is slow in comparison with the rate of its reaction the term $k_1[\mathrm{C}]_0 + k_1[\mathrm{S}]_0$ may be neglected; the rate equation then becomes

$$-\frac{\mathrm{d}[\mathrm{S}]}{\mathrm{d}t} = \frac{k_1 k_2[\mathrm{C}]_0[\mathrm{S}]_0[\mathrm{W}]}{k_{-1}[\mathrm{Y}] + k_2[\mathrm{W}]} \tag{27}$$

Two special cases of this are important.

Case 1: If $k_2[\mathrm{W}] \gg k_{-1}[\mathrm{Y}]$ the rate becomes:

$$-\frac{\mathrm{d}[\mathrm{S}]}{\mathrm{d}t} = k_1[\mathrm{C}]_0[\mathrm{S}]_0 \tag{28}$$

The rate is thus completely controlled by the first step, and there is general acid catalysis.

Case 2: If $k_{-1}[\mathrm{Y}] \gg k_2[\mathrm{W}]$ the rate is given by:

$$-\frac{\mathrm{d}[\mathrm{S}]}{\mathrm{d}t} = \frac{k_1 k_2}{k_{-1}} \frac{[\mathrm{C}]_0[\mathrm{S}]_0[\mathrm{W}]}{[\mathrm{Y}]} \tag{29}$$

However, all of the acidic and basic species (other than the substrate) present in solution are at equilibrium, and in particular (*cf.* equation 19)

$$\frac{[\mathrm{C}]_0[\mathrm{W}]}{[\mathrm{Y}]} = \frac{[\mathrm{Z}]}{K'} \tag{30}$$

TABLE 2

Summary of kinetic behavior in acid and base catalysis

TYPE OF CATALYSIS	NATURE OF W	DEPENDENCE OF RATE ON CATALYST CONCENTRATION ASSUMING			
		Equilibrium theory		Steady-state theory	
		Low concentration	High concentration	(All concentrations) $k_2[\mathrm{W}] \gg k_{-1}[\mathrm{Y}]$	$k_{-1}[\mathrm{Y}] \gg k_2[\mathrm{W}]$
Acid .	Solvent	$[\mathrm{H_3O^+}]$	No dependence	Σ[acid]	$[\mathrm{H_3O^+}]$
Acid	Solute	Σ[acid]	Σ[acid]	Σ[acid]	Σ[acid]
Base	Solvent	$[\mathrm{OH^-}]$	No dependence	Σ[base]	$[\mathrm{OH^-}]$
Base	Solute	Σ[base]	Σ[base]	Σ[base]	Σ[base]

since $[\mathrm{C}]_0$ is in this case approximately equal to [C]. The rate equation therefore becomes:

$$-\frac{\mathrm{d}[\mathrm{S}]}{\mathrm{d}t} = \frac{k_1 k_2}{k_{-1}} \frac{[\mathrm{S}_0][\mathrm{Z}]}{K'} \tag{31}$$

In acid catalysis Z may be either the lyonium ion (if W is the solvent) or a solute acid (if W is a solute); there is therefore either specific or general acid catalysis according as W is the solvent or a solute.

In the steady-state case there is linear dependence of the rate on catalyst concentrations at all concentrations, in contradistinction to the equilibrium case for which there is nonlinear dependence if W is the solvent.

The variation of the rate with catalyst concentration is shown for the various cases in table 2, in which Σ [acid] and Σ [base] indicate general acidic and basic catalysis. Whether equilibrium or steady-state theory is the valid one, the results can be summarized as follows:

(*1*) If the mechanism is prototropic, i.e., if W is a solute, there is general acid catalysis and the rate is always linear in the catalyst concentrations.

(*2*) If the mechanism is protolytic, there may be either general or specific catalysis and, in the latter case only, the rate may sometimes (if equilibrium theory is applicable) become independent of the catalyst concentration.

The fact that the kinetic behavior depends upon the nature of W has long been recognized in the distinction between prototropic reactions and protolytic reactions. According to the present treatment protolytic reactions may be said to be those in which W is the solvent, and prototropic reactions those in which it is a solute. The above analysis has shown that protolytic reactions may show either general or specific catalysis according to the relative magnitudes of $k_2[W]$ and $k_{-1}[Y]$, while a prototropic reaction always exhibits general catalysis whatever the relative magnitudes. It is difficult on the experimental side to distinguish between the two types of reaction however, since failure to detect general catalysis, which might be taken as evidence for a protolytic mechanism, does not necessarily imply that acids other than the hydrogen ion have absolutely no catalytic action.

SUMMARY

The kinetic equations for catalyzed reactions involving a single substrate are developed in a generalized form, the object being to demonstrate analogies between the behavior of surface-catalyzed, enzyme-catalyzed, and acid–base-catalyzed reactions. Both the equilibrium and the steady-state treatments are used, and it is shown that, where the former is applicable, the rate becomes limiting at high substrate concentrations for both surface-catalyzed and enzyme-catalyzed reactions; with acid–base catalysis, on the other hand, the rate is always linear in the substrate concentration. A nonlinear dependence of the rate on the catalyst concentration is found to be possible for all types of catalysis; examples are quoted, and the necessary conditions defined. It is shown that in acid–base catalysis the general type of kinetic behavior does not depend upon the nature of the catalyst which initially interacts with the substrate, except as to whether it is acidic or basic, but depends in a critical manner on the nature of the species which reacts with the intermediate complex to form the final products.

REFERENCES

(1) BJERRUM, N.: Z. physik. Chem. **108**, 82 (1924).
(2) BRIGGS, G. E., AND HALDANE, J. B. S.: Biochem. J. **19**, 338 (1925).
(3) BRØNSTED, J. N.: Chem. Revs. **5**, 231 (1928).
(4) CHANCE, B.: J. Biol. Chem. **131**, 553 (1943); Science **109**, 204 (1949).
(5) EULER, H. VON: Svensk. Vet. Akad. Forh. **No. 4** (1899); Z. physik. Chem. **28**, 619 (1899); **32**, 384 (1900); **36**, 641 (1901).
(6) EULER, H. VON, AND OLANDER, A.: Z. physik. Chem. **131**, 107 (1927).
(7) HERZFELD, K. F.: Z. physik. Chem. **98**, 161 (1921).
(8) HINSHELWOOD, C. N.: *Kinetics of Chemical Change in Gaseous Systems*. Oxford University Press, London (1926, 1929, 1933, 1941).
(9) LANGMUIR, I.: J. Am. Chem. Soc. **40**, 1361 (1918).
(10) MICHAELIS, L., AND MENTEN, M. L.: Biochem. Z. **49**, 333 (1913).
(11) SEYER, W. F., AND YIP, C. W.: Ind. Eng. Chem. **41**, 378 (1949).
(12) SOCQUET, I. M., AND LAIDLER, K. J.: Arch. Biochem. **25**, 171 (1950).
(13) STERN, K. G.: J. Biol. Chem. **114**, 473 (1936).
(14) STRAUB, F. B.: Enzymologia **9**, 143 (1941).

KINETIC LAWS IN CATALYZED SYSTEMS. II

REACTIONS INVOLVING TWO SUBSTRATES OR A SUBSTRATE AND A COENZYME

K. J. LAIDLER AND IRENE M. SOCQUET

Department of Chemistry, The Catholic University of America, Washington, D. C.

Received July 25, 1949

In Part I of this series of papers (14) we have considered, on the basis of both the equilibrium and the steady-state treatments, the kinetic laws obeyed by catalyzed systems in which there is only one substrate. The laws will now be developed for the case of reaction involving the formation of a ternary complex consisting of the catalyst molecule and two other molecules. These two molecules may be substrate molecules in the ordinary sense; an example is to be found in catalyzed esterification, in which is formed a complex involving the catalyst, the acid, and the alcohol. Another important case which is included in the present treatment arises in enzymatic hydrogenations, in which reaction occurs between a substrate and a coenzyme molecule which together form a ternary complex with the enzyme molecule; an example is to be found in lactic dehydrogenase, which catalyzes the transfer of two hydrogen atoms from lactic acid to coenzyme I. A third important type of reaction which will be covered in the present paper comprises those in which the solvent itself acts as a second substrate; sometimes these systems behave kinetically as one substrate system, but in other cases a special type of competitive inhibition has to be taken into account (13).

From the standpoint of the kinetic laws it makes no difference whether there are two substrates or a substrate and a coenzyme; in the treatment which follows we shall refer to two substrates S_1 and S_2, and it is to be understood that one of these (S_2) may be a coenzyme. It is supposed that in order for reaction to occur substrate S_1 must be attached to a particular active site on the catalyst, while S_2 must be attached to a neighboring active site; molecular rearrangement can then occur with the formation of the reaction products. The simplest case to consider is the one in which S_1 and S_2 do not interfere with one another; i.e., S_1 has no tendency to become adsorbed on the site reserved for S_2, and *vice versa*. When this is the case, it is found (*cf.* equation 7 below) that the rate varies with each substrate concentration in the same manner as in single-substrate systems; with increasing catalyst concentration, on the other hand, the rate increases to a maximum and then decreases. A more complex case arises when there is competitive adsorption of the two substrates; for example, S_1 may be to some extent adsorbed on the site reserved for S_2. Either or both of the substrates may act in this way, and it will be seen that as the concentration of such a substrate increases the rate first rises to a maximum and then decreases. An example in which one substrate (S_2) is the solvent is to be found in the hydrolysis of urea catalyzed by urease (7, 8, 13); here, in agreement with experiment, the theory indicates that with increasing S_1 concentration the rate increases to a maximum and then decreases, this effect being due to the encroachment by the urea molecules on the water sites.

The kinetic laws will now be developed for the three main cases considered: namely, (*1*) noncompetitive adsorption, (*2*) competitive adsorption, and (*3*) competitive adsorption in the special case that one substrate is the solvent. The treatment will be worked through for the equilibrium case only: the development is simpler for this case, and the final expressions are of much the same form for the two cases. Previous treatments along similar lines have been presented by LuValle and Goddard (16) and by Hearon (6), but general expressions were not obtained by these workers; moreover, their kinetic mechanisms are not as simple and clear-cut as the present ones and do not appear to account for the main features of the behavior found experimentally.

The present work represents to some extent an extension and generalization of part of the treatment of surface reactions given by Laidler, Glasstone, and Eyring (11, 12).

NONCOMPETITIVE ADSORPTION

In the case of noncompetitive adsorption the substrate S_1 can be adsorbed only on sites of type 1, while S_2 can be adsorbed only on sites of type 2. Let θ_1 be the fraction of the sites of type 1 which are covered by S_1; the equilibrium condition is therefore given by the Langmuir adsorption isotherm

$$\frac{\theta_1}{1-\theta_1} = K_1[S_1] \tag{1}$$

where K_1 is the equilibrium constant for the formation of the binary complex between the enzyme and S_1. The concentration $[S_1]$ is given initially by

$$[S_1] = [S_1]_0 - [C]_0\theta_1 \tag{2}$$

where $[S_1]_0$ is the amount of substrate added and $[C]_0$ is the total amount of catalyst; $[C]_0\theta_1$ is thus the amount of substrate in the form of complex. Therefore

$$\frac{\theta_1}{1-\theta_1} = K_1([S_1]_0 - [C]_0\theta_1) \tag{3}$$

whence

$$\theta_1 = \frac{K_1[S_1]_0}{1 + K_1[C]_0 + K_1[S_1]_0} \tag{4}$$

In a precisely similar way, for the adsorption of S_2 on sites of type 2, the fraction covered is given by

$$\theta_2 = \frac{K_2[S_2]_0}{1 + K_2[C]_0 + K_2[S_2]_0} \tag{5}$$

where K_2 is now the equilibrium constant for the formation of the binary complex between the enzyme and S_2.

The concentration of ternary complexes, i.e., those in which S_1 and S_2 are adsorbed simultaneously on a catalyst molecule, is $[C]_0\theta_1\theta_2$; if k_2 is the specific rate constant for the decomposition of the complex into the products, the rate is therefore

$$v = k_2[\mathrm{C}]_0\theta_1\theta_2 \tag{6}$$

Using equations 4 and 5 this becomes:

$$v = \frac{k_2 K_1 K_2[\mathrm{C}]_0[\mathrm{S}_1]_0[\mathrm{S}_2]_0}{(1 + K_1[\mathrm{C}]_0 + K_1[\mathrm{S}_1]_0)(1 + K_2[\mathrm{C}]_0 + K_2[\mathrm{S}_2]_0)} \tag{7}$$

The variation of the rate with the substrate concentrations is shown to be of the same type as in a one-substrate system (*cf.* equation 8 and figure 2 of Part I). Thus when $[\mathrm{S}_1]_0$ is sufficiently small, $K_1[\mathrm{S}_1]_0 \ll 1 + K_1[\mathrm{C}]_0$, and the denominator of equation 7 does not involve $[\mathrm{S}_1]_0$; the rate of reaction is therefore directly proportional to $[\mathrm{S}_1]_0$. At high substrate concentrations on the other hand $K_1[\mathrm{S}_1]_0 \gg 1 + K_1[\mathrm{C}]_0$, so that the denominator of equation 7 is proportional to $[\mathrm{S}_1]_0$; the rate is therefore independent of $[\mathrm{S}_1]_0$. The same arguments apply to S_2.

In enzyme-catalyzed reactions this type of variation of rate in two-substrate and substrate–coenzyme systems has been found experimentally for both substrate (*cf.* reference 3) and coenzyme (*cf.* reference 15). It also seems likely that the same type of behavior is to be found in surface-catalyzed reactions, although there seem to be no clear-cut examples. For the adsorption of the two substrates to be noncompetitive it is required that there be two types of active centers on the surface, one type adsorbing only the substrate S_1 and the other only S_2; such a situation is to be expected particularly with catalysts of the composite type.

The variation of the rate with increasing catalyst concentration is different from the above. At low catalyst concentrations the rate is again proportional to $[\mathrm{C}]_0$, since $K_1[\mathrm{C}]_0 \ll 1 + K_1[\mathrm{S}_1]_0$ and $K_2[\mathrm{C}]_0 \ll 1 + K_2[\mathrm{S}_2]_0$; at high concentrations $K_1[\mathrm{C}]_0 \gg 1 + K_1[\mathrm{S}_1]_0$ and $K_2[\mathrm{C}]_0 \gg 1 + K_2[\mathrm{S}_2]_0$, so that the rate becomes equal to

$$v = k_2[\mathrm{S}_1]_0[\mathrm{S}_2]_0/[\mathrm{C}]_0 \tag{8}$$

and is inversely proportional to the catalyst concentration. At intermediate catalyst concentrations the rate passes through a maximum.

This type of behavior has not often been observed, since the catalyst concentrations used are seldom sufficiently high. However, Straub (19) has found a maximum in the lactic dehydrogenase system (actually a case of competitive adsorption, see below), and in a reinvestigation of the system (18) we have found evidence that the behavior can be explained in terms of the rate equation (equation 7); an alternative explanation had been given by Straub. The existence of a maximum does not seem to have been observed with surface catalysis.

The physical explanation of the decrease in rate at high catalyst concentrations is that, under these conditions, the substrate molecules are spread out over a large number of sites, so that the probability of an S_1 and an S_2 molecule becoming adsorbed on neighboring sites is decreased.

The value of $[\mathrm{C}]_0$ at the maximum is given by differentiating equation 7 and setting $\mathrm{d}v/\mathrm{d}[\mathrm{C}]_0$ equal to zero; this gives rise to

$$[\mathrm{C}]_{0_{\max}} = 1/(K_1K_2)^{1/2} \tag{9}$$

COMPETITIVE ADSORPTION

In this case it is again postulated that, for reaction to be possible, S_1 must be adsorbed on a site of type 1 and S_2 on a site of type 2; however, there is now the possibility of a special type of inhibition, since S_1 may become adsorbed on sites of type 2 and S_2 on sites of type 1. Reaction can *not* occur between S_1 on site 2 and S_2 on site 1.

As before, let θ_1 be the fraction of sites 1 covered by S_1, and K_1 the corresponding equilibrium constant; similarly, let θ_2 and K_2 be for S_2 on sites 2. Let θ_1' be the fraction of sites 1 covered by S_2, θ_2' the fraction of sites 2 covered by S_1, and K_1' and K_2' the corresponding equilibrium constants.

For the sites of type 1 the fraction covered by S_1 is θ_1 and the fraction bare is $1 - \theta_1 - \theta_1'$. The equilibrium involving S_1 and sites 1 is therefore given by

$$\frac{\theta_1}{1 - \theta_1 - \theta_1'} = K_1[\mathrm{S}_1] \tag{10}$$

$$= K_1([\mathrm{S}_1]_0 - [\mathrm{C}]_0\theta_1 - [\mathrm{C}]_0\theta_2') \tag{11}$$

The equilibrium involving S_2 and sites 1 is similarly

$$\frac{\theta_1'}{1 - \theta_1 - \theta_1'} = K_1'[\mathrm{S}_2] \tag{12}$$

$$= K_1([\mathrm{S}_2]_0 - [\mathrm{C}]_0\theta_2 - [\mathrm{C}]_0\theta_1') \tag{13}$$

In the same way, for S_2 adsorbed on sites of type 2,

$$\frac{\theta_2}{1 - \theta_2 - \theta_2'} = K_2([\mathrm{S}_2] - [\mathrm{C}]\theta_2 - [\mathrm{C}]\theta_1') \tag{14}$$

and for S_1 on sites of type 2,

$$\frac{\theta_2'}{1 - \theta_2 - \theta_2'} = K_2'([\mathrm{S}_1]_0 - [\mathrm{C}]_0\theta_1 - [\mathrm{C}]_0\theta_2') \tag{15}$$

The exact solution of equations 11, 13, 14, and 15 is laborious and yields clumsy expressions for θ_1 and θ_2; however, an approximate treatment gives rise to

$$\theta_1 = \frac{K_1[\mathrm{S}_1]_0}{1 + [\mathrm{C}]_0(K_1 + K_1') + K_1[\mathrm{S}_1]_0 + K_1'[\mathrm{S}_2]_0} \tag{16}$$

and

$$\theta_2 = \frac{K_2[\mathrm{S}_2]_0}{1 + [\mathrm{C}]_0(K_2 + K_2') + K_2'[\mathrm{S}_1]_0 + K_2[\mathrm{S}_2]_0} \tag{17}$$

The concentration of ternary complexes of the type that give rise to reaction, having S_1 on site 1 and S_2 on site 2, is $[C]_0\theta_1\theta_2$, and the rate of reaction is therefore $k_2[C]_0\theta_1\theta_2$, where k_2 is the rate constant for the decomposition of the complex; hence the reaction rate is

$$v = \frac{k_2 K_1 K_2 [C]_0 [S_1]_0 [S_2]_0}{(1 + [C]_0(K_1 + K_1') + K_1[S_1]_0 + K_1'[S_2]_0)(1 + [C]_0(K_2 + K_2') + K_2'[S_1]_0 + K_2[S_2]_0)} \tag{18}$$

This expression is to be compared and contrasted with equation 7, to which, as is to be expected, it reduces if K_1' and K_2' are zero, i.e., if there is no competitive adsorption. The two equations are seen to predict the same type of variation of the rate with the catalyst concentration, the rate passing through a maximum and then diminishing. An important difference between the two expressions arises in connection with the influence of substrate concentration; according to equation 7 the rate reaches a limiting value at high concentrations of either substrate, but according to equation 18 it passes through a maximum and finally diminishes towards zero; thus at sufficiently high values of $[S_1]_0$ the rate becomes inversely proportional to $[S_1]_0$. Examples of this type of behavior are not common, but we have found a case of it in the reaction between lactic acid and coenzyme I catalyzed by lactic dehydrogenese (18); the rate was found to pass through a well-defined maximum value as the coenzyme concentration was increased. It was found, on the other hand, that there was no maximum with increasing lactic acid concentration, indicating that there is little adsorption of lactic acid (S_1) on sites of type 2, i.e., that K_2' is very small.

That the rate of this reaction passes through a maximum with increasing enzyme concentration (18, 19) has already been noted.

With surface reactions the case of competitive adsorption is probably more common than that of noncompetitive adsorption, which was seen to be possible only when there are two different types of active centers. When there is only one type, each substrate can be adsorbed on any site, and the kinetic law obtained (*cf.* reference 12, pp. 669–71; reference 5, pp. 377–81) is then equivalent to equation 18. Several examples are available of reactions obeying this law, although the data are seldom complete. A maximum in the rate with increasing substrate concentration has been observed in the reaction between hydrogen and carbon dioxide on platinum (9). Under certain circumstances the rate of the reaction between carbon monoxide and oxygen on the surface of quartz (2) and of platinum (10) is inversely proportional to the concentration of carbon monoxide, while in the reaction between hydrogen and oxygen on platinum (17) the rate is sometimes inversely proportional to the hydrogen pressure. The reaction between ethylene and hydrogen on copper (1) shows similar behavior.

COMPETITIVE ADSORPTION: S_2 IS THE SOLVENT

An important variation of the above treatment arises when one of the substrates, S_2, is the solvent; this is the case particularly in hydrolyses. The essential difference between this case and the preceding one is that the sites cannot be bare with respect to the substrates; e.g., if site 1 is not covered by an S_1 molecule it must be covered by a solvent S_2 molecule. Let θ_1 be the fraction of sites 1 covered by S_1; then $1 - \theta_1$ is the fraction covered by S_2. Similarly, if θ_2 is the fraction of sites 2 covered by S_1, $1 - \theta_2$ is the fraction covered by the solvent molecules.

The equilibrium equations are now as follows:

for site 1:

$$\frac{\theta_1}{1 - \theta_1} = K_1([S_1]_0 - [C]_0\theta_1 - [C]_0\theta_2) \tag{19}$$

and for site 2:

$$\frac{\theta_2}{1 - \theta_2} = K_2([S_1]_0 - [C]_0\theta_1 - [C]_0\theta_2) \tag{20}$$

Approximate solutions of these equations are

$$\theta_1 = \frac{K_1[S_1]_0}{1 + K_1[C]_0 + K_1[S_1]_0} \tag{21}$$

$$\theta_2 = \frac{K_2[S_1]_0}{1 + K_2[C]_0 + K_2[S_1]_0} \tag{22}$$

The concentration of active complexes, having S_1 adsorbed on sites 1 and S_2 on sites 2, is now $[C]_0\theta_1(1 - \theta_2)$, and the rate is therefore

$$v = k_2[C]_0\theta_1(1 - \theta_2) \tag{23}$$

$$= \frac{k_2K_1K_2[C]_0[S_1]_0(1 + K_2[C]_0)}{(1 + K_1[C]_c + K_1[S_1]_0)(1 + K_2[C]_0 + K_2[S_1]_0)} \tag{24}$$

At low catalyst concentrations this equation becomes

$$v = \frac{k_2K_1K_2[C]_0[S_1]_0}{(1 + K_1[S_1]_0)(1 + K_2[S_1]_0} \tag{25}$$

an equation that was derived by Laidler and Hoare (13) with reference to the urease-catalyzed hydrolysis of urea.

The most interesting feature of this equation is that it accounts for a maximum rate with increasing S_1 concentration; the physical significance of this is that the substrate becomes more and more adsorbed on sites of type 2, and so inhibits reaction. A very clear-cut example of this is to be found in the urea–urease system, for which such a maximum has been well established (7, 8, 13). The effect has been shown not to be due to a decrease in the activity of the water at high urea concentrations (7), and the kinetic data have been fitted to equation 25 with fair accuracy; it has been found that the fit is best with K_1 equal to K_2, indicating that the urea is equally well adsorbed on the two sites. Equation 24 would predict a linear variation of the rate with catalyst concentration provided the concentration is not too high; this has been demonstrated experimentally. Work at high molar concentrations of the enzyme cannot be carried out, owing to the limited solubility and high molecular weight; however, equation 24 would predict the attainment of a limiting rate, rather than a maximum one as given by equation 18.

A maximum rate with increasing substrate concentration has also been found in the acid-catalyzed hydrolysis of acetamide (4) (*cf.* Part I). This effect may be accounted for in terms of the present treatment, but it is perhaps more likely due to a decrease in the activity of the water with increasing acetamide concentration. More experimental work is required to distinguish between these possibilities.

SUMMARY

Expressions are worked out for the rates of catalyzed reactions involving two substrates, or a substrate and a coenzyme. The expressions are shown to account for the main features of the relevant experimental results. Three cases are considered: (*1*) noncompetitive adsorption of the substrate molecules on neighboring active sites of the catalyst molecule, (*2*) competitive adsorption of the substrate molecules, i.e., one or both can be adsorbed on each type of site, and (*3*) competitive adsorption in which one substrate is the solvent.

It is found that in cases (*1*) and (*2*) the rate passes through a maximum with increasing catalyst concentration, but that in case (*3*) it attains a limiting value. In case (*1*) the rate reaches a limiting value with increasing concentration of either substrate and in case (*2*) it passes through a maximum, while in case (*3*) it passes through a maximum with increasing concentration of the solute substrate.

REFERENCES

(1) Benton, A. F., and Williams, T. L.: J. Phys. Chem. **30,** 1487 (1926).
(2) Bodenstein, M., and Ohlmer, F.: Z. physik. Chem. **53,** 166 (1905).
(3) Dann, W. J.: Biochem. J. **25,** 178 (1931).
(4) Euler, H. von, and Olander, A.: Z. physik. Chem. **131,** 107 (1927).
(5) Glasstone, S., Laidler, K. J., and Eyring, H.: *The Theory of Rate Processes.* McGraw-Hill Book Company, Inc., New York (1941).
(6) Hearon, J. Z.: Bull. Math. Biophys. **11,** 29, 83 (1949).
(7) Hoare, J. P., and Laidler, K. J.: J. Am. Chem. Soc., in press.
(8) Howell, S. F., and Sumner, J. B.: J. Biol. Chem. **104,** 619 (1934).
(9) Hinshelwood, C. N., and Prichard, C. R.: J. Chem. Soc. **127,** 806 (1925).
(10) Langmuir, I.: Trans. Faraday Soc. **17,** 621 (1922).
(11) Laidler, K. J., Glasstone, S., and Eyring, H.: J. Chem. Soc. **8,** 659 (1940).
(12) Laidler, K. J., Glasstone, S., and Eyring, H.: J. Chem. Phys. **8,** 667 (1940).
(13) Laidler, K. J., and Hoare, J. P.: J. Am. Chem. Soc. **71,** 2699 (1949).
(14) Laidler, K. J., and Socquet, I. M.: J. Phys. & Colloid Chem. **54,** 519 (1950).
(15) Lipmann, F.: Cold Spring Harbor Symposia Quant. Biol. **7,** 248 (1939).
(16) LuValle, J. E., and Goddard, D. R.: Quarterly J. Biol. **23,** 197 (1948).
(17) Pease, R. N.: J. Am. Chem. Soc. **45,** 1196 (1923).
(18) Socquet, I. M., and Laidler, K. J.: Arch. Biochem. **25,** 171 (1950).
(19) Straub, F. B.: Enzymologia **9,** 143 (1941).

THERMODYNAMICS OF ADSORPTION FROM SOLUTIONS. III

Adsorption at Liquid–Air Interfaces

YING FU AND F. E. BARTELL

Department of Chemistry, University of Michigan, Ann Arbor, Michigan

Received May 31, 1949

INTRODUCTION

The thickness of adsorbed films of soluble substances on the surface of dilute solutions has generally been accepted to be monomolecular (2). The evidence for such monomolecular films on more concentrated solutions has been less conclusive. From surface tension measurements Butler and Wightman (8) advanced the opinion that for concentrated aqueous solutions of ethyl alcohol the adsorbed film is more than one molecule thick, but in their calculations one of the equations used is of doubtful validity. In previous publications from this laboratory (10, 11, 17) evidence was presented to show that the adsorbed layers at solid–liquid interfaces might be either monomolecular or multimolecular. The conclusions were based on the comparison of the molecular areas of the adsorbates deduced from adsorption data and those obtained from crystal structure studies, and on the correlation between various thermodynamic quantities, such as activity coefficients and free surface energy changes, with the amount adsorbed. It seemed desirable to obtain similar evidence for adsorption at liquid–air interfaces to determine whether parallelism exists between the adsorptions at these two kinds of interfaces. If such a parallelism is found to exist, it would then be possible to make a reasonable inference as to the thickness of the adsorbed layer at liquid–air interfaces.

PROCEDURE AND RESULTS

In a study of the adsorption at liquid–solid interfaces the directly measured quantity is the surface excess, from which all thermodynamic quantities are derived. In the case of liquid–air interfaces, the quantity most easily accessible to accurate direct measurement is the surface tension, and the surface excess is derived from surface tension measurements by applying Gibbs' adsorption equation. Once the surface excess, Γ, has been obtained, various thermodynamic quantities can be calculated as was done in the case of solid–liquid interfaces. For the present investigation, aqueous solutions of butyric, valeric, and caproic acids, phenol, butyl alcohol, and resorcinol were used. This list was selected partly because parallel studies (except for resorcinol) have been made previously for solid–liquid interfaces (10, 11, 17), and partly because activity values for these systems are either available or can be calculated from appropriate data reported in the literature. The importance of using the exact form of the Gibbs equation, i.e., expressing the chemical potentials in terms of activities instead of concentrations, deserves special emphasis because, unless the solutions are very dilute, the Γ-values derived from the exact and from the approximate form of Gibbs' equation may differ to such an extent that not only the quantitative but also the qualitative aspect of the adsorption isotherm may be altered.

In the calculations[1] the surface tension data were taken from the following sources:

SUBSTANCE	SOURCE OF DATA
Butyl alcohol	Bartell and Davis (4)
Butyric acid	Harkins and King (20)
Valeric acid	Szyzkowski (24)
Caproic acid	Rehbinder (23)
Phenol and resorcinol	Harkins and Grafton (19)

The sources of activity data are:

SUBSTANCE	SOURCE OF DATA
Butyl alcohol	Harkins and Wampler (21)
Phenol	Jones and Bury (22)
Valeric acid	Freezing-point data of Giacolone (13)
Resorcinol	Freezing-point data of Bourion and Tuttle (5)

Neither the activity values nor any other appropriate data for caproic acid are available. Since the caproic acid solution used was extremely dilute, it is believed that the approximate form of Gibbs' equation can be used in this case without serious error.

The calculations were based on the following equations[1]:

---

[1] The meanings of the different symbols are as follows:
$\Gamma_2^{(1)}$ = the classical surface excess of Gibbs,
$\Gamma_2^{(v)}$ = the surface excess on volume basis,
γ_0 and γ = surface tension of water and the solution, respectively,
a = activity of the solute in the bulk phase,
$\bar{v}$ = molal volume of the solution,
$\bar{v}_1$ and $\bar{v}_2$ = partial molal volume of the solvent and the solute, respectively,
m^s = molality of the adsorbate in the adsorbed layer,
f^s = activity coefficient of the adsorbate in the adsorbed layer,
$\Delta\mu^0 = RT \underset{a\to 0}{\log_e}(m^s/a)$ = change of standard chemical potential of the adsorbate,
t = thickness of the adsorbed layer,
c = equilibrium concentration, in moles per liter, of the solution,
H_2O^0 = original number of moles of water in the surface layer,
ϕ = surface pressure,
A = area per molecule of the adsorbate in the adsorbed layer,
Z_2 = total number of molecules of adsorbate per unit area, and
N = Avogadro's number.

$$\Gamma_2^{(1)} = -\mathrm{d}\gamma/2.3RT\ \mathrm{d}\log a \qquad (1)$$

$$\Gamma_2^{(v)} = (\bar{v}_1/\bar{v})\Gamma_2^{(1)} \quad (16) \qquad (2)$$

$$m^s = (\Gamma_2^{(v)} + tc/1000)/(\mathrm{H_2O}^0 - (\bar{v}_2/\bar{v}_1)\Gamma_2^{(v)}) \times 55.5 \quad (12) \qquad (3)$$

$$\log f^s = \Delta\mu^0/2.3RT + \log a - \log m^s \quad (10) \qquad (4)$$

$$\phi = \gamma_0 - \gamma \qquad (5)$$

$$A = 1/Z_2 = 1/N(\Gamma_2^{(v)} + tc/1000) \quad (3) \qquad (6)$$

The data obtained are given in table 1.

DISCUSSION

In evaluating the activity coefficients of valeric acid and resorcinol from freezing-point data, the convention of Jones and Bury (22) was adopted. This convention differs from the more commonly used one of Lewis and Randall in that a convenient concentration instead of infinite dilution was chosen as the standard state. This procedure was expedient in the present case because no data covering the most dilute range were available. Since the activity coefficients so obtained differ from those obtained by the Lewis–Randall convention only by a multiplicative constant, the slope of the γ *vs.* log a curve is in no way affected. Of these two series of activity coefficient values, that of valeric acid is probably the less accurate because the freezing-point data used are less precise. Fortunately, highly accurate activity values are not absolutely necessary for the calculation of surface excesses. A comparison of the adsorption isotherms of valeric and caproic acids (figure 1) shows that they are of the same type, as would be expected from the previous studies on the adsorption of these two substances by graphites and sugar char (17), an indication that the isotherm for valeric acid is at least qualitatively correct.

For the calculation of surface molality, m^s, and the molecular area, A, it is necessary to know the total number of the adsorbate molecules in the adsorbed layer. This problem has been studied from time to time by various investigators. Harkins and coworkers (18, 21) obtained this number by adding to $\Gamma_2^{(1)}$ the two-thirds power of the number of solute molecules per unit volume of the bulk solution. The unsatisfactory nature of this procedure has been pointed out by Butler (7). Butler and Wightman (8) and Guggenheim and Adam (16) used the equation

$$Z_1A_1 + A_2A_2 = 1 \qquad (7)$$

together with a specialized form of equation (515) of Gibbs (14):

$$-\frac{\partial\gamma}{\partial\mu_2} = \Gamma_2^{(1)} = Z_2 - Z_1\ x_2/x_1 \qquad (8)$$

where x_2 and x_1 represent the mole fractions. By choosing reasonable values for the molecular areas, these two equations can be solved simultaneously for the Z's. As pointed out by Davis (9), equation 7 is valid only under very special conditions, because it implies that the adsorbed layer is monomolecular with respect

TABLE 1

Adsorption at water–air interfaces

c	a	$\Gamma_2^{(1)} \times 10^{10}$	$\Gamma_2^{(v)} \times 10^{10}$	$Z \times 10^{10}$	A	ϕ	ϕA	m^s	f^s
Butyl alcohol									
0.028	0.0275	2.41	2.40	2.42	68.6	6.3	429	5.36	1.005
0.055	0.0534	3.54	3.52	3.56	46.7	11.2	522	10.3	1.02
0.109	0.103	4.50	4.46	4.53	36.6	18.3	671	17.3	1.17
0.216	0.201	5.27	5.18	5.32	31.2	26.7	833	27.6	1.43
0.323	0.297	5.60	5.44	5.66	29.4	31.6	928	34.5	1.68
0.430	0.392	5.80	5.59	5.87	28.3	35.3	999	40.0	1.92
0.537	0.485	5.89	5.62	5.97	27.8	38.3	1065	43.9	2.16
0.640	0.572	5.99	5.66	6.08	27.3	40.8	1114	47.6	2.37
0.738	0.662	5.99	5.62	6.12	27.2	43.0	1169	49.4	2.62
Butyric acid									
0.033	0.040	2.18	2.17	2.19	75.9	5.3	405	4.46	1.16
0.050	0.063	3.21	3.19	3.22	51.6	8.6	442	7.88	1.04
0.083	0.100	3.84	3.91	3.87	42.9	12.5	539	10.9	1.19
0.116	0.141	4.21	4.17	4.25	39.1	15.8	620	13.2	1.39
0.165	0.200	4.46	4.41	4.52	36.7	19.5	715	15.1	1.72
0.208	0.251	4.67	4.59	4.73	35.2	22.0	773	16.7	1.95
0.263	0.316	4.79	4.68	4.86	34.2	24.6	843	18.0	2.29
0.335	0.398	4.91	4.78	5.01	33.2	27.3	906	19.4	2.70
0.428	0.501	5.00	4.82	5.11	32.5	30.1	978	20.5	3.18
0.550	0.631	5.11	4.87	5.25	31.6	33.9	1070	22.1	3.72
0.708	0.794	5.22	4.89	5.37	30.9	35.8	1106	23.8	4.34
0.922	1.000	5.30	4.89	5.52	30.1	38.7	1166	25.8	5.06
Phenol									
0.010	0.010	0.52	0.52	0.52	322	1.3	402	0.95	0.93
0.016	0.016	0.82	0.82	0.82	202	2.0	404	1.58	0.88
0.026	0.025	1.29	1.28	1.29	128.6	3.2	404	2.78	0.79
0.041	0.040	2.06	2.05	2.07	80.2	5.0	401	5.02	0.70
0.065	0.063	3.10	3.08	3.12	53.2	7.7	410	9.62	0.58
0.103	0.100	4.10	4.06	4.12	40.3	11.7	472	17.3	0.51
0.166	0.159	4.71	4.64	4.74	35.0	16.8	588	25.5	0.55
0.212	0.200	4.87	4.78	4.91	33.8	19.5	659	28.7	0.58
0.273	0.251	5.07	4.95	5.11	32.5	22.4	728	33.8	0.66
0.356	0.316	5.24	5.08	5.29	31.4	25.3	795	38.6	0.72
0.473	0.398	5.35	5.13	5.41	30.7	28.3	868	42.9	0.82
Resorcinol									
0.033	0.050	0.30	0.30	0.32	519	0.8	415	0.65	1.0
0.053	0.079	0.47	0.47	0.50	332	1.3	415	1.05	1.0
0.067	0.100	0.57	0.57	0.61	275	1.5	423	1.29	1.0
0.085	0.126	0.70	0.69	0.73	226	1.9	430	1.61	1.01
0.109	0.159	0.84	0.83	0.89	187	2.4	450	2.00	1.03
0.139	0.200	0.99	0.98	1.06	156	3.0	468	2.49	1.04
0.179	0.251	1.15	1.13	1.22	136	3.6	488	2.96	1.10

TABLE 1—*Concluded*

c	a	$\Gamma_2^{(1)} \times 10^{10}$	$\Gamma_2^{(v)} \times 10^{10}$	$Z \times 10^{10}$	A	ϕ	ϕA	m^s	f^s
Resorcinol									
0.229	0.316	1.30	1.27	1.39	119	4.3	514	3.49	1.18
0.299	0.399	1.43	1.39	1.55	107	5.0	535	4.03	1.29
0.385	0.501	1.58	1.53	1.73	96	5.9	566	4.70	1.38
0.507	0.631	1.75	1.67	1.94	85.8	6.8	583	5.54	1.48
0.677	0.794	2.01	1.87	2.22	74.8	7.8	584	6.84	1.51
0.917	1.000	2.36	2.17	2.65	62.7	9.1	570	9.19	1.41
1.126	1.150	2.65	2.39	2.98	55.7	9.9	551	11.5	1.29
Valeric acid									
0.013	0.016	2.73	2.73	2.74	60.8	7.2	438	5.06	1.01
0.021	0.025	3.52	3.51	3.53	47.0	10.7	503	7.68	1.05
0.033	0.040	4.18	4.17	4.19	39.6	14.9	590	10.6	1.21
0.053	0.063	4.77	4.74	4.78	34.7	19.9	691	14.2	1.43
0.068	0.079	5.04	5.00	5.06	32.8	22.6	741	16.5	1.55
0.086	0.100	5.32	5.27	5.34	31.1	25.5	793	19.2	1.68
0.142	0.159	5.86	5.78	5.89	28.2	31.6	891	26.4	1.94
0.185	0.200	6.33	6.21	6.36	26.1	35.0	914	36.0	1.83
0.241	0.251	6.85	6.68	6.88	24.1	38.7	932	54.9	1.47
0.279	0.282	7.30	7.10	7.33	22.6	40.6	918	93.1	0.97
Caproic acid									
0.0020		1.65		1.65	100.6	4.0	402	2.18	1.00
0.0040		2.70		2.70	61.5	7.5	461	4.26	1.02
0.0063		3.45		3.46	48.1	10.9	525	6.33	1.09
0.0079		3.80		3.81	43.6	13.0	568	7.55	1.15
0.0100		4.14		4.15	40.0	15.2	606	8.93	1.19
0.0126		4.53		4.54	36.7	17.6	648	10.8	1.27
0.0159		4.98		5.00	33.5	20.3	680	13.7	1.26
0.0212		5.72		5.74	28.9	23.9	694	20.7	1.11
0.0251		6.31		6.33	26.2	26.5	695	30.6	0.90
0.0298		6.98		7.01	23.7	28.4	674	55.2	0.59

to both components. As the assignment of a definite value to the molecular area of one of the components automatically fixed the thickness of the adsorbed layer, the condition of simultaneous monomolecularity with respect to both components can be fulfilled only when the two molecular species are of equal length. Since this is very seldom the case, equation 7 is too restricted to be of general use. In a previous paper from this laboratory (10) Z_2 was taken to be $\Gamma_2^{(v)} + B$, where B, the original number of adsorbate molecules present on the surface without adsorption, was assumed to be the product of the total number of molecules of both components in the adsorbed layer by the mole fraction of the solute in the bulk solution. It has been pointed out in a recent note (12) that this procedure is rigorously applicable only when the molecules of both species are of the same size. This method, therefore, has the same shortcoming as the one mentioned above. It seems that, of all the methods proposed for this purpose, the one of Bartell and Benner (3) is probably the most suitable. They assumed the adsorbed molecules to be oriented, which assumption is similar to that made by Butler and Wightman and by Guggenheim and Adam. The number of adsorbate molecules present in the adsorbed layer in case of no adsorption is, then, simply the product of the concentration of the bulk solution by the thickness of the layer, which is, of course, the length of the adsorbate molecule. Even though the assumption of complete orientation may not be rigorously true when the adsorption is very low, the error so resulting is too small to be of any consequence because the correction term, B, is very small for such dilute solutions. The lengths of the adsorbate molecules were deduced from the partial molal volumes and the molecular areas as given by Adam (1).

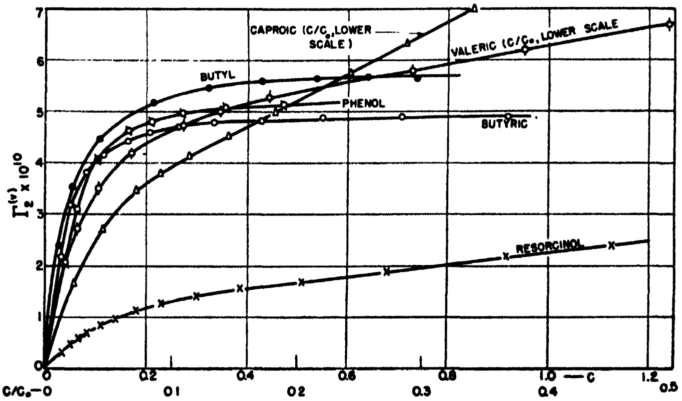

FIG. 1. Comparison of the adsorption isotherms of phenol, resorcinol, butyl alcohol, and butyric, caproic, and valeric acids.

TABLE 2

Adsorption of caproic acid

c	c/c_0	Γ_{calcd}	Γ_{exptl}	ϕ_{calcd}	φ_{exptl}
0.002	0.0228	1.63	1.65		
0.005	0.0571	2.91	3.07	9.6	9.1
0.010	0.114	4.07	4.12	15.5	15.3
0.015	0.171	4.86	4.88	19.9	19.6
0.020	0.228	5.55	5.58	23.5	23.2
0.025	0.285	6.23	6.26	26.7	26.4
0.030				29.6	29.5

An inspection of the adsorption isotherms (figure 1) shows that they belong to two distinct types. Butyl alcohol, butyric acid, and phenol belong to the monolayer type of Langmuir, while resorcinol, valeric acid, and caproic acid belong to type II of the B.E.T. classification (6). The first three isotherms can be satisfactorily represented by Langmuir's equation. The valeric acid isotherm can be represented by neither the Langmuir nor the simple B.E.T. equation. This is probably due to the inaccurate Γ-values resulting from inaccurate activity data. The isotherm for caproic acid follows the simple B.E.T. equation quite closely, as can be seen from table 2. For the calculations in this table, the following equations and constants were used: $\Gamma_m = 5.00$; $b = 20.0$; c_0 (solubility of caproic acid) $= 0.0876$;

$$\Gamma = \frac{\Gamma_m bc}{(c_0 - c)\left\{1 + (b - 1)\frac{c}{c_0}\right\}}$$

and

$$\phi = 2.3RT\Gamma_m \log \frac{c_0 + (b - 1)c}{c_0 - c}$$

The relative concentrations of the resorcinol solution are so low that any attempt to decide the molecularity of the adsorbed layer from the isotherm alone would not be conclusive.

The fact that some isotherms follow the B.E.T. equation suggests but does not prove the multilayer nature of the adsorbed layers at the liquid–air interfaces. More especially is further corroborative evidence required, since the minimum areas per molecule are higher than those observed with condensed films. It has been shown previously (10, 11) that for solid–liquid interfaces the mono- and multi-layer adsorptions can be distinguished from the curves correlating some thermodynamical quantities with the surface excesses. The characteristics of such curves are as follows:

CURVE	MONOLAYER	MULTILAYER
f^s *vs.* Γ	Parabolic	Parabolic at low Γ, then bending downward at completion of monolayer
ϕ *vs.* Γ	Parabolic	S-shaped
ϕA *vs.* ϕ	Linear	First portion linear, then developing negative curvature, finally bending downward

When corresponding curves were plotted for the systems of the present investigation (figures 2–4), butyl alcohol, butyric acid, and phenol showed the monolayer characteristics, while resorcinol, valeric acid, and caproic acid followed the multilayer curves. The breaks of the f^s *vs.* Γ curve and the inflection points of the ϕ *vs.* Γ curves come at approximately the *B* points (used by Brunauer and Emmett) of the isotherm curves. In the case of caproic acid, the Γ_m-value, which represents the number of moles required to form a completely saturated monolayer, obtained from the curves is about 4 per cent lower than that calculated by the B.E.T. equation. Considering the degree of accuracy attainable from the slope of the surface tension–concentration curve, the agreement is quite satisfactory.

Even though the phenol isotherm is qualitatively the same as those for butyl

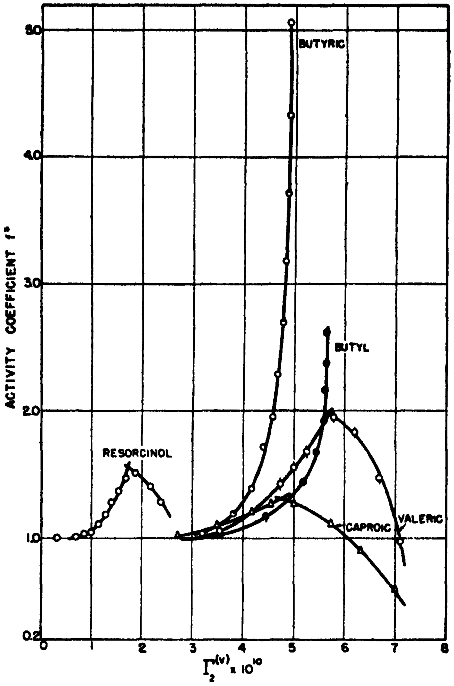

FIG. 2. f^s *vs.* Γ curve for resorcinol, butyl alcohol, and butyric, caproic, and valeric acids

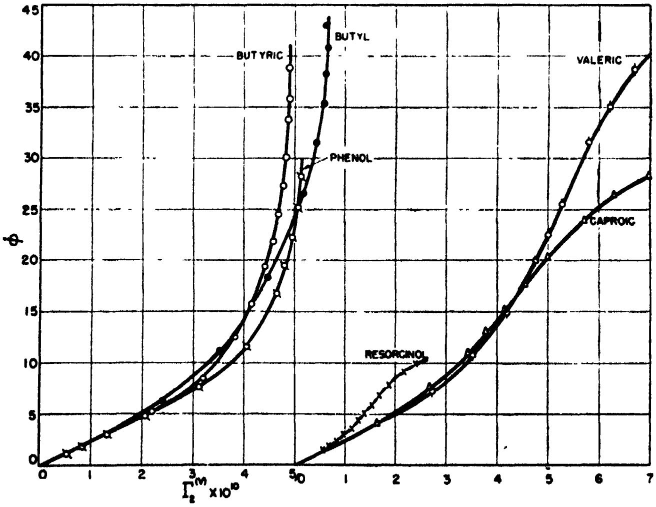

FIG. 3. ϕ *vs.* Γ curves for phenol, resorcinol, butyl alcohol, and butyric, caproic, and valeric acids.

alcohol and butyric acid, it differs from the latter in that the amount adsorbed varies linearly with concentration up to about $c \approx 0.06$ M. The same qualitative results were obtained when surface excesses were calculated from the surface tension data of Goard and Rideal (15). In terms of surface concentrations, this means that the surface solution remains ideal up to about 10 molal. The activity coefficient–surface molality curve shows the characteristics similar to those often observed with bulk solutions. When the molality of the adsorbate in the adsorbed layer, m^s, is low, the activity coefficient of the adsorbate in the adsorbed layer reaches a minimum at about $m^s \approx 16$ and then starts to rise parabolically. The last portion of this curve is similar to the curves for butyl alcohol and butyric acid. Probably the phenol-type curve is general for all systems. The reason that this has not been observed with other systems is because the downward portion is too small to be detected. The fact that the activity coefficients are not unity when the surface solution remains ideal does not invalidate the defining equation of $\Delta\mu_0$, because molalities instead of mole fractions were used to express chemical potentials. As is well known, the activity coefficient will remain unity for an ideal solution of finite concentration only when mole fractions are used.

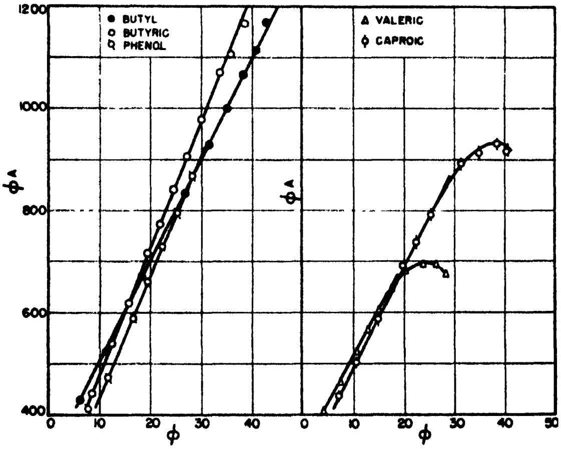

FIG. 4. ϕA vs. ϕ curves for phenol, butyl alcohol, and butyric, caproic, and valeric acids

Of the four quantities, f^s, m^s, ϕA, and ϕ, the values of the first three depend on the thickness assumed for the adsorbed layer, while the surface pressure, ϕ, of course, does not. In calculating f^s, m^s, and A (the area per molecule of adsorbate in adsorbed layer), it was assumed that all the solute molecules adsorbed are in the monolayer. This, of course, is not true if the adsorption is multilayer. Therefore, when the f^s *vs.* Γ, ϕ *vs.* Γ, or ϕA *vs.* ϕ curves deviate from the normal course, the point of departure may be used to detect the completion of the monolayer or the presence of multilayers. The downward trend of the f^s *vs.* Γ curve is caused by the change of the standard chemical potential of the adsorbed molecules (10), while the downward trend of the ϕA *vs.* ϕ curve is due to the fact that available areas assigned to the molecular values are smaller than the true values. Since there is no means to determine the distribution of the adsorbate molecules among the various layers, it is easy to realize why no really satisfactory equation of state for the adsorbed layers has ever been proposed.

SUMMARY

Adsorption of butyl alcohol, butyric acid, phenol, resorcinol, valeric acid, and caproic acid at water–air interfaces has been calculated from surface tension data by means of the exact form of Gibbs' equation.

Activity coefficients, surface molalities, molecular areas, and surface pressures have been calculated and plotted. These curves are entirely similar to those obtained for the solid–liquid interfaces.

The adsorption of butyl alcohol, butyric acid, and phenol is monolayer; that of resorcinol, valeric acid, and caproic acid is multilayer.

REFERENCES

(1) ADAM: *The Physics and Chemistry of Surfaces*, p. 50. Oxford University Press, London (1941).
(2) Reference 1, p. 118.
(3) BARTELL AND BENNER: J. Phys. Chem. **46,** 847 (1941).
(4) BARTELL AND DAVIS: J. Phys. Chem. **45,** 1321 (1941).
(5) BOURION AND TUTTLE: J. Chem. Phys. **26,** 292 (1929).
(6) BRUNAUER: *The Adsorption of Gases and Vapors. Vol. I. Physical Adsorption*, p. 150. Princeton University Press, Princeton, New Jersey (1943).
(7) BUTLER: Proc. Roy. Soc. (London) **A135,** 348 (1932).
(8) BUTLER AND WIGHTMAN. J. Chem. Soc. **1932,** 2095.
(9) DAVIS: Thesis, University of Michigan, 1941.
(10) FU, HANSEN, AND BARTELL: J. Phys. & Colloid Chem. **52,** 374 (1948)
(11) FU, HANSEN, AND BARTELL: J. Phys. & Colloid Chem. **53,** 1141 (1949).
(12) FU, HANSEN, AND BARTELL. J Phys & Colloid Chem. **53,** 454 (1949).
(13) GIACOLONE: Gazz chim. ital. **70,** 47 (1940).
(14) GIBBS· *Collected Works*, Vol. I, p. 236. Longmans, Green and Company, New York (1928).
(15) GOARD AND RIDEAL: J. Chem. Soc. **127,** 1672 (1925).
(16) GUGGENHEIM AND ADAM· Proc. Roy. Soc. (London) **A139,** 218 (1933).
(17) HANSEN, FU, AND BARTELL: J. Phys. & Colloid Chem. **53,** 769 (1949).
(18) HARKINS AND FOWKES· J. Am. Chem. Soc. **62,** 3377 (1940).
(19) HARKINS AND GRAFTON: J. Am. Chem. Soc. **47,** 1329 (1925).
(20) HARKINS AND KING: Kansas State Agr Coll. Tech. Bull. **No. 9.**
(21) HARKINS AND WAMPLER: J. Am. Chem. Soc. **53,** 850 (1931).
(22) JONES AND BURY. Phil. Mag. **4,** 1125 (1927).
(23) REHBINDER: Z. physik. Chem. **111,** 447 (1924).
(24) SZYZKOWSKI: Z. physik. Chem. **64,** 385 (1908).

PARAMETRIC EQUATIONS IN THE TREATMENT OF MULTICOMPONENT SYSTEMS

L. A. DAHL[1]

National Bureau of Standards, Washington, D.C.

Received May 11, 1949

INTRODUCTION

A system of n components in an N-component system can be defined analytically by N parametric equations involving $n - 1$ parameters.[2] In each of these equations the percentage of a component is equated to an expression which is linear with respect to the parameter or parameters. This is advantageous, since it affords a means of direct computation of mixtures in the n-component system by assigning values to the parameters. Parametric equations are particularly useful when n is small and N is large. For example, the parametric equations for a binary system in a system of many components are just as simple as the equations of a binary system in a ternary system, and are as simply derived. Equations of this type are useful in planning mixtures for study in phase equilibrium investigations of multicomponent systems.

Interpretation of phase equilibrium data requires consideration of nonlinear relations, since curved lines, curved surfaces, etc., appear in phase diagrams and space models representing equilibrium conditions. However, this paper will be concerned only with equations which are linear with respect to the parameters.

In a previous paper (1) equations were derived for estimating proportions of phases at equilibrium in mixtures in the quaternary system CaO–$5CaO \cdot 3Al_2O_3$–$4CaO \cdot Al_2O_3 \cdot Fe_2O_3$–$2CaO \cdot SiO_2$, a system of interest in portland cement technology. The equations were derived by the methods described in this paper from the data obtained by Lea and Parker (4, 5) in their investigation of the system. By substituting quaternary portland cement compositions in the equations the proportions of crystalline phases and liquid are obtained when the liquid is at an invariant point, on a univariant curve, or on an isotherm on a bivariant surface. With the exception of equilibrium at an invariant point, the methods used in deriving the equations were not described and appear here for the first time.

TERMINOLOGY AND NOTATION

The entire range of compositions which may be formed by varying the proportions of any given set of substances (components) will be referred to as a system. In the broad sense in which the term "system" is used in this paper, the only restriction as to the substances which may be taken as components is that no one of them should be capable of being formed from two or more of the others in any proportions, positive or negative. In considering systems within a system, the latter will be referred to as the *primary system* and its components as *primary components*. Systems within the primary system will be referred to as *subordinate systems* and their components as *subordinate components*. The number of components in a primary system and the number in a subordinate system will be designated as N and n, respectively. When $n = N$, the subordinate system is also termed a *secondary system* (2).

---

[1] Research Associate, National Bureau of Standards, Washington, D.C.

[2] A parameter may be defined as "an independent variable through functions of which may be expressed other variables." (Webster) For example, a curve in space may be expressed by three equations, in each of which one of the coördinates, x, y, and z, is equated to a function of p, a parameter. Equations of this type are parametric equations.

The systems to be considered in illustrative examples will involve various combinations of the oxides CaO, Al_2O_3, Fe_2O_3, SiO_2, MgO, Na_2O, and K_2O as primary components. These will be designated as C, A, F, S, M, N, and K, respectively. Percentages of these oxides will be designated by corresponding letters in italics: the symbol A will represent the percentage of A, that is, of Al_2O_3, etc. Compounds will be designated by formulas in which the oxides are treated as elements. For example, the compound $CaO \cdot Al_2O_3 \cdot 2SiO_2$ is designated as CAS_2.

PARAMETERS AND PARAMETRIC EQUATIONS

Any curve, surface, or other geometrical figure which may be defined by an equation or equations involving variables representing distances from coördinate axes may also be defined by a series of parametric equations. These equations define each of the variables in terms of one or more independent variables or parameters. To illustrate, let us consider the parabola,

$$x^2 + y^2 - 12x - 13y - 2xy + 86 = 0 \qquad (1)$$

The curve may also be represented by the pair of parametric equations,

$$x = p^2 + 3p + 4 \qquad (2)$$
$$y = p^2 - 2p + 3 \qquad (3)$$

in which p is the parameter. If $p^2 + 3p + 4$ and $p^2 - 2p + 3$, respectively, are substituted for x and y in equation 1, all terms drop out, leaving the equation $0 = 0$. It follows that if any value assigned to p is substituted in equations 2 and 3, the values of x and y so obtained will satisfy equation 1.

The parameter p must have a definite significance, since it is a function of the coördinates of points on the curve. In some instances a variable of known significance may be selected as a parameter, but this is not necessary. In the example given above it would be difficult to ascribe a simple and readily visualized significance to p, and it is sufficient to consider p to be merely an independent variable introduced to define the values of x and y at every point on the curve.

It will be noted that only one parameter appears in equations 2 and 3. This is true for any set of parametric equations defining the coördinates of points on a curved or straight line, regardless of the number of coördinates required for geometric representation. Let us now consider the line which is the intersection of the planes represented by the equations:

$$3x - 4y + z + 10 = 0 \qquad (4)$$
$$6x - 2y - z - 7 = 0 \qquad (5)$$

The x, y, and z coördinates of any point on the line satisfy both equations. The line may also be defined by the parametric equations,

$$x = \frac{2d}{7} + 3 \tag{6}$$

$$y = \frac{3d}{7} + 5 \tag{7}$$

$$z = \frac{6d}{7} + 1 \tag{8}$$

in which d is the distance of any given point on the line from the point (3,5,1), which is also on the line.

It will be noted that equations 4 and 5 are linear, and that parametric equations 6–8, representing the same line, are also linear. In general, parametric equations in linear form may be derived to represent any relation capable of being expressed by linear equations in terms of coördinates. On the other hand, if nonlinear equations in terms of coördinates are required to express a given relation; at least one of the corresponding parametric equations is nonlinear.

DEGREES OF FREEDOM

Considering any set of variables, the number of degrees of freedom, F, is the number of variables which may be independently altered. For example, if x, y, and z are the variables, and there exists no relation between them, $F = 3$. An equation involving one or more of the variables reduces the number of degrees of freedom by one, so that $F = 2$. That is, values may be assigned to only two of the variables, the value of the third then being fixed. Similarly, two equations further reduce the number of degrees of freedom, so that $F = 1$.

In treatises on the phase rule and its applications the number of degrees of freedom is usually defined as the number of variables—composition, pressure, and temperature—which may be altered independently without causing the disappearance of a phase or the appearance of a new phase. This definition is restricted to the variables involved in phase equilibria. In this study the number of degrees of freedom is considered in a more general sense, as we shall have occasion to deal with composition relations without reference to equilibrium between phases.

The number of degrees of freedom possessed by any geometrical figure may be defined as the number of dimensions in that figure. Regardless of the number of dimensions in the space in which a curve lies, a curve has only one dimension and therefore possesses one degree of freedom. A surface has two dimensions and therefore possesses two degrees of freedom. In dealing with multicomponent systems it is important to bear in mind that a curve represents a univariant condition in any system, regardless of the number of components in the system, or the number of dimensions required for geometrical representation of the system and the additional variables of temperatures and pressure. Considered with reference to composition relations alone—that is, without these additional variables—a system may be said to possess a definite number of degrees of freedom.

For example, a binary system, represented geometrically by a straight line, possesses one degree of freedom, whether it is in a ternary or quaternary system, or in a multicomponent system.

The number of parameters required to define a given geometrical figure represented by one or more equations is equal to the number of degrees of freedom possessed by the figure. For example, one parameter is required to define a curve, and two parameters to define a surface, regardless of the number of dimensions of the space in which the curve or surface lies.

An n-component system is represented geometrically in $n - 1$ dimensions, since the sum of the percentages of the components is 100 and there are therefore $n - 1$ independent variables. Considered only with reference to composition, the system has $n - 1$ degrees of freedom, and may therefore be defined by a series of parametric equations involving $n - 1$ parameters. Equations representing an n-component system are linear.

DERIVATION AND PROPERTIES OF PARAMETRIC EQUATIONS

The general method of deriving parametric equations involves four successive steps: (*1*) determination of the number of parameters required; (*2*) selection of parameters; (*3*) setting up the equations with literal constants; and (*4*) evaluation of the constants. This procedure may be followed for either linear or nonlinear relations. The parameters may have no readily defined physical significance, or they may represent such variables as temperature, pressure, or the concentrations of primary or subordinate components. When the weight fractions or percentages of subordinate components are taken as parameters, a more direct method may be used. This method will be described first.

DIRECT METHOD: PRIMARY COMPONENTS IN TERMS OF SUBORDINATE COMPONENTS

In the investigation of phase equilibria in a multicomponent system it is convenient to study one subordinate system at a time. For each subordinate system mixtures are planned for heat treatment or other experimental procedures. Weight fractions or percentages of $(n - 1)$ subordinate components may be selected as parameters, with the advantage that limits on values of the parameters are easily formulated. To illustrate the direct method, let us derive equations for the ternary system KAS_2–CMS_2–C_2AS in the quinary system K–C–M–A–S (the system K_2O–CaO–MgO–Al_2O_3–SiO_2). Let r and s represent weight fractions of KAS_2 and CMS_2, respectively, in any mixture of the three subordinate components. Then the weight fraction of C_2AS is $1 - r - s$. The percentage compositions of the subordinate components are given in table 1.

The parametric equation for any given primary component is found by adding the products obtained by multiplying the percentage of that component in each subordinate component by the corresponding weight fraction. That is,

$$\begin{aligned}
K &= 29.78r \\
C &= 25.90s + 40.91(1 - r - s) \\
M &= 18.62s \\
A &= 32.24r + 37.18(1 - r - s) \\
S &= 37.98r + 55.48s + 21.91(1 - r - s)
\end{aligned}$$

Simplifying,

$$\begin{aligned} K &= 29.78r & (9)\\ C &= -40.91r - 15.01s + 40.91 & (10)\\ M &= 18.62s & (11)\\ A &= -4.94r - 37.18s + 37.18 & (12)\\ S &= 16.07r + 33.57s + 21.91 & (13) \end{aligned}$$

Any assigned values of r and s substituted in equations 9–13 will give a composition in the system KAS_2–CMS_2–C_2AS or in an extension of that system. Compositions will be restricted to that system if neither r nor s is negative and $r + s$ does not exceed 1.

Upon adding equations 9–13, it is found that the terms involving parameters drop out, leaving the relation:

$$K + C + M + A + S = 100.00$$

TABLE 1

PRIMARY COMPONENTS	SUBORDINATE COMPONENTS		
	KAS_2	CMS_2	C_2AS
	per cent	*per cent*	*per cent*
K	29.78		
C		25.90	40.91
M		18.62	
A	32.24		37.18
S	37.98	55.48	21.91
	WEIGHT FRACTION		
	r	s	$1 - r - s$

This constitutes a check on the accuracy of the computations required in deriving the equations.

Equations in which the parameters are weight fractions or percentages of subordinate components are useful in many problems requiring the computation of mixtures in a given subordinate system. Their application to such problems is simplified through the fact that limits on values of the parameters are readily seen. The range of values which may be assigned to the parameters are not mutually independent, since their sum must not exceed 1.00 when weight fractions are used, or 100 when percentages are used. For instance, in this example, if $r = 0.2$, s may have values from 0.0 to 0.8. When variables other than subordinate components are taken as parameters the ranges of values of parameters are similarly dependent upon one another, but they are not so simply expressed nor so easily found.

SUBORDINATE COMPONENTS IN TERMS OF PRIMARY COMPONENTS

In the foregoing example the equation for each primary component is expressed in terms of the parameters r and s. To obtain equations for the weight fractions or percentages of the subordinate components in terms of two of the primary components, any two of these equations may be solved for r and s. The pair of equations selected should be those defining the primary components which are intended to appear in the final equations. Equations in terms of K and M are obtained directly, since $K = 29.78r$ and $M = 18.62s$ (equations 9 and 11). That is,

$$\begin{aligned}\text{Per cent } KAS_2 &= 100r = 3.3580K\\ \text{Per cent } CMS_2 &= 100s = 5.3706M\end{aligned}$$

By difference,

$$\text{Per cent } C_2AS = 100 - 3.3580K - 5.3706M$$

Equations in terms of C and S will be needed in a problem to be considered presently. These may be derived from equations 10 and 13, which are repeated below, with terms transposed.

$$40.91r + 15.01s = -C + 40.91 \qquad (10)$$

$$16.07r + 33.57s = S - 21.91 \qquad (13)$$

Solving for r and s,

$$\text{Per cent } KAS_2 = 100r = -1.3258S - 2.9652C + 150.35 \qquad (14)$$

$$\text{Per cent } CMS_2 = 100r = 3.6135S + 1.4194C - 137.24 \qquad (15)$$

By difference,

$$\text{Per cent } C_2AS = -2.2877S + 1.5458C + 86.89 \qquad (16)$$

GENERAL METHOD

The general method, involving the successive steps indicated on page 550, may be applied in any case, including those previously discussed. The variables selected as parameters may be composition variables, or they may be other variables, such as temperature and pressure. To illustrate the general method of deriving parametric equations, let us derive equations for the binary system CAS_2–C_2AS in the ternary system C–A–S (the system CaO–Al_2O_3–SiO_2). In table 2 the percentage compositions of the subordinate components are given. Only one parameter is required for a binary system, and primary component S is selected. The percentages of S are indicated in the table as values of the parameter for each of the subordinate components.

The literal equations for C and A are in the form indicated below for C,

$$C = aS + b \qquad (17)$$

in which a and b are constants to be evaluated. Substituting in equation 17 the values of C and S in the two subordinate components, the following equations are obtained:

$$\begin{aligned}43.18a + b &= 20.17\\ 21.91a + b &= 40.91\end{aligned}$$

Solving for a and b, and substituting in equation 17:

$$C = -0.9751S + 62.27 \tag{18}$$

By the same procedure for A:

$$A = -0.0249S + 37.73 \tag{19}$$

Substitution of any assigned value of S in equations 18 and 19 will lead to a composition in the binary system CAS_2–C_2AS or in an extension of that system.

TABLE 2

PRIMARY COMPONENTS	SUBORDINATE COMPONENTS	
	CAS_2	C_2AS
	per cent	*per cent*
C	20.17	40.91
A	36.65	37.18
	PARAMETER	
S	43.18	21.91

TABLE 3

PRIMARY COMPONENTS	SUBORDINATE COMPONENTS		
	KAS_2	CMS_2	C_2AS
	per cent	*per cent*	*per cent*
K	29.78	0.00	0.00
M	0.00	18.62	0.00
A	32.24	0.00	37.18
	PARAMETERS		
S	37.98	55.48	21.91
C	0.00	25.90	40.91

Since the percentages of S in C_2AS and CAS_2 are 21.91 and 43.18, respectively, compositions may be restricted to the system CAS_2–C_2AS by limiting S to values from 21.91 to 43.18.

DETERMINATION OF LIMITS ON PARAMETERS

It was mentioned previously (page 551) that when two or more parameters are required the ranges of values of the parameters are not mutually independent. As a basis for discussing the determination of limits on the values which may be assigned to parameters, we shall consider a ternary subordinate system, which requires two parameters. We shall again derive equations for the ternary system KAS_2–CMS_2–C_2AS in the quinary system K–C–M–A–S, this time selecting S and C as parameters. The data are given in table 3.

The parametric equations have the form indicated below for K.

$$K = aS + bC + c$$

in which a, b, and c are constants to be evaluated. The procedure is the same as in the preceding example. The equations derived by that procedure are given below:

$$K = -0.3948S - 0.8830C + 44.78 \tag{20}$$
$$M = 0.6728S + 0.2643C - 25.56 \tag{21}$$
$$A = -1.2780S - 0.3813C + 80.78 \tag{22}$$

Limits can be assigned to one of the parameters by observing the maximum and minimum values shown in table 3 for that parameter. Since C has the wider range of values, from 0.00 to 40.91, these may be taken as limits on the values of C. The limits on S must now be defined in terms of C. The limits on S must restrict all compositions to the system KAS_2–CMS_2–C_2AS. They are therefore determined from equations of the subordinate components of this system in terms of S and C. These equations were obtained in a previous example involving the same primary and subordinate systems (page 552) and are repeated below.

$$\text{Per cent } KAS_2 = -1.3258S - 2.9652C + 150.35 \tag{14}$$
$$\text{Per cent } CMS_2 = 3.6135S + 1.4194C - 137.24 \tag{15}$$
$$\text{Per cent } C_2AS = -2.2877S + 1.5458C + 86.89 \tag{16}$$

The percentages of the subordinate components are positive or zero for all compositions in the subordinate system. To meet this condition in equation 14,

$$1.3258S \ngtr 150.35 - 2.9652C$$

or,

$$S \ngtr 113.40 - 2.2365C \tag{23}$$

Similarly, from equations 15 and 16:

$$S \nless 37.98 - 0.3928C \tag{24}$$
$$S \ngtr 37.98 + 0.6757C \tag{25}$$

For any given value of C there is only one minimum and one maximum value of S. Inequalities 23 and 25, which express maximum values of S, must therefore apply to different ranges of values of C. By equating the right-hand members of these inequalities, and solving for C, we obtain $C = 25.90$. For this value of C both inequalities indicate the same maximum value of S. By trial of a single value of C less than 25.90 it is found that inequality 25 gives a smaller quantity for the maximum value of S than does inequality 23. Inequality 25 therefore applies when C is less than 25.90, while inequality 23 applies for larger values of C. The limits on C and S may be stated as follows.

C from 0.00 to 25.90:

$$S \nless 37.98 - 0.3928C$$
$$S \ngtr 37.98 + 0.6757C$$

C from 25.90 to 40.91:

$$S \nless 37.98 - 0.3928C$$
$$S \ngtr 113.40 - 2.2365C$$

PARAMETERS OTHER THAN COMPOSITION

In the foregoing study we have derived linear equations in which each of the parameters represents the quantity of a component. Other variables may be selected as parameters. The analytical treatment of systems with reference to phase equilibria involves temperature or pressure, or both, as variables. Relations between these variables and composition are seldom linear, so that when such relations are involved the use of linear equations must be restricted to cases in which the relations are approximately linear. For example, a curve may be so short that it can be taken as a straight line without appreciable error. Or, if a curve as a whole may not be treated as a straight line, it may be possible to divide the curve into segments, treating each segment as a straight line. This mode of attack is frequently advantageous because of the simplicity of linear equations.

The derivation of linear equations involving parameters other than composition variables will be illustrated in the case of a segment of the boundary between the C_3S and C_2S primary phase regions in Rankin and Wright's phase diagram of the ternary system CaO–Al_2O_3–SiO_2 (6). This boundary is curved, but segments representing intervals of 100°C. are approximately straight lines. Furthermore, points at 100° intervals on the curve are nearly equally spaced, which is evidence that 100° segments of the corresponding curve in the space model of the system are approximately straight lines. Parametric equations will be derived for the segment between 1500° and 1600°C. Let us designate the compositions at the 1500° and 1600°C. points as X and Y, respectively. The data required for deriving parametric equations, with T (temperature) as a parameter, are given in table 4.

The form of the equation is that shown below for C.

$$C = aT + b$$

Proceeding by the general method, the following equations are obtained.

$$\begin{array}{lrr} C = & +\,0.033T + & 9.1 \\ A = & -\,0.069T + & 135.8 \\ S = & +\,0.036T - & 44.9 \\ \hline \text{Total} & & 100.0 \end{array}$$

METHODS OF APPLICATION

The examples which have been considered in describing the derivation and properties of parametric equations suggest some applications to the analytical treatment of multicomponent systems. More complex problems may be solved when a knowledge of the derivation and properties of parametric equations is accompanied by experience in performing algebraic operations. To demonstrate the manner in which the application of the equations may be extended, two examples will be considered in this section, one dealing with the planning of mixtures for use in an investigation of phase equilibria, the other with the analytical treatment of phase equilibria data.

In a previous paper (2) the derivation and properties of intrinsic equations were described. It was pointed out that the difficulty of applying intrinsic equations increases with $N - n$, while this situation is reversed in the case of parametric equations. To illustrate, relations in a quaternary system within a quinary system may be expressed by a single intrinsic equation in simple form, and for many purposes this type of equation is to be preferred. On the other hand, a binary system within a quinary system is much more easily treated by means of parametric equations.

TABLE 4

PRIMARY COMPONENTS	SUBORDINATE COMPONENTS*	
	X	Y
	per cent	*per cent*
C	58.6	61.9
A	32.3	25.4
S	9.1	12.7
	PARAMETER	
T	1500	1600

* Estimated from phase diagram.

PLANNING MIXTURES IN THE INVESTIGATION OF A QUINARY SYSTEM

Composition relations in a quinary system can not be represented in a phase diagram or space model, since four dimensions are required. A plan followed by Eubank (3) in an investigation of a portion of the system N–C–A–F–S (the system Na_2O–CaO–Al_2O_3–Fe_2O_3–SiO_2) was to study phase equilibria in a series of sections through the quinary system, represented by triangular diagrams, in each of which the percentages of two components were arbitrarily fixed. By a systematic choice of the percentages of the two components, the series of diagrams can be arranged in columns with reference to one of the components and in rows with reference to the other, for convenient study and comparison. The planning of mixtures in the various sections investigated by Eubank will be considered as an example of the application of parametric equations. His problem was to investigate the effect of the addition of Na_2O, in the form of NC_8A_3, to compositions in a portion of the system CaO–C_5A_3–C_2F–C_2S. This portion of the system is defined by a tetrahedron with vertices as indicated in table 5. The compound NC_8A_3 and the compositions at the vertices of the tetrahedron define a quinary system. The problem that we shall consider is the calculation of mixtures in the plane (triangular) sections through the quinary system, in which two components vary from plane to plane but are constant in each plane. The required data are shown in table 6.

TABLE 5

COMPONENTS	VERTEX			
	1	2	3	4
	per cent	*per cent*	*per cent*	*per cent*
C	20	0	0	0
C_2S	15	15	35	15
C_5A_3	39	59	39	39
C_2F	26	26	26	46

TABLE 6

PRIMARY COMPONENTS	SYMBOL	SECONDARY COMPONENTS				
		V	W	X	Y	Z
		per cent	*per cent*	*per cent*	*per cent*	*per cent*
C	B	20	0	0	0	0
C_2S	D	15	15	35	15	0
C_5A_3	E	39	59	39	39	0
C_2F	G	26	26	26	46	0
NC_8A_3	H	0	0	0	0	100
		WEIGHT FRACTION				
		v	w	x	y	$1 - v - w - x - y$

This investigation is confined to a portion of the system C–C_2S–C_5A_3–C_2F–NC_8A_3, and the components of this system are prepared in quantity for use in making mixtures. It is therefore convenient to treat these compounds as primary components. As a preliminary step we shall derive equations for the system V–W–X–Y–Z in the system B–D–E–G–H by the direct method previously described (page 550). The equations so derived are as follows:

$$\text{Per cent C} = B = 20v \tag{26}$$

$$\text{Per cent } C_2S = D = 15v + 15w + 35x + 15y \tag{27}$$

$$\text{Per cent } C_5A_3 = E = 39v + 59w + 39x + 39y \tag{28}$$

$$\text{Per cent } C_2F = G = 26v + 26w + 26x + 46y \tag{29}$$

$$\text{Per cent } NC_8A_3 = H = -100v - 100w - 100x - 100y + 100 \tag{30}$$

Now let us arbitrarily select C_5A_3 and NC_8A_3 as the components to be constant in each triangular diagram representing a plane section through the quinary system. Equations 28 and 30 give the percentages of these components but involve four parameters, whereas only two parameters are required for a ternary subordinate system. Let us choose x and y as the parameters to be retained, and let E_1 and H_1 represent the constant values of E and H, respectively, in any given diagram. Transposing terms in equations 28 and 30, and substituting E_1 and H_1, respectively, for E and H, we obtain the equations:

$$\begin{aligned} 39v + 59w &= E_1 - 39x - 39y \\ 100v + 100w &= -H_1 - 100x - 100y + 100 \end{aligned}$$

Solving for v and w:

$$v = -0.05E_1 - 0.0295H_1 - x - y + 2.95 \tag{31}$$
$$w = 0.05E_1 + 0.0195H_1 - 1.95 \tag{32}$$

Since the parameters v and w are to be eliminated through the substitutions which follow, we must now consider the requirement that neither of these variables can be less than zero. From the above equations we obtain the following inequalities expressing this condition:

$$x + y \ngtr 0.0295(100 - H_1) - 0.05E_1 \tag{31a}$$
$$E_1 \nless 0.39(100 - H_1) \tag{32a}$$

Substituting in equations 26, 27, and 29 the values of v and w in equations 31 and 32, we obtain the equations,

$$\text{Per cent CaO} = B = 0.59(100 - H_1) - E_1 - 20(x + y) \tag{33}$$
$$\text{Per cent } C_2S = D = 0.15(100 - H_1) + 20x \tag{34}$$
$$\text{Per cent } C_2F = G = 0.26(100 - H_1) + 20y \tag{35}$$

By substituting for E_1 and H_1 the percentages of C_5A_3 and NC_8A_3 to be constant in a particular diagram representing a section through the quinary system, parametric equations are obtained for calculating mixtures in that section. For example, let $E_1 = 45$ and $H_1 = 8$. These values satisfy inequality 32a. Substituting in equations 33–35,

$$\text{Per cent CaO} = B = 9.28 - 20(x + y) \tag{33a}$$
$$\text{Per cent } C_2S = D = 13.80 + 20x \tag{34a}$$
$$\text{Per cent } C_2F = G = 23.92 + 20y \tag{35a}$$

The value of B in equation 33a will be negative if $x + y$ is greater than 9.28/20, or 0.464. We may therefore assign limits to the parameters x and y by stating that x and y must be zero or positive, and that their sum must not exceed 0.464. Within these limits, compositions obtained by substituting assigned values of x and y in the equations will be restricted to the secondary system V–W–X–Y–Z.

In drawing a series of triangular diagrams, each with constant percentages of C_5A_3 and NC_8A_3, it is necessary to determine the composition at each vertex in terms of the three remaining primary components, as a basis for extimating the composition at any point in the diagram. This may be done by assigning limiting values to x and y. In this case, when one of these variables is equal to zero, the maximum value of the other variable is 0.464. We therefore have three pairs of values of x and y representing the vertices, as indicated in table 7.

ESTIMATION OF PROPORTIONS OF PHASES

The interpretation of phase equilibrium data represented by a phase diagram involves determination of the phases present under any given condition, and estimation of the proportions of those phases. In the case of systems represented in a plane diagram, these operations are performed graphically. Parametric equations provide a convenient means of performing the same operations analytically, as will be shown in a specific example.

Before considering the example illustrating the application of parametric equations, we shall discuss a rule of procedure which is important in applying analytical methods to the interpretation of phase equilibrium data. Let us consider an invariant point L at which three solid phases, A, B, and C, are capable of coexisting with the liquid at temperature T_1. During slow fusion of a mixture in the system A–B–C the temperature remains constant at temperature T_1 while the quantity of liquid increases and the proportions of solid phases change. The quantity of liquid reaches a maximum, at which point one of the solid phases disappears, or two or more disappear simultaneously. The maximum quantity of liquid which can form at that temperature is present when one of the solid phases disappears, or when two or more disappear simultaneously. Further formation of liquid L is impossible, since it would leave a solid residue which can not be composed of solid phases with which liquid L can coexist. The problem of determining the maximum amount of liquid at an invariant point is therefore one of determining the quantity of liquid present when one of the solid phases disappears. A convenient method of accomplishing this is to express the compositions of the liquid and the mixture under study in terms of the solid phases capable of coexisting with the liquid. Let us suppose that the percentages of A, B, and C in this expression of composition of the liquid are A_1, B_1, and C_1, respectively. Then the percentages of A, B, and C in the mixture are reduced $0.01A_1$, $0.01B_1$, and $0.01C_1$, respectively, by each per cent of liquid formed. It is then a

TABLE 7

VERTEX	VALUES OF PARAMETERS		COMPOSITION AT VERTEX*		
	x	y	CaO	C_2S	C_2F
			per cent	*per cent*	*per cent*
1	0.00	0.00	9.28	13.80	23.92
2	0.00	0.464	0.00	13.80	33.20
3	0.464	0.00	0.00	23.08	23.92

* By substitution in equations 33a–35a.

simple matter to determine the percentage of liquid which will lead to the disappearance of a solid phase, and to determine the percentages of the solid phases then present. The rule to be followed in estimating the proportions of solid phases and liquid in a mixture in a state of equilibrium may be stated as follows: Compositions of the mixture and the liquid should be expressed in terms of the solid phases capable of coexisting with the liquid and, when necessary, such additional substances as are needed to make a total of N substances. The significance of the latter part of this rule will be clear when it is presently applied.

The foregoing rule will be applied in the solution of a problem pertaining to mixtures in the system CAS_2–C_2AS–CS in the ternary system CaO–Al_2O_3–SiO_2, using data obtained by Rankin and Wright (6) in their investigation of the system. When mixtures in the system CAS_2–C_2AS–CS are slowly fused, the first stable liquid is formed at 1265°C., at the invariant point 38 per cent CaO, 20 per cent Al_2O_3, 42 per cent SiO_2. This point will be designated as X. Liquid of composition X is capable of coexisting with solid CAS_2, C_2AS, and CS at 1265°C. The first two phases are essentially pure compounds, while the CS phase probably contains a small quantity of other constituents in solid solution. However, since the actual composition of the CS phase which is capable of coexisting with liquid X is not known, it will be treated here as a pure compound. Following the above rule, the composition of the liquid is converted into terms of CAS_2, C_2AS, and CS, obtaining the "potential composition," 30.30 per cent CAS_2, 23.92 per cent C_2AS, 45.78 per cent CS. Let B_1, D_1, and G_1 represent the potential percentages of CAS_2, C_2AS, and CS, respectively, in any given mixture. Then for any state of equilibrium at 1265°C. the percentages of the solid phases may be found from the equations,

$$\text{Per cent solid } CAS_2 = B_1 - 30.30m \tag{36}$$
$$\text{Per cent solid } C_2AS = D_1 - 23.92m \tag{37}$$
$$\text{Per cent solid CS} = G_1 - 45.78m \tag{38}$$

in which m is the weight fraction of liquid X in the mixture. All three of the solid phases may be present at 1265°C., but as heat is supplied the quantity of liquid X increases, and each of the solid phases decreases in quantity, until one of the solid phases disappears. The quantity of liquid has then reached the maximum which may be present at that temperature. Further introduction of heat causes the liquid to leave point X, and the temperature rises. To determine the maximum quantity of liquid at the invariant point temperature, we equate the right-hand members of the equations to zero and solve each of the resulting equations for m. The lowest value of m so obtained is the maximum weight fraction of liquid at the invariant point temperature. Upon substituting this value of m in equations 36–38 the percentages of solid phases present when the liquid leaves point X is obtained. The course of the liquid phase upon leaving X is also learned by this procedure. For example, if equation 36 gives the lowest value of m, CAS_2 is the disappearing phase, and the liquid leaves point X to follow the univariant curve for C_2AS and CS. Similarly, if equations 36 and 37 give identical values of m, lower than that obtained from equation 38, CAS_2 and C_2AS disappear simultaneously, and the liquid passes into the CS primary phase region, in a direction toward the composition point for CS.

From the foregoing considerations it may be seen that equations 36–38 provide a means of classifying mixtures in the system CAS$_2$–C$_2$AS–CS, with reference to the course which the liquid will follow upon leaving point X. To describe the method of estimating proportions of phases when the liquid is on a univariant curve we shall select the range of compositions for which equation 38 gives the lowest value of m. For mixtures in this range, $m = G_1/45.78$ when the liquid starts to follow the univariant curve for CAS$_2$ and C$_2$AS. This curve appears as a straight line in the phase diagram of the system. It extends from point X, which we have already considered, to the invariant point for CAS$_2$, C$_2$AS, and Al$_2$O$_3$, which we shall designate as Y. The univariant curve may then be designated as the line XY. The data required for estimating proportions of phases when the liquid is on the line XY are shown in table 8.

TABLE 8

COMPONENTS	SYMBOL	X*	Y†
		OXIDE COMPOSITION	
		per cent	*per cent*
CaO		38.	29.2
Al$_2$O$_3$		20.	39.0
SiO$_2$		42.	31.8
		POTENTIAL COMPOSITION	
CAS$_2$	B	30.30	54.42
C$_2$AS	D	23.92	51.24
CS	G	45.78	−5.66

* Invariant point for CAS$_2$, C$_2$AS, and CS (6).

† Invariant point for CAS$_2$, C$_2$AS, and Al$_2$O$_3$ (6).

At present we are concerned with equilibria in which the only solid phases are CAS$_2$ and C$_2$AS. The potential compositions of the liquid phase and any mixture under consideration must therefore be expressed in terms of CAS$_2$, C$_2$AS, and a third substance, since the system is ternary. The third substance may be selected arbitrarily, without influencing estimates of the proportions of phases. However, whenever it is possible, it is convenient to select components of the system in which mixtures under consideration lie. We have therefore selected CS as the third component in the potential compositions given in table 8. Potential compositions are expressed to a higher degree of accuracy than the oxide compositions merely to insure consistency in the results. This applies also to the computations which follow.

For the parameter in equations for the line XY we may select B, D, or G. However, later operations in which the parametric equations are used are somewhat simplified by selecting G, as will presently be seen. Following the general method described on page 552 the following parametric equations for the line XY are obtained:

$$\begin{aligned}\text{Per cent } CAS_2 &= B = -0.4689G + 51.77 && (39)\\ \text{Per cent } C_2AS &= D = -0.5311G + 48.23 && (40)\\ \text{Per cent CS} &= G = G && (41)\end{aligned}$$

Let B_1, D_1, and G_1 represent the potential percentages of CAS_2, C_2AS, and CS in any given mixture. If m is the weight fraction of liquid, the percentages of the solid phases are given by the following equations, in which the coefficients of m are the values of B, D, and G in equations 39–41.

$$\begin{aligned}\text{Per cent solid } CAS_2 &= B_1 - (51.77 - 0.4689G)m && (42)\\ \text{Per cent solid } C_2AS &= D_1 - (48.23 - 0.5311G)m && (43)\\ \text{Per cent solid CS} &= G_1 - Gm && (44)\end{aligned}$$

However, solid CS cannot exist in equilibrium with liquid on the line XY, so that $G_1 - Gm = 0$, or $G = G_1/m$. Substituting G_1/m for G in equations 42 and 43, and simplifying, we obtain equations 45 and 46 (below) for all equilibrium states in which the liquid phase is on the line XY.

$$\begin{aligned}\text{Per cent solid } CAS_2 &= B_1 + 0.4689G_1 - 51.77m && (45)\\ \text{Per cent solid } C_2AS &= D_1 + 0.5311G_1 - 48.23m && (46)\\ \text{Per cent liquid} &= 100.00m && (47)\end{aligned}$$

It was shown previously (page 561) that $m = G_1/45.78$ when the liquid leaves point X to follow the line XY. This is therefore the minimum value of m which may be substituted in equations 45–47. As the value of m increases, the percentages of CAS_2 and C_2AS decrease, until at some point one of these phases disappears. At this point the liquid leaves the line XY and passes into the primary phase region for the solid phase which remains. The maximum value which may be assigned to m is therefore found after substituting the composition of a mixture in equations 45 and 46, by choosing the lower of the two values obtained when the right-hand members of these equations are equated to zero, and solved for m. Interest is usually confined to the proportions of phases when the minimum and maximum weight fractions of liquid are substituted in equations similar to equations 45–47.

ESTIMATION OF PHASES IN THE NEIGHBORHOOD OF A PERITECTIC POINT

In the foregoing example invariant point X is a eutectic point, and its potential composition can be expressed in positive percentages of the solid phases with which liquid X may coexist. That is, the invariant point is in the system CAS_2–C_2AS–CS. The portions of the univariant curves involved in estimating proportions of phases in mixtures in that system are also located in the system. On the other hand, a peritectic point is outside of the system whose components are the solid phases capable of coexisting with the liquid. Univariant curves leading from a peritectic point in a direction of higher temperatures are also outside of the system in the neighborhood of the peritectic point. Both positive and negative values therefore appear in the potential compositions of such liquids. The fact that negative values appear does not interfere with the application of the method which has been described for equilibria at eutectic point X and for points on the univariant curve for CAS_2 and C_2AS. This may be illustrated by considering a hypothetical case in which the invariant point is a peritectic. Let us suppose that the peritectic point P represents a liquid capable of coexisting with the solid phases A, B, and C, and that its potential composition, expressed in terms of the solid phases, is $A = 65$, $B = -25$, $C = 60$. Then if A_1, B_1, and C_1 are the potential percentages of A, B, and C, respectively, in any given mixture, and m is the weight fraction of liquid P,

$$\begin{aligned}\text{Per cent solid A} &= A_1 - 65m\\ \text{Per cent solid B} &= B_1 + 25m\\ \text{Per cent solid C} &= C_1 - 60m\end{aligned}$$

These equations are similar to equations 36–38, except that the coefficient of m in the second equation is positive. From this it is seen that the quantity of solid B increases as the quantity of liquid increases, and that this phase consequently does not disappear. There are only two univariant curves leaving point P in a direction of higher temperatures, the curves for A and B and for B and C. The value of m when one of the solid phases, A or C, disappears is determined in the same manner as in the case of a eutectic point. Estimation of the proportions of phases when the liquid is on one of the univariant curves is accomplished in the same manner as in the preceding example. It is not necessary to give separate treatment to the portions of the univariant curves inside and outside of the system A–B–C, since the signs appearing in the potential composition at any point on these curves take care of the situation.

NONLINEAR RELATIONS

Estimation of proportions of phases when the liquid phase is on a univariant curve has been illustrated by an example in which the curve appears as a straight line in the phase diagram. Curved lines may be represented by nonlinear parametric equations. However, the use of nonlinear equations leads to difficulties in both the derivation of equations and application to individual mixtures. It is much more simple to treat the curve as being composed of a series of straight lines. Usually the degree of accuracy with which the location of a curve has been established is not so great that nonlinear equations can be considered to be much more accurate than a successive series of linear equations representing segments of the curve treated as straight lines. There may be instances in which curvature is so great that this mode of treatment is not satisfactory, but it is usually the most practical method of dealing with nonlinear relations.

SUMMARY

The derivation and use of parametric equations in problems encountered in the investigation of phase equilibria are described. These problems are of two kinds: (*1*) the design of mixtures to be subjected to heat treatment or other ex-

perimental operations in the course of an investigation, and (*2*) analytical interpretation of the data obtained. Advantages of parametric equations are their simplicity when dealing with a system of a small number of components within a multicomponent system, and their form, which permits direct computation of the quantity of each component when values are assigned to the parameters. The form of the equations also simplifies the operations required in deriving equations for estimating percentages of phases under specified conditions of equilibrium.

REFERENCES

(1) Dahl, L. A.: Rock Products **41–42** (1938–39).

(2) Dahl, L. A.: J. Phys. & Colloid Chem. **52,** 698 (1948).

(3) Eubank, W. R.: Dissertation, The Johns Hopkins University, 1947.

(4) Lea, F. M., and Parker, T. W.: Phil. Trans. Roy. Soc. (London) **A234** (No. 731), 1 (1934).

(5) Lea, F. M., and Parker, T. W.: Dept. Sci. Ind. Research, Building Research Tech. Paper No. **16,** 52 pp. (1935).

(6) Rankin, G. A., and Wright, F. E.: Am. J. Sci. **39,** 1 (1915).

SOME BINARY SYSTEMS OF ANALOGOUS ORGANIC CHALCOGEN DERIVATIVES[1]

GIUSEPPE CILENTO[2]

Departamento de Química, Faculdade de Filosofia, Ciências e Letras, Universidade de São Paulo, São Paulo, Brasil

Received June 27, 1949

In this paper are reported solidus–liquidus binary systems between *o*-phthaloyl derivatives (Ia: X = O, S, Se, NH) and also between triaryl phosphates (II: R = H, CH_3; X = O, S, Se). They constitute part of a systematic research undertaken by H. Rheinboldt *et al.* in the isomorphogenic relationships of organic oxygen, sulfur, selenium, and tellurium compounds.

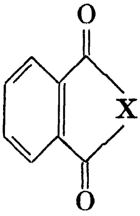

Ia

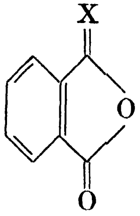

Ib

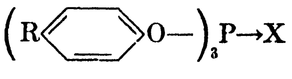

II

---

[1] Part of the thesis submitted by Giuseppe Cilento in partial fulfillment of the requirements for the degree of Doctor of Science at the Universidade de São Paulo, Brasil, October, 1946.

[2] Present address: Fundação Andrea e Virginia Matarazzo, Faculdade de Medicina, Universidade de São Paulo, Caixa Postal 100-B, São Paulo, Brasil.

EXPERIMENTAL

Phthalic anhydride, phthalimide, and triphenyl phosphate were available in our laboratories. All other compounds were prepared by current methods. Phthalic anhydride and phthalimide were purified by sublimation. Thiophthalic anhydride was recrystallized several times from ethanol and petroleum ether, while the selenophthalic anhydride was recrystallized from carbon tetrachloride. All other compounds were purified by successive recrystallizations from ethanol. Triphenyl thiophosphate was also recrystallized from petroleum ether.

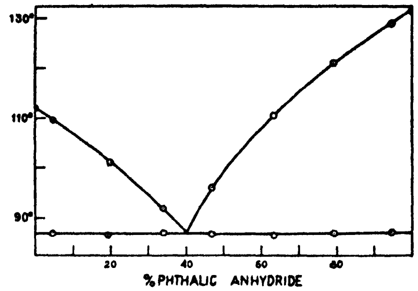

FIG. 1.

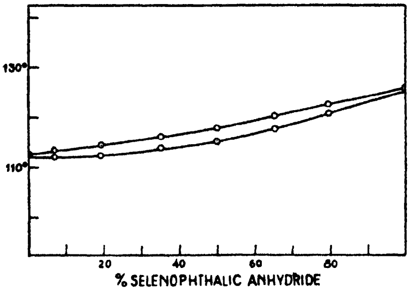

FIG. 2.

FIG. 1. Binary system phthalic anhydride (A)–thiophthalic anhydride

Per cent A	0.0	4.6	19.3	34.1	46.9	63.5	79.4	94.8	100.0
Thawing point	111.8	87.0	86.6	87.0	86.8	86.6	87.0	87.2	130.6
Melting point	112.1	109.8	101.3	91.9	96.2	110.5	121.0	129.2	131.6

Simple eutectic system without mixed crystals. Eutectic point at 40 per cent cent A and 87.0°C

FIG. 2. Binary system selenophthalic anhydride (A)–thiophthalic anhydride

Per cent A	0.0	6.8	19.3	35.2	50.0	65.3	79.6	100.0
Thawing point	111.8	112.0	112.2	113.8	115.0	117.6	120.8	125.8
Melting point	112.4	113.5	114.3	116.2	117.7	120.4	122.8	126.0

Continuous mixed-crystal series of type I of Bakhuis-Roozeboom's classification (2).

Solid-liquid phase diagrams of the binary systems were worked out by the "thaw-melting method" described by H. Rheinboldt (10).

All mixtures of the components, except those of the binary system triphenyl phosphate–triphenyl thiophosphate (figure 5), were prepared by melting and, after solidification, ground in an agate mortar.

Compositions indicated in the tables and figures are in weight per cent. Ordinates are temperature in °C. The heating rate was 1°C. or less per minute. Thaw points and melting points are accurate to less than 1°C., while the accuracy of the thermometer was ±0.1°C.

DISCUSSION

The failure of mixed-crystal formation between phthalic and thiophthalic anhydrides (figure 1) is a somewhat unexpected result, since when oxygen and sulfur are members of a rigid ring, isomorphism is favored. Moreover, approximately alike intermolecular forces may exist in both anhydrides, since they distil at the same temperature (b.p. = 284°C./760 mm.).

It must be pointed out that thiophthalic anhydride has also been formulated as Ib (X = S)(3), and this structure might explain the reciprocal insolubility in the solid state with phthalic anhydride, as, in general, $>C{=}O$ and $>C{=}S$ analogous organic derivatives are not isomorphous (11). However, when the relative energies of structures Ia and Ib are considered, it follows that the former structure is far more stable than the latter.

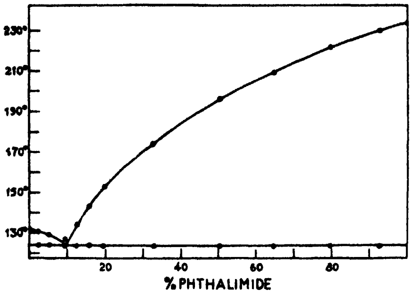

FIG. 3.

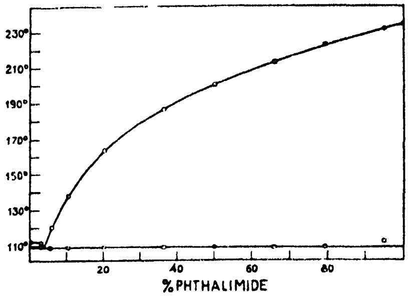

FIG. 4.

FIG. 3. Binary system phthalimide (A)–phthalic anhydride

Per cent A	0.0	2.3	5.1	9.4	12.5	15.9	19.7	32.7	50.4	64.6	79.6	92.6	100.0
Thawing point	130.6	124.0	124.2	124.0	124.2	124.2	124.0	124.1	124.2	124.3	124.4	124.4	233.2
Melting point	131.6	130.8	129.6	126.8	134.2	143.2	153.0	174.4	196.2	209.5	222.4	230.7	234.4

Simple eutectic system without mixed crystals. Eutectic point at 10 per cent A and 124.2°C.

FIG 4. Binary system phthalimide (A)–thiophthalic anhydride

Per cent A .. .	0.0	2.9	5.9	10.4	20.4	36.3	50.0	66.1	79.4	94.9	100.0
Thawing point	111.8	109.2	109.4	109.3	109.3	109.2	109.3	109.6	109.2	113.4	233.2
Melting point	112.1	111.7	120.4	138.2	163.6	186.2	200.0	212.8	223.0	231.6	234.4

Simple eutectic system without mixed crystals. Eutectic point at 4 per cent A and 109.3°C.

Thus, as one can deduce from bond energy values (8) passing from structure $-\underset{\underset{O}{\|}}{C}-S-C$ to $-\underset{\underset{S}{\|}}{C}-O-C$ there is an increase of 15 kcal. in the molar energy.

Acting in the same direction is the difference between the resonance energy of Ia (X = S) and Ib (X = S), since in the latter structure some contributions, such as the resonance in the anhydride group, would be greatly reduced.

Finally, the pentacyclic ring strain, being inversely related to the radius of the heteroatom, would be increased in structure Ib.

Thus, thiophthalic anhydride should have structure Ia. Therefore it would appear that there should exist a remarkable dissimilarity in the geometrical structures of phthalic and thiophthalic anhydrides, which prevents isomorphism.

For selenophthalic anhydride structure Ia (X = Se) must be a still far more stable structure than Ib (X = Se). Moreover, it can readily be deduced on geometric grounds that little, if any, strain exists in the pentacyclic ring, the intervalency angle of selenium being around 90°. The observed isomorphism with the thioanhydride (figure 2) is the expected result and suggests that both molecules have a very similar structure.

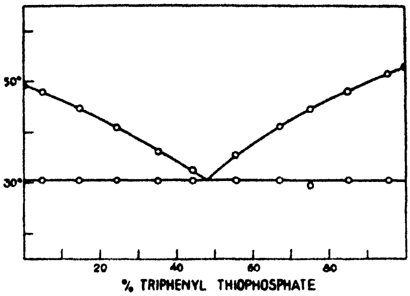

FIG. 5.

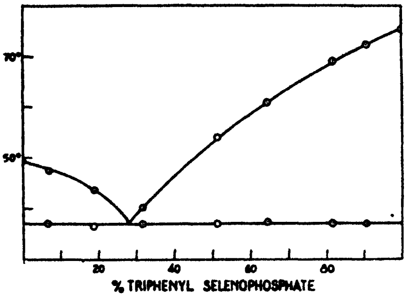

FIG. 6.

FIG. 5. Binary system triphenyl thiophosphate (A)–triphenyl phosphate

Per cent A ..	0.0	5.0	14.7	24.5	35.3	44.5	55.7	67.2	75.2	85.1	95.5	100.0
Thawing point .	48.5	30.5	30.6	30.4	30.3	30.2	30.4	30.4	29.5	30.4	30.4	52 0
Melting point	49.3	48.0	44.8	41.0	36.2	32.6	35.6	41.1	44.4	48.2	51.7	53.2

The mixtures of the substances were prepared by close grinding of the components in an agate mortar. Simple eutectic system without mixed crystals. Eutectic point at 48 per cent A and 30.4°C. By cooling the mixtures essentially the same liquidus curve is obtained.

FIG. 6. Binary system triphenyl selenophosphate (A)–triphenyl phosphate

Per cent A	0.0	6.9	19.0	31.9	51.3	64.4	81.7	90.6	100.0
Thawing point	48.5	37.1	36.6	37.1	37.2	37.4	37.2	37.2	75.2
Melting point	49.3	47.3	43.6	40.2	54.0	60.8	69.0	72.4	75.5

Simple eutectic system without mixed crystals. Eutectic point at *ca.* 29 per cent A and 37.2°C.

The binary system phthalimide–phthalic anhydride has been investigated by Grimm *et al.* (6). The observed eutectic (figure 3) is consistent with the different structure of those molecules, as is suggested by dipole-moment measurements (4, 9).

On account of the mutual insolubility of phthalic anhydride and phthalimide it is not surprising that the latter compound fails also to form solid solutions with thiophthalic anhydride (figure 4).

As far as the isomorphous relationships of oxygen, sulfur, and selenium are concerned, the foregoing results are a further proof that sulfur resembles selenium much more than oxygen (5). The reciprocal insolubility of triphenyl phosphate with triphenyl thiophosphate (figure 5) or selenophosphate (figure 6) and the isomorphogeny of the latter two compounds (figure 7) can also be explained along those lines. However, P. Pascal (7) found a continuous mixed-crystal formation between triphenyl phosphate and a triphenyl thiophosphate which melted at 63°C., the reported melting points in the literature ranging from 48°C. to 53°C. Unless Pascal used a hitherto unknown polymorphic modification of triphenyl thiophosphate his results are in doubt. Moreover, the p-methyl derivatives also fail to form solid solutions (figure 8).

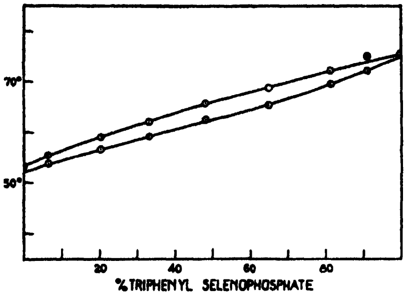

FIG. 7.

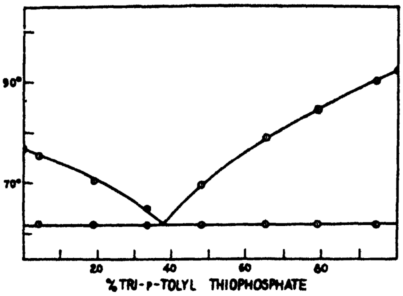

FIG. 8.

FIG. 7. Binary system triphenyl selenophosphate (A)–triphenyl thiophosphate

Per cent A	0.0	6.6	20.3	33.3	48 2	65.1	81 3	91.1	100.0
Thawing point.	52.0	53.8	56.6	59.2	62.6	65 4	69 6	72.2	75.2
Melting point	53.2	55.5	59.0	62.1	65.8	68 8	72.2	75.0	75.5

Continuous mixed-crystal series of type I of Bakhuis-Roozeboom's classification (2).

FIG. 8. Binary system tri-p-tolyl thiophosphate (A)–tri-p-tolyl phosphate

Per cent A	0.0	4.2	18.9	33.7	48 2	65.3	79.0	94.4	100.0
Thawing point	75.8	62.0	61.8	61.7	61.9	61.7	61.8	61.8	91 4
Melting point	76.8	75.5	70.4	65.0	69.6	79.0	84 8	90.3	92.4*

Simple eutectic system without mixed crystals. Eutectic point at 38 per cent A and 61.8°C

* Reported melting point: 87°C. (1); 93–94°C. (12).

SUMMARY

Solidus–liquidus binary systems between analogous organic derivatives of oxygen, sulfur, and selenium have been studied. The periodical isomorphogeny of those elements has been ascertained. The structure of thiophthalic and selenophthalic anhydrides is discussed.

REFERENCES

(1) AUTENRIETH, W., AND MEYER, W.: Ber. **58**, 840 (1925).
(2) BAKHUIS-ROOZEBOOM, H. W.: Z. physik. Chem. **30**, 385 (1899).
(3) BEILSTEIN: *Handbuch der organischen Chemie*, 4th edition, Vol. XVII, p. 486. Julius Springer, Berlin (1933).
(4) COWLEY, E. G., AND PARTINGTON, J. R.: J. Chem. Soc. **1936**, 47.

(5) Cullinane, N. M., and Plummer, A. J.: J. Chem. Soc. **1938,** 63.
(6) Grimm, H., Guenther, M., and Tittus, H.: Z. physik. Chem. **14B,** 169 (1931).
(7) Pascal, P.: Bull. soc. chim. [4] **33,** 178 (1923).
(8) Pauling, L.: Quoted from G. E. K. Branch and M. Calvin, *The Theory of Organic Chemistry,* p. 274. Prentice-Hall, Inc., New York (1944).
(9) Rau, M. A. G., and Anatanarayanan, N.: Proc. Indian. Acad. Sci. **5A,** 185 (1937).
(10) Rheinboldt, H., *et al.*: J. prakt. Chem. [2] **111,** 242 (1925); **112,** 187, 199 (1926); **113,** 348 (1926); Ber. **74,** 756 (1941)
(11) Reinboldt, H., *et al.*: Ber. **73,** 433 (1940); other unpublished results.
(12) Strecker, W., and Grossmann, C. · Ber. **49,** 81 (1916)

RADIOACTIVE TRACER STUDY OF AN ALIPHATIC ACID IN HYDROCARBON OIL

ANDREW GEMANT

Research Department, The Detroit Edison Company, Detroit, Michigan

Received July 5, 1949

The author had previously found (1) that when an aliphatic acid, an amine, and a phenol are added to hydrocarbon oils, the resulting solutions have high electrical conductivity. The negative ions in such solutions were shown, by means of E.M.F. measurements (2), to be the anions of the aliphatic acid. All evidence indicated that these are molecularly dispersed solutions containing aggregates of relatively low molecular weight. It seemed desirable, however, to obtain direct experimental proof of this statement, the more so since in many other instances high conductivity is associated with the appearance of a second phase, i.e., particles of at least colloidal dimensions, as was shown by J. D. Piper and coauthors (5).

This experimental evidence was obtained by determining the diffusion rate of a C^{14}-labelled aliphatic acid. Tridecanoic acid, labelled in the carboxyl group, was synthesized (4) for the purpose. Using a technique developed by the author (3) with the present application in mind, the diffusion coefficient k of the aliphatic acid was measured. From the diffusion coefficient the molecular radius r can be estimated from Stokes' relation:

$$r = \mathbf{k}T/6\pi\eta k \qquad (1)$$

where $\mathbf{k}$ = Boltzmann's constant, T = absolute temperature, and η = the viscosity of the solution.

The scope of the investigation was enlarged beyond that just indicated. Information on the adsorption of the acid from solution and on the oxidation process of the oil was also obtained. The results of the complete investigation are reported in this paper.

The experimental diffusion assembly is shown in figure 1. The radioactive solution is contained in the cylindrical aluminum cell with handle. The solvent is contained in a thin fiberglass mat which is built into the bottom of the metal holder to be seen on top of the aluminum cell. On top of the holder is a Geiger–Müller counter tube. As the solute diffuses into the solvent, the counts increase as a result of the reduced absorption effect. Since the range of 0.15-M.e.v. betas is 20 mg./cm.^{2}, the concentration near the free surface will determine the activity. From the theoretical diffusion equation valid for this case (3) the relative counts per minute, f, for a soft beta emitter such as carbon 14 was computed and is shown in figure 2 as a function of the argument kt/l^2, where t = time and l = thickness of the fiberglass mat. The ordinate is unity for $t = \infty$. Experimental curves relating the counts to time permit computation of the diffusion coefficient k if l is known, as will be shown.

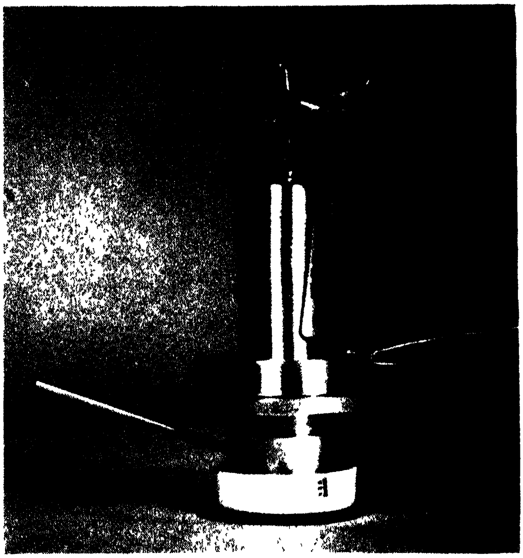

FIG. 1 Cell for diffusion measurement by means of a radioactive tracer

In the subsequent measurements, a hydrocarbon oil of viscosity 0.17 poise at 25°C. was used. The concentration of tridecanoic acid was 0.005 N. With few exceptions, a mat of 0.050-cm. thickness was used. Since the measurements involved relative counts only, no corrections, except for background, were necessary. The activity of the sample was such that the mat saturated with the solution yielded about 240 counts/min.

Before measuring the diffusion rate of the acid in the electrically conducting solutions, a series of measurements was made on oil containing only the acid. Figure 3 shows two sets of data, obtained from the same solution, giving f as a function of time in days. The curve was drawn through the experimental points and the evaluation of k in square centimeters per day is shown in table 1. For a few arbitrarily chosen times, f was read. The corresponding values of kt/l^2 from figure 2 are listed. These figures multiplied by l^2/t give k, which is reasonably constant; its average value is 0.032 cm.^{2}/day.

From equation 1 one has

$$r = 1.88 \times 10^{-2}/\eta k \text{ in Ångström units} \tag{2}$$

giving, with $\eta = 0.17$, $r = 3.5$ Å. as the equivalent radius of the tridecanoic acid molecule in hydrocarbon oil. From the density (0.88) of the crystalline acid and its molecular weight (214) the distance between molecules is 6.8 Å., a value which is in agreement with the molecular diameter as measured. The dispersion of the acid in the solution, if alone, is therefore molecular.

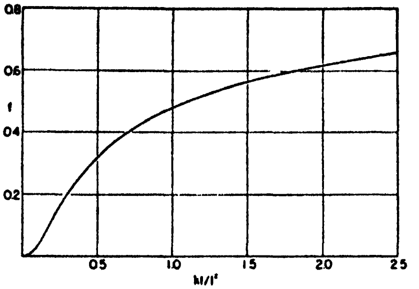

FIG. 2.

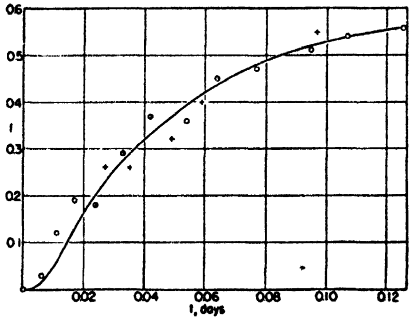

FIG. 3.

FIG. 2. Theoretical relation between relative counts f and the argument kt/l^2 for a soft beta emitter.

FIG. 3. Relative counts *vs.* time for C^{14}-labelled 0.005 N tridecanoic acid dissolved in hydrocarbon oil.

TABLE 1

Evaluation of the diffusion coefficient for tridecanoic acid in oil

t	f	kt/l^2	k
days			*cm.²/day*
0.02	0.16	0.25	0.031
0.04	0.32	0.51	0.032
0.06	0.42	0.76	0.032
0.08	0.49	1.05	0.033
0.10	0.53	1.27	0.032
0.12	0.55	1.44	0.030

The same solution was measured also with mats of different thicknesses and, in one case, with an addition of liquid paraffin in order to increase the viscosity of the solution. The results from these various tests are summarized in table 2. The figures in the last column are reasonably constant, as is to be expected.

As a second series, solutions of tridecanoic acid with the addition of an amine and a phenol were investigated, as mentioned in the introduction. Figure 4 shows test results on a solution containing, besides the acid, 0.3 N tributylamine and 0.4 N *o*-cresol. Of the three curves relating relative counts f to time, t, curve 1 was obtained immediately after the solution was prepared, curve 2 after 2 weeks, and curve 3 after 4 weeks. As time progresses, the rate of diffusion decreases, indicating an association of molecules. In case the acid is distributed among aggregates of different sizes, the method yields, of course, an average size. Because of the considerable excess of the amine and phenol over the acid in the present test, it may be assumed that, because of the mass action law, a large fraction of the acid is present in the associated state.

The results of this group of tests are summarized in table 3. The viscosity of the solution was 0.14 poise. With the addition of the amine alone, no noticeable association takes place. From the increase of the molecular radius in the presence of *o*-cresol, a rough estimate of the total number of molecules participating in the compound formation can be made. This number is 4 for r = 6.1 Å. and 11 for r = 8.4 Å. These figures are in reasonable agreement with previous estimates (2), according to which three molecules of amine, two molecules of acid, and five molecules of phenol form a compound molecule. These solutions which, as previously mentioned, are electrically conducting contain, therefore, moderately large compound molecules and the sizes of the ions formed from them are very likely of the same order of magnitude. Whereas a direct proof of this latter statement would be desirable, it follows from the probable structure of these compounds (1), as well as from observations on electrolytic ions in general.

TABLE 2

Diffusion coefficient and molecular radius of tridecanoic acid in oil

l	η	k	r
cm.	*poises*	*cm.²/day*	*Å.*
0.038	0.17	0.030	3.7
0.050	0.17	0.032	3.5
0.108	0.17	0.028	3.9
0.050	0.32	0.018	3.3

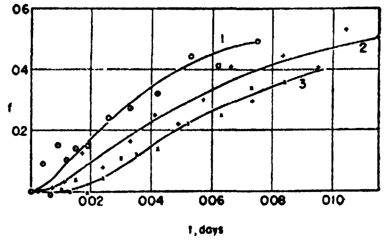

FIG. 4.

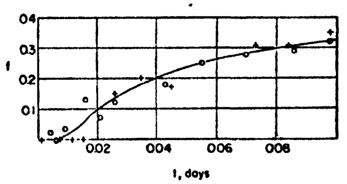

FIG. 4.

FIG. 4. Relative counts *vs.* time for 0.005 N tridecanoic acid, 0.3 N tributylamine, and 0.4 N *o*-cresol in oil. Curve 1 (○) obtained directly after making of solution, curve 2 (+) 2 weeks later, curve 3 (×) 4 weeks later.

FIG. 5. Relative counts *vs.* time for 0.005 N tridecanoic acid and 1.0 per cent colloidal graphite in oil.

Next, tests were made to determine whether the same method might be used for the investigation of adsorption of the tridecanoic acid from solution. Ten per cent, by volume, of Oildag, a colloidal graphite preparation in mineral oil, was added to the solution. Since the concentration of graphite in Oildag was about 10 per cent, its concentration in the solution was about 1.0 per cent. The result of the diffusion test is shown in figure 5, two sets of data with the same solution being recorded. If the fraction a of the total acid is adsorbed, the fraction $(1 - a)$ is free to diffuse. Table 4 shows the evaluation of a from figure 5. For arbitrary values of t, f was read from the figure and kt/l^2 calculated with the known value of k, 0.032. Next, from figure 2, corresponding counts f_0 are listed which should have been observed if no adsorption had taken place. The ratios f/f_0 give the fraction free to diffuse, which is equal to $(1 - a)$. The last column then gives a, which is constant as is to be expected.

TABLE 3

Diffusion coefficient of tridecanoic acid in the presence of an amine and a phenol

NORMALITY OF		TIME OF MEASUREMENT AFTER PREPARATION	k	r
Tributylamine	o-Cresol			
		weeks	*cm.²/day*	Å.
0.30		0	0.033	4.1
0.30		3	0.033	4.1
0.30	0.40	0	0.035	3.8
0.30	0.40	2	0.022	6.1
0.30	0.40	4	0.016	8.4

TABLE 4

Evaluation of adsorbed fraction a from diffusion of tridecanoic acid

t	f	kt/l^2 WITH k = 0.032	f_0 FROM FIGURE 2	f/f_0	a
days					
0.02	0.100	0.26	0.165	0.61	0.39
0.04	0.200	0.51	0.325	0.62	0.38
0.06	0.260	0.77	0.425	0.62	0.38
0.08	0.295	1.02	0.485	0.61	0.39
0.10	0.325	1.28	0.530	0.62	0.38

A similar experiment was carried out with Gilsonite, an asphalt, instead of graphite; the significant data of both tests are summarized in table 5. The specific adsorption appears to be similar in the two cases.

The calculation was carried out on the basis of a viscosity 0.17 that of the solvent into which the acid diffused. The viscosities of the colloidal solutions in the two cases were 0.23 and 0.19. A more accurate determination with identical viscosities throughout would yield lower values for the adsorbed fractions.

Apart from an increase in the macroscopic viscosity of the solution, the microscopic mobility of the acid in the presence of the colloidal particles might also be reduced. Such an effect might account for part of the observed reduction in diffusion rate.

The technique described above may be used also to study exchange reactions. The diffusion of the acid was measured in a sample to which copper acetate crystals had been added. The solubility of this compound in hydrocarbon oil at room temperature is practically zero. The diffusion rate of the acid in this system, measured 6 hr. after preparation, was found to be reduced; this may be explained by means of an equilibrium according to the following reaction:

$$(CH_3COO)_2Cu + 2C_{12}H_{25}\overset{*}{C}OOH \rightleftarrows (C_{12}H_{25}\overset{*}{C}OO)_2Cu + 2CH_3COOH$$

It is known (5) that the solubility of copper salts of higher-molecular-weight, saturated aliphatic acids in hydrocarbon oil below 40°C. is very limited. Hence, the copper salt of the labelled acid is probably in a colloidal state and does not contribute noticeably to the diffusion. From the data obtained it was computed, according to the method shown in table 4, that 25 per cent of the acid was present in the form of its copper salt.

TABLE 5

Adsorbed fractions of tridecanoic acid from solution in oil

ADSORBENT	CONCENTRATION OF ADSORBENT	f/f_0	a
	per cent		
Graphite (Oildag)	1.0	0.62	0.38
Asphalt (Gilsonite) . . .	0.9	0.54	0.46

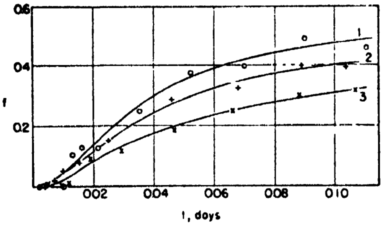

FIG. 6. Relative counts *vs.* time for 0.005 N tridecanoic acid and copper catalyst in oil. Oxidized at 150°C. Curve 1 (○) after 24 hr., curve 2 (+) after 64 hr , curve 3 (×) after 176 hr. of oxidation.

The final series of experiments were concerned with the oxidation and sludge formation of hydrocarbon oil. It is known that in the early stages of oxidation acids are formed. By adding a labelled acid, it is possible to elucidate their further function in the process. The solution containing 0.005 N radioactive tridecanoic acid in oil was oxidized at 150°C. in Sligh oxidation flasks. Diffusion measurements were carried out after certain times of oxidation. Figure 6 gives the results for a sample containing copper as catalyst. It can be seen that the diffusion rate becomes less as time progresses. Curves of this kind may be evaluated according to either of the two principles, as shown in tables 1 and 4. The first assumes an average diffusion coefficient of reduced magnitude; the second assumes that a fraction of the substance diffuses at the original rate, the balance at an appreciably lower rate. When it is not obvious which of the two conditions prevails, both calculations may be tried and the one yielding a more constant result should be retained. When this technique was used in connection with the data of figure 6, *a* showed a markedly better constancy than did *k*. The values of *a* give the fraction of the acid that in the course of oxidation forms macromolecules so large that their diffusion becomes unmeasurable during the times employed. These data, among others, are summarized in table 6. The total activity of the oil was also checked; it remains practically unchanged during the process of oxidation, notwithstanding pronounced sludge formation. The sludge was collected by repeated centrifuging of the oil in solvent naphtha; after drying it was weighed and its activity measured. The sample (14.0 mg.) was spread over an area of 3.5 cm.^{2} At a distance of 0.6 cm. from a Geiger–Müller counter it produced a count of 907 per minute. After absorption and geometry corrections, a simple formula (4) permits computation of the sample activity, which in this case was 19×10^3 counts/min. The total activity of the solution, determined in an analogous manner, was 6.7×10^6 counts/min. The acid present in the sludge was then 0.28 per cent of the total. Hence, in oxidizing an oil that contains an aliphatic acid, it is seen that the acid takes part in the formation of polymer molecules, but (up to about 200 hr.) only to a small extent in the formation of the solid precipitate.

TABLE 6

Polymerization of tridecanoic acid due to oxidation of oil

COPPER INGREDIENT	HOURS OF OXIDATION	*a*, FRACTION POLYMERIZED	AVERAGE *k*	FRACTION IN PRECIPITATE
Copper metal	24	0.08		
	64	0.24		
	176	0.44		0.0028
None	16		0.035	
	48		0.033	
	184		0.025	0.0007

Table 6 presents, in addition to the data mentioned, results of a series of tests without the copper catalyst. In this instance, the evaluation with respect to an average *k* showed a better constancy than with respect to *a*. The polymerization of the acid is first not noticeable, and only at the end of the test, after 184 hr. of oxidation, does the diffusion constant drop from its initial value of 0.035 to 0.025, corresponding to a radius of 4.4 Å. The total activity of the solution was not diminished, and the activity of the solid precipitate was only 0.07 per cent of the total. By using this technique, a better insight into the function of a copper catalyst is obtained.

SUMMARY

The diffusion rate of C^{14}-labelled tridecanoic acid in hydrocarbon oil was measured by means of a Geiger–Müller counter. Knowledge of the diffusion rate per-

mits the investigation of a variety of problems connected with hydrocarbon oils, as typified by the following results:

Tridecanoic acid, a typical aliphatic acid, was found to be molecularly dispersed in oil, the molecular radius being 3.5 Å. If an amine and a phenol are added, electrically conducting oils are produced; the compounds found in such a solution are moderately large molecules of 6–8 Å. radius.

The degree of adsorption, by graphite or asphalt, of the acid from solution was determined, as well as the extent of its exchange reaction with copper acetate added to the oil.

When an oil containing the acid was oxidized, it was found that a large fraction of the acid takes part in the formation of polymer molecules, but, up to 200 hr., only to a small extent in the formation of the solid precipitate.

REFERENCES

(1) Gemant, Andrew: J. Chem. Phys. **14**, 424 (1946).
(2) Gemant, Andrew: J. Electrochem. Soc. **94**, 160 (1948).
(3) Gemant, Andrew: J. Applied Phys. **19**, 1160 (1948).
(4) Hines, Edward, and Gemant, Andrew: Science **110**, 19 (1949).
(5) Piper, J. D., *et al.*: Ind. Eng. Chem. **31**, 307 (1939); **32**, 1510 (1940).

ON COMPACT-DISPERSED SILVER

GEORGE-MARIA SCHWAB

Department of Inorganic, Physical, and Catalytic Chemistry, Institute Nicolaos Canellopoulos, Piraeus, Greece

Received June 27, 1949

INTRODUCTION

Compact-dispersed substances (3) consist of discrete particles bound together at single surface points and kept in fixed relative positions by this binding. Many real adsorbents and catalysts, e.g., charcoal, fritted metal powders, skeleton contacts (Raney), belong to this class. They exhibit a manifold larger and often more active surface for reactions, adsorption, and catalysis than do ordinary compact substances, and therefore they must be classified as active substances. Fricke (1) enumerates fifteen methods for the preparation of active substances, but does not include the essentially electrolytic method described below.

PREPARATION

In the recovery of metallic silver from halide residues by the usual method of reduction in suspension with zinc and acid we were surprised by the great velocity of this process, in view of its heterogeneous nature. We first considered an action of atomic hydrogen, diffusing from the zinc surface to remote halide particles, but the reaction proceeds equally well in neutral media where no hydrogen is evolved. Diffusion of silver ions or atoms or even of electrons through the halide particles is precluded at room temperature. A review of the scarce data (2) existing on the series of action of different metals other than zinc shows that it follows well the series of electrolytic potential. Hence, the mechanism is an electrolytic one: zinc forms the anode of local elements at the contact points; zinc is dissolved and silver is deposited on the already formed silver cathodes from the solution which contains, at least near the halide surface, silver ions owing to the solubility of the silver halide.

A microscopic examination confirmed this view: Foils or rods, cast from fused silver chloride, were brought into contact with a piece of zinc, iron, nickel, or cadmium in solutions of hydrochloric acid, sulfuric acid, sodium chloride, or sodium sulfate. Then, it was seen that a silver front proceeded from the contact point gradually over the whole surface of the halide body and even into its interior. Obviously, the silver front at every moment forms the cathode of the short-circuited element, current flowing through the solution from the zinc to the silver front. The important point is that the growth is three-dimensional, which means that the silver body formed is porous and contains conductive electrolyte within its pores. This is due to the fact, directly observed, that the silver body forms an exact pseudomorph with all the details of shape and surface of the original halide body. Now, the molal volume of silver chloride is 25.9 ml., and the atomic volume of silver 10.3 ml. only. Consequently, the pseudomorph is bound to have an overall porosity of $\delta = 0.6$.

Pieces of compact-dispersed silver up to a size of a few millimeters could be obtained; the larger ones sometimes show deep cracks due to internal stress. The Brinell hardness is of the order of 1 kg./mm.^{2} These preparations, in view of their origin, somewhat correspond to Gomberg's "molecular silver," as used in the preparation of free organic radicals. The compact-dispersed appearance, however, gives a better possibility for dispersoid characterization.

PORE SIZE FROM CATALYTIC ACTION

In order to determine, in addition to the porosity, the true average pore diameter, one additional measurement is needed. We chose the catalytic action of the compact-dispersed silver in the dehydrogenation of formic acid vapor. This is a zero-order reaction, and its velocity is proportional to the true total accessible surface, provided the activity distribution of the active centers can be taken as constant. For compact bulk silver, in former work (6), the velocity

$$\log v = 7.03 - 17{,}600/4.57T$$

has been measured for a surface of 15 cm.^{2} We measured on two samples of compact-dispersed silver, prepared with zinc,

$$\log v = 10.2 - 23{,}000/4.57T$$

Thus, the surface of our preparation is not more active than that of ordinary silver, but, on the contrary, shows an increased activation energy. According to our former findings (6), this can be due to a certain zinc content of the silver, taken up during its deposition, as 1 atom per cent of zinc increases the activation energy by 1 kcal./mole. Then, our value of 23 kcal./mole would correspond to a zinc content of 5.4 atom per cent. In fact, an x-ray examination of the sample disclosed the corresponding diminution of the lattice spacings. Now, a compact silver alloy of this composition, because of the general relation between activation energy and frequency factor (F), would give a velocity of

$$\log v = 8.2 - 23{,}000/4.57T$$

A comparison of the frequency logarithms 8.2 and 10.2 showed that our preparation has a true accessible surface, γ, *100 times* larger than compact particles of the same size. Measurements of the catalytic dehydrogenation of ethanol gave an identical result.

From this and the porosity value an approximate estimate of the pore diameter is possible as follows:

Let

a = the edge length of a single, say cubic, piece of the catalyst,
b = the edge length of the small cubic particles of which it is supposed to consist,
V_a = the apparent volume of a catalyst piece,
V_b = the total true volume of silver in it,
$\beta = 1 - \delta$, the fractional volume occupied by silver,
O_a = the geometrical surface of a catalyst piece,
O_b = the true total surface of the small silver cubes,
γ = the "roughening", i.e., the surface increase factor, measured catalytically, and
N = the number of small silver cubes contained in one piece of the catalyst.

Then

$$V_b = \beta V_a = \beta a^3 = Nb^3 \tag{1}$$

hence

$$b = a\sqrt[3]{\beta/N} \tag{2}$$

and

$$O_b = \gamma O_a = 6\gamma a^2 = 6Nb^2 \tag{3}$$

hence

$$b = a\sqrt[2]{\gamma/N} \tag{4}$$

and from equations 2 and 4:

$$N = \beta^{-2}\gamma^3 \tag{5}$$

or

$$b = a\beta/\gamma \tag{6}$$

With the experimental values $a = 0.1$ cm., $\beta = 0.4$, and $\gamma = 100$, we obtain $b = 4 \times 10^{-4}$ cm.

As the porosity is nearly 50 per cent, the pore diameter is nearly equal to the cube edge, and we obtain for the pore radius:

$$r \approx 2 \times 10^{-4} \text{ cm.}$$

PORE SIZE FROM SPECIFIC PENETRATION

According to Manegold (4) for a porous diaphragm a specific flow penetration ("Durchlässigkeit," in contradistinction to the diffusion permeability), independent of the flowing substance, can be defined by:

$$D_s = \frac{VL\eta}{Ft\Delta p} \text{ cm.}^2 \tag{7}$$

where V is the volume of a substance of the viscosity η passed during the time t through a sample of the length L and the cross section F under the pressure difference Δp (absolute units). By means of the Hagen–Poisseuille law, D_s is related to the porosity δ and the average pore radius r by

TABLE 1

Measurement of specific penetration

SAMPLE NO.	V	t	L	F	η	Δp		$D_s \times 10^{10}$	$r \times 10^4$
						Mm. H_2O	Bar		
	ml.	*sec.*	*cm.*	*sq. cm.*	*poises*				
1	1.45	61200	0 4	0.0154	0.01	20	2×10^4	3.08	0.6
2	1.40	18000	0.23	0.04				2.24	0.5
3	1.8	16560	0.27	0.0158				9.3	1.2
Mean value									0.8

$$D_s = \frac{r^2\delta}{8} \tag{8}$$

hence

$$r = \sqrt[2]{\frac{2VL\eta}{Ft\Delta p\delta}} \tag{9}$$

Compact-dispersed silver plugs were prepared by reducing *in situ* silver halide columns fused in the bottom of glass tubes, and water was passed through them. Table 1 gives the results.

The mean value obtained, $r \sim 1 \times 10^{-4}$ cm., coincides well with the result of the catalytic measurements, $r \sim 2 \times 10^{-4}$ cm., especially in view of the fact that the influence of the pore shape and pore distribution has not been taken into account and this effect certainly acts differently in both cases. The pore size is just at the limit of microscopic visibility, in agreement with the somewhat coarse metallic appearance of the compact-dispersed silver surface.

PARTICLE SIZE BY X-RAYS

The Debye–Scherrer lines of the preparations are sharp but entirely smooth; this indicates that no particles above 10^{-4} cm. nor below 10^{-5} cm. are present. Thus the secondary particles, indicated by the b-value, are identical with the primary crystallites.

It may be mentioned here that rods of compact-dispersed silver, prepared from single crystals of silver chloride, showed no lattice orientation with respect to the original crystal; this agrees with the finding (5) that silver prepared by the superficial photographic processing of chloride or bromide single crystals is also randomly crystallized, corresponding to the general rules concerning lattice orientation in coating films (*loc. cit.*).

CONCLUSIONS

The good agreement of three independent methods for the estimate of the secondary structure is of importance for the comparison of these methods, especially of the catalytic one. Once more it shows that the catalytic reaction velocity is not a casual magnitude but can be predicted in a quantitative manner. As for the compact-dispersed silver, the measurements show that it is relatively little dispersed and by no means possesses specific surface properties, say like a Raney catalyst. Thus, the "molecular silver" acts on radical halides simply by virtue of its enlarged surface and not as a result of any sort of "molecular" dispersity.

REFERENCES

(1) Fricke, R.: Hedvall Festskrift, p. 189 (Göteborg, 1948).
(2) *Gmelin's Handbuch der anorganischen Chemie*, 7th edition. Carl Winter, Heidelberg (1920).
(3) Kohlschütter, H. W.: Kolloid-Z. **77**, 229 (1936); idem in G.-M. Schwab's *Handbuch der Katalyse*, Vol. 4, p. 391, J. Springer, Vienna (1943).
(4) Manegold, E.: Kolloid-Z. **81**, 164 (1937); see E. Zimens in G.-M. Schwab's *Handbuch der Katalyse*, Vol. 4, p. 243, J. Springer, Vienna (1943).
(5) Schwab, G.-M.: Trans Faraday Soc. **43**, 715, 724, (1947); also previous papers.
(6) Schwab, G.-M.: Trans. Faraday Soc. **42**, 689 (1946).
Schwab, G.-M., and Holz, G.: Z. anorg. Chem. **252**, 205 (1944).
(7) Schwab, G.-M., and Theophilides, N.: J. Phys. Chem. **50**, 427 (1946).

APPLICATIONS OF REACTION KINETICS TO METALLOGRAPHIC PROBLEMS

GEORGE-MARIA SCHWAB AND GEORGE PETROUTSOS

Department of Inorganic, Physical, and Catalytic Chemistry, Institute Nicolaos Canellopoulos, Piraeus, Greece

Received June 27, 1949

INTRODUCTION

In previous papers from this laboratory (17, 21) it has been shown that the activation energy of the gas-phase dehydrogenation of formic acid with Hume-Rothery alloys as catalysts is a function of their electron concentration, being higher according to the degree to which the first Brillouin zone of electron levels in these alloy structures is filled with free electrons. This has been confirmed for all the Hume-Rothery phases for which calculations of the zone exist (10).

In alloys other than Hume-Rothery, where covalent or polar bonds exist in addition to the metallic bond, the concentration of the free electrons can no longer be calculated on the basis of the chemical formula, so that theoretical predictions about the degree of saturation of the Brillouin zone are impossible. However, as the dehydrogenation clearly depends only on the free electrons, it was thought possible to reverse the argument and to determine experimentally the degree of saturation of the first Brillouin zone by measuring the activation energy of the catalyzed gas reaction. The information gained in this way may be useful in the discussion of the forces acting in certain alloys. In this paper some applications of this idea are reported. (Probably the measurement of the electrical resistance could lead to similar results, but with nonworkable alloys the activation energy is more easily measured.)

GENERAL PROCEDURE

The measurement of the formic acid dehydrogenation was carried out as previously described (17, 21). In a reflux system formic acid vapor was streamed at atmospheric pressure over a catalyst of measured and continuously varied temperature, and the rate of product formation ($CO_2 + H_2$) was measured by a Riesenfeld flowmeter. The curves taken at rising and falling temperatures were coincident and reproducible over a range of about tenfold variation of the velocity. Most of the catalysts were used in the form of broken lumps of about 1 mm. size, and their geometrical surface estimated on the basis of the size statistics. Iron and steel, copper and gold were used as foils. Activation energies q and frequency logarithms B of the equation

$$\log v = B - q/RT \tag{1}$$

were taken from logarithmic plots. Two samples at least were used of every catalyst.

I. GOLD–IRON ALLOYS

The phase diagram of the system gold–iron, as given by Hansen (6), is reproduced in figure 1. Our original purpose was to elucidate the character of the compound $AuFe_3$, this being the only compound reported of a Group IB and a Group VIII metal. However, an x-ray examination of preparations of the respective composition showed that even after many hours of annealing at 700–750°C. and considerable recrystallization only the diagrams of iron-saturated gold (15 weight per cent) and of metallic iron were present. Thus, the existence of the compound $AuFe_3$, assumed by Wever according to an occasional communication of L. Nowack (6), is to be discarded.

However, the kinetic investigation of this system led to other interesting results concerning the question whether, in gold–iron alloys, the 4*s* electrons of iron contribute to the electron gas or the 6*s* (and 5*d*) electrons of gold enter the empty 3*d* levels of iron atoms. The results of magnetic observations will be discussed below.

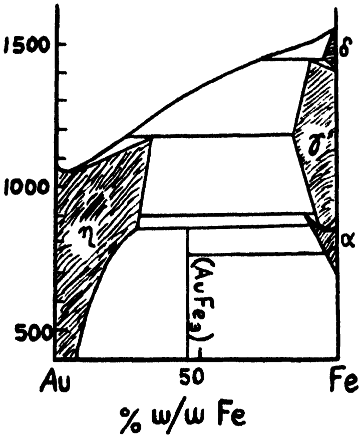

FIG. 1. Phase diagram of the system gold–iron as given by Hansen (6)

Materials

(*1*) *Gold:* Although in previous work (17, 21) reproducible catalytic data have been obtained with gold samples purified by Krüss's reprecipitation method (see 21), for this investigation the gold was purified once more by ether extraction of chloride solutions according to Mylius (11). This preparation did not differ catalytically from the former; thus, the *B* and *q* data obtained can be considered as those of the pure element. Gold measurements were regularly repeated throughout the present investigation as a standard for control of the arrangement, purity, etc.

(*2*) *Iron:* Iron powder "purissimum" Kahlbaum, fused in a gas–oxygen furnace under barium chloride in a double porcelain crucible and rolled to foils, was used as catalyst and as component in the alloys.

(*3*) *The alloys:* An alloy of a final content of 41 weight per cent iron was fused as above under sodium metaborate by heating the components together to 1400°C. Similarly, a 14 weight per cent iron alloy was prepared, and from this the 8 per cent and 4 per cent alloys by dilution with pure gold. The composition of the 14, 8, and 4 per cent alloys was checked by x-ray photographs (as for the 41 per cent alloy, see above). Thus, three points within the homogeneous η-region, one in the heterogeneous field, and α-iron were measured. Between duplicate runs the alloys were heated to 600°C. in a hydrogen stream.

TABLE 1

Formic acid decomposition on gold–iron alloys

PERCENTAGE OF IRON		q	$10^3/T$ ($v = 10$)	F	B (15 SQ. CM.)	q_m	B_m	BRINELL HARDNESS	
By weight	In atoms							Before annealing	After annealing
		kcal.		*sq. cm.*		*kcal.*		*kg./mm.*^{2}	*kg./mm.*^{2}
0	0	12.7	1.69	15.1	5.7	12	5.2		15
		11.0	1.62	15.1	4.9				
		12.0	1.56	15.1	5.1				
4	13	21	1.36	19.5	7.8	23	8.0	102	33
		24.5	1.36	19.5	8.2				
8	24	19	1.575	15	7.5	19	7.5	72	67
14	39	24	1.58	8.7	9.5	21	8.4		
		17.5	1.66	8.7	7.6				
		17	1.84	8.7	8.1				
41	71	21	1.55	6.2	8.5	22	9.0	180	129
		22	1.58	6.2	9.0				
		26	1.603	6.2	10.5				
		20.5	1.68	6.2	9.0				
100	100	22	1.70	12.2	9.2	22	9.4	103	57
		23	1.71	12.2	9.6				

Results

Some difficulty was encountered in the determination of the activation energy with pure iron as catalyst. It is very sensitive to casual poisoning. Under poison-free conditions, it was generally found that the reaction does not obey the simple Arrhenius law of equation 1 but that the temperature increment decreases at higher temperatures. A more detailed investigation to be described below (see Section II) disclosed later that the increment above 310°C. has to be considered as the true value for iron. The measurements given in table 1 were made before this was known, and therefore not under the best conditions. The preliminary value given, however, is sufficient for a comparison with the gold alloys.

The results are contained in table 1. The term q (zero-order reaction) is the true activation energy, $10^3/T$ ($v = 10$) indicates the temperature at which the velocity attains a value of 10 ml. of hydrogen per minute (which is within the upper third of the interval used), F is the geometrical surface, and B the decadic logarithm of the temperature-independent (frequency) factor of the Arrhenius equation, referred to a standard surface of 15 cm.^{2} The index m indicates mean values. The table contains, in addition, the Brinell hardness measured with a sphere diameter of 6.5 mm., a load of 35 kg., and in 1 min.

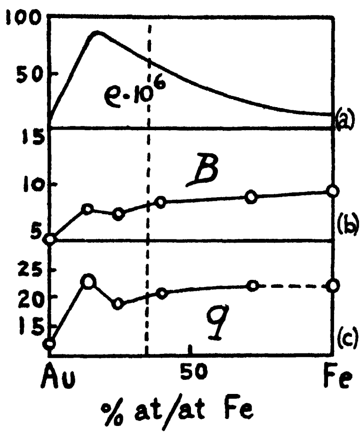

FIG. 2

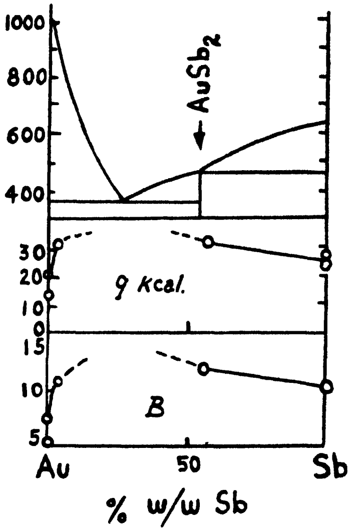

FIG. 3

FIG. 2. (a) Plot of specific resistance of alloys *vs.* atomic composition. (b) Plot of B-values *vs.* atomic composition. (c) Plot of activation energy *vs.* atomic composition.

FIG. 3. The gold-antimony system

Discussion

In figure 2 our values of the activation energy are plotted against the atomic composition. The dotted line indicates the solubility limit of the gold phase (η in figure 1) for the preparation temperature of 700°C. which has been shown to hold for our supercooled alloys. A sharp increase of the activation energy of gold is effected by the first few per cents of iron, followed by a flat minimum, still within the homogeneous region. The B-values, as usual (see, e.g., 21), follow this behavior, as is shown in figure 2 (middle). At the top of figure 2 the specific resistance of the alloys is plotted, mainly according to measurements of Linde (9). The maximum is found here again, but the minimum is not, because of the low resistance of pure iron. Thus, certainly, the maximum is connected with the electronic structure of the dilute alloys.

E. Vogt (25) measured the paramagnetism of iron dissolved in gold up to 7 weight per cent and found an atomic moment of 5.2 Bohr magnetons (by omitting the Curie–Weiss correction, W. Klemm (8) calculates an "effective" moment of

4.4 magnetons). This value very nearly corresponds to the doubly charged state of iron, Fe^{++} (4.9 magnetons). This requires that every dissolved iron atom contribute two valence electrons to the first Brillouin zone of the gold lattice. In fact, we find a corresponding large increase of the activation energy, Brinell hardness (see Schwab (18)), and specific resistance. The "atomic inactivation," i.e., the increase of activation energy in kilogram-calories per atom per cent is 85×10^{-2}; for gold–cadmium (21) it is 120×10^{-2}, and for copper–zinc (20) 100×10^{-2}. A more detailed comparison is not possible, as it has been found (20, 21) that not only the valence but also the period number of the solute element is of influence.

On the other hand, Pan, Kaufmann, and Bitter (13) measured the ferromagnetism of a homogeneous alloy with 37 atom per cent iron and found an absolute saturation moment of 1 Bohr magneton per atom. They conclude that in this alloy valence electrons of gold compensate the magnetic moment of iron. This would involve a decrease of the concentration of free electrons, and, in fact, at this iron concentration the activation energy as well as the resistance is lower and so is the hardness of the quenched 24 atom per cent alloy (after annealing it is biphasic (see figure 1)).

Thus, for this system the kinetic method is able to discover a deviation from the simple Hume-Rothery rules, confirmed by electric and explained by magnetic data.

II. IRON–CARBON ALLOYS

As already mentioned above for a special case, it has generally been found (18, 19) that the activation energy and the Brinell hardness of Hume-Rothery alloys show a common systematic dependence on the electron concentration, parallel to that of the electric resistance. In homogeneous phases the hardness increases with approaching saturation of the first Brillouin zone. An explanation, common to the three properties, was found (*loc. cit.*) in the fact that the (free) energy content of a structure rises abruptly when the coördinated wave length of the fastest electrons approaches the double distance of the first intensely reflecting lattice planes. Acceleration of electrons by an external field or entry of valence electrons from a catalyzed reactant brings the shortest wave length nearer to the double lattice distance and hence will be difficult in the case of a nearly saturated zone. This explains the behavior of resistance and of activation energy. A similar difficulty must be encountered in a local increase of the lattice distances. The critical step in plastic deformations is the formation of a dislocation in the lattice, which certainly implies a local increase of certain atomic distances. Thus, one may well understand the observation that this step requires a higher activation energy, resulting in higher hardness, in structures with a nearly saturated conductivity zone.

It was thought that this viewpoint might be applicable to the hardness of martensite in steel. Martensite, similar to the very hard carbides and nitrides of the tungsten carbide type, is an interstitial solution, the carbon atoms occupying interlattice sites in a tetragonally deformed body-centered α-iron lattice. Hence, every carbon atom adds four electrons to the zone without adding anything to the number of lattice atoms, and a considerable increase of the electron concentration results (0.19 per weight per cent of carbon). In the above example gold–iron, an increase of the electron concentration of gold by 0.13 (4 per cent iron by weight) brings about a sevenfold hardness increase, and exactly the same increase was found (21) for a gold–cadmium alloy of equal electron concentration. These effects nearly correspond to what is observed with a quenched 0.7 per cent carbon steel having the same increase of electron concentration. Thus, it is not out of reason that, perhaps besides the effect of microstresses, a considerable part of the hardness of martensite, as compared with pure or annealed iron, is due to the increased electron concentration. In this case, it is to be expected that also the activation energy of the formic acid dehydrogenation would be higher on hard steel than on soft, pure or annealed, iron.

Materials

The fused, chemically pure iron described above was used. The carbon alloys were prepared by heating 0.03–0.04 mm. foils in a charcoal bed to 900°C. for 2 hr. The carbon content was determined on the basis of the weight increase. The foils were hardened by heating them in a hydrogen atmosphere to about 600°C. for 5 min. and quenching in water under hydrogen. Before use, all the catalysts were rubbed with emery paper.

Results

In the beginning all the experiments were negative. No difference could be discovered between the curves of pure iron, hardened samples of iron containing 0.3–1.8 weight per cent carbon, and the same samples after annealing. It was thought that the martensite had disappeared during the measurement proper, as at temperatures between 280° and 350°C., as used here, and during 1 hr. a considerable martensite–perlite transition is possible (3). This seemed to be confirmed by the fact that the very first measurement with a fresh specimen always exhibited a higher activation energy than the later, reproducible curves. But it was found that this phenomenon is independent of the carbon content and occurs equally after previous annealing. Thus, it is merely due to an activation of the surface during the first rising run. Moreover, the catalysts did not always lose their hardness during one run, and the failure of the first experiments was to be sought elsewhere.

A survey of sixteen runs made with seven different catalysts containing between 0 and 1.8 weight per cent carbon, mostly after annealing, showed that the reaction on iron catalysts (see above) did not obey the simple Arrhenius law of equation 1 but all the log v *vs.* $1/T$ plots show a reproducible sharp break at 313°C. ± 3°. Below this temperature the lines are not ideally straight and reproducible, and only in a first approximation can they be represented by

$$\log v = 12.2 - 30{,}600/4.57T$$

Above the transition temperature, the Arrhenius law holds strictly with an average of

$$\log v = 8.1 - 19{,}600/4.57T$$

both equations referring to a 15 cm.^{2} surface.

The change of slope can not be explained by a change of the rate-determining step, as is usual in similar cases. The respective formulations would give a transition much smoother than the abrupt break observed. For the exact determination of the high-temperature increment and its eventual dependence on the martensite present, the amount of catalyst was diminished so that the transition temperature fell at the lower end of the temperature scale and the whole interval of reaction velocities available (1–30 ml./min.) was in the region of the high-temperature increment. In fact, by this measure, the effect sought for was discovered at once, as is shown in table 2.

TABLE 2

Formic acid decomposition on iron and steel

CATALYST	q	$10^3/T$ ($v = 10$)	F	B (15 SQ. CM.)
	kcal.		*sq. cm.*	
Pure iron	22	1.542	2.5	9.5
Iron alloy containing 3 weight per cent carbon, freshly hardened	25	1.575	2.7	10.4
The same, annealed at 300–400°C. . .	21	1.591	2.7	9.1

The effect, although distinct, perhaps appears small as compared with the well-known large hardness difference. However, it must be remembered that probably, because of the inevitable partial annealing during the measurement, only some residual increase of the activation energy is observed, and, secondly, in the hardness of steel the grain structure factor, as well as the intrinsic hardness of martensite, plays a part. Thus it appears justifiable to trace the martensite hardness, at least in part, to the increased electron concentration. It is equally well known that the electric resistance of iron is increased by dissolved carbon in a much higher degree than by cementite carbon. Thus, the parallelism of resistance, activation energy, and hardness holds also for the system iron–carbon.

III. GOLD–ANTIMONY ALLOYS

In the system gold–antimony the compound $AuSb_2$ is formed as a single phase at the stoichiometric composition of 66.7 atom per cent = 55 weight per cent antimony (see the phase diagram at the top of figure 3). This compound is reported to have the face-centered cubic structure of iron pyrite (FeS_2), with a cube edge of 6.63 Å. (12). We found this confirmed for our preparation of 56 weight per cent antimony. This is in accordance with the well-known rule that at electron concentrations as high as 3.67 salt-like structures are formed. Antimony in this compound is to be considered as prevailingly existing as negative ions or, at most, neutral atoms, bound in pairs by covalent forces. The covalent bond will absorb some of the five valence electrons of antimony, so that the actual concentration of conductivity electrons is considerably lowered.[1] The question to be answered is, whether the residual conductivity electrons fill up most of the available levels of the structure or leave many levels empty.

Materials

(*1*) *Gold:* The samples described above were used. As antimony alloys produce a permanent poisoning of the apparatus, removable only by thorough cleaning with nitric acid, many gold test runs were necessary between the alloy runs, and, for this, fresh gold samples were prepared from the iron alloys by the method described. They behaved identically.

(*2*) *Antimony:* Kahlbaum's antimony "pro analysi" was used.

(*3*) *The alloys:* The compound $AuSb_2$ was prepared by melting together the components under sodium metaphosphate in a porcelain crucible on a Bunsen burner, from this a 3 weight per cent alloy by dilution with pure gold, and from this the eutectic 25 weight per cent alloy by dilution with pure antimony in the same way.

Procedure

Gold and the compound $AuSb_2$ could be measured in the usual manner. The 3 weight per cent alloy had so little catalytic action below the limiting eutectic temperature of 360°C. (figure 3) that a smaller model of the same apparatus (24) had to be used, giving a seventeen times greater sensitivity. The catalytic action of the empty glass vessel, being of the same order of magnitude, had to be subtracted. This operation was checked by a subsequent run with gold which gave the same result as poisoned gold in the large apparatus. The reaction on the eutectic alloy could not even be measured in this manner.

---

[1] The usual treatment (10) is to consider all the electrons external to a closed shell as belonging to one zone, e.g., in the case of selenium the two electrons per atom engaged in the bonds of the atomic chains are taken together with the four "free" electrons as nearly filling a zone of six electrons per atom, and in graphite the three electrons per atom engaged in the bonds within the basic layers are placed, together with the fourth, metallic electron, in a flat hexagonal zone containing four electrons per atom. This is effected by selecting out of the reflecting planes a set bounding a zone volume corresponding to the total number of electrons external to a closed shell, Electrons in lower, closed shells of the atomic cores, e.g., $3d$ of copper, are considered as belonging to other and filled zones.

An alternative treatment would be to consider electrons engaged in covalent bonds as belonging to complete zones in a similar way as inner electrons of atomic cores, and to select the planes bounding the zone volume according to the residual number of conductivity electrons (one for graphite, four for selenium; e.g., for graphite this zone is bounded by (1100) and (0002)). The results would not differ as for the electrical properties, but give a more adequate picture of some chemical facts. It is in this sense that the discussions of Sections III and IV are meant.

Results

The results are tabulated in table 3.

Discussion

In figure 3 the dependence of B (below) and of q (middle) on the weight composition of the alloys is plotted. For pure gold, naturally, the results coincide with those reported above (page 584). Pure gold, inserted in the apparatus immediately after an antimony alloy, in the beginning gives the data of pure gold, and in the course of a run (five to six up-and-down measurements) the curves decay gradually to a final set of values, somewhat reproducible. Gold specimens in this poisoned state were considered and tabulated as an alloy of a very small antimony content. The increase of activation energy exhibited by them is considerable and comparable to that produced by traces of lead (17, 20). At 3 weight

TABLE 3

Formic acid decomposition on gold–antimony alloys

PERCENTAGE OF ANTIMONY IN CATALYST		STATE	q	$10^3/T$ ($s = 10$)	F	B (15 sq. cm.)	APPARATUS	q_m	B_m	BRINELL HARDNESS	
By weight	In atoms									Before annealing	After annealing
			kcal.		*sq. cm.*			*kcal.*		*kg./mm.²*	*kg./mm.²*
0	0	Pure	11	1.462	15.1	4.52	Large scale				
		Pure	11	1.594	16.6	4.79	Large scale	$11._1$	4.7		15
		Pure	10	1.676	16.6	4.63	Large scale				
		Pure	12.5	1.376	16.6	4.73	Large scale				
Trace	Trace	Poisoned	22		15.1	7.14	Small scale				
Trace	Trace	Poisoned	19	1.476	15.1	7.14	Large scale	20	7.2_6		
Trace	Trace	Poisoned	23	1.475	16.6	8.39	Large scale				
Trace	Trace	Poisoned	17	1.432	15.1	6.33	Large scale				
3	4.8		31	(1.450) Extrapolated	21	10.84	Small scale	31	10.8	80	19
25	35	Eutectic	Not measurable		7		Small scale			139	104
56	67.4	$AuSb_2$	32	1.512	12.2	11.67	Large scale	32	11.7	Broke	
		$AuSb_2$	32	1.515	12.2	11.69	Large scale				
100	100	Ref. 20	23.7				Large scale	25	∼10		∼60 (literature
		Ref. 17	27			∼10	Large scale				

per cent antimony it attains 20 kcal., the highest value ever recorded for a homogeneous alloy (no appreciable solubility of antimony in gold is recorded in the literature (6). Hence, this alloy probably is already heterogeneous. However, as the compound $AuSb_2$ has an activation energy of 32 kcal., the very nearly equal value of the 3 per cent alloy must be nearly that of the saturated gold crystals). The hardness is in qualitative agreement with the activation energies.

The point of interest is that the compound $AuSb_2$ does not differ from the saturated α-phase. So it behaves like a β- or ε-phase rather than like a γ-phase, and this means that in its first Brillouin zone many energy levels are left free.

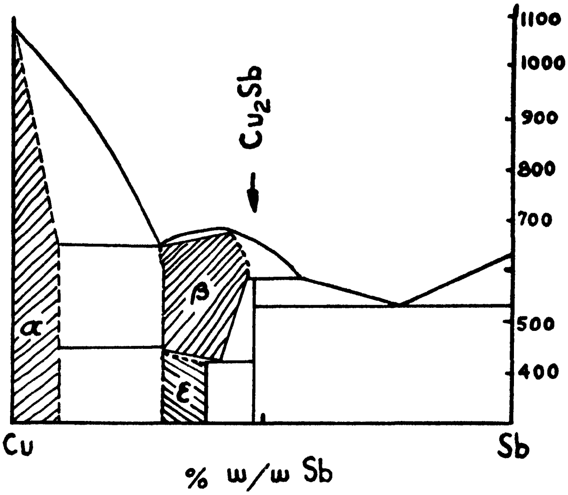

FIG. 4. The copper–antimony system

IV. COPPER–ANTIMONY ALLOYS

This system (see the phase diagram of figure 4), in the temperature region of catalysis, besides the Hume-Rothery phases α and ε, forms a new type of intermetallic compound at the composition Cu_2Sb. Its structure, according to Westgren, Hägg, and Erikson (26) and Howells and Morris-Jones (7), is identical with that of Fe_2As as determined by Hägg (5). It is tetragonal with $a = 3.99$ Å. and $c/a = 1.55$. The structure may be represented by layers of copper atoms, separated by undulated double layers of equiatomic composition. Every antimony atom has three copper neighbors at nearly equal distances, but no antimony neighbors in the first sphere. Thus, no covalent bond between antimony atoms is possible, and, if the actual electron concentration of this phase is found to be relatively low, this will indicate that antimony does not contribute its 5*s* and 5*p* electrons to the conductivity zone, but is neutral or even consumes 4*s* electrons of copper, acting as a negative partner. We examined a 46 weight per cent antimony alloy which gave the x-ray diagram of Cu_2Sb. For comparison, a 34 weight per cent antimony alloy, corresponding to phase ε, was examined. The x-ray diagrams showed that the phase β, at first formed from the melt, goes readily over to ε without supercooling. The 5 weight per cent antimony alloy had a slightly enlarged copper lattice, some superstructure lines being visible.

Materials

(*1*) *Antimony* was prepared by reduction of "pro analysi" antimony pentoxide with charcoal under calcium chloride and sodium chloride.

(*2*) *Copper:* Technical wire was used as a component for all the alloys. It was fused and rolled to foil.

TABLE 4

Formic acid decomposition on copper–antimony alloys

PERCENTAGE OF ANTIMONY IN CATALYST		PHASE	q	$10^3/T$ ($v = 10$)	F	B (15 SQ. CM.)	q_m	B_m	BRINELL HARDNESS	
By weight	In atoms								Before annealing	After annealing
			kcal.		*sq. cm.*		*kcal.*		*kg./mm.²*	*kg./mm.²*
0	0	Cu	18	1.493	15	6.89	18	6.9		35
5.1	2.7	α	17.5	1.498	20	6.62				
		α	26	1.500	16	9.52	21.5	8.0	94	67
		α	21	1.498	16	7.86				
34	21	ε	22	1.395	13.2	7.78				
		ε	21	1.423	18.9	7.44	21.5	7.6		>300
46	31	Cu_2Sb	20	1.368	17	6.90				
		Cu_2Sb	23.5	1.404	12.4	8.31	22	7.8		157
		Cu_2Sb	23.5	1.448	12.4	8.54				
			20.5	1.388	13.2	7.29				
100	100	Sb	(See table 3, below)				25	∼10		∼60

(*3*) *The alloys:* The components were fused together in crucibles under a eutectic sodium chloride–calcium chloride mixture. The α-phase could be rolled to flat plates; the other alloys were broken to lumps.

Results

The results are given in table 4.

Discussion

The reproducibility is not very satisfactory, especially for the α-phase, but it is felt that the mean values given are not very far from correct. For copper wire a value of 18 kcal. has been found, in good agreement with further measurements to be described below. (Formerly (23) in this laboratory, values of 23–24 kcal. were found on Kahlbaum's copper lathe chips. We repeated and confirmed these measurements. Naturally, the alloys must be compared with the copper specimen used in their preparation.)

The increase of the activation energy in the homogeneous α-phase is surprisingly small, and so it is in the phase ε. About the same has been found in the system copper–tin (17). But it is remarkable that the compound Cu_2Sb does not show any exaltation of activation energy comparable with, e.g., the γ-phase of copper–tin (Δq = 9 kcal.). This confirms the assumption that antimony in this compound is existing as an anion or a neutral component. The hardness of the compound, being even lower than that of the ε-phase, is another indication in this sense.[2]

V. COPPER–MAGNESIUM ALLOYS

Copper and magnesium (see the phase diagram in figure 5, left ordinate) form, besides the solid solution α, two intermetallic compounds, Cu_2Mg at 16 weight per cent magnesium, and $CuMg_2$ at 43.3 weight per cent magnesium (2, 4, 6, 16). The structure of the first is fully known. It is a cubic face-centered lattice of magnesium atoms in which four of the eight subcubes are body-centered by magnesium, and the other four contain tetrahedra of four copper atoms. The other compound is rhombic or orthohexagonal, but the atom parameters are unknown. We found both structures by x-rays in our respective preparations.

Between copper and magnesium neither polar nor covalent bonds are probable; hence their compounds are to be considered as true metals. This view is strongly supported by the nearly exact additivity of the third root of the molecular volumes in both structures (Vegard's rule). Also, the distances copper–copper, magnesium–magnesium, and copper–magnesium in Cu_2Mg are nearly equal to the sums of the neutral atom radii, as taken from the close-packed lattices of the elementary metals.

Under these circumstances, Cu_2Mg ought to be a saturated Hume-Rothery α-phase, and $CuMg_2$ an ε-phase. Actually, however, the α-phase breaks down at the low concentration of 7.5 atom per cent magnesium, and instead of the expected phases two new structures within very narrow regions of concentration (at most ± 2 weight per cent) occur, because the extreme atomic radius ratio of 0.8 is at the boundary of all the Hume-Rothery systems. This causes these ordered structures to be more stable than the Hume-Rothery random arrangements. Thus, the concentration range of stability of these phases is determined by the atomic radius ratio. Nevertheless, their electric and catalytic properties are bound to depend rather on the degree of saturation of the Brillouin zone and, for this, some new information is available from a measurement of the activation energy.

Materials

(*1*) *Copper* as before.

(*2*) *Magnesium:* Lathe chips for the Grignard reaction and flashlight ribbon were examined. The emery-rubbed ribbon did not act on formic acid at all, whereas with the chips a slight reaction was observed. It was supposed to be due to a superficial oxide layer, and magnesium oxide pellets were examined comparatively. In fact, the activation energy was the same in both cases, and it was further found that both reactions are nearly 100 per cent dehydrogenation, at most 10 per cent carbon monoxide being formed. Thus, the catalytic action of metallic magnesium could not be measured in our experiments.

---

[2] With nickel–antimony alloys it has been observed (22) that they are transformed into nickel catalysts during the reaction of formic acid owing to removal of antimony. An analogous reaction would explain the smallness of the activation energy differences in the copper–antimony alloys. This is precluded by the plain absence of any slow variation of the catalytic action in the course of the runs, in contradistinction to the nickel alloys.

TABLE 5

Formic acid decomposition on copper–magnesium alloys

PERCENTAGE OF MAGNESIUM IN CATALYST		PHASE	q	$10^3/T$ ($v = 10$)	F	B (15 SQ. CM.)	q_m	B_m
By weight	In atoms							
			kcal.		*sq. cm.*		*kcal.*	
0	0	Cu	19	1.560	17.2	7.43	20	7.7
		Cu	21	1.522	15.5	7.99		
12	26	$\alpha + Cu_2Mg$	23.2	1.651	10.3	9.55	22	9.2
		$\alpha + Cu_2Mg$	21.5	1.642	9.6	8.92		
20	39.5	Cu_2Mg	25	1.578	8.0	9.92	24	9.7
		Cu_2Mg	23	1.619	6.1	9.54		
35	58.5	$Cu_2Mg + CuMg_2$	16	1.450	7.2	6.40	17	6.8
		$Cu_2Mg + CuMg_2$	18	1.462	6.9	7.10		
45	68.2	$CuMg_2$	14.5	1.446	9.7	5.78		
		$CuMg_2$	17.5	1.490	10.3	6.87	15.5	6.2
		$CuMg_2$	15.5	1.422	9.7	6.02		
78.5	90.0	$CuMg_2 + Mg$	12.5	1.292	6.5	4.80	13	5.0
		$CuMg_2 + Mg$	14	1.334	10.6	5.24		
100	100	Mg + MgO	26	1.492	5.0	9.98	25	9.7
(Grignard)		Mg + MgO	24	1.442	6.0	9.08		
MgO	MgO	MgO	26	1.568	9.4	10.13		
		MgO	25	1.503	9.4	9.43		

(*3*) *The alloys:* Easy oxidation and low specific gravity of the magnesium alloys offer great difficulty in their preparation. Finally, a great excess of magnesium was melted within a protective sodium chloride–calcium chloride mixture and copper wire dissolved in the drops which finally gathered to a regulus at the bottom. The composition of the reguli was determined by measuring the specific gravity and interpolating between the x-ray gravities of Cu, Cu_2Mg, $CuMg_2$, and Mg, respectively. Hardness measurements were impossible; all the alloys are very hard, but brittle.

Results

The results of the catalytic measurements are given in table 5 (the arrangement was repeatedly checked with gold).

Discussion

In figure 5 (right ordinate, upper curve) the activation energies are plotted as a function of the atomic composition of the alloys. The activation energy of the compound Cu_2Mg is considerably higher than that of copper, and the eutectic mixture of both shows an intermediate value. This is consistent with the view expressed above that the compound Cu_2Mg is a true metal. Being a cubic face-centered structure of close-packed coördination, it is likely to behave about like a Hume-Rothery α-phase of the same electron concentration.

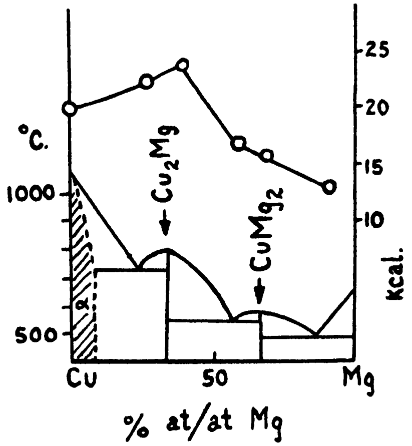

Fig. 5. The copper-magnesium system

The other compound, $CuMg_2$, shows an activation energy heavily diminished, even lower than that of pure copper. An ε-phase (which would be the Hume-Rothery phase corresponding to this composition) would, as found in numerous other examples, give a value nearly equal to that of the saturated α-phase or its substitute. Thus, the degree of saturation of the first Brillouin zone in this structure must be still considerably lower than in the ε-phases, where it amounts to about 74 per cent (10).

Unfortunately, the exact details of the structure are not known, so that a quantitative calculation is not possible at the present time. But the following argument can be brought forward on the basis of the Mott-Jones theory (10): In the debyeogram of $CuMg_2$ the only intensive reflexes are (204) and (224). Hence, in the "*k*-space" the first Brillouin zone is essentially limited by these planes. They have, because of the rhombic type of the lattice, the low frequency numbers of 4 and 8, respectively. Thus, the zone is represented by a rhombic dodecahedron, which is less spherical in shape than the zones of all the cubic and hexagonal Hume-Rothery phases, and the inscribed sphere of electron impulses will leave more empty space than in any of them. This causes ample electron levels to be available for the entrance of valency electrons from formic acid molecules (see 17), and the activation energy must be lower than in the Hume-Rothery phases, as is found.

VI. GOLD–LEAD ALLOYS

Besides the compound Bi_2K, which is not practicable for our purposes, one alloy exists on which part of the above results can be duplicated: the system gold–lead at 34.5 weight per cent lead forms the compound Au_2Pb, which is of the same cubic structure as Cu_2Mg (15). What has been said above about atomic radius ratio and distance additivity is equally true here; thus, we have to expect an increased activation energy for this compound too. Schwab and Holz (20) have found that gold, prepared by cupellation with lead, shows an activation energy of 20 kcal. instead of 12, and that this value can be increased to 24 kcal. by intentional contamination of pure gold with traces of lead, although the solubility is negligibly small. Thus, a rather large increase should result in the compound. We examined a 33.75 weight per cent lead alloy which, after annealing, showed the expected x-ray diagram. Alloys of higher lead content, including the compound $AuPb_2$, can not be subjected to the catalytic measurements because of the low peritectic and eutectic temperatures of 254°C. and 215°C. (6).

Materials

Gold as before and lead "purissimum" Kahlbaum. The alloy was prepared by fusing together the components under a protective eutectic of sodium chloride and calcium chloride and some borax.

Procedure

The peritectic dissociation of Au_2Pb at 418°C. (6) prevents the use of higher temperatures, so that the small-scale apparatus had to be used. The activity of the glass in this case gave only an insignificant correction. On this occasion an observation, made previously in this laboratory (20, 23) on pure lead and lead-rich silver alloys, was confirmed: During the first rise of temperature at about 260°C. a reaction sets in, reaches a maximum of about 12 ml. of hydrogen per minute at about 300°C., and falls to zero at about 350°C., when the catalysis proper begins. It is probable (*loc. cit.*) that this pre-reaction is a decomposition of superficial formate. Moreover, we found that, after removal of the catalyst, the empty glass apparatus retains for several runs the catalytic characteristics of the lead alloy, including the pre-reaction, and cleaning with nitric acid restores its former state. It appears that during the catalysis some lead hydride is volatilized by the nascent hydrogen (Paneth (14)) and traces of lead are deposited on the walls on its decomposition.

Results

The results of the measurement, together with some new gold values and with the values of lead-contaminated gold, mentioned above, are contained in table 6.

Discussion

The expected large increase of the activation energy is found, and thus the views regarding this structure are once more confirmed. Also, the hardness shows a corresponding increase.

VII. THE FREQUENCY FACTORS

Hitherto, only the activation energies and their dependence on the alloy structure have been discussed, because (see 17 and 24) the frequency factors or their logarithms B are a function of the activation energy. This function is represented in figure 6, all the B_m-values of tables 1–6 having been plotted against the corresponding q_m-values. The full circles refer to pure gold and copper and their α-alloys (solid solutions of the cubic face-centered type). The full line is not the mean line, but has been found in earlier work (17, 20), mainly with α-silver alloys. It is seen that it holds equally well for the new α-phases studied here. The empty circles, differently marked, refer to all the catalysts other than α, pure metals as well as compounds and heterogeneous biphasic alloys. With two exceptions (copper–antimony) they lie on a different straight line of a greater

TABLE 6

Formic acid decomposition on gold–lead alloys

PERCENTAGE OF LEAD IN CATALYST		PHASE	q	$10^3/T$ ($v = 10$)	F	B (15 SQ. CM.)	q_m	B_m	BRINELL HARDNESS	
By weight	In atoms								Before annealing	After annealing
			kcal.		*sq. cm.*		*kcal.*		*kg./mm.²*	*kg./mm.²*
0	0	Au	11.5	1.450	15.1	4.65				
		Au	11.5	1.359	15.1	4.42	12	4.8		15
		Au	12	1.500	15.1	4.95				
		Au	12	1.613	18.2	5.08				
Trace	Trace	α	20	(1.425)	(15)	7.24	20	7.2		
More	More	α	24	(1.210)	(15)	7.35	24	7.4		
33.75	32.7	Au_2Pb	30	1.556	11	11.35	30	11.4	80	67

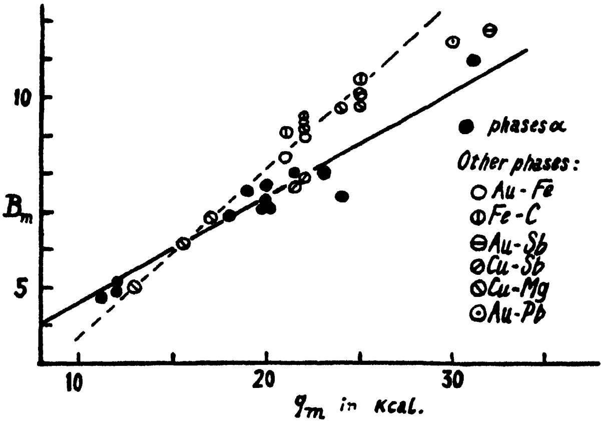

FIG. 6. Plot of B_m-values *vs.* corresponding q_m-values

slope. This phenomenon, formerly observed by us with copper–tin, silver–antimony, and gold–cadmium alloys (21 and earlier work, cited there) is thus confirmed on a broader material. The general increase of B on increasing q is explained (17, 19, 24; see also 1) by the statistical quality distribution of the active centers, and the steeper slope of the non-α-alloys by their increasingly rougher breaking surface due to the parallel between hardness and activation energy (18). This latter point of view can be maintained, although the points of the copper–magnesium alloys lie on or even beneath the α-line. These alloys differ from all the others in giving very smooth and bright breaking surfaces.

SUMMARY

The systematic variation of the activation energy of the formic acid vapor dehydrogenation in Hume-Rothery alloys as catalysts has been extended to other types of alloys, for the purpose of obtaining information about the degree of electron saturation of the first Brillouin zone.

For this purpose the activation energy has been measured in six alloy systems at different compositions. The results are in general agreement with the basic assumptions.

In the system gold–iron they agree with conclusions drawn from electric and magnetic data. In the system iron–carbon the hardness of martensite can be traced to its increased electron concentration. In the system gold–antimony the compound $AuSb_2$ of pyrite type has a relatively empty zone, and in the system copper–antimony the compound Cu_2Sb behaves similarly. In the system copper–magnesium the compound Cu_2Mg corresponds to a saturated α-phase, while the compound $CuMg_2$ has an extremely low degree of zone saturation. In the system gold–lead the compound Au_2Pb, isomorphous to Cu_2Mg, corresponds to it also in its electron distribution.

The frequency factors measured during this work confirm the systematic influence of the activation energy and lattice type stated previously.

REFERENCES

(1) ELEY, D. D.: Trans. Faraday Soc. **44**, 216 (1948).
(2) FRIAUF, I. B.: J. Am. Chem. Soc. **49**, 3107 (1927).
(3) *Gmelin's Handbuch der anorganischen Chemie*, 8th edition, Fe. Verlag Chemie, Berlin (1936).
(4) GRIMME, G., AND MORRIS-JONES, W.: Phil. Mag. **7**, 1113 (1929).
(5) HÄGG, G.. Z. Krist. **71**, 135 (1929); Arkiv Kemi, Mineral. Geol. **B12**, No. 1 (1935).
(6) HANSEN, M.: *Der Aufbau der Zweistofflegierungen.* J. Springer, Berlin (1936).
(7) HOWELLS, E. V., AND MORRIS-JONES, W.: Phil. Mag. [7] **9**, 993 (1930).
(8) KLEMM, W.: *Magnetochemie. Vol. I. Physik und Chemie*, p. 211. Akademische Verlagsgesellschaft, Leipzig (1936).
(9) LINDE, J. O.: *Elektrische Widerstandseigenschaften der verdünnten Legierungen des Kupfers, Silbers und Goldes*, Chap. 10, "Ergebnisse der Untersuchung des Gold-Eisen Systems." Ohlsson, Lund (1939).
(10) MOTT, N. F., AND JONES, H.: *The Theory of the Properties of Metals and Alloys.* University Press, Oxford (1936).
(11) MYLIUS, F.: Z. anorg. Chem. **70**, 215 (1911).

(12) Oftedal, I.: Z. physik. Chem. **135,** 291 (1928).
Nial, O., Almin, A., and Westgren, A.: Z. physik. Chem. **B14,** 81 (1931).

(13) Pan, S. T., Kaufmann, A. R., and Bitter, F.: Phys. Rev. [2] **57,** 569 (1940).

(14) Paneth, F., and Nörring, O.: Ber. **53,** 1693, 1710 (1920).

(15) Perlitz, H.: J. Inst. Metals **2,** 15, 222 (1935); Chem. Zentr. **1935, I,** 783.

(16) Runquist, A., Arnfelt, H., and Westgren, A.: Z. anorg. Chem. **175,** 43 (1928).

(17) Schwab, G.-M.: Trans. Faraday Soc. **42,** 689 (1946).

(18) Schwab, G.-M.: Experientia **2,** 103 (1946).

(19) Schwab, G.-M.: Proc. Intern. Congr. Chemistry, 11th Congress London, 1947; Göteborg Handlingar, 1949; Trans. Faraday Soc. **45,** 385 (1949).

(20) Schwab, G.-M., and Holz, G.: Z. anorg. Chem. **252,** 205 (1944).

(21) Schwab, G.-M., and Pesmatjoglou, S.: J. Phys. & Colloid Chem. **52,** 1046 (1948).

(22) Schwab, G.-M., and Pesmatjoglou, S.: Hedvall Festskrift, p. 533 (Göteborg, 1948).

(23) Schwab, G.-M., and Schwab-Agallidis, E.: Ber. **76,** 1228 (1943).

(24) Schwab, G.-M., and Theophilides, N.: J. Phys. Chem. **50,** 427 (1946).

(25) Vogt, E.: Angew. Chem. **48,** 734 (1935).

(26) Westgren, A., Hägg, G., and Erikson, S.: Z. physik. Chem. **B4,** 453 (1929).

BOOKS RECEIVED

Booth, Harold Simmons, and Martin, Donald Ray. *Boron Trifluoride and its Derivatives.* John Wiley and Sons, Inc., 440 Fourth Ave., New York 16. 1949. 315 pp. Price: $5.00.

Glocker, Richard. *Röntgen- und Radiumphysik fur Mediziner.* Georg Thieme Verlag, Stuttgart. Agents for the United States: Grune & Stratton, Inc., New York. 1949. 273 pp. Price: 19.20 RM.

Guthrie, A., and Wakerling, R. K. (Editors). *The Characteristics of Electrical Discharges in Magnetic Fields.* (National Nuclear Energy Series. Manhattan Project Technical Section. Division I–Vol. 5.) McGraw-Hill Book Company, Inc., 330 West 42nd St., New York 18. 1949. 376 pp. Price· $3.50.

Guthrie, A., and Wakerling, R. K. (Editors). *Vacuum Equipment and Techniques.* (National Nuclear Energy Series. Manhattan Project Technical Section. Division I–Vol. 1). McGraw-Hill Book Company, Inc., 330 West 42nd St., New York 18. 1949. 263 pp. Price: $2.50.

Haward, R. N. *The Strength of Plastics and Glass.* Interscience Publishers, Inc., 215 Fourth Ave., New York 3. 1949. 245 pp. Price: $5.50.

Houwink, R. *Fundamentals of Synthetic Polymer Technology.* Elsevier Publishing Company, Inc., 215 Fourth Ave., New York. 1949. 258 pp. Price: $3.75.

Laubengayer, A. W. *Laboratory Manual and Problems in General Chemistry.* Rinehart and Company, Inc.. New York. 1949. 229 pp. Price: $2.25.

Lecat, Maurice. *Tables azéotropiques. Azéotropes binaires orthobares.* Vol. I. Second edition. Chez l'Auteur, Uccle-Bruxelles, 29, Rue Auguste Danse. 1949. 406 pp. Price: 1000 frs. belges.

Matz, Werner. *Die Thermodynamik der Wärme- und Stoffaustausches in der Verfahrenstechnik.* Steinkopff, Frankfurt am Main. 1949. 355 pp. Price: 26 DM.

Pringsheim, Peter. *Fluorescence and Phosphorescence.* Interscience Publishers, Inc., 215 Fourth Ave., New York 3. 1949. 794 pp. Price: $15.00.

Ritchie, Patrick D. *A Chemistry of Plastics and High Polymers.* Interscience Publishers, Inc., 215 Fourth Ave., New York 3. 1949. 288 pp. Price: $4.50.

Snell, Foster Dee, and Snell, Cornelia T. *Colorimetric Methods of Analysis, Including Some Turbidimetric and Nephelometric Methods. Vol. II. Inorganic.* Third edition. D. Van Nostrand Company, Inc., New York. 1949. 950 pp. Price: $12.00.

Sullivan, William H. *Trilinar Chart of Nuclear Species.* John Wiley and Sons, Inc., 440 Fourth Ave., New York 18. 1949. Six charts. Price: $2.50.

THE TEMPERATURE FUNCTION OF THE INTERNAL HEAT OF EVAPORATION

J. C. DE WIJS

Meerkolstraat 5, Nijmegen, Holland

Received September 28, 1949

Some years ago the author proved (1) an empirical relation between the heat of evaporation of liquids and the temperature:

$$L = K_1(T_k - T)^m \tag{1}$$

in which L is the latent of evaporation at the temperature T and T_k the critical temperature, while K_1 and m are two constants dependent on the nature of the substances under investigation, the average value of m being 0.400. This formula holds good for a great number of liquids between the melting point and the critical temperature, with the exception of those liquids whose critical temperature is very low, such as the liquid gases.

It is now found that a similar empirical formula holds for the *internal* heat of evaporation, λ:

$$\lambda = K_2(T_k - T)^n \tag{2}$$

The constants K_2 and n are again in general dependent on the nature of the substances.

To examine this formula only those substances may be used for which the internal heat is known in a wide range between the melting point and the critical temperature. Such substances are, with the exception of the liquid gases, chiefly organic compounds (hydrocarbons, alcohols, esters, benzene, and derivatives, and some others) for which the data for the internal heat up to a few degrees below the critical point has been published by Mills (2) according to measurements of Sydney Young and coworkers. For five substances as representatives of some important classes of compounds we have calculated the constants K_1 and n and with these data the values of λ in formula 2. The results are compiled in table 1, in which λ is given in calories per gram.

From table 1 it appears that in all cases the agreement between the observed and calculated data is very satisfactory. Most of the differences do not exceed 2 per cent, which is of about the same order as usually found for empirical relations of this kind.

van Laar (3) has already proved that formula 2 holds for benzene but, owing to the use of other values for the internal heat, his constants differ slightly from ours: namely, $K_2 = 9.157$ and $n = 0.42$.

Besides the examples given here the formula is also valid within the same degree of accuracy for a large number of other substances, but again with the exception of the liquid gases.

TABLE 1

Observed and calculated data for λ in calories per gram

T	2,3-DIMETHYLBUTANE		n-PENTANE		METHANOL		ETHYL ACETATE		BENZENE	
	T_k = 500.5°K. K_2 = 8.3250 n = 0.4094		T_k = 470.3°K. K_2 = 9.2984 n = 0.4146		T_k = 513.1°K. K_2 = 29.901 n = 0.4068		T_k = 523.8°K K_2 = 8.2532 n = 0.4377		T_k = 561.6°K. K_2 = 9.5574 n = 0.4099	
	Observed	Calculated	Observed	Calculated	Observed	Calculated	Observed	Calculated	Observed	Calculated
°*K*.										
273	78.81	76.63	85.85	83.18	272.4	278.0	94.45	92.64	99.16	97.52
293					266.5	268.3				
313			76.16	77.47	258.9	258.1				
333	68.86	67.61	71.69	71.57	249.7	247.3				
353	65.08	64.18	66.86	67.04	238.5	235.7	78.25	78.29	86.70	85.37
373	60.64	60.46	61.57	62.04	225.2	223.2	74.36	74.15	82.37	81.91
393	56.03	56.39	56.33	56.39	211.0	209.7	69.64	69.66	77.39	78.23
413	51.12	51.83	49.08	49.80	195.4	194.7	64.42	64.78	73.45	74.29
433	45.78	46.61	40.89	41.69	178.2	177.8	58.36	59.30	69.48	70.00
453	39.60	40.37	30.02	30.33	158.1	158.2	52.68	53.26	65.21	65.33
468			13.38	13.44						
473	31.92	32.21			134.9	134.2	46.11	46.06	59.75	60.09
493	18.95	18.98			99.6	101.4	37.21	37.00	53.76	54.11
498	12.46	12.11								
503					74.60	76.61				
509					54.39	53.09				
513							23.55	23.38	46.53	46.97
520							14.82	14.80		
533									37.55	37.80
553									23.45	23.10

TABLE 2

Values of $m - n$ and m/n

SUBSTANCE	$m - n$	m/n
2,3-Dimethylbutane	−0.015	0.961
n-Pentane	−0.015	0.964
Methanol	−0.016	0.961
Ethyl acetate	−0.017	0.963
Benzene	−0.016	0.961

As a first approximation, the constant n is the same for all substances, as is also the case with m of formula 1. There is, therefore, for these substances a relation between the exponents of both formulas. With the average values for m =

0.400 and $n = 0.416$ we have $m - n = -0.016$ and $m/n = 0.962$. As table 2 shows, this holds good for the substances cited.

SUMMARY

An empirical formula for the internal heat of evaporation as a function of the temperature is given. This relation is valid between the melting point and the critical temperature of the substance.

REFERENCES

(1) DE WIJS, J. C.: Rec. trav. chim. **62**, 459 (1943).
(2) MILLS, J. E.: J. Am. Chem. Soc. **31**, 1099 (1909).
(3) VAN LAAR, J. J.: *Die Zustandsgleichung von Gasen und Flüssigkeiten*, p. 263. Leopold Voss, Leipzig (1924).

THE THERMODYNAMIC PROPERTIES OF SULFUR DIOXIDE

JAMES R. WEST[1] AND GINO P. GIUSTI[2]
Mellon Institute, Pittsburgh, Pennsylvania

Received July 20, 1949

INTRODUCTION

In the petroleum and the chemical industries the use of sulfur dioxide is increasing. At the same time the industries which roast sulfide ores, make sulfuric acid, manufacture sulfur from hydrogen sulfide, and burn sulfur to sulfur dioxide have an interest in the properties of sulfur dioxide at elevated temperatures.

Relatively pure sulfur dioxide may be produced by burning sulfur with oxygen from the tonnage oxygen plants now coming on the market. The combustion may also be carried out under pressure so as to produce, in one operation, a relatively pure compressed gas. Such a process awaits the development of a suitable combustion unit.

Because of the present and possible future need for data on the thermodynamic properties at elevated temperatures, the writers have extended to 2000°F. the information presented by D. F. Rynning and C. O. Hurd (4). Since Rynning and Hurd prepared their article after a critical evaluation of the various publications on this subject, their work is considered the most reliable. The results of the new calculations have been added to those of Rynning and Hurd, so that the tables and graphs shown here are complete and coherent.

[1] Senior Fellow, Mellon Institute, Pittsburgh, Pennsylvania, on the Multiple Fellowship sustained by the Texas Gulf Sulphur Company, New York, New York.

[2] Research Assistant (on the same project).

EVALUATION OF THE ENTHALPY[3] ABOVE 500°F.

Values of the enthalpy of sulfur dioxide were computed at 15 p.s.i.a. from the following equation. The value of 214.1 B.T.U. per pound[4] used in this equation

$$H^* = \int_{298}^{T} \left(0.320 + 3.98 \times 10^{-5} T - 5.75 \times 10^{3} \frac{1}{T^2}\right) dT + 214.1$$

was estimated from the work of Rynning and Hurd.

Then, starting at 500°F. and using 100°F. steps, the corrections for deviation from ideality with increasing pressure were found by the use of figure 106 in the charts published by O. A. Hougen and K. M. Watson (1). Next, isotherms of the enthalpy of the actual gas were plotted as a function of the pressure in order to smooth the data. Cross-plots of isobars of the enthalpy *versus* temperature were also made.

At 500°F. the maximum deviation of these values from the corresponding ones of Rynning and Hurd was 0.15 per cent at 600 p.s.i.a.

EVALUATION OF THE ENTROPY ABOVE 500°F.

Values of the entropy of sulfur dioxide were calculated at 15 p.s.i.a. from the following equation. The value of 0.4617 B.T.U. per pound per °F. used in this

$$S^* = \int_{298}^{T} \left(0.178 + 2.21 \times 10^{-5} T - 3.20 \times 10^{3} \frac{1}{T^2}\right) \frac{dT}{T} + 0.4617$$

equation was estimated from the work of Rynning and Hurd.

To obtain the entropy values for the actual gases at various pressures the following equation was employed. The Mehl equation of state (3) was used to

$$S = S^* - \int_{P_0}^{P} \left(\frac{\partial V}{\partial T}\right)_P dP$$

determine the last term in this relation.

Starting at 500°F. and proceeding in 100°F. steps, isotherms of the entropy were graphed as a function of the pressure. Cross-plots of isobars of the entropy *versus* temperature were also made.

At 500°F. the maximum deviation of these values from the corresponding ones of Rynning and Hurd was 3.3 per cent at 1000 p.s.i.a.

---

[3] Notation:

H^* = enthalpy of superheated vapor at 15 p.s.i.a, in B.T.U. per pound
P = pressure of superheated vapor, in p.s.i.a.
P_0 = reference pressure of 15 p.s.i.a.
R = gas law constant
S^* = entropy of superheated vapor at 15 p.s.i.a., in B.T.U. per pound per °F.
S = entropy of superheated vapor, in B.T.U. per pound per °F.
T = absolute temperature, in °K.
V = volume of superheated vapor, in cubic feet per pound
Z = correction factor for ideal gas law.

[4] The heat capacity equation of P. C. Cross (J. Chem. Phys. **3**, 825 (1935)) was modified so that the enthalpy is expressed as B.T.U. per pound.

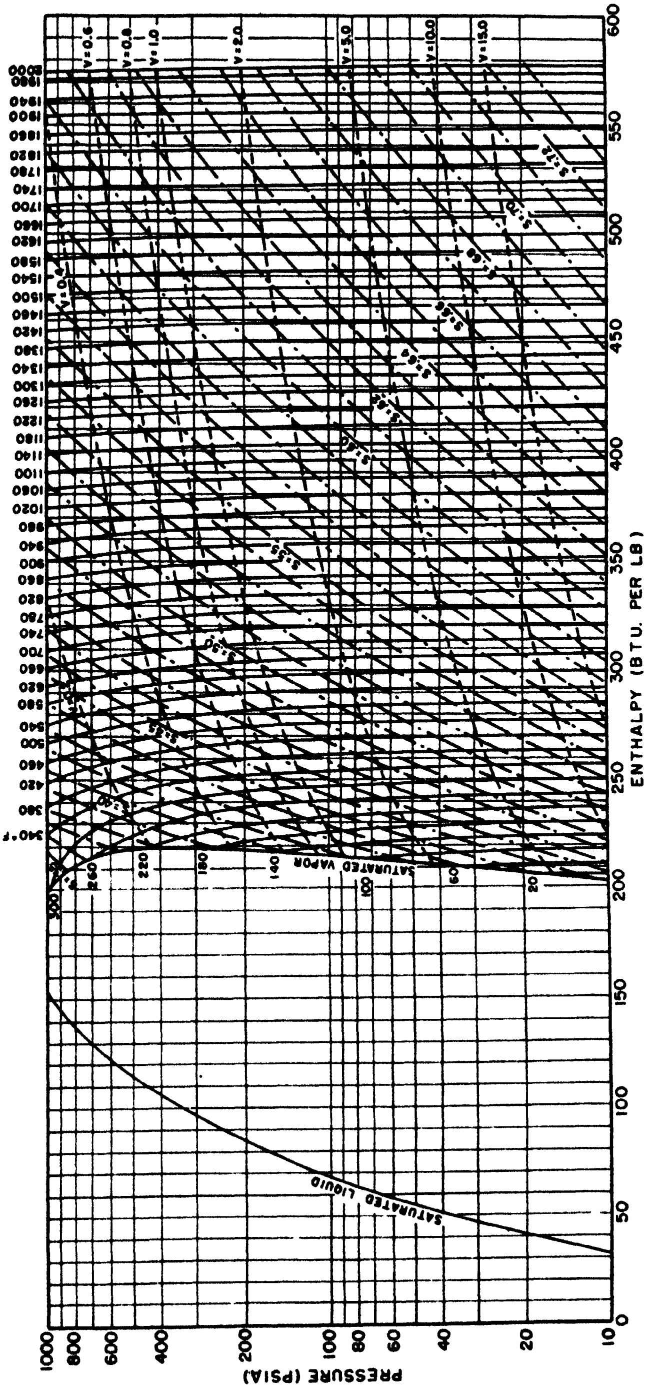

FIG. 1. Pressure–enthalpy diagram for sulfur dioxide

EVALUATION OF THE VOLUME ABOVE 500°F.

Values of the volume of sulfur dioxide were figured from the following equation. For the desired temperatures and pressures, values of Z were procured from

$$V = \frac{ZRT}{P}$$

figure 103 in the charts published by Hougen and Watson (1). Starting at 500°F. and proceeding in 100°F. steps, isotherms of the volume were graphed as a function of the pressure in order to smooth the data. Cross-plots of isobars of the volume *versus* temperature were also made.

At 500°F. the maximum deviation of these values from the corresponding ones of Rynning and Hurd was 3.1 per cent at 300 p.s.i.a.

EVALUATION OF THE FUGACITY COEFFICIENT ABOVE 500°F.

For the pressure range of 15 to 1000 p.s.i.a. and the temperature interval of 500° to 2000°F., values of the fugacity coefficient were derived from figure 142 of the charts published by Hougen and Watson (1).

At 500°F. the maximum deviation of these values from the corresponding ones of Rynning and Hurd was 1.3 per cent at 800 p.s.i.a.

RESULTS[5]

The properties of saturated sulfur dioxide are listed in table 1. These data, taken from the article by Rynning and Hurd, are included for the sake of completeness.

The properties of the superheated vapor are tabulated in table 2. The pressure ranges from 0.294 to 1000 p.s.i.a.; and the temperature, from −100° to 2000°F. The information at 500°F. and below is given in the article by Rynning and Hurd.

The compilations of tables 1 and 2 are illustrated in figure 1 as a Mollier chart.

The heat, the standard free energy, and the entropy of formation of gaseous sulfur dioxide from rhombic sulfur and gaseous oxygen are presented in table 3 as a function of temperature (2). In table 4 the same data are given for the case where diatomic sulfur vapor has replaced the rhombic form (2).

SUMMARY

In the literature the thermodynamic properties of sulfur dioxide now extend from −100° to 500°F. and from 0.294 to 1000 p.s.i.a. Data to 2000°F. are given in this paper.

---

[5] Because of space limitations, the tables described in this section are not published with this version of the article. For the detailed paper order Document 2708 from American Documentation Institute, 1719 N Street, N. W., Washington 6, D. C., remitting $0.50 for microfilm (images 1-in. high on standard 35-mm. motion picture film) or $2.00 for photocopies (6 x 8 in.) readable without optical aid.

This article was made possible through the kind support of the Texas Gulf Sulphur Company. To W. A. Hamor and L. H. Cretcher of Mellon Institute and to W. W. Duecker of the Texas Gulf Sulphur Company the authors are indebted for good advice.

REFERENCES

(1) Hougen, O. A., and Watson, L. M.: *Chemical Process Principles Charts.* John Wiley and Sons, Inc., New York (1946).

(2) Kelley, K. K.: U. S. Bur. Mines Bull. No. **406**, pp. 12–13 (1937).

(3) Mehl, W.: Bull. Intern. Inst. Refrig. **15**, 33A (1934).

(4) Rynning, D. F., and Hurd, C. O.: Trans. Am. Inst. Chem. Engrs. **41**, 265 (1945).

THE EFFECT OF PREVIOUS HEAT TREATMENT ON SOME OF THE ADSORPTION PROPERTIES OF SUGAR CARBON[1]

EDWARD R. LINNER and ARDIS PAUL WILLIAMS

Sanders Laboratory of Chemistry, Vassar College, Poughkeepsie, New York

Received July 25, 1949

INTRODUCTION

Early experiments demonstrating the difference in the adsorption properties of carbons activated at different temperatures are due to Lemon (20). Repeated activations at 650°C. increased the ability of the carbon to adsorb air. Such an ability was decreased, however, if the carbon had been heated at temperatures of from 800° to 900°C. Philip and Jarmon (27) carbonized birch wood at a series of temperatures from 350° to 850°C. for a definite period of time, testing the power of the char to adsorb iodine, oxalic acid, methylene blue, tartar emetic, and quinine sulfate. For the different carbons produced, it was found that maximum adsorption varied with the adsorbate used and not with the temperature of carbonization. It was noted, however, that with an increased amount of air available during carbonization at higher temperatures, a carbon of increased activity was produced. Other workers, notably Griffin and coworkers (13), Firth (11), Firth and Watson (12), Bhatagnar and coworkers (3), and Burrage (5), using various carbons and adsorbates, found much the same effect of temperature and time of activation on the adsorption properties of the carbon.

It has been well known for a number of years that adsorption of the members of an homologous series of organic compounds increases regularly with increase in molecular weight. Divergencies from this generalization, known as Traube's rule, have been observed frequently in the case of the interface between an aqueous solution of an aliphatic acid solution and carbon. Nekrassov (24) and

---

[1] This article is based in part on a thesis submitted by Ardis Paul Williams (née Ardis M. Paul) to the Faculty of Vassar College in partial fulfillment of the requirements for the M.A. degree, June, 1946.

Sabalitschka (28) did some of the early work which indicated that under certain conditions Traube's rule did not hold. Some of this work suggested a relationship between temperature of activation of the carbon and its subsequent behavior. These initial suggestions of the problem were followed by a series of papers by Dubinin (7–10), in which he showed that carbons heated at different temperatures behaved very differently as adsorbents. For example, he discovered that carbons heated at 500°C. followed Traube's rule, while those activated at 800°C. showed a reversal of the rule. Dubinin's data were variously interpreted. Dubinin himself at first believed that carbon heated at 500°C. had an amorphous structure, while that treated at 800°C. had a crystalline structure. Later he came to the conclusion that differences could be accounted for on the basis of the formation of suboxides of carbon. Bruns (4) showed experimentally that Dubinin's results depended upon the porosity of the carbon, a conclusion that Dubinin (9) had also reached.

These studies, and those of Shilov and coworkers (29, 30), led to a more detailed study of the surface structure of carbon and to the relation of the structure to the temperature of activation. In the few years following Shilov's suggestion of surface oxides, the theory was questioned by many scientists in the field, though Miller (23) found evidence for the existence of surface oxides in electrodialysis experiments. Later, pH studies and their relation to adsorption carried on by King and coworkers (16, 17) seemed to indicate the existence of acidic and basic oxides which influence adsorption fundamentally. Weller and Young (32) treated low-ash carbons with oxygen at 400°C. and showed that such treatment resulted in a carbon with an increased ability to remove alkali from solution but a decreased ability to remove acid. They reported that the amount of acid and base removed by a charcoal increases with time of immersion, and suggested that time is required for diffusion through the pore system of the charcoal.

Ogawa (25) had already shown that there was an increase in adsorption upon the disintegration of carbon. Dubinin and others had interpreted changes in adsorption on the basis of increases in surface. Later, Ockrent (26) demonstrated that grinding increased the surface available for larger molecules and decreased that available for smaller molecules. He suggested that besides the increase in surface due to disintegration, there may be an increase dependent upon pore size. The ultraporosity theory proposed by Herbst (14) was apparently verified by Ockrent (26), but it was questioned by Cohan (6) on the basis of experimental evidence obtained from electron microscope studies of carbon black. The photomicrographs indicate a smooth carbon surface. Any pores or fissures present in such material were found to be too small to admit nitrogen molecules, since the area determined from adsorption methods using nitrogen agreed with the area calculated from the electron micrographs and x-ray and electron diffraction data. Lemieux and Morrison (19) studied the adsorption of acetic, propionic, butyric, and valeric acids from aqueous solution by steam-activated carbons. Comparisons of the maximum amount of each adsorbed acid with one another and with the surface areas presented to gaseous nitrogen seem to indicate that the acids were adsorbed on a part of the carbon surface. The differences were interpreted as due to differences in the relative sizes of pores and fissures in the carbon.

Most discussions dealing with surface structure have implied that changes in heat treatment could cause changes of surface from one type to another and changes in the amount of surface available for adsorption. Reports on this phase of the problem are both incomplete and contradictory. King (16, 17) carried out a series of experiments to determine the influence of temperature of activation on the adsorption of acids and bases by charcoal. Although he made allowance for increased adsorption due to surface extension, he ascribed most of the variation to changes in the constitution of the oxide surface produced at the temperature to which the carbon has been heated. The results of his experiments with carbons that were heated above 850°C. were in disagreement with results obtained by Bartell and Miller (2) and Dubinin (7).

Many of the observations made of the effect of heat treatment on the adsorption properties involve single concentration studies. This is particularly true of those in which aqueous solutions of the aliphatic acids were used. In order to obtain more completely representative data, Heuchling (15) investigated the adsorption of aliphatic acids of low molecular weight from aqueous solutions over a range of concentrations, with norite as the adsorbent. Samples of the norite were subjected to heat treatment at 100° intervals between 500° and 1100°C. before it was used. These experiments showed differences among the various carbons used and each acid showed a trend, with maximum adsorption occurring with carbons preheated at 800°C. and 900°C. There is a reasonable doubt cast upon these results in spite of the definite trends observed, since norite is a substance which has already been activated. The present study was undertaken to evaluate Heuchling's results, using purified sugar carbon as the adsorbent with the monocarboxylic acids as adsorbates.

EXPERIMENTAL

Materials

The adsorbate: Four aliphatic acids—acetic, propionic, butyric, and valeric—and iodine were employed throughout this study. All were of satisfactory purity.

The adsorbent: The adsorbent used was a large sample of carbon prepared from pure cane sugar by carbonization with sulfuric acid. After carbonization, the product was washed free of sulfate ions. It was then dried, ground, and screened. To insure complete carbonization, it was heated at 400°C. for 8 hr. This heating was followed by treatment with hydrofluoric and hydrochloric acids to insure the removal of any silica which might have been picked up in the ball mill during grinding. A thick paste was made with the acids and carbon in platinum dishes and the mass was dried on an electric hot plate. This dried material was washed twice with concentrated hydrochloric acid and then with hot water until there was no test for chloride ions. Further purification was accomplished by electrodialyzing the mass until no chloride ion was detected in the solution about the anode. The resulting product was screened when dry and the portion which passed through the 100-mesh sieve was retained for analysis and the adsorption studies. Analysis showed that the carbon contained 0.522 per cent ash, of which 5.40 per cent was silica and 81.5 per cent iron. Calcium was also present in the ash but in such small quantities that a determination was not considered necessary. The adsorption studies involved several different samples of this 100-mesh carbon, each of which was heated at a different temperature before it was used for adsorption measurements. The temperature ranged from 500°C. to 1100°C. at intervals of 100°C. The carbon to be heated was placed in quartz crucibles and covered with flat, quartz plates in such a way that only the air between the surface of the carbon and the plate cover was in contact with it. The crucible and its contents were put in an electric furnace, brought to the desired temperature and kept there for 12 hr., after which they were removed and cooled in a desiccator. Only a small amount of carbon was lost during the heating process even at the higher temperatures. The heat-treated carbon was used for adsorption experiments within 4 hr. of cooling.

Experimental procedure

The actual adsorption studies involving the aliphatic acids followed the procedure described by Linner and Gortner (21). The trend of adsorption was studied over a range of concentrations from 0.025 to 0.25 molar, using 1 g. of the heat-treated carbon as adsorbent in 75 ml. of solution. Solutions and carbon were shaken for at least a half-hour and allowed to stand overnight at room temperature. The concentration of each filtered equilibrium solution was determined by the titration of duplicate aliquots with standard base, using the usual analytical procedure. The millimoles of acid adsorbed from 75 ml. of solution per gram of carbon was calculated for each dilution. Duplicate results agree within two parts per thousand. Equilibrium concentrations were calculated to moles per liter.

For iodine adsorption, 1 g. of each of the carbons was shaken with 100 ml. of 0.1 molar iodine in potassium iodide (0.15 molar). The flasks were shaken for one half-hour and allowed to stand for one half-hour before they were centrifuged. Two 20-ml. portions were withdrawn from each of the centrifuged systems and titrated with standard sodium thiosulfate solution.

The Langmuir equation (18)

By rearrangement of this equation

$$C/a = C/\beta + 1/\alpha\beta$$

in which C is the equilibrium concentration in moles per liter and a is the number of millimoles of reagent adsorbed by 1 g. of carbon from 75 ml. of solution. The values of the constants α and β are determinable by plotting C/a against C. When the data obtained from these experiments were so plotted, straight lines resulted in all cases. The constants for the equations representing each of these lines were calculated by the method of least squares. The values of α and β were determined from these constants and are contained in table 1, together with the per cent standard deviation between the observed values of a, the quantity adsorbed, and those calculated by the equation derived for each isotherm. For low equilibrium concentrations, the Langmuir relationship predicts an adsorption which is invariably less than that observed. Hence, the equations are somewhat less successfully applied to the first data of each run. The constant

TABLE 1

Showing values of α and β of the Langmuir equation, $a = \alpha\beta C/(1 + \alpha C)$, for various systems of carbon and organic acid at equilibrium

Each carbon is considered separately and is designated by the temperature to which it had been heated, i.e., 500°-carbon, 600°-carbon, etc.; the standard deviation given in column 5 considers seven points in each case

	ACID	α	β	STANDARD DEVIATION BETWEEN OBSERVED AND CALCULATED a
				per cent
500°-carbon.....	Acetic	0.3949	1.943	5.08
	Propionic	0.8878	2.030	7.40
	Butyric	2.057	1.708	4.16
	Valeric	2.239	1.428	4.39
600°-carbon.....	Acetic	0.4805	1.970	5.08
	Propionic	1.074	1.983	5.27
	Butyric	3.984	1.640	1.64
	Valeric	6.803	1.295	1.63
700°-carbon.....	Acetic	0.5071	1.986	5.71
	Propionic	0.9863	2.068	5.62
	Butyric	2.189	1.753	5.07
	Valeric	2.571	1.363	5.00
800°-carbon..	Acetic	0.5884	2.055	3.32
	Propionic	0.8060	2.200	6.61
	Butyric	5.462	1.722	5.31
	Valeric	1.940	1.550	9.41
900°-carbon..	Acetic	0.4909	1.788	3.55
	Propionic	0.7268	1.614	5.67
	Butyric	4.314	1.246	5.99
	Valeric	3.765	1.043	3.86
1000°-carbon.	Acetic	0.2180	0.7718	8.69
	Propionic	0.6151	0.6180	3.73
	Butyric	0.5535	0.6857	9.88
	Valeric	0.8480	0.6527	6.96
1100°-carbon....	Acetic	0.3758	0.9856	0.33
	Propionic	0.4852	0.8230	6.64
	Butyric	0.9309	0.7551	3.33
	Valeric	3.001	0.6071	1.60

β is of especial interest, since it is used as a basis of comparison of the adsorptive powers of the various carbons for the different acids. Linner and Gortner (21) have shown that this constant has the dimensions of surface and, since it represents the maximum adsorbed, they have demonstrated that β will serve as a more logical basis for comparison than will α or the constants of the Freundlich equation. For this reason, the latter equation has not been applied to the data of these studies. The variation of the values of β of the isotherms for each carbon, when used as the adsorbent for an individual acid, is shown in figure 5b. Here the values of the constant are plotted against the temperature to which the carbon has been heated before it was used in the study. Since, as stated above, β represents the maximum amount of the acid adsorbed, it is to be expected that the position of each value of this constant when so plotted will be the same as the relative positions of the isotherms obtained when a is plotted against C (figures 1–4). This is substantiated. Figure 5b also makes it clear that a highest maximum is reached with the 800°-carbon with all acids except butyric, in which

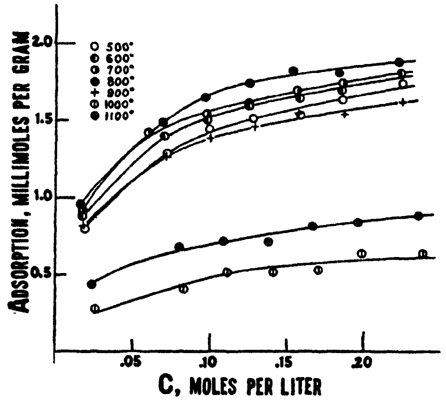

FIG. 1. Isotherms of acetic acid

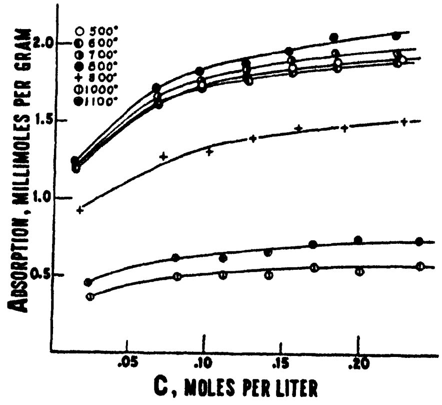

FIG. 2 Isotherms of propionic acid

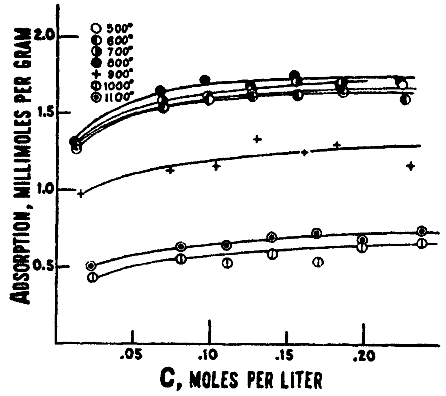

FIG. 3 Isotherms of butyric acid

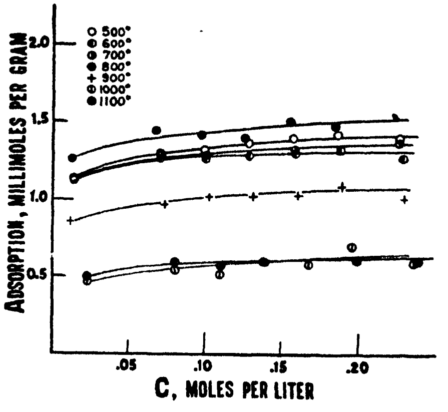

FIG. 4. Isotherms of valeric acid

case little if any difference can be made between the adsorptive power of either the 700°- or the 800°-carbon. In fact, the Langmuir equations representing the adsorption of butyric acid by the 700°- and 800°-carbons may be used interchangeably. The values of β for the equations applicable to the adsorption of the 1000°- and 1100°-carbons are interesting. The respective values for acetic and propionic acids are quite different, that for the 1100°-carbon being greater than that for the 1000°-carbon. Neither is as great as that for the 900°-carbon. These observations are also to be made when the data obtained with butyric acid are studied, except that differences are much less marked. The values of β for the adsorption isotherms of valeric acid obtained with the 1000°- and 1100°-carbons are 0.653 and 0.607, respectively. This indicates a small drop in the maximum adsorbed by the 1100°-carbon. Yet the values of a and C for each run are such that the Langmuir equations for the 1000°- and 1100°-carbons are not interchangeable.

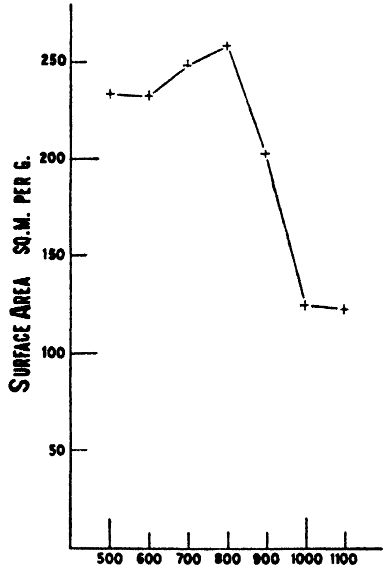

FIG. 5a

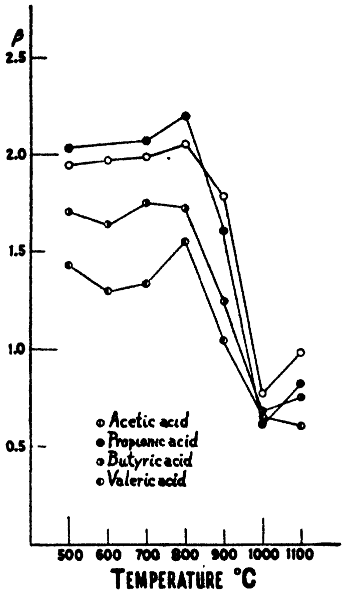

FIG. 5b

Fig. 5a. Variation of surface area of carbon available for iodine adsorption with the temperature to which the carbon was heated before adsorption measurements.

FIG. 5b. Variation of values of B, the maximum of acid adsorbed by the various carbons, with the temperature to which each was heated before the study was made.

pH of aqueous suspensions of the carbons

Ten-gram samples of each of the carbons were thoroughly wetted with freshly distilled water and then mixed with enough of the water to make the total volume of the latter 100 ml. The pH values of such suspensions were determined with the Beckman pH meter at 32–33°C. A blank with distilled water alone was treated in the same fashion and was found to have a pH of 6.5 at 32°C. The pH values of the aqueous carbon suspensions are as follows: 500°-carbon, 6.4; 600°-carbon, 6.7; 700°-carbon, 7.0; 800°-carbon, 8.0; 900°-carbon, 7.6; 1000°-carbon, 7.5; 1100°-carbon, 8.5.

Calculation of the extent of surface available for adsorption

The surface of the several carbons was determined by the method suggested by Smith, Thornhill, and Bray (31), based upon the adsorption of iodine. These investigators assigned 100 sq. m. of surface to 130 mg. of iodine. Table 2 gives the number of millimoles of iodine adsorbed per gram of each of the heat-treated carbons together with the surface of each determined upon this basis. From a study of these values, it is evident that the amount of surface that is available for iodine adsorption depends upon the previous treatment to which the adsorbent has been subjected. A maximum is reached with the 800°-carbon; a marked decrease in surface is encountered with the 900°-carbon and a further extreme decrease is observed in the surface of the 1000°- and 1100°-carbons with but a slight difference between the available surfaces of these two. When the square meters of available surface calculated from the iodine adsorption are plotted against the temperature to which the carbon has been subjected, a curve is obtained that is strikingly similar to each of those obtained when the values of β for the various acids are plotted in this fashion. Figure 5 demonstrates this clearly.

TABLE 2

Showing the maximum quantity of iodine adsorbed by each of the various carbons and the surface area of each which is available for the adsorption of iodine

TEMPERATURE OF HEAT TREATMENT OF CARBON	ADSORBED PER GRAM OF CARBON		AVAILABLE SURFACE
	Grams	Millimoles	
°C.			*sq. m./gram*
500	308.0	1.213	237
600	301.0	1.186	232
700	322.6	1.272	248
800	334.0	1.316	258
900	263.5	1.039	202
1000	161.3	0.635	124
1100	157.5	0.620	122

Because of the striking similarity in these curves it seemed well to attempt an approximation of the surface available to the fatty acid molecules. The value 25.1 sq. Å., which is that assigned to $-CH_2CH_2COOH$ by Adam (1), was chosen as the cross-sectional area. If we assume that this is the average cross-sectional area of each of the aliphatic acid molecules, then the area of the adsorbent in square meters is given by $25.1 \times 6.03 \times \beta$, where 6.03 is the number of molecules in 10^{-23} moles. It is necessary, however, that one bear in mind the method utilized in determining the value 25.1 sq. Å., because it will be apparent that, since the values given in table 3 depend upon this area, they may possess validity when they are compared with each other. It may be well, therefore, to refer to them as the relative surfaces available for the adsorption of acid molecules. Nevertheless, it is profitable to compare the values so obtained with the area assigned to the iodine molecule, which is based on the atomic diameter of iodine determined by Mack (22) from diffusion studies. It will be noted that the relative surface available for the adsorption of all of the acids but valeric is larger in most instances than that available for iodine adsorption. This is to be expected, perhaps, since the maximum quantities of the three acids adsorbed by each of the carbons expressed in millimoles per gram are greater than those for iodine. Valeric acid maxima are slightly greater, too, except for the 1000°- and 1100°-carbons, yet in most cases the surface areas available for adsorption of the valeric acid molecules as calculated are somewhat less than those assigned to the iodine.

TABLE 3

Showing the surface areas available for the adsorption of the aliphatic acid molecules, based upon an average cross-sectional area of 25.1 sq. Å., compared with those available for iodine (130 mg. of iodine associated with 100 sq. m. of surface)

TEMPERATURE OF HEAT TREATMENT OF CARBON	IODINE	ACETIC ACID	PROPIONIC ACID	BUTYRIC ACID	VALERIC ACID
°C.					
500	237	294	307	258	216
600	232	298	301	248	196
700	248	301	313	265	206
800	258	311	330	261	234
900	202	271	244	189	158
1000	124	117	94	104	95
1100	122	149	125	114	92

Comparisons among the acids themselves reveal that the surface available for the adsorption of propionic acid on the 900°- 1000°-, and 1100°-carbons is less than that for acetic acid. In the case of butyric and valeric acids, the differences are most marked. Furthermore, the space available to butyric acid on all of the carbons is generally somewhat smaller than that available to propionic acid. Since the results are based upon β, i.e., each area is obtained by multiplying β by a constant, all of these comparisons are essentially comparisons among the values of β, the maximum adsorbed. It must be pointed out that the relative surface available to longer molecules is smaller and that the longer molecules are adsorbed to a lesser degree than are the shorter molecules. This latter fact is not in agreement with the general observation summarized in Traube's rule. The magnitude of adsorption of the fatty acids by all of the carbons used in this study and at all concentrations investigated is such that generally the rule is reversed.

DISCUSSION

Of the theories advanced to explain the changes undergone by carbon during a activation process involving heating, two will be applied to interpret the results obtained with the present experiments. One of these theories concerns itself with the formation of oxides at the surface of the carbon during the heat treatment, the other with changes in the available surface. The former seems to be an unsatisfactory explanation for the results obtained; the latter more adequately explains experimental facts.

If the possibility of the existence of surface oxides is considered, only a partial explanation can be given for the shape of the β-curves. King (16) has studied the pH of aqueous suspensions of various charcoals and has attributed the various pH values obtained to the existence of basic and acidic oxides on the surface of the adsorbents. He assumed that a certain pH and, therefore, a certain type of oxide surface are characteristic of the temperature at which the carbon has been activated. In the present study, in which the heating of the carbon was carried out in a very limited supply of air, it was found that the pH of aqueous suspensions of the sugar carbons increased as the temperature to which the carbon was subjected was increased, with but slight variation in values of the 800°-, 900°-, and 1000°-carbons. A maximum pH value of 8.5 was obtained with the suspension of the 1100°-carbon. The results obtained with carbons up to the 800°-carbon are similar to those obtained by King, but beyond this point there is no correlation between the pH of the suspension of a carbon and its adsorptive capacity for the aliphatic acids. The 900°- and 1000°-carbons of pH values 7.6 and 7.5, respectively, are widely different in adsorptive capacity. They in no wise resemble that of the 800°-carbon. Furthermore, the pH of the aqueous suspension of the 1100°-carbon is the highest of all of those studied, and yet its adsorptive capacity ranks with that of the 1000°-carbon and is well below that of any of the other carbons studied. Such observations throw doubt upon the validity of the idea that pH can be used as an indication of the chemical nature of the surface and that it can be used to predict the adsorption capacity of these sugar carbons for the four aliphatic acids used in the experiments. If pH as determined is any indication of the type of oxide existing at the surface of the carbon, the basicity is shown to increase with the increased temperature of heat treatment, a change from a somewhat acid oxide formed at the lower temperatures of heat treatment to a distinctly basic oxide at the highest temperature. Nevertheless, maximum adsorption capacity of the acids is not reached with the carbon which yielded the most basic suspension, but it is reached with the 800°-carbon, which is somewhat less basic. More strongly in contradiction to the supposition that pH and the character of surface oxide are interrelated is the magnitude of the adsorption of the acids by the 500°-, 600°-, and 700°-carbons. These carbons are relatively excellent adsorbents for the acids, yet the pH values of the suspensions are either somewhat acid or nearly neutral. One may conclude that if surface oxides are formed on the carbon during the heating process, the pH of suspensions of these carbons does not indicate the type of oxide, since increased basicity is not accompanied by increased adsorption.

King (17) believed that iodine adsorption is not influenced by the nature of the surface. Smith, Thornhill, and Bray (31) have compared iodine adsorption and the surface area of carbons and have concluded that such adsorption is independent of the specific nature of the carbon surface and that it is primarily a function of the total extent of surface. If this is the case, and there is little reason to doubt it, the similarity of the curves represented in figures 5a and 5b throws further doubt upon the value of considering the pH of aqueous suspensions of the carbons as an index of adsorption capacity. If the surface area alone determines the amount of iodine adsorbed—and hence the shape of the iodine adsorption–temperature curve (figure 5a)—then surface area alone may conceivably determine the shape of the β-curves. These curves are in a different position for each acid, showing that the surface area available to each acid is different. This is dependent upon a number of variable factors inherent in the acid molecules themselves, such as average orientation, cross-sectional area, and length of chain. These variables do not come into play when the curve of one acid alone is considered. The nature and extent of surface are the possible determining properties. If it is true that iodine adsorption is not influenced by the nature of the surface, then the part played by the nature of the surface in determining the adsorption of the aliphatic acids—and therefore the shape of the β-curve—is also not significant. On this basis, one may conclude that the relative values of β for one acid are dependent upon the surface area alone.

In connection with this, a significant observation is to be made in studying tables 1 and 2 and figures 1 to 5. This is the general reversal of Traube's rule, except for the adsorption of acetic and propionic acids by the carbons heated below 900°C. In each of these four cases, however, there is but a slight difference among the values of β, the maximum acid adsorbed, for each acid for each carbon. It is possible that these reversals and the changes in the surface available for adsorption may be explained in the same way. Reference has been made to the relative available surface area assigned to each of the acid molecules on each of of the several carbons used in these experiments. Each is based upon the assumption that the molecules of all four aliphatic acids have the same average cross-sectional area. No account has been taken of the length of the chain of the molecule and the effect of lengthening the chain upon the relative surface available for the adsorption of the molecule. Ockrent (26) has demonstrated that active charcoal is an assembly of ultrapores of molecular dimensions and that the surface available for adsorption is determined by the dimensions of the adsorbed molecules. Lemieux and Morrison (19) have concluded from their experiments with steam-activated charcoals that acids are adsorbed on only a part of the actual surface, since the pores in the carbon are of such a size as to permit only the short acetic acid molecule to reach the pore walls and to be adsorbed upon them. The same pore walls are not available to molecules of greater length, even if these molecules have the same average cross-sectional area. One may assume that pores and fissures exist in the sugar carbons used in the present experiments. In those subjected to lower temperatures during the heat treatment, i.e., below 800°C., the same average number of pores are of such a size that they are available to both acetic and propionic acid molecules; fewer of these pores are of such a size that the acid of higher molecular weight can enter. A study of the Fisher–Hirschfelder–Taylor models of these four aliphatic acid molecules makes it quite apparent that as —CH_2— groups are added to the chain, the length of the chain as well as the cross-sectional area may be a determining factor in predicting the surface area available for the adsorption of the molecule. The addition of —CH_2— groups to the molecule makes it much less free to enter the pores, with the result that the surface available to these acids is decreased and, therefore, less of the longer chain acids are adsorbed. As the chain is lengthened, there are fewer pores of proper dimensions to permit the entry of an acid molecule of the length of that of butyric acid and there are fewer still for valeric acid. Therefore, a smaller number of pore walls is available to butyric acid than to acetic and propionic acids and a still smaller number is available to valeric acid molecules. This interference due to each added —CH_2— group may be anticipated. Vertical orientation of the molecule at the solid–liquid interface will result in a smaller number of millimoles of acid adsorbed when comparison is made between a given aliphatic acid and the next higher member of the series with any one carbon adsorbent. This will result in observations which will be the reverse of those anticipated from Traube's rule.

Heat treatment of the adsorbent up to 800°C. gives rise to pores and fissures of slightly larger size; or, perhaps, it may result in the opening up of a few new ones so that the general result is a slight increase in the surface available to all of the acids in the same relative order. Such changes in the surface of the carbon are essentially very small except in the case of the 800°-carbon, where there are marked increases in adsorption. Heat treatment above 800°C. to a temperature of 1100°C. gives rise to carbons with much less available surface. This decrease can be accounted for if a sintering effect is assumed to have taken place during the period of heat treatment. This sintering results in a collapse of some of the pores and fissures, filling in some of them so that actually there is a reduction of the available surface. Hence, the amounts of the acids adsorbed are decreased again in the same general order though it should be noted that now apparently more pores are available to acetic acid molecules than to propionic acid molecules, since the former acid is adsorbed to the greater extent. On the basis of this reasoning, heating the carbon at relatively high temperatures reduces the number and size of the pores and fissures to such a degree that fewer molecules can enter and be adsorbed on the walls.

The variation of the surface available for iodine adsorption on the various carbons may also be explained in the same way. It seems reasonable to suppose that fewer molecules of iodine will be adsorbed than of the aliphatic acids, since the iodine molecule has a larger cross-sectional area than does any of the aliphatic acid molecules investigated. Molecules of iodine may enter fewer of the pores and fissures; hence the surface available to them is smaller than to the acids.

The existence of pores in the carbon and the changes in pore size during heat treatment explain both the reversals of Traube's rule found generally in this study and also the lowered adsorption capacity of carbons subjected to higher temperatures during the heat treatment.

The greatly lowered capacity of the 1000°- and 1100°-carbons for the adsorption of the aliphatic acids is worth pointing out, for though Heuchling (15) found that norite decreased in adsorptive capacity when heated at these temperatures, the changes were not nearly so dramatic as those observed in these experiments. However, the maximum adsorption observed in the experiments of this study is in general agreement with the results of Heuchling.

SUMMARY

The adsorption of four monobasic fatty acids of low molecular weight has been studied. Purified sugar carbon which had been subjected to heat treatment at various temperatures within the range 500–1100°C. was used as the adsorbent. The constants of the Langmuir equation have been determined for each acid with each sample of carbon. The constant β, which is the maximum amount of acid adsorbed, was used to estimate the relative surface areas on each carbon available to each of the acids. Comparisons of these areas with those available for iodine adsorption were made. The changes in the adsorption capacity of the carbon with the intensity of heat treatment and the reversals of Traube's rule observed in these experiments were explained on the basis of changes in surface area.

REFERENCES

(1) Adam, N. K.: J. Phys. Chem. **29**, 87 (1925).
(2) Bartell, F. E., and Miller, E. J.: J. Am. Chem. Soc. **44**, 1866 (1922).
(3) Bhatagnar, S. S., Kapur, P. L., and Luthra, R. K.: Kolloid-Z. **80**, 265 (1937).
(4) Bruns, B.: Kolloid-Z. **54**, 33 (1931).
(5) Burrage, J. L.: Trans. Faraday Soc. **29**, 445, 564, 665 (1933).
(6) Cohan, L. H.: Chem. Eng. News **23**, 2078 (1945).
(7) Dubinin, M. M.: J. Russ. Phys. Chem. Soc. **61**, 587 (1929).
(8) Dubinin, M. M.: Z. physik. Chem. **A140**, 81 (1929).
(9) Dubinin, M. M.: Z physik. Chem. **A150**, 145 (1930).
(10) Dubinin, M. M.: J. Russ. Phys. Chem. Soc. **62**, 1829 (1930).
(11) Firth, J. B.: J. Soc. Chem. Ind. **42**, 242T (1923).
(12) Firth, J. B., and Watson, F. S.: J. Phys. Chem. **29**, 987 (1925).
(13) Griffin, K. M., Richardson, R. L., and Robertson, P. W.: J. Chem. Soc. **131**, 2705 (1928).
(14) Herbst, H.: Kolloid-Z. **38**, 314 (1926).
(15) Heuchling, A.: Master's dissertation, Vassar College, Poughkeepsie, New York.
(16) King, A.: J. Chem. Soc. **1935**, 889.
(17) King, A.: J. Chem. Soc. **1937**, 1489.
(18) Langmuir, I.: J. Am. Chem Soc. **40**, 1362 (1918).
(19) Lemieux, R. U., and Morrison, J. L.: Can. J. Research **25B**, 440 (1947).
(20) Lemon, H. B.: Phys. Rev. **14**, 281 (1919).
(21) Linner, E. R., and Gortner, R. A.: J. Phys. Chem. **39**, 35 (1935).
(22) Mack, E.: J. Am. Chem. Soc. **47**, 2468 (1925).
(23) Miller, E. J.: J. Phys. Chem. **36**, 2967 (1932).
(24) Nekrassov, B.: Z. physik. Chem. **136**, 18, 379 (1928).
(25) Ogawa, I.: Biochem. Z. **161**, 275 (1925).
(26) Ockrent, C.: J. Chem. Soc. **1932**, 1864.
(27) Philip, J. C., and Jarmon, J. J.: J. Phys. Chem. **28**, 346 (1924).
(28) Sabalitschki, Th.: Pharm. Ztg. **74**, 382 (1929).

(29) SHILOV, N., AND CHMUTOV, K.: Z. physik. Chem. **A148**, 233 (1930).
(30) SHILOV, N., SCHATUNOVSKA, H., AND CHMUTOV, K.: Z. physik. Chem. **A149**, **211** (1930).
(31) SMITH, W. R., THORNHILL, F. S., AND BRAY, R. I.: Ind. Eng. Chem. **33**, 1303 (1941).
(32) WELLER, S., AND YOUNG, T. L.: J. Am. Chem. Soc. **70**, 4155 (1948).

REARRANGEMENT PEAKS OBSERVED IN SOME MASS SPECTRA[1]

ALOIS LANGER
Westinghouse Research Laboratories, East Pittsburgh, Pennsylvania

Received June 13, 1949

INTRODUCTION

When some compounds are examined in a mass spectrometer there are observed, among the products of dissociation due to electron impact, fragments whose origin cannot be explained by the simple assumption of bond scission, as is done in most cases of molecular decomposition. In describing the mechanism of the formation of these ions one is still guided by established classical valence-bond formulae of the compound, assuming that any of the bonds can be broken and that under the conditions of investigation these structures are physically stable enough to be detected.

From the standpoint of conventional molecular structures such anomalous fragments were recorded, probably for the first time, in a paper by Delfosse and Bleakney (4) reporting the dissociation of allene and were recognized as fragments one would not expect in mass spectra somewhat later by Stevenson and Hipple (9) in their paper on *n*-butane and isobutane. Scattered attention has been given to these peaks since that time (2), although the phenomenon of rearrangement in mass spectra seems to be quite a common one.

The interaction of a moving electron with a complex molecule is not a simple process. The positive-ion formation is the more abundant and better known reaction, giving rise as far as is known in mass spectra to several distinct kinds of peaks. Besides singly charged ionization and dissociation fragments there are peaks due to multiple, mainly doubly charged, ions. The doubly charged ions appear at integral or half masses, usually have low abundance, and can easily be recognized by the much higher appearance potential. There are peaks due to the isotope contribution of the constituent elements. These peaks are at integral masses and their location and height can be predicted from the known isotopic composition of the elements in the compound. By their shape and location one can easily recognize peaks caused by metastable transitions or peak broadening due to kinetic energy. The peaks assigned to rearrangements appear at integral masses, have a normal shape, and are not explainable by the isotope contribution of the elements, because they sometimes have very high relative intensities. Because of their shape and their appearance potential they likewise can hardly be due to kinetic energy solely (7, 8, 9).

---

[1] **Presented before the Division of Physical and Inorganic Chemistry at the 115th Meeting of the American Chemical Society, which was held in San Francisco, California, March 27–April 1, 1949.**

Since it can be also assumed that peaks due to such secondary reactions as recharging, or other collision processes of the gas molecules or ions with each other or with the wall of the instrument, are negligible in present-day spectra, because the instruments are operated at a rather low pressure, the rearrangement peaks must be associated with the primary process of dissociation caused by the impinging electron.

EXPERIMENTAL PROCEDURE

The investigations were made with a 90° sector-type instrument with an attached pen recording device. The whole mass spectrometer tube was heated to 60°C. to facilitate evacuation. The substances were ionized with an electron beam of 50-e.v. energy. The necessary precautions for taking calibration spectra for chemical analysis were observed in this investigation. The height of the peaks obtained—in other words, the probability of forming a certain fragment—is represented graphically, since more precise numerical values have significance only in relation to a single type of instrument, because the abundance of a fragment is not only dependent on the energy of the electrons and on the temperature of the tube, but also to some extent on the discrimination of masses in a given instrument. Usually the general pattern is preserved and can be recognized as belonging to a certain compound for any of the existing instruments, although the relative intensities might vary considerably. It also should be mentioned that the absolute purity of the substances introduced was not known. The purest compounds obtainable were used without further purification.

EXPERIMENTAL RESULTS

Figure 1 represents a graphical compilation of the dissociation patterns of the C_1 to C_7 saturated hydrocarbons (3). The relative intensities are expressed in per cent of the highest peak in the spectrum. From this figure one immediately gains the impression that certain fragments are obtained in approximately constant proportions from all the hydrocarbons studied, although they have a varying chain structure and chain length. These peaks are the masses 29, 43, 57, and 71, representing the masses of stable hydrocarbons which have lost one hydrogen. It can be seen that the $C_3H_7^+$ (43) fragment seems to be formed with special ease. However, the more striking observation is that these masses are produced in a comparable proportion in many cases from molecular structures which cannot produce them without first undergoing some sort of rearrangement process.

From figure 1 it is observed that isobutane produces a mass 29 which cannot be obtained by direct splitting of the isobutane molecule. The next molecule to show rearrangement is neopentane. Three mass peaks are formed,—28, 29, and 43. The formation of the mass 29, which is the largest of the rearrangement peaks, requires the simultaneous acquisition of two mass units, whereas masses 28 and 43 can be formed by the addition of one unit only. It should be noticed that mass 43 is present only in small abundance in neopentane, while in *n*-pentane

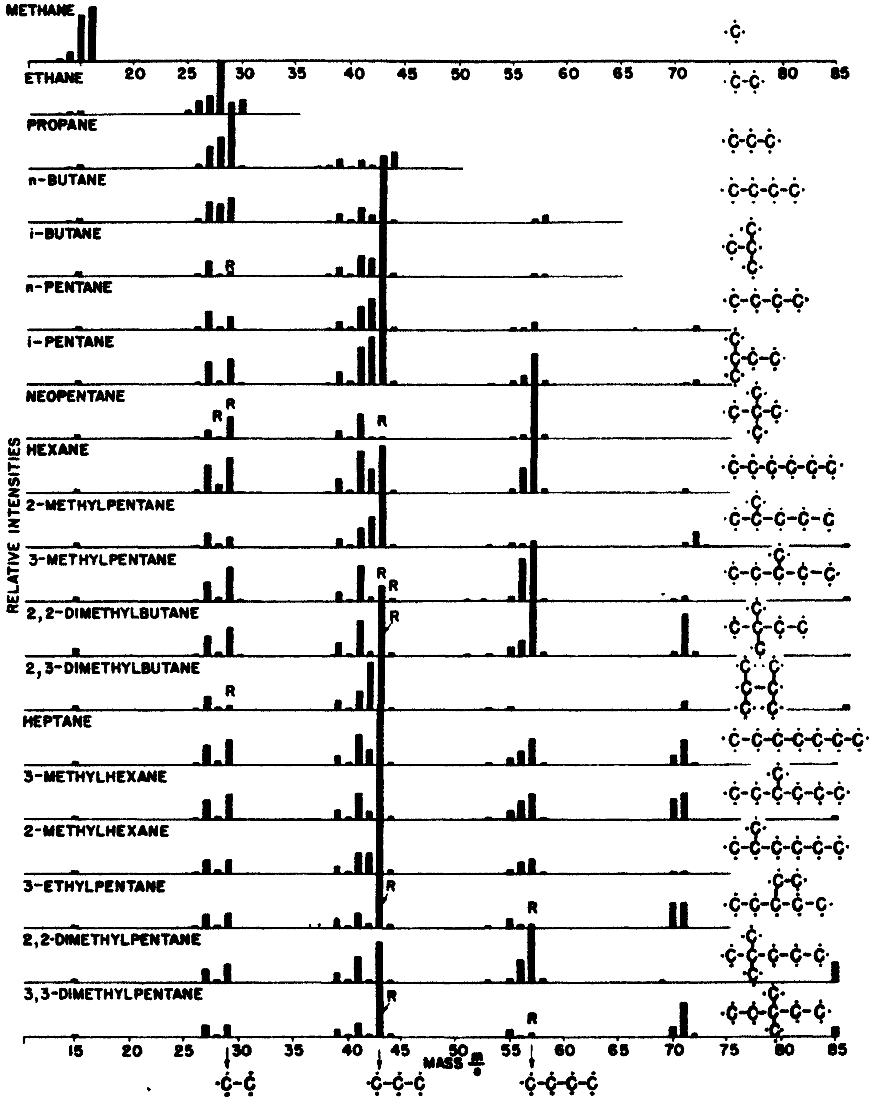

FIG. 1. Mass spectra: dissociation patterns of the C_1 to C_7 hydrocarbons

and isopentane it is the largest peak in the spectrum. On the other hand, peak 29 is comparable in size in all the pentanes. In the same way 3-methylpentane forms a large peak 43, but also a smaller one at 44 requiring two hydrogens for their formation, as does mass 43 in 2,2-dimethylbutane, which is the largest peak in the whole spectrum. It is interesting also to note that in 2,3-dimethylbutane a peak at mass 29 is observed, but an expected peak at 57 is missing. Rearrangement peaks of mass 43 are observed in 3-ethylpentane and 3,3-dimethylbutane in great abundance, whereas mass 57 in those two molecules is relatively small.

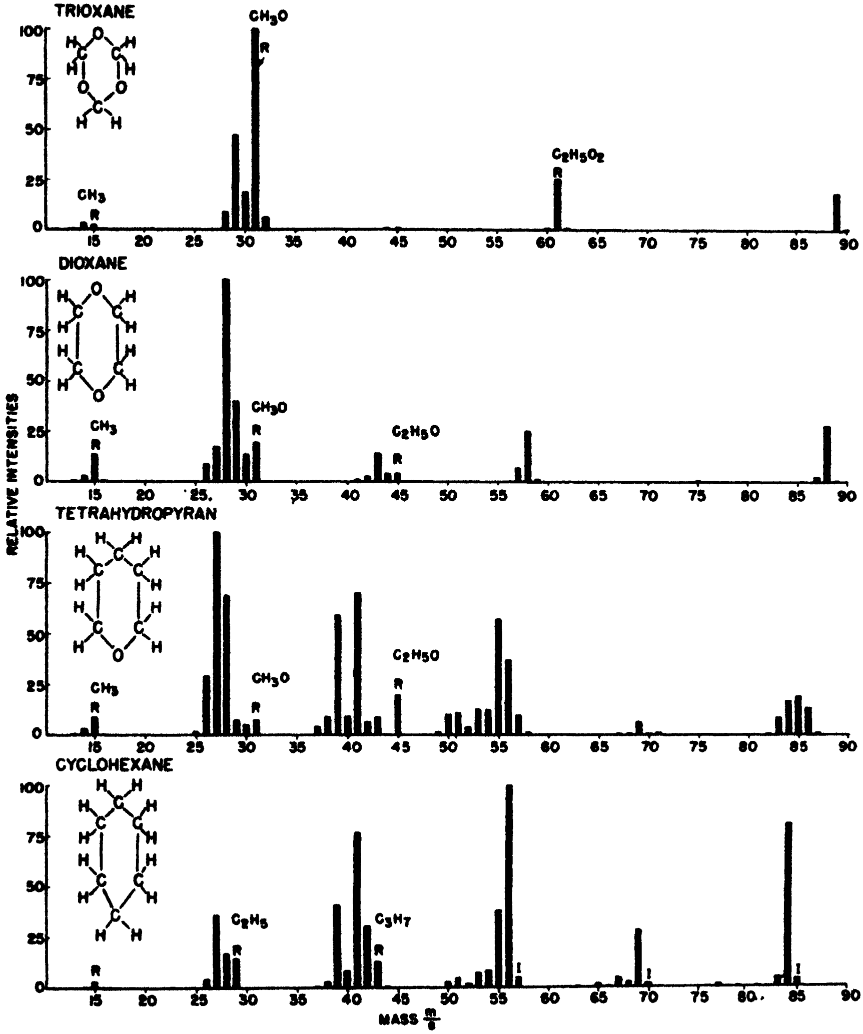

FIG. 2. Mass spectra of trioxane, dioxane, tetrahydropyran, and cyclohexane

It should be mentioned that in the spectra of all the hydrocarbons a peak at mass 16 is also observed. This mass is present in larger amounts than can be accounted for by the contribution of the carbon isotopes and is probably due to a rearrangement process, although some may come from methane present as impurity in the samples or be created by thermal cracking of the compounds on the hot filament of the tube.

The formation of rearrangement peaks is observed not only in saturated hydrocarbons but also in unsaturated ones as well. Thus *cis*- and *trans*-2-butenes have a peak at mass 29 which differs even slightly in abundance, and isobutene (2-methyl-2-propene) has peaks at masses 28 and 29. One can also find rearranged masses in *cis*- and *trans*-2-pentenes and in a few others. Dimethylacetylene is somewhat peculiar, in that a mass 28 is produced, indicating that a hydrogen

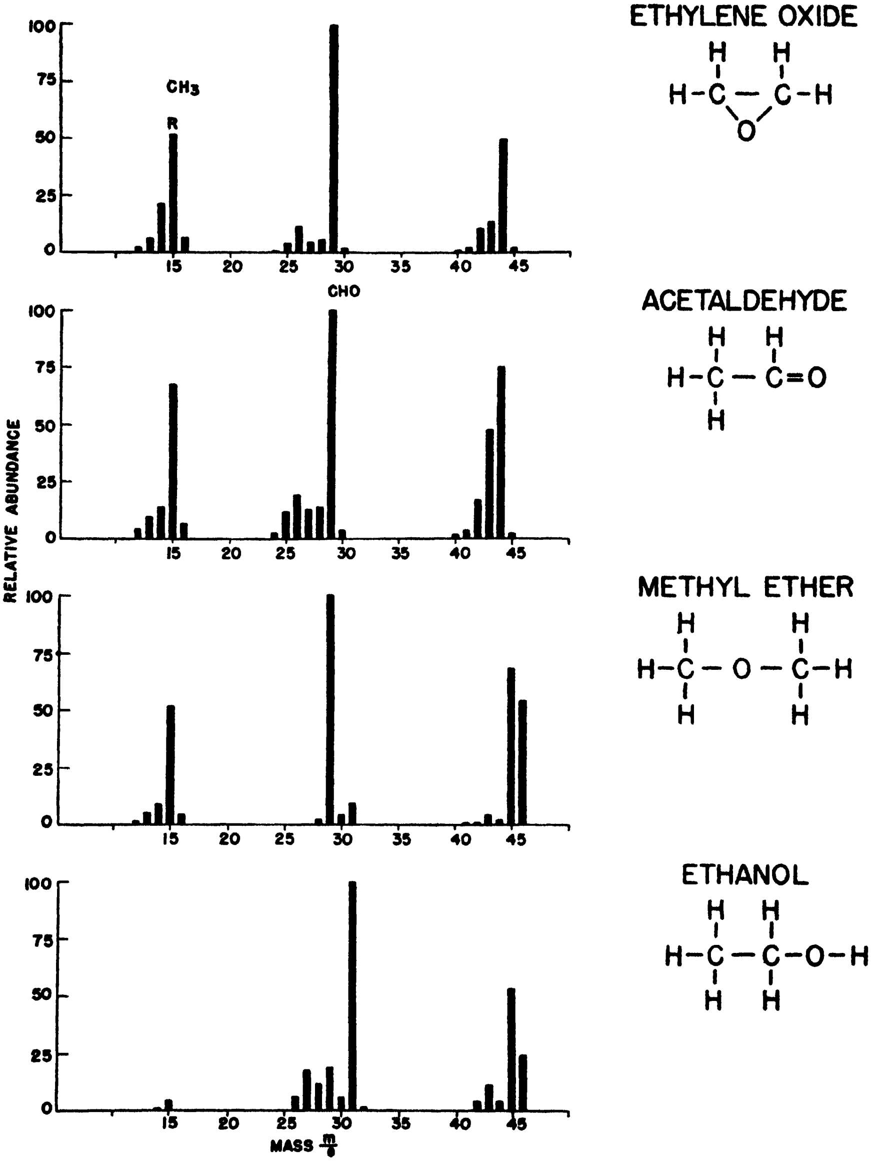

FIG. 3. Mass spectra of ethylene oxide, acetaldehyde, methyl ether, and ethanol

can be obtained not only from a neighboring carbon atom which has them available but also from a more distant one.

Among the oxygen-containing compounds trioxane was first studied. The result is indicated in figure 2, showing that it gives three major rearrangement peaks at massss 61, 31, and 15. Peak 31 is the largest one in the spectrum.

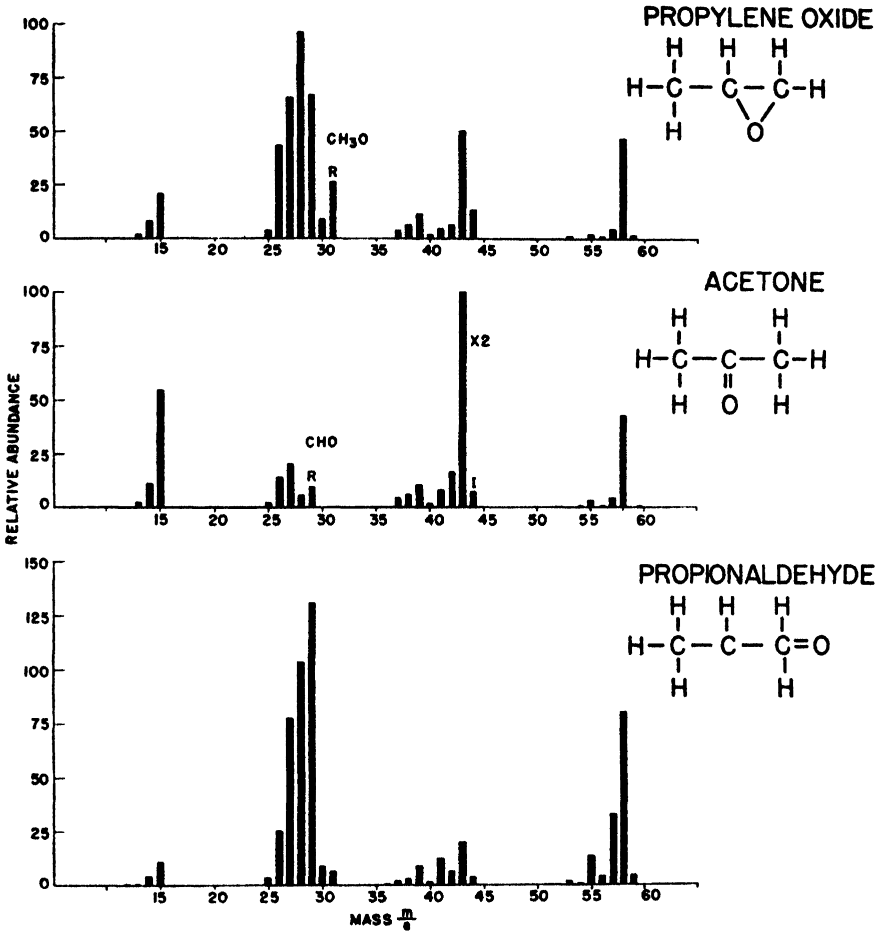

FIG. 4. Mass spectra of propylene oxide, acetone, and propionaldehyde

These peaks were checked and rechecked many times independently, so that no mistake in mass assignment is likely. It was therefore of some interest to investigate dioxane, which has only two oxgyens in the ring. It likewise has rearrangement peaks, the one at mass 15 being relatively larger than in trioxane. While peak 31 is present it is not the dominant one in the spectrum. In addition dioxane contains a peak at a mass 45 corresponding to a fragment $C_2H_5O^+$. The third molecule represents tetrahydropyran with one oxygen in the ring. Even this compound gave a peak at 15, one at 31, and a quite large one at mass 45. In order to complete the series, cyclohexane was run. It was quite surprising to find rearrangement peaks corresponding to masses 15, 29, and 43.

In order to gain more insight into these reactions a much simpler ring structure was examined next: namely, ethylene oxide. As shown in figure 3, a relatively large rearrangement peak 15 is observed and the peak which was expected as being the largest—namely, mass 30—resulting from fission across the two bonds is missing. In fact, it was found that the spectrum of ethylene oxide resembles so closely the spectrum of acetaldehyde that the two compounds at first glance would be hardly distinguishable from each other.

It was therefore interesting to determine the mass spectrum of propylene oxide. As a result of the previous finding, one might expect that it would have a spectrum like that of acetone or propionaldehyde. The mass spectra as indicated in figure 4 reveal that propylene oxide bears a closer resemblance to propionaldehyde but a relatively large peak 31 is also observed.

DISCUSSION

The spectrum of trioxane was the one which aroused the present interest in the rearrangement peaks. It was found unusual that trioxane, a cyclic trimer of formaldehyde, does not part under electron impact into formaldehyde again, although under certain conditions this process can be chemically accomplished. Because formaldehyde gives comparatively abundant masses only below 30, one might at first assume that trioxane is made purely of hydrogen bond bridges and assign a new structure to it.

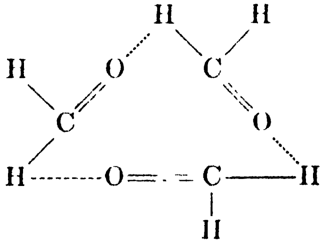

Although from this structure fragments 31 and 61 could be produced by direct bond cleavage, this formulation could of course not explain why there is also a mass 15 observed corresponding to a CH_3^+ ion. However, the evidence from many physical measurements to which trioxane has been subjected has established definitely that it has a hexagonal ring of the cradle structure. On account of this fact it will be assumed that the conventional structures are valid in all the other compounds investigated and that the rearrangement peaks are due to the electron impact, rather than the result of an inadequate formula assigned to the molecule.

In general, the meaning of the mass spectrometer rearrangements differs from the chemical rearrangements to which we are accustomed in organic chemistry. In chemical rearrangement a new compound of high stability is formed, so that it can be isolated, whereas in this case rearrangement is indicated only by the relation of the masses of some ions to the structure of the parent molecule.

For the formation of rearrangement peaks several procedures can be devised, in some respects identical with the one already proposed for chemical rearrangements (10). Owing to the conditions in the mass spectrometer tube the rearranging part of the molecule can hardly exist kinetically free even momentarily and then be reattached to another part of the molecule, because any separate charged particle formed would be pulled immediately away in the electrostatic field in the instrument. Even if the fragments were neutral free radicals they would have a very low recombination probability, owing to the low pressure in the tube. For this reason radical mechanisms or chain reactions are not probable.

These peaks therefore must be associated with the primary process of dissociation; in other words, they are intramolecular in nature. There are several ways in which such a process might happen intramolecularly.

First, by a rearrangement whereby the skeleton of the molecule is regrouped by some process to an isomeric compound. The neutral molecule or the ion already formed could undergo such change, which would require hydrogenation or dehydrogenation of some parts of the new skeleton configuration. The new compound would split later at its chemical bonds.

Further, by a process of sharing electron migration, simply by shifting the binding electrons from one atom or atomic group to another. Such a shifting could involve the hydrogen atoms only, resulting in an apparent free migration of the hydrogens in the molecule, or could involve the whole or only part of the skeleton as well. In the latter case the structural bonds of the molecule would have lost their directional properties and a regrouping to the different dissociation fragments could be governed more or less by chance.

Although these processes are identical as to their result observed in the mass spectrometer, in order to see the difference let us examine the possible formation of mass 29 in isobutane.

In the isomerization process isobutane is first rearranging at least partly to normal butane, which splits apart later giving a $C_2H_5^+$ ion.

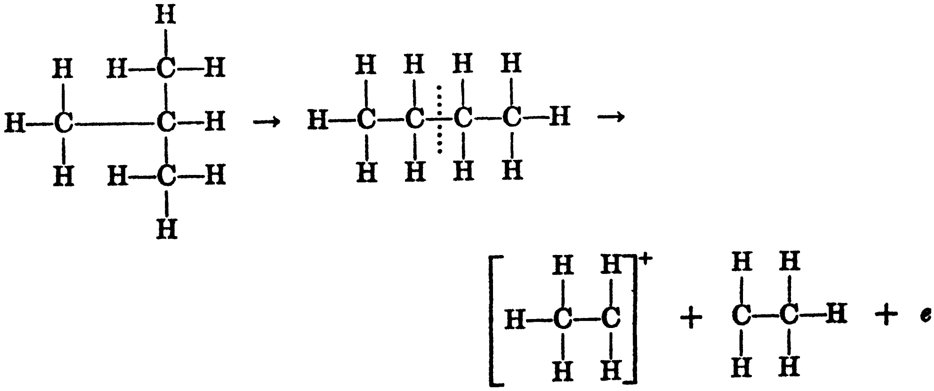

By the theory of hydrogen migration one can assume that at the instant the molecule splits, a proton will be acquired from the surrounding hydrogen cloud by the central carbon atom:

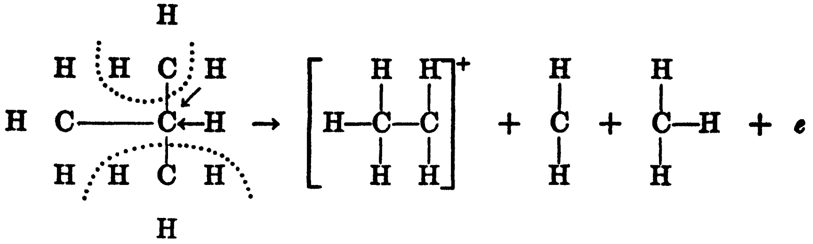

As a third possibility all directed bonds in the molecule have vanished and the regrouping can occur statistically. The process can be indicated as follows:

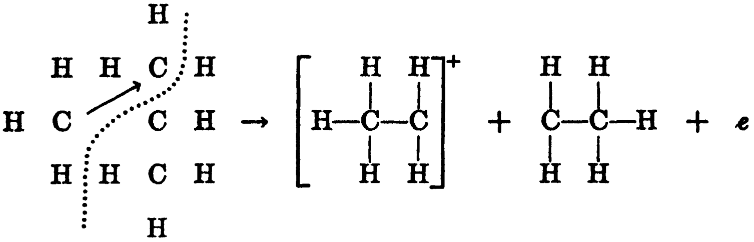

Postulating the formation of an intermediate compound and later splitting as a step-by-step process, an excited molecule probably has to maintain its identity for several vibrational or even rotational periods. But since this time is still shorter than the time necessary for the molecule to drift out from the sensitive region of the instrument, assuming average molecular speeds, such a mechanism should be still possible. Actually, the occurrence of metastable ions indicates that the time of instability can be appreciable.

With the shifting of binding electrons the rearrangement process could occur with the rapidity of the electron jumps. It has been shown in the early work on hydrogen and other simple molecules that the dissociation under electron impact can be explained by the Franck–Condon principle, postulating the actual immobility of the nuclei in the molecule and determining the dissociation solely by what happened to the electronic states. On this basis one has to assume that the rearranging parts do not move from their positions before dissociation. For this reason electronic transitions resulting in binding will be possible only when the atoms are already in such a location that a sharing of the electron can take place relatively free from steric strain. This bond is newly created by the electron impact, since it is normally assumed that structures like *n*-butane and isobutane do not resonate. There are indications that chemical isomerization by the aid of a catalyst is proceeding by a chain reaction.

Under certain assumptions one should be able to make a decision between the proposed theories by using isotope-labeled compounds (1). Such experiments have recently been reported by Honig (6) on the butanes. The interpretation of these tests given by Honig indicates that the isomerization mechanisms definitely should be favored. However, there are observations which contradict this interpretation in other molecules. For example, if neopentane should isomerize under electron impact to such an extent that a large rearranged peak 29 is observed, then also a large 42 and a rearranged 43 peak should appear in the spectrum, which is not the case. One would have to assume different modes of splitting for *n*-pentane or isopentane, whichever is formed by the isomerization process.

Without going further into discussion of the other hydrocarbons let us review the results with the oxygen-containing compounds.

In the case of trioxane two of the rearrangement peaks could be derived by assuming that some sort of a hydrogen binding in the chelation sense of a residual valence does exist between the hydrogen and oxygen, which would during the dissociation process develop into a main bond, so that an additional hydrogen would be carried with the oxygen-containing part, thus producing a fragment of mass 31 and also one of 61. However, the mass 15 which is also observed could not be formed in this way. All the observed peaks can be explained by assuming the migration of one hydrogen from one carbon to another. This attachment would have to occur across the oxygen bridge, but from the evidence gained in dimethylacetylene such a shifting should not be improbable. Assuming that one hydrogen can be located close to the other carbon, if cleavage occurs at lines 1 and 2 mass 15 is formed; if it is between lines 1 and 3, mass 31 is obtained; and if it is at lines 1 and 4, mass 61 results.

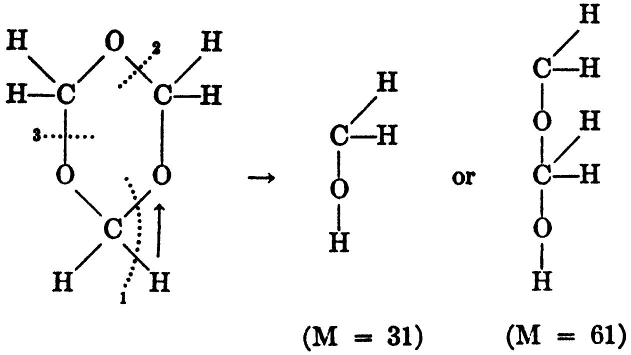

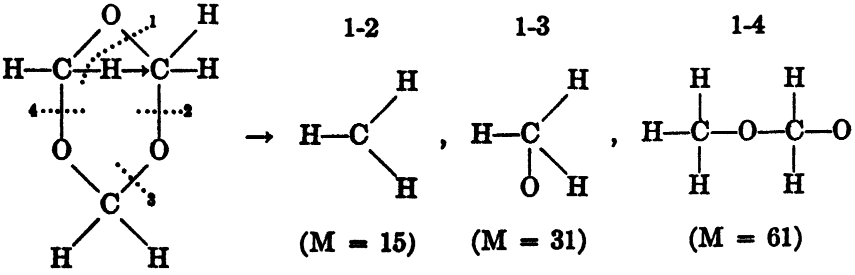

In a similar way one can explain the occurrence of the rearranged peak in dioxane, tetrahydropyran, and cyclohexane.

If one attempts to explain the formation of these masses by an isomerization process, it is necessary to assume the formation first of a molecule such as shown below, which later splits at the dotted lines 1, 2, and 3.

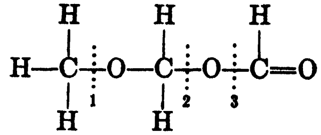

In the case of ethylene oxide the finding could be interpreted on the basis of the ethylene oxide isomerizing into acetaldehyde, which can easily split into mass 15 and mass 29. But the same result can be obtained by assuming that during the splitting the oxygen molecule migrates to one carbon permanently, while the hydrogen attaches to the other carbon atom. Peaks 15 and 29 are so formed that either the right-hand or the left-hand side carries the charge.

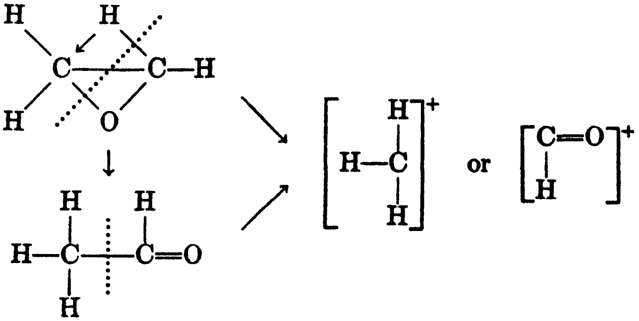

As can be seen, the two possibilities differ in these cases of oxygenated compounds only as to the physical presence of the rearranged compounds as intermediate.

Since the spectrum of ethylene oxide can be explained on the basis of the oxygen attaching to one carbon while one hydrogen drifts to the other, it was interesting to determine in which way the shift occurs in propylene oxide. Either the oxygen is carried by the central carbon, in which case an acetone-like spectrum should be obtained, or the oxygen goes to the end carbon giving a propionaldehyde-like spectrum. The actual mass spectra reveal, if such a comparison is justified at all, that the aldehyde spectrum bears a closer resemblance to that of propylene oxide. But the process must be still more complicated and another rearrangement possible whereby both hydrogen and oxygen are attached to the end carbon, because a relatively large peak at mass 31 is also observed.

This evidence points to a more complicated nature of regrouping in support of the assumption discussed previously: namely, that the molecule has lost its structural identity owing to the electron impact. On this basis one could also explain other phenomena, such as some of the fragments appearing in great abundance in a whole series of different compounds and thus indicating some unique stability of these groups. However, this mechanism alone still does not explain why there is a difference in the spectra of isomeric compounds at all, as, for example, why the largest peak in ethanol is two units higher than in methyl ether (figure 4). In order to account for the relative distribution of these peaks, yet unknown steric factors would have to be considered.

Another observation is quite interesting: namely, that many of the rearrangement peaks are metastable. In the hydrocarbons at least a part of all the rearrangement peaks 29 and 43 drop in time one hydrogen molecule and go over to mass 27 and 41.

The observed rearrangements in the stable molecules lend credence to the assumption that such processes play a part in the splitting of metastable ions, which have been studied with the aid of the mass spectrometer (5). Thus, for example, a small peak at a mass 30.4 in *n*-butane can be explained on the basis of the ionic fragment 58^+ undergoing a transition in time, dropping a methane molecule and forming a charged mass 42^+ ($58^+ \rightarrow 42^+ + 16$). Similarly, mass 25.5 in pentane can be regarded as due to mass 41^+ expelling mass 16, whereas mass 24.5, as can be calculated, should result from the ion 72^+ losing an ethane molecule and changing into mass 42^+. It is evident from the structure of the ions that masses 16 and 30 must be formed again by a rearrangement process if one excludes double ionization into $CH_3 + H$ for mass 16.

It is obvious that much more experimental evidence has to be gathered before the problem of rearrangement can be understood. The paper is presented to indicate the extent of the problem and some avenues of further attack.

SUMMARY

Electron impact in a mass spectrometer creates in some compounds dissociation fragments whose origin cannot be accounted for by bond fission along classical valence lines. These peaks have a normal shape, appear at integral masses, and are not explainable by the isotope contribution. They have sometimes a high relative intensity.

The occurrence of these peaks has been summarized for some hydrocarbons and studied in certain oxygen-containing compounds. The process seems to be intramolecular in nature. Possible mechanisms of formation are discussed.

REFERENCES

(1) Beeck, O., Otvos, J. W., Stevenson, D. P., and Wagner, C. D.: J. Chem. Phys. **16**, 252 (1948).

(2) Bloom, E. G., Mohler, F. L., Sengel, J H., and Wise, C. E.: J. Research Natl. Bur. Standards **14**, 129 (1948).

(3) *Catalog of Mass Spectral Data*. American Petroleum Institute, Research Project 44, National Bureau of Standards, Washington, D. C.

(4) Delfosse, J., and Bleakney, W.: Phys. Rev. **56**, 256 (1939).

(5) Hipple, J. A., Fox, R. E., and Condon, Ed.: Phys. Rev. **69**, 347 (1946).

(6) Honig, R. E.: Bull. Am. Phys. Soc. **24**, No. 1, R12 (1949).

(7) Koffel, M. B., and Lad, R. A.: J. Chem. Phys. **16**, 420 (1948).

(8) Mitchel, J. J., and Coleman, F. F.: J. Chem. Phys. **17**, 44 (1949).

(9) Stevenson, D. P., and Hipple, J. A.: J. Am. Chem. Soc. **64**, 1588 (1942).

(10) Wallis, E. S.: "Molecular Rearrangements", in *Organic Chemistry*, edited by Henry Gilman. John Wiley and Sons, Inc., New York (1943).

REVERSIBILITY AND IRREVERSIBILITY OF ELECTRODE REACTIONS IN OSCILLOGRAPHIC POLAROGRAPHY

THE VALIDITY OF THE WAVE HEIGHT EQUATION

PAUL DELAHAY[1]

Department of Chemistry, University of Oregon, Eugene, Oregon

Received July 25, 1949

The theory of the diffusion process taking place in oscillographic polarography has been discussed in two recent papers by Randles (7) and by Sevcik (8). Randles derived the following expression for the height of an oscillographic wave corresponding to a reversible electrode reaction

$$I = \frac{1.24\pi\mathfrak{F}}{(0.0118)^{1/2}\,10^3}\,n^{3/2}\gamma^{2/3}\tau^{2/3}v^{1/2}D^{1/2}C \qquad (1)$$

in which I = the height of the oscillographic wave in amperes,

$\mathfrak{F}$ = the faraday,

n = the number of electrons involved in the reaction,

γ = related to the radius r of the mercury drop by the relation $r^3 = \gamma\tau$,

τ = the time of the drop life at which the peak current occurs,

v = the rate of potential change in volts per second,

D = the diffusion coefficient of the substance reacting at the dropping mercury electrode in square centimeters per second, and

C = the concentration of the substance reacting at the electrode in moles per liter.

Equation 1 can be transformed into a more convenient form in the following manner. By expressing the weight of the mercury drop as a function of m, the rate of flow of mercury, one obtains

$$\frac{4}{3}\pi\gamma\tau\delta = m\tau \qquad (2)$$

δ being the density of mercury. Thus

$$\gamma = 0.01764m \qquad (3)$$

m being expressed in grams per second.

Substituting this value of γ in formula 1 one obtains, after grouping the numerical constants,

$$I = 2{,}344n^{3/2}m^{2/3}\tau^{2/3}v^{1/2}D^{1/2}C \qquad (4)$$

in which the following units are used: I in microamperes, m in milligrams per second, τ in seconds, v in volts per second, D in square centimeters per second, C in millimoles per liter.

---

[1] Present address: Department of Chemistry, Louisiana State University, Baton Rouge 3, Louisiana.

For practical purposes, the factor τ of formula 4 may be taken as equal to the drop time when only the wave corresponding to the maximal area of the mercury drop is taken into consideration, a fairly large number of waves being recorded during the life of a single drop. The current corresponding to the maximal area of the drop has been called "maximal peak current" by the author of the present paper.

On the other hand, Sevcik (8) has derived the following equation for the height of an oscillographic wave written with the notations of formula 1:

$$I = 0.361 \frac{\mathfrak{F}^{3/2}}{(RT)^{1/2}} n^{3/2} A v^{1/2} D^{1/2} C' \tag{5}$$

in which R and T have their usual significance, A is the area of the mercury drop at the time of the drop life at which the peak current occurs, expressed in square centimeters, and C' is expressed in moles per milliliter.

Expressing the area A as a function of m and τ one obtains

$$A = 4\pi \left(\frac{3}{4\pi\delta}\right)^{2/3} m^{2/3} \tau^{2/3} \tag{6}$$

$$= 0.8515 m^{2/3} \tau^{2/3} \tag{7}$$

m being expressed in grams per second.

Substituting this value of A in formula 5 and grouping the numerical constants one obtains an equation identical with formula 4 except for the numerical constant, which becomes 1,852.

In evaluating the reliability of either result it should be pointed out that Randles determined the height of a few oscillographic waves and found them in good agreement with the values calculated by application of his formula. On the other hand, Sevcik limited his experimental work to the verification of the proportionality between the wave height and the factors v and C. Moreover, the results obtained in the present paper tend to confirm Randles' equation rather than Sevcik's. Therefore, all calculations described in the present paper have been carried out according to Randles' equation (formula 4).

Equation 4 has been derived by assuming that the electrode reaction is reversible. The correctness of equation 4 was verified experimentally by Randles for rates of potential change not exceeding 1 volt per second. It is the purpose of the present paper to extend this verification to higher rates of potential change and also to examine the case of irreversible electrode reactions.

The experimental arrangement has been previously described (4) and does not need any further comment. All results correspond to measurements carried out at 25°C.

DEPENDENCE OF THE MAXIMAL PEAK CURRENT ON THE FACTORS m AND τ

According to formula 4 the maximal peak current I is proportional to the quantity $(m\tau)^{2/3}$. Since the product $m\tau$ is independent of the pressure on the dropping electrode (5, p. 70) within a few per cent, the maximal peak current should be practically independent of that pressure. We found that this was indeed the case for the reduction of zinc ion (3). However, an extensive study

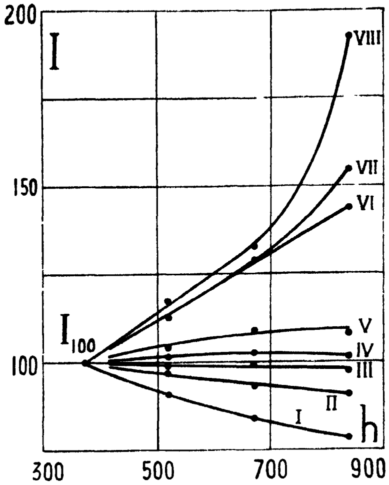

FIG. 1. Variation of the maximal peak current with the mercury head h = head of mercury (in mm.); no correction for the back pressure. I = maximal peak current (in per cent).

Curve I .	$SbCl_3$(10^{-3} mole/liter) in H_2SO_4 (0.5 mole/liter); f = 12 sweeps/sec.; v = 24 9 v./sec.; I_{100} = 494 microamp
Curve II.	$Pb(NO_3)_2$ (10^{-3} mole/liter) in KNO_3 (0 5 mole/liter); f = 20 sweeps/sec ; v = 68.1 v./sec ; I_{100} = 343 microamp
Curve III.	$CdSO_4$ (10^{-3} mole/liter) in KCl (1 mole/liter); f = 12 sweeps/sec.; v = 29.9 v./sec.; I_{100} = 239 microamp.
Curve IV.	$TlNO_3$ (10^{-3} mole/liter) in KNO_3 (0.5 mole/liter); f = 12 sweeps/sec. v = 34.8 v./sec.; I_{100} = 189 microamp.
Curve V.	KIO_3 (10^{-3} mole/liter) in H_2SO_4 (0 5 mole/liter); f = 20 sweeps/sec ; v = 68.1 v./sec ; I_{100} = 383 microamp.
Curve VI.	$NiSO_4$ (10^{-3} mole/liter) in $(CH_3)_4NBr$ (0.1 mole/liter); f = 20 sweeps/sec.; v = 44.0 v./sec.; I_{100} = 25 2 microamp
Curve VII. .	KIO_3 (10^{-3} mole/liter) in NaOH (0.1 mole/liter); f = 20 sweeps/liter; v = 68.1 v./sec.; I_{100} = 179 microamp.
Curve VIII. . ..	HCl (10^{-3} mole/liter) in LiCl (0.5 mole/liter); f = 20 sweeps/sec.; v = 51.1 v./sec.; I_{100} = 63.5 microamp.

has shown that, in general, there is a dependence of the maximal peak current on the head of mercury. The maximal peak current either increases or decreases when the head of mercury is increased, although an increase in the current is more frequently observed.

The variations of the maximal peak current with the head of mercury are rather small for electrode reactions which are known to occur reversibly or almost reversibly. This is the case for the reduction of cadmium and thallous ions (curves III and IV of figure 1).

For irreversible electrode reactions the variations of the maximal peak current with the head of mercury are very large (figure 1). When the overvoltage required for the reduction of a substance changes with the nature of the supporting electrolyte, it is observed that the reaction occurring with the lowest overvoltage also shows the smallest variation of the maximal peak current with the head of mercury. This conclusion is verified in figure 1 for the reduction of iodate ion, which is less irreversible in acid (curve V) than in alkaline solution (curve VII) (5, p. 320). In the case of an irreversible reaction it is also observed that the variations of the maximal peak current with the mercury head increase in amplitude with the rate of potential change (table 1).

TABLE 1

Variation of the maximal peak current with the head of mercury in the case of a 10^{-3} molar cobaltous nitrate solution in 1 molar potassium chloride

HEAD OF MERCURY	MAXIMAL PEAK CURRENT EXPRESSED IN PER CENT OF THE VALUE FOR A HEAD OF MERCURY OF 375 MM			
	f = 7.5 sweeps/sec. v = 20.5 v./sec I_{100} = 45.7 microamp	f = 15 sweeps/sec v = 43.3 v./sec I_{100} = 51.2 microamp.	f = 30 sweeps/sec v = 96.5 v./sec I_{100} = 60.8 microamp	f = 60 sweeps/sec v = 195 v./sec I_{100} = 69.5 microamp
mm	*per cent*	*per cent*	*per cent*	*per cent*
375	100	100	100	100
519	122	124	129	133
669	152	150	158	164
841	183	189	202	209

The dependence of the maximal peak current on the head of mercury in the case of an irreversible electrode reaction implies that equation 4 is no longer applicable. It might be thought that the experimental results could be interpreted by a formula similar to equation 4, in which the factors m and τ would be affected with arbitrary exponents x and y. These exponents could be calculated from the results of a set of three experiments carried out with three different values of the head of mercury. Such calculations have been carried out for some of the reactions mentioned in figure 1, but it was found that the exponents x and y vary widely with the head of mercury. Therefore it is not possible to extend the application of formula 4 to irreversible electrode reactions by merely changing the value of the exponents of the factors m and τ.

Because of the dependence of the maximal peak current on the head of mercury, maximal peak currents recorded with different dropping electrodes cannot be correlated with one another in the case of an irreversible electrode reaction. On the other hand, in the case of a reversible electrode reaction the results obtained with different values of m and τ can be compared with one another by application of formula 4. However, before doing so one should verify that the maximal peak current actually does not depend on the head of mercury.

The study of the variations of the maximal peak current with the head of mercury gives us a very simple method of determining whether an electrode reaction occurs reversibly or irreversibly. In the case of a reversible electrode process the maximal peak current will practically not depend on the mercury head, while in the case of an irreversible electrode reaction the maximal peak current will change appreciably with the value of the head of mercury.

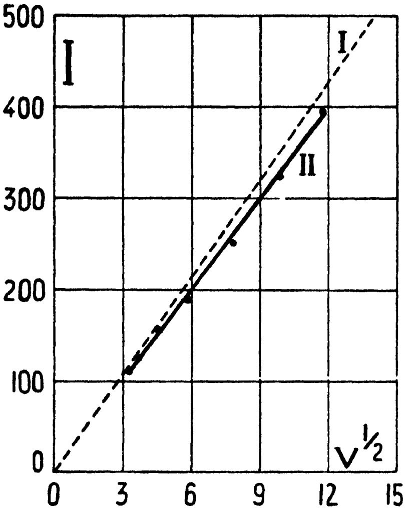

FIG. 2

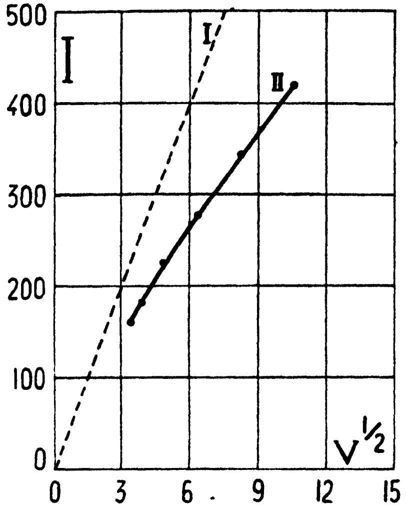

FIG. 3

FIG. 2. Variation of the maximal peak current with the rate of potential change in the case of a "reversible" electrode reaction. v = rate of potential change (v./sec.); I = maximal peak current (microamp.). $TlNO_3$ (10^{-3} mole/liter) in KNO_3 (0.5 mole/liter); m = 1.41 mg./sec.; τ = 4.40 sec. Curve I, calculated by application of formula 4, $I = 35.4v^{1/2}$. Curve II, experimental results.

FIG. 3. Variation of the maximal peak current with the rate of potential change in the case of a "reversible" electrode reaction. $Pb(NO_3)_2$ (10^{-3} mole/liter) in KNO_3 (0.5 mole/liter); m = 1.41 mg./sec.; τ = 4.00 sec. Curve I, calculated by application of formula 4, $I = 66.0v^{1/2}$. Curve II, experimental results.

DEPENDENCE OF THE MAXIMAL PEAK CURRENT ON THE RATE OF POTENTIAL CHANGE

Experimental results

According to formula 4 the maximal peak current is proportional to the square root of the rate of potential change in the case of a reversible electrode reaction. This relationship has been verified experimentally and a few typical results are shown in figures 2–4. In these diagrams the dotted line corresponds to the maximal peak current as calculated by application of formula 4; the solid line corresponds to the experimental results.

The values of the diffusion coefficient used in this calculation are those corresponding to infinite dilution (5, p. 45). For the Tl^+ solution (figure 2) equation 4 is essentially correct over the investigated range of rates of potential change.

On the other hand, for Pb^{++} and Cd^{++} solutions (figures 3–4) one observes a marked departure from the calculated values. It could be objected that a calculation based on the value of the diffusion coefficient at infinite dilution certainly yields too high a value for the maximal peak current. This circumstance could account partially for the discrepancy observed between the calculated and experimental results. However, the ratio of the experimental value of the maximal peak current to the calculated value decreases as the rate of potential change increases (table 2), and this effect can not be explained by any error in the value of the diffusion coefficient. The reason underlying the existence of this effect will be given below.

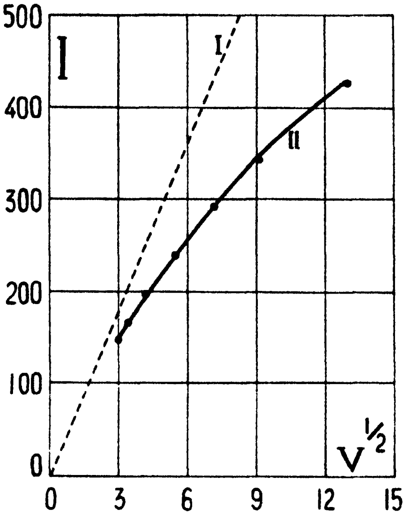

FIG. 4

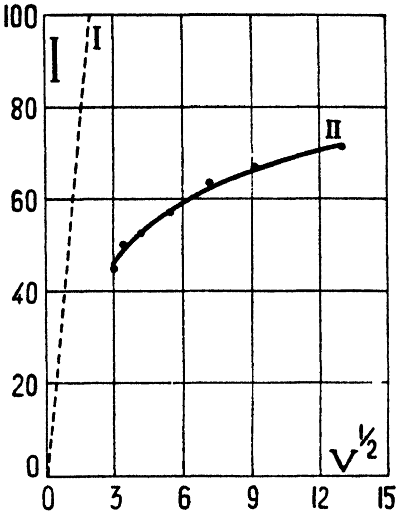

FIG. 5

FIG. 4. Variation of the maximal peak current with the rate of potential change in the case of a "reversible" electrode reaction. $CdSO_4$ (10^{-3} mole/liter) in KCl (1 mole/liter); $m = 1.41$ mg./sec.; $\tau = 4.40$ sec. Curve I, calculated by application of formula 4, $I = 60.2v^{1/2}$. Curve II, experimental results.

FIG. 5. Variation of the maximal peak current with the rate of potential change in the case of an "irreversible" electrode reaction. HCl (10^{-3} mole/liter) in LiCl (0.5 mole/liter); $m = 1.41$ mg./sec.; $\tau = 2.40$ sec. Curve I, calculated by application of formula 4, $I = 51.3v^{1/2}$. Curve II, experimental results.

A few irreversible electrode reactions have also been investigated; the results are shown in figures 5–7. The experimental currents are much smaller than the calculated values (table 2). Therefore equation 4 is by no means applicable even at a rate of potential change of a few volts per second.

Interpretation of the diagram $I = f(v^{1/2})$

The diagram $I = f(v^{1/2})$ can be interpreted in a satisfactory manner by assuming that the rate of the electrode reaction is a factor controlling the strength of the maximal peak current in the case of an irreversible electrode reaction. This influence of the reaction rate is the more pronounced the higher the rate of potential change. Consequently, a curvature appears in the diagram $I = f(v^{1/2})$ and the ratio $I_{\text{exptl.}}/I_{\text{calcd}}$ of the experimental current to the calculated value (formula 4) decreases as v increases (table 2). The magnitude of the rate effect depends on the nature of the electrode process.

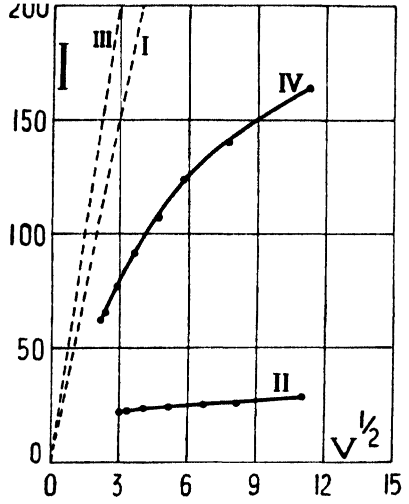

FIG. 6

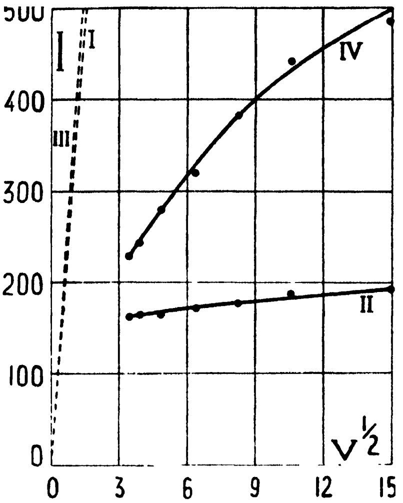

FIG. 7

FIG. 6. Variation of the maximal peak current with the rate of potential change in the case of an "irreversible" electrode reaction.

Curves I, II: $NiSO_4$ (10^{-3} mole/liter) in $(CH_3)_4NBr$ (0.1 mole/liter); m = 2.17 mg./sec.; τ = 1.80 sec. Curve I, calculated by application of formula 4, $I = 43.4v^{1/2}$. Curve II, experimental results.

Curves III, IV: $NiSO_4$ (10 ^{3} mole/liter) in KCNS (0.5 mole/liter); m = 2.17 mg./sec ; τ = 3.50 sec. Curve III, calculated by application of formula 4, $I = 67.7v^{1/2}$. Curve IV, experimental results.

FIG. 7. Variation of the maximal peak current with the rate of potential change in the case of an "irreversible" electrode reaction.

Curves I, II: KIO_3 (10^{-3} mole/liter) in NaOH (0.1 mole/liter); m = 1.41 mg./sec.; τ = 3.30 sec. Curve I, calculated by application of formula 4, $I = 318v^{1/2}$. Curve II, experimental results.

Curves III, IV: KIO_3 (10^{-3} mole/liter) in H_2SO_4 (0.5 mole/liter); m = 1.41 mg./sec.; τ = 4.00 sec. Curve III, calculated by application of formula 4, $I = 361v^{1/2}$. Curve IV, experimental results.

For a reversible electrode reaction no rate effect should be observed, and formula 4 is applicable for any value of the rate of potential change. This is the case of the reduction of thallous ion (figure 2).

For an irreversible electrode reaction the rate effect will depend on the free energy of activation of the process involved. This dependence can be shown in a qualitative manner by considering the relation connecting the free energy of activation with the current density at an electrode on which the reaction is taking place. In the case for which the rate of the electrochemical process is the

TABLE 2

Calculated and experimental maximal peak currents at different rates of potential change

SUBSTANCE	REFERENCE	v_{lowest}	$\frac{I_{\text{exptl.}}}{I_{\text{calcd}}}$	v_{highest}	$\frac{I_{\text{exptl.}}}{I_{\text{calcd.}}}$
		volts/sec.	*per cent*	*volts/sec.*	*per cent*
$TlNO_3$	Figure 2	10.4	97.4	138	94.7
$Pb(NO_3)_2$	Figure 3	11.9	70.4	110	60.3
$CdSO_4$	Figure 4	8.90	82.3	168	54.6
HCl	Figure 5	8.90	29.3	168	10.7
$NiSO_4$ in $(CH_3)_4Br$	Figure 6	9.00	16.9	120	5.95
$NiSO_4$ in KCNS	Figure 6	4.50	42.9	126	23.0
KIO_3 in NaOH	Figure 7	11.8	14.8	223	4.06
KIO_3 in H_2SO_4	Figure 7	11.8	18.4	223	8.97

only factor controlling the current, the following equation for the current density has been derived recently by Van Rysselberghe (9):[2]

$$i_{\text{C.D.}} = \frac{kT}{h} n\mathfrak{F}ae^{-[\Delta F^{\ddagger}+n\mathfrak{F}(\psi_a-\psi_s)]/RT} \tag{8}$$

in which $i_{\text{C.D.}}$ = the current density in amperes per square centimeter,
n = the number of electrons involved in the reaction,
$\mathfrak{F}$ = the Faraday,
a = the activity of the substance reacting at the electrode, expressed in moles per liter,
$\Delta F^{\ddagger}$ = the free energy of activation of the process taking place at the electrode, expressed in calories,
ψ_s = the electrical potential of the reacting species in solution, in volts,
ψ_a = the electrical potential of the reacting species in its activation position closest to the electrode, in volts, and
e, k, h, T, and R have their usual significance.

The term $(\psi_a - \psi_s)$ appearing in relation 8 is not known exactly, but it can be expressed in terms of the potential difference between the electrode and the solution by introducing the notion of transfer coefficient. However, these developments are not needed here.

Formula 8 thus gives the maximum current density at which the electrode process is taking place for a given value of $(\psi_a - \psi_s)$.

In oscillographic polarography there is concentration polarization at the dropping mercury electrode and the maximal peak current cannot be calculated by application of formula 8. Nevertheless, formula 8 shows that the maximal peak current depends on the free energy of activation of the electrode process and, furthermore, that the higher the free energy of activation the smaller the strength of the maximal peak current will be, all other conditions being the same.

The correctness of this statement can be proved experimentally by studying the reduction of iodate ion in various media. It is known from ordinary polarography that the reduction of iodate ion involves a smaller free energy of activation in acid medium than in alkaline solution (5, p. 320). It follows from formula 8 that the maximal peak current of a potassium iodate solution should be larger in an acid supporting electrolyte than in an alkaline medium, all other conditions being the same. The results indicated on figure 7 and in table 2 show that this is indeed the case.[3]

---

[2] The reverse reaction is neglected in relation 8.

The reduction of the nickel ion in various supporting electrolytes is similar to the case of the reduction of iodate ion. It is known from ordinary polarography that the reduction of the nickel ion in a potassium thiocyanate solution involves a smaller free energy of activation than in a potassium chloride solution (5, p. 281). As a result, the maximal peak current of a nickel ion solution in a thiocyanate medium is larger than in a potassium chloride solution, all other conditions being the same (figure 6, curves II and IV).

APPLICATION TO THE DETERMINATION OF THE REVERSIBILITY OF AN ELECTRODE PROCESS

The comparison of the experimental diagram $I = f(v^{1/2})$ with the theoretical one as calculated by application of formula 4 gives us a method of deciding whether an electrode reaction occurs reversibly or irreversibly.[4]

The shape of the diagram $I = f(v^{1/2})$ is also a criterion of reversibility, because a curvature in the diagram indicates the irreversibility of the electrode process. Figures 2 to 7 are examples of application of this method. Among these cases the reduction of cadmium ion is of special interest because this reaction is supposed to occur reversibly (5, p. 269) at the dropping mercury electrode, while the oscillographic method shows definitely that the reduction is actually slightly irreversible. This irreversibility does not appear in ordinary polarography, because it could be detected only by certain effects which are beyond the accuracy of measurement or calculation. On the other hand, this slight irreversibility appears in oscillographic polarography because of the very short duration of the wave recording.[5]

IMPLICATIONS FOR ANALYTICAL APPLICATIONS OF THE OSCILLOGRAPHIC METHOD

From the discussion in the previous section it is obvious that any factor affecting the rate of the electrode reaction will modify the strength of the maximal peak current. If such a modification of the reduction rate is taking place when the experimenter is unaware of it, the maximal peak current may be seriously in error. Therefore, it is essential to work in conditions such that the rate of the electrode reaction is well defined. This condition brings about a difficulty which is not encountered in ordinary polarography.

---

[3] It should be pointed out that curves II and IV have not been recorded with the same drop time, although the difference between the drop times, which are respectively 3.30 and 4.00 sec., is not large enough to account for a wide difference between curves II and IV.

[4] The value of the diffusion coefficient appearing in formula 4 can be easily determined by running an ordinary polarogram and by calculating D from the value of the diffusion current (Ilkovič equation).

[5] This effect should not be confused with the "rate current" observed in ordinary polarography in some cases, for which the diffusion current is limited by the rate of transformation of one substance into another (1, 2, 6).

For example, the oscillographic determination of the iodate-ion concentration in an unbuffered supporting electrolyte would not be very reliable, since a modification of the pH of the solution would result in a variation of the maximal peak current, as we have seen previously. It is therefore essential in the present case to record the iodate wave in a buffered medium. In ordinary polarography this would not be necessary, since a slight variation in the pH of the supporting electrolyte would not appreciably affect the value of the diffusion coefficient of the iodate ion.

SUMMARY

The equations obtained by Randles and by Sevcik for the height of an oscillographic polarogram have been recalled. After transformation these equations were found to be identical except for a difference in a numerical constant.

Several of the factors appearing in the equation have been investigated experimentally. For a reversible electrode reaction Randles' equation was found to be correct. For an irreversible electrode process the rate of the reaction is a controlling factor of the current and the experimental results cannot be predicted by Randles' equation.

The dependence of the wave height on the rate of the electrode reaction is interpreted in terms of the free energy of activation of the electrode process involved. Experimental implications of the reaction rate dependence are discussed.

It is concluded from the experimental data that some electrode processes which are usually considered as occurring reversibly, actually involve a small free energy of activation.

This work is part of a research project entitled "Polarographic Study of Corrosion Phenomena" carried out at the University of Oregon under contract with the Office of Naval Research. The author is indebted to Professor Pierre Van Rysselberghe, Director of the project, for very helpful discussions on overvoltage theories as well as for the discussion of the contents of the present paper.

REFERENCES

(1) Brdička, R.: Collection Czechoslov. Chem. Commun. **12**, 212 (1947).

(2) Brdička, R., and Wiesner, K.: Collection Czechoslov. Chem. Commun. **12**, 138 (1947).

(3) Delahay, P.: J. Phys. & Colloid Chem. **53**, 1279 (1949).

(4) Delahay, P.: J. Phys. & Colloid Chem. **54**, 402 (1950).

(5) Kolthoff, I. M., and Lingane, J. J.: *Polarography*. Interscience Publishers, Inc., New York (1941).

(6) Koutecky, J., and Brdička, R.: Collection Czechoslov. Chem. Commun. **12**, 337 (1947).

(7) Randles, J. E. B.: Trans. Faraday Soc. **44**, 327 (1948).

(8) Sevcik, A.: Collection Czechoslov. Chem. Commun. **13**, 349 (1948).

(9) Van Rysselberghe, P.: J. Chem. Phys. **17** (December, 1949).

THE SEPARATION OF THORIUM AND RARE EARTH SALTS BY SOLVENT EXTRACTION[1, 2]

G. F. ASSELIN, L. F. AUDRIETH, AND E. W. COMINGS

W. A. Noyes Laboratory of Chemistry, University of Illinois, Urbana, Illinois

Received June 27, 1949

The separation of the rare earth elements and thorium from the natural mixtures has long taxed the ingenuity of chemists. Even today separation procedures are unduly tedious, time consuming, and wasteful of materials. An attempt was therefore made to develop a fractionation scheme based on selective solvent extraction, which would possess all of the inherent advantages of a continuous counter-current method. Remarkable success was achieved in separating thorium from the rare earth group by the preferential extraction of the former in 1-pentanol from an aqueous solution of the mixed nitrates and ammonium thiocyanate.

HISTORICAL

The literature dealing with the solvent fractionation of thorium and rare earths is quite meager. Fischer *et al.* (2) report briefly on the distribution of rare earth halides between water and such organic solvents as alcohols, ketones, and ethers. Selwood and Appleton (5) present preliminary data on the solubility of a variety of rare earth salts in a large number of organic solvents. They also carried out a few batch extractions to separate neodymium from praseodymium. Leventhal (3) determined equilibrium distribution ratios for a number of rare earth salts between water and 1-butanol. Fischer and Bock (1) studied the purification of scandium by ether extraction from aqueous solutions of various metal salts containing ammonium thiocyanate and extended their work in a preliminary fashion to the rare earths and thorium. The few data which they present indicate that thorium should be extracted preferentially from the rare earths under these conditions and that very large quantities of ether would be required to purify any reasonable amount of thorium.

More recently, Templeton and Hall (6) determined the solubility of thorium nitrate tetrahydrate in some sixty-five organic solvents. They then extended (4) the investigation to cover the separation of thorium nitrate from rare earth nitrates. Equilibrium distribution data and preliminary batch extractions of thorium–rare earth mixtures indicate that it should be feasible to effect such separations by preferential solvent extraction.

THEORETICAL

The present investigation was guided by two theoretical postulates based on expected differences in behavior among the rare earths and thorium. Neither

---

[1] This paper was abstracted from a thesis submitted by G. F. Asselin to the Graduate College of the University of Illinois in partial fulfillment of the requirements for the degree of Master of Science in Chemical Engineering, June, 1947.

[2] Publication of this paper has been approved by the Chemistry Branch of the Office of Naval Reserve, Washington, D. C., and by the United States Atomic Energy Commission.

working hypothesis proved to be entirely correct, but each will be mentioned briefly. First, since the ionic radii of the rare earths decrease gradually with increasing mass (atomic number), it was anticipated that salts of the heavier rare earths should be less ionic in character and hence more soluble in organic solvents than the lighter ones. It should then be possible to extract the heavier earths preferentially from an aqueous solution by employing an immiscible organic solvent. Secondly, with increasing mass and nuclear charge, the rare earths might be expected to display an increasingly greater tendency toward the formation of both cationic and anionic complexes. Since such complexes are generally more soluble in organic liquids than simple ionic compounds, it was expected that the differences in solubility among the rare earths anticipated by the first hypothesis would thereby be augmented.

EXPERIMENTAL

Data were obtained for the equilibrium distribution of various rare earth and thorium salts between aqueous and solvent phases by standard techniques. Measured volumes of solvent and of aqueous solutions of solutes were placed in separatory funnels at room temperature and agitated until equilibrium had been attained. The phases were then allowed to settle, were separated, and were subsequently analyzed for solute content. The organic solvent was removed from all samples by steam distillation prior to analysis.

Rare earth determinations were generally made by precipitation with oxalic acid and ignition to the oxide, although a few samples were checked also by precipitation with ammonia and subsequent ignition. Thorium was usually determined by precipitation with ammonia and ignition to the oxide, but a few samples were checked by precipitation with oxalic acid. In all cases the agreement between the two methods was entirely satisfactory.

Mixtures of thorium and neodymium were analyzed by determining the neodymium content of the solution spectrophotometrically after removal of thiocyanate by silver nitrate, since the thiocyanate affects the absorption spectrum of neodymium. The thorium content was then obtained by difference after precipitation of both thorium and neodymium as hydroxides by addition of ammonia and ignition to the mixed oxides.

Thiocyanate-ion concentrations were checked by use of the standard Volhard procedure.

All rare earths were obtained from the University of Illinois stocks and were of high purity, with the exception of the erbium sample which had an apparent atomic weight of approximately 150. The oxides were dissolved in a slight excess of the acid whose salt it was desired to prepare, and the excess acid was removed by evaporating the solution to dryness on a steam bath. The dry material was then redissolved in sufficient water to yield a stock solution of the desired strength from which test samples of various concentrations were prepared by dilution. All stock solutions had a pH lying in the range between 3 and 4.

Thorium nitrate was supplied by the Lindsay Light and Chemical Company and was dissolved in water to give a stock solution with a pH of 1.8. Cerous chloride was used as obtained from the G. F. Smith Chemical Company.

PRESENTATION AND DISCUSSION OF DATA

General

With the objective of developing an improved method for isolating salts of pure individual rare earths and thorium from mixtures of these by liquid–liquid extraction, experiments were directed primarily toward the fractionation of mixtures readily obtainable from natural rare earth ores. The design of equipment for such a commercial process requires phase equilibrium data for a system consisting of two solvents and two or more solutes. The determination of complete equilibrium data for such a complex system is an almost prohibitive task and certainly would not be undertaken without preliminary assurance that separations could be effected.

It was considered probable that data on the distribution of individual solutes as a function of concentration would be indicative of the possible success of such a method, provided no interaction occurs between the solutes when they are present in a mixture. If the distribution curves for the pure salts of two rare earths which are widely separated in position in the series coincide for a given set of conditions, then it is quite unlikely that any separation can be achieved by extracting a solution containing a mixture of these salts under these conditions. On the other hand, if such equilibrium curves are found to be markedly different under the same conditions, then further investigation is warranted to ascertain whether or not the distribution of one pure component is affected by the presence of the other in a mixture of the two. It was anticipated that such an effect would be found, but even so it was felt that the distribution curves for the pure salts might be used as first approximations to estimate the feasibility of achieving a separation.

Water was naturally selected as one solvent. 1-Butanol was considered as the second solvent, as Leventhal (3) had found that it extracts appreciable quantities of rare earth salts from aqueous solutions and posesses some degree of selectivity. A number of other solvents were tested qualitatively for extraction capacity to find one less miscible with water than 1-butanol, because it was believed that greater selectivity would be realized from such a solvent. Those tested included 1-butanol, 1-pentanol, diethyl ether, dibutyl ether, chloroform, nitromethane, nitrobenzene, ethyl acetate, and amyl acetate. Only 1-butanol and 1-pentanol extracted satisfactory amounts of rare earth salts. 1-Butanol extracted larger quantities than 1-pentanol with apparently no great difference in selectivity and it was chosen as a suitable, although not necessarily the best, solvent for the initial work.

1-Butanol as solvent

Data for the equilibrium distribution of neodymium chloride and of the chloride of an erbium-rich mixture between water and 1-butanol are represented graphically in figure 1. In this and all subsequent graphs, concentrations are expressed as *grams* of *metal* per liter. It will be noted from figure 1 that very little of either material is extracted by the alcohol and that the difference between the distributions of the two salts lies within the accuracy of the data, so that two distinct curves cannot be drawn. The separation expected on the basis of these data was too slight to warrant further investigation of the chlorides, especially since neodymium and erbium are so widely spaced in the rare earth series.

Leventhal (3) showed that nitrates are more soluble in 1-butanol than chlorides and they were investigated next. Data for the distribution between water and 1-butanol of the nitrates of thorium, neodymium, yttrium, ytterbium and an erbium-rich mixture are presented in figure 2. Nitrates are seen to be roughly four times as soluble as chlorides in the alcohol phase at comparable concentrations in the aqueous phase (i.e., four times as "extractable"), and there are measurable differences in extractability among the various materials. Contrary to the original hypothesis, the lighter rare earths are extracted more readily than the heavier ones.

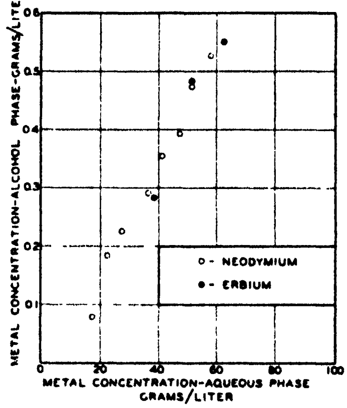

FIG. 1

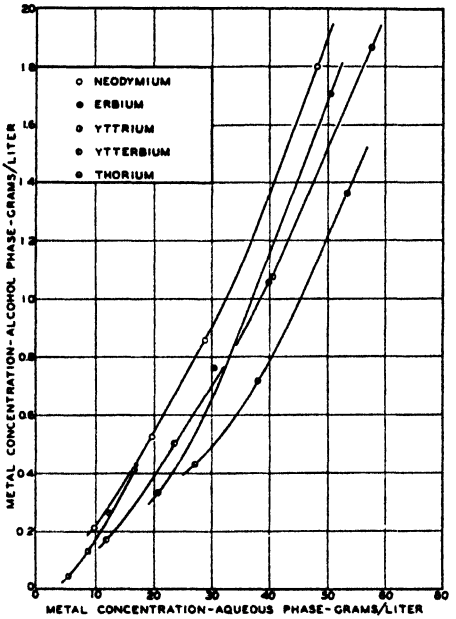

FIG. 2

Fig. 1. Distribution of rare earth chlorides between water and 1-butanol
FIG. 2. Distribution of rare earth nitrates between water and 1-butanol

To determine the possible effect of complex formation, batch extractions were made with 1-butanol and aqueous solutions of rare earth chlorides containing ammonium thiocyanate in the amount of 6 moles of thiocyanate to 1 mole of rare earth. This ratio was selected arbitrarily as corresponding to a likely coordination number for any complex which might form. The equilibrium distribution of both neodymium and an erbium-rich mixture was determined under these conditions. Erbium was found to be measurably but not significantly more extractable than neodymium in the presence of thiocyanate, as may be seen from figure 3. Water and 1-butanol were later discovered to be completely miscible in the presence of a sufficiently high thiocyanate concentration and appreciably miscible at lower concentrations. This behavior limits the practical usefulness of 1-butanol in a process employing thiocyanate.

1-Pentanol as solvent

Preliminary qualitative extractions indicated that 1-pentanol extracts slight amounts of rare earth salts from aqueous solutions. Its miscibility with water in the presence of high thiocyanate concentrations is low; consequently, further tests were made with it.

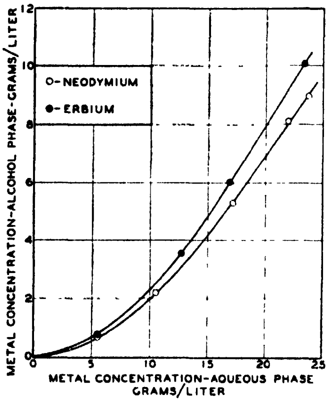

FIG. 3

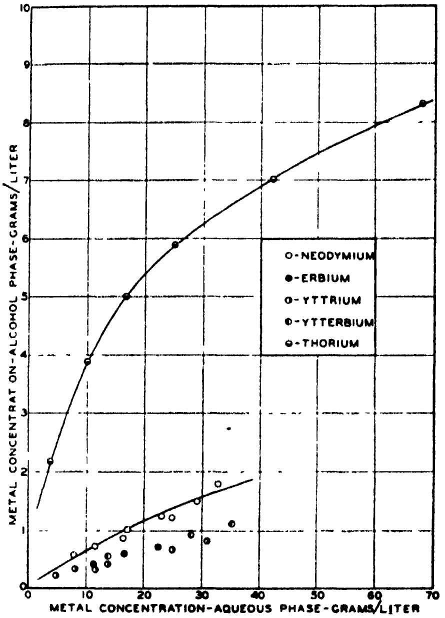

FIG. 4

FIG. 3. Distribution of rare earth chlorides between water and 1-butanol in the presence of ammonium thiocyanate. Conditions of test · 50 ml. of aqueous solution containing rare earth chloride and 6 moles of ammonium thiocyanate per mole of rare earth in contact with 50 ml. of 1-butanol.

FIG. 4. Distribution of rare earth nitrates between water and 1-pentanol in the presence of ammonium thiocyanate. Conditions of test: 40 ml. of aqueous solution containing rare earth nitrate and 0.0376 mole of ammonium thiocyanate in contact with 75 ml. of 1-pentanol.

Equilibrium distribution data for the nitrates of neodymium, yttrium, an erbium-rich mixture, ytterbium, and thorium in the presence of fixed amounts of ammonium thiocyanate were determined as a function of concentration and are presented in figure 4. The concentration of thiocyanate in the aqueous phase when equilibrium is established varies somewhat, since only the amount of thiocyanate in the aqueous phase before extraction was maintained constant, while its distributition between the phases is affected by the concentration of the other salts present. This variation is shown in figure 6, which presents data on the distribution of thiocyanate between water and 1-pentanol in the presence of varying amounts of thorium and neodymium nitrates and mixtures of these at the overall concentration employed in the above series of tests and at a higher overall concentration used in tests which will be described later.

It will be noted from figure 4 that the differences in extractability among the various rare earths are not sufficient to afford an easy means of separation. Further, the order of extractability by 1-pentanol in the presence of thiocyanate is essentially the same as that observed for 1-butanol in its absence, so that no definite conclusions can be drawn from these data as to whether or not the heavier rare earths form complexes more readily than the lighter ones.

The distribution of thorium is much more interesting. It will be recalled that thorium is extracted by 1-butanol to a lesser extent than any rare earth and presumably this would also be the situation with 1-pentanol. However, in the presence of thiocyanate, thorium is extracted by 1-pentanol three or four times as readily as neodymium, one of the most extractable of the rare earths. This behavior is considered strong evidence of the formation of some type of thiocyanate complex by thorium.

The data presented in figure 4 indicate that it should be easy to separate thorium from the rare earths by preferential extraction of the former with 1-pentanol from an aqueous solution of the mixed nitrates containing thiocyanate, provided no interaction which would affect their distribution occurs between the salts when they are present together in a mixture. Because these data appeared promising, further tests were made to verify the expected separation of thorium from the rare earths under these conditions. Neodymium was selected as a representative rare earth which should be one of the most difficult to separate from thorium. Neodymium is also fairly abundant in purified form and is easy to determine spectrophotometrically.

The distribution of neodymium and thorium nitrates and of cerous chloride between water and 1-pentanol in the presence of a greater amount of ammonium thiocyanate than was used in obtaining the data in figure 4 was investigated and these data are presented graphically in figure 5. A comparison of figures 4 and 5 shows that the extractability of neodymium and thorium increases with increasing thiocyanate concentration. The distribution of cerium, the lightest rare earth, was investigated to justify the use of neodymium to represent the rare earth most difficult to separate from thorium. Figure 5 shows that the distribution of cerous chloride is very nearly the same as the other rare earth nitrates in the presence of comparable amounts of thiocyanate; hence, cerium should not be more difficult to separate from thorium than neodymium. Although it was shown previously that chlorides are generally less extractable than nitrates, it is felt that the comparison of chlorides and nitrates in the presence of thiocyanate is valid because the effect of thiocyanate far overshadows any differences which would otherwise exist betwen the extractabilities of chlorides and nitrates alone.

Cerium is present to an appreciable extent in the tetravalent state in natural rare earth mixtures and must be reduced to the cerous state prior to extraction in the presence of thiocyanate. Ceric cerium is known to oxidize the thiocyanate radical to free thiocyanogen, which subsequently polymerizes and yields a yellow to orange precipitate of what is presumed to be the polymeric modification. Free thiocyanogen also undergoes rapid hydrolysis to yield sulfuric acid and hydrogen cyanide. An attempt was made to extract a natural mixture of thorium and the rare earths, but the addition of thiocyanate to this mixture resulted in the immediate evolution of hydrogen cyanide gas and the prompt formation of a yellow precipitate. This difficulty is readily obviated by reducing cerium to the cerous state with hydrogen peroxide and removing the excess peroxide by acidification and boiling.

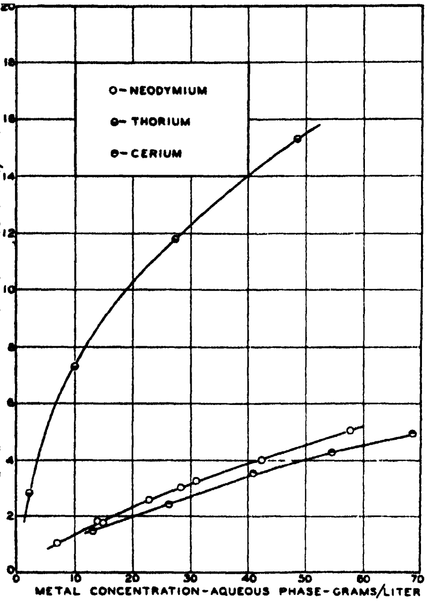

FIG. 5

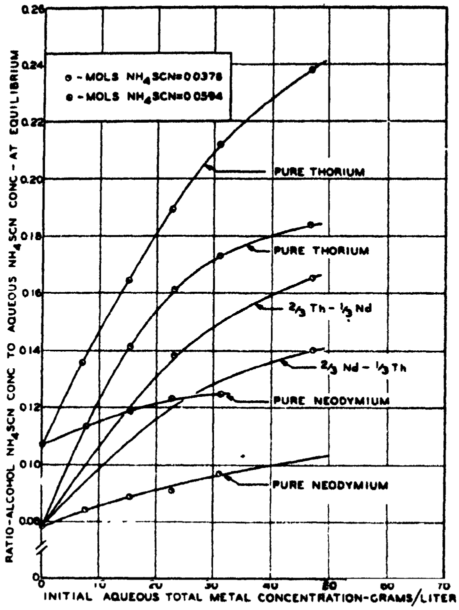

FIG. 6

FIG. 5. Distribution of neodymium and thorium nitrates and cerous chloride between water and 1-pentanol in the presence of ammonium thiocyanate. Conditions of test: 40 ml. of aqueous solution containing rare earth salt and 0.0594 mole of ammonium thiocyanate in contact with 75 ml. of 1-pentanol.

FIG. 6. Effect of neodymium and thorium nitrates on the distribution of ammonium thiocyanate between water and 1-pentanol. Conditions of test: 40 ml. of aqueous solution containing 0.0376 or 0.0594 mole of ammonium thiocyanate and mixtures of thorium and neodymium nitrates in contact with 75 ml. of 1-pentanol.

Separation of thorium–neodymium mixtures

To verify the expectation based on the distribution of pure salts that thorium could be separated easily from the rare earths in the presence of thiocyanate, synthetic mixtures of thorium and neodymium nitrates of varying concentrations and proportions of thorium and neodymium were prepared and extracted by 1-pentanol in the presence of two different fixed amounts of ammonium thiocyanate. The data are presented in table 1. The distribution of thiocyanate between the phases was determined for some of these samples and the data are included in figure 6, from which it is evident that the distribution of thiocyanate between the phases is affected markedly by the amounts of thorium and neodymium present.

The data in table 1 definitely prove the feasibility of the method for separating thorium from the rare earths. This is most readily apparent from a comparison of the first and the last two columns, which shows clearly the separations obtained in single batch extractions. In view of the excellent separations obtained in single steps, relatively few counter-current extraction stages would be required to separate thorium completely from the rare earths. The fourth and sixth columns show that the organic solvent has a very high extraction capacity and hence reasonable quantities of solvent would be required for practical separations.

TABLE 1

Extraction of 40-ml. portions of aqueous solutions of neodymium and thorium nitrate mixtures containing ammonium thiocyanate by 75 ml. of 1-pentanol

INITIAL THORIUM (DRY BASIS)	NH_4SCN	EQUILIBRIUM CONCENTRATION				THORIUM AFTER EXTRACTION (DRY BASIS)	
		Aqueous phase		Alcohol phase			
		Neodymium	Thorium	Neodymium	Thorium	Aqueous phase	Alcohol phase
per cent	*moles*	*g./l.*	*g./l.*	*g./l.*	*g./l.*	*per cent*	*per cent*
80	0.0376	8.31	21.8	0.209	5.74	66.5	96.5
66.7	0.0376	17.2	24.7	0.385	3.72	59.0	90.7
66.7	0.0376	25.4	40.8	0.560	7.24	62.6	92.9
50.0	0.0376	19.8	12.4	0.698	4.04	38.3	85.5
33.3	0.0376	16.4	4.20	0.765	1.78	20.4	69.5
33.3	0.0376	44.5	22.0	1.47	4.90	33.1	77.0
20	0.0376	31.5	7.06	1.35	2.08	17.8	60.7
66.7	0.0594	7.09	5.56	1.37	6.60	44.0	82.9
66.7	0.0594	13.6	12.8	1.88	12.1	48.5	86.7
66.7	0.0594	22.2	20.6	2.12	21.0	48.2	91.0
33.3	0.0594	11.9	3.80	2.70	2.22	8.1	45.1
33.3	0.0594	26.2	8.05	4.24	6.75	23.5	61.3
33.3	0.0594	46.8	12.5	5.77	9.69	23.0	62.7

If the equilibrium concentrations of thorium and neodymium given in table 1 are plotted on figures 4 and 5, the points will not fall on the curves drawn for pure thorium and neodymium under comparable conditions. It is believed that the difference is due primarily to interaction between neodymium and thorium when they are present together in a mixture. For this reason, the data presented are not sufficient to permit accurate engineering design calculations, but they do show that such a separation procedure is practical.

SUMMARY

1. Rare earth chlorides are extracted very slightly from aqueous solutions by 1-butanol and no separation is feasible under these conditions.

2. Rare earth and thorium nitrates are extracted to a significant extent from aqueous solutions by 1-butanol. The order of decreasing extractability is given by neodymium through ytterbium and then thorium. Sufficient differences in the extractabilities of the various materials exist to offer some possibility of separation, but the system was not investigated fully.

3. Rare earths are extracted to a reasonable extent by 1-pentanol from aqueous solutions containing ammonium thiocyanate. Thorium is so much more extractable than any of the rare earths that a simple, very effective means of separating thorium from the rare earths is thereby afforded. Cerium usually present in natural thorium ores must be reduced to the trivalent state prior to the addition of thiocyanate.

4. The more basic rare earths are the most difficult to separate from thorium in the preceding process. Single-step extractions of synthetic neodymium–thorium mixtures were carried out at two fixed thiocyanate concentrations and very good separations were obtained. No marked difference in selectivity for one thiocyanate concentration over the other was found to exist.

5. The equilibrium distribution of thorium between water and 1-pentanol is influenced by the presence of neodymium and *vice versa*.

Therefore, distribution curves for the pure materials cannot be used to predict accurately the behavior of mixtures, although they may be used as first approximations.

The authors wish to acknowledge the financial support given the present investigation by the Office of Naval Research. They also desire to express their appreciation to Messrs. Frank Etges and William Mann, who performed some of the laboratory work, and to Mr. Calvin Brantley, who carried out the spectrophotometric analyses.

REFERENCES

(1) Fischer and Bock: Z. anorg. allgem. Chem. **249**, 146 (1942).
(2) Fischer, Dietz, and Jueberman: Naturwissenschaften **25**, 348 (1937).
(3) Leventhal, H. L.: "Liquid-Liquid Extraction of Rare Earths," M.S Thesis, University of Illinois, 1941.
(4) Rothschild, Templeton, and Hall: J. Phys. & Colloid Chem. **52**, 1006 (1948).
(5) Selwood and Appleton: J. Am. Chem. Soc. **63**, 2049 (1941).
(6) Templeton and Hall: J. Phys. & Colloid Chem. **51**, 1441 (1947).

SOME ASPECTS OF DIFFUSION IN SOLUTION AND A DEFINITION OF A COLLOIDAL PARTICLE

ALFRED POLSON

Veterinary Research Institute, Onderstepoort, Transvaal, Union of South Africa

Received July 28, 1949

The theoretical treatment of diffusion constants of low-molecular-weight substances in solution in terms of molecular dimension is extremely difficult, as the laws of hydrodynamics for the macroscopic state, where the dispersion medium is regarded as continuous, are no longer applicable. This is because the sizes of the molecules of low-molecular-weight substances are comparable in magnitude to those of the dispersion medium.

The object of this paper is to consider the friction of the molecules against the medium in terms of molecular size and to point out some interesting conclusions that can be drawn from diffusion constants.

For an arbitrary molecule we have the well-known equation of Einstein

$$D = \frac{RT}{f}$$

where D is the diffusion constant, R is the gas constant, T is the absolute temperature, and f is the frictional constant per mole. For a spherical unhydrated molecule the frictional constant f_0 can be expressed by the equation

$$f_0 = 6\pi\eta N \left(\frac{3MV}{4\pi N}\right)^{1/3} \tag{1}$$

where η is the viscosity of the solvent, N is the Avogadro number, M is the molecular weight, and V is the specific volume of the solute.

Combining these equations we get

$$M\left(\frac{f}{f_0}\right)^3 = \frac{R^3T^3}{162\pi^2N^2\eta^3}\cdot\frac{1}{D^3V} = \frac{k}{D^3V}$$

or

$$D = \left(\frac{k}{MV}\right)^{1/3}\left(\frac{f_0}{f}\right)$$

In this equation k is a constant and equal to

$$\frac{R^3\,T^3}{162\pi^2N^2\,\eta^3}$$

If $V^{1/3}$ be regarded as constant as a first approximation for organic substances we get:

$$D = \frac{C}{M^{1/3}} \tag{2}$$

In this equation C is also a constant and its value can be calculated from diffusion constant and molecular weight data of proteins with low f/f_0 values. These values of f/f_0 are tabulated by Svedberg and Pedersen (8). Values for low-molecular-weight organic molecules of condensed structure can be calculated from the data available in the literature.

In table 1 such diffusion data are tabulated, together with some unpublished results. These determinations were all made with the help of the scale method of Lamm (3). The last column presents the C-values as calculated.

From table 1 it is evident that C is constant for substances of molecular weights larger than that of gramicidin S. From the molecular weight of gramicidin S downwards the value of C increases.

TABLE 1

C-values for various substances

SUBSTANCE	MOLECULAR WEIGHT	DIFFUSION CONSTANT × 10^7	$C \times 10^5$	REFERENCE
		cm.²/sec.		
Excelsine	294000	4.26	2.80	(8)
Serum albumin	70100	6.17	2.54	(8)
Hemoglobin	63000	6.90	2.74	(8)
Ovalbumin	43800	7.76	2.73	(8)
Lactalbumin	17500	10.57	2.74	(8)
Myoglobin	17200	11.25	2.90	(8)
Tyrocidine	2473	21.3	2.88	(5)
Tannic acid	1700	22.0	2.63	
Gramicidin S	1140	26.0	2.72	(5)
Transvaalin	700	32.9	2.92	(4)
Sucrose	346	46.0	3.22	(7)
Citric acid	208	61.1	3.62	
Tryptophan	208	62.0	3.68	(7)
Proline	125	80.2	4.01	(7)
Formaldehyde	30	140.1	4.35	
Deuterium oxide	20	200.0	5.43	(3)

The data of table 1 are presented in graphical form in figure 1. The lower curve was calculated from equation 2 and the upper curve gives the relationship between molecular weight and diffusion constants as tabulated in table 1. For high-molecular-weight substances the two curves coincide, but in the region of molecular weight 1000 they start to deviate. This deviation increases as the molecular weights decrease.

The explanation for this departure in the low-molecular-weight regions must be sought from equation 1. For low-molecular-weight substances the molecules of the solute become comparable in size to that of the solvent and the solvent cannot, therefore, be regarded as exerting continuous friction on such solute molecules. As a result of this the molecules of the solvent will experience less resistance to its movements as a certain amount of slipping between the molecules of the solvent can take place. The factor $6\pi\eta Nr$ in equation 1, in which r is the radius of the molecule, will thus become smaller, which will cause the molecules to diffuse faster than can be calculated from the equation of Einstein.

Molecules that cannot be regarded as condensed, like the aliphatic amino acids, have diffusion constants considerably smaller than molecules of corresponding molecular weights but of more compact structures. A curve showing the relationship between molecular weights and diffusion constants of such molecules is omitted, as it falls outside the scope of this work. It may be pointed out, however, that the extent of the departure from the curve of the compact or condensed molecules may furnish valuable information regarding structures of molecules of unknown constitution.

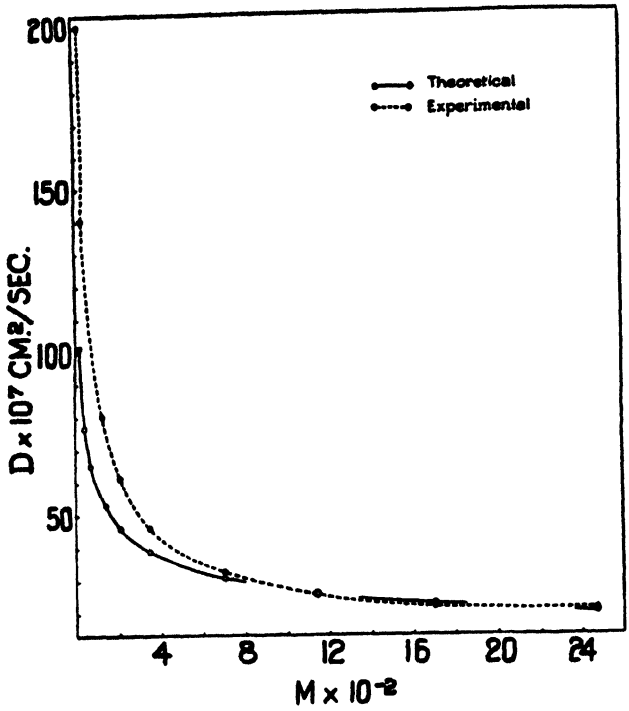

FIG. 1. The relationship between diffusion constants of compact molecules and molecular weight. ——, theoretical curve; ----, experimental curve.

The very regular behavior of molecules of condensed structure, as shown in figure 1, can be explained by the work of Herzog, Illig, and Kudar (1) and by that of Perrin (6). These authors have shown that the shape of a molecule can depart appreciably from the spherical without causing much change in the factor f/f_0 or its equivalent D_0/D, where D is the diffusion constant of a molecule and D_0 is that of a spherical particle of the same molecular weight and density.

The curve in figure 1 can be of some use in the determination of molecular weights of substances of unknown constitution. This method will necessarily yield values that can be considered maximum, as any departure from the condensed state will increase the frictional constant of the particle with a resultant lowering of the diffusion constant.

The usefulness of this diffusion method for determining molecular weights can be illustrated here on the estimation of the molecular weight of gramicidin. According to Pedersen and Synge (5) the diffusion constant of this substance is 18.9×10^{-7} cm.^{2}/sec. at 20°C. When this figure is interpolated in the curve of figure 1 a molecular weight of 3000 is found. This value agrees very well with the values estimated from the sulfur content of the flavianate, i.e., 2986 ± 300 and from the carbon content of the flavianate, i.e., 3036 ± 300, found by Tishler, Stokes, Trenner, and Conn (8) (see Hotchkiss (2)). It is very unlikely that the molecular weight of gramicidin is greater than 3000, as in that case its structure must be more compact than that of any of the substances given in table 1.

A DEFINITION FOR THE COLLOIDAL STATE

For lack of a better definition in the past a dispersion was considered colloidal if the particles of which it is composed are larger than 1 mμ. This limit was chosen quite arbitrarily and has no bearing on any change of properties of a solution. To the mind of the author a much more suitable definition will be if a colloidal particle be defined as of such dimension that it exerts macroscopic friction against its dispersion medium. From a consideration of figure 1 this will be at the position of the departure of the two curves, which is in the region of molecular weight 1000. Thus a molecule must be considered of colloidal dimension if it is compact in structure and of molecular weight greater than 1000. This figure will depend on the dispersion medium, in that if the difference in size between the solute and solvent molecules becomes smaller, slipping or inhomogeneous friction will again take place. It must thus be considered as having bearing on watery solutions alone.

SUMMARY

The relationship between the diffusion constants and molecular weights of electrically neutral organic substances of condensed structure can be presented by a very smooth curve. The equation of this curve for molecular weights greater than 1000 is $D = C/M^{1/3}$, where C is a constant and of value 2.74×10^{-5}. This equation does not hold good for substances of molecular weight smaller than 1000. This molecular weight marks the position above which a molecular dispersion can be regarded as colloidal.

The smooth curve offers a means of estimation of molecular weights of organic substances of condensed structure.

REFERENCES

(1) Herzog, R. O., Illig, R., and Kudar, H.: Z. physik. Chem. **167**, 330 (1933).
(2) Hotchkiss, R. D.: Advances in Enzymol. **4**, 162 (1944).
(3) Lamm, O.: Thesis, Upsala, 1937.
(4) Louw, P. G. J.: Nature **163**, 30 (1949).
(5) Pedersen, K. O., and Synge, R. L. M.: Acta Chem. Scand. **2**, 408 (1948).
(6) Perrin, F.: J. phys. radium [7] **7**, 1 (1936).
(7) Polson, A.: Biochem. J. **31**, 1903 (1937).
(8) Svedberg, T., and Pedersen, K. O.: *The Ultracentrifuge*. The Clarendon Press, Oxford (1940).
(9) Tishler, M., Stokes, J. L., Trenner, N. R., and Conn, J. B.: J. Biol. Chem. **141**, 1947 (1941).

SURFACE ROUGHNESS AND CONTACT ANGLE

J. J. BIKERMAN

Research Laboratories, Merck and Company, Inc., Rahway, New Jersey

Received August 5, 1949

I. INTRODUCTION

It has been reported (1) that contact angles on rough solids are greater than on relatively smooth surfaces and that hysteresis of wetting increases with the degree of roughness. However, in almost all publications known to the author, surface roughness was characterized in qualitative terms only (such as "highly polished," "ground," etc.). Parker and Smoluchowski (4) mentioned a quantitative parameter of roughness of their iron plates but gave no numerical value for the wetting observed. In the present work, contact angles have been measured using solid surfaces the profile of which was determined with a tracer instrument.

The system investigated comprised drops of distilled water in air on 18-8 stainless steel plates of different finishes. The chemical composition of all plates and, presumably, of their surfaces is stated to be identical.

II. EXPERIMENTAL PROCEDURE

There are six standard sheet finishes of 18-8 stainless steel on the market. Their preparation is described in the booklet entitled "Fabrication of U.S.S. Stainless and Heat-Resisting Steels" (1947) and distributed by the United States Steel Corporation. A summary of this description is given below, together with the "root-mean-square elevations" (h_{rms}) of the finishes, determined by means of a tracer instrument.[1] The root-mean-square elevations were obtained as follows: A diamond needle, the tip of which has the radius of 13 × 10^{-4} cm., was moved along the surface to be explored. In this movement it fell h_1 cm. into a depression, rose h_2 cm. to reach the summit of the next hill, fell h_3 cm. into the next valley, etc. The h_{rms}, defined as $\frac{1}{2}(h_1^2 + h_2^2 + h_3^2 + \cdots)^{1/2}$, was computed by an electrical apparatus. A record of the actual movement of the needle, i.e., the profile of the surface, on finish No. 1 has been published (3).

These profiles and the values of h_{rms} given in table 1 refer to the set of plates (7 x 5 x 0.08 cm.) designated in the following as set I; it was supplied with a copy of the above booklet. Set II comprised plates (same dimensions) taken from another copy of the booklet. The description of their preparation given in table 1 is valid for both set I and set II, but the h_{rms} was not determined for the latter.

The plates were washed with soap and hot water, rinsed with distilled water, rubbed with cotton soaked with acetone, rinsed with acetone, rubbed with cotton soaked in carbon tetrachloride, rinsed with carbon tetrachloride, and allowed to dry in air protected from dust.

---

[1] These determinations have been carried out in the laboratories of the Norton Company, Worcester 6, Massachusetts, through the courtesy of Dr. S. S. Kistler. Two lines on each sample were scanned, whence two values of h_{rms} for each finish.

The contact angles formed by water drops on the plates "cleaned" in this manner were determined by a modification of the previous method (2). Drops of the volume v were deposited on the plates and the mean diameters (Δ) of their bases were at once (before a noticeable evaporation took place) measured in a microscope at a magnification of about 20. The ratio Δ^3/v was extrapolated to $v = 0$, and the contact angle θ (through water) was calculated from this extrapolated value (Δ_0^3/v) by means of the equation:

$$\frac{\Delta_0^3}{v} = \frac{24 \sin^3 \theta}{\pi(2-3 \cos \theta + \cos^3 \theta)} \tag{1}$$

A numerical table for the right-hand term of this equation can be found in reference 2.

TABLE 1

Values of h_{rms} for plates of set I

FINISH	PREPARATION	h_{rms}
		cm.
Finish No. 1	Hot rolled, annealed, and pickled	3.1×10^{-4} 3.1×10^{-4}
Finish No. 2D	Cold rolled, annealed, and pickled	0.8×10^{-4} 1.0×10^{-4}
Finish No. 2B	Produced by final light cold rolling	0.25×10^{-4} 0.40×10^{-4}
Finish No. 4	Polished with No. 120 grit and a lubricant	0.033×10^{-4} 0.045×10^{-4}
Finish No. 6	Produced by brushing a No. 4 surface with a rotating brush of tampico fibre loaded with fine abrasive and oil	0.084×10^{-4} 0.10×10^{-4}
Finish No. 7	Polished with No. 320 grit and a viscous lubricant	0.020×10^{-4} 0.030×10^{-4}

The droplets were deposited either from a microburet (the tip of which was waxed), the volumes being 0.008, 0.004, and 0.002 ml., or from a micrometer syringe, the volumes being 0.008, 0.004, 0.002, and 0.001 ml. In each series eight droplets of each size were measured. Because the spread of the Δ^3/v values rendered extrapolation based on an individual series of droplets inexact, a formula was derived which approximately represented the average dependence of Δ^3/v on v for all the observations in this work. It is

$$\frac{\Delta^3}{v} = \frac{\Delta_0^3}{v}(1 + 28.3v - 1670v^2) \tag{2}$$

v being expressed in milliliters. It follows from this equation that the values of Δ^3/v found for droplets of 0.008, 0.004, 0.002, and 0.001 ml. must be divided by 1.120, 1.087, 1.050, and 1.027, respectively, to obtain Δ_0^3/v. In this manner, every series of droplets yielded three or four values of Δ_0^3/v. The mean of these values was used to calculate θ.

The precision of these values of θ is limited chiefly by (*a*) the deviation of the base of the drops from a perfect circle (see reference 2 and Section IV, below) and (*b*) the poor reproducibility of solid surfaces. In spite of the standardized pretreatment of all plates, the same plate in a duplicate experiment and even the right and the left halves of a plate in one experiment yielded θ-values differing by 5° or more. The errors due to (*a*) and (*b*) are believed to be much greater than the error which may be due to using the empirical equation 2.

TABLE 2

Contact angles (through water) between air, water drops, and steel plates of various degrees of roughness

	FINISH NO.					
	1	2D	2B	6	4	7
	Set I					
Drops from microburet	90° 90°	82° 76°	93° 87°	65° 57°	70° 71°	91° 87°
Drops from syringe	87°	84°	93°	58°	70°	89°
Mean	89°	81°	91°	60°	70°	89°
	Set II					
Drops from microburet	89° 93°	68° 71°	71° 75°	75° 74°	81° 77°	86° 91°
Drops from syringe	100°	78°	81°	70°	89°	91°
Mean	94°	72°	76°	73°	82°	89°

III. RESULTS

The values obtained for the contact angles θ are collected in table 2.

Comparison of the different columns of table 2 shows that surface roughness has no definite effect on θ. The contact angles on finish No. 1 and finish No. 7 are identical or nearly identical, although h_{rms} of the former is more than 100 times that of the latter (in set I).

Comparison of the upper and lower parts of table 2 demonstrates that two specimens of supposedly identical finishes may differ more than two specimens of quite different roughness; thus, the difference between the θ of two specimens of finish 2B was 15°.

The two lines marked "microburet" exemplify the reproducibility of contact angles on the same plate subjected to, as far as possible, identical treatment. The greatest difference observed here is 8°, i.e., again greater than that between the coarsest and the finest finish.

There is no systematic difference between droplets from a microburet and those from a micrometer syringe, showing that slight changes in the procedure of deposition have no noticeable effect on wetting. This was confirmed also by special experiments: drops from the microburet were either first formed at the waxed tip and then transferred onto the plate, or formed on the plate, which was almost in contact with the tip of the microburet, at different rates of flow; no definite effect on θ was recognizable.

IV. WETTING OF ANISOTROPIC SURFACES

Of the six commercial finishes, No. 4 is the most anisotropic. Its surface is covered with parallel grooves clearly visible at a magnification as small as 20. The h_{rms} values given for it above were obtained by moving the diamond needle *along* the grooves. Water droplets on No. 4 surfaces are elongated in the direction of the grooves. The ratio of the major axis a to the minor axis b of the bases of these droplets usually was between 1.15 and 1.20, although also ratios above 1.50 occurred. The roughly elliptical shape of the base undoubtedly causes an error in the above calculation of θ, in which the base is assumed to be circular and Δ is taken as $\frac{1}{2}(a + b)$.

Elongated droplets can be formed also on a reasonably isotropic surface, such as 2D or 2B, e.g., by depositing two droplets almost in contact with each other and then causing their coalescence by adding a third droplet. Comparison of these droplets with circular drops on the same surface shows that Δ of the latter is always less than $\frac{1}{2}(a + b)$ of the former. Sometimes Δ is almost equal to b; in other instances, $\Delta = \sqrt[3]{ab^2}$. If the last-mentioned equation is assumed, the Δ_0^3/v values for No. 4 are reduced by about 10 per cent and the θ-values of table 2 are increased by 3–4°. The uncorrected values are given in table 2 because the correction has no theoretical foundation. Unfortunately, exact calculation of the shape of elongated drops would be extremely tedious.

The drops on No. 4 finish (and sometimes also on No. 6 and No. 7) had also another peculiarity: the longer sides of their bases were straight along a good part of the contour (see figure 1, in which the direction of the grooves is indicated by an arrow). Apparently, movement of the drop (expansion or contraction) was checked by a microscopic ridge and stopped along its slope.

V. WETTING AND ROUGHNESS

Roughness may be expected to affect wetting differently according to whether (*a*) the surface is grooved or ridged, (*b*) the drops expand or contract, and (*c*) the equilibrium contact angle is acute, right, or obtuse. The difference between grooved and ridged surfaces, as these terms are meant here, is that in the former the depressions are connected with each other and enclose elevated islands, while in the latter the ridges enclose disconnected depressions.

If the hysteresis of wetting is small, the behavior of a drop on a grooved surface would be determined by the equilibrium contact angle. If this angle is acute, the liquid would spread along the grooves and the observable θ would be small; an obtuse contact angle would be made even more obtuse, and a right angle would not be affected. On a ridged surface, hysteresis of wetting would determine the behavior. Both spreading and contraction of a drop would be obstructed as long as the equilibrium contact angle is not too small (at $\theta = 0$ liquid would spread over surfaces of any kind and degree of roughness), i.e., for obtuse, right, and large acute angles. Apparently, there is no experimental proof for this obstruction on the microscopic scale but figure 2 makes its existence highly probable. The main assumption on which figure 2 is based is that the true contact angle, i.e., that between air, liquid, and the actual solid surface (as distinct from its main plane), remains constant during spreading or contraction of a drop. If this assumption is granted, figure 2 shows that climbing of the drop front over ridges would involve contortion of the liquid–air interface and, consequently, an increase in the surface energy of the system, which contortion may be associated with lifting of the center of gravity of the drop, i.e., an increase also in the gravitational energy. If the drop does not possess this additional energy, its movement would cease at a ridge. On a surface which is neither purely "grooved" nor purely "ridged" but a mixture of both, the behavior of a drop is difficult to predict in general terms. It is clear, however, that the enhancement of spreading by depressions may be offset by its obstruction due to elevations, thus making the extent of spreading independent of roughness.

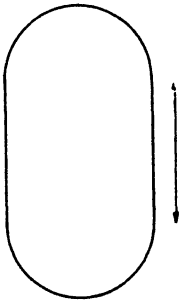

FIG. 1

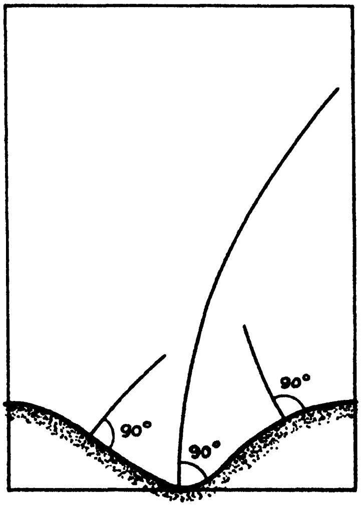

FIG. 2

FIG. 1. Approximate shape of drops on the anisotropic surface No. 4. The arrow indicates the direction of the grooves.

FIG. 2 Movement of drop front over a ridge. The real contact angle is constant and, in the drawing, is 90°. The position in the bottom of a valley is stable in this instance. Movement either to the right (contraction) or to the left (spreading) results in contortion of the drop, which increases the surface energy of the system and may also lift its center of gravity.

Although this discussion is of necessity qualitative only, it may be used to account for some of the observations made in this work. The mutual cancellation of the effects produced by grooves and ridges can be made responsible for θ being independent of roughness, as shown by finishes No. 1 and No. 7 in table 2. The relatively good wettability of No. 6 finish would indicate its nature as a "grooved" surface. Because the effect of roughness in this work was generally small, accidental impurities often determined the θ observed (see the last paragraph in the section on experimental procedure).

The ratio $a:b$ of droplets deposited with a microsyringe on No. 4 finish was 1.09–1.24 (mean, 1.17) for set I and 1.14–1.25 (mean, 1.19) for set II, while θ was 70° for set I and 89° for set II. As the ratio $a:b$ was independent of contact angle, ridges, in this instance at least, appear to have greater importance than grooves whose effects for $\theta = 70°$ would be much greater than for $\theta = 89°$. As mentioned in the section on wetting of anisotropic surfaces, the peculiar shape of drops on No. 4 also seems to be due to ridges.

The author thanks Dr. P. K. Frolich, Vice President for Research and Development, for permission to carry out the work here reported in the laboratories of Merck and Company, Inc., and Dr. S. S. Kistler, Norton Company, for the roughness data on the samples used.

REFERENCES

(1) Bikerman, J. J.: *Surface Chemistry for Industrial Research*, p. 332. Academic Press, New York (1948).
(2) Bikerman, J. J.: Ind. Eng. Chem., Anal. Ed. **13**, 443 (1941).
(3) Bikerman, J. J.: J. Applied Phys. **20**, 971 (1949).
(4) Parker, E. R., and Smoluchowski, R.: Trans. Am. Soc. Metals **35**, 362 (1945).

A DETERMINATION OF THE SOLUBILITY OF POTASSIUM ZINC FERROCYANIDE

M. W. GRIEB and W. H. CONE

Department of Chemistry, University of Idaho, Moscow, Idaho

Received August 5, 1949

The use of diphenylbenzidine as an indicator for the titration of zinc with potassium ferrocyanide (1) depends on the ratio of the solubility of zinc ferricyanide to that of potassium zinc ferrocyanide. Because the only available reference (5) to the solubility of the latter compound was somewhat ambiguous and not in accordance with observations, a determination of its solubility was undertaken.

The method employed was a measurement of the oxidation potential of a solution saturated with both zinc ferricyanide and potassium zinc ferrocyanide, which potential is dependent upon the activities of the ferricyanide and ferrocyanide ions as expressed by the equation:

$$E = E^0 - \frac{RT}{nF} \ln \frac{a_{\text{Ferro}}}{a_{\text{Ferri}}}$$

From the measured potential, the ratio of the concentration of the ferrocyanide ion to the concentration of the ferricyanide ion may be calculated if the assumption is made that the concentrations are equal to the activities. The solubility of the potassium zinc ferrocyanide was then calculated from the solubility of zinc ferricyanide.

METHOD

Yellow zinc ferricyanide, having the formula $Zn_3[Fe(CN)_6]_2$, is precipitated in a practically pure state from hot solutions of zinc salts upon addition of potassium ferricyanide. Below 69–70°C. it exists as the brown dodecahydrate and its solubility at ordinary temperature, determined iodometrically, is given as 1.24×10^{-4} moles per liter (2).

A redetermination of the solubility of this compound at 25°C. was made by comparison, by means of a photoelectric colorimeter, of the intensity of yellow color imparted to saturated solutions by the ferricyanide ion, with the colors of standard solutions of potassium ferricyanide. Six samples of zinc ferricyanide were prepared from zinc sulfate and potassium ferricyanide by slow addition of a hot solution of one to a hot, rapidly stirred solution of the other. The reagents were used in stoichiometric ratios of 1:1, 2:1, and 1:2, with both orders of addition being used for each combination. The samples were thoroughly washed by decantation. Those samples precipitated with excess ferricyanide showed a higher ferricyanide-ion concentration in their saturated solutions than did the others, as long as the washings were made with cold water. A boiling treatment brought their indicated concentrations into agreement.

The average of forty-two determinations, with a relative mean deviation of 3.2 per cent, indicated a solubility of 1.65×10^{-4} moles per liter.

Saitô (9) has determined by means of potentiometric titrations that in the reaction between a soluble zinc salt and potassium ferrocyanide, zinc ferrocyanide, $Zn_2Fe(CN)_6$, forms fairly rapidly at first, followed by the irreversible formation of potassium zinc ferrocyanide, $K_2Zn_3[Fe(CN)_6]_2$, at a somewhat slower rate. The rate of the second reaction is accelerated by weak solutions of hydrochloric and sulfuric acids, but retarded by acetic acid. The composition of potassium zinc ferrocyanide has been determined thermometrically by Paris (8) and by others (3, 7).

Potassium zinc ferrocyanide was prepared by adding the stoichiometric quantity of potassium ferrocyanide to a solution of zinc sulfate. This precipitate was thoroughly washed with oxygen-free water under a nitrogen atmosphere and then combined in a flask with a precipitate of zinc ferricyanide. These mixed precipitates were again thoroughly washed with oxygen-free water before being transferred to the electrode vessels. The electrode vessels were placed in a constant-temperature bath which was kept at 25°C. ± 0.05°, where they were allowed to stand for at least 2 days before measurements were made.

Twenty-two half-cells were prepared and their potentials were measured. In half of these the electrodes were bright platinum; in the other half they were platinized platinum. There was no observable difference between the potentials of these two types of electrodes. The average value of these cells, measured against a saturated calomel electrode, was 0.710 v., with maximum and minimum values of 0.724 and 0.694 v.

The potential of the saturated calomel cell was taken as 0.246 v. (4, 10). The E^0 value for the cell $Fe(CN)_6^{-4}$, $Fe(CN)_6^{-3}$, Pt was taken as 0.356 v. (6). For the cell:

$$\text{Saturated calomel} \parallel (Fe(CN)_6^{-4}, Fe(CN)_6^{-3})\ Pt$$

$$0.710 = 0.356 - 0.0591 \log \frac{Fe(CN)_6^{-4}}{Fe(CN)_6^{-3}} - 0.246$$

$$\frac{0.60}{0.0591} = -\log \frac{Fe(CN)_6^{-4}}{Fe(CN)_6^{-3}}$$

The ratio of ferrocyanide to ferricyanide is 7.1×10^{-11}. Since zinc ferricyanide and potassium zinc ferrocyanide each give two of the complex anions per molecule, the ratio of their molar solubilities is the same as the ratio of the ion concentrations. Multiplying the above ratio by the solubility of zinc ferricyanide gives 1.2×10^{-14} moles per liter for the solubility of potassium zinc ferrocyanide.

SUMMARY

1. The solubility of potassium ferricyanide was determined colorimetrically to be 1.65×10^{-4} moles per liter.

2. The ratio of the solubility of potassium zinc ferrocyanide to zinc ferricyanide, measured potentiometrically, was 7.1×10^{-11}.

3. The solubility of potassium zinc ferrocyanide was calculated to be 1.2×10^{-14} moles per liter.

4. The ratio 7.1×10^{-11} is sufficient to account for satisfactory use of diphenylbenzidine as an indicator in the titration of zinc.

REFERENCES

(1) CONE, W. H., AND CADY, L. C.: J. Am. Chem. Soc. **49**, 356 (1927).
(2) ČŮTA, F.: Collection Czechoslov. Chem. Commun. **1**, 538 (1929).
(3) ERISTAVI, D. I., AND BARNABISHVILI, D. N.: J. Gen. Chem. (U.S.S.R.) **9**, 1880 (1939).
(4) FALES, H. A., AND MUDGE, W. A.: J. Am. Chem. Soc. **42**, 2434 (1920).
(5) GUÉRON, J.: Ann. chim. anal. [2] **14**, 393 (1932).
(6) KOLTHOFF, I. M., AND TOMSICEK, W. J.: J. Phys. Chem. **39**, 945 (1935).
(7) MEURICE, R.: Ann. chim. anal. **18**, 342 (1913).
(8) PARIS, R.: Compt. rend. **199**, 863 (1934).
(9) SAITÔ, S.: Bull. Inst. Phys. Chem. Research (Tokyo) **8**, 921 (1923).
(10) VELINGER, E.: Arch. phys. biol. **2**, 119 (1926).

THE ADSORPTION OF SULFANILAMIDE ON SILK FIBROIN[1]

JANE COULOMBRE AND WALTER J. MOORE
Department of Chemistry, The Catholic University of America, Washington, D. C.

Received August 8, 1949

There have been a number of studies of the combination of organic anions with proteins in buffered solutions. For example, in the work of Klotz and Urquhart (6) a study was made of the binding of methyl orange and azosulfathiazole by bovine serum albumin at 0°C. and 25°C. in acetate and phosphate buffers. A small temperature coefficient was observed, corresponding to a heat of binding of the first anion of around 2000 cal./mole. A positive entropy of binding of around 15 E.U. was found. These results suggest that the binding process is an ion exchange between buffer anion and dye anion. Such positive entropies of adsorption have been noted in ion exchange of cations by organic zeolites (1).

In the present investigation the authors have studied the adsorption of sulfanilamide on silk fibroin in unbuffered solutions. The results have been treated by straightforward analysis of the adsorption isotherm. Since fibroin is an insoluble protein of well-defined composition, it is an ideal substrate for these studies.

EXPERIMENTAL

The fibroin was obtained by degumming raw silk by the procedure of Sookne and Harris (8). The sulfanilamide was an Eimer and Amend product, twice recrystallized.

The adsorption runs were carried out by adding a weighed portion (about 0.5 g.) of vacuum-dried fibroin to 100 ml. of sulfanilamide solution in an Erlenmeyer flask. The solution was maintained in a thermostat at 0.1°, 16.3°, or 34.4°C. for 4–8 hr. (It was found that standing for 48 hr. did not further increase the measured adsorption.) A sample of solution was then drawn off and analyzed for sulfanilamide by the method of Solts (7), i.e., bromination and titration with 0.1 N potassium bromate.

A few experiments were also made on a sample of fibroin that had been dispersed by dissolving in copper ethylenediamine and precipitating with methanol and hydrochloric acid (4).

RESULTS

The experimental isotherms are plotted in figure 1 as milligrams of sulfanilamide adsorbed per gram of protein *vs.* the ratio of the sulfanilamide concentration to the saturation concentration, C_0, at the particular temperature. As determined in separate experiments the values of C_0 in grams per 100 ml. of solution are 1.261 at 34.4°C., 0.561 at 16.3°C., and 0.245 at 0.1°C. (extrapolated).

The isotherms in figure 1 were measured at a pH of from 5.7 to 6.0. Lowering the pH to 5.0 changed the observed isotherm slightly in the direction of decreased adsorption, but further pH variations were not investigated.

---

[1] This article is based upon a dissertation submitted by Jane Coulombre to the Faculty of The Catholic University of America in partial fulfillment of the requirements for the degree of Master of Science, June, 1949.

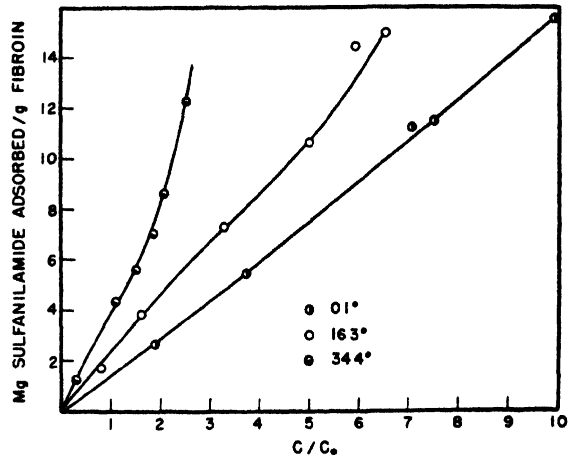

FIG. 1. Adsorption isotherms of sulfanilamide on fibroin

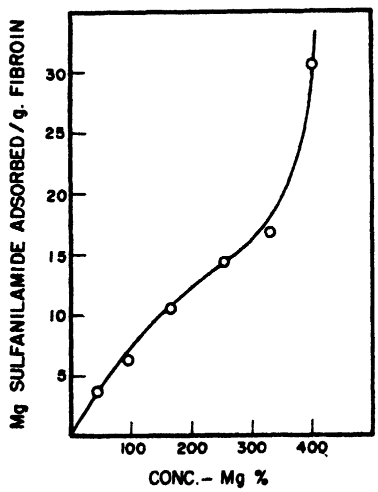

FIG. 2

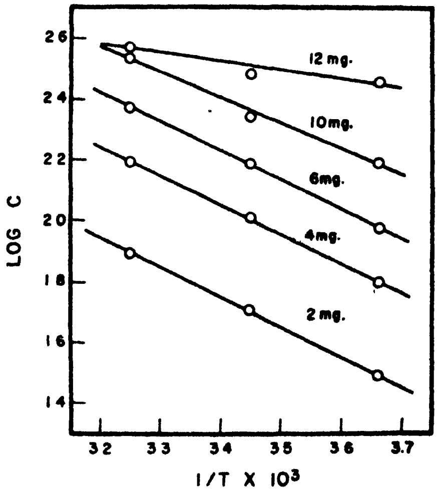

FIG. 3

FIG. 2. An isotherm at 25°C. on dispersed fibroin

FIG. 3. Adsorption isosteres at various coverages in milligrams per 100 g. of protein

The adsorption isotherm on dispersed fibroin at 25.1°C. and pH 6.1–6.4 is shown in figure 2. It resembles somewhat the sigmoid isotherms observed for the physical adsorption of inert gases on finely divided solids (2).

If we plot the logarithms of the equilibrium concentrations at constant adsorption against the reciprocal of the absolute temperature, the absorption isosteres shown in figure 3 are obtained. The adsorption of sulfanilamide in milligrams per gram of fibroin is noted on each isostere. From the slopes of these lines the differential heat of adsorption at constant coverage is calculated. This calculation implies the substitution of a concentration ratio for an activity ratio. Since the sulfanilamide, under the conditions of this experiment, exists predominantly as uncharged molecules, the activity coefficients in the dilute solutions may not depart appreciably from unity.

The $\Delta \bar{F}^0$ for adsorption can then be estimated from $-\Delta \bar{F}^0 = RT \ln C$, where C is the equilibrium concentration in moles per liter. The $\Delta \bar{S}^0$ is $(\Delta \bar{H}^0 - \Delta \bar{F}^0)/T$. These thermodynamic data are summarized in table 1. The negative entropies are in accord with the usual experience in adsorption.

TABLE 1

Thermodynamic data for adsorption of sulfanilamide on fibroin

SULFANILAMIDE ADSORBED PER GRAM OF FIBROIN	ΔF^0	$\Delta \bar{H}^0$	$\Delta \bar{S}^0$
mg.			
2	−3320	−4500	−4.0
4	−2920	−4500	−5.3
6	−2680	−4400	−5.8
10	−2460	−3800	−4.5
12	−2340	−1220	+3.8

DISCUSSION

It will be noted that the heat of adsorption remains practically constant at 4500 cal./mole until an adsorption of 0.0058 mole of sulfanilamide per 100 g. of protein is reached. Thereafter it decreases rapidly. The basic amino acids in fibroin occur to the following extents (3):

ACID	MOLES/100 G. PROTEIN	pK_a
Histidine	0.00045	5.6–7.0
Lysine	0.00171	9.4–10.6
Arginine	0.00436	11.6–12.6
Total	0.00652	

Although sulfanilamide ($pK_a = 10.43$) is only slightly dissociated at pH 6.0, it is probable that it is bound to the basic side chains of the protein as the sulfanilamide anion. If one excludes the imidazolium groups of histidine the observed adsorption of 0.0058 mole/100 g. is very close to the lysine plus arginine content of 0.0061.

Since the heat of adsorption remains practically constant until these groups are covered, it seems likely that they are fairly well separated in the fibroin chain; otherwise electrostatic repulsions would lower the ΔH. The fact that all the basic groups in fibroin are readily accessible is in itself worth remarking. Either the interior of the fibre is freely accessible to large molecules or the basic side chains are all directed outwards.

The considerably enhanced adsorption of the dispersed fibroin is more than can be accounted for by the available basic groups. We may recall that the model for the dispersion of fibroin proposed by Coleman and Howitt (4) was a bending around a molecular hinge consisting of a prolyltyrosylprolyl segment. Even after reprecipitation the fibroin that has been dispersed may have more tyrosine residues available for binding. The large van der Waals forces between the benzene ring of tyrosine and that of sulfanilamide might cause considerable binding.

Whether or not the bacteriostatic action of the sulfonamides arises from a competition with *p*-aminobenzoic acid (5, 9), the site of the enzyme inhibition may well be localized in the arginine or lysine residues of the enzyme protein. If the inhibited enzyme is one concerned with protein synthesis, it is reasonable to believe that it acts as an acid-base catalyst.

SUMMARY

The adsorption of sulfanilamide on silk fibroin has been measured in unbuffered solutions (pH = 6.0) at 0.1°, 16.3°, and 34.4°C. The calculated differential heat of adsorption remains practically constant at 4500 cal./mole until an adsorption of 0.0058 mole of sulfanilamide per 100 g. of protein is reached; thereafter it decreases rapidly. The arginine and lysine side chains in fibroin amount to 0.0061 mole per 100 g. of protein. The entropies of adsorption are negative, in contrast to the usual experience in buffered solutions where adsorption probably occurs by an ion exchange.

REFERENCES

(1) Boyd, G. E., Schubert, J. and Adamson, A. W : J. Am. Chem. Soc **69,** 2818 (1947).

(2) Brunauer, S.: *Physical Adsorption* Princeton University Press, Princeton, New Jersey (1943).

(3) Cohn, E. J., and Edsall, J. T *Proteins, Amino Acids, and Peptides*, pp. 358, 445. Reinhold Publishing Corporation, New York (1943).

(4) Coleman, D., and Howitt, F. O.· Proc Roy. Soc. (London) **A190,** 145 (1947).

(5) Klotz, I. M.: J. Am. Chem. Soc. **66,** 459 (1944).

(6) Klotz, I. M., and Urquhart, J.: J. Am. Chem. Soc. **71,** 847 (1949).

(7) Solts, F. M.. Ukrain. Gosudarst. Inst. Eksptl. Farm. (Kharkov) Konsul'tats. Materialy **1940,** No. 1, 31–2; Chem. Abstracts **36,** 3000 (1942).

(8) Sookne, A. M., and Harris, M.. J. Research Natl. Bur. Standards **23,** 294 (1939).

(9) Woods, D. D.: Brit. J. Exptl. Path. **21,** 74 (1940).

THE SOLUBILITY OF SOLID ETHANE, ETHYLENE, AND PROPYLENE IN LIQUID NITROGEN AND OXYGEN

ANNA LUCILE COX[1] AND THOMAS DE VRIES

Department of Chemistry, Purdue University, Lafayette, Indiana

Received August 11, 1949

Hildebrand (5) has contributed to the understanding of intermolecular forces in the liquid state by developing an equation which he has successfully applied to many solutions of nonpolar substances. Such solutions have a random arrangement, because any tendencies toward molecular association are sufficiently weak to be overcome by thermal agitation. These solutions are designated "regular" solutions. The treatment of these solutions is more complicated than for ideal solutions, since consideration must be given to the differences in molal volumes and also to the differences in internal pressures of the two components.

Relatively few data are available on solutions of nonpolar solids in nonpolar liquids at low temperatures. Solutions of krypton and xenon (15), of argon (7), and of ethane (6) in liquid oxygen have been investigated, as well as solutions of acetylene and carbon dioxide (4, 9), ethylene and propylene (6, 16), and methane (3) in liquid nitrogen and in liquid oxygen.

The purpose of the present investigation has been to obtain more solubility data on solutions at low temperatures and to study their deviations from Hildebrand's equation for regular solutions. The systems investigated were ethane in liquid nitrogen, and ethane, ethylene, and propylene in liquid oxygen.

EXPERIMENTAL

The oxygen used as solvent was prepared by heating potassium permanganate; it was purified by passing it first over soda lime and then over phosphorus pentoxide (A, B, C in figure 1).

The nitrogen used as solvent was obtained from a cylinder of Linde dry nitrogen. It was bubbled through concentrated sulfuric acid, passed over hot copper wire, and then over soda lime and phosphorus pentoxide.

The ethane, ethylene, and propylene used as solutes were of technical grade and, after preliminary treatment with sulfuric acid and 50 per cent potassium hydroxide, were subjected to repeated fractional condensation until their vapor pressures did not change on further fractionation.

Solubilities were determined at different temperatures by measurement of the lowering of the vapor pressure of the solvent in a saturated solution in the presence of excess solute. This method is based upon the assumption, which was experimentally verified, that the solution obeys Raoult's law and that the vapor pressure of the solute is negligible. The differential manometer, D in figure 1, registered the difference between the vapor pressure of the pure solvent, contained in E, and that of the solution in the solubility cell, G. The oxygen vapor-tension thermometer, P, gave both the temperature of the bath and the vapor pressure of the pure solvent. A rotating magnet, R, operated the bath stirrer, Q.

---

[1] This paper is an abstract of the thesis submitted by A. Lucile Cox to the Faculty of the Graduate School of Purdue University as partial fulfillment of the requirements for the degree of Doctor of Philosophy, August, 1948.

All readings were made with a Gaertner cathetometer reading to 0.05 mm. and were corrected for capillary depression of mercury in glass as well as the usual corrections for the thermal expansion of mercury. Readings were made after 3 hr. of intermittent stirring of the solution. Each reading was preceded by a period of 20 min. of stirring and then 15 min. standing with the stirrer held above the solution by a small permanent magnet, I. This procedure was necessary, since the cell stirrer conducted heat to the solution causing its vapor pressure to be slightly too high.

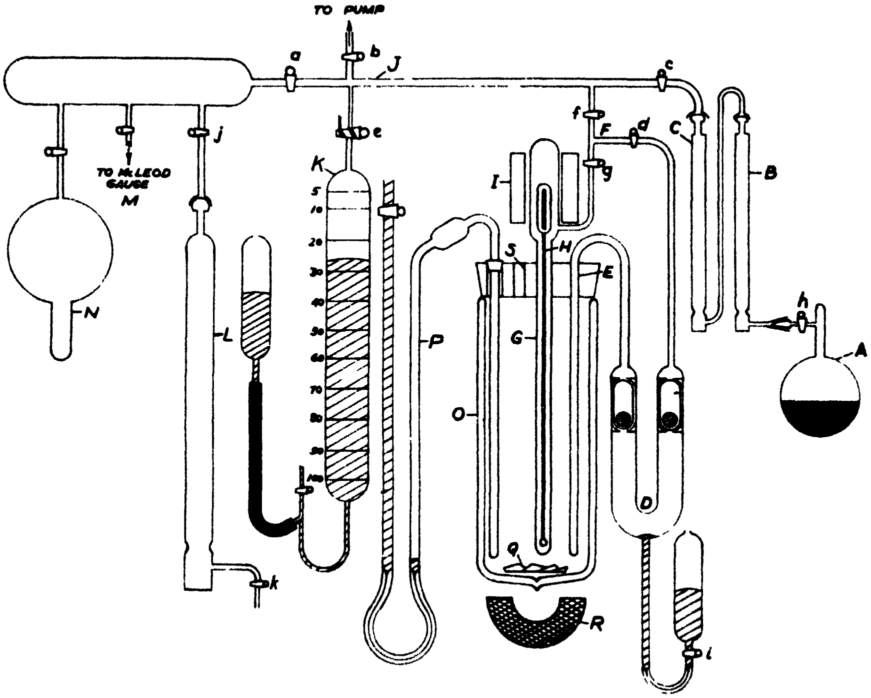

FIG. 1. Vapor pressure apparatus

The concentration of solute was sufficiently dilute so that the vapor pressure of the solvent would obey Raoult's law, but experiments were conducted to confirm this fact. For this part of the work, known but increasing amounts of the solvent were added to a known amount of the solute to produce unsaturated solutions of different concentrations. The amounts of solute and solvent were determined by pressure–volume measurements in a gasometer (K in figure 1). The known mole fraction was compared with that calculated from the lowering of the vapor pressure. The data tabulated in table 1 show that, within the limits of experimental error, the vapor pressure of the solvents obeyed Raoult's law.

RESULTS

In order to make a quantitative test of Hildebrand's equation for regular solutions, observed solubility data were used to calculate $(\Delta E/V)^{1/2}$, the internal pressure, which has also been called the "solubility parameter" by Hildebrand and denoted by δ, and such values were compared with values calculated from energies of vaporization data. Hildebrand's equation is

TABLE 1

Test of validity of Raoult's law for the solvent

SOLUTION	°K.	ΔP	N_2 (EXPERIMENTAL)	N_2 (CALCULATED)	$N_{2\,\text{exptl.}}/N_{2\,\text{calcd.}}$
		mm.			
Ethane in oxygen	85.96	10.93	0.0229	0.0224	1.03
	86.15	8.62	0.0177	0.0184	0.95
Ethylene in oxygen	90.10	7.35	0.00973	0.00969	1.003
	90.14	5.13	0.00679	0.00668	1.017
Ethane in nitrogen	77.24	4.72	0.0063	0.00667	0.95
	77.26	2.74	0.0037	0.00403	0.91

TABLE 2

Logarithm of ideal solubility, a_2, as mole fraction

°K.	ETHANE	ETHYLENE	PROPYLENE
70	−0.643	−0.813	−0.457
75	−0.504	−0.646	−0.307
80	−0.382	−0.502	−0.176
85	−0.275	−0.372	−0.061
90	−0.179	−0.258	
95	−0.0926	−0.155	
T_f, °K.	101.2*	103.7*	87.9*
ΔH_f, cal. per mole	668†	801‡	718§

* Reference 12.
† Reference 17.
‡ Reference 1.
§ Reference 14.

$$RT \ln (a_2/N_2) = V_2\left(\frac{N_1V_1}{N_1V_1 + N_2V_2}\right)^2 (\delta_2 - \delta_1)^2$$

where N_1 and N_2 are the mole fractions of solvent and solute, respectively, and V_1 and V_2 are the corresponding molal volumes. The activity, a_2, of the solute is given by the well-known equation $\ln a_2 = \Delta H/R\ (1/T_f - 1/T)$, in which ΔH is the heat of fusion of the solute and T_f is its melting point. The results of such a calculation are given in table 2 for the ideal solubilities of ethane, ethylene, and propylene together with the data required for the calculations. The calculated values of the "solubility parameters" of the solutes and solvents are tabulated in table 3. For these calculations the molal volumes were calculated from densities of the liquids (2) which, in some cases, had to be extrapolated over more than a 100° range. The energies of vaporization were obtained from various sources. For ethane, the expression $\Delta E = 4753 - 9.92T$ was obtained, using the ΔH values of Porter (13) at 184.5°K. and heat capacities of the liquid and vapor given by Wiebe (17) and by Kistiakowsky (10) and their coworkers. For ethylene, the expression $\Delta E = 4677 - 10.31T$ was derived from the extensive thermodynamic data of York and White (18). For propylene, the expression $\Delta E = 7011 - 15.43T$ was obtained from the ΔH value of Powell and Giauque (14), and the heat capacity data of Kistiakowsky and coworkers (11). For nitrogen and oxygen, the expressions $\Delta E = 1973 - 10.3T$, and $\Delta E = 2217 - 8.5T$ were used, obtained from heats of vaporization given in the literature (8).

TABLE 3

Molal volumes and values of $(\Delta E/V)^{1/2}$

GAS	MOLAL VOLUMES				SOLUBILITY PARAMETER			
	70°K.	75°K.	80°K	85°K.	70°K.	75°K.	80°K.	85°K.
Ethane	43.20	43.61	44.02	44.44	9.70	9.58	9.48	9.38
Ethylene	39.75	40.14	40.54	40.95	9.97	9.86	9.74	9.63
Propylene	52.25	52.67	53.09	53.51	10.65	10.52	10.42	10.31
Nitrogen	33.28	34.20	35.18	36.22	6.14	5.93	5.72	5.51
Oxygen	25.79	26.28	26.80	27.34	7.94	7.75	7.57	7.39

TABLE 4

Experimental solubilities and solubility parameters

SOLUTION	°K.	ΔP	LOG N_2	LOG a_2	$(\delta_2 - \delta_1)^2$	$(\delta_2 - \delta_1)$ (OBSERVED)	$(\delta_2 - \delta_1)$ (CALCULATED)
		mm.					
Ethane in oxygen	77.3	2.55	−1.784	−0.445	11.4	3.38	1.87
	80.0	6.14	−1.564	−0.382	10.8	3.28	1.91
	81.1	7.83	−1.526	−0.350	10.9	3.30	1.93
	85.3	24.80	−1.250	−0.264	10.4	3.22	1.99
Ethylene in oxygen. ..	81.1	1.17	−2.350	−0.471	17.4	4.17	2.19
	82.3	1.79	−2.230	−0.438	16.9	4.12	2.20
	86.9	6.13	−1.939	−0.326	16.2	4.03	2.27
	87.6	7.03	−1.903	−0.310	16.1	4.02	2.28
	89.9	9.95	−1.870	−0.257	16.7	4.08	2.31
Propylene in oxygen .	83.0	0.46	−2.85	−0.106	19.6	4.43	2.89
	83.3	0.88	−2.64	−0.105	18.3	4.28	2.90
	86.8	3.23	−2.21	−0.023	16.6	4.07	2.95
	87.4	3.70	−2.18	−0.010	16.6	4.07	2.95
Ethane in nitrogen	77.3	5.87	−2.11	−0.445	13.7	3.70	3.70
	78.1	6.62	−2.09	−0.426	13.8	3.72	3.72
	78.6	8.37	−2.04	−0.414	13.6	3.69	3.73

Representative results of the experimental work are given in table 4, together with a graph of the solubility of ethane in liquid oxygen and in nitrogen in figure 2. Our experimental results agree with those obtained by Tsin (16) for the solubility of ethylene in liquid oxygen, using an analytical method, but they differed greatly from his results for the solubility of propylene in liquid oxygen. He reported a value of 0.079 mole fraction at 83°K. In the present work it was noted that two liquid layers were present throughout the experiments with saturated solutions. Tsin's method for determining solubilities depends upon filtering a mixture of the saturated solution and excess solute, followed by analysis of the filtrate. The presence of two liquid layers would give erroneous results in such a procedure.

The quantity $(\delta_2 - \delta_1)$ was calculated from the solubility data by using Hildebrand's equation; such values are given and compared in the last two columns of table 4 with values based on thermodynamic data (see table 3). The results indicate that a solution of solid ethane in liquid nitrogen appears to be a "regular" solution. The agreement for the $(\delta_2 - \delta_1)$ values is better than one would expect.[2] However, the solubilities in liquid oxygen gave values larger than those calculated: namely, differences of 1.4 for ethane, 1.8 for ethylene, and 1.3 for propylene solutions. Such a value means that the solubilities are less than that given by Hildebrand's equation, a deviation which may be ascribed to strong intermolecular repulsions. Hildebrand's derivation assumed that such repulsions were negligible. Because the molar volume of liquid oxygen is appreciably less than that of liquid nitrogen, the molecules in liquid oxygen solution would be

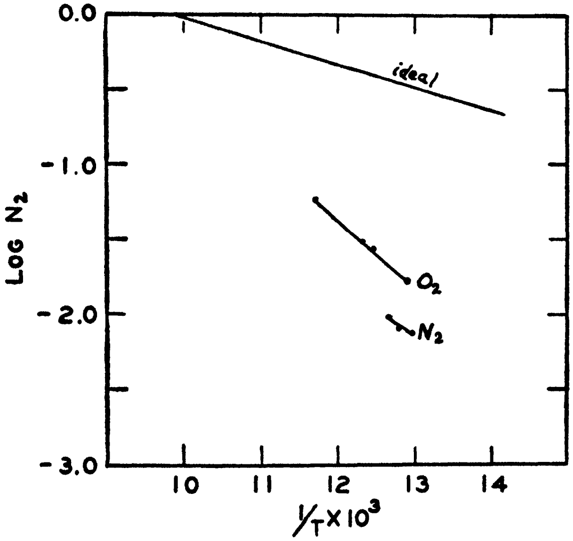

FIG. 2. Solubility of ethane in liquid nitrogen and oxygen

closer together and this might lead to stronger intermolecular repulsions. It has been observed (3) that the solubility of methane in liquid oxygen deviated more from ideal solubility than that of methane in liquid nitrogen.

---

[2] The solubility of ethylene was too small to measure at the boiling point of nitrogen. Propylene gave a lowering of 0.25 mm., which corresponds to 0.00033 mole fraction, a value too small to be reliable.

It also seems logical that larger deviations would be observed at low temperatures when the kinetic energy of the solvent molecules might be unable to overcome the intermolecular forces between the solute molecules. In fact, the data show such a trend of smaller deviations at higher temperatures. An extended theory of solubility ought to consider the effect of intermolecular forces.

SUMMARY

The solubility of solid ethane, ethylene, and propylene in liquid oxygen is less than that calculated from Hildebrand's equation for regular solutions. The solubility of solid ethane in liquid nitrogen agrees well with theory. An explanation is offered, based on the concept of intermolecular repulsions between the solute molecules.

REFERENCES

(1) EGAN, C. J., AND KEMP, J. D.: J. Am. Chem. Soc. **59**, 1264 (1937).
(2) EGLOFF, G.: *Physical Constants of Hydrocarbons*, Vol. I, Reinhold Publishing Corporation, New York (1939); *International Critical Tables*, Vol. III, pp. 20, 21, McGraw-Hill Book Company, Inc., New York (1928).
(3) FASTOVSKIĬ, V. G., AND KRESTINSKIĬ, YU. A.: J. Phys. Chem. (U.S.S.R.) **15**, 525 (1941).
(4) FEDEROVA, M. F.: J. Phys. Chem. (U.S.S.R.) **14**, 422 (1940).
(5) HILDEBRAND, J. H.: *Solubility of Nonelectrolytes*, 2nd edition, American Chemical Society Monograph Series, Reinhold Publishing Corporation, New York (1936).
(6) HUNTER, M. A.: J. Phys. Chem. **10**, 330 (1906).
(7) INGLIS, J. K. H.: Phil. Mag. [6] **11**, 656 (1906).
(8) *International Critical Tables*, Vol. V, p. 135. McGraw-Hill Book Company, Inc., New York (1929).
(9) ISHKIN, I. P., AND BURBO, P. Z.: J. Phys. Chem. (U.S.S.R.) **13**, 1337 (1939).
(10) KISTIAKOWSKY, G. B., AND RICE, W. W.: J. Chem. Phys. **7**, 281 (1939).
(11) KISTIAKOWSKY, G. B., RICE, W. W., LACHER, J. R., AND RANSOM, W. W.: J. Chem. Phys. **8**, 610, 970 (1940).
(12) MAASS, O., AND WRIGHT, C. H.: J. Am. Chem. Soc. **43**, 1098 (1921).
(13) PORTER, F.: J. Am. Chem. Soc. **48**, 2055 (1926).
(14) POWELL, T. M., AND GIAUQUE, W. F.: J. Am. Chem. Soc. **61**, 2366 (1939).
(15) STACKELBERG, M. v.: Z. physik. Chem. **A170**, 262 (1934).
(16) TSIN, M. N.: J. Phys. Chem. (U.S.S.R.) **14**, 418 (1940).
(17) WIEBE, R., HUBBARD, K. H., AND BREVOORT, M. J.: J. Am. Chem. Soc. **52**, 615 (1930).
(18) YORK, R., AND WHITE, E. F.: Trans. Am. Inst. Chem. Engrs. **40**, 227 (1944).

STUDIES IN THE IONIZATION OF MAGNESIUM, CALCIUM, AND BARIUM CLAYS[1]

B. CHATTERJEE AND C. E. MARSHALL

Department of Soils, Missouri Agricultural Experiment Station, Columbia, Missouri

Received August 15, 1949

INTRODUCTION

The development of clay membrane electrodes sensitive to divalent cations as well as to monovalent has made possible studies of the ionization of a variety of single cations from colloidal systems. The clay minerals are of especial interest from two points of view. Their importance in soil chemistry and hence in the uptake of nutrients by plants is evidenced by the fact that they contribute greatly to the chemical environment of plant roots. Further, they are of great inherent interest as examples of colloidal electrolytes, using the term in its most general sense. Experience has shown also that the study of their electrochemical properties is likely to be of importance in the identification of clay minerals.

The first direct evidence on the extent of ionization of calcium clays was afforded by some preliminary measurements by Marshall in 1942 (1), carried out on Putnam clay (beidellite). Calcium was found to give an extremely small fraction active, of the order of 0.01–0.04 as compared with 0.06–0.2 for alkali metal cations. The methods of determining calcium and magnesium were explored by Marshall and Ayers (3, 4) and Marshall and Eime (5), and some calcium hydroxide titration curves on Putnam clay were reported (3). Marshall and McLean examined the influence of clay concentration on calcium-ion activities for four clay minerals,—a montmorillonite (Wyoming bentonite), a beidellite (Putnam clay), an illite (Grundite), and a kaolinite (7). In a discussion of the ionization of calcium from soil colloids, data for Putnam clay, montmorillonite, and kaolinite were compared (2). A remarkable feature was shown by the titration curves of the clay acids with calcium hydroxide: namely, that over a considerable range from about 20 to 80 per cent neutralization additions of base caused no appreciable rise in the calcium-ion activity

The present investigation was designed to amplify this information by providing complete titration curve data for magnesium, calcium, and barium using several clay minerals.

EXPERIMENTAL METHODS

The general procedure has been described previously (4, 5, 6). The following notes cover special details used in the present series.

A. Magnesium-ion activities

Based on the work of Marshall and Eime (5), the electrodes chosen were of hydrogen bentonite (fraction < 200 mμ Wyoming bentonite). (It should be noted that in the work referred to, the legends attached to the graphs were wrongly assigned and should have been as follows: Fig. 1. Hydrogen Putnam; Fig. 2. Calcium Putnam; Fig. 3. Calcium bentonite; Fig. 4. Hydrogen bentonite.) The temperature of pretreatment was 410°C. Because of their favorable properties these membranes were used also for the measurements of calcium ion and barium-ion activity here reported. Experience in their use for magnesium ion showed that at low activities they gave better agreement with the Nernst equation than was found by Marshall and Eime. Down to 10^{-4} molal the results are comparable with those in the calcium and barium series. Below this they deteriorate by comparison, and at 10^{-5} molal errors in magnesium-ion activity up to 30 per cent may be present. The magnesium chloride solution used as standard inside the membrane tubes was generally 0.0009 a_{Mg}; one series was carried through using 0.0003 a_{Mg} as standard.

---

[1] Journal Series Paper No. 1160 from the Department of Soils, Missouri Agricultural Experiment Station.

Hydrogen-ion activities were measured in all systems with the glass electrode. The mobility ratio $U_{\mathrm{H}}/U_{\mathrm{Mg}}$ was determined by the simplified equation

$$E = \frac{RT}{2F} \ln \frac{2a^{\mathrm{I}}_{\mathrm{Mg}}}{U_{\mathrm{H}}/U_{\mathrm{Mg}} \cdot a^{\mathrm{II}}_{\mathrm{H}}}$$

which applies when $a^{\mathrm{I}}_{\mathrm{Mg}} \gg a^{\mathrm{II}}_{\mathrm{H}}$. It was found to be 1.10 for the 410°C. membranes used. Whenever necessary, the hydrogen-ion activity of the clay system was used in conjunction with the membrane mobility ratio, $U_{\mathrm{H}}/U_{\mathrm{Mg}}$, to calculate the actual magnesium-ion activity. Successive approximations were applied in the equation

$$E = \frac{RT}{F}\left[\frac{a^{\mathrm{I}}_{\mathrm{Mg}} - a^{\mathrm{II}}_{\mathrm{Mg}} - U_{\mathrm{H}}/U_{\mathrm{Mg}} \cdot a^{\mathrm{II}}_{\mathrm{H}}}{2(a^{\mathrm{I}}_{\mathrm{Mg}} - a^{\mathrm{II}}_{\mathrm{Mg}}) - U_{\mathrm{H}}/U_{\mathrm{Mg}} \cdot a^{\mathrm{II}}_{\mathrm{H}}} \ln \frac{2a^{\mathrm{I}}_{\mathrm{Mg}}}{2a^{\mathrm{II}}_{\mathrm{Mg}} + U_{\mathrm{H}}/U_{\mathrm{Mg}} \cdot a^{\mathrm{II}}_{\mathrm{H}}}\right]$$

in which $a^{\mathrm{I}}_{\mathrm{Mg}}$ refers to the standard solution inside the electrode tube, $a^{\mathrm{II}}_{\mathrm{Mg}}$ is the unknown magnesium-ion activity, and $a^{\mathrm{II}}_{\mathrm{H}}$ is the measured hydrogen-ion activity in the clay system. Similar procedures were used for calcium and barium wherever hydrogen-ion corrections were called for.

In measuring magnesium-ion activities in clay systems the electrodes were in contact with the clay suspension for ½–2 hr. before the saturated calomel electrodes were inserted and readings taken. Single clay systems were prepared for each point on the titration curve and each was read with two different clay membrane electrodes. The clay systems were agitated before and between readings.

B. Calcium-ion activities

The same type of electrodes were employed as for magnesium. The mobility ratio $U_{\mathrm{H}}/U_{\mathrm{Ca}}$ was determined. Most of the determinations were made with a set of electrodes for which $U_{\mathrm{H}}/U_{\mathrm{Ca}} = 1.10$. The known solutions of calcium chloride corresponded to $a^{\mathrm{I}}_{\mathrm{Ca}} = 0.0009$ and $a^{\mathrm{I}}_{\mathrm{Ca}} = 0.0003$. The calcium activities are probably accurate to 2 per cent down to 0.0001 and to 10 per cent at 0.00001. In other respects the determinations were similar to those carried out with magnesium.

C. Barium-ion activities

Since no previous work had been done with barium, it was necessary first to investigate membrane behavior with regard to this cation. Standard barium chloride solutions were prepared giving a series of barium-ion activities in which adjacent members differed by a factor of 3.000. The appropriate concentrations were calculated by the method previously described for calcium. The activity coefficients for barium chloride were taken from Dole.[2] Table 1 gives the activity and concentration data. Excellent behavior with regard to the Nernst equation was found in the range 0.01–0.0001 molal, the falling off at 0.0001 being very slight (table 2). At 0.00003 molal the uncertainty is no more than 4 per cent and at 0.00001 no more than 10 per cent.

TABLE 1

Barium-ion activity and barium chloride concentration data

A_{Ba}	MOLALITY OF $BaCl_2$	$BaCl_2 \cdot 2H_2O$ PER 1000 G. WATER
		grams
0.0001	0.000105	0.02565
0.0003	0.000320	0.07818
0.0009	0.001021	0.2494
0.0027	0.00385	0.9406
0.0081	0.01818	4.4416
0.0243	0.0940	22.9651

TABLE 2

Potentials obtained with 410°C. hydrogen bentonite membranes in standard barium chloride solutions

Values corrected to 25°C.; theoretical value for $a_1/a_2 = 3.00$ is 14.1 mv ; potentials are averages of six electrodes not differing by more than 0.5 mv.

BARIUM-ION ACTIVITY a_1	BARIUM-ION ACTIVITY a_2	MEMBRANE POTENTIAL
		mv.
0.0003	0.0001	13.9
0.0009	0.0003	14.1
0.0027	0.0009	14.1
0.0081	0.0027	14.1
0.0243	0.0081	9.5

In correcting for the presence of hydrogen ions the mean mobility ratio U_H/U_{Ba} for the 410°C. hydrogen bentonite membranes was determined to be 3.61. This is considerably higher than the U_H/U_{Mg} and U_H/U_{Ca} values and it consequently enhances the magnitude of the corrections. Using this same membrane material other mean mobility ratios determined gave the following values: U_{Mg}/U_{Ba} =

---

[2] Dole, M.: *Theoretical and Experimental Electrochemistry*, 1st edition, p. 273. McGraw-Hill Book Company, Inc., New York (1935).

0.82; $U_{Ca}/U_{Ba} = 1.14$; $U_K/U_{Ba} = 0.71$. In each case there was a small but measurable variation with concentration. The standard solutions used for measurements with clays corresponded to $a^{I}_{Ba} = 0.0009$ and $a^{I}_{Ba} = 0.0003$.

D. Preparation of clay systems

These were identical with the systems previously reported on (6). All were freshly electrodialyzed. Barium and calcium hydroxides were added in solution and 48 hr. was allowed for equilibrium. Magnesium was introduced as the oxide. Six days' contact with intermittent shaking was needed to attain equilibrium. Clay content and total volume were held constant in each series. The clays were as follows:

CLAY	FRACTION
	µ
Montmorillonite, Wyoming bentonite	<0.2
Beidellite, Putnam subsoil clay	<0.2
Illite, Grundite from Illinois	<2
Kaolinite, North Carolina	<2

The neutralization capacities for sodium hydroxide at the inflexion points of the pH titration curves were: montmorillonite, 100 milliequiv./100 g.; beidellite, 70 milliequiv./100 g.; illite, 27.5 milliequiv./100 g.; kaolinite, 3.00 milliequiv./100 g.

RESULTS

In order to make the data less voluminous and to facilitate comparisons, not all the titration curves are given. The graphs include only the data obtained at a single concentration of each clay (generally the highest). From them it is easy to see how the titration curves for magnesium, calcium, and barium are related for each clay mineral. In table 4 comparisons between the different clays at fixed stages of base saturation can readily be made.

pH titration curves

The points of inflexion are shifted to lower pH values as compared with the monovalent cases. Table 3 summarizes the results and indicates that very appreciable variations may be found, especially in the case of kaolinite. When titration curves for different concentrations of a single clay are compared, they agree well as regards the inflexion points. The curves often lie closer together than for monovalent cations, although in the case of the swelling clays there is an appreciable displacement with concentration below the inflexion point.

Cationic activities

As may be seen from figures 1, 2, 3, 4, and 5, the activities of divalent cations are extremely low below 80 per cent saturation with base. They then rise very rapidly in all cases through the point of equivalence. Over a considerable region there is virtual constancy in the cationic activity. At degrees of saturation below

40 per cent a considerable number of instances have been found in which the activity falls with increasing amounts of base. This is difficult to explain except on the assumption that, as the titration proceeds further, a redistribution of the calcium already present is facilitated. The effect has been noticed with all four clays and at pH values up to 5. It is not entirely due to an underestimation of the hydrogen-ion correction, since in some well-established cases the fall in calcium-ion activity with increasing amounts of base is greater than the maximum possible correction for hydrogen-ion activity.

TABLE 3

Inflexion point data for pH titration curves

CLAY	MAGNESIUM		CALCIUM		BARIUM	
	Milliequivalents of base	pH	Milliequivalents of base	pH	Milliequivalents of base	pH
Montmorillonite	101	6.4	97	7.9	97	8.35
Beidellite	68	6.6	60	6.6	62	6.75
Illite	33	6.2	30	7.75	31	8.25
Kaolinite	2.65	6.5	2.2	6.8	2.2	6.85

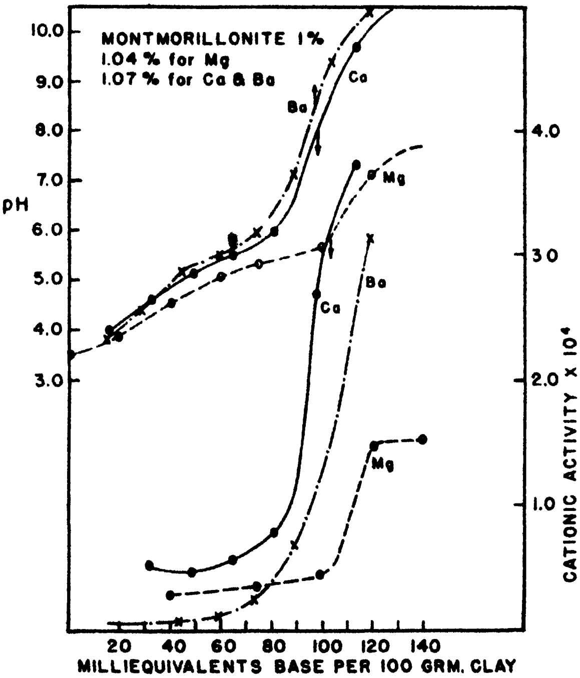

FIG. 1. pH (upper) and cationic activity curves (lower) for montmorillonite (Wyoming bentonite). Inflexions on pH curves indicated by arrows.

(*a*) *Montmorillonite:* Comparing the activity curves at about 1 per cent clay concentration (figure 1), it can be seen that the order of dissociation of the three cations up to 80 per cent saturation is Ba < Mg < Ca. At the inflexion point of the pH curves (i.e. ~ 100 milliequiv./100 g.) it has changed to Mg < Ba < Ca, this order persisting for still higher additions of base. The low ionization of magnesium is remarkable. Its persistence over a broad pH range indicates that the magnesium ion is actually responsible and not complex cations such as $MgOH^+$, although conceivably the latter may account for the flattening of the activity curve at pH values over 7.

(*b*) *Beidellite:* Only magnesium and calcium can be strictly compared at 5 per cent clay concentration (figure 2). Up to about 80 per cent equivalence, magnesium ionizes more than calcium; beyond this the order is reversed. It is very evident from the figures for barium, which can be compared with magnesium using 1.4 per cent clay (figure 3), that ionization is considerably less than for magnesium up to 80 per cent saturation. The curves cross at about 55 milliequiv. Calcium can be included in the comparison at 1.4 per cent clay concentration by rough interpolations from the 5 per cent and 1 per cent suspensions. It is found to be considerably more ionized than either magnesium or barium.

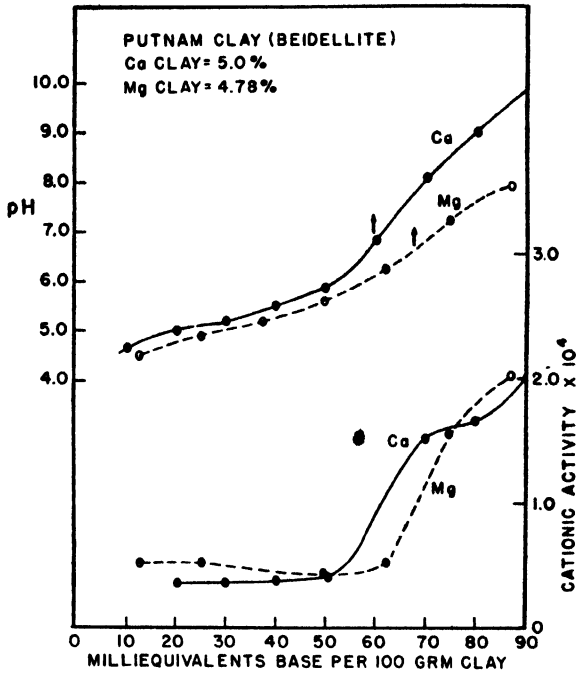

FIG. 2. pH (upper) and cationic activity curves (lower) for beidellite (Putnam clay) Inflexions on pH curves indicated by arrows.

(*c*) *Illite:* Comparable titration curves for magnesium, calcium, and barium were obtained for 4.86 per cent clay suspensions (figure 4). The order of degree of ionization is consistently Ba < Mg = Ca, with Mg and Ca closely alike up to 20 milliequiv. of base, the calcium thereafter gaining markedly relative to the magnesium. At high alkalinities the activity curve for barium finally crosses the

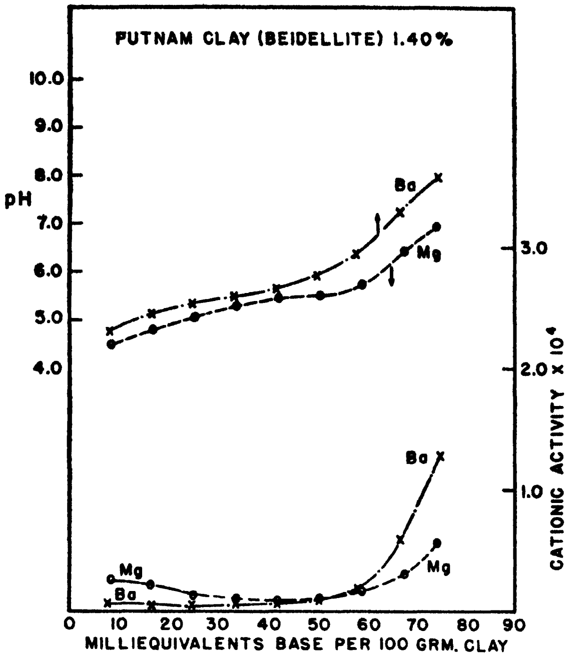

Fig. 3. pH (upper) and cationic activity curves (lower) for beidellite (Putnam clay). Inflexions on pH curves indicated by arrows.

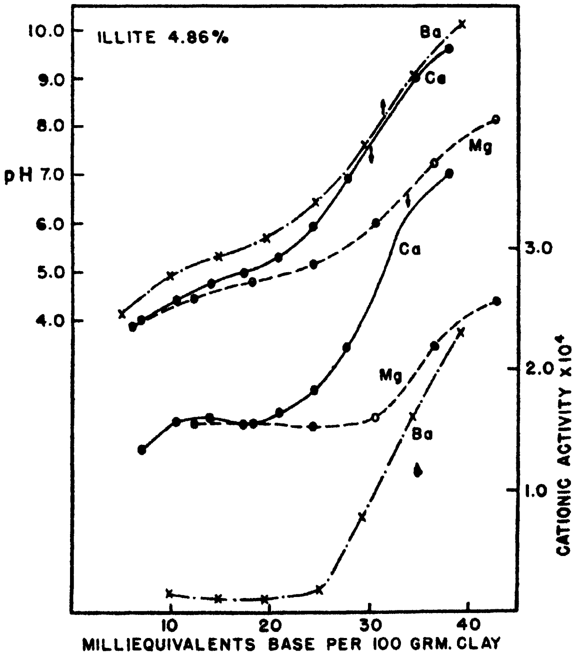

Fig. 4. pH (upper) and cationic activity curves (lower) for illite (Grundite). Inflexions on pH curves indicated by arrows.

curve for magnesium. The extremely low fraction active for barium indicates that stereochemical factors are probably playing a part. The barium ion is of about the same size as potassium and would, like the latter, fit closely into the Si_2O_3 sheets of the mica structure. It will be recalled that Page and Baver (8) found strong fixation effects for barium in the case of montmorillonite.

(*d*) *Kaolinite:* Nine per cent clay suspensions were compared (figure 5). The order of dissociation is Mg < Ca < Ba, the two latter being close together throughout. The fraction active for magnesium is considerably lower than that of the other cations, in spite of the fact that more magnesium is required to attain the inflexion on the pH curve.

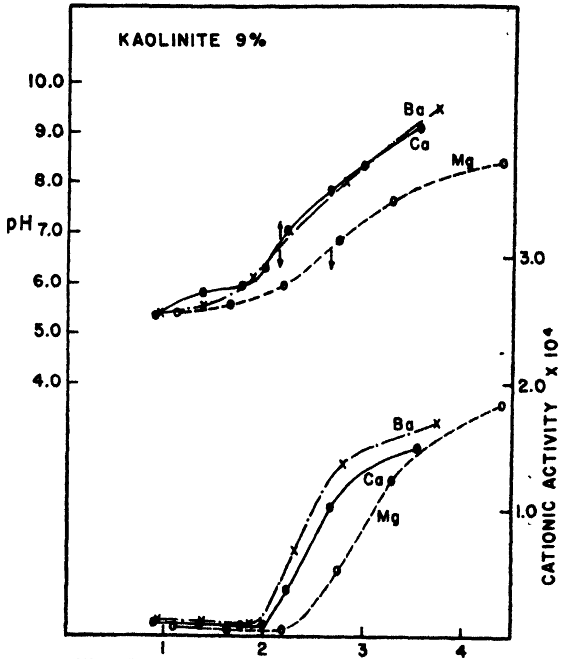

FIG. 5. pH (upper) and cationic activity curves (lower) for kaolinite. Inflexions on pH curves indicated by arrows.

(*e*) *Uses in identification:* A number of features shown by the activity curves could conceivably lead to electrochemical methods for the identification of clay minerals. At present we have insufficient evidence on different members of the clay groups here represented to make this certain. In the case of the illite clay, the very low activities found for barium as compared with calcium and magnesium might provide a diagnostic property. Kaolinite is the only clay here studied showing an invariable ionization order: Mg < Ca < Ba. The magnitude of the fraction active might also be used in certain cases, although it varies greatly with a given clay according to the extent of neutralization and to some extent also with concentration.

Comparison of the four clays

Table 4 shows the cationic fraction active at various stages of neutralization with base. Strictly speaking, valid comparisons of the ionization behavior of the different clays can only be made at comparable total cation concentrations. Thus 1.07 per cent montmorillonite and 1.4 per cent beidellite are reasonably comparable. The 4.86 per cent illite cannot be directly compared with either of the

TABLE 4

The cationic fraction active at different stages of neutralization of the acid clays

CLAY	EQUIVALENCE	CONCENTRATION	CATION	FRACTIONS ACTIVE AT THE FOLLOWING PERCENTAGES OF NEUTRALIZATION					
				20	40	60	80	100	120
		per cent							
Montmorillonite...	101	1.07	Mg	0.069	0.014	0.010	0.008	0.010	0.024
		2.14	Mg	0.180	0.042	0.019	0.011	0.013	0.021
Beidellite.......	68	1.40	Mg		0.007	0.003	0.003	0.006	
		4.78	Mg	0.016	0.008	0.005	0.003	0.006	0.009
Illite	33	4.86	Mg	0.125	0.050	0.034	0.025	0.022	0.025
		9.73	Mg	0.091	0.047	0.031	0.024	0.024	0.028
Kaolinite .	2.65	9.0	Mg		0.015	0.008	0.006	0.029	0.081
Montmorillonite. .	97	0.43	Ca	0.145	0.029	0.018	0.014	0.036	0.069
		1.07	Ca	0.066	0.023	0.016	0.017	0.052	0.065
Beidellite*... ...	62	9.0	Ca		0.005	0.004	0.004	0.007	0.010
		5.0	Ca		0.006	0.004	0.003	0.005	0.008
		1.0	Ca		0.020	0.013	0.007		0.025
Illite.	30	0.97	Ca	0.266	0.063	0.044	0.034	0.065	0.093
		4.86	Ca	0.208	0.056	0.036	0.031	0.042	0.040
Kaolinite....... ..	2.2	2.1	Ca		0.126	0.091	0.069	0.075	0.160
		9.0	Ca		0.028	0.015	0.011	0.030	0.082
Montmorillonite...	97	0.43	Ba	0.075	0.010	0.005	0.006	0.024	0.052
		1.07	Ba		0.004	0.003	0.008	0.022	0.043
Beidellite.. ..	62	1.40	Ba	0.006	0.002	0.002	0.003	0.006	0.022
		3.41	Ba	0.003	0.005	0.004	0.003	0.007	0.012
Illite.... ..	31	0.97	Ba	0.149	0.023	0.015	0.022	0.049	0.072
		4.86	Ba	0.146	0.005	0.003	0.004	0.014	0.023
Kaolinite.... ..	2.2	2.1	Ba		0.163	0.103	0.081	0.162	0.227
		9.0	Ba		0.034	0.031	0.014	0.053	0.090

* Results for Putnam clay (beidellite) with calcium hydroxide by A. D. Ayers.

concentrations of montmorillonite or beidellite. It would correspond to about 1.6 per cent montmorillonite, which is halfway between the 1.07 and 2.14 series. We can therefore interpolate the comparable figures for the fractions active from table 4. As regards kaolinite the best comparisons appear to be those between 9 per cent kaolinite and 0.97 per cent illite and between 9 per cent kaolinite and 0.43 per cent montmorillonite. We find in this way a consistent series: illite > montmorillonite > beidellite. Kaolinite varies in its relative position according to the nature of the cation and the extent of neutralization. It is somewhat less dissociated than illite or montmorillonite for calcium. With magnesium it is less dissociated than illite or montmorillonite up to 80 per cent saturation, but above this it is more dissociated. With barium it is generally more dissociated than illite or montmorillonite.

As compared with the order for monovalent cations (Na, K, NH_4), which consistently gave kaolinite > montmorillonite > beidellite > illite, we find the position of illite entirely shifted. It is the least ionized of the four clays with monovalent cations, and the most ionized with divalent (except that kaolinite surpasses it with barium).

The situation as regards kaolinite is complicated by the much lower inflexion points for calcium and barium than for sodium and potassium. If the equivalence for monovalent cations is chosen as the basis of comparison, then the fraction active with divalent cations is greatly raised over the figures given in table 4. The conclusion one then arrives at is that kaolinite, over a range from pH 6 onwards, is the most highly ionized of the four clays under consideration. This detailed examination shows that the preliminary data for kaolinite discussed in a previous paper (2) were at variance with our present series, in one respect. The calcium-ion activities measured at 1.2 and 1.7 milliequiv. Ca/100 g. kaolinite were considerably higher than we now find, thus making it appear that there was no region of very low fraction active. The more detailed curves now obtained show that for this clay also there is a considerable zone in which no increase in calcium activity with successive additions of the hydroxide can be detected. Within this range kaolinite is definitely less dissociated than illite or montmorillonite. Near the inflexion point of the pH curve the calcium-ion activity rises extremely rapidly, so that comparisons then lead to the order kaolinite > illite > montmorillonite.

GENERAL DISCUSSION

In all the activity curves here presented three distinct regions are readily apparent, and two others may reasonably be inferred. Over a broad zone in the middle range, varying somewhat in extent with the clay and with the cation, addition of a divalent base causes practically no increase in cationic activity. Then starting at 70–80 per cent neutralization we enter a region of very rapid increase of cationic activity, which extends through the point of equivalence and somewhat beyond it. With still further additions of base it seems that the slope of the activity curves decreases again. One could anticipate that eventually, with still larger additions of base, the curves would become steeper, after all acidic groups have reacted. From the positions of the activity curves at low degrees of saturation it can be seen that a part of the early additions of base must cause a definite increase in cationic activity before the region of constancy is reached. This zone is ill defined at present because of the difficulty of measuring minute activities of divalent cations in the presence of comparable or larger amounts of hydrogen. The difficulties are not nearly so great with the monovalent cations. In these cases also it was concluded that the first small additions of base caused proportionately greater increases in cationic activities than moderate additions (6).

It is therefore evident, as has already been pointed out (2), that the bonding energies of cations on clays cover a broad range in each case. The calculation of these energies and their comparison with one another will form the subject of a separate communication.

REFERENCES

(1) Marshall, C. E.: Soil Sci. Soc. Am. Proc. **7**, 182 (1942).
(2) Marshall, C. E.: Soil Sci. **65**, 57 (1948).
(3) Marshall, C. E., and Ayers, A. D.: Soil Sci. Soc. Am. Proc. **11**, 171 (1946).
(4) Marshall, C. E., and Ayers, A. D.: J. Am. Chem. Soc. **70**, 1297 (1948).
(5) Marshall, C. E., and Eime, L. O. J. Am. Chem. Soc. **70**, 1302 (1948).
(6) Marshall, C. E., and Krinbill, C. A.: J. Phys. Chem. **46**, 1077 (1942).
(7) Marshall, C. E., and McLean, E. O.: Soil Sci. Soc. Am. Proc. **12**, 172 (1947).
(8) Page, J. B., and Baver, L. D.: Soil Sci. Soc. Am. Proc. **4**, 150 (1939).

INFLUENCE OF CERTAIN SURFACE-ACTIVE COMPOUNDS UPON THE HYDROGEN PERMEABILITY OF A PALLADIUM CATHODE[1]

R. D. MISCH, R. B. BERNSTEIN, and H. J. McDONALD[2]

Department of Chemistry, Illinois Institute of Technology, Chicago, Illinois

Received August 24, 1949

Preliminary investigations were carried out to study the influence of organic additives upon the process of electrodeposition of hydrogen upon a palladium cathode. These experiments consisted of measurements of the rate of diffusion of hydrogen through the cathode in an electrolyte of 0.2 *N* sulfuric acid containing small concentrations of organic compounds. Previous work has dealt primarily with the properties of clean palladium surfaces. The dependence of the diffusion rate of hydrogen on the current density has been evaluated (2, 4, 5), and the potentials of palladium containing dissolved hydrogen have been reported (6, 8). The influence of surface-active agents, however, has only been considered indirectly from the viewpoint of inhibition of corrosion, where the production of hydrogen embrittlement in iron and steel has been studied (1, 7, 9).

---

[1] The work reported in this paper was done under Contract N7-onr-329, Task Order 1, with the Office of Naval Research, United States Navy Department.

[2] Present address: Stritch School of Medicine of Loyola University, Chicago, Illinois.

The rate of diffusion of hydrogen through a palladium cathode is a function of the steady-state concentration of hydrogen atoms at the surface. The existence of an equilibrium between atomic and molecular hydrogen at the surface is indicated by the observed dependence of the diffusion rate of cathodic hydrogen upon the square root of the current density (3). It might be expected that, at a given current density, the ratio of the concentration of atomic hydrogen to that of molecular hydrogen could be altered in the presence of a new molecular species. For example, if a surface film is found, it may be considered to present a barrier to the escape of molecular hydrogen, in which case an increased concentration of hydrogen atoms might be maintained at the interface with a resultant increase in the ratio of diffused to evolved hydrogen. The presence of a film should also be expected to increase the potential required to maintain a given rate of hydrogen deposition. Measurements of the fractional transmission of cathodic hydrogen as a function of the nature and thickness of the surface films, together with data on the characteristics of the overvoltage current, should prove helpful in elucidating the theory of overvoltage.

Several experiments were performed in this study which demonstrate the rather marked influence of certain organic additives upon the quantity of hydrogen which diffused through a hollow palladium cathode of 7.6 cm.^{2} area at a given current density. The cathode was connected to a glass apparatus for measuring the volume of hydrogen transmitted at 1 atm. during a suitable time interval. A constant volume of 400 ml. of 0.2 N sulfuric acid was employed for all the measurements, which were made at 26°C.

The behavior of the palladium was first compared with the data of other investigators by obtaining the dependence of transmitted hydrogen on current density. The resulting curve provided a standard by which the effect of additions of surface-active materials to the solution could be easily judged. The percentage transmission (fraction of total hydrogen) was found to decrease rapidly with current density at low currents and then varied slowly in the range 10–25 ma./cm.^{2} Most of the data were obtained at 13 ma./cm.^{2} Sufficient time was always allowed for a constant value of the diffusion rate to be reached. Observations of the percentage transmission were reproducible to a precision of $\pm$ 1 per cent.

To investigate a variety of conditions, a number of salts as well as organic compounds were added to the electrolyte. Copper and mercuric ions, which plate out on the surface, were found to produce a severe decrease in the transmission. Relatively inactive compounds such as ethanol, gelatin, and *n*-butylamine were also added. Ethanol, in concentrations up to 0.4 M, produced no measurable effect; it was therefore used as a solvent for certain other additives to the solution. Gelatin (0.1 per cent) produced a slight decrease in percentage transmission, while concentrations of *n*-butylamine up to 0.02 M were found to cause a larger decrease in the transmission, which changed from 88 per cent to 78 per cent with increasing concentration.

The most significant effects were obtained with capillary-active compounds, which included thiourea, diisopropylthiourea, butyl iodide, styrene, and benzyl sulfide. A few results were also obtained with carbon disulfide and paraffin which showed qualitative agreement with the other data.

The behavior of thiourea and benzyl sulfide was of special interest, since these compounds differ considerably in polar character and solubility. Figure 1 shows the variation of the observed percentage transmission as a function of the concentration of the added material. The general features of the curve for benzyl sulfide were found to be characteristic of the other nonpolar, slightly soluble organic compounds. Butyl iodide, styrene, and diisopropylthiourea were all found to produce an initial increase in transmission at concentrations below about 10^{-5} M and a subsequent decrease at higher concentrations. It is suggested that the decrease at higher concentrations is related to an increase in adsorbed film thickness, although a detailed interpretation cannot be made without a knowledge of the adsorption isotherms for these compounds. This point was further investigated by experiments in which monolayer films of stearic acid were directly deposited in succession upon the dry electrode before electrolysis.

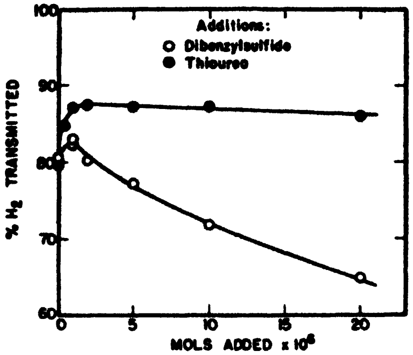

FIG. 1

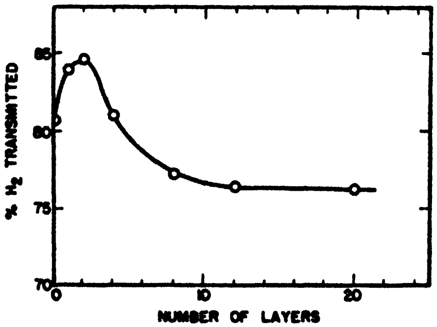

FIG. 2

FIG. 1. Percentage transmission as a function of the concentration of additive
FIG. 2. Percentage transmission as a function of the number of layers of stearic acid

Figure 2 shows the dependence of the transmission upon the number of layers placed on the surface. At the conclusion of the experiment, the electrolyte was discarded and a solution of 0.2 N sulfuric acid which had been previously saturated with stearic acid was substituted. The transmission then observed was found to agree with the values obtained at nominal thicknesses above ten layers, which may thus be the upper limit on the number of layers of stearic acid in equilibrium with the aqueous solution.

By analogy with the results for stearic acid, a possible interpretation for the data obtained with benzyl sulfide is provided. The initial increase may be attributed to the presence of one or two layers adsorbed upon the electrode, with further layers producing a decrease in the transmission.

The results for thiourea would suggest a monolayer type of adsorption isotherm. The percentage transmission increases to a constant value, even up to concentrations as high as 0.1 per cent (not shown on figure 1). The structure of thiourea suggests the possible formation of an oriented monolayer with the polar amine groups directed out from the electrode.

The changes in the percentage of diffused hydrogen are thus shown to be a function of the nature and concentration of organic additives in the solution. These changes are related to the surface concentration of atomic hydrogen, and it is suggested that the presence of surface films is responsible for the observed effects.

SUMMARY

Experiments are reported in which the presence of various organic additives is shown to influence the process of hydrogen discharge on a palladium cathode. At constant current density, the steady-state hydrogen diffusion rate through a hollow palladium cathode was found to be a function of the nature and concentration of the additive.

Measurements were made with current densities of 15 ma./cm.^{2}, employing an electrolyte of 0.2 N sulfuric acid. The ratio of diffused to evolved hydrogen was observed to increase when additions of thiourea, diisopropylthiourea, butyl iodide, styrene, and benzyl sulfide were made in concentrations up to about 10^{-4} M. Further increases in the concentrations of additives, with the exception of thiourea, produced a large decrease in the fraction diffused. Successive layers of stearic acid gave similar results when deposited directly upon the palladium before electrolyzing.

REFERENCES

(1) Bablick, H.: Sheet Metal Inds. **24**, 307 (1947).
(2) Barrer, R. M.: Trans. Faraday Soc. **36**, 1235 (1940).
(3) Barrer, R. M.: *Diffusion in and through Solids*. The Macmillan Company, New York (1941).
(4) Bodenstein, M.: Z. Elektrochem. **28**, 517 (1922).
(5) Borelius, G., and Lindblom, S.: Ann. Physik **82**, 201 (1927).
(6) Frumkin, A.: Acta Physicochim. U.R.S.S. **19**, 1 (1944).
(7) Morris, T.: J. Soc. Chem. Ind. (London) **54**, 7 (1935).
(8) Stout, H. P.: Faraday Society Discussions **1**, 107 (1947).
(9) Zapffe, C. A., and Haslam, M. E.: Wire and Wire Products **23**, 933 (1948).

SPECIFIC ADSORPTION ISOTHERMS OF THIOCYANATE AND HYDROGEN IONS AT THE FREE SURFACE OF AQUEOUS SOLUTIONS[1]

PHILIP B. LORENZ[2]

Mallinckrodt Chemical Laboratory, Harvard University, Cambridge, Massachusetts

Received August 19, 1949

INTRODUCTION

Although most inorganic electrolytes increase the surface tension of pure solvents in a roughly linear manner, the slopes of the curves for different electrolytes are quite different, and many acids even lower the surface tension of water. To a certain extent the individuality is an additive function of the ion species present. This can be seen in table 1 by comparing the differences between any two rows or columns. Magnesium sulfate is an exception, to be sure, and the surface tension of solutions of organic electrolytes is not at all additive. Nevertheless, within certain limits additivity is a fair approximation, and it undoubtedly reflects the different adsorption tendencies of the various ions. If adequate data were available, somewhat more regularity might appear in the actual adsorptions of electrolytes at the free surface.

The influence of different ions on surface tension does not seem to be correlated with the size of ions in solution as derived from electric mobility or the Debye–Hückel treatment of activity. Let us suppose that the adsorption is the sum of two effects: (*1*) the electrostatic (negative) adsorption of ions as charged spheres near the boundary of a dielectric medium; and (*2*) the specific adsorption of ions as chemical species. Probably in the case of those electrolytes which cause the greatest increase in surface tension within a given valence type, such as the alkali hydroxides and chlorides in table 1, there is little specific adsorption of either ion. The electrostatic adsorption has been estimated theoretically for low concentrations (18) and is not very dependent on ionic size. Therefore, neglecting the effect of ionic size altogether, the specific adsorption of an electrolyte can be obtained approximately by comparing its total adsorption with that of a nearly ideal electrolyte whose adsorption is largely electrostatic.

If we assume potassium chloride to be such an electrolyte, the electrostatic adsorption can be canceled by subtracting the adsorption of potassium chloride from that of the electrolyte whose specific adsorption is sought. If one of the ions of the latter is potassium or chloride, whatever small contribution is made by this common ion will be canceled as well (insofar as the ions make separate contributions), and the result may be regarded as an estimate of the specific adsorption of the other ion.

---

[1] This paper is based on a thesis submitted by Philip B. Lorenz to the Faculty of Arts and Sciences of Harvard University in partial fulfillment of the requirements for the degree of Doctor of Philosophy, June, 1949.

[2] Present address: Petroleum Experiment Station, U. S Bureau of Mines, Bartlesville, Oklahoma.

THE SPECIFIC ADSORPTION OF THIOCYANATE ION

The only suitable electrolyte for which sufficiently accurate and comprehensive surface-tension data have been reported is potassium thiocyanate. Table 2 gives its adsorption, together with that of potassium chloride, as calculated from the Gibbs equation, which may be written in the form:

TABLE 1

Increase in surface tension (dynes per centimeter) on dissolving 1 mole of electrolyte in 1000 g. of water, at 20–30°C.

	SO_4^{--}	OH^-	Cl^-	NO_3^-	ClO_4^-
H	0.7 (19)		−0.1 (3)	−0.8 (20)	−1.5 (17)
Na	2.7 (20)	1.9 (20)	1.7 (14)	1.3 (10)	0.4 (4)
K	2.9 (12)	1.8 (20)	1.7 (12)	1.2 (10)	
Mg	2.2 (15)		3.3 (10)	2.6 (10)	

TABLE 2

The specific adsorption of thiocyanate ion at the free surface of aqueous solutions at 25°C.

m	KCNS			KCl			$RT(\Gamma_{KCNS} - \Gamma_{KCl})$
	$\frac{d\sigma}{dm}$ (13)	$\frac{d \log \gamma_\pm}{d \log m}$ (9)	$-RT\Gamma$	$\frac{d\sigma}{dm}$ (12)	$\frac{d \log \gamma_\pm}{d \log m}$ (8)	$-RT\Gamma$	
0.05	0.60	(−0.078)	0.016	2.06	−0.078	0.056	0.040
0.10	0.54	−0.087	0.030	1.79	−0.118	0.101	0.071
0.20	0.40	−0.112	0.045	1.70	−0.128	0.195	0.15
0.50	0.33	−0.114	0.093	1.48	−0.130	0.425	0.33
1.00	0.48	−0.102	0.27	1.56	−0.113	0.88	0.61
2.00	0.65	−0.093	0.72	1.77	−0.065	1.90	1.18

$$-RT\Gamma = \frac{m\, d\sigma/dm}{\nu(1 + d \log \gamma_\pm / d \log m)}$$

where Γ = salt adsorption, in moles per square centimeter, with reference to the surface for which $\Gamma_{H_2O} = 0$

m = molal concentration

σ = surface tension, dynes per centimeter

ν = number of gram-ions per mole and

$\gamma_\pm$ = mean ionic activity coefficient.

Calculations were not carried below 0.05 *M* because of the lack of activity data and the increasing uncertainty of the slopes of the surface-tension curves. The last column of table 2 is plotted in figure 1. The specific adsorption isotherm is seen to be slightly convex upward in the range 0.05 *M* to 2.00 *M*.

THE SPECIFIC ADSORPTION OF HYDROGEN ION

Of all inorganic cations, only hydrogen ion exhibits pronounced specific adsorption at the free surface. New measurements of the surface tension of hydrochloric acid solutions are reported below and compared with potassium chloride for the estimation of the specific adsorption isotherm of hydrogen ion.

Previous measurements of the surface tension of hydrochloric acid (3, 11, 20) are not in perfect agreement and do not extend to low enough concentrations for satisfactory calculation of adsorption in the region where molecular hydrogen chloride is negligible. The present measurements extend the range of values down to 0.02 *M*. Secondary effects interfere at lower concentrations.

EXPERIMENTAL

The method and apparatus[3] of Jones and Ray (12) were used. Samples of hydrochloric acid for measurement were prepared from stock solution by weight dilution with conductivity water, and freed from surface-active materials by successive fractional transfers through siphons or taps. During preparation the sample came into contact only with glassware which had been cleaned with boiling nitric acid, steamed, and stored in an electric oven at 150°C. Stock solutions were prepared from reagent-grade acid. The concentration was evaluated azeotropically (5) and also by comparing density measurements with established density values (2). All measurements were made at 25.00°C. In each experiment, surface tension relative to that of water was calculated from weight according to formula 11 of Jones and Ray (12), and from direct observation of capillary height. There is an average discrepancy of 0.00013 between the two calculations. This is about equal to the average probable error of the measurements, and should be a reasonable estimate of their accuracy.

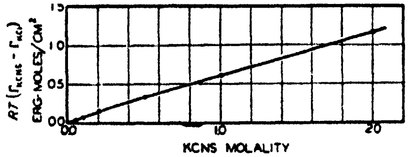

FIG. 1. Specific adsorption isotherm of thiocyanate ion at the free surface of aqueous solutions at 25°C.

RESULTS

The results are summarized in table 3 and plotted in figure 2. At the higher concentrations they are in fair agreement with those of Belton (3). Below about 0.3 *M* the surface tension of hydrochloric acid solutions exceeds that of water. This is contrary to what has usually been assumed, although it might have been anticipated from consideration of the fact that hydrochloric acid is approaching

---

[3] The quartz capillarimeter and thermostat used in this work were generously provided by the late Professor Jones.

TABLE 3

Surface tension of hydrochloric acid solutions at 25°C., relative to that of water

Averaged over restricted concentration ranges: n = number of data in average; P.E. = $0.67\sqrt{\Sigma(\text{deviations})^2/(n-1)}$

MOLAL CONCENTRATION	DENSITY	RELATIVE SURFACE TENSION					
		From height	n	P.E. $\times 10^5$	From weight	n	P.E. $\times 10^5$
	g./cc.						
0.00072–0.00080		0.99973	6	16	0.99968	6	14
0.00084–0.00096		0.99980	6	8	0.99978	4	8
0.00121–0.00123		0.99990	4	12	0.99986	4	9
0.00247–0.00269		1.00006	3	15	0.99987	3	7
0.00435–0.00449		0.99996	6	4	0.99978	5	9
0.01000–0.01006		0.99986	5	8	0.99992	5	7
0.02189–0.02244		0.99999	9	9	0.99997	8	9
0.0299 –0.0301		1.00000	4	4	0.99997	4	8
0.049 –0.05537		1.00005	3	2	1.00000	2	10
0.1022	0.998914	1.00034	1				
0.1559	0.999883	1.00012	1				
0.2837	1.002145	1.00001	1				
0.5146	1.006042	0.99935	1		0.99932	1	
0.9505	1.013504	0.99844	1		0.99865	1	
1.875	1.028366	0.99702	1		0.99717	1	

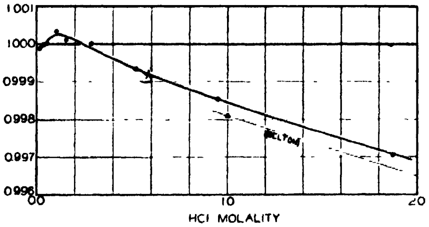

FIG. 2

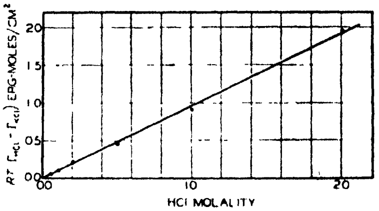

FIG. 3

FIG. 2. Surface tension of hydrochloric acid solutions at 25°C. relative to that of water

FIG. 3. Specific adsorption isotherm of hydrogen ion at the free surface of aqueous solutions at 25°C.

TABLE 4

The specific adsorption of hydrogen ion at the free surface of aqueous solutions at 25°C.

HCl				
m	$\frac{d\sigma}{dm}$	$\frac{d \log \gamma_\pm}{d \log m}$	$RT\Gamma$	$RT(\Gamma_{HCl} - \Gamma_{KCl})$
0.05	+0.4	−0.061	−0.01	0.05
0.10	0	−0.058	0	0.1
0.20	−0.2	−0.041	+0.02	0.22
0.50	−0.14	+0.042	+0.034	0.46
1.00	−0.115	+0.262	+0.045	0.92
2.00	−0.11	+0.605	+0.07	1.97

the behavior of an ideal electrolyte. Below 0.03 *M* the data show a pronounced "Jones–Ray effect" (*cf.* 16).

The specific adsorption of hydrogen ion is calculated in table 4 and plotted in figure 3. The adsorption isotherm is nearly a straight line from 0.05 *M* to 2 *M*. This result is, of course, dependent on the choice of potassium chloride as a standard.

DISCUSSION

To a certain extent the tendency for large hydrophobic ions like thiocyanate to appear at the surface can be correlated with crystallographic size and low energy of solution (*cf.* 6). The correlation is far from perfect, but hydrogen ion is so far out of line as to lend weight to the suggestion (1) that the mechanism involves oriented water molecules and proton bonds. Although the difference between the specific adsorption isotherms of hydrogen ion and thiocyanate ion is small, the latter has more of the character of typically capillary-active substances even though its specific adsorption is much weaker than that of hydrogen ion. This also supports the theory that there is a unique mechanism for specific adsorption of hydrogen ion.

The limiting law for electrostatic adsorption can be written

$$A_e = -a_e c \log c$$

If the specific adsorption obeyed the classical isotherm

$$A_s = a_s c^{1/n}$$

down to low concentrations, it is evident that $\lim_{c \to 0} A_s/A_e$ would vanish only if $n \leqslant 1$, but would approach infinite values if $n > 1$. In the latter case the specific adsorption would dominate even at low concentrations and the electrical limiting law would not be approached. Probably all adsorption isotherms must become linear ($n = 1$) at infinite dilution, but according to the above data the specific adsorption isotherm of hydrogen ion is linear up to higher concentrations than that of thiocyanate ion. The surface tension of acids can be expected to approach ideal electrolytic behavior at low concentrations more rapidly than the surface tension of specifically adsorbed salts.

SUMMARY

1. For many inorganic electrolytes the surface tension of molar aqueous solutions is an additive function of the ion species.
2. Assuming that the adsorption of potassium chloride at the free surface is largely electrostatic, it is compared with that of potassium thiocyanate to estimate the "specific adsorption isotherm" of thiocyanate ion.
3. Measurements are reported of the surface tension of hydrochloric acid solutions from 10^{-3} *M* to 2 *M*, with a probable accuracy of about 0.01 per cent. Below 0.3 *M* the surface tension exceeds that of pure water.
4. The specific adsorption isotherm of hydrogen ion at the free surface is calculated and found to be nearly a straight line.

The author is grateful to Dr. A. S. Coolidge for his encouragement and guidance in this work.

REFERENCES

(1) **Ariyama, K.**: Bull. Chem. Soc. Japan **12**, 109 (1937).
(2) **Beattie, J. A.**: *International Critical Tables*, Vol. III, p. 54. McGraw-Hill Book Company, Inc., New York (1928).
(3) **Belton, J. W.**: Trans. Faraday Soc. **31**, 1413 (1935).
(4) **Belton, J. W.**: Trans. Faraday Soc. **32**, 1717 (1936).
(5) **Foulk, C. W., and Hollingsworth, M.**: J. Am. Chem. Soc. **45**, 1220 (1923).
(6) **Frumkin, A., Reichstein, S., and Kulvarskaya, R.**: Kolloid-Z. **40**, 9 (1926).
(7) **Harned, H. S., and Owen, B. B.**: *The Physical Chemistry of Electrolytic Solutions*, p. 547. Reinhold Publishing Corporation, New York (1943).
(8) Reference 7, p. 558.
(9) Reference 7, p. 563.
(10) **Herz, W., and Knaebel, E.**: Z. physik. Chem. **A131**, 389 (1928).
(11) **Howell, O. R.**: J. Chem. Soc. **1927**, 2309.
(12) **Jones, G., and Ray, W. A.**: J. Am. Chem. Soc. **59**, 187 (1937).
(13) **Jones, G., and Ray, W. A.**: J. Am. Chem. Soc. **63**, 288 (1941).
(14) **Jones, G., and Ray, W. A.**: J. Am. Chem. Soc. **63**, 3262 (1941).
(15) **Jones, G., and Ray, W. A.**: J. Am. Chem. Soc. **64**, 2744 (1942).
(16) **Langmuir, I.**: Science **88**, 430 (1938).
(17) **Neros, C. A., and Eversole, W. G.**: J. Phys. Chem. **45**, 388 (1941).
(18) **Onsager, L., and Samaras, N. N. T.**: J. Chem. Phys. **2**, 528 (1934).
(19) **Suggitt, R. M., Aziz, P. M., and Wetmore, F. E. W.**: J. Am. Chem. Soc. **71**, 676 (1949).
(20) **Young, T. F., and Harkins, W. D.**: *International Critical Tables*, Vol. II, p. 464. McGraw-Hill Book Company, Inc., New York (1928).

THE FLUORIDE ION AS A BASE IN HIGH-TEMPERATURE REACTIONS WITH POLYPHOSPHATES[1]

O. F. HILL[2, 3] AND L. F. AUDRIETH

Noyes Laboratory of Chemistry, University of Illinois, Urbana, Illinois

Received August 17, 1949

Reactions involving "molecular dehydration" of the mono- and di-hydrogen phosphates at higher temperatures may be regarded as examples of polyanionic aggregation, the extent of such aggregation being dependent upon the potential acidity of the starting materials and the temperature. Thermal methods for the preparation of the poly- and meta-phosphates are usually represented by equations 1, 2, and 3. Since these equations do not, however, reveal their true nature as acid–base reactions they have been represented (in parentheses) as reactions

---

[1] Presented at the 114th Meeting of the American Chemical Society, which was held in Portland, Oregon, September, 1948.

[2] Abstracted from a thesis submitted by O. F. Hill to the Faculty of the Graduate School of the University of Illinois in partial fulfillment of the requirements for the Ph.D. degree, January, 1948.

[3] Victor Chemical Works Research Fellow at the University of Illinois, 1946–48.

	RATIO H^+/PO_4^{-3}
1. $2HPO_4^{-2} \rightarrow P_2O_7^{-4} + H_2O$ $(2H^+ + 2PO_4^{-3} \rightarrow P_2O_7^{-4} + H_2O)$	1.00
2. $H_2PO_4^- + 2HPO_4^{-2} \rightarrow P_3O_{10}^{-5} + 2H_2O$ $(4H^+ + 3PO_4^{-3} \rightarrow P_3O_{10}^{-5} + 2H_2O)$	1.33
3. $XH_2PO_4^- \rightarrow XH_2O + (PO_3)^-$ $(2H^+ + PO_4^{-3} \rightarrow PO_3^- + H_2O)$	2.00

$X = 3$ and X.

involving increasingly greater aggregation as the potentially available proton concentration is increased. The hydrogen ion:phosphate ion ratio is given in each case. These reactions are therefore similar to the better known examples of polyanionic aggregation which chromates, tungstates, molybdates, and vanadates undergo as the hydrogen-ion concentration is increased but differ in that condensation polymerization of the phosphate ion does not take place in aqueous solution. Structurally, conversion of the orthophosphates into poly- and metaphosphates involves the joining together of phosphate tetrahedra by removal of oxide ions to form either chain or cyclic structures. The polyanionic species which are thus formed become increasingly more "acidic" in character as their composition approaches that of phosphorus(V) oxide.

Of particular interest is the formation of the polymetaphosphate when the crystalline sodium metaphosphates (or dihydrogen phosphates) are fused and cooled rapidly to give the glassy product known as Graham's Salt and incorrectly designated as hexametaphosphate. This particular product dissolves readily in water, yielding solutions containing particles with an average ionic molecular weight of 10,000–20,000. The depolymerization of such polymetaphosphate aggregates takes place in aqueous solution by the process known as reversion. In these instances the larger ionic species undergo hydration with the eventual formation of the orthophosphate ion. Obviously this reversion reaction must involve rupture of the P—O—P linkages which hold together the phosphate tetrahedra.

Such depolymerization reactions also take place in ansolvous systems at higher temperatures. The metaphosphate bead test is based upon the fact that metallic oxides dissolve in fused sodium metaphosphate to form ortho- and/or pyro-phosphates (4, 14). While simple equations are usually written to represent these processes, it is evident that the polymetaphosphate in the fused state undergoes depolymerization. These reactions represent from our point of view examples of high-temperature acid–base reactions in which a polyanionic acid is converted to the more basic species represented by the pyrophosphate and phosphate ions, much as the polychromates undergo conversion to smaller ionic particles with increase in pH.

While we have preferred to interpret such reactions from the Lewis[4] point of view, it may be well in this connection to call attention to the alternative proposal first presented by Lux (13) and later developed by Flood and coworkers (6, 7, 8). Lux defines acid–base relationships in high-temperature oxide systems as involving essentially transfer of oxide ions, much as the Brønsted concept places emphasis on proton transfer.

---

[4] The Lewis concept in a very general way defines bases as electron-pair donors and acids as electron-pair acceptors. Neutralization involves formation of a coördinate coval-

$$\text{Lux–Flood:}\quad B \rightleftharpoons A + O^{-2}$$
$$\text{Brønsted:}\quad A \rightleftharpoons B + H^{+}$$

Acids in such systems may be defined as oxide-ion acceptors and bases as potential oxide-ion donors. The application of this concept to polyanionic complexes is outlined by the statement, "The transition of a polyacid to its corresponding base consists in a breaking of an oxygen bridge and the simultaneous binding of an oxygen atom. . . . The acid-base reaction is thus connected with a disintegration of the macro-molecular structure." (8)

In our opinion, however, the Lux–Flood concept is entirely too limited, and is in fact merely a specialized case of the more generalized electronic theory, as extended to high-temperature reactions by Audrieth and coworkers (2). Reference has already been made to the fact that metaphosphate, acting as an acid in fused systems, undergoes depolymerization when allowed to react with a metallic oxide, that is, a compound capable of furnishing the base, the oxide ion. Several other examples of such reactions involving anionic bases may be cited.

$$(PO_3^-)_x + XO^{-2} \rightleftharpoons XPO_4^{-3}$$

Thus, polymetaphosphates can be depolymerized to orthophosphates by heating with hydroxides and/or carbonates (15). Sodium monothiophosphate (17) is obtained by fusion of equimolecular quantities of sodium metaphosphate with sodium sulfide. From the Lewis point of view, the oxide, hydroxide, carbonate, and sulfide ions are bases or electron-pair donors.[5] No previous effort had been made, however, to extend these high-temperature reactions to other typical anionic bases, such as the fluoride ion. The experimental results which are presented below demonstrate that fusion of sodium polymetaphosphates with sodium fluoride leads to depolymerization of the metaphosphate aggregate with the formation of sodium monofluophosphate.

$$(PO_3)_x^- + XF^- \rightleftharpoons XPO_3F^{-2}$$

The experimental accomplishment of this objective constitutes not only an unquestionable proof of the usefulness of the generalized electronic concept of acids and bases as

---

ent bond between the reacting species. As examples of typical bases there may be cited molecules such as ammonia and the amines and ions such as oxide, sulfide, and fluoride. Typical molecular acids include CO_2, SO_3, SiO_2, BF_3, and $AlCl_3$. Ionic acids include the proton and metallic ions, in general. See reference 12 for an extended exposition of the Lewis concept.

[5] Reactions of acids with CO_3^{--} and OH^- may also be regarded as displacement reactions in which the weaker acids, CO_2 and H_2O, are displaced by a stronger acid in accordance with simplified equations:

$$PO_3^- + CO_3^{--} \rightleftharpoons PO_4^{---} + CO_2$$
$$PO_3^- + 2OH^- \rightleftharpoons PO_4^{---} + H_2O$$

applied to high-temperature reactions, but also affords a simple and convenient method for the preparation of disodium monofluophosphate, heretofore available only by a somewhat difficult preparative procedure.

EXPERIMENTAL

Sodium polymetaphosphate

This material, known as Graham's Salt, was prepared either by fusion of sodium dihydrogen phosphate at 700–800°C. for at least 2 hr. or by fusion of anhydrous sodium trimetaphosphate, $Na_3P_3O_9$. Melts in both cases were quenched by cooling between steel plates to produce the metaphosphate glass. All fusions were carried out in platinum dishes in electrically heated muffle furnaces.

Analytical methods

Standard analytical procedures were employed for the determination of each of the following: (*a*) *orthophosphate*, by the colorimetric molybdenum blue procedure (5); (*b*) *pyrophosphate*, by precipitation as zinc pyrophosphate at pH 3.8 (this procedure can be used to determine pyrophosphate in the presence of monofluophosphate) (3); (*c*) *polymetaphosphate*, by precipitation of the barium salt at pH 3, followed by solution of the precipitate in 1:1 nitric acid and boiling to convert to orthophosphate, after which total phosphorus was determined (9); (*d*) *total phosphorus*, by hydrolysis of the sample to orthophosphate and precipitation as ammonium phosphomolybdate, solution of the precipitate in standard sodium hydroxide, and back-titration of excess base with standard acid (1); (*e*) *fluorine*, by the Willard–Winter procedure (16).

In addition to analytical methods, x-ray diffraction techniques were employed to confirm the identity of the sodium and silver salts of monofluophosphoric acid prepared (*a*) by the older method of Lange (10, 11) and (*b*) by the new procedure outlined below. The characteristic silver salt of monofluophosphoric acid precipitates from a solution, from which other phosphates have been removed by preliminary treatment with a dilute silver-ion reagent, upon addition of solid silver nitrate. This test serves for the qualitative identification of the monofluophosphate ion.

Fusion of sodium polymetaphosphate with sodium fluoride

Disodium monofluophosphate is obtained as the principal reaction product when the following mixtures are heated to approximately 800°C. to effect fusion and the resulting melts cooled rapidly: (*a*) equimolecular mixtures of sodium fluoride and Graham's Salt (represented as $NaPO_3$), and (*b*) a mixture of sodium trimetaphosphate, $Na_3P_3O_9$, and sodium fluoride, in the molar ratio of 1:3. The fluophosphate is also obtained by adding solid sodium fluoride directly to a melt of either the glass or the trimetaphosphate. Significantly, solution of the fluoride in the fused metaphosphate is accompanied by a marked decrease in viscosity. Observations based on numerous preliminary experimental trials have led to the development of the following procedure for the preparation of disodium monofluophosphate:

An intimate mixture of 40 g. of anhydrous sodium trimetaphosphate (or glassy polymetaphosphate) and 16.48 g. of anhydrous sodium fluoride is placed in a 100-ml. platinum dish and heated in a muffle furnace at 800°C. for about 6 min., but no longer than to effect complete fusion. The melt is removed from the furnace, allowed to cool below red heat in the open air, and then to room temperature in a desiccator.[6] The crude product is ground and dissolved in 200 ml. of distilled water. One to two grams of solid silver monofluophosphate is then added to the solution to effect precipitation of pyro- and ortho-phosphates, which are removed by filtration. The resulting filtrate is treated with a slight excess of sodium hydroxide to remove excess silver ions. The solution is then treated with an equal volume of ethyl alcohol and agitated, after which the mixture is allowed to separate into two liquid layers. The upper liquid layer is decanted and rejected. The lower aqueous layer is again treated with an equal volume of alcohol, extraction, agitation, and decantation being repeated until crystallization occurs. The extraction procedure removes all the water and excess caustic soda to yield 45.7 g. of Na_2PO_3F (81.1 per cent of theoretical). Analysis: calculated for Na_2PO_3F: F, 13.19; P, 21.53. Found: F, 13.17; P, 21.53.

When, however, mixtures of metaphosphate and sodium fluoride are fused for longer periods of time (1 hr. or longer) at 700°C. or higher, no monofluophosphate is found in the fusion residues. The polymetaphosphate is completely depolymerized and the fusion residue consists primarily of sodium pyrophosphate and some fluoride. Since the analogous fluosulfates have been shown to decompose at higher temperatures to give sulfuryl fluoride, it was first assumed that sodium monofluophosphate had undergone decomposition to give phosphorus(V) oxyfluoride. Analysis of the fusion residues showed that but little phosphorus had been lost, but that appreciable quantities of fluorine had disappeared. Since these fusions were carried out in a platinum dish in contact with the atmosphere, the possibility of high-temperature hydrolysis suggested itself. The data presented in table 1 indicate that results of prolonged fusions agree fairly well with the overall equation:

$$2NaPO_3 + 2NaF + H_2O \rightarrow Na_4P_2O_7 + 2HF$$

Fusion of sodium fluoride with polyphosphates

When sodium triphosphate is heated to the fusion temperature it undergoes disproportionation into pyrophosphate and polymetaphosphate. If a mixture of sodium triphosphate and sodium fluoride is fused quickly (3 min. at 800°C.) and the melt cooled rapidly, the qualitative presence of monofluophosphate in the reaction mixture can be demonstrated. Longer fusion again gives products containing none of the desired monofluophosphate.

---

[6] The resulting product contains about 85 per cent Na_2PO_3F and 10 per cent $Na_4P_2O_7$, the remainder consisting largely of sodium orthophosphate. X-ray diffraction patterns of the crude products reveals the presence of the disodium monofluophosphate, demonstrating beyond a question its formation under the indicated conditions.

Efforts to prepare the monofluophosphate by fusing sodium pyrophosphate with sodium fluoride (in 1:1 ratios or greater) met with failure, no fluophosphate being found among the reaction products. On the other hand, the longer the time of fusion and the higher the temperature, the greater is the amount of orthophosphate formed (see table 2), indicating that some depolymerization of the pyrophosphate does take place. The primary reaction undoubtedly can be represented by the equation: $Na_4P_2O_7 + NaF \rightarrow Na_2PO_3F + Na_3PO_4$. The rate of depolymerization of pyrophosphate is evidently much slower than the rate of decomposition (or hydrolysis) of sodium monofluophosphate which is formed as the intermediate product.

TABLE 1

Fusion of sodium fluoride–sodium metaphosphate mixtures

Time of fusion, 1 hr.

	FUSION TEMPERATURE	$(NaPO_3)_x$	NaF	P	F
	°C.				
Initial composition of mixtures (in grams)	800	3.09	1.24	0.979	0.554
	860	10.00	4.12	3.15	1.86
Final content of fusion residues	800			0.951	0.102
	860			3.12	0.315
Loss during fusion (by difference)	800			0.028	0.452
	860			0.03	1.54
		OBSERVED		THEORETICAL*	
Tetrasodium pyrophosphate content after fusion	800	3.17		3.08	
	860	10.78		10.68	

* Based on the overall equation: $2NaPO_3 + 2NaF + H_2O \rightarrow Na_4P_2O_7 + 2HF$.

TABLE 2

Fusion of mixtures of tetrasodium pyrophosphate and sodium fluoride

MOLE RATIO NaF TO $Na_4P_2O_7$	FUSION TEMPERATURE	TIME OF FUSION	PER CENT CONVERSION TO Na_3PO_4
	°C.		
1:1	450*	17 hr.	
1:1	700	60 min.	6.07
1:1	900	70 min.	32.0
1:1	1050	3 min.	†
4:1	700	60 min.	10.8
4:1	800	60 min.	26.2
4:1	900	60 min.	52.6
4:1	1000	60 min.	56.4

* No fusion or sintering occurs at this temperature.

† No monofluophosphate found in reaction mixture.

DISCUSSION

The experimental data presented above demonstrate conclusively that the fluoride ion behaves as a strong anionic base in effecting the high-temperature depolymerization of the polymetaphosphate and polyphosphate ions in the fused state. Formation of the monofluophosphate under the indicated conditions must involve rupture of the P—O—P bonds linking together the phosphate tetrahedra in the structures of the condensed phosphate. The noticeable reduction in viscosity as solution of fluoride in fused polymetaphosphate takes place must be regarded as further qualitative evidence of such depolymerization, especially since the fluorine atom in a fluophosphate cannot serve as a bridging group.

Since other anionic bases, such as the oxide and sulfide ion, undergo similar reactions with polyanionic acids, it would seem apparent that the concept presented by Lux and Flood dealing specifically with acidic and basic properties of oxides represents merely a specialized case of the Lewis concept as extended by Audrieth and Moeller (8) to high-temperature ansolvous systems.

The assistance of Dr. Howard Adler, Mr. W. H. Woodstock, and Mr. Russell Bell of the Research Laboratories of the Victor Chemical Works, Chicago Heights, Illinois, in facilitating the present study is gratefully acknowledged.

REFERENCES

(1) Association of Official Agricultural Chemists *Methods of Analysis of the Association of Official Agricultural Chemists*, 6th edition, p. 22. George Banta Publishing Company, Menasha, Wisconsin (1945).

(2) Audrieth, L. F., and Moeller, T.: J. Chem Education **20,** 219 (1943).

(3) Bell, R. N.. Anal. Chem. **19,** 97 (1947)

(4) Cohn, T.: Chem. News **129,** 32 (1924).

(5) Fiske, C. H , and Subbarow, Y.: J Biol. Chem **66,** 375 (1925).

(6) Flood, H., and Förland, T. Acta Chem. Scand. **1,** 592 (1947).

(7) Flood, H., and Förland, T.: Acta Chem. Scand. **1,** 781 (1947).

(8) Flood, H., Förland, T., and Roald, B . Acta Chem Scand. **1,** 790 (1947).

(9) Jones, L. T.. Ind. Eng Chem., Anal Ed **14,** 536 (1942).

(10) Lange, W : Ber. **62B,** 786, 793 (1929).

(11) Lange, W., and Livingston, R.: J. Am. Chem. Soc. **69,** 1073 (1947).

(12) Luder, W. F., and Zuffanti, S *The Electronic Theory of Acids and Bases*. John Wiley and Sons, Inc., New York (1946)

(13) Lux, H.: Z. Elektrochem. **45,** 303 (1939).

(14) Wallroth, K. A.: Bull. soc. chim [2] **39,** 316 (1883)

(15) Weinberg, E. L.: Thesis, University of Illinois, 1947

(16) Willard, H. H , and Winter, D. B.: Ind. Eng. Chem., Anal Ed. **5,** 7 (1933).

(17) Zintl, E., and Bertram, A.: Z. anorg. allgem. Chem **245,** 16 (1940).

COVALENT ADSORPTION ON BASE-EXCHANGE RESINS. II

ADSORPTION FROM BUFFER SOLUTIONS OF STRAIGHT-CHAIN ACIDS

JOHN A. BISHOP

Department of Chemistry, Newark College of Engineering, Newark, New Jersey

Received August 24, 1949

In the first paper of this series (1), it was suggested that the ion product should be substituted for the total concentration in plotting the Freundlich isotherm when acid adsorption was being studied. The adsorption equation becomes

$$\log X = k \log a_{\mathrm{H}^+} \cdot a_{\mathrm{A}^-} + \text{constant} \qquad (1)$$

where X is the adsorption in millimoles of acid per gram of resin adsorbent.

If this equation holds, adsorption from buffer solutions should be greater than from nonbuffered solutions of the same acids, and should increase with increasing salt concentration when the pH is held constant. In addition, the points for a given acid should all fall on the same line regardless of pH or salt concentration. To check this equation and to find out whether all acids would fall on the same line regardless of degree of ionization, it was decided to run adsorption isotherms of two acids which were far enough apart in pK that they would not fall on the same line fortuitously. Acetic acid and chloroacetic acid were chosen.

EXPERIMENTAL

Materials

The ion exchanger used in these experiments was Amberlite IR-400 A.G., which is produced by Rohm and Haas Company, and has been sized for use in analytical determinations. The resin was washed by extraction as explained previously (1), since it was found that a pronounced color developed which increased with increased acid and/or increased salt concentration. Jenny (4) has remarked on this, but Kunin and Meyers (5) made no mention of it. The acids used were of C.P. grade and gave no test for chloride.

Method of analysis

Solutions were made up from a concentrated solution of the acid, and were buffered either by partial neutralization with sodium hydroxide, or by adding a solution of the sodium salt of the acid. The initial solutions were titrated for total acidity, and the pH determined using a line-operated pH meter. The apparent concentration of the anion was calculated from these measurements, since

$$\log a_{\mathrm{A}^-} = \mathrm{pH} - \mathrm{p}K + \log a_{\mathrm{HA}} \qquad (2)$$

where pK was the thermodynamic pK. The concentration of unionized acid was used in place of the activity. This was not used with the idea of obtaining the individual ion activity, but simply to correct for the slight variations of anion between individual solutions.

After 100.0 ml. of the solution had been allowed to come to equilibrium with 1.000 g. of the washed and dried resin, samples were taken and analyzed for pH and for total acidity. In making the plots of log X *vs.* log $a_{H^+} \cdot a_{A^-}$, the final pH was combined with the value of log a_{A^-} from equation 2. In the case of chloroacetic acid a correction was made for the concentration of anion due to the dissociation of the acid.

DISCUSSION OF RESULTS

In figures 1 and 2 adsorption is plotted against pH for varying buffer ratios. From these graphs it can be seen that addition of buffering salt does increase the adsorption for any pH. Kunin and Meyers (5) have shown that the same thing is true for the adsorption of hydrochloric acid from potassium chloride solution, also using a base-exchange resin. Previously it was found that salts having an anion ion in common with the acid also increase adsorption of acids on both activated charcoal and activated alumina (2, 6).

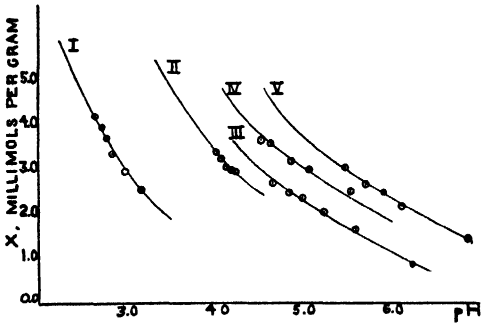

FIG. 1

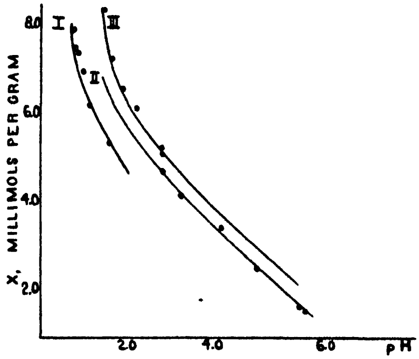

FIG. 2

FIG. 1. The effect of buffer salt concentration on adsorption of acetic acid on Amberlite IR-400. Curve I, no buffer; curve II, acetic acid + sodium acetate (0.02 *M*); curve III, acetic acid + sodium acetate (0.04 *M*); curve IV, acetic acid + sodium acetate (0.227 *M*); curve V, acetic acid + sodium acetate (0.453 *M*).

FIG. 2. The effect of buffer salt concentration on adsorption of chloroacetic acid on Amberlite IR-400. Curve I, no buffer; curve II, chloroacetic acid + sodium chloroacetate (0.10 *M*); curve III, chloroacetic acid + sodium chloroacetate (0.50 *M*).

Figures 3 and 4 show the result of using equation 1 as the basis for plotting adsorption from buffers. In figure 5 a graph has been made using the results of Kunin and Meyers (5). Points were taken from their graph at rounded pH values, using dividers, since they gave no data. The chloride concentration was taken as that of the salt, except for the pure acid. In that case, as with acetic and chloroacetic acids, the pH was doubled to get $-\log a_{H^+} \cdot a_{A^-}$. These graphs show clearly that equation 1 can be used for solutions of acids containing a salt with an anion in common with the acid. Figure 6 shows the data of Graham and Horning for the adsorption of oxalic acid on hydrous alumina from various concentrations of potassium oxalate. They started with a neutral solution of potassium oxalate (pH = 7) and observed the change in pH (2). From this change the author of the present paper has calculated the amount of acid adsorbed; the resulting plot is shown in figure 6. This would indicate that there is a possibility that equation 1 may be applied to general acid adsorption.

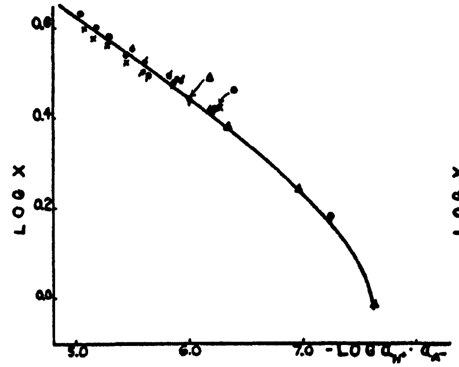

FIG. 3

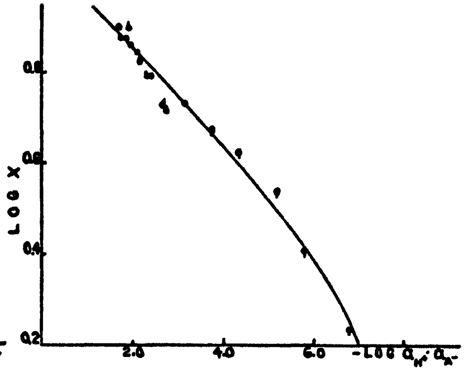

FIG. 4

FIG. 3. Adsorption of acetic acid from buffer solutions on Amberlite IR-400. ⊙, no buffer; ȯ, acetic acid + sodium acetate (0.02 *M*); △, acetic acid + sodium acetate (0.04 *M*); ×, acetic acid + sodium acetate (0.227 *M*); ♀, acetic acid + sodium acetate (0.453 *M*).

FIG. 4. Adsorption of chloroacetic acid from buffer solutions on Amberlite IR-400. ⊙, chloroacetic acid, no salt; ♀, chloroacetic acid + 0.10 *M* sodium chloroacetate; ȯ, chloroacetic acid + 0.50 *M* sodium chloroacetate.

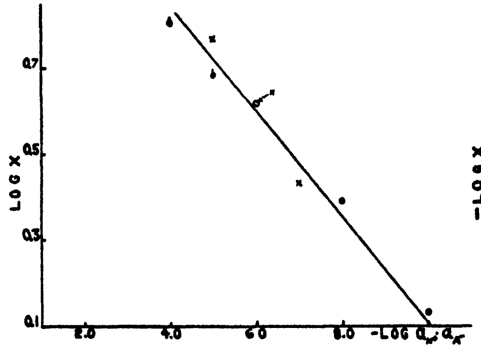

FIG. 5

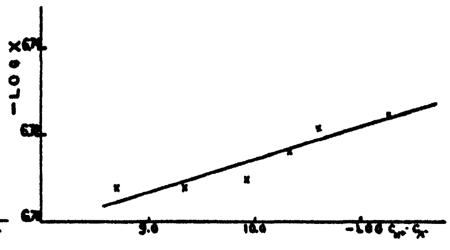

FIG. 6

FIG. 5. Adsorption of hydrochloric acid from potassium chloride solutions on Amberlite IR-400. ⊙, no salt; ×, hydrochloric acid + potassium chloride (0.01 *M*); ȯ, hydrochloric acid + potassium chloride (1.0 *M*).

FIG. 6. Adsorption of oxalic acid from potassium oxalate on alumina

In the previous paper (1) the author suggested that the acids were held to the exchangers by covalent adsorption of the hydrogen to the nitrogen of the adsorber, with the anion being held by electrostatic attraction. Kunin and Meyers (5) objected to this, interpreting it as a "mechanism" of adsorption. They proposed that the adsorption of the anion was simply a matter of displacement of the hydroxide ion of the resin by the anion in question, with subsequent reaction of the hydroxide ion with the hydronium ion of the acid solution. They quoted Jenny (4), who has called attention to the large amount of water adsorbed by these resins when used with water solutions. This has been pointed out by others (1, 7). Since mechanism can not be determined from equilibrium measurements, it seems to be a matter of opinion as to whether displacement or neutralization takes place first. The brief discussion by Heyman and O'Donnell (3) seems to cover this point adequately.

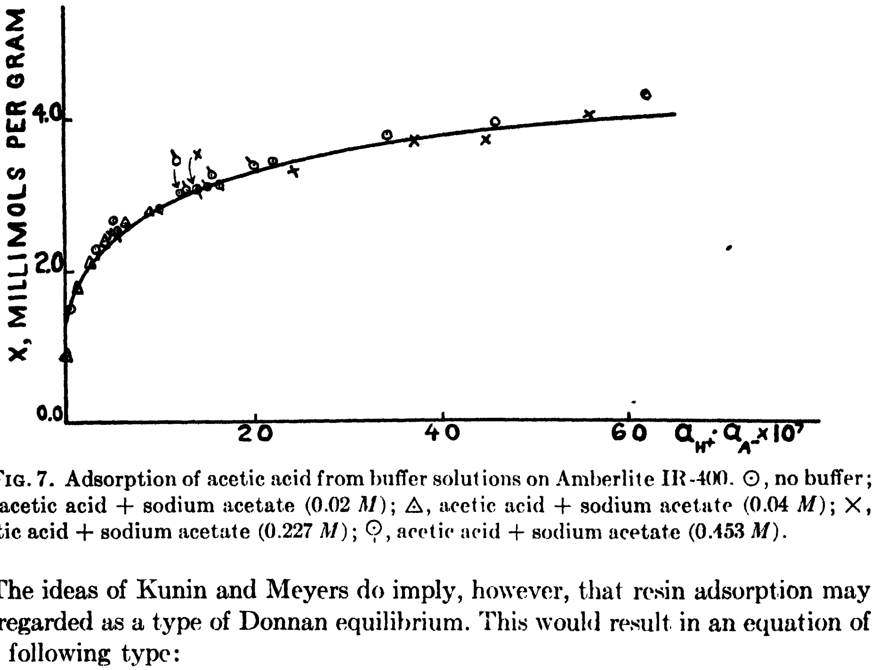

FIG. 7. Adsorption of acetic acid from buffer solutions on Amberlite IR-400. ⊙, no buffer; ȯ, acetic acid + sodium acetate (0.02 *M*); △, acetic acid + sodium acetate (0.04 *M*); ×, acetic acid + sodium acetate (0.227 *M*); ọ, acetic acid + sodium acetate (0.453 *M*).

The ideas of Kunin and Meyers do imply, however, that resin adsorption may be regarded as a type of Donnan equilibrium. This would result in an equation of the following type:

$$\frac{X}{(a_{OH^-})_r} = \frac{a_{A^-}}{(a_{OH^-})_s} \tag{3}$$

where X = adsorption of acid in millimoles per gram of adsorbent
$(a_{OH^-})_r$ = activity of hydroxide ions on the resin
$(a_{OH^-})_s$ = activity of hydroxide ions in solution
a_{A^-} = activity of the anion of the acid adsorbed.

If both numerator and denominator are multiplied by a_{H^+}, the right-hand member of the equation is changed into the ion product divided by K_w, resulting in equation 4:

$$\frac{X}{(a_{OH^-})_r} = \frac{(a_{H^+} \cdot a_{A^-})}{K_w} \tag{4}$$

If X is plotted against the ion product, a curve should result which should not be a straight line, and the slope of which should be equal to $(a_{OH^-})/K_w$. This has been done for the solutions which were plotted above, the results being shown in figures 7, 8, and 9. It is again noticeable that all solutions for one acid fall on the same curve. Values of the slope were determined and $(a_{OH^-})_r$ calculated (table 1).

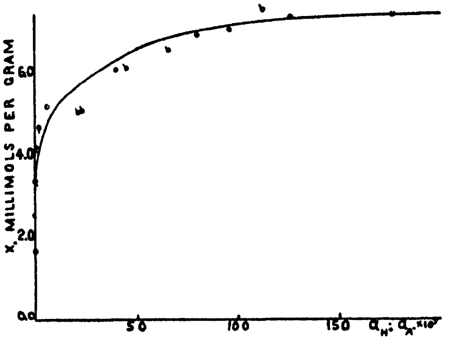

FIG. 8

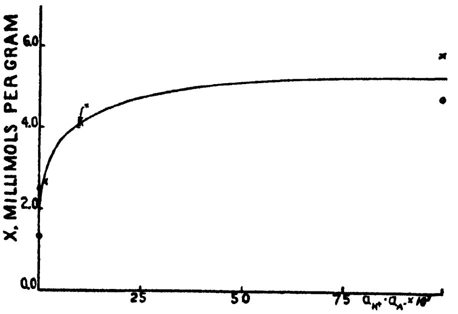

FIG. 9

FIG. 8. Adsorption of chloroacetic acid from buffer solutions on Amberlite IR-400. ⊙, chloroacetic acid, no salt; ⊙, chloroacetic acid + 0.10 *M* sodium chloroacetate; ⊙, chloroacetic acid + 0.50 *M* sodium chloroacetate.

FIG. 9. Adsorption of hydrochloric acid from potassium chloride solutions on Amberlite IR-400. ⊙, no salt; ×, hydrochloric acid + potassium chloride (0.01 *M*); ⊙, hydrochloric acid + potassium chloride (1.0 *M*).

TABLE 1

Values of $(a_{OH^-})_r$

CH_3COOH		$CH_2ClCOOH$		HCl	
X	$(a_{OH^-})_r \times 10^9$	*X*	$(a_{OH^-})_r \times 10^9$	*X*	$(a_{OH^-})_r \times 10^9$
0 48	418	0.86	120	0.86	$1\ 35 \times 10^5$
1.35	100	2.20	10.0	1.91	1.13×10^3
1.90	25	3.00	2.65	3.50	20.0
2.30	15	3.50	1.45	4.00	10.0
3.60	5.1	4.00	0.53	5.20	4.3
3.60	3.27	5.00	0.10		

In the previous paper (1) an equation was obtained by considering the adsorption as one of salt formation:

$$\frac{X}{T - X} = \frac{C_{H^+} \cdot C_{A^-}}{K_{a^+}} \tag{5}$$

where $T - X$ represents the total number of millimoles of possible adsorption minus the amount adsorbed (per gram of resin). At first glance K_{a^+}, which is really the classical hydrolysis constant of the salt formed, would appear to be equal to K_w, from the resemblance of equations 4 and 5. Actually this would be true only if $T - X$ were composed entirely of ionized hydroxide ions, held to the resin by electrostatic forces. That this is not so can be seen by comparing the values of the total possible adsorption on resins with the values of the hydroxide-ion "activity" calculated from the above equation and tabulated in table 1.

It would seem therefore that there may be adsorption due to direct reaction as well as adsorption due to reaction with displaced hydroxide ions.

If the logarithm of both sides of equation 4 is taken, an equation is obtained which resembles equation 1:

$$\log X = \log a_{\mathrm{H}^+} \cdot a_{\mathrm{A}^-} + \log (a_{\mathrm{OH}^-})r/K_w \tag{6}$$

Since the hydroxide-ion activity varies as the value of X changes, this may explain why there is always a constant in the logarithmic equations for adsorption. The intercept changes continuously; consequently the slope will be expected to change. Since the value of the last term in equation 6 will vary only gradually as X changes, it may also be expected that there will be a close approximation to a straight line if the range of concentrations is not too great.

SUMMARY

The equation proposed previously in which weight adsorbed is plotted against ion product, using a log–log plot, has been tested for buffer solutions. It has been found that results predicted from this equation are obtained experimentally, and that all points for a single acid fall on the same curve, both those for the acid solutions and those for the buffers. Further support for the method of plotting has been found using the data of other observers. A reason why the slope is not unity has been suggested, based on the similarity of the equation to one which may be obtained by considering the adsorption as a type of Donnan equilibrium.

REFERENCES

(1) Bishop: J. Phys. Chem. **50**, 6 (1946).
(2) Graham and Horning: J. Am. Chem. Soc. **69**, 1214 (1947).
(3) Heyman and O'Donnell: J. Colloid Sci. **3**, 479 (1948).
(4) Jenny: J. Colloid Sci. **1**, 33 (1946).
(5) Kunin and Meyers: J. Am. Chem. Soc. **69**, 2874 (1947).
(6) Svedberg: *Colloid Chemistry*, p. 243. The Chemical Catalog Company, Inc., New York (1928).
(7) Walton: J. Phys. Chem. **47**, 371 (1943).

FURTHER STUDIES ON THE REVERSIBLE PHOTOBLEACHING OF CHLOROPHYLL A[1, 2]

J. D. KNIGHT[3] AND ROBERT LIVINGSTON

School of Chemistry, Institute of Technology, University of Minnesota, Minneapolis 14, Minnesota

Received August 29, 1949

Since the discovery by Porret and Rabinowitch (17) that solutions of chlorophyll in methanol undergo reversible bleaching when illuminated in the absence of air, a number of investigations (7, 13) have been conducted to obtain information on the characteristics of the underlying reactions.

The present work has been directed along three general lines: (*1*) a reëxamination of the reversible photobleaching of oxygen-free solutions of pure chlorophyll a in various solvents and solvent combinations; (*2*) measurements of the extent of reversible and irreversible photobleaching as a function of oxygen concentration; (*3*) a measurement and analysis of the bleaching reaction in the presence of iodine and certain inorganic salts.

EXPERIMENTAL METHODS AND MATERIALS

Bleaching was measured by a differential photometer of the type described by McBrady and Livingston (13). The optical and electrical systems were used in essentially the same form, with minor adjustments to improve stability of operation. The actinic light was obtained from a 1000-watt projection lamp filtered through a copper sulfate cell and a Corning filter No. 348, thereby eliminating the blue, ultraviolet, and most of the infrared from the white light. The scanning light, coming from a battery-powered 108-watt projection lamp, was passed through a filter combination consisting of a Corning filter No. 352 in front of the reaction cells and a Corning filter No. 241 and 2 cm. of a 5 per cent copper sulfate solution in front of the photocell; this combination transmitted a narrow band peaked at about 6550 Å., corresponding closely to the red absorption maximum of the chlorophyll. The temperature of the reaction cells was controlled by circulating the jacket water supply through a coil of copper tubing immersed in a thermostat.

The extent of bleaching was measured by means of galvanometer deflections, these in turn being interpreted in terms of chlorophyll concentration changes by means of a calibrated glass comparator (7). Light absorption of the chlorophyll solutions deviated somewhat from Beer's law over the range of concentrations used in this work, owing presumably to the finite width of the wave length band

---

[1] This work was made possible by the support of the Office of Naval Research under Contract N6ori-212, Task Order I, Project 059,028.

[2] This paper is based upon a dissertation submitted by J. D. Knight to the Faculty of the Graduate School of the University of Minnesota in partial fulfillment of the requirements for the degree of Doctor of Philosophy, January, 1948.

[3] Present address: Los Alamos Scientific Laboratory, Los Alamos, New Mexico.

of the scanning light; the effective extinction coefficient for 5×10^{-6} M solutions was about 0.7 of that for 1×10^{-6} M solutions. Accordingly, separate concentration calibrations were made and employed for each of the chlorophyll concentration ranges studied.

The chlorophyll a was extracted from fresh spinach and isolated by a modification (11) of the method developed by Zscheile (21). Its concentration and purity with respect to pheophytin and chlorophyll b content were determined with a Beckmann spectrophotometer. The stock solutions of chlorophyll a used in this investigation were made up from preparations with a "purity ratio" (21) of 44 or better.

The methanol was purified as described previously (13). The benzene used in the experiments on the solvent effect was prepared from C.P. thiophene-free material by crystallization, drying over sodium, and fractionation through a high-efficiency column; the middle fraction, boiling within a temperature range of 0.1°C., was saved for use.

Because of the pronounced effect on bleaching of trace impurities occurring in the common reagent-grade carbon tetrachloride, a special batch of this solvent was prepared by the following procedure. A sample of Baker and Adamson reagent-grade carbon tetrachloride was saturated with chlorine gas, illuminated with strong artificial light overnight, again saturated with chlorine, and allowed to stand in normal daylight for 2 days. The bulk of the dissolved chlorine was then driven out by prolonged reflux in an all-glass apparatus; the remainder was removed by thorough shaking with six successive portions of 1 per cent sodium hydroxide, followed by four shakings with water to rinse out the residual base. After drying over anhydrous sodium carbonate, the carbon tetrachloride was fractionated in a high-efficiency still and the middle fraction was saved for use.

All inorganic reagents used were of reagent grade unless otherwise noted. The cerous chloride was obtained by reducing ceric sulfate with sodium sulfite, destroying the excess sulfite with hydrochloric acid, and converting the residual sulfate ion to chloride with barium chloride. The lanthanum chloride[4] was prepared from the Eimer and Amend C.P. product, and had been especially treated to free it from cerium.

The chlorophyll a was used at three concentrations: 1×10^{-6}, 2×10^{-6}, and $5 \times 10^{-6}M$. Solutions were prepared from the ether concentrate in the following manner: an aliquot (~0.5 ml.) of the concentrate was pipetted into a specially designed suction flask, 25–30 ml. of the purified solvent was added, and at room temperature the solution was evaporated under vacuum to about 2 ml. to boil out most of the ether. A second portion of the solvent was added and the evaporation was repeated; then, or after a third addition of solvent and evaporation if necessary, the final concentrate was transferred to a volumetric flask and diluted to the appropriate volume. All operations with the chlorophyll solutions were carried out in subdued light, and the solutions were stored in the dark in a refrigerator when not in use. For experiments under oxygen-free conditions, the solutions were deaerated in the reaction cells by adding an equal volume of the pure solvent and then boiling off the excess solvent under vacuum.

---

[4] We are indebted to Dr. G. Matsuyama for providing us with a sample of this reagent.

EXPERIMENTAL RESULTS

Photobleaching of oxygen-free solutions

In most of the experiments the chlorophyll a was used at a concentration of $2 \times 10^{-6}\ M$. As a check on the chlorophyll preparations and on the performance of the differential photometer, a set of preliminary experiments was carried out on solutions of chlorophyll in methanol which had been degassed by the boiling-off technique described above. The observations on these solutions were in general agreement with those of McBrady and Livingston (13). Irreversible bleaching was zero within experimental error; reversible bleaching amounted to approximately 10^{-8} moles per liter at the steady state under full illumination. From semiquantitative observations at the beginning and end of illumination periods, the bleaching and debleaching reactions were estimated to be at least 90 per cent complete within 1 sec., the resolving time of the galvanometer.

TABLE 1

The dependence of steady-state bleaching on chlorophyll concentration at constant intensity of incident light

CHLOROPHYLL CONCENTRATION	TEMPERATURE	STEADY-STATE BLEACHING
(moles/liter) $\times 10^{6}$	°C.	*(moles/liter)* $\times 10^{3}$
1.0	30.9	0.013
2.0	31.2	0.010
5.0	32.3	0.010

To provide a further check on the efficiency of oxygen removal by the boiling-off technique, a comparison run was made with a solution which had been deoxygenated by sweeping out the contents of the reaction cell with pure nitrogen (rendered oxygen-free by passing tank nitrogen through a heated column containing copper on kieselguhr (14, 16)). The extent of reversible bleaching was the same within experimental error, confirming the adequacy of the standard Thunberg technique.

Additional measurements, carried out at several temperatures, showed that the extent of steady-state bleaching is practically independent of temperature. The relative values of the steady-state bleaching at 13.3°, 27.3°, and 39.5°C. were, respectively, 1.10, 1.00, and 0.98.

The measurements summarized in table 1 were performed, with constant intensity of incident light, to determine the effect of chlorophyll concentration upon the steady-state bleaching. The solutions were prepared from a common stock chlorophyll solution and the same batch of methanol. These data show that the extent of steady-state bleaching is substantially independent of chlorophyll concentration. If the fraction of the incident actinic light absorbed is proportional to the chlorophyll concentration (and for the concentrations and the experimental arrangement used, this is a good approximation), the extent of the steady-state bleaching must be inversely proportional to the chlorophyll concentration. Since this conclusion is contrary to the earlier results of McBrady and Livingston (13), additional experiments were carried out with 2×10^{-6} and 5×10^{-6} M solutions made up from a different chlorophyll stock solution. Again, the two solutions exhibited the same bleaching within experimental error, although the extent of steady-state bleaching for both was slightly smaller. There is no immediately apparent reason for this discrepancy.

Previous investigations (7, 13) have shown that the amount of reversible bleaching and the rate of the back-reaction are sensitive to the purity of the solvent. Comparatively little attention, however, has been given to the effect of the solvent itself. Accordingly, a number of experiments were devoted to a more detailed examination of the solvent effect. The results are summarized in table 2.

TABLE 2

The effect of solvent on bleaching of oxygen-free chlorophyll solutions
Chlorophyll concentration = $2 \times 10^{-6}M$

SOLVENT	STEADY-STATE REVERSIBLE BLEACHING	RATE OF IRREVERSIBLE BLEACHING
	(moles/liter) × *10^6*	*(moles/liter/second)* × *10^6*
Methanol	1.0	0.000
98 per cent methanol + 2 per cent water	1.7	0.007
Benzene	0.0	0.037
99 per cent benzene + 1 per cent methanol	0.4	0.007
Carbon tetrachloride	0.0	0.93

It may be seen first that, of the solvents tried, only methanol gave no irreversible bleaching. Reversible bleaching is observed only in the presence of polar solvents. Only a very small amount of methanol is required to produce a steady-state reversible bleaching of the same order of magnitude as found in pure methanol. This effect is of interest in connection with the "activation" (12) of fluorescence of chlorophyll in nonpolar solvents by traces of hydrogen-bonding compounds. The addition of water enhances the reversible bleaching, but tends also to produce a slow irreversible bleaching.

A further contrast in behavior between polar and nonpolar solutions was provided by the results with a pure carbon tetrachloride solvent. Although the solution had been degassed by the standard method used with the other solvents, the irreversible reaction during illumination was extremely rapid; a total of 3 min. of illumination with the actinic light at full intensity was sufficient to bring about complete bleaching of the solution to a faint straw-yellow color. In the absorption spectrum of the final bleached product, the characteristic chlorophyll a peaks at 6650 Å. and 4300 Å. were replaced by a sharp absorption at 4300 Å., in qualitative resemblance to the spectrum found by Aronoff and Mackinney (1) for chlorophyll which had undergone photoöxidation in acetone.

Very small amounts of oxygen are known (7, 13, 17) to inhibit reversible bleaching and to bring about comparatively rapid irreversible bleaching during illumination. In order to determine the oxygen concentration range in which this effect sets in, and to establish if possible a quantitative relationship between oxygen concentration and bleaching, a series of experiments was performed with 2×10^{-6} *M* solutions of chlorophyll in methanol containing known concentrations of oxygen. The data from a typical run are plotted in figure 1. In this run, as in others at low oxygen concentrations, the slope of the $\Delta[C]$ *versus* time curve has its greatest value during the first illumination period and gradually decreases during the succeeding illumination periods. This effect is probably to be attributed to the consumption of both chlorophyll and oxygen by the irreversible bleaching.

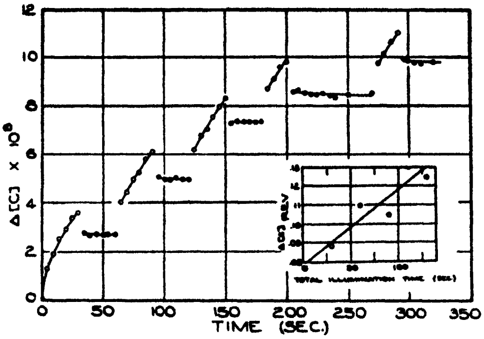

FIG. 1. Reversible and irreversible bleaching of 2×10^{-6} *M* chlorophyll a solution in the presence of 1.2×10^{-6} *M* oxygen.

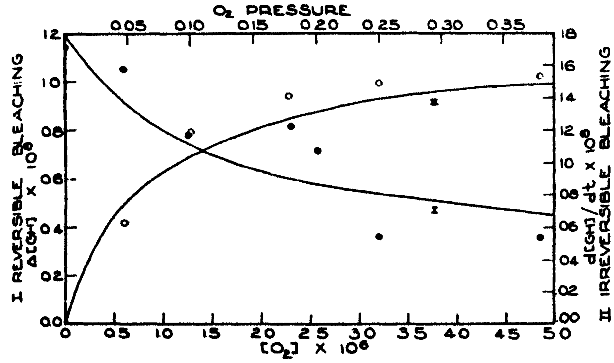

FIG. 2. The extent of the steady-state reversible bleaching and the rate of the irreversible bleaching as functions of oxygen concentration.

The results of reversible and irreversible photobleaching measurements at various oxygen concentrations[5] are plotted in figure 2, the reversible measure-

---

[5] Oxygen concentration was controlled by admitting a known quantity of air to the degassed solution in the reaction vessel and shaking to equilibrate liquid and gas phases. The absorption coefficient

$$\lambda = \frac{\text{volume of gas absorbed}}{\text{volume of absorbing liquid}}$$

was taken from the tables of Seidell (20).

ments being indicated by dots and the irreversible by circles. The curves are plots of theoretical equations, which are discussed later in this paper. The rate of irreversible bleaching is proportional to oxygen concentration at low concentrations, but approaches at higher concentrations a limiting value of 0.17×10^{-8} moles/liter/second. The extent of reversible bleaching, though less accurately known (because of the difficulty of measuring small changes in chlorophyll concentration in the presence of large drifts due to the irreversible relation), decreases approximately linearly with increasing oxygen concentration in the low concentration range, tailing off more slowly to zero at higher pressures.

The temperature dependence of the irreversible bleaching rate was determined by measurements over a 20°C. range on solutions of (2×10^{-6} M) chlorophyll in methanol which had been saturated with air at room temperature. The rates of irreversible bleaching at 16.4, 27.3, and 36.4°C. were, respectively, 0.190, 0.172, and 0.162 (moles/liter/second) $\times 10^{8}$.

Rabinowitch and Weiss (19) found that the addition of ferric chloride to methanol solutions of chlorophyll or alkyl chlorophyllides brings about a color change from green to yellow (with almost complete disappearance of the characteristic chlorophyll absorption band at 6650 Å.), which can be reversed by immediate addition of ferrous ion or other reducing agents. A similar result was obtained with ceric ammonium nitrate as the oxidizing agent. They also found that the addition of ferrous chloride alone to chlorophyll solutions inhibited the photobleaching.

It appeared worthwhile, therefore, to extend these results by examining the photobleaching of chlorophyll in the presence of cerous ion, and as a check on the ionic charge effect, with lanthanum and with barium salts. Several runs were carried out with chlorophyll in methanol containing these salts in concentrations of 2×10^{-5} to 2×10^{-4} moles/liter. Reversible bleaching was found to be enhanced greatly by the cerous and lanthanum salts and to a lesser extent by the barium. The back-reactions in the first two instances were nearly first order, with half-periods of the order of 7 to 8 sec. in the case of cerium and 20 sec. in the case of lanthanum. Semiquantitative measurements indicated that a tenfold increase in cerium concentration was accompanied by a fivefold increase in steady-state bleaching. The bleaching varied approximately as the square root of incident light intensity; this result, though seemingly inconsistent with the first-order decay of the bleached product, has been observed with other reagents. The reversible bleaching was accompanied by an irreversible increase in the absorption (rather than the usual bleaching) of the solutions during the course of illumination. It is apparent that the irreversible reaction in the presence of cerous chloride or lanthanum chloride leads to the formation of one or more products which are more strongly absorbing at 6650 Å. than the pure chlorophyll. The photobleaching in the presence of barium chloride, on the other hand, was largely reversible and no abnormal reactions were noted.

It has been reported (13) that chlorophyll a solutions containing iodine in concentrations as low as 10^{-5} M exhibit greatly enhanced reversible bleaching, a slow back-reaction, and the suppression of the irreversible bleaching ordinarily associated with the presence of small amounts of oxygen. This effect has been verified in the present work. Experiments were performed with 2×10^{-6} *M* chlorophyll in mechanol solutions to which various amounts of iodine had been added. It was found necessary to start the bleaching runs within an hour after addition of the iodine in order to obtain consistent and reproducible measurements.

Bleaching and dark-reaction curves for one illumination cycle for a typical iodine-containing solution are shown in figure 3. The back-reaction at cessation of illumination was found to be first order; its half-period at 30°C. was fairly constant at about 25 ± 5 sec., independent of iodine concentration in the range 10^{-5} to 10^{-6} *M*. The extent of reversible bleaching was directly proportional to the iodine concentration over the same range. A number of lines of evidence indicate, however, that the reversible bleaching effect in these cases is more complex than was first assumed. First of all, it was found, as may be seen from figure 3, that the approach to steady-state bleaching during the first part of the illumination cycle was considerably more rapid than should be expected for a first-order reaction throughout. Secondly, the extent of steady-state reversible bleaching was not proportional to the first power of the absorbed light intensity, as should follow from a first-order limiting process. A series of measurements performed with incident light varying from 7 per cent intensity to full strength showed the extent of bleaching to be very nearly proportional to the square root of the absorbed light intensity.

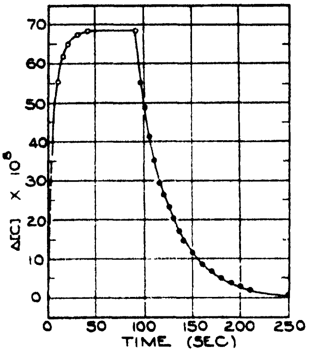

FIG. 3. Reversible photobleaching of 2×10^{-6} *M* chlorophyll a solution containing 2×10^{-5} *M* iodine.

A complicating feature in the above measurements was the presence of irreversible reactions, taking place slowly in the dark and somewhat more rapidly after prolonged irradiation. In a series of illuminations with the same solution, the extent of steady-state bleaching became slightly smaller with each succeeding illumination period, and the decay half-period of the bleached state underwent a similar decrease, although the reaction appeared to be reversible for any one cycle. It was necessary, therefore, to carry out the runs with fresh solutions in order to obtain consistent and reproducible results. In view of the observation, previously cited, that the half-life of the back reaction is sensibly independent of iodine concentration for fresh solutions, the change in behavior with long-illuminated solutions must be attributed to the influence of products from the reaction of the iodine with the solvent or with the chlorophyll itself.

Subsequent to these experiments, researches[6] by Dr. W. W. Watson have shown that iodine in low concentrations brings about a rapid allomerization of chlorophyll in methanol solutions. This allomerization is accompanied by changes in the absorption spectrum and intensity of the fluorescence of the chlorophyll. Undoubtedly, allomerization of chlorophyll influences its reversible photobleaching. However, the fact that increasing the concentration of iodine well in excess of stoichiometric proportions continues to enhance the reversible bleaching is evidence that iodine (and probably lanthanum chloride, etc.) has some additional influence on the photochemical properties of chlorophyll solutions.

CALCULATIONS AND DISCUSSION OF RESULTS

The overall efficiencies of the reversible and irreversible photobleaching reactions may be calculated on the basis of the data given in the preceding section.

A lower limit for the quantum yield for reversible bleaching of chlorophyll in methanol solutions may be obtained from these data, together with a determination, from another experiment, of the absolute intensity of the actinic light absorbed. Figure 2 shows that the steady-state reversible bleaching at zero oxygen concentration for $2 \times 10^{-6}\ M$ chlorophyll is approximately 1.2×10^{-8} moles/liter at maximum incident light intensity. The debleaching back-reaction appears to be at least 90 per cent complete in 1 sec. For the actinic light source and filter arrangement used in the present work, McBrady and Livingston (13) obtained a value of 2.3×10^{19} quanta/second/liter of light absorbed by a $2 \times 10^{-6}\ M$ solution of chlorophyll in methanol under full illumination.

If, as indicated by the intensity–bleaching relationship, the debleaching reaction follows a second-order law,

$$-\frac{d(\Delta[C])}{dt} = k(\Delta[C])^2$$

$$k = \frac{1}{t}\left[\frac{1}{(\Delta[C])_t} - \frac{1}{(\Delta[C])_0}\right]$$

$(\Delta[C])_t$ is the extent of bleaching (change in chlorophyll concentration in moles/liter) at any time, t, after cessation of illumination, I_{abs} is the intensity of the absorbed light, and φ_{rev} is the quantum yield for the reversible bleaching reaction. At steady-state bleaching,

$$k(\Delta[C])_0^2 = \varphi_{\mathrm{rev}} I_{\mathrm{abs}}$$

These expressions may be combined to give:

$$\varphi_{\mathrm{rev}} = \frac{(\Delta[C])_0^2}{I_{\mathrm{abs}}t}\left[\frac{1}{(\Delta[C])_t} - \frac{1}{(\Delta[C])_0}\right]$$

---

[6] A preliminary account of these results has been reported by R. Livingston (9). Details will be published elsewhere.

Substituting the numerical values given above,

$$\varphi_{\text{rev}} > \frac{1.2 \times 10^{-8} \text{ moles liter}^{-1} \times 6 \times 10^{23} \text{ quanta mole}^{-1}}{2.3 \times 10^{-9} \text{ quanta second}^{-1} \text{ liter}^{-1} \times 1 \text{ second}} \times (10 - 1)$$

$$\geq 2.9 \times 10^{-3}$$

This value is about sevenfold greater than the limiting quantum yield calculated by McBrady and Livingston (13). A comparison of the respective data shows that the major part of the discrepancy arises from somewhat smaller values for steady-state bleaching found in their work; their observed $(\Delta[C])_0$ was 0.55×10^{-8} moles/liter under the same illumination conditions. Since this term is squared in the expression above, the calculated quantum yield is sensitive to differences in observed values for steady-state bleaching. Runs in the current work have given a $(\Delta[C])_0$ as low as $\sim 0.5 \times 10^{-8}$ moles/liter, depending on the batch of chlorophyll concentrate used in preparing the solutions. These variations may be due to differences in concentration of trace impurities or to some difference in the state of the chlorophyll. Since the greatest bleaching seemed to be found with fresh preparations, the larger figure was taken as representing the optimum bleaching in pure chlorophyll solutions.

The quantum yield for irreversible photobleaching in the presence of oxygen may be computed in a similar manner. The rate of irreversible bleaching of 2×10^{-6} *M* chlorophyll reaches a limiting value of 1.7×10^{-9} moles/liter/second at high oxygen concentrations and under full illumination. The corresponding quantum yield is $\varphi_{\text{irrev}} = 4.5 \times 10^{-5}$ moles of chlorophyll destroyed per quantum absorbed. This value is in good agreement with the corresponding figure of 4×10^{-5} obtained by McBrady and Livingston (13).

A comparison of the quantum yields shows that the reversible reaction is at least sixtyfold more efficient, under these conditions, than the irreversible reaction. The irreversible photobleaching of chlorophyll in carbon tetrachloride solution was considerably more rapid, even in the absence of oxygen, than in the methanol solutions, but its quantum yield as calculated by the same method was about 2.5×10^{-4}, which is still only ~9 per cent of the minimum yield for reversible bleaching in methanol.

It is of some interest to compare the reversible bleaching quantum yield for "pure" chlorophyll solutions with their counterparts for solutions to which iodine was added. From figure 3 the observed steady-state bleaching is 0.7×10^{-6} moles/liter. Inclusion of a correction factor to allow for the bleaching effect of the scanning light (*cf.* reference 13) raises this figure to 0.8×10^{-6}. Assuming that the debleaching reaction is first order with a rate constant of 0.028 sec.$^{-1}$, and allowing also for decreased light absorption due to partial bleaching of the solution, one obtains $\varphi \simeq 10^{-3}$. Since this limiting value for the yield is slightly less than that observed for the system in the absence of iodine, the great increase in the steady-state bleaching must be due entirely to the decreased rate of the back-reaction.

The new finding, that at constant intensity of observed light the extent of the steady-state bleaching is inversely proportional to the concentration of chlorophyll, requires some revision of the mechanism of photobleaching which was presented by McBrady and Livingston (13). A simple mechanism which is consistent with the present data can be obtained by postulating that, at concentrations of chlorophyll equal to or greater than $10^{-6}\,M$, the long-lived state, HG, is degraded to the ground state by an interaction with a normal chlorophyll molecule rather than by a spontaneous process of internal conversion (3). This postulated mechanism for the degradation of the long-lived state, HG, is directly analogous to the self-quenching of the fluorescent (excited singlet) state, GH* (15, 22). The occurrence of self-quenching of HG in dilute chlorophyll solutions, where self-quenching of fluorescence is negligible (23), may be attributed to the much longer life of HG. It has been suggested by M. Kasha (5) that the general absence of phosphorescence in fluid solutions is due to this type of self-quenching of the phosphorescent (triplet?) state. This hypothesis is also consistent with the measurements of Gaffron (4) on the effect of the chlorophyll concentration upon the quantum yield of the chlorophyll-sensitized autoöxidation of allylthiourea. Accepting this hypothesis, we may revise McBrady and Livingston's mechanism for photobleaching as follows:

$$\begin{array}{lrl}
(1) & \mathrm{GH} + h\nu \rightarrow \mathrm{GH}^* & V_1 = I_{\mathrm{abs}} \\
(2) & \mathrm{GH}^* \rightarrow \mathrm{GH} + h\nu_f & V_2 = k_2(\mathrm{GH}^*) \\
(3) & \mathrm{GH}^* \rightarrow \mathrm{HG} & V_3 = k_3(\mathrm{GH}^*) \\
(4) & \mathrm{HG} + \mathrm{GH} \rightarrow 2\mathrm{GH} & V_4 = k_4(\mathrm{GH})(\mathrm{HG}) \\
(5) & \mathrm{HG} + \mathrm{B} \rightarrow \mathrm{C} + \mathrm{D} & V_5 = k_5(\mathrm{B})(\mathrm{HG}) \\
(6) & \mathrm{C} + \mathrm{D} \rightarrow \mathrm{GH} + \mathrm{B} & V_6 = k_6(\mathrm{C})(\mathrm{D})
\end{array}$$

The symbol GH indicates normal chlorophyll; GH* is chlorophyll in its first electronically excited singlet state; and HG is a long-lived activated form of chlorophyll, probably the lowest triplet state. I_{abs} represents the intensity of the absorbed light, in appropriate units. V_i is the rate of the i^{th} reaction step. B is some substance present in the solution, which reacts with HG to yield two products, C and D. C and D, which are probably radicals, recombine to regenerate normal chlorophyll and the original reactant, B. Either C or D constitutes most, and probably all, of the bleached chlorophyll.[7]

The nature of the reactant B is as yet unknown. B has been assumed (2, 7, 8, 13, 18) variously to be the solvent, an oxidizing or reducing impurity in the solution, or chlorophyll itself. The last alternative, which in some respects is the simplest and most attractive (7), can be ruled out on kinetic grounds (see equation 4), since the steady-state bleaching is an inverse function of the chlorophyll concentration. The hypothesis that the solvent molecules act as B, while possible, is improbable for two reasons. First, it is unlikely that a reaction such as step 5 would have practically the same rate for a variety of solvent molecules (i.e., B), including methanol, ethanol, and acetate. Second, the observation that reversible bleaching is either absent or very small in benzene but is nearly normal in benzene containing 1 per cent methanol, appears inconsistent with the concentration dependence implied by reaction 5. The observation that reversible bleaching is enhanced by oxidizing agents and unaffected by most reducing agents suggests that B is an oxidizing impurity. Since solvent purification procedures which are rigorous by usual laboratory standards may still leave untouched organic impurities at concentration levels well in excess of the chlorophyll concentrations employed in this work, substance B might plausibly be some such undetected organic oxidant.

---

[7] The long-lived state might be expected (6) to have an absorption spectrum differing appreciably from that of the ground state and so contribute substantially to the bleached form. However, the dependence of the steady-state bleaching upon the square root of the intensity of the absorbed light practically excludes this possibility. A comparison (10) of the quantum yield for photosensitized reactions and the maximum fluorescent yield (~0.08) with the estimated low yield (10^{-3}) for the reversible bleaching constitutes sufficient independent grounds for rejecting the view that HG is (or contributes substantially to) the bleached form of chlorophyll.

The concentrations of the various intermediates may be calculated upon the usual assumption that a steady state exists, to be as follows:

$$\mathrm{HG} = \frac{k_3}{(k_2 + k_3)[k_4(\mathrm{GH}) + k_5(\mathrm{B})]} I_{\mathrm{abs}} \tag{1}$$

and

$$(\mathrm{C}) = (\mathrm{D}) = \left(\frac{k_5}{k_6}\right)^{1/2} (\mathrm{B})^{1/2}(\mathrm{HG})^{1/2}$$

$$= \left[\frac{k_3 k_5(\mathrm{B})}{k_6(k_2 + k_3)[k_4(\mathrm{GH}) + k_5(\mathrm{B})]}\right]^{1/2} I_{\mathrm{abs}}^{1/2} \tag{2}$$

These expressions may be simplified by the following approximations: first, since the maximum fluorescence yield is known to be about 8 per cent, we may take $k_2 + k_3 \approx k_3$; also, since step 4 must be considerably more rapid than step 5, $k_4(\mathrm{GH}) + k_5(\mathrm{B}) \approx k_4(\mathrm{GH})$. With the incorporation of these approximations, the expressions above reduce to:

$$(\mathrm{HG}) = \frac{1}{k_4(\mathrm{GH})} I_{\mathrm{abs}} \tag{3}$$

and

$$(\mathrm{C}) = (\mathrm{D}) = \left(\frac{k_5(\mathrm{B})}{k_4 k_6(\mathrm{GH})}\right)^{1/2} I_{\mathrm{abs}}^{1/2} \tag{4}$$

On the basis of this analysis, with C representing most of the bleached product, the extent of reversible bleaching in oxygen-free solutions is directly proportional to the square root of absorbed actinic light intensity and inversely proportional to the square root of chlorophyll concentration, in agreement with the experimental data. Substitution of (GH) for (B), as required when chlorophyll is the second reaction partner in step 5, would on the other hand lead to prediction of a bleaching effect independent of chlorophyll concentration for a given absorbed light intensity, contrary to our findings. It appears that the assumption that B is an impurity (or possibly a solvent molecule) is the only one consistent with the present kinetic measurements.

The quantum yield for reversible bleaching, in terms of the present mechanism, is given by:

$$\varphi_{\mathrm{rev}} = \frac{k_6(\mathrm{C})^2}{I_{\mathrm{abs}}} \cong \frac{k_3}{k_2 + k_3} \times \frac{V_5}{V_4} \qquad (5)$$

To a good approximation, then, $\varphi_{\mathrm{rev}} \simeq V_5/V_4$, and the reversible bleaching quantum yield turns out to be about equal to the ratio of the rates of steps 4 and 5.

For reversible and irreversible bleaching processes in chlorophyll solutions containing oxygen, several possible mechanisms have been discussed by McBrady and Livingston (13). The following reaction scheme is probably in best agreement with the data given in figure 2:

(7) $\mathrm{H\dot{G} + O_2 \rightarrow HGO_2}$ $V_7 = k_7(\mathrm{H\dot{G}})(\mathrm{O_2})$

(8) $\mathrm{HGO_2 \rightarrow GH + O_2}$ $V_8 = k_8(\mathrm{HGO_2})$

and for irreversible bleaching

(9) $\mathrm{HGO_2 + GH \rightarrow GH + GHO_2}$ $V_9 = k_9(\mathrm{HGO_2})(\mathrm{GH})$

or

(10) $\mathrm{HGO_2 \rightarrow GHO_2}$ $V_{10} = k_{10}(\mathrm{HGO_2})$

Step 7, a combination of the excited form $\mathrm{H\dot{G}}$ with oxygen to give an unstable mole-oxide, is presumed to have an efficiency comparable with that of step 4. The mole-oxide, as seen above, may then either dissociate to normal chlorophyll and oxygen (step 8) or, with much lower efficiency, bring about irreversible bleaching by rearranging to a permanent oxidation product (step 10) or by oxidizing another chlorophyll molecule (step 9). Evidence of the efficiency of chlorophyll as a photosensitizer for the oxidation of other substrates in solution (15) favors step 9. Use of the symbol $\mathrm{GHO_2}$ is intended only to indicate that permanent oxidation has occurred, without stipulation as to nature or possible variety of oxidation products.

If it is assumed that $\mathrm{GHO_2}$ (and possibly $\mathrm{HGO_2}$) is bleached by present criteria, the reversible bleaching in oxygen-containing solutions can be represented as the sum of the C and $\mathrm{HGO_2}$ effects. A kinetic analysis of steps 1 to 10, including the simplifying assumptions previously employed, leads to the result:

$$(\mathrm{C}) = \left[\frac{k_5(\mathrm{B})}{k_6[k_4(\mathrm{GH}) + k_7(\mathrm{O_2})]}\right]^{1/2} I_{\mathrm{abs}}^{1/2} \qquad (6)$$

and

$$(\mathrm{HGO_2}) = \left\{\frac{k_7(\mathrm{O_2})}{[k_8 + k_9(\mathrm{GH})]\,[k_4(\mathrm{GH}) + k_7(\mathrm{O_2})]}\right\} I_{\mathrm{abs}} \qquad (7)$$

Where step 10 is taken in place of step 9, the term $k_9(\mathrm{GH})$ in the above expressions is replaced by k_{10}.

The rate of irreversible bleaching is given by:

$$\frac{-\mathrm{d(GH)}}{\mathrm{d}t} = \left[\frac{k_7 k_9(\mathrm{GH})(\mathrm{O_2})}{[k_8 + k_9(\mathrm{GH})][k_4(\mathrm{GH}) + k_7(\mathrm{O_2})]}\right] I_{\mathrm{abs}} \qquad (8)$$

Inspection of this equation shows that, at constant chlorophyll concentration and constant light intensity, steps 9 and 10 both lead to rate equations of the form:

$$-\frac{\mathrm{d(GH)}}{\mathrm{d}t} = \frac{(\mathrm{O_2})}{a + b(\mathrm{O_2})} \qquad (9)$$

so that rate *vs.* oxygen concentration data alone do not offer a means of making a choice. However, the validity of the general irreversible bleaching rate expression may be checked by reference to figure 2. Since the data were obtained at a single chlorophyll concentration, all the rate constants and the (GH) may be lumped in one constant a' and the equation may be rewritten as:

$$-\frac{\mathrm{d(GH)}}{\mathrm{d}t} = \frac{a'(\mathrm{O_2})}{\frac{k_4}{k_7}(\mathrm{GH}) + (\mathrm{O_2})} \qquad (10)$$

From figure 2, the limiting irreversible bleaching rate for 2×10^{-6} *M* chlorophyll in methanol at high oxygen concentrations is 0.17×10^{-8} moles/liter/second. The irreversible bleaching rate reaches half its limiting value at $(\mathrm{O_2}) \approx 0.8 \times 10^{-6}$ moles/liter. Insertion of these two data in the formula above leads to the value $k_4/k_7 \approx 0.4$, and thus the numerical expression becomes:

$$-\frac{\mathrm{d(GH)}}{\mathrm{d}t} = \left(\frac{(\mathrm{O_2})}{0.8 \times 10^{-6} + (\mathrm{O_2})}\right) \times 0.17 \times 10^{-8} \text{ moles/liter/second} \qquad (11)$$

when the chlorophyll concentration is 2×10^{-6} moles/liter. The numerical expression for reversible bleaching, calculated by a similar method, turns out to be:

$$(\mathrm{C}) = \left(\frac{1}{1 + 1.25 \times 10^{6}(\mathrm{O_2})}\right)^{1/2} \times 1.2 \times 10^{-8} \text{ moles/liter} \qquad (12)$$

In figure 2 the curves are plots of equations 11 and 12. It will be recalled that two experimental values, the limiting irreversible bleaching rate and the oxygen concentrations at half the limiting rate, were needed to specify uniquely the calculated curve for irreversible bleaching. One additional value $(\mathrm{C})_0$, for zero oxygen concentration, was needed to determine the reversible bleaching curve.

The curve for irreversible bleaching is in good agreement with the experimental data. The departure of the calculated curve from the data for reversible bleaching is probably outside the range of experimental error, and may be due either to basic inaccuracies in the proposed mechanism or to neglect of contributions from the mole-oxide. An examination of the expression for the rate of irreversible bleaching may now be used to locate the source of the low quantum yield for this process. The quantum yield is given by the ratio of V_9 to V_1, and may be written as:

$$\varphi_{\text{irrov}} = \frac{k_9 k_3 k_7(\text{GH})(\text{O}_2)}{[k_2 + k_3][k_8 + k_9(\text{GH})][k_4(\text{GH}) + k_5(\text{B}) + k_7(\text{O}_2)]}$$

At high oxygen concentrations, the HG-removal steps 4 and 5 become negligible compared to step 7, and the above formula reduces to:

$$\varphi_{\text{irrov}} = \frac{k_9(\text{GH})}{k_8 + k_9(\text{GH})}$$

Since φ_{irrev} approaches a value of 4.5×10^{-5} for high oxygen concentrations, it follows that $k_8 \gg k_9(\text{GH})$; therefore under these conditions $V_7 \simeq V_8$. The oxygen, in effect, acts as a catalyst for the conversion of species HG to normal chlorophyll; the estimate of the ratio k_4/k_7 as 0.4 indicates that oxygen is about 2.5 times as effective a catalyst for the purpose as chlorophyll itself. Where the oxygen exceeds the chlorophyll concentration, most of the initially excited molecules GH pass through a reaction sequence consisting of steps 3, 7, and 8; at lower oxygen concentrations, where step 7 is cut down, the bulk of the species HG is drawn off through the high-efficiency step 4, with step 5 remaining as a small-scale parasitic reaction which constitutes the reversible bleaching. It is possible that reversible bleaching is still further reduced at moderate oxygen concentrations by destruction of the radicals C and D by O_2 or by the oxidant HGO_2, though a lack of knowledge as to the nature of the various oxidation products in bleached solutions prevents a more detailed analysis of the reactions taking place.

SUMMARY

In air-free methanol solutions of chlorophyll a, at a concentration of 2×10^{-6} *M*, the quantum yield of the reversible photobleaching has an (estimated) value $\geqslant 3 \times 10^{-3}$. The extent of the steady-state reversible bleaching is proportional to the square root of the intensity of the absorbed light, inversely proportional to the square root of the chlorophyll concentration, and sensibly independent of temperature. The reversible bleaching is suppressed by oxygen, falling to a value of half of its (oxygen-free) maximum at an oxygen concentration of about 3×10^{-6} *M*. Chlorophyll dissolved in purified benzene or carbon tetrachloride exhibits no reversible bleaching. However, the addition of 1 per cent of methanol to a benzene solution restores the reversible bleaching to about half of its maximum value.

The irreversible bleaching approaches a maximum quantum yield of about 5×10^{-5} at high concentrations of oxygen. It is negligible in oxygen-free (methanol) solutions, and has a value of 2.5×10^{-5} when the oxygen concentration is 1×10^{-6} *M*. The yield decreases by about 15 per cent as the temperature is increased from 16° to 36°C.

The addition of small amounts (2×10^{-4} to 2×10^{-5} *M*) of lanthanum or cerous chloride to chlorophyll solutions results in a greatly increased reversible bleaching, with a slow first-order back-reaction. Traces of iodine produce similar but even more marked effects. In part, these effects appear to be related to the allomerization of chlorophyll (9).

REFERENCES

(1) Aronoff, S., and MacKinney, G.: J. Am. Chem. Soc. **65,** 956 (1943).

(2) Franck, J., and Livingston, R.: J. Chem. Phys. **9,** 184 (1941).

(3) Franck, J., and Sponer, H.: *Contribution à l'étude de la structure moléculaire*, p. 169. Desoer, Liège, Belgium (1948).

(4) Gaffron, H.: Ber. **60B,** 775 (1927).

(5) Kasha, M.: Unpublished communication, 1947.

(6) Lewis, G. N., Lipkin, D., and Magel, T.: J. Am. Chem. Soc. **64,** 1774 (1942).

(7) Livingston, R.: J. Phys. Chem. **45,** 1312 (1941).

(8) Livingston, R.: J. Phys. & Colloid Chem. **52,** 527 (1948).

(9) Livingston, R.: *Photochemistry of Chlorophyll in Photosynthesis in Plants*, p. 179. Iowa State College Press (1949).

(10) Livingston, R.: J. Soc. Dyers Colourists **65,** 781 (1949).

(11) Livingston, R., Sickle, D., and Uchiyama, A.: J. Phys. & Colloid. Chem. **51,** 775 (1947).

(12) Livingston, R., Watson, W., and McArdle, J.: J. Am. Chem. Soc. **71,** 1543 (1949).

(13) McBrady, J., and Livingston, R.: J. Phys. & Colloid. Chem. **52,** 662 (1948).

(14) Meyer, F., and Ronge, G.: Z. angew. Chem. **52,** 637 (1939).

(15) Perrin, F.: Compt. rend. **178,** 1978 (1924).

(16) Pollack, M., Pringsheim, P., and Terwoord, D.: J. Chem. Phys. **12,** 295 (1944).

(17) Porret, D., and Rabinowitch, E.: Nature **140,** 321 (1937).

(18) Rabinowitch, E.: *Photosynthesis*, Vol. I, p. 484 ff. Interscience Publishers, Inc., New York (1945).

(19) Rabinowitch, E., and Weiss, J.: Nature **138,** 1098 (1936), Proc. Roy. Soc. (London) **A162,** 251 (1937)

(20) Seidell, A.: *Solubilities of Inorganic and Metal Organic Compounds*, p. 1355. D. Van Nostrand Company, Inc., New York (1940).

(21) Zscheile, F., and Comar, G. Botan. Gaz. **102,** 463 (1941).

(22) Vavilov, S. I.: J. Phys. (U.S.S.R.) **7,** 141 (1943).

(23) Watson, W., and Livingston, R.: Nature **162,** 452 (1948).

THE SEPARATION OF THE ISOMERS OF IN^{114} AND IN^{112} IN AN ELECTRIC FIELD[1,2]

G. J. GOLDSMITH and E. BLEULER

Department of Physics, Purdue University, Lafayette, Indiana

Received September 1, 1949

The changes induced in a molecule by the isomeric transition of one of its member nuclei produce ions which can be collected on an electrode placed in a nonconducting solution of the compound. In^{114} dissolved in chloroform as the 8-hydroxyquinolinate was subjected to fields of the order of 7500 v./cm. for various periods up to 20 min. The deposit on the *anode* was found to have the expected half-life of 72 sec. of the ground state superimposed on a weak back-

---

[1] This article contains material from the thesis submitted by G. J. Goldsmith to the Faculty of the Graduate School of Purdue University in partial fulfillment of the requirements for the M. S. degree, August, 1948.

[2] This work was supported in part by the Office of Naval Research under Contract N6ori-222.

ground due to the long-lived upper state. In the case of the In^{112} isomers it was established by this method that the half-life of 10 min. must be ascribed to the ground state and the 21.5-min. period to the excited state.

INTRODUCTION

It is known that a change in the chemical state of an atom produced by an isomeric transition may make possible the separation of the ground state atoms from an equilibrium mixture of ground state and excited state. Segrè, Halford, and Seaborg (6) were the first to report such an effect, using it to separate the isomers of bromine by a chemical method. Williams (10) found a change in the oxidation state of tellurium caused by the isomeric transition.

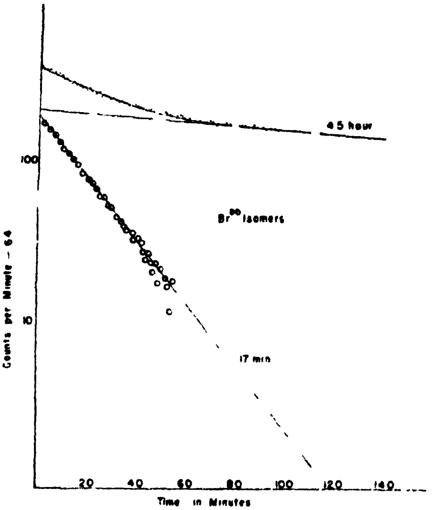

FIG. 1

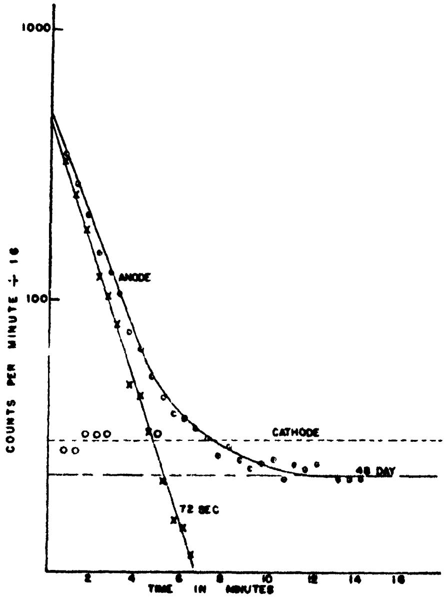

FIG. 2

FIG. 1. Separation of Br^{80} isomers in an electric field
FIG. 2. In^{114} isomers

An internally converted isomeric transition may lead to a considerable electron loss (ionization) because of cascading Auger effects which may follow the conversion itself (3, 9). If the active atom is contained in a molecule, this ionization may lead to the rupture of one or more molecular bonds. It should be possible then to collect the ionized fragments by subjecting them to an electric field and thus to concentrate the ground-state atoms. One requirement for the success of this method is that it be possible to prepare a solution of molecules containing the isomeric nuclei in which there is very little random ionization.

The first reported separation of isomers by an electric field from the liquid phase was that by Capron, Stokkink, and van Meerssche (1), who succeeded in separating the ground-state isomer of Br^{80} using 1,2-dibromoethane, silver electrodes, and a field of 150 v./cm. This result has been confirmed by Roussinow and Karamian (5) and also in our laboratory (figure 1). DeVault and Libby (9) succeeded in separating the Br^{80} isomers from the gas phase between parallel charged plates. Equal enrichment was found on both electrodes in this case.

IN^{112} AND IN^{114}

The existence of an isomeric pair for In^{112} has been reported by Smith (7) and by Tendam and Bradt (8), who found the characteristic growth-curve of a parent–daughter pair of nuclei with half-lives of 23 min. for the excited state and 9 min. for the ground state (8). More recent measurements (2) alter these values to 21.5 and 10 min., respectively. The excitation energy (2) is 154 Kev., and about 90 per cent of the transitions are internally converted. It was the original purpose of this research to confirm the half-life assignments by separating the isomers.

In^{112} can most conveniently be produced with the Purdue cyclotron in either of two manners: by alpha-particle bombardment of silver or by deuteron bombardment of cadmium. The alpha reaction on silver was found to be more satisfactory, since it produces fewer contaminating activities (table 1).

TABLE 1

Reactions of silver with alpha particles

REACTION	HALF-LIFE	RADIATIONS
$Ag^{107}(\alpha, n)\ In^{110}$	66 min.	β^+, K, γ
$Ag^{109}(\alpha, n)\ In^{112}$	21.5 min.	γ, e^-
	10 min.	β^-, β^+, K
$Ag^{107}(\alpha, 2n)\ In^{109}$	5.2 hr.	β^+, K, γ
$Ag^{109}(\alpha, 2n)\ In^{111}$	2.7 days	K, γ
$Ag^{107}(\alpha, p)\ Cd^{110}$	Stable	
$Ag^{109}(\alpha, p)\ Cd^{112}$	Stable	

For preliminary study of the separation process, In^{114} (produced in the Clinton Pile) was chosen in preference to In^{112} because of the longer half-life of the excited state of In^{114} (48 days). The energy of this excited state is 190 Kev., conveniently close to the energy of the 112 transition as reported above. Furthermore, the short period of the ground state (72 sec.) facilitates the observation of a separation.

CHEMICAL PROCEDURE

The problem at the outset was to find a suitable compound of indium which has the desired characteristics and which can be prepared rapidly. Our final choice was the 8-hydroxyquinolinate of indium (in chloroform solution), which has been utilized in an analytical procedure for the determination of indium reported by Moeller (4). Moeller's procedure for preparing this substance was followed almost exactly, except that at the end of the extraction, before subjecting it to the electric field, the chloroform solution of indium 8-hydroxyquinolinate was dried with silica gel.

In dealing with In^{112} produced by alpha-particle bombardments of silver, it was found desirable to add indium carrier to the target material and carry out a conventional separation of the indium previous to the preparation of the 8-hydroxyquinolinate.

EXPERIMENTAL RESULTS

It was found in the case of In^{114} that a field intensity of about 7500 v./cm. applied for 1 min. across 2 mm. between 2 x 3 cm. nickel electrodes produced the most satisfactory results. The 72-sec. period of the ground state was apparent for about 7 min. The separation factor, defined as the ratio of initial 72-sec. activity to 48-day background, was about 25. The maximum collection efficiency obtained was of the order of 1 per cent, i.e., approximately 1 per cent of the ground-state atoms produced by the isomeric transition during the collecting time were deposited on the electrode. It should be emphasized (figure 2) that this collection was obtained on the *anode;* the cathode showed only an equilibrium activity at a level comparable to the anode background.

The background activity resulting from collection of the equilibrium mixture of nuclei must be explained by random ionization due to causes other than the isomeric transition. The *rate* of collection of the background activity is found to *decrease* during the early stage of the collection. This is brought out by the fact that even after 10 min. of field application the separation factor remains rather high, roughly 10 to 15. (If the rate of collection were constant, a linear increase of the background activity with time would be observed, and would result, for example, in a 4:1 drop in the measured separation factor if the collection time were increased from 1 min. to 10 min.). The field therefore seems to have some sort of cleaning effect upon the solution. Attempts to put the conditions on a quantitative basis failed, apparently because it was not possible to control all the contributing factors in the solution. It was definitely established, however, in a series of about fifty separations, that lower fields and, for constant field, greater spacings, result in poorer separations.

When these optimum conditions were established, the procedure was applied to In^{112}, with the modification that the collection time was increased to 20 min. because of the longer half-life of the ground state. The time chosen represents a compromise: the total activity and therefore the statistical accuracy increase with the collection period, whereas the separation factor decreases slightly.

The analysis of the decay curves of the deposited activities is complicated by the presence of all radioactive indium isotopes listed in table 1. After subtraction of the 5.2-hr. and 2.7-day half-lives, the activity on the *anode* shows, superimposed on a 66-min. and 21.5-min. background, the 10-min. period of the ground state of In^{112} (figure 3). The separation factor obtained is considerably smaller than in the case of In^{114}. This may arise in part from the inferior purity of the cyclotron-produced preparations, but the main reason is the difference in half-lives of the two *ground* states. The effect may be easily illustrated by assuming a long half-life for the upper state and a short collection time T. Then simple but plausible considerations show that both the equilibrium activity B on the electrode and the number of ground-state ions N produced by isomeric transitions and deposited on the electrode would be proportional to the activity S of the solution and to the collection time: $B = c_1TS$, $N = c_2TS$ (c_1, c_2 = constants). The initial activity A (i.e., after the field is switched off) of the ground-state period (decay constant λ) would be $A = \lambda N = \lambda c_2TS$. The separation factor, defined as the ratio of the initial activities, then is

$$A/B = \lambda c_2/c_1$$

A closer analysis shows that λ must be replaced by the difference between the decay constants of the lower and upper states, if the half-lives are comparable.

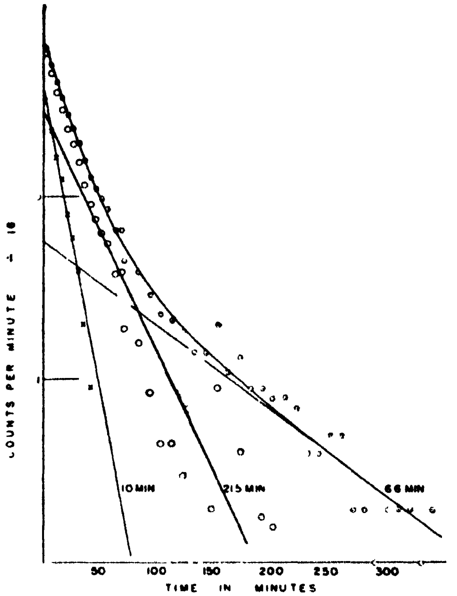

FIG. 3

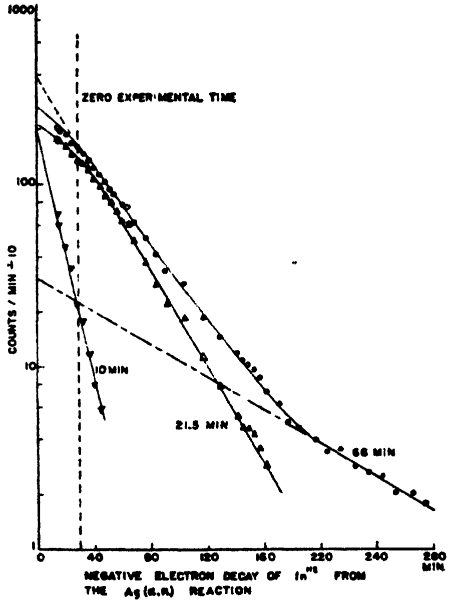

FIG. 4

FIG. 3. In^{112} isomers. ○, gross activity after subtraction of very long periods. ⊙, gross activity after subtraction of the 66-min. activity. ×, remaining 10-min. activity after subtraction of 21.5-min. period.

FIG. 4. Decay of In^{112} immediately after bombardment, showing growth curve. Measured on a sample of silver without further treatment after bombardment. "Zero experimental time" = time after bombardment that chemical purification of the indium is completed on the chemically treated samples. The 10-min. period is obtained from the difference between a true 21.5-min. curve and the experimental curve.

Then the expected separation factor for In^{112} is 6.4 per cent of the one for In^{114}. This result should be further modified by taking into account decay during the collection time and the observed diminution of the rate of background deposition with time. A detailed analysis was not possible, however, because of inadequacies in both experimental and theoretical knowledge.

No indication of any enrichment was obtained on the cathode. Similarly, the decay curve of the unseparated mixture, measured at the same time, showed no deviation from the 21.5-min. period (figure 4). (Immediately after bombardment, however, a growth curve is observed.)

These results show conclusively that the 10-min. period, enriched by the separation, represents the ground state of the isomeric pair of In^{112}.

THE SEPARATION MECHANISM

Because of the fact that the isomeric transition leads to the loss of at least several electrons, one might expect that the ground-state atoms are collected at the cathode. In both cases—the separation of Br^{80} from 1,2-dibromoethane and the extraction of $In^{112, 114}$ from indium 8-hydroxyquinolinate—the enrichment has been found on the *anode*. It would seem then, that not the initial charge of the fragment, but its subsequent history determines on which electrode it will be deposited.

In the case of bromine, it is probable that due to the electron loss a Br^+ ion is ejected from the molecule, since the bromine is bound by a single covalent bond. It must be assumed that it acquires a negative charge while drifting through the liquid. The reduction of a Br^+ ion to the Br^- state is precisely what one would expect in an aqueous solution. It may be possible that the dielectric constant of 1,2-dibromoethane (4.9) is sufficiently high to permit the same process. An alternate explanation may be that in a small percentage of the transitions the liberated Br has a negative charge and is deposited on the anode, while the Br^+ ions produced in most of the decays are merely neutralized (if neutralization only is possible but not a subsequent reduction to Br^-). The low collection efficiency is at least not incompatible with this assumption.

In the indium 8-hydroxyquinolinate molecule there is found a somewhat different situation. Here the indium occupies the center of an octahedron in the corners of which are alternate oxygen and nitrogen atoms. It is difficult to visualize how the processes of electron loss could result in the ejection of an unbound indium ion from the molecule. The experimental evidence (i.e., the fact that the ground-state atoms are found on the anode) further confirms this point of view, since we cannot conclude that a single unbound indium ion would have any tendency whatever to form a negative ion. One plausible explanation is that the internal conversion and Auger effect serve to alter the electronic structure in the vicinity of the indium atom in such a way that the rigid octahedral structure is destroyed. This distorted array of atoms may then collect electrons so that a negative ion is formed. An alternate explanation is that the electron loss results in decomposition of the molecule in such a manner as to leave an InO_n fragment which may either occasionally be formed as a negative ion or acquire a negative charge.

CONCLUSION

It has been shown that the separation of nuclear isomers of a metal is possible by subjecting an organic compound of the metal in a nonconducting solution to a high electric field. In the case of the In^{112} isomers, the assignment of half-lives to the two levels has been confirmed unambiguously. The mechanism of the separation is not clearly understood; it is felt that further investigation of simple cases, like the Br^{80}-separation, is highly desirable.

In In^{114} used in this research was supplied by the Clinton Laboratories of the Carbide and Carbon Chemicals Corporation, Oak Ridge, Tennessee, and obtained on allocation from the Isotopes Division, United States Atomic Energy Commission.

The authors wish to express their appreciation to H. L. Bradt for suggesting the problem, to D. J. Tendam for producing the many In^{112} samples necessary, and to T. H. Davies, K. Lark-Horovitz, W. F. Libby, and D. C. de Vault for helpful suggestions and discussions.

REFERENCES

(1) Capron, P. C., Stokkink, G., and Meerssche, M. van: Nature **157**, 806 (1946).
(2) Chowdary, S. A.: Unpublished thesis, Purdue University, 1949.
(3) Cooper, E. P.: Phys. Rev. **61**, 1 (1942).
(4) Moeller, T.: Ind. Eng. Chem., Anal. Ed. **15**, 270 (1943).
(5) Roussinow, L. I., and Karamian, A. S.: Compt. rend. acad. sci. U.R.S.S. **55**, No. 7, 599 (1947).
(6) Segrè, E., Halford, R. S., and Seaborg, G. T.: Phys. Rev. **55**, 321 (1939).
(7) Smith, R. N.: Phys. Rev. **61**, 389 (1942).
(8) Tendam, D. J., and Bradt, H. L.: Phys. Rev. **72**, 1118 (1947).
(9) Vault, D. C. de, and Libby, W. F.: J. Am. Chem. Soc. **63**, 3216 (1941).
(10) Williams, R. R., Jr.: J. Chem. Phys. **16**, 153 (1948).

REACTION OF POLYORGANOSILOXANE MONOLAYERS WITH AQUEOUS SUBSTRATES[1]

H. W. FOX, E. M. SOLOMON, AND W. A. ZISMAN

Naval Research Laboratory, Washington, D. C.

Received September 7, 1949

INTRODUCTION

In connection with a previous study of the surface-active properties of the polyorganosiloxanes or "silicones" (2) it was noted that the critical spreading pressure and the force–area (*F–A*) curves of all the substances investigated changed slowly with the time of contact of the monolayer with the water substrate. Preliminary experiments showed that the presence of acid or base in the substrate accelerated the change and could profoundly alter the shape of the *F–A* curves. This is a report of the investigation of the effects of time, pH, and various aqueous ions in the substrate on polyorganosiloxane monolayers adsorbed at the air–water interface.

The only difference in this investigation from the technique employed previously was the use of polytetrafluoroethylene ribbons 0.0005 in. thick to connect the waxed mica float to the sides of the tray of the Langmuir balance (3). The compounds used in this investigation were the same as before, with the addition of the ethoxy end-blocked siloxanes kindly supplied by Drs. M. J. Hunter and Shailer Bass of the Dow-Corning Corporation. The water of the substrate was distilled using a block-tin condenser. Allowing the filled tray with no film on it to stand for 21 hr. produced only 0.2–0.4 dyne/cm. pressure when the area was reduced to 1/30th, so that the increases in pressure observed were not due to accidental contamination. All measurements were made in a room kept at 20°C. ± 0.25°. All pH measurements were made with a line-operated Beckman pH meter.

---

[1] The opinions or assertions contained in this paper are those of the authors and are not to be construed as official or reflecting the views of the Navy Department.

FILMS ON PURE WATER

Figure 1 shows the effect of aging several types of monolayers in contact with water. There is a change with time in the *F–A* curves regardless of the type of polyorganosiloxane. The 2-hr. curve of figure 2 for the polymethylsiloxane heptadecamer shows that the change on water was slow enough to justify regarding the initial curves on water (usully taken within 15 min.) as reference curves. The noteworthy details of the observed changes are the gradual shortening of the highly compressible region and the increase in pressure at a given area for areas to the left of the "kink point" (small specific areas). There was no indication that the reaction causing the changes in the *F–A* curves was complete even after 93 hr.

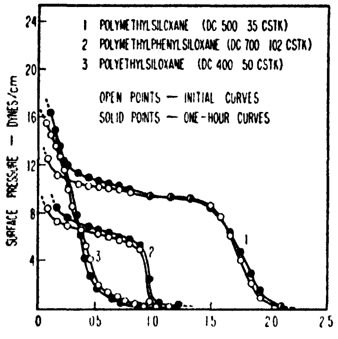

FIG. 1

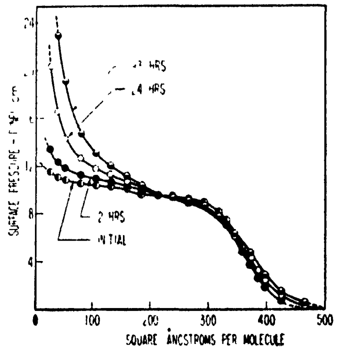

FIG. 2

FIG. 1. The force-area curves of polyorganosiloxane monolayers on distilled water
FIG. 2. Polymethylsiloxane heptadecamer aged on distilled water

A monolayer of the heptadecamer was aged on water at 35°C. to increase the rate of reaction. The salient difference in the curves obtained at this temperature was an observable reduction in limiting area (about 10 per cent in the first hour), whereas at 20°C. there was no change within experimental error even in 93 hr.

EFFECT OF ACID SUBSTRATES

Films of the same compound on 0.1 *N* sulfuric acid gave the *F–A* curves of figure 3. On this substrate, even the initial curve has lost its resemblance to the typical polymethylsiloxane curve on water. The initial curve resembles the initial curve for the polymethylsiloxane octamer on water (see figure 4). The plateau in the typical curve for a higher polymethylsiloxane is now only suggested by the inflection in the middle of the curve. An added feature is the progressive reduction of the limiting area, until after 24 hr. the film has disappeared. This effect was not peculiar to the heptadecamer but occurred with every polyorganosiloxane tried. It was established that the change was not caused by mechanical working of the film, since films allowed to remain in contact with the acid substrate for a given length of time before the first compression gave limiting areas comparable to those which had been worked several times to obtain a series of curves. An *F–A* curve was determined for a film allowed to remain on the acid substrate at pH 1.4 for 90 min. The acid in the substrate was carefully neutralized with potassium hydroxide and the *F–A* curve on the neutral substrate was the same as immediately before neutralization. Hence the state of the aged film was due to irreversible changes. The curves of figure 3 given by aged films resemble the curves of the polyethylsiloxanes on water of the earlier investigation (2), those for ethoxy end-blocked materials on acid reported by Hunter *et al.* (5), as well as those of the polyacrylates reported by Crisp (1). Curves for the linear octamer on 0.1 *N* sulfuric acid given in figure 4 show the same characteristics and indicate that the effect is general. Similar curves were obtained using DC 500 (35 centistokes) polymethylsiloxane fluid to produce the monolayer.

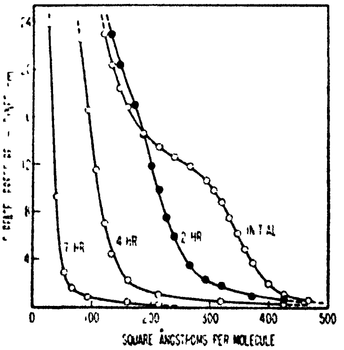

FIG. 3

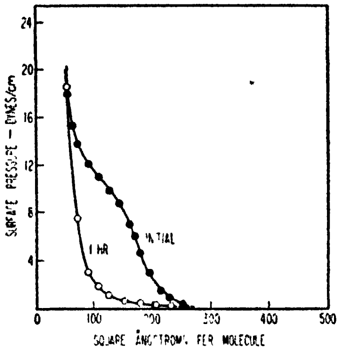

FIG. 4

FIG. 3. Polymethylsiloxane heptadecamer on 0.1 *N* sulfuric acid
FIG. 4. Polymethylsiloxane octamer aged on 0.1 *N* sulfuric acid

Figures 5 and 6 show the effect of weaker concentrations of sulfuric acid on films of the heptadecamer. On 0.001 *N* acid the change in shape of the curve is barely more rapid than on water. On 0.01 *N* acid the rate of change in shape of the curve is intermediate between that of the 0.1 *N* and 0.001 *N* acids.

A study of polymethylsiloxanes on substrates containing acids with other anions, such as nitric, hydrochloric, and orthophosphoric acids, gave similar results. Clearly, the rates of reaction, as measured by the rate of reduction of the limiting area (A_L), depend on pH rather than normality. In figure 7 are the curves obtained for the polymethylsiloxane heptadecamer on 0.1 *N* phosphoric acid (pH 1.9). The changes illustrated by these curves are like those shown for sulfuric acid, but they take place more slowly. The curves on 0.01 *N* acetic acid resembled those on water. It was not possible to obtain comparable results with

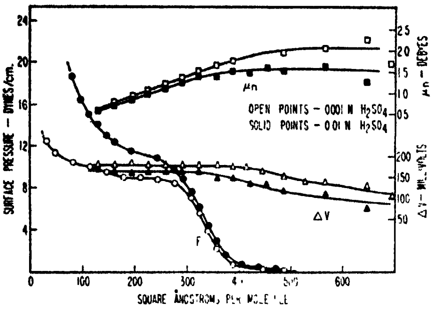

Fig. 5

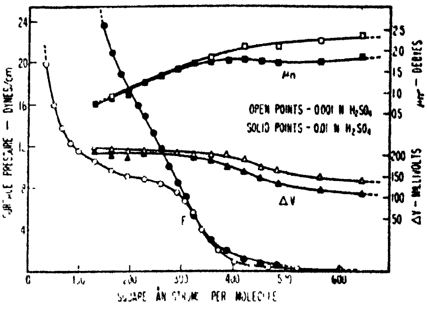

Fig. 6

Fig. 5. Initial curves of polymethylsiloxane heptadecamer on sulfuric acid
Fig. 6. Polymethylsiloxane heptadecamer aged 1 hr. on sulfuric acid

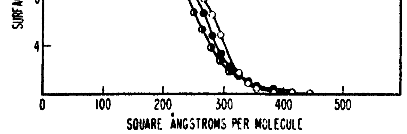

Fig. 7

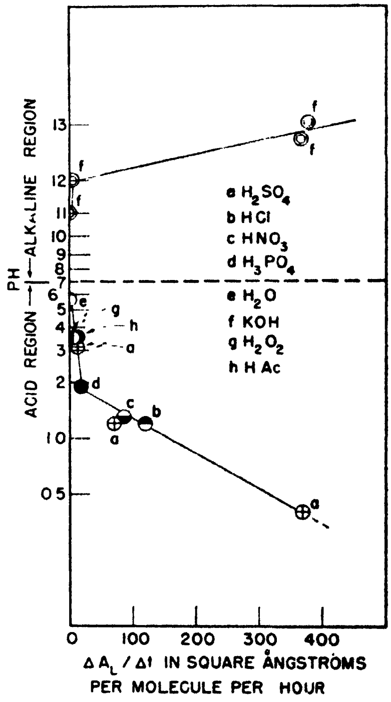

Fig. 8

Fig. 7. Polymethylsiloxane heptadecamer on 0.1 *N* phosphoric acid
Fig. 8. The rate of change of limiting area with time during the first hour for the polymethylsiloxane heptadecamer on various substrates.

0.1 *N* acetic acid, since at this concentration the acid depressed the surface tension of the water substrate by an amount (2–3 dynes) which obscured the movement at the plateau of the *F–A* curves. Displacements of the limiting areas with time were recorded for the ethoxy end-blocked decamer on both sulfuric and hydrochloric acid.

The dependence of $\Delta A_L/\Delta t$ on pH for the polymethylsiloxane heptadecamer is shown in figure 8 for a number of substances, the rate $\Delta A_L/\Delta t$ falling off sharply as the pH rises from 1.3 to 2.0. Figure 8 was arranged to show the symmetry of the effects of acid and alkali by cutting the logarithmic ordinate at pH 7 and continuing with an inverted pH scale. Acetic acid and hydrogen peroxide at pH 3.6 gave rates close to zero. An extrapolation of the curve to zero intersects the pH axis at pH 5.7, which is the pH of water in equilibrium with the carbon dioxide in air.

If the compressibilities of the films at considerable pressures (say 18 dynes/cm.) are compared, it is found that the rate of change of compressibility with time varies roughly as the rate of change of limiting area with time, being greater for values of pH near 1.2 than for values near 2.0, and again being dependent on pH rather than on the nature of the ions dissolved in the substrate. The compressibility of the compounds of shorter chain length is always smaller at high pressures than is that of the long-chain compounds. However, when these latter compounds are spread on acid at pH 1.2, their compressibilities quickly decrease to values comparable to those of compounds of shorter chain length.

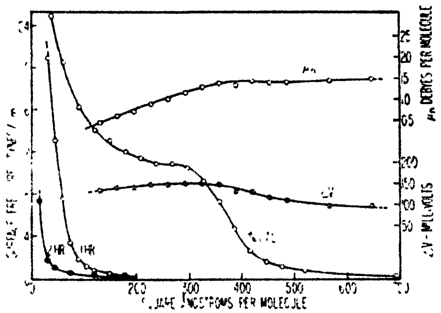

FIG. 9. Polymethylsiloxane heptadecamer aged on 0.1 *N* potassium hydroxide

The polymethylsiloxane octamer was shown in the earlier investigation not to coil, since its *F–A* curve lacked the plateau and kink-point characteristic of the homologs of longer chain length (2). The octamer films on water did not change in shape with time, but the whole curve was shifted to the left, i.e., to smaller limiting areas. A drop of the octamer held near a talc-covered water surface scattered the talc, showing that the octamer was appreciably volatile. Thus the shift in the curve could have been due to loss of material from the film by evaporation. On 0.1 *N* sulfuric acid, the octamer curve changed shape as well as became reduced in limiting area (figure 4), the shape of the 1-hr. curve resembling those given by the higher homologs under the same conditions.

EFFECT OF ALKALINE AND OTHER SUBSTRATES

The behavior of the heptadecamer monolayers on 0.1 *N* potassium hydroxide at pH 12.8 is shown in figure 9. The change in shape of the curves is like that on acid, but the reduction in limiting area with time is greater. At pH 12.0 (0.01 *N* potassium hydroxide) the rate of change is much slower. Indeed, it is only a little more rapid than on water (figure 8). At concentrations less than 0.1 *N*, acid is more effective than base, but at higher concentrations the reverse becomes true. At the highest pH obtainable with ammonium hydroxide (*ca.* 12.0) no significant acceleration of reaction was observed.

F–A curves were also obtained on substrates containing dissolved salts (sodium sulfate, sodium chloride, calcium chloride, ammonium acetate, ammonium chloride, copper sulfate, all at 0.1 *N*; ammonium molybdate, 0.01 *N*; and hydrogen peroxide (3 per cent). No effects could be observed other than those attributable to the pH.

ELECTRICAL PROPERTIES OF MONOLAYERS

Given in figures 5, 6, and 9 are surface potential *vs.* area data (ΔV–*A*) and the normal component (μ_n) of the apparent dipole moment *vs.* area (μ_n–*A*) obtained for the heptadecamer simultaneously with the *F–A* curves. In contrast to earlier measurements on distilled water (2), where μ_n for the uncompressed films was zero, μ_n for uncompressed films on acid or basic solutions was finite and remained nearly constant as the film was compressed. This initial surface-potential difference was present even on 0.001 *N* sulfuric acid,—a concentration which showed essentially no acceleration in rate of change of the *F–A* curves. The slow rate of change of the ΔV–*A* curves is reflected in the μ_n–*A* curves. There is no longer the maximum at close packing observed earlier (2). Instead, the μ_n–*A* curve remains rather flat until the film is close-packed and then begins to drop off linearly. There is a slight increase in moment as the film ages, but its significance has not been established. With the electrodes used in this study, the potential difference between a water surface or an acid surface and the electrode was positive, whereas if the substrate contained a base the potential difference was negative. The effect of spreading a polyorganosiloxane monolayer on the surface was always to decrease the potential difference. That is, the sign of ΔV was the same regardless of the nature of the substrate; hence the normal moment vector, μ_n, of each silicone monomer was always directed *away* from the water interface into the air.

DISCUSSION

The slow changes in the *F–A* curves around pH 7.0 at 20°C., at a rate essentially independent of the nature of the ion present in the substract, are probably the result of limited adsorption of hydrated hydrogen (or hydroxide) ions. That it is not the result of extensive adsorption of ions is shown by the fact that the *F–A* and ΔV–*A* curves below 9 dynes/cm. pressure (at specific areas larger than that represented by the kink-point) do not change with time and are reversible. Extensive adsorption of ions would also result in an increase in the pressure required to pull the adsorbed polymer chains out of the water into the coiled configuration, thus requiring a shift toward higher pressures in the plateau of the curve. On the other hand, it becomes more difficult to tilt the coils out of the interface, as shown by the constantly increasing pressures at specific areas less than that represented by the kink-point. This may be due either to the presence of the few adsorbed ions which exert a measurable repulsion toward each other when removed from the "neutralizing" influence of the neighboring ions in the water or, possibly, to the adsorption of water molecules on the siloxane chain. At 35°C. the reaction is significantly accelerated, so that the limiting area starts to fall and the shape of the curve changes, as is the case with films on acid or basic substrates.

Below pH 3 (or above pH 11) another mechanism prevails. The instantaneous reduction in ability to coil, shown by the difference in shape of the initial *F–A* curves, is probably due to extensive adsorption of hydrated hydrogen (or hydroxide) ions. The subsequent irreversible shift in the limiting area of the curves is undoubtedly due to hydrolysis of the polymer catalyzed by the adsorbed ions and resulting in scission of the polymer chains. The recent literature gives many instances of the rupture of the Si—O bond by concentrated acid and base (6, 7). These scissions produce disproportionation and are used to adjust the average chain length of the polymers where recondensation follows the rupture. On the film balance, however, the situation of a monolayer on an aqueous substrate is such that recondensation following rupture is unlikely. Every Si—O bond is in contact with an ideal hydrolyzing medium at close packing, and it is reasonable to visualize the mechanism as involving a rupture of the Si—O linkage with the formation of two terminal —OH groups which recondense only infrequently, thus:

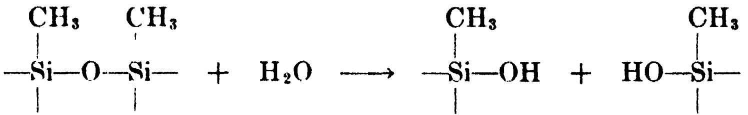

$$-\underset{\mathrm{CH_3}}{\overset{\mathrm{CH_3}}{\mathrm{Si}}}-\mathrm{O}-\underset{\mathrm{CH_3}}{\overset{\mathrm{CH_3}}{\mathrm{Si}}}- \;+\; \mathrm{H_2O} \longrightarrow -\underset{\mathrm{CH_3}}{\overset{\mathrm{CH_3}}{\mathrm{Si}}}-\mathrm{OH} \;+\; \mathrm{HO}-\underset{\mathrm{CH_3}}{\overset{\mathrm{CH_3}}{\mathrm{Si}}}-$$

Additional evidence for the presence of strongly hydrophilic groups on the polymer molecules is the decreasing compressibility. Eventually the fragments will become short enough so that each fragment will be solubilized by the two hydroxyl groups attached. In this way the loss of material from the film is explained. It is unlikely that the small fragments would volatilize, since the presence of two hydroxyl groups on each should reduce the vapor pressure to a small value. There was no way of ascertaining whether the Si—C bond was attacked. Any cyclic structures formed during these processes probably react further leaving no residue, since the film disappears entirely when the reaction goes to completion.

This conception of the rupture of the siloxane chains, resulting in fragments terminated by hydroxyl groups, is lent additional weight by the similarity in shape of the curves obtained by us for a partially degraded polymer to that of the curves obtained by Hunter *et al.* (5) for the ethoxy end-blocked silicones on 0.01 *N* hydrochloric acid. In the presence of acid or base, the ethoxyl radical can be expected to hydrolyze very quickly to hydroxyl to give polymers which have terminal hydroxyl groups similar to those produced by scissions of the chain.

Figure 8 shows that the rate of reduction of limiting area (a measure of the rate of reaction) is about twice as great for the potassium hydroxide substrate at pH 13 as for the mineral acid substrates at pH 1.0. This is not unreasonable if we can draw an analogy between the hydrolysis of the silicones and the well-known mechanisms for hydrolysis of esters (4). Acid hydrolysis, given the proper environment, would be reversible, since the two terminal hydroxyl groups produced by each scission can recondense with the elimination of water. The excess of water present in the film-balance experiments drives the equilibrium in the direction of hydrolysis. The net excess of scissions over recondensations produces the rate of reaction noted in the curves. If it is assumed that the rates of scission at equivalent concentrations of OH^- and H^+ are the same, alkaline hydrolysis should be faster, since it is irreversible. The hydroxyl groups produced by the scissions in this case react immediately with the alkali present to form negatively charged, substituted silicate ions which cannot recondense. Moreover, to produce solubility in the presence of alkali, it is probably not necessary to reduce the fragments to as small a size as is the case in the presence of acid. Thus the number of scissions needed to lose a given fraction of the film is smaller for alkali than for acid. The sum of these two effects, then, probably is responsible for the observed greater reaction velocity in the presence of strong potassium hydroxide.

In reviewing the surface-potential data described above, several salient points appear. According to figures 5, 6, and 9, the value of μ_n per heptadecamer molecule is 1.5 debyes for the uncompressed films when spread on acid or base even at such dilutions as 0.001 *N*. This is in contrast to the zero moment found for films spread on distilled water at large areas (2). But the maximum moment found on water (at close packing) was also 1.5 debyes. The moment is constant at 1.5 debyes until the limiting area is reached (*ca.* 400 Å.^{2}/molecule) and then decreases so that μ_n extrapolated to zero area is zero for all the curves measured. The most noteworthy change in μ_n with time was the reduced scatter of the measurements on acid and basic substrates at low pressures. Within the precision of the measurements, the value of ΔV remained essentially unchanged at low pressures.

The μ_n–A curves corroborate and extend this picture of the behavior of polyorganosiloxane films on neutral, acidic, and basic solutions. At low pressures on neutral solution, where adsorption is small, the polymer chains are oriented at random on the water, so that on the average no net vertical component of the electric moment exists. When the molecules begin to be confined by increasing pressure, each must straighten out into a rod-like shape so oriented that every oxygen atom is in the water; the silicon atoms are arranged immediately above in a slight zig-zag alternately on either side of a vertical plane passed through the line formed by the oxygen atoms. This arrangement evidently results in the maximum vertical moment at close packing. Increase in pressure can result only in disorganization by buckling out of the interface with accompanying decrease in moment. On acids or bases, however, all the monomeric dipoles are completely oriented, even at low surface pressures, probably because of the local electrical fields of the adsorbed hydrogen or hydroxide ions which increase the attraction of the siloxane chain for the interface. This orientation, which would produce the maximum moment at all areas larger than the limiting area, is shown here by the constancy of the moment until the limiting area is reached.

CONCLUSIONS

It may be concluded that the silicones are subject to degradation by water, especially in the presence of dilute or concentrated acid or base, or at high temperature. For the rate of degradation to be appreciable, however, there must be a large interface between the silicone and the water, as is the case on a film balance. Such an interface may be present in an emulsion, aerosol, or a porous polymeric form.

REFERENCES

(1) Crisp, D. J.: J. Colloid Sci. **49**, 161 (1946).
(2) Fox, H. W., Taylor, P. W., and Zisman, W. A.: Ind. Eng. Chem. **39**, 1401 (1947).
(3) Fox, H. W., and Zisman, W. A.: Rev. Sci. Instruments **19**, 274 (1948).
(4) Hammett, L. P.: *Physical Organic Chemistry*, p. 356. McGraw-Hill Book Company, Inc., New York (1940)
(5) Hunter, M. J., Gordon, M. S., Barry, A. J., Hyde, J. F., and Heidenreich, R. D.: Ind. Eng. Chem. **39**, 1389 (1947).
(6) Kreible, R. H., and Elliott, J. R.: J. Am. Chem. Soc. **68**, 2291 (1946).
(7) Patnode, W., and Wilcock, D. F.: J. Am. Chem. Soc. **68**, 358 (1946).

THE ENTROPY OF THE CHLORIDE ION AT 12.5°C.

H. D. CROCKFORD AND J. L. HALL

Venable Chemical Laboratory, University of North Carolina, Chapel Hill, North Carolina

Received September 14, 1949

Eastman (2), from the data obtained by Richards from thermal cell studies using mercury–mercurous chloride electrodes and electrolytes of 0.01 *m* solutions of hydrochloric acid, lithium chloride, sodium chloride, and potassium chloride, calculated a value of 28.0 E.U. for the chloride ion at 15°C. Bernhardt and Crockford (1), using silver–silver chloride electrodes in solutions of the above electrolytes and in addition potassium chloride, rubidium chloride, and cesium chloride, determined the entropy of the chloride ion in various concentrations of the electrolytes at 30°C. The average value for 0.01 *m* solutions was 27.1 E.U., a lower value than that obtained by Eastman at 15°C.

The purpose of the work reported in this paper was to determine the entropies of the chloride ion at the same concentrations employed by Crockford and Bernhardt, but at a temperature of 12.5°C. Such a study would give a check on the lower value obtained by Eastman and would give an indication of the effect of temperature change on the entropy of the ion.

EXPERIMENTAL PROCEDURE

For this work the silver–silver chloride electrode was used. The apparatus, methods of purification, methods of calculation, and general procedures used by Crockford and Bernhardt (1) were employed. The concentration ranges were from 0.01 to 1.00 *m*. The two temperatures were 0° and 25°C., thus giving data for the calculation of the ionic entropy at a mean temperature of 12.5°C.

TABLE 1

Electromotive force data

MOLALITY	E.M.F.	MOLALITY	E.M.F.
NaCl		KCl	
0.0107	0.01568	0.0102	0.01622
0.0254	0.01429	0.0263	0.01478
0.0519	0.01285	0.0500	0.01353
0.2518	0.00949	0.2506	0.01025
0.5011	0.00791	0.4806	0.00887
1.0033	0.00607	1.0001	0.00734
NH_4Cl		HCl	
0.0101	0.01718	0.0108	0.00837
0.0268	0.01478	0.0251	0.00685
0.0500	0.01438	0.0594	0.00531
0.2610	0.01127	0.2693	0.00272
0.5003	0.01004	0.4956	0.00163
0.9979	0.00874	0.9870	0.00050

TABLE 2

Summary of entropy values

ELECTROLYTE	MOLALITY					
	0.01	0.025	0.050	0.250	0.500	1.000
	E.U.	E.U.	E.U.	E.U.	E.U.	E.U.
NaCl ...	27.4	26.1	24.8	21.6	20.1	18.5
KCl .	27.9	26.7	25.4	22.4	21.1	19.7
NH_4Cl.	28.3	26.9	25.7	22.9	21.7	20.5
HCl	28.1	26.4	25.4	22.7	21.5	20.5
Average at 12.5°C.	27.9	26.5	25.3	22.4	21.1	19.8
Average at 30.0°C.	27.1	25.4	24.2	21.4	20.0	18.8

In the calculations the entropies of transfer calculated by Eastman were used. The entropies of silver and silver chloride at 12.5°C. were calculated from the specific heat data of Eastman and Milner (3) and of Rodebush and Rodebush (4). The values obtained were 22.21 E.U. for silver chloride and 9.75 E.U. for silver.

DATA AND RESULTS

The values of the E.M.F. obtained for cells using various molalities of the electrolytes are given in table 1. The entropy values obtained from the data of table 1 were plotted and the entropy values at rounded molalities were obtained. These values are given in table 2, together with the average values obtained by Crockford and Bernhardt at 30°C. The values obtained by Eastman at 15°C. for the 0.01 *m* solutions were: sodium chloride, 27.7 E.U.; potassium chloride, 27.6 E.U.; hydrochloric acid, 28.2 E.U. Figure 1 shows the entropy values obtained at 12.5°C. and at 30°C. by Bernhardt and Crockford plotted as a function of temperature. This curve is typical of the curves obtained for the other electrolytes.

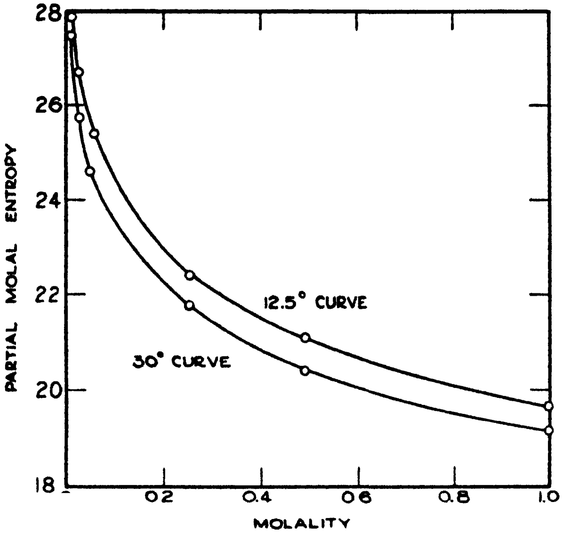

FIG. 1 Entropy-concentration relationships in potassium chloride solutions

An examination of the data shows that our values obtained at 12.5°C. for the entropy of the chloride ion in 0.01 *m* sodium chloride, potassium chloride, and hydrochloric acid, using the silver–silver chloride electrode, agree well with those obtained by Eastman from data based on the use of the mercury–mercurous chloride electrode at 15°C. The values obtained by us at 12.5°C. are consistently higher in value than those obtained by Crockford and Bernhardt at 30°C., a somewhat unexpected result, although a conclusion indicated by the Eastman and the Crockford and Bernhardt data. The variation is less in the cases of sodium chloride and potassium chloride, especially at the lower concentrations, than in the cases of ammonium chloride and hydrochloric acid. The average difference is about 1 E.U.

SUMMARY

The absolute entropy of the chloride ion in six different concentrations of hydrochloric acid, ammonium chloride, sodium chloride, and potassium chloride at a mean temperature of 12.5°C. has been calculated from data obtained from thermocells, using silver–silver chloride electrodes.

REFERENCES

(1) **Bernhardt, H. A., and Crockford, H. D.**: J. Phys. Chem. **46**, 473 (1942).

(2) **Eastman, E. D.**: J. Am. Chem. Soc. **50**, 292 (1928).

(3) **Eastman, E. D., and Milner, R. T.**: J. Chem. Phys. **1**, 450 (1933).

(4) **Rodebush, W. H., and Rodebush, Esther**: *International Critical Tables*, Vol. V, p. 84. McGraw-Hill Book Company, Inc., New York (1929).

STUDIES IN VAPOR-LIQUID EQUILIBRIA. II

The Binary System Triethylene Glycol–Water[1]

HENRY WISE,[2] THEODORE T. PUCK,[3] AND CRAWFORD F. FAILEY

Departments of Medicine and Biochemistry, University of Chicago, Chicago 37, Illinois

Received August 4, 1949

In a previous report (2) a new dynamic method for the determination of vapor pressures of liquids was described, which proved particularly useful for measurements in the region of low pressures. This method has now been extended to the study of vapor–liquid equilibria of two-component systems. As in the previous case, the experimental procedure involves impingement of a vapor-laden gas stream on a polished mirror maintained at a constant temperature. A simple means is provided for progressive variation of the concentrations of the condensible components in the gas stream until a composition is found at which a condensate just begins to form on the mirror surface or just tends to disappear from it. Measurements carried out in this way yield the equilibrium vapor density of each component at the temperature of the target. From these data the fugacities may be computed by means of the gas laws. This procedure has been applied to the binary system triethylene glycol[4]–water, for which the equilibrium compositions in the vapor phase have been determined experimentally and for which the composition of the liquid phase in equilibrium with the vapor mixture has been calculated with the aid of a graphical procedure based on Gibbs' equation for the variation in partial molal quantities with composition (1).

---

[1] This work was aided in part by the Bartlett Memorial Fund and in part by a grant from the Dr. Wallace C. and Clara A. Abbott Memorial Fund of the University of Chicago.

[2] Present address: Jet Propulsion Laboratory, California Institute of Technology, Pasadena 4, California.

[3] Present address: Department of Biophysics, University of Colorado Medical Center, Denver 7, Colorado.

[4] Triethylene glycol = 2,2′-ethylenedioxydiethanol.

PROCEDURE

The apparatus used for the measurement of the vapor–vapor equilibria of the binary system is shown schematically in figure 1. Its component parts have previously been described in detail (2). Each liquid is delivered to a vaporizing heater at a constant predetermined rate by a syringe whose piston is advanced by a synchronous motor attached to a variable-speed gear mechanism. A carrier stream of dry nitrogen gas whose flow is accurately regulated and measured passes successively over the water and glycol vaporizers and transports the volatilized materials to the thermostated mirror which reveals the occurrence of condensation. Since the rates of vaporization of each liquid and the rates of flow of nitrogen gas (measured by the differential-type flowmeters) can be accurately known, the composition of the resulting vapor mixture impinging on the target can be readily calculated.

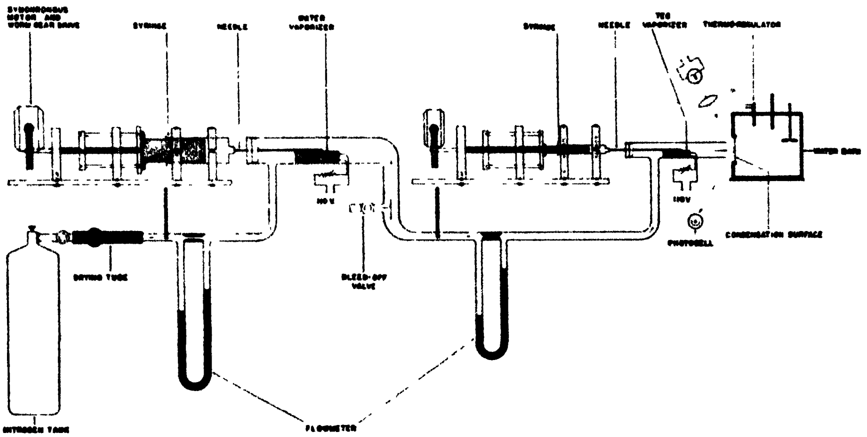

FIG. 1. The apparatus

In order to permit rapid changes in the composition of the vapor mixture carried toward the target by the inert gas stream, a simple bleed-off valve has been inserted between the two flowmeters. By this means any desired aliquot of the gas mixture containing a known amount of the first vapor may be admitted to the second vaporizing chamber through the second flowmeter. Thus, in the diagram of figure 1, any desired degree of dilution of the glycol vapor by a stream containing a definite amount of water vapor can be effected. The experimental technique is thereby reduced to a determination of the volume of nitrogen gas of known relative humidity required to produce a saturated composition when mixed with a given quantity of glycol vapor and brought to the temperature of the target.

To determine a point on the vapor–vapor equilibrium curve, the nitrogen flow is begun and both vaporizers are started. The rates of vaporization may be arbitrary at first, just so neither component is introduced in an amount sufficient to saturate by itself the carrier gas stream. The bleed-off valve is then adjusted until the final mixture achieves a composition equivalent to the saturation point at the temperature of the mirror, as evidenced by the fact that it becomes possible to form or to remove a condensate by very small successive adjustments of the bleed-off valve in opposite directions. As shown in the previous discussion (2), this condition indicates the attainment of equilibrium between the condensate and the gas stream at the temperature of the mirror. In the measurements described here, the formation and disappearance of a condensate were determined by means of a recording milliammeter attached to the output of a photocell which was illuminated by a light beam reflected from the mirror's surface. An undersaturated gas stream removes condensate from the mirror and thus raises the reflectivity of its surface, so increasing the photoelectric current; similarly, a composition corresponding to supersaturation depresses it. The existence of an equilibrium composition is indicated by constancy of the photocell output for 5 or 10 min. while the stream continues to flow against the mirror on which a small film of condensate is already deposited. Hence equilibrium is approached from both sides by alternately supersaturating and undersaturating the gas mixture. Each such determination provides a single point on the vapor–vapor equilibrium curve. Additional points are obtained by repeating the procedure with different rates of vaporization of the two components.

RESULTS

The water and triethylene glycol were purified by distillation, the latter at reduced pressure. The boiling point of the glycol fraction selected was 177-178°C. (corr.) at 22.5 mm. of mercury. Measurement of the saturated vapor densities was carried out at temperatures of 20.00°C., 25.03°C., and 29.05°C., respectively. The experimental results are summarized in column A of table 1. From these data the corresponding partial pressures and activities have been calculated by means of the gas laws (columns B and C). The partial pressures of triethylene glycol covered by these measurements lie in the region of 10^{-3} to 10^{-4} mm. of mercury, while those of the water are between 2 and 30 mm. of mercury. Each of the recorded points gave a clear definition of the end-point.

The values for the vapor pressure of pure triethylene glycol at the three experimental temperatures obey the relationship

$$\log_{10} P = \frac{-3170}{T} + 7.758 \tag{1}$$

and the average heat of vaporization over the interval 20–29°C., calculated on this basis, is 14.5 kilocal. per mole.

DETERMINATION OF THE EQUILIBRIUM COMPOSITION OF THE LIQUID PHASE

The composition of the liquid solution in isothermal equilibrium with the vapor mixture may be obtained from the resulting vapor–vapor curve by use of the relationship

$$N_1 \, d(\ln a_1) + N_2 \, d(\ln a_2) = 0 \tag{2}$$

TABLE 1

Experimental determination of saturated vapor densities of the binary system triethylene glycol–water at three temperatures

A EQUILIBRIUM VAPOR DENSITY		B PARTIAL PRESSURE		C $\frac{p}{p^0}$ = ACTIVITY	
Triethylene glycol	Water	Triethylene glycol	Water	Triethylene glycol	Water
Temperature, 20.00°C. ± 0.04°					
(*g./l.*) × *10*³	(*g./l.*) × *10*³)	*mm.* Hg	*mm.* Hg		
0.00711	0	0.000866	0	1.000	0
0.00617	2.20	0.000751	2.24	0.867	0.128
0.00359	5.20	0.000437	5.28	0.505	0.301
0.00296	7.02	0.000360	7.13	0.416	0.407
0.00196	9.05	0.000238	9.19	0.275	0.524
0.00139	10.84	0.000170	11.01	0.196	0.628
0.00117	11.63	0.000142	11.82	0.164	0.674
		0	17.535*	0	1.000
Temperature, 25.03°C. ± 0.04°					
0.01082	0	0.00134	0	1.000	0
0.00853	2.45	0.00106	2.53	0.791	0.106
0.00617	4.25	0.000763	4.38	0.569	0.184
0.00442	8.75	0.000547	9.00	0.408	0.379
0.00363	11.12	0.000450	11.50	0.336	0.483
0.00277	13.96	0.000343	14.41	0.256	0.605
0.00235	15.43	0.000291	15.90	0.217	0.668
0.00190	17.29	0.000235	17.80	0.175	0.748
		0	23.80*	0	1.000
Temperature, 29.05°C. ± 0.04°					
0.01417	0	0.00178	0	1.000	0
0.01158	2.54	0.00145	2.65	0.816	0.088
0.01038	3.12	0.00130	3.27	0.731	0.109
0.00958	4.63	0.00120	4.84	0.675	0.161
0.00752	9.00	0.000944	9.42	0.531	0.313
0.00617	12.77	0.000774	13.38	0.435	0.444
0.00498	16.27	0.000625	17.07	0.352	0.567
0.00242	21.16	0.000304	22.12	0.171	0.734
		0	30.13*	0	1.000

* *International Critical Tables.*

which defines the effect of isothermal changes in composition on the escaping tendency of the two constituents in the mixture (1). At equilibrium the composition of the film which forms on the mirror must obey the equation:

$$N_2 = \frac{1}{1 - \frac{d(\log a_2)}{d(\log a_1)}} \tag{3}$$

TABLE 2

Activities of binary system triethylene glycol–water

Component 1 is water; component 2 is triethylene glycol

a_2	a_1	$-\log a_2$	$-\log a_1$
t = 20.02°C. ± 0.04°			
1	0	0	∞
0.867	0.128	0.062	0.893
0.505	0.301	0.297	0.521
0.416	0.407	0.381	0.390
0.275	0.524	0.561	0.281
0.196	0.628	0.708	0.202
0.164	0.674	0.785	0.171
0	1	∞	0
t = 25.03°C. ± 0.04°			
1	0	0	∞
0.791	0.106	0.102	0.975
0.569	0.184	0.245	0.735
0.408	0.379	0.389	0.421
0.336	0.483	0.474	0.316
0.256	0.605	0.592	0.218
0.217	0.668	0.663	0.175
0.175	0.748	0.757	0.126
0	1	∞	0
t = 29.05°C. ± 0.04°			
1	0	0	∞
0.816	0.088	0.088	1.055
0.731	0.109	0.136	0.963
0.675	0.161	0.171	0.793
0.531	0.313	0.275	0.504
0.435	0.444	0.361	0.353
0.352	0.567	0.453	0.246
0.171	0.734	0.767	0.134
0	1	∞	0

$$N_1 = \frac{1}{1 - \dfrac{d(\log a_1)}{d(\log a_2)}} \tag{3'}$$

Consequently, since the rate of change of the activity of one component with respect to that of the other may be calculated from the experimental measurements, the corresponding mole fraction of each component in the liquid phase can be computed.

In table 2 values of log a_1 and log a_2 are listed for the three experimental temperatures. These have been plotted in figure 2 (upper curve) and a single curve has been drawn through them ignoring temperature differences. This seems permissible since the points obviously scatter, with the 25° points lying sometimes between the 20° points and the 29° points, and sometimes above or below them. It may also be seen from a plot of a_1 *versus* a_2 that those curves are roughly parallel, with no definite temperature coefficient. Great care must be exercised in the preparation of the log a_1 *vs.* log a_2 plot, because of its sensitivity to small errors in the experimental measurements. Any uncertainty of the data will become especially pronounced near the two extremes of the curve. The logarithmic plot is governed by the condition that

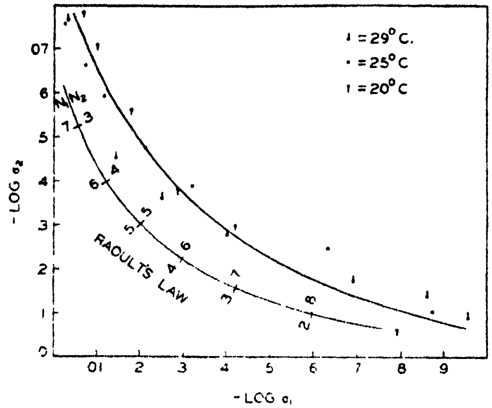

FIG. 2

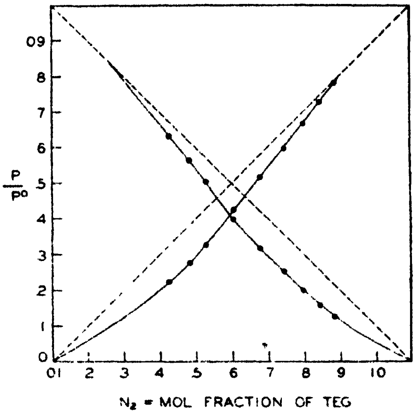

FIG. 3

FIG. 2. Logarithmic plot of activities of triethylene glycol (a_2) and water (a_1) in temperature range from 20.0°C. to 29.0°C.

FIG. 3. Vapor–liquid phase diagram for the binary system triethylene glycol–water

TABLE 3

Calculation of the composition of liquid phase in equilibrium with the vapor

$-\log a_1$	$-\log a_2$	a_1	a_2	$-\frac{d \log a_2}{d \log a_1}$	N_2
0.2	0.653	0.631	0.222	2.070	0.326
0.25	0.562	0.562	0.274	1.617	0.382
0.3	0.489	0.501	0.324	1.350	0.429
0.4	0.374	0.398	0.423	0.995	0.501
0.5	0.287	0.316	0.516	0.733	0.577
0.6	0.225	0.251	0.596	0.552	0.644
0.7	0.176	0.200	0.667	0.435	0.697
0.8	0.137	0.159	0.730	0.345	0.743
0.9	0.107	0.126	0.782	0.275	0.784

$$\frac{d^2(\ln a_2)}{d(\ln a_1)^2} = \frac{d\left(-\frac{N_1}{N_2}\right)}{d(\ln a_1)} \tag{4}$$

so that this second derivative is always negative and less than zero, since

$dN_1/d(\ln a_1)$ must always be greater than zero for a stable solution. The slope of the curve therefore continually decreases with no straight portions or inflexions, and asymptotically approaches the theoretical curve based on Raoult's law (figure 2), since a_1/N_1 and a_2/N_2 approach unity for pure liquids. Values for N_1 and N_2 computed with the aid of the chord-area method (3) for the evaluation of the derivatives which appear in the denominator of equations 3 and 3′ are listed in table 3. On the basis of these results the vapor–liquid phase diagram shown in figure 3 was constructed. In view of the nature of the graphical procedure used for the evaluation of the composition of the liquid phase, its composition cannot be known with the same degree of accuracy as that of the vapor. Because of the sensitivity of the plot to small fluctuations in the measured points, some ambiguity exists in drawing the curve through the experimental points of figure 2. However, these calculations show that the system triethylene glycol–water exhibits negative deviations from Raoult's law.

DISCUSSION

The procedure described above is of greatest value in the determination of equilibrium composition data for solutions with at least one slightly volatile constituent, for it eliminates the necessity for direct measurement of very small vapor densities which is the major source of inconvenience and error when conventional methods are employed. However, a plot of the activity of one component against that of the other and the deviations from a straight line observed in such a diagram are not indicative of the sign of the deviation from Raoult's law. A straight line is approached by the curve as the solution becomes more nearly ideal, and deviations from a straight line are merely an index of the relative deviation from ideality of one component with respect to that of the other. Under these circumstances the graphical method for the computation of the composition of the liquid phase in equilibrium with the vapor mixture becomes useful, since it eliminates the need for additional experimental measurements.

For this purpose figure 2 may be also used as a kind of nomogram for the rapid estimation of the composition of the liquid phase. In this figure a lower curve is added corresponding to Raoult's law; the numbers above it give values of N_2 and those below, N_1. For any point on the experimental curve the composition of the liquid phase may be obtained by using a pair of triangles to find that point on the Raoult's law curve whose tangent is parallel to the tangent through the chosen experimental point. The activities may also be read from the Raoult's law curve, using the fact that the intersection of any ordinates with the two curves represents equal values of a_2, while intersection of any abscissa with the two curves defines two points with the same a_1. Such procedures are less accurate but more rapid than computation and enable one to estimate the general properties of the system.

A system with two coexistent liqud phases would present a log a_2 *vs.* log a_1 curve with a break at the fixed values of a_1 and a_2 corresponding to the coexistence of the two liquid phases. The composition of each phase may be obtained from the slope of the curve on the appropriate side of the discontinuity.

SUMMARY

A dew-point method for experimental measurement of the saturated vapor densities of each component of a binary system over the entire range of composition is described. It is particularly applicable to solutes of slight volatility. The equilibrium vapor-phase compositions of aqueous triethylene glycol solutions have been determined by this method. Good definition of the end-point was obtained for partial pressures of triethylene glycol as low as 10^{-4} mm. of mercury.

A method of analysis of these data is described which permits computation of the composition of the liquid phase in equilibrium with any saturated vapor mixture. The method depends upon evaluation of the derivatives of the activities of the components with respect to each other. Such an analysis of the triethylene glycol-water system indicates the existence of negative deviations from Raoult's law.

REFERENCES

(1) LEWIS AND RANDALL *Thermodynamics and the Free Energy of Chemical Substances.* McGraw-Hill Book Company, Inc., New York (1923).

(2) PECK AND WISE: J. Phys. Chem. **50**, 329 (1946).

(3) YOUNG AND VOGEL. J. Am. Chem. Soc. **54**, 3025 (1932).

RATE OF DISSOCIATION OF MONOMETHYLOLUREA IN HYDROCHLORIC ACID SOLUTIONS

LAURANCE H. DONNALLY

Donnally Research and Consulting Laboratory, 484 Fourth Avenue, San Francisco, California

Received August 8, 1949

INTRODUCTION

Urea and formaldehyde react reversibly in aqueous solutions to form various crystalline substances, such as monomethylolurea and dimethylolurea. Smythe (4) has investigated the kinetics of formation of monomethylolurea in the absence of buffers and in the range of pH from 4 to 6; his initial concentrations were 1.88–2.52 moles per liter. Crowe and Lynch (1) have measured the equilibrium and rates of association and dissociation of monomethylolurea at a single hydroxide-ion concentration of 0.05 M by a polarographic method. It is the purpose of this investigation to present the rates of dissociation of monomethylolurea at hydrochloric acid concentrations of 0.005 to 0.25 M, with added salt concentrations to 0.35 M in potassium chloride.

The dissociation and formation of monomethylolurea may be represented as follows:

$$H_2NCONHCH_2OH \rightleftharpoons H_2NCONH_2 + HCHO \tag{1}$$

However, there are evidently side reactions also since, at concentrations of monomethylolurea higher than approximately 0.01 M, a white precipitate is formed. For this reason the measurements were all made at a concentration of approximately 0.0057 M.

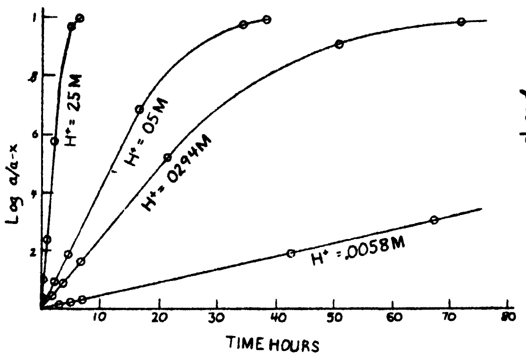

FIG. 1.

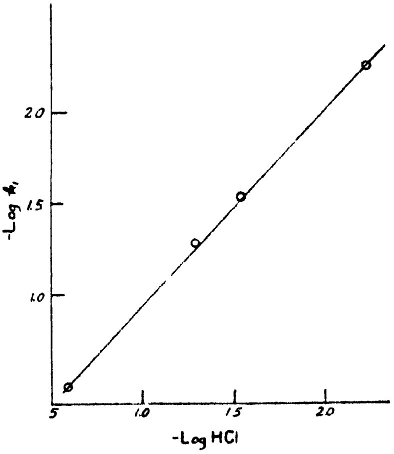

FIG. 2.

FIG. 1. Dissociation of monomethylolurea at various hydrogen-ion concentrations, where a is the initial monomethylolurea concentration at 18.8°C.

FIG. 2. Plot of $-\log k_1$ *versus* $-\log$ (HCl)

TABLE 1

The specific rate of dissociation of monomethylolurea in hydrochloric acid solutions, with and without added potassium chloride, at 18.8°C.

KCl	HCl, MOLES PER LITER			
	0.0058	0.029	0.050	0.25
moles/liter				
None	0.0056	0.028	0.052	0.32
0.35	0.0068		0.061	
0.23		0.034		
0.25				0.33

EXPERIMENTAL

Monomethylolurea was synthesized by the method of Einhorn and Hamburger (3). The melting point of the thoroughly dried material was 111°C. (uncorr.) The rate of the dissociation was followed by measurements of the formaldehyde concentration by a method of Donnally (2) which consists in neutralizing the sample to approximately pH 7 with sodium bicarbonate, adding excess sodium bisulfite, allowing to stand for 15 min., adding acid to pH 3, titrating the excess bisulfite with iodine solution, finally adding sodium carbonate solution, and titrating the formaldehyde bisulfite compound. The total amount of the monomethylolurea was measured by adding to the sample sufficient of an equimolal mixture of disodium hydrogen phosphate and sodium dihydrogen phosphate to make the total phosphate concentration 0.3 M. The sample was then heated on a steam bath for 1 hr. and finally assayed for formaldehyde as before. The monomethylolurea concentration should be below 0.006 M for 99 per cent dissociation of the compound under these conditions.

In figure 1 is shown a plot of log $a/(a - x)$, where a is the initial concentration of monomethylolurea and x is the concentration of formaldehyde at time t against the time in hours. Initial monomethylolurea concentrations varied from 0.0054 to 0.0061 M and the hydrochloric acid concentrations in different experiments were 0.0058, 0.0295, 0.05, and 0.25 M. Owing to the formation reaction and perhaps also to the side reactions the plots deviate toward the end of the reactions from a straight line. However, it is possible to compare the reaction rate constants, k_1, by use of the slope of the curve at zero time.

In figure 2 is shown a plot of log k_1 against log (HCl). In table 1 the data are tabulated; also included are values obtained at concentrations of potassium chloride up to 0.35 M.

SUMMARY

The rate of dissociation of monomethylolurea at hydrochloric acid concentrations of 0.0058 to 0.25 M and at 18.8°C. was measured. The rate was found to be directly proportional to the concentration of hydrochloric acid in that range of hydrogen-ion concentration.

REFERENCES

(1) Crowe, G. A., Jr., and Lynch, C. C.: J. Am. Chem. Soc. **70**, 3795 (1948).
(2) Donnally, L. H.: Ind. Eng. Chem., Anal. Ed. **5**, 91 (1933).
(3) Einhorn, A., and Hamburger, A.: Ber. **41**, 24 (1908).
(4) Smythe, Lloyd E.: J. Phys. & Colloid Chem. **51**, 369 (1947).

COMMUNICATION TO THE EDITOR

ADDITION TO THE PAPERS "THE ORIGIN OF THE BI-IONIC POTENTIAL ACROSS POROUS MEMBRANES OF HIGH IONIC SELECTIVITY. I AND II."

J. Phys. & Colloid Chem. **53**, 1211, 1226 (1949)

In reviewing the literature on the bi-ionic potential (B.I.P.) important work by K. H. Meyer and P. Bernfeld (Helv. Chim. Acta **28**, 962, 980 (1945)) was missed.

These investigators have reported some additional measurements on B.I.P. chains which check with those of previous workers. More important, they have applied the fixed-charge theory to this problem, anticipating thereby, in a somewhat different terminology, major aspects of our later much more extensive treatment of this topic. Readers interested in the B.I.P. will find it illuminating and well worthwhile to refer to the quoted papers by Meyer and Bernfeld.

KARL SOLLNER.

Laboratory of Physical Biology
Experimental Biology and Medicine Institute
National Institutes of Health
Bethesda 14, Maryland
February, 1950

BOOKS RECEIVED

THEILHEIMER, W. *Synthetic Methods of Organic Chemistry, A Thesaurus.* Vol. II. Translated from the German by A. Ingberman in collaboration with the author. Interscience Publishers, Inc., 215 Fourth Ave., New York 3. 1949. 324 pp Price: $7.50.

WEISSBERGER, ARNOLD (Editor). *Technique of Organic Chemistry. Vol. I, Part II. Physical Methods of Organic Chemistry.* Interscience Publishers, Inc., 215 Fourth Ave., New York 3. 1949. 1023 pp. Price: $12.50

WYCKOFF, RALPH W. G. *Electron Microscopy. Technique and Applications.* Interscience Publishers, Inc., 215 Fourth Ave., New York. 1949. 248 pp.; 202 illustrations. Price: $5.00.

ZWIKKER, C., AND **KOSTEN,** C. W. *Sound Absorbing Materials.* Elsevier Publishing Company, Inc., 215 Fourth Ave., New York 3. 1949. 174 pp. Price: $3.00.

Colloid Science. Vol. II. Reversible Systems. Edited by H. R. Kruyt. Elsevier Publishing Company, Inc., 215 Fourth Ave., New York 3. 1949. 753 pp. Price: $11.50.

Organic Syntheses. Vol. 29. C. S. Hamilton (Editor-in-Chief). John Wiley and Sons, Inc., 440 Fourth Ave., New York 18. 1949. 119 pp. Price: $2.00.

"Surface Chemistry." Papers presented for a discussion at a joint meeting of the Société de Chimie Physique and the Faraday Society held at Bordeaux from October 5 to October 9, 1947. Interscience Publishers, Inc., 215 Fourth Ave., New York 3. 1949. 334 pp. Price: $6.00.

PENETRATION OF CELLULOSE FIBERS[1]

ALFRED J. STAMM AND HAROLD TARKOW

Forest Products Laboratory,[2] Forest Service, U. S. Department of Agriculture

Received April 27, 1949

INTRODUCTION

Some liquids can penetrate only the fiber cavities and interfiber spaces of natural and synthetic cellulosic materials, while others can penetrate the fibers themselves. Some liquids which by themselves cannot penetrate fibers can, however, replace other liquids within a fiber. These phenomena, which are closely related to swelling and shrinking, will be described and an attempt made to explain why the various systems differ.

All natural and most synthetic cellulosic materials are formed in an aqueous medium. The natural state is therefore that in which the fibers are completely swollen in water. It has been shown, in the case of both cotton (3) and wood (17), that the shrinkage of the fiber substance on drying is practically equal to the volume of water lost. This means that the water held within a fiber is not held in rigid capillaries. On the basis of a capillary theory, the capillaries must be considered distortable to the degree that their volume always coincides with the volume of liquid which they contain. To avoid confusion with normal rigid capillaries, one of the authors has called these "transient capillaries" (19, 20). Saying that water is held in transient capillaries approaching molecular dimensions is equivalent to saying that water is held in solid solution. The term "solid solution" may be preferred by many, as it immediately implies the flexibility of the discrete minute volumes of liquid that are dispersed throughout the solid.

PENETRATION INVOLVED IN SPECIFIC VOLUME DETERMINATIONS

Regardless of the concept for the mechanism of penetration, water practically adds its volume to the volume of the dry cellulosic material up to the fiber-saturation point. A slight decrease in volume of the fiber–water system is, however, believed by many to occur as a result of a slight compression of the surface-held water or a more compact orientation of the surface-adsorbed water. Those who object to the concept of water being compressively adsorbed do so on the basis of some data giving unbelievably high compression values.

Hermans (9) contends that the slight decrease in volume of the fiber–water system is not due to compression of the water, but to the existence of submicroscopic voids of relatively small total volume in the cell-wall substance, into which water can enter without contributing to the overall volume. The high heat of adsorption and the large decrease in entropy of the initially adsorbed water suggest, however, that something does occur to decrease its specific volume.

---

[1] Presented before the Fiber Symposium which was held under the joint auspices of the Divisions of Colloid Chemistry and Cellulose Chemistry at the 115th Meeting of the American Chemical Society, San Francisco, California, March 28, 1949.

[2] Maintained at Madison, Wisconsin, in coöperation with the University of Wisconsin.

This question concerning the specific volume of water adsorbed on cellulose is not an easy one to answer. The whole problem hinges on what medium should be used to determine the true dry specific volume of cellulose or lignocellulosic substance. The medium must completely penetrate all natural voids of a fiber without being attracted with so large a force that it could be compressed. Helium will meet the second requirement, but there is still controversy as to whether it meets the first requirement. Stamm and Hansen (22) have obtained a value of 0.632 for the specific volume of alpha cellulose from cotton linters in helium. Lyons (11) has shown that this value agrees exceedingly well with a value calculated from Meyer and Mische's (12) most recent x-ray crystal structure data. Walker[3] obtained a quite similar value for standard cotton of 0.634. Specific volume values for cellulose determined in water are somewhat lower, and values determined in benzene and toluene are somewhat higher (4, 6, 13, 22, 26). On the basis of helium giving the true values of specific volume, water must either be compressively adsorbed or become so oriented on adsorption as to occupy a smaller volume, and benzene and toluene must give incomplete penetration. In this case, the average density of the adsorbed water up to the fiber-saturation point should range from about 1.05 to 1.11 for the different cellulosic and lignocellulosic materials, according to the various available data (19, 20, 22). If water gives the true volume, helium, as well as benzene and toluene, does not penetrate the fiber completely.

EXPERIMENTAL MEANS OF DETERMINING FIBER PENETRATION

The total amount of a liquid lost from or taken up by a cellulosic material on drying or soaking can be readily followed by determining its change in weight. This is not a gage of the amount of liquid that leaves or penetrates the fiber walls, as it also includes changes in the amount of liquid held in the permanent capillary structure, such as the fiber cavities and interfiber spaces. The amount taken up by the cell wall can, however, be followed by adsorption measurements from the vapor phase or shrinking and swelling measurements of the isolated cell walls.

Although the fiber cavities and interfiber spaces are sufficiently small to depress the vapor pressure of a liquid slightly, condensation will normally occur in them only at relative vapor pressures of 0.999 and greater (19). Hence, if adsorption measurements are made at several experimentally controllable high relative vapor pressures and the corresponding moisture content–relative vapor pressure curve is extrapolated to unit relative vapor pressure, the moisture content value so obtained is within experimental error of the value believed to correspond to the saturation point of the fiber walls. In the case of wood, data for moisture content and relative vapor pressure extrapolated through the last accurately controllable relative vapor pressure point, about 0.98, give a fiber-saturation point of about

---

[3] F. Walker: Ph. D. Thesis, Department of Chemistry, McGill University, Montreal, Canada, 1937.

30 per cent. Theoretically, at unit relative vapor pressure the entire capillary structure should be saturated, which for woods of different specific gravities should range from 200 to 300 per cent. This means that a sharp upward break must occur in the curve above a relative vapor pressure of 0.98, which is presumably due to a break in the size-volume relationship of the capillaries when going from the larger transient cell-wall capillaries to permanent structural capillaries. This would be expected in the light of knowledge of the microstructure of wood (20).

In a lignocellulosic material like wood, in which the fibers are held together in a continuous structure by means of the lignin middle lamella, shrinkage normally begins when the moisture content falls below the fiber-saturation point. If the rate of moisture removal is too great, shrinkage stresses may occur at the surface even though the overall moisture content exceeds the fiber-saturation point. Furthermore, if some of the cell cavities are completely filled with water—that is, if they contain no air bubbles—the water in the cavities will evaporate only when the outside relative vapor pressure has dropped below a value corresponding to the relative vapor pressure of water in the permanent pores of the pit membranes. In the meantime, however, some moisture will have left the cell walls; thus shrinkage will occur although the moisture content exceeds the fiber-saturation point.

In the case of less structurally bonded cellulosic materials, such as paper and fabrics, shrinkage may begin, especially in the original cycle of dehydration above the fiber-saturation point as a result of drawing together of the fibers. With such materials, it is preferable to determine fiber penetration by adsorption measurements from the vapor phase.

In the case of thin cross sections of wood, the volumetric shrinking and swelling transmitted to the external dimensions are practically equal to the dimension change of the total lignocellulose material contained in the specimen, when water and other liquids that do not swell wood more than water does are removed from or adsorbed by the wood. This is true because the fiber cavities do not, on the average, change in volume as wood shrinks and swells, except when the swelling is beyond that in water (2, 14, 17). This has been proven by the constancy of the permeability of thin cross sections of wood to air of different relative humidity (18), and by the fact that the shrinkage of such sections, S, is equal, on the basis of volume of water per unit weight of dry wood (17, 24), to the green volume, dry-weight specific gravity of the wood, G, times the fiber-saturation point of wood, f, thus:

$$S = fG \tag{1}$$

The constancy of the dimensions of the cell cavities on swelling and shrinking is undoubtedly due to the peculiar orientation of the micells in the cell walls. There is evidence that a thin lamina exists adjacent to the lumen or the fiber cavity in which the micellar orientation is approximately at right angles to the long cell axis (1, 27). Such an orientation would tend to restrain dimensional changes of the fiber cavity. Furthermore, the micells in this lamina may be reinforced by proteinaceous material of the dead protoplasm. Internal buckling may be observed during pronounced swelling beyond the water-swollen condition. In the case of wood fibers swelling in concentrated sodium hydroxide, the fiber cavities become almost completely closed as a result of internal swelling.

CORRELATION OF SWELLING WITH PROPERTIES OF THE LIQUID

With this background in mind, it is interesting to compare the penetration of various liquids into the fibers of cellulose and wood.

Nonpolar liquids, such as straight-chain, aromatic, and terpene hydrocarbons, carbon bisulfide, and carbon tetrachloride, penetrate cellulosic fibers and swell them to only a slight extent. Somewhat more polar liquids, such as ethyl ether, chloroform, benzaldehyde, aniline, chlorobenzene, and bromobenzene, penetrate and swell cellulosic fibers more, but still to a limited degree. The presence of traces of water enhances their penetrating and swelling power greatly. Hermans (9) has strikingly shown the effects of small quantities of water in glycerol on the swelling of cellulose in glycerol. He demonstrated visibly that the water diffuses first, thus making an easier pathway for the glycerol. Acetone and various esters of low fatty acids penetrate and swell fibers to a still higher degree. Alcohols and fatty acids vary greatly in their penetrating and swelling power, according to their molecular weight. Methanol is adsorbed by cellulose and swells wood almost as much as water (figure 1). The penetrating and swelling power falls off rapidly, however, when advancing in the homologous alcohol series from one to five carbon atoms. A similar but less rapid decrease in penetrating and swelling power occurs when advancing in the fatty acid homologous series.

Only a few organic liquids have been found to swell wood beyond the swelling in water: namely, formic acid, formamide, lower primary amines, pyridine, and some of its related compounds.

The differences in penetrating and swelling power of these various liquids for cellulosic fibers have been chiefly attributed to differences in polarity of the liquids. DeBruyne (5), using the swelling data of Hasselblatt (8) for birch, found that by plotting $(\epsilon-1)^{1/2}$, in which ϵ is the dielectric constant of the liquid, against the volumetric swelling, he obtained a linear relationship passing through the origin. If, however, water is more thoroughly removed from some of these liquids and others are added to the experiment, the relationship is no longer valid (19).

Figure 2 gives the volumetric swelling of thin cross sections of wood in a large number of water-free organic liquids plotted against the dielectric constant of the liquids. If each compound type is considered separately, there is a rough correlation between swelling and dielectric constant, especially in the case of benzene derivatives, but collectively the correlation is poor. Poor correlation is also obtained when the dipole moment is plotted against the swelling, again excepting the benzene derivatives, as is shown in figure 3. The relationship between the surface tension of the liquid and the swelling (figure 4) also gives poor correlation, except in the case of benzene derivatives. Interfacial surface tension, which is a measure of the attractive force of cellulose and lignocellulosic materials for the liquid rather than the attractive force of the liquid for itself, as in the case of

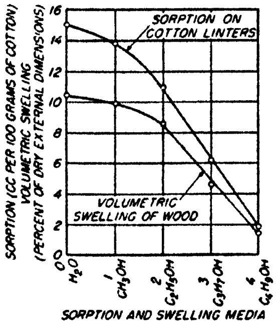

FIG. 1

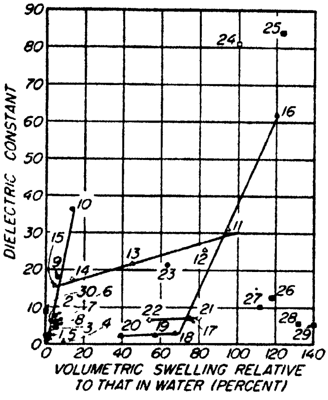

FIG. 2

FIG. 1. Sorption of water and monohydric alcohols by cotton and by white pine wood (15, 17).

FIG. 2. Volumetric swelling of pine and spruce wood in organic liquids plotted against the dielectric constants of the liquids (19).[4]

○ 1, carbon tetrachloride; 2, chloroform; 3, ethyl ether

● 4, benzene; 5, toluene; 6, aniline; 7, chlorobenzene; 8, bromobenzene; 9, benzaldehyde; 10, nitrobenzene

△ Alcohols: 11, methyl; 12, ethyl; 13, propyl; 14, *n*-butyl; 15, amyl

▲ Acids: 16, formic; 17, acetic; 18, propionic; 19, valeric; 20, oleic

◇ Acetates: 21, methyl; 22, ethyl

◆ 23, acetone

□ 24, water

■ Nitrogen compounds: 25, formamide; 26, pyridine; 27, 2-picoline; 28, piperidine; 29, *n*-butylamine; 30, quinoline

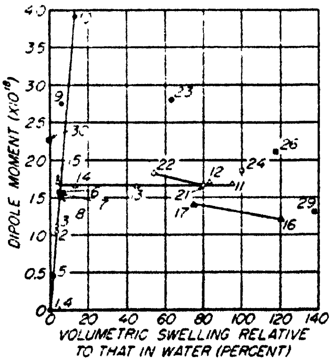

FIG. 3

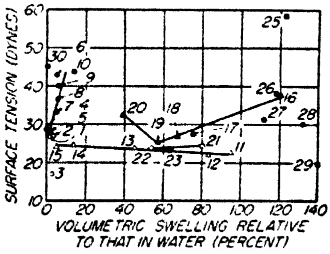

FIG. 4

FIG. 3. Volumetric swelling of pine and spruce wood in organic liquids plotted against the dipole moments of the liquids (19).[4] Symbols and numbers have the same significance as in figure 2.

FIG. 4. Volumetric swelling of pine and spruce wood in organic liquids plotted against the surface tension of the liquids (19).[4] Symbols and numbers have the same significance as in figure 2.

---

[4] A. N. Nayer: Ph.D. Thesis, University of Minnesota, Minneapolis, Minnesota, 1948.

surface tension, should give better correlation. Unfortunately, however, no one has found a method of making the measurements for such systems.

The most successful correlation between penetrating power or swelling and a property of the liquid appears to be with the tendency for the liquid to form hydrogen bonds. Unfortunately, only limited data are available for the relative tendency for liquids to form hydrogen bonds with methanol (7). Figure 5 gives the relationship between the intensity of hydrogen bonding of different liquids for hydroxyl groups and the volumetric swelling of wood in these liquids. The intensity of hydrogen bonding is measured by the amount of shift in characteristic vibration frequency of the hydroxyl group in methanol when methanol is brought in contact with the liquids in question. Except for a few points the correlation is good.

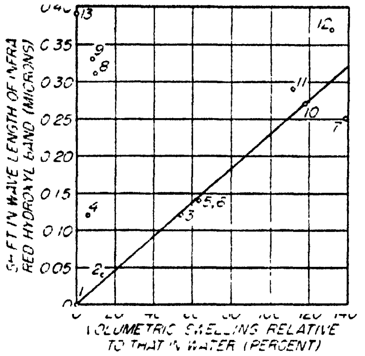

FIG. 5

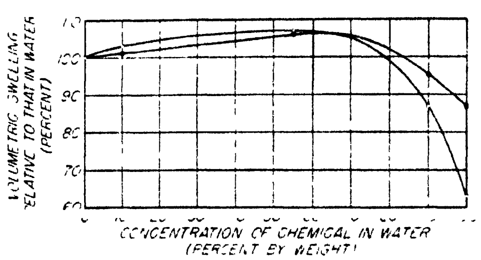

FIG. 6

FIG. 5. Relationship between the intensity of hydrogen bonding of different liquids for hydroxyl groups and the volumetric swelling of wood in these liquids (7).[4] 1, benzene; 2, nitrobenzene; 3, ethyl acetate; 4, benzadeldehyde; 5, acetone; 6, dioxane; 7, *n*-butylamine; 8, di-*n*-butylamine; 9, tri-*n*-butylamine; 10, pyridine; 11, 2-picoline; 12, piperidine; 13, quinoline.

FIG. 6. Volumetric swelling of cross sections of Sitka spruce in water-acetone and water-ethylene glycol monoethyl ether systems.[5]

According to the literature (6), di-*n*-butylamine and tri-*n*-butylamine show a large tendency to form hydrogen bonds with hydroxyl groups and thus, like *n*-butylamine, would be expected to give high swelling. The fact that they do not is perhaps explainable on the basis of steric hindrance. If the tendency for hydrogen bonding as determined by Gordy (7) had been determined with only slightly flexible polyhydroxides, such as cellulose, instead of the mobile monohydroxide methanol, he might have found lower values for the shift in vibration frequency for the amines containing more than one butyl group, as then the added groups might have prevented the amine group from approaching sufficiently near to the immobile hydroxyl groups of cellulose. The same argument could be applied to quinoline in contrast to pyridine, but it does not apply to benzaldehyde. No explanation is at present available for the low swelling by this liquid.

Although the correlation of swelling with the tendency to form hydrogen bonds is quite good, there is little question that molecular size is also of importance in controlling penetration and swelling. The fact that the secondary and tertiary amines and quinoline swell wood to such a small degree may also be due to their large molecular volumes. This is illustrated in figures 1 to 4 by the data for methyl to amyl alcohols. These alcohols would not be expected to have greatly different hydrogen-bonding tendencies, but they do show large differences in their adsorption by cellulose and their swelling of wood.

---

[5] Obtained by L. V. Peakes while at the Forest Products Laboratory.

PENETRATION OF SOLUTIONS INTO FIBERS

Solutions may act quite differently in penetrating and swelling fibers than does the solvent alone. In some cases, the rate of penetration is materially decreased even though the final equilibrium swelling may be increased (14, 15). An extreme case which illustrates this was obtained in a series of tests to determine the penetration of a saturated solution of magnesium chloride into thin, oven-dry cross sections of wood. It took 58 days to swell them to the same degree that matched sections are swollen in water in 1 day. When the water-swollen sections were transferred to a saturated solution of magnesium chloride containing sufficient excess magnesium chloride to saturate the water in them, the sections swelled to an equilibrium value of about 1 per cent beyond that attained in water in 9 days. In contrast, the sections swollen directly in the saturated magnesium chloride solution had not attained this equilibrium swelling in 100 days.

Saturated magnesium chloride, when placed on the surface of dry wood, remains there as spherical drops. It is quite apparent then that a saturated magnesium chloride solution does not tend to wet wood. The magnesium chloride has a very high affinity for water, as shown by the fact that the vapor pressure of water in a saturated solution is reduced to one-third of normal (16). It appears that the magnesium chloride solution does not penetrate the fiber and that only small increments of water can be taken away from the solution at a time to penetrate the fiber. Magnesium chloride then diffuses into this small amount of water, and the cycle is repeated. The process is slow because diffusion is into molecularly held rather than bulk water. When the wood is first swollen completely in water, the structure is opened up, so that diffusion readily occurs into polymolecularly held water, in which case the blocking effect is small.

The penetration and the swelling of the fibers beyond the swelling in water alone can be explained on the basis of an equilibrium being established between the force of adsorption of the fiber for the solvent, the solution pressure of the solute in the solvent, and the structural resistance of the fiber to swelling (17, 19). It has been shown that the equilibrium swelling of fibers beyond the swelling in water is a function of the specific volume of salt in solution. The swelling in all cases is less than the volume of salt taken up, thus indicating that some water is displaced. Salt is at first taken up without any appreciable swelling occurring. Both the solution pressure of the salt and the structural resistance of the wood exceed the force with which the last few increments of water are held by the wood. Water is hence displaced as salt diffuses into the fiber. The work necessary to displace more water increases with each increment of water displaced below the fiber-saturation point, as is indicated by an increased reduction in the equilibrium vapor pressure. The resistance to displacement of water finally exceeds the structural resistance force, and the fiber swells. The solution pressure of appreciably soluble salts in high concentration is the predominating force which becomes satisfied by diffusion, tending to make the salt concentration within the fiber equal to that outside of the fiber. This is done at first by displacing water from the fiber by overcoming the attractive force of the fiber for water and then by overcoming structural resistance (17).

This mechanism for the swelling of fibers in aqueous solutions beyond that attained in water applies not only to swelling in inorganic salt solutions, but may also apply to swelling in aqueous solutions of organic compounds that have an appreciable solution pressure. Figure 6 gives data[5] for the volumetric swelling of cross sections of Sitka spruce in water–acetone and water–ethylene glycol monoethyl ether systems.

REPLACEMENT OF PENETRATING AGENTS BY NONPENETRATING AGENTS

Although nonpolar liquids do not penetrate fibers by themselves, they can replace polar liquids in which they are soluble. The same is true for large polar molecules, which penetrate wood only partially by themselves. The case of *n*-butyl alcohol replacing methyl alcohol may again be cited.

It has been shown that, when the liquid replacing water is a polar one, such as acetone or ethylene glycol monoethyl ether, the replacement may be made complete (21). When such liquids are in turn replaced by a nonpolar liquid, such as benzene, toluene, petroleum ether, or waxes, the replacement is not complete (21). The amount of intermediate mutual solvent that cannot be replaced with nonpolar liquids has a volume equal to the volume of water originally held in the first monomolecular layer of the completely water-swollen wood. This is about 20 per cent of the volume of the water held within the fiber. The fiber-saturation point of wood is, on the average, 30 per cent (19). The amount of monomolecularly held water is believed to be about 6 per cent from sorption studies (19) and determinations of the amount of water within the cell wall that does not act as a solvent for sodium chloride, glycerol, and sucrose (23). This is 20 per cent of the amount of water held at the fiber-saturation point, in good agreement with the percentage of polar liquid that cannot be replaced by a nonpolar liquid. When the nonpolar liquid is a nonvolatile molten wax, the intermediate liquid can be removed by distilling it off. If the molecular size of the wax is so large as to prevent diffusion into the transient capillaries, the wood then shrinks by an amount equal to the volume of intermediate liquid lost from the cell walls.

Kistler (10) has shown that aerogels can be made from silica gel by replacing the water in the gel with intermediate polar liquids and the latter with petroleum ether. When the petroleum ether is flash dried from the gel, evaporation takes place without setting up the normal contracting forces. A dry slice with the volume of the original gel is thus obtained. In the case of wood, the final replacement cannot be made complete, so that at least 20 per cent of the possible shrinkage takes place. It is hence not possible to make a completely expanded aerogel from wood, but a partial aerogel is theoretically possible. When the wood aerogel is soaked in water to allow water to penetrate the cell-wall structure, and then dried, the full normal shrinkage of the wood results.

CONCLUSIONS

Fibers of pure cellulose and lignocellulosic materials such as wood can be directly penetrated only by polar liquids. These liquids, except for a small correction for adsorption compression, add their volume to the volume of the cell walls, indicating that they are not entering existing voids but are forming a solid solution with the fibers.

The extent to which a liquid will penetrate fibers and swell them appears to be dependent upon the ability of the liquid to form hydrogen bonds with the hydroxyl groups of cellulose and the lignin, and also upon the size of the liquid molecules.

Although solutions may penetrate the fibers much more slowly than the solvent in a number of cases, they eventually swell wood more than does either component alone. This enhanced swelling can be explained on the basis of an equilibrium between sorption, solution pressure, and structural resistance.

Nonpolar liquids, which do not by themselves penetrate fibers, can replace polar liquids already in the fibers except for the monomolecularly held portion of the polar liquid. Only partially expanded aerogels can thus be made from cellulosic fibers.

REFERENCES

(1) Bailey, I. W., and Kerr, T.: J. Arnold Arboretum (Harvard Univ.) **16**, 273 (1935).
(2) Beiser, W.: Kolloid-Z. **65**, 203 (1933).
(3) Collins, G. E.: J. Textile Inst. **21**, T311 (1930).
(4) Davidson, G. F.: J. Textile Inst. **18**, T175 (1927).
(5) DeBruyne, N. A.: Nature **142**, 570 (1938).
(6) Filby E. A., and Maass, O.: Can. J. Research **7**, 162 (1932).
(7) Gordy, W.: J. Chem. Phys. **7**, 93 (1939).
(8) Hasselblatt, M.: Z. anorg. allgem. Chem. **154**, 375 (1926).
(9) Hermans, P. H.: *Contributions to the Physics of Cellulose Fibres*. Elsevier Publishing Publishing Company, Holland and New York City (1946).
(10) Kistler, S. S.: J. Phys. Chem. **36**, 52 (1932).
(11) Lyons, W. J.: J. Chem. Phys. **9**, 377 (1941).
(12) Meyer, K. H., and Misch, L.: Helv. Chim. Acta **20**, 232 (1937).
(13) Russell, J. K., Maass, O., and Campbell, W. B.: Can. J. Research **15B**, 13 (1937).
(14) Schwalbe, C. G., and Beiser, W.: Papierfabr. **50**, 655 (1933).
(15) Sheppard, S. E., and Newsome, P. T.: J. Phys. Chem. **36**, 2306 (1932).
(16) Stamm, A. J.: J. Am. Chem. Soc. **56**, 1195 (1934).
(17) Stamm, A. J.: Ind. Eng. Chem. **27**, 401 (1935).
(18) Stamm, A. J.: Physics **6**, 334 (1935).
(19) Stamm, A. J.: Part 4 in *Wood Chemistry*, edited by L. E. Wise. Reinhold Publishing Corporation, New York (1944).
(20) Stamm, A. J.: "Passage of Liquids, Vapors and Dissolved Materials through Softwoods," U. S. Dept. Agr. Tech. Bull. No. **929** (1946).
(21) Stamm, A. J., and Hansen, L. A.: Ind. Eng. Chem. **27**, 1480 (1935).
(22) Stamm, A. J., and Hansen, L. A.: J. Phys. Chem. **41**, 1007 (1937).
(23) Stamm, A. J., and Hansen, L. A.: J. Phys. Chem. **42**, 209 (1938).
(24) Stamm, A. J., and Loughborough, W. K.: Trans. Am. Soc. Mech. Engrs. **64**, 379 (1942).
(25) Stamm, A. J., and Millett, M. A.: J. Phys. Chem. **45**, 43 (1941).
(26) Stamm, A. J., and Seborg, R. M.: J. Phys. Chem. **39**, 133 (1934).
(27) Stamm, A. J., and Tarkow, H.: J. Phys. & Colloid Chem. **53**, 251 (1949).

POLAROGRAPHIC OBSERVATIONS ON PERCARBONIC ACIDS AND PERCARBONATES[1]

PIERRE VAN RYSSELBERGHE, PAUL DELAHAY,[2] ARMIN H. GROPP,[3] JOHN M. McGEE, AND ROBERT D. WILLIAMS[4]

Department of Chemistry, University of Oregon, Eugene, Oregon

Received May 2, 1949

In the course of a program of research dealing with the polarographic study of corrosion phenomena[5] it was noticed that polarograms obtained with solutions containing simultaneously carbon dioxide and oxygen or hydrogen peroxide exhibited, between the two well-known oxygen reduction steps, a new wave which, as far as we were able to ascertain, had not been reported by other workers. This finding led us to the separate investigation reported in the present paper. The initial observations and some of their possible implications from the point of view of corrosion are presented elsewhere (18).

EXPERIMENTAL METHOD

The polarograms were taken by means of the Sargent photographic polarograph Model XII and by means of a manual polarograph assembled from standard physical-chemical equipment. Various types of cells were used, including the Heyrovský cells and those specially designed for our experiments (18). All supporting electrolytes were "polarographically" pure, i.e., they did not exhibit, in the absence of dissolved oxygen, any reduction wave before their own final reduction currents. In order to achieve this, some electrolytes, in particular tetramethylammonium bromide, had to be carefully and repeatedly recrystallized. Some C.P. electrolytes were satisfactory as obtained. A number of buffers prepared according to Kolthoff and Laitinen (10) were used to study the influence of pH on the newly observed wave. In a number of cases both the oxygen and the carbon dioxide concentrations of the solutions studied were determined analytically by means of the Winkler method for oxygen and by means of a specially designed barium hydroxide titration device for carbon dioxide (18).

In order to suppress the sharp maximum of the first oxygen wave a number of surface-active substances were used, such as methyl red, thymol, etc. (18). In the presence of sodium fluoride used as supporting electrolyte the oxygen peak does not appear and the new wave can be studied in the absence of any maximum suppressor. This was also the case in some electrolyte mixtures containing certain minimum amounts of magnesium ion. By the simple device of passing the solution through filter paper when introducing it in the polarographic cell, as is done, for instance, by Heyrovský (9) and by Brdička and Wiesner (1), it was possible to study the new wave without any addition of a maximum suppressor. It might be noted in passing that, when the oxygen concentration falls appreciably below the 10 mg./l. corresponding to saturation with air, a maximum suppressor is usually unnecessary.

---

[1] Paper presented before the Division of Physical and Inorganic Chemistry at the 115th Meeting of the American Chemical Society, which was held in San Francisco, California, March 27 to April 1, 1949.

[2] Present address: Department of Chemistry, Louisiana State University, Baton Rouge, Louisiana.

[3] Present address: Department of Chemistry, University of Florida, Gainesville, Florida.

[4] Present address: Research Laboratories, Aluminum Company of America, New Kensington, Pennsylvania.

[5] Research project under contract between the University of Oregon and the Office of Naval Research, United States Navy Department.

The capillaries used were such that the $m^{2/3}\ t^{1/6}$ product of the Ilkovič equation was always close to 2.5 in the range of potentials corresponding to the new wave, i.e., at a few tenths of a volt negative with respect to the saturated calomel electrode.

The temperature was close to 25°C. or to 20°C. The electrotitration experiments were run at 0°C.

In some crucial experiments designed to identify the nature of the new wave we used two different preparations of Kahlbaum potassium percarbonate and some percarbonate which we prepared electrolytically by the method of Constam and von Hansen (4, 8). Attempts at preparing percarbonates by other methods, in particular that of Wolffenstein and Peltner (19), gave products exhibiting a polarographic behavior different from that of the Kahlbaum compound and from that of our own electrolytic product. Similarly, the sodium carbonate peroxide, $2Na_2CO_3 \cdot 3H_2O_2$, of the Buffalo Electrochemical Company gave polarograms different from those obtained with the true percarbonates.

The hydrogen peroxide used in this work was obtained by diluting C.P. acid-free 30 and 90 per cent hydrogen peroxide obtained from the Buffalo Electrochemical Company. All pH measurements and the electrotitration experiments on percarbonic acid were carried out by means of a Beckman pH meter.

The carbon dioxide used was obtained from cylinders supplied by Pure Carbonic, Inc.

RESULTS

1. *Air-saturated solutions with various additions of carbon dioxide*

As previously reported (18) many air-saturated 0.1 *N* solutions of unbuffered electrolytes such as potassium chloride, potassium nitrate, tetramethylammonium bromide, etc. containing approximately 0.4 mg. carbon dioxide per liter gave polarograms exhibiting a small intermediate wave between the two reduction steps of oxygen. When methyl red is used as a maximum suppressor this new reduction step is almost always present and its height increases when additional amounts of carbon dioxide are dissolved. With thymol the step appears only in the alkaline range with air-saturated solutions but with sufficient addition of carbon dioxide it appears also in unbuffered neutral solutions. In both cases these waves, including the initial ones, are not waves of the maximum suppressors. With solutions which do not require a maximum suppressor the step may not be immediately apparent, but it always develops upon addition of carbon dioxide. As this wave increases in height the second oxygen wave decreases and the sum of the two waves remains equal to the original height of the second oxygen wave. The first oxygen wave remains unaltered except when the pH becomes smaller than 5.5, at which point the new intermediate wave becomes an extension of the first oxygen wave on account of a shift of half-wave potential towards less cathodic values (see below). Several typical polarograms obtained by the manual method have been presented previously (18) for qualitative discussion. In table 1 we give the ratios of the heights of the new wave to the original height of the second oxygen wave for different concentrations of oxygen and carbon dioxide analytically determined, the supporting electrolyte being 0.1 *N* tetramethylammonium bromide. In table 2 similar data are given for 0.1 *N* potassium chloride. Since it was immediately noticed that, at very small carbon dioxide concentrations, the height of the new wave was much larger than could be expected for a two-electron reduction of some compound derived from the carbon dioxide present, we computed an apparent number of electrons *n* per molecule of carbon dioxide by taking the ratio of the two limiting currents (that of the new wave, i_{CO_2}, and the one corresponding to the total second oxygen wave, i_{O_2}) derived from the Ilkovič equation:

TABLE 1

Apparent number of electrons per molecule of carbon dioxide in the new reduction wave

0.1 *N* tetramethylammonium bromide

CO_2	O_2	i_{O_2}/i_{CO_2}	*n*	CO_2	O_2	i_{O_2}/i_{CO_2}	*n*
mg./l.	*mg./l.*			*mg./l.*	*mg./l.*		
0.4	9.5	6.01	10.6	5.8	9.2	5.37	0.88
0.4	9.3	7.34	9.4	9.7	9.8	5.23	0.56
0.8	10.0	6.85	5.3	17.4	9.4	5.00	0.31
1.3	9.2	6.54	3.2	23.7	9.4	1.32	0.95
3.4	9.2	6.92	1.2	23.7	8.8	1.24	0.90
4.1	9.5	8.59	0.78	47.8	9.0	1.26	0.44
4.3	10.0	6.89	0.98	67.5	9.4	1.18	0.34

TABLE 2

Apparent number of electrons per molecule of carbon dioxide in new reduction wave

0.1 *N* potassium chloride

CO_2	O_2	i_{O_2}/i_{CO_2}	*n*	CO_2	O_2	i_{O_2}/i_{CO_2}	*n*
mg./l.	*mg./l.*			*mg./l.*	*mg./l.*		
0.4	9.8	6.80	8.4	2.2	10.5	5.69	2.4
1.0	10.1	6.60	4.7	2.9	9.6	6.81	1.4
1.1	10.5	7.31	3.5	17.5	9.6	10.2	0.16
1.6	9.3	6.63	2.6	50.0	9.7	4.54	0.12
2.0	9.7	5.73	2.5				

$$\frac{i_{CO_2}}{i_{O_2}} = \frac{n}{2} \cdot \frac{C_{CO_2}}{C_{O_2}} \cdot \frac{D^{1/2}_{CO_2}}{D^{1/2}_{O_2}} \qquad (1)$$

in which C_{CO_2} and C_{O_2} are the molar concentrations of carbon dioxide and oxygen and D_{CO_2} and D_{O_2} are their diffusion coefficients; the ratio of their square roots was taken constant and such that

$$n = 2.16 \frac{C_{O_2}}{C_{CO_2}} \cdot \frac{i_{CO_2}}{i_{O_2}} \tag{2}$$

Values of n much larger than 2 would tend to indicate that each molecule of carbon dioxide is involved several times in the reduction process and very small values of n would indicate that only a small fraction of the carbon dioxide present is involved in the process. The flattening of the wave with the establishment of an apparent diffusion current would be due to the disappearance, by reduction to water, of the other compound essential to the occurrence of the new wave: namely, the hydrogen peroxide resulting from the first reduction step of oxygen.

Other experiments, with appreciably higher carbon dioxide concentrations, showed that, in tetramethylammonium bromide solutions, the second oxygen wave can be nearly entirely replaced by this new wave while, in potassium chloride solutions, it is much more difficult to reach these high carbon dioxide concentrations and the replacement of the second oxygen wave by the new wave is always far from complete. Our experience with solutions of electrolytes containing carbon dioxide shows that quaternary ammonium salts are able to keep carbon dioxide at supersaturation much more easily than all other salts.

The foregoing results will be discussed below but it is already apparent that the new wave results from the formation and the subsequent reduction of a compound involving carbon dioxide and the hydrogen peroxide resulting from the reduction of oxygen along the first oxygen wave.

A typical polarogram showing the phenomena described above is given in figure 1. In figure 2 the previously observed reduction of carbon dioxide (15, 16, 17) at a half-wave potential of 2.16 v. with respect to the saturated calomel electrode appears in addition to the new wave observed at low potentials.

2. *Solutions of hydrogen peroxide with various additions of carbon dioxide*

When dilute solutions of hydrogen peroxide in 0.1 N unbuffered electrolytes are treated with pure nitrogen to remove all or most of the oxygen, polarographic reduction waves of the type of the first curve on the left of figure 3 are obtained. No maximum suppressor is needed in this case. When carbon dioxide is gradually added to such solutions the hydrogen peroxide wave is split into two fragments and, with sufficient addition of carbon dioxide, it is finally entirely replaced by the new wave already observed on polarograms of mixtures of oxygen and carbon dioxide.

In mixtures of hydrogen peroxide and carbon dioxide the reducible compound is present in bulk concentration, while in mixtures of oxygen and carbon dioxide the compound is formed at the dropping cathode through reaction between carbon dioxide and hydrogen peroxide. In mixtures of hydrogen peroxide and carbon dioxide the simplest compound one could expect is the percarbonic acid (H_2CO_4) formed by direct addition of carbon dioxide to hydrogen peroxide.

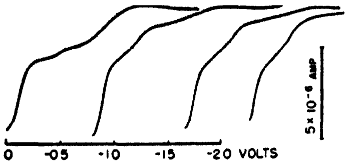

FIG. 1. Gradual addition of carbon dioxide to a 0.1 *N* solution of tetramethylammonium bromide saturated with air. First curve on left has no added carbon dioxide. Last curve on right shows maximum transformation of second oxygen wave to intermediate wave with slight decrease of first oxygen wave due to displacement by carbon dioxide. Drop of methyl red used. Recording by Sargent Polarograph Model XII. Picture is tracing of original polarogram with minute galvanometer oscillations left out.

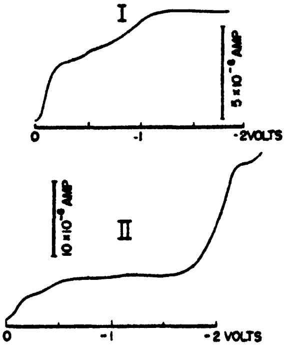

FIG. 2. Curve I is similar to curve on the left of figure 1. Curve II is the result of the addition of a large amount of carbon dioxide to an air-saturated solution of 0.1 *N* tetramethylammonium bromide with both the low and high potential waves due to carbon dioxide observable. Recording by Sargent Polarograph Model XII. Picture is tracing of original polarogram with minute galvanometer oscillations left out.

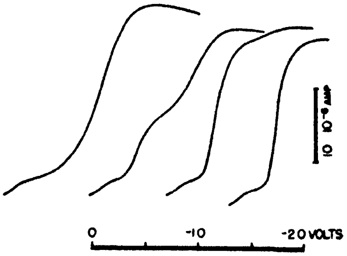

FIG. 3. Gradual addition of carbon dioxide to 0.1 *N* solution of tetramethylammonium bromide containing one drop of 3 per cent hydrogen peroxide per 10 ml. of solution. First curve on left has no added carbon dioxide. Last curve on right shows maximum transformation of hydrogen peroxide wave to new wave. No methyl red used. Recording by Sargent Polarograph Model XII. Picture is tracing of original polarogram with minute galvanometer oscillations left out.

Other percarbonic acids could also be expected, such as H_2CO_5 and $H_2C_2O_6$. Our previous polarographic studies on carbon dioxide (15, 16, 17) have shown that, in the absence of oxygen or hydrogen peroxide, the new wave now being discussed is not observed. We are definitely dealing with the reduction of a compound formed by reaction of carbon dioxide with hydrogen peroxide.

3. *Buffered solutions*

In eight different buffers prepared according to Kolthoff and Laitinen (10) and saturated with air at 20°C. the new wave was registered and its half-wave potential was determined for each pH. Mixtures of carbon dioxide and hydrogen peroxide were added to samples of the same buffers. At the pH's which were studied these solutions exhibited percarbonic waves of about the same height as in air-saturated solutions. In all cases very satisfactory percarbonic waves were registered by using the higher sensitivities of the Sargent polarograph. It was immediately noticed that an increase of acidity shifts the half-wave potential to lower cathodic values. When the pH becomes smaller than 5.5 the new wave is no more distinguishable from the first oxygen wave of which it becomes an extension with a short inflection connecting the two segments of curves. The half-wave potentials observed at 20°C. are plotted on figure 4. By interpolation one finds that at pH = 7 the half-wave potential is 0.37 v. negative with respect to the saturated calomel electrode. In the range pH = 5.50 to pH = 9.71 the following relation holds:

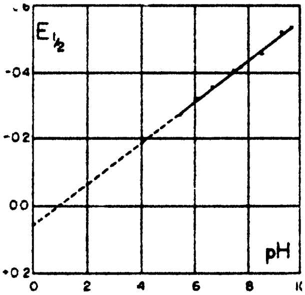

FIG. 4. Variation of the half-wave potential of the percarbonic wave with pH at 20°C. Zero of potential scale corresponds to standard hydrogen electrode.

$$E_{1/2} = 0.06 - 0.061 \text{ pH} \tag{3}$$

If the extrapolation shown on figure 4 to pH = 0 is assumed to have at least theoretical meaning one may conclude that at activity 1 of hydrogen ion the half-wave potential is +0.06 v. against the saturated calomel electrode or +0.31 v. against the standard hydrogen electrode. It will be remembered that the half-wave potentials of both the first and the second oxygen waves do not vary with pH but are slightly affected by the nature of the buffers (11, 12), while the half-wave potential of the intermediate wave observed by us in the case of the buffered solutions and due to the presence of carbon dioxide does depend linearly on pH. The slope $\Delta E/i_d$ at the half-wave is 0.055 ± 0.003 in the case of the waves obtained in buffers. This would be in agreement with a two-electron reduction per molecule (15). The potential interval ΔE and the diffusion current i_d

are the horizontal and vertical sides of a rectangular triangle whose hypotenuse is the tangent at the half-wave. These properties of the waves make it possible that we are dealing with a reversible reduction. However, with percarbonic waves obtained with mixtures of carbon dioxide and hydrogen peroxide and with unbuffered solutions the slope is often quite different from that required for a two-electron reversible reduction.

4. *Solutions of potassium percarbonate*

The interpretation of the nature of this intermediate reduction step between the two oxygen waves was greatly helped by crucial observations on solutions containing the potassium percarbonate, $K_2C_2O_6$. A Kahlbaum bottle of this product, which had never been opened, was available in our laboratory. Although no formula was given on the label it seems certain that this product was obtained by the electrolytic process (4, 8), which is known to give percarbonates of the $K_2C_2O_6$ type. Solutions containing small amounts of this salt in 0.1 *M* potassium nitrate gave the waves shown in figure 5. We note that, with polarograms taken at intervals of 10 min., the height of the percarbonic acid step increases with time. In the alkaline solutions resulting from the dissolution of the percarbonate the reduction must be that of the negative ion CO_4^{--} formed by the relatively slow hydrolysis reaction (13):

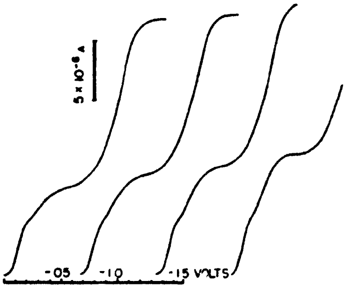

FIG. 5. Polarographic waves of potassium percarbonate taken at 10-min. intervals. On each curve the intermediate wave is that of percarbonate. The first wave is that of oxygen; the third wave includes oxygen and hydrogen peroxide. Supporting electrolyte is 0.1 *N* potassium nitrate. Each curve begins at zero applied potential. Recording by Sargent Polarograph Model XII. Picture is tracing of original polarogram, with minute galvanometer oscillations left out.

$$K_2C_2O_6 + H_2O \rightarrow K_2CO_4 + H_2CO_3 \qquad (4)$$

In later experiments it was found that the percarbonate had quickly deteriorated after the bottle had been opened for the first time. A second bottle of Kahlbaum percarbonate was located and similar observations were made with its contents. Attempts at preparing percarbonates resulted in compounds which gave only hydrogen peroxide waves or at most negligible intermediate waves, unless some acid was added, in which case what must have been a percarbonic acid was formed between carbon dioxide and hydrogen peroxide. In particular the methods of Wolffenstein and Peltner (19) for the preparation of both Na_2CO_4

and $Na_2C_2O_6$ were used but resulted in compounds which gave only hydrogen peroxide waves. This leads us to the opinion that these percarbonates were actually addition products of carbonate and hydrogen peroxide. The same situation holds for the sodium carbonate peroxide, $2Na_2CO_3 \cdot 3H_2O_2$, of the Buffalo Electrochemical Company. It must be concluded from these and many other similar attempts that only the Kahlbaum product was a true percarbonate.

On the other hand, some potassium percarbonate which we prepared ourselves by the electrolytic method of Constam and von Hansen (4, 8) and which, in accordance with the description given by these authors, was of a light sky-blue color, gave the intermediate waves shown on the three polarograms of figure 6.

5. *Percarbonic acids and their titration*

It can be deduced from these observations that the new wave is due to one or several of the possible forms of percarbonic acid: H_2CO_4, H_2CO_5, $H_2C_2O_6$, or their ions. In the case of air-saturated solutions percarbonic acid would be formed between carbon dioxide and the hydrogen peroxide accumulating near the dropping mercury cathode during the first oxygen wave. The resulting percarbonic acid would then be reducible at potentials smaller than those required for the reduction of hydrogen peroxide and for the complete reduction of oxygen to water. In the case of mixtures of hydrogen peroxide and carbon dioxide percarbonic acid is present before polarographic reduction. This has been confirmed by the electrotitration of solutions of percarbonic acid obtained by mixing carbon dioxide with an excess of acid-free hydrogen peroxide. After 24 hr. at 0°C. these solutions have reached equilibrium and constant acid strength. They also have lost most of the unreacted carbon dioxide. The mathematical analysis of the titration curves according to the treatment of Britton (2), assuming that only one dibasic acid is present, was attempted. Further work will be needed to obtain accurate ionization constants. The only statement we shall make at present is that percarbonic acid is stronger than carbonic acid, in agreement with the statement of Charlot (3).

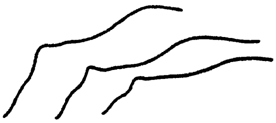

FIG. 6. Identification of the intermediate wave as percarbonic wave with solution of potassium carbonate containing some percarbonate formed by electrolysis. Middle curve obtained with solution as removed from electrolysis cell. Curve on right obtained with same solution after removal of some oxygen by nitrogen. Curve on left is repeat run at higher sensitivity. Recording by Sargent Polarograph Model XII. Picture is tracing of original polarogram with minute galvanometer oscillations left out.

DISCUSSION

If the experiments carried out with percarbonates can be regarded as definitely proving that the new wave is due to one or several percarbonic acids or their ions, it becomes of interest to inquire into the nature of the reduction reaction.

If one assumes that the equilibrium constant for the formation of H_2CO_4 from hydrogen peroxide and carbon dioxide is of the same order of magnitude as those observed by d'Ans and Frey (5, 6) for peracids such as performic and peracetic, i.e., of the order of unity, one could estimate the free energy of formation of H_2CO_4 as being -124 kcal. (-31.5 for H_2O_2 aq.; -92.3 for CO_2 aq.). The reduction

$$H_2CO_4 + 2H^+ + 2e^- \rightarrow CO_2 + 2H_2O \qquad (5)$$

involves a free energy decrease of -82 kcal. at pH $= 0$, while the energy corresponding to the polarographic potential is -14 kcal. One may conclude either that reaction 6 occurs irreversibly with an overvoltage of the order of 1.5 v. or that it occurs reversibly with respect to the formation of orthocarbonic acid, $C(OH)_4$, which would decompose spontaneously into CO_2 and $2H_2O$. Starting with the free energy of formation of methanol, -40 kcal., and using the value -34 kcal. for each substitution of H to OH (Parks and Huffman (14)) one arrives at -142 kcal. for the free energy of formation of $C(OH)_4$. The difference $-142 - (-124)$ is -18 kcal., which is similar to the -14 kcal. derived from the polarographic potential. It is possible that this polarographic potential corresponds to the activation energy of a complex having the gross formula $C(OH)_4$ but properties quite different from those of the hypothetical orthocarbonic acid. An explanation based upon a reduction to performic acid was examined but not retained. We found experimentally that performic acid is itself reducible at potentials corresponding to the reduction of percarbonic acid. Performic acid has been reported as unstable by d'Ans and Frey (5, 6) and quite recently by Greenspan (7). Since carbon dioxide is apparently formed again by reduction of percarbonic acid, one may expect in the experiments with air-saturated solutions, where the acid is formed at the dropping electrode, that the carbon dioxide will react again with hydrogen peroxide and possibly go through several successive cycles of reaction and reduction, leading to a wave height much greater than would be expected from the concentration of carbon dioxide. That this is indeed the case is shown by the fact that, in air-saturated solutions containing about 0.4 mg. of carbon dioxide and 10 mg. of oxygen per liter, the ratio of the height of the percarbonic wave to that of the first oxygen wave was found to vary, in one series of runs, from 0.242 to 0.214 as the drop time of the mercury cathode was changed from 3.05 to 0.54 sec. If the carbon dioxide present were involved in only one cycle of reaction with hydrogen peroxide and reduction back to CO_2 through $C(OH)_4$, the ratio of these wave heights should be of the order of 0.05. It is evident that the amount of hydrogen peroxide available determines the maximum height of the percarbonic wave which can never be larger than the original hydrogen peroxide wave in the absence of carbon dioxide. We hope to obtain more precise information concerning these cycles of formation and reduction by means of an oscillographic method being developed by one of us (P.D.).

An interesting observation for which we have no complete explanation is the following: basic air-saturated solutions give percarbonic waves of about the same height as neutral solutions, in spite of the fact that the carbon dioxide concentration is then greatly decreased. Apparently reducible percarbonate ions are readily formed with the hydrogen peroxide formed at the dropping cathode, while the mixing of hydrogen peroxide with a carbonate or a bicarbonate solution does not lead to any detectable formation of percarbonates. Addition of acid to such mixtures immediately results in the formation of percarbonic acid. One might assume that the hydrogen peroxide formed at the dropping cathode is in some sort of activated state with greater reactivity. The possibility of the formation of other reduction products, such as OH or O_2^-, which would react readily with carbonate and bicarbonate ions might be considered, but there are thermodynamic difficulties involved in the postulation of such mechanisms.

SUMMARY

A new polarographic wave is observed between the two oxygen waves whenever carbon dioxide is present with oxygen or hydrogen peroxide in solution. Percarbonates exhibit the same wave, which is thus ascribed to one or several of the possible percarbonic acids or their ions.

The characteristics of the new wave, i.e., variation of half-wave potential with pH, slope, height, and possible reversibility or irreversibility, are discussed.

This work was carried out as part of a research project sponsored by the Office of Naval Research, United States Navy Department, to which the authors express their gratitude.

REFERENCES

(1) Brdička, R., and Wiesner, K.: Collection Czechoslov. Chem. Commun. **12**, 39 (1947).
(2) Britton, H. T. S.: *Hydrogen Ions*, Vol. I, p. 198. D. Van Nostrand Company, Inc., New York (1943).
(3) Charlot, G.: *Théorie et méthode nouvelle d'analyse qualitative*, p. 251. Masson, Paris (1946).
(4) Constam, E. J., and Hansen, A. von: Z. Elektrochem. **3**, 137 (1896).
(5) d'Ans, J., and Frey, W.: Ber. **45**, 1845 (1912).
(6) d'Ans, J., and Frey, W.: Z. anorg. allgem. Chem. **84**, 145 (1914).
(7) Greenspan, F. P.: J. Am. Chem. Soc. **68**, 907 (1946).
(8) Hansen, A. von: Z. Elektrochem. **3**, 445 (1896).
(9) Heyrovský, J.: *Polarographie*, p. 409. Springer Verlag, Vienna (1941).
(10) Kolthoff, I. M., and Laitinen, H. A.: *pH and Electrotitrations*, pp. 34–5. John Wiley and Sons, Inc., New York (1941).
(11) Kolthoff, I. M., and Lingane, J. J.: *Polarography*, pp. 307–12. Interscience Publishers, Inc., New York (1941).
(12) Kolthoff, I. M., and Miller, C. S.: J. Am. Chem. Soc. **63**, 1013 (1941).
(13) Latimer, W. M.: *The Oxidation States of the Elements and their Potentials in Aqueous Solutions*, p. 124. Prentice-Hall, Inc., New York (1938).
(14) Parks, G. S., and Huffman, H. M.: *The Free Energies of Some Organic Compounds*, Table 40, p. 210. The Chemical Catalog Company, Inc., New York (1932).
(15) Van Rysselberghe, P.: J. Am. Chem. Soc. **68**, 2047 (1946).
(16) Van Rysselberghe, P., and Alkire, G. J.: J. Am. Chem. Soc. **66**, 1801 (1944).
(17) Van Rysselberghe, P., Alkire, G. J., and McGee, J. M.: J. Am. Chem. Soc. **68**, 2050 (1946).
(18) Van Rysselberghe, P., McGee, J. M., Gropp, A. H., Williams, R. D., and Delahay, P.: Corrosion and Material Protect. **5**, No. 2, 11 (1948).
(19) Wolffenstein, R., and Peltner, E.: Ber. **50**, 280 (1908).

ON THE SIGNIFICANCE OF THE SLOPE OF THE POLAROGRAPHIC WAVE[1]

HOWARD K. ZIMMERMAN, JR.,[2] AND ARMIN H. GROPP

Departments of Chemistry, University of Utah, Salt Lake City, Utah, and University of Florida, Gainesville, Florida

Received June 24, 1949

INTRODUCTION

During recent years much work has been performed in the direction of employing directly the geometric properties of polarographic waves as a means of extracting from the experimental data themselves the greatest possible amount of fundamental information regarding the nature of polarographic processes. One of the most important results of this sort of work has been the trend toward a fuller appreciation of the basic role of adsorptive phenomena in processes at the dropping mercury electrode. Particularly in Europe, the investigations of Frumkin and of Brdička into the properties of mercury drops and the bearing of those properties on the problem of polarography have been of outstanding value in that direction. In this country also, efforts have been made to include, in the interpretation of polarographic waves, a consideration of the phenomenon of adsorption (5).

A second important development coming out of the study of the geometry of polarographic waves has been a closer consideration of the meaning of polarographic reversibility. Detailed analysis of this question serves to emphasize the fundamental distinction which must be drawn between true thermodynamic reversibility and the reversibility criteria applied to the totality of processes at the dropping electrode.

It has been found that the analytical method which is to be presented here affords not only a means of detecting information heretofore not observed in polarographic waves, but also an especially graphic and convincing way of presenting the question of reversibility and of the manner in which neglect of adsorptive effects has tended to obscure its full understanding.

THEORETICAL

In the course of studying the geometry of current–voltage curves obtained from the photographically recording polarograph manufactured by E. H. Sargent and Company, it was found that in many cases an accurate determination of the point of inflection of the wave is extremely difficult, if not impossible. Since a knowledge of this point is vital to the precision of the mathematical analysis which was in use (5), means were sought to improve its measurement. It was of course well known that the point of inflection represents that spot at which the rate of change of the slope of the wave vanishes. Therefore, it was thought that a continuous plot of the slope of the wave *versus* potential might be of value in obtaining the desired precision. Accordingly, such plots were attempted, it being found that they could be constructed in the following manner. Employing a ruler with 0.5-mm. graduations, the exact values of the current are measured at intervals of 2 mm. along the voltage axis. The difference between any two successive values of current then provides the increment of current over that interval of voltage. Since the voltage interval is kept constant, this increment gives the value of $\Delta i/\Delta E$ for the range of voltage in question. This value may now be plotted against the voltage to give a series of points through which a continuous line may be drawn. The curve so constructed thus gives the variation of di/dE with E, potential. The constructed curve may of course be laid out on any scale desired. More specifically, the voltage axis may be sufficiently expanded to give a highly accurate location of any point on the curve,—within the limits of experimental error, of course.

---

[1] Presented in part by A. H. Gropp at the January 1947 meeting of the Oregon Academy of Sciences in Portland, Oregon, and by H. K. Zimmerman, Jr., before the 115th Meeting of the American Chemical Society, which was held in San Francisco, California, March 27 to April 1, 1949.

[2] Present address: Department of Chemistry, University of Kentucky, Lexington, Kentucky.

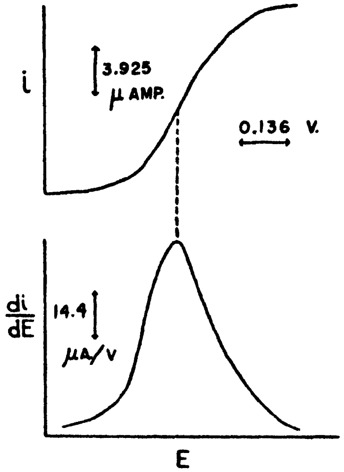

FIG. 1

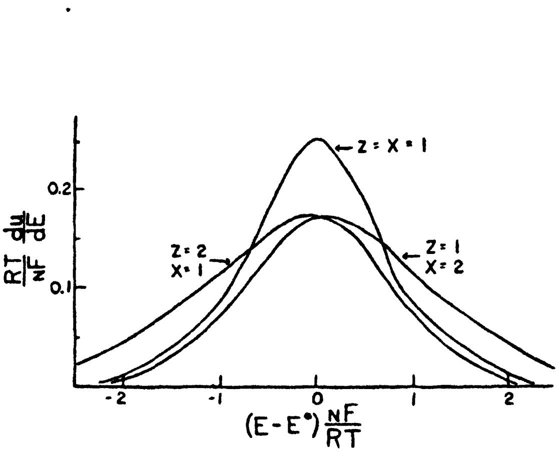

FIG. 2

FIG. 1. A typical polarographic wave and the differentiated form

FIG. 2. Differentiated curves showing the relationship between z and x and the symmetry of the curves.

A typical result of this analysis is shown in figure 1, together with the original wave from which it was obtained. It is seen that the constructed curve rises to a maximum and falls off asymptotically toward zero on both sides. According to the elementary theory of maxima and minima, therefore, it is obvious that the maximum corresponds in potential to the position of the point of inflection of the original wave. This point may consequently be established to a high degree of accuracy.

Now it is doubtless apparent at this point that an analysis of any great number of waves by the method described is an extremely tedious undertaking. However, it is not always necessary to perform the construction in the manner outlined. Delahay (2) has recently designed an auxiliary electric circuit which is capable of performing the differentiation electrically and which yields a curve identical to that which has been described.

At first glance, it would appear that the form of the constructed (or differentiated) curve is that of a Boltzman-type distribution function. That this is not the correct interpretation, however, may be shown from a mathematical analysis of the geometric procedure given above. For such an analysis it is convenient to start with the general equation of the polarographic wave, including adsorptive effects, which has been given by Van Rysselberghe (5):

$$E = E^* + \frac{RT}{n\mathfrak{F}} \ln \frac{u^z}{(1 - u)^x} \tag{1}$$

Here E = potential applied to the dropping mercury cathode,
E^* = a constant which includes the standard reduction potential,
R = the general gas constant,
T = absolute temperature,
n = the number of electrons involved in the reduction,
$\mathfrak{F}$ = the faraday,
u = i/i_d, the ratio of actual current at any potential to the diffusion current (Use of this terminology is deemed convenient in that it allows one to regard the current at any part of the wave as a fraction of the total wave, thus divorcing the geometric discussion from any confusion which might arise from the fact that diffusion currents—and hence all other currents—vary with concentration of the reducible substance.),
z = the Freundlich adsorption exponent for the product of the reduction on the surface of the mercury drop, and
x = the stoichiometric coefficient of the reducible substance in the reaction with n electrons. (For present purposes, however, x and z may, if desired, be regarded merely as parameters. In unbuffered acids, one replaces x by $x + 1$, in which the new x still has the same meaning as that given above.)

Since the differentiated curves presented herein involve $\mathrm{d}u/\mathrm{d}E$, the variation of u with respect to E, it is desirable to rewrite equation 1 in the form

$$\frac{u^z}{(1 - u)^x} = \exp\left[\frac{n\mathfrak{F}}{RT}(E - E^*)\right] \tag{2}$$

although identical results may also be obtained with ease directly from equation 1. Equation 2 is to be regarded as defining the dependence of u on E throughout the present discussion. Differentiation of equation 2 with respect to E then leads to the following expression:

$$\frac{\mathrm{d}u}{\mathrm{d}E} = \frac{(1 - u)^x}{u^{z-1}\left[z + \frac{xu}{1 - u}\right]} \frac{n\mathfrak{F}}{RT} \exp\left[\frac{n\mathfrak{F}}{RT}(E - E^*)\right] \tag{3}$$

Substituting from equation 2 into equation 3 this may be simplified to the following form:

$$\frac{du}{dE} = \frac{n\mathfrak{F}}{RT}\left[\frac{n(1 - u)}{z + (x - z)u}\right] \tag{4}$$

Despite the fact that it is not practicable to write equation 4 in its analytical form as a function of E, the fact that u itself is a function of E as given in equation 2 permits one to regard equation 4 as such a function of E. If this be done, equation 4 reflects in a most striking manner the nature of symmetry in the polarographic wave, and its dependence on the parameters, x and z, which are constants for waves produced by any given substance. For example, in the special case where $z = x$, it is a simple matter to demonstrate that

$$\frac{du}{dE} = \frac{1}{\exp\left[\frac{n\mathfrak{F}}{xRT}(E - E^*)\right] + \exp\left[\frac{-n\mathfrak{F}}{xRT}(E - E^*)\right] + 2}\,\frac{n\mathfrak{F}}{xRT} \tag{5}$$

from which an elementary analysis clearly illustrates the symmetry of the differentiated curve and hence of the original wave.

On the other hand, for the more general case where $z \neq x$, the curves shown in figure 2 reflect just as clearly the manner in which the inequality leads to asymmetry in the differentiated curve, and consequently in the original wave. It will be noted that when $z = x$, the point of inflection (maximum of the curve) coincides with the value, $E = E^*$. When $z \neq x$, on the other hand, the curves indicate a slight displacement of this point from the value, $E = E^*$. In most of the asymmetric cases which will be encountered in polarographic practice, this displacement will be so small as to be negligible in the light of the other sources of experimental error which exist.[3] However, a more precise evaluation of the deviation may be established if we note that at the point of inflection,

$$u = \frac{1}{\frac{x}{z} + 1} \tag{6}$$

as Marker has shown. Utilizing this relation in equation 1, we may write:

$$(E - E^*)\frac{n\mathfrak{F}}{zRT} = \frac{\left[\frac{x}{z} - 1\right]\ln\left[\sqrt{\frac{x}{z}} + 1\right]}{\frac{x}{z}\ln\sqrt{\frac{x}{z}}} \tag{7}$$

Equation 7 therefore gives us a precise way of determining the deviation of the point at which $E = E^*$ from the point of inflection. Consequently we are able to determine the value of E^* in every possible case.

With these facts well in mind, it is possible to draw a series of very important fundamental conclusions about the polarographic wave. In the first place, it would appear that, in the characterization of reducible substances, the potential at which the point of inflection occurs is a far more reliable and natural criterion than is the customary half-wave potential. As a matter of fact, in the general case half-wave potential is of no more significance in determining E^* than is the potential at any other random point on the wave, since the half-wave potential will in general include the term, $\ln 2^{z-x}$, in addition to the other constants already present in E^*. Only in the fortuitous case where $z = x$ does the logarithmic term of equation 1 vanish for $u = \frac{1}{2}$ and thus lead directly to the true value of E^*. At the point of inflection, on the other hand, the measured potential coincides with E^* in the symmetric case and can be made to coincide in all other cases by application of the correction discussed above.

---

[3] This interesting lack of invariance in the point of inflection about the quantity $E - E^*$ was pointed out to us by Mr. Leon Marker, of the University of Utah, who has carried out a rigorous mathematical proof.

The other conclusions which may be drawn from the results given above involve the interpretation of the symmetry (or lack of it) in the wave, and lead in a most natural way to a very considerable clarification of the question of reversibility. For example, one criterion of reversibility which has been favored in the past has been the statement that, in order to be considered reversible, the wave must be symmetric. However, equation 4 and its consequences clearly indicate that this criterion is illusory. To be sure, the symmetric case *does* follow from the conditions of thermodynamic reversibility, but this circumstance is far from unique. The asymmetric cases also follow with equal validity from the same conditions. Furthermore, consider the criterion of reversibility originally suggested by Tomes (4). It may be expressed in the form,

$$E_{3/4} - E_{1/4} = \frac{-0.058}{n'} \tag{8}$$

where, for reversibility, n' must be integer. Yet it is a simple matter to show even in the symmetric case where $z = x \neq 1$ that $n' = n/x$, where although n and x are integers, n' plainly cannot be an integer except in special cases.

Such a discussion might perhaps be continued further. However, the considerations which have been set forth are sufficient to show very clearly that it is meaningless to attach any special significance to the phenomenon of symmetry in a polarographic wave aside from the fact that $z = x$. In the general case, the wave may be asymmetric to almost any possible degree without that fact having any particular bearing on the question of its reversibility.

The other principal criterion of reversibility which has been in common use requires that, in order that a reduction may be classified reversible, the cathodic (or reduction) wave must coincide in half-wave potential with the same potential of the anodic (or oxidation) wave of the reduction product. Now the foregoing discussion has shown that in general the position of the half-wave is of much less significance than the position of the point of inflection. Hence, it would appear at the start that the attachment of any great significance to the half-wave potential is of doubtful value at best. Even beyond that, however, it should be recognized that there is a fundamental fallacy in applying any such criterion to determine the thermodynamic reversibility of the polarographic process. It has been pointed out before in the literature (1, 3) that it is perfectly possible to have a reversible electrode reaction whose product is unstable, being irreversibly transformed into another substance. Thus an application of the present criterion to such a case will show truly that the overall reaction is irreversible, but by its very nature it will show nothing whatever about the reversibility of the electrode process which, after all, is the only reaction which the current–voltage curve measures.

From the foregoing discussion it appears that one must recognize two kinds of reversibility in dealing with polarographic data. In the first place, there is the question of the reversibility of the single process, transfer of electrons from the dropping cathode to the reducible substance. This we prefer to term thermodynamic reversibility, and it is governed by the usual Nernst-type formulae, derived directly from the thermodynamics of reversible processes. In the second place, there is the question of the reversibility of the totality of processes occurring at the dropping cathode, of which the above-mentioned electron transfer is but one. This we would call polarographic reversibility, and it is established by most of the usual criteria at present in use in polarographic practice.

It is therefore of paramount importance that a careful distinction be made between what is meant by thermodynamic and by polarographic reversibility. According to the usual practice of determining polarographic reversibility on the basis of the behavior of half-wave potentials (or more properly, points of inflection) as described above, one is led to the inescapable conclusion that this type of reversibility is applicable only to a judgment of the nature of the overall reaction, including the electrode process and all those processes which may spontaneously follow it. That information of this kind is of importance cannot be denied. It is erroneous, however, to attempt to use such information to make a decision regarding the thermodynamic reversibility of the actual electrode process itself. This latter type of reversibility may be considered to exist only if the experimental data, as reflected by the actual geometry of a given wave, satisfy a theoretical expression, such as equation 1, the antecedents of which expressly include the conditions of thermodynamic reversibility.

APPLICATIONS

In an effort to assess the value of the differentiated curve in the practical evaluation of polarographic waves, a large number of such constructions have been performed. A number of typical results are collected in figures 3 and 4. As is to be expected, a large variety of aspects of the asymmetry of the waves appears, depending on the nature of the substance in question. But in every case the maximum of every differentiated curve is clear and well-defined, leading to the location of E^* for every molecular or ionic species under reduction at the dropping mercury electrode.

In figure 5 there is reproduced the result of the analysis applied to the wave arising from the reduction of a mixture of chlorophyll and carbon dioxide. Here one is able to observe the occurrence of a rather remarkable effect, for despite the fact that the original wave appears to be a single, well-defined curve, the differentiated curve shows two distinct maxima which correspond to two distinct points of inflection in the original wave. In view of the preceding theoretical discussion, therefore, it would appear that the experimental wave represents the reduction of two separate species of molecules. This phenomenon apparently has

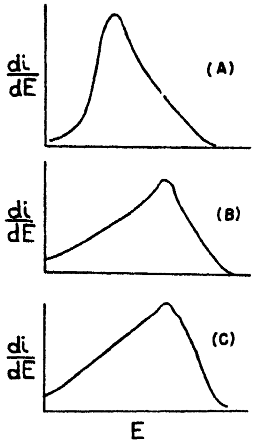

FIG. 3

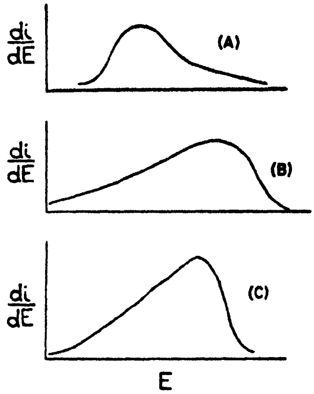

FIG. 4

FIG. 3. Representative differentiated curves for various ions: (A) NH_4^+; (B) $C_2H_5N(CH_3)_3^+$; (C) *i*-$C_3H_7N(CH_3)_3^+$.

FIG. 4. Representative differentiated curves for various substances. (A) chlorophyll; (B) carbon dioxide; (C) *i*-$C_4H_9N(CH_3)_3^+$.

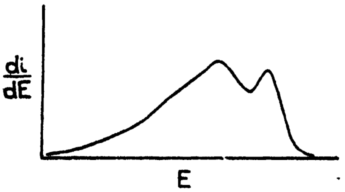

FIG. 5

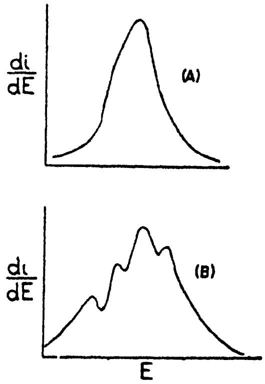

FIG. 6

FIG. 5. The differentiated curve from the reduction wave produced by a mixture of chlorophyll and carbon dioxide.

FIG. 6. The differentiated curves from the two reduction waves produced by oxygen: (A) first wave; (B) second wave.

never been detected in any previous work. In the absence of complex formation between the two reducible constituents, it might tentatively be suggested from a comparison of the shape of figure 5 with the shapes of the separate differentiated curves for the two substances (*cf.* figure 4), that the left-hand maximum could be attributed to chlorophyll, and the right-hand one to carbon dioxide. Any positive identifications, of course, must be deferred until a more detailed study of the system, with varying amounts of the two active components, can be carried out.

But despite the manifest difficulty of making any precise assignments of two points of inflection, the mere fact that they can be detected in this way is of great importance, since if this can be shown to be a result to be expected generally when more than one substance is being reduced in a given polarographic wave, one then has at his disposal a very powerful tool for the detection of hitherto unsuspected electrode processes.

Indeed, a second and even more complex example of this kind is to be found in the analysis of the reduction waves of oxygen. This substance yields two successive polarographic waves, the differentiated curves of which are given in figure 6. From these curves one notes the remarkable fact that, while the first wave appears to be due to the reduction of only one species (presumably oxygen), the second wave seems to contain about four points of inflection. Upon the basis of the foregoing analysis and examples, therefore, one is led to the conclusion that the second oxygen wave is the result of the reduction at approximately the same potential of a relatively tremendous number of molecular and/or ionic species, the exact nature of which are completely unknown. The complexity of the problem of assigning these reductions to their proper reductant is such that its solution cannot even be attempted here.

However, in the light of work done by others (6) subsequent to the construction of the first differentiated curves which were made for oxygen, it now appears that the first maximum which is observed in these curves is due to the reduction of a minute amount of percarbonic acid which forms near the mercury drop due to a reaction between dissolved carbon dioxide and the small amount of hydrogen peroxide which is the product of the reduction of oxygen which gives rise to the low-potential oxygen wave.

SUMMARY

A method is described for determining the point of inflection of a polarographic wave. The use of this point for determining the value of E^*, the linear constant in the equation for the wave, is discussed. Some criteria for determining the reversibility of the polarographic wave on the basis of its symmetry characteristics are examined critically, and it is concluded that in dealing with polarographic data two kinds of reversibility must be distinguished. These are defined. Several examples of the application of the method to different kinds of substances are presented. It is found that, for some polarographic curves, the present method discloses the presence of previously unsuspected points of inflection. These new points of inflection are attributed to the existence of electrode processes which have never before been detected.

REFERENCES

(1) Bieber, R., and Trümpler, G.: Helv. Chim. Acta **30**, 706 (1947).

(2) Delahay, P.: Anal. Chim. Acta **1**, 19–32 (1947).

(3) Smith, L. I., Kolthoff, I. M., Wawzonek, S., and Ruoff, P. M.: J. Am. Chem. Soc. **63**, 1018 (1941).
(4) Tomeš, J.: Collection Czechoslov. Chem. Commun. **9**, 12, 81, 150 (1937).
(5) Van Rysselberghe, P.: J. Am. Chem. Soc. **68**, 2047 (1946).
(6) Van Rysselberghe, P., McGee, J. M., Gropp, A. H., Williams, R. D., and Delahay, P.: Corrosion **5**, No. 2, 11–16 (1948).

THE EXCHANGE OF RADIOACTIVE ZINC BETWEEN CELLULOSE AND SODIUM HYDROXIDE-SODIUM ZINCATE SOLUTIONS

KARL BORGIN[1] AND ALFRED J. STAMM

Forest Products Laboratory,[2] Forest Service, U. S. Department of Agriculture

Received July 5, 1949

The nature of the interaction of concentrated aqueous solutions of alkali hydroxides with cellulose is still but vaguely understood even though these systems have been studied for years. Some investigators maintain that a definite chemical reaction occurs (3, 4, 6, 11, 12). Others believe that the swelling and solution can be accounted for on the basis of adsorption, hydration of ions, and swelling pressure (1, 5, 7, 8). Neale (9, 10) believes the action to be due to a combination of physical and chemical phenomena.

Davidson (2) has shown that the addition of relatively small amounts of zinc oxide to concentrated solutions of sodium hydroxide, forming a sodium zincate solution, greatly increases the swelling and solvent power of the alkali for cellulose. The question arises as to whether the zinc complex is physically adsorbed or whether it reacts chemically with cellulose. Experiments were conducted on the exchange of radioactive Zn^{65} in an attempt to answer this question.

Cotton was used in these preliminary experiments, as most of the available swelling and solubility data are for cotton and because a small wad of it was so easily handled with long tongs to transfer it from one solution to another.

The cotton was supplied by the Cotton Fiber Research Division, Southern Regional Research Laboratory, and had the following analysis:

Cellulose	95.3 per cent (dry basis)
Estimated degree of polymerization	2,160
Fluidity (reciprocal poises)	2,172
Protein (N × 1.65)	1 per cent
Ash	0.86 per cent
Wax	0.75 per cent

The cotton was extracted with benzene and ether–alcohol for 24 hr. before use.

---

[1] Foreign collaborator. Research fellow of the Norwegian Government, Department of Education. Present address: Borregaard A-S, Cellulose Derivatives Laboratory, Sarpsborg, Norway.

[2] Maintained at Madison, Wisconsin, in coöperation with the University of Wisconsin.

The radioactive Zn^{65} was supplied from Oak Ridge, Tennessee, in the form of an acid solution of zinc chloride, 1 ml. of which contained 184.2 mg. in 0.02 *M* hydrochloric acid. Zinc hydroxide, both active and inactive, was simultaneously prepared by precipitating 0.4 ml. of solutions of identical concentration with ammonium hydroxide, by centrifuging it several times, and then decanting off the supernatant liquid and drying at 100°C. Although the precipitation is not quantitative, this method of preparation was preferred over others tried because of its simplicity. Each of the zinc oxide preparations was dissolved in sufficient 5 *M* sodium hydroxide to give a solution containing 43.75 mg. of zinc oxide per milliliter (0.538 *M* in zinc oxide). The solution containing radioactive zinc gave a Geiger count of 6325 per milligram of zinc oxide per milliliter per minute when a 0.01-ml. sample (taken for count) was placed on a microscope slide and dried under an infrared lamp. Dilutions with the inactive solution showed that this ratio holds down to the lowest measurable concentration; therefore the coincidence error was negligible. Counts were usually made for 10 min. Corrections were made for background counting, but not for radioactive decay, as the half-life of the radioactive zinc is 250 days.

The radioactive zinc solution was found to be more active than needed. Hence, for all of the experiments 0.8 ml. was added to 9.2 ml. of the inactive solution. The labeled zinc concentrations were therefore 8 per cent of the total, or 3.58 mg. per milliliter in all of the following experiments.

A 200-mg. sample of desiccator-dried cotton was soaked in 10-ml. portions of both the active and the inactive solutions for 24 hr. at room temperature (about 22°C.). The cotton was removed from the inactive solution, blotted between sheets of filter paper, and weighed. The increase in weight averaged 227 per cent for several determinations. The cotton from the active solution was similarly blotted and was transferred to the inactive solution from which the cotton had just been removed, and the time was recorded. An inactive solution in which the same weight of cotton had soaked was used instead of a fresh solution, so as to make the inactive solution equal in concentration to the free active solution in the test cotton, even though some selective adsorption may have occurred. The inactive solution was stirred, and, at appropriate intervals (5 min. to 48 hr.), 0.01 ml. was removed and the amount of active zinc originally in the cotton that exchanged with the inactive zinc in the solution was determined from the Geiger count. The experiment was repeated with an inactive 6.25 *M* solution of sodium hydroxide containing the same increased proportion of zinc oxide:

$$\frac{6.25}{5.0} \times 0.538 = 0.672\ M \text{ in zinc oxide}$$

The data for the two experiments are given in figure 1. Both give smooth curves and indicate that exchange alone (figure 1B) and inward diffusion of inactive zinc and sodium hydroxide superimposed upon exchange (figure 1A) are very nearly complete in 1 hr.

These experiments give no information as to the amount of radioactive zinc remaining in the cotton. The exchange might only be between the free active zinc within the coarse capillary structure and the bulk inactive solution. In

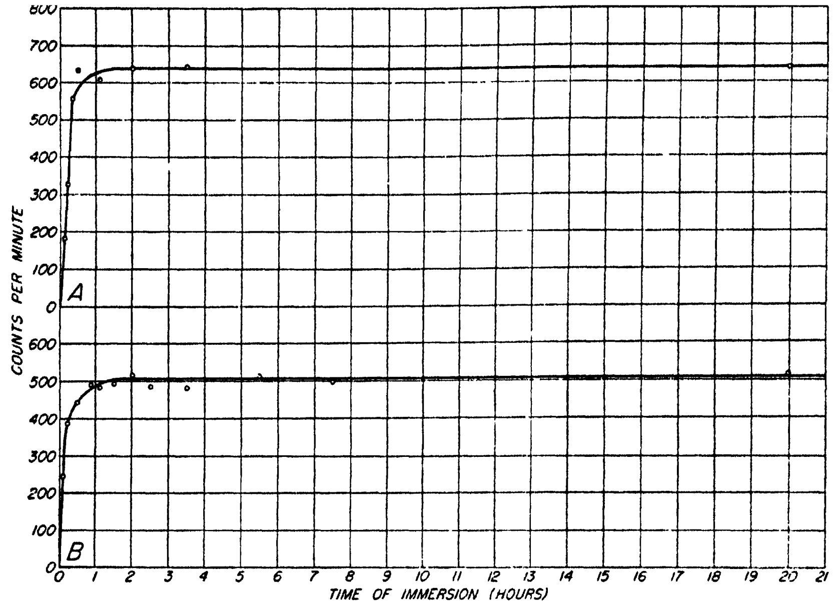

FIG. 1. Rate of exchange of radioactive zinc from cotton into media of (A) higher concentration and (B) identical concentration.

TABLE 1

Radioactivity of consecutive 10-ml. immersion solutions and the calculated remaining radioactivity of 200 mg. of cotton after immersion in two different concentrations

TIME OF IMMERSION	INACTIVE SOLUTION OF IDENTICAL CONCENTRATION		INACTIVE SOLUTION OF HIGHER CONCENTRATION		WATER	
	Activity of solutions after immersion	Activity remaining in cotton	Activity of solutions after immersion	Activity remaining in cotton	Activity of solutions after immersion	Activity remaining in cotton
min.	*counts per minute*	*per cent*	*counts per minute*	*per cent*	*counts per minute*	*per cent*
1	7275	18.3	6388	25.2	7892	10.4
4	1308	3.6	1862	3.7	509	4.7
5	266	0.6	262	0.6	361	0.6
15	50	0.0	50	0.0	50	0.0
60	approx. 0		approx. 0		approx. 0	
Total	8900		8562		8812	

order to determine the increments of active zinc lost from the cotton and the final amount retained, the following experiments were performed. Cotton was soaked in the active and in the inactive solutions as before. The cotton containing the

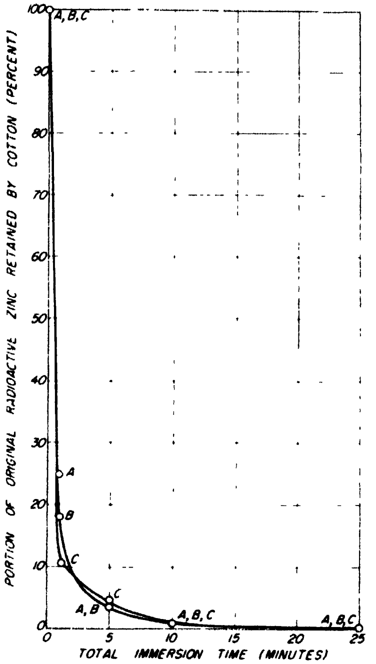

FIG. 2. Portion of original radioactive zinc retained by cotton after repeated transfers into fresh media of (A) higher concentration, (B) identical concentration, and (C) water.

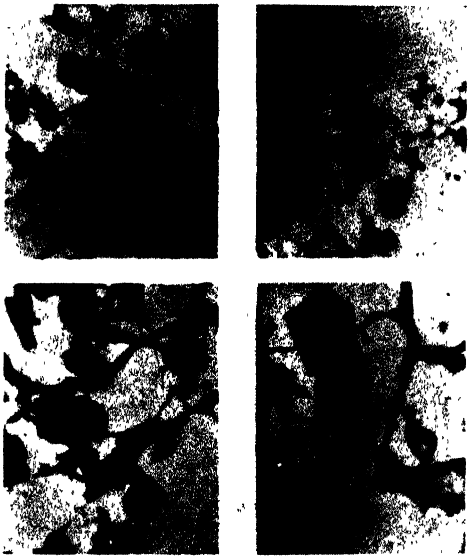

FIG. 3. Electron photomicrographs of cotton containing zinc oxide precipitated by water; magnification, 6000.

radioactive solution was, however, transferred to fresh inactive solution at intervals, with blotting between each transfer and determination of the Geiger count on the solutions. The experiment was also performed by making the transfers into the more concentrated inactive solution and into water. Table 1 gives the results of these experiments. Figure 2 gives the same data expressed in terms of the fraction of the radioactive zinc remaining in the cotton after various periods of time, calculated from the summation of the counts from the different transfers.

From the average solution content of the blotted cotton (227 per cent of the desiccator dry weight of the cotton), the specific gravity of the active solution (1.20), the original content of labeled zinc oxide per milliliter of the starting solution (3.5 mg.), and the count per milligram of active zinc per milliliter per minute (6325), the original count of the cellulose should be 8412. This value is slightly less than the summation of counts given in table 1 for the radioactive zinc actually lost. The differences between the values are probably caused by slight variations in the solution content of the different samples of cotton, due presumably to variations in blotting. Although these experiments indicate that radioactive zinc is entirely removed from the cotton, further tests were made to confirm this by dissolving the final cotton samples after the final exchange of 60 min. (total exchange time of 85 min.) in 2 ml. of concentrated sulfuric acid. In the case of the exchange into equal and more concentrated inactive solutions, counts on 0.01-ml. portions were within experimental error of the background count. In the case of the cotton transferred into water, 53 counts per minute were obtained. This appreciable amount of residual zinc was shown to be due to the precipitation of zinc oxide on dilution with water. When 6 10 volumes of water were added to 1 volume of the inactive solution, the light transmission of the solution dropped to 10 per cent of the original value after standing for 16 min. Electron microscope pictures (figure 3) indicate that a crystalline precipitate is actually formed within the fibers.

DISCUSSION AND CONCLUSIONS

Radioactive Zn^{65} in the form of sodium zincate dissolved in concentrated sodium hydroxide can be rapidly removed from cotton by exchange into an inactive solution of identical concentration and by exchange into a more concentrated solution counter to the inward diffusion under a concentration gradient. In the latter case, inward diffusion hinders exchange for the first minute, while equalization of concentrations is occurring. Exchange during the next 4 min. into the second solution is relatively faster, as more radioactive zinc remains in the cotton for exchange. Exchange into the third and fourth solutions is about the same. Diffusion into water is more rapid at first than the exchange into the same concentration of inactive solution because of the diffusion potential. Diffusion slows down, however, as both sodium hydroxide and sodium zincate are removed from the cotton as a result of the shrinkage of the cotton and a reduction in the cross section effective for diffusion.

In no case do breaks occur in the curves that would result if slowly dissociating zinc compounds were formed. If compound formation does occur, the reaction must be more rapidly reversible than the exchange and the diffusion (96 per cent complete in 5 min.).

The authors wish to thank Professor John E. Willard of the Department of Chemistry of the University of Wisconsin for making available the facilities of his radioactive tracer laboratory.

REFERENCES

(1) Bancroft, W. D., and Calkin, J. B.: J. Phys. Chem. **39**, 1 (1935).
(2) Davidson, G. F.: J. Textile Inst. **28**, T27 (1937).
(3) Gladstone, J.: Jahresber. Chem. **5**, 823 (1852).
(4) Hess, K.: Z. angew. Chem. **38**, 230 (1925).
(5) Joyner, R. A.: J. Chem. Soc. **121**, 1511 (1922).
(6) Kolthoff, I. M.: Pharm. Wochenblatt **57**, 1571 (1920); **58**, 46 (1921).
(7) Leighton, A.: J. Phys. Chem. **20**, 32 (1916).
(8) Miller, D.: Ber. **40**, 4903 (1907).
(9) Neale, S. M.: J. Textile Inst. **20**, 373T (1929).
(10) Neale, S. M.: J. Soc. Chem. Ind. **50**, 177 (1931).
(11) Thiele, E.: Chem. Ztg. **25**, 610 (1901).
(12) Viewig, W.: Ber. **40**, 3876 (1907).

THE KINETICS OF ISOTOPIC EXCHANGE REACTIONS[1]

T. H. NORRIS

Department of Chemistry, Oregon State College, Corvallis, Oregon

Received July 5, 1949

It has been shown (4, 8) that, in a radioactive (or separate isotope) tracer study of the rate of an exchange reaction carried out at chemical equilibrium (as is normally the case), no matter what the actual kinetics, the course of any given run will be governed by a first-order rate law. Duffield and Calvin (4) have given an equation which may be used in computing the rate of an exchange reaction, but since, in practice, we have found that the application of this equation and others like it tends to become rather confusing, it has seemed worthwhile to discuss this topic in some detail.

Following the usage of Duffield and Calvin, we represent our exchange reaction by the equation (the asterisks having their usual significance):

$$\mathrm{BX^* + AX = AX^* + BX}$$

in which the concentrations are represented by

$$x = (\mathrm{AX^*}) \qquad a = (\mathrm{AX^*}) + (\mathrm{AX})$$
$$y = (\mathrm{BX^*}) \qquad b = (\mathrm{BX^*}) + (\mathrm{BX})$$

$$x_0 = x \text{ and } y_0 = y \text{ at } t = 0$$
$$x_\infty = x \text{ and } y_\infty = y \text{ at } t = \infty$$

---

[1] Published with the approval of the Oregon State College Monographs Committee. Research Paper No. 154, Department of Chemistry, School of Science, Oregon State College.

and for which R = rate of reaction, F = fraction of exchange equilibrium, and $\boldsymbol{x} = x/a$; $\boldsymbol{y} = y/b$ (see table 1).

The equation given by Duffield and Calvin is equivalent to

$$R = -\frac{2.3}{t}\left(\frac{ab}{a+b}\right)\log(1-F) \tag{1}$$

where F, the fraction of exchange equilibrium which has been attained at time t, is given by

$$F = \frac{x}{x_\infty} \qquad \text{when} \quad x_0 = 0 \tag{2}$$

or

$$F = \frac{x - x_0}{x_\infty - x_0} \qquad \text{when} \quad x_0 \neq 0 \tag{2'}$$

Equation 2 is a special case of equation 2′. In actual practice one would most frequently employ equation 2′ for separated isotope tracers and equation 2 for radioactive isotopes.

It often happens in practice that one of the reactants is present in large excess. Obviously, in such a case, equation 1 may be simplified to:

$$R = -\frac{2.3a}{t}\log(1-F) \qquad b \gg a. \tag{1'}$$

$$R = -\frac{2.3b}{t}\log(1-F) \qquad a \gg b \tag{1''}$$

R, the rate of the reaction between AX (+ AX*) and BX (+ BX*), represents the *total* number of "exchanges," both radioactive and nonradioactive, per unit time, in terms of the concentration units being used, e.g., moles per liter. It is, therefore, quite independent of the concentration of the tracer and evidently remains constant throughout a run. It is not, however, in any sense a "rate constant," but is some function of any of the factors which may govern the rate of a chemical reaction, such, for example, as the concentrations a and b. Notice, though, that a possible functional dependence on a and b is quite apart from the existence of these quantities in equation 1, 1′, or 1″. Any kinetic study has as its object the ascertainment of the nature of this function; this is done by conventional kinetic methods, R being directly comparable from one run to another. For example, were two runs identical in all significant respects except concentrations, R should be the same in both if the reaction is zero order, but not otherwise. Were our reaction bimolecular we would get $R = (ab)$ (constant).

In equations 2 and 2′ the x's, of course, are defined as concentrations, but, since they occur as a dimensionless ratio, they may be expressed in any units which, for a given run (but not necessarily from one run to another), are proportional to the concentration of the radioactive molecules being formed in the reaction. In practice this means either the total activity or the specific activity of the initially inactive fraction, where the units might be respectively, for example, counts per minute, and counts per minute per mole (or, if all activities are measured in a common chemical form such as $BaCO_3$, the latter might be counts per minute per milligram). Alternatively, if the tracer is a separated isotope, such as C^{13} or O^{18}, the x's refer to that compound which initially had the normal isotopic composition and, if equation 2 is used, will be expressed as mole fraction excess, i.e., mole fraction of the separated isotope minus the normal mole fraction as it occurs in nature. This amounts to the same thing, of course, as substituting mole fractions for the x's in equation 2′.

TABLE 1

Expressions for F in various units

TOTAL ACTIVITIES	SPECIFIC ACTIVITIES OR MOLE FRACTION EXCESS	RESTRICTION
(1) $\frac{x}{x_\infty}$	(1′) $\frac{x}{x_\infty}$†	
(2) $\left(1 + \frac{b}{a}\right)\frac{x}{y_0}$*	(2′) $\left(1 + \frac{a}{b}\right)\frac{x}{y_0}$*	
(3) $\frac{b}{a} \cdot \frac{x}{y_0} = \frac{b}{a} \cdot \frac{x}{y_\infty}$	(3′) $\frac{x}{y_0} = \frac{x}{y_\infty}$*	$b \gg a$
(4) $\frac{x}{y_0}$*	(4′) $\frac{a}{b} \cdot \frac{x}{y_0}$	$a \gg b$
(5) $\frac{y_0 - y}{y_0 - y_\infty}$	(5′) $\frac{y_0 - y}{y_0 - y_\infty}$†	
(6) $\left(1 + \frac{b}{a}\right)\left(1 - \frac{y}{y_0}\right)^*$	(6′) $\left(1 + \frac{b}{a}\right)\left(1 - \frac{y}{y_0}\right)^*$	
(7) $\frac{b}{a}\left(1 - \frac{y}{y_0}\right)$	(7′) $\frac{b}{a}\left(1 - \frac{y}{y_0}\right)$	$b \gg a$
(8) $\left(1 - \frac{y}{y_0}\right)^*$	(8′) $\left(1 - \frac{y}{y_0}\right)^*$	$a \gg b$
(9) $\left[1 - \frac{y - (b/a)x}{y_0}\right]^*$	(9′) $\left[1 \quad \frac{y - x}{}\right]^*$	

* Expressions most often useful.

† In terms of *mole fractions*, these expressions become

$$F = \frac{x - x_0}{x_\infty - x_0} = \frac{y_0 - y}{y_0 - y_\infty}$$

The expressions for F contain the quantity x_∞, which is often not determined experimentally,[2] so it is perhaps worthwhile to set down in table 1 a number of alternative expressions for F which may be used in order to obtain a value for

---

[2] The determination of x_∞ is required in some work and is always useful as a further test of the experimental method.

R from equation 1. These are all readily derived from the self-evident relationships[3, 4]

$$y_0 + x_0 = y + x = y_\infty + x_\infty \tag{3}$$

$$\frac{x_\infty}{a} = \frac{y_\infty}{b} \tag{3'}$$

and the defining equations for F, equation 2 or 2′.

Since, under normal counting conditions, the units of x and y, i.e., concentrations, are proportional to total activities (in any given experiment), x and y may equally well be expressed in terms of the latter, as indicated by the heading of the first column. The second column is given in terms of the quantities $\mathbf{x} = x/a$ and $\mathbf{y} = y/b$, which, then, represent specific activities. Alternatively, the latter expressions apply if the units are mole fraction excess of stable tracer isotope (excess over the "natural" mole fraction). The subscripts have the same meaning as hitherto.

In table 1 expressions 1 to 4′ correspond to cases where the rate of exchange is followed by measuring the activity (or isotopic composition) of the substance initially inactive (or of normal isotopic composition), whereas expressions 5 to 8′ correspond to the alternative procedure of following the decrease in activity of the substance initially active. Expressions 9 and 9′ correspond to the procedure of following the activity of both of these fractions. This last may be used as an aid in testing the experimental procedure. Expressions 3 to 4′ and 7 to 8′ correspond, as indicated, to a large excess concentration of one of the reactants. The equalities in expressions 3 and 3′ correspond to the fact that for $b \gg a$, y or $\mathbf{y}$ remains constant and equal to y_0 or $\mathbf{y}_0$. For this same reason expressions 7 and 7′ are of no practical value; they are included for the sake of completeness only. Likewise expressions 3 and 4′ will frequently be of no value, since the ratio b/a or *vice versa*, may be difficult to establish accurately, if the concentration of the excess component is unknown (*cf.* the last paragraph of this paper). It is to be noted that in these cases, this (excess) concentration is not needed, since it drops out of equations 1′ and 1″ for R. Since, in addition, x_∞ and y_∞ are not normally measured directly, expressions containing them are of secondary importance. (One may determine x_∞ or y_∞ indirectly, but this is tantamount to using one of the other expressions for F.) Thus we find, as the expressions which most fre-

---

[3] Throughout this paper, it is assumed that radioactive decay is corrected for in conventional fashion.

[4] These relations and, in general, the quantitative validity of tracer methods depend on the assumption that the tracer and "traced" isotopes are chemically identical. It has long been recognized that such an assumption in the case of the hydrogen isotopes is far from valid. Recent work has shown that other isotopes, with higher atomic weights, such as C^{13} and C^{14}, may also, in certain cases, exhibit a surprisingly large isotope effect, although the magnitude of the effect in various reactions is not yet clearly established (1, 2, 7, 9, 12, 13, 14). For instance, Yankwich and Calvin (14) report an effect in the decarboxylation of C^{14}-labelled bromomalonic acid which, if correct, could never be ignored. It is evident that in quantitative tracer studies, where such an effect is appreciable, it may not be neglected but should be corrected for.

quently will be used, those marked with an asterisk. Substitution of expressions 6 and 6′ in equation 1 leads with slight rearranging to the equation given by Davidson and Sullivan[6] (3).

Discussing now the concentrations a and b: inspection of the equations in which they occur indicates that these quantities must always be expressed in the same units. Furthermore, these must be gram-atom units (see the discussion below in regard to molecules such as AX_2, etc.), e.g., pressure at some standard temperature, gram-atoms per liter, etc.

Since we are here dealing with a first-order rate law, it is possible to obtain a value of R from the slope of a semilogarithmic plot giving the rate of approach to equilibrium, but it is to be noticed that R is not equal to this slope, as may be seen from equation 4 below. This procedure has the advantage that no knowledge of a zero time is necessary, but it entails a measurement of the extent of exchange for fixed conditions at *at least* two different values of t. From equation 1 we obtain

$$R = -2.3\left(\frac{ab}{a+b}\right)\frac{\mathrm{d}\log(1-F)}{\mathrm{d}t} = -2.3\left(\frac{ab}{a+b}\right)\frac{\mathrm{d}\log Q}{\mathrm{d}t} \qquad (4)$$

$$R = -2.3a\,\frac{\mathrm{d}\log(1-F)}{\mathrm{d}t} = -2.3a\,\frac{\mathrm{d}\log Q}{\mathrm{d}t} \qquad b \gg a \qquad (4')$$

$$R = -2.3b\,\frac{\mathrm{d}\log(1-F)}{\mathrm{d}t} = -2.3b\,\frac{\mathrm{d}\log Q}{\mathrm{d}t} \qquad a \gg b \qquad (4'')$$

For Q we may substitute, besides $(1 - F)$, $(x_\infty - x)$ or $(y - y_\infty)$, where the x's and y's may be expressed as concentrations, mole fractions, specific activities, or total activities. Values for $(1 - F)$ may be obtained from table 1, but it is perhaps worth noting that in many such cases the expression can be rearranged to a form with a constant denominator. In such a case, of course, only the numerator need be substituted for Q in equation 4. Thus, for instance, application of expression 4 (table 1) leads to a value for Q of $(y_0 - x)$.

The foregoing discussion has general validity for a homogeneous exchange reaction between a pair of molecules each containing one exchangeable atom. Friedlander and Kennedy (5) discuss the case where one or both of these molecules have more than one exchangeable atom (e.g., AX_2 or BX_n). As these authors indicate, the applicability of the treatment here under discussion remains unaltered, so long as all the X atoms in a given molecule are, at least in an exchange sense, equivalent and concentrations are expressed in gram-atoms per unit volume of X (in either exchanging molecule). Nonequivalent X atoms in a given molecule will, in the general case, exchange at different rates. The observed total rate is then a superposition of two or more first-order rates, and the present simple treatment cannot be applied, unless the different rates are of completely different orders of magnitude.

For heterogeneous exchange reactions, the expressions in this paper have only limited validity. Zimens (15) has discussed the kinetics of such cases. His treatment has particular reference, but is not limited, to exchange between a solid and a liquid (or gas) phase. Expressions are derived, applicable to rate determination by three different alternative processes: (*1*) diffusion through a layer of the less dense phase adsorbed on the surface of the more dense; (*2*) chemical reaction at the interface; (*3*) diffusion within the solid phase. The expressions for the first two cases, while more directly applicable to the study of heterogeneous systems, are equivalent to those in this paper; hence these remain valid. The present treatment, however, cannot be applied to Zimens' third process. This is because the atoms in the interior of the solid are not equivalent to those on the surface and consequently exchange at different rates. The rate law becomes a summation of several rate terms, as for the case in the previous paragraph.[6]

---

[6] The terminology used by Davidson and Sullivan differs somewhat from that used in the present paper.

Zimens (15) gives experimental criteria for distinguishing between the different rate-determining processes. Here, however, our primary concern is whether the simple first-order rate law is applicable. The test lies in a plot, for a given run, of log $(1 - F)$ *versus* t, using several different values of F (and t). A straight line indicates applicability. In certain cases, this straight line may not run through the origin, as, for example, was observed by Prestwood and Wahl (11) (where separation errors, or separation-induced exchange occurred). A curved-line plot indicates a lack of equivalence of exchanging atoms, heterogeneous exchange, or faulty technique.

For heterogeneous systems the units in which a and b should be expressed tend to become confusing. Following Zimens (15), one may express them as *amounts* (e.g., gram-atoms); R is then obtained in corresponding units (amounts/time). Alternatively, if concentrations are used, it should again be emphasized that the units of a and b must be identical. Thus, considering the exchange between two substances dissolved each in different, immiscible liquids, a and b cannot be expressed as concentration of each substance in its own phase; rather they might be given as amounts per unit volume of either one phase (or per unit volume of both phases taken together). From this it follows, as a corollary for such a case, that successive runs, to be comparable, must duplicate not only the concentration of each reactant in its own phase but the phase volume ratio as well.

The last statement, based entirely on the equations given for R, involves no assumption, other than the applicability of these equations, concerning the mechanism or rate law of the heterogeneous reaction. It can, however, be supported and extended by arguments involving the inherent nature of such reactions. Heterogeneous rate laws are dimensionally different from homogeneous ones. Thus it is commonly recognized that such geometrical factors as surface–volume ratios will affect the rates. Fuzek and Smith (6) have studied certain catalytic hydrogenations and shown that the total volume of the system must be included as a term in the rate law. Evidently, then, in order for different runs in a heterogeneous kinetic study to be comparable, geometrical factors in general must be maintained constant. This implies, for the example of the previous paragraph, that the phase volume ratio, as before, and, in addition, the total volume of the system must be kept constant. Or again, considering an exchange study between a gas and a liquid, runs being made in sealed bomb tubes: the total tube volume for comparable runs must always be the same. If this is impractical, assumptions about the dependence of R on the volume become necessary.

---

[6] For an experimental illustration of this phenomenon see, for example, the paper by Polessitsky (10).

In heterogeneous reactions it is sometimes inconvenient, difficult, or impossible to express the concentrations of both a and b in the same units. Here, though, it will often be obvious that one of the reactants is present in large excess (i.e., $a \gg b$ or *vice versa*). In such a case the equation which will be used (equation 1′, 1″, 4′, or 4″ plus an appropriate expression for F from table 1) will contain only the concentration of the component present in small amounts and not the other concentration. Here any reasonable concentration units may be employed.

SUMMARY

An isotopic exchange reaction must proceed toward equilibrium according to a first-order rate law or according to concurrent first-order laws. A discussion is given of the implications of this concept for the experimental study of the kinetics of exchange reactions. Expressions are tabulated for the fraction of exchange equilibrium, F, attained at any time, t, in terms of quantities which are experimentally determinable.

REFERENCES

(1) Beeck, O., Otvos, J. W., Stevenson, D. P., and Wagner, C. D.: J. Chem. Phys. **16**, 255 (1948).
(2) Bigeleisen, J., *et al.*: Science **110**, 14, 149 (1949); J. Chem. Phys. **17**, 344, 425, 998 (1949).
(3) Davidson, Norman, and Sullivan, John H.: J. Am. Chem. Soc. **71**, 739 (1949).
(4) Duffield, R. B., and Calvin, M.: J. Am. Chem. Soc. **68**, 557 (1946).
(5) Friedlander, G., and Kennedy, J. W.: *Introduction to Radiochemistry*, p. 288. John Wiley and Sons, Inc., New York (1949).
(6) Fuzek, J. F., and Smith, H. A.: J. Am. Chem. Soc. **70**, 3743 (1948).
(7) Lindsay, J. G., McElcheran, D. E., and Thode, H. G.: J. Chem. Phys. **17**, 589 (1949).
(8) McKay, H. A. C.: Nature **142**, 997 (1938).
(9) Pitzer, K. S.: J. Chem. Phys. **17**, 1341 (1949).
(10) Polessitsky, A.: Compt. rend. acad. sci. U.R.S.S. **28**, 441 (1940).
(11) Prestwood, R. J., and Wahl, A. C.: J. Am. Chem. Soc. **71**, 3137 (1949).
(12) Stevenson, D. P., Wagner, C. D., Beeck, O., and Otvos, J. W.: J. Chem. Phys. **16**, 993 (1948).
(13) Weigl, J. W., and Calvin, M.: J. Chem. Phys. **17**, 210 (1949).
(14) Yankwich, P. E., and Calvin, M.: J. Chem. Phys. **17**, 109 (1949).
(15) Zimens, K. E.: Arkiv Kemi, Mineral. Geol. **A20**, No. 18 (1945); **A21**, No. 16 (1946).

ADSORPTION-DESORPTION HYSTERESIS IN RELATION TO CAPILLARITY OF ADSORBENTS[1]

CONWAY PIERCE AND R. NELSON SMITH

Department of Chemistry, Pomona College, Claremont, California

Received July 19, 1949

The phenomenon of hysteresis in the desorption[2] of vapors from solid surfaces is generally assumed to be related to the emptying of capillaries. In fact, the occurrence of hysteresis is usually taken as evidence for capillary condensation.

Several theories have been advanced to account for a difference in the manner in which the vapor condenses in and evaporates from capillaries. All but the more recent ones of Juhola and Wiig (10), Hill (7), and Gleysteen and Deitz (6) have been summarized by Brunauer (3).

In recent studies with some nonporous adsorbents we have found hysteresis to occur in desorptions from surfaces where there is evidence against the existence of capillaries. This has led us to inquire into a possible mechanism for hysteresis that does not require capillary condensation of the adsorbate. A new hypothesis has been developed which we believe gives an adequate explanation of hysteresis both from plane surfaces and from capillaries. It also takes into account the occurrence of hysteresis with some adsorbates while other adsorbates show none from the same capillary pores. This hypothesis is herein presented.

EXPERIMENTAL

Adsorption and desorption isotherms were determined for ethyl chloride and water on graphite NC-1, Graphon, and activated charcoal S84.

Graphite NC-1 was obtained from the National Carbon Company.[3] It has a nitrogen area of 4 sq. m./g. and has less than 0.001 per cent ash. This is the same sample as was used for other studies in this laboratory (11, 12, 13).

Graphon is partially graphitized Spheron Grade 6 carbon black, obtained from Godfrey L. Cabot Company.[4] It is from the same lot used by Beebe, Biscoe, Smith, and Wendell (2) and by Joyner and Emmett (8). The nitrogen area is given by the latter as 80 sq. m./g.

S84 is a highly activated charcoal prepared in this laboratory by carbonization of sheet Saran at 600°C. and steam activation at 900°C. until there is 84 per cent weight loss of the carbonized material. It has an adsorptive pore volume near 1.1 ml./g.

---

[1] This is a progress report of work conducted under Contract N8 onr 54700 with the Office of Naval Research, United States Navy Department.

[2] In this paper we are speaking only of reversible hysteresis. Brunauer (3) defines hysteresis as reversible if on repetition of the experiment the adsorption isotherm is completely reproduced. When the adsorbent itself is altered by adsorption and desorption of vapor the explanation must be somewhat different than when there is no alteration of the adsorbent structure.

[3] Through the courtesy of Dr. Lester L. Winter.

[4] Through the courtesy of Dr. Walter R. Smith.

All isotherms were determined gravimetrically by removing and weighing the sample bulb after equilibrium was attained at each pressure. Experimental details are given in previous papers.

When the isotherm temperatures are below room temperatures, there is alternate desorption and readsorption of vapor as the sample tube is removed for weighing and then re-cooled in the bath. This amounts to "scanning" the hysteresis loop in desorptions and may have the effect of diminishing the apparent amount of hysteresis. When the isotherm temperature is below room temperature it is necessary to reëquilibrate the sample to a pressure near p_0 after each removal for weighing.

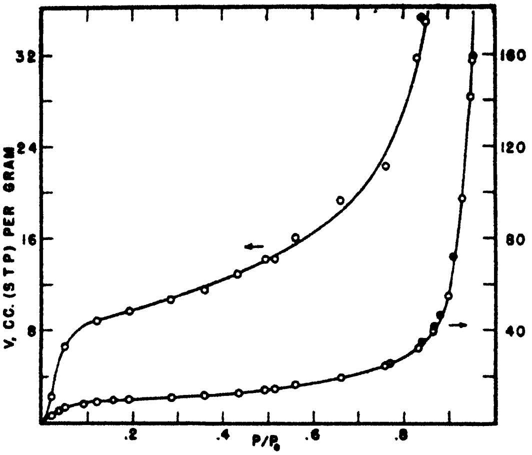

FIG. 1

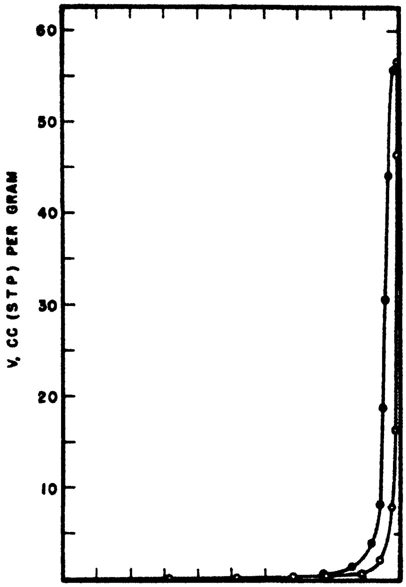

FIG. 2

FIG. 1. Ethyl chloride at 0°C. on Graphon. ●, desorption. At 0.997 p_0 a volume of 293 ml. is adsorbed.

FIG. 2. Water on Graphon at 28.9°C.; ●, desorption

The isotherms are shown in figures 1 to 4.

DISCUSSION

The ethyl chloride isotherm in figure 1 indicates, as discussed later, that the adsorbent, Graphon, has no capillaries. The water isotherm of figure 2 shows, however, a pronounced desorption hysteresis. If we are correct in concluding that Graphon has no capillaries, it follows that none of the previous theories (all of which are based upon capillary condensation) are adequate to explain the water desorption hysteresis. We have therefore sought an explanation which is applicable for adsorption-desorption in capillaries and on plane surfaces.

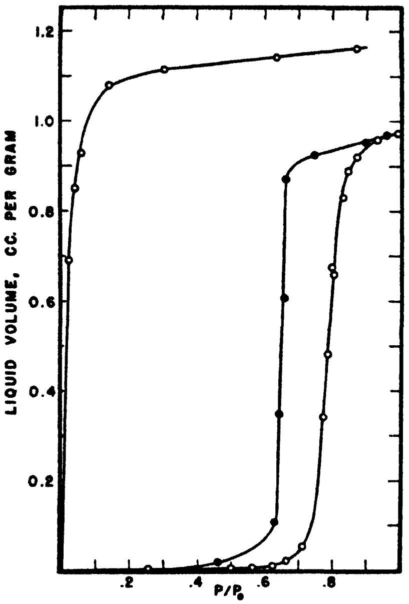

FIG. 3

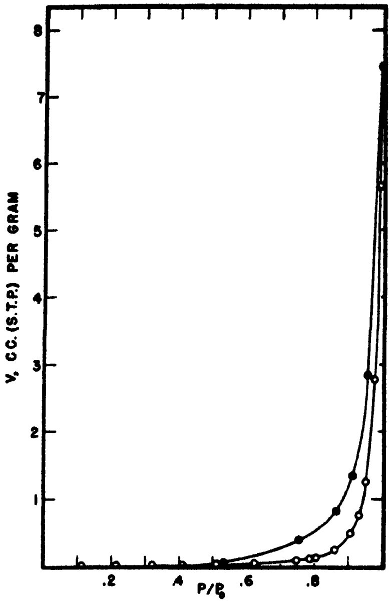

FIG. 4

FIG. 3. Ethyl chloride at −78°C. (left) and water at 28.9°C. on Charcoal S84. Plotted as liquid volume adsorbed. ●, desorption.

FIG. 4. Water on graphite NC-1 at 28.9°C.; ●, desorption

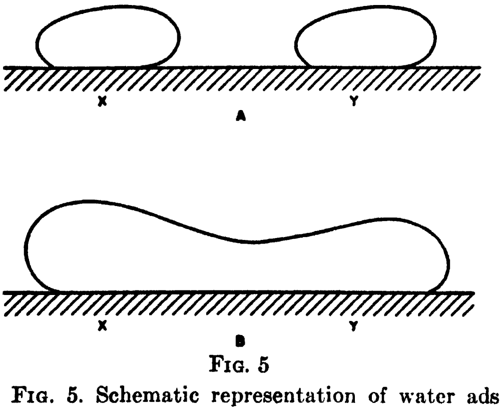

FIG. 5

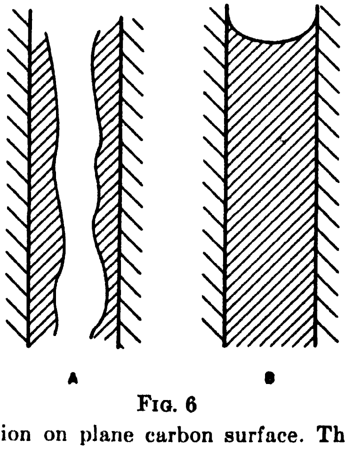

FIG. 6

FIG. 5. Schematic representation of water adsorption on plane carbon surface. The droplets first formed at active sites X and Y (A) later merge (B) as pressure is increased.

FIG. 6. Schematic representation of adsorption in large capillary. A multilayer film is first formed on each wall (A) and then merges at higher pressure (B) to fill the capillary.

PROPOSED THEORY

If there is stable equilibrium in the desorption part of the cycle (which we believe to be the case), it means that the adsorbed molecules are more strongly held during desorption than at the corresponding degree of saturation during adsorption. In other words, a change has occurred in the nature of the adsorbed layer. Such a change is readily accounted for by the assumption that adsorption occurs in isolated clumps that later merge. When two clumps merge the forces on all molecules are increased, as specifically discussed below.

First, we consider adsorption on a plane surface of nonuniform activity, as illustrated in figure 5A. Two active sites, X and Y, each hold a multilayer clump of molecules. As adsorption proceeds the clumps may meet and merge, as in figure 5B. When this happens *all* molecules of the combined clump are held by long-range forces from *both* active sites, whereas before merging the molecules in each clump were held only by forces from the active site on which the clump is adsorbed. Thus the vapor pressure is lowered after the clumps merge, and desorption hysteresis will occur. This hysteresis will persist until a point is reached at which the clump breaks up into two separate clumps; at this point the desorption branch of the isotherm rejoins the adsorption branch, since conditions are now exactly as they were at this degree of saturation in adsorption.

A condition similar to that described above exists when wide capillaries are filled by multilayer adsorption on opposite walls, followed by eventual merging of the films. The conditions before and after merging are illustrated in figures 6A and 6B. Prior to merging, the layers are held by surface forces from a single wall, but after merging surface forces from both walls affect all molecules. This reduces the fugacity and there is desorption hysteresis which persists either until the capillary contains only a monolayer on each wall or until the remaining adsorbate breaks up into two separate multilayer films.

In figure 6 we have, for simplicity, represented the capillary as a fissure between two plane parallel walls. This is, of course, an oversimplification but is chosen to show that one need not assume constrictions, bottle necks, or closed-end capillaries to account for hysteresis. The single multilayer films on opposite walls before merging (figure 6A) are represented as of variable thickness, in keeping with our view that the most active sites will hold more molecules than less active ones.

The present theory is based on two assumptions: (*a*) that many surfaces are of nonuniform activity and (*b*) that long-range forces from a surface may extend to great distances through a liquid-like film but not to the same distances in the absence of a film. There is much evidence from heats of adsorption for the first assumption; in fact, we know of no heat of adsorption data which indicate uniform surfaces. As to the second, it is obvious from multilayer adsorption data that surface forces can extend to great distances *in a film*. The ethyl chloride isotherm of figure 1 shows adsorption of some 32 statistical layers before saturation is reached. This means that surface forces can lower adsorbate vapor pressures through a film of some 150 Å. in depth. It appears reasonable then to assume that when two films merge all molecules are acted upon by additional forces, since all now have contact through the film with additional surface sites. In absence of a film it is generally assumed that van der Waals forces fall off inversely with the seventh power of distance. Consequently the surface forces exert negligible effect in space at distances of the order of several molecular diameters. In the situation of figure 6A the film on one wall is not affected by forces from the other wall until the two films merge.

APPLICATIONS

In applying the present theory to experimental data it must be kept in mind that hysteresis occurs only when the mechanism of adsorption is such that discrete clumps or films merge. This is the determining factor rather than the presence or absence of capillaries. In fact, as shown later, given capillaries may with some adsorbates yield isotherms that exhibit desorption hysteresis while with other adsorbates there is no hysteresis.

We consider now various examples of hysteresis.

1. Water shows hysteresis in desorption from Graphon but ethyl chloride does not. The difference is due to the way in which the two adsorbates are held. Ethyl chloride gives a typical Type II isotherm, with a monolayer apparently completed at low relative pressure. This must mean that the entire surface can hold ethyl chloride molecules firmly, even though some sites have greater activity than others. The first layer is completed before there is appreciable multilayer adsorption. Therefore the condition of figure 5 does not apply; no change takes place in the nature of the adsorbed film as adsorption proceeds and there is no desorption hysteresis. Water, on the other hand, is poorly held by carbon. A relative pressure of 0.99 is needed to adsorb a statistical monolayer and at 0.997 p_0 only two statistical monolayers are held. We think that this behavior indicates a condition like that of figure 5. Only the more active sites hold adsorbate, and multilayers build up as discrete clumps at these sites. At high relative pressure some of these clumps merge, thereby changing the condition of the adsorbed molecules, and hysteresis is shown on desorption.

Our assumption that adsorption of water occurs only at certain active sites is in keeping with known properties of the carbon–water system. First, as previously discussed (12), water lacks mobility on a carbon surface, while other adsorbates appear to have such mobility There can be surface mobility only when all sites can hold adsorbate; otherwise the adsorbate molecule evaporates when it reaches a site that cannot retain it. Second, the heat of emersion data of Basford, Jura, and Harkins (1) indicate that a saturated graphite surface is not completely covered by a water film. When a saturated sample of titanium dioxide is immersed there is a heat evolution of 119 ergs/sq. cm. due to disappearance of water surface. But when a nearly saturated graphite sample is immersed, approximately 86 ergs/sq. cm. is absorbed; in other words, there is not a complete water film over the surface. From the adsorption isotherm and these other considerations then, we believe that water is adsorbed in clumps rather than over the whole surface.

2. Desorption from capillaries may or may not give hysteresis. This is shown in the isotherms of water and ethyl chloride on charcoal S84, in figure 3. Here the amount adsorbed is plotted as liquid volume. As discussed in a previous paper (12), if water is held by capillary condensation then ethyl chloride must

also be held by condensation in the same capillaries; the point B volume[5] of ethyl chloride is greater than the saturation volume of water. Yet the water isotherm shows hysteresis and the ethyl chloride isotherm does not (no Type I isotherms give desorption hysteresis). The difference is readily explained by the theory given above. Ethyl chloride does not fill the capillaries by first forming a multilayer film on opposite walls and eventual merging of these films. Most of its adsorption occurs at low relative pressures, too low for appreciable multilayer adsorption. This is seen by comparing the isotherms of Graphon and S84. It must be, then, that ethyl chloride fills the capillaries by adsorption at a meniscus which starts at the narrowest places, as discussed in our previous paper. If so, there is at all times a wall-to-wall film and the process of figure 6 does not apply. On desorption all molecules are held exactly as they were on adsorption and there is no hysteresis. Water, on the other hand, is poorly held by carbon. Discrete clumps are adsorbed at the most active sites and these later merge to fill the capillaries. This merging leads to hysteresis for water desorption.

3. Desorption from wide capillaries is always attended by hysteresis, regardless of the adsorbate employed. When the walls are too far apart to cause the capillary to fill at low relative pressure there is multilayer adsorption on the separate walls at high relative pressure and eventual meeting and merging of the films, as shown in figure 6. Whenever this happens the isotherm is of Type IV. Such isotherms show the rise beginning at the relative pressure region near 0.4 that is characteristic of multilayer adsorption. It is only when capillaries fill in the higher relative pressure region that multilayer adsorption on separate walls can occur. We know from many Type II isotherms that appreciable multilayer adsorption does not begin until the relative pressure is near 0.4 or greater.

Gleysteen and Deitz (6) gave some years ago a clear explanation of hysteresis from capillaries that fill by multilayer adsorption. They were the first to "attribute hysteresis to some fundamental change in the adsorbed layer that takes place at a relative pressure near saturation" and to point out that molecular clusters may form at many points on a surface and then be modified by merging. In essence our explanation is like theirs but we differ in some important details. First, after showing that the heat of desorption is greater than that of adsorption for isotherms that show hysteresis, they related this excess heat to the heat of adsorption of the last layer, Q, first proposed by Brunauer, Deming, Deming, and Teller (4). According to our view, the excess heat of desorption is not the heat of adsorption of the last layer, as incorporated in the B.D.D.T. treatment. Rather it is due to the fact that after the separate films merge all molecules within the film are more strongly held than before merging. Second, the Gleysteen and Deitz explanation applies only to hysteresis in desorption from capillaries, not to desorption from a plane surface. Finally, they take no account of capillaries that may be emptied without hysteresis.

Joyner and Emmett (9) have determined isosterically the excess heat of desorption for nitrogen on a porous glass sample. Over most of the hysteresis loop the excess heat is some 200–250 cal./mole, but it is not constant. Even with these small heat values there is obtained quite a large hysteresis loop, i.e., a much lower equilibrium pressure for desorption than for adsorption. We believe their data to be quite in keeping with our theory that after the capillary has filled by merging of separate films all molecules are more tightly held than when the films are separate; the small excess heat values show that a small additional force on the molecules may appreciably lower their equilibrium vapor pressures.

---

[5] By point B we mean the beginning of the linear portion of the isotherm, which is generally assumed to be closely related to the completion of the first layer.

CLASSIFICATION OF CAPILLARIES

It is convenient to classify the adsorption–desorption characteristics of capillaries according to their method of filling and their hysteresis properties.

Class I: A capillary which fills at the low relative pressures usually associated with monomolecular adsorption and which shows no desorption hysteresis is designated as Class I. Such capillaries probably do not exceed a few molecular diameters in width. The walls are so close together that their coöperative effect lowers the vapor pressure of contained molecules to the relative pressure region usually associated with adsorption in the first layer on plane surfaces.

The isotherms for Class I capillaries are of Type I. An example is the ethyl chloride isotherm of figure 3. In the past the interpretation of such isotherms has been that the capillaries are so narrow that the adsorption of a monolayer on each wall will fill the opening. But, as shown in a previous paper (12), there is considerable evidence that such capillaries are wider than two molecular diameters; in the case of charcoal S84 the width must be at least 12–15 molecular diameters. (The preceding paper should be consulted for details.)

Class II: When a capillary fills by first adsorbing separate multimolecular clumps or films which later merge it shows desorption hysteresis. Such capillaries are designated as Class II. They fill only in the higher relative pressure region, since multilayer films are formed only at higher relative pressures. Their isotherms are usually of Type IV or V.

Some capillaries may act as Class I with well-adsorbed molecules and Class II with poorly held molecules. The capillaries of charcoal S84 are examples of such. Toward ethyl chloride they behave as Class I but toward water as Class II, as shown in the isotherms of figure 3.

CRITERIA FOR DETECTION OF CAPILLARY ADSORPTION

It has been assumed that when there is capillary condensation of adsorbate there is desorption hysteresis. Conversely, the existence of hysteresis is believed to indicate capillarity. Since, however, Class I capillaries do not give isotherms that exhibit hysteresis and since hysteresis may occur in the absence of capillaries, we should reëxamine the criteria by which it is deduced whether a given adsorbent is porous. There are several lines of evidence that should be considered for such an evaluation.

1. If an isotherm is of Type I it is almost conclusive evidence that there are narrow, Class I capillaries. We believe that such capillaries are several molecular diameters in width.

2. The existence of a Type IV or Type V isotherm indicates capillaries whose filling prevents further multilayer adsorption and causes the isotherm to flatten at high relative pressures. Such isotherms show desorption hysteresis in all cases.

3. In Type II isotherms a comparison of the V_m-value (point B) with the adsorption near p_0, V_s, may sometimes indicate the presence of small Class I capillaries that fill at low relative pressure. As shown by figure 1, multilayers often build up to as many as 20–30 or more statistical layers, as p_0 is approached. If there are Class I capillaries they add to the low-pressure adsorption and make the apparent value of V_m much higher than the true monolayer value. Consequently, the ratio V_s/V_m is made to become too small. When this ratio is smaller than 10–20 there is reason to suspect Class I capillaries.

Some adsorbents appear to possess both Class I and Class II capillaries. They yield a Type IV isotherm and such an isotherm does not indicate whether the low-pressure adsorption is due to formation of a monolayer or to capillary condensation. This is the situation for the charcoals studied by Gleysteen and Deitz (6). We suspect, because of the high apparent V_m-values, that these charcoals have small pores that become filled at low relative pressure and that the true surface area is much smaller than that estimated from the adsorption at point B.

4. Use of different adsorbates may sometimes aid in detecting the presence of capillaries. For example, capillaries in charcoal which behave as Class I towards most adsorbates may be Class II with respect to water and thereby their presence can be recognized. One might use water adsorption to show whether or not the low-relative-pressure nitrogen adsorption found by Gleysteen and Deitz is due to capillaries.

5. The existence of hysteresis in the high-pressure region of a Type II isotherm indicates the presence of very wide capillaries. A case in point is graphite NC-1. Its ethyl chloride isotherm (11) shows some hysteresis at very high relative pressures. Nevertheless the isotherm does not flatten as p_0 is approached. Therefore we reason that either there are few capillaries and most of the adsorption is on exposed surface, or else that the capillaries are so wide that they fill only at pressures very near p_0.

The suspected presence of large capillaries in NC-1 was further confirmed by determination of a water isotherm, shown in figure 4. This isotherm shows more hysteresis than was found for Graphon, i.e., the hysteresis loop persists to lower relative pressure than was the case with Graphon. Both the water and the ethyl chloride isotherms therefore lead us to suspect, contrary to our previous opinion, that sample NC-1 does have some large capillaries. Graphon, however, is thought to be nonporous. None of its isotherms indicate porosity.

APPLICABILITY OF THE KELVIN EQUATION TO PORE-SIZE DISTRIBUTION

Numerous estimations of capillary pore sizes have been made by application of the Kelvin equation

$$\ln \frac{p}{p_0} = \frac{-2\sigma v \cos \theta}{rRT}$$

to adsorption or desorption isotherms. Here θ is the angle of wetting, σ is the surface tension, v the molar volume, r the capillary radius, R the gas constant, and T the absolute temperature. Previously (12) we questioned the application of this equation for menisci of molecular dimensions. At the present time we are even more skeptical, particularly as to use of the Kelvin equation for water isotherms of charcoals. As shown above, water and ethyl chloride fill the same capillaries. If the Kelvin equation were applicable to either, one would think it more so to ethyl chloride than to water isotherms because the former apparently wets all the surface, the latter only certain active sites. It is implicit in the equation that adsorbate molecules be strongly held at all surface atoms, since the equation relates vapor pressure lowering to the curvature of a meniscus, which is caused by the attraction of surface for adsorbate. Ethyl chloride is much more strongly attracted by carbon than is water, as shown by comparison of their isotherms. But it happens that application of the Kelvin equation to ethyl chloride or similar isotherms leads to computed radii smaller than one molecular diameter, while application to water isotherms does give computed radii of the order of 3–5 molecular diameters. This we believe to be misleading. There is more justification for using the Kelvin equation for wide capillaries that fill by merging of multilayer films from opposite walls, if an adsorbate is selected which wets the surface well. Here the meniscus is wide in comparison to the diameter of a single molecule and its radius of curvature has more meaning than for capillaries only a few molecular diameters in width.

Emmett and Cines (5) have studied glasses with wide capillaries, comparing the pore diameters computed by the Kelvin equation with those computed by the surface–volume ratio. The isotherms are all of Type IV. They find that radii computed by the Kelvin equation applied to the steepest part of the adsorption isotherm are in fairly good agreement among the various adsorbates used, all of which appear to wet the surface well. The Kelvin radii tend to be somewhat larger than r_v, the radius computed from the surface–volume ratio. One cannot, however, say that the agreement proves the correctness of the estimated radii. There are two factors which are not taken into account. One is that the Kelvin equation is for cylindrical pores. It must be modified for pores of other shapes. The other factor, of perhaps greater importance, is that the r_v-values are based on the assumption that all of the adsorption at point B is monomolecular, i.e., that V_m is determined by the point B adsorption. If there are any Class I capillaries which are filled at low relative pressure the effect is to make the V_m-value too large and therefore the r_v-value too small. One cannot tell from the isotherms whether such Class I capillaries are present or not.

We feel, therefore, that there is not yet any reliable method for estimation of pore sizes and it is possible that all present estimates are not even correct as to the order of magnitude. Indeed, if one considers the possible mechanisms for pore formation in such materials as charcoal and silica gel it appears that pores must be highly irregular openings as to both size and shape. It may well be that except for saturation values, which are determined by the total pore volume, other properties of isotherms are determined by pore widths at constrictions and not by average pore widths. If so, the concept of average width ceases to have meaning.

SCANNING OF ISOTHERMS

The proposed theory affords a satisfactory qualitative explanation of the phenomena observed when a hysteresis loop is scanned. For simplicity we shall consider first a single large pore of uniform cross section and surface activity. At the start of adsorption there is formation of the first layer, at low relative pressure; the isotherm is just like that for a plane surface. As pressure is increased, a multilayer is formed on each wall—again just as for a plane surface. At the relative pressure where the multilayers on opposite walls become thick enough to meet, the pore becomes filled. No further adsorption can occur, and the isotherm now becomes flat. At the point where the films meet there is a decrease in the vapor pressure of all molecules in the pore. If now pressure is reduced no evaporation occurs until the equilibrium pressure of the filled pore is reached. At this point an infinitesimal decrease in pressure causes evaporation and the desorption branch drops almost vertically until it meets the adsorption branch. This may occur when only a monolayer remains on each wall or the meniscus may break at a point when the adsorbed film on each wall is somewhat greater than monomolecular.

If the ideal capillary is partially emptied by desorption, readsorption will follow the desorption branch. That is, condensation will occur at the meniscus until the capillary is again filled; the vapor pressure at the meniscus is lower than that required to form separate films on each wall, since the meniscus molecules are subjected to forces from both walls. In other words, for a single uniform capillary we do not obtain the usual type of scanning loop.

Now, in an actual sample there is a distribution of pore widths and of surface activity and each pore has irregular width. The adsorption branch tends to become flatter than for a nonporous adsorbent because the smaller pores fill and their surface disappears while there is still multilayer adsorption on the walls of wide pores. Eventually all pores fill and the isotherm becomes flat. Now on desorption the drop is not completely vertical, for the larger pores have highest vapor pressures and start to desorb before the narrower ones. Nevertheless one can obtain isotherms in which there is quite a sharp drop, such as shown by Emmett and Cines (5).

If after partial desorption one now begins a readsorption, there will be two types of pores present. Some will be empty, except for a monolayer on each wall; others will still have a wall-to-wall meniscus. The empty pores will adsorb separate multilayer films on opposite walls, at the equilibrium pressures that correspond to the adsorption branch of the isotherm. Those pores that still have a wall-to-wall meniscus will have vapor pressures corresponding to the desorption branch. The resultant effect will be that found in scanning a loop; the new adsorption branch will lie between the original adsorption and desorption branches. As the partially empty pores again become full the isotherm approaches the original adsorption branch, which it finally meets. On desorption scanning, a reverse situation is true; some pores are filled, others have unjoined films. Here too the scanning branch lies between the adsorption and desorption loops.

SUMMARY

It is shown that desorption hysteresis does not require prior capillary condensation, but may also occur when adsorbate is held on a plane surface. Hysteresis is found when adsorption occurs by merging of clumps of molecules on separate sites. After clumps merge all molecules are held by forces from all active sites touched by the merged clump. Forces are therefore stronger than when the clumps were separate; the vapor pressures of all molecules are lowered and there is desorption hysteresis. The most common case of hysteresis is when capillaries are filled by the meeting of multilayer films on opposite walls. After the films meet, all molecules are held by surface forces from both walls.

Small capillaries may fill by condensation which starts at the narrowest places, owing to effects of both walls on lowering the vapor pressure in the meniscus. Such capillaries undergo no change of the adsorbed layer as condensation proceeds and show no hysteresis. They are designated as Class I. Capillaries which fill by meeting of multilayer films on opposite walls are called Class II. They show hysteresis.

Criteria are suggested for the recognition of capillary condensation in adsorption. In some cases it is not possible to tell from isotherms whether or not there is capillary condensation.

The validity of using the Kelvin equation to compute pore sizes is discussed.

An explanation is offered for the phenomena observed in scanning a hysteresis loop.

REFERENCES

(1) Basford, Jura, and Harkins: J. Am. Chem. Soc. **70**, 1444 (1948).
(2) Beebe, Biscoe, Smith, and Wendell: J. Am. Chem. Soc. **69**, 95 (1947).
(3) Brunauer: *The Adsorption of Gases and Vapors*. Princeton University Press, Princeton, New Jersey (1943).
(4) Brunauer, Deming, Deming, and Teller: J. Am. Chem. Soc. **62**, 1723 (1940).
(5) Emmett and Cines: J. Phys. & Colloid Chem. **51**, 1248 (1947).
(6) Gleysteen and Deitz: J. Research Natl. Bur. Standards **35**, 285 (1945).
(7) Hill: J. Chem. Phys. **15**, 767 (1947).
(8) Joyner and Emmett: J. Am. Chem. Soc. **70**, 2353 (1948).
(9) Joyner and Emmett: J. Am. Chem. Soc. **70**, 2359 (1948).
(10) Juhola and Wiig: J. Am. Chem. Soc. **71**, 2069 (1949).
(11) Pierce and Smith: J. Phys. & Colloid Chem. **52**, 1111 (1948).
(12) Pierce, Wiley, and Smith: J. Phys. & Colloid Chem. **53**, 669 (1949).
(13) Smith and Pierce: J. Phys. & Colloid Chem. **52**, 1115 (1948).

HEATS OF ADSORPTION. IV

ENTROPY CHANGES IN ADSORPTION[1]

CONWAY PIERCE AND R. NELSON SMITH
Department of Chemistry, Pomona College, Claremont, California

Received August 6, 1949

In recent papers by Davis and DeWitt (5) and Joyner and Emmett (7), entropy changes are discussed for the process:

Bulk liquid (vapor at p_0) + solid surface = adsorbed film (vapor at p)

The conclusions of these two papers appear at first sight to be contradictory. Davis and DeWitt find the entropy to increase at the start of adsorption and to become that of bulk liquid before a monolayer is adsorbed. Joyner and Emmett, on the contrary, show that for most of the adsorption in the first layer there is a decrease in entropy and that after completion of the first layer the entropy change approaches zero. For Graphon they find an initial region of entropy increase, but for carbon black they report no region of entropy increase. Neither paper considers the entropy changes in the region of multimolecular adsorption at high relative pressures.

In connection with our adsorption studies we have experimentally obtained differential heats of adsorption over the entire relative pressure range for several systems. In view of the apparent discrepancies between the two papers cited, plus the fact that neither has considered the region of high relative pressures, we have used our heat data to compute entropy changes for several adsorption systems and we find what we believe to be relations of general applicability, which are herein reported.

EXPERIMENTAL

Ethyl chloride isotherms were determined at temperatures of 0°C. and −78°C. for Carbolac I. This is presumably a nonporous black[2] of surface area near 1000 sq. m./g. The amount adsorbed was followed gravimetrically by weighing the sample bulb after each addition. Details are given in previous papers (8, 11). A McLeod gage was used to determine vapor pressures for the −78°C. isotherm.

Water isotherms for temperatures of 0°C. and 28.6°C. were determined for Graphon.[2] This is a partially graphitized carbon black of surface area near 80 sq. m./g. It appears to be completely nonporous (10). Before use, it was treated with hydrogen at 1100°C., to eliminate the possibility that oxygen complexes on the surface might affect the water adsorption.

The amount of water adsorbed was determined gravimetrically. Pressures were read on silicone-filled manometers. These were freshly pumped before each reading, since it was found that if allowed to stand in contact with water vapor the readings slowly changed. A p_0 reading was taken immediately following each adsorption reading; constant p_0 values were found.

---

[1] This is a progress report of work done under Contract N8 onr 54700 with the Office of Naval Research, United States Navy Department.

[2] We desire to thank Dr. W. R. Smith of the Godfrey L. Cabot Company, Boston, Massachusetts, for furnishing the samples. The properties of the two samples have been described by Smith, Thornhill, and Bray (12).

The Graphon sample was of the same lot used by Joyner and Emmett (7) and by Beebe, Biscoe, Smith, and Wendell (3).

The nitrogen isotherm given by Joyner and Emmett for Graphon shows an unusual hump in the multilayer region, starting at about 0.3 p_0. This hump has been observed by others for low-temperature adsorption of small molecules[3] but did not show up in various isotherms determined in this laboratory, with large organic molecules. The hump does not seem to be the cause of the unusual entropy change at 1–1.5 V_m reported by Joyner and Emmett and discussed later, since its maximum occurs at about 2 V_m. To the best of our knowledge no other nonporous adsorbent has ever shown a hump of this type in its isotherm. We know of no satisfactory explanation to account for it.

COMPUTATION OF ENTROPY CHANGE IN ADSORPTION

We have followed the method used in the other papers cited for computation of $T\Delta S$ values in the adsorption process. The entropy change is given by the relation:

$$T\Delta S = \Delta H - \Delta F \qquad (1)$$

Here ΔH is the measured quantity $-(E - E_L)$ or the differential heat of adsorption. Since $E - E_L$ is customarily given a plus sign when heat is evolved, it is necessary to use a minus sign when following thermodynamic conventions.

The free energy change, ΔF, is computed by

$$\Delta F = RT \ln p/p_0 \qquad (2)$$

Experimental ΔH and computed ΔF values are plotted as functions of relative pressure. Graphical subtraction then yields a $T\Delta S$ curve for the process.

In using this method certain precautions are necessary which are not explicitly stated in either of the other papers. In order to make the computation of ΔF it is necessary to relate the ΔH values, which are computed for given volumes adsorbed, to relative pressure. This is done (approximately at least) by using the average relative pressure for each volume. For example, 70 ml./g. is adsorbed by Carbolac at relative pressures of 0.015 at −78°C. and 0.07 at 0°C. The average relative pressure is 0.0425. This is the value used to compute ΔF for an adsorption of 70 ml. This pressure corresponds to an average isotherm determined at the mean temperature, −39°C. Therefore this mean temperature is used to compute ΔF.

It is apparent that this method for computing the entropy change in adsorption neglects any change which may take place in the entropy of the surface itself as an adsorbed film is formed. This we believe to be proper, since the forces holding surface atoms of a solid are very large in comparison to the forces between surface atoms and adsorbate molecules. In other words, it is reasonable to assume that the thermal vibrations of surface atoms are but slightly affected by the presence of an adsorbed layer on the surface. We are therefore assuming no change in entropy for the surface itself and computing only the entropy changes for adsorbed molecules as they pass from bulk liquid to adsorbed film.

---

[3] Private communications from Professor R. A. Beebe of Amherst College and Dr. M. L. Corrin of the University of Chicago.

Differential ΔH, ΔF, and $T\Delta S$ values for the adsorption of ethyl chloride by Carbolac 1 are plotted as functions of relative pressure in figure 1. The isotherms from which the values are computed are given in Figure 2.

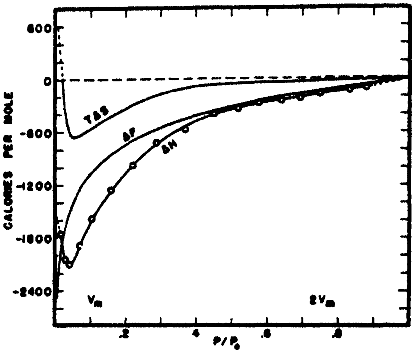

FIG. 1

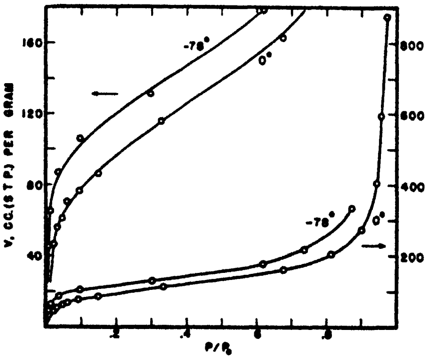

FIG. 2

FIG. 1. Differential free energy, net heat, and entropy changes for adsorption of ethyl chloride by Carbolac I. The approximate pressures are indicated at which statistical first and second layers are completed.

FIG. 2. Isotherms of ethyl chloride on Carbolac I at 0°C. and −78°C. At 0.995 p_0 the volume adsorbed at 0°C. is 1650 ml. (S.T.P.).

INTERPRETATION AND APPLICATIONS OF ENTROPY CURVE

We find for the Carbolac–ethyl chloride system some relations which we believe to be of general applicability for all physical adsorption. The $T\Delta S$ curve shows three separate regions, as follows:

1. At the start of adsorption there is an increase in entropy. That such must always be true is shown by equation 1. As pressure approaches zero, $-\Delta F$ approaches infinity; ΔH, however, must be finite for physical adsorption. Consequently, $T\Delta S$ must have a positive sign at the region near zero pressure and all $T\Delta S$ curves must tend towards + infinity at zero pressure The region of entropy increase may or may not be found in experimental curves. Davis and DeWitt show only this region; Joyner and Emmett find it for one system but not for another. Whether or not the region can be experimentally observed depends upon the magnitude of ΔH at low relative pressure. When an isotherm rises very steeply at the start the ΔH curve may be so steep that it crosses the ΔF curve at pressures too low for accurate measurement, and the positive $T\Delta S$ region is not observed.

2. Starting at something less than 0.5 V_m the entropy curve shows an abrupt

change from positive to negative and it goes through a minimum somewhere near the point at which a first layer is completed.

3. Near the point at which the first layer is completed there is an abrupt rise in entropy, which now approaches that of bulk liquid. There is, however, an entropy decrease throughout the region of multilayer adsorption and the entropy becomes that of bulk liquid only at saturation.

These three regions have been observed for the entropy changes in a variety of adsorption systems. There are, of course, variations in the magnitudes observed and in the pressures at which the transition from positive to negative entropies occur, but the general shapes of the curves are like that of the $T\Delta S$ curve of figure 1. Among the systems for which we have computed the entropy changes are the following:

1. Butane on glass spheres, using the data of Davis and DeWitt (5) Our numerical values are somewhat smaller than they give; apparently they did not use average relative pressures in relating adsorbed volumes to pressure. Rather, it appears that they used the relative pressures corresponding to the isotherm at the lower temperature in computing ΔF.
2. Ethyl chloride on Graphon.
3. Benzene on Graphon.
4. Cyclohexane on Graphon.
5. Methanol on Graphon. The isotherm for this system is Type VI (9).

The results of Davis and DeWitt and of Joyner and Emmett are both in accord with the general entropy curve. The apparent discrepancies in their findings are due to the fact that each considered only narrow regions, Davis and DeWitt the initial region where there is an increase in entropy, and Joyner and Emmett the second region where there is a decrease in entropy (for one system they did note part of the first region). Both Davis and DeWitt and Joyner and Emmett seem to have tacitly assumed that ΔS is zero in the region of multilayer adsorption.

The three distinct regions of the general entropy curve are precisely what one might predict in advance, from considerations of the relative degrees of order of molecules in adsorbed films and in bulk liquid. At the start of adsorption the first molecules are randomly distributed over the adsorbent surface, at the most active sites. With respect to one another, the adsorbate molecules are much less ordered than in bulk liquid and consequently the process is accompanied by an increase in entropy. As more molecules are adsorbed in the first layer they begin to crowd together in a two-dimensional lattice. The arrangement now is more ordered than in bulk liquid; surface forces hold the molecules rather tightly to the surface and they have less mobility with respect to one another than in bulk liquid. This greater order leads to the entropy decrease found in the second portion of the $T\Delta S$ curve, with the minimum at or near the point at which the first layer is completed. As soon as adsorption begins in the second layer the degree of order is markedly decreased, for the situation is now more like that of bulk liquid. This is the point at which the $T\Delta S$ curve rises rapidly to a value near zero. Finally, for adsorption in multimolecular layers, one would expect the degree of order to approach that of bulk liquid but that film molecules would, because of the influence of forces from the solid surface, be still slightly more ordered than in bulk liquid. This too is found in the $T\Delta S$ curve.

THERMODYNAMICS OF WATER ADSORPTION BY CARBON

One of the puzzling phenomena of adsorption is the behavior of water on carbon surfaces. Coolidge (4) measured isosteric heats for charcoals and came to the conclusion that $E - E_L$ is zero for the first portions adsorbed but greater than zero for the bulk of adsorption. We have (figure 3) determined the isotherms of water on Graphon at temperatures of 0°C. and 28.6°C. These isotherms show less adsorption per unit area than any previously reported water isotherms for nonporous carbon surfaces. We believe that this is due to the absence of oxygen complex. A relative pressure of 0.99 is required to form a statistical monolayer (30 ml.) and at 0.997 p_0 only two statistical monolayers are adsorbed—quite in contrast to the behavior of other adsorbates on this sample, which holds some 32 statistical layers of ethyl chloride at 0.997 p_0.

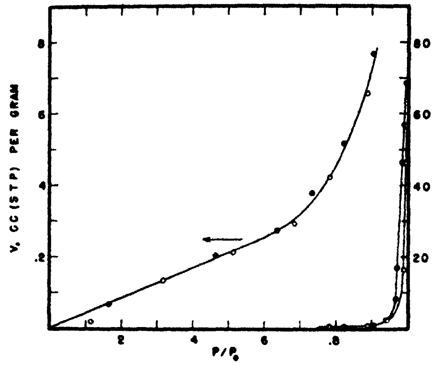

Fig. 3

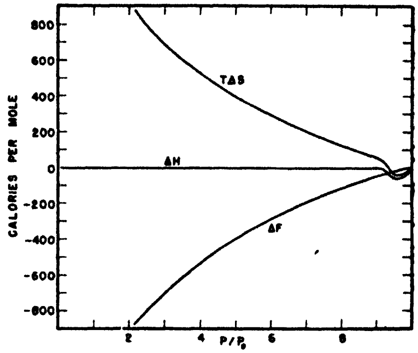

Fig. 4

Fig. 3. Isotherms for water on Graphon: ○, at 28.6°C.; ●, at 0°C.

Fig. 4. Differential free energy, net heat, and entropy changes for adsorption of water by graphite.

We believe that the isotherms at 0°C. and 28.6°C. are identical up to about 0.93 p_0. In other words $E - E_L = 0$ for this region. Above 0.93 p_0 the 0°C. isotherm is definitely displaced to the left of the 28.6°C. isotherm, or $E - E_L$ is positive. Thus our findings in this temperature range are in agreement with those of Coolidge for an activated charcoal.

We find it necessary, therefore, to modify our previously stated view that adsorption occurs only when $E > E_L$. For the most part this view is correct, but apparently some water does adsorb with zero net heat. An explanation is suggested by the general shape of the entropy curve for adsorption. Water is, in comparison to other adsorbates, poorly adsorbed and the region of entropy increase extends to much higher relative pressure than for other adsorbates. At 0.93 p_0 less than one-tenth of a statistical monolayer is held. Up to this relative pressure, therefore, we may have spontaneous adsorption with zero net heat, since the increase in entropy permits a free energy decrease. Above 0.93 p_0 the isotherm for 0°C. lies to the left of that for 28.6°C., or $E > E_L$. It is illogical to assume that now a portion of the surface can adsorb with positive net heat, which could not adsorb at lower relative pressure. Rather one is forced to the conclusion that the increased heat of adsorption above 0.93 p_0 is due to lateral interactions with previously adsorbed molecules, as discussed by Barrer (1) and by Halsey (6), and that the net heat of interaction of water molecules with surface atoms remains zero. When coöperative adsorption sets in the entropy becomes negative in sign, but now the net heat is positive and a spontaneous process is still possible.

The ΔH and $T\Delta S$ curves for water (figure 4) are in line with this interpretation. The region of entropy decrease is confined to the relative pressure region 0.93–1.0, but it is in this region that 95 per cent of the adsorption occurs. Thus, while some adsorption can occur with zero or negative net heat, because of the contribution of the entropy term to the free energy of the process, the bulk of the adsorption must occur when $E > E_L$.

The incidence of coöperative adsorption when less than 10 per cent of a statistical monolayer has formed is indirectly further evidence for our previously stated view (11) that water adsorption on carbon occurs only at the most active sites and that probably the entire surface is never covered. The small adsorption at saturation also favors this view. We think that at saturation there are multilayer clumps of adsorbate at the more active sites while other portions of the surface hold no adsorbate.

In connection with the ΔH and $T\Delta S$ curves of figure 4, it should be noted that the small adsorption of water at low relative pressures makes the experimental precision poor. It is not absolutely certain that the isotherms for the two temperatures coincide up to 0.93 p_0, but this is the best interpretation we can give our data. Certainly one is not justified in saying that the 0°C. curve is displaced to the left of the 28.6°C. curve below 0.93 p_0 or that for this region $E > E_L$. Actually, it is for the present discussion immaterial whether there is a small positive net heat or a zero net heat in the lower pressure region. In either case it is possible to have a spontaneous adsorption only because there is a large increase in entropy for the region. It is significant that such an increase in entropy is of general occurrence in all adsorptions and need not be specifically invoked to explain the water–carbon system. The interpretation of this system now falls into the general theory which holds for all adsorption systems.

On the basis of heat of emersion measurements Basford, Jura, and Harkins (2) concluded that there is an initial high heat of adsorption for water on graphite and that even at as much adsorption as 0.18 V_m there is a net heat of some 20,000 cal./mole. Such cannot be true for the sample we used. If there were a net heat of even a few hundred calories per mole, the lower pressure portion of the isotherms of figure 3 would show a marked displacement for the two temperatures. Within experimental limits we find no displacement in this region. Even on an expanded scale (left-hand curve) the two isotherms are identical.

ISOSTERIC HEATS OF ADSORPTION

The preceding discussion of the three general regions for the entropy of adsorption is based largely upon isosteric measurements of heats of adsorption. Calorimetric measurements are usually possible only up to V_m or at best 2 V_m, because of the small net heat effects after the first layer is completed. In the region of multilayer adsorption the net heat can be measured only by application of the Clapeyron equation to isotherms at two different temperatures. This procedure has led to the conclusion that $E - E_L$ is positive up to saturation, and to the generalizations we have made concerning entropies of adsorption. It is important then to reëxamine the validity of using the Clapeyron equation.

The basic equation

$$\frac{dp}{dT} = \frac{\Delta H}{T\Delta V} \tag{1}$$

is undoubtedly rigorous when applied to vapor pressures of adsorbed films. In practice, however, one uses the approximate integrated form

$$\Delta H = \frac{RT_1T_2}{T_1 - T_2} \ln \frac{p_1}{p_2} \tag{2}$$

and ΔH is computed from the vapor pressure at T_1 and T_2 of a given weight of adsorbate. If the N molecules of adsorbate occupy the same surface sites at the two temperatures equation 4 should apply, at least as a good approximation, but if the situation is such that the given N molecules do not occupy the same sites at two temperatures, there may be doubt as to its applicability. Such a case is found just after completion of the first layer. If the N molecules just cover the surface at the lower temperature T_2 they cannot all be held in the first layer at the higher temperature T_1. As the temperature rises the area per molecule must increase and at T_1 some of the molecules must be in a second layer, where they are less tightly held than in the first layer. For such molecules dp/dT may have a different value than for first-layer molecules. So we question the exact validity of the isosteric heat values just past V_m.

It is possible that this effect has caused the very peculiar entropy values reported by Joyner and Emmett (7) for adsorption of nitrogen by Graphon. Just past V_m they find a small region in which the calculated ΔS values are positive. As pointed out in their paper, this is difficult to explain. It seems highly improbable that there is greater disorder in this adsorption region than in bulk liquid, and that a region of entropy increase from 1 to 1.5 V_m could then be followed by a region of entropy decrease.

Another region in which the Clapeyron equation must be used with caution is near saturation for porous adsorbents whose isotherms are type I. At the lower temperature V_s is greater than for the higher and the isotherms tend to become parallel and nearly horizontal at high relative pressure. In such a situation it is customary to use vapor pressure ratios for equal fractions of saturation (equal pore volumes filled) in the application of equation 4. There may be some doubt as to the validity of this procedure, but it does lead to what appear to be self-consistent heat values.

In isotherms for nonporous solids the Clapeyron equation seems to be applicable right up to p_0 if the isotherm is Type II. For several such isotherms we have found that the V_s value is almost independent of the temperature, or the isotherms for two different temperatures converge as p_0 is approached. This is not true for the Type III water isotherm of figure 3, however. The V_s adsorption at 0°C. is considerably greater than that for 28.6°C. This indicates that the last molecules are held differently at the two temperatures, and raises a question as to the validity of isosteric heats at high relative pressures. We believe that the separation of the two isotherms above 0.93 p_0 does indicate a positive net heat, but we do not consider the heat values reliable except as to order of magnitude.

In the low-pressure region of an isotherm isosteric heats seem theoretically sound, since if the surface is only partially covered a given N molecules should occupy the same sites, regardless of the temperature. Another difficulty arises in this region. At very low relative pressures the ratio of pressures at T_1 and T_2 is more difficult to measure accurately than at higher pressures and any error introduces a corresponding error into the computed net heat. Therefore values in this region are less reliable than in the higher pressure regions of multilayer adsorption. To illustrate, at -78°C. p_0 for ethyl chloride is only 3.44 mm., while at 0°C. it is 471 mm. (mercury manometer, not corrected for temperature). At an adsorption of 70 ml. per gram of Carbolac the actual pressures at 0° and -78°C. are respectively 33 and 0.0517 mm. Obviously any error in the measured pressure at -78°C. would have a large effect on the computed net heat.

Because of experimental uncertainty in isosteric heats at low relative pressures we have indicated the lower end of the ΔH curve of figure 1 by a dotted line. Whether or not this represents the true heat is, however, immaterial insofar as the general shape of the entropy curve is concerned. In any event, the ΔF curve must cross the ΔH curve and a positive value of ΔS must result.

Another point which we have considered is whether the minimum of the ΔH curve of figure 1 is real or not. We have found a similar minimum in all the Type II isotherms cited above. It corresponds to the maximum in the $E - E_L$ curve found calorimetrically by Beebe and associates (3) and isosterically by Joyner and Emmett for nitrogen on Graphon. But no other calorimetric heat curves show this minimum ΔH near V_m. If real it is readily accounted for by the coöperative effect of neighboring molecules, which should be most pronounced in the region 0.5 V_m to V_m. But there exists the possibility that this minimum is in some way associated with a defect in the isosteric heat values. There again, however, it is immaterial, insofar as the entropy curve is concerned, whether the minimum is real or not. In either case the entropy curve shows a minimum near V_m. It is hoped that as more calorimetric data are obtained it will be possible to find whether the minimum is real.

Despite the various uncertainties that are possibly inherent in the measurements of isosteric heats, it appears that in the main these are quite reliable, at least as to order of magnitude. The excellent agreement obtained by Joyner and

Emmett with the calorimetric values previously reported for the same systems lend confidence to the use of isosteric heats.

SUMMARY

Entropy changes for the adsorption process are computed by the relation $T\Delta S = \Delta H - \Delta F$. It is found that the $T\Delta S$ *vs.* relative pressure curve is characterized by three regions. First there is a region of entropy increase as the first molecules are adsorbed in a disorderly array. This is followed by a region of entropy decrease and very orderly arrangement of molecules as the surface becomes covered by a monolayer. Finally, in the region of multilayer adsorption there is a small entropy decrease which approaches zero as p approaches p_0.

An interpretation is suggested for the isotherm of water on a plane carbon surface, the only known example of a Type III isotherm. The first molecules are adsorbed at the most active sites with zero or very small net heats but with a large increase in entropy. On further adsorption there is a larger net heat, due to lateral interactions, and a decrease in entropy.

The limitations which may apply to use of the Clapeyron equation for computing heats of adsorption are discussed.

REFERENCES

(1) Barrer: Proc. Roy. Soc. (London) **161A,** 476 (1937).
(2) Basford, Jura, and Harkins: J. Am. Chem. Soc. **70,** 1444 (1948).
(3) Beebe, Biscoe, Smith, and Wendell: J. Am. Chem. Soc. **69,** 95 (1947).
(4) Coolidge: J. Am. Chem. Soc. **49,** 708 (1927).
(5) Davis and DeWitt: J. Am. Chem. Soc. **70,** 1135 (1948).
(6) Halsey: J. Chem. Phys. **16,** 931 (1948).
(7) Joyner and Emmett: J. Am. Chem. Soc. **70,** 2353 (1948).
(8) Pierce and Smith: J. Phys. & Colloid. Chem. **52,** 1111 (1948).
(9) Pierce and Smith: J. Phys. & Colloid Chem. **54,** 354 (1950).
(10) Pierce and Smith: J. Phys. & Colloid Chem. **54,** 784 (1950).
(11) Smith and Pierce: J. Phys. & Colloid Chem. **52,** 1115 (1948).
(12) Smith, Thornhill, and Bray: Ind. Eng. Chem. **33,** 1303 (1941).

ROLE OF INDIFFERENT ELECTROLYTES IN ELECTRODE KINETICS

K. S. GURURAJA DOSS

Indian Institute of Sugar Technology, Kanpur, India

AND

H. P. AGARWAL

D. A. V. College, Kanpur, India

Received July 18, 1949

A new and interesting method for studying the kinetics of electrode reactions has been worked out by Randles (2). The method is based on the application of an alternating potential of small amplitude to a microelectrode at which the relevant electrode reaction is in equilibrium. The microelectrode consists of a capillary dropping electrode similar to the polarographic electrode, except that a dilute amalgam of the metal under consideration replaces the mercury. The microelectrode is in contact with an aqueous solution containing an indifferent electrolyte like potassium nitrate, potassium bromide, etc. at molar concentration (to avoid migration effects) in addition to the metal ions taking part in the electrode reaction. The theory of the method has been completely worked out by Randles.

By combining (*a*) Fick's law of diffusion, (*b*) Faraday's laws of electrolysis, and (*c*) the theory of absolute reaction rates (1), as applied to electrode processes, Randles has shown that the microelectrode system can be considered as equivalent to a capacity and a resistance in series, inasmuch as a phase shift is caused by the microelectrode in the alternating current passing through the system. By measuring the phase shift and the alternating current passing through the system by the help of an oscillograph, it is possible to calculate the equivalent resistive and capacitative impedances of the system. Randles has worked out equations by means of which one can calculate the rate constants of electrode processes from the values of the impedances. He has applied the method to a number of systems and has obtained interesting correlations. One of the observations made by him is that the rate constant for the discharge of zinc ions at the dropping amalgam electrode depends upon the nature of the indifferent electrolyte. He finds that the rate constant increases in the order:

$$KNO_3 < KCl < KBr < KCNS < KI$$

He attributes this to the increase in covalency of bondage between the metal ion and its addenda, which is supposed to lower the activation energy for discharge of the ion.

It is the object of the present paper to examine critically the cause of this interesting phenomenon.

Applying the theory of absolute reaction rates, Randles puts for the current *i*,

$$i = NFA[K_2c_2^0e^{\alpha vnF/RT} - K_1c_1^0e^{-(1-\alpha)vnF/RT}] \qquad (1)$$

where c_1^0 and c_2^0 are the respective concentrations of the metal in the amalgam and that of the metal ion in the aqueous solution, close to the interface; K_1 and K_2 are the rate constants for the two reactions; v is the potential of the aqueous solution relative to the mercury; α is the fraction of the potential difference operative on the aqueous solution side of the energy barrier; n is the valency of the metal ion; F is the faraday; A is the area of the electrode; R is the gas constant; and T is the absolute temperature.

Further Randles assumes that $v = 0$ for the equilibrium potential of the electrode when $c_1^0 = c_2^0 = c$, whence he gets $K_1 = K_2 = K$, where K defines the rates of opposing reaction at the equilibrium potential, as Kc moles per second per unit area of the electrode surface. The exact significance of K of Randles becomes clear by a careful consideration of the theory of absolute reaction rates. According to the theory, the rates of the opposing reactions at equilibrium at any electrode where $c_1^0 = c_2^0 = c$, are given by the expressions,

TABLE 1

INDIFFERENT ELECTROLYTES	$K \times 10^{-3}$	$-(v_e - v_e')$
		mv.
NO_3^-	4.3	0
Cl^-	6	8.5
Br^-	11	24
CNS^-	17	35
I^-	93	79

$$K_1 c\gamma_1 e^{-v_e nF(1-\alpha)/RT} = K_2 c\gamma_2 e^{v_e nF\alpha/RT} \tag{2}$$

where the first expression is for the rate of discharge and the latter is for the rate of conversion of the atom of the metal into an ion in solution. In these γ_1 and γ_2 are the activity coefficients of the metal in the amalgam and the metal ion in the solution, respectively. Therefore

$$K = K_1\gamma_1 e^{-v_e nF(1-\alpha)/RT} = K_2\gamma_2 e^{v_e nF\alpha/RT} \tag{3}$$

If for the system Zn, Hg | Zn^{++}, NO_3^- we represent the Randles rate constant by K' and the equilibrium potential by v_e' we get

$$K' = K_1\gamma_1 e^{-(1-\alpha)nFv_e'/RT} \tag{4}$$

and in the general case for the zinc amalgam electrode dipped in other media, we put:

$$K = K_1\gamma_1 e^{-(1-\alpha)nFv_e/RT} \tag{5}$$

Combining equations 4 and 5 we get,

$$\frac{RT}{nF} \ln K/K' = -(1 - \alpha)(v_e - v_e') \tag{6}$$

an important relation showing how the rate constants depend upon the equilibrium potential values.

If α is put equal to 0.5, it is possible to calculate the values of $v_e - v'_e$; the values so obtained are given in table 1.

Some of the rate constant values used in the calculations in table 1 were inadvertently left out in Randles' paper. Our thanks are due to Randles, who gave us all the details in a private communication. One can see from the values that they appear to be plausible and explain why the rate constants vary when the indifferent electrolyte is changed.

It is to be noted however that $v_e - v'_e$ is experimentally measurable, though, of course, there will be the interference by the liquid-junction potential. If the latter could be eliminated it would then be possible to calculate exactly the value of α. It appears also possible to estimate the values of $v_e - v'_e$ by the knowledge of activity coefficients; but the time effects coming up at the dropping electrode, combined with the fundamental difficulty in the evaluation of the activity coefficients of individual ions, may render this procedure difficult.

SUMMARY

By studying the kinetics of electrode processes Randles observed that the rate constant for the discharge of the zinc ion depended upon the nature of the indifferent electrolyte used in the experiment. It is shown that the variation in the rate constants can be interpreted plausibly on the basis of the variation of the equilibrium potential of the different systems.

REFERENCES

(1) Glasstone, Laidler, and Eyring: *Theory of Rate Processes*, p. 575. McGraw-Hill Book Company, Inc., New York (1941).
(2) Randles: Faraday Society Discussion **1**, 11 (1947).

GELATION OF SODIUM SILICATE

Effect of Sulfuric Acid, Hydrochloric Acid, Ammonium Sulfate, and Sodium Aluminate

REYNOLD C. MERRILL and ROBERT W. SPENCER
Philadelphia Quartz Company, Philadelphia, Pennsylvania

Received September 12, 1949

The addition to sodium silicate solutions of acids, acid-forming compounds, ammonium salts, and sodium aluminate produces a silica or silica alumina gel. Such gels are produced from a sodium silicate solution containing approximately 8.9 per cent sodium oxide and 28.7 per cent silica corresponding to a silica-to-alkali (Na_2O) molecular ratio of 3.3, by reaction with an acid, usually sulfuric. Silica alumina gels may be made by reaction of the silicate with either an aluminum salt such as the sulfate or with sodium aluminate.

This paper reports the time required to form gels when sulfuric acid, hydrochloric acid, ammonium sulfate, and three commercial sodium aluminates are added to solutions of a 3.3 ratio sodium silicate. Several previous investigators (1, 2, 4, 6, 8, 10, 11, 12, 13) have studied the time for gelation of sodium silicates in the presence of sulfuric or hydrochloric acid but none reported quantitative data over the entire range of concentrations and acid–silicate ratios of interest to us. Hay shows some gel times for silicate–ammonium sulfate mixtures in his patent on the preparation and use of activated silica sols produced by reaction with ammonium salts (3). No systematic data have been located in the literature on the gel times of silicate–sodium aluminate mixtures.

EXPERIMENTAL

The silicate used in all of the work reported here was a commercial sodium silicate which contains 8.90 per cent Na_2O, 28.7 per cent SiO_2, and 62.4 per cent H_2O. The acids and ammonium sulfate were reagent-grade chemicals. Distilled water was used for diluting the commercial silicate and making up solutions. Our analysis showed that one reagent-grade sodium aluminate powder contained 34.9 per cent Na_2O and 40.6 per cent Al_2O_3, corresponding to a molecular alumina-to-alkali weight ratio of 0.707 instead of the theoretical ratio of 1.00 required by the formula $NaAlO_2$. Another sodium aluminate had 43.3 per cent Na_2O and 54.4 per cent Al_2O_3 with a corresponding molecular ratio of 0.763. A third sodium aluminate contained 34.5 per cent Na_2O and 44.7 per cent Al_2O_3, giving a corresponding ratio of 0.788. All of these products contained more sodium hydroxide than required by the theoretical formula $NaAlO_2$ for sodium aluminate. Presumably this is done to stabilize the product against hydrolysis and precipitation of alumina. The alkali was determined by titration with standardized hydrochloric acid to the bromthymol blue end-point. Alumina was determined gravimetrically.

Gel times were determined by adding a dilute solution of the gel-forming reagent to the sodium silicate solution, mixing well, and allowing the mixture to stand in a 4-oz. bottle kept in a 25.0°C. thermostat until it gelled. The mixing time was a negligible proportion of the gel time. The criteria of gelation were loss of uniform fluid flow, the appearance of breakage planes when the mixture was tilted, and the adherence of solid gel to the glass wall. Gel times obtained in this manner were reproducible within 2 per cent and should correspond fairly closely to the "time of set" determined by the "tilted rod" method extensively used by Hurd and collaborators (7). In order to save space all data are presented graphically. When a solution gelled during the night, the maximum and minimum possible gel times are indicated on the graphs and the two points connected by a line. The mole ratios given in the figures are the number of moles of acid, or ammonium sulfate per mole of sodium oxide in the silicate.

GEL TIMES

Sulfuric acid: Figure 1 shows on a semilogarithmic scale the gel times at 25.0°C. of 3.3 ratio sodium silicate–sulfuric acid mixtures containing 1.00, 1.50, 2.00, 2.50, 3.00, 3.50, and 4.00 per cent SiO_2.

In figure 2 the gel times for these mixtures are shown as a function of the pH of the mixture determined with a Beckman pH meter using the glass electrode within 2 min. after mixing. The acid-to-silicate mole ratio at minimum gel time decreases from 0.98 at a concentration of 1.0 per cent SiO_2 to 0.92 at 3.0 per cent SiO_2. Similarly, the pH at minimum gel time increases from 7.0 at 1.0 per cent SiO_2 to 7.7 at 3.0 per cent SiO_2. The pH values of the acid-silicate mixtures gradually increase on standing below a molecular acid-to-silicate ratio of 1.0 by as much as 0.7 pH unit. Above 100 per cent neutralization of the silicate alkalinity there appears to be a decrease in pH on standing.

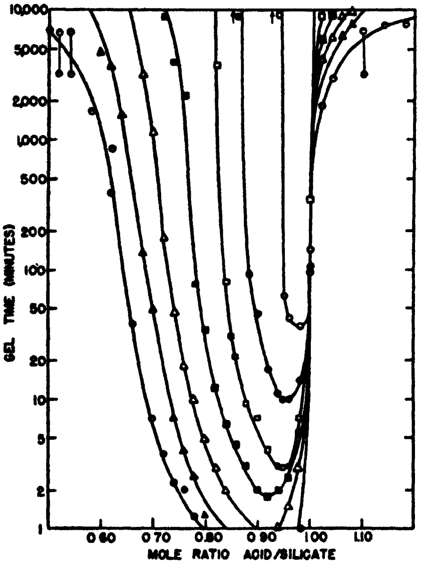

FIG. 1

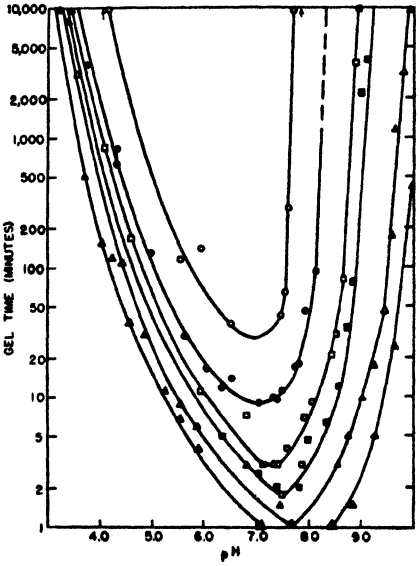

FIG. 2

FIG. 1. Gel times at 25.0°C. of 3.3 ratio sodium silicate–sulfuric acid mixtures as a function of acid–silicate molecular ratio.

O, 1.00% SiO_2; ●, 1.50% SiO_2; □, 2.00% SiO_2; ▲, 3.50% SiO_2
■, 2.50% SiO_2; △, 3.00% SiO_2; ◒, 4.00% SiO_2

Fig. 2. Gel times at 25.0°C. of 3.3 ratio sodium silicate–sulfuric acid mixtures as a function of initial pH of mixture.

O, 1.00% SiO_2; ●, 1.50% SiO_2; □, 2.00% SiO_2; ▲, 3.50% SiO_2
■, 2.50% SiO_2; △, 3.00% SiO_2; ◒, 4.00% SiO_2

At a molecular acid-to-silicate ratio of 1.10, a 3.3 ratio sodium silicate–sulfuric acid mixture containing 5 per cent SiO_2 will gel in about 59 hr., one containing 10 per cent SiO_2 in 13–19 hr., and a mixture with 15 per cent SiO_2 in 2 hr. or less. At these high concentrations the exact gel time depends somewhat on the order of mixing. Gel times in this region are higher if the silicate is added to the acid rather than *vice versa.*

Our data agree with those expected from the "times of set" given by Hurd, Frederick, and Haynes (8) for a 3.3 ratio silicate solution containing 3.98 per cent SiO_2 at pH's of 3 to 5.

Hydrochloric acid: The gel times at 25.0°C. for 3.3 ratio sodium silicate–hydrochloric acid mixtures containing 2.00 per cent SiO_2 are shown in figure 3. The minimum gel time is for a mixture containing 0.95 equivalence of acid per mole of silicate, as with sulfuric acid. Comparison with figure 1 shows that at comparable degrees of neutralization sulfuric acid–silicate mixtures gel more slowly than those with hydrochloric acid, as has been found by others (1, 2, 6, 8). More concentrated silicate–hydrochloric acid mixtures also gel more rapidly than those with sulfuric acid, and the time to form a gel depends on the order of mixing. For example, at a molecular acid-to-silicate ratio of 1.10, a 3.3 ratio silicate solution containing 5 per cent SiO_2 will gel in 96 hr., one containing 10 per cent SiO_2 gels in 12–16 hr., whereas a 15 per cent SiO_2 system gels practically instantaneously. When the acid is added to the silicate containing 5 per cent SiO_2, a gel forms in between 80 and 90 hr., whereas 96 hr. are required when the silicate is added to the acid.

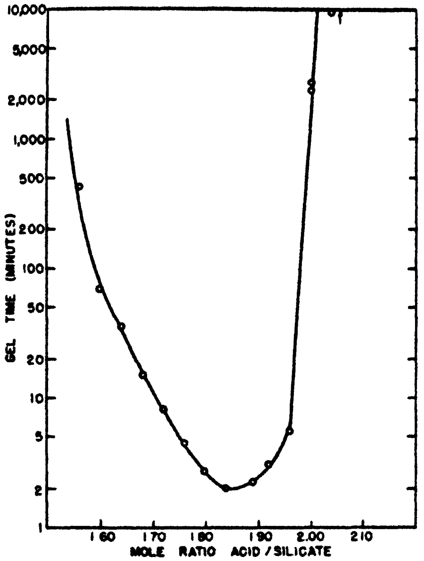

FIG. 3

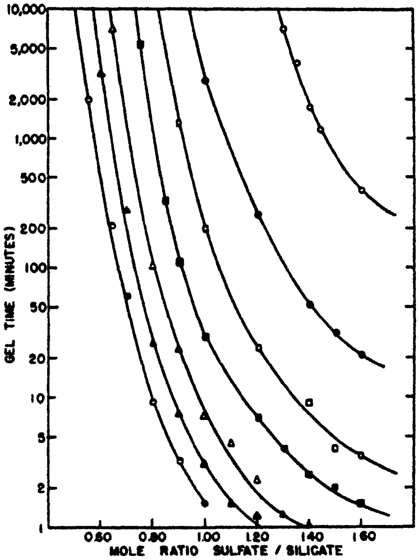

FIG. 4

Fig. 3. Gel times at 25.0°C. of 3.3 ratio sodium silicate–hydrochloric acid mixtures containing 2.00 per cent SiO_2 as a function of acid–silicate molecular ratio.

Fig. 4. Gel times at 25.0°C. of 3.3 ratio sodium silicate–ammonium sulfate mixtures as a function of sulfate–silicate molecular ratio.

○, 1.00% SiO_2; ●, 1.50% SiO_2; □, 2.00% SiO_2; ▲, 3.50% SiO_2
■, 2.50% SiO_2; △, 3.00% SiO_2; ◐, 4.00% SiO_2

Ammonium sulfate: Figure 4 shows the gel times at 25.0°C. of mixture of ammonium sulfate with 3.3 ratio sodium silicate. The pH's of these mixtures were all between 9.5 and 10.5 and decreased gradually with increase in sulfate-to-silicate ratio (*cf.* Fig. 1, reference 9). For example, the mixture containing 3.5% SiO_2 with sulfate–silicate molecular ratio of 0.6 has a pH of 10.36, and the addition of more sulfate to a ratio of 1.2 decreases the pH only to 9.66.

A comparison of the speed of gelation of the silicate with sulfuric acid and ammonium sulfate as a function of silica concentration is given in figure 5. The longer gel times obtained with the ammonium salt are clearly evident.

Sodium aluminate: Gel times of mixtures of 3.3 ratio sodium silicate containing 1.50 per cent SiO_2 with three commercial sodium aluminates are shown in figure 6 as a function of the molecular ratio on a sodium oxide basis of aluminate to silicate. Mixtures containing the more alkaline aluminates have longer gel times at comparable molecular ratios. All of the silicate–aluminate mixtures had pH's above 13 and were thus more alkaline than the silicates alone.

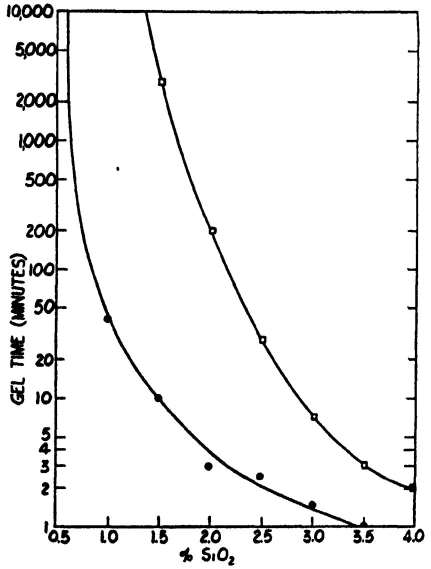

FIG. 5

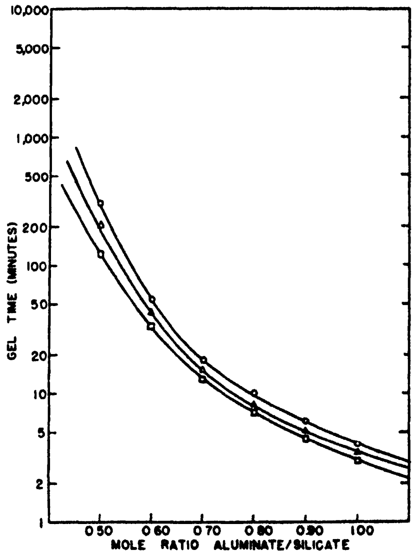

FIG. 6

Fig. 5. Gel times at 25.0°C. of mixtures of 3.3 ratio sodium silicate with ammonium sulfate and sulfuric acid as a function of silica concentration. □, ammonium sulfate mixtures, mole ratio = 1.0; ●, sulfuric acid mixtures, mole ratio = 0.96 (results at a ratio of 1.0 are somewhat erratic; a small change in ratio around 1.0 makes a large change in gel time; *cf.* figure 1).

Fig. 6. Gel times at 25.0°C. of 3.3 ratio sodium silicate–sodium aluminate mixtures containing 1.50 per cent SiO_2 as a function of molecular aluminate–silicate ratio. ○, $Na_2O:0.707Al_2O_3$; △, $Na_2O:0.763Al_2O_3$; □, $Na_2O:0.788Al_2O_3$.

DISCUSSION

Our data show that in general the rates of gelation of mixtures of 3.3 ratio sodium silicate with the various gelling agents increase in the order ammonium sulfate, sulfuric acid, hydrochloric acid, and sodium aluminates, although under several conditions this order does not hold. Both the ammonium sulfate and the sodium aluminates behave differently from the two acids. The mole ratio of gelling reagent to the alkali of the silicate does not affect the gel time as much with the aluminate and ammonium salt as with the acids. For example, the 3.3

ratio silicate–ammonium sulfate or acid containing 2.0 per cent SiO_2 did not gel in 1 week when the mole ratio of gelling agent to silicate was 0.8. When the ratio was 0.9, the mixture with sulfuric acid gelled in 6 min., whereas that with ammonium sulfate did not gel for 24 hr.

While the data in this paper are for a temperature of 25.0°C., they may be used to estimate gel times for other temperatures when the "activation energy" or temperature coefficient of the process is known. Hurd and collaborators have reported that the energy of activation for the setting reaction of silicic acid gels at pH's from 3.0 to 5.5 is about 17,000 cal./mole (8), and for sulfuric and hydrochloric acids at pH's of +0.5 to −0.5 is 11,000 and 9,000 cal./mole, respectively (6). The activation energies of the setting reactions with ammonium sulfate and sodium aluminate are apparently not known but are probably different from those with the acids.

According to the theory most widely accepted at the present time (*cf.* 5), a silica gel consists of a heavily hydrated interlaced fibrillar or brush heap structure of very large polysilicic acid molecules with the spaces filled with water or dilute silicate solution. These chains are formed by the condensation of molecules of simpler silicic acids or hydroxides, forming water and high-polymeric polysilicic acids. Assuming that the gelation is due to a condensation reaction of this type, fastest gelling should occur near the pH of least ionization, where there is a minimum of repulsion forces between similarly charged silicic acids or hydroxides, or an equal number of positively and negatively charged species containing silicon hydroxides. That such a maximum rate of gelation occurs at an initial pH of approximately 7 is evidence that the silicic acids are much stronger than ordinarily supposed. The increase in pH during aging and gelation indicates that the polysilicic acids forming are weaker and more extensively hydrolyzed.

Our data show clearly that the gelling power of ammonium salts is not entirely due to acid formed by hydrolysis, for they form gels at pH's only slightly less alkaline than those of the sodium silicates themselves. Systems of silicates with acids do not form gels at these pH's. The sodium aluminate–silicate mixtures have higher pH's than silicate solutions. The ability of ammonium salts to gel sodium silicates is therefore probably due to the formation of slightly ionized, heavily hydrated insoluble gelatinous salts. The sodium silico-aluminate gels formed when sodium silicates and aluminates are mixed contain interstitial sodium ions which are not removable by extensive washing with water. These sodium ions are replaced with other cations such as calcium and magnesium ions. Such products, usually termed "artificial zeolites," are used extensively in water treatment. Since aluminum or aluminate ions as well as the silicates can be regarded as polyfunctional, the formation of a silica alumina gel probably involves a copolymerization reaction.

SUMMARY

The times required for mixtures of a 3.3 ratio sodium silicate with sulfuric and hydrochloric acids, ammonium sulfate, and sodium aluminates to form gels at various concentrations and ratios of gelling agent to silicate are given. The

data show that different mechanisms are involved in gelation by acids, ammonium salts, and sodium aluminate. Gel formation with the latter reagents probably involves the formation of unionized (or slightly ionized), heavily hydrated gelatinous salts as well as copolymerization.

REFERENCES

(1) Davis, H. L., and Hay, K. D.: J. Am. Chem. Soc. **61**, 1020 (1939).
(2) Flemming, W.: Z. physik. Chem. **41**, 427 (1902).
(3) Hay, H. R.: U. S. patent 2,444,774 (July 6, 1948).
(4) Holmes, H. N.: J. Phys. Chem. **22**, 510 (1918).
(5) Hurd, C. B.: Chem. Revs. **22**, 403 (1938).
(6) Hurd, C. B., and Barclay, R. W.: J. Phys. Chem. **44**, 847 (1940).
(7) Hurd, C. B., and Miller, P. S.: J. Phys. Chem. **36**, 2194 (1932).
(8) Hurd, C. B., Frederick, K. J., and Haynes, C. R.: J. Phys. Chem. **42**, 85 (1938).
(9) Merrill, R. C.: Ind. Eng. Chem. **40**, 1355 (1948).
(10) Prasad, M.: J. Indian. Chem. Soc. **10**, 119 (1933).
(11) Prasad, M., and Hattiangadi, P. B.: J. Indian. Chem. Soc. **6**, 653, 893 (1929).
(12) Ray, R. C., and Ganguly, P. B.: J. Phys. Chem. **34**, 352 (1930).
(13) Ray, R. C., and Ganguly, P. B.: J. Phys. Chem. **35**, 596 (1931).

MATHEMATICS OF ADSORPTION IN BEDS. II

NEAL R. AMUNDSON

Department of Chemical Engineering, School of Chemistry, University of Minnesota, Minneapolis 14, Minnesota

Received September 15, 1949

The mathematical solution of problems of adsorption of a solute by a solid from a solution depends upon the mechanism assumed to be controlling in the bed. There is a fundamental difference in the mathematical analysis, depending upon whether one assumes that equilibrium obtains or whether one assumes a kinetic approach of some kind. In the first case the basic problem is the solution of a first-order partial differential equation. Since the definition of linearity for first-order equations is somewhat more liberal than it is for second-order equations, it develops that solutions in the first case can be obtained for general isotherms. This problem has been considered by a great number of writers. In the second case the problem is not quite as simple, since the equations which are to be solved are of second order and only very special cases can be solved analytically. Similarly, this problem has been considered by many writers. In a previous paper (1) the author considered one problem of the second category in full generality. It is the purpose of this paper to solve two additional problems completely.

If we assume that we have an adsorbent bed of unit cross section where depths (or heights) are measured as z and if

c = concentration in moles of adsorbate per unit volume of solution in the fluid stream,

n = amount of adsorbate in bed in moles per unit volume of bed,
V = velocity of fluid through interstices of the bed,
α = fractional void volume of bed, and
t = time,

then on considering an elemental thickness of bed Δz we obtain the equation (see Klotz (6)):

$$V\frac{\partial c}{\partial z}+\frac{\partial c}{\partial t}+\frac{1}{\alpha}\frac{\partial n}{\partial t}=0 \tag{1}$$

Previously the author considered, after Bohart and Adams (3), that the local rate of removal in the bed was governed by

$$\frac{1}{\alpha}\frac{\partial n}{\partial t}=kc(N_0-n)$$

where N_0 is the saturation capacity of the bed and k is the velocity constant.

In this paper two additional cases will be discussed.

Case A:
$$\frac{1}{\alpha}\frac{\partial n}{\partial t}=k_1c-k_2n \tag{2}$$

Case B:
$$\frac{1}{\alpha}\frac{\partial n}{\partial t}=k_1c(N_0-n)-k_2n \tag{3}$$

Special cases for Case A have been considered previously. It is to be noted in this case that such a kinetic assumption covers both the cases where there is a mass transfer resistance and also where adsorption itself may be controlling. Either of these conditions merely requires a redefinition of k_1 and k_2. Case B was first considered by Thomas (10) for ion exchange. Here we shall solve these problems for arbitrary initial condition of the column and for arbitrary inlet feed composition to the column. Also the term $\partial c/\partial t$ will not be neglected, as has often been done.

Although the method of Riemann is applicable in the mathematical solution of these problems, the author prefers the use of the La Place transformation. For this method any one of several good books in the field may be consulted; however, the author recommends the book of Churchill (4). The transform operator will be denoted by L and the transform variable corresponding to time (or better, distance along the bed) as p. Therefore $L[f(t)] = g(p)$, where $g(p)$ is the transform of $f(t)$. Tables needed for finding inverse transforms are available in Churchill's book and no further reference to these tables will be made.

CASE A

In this case the complete statement of the problem is

$$V\frac{\partial c}{\partial z}+\frac{\partial c}{\partial t}+\frac{1}{\alpha}\frac{\partial n}{\partial t}=0 \tag{1}$$

$$\frac{1}{\alpha}\frac{\partial n}{\partial t}=k_1c-k_2n \tag{2}$$

$$c(z, t) = c_0(t), \quad \text{where } z = 0 \tag{4}$$

$$n(z, t) = n_0(z), \quad \text{where } t \leqq \frac{z}{V} \tag{5}$$

This case has been called by Thomas (11) the case of linear kinetics. Equation 4 indicates that the concentration in the feed stream can be a function of the time and can therefore vary in an arbitrary manner throughout the course of any run. Equation 5 states that the amount of adsorbate already on the column can be a function of the space variable z. From this condition we see that the solution of this system will resolve the problems of adsorption and desorption simultaneously. It follows that we are seeking two functions which will satisfy equations 1, 2, 4, and 5.

In order to facilitate the solution we shall make the following changes of variable. Let

$$x = z/V$$

$$y = \alpha(t - z/V)$$

Then equations 1, 2, 4, and 5 become

$$\frac{\partial n}{\partial y} + \frac{\partial c}{\partial x} = 0 \tag{6}$$

$$\frac{\partial n}{\partial y} = k_1 c - k_2 n \tag{7}$$

$$c(z, t) = c_0(y/\alpha) = c_1(y) \quad \text{when } x = 0 \tag{8}$$

$$n(z, t) = n_0(Vx) = n_1(x) \quad \text{when } y = 0 \tag{9}$$

Note that condition 6 states that

$$\frac{\partial n}{\partial y} = -\frac{\partial c}{\partial x}$$

and hence there exists a function $f(x, y)$ such that

$$df(x, y) = n\, dx - c\, dy$$

and therefore

$$n = \frac{\partial f}{\partial x}, \qquad c = -\frac{\partial f}{\partial y} \tag{10}$$

Utilizing this fact it follows from equation 7 that

$$\frac{\partial^2 f}{\partial x\, \partial y} + k_1 \frac{\partial f}{\partial y} + k_2 \frac{\partial f}{\partial x} = 0 \tag{11}$$

It is well known that the change of dependent variable

$$f(x, y) = e^{-k_1 x - k_2 y} \phi(x, y) \tag{12}$$

reduces equation 11 to

$$\frac{\partial^2 \phi}{\partial x\,\partial y} - k_1 k_2 \phi(x, y) = 0 \tag{13}$$

If we combine equations 10 and 12 with equations 8 and 9 we obtain:

$$n_1(x) = -k_1 e^{-k_1 x}\phi(x, 0) + e^{-k_1 x}\frac{\partial \phi(x, 0)}{\partial x}$$

$$-c_1(y) = -k_2 e^{-k_2 y}\phi(0, y) + e^{-k_2 y}\frac{\partial \phi(0, y)}{\partial y}$$

We note that these are ordinary differential equations, linear and of the first order, whose solution can be written

$$\phi(x, 0) = e^{k_1 x}\int_0^x n_1(\xi)\,\mathrm{d}\xi = f(x) \tag{14}$$

$$\phi(0, y) = -e^{k_2 y}\int_0^y c_1(\eta)\,\mathrm{d}\eta = g(y) \tag{15}$$

which equations define $f(x)$ and $g(y)$ and where we have set $\phi(0, 0) = 0$. This is legitimate, since $f(x, y)$ occurs only as a derivative.

It follows that we have reduced our original problem to the solution of equations 13, 14, and 15. In order to solve this system it is convenient to reduce it to two others. Consider the two problems:

$$\frac{\partial^2 u}{\partial x\,\partial y} - k_1 k_2 u = 0 \tag{16a}$$

$$u = f(x), \quad \text{when } y = 0$$

$$u = 0, \quad \text{when } x = 0$$

$$\frac{\partial^2 y}{\partial x\,\partial y} - k_1 k_2 v = 0 \tag{16b}$$

$$v = 0, \quad \text{when } y = 0$$

$$v = g(y), \quad \text{when } x = 0$$

Note that the sum $u + v$ satisfies equation 13 and also equations 14 and 15, so that $\phi = u + v$ is the desired solution. Let $L[u(x, y)] = U(p, y)$. Hence

$$p\,\frac{\mathrm{d}U}{\mathrm{d}y} - k_1 k_2 U = 0$$

$$U = F(p) \text{ when } y = 0$$

where $L[f(x)] = F(p)$. The solution of this system is

$$U = F(p)\exp(k_1 k_2 y/p)$$

It can be shown that because $f(0) = 0$, the inverse transform of this expression is a convolution of $f'(x)$ and $I_0(2\sqrt{k_1 k_2 xy})$ or

$$u(x, y) = \int_0^x f'(\xi) I_0(2\sqrt{k_1 k_2 y(x - \xi)})\, d\xi$$

where $f'(x)$ is the derivative of $f(x)$ and $I_0(z)$ is the Bessel function of the zero$^{\text{th}}$ order with imaginary argument.

The solution of equation 16b can be obtained in an analogous manner by taking the transform with respect to y. There results

$$v(x, y) = \int_0^y g'(\eta) I_0(2\sqrt{k_1 k_2 x(y - \eta)})\, d\eta$$

Hence

$$f(x, y) = e^{-k_1 x - k_2 y}\left[\int_0^x f'(\xi) I_0(2\sqrt{k_1 k_2 y(x - \xi)}\, d\xi \right. \\ \left. + \int_0^y g'(\eta) I_0(2\sqrt{k_1 k_2 x(y - \eta)})\, d\eta \right] \tag{17}$$

In order to compute $c(z, t)$ and $n(z, t)$ it is necessary to compute the partial derivatives of $f(x, y)$, as shown in equation 10, and to revert to the original variables. After some manipulation with Bessel functions the following formulae result.

$$\begin{aligned} \exp(k_1 x + k_2 y)\frac{\partial f}{\partial y} = &- k_2 \int_0^x f'(\xi) I_0(2\sqrt{k_1 k_2 y(x - \xi)})\, d\xi \\ &+ \int_0^x f'(\xi) \sqrt{\frac{k_1 k_2 (x - \xi)}{y}}\, I_1(2\sqrt{k_1 k_2 y(x - \xi)})\, d\xi \\ &- k_2 \int_0^x g'(\eta) I_0(2\sqrt{k_1 k_2 x(y - \eta)})\, d\eta \\ &+ \int_0^y g'(\eta) \sqrt{\frac{k_1 k_2 x}{y - \eta}}\, I_1(2\sqrt{k_1 k_2 x(y - \eta)})\, d\eta \\ &+ g'(y) \end{aligned} \tag{18}$$

and

$$\begin{aligned} \exp(k_1 x + k_2 y)\frac{\partial f}{\partial x} = &- k_1 \int_0^x f'(\xi) I_0(2\sqrt{k_1 k_2 y(x - \xi)})\, d\xi \\ &+ \int_0^x f'(\xi) \sqrt{\frac{k_1 k_2 y}{x - \xi}}\, I_1(2\sqrt{k_1 k_2 y(x - \xi)})\, d\xi \\ &- k_1 \int_0^y g'(\eta) I_0(2\sqrt{k_1 k_2 x(y - \eta)})\, d\eta \\ &+ \int_0^y g'(\eta) \sqrt{\frac{k_1 k_2 (y - \eta)}{x}}\, I_1(2\sqrt{k_1 k_2 x(y - \eta)})\, d\eta \\ &+ f'(x) \end{aligned} \tag{19}$$

where we have written the exponent on the left-hand side to simplify the writing. $c(z, t)$ and $n(z, t)$ can be obtained from the above by substituting $x = z/V$ and $y = \alpha(t - z/V)$ and where

$$f'(x) = \left[n_0(xV) + (k_1/V) \int_0^{xV} n_0(\xi)\, d\xi\right] \exp(k_1 x)$$

and

$$g'(y) = \left[-c_0(y/\alpha) - k_2\alpha \int_0^{y/\alpha} c_0(\eta)\, d\eta\right] \exp(k_2 y)$$

Rather than convert equations 18 and 19 into the original z and t variables it is generally easier to convert experimental data into the x and y coördinates. These formulae are rather complex but their numerical use would not pose too many problems, since the functions involved are well tabulated so that numerical integrations either manually or by new high-speed computing machines would be relatively easy. These formulae are perfectly general and it can be shown that all previous solutions (see references 2, 5, 7, 8, and 9), assuming kinetics of the kind assumed here, are special cases of equations 18 and 19.

CASE B

This case is a mathematical generalization of a problem previously considered by the author; however, it involves a different physical assumption since it assumes that adsorbed adsorbate exerts a back pressure. Thomas (10, 11), in his treatment of ion exchange, solved a special case of what follows. The system to be solved is

$$V\frac{\partial c}{\partial z} + \frac{\partial c}{\partial t} + \frac{1}{\alpha}\frac{\partial n}{\partial t} = 0 \tag{1}$$

$$\frac{1}{\alpha}\frac{\partial n}{\partial t} = k_1 c(N_0 - n) - k_2 n \tag{3}$$

$$c(z, t) = c_0(t) \quad \text{when } z = 0 \tag{4}$$

$$n(z, t) = n_0(z) \quad \text{when } t = z/V \tag{5}$$

Thomas has called this case adsorption with Langmuir-type kinetics, since in the limit $\partial n/\partial t = 0$ and therefore

$$n = \frac{k_1 N_0 c}{k_2 + k_1 c}$$

We proceed, in the solution, as in the first case, by making the same changes of variable. A function $f(x, y)$ can once again be defined such that

$$\frac{\partial^2 f}{\partial x \partial y} + k_1 N_0 \frac{\partial f}{\partial y} + k_2 \frac{\partial f}{\partial x} - k_1 \frac{\partial f}{\partial x}\frac{\partial f}{\partial y} = 0 \tag{20}$$

Although this is a nonlinear equation it can be linearized by the substitution:

$$f(x, y) = -\frac{1}{k_1} \log\left[\phi(x, y) \exp(-k_1 N_0 x - k_2 y)\right]$$

Equation 20 then reduces to

$$\frac{\partial^2 \phi}{\partial x \partial y} - k_1 k_2 N_0 \phi(x, y) = 0 \tag{21}$$

and equations 4 and 5 to

$$-c_1(y) = \frac{k_2}{k_1} - \frac{1}{k_1} \frac{\partial \log \phi(0, y)}{\partial y}$$

$$n_1(x) = N_0 - \frac{1}{k_1} \frac{\partial \log \phi(x, 0)}{\partial x}$$

These equations can be solved as ordinary differential equations whose solutions are, after defining $\phi(0, 0) = 1$,

$$\phi\ (0, y) = \exp \int_0^y [k_1 c_1(\eta) + k_2]\, d\eta = G(y) \tag{22}$$

$$\phi(x, 0) = \exp \int_0^x [- n_1(\xi) + N_0]\, k_1\, d\xi = F(x) \tag{23}$$

which equations define $G(y)$ and $F(x)$. Note that $G(0) = 1 = \mathrm{F}(0)$. Hence the problem to be solved is similar to that under Case A; however, it must be handled in a slightly different manner. Consider the two problems:

$$\frac{\partial^2 u}{\partial x \partial y} - k_1 k_2 N_0 u = 0 \tag{24a}$$

$$u(0, y) = G(y) \quad \text{when } x = 0$$

$$u(x, 0) = 1 \quad \text{when } y = 0$$

$$\frac{\partial^2 y}{\partial x \partial y} - k_1 k_2 N_0 v = 0 \tag{24b}$$

$$v(0, y) = 0 \quad \text{when } x = 0$$

$$v(x, 0) = F(x) - 1 \quad \text{when } y = 0$$

Note that $u + v$ satisfies all the conditions that ϕ satisfies. Splitting this problem up into two in such a peculiar fashion is desirable to preserve the continuity at the origin. If the method of Case A is used, u and v are discontinuous at the origin and some care must be exercised. Let $L[u(x, y)] = U(x, p)$, $L[v(x, y)] = V(q, y)$, $L[G(y)] = P(p)$, $L[F(x)] = Q(q)$; then equations 24a and 24b become respectively

$$p \frac{dU}{dx} - k_1 k_2 N_0 U = 0$$

$$U = P(p) \quad \text{when } x = 0$$

and

$$q\frac{dV}{dy} - k_1k_2N_0V = 0$$

$$V = Q(q) - \frac{1}{q} \quad \text{when } y = 0$$

whose solutions are

$$U = P(p) \exp\left(\frac{k_1k_2N_0x}{p}\right)$$

$$V = \left[Q(q) - \frac{1}{q}\right] \exp\left(\frac{k_1k_2N_0y}{q}\right)$$

The inverse transforms of these can be written after some manipulation as:

$$u = I_0(2\sqrt{k_1k_2N_0xy}) + \int_0^y G'(\eta)I_0(2\sqrt{k_1k_2N_0x(y-\eta)})\,d\eta$$

and

$$v = \int_0^x F'(\xi)I_0(2\sqrt{k_1k_2N_0y(x-\xi)})\,d\xi$$

where

$$F'(x) = [k_1c_0(y/\alpha) + k_2] \exp\left[\alpha\int_0^{y/\alpha} (k_1c_0(\eta) + k_2)d\eta\right]$$

$$G'(y) = k_1[-n_0(xV) + N_0] \exp\left[\frac{k_1}{V}\int_0^{xV} (-n_0(\xi) + N_0)d\xi\right]$$

Then

$$\phi(x, y) = I_0(2\sqrt{k_1k_2N_0xy}) + \int_0^y G'(\eta)I_0(2\sqrt{k_1k_2N_0x(y-\eta)}\,d\eta$$

$$+ \int_0^x F'(\xi)I_0(2\sqrt{k_1k_2N_0y(x-\xi)})\,d\xi$$

Now to calculate c and n in terms of x and y variables we need

$$\frac{\partial f}{\partial x} = N_0 - \frac{1}{k_1}\frac{\partial \phi}{\partial x}\frac{1}{\phi} \tag{25}$$

and

$$\frac{\partial f}{\partial y} = \frac{k_2}{k_1} - \frac{1}{k_1}\frac{\partial \phi}{\partial y}\frac{1}{\phi} \tag{26}$$

The derivatives $\partial\phi/\partial x$ and $\partial\phi/\partial y$ can be calculated in a manner analogous to that in Case A; hence $c(z, t)$ and $n(z, t)$ can be obtained after reversion to the old variables. Again, it would probably be better to convert the experimental data to x and y variables if these formulae were to be used. It can be shown that previous solutions (see references 1, 3, 10, and 11) reduce to equations 25 and 26. These formulae are cumbersome and their use would be enhanced by some reduction to simpler form. However, since the problem solved was a general one, no simplification can be expected and yet retain the generality. Experimental work is now being carried on in these laboratories, and it is hoped that verification of these results will be forthcoming. This solution, so far as the author is aware, has not appeared in the literature in connection with adsorption, although, as mentioned, Thomas considered a somewhat simpler problem for ion exchange.

SUMMARY

General equations are developed for adsorption in beds of adsorbent which cover simultaneously adsorption and desorption. The bed may have an arbitrary distribution of adsorbate adsorbed on it, and the inlet solution concentration may have an arbitrary dependence upon the time. These equations are developed for two different cases depending upon the mechanisms assumed to be controlling in the bed. The first is that originally used by Bohart and Adams (3), while the second is that which Thomas (10) called Langmuir kinetics. No simplifying approximations are made; hence the solution is mathematically exact for the cases considered.

This paper was prepared while the author was on a Summer Research Fellowship from the Graduate School of the University of Minnesota.

REFERENCES

(1) Amundson, N. R.: J. Phys. & Colloid Chem. **52**, 1153 (1948).
(2) Anzelius, A.: Z. angew. Math. Mech. **6**, 291 (1926).
(3) Bohart, G. S., and Adams, E. Q.: J Am. Chem. Soc. **42**, 543 (1920).
(4) Churchill, R. V.: *Modern Operational Mathematics in Engineering*. McGraw-Hill Book Company, Inc., New York (1944).
(5) Furnas, C. C.: U. S. Bur. Mines Bull. No. **361** (1932).
(6) Klotz, I. M.: Chem. Revs. **39**, 241 (1946).
(7) Nusselt, W.: Z. Ver. deut. Ing. **71**, 85 (1927).
(8) Schumann, T. E. W.: J. Franklin Inst. **208**, 405 (1929).
(9) Thiele, E. W.: Ind. Eng. Chem. **38**, 646 (1946).
(10) Thomas, H. C.: J. Am. Chem. Soc. **66**, 1664 (1944).
(11) Thomas, H. C.: Ann. N. Y. Acad. Sci. **49**, 161 (1948).

MATHEMATICS OF ADSORPTION IN BEDS. III

RADIAL FLOW

LEON LAPIDUS AND NEAL R. AMUNDSON

Department of Chemical Engineering, School of Chemistry, University of Minnesota, Minneapolis 14, Minnesota

Received September 15, 1949

In the formation of a radial chromatogram a solution is added to an adsorbent disc of uniform thickness through a central hole whereby the solutes are adsorbed in the form of a symmetrical band. The chromatogram is then developed by adding a sufficient quantity of pure solvent to cause the solutes to move radially through the adsorbent. During development the front and rear portions of the band or bands may exhibit various concentration gradients (sharp or diffuse boundaries).

Numerous papers have appeared in the literature dealing with the application of radial chromatography to laboratory (5, 9) and commercial (2, 4) analysis. However, a theoretical approach to this process has been almost completely neglected. Wilson (10) and Thomas (7) briefly mentioned the procedure necessary to extend their vertical chromatographic equations to the case of a radial disc. Sanborn and Amundson (6) have indicated a few of the basic equations necessary in the analysis. It is the purpose of this paper to present a mathematical solution of single-solute radial chromatography where the relation between the solution concentration and the adsorbate concentration can be expressed in two ways depending upon the mechanism assumed to be controlling: (*1*) by an adsorption isotherm, and (*2*) by a kinetic equation.

FUNDAMENTAL DIFFERENTIAL EQUATION

Consider an adsorbent bed in the form of an infinite plate of thickness h, with a circular hole of radius R with center at the origin into which the solution is introduced. Also let

r = distance from the origin to any point in the disc
c = amount of solute in solution per unit volume solution
n = amount of solute adsorbed per unit volume of bed
$f(c) = n/A$ = adsorption isotherm
A = amount of adsorbent per unit volume of bed
$\bar{v}$ = volume rate of flow of solution or solvent (assumed constant)
V = total volume of solvent poured into disc up to time t
V_0 = total volume of original solution poured into disc
D = diffusion constant of solute in solution
m = porosity of adsorbent bed.

For a cylindrical layer of adsorbent of thickness Δr, a material balance demands that the amount of solute entering at r by fluid flow and diffusion minus that leaving at $r + \Delta r$ must be equated to the concentration change which occurs in the solution plus that change which occurs in the solute adsorbed. Thus, neglecting any vertical concentration gradient one finds

$$(\bar{v}c)_r - (\bar{v}c)_{r+\Delta r} + \left(-2\pi rhmD\frac{\partial c}{\partial r}\right)_r - \left(-2\pi rhmD\frac{\partial c}{\partial r}\right)_{r+\Delta r}$$

$$= 2\pi rh\Delta r\left(\frac{\partial n}{\partial t}\right)_{\bar{r}} + 2\pi rhm\Delta r\left(\frac{\partial c}{\partial t}\right)_{\bar{r}}, \; r < \bar{r} < r + \Delta r \quad (1)$$

Divide equation 1 by Δr, assume $\bar{v}$, D, and m are constant and let Δr pass to the limit of zero:

$$\bar{v}\frac{\partial c}{\partial r} + 2\pi rh\frac{\partial n}{\partial t} + 2\pi rhm\frac{\partial c}{\partial t} = 2\pi hmD\frac{\partial}{\partial r}\left(r\frac{\partial c}{\partial r}\right) \quad (2)$$

If diffusion in the radial direction is neglected, the fundamental differential equation results:

$$\bar{v}\frac{\partial c}{\partial r} + 2\pi rh\frac{\partial n}{\partial t} + 2\pi rhm\frac{\partial c}{\partial t} = 0 \quad (3)$$

EQUILIBRIUM THEORY FOR SINGLE SOLUTES

If the assumption is made that instantaneous equilibrium occurs at every point in the disc between solution and adsorbent, the amount of solute adsorbed can be related to the solution concentration by the adsorption isotherm

$$n = 4f(c) \quad (4)$$

Equation 3 thus becomes

$$\bar{v}\frac{\partial c}{\partial r} + 2\pi rh[m + Af'(c)]\frac{\partial c}{\partial t} = 0 \quad (5)$$

where $f'(c)$ is the derivative of $f(c)$. But as $V = \bar{v}t$, equation 5 may be alternately written as:

$$\frac{\partial c}{\partial r} + 2\pi rh[m + Af'(c)]\frac{\partial c}{\partial V} = 0 \quad (6)$$

To this equation must be appended the initial condition of the column and the equation which describes the condition of the entering solution. These are

$$\begin{aligned} c(r, V) &= c_0(V), \quad \text{when } r = R \\ n(r, V) &= n_0(r), \quad \text{when } V = \pi hm(r^2 - R^2) \end{aligned} \quad (7)$$

However, the solution of equation 6 is complicated by the fact that one boundary value must be at $r = R$. To circumvent this difficulty, the substitution is made that

$$y = r - R$$

and equation 6 becomes

$$\frac{\partial c}{\partial y} + 2\pi h(y + R)[m + Af'(c)]\frac{\partial c}{\partial V} = 0 \quad (8)$$

Now a solution can be obtained at the much more convenient $y = 0$. Also note that

$$r^2 - R^2 = y^2 + 2Ry \tag{9}$$

We shall now proceed to derive equations, using the method of the La Place transform, which will completely describe the movements of a solute within the disc for the case of the linear isotherm:

$$n = bc \tag{10}$$

The more general isotherm will be treated in a later communication.

While the linear isotherm has often been referred to as impractical, the authors have examined experimental data (8) which indicate that equation 10 holds for a number of systems and in some cases a large range of concentrations.

To facilitate the solution we make a change of variable in equation 8 by letting

$$z = \bar{v}t - \pi hm(r^2 - R^2) \tag{11}$$

and then by further substituting equation 10, there results

$$\frac{\partial c}{\partial y} + 2\pi hb(y + R)\frac{\partial c}{\partial z} = 0 \tag{12}$$

The boundary conditions necessary using these variables in forming a chromatogram are

$$\begin{aligned} c(0, z) &= c_0 \\ c(y, 0) &= 0 \end{aligned} \tag{13}$$

Taking the La Place transform of c with respect to z, $L[c(y, z)] = M(y, p)$, equations 12 and 13 become:

$$\frac{dM}{dy} + 2\pi hb(y + R)pM = 0 \tag{14}$$

$$M = \frac{c_0}{p}, \qquad y = 0 \tag{15}$$

But equation 14 is a simple linear differential equation whose solution is

$$M = C_1 \exp(-\pi hb(y^2 + 2Ry)p)$$

where C_1 is an arbitrary constant. Applying equation 15,

$$C_1 = \frac{c_0}{p}$$

and thus

$$M = \frac{c_0}{p} \exp(-\pi hb(y^2 + 2Ry)p) \tag{16}$$

To take the inverse transform of equation 16, we note that Churchill (3) gives the inverse transform of $m \exp(-kp)/p$ as being the stepwise function:

$$S_k(t) = \begin{cases} 0 & 0 < t < k \\ m & t > k \end{cases}$$

Thus we have:

$$c(y, z) = \begin{cases} 0 & 0 < z < \pi hb(y^2 + 2Ry) \\ c_0 & z > \pi hb(y^2 + 2Ry) \end{cases}$$

Changing back to the original set of variables and using equation 9, there results:

$$c(r, V) = \begin{cases} 0 & r > \left[\dfrac{V_0}{\pi h(m + b)} + R^2\right]^{1/2} \\ \\ c_0 & r < \left[\dfrac{V_0}{\pi h(m + b)} + R^2\right]^{1/2} \end{cases} \tag{17}$$

For developing the band equations 10 and 12 are used again, but in the form:

$$\frac{\partial n}{\partial y} + 2\pi hb(y + R)\frac{\partial n}{\partial z} = 0 \tag{18}$$

The appropriate boundary values are

$$\begin{aligned} c(0, z) &= 0 \\ n(y, 0) &= 0 \quad \text{for} \quad y > a \\ n(y, 0) &= n_0 \quad \text{for} \quad y < a \end{aligned} \tag{19}$$

where a is the width of the original band from $r = R$ to $r = R + a$. Also, since $c = 0$ when $y = 0$, it follows from the isotherm that $n = 0$ when $y = 0$. We take the La Place transform with respect to z again, letting $L[n(y, z] = N(y, p)$. Then

$$\frac{dN}{dy} + 2\pi hb(y + R)[pN - n(y, 0)] = 0$$

where $n(y, 0)$ is as defined in equation 19. This can be written as

$$\frac{dN}{dy} + 2\pi hb(y + R)pN = 2\pi hb(y + R)n(y, 0) \tag{20}$$

The function $E(y, P) = \exp[\pi hb(y^2 + 2Ry)p]$ is an integrating factor, so that the solution can be written immediately as

$$N = E(y,-p)\int_0^y 2\pi hb(s + R)n(s,0)E(s,p)\,ds \tag{21}$$

where s is the variable of integration.

If we split the integral into two pieces, the first from 0 to a and the second from a to y, then in the first portion $n(y, 0) = n_0$ and in the second portion $n(y, 0) = 0$. Thus

$$N = n_0 E(y,-p) \int_0^a 2\pi hb(s + R)E(s,p)\, ds$$

The integration can now be performed and there results

$$N = \frac{n_0}{p} \{ -\exp[-\pi hb(y^2 + 2Ry)p] + \exp[-\pi hb(y^2 + 2Ry - a^2 - 2Ra)p]\} \quad (22)$$

But the inverse transform of the function

$$\frac{n_0}{p} [\exp(-k_1 p) - \exp(-k_2 p)]$$

is the stepwise function

$$S_k(t) = \begin{cases} 0 & 0 < t < k_1 \\ n_0 & k_1 < t < k_2 \\ 0 & k_2 < t \end{cases}$$

Hence

$$n(y, z) = \begin{cases} 0 & 0 < z < \pi hb(y^2 + 2Ry - a^2 - 2Ra) \\ n_0 & \pi hb(y^2 + 2Ry - a^2 - 2Ra) < z < \pi hb(y^2 + 2Ry) \\ 0 & \pi hb(y^2 + 2Ry) < z \end{cases} \quad (23)$$

or on changing back to the original variables, there results:

$$n(r, V) = \begin{cases} 0 & r < \left[\dfrac{V}{\pi h(m + b)} + R^2\right]^{1/2} \\ n_0 & \left[\dfrac{V}{\pi h(m + b)} + R^2\right]^{1/2} < r < \left[\dfrac{V + \pi hb(a^2 + 2Ra)}{\pi hb(m + b)} + R^2\right]^{1/2} \\ 0 & \left[\dfrac{V + \pi hb(a^2 + 2Ra)}{\pi h(m + b)} + R^2\right]^{1/2} < r \end{cases} \quad (24)$$

Of course, a can be found directly from equation 17. Note that the original sharp band formed moves out from the center of the disc and decreases in width.

KINETIC THEORY FOR SINGLE SOLUTES

The assumption is made in this section that the local rate of removal of adsorbate is governed by the kinetic equation (see Thomas (7)):

$$\frac{\partial n}{\partial t} = k_1 c(N_0 - n) - k_2 n \quad (25)$$

where N_0 is the saturation capacity of a unit volume of bed and k_1 and k_2 are velocity constants.

To equations 8 and 25 certain boundary values must be added:

$$n(r, t) = n_0(r), \quad \text{when } \bar{v}t \leqq \pi hm(r^2 - R^2) \tag{26}$$

$$c(r, t) = c_0(t), \quad \text{when } r = R \tag{27}$$

Equation 26 gives the initial distribution of solute in the bed as a function of r, and equation 27 gives the inlet concentration of the solution as a function of t. Once again, making the following substitutions

$$y = r - R$$

$$z = \bar{v}t - \pi hm(r^2 - R^2)$$

equations 4, 25, 26, and 27 become

$$\frac{\partial c}{\partial y} + 2\pi h(y + R)\frac{\partial n}{\partial z} = 0 \tag{28}$$

$$\bar{v}\frac{\partial n}{\partial z} = k_1c(N_0 - n) - k_2n \tag{29}$$

$$n(r, t) = n_1(y), \quad \text{when } z = 0 \tag{30}$$

$$c(r, t) = c_1(z), \quad \text{when } y = 0 \tag{31}$$

where $c_1(z) = c_0(z/V)$ and $n_1(y) = n_0(y + R)$. But equation 28 says that

$$\frac{\partial c}{\partial y} = -2\pi h(y + R)\frac{\partial n}{\partial z} \tag{32}$$

which implies that there exists a function F, such that

$$\mathrm{d}F = c\,\mathrm{d}z - 2\pi h(y + R)n\,\mathrm{d}y \tag{33}$$

and

$$c = \frac{\partial F}{\partial z}, \qquad n = -\frac{1}{2\pi h(y + R)}\frac{\partial F}{\partial y} \tag{34}$$

Substituting equation 34 into equation 29, we obtain

$$\frac{\partial^2 F}{\partial z \partial y} + A(y + R)\frac{\partial F}{\partial z} + B\frac{\partial F}{\partial z}\frac{\partial F}{\partial y} + D\frac{\partial F}{\partial y} = 0 \tag{35}$$

which is a nonlinear hyperbolic differential equation in which

$$A = \frac{k_1N_02\pi h}{\bar{v}}; \qquad B = \frac{k_1}{\bar{v}}; \qquad D = \frac{k_2}{\bar{v}}$$

By letting

$$BF = \log\{U(z, y)\exp[-Dz - \frac{A}{2}(y^2 + 2yR)]\} \tag{36}$$

equations 34 and 35 become

$$c = \frac{1}{B}\left(\frac{1}{U}\frac{\partial U}{\partial z} - D\right) \tag{37}$$

$$n = \frac{A}{2\pi hb} - \frac{1}{2\pi h(y + R)BU}\frac{\partial U}{\partial y} \tag{38}$$

$$\frac{\partial^2 U}{\partial z \partial y} = AD(y + R)U \tag{39}$$

From equations 37 and 38 it is seen that the auxiliary conditions 30 and 31 are

$$\frac{\partial \log U(z, 0)}{\partial z} = Bc_1(z) + D \tag{40}$$

$$\frac{\partial \log U(0, y)}{\partial y} = [A - n_1(y)2\pi hB][y + R] \tag{41}$$

which integrate into

$$\log U(z, 0) = \int_0^z [Bc_1(s) + D]\, \mathrm{d}s + \log U(0, 0)$$

$$\log U(0, y) = \int_0^y [A - n_1(s)2\pi hB][s + R]\, \mathrm{d}s + \log U(0, 0)$$

where s is the variable of integration. Defining $U(0, 0) = 1$ (see Amundson (1) and Thomas (7)), we find that

$$U(z, 0) = \exp\left\{\int_0^z [Bc_1(s) + D]\, \mathrm{d}s\right\} = f_2(z) \tag{42}$$

$$U(0, y) = \exp\left\{\int_0^y [A - n_1(s)2\pi hB][s + R]\, \mathrm{d}s\right\} = f_1(y) \tag{43}$$

A solution must now be found which satisfies differential equation 39 and the boundary conditions given by equations 42 and 43. This can be accomplished by means of the La Place transform. Let

$$L[U(y, z)] = u(y, p)$$

and equations 39, 42, and 43 become

$$\frac{\mathrm{d}u}{\mathrm{d}y} - \frac{AD}{p}(y + R)u = \frac{f'(y)}{p} \tag{44}$$

$$u = f_3(p), \qquad y = 0 \tag{45}$$

where $f_3(p)$ is the transform of $f_2(z)$. But equation 44 is a simple linear differential equation whose solution is

$$u = \exp\left[\frac{AD}{2p}(y^2 + 2yR)\right]\left\{\int_0^y \frac{f_1'(s)}{p}\exp\left[-\frac{AD}{2p}(s^2 + 2sR)\right]\mathrm{d}s + C_1\right\}$$

Substituting equation 45, we find:

$$C_1 = f_3(p)$$

Thus the complete solution, after algebraic manipulation, is

$$u = \int_0^y \frac{f_1'(s)}{p} \exp\left[\frac{AD}{2p}(y^2 - s^2 + 2(y - s)R)\right] ds$$

$$+ \frac{(pf_3(p) - 1)}{p} \exp\left[\frac{AD}{2p}(y^2 + 2yR)\right] + \frac{1}{p}\exp\left[\frac{AD}{2p}(y^2 + 2yR)\right] \tag{46}$$

To take the inverse transform, we note that

$$L^{-1}\left[\frac{\exp(k/p)}{p}\right] = I_0(2\sqrt{kz})$$

and

$$L^{-1}[pf_3(p) - 1] = f_2'(z)$$

where I_0 is the modified Bessel function of the zero$^{\text{th}}$ order. Thus:

$$U(y, z) = \int_0^y f_1'(s) I_0(\sqrt{2ADz[y^2 - s^2 + 2(y - s)R]})\, ds$$

$$+ \int_0^z f_2'(s) I_0(\sqrt{2AD(y^2 + 2yR)(z - s)})\, ds$$

$$+ I_0\,(\sqrt{2ADz(y^2 + 2yR)}) \tag{47}$$

From equation 47 there results

$$\frac{\partial U}{\partial y} = f_1'(y) + \int_0^y f_1'(s)(y + R)\left[\frac{2ADz}{y^2 - s^2 + 2(y - s)R}\right]^{1/2} \cdot$$

$$\cdot\, I_1\,(\sqrt{2ADz[y^2 - s^2 + 2(y - s)R]})\, ds$$

$$+ \int_0^z f_2'(s)(y + R)\left[\frac{2AD(z - s)}{y^2 + 2yR}\right]^{1/2} I_1\,(\sqrt{2AD(y^2 + 2yR)(z - s)})\, ds$$

$$+ (y + R)\left[\frac{2ADz}{y^2 + 2yR}\right]^{1/2} I_1\,(\sqrt{2ADz(y^2 + 2yR)}) \tag{48}$$

$$\frac{\partial U}{\partial z} = \int_0^y f_1'(s)\left[\frac{AD(y^2 - s^2 + 2(y - s)R)}{2z}\right]^{1/2}$$

$$\cdot\, I_1\,(\sqrt{2ADz[y_2 - s^2 + 2(y - s)R]})\, ds$$

$$+ f_2'(z) + \int_0^z f_2'(s)\left[\frac{AD(y^2 + 2yR)}{2(z - s)}\right]^{1/2} I_1(\sqrt{2AD(y^2 + 2yR)(z - s)})\, ds$$

$$+ \left[\frac{AD(y^2 + 2yR)}{2z}\right]^{1/2} I_1(\sqrt{2ADz(y^2 + 2yR)}) \tag{49}$$

Now equations 38 and 39, which give the values of c and n as a function of the time and the position in the bed, can be written easily. However, their complexity is such as to deter their being written here.

Experimental work is being carried out at the present time to verify the above equations.

SUMMARY

The general equations for radial flow adsorption columns are derived and their solution obtained for two different cases. The first case is that in which equilibrium is established. The solution is obtained by means of the La Place transform for the case of a linear isotherm. This method is not of use for nonlinear isotherms. The second case covers the nonequilibrium situation, and in it the authors assume a kinetic equation of the Langmuir type. General solutions are obtained for this case. No experimental confirmation of these equations is presented but work is proceeding in this direction.

REFERENCES

(1) Amundson, N. R.: J. Phys. & Colloid Chem. **52**, 1153 (1948).
(2) British patent 611,080 (October 25, 1948).
(3) Churchill, R. V.: *Modern Operational Mathematics in Engineering*. McGraw-Hill Book Company, Inc., New York (1944).
(4) Hopf, P. P.: Ind. Eng. Chem. **39**, 938 (1947).
(5) Meinhard, J. E., and Hall, N. F.: Anal. Chem. **21**, 185 (1949).
(6) Sanborn, C. E., and Amundson, N. R.: Am. Math. Monthly **56**, 217 (1949).
(7) Thomas H. C.: Ann. N. Y. Acad. Sci. **49**, 161 (1948).
(8) Trueblood, K. N.: "An Experimental Study of Chromatography on Silicic Acid-Celite", in press.
(9) Williams, T. I.: *Introduction to Chromatography*. Blackie and Son, Glasgow (1947).
(10) Wilson, J. N.: J. Am. Chem. Soc. **62**, 1583 (1940).

INDIRECT COLORIMETRY

The Determination of the Apparent Dissociation Constants of Mononitroquinol, 2,6-Dinitroquinol, and 3-Alizarinsulfonic Acid

LUIGI SACCONI

Institute of Physical Chemistry, University of Florence, Florence, Italy

Received February 25, 1949

THEORY

It is well known that if two colored substances, A and B, each absorbing light independently, are present in a homogeneous system (e.g., solution) the ratio c_A/c_B of their concentrations can be determined colorimetrically if the following conditions are fulfilled: (*a*) the total stoichiometric concentration is known; (*b*) both A and B can be isolated in order to prepare two standard solutions for comparison with solutions containing the substances in an unknown ratio c_A/c_B.

This last condition is not always satisfied. In a system of the type:

$$pA + qX + \cdots \rightleftharpoons pB + rY + \cdots \tag{1}$$

where A and B are the only colored components, the equilibrium cannot always be completely displaced to one side or the other. Moreover, in the attempt to isolate either A or B, reactions may occur which alter the system itself.

The object of this study is to point out that, even when it is not possible or convenient to isolate the components A and B, the problem can be solved under the following condition: the ratio of the stoichiometric concentrations of the two components must be a function of a variable a which may be directly measured, or evaluated in terms of other known quantities characteristic of the system.

In other words, for any ratio, c_A/c_B we must have

$$\frac{c_A}{c_B} = f(a) \tag{2}$$

where f represents an unknown function (otherwise the c_A/c_B value could be directly determined by calculation). One typical system where such a condition holds is the solution of an acid-base indicator, the equilibrium of which may be represented as follows: $HI \rightleftharpoons H^+ + I^-$. In fact, the system is described in general by a function F which relates the ratio of the concentrations of both HI and I^- to the reciprocal of the hydrogen-ion activity according to the following equation:

$$\frac{c_{I^-}}{c_{HI}} = F\left(\frac{1}{a_{H^+}}\right) \tag{3}$$

in which the function F represents the apparent dissociation constant K_I, constant for constant ionic strength and defined by the well-known relation:

$$K_I = a_{H^+}\cdot\frac{c_{I^-}}{c_{HI}} = a_{H^+}\cdot\frac{\alpha}{1-\alpha}$$

In the case of an indicator, it is often impossible to isolate both the optical HI and I^- forms. To this the solution must usually be brought to a high alkalinity or acidity, which may cause either the decomposition of the indicator or give rise to a salt error. Moreover, for an indicator behaving as a dibasic acid according to the scheme: $H_2I \rightleftharpoons H^+ + HI^- \rightleftharpoons 2H^+ + I^{--}$, the two color changes may be superposed. In the latter case, the intermediate form HI^-, for any given pH value, never exists alone in the solution, and hence cannot be isolated to prepare the standard solution of the pure HI^- form.

In these circumstances it is impossible to determine the value of c_{I^-}/c_{HI} by the usual colorimetric methods, or, for a double color change, the values of c_{HI^-}/c_{H_2I} and $c_{I^{--}}/c_{HI^-}$, as well as the value of pK, or for a double color change, of pK_1 and pK_2.

By the following method of indirect colorimetry, all these determinations can be carried out.

METHOD OF DOUBLE INCOMPLETE COLOR CHANGE

Case I: Neither of the two forms HI *and* I^- *of the indicator can be isolated.*

When three values of the hydrogen-ion activity a_{1H^+}, a_{2H^+}, a_{3H^+}, are known for three different equilibrium conditions of the system, the following equations hold:

$$K_I = a_{1H^+} \cdot \frac{c_{1I^-}}{c_{1HI}} = a_{2H^+} \cdot \frac{c_{2I^-}}{c_{2HI}} = a_{3H^+} \cdot \frac{c_{3I^-}}{c_{3HI}} \tag{4}$$

This indeterminate system of three equations with four unknowns can become determinate in the following manner. Suppose that a colorimeter (figure 1) is formed by two joined wedge cells 1 and 2 and a movable cell 3, and suppose that the solutions of the indicator contained in the three cells have the same concentrations. Let $a_{1H^+} > a_{3H^+} > a_{2H^+}$ be, respectively, the hydrogen-ion activities of the three solutions, and c_{1I^-}/c_{1HI}, c_{2I^-}/c_{2HI}, c_{3I^-}/c_{3HI} be, respectively, the ratios of the concentrations of the two forms in the three solutions; then the dissociation constant K_I will be defined by relation 4.

Now let the cell 3 be adjusted over cells 1 and 2 until its color matches the color resulting from the two joined cells. In figure 1, *MN* represents the optical path through the cells. Suppose the two forms HI and I^- are separated in cells 1 and 2 by two imaginary planes (the traces of which are dotted in figure 1) drawn from the corners *A* and *C*, and so arranged as to delimit in each cell two zones in which the respective concentrations of the HI and I^- forms are equal: the segment *MN* will cut the two traces of these planes and the trace of the boundary wall between the two wedge cells in the points *P*, *S*, *Q*. If $MQ = b$, $MP = x$, $QN = c$, $SN = y$, then:

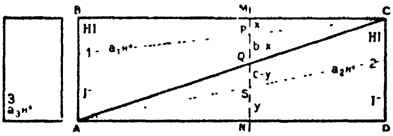

FIG. 1

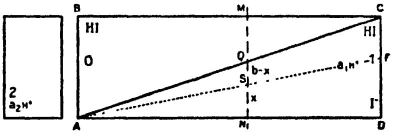

FIG. 2

FIG. 1. Scheme of the double incomplete color change method
FIG. 2. Scheme of the simple incomplete color change method

$$\frac{b-x}{x} = \frac{c_{1I^-}}{c_{1HI}}; \qquad \frac{y}{c-y} = \frac{c_{2I^-}}{c_{2HI}}; \qquad \frac{b-x+y}{c-y+x} = \frac{c_{3I^-}}{c_{3HI}} \tag{5}$$

On substituting these values in equations 4 we find:

$$K_I = a_{1H^+} \cdot \frac{b-x}{x} = a_{2H^+} \cdot \frac{y}{c-y} = a_{3H^+} \cdot \frac{b-x+y}{c-y+x} \tag{6}$$

Now, *b* and *c* are given by colorimetric measurements, and if a_{1H^+}, a_{2H^+}, a_{3H^+} are known, the system of three equations with three unknown quantities (K_I, x, y) can be solved.

By dividing the members of the equations 6 by a_{1H^+} and putting $a_{2H^+}/a_{1H^+} = h_2$, $a_{3H^+}/a_{1H^+} = h_3$, we find:

$$h_2 \cdot \frac{y}{c-y} = \frac{b-x}{x}; \qquad h_3 \cdot \frac{b-x+y}{c+x-y} = \frac{b-x}{x} \tag{7a, 7b}$$

From the first equation we obtain:

$$y = \frac{c(b - x)}{h_2 x + b - x} \tag{8}$$

On substituting the value of y in equation 7b, rearranging, and simplifying, we find:

$$h_2h_3x^2 - h_3x^2 - h_2x^2 + x^2 + h_3bx - h_2cx + h_3cx - bx = 0$$

hence, dividing by x and solving with respect to this unknown quantity we obtain:

$$x = \frac{b + h_2c - h_3(b + c)}{h_2h_3 - (h_2 + h_3) + 1} \tag{9}$$

Substitution of x in equation 8 gives y, and from equation 5 we obtain the value of the three unknown ratios $c_{I^-}/c_{HI} = \alpha/(1 - \alpha)$ for the three solutions in the three cells. By substituting the x- and y-values in one of equations 6, the values of K_I and pK are finally obtained. For example, from

$$K_I = a_{{}^3H^+} \cdot \frac{b - x + y}{c + x - y}$$

by putting $pH_3 = -\log a_{{}^3H^+}$, we obtain:

$$pK = pH_3 - \log \frac{b - x + y}{c + x - y}$$

Case II: In the case of the equilibrium in a buffer–indicator system of the type: $I^- + HA \rightleftarrows HI + A^-$, which defines the concentration equilibrium constant (8):

$$K = \frac{c_{I^-} \cdot c_{HA}}{c_{HI} \cdot c_{A^-}}$$

which is constant for a constant ionic strength, being $c_{I^-}/c_{HI} = F(c_{A^-}/c_{HA})$, it is, similarly, possible to determine by indirect colorimetry the values of the ratio c_{I^-}/c_{HI} and the K-value, even in the case when neither of the I^- and HI forms can be isolated.

In fact, if three values of the ratio c_{HA}/c_{A^-} are known, we can write the system of equations:

$$K = \frac{c^1_{I^-} \cdot c^1_{HA}}{c^1_{HI} \cdot c^1_{A^-}} = \frac{c^2_{I^-} \cdot c^2_{HA}}{c^2_{HI} \cdot c^2_{A^-}} = \frac{c^3_{I^-} \cdot c^3_{HA}}{c^3_{HI} \cdot c^3_{A^-}}$$

Assuming the above explanation and setting $c^1_{HA}/c^1_{A^-} = R_1$, $c^2_{HA}/c^2_{A^-} = R_2$, $c^3_{HA}/c^3_{A^-} = R_3$, $R_2/R_1 = r_2$, $R_3/R_1 = r_3$, we obtain in a similar way:

$$x = \frac{b + r_2c - r_3(b + c)}{r_2r_3 - (r_2 + r_3) + 1}, \qquad y = \frac{c(b - x)}{r_2x + b - x}$$

and if x and y are known, the three ratios c_{I^-}/c_{HI} can be determined, as well as the value of K, from equation 5 and from the following:

$$K = R_1 \frac{b - x}{x} = R_2 \frac{y}{c - y} = R_3 \frac{b - x + y}{c - y + x}$$

METHOD OF SIMPLE INCOMPLETE COLOR CHANGE

Case I: Only the acid form HI *can be isolated.* Let the acid solution be placed in the cell 0 (figure 2) and a solution of hydrogen-ion activity $a_{1_{H^+}}$ be placed in cell 1. Let the ratio of the alkaline to the acid form in this solution be $c_{1_{I^-}}/c_{1_{HI}}$ and the corresponding values for the solution in the cell 2 be respectively $a_{2_{H^+}}$ and $c_{2_{I^-}}/c_{2_{HI}}$ ($a_{2_{H^+}} > a_{1_{H^+}}$). The resulting system of two equations with three unknown quantities:

$$K_I = a_{1_{H^+}} \cdot \frac{c_{1_{I^-}}}{c_{1_{HI}}} = a_{2_{H^+}} \cdot \frac{c_{2_{I^-}}}{c_{2_{HI}}} \qquad (10)$$

is indeterminate.

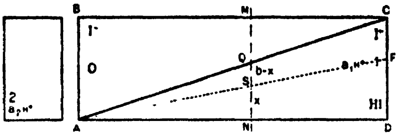

FIG. 3

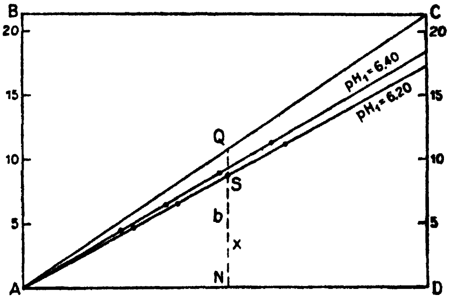

FIG. 4

FIG. 3. Scheme of the simple incomplete color change method
FIG. 4. Graphic verification for 3-alizarinsulfonic acid

If we find the match between cell 2 and the joined wedge cells 0 and 1, and mark the trace of the imaginary boundary plane between the two I^- and HI forms in the cell 1, the above treatment will give:

$$c_{1_{I^-}}/c_{1_{HI}} = SN/SQ, \qquad c_{2_{I^-}}/c_{2_{HI}} = SN/MS$$

Setting $MN = d$, $QN = b$, $SN = x$, $QS = b - x$, and substituting in equations 10, we obtain:

$$K_I = a_{1_{H^+}} \cdot \frac{x}{b - x} = a_{2_{H^+}} \cdot \frac{x}{d - x} \qquad (11)$$

when $a_{1_{H^+}}$, $a_{2_{H^+}}$, and d (thickness of the solution layers) are known, the measurement of b makes the system determinate. For, putting $a_{2_{H^+}}/a_{1_{H^+}} = q$, from equation 11 we have:

$$x = \frac{qb - d}{q - 1}, \qquad K_I = a_{1_{H^+}} \cdot \frac{qb - d}{d - b}$$

Case II: Only the alkaline form can be isolated. Let its solution be placed in the cell 0 (figure 3), and two solutions with hydrogen-ion activities $a_{1_{H^+}}$ and $a_{2_{H^+}}$ ($a_{1_{H^+}} > a_{2_{H^+}}$), respectively, be placed in cells 1 and 2. If the ratios between the two forms in the solutions are $c_{1\mathrm{I}^-}/c_{1\mathrm{HI}}$, $c_{2\mathrm{I}^-}/c_{2\mathrm{HI}}$, respectively, then the above treatment gives:

$$c_{1\mathrm{I}^-}/c_{1\mathrm{HI}} = QS/SN = (b - x)/x; \qquad c_{2\mathrm{I}^-}/c_{2\mathrm{HI}} = MS/SN = (d - x)/x$$

If

$$a_{1\mathrm{H}^+}/a_{2\mathrm{H}^+} = Q: \qquad x = \frac{Qb - d}{Q - 1}, \quad K_{\mathrm{I}} = a_{1\mathrm{H}^+} \cdot \frac{d - b}{Qb - d}$$

Thus by the double incomplete color change method, in place of two standard solutions, each containing one of the two pure colored forms, two *fictitious* standard solutions, included within the range of the color change, are employed. In the simple incomplete color change method, when only one optical form can be isolated, then in place of the standard solution of the form which cannot be isolated, a *fictitious* standard, within the range of the color change, is employed.

It could also be shown that the indirect method can be applied with a Gillespie colorimeter (4). The validity and accuracy of the method have been tested and established in previous researches (14).

EXPERIMENTAL

The wedge colorimeter used was of the Bjerrum–Kolthoff type (2). The upper field of the movable cell and the lower of the joined wedge cells are brought to optical contiguity by a prism arrangement. In the calculations, instead of the whole thickness of the two absorbing layers in the two joined cells, the breadth AD of the cells is used (AD = 21.20 cm.; 21.35 cm). In place of b- and c-values, corresponding to the parts in which the segment MN is divided by the wall AC, as indicated in the previous scheme, the proportional values ND and AN are used. The scale AD is graduated in 0.5 mm. Combinations of blue and green filters were used to make the transmitted light as nearly as possible a neutral grey.

McIlvaine's buffer solutions (10) (0.1 M citric acid and 0.2 M disodium hydrogen phosphate) were used for the first color change of the dinitroquinol and 3-alizarinsulfonic acid. A Kolthoff buffer (6) was used for the first color change of mononitroquinol. For the second color change of the mono- and di-nitroquinols 0.1 M sodium carbonate + 0.1 M boric acid + 0.1 N potassium chloride buffers (7) were used. For the second color change of the Alizarin S Ringer buffers (9) (0.15 M disodium hydrogen phosphate and 0.1 M sodium hydroxide) were used. It is assumed that the difference in the observed values caused by inconstant ionic strength falls within the experimental errors.

The mononitroquinol was prepared according to Richter (13), and was recrystallized to constant melting point (133°C.). The dinitroquinol was prepared according to Nietzki (11) and recrystallized to constant melting point (134–136°C.). Alizarin S from Grubler and Co., Leipzig, was used. The indicator solutions used were: mono- and di-nitroquinols, 0.1 per cent in 20 per cent alcohol + 80 per cent water mixture; Alizarin S, 0.1 per cent solution in water.

DISCUSSION, PROCEDURE, AND RESULTS

The mono- and di-nitroquinols, in strong acid solutions, show a greenish yellow color. The color of mononitroquinol turns to orange within the 5.5–9.2 pH range, and to violet within the 9.2–11.2 pH range. For the 2,6-dinitroquinol (5) the color change towards orange takes place within the 3.0–5.8 pH range, and the orange to violet color change within the 8.0–10.0 pH range.

The electrometric determinations of pK values of these substances gave nonreproducible values because of decomposition (3). Prideaux and Nunn (12), in a colorimetric method, assumed the existence of three optical forms, yellow, orange, violet (in addition to the acid one), corresponding to three colorimetric constants, the values of which are found to be: for mononitroquinol pK_1 = 3.25, pK_2 = 7.2, pK_3 = 10.2; for 2,6-dinitroquinol pK_1 = 2.8, pK_2 = 5.2, pK_3 = 9.05.

The yellow form was not actually isolated to prepare its corresponding standard solutions, but the alkaline form of dinitrophenol was arbitrarily employed in its place. Further, the color changes being multiple and probably superimposed, the existence of the pure orange form in the orange standard solutions used was not assumed, as it was not demonstrated that some solutions used as standard (e.g., mononitroquinol at pH = 5.5, at the beginning of the color change towards orange) contain only one pure form. Since the violet form of both indicators, existing in a strongly alkaline solution, easily decomposes, the standards of the pure alkaline form are unstable.

It is thought that indirect colorimetry is suitable for the determination of the pK values of these substances.

DETERMINATION OF PK_1 OF THE MONO- AND DI-NITROQUINOLS

Mononitroquinol

A standard solution, containing the pure greenish yellow (acid) form of the substance (Solution 0, 0.1 N hydrochloric acid) was prepared. As a fictitious orange standard, a series of solutions was used of such pH that the color change towards orange could not be fully achieved (Solution 1, pH$_1$ = 7.60–7.80–8.0). Suitable intermediate solutions (Solution 2, pH$_2$ = 7.00–7.20–7.40–7. 60) were used. Solution 2 was matched with 0 and 1 conjointly so that the $x/(b - x) = \alpha/(1 - \alpha)$, $K_I = a_{1\text{H}^+} \cdot \frac{x}{b - x}$ values were found. The fact that the pK values found are, within the experimental errors, close to the same value (7.63) shows that the color change from greenish yellow to orange is simple (see table 1). In fact, if the indicator had two different greenish yellow–yellow and yellow–orange color changes, the fictitious standard Solution 2 would result as a mixture of the two forms, the yellow and the orange one. Then for each pH value of Solution 2, a different pK value would be obtained, situated between the value of a pK corresponding to the greenish yellow–yellow color change and the value of a pK corresponding to a yellow–orange color change.

By the double incomplete color change method (see table 2) it has been definitely demonstrated that the color change from greenish yellow to orange is simple. As a fictitious acid standard, a solution with a weak but definite concentration of the orange form was chosen, *viz.*, a solution the color of which lies at the beginning of the color change from greenish yellow to orange (or from yellow to orange, if the yellow form exists) (Solution 1, $pH_1 = 6.80$). As a fictitious orange standard, a series of solutions was used with such a pH (Solution 2, $pH_2 = 8.20$–8.40) as to allow the larger part of the indicator to exist in the orange form and the smaller in the acid one (greenish yellow or yellow). Intermediate solutions (Solution 3, $pH_3 = 7.40$–7.80) were employed. Since the orange form always exists in the two fictitious standards, the solutions will always remain in the range of the greenish yellow–orange or within the range of the yellow–orange color change, if the yellow form exists. In the last case the determined constant should correspond to a yellow–orange color change, and therefore it should be different from that previously determined for the color change from greenish yellow to orange. Actually, the pK_1 value found is identical, within the experimental errors, with that determined by the simple incomplete color change method. We therefore conclude that the color change from greenish yellow to orange is simple and that a yellow form does not exist.

TABLE 1

pK_1 value of mononitroquinol determined by the simple incomplete color change method

Stoichiometric concentration of indicator = 1.03×10^{-7}; $T = 21.0°C$.

pH_1	$a_{1H^+} \times 10^8$	pH_2	$a_{2H^+} \times 10^7$	q	b	d	x	$\frac{x}{b} \times 100$	pK_1
7.60	2.51	7.00	1.000	3.98	8.32	21.20	3.99	48.0	7.63
8.00	1.00	7.60	0.251	2.51	14.51	21.20	10.07	69.4	7.64
8.00	1.00	7.40	0.396	3.98	11.44	21.20	8.16	71.3	7.61
8.00	1.00	7.20	0.631	6.31	8.16	21.20	5.71	70.0	7.64
8.00	1.00	7.00	1.000	10.00	5.90	21.20	4.20	71.2	7.61
7.80	1.58	7.00	1.000	6.31	6.73	21.20	4.00	59.4	7.63
7.80	1.58	7.20	0.631	3.98	9.43	21.20	5.48	58.1	7.66
Mean value									7.63±0.02

TABLE 2

pK_1 value of mononitroquinol determined by the double incomplete color change method

Stoichiometric concentration of indicator = 1.03×10^{-7}; $T = 21.0°C$.

pH_1	$a_{1H^+} \times 10^7$	pH_2	$a_{2H^+} \times 10^9$	pH_3	$a_{3H^+} \times 10^8$	b	c	x	y	$\frac{b-x+y}{c+x-y}$	pK_1
6.80	1.58	8.40	3.98	7.60	2.51	11.16	10.04	9.82	8.47	0.862	7.66
6.80	1.58	8.20	6.31	7.60	2.51	9.89	11.31	8.64	8.87	0.913	7.64
6.80	1.58	8.20	6.31	7.40	3.98	13.79	7.41	12.21	6.21	0.581	7.64
6.80	1.58	8.20	6.31	7.80	1.58	6.25	14.95	5.47	11.69	1.430	7.65
6.80	1.58	8.40	3.98	7.80	1.58	8.00	13.20	7.08	11.06	1.301	7.68
Mean value											7.65 ±0.02

2,6-Dinitroquinol

Two series of measurements were made. In the first, a greenish yellow (acid) standard solution (Solution 0, 0.1 *N* hydrochloric acid) and a fictitious orange standard (Solution 1, $pH_1 = 4.40–4.80–5.20$) were used. In the second series, an actual orange standard (Solution 0, $pH = 6.80$) and a fictitious acid standard (Solution 1, $pH_1 = 3.40–3.60$) were used. The last solution is ranged at the beginning of the greenish yellow–orange color change (or yellow–orange if the yellow form exists).

TABLE 3

pK_1 value of 2,6-dinitroquinol determined by the simple incomplete color change method

Stoichiometric concentration of indicator = 0.8×10^{-7}; $T = 21.0°C$.

pH_1	$a_{1_{H^+}} \times 10^5$	pH_2	$a_{2_{H^+}} \times 10^4$	q	b	d	x	$\frac{x}{b} \times 100$	pK_1
4.80	1.58	4.00	1.000	6.31	8.50	21.20	6.11	71.9	4.40
4.80	1.58	4.40	0.398	2.51	14.63	21.20	10.28	70.3	4.43
4.80	1.58	3.80	1.580	10.00	5.47	21.20	3.72	68.1	4.43
5.20	0.63	4.20	0.631	10.00	9.44	21.20	8.13	86.2	4.41
4.40	3.98	3.60	2.510	6.31	5.69	21.20	2.77	48.6	4.42
Mean value									4.42 ±0.02

TABLE 4

pK_1 value of 2,6-dinitroquinol determined by the simple incomplete color change method

Stoichiometric concentration of indicator = 0.8×10^{-7}; $T = 21.0°C$.

pH_1	$a_{1_{H^+}} \times 10^4$	pH_2	$a_{2_{H^+}} \times 10^5$	Q	b	d	x	$\frac{x}{b} \times 100$	pK_1
3.40	3.98	4.20	6.31	6.31	14.72	21.20	13.51	91.8	4.44
3.40	3.98	4.40	3.98	10.00	12.31	21.20	11.32	92.0	4.46
3.40	3.98	4.60	2.51	15.86	9.10	21.20	8.29	91.1	4.41
3.60	2.51	4.60	2.51	10.00	9.52	21.20	8.22	86.4	4.40
Mean value									4.43 ±0.03

The pK_1 values found are the same in both series (see tables 3 and 4); hence it is concluded that a yellow form of 2,6-dinitroquinol does not exist, and therefore the greenish yellow–orange color change is simple.

Both the nitro compounds behave as dibasic acids, following the scheme: $H_2I \leftrightarrows H^+ + HI^- \leftrightarrows 2H^+ + I^{--}$, where H_2I corresponds to the greenish yellow form, HI^- to the orange, and I^{--} to the violet.

The indirect method offers a control which makes it possible, in the case of multiple color change, to avoid using, as a standard, a solution containing also a form situated outside the investigated color change (e.g., the violet form which may be present in the standard orange solution). In fact, using filters of a color complementary to that leaving the colorimeter, it can easily be seen if the color of the intermediate solution fails to match the color from the solutions of the joined wedge cells.

DETERMINATION OF pK_2 VALUES OF MONONITROQUINOL AND 2,6-DINITROQUINOL

Mononitroquinol

The double incomplete color change method (see table 5) was used for the orange–violet color change, to avoid a strong alkalinity causing the decomposition of the only existent violet form. For this reason, a fictitious violet (alkaline) standard at pH_2 = 10.80 (Solution 2) such that the color change toward violet should not be complete was employed. Since the contiguity of the greenish yellow–orange color change to the orange–violet one does not allow the rigorous isolation of the pure orange form, a fictitious orange standard solution (Solution 1, pH_1 = 9.20) was used in place of an orange standard. This pH is within the range of the orange–violet color change; hence this solution contains only the orange and violet forms. The pH values of the intermediate solution (pH_3, Solution 3) are 9.00–10.00–10.20.

TABLE 5

pK_2 value of mononitroquinol determined by the double incomplete color change method

Stoichiometric concentration of indicator = 0.64×10^{-7}; T = 21.0°C.

pH_1	$a_{1_{H^+}} \times 10^{10}$	pH_2	$a_{2_{H^+}} \times 10^{11}$	pH_3	$a_{3_{H^+}} \times 10^{10}$	b	c	x	y	$\frac{b-x+y}{c+x-y}$	pK_2
9.20	6.31	10.8	1.58	9.8	1.580	14.00	7.20	12.34	6.04	0.571	10.04
9.20	6.31	10.8	1.58	10.0	1.000	11.28	9.92	9.96	8.38	0.843	10.07
9.20	6.31	10.8	1.58	10.2	0.631	7.96	13.24	7.03	11.14	1.323	10.08
Mean value											10.06 ±0.02

It can be seen that pK_2 − pK_1 = 10.06 − 7.64 = 2.42. According to the general equation for indicator equilibrium, pH − pK = $\log \alpha/(1-\alpha)$, for a pH = 8.85, halfway between 7.64 and 10.06, we obtain: 8.85 − 7.64 = $\log \alpha'/(1-\alpha')$, $1-\alpha'$ being the fraction of indicator which has not been transformed into the orange form = 1/17; 10.06 − 8.85 = $\log (1-\alpha'')/\alpha''$, α'' being the fraction of the indicator transformed into the violet form = 1/17, respectively, for the first and the second color changes. We can therefore assume that an orange solution with pH = 8.85 contains 1/17 of both greenish yellow and violet forms. In this case, it is demonstrated that the ranges of both color changes are superimposed and that the standard solution of the pure orange form cannot be prepared. If we calculate the amount of the violet form in the fictitious orange standard at pH = 9.20, above employed, we find that $\alpha'' = c_{\text{I}^{--}}/(c_{\text{I}^{--}} + c_{\text{HI}^{-}})$ $= (b-x)/b$ = 10.5 per cent, and the concentration of the orange form must be 89.5 per cent. It is thus confirmed that the solution at pH = 9.5, used in the investigations reported (12) as standard of the pure orange form, does not contain only this last form. In fact, at pH = 9.5 the concentration of the violet form is certainly larger than that which must exist at pH = 9.20 (10.5 per cent).

2,6-Dinitroquinol

For the orange–violet color change which ranges far from the greenish yellow–orange one, an actual orange standard (pH = 6.80–6.90) is employed. To avoid decomposition of the substance in strongly alkaline solution, a series of fictitious standards (Solution 1, pH_1 = 9.20–9.40–9.60) is used. These solutions, where both orange and violet forms exist, are stable enough to allow a series of measurements (see table 6). The pH_2 values of the intermediate solutions (Solution 2) are 8.60–8.80–9.00.

Summarizing:

Mononitroquinol: $pK_1 = 7.64 \pm 0.03$; $pK_2 = 10.06 \pm 0.02$
2,6-Dinitroquinol: $pK_1 = 4.43 \pm 0.03$; $pK_2 = 9.14 \pm 0.03$

TABLE 6

pK_1 value of 2,6-dinitroquinol determined by the simple incomplete color change method

Stoichiometric concentration of indicator = 0.5×10^{-7}; T = 21.0°C.

pH_1	$a_{1H^+} \times 10^{10}$	pH_2	$a_{2H^+} \times 10^9$	q	b	d	x	$\frac{x}{b} \times 100$	pK_2
9.60	2.51	8.60	2.51	10.00	6.16	21.20	4.49	72.8	9.17
9.60	2.51	8.80	1.58	6.31	8.98	21.20	6.67	75.5	9.14
9.40	3.98	9.00	1.00	2.51	14.12	21.20	9.43	66.7	9.10
9.40	3.98	8.80	1.58	3.98	10.06	21.20	6.32	62.8	9.17
9.20	6.31	8.60	2.51	3.98	8.95	21.20	4.84	54.1	9.13
9.20	6.31	8.80	1.58	2.51	12.25	21.20	6.32	51.6	9.17
Mean value....................									9.14 ±0.03

DETERMINATION OF THE pK_1 AND pK_2 VALUES OF 3-ALIZARINSULFONIC ACID

This substance, the sodium salt of which is called Alizarin Red S, shows in strong acid solutions a greenish yellow color. With decreasing hydrogen-ion concentration the color turns brown, reaching violet, through red and lilac, in strongly alkaline solution.

A. K. Babko (1) found the following values for the two dissociation constants: $K_1 = 3 \times 10^{-6}$, $pK_1 = 5.52$; $K_2 = 3 \times 10^{-10}$, $pK_2 = 9.52$. Salm (15) by a semiquantitative investigation found that the transitory lilac color appears at pH $\cong$ 11.

In view of this discrepancy, to avoid a strong alkalinity of the standard solutions containing the only pure violet form (pH > 12), which causes decoloration, the indirect colorimetric method was used.

Greenish yellow–red color change

Acid standard (Solution 0, 0.1 *N* hydrochloric acid); fictitious red standard (Solution 1, pH_1 = 6.20–6.40); intermediate solution (Solution 2, pH_2 = 5.00–5.20–5.40–5.60). (See table 7.)

Red–violet color change

Red standard (Solution 0, pH = 7.60). Violet fictitious standard (Solution 1, pH_1 = 11.77–12.06). Intermediate solutions (Solution 2, pH_2 = 10.97–11.29). (See table 8.)

This value obtained is very different from Babko's, and confirms Salm's semiquantitative investigation.

TABLE 7

pK_1 value of 3-alizarinsulfonic acid determined by the simple incomplete color change method

Stoichiometric concentration of indicator = 0.56×10^{-7}; T = 19°C.

pH_1	$a_{1H^+} \times 10^7$	pH_2	$a_{2H^+} \times 10^6$	q	b	d	x	$\frac{x}{b} \times 100$	pK_1
6.20	6.31	5.00	10.00	15.85	5.82	21.35	4.77	82.0	5.54
6.20	6.31	5.20	6.31	10.00	8.09	21.35	6.62	81.8	5.55
6.20	6.31	5.40	3.98	6.31	10.78	21.35	8.78	81.5	5.55
6.20	6.31	5.60	2.51	3.98	13.78	21.35	11.24	81.5	5.55
6.40	3.98	5.00	10.00	25.12	5.28	21.35	4.61	87.3	5.56
6.40	3.98	5.20	6.31	15.85	7.52	21.35	6.59	87.6	5.55
6.40	3.98	5.40	3.98	10.00	10.28	21.35	9.05	88.0	5.54
6.40	3.98	5.60	2.51	6.31	12.95	21.35	11.37	87.8	5.54
Mean value									5.54 ±0.01

TABLE 8

pK_2 value of 3-alizarinsulfonic acid determined by the simple incomplete color change method

Stoichiometric concentration of indicator = 0.46×10^{-7}; T = 19°C.

pH_1	$a_{1H^+} \times 10^{12}$	pH_2	$a_{2H^+} \times 10^{11}$	q	b	d	x	$\frac{x}{b} \times 100$	pK_2
12.06	0.871	11.29	0.513	5.89	14.75	21.20	13.43	91.1	11.05
11.77	1.700	11.29	0.513	3.02	16.35	21.20	13.96	85.4	11.01
12.06	0.871	10.97	1.070	12.28	11.36	21.20	10.48	92.3	10.98
Mean value									11.01 ±0.04

GRAPHIC VERIFICATION OF THE METHOD

Let us consider the determination of pK_1 value for 3-alizarinsulfonic acid. Let $ABCD$ be the wedge colorimeter (figure 4), where $AB = CD = d$. Let the triangle ABC correspond to the cell 1 containing the solution 1. For pH_1 = 6.20 draw a segment QN perpendicular to AD, such that its length may be equal to the measured value of b. On this segment take a point S such that $SN = x$. The same operation is carried out for all the values of b and x measured and calculated at pH_1 = 6.20. It is repeated at pH_1 = 6.40, and two series of points are obtained, which (within the experimental errors) lie on two straight lines drawn from A and representing the traces of the two imaginary planes previously assumed in order to demonstrate the method.

SUMMARY

The theory of indirect colorimetry is summarized.

The values of pK of mononitroquinol, 2,6-dinitroquinol, and 3-alizarinsulfonic acid were determined by an indirect colorimetric method and the values found by the usual methods corrected.

It is shown that, if it is not possible to isolate the pure optical forms, the usual colorimetric methods are not suitable.

REFERENCES

(1) Babko, A. K.: Univ. état Kiev, Bull. sci., Rec. chim. No. **3**, 49–67; Chem. Zentr. **1940, II,** 1184.
(2) Bjerrum, N.: Z. anal. Chem. **56**, 81 (1917).
Kolthoff, I. M.: Rec. trav. chim. **43**, 144 (1924).
(3) Gilbert, F. L., Laxton, F. C., and Prideaux, E. B. R.: J. Chem. Soc. **129**, 2295 (1927).
(4) Gillespie, L. J.: J. Bact. **6**, 399 (1921); J. Chem. Soc. **122**, 157 (1922).
(5) Henderson, L. J., and Forbes, A.: J. Am. Chem. Soc. **32**, 687 (1910).
(6) Kolthoff, I. M.: Biochem. Z. **189**, 191 (1927).
(7) Kolthoff, I. M.: *Saüre-Basen Indicatoren*, p. 263. Springer, Berlin (1932).
(8) Kolthoff, I. M., and Guss, L. S.: J. Am. Chem. Soc. **60**, 2516 (1938).
(9) Lehmann, G.: *Die Wasserstoffionenmessung*, p. 50. J. A. Barth, Leipzig (1942).
(10) MacIlvaine, T. C.: J. Biol. Chem. **49**, 183 (1921).
(11) Nietzki, R.: Ann. **215**, 125 (1882).
(12) Prideaux, E. B. R., and Nunn, G. R.: J. Chem. Soc. **125**, 2110 (1924).
(13) Richter, M. M.: Ber. **49**, 1398 (1916).
(14) Sacconi, L.: Gazz. chim. ital. **78**, 192, 303, 674 (1948).
(15) Salm, E.: Z. physik. Chem. **57**, 471 (1907).

ELECTROLYTIC DISSOLUTION OF COPPER IN AMMONIACAL ELECTROLYTES

FRED A. SCHIMMEL

Department of Chemistry, Fisk University, Nashville, Tennessee

Received March 24, 1949

I. INTRODUCTION

It is known that copper can be dissolved electrolytically in ammoniacal electrolytes. A process based on this fact has been used recently with success, e.g., for the recovery of copper from copper-plated iron scrap on a commercial scale in Germany. When electrolytically dissolved, copper as an anode sends cuprous or/and cupric ions into solution and can be deposited on the cathode from monovalent or/and bivalent ions. The purpose of the present investigation was to determine the conditions under which copper can be dissolved anodically in the cuprous form and also deposited cathodically from the monovalent state using an ammoniacal electrolyte.

II. EXPERIMENTAL

A. Electrolyses

Several electrolytes were tried under various conditions. A copper coulometer was always connected in series. Except for a few experiments described below, air was excluded as far as possible from the electrolyte by passing a neutral gas stream through the solution, preferably around the anode to limit at the same time polarization due to low concentration of the solution in the layer around the anode. Also, covering the surface of the electrolyte with paraffin oil proved advantageous.

The valence ratio by which copper was dissolved anodically was determined from the loss in weight of the anode in the electrolyte and the gain in weight of the cathode in the coulometer. The amount of copper which goes into solution without the aid of the electric current was usually determined separately by running a blank and subtracted from the loss of the anode. This discrepancy is due to minute traces of oxygen which could not be excluded from the electrolyte and which were in most cases too small to cause a readily visible coloration. The valence ratio is expressed in the last but one column of tables 1 to 3 as current efficiency based on the reaction Cu → Cu^+, so that an efficiency of 100 per cent corresponds to the exclusive formation of cuprous ions, and one of 50 per cent to the exclusive formation of cupric ions. This was permissible, since no other electrochemical reactions were perceptible.

TABLE 1

Electrolyte: Ammonia solutions of various concentrations

Agitation with hydrogen gas in Nos. 12, 14, 15, with air in Nos. 31, 32, 37, or with carbon dioxide gas in Nos. 41, 45, 49, 51

Anode: One rectangular anode of electrolytic copper, 2 x 5 cm.

Cathode: Two rectangular cathodes of copper, 2 x 5 cm., each 2 cm. from the anode

NUMBER OF EXPERIMENT	GAIN OF CATHODE IN COULOMETER	LOSS OF ANODE IN ELECTROLYTE	LOSS OF ANODE WITHOUT CURRENT	AMPERAGE	CURRENT DENSITY	CURRENT EFFICIENCY	COLOR OF ELECTROLYTE
	grams	*grams*	*grams*	*amperes*	*amp.* $\times 10^{-4}$/*cm.*^{2}	*per cent*	
12.	0.0592	0.1240	0.0045	0.049	24.5	100	Colorless
14.	0.0696	0.1388	0.0045	0.058	29.0	95.7	Very faintly blue
15.	0.0948	0.1840	0.0045	0.080	40.0	94.6	Very faintly blue
31.	0.0574	0.1286	0.0142	0.0484	24.2	100	Dark blue
32.	0.0638	0.1438	0.0142	0.054	27.0	95	Dark blue
37.	0.2920	0.3296	0.0142	0.246	123.0	53.8	Dark blue
41.	0.1548	0.3238	0.0224	0.130	65	100	Faintly blue
45.	0.2173	0.4570	0.0224	0.183	91.5	100	Faintly blue
49.	0.5212	1.0476	0.0224	0.439	219.5	100	Faintly blue
51.	0.6050	1.1928	0.0224	0.510	255	98	Faintly blue

The anode was made of electrolyte copper and the cathode of platinum. In cases where the dissolution of copper was of prime importance, one anode was placed between two cathodes at a distance of 2 cm. from each. Otherwise two anodes and one cathode were used. Each electrode had a total surface of 20 cm. The time of each electrolysis was about 60 min. The exact amount of ampere-seconds applied in each electrolysis was indicated by the coulometer. These first experiments were carried out at room temperature.

The following results were obtained: If ammonia solutions are used as electrolytes the concentration of ammonia has no influence upon the potential of the copper, Cu^+/Cu^{++}. Applying hydrogen (experiments No. 12, 14, 15) or air (experiments No. 31, 32, 37) as an agitating medium, copper is dissolved exclusively in the monovalent form up to a current density of about 25×10^{-4} amp./cm.^{2} At a current density of 40×10^{-4} amp./cm.^{2}, the deviation from monovalency is 2×5.4 per cent.

When air was used the electrolyte was blue, owing to oxidation:

$$2Cu(NH_3)_2(OH) + 4NH_3 + H_2O + \tfrac{1}{2}O_2 = 2Cu(NH_3)_4(OH)_2$$

At higher current densities cuprous ions are formed together with cupric ions in a diminishing ratio, until at around 150×10^{-4} amp./cm.^{2} copper is dissolved in the bivalent form only.

In another series of experiments carbon dioxide was taken as the agitating gas. The ammonia of the electrolyte was now present as bicarbonate, which has a lower ammonia tension, so that the loss of ammonia during electrolysis is considerably reduced. This electrolyte permitted the dissolution of copper as cuprous ions up to a current density of 250×10^{-4} amp./cm.^{2} (experiments No. 41, 45, 49, 51).

Ammonium sulfate was tried as a conductance salt, but it has apparently no influence upon the electrolytic potentials of copper. The results obtained in this series were practically identical with those in experiments 41 to 51.

The addition of ammonium chloride as a conductance salt gave better results as to the limiting current density, and because it has also been used commercially the results may be reported in more detail. Agitation was provided by a current of carbon dioxide; the anode, cathode, anodic surface, temperature, and time of each run were the same as above. The concentrations of ammonia and ammonium chloride were 2 *N*. In this series (see table 2) it was possible to obtain an anodic current efficiency with respect to cuprous ions of over 95 per cent even at current densities of about 450 amp./m.^{2}

The copper deposit on the cathode in the last series tended to be spongy, particularly at higher current densities. Therefore, in order to improve the structure of the deposit, copper was added to the electrolyte in the form of cuprous chloride. The conditions of this group of electrolyses are given in table 3. During these electrolyses the solutions remained completely colorless, thus indicating that copper was dissolved in the monovalent form. Likewise the copper was deposited from monovalent ions. The deposit had the rosy color of pure electrolytic copper. The cathodic deposit was coarsely crystalline at the lower current densities and spongy at densities above 130×10^{-4} amp./cm.^{2} in the 25°C. runs. The copper crystals were then rather loosely attached to the cathode. An increase of the temperature of the bath to 45°C. or still better to 60°C. greatly improves the structure of the copper. The copper adheres now to the cathode and possesses a fine crystalline structure.

TABLE 2

Electrolyte: 2 N NH_3 as ammonium bicarbonate, 2 N NH_4Cl
Agitation with carbon dioxide gas
Anode: One rectangular anode of electrolytic copper, 2 x 5 cm.
Cathode: Two rectangular cathodes of copper, 2 x 5 cm., each 2 cm. from the anode

NUMBER OF EXPERIMENT	GEIN OF CATHODE IN OULOMETER	LOSS OF ANODE IN ELECTROLYTE	LOSS OF ANODE WITHOUT CURRENT	AMPERAGE	CURRENT DENSITY	CURRENT EFFICIENCY	COLOR OF ELECTROLYTE
	grams	*grams*	*grams*	*amperes*	*amp.* × 10^{-4}*/cm.*^{2}	*per cent*	
61	0.1020	0.2622	0 0582	0.086	43.0	100	Colorless
63	0.1575	0.3732	0.0582	0.133	66.5	100	Colorless
65	0.2520	0.5625	0.0582	0.212	106	100	Colorless
66	0.3520	0.7622	0.0582	0.296	148	100	Colorless
67	0.5272	1.1164	0.0582	0.444	222	100	Colorless
68	0.6000	1.2597	0.0582	0.505	252	100	Colorless
69	0.7000	1.4530	0.0582	0.589	294.5	96.5	Colorless
70	0.8108	1.6568	0.0582	0.682	341	98.5	Very faintly blue
71	1.0528	2.0896	0.0582	0.885	442	96.8	Very faintly blue

TABLE 3

Electrolyte: 2 N NH_3 as ammonium bicarbonate, 2 N NH_4Cl, 0.25 N CuCl as cuprous ammonium chloride
Agitation with carbon dioxide gas
Anode: Two rectangular anodes of electrolytic copper, 2 x 5 cm. and 4 cm. apart
Cathode: Platinum, 2 x 5 cm., surface 20 cm.^{2}

NUMBER OF EXPERIMENT	GAIN OF CATHODE IN COULOMMETER	LOSS OF ANODE IN ELECTROLYTE	GAIN OF CATHODE IN ELECTROLYTE	TIME OF ELECTROLYSIS	TEMPERATURE	CATHODIC CURRENT DENSITY	CURRENT EFFICIENCY	COLOR OF ELECTROLYTE
	grams	*grams*	*grams*	*hours*	°C.	*amp.* × 10^{-4}*/cm.*^{2}	*per cent*	
73	0.7061	1.4128	1.4118	4⅓	25	69	100	Colorless
74	3.3218	6.6675	6.6654	22	25	63.7	100	Colorless
75	1.2286	2.4580	2.4518	4	25	128.5	100	Colorless
76	2.8073	5.6968	5.6293	19	45	62.5	100	Colorless
80	1.5500	3.1415	3.0526	5	60	130	100	Colorless
81	6.2000	12.4800	12.3896	10	60	260	99	Colorless

In some further experiments the chloride ion in the electrolyte was displaced by the sulfate ion with the result that the copper deposit on the cathode showed now a considerably finer grain structure. In this respect a further improvement was possible when using carbonates. As a conductance salt potassium bicarbonate had then been added. While the chloride-containing electrolyte was saturated with respect to $Cu(NH_3)_2Cl$, the sulfate- and carbonate-containing electrolytes would have permitted a higher concentration.

The conditions in table 3 are approximately those under which the process of G. Haensel (2) works. This process has been fully described previously (7).

B. Potentials

In contact with its normal salts the potential of Cu/Cu^{++} is equal to $E_H = +0.348$ v., while the Cu/Cu^{+} potential equals $E_H = +0.528$ v. under the assumption that the concentration of the copper ions in the solution is normal in both cases (4, 5). If copper is dissolved in the monovalent form in an ammoniacal solution, the potential Cu/Cu^{+} must now have become more negative than the potential Cu/Cu^{++}. It seemed desirable to have more information through a few measurements of the potentials involved, which also should disclose the amount of polarization during solution and deposit of copper. Since only those potentials at which electrolyses at the different current densities could be carried out continually were of interest, the so-called direct method was preferred to the commutator method (1). The measurements were carried out at 60°C. in an atmosphere of carbon dioxide. The composition of the electrolyte was the same as described in table 3. The 0.1 *N* calomel electrode was used as a reference electrode. The arrangement was the customary one, as first described by Ostwald, whereby a capillary electrometer was used as a zero instrument. Cathode and anode, 2 x 5 cm. in size, were made of electrolytic copper; their reverse sides were covered with picein.

TABLE 4

ANODE POTENTIAL, E_H		CATHODE POTENTIAL, E_H		CURRENT DENSITY
Circuit open	Circuit closed	Circuit open	Circuit closed	
volts	*volts*	*volts*	*volts*	*amp.* × 10^{-4}/*cm*^{2}
−0.036	−0.006	−0.036	−0.053	12.5
−0.036	−0.002	−0.035	−0.059	25.0
−0.035	+0.001	−0.037	−0.070	50.0
−0.037	+0.015	−0.036	−0.082	100.0
−0.036	+0.019	−0.035	−0.092	150.0

The experiment was performed in the following manner: first, the potential of the anode was measured, the circuit being open; second, the cathode potential was measured at the various current densities; third, the potential at the cathode was measured, the circuit being open; and last, the cathode potential at the various current densities. Between each measurement was a time interval of 10 min. The values thus found are given in table 4 and figure 1.

Through complex formation the potential of copper is 0.036 v. more negative than the hydrogen electrode. The cathode potential becomes more negative, the anode potential more negative with increasing current densities, whereby more vigorous agitation of the electrolyte did not change the values found, indicating that the overvoltage of the electrodes is probably not due only to concentration polarization. Another factor influencing the overvoltage might be the fact that the formation of the copper ammonia complex at the anode and its disruption at the cathode take a finite time interval. That the reaction $Cu^{++} + 5H_2O = Cu(H_2O)_5^{++}$ is in all probability a time reaction was first pointed out by Le Blanc (6; see also 3).

If carbon dioxide as an agitating gas is replaced by hydrogen, the potential of copper is found to be $E_H = -0.140$ v., indicating that the carbon dioxide under the prevailing conditions makes the copper appear nobler by about 0.1 v. Carbon dioxide can obviously not destroy the cuprous ammonia complex, but increases the concentration of the free copper ions in solution by neutralizing the free ammonia in the electrolyte.

It might be mentioned here, that measurements of copper potentials using the same concentrations and temperatures except that copper was in the bivalent form gave the value of $E_H = -0.08$ v. in the absence of carbon dioxide, and $E_H = +0.04$ v. in the presence of carbon dioxide. The situation is analogous to that in the preceding paragraph. The presence of carbon dioxide increases the concentration of the copper ions without destroying completely the copper ammonia complex. The complex formation between cuprous ion and ammonia appears to be stronger than that between cupric ion and ammonia. This is not in conformity with the general rule that the higher state of oxidation forms the stronger coördinate bond.

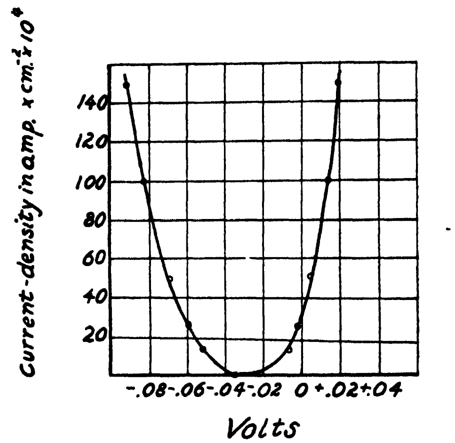

FIG. 1. Curve of current density plotted against potential

III. SUMMARY

The valence with which copper is deposited from and enters various ammoniacal solutions has been determined as a function of the current density. Some determinations of potentials of copper in ammoniacal electrolytes were made and the results discussed.

REFERENCES

(1) GLASSTONE, S.: J. Chem. Soc. **125**, 250 (1924).
(2) HAENSEL, G.: German patent 688,696 (1940).
(3) HARING, H. E.: Trans. Am. Electrochem. Soc. **49**, 417 (1926).
(4) HEINERT, E.: Z. Elektrochem. **37**, 61 (1931).
(5) *International Critical Tables*, Vol. III. McGraw-Hill Book Company, Inc., New York (1928).
(6) Abhandlungen der deutschen Bunsengesellschaft, No. 3 (1910).
(7) SCHIMMEL, F. A.: "Über die elektrolytische Kupferraffination aus ammoniakalischer Kuprosalzlösung," Dissertation, Darmstadt, 1928.

SYMPOSIUM ON KINETICS OF PROPELLANTS

INTRODUCTORY REMARKS[1]

R. E. GIBSON

Applied Physics Laboratory, The Johns Hopkins University, Silver Spring, Maryland

Received January 9, 1950

ORIGIN AND GENERAL SIGNIFICANCE OF STUDY OF KINETICS OF PROPELLANTS

In these introductory remarks I propose to outline the origin and general significance of the study of the kinetics of propellants and to present some of the elementary ideas which underlie the discussions that are to follow.

Propulsion

This symposium deals with a very special aspect of a field of study which has a very widespread appeal and importance: namely, the study of how to move massive bodies from one place to another with ever-increasing velocities. As applied to transportation, the science and art of propulsion is basic to our present-day type of civilization; as applied to ballistics, it provides our most potent weapons in time of war. Although the various engines used for propulsion appear upon superficial examination to differ greatly, e.g., aeroplane engines, locomotives, guns, or rockets, they all depend basically on the controlled conversion of chemical energy into the elastic energy of a gas, which in turn is transformed into energy of directed motion by an engine devised to suit the particular application. Walking is the only common form of propulsion that does not depend on this principle. Furthermore, up to the present, the chemical reactions involved in practical propulsion have all been limited to interactions in the system carbon, hydrogen, nitrogen, oxygen. Thus, although our discussions will be limited to a very restricted field, the physical-chemical results will certainly be of much wider application.

---

[1] Presented at the Symposium on Kinetics of Propellants which was held under the auspices of the Division of Physical and Inorganic Chemistry at the 112th Meeting of the American Chemical Society, New York City, September 15, 1947.

Solid propellants

The chemical reactions which produce the hot compressed gases in propulsion reactions are so frequently oxidation reactions that it has become common practice to divide each propulsion chemical system into two main components: (*1*) the fuel or substance to be oxidized; (*2*) the oxidizer or oxidizing substance. Together these constitute a propellant. The interaction of these two components makes available the energy that is required. Generally speaking, these two components are stored separately and mixed mechanically at the time, and in the vessel, where the propulsion reaction takes place. For example, fuels such as coal, petroleum, or gas are mixed with air, the most common oxidizer, just prior to combustion. Likewise, in large rockets having a liquid propulsion system, the fuel and the oxidizer are kept in separate containers until they are mixed in the combustion chamber, where they react at once. In such rockets, aniline, alcohol, gasoline, or hydrazine hydrate are used as fuels, whereas concentrated nitric acid, liquid oxygen, hydrogen peroxide, etc., are used as oxidizers. However, in solid propellants, which find their chief application in rockets or guns, the fuel and oxidizer are intimately mixed at the time of manufacture and the solid remains in a condition of thermodynamic metastability until the proper energy of activation is supplied through the mechanism of ignition. It is convenient to distinguish two classes of solid propellants.

(*1*) *Composite or heterogeneous propellants:* In propellants of this class the fuel and oxidizer occur as separate phases, such as a mixture of finely divided crystals held together by a suitable bond. Ordinary black powder is the most common composite propellant—the fuel being sulfur and carbon, and the oxidizer potassium nitrate. During the war a number of composite propellants were developed: for example, mixtures of ammonium picrate and sodium or potassium nitrate, held together with plastic binders, gave propellants of high power and excellent burning characteristics.

(*2*) *Colloidal or homogeneous propellants:* In propellants of this class the fuel and oxidizer form one phase and, indeed, the fuel and oxidizer are frequently present in each molecule. The chemical constituents of a colloidal propellant are (*1*) a high polymer capable of self-combustion, i.e., containing sufficient oxygen to oxidize the carbon and hydrogen to carbon monoxide or carbon dioxide and water, e.g., nitrocellulose; (*2*) an explosive plasticizer which is compatible with the high polymer and also rich in oxygen, e.g., nitroglycerin or similar nitrates; (*3*) other nonexplosive plasticizers to permit adjustment of the fuel–oxidizer ratio; (*4*) inorganic salts; (*5*) a stabilizer to absorb decomposition products and prevent autocatalytic increases in decomposition rates.

In the class of colloidal propellants, ordinary single-base smokeless powder, consisting of gelatinized nitrocellulose with nonexplosive plasticizers, salts, and stabilizers, has been the most common type in use in this country. However, the most versatile members in this class are the double-base powders, which have long been used in guns by other countries and which have proved to be very valuable as rocket propellants. Double-base powders contain nitrocellulose and nitroglycerin or other explosive plasticizers as the main constituents, with nonexplosive plasticizers, salts, and stabilizers as minor constituents. A typical double-base powder useful for rockets will contain approximately 50 per cent nitrocellulose, 30–40 per cent nitroglycerin, and 10–20 per cent other constituents. It forms a hard horny colloid which is quite tough. This symposium will be concerned mainly with propellants of this composition.

THE ORIGIN OF KINETIC PROBLEMS OF PROPELLANTS

It is of interest to note that all the investigations to be discussed today arose from extremely practical problems connected with the internal ballistics of guns and especially of rockets. The art of making and using solid propellants for guns has been promoted for many decades and reached a high state of perfection long ago. Although scientific principles and knowledge were applied to this art from time to time in a spasmodic manner, it must be recognized that it was the empirical ballisticians who developed in gun propellants those qualities of reliability, reproducibility, and effectiveness that gave the high standards of safety and accuracy now required from all types of guns.

When the development of rockets for military purposes was seriously considered, propellants of higher power (i.e., higher specific impulse) than black powder were required, and it was natural for the developers to turn to available gun propellants for their source of supply. Double-base powder of high nitroglycerin content was found to be most suitable. Its performance in rockets, however, raised a number of serious problems, and it soon became evident that a planned scientific attack on the physics and chemistry of rocket propellants must replace the empirical approach, if those problems were to be solved in a short enough time. Indeed, it was decided that quicker and surer progress would be possible if the planned program contained fundamental research studies designed to lead to an understanding of the physical chemistry of propellant reactions, as well as more short-range developmental studies. Subsequent events have shown that this course was a wise one.

These studies of propellants raised important research problems in all three of the recognized fields of physical chemistry. Studies of such important engineering qualities as the specific impulse, i.e., the thrust produced by unit mass rate of discharge of propellant gas, the temperature of the gases, the discharge coefficient, etc., led to important applications of *chemical thermodynamics* to propellant gas systems under extreme conditions of pressure and temperature. Questions arising in the fabrication of rocket propellants in different sizes and shapes and their ability to withstand the peculiar stresses set up under service conditions led to work in the field of the *structure and physical properties of solids*—particularly plastics. Both in guns and in rockets the exact control of the rate of evolution of hot gas is a problem of prime importance in determining the thrust and the equilibrium pressure, and this leads at once to a study of the *chemical kinetics* of the complex series of reactions commonly called the "burning of the propellant." Time and the occasion permit me to speak only of this third class of problem.

Elementary ideas concerning the burning of solid propellants

It has long been known that a solid propellant is satisfactory only if it obeys the *law of burning in parallel layers*; this is to say that the self-oxidation reaction, i.e., the "burning," takes place only on the exposed surfaces and that the rate at which the burning surface progresses normal to itself into the powder grain is the same at all points. This rate of progression is called the *linear burning rate* of the powder. If these conditions hold, it is possible to calculate the geometry of the powder grain and hence the area of the burning surface at any instant during the reaction. If r is the linear burning rate (inches per second) at any time, S is the area of the burning surface (in square inches), and ρ is the density in pounds per cubic inch, then $rS\rho$ is the rate of evolution of gas in pounds per second. It has also been known for a long time that the linear burning rate as defined above depends strongly on the pressure under which the burning takes place. For practical purposes equations such as

$$r = a + bP \tag{1}$$

or

$$r = cP^n \tag{2}$$

represent the data very well over a considerable range of pressures. In these equations a, b, and c are constants for a given temperature, r is the linear burning rate, P is the pressure, and n is a constant. Investigations during the war increased enormously the variety of propellants for which good burning-rate data are available and have established the validity and utility of these equations, especially equation 2, over a wide range of powder compositions. A typical example is given in figure 1.

Although there is considerable uncertainty about the superiority of either of the above equations over the other, or even about the most suitable form of pressure equation, it has been found that equation 2 is easier to handle in some ways and does not lead to misleading results.

Simple equilibrium equation

In order to illustrate the practical significance of kinetic problems in the design of rockets, we may consider the simple equation for the equilibrium pressure generated in a rocket when the burning-rate law (equation 2) is obeyed and where all other factors affecting the rate of burning are kept constant. This equation is

$$P_{\text{equil}} = \left[\frac{Sc(\rho - \rho_g)}{A_t C_D}\right]^{1/(1-n)} \tag{3}$$

where S is the area of the burning surface, c and n are the constants in equation 2, ρ is the density of the powder, ρ_g is the density of the powder gas, A_t is the area of the nozzle, and C_D is the discharge coefficient. This equation illustrates at least one kinetic problem—the value of a search for a low-pressure exponent.

If $n = 1$, a stable equilibrium pressure is impossible; if $n = 0$, the equilibrium pressure varies linearly with the various parameters inside the bracket. For powders available in the past, $n = 0.75$ approximately, which means that the equilibrium pressure depended on the fourth power of these parameters, a circumstance which led all too readily to uncontrollable pressures. An understanding of the effect of pressure on the linear burning rates and a knowledge of means of making it as small as possible were much to be desired.

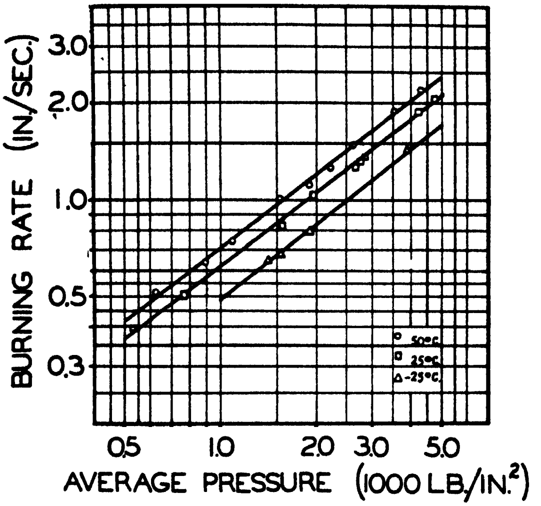

FIG. 1. Burning-rate data for powder composition 14400

Powder composition 14400

Nitrocellulose	59.92
including per cent nitrogen	13.22
Nitroglycerin	38.96
Ethyl centralite	0.94
Total volatiles	1.18
Diphenylamine	0.18
Heat of explosion	1257 cal/g.

Burning-rate data

TEMPERATURE	n	$\frac{c}{10^{-4}}$	BURNING RATE AT PRESSURES OF			
			1000 lb./in.²	2000 lb./in.²	3000 lb./in.²	4000 lb./in.²
°C.			in./sec.	in./sec.	in./sec.	in./sec.
50	0.76	3.70	0.71	1.20	1.64	2.04
25	0.76	3.31	0.62	1.04	1.42	1.76
−25	0.78	2.24	0.49	0.84	1.15	1.44

$\bar{n}$	0.77
c'	0.595
T_1	226

Effect of chemical composition

The linear rate of burning of powders also depends on their chemical composition, a dependence which seems to work through the adiabatic flame temperature of the propellant gas. In general, the hotter the powder, the faster its rate of burning under a given pressure. Studies of the effect of composition on the rates of burning have proved to be very fruitful in suggesting or verifying hypotheses used in theoretical descriptions of the process. Figure 2 shows the burning rates of a few powders as a function of their heat of explosion. The relationship depicted is valuable but should not be overrated. You will notice the general order of magnitude of the linear burning rates of powders in the nitrocellulose–nitroglycerin double-base family.

Effect of temperature

At constant pressure, the linear burning rate of a given powder increases with its initial temperature, a circumstance which can be compensated for by a slight correction in guns but which created a profoundly disturbing effect in rockets. The constant n in equation 2 is not much affected by temperature, so that the whole effect of temperature on the equilibrium pressure may be followed through its influence on the constant c. Relations such as

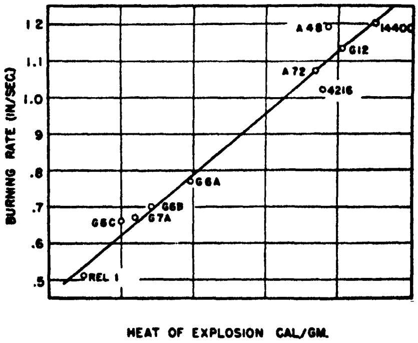

FIG. 2. Burning rates of various double-base powders at 25°C. and 2500 lb./in.² as functions of the heat of explosion.

$$v = \frac{c'}{T_i - T} \tag{4}$$

where c' and T_i are constants, have been used successfully to express this variation. If the exponent n is close to 1, it will be seen that variations in c with temperature can cause profound changes in the equilibrium pressure. The temperature coefficient of the linear burning rate is, therefore, a quantity which must be understood and controlled, if successful practical applications in rockets are to be made.

Effect of radiation

The radiation falling on a burning grain of powder from the enveloping hot gases also affects the linear rate of burning. The hotter the adiabatic flame temperature, the greater is this effect. The effect of radiation on the burning rate may be treated by the hypothesis that the radiation penetrates into the powder beyond the burning surface and upon absorption raises the temperature of the solid with consequent increase in its burning rate. By the addition of suitable absorbing material into the propellant, the penetration of the radiation can be controlled and even used to advantage.

Effect of gas velocity

Under comparable conditions of pressure and temperature the burning rate of a powder of given composition increases as the velocity of the propellant gas parallel to the burning surface increases. The contribution of this effect to the overall burning is called "*erosive burning*" and becomes especially significant in rockets, where the channel available for the movement of the hot gases is narrower and where the gases flow over a considerable length of burning surface. Especially the effect of erosive burning may be described by an equation of the form

$$r = cP^n(1 + kv) \tag{5}$$

where the symbols are the same as in equation 2 with the addition of k (a constant) and v (the velocity of the gas over the powder).

Summary of factors influencing gas evolution

It will be seen from the foregoing that control of the rate of generation of hot gases by a solid propellant is definitely a complicated problem. Basically the principal factors involved are ρSr, the product of the density, the burning surface, and the linear burning rate. The burning surface S is controlled by the geometry of *each single grain* of the propellant charge and must be known at every instant of the reaction. The linear burning rate depends on the following factors and is under control only when all these factors are under control: (*1*) chemical composition; (*2*) chamber pressure; (*3*) initial powder temperature; (*4*) radiation from environment; and (*5*) tangential velocity of propellant gases. It is only recently that the significance of these last three variables has been recognized and investigated. Generally speaking, the empirical understanding of these factors has advanced to a point where an equation similar to equation 3 but taking all effects into account, can be set up to give quite accurately the equilibrium pressure in a rocket from a knowledge of properties of the propellant. On the basis of this work, it has been possible to design successful rockets in which gas is generated at rates of the order of 500 lb./sec.—a very brisk reaction.

Theoretical and experimental studies of the physical-chemical mechanism of the burning of propellants are the ultimate source of a basic understanding of this complex process. As the symposium proceeds, we shall see what progress has been made in this direction. I should like to emphasize this work as a field which presents challenging and interesting problems to the serious student of kinetics. The problems are difficult and the phenomena too susceptible to practical test to permit oversimplification masquerading as basic knowledge. However, the applications of the result are far-reaching, and the interest and discipline of the investigation cannot fail to inspire the enthusiastic physical chemist.

THE MECHANISM OF THE BURNING OF DOUBLE-BASE PROPELLANTS[1, 2]

BRYCE L. CRAWFORD, Jr., CLAYTON HUGGETT,[3, 4] and J. J. McBRADY[5]

School of Chemistry, Institute of Technology, University of Minnesota,
Minneapolis 14, Minnesota

Received January 9, 1950

The application of double-base propellants to jet propulsion devices during and since the recent war focused attention on the burning behavior of these materials at low and medium pressures, up to 5000 lb./in.^{2} The burning behavior in this pressure range cannot be described by simple extrapolation from the higher pressures previously studied in guns. As a consequence, the burning mechanism has been the subject of a number of recent investigations with their goal the improvement of propellant characteristics for low-pressure applications. Since these researches have resulted in a considerable increase in our knowledge of the burning process, it seems worth while to present in broad outline our picture of the complex sequence of reactions which constitutes the mechanism of burning. The supporting experiments will be described only briefly.

We shall confine our attention to double-base propellants, i.e., nitrocellulose plasticized with nitroglycerin, together with various minor constituents. Much of our experimental work was done with a powder having the following simple composition:

	per cent
Nitrocellulose (13.25 per cent nitrogen)	54
Nitroglycerin	43
Ethyl centralite	3

The centralite, *s*-diethyldiphenylurea, is present as a stabilizer. Frequently, other constituents were added to this basic composition in order to study their effect on the burning process.

Such propellants burn "by parallel layers," that is, the burning surface tends to maintain its original geometrical form during burning. Thus, for ballistic purposes, the mass burning rate and the burning time may be controlled within

---

[1] This paper is based on work done for the Office of Scientific Research and Development under Contract OEMsr-716 with the University of Minnesota and to some extent on work done for the United States Navy Department under Contract NOrd-9680.

[2] Presented at the Symposium on Kinetics of Propellants which was held under the auspices of the Division of Physical and Inorganic Chemistry at the 112th Meeting of the American Chemical Society, New York City, September 15, 1947.

[3] This paper is based in part on a thesis submitted by Clayton Huggett to the Graduate Faculty of the University of Minnesota in partial fulfillment of the requirements for the degree of Doctor of Philosophy, February, 1945.

[4] Present address: Rohm and Haas Company, 5000 Richmond Street, Philadelphia, Pennsylvania.

[5] Present address: Central Research Laboratory, Celanese Corporation of America, Summit, New Jersey.

limits by the geometry of the propellant grain, independent of the linear burning rate of the particular propellant used. Thus, also, a long cylindrical powder strand, ignited at one end, can be made to burn with a flat burning surface if the sides of the strand are suitably coated to prevent spreading of the flame. We may, neglecting edge effects, consider the burning of such a grain as a one-dimensional process, starting within the solid propellant and proceeding through the burning surface and reacting flame to the final gaseous products. Such end-burning strands, usually in a pressure vessel charged with nitrogen, were used in most of our experiments and permitted a number of significant observations.

REACTIONS IN THE SOLID PHASE

The thermal decompositions of nitrocellulose, nitroglycerin, and a variety of other nitrate esters have been studied by a number of investigators (1, 6, 8). In each case the experimental evidence indicates that the initial step in the decomposition is the unimolecular breaking of the nitrogen–oxygen bond to give nitrogen dioxide and a free radical. The activation energy of this process is found to be about 40 kcal./mole. The products of this initial step react further to give the complex mixture of products usually observed in such decomposition experiments.

Reactions of this type undoubtedly take place in the heated powder layers close to the burning surface. The presence of stabilizers, aromatic compounds which are ready acceptors for nitrogen dioxide and which may react directly with nitrate esters, contributes to these solid-phase reactions.

If a grain of powder is heated at a temperature too low to produce instantaneous ignition, the temperature within the interior of the grain, measured by a thermocouple embedded in the grain, will rise above that of the surroundings. At sufficiently high heating temperatures, this self-heating will cause the grain to ignite. The "ignition temperatures" determined in this manner are in the neighborhood of 200°C. While the significance of this figure is debatable, it must certainly set a lower limit to the temperature of the burning surface. It is in good agreement with the ignition temperature observed for pure nitroglycerin (9).

This self-heating effect is greater in powders containing large amounts of stabilizers. Such powders will burn smoothly in an inert atmosphere at atmospheric pressure and 35°C., whereas powders containing only nitrocellulose and nitroglycerin will not burn at pressures below 200 lb./in.^{2} at 35°C. These exothermic reactions, taking place within the solid phase beneath the burning surface, must contribute a significant part of the energy necessary to decompose the surface layers of the propellant and transport it to the flame reaction zone.

THE POWDER FLAME

When a powder strand is ignited in air by an open flame, the strand burns with a large luminous flame and the burning surface assumes a conical form as the reaction moves down the sides of the strand (figure 1). If the strand is ignited in an inert atmosphere, or even in air by gentle ignition, such as a glowing wire, it burns quietly with a nonluminous flame (figure 2). The burning surface is flat and normal to the axis of the strand. The products of this nonluminous reaction, when mixed with air and ignited, burn with a luminous flame whose spectrum is similar to that of the luminous powder flame.

The nonluminous burning has a heat of reaction of about 500 cal./g., while the luminous combustion in air evolves about 3000 cal./g. In spite of this difference, the burning rate of the powder, when proper allowance is made for the increased burning surface associated with the luminous burning, is approximately the same in the two cases. At this low pressure the burning rate must be controlled by reactions associated with the nonluminous stage, taking place close to and within the burning surface. Little of the energy from the more vigorous luminous reaction returns to the burning surface to affect the rate-controlling process.

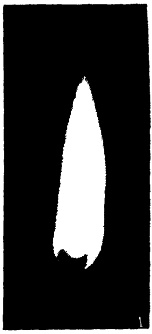

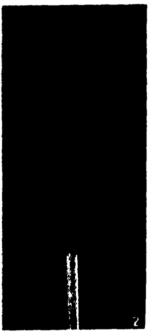

Fig 1. A strand of double-base powder (ignited by a match) burning in air
Fig. 2. The same powder as in figure 1 (ignited by a hot wire) burning in air

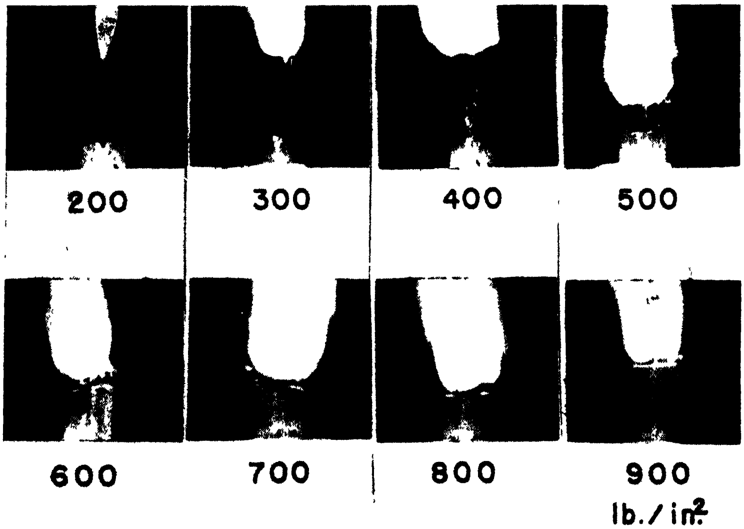

Fig. 3. Strands of double-base powder burning in nitrogen at various pressures

As the pressure of inert gas surrounding the burning strand is increased to 200 or 300 lb./in.^{2}, a luminous region appears in the flame at some distance from the burning surface. Further increases in pressure cause the luminous flame to approach the surface more closely, until at 1000 lb./in.^{2} it is difficult to detect the dark zone between the powder surface and the luminous flame (figure 3). The length of the dark zone was determined at various pressures from motion picture films of the burning strands. The pressure dependence can be represented quite accurately by the expression:

$$s = c/P^3 \tag{1}$$

in which s is the length of the dark zone, c is a constant whose value depends somewhat on the powder composition, and P is the pressure of inert gas. At 1000 lb./in.^{2} the luminous flame is about 0.25 mm. from the burning surface. The interpretation of this pressure dependence is complicated by the uncertain effect of diffusion of the inert gas into the reaction zone under the conditions of our experiments. However, the occurrence of the dark and the luminous reaction zones indicates that the gas-phase reactions take place in at least two well-defined stages. The rate of the second, at least, shows a strong dependence on pressure.

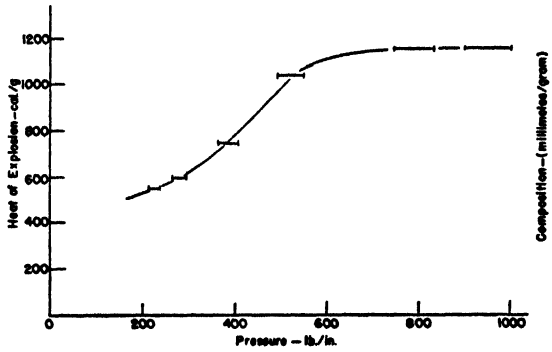

FIG. 4

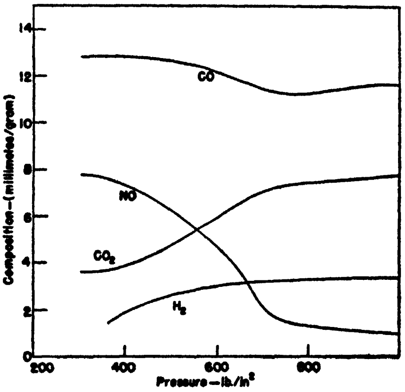

FIG. 5

FIG. 4. Variation of the heat of explosion with pressure
FIG. 5. Variation of the gaseous products of explosion with pressure

THE HEAT OF EXPLOSION

Further evidence for the stepwise nature of the flame reaction is found in the variation of the heat of explosion with pressure. Fennimore and Kuhn (3) have shown that nitrocellulose does not develop its full heat of explosion at low loading densities. Double-base powders behave similarly. Our experiments were carried out by pressurizing the calorimeter with nitrogen and keeping the density of loading constant and low enough so that burning took place at nearly constant pressure. The result of a typical series of measurements is shown in figure 4.

The heat of reaction remains nearly constant at about one-half of its maximum value from below atmospheric pressure to the point at which the luminous flame appears, 300–400 lb./in.^{2} At this point it increases sharply and approaches the maximum value observed at high pressures. About one-half of the total energy of the propellant must come from reactions taking place in the luminous flame zone.

THE PRODUCTS OF REACTION

As is to be expected, the products of reaction show a corresponding change with pressure. Figure 5 shows the results of a series of analyses of the gaseous reaction products at various pressures. As in the calorimetric experiments, the sample in the form of an end-burning strand was burned in nitrogen at a low loading density. At low pressures an oily residue remains in the combustion chamber. Similar residues have been analyzed by others and found to consist largely of glyoxal and other low-molecular-weight oxygenated organic compounds (10). At higher pressures this residue disappears along with the nitric oxide. The amounts of carbon monoxide and carbon dioxide increase with the appearance of the luminous flame, and more hydrogen is formed by the water-gas reaction. In one experiment at 1000 lb./in.^{2} the concentrations of hydrogen, water, carbon monoxide, and carbon dioxide were found to correspond to the water-gas equilibrium value at 1750°K. This presumably represents the temperature at which equilibrium is frozen on cooling, since the calculated flame temperature is much higher, in the neighborhood of 3000°K. At high pressures and high loading densities, the products are known to be in approximate thermodynamic equilibrium.

THE BURNING RATE

Measurements of burning rate were made on long end-burning strands at constant pressure. Burning times were observed visually at low pressures and recorded electrically at higher pressures. Details of the experimental method have been reported elsewhere (2).

The burning rate is determined by three fundamental variables: pressure, temperature, and powder composition. Secondary effects, such as those due to radiation and to erosive burning, depend on the geometry of the propellant grain and the combustion chamber and were not important in our experiments.

It is customary, for the purpose of ballistic calculation, to express the dependence of the burning rate on the pressure at constant temperature by one of the two equations:

$$r = a + bP \tag{2}$$

$$r = cP^n \tag{3}$$

where a, b, c, and n are constants characteristic of the powder composition. The two forms reproduce the available high-pressure data about equally well. Our own more precise measurements at pressures up to 6500 lb./in.^{2} show that the burning rates of conventional double-base compositions can be represented very accurately down almost to atmospheric pressure by the expression:

$$r = a + bP^n \tag{4}$$

where *n* is approximately unity. Figure 6 is a logarithmic plot of the burning rate over the entire pressure range covered in these experiments. Figure 7 shows how well equation 4 fits the experimental data. It is significant that the burning rate

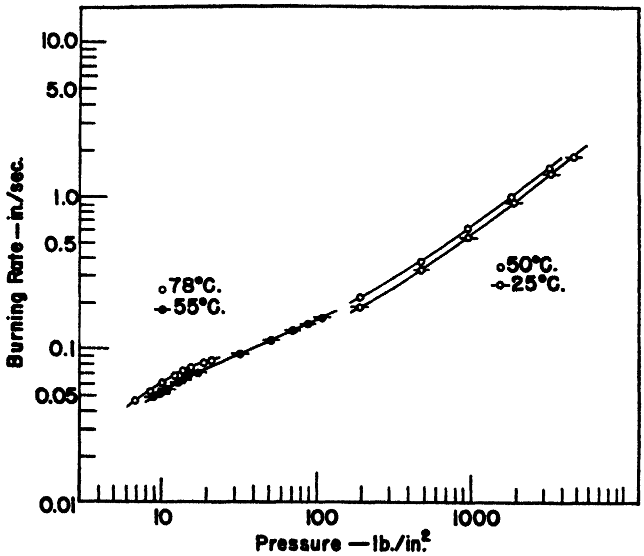

FIG. 6. The burning rate of a double-base powder as a function of pressure: log *r* *vs.* log *p*.

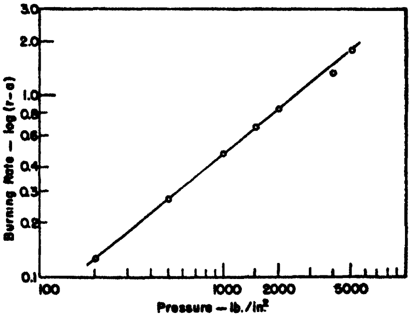

FIG. 7

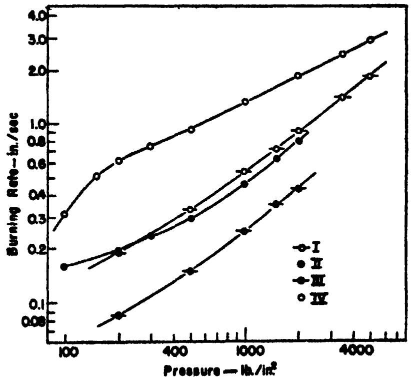

FIG. 8

FIG. 7. The burning rate of a double-base powder as a function of pressure: log $(r - a)$ *vs.* log *p*.

FIG. 8. The burning rate of various powders as a function of pressure

increases smoothly through the pressure region where the heat of reaction, the products of reaction, and the character of the flame are undergoing a rather abrupt change (compare figures 3, 4, and 5 with figures 6 and 7). The final stages of the reaction which are responsible for these changes have little effect on the burning rate in this low-pressure region.

The burning rate at low pressures becomes nearly independent of pressure, in accord with equation 4. However, the burning rate falls off suddenly at about atmospheric pressure, and the strands fail to burn at much lower pressures, even at elevated temperatures. We cannot suggest a reason for this abrupt change at this time, since we were unable to observe any discontinuity in the other properties of the reaction in this pressure region.

We are tempted to associate the pressure-independent term in the burning rate equation with the energy liberated by the reactions taking place within the solid powder surface. The pressure-dependent term can be associated in similar fashion with the pressure-dependent transfer of energy from the hot flame zone to the burning surface. Such a picture undoubtedly represents a considerable oversimplification of the process.

It has been pointed out that at high pressures an approximate linear relationship holds between the heat of explosion and the linear burning rate at constant temperature and pressure (4). A correlation of burning rate and flame temperature, which roughly parallels the heat of explosion, should be more sound, since at high pressures the burning rate is largely controlled by energy transfer to the burning surface from the flame. However, at lower pressures, as we have shown, powders may develop only a fraction of their heat of explosion, or the flame temperature may reach its ultimate value only at a considerable distance from the burning surface. Under these conditions, reactions taking place beneath the burning surface or in the gas layers close to the surface may contribute a major portion of the energy necessary to support the reaction. Consequently, it is not surprising that we have found powders with similar total heats of explosion but widely different compositions to have burning rates differing by more than a factor of 2 at 1000 lb./in.^{2} The heat of explosion and flame temperature may be useful guides in predicting the effect of small variations in composition on the burning rate, but their usefulness is questionable when considering major changes in composition or low-pressure burning.

THE BURNING PROCESS

The experimental results described in the preceding section provide us with a qualitative picture of the burning process. This model has been the subject of theoretical investigations by others (5, 7).

The heated surface layers of the propellant grain decompose into volatile fragments and pass into the gaseous flame region. The energy necessary to bring about this initial decomposition is supplied in part by exothermic reactions taking place within the surface layers and in part by energy transferred to the surface from the hotter flame zone. The burning surface probably reaches a temperature in the neighborhood of 300°C. before decomposition is complete. The rate of volatilization of the surface layers, the burning rate, is controlled by the rate at which energy is supplied to the reacting powder layers from all sources.

These primary fragments react further in the gas phase very close to the powder surface. The products are nitric oxide and simple organic molecules, such as glyoxal, together with some of the stable end products: nitrogen, water, carbon monoxide, and carbon dioxide. Approximately half of the total heat of reaction is liberated up to this point and the temperature of the reaction zone rises to perhaps 1500°K.

In the final stages of the reaction, nitric oxide reacts with the remaining oxidizable material and the products approach thermodynamic equilibrium. The flame temperature reaches its maximum value, perhaps 3000°K., and the reaction zone is brightly luminous. This high-temperature region is too far from the burning surface at low pressures to supply much of the energy from the primary decomposition; radiation is of minor importance compared to conduction in the powder flame. However, at high pressures the high-temperature luminous flame zone approaches close enough to the burning surface to become a controlling factor in determining the burning rate.

It should be pointed out that while most of our experiments were carried out with pressure as the variable, time or distance in the reaction zone is probably the more fundamental quantity. Under the conditions of our experiments, using slender end-burning strands in an atmosphere of nitrogen, reactions undoubtedly failed to go to completion, because they were quenched by the diffusion of cool inert gas into the reaction zone before sufficient time had elapsed for reaction. A grain of powder burning under the pressure of its decomposition products instead of under pressure of nitrogen might give different results, although data on the burning rate show no significant difference. At the same time, our experimental technique allowed us to isolate the intermediate reaction steps which otherwise would be difficult to observe. There can be little doubt that the sequence of reactions described here actually takes place, perhaps with a slightly modified scale of distances, when a propellant grain functions at high pressures.

The function of an increase in pressure is to compress the reaction zone into a smaller distance about the burning surface. This takes place through an acceleration of chemical processes and also through the compression of the gaseous products. The detailed structure of the reaction zone and the form of the temperature gradient through it will depend on the composition of the propellant. Through a consideration of this dependence of the structure of the reaction zone on composition, we are able to predict, in a qualitative way, the effect of specific compositional changes on the burning rate and the pressure dependence of the burning rate.

Compositional changes which favor the exothermic solid-phase reactions should increase the burning rate at low pressures and thus decrease the effect of pressure on the burning rate in this region. Stabilizers, such as centralite and diphenylamine, are effective; *p*-phenylenediamine has been found to be even more reactive. In figure 8 the burning rate of the standard composition (curve I) is compared to that of a sample to which 5 per cent of *p*-phenylenediamine has been added (curve II). Although this addition decreases the heat of explosion, the burning rate at low pressures is increased, and the pressure dependence of the burning rate is significantly lower. At high pressures the burning rate of the *p*-phenylenediamine powder is lower than that of the standard because of the lower heat of explosion, but the pressure dependence, which is controlled primarily by the flame reaction, is normal.

Cooling the burning surface by the addition of some substance which decomposes with the absorption of energy should have the opposite effect, reducing the burning rate at low pressures and increasing the pressure dependence. Curve III of figure 8 shows the effect on the burning rate of adding 5 per cent of paraformaldehyde to the standard composition. The paraformaldehyde presumably dissociates to formaldehyde and then to hydrogen and carbon monoxide close to the burning surface, absorbing some 400 cal./g. in the process. This powder fails to burn at low pressures, but since the final flame temperature is less affected than the surface temperature, the burning rate increases rapidly as the hot flame zone is forced closer to the burning surface by increased pressure.

The addition of a strong oxidizing agent, such as potassium perchlorate, causes the final step in the reaction to take place closer to the burning surface. As a result, the burning rate increases rapidly in the low-pressure region and attains a relatively high value. Thereafter it increases only slowly, since increased pressure can have little further effect on the structure of the reaction zone. Curve IV of figure 8 shows the burning rate of a sample containing 40 per cent of a mixture containing 85.2 per cent perchlorate and 14.8 per cent carbon black.

It appears that at high pressures the burning rates of the various powders shown in figure 8 draw together, when due allowance is made for small differences in the heats of explosion. The flame temperature is undoubtedly the most important factor in determining the burning rate at high pressures.

SUMMARY

The results of experiments dealing with various aspects of the burning of double-base powders at pressures between 10 and 6500 lb./in.^{2} are described.

Based on these experimental results, a qualitative picture of the burning process is presented.

This mechanism is shown to account for the observed effects of various compositional changes on the burning rate and the pressure dependence of the burning rate.

REFERENCES

(1) Appin, A., Todes, O., amd Khariton, Yu. B.: J. Phys. Chem. (U.S.S.R.) **8**, 866 (1936).
(2) Crawford, B. L., Jr., Huggett, C., Daniels, F., and Wilfong, R. E.: Anal. Chem. **19**, 630 (1947).
(3) Fennimore, C., and Kuhn, L.: Unpublished work.
(4) Gibson, R. E.: Unpublished work.
(5) Parr, R. G., and Crawford, B. L., Jr.: J. Phys. & Colloid Chem. **54**, 929 (1950).
(6) Phillips, H.: Nature **160**, 753 (1947).
(7) Rice, O. K., and Ginell, R.: J. Phys. & Colloid Chem. **54**, 885 (1950).
(8) Roginsky, S.: Physik. Z. Sowjetunion **1**, 640 (1932).
(9) Snelling, W. O., and Storm, C. G.: U. S. Bur. Mines Techn. Paper No. **12** (1912).
(10) Wolfrom, M. L., and collaborators: Unpublished work.

AN HYPOTHESIS FOR PROPELLANT BURNING[1]

ROBERT E. WILFONG,[2] STANFORD S. PENNER,[2] AND FARRINGTON DANIELS

Department of Chemistry, University of Wisconsin, Madison, Wisconsin

Received January 9, 1950

When nitrocellulose "burns" the surface undergoes violent decomposition and evolves large quantities of hot gases which can be used for propulsion purposes. As the surface molecules are decomposed and ejected, fresh layers of molecules are exposed successively deeper and deeper in the propellant. The rate of regression, or "peeling-off" of one molecular layer after another, has been measured directly and found to be of the order of 2 cm./sec. at a pressure of 1500 lb./in.^{2} A small bomb was developed (2) for the rapid determination of the linear burning rate of experimental propellants under pressure, making use of fuse wires and timing circuits. The linear rate of burning depends greatly on the pressure of the gases surrounding the propellant and to a small extent on the initial temperature of the propellant.

The purpose of this investigation was to try to explain the mechanism and predict the behavior of propellant burning in the simplest possible way from general concepts of chemical kinetics. Most of the experiments were carried out with double-base powder containing 54 per cent nitrocellulose (13.25 per cent nitrogen), 43 per cent nitroglycerin, and 3 per cent *s*-diethyldiphenylurea. The laboratory facts and many field observations are in accord with the following simple but obviously incomplete hypothesis.

The rate-determining step in the burning of the propellant is the decomposition of the molecules at the surface. It is an unimolecular reaction which involves merely the endothermic breaking of the oxygen–nitrogen bond in the nitrate group of nitrocellulose or nitroglycerin. The fragments of NO_2 and organic radicals, similar to (CHO), are thrown out from the surface and then react in the gas phase. The heat from this exothermic gas reaction is transferred to the propellant by diffusion, convection, and radiation, raising the temperature of the surface molecules to a temperature in the neighborhood of 1000°C.

Nitrocellulose and nitroglycerin contain the following structural unit:

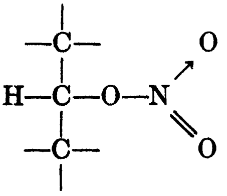

---

[1] This paper is based on work carried out at the University of Wisconsin under Contract OEMsr-762 with the Office of Scientific Research and Development and described in part in OSRD Reports 6559 and 3206. A portion of this material was presented at the Symposium on Kinetics of Propellants which was held under the auspices of the Division of Physical and Inorganic Chemistry at the 112th Meeting of the American Chemical Society, New York City, September 15, 1947.

[2] Present address: E. I. du Pont de Nemours and Company, Waynesboro, Virginia.

Of the various bonds in this unit the weakest is the O—N bond. Less energy is required to break the O—N bond than the other bonds, C—H, C—C, C—O, and N═O, and the rate of breaking these O—N bonds, which are at the surface, can be estimated at a given temperature with the simple formulas of chemical kinetics and making use of independent constants.

The effect of pressure on the rate of burning of a propellant is very large and cannot be calculated *a priori* on the hypothesis proposed here. The simple assumption is made that the heat transferred back to the freshly exposed surface is constant at constant pressure, thus giving conditions for a unimolecular stage of the reaction at an elevated but constant temperature. A steady state is reached in which the heat transferred from the exothermic gas reaction is equal to the endothermic heat of the bond breaking. Qualitatively it can be seen that if the exothermic reaction between the fragments in the gaseous envelope surrounding the propellant is bimolecular in nature, it will increase in rate with an increase in pressure. Moreover, the envelope of burning gases will be driven closer to the surface of the propellant. An increase in the rate of the gaseous reaction increases the rate at which heat is evolved and transferred back to the surface. A higher pressure then gives a higher temperature, which in turn gives a faster reaction at the surface and the faster reaction gives a greater rise in pressure in a closed space and so on,—leading to an explosion.

However, this explosion is not a detonation in which all molecules decompose instantly throughout the mass; the decomposition is still confined to the surface molecules. With the help of empirically determined constants determined from measurements of the burning rate of the propellant, O. K. Rice (5) has developed a broader theory which gives the effect of pressure on the burning rate. Boys and Corner (1) have developed a theory emphasizing the importance of the exothermic gas reaction as the rate-determining step in the steady state, whereas the hypothesis offered here emphasizes the importance of the endothermic unimolecular surface reaction as the rate-determining step. Both are different views of the same phenomenon. The Rice theory is broad enough to include both views, and it can give ouantitative calculations making use of constants which are determined empirically from experiments on the burning rates.

Experimental measurements and general observations will now be cited in support of the simplified hypothesis proposed here.

THE UNIMOLECULAR SURFACE REACTION

The rate-determining step is the isothermal unimolecular rupture of the oxygen-nitrogen bonds at the surface. The general equation for a unimolecular reaction is

$$k = \frac{RT}{Nh} e^{\Delta S_{\text{act}}/R} e^{-\Delta H_{\text{act}}/RT} \tag{1}$$

where k is the specific reaction rate, R, T, N, and h are the gas constant, absolute temperature, Avogadro's number, and Planck's constant, respectively, and ΔS_{act}

---

[3] Present address: Jet Propulsion Laboratory, California Institute of Technology, Pasadena, California.

and ΔH_{act} are the entropy and heat of activation. ΔS_{act} may be regarded as essentially zero for the breaking of a bond, and at 1000°C. the formula[4] becomes:

$$k = 3 \times 10^{13} e^{-\Delta H_{act}/RT} \tag{2}$$

A lower limit for the activation energy is the energy required to break the weakest bond in the molecule, i.e., the heat of dissociation of the O—N bond. This bond strength has been given various values but is probably not far from 45,000 cal./mole. Inasmuch as the fragments of the rupture involve free radicals which require very small activation energy for recombination, the activation energy for rupture is probably not much greater than the heat of reaction as given by the bond strength. Experiments with nitrocellulose at elevated temperatures gave 46,700 cal./mole, as described in a later section. With this value for the activation energy, equation 2 gives at 1000°C.

$$k = 5.5 \times 10^{5} \tag{3}$$

where k is expressed in reciprocal seconds.

The significance of k and the frequency factor can be interpreted in terms of the mechanical picture of the surface reaction. The specific rate constant k is defined by the equation

$$-\frac{dn}{dt} = kn \tag{4}$$

where n is the number of potentially reactable molecules, i.e., the number of O—N bonds at the surface of the propellant, and dn/dt is the rate in seconds of the number being broken.

A minimum value of the number of O—N bonds at the surface can be calculated from the density and the chemical composition. A cube of the propellant, 1 cm. on an edge, weighs 1.63 g. It contains 54 per cent by weight of nitrocellulose (13.25 per cent of which is nitrogen) and 43 per cent of nitroglycerin (18.5 per cent of which is nitrogen). There is then 0.246 g. of nitrogen or 1.07×10^{22} atoms of nitrogen per milliliter. Each atom of nitrogen provides one oxygen-nitrogen bond, giving 1.07×10^{22} bonds per milliliter. When the 1 cm. cube of propellant burns, the linear rate of regression involves burning inward from one surface which contains $(1.07 \times 10^{22})^{2/3}$ or 4.8×10^{14} oxygen-nitrogen bonds per square centimeter, provided the surface is perfectly smooth. Rough surfaces and cracks will, of course, increase this surface. A minimum rate of burning in seconds at a constant surface temperature of 1000°C. then is given by equations 3 and 4:

$$-\frac{dn}{dt} = kn = (5.5 \times 10^{5}) \times 4.8 \times 10^{14} = 2.6 \times 10^{20}\ \text{sec.}^{-1} \tag{5}$$

where n is the number of O—N bonds per square centimeter. The value of n remains constant, because when a surface molecule is decomposed with expulsion of its fragments another molecule just below it is exposed. Accordingly the rate remains constant as long as the steady state is maintained, with a constant gas pressure and constant surface temperature. The reaction is then apparently of zero order, since the concentration of reactants remains constant.

---

[4] This formula and its application have been discussed in general terms by Daniels (3).

This rate of breaking O—N bonds along a propellant 1 cm.^{2} in cross section can be translated into a linear burning rate by dividing by the number of bonds per centimeter of length, 1.07×10^{22}. Thus equation 5, expressed in number of bonds broken per second, becomes equation 6 when expressed in centimeters per second.

$$-\frac{dn}{dt} = \frac{2.6 \times 10^{20}}{1.07 \times 10^{22}} = 2.4 \times 10^{-2} \text{ cm. sec.}^{-1} \qquad (6)$$

if the surface is assumed to be molecularly flat. The experimentally determined rate of burning is much faster than this—about 2 cm. per second at a pressure of 1500 lb./in.^{2} The effective surface area is certainly much greater than the ideal, molecularly flat surface calculated by taking the two-thirds power of the volume. Boiling or bubbling of a liquid at the surface could well increase the number of molecules in the surface by a factor of 100 and bring the burning rate up to the experimentally observed value; and there is evidence also for cracks in the surface which expose an additional number of O—N bonds. In fact, the "effective" surface may even extend out a short distance from the geometrical surface as particles of the propellant are shot forth into the gas space.

The burning surface was suddenly quenched by blowing out a rupture disc in the bomb, and the propellant surface and suitable controls were then allowed to stand in dye solution, the solution was evacuated, and the vacuum was broken. The dyes methyl violet, gentian violet, and basic fuchsin were found to be suitable for diffusion into minute cracks in colloidal nitrocellulose or double-base powder. They penetrated as a dense layer 0.0125–0.017 cm. thick in the surface which had been burnt, as revealed by microscopic examination of their sections. The penetration of the surface caused by the arrested burning is due to cracks, and if these cracks were present at the time of burning, it can be estimated that they could expose 2×10^4 O—N bonds along the cracks per square centimeter (8). It is possible, of course, that the cracks may have been produced by the rapid cooling of the surface as well as by the quick heating. If part of these surfaces of cracks is added to the flat surface the calculated burning rate can be made to increase over 100-fold and to check with the observed burning rate.

ACTIVATION ENERGY OF NITROCELLULOSE[5]

The activation energy was calculated from measurements on the rate of decomposition of nitrocellulose at different temperatures in the neighborhood of 160°C., using the apparatus shown in figure 1.

About 2.0 g. of nitrocellulose containing 13.4 per cent nitrogen was deposited from acetone solution onto glass pearls in a glass vessel. The small spheres gave rapid heat exchange with a flowing stream of nitrogen and assured isothermal conditions even during the exothermic reaction. The uniform film of nitrocellulose, after drying, was of the order of 1000 molecules in thickness. The glass inlet coil and the reaction chamber were immersed in the thermostat, and purified nitrogen from a tank was passed through, but measurements of the decomposition were not made until the two thermometers gave the same reading. The exit nitrogen, which contained the products of the decomposition of nitrocellulose, was passed through a pair of absorption towers containing sodium hydroxide. Several outlets permitted collection of successive samples.

---

[5] More details are given in part of a Ph. D. thesis presented by S. S. Penner at the University of Wisconsin in 1946.

An excess of acidified 0.02 *N* potassium permanganate was then added in known quantity and allowed to stand for 15 min., after which an excess of potassium iodide was added and the solution was tirated with sodium thiosulfate.

The volume of potassium permanganate used up (i.e., the difference in volume of thiosulfate solution for successive samples) is a measure of the amount of nitrogen dioxide and organic reducing material liberated, which in turn is a measure of the amount of nitrocellulose decomposed. The reaction is apparently of zero order, because there is a very large number of potentially decomposable molecules at the surface and because when a molecule at the surface decomposes ts place is taken by another one just under it.

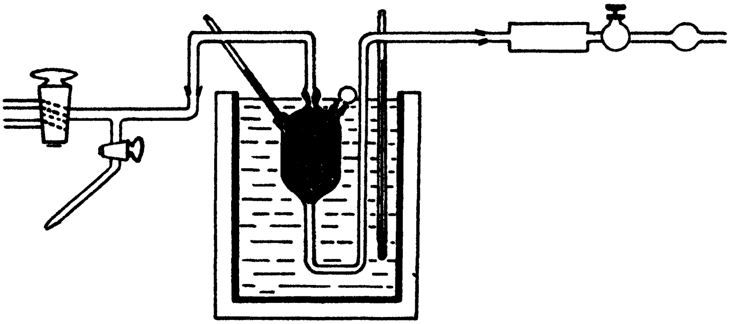

FIG. 1. Apparatus for measuring the rate of decomposition of nitrocellulose

For the calculation of the activation energy the number of milliliters of sodium thiosulfate required per unit of time in the titration may be used as a measure of the decomposition rate, d*c*/d*t*, at a given temperature. Sample data are given in table 1. Ninety milliliters of 0.2 *N* sodium hydroxide was used for absorption and 15 ml. of 1:5 sulfuric acid and 10 ml. of potassium permanganate (equivalent to 13.95 ml. of sodium thiosulfate) were added.

These data are plotted in a log d*c*/d*t* *vs.* $1/T$ graph in figure 2, where it is seen that a straight line is obtained with a slope which multiplied by $-2.303\ R$ gives an activation energy of 47,400 cal./mole. It is gratifying to note that the last measurement (No. 5) was obtained after the nitrocellulose had been heated to higher temperatures and brought back to lower temperature. The fact that this point falls on the line shows that the reacting system is reproducible and that it has not changed with time and temperature.

The upper dotted line gives a qualitative insight into some of the complications involved in the gaseous products which are evolved. Air was used instead of nitrogen in these experiments, and the larger amounts of potassium permanganate reduced at the higher temperatures can probably be explained on the assumption that the oxygen oxidized some of the organic material at the higher temperatures and thus prevented the reduction of some nitrogen dioxide. The larger amount of nitrogen dioxide remaining in the gases leads to a larger difference in the titration with sodium thiosulfate.

Three sets of determinations were made, giving 46,000, 46,700, and 47,400 cal./mole for the energy of activation. The average value is 46,700.

In attempting to study the primary step in the decomposition of nitrocellulose or double-base powder at an elevated temperature it is essential to sweep out the products of decomposition as fast as they are formed. When such propellants stand for long periods of time at room temperature, enough nitrogen dioxide accumulates to give definite color and odor. In fact, a test for nitrogen dioxide with special paper is a standard test for the instability of an old propellant, and stabilizers such as diphenylamine are introduced which combine directly with nitrogen dioxide. At elevated temperatures however, the nitrogen dioxide undergoes chemical reaction with the residual organic matter. This reaction leads to the production of nitric oxide and nitrogen and a variety of partially oxidized

TABLE 1

Rate of decomposition of nitrocellulose

	(1)	(2)	(3)	(4)	(5)
Temperature in °C.	130.5	140.0	149.5	155.0	146.5
Time of decomposition in hours..	1.00	0.50	0.50	0.50	0.50
Back-titration, $Na_2S_2O_3$ in milliliters	13.55	12.95	10.85	7.40	11.75
dc/dt in terms of milliliters of $Na_2S_2O_3$ per hour	0.40*	2.00	6.20	13.10	4.40

* 13.95 − 13.55 = 0.40 ml. of sodium thiosulfate consumed for the decomposition during 1 hr.

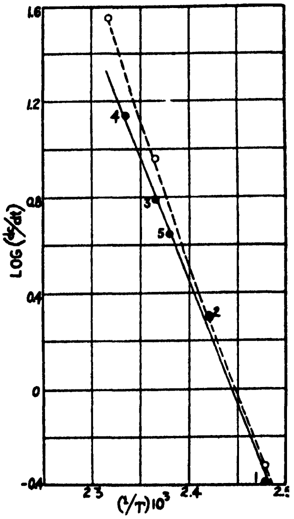

FIG. 2. Determination of the activation energy for the decomposition of nitrocellulose

organic materials which have been the object of considerable study in several laboratories. At the higher temperatures which prevail in normal propellant burning at high pressures the nitric oxide and the organic material react further to give chiefly nitrogen, water, and carbon dioxide (and carbon monoxide if there is insufficient oxygen). Only under these conditions is the full heat of the propellant burning realized and only then can the high surface temperature be maintained. When the reduction of the nitrogen dioxide to nitrogen is not complete the burning will be abnormally slow, as in "fizz burning" at low pressures in the laboratory or in intermittent "chuffing" in field tests.

Although nitrogen dioxide is readily observed in the slow decomposition of nitrocellulose at room temperature and at 160°C., attempts to find it in the products of high-temperature "burning" were unsuccessful. At the higher temperature it probably decomposes or reacts with the organic material before it can be isolated by quick chilling. It is unimportant from a *practical* standpoint whether nitrogen dioxide is formed in the first step and later reduced to nitric oxide and nitrogen in the gaseous reactions which follow the initial unimolecular decomposition, but since the O—N bond is the weakest bond it seems likely that the primary step, at high temperatures as well as at low temperatures, is the breaking of this bond and the initial production of nitrogen dioxide.

Experiments were carried out with the addition of materials designed to explore the possibility of chain reactions. Lead tetraethyl and iron pentacarbonyl incorporated in the propellant had only a slight effect in reducing the burning rate, indicating the absence of long chains in the propellant or the gaseous reactions. Inert materials like carbon dioxide and magnesium oxide reduced the burning rate by increasing the heat capacity and lowering the temperature.

The decomposition of nitrocellulose becomes complicated and abnormal if the products of decomposition are not removed from the surface. The nitrocellulose decomposition vessel was prepared as it was in the experiments shown in figure 1, but before taking the measurements it was allowed to stand at 160°C. for several days without sweeping any gas through the vessel. The log dc/dT *vs.* $1/T$ line was not straight and it changed slope markedly with successive heating and cooling, giving lower activation energies. Some of the activation energies given in the literature (6, 7) agree with the value (46,700) obtained in this investigation and others are considerably lower. Complications due to the accumulation of intermediate products of the decomposition may have been involved.

When the propellant burns under field conditions the decomposition products are quickly swept away from the surface by the large volume of gases evolved, thus meeting the requirements for the hypothesis proposed here.

SURFACE TEMPERATURE AND EFFECT OF INITIAL TEMPERATURE

The hypothesis offered here suggests that the extreme surface layer is at a high temperature. Experimental evidence of such a high temperature was sought by incorporating temperature-indicating substances in the propellant, burning the propellant in a bomb, and quenching by the rupture of a thin metal disc when the pressure reached 1500 lb./in.^{2} The standard double-base powder was mixed with acetone, and extruded after introducing finely divided copper powder.

A study of microphotographs showed that although some larger cubical particles remained unmelted, all copper particles smaller than 0.0004 cm. which were in the surface were melted into spheres. This fact showed that the particles had attained a temperature of at least 1083°C., which is the melting point of copper. The smallest sphere had a diameter of 0.00025 mm.

In other experiments finely powdered alkaline earth carbonates were incorporated in the propellant, and after arrested burning the surface was treated with phenolphthalein. A red color is produced if the carbonate has decomposed thermally to leave the oxide. Experiments showed over one-fourth of the particles of calcium carbonate had been decomposed, whereas practically none of the barium carbonate particles had been decomposed. These experiments support the view that the extreme surface temperature was hot enough to dissociate calcium carbonate.

TABLE 2

Specific reaction rates of unimolecular reactions

TEMPERATURE	ACTIVATION ENERGY (CAL./MOLE)	35,000	40,000	45,000	50,000
°K.					
1000	k	7×10^5	5×10^4	4×10^3	4×10^2
	$\frac{k_{1004}}{k_{1000}}$	1.07	1.08	1.09	1.11
1200	k	2×10^7	2×10^6	2×10^5	3.0×10^4
	$\frac{k_{1204}}{k_{1200}}$	1.05	1.05	1.06	1.07
1400	k	1.0×10^8	2×10^7	4×10^6	7×10^5
	$\frac{k_{1404}}{k_{1400}}$	1.04	1.04	1.05	1.05
1600	k	8×10^8	2×10^8	4×10^7	8×10^6
	$\frac{k_{1604}}{k_{1600}}$	1.03	1.03	1.04	1.04

A surface temperature above 1000°C. can be calculated theoretically by dividing the heat of reaction by the heat capacity. Moreover the heat conductivity of the double-base powder is low, less than that of fire brick and one-tenth that of paraffin wax. The outermost molecular layer peels off the propellant surface in about one-millionth of a second, so that it has little chance to conduct the heat returned from the hot gases back into the cool interior. The heat from the envelope of burning gases then is used chiefly in raising the temperature of the outermost molecular layers.

There is another argument for a high surface temperature. Two criteria must be met in the propellant burning at 1500 lb./in.^{2}: the burning rate is about 2 linear centimeters per second and it increases about 0.5 per cent per degree rise in initial temperature. It will be shown in table 2 that those two criteria can be met only if the surface temperature is high.

A high initial temperature, T_i, will lead to a high surface temperature, T_s, for burning. If one sample of a given propellant has an initial temperature 1.0°C. higher than a second one, and both are subjected to the same amount of heat from the burning gases, the first one will have a higher surface temperature than the second and will burn faster. It will not be 1.0°C. higher, but in the neighborhood of 1000°C. it will be about 0.4°C. higher, because the heat capacities of both increase at higher temperatures as new modes of vibration are brought into play. The heat capacity cannot be measured at these high temperatures where the material has only a transitory existence. It is estimated by analogy with specific heat data for hydrocarbons (4) that the heat capacity will increase from 62.8 cal.deg.$^{-1}$ mole^{-1} at room temperature to 164 cal.deg.$^{-1}$ mole^{-1} at 1000°C.

In table 2 values of k are calculated with the formula

$$k = 3 \times 10^{13} e^{-\Delta H_{\text{act}}/RT}$$

for various activation energies and temperatures and the effect of inital temperatures is indicated by

$$\frac{k_{T_i+10}}{k_{T_i}} \quad \text{or} \quad \frac{k_{T_s+4}}{k_{T_s}}$$

The term k_{T_s+4}/k_{T_s} should have values of about 1.05 to be in agreement with the 0.5 per cent increase in rate per degree rise in temperature. These values occur only above 1000°A. or 1373°K. for activation energies between 45,000 and 50,000 cal./mole. Values of k of about 5×10^7 are required to give linear burning rates of 2 cm. per second, as shown in equations 3 and 6, if the burning surface is molecularly flat. As pointed out before, this large value of k can be obtained only at unreasonably high temperatures and it is necessary to allow for a rougher surface. An effective surface factor of 100 seems reasonable and in agreement with evidence from the penetration of dyes. Combining this surface factor with a calculated value of k of about 5×10^5, a numerical value of 5×10^7 is obtained which gives a rate of burning of 2 cm. per second. Table 2 shows that this value of k is obtained at a surface temperature of about 1000°C. when the activation energy is between 45,000 and 50,000 cal./mole. This correction for effective surface area is unsatisfactory, but it permits an hypothesis of burning based on simple concepts of kinetics. The surface temperature, like the surface factor, is somewhat indefinite and may be interpreted to be the effective temperature of the outer surface of the propellant and to include even a small gas layer adjacent to the propellant. Further investigations should be carried out to ascertain more definitely the *true* temperature of the outside layer of molecules during the microsecond in which the molecules are decomposing at very high temperature, in the neighborhood of 1000°C. Ordinary temperature-measuring devices do not easily record the temperature of a thin outer layer of molecules, on account of the conduction of heat by the instrument itself. Studies of the rate of burning of propellants in a very rapid stream of hot inert gas would be helpful.

SUMMARY

1. An hypothesis is offered for the burning of propellants in which it is assumed that the rate-determining step is the breaking of the O—N bonds at the extreme surface of the propellant. It is assumed that the effective surface temperature is of the order of 1000°C., maintained in a steady state by the heat coming back from an envelope of gases which are undergoing violent exothermic action. These gases include nitrogen oxides and organic fragments.

2. Experimental evidence is offered for the high surface temperature and for an activation energy of 46,700 cal./mole.

3. Applying the simple formula for a unimolecular bond-breaking process, calculations are made for the linear burning rate and for the influence of the initial temperature of the propellant.

REFERENCES

(1) Boys, S. F., and Corner, J.: Confidential report.
(2) Crawford, B. L., Jr., Huggett, C., Daniels, F., and Wilfong, R. E.: Anal. Chem. **19**, 630 (1947).
(3) Daniels, F.: Ind. Eng. Chem. **35**, 504–10 (1943).
(4) Parks, G. S., and Huffman, H. M.: *Free Energies of Some Organic Compounds*, p. 68. The Chemical Catalog Company, Inc., New York (1932).
(5) Rice, O. K. and Ginell, Robert. J. Phys. & Colloid Chem. **54**, 885 (1950).
(6) Robertson, R., and Napper, S. S.: J. Chem. Soc. **91**, 764 (1907).
(7) Roginsky, S.: Physik. Z. Sowjetunion **1**, 640 (1932).
(8) Wilfong, R. E.. Ph. D. Thesis, University of Wisconsin, 1944, pp. 13 and 49.

THERMAL THEORY OF IGNITION OF SOLID PROPELLANTS[1]

J. H. FRAZER and B. L. HICKS

Ballistic Research Laboratories, Aberdeen Proving Ground, Maryland

Received January 9, 1950

1

The ignition processes in a solid propellant are closely connected with the flow of heat in the propellant. It should therefore be possible to describe some aspects of ignition in terms of a purely thermal model in which rate of reaction is a function only of the temperature. A number of calculations have been made during the past two years of temperature as a function of position and time for a simple thermal model of ignition for which the external heating rate conforms approximately to the course of heating by the igniter of the propellant in a rocket. In this preliminary note only the more important results of the calculations will be discussed. The data presented are not final.

---

[1] Presented at the Symposium on Kinetics of Propellants which was held under the auspices of the Division of Physical and Inorganic Chemistry at the 112th Meeting of the American Chemical Society, New York City, September 15, 1947.

2

The model consists of the half space $x > 0$ filled with propellant which is being heated externally by a gas at temperature T_g and internally by heat released in chemical reaction. The mathematical formulation adopted is:

$$c\rho \frac{\partial T}{\partial t} = K \frac{\partial^2 T}{\partial x^2} + Qe^{-E/RT} \qquad x > 0;\ t > 0 \qquad (1)$$

$$-K \frac{\partial T}{\partial x} = h(T_g - T) \qquad x = 0;\ t > 0 \qquad (2)$$

$$-K \frac{\partial T}{\partial x} = 0 \qquad x \to \infty;\ t \geq 0 \qquad (3)$$

$$T = T^{(0)} \qquad x \geq 0;\ t = 0 \qquad (4)$$

The quantities $(c\rho)$, K, Q, E/R, h, and $T^{(0)}$ are constants. The gas temperature varies as follows:

$$\left.\begin{aligned} T_g &= T_g^{(1)} & 0 < t \leq t_0 \\ &= T_g^{(2)} \ll T_g^{(1)} & t_0 < t \end{aligned}\right\} \qquad (5)$$

in which t_0 then corresponds, in the case of a rocket, to the duration of heating of the propellant by the igniter.

The number of independent parameters in the problem is reduced by transformations to the reduced variables u, τ, ξ, h:

$$T = (E/R)u \qquad (6)$$

$$t = [(c\rho)(E/R)/Q]\tau \qquad (7)$$

$$x = [K(E/R)/Q]^{1/2}\xi \qquad (8)$$

$$h = [QK/(E/R)]^{1/2}H \qquad (9)$$

leading to:

$$\frac{\partial u}{\partial \tau} = \frac{\partial^2 u}{\partial \xi^2} + e^{-1/u} \qquad \xi > 0;\ \tau > 0 \qquad (10)$$

$$-\frac{\partial u}{\partial \xi} = H(u_g - u) \qquad \xi = 0;\ \tau > 0 \qquad (11)$$

$$-\frac{\partial u}{\partial \xi} = 0 \qquad \xi \to \infty;\ \tau \geq 0 \qquad (12)$$

$$u = u^{(0)} \qquad \xi \geq 0;\ \tau = 0 \qquad (13)$$

$$\left.\begin{aligned} u_g &= u_g^{(1)} & 0 < \tau \leq \tau_0 \\ &= u_g^{(2)} & \tau_0 < \tau \end{aligned}\right\} \qquad (14)$$

3

The set of equations 10–14 has been solved approximately by numerical integration with desk machines for several combinations of the parameters $u^{(0)}$, H, τ_0, as indicated in table 1.

From these solutions, the ignition time and temperature and the ignition delay can be computed. A typical heating curve is given in figure 1, in which the ordinate u is the reduced temperature at the surface of the propellant and the abscissa τ is the reduced time. It is reasonable to define $u = u_i = 0.05$ as the temperature at which "ignition" has been completed, since when u is this high the temperature rise has become very rapid. For $\log_{10} \tau_0 = 8.92$, as given in figure 1, $\log_{10} \tau_i = 9.52$ and the ignition delay $\log_{10}(\tau_i - \tau_0) = 9.4$. As τ_0 increases, τ_i decreases until they become equal to each other and to the "minimum ignition time," τ_{im}. If τ_0 decreases, however, τ_i increases very rapidly until it reaches the "adiabatic ignition time," τ_{ia}, corresponding to self-heating of the propellant with negligible heat flow in the neighborhood of the point of maximum temperature in the solid. That heating time is denoted by τ_c, for which $\tau_i \cong \tau_{ia}$. For all $\tau_0 \leq \tau_c$ then, $\tau_i \cong \tau_{ia}$.

TABLE 1

Range of dimensionless parameters considered

H	$\log_{10} \tau_0$			
	$u^{(0)} = 0.017$	$u^{(0)} = 0.024$	$u^{(0)} = 0.031$	$u^{(0)} = 0.034$
2×10^{-10}	~16.5	14.4–14.7		
2×10^{-8}	13.9–14.1	12.4–12.6	10.6–11.0	
2×10^{-6}	9.6–9.7		8.9–9.0	8.5–8.8

$u_g^{(1)} = 0.18$; $u_g^{(2)} = 0.021$

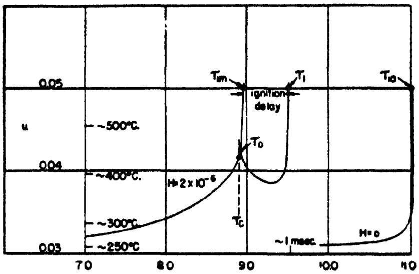

FIG. 1. Reduced temperature *vs.* reduced time for $u^{(0)} = 0.031$, $u_g^{(1)} = 0.18$, $u_g^{(2)} = 0.021$

4

Unless $u^{(0)}$ and H are such that τ_{im} is almost as large as τ_{ia}, which sometimes can occur, $(\tau_{im} - \tau_c)/\tau_{im}$ is generally small compared to unity. Therefore it is sufficient, for qualitative purposes, to plot only τ_{im} and τ_{ia} against $u^{(0)}$ and H, as is done in figure 2. The values of τ_{ia} are computed from equations 10 and 13 with $\partial^2 u/\partial\xi^2$ put equal to zero, and values of τ_{im} from the numerical solutions of the equations described above. The stepwise integrations necessary in order to obtain these solutions are quite laborious (about 20,000 net points used in the hand calculations so far). It is therefore encouraging that a simpler analytical method for estimating the τ_{im} curves has been found (no exact solution is possible at present of these nonlinear equations) which appears to be accurate enough for many practical and theoretical purposes. Details of the analytical method will be reported later.

From figure 2 there are seen to be two types of behavior: for sufficiently low initial temperature the ignition time is determined by the rate of external heating, but for higher initial temperatures it is determined primarily by the initial temperature. The ignition time is a sensitive function of the heating time and it is easy to construct rough plots of τ_i *vs.* τ_0, a few examples being given in figure 3. The horizontal segments of the curves correspond to the adiabatic ignition process and the intercepts on the 45° line to the minimum ignition time. The parts of the curves between τ_{ia} and τ_{im}, corresponding to ignition with varying amounts of delay, are affected considerably by the detailed variation of the rate of external heat transfer to the propellant as are also, to some extent, the values of τ_{im}.

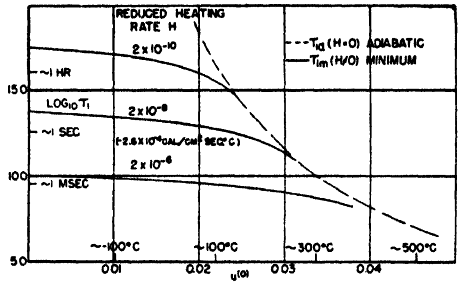

FIG. 2

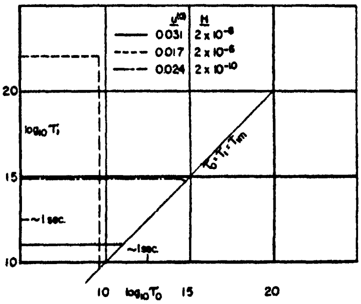

FIG. 3

FIG. 2. Ignition time *vs.* initial temperature and heating rate (reduced variables); $u_g^{(1)} = 0.18$.

FIG. 3. Ignition time *vs.* heating time (reduced variables)

The data given in terms of u, τ, and H can easily be translated into measures of T, t, and h. Consider a propellant ignition process with the following characteristics:

$$c\rho = 0.48 \text{ cal./cm.}^3 \text{ °C.}$$

$$K = 10^{-4} \text{ cal./cm. sec. °C.}$$

$$(E/R) = 1.7 \times 10^4 \text{ (°C.)}$$

$$Q = 2.9 \times 10^{16} \text{ cal./cm.}^3 \text{ sec.}$$

Equations 6–9 may be rewritten:

$$T \sim 1.7 \times 10^4\, u\ ^\circ\text{K}. \tag{15}$$

$$t \sim 2.9 \times 10^{-13}\, \tau \text{ sec.} \tag{16}$$

$$x \sim 7.7 \times 10^{-9}\, \xi \text{ cm.} \tag{17}$$

$$h \sim 1.3 \times 10^4\, H \text{ cal./sec. cm.}^2\ ^\circ\text{C.} \tag{18}$$

From these equations the values of the dimensional parameters corresponding to the dimensionless parameters in table 1 can be computed and are shown in table 2. Correspondingly, on figure 2, values of T and t are marked in customary units.

TABLE 2

Sample range of dimensional parameters

h	LOG t_0 (IN SECONDS)			
	$T^{(0)} = 16$°C.	$T^{(0)} = 135$°C.	$T^{(0)} = 254$°C.	$T^{(0)} = 306$°C.
cal./cm.²/sec. °C.				
2.6×10^{-6}	4.0	1.9-2.2		
2.6×10^{-4}	1.4-1.6	(−0.1)-(0.1)	(−1.9)-(−1.5)	
2.6×10^{-2}	(−2.9)-(−2.8)		(−3.6)-(−3.5)	(−4.0)-(−3.8)

It must be remembered that the temperature scale (i.e., correspondence between u and T) is dependent upon (E/R) and that the time scale is strongly dependent on Q and the other parameters. The value of (E/R) may range from 1.2 to 2.5×10^4 (°C.)$^{-1}$, while Q may vary by a factor of 10^2 or more.

Recently, calculations of ignition curves for the same model with other heat input curves have been completed on the Bell Relay Computer. The first object of these calculations was to establish the level of accuracy of the very extensive stepwise integrations required in this nonlinear problem. It is hoped that further calculations on the Bell machine will establish curves such as those in figures 1–3 with a uniform and known accuracy. In current investigations diffusion as well as heat flow is being investigated.

DETERMINATION OF THE THERMAL STRUCTURE OF A COMBUSTION WAVE BY FINE THERMOCOUPLES[1,2,3]

RALPH KLEIN,[4] MORRIS MENTSER,[5] GUENTHER von ELBE,[6] AND BERNARD LEWIS[7]

Central Experiment Station, U. S. Bureau of Mines, Pittsburgh, Pennsylvania

Received January 9, 1950

A combustion wave propagating through an explosive gas mixture or into a grain of propellant powder presents complex problems of heat transfer, diffusion, and chemical reaction. In view of the difficulties of theoretical treatment an experimental method for probing into the structure of the combustion wave is desirable. It is feasible to mount a fine thermocouple of high-melting wires in a strand of smokeless powder and to register the rise of E.M.F. with time as the combustion wave passes over the thermocouple. Measurement of the burning velocity then permits determination of the temperature distribution in the combustion wave. This paper reports the technique used and some results obtained.

When a strand of propellant powder is ignited at one end, combustion may propagate as a plane wave normal to the axis of the strand. At constant pressure and ambient temperature the combustion wave is in a steady state, that is, both the wave velocity and the thermal structure of the wave are constant. The combustion wave is characterized by three distinct zones. The first, the region of liquefaction and gas formation, is called the "foam" zone. The second, a gaseous region of very faintly luminous decomposition products capable of further reaction and heat liberation, is called the "fizz" zone. The third is the strongly luminous region of final reaction, known as the "flame" zone. The foam zone is very narrow—of the order of 10 μ. Figure 1 is a photograph of a strand burning at 500 p.s.i.g. in a nitrogen atmosphere in which the fizz and flame zones are evident. The incandescence at the base of the fizz zone is attributable to the presence on the strand of an inert coating of vinylite plastic which fritters away, forming an irregular luminous ring as the strand burns down.

---

[1] Approved for publication by the Public Information Division, National Defense Department.

[2] Presented at the Symposium on Kinetics of Propellants which was held under the auspices of the Division of Physical and Inorganic Chemistry at the 112th Meeting of the American Chemical Society, New York City, September 15, 1947

[3] This research is part of the work being done at the Bureau of Mines on Project TM1-5006A, supported by the Office of the Chief of Ordnance, Department of the Army.

The material in this publication is part of a thesis submitted by Ralph Klein to the Faculty of the Graduate School of the University of Pittsburgh in partial fullfillment of the requirements for the degree of Doctor of Philosophy.

[4] Physical Chemist, Physical Chemistry and Physics Section, Explosives Branch, Bureau of Mines, Pittsburgh, Pa.

[5] Physical Chemist, Physical Chemistry and Physics Section, Explosives Branch, Bureau of Mines, Pittsburgh, Pa.

[6] Supervising Chemist, Physical Chemistry and Physics Section, Explosives Branch, Bureau of Mines, Pittsburgh, Pa.

[7] Physical Chemist, Chief, Explosives Branch, Bureau of Mines, Pittsburgh, Pa.

EXPERIMENTAL

Thermocouples were prepared from 0.0005-in. Wollaston wires of platinum and platinum–10 per cent rhodium. A length of about 2 in. of each of the silver-sheathed wires was soldered to a copper wire and $\frac{1}{2}$ in. of the silver sheath was dissolved with nitric acid. The thermocouple junction was formed by momentary application of a small gas-oxygen flame to the crossed wire ends. Micromanipulation technique was unnecessary. Some early results which were obtained with bare thermocouples showed evidence of catalytic activity of the platinum. To inhibit this the couples were dipped in molten borax, which adhered to the wire in a very thin layer. The couples were mounted in both strips and cylindrical strands. In the earlier work two strips—0.027 in. thick, 0.75 in. wide, and 4 in. long—were moistened with acetone and pressed together with the thermocouple sandwiched between them. When using cylindrical strands ($\frac{1}{8}$ in. in diameter) the thermocouples were mounted by cutting the strands at 20 degrees oblique to the longitudinal axis, wetting the cut faces with acetone, placing the couple on one face in such a position that the tip of the couple entered the burning front first, and finally pressing the two faces together. The method adopted later

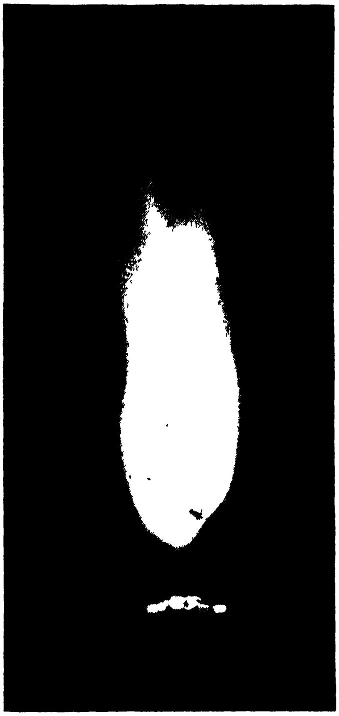

FIG. 1

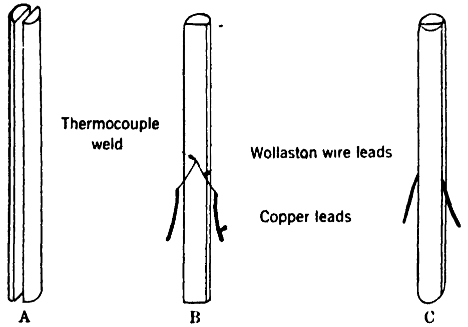

FIG. 2

FIG. 1. Propellant strand burning in nitrogen at 500 p.s.i.g.

FIG. 2. The mounting of a thermocouple in a propellant powder strand. A, strand cut lengthwise; B, thermocouple cemented on cut face with ethyl acetate; C, two halves cemented together.

consisted in cutting the powder strand in half lengthwise and cementing the halves together again with ethyl acetate after the thermocouple had been inserted in the center of the strand. Figure 2 is a diagram of a thermocouple mounted in this way. After a drying period of at least 6 days at 60°C., the samples were surface-inhibited with plastic coatings such as polyvinyl alcohol or vinylite to prevent uneven burning over the exposed strand surface (4).

The propellant strands were burned in a nitrogen atmosphere in a bomb provided with a window for visual observation. A thermostated water bath controlled the temperature to ±0.2°C. Pressure control of 1 per cent of gauge setting was obtained by a magnetic release valve operated by electrical contacts on the pressure gauge. The powder strands were mounted vertically in the bomb with outlets for the thermocouple leads and ignited at the upper end with an electrically heated wire. The E.M.F. time curves were recorded photographically with a string galvanometer (1) (Hindle-type electrocardiograph), an instrument which possesses advantages of rapid response and ease of recording, which was especially adaptable for this work. The frequency response characteristics at the string tension used were checked with an audio frequency oscillator and showed no appreciable efficiency loss up to 150 cycles per second.

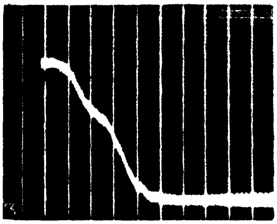

FIG. 3

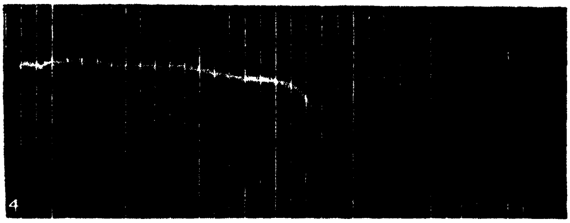

FIG. 4

FIG. 3. E.M.F.-time curve for M-2 powder strand burning at 150 p.s.i.g. at 39°C. in nitrogen. Bare thermocouple used. Vertical time lines are 1/25 sec. apart. Ten horizontal divisions equal 5 mv.

FIG. 4. E.M.F.-time record for nitrocellulose strand at 400 p.s.i.g. at 25°C.

EXPERIMENTAL RESULTS AND THEORETICAL TREATMENT

Figure 3 shows a typical record of E.M.F. *versus* time of a bare thermocouple embedded in a strand of M-2 powder (a double-base powder containing 20 per cent nitroglycerin) burning under a nitrogen pressure of 150 p.s.i.g. and at 39°C. The temperature record is obtained in the solid phase and in all or part of the fizz zone. The flame zone was either entirely absent in these experiments or the thermocouple was destroyed by melting before entering the zone. The reproducibility of such records was not satisfactory. However, they all show two stages of burning, the temperature at the end of the first stage being 1100°C. ± 50° with a temperature subsequently rising to at least 1773°C., the melting point of platinum. The entire temperature rise from the beginning of detectability on the record of figure 3 to the melting of the couple took place within 0.6 mm.

Failure of reproducibility of the earlier records was found to be in large part due to the method of mounting the thermocouples in the powder strands. Good reproducibility was obtained by the method developed later and shown in figure 2.

It was suspected that the second stage of burning was a manifestation of catalytic activity of the bare platinum wire in the gases of the fizz zone. Analysis showed the fizz gas to consist principally of carbon dioxide, carbon monoxide, nitric oxide, water vapor, hydrogen, and nitrogen. The catalytic effect of platinum on the water gas reaction and the nitric oxide–hydrogen reaction is well known (2, 5, 7). When the thermocouples were coated with borax as described above, the second stage disappeared.

Figure 4 is a record of E.M.F. *versus* time of a borax-coated thermocouple embedded in a strand of 13.15 per cent nitrogen nitrocellulose containing 1 per cent stabilizer burning under a pressure of 400 p.s.i.g. at 25°C. As a check on the efficiency of the thermocouple coating, mixtures of the various gases found in the fizz zone were prepared and metered past two thermocouples, one coated with various substances, the other uncoated, to simulate the temperature and flow conditions in the fizz zone of the burning propellant. Of the coating substances tried, borax proved most satisfactory. Table 1 gives the results of a typical experiment.

TABLE 1

Comparison of uncoated and borax-coated thermocouples

	TEMPERATURE BEFORE FLOW	TEMPERATURE DURING NITROGEN FLOW	TEMPERATURE DURING FLOW OF NITRIC OXIDE + 5 PER CENT HYDROGEN
	°C	°C	°C
Coated couple	995	995	1034
Uncoated couple	995	995	1416

Using borax-coated thermocouples, strands of 13.15 per cent nitrogen nitrocellulose were burned at fixed pressures and temperatures and records of temperature *versus* time (E.M.F.–time) were obtained. To convert such records to temperature–distance curves the burning velocity was determined by an electrical timing method (4) by which the burning time was measured between two fuse wires placed at a fixed distance apart in the strand. Figure 5 shows curves of burning velocity *versus* pressure, at various strand temperatures. Figure 6 shows the temperature–distance curve for the strand whose E.M.F.–time curve is shown in figure 4. The observed temperatures were corrected for the temperature difference between the wire and the gas by an extension of the equation used by Klaukens and Wolfhard (6), to include a correction for the nonsteady state:

$$T_2 = T_1 + \frac{cV\rho}{\alpha S}\frac{dT_1}{dt} + \frac{\sigma T_1^4 e}{\alpha}$$

where c is the specific heat of the couple, α is a coefficient depending on the Nusselt number, σ is Stefan's constant, S is the surface area of the couple bead, V is the volume of the couple bead, ρ is the density of the couple material, e is the emissivity, and T_1 and T_2 are the observed and true temperatures, respectively. Radiation of the gas to the couple and the effects due to the borax coating are neglected as these are considered to be small. It is seen (figure 6) that the difference between T_1 and T_2 is so small that it can be ignored in evaluations of the temperature records.

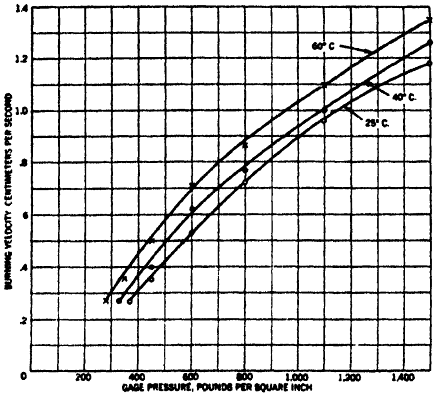

FIG. 5

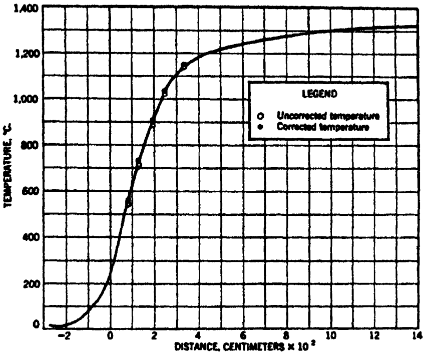

FIG. 6

FIG. 5. Burning velocities in nitrogen for vinylite-coated strands of 13.15 per cent nitrogen nitrocellulose plus 1 per cent ethyl centralite.

FIG. 6. Temperature–distance curve for burning strand whose E.M.F.-time curve is shown in figure 4.

For the analysis of the temperature–distance curves the steady-state equation

$$\frac{\partial}{\partial x}\left(\lambda \frac{\partial T}{\partial x}\right) - M \frac{\partial}{\partial x}(cT) + q(x) = 0 \tag{1}$$

expressing the heat balance in any plane x of the combustion wave, is used. x is the distance from an arbitrary reference point, λ the coefficient of thermal conductivity, M the mass burning rate, and c the specific heat at constant pressure. The first term in the equation represents the rate of change of heat per unit volume due to heat conduction; the second term is the rate of change of heat due to mass flow; and the third term is the rate of heat release by chemical reaction. For purposes of simplification, λ and c may be regarded either as constant or as step functions. Assuming λ and c to be constant the equation then becomes:

$$\lambda \frac{\partial^2 T}{\partial x^2} - Mc \frac{\partial T}{\partial x} + q(x) = 0 \tag{2}$$

In the low-temperature portion of the temperature–distance curve, the increase of heat content must be due primarily to heat conduction and mass flow, since $q(x)$ is very small. There can be no appreciable heat production in the solid phase of the combustion wave except very close to the surface because of the strong Arrhenius dependence of the exothermic reaction coupled with the low

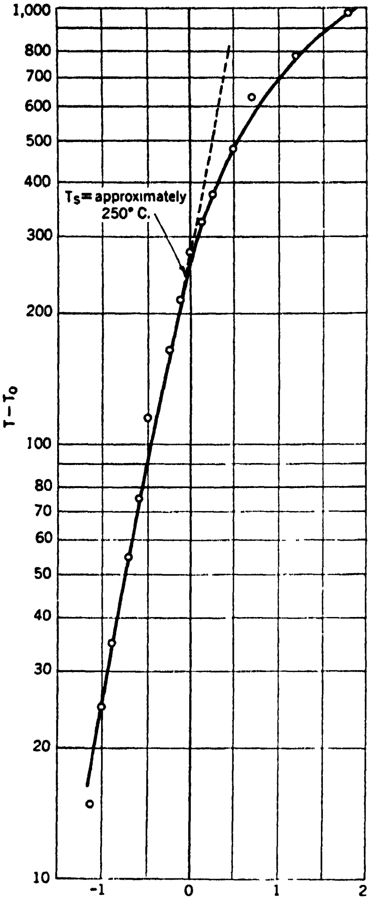

FIG. 7

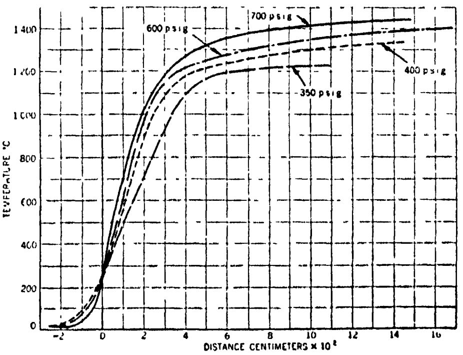

FIG. 8

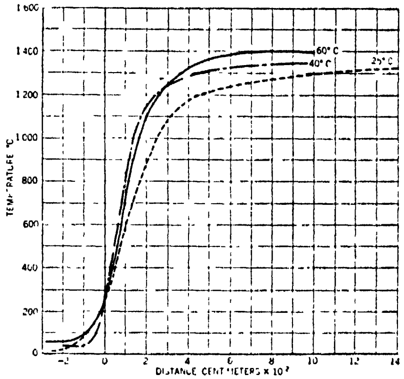

FIG. 9

FIG. 7. The surface temperature of a burning nitrocellulose strand derived graphically from a plot of log $(T - T_0)$ *versus* distance with heat production term equal to zero. The point of departure from linearity is taken as the surface temperature. Nitrogen pressure, 400 p.s.i.g.; temperature, 60°C.

FIG. 8. Temperature distribution in the combustion wave of 13.15 per cent nitrogen nitrocellulose plus 1 per cent ethyl centralite strands at 25°C. in the pressure region 350–700 p.s.i.g. (The lower portion of the 600-p.s.i.g. curve appears to overlap with the 350-p.s.i.g. curve.)

FIG. 9. Temperature distribution in the combustion wave of 13.15 per cent nitrogen nitrocellulose plus 1 per cent ethyl centralite at 400 p.s.i.g. in the temperature region 25–60°C.

thermal conductivity and the almost thermally neutral process of gasification. If the surface temperature is designated by T_s and the zero point of the x-axis is placed at the surface, the heat flow equation, integrated with $q(x) = 0$, and $T = T_s$ at $x = 0$, becomes

$$T - T_0 = (T_s - T_0)e^{Mcx/\lambda} \tag{3}$$

where T_0 is the temperature of the strand before ignition.

Figure 7 is a plot of ln $(T - T_0)$ *versus* x. It shows an initial linear portion, followed by a departure from linearity which represents the plane in the combustion wave where heat production becomes important. The surface temperature is given by the point of departure from linearity. This analysis has been made for a number of records; although lacking in precision, it was found to yield surface temperatures of about 250°C., in agreement with other observations (3). The initial slope of the curves of ln $(T - T_0)$ *versus* x gives Mc/λ. Using a value of 0.3 for c and the observed value of M, the value of λ in all curves was found to be of the correct order of magnitude, ranging from 0.0006 to 0.001 cal./cm. °C. sec. Direct measurements of λ yielded the value of 0.0005 cal./cm.°C. sec.

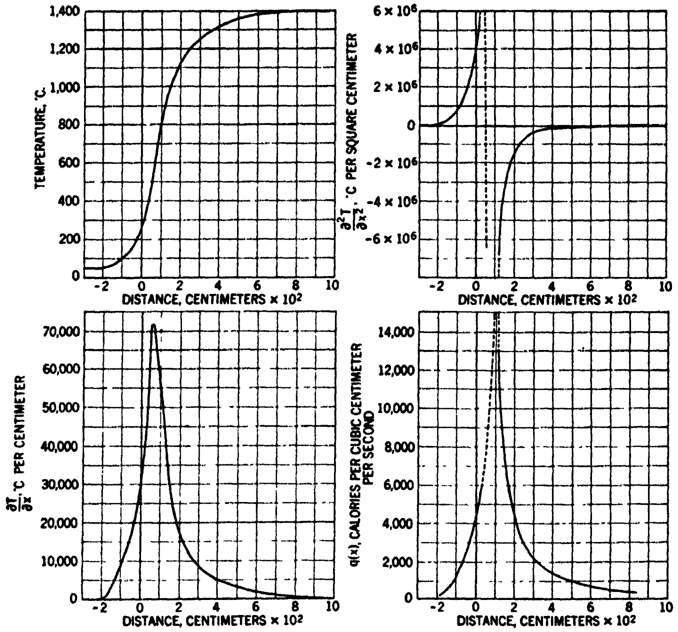

FIG. 10. Graphical development of the temperature distribution curve for the combustion wave of a nitrocellulose strand at 400 p.s.i.g., and 60°C. from the heat flow equation.

Figure 8 shows experimental curves of temperature and distance for the nitrocellulose–1 per cent stabilizer strands at 25°C. initial temperature and for the pressure region from 350 to 700 p.s.i.g. The zero point for these curves is chosen at $T = 250$°C. Increase of pressure is accompanied by a narrowing of the wave and an increase of the final fizz zone temperature. Fgure 9 shows the effect of varying the initial temperature at a pressure of 400 p.s.i.g. Figure 10 shows an analysis of the 400 p.s.i.g. 60°C. curve of figure 9, in which first and second differential quotients of the T *versus* x curve were determined graphically. Substitution of these values in the heat flow equation (equation 2) permits a plot of the $q(x)$ function. It is seen that the reaction rate attains a steep maximum somewhat beyond the solid phase and then tapers off gradually to zero at the end of the fizz zone.

SUMMARY

An experimental technique for the determination of the thermal structure of a combustion wave in a burning propellant strand is described. The method involves the use of fine thermocouples in conjunction with a string galvanometer. Temperature–time curves together with measurements of burning velocity allow determination of the temperature–distance curves. The results of measurements with nitrocellulose strands clearly show the effects of pressure and temperature on the temperature distribution in the wave. The analysis of a typical curve by means of the approximate equation

$$\lambda \frac{\partial^2 T}{\partial x^2} - Mc \frac{\partial T}{\partial x} + q(x) = 0$$

for the heat balance in the combustion wave qualitatively demonstrates the distribution of the chemical reaction rate throughout the combustion wave.

REFERENCES

(1) Adcock, F., and Wells, E. H.: Phil. Mag. **45**, 532 (1923).
(2) Andrussov, L.: Ber. **60**, 536 (1927).
(3) Aristova, Z. I., and Leipunskiĭ, O. I.: J. Phys. Chem. (U.S.S.R.) **20**, 1391 (1946).
(4) Crawford, B. L., Jr., Huggett, C., Daniels, F., and Wilfong, R. E.: Anal. Chem. **19**, 630 (1947).
(5) Green, T. E., and Hinshelwood, C. N.: J. Chem. Soc. **1926**, 1709.
(6) Klaukens, H., and Wolfhard, H. G.: Proc. Roy. Soc. (London) **A193**, 512 (1948).
(7) Prichard, C. R., and Hinshelwood, C. N.: J. Chem. Soc. **127**, 806 (1925).

THE THEORY OF THE BURNING OF DOUBLE-BASE ROCKET POWDERS[1]

O. K. RICE AND ROBERT GINELL[2]

Department of Chemistry, University of North Carolina, Chapel Hill, North Carolina

Received April 20, 1949

I. INTRODUCTION

The burning of double-base rocket powder offers a number of features of scientific interest. These powders are essentially homogeneous mixtures of nitrocellulose and nitroglycerin with small additions of other material. They are self-combustible, that is, one portion of the powder is oxidized by another portion, which may even be a part of the same molecule, no external source of oxygen being required. In the experiments that we shall consider, the burning takes place in an inert atmosphere. It consists of a rather complex series of reactions, starting at the solid surface or within the solid, and continuing in the gas phase. Gas is ejected normally to the surface, and in the ordinary type of burning the surface recedes in a direction perpendicular to itself. The rate at which the burning proceeds normal to the surface, and the way in which it is affected by the room temperature, the pressure exerted by the surrounding inert gas, and the composition are the subjects of the present paper.

The qualitative features of the burning process are summarized in figure 1, which also serves to fix the terminology. In figure 1 it is assumed that the solid stick of powder is burning from the end only, as in the experimental arrangement of Crawford and his collaborators (5), upon whose data we largely rely. We designate distances along the axis of the stick of powder by x, the powder surface being at $x = 0$. In the steady state, the powder stick may be assumed to be fed into the flame so that the surface at $x = 0$ remains stationary. Then M grams of material cross *any* cross section ($-\infty < x < \infty$) per square centimeter per second, M being the burning rate.

The burning of the powder appears to occur in three stages, all with evolution of heat. The first stage occurs at the surface of, or just within, the solid powder, and results in the formation of unsaturated fragments which are ejected into the gas phase normal to the surface. In the second stage, these fragments react in the gas phase (at average distance x_1) in an assumed second-order reaction.

---

[1] This paper is based in large part on material presented in OSRD Reports 5224 (June, 1945) and 5574 (November, 1945) and some earlier monthly reports by O. K. Rice and Robert Ginell which were prepared under Contract OEMsr-976 between the Office of Scientific Research and Development and the University of North Carolina.

A preliminary report on this work was presented at the Symposium on Kinetics of Propellants which was held under the auspices of the Division of Physical and Inorganic Chemistry at the 112th Meeting of the American Chemical Society, New York City, September 15, 1947. Since then the material on the effect of diffusion has been added and the calculations have been reworked.

[2] Present address: Brooklyn College, Brooklyn, New York.

These two stages together constitute what has been called "fizz burning"; the gases produced are still capable of further reaction. At low pressures (from one to a few atmospheres) the only heat reaching the surface is that produced by the reaction at the surface, which is thus self-sustaining at a definite (limiting low-pressure) rate.[3] At higher pressures heat generated from the gas phase reaction reaches the surface and the reaction rate then increases with pressure. The reactions thus far considered produce no visible light.

The third stage of the reaction consists of the flame, which appears only at pressures exceeding about 20 atm., and apparently does not affect the rate of reaction below about 100 atm. The flame exhibits a very striking appearance. The edge of the luminous zone is fairly sharp; it is located in figure 1 at x_2. The base of the flame at the burning end of a long cylindrical stick of powder appears no larger in diameter than the powder. Beyond this, however, the flame flares out, frequently exhibiting signs of turbulence. This appearance suggests that the second gas-phase reaction resembles a branching-chain explosion. We can imagine that as the gas leaves the fizz-burning zone there develops a concentration of some active particles. When this concentration reaches some defi-

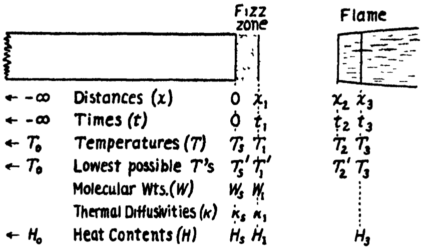
Fizz zone
Flame
← -∞ Distances (x) 0 x_1 x_2 x_3
← -∞ Times (t) 0 t_1 t_2 t_3
← T_0 Temperatures (T) T_s T_1 T_2 T_3
← T_0 Lowest possible T's T_s' T_1' T_2' T_3
Molecular Wts.(W) W_s W_1
Thermal Diffusivities (κ) κ_s κ_1
← H_0 Heat Contents (H) H_s H_1 H_3

FIG. 1

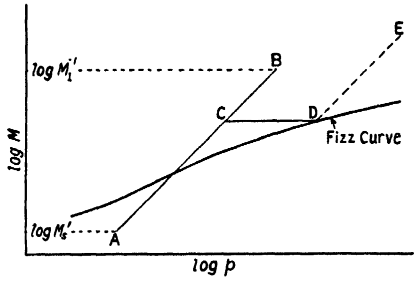

FIG. 2

FIG. 1. Schematic sketch of a stick of burning powder, illustrating notation and use of subscripts. The quantities in the last three lines with subscripts s, 1, and 3 designate properties of the gas just to the right of the position indicated. Primes are to be added to the H symbols for specific temperatures T_s', T_1', and T_3'. For the relation between τ_1, τ_1', and t_1 see subsection "Effect of Diffusion" of Section IV. The following list will be a guide to other frequently used symbols (the number in the parentheses gives the equation where first used): A (12), B_0 (48), B_b (47a), B_c (47b), B_d (47c), D_s (15), E_s (12), k_1 (13), K (39), m (36), M (1), M_1' (28), M_s' (28), n_2 (35), p (6), $\bar{r}$ (31), u (3), z_1 (8), Z_1 (22), z_2 (41), Z_3 (44), β_1 (10), β_1' (46a), β_2 (42), β_3 (45), λ (1), ρ (3), τ_3 (44). (In general $T_2' = T_1'$; see following equation 45.)

FIG. 2. Schematic diagram to illustrate construction of the fizz curve (line DE is used in calculating the effect of the flame; see Section VIII).

---

[3] Below 1 atm. the rate falls off again. This phenomenon is not treated here, but has been considered by Parr and Crawford (17). In some cases the burning-rate pressure curve above 1 atm. seems to merge with that below 1 atm., without showing the approach to constancy in the region just above 1 atm. This, in fact, is the case with the powder considered in detail here (see figure 4). However, there are enough cases in which the burning rate–pressure curve appears to flatten out at low pressures (above 1 atm.), so that we believe that this is a general phenomenon which is accidentally masked in some cases.

nite value, which occurs at a definite distance x_2 from the surface in the steady state, the gas proceeds to react, this reaction occuring at an average distance x_3. This resembles the nature of the phenomena observed in branching-chain explosions in gases contained in ordinary reaction vessels; for example, gas mixtures can be made which will show a definite induction period, during which no apparent reaction takes place and at the end of which the mixture suddenly explodes. As will appear later (see equation 39 and accompanying discussion) another reason for believing that the initiation of the flame may involve a branching-chain explosion is the great dependence of x_2 on the pressure.

At the lowest pressures, where only the surface reaction occurs, the temperature of the surface is designated as T'_s. At higher pressures, where heat gets back to the surface from the gas, T_s rises above T'_s. If only fizz burning occurred the gases would emerge from the fizz zone with temperature T'_1. At high pressures, around 100 atm., where heat from the flame gets back to the fizz zone, T_1 rises above T'_1. The temperature at which the flame starts is taken as T_2 (this is in general higher than T_1 because the flame does not start where the fizz zone ends) and the gases finally emerge at T_3, if the full heat of reaction is developed. Over the pressure range in which the flame develops the heat of reaction rises from that characteristic of fizz burning alone, around 500 cal./g., to its full value, about 800 to 1300 cal./g., depending on the powder.

II. TYPES OF THEORY

There are two distinct possibilities as regards the gas-phase reactions, which will make a considerable difference in the nature of the theory to be applied: (*1*) If the energy of activation of a gas-phase reaction is small, the average distance from the surface and the average time at which it will occur will be determined by a reaction rate which will not depend strongly on the temperature. (*2*) If the energy of activation is high the average distance and time will not depend directly on the rate constant, but rather on the time required for any particular portion of the gas to be carried into a region where the temperature is high enough for reaction to occur at an appreciable speed.

Case 1 will be the theory considered in this paper. Among recent developments of this type may be mentioned the work of Daniels (12).

Case 2 has been considered in detail by Boys and Corner (2). In this case, the gas-phase reaction is completely rate-determining; the zone of reaction merely moves toward or away from the surface, so that the temperature of the latter is adjusted to eject reactive fragments into the gas, at the required rate for maintenance of a steady state. This theory makes the slope of the log M *vs.* log p curve (p = pressure) equal to one-half the order of the gas-phase reaction (2; 19, pp. 70 ff.), while the theory of Case 1 indicates that the slope of the curve may be a much more complicated matter.

We shall present some reasons for supposing that Case 1 corresponds more closely to the experimental facts, considering separately the fizz reaction and the flame reaction.

The fizz reaction: According to the theory of Boys and Corner, at low pressures the reaction would recede from the surface and the temperature of the surface would drop. But it cannot drop below T'_s, and at the pressure at which this temperature was reached there would be a *sudden* change of the rate-pressure law, since below this pressure the rate would simply remain constant. Below this pressure, the rate of reaction at the surface would be too fast for the reaction in the gas phase, the zone of the latter would, therefore, be pushed out to infinity, and the gas-phase part of fizz burning would cease. There appears, however, to be no particular reason to suppose that it does stop or change its character. Crawford, Huggett, and McBrady (5) have conducted a rather extensive investigation of the burning of a cordite powder at low pressures. This powder starts its increase in burning rate at around 4 or 5 atm., but does not show a marked increase up to 6 atm. The heat of burning does not show any sudden or very great change in the region of low pressures, up to the pressure at which the effects of flame burning begin to be felt. The percentages of carbon monoxide and carbon dioxide in the product gases change only gradually through this pressure region and up to high pressures. The percentage of hydrogen does show an apparent increase of 50 to 100 per cent between about 3 and 5 atm., and then changes gradually up into the higher pressure range. It is difficult to know whether to assign any particular significance to this, but on the whole there does not at any point appear to be any very abrupt and marked change in the character of the burning in the region in which such would be expected if Case 2 applied.

The flame reaction: In this case the situation seems to be even more clear-cut. The flame exists and approaches the surface according to a regular law in the range of pressures from 20 to 100 atm., where it has little or no effect on the rate of burning, presumably because no heat reaches the surface. (This conclusion results from study of a catalyzed powder, in which the flame is much closer to the surface, but which burns at about the same rate as an uncatalyzed powder until the flame approaches to a distance corresponding to that in the uncatalyzed powder at 100 atm.; see Section VIII). If no heat from the flame reaches the surface, and the rate of reaction is controlled by the fizz burning, the rate will in general be either too fast for the flame, or too slow, assuming the position of the flame to be controlled by the mechanism of Case 2. In the former case it would recede to infinity; in the latter it would approach the surface and proceed to control the rate. As it does neither of these things, we conclude that the position of the flame is controlled by a reaction starting at the surface in the fizz zone, as envisioned in Case 1.

III. THE LAW OF STEADY HEAT FLOW

The problem which we have to solve is essentially a problem in heat conduction, chemical kinetics, and diffusion. When a steady state has been attained (in which the powder stick is fed into the flame so that the position of the burning surface is fixed at $x = 0$), we may make use of the "law of steady heat flow," established by Boys and Corner (2) and independently discovered, though not published, by J. E. Mayer. This law states that the amount of heat crossing any given plane x per unit time is the same as that crossing any other; otherwise there would be accumulations of heat and changes in temperature.

Heat is transferred by mass transport and by conduction. The heat crossing any x per unit time per unit cross section from left to right by mass transport is MH, where H is the heat content per gram; by conduction it is $-\lambda \mathrm{d}T/\mathrm{d}x$, where λ is the heat conductivity. The total is thus $MH - \lambda \mathrm{d}T/\mathrm{d}x$. Now $\mathrm{d}T/\mathrm{d}x$ is zero at $x \ll 0$, where the powder is at the uniform room temperature T_0, with $H = H_0$. $\mathrm{d}T/\mathrm{d}x$ is also zero for x greater than the last point at which an exothermic reaction occurs, since the final temperature of the gas must be that to which it can be raised by the heat of reaction. Hence

$$MH - \lambda \mathrm{d}T/\mathrm{d}x = MH_0 = MH'_s = MH'_1 = MH_3 \tag{1}$$

where H'_s, H'_1, and H_3 are heat contents of the gas, as indicated in figure 1, at the respective distances 0, x_1, and x_3 and the respective temperatures T'_s, T'_1, and T_3. These are the temperatures reached at the respective values of x if no reaction takes place at a greater value of x, and if, consequently, $\mathrm{d}T/\mathrm{d}x$ has become zero at that value of x. The fact that the heat contents H_0, H'_s, H'_1, H_3 are all equal means that after any complete reaction the loss in heat content due to heat of reaction is equal to the increase in heat content due to increase in temperature.

IV. THEORY OF FIZZ BURNING

We shall now apply the law of steady heat flow to the fizz-burning process, assuming provisionally that all the reaction occurs in the single plane at x_1, where the gas reaches the temperature T_1. If there were no flame, we would have $T_1 = T'_1$; however, we can just as easily treat the more general case.

The heat content per gram of the gas at a point for which $x < x_1$ (i.e., before reaction takes place) and for which the temperature is T (whether the surface temperature is T'_s or greater) is $H = H'_s + C_p(T - T'_s)$, where C_p is the average specific heat of the gas between T and T'_s. Applying equation 1 we have

$$MC_p(T - T'_s) - \lambda \mathrm{d}T/\mathrm{d}x = 0 \tag{2}$$

Provisionally neglecting the effect of diffusion, we fix our attention on a small disc of gas moving outward with the velocity u of the stream.

$$u = \mathrm{d}x/\mathrm{d}t = M/\rho \tag{3}$$

where t is the time after leaving the surface and ρ is the density of the gas. This disc of gas will find itself in regions of continually increasing temperature; by equations 2 and 3

$$\mathrm{d}T/\mathrm{d}t = (\mathrm{d}T/\mathrm{d}x)(\mathrm{d}x/\mathrm{d}t) = M^2(T - T'_s)/\rho^2\kappa \tag{4}$$

where

$$\kappa = \lambda/C_p\rho \tag{5}$$

is what we shall call the thermal diffusivity (defined in terms of an average C_p). The gas density ρ is related to p by the equation of state, which we assume to be the perfect gas law,

$$\rho = pW/RT \tag{6}$$

where W is the molecular weight and R the gas constant.

Examination of experimental data on thermal conductivities (see, e.g., the Landolt-Börnstein tables) indicates that the variation of κ with temperature will not be far from canceling that of ρ in equation 4 at a given pressure, so that we can substitute ρ_s and κ_s in equation 4. Integrating equation 4 then from $t = 0$ and $T = T_s$ at $x = 0$ to $t = t_1$ and $T = T_1$ at $x = x_1$, we get:

$$t_1 = \frac{\rho_s^2 \kappa_s}{M^2} \ln \frac{T_1 - T_s'}{T_s - T_s'} \tag{7}$$

Applying equation 6 to the gas emerging from the surface, setting

$$z_1^2 = \ln \frac{T_1 - T_s'}{T_s - T_s'} \tag{8}$$

and rearranging, we obtain from equation 7:

$$p = (MRT_s/W_s z_1)(t_1/\kappa_s)^{1/2} \tag{9}$$

We shall often wish to use the logarithmic form:

$$\ln p = \ln M - \ln z_1 + \ln [(R/W_s)(T_s^2 t_1/\kappa_s)^{1/2}] \tag{9a}$$

We also write

$$\beta_1 = (T_s - T_s')/(T_1 - T_s') \tag{10}$$

hence

$$\beta_1 = \exp(-z_1^2) \tag{11}$$

M, we assume, can be expressed in the form of an Arrhenius relation for the reaction that takes place at the surface of (or just within) the solid:

$$M = Ae^{-E_s/RT_s} \tag{12}$$

where A is a "frequency factor" and E_s is the energy of activation.

If Case 1 of Section II applies, and if the reaction of the fragments leaving the surface is of the n^{th} order, we may write

$$t_1 = 1/k_1 p^{n-1} \tag{13}$$

where k_1 is a reaction rate constant, which to a first approximation is independent of temperature. Since κ_s is inversely proportional to p, it is readily seen from equation 9 that in this case, as in the Boys–Corner theory, we would have the slope of the log M *vs.* log p curve equal to $n/2$, except that z_1 is not constant.

We shall assume the fizz reaction to be bimolecular, $n = 2$, and since κ_s is proportional to p^{-1} and at least roughly to T_s^2, we may consider $T_s^2 t_1/\kappa_s$ to be a constant parameter. We then have a set of four equations, equations 9, 10, 11, and 12 with five unknowns, T_s, p, M, z_1, and β_1 and a number of parameters. Of the parameters we may state:

$$W_s,\ T_s^2 t_1/\kappa_s,\ A,\ E_s \text{ are constants} \qquad \text{(A)}$$

In the remainder of this section we shall consider the case of sufficiently low pressures so that no heat gets back from the flame, and hence $T_1 = T_1'$. We can then make the following statement:

$$T_s',\ T_1' \text{ are functions of } T_0 \qquad \text{(B)}$$

If we can evaluate the parameters we can eliminate T_s, z_1, and β_1 between the five equations and determine M as a function of p for any T_0; thus,

$$M,\ T_s,\ z_1,\ \beta_1 \text{ are functions of } T_0 \text{ and } p \qquad \text{(C)}$$

It will also be useful for future reference to note that, since β_1 and T_s are both functions of T_0 and p, we can state:

$$\beta_1 \text{ is a function of } T_0 \text{ and } T_s \qquad \text{(D)}$$

We now indicate the method of solving the four simultaneous equations. Assuming that the parameters can be determined, we will know T_s' and T_1', and the corresponding values of M, which we call M_s' and M_1'. We then make a preliminary plot of log M against log p, taking M between M_s' and M_1' and assuming z_1 is constant (line AB of figure 2). Choosing any value of β_1 we can, from equation 10, find the corresponding value of T_s, and then from equation 12 the corresponding value of M, which we locate on the preliminary curve (e.g., point C in figure 2). Since we can calculate z_1 from equation 11 it is now possible, from equation 9a, to make a correction for log p at this value of log M (e.g., length of CD in figure 2 is equal to[4] log z_1 for the corresponding β_1). In this way we construct the fizz curve, as shown in figure 2. The fizz curve can then be shifted horizontally to make it coincide with the experimental data, for this amounts, assuming κ_s and W_s to be known, to determining t_1, for which independent data are not available.

In the foregoing we have assumed that all the reaction occurs at the plane x_1. It can be shown (see Appendix I) that, with a bimolecular reaction, the finite reaction zone can be taken care of simply by retaining equation 10 but replacing equation 11 by equation 11a:

$$\beta_1 = 1 - z_1^2 \exp(z_1^2) \int_{z_1}^{\infty} e^{-y} y^{-1} \mathrm{d}y \qquad \text{(11a)}$$

The integral can be evaluated from tables or, for large z_1, by means of the asymptotic formula (16). No additional difficulty in the calculation is caused by use of equation 11a instead of equation 11. Values of z_1 as a function of β_1, calculated from equations 11 and 11a, are to be found in table 1, together with some other values which will be used later.

---

[4] In the modified theory, taking diffusion into account (see below), log z_1 is replaced by log Z_1.

Effect of diffusion

In obtaining equation 11a the assumption has been made that the reactive particles are carried away from the surface solely by the outward streaming motion of the gas, any effect of diffusion being neglected. Actually the latter is far from negligible. Diffusion of the reactive particles away from the place where they are formed tends to reduce their concentration, and so to increase the time necessary for reaction and to make the seat of reaction recede from the surface. We shall take care of the effect of diffusion by a very rough but, it is believed, adequate calculation.

TABLE 1

β_1	z_1 (EQUATION 11)	z_1 (EQUATION 11a)	z_1 (EQUATION 69)	Z_1 (EQUATIONS 11a, 22, 23)*
0.05	1.73	4.25	3.17	2.90
0.1	1.518	2.87	2.23	1.636
0.15		2.22	1.83	1.080
0.2	1.268	1.835	1.58	0.774
0.3	1.100	1.325	1.27	0.413
0.4	0.957	1.010	1.06	0.230
0.5	0.834	0.782	0.895	0.1257
0.6	0.715	0.600	0.750	0.0645
0.8	0.473	0.314	0.470	0.0108

* $\mu D_s/\kappa_s$ has been estimated, with the aid of data in the Landolt-Börnstein tables, as 2.67.

We shall again provisionally assume that the gas-phase reaction takes place at a definite plane x_1. Then equation 9 will still hold provided t is introduced into the equation of heat flow merely as a quantity related to x by equation 3. t_1 is then equal to $x_1/\bar{u}$, where $\bar{u}$ is an average velocity of flow. The actual time of reaction, which we shall designate as τ_1', will now be different from t_1. In the time τ_1' the reactive particles will have been displaced on account of diffusion by an average amount of about $\mu^{1/2}\overline{D^{1/2}}\tau_1'^{1/2}$, where $\overline{D^{1/2}}$ is an average between $x = 0$ and $x = x_1$ of the square root of the diffusion constant, and μ is a numerical constant;[5] they will also have been displaced on account of streaming of the gas by an amount $\bar{u}\tau_1'$, where $\bar{u}$ is at least roughly the same average of u as is involved in the relation between x_1 and t_1. Hence we may write

---

[5] This is inferred from the expression for the distribution of particles which have diffused from an instantaneous plane source. After a time τ the particles originally in the plane are distributed according to the law, const. $\times\ \tau^{-1/2} \exp(-\xi^2/4D\tau)$, where ξ is the distance from the plane. The average value of $|\xi|$ is $(4D\tau/\pi)^{1/2}$, which suggests $\mu \sim 4/\pi$. The value of $\mu D_s/\kappa_s$ used in table 1 may slightly overestimate the effect of diffusion, but this should not be too important, as the results are not sensitive to μ (see also the end of Appendix II).

$$x_1 = \bar{u}t_1 = \mu^{1/2}\overline{D^{1/2}}\,\tau_1'^{1/2} + \bar{u}\tau_1' = \mu^{1/2}\overline{D^{1/2}}\tau_1'^{1/2}(1 + \alpha) = \bar{u}\tau_1'(1 + \alpha)/\alpha \quad (14)$$

where α is defined by the equation.

At constant pressure, D varies roughly as T^2. Since u is proportional to T, by equations 3 and 6, the dependence of $D^{1/2}$ and u on T is similar, and it will be safe to replace $\bar{u}$ and $\overline{D^{1/2}}$ in equation 14 by the values at the surface, writing

$$u_s t_1 = \mu^{1/2}D_s^{1/2}\tau_1'^{1/2} + u_s\tau_1' = \mu^{1/2}D_s^{1/2}\tau_1'^{1/2}(1 + \alpha) = u_s\tau_1'(1 + \alpha)/\alpha \quad (15)$$

From equation 15 or 14:

$$\tau_1' = \alpha(1 + \alpha)^{-1}t_1 \quad (16)$$

We can obtain another relation between τ_1' and t_1. The density of active particles in the region between $x = 0$ and $x = x_1$ will be equal to the number of active particles leaving unit area of surface in time τ_1' divided by x_1. The number leaving unit surface per unit time will be c_0u_s, where c_0 is a constant of proportionality. Hence the density is $c_0u_s\tau_1'/x_1$. Had no diffusion occurred it would have required a time t_1 for the active particles to get to x_1, and the density would have been $c_0u_st_1/x_1$. Let τ_1 be the average life-time of the reactive fragments if no diffusion had occurred. This is a quantity which is inversely proportional to the pressure, if the reaction is bimolecular, since if there is no diffusion the gas at the burning surface consists solely of reactive fragments. Under these circumstances we may put

$$\tau_1 = 1/k_1p \quad (17)$$

which is analogous to equation 13. Assuming bimolecularity, the time of reaction is inversely proportional to the density of the reactive particles, which are diluted by already reacted gas when diffusion occurs; hence

$$\tau_1/\tau_1' = (c_0u_s\tau_1'/x_1)/(c_0u_st_1/x_1) \quad (18)$$

and

$$\tau_1'^2 = \tau_1t_1 \quad (19)$$

In obtaining this equation we have not taken into account all the details of the behavior of the system and the variation in conditions between $x = 0$ and $x = x_1$; however, we believe it will be a reasonably good approximation. We may now use equation 19 to evaluate $\tau_1'^{1/2}$ in the third member of equation 15, and we use equations 3 and 6 to evaluate u_s in the first member. Squaring each of these members we then have

$$\mu(1 + \alpha)^2D_s\tau_1^{1/2}t_1^{1/2} = (MRT_s/pW_s)^2t_1^2$$

or (20)

$$p^2 = \left(\frac{MRT_s}{W_s}\right)^2 \frac{t_1^{3/2}}{\mu(1 + \alpha)^2 D_s\tau_1^{1/2}}$$

Now, as we have already noted, equation 9 is still valid. We cube both sides of equation 9 and divide by equation 20. This gives

$$p = \frac{MRT_s}{W_s z_1^3} \frac{\mu(1 + \alpha)^2 D_s \tau_1^{1/2}}{\kappa_s^{3/2}} = (MRT_s/W_s Z_1)(\tau_1^{1/2}/\kappa_s^{1/2}) \qquad (21)$$

where

$$Z_1 = z_1^3 \kappa_s/\mu(1 + \alpha)^2 D_s \qquad (22)$$

It is now seen that equation 21, if used with equation 17, is effectively identical with equation 9 used with equation 13 (setting $n = 2$), except that z_1 of equation 9 is replaced by Z_1 of equation 21. We have, therefore, again succeeded in reducing the problem to one of finding a certain parameter, this time Z_1 as a function of β_1. But if z_1 is known as a function of β_1, we may use equation 22 to find Z_1 as a function of β_1 provided α can be found. α can be found by comparing the middle member of equation 21 with the right-hand member of equation 9 and substituting for t_1 in the latter from equation 16 and 19. This gives

$$\mu(1 + \alpha)^2 D_s \tau_1^{1/2}/\kappa_s^{3/2} z_1^3 = (1 + \alpha)\alpha^{-1}\tau_1^{1/2}/z_1 \kappa_s^{1/2}$$

whence

$$\alpha(1 + \alpha) = z_1^2 \kappa_s/\mu D_s \qquad (23)$$

which provides the desired relation if κ_s, D_s, and μ are known. D_s has very approximately the same variation as κ_s, so we can consider the right-hand side of equation 23 to be independent of temperature and pressure.

Though we have set forth the above development on the assumption that all the reaction takes place at x_1, it remains essentially unaltered if the reaction takes place over a range of values of x, the average distance being x_1. We again have only to substitute for equation 11 the proper relation between z_1 and β_1. Equation 11a will not be quite right, because the distribution of heat sources is altered by diffusion. Diffusion tends to make them more uniformly distributed, at least near the surface. We have therefore carried out calculations (see Appendix I) assuming a uniform distribution of heat sources between $x = 0$ and $x = 2x_1$, with no heat source beyond $x = 2x_1$ (the average distance thus being x_1). This gives values of z_1 which are also shown in table 1. These do not differ significantly from those given by equation 11a up to $\beta_1 = 0.6$, and, as we shall see later, values of β_1 greater than 0.6 do not appreciably affect the rate–pressure curve. It seems in any event that the assumptions made in obtaining equation 11a should be more nearly correct than the assumption of uniformly distributed heat sources, and the truth probably lies between. We shall, therefore, use equation 11a to determine z_1 as a preliminary to the determination of Z_1 from equations 22 and 23. Z_1 is also given in table 1. Once Z_1 is given it is just as easy as before to apply figure 2 to obtain the rate–pressure curve. It is convenient to write equation 21 in the logarithmic form:

$$\ln p = \ln M - \ln Z_1 + \ln [(R/W_s)(T_s^2 \tau_1/\kappa_s)^{1/2}] \qquad (24)$$

Pressure coefficient

The above procedure gives M as a function of p for any T_0. It is, however, often useful to have an explicit expression for the pressure coefficient $(\partial \ln M/\partial \ln p)_{T_0}$. This can be obtained with the aid of the formal statements shortly following equation 13 (in which τ_1 should now replace t_1). By differentiating equation 24, noting statement A, we have:

$$\left(\frac{\partial \ln p}{\partial \ln M}\right)_{T_0} = 1 - \frac{\mathrm{d} \ln Z_1}{\mathrm{d}\beta_1}\left(\frac{\partial\beta_1}{\partial \ln M}\right)_{T_0} \tag{25}$$

Since M is a function only of T_s,

$$(\partial\beta_1/\partial \ln M)_{T_0} = (\partial\beta_1/\partial T_s)_{T_0}(\mathrm{d}T_s/\mathrm{d} \ln M) \tag{26}$$

and we find from equation 10, with $T_1 = T_1'$, and equation 12:

$$\left(\frac{\partial \ln M}{\partial \ln p}\right)_{T_0} = \left[1 - \frac{\mathrm{d} \ln Z_1}{\mathrm{d}\beta_1}\,\frac{RT_s^2}{E_s(T_1' - T_s')}\right]^{-1} \tag{27}$$

Equation 27 shows the factors influencing the pressure coefficient. At any given value of β_1 we see that $(\partial \ln M/\partial \ln p)_{T_0}$ is greater the greater $E_s(T_1' - T_s')/RT_s^2$, for $\mathrm{d} \ln Z_1/\mathrm{d}\beta_1$ is always negative. From equation 12, evaluating at $T_s = T_s'$ where $M = M_s'$, and at $T_s = T_1'$ where $M = M_1'$, we find:

$$\ln (M_1'/M_s') = E_s(T_1' - T_s')/RT_s'T_1' \tag{28}$$

For any given value of β_1 it is clear that $T_s'T_1'$ will be approximately proportional to T_s^2. So we can consider that for a given value of β_1, or, e.g., speaking roughly, for the middle of the fizz-burning range, the pressure coefficient is determined in large measure solely by the ratio M_1'/M_s', and since the logarithm of the ratio is involved, the pressure coefficient is not very sensitive to M_1'/M_s'. For a typical calculation based on equation 27 see table 5 of Section VIII.

Temperature coefficient

As a preliminary to the calculation of this quantity, $(\partial \ln M/\partial T_0)_p$, for the case of $T_1 = T_1'$, we note (since $\mathrm{d}H = C_p\mathrm{d}T$) that from equation 1

$$C_{p,s}'\mathrm{d}T_s' = C_{p,1}'\mathrm{d}T_1' = C_{p,0}\mathrm{d}T_0 \tag{29}$$

where the C_p's are the respective specific heats at the temperatures indicated (not, in this case, average specific heats). If we set

$$C_{p,0}/C_{p,s}' = r_s' \text{ and } C_{p,0}/C_{p,1}' = r_1'$$

we can write

$$\mathrm{d}T_s'/\mathrm{d}T_0 = r_s' \text{ and } \mathrm{d}T_1'/\mathrm{d}T_0 = r_1' \tag{30}$$

We now see that from equation 10, with $T_1 = T_1'$, we have

$$(\partial T_s/\partial T_0)_{\beta_1} = r_s' + (r_1' - r_s')\beta_1 = \bar{r} \tag{31}$$

where $\bar{r}$ is defined by the equation. From statement D, above, we see that

$$(\partial\beta_1/\partial T_0)_{T_s} = -(\partial\beta_1/\partial T_s)_{T_0}(\partial T_s/\partial T_0)_{\beta_1} = -\bar{r}(T_1' - T_s')^{-1} \tag{32}$$

the last expression coming from equations 10 and 31.

To calculate the temperature coefficient we differentiate equation 24, holding T_s, and hence M, constant. We obtain

$$(\partial \ln p/\partial T_0)_M = -(\partial \ln Z_1/\partial T_0)_M = -(\mathrm{d} \ln Z_1/\mathrm{d}\beta_1)(\partial\beta_1/\partial T_0)_{T_s} \tag{33}$$

the last expression arising because Z_1 is a function of β_1 only. Hence, since

$$(\partial \ln p/\partial T_0)_M = -(\partial \ln p/\partial \ln M)_{T_0}(\partial \ln M/\partial T_0)_p$$

we get, using equation 32:

$$\left(\frac{\partial \ln M}{\partial T_0}\right)_p = -\frac{\mathrm{d} \ln Z_1}{\mathrm{d}\beta_1}\,\frac{\bar{r}}{T_1' - T_s'}\left(\frac{\partial \ln M}{\partial \ln p}\right)_{T_0} \tag{34}$$

Another expression for the temperature coefficient is the following:

$$\left(\frac{\partial \ln M}{\partial T_0}\right)_p = \frac{E_s\bar{r}}{RT_s^2}\left[1 - \left(\frac{\partial \ln M}{\partial \ln p}\right)_{T_0}\right] \tag{34a}$$

If equation 27 is substituted into equations 34 and 34a they are readily seen to be equal. From equation 34 it is seen that, in comparing one powder with another, we may expect the temperature coefficient to parallel the pressure coefficient, but the factor $T_1' - T_s'$ is equally important. We can easily show that $\mathrm{d} \ln Z_1/\mathrm{d}\beta_1$ tends toward infinity in the lower range of β_1, while at the same time $(\partial \ln M/\partial \ln p)_{T_0}$ tends toward zero. Under these circumstances equation 34 is not convenient, but equation 34a can be used.

Equation 34 was derived on the assumption that τ_1 is independent of temperature. If τ_1 may be supposed to depend only on T_s, however, equation 34 still holds, because, by virtue of equation 12, τ_1 may then be alternatively assumed to depend only on M, and equation 33 will remain valid. All other equations involved in obtaining equation 34 also remain unchanged. However, $(\partial \ln M/\partial \ln p)_{T_0}$ will be changed (see Appendix II), and equation 34a will be altered also.

V. THE EFFECT OF THE FLAME

The effect of the flame can be taken into account by adding certain equations to those of the last section. We have already noted that we believe that the flame is to be considered as a manifestation of a branching-chain explosion. Let us assume that the flame starts when certain constituents which are formed in the gas, starting from the fizz zone, reach a certain critical concentration. The rate at which these active particles are formed will depend on the pressure but not, at least greatly, on the temperature, as we believe Case 1 of Section II to hold here also. The critical concentration may also depend on the pressure. If we let c_2 be the concentration of active particles, we have

$$\mathrm{d}c_2/\mathrm{d}t = k_2p^{n_2} \tag{35}$$

where k_2 is a rate constant and n_2 the order of the reaction. (The reaction rate would depend on the concentration rather than on p, but the difference is negligible, especially as we neglect the temperature dependence of k_2 anyhow.)

If the critical concentration of c_2 is of the form B/p^m, where B and m are constants, then the time necessary for the development of the critical concentration and hence for the flame to start is

$$t_2 - \tau_1' = B/k_2p^{m+n_2} \tag{36}$$

Here we retain as the zero of time that time at which the particular observed portion of gas left the surface, and subtract from t_2 the time τ_1' which actually elapses before reaction takes place at the average distance x_1. Usually τ_1' will be small compared to t_2.

In considering the development of the flame we neglect effects of diffusion, since our main purpose is to give a general picture of the situation, and the constants in the final equation will be determined empirically in any event. On this basis we write

$$x_2 - x_1 = u_1(t_2 - \tau_1') \tag{37}$$

where u_1 is the velocity (assumed constant) of the gas between x_1 and x_2. Also

$$u_1 = M/\rho_1 = MRT_1/pW_1 \tag{38}$$

where the temperature is assumed to have a constant value of T_1, and ρ_1 is the density and W_1 the molecular weight in the region x_1 to x_2. We therefore write

$$x_2 - x_1 = MRT_1B/W_1k_2p^{m+n_2+1} = KT_1M/p^{m+n_2+1} \tag{39}$$

where K is a constant determined by the equation.

Crawford, Huggett, and Parr (8) have measured the length of the dark zone, essentially x_2, or very approximately $x_2 - x_1$, and their measurements will be applied later in evaluating the constants in this equation.

If equation 39 is considered to be verified empirically we can take $t_2 - \tau_1'$ as being defined in terms of $x_2 - x_1$ by equation 37, just as we earlier used equation 3 to define t in terms of x, and even if diffusion is of importance, write from equations 37, 38, and 39:

$$t_2 - \tau_1' = KW_1/Rp^{m+n_2} \tag{40}$$

Now an equation exactly similar to equation 9 of Section IV may be derived for the region between x_1 and x_2 instead of for the fizz reaction occurring between $x = 0$ and x_1, except that all quantities evaluated at $x = 0$ will be replaced by quantities evaluated at $x = x_1$, and the quantities evaluated at $x = x_1$ will be replaced by the corresponding quantities at $x = x_2$. In particular $t_2 - \tau_1'$ will replace t_1, T_2 will replace T_1, and T_1' will replace T_s'. We substitute for $t_2 - \tau_1'$ from equation 40 and obtain in logarithmic form (similar to equation 24)

$$\tfrac{1}{2}(m + n_2 + 1) \ln p = \ln M - \ln z_2 + \ln \sqrt{KRT_2^{\prime 2}/W_1\kappa_1p} \tag{41}$$

where, in view of the properties of κ_1 and the constancy of K, the square root under the last logarithm can be taken as approximately independent of both temperature and pressure.

If we set

$$\beta_2 = (T_1 - T_1')/(T_2 - T_1') \tag{42}$$

it seems reasonable in this case to use an equation analogous to equation 11 rather than equation 11a, because the base of the flame does occur at a fixed distance, x_2. Thus

$$\beta_2 = \exp(-z_2^2) \tag{43}$$

Thus far we have not considered the finite reaction zone (x_2 to x_3) in the flame. This is of considerable importance to us, since the heat of the flame is actually produced here. If the reaction within the flame depends less strongly on pressure than that in the dark zone, as seems altogether probable, the reaction zone, $x_3 - x_2$, in the flame may well exceed the dark zone, $x_2 - x_1$, at the higher pressures at which an appreciable amount of heat from the flame reaches the surface; in this case $x_3 - x_2$ is rate-determining. It seems necessary to suppose that $x_3 - x_2$ does ultimately exceed $x_2 - x_1$, in order to avoid too sharp a rise of the burning rate with pressure. We shall assume that $\tau_3 - t_2$ (where τ_3 is the time at which reaction would occur if there were no diffusion) varies as p^{-1} as for a bimolecular reaction, as application to the experimental results will indicate that this is satisfactory. We obtain another equation like equation 24:

$$\ln p = \ln M - \ln Z_3 + \ln\left[(R/W_1)\sqrt{T_1^2(\tau_3 - t_2)/\kappa_1}\right] \tag{44}$$

It is legitimate to use W_1 and κ_1 because in the dark zone the physical properties of the gas will not change appreciably if all that is happening is the building up of a small concentration of active particles. Of course the temperature changes between x_1 and x_2, but since the term under the square-root sign is again constant this will not matter.

In this case Z_3 is related to

$$\beta_3 = (T_2 - T_1')/(T_3 - T_1') \tag{45}$$

in the same way that Z_1 is related to β_1. If no appreciable amount of heat is generated during the induction period as the gas goes from x_1 to x_2, the lowest value for T_2 is T_1', which is the temperature x_2 would have if the reaction zone in the flame were so long that no appreciable heat got back to x_2 from it. T_1' therefore takes the place of T_s' in equation 10. As the gas reaches its final temperature T_3 beyond x_3, we see that T_3 is the upper limit.

Equations 10, 42, and 45 can be combined by solving for T_2 in equation 45, inserting it in equation 42, then solving for T_1 in equation 42 and inserting the result in equation 10. The result is

$$T_s = T_s' + (T_1' - T_s')\beta_1 + (T_3 - T_1')\beta_1\beta_2\beta_3 \tag{46}$$

The term $(T_3 - T_1')\beta_1\beta_2\beta_3$ represents the contribution to the temperature of the surface arising from the heat which reaches it from the flame. Actually this heat is all fed in at the point $x = x_1$; consequently it would be better to replace[6] β_1 by β_1', where β_1' is related to z_1 by equation 11 rather than by equation 11a. (z_1 is related to Z_1, as before, by equation 22.) We, therefore, replace equation 46 by

$$T_s = T_s' + (T_1' - T_s')\beta_1 + (T_3 - T_1')\beta_1'\beta_2\beta_3 \tag{46a}$$

We can now summarize the problem of determining M as a function of p when the effect of the flame is included. We have nine equations, *viz.*, equations 24, 12, 41, 43, 44, 46a, the relations giving Z_1 and β_1' as functions of β_1, and that giving Z_3 in terms of β_3. There are ten unknowns M, p, T_s, β_1, β_1', Z_1, β_2, z_2, β_3, and Z_3. We eliminate all but M and p, and so obtain finally a relation between these two. The complete list of parameters is now as follows:

$$T_s',\ T_1',\ T_3,\ m + n_2,\ A,\ E_s, \text{ and}$$

$$B_b = (R/W_s)\sqrt{T_s^2\tau_1/\kappa_s} \tag{47a}$$

$$B_c = \sqrt{KRT_1^2/W_1\kappa_1 p} \tag{47b}$$

$$B_d = (R/W_1)\sqrt{T_1^2(\tau_3 - t_2)/\kappa_1} \tag{47c}$$

The combinations designated as B's may be considered as constants, on account of the behavior of the κ's, and so may be considered as units. It will also be found convenient to define

$$B_0 = 2(m + n_2 - 1)^{-1}[\ln B_c - \tfrac{1}{2}(m + n_2 + 1)\ln B_b] \tag{48}$$

VI. COMPOSITION AND SPECIFIC HEAT OF THE GASES

In the evaluation of a number of parameters we shall need information concerning the composition and specific heats of the gases formed in various stages of the burning process. Crawford, McBrady, and Hanson (9) have analyzed the products of reaction of HES 4016, a powder much used in the experimental work, over a range of pressures for carbon dioxide, hydrogen, carbon monoxide, and nitric oxide; other constituents are guessed at by effecting a material balance. At the highest pressure the flame is well developed, and the products are presumably the products of flame burning. At the lowest pressure used we assume that the products are those of fizz burning. This is supported by the fact that earlier work at still lower pressures (this time on a slightly different powder) indicated only small changes in composition below this pressure—only the hydrogen seems to be in a little doubt. We give in table 2 the results of these analyses and estimates.

---

[6] This will be most easily understood by reference to Appendix I, where β is described (equation 57) as the ratio of the temperature increase at the surface to the temperature increase at some point in the gas due to heat thrown in at that point. The total temperature increase is obtained on the basis of the superposition principle, which results in the integral, equation 58, which is entirely equivalent to the term $(T_1' - T_s')\beta_1$ in equation 46a. If a special increment of heat is thrown in at the point x_1, it results in a term (i.e., the last term in equation 46a) which may merely, by the superposition principle, be added to the integral; this is proportional to the value of β at x_1 related to z_1 by equation 64 or equation 11.

The specific heats of these gas mixtures, given in table 3, were obtained from thermal data given by Hirschfelder, McClure, Curtiss, and Osborne (14). The specific heat of formaldehyde was calculated from the vibrational frequencies (21, p. 86). We have included specific heats for a 20 per cent PF powder (80 per cent of the powder of table 2, 20 per cent paraformaldehyde), assuming that the paraformaldehyde is completely decomposed to formaldehyde in the fizz gas and to hydrogen and carbon monoxide in the flame gas.

TABLE 2

Composition of product gases in millimoles per gram of powder[*] burned

CONSTITUENT	AMOUNT IN FIZZ BURNING	AMOUNT IN COMPLETE BURNING
CO_2	3.65	7.7
CO	12.85	11.4
H_2	2.0	3.5
NO	7.82	0.7
H_2O	6.4	9.45
N_2	0.95	5.15
NH_3	1.3	
H_2CO	2.6	

[*] Elementary composition of powder in millimoles per gram: C, 19.09; H, 25.90; N, 11.02; O, 36.96.

Powder consists of nitrocellulose (13.25 per cent nitrogen), 54.0 per cent; nitroglycerin, 43.0 per cent; centralite, 3.0 per cent.

In addition we require the specific heat of the primary fragments produced at the surface of the powder. To obtain this we speculate somewhat, following Daniels (12). We assume that the original gases consist of 0.011 mole per gram of nitrogen dioxide and a hydrocarbon with three carbon atoms, presumably a free radical, which would have the average composition of $C_3H_4O_{7/3}$ and be present in the amount of 0.0064 mole per gram to effect the material balance. The vibration frequencies (21, p. 78) of nitrogen dioxide are 1370, 1615, and 640 $cm.^{-1}$ The vibration frequencies of $C_3H_4O_{7/3}$ were estimated as 800 ($4\frac{1}{3}$) (C—C stretching and C—O stretching); 3000 (4) (C—H stretching); 400 ($6\frac{2}{3}$) (heavy-atom bending); 1450 (7) (C—H bending).[7] (Actually there should be 8 C—H bendings and $5\frac{2}{3}$ heavy-atom bendings, but we used the assignment indicated to allow a little for a possible looseness in the binding of the free radical.) On this basis we found the specific heats listed in table 3. It must be admitted that there is considerable uncertainty as to the composition of this gas. Some of the carbon is almost certainly in the form of carbon monoxide or carbon dioxide, but, on the other hand, there may be some molecules or radicals of higher molecular weight than our assumed three-carbon compound. Also it seems likely that some of the nitrogen dioxide must be reduced to nitric oxide. However, the insensitivity of the specific heat to the exact composition, evidenced in table 3, indicates that our estimate cannot be far wrong.

---

[7] The numbers in parentheses give the degeneracy.

To calculate the specific heat of the primary fragments in the PF powder we assumed that the paraformaldehyde had already dissociated to formaldehyde.

TABLE 3

Specific heats of product gases in calories per gram

TEMPERATURE	ORIGINAL FRAGMENTS		FIZZ GAS		FLAME GAS	
	0% PF	20% PF	0% PF	20% PF	0% PF	20% PF
°K.						
400	0.272	0.284	0.294	0.301	0.299	0.332
600	0.328	0.342	0.315	0.332	0.319	
800	0.368	0.386	0.337	0.361	0.339	
1000	0.396		0.355	0.384	0.356	
1200	0.415		0.370	0.403	0.370	
1400	0.428		0.382	0.418	0.381	
∞					0.431	0.464

TABLE 4

Values of parameters (T_0 = 300°K.)

PARAMETER	UNITS	HES 4016	5 PER CENT PF	20 PER CENT PF
T'_s	°K.	700	622	367
T'_1	°K.	1400	1288	957
T_3	°K.	3370	3120	2405
$m + n_2$		2.5	2.5	2.5
A	g. cm.$^{-2}$ sec.$^{-1}$	1.4×10^4	1.4×10^4	1.4×10^4
E_s/R	degrees	8000	8000	8000
B_b		16.4	18.0	23.5
B_e		1980	·	
B_0		3.60	3.60	3.60
B_d/B_h		0.0712	0.0712	0.0712

Units for quantities in the *B*'s: applied pressures (whether appearing directly, or indirectly as in *R* and *K*) in atmospheres; temperatures in °K.; otherwise C.G.S. units.

VII. EVALUATION OF THE PARAMETERS

The *B*'s all contain factors, τ_1, K, and $\tau_3 - t_2$, respectively, depending on rates of reaction in the gas phase. They have been considered as parameters which may be fixed to give the best agreement with the burning-rate data, and the values used are as given in table 4.

The value of $m + n_2$ is obtained from measurements of Crawford, Huggett, and Parr (8). Early measurements of the length of the dark zone ($x_2 - x_1$)

indicated that it varies about as p^{-3}. Making some allowance for the pressure variation of M, this suggested the value $m + n_2 = 2.5$, which was used.

Some later measurements of Crawford and his collaborators (11) indicated a possible higher value of $m + n_2$. These were performed because it was suggested by Powell (18) that the length of the dark zone might vary only as p^{-2} if diffusion to the sides of the burning gas system could be avoided. It was found that with powder sticks of larger diameter, to avoid diffusion, the length of the dark zone did seem to vary as p^{-2} at low pressures. But at higher pressures, where diffusion would not be important in any event, the thickness of the dark zone appeared to decrease much more rapidly than had been observed in the first series of experiments. This led us to make some calculations (20) with $m + n_2 = 4.5$, but the shape of the rate–pressure curves thus obtained was not as good as with $m + n_2 = 2.5$, though the difficulty connected with the value of B_c, discussed at the end of Section VIII, was somewhat lessened. It should be noted that in any event both the values of K and of $m + n_2$ used in the theory are an extrapolation, since it is impossible to extend the measurements to dark-zone lengths which are sufficiently small so that an appreciable amount of heat from the flame gets back to the surface.

T'_s is simply estimated as 700°K. This is not far from other estimates, and is slightly less than what might be indicated as an upper limit by the fact that a strand of powder, which has been made very opaque by adding 0.5 per cent of carbon black, does not show a red glow when fizz burning in a darkened room (communicated by Dr. B. L. Crawford, Jr.)

We have noted in Section IV that equations 27 and 28 indicate that the pressure coefficient in the fizz-burning range is largely determined by M'_1/M'_s. If the pressure coefficient is given correctly by any set of parameters, then it is clear from equation 34 that $T'_1 - T'_s$ is pretty well determined by the temperature coefficient. We shall show later that the temperature coefficient is consistent with our value of $T'_1 - T'_s$. We also note that, knowing T'_1, T'_s, and M'_1/M'_s, the value of E_s is fixed.

We thus have accounted for the values of E_s and T'_1 which we have used; there are, however, a couple of lines of experiment which may throw some light on T'_1. Daniels (12) investigated the temperature of the surface by imbedding small particles of copper in the powder. He observed that they melted, which led him to conclude, from the melting point of copper, that the temperature of the surface, or of the gas within about 2×10^{-4} cm. of it, was at least 1300–1400°K. He also concluded that the surface temperature was between 1100°K. and 1600°K. from the decomposition of certain carbonates which he imbedded in the powder. Most of his experiments were done around 100 atm., where T_s is around 950°K. However, as shown in Section IX, the thickness of the fizz zone is only of the order of 3×10^{-4} cm. at this pressure, so we might expect Daniels' experiments to register a temperature somewhere between T_s and T'_1. On this basis our value of T'_1 might possibly seem a little low, but it certainly is in the right neighborhood.

The second line of experiment is the measurement by Crawford and his collaborators (7) of the heat of reaction of a number of powders over a range of pressures. The heat of reaction usually has a characteristic value at low pressures of about 500 cal./g., which may be taken as the heat of fizz burning, as no flame is present. Actually, at the lowest pressures used in the later work, the heat of reaction was slightly over 500, but the indications are that the limiting low-pressure value would be a little below 500. But this value is the value obtained in a calorimeter, where some of the products are condensed. The heat of condensation of the water indicated in the fizz products in table 2 amounts to 67 cal./g. of powder, and the heat of reaction of ammonia, in the amount indicated in table 2, with liquid water and carbon dioxide to give ammonium bicarbonate is 38 cal./g. In addition, there might be heat given out by polymerization of formaldehyde; alternatively there may be some condensation of ammonia and formaldehyde. However, these last products and, therefore, their reactions, are highly uncertain. Nevertheless, we believe that a heat of fizz burning somewhat under 400 cal./g. cannot be far wrong. If the fizz gas has an average specific heat of 0.34 cal. $g.^{-1}$ $deg.^{-1}$, it will require about 375 cal. to raise its temperature from 300° to 1400°K. This offers excellent confirmation of our value of T_1'.

Our estimate of T_3 can be rather rough, as this is not a very critical parameter. On the basis of the heat of reaction (given by Huggett (15) as 1260 cal./g.; probably about 1160 cal./g. if allowance is made for the fact that Huggett's calculations were presumably based on condensed rather than gaseous water) and the specific heat of the gases we estimate 3370°K.

Catalyzed powder

We shall wish to compare the ordinary double-base powder with several other powders with special properties. One of these is a catalyzed powder, in which a small amount of nickel is chemically combined with the nitrocellulose (6). At low pressures the catalyzed powder burns very slightly slower than the uncatalyzed. On the other hand, the flame is greatly promoted by the catalyst, and at any given pressure the dark zone is only about 1/13 as long. This is taken care of reasonably well by dividing K by 13, and changing B_c accordingly. It is assumed that this is the only difference between the catalyzed and the uncatalyzed powders.

Paraformaldehyde powders

Huggett (15) has studied HES 4016 containing added paraformaldehyde. Paraformaldehyde (PF) decomposes, probably while still in the solid powder, into formaldehyde, with the absorption, according to Huggett, of about 391 cal. per gram of PF. Since formaldehyde is similar to materials which emerge from fizz burning, it may probably be considered as an inert ingredient in the fizz zone. These facts give the basis for calculating parameters for PF powders.

We set up the following definitions:

α_P = fraction of PF by weight,

α_R = fraction of reactive material by weight = $1 - \alpha_P$,

Q_s = total heat evolved at room temperature per gram of powder from the reaction at the powder surface = $H_0 - H_s$ (where H_s is evaluated at room temperature),

Q_1 = heat evolved at room temperature per gram of powder in the complete fizz reaction (including the surface reaction) = $H_0 - H_1$ (where H_1 is evaluated at room temperature), and

Q_3 = total heat evolved in the formation of final flame products from solid powder (all at room temperature).

We have

$$\begin{aligned} T'_s - T_0 &= Q_s/C_{p,s} \\ T'_1 - T_0 &= Q_1/C_{p,1} \\ T_3 - T_0 &= Q_3/C_{p,3} \end{aligned} \tag{49}$$

where the C_p's are average specific heats of the respective product gases, as obtained from table 3.

The values of T'_s, T'_1, and T_3 given in table 4 for 0 per cent PF, $\alpha_p = 0$, correspond to $Q_s = 120$, $Q_1 = 372.2$, and $Q_3 = 1160$ cal.g.$^{-1}$ deg.$^{-1}$, respectively. From these figures and the values 391 cal./g. and 453 cal./g. for the heat absorbed in the decomposition of paraformaldehyde into formaldehyde (presumably the product in the fizz gas) and carbon monoxide plus hydrogen (presumably the products in the flame), respectively, we have:

$$\begin{aligned} Q_s &= 120\alpha_R - 391\alpha_P \\ Q_1 &= 372.2\alpha_R - 391\alpha_P \\ Q_3 &= 1160\alpha_R - 453\alpha_P \end{aligned} \tag{50}$$

From these we calculate T'_s, T'_1, and T_3 for the PF powders.

The mole fractions of PF and the molecular weight of the gaseous products at the various stages are readily obtained from table 2, knowing the amount of formaldehyde or hydrogen plus carbon monoxide to be added. As noted, we assume that the formaldehyde goes through the fizz zone without change, but it seems likely that it is changed to hydrogen and carbon monoxide early enough in the flame, so that we can consider that an equivalent amount of hydrogen and carbon monoxide is added to the fizz products, which are fed into the flame. Since the average molecular weight of hydrogen and carbon monoxide is about half that of the fizz products and the molecular weight of formaldehyde is about half that of the reactive fragments, we may assume that there is roughly the same proportional change in molecular weight and mole fraction of active material in the flame and in the fizz zone. Thus it seems reasonable to suppose that B_d/B_b is unchanged by the presence of PF, since τ_1 and $\tau_3 - t_2$ should both be inversely proportional to the mole fraction of active material. This conclusion may not be strictly correct, but in any event is probably within the limits of other inaccuracies in our calculations. The changes noted in τ_1 and W_s serve as the basis of the altered values of B_b itself listed in table 4.

B_0 involves K and t_1 in a fairly complicated way, but both of them might be expected to be greater for a PF powder, on account of the dilution by paraformaldehyde, and the effect of K and t_1 will at least partially cancel. Lacking more certain knowledge, therefore we assume B_0 also, as well as A and E_s, to be unaltered for the PF powders.

VIII. CALCULATIONS AND RESULTS

The first step in the solution of the equations is the construction of the fizz curve as indicated in figure 2. This curve is continued into the high-pressure region as though the flame did not exist, and the various values of β_1 are located on it.

In order to take care of the effect of the flame we derive slightly modified relations from equations 24 and 44. Using the notation of equations 47 we see at once that

$$Z_3/Z_1 = B_d/B_b \tag{51}$$

which shows that the ratio Z_3/Z_1 is a constant. Eliminating log p between equations 24 and 41 we find, using equation 48:

$$\ln M = (m + n_2 + 1)(m + n_2 - 1)^{-1} \ln Z_1 - 2(m + n_2 - 1)^{-1} \ln z_2 + B_0 \tag{52}$$

Having decided on the best value of B_d/B_b, we calculate Z_3 as a function of Z_1, hence from table 1, β_3 as a function of β_1. We can then use equations 12 and 46a to get M as a function of β_2 for various fixed values of β_1. Curves giving log M as a function of β_2 for fixed values of β_1 can also be obtained from equations 52 and 43. The intersection of a curve from equation 51 with the corresponding curve from equation 52 gives the values of β_1, β_2, and M for a solution of the set of simultaneous equations. (It is possible for there to be three intersections and hence three solutions; this produces a steep section in the log M *vs.* log p curve.) Some sample curves and intersections are shown in figure 3.

Since equation 24 holds and Z_1 is a function only of β_1 regardless of whether there is a flame or not, the point determined by an intersection in figure 3 can be located in a figure such as figure 2 on a straight line of slope 1 passing through the point of the fizz curve corresponding to the given value of β_1 (e.g., in figure 2, on the line DE for value of β_1, corresponding to C and D).

The final curves are compared with some typical experimental data in figure 4. It is seen that we get good agreement with experiment with a very reasonable set of parameters. It is true that the B's are chosen to give the best fit, but they do not affect the slope of the curves in figure 4 nor, to any great extent, the comparison between the powders having different amounts of PF. Particularly interesting is the curve for the 20 per cent PF powder, with its very low fizz portion, and the rather extreme effect of the flame, which seems to accord rather well with the data, as far as the latter go. It was not possible to get the 20 per cent PF powder to burn at low pressures. Experiments on compositions between 5 per cent and 20 per cent would be interesting, especially if carried to as low pressures as possible, using high temperatures if necessary.

In this connection it may be of interest to note that there are some other powders, generally containing a considerable amount of coolant, which show the break as the flame comes in very markedly, though this sometimes depends on such apparently irrelevant factors as the way the powder is mixed (1). That the effect may be fairly complex is indicated by the fact that at least one powder has been stated to show a minimum in the burning rate just before the effect of the flame comes in. It was suggested that this was due to the coolant reacting with absorption of heat out in the gas. With an *ad hoc* distribution of heat sources and sinks, of course, any burning-rate law could be explained. In another still more anomalous and unexplained case a German powder, studied at the California Institute of Technology, showed a dip in the rate–pressure curve at a relatively low pressure. This dip increased with temperature, so that over a short pressure range the rate of burning showed a negative temperature coefficient.

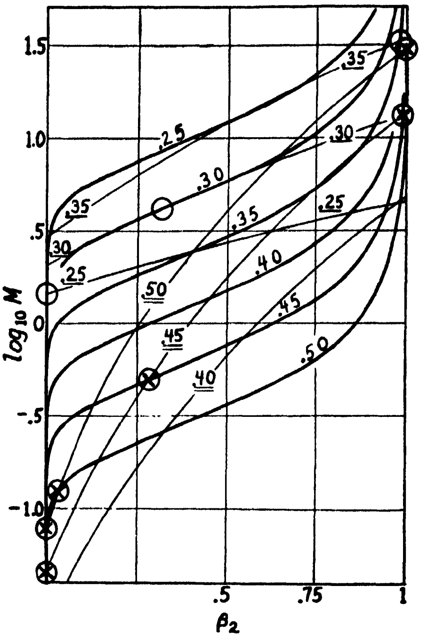

FIG. 3. Sample construction curves for preparation of figure 4. The heavy curves are from equation 52; the numbers on the curves give values of β_1. The lighter curves are from equation 51; the numbers again give β_1, the curves with singly underlined numbers being for 0 per cent PF powder and the curves with doubly underlined numbers being for 20 per cent PF powder. Intersections of curves for equation 51 and equation 52 are circled: open circles for 0 per cent PF powder, and circles with crosses inside for 20 per cent PF powder.

Temperature coefficient

We have previously noted that the temperature coefficient of burning is of importance, and that the parameters must be chosen so that the temperature coefficient is correctly reproduced. In table 5 we give the temperature coefficient at several pressures as calculated from equations 34 and 27. These calculated values of $(\partial \ln M/\partial T_0)_p$ fit in very well with the experimental values (10). Though the experiments are not too precise, there is some indication that the rise in temperature coefficient with decreasing pressure may also be observed.

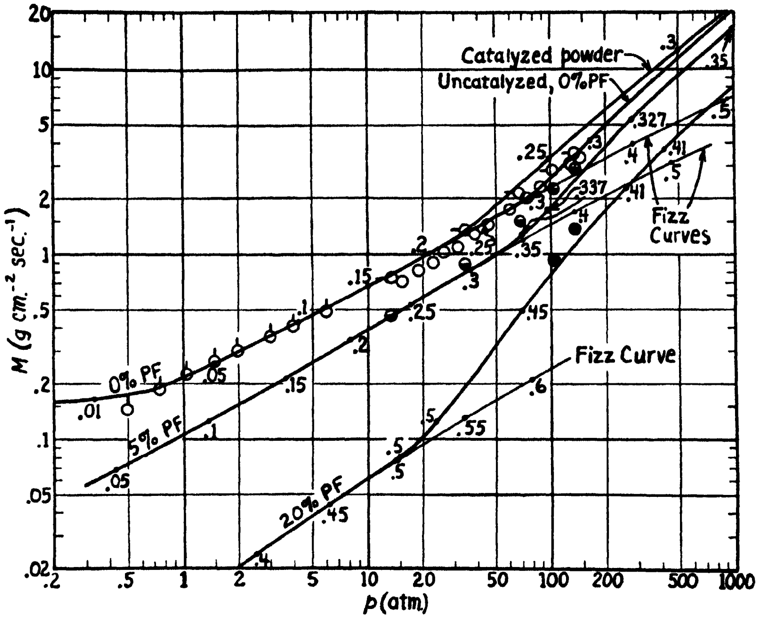

FIG. 4. Comparison of experimental data at 25°C. for the powder of table 2 and this powder mixed with PF, with the theoretical curves. Numbers near the curves give the values of β_1 at the points indicated. ○, data for 0 per cent PF powder (ϕ, values extrapolated to 25°C. from data at higher temperatures; -○, values from samples taken from a different batch of the same kind of powder); ⊖, data for 5 per cent PF; ●, data for 20 per cent PF. No data are shown for the catalyzed powder, but this is discussed in the text. Data are from B. L. Crawford, Jr., (10) and Clayton Huggett (15). To calculate M from the linear burning rate we have taken the density of the solid powder as 1.6 g./cc. in all cases.

TABLE 5

Temperature and pressure coefficients for pure HES 4016 (fizz burning only)

β_1	p	T_s	$-\frac{d \ln Z_1}{d\beta_1}$	$\frac{RT_s^2}{E_s(T_1' - T_s')}$	$\left(\frac{\partial \ln M}{\partial \ln P}\right)_{T_0}$	$\bar{r}$	$\left(\frac{\partial \ln M}{\partial T_0}\right)_p$
	atm.	°*K.*					
0.1	4.2	770	9.40	0.1060	0.501	1.043	0.0070
0.2	22	840	6.60	0.1260	0.547	1.034	0.0053
0.3*	82	910	5.90	0.1478	0.532	1.024	0.0046

* Calculated as though flame did not exist.

$\bar{r}$ is based on specific heat of solid at room temperature of 0.367.

Comparison of the catalyzed and uncatalyzed powders

Experimentally (6), the catalyzed powder burns slightly more slowly at lower pressures, passes the uncatalyzed powder at around 40 atm., is about 11 per cent faster than the uncatalyzed rate at 68 atm., 17 per cent at 102 atm., and 15 per cent at 136 atm. In figure 4 the catalyzed powder is assumed to have the same rate as the uncatalyzed at low pressures, starts to depart from it at about 30 atm., and the greatest deviation between the two theoretical curves is of the order of 30 per cent. Data at higher pressures would be of great interest, as they would show whether the burning rate of the catalyzed powder actually approaches that of the uncatalyzed again, as suggested by figure 4.

The values of B_c have actually been determined so as to make the effect of the flame in the catalyzed powder come in at the right pressure, remembering that K is about 1/13 and B_c, therefore, about $\sqrt{1/13}$ the respective values for the uncatalyzed powder. It should, however, be possible to evaluate B_c from equation 47b. W_1 is found to be 27 from table 2. K may be found by the use of equation 39 in conjunction with the dark-zone data (8, 11) and the burning-rate data. It is estimated at 35 atm.$^{3.5}$ cm.^{3} sec. g.$^{-1}$deg.$^{-1}$ if $m + n_2 = 2.5$. κ_1 may be estimated from values of the heat conductivity of different gases given in the Landolt-Börnstein tables, making due allowance for the temperature. We estimate $\lambda_1 = 3 \times 10^{-4}$ cal. cm.$^{-1}$ sec.$^{-1}$ deg.$^{-1}$ at 1400°, and from this we get $\kappa_1 = \lambda_1/C_{p,1}\rho_1 = 3.34/p$ cm.^{2} sec.$^{-1}$, the pressure p being in atmospheres. The value thus found for B_c is 7920. This value is appreciably greater than that given in table 4. If we refer this discrepancy to λ_1, the least certain of the quantities involved, it is found that λ_1 must be about 16 times as great as estimated from the Landolt-Börnstein table. This means that when the flame does begin to have an effect on the burning rate, it is still too far from the surface for heat from it to reach the surface in appreciable quantities, unless the heat conductivity is greater than one might suppose, or unless there is heat produced in the dark zone. It may be that atoms are formed in the flame, and that these, diffusing readily in the region preceding the flame, recombine there, thus effectively moving part of the heat source to a position closer to the powder surface (or effectively increasing the heat conductivity, however one may wish to look at it). There is, also, perhaps some possibility that the effective heat conductivity is increased, or that the hot gases at the base of the flame effectively moved closer to the surface, by turbulence transmitted from the base of the flame as it flares out. This might be related to the well-known phenomenon of erosion, or increased rate of burning, arising when gases are forcibly blown across the powder parallel to the surface. Finally, part of the discrepancy may be connected with the choice of the value of $m + n_2$. (In this connection see the remarks in Section VII.)

IX. REACTION TIMES AND DISTANCES AND THEIR INTERPRETATION

The reaction in the surface

We have assumed that the reaction in the surface follows equation 12 and have evaluated A as 1.4×10^4 g. cm.$^{-2}$ sec.$^{-1}$ This may be compared with what would be expected theoretically if the rate-determining step consists of the breaking off of NO_2 groups at the burning surface. There being 0.011 gram-atom of nitrogen, hence very approximately 0.011 mole of NO_2 groups per gram in HES 4016 (see table 2), we may state that the number of NO_2 groups detached per second per square centimeter is

$$1.4 \times 10^4 e^{-E_s/RT_s} \times 0.011 \times 6.02 \times 10^{23} = 9.3 \times 10^{25} e^{-E_s/RT_s} \tag{53}$$

Daniels (12) has estimated that there are about 5×10^{14} NO_2 groups exposed at a square centimeter of the powder surface. Hence, the rate of detachment per exposed NO_2 is

$$9.3 \times 10^{25} e^{-E_s/RT_s}/5 \times 10^{14} = 1.9 \times 10^{11} e^{-E_s/RT_s} \tag{54}$$

If the action is of the nature of an ordinary unimolecular reaction, a frequency factor of around 10^{13} might be expected. 1.9×10^{11} is in reasonably good agreement. It should be borne in mind that this is a rough result, and it could be changed appreciably by moderate changes in the parameters.

Though this analysis indicates that the value of A is reasonable, there is some evidence to indicate that some reaction, at any rate, takes place in the solid below the surface. Daniels (12) has examined grains of powder which were partially burned and quenched, and has found, by the use of dyes, that there is a changed layer near the surface of the powder which is perhaps 0.015 cm. deep and is strongly altered for a depth of about 0.005 cm. We may assume that the powder was appreciably heated to this depth. If we suppose that all the heat is produced at the surface and that the interior is heated only by conduction, equation 2 can be applied to the solid and written in the form

$$\lambda \mathrm{d}T/\mathrm{d}x = MC_p(T - T_0) \quad . \tag{55}$$

where T is the temperature at any point in the solid and C_p is the average specific heat between T and T_0. From this equation it is clear that the thickness of the heated layer should be of the order of magnitude of λ/MC_p. We may take λ to be about 3×10^{-4} cal./cm. sec. deg. Since C_p increases rather rapidly with the temperature, we may estimate an average value as 0.5 cal./g. deg. Since the powder is quenched, and the rate of burning has, therefore, at the last moment dropped to zero, we are a little embarrassed in choosing an appropriate value of M. However, work of Frazer and his collaborators (13), using powder impregnated with dyes which change color with temperature, indicates that there is a heated layer in the powder of the order of magnitude found by Daniels even when the powder is burning. If we give M its low-pressure value, about 0.25 g./cm.^{2} sec., we find $\lambda/MC_p = 0.0024$ cm. This is considerably smaller than the actual thickness of the altered layer, which indicates that this layer is being heated within itself as well as obtaining heat from the surface. On the other hand, when powder was quenched at around 10 atm., the altered layer was only about 0.001 cm. thick (4). M is about 0.65 g./cm.^{2} sec. at this pressure, and λ/MC_p comes out about equal to the observed thickness.

It has been observed by Crawford and by Frazer that the altered layer is full of gas bubbles, another indication that reaction is occurring there. However, this too is more important at low pressures.

So it is quite possible that at the higher pressures the reaction is really controlled by some process taking place at the surface, such as the breaking off of NO_2 groups. If, however, we must consider a reaction occurring throughout the body of the solid as rate-determining, it is still probable that, except at very low pressures, it will depend in a fairly normal way on the surface temperature, and that there will be an apparent activation energy based on this temperature, so that equation 12 can still be used. If the reaction in the solid is of a simple type, it should be possible to treat it by the Boys and Corner method. In this case E_s would be an effective activation energy, which can be shown to be just one-half the true activation energy of the reaction occurring in the solid (2; 19, pp. 70 ff.)

The reaction in the gas phase

The time τ_1 for the fizz reaction can be evaluated from equation 47a, knowing B_b. W_s is about 57 (Section VI) and we estimate that $\lambda_s = 10^{-4}$ cal. cm.$^{-1}$ sec.$^{-1}$ deg.$^{-1}$ at 700°K. which enables us to evaluate κ_s as 0.29 cm.^{2} sec.$^{-1}$ at 700°K. and 1 atm. (T^2/κ_s, it will be recalled, is to be assumed independent of temperature, so any convenient value can be used for T_s.) τ_1 then turns out to be 7.8 $\times$ $10^{-5}/p$, with p in atmospheres, which is found to be about 1.5 $\times$ 10^5 times the time between collisions at 1000°K., assuming an ordinary kinetic theory diameter of 3 $\times$ 10^{-8} cm. This factor corresponds to an activation energy of about 24,000 cal./mole reaction at 1000°K. This is larger than E_s, and would mean that the gas-phase reaction-rate constant would be about 5500 times as great at T_1' as at T_s'. The theory would go over into the Boys–Corner form at low pressures, and the advantages of the form of theory we are presenting would be eliminated. However, if there is a steric factor of around 10^{-4} (including allowance for collisions with molecular species incapable of reacting), which is not at all unreasonable, the activation energy would be only around 5500, which would give only a seven- or eight-fold change in the reaction-rate constant between T_s' and T_1'. This seems fairly reasonable and, on the basis of the theory presented, would make only a relatively small difference in the shape of the curves shown in figure 4. This is discussed in Appendix II.

TABLE 6

Length of fizz zone

β_1	p	T_s	M	x_1
	atm.	*°K.*	*g. cm.$^{-2}$ sec.$^{-1}$*	*cm.*
0.1	4.2	770	0.42	63 $\times$ 10^{-4}
0.2	22	840	1.01	11.4 $\times$ 10^{-4}
0.3*	82	910	2.10	3.1 $\times$ 10^{-4}
0.3	162	985	4.1	1.8 $\times$ 10^{-4}

* Calculated as though the flame did not exist.

Length of the fizz zone

It will be of interest to tabulate calculated values of this quantity, x_1, for purposes of orientation. x_1 may be calculated roughly by eliminating t_1 and τ_1' between equations 14, 16, and 19. Thus

$$x_1 = \bar{u}(1 + \alpha)^2\alpha^{-2}\tau_1 = (MRT_s/k_1p^2W_s)\,(1 + \alpha^2)\alpha^{-2} \tag{56}$$

using equation 17 to evaluate τ_1 and equations 3 and 6 to evaluate $\bar{u}$, assumed equal to u_s (which means that x_1 will be slightly underestimated). Results are tabulated in table 6. There are, of course, no experimental values with which these may be compared, but they are undoubtedly of the right order of magnitude.

SUMMARY

To explain the characteristics of the burning of double-base powders, a theory is developed in which flow of heat from the reacting gases beyond the burning surface to that surface plays an important role. In the early part of the paper, this type of theory is contrasted to theories in which it is supposed the only rate-determining process is a reaction in the gas phase.

The burning of the powder appears to occur in three stages, all with evolution of heat. The first stage occurs at, or just within, the surface of the solid powder and results in the formation of unsaturated fragments which are ejected into the gas phase normal to the surface; it is responsible for a limiting low rate of burning at low pressures. In the second stage, the fragments react in the gas phase; heat from this reaction reaches the surface in increasing amounts as the pressure is increased. The first two stages together constitute fizz burning; the gases produced are still capable of further reaction. This further reaction occurs, however, only at relatively high pressures; it constitutes the flame, which appears to be of the nature of a branching-chain explosion.

The behavior of these reactions and their effect on the burning rate are handled with the aid of the laws of chemical kinetics, of flow of heat in a moving medium, and of diffusion. The theory serves to correlate the effect of pressure and temperature on the burning rate, the comparative behavior of the flame and its distance from the surface in ordinary double-base powders and in powders containing a catalyst, and the effect of coolants—in particular, paraformaldehyde—on the burning rate. There is some difficulty in accounting for the high magnitude of the rate of transfer of heat from the flame to the surface.

In making the calculations various parameters had to be evaluated with the help of the known properties of the powder. In some cases, the rate of burning, itself, entered into this evaluation. This was true in the determination of the energy of activation of the surface (solid-phase) reaction as 16,000 cal./mole reaction, the determination of the lowest possible temperature, T_s' of the burning surface as 700°K., and the determination of the lowest possible temperature T_1' of the fizz gases (after the completion of the fizz reaction, but without receiving

any heat from the flame) as 1400°K. All these values are shown to be very reasonable. Other characteristics of the reaction at the solid surface, and reactions in the gas phase are discussed, and, in particular, the length of the fizz-burning zone is estimated to range from about 60×10^{-4} to about 3×10^{-4} cm. between 4 and 100 atm.

In concluding it may be remarked that the ideas developed in this paper have helped in the exposition of a qualitative theory for the burning of composite propellants, consisting of potassium perchlorate and carbon black in a matrix of double-base powder. These are of interest as they are an example of the burning of a heterogeneous mixture, but as there seems to be nothing to add at the present time, and this discussion is available elsewhere (20), it is not proposed to publish further on the matter.

We wish to express our appreciation to Dr. B. L. Crawford, Jr., Dr. Clayton Huggett, Dr. R. G. Parr, and others at the University of Minnesota. Their comments have done much to improve this work, and their coöperation in the providing of experimental data has been of great assistance.

REFERENCES

(1) Avery, W. H., and Higbie, H.: Private communication (1945).
(2) Boys, S. F., and Corner, J.: Proc. Roy. Soc. (London) **A197**, 90 (1949).
(3) Chapman, S., and Cowling, T. G.: *The Mathematical Theory of Non-Uniform Gases*, Chap. 16. Cambridge University Press, London (1939).
(4) Comley, E. A., and Crawford, B. L., Jr.: Private communication (1945).
(5) Crawford, B. L., Jr., Huggett, C., and McBrady, J. J.: OSRD Report 3544 (April, 1944).
(6) Crawford, B. L., Jr., Huggett, C., and McBrady, J. J.: University of Minnesota report (August, 1944).
(7) Crawford, B. L., Jr., Huggett, C., McBrady, J. J., and Hanson, M.: University of Minnesota report (1944).
(8) Crawford, B. L., Jr., Huggett, C., and Parr, R. G.: University of Minnesota report (1944).
(9) Crawford, B. L., Jr., McBrady, J. J., and Hanson, M.: University of Minnesota report (1945).
(10) Crawford, B. L., Jr., and others: University of Minnesota report (1944).
(11) Crawford, B. L., Jr., and others: University of Minnesota report (1945).
(12) Daniels, F., Wilfong, R. E., and Penner, S. S.: J. Phys. & Colloid Chem. **54**, 863 (1950); OSRD Report 3206 (1944).
(13) Frazer, J. H.: J. Phys. & Colloid Chem. **54**, 872 (1950) and earlier reports.
(14) Hirschfelder, J. O., McClure, T., Curtiss, C. F., and Osborne, D. M.: OSRD Report 1087 (1942), available from Office of Technical Services, Washington, D. C.
(15) Huggett, C.: University of Minnesota report (1945).
(16) Jahnke, E., and Emde, F.: *Tables of Functions*. Dover Publications, New York (1943).
(17) Parr, R. G., and Crawford, B. L., Jr.: J. Phys. & Colloid Chem. **54**, 929 (1950).
(18) Powell, R. E.: (1945).
(19) Rice, O. K., OSRD Report 5224 (1945), available from Office of Technical Services, Washington, D. C.
(20) Rice, O. K.: OSRD Report 5574 (1945), available from Office of Technical Services, Washington, D. C.
(21) Sponer, H.: *Molekülspektren*, Vol. I. Julius Springer, Berlin (1935).

APPENDIX I. EFFECT OF FINITE REACTION ZONE

In the detailed discussion in the text of this paper, we supposed that all the heat of fizz burning was produced at a fixed distance from the surface of the powder. Actually it is produced over a range of distances, and the results to be expected depend upon the distribution of the real heat sources. We shall show that the exact way in which they are distributed is not very crucial, and so we shall feel justified in making certain assumptions: namely, that the specific heat, heat conductivity, and velocity of the gas are constant. Then we can assume that we have a series of plane heat sources, and that the temperature distribution arising from any given source is independent of all others, and their effects are therefore additive (superposition principle).

We shall take up first the case of no diffusion, and assume a bimolecular reaction in the gas phase. We consider a little disc of gas moving outward from the surface and suppose that a fraction f of the heat evolved by it has appeared by the time t after it leaves the surface (f is also equal to the fraction of molecules which have reacted). The fraction of heat evolved between t and $t + \mathrm{d}t$ is $(\mathrm{d}f/\mathrm{d}t)\mathrm{d}t$. Suppose this amount of heat is sufficient to raise the temperature of the gas from T to $T + \mathrm{d}T$ and that the temperature of the surface, due to conduction of heat back to the surface from the part of the reaction which takes place between t and $t + \mathrm{d}t$, is $T'_s + \mathrm{d}T_s$. Then we may define β for the region between t and $t + \mathrm{d}t$ as

$$\beta = \mathrm{d}T_s/\mathrm{d}T \tag{57}$$

which is exactly analogous to equation 10. For the total increase of temperature at the surface, $T_s - T'_s$, we have then

$$T_s - T'_s = \int_{T'_s}^{T_1} \beta\,\mathrm{d}T \tag{58}$$

since the total change of temperature of the gas is from T'_s to T_1. We can, however, write

$$C_p\mathrm{d}T = Q_1(\mathrm{d}f/\mathrm{d}t)\mathrm{d}t \tag{59}$$

where Q_1 is the total heat of fizz burning, since both sides of this equation must be equal to the heat evolved by the little disc of gas between t and $t + \mathrm{d}t$. Thus equation 58 becomes

$$T_s - T'_s = \int_0^{\infty} \beta(Q_1/C_p)(\mathrm{d}f/\mathrm{d}t)\mathrm{d}t \tag{60}$$

Since

$$T_1 - T'_s = \int_{T'_s}^{T_1} \mathrm{d}T = \int_0^{\infty} (Q_1/C_p)(\mathrm{d}f/\mathrm{d}t)\mathrm{d}t \tag{61}$$

we have

$$\beta_1 = \int_0^{\infty} \beta C_p^{-1}(\mathrm{d}f/\mathrm{d}t)\mathrm{d}t \Big/ \int_0^{\infty} C_p^{-1}(\mathrm{d}f/\mathrm{d}t)\mathrm{d}t \tag{62}$$

where β_1 now has exactly the same definition as in equation 10. It does not seem that too much error should be made in the evaluation of the quotient of these integrals by setting C_p constant. Therefore, since by the definition of f we must have $\int_0^\infty (\mathrm{d}f/\mathrm{d}t)\mathrm{d}t = 1$, we see that to a good approximation:

$$\beta_1 = \int_0^\infty \beta(\mathrm{d}f/\mathrm{d}t)\mathrm{d}t \tag{63}$$

We now note that since each plane source has a temperature distribution independent of the other plane sources, its (relative) temperature distribution will be of just the same form as that discussed at the beginning of Section IV. We can thus write

$$\beta = \exp(-z^2) \tag{64}$$

and we shall have a relation of the same form as equation 9, with z substituted for z_1 and t for t_1. If we assume that T_s^2/κ_s is constant, then for any given case (constant p) we may write from equation 9

$$z'^2/z''^2 = t'/t'' \tag{65}$$

where z' and z'' are the values of z at two different times t' and t''.

Assuming the fizz reaction to be bimolecular, the rate of change of the concentration c_1 is given by $-\mathrm{d}c_1/\mathrm{d}t = k_1c_1^2$, where k_1 is the rate constant. If c_0 is the initial concentration, then $c_1/c_0 = 1 - f$, and

$$\mathrm{d}f/\mathrm{d}t = k_1c_0(1 - f)^2 \tag{66}$$

Integrating this equation, with due regard to the initial condition ($f = 0$ when $t = 0$), we obtain

$$(1 - f)^{-1} = k_1c_0t + 1 \tag{67}$$

It will be noted that half of the reaction is over when $t = (k_1c_0)^{-1}$ and we may call this the average time of reaction. This is the closest analogy to t_1 in the simple theory, so we rewrite equation 67

$$(1 - f)^{-1} = 1 + t/t_1 \tag{68}$$

and we also set z equal to z_1 when $t = t_1$ in analogy to the simple theory. From equation 65, $z^2 = z_1^2t/t_1$. Therefore, using equations 64 and 66, with $k_1c_0 = t_1^{-1}$, and equation 68 in equation 63, we obtain

$$\begin{aligned}\beta_1 &= t_1\int_0^\infty (t + t_1)^{-2}\exp(-z_1^2t/t_1)\,\mathrm{d}t\\ &= z_1^2\int_0^\infty (z^2 + z_1^2)^{-2}\exp(-z^2)\mathrm{d}z^2 \text{ (substituting } z^2 \text{ as variable)}\\ &= z_1^2e^{z_1^2}\int_{z_1^2}^\infty e^{-y}y^{-2}\mathrm{d}y \text{ (setting } y = z^2 + z_1^2)\end{aligned}$$

Integrating once by parts we obtain equation 11a. Equation 9 holds between z_1 and t_1, as for any z and the corresponding t, and can be used unchanged if equation 11a is substituted for equation 11.

Thus far we have neglected diffusion. However, we can, as in the text, assume the time t to be defined in terms of the distance x from the surface and the gas velocity u (in this case assumed uniform as an approximation) as $t = x/u$, so t is really a measure of the distance from the surface, the distribution of heat sources being determined by equation 67. The effect of diffusion can then be handled as in the text, but it may have the additional effect of changing the distribution of heat sources.

If we suppose that, instead of being controlled by equation 67, reaction occurs uniformly, i.e., df/dt = constant, up to $x = 2x_1$ or $t = 2t_1$, and then breaks off suddenly, we obtain instead of equation 11a:

$$\beta_1 = (2z_1^2)^{-1}(1 - e^{-2z_1^2}) \tag{69}$$

The results embodied in equations 11a and 69 have been tabulated in table 1. They are similar enough to indicate that the burning rate will not depend very strongly on the exact distribution of heat sources in the gas.

APPENDIX II. SOME ERRORS AND CORRECTIONS

A number of assumptions and approximations, which may not in all cases have been explicitly mentioned, are implicit in our calculations. It will be well to list these, and to consider the most important of them.

We have neglected any effect of thermal expansion or compressibility of the solid powder. These effects we believe to be negligible.

We believe any effect of radiation to be negligible, under the conditions of the experiments performed by Crawford and his collaborators, in which powder strands a couple of millimeters in diameter are burned from the end. In the first place, the flame apparently has no effect on the rate until it is closer than about 0.5 mm.; if direct radiation from the flame were effective, its influence should be noticeable even at greater distances. On the other hand, if the hot gases in the flame acted as a black body at around 3300°K., enough radiation might reach the surface to have some effect on the rate. At 3300°K. radiation would be emitted by a black body at the rate of about 160 cal.sec.$^{-1}$cm.$^{-2}$ At 100 atm. the powder burns at the rate of about 3 g.sec.$^{-1}$cm.$^{-2}$, and so there would be enough radiation to raise the temperature of the surface by about 150°. But it seems most unlikely that the gases in a layer about 2 mm. thick (equivalent to about 2 cm. at normal temperature and pressure if the gas is at 100 atm. and 3300°K.), which is about the thickness which could be effective in sending much radiation to a surface 2 mm. in diameter, could have an emissivity of more than a few per cent of the black body emissivity. It is true that some of these gases in the flame have strong infrared absorption bands, but these extend over a relatively limited range of frequencies.

We have neglected effects of gas imperfection. These may have a direct effect on the relation between density and pressure; they may also have an indirect effect, because of the rate of collision which increases more than proportionally with the pressure when the gas is dense. An increased rate of collision will increase the reaction rate and the heat conductivity, both in somewhat the same way. And it will be noted (see equations 24, 41, and 44) that these quantities enter our equations in the same way. At the same time, however, the diffusion coefficient will be lowered ("cage effect") to roughly the same extent as the heat conductivity is raised. This will mean that diffusion is somewhat less important at the higher pressures. Some rough calculations, based on equations and data reproduced by Chapman and Cowling (3), indicate that these effects may not be entirely negligible, but will probably not be of great importance up to 200 atm. (For a more detailed discussion of some of the effects of gas imperfections see Appendix III of reference 19.)

Probably more important than the neglect of gas imperfections is the neglect of any activation energy of the gas-phase reactions. Since both T_s and the temperature of the reacting gases increase with increasing pressure, it is seen that these two effects will actually operate in somewhat the same way. We shall, therefore, consider the effect on fizz burning of the more important of them in some detail.

The simplest way to test the effect of an activation energy for the fizz reaction is to find out how much it can affect the pressure coefficient toward the middle of the fizz-burning range. We shall assume that the reaction time τ_1 depends only on T_s, being proportional to e^{E_1/RT_s} where E_1 is the activation energy. This will overestimate the effect, since actually the reaction will take place beyond the surface at some temperature between T_s and T_1, and, therefore, will not depend as strongly as indicated on T_s as T_s increases and finally approaches T_1.

If we take into account such a dependence of τ_1 on T_s we obtain, instead of equation 25,

$$\begin{aligned}\left(\frac{\partial \ln p}{\partial \ln M}\right)_{T_0} &= 1 - \frac{\mathrm{d} \ln Z_1}{\mathrm{d}\beta_1}\left(\frac{\partial \beta_1}{\partial \ln M}\right) + \frac{1}{2}\frac{\mathrm{d} \ln \tau_1}{\mathrm{d}T_s}\frac{\mathrm{d}T_s}{\mathrm{d} \ln M} \\ &= 1 - \frac{\mathrm{d} \ln Z_1}{\mathrm{d}\beta_1}\left(\frac{\partial \beta_1}{\partial \ln M}\right)_{T_0} - \frac{E_1}{2E_s}\end{aligned} \tag{70}$$

the last equation following from the discussion of the preceding paragraph and equation 12. In the same way that we derived equation 27 we now obtain:

$$\left(\frac{\partial \ln M}{\partial \ln p}\right)_{T_0} = \left[1 - \frac{\mathrm{d} \ln Z_1}{\mathrm{d}\beta_1}\frac{RT_s^2}{E_s(T_1' - T_s')} - \frac{E_1}{2E_s}\right]^{-1} \tag{71}$$

In Section IX it was suggested that E_1 might be reasonably taken as 5500 cal./mole reaction. This would change $(\partial \ln M/\partial \ln p)_{T_0}$ at $\beta_1 = 0.2$ from 0.547 to 0.604. As noted above, however, this overestimates the effect. If $E_1 = 20{,}000$ and we make the calculation on the same basis, $(\partial \ln M/\partial \ln p)_{T_0}$ becomes 0.84. If E_1 is as large as this, we shall be getting into a region in which Case 2 of Section II would begin to apply, but, in spite of this, equation 24 will still be approximately valid, as it does not depend on any assumed mechanism of reaction, and equation 71 will still give an overestimate for $(\partial \ln M/\partial \ln p)_{T_0}$. An approximate method of handling the case of moderately large values of E_1 has recently been formulated by R. G. Parr. We believe, however, that the above calculation indicates that our neglect of E_1 is not likely to result in too great an error. It might result in E_s and some of our temperature parameters being assigned incorrect values, in spite of the fact that the latter, in particular, appear so reasonable. However, we do not believe the effect will be as great as that caused by neglecting diffusion entirely. If diffusion is not considered we get (19) $T'_s = 770$, $T'_1 = 1100$, and $E_s = 17{,}000$, but with these parameters the curves fit the data about as well as is indicated in figure 4. The values of T'_s and T'_1 used here seem much more probable.

RADIATION EFFECTS IN PROPELLANT BURNING[1]

W. H. AVERY

The Applied Physics Laboratory, The Johns Hopkins University, Silver Spring, Maryland

Received January 9, 1950

INTRODUCTION

When the development of military rockets was begun in the United States in 1941, ballistic considerations required the use of powder grains[2] having dimensions greatly exceeding those common for use in guns. Grains with web thicknesses[3] of the order of half an inch and burning times of 1 sec. or more became necessary.

Although English experience with Cordite SC, which is a transparent propellant, showed that good performance could be obtained with that powder in rockets, American experience with hotter (i.e., higher flame temperature) compositions showed that transparent grains of these powders on burning developed a pitted, termitic looking surface, leading to a greatly increased gas production and excessive rocket pressures. The effect was particularly pronounced in propellants containing inorganic salts. After the usual mystical explanations of the phenomenon had been rejected, it was proved conclusively that the effect was caused by subsurface heating and ignition of powder in contact with radiation-absorbing specks of foreign material unavoidably present in the propellant.

---

[1] Presented at the Symposium on Kinetics of Propellants which was held under the auspices of the Division of Physical and Inorganic Chemistry at the 112th Meeting of the American Chemical Society, New York City, September 15, 1947.

[2] A powder grain is defined to be one piece of propellant. A propellant grain for use in rockets may weigh upwards of 100 lb.

[3] The web thickness is defined as the distance through which burning takes place in the consumption of a propellant grain.

The obvious (and successful) solution to the difficulty was to include in the propellant composition sufficient darkening material, e.g., carbon black, to prevent significant penetration of radiation beyond the burning surface. When this was done, it was found that powders containing only small amounts of darkening material displayed pressure–time curves with a pronounced tendency to curve up toward the end of burning, in some cases even rising to a high peak. Qualitatively it appeared evident that the phenomenon could be explained by internal heating of the powder by the hot propellant gases. It was desirable, however, to investigate the nature of the effect quantitatively in order to make use of it in the design of neutral-burning charges and in the estimation of the effect of variations in salt content or amount of darkening agent in a service propellant.

EXPERIMENTAL

In the charges employed in experimental rockets, the surface decreased nearly uniformly during burning, so that the pressure–time curve of a powder grain which did not show the radiation effect would be of the form shown in figure 1, while that typical of hot, salted powders with a small amount of darkening agent would be of the form shown in figure 2.

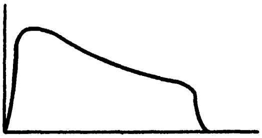

FIG. 1

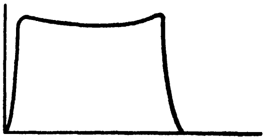

FIG. 2

FIG. 1. Pressure–time plot of unsalted propellant
FIG. 2. Pressure–time plot of salted propellant

For service rockets it was desired to have the more nearly rectangular pressure–time curve exhibited by the salted powders since, with this type of curve, a desired value of the average thrust could be obtained with a minimum strength of the rocket chamber.

The propellant grains used in the studies described in this report were tubular, the dimensions being approximately those shown in figure 3. For the grain shown, the initial surface area is 22.3 in.^{2}, and the area at the end of burning is 20.1 in.^{2}

The grains were burned in rocket motors, adapted for static experiments and equipped with instruments which recorded the pressure in the rocket chamber as a function of burning time (figures 1 and 2). From the pressure–time curve, the burning rate at any instant was obtained as follows:

At any instant, the mass rate of consumption of propellant is

$$\dot{m}_b = rS\rho \qquad (1)$$

in which r = burning rate normal to burning surface,
S = area of burning surface, and
ρ = propellant density.

The burning propellant generates gas at a pressure, P, part of which may remain within the rocket chamber, the remainder being discharged through the nozzle. That is,

$$\dot{m}_b = \dot{m}_c + \dot{m}_d$$

The rate of change of mass within the rocket chamber is:

$$\begin{aligned} \dot{m}_c &= \frac{\mathrm{d}}{\mathrm{d}t}(\rho_g V_t) = \rho_g \frac{\mathrm{d}V_t}{\mathrm{d}t} + V_t \frac{\mathrm{d}\rho_g}{\mathrm{d}t} \\ &= \rho_g r S + \alpha V_t \frac{\mathrm{d}P}{\mathrm{d}t} \end{aligned} \tag{2}$$

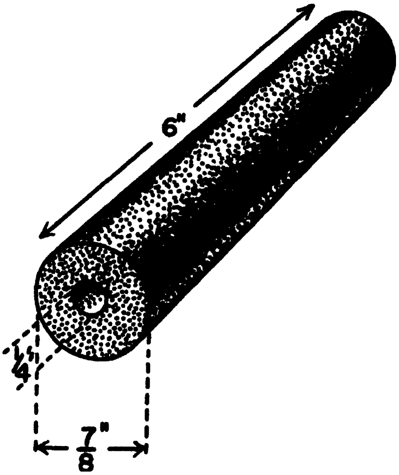

FIG. 3

in which α = constant factor for converting density to pressure for the particular propellant composition and gas temperature,

ρ_g = gas density, and

$V_t = V_c - V_{pt}$ = volume of rocket chamber minus propellant volume at time t.

The mass rate of discharge of gas from the rocket chamber is

$$\dot{m}_d = C_D P A_t \tag{3}$$

in which C_D = discharge coefficient[4] and A_t = area of rocket nozzle throat. Equating equation 1 to equations 2 and 3 and solving for r:

$$r = \frac{1}{(\rho - \alpha P)S_t}\left(\alpha V_t \frac{\mathrm{d}P}{\mathrm{d}t} + C_D P A_t\right) \tag{4}$$

---

[4] The discharge coefficient varies slightly with the pressure. For the pressure used in these studies the variation was small enough to be neglected.

Equation 4 may be used to obtain the value of the burning rate at any instant during burning if the surface area and instantaneous volume may be expressed as a function of the burning time. This may be done as follows: At the time, t_b, at which the propellant is entirely consumed

$$\int_0^{t_b} \dot{m}_b\,dt = M = C_D A_t \int_0^{t_b} P\,dt + \alpha V_c P_e \tag{5}$$

in which V_c = volume of the empty rocket chamber,
P_e = pressure at the end of burning, and
M = initial mass of propellant.

At any time, t, during burning the mass of propellant that has been burned will be:

$$m_b = C_D A_t \int_0^{t} P\,dt + \alpha P V_t \tag{6}$$

Thus the fraction, f_{vt}, of the mass burned at time t will be

$$f_{vt} = \frac{m_b}{M} = \frac{\int_0^{t} P\,dt + \alpha P V_t}{\int_0^{t_b} P\,dt + \alpha P_e V_c} \tag{7}$$

For a grain of the type shown in figure 3 it may easily be shown that

$$S_t = \pi(D_1 + D_2)[l + W(1 - 2f_{wt})] \tag{8}$$

in which f_{wt} is given implicity by the relation

$$f_{vt} = f_{wt}\left(\frac{W^2(1 - f_{wt})}{lW} + 1\right)$$

in which f_{wt} = fraction of the web burned at time t,
W = web thickness,
l = length of the propellant grain, and

$$V_t = V_c - \frac{\pi}{2}(D_2 + D_1)(l - W f_{wt}) W (1 - f_{wt}) \tag{9}$$

Equations 4 through 9 permit the burning rate at successive times during burning of a given round to be expressed as a function of the instantaneous pressures.

If several rounds are fired at various pressures, it is possible also to obtain a plot by the usual means of *average* burning rate *vs. average* pressure.

If the instantaneous rates obtained for the given round are then compared with the *average* rate for the same pressures, it is found that salted powders show a progressive increase in instantaneous rate relative to average rate, as the powder burns. Typical curves obtained in this manner for two rounds of a standard salted powder are shown in figure 4.

It is apparent that there is an increase in rate (referred to constant pressure) of about 5 per cent. Owing to the sensitivity of the rocket pressure to changes in propellant burning rate, this 5 per cent rate increase produces an increase in pressure of about 20 per cent.

THEORETICAL

To explain a change in the burning rate with burning time, it is necessary to find a factor, on which the rate depends, that does not reach an equilibrium value at the same time as the pressure does. Apart from the powder composition, the variables which conceivably can affect the burning rate at constant pressures are: (*1*) the gas temperature, (*2*) the gas velocity parallel to the powder surface, (*3*) the powder temperature, (*4*) the intensity of radiation impinging on the powder surface, and (*5*) the gas composition.

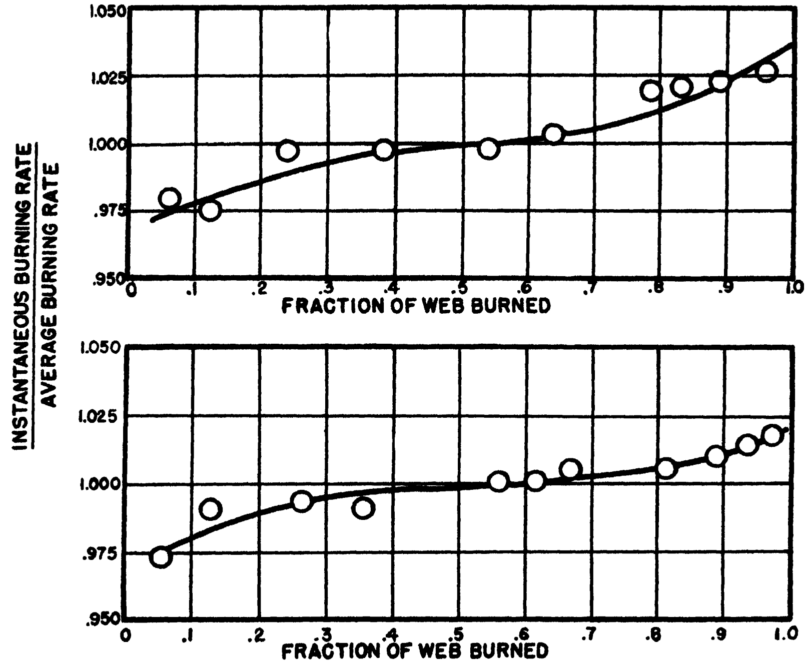

FIG. 4a. Observed curve, round 1
FIG. 4b. Observed curve, round 2

The gas temperature and composition are constant at constant pressure. Since the port area increases, the gas velocity decreases as burning progresses and this should reduce the rate. However, the temperature of the powder can be expected to increase as burning progresses, because heat is conducted into the interior from the hot surface and because at least some of the radiation emitted by the powder gases penetrates the surface layer and is absorbed in the inside of the web; finally, the radiation intensity will, in general, increase because the thickness of the radiating layer increases. Of the possibilities enumerated, it appears that only the last two provide possible explanations of the progressive nature of the curves.

WARMING OF POWDER BY HEAT CONDUCTION

It can be shown that the temperature increment produced by conducted heat at a point inside a grain burning normal to the surface, at a rate, r, is given by

$$T_z = T_s e^{-(\rho C/K)rz} \qquad (10)$$

provided a steady state has been reached. Here

T_z = temperature at a depth of z centimeters below the burning surface,
T_s = surface temperature,
K = thermal conductivity of the powder,
C = heat capacity of the powder,
ρ = density, and
z = the distance of a given point in the powder from the surface.

TABLE 1

Temperature increment produced by heat conduction at various depths below the burning surface

Z DEPTH	T_z TEMPERATURE RISE	Z DEPTH	T_z TEMPERATURE RISE
cm.	°*C.*	*cm.*	°*C.*
1	10^{-10^3}	0.001	60
0.1	10^{-10^2}	0.0005	236
0.01	$10^{-9.2}$	0.0001	760
0.002	4		

In table 1 are listed values for the temperature rise at various distances below the burning surface. The surface temperature is assumed to be 1000°K., the thermal conductivity to be 5×10^{-4} cal./cm.^{2} sec. deg./cm., the density to be 1.6 g./cm.^{3}, and the burning rate to be 2.5 cm./sec. This table shows that the temperature increment is insignificant at depths greater than about 10 microns. Therefore, temperature equilibrium with respect to conducted heat is attained almost immediately after ignition, and heat conduction into the web does not provide an explanation of progressive burning.

WARMING OF POWDER BY RADIANT ENERGY

Although insufficient data are available to permit an exact evaluation of the warming of the powder by radiation, it is possible to calculate rather simply the approximate change in burning rate to be expected. Consider a layer of powder parallel to the burning surface, of unit cross section and thickness dx, and at a depth of b cm. (figure 5). Assume also that radiation of intensity I_0 ergs/(cm.^{2} sec.) is impinging normally on the surface of the powder. We wish to determine the warming of the layer at an original depth b by radiation passing through the surface, during the time that the burning surface progresses from its position at zero time until the surface reaches the thin layer under consideration. If we let X represent the position of the surface at any time with respect to the position of the layer dx, then

$$X = b - rt \tag{11}$$

where r is the burning rate of the powder and t is the time.

Provided the radiation intensity and burning rate are constant, it is easily shown that the energy absorption per unit volume during the time the burning progresses to the depth b is

$$E_1 = \frac{I_0}{r}(1 - e^{-kb})$$

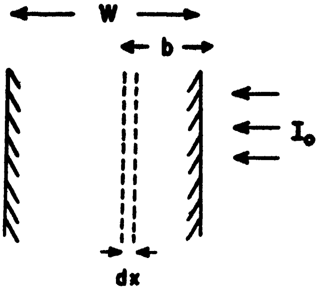

FIG. 5

The rise in temperature of the layer during this time is[5]

$$\Delta T_1 = \frac{I_0}{rC\rho}(1 - e^{-kb})$$

in which C = heat capacity and ρ = density.

In a burning tubular grain of propellant, radiation penetrates the propellant from the perforation as well as from the outside surface. If the web thickness is W, then a surface initially at a depth b from one surface, is at a depth $W - b$ from the other surface. The total energy that is absorbed during the time burning progresses to a depth b (where b is less than $W/2$) is then

$$E = E_1 + E_2 = \frac{I_0}{r}(e^{kb-1})[e^{-kb} + e^{-k(W-b)}]$$

and the temperature rise is

$$\Delta T = \frac{I_0}{rC\rho}(e^{kb} - 1)[e^{-kb} + e^{-k(W-b)}]$$

The fraction of the web burned when the burning has proceeded to the depth b is

$$f = 2b/W \tag{12}$$

---

[5] Heat conduction is neglected.

Substituting for b:

$$\Delta T = \frac{I_0}{rC_p}(1 - e^{-kWf/2})[1 + e^{-kW(1-f)}] \tag{13}$$

Equation 13 may be rearranged to give:

$$\frac{\Delta TrC_p}{I_0} = [1 - e^{-kWf/2}][1 + e^{-kW(1-f)}] \tag{14}$$

Values of the quantity $\Delta TrC_p/I_0$ are plotted in figure 6 as a function of f for values of k ranging from 1 to 100. The web was taken to be 0.3 in. The figure shows that if I_0 and r remain constant during burning, the temperature just below the burning surface increases nearly linearly with the fraction of the web burned for low values of k. But if k is large, the temperature rises rapidly to a value which may be much above the initial value, remains at this value until the web is nearly burned through, and then again rises steeply to a value twice the initial increase.

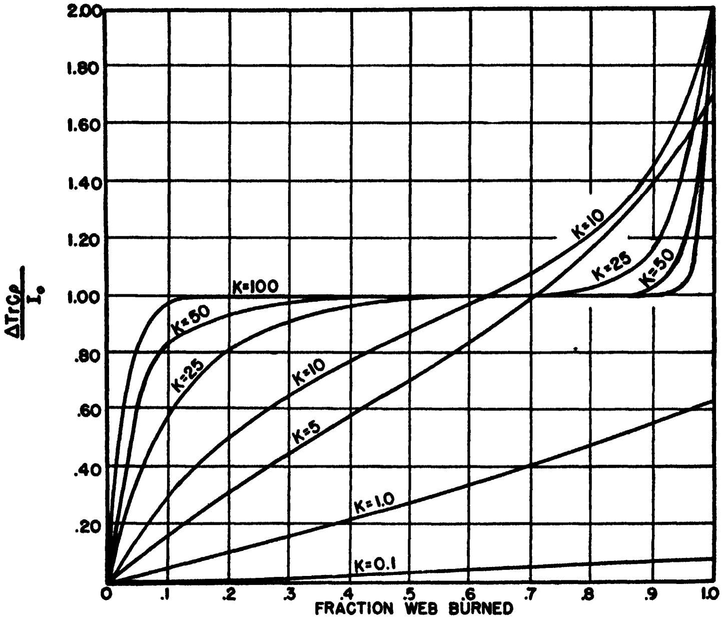

FIG. 6. $\Delta TrC_p/I_0$ *vs.* fraction of web burned for various absorption coefficients

In figure 7 the quantity $\Delta TrC_p/I_0$ is plotted as a function of k for values of f varying in intervals of 0.1 from 0 to 1.0. It is interesting to note that the temperature increase for the last sections of the web burned has a maximum for values of k in the neighborhood of 8.

In the above treatment of the temperature increment at constant burning rate, two important factors have been neglected: (*1*) the dependence of k and I_0 on the wave length of the radiation, and (*2*) the variation of I_0 with the pressure and depth of the emitting layer.

The first factor may be dealt with rather easily by dividing the radiation spectrum into segments narrow enough so that the radiant energy and absorption coefficients of the powder may be considered constant within a given segment. The temperature increment is computed from energy absorption in each segment and the temperatures so obtained are summed over all segments. When this is done equation 13 becomes:

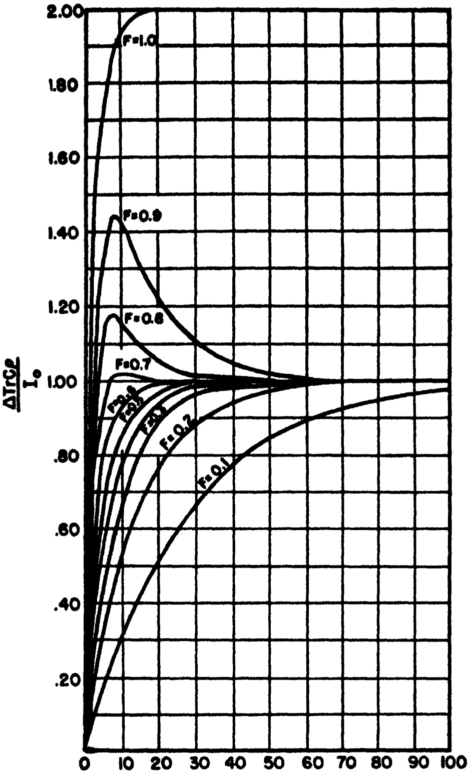

FIG. 7

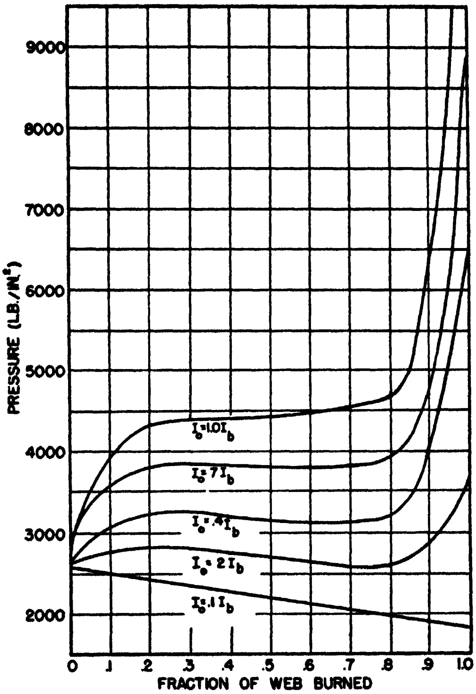

FIG. 8

FIG. 7. $\Delta TrCp/I_0$ *vs.* absorption coefficient for various fractions of the web burned.

FIG. 8. Curves of pressure *vs.* fraction of the web burned at various intensities of radiation.

$$\Delta T = 1/rcp \sum_i I_i[1 - e^{-k_i w f/2}][1 - e^{-k_i w(1-f)}] \qquad (15)$$

For this calculation it is necessary to know the energy distribution and the absorption coefficient of the powder as functions of the wave length. If the powder emits as a "gray" or black body, the energy distribution is given by Planck's function. Average values of the energy emitted by a black body at 3000°K. for wave-length intervals covering the spectrum are listed in table 2 along with the absorption coefficients of a typical propellant for the same spectral regions. The data are taken from curves obtained by Dr. J. Beek (0.04–

1.0 μ) and Professor Farrington Daniels (1.0–5.0 μ). The absorption coefficient in the region 5–10 μ has been estimated.

PRESSURE FRACTION OF WEB CURVES AT CONSTANT RADIATION DENSITY

The data obtained above may be used to calculate the change in the shape of a pressure *vs.* time curve (or more conveniently, pressure *vs.* fraction-of-the-web-burned curve) that would be associated with different intensities of radiation striking the powder surface. This is done as shown below.

TABLE 2

Radiation emitted by a black body at 3000°K. and absorption coefficients of JPT powder

WAVE-LENGTH INTERVAL	BLACK-BODY RADIATION AT 3000°K.			ABSORPTION COEFFICIENT*
	E	$E_\lambda d_\lambda$	$E_\lambda d_\lambda$	
μ	*ergs/cm.² sec.*	*ergs*	*calories*	*cm.⁻¹*
0.3– 0.4	1.27×10^{12}	1.3×10^7	0.30	
0.4– 0.5	5.38	5.4	1.29	56
0.5– 0.6	12.50	12.5	2.99	34
0.6– 0.7	20.30	20.3	4.85	23
0.7– 0.8	26.45	26.5	6.32	17
0.8– 1.0	30.20	60.4	14.43	12
1.0– 2.0	21.56	215.6	51.51	13
2.0– 3.0	7.76	77.6	18.54	42
3.0– 4.0	2.74	27.4	6.55	64
4.0– 5.0	1.16	11.6	2.77	31
5.0–10.0	0.40	20.0	4.78	40

* These values for $k = d^{-1} \log_e I_0/I$ are approximate because corrections for light scattering, reflections, and refraction at the powder surface have been neglected. Dr. Beek has estimated that reflection would decrease the intensity of the radiation penetrating the surface by about 10 per cent and that the effect of refraction could be approximated by increasing the value of k by 13 per cent. The uncertainty in the absorption coefficient makes these refinements superfluous.

Studies of a large number of propellants of the type under discussion show that the dependence of the average burning rate on the average ambient pressure and initial propellant temperature may be represented by the equation

$$r = \frac{C'P^n}{T_1 - T_p} \tag{16}$$

in which C', n, and T_1 are constants characteristic of the propellant composition and T_p is the initial propellant temperature. Since the effect of radiation is to raise the temperature of the burning layer of propellant, the instantaneous rate may be expressed by the equation

$$r = \frac{C''P^{n'}}{T_1' - (T_p + \Delta T_f)} \tag{17}$$

in which ΔT_f is the increase in propellant temperature at the burning layer and C'', n', and T_1' will have slightly different values from those found by use of the average dependence of rate on *average* pressure and *initial* temperature.[6]

Assuming that the rate is given by equation 17, and equating this to equation 4, we have:

$$\frac{C'P^n}{T_1' - (T_p + \Delta T_f)} = \frac{1}{(\rho - \alpha P)S_t}\left[\alpha V_t \frac{dP}{dt} + C_D P A_t\right] \tag{18}$$

In this equation C', n, T_1', ρ, α, and C_D are dependent only on the propellant composition and, for the propellant considered, had the values:

$$C' = 2.085\ (\text{cm./sec.})(\text{lb. in.}^2)^n,$$
$$n = 0.72,$$
$$\rho = 1.6\ \text{g./cm.}^3, \text{ and}$$
$$\alpha = 7.25 \times 10^{-6}P\ (\text{g./cm.}^3).$$

For a typical rocket the gas density is less than 0.5 per cent of the propellant density, and the rate of change of mass in the chamber is less than 0.5 per cent of the rate of discharge. Neglecting the small terms, the pressure may then be expressed as a function of the fraction of the web burned by the formula

$$P = \frac{C'}{T_1' - (T_p + \Delta T_f)}\,\frac{\rho}{C_D}\,\frac{S_0}{A_t}\left[1 - \frac{2Wf_{wt}}{l+W}\right]^{1/(1-n)} \tag{19}$$

in which S_0 is the initial surface area.

Curves for pressure *versus* fraction of web burned may then be constructed by selecting initial conditions to give a desired pressure, computing the appropriate rate of equation 17, determining the temperature rise when a small fraction f is consumed, calculating the pressure and rate corresponding to this temperature, and repeating at appropriate intervals until the powder is consumed.

Figure 8 presents a series of pressure *vs.* fraction-of-the-web-burned curves obtained by the above method. The different curves correspond to different values of the radiation intensity, i.e., different fractions of the energy that would be produced by a black body at 3000°K.

The curves bring out three important points: (*1*) radiation can have an appreciable effect on the pressure–time curve even when the emissivity of the powder gases is as low as 20 cal./(cm.² sec.); (*2*) all of the curves except the first, in which there is no radiation, exhibit the "end-peaks" characteristic of salted powders; (*3*) the assumption of constant emissivity is not a good approximation to the actual conditions, since the formula derived on this basis does not predict pressure–time curves that are markedly progressive over the entire course of the curve even for the case of maximum possible radiation.

---

[6] It is evident that the principal change will be in the value of T_1, since $T_1' \cong T_1 + \overline{\Delta T_f}$. The values of n and C' change slightly since the burning time, and hence the average value of ΔT_f, changes with pressure. To the approximation considered here it has been assumed that $n' = n$, $C'' = C'$.

The treatment of the radiation effect may be further extended to take account of changes in radiation density due to increase in the depth of the emitting layer and to changes in pressure. The resulting formulas are complicated and of too specialized applicability to make it worthwhile to present them here. However, incorporation of these refinements leads to satisfactory qualitative agreement between the form of the observed dependence of rate on fraction burned and that calculated. It appears that quantitative agreement would necessitate the use of somewhat lower values of the gas emissivity than those that were employed in the calculations.

SUMMARY

In an effort to explain the action of added potassium salts upon the burning rates of rocket propellants, an examination is made of the factors which can affect the shape of the pressure–time curve of a rocket fired statically under standard conditions. Of the variables considered, it is most reasonable to assume that warming of the powder (*1*) through heat conduction or (*2*) through radiation causes the burning rate, and hence the pressure, to increase with time of burning.

A roughly quantitative treatment is made which shows that the effect of heat conduction is negligible but that the warming of the powder by radiation may be appreciable. The radiation effect is studied in some detail and the changes in shape of the pressure–time curves investigated theoretically for two cases in which the postulated conditions are: (*a*) a constant radiation intensity and constant absorptivity of the powder; (*b*) a radiation intensity constant with time but distributed spectrally according to Planck's radiation law for a black body at 3000°K., the absorption coefficient of the powder being given as a function of the wave length from experimental data.

Pressure–time curves calculated by the formulas developed are presented for radiation intensities corresponding to several different fractions of the radiation from a black body at 3000°K.

I wish to express my thanks to Professors Farrington Daniels and Bryce L. Crawford, Jr., for supplying data on the absorption coefficient of the propellant and the emissivity of the gas. I am also indebted to Drs. F. T. McClure and John Beek for helpful discussions. The work described was done at the Allegany Ballistics Laboratory operated by George Washington University under Contract OEMsr-273 with the Office of Scientific Research and Development.

A PHYSICAL THEORY OF BURNING OF DOUBLE-BASE ROCKET PROPELLANTS. I[1]

ROBERT G. PARR[2] AND BRYCE L. CRAWFORD, JR.

School of Chemistry, University of Minnesota, Minneapolis, Minnesota

Received August 15, 1949

I. INTRODUCTION

Considerable experimental evidence (3, 4) indicates that the burning of double-base (nitrocellulose–nitroglycerin) propellants is a stepwise process. It is generally believed (3, 4, 5) that three main stages are involved (a "stage" may consist of several elementary processes): (*a*) primary solid-phase decomposition giving organic fragments and nitrogen dioxide, (*b*) nonluminous gas-phase reaction of the products of (*a*) to give nitric oxide and aldehydic[3] molecules, and (*c*) luminous gas-phase reaction of the products of (*b*) to give the final products. These stages may be called the *foam*, *fizz*, and *flame reactions*, respectively.

The task of treating this burning mechanism quantitatively is really twofold. A definite model must first be set up, and then means must be devised for treating it mathematically. The model must include detailed kinetics of individual steps and various thermal quantities—several unknown parameters—and hence at best can be only a crude approximation; we can ask more of the mathematics. Starting from an assumed model, we shall obtain theoretical results which we can try to make fit experiment by varying the parameters. If we are successful at this (getting reasonable values for the parameters) we may claim that our model has some use; if we are not, we may still hope that our mathematical treatment of the model will have value elsewhere.

II. MATHEMATICAL DEVELOPMENT OF THE THEORY

A. *Statement of the problem*

The one-dimensional model for the reaction zones which we shall consider is shown in figure 1. We will suppose that the foam, fizz, and flame reactions are exothermic by Q_a, Q_b, and Q_c calories per gram (assumed independent of temperature), and that foam and fizz reactions are of first and second order, respectively.[4] Experiment indicates that these three stages are fairly well separated in space (3, 4). We take advantage of these indications, and postulate as complete separation as possible. No reaction (of finite order) is ever complete in a finite time, so that we cannot require the foam reaction to be 100 per cent complete before the fizz reaction starts. However, writing ϵ_a for the fraction of the foam reaction completed (a function of y), and similarly ϵ_b, ϵ_c, we can demand that

---

[1] This paper is based on work done at the University of Minnesota under Contract OEMsr-716 with the Office of Scientific Research and Development, and under Contract NOrd-9680 with the Bureau of Ordnance of the United States Navy Department.

[2] Present address: Department of Chemistry, Carnegie Institute of Technology, Pittsburgh 13, Pennsylvania.

[3] The exact nature of these partially oxidized intermediates is by no means proven; some investigators feel that aldehydes are not formed in the fizz reaction but earlier.

[4] The flame reaction will not be treated in detail in this paper. It would seem that its order must be higher than that of the fizz reaction, however, if a stable separate zone is to appear.

$$\epsilon_b = 0, \qquad \epsilon_a = 1 - \delta_a, \qquad \text{at } y = 0 \tag{1}$$

where δ_a is some very small number whose value must be determined. (The surface plane $y = 0$ is defined by this boundary condition.) Similarly we demand

$$\epsilon_c = 0, \qquad \epsilon_b = 1 - \delta_b, \qquad \text{at } y = y_1 \tag{2}$$

where δ_b is another small number.

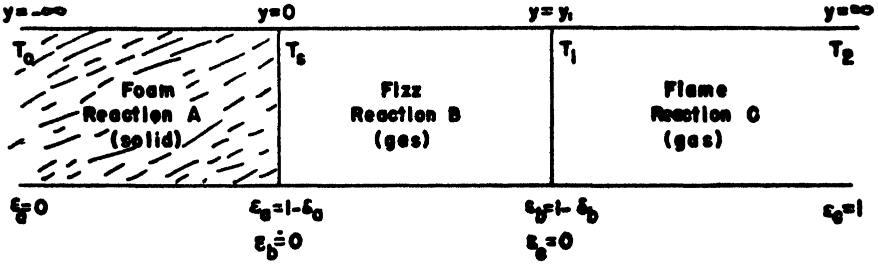

FIG. 1. Model for the reaction zones

The fundamental differential equation which we shall solve is that giving the heat balance in the steady state for a moving medium in which heat sources are distributed:

$$\frac{d}{dy}\left(\lambda \frac{dT}{dy}\right) - M \frac{d}{dy}(cT) + q = 0 \tag{3}$$

where $T(y)$ = temperature, deg.,
$\lambda(y)$ = thermal conductivity, cal. sec.$^{-1}$ cm.$^{-1}$ deg.$^{-1}$,
M = mass burning rate, g. sec.$^{-1}$ cm.$^{-2}$,
$c(y)$ = constant pressure heat capacity, cal. g.$^{-1}$ deg.$^{-1}$, and
$q(y)$ = source strength, cal. sec.$^{-1}$ cm.$^{-3}$

This equation is applicable to more complex (and more nearly correct) models than ours; it holds provided radiation and diffusion due to concentration gradients may be ignored and pressure may be assumed constant throughout the reaction zones. It can indeed be shown without difficulty that the radiation effect is trivial and that pressure is near constant (3); the only serious limitation of equation 3 is its neglect of diffusion. Diffusion in the solid is probably not important, but diffusion in the gaseous zones cannot be dismissed so easily. We shall consider the latter in detail in a later paper—the results we obtain now will be strictly valid only when diffusion coefficients are zero.[5]

---

[5] Both Corner (1, 2) and Rice and Ginell (5) also consider the case of zero diffusion first.

Assumptions 1 and 2 simplify the solution of equation 3 enormously. They permit us to resolve the problem into three parts, in each of which we need consider only one reaction variable. The three parts are joined by thermal boundary conditions expressed in terms of the temperatures $T_s \equiv T(0)$ and $T_1 \equiv T(y_1)$, and by the mass-balance requirement that M be a constant. Our separated mathematical problems then are:

A. To find a relation between M, the pressure P, and T_s by studying the solid-phase reaction A.

B. To find a relation between M, P, T_s, and T_1 by investigating the effect of reaction B on T_s.

C. To find a relation between M, P, and T_1 by investigating the effect of reaction C on T_1.

Having found these relations, we may eliminate T_s and T_1 to obtain the relation between M and P—the burning rate law.

Our model is a slight extension of that of Rice and Ginell (5). They suppose that reaction A takes place entirely at the surface $y = 0$; we allow it to occur in a region of finite width. We shall see that this difference affects the results only at low pressures.

B. The foam reaction

Quite generally, the rate (g. cm.$^{-3}$ sec.$^{-1}$) of the solid-phase reaction may be written

$$\text{Rate} = M(\mathrm{d}\epsilon_a/\mathrm{d}y) \tag{4}$$

so that

$$q(y) = MQ_a(\mathrm{d}\epsilon_a/\mathrm{d}y) \tag{5}$$

If we substitute equation 5 in equation 3, assign constant values c_a and λ_a to c and λ (these are secondary parameters and we may as well assume them constant), and perform a first integration subject to the boundary condition

$$(\mathrm{d}T/\mathrm{d}y) = 0 \text{ at } T = T_0 \tag{6}$$

where T_0 is the ambient temperature, we obtain

$$\lambda_a(\mathrm{d}T/\mathrm{d}y) = MQ_a(1 - \delta_a - \epsilon_a) + Mc_a(T - T_a) \tag{7}$$

where

$$T_a = T_0 + (Q_a/c_a)(1 - \delta_a) \cong T_0 + (Q_a/c_a) \tag{8}$$

T_a is the temperature the surface $y = 0$ would have if no heat reached it from the fizz and flame reaction zones.

Since the solid-phase reaction is first order (by hypothesis), its rate will be given by

$$M(\mathrm{d}\epsilon_a/\mathrm{d}y) = B_a\rho_f(1 - \epsilon_a)\exp(-A_a/T) \tag{9}$$

where B_a = frequency factor, sec.$^{-1}$,
A_a = activation energy E_a divided by gas constant R, deg., and
ρ_f = density (a function of ϵ_a and T), g. cm.$^{-3}$

Now the products of this reaction are gases, the same gases which later react in the first gas-phase reaction; while they will dissolve in the solid to some extent, it is reasonable to suppose that they will form bubbles.[6] This suggests that we write the specific volume as

$$(1/\rho_f) = (1/\rho)(1 - \epsilon_a) + (RT/PW_a)\epsilon_a \tag{10}$$

where ρ = powder density (g. cm.$^{-3}$) and W_a = average molecular weight of products of foam reaction. Equation 9 then becomes

$$M\frac{d\epsilon_a}{dy} = \frac{B_a\rho(1 - \epsilon_a)\exp(-A_a/T)}{[1 + (\rho RT/PW_a)\epsilon_a - \epsilon_a]} \tag{11}$$

which divided by equation 7 yields:

$$\frac{d\epsilon_a}{dT} = \frac{\lambda_a B_a \rho(1 - \epsilon_a)\exp(-A_a/T)}{M^2[1 + (\rho RT/PW_a)\epsilon_a - \epsilon_a][Q_a(1 - \delta_a - \epsilon_a) + c_a(T - T_a)]} \tag{12}$$

We must integrate this equation under the boundary conditions

$$\epsilon_a = 0 \text{ at } T = T_0 \tag{13}$$

and

$$\epsilon_a = 1 - \delta_a \text{ at } T = T_s \tag{14}$$

As a first approximation,[7] which will be at its best in the region where most of the reaction is taking place (near the surface), we set $T = T_s$ in the exponential and in the first coupling term in the denominator of equation 7. The resulting differential equation is linear, and has the solution satisfying equation 14:

$$\begin{aligned}\eta = {} & -\xi^{-\alpha}\exp(\alpha r\xi)\int_{\delta_a}^{\xi}\xi^{\alpha}\exp(-\alpha r\xi)d\xi + \xi[1 - (\delta_a/\xi)^{\alpha+1}\exp(-\alpha r\delta_a + \alpha r\xi)] \\ & + [(c_a/Q_a)(T_s - T_a) - \delta_a][1 - (\delta_a/\xi)^{\alpha}\exp(-\alpha r\delta_a + \alpha r\xi)]\end{aligned} \tag{15}$$

where

$$\eta = (c_a/Q_a)(T_s - T), \qquad \xi = 1 - \epsilon_a \tag{16}$$

$$r = 1 - (PW_a/\rho RT_s) \tag{17}$$

and

$$\alpha = (c_a M^2 RT_s/\lambda_a B_a PW_a)\exp(A_a/T_s) \tag{18}$$

As the second approximation, we use equation 15 to express each of the coupling terms in the denominator of the right side of equation 12 in terms of ξ alone, and integrate again, imposing both of the conditions 13 and 14. We find

---

[6] This is borne out by various experimental observations on the "altered layer" (3).

[7] The integrations by successive approximations employed in this paper are patterned after those carried out by Boys and Corner (1).

$$\begin{aligned}
(1/2\alpha)I(T_s) = {} & (Q_a/c_a)^2 \Bigg\{ \int_{\delta_a}^{1} (1 - \xi)\xi^{-(2\alpha+1)} \exp(2\alpha r\xi) \left[\int_{\delta_a}^{\xi} \xi^{\alpha} \exp(-\alpha r\xi) \mathrm{d}\xi \right]^2 \mathrm{d}\xi \\
& + \int_{\delta_a}^{1} \xi^{-(\alpha+1)} \exp(\alpha r\xi) \left[\int_{\delta_a}^{\xi} \xi^{\alpha} \exp(-\alpha r\xi) \mathrm{d}\xi \right] [(\delta_a - \xi)(1 - \xi)] \mathrm{d}\xi \Bigg\} \\
& + (Q_a/c_a) \Bigg\{ \int_{\delta_a}^{1} \xi^{-(\alpha+1)} \exp(\alpha r\xi) \Bigg[\int_{\delta_a}^{\xi} \xi^{\alpha} \exp(-\alpha r\xi) \mathrm{d}\xi][T_s(1 - r)\xi \\
& + T_a(1 - \xi) + 2(T_s - T_a)(1 - \xi)(\delta_a/\xi)^{\alpha} \exp(\alpha r\xi - \alpha r\delta_a)] \mathrm{d}\xi \Bigg\} \\
& + (T_s - T_a) \Bigg\{ \int_{\delta_a}^{1} (\delta_a/\xi)^{\alpha} \exp(\alpha r\xi - \alpha r\delta_a)\xi^{-1}[T_s(1 - r)\xi \\
& + T_a(1 - \xi) + (Q_a/c_a)(\delta_a - \xi)(1 - \xi) \\
& + (T_s - T_a)(1 - \xi)(\delta_a/\xi)^{\alpha} \exp(\alpha r\xi - \alpha r\delta_a)] \mathrm{d}\xi \Bigg\}
\end{aligned} \tag{19}$$

where

$$I(T_s) = 2T_s \exp(A_a/T_s) \int_{T_0}^{T_s} \exp(-A_a/T) \mathrm{d}T \tag{20}$$

Equation 19 may be greatly simplified by the assumption that δ_a is small. Indeed, if δ_a is neglected everywhere it occurs in combination with quantities of the order of magnitude of unity, and if moreover α is allowed to approach zero in the coefficient of δ_a^{α} (when δ_a is small, δ_a^{α} is appreciable only for small α), there results:[8]

$$\begin{aligned}
(Q_a/c_a)^2[L_0 - L_1 + H_2 - H_1] + (Q_a/c_a)[T_s(1 - r)H_1 + T_a(H_0 - H_1)] & \\
+ (1/2)[T_s^2 - I(T_s) - (T_a + [T_s - T_a]\delta_a^{\alpha})^2] = 0 &
\end{aligned} \tag{21}$$

where

$$H_k = H_k(\alpha, r) = \alpha(\alpha r)^{-(\alpha+1)} \int_0^1 \gamma(\alpha + 1, \alpha r\xi) \exp(\alpha r\xi)\, \xi^{k-\alpha-1} \mathrm{d}\xi \tag{22}$$

$$L_k = L_k(\alpha, r) = \alpha(\alpha r)^{-2(\alpha+1)} \int_0^1 \gamma^2(\alpha + 1, \alpha r\xi) \exp(2\alpha r\xi)\xi^{k-2\alpha-1} \mathrm{d}\xi \tag{23}$$

and

$$\gamma(\alpha + 1, \alpha r\xi) = \int_0^{\alpha r\xi} x^{\alpha} e^{-x} \mathrm{d}x \tag{24}$$

We may obtain a final reduction by noting that at moderate pressures the specific volume of the solid reactants is negligible compared to that of the gaseous products; *viz.*,

$$r = 1 \tag{25}$$

---

[8] In passing from equation 19 to equation 21 the limit as $\delta_a \to 0$ is *not* taken This limit exists but is not uniform in α.

When this condition is imposed, it can be shown that equation 21 becomes

$$\{1 - (Q_a/c_aT_a)F(\alpha)\}^2 - \{1 + (T_s/T_a)^2 - I(T_s)/T_a^2\} + \{1 + [(T_s/T_a) - 1]\delta_a^\alpha\}^2 = 0 \quad (26)$$

where

$$F(\alpha) = 1 - \alpha^{-(\alpha+1)}e^\alpha\gamma(\alpha + 1, \alpha) \quad (27)$$

Problem A is now solved except for arithmetical details, for equation 26 gives α as an implicit function of T_s. This equation may be contrasted to the simpler one employed by Rice and Ginell: namely,

$$M = B_0 \exp(-A_a/T_s) \quad (28)$$

where B_0 is a frequency factor in g. sec.$^{-1}$ cm.$^{-2}$

C. The fizz reaction

Assuming the fizz reaction to be a second-order reaction whose reactants and products have the molecular weights W_a and W_b, we may write the rate of reaction as

$$M(\mathrm{d}\epsilon_b/\mathrm{d}y) = [B_b(1 - \epsilon_b)^2/V^2] \exp(-A_b/T) \quad (29)$$

where B_b = frequency factor, cm.^{3} g.$^{-1}$ sec.$^{-1}$, and
A_b = activation energy E_b divided by R, deg.,
and V is the specific volume, given by

$$V = [(1 - \epsilon_b)/W_a + \epsilon_b/W_b](RT/P) = (1 + n\epsilon_b)(RT/PW_a) \quad (30)$$

where

$$n = (W_a/W_b) - 1 \quad (31)$$

In analogy with equation 7 the equation representing the conservation of energy in this reaction zone is

$$\lambda_b(\mathrm{d}T/\mathrm{d}y) = MQ_b(1 - \delta_b - \epsilon_b) + Mc_b(T - T_b) \quad (32)$$

where c_b and λ_b are suitable average values for the heat capacity and thermal conductivity, and T_b is the value T_1 would have if no heat reached the fizz zone from the flame reaction; i.e.,

$$T_b = T_a + (Q_b/c_b)(1 - \delta_b) \cong T_a + (Q_b/c_b) \quad (33)$$

Division of equation 29 by equation 32 and use of equation 30 yields

$$\frac{\mathrm{d}\epsilon_b}{\mathrm{d}T} = \frac{\lambda_b B_b P^2 W_a^2(1 - \epsilon_b)^2 \exp(-A_b/T)}{M^2 R^2 T^2(1 + n\epsilon_b)^2[Q_b(1 - \delta_b - \epsilon_b) + c_b(T - T_b)]} \quad (34)$$

which we must integrate subject to

$$\epsilon_b = 0 \text{ at } T = T_s \quad (35)$$

and

$$\epsilon_b = 1 - \delta_b \text{ at } T = T_1 \tag{36}$$

As the first approximation, we set

$$\frac{\exp(-A_b/T)}{T^2(1 + n\epsilon_b)^2} = \frac{\exp(-A_b/T_1)}{T_1^2(1 + n)^2} \tag{37}$$

Integration of equation 34 and application of 36 then gives

$$\eta = \beta \exp(\beta/\xi)[-E_i(-\beta/\xi) + E_i(-\beta/\delta_b)] + [(c_b/Q_b)(T_1 - T_b) - \delta_b]\,[1 - \exp(\beta/\xi)\exp(-\beta/\delta_b)] \tag{38}$$

where

$$\eta = (c_b/Q_b)(T_1 - T), \qquad \xi = 1 - \epsilon_b \tag{39}$$

$$\beta = [c_b M^2 R^2 T_1^2 (1 + n)^2/\lambda_b B_b P^2 W_a^2] \exp(A_b/T_1) \tag{40}$$

and

$$-E_i(-x) = \int_x^\infty x^{-1} e^{-x} dx \tag{41}$$

is the exponential integral. If we wished to stop with this approximation, we would set $T = T_s$, $\xi = 1$, and find, with the aid of equation 33 and the fact that δ_b is very small,

$$T_s - T_a = (Q_b/c_b)\,\{1 - \beta \exp(\beta)\,[-E_i(-\beta)]\} + (T_1 - T_b)\exp(\beta)\exp(-\beta/\delta_b) \tag{42}$$

which to this degree of approximation is the solution of Problem B.

It is interesting to compare equation 42 with the equation obtained by Rice and Ginell by a different method (5): namely,

$$T_s - T_a = (Q_b/c_b)\,\{1 - z_1^2 \exp(z_1^2)\,[-E_i(-z_1^2)]\} \tag{43}$$

where z_1 is a parameter proportional to (M/P). Equations 42 and 43 are identical for the case $T_1 = T_b$ and otherwise differ only by the last term in equation 42. This is as it should be, for in his derivation Rice assumes (*1*) constant ratio of conductivity to square of specific volume, and (*2*) zero activation energy, which are essentially equivalent to what we assume in equation 37; and in addition (*3*) all heat reaching the surface from the plane $y = y_1$ may be regarded as originating at that plane (i.e., the temperature gradient at $y = y_1$ is zero), which causes equation 43 to lack the last term of equation 42. Indeed, the dependence of this term on δ_b is just what one would predict, for it is to be expected that the smaller δ_b is taken, the smaller will be the amount of heat that gets back to the surface from the flame reaction at a given pressure, the point $\epsilon_b = 1 - \delta_b$ being by equation 2 the point where the flame reaction begins.

If we wish to perform the integration of equation 34 in two steps rather than one, we employ as the first approximation

$$\frac{\exp(-A_b/T)}{T^2(1 + n\epsilon_b)^2} = \frac{\exp(-A_b/T_1)}{\chi T_1^2(1 + n)^2} \tag{44}$$

where χ is a parameter depending on A_b whose value is to be determined.[9] The first integration gives an equation identical with equation 38 except that β is replaced by $\chi\beta$. When this is substituted back in the coupling term of equation 34, a second integration between the limits 35 and 36 may be carried out. After use is made of the fact that δ_b is small, there results

$$h_n(\chi\beta) + (c_b/Q_b)(T_1 - T_b)[1 - \exp(-\chi\beta/\delta_b)] = \chi f(T_s) \tag{45}$$

where

$$h_n(x) = g_1(x) - 2n(1 + n)^{-1}g_2(x) + n^2(1 + n)^{-2}g_3(x) \tag{46}$$

$$g_k(x) = x^k \int_x^\infty [1 + u \exp(u)E_i(-u)]u^{-k}\mathrm{d}u \tag{47}$$

and

$$f(T_s) = (c_bT_1/Q_b)(T_1/A_b)[1 - \exp(-A_b/T_s) \exp(A_b/T_1)] \tag{48}$$

The evaluation of χ can be accomplished by means of the relations

$$[T_s]_{(p=0)} = T_a \tag{49}$$

$$[T_1)_{(p=0)} = T_b \tag{50}$$

which are proved in Appendix I. From equations 45, 49, and 50, we find

$$\chi = H(n)/f(T_a) \tag{51}$$

where

$$\begin{aligned} H(n) &= \lim_{p\to 0} h_n(\chi\beta) = \lim_{x\to\infty} h_n(x) \\ &= (1 + n + n^2/3)(1 + n)^{-2} \end{aligned} \tag{52}$$

Substituting this in equation 45, we then find

$$\begin{aligned} &h_n(\chi\beta) + (c_b/Q_b)(T_1 - T_b)[1 - \exp(-\chi/\delta_b)] \\ &\qquad = H(n)\left[\frac{1 - \exp(-A_b/T_s)\exp(A_b/T_1)}{1 - \exp(-A_b/T_a)\exp(A_b/T_1)}\right] \end{aligned} \tag{53}$$

This equation gives β as a function of T_s, and so represents a second and better approximation to the solution of Problem B.

III. RESULTS

A. The burning rate law for fizz burning

The equations developed above suffice for the determination of the M–P relation for pressures of which the flame reaction can be neglected (fizz burning).

---

[9] It would be desirable to let χ depend upon P as well as A_b, but the problem of finding its value then becomes intractable.

We need only set $T_1 = T_b$ in equation 53 (or 42) and eliminate T_s between it and equation 26.

In tables 1 and 2 we have tabulated as functions of T_a/T_s the quantities

$$\begin{aligned} X &= -\log\,[\alpha(T_a/T_s)\exp(-A_a/T_s)] \\ &= \log P - 2\log M + \log(\lambda_a B_a W_a/c_a R T_a) \end{aligned} \tag{54}$$

and

$$Y = \log\,(\chi\beta)$$

$$= -2\log P + 2\log M + \log\,[(\chi c_b R^2 T_b^2(1+n)^2/\lambda_b B_b W_a^2)\exp(A_b/T_b)] \tag{55}$$

calculated from equations 26 and 53 for a wide range of values of the parameters T_a, T_b, A_a, A_b, δ_a, and two values of the ambient temperature T_0. For lack of a better value, we have assigned to n the value 1, corresponding to a 50 per cent decrease of average molecular weight in the fizz reaction. Entries in the tables are in error at most a few units in the last place.[10]

M and P may be found as functions of T_a/T_s, and hence of each other, from the formulas

$$\log M' = \log k_m M = -(X + \tfrac{1}{2}Y) \tag{56}$$

and

$$\log P' = \log k_p P = -(X + Y) \tag{57}$$

where

$$k_m = [cT_a\lambda_b^{1/2}B_b^{1/2}/\chi^{1/2}c_b^{1/2}T_b\lambda_a B_a(1+n)]\exp(-A_b/2T_b) \tag{58}$$

and

$$k_p = [cT_a\lambda_b B_b W_a/\chi c_b R T_b^2\lambda_a B_a(1+n)^2]\exp(-A_b/T_b) \tag{59}$$

Here λ_a/c_aT_a and $\lambda_b/c_bT_b^2$ are roughly independent of the ambient temperature,[11] so that

$$k_m \cong k_m'\chi^{-1/2}\exp(-A_b/2T_b) \tag{60}$$

and

$$k_p \cong k_p'\chi^{-1}\exp(-A_b/T_b) \tag{61}$$

where k_m' and k_p' do not depend on T_0.

The calculations which lead to tables 1 and 2 are tedious but for the most part straightforward, and consequently need not be described in detail. The only unfamiliar functions entering these calculations are the $g_k(x)$, the computation of which is discussed in Appendix II.

[10] This refers to the precision of the calculations based on equations 26 and 53, not to the accuracy of those approximate equations compared to "true" solutions of the differential equations 12 and 34. The latter could be tested only by numerical integration.

[11] This does not contradict the assumption of constant heat capacities and conductivities made in earlier sections. There these quantities were assigned average values through the reaction zones; here a dependence on T_0 is ascribed to those average values.

TABLE 1

X as a function of T_a/T_s

$T_0 = 298$

δ_a	$10^{-3}A_a$	T_s	T_a/T_s 1.000	0.996	0.992	0.988	0.984	0.98	0.97	0.96	0.95	0.94	0.93	0.92	0.91	0.9	0.8	0.7	0.6	0.5	0.4	0.3	0.2
e^{-8}	2	400	1.489	1.508	1.525	1.541	1.560	1.579	1.624	1.674	1.722	1.771	1.824	1.879	1.935	1.994	2.468	2.527	2.478	2.385	2.268	2.129	1.951
		700	0.855	0.862	0.867	0.874	0.880	0.886	0.901	0.917	0.934	0.952	0.969	0.987	1.005	1.025	1.262	1.491	1.582	1.595	1.562	1.453	
		1000	0.391	0.395	0.399	0.403	0.408	0.412	0.424	0.435	0.445	0.457	0.468	0.480	0.493	0.506	0.635	0.783	0 927	0.985	0.783		
		1300	0.065	0.068	0.073	0.076	0.079	0.083	0.090	0.098	0.106	0.113	0.120	0.127	0.134	0.142	0.216	0.270	0.265	0.059			
	8	400	8.971	8.988	9.004	9.018	9.038	9.055	9.094	9.115	9.124	9.118	9 100	9 072	9.042	9.003	8.453	7.768	7.032	6.266	5.485	4.696	3.900
		700	5.421	5.426	5.431	5.436	5.440	5.444	5.455	5.465	5.470	5 475	5 475	5.470	5 463	5.454	5.244	4.927	4.560	4.169	3.762	3.345	
		1000	3.866	3.871	3.875	3.879	3.883	3.888	3.901	3.912	3.922	3 932	3.941	3 949	3.952	3.956	3.890	3.726	3.510	3 271	3.015	2.747	
		1300	2.986	2.991	2.996	3.000	3.005	3.009	3.021	3.032	3.046	3.059	3.071	3.082	3.093	3 102	3.120	3.040	2.910	2.753	2.577	2.389	
	14	400	15.783	15.789	15.793	15.791	15.791	15.783	15.752	15.696	15.628	15 546	15 456	15.355	15.252	15.146	13.917	12.575	11.184	9.764	8.328	6.879	5.432
		700	9.413	9.409	9.406	9.402	9 396	9.388	9.368	9.342	9.309	9 273	9 234	9.189	9.139	9 088	8.488	7.786	7.041	6.271	5.488	4.698	3.901
		1000	6.742	6.744	6.742	6.739	6 736	6 733	6.729	6 720	6 706	6.692	6 674	6.651	6.626	6.600	6.251	5.810	5.326	4.818	4.297	3.768	
		1300	5.264	5.264	5.267	5 269	5 270	5.271	5 270	5 268	5.268	5 263	5.256	5 246	5 236	5 224	5 011	4.713	4.369	4.005	3.623	3.235	
	20	400	22.475	22.462	22.443	22.417	22.391	22 358	22.256	22.136	21.998	21 846	21.686	21 521	21.351	21.178	19 290	17 293	15.247	13.174	11.085	8.985	6.882
		700	13.301	13 286	13.271	13.252	13.233	13.201	13.154	13.093	13 021	12.948	12 870	12 887	12.700	12 612	11.627	10.548	9.430	8.284	7.127	5.962	4.792
		1000	9.514	9.507	9.496	9.485	9.474	9.463	9.435	9.398	9 361	9 321	9.272	9 223	9.172	9.120	8 500	7.793	7.045	6.273	5.489	4.698	3.901
		1300	7.434	7.430	7.428	7.424	7.418	7.412	7.393	7 377	7 356	7 330	7.301	7.273	7.242	7.207	6.781	6.277	5.728	5.160	4.576	3.987	
e^{-16}	2	400	1.489	1.308	1.525	1.541	1.560	1 579	1.624	1.674	1.722	1.771	1 824	1.879	1 935	1.995	2 711	2.810	2.772	2.682	2.566	2.429	2.251
		700	0.855	0.862	0.867	0.874	0.880	0.886	0.901	0.917	0.934	0.952	0.969	0.987	1.005	1.025	1.271	1.651	1.831	1.870	1.846	1.736	
		1000	0.391	0.395	0.399	0 403	0.408	0.412	0.424	0.435	0.445	0 457	0 468	0.480	0.493	0.506	0.635	0.785	0.951	1.051	0.791		
		1300	0.065	0.068	0.073	0.076	0.079	0 083	0.090	0 098	0.106	0 113	0.120	0.127	0 134	0.142	0.216	0.270	0.265	0.059			
	8	400	8.971	8.990	9.009	9.029	9.056	9.088	9.177	9 257	9.305	9 328	9.329	9.317	9.291	9.262	8.739	8.061	7.239	6.565	5.785	4.997	4.201
		700	5.421	5.428	5.436	5.445	5.453	5.462	5.492	5.525	5.560	5 590	5.616	5.633	5.645	5.650	5.508	5.210	4.850	4.464	4.060	3.645	3.225
		1000	3.866	3.872	3.877	3.882	3.889	3.898	3.918	3.940	3.966	3.994	4.024	4 054	4.081	4.103	4.136	4.000	3.796	3.564	3.311	3.045	2.715
		1300	2.986	2.992	2.997	3.002	3.008	3.014	3.029	3.045	3.068	3.092	3.116	3.145	3.174	3.201	3.347	3.306	3.192	3.043	2.872	2.686	
	14	400	15.783	15.803	15.824	15.847	15.871	15.881	15.915	15.897	15.850	15.784	15 703	15.614	15.514	15.411	14.205	12.858	11.462	10.046	8.606	7.164	5.729
		700	9.413	9.418	9.426	9.433	9.437	9.438	9.460	9.465	9.460	9.447	9.423	9.392	9.357	9.317	8.758	8.071	7.334	6.568	5.787	4.997	4.201
		1000	6.742	6.749	6.753	6.757	6.763	6.771	6.791	6.809	6.820	6.828	6.830	6.825	6.816	6.803	6.511	6.089	5.616	5.111	4.593	4.067	
		1300	5.264	5.268	5.275	5.281	5.287	5.293	5.211	5.333	5.353	5.370	5.385	5.394	5.401	5.403	5.264	4.989	4.657	4.298	3.920	3.534	

	20	400	22.475	22.487	22.500	22.509	22.512	22.500	22.443	22.348	22.228	22.088	21.940	21.782	21.615	21.446	19.560	17.582	15.545	13.473	11.385	9.281	7.163
		700	13.301	13.301	13.302	13.297	13.297	13.285	13.271	13.240	13.192	13.139	13.073	13.004	12.928	12.844	11.901	10.832	9.712	8.568	7.414	6.255	5.092
		1000	9.514	9.516	9.516	9.518	9.523	9.522	9.525	9.518	9.504	9.484	9.451	9.417	9.379	9.335	8.766	8.075	7.336	6.568	5.787	4.997	4.201
		1300	7.434	7.438	7.444	7.448	7.449	7.449	7.463	7.471	7.474	7.472	7.461	7.449	7.429	7.405	7.042	6.557	6.017	5.454	4.873	4.286	
e^{-24}	2	400	1.489	1.508	1.525	1.541	1.560	1.579	1.624	1.674	1.722	1.771	1.824	1.879	1.935	1.995	2.858	2.979	2.944	2.857	2.742	2.604	2.400
		700	0.855	0.862	0.867	0.874	0.880	0.886	0.901	0.917	0.934	0.952	0.969	0.987	1.005	1.025	1.271	1.697	1.983	2.035	2.015	1.908	
		1000	0.391	0.395	0.399	0.403	0.408	0.412	0.424	0.435	0.445	0.457	0.468	0.480	0.493	0.506	0.635	0.785	0.951	1.054	0.791		
		1300	0.065	0.068	0.073	0.076	0.079	0.083	0.090	0.098	0.106	0.113	0.120	0.127	0.134	0.142	0.216	0.270	0.265	0.059			
	8	400	8.971	8.990	9.010	9.030	9.060	9.092	9.206	9.334	9.420	9.462	9.474	9.468	9.448	9 420	8.911	8.236	7.502	6.738	5.959	5.172	4.375
		700	5.421	5.428	5.437	5.446	5.455	5.464	5.502	5.544	5.598	5.652	5.700	5.734	5.761	5.776	5.669	5.379	5.025	4.639	4.236	3.820	
		1000	3.866	3.872	3.877	3.882	3.890	3.898	3.920	3.945	3.979	4.017	4.060	4.106	4.150	4.189	4.289	4.166	3.968	3.737	3.486	3.220	
		1300	2.986	2.992	2.997	3.002	3.008	3.014	3.029	3.047	3.071	3.097	3.125	3.160	3.199	3.240	3 489	3.468	3.361	3.215	3.046	2.861	
	14	400	15.783	15.804	15.830	15.869	15 913	15.955	16.023	16 027	15 994	15.934	15.860	15.774	15.675	15 574	14 378	13 042	11.657	10.241	8.804	7.357	5.910
		700	9.413	9.419	9.431	9.443	9.455	9.471	9.512	9.542	9.560	9.561	9.549	9.527	9.498	9.462	8.924	8.243	7.506	6.740	5.960	5.173	4.376
		1000	6.742	6.751	6.756	6.761	6.770	6.782	6.816	6.853	6.888	6.914	6.932	6.940	6.939	6.934	6.672	6.259	5.787	5.285	4.768	4.243	
		1300	5.264	5.268	5.275	5.283	5.291	5.299	5.324	5.357	5.394	5.429	5.461	5.486	5.505	5.518	5.420	5.156	4.827	4.472	4.096	3.709	
	20	400	22.475	22.496	22.525	22.557	22.581	22.595	22.567	22.489	22.378	22.243	22.100	21.942	21.780	21.613	19.752	17.757	15.721	13.650	11.561	9.460	7.360
		700	13.301	13.308	13.316	13.321	13.334	13.332	13.350	13.340	13.306	13.265	13.209	13.145	13.074	12 994	12.067	11.008	9.896	8.753	7.599	6.437	5.266
		1000	9.514	9.520	9.523	9.532	9.540	9.549	9.575	9.594	9.598	9.592	9.573	9.546	9.516	9.476	8.929	8.245	7.507	6.741	5.960	5.173	4.376
		1300	7.434	7.440	7.448	7.456	7.463	7.472	7.501	7.528	7.549	7.564	7.567	7.564	7.555	7.538	7.202	6.725	6.189	5.629	5.050	4.460	
e^{-48}	2	400	1.489	1.508	1.525	1.541	1.560	1.579	1.624	1.674	1.722	1.771	1.824	1.879	1.935	1.995	3.052	3.196	3.164	3.078	2.963	2.827	2.651
		700	0.855	0.862	0.867	0.874	0.880	0.886	0.901	0 917	0.934	0.952	0.969	0.987	1.005	1.025	1.271	1.755	2.183	2.250	2.236	2.124	
		1000	0.391	0.393	0.399	0.403	0.408	0.412	0.424	0 435	0.445	0.457	0.468	0.480	0.493	0.506	0.635	0.785	0.951	1.055	0.791		
		1300	0.065	0.068	0.073	0.076	0.079	0.083	0.090	0.098	0.106	0.113	0.120	0.127	0.134	0.142	0.216	0.270	0.265	0.059			
	8	400	8.971	8.990	9.010	9.030	9.060	9.093	9.220	9.419	9.572	9.641	9.667	9.667	9.655	9.629	9.126	8.455	7.724	6.963	6.183	5.391	4.600
		700	5.421	5.428	5.437	5.446	5.455	5.465	5.503	5.552	5.621	5.710	5.798	5.866	5.916	5.945	5.878	5.594	5.245	4.858	4.456	4.043	3.622
		1000	3.866	3.872	3.877	3.882	3.890	3 898	3.920	3.945	3.981	4.023	4.077	4.141	4.213	4.287	4.490	4.378	4.186	3.956	3.706	3.442	3.112
		1300	2.986	2.992	2.997	3.002	3.008	3.014	3.029	3.047	3.071	3.097	3.126	3.167	3.211	3.263	3.677	3.676	3.577	3.432	3.265	3.081	
	14	400	15.783	15.806	15.832	15.880	15.943	16.024	16.168	16.205	16.187	16.133	16.064	15.979	15.887	15.789	14.599	13.266	11.875	10.456	9.022	7.581	6.128
		700	9.413	9.421	9.433	9.449	9.465	9.491	9.567	9.643	9.694	9.718	9.720	9.709	9.687	9.654	9.133	8.458	7.726	6.965	6.184	5.392	4.600
		1000	6.742	6.751	6.756	6.763	6.777	6.791	6.834	6.895	6.965	7.025	7.068	7.095	7.108	7.111	6.881	6.474	6.006	5.508	4.991	4.462	
		1300	5.264	5.268	5.275	5.283	5.292	5.300	5.327	5.372	5.424	5.486	5 551	5.604	5.646	5 674	5.624	5.368	5.047	4.692	4.317	3.931	
	20	400	22.475	22.501	22.546	22.609	22.678	22.724	22.742	22.678	22.574	22.449	22.304	22.152	21.993	21.823	19.972	17.983	15.938	13.866	11.778	9.684	7.578
		700	13.301	13.312	13.327	13.345	13.372	13.389	13.455	13.479	13.470	13.439	13.391	13.335	13.267	13.192	12.276	11.223	10.115	8.979	7.824	6.655	5.491
		1000	9.514	9.521	9.528	9.544	9.560	9.577	9.637	9.693	9.728	9.743	9.738	9.723	9.698	9.663	9.136	8.560	7.727	6.965	6.184	5.392	4.600
		1300	7.434	7.441	7.450	7.459	7.469	7.481	7.528	7.589	7.644	7.687	7.712	7.724	7.725	7.717	7.408	6.937	6.410	5.849	5.272	4.683	

TABLE 1—*Concluded*

X as a function of T_a/T_s

$T_0 = 323$

δ_a	$10^{-8}A_a$	T_a	T_a/T_s 1.000	0.996	0.992	0 988	0.984	0.98	0.97	0.96	0.95	0.94	0.93	0 92	0.91	0.9	0.8	0.7	0.6	0.5	0.4	0.3	0.2
e^{-8}	2	425	1.249	1.269	1.289	1.309	1.330	1.350	1.399	1.451	1.500	1.552	1.606	1 662	1.721	1.783	2 317	2.405	2.371	2.291	2.184	2.059	1.886
		725	0.746	0.752	0.759	0.765	0.771	0.778	0.794	0.812	0.829	0 848	0 868	0.887	0.907	0.927	1.156	1 411	1.523	1.545	1.515	1.390	
		1025	0.319	0.324	0.327	0.332	0.336	0.339	0.350	0.361	0 372	0 383	0.396	0.408	0.420	0.432	0.565	0.708	0.848	0.899	0.621		
		1325	0.006	0.009	0.012	0.015	0.019	0 022	0.029	0.037	0 045	0.054	0.062	0.069	0.076	0.084	0.158	0.203	0.186	0.044			
	8	425	8.387	8.406	8.423	8.440	8 464	8.484	8.533	8.569	8.597	8.589	8.582	8.561	8 536	8.504	8.012	7.379	6 700	5 986	5.257	4.516	3.774
		725	5.211	5.217	5.222	5.230	5 236	5.240	5.252	5 266	5 274	5 280	5.285	5.285	5 280	5 273	5 088	4 790	4 441	4.068	3.678	3.280	
		1025	3.753	3.760	3.765	3.769	3.773	3.778	3.792	3 806	3 817	3.828	3 839	3.848	3 853	3.858	3 808	3.654	3.448	3.217	2.969	2.711	
		1325	2.914	2 918	2 924	2 929	2.933	2.938	2.951	2 963	2.977	2 992	3 004	3 017	3 028	3.036	3 066	2.993	2.870	2.718	2.547	2.366	
	14	425	14 827	14.836	14 845	14 851	14 854	14 855	14 835	14 793	14 736	14 665	14 588	14 498	14 403	14 307	13 175	11.923	10 621	9.290	7.942	6.585	5.226
		725	9 079	9.076	9 073	9 072	9 069	9 062	9 045	9 026	8 996	8 964	8 931	8.892	8.845	8.797	8.230	7 559	6.847	6 107	5.355	4.593	3.287
		1025	6.569	6.572	6 572	6.570	6 568	6 566	6 563	6 557	6.546	6 533	6 517	6 497	6 473	6.450	6 119	5 693	5 226	4 734	4.228	3.713	
		1325	5.155	5.156	5 159	5 162	5.163	5.166	5.166	5 166	5 166	. 164	5.159	5 150	5.141	5 131	4 927	4.641	4.307	3.950	3.579	3.203	
	20	425	21.138	21.133	21.122	21.102	21 086	21.059	20 973	20 867	20 745	20 608	20 465	20 313	20 156	19 996	18 238	16.370	14 451	12 509	10 546	8.576	6.598
		725	12.844	12.826	12.814	12 800	12 783	12 763	12.713	12 657	12 590	12 523	12 450	12 371	12 289	12 205	11 267	10 232	9.158	8 056	6 942	5 819	4.693
		1025	9.280	9.274	9.265	9.255	9 243	9 233	9 209	9 172	9.141	9 102	9 058	9.011	8 962	8.912	8 318	7.633	6.907	6.157	5.395	4 624	3.849
		1325	7.288	7.286	7.284	7.281	7 277	7.272	7.255	7 239	7 221	7.197	7.170	7 143	7 113	7 081	6 670	6.180	5 644	5 088	4 517	3 942	
e^{-10}	2	425	1 249	1.269	1.289	1.309	1.330	1 350	1.399	1 451	1 500	1.552	1 606	1.662	1 721	1.783	2.547	2.685	2.663	2.587	2 484	2.359	2.186
		725	0.746	0 752	0.759	0.765	0 771	0 778	0.794	0.812	0 829	0.848	0.868	0.887	0.907	0 925	1.163	1.545	1 764	1 820	1 799	1.672	
		1025	0 319	0.324	0.327	0.332	0.336	0.339	0 350	0 361	0 372	0 383	0.396	0 408	0.420	0 432	0.565	0.709	0.857	0.928	0.622		
		1325	0.006	0.009	0 012	0.015	0 019	0.022	0 029	0 037	0 045	0.054	0.062	0 069	0 076	0 084	0.158	0.203	0.186	−0.044			
	8	425	8.387	8.406	8.426	8 448	8.475	8.506	8.601	8.698	8.762	8 796	8 808	8.805	8.787	8 764	8.298	7.673	6.996	6.285	5.556	4.817	4.075
		725	5.211	5.219	5.226	5.237	5 246	5 255	5.285	5.321	5 358	5 392	5 422	5 444	5 460	5 469	5.352	5.073	4.732	4.363	3.976	3.580	3.175
		1025	3.753	3.761	3.767	3.772	3.778	3.787	3.808	3.831	3 857	3 888	3 919	3.950	3.977	4.002	4.053	3.928	3.735	3.510	3.266	3.009	
		1325	2.914	2.919	2.925	2.930	2.936	2.942	2.958	2.975	2.996	3 022	3.046	3.075	3.104	3 133	3.292	3.259	3.152	3.008	2.842	2.663	
	14	425	14.827	14.846	14.871	14 897	14 927	14.946	14.996	14.994	14.958	14.907	14 835	14.759	14.667	14 573	13.464	12.206	10.897	9.569	8.220	6.872	5.526
		725	9.079	9.084	9.092	9.102	9.109	9.111	9.136	9 148	9.148	9 138	9.121	9.094	9 062	9.026	8.500	7.843	7 140	6.403	5 653	4.892	4.127
		1025	6.569	6.577	6.582	6.587	6.592	6 601	6.623	6 642	6.659	6 668	6 673	6 671	6.663	6.653	6.378	5.972	5.516	5.028	4.525	4.012	
		1325	5.155	5.160	5.167	5.174	5.180	5.187	5.205	5 229	5.250	5.269	5.285	5 297	5 305	5.308	5.179	4.917	4.595	4.243	3.876	3.501	

	20	425	21.138	21.152	21.170	21.189	21.202	21.200	21.162	21.083	20.979	20.855	20.720	20.576	20.422	20.266	18.511	16.660	14.749	12.808	10.846	8.871	6.880
		725	12.844	12.841	12.845	12.845	12.844	12.842	12.828	12.803	12.760	12.713	12.652	12.587	12.517	12.440	11.541	10.516	9.442	8.342	7.231	6.113	4.994
		1025	9.280	9.283	9.284	9.285	9.290	9.291	9.296	9.291	9.283	9.265	9.238	9.206	9.171	9.130	8.583	7.914	7.918	6.453	5.693	4.923	4.150
		1325	7.288	7.293	7.299	7.304	7.308	7.308	7.325	7.334	7.339	7.337	7.329	7.319	7.301	7.280	6.931	6.460	5.934	5.381	4.814	4.241	
ε^{-24}	2	425	1.249	1.269	1.289	1.299	1.330	1.350	1.399	1.451	1.500	1.552	1.606	1.662	1.721	1.783	2.689	2.853	2.835	2.762	2.658	2.534	2.345
		725	0.746	0.752	0.759	0.761	0.771	0.778	0.794	0.812	0.829	0.848	0.868	0.887	0.907	0.927	1.163	1.582	1.912	1.983	1.966	1.837	
		1025	0.319	0.324	0.327	0.329	0.336	0.339	0.350	0.361	0.372	0.383	0.396	0.408	0.420	0.432	0.565	0.709	0.857	0.928	0.622		
		1325	0.006	0.009	0.012	0.013	0.019	0.022	0.029	0.037	0.045	0.054	0.062	0.069	0.076	0.084	0.158	0.203	0.186	−0.044			
	8	425	8.387	8.406	8.426	8.437	8.476	8.509	8.620	8.762	8.871	8.928	8.953	8.957	8.946	8.924	8.471	7.849	7.171	6.459	5.731	4.993	4.250
		725	5.211	5.219	5.227	5.233	5.248	5.256	5.291	5.336	5.391	5.446	5.500	5.542	5.573	5.593	5.513	5.242	4.904	4.539	4.153	3.754	3.351
		1025	3.753	3.761	3.767	3.770	3.778	3.786	3.809	3.835	3.865	3.903	3.947	3.995	4.041	4.083	4.206	4.094	3.905	3.684	3.441	3.184	
		1325	2.914	2.919	2.925	2.927	2.936	2.942	2.958	2.975	2.998	3.026	3.053	3.088	3.127	3.167	3.433	3.420	3.321	3.181	3.015	2.838	
	14	425	14.827	14.845	14.876	14.893	14.960	15.011	15.100	15.124	15.102	15.055	14.991	14.919	14.830	14.740	13.634	12.391	11.082	9.767	8.420	7.062	5.705
		725	9.079	9.086	9.098	9.105	9.124	9.139	9.184	9.224	9.245	9.250	9.246	9.228	9.202	9.171	8.666	8.016	7.312	6.576	5.827	5.068	4.302
		1025	6.569	6.578	6.585	6.588	6.599	6.612	6.645	6.682	6.723	6.752	6.772	6.784	6.785	6.783	6.540	6.142	5.688	5.201	4.699	4.188	
		1325	5.155	5.160	5.167	5.171	5.184	5.192	5.215	5.251	5.287	5.325	5.359	5.387	5.408	5.422	5.336	5.084	4.765	4.418	4.052	3.676	
	20	425	21.138	21.162	21.193	21.212	21.268	21.291	21.287	21.224	21.129	21.009	20.880	20.735	20.585	20.432	18.698	16.840	14.926	12.987	11.024	9.050	7.078
		725	12.844	12.847	12.857	12.862	12.878	12.887	12.903	12.901	12.875	12.839	12.788	12.728	12.663	12.591	11.707	10.691	9.623	8.526	7.415	6.295	5.167
		1025	9.280	9.286	9.290	9.293	9.306	9.317	9.346	9.364	9.376	9.372	9.359	9.334	9.307	9.271	8.747	8.805	7.370	6.625	5.867	5.099	
		1325	7.288	7.295	7.304	7.307	7.320	7.327	7.359	7.388	7.412	7.428	7.435	7.434	7.426	7.413	7.091	6.628	6.104	5.557	4.991	4.416	
ε^{-40}	2	425	1.249	1.269	1.289	1.299	1.330	1.350	1.399	1.451	1.500	1.552	1.606	1.662	1.721	1.783	2.872	3.070	3.057	2.983	2.881	2.755	2.583
		725	0.746	0.752	0.759	0.761	0.771	0.778	0.794	0.812	0.829	0.848	0.868	0.887	0.907	0.927	1.163	1.590	2.107	2.191	2.180	2.056	
		1025	0.319	0.324	0.327	0.329	0.336	0.339	0.350	0.361	0.372	0.383	0.396	0.408	0.420	0.432	0.565	0.709	0.857	0.928	0.622		
		1325	0.006	0.009	0.012	0.013	0.019	0.022	0.029	0.037	0.045	0.054	0.062	0.069	0.076	0.084	0.158	0.203	0.186	−0.044			
	8	425	8.387	8.406	8.426	8.437	8.476	8.509	8.625	8.819	9.061	9.103	9.144	9.156	9.153	9.133	8.689	8.071	7.389	6.681	5.952	5.212	4.472
		725	5.211	5.219	5.227	5.233	5.248	5.257	5.292	5.342	5.409	5.493	5.587	5.667	5.723	5.760	5.722	5.456	5.126	4.759	4.373	3.977	3.572
		1025	3.753	3.761	3.767	3.770	3.778	3.786	3.809	3.835	3.867	3.908	3.959	4.024	4.097	4.173	4.407	4.306	4.124	3.903	3.661	3.406	
		1325	2.914	2.919	2.925	2.927	2.936	2.942	2.958	2.975	2.998	3.026	3.054	3.092	3.134	3.184	3.620	3.631	3.537	3.398	3.235	3.058	
	14	425	14.827	14.849	14.876	14.896	14.979	15.063	15.240	15.300	15.296	15.256	15.199	15.125	15.042	14.954	13.857	12.613	11.315	9.985	8.641	7.288	5.927
		725	9.079	9.087	9.099	9.108	9.132	9.154	9.231	9.317	9.376	9.407	9.416	9.409	9.392	9.364	8.877	8.233	7.530	6.799	6.049	5.286	4.525
		1025	6.569	6.578	6.585	6.589	6.607	6.618	6.659	6.721	6.793	6.858	6.907	6.937	6.954	6.960	6.748	6.358	5.905	5.423	4.921	4.406	
		1325	5.155	5.160	5.167	5.171	5.185	5.193	5.218	5.265	5.314	5.377	5.444	5.502	5.546	5.577	5.540	5.295	4.986	4.639	4.274	3.898	
	20	425	21.138	21.165	21.206	21.239	21.354	21.415	21.456	21.413	21.328	21.215	21.083	20.944	20.800	20.646	18.923	17.062	15.147	13.203	11.245	9.276	7.299
		725	12.844	12.850	12.867	12.876	12.913	12.940	13.007	13.038	13.037	13.013	12.970	12.921	12.858	12.788	11.918	10.908	9.842	8.749	7.637	6.512	5.391
		1025	9.280	9.287	9.294	9.299	9.325	9.343	9.404	9.460	9.506	9.522	9.524	9.512	9.490	9.458	8.955	8.301	7.588	6.848	6.089	5.316	4.548
		1325	7.288	7.296	7.306	7.310	7.326	7.336	7.385	7.446	7.504	7.550	7.579	7.594	7.597	7.591	7.297	6.840	6.326	5.778	5.213	4.638	

TABLE 2

Y as a function of T_a/T_s

$T_0 = 298$

T_a	T_b	$10^{-3}A_b$	X	T_a/T_s																
				0.996	0.992	0.988	0.984	0.98	0.97	0.96	3.95	0.94	0.93	0.92	0.91	0.9	0.8	0.7	0.6	0.5	0.4	0.3
400	700	0	0.3333	1.92	1.61	1.42	1.29	1.18	0.980	0.834	0.716	0.614	0.524	0.442	0.366	0.297	−0.280	−0.852	−1.900			
		8	2.8577	4.697	4.378	4.184	4.041	2.926	3.703	3.529	3.382	3.251	3.131	3.019	2.912	2.810	1.88	0.935	−0.506			
		14	5.0000	7.233	6.900	6.692	6.534	6.404	6.141	5.925	5.733	5.554	5.385	5.221	5.061	4.903	3.379	1.84	−0.053			
	1000	0	0.2333	2.07	1.76	1.57	1.45	1.34	1.15	1.01	0.889	0.797	0.715	0.642	0.573	0.511	0.032	−0.358	−0.762	−1.305		
		8	2.8000	6.186	5.867	5.673	5.530	5.415	5.192	5.018	4.872	4.741	4.622	4.510	4.404	4.301	3.377	2.49	1.61	0.633		
		14	4.9000	9.839	9.506	9.298	9.140	9.010	8.747	8.530	8.338	8.160	7.991	7.827	7.666	7.509	5.976	4.455	2.935	1.38		
	1300	0	0.1795	2.13	1.82	1.64	1.51	1.41	1.22	1.08	0.963	0.871	0.792	0.720	0.657	0.595	0.146	−0.202	−0.539	−0.915	−1.46	
		8	2.4852	6.988	6.669	6.475	6.332	6.217	5.994	5.820	5.673	5.543	5.423	5.312	5.205	5.103	4.179	3.303	2.42	1.54	0.543	
		14	4.3491	11.242	10.909	10.701	10.543	10.413	10.150	9.934	9.741	9.563	9.394	9.230	9.070	8.912	7.379	5.858	4.338	2.815	1.26	
	1600	0	0.1458	2.17	1.86	1.68	1.55	1.45	1.26	1.12	1.01	0.912	0.833	0.763	0.701	0.642	0.205	−0.128	−0.433	−0.762	−1.174	−1.90
		8	2.1875	7.489	7.170	6.976	6.833	6.718	6.495	6.321	6.174	6.044	5.925	5.813	5.706	5.604	4.680	3.805	2.934	2.06	1.15	−0.053
		14	3.8281	12.119	11.786	11.578	11.420	11.290	11.027	10.810	10.618	10.440	10.271	10.107	9.946	9.789	8.256	6.735	5.215	3.695	2.17	0.484
700	850	0	0.4804	1.52	1.20	0.996	0.849	0.731	0.498	0.368	0.160	0.015	−0.120	−0.247	−0.382	−0.512	−1.38 T_a/T_s = 0.85					
		8	1.1175	2.03	1.71	1.52	1.38	1.26	1.04	0.857	0.708	0.568	0.437	0.308	0.180	0.046	−0.865					
		14	1.7467	2.48	2.17	1.97	1.83	1.71	1.48	1.29	1.13	0.981	0.839	0.703	0.563	0.419	−0.536					
	1000	0	0.4083	1.76	1.44	1.26	1.12	1.01	0.797	0.642	0.510	0.397	0.297	0.205	0.117	0.032	−0.762	−1.305 T_a/T_s = 0.75				
		8	1.4470	2.693	2.38	2.20	2.06	1.95	1.74	1.59	1.46	1.34	1.24	1.15	1.06	0.967	0.367	−0.470				
		14	2.4561	3.579	3.280	3.065	2.921	2.805	2.581	2.40	2.26	2.13	2.01	1.90	1.78	1.68	0.606	−0.049				
	1150	0	0.3551	1.88	1.56	1.38	1.25	1.14	0.931	0.785	0.666	0.560	0.468	0.385	0.307	0.235	−0.384	−1.057				
		8	1.6062	3.158	2.846	2.659	2.52	2.41	2.22	2.06	1.94	1.83	1.73	1.64	1.56	1.48	0.786	0.004				
		14	2.7799	4.373	4.055	3.860	3.717	3.602	3.378	3.204	3.057	2.926	2.806	2.694	2.586	2.48	1.54	0.531				
	1300	0	0.3141	1.95	1.64	1.46	1.32	1.22	1.02	0.871	0.756	0.657	0.565	0.486	0.413	0.346	−0.202	−0.718	−1.46			
		8	1.6653	3.510	3.199	3.012	2.879	2.771	2.567	2.41	2.29	2.19	2.09	2.00	1.92	1.84	1.19	0.552	−0.340			
		14	2.8997	4.984	4.665	4.471	4.328	4.212	3.989	3.816	3.669	3.538	3.418	3.306	3.200	3.097	2.17	1.26	0.138			

	1600	0	0.2552	2.04	1.73	1.54	1.41	1.31	1.12	0.971	0.859	0.763	0.680	0.604	0.535	0.470	−0.023	−0.432	−0.883	−1.58	
		8	1.6433	4.013	3.702	3.516	3.383	3.275	3.073	2.920	2.796	2.689	2.594	2.50	2.42	2.35	1.72	1.17	0.555	−0.331	
		14	2.8711	5.860	5.542	5.348	5.205	5.090	4.866	4.693	4.546	4.416	4.296	4.184	4.078	3.975	3.050	2.17	1.27	0.152	
1600	1150	0	0.5072	1.38	1.05	0.839	0.689	0.559	0.307	0.100	−0.089	−0.264	−0.439	−0.625	−0.824	−1.058	-1.35^a	-1.79^b			a: $T_a/T_s=0.81$
		8	0.8171	1.63	1.31	1.10	0.949	0.828	0.584	0.381	0.203	0.027	−0.147	−0.329	−0.529	−0.762	−1.06	−1.51			b: $T_a/T_s=0.88$
		14	1.1041	1.83	1.52	1.32	1.17	1.04	0.791	0.596	0.414	0.243	0.067	−0.120	−0.322	−0.561	−0.862	−1.33			
	1300	0	0.4487	1.64	1.32	1.13	0.986	0.870	0.657	0.486	0.346	0.222	0.108	−0.001	−0.105	−0.202	−1.46	-0.719^a	-2.12^b		a: $T_a/T_s=0.85$
		8	0.9837	2.10	1.79	1.60	1.46	1.35	1.14	0.973	0.838	0.721	0.611	0.505	0.405	0.307	−0.984	−0.206	−1.66		b: $T_a/T_s=0.78$
		14	1.5094	2.51	2.205	2.01	1.87	1.76	1.54	1.37	1.24	1.11	0.992	0.880	0.777	0.673	−0.681	0.130	−1.40		
	1450	0	0.4023	1.77	1.46	1.27	1.13	1.02	0.813	0.661	0.531	0.418	0.320	0.229	0.143	0.060	−0.704	−2.31			
		8	1.0898	2.41	2.11	1.92	1.79	1.68	1.48	1.33	1.20	1.09	0.993	0.900	0.818	0.738	−0.039	−1.74			
		14	1.7709	3.014	2.699	2.51	2.37	2.26	2.05	1.89	1.76	1.64	1.53	1.44	1.34	1.25	0.388	−1.44			
	1600	0	0.3646	1.86	1.55	1.36	1.23	1.12	0.911	0.763	0.643	0.535	0.442	0.359	0.279	0.204	0.432	−1.174			
		8	1.1511	2.660	2.35	2.17	2.03	1.93	1.73	1.58	1.46	1.35	1.26	1.18	1.10	1.03	0.688	−0.415			
		14	1.9242	3.412	3.098	2.909	2.770	2.660	2.44	2.29	2.16	2.04	1.94	1.85	1.76	1.67	0.902	−0.001			
1300	1450	0	0.5250	1.27	0.928	0.718	0.554	0.417	0.143	−0.097	−0.319	−0.545	−0.789	−1.079	−1.48	−2.31					
		8	0.7070	1.42	1.09	0.875	0.717	0.584	0.313	0.082	−0.139	−0.363	−0.605	−0.893	−1.30	−2.14					
		14	0.8674	1.54	1.21	1.00	0.841	0.712	0.442	0.214	−0.005	−0.225	−0.470	−0.765	−1.171	−2.03					
	1600	0	0.4740	1.54	1.23	1.03	0.879	0.764	0.535	0.356	0.205	0.066	−0.066	−0.187	−0.311	−0.432	−1.175	$T_a/T_s = 0.85$			
		8	0.7989	1.82	1.51	1.31	1.17	1.06	0.832	0.663	0.512	0.381	0.255	0.135	0.013	−0.109	−0.849				
		14	1.1036	2.06	1.74	1.55	1.41	1.30	1.07	0.896	0.750	0.618	0.489	0.369	0.249	0.127	−0.635				

TABLE 2—*Concluded*

Y as a function of T_a/T_s
$T_0 = 323$

T_s	T_b	$10^{-3}A_b$	χ	T_a/T_s																		
				0.996	0.992	0.988	0.984	0.98	0.97	0.96	0.95	0.94	0.93	0.92	0.91	0.9	0.8	0.7	0.6	0.5	0.4	0.3
425	725	0	0.3420	1.90	1.59	1.40	1.28	1.16	0.961	0.815	0.697	0.593	0.501	0.419	0.343	0.274	−0.318	−0.922	−2.305			
		8	2.6646	4.381	4.066	3.874	3.731	3.617	3.398	3.228	3.083	2.957	2.841	2.733	2.630	2.532	1.64	0.715	−1.073			
		14	4.6611	6.667	6.337	6.130	5.974	5.845	5.588	5.378	5.193	5.022	4.859	4.703	4.550	4.401	2.953	1.50	−0.679			
	1025	0	0.2419	2.05	1.75	1.56	5.43	1.33	1.14	0.995	0.878	0.784	0.702	0.627	0.558	0.494	0.011	−0.388	−0.807	−1.39		
		8	2.6651	5.783	5.469	5.277	1.134	5.020	4.800	4.630	4.486	4.359	4.244	4.136	4.033	3.935	3.054	2.23	1.38	0.396		
		14	4.6639	9.122	8.791	8.584	8.428	8.300	8.043	7.833	7.647	7.476	7.314	7.157	7.005	6.855	5.409	3.978	2.547	1.06		
	1325	0	0.1871	2.12	1.81	1.63	1.50	1.40	1.21	1.07	0.955	0.861	0.781	0.710	0.646	0.584	0.131	−0.221	−0.567	−0.955	−1.55	
		8	2.3923	6.551	6.236	6.044	5.901	5.787	5.568	5.398	5.254	5.127	5.011	4.903	4.800	4.702	3.823	2.995	2.18	1.33	0.321	
		14	4.1865	10.465	10.134	9.927	9.771	9.643	9.386	9.176	8.990	8.819	8.657	8.501	8.348	8.198	6.752	5.321	3.890	2.45	0.954	
	1625	0	0.1526	2.16	1.85	1.67	1.54	1.44	1.25	1.11	0.994	0.903	0.825	0.755	0.692	0.634	0.193	−0.142	−0.450	−0.789	−1.221	−2.05
		8	2.1207	7.035	6.720	6.529	6.385	6.271	6.052	5.882	5.737	5.611	5.495	5.387	5.284	5.186	4.309	3.480	2.658	1.83	0.952	−0.322
		14	3.7112	11.312	10.981	10.775	10.618	10.490	10.233	10.023	9.837	9.666	9.504	9.348	9.195	9.046	7.599	6.168	4.737	3.306	1.87	1.65
725	875	0	0.4833	1.51	1.18	0.980	0.834	0.715	0.480	0.347	0.138	−0.009	−0.147	−0.280	−0.416	−0.553	−1.50 $T_a/T_s = 0.85$					
		8	1.0766	1.97	1.66	1.47	1.33	1.21	0.980	0.805	0.654	0.509	0.375	0.246	0.111	−0.028	−1.01					
		14	1.6606	2.40	2.09	1.89	1.74	1.63	1.39	1.21	1.05	0.894	0.755	0.614	0.471	0.325	−0.714					
	1025	0	0.4126	1.75	1.43	1.25	1.10	0.994	0.784	0.627	0.495	0.382	0.281	0.187	0.097	0.011	−0.811	−1.40 $T_a/T_s = 0.75$				
		8	1.3874	2.616	2.31	2.12	1.98	1.88	1.67	1.52	1.38	1.27	1.17	1.07	0.981	0.891	0.258	−0.615				
		14	2.3402	3.445	3.125	2.931	2.787	2.671	2.44	2.28	2.13	2.00	1.88	1.77	1.66	1.56	0.519	−0.210				
	1175	0	0.3599	1.87	1.55	1.37	1.24	1.13	0.921	0.774	0.655	0.547	0.455	0.371	0.293	0.220	−0.407	−1.113				
		8	1.5436	3.063	2.752	2.567	2.42	2.32	2.12	1.97	1.85	1.74	1.64	1.55	1.47	1.39	0.702	−0.108				
		14	2.6635	4.204	3.885	3.691	3.547	3.433	3.211	3.039	2.895	2.765	2.646	2.536	2.429	2.33	1.41	0.394				
	1325	0	0.3192	1.94	1.63	1.45	1.31	1.21	1.01	0.861	0.747	0.647	0.555	0.475	0.402	0.333	−0.221	−0.752	−1.55			
		8	1.6057	3.402	3.092	2.907	2.773	2.666	2.46	2.31	2.19	2.08	1.99	1.90	1.82	1.74	1.10	0.465	−0.483			
		14	2.7915	4.790	4.471	4.278	4.134	4.020	3.798	3.626	3.481	3.353	3.235	3.125	3.020	2.920	2.02	1.13	−0.035			

	1625	0	0.2603	2.03	1.72	1.54	1.41	1.30	1.11	0.963	0.850	0.755	0.672	0.596	0.526	0.461	−0.036	−0.451	−0.915	−1.67	
		8	1.5941	3.888	3.580	3.395	3.261	3.155	2.953	2.803	2.681	2.574	2.47	2.39	2.31	2.24	1.62	1.07	0.460	−0.474	
		14	2.7835	5.637	5.318	5.125	4.981	4.867	4.645	4.474	4.329	4.201	4.083	3.973	3.869	3.769	2.870	2.02	1.135	−0.018	
1025	1175	0	0.5089	1.37	1.04	0.829	0.677	0.546	0.293	0.083	−0.109	−0.289	−0.467	−0.659	−0.866	−1.114	−1.435[a]	−1.97[b]			a: $T_a/T_s = 0.89$
		8	0.8038	1.61	1.28	1.08	0.925	0.803	0.566	0.353	0.171	−0.007	−0.185	−0.377	−0.585	−0.830	−1.16	−1.70			b: $T_a/T_s = 0.88$
		14	1.0752	1.80	1.48	1.28	1.13	1.01	0.760	0.557	0.374	0.198	0.016	−0.173	−0.389	−0.639	−0.970	−1.53			
	1325	0	0.4513	1.63	1.31	1.12	0.976	0.860	0.646	0.475	0.333	0.209	0.093	−0.018	−0.122	−0.221	−1.55	−0.751[a]	−2.39[b]		a: $T_a/T_s=0.88$
		8	0.9617	2.07	1.76	1.57	1.43	1.32	1.11	0.940	0.806	0.687	0.574	0.467	0.367	0.269	−1.086	−0.258	−1.98		b: $T_a/T_s=0.78$
		14	1.4618	2.45	2.15	1.96	1.82	1.70	1.49	1.32	1.18	1.055	0.935	0.829	0.725	0.618	−0.805	+0.063	−1.74		
	1475	0	0.4054	1.76	1.45	1.26	1.12	1.02	0.805	0.651	0.520	0.407	0.308	0.217	0.130	0.046	−0.733	−2.67			
		8	1.0636	2.38	2.07	1.89	1.75	1.64	1.44	1.29	1.16	1.05	0.952	0.861	0.778	0.699	−0.116	−2.17			
		14	1.7158	2.949	2.630	2.44	2.30	2.20	1.985	1.825	1.69	1.57	1.47	1.37	1.28	1.19	0.318	−1.89			
	1625	0	0.3680	1.85	1.54	1.35	1.22	1.11	0.902	0.755	0.633	0.525	0.432	0.348	0.268	0.193	−0.453	−1.221			
		8	1.1233	2.617	2.31	2.13	1.99	1.88	1.69	1.54	1.42	1.31	1.22	1.13	1.05	0.979	0.623	−0.490			
		14	1.8677	3.329	3.017	2.829	2.691	2.580	2.36	2.22	2.08	1.97	1.87	1.78	1.68	1.60	0.833	−0.091			
1325	1475	0	0.5240	1.26	0.921	0.710	0.544	0.407	0.130	−0.112	−0.338	−0.570	−0.820	−1.126	−1.56	−2.67					
		8	0.7013	1.41	1.07	0.859	0.702	0.568	0.295	0.060	−0.163	−0.393	−0.644	−0.945	−1.39	−2.52					
		14	0.8550	1.53	1.20	0.980	0.821	0.692	0.421	0.188	−0.035	−0.261	−0.515	−0.821	−1.28	−2.42					
	1625	0	0.4756	1.53	1.22	1.02	0.871	0.756	0.525	0.346	0.194	0.053	−0.079	−0.202	−0.329	−0.451	−1.22				
		8	0.7890	1.81	1.49	1.30	1.15	1.04	0.813	0.642	0.491	0.359	0.232	0.109	−0.015	−0.138	−0.906				$T_a/T_s=0.85$
		14	1.0816	2.04	1.72	1.52	1.38	1.27	1.045	0.867	0.722	0.586	0.459	0.334	0.214	0.088	−0.700				

B. Pressure and temperature coefficients of fizz burning

Unfortunately, equations 26 and 53 are too complicated to allow the derivation of simple analytical expressions for the pressure coefficient

$$\pi = (\partial \log M/\partial \log P)_{T_0} \tag{62}$$

and temperature coefficient

$$\tau = (\partial \log M/\partial T_0)_P \tag{63}$$

of the burning rate, even in the case of fizz burning. We can obtain useful expressions for them in terms of quantities approximately determinable from tables 1 and 2, however. Let

$$\left.\begin{aligned} \delta_s X &= [\partial X/\partial(T_a/T_s)]_{T_0} \\ \delta_s Y &= [\partial Y/\partial(T_a/T_s)]_{T_0} \\ \delta_0 X &= [\partial X/\partial T_0]_{T_a/T_s} \\ \delta_0 Y &= [\partial(Y - \log \chi)/\partial T_0]_{T_a/T_s} \end{aligned}\right\} \tag{64}$$

Equations 56–61 then give

$$\pi = (\delta_s X + \tfrac{1}{2}\delta_s Y)(\delta_s X + \delta_s Y)^{-1} \tag{65}$$

and

$$\begin{aligned} \tau &= [\partial \log M/\partial T_0]_{T_a/T_s} - \frac{[\partial \log M/\partial(T_a/T_s)]_{T_0}[\partial \log P/\partial T_0]_{T_a/T_s}}{[\partial \log P/\partial(T_a/T_s)]_{T_0}} \\ &= \pi[\delta_0 X + \delta_0 Y + (\mathrm{d} \log \chi k_p/\mathrm{d}T_0)] - [\delta_0 X + \tfrac{1}{2}\delta_0 Y + (\mathrm{d} \log \chi^{1/2} k_m/\mathrm{d}T_0) \\ &\cong (\pi - \tfrac{1}{2})[\delta_0 X + \delta_0 Y + (A_b/2.303 T_b^2)] - \tfrac{1}{2}\delta_0 X \end{aligned} \tag{66}$$

The last equation is approximate because equations 60 and 61 are only approximate.

Now define, for a fixed T_0 and T_a/T_s between T_a/T'_s and T_a/T''_s,

$$\left.\begin{aligned} \Delta_s X &= X_{T_a/T''_s} - X_{T_a/T'_s} \\ \Delta_s Y &= Y_{T_a/T''_s} - Y_{T_a/T'_s} \end{aligned}\right. \tag{67}$$

Equation 65 then yields

$$\pi \cong (\Delta_s X + \tfrac{1}{2}\Delta_s Y)(\Delta_s X + \Delta_s Y)^{-1} \tag{68}$$

which gives the pressure coefficient in terms of horizontal differences in tables 1 and 2. Similarly, for a fixed T_a/T_s, let

$$\begin{aligned} \Delta_0 X &= X_{323} - X_{298} \\ \Delta_0 Y &= Y_{323} - Y_{298} - \log[(\chi)_{323}/(\chi)_{298}] \end{aligned} \tag{69}$$

Then if Δ is the difference between the logarithms of the burning rates at 25°C.

and 50°C. at the pressure corresponding to the given value of T_a/T_s, equation 66 gives

$$\Delta \cong (\pi - \tfrac{1}{2})[\Delta_0 X + \Delta_0 Y + (25A_b/2.303T_b^2)] - \tfrac{1}{2}\Delta_0 X \tag{70}$$

In the limit of very low pressures, T_s approaches T_a, so that equation 18 reduces to an equation of the form

$$M^2 = \text{constant} \times P \tag{71}$$

TABLE 3

Limiting low-pressure temperature coefficients

δ_a	A_a	$[T_a]_{25^\circ\text{C.}}$	$\Delta_{P=0} = \lim_{P\to 0}[\log(M_{50^\circ\text{C.}}/M_{25^\circ\text{C.}})]$
Any value	2000	400	0.120
		700	0.054
		1000	0.036
		1300	0.030
	8000	400	0.292
		700	0.105
		1000	0.056
		1300	0.036
	14000	400	0.478
		700	0.167
		1000	0.086
		1300	0.055
	20000	400	0.668
		700	0.229
		1000	0.117
		1300	0.074

Consequently,

$$\pi_{P=0} = \tfrac{1}{2} \tag{72}$$

and

$$\Delta_{P=0} = \tfrac{1}{2}[\Delta_0 X]_{(T_a/T_s=1)} \tag{73}$$

Values of $\Delta_{P=0}$ for various values of the foam parameters are given in table 3. The experimental value for a typical ballistite (HES 4016) is 0.03.

C. Fit to a powder

Experimental burning rate–pressure data for a typical powder, HES 4016, are plotted in figure 2.[12] By proper choice of the several parameters, theoretical curves can be drawn which agree very well with these experimental ones. For

---

[12] Below 100 p.s.i. this powder would not burn at room temperature. The points given are extrapolated from data taken at 79° and 55°C.

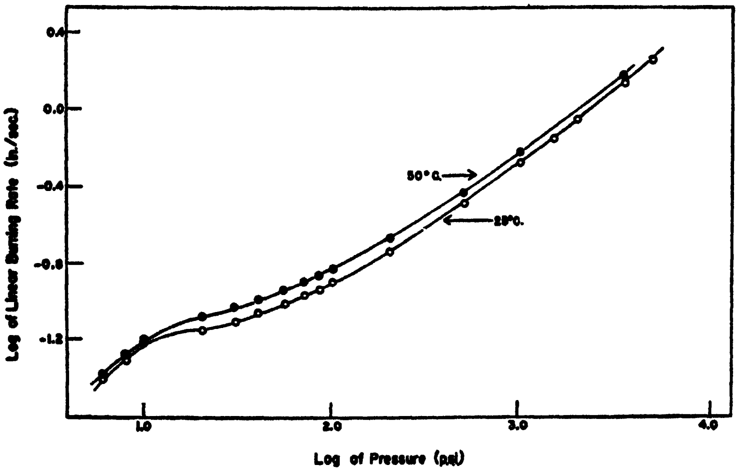

FIG. 2. Burning rates of a typical powder, HES 4016. Data from UM/31 and UM/40 (reference 3). Points for which P is less than or equal to 100 p.s.i. are extrapolated from data at higher temperatures.

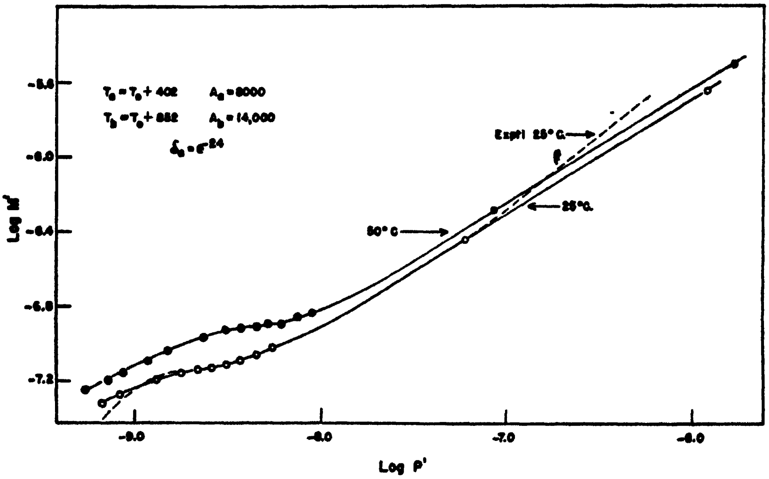

FIG. 3. Theoretical burning rates. The 50°C. theoretical curve has been translated as required by equations 60 and 61 so that the 25°C. and 50°C. curves are correctly related to each other.

example, figures 3 and 4 show theoretical curves for the parameter values:

$$T_a = T_0 + 402, \quad T_b = T_0 + 852, \quad A_a = 8000, \quad A_b = 14000, \quad \delta_a = e^{-24} \qquad (1)$$

$$T_a = T_0 + 702, \quad T_b = T_0 + 1002, \quad A_a = 8000, \quad A_b = 14000, \quad \delta_a = e^{-24} \qquad (2)$$

These represent the best fits obtainable with $T_a - T_0 = 402$ and 702.

Results of varying one parameter at a time are as follows:

(*1*) Increase in A_a increases the pressure coefficient except at low pressures, increases the temperature coefficient over the whole range, and decreases the burning rate at a given pressure.

(*2*) Increase in A_b increases the temperature coefficient at the high-pressure end of the curve, decreases the temperature coefficient in the flat portion of the curve, and decreases the pressure coefficient slightly at high pressures.

(*3*) Increase in T_a (in the heat of the foam reaction) increases the burning rate at a given pressure, damps the effect of the fizz reaction, and markedly decreases the temperature coefficient over the whole range.

(*4*) Increase in T_b (in the heat of the fizz reaction) decreases the temperature coefficient at high pressures, increases the temperature coefficient in the flat portion of the curve, and increases the burning rate at very high pressures.

(*5*) Increase in δ_a decreases the low-pressure "hump."

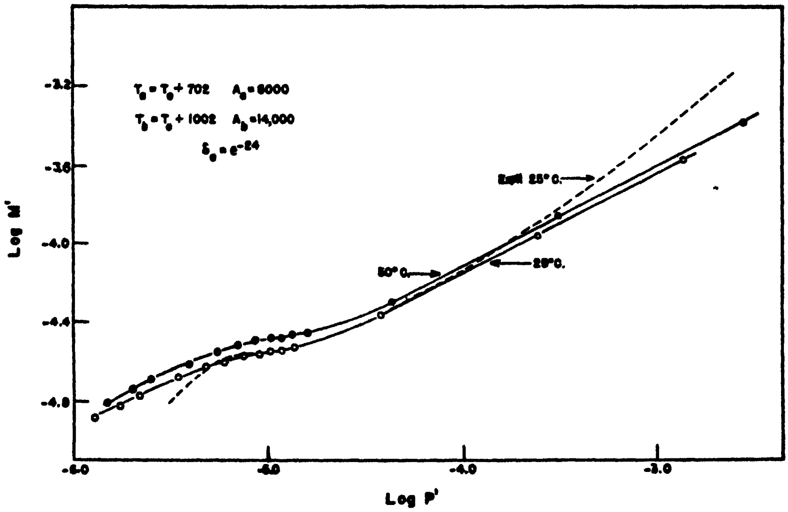

FIG. 4. Theoretical burning rates. The 50°C. theoretical curve has been translated as required by equations 60 and 61 so that the 25°C. and 50°C. curves are correctly related to each other.

Most of these effects could have been predicted qualitatively without recourse to calculation, but we examined an appropriate family of computed curves in each case. Effect No. 5 is illustrated in figure 5.

Any fit based on the model we have set up will give a limiting very low pressure coefficient of 0.50 (see equation 72), while the experimental value is about 0.75 (see figure 2). A good fit in the very low pressure range therefore cannot be expected. At best, one hopes for reproduction of the observed pressure and temperature coefficients at high pressures, pressure coefficient and increase of temperature coefficient on the flat low-pressure portion of the curve, and decrease of temperature coefficient at very low pressures.

The flame reaction becomes important for HES 4016 at about 1000 p.s.i.

(3, 4). We therefore want our calculated fizz-burning curves to begin falling below the experimental curves in the neighborhood of this pressure, as the curves in figures 3 and 4 indeed do.

Experimentally, one can say little about A_a and A_b—these are effective activation energies for complexes of single steps and should only be compared very carefully with activation energies for single steps (even if data on the latter were available). The situation as regards T_a and T_b is not much better—here a great deal of experimental work has been done but its interpretation is an extremely delicate matter. Our feeling is that T_a is nearer 700°K. than 400° or 1100° and T_b nearer 1150°K. than 1000° or 1300°.

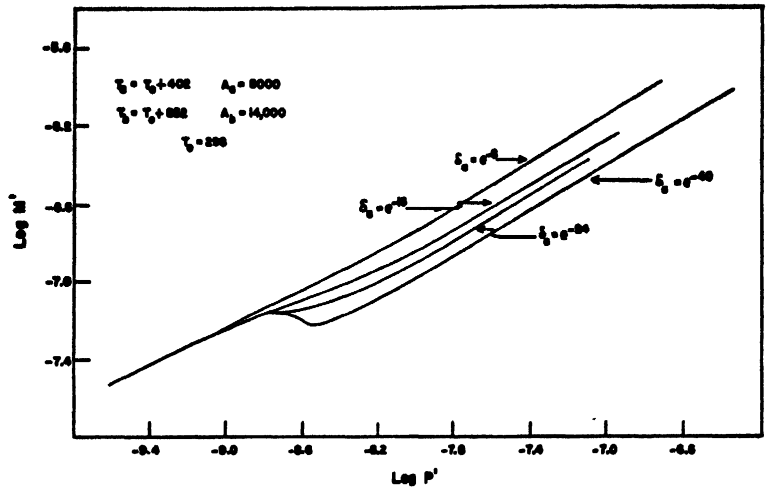

FIG. 5. Effect of varying δ_a

TABLE 4

Best values of the parameters at 25°C., diffusion neglected

T_a = 700°K.; T_b = 1100°K.
A_a = 10,000°K.; A_b = 15,000°K.
E_a = 20 kcal./mole; E_b = 30 kcal./mole
$\delta_a = e^{-24}$

Taking all of these things into consideration, we estimate the "best" values of the parameters which are given in table 4. The table may have to be revised when diffusion is taken into account and so should be regarded as tentative.

IV. DISCUSSION

As mentioned in Section III, the qualitative results of our calculation give us nothing new; the effect of varying, say, the heat of the fizz reaction can be seen directly from the model. What our work does offer is, first, some confirmation of our model in the sense that it will quantitatively reproduce the experimental observations, with reasonable values for the parameters, and second, a basis for further extension and refinement.

Our results indicate that the observed low-pressure drop-off of burning rate curves can be accounted for on the basis of a solid-phase reaction zone of finite thickness. They coalesce with Rice and Ginell's zero-diffusion results for high pressures, however (we have verified this by detailed quantitative comparisons), which means that the model chosen for the solid-phase reaction zone is of little importance in the higher pressure (and ballistically more significant) regions. In this connection, we might point out that our Problem B is identical with the problem Rice and Ginell posed concerning the fizz reaction, so that our analytical and numerical results could be carried over to the Rice and Ginell model *in toto*. In particular, our second approximation results—equation 53 and table 2—provide an estimate of the effect of the activation energy of the fizz reaction, which Rice and Ginell did not consider in so detailed a fashion.

With regard to the "parameters" δ_a, δ_b, the formal physical interpretation, as extent of reaction incomplete, is not to be taken seriously. These δ's are strictly mathematical artifices, made necessary by our sharp division of reaction zones. In a sense, equations 1 and 2 give us "theorems of the mean" whereby we avoid treating overlapping zones; the δ's are the "mean value" parameters. Clearly we should be able to calculate the correct values of the δ's, if only we could solve the true overlapping-zone problem. The fact that part of the burning rate curve, *viz.*, the low-pressure hump, is sensitive to the value of δ_a perhaps indicates some significant effects of the overlapping between foam and fizz reactions.

With regard to extension of the theory, it is clear that it can be applied immediately to the flame zone; this would enable us to carry the curves up to higher pressures. We can also change the kinetics in any zone of our model, with little trouble; indeed, the low-pressure results indicate that we should do better to take our foam reaction with order 1.5, rather than 1.0. It does appear to us that the successive reaction zones must have increasing orders; i.e., with a fizz reaction of order 2, the foam reaction must have smaller order (1.0 or 1.5, say), and the flame reaction higher (3.0 or 2.5). Two successive zones of the same reaction order would behave simply as a single zone.

The extensions suggested above are mere matters of calculation; the methods we have used would suffice. More serious is the extension to include diffusion; we are now carrying this out, following the lead of Corner in his work on single-zone flames (2). Corner's work indicates that the effect of diffusion is by no means negligible.

Another highly desirable extension would be to include overlapping zones. This would get us away from such tricks as our δ's and, more important, would enable us to write into our theory the actual separate steps of each reaction stage. So far, experimental analysis has given us almost no data on these separate steps, but it would be pleasing to have the theory ready to use such data when they become available.

Meanwhile, the present theory encourages our belief that our model of the burning zone is not too far off. The methods we use should be applicable to any adiabatic reaction stream where the consecutive reactions occur in non-overlapping or slightly overlapping zones.

We are indebted to Professor O. K. Rice for much helpful comment, Dr. C. F. Curtiss for proof of the elusive lemma of Appendix I, Dr. Clayton Huggett for encouragement and advice, and Mr. A. Levy and Mr. T. Yamada for computational assistance.

REFERENCES

(1) Boys, S. F., and Corner, J.: Proc. Roy. Soc. (London) **A197,** 90 (1949).

(2) Corner, J.: Proc. Roy. Soc. (London) **A198,** 388 (1949).

(3) Crawford, B. L., Jr., *et al.*: OSRD Report 5224 (1945).

(4) Crawford, B. L., Jr., Huggett, C., and McBrady, J.: J. Phys. & Colloid Chem. **54,** 854 (1950).

(5) Rice, O. K., and Ginell, R.: J. Phys. & Colloid Chem. **54,** 885 (1950).

APPENDIX I. THE FIZZ REACTION AT ZERO PRESSURE[13]

Let us consider the solution $T(\epsilon_b)$ of the differential equation

$$\frac{dT}{d\epsilon_b} = \frac{M^2R^2T^2(1+n\epsilon_b)^2[Q_b(1-\delta_b-\epsilon_b)+c_b(T-T_b)]}{\lambda_bB_bP^2\,W_a^2(1-\epsilon_b)^2\exp(-A_b/T)} \tag{A1}$$

which satisfies the condition

$$T(1-\delta_b) = T_1 \tag{A2}$$

The existence, uniqueness, and analyticity of this solution in the interval $0 \leq \epsilon_b \leq 1 - \delta_b$ is assured by an existence theorem from the theory of differential equations.[14] Equations A1 and A2 therefore uniquely determine a temperature $T(0)$ which may be identified with the surface temperature T_s provided that

$$T(\epsilon_b) \geq T_a \text{ for } 0 \leq \epsilon_b \leq 1 - \delta_b \tag{A3}$$

This inequality must be explicitly proved, for if it failed to hold at some pressure, one might suppose the true situation to be

$$T \equiv T_a, \qquad \epsilon_b \equiv 0 \tag{A4}$$

which would mean that the fizz reaction did not take place at that pressure.

Because of equation 33, equation A3 will be established if it can be shown that, irrespective of the value of P, $T(\epsilon_b)$ satisfies the inequality:

$$Q_b(1-\delta_b-\epsilon_b) + c_b(T-T_b) \geq 0 \text{ for } 0 \leq \epsilon_b \leq 1-\delta_b \tag{A5}$$

To prove this, one may first note that the approximate solution, equation 42, which is exact near $\epsilon_b = 1 - \delta_b$, gives:

$$\begin{aligned} Q_b(1-\delta_b-\epsilon_b) + c_b(T-T_b) \equiv {} & Q_b\xi\{1 - (\beta/\xi)\exp(\beta/\xi)[-E_i(-\beta/\xi)]\} \\ & + c_b(T_1 - T_b)\exp(\beta/\xi)\exp(-\beta/\delta_b) \geq 0] \end{aligned} \tag{A6}$$

---

[13] The key theorem of this appendix, equation A3, was first proved by C. F. Curtiss, using essentially the method given here.

[14] See, for example, Ince, *Ordinary Differential Equations*, p. 281. The special case $\delta_b = 0$, $T_1 = T_b$ requires a less well-known theorem due to Bendixon (Ofv. Vet.-Akad. Stockholm **55,** 69 (1898)).

Hence equation A5 holds in the neighborhood of $\epsilon_b = 1 - \delta_b$. But if it holds in this neighborhood, it must hold throughout $0 \leq \epsilon_b \leq 1 - \delta_b$. For, equation A1 requires that $(dT/d\epsilon_b)$ be zero whenever

$$Q_b(1 - \delta_b - \epsilon_b) + c_b(T - T_b) = 0 \tag{A7}$$

and no analytic function $T(\epsilon_b)$ which starts out from the origin $T = T_1$, $\epsilon_b = 1 - \delta_b$ below the line A7 of positive slope can ever cross that line if $dT/d\epsilon_b$ is zero wherever the function and line coincide.

As an immediate corollary to equation A3, we have

$$[T(0)]_{(P=0)} = [T_s]_{(P=0)} \geq T_a \tag{A8}$$

But

$$[T_s]_{(P=0)} \leq T_a \tag{A9}$$

since in the limit of zero pressure no heat can get back to the surface from the gas-phase zones.[15] Thus

$$[T(0)]_{P=0} = [T_s]_{P=0} = T_a \tag{A10}$$

Finally, we find from equations A5 and A10 that

$$Q_b(1 - \delta_b - \epsilon_b) + c_b(T - T_b) \equiv 0 \text{ when } P = 0 \tag{A11}$$

whence

$$[T_1]_{P=0} \equiv T_b \tag{A12}$$

APPENDIX II. CALCULATION OF THE $g_k(x)$

To obtain a representation of $g_k(x)$ convenient for large values of x, we substitute in equation 47 the asymptotic expansion

$$-u \exp(u) E_i(-u) \sim 1 - \frac{1}{u} + \frac{1}{u^2} - \frac{2!}{u^3} + \cdots \tag{A13}$$

and integrate term by term. We obtain

$$g_k(x) \sim \frac{1}{k} - \frac{1}{k+1}\left(\frac{1}{x}\right) + \frac{2!}{k+2}\left(\frac{1}{x}\right)^2 - \cdots \tag{A14}$$

When x is small, we dispose of two of the needed $g_k(x)$ by use of the identities

$$g_1(x) = -x\exp(x)\, E_i(-x) \tag{A15}$$

$$g_3(x) = x\,[g_2(x) - g_1(x) + \tfrac{1}{2}] \tag{A16}$$

and calculate the third from the formula

$$\begin{aligned} x^{-2}g_2(x) &= x^{-1} - \gamma \ln x - \tfrac{1}{2}\ln^2 x + E_i(-x)\ln x + \gamma E_i(-x) \\ &\quad - E_i(-x)E_i(x) - \sum_{n=1}^{\infty}\frac{(-x)^n}{n^2\, n!} + \sum_{m=1}^{\infty}\sum_{n=0}^{\infty}\frac{(-x)^n x^m}{m\, m!\, n!\,(n+m)} - 2.633980 \end{aligned} \tag{A17}$$

---

[15] Mathematical proof of this is straightforward but cumbersome.

where $\gamma = 0.5772157$ is Euler's constant and

$$2.633980 = (\pi^2/6) + \sum_{n=1}^{\infty} \frac{(-1)^{n-1}}{n^2 n!} + \int_1^{\infty} \ln x \exp(-x) x^{-1}\, dx \qquad \text{(A18)}$$

To verify equation A17, one may insert into equation 47 the series

$$-E_i(-x) = \gamma - (1/4) \ln x^4 - \sum_{n=1}^{\infty} \frac{(-x)^n}{n n!} \qquad \text{(A19)}$$

and integrate term by term.

THORIUM NITRATE. IV

LEACHING WITH HIGHER ALCOHOLS AND KETONES AS A MEANS OF ENRICHING MIXED NITRATES IN THORIUM[1]

CHARLES C. TEMPLETON[2] AND NORRIS F. HALL

Department of Chemistry, University of Wisconsin, Madison, Wisconsin

Received September 14, 1948

In earlier papers (5, 6, 7) of this series we have considered the possibilities of both liquid–liquid extraction and leaching with a single solvent. Liquid–liquid extraction may be used as a fractionation process and theoretically allows the enrichment in the desired component to be carried to any desired value by the use of a sufficient number of cycles. A leaching process for the separation of two substances, on the other hand, if the system is allowed to come to equilibrium, obviously attains its maximum enrichment in a single step. Only such equilibrium leaching has been considered in this study.

In view of these considerations, leaching is applicable only as a process for the initial enrichment of materials in thorium, and would be practical only if a great enrichment in thorium were achieved in a single step. This investigation shows that for higher alcohols and ketones (of six carbon atoms and over) such is the case. Further, we have previously shown (5) that a single wash with an equal volume of water is sufficient to remove practically all the extracted material from the saturated leaching solution.

Our general investigation of the solvent extraction of thorium from mixtures with the rare earths has been confined to simple systems without the addition of any special anion to cause the thorium to form a complex in the organic phase. We have succeeded only because we chanced to study the distribution of thorium nitrate between water and an organic solvent in the *concentrated* range of aqueous solutions (60–100 per cent saturated in thorium nitrate). This led directly to the leaching idea.[3] Our entire investigation is thus in contrast to those of other authors (1, 2) who, confining their studies of the separation of actinide from lanthanide nitrates by liquid–liquid extraction to the range of quite *dilute* solutions, have to add special complex-forming agents to make the actinide preferentially enter the organic phase.

---

[1] This paper is based upon the thesis submitted by C. C. Templeton to the Graduate Faculty of the University of Wisconsin in partial fulfillment of the requirements for the degree of Doctor of Philosophy, June, 1948.

[2] Present address: Department of Chemistry, University of Michigan, Ann Arbor, Michigan.

EXPERIMENTAL

For this study, we define "thorium enrichment" as the percentage of thoria in the total metal oxides in the material. For equilibrium leaching, the attainable enrichment in thorium would be that of the total material in an organic solution saturated with respect to both $Th(NO_3)_4 \cdot 4H_2O$ and the rare earth nitrate of interest.

The organic solvents used were all of Eastman Kodak Company "practical" grade. The thorium nitrate (C.P. $Th(NO_3)_4 \cdot 4H_2O$) was purchased from the J. T. Baker Chemical Company. We chose to leach thorium from a mixture of the nitrates of thorium and several rare earths. The mixed rare earth nitrate used, obtained from the University of Wisconsin stocks, was of the following relative composition (percentages as metal in an oxalate sample):

ELEMENT	PER CENT	ELEMENT	PER CENT	ELEMENT	PER CENT
La	7.0	Eu	0.05	Er	0.5
Ce	0.0	Gd	1.5	Tm	0.1
Pr	5.7	Tb	0.2	Yb	0.5
Nd	12.5	Dy	1.0	Y	10.0
Sm	3.0	Ho	0.3		

Studies were made of four alcohols and of five methyl ketones. In each case 5–10 ml. of solvent was mixed in a test tube with appropriate amounts of both thorium nitrate and the mixed rare earth nitrates. The samples were then rotated end over end at 30 R.P.M. at room temperature for 5 days. Saturation was assured by the presence of distinct white (thorium) and pink (neodymium) lumps in the final solid phase. Each solution was then filtered, and the "total solubility" (grams of total metallic oxides per 100 g. of solution) was determined. This was done in our usual manner by weighing out about 1 ml. of solution into a tared platinum crucible, burning off the solvent, and igniting to the oxides. The remaining solution was decomposed to yield the dissolved material in solid form. For methyl and *n*-propyl alcohols, and for acetone and methyl ethyl ketone, the decomposition was accomplished by pouring the solution into water and boiling until only an aqueous solution remained, followed by the addition of a little nitric acid, evaporation, and crystallization. For the higher alcohols and ketones, the organic solution was washed with about twice its volume of water, and the solid nitrates were crystallized from the aqueous extract. No metallic nitrates could be detected in 1 ml. of the washed organic solutions.

---

[3] Although most current work in this field of solvent extraction has been concerned with liquid–liquid systems, leaching of mixed solids with a single organic solvent has often been investigated. Misciattelli (4) studied the system uranyl nitrate–thorium nitrate–ethyl ether at various temperatures and claimed to have prepared the anhydrous nitrates. Regardless of whether he actually had the anhydrous salts, his systems at least had a very low water content. He found that at any temperature above 20°C. only uranyl nitrate dissolved in the anhydrous ether, provided sufficient uranyl nitrate was present to insure saturation. If insufficient uranyl nitrate was present, some thorium nitrate also dissolved.

TABLE 1

Thorium enrichments attainable in organic solutions saturated in both thorium and rare earth nitrates

SOLVENT	THORIUM ENRICHMENT (PER CENT ThO_2 IN TOTAL OXIDES)		RATIO OF ThO_2 TO $(R.E.)_2O_3$	TOTAL SOLUBILITY	
	Single determinations	Average		Total oxides per 100 g. solution	$Th(NO_3)_4$ per 100 g. solution
	per cent	*per cent*		*grams*	*grams*
Acetone	71.1 70.6	70.8	2.42	35.6	45.7
Methyl ethyl ketone	79.1	79.1	3.78	32.0	46.0
Methyl isobutyl ketone	88.4 88.6	88.5	7.7	24.0	38.5
Methyl *n*-amyl ketone	90.4	90.4	9.4	21.4	35.1
Methyl *n*-hexyl ketone	93.2 93.0	93.1	13.5	17.8	30.2
Methyl alcohol	54.6 54.8	54.7	1.21	36.2	36.0
n-Propyl alcohol	76.7 76.8	76.8	3.3	28.4	39.6
Isoamyl alcohol	90.4	90.4	9.4	22.0	36.1
n-Hexyl alcohol	92.3	92.3	12.0	19.5	32.7
Ethyl butyrate (7 days' agitation)	91.0	91.0	10.1	18.5	30.5

The solid nitrates were in an indefinite state of hydration, but this uncertainty was cancelled out in the analytical scheme. In each case two samples were weighed out rapidly enough for both to be in the same condition. In one of these, the amount of total oxides was determined by precipitating the hydroxides with ammonia, filtering, and igniting. In the other, thoria was determined after separating thorium and the rare earths by the iodate method (3). Thorium enrichments were then calculated as the percentage of thoria in the total oxides.

The total solubilities and the thorium enrichments are listed in table 1. From these have been calculated the ratio of thoria to rare earth oxides and the total amount of thorium nitrate extracted per gram of resultant leaching solution. The results on ethyl butyrate already reported are included for comparison.

DISCUSSION

The type of leaching being considered consists simply in agitating the solid mixed nitrates with an appropriate amount of any of the higher alcohols or ketones. A batch of saturated solution is withdrawn and agitated with an equal volume of water until practically all the extracted nitrates enter the aqueous phase. The product is crystallized from the aqueous phase by evaporation and the washed organic solvent saved for re-use.

The increase in thorium enrichment with increasing molecular weight of the solvent in either homologous series is apparent from the data in table 1. The thorium nitrate content of all the solutions is only slightly less than the solubility of $Th(NO_3)_4 \cdot 4H_2O$ alone in the same solvent (6). The increase in thorium enrichment is thus due to the greater decrease in solubility of rate earth nitrates, as compared to thorium nitrate, with increasing molecular weight of the solvent.

SUMMARY

1. Mixed nitrates of thorium and rare earths may be enriched to over 80 per cent in thorium nitrate by leaching with any of several alcohols or ketones.

2. The attainable thorium enrichment increases within an homologous series of alcohols or ketones with increasing molecular weight.

This research was supported in part by the Research Committee of the University of Wisconsin Graduate School from funds obtained from the Wisconsin Alumni Research Foundation.

REFERENCES

(1) Audrieth, L. F.: Private communication to N. F. Hall.

(2) Harvey, Heal, Maddock, and Rowley: J. Chem. Soc. **1947,** 1010.

(3) Hillebrand and Lundell: *Applied Inorganic Analysis.* John Wiley and Sons, Inc., New York (1929).

(4) Misciattelli: Phil. Mag. [7] **7,** 670 (1929).

(5) Rothschild, Templeton, and Hall: J. Phys. & Colloid Chem. **52,** 1006 (1948).

(6) Templeton and Hall: J. Phys. & Colloid Chem. **51,** 1441 (1947).

(7) Templeton, Rothschild, and Hall: J. Phys. & Colloid Chem. **53,** 838 (1949).

THORIUM NITRATE. V

EXTRACTION FROM AQUEOUS SOLUTION BY ORGANIC SOLVENTS AS A MEANS OF ENRICHING MIXED NITRATES IN THORIUM[1]

CHARLES C. TEMPLETON[2] AND NORRIS F. HALL

Department of Chemistry, University of Wisconsin, Madison, Wisconsin

Received September 14, 1948

We have shown (4) that leaching of mixed solid thorium and rare earth nitrates with higher alcohols and ketones results in a considerable increase in the proportion of thorium nitrate. The present paper demonstrates that the last 10–20 per cent of rare earth nitrates can be removed by a liquid–liquid extraction process.

EXPERIMENTAL

Apparatus and method

An all-glass extraction apparatus (figure 1) was used. Each of the vessels had a total capacity of about 200 ml. Vessels II and IV had volumes of about 160 ml. below the overflow arms. All solvent flow was by gravity. Vessel I was initially filled with the desired organic extraction solvent. Vessel II was filled, to within ½ to ¾ in. of the overflow, with a concentrated aqueous solution of the starting mixed nitrates. Vessel III was an overflow reservoir. Vessel IV was filled, to within ½ to ¾ in. of the overflow, with distilled water. The appropriate stopcocks were adjusted so that a steady drop rate was maintained at both overflow tubes. The flow rate was usually about 100 ml. per hour, although it could not conveniently be kept absolutely constant. Layers of organic solvent formed above the aqueous phases in both vessels II and IV. A motor-driven stirrer, adjusted to about 50 to 100 R.P.M., was arranged to agitate the aqueous phase in vessel IV without disturbing the supernatant organic layer. No means of stirring was provided in vessel II inasmuch as, without stirring, more material was extracted than could be completely washed out in vessel IV even with stirring. The washed solvent which overflowed was returned to vessel I; in no run was the total amount of solvent required more than the initial 200 ml. Thus all of the solvents investigated remained nearly immiscible with water during the entire process.

Owing to the nature of the relation governing the distribution of thorium nitrate between water and any of these organic solvents (1, 3, 5), at a maximum only about 20 per cent of the thorium nitrate could be practically extracted from an initially saturated aqueous solution. Consequently, for each run vessel II was originally filled with an almost saturated solution, and solvent was run through the system until the accumulated material in vessel IV represented 5–10 per cent of the original nitrates. At this point vessel IV was drained, and the aqueous solution evaporated to obtain the yield in solid form.

---

[1] This paper is based upon the thesis submitted by Charles C. Templeton to the Graduate Faculty of the University of Wisconsin in partial fulfillment of the requirements for the degree of Doctor of Philosophy, June, 1948.

[2] Present address: Department of Chemistry, University of Michigan, Ann Arbor, Michigan.

Analytical methods

Two samples of a given nitrate mixture were weighed out at the same time. One sample was ignited in a platinum crucible to give the percentage of total oxides. The amount of Nd_2O_3 was determined by measuring the absorption of light at 525 and 579 millimicrons by a solution of the other sample in 2 N nitric acid, using the Beckman Model DU quartz spectrophotometer. Results were read from an empirical calibration curve, based on measurements made on solutions prepared from pure $Nd(NO_3)_3 \cdot 6H_2O$. For those runs where a mixture of the rare earths was used in the starting material, neodymium was determined as above and the total rare earth oxides were calculated on the assumption that the proportions of the various rare earths were not changed during the extraction. That this assumption does not seriously affect the results in question (runs B and I) may be seen from the fact that the separation factor for fractionating neodymium and lanthanum nitrates with n-hexyl alcohol is about 1.5 (2). En-

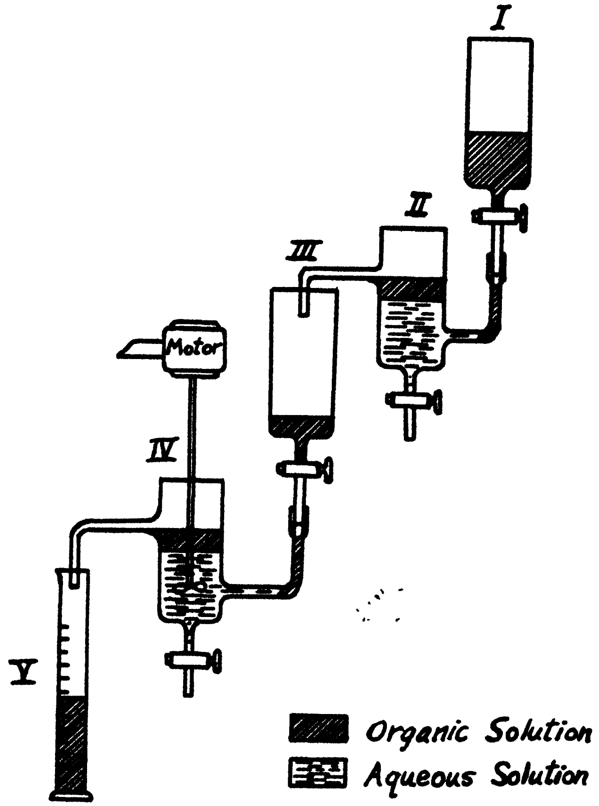

FIG. 1. Continuous liquid-liquid extraction apparatus

richments in thorium and neodymium were then calculated as the percentage of the respective oxide in the total oxides.

DATA

A preliminary test[3] of the apparatus was made using *n*-hexyl alcohol, first with pure thorium nitrate as the starting material (run A), and then with a mixture of thorium and mixed rare earth[4] nitrates as the starting material (run B).

In run I methyl *n*-hexyl ketone was used to enrich a mixture of thorium and mixed rare earth nitrates of an initial thorium enrichment of 84.9 per cent. For runs II, III, and IV the starting material was a mixture of thorium and neodymium nitrates only, the solvents being methyl *n*-hexyl ketone, methyl isobutyl ketone, and ethyl butyrate, respectively. The detailed data are given in table 1. Yields are given as percentages of the total weight of hydrated nitrates used in the starting material. Separation factors have been calculated as the ratio of thoria to rare earth oxides in the yield divided by the same ratio in the starting material.

DISCUSSION

These data show that the separation of thorium from the rare earths by extraction from aqueous solution with organic solvents is feasible. The major consideration is that the aqueous phase must be quite concentrated (80 per cent or more of saturation) in thorium nitrate for any appreciable portion of the thorium to enter the organic phase. It is a corollary that any organic solution of thorium nitrate will surrender its solute almost completely to an equal volume of water, if given a reasonable amount of time and agitation. The periodic removal and resaturation of the starting aqueous nitrate solution is an inherent feature of the process. In view of this feature, the apparently low yields of 5–10 per cent are not significant, since eventually most of the thorium may be extracted with a reasonable number of resaturations of the starting solution.

In this work, no trouble was encountered due either to indistinct phase boundaries or to loss of organic solvent because of increased miscibility with the aqueous phase.

CONCLUSIONS

1. The extraction of thorium nitrate from aqueous solutions also containing the nitrates of the rare earths by the use of higher organic solvents has been shown to be possible. Appreciable yields of thorium nitrate of high purity were obtained.

2. The only condition which is critical to the process is that the starting aqueous solution must be kept quite near to saturation with respect to thorium nitrate. The method is mainly applicable to materials which have been enriched to about 80 per cent in thorium by some other means, such as the leaching scheme previously described (4).

---

[3] This test was performed by Mr. Bill F. Rothschild.

[4] The mixed rare earth nitrates were from the lot used in the work described in reference 4.

TABLE 1

Liquid–liquid extractions with organic solvents

Run A

Solvent: *n*-hexyl alcohol (Eastman Kodak Company, practical)
Starting material: C.P. $Th(NO_3)_4 \cdot 4H_2O$
Flow rate: about 50 ml./hr.
Vessel II: 130 ml. aqueous thorium nitrate solution
Vessel IV: 120 ml. water

TOTAL SOLVENT FLOW	CONCENTRATION CHANGES PERCENTAGES OF $Th(NO_3)_4$ IN SOLUTION			
	Vessel II	Vessel III	Vessel IV	Vessel V
ml.	*per cent*	*per cent*	*per cent*	*per cent*
0	60.81	0.0	0.0	0.0
100	59.02	3.81	0.43	0.72
150	57.65	3.38	1.84	1.88
200		4.16	3.05	1.42
250		6.53	3.81	1.85
300		4.58	5.12	1.67
350	54.54	5.13	6.35	1.75

Run B

Solvent: *n*-hexyl alcohol (Eastman Kodak Company, practical)
Starting material: mixture of $Th(NO_3)_4 \cdot 4H_2O$ and mixed rare earth nitrates; enrichment, 83.0 per cent
Flow rate: 50 ml./hr.
Vessel II: 130 ml. aqueous mixed nitrate solution
Vessel IV: 120 ml. water

TOTAL SOLVENT FLOW	CONCENTRATION CHANGES PERCENTAGES OF TOTAL OXIDES IN SOLUTION		
	Vessel II	Vessel IV	Vessel V
ml.	*per cent*	*per cent*	*per cent*
0	29.12	0.0	0.0
100		0.08	0.51
150		0.36	0.81
200		0.73	0.67
250		1.02	0.59
300		1.31	0.45
350	28.86	1.51	0.39

Total solvent flow: 350 ml.
Yield: 2.5 per cent
Thorium enrichment: 96.2 per cent
Separation factor: 5.2

TABLE 1—*Continued*

Liquid-liquid extractions with organic solvents

Run I

Solvent: methyl *n*-hexyl ketone (b.p., 172–173°C.)
Starting material: 160 g. mixture of $Th(NO_3)_4 \cdot 4H_2O$ and mixed rare earth nitrates; thorium enrichment, 84.9 per cent
Flow rate: about 100 ml./hr.
Vessel II: 130 ml. aqueous mixed nitrate solution
Vessel IV: 130 ml. water

TOTAL SOLVENT FLOW	CONCENTRATION CHANGES PERCENTAGES OF TOTAL OXIDES IN SOLUTION		
	Vessel II	Vessel IV	Vessel V
ml.	*per cent*	*per cent*	*per cent*
0	32.9	0.0	0.0
50		0.40	0.57
100		0.91	0.77
150		1.11	0.49
250		1.58	0.72
400		1.92	0.76
600		2.46	0.68
1000		3.37	0.21

Total solvent flow: 5200 ml.

PORTION OF PROCESS	YIELDS AS HYDRATED NITRATES	RARE EARTH ENRICHMENT	THORIUM ENRICHMENT (BY DIFFERENCE)
	grams	*per cent*	*per cent*
0 to 1100 ml.	10.0	0.3	99.7
1100 to 2100 ml.	3.3	1.1	98.9
2100 to 5200 ml.	6.8	0.4	99.6

Total yield: 12.6 per cent
Separation factor: 44

Run II

Solvent: methyl *n*-hexyl ketone (b.p., 172–173°C.)
Starting material: 142 g. mixed $Th(NO_3)_4 \cdot 4H_2O$ and $Nd(NO_3)_3 \cdot 6H_2O$; thorium enrichment, 97.1 per cent
Flow rate: about 100 ml./hr.
Vessel II: 100 ml. aqueous mixed nitrate solution
Vessel IV: 100 ml. water

CONCENTRATIONS IN	PER CENT TOTAL OXIDES IN SOLUTION
Vessel II (initial)	34.1
Vessel IV (final)	2.86

Total solvent flow: 3240 ml.
Yield: 5.5 per cent
Thorium enrichment: 99.92 per cent
Neodymium enrichment: 0.08 per cent
Separation factor: 37

TABLE 1—*Concluded*

Liquid–liquid extractions with organic solvents

Run III

Solvent: methyl isobutyl ketone (Eastman Kodak Company, practical)
Starting material: 155 g. mixed $Th(NO_3)_4 \cdot 4H_2O$ and $Nd(NO_3)_3 \cdot 6H_2O$; thorium enrichment, 97.0 per cent
Flow rate: about 100 ml./hr.
Vessel II: 110 ml. aqueous mixed nitrate solution
Vessel IV: 120 ml. water

CONCENTRATIONS IN	PER CENT TOTAL OXIDES IN SOLUTION
Vessel II (initial)	34.0
Vessel IV (final)	5.5

Total solvent flow: 1280 ml.
Yield: 10.3 per cent
Thorium enrichment: 99.7 per cent
Neodymium enrichment: 0.3 per cent
Separation factor: 10.3

Run IV

Solvent: ethyl butyrate (Eastman Kodak Company, practical)
Starting material: 160 g. mixed $Th(NO_3)_4 \cdot 4H_2O$ and $Nd(NO_3)_3 \cdot 6H_2O$; thorium enrichment, 97.0 per cent
Flow rate: about 100 ml./hr.
Vessel II: 115 ml. aqueous mixed nitrate solution
Vessel IV: 120 ml. water.

CONCENTRATIONS IN	PER CENT TOTAL OXIDES IN SOLUTION
Vessel II (initial)	33.9
Vessel IV (final)	1.02

Total solvent flow: 2000 ml.
Yield: 1.4 per cent
Thorium enrichment: 99.97 per cent (limit of analytical method)
Neodymium enrichment: 0.03 per cent (No neodymium was detectable)
Separation factor: 103

This research was supported in part by the Research Committee of the University of Wisconsin Graduate School from funds obtained from the Wisconsin Alumni Research Foundation.

REFERENCES

(1) Rothschild, Templeton, and Hall: J. Phys. & Colloid Chem. **52,** 1006 (1948).
(2) Templeton: J. Am. Chem. Soc. **71,** 2187 (1949).
(3) Templeton and Hall: J. Phys. & Colloid Chem. **51,** 1441 (1947).
(4) Templeton and Hall: J. Phys. & Colloid Chem. **54,** 954 (1950).
(5) Templeton, Rothschild, and Hall: J. Phys. & Colloid Chem. **53,** 838 (1949).

COMMUNICATIONS TO THE EDITOR

FLEXIBILITY OF NITROCELLULOSE MOLECULES IN ACETONE

It has been previously reported (R. M. Badger and R. H. Blaker: J. Phys. & Colloid Chem. **53,** 1056 (1949)), largely on the basis of light-scattering, viscosity, and diffusion measurements, that the hydrodynamic equations for flexible macromolecules of Kirkwood and Riseman (J. G. Kirkwood and J. Riseman: J. Chem. Phys. **16,** 565 (1948); J. Riseman and J. G. Kirkwood: J. Chem. Phys. **17,** 442 (1949)) offered promise as being applicable to solutions of cellulose and its derivatives possessing degrees of polymerization, Z, greater than 100.

This writer would like to mention that he had considered the applications of the Kirkwood–Riseman theory to cellulose nitrate in acetone, employing published sedimentation data, and had similarly concluded that for large molecular weights the theory might serve, at least to a first approximation, as a satisfactory formalism interrelating translational and rotatory diffusion, viscosity, and sedimentation. The validity of the theoretical equations in the case of polystyrene has been experimentally demonstrated (J. G. Kirkwood and J. Riseman: *loc. cit.*; S. Newman, J. Riseman, and F. Eirich: Rec. trav. chim. **68,** 921 (1949)).

Because of the greater precision of sedimentation measurements as compared to those of diffusion, and because of the convenience of the former in computing the molecular parameters b, the effective bond length, and ζ, a frictional coefficient, which appear in the Kirkwood–Riseman theory, we had considered the sedimentation data of H. Mosimann (Helv. Chim. Acta **26,** 61 (1943)) and I. Jullander (Arkiv Kemi, Mineral. Geol. **21A,** 1 (1945)) on nitrocellulose in acetone. It was found, upon neglecting small differences in the degrees of esterification, that for five fractions (Mosimann) the sedimentation constants extrapolated to infinite dilution bore, to a good approximation, the following relation to the degree of polymerization:

$$S_0 = 2.2 \times 10^{-13} + 0.58 \times 10^{-13}\, Z^{0.5}$$

Solving for b and ζ from the equation[1]

$$S_0 = M_0(1 - \bar{V}\rho)\,[1 + (8\lambda_0/3)Z^{0.5}]/\zeta N$$
$$\lambda_0 = \zeta/(6\pi^3)^{0.5}\,\eta_0 b$$

where M_0 is the relative monomer weight, N is Avogadro's constant, $(1 - \bar{V}\rho)$ is the buoyancy factor, and η_0 is the viscosity coefficient of the solvent, we have obtained the values reported in table 1. For comparison, the results of Badger and Blaker from diffusion and light scattering on samples of somewhat higher nitrogen content are included.

Values of the parameters calculated from sedimentation data of Jullander for unfractionated samples containing approximately 12.5 per cent nitrogen lead to substantially the same results as those of Mosimann, which contain approximately 12.0 per cent nitrogen. The samples of Badger and Blaker were nitrated to slightly more than 13 per cent nitrogen.

---

[1] The original published equation (J. G. Kirkwood and J. Riseman: J. Chem. Phys. **16,** 565 (1948)) contains a typographical error.

We have computed with the Kirkwood–Riseman equations the intrinsic viscosity of the samples of Badger and Blaker, using the b- and ζ-values calculated from sedimentation data and reported above, and have compared them with the experimental intrinsic viscosity values (see table 2).

Considering sample inhomogeneity and differences in degrees of nitration, a satisfactory agreement between observed and calculated values is noted. This agreement suggests that of the range of values for b reported by Badger and Blaker, the lowest ones approximating those we have used would seem to be more appropriate for the samples they have studied and which are discussed here.

TABLE 1

Molecular parameters for nitrocellulose in acetone

METHOD	b	$10^{10}\zeta$
	Å.	g./sec.
Sedimentation	30	11.9
Diffusion	46	8.0
Light-scattering	32–57	

TABLE 2

Comparison of observed and calculated intrinsic viscosities

SAMPLE	MOLECULAR WEIGHT	INTRINSIC VISCOSITY	
		Observed	Calculated
S-4,3	9,400	0.30	(0.51)
S-3,4	35,000	1.30	1.50
S-1,1–4	50,000	2.22	1.98
P-3,2	93,000	2.98	3.14
P-4,2	319,000	6.86	7.45

While the agreement noted in table 2 may be fortuitous, we believe rather that for high molecular weights there is sufficient "bending" in the molecule to permit an approximate application of the Kirkwood–Riseman theory, even though it was not intended for so "stiff" a molecule. Coördinate measurements on homogeneous samples are required for a quantitative study of the limits of applicability of the theory in its present state.

Since it is postulated that for a rod-like molecule S_0 is proportional to log Z,[2] and for the sedimentation data cited here such a plot approaches linearity only for $Z < 100$, we had tentatively concluded that a theory based on a flexible macromolecule would be inapplicable in this lower range; this confirms the conclusions of Badger and Blaker.

---

[2] Private communication from Dr. J. Riseman.

SEYMOUR NEWMAN.

Southern Regional Research Laboratory
Agricultural Research Administration
U. S. Department of Agriculture
New Orleans, Louisiana

February 2, 1950

A METHOD FOR DETERMINING THE PROPERTIES OF MICELLES

We have found it possible to obtain thermodynamic and kinetic data about micelles formed by association colloids by "tagging" the micelles with a minute amount of a solubilized material such as a dye. In aqueous solutions of soap, for example, water-insoluble dyes are taken up by micelles alone (J. W. McBain: *Frontiers in Colloid Chemistry*, Interscience Publishers, Inc., New York (1950)) and the movement of the dyes, and therefore of the micelles, may be observed under the influence of various forces. Thus the self-diffusion coefficient of the micelle (or at least of the average solubilizing micelle), its electrophoretic mobility, sedimentation equilibrium, etc. may be determined. These lead by well-known methods (Alexander and Johnson: *Colloid Science*, Oxford University Press (1949)) to an estimate of the molecular weight, charge, and approximate shape of the micelle. The method is generally applicable to solubilizing particles in both aqueous and nonaqueous solutions and may be used with any solvent-insoluble tracer as well as with dyes.

In preliminary experiments we have estimated the electrophoretic mobility and the diffusion constant of the micelle in 5 per cent potassium laurate containing 4 mole per cent potassium hydroxide on the soap, using Sudan IV, a water-insoluble dye, as a tracer. We have also observed the sedimentation in a centrifugal field of micelles of sodium lauryl sulfate containing Sudan IV.

The electrophoretic movement of ascending and descending boundaries between the tagged and the dye-free solutions of the same concentration was observed in a standard Tiselius apparatus made available through the kindness of Dr. E. Jameson. Owing to the absence of density differences, a parabolic boundary is obtained. Diffusion was observed between two similar solutions in an unstirred sintered-glass diaphragm cell made available by Professor A. Adamson. Sedimentation was observed qualitatively in a McBain–Ford air-driven opaque centrifuge.

The values obtained were $D = 0.04$ cm.^{2}/day and $u = 2.3 \times 10^{-4}$ cm.^{2}/volt sec. The only comparable, although differently interpreted, measurement is $D = 0.06$ cm.^{2}/day obtained by Dean and Vinograd (J. Phys. Chem. **46**, 1091 (1942)) for Yellow AB in Aerosol OT.

On the basis of our values, it appears that the average solubilizing micelle in 5 per cent potassium laurate has effectively 12 negative charges, an equivalent spherical radius of about 25 Å., and a molecular weight of at most 40,000, corresponding to 170 soap molecules.

We are indebted to the Bristol Myers Company for support which made this work possible.

Department of Chemistry
University of Southern California
Los Angeles 7, California
March 22, 1950

Horst W. Hoyer.
Karol J. Mysels.

BOOKS RECEIVED

Bravais, M. A. *On the Systems Formed by Points Regularly Distributed on a Plane or in Space.* Translated by Amos J. Shaler. The Crystallographic Society of America Memoir No. 1. May be obtained from W. Parrish, Crystallographic Laboratory, Philips Laboratories, Inc., Irvington-on-Hudson, New York City. 1949. 113 pp. Price: \$3.40 to members, \$3.90 to nonmembers of the Society.

Daniels, Farrington, Mathews, Joseph Howard, Williams, John Warren, Bender, Paul, Murphy, George W., and Alberty, Robert A. *Experimental Physical Chemistry.* 4th edition. McGraw-Hill Book Company, Inc., 300 West 42nd St., New York 18. 1949. 568 pp. Price: \$4.50.

Karve, D. D. *An Elementary Textbook of Organic Chemistry.* Dastane Brothers' Home Service, Ltd., 456 Raviwar Peth, Poona 2, India. 1949. 192 pp. Price: Rs. 2-12-0.

Karve, D. D., and Advani, G. D. *Selected Topics from Organic Chemistry.* Dastane Brothers' Home Service, Ltd., 456 Raviwar Peth, Poona 2, India. 1947. 418 pp. Price: Rs. 10/—.

Kirk, Paul L. *Quantitative Ultramicroanalysis.* John Wiley and Sons, Inc., 440 Fourth Ave., New York 16. 1950. 310 pp. Price: \$5.00.

Niven, William W., Jr. *The Fundamentals of Detergency.* Reinhold Publishing Corporation, 330 West 42nd St., New York. 1950. 256 pp. Price: \$5.50.

Partington, J. R. *An Advanced Treatise on Physical Chemistry. Vol. I. Fundamenta Principles, The Properties of Gases.* Longmans, Green and Company, Inc., 55 Fifth Ave., New York. 1949. 943 pp. Price: \$16.00.

Reiner, Markus. *Deformation and Flow.* H. K. Lewis and Company, Ltd., London. 1949. 346 pp. Price: \$6.50.

Third Symposium on Combustion and Flame and Explosion Phenomena. Published under the auspices of the Standing Committee on Combustion Symposia: Bernard Lewis, *Chairman,* Hoyt C. Hottel, *Secretary,* and A. J. Nerad. The Williams & Wilkins Company, Baltimore 2, Maryland. 1949. 748 pp. Price: \$13.50.

Frontiers in Chemistry. Vol. VIII. Frontiers in Colloid Chemistry. Edited by R. E. Burk and Oliver Grummitt. Interscience Publishers, Inc., 215 Fourth Ave., New York 3. 1950. 157 pp.

(To April 4, 1950)

Adams, Douglas P. (Compiler and Editor). *An Index of Nomograms.* Published jointly by The Technology Press of The Massachusetts Institute of Technology and John Wiley and Sons, Inc., New York. 1950. 174 pp. Price: \$4.00.

BERL, WALTER G. (Editor). *Physical Methods in Chemical Analysis.* Vol. I. Academic Press, Inc., New York. 1950. 664 pp. Price: $12.00.

BURK, R. E., AND GRUMMITT, OLIVER (Editors). *Frontiers in Chemistry. Vol. VIII. Frontiers in Colloid Chemistry.* Interscience Publishers, Inc., 215 Fourth Ave., New York 3. 1950. 157 pp.

FARKAS, ADALBERT (Editor). *Physical Chemistry of Hydrocarbons.* Vol. I. Academic Press, Inc., New York. 1950. 453 pp. Price: $8.50.

HARNED, HERBERT S., AND OWEN, BENTON B. *The Physical Chemistry of Electrolytic Solutions.* Second edition. Reinhold Publishing Corporation, 330 West 42nd St., New York 18. 1950. 645 pp. Price: $10.00.

HOUWINK, R. (Editor). *Elastomers and Plastomers. Vol. I. General Theory.* Elsevier Publishing Company, Inc., 215 Fourth Ave., New York 3. 1950. 495 pp. Price: $7.00.

KARRER, PAUL. *Organic Chemistry.* Original translation by A. J. Mee. Fourth English edition, revised and enlarged in accordance with the 11th German edition by H. V. Simon and N. G. Bisset. Elsevier Publishing Company, Inc., 215 Fourth Ave., New York 3. 1950. 973 pp. Price: $8.50.

REINER, MARKUS. *Twelve Lectures on Theoretical Rheology.* Interscience Publishers, Inc., 215 Fourth Ave., New York 3. 1949. 162 pp. Price: $4.00.

UBER, FRED M. (Editor). *Biophysical Research Methods.* Interscience Publishers, Inc., 215 Fourth Ave., New York 3. 1950. 667 pp. Price: $9.50.

WEISSBERGER, ARNOLD (Editor). *Technique of Organic Chemistry.* Vol. III. Heating and Cooling; Mixing; Centrifuging; Extraction and Distribution; Dialysis and Electrodialysis; Crystallization and Recrystallization; Filtration; Solvent Removal, Evaporation, and Drying. Interscience Publishers, Inc., 215 Fourth Ave., New York 3. 1950. 661 pp. Price: $10.00.

ON THE GROWTH AND PROPERTIES OF THE CUPRENE FIBER

JOHN H. L. WATSON

Edsel B. Ford Institute for Medical Research, Detroit 2, Michigan

AND

A. E. LÉGER AND C. OUELLET

Laval University, Québec, Canada

Received October 3, 1949

INTRODUCTION

Cuprene growths are interesting, because their presence is thought to inhibit catalysis in many chemical reactions, because information concerning the general problems of polymer formation and its kinetics may be gained by their study, and because fundamentals can be investigated by the comparison of these acetylene polymers produced chemically with those formed by the action of radiations upon acetylene gas (5, 6). Recently, samples[1] of cuprene prepared under controlled conditions were studied by electron microscope and x-ray diffraction. A number of observations concerning the structure and composition of cuprene and the mechanism of its formation are reported briefly here from this investigation.

Cuprene is a polymer of acetylene formed in the presence of cuprite and other copper oxides or metallic copper as a catalyst. Compared with cuprite, copper is a relatively poor catalyst, possibly because cuprite being very friable breaks up to offer great surface multiplication. Since the polymerization is very much faster on cuprite, this substance is used whenever speed is a factor. Another explanation for the increased activity of cuprite over solid copper (in the form of a wire, say) is given in this paper: *viz.*, that cuprite is reduced by hydrogen from the acetylene in the reaction to set free finely divided copper which offers an enlarged active surface.

SEEDING EXPERIMENTS

Cuprene is seeded in a manner similar to that by which the popcorn polymer, polybutadiene, is seeded by Winkler (2, 3). A small amount of original cuprene, taken from a portion of the growth far from the original cuprite catalyst so that it can contain none of the cuprite, will act in a second reaction chamber as a seed for a new growth of cuprene when acetylene at the usual temperatures is introduced into the chamber without catalyst. The seeding process is repeatable many times, but the growth becomes much less rapid with continued seeding and there are certain changes in the morphology of the fibers, some of which are

---

[1] The samples were prepared under a grant-in-aid to Laval University from the National Research Council of Canada, through the Association Committee for Synthetic Rubber Research.

described in the following. The observations were reproduced for three seeding series, for which experimental data are given in table 1.

From each sample studied, except No. 3 (table 1), a strong x-ray diffraction pattern (table 2) of metallic *copper* is obtained, agreeing in this regard with the observation reported earlier (7) from electron diffraction. This was true regardless of whether the cuprene was formed originally in the presence of cuprite or of copper and suggests strongly that metallic copper, not the combination with oxygen, is the dominant factor in the catalysis of the polymer. It is thought that low intensity alone, due to the greatly reduced amount of copper, explains the lack of a pattern in sample No. 3.

From almost all of the *original* cuprenes (see tables 2 and 3) very weak cuprite lines were detected in addition to the strong copper pattern, again regardless of whether copper or cuprite was originally present. Thus, in table 2, the samples of original cuprene in the seeded series, Nos. 1, A1, and B1, each show weak cuprite lines. In addition, samples from the temperature series to be described later (Nos. 39, 45, 63, 59, and 67) demonstrate the presence of cuprite. Presumably, Nos. 37 and 69 should also have cuprite, except for anomalies in the preparation and exposure of the specimens.

TABLE 1

Experimental data for seeding series with cuprite as catalyst

SERIES	SAMPLE NO	REACTION TEMPERATURE	SEEDING	PRESSURE OF C_2H_2		REACTION TIME
				Initial	Final	
		°C.		cm. Hg	cm. Hg	hours
I	1	250–260	Original	29	25	24
	2	250–260	First	30	25	24
	3	250–260	Fifth	30	29	96
II	A1	260–265	Original	30	15	15
	A2	260–265	First	30	20	24
	A3	260–265	Second	30	29	96
III	B1	260–265	Original	30	20	3
	B2	260–265	First	30	25	3
	B3	260–265	Second	30	28	3
	B4	260–265	Third	30	29	10
	B5	260–265	Fourth	30	29	24

No cuprite lines were seen in seeded, as distinguished from original, specimens but the presence of microscopic amounts of cuprite in these cannot be ruled out on this evidence alone, since the amounts would be extremely small and line intensities negligible.

On the basis of these observations it is concluded that copper is the dominant catalytic member in the reaction and that the reduction of the oxide when cuprite is used is a separate but significant reaction which occurs prior to the actual

TABLE 2

X-ray diffraction data for cuprene

SAMPLE NO.*	EXPOSURE	COPPER PRESENT	RELATIVE INTENSITY†	CUPRITE PRESENT	RELATIVE INTENSITY	NUMBER OF Cu LINES	NUMBER OF Cu_2O LINES
	hours						
1	4	Yes	S	Yes	W	C	2
2	4.2	Yes	W	No		6	
3	3.5	No		No			
37	2.1	Yes	W	Doubtful		6	
39	2.0	Yes	S	Yes	W	C	2
45	2.0	Yes	S	Yes	W	C	2
63	3.0	Yes	S	Yes	M	C	2
69	1.9	Yes	S	No		C	
59	2.1	Yes	S	Yes	M	C	2
67	1.9	Yes	VS	Yes	S	C	2
A1	2.0	Yes	M	Yes	W	C	2
A2	2.0	Yes	VVW	No		1	
A2	2.0	Yes	VW	No		4	
A3	2.0	No		No			
A3	3.0	Yes	VVW	No		1	
B1	2.0	Yes	VS	Yes	S	C	5
B2	2.0	Yes	M	Doubtful		C	
B3	3.0	Yes	M	No		C	
B4	2.9	Yes	VW	No		1	

* Description of sample numbers is given in tables 1 and 4.

† VS = very strong; S = strong; M = medium strong; W = weak; C = complete copper pattern.

TABLE 3

X-ray diffraction data for cuprene

LINE NO.	MEASURED *d*-VALUES	I/I_1	STANDARD *d*-VALUES			
			Cu	I/I_1	Cu_2O	I/I_1
1	2.48	0.7			2.45	1.0
2	2.31	0.1	β of No. 4			
3	2.14	0.3			2.12	0.3
4	2.09	1.0	2.08	1.0		
5	1.81	0.8	1.81	0.8		
6	1.51	0.3			1.51	0.4
7	1.28	0.7	1.28	0.8	1.28	0.3
8	1.23	0.1			1.23	0.05
9	1.09	0.8	1.09	0.8		
10	1.05	0.4	1.04	0.5		
11	0.905	0.2	0.902	0.3		
12	0.830	0.4	0.828	0.4		
13	0.830	0.3	0.828			
14	0.809	0.4	0.808	0.4		
15	0.809	0.3	0.808			

growth of the cuprene to provide a finely divided, highly active copper catalyst. The fibers carry the copper (7) and trace amounts of cuprite with them as they grow, and the reaction continues at the interface of these and the fibers. This effect accounts for the success of the seeding process and suggests that the growth occurs at the tip, not at the base, of a fiber.

When cuprite is used as an original catalyst, a first reaction, perhaps incident to the growth, may be a reduction of the oxide at the reaction temperature to form water, free carbon, and copper:

$$Cu_2O + C_2H_2 \rightarrow H_2O + 2C + 2Cu$$

Kinetic experiments have indicated that oxygen plays a role somewhere. That this is in the induction period is suggested by the fact that this period is sensitive to the presence of oxygen and nitric oxide in a manner quite different from the later courses of the reaction (4). Although the major catalytic action is probably due to copper itself, cuprite may also be a factor. It may be that the copper–copper oxide interface is the initiator and that this explains the increased activity of cuprite over copper alone as a catalyst, or it may be that copper reduced from cuprite is in a much finer state than a copper wire or other solid form and is able to offer greater free surface to the reaction. That the copper held by the fibers is in a finely dispersed state is evident from the general character of the diffraction lines.

The dark grey color of the original cuprene grown with the cuprite as compared with the yellow-brown solids which are formed later from seeding indicates indirectly that free carbon is present. X-ray diffraction detects no carbon pattern, and it is concluded that any carbon is present in small quantities in a finely divided, amorphous state. With continued seedings the product continues to grow lighter in color, and cuprene grown with copper as the original catalyst is also light in color. No reduction process would be possible under these conditions.

A number of qualitative observations were made on the seeded series with the electron microscope (figures 1, 2, and 3), and the differences in appearance between the original and the seeded samples in a series were striking. The original cuprenes (figure 1) had the usual morphology although the fibers were more friable than usual, an observation which seems to be true of cuprenes in general when they are formed at intermediate temperatures in the presence of adequate amounts of catalyst and acetylene and which may be a manifestation of relatively short polymer chains and lower fiber strengths at these temperatures. After one seeding the fibers had changed radically (figure 2) and were no longer fragile or thin. There was less structure visible over their surfaces because of increased fiber thickness and resultant electron opacity. They were longer and less broken and where the original was composed mostly of tubular fibers with other forms, as described in reference 7, the seeded samples showed a preponderance of ribbon-like forms. All of these characteristics of seeded material were merely emphasized in the fifth seeding sample (figure 3). Throughout the original samples it is usual to see high-scattering particles which are not noticeable in the seeded specimens and which are thought to be copper. In agreement with this observa-

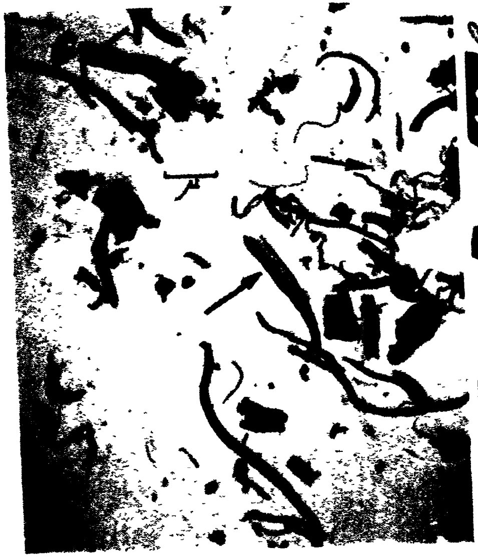

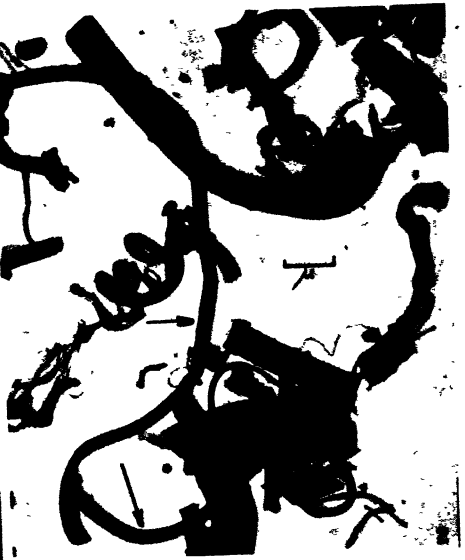

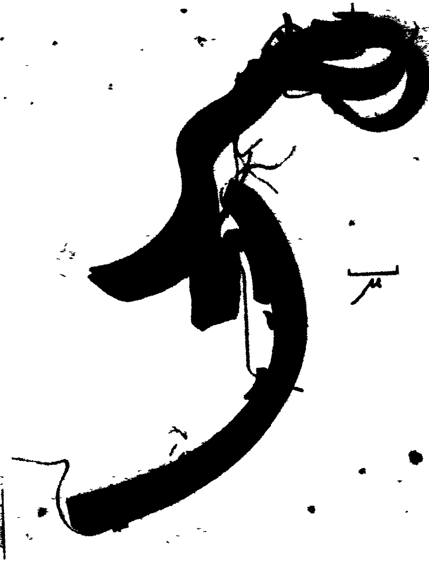

3

Fig 1 Sample No. 1: an original cuprene obtained with cuprite as catalyst at 250-260°C. × 7000.

Fig 2 Sample No. 2: cuprene from a first seeding of the sample in figure 1. × 7000.

Fig. 3 Sample No 3 cuprene from a fifth seeding of the sample in figure 2. × 7000.

tion, the x-ray diffraction copper lines diminish in intensity as seeding proceeds (table 2) and are not detectable in a sample formed by a fifth seeding. A typical copper pattern from cuprene is shown in figure 4. In it, the locations of the weak cuprite lines are indicated at the arrows. Observed lines together with comparison standards are given in table 3.

Since the amount of copper decreases with continued seeding, while the opacity of fibers of all widths increases, it is concluded that the wall thickness of the seeded fibers is greater than that of the originals. The explanation for the noticeable increase in fiber density may be that with less catalyst but adequate acetylene the growth occurs more slowly in fewer places and a denser fiber is achieved as well as a thicker one. The reverse would appear to be true of the original cuprenes where there are many catalytic centers, since the growth would take place rapidly in many localities, the available acetylene would be used up quickly, and the fibers would not develop as well.

Ouellet and Léger have observed (4) that in later stages of the seeding reaction the rate seemed to be governed chiefly by the number of seedings (the age) of the cuprene. This result is confirmed here. The first growth is thought from this work to be rapid and disorderly because the catalyst is abundant, easily accessible, and evenly distributed. In seeding stages the catalyst is naturally greatly diluted in the large mass, so that diffusion processes take control and lead to the smoother, more symmetrical forms which are seen. To explain the few fine fibrils which exist in seeded specimens, it might be hypothesized that when the reaction has become uniform and quiet, a few spots which have remained more active than average can develop local pressures and extrude themselves from the main fibers. Again they would have free access to the gas and would rapidly bring their catalyst to limiting dilution by growing a fine fibril reminiscent of their youthful forms. It is cônceivable that such fibrils could again reach a milieu where both acetylene and catalyst would be more plentiful and could start a more vigorous life, growing into the larger fiber forms. It is our opinion that the larger, well-developed, denser, stronger fibers are more mature than the smaller, fragile ones.

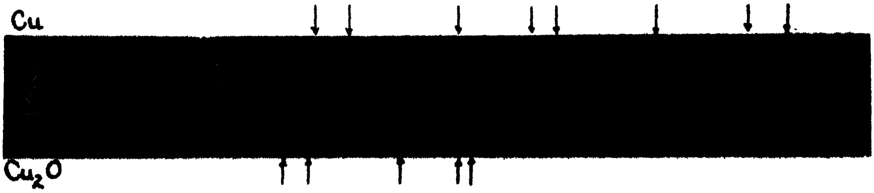

FIG. 4 Typical copper x-ray diffraction pattern from a cuprene sample grown with either cuprite or copper as catalyst.

REACTION TEMPERATURE

The catalyst in each reaction of the temperature series was a medium, hard-drawn, copper wire, No. 18 B. & S. There was no pretreatment of the copper outside of washing it with ether for a few minutes. The oxygen was added at the beginning of the reaction within 5 sec. after the introduction of the acetylene into the reaction chamber. Shadow casting was done at an angle whose tangent was about 0.73.

Léger and Ouellet report that a sharp break occurs in the kinetic curves at about 278°C., the energy of activation passing abruptly from 10 to 40 kcal./mole. However, no obvious structural differences were detected by electron microscopy to correspond with this temperature, but a fragility of fibers and a significant decrease in their mean diameter did take place at intermediate temperatures of 270°C. for the oxygenated reactions and 230°C. for those which were not oxygenated (see table 4) in a manner similar to that for cuprene grown on cuprite in seeding experiments at 250-260°C.

No striking differences in morphology great enough to be observed or measured were introduced by the addition of oxygen, except that the fiber diameters in the oxygenated cases tended to be lower for the same order of temperature. At the same time certain effects of oxygen which were substantially consistent with the conclusions and observations from microscopy and diffraction were noted in the kinetic experiments: (*1*) pronounced oxidation of the copper catalyst at high temperatures before introduction of the acetylene increased the reaction velocity and did not increase the induction period; (*2*) oxygen added after the acetylene had been introduced produced a slight decrease in reaction velocity at oxygen concentrations, due possibly to a dilution effect; and (*3*) oxygen added a few seconds before the acetylene increased the induction period and caused a decrease in reaction velocity.

TABLE 4

Data for cuprene samples prepared on a copper catalyst at a series of temperatures with and without oxygen

SAMPLE NO	REACTION TEMPERATURE	ADDED OXYGEN	MEAN FIBER DIAMETER	STANDARD DEVIATION
	°C	*per cent*	*microns*	*microns*
37	210	None	0.145	0.055
39	230	None	0.095	0.017
45	250	None	0.154	0.046
59	292	None	0.142	0.036
63	250	0.7	0.130	0.036
69	270	0.7	0.106	0.023
67	324	0.7	0.134	0.035

Three general types of fiber material are observed over the specimens: (*1*) membrane-like material which shows considerable structure and is quite transparent, as in figure 1 at the arrow; (*2*) well-formed smaller fibers which may be partially transparent but which have little apparent structure, as in figure 2; and (*3*) thick opaque fibers with no visible structure, such as those in figure 3.

X-ray diffraction patterns were again indicative of the strong presence of copper with traces of cuprite in all specimens. The change in color from a light brown to dark grey with continued rise in reaction temperature suggests that carbon is formed from the acetylene at the higher temperatures, but no carbon was detectable by either microscope or diffraction techniques. Higher temperatures were not used in the series, since the explosive limit at 325°C. for catalyzed reactions of cuprene was just about reached (1).

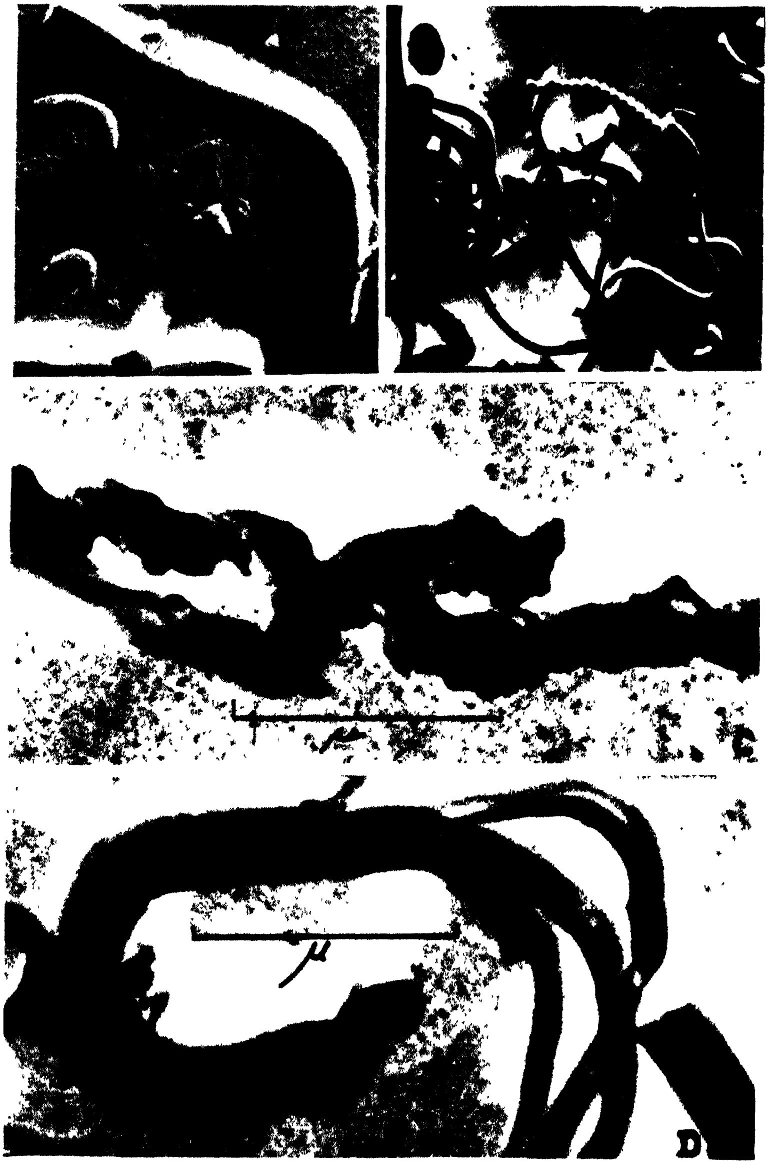

FIG. 5. Cuprene fibers showing component fibrils and spiralling. A, sample No. 39, × 35,000; B, sample No. 59, × 7,000; C, sample No. 69, × 35,000; D, sample No. 69, × 35,000

The fragility of the fibers at some temperatures suggests that there is an optimum intermediate temperature where the growth is rapid and imperfect and where short weak chains are the result. Figures 1, 2, and 3 are not only descriptive of the growths observed in a seeding series but are very similar to those observed in a temperature series where figure 2 represents the material at either extreme and figure 1 represents the friable fibers at the intermediate temperature.

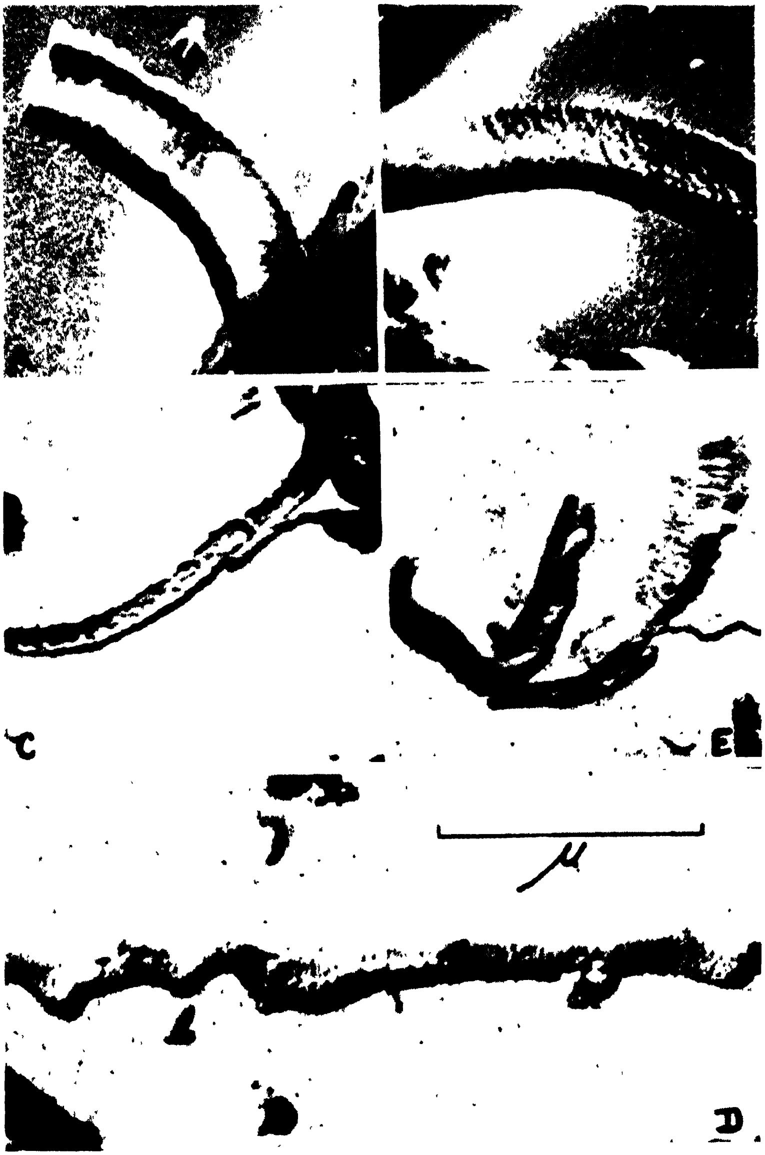

FIG. 6 Cuprene fiber segments from sample No. 1 showing hollow nature and macroscopic periods. × 35,000.

FINE STRUCTURE OF THE FIBERS

The following discussion records some of the fine structures observed in shadow-cast specimens. Much of the longitudinal structure reported in reference 7 is observed from shadow casting to be a manifestation of two or more fibers lying close together and parallel in a plane or bundle (figure 5A). A different type of spiral in addition to the usual one in figure 5B is shown in figure 5C, where several small fibers are wound in such a way as to form a large spiral in which the recognizable spiral locations seem to be periodic. Figure 5D shows a single fiber which breaks into at least three recognizable components.

The hollow nature of the fibers is clearly seen in many shadow casts of segments (figures 6A, 6B, and 6C). These figures also show the transparent nature of the thin walls as well as the inherent structures in them. The transverse structures, similar to those discussed in reference 7, are shown well in figures 6D and 6E and are periodic with an average height-to-height dimension of about 235 Å. in figure 6D and about 310 Å. in figure 6E. The periodicity is not observed in all fibers which show transverse structure, so that one is forced to conclude either that it is not present in each one or else that the fiber itself is asymmetric to some extent and has to be viewed at particular angles before the structure is seen. The latter view is supported somewhat by the fact that while there is a certain periodicity of structure in figures 6A and 6B, it is at an angle to the axis rather than accurately transverse. The periodicity of figure 6B averages about 385 Å. In each case where transverse structure is seen, the periodicity is lent also to the roughness of the fiber edge. It is not a function of the supporting film but a real property of the cuprene.

These macroscopic periodicities may offer additional insight into the mechanism of the growth. Although similar structures are not observed as frequently in larger, more mature fibers, probably owing to opacity effects, it is reasonable to suppose that they too have somewhat the same inherent structure but that the slower, more methodical growth introduces much smaller periods.

SUMMARY

Cuprene polymers prepared by seeding and at a series of temperatures have been examined by the methods of electron microscopy and x-ray diffraction and the observations discussed with reference to certain studies made on the kinetics of the reactions. It is found that copper is present in relatively large amounts in all of the samples and that cuprite (Cu_2O) is present, at least in the original samples, in trace amounts. These facts, plus the processes of the seeding, confirm that copper and probably some cuprite are carried along as the fiber grows. This could account for the success of the seeding operation, and it indicates that the fiber grows from its tip rather than from its base. When cuprite is used as a catalyst, the reduction of the oxide to free copper is a first reaction, probably incident to the growth.

Effects of seeding on the morphology of the fibers are discussed. Large opaque fibers seem to be the more mature forms. No striking differences in morphology

were discovered with oxygen added, nor by changing the reaction temperature, except that at an optimum intermediate temperature the fibers are smaller and more friable. Their fine structure is described from shadow-cast specimens. Compound fibers are seen and a transverse, macroscopic periodicity is measured.

REFERENCES

(1) Calhoun, J. M.: Can. J. Research **15**, 208 (1937).
(2) Devins, J. C., and Winkler, C. A.: Can. J. Research **B26**, 356 (1948).
(3) Graham, W., and Winkler, C. A.: Can. J. Research **B26**, 564 (1948).
(4) Ouellet, C., and Léger, E. A.: Unpublished results.
(5) Watson, John H. L.: J. Phys. & Colloid Chem. **51**, 634 (1947).
(6) Watson, John H. L.: J. Phys. & Colloid Chem. **52**, 470 (1948).
(7) Watson, John H. L., and Kaufmann, K.: J. Applied Phys. **17**, 996 (1946).

THE ELECTROLYTIC TRANSFERENCE PROPERTIES OF POLYMERIC ACIDS[1]

FREDERICK T. WALL, GUNTHER S. STENT,[2] AND JOHN J. ONDREJCIN
Noyes Chemical Laboratory, University of Illinois, Urbana, Illinois

Received October 3, 1949

THEORY

1. *Introduction*

Numerous investigations have shown that polymeric electrolytes possess properties which are strikingly different from those of either nonionic polymers or simple electrolytes. For example, it has been shown by Staudinger (7) and by Fuoss and Strauss (4) that the viscosities of polyelectrolyte solutions have an abnormal dependence on concentration. Moreover the conductance and ionization of solutions of such substances do not obey the laws valid for ordinary electrolytes, such as Ostwald's dilution law (3, 9).

To characterize further the behavior of polymeric electrolytes, we undertook the study of the electrolytic transference properties of polymeric ions. Conductance measurements by Wall and deButts (9) on polymeric acids indirectly indicated that the mobility of a slightly ionized polymeric anion is very small compared to that of hydrogen ions. The purpose of the investigation here reported was to determine the actual magnitude of such mobilities by transference studies and to use electrolytic means for the fractionation of polymeric ions.

---

[1] This work was carried out under sponsorship of the Office of Rubber Reserve, Reconstruction Finance Corporation, in connection with the Synthetic Rubber Program of the United States Government.

[2] Present address: Kerckhoff Laboratories of Biology, California Institute of Technology, Pasadena 4, California.

2. *Ionic mobility*

To provide a basis for deriving theoretical formulas relating to mobility, we shall assume that a polymer molecule can be represented by a string of beads, as in Debye's simple viscosity theory (2). The present theory will, of course, be subject to the limitations inherent in Debye's theory, since identical assumptions are made with respect to the viscous interactions of "beads" with the solvent. A polymer molecule of the type assumed, consisting of N beads and moving through the solvent with constant velocity v, will experience a total frictional resistance

$$Q = Nfv \tag{1}$$

where f is Debye's frictional force coefficient per bead. We shall identify the beads with monomeric units and N with the degree of polymerization and assume that f remains the same whether or not a monomer unit is ionized.

Let us define the mobility μ of an ion moving with velocity v under the influence of an electrical potential gradient ϕ by the relation:

$$v = \mu\phi \tag{2}$$

Substituting equation 2 in equation 1, one obtains:

$$Q = Nf\mu\phi \tag{3}$$

But if the ion carries a charge z, then the electrical force acting on it will be

$$Q = z\phi \tag{4}$$

Equating equations 3 and 4 we obtain the mobility of a polymeric anion:

$$\mu = z/Nf \tag{5}$$

But if s is the number of ionizable groups per monomer unit and α the degree of ionization, then

$$z = Ns\alpha \tag{6}$$

and equation 5 becomes

$$\mu = \alpha s/f \tag{7}$$

Thus it appears that the mobility of a polymeric anion is a function only of the ratio of the degree of ionization to the molecular friction coefficient, and not of the degree of polymerization, except implicitly as the latter affects the degree of ionization (9).

3. *Transference numbers*

Let us consider a solution of one species of cation and k species of anions of degrees of polymerization N_1, N_2, . . . N_k in molar concentrations c^+ and c_1, c_2, . . . c_k, respectively, such as would be encountered in a mixture of polymeric acids. Let us further assume that there correspond to each species electrical charges of z^+e and $-z_1e$, $-z_2e$, . . . $-z_ke$. When an electric current is passed through this solution, the different species will, in general, carry different fractions of the current, and these fractions are the transference numbers of the constituent species.

If we now assume that these ions move independently of each other, the current carried by the i^{th} species in a cell of cross-sectional area A filled with such an electrolytic solution is

$$I_i = A\mu_i c_i z_i eF\phi \tag{8}$$

where μ_i is the ionic mobility of that species and F is the number of coulombs per faraday. The total current, I, flowing through the solution will be given by

$$I = AeF\phi\left\{\sum_i \mu_i c_i z_i + \mu^+ c^+ z^+\right\} \tag{9}$$

where μ^+ is the cationic mobility. From equation 9 it will be seen that the fraction of the current carried by the j^{th} species, i.e., the transference number, t_j, is

$$t_j = \frac{\mu_j c_j z_j}{\sum_i \mu_i c_i z_i + \mu^+ c^+ z^+} \tag{10}$$

and the total transference number of negative ions will be

$$t^- = \sum_i t_i$$

But since the solution is electrically neutral, it follows that

$$\sum_i c_i z_i = c^+ z^+ \tag{11}$$

In the special case of a homogenous polymer solution, i.e., where $k = 1$, substitution of equation 11 into equation 10 gives the ordinary equation:

$$t^- = \mu^- / (\mu^+ + \mu^-) \tag{12}$$

Actually, it turns out that the mobilities of polymeric anions are very much less than that of the hydrogen ion, i.e., $\mu_i \ll \mu^+$, for all i. Then, from equation 11 it is evident that

$$\sum_i \mu_i c_i z_i \ll \mu^+ c^+ z^+ \tag{13}$$

so that equations 10 and 11 can be approximately written

$$t_j = \frac{\mu_j c_j z_j}{\mu^+ c^+ z^+} \tag{10a}$$

and

$$t^- = \mu^- / \mu^+ \tag{11a}$$

There are several methods for the determination of transference numbers, but that of Hittorf (5) is the most direct and appeared most practical for the present work. The electrolyte solution is divided into three compartments, anode, middle, and cathode, and the concentration changes occurring in each of the compartments during electrolysis are measured. When analyses of the middle compartment yield the same values before and after the experiment, it is assumed that no mixing by ordinary diffusion has taken place. If during the electrolysis n_i equivalents of the i^{th} species have migrated into a given compartment while a total of n_e equivalents of electricity have passed through the cell, then

$$t_i = n_i/n_e \tag{14}$$

When an aqueous solution of a substance such as a polyacrylic acid is placed in a cell between platinum electrodes and a potential difference applied, the polymeric anions will, of course, move towards the anode and the hydrogen ions will move towards the cathode. Now if there has been an increase of Δw_i grams of polymer solute of the i^{th} species in the anode compartment, the number of equivalents of electricity carried by that species is

$$n_i = \Delta w_i \alpha_i / M_i \tag{15}$$

where M_i is the equivalent weight of a monomer unit in the i^{th} species and μ_i the degree of ionization of the i^{th} species. From equation 14 we can arrive at the transference number:

$$t_i = \Delta w_i \alpha_i / M_i n_e \tag{16}$$

It can readily be shown from simple mass law considerations that the degree of ionization of a weak acid at a fixed pH is independent of the presence of other acids, if the activity coefficients remain unaffected by the presence of other species. The quantity μ_i appearing in equation 16 can thus be obtained from pH measurements, since

$$\alpha_i = (M_i/w_i)10^{-\text{pH}} \tag{17}$$

where w_i is the weight concentration of the i^{th} species in grams per liter in a solution of pure i having the same pH as the mixture being electrolyzed.

4. Homogeneous polymers

We now return to the case of a homogeneous polymer sample and substitute equation 7 into equation 11a, which yields:

$$t^- = s\alpha/f\mu^+ \tag{18}$$

If we equate equations 18 and 16, then

$$\Delta w/n_e = Ms/f\mu^+ \tag{19}$$

From this it appears that the change in grams of solute in each compartment per faraday of electricity passed, a quantity readily determinable in practice, should be independent of the degree of polymerization of the molecule. If equation 19 is substituted back into equation 16, it is seen that t^- is proportional to α,

$$t^- = (s/f\mu^+)\alpha = K\alpha \tag{20}$$

where K, the proportionality factor, depends only on the nature of the monomeric unit and the mobility of the hydrogen ion, and not on the degree of polymerization.

5. Fractionation

Let us now consider the possibility of electrolytic fractionation of mixtures of polymeric electrolytes. The different species can be made up of different monomer units or of the same units with different degrees of polymerization. Consider the i^{th} species of a mixture being electrolyzed and substitute equations 6 and 7 into 10a, which yields:

$$t_i = \frac{\alpha_i^2 s_i^2 c_i N_i}{f_i \mu^+ c^+ z^+} \tag{21}$$

We now recognize that f_i and s_i can depend upon the kind of monomer unit. By equating equations 21 and 16, we then obtain

$$\Delta w_i/n_e = \frac{\alpha_i s_i^2 M_i N_i c_i}{f_i \mu^+ c^+ z^+} \tag{22}$$

or, since the weight concentration of polymer, $w_i = s_i M_i N_i c_i$,

$$\Delta w_i/n_e = \frac{\alpha_i s_i w_i}{f_i \mu^+ c^+ z^+} \tag{23}$$

From equation 23 we can estimate directly the ratio of the relative enrichment or depletion of two species a and b in an electrode compartment at any stage of the electrolysis as:

$$\frac{\Delta w_a/w_a}{\Delta w_b/w_b} = \frac{\alpha_a s_a f_b}{\alpha_b s_b f_a} \tag{24}$$

If the species which are to be fractionated are polymers of the same monomeric unit, differing only in the degree of polymerization, then equation 24 simplifies to

$$\frac{\Delta w_a/w_a}{\Delta w_b/w_b} = \frac{\alpha_a}{\alpha_b} \tag{25}$$

which means that the relative fractionation should be in the ratio of the degrees of ionization. Accordingly, a fractionation by molecular weight can be expected only if the degree of ionization depends upon molecular weight.

A relation between the degree of ionization, α, and the degree of polymerization in homologous series of polymers has been recently derived (9), and it is concluded that α decreases with increasing degree of polymerization. Thus, during electrolysis an enrichment of the lower molecular weight species in the anode compartment is to be expected. Likewise, the average molecular weight of the cathode compartment solute is expected to increase, since relatively more of the less ionized, higher molecular weight material remains behind. Thus by studying the average molecular weight changes in the anode (or cathode) compartment as a function of n_e, it should be possible, in principle at least, to arrive at a molecular weight distribution for the mixture examined.

EXPERIMENTAL

1. Acids used

The experiments were carried out on three polyacrylic acids and on a hydrolyzed copolymer of maleic anhydride and styrene. The polyacrylic acids were prepared from Minnesota Mining and Manufacturing Company research grade acrylic acid by a method similar to that of Condo, Krister, and Lundquist (1), and the copolymer was prepared by the same method from twice-recrystallized maleic anhydride and redistilled styrene.[3]

The polymers were extracted with benzene in a Soxhlet extractor for several days in order to remove traces of monomer. After this extraction, the samples were dried at 60°C. in a vacuum oven for 24 hr. Solutions of these acids were prepared using conductivity water as the solvent.

The polyacrylic acids (numbered 1, 2, and 3) had different degrees of polymerization, increasing in the order indicated. This conclusion was reached by comparing solution viscosities of the different acids at various concentrations. For each concentration, acid No. 3 had a higher viscosity than acid No. 2, which in turn had a value higher than that of acid No. 1. A very crude estimate of the degrees of polymerization of acids Nos. 1 and 3 was obtained by the method of Staudinger and Trommsdorff (8), which involves the measurement of viscosities in the presence of excess base. From these measurements it appeared that the degrees of polymerization were approximately 560 and 2000 for acids No. 1 and No. 3, respectively.

2. Transference numbers

For purposes of studying transference numbers, the modified Hittorf method described by MacInnes (6) was applied. The transference cell especially designed for these experiments is shown in figure 1. It permits the withdrawal without mixing of solutions from the anode, middle, and cathode compartments, when stopcock No. 1 is opened and the hydrostatic head AB relieved. This cell avoids the necessity of incorporating large-bore stopcocks into the equipment, such as those described by MacInnes. Platinum electrodes were used. A milliammeter and a silver coulometer were connected in series with the cell to obtain duplicate measurements of the number of faradays passed.

The contents of the compartments were drained through the bottom stopcocks into weighing bottles and the weight of solution in each determined. The concentrations of the initial solution and of the solutions in the compartments at the end of each experiment were obtained in duplicate by weighing 10- or 20-ml. portions of the solutions and then evaporating them to dryness in a 90°C. oven for 48 hr. From the weights of the residues the concentrations could be readily calculated. It was found for all the experiments that the concentration of the middle compartment remained substantially constant.

---

[3] These polymerizations were devised and carried out by E. H. deButts and H. Levine, for whose assistance the authors express grateful appreciation.

From the amounts of solute initially and finally present in each compartment the weight of polymer that migrated is readily calculated. The total equivalents of electricity passed were so small (about 10^{-4} faradays) that corrections for concentration changes due to the electrolytic decomposition of water were unnecessary.

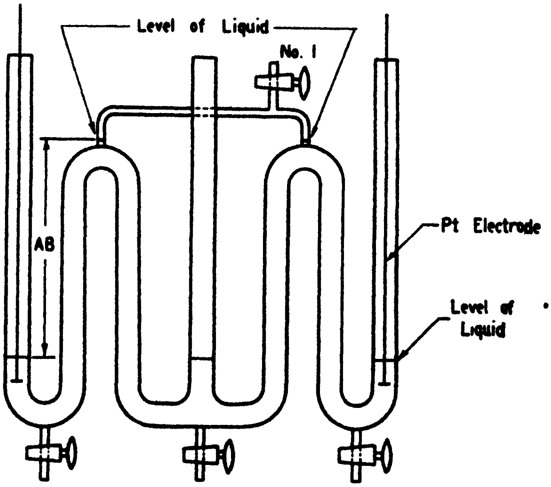

FIG. 1. Transference cell

3. *Determination of pH*

The pH was measured in a Beckman pH meter, Model 3, using a type 270-E glass electrode for pH ranges above 9.

4. *Fractionation*

Three fractionation experiments were carried out in the same type of cell as was employed for measurement of transference numbers. Viscosities were determined for the anode and cathode compartments before and after fractionation; for two of the experiments, all pH values were measured.

RESULTS AND DISCUSSION

1. *Transference experiments*

Measurements of the transference numbers of the polymeric anions were made on the three polyacrylic acids at various concentrations, and on the hydrolyzed copolymer of maleic anhydride and styrene. All of these substances were assumed to be homogeneous for purposes of calculation.

Tables 1, 2, and 3 summarize the results of the experiments carried out with polyacrylic acids Nos. 1, 2, and 3, and figure 2 presents graphically the dependence of the transference number on the concentration. In figure 3 the transference number is plotted against the degree of ionization, and it is seen that equation 20 is roughly obeyed, i.e., the transference number seems to be proportional to the degree of ionization. Furthermore, it can be seen from the tables that the quantity $\Delta w/n_e$ is approximately constant as predicted, except for the most concentrated solutions examined, where it is definitely lower. It will be observed that the transference numbers vary from about 0.01 to 0.035 over the concentration range investigated. These low values are consistent with the conductance measurements of Wall and deButts (9).

TABLE 1

Transference experiments

Polyacrylic acid No. 1

	EXPRIMENT 1		EXPERIMENT 2		EXPERIMENT 3		EXPERIMENT 4	
	Initial	Middle	Initial	Middle	Initial	Middle	Initial	Middle
pH.......	2.47	2.47	2.73	2.71	2.86	2.86	3.08	3.08
Concentration, in grams per 1000 g........	23.78	23.71	11.54	11.59	5.681	5.664	2.766	2.756
	Anode	Cathode	Anode	Cathode	Anode	Cathode	Anode	Cathode
pH	2.48	2.47	2.70	2.73	2.89	2.89	3.02	3.13
Weight of compartment	46.21	45.56	50.64	48.81	48.24	46.44	49.63	49.90
Concentration, in grams per 1000 g...... .	24.19	23.25	11.80	11.26	6.223	5.106	3.208	2.347
Δw...... .	0.0185	0.0225	0.0171	0.0130	0.0263	0.0260	0.0218	0.0207
$\overline{\Delta w}$.... .	0.0205		0.0150		0.0262		0.0212	
α.. ...	0.0104		0.012		0.01736		0.0217	
n_e.	2.456×10^{-4}		1.79×10^{-4}		2.45×10^{-4}		1.855×10^{-4}	
t^-......	0.0121		0.0140		0.0259		0.0345	
$\overline{\Delta w}/n_e$.....	83.4		83.9		111.2		114.2	

The results of a transference experiment on the maleic acid–styrene copolymer are summaried in table 4. For the anion of this acid, the transference number is about 0.056, a value which is higher than that for the polyacrylic acids. However, $\Delta w/n_e$ has roughly the same value as for polyacrylic acid. This is purely coincidental but not too unreasonable, for it implies (see equation 19) that the frictional coefficients of the two kinds of "beads" are in the same ratio as their masses. This conclusion should not, however, be considered generally valid.

2. Fractionation experiments

Three fractionation experiments were also carried out, but satisfactory quantitative results were not obtained either to substantiate or to contradict the theory. Qualitatively, however, the observations were in line with expectations.

In the first experiment, the copolymer of maleic acid and styrene was subjected to electrolysis. To characterize the solutions before and after electrolysis, the apparent intrinsic viscosities were measured, all at the same concentrations. As expected, the polymer concentration decreased in the cathode compartment and increased in the neighborhood of the anode. The apparent intrinsic viscosity in the neighborhood of the cathode increased, whereas that of the anode decreased.

TABLE 2

Transference experiments

Polyacrylic acid No. 2

	EXPERIMENT 1		EXPERIMENT 2		EXPERIMENT 3		EXPERIMENT 4	
	Initial	Middle	Initial	Middle	Initial	Middle	Initial	Middle
pH	2.66	2.65	2.73	2.73	2.99	2.99	3.22	3.24
Concentration, in grams per 1000 g.	14.521	14.569	7.720	7.720	3.842	3.879	1.921	1.894
	Anode	Cathode	Anode	Cathode	Anode	Cathode	Anode	Cathode
pH	2.62	2.66	2.71	2.75	2.95	3.02	3.15	3.29
Weight of compartment	50.27	48.55	47.75	46.22	46.46	49.24	48.05	46.87
Concentration, in grams per 1000 g.	15.009	14.094	8.150	7.276	4.211	3.516	2.322	1.542
Δw	0.0249	0.0210	0.0229	0.0206	0.0173	0.0162	0.0193	0.0178
$\overline{\Delta w}$	0.0230		0.0218		0.0168		0.0186	
α.	0.01129		0.0176		0.0192		0.0227	
n_e.	2.37×10^{-4}		1.87×10^{-4}		1.51×10^{-4}		1.67×10^{-4}	
t^-	0.0152		0.0283		0.0295		0.0350	
$\overline{\Delta w}/n_e$	97.1		111.2		111.2		111.3	

For the second experiment a mixture of the copolymeric acid and the polyacrylic acid was electrolyzed. Here the changes in apparent intrinsic viscosities were even more pronounced, presumably because of compositional hetero-

TABLE 3

Transference experiments

Polyacrylic acid No. 3

	EXPERIMENT 1		EXPERIMENT 2		EXPERIMENT 3		EXPERIMENT 4	
	Initial	Middle	Initial	Middle	Initial	Middle	Initial	Middle
pH	2.50	2.50	2.61	2.61	2.86	2.82	3.12	3.14
Concentration, in grams per 1000 g.		26.76	13.06	13.04	6.357	6.306	2.710	2.706
	Anode	Cathode	Anode	Cathode	Anode	Cathode	Anode	Cathode
pH	2.50	2.51	2.60	2.67	2.88	2.80	3.08	3.20
Weight of compartment	45.97	44.54	43.51	41.54	47.04	45.00	52.69	49.27
Concentration, in grams per 1000 g.	27.86	25.38	12.20	13.88	6.784	5.810	3.202	2.195
Δw	0.0577	0.0468	0.0346	0.0348	0.0197	0.0245	0.0258	0.0252
$\overline{\Delta w}$	0.0522		0.0347		0.0221		0.0255	
α	0.00859		0.0136		0.0157		0.0203	
n_e	6.10×10^{-4}		3.45×10^{-4}		1.95×10^{-4}		2.04×10^{-4}	
t^-	0.0101		0.0190		0.0248		0.0352	
$\overline{\Delta w}/n_e$	85.6		100.5		113.2		125.0	

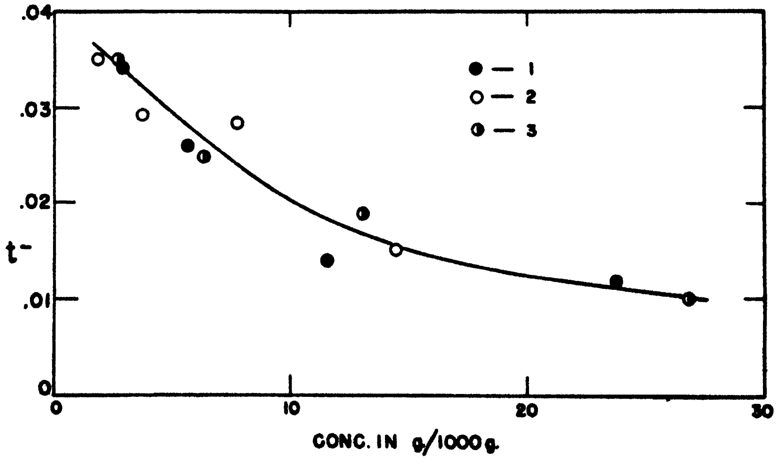

FIG. 2. Transference number plotted against concentration for three different polyacrylic acids.

geneity as well as molecular weight differences. These changes left no doubt that fractionation occurred, but we are unable to characterize the extent of fractionation quantitatively.

The last experiment involved the electrolysis of a mixture of polyacrylic acids No. 1 and No. 3. In this instance no fractionation was observed, but the result is not inconsistent with the theory. The polyacrylic acid solutions which were mixed for this experiment had the same pH values and same degrees of ionization. Therefore, upon mixing the pH and degrees of ionization remained unchanged; hence from equation 25 we would expect no fractionation. Other experiments are being planned which will surmount some of the experimental difficulties and provide a rigorous test of the theory.

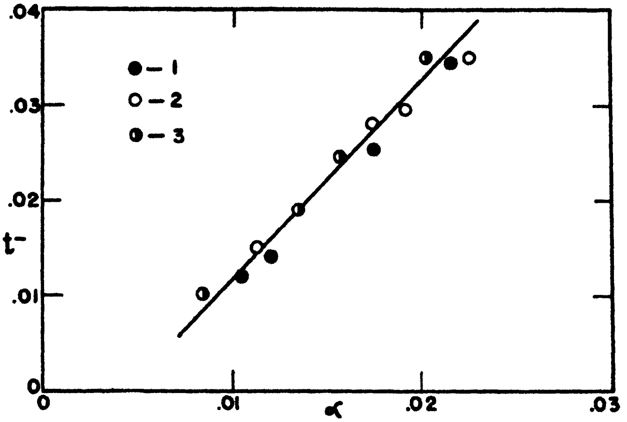

FIG. 3. Transference number plotted against degree of ionization for three different polyacrylic acids.

TABLE 4

Transference experiment

Maleic acid–styrene copolymer

	INITIAL	MIDDLE	ANODE	CATHODE
pH	2.70	2.70	2.69	2.71
Concentration, in grams per 1000 g.	4.000	3.994	4.228	3.796
Weight of compartment			47.19	46.63
Δw			0.0108	0.0095
$\overline{\Delta w}$			0.0102	
α			0.0555	
n_e			0.916×10^{-4}	
t^-			0.0559	
$\overline{\Delta w}/n_e$			111.2	

SUMMARY

A simple theory is developed for the electrical transference properties of polymeric ions, using Debye's model of a polymer molecule as a string of beads. It is also shown theoretically that electrolytic fractionation can be expected when the degrees of ionization of the polymers in the mixture are different.

Experiments have been carried out on three samples of polyacrylic acid and on the hydrolyzed copolymer of maleic anhydride with styrene. The results are in qualitative agreement with the theory. It is found that the transference numbers of polymeric anions are in the neighborhood of a few hundredths and also that electrolytic fractionation is possible.

REFERENCES

(1) Condo, Krister, and Lundquist: U. S. patent 2,286,062 (1942).
(2) Debye: J. Chem. Phys. **14,** 636 (1946).
(3) Fuoss and Strauss: J. Polymer Sci. **3,** 246 (1948).
(4) Fuoss and Strauss: J. Polymer Sci. **3,** 602-3 (1948).
(5) Hittorf: Ann. Physik **103,** 1 (1853).
(6) MacInnes: *The Principles of Electrochemistry*, p. 65 ff. Reinhold Publishing Corporation, New York (1939).
(7) Staudinger: *Die hochmolekularen organischen Verbindungen*, p. 333 ff. Julius Springer, Berlin (1932).
(8) Staudinger ahd Trommsdorff: Ann. **502,** 201 (1933).
(9) Wall and deButts: J. Chem. Phys. **17,** 1330 (1949).

THE CONCEPT OF CRITICAL ZETA POTENTIAL FOR HYDROPHOBIC SOLS. I

HARRY B. WEISER and PAUL MERRIFIELD

Department of Chemistry, The Rice Institute, Houston, Texas

Received October 17, 1949

I. INTRODUCTION

The stability of typical hydrophobic sols is attributed to the electrokinetic or ζ-potential of the colloidal particles as given by the Helmholtz-Smoluchowski equation,

$$\zeta = 4\pi\eta u/HD$$

in which u is the migration velocity of the particles moving under a potential H in a medium of viscosity η and dielectric constant D. The addition of electrolytes to hydrophobic sols lowers the ζ-potential to the point where agglomeration and precipitation of the colloidal particles take place. It has been found that the ζ-potential of the particles need not be reduced to zero in order to bring about coagulation. This observation has led to the concept of a critical

ζ-potential above which the sol is relatively stable and below which it coagulates rapidly. Since ζ-potential is proportional to mobility, and ζ-potential cannot be determined directly, McBain (12) and others prefer to speak of a critical mobility rather than of a critical ζ-potential. The concept of critical ζ-potential was proposed by Powis (16) as a result of his observations on oil drops and on arsenic trisulfide sol. In table 1 are given the ζ-potentials at the surface of arsenic trisulfide particles and ferric oxide particles when just enough of the several electrolytes is added to cause rapid coagulation. It will be noted that the critical ζ-potential for the negative arsenic trisulfide sol is about 26 mv. for all multivalent cations, and that for the positive ferric oxide sol it is approximately 32 mv. for all anions. The critical mobility and ζ-potential of arsenic trisulfide in the presence of potassium chloride are appreciably higher than for the other salts. A similar behavior was observed with salts of the potassium chloride type on silver iodide sol. This is not a question of the univalence of potassium ion, since Briggs (2) showed that the critical mobility of univalent new fuchsin and strychnine cations for arsenic trisulfide sol is the same as for bivalent barium. On the other hand, Briggs obtained an S-shaped curve on plotting potassium chloride concentration against the mobility (or ζ-potential) of arsenic trisulfide particles. In some instances with salts of the potassium chloride type, the curve increases from the start to a maximum and then falls off; in others it decreases from the start (10); in still others it decreases to a minimum and then rises (5, 13).

TABLE 1

Critical ζ-potentials of particles in sols

SOL	ELECTROLYTE	CONCENTRATION	ζ-POTENTIAL
		milliequiv./liter	*mv.*
Arsenic trisulfide sol (—)	KCl	40.0	44
	$BaCl_2$	1.0	26
	$AlCl_3$	0.15	25
	$Th(NO_3)_4$	0.20	27
	$Th(NO_3)_4$	0.28	26
	$Th(NO_3)_4$	0.40	24
Ferric oxide sol (+)	KCl	100.0	33.7
	NaOH	7.5	31.5
	K_2SO_4	6.6	32.5
	Aniline sulfate	8.0	31.4
	$K_2C_2O_4$	6.5	32.5
	$K_3Fe(CN)_6$	0.65	30.2

Kruyt and coworkers (10, 11) postulate a decrease in dielectric constant to account for the lower critical mobility and the corresponding higher critical ζ-potential for salts of the potassium chloride type. Mukherjee and coworkers (14) and Ghosh (6) believe that a decrease in dielectric constant alone would not account for the observed results, and suggest that the anomalous behavior is due in part to the stabilizing action of the adsorbed chloride which opposes the precipitating action of the potassium ion.

Because of the anomalous effect of certain coagulating electrolytes on the mobility of sol particles, Mukherjee contends that one should not speak of a critical mobility or critical ζ-potential. This point of view seems a bit extreme under the circumstances. In most instances electrolytes effect coagulation at a critical mobility or ζ-potential. The fact that we do not know enough at present to interpret adequately the behavior with certain salts is no reason to abandon the whole concept of critical mobility or ζ-potential. This is especially true when we consider that the anomalous behavior is usually encountered only with salts that precipitate in high concentration, and not always with these. For example, Ghosh observed a normal behavior of potassium chloride with his ferric oxide sol (table 1). Similarly, Jenny and Reitemeier (8) found a normal behavior with clay hydrosols, and Bikerman (1) with arsenic trisulfide sol in ethyl acetoacetate.

Eilers and Korff (3) have recently criticized some of the data on which the relation between ζ-potential and the stability of hydrophobic sols is based. They concluded that the assumption of a critical potential has no adequate foundation but that the factor which determines the stability of such systems is the energy required to bring two particles of the sol together against the action of their electric field. This energy A is expressed by the following formula:

$$A = C\frac{\zeta^2}{K}$$

in which K is the Boltzmann constant. $1/K$ represents the average thickness of the ion sphere occurring in the Debye–Hückel equation. According to this hypothesis, the stability of a sol system is determined not only by the electrokinetic potential, but also by the concentration and valency of the ions present in the aqueous phase. It is pointed out that rather small quantities of electrolytes will have little effect on the ζ-potential but will influence greatly the value of K.

This hypothesis was tested by Eilers and Korff for several sol systems in which ζ at the coagulation point was not constant (e.g., the experiments of Powis on arsenic trisulfide sol (table 1)). In the cases tested it was found that the value of ζ^2/K was more nearly constant at the coagulation point for different electrolytes than was the value of ζ.

Although the views of Eilers and Korff deserve careful consideration, one should not overlook the cases referred to above in which the ζ-potential was constant at the coagulation point for electrolytes with ions of varying valences. It is obvious that in such cases the value of ζ^2/K would not be constant.

In view of the conflicting evidence for and against the concept of a critical ζ-potential as defined by the Smoluchowski equation, it was decided to test the concept with monodisperse sols in order to determine whether variation in particle size in a given sol influenced the relationship between ζ-potential and stability toward electrolytes. The experimental part of this report describes the preparation of monodisperse sols of various kinds and the results of preliminary mobility studies on the sols in the presence of varying amounts of coagulating electrolytes.

II. EXPERIMENTAL

A. Preparation of sols

The following methods of preparation of the sols to be investigated were chosen with two significant properties of the resulting sols in view: namely, that the sols produced be monodisperse in character, and that dialysis be not required for purification or stabilization. Monodispersity was naturally a necessity, since the whole problem hinged on the assumption that the sols investigated were of uniform particle size. Selections of preparatory methods were made from a wide variety listed by Weiser (18).

The aversion to employing dialysis in the methods of preparation was based on the research of Holliday (7), who showed that the mobility and therefore the ζ-potential of nuclear gold sols changed during dialysis.

Gold sol: A gold sol was prepared by the classic method of Faraday (4) with a saturated solution of phosphorus in ether as the reducing agent. To 1200 ml. of pure water were added 25 ml. of 0.6 per cent chloroauric acid and 30 ml. of 0.18 *N* sodium carbonate followed by the addition of 10 ml. of the reducing agent. After 15 min. the reduction mixture was boiled to remove the excess ether and a clear red gold sol containing 0.52 g. of gold per liter was obtained. Excess phosphorus was removed by oxidation with a current of air.

The colloidal particles formed by this method are so fine that they cannot be seen in the ultramicroscope. This inability of the ultramicroscope to detect the particles places the particle size at less than 10 mμ in diameter. It also indicates that the gold sol is sufficiently monodisperse.

Selenium sol: Preparation of a selenium sol of uniform particle size involved a slight modification of the method of Kruyt and van Arkel (9). In a Pyrex beaker, 550 ml. of pure water containing 30 ml. of a 1.2 *M* solution of hydrazine hydrate was brought to the boiling temperature and 25 ml. of a 0.1 *M* solution of sodium selenite was quickly added. After the sol reached a yellow color, 5 ml. more of the sodium selenite was added. The sol was allowed to cool for 15 min. and then was diluted to 3.5 times its original volume. In appearance, the sol had a rich salmon-red color, and analysis showed that it contained 0.40 g. of selenium per liter.

B. Electrophoresis apparatus

The electrophoretic mobility measurements observed in this research were determined by the microscopic moving boundary technique, with a modified Burton U-tube apparatus developed by Price and Lewis (17). A diagram of the apparatus is shown in figure 1.

The main U-tube has two side arms whose object is to prevent polarization products of the main electrodes from migrating into the center section. The side arms are of sufficient length so that hydroxyl ions liberated at the cathode and zinc ions formed at the anode will not migrate into the main tube during the time required for a "run." Therefore any change in ionic concentration or resistance is confined to the side arms. Under a potential gradient of 1.3 v./cm., which was the gradient in all cases, the hydroxyl ions, which are the faster moving, migrate 5 cm. in 30 min. (time of duration of a "run"). The length of each side arm is approximately 18 cm.

Gassing at the main electrodes is prevented by using a solid zinc cylinder as the anode and a hollow lead cylinder on which lead dioxide was formed as the cathode. This choice of electrodes prevents the liberation of hydrogen and oxygen, since at the cathode the conversion of lead dioxide to lead monoxide and at the anode the conversion of zinc to zinc ion take preference over the usual reactions in the electrolysis of water.

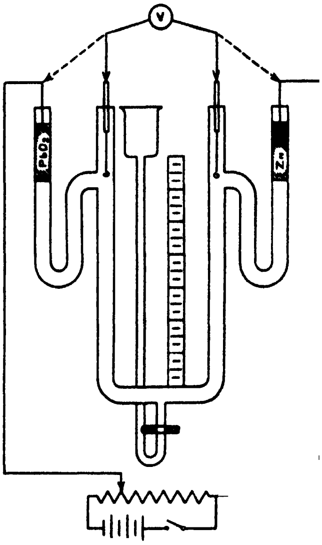

FIG. 1. The apparatus

The electrodes in the main tube are small platinum wires and are connected to a voltmeter which serves a dual purpose. At the beginning of a "run" the voltmeter is used to determine the potential applied at the main electrodes. This potential was always 100 v. During the "run" the voltmeter is used to check the constancy of the potential gradient across the main tube and any deviation is corrected by varying slightly the resistance in the primary circuit. This compensates for any change in resistance in the side arms due to formation of electrolysis products at the main electrodes.

The filling tube is equipped with a stopcock to control the rate at which the sample flows into the U-tube. The scale used to measure the distance traversed by the boundary is a Beckmann thermometer scale which was calibrated with a cathetometer. It was found that the scale was linearly graduated, with each division equal to 0.0432 cm. The scale is viewed through a telescope capable of moving in any vertical plane. The whole apparatus is illuminated with an intense beam of light.

C. *Mobility measurements*

The actual measurements of the mobility of the colloidal particles were made on a 22-ml. sample of the sol to be investigated. A boundary was formed between the sol and its ultrafiltrate, which in all cases was the liquid above the sol, and the distance through which the boundary moved in 30 min. under a potential gradient of 1.3 v./cm. was observed through the telescope. The formation of a boundary was facilitated by the addition of 2 ml. of 0.2 *M* sucrose solution to 20 ml. of the sol. This is in accordance with experiments performed by Northrop and Cullen (15), who showed that sucrose solutions up to 0.5 *M* concentration produced no change in the mobility of colloidal particles. To confirm their experiments, two measurements were made with gold sol samples to which no sucrose was added; agreement with measurements made in the presence of sucrose was within the margin of experimental error (see table 2).

TABLE 2

Coagulation values after 8 hr. for the various sols with the electrolytes used

(Values are given in millimoles per liter)

SALT	GOLD SOL	SELENIUM SOL
KCl	45.0	100.0
$BaCl_2$	0.26	2.05

The ultrafiltrate was used as the supernatant liquid above the sol, since it has the same conductivity as the sol itself. Ultrafiltration was accomplished by passing the sol through a cellophane membrane supported by a nickel screen under a pressure of 100 lb. of nitrogen per square inch.

Increasing concentrations of electrolytes were added to the sol and ultrafiltrate and the decrease in mobility up to and beyond the coagulation point was measured. It was possible to obtain values beyond the coagulation point, as coagulation values were determined over an 8-hr. period and therefore concentrations of electrolyte in excess of that necessary to produce coagulation could be added and the sol would still be stable during the duration of a run. However, the mobility and ζ-potential values were at their minimum, and so values beyond the coagulation point were merely checks on the critical ζ-potential.

The following relationships are those involved in the calculations of mobilities and ζ-potentials. Migrational velocity is the average rate of motion of the boundaries in the U-tube, or $u = \frac{1}{2}(d_1 + d_2)c/t$, where d_1 and d_2 are the observed number of scale divisions moved by the rising and falling interfaces, c is the number of centimeters per scale division, and t is the time in seconds during which the migration was allowed to continue. The electrophoretic mobility is merely the migrational velocity under a potential gradient of 1 v./cm., or $v = u/H$, where H is the potential drop through the liquid.

The ζ-potential is related to the migrational velocity by the following equation:

$$\zeta = 4\pi\eta u/HD$$

where η is the viscosity of the medium in which the sol is prepared, D is the dielectric constant of this medium, and u and H are as previously defined. The variables in this equation, since H was maintained constant for all "runs," are the migrational velocity and the viscosity. When the constants are evaluated, the practical equation for calculating the ζ-potential becomes $\zeta = 0.121\eta u$. Viscosity varies with temperature, thus requiring an observation of the temperature at the end of each run.

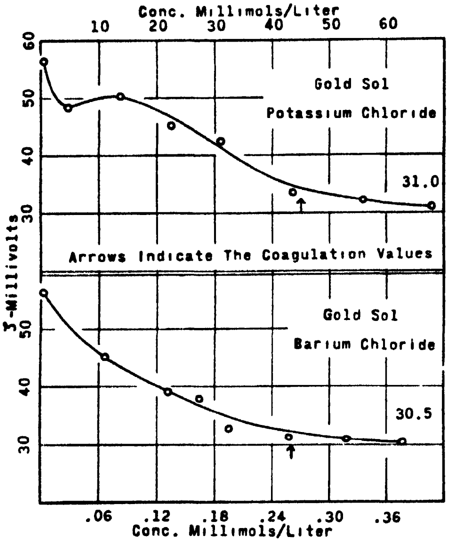

FIG. 2

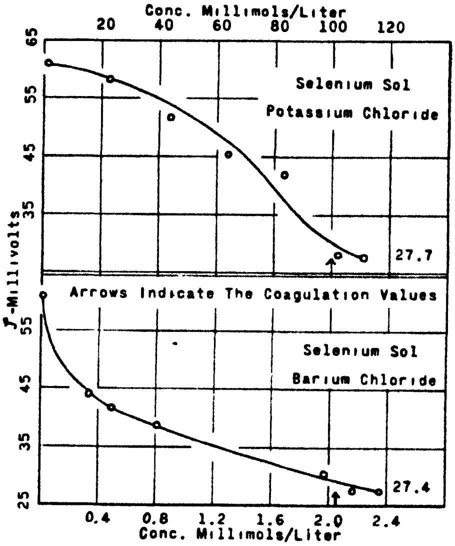

FIG. 3

FIG. 2. Plot of ζ-potential against concentration of added electrolyte for gold sol

FIG. 3. Plot of ζ-potential against concentration of added electrolyte for selenium sol

The sols investigated were negatively charged; therefore the migration was downward in the left-hand side of the U-tube and upward in the right. Duplicate measurements were made in several instances, and it was found that values of the ζ-potential were reproducible to within 1 mv.

III. RESULTS

The results obtained are presented in tables 3 and 4 in figures 2 and 3. The tables are self-explanatory, but the graphs may require slight clarification. The ζ-potential is plotted on the same scale in a vertical direction, but the electrolyte concentration along the horizontal axis differs in scale with each graph, depending on the relative magnitude of the concentrations used. The ζ-potential

TABLE 3

ζ-Potential of gold sol

20 ml. sol + 2 ml. 0.2 *M* sucrose + KCl; $\zeta = 0.121\ \eta u$

KCl CONCENTRATION	TIME	DISTANCE	VELOCITY/ SECOND	TEMPERATURE	VISCOSITY	ζ
millimoles/liter	*sec.*	*cm.*		*°C.*	*cp.*	*mv.*
4.53	1950	1.015	5.21	32.0	0.7679	48.4
13.5	1830	0.994	5.42	32.0	0.7679	50.4
22.2	1830	0.907	4.95	33.0	0.7523	45.1
30.8	1860	0.843	4.53	31.5	0.7760	42.6
43.5*	1980	0.692	3.49	33.0	0.7523	33.5
55.8*	1800	0.605	3.36	33.0	0.7523	32.2
67.8*	1800	0.583	3.24	33.0	0.7523	31.0

20 ml. sol + 2 ml. 0.2 *M* sucrose + $BaCl_2$; $\zeta = 0.1274\ \eta u$

$BaCl_2$ CONCENTRATION	TIME	DISTANCE	VELOCITY/ SECOND	TEMPERATURE	VISCOSITY	ζ
millimoles/liter	*sec.*	*cm.*		*°C.*	*cp.*	*mv.*
0.000†	1800	1.080	6.00	31.5	0.7760	56.3
0.000	1800	1.123	6.24	33.0	0.7523	56.8
0.067	1740	0.843	4.84	32.0	0.7679	45.0
0.132†	1860	0.778	4.18	31.0	0.7840	39.6
0.132	1830	0.778	4.25	33.0	0.7523	38.7
0.164	1860	0.756	4.06	32.0	0.7679	37.8
0.195	1800	0.626	3.48	31.5	0.7760	32.6
0.257	2040	0.670	3.28	31.0	0.7840	41.1
0.317	1860	0.605	3.25	31.0	0.7840	30.8
0.376	1860	0.605	3.25	31.5	0.7760	30.5

* $H = 1.22$.

† No sucrose added to sol.

TABLE 4

ζ-Potential of selenium sol

20 ml. sol + 2 ml. 0.2 *M* sucrose + KCl; $\zeta = 0.121\ \eta u$

KCl CONCENTRATION	TIME	DISTANCE	VELOCITY/ SECOND	TEMPERATURE	VISCOSITY	ζ
millimoles/liter	*sec.*	*cm.*		*°C.*	*cp.*	*mv.*
22.2	1830	1.166	6.37	33.0	0.7523	58.0
43.5	1890	1.080	5.72	33.5	0.7447	51.5
63.8	1800	0.907	5.04	33.5	0.7447	45.4
83.4	1800	0.864	4.80	34.0	0.7371	42.8
102	1800	0.583	3.24	35.5	0.7155	28.1
111	1950	0.605	3.10	34.0	0.7371	27.7

20 ml. sol + 2 ml. 0.2 *M* sucrose + $BaCl_2$

$BaCl_2$ CONCENTRATION	TIME	DISTANCE	VELOCITY/ SECOND	TEMPERATURE	VISCOSITY	ζ
millimoles/liter	*sec.*	*cm.*		*°C.*	*cp.*	*mv.*
0.000	1920	1.253	6.53	32.0	0.7679	60.7
0.337	1830	0.864	4.72	32.0	0.7679	43.8
0.489	1920	0.864	4.50	32.5	0.7601	41.4
0.807	1800	0.756	4.20	32.5	0.7601	38.6
1.59	1800	0.605	3.36	31.0	0.7840	31.9
1.97	1800	0.583	3.24	31.5	0.7760	30.4
2.16	2100	0.626	2.98	32.0	0.7679	27.7
2.34	1830	0.540	2.95	32.0	0.7679	27.4

is plotted instead of the customary mobility, because in the absence of a constant-temperature bath the ζ-potential values are more significant, as they include the variation with viscosity.

IV. DISCUSSION

As pointed out in the introductory section of this paper, attempts have been made to rationalize the abnormal behavior of sols toward uni-univalent salts by attributing the stability of hydrophobic colloids to factors other than the ζ-potential, and by deriving other and more complete equations than the Helmholtz–Smoluchowski equation to minimize the inconsistencies. Since the abnormalities vanish if the sols are monodisperse it would appear that the ζ-potential, as defined by the Helmholtz–Smoluchowski equation, is the primary stabilizing factor for lyophobic sols.

V. SUMMARY

1. Sols have given inconsistent critical ζ-potential values when coagulated with uni-univalent salts. The abnormal behavior is attributed to the polydisperse character of the sol investigated.
2. Monodisperse sols of gold and selenium were prepared and their mobilities were measured in a modified Burton U-tube by the microscopic moving boundary method.
3. The calculated critical ζ-potential values of the monodisperse sols were constant irrespective of the electrolyte used.
4. With sols of uniform particle size there is no anomalous behavior of the critical ζ-potential values with uni-univalent electrolytes.
5. A return to the concept of the ζ-potential given by the Helmholtz–Smoluchowski equation as the stabilizing factor of lyophobic colloids is advocated.

REFERENCES

(1) Bikerman: Z. physik. Chem. **115**, 261 (1925).
(2) Briggs: J. Phys. Chem. **34**, 1326 (1930).
(3) Eilers and Korff: Trans. Faraday Soc. **36**, 229 (1940).
(4) Faraday: Phil. Trans. **147**, 145 (1837).
(5) Freundlich and Zeh: Z. physik. Chem **114**, 84 (1925).
(6) Ghosh: J. Chem. Soc. **1929**, 2693.
(7) Holliday: Trans. Faraday Soc. **43**, 661 (1947).
(8) Jenny and Reitemeier: J. Phys. Chem. **39**, 593 (1935).
(9) Kruyt and van Arkel: Kolloid-Z. **32**, 29 (1923).
(10) Kruyt and van der Willigen: Z. physik. Chem. **130**, 170 (1927).
(11) Kruyt and coworkers: Colloid Symposium Monograph **4**, 493 (1927).
(12) McBain: J. Indian Chem. Soc. (Ray Commemoration Volume), p. 67 (1933).
(13) Mukherjee and Chaudhury: J. Indian Chem. Soc. **2**, 296 (1925); **4**, 493 (1927).
(14) Mukherjee and coworkers: J. Indian Chem. Soc. **5**, 735 (1928); **7**, 465 (1930); **10**, 26 (1933); Nature **122**, 960 (1928); Science and Culture **1**, 111 (1935).
(15) Northrop and Cullen: J. Gen. Physiol. **4**, 635 (1921–22).
(16) Powis: J. Chem. Soc. **109**, 734 (1916).
(17) Price and Lewis: Trans. Faraday Soc. **29**, 775 (1933).
(18) Weiser: *Inorganic Colloid Chemistry. I. The Colloidal Elements.* John Wiley and Sons, Inc., New York (1933).

SOME PHYSICOCHEMICAL STUDIES ON GALLIUM(III) SALT SOLUTIONS[1]

THERALD MOELLER AND GLENDALL L. KING[2]
Noyes Chemical Laboratory, University of Illinois, Urbana, Illinois

Received October 20, 1949

INTRODUCTION

Among the characteristics of the gallium–indium–thallium family essential to its systematic study are trends and variations in basicity. The combined effects of small size and comparatively high charge among the tripositive ions of these elements should render all of them quite highly acidic, but significant differences should be discernible as these factors vary. Variations in basicity have been studied as part of a general investigation of comparative properties in this family. It is the purpose of this communication to summarize results obtained with gallium(III) compounds by the techniques of electrometric titration with alkali and measurement of pH as a function of salt concentration and to compare them with existent data for indium(III) compounds.

Previously reported measurements of these types have been limited in number and lacking in agreement. Fricke and Meyring (3) obtained data, based upon a hydrogen electrode study of titration of gallium(III) chloride solutions with sodium and potassium hydroxides, which indicate precipitation of the hydrous oxide (9) in the vicinity of pH 2.8–3.1. Von Bergkampf (15) reported precipitation from hydrochloric acid solution at pH 3.4 and from sodium hydroxide solution at pH 9.7 as a result of single titrations of 0.1 *N* gallium(III) chloride solutions, a quinhydrone electrode being used. More recently Ivanov-Emin and Rabovik (5) found from a hydrogen electrode study that precipitation from 0.01 *M* gallium(III) chloride solutions began at pH 3.48–3.50 with 2.6 equivalents of sodium hydroxide added and was complete at pH 6.7–6.8 with 2.8–2.9 equivalents. With 0.005 *M* gallium(III) sulfate solutions, however, precipitation began at pH 3.40–3.45 with 0.2 equivalent and was complete at pH 4.7–4.8 with 2.5–2.6 equivalents. Dissolution of the hydrous precipitate at pH 9.6–9.7 after addition of 4.0–4.2 equivalents of alkali was considered evidence for the formation of the species $[Ga(OH)_4]^-$ in solution. Lacroix (8) obtained precipitation from 0.007 *M* gallium(III) chloride solution at *ca.* pH 3.2 and dissolution of the hydrous oxide over a broad range above pH 6.

Hydrolysis studies on gallium(III) salt solutions appear limited to those of Fricke and his coworkers (2, 3). A preliminary measurement (2) of hydrogen-ion concentration showing 0.1875 *N* gallium(III) chloride solution to be 32.9 per cent hydrolyzed was followed (3) by similar measurements as functions of gallium concentration. Values of pH from 3.362 for 0.00314 *M* to 1.624 for 0.0951 *M* solutions were in agreement with a first hydrolysis constant, corresponding to the formation of $Ga(OH)^{++}$ ions, of 1.4×10^{-3}. Electrometric titration data (3) led to a value of 3.5×10^{-4} for a second hydrolysis constant corresponding to the formation of $Ga(OH)_2^+$ ions. Correspondingly, the first and second stages in the hydrolysis of sodium gallate solutions were characterized, respectively, by the constants 3×10^{-3} and 1.2×10^{-4}.

---

[1] Presented in part at the 114th National Meeting of the American Chemical Society, which was held in Portland, Oregon, September, 1948.

Reproduction in whole or in part permitted for any purpose of the United States Government.

[2] Present address: Los Alamos Scientific Laboratory, Los Alamos, New Mexico.

Lack of agreement and comprehensiveness in these data warrants more nearly complete studies. The data reported here were obtained from electrometric titration studies on gallium(III) sulfate, bromide, chloride, and nitrate solutions and from hydrolysis studies on bromide, chloride, and nitrate solutions.

EXPERIMENTAL

A. Materials

The gallium compounds used in this investigation were prepared from a sample of the metal[3] containing only spectroscopic traces of other elements. Pure gallium(III) sulfate was obtained by dissolving a sample of the metal in a mixture of concentrated nitric and sulfuric acids and evaporating off the excess acids to leave a crystalline product. Anhydrous gallium(III) bromide was prepared by passing nitrogen laden with bromine over gallium metal at 300°C. (7) and repeatedly subliming the product in dry nitrogen. Anhydrous gallium(III) chloride was prepared by passing dry hydrogen chloride over gallium metal at 200°C. (6) and repeatedly subliming the product in dry nitrogen. Both bromide and chloride samples were sealed in nitrogen in glass ampoules which could be broken just prior to use. Gallium(III) nitrate was obtained by dissolving the metal in dilute nitric acid solution, concentrating the resulting solution on the steam bath, cooling, and drying the crystallized product for several days in a desiccator over calcium chloride. Solutions obtained by dissolving these gallium compounds in carbon dioxide-free distilled water were standardized by gravimetric determination of gallium as either the oxide or the 8-hydroxyquinoline derivative (13). Stock solutions were diluted to desired concentrations with carbon dioxide-free water.

Tenth-normal solutions of sodium hydroxide were prepared by dilution of a concentrated, carbonate-free solution with carbon dioxide-free water and were standardized against the primary standard potassium acid phthalate. These solutions were protected from atmospheric carbon dioxide with soda lime.

B. Procedure

For all measurements, solutions were maintained within ±0.2°C. of the stated temperature by thermostating. Electrometric titration data were obtained by the standard procedure (11), using a Beckman Model H pH meter the glass electrode of which was checked frequently against a 0.05 *M* potassium acid phthalate buffer. Hydrolysis measurements were made by determining pH values as functions of concentration (10, 12).

---

[3] Obtained from the Eagle-Picher Company, Joplin, Missouri.

RESULTS AND DISCUSSION

A. Electrometric titration studies

Data were obtained for electrometric titrations with sodium hydroxide of gallium(III) sulfate solutions varying from 0.099 to 0.229 *M* in gallium ion at temperatures of 10°, 25°, and 40°C. Corresponding data were obtained at 25°C. for 0.020–0.180 *M* gallium(III) bromide solutions, 0.010–0.150 *M* gallium(III) chloride solutions, and 0.010–0.123 *M* gallium(III) nitrate solutions. Some back-titration studies with standard acids were also carried out.

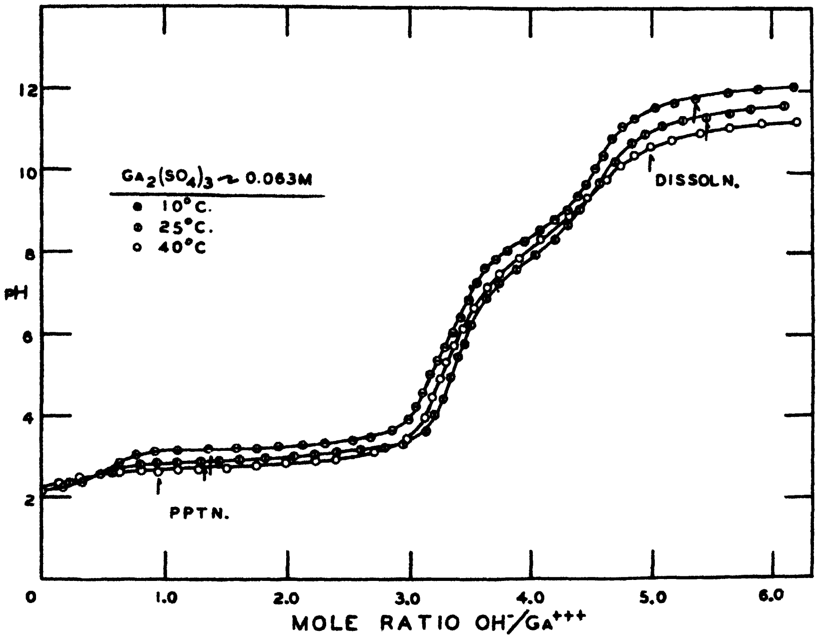

Fig. 1. Titration of gallium (III) sulfate solutions with sodium hydroxide

Representative data for 0.063 *M* gallium(III) sulfate solutions (0.125 *M* in gallium ion) at the three temperatures are given in figure 1, plotted as pH *vs.* the ratio of moles of hydroxyl ion added to moles of gallium ion initially present. Points at which precipitation began and dissolution of the precipitate was complete are indicated by small arrows. Data at other concentrations gave exactly similar plots, the displacements of the curves with increasing temperature as shown in figure 1 being characteristic of all plots for solutions of a given concentration.

Significant data characterizing these titrations are summarized in table 1. It is apparent that, regardless of temperature, roughly 1 mole of hydroxyl ion to each mole of gallium ion was necessary for precipitation incidence. The average values for these ratios are 1.23 at 10°C., 1.11 at 25°C., and 0.93 at 40°C. Comparison of these ratios with the corresponding ones of 0.94, 0.84, and 0.73 for indium(III) sulfate solutions (11) suggests a greater tendency for aggregation in the gallium solutions on addition of hydroxyl ion. It was impossible to obtain precipitation at lower ratios as reported by Ivanov-Emin and Rabovik (5).

Precipitation pH values are essentially independent of concentration at a given concentration but decrease significantly with temperature increase. Average values of 3.03 at 10°C., 2.80 at 25°C., and 2.68 at 40°C. are again to be compared with 3.56, 3.43, and 3.15, respectively, for indium(III) sulfate solutions at the same temperature (10). A somewhat greater acidity for the gallium(III) ion is thus indicated.

TABLE 1

Effect of gallium-ion concentration on titrations of gallium(III) sulfate solutions

INITIAL Ga^{+++} CONCENTRATION	PRECIPITATION INCIDENCE		DISSOLUTION OF PRECIPITATI	
	pH	OH^-/Ga^{+++}	pH	OH^-/Ga^{++}
	10°C.			
moles/liter				
0.125	3.19	1.29	11.90	5.40
0.150	3.00	1.19	11.85	5.42
0.195	3.02	1.22	12.08	5.40
0.229	2.89	1.21	11.85	5.41
Average.	3.03	1.23	11.92	5.41
	25°C.			
0.125	2.85	1.14	11.40	5.41
0.150	2.78	1.05	11.48	5.17
0.195	2.78	1.11	11.85	6.31
0.229	2.79	1.13	11.76	6.07
Average......	2.80	1.11	11.62	5.74
	40°C.			
0.125	2.69	0.95	10.57	4.92
0.150	2.65	0.93	10.65	4.90
0.195	2.65	0.92	10.85	5.00
Average.	2.68	0.93	10.69	4.94

Data characterizing complete dissolution of the precipitates are subject to somewhat greater variations. In general, between 5 and 6 moles of hydroxyl ion were required per mole of gallium ion to cause dissolution. These mole ratios are probably without real significance, for dissolution, like precipitation, was undoubtedly spread over a considerable interval. The lack of significant breaks in the titration curves in this region (see figure 1) may be cited as evidence in support of this conclusion. It seems reasonable to expect considerable hydrolysis in gallate solutions, and the total quantity of hydroxyl ion required to effect complete dissolution is doubtless the sum of the quantity necessary for gallate formation and the quantity necessary to prevent precipitation by hydrolysis. The slight breaks in the titration curves (figure 1) in the vicinity of mole ratio 4 may indicate gallate formation involving four hydroxyls to one gallium. Ivanov-Emin and Rabovik (5) suggest this to be true, and the data of Fricke and Meyring (3) are not inconsistent with this conclusion.

TABLE 2

Solubility product and solubility data, calculated from titrations of gallium(III) sulfate solutions

TEMPERATURE	INITIAL Ga^{+++} CONCENTRATION	SOLUBILITY PRODUCT × 10^{35}	SOLUBILITY
°C.	*moles/liter*		*(moles/liter)* × 10^{10}
10	0.125	0.17	4.9
	0.150	0.08	4.1
	0.195	0.10	4.3
	0.229	0.04	3.4
Average		0.10	4.2
25	0.125	0.68	7.0
	0.150	0.70	7.0
	0.195	0.58	6.8
	0.229	0.85	7.4
Average		0.70	7.1
40	0.125	8.4	13.1
	0.150	7.3	12.6
	0.195	12.5	14.4
Average		9.4	13.4

The curves in figure 1 indicate completion of precipitation when the mole ratio of OH^- to Ga^{+++} reaches 3, corresponding to the formation of the hydrous hydroxide or oxide. Formulation of the precipitation product as the latter is more consistent with the data of Milligan and Weiser (9), although for convenience in evaluation of the solubility product constant and water solubility, consideration of the material as hydroxide is useful. Application of the conventional treatment (e.g., 11, 14) without use of activities at various OH^- to Ga^{+++} ratios in the precipitation regions of the titrations yielded the data summarized in table 2, the ion product of water being taken as 0.295×10^{-14}, 1×10^{-14}, and 3.02×10^{-14} at 10°, 25°, and 40°C., respectively. Calculated solubility product constants increase markedly in magnitude with temperature but are of the general order of magnitude of 10^{-35}. By a similar approach using a chloride solution, Lacroix (8) obtained a value of $10^{-36.5}$. Corresponding water solubilities of the order of 10^{-10} gram-mole per liter agree quite closely with an average of 6.3×10^{-10} reported by Oka (14). Corresponding calculations (11) for indium hydroxide gave 10^{-33} for the solubility product constant and 10^{-9} gram-mole per liter for the water solubility, variation with temperature being a little less striking.

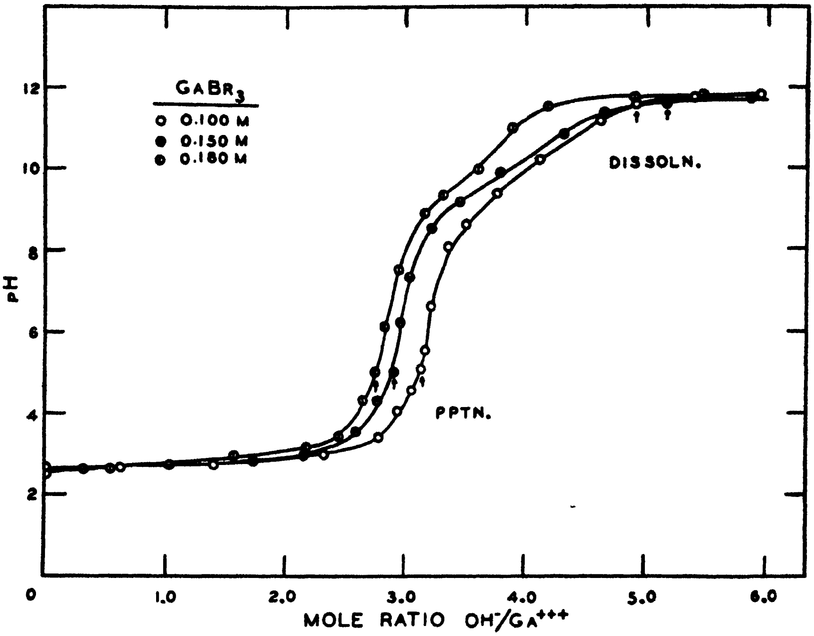

FIG. 2. Titration of gallium(III) bromide solutions with sodium hydroxide

Plotted in figures 2, 3, and 4 are representative titration data for gallium(III) bromide, chloride, and nitrate solutions, respectively, at 25°C. Numerical values significant to these titrations are summarized in table 3.

While the curves obtained for the bromide, chloride, and nitrate are similar to those obtained with sulfate solutions, precipitation incidence is markedly different. With bromide, chloride, and nitrate, nearly 3.0 moles of hydroxyl ion were required per mole of gallium ion before visible precipitation occurred, yet the plateaus in the titration curves indicate steady consumption of hydroxyl ion up to these points. At the points of precipitation incidence shown in figures 2, 3, and 4 and recorded in table 3, complete flocculation occurred, but it was never possible to obtain indications of cloudiness in solutions containing less hydroxyl ion. It appears that either excessive ion aggregation occurs under such conditions or that peptization by excess gallium(III) ion takes place as hydroxyl ion is added, the bromide, chloride, and nitrate ions having negligible flocculating effects on the sols produced. It is significant that Ivanov-Emin and Rabovik (5) reported precipitation from gallium(III) chloride solutions only after addi-

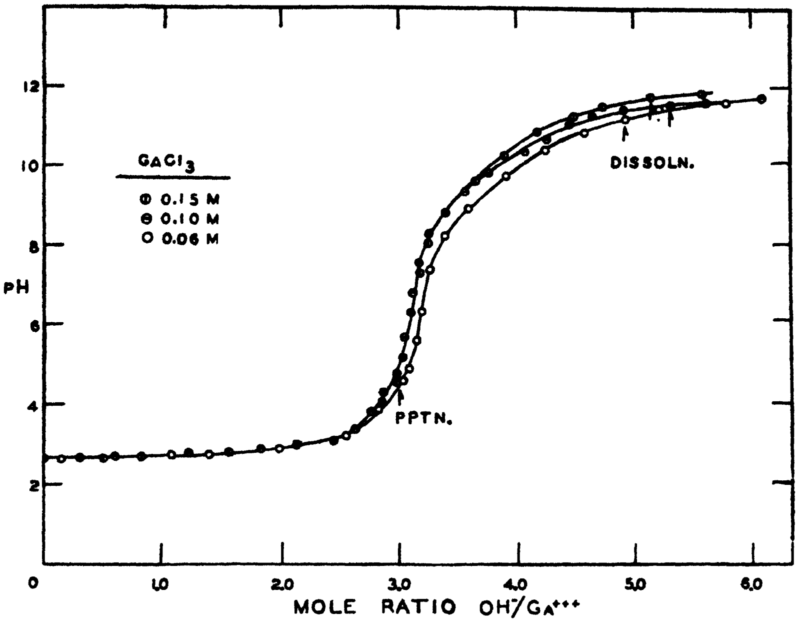

Fig. 3. Titration of gallium(III) chloride solutions with sodium hydroxide

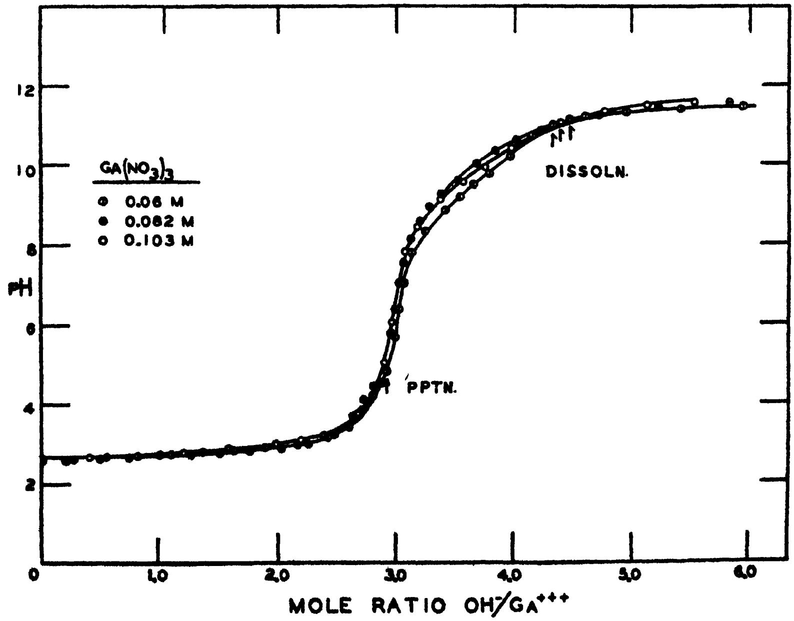

Fig. 4. Titration of gallium(III) nitrate solutions with sodium hydroxide

TABLE 3

Effects of gallium-ion concentration on titrations of bromide, chloride, and nitrate solutions at 25°C.

INITIAL Ga^{+++} CONCENTRATION	PRECIPITATION INCIDENCE		DISSOLUTION OF PRECIPITATE	
	pH	OH^-/Ga^{+++}	pH	OH^-/Ga^{+++}
	Gallium(III) bromide			
moles/liter				
0.020	5.60	3.63	11.43	6.05
0.030	5.30	3.63	11.28	5.62
0.060	5.05	3.50	11.42	6.05
0.100	5.09	3.14	11.57	4.92
0.125	5.02	2.98	11.50	4.96
0.150	4.99	2.90	11.65	5.53
0.180	5.00	2.81	11.63	4.81
Average .	5.15	3.23	11.50	5.42
	Gallium(III) chloride			
0.010	5.50	3.21	10.90	4.80
0.015	5.25	3.19	11.05	4.94
0.020	5.15	3.14	11.11	5.06
0.030	5.22	3.13	11.05	4.72
0.040	5.00	3.12	11.10	5.06
0.060	4.91	3.07	11.25	4.89
0.100	4.80	2.98	11.50	5.26
0.125	4.71	2.94	11.62	5.19
0.150	4.51	2.97	11.68	5.13
Average . .	5.01	3.08	11.24	5.01
	Gallium(III) nitrate			
0.010	5.25	3.02	10.80	4.49
0.020	5.25	2.95	11.20	4.52
0.030	5.35	2.92	11.22	4.48
0.040	5.38	2.92	10.90	4.48
0.050	5.25	2.78	11.12	4.52
0.060	5.15	2.93	11.05	4.31
0.070	5.08	2.91	10.98	4.34
0.082	4.78	2.86	11.18	4.45
0.103	4.80	2.85	11.05	4.32
0.123	4.84	2.86	11.10	4.44
Average	5.11	2.90	11.06	4.44

tion of 2.6 equivalents of sodium hydroxide, although Fricke and Meyring (3) obtained precipitates shortly after the addition of single equivalents. An investigation of these phenomena will be reported in a subsequent communication.

Because of the uncertainties characterizing precipitation from bromide, chloride, and nitrate solutions, evaluations of solubility product constants were not attempted. The major inflections in the curves in figures 2, 3, and 4 again indicate completion of precipitation at an OH^- to Ga^{+++} ratio of 3.0 and suggest that the hydrous oxide (or hydroxide) is the ultimate precipitate. Data on dissolution of the precipitates in excess hydroxyl ion are in excellent agreement with those given for the sulfate solutions. Alterations in initial gallium-ion concentration are without major effect at any place in the titrations.

A few back-titrations with standard acid were carried out to cast light on the nature of the gallate solutions. Plotted in figure 5 are data for titration of 0.02 M gallium(III) nitrate solution with 0.1 N sodium hydroxide followed by back-titration of the strongly alkaline solution with 0.1 N nitric acid. As acid is added, hydrogen ion is consumed regularly by excess hydroxyl ion. However, the curve breaks significantly just before the hydrous precipitate reappears, and the position of this break suggests rather conclusively that four hydroxyls are associated with a single gallium in the gallate. The remainder of the curve is essentially a reproduction, although at slightly lower pH values, of the original titration curve. Studies at other concentrations gave the same results.

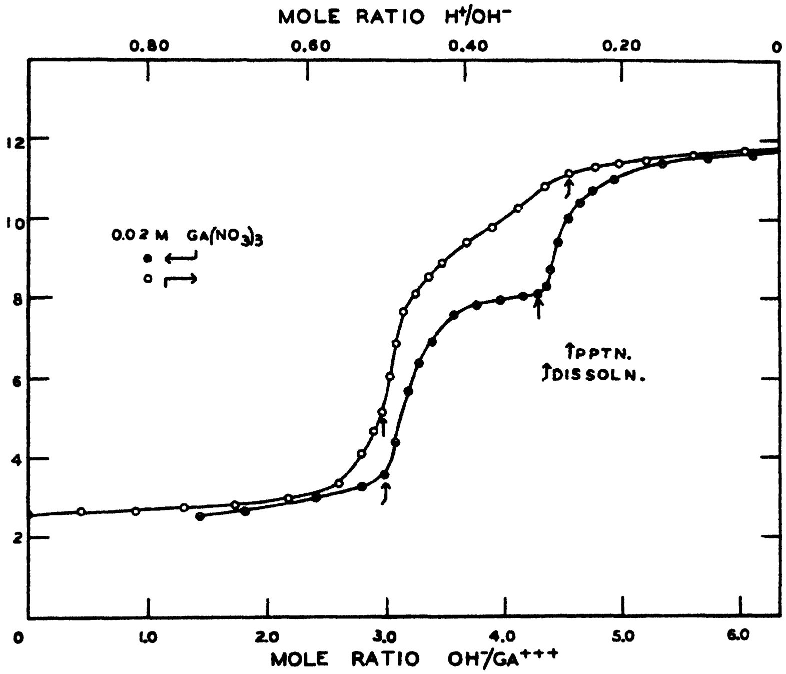

FIG. 5. Titration and back-titration of a gallium (III) nitrate solution

B. Hydrolysis studies

Hydrolysis studies were limited to gallium(III) bromide, chloride, and nitrate solutions at 25°C. Bromide, chloride, and nitrate were selected as being sufficiently weakly basic in character to contribute comparatively nothing to any observed alterations in the hydrogen-ion concentrations in the solutions. Under these conditions then, any such alterations could be ascribed to the acidic characteristics of the gallium(III) ion.

It may be assumed, as a first approximation, that the governing hydrolytic process in dilute solutions may be formulated as either

$$Ga^{+++} + H_2O \rightleftharpoons GaOH^{++} + H^+ \tag{1}$$

or

$$Ga^{+++} + H_2O \rightleftharpoons GaO^+ + 2H^+ \tag{2}$$

ionic hydration and complex-ion formation being neglected in all cases. The first of these reactions is characteristic of a number of other tripositive ions, among them indium (4, 10, 12), and has been suggested for gallium (3, 8). The second is probably never a primary process, but a product such as GaO^+ (or its hydrate, $Ga(OH)_2{}^+$) may result from the secondary hydrolysis of $GaOH^{++}$.

Applications of conventional treatments (1) to these equations yields the expression

$$K_h = \frac{cx^2}{1 - x} = \frac{[GaOH^{++}][H^+]}{[Ga^{+++}]} \tag{3}$$

for equation 1 and the expression

$$K'_h = \frac{4c^2x^2}{1 - x} = \frac{[GaO^+][H^+]^2}{[Ga^{+++}]} \tag{4}$$

for equation 2, where K_h and K'_h are the respective hydrolysis constants, c the molar concentration of gallium ion, and x the degree of hydrolysis. The degree of hydrolysis, in turn, may be evaluated for reactions 1 and 2 as

$$x = c_{H^+}/c \qquad \text{and} \qquad x = c_{H^+}/2c$$

respectively. Both equations 3 and 4 are of such form that if the hydrolytic process be represented by either equation 1 or equation 2, linear relationships should exist between pH and log c.

Data showing the existence of such relations at least up to $c = 0.1$ are plotted for bromide, chloride, and nitrate solutions in figure 6. Agreement among bromide, chloride, and nitrate data is excellent and suggests the three anions to be of equal influence or lack of influence in governing hydrolysis. Deviations at higher concentrations are not unexpected since activities have been neglected, while those at very low concentrations doubtless result from lack of absolute accuracy in pH measurement.

Decision as to the mechanism governing the hydrolytic process is best based upon the constancy of the hydrolysis constant as calculated from experimental data. In all cases a greater degree of constancy is obtained by application of equation 3, and it may be assumed, therefore, that reaction 1 is governing. Data tabulated in tables 4, 5, and 6 summarize experimental observations on bromide, chloride, and nitrate solutions and calculated values for the degree of

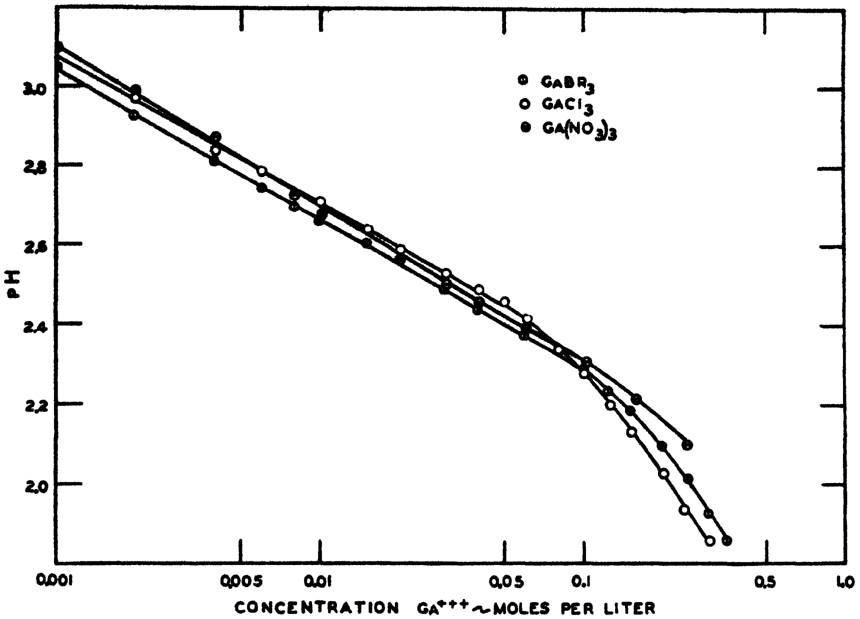

FIG. 6. Hydrolysis of gallium(III) bromide, chloride, and nitrate solutions

TABLE 4

Hydrolysis of gallium(III) bromide solutions at 25°C.

INITIAL Ga^{+++} CONCENTRATION	pH	DEGREE OF HYDROLYSIS (x)	HYDROLYSIS CONSTANT $\times 10^4$	INITIAL Ga^{+++} CONCENTRATION	pH	DEGREE OF HYDROLYSIS (x)	HYDROLYSIS CONSTANT $\times 10^4$
moles/liter				*moles/liter*			
1.116	0.92	0.103	144.	0.1000	2.29	0.0512	2.86
1.042	0.97	0.102	123.	0.0800	2.33	0.0583	2.90
0.9000	1.18	0.0741	52.6	0.0600	2.38	0.0695	3.10
0.8000	1.28	0.0657	36.8	0.0400	2.45	0.0888	3.48
0.7000	1.39	0.0581	25.1	0.0300	2.50	0.106	3.70
0.6000	1.51	0.0515	16.7	0.0200	2.58	0.131	4.03
0.5000	1.66	0.0438	10.0	0.0150	2.62	0.160	4.43
0.4000	1.80	0.0398	6.66	0.0100	2.67	0.214	5.72
0.3500	1.86	0.0395	5.61	0.0080	2.70	0.249	6.60
0.3000	1.93	0.0394	4.80	0.0060	2.75	0.297	7.92
0.2500	2.02	0.0382	3.80	0.0040	2.81	0.388	12.0
0.2000	2.10	0.0398	3.26	0.0020	2.93	0.585	13.7
0.1500	2.19	0.0429	2.87	0.0010	3.08	0.830	34.4
0.1250	2.24	0.0459	2.76				

hydrolysis and hydrolysis constant based on application of the principles outlined above to equation 1. Agreement among average values over the concentration range 0.004–0.25 M of 4.6×10^{-4}, 4.1×10^{-4}, and 3.7×10^{-4} for the hydrolysis constants for bromide, chloride, and nitrate solutions, respectively, is excellent. Indium(III) bromide and chloride solutions, by comparison, are uniformly less hydrolyzed at 25°C. and are characterized by mean hydrolysis constants of 1.4×10^{-5} and 1.2×10^{-5}, respectively (10, 12), again illustrating the greater acidity of the gallium(III) ion. The data of Fricke and his coworkers (2, 3) indicate considerably greater hydrolysis for gallium(III) chloride solutions than do the data presented here, but those values were obtained with solutions containing free hydrochloric acid, which may not have been completely corrected for, and were not obtained at any stated temperature.

TABLE 5

Hydrolysis of gallium(III) chloride solutions at 25°C.

INITIAL Ga^{+++} CONCENTRATION	pH	DEGREE OF HYDROLYSIS (x)	HYDROLYSIS CONSTANT $\times 10^4$	INITIAL Ga^{+++} CONCENTRATION	pH	DEGREE OF HYDROLYSIS (x)	HYDROLYSIS CONSTANT $\times 10^4$
moles/liter				*moles/liter*			
0.3334	1.81	0.0465	7.56	0.0400	2.49	0.0810	2.86
0.3000	1.86	0.0470	6.96	0.0300	2.53	0.0983	3.22
0.2500	1.94	0.0460	5.55	0.0200	2.59	0.1285	3.78
0.2000	2.03	0.0467	4.57	0.0150	2.64	0.153	4.12
0.1500	2.13	0.0494	3.88	0.0100	2.71	0.193	4.73
0.1250	2.20	0.0505	3.35	0.0080	2.74	0.227	5.36
0.1000	2.28	0.0525	2.91	0.0060	2.79	0.270	6.00
0.0800	2.34	0.0572	2.77	0.0040	2.84	0.363	8.25
0.0700	2.38	0.0596	2.65	0.0020	2.97	0.535	12.3
0.0600	2.42	0.0633	2.57	0.0010	3.11	0.776	18.6
0.0500	2.46	0.0694	2.59				

TABLE 6

Hydrolysis of gallium(III) nitrate solutions at 25°C.

INITIAL Ga^{+++} CONCENTRATION	pH	DEGREE OF HYDROLYSIS (x)	HYDROLYSIS CONSTANT $\times 10^4$	INITIAL Ga^{+++} CONCENTRATION	pH	DEGREE OF HYDROLYSIS (x)	HYDROLYSIS CONSTANT $\times 10^4$
moles/liter				*moles/liter*			
0.2620	2.09	0.0310	2.61	0.0400	2.46	0.0868	3.30
0.2450	2.10	0.0324	2.65	0.0300	2.50	0.105	3.72
0.2050	2.15	0.0345	2.53	0.0200	2.55	0.141	4.62
0.1640	2.21	0.0376	2.41	0.0100	2.67	0.214	5.83
0.1230	2.27	0.0437	2.44	0.0080	2.72	0.238	6.00
0.1030	2.31	0.0476	2.45	0.0060	2.80	0.265	5.74
0.0820	2.34	0.0557	2.70	0.0040	2.88	0.330	6.61
0.0700	2.37	0.0610	2.78	0.0020	2.99	0.510	10.6
0.0600	2.39	0.0679	2.96	0.0010	3.10	0.794	30.6
0.0500	2.42	0.0760	3.13				

SUMMARY

1. The acidic characteristics of gallium(III) ion in aqueous solution have been studied by electrometric titrations with sodium hydroxide and by hydrogen-ion determinations as functions of concentration.

2. In the presence of sulfate ion, electrometric titration has shown the hydrous oxide to begin precipitating when the mole ratio of added hydroxyl ion to gallium ion approximates 1 and to be complete when this ratio reaches 3. At 25°C. the average pH for precipitation is 2.80.

3. In the presence of bromide, chloride, and nitrate ion, apparent precipitation is delayed until the OH^- to Ga^{+++} ratio reaches 3, where complete flocculation occurs. The pH values characterizing these changes are not too consistent.

4. In all cases, dissolution of the precipitates in excess hydroxyl ion occurs only after addition of 5–6 moles of hydroxyl ion, although the gallate ion has the composition $[Ga(OH)_4]^-$.

5. Solubility product constants for the hydrous hydroxide of the order of 10^{-35} and corresponding water solubilities of the order of 10^{-10} M have been evaluated from data on sulfate solutions.

6. Hydrolysis in dilute gallium(III) bromide, chloride, and nitrate solutions has been shown to be governed by formation of $GaOH^{++}$ ions and to correspond to hydrolysis constants of 4.6×10^{-4}, 4.1×10^{-4}, and 3.7×10^{-4}, respectively, at 25°C.

7. Gallium(III) ion has been shown by these data to be somewhat more acidic than indium(III) ion.

The authors wish to express appreciation to the Office of Naval Research for support received during this investigation.

REFERENCES

(1) Britton: *Hydrogen Ions*, 3rd edition, Vol. I, pp. 208–11. Chapman and Hall, Ltd., London (1942).

(2) Fricke and Blenke: Z. anorg. allgem. Chem. **143**, 183 (1925).

(3) Fricke and Meyring: Z. anorg. allgem. Chem. **176**, 325 (1928).

(4) Hattox and de Vries: J. Am. Chem. Soc. **58**, 2126 (1936).

(5) Ivanov-Emin and Rabovik: J. Gen. Chem. (U.S.S.R.) **14**, 781 (1944).

(6) Johnson and Haskew: *Inorganic Syntheses*, Vol. I, pp. 26–7. McGraw-Hill Book Company, Inc., New York (1939).

(7) Klemm and Tilk: Z. anorg. allgem. Chem. **207**, 161 (1932).

(8) Lacroix: Dissertation, University of Paris, Paris, France (1948).

(9) Milligan and Weiser: J. Am. Chem. Soc. **59**, 1670 (1937).

(10) Moeller: J. Am. Chem. Soc. **63**, 1206 (1941).

(11) Moeller: J. Am. Chem. Soc. **63**, 2625 (1941).

(12) Moeller: J. Am. Chem. Soc. **64**, 953 (1942).

(13) Moeller and Cohen: Anal. Chem. **22**, 686 (1950).

(14) Oka: J. Chem. Soc. Japan **59**, 971 (1938).

(15) von Bergkampf: Z. anal. Chem. **90**, 333 (1932).

THE EFFECT OF ADDED HYDROCARBONS UPON CRITICAL CONCENTRATIONS OF SOAP AND DETERGENT SOLUTIONS

H. B. KLEVENS[1]

Received March 29, 1950

It has been observed that the solubilization of hydrocarbons by soap solutions at room temperature is a relatively slow process, often taking days to reach equilibrium (5, 9, 12). The results of Powney and Addison on interfacial tensions of various sodium alkyl sulfates against xylene (14) were shown to be nonequilibrium values (10). The equilibrium values of the interfacial tension of alkyl sulfonates and benzene were obtained only after a number of days (10), a result which was in accord with the findings that solubilization, as determined by light scattering (5), is a slow process.

A number of reports have dealt with the effect of polar compounds, alcohol, a second soap, dyes, and amines on the critical micelle concentration (C.M.C.) (1, 6, 7, 15, 18) and have shown that the C.M.C. decreases upon the addition of long-chain soaps and alcohols, owing to the formation of mixed micelles. Except for a small table (10) which contains final equilibrium values of the effect of added hydrocarbons on C.M.C., no data are available concerning the change in C.M.C. with time upon the addition of a hydrocarbon or the effect of increment addition of hydrocarbons. Recently, Ralston and Eggenberger have found a small but definite decrease in C.M.C. in the presence of benzene and hexane by conductivity studies (15).

EXPERIMENTAL

A rather simple method, based on one discussed briefly by Hartley (4) and applied to gelatin and to soap systems (2, 16), has been used here to follow changes in the C.M.C. in the presence of added hydrocarbons. Essentially, this method involves the observation of a change in the color or fluorescence of a dye solution visually or spectrophotometrically. This change in color of the dye occurs at the C.M.C., and it is this property which makes it possible to follow various external effects with relative ease.

The dyes used for the anionic soaps were pinacyanol chloride and anisolein. The fatty acid soaps were prepared by fractionation of the ethyl esters of the corresponding fatty acids, followed by saponification and repeated recrystallization. The sodium alkyl sulfonates were those used previously (6, 7). All soap-water solutions (alkali added to pH 8.0) were made up by weight such that the concentration of the soap was just above the C.M.C., the benzene was then added, the tubes sealed off, and the samples shaken for as long as 300 hr. Titration with dye solution to determine the C.M.C. was then carried out. The dyes used were so chosen because, in addition to having a charge opposite to that of the long-chain soap ion, they were virtually insoluble in benzene, and thus any color changes observed would not be masked by solubility of the dye in the hydrocarbon. Original dye concentrations were such that $6 \pm 1 \times 10^{-5}$ *M* was the dye concentration after titration.

---

[1] Address: Division of Agricultural Biochemistry, University of Minnesota, St. Paul, Minnesota.

DATA

The data showing the change in C.M.C. at 25°C. with time upon addition of 0.15 g. benzene to 100 g. of 0.008 *M* potassium myristate are plotted in figure 1. Titrations were made with dye solutions containing 1.5 g. benzene per 1000 g. of dye solution. The solubility of benzene has been determined by light scattering to be 1.82 g. per liter of water at 25°C. The present technique has not as yet proven to be sufficiently sensitive to allow more than a qualitative statement as to the time necessary to reach equilibrium, but it has been noticed in these experiments that various soaps require different times; usually the more soluble soaps require less time.

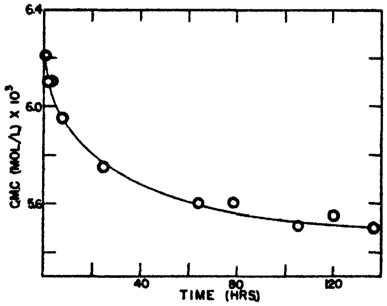

FIG. 1

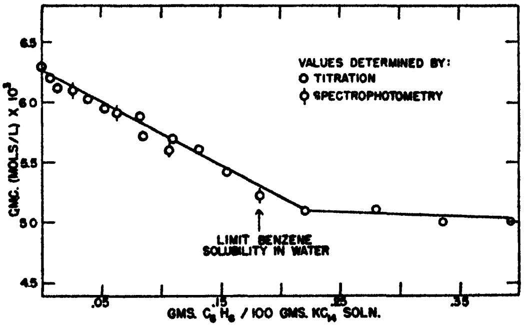

FIG. 2

FIG. 1. Change of critical micelle concentration of potassium myristate with time upon addition of 1.5 g. benzene per 1000 g. of soap solution (T = 25°C.)

FIG. 2. Change of critical micelle concentration of potassium myristate upon addition of benzene.

In figure 2 the effect of increment addition of benzene on the C.M.C. of potassium myristate is shown. Initially, these solutions contained larger amounts of benzene, and the values of added benzene in figure 2 have been corrected for the addition of the small amount of dye solution used in titration. Most of the points on this curve were determined by visual observation of changes in color and fluorescence. To check the accuracy of the titrated points, a number of the C.M.C. values were determined spectrophotometrically by a method similar to that used previously (2). The two sets of values were found to check reasonably well and to fall on the same curve.

A linear decrease in the C.M.C. of potassium tetradecanoate at 25°C. is observed upon the addition of hydrocarbon up to about 2.1 g. benzene per 1000 g. of soap solution, a value somewhat larger than the limit of solubility of benzene in water (1.82 g. per liter). At this point the C.M.C. remains almost constant and changes by only a few per cent up to 4.0 g. benzene per liter. Similar curves were obtained for potassium dodecanoate, potassium decanoate, and potassium octanoate, all at 25°C. It was noted that the more soluble the soap (the higher the C.M.C.), the smaller was the change observed upon the addition of benzene until, in the case of potassium octanoate, the decrease in C.M.C. amounted to only a few per cent. Similar data have been obtained for a series of sodium alkyl sulfonates, as seen in table 1. These data are equilibrium values for all points given in the tables, and are averages of duplicates which were measured at time intervals of approximately 100 hr. The C.M.C. values of the alkyl sulfonates are essentially equal to those obtained by solubility–temperature (17), conductivity (19), and refraction (7) measurements. The percentage decreases in C.M.C. due to the presence of benzene as determined by the dye spectral method are somewhat smaller than those determined by the surface tension and interfacial tension methods (10). It should be noted that the actual decreases in the case of the sodium alkyl sulfonates are in agreement within a few per cent in comparing surface tension–interfacial tension and dye spectral methods. The small variations observed are probably functions of the methods used, for the C.M.C. of the alkyl sulfonates varies somewhat depending on the method of measurement.

TABLE 1

Effect of added hydrocarbon on critical micelle concentrations as determined by titration with pinacyanol chloride

(2.2 g. benzene per liter of soap solutions; 25°C.)

SOAP	C.M.C.		DECREASE
	No benzene added	Benzene added	
	Potassium fatty acid soaps		
	moles/liter	*moles/liter*	*per cent*
Octanoate	0.395	0.384	(3)
Decanoate	0.100	0.093	7
Dodecanoate	0.024	0.020	13
Tetradecanoate	0.0063	0.0051	19
	Sodium alkyl sulfonates		
Decanoate	0.038	0.034	10
Dodecanoate	0.0092 (33.5°C.)	0.0075	19
Tetradecanoate	0.0025 (42.5°C.)	0.0018	28

DISCUSSION

An increase in size and weight of a hydrocarbon-saturated micelle has been calculated by Mattoon from his extensive x-ray data on soap solutions (13). It is obvious that mixed micelles of the type observed in soap–soap and soap–alcohol systems, in which polar groups of both soap and alcohol are oriented toward the water and the hydrocarbon tails toward the inner portion of the micelle, are completely different from soap–hydrocarbon systems in which the soap is oriented as above but the hydrocarbon is in the hydrocarbon-like interior of the micelle (3, 8). The much larger decrease in C.M.C. reported in the case of mixtures of soap and alcohol (1, 15) and soap and soap (6) is not observed here upon the addition of benzene to soap solutions. The small decrease observed in C.M.C. must be due to the benzene, which is originally solubilized at soap concentrations above the C.M.C. (before titration with dye solution). Since an extremely small amount of benzene, not determinable because the distribution of benzene between micelle and water is not known in the vicinity of the C.M.C., is in the micelle, only small decreases in C.M.C. can be expected. This agrees with the observed changes in C.M.C. Larger decreases in C.M.C. should not be expected for, as pointed out by McBain (11), the complete colloid property (maximum solubilization of dye) of potassium laurate (C.M.C. = 0.025 *M*) is not reached until about 0.1 *M*. The observed decreases in C.M.C. in those cases where long-chain alcohols or less soluble soaps are the additives is probably due to an enhancement in the attraction forces (short-range van der Waals forces) necessary to overcome the long-range electrostatic repulsive forces. An equilibration of these forces is necessary for micelle formation. The addition of a hydrocarbon to a soap solution in the region of the C.M.C. apparently has no or only a minor effect on these forces, a result which is in accord with the small decrease in C.M.C. noted.

SUMMARY

1. Increment addition of benzene to soap solutions causes a very small decrease in the critical micelle concentration. Equilibrium values were obtained in certain systems only after 100 hr. or more.

2. The largest percentage decrease in critical micelle concentration was noted in those systems in which the soap has the lowest critical concentration.

3. The small decreases upon the addition of hydrocarbons, as compared with those which occur when polar compounds are the additives, can be explained on the region of the micelle occupied by these additives as well as on their contribution to the forces involved in micelle formation.

REFERENCES

(1) Corrin, M. L., and Harkins, W. D.: J. Chem. Phys. **14**, 642 (1946).
(2) Corrin, M. L., Klevens, H. B., and Harkins, W. D.: J. Chem. Phys. **14**, 480 (1946).
(3) Harkins, W. D., Mattoon, R. W., and Mittelmann, R.: J. Chem. Phys. **15**, 763 (1947).
(4) Hartley, G. S.: *Aqueous Solutions of Paraffin-Chain Salts*. Hermann et Cie, Paris (1936).
(5) Heller, W., and Klevens, H. B.: J. Chem. Phys. **14**, 567 (1946).
(6) Klevens, H. B.: J. Chem. Phys. **14**, 742 (1946).
(7) Klevens, H. B.: J. Phys. & Colloid Chem. **52**, 130 (1948).
(8) Klevens, H. B.: J. Am. Oil Chemists' Soc. **26**, 456 (1949).
(9) Lambert, J. M., and Busse, W. F.: J. Chem. Phys. **16**, 847 (1948).
(10) Lingafelter, E. C., Wheeler, O. L., and Tartar, H. V.: J. Am. Chem. Soc. **68**, 1490 (1946).

(11) McBain, J. W.: *Advances in Colloid Science*, Vol. I. Interscience Publishers, Inc., New York (1942).

(12) McBain, J. W., and Johnson, K. E.: J. Am. Chem. Soc. **66**, 9 (1944).

(13) Mattoon, R. W., Stearns, R. S., and Harkins, W. D.: J. Chem. Phys. **16**, 644 (1948).

(14) Powney, J., and Addison, C. C.: Trans. Faraday Soc. **34**, 372, 635 (1938).

(15) Ralston, A. W., and Eggenberger, D. N.: J. Am. Chem. Soc. **70**, 983 (1948).

(16) Sheppard, S. E., and Geddes, A. L.: J. Chem. Phys. **13**, 63 (1945).

(17) Tartar, H. V., and Wright, K. A.: J. Am. Chem. Soc. **61**, 539 (1939).

(18) Ward, A. F. H.: Proc. Roy. Soc. (London) **A176**, 412 (1940).

(19) Wright, K. A., Abbott, A. D., Sivertz, V., and Tartar, H. V.: J. Am. Chem. Soc. **61**, 549 (1939).

METHOD OF MEASURING THE ABSOLUTE POTENTIAL OF AQUEOUS HALF-CELLS

WALTER A. PATRICK and CLARENCE L. LITTLER

Department of Chemistry, The Johns Hopkins University, Baltimore, Maryland

Received November 3, 1949

The experimental and theoretical difficulties associated with the absolute potential of single electrodes have led most people to the conclusion that the problems are fundamentally insoluble. In fact, some go so far as to assert that even the concept of such a potential is incapable of thermodynamic expression (8). The purpose of this paper is to present a new method of measuring such potentials, which is based upon the following sequence of ideas: When silver metal is immersed into a solution containing silver ions, the latter, if present in concentrations exceeding a certain critical value, pass from the solution to the metal, until the accumulative positive charge on the metal and the negative charge in the solution stop further transfer of ions. That is to say, an initial potential difference exists between metallic silver and solutions containing silver ions which causes a transfer of matter at the interface, until the so-called Helmholtz layer is formed. If an area of metallic silver sufficiently large to accommodate 1 gram-atom of silver ions in the form of such a layer were brought in contact with a very large volume of solution, it would be possible to write down a numerical value for the energy associated with such a change of state. In this manner, it is possible to characterize thermodynamically a single electrode potential.

The Helmholtz layer may be formed by reactions of the electrode with either cations or anions. For example, if metallic silver be immersed into a solution containing chloride ions, the metal acquires a negative charge owing to the formation of silver chloride, the layer at the interface now consisting of electrons in the metal and the cations initially associated with the chloride ion. The formation of such layers is found to obey the ordinary thermodynamic rules, and definite changes of enthalpy and entropy are associated with such transfers of matter. Furthermore, following the usual criteria of equilibria, it is possible to select a particular concentration of the aqueous reactive ion such that no layer is formed. A solution of such ion concentration, or partial molar ion entropy, should exhibit zero potential against the metal electrode.

Experimentally a study is made of the transient current between a stationary electrode immersed in an aqueous solution containing a reactive ion and a similar electrode freshly dipped into the same solution. This current and its direction measure the flow of electrons necessary for the formation of the Helmholtz layer. As will be shown, not all electrodes and solutions exhibit these phenomena in such a manner as to allow for the change to be definitely characterized. The changes may be obscured by overlapping kinetic disturbances. If, however, a few or even a single electrode reaction may be formed that answers to a reversible thermodynamic equilibrium, all single potentials may be represented on an absolute scale. It must also be noted that the selection of such a scale, valid for various temperatures, demands a knowledge of the electrode reaction.

The first attempts to find a single potential were those of Lippmann (10) and others with the capillary electrometer and dropping mercury electrode. Later, Bennewitz and Schulz (3) scraped one silver electrode of a pair connected through a galvanometer and observed the direction of current in solutions of different concentrations of silver ion. Bennewitz (2) confirmed his previous value by measuring the interfacial tension of mercury in different concentrations of mercurous nitrate. Billitzer (5) observed the motion of fine metallic particles suspended in a solution subjected to a potential gradient, while Garrison (7) observed the motion of a silver needle under similar conditions. Andauer (1) measured the calomel half-cell potential with a second electrode in the air above the solution.

These direct experimental methods led to one of two values for the single potential of the normal calomel half-cell. The capillary electrometer and dropping electrode gave the value −0.56 v., while the methods of Bennewitz, Billitzer, and Garrison all yielded approximately +0.19 v. Andauer reported first one and then the other of these two, widely divergent potentials.

Indirect methods have also been applied to obtain the value of the single potential. For example, a hypothetical mixture of gaseous metal ions, electrons at an energy level lower than gaseous electrons by an amount equal to the work function, and liquid water molecules constitutes an unstable system. Two changes are possible producing more stable states: the ions may unite with the electrons and condense to form the metal, or the ions may neutralize their charge by clustering about themselves the polar water molecules. The single potential is the difference between these two energy paths. All the necessary energy changes are known for the calculation of the single potential except the hydration energy of the ions.

Born (6) has pointed out that the energy of hydration of a gaseous ion should be given by the expression

$$\Delta E = \frac{ze^2}{2r_e} \cdot \frac{D-1}{D}$$

where r_e is the ion radius and D the dielectric constant. Debye has shown that one would not expect this to hold except where the dielectric does not approach saturation in the vicinity of the ion.

Webb (13) has developed the hydration energy as a sum of the electrical work of charging an ion in a molecular medium plus a term due to the compression of the solvent in the vicinity of an ion. Makishima (11) has used Webb's results to calculate single potentials and reports −0.51 v. for the normal calomel electrode.

Philpot (12), while investigating the nature of the diffuse double layer, calculated a single potential value of silver in 0.1 *N* sodium chloride as −0.47 v.; this would place the potential of the normal calomel electrode at −0.59 v.

Bernal and Fowler (4) calculated the individual hydration energies of ions in terms of the mutual potential energy of ion and water molecules, the changed orientation of water in the vicinity of an ion, and the energy of the coördination sphere. They assumed that potassium and fluoride ions, having the same radii and the same mutual potential energy, should have the same hydration energy. They then split the known hydration energy of the ion pair and used the value as the starting point for calculating hydration energies of other ions. Although the authors made no calculations of potential, an acceptance of their hydration energies leads to a single potential of +0.18 v. for the calomel electrode.

Recently Latimer (9) has shown that the addition of an arbitrary constant to the radii of the positive ions, and another smaller one to the negative ions, leads to agreement with the Born equation with the dielectric constant taken as that of normal water. He then calculated the single potential of the normal calomel electrode to be −0.50 v.

It is curious indeed that all determinations, both theoretical and experimental, have led to normal calomel electrode potentials in agreement with one or another of the two widely separated values −0.56 v. or +0.19 v. Nearly all of the methods so far proposed are open to objections. The direct determination by electrocapillary curves will subsequently be shown to be in error, owing to the presence of complex mercuric ions, which have heretofore been lost sight of. The dropping mercury electrode gives erroneous results, owing to its operation under conditions that do not allow the mercury sufficient time to form its equilibrium layer.

The following method has been used to determine the single potential of the calomel electrode: A cathode-ray oscillograph, with triple amplification of the input signal, proved to be satisfactory for the detection of these transient currents. Using this device, deflections were observed for a large number of electrodes, and reversal points were determined for several systems. The potentials of electrodes in solutions of proper concentration for reversal of the direction of deflection were then measured against a calomel half-cell. The overall potential was taken to be the single potential of the calomel electrode. The reversal point with different electrodes occurred at approximately the same potential, though absolute concordance was not obtained.

APPARATUS AND MATERIALS

The cathode-ray oscillograph was an R.C.A. instrument, type T.M.V. 122B. It has been modified for the detection of direct current potentials by a previous investigator in this laboratory. The essential changes in design are shown in figure 1. The heavy lines are a reproduction of part of the schematic diagrams

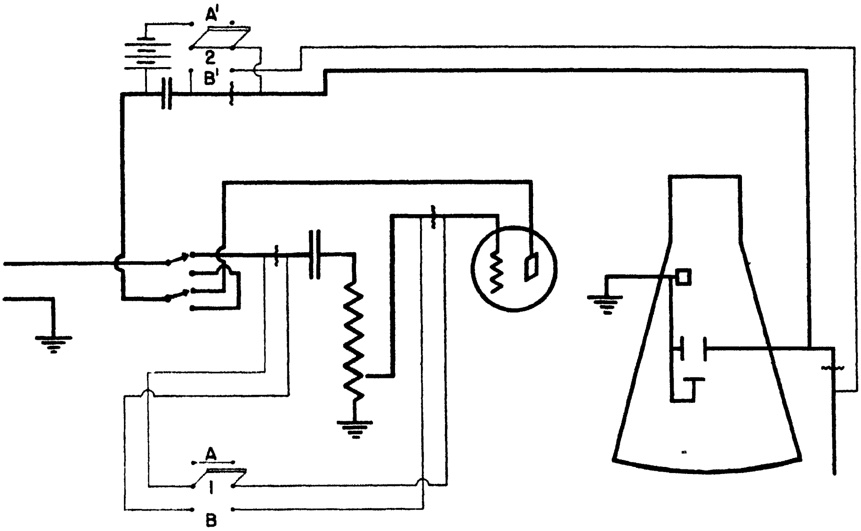

FIG. 1. Diagram of the cathode-ray oscillograph

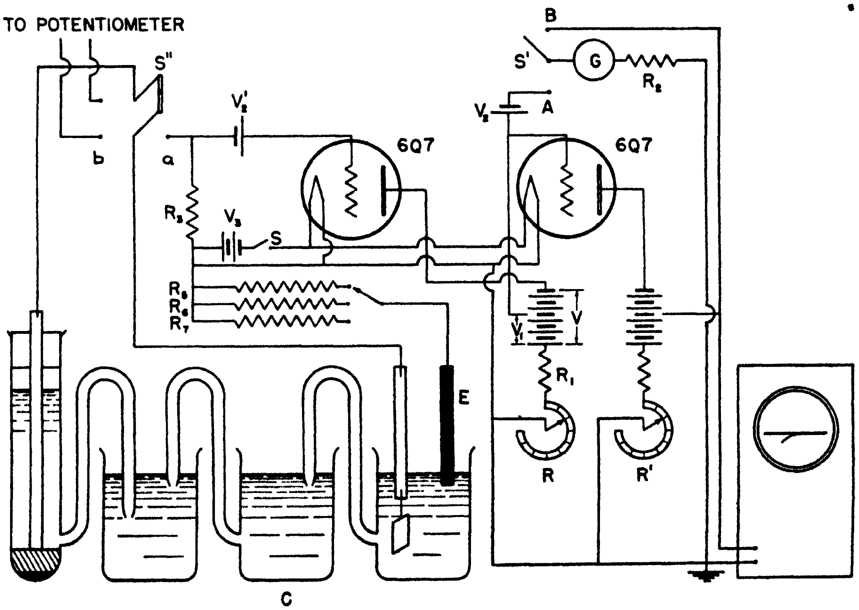

FIG. 2. Complete wiring diagram for the experimental set-up

furnished with the instrument, while the light lines show the modifications introduced. Breaks in the original circuit are shown by wavy lines. When switch 1 is in position A, the condenser and gain control are by-passed. When it is in position

B, the connections are the same as in the original instrument. When switch 2 is in position A′, the vertical beam shift is disconnected and the condenser by-passed. A battery of 180 v. serves to keep the beam in the center of the screen. When the switch is in position B′, the original connections are restored. The present work was done with the switches in positions A and A′, respectively, and the vertical amplifier of the instrument on. The saw-tooth sweep was used on the horizontal plates with a frequency of 120 cycles per second. The input signal was amplified by an auxiliary amplifier before connection with the oscillograph.

The complete wiring diagram for the experimental set-up is shown in figure 2. All equipment, including the cells, was carefully shielded. The method of operation was as follows: After closing switch S and allowing some time for the filaments to get hot, switch S′ was thrown to position A and the resistance R varied until the galvanometer G showed no deflection. S′ was then thrown to position B and R′ adjusted until G showed no deflection. S″ was thrown to a, connecting the fixed electrode to the grid of the amplifier. The identical electrode E could be connected through 2, 5, or 10 megohms. These resistances had to be large compared to that connecting the grid to ground, or there would be a permanent shift of the oscillograph beam when the parallel circuit was completed by immersing E. This indicated that a slight current was flowing between filament and grid at all times in spite of the negative potential of the latter. With the ratios shown, however, no permanent shift could be detected; yet the deflections produced by electrodes far removed from the reversal point were sufficient to throw the beam completely off the oscillograph screen, even with the 10-megohm resistor. Calibration with permanent applied E.M.F.'s between a and E gave the following results:

RESISTANCE IN OHMS	MILLIVOLTS PER MILLIMETER DEFLECTION
2×10^6	1.0
5×10^6	2.3
10×10^6	4.5

This varied somewhat, however, with the aging and replacement of batteries.

Switch S″ of figure 2 could be thrown to position b and the potential of the stationary electrode measured against a normal calomel half-cell with a potentiometer. An intermediate bridge of 1 *N* potassium nitrate was placed at C to prevent difficulties through the formation of insoluble chlorides. This introduced an additional junction potential, but the overall accuracy of the method did not justify any attempts to determine its magnitude.

A Leeds & Northrup type K potentiometer was used at first, but was later replaced by the ordinary student type.

Solutions were prepared with C.P. salts and water that had been redistilled from a phosphoric acid–potassium permanganate mixture in a Pyrex still. Since the solutions had to stand many hours in glass during the course of a determination, no further precautions were deemed worth while.

Electrodes were prepared from the purest metals obtainable and always from the same piece to avoid permanent differences of potential due to different structure or differing amounts of impurities. In all cases where a reversal of deflection was observed with a given metal, four or five electrodes were used, with frequent exchanges of stationary and moving electrodes to assure that no spurious reversal was being observed.

EXPERIMENTAL

The validity of the method was first tested qualitatively by observing the deflections of silver electrodes in strong silver nitrate solution and zinc electrodes in zinc sulfate solution. One electrode of the metal under consideration was immersed and connected to the high side of the amplifier. Another identical electrode was connected through the 10-megohm resistance to ground and suddenly dipped into the solution. In agreement with the initial hypothesis, the observed oscillograph deflections were in opposite directions and in accord with the charge one might expect to be present on the stationary electrode, i.e., as if zinc acquired a negative charge in solution and silver a positive charge. The deflections died out rapidly in both cases, a single sweep being sufficient for most of the potential difference to disappear.

TABLE 1

Current deflections between moving and stationary electrodes

SYSTEM	REVERSAL POINT E_H
Zn, Zn^{++}	No reversal; electrode always negative
Cd, Cd^{++}	No reversal; electrode always negative (?)*
Tl, Tl^{+}	No reversal; electrode always negative
Co, Co^{++}	No reversal; electrode always negative
Ni, Ni^{++}	No reversal; electrode always positive
Sn, Sn^{++}	No reversal; electrode always negative
Pb, Pb^{++}	No reversal; electrode usually negative (?)
Cu, Cu^{++}	No reversal; electrode always positive
	volts
Ag, Ag_2O, NH_4OH	−0.46 ± 0.01
Ag, $AgIO_3(s)$, KIO_3	−0.47 ± 0.01
$\left.\begin{matrix}\text{Au}\\ \text{or}\\ \text{Pt}\end{matrix}\right\}$, Fe^{++}, Fe^{+++}, SO_4^{--} H^+	−0.47 ± 0.01
$\left.\begin{matrix}\text{Au}\\ \text{or}\\ \text{Pt}\end{matrix}\right\}\begin{matrix}\text{quinhydrone}\\ ,\\ H^+, Na^+, CH_3COO^-\end{matrix}$	−0.47 ± 0.01
Au, $\begin{matrix}K_4Fe(CN)_6\\ K_3Fe(CN)_6\end{matrix}$ KNO_3	−0.46 ± 0.01

* The (?) on the cadmium and lead systems indicates that the results were occasionally erratic.

Following this encouraging result a large number of electrode systems (see table 1) were investigated in an attempt to find those that would show a reversal of deflection with change in solution concentration. When such a system was found, the stationary electrode was used as one electrode of a cell having a normal calomel electrode as the other terminal and the overall potential was measured with the potentiometer.

Certain characteristics of behavior were found to be common to nearly all of the systems studied. The speed of immersion or the area touching the solution had no observable effect on the magnitude or duration of the deflection. A sudden increase in the interfacial area after the initial immersion would cause a slight momentary deflection, but of much lower magnitude than that observed initially. Shaking an electrode caused "motor electric" potentials that were much smaller than the deflection on immersion. Some electrodes such as nickel and cobalt gave relatively permanent residual potential differences, due undoubtedly to their hardness and apparent lack of reversibility. All systems except those reversible to anions showed relatively permanent deflections when the concentration of metal ion dropped below 10^{-5} *M*. In solutions approaching saturation in fairly soluble salts the deflections frequently could not be detected. With zinc, however, deflections were readily apparent even in saturated solution.

ELECTRODE SYSTEMS STUDIED

The Zn–$ZnSO_4$ *couple*

Cast zinc electrodes were rubbed with fine emery before use. In all concentrations of zinc ion deflections were very strong, the beam being thrown completely off the screen. Return to the original base line was rapid in solutions stronger than 10^{-5} *M*, being complete in one or two sweeps of the oscillograph. Highly diluted solutions led to smaller residual potential differences after the initial large deflection that would sometimes require nearly a minute to die out. The large jump was always in such a direction as to indicate a negative charge in the stationary electrode, but residual potentials were erratic, lying on either side of the base line. Heating an electrode before use to assure a heavy oxide coating had no effect upon the nature of the deflection.

The Cd–$Cd(NO_3)_2$ *couple*

Cast cadmium electrodes buffed with emery were also used in this determination. In solutions of concentration less than 1 *N* there was a rapid deflection indicating a negative charge on the stationary electrode, followed immediately by a relatively permanent potential difference of opposite sign that died out slowly. As the solution was made more concentrated, the initial deflection of opposite sign was apparent. This die-out constitutes an actual reversal, since there was no growth of a *rapid* deflection of opposite sign. The indication was merely that high concentration permitted adjustment of potential more rapidly than the oscillograph could follow.

The Tl–$TlC_2H_3O_2$ *couple*

This system was tried only in 1 N solution. Deflections were always such as to indicate a negative charge on the stationary electrode.

The Co–$CoSO_4$ *couple*

Tested in 0.1 N, 1.0 N, and saturated solutions this couple always showed a negative charge. Return to equilibrium was always rapid, yet the potential in saturated solution was $E_H = +0.200$ v., a value far from the reversible potential.

The Ni–$NiSO_4$ *couple*

Nickel electrodes were prepared from heavy nickel wire and buffed with emery before use. The potential of such an electrode in 1 N nickel sulfate was found to be $E_H = -0.07$ v., a value far more noble than the reversible potential. Deflections also were relatively permanent, lasting 15–20 min. before equilibrium was attained. In all cases deflections were in such direction as to indicate a positive charge. Owing to the apparent irreversibility of this system the positive potential was not considered significant.

The Sn–Sn^{++} *couple*

Both stannous chloride in hydrochloric acid and stannous perchlorate were used as test solutions. In all concentrations tin electrodes showed a consistently negative charge.

The Pb–$Pb(NO_3)_2$ *couple*

Erratic results were obtained with this system. Emery-buffed electrodes sometimes made the stationary electrode appear positively charged, while those that were merely washed and wiped briskly with a towel gave the opposite effect. This was the first evidence that the preliminary treatment of the dipping electrode could alter the result obtained. It was not consistent in the case of lead, however. Regardless of treatment of the dipping electrode, the stationary one appeared negative about 80 per cent of the time. No method could be devised to eliminate the variability of this soft metal and produce a reproducible surface, so experiments were discontinued.

The Ag–Ag^+ *couple*

This system was first tested in silver iodide–potassium iodide solution because the potential could be raised above that of lead. Silver iodide was precipitated from silver nitrate with potassium iodide and, after washing, was left in distilled water for 2 weeks. Crystals of potassium iodide were dissolved in this solution before use. In spite of the low silver-ion concentration, equilibrium was established rapidly as long as the iodide-ion concentration was reasonably high. Apparently the system behaved reversibly with respect to iodide ion, even though the electrodes were initially free of silver iodide.

Silver electrodes were prepared from heavy silver wire. The wire was covered with a thin oxide layer when first obtained. This was reduced by heating in a flame to a dull red heat, leaving a white layer of silver on the electrode. After being used once, the electrodes were washed in distilled water and then dipped in nitric acid to remove any iodide remaining on the surface. A second washing, followed by heating, restored a pure silver surface.

Deflections indicated that the stationary electrode was negatively charged in all concentrations of iodide ion. This served to confirm the opinion that silver was probably negatively charged.

Silver electrodes were then tried in silver chloride–1 *N* chloride and finally in 0.1 *N* silver nitrate. The stationary electrode was negatively charged in the former solution and positively charged in the latter. This indicated definitely that a reversal point lay somewhere between these extremes.

A semisaturated silver oxide solution, prepared by boiling silver oxide in water for 20 min., was found to charge silver positively. The potential initially was $E_H = -0.59$ v. Dilute ammonia solution was added drop by drop and the deflections observed. In this experiment electrodes were reactivated by heating to red heat only, since the substances forming the ion layer are all decomposed or driven off by heat. In addition to the rapid initial deflection there was always a small residual potential difference that interfered with observation as the principal deflection became smaller. Nevertheless it was possible to observe a definite reversal of direction of deflection in the potential range $E_H = -0.45$ to -0.47 v.

Since the above solution was essentially the same as that used by Bennewitz and Schulz, who report the same reversal point, it appeared desirable to select one in which total salt concentration would be higher and thus eliminate the possible objection that deflections might be due to a zeta potential. A reversal was obtained successfully in a solution containing silver iodate and potassium iodate, although it was more difficult to observe because of relatively large, permanent potential differences. The potential at reversal appeared to lie in the range $E_H = -0.47$ to -0.48 v.

The $Hg-Hg_2^{++}$ *couple*

Gold wires were fused to a bead on the tip and sealed into glass tubing. The beads were dipped into mercury that had been purified with great care. The amalgamated beads so obtained were transferred rapidly from mercury vessel to test solution to avoid as much as possible the formation of oxide and diffusion of gold to the surface. The solutions tested were mercurous chloride–potassium chloride, mercurous iodide–potassium iodide, and mercurous bromide–potassium bromide. The halides gave uniform deflections in such a direction as to indicate that the stationary electrode was positively charged. Even in a solution saturated with potassium iodide the deflection was not changed.

The $Fe^{++}-Fe^{+++}$ *couple*

A solution of ferrous ammonium sulfate was acidified with sulfuric acid and left in contact with zinc for a few minutes to ensure removal of oxidized iron. A large gold foil was used as the stationary electrode and No. 22 gold wire as the dipping electrode. Some difficulty was encountered in the reactivation of such electrodes after use. Heating in a flame to redness leaves no appreciable layer of finely divided gold, as in the case with silver or copper in hydrogen. Attempts to use this method without modification led to fast fleeting deflections, too fast for the camera to record, which were in such direction as to indicate that the stationary electrode was negatively charged down to a potential of $E_H = -0.73$ v., attained by adding first ferric sulfate and finally potassium dichromate. Since these were not full-bodied deflections, such as had been obtained previously, a study was made of the effect of different electrode treatment. As with other metals, scratching with emery raised the potential at reversal to a value above that for silver. Washing and wiping without heating gave a reversal at -0.47 v., in agreement with silver, but the possibility of ions from the solution being retained was too great to justify this procedure. To remove adsorbed ions the electrodes were washed, dipped in aqua regia, rinsed, heated to redness, and then rubbed gently on a soft cloth. This sufficed to insure a clean surface that was unscratched and yet the fleeting deflections were overcome. With this treatment the reversal point lay between -0.47 and -0.48 v.

The reversal with this system could be attained from either side by using stannous chloride to raise the potential after lowering with ferric sulfate. The presence of stannous chloride caused some semipermanent potential difference, however, that tended to obscure the exact point of reversal when changing toward less noble potentials.

The quinone–hydroquinone | gold couple

A saturated water solution of quinhydrone was acidified with acetic acid, and sodium acetate was used to lower the hydrogen-ion concentration. Reversal of deflection occurred at -0.47 ± 0.01 v. There was very little base-line shift with this system, equilibrium being attained quite rapidly. In any single determination it appeared possible to place the reversal point within a few millivolts, yet there was enough fluctuation between successive determinations and between different gold electrodes to introduce a greater degree of uncertainty. Platinum electrodes yielded essentially the same reversal point, but more often gave semipermanent potential differences that made observation difficult.

The $\mathrm{Fe(CN)_6^{4-}}$–$\mathrm{Fe(CN)_6^{3-}}$ | Au *couple*

A 1 *N* potassium nitrate solution was used as a supporting electrolyte in this determination; 0.1 *N* solutions of potassium ferrocyanide were added in small amounts, 0.5–1.0 ml. to 30 ml. of the potassium nitrate solution. The reversal point was established at $E_H = -0.46 \pm 0.01$ v. This system was the most perfect one studied from the standpoint of rapid attainment of equilibrium. Reversal could be obtained by shifting the potential in either direction, and great accuracy was prevented only by lack of a perfectly reproducible method of reactivating electrodes. A typical set of photographs of deflections is shown in figure 3. They illustrate the gradual decrease in magnitude of deflection with change in the potential, the shift through zero, and the build-up on the opposite side.

The behavior of fresh mercury surfaces against halide solutions appears anomalous, for, from the absolute potential of the calomel solution (+0.19 v.), one should expect a negative charge on the metal. However, the initial transient current as detected by the oscillograph indicates a positive charge on the mercury. This action may be explained by assuming the initial effect to be a reduction of the adsorbed mercury complexes which is subsequently followed by a slower re-formation of the same. The situation may be approximated by means of the following equilibria:

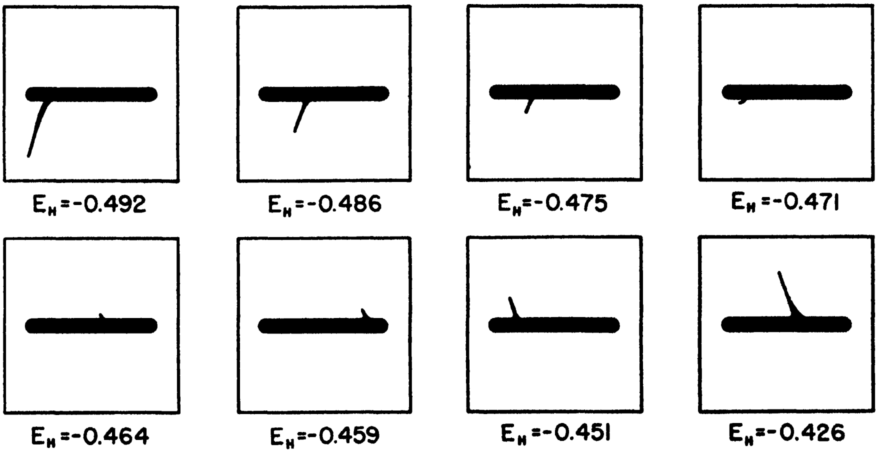

$E_H = -0.492$ $E_H = -0.486$ $E_H = -0.475$ $E_H = -0.471$

$E_H = -0.464$ $E_H = -0.459$ $E_H = -0.451$ $E_H = -0.426$

FIG. 3. Typical set of photographs of deflections

$$Hg_2Cl_2 \rightleftarrows Hg_2^{++} + 2Cl^- \qquad K = 1.1 \times 10^{-18}$$

$$Hg_2^{++} \rightleftarrows Hg + Hg^{++} \qquad K = 1/80$$

$$HgCl_4^{--} \rightleftarrows Hg^{++} + 4Cl^- \qquad K = 1 \times 10^{-16}$$

from which it follows that the $HgCl_4^{--}$ ion concentration in 1 *N* calomel solution is of the order of 10^{-4} mole per liter. It is to be noted that the latter concentration is 10^{14} times as great as the mercurous-ion concentration. In the adsorbed layer of the complex the initial reduction must take place, and this reduction is indicated by the oscillograph.

The presence of such high concentrations of the mercuric complexes is also responsible for the failure of the capillary electrometer to measure absolute potentials correctly. This latter instrument is essentially a concentration cell with diminishing concentration of the mercury complex in the capillary as the polarization potential is increased. An accurate evaluation of the effect would require an exact knowledge of the stability of the complexes as well as the transference numbers of the same. In other words, one should know whether the complex is $HgCl_3^-$, $HgCl_4^{--}$, or $HgCl_6^{---}$, etc., the equilibrium concentrations, and their transference numbers before one could evaluate the potential of the concentration cell. It is hardly necessary to say that such knowledge is not available at present; furthermore such data are unnecessary, as long as we realize that the potential applied to a capillary electrometer does something more than merely change the interfacial surface energy. The latter change is associated with the reduction in concentration of the mercury complex. It is incorrect to assume that the electrical energy is equal to the change in surface energy.

The method used for obtaining the zero point in the present work appears to be less objectionable than any that has been employed heretofore. In addition, the results agree with the theoretical work, which has taken the most detailed account of the structure of the solvent medium. The results do not agree with the theoretical results of Born and Webb, both of whom treat the solvent as a continuous dielectric medium of unchanging properties. On the basis of the cited facts it is probable that the zero of single potentials actually lies near $E_H = +0.47$ v. rather than at $E_H = +0.28$ v., the value that has been most commonly accepted in the past.

There are two major objections that appear if one tries to interpret the present results as manifestations of electrokinetic potential: first, the magnitude of the deflections; second, the wide range of electrolyte concentrations used. With any electrode far removed from the reversal point the deflections indicate potential differences that are much greater than any known electrokinetic potentials. Furthermore the solution may greatly vary in ionic strength, with no apparent effect upon the reversal point. Electrokinetic potentials, on the other hand, are most sensitive to variation of ionic strength, practically disappearing in concentrated electrolyte solutions.

REFERENCES

(1) ANDAUER, M.: Z. physik. Chem. **125**, 135 (1927); **138**, 375 (1928).
(2) BENNEWITZ, K.: Z. physik. Chem. **125**, 114 (1927).
(3) BENNEWITZ, K., AND SCHULZ, J.: Z. physik. Chem. **124**, 115 (1926).
(4) BERNAL, J. D., AND FOWLER, R. H.: J. Chem. Phys. **1**, 515 (1933).
(5) BILLITZER, J.: Z. physik. Chem. **48**, 513 (1904); **51**, 166 (1905).
(6) BORN, M.: Z. Physik **1**, 45 (1920).
(7) GARRISON, A.: J. Am. Chem. Soc. **45**, 37 (1923).
(8) GUGGENHEIM, E. A.: *Commentary on the Scientific Writings of Willard Gibbs*, Vol. I, Chap. E. Yale University Press, New Haven, Connecticut (1936).
(9) LATIMER, W. M., PITZER, K. S., AND SLANSKY, C. M.: J. Chem. Phys. **7**, 108 (1939).
(10) LIPPMANN, G.: Ann. Physik **179**, 494 (1875).
(11) MAKISHIMA, S.: J. Chem. Soc. Japan **56**, 1192 (1935).
(12) PHILPOT, J. ST. L.: Phil. Mag. **13**, 775 (1932).
(13) WEBB, T. J.: J. Am. Chem. Soc. **48**, 2589 (1926).

ON THE CONCENTRATION DEPENDENCE OF THE RATES OF DIFFUSION OF MACROMOLECULES IN SOLUTION

An Investigation of Fractions of Polystyrene[1]

ANITA F. SCHICK AND S. J. SINGER[2]

Department of Chemistry, Polytechnic Institute of Brooklyn, Brooklyn, New York

Received October 27, 1949

I. INTRODUCTION

In investigations of the properties of asymmetric protein and polymer molecules in dilute solution, one is constantly made aware of the strong dependence upon concentration which most physical properties exhibit. Whether these are equilibrium properties, such as osmotic pressure, or kinetic properties, such as sedimentation rate, the appropriate parameters must be extrapolated to infinite dilution to be interpreted as constants characteristic of the single molecules. It has therefore been somewhat puzzling to note that while sedimentation rates are often strongly concentration dependent, diffusion rates are often not particularly so; and that while sedimentation rates always decrease with increasing concentration, as is easily understood, diffusion rates usually increase, but with certain systems decrease, with increasing concentration. The basis for explaining these facts was established by Beckmann and Rosenberg (2), who showed that the general diffusion equation developed by Onsager and Fuoss (18), when interpreted for the systems under consideration, contains the answer to the problem. Two factors contribute to the concentration dependence of the diffusion rate of macromolecules in solution: the thermodynamic factor, which usually, but not always, tends to increase it, and the hydrodynamic factor, which always decreases it, with increasing solute concentration. The relative magnitudes of these factors determine the variation of the diffusion rate. This hypothesis was tested experimentally by Singer (24) with a series of fractions of cellulose acetate in acetone by means of coöperative osmotic pressure, sedimentation, and diffusion measurements, and was found to hold within the experimental errors encountered. In order to verify the hypothesis more generally and contribute to a better understanding of its molecular basis, it is desirable to extend these investigations to more flexible molecules than cellulose derivatives, and to study the effects of different solvents on the various factors involved.

We have therefore investigated a series of four polystyrene fractions in butanone and carbon tetrachloride and another fraction in six solvents, by diffusion, viscosity, osmotic pressure, and sedimentation experiments.

---

[1] Taken in part from the thesis presented by A. F. Schick in partial fulfillment of the requirements for the Ph.D. degree at the Polytechnic Institute of Brooklyn, June, 1948. Presented before the 115th Meeting of the American Chemical Society, which was held in San Francisco, April, 1949.

[2] Present address: Gates and Crellin Laboratories, California Institute of Technology, Pasadena, California.

II. THEORETICAL

For a detailed account of the hypothesis under consideration, the reader is referred to the papers by Beckmann and Rosenberg (2) and Singer (24). It was shown that the diffusion constant in dilute solutions of large molecules can be given by the equation:

$$D_c = \frac{RT[1 + (2BM/RT)c]}{f_0(1 + k_s c)} \cong D_0(1 + k_D c) \tag{1}$$

in which D_0 is the diffusion constant and f_0 the molar frictional coefficient at infinite dilution; B is the coefficient of the quadratic term in the power series expressing the osmotic pressure as a function of concentration; M is the molecular weight of the solute (number-average for a polydisperse system), and c is its concentration; k_s is the empirical constant obtained from sedimentation experiments (equation 2 below), and k_D is the empirical constant obtained from diffusion measurements.

Three assumptions were made in deriving equation 1: (*a*) that the gradient of the free energy of dilution of the system is the driving force of the diffusion process; (*b*) that the molar frictional coefficient at a finite concentration in a given system is the same in sedimentation and diffusion; and (*c*) that the frictional coefficient at the concentration c is given by the equation:

$$f_c = f_0(1 + k_s c) \tag{2}$$

The first two assumptions are certainly reasonable, and can be tested by the accuracy with which equation 1 represents the data. Justification was found for the assumption of a linear increase of f with c in dilute solutions from the fact that much sedimentation data on polymer solutions seemed to indicate it, and from the theory of Burgers (5) predicting such a linear dependence in dilute solutions of spheres. Recently, however, Bueche (4) has developed a theory indicating that in very dilute solutions of large molecules f is proportional to $c^{1/2}$ and, at somewhat higher concentrations, to c. The exact nature of this dependence, while of considerable interest, is not vital to an experimental test of the quantitative dependence of k_D on the variations of osmotic pressure and frictional coefficient with concentration. Since the sedimentation data reported in this paper seem to satisfy equation 2 in the concentration range studied, we have continued to use the relation although we do not necessarily attach theoretical significance to it.

The value of B in solutions of macromolecules has been the subject of many theoretical investigations in the past few years. This parameter measures the departure of the free energy of dilution of the system from its ideal value. In the case of protein solutions away from the isoelectric point, electrostatic interactions and differential salt distributions contribute markedly to its magnitude (19). With nonionic polymer solutions in which there are small heats of mixing, the relatively large values of B which are often observed are due mainly to large entropies of dilution, which in turn are related to the large volume fractions occupied by the molecules in solution (8, 28). As is indicated in equation 1, in order to interpret k_D theoretically we must know the relation between B and k_s. For these polymer solutions, however, there has not yet been developed a comprehensive theory correlating B with the molecular dimensions of the solute and, in turn, with kinetic parameters such as intrinsic viscosity and k_s. Lacking this theory, we can say little more concerning the anticipated variation of k_s with B, hence k_D, with a change in the solvent other than that the two parameters should vary in the same direction. It develops that B increases somewhat more rapidly than k_s in the polystyrene solutions which we have investigated.

TABLE 1

*Characterization of polystyrene fractions**

FRACTION	$[\eta]_{but}$	$[\eta]_{tol}$	$s_0 \times 10^{13}$†	$D_0 \times 10^7$†	M_n	M_s
D-8.......	0.29	0.45	9.8	9.6	82,000	95,000
D-2..... ..	0.44	0.74	13.3	5.1	140,000	240,000
B-72-18....	0.80	1.46	20.0	3.3	480,000	560,000
B-72-9....	1.09	2.07	25.0	2.5	1,100,000	910,000
PSAF	1.22	2.25	2.73‡	0.50‡	770,000	680,000‡
			9.5§	0.96§		1,140,000§

* The results in the columns headed $[\eta]_{but}$, $[\eta]_{tol}$, and M_n, except for those obtained with fraction PSAF, were determined by Goldberg (9) or Goldberg, Hohenstein, and Mark (10). The viscosity measurements on the first four fractions in butanone were performed at 40.3°C., and in toluene at 30°C. PSAF viscosity determinations in butanone and toluene were made at 27°C.

† The sedimentation results were corrected to 27°C. by the usual procedure (27), while the diffusion constants were all determined at that temperature. The diffusion measurements of the first four fractions were performed in butanone solution.

‡ Determined in decalin solution.

§ Determined in ethylbenzene solution.

III. EXPERIMENTAL

A. Materials

Polystyrenes D-8 and D-2 are fractions of a solution-polymerized material which was prepared as follows: one hundred fifty grams of styrene which had been alkali-washed and vacuum-distilled was polymerized at 60°C. in the presence of 0.5 per cent benzoyl peroxide and 150 g. of toluene for 70 hr. The degree of conversion was 72 per cent and the intrinsic viscosity of the polymer in toluene at 28°C. was 0.45. The polymer was fractionated by Dr. A. Goldberg according to the procedure described by Goldberg, Hohenstein, and Mark (10). Polystyrenes B-72-18 and B-72-9[3] are fractions of an emulsion-polymerized material, the preparation and fractionation of which have been reported by Goldberg, Hohenstein, and Mark. Polystyrene PSAF is a somewhat more polydisperse fraction, refractionated from a solution-polymerized polystyrene fraction by the same methods used to obtain the polymers discussed above. The data characterizing these fractions are recorded in table 1.

---

[3] These fractions are designated e and c, respectively, in the paper by Goldberg, Hohenstein, and Mark (10).

The solvents were distilled from C.P. grade materials, and their boiling points, densities, and refractive indices agreed with the best recorded values (20).

B. *Molecular weight determinations*

The number-average molecular weights, M_n, of fractions D-8 and D-2 were determined by Goldberg (9) and those of fractions B-72-18 and B-72-9 by Goldberg, Hohenstein, and Mark (10) from osmotic pressure data obtained with the osmometer designed by Zimm and Myerson (29). That of fraction PSAF in butanone was determined in a similar manner. The osmotic pressure data for this fraction are graphed in figure 1.

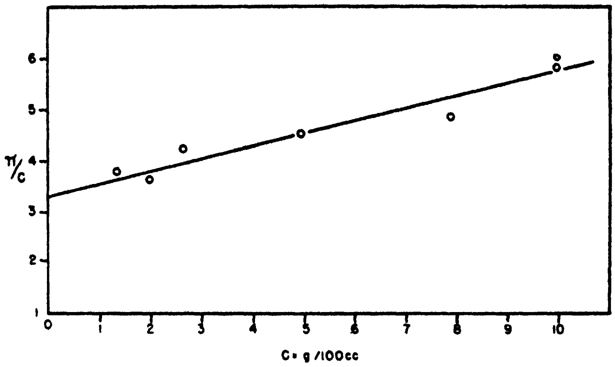

FIG. 1: Osmotic pressure data for fraction PSAF in butanone at 27°C. π is expressed in grams per square centimeter.

The molecular weights, M_s, obtained by combining sedimentation velocity and diffusion measurements were calculated by means of the Svedberg equation:

$$M_s = \frac{RTs}{D(1 - \bar{V}d)} \tag{3}$$

in which s and D are the sedimentation and diffusion constants extrapolated to infinite dilution, $\bar{V}$ is the partial specific volume of the solute, and d is the density of the solvent. The sedimentation experiments were performed in an air-driven ultracentrifuge of the Beams–Pickels type, the operation of which has been described elsewhere (24, 25).

C. *The diffusion apparatus*

The diffusion experiments were performed in all-glass cells, described by Stern, Singer, and Davis (26). In operating this cell the boundary between solvent and solution is created at a stopcock, and this boundary is then carefully raised by hydrostatic pressure into the optical chamber of the cell. The scale method of Lamm (16), in conjunction with a conventional optical system, was utilized for the observation of the refractive-index gradients in the diffusing systems.

The experiments were carried out in an apparatus designed to permit the simultaneous performance of several lengthy experiments. The thermostat bath in which three diffusion cells were mounted could be moved in a direction perpendicular to the stationary optical system so that one cell at a time could be moved into the optical path. The movement of the bath was designed to be as free of vibration as possible, and independent experiments on solutions of mannitol in water indicated that the motion of the bath did not disturb the diffusion process to any significant extent. A detailed description of the apparatus and its operation will be published elsewhere.

D. Calculation of the diffusion constant

The standard methods of calculation of the diffusion constants from free diffusion measurements as described by Lamm (16) were followed. For comparison, two values of the constant, the area–maximum ordinate value, D_A, and the second-moment value, $D_{2,0}$, were determined. These were obtained from the equations:

$$D_A = \frac{A^2}{4\pi t H^2} F^2 \tag{4}$$

$$D_{2,0} = \frac{\sigma^2}{2t} F^2 \tag{5}$$

In these equations A is the area, H the maximum ordinate, and σ the standard deviation of the diffusion curve at the time t after the start of diffusion. F is an apparatus constant, determined by various optical distances in a given experiment. The second-moment diffusion constant, under certain circumstances a weight-average value (11, 14), was utilized in calculating molecular weights by means of equation 3.

The value of t was in most cases a corrected value obtained in the manner followed by Stern, Singer, and Davis (26). $(A/H)^2$ and σ^2 were plotted against t', the time after the formation of the boundary between solvent and solution. Straight lines drawn through these points usually intercepted the time axis at some negative value, and the absolute magnitude of this time correction was then added to t' to give t. As has been observed frequently, the process of moving the solvent–solution boundary from the position of its formation into the optical part of the cell results in a slight disturbance of the boundary, which can be corrected for in the above-mentioned manner. Typical plots for the zero-time corrections are shown in figure 2.

The best criterion for the reliability of a given experiment is obtained when the experimental diffusion curves are transformed to a set of normal coördinates, as was suggested by Lamm (16). The normal coördinates X and Y are derived from the experimental coördinates z and Z, which are obtained from the scale photographs by the following equations:

$$X = \frac{Z}{2\sigma} \qquad Y = \frac{5\sigma Z}{\int Z dz} \tag{6}$$

This transformation eliminates the variables of time, concentration, and optical constants, and in a perfect experiment the experimental points obtained at different times will fall on the same normalized curve. The choice of the normalized ideal curve is arbitrary. We have followed the procedure of Beckmann and Rosenberg (2) in choosing a normal curve of 2.5 square units and maximum ordinate of 2. Examples of the normalized diffusion curves which we obtained are given in figure 3, in which the dashed curves represent the normalized ideal curves.

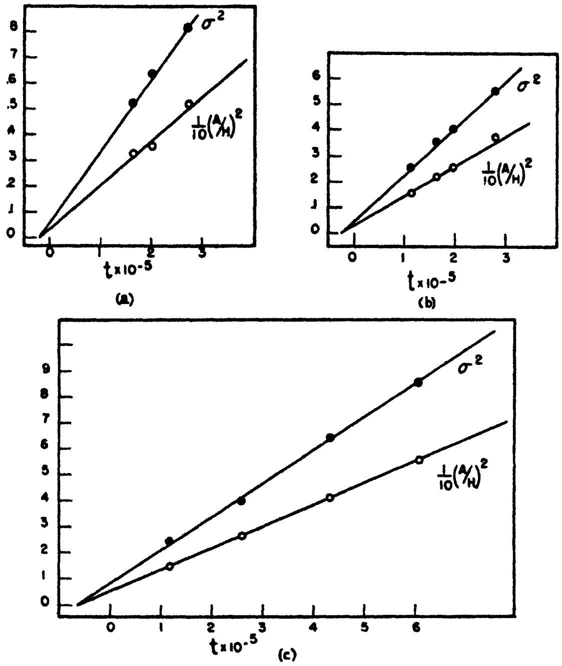

FIG. 2: Zero-time correction plots for (a) fraction D-8, (b) fraction D-2, and (c) fraction B-72-18, all in butanone.

E. The evaluation of k_D from diffusion data

The deviation of the experimental normalized curve from the ideal serves as a measure of the concentration dependence of the diffusion constant. Qualitatively, a positive concentration dependence is manifested by a displacement or skewness of the experimental curve toward the solvent side (to the left of the original boundary in figure 3), while the curves with a negative concentration dependence are displaced toward the solution side.

Quantitatively, the concentration dependence of the diffusion constant was calculated by two methods. The procedure suggested by Gralén (11) assumes a linear dependence of D upon c, while that of Beckmann and Rosenberg (2) does not introduce this assumption. The value obtained by the former method is given in terms of the normal coördinates by:

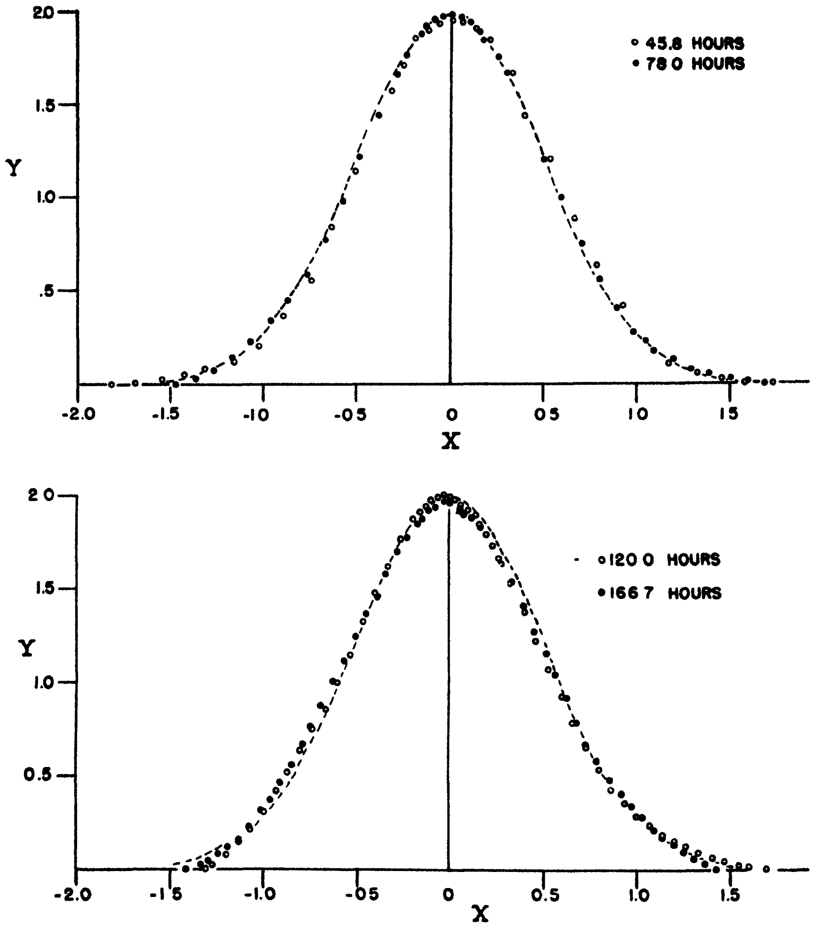

FIG. 3: Normalized diffusion curves for (a) fraction PSAF and (b) fraction B-72-9 in butanone.

$$k_D = \frac{10}{c_0}\frac{D_{2,0}}{D_0}\frac{X_{\max}}{Y_{\max}} \tag{7}$$

$$D_0 = D_{2,0}\left(1 + \frac{5X_{\max}}{Y_{\max}}\right) \tag{8}$$

where X_{max} is the value of X at which Y has its maximum value, Y_{max}, and c_0 is the initial concentration of the solution. The Beckmann and Rosenberg procedure involves plotting $D_c/D_{2,0}$ as a function of $2c/c_0$, where

$$\frac{D_c}{D_{2,0}} = \frac{Y^0}{Y}\left[1 - \frac{4}{Y^0}\int_{-\infty}^{X} X\Delta Y\,\mathrm{d}X\right] \tag{9}$$

$$\frac{2c}{c_0} = \frac{4}{5}\int_{-\infty}^{X} Y\mathrm{d}X \tag{10}$$

in which Y^0 is the ordinate of the ideal normalized curve and $\Delta Y = Y - Y^0$. The curves so obtained in our experiments were usually linear near the value $2c/c_0 = 1$, and k_D was evaluated from this portion of the curves.

The values of k_D obtained independently by these two methods checked closely, indicating that the concentration dependence of the diffusion constant is essentially linear in the systems studied.

F. The calculation of k_D from sedimentation and osmotic pressure data

The indirect calculation of k_D from sedimentation and osmotic pressure data according to equation 1 requires the knowledge of the parameters B, M, and k_s. The values of B for the systems studied were obtained from the osmotic pressure data of M. Schick (21). The values of M used were the number-average molecular weights recorded in table 1. k_s was evaluated by plotting the reciprocal of the sedimentation constant against concentration (11); the fact that linear relationships were usually obtained from such plots justifies the use of equation 2 for the purposes of these experiments.

G. Viscosity determinations

In order to aid in characterizing the systems investigated, viscosity measurements were made on solutions of fraction PSAF in the solvents used in the diffusion studies. Ostwald viscosimeters (5-ml. capacity) were employed, and the small kinetic energy corrections were neglected.

IV. RESULTS

The data obtained from the analysis of the diffusion curves are listed in table 2. In figure 2 are shown several graphs from which the zero-time corrections were obtained, while in figure 3 are represented several normalized diffusion curves.

Comparison of k_D values obtained by the Gralén and the Beckmann and Rosenberg methods is made in tables 3 and 5. It may be seen that the two values generally agree quite well. In figure 4 we have reproduced a few examples of plots according to the Beckmann and Rosenberg procedure for evaluating k_D.

Sedimentation experiments were performed with fractions D-8, D-2, B-72-18, and B-72-9 in butanone, and with fraction PSAF in ethylbenzene and decalin. The results of these measurements are given in table 4, and are plotted in figure 5. Measurements of the partial specific volume were made pycnometrically

TABLE 2

Data obtained from the analysis of the diffusion curves

FRACTION AND SOLVENT	DIFFUSION TIME (CORRECTED)	AREA	MAXIMUM ORDINATE	σ^2	$D_{1,0} \times 10^7$	$D_A \times 10^7$
c = 0.3918 g./100 cc.; F = 0.7456; zero-time correction = 20,000 sec.						
	seconds	*cm.²*	*cm.*	*cm.²*		
Fraction D-8 in butanone	185,060	0.06165	0.0342	0.5190	7.80	7.77
	222,380	0.06013	0.0319	0.6364	7.96	7.07
	294,680	0.06200	0.0272	0.8173	7.71	7.80
Average					7.8_2	7.5_4
c = 0.4168 g./100 cc.; F = 0.7446; zero-time correction = 30,000 sec.						
Fraction D-2 in butanone	142,620	0.06387	0.0514	0.2597	5.05	4.78
	194,940	0.06311	0.0424	0.3568	5.07	5.01
	226,380	0.06358	0.0395	0.4045	4.95	5.05
	310,800	0.06452	0.0334	0.5550	4.95	5.30
Average					5.0_1	5.0_4
c = 0.3977 g./100 cc.; F = 0.7452; zero-time correction = 65,000 sec.						
Fraction B-72-18 in butanone	179,780	0.05861	0.0488	0.2471	3.91	3.63
	321,800	0.05660	0.0348	0.3994	3.53	3.63
	496,520	0.05715	0.0282	0.6415	3.59	3.65
	672,620	0.05767	0.0245	0.8579	3.54	3.64
Average					3.6_4	3.6_4
c = 0.4030 g./100 cc.; F = 0.7441; zero-time correction = 140,000 sec.						
Fraction B-72-9 in butanone	315,380	0.05351	0.0417	0.2980	2.62	2.30
	396,680	0.05517	0.0359	0.4410	3.15	3.30
	571,880	0.05348	0.0284	0.5652	2.74	2.73
	740,240	0.05622	0.0246	0.7822	2.93	3.11
Average					2.8_6	2.8_6
c = 0.4062 g./100 cc.; F = 0.7359; zero-time correction = 0						
Fraction PSAF in butanone	164,940	0.06052	0.0615	0.1468	2.47	2.59
	260,220	0.06089	0.0498	0.2280	2.43	2.53
	280,500	0.06214	0.0484	0.2563	2.53	2.59
	339,600	0.06076	0.0433	0.3204	2.61	2.56
Average					2.5_1	2.5_7
c = 0.4022 g./100 cc.; F = 0.7359; zero-time correction = 250,000 sec.						
Fraction D-8 in CCl_4	406,600	0.03615	0.0196	0.5475	3.25	3.21
	499,120	0.03736	0.0186	0.6368	3.14	3.03
	586,480	0.03785	0.0180	0.7974	3.39	3.00
Average					3.2_6	3.0_8

TABLE 2—*Continued*

FRACTION AND SOLVENT	DIFFUSION TIME (CORRECTED)	AREA	MAXIMUM ORDINATE	σ^2	$D_{2,0} \times 10^7$	$D_A \times 10^7$
c = 0.4001 g./100 cc.; F = 0.7337; zero-time correction = 300,000 sec.						
	seconds	*cm.²*	*cm.*	*cm.²*		
Fraction D-2 in CCl_4	548,760	0.03875	0.0223	0.4771	2.34	2.36
	636,540	0.03868	0.0207	0.5258	2.22	2.35
	803,580	0.03813	0.0182	0.6712	2.25	2.34
Average					2.2_7	2.3_5
c = 0.4028 g./100 cc.; F = 0.7371; zero-time correction = 100,000 sec.						
Fraction B-72-18 in CCl_4	303,640	0.03998	0.0408	0.1575	1.41	1.37
	358,180	0.03939	0.0367	0.1875	1.42	1.39
	459,760	0.03955	0.0324	0.2323	1.37	1.40
	612,760	0.04073	0.0286	0.3194	1.42	1.43
Average					1.4_1	1.4_0
c = 0.6206 g./100 cc.; F = 0.7370; zero-time correction = 395,000 sec.						
Fraction B-72-9 in CCl_4	561,320	0.06250	0.0575	0.2498	1.21	0.91
	754,880	0.06453	0.0466	0.3431	1.23	1.10
	907,220	0.06377	0.0416	0.4039	1.20	1.12
	1,099,880	0.06285	0.0372	0.4727	1.17	1.12
Average					1.2_0	1.0_6
c = 0.6602 g./100 cc.; F = 0.7371; zero-time correction = 500,000 sec.						
Fraction PSAF in CCl_4	666,920	0.06558	0.0514	0.2787	1.14	1.06
	860,180	0.06643	0.0439	0.3709	1.17	1.15
	1,012,940	0.06550	0.0395	0.4170	1.19	1.17
	1,205,000	0.06500	0.0364	0.4874	1.10	1.14
Average					1.1_5	1.1_3
c = 0.7952 g./100 cc.; F = 0.7355; zero-time correction = 100,000 sec.						
Fraction PSAF in ethylbenzene	352,300	0.05805	0.0530	0.1923	1.48	1.47
	426,820	0.05745	0.0475	0.2228	1.41	1.48
	529,780	0.05663	0.0422	0.2744	1.40	1.46
	688,540	0.05823	0.0365	0.3819	1.50	1.26
Average					1.4_5	1.4_2
c = 0.8424 g./100 cc.; F = 0.7350; zero-time correction = 80,000 sec.						
Fraction PSAF in toluene	333,200	0.06113	0.0529	0.2083	1.69	1.72
	510,560	0.06220	0.0424	0.3314	1.75	1.81
	668,540	0.06160	0.0367	0.4064	1.59	1.76
	927,560	0.06040	0.0309	0.5556	1.58	1.77
Average					1.6_5	1.7_7

TABLE 2—*Concluded*

FRACTION AND SOLVENT	DIFFUSION TIME (CORRECTED)	AREA	MAXIMUM ORDINATE	σ^2	$D_{2,0} \times 10^7$	$D_A \times 10^7$
c = 0.4040 g./100 cc.; F = 0.7395; zero-time correction = 12,500 sec.						
	seconds	*cm.²*	*cm.*	*cm.²*		
Fraction PSAF in ethyl acetate	150,620	0.06194	0.0665	0.1436	2.61	2.51
	173,780	0.06294	0.0621	0.1820	2.86	2.57
	246,500	0.06161	0.0530	0.2366	2.63	2.39
Average					2.7_0	2.4_9
c = 0.7967 g./100 cc.; F = 0.7347; zero-time correction = 120,000 sec.						
Fraction PSAF in decalin	708,420	0.06906	0.0781	0.1237	4.71	4.74
	967,440	0.06856	0.0666	0.1744	4.87	4.71
	1,314,420	0.06892	0.0578	0.2157	4.53	4.65
Average					4.7_0	4.7_0

TABLE 3

Variation of D_0 and k_D with molecular weight

FRACTION	SOLVENT	B. AND R METHOD		GRALÉN METHOD	
		$D_0 \times 10^7$	k_D	$D_0 \times 10^7$	k_D
D-8	Butanone	9.58	−0.92	9.40	−0.86
D-2		5.14	−0.12	5.14	−0.12
B-72-18		3.28	0.55	3.32	0.49
B-72-9		2.53	0.64	2.64	0.40
PSAF		2.51	0	2.51	0
D-8	CCl_4	4.43	−1.31	4.40	−1.27
D-2		2.27	0	2.27	0
B-72-18		1.41	0	1.41	0
B-72-9		1.04	0.50	1.06	0.48
PSAF		1.10	0.13	1.12	0.08

(27), and $\bar{V}$ for polystyrene was found to be 0.90 ± 0.02 in butanone and 0.91 ± 0.02 in ethylbenzene. Signer and Gross (22) have determined $\bar{V}$ = 0.91 ± 0.03 for polystyrene in decalin.

The sedimentation and diffusion constants extrapolated to infinite dilution, combined with the measurements of partial specific volume, were used to evaluate molecular weights by equation 3. These are the M_s values recorded in table 1.

Comparison of k_D values obtained directly from diffusion measurements with those obtained indirectly through sedimentation and osmotic pressure measurements according to equation 1 is made in table 6. k_D (calculated) was obtained by evaluating the ratio $[1 + (2BM/RT)c]/1 + k_s c$ at $c = 0.5$ g./100 cc. from the experimentally determined values of B, M, and k_s, and then calculating k_D from equation 1.

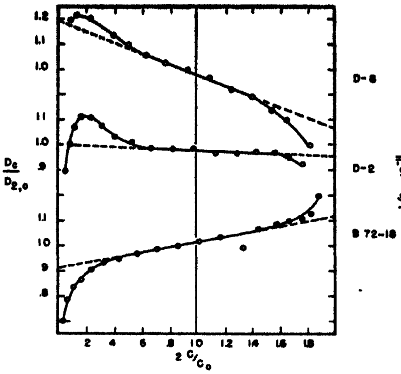

FIG. 4

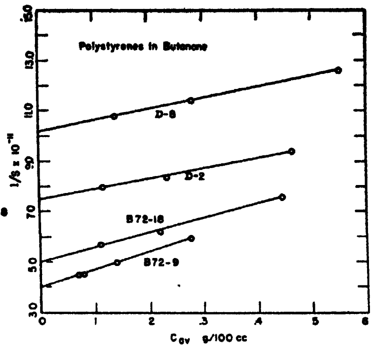

FIG. 5

FIG. 4: Diffusion data obtained in butanone solution plotted according to the Beckmann and Rosenberg procedure for determining k_D. The dashed lines are drawn through the linear portions around $2c/c_0 = 1$.

FIG. 5: Sedimentation data for polystyrene fractions in butanone solution corrected to 27°C.

TABLE 4

Sedimentation data on polystyrenes

SOLVENT	POLYMER	c_0	c_{av}	$S_{27} \times 10^{13}$	k_s
		g./100 cc.	*g./100 cc.*		
Butanone.......	D-8	0.600	0.552	7.9	0.43
		0.300	0.279	8.8	
		0.150	0.140	9.3	
		0.000		9.8*	
	D-2	0.501	0.466	10.9	0.48
		0.251	0.233	12.0	
		0.125	0.116	12.7	
		0.000		13.3*	
	B-72-18	0.480	0.446	13.4	1.11
		0.240	0.221	16.2	
		0.120	0.110	17.7	
		0.000		20.0*	
	B-72-9	0.300	0.276	16.9	1.75
		0.150	0.140	20.1	
		0.086	0.079	22.2	
		0.075	0.070	22.6	
		0.000		25.0*	
Ethylbenzene.....	PSAF	0.402		3.90	3.55
		0.200		5.55	
		0.167		6.30	
		0.082		7.40	
		0.044		8.10	
		0.000		9.5*	
Decalin...........	PSAF	0.400		2.13	0.73
		0.202		2.41	
		0.076		2.62	
		0.000		2.73*	

* Extrapolated.

TABLE 5

k_D values for fraction PSAF

SOLVENT	μ*	$[\eta]$	B. AND R. METHOD		GRALÉN METHOD	
			k_D	$D_0 \times 10^7$	k_D	$D_0 \times 10^7$
Toluene	0.430	2.25	0.96	1.22	0.92	1.19
Ethylbenzene	0.434	2.10	1.3	0.96	1.1	1.02
Carbon tetrachloride	0.445	2.20	0.13	1.10	0.08	1.12
Butanone	0.484	1.22	0	2.51	0	2.51
Ethyl acetate	0.485		0.12	2.64	0.12	2.64
Decalin	0.495†	0.87	−0.15	0.50	−0.18	0.51

* μ values obtained from M. Schick (21).

† Interpolated in the values of Boyer and Spencer (3) obtained from swelling pressure measurements, assuming a constant difference between μ values so obtained and those derived from osmotic pressure measurements.

TABLE 6

Concentration dependence of D

FRACTION	SOLVENT	$1 + \frac{2BM}{RT} c$*	$1 + k_s c$*	$\frac{1 + \frac{2BM}{RT} c^*}{1 + k_s c}$	k_D (CALCULATED)	k_D (OBSERVED)
D-8	Butanone	1.12	1.21	0.92	−0.16	−0.92
D-2	Butanone	1.21	1.24	0.97	−0.06	−0.12
B-72-18	Butanone	1.71	1.56	1.10	0.20	0.55
B-72-9	Butanone	2.63	1.88	1.40	0.80	0.64
PSAF	Ethylbenzene	4.39	2.78	1.58	1.2	1.3
PSAF	Decalin	1.20	1.37	0.88	−0.24	−0.15

* Calculated at the concentration $c = 0.5$ g./100 cc.

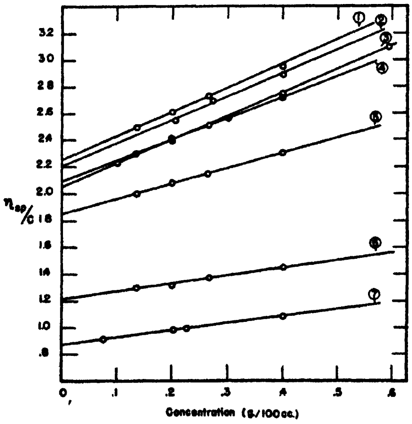

FIG. 6

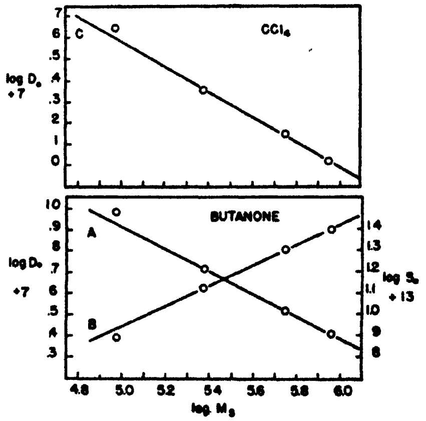

FIG. 7

FIG. 6: Viscosity data for fraction PSAF in the following solvents at 27°C.: (1) toluene; (2) carbon tetrachloride; (3) ethylbenzene; (4) dioxane; (5) morpholine; (6) butanone; (7) decalin.

FIG. 7: Dependence of the diffusion constant on molecular weight for polystyrene fractions in butanone and carbon tetrachloride, and of the sedimentation constant on molecular weight in butanone. Curve B represents the sedimentation data.

In the terminology of the theory of polymer solutions based on the quasi-lattice model (7, 13), the parameter B is related to the compatibility constant, μ, by the equation:

$$B = \frac{(0.5 - \mu)RT}{V_1 d_2^2} \tag{11}$$

where V_1 is the partial molal volume of solvent, d_2 is the density of pure solute, and μ is a constant characteristic of a given solute–solvent system. In table 5 are listed the μ and B values, calculated using the value $d_2 = 1.096$ for polystyrene at 27°C., along with the intrinsic viscosities obtained from the viscosity data plotted in figure 6.

V. DISCUSSION

A. Concentration dependence of the diffusion constant

The results listed in table 6 indicate that in those systems for which sedimentation as well as diffusion and osmotic pressure data were obtained, the concentration dependence of the diffusion constant is given by equation 1 within the experimental errors. The only serious exception occurs with the lowest-molecular-weight fraction, D-8, in butanone, in which the observed concentration dependence appears to be larger than that calculated. This may be due to some unknown peculiarity of this fraction, since a similarly large negative concentration dependence is observed in the experiment in carbon tetrachloride solution. On the whole, however, the theoretical development which was outlined earlier in this paper appears to be confirmed by our data.

The occurrence of negative values of k_D for some of the systems investigated, indicating that the rate of diffusion of the solute is slower in more concentrated solutions, is particularly interesting. Jullander (14), studying the diffusion of some low-molecular-weight nitrocelluloses in acetone, observed negative k_D values but attributed them to experimental errors. Neurath and Saum (17) found that a large negative k_D existed with solutions of tobacco mosaic virus protein in phosphate buffer, and suggested that intermolecular interference diminished the diffusion rate. Our results establish the significance of a decrease in diffusion rate with increasing concentration, and indicate that it may be expected to occur whenever a combination of factors makes $2BM/RT$ smaller than k_s.

B. The effect of molecular weight on k_D

In terms of the hypothesis that is being tested in this investigation, the problem of the dependence of k_D on molecular weight must be resolved into the two independent problems of the effects of molecular weight on the two terms $2BM/RT$ and k_s. Since B is essentially independent of molecular weight (28), the former of these terms varies linearly with M. If we express k_s as a function of M by the following empirical equation:

$$k_s = \text{constant} \cdot M^p \tag{12}$$

and use the number-average molecular weights of the first four polystyrene fractions, we find from our sedimentation data in butanone that $p = 0.6 \pm 0.1$. From equation 1 it follows that k_D should increase with molecular weight, as is observed experimentally.

In investigations of the diffusion properties of nitrocelluloses in acetone and amyl acetate, Jullander (14) found that k_D increased gradually with molecular weight. Our studies indicate similar trends for polystyrene fractions in butanone and carbon tetrachloride. It should be emphasized, however, that for a given system the variation of k_D with M depends entirely on the independent variation of k_s with M. With the system cellulose acetate in acetone, Singer (24) found that k_s varies approximately linearly with M in the molecular weight range 10,000–200,000 and although quantitative calculations of k_D were not performed, it might be inferred that k_D is therefore independent of M in this system.

The characteristics of the dependence of k_s upon M are apparently similar to those of the dependence of the intrinsic viscosity upon M. For polymer solutions it has been demonstrated experimentally and theoretically that if the $[\eta]$–M relation is expressed as follows:

$$[\eta] = KM^a \tag{13}$$

a varies from the value 0.5 in poor solvents (barring association effects) to the value 1.0 in good solvents. In the polystyrene–butanone system (10) $a = 0.53$, while in the cellulose acetate–acetone system (1) $a = 0.82$. It is therefore reasonable to expect that the exponent p in equation 12 should be larger for the cellulose acetate–acetone system than for the polystyrene–butanone system.

C. The effect of solvent on k_D

Our data suggest an interesting effect produced by varying the solvent, which should be tested by other diffusion measurements on a variety of systems. In table 5 are listed values of k_D for fraction PSAF in various solvents. It appears that k_D varies from a value around zero in poor solvents to 1.0 in good solvents for this particular polymer. Since M does not change in these systems, these results suggest that B varies more rapidly in going from poor to good solvents than does k_s. This is confirmed independently by the determination of k_s by sedimentation experiments in ethylbenzene and decalin.

It is not possible at present to understand this fact in detail, owing to the absence of a suitable theory correlating k_s and B. Qualitatively, we may say that as the solvent becomes poorer, i.e., as the free energy of dilution for the system at a given low concentration becomes smaller, associated changes occur in the configurations of the polystyrene molecules, reducing their average lengths and penetrability to solvent. The hydrodynamic interference term, k_s, may therefore be expected to decrease as the solvent becomes poorer and as B decreases. The exact nature of this decrease is a matter for future developments in the theory of polymer solutions to explain.

D. Molecular weight determinations by sedimentation and diffusion measurements

Although considerable research has been performed with cellulose derivatives, and molecular weights calculated by the Svedberg equation (equation 3) have been shown to apply in general within the experimental errors, little investigation has been made of the more flexible polymers such as polystyrene. Signer and Gross (22) performed equilibrium and rate sedimentation, but no diffusion, experiments on some unfractionated polystyrenes; recently, Gralén and Lagermalm (12) have reported sedimentation rate experiments with polystyrene fractions and plan diffusion experiments with them.

The molecular weights calculated by equation 3 are rather complicated average values, usually falling between the number-average and the weight-average values (14, 23). In general the molecular weights, M_s, listed in table 1 therefore compare favorably with the number-average values, M_n. For fraction B-72-9 $M_s < M_n$, but the difference is probably within the experimental errors for this high-molecular-weight fraction, for which the limiting osmotic pressure is difficult to determine accurately. The value of M_s for fraction PSAF in ethylbenzene is 1,140,000, while $M_n = 770,000$. Here the indication is that PSAF is more heterogeneous than the other fractions. This is confirmed by the relatively large values of $[\eta]$ for this fraction in butanone and toluene (table 1). Since $[\eta]$ is nearly a weight-average quantity, it reflects the presence of high-molecular-weight species. The value $M_s = 680,000$ for PSAF in decalin solution is too low, apparently owing to a value of D_0 which is somewhat too large.

E. The dependence of D upon M

Recently, theories have been developed relating the diffusion and sedimentation rates as well as the intrinsic viscosity to the molecular weight of flexible long-chain molecules. In figure 7, log D_0 is plotted against log M_s for the four sharp polystyrene fractions in butanone and carbon tetrachloride. In butanone the curve is represented empirically by

$$D_0 = \text{constant}\cdot M_s^{-0.53} \tag{14}$$

and in carbon tetrachloride by

$$D_0 = \text{constant}\cdot M_s^{-0.59} \tag{15}$$

The values of the exponents are in agreement with the values predicted by Debye and Bueche (6) and by Kirkwood and Riseman (15) and others, of -0.5 to -1.0, where the higher values correspond to the more extended configurations of the solute molecules and hence to the better solvent. The experimental errors are such that the value -0.53 is not quite significantly different from -0.59, but it is interesting that thermodynamically carbon tetrachloride is a better solvent for polystyrene than is butanone. More extensive measurements are required, however, to evaluate the exponents more accurately.

VI. SUMMARY

The formulation of the concentration dependence of the diffusion constant in terms of two independently measurable quantities, the increase in osmotic pressure and in the frictional coefficient with concentration, has been verified. This indicates that the basic assumptions involved in this formulation are satisfied: namely, that the gradient of the free energy of dilution is the driving force of the diffusion process, and that the frictional coefficients in sedimentation and diffusion are the same.

Both positive and negative values of the concentration dependence of the diffusion rate have been found for polystyrene solutions. This has been shown to be possible, depending on the relative contributions of the hydrodynamic and thermodynamic factors to the diffusion rate.

The variation of the concentration dependence of the diffusion constant with respect to molecular weight and solvent power has also been discussed.

The authors wish to express their gratitude to Professor K. G. Stern, who supervised the construction of the diffusion apparatus employed in this study. The polystyrene fractions D-8, D-2, B-72-18, and B-72-9 were obtained through the kind coöperation of Dr. A. I. Goldberg.

REFERENCES

(1) Badgley, W., and Mark, H.: J. Phys. & Colloid Chem. **51,** 58 (1947).
(2) Beckmann, C. O., and Rosenberg, J.: Ann. N. Y. Acad. Sci. **46,** 209 (1945).
(3) Boyer, R. F., and Spencer, R. S.: J. Polymer Sci. **3,** 913 (1948).
(4) Bueche, A. M.: Personal communication.
(5) Burgers, J. M.: Proc. Acad. Sci. Amsterdam **44,** 1045, 1177 (1941); **45,** 9, 126 (1942).
(6) Debye, P., and Bueche, A. M.: J. Chem. Phys. **16,** 573 (1948).
(7) Flory, P. J.: J. Chem. Phys. **10,** 51 (1942).
(8) Flory, P. J.: J. Chem. Phys. **13,** 453 (1945).
(9) Goldberg, A. I.: Personal communication.
(10) Goldberg, A. I., Hohenstein, W. P., and Mark, H.: J. Polymer Sci. **2,** 503 (1947).
(11) Gralén, N.: Inaugural Dissertation, Uppsala, 1944.
(12) Gralén, N., and Lagermalm, G.: Festskr. J. Arvid Hedvall **1948,** 215.
(13) Huggins, M. L.: Ann. N. Y. Acad. Sci. **43,** 1 (1942).
(14) Jullander, I.: Arkiv Kemi, Mineral. Geol. **21A,** No. 8 (1945).
(15) Kirkwood, J. G., and Riseman, J.: J. Chem. Phys. **16,** 565 (1948).
(16) Lamm, O.: Nova Acta Regiae Soc. Sci. Upsaliensis **10,** 1 (1937).
(17) Neurath, H. and Saum, A. M.: J. Biol. Chem. **126,** 435 (1938).
(18) Onsager, L. and Fuoss, R. M.: J. Phys. Chem. **36,** 2689 (1932).
(19) Scatchard, G.: J. Am. Chem. Soc. **68,** 2315 (1946).
(20) Schick, A. F.: Ph. D. Thesis, Polytechnic Institute of Brooklyn, June, 1948.
(21) Schick, M. J.: Ph. D. Thesis, Polytechnic Institute of Brooklyn, June, 1948.
(22) Signer, R., and Gross, H.: Helv. Chim. Acta **17,** 59 (1934).
(23) Singer, S. J.: J. Polymer Sci. **1,** 445 (1946).
(24) Singer, S. J.: J. Chem. Phys. **15,** 341 (1947).
(25) Stern, K. G., Singer, S. J., and Davis, S.: Polymer Bull. **1,** 31 (1945).
(26) Stern, K. G., Singer, S. J., and Davis, S.: J. Biol. Chem. **167,** 321 (1947).
(27) Svedberg, T., and Pedersen, K. O.: *The Ultracentrifuge.* Oxford University Press, London (1940).
(28) Zimm, B. H.: J. Chem. Phys. **14,** 164 (1946).
(29) Zimm, B. H., and Myerson, I.: J. Am. Chem. Soc. **68,** 911 (1946).

THE ADHESION OF PHOSPHORS ON CATHODE-RAY SCREENS[1]

WM. STERICKER

Philadelphia Quartz Company, Public Ledger Building, Philadelphia 6, Pennsylvania

AND

FRED HAZEL

Department of Chemistry and Chemical Engineering, University of Pennsylvania, Philadelphia 4, Pennsylvania

Received October 5, 1949

The settling method of producing screens of fluorescent materials in glass bulbs to be used as cathode-ray tubes is used almost universally at the present time (5). The details of the methods vary, but in general the process is as follows: A layer of water is introduced into the clean bulbs, followed by a suspension of the phosphor and solutions of potassium silicate and some other soluble salt. The phosphor suspension may be prepared in the silicate solution, or the silicate and neutral salt solutions may be mixed before being added. Care is taken to make sure that the suspension is spread evenly. The bulb is allowed to stand until the phosphor has settled and adhered to the glass. The time required to get good adhesion varies considerably. During the settling period the bulb must not be disturbed if a uniform screen is to be obtained. At the end of the settling period the bulb usually is placed on a tilting table and the aqueous layer is poured off by turning the table slowly and uniformly. After draining and drying the bulb is ready for further operations.

This work was undertaken to try to determine the reason why the phosphor adhered to the glass. At the time when it was started there was a question as to whether the surface phenomena might be due to electrical (1) or to chemical effects. It was found that both of these are important in the settling period, but that the primary cause of adhesion is the bridge formed by polymerization of the silicate adsorbed on the glass and on the phosphor surfaces.

METHOD

The settling tests were carried out in both Erlenmeyer flasks and beakers. The shape of an Erlenmeyer flask is somewhat similar to the shape of a small cathode-ray tube. For the photographs it was found better to use beakers. The results obtained in the two containers were similar. Details of the methods will be given as the experiments are described.

MATERIALS

A number of different phosphors were tried in the settling tests. These included zinc sulfides and zinc silicates. The phosphors also differed in particle size, some of them being in the range around 5 microns and some around 15. The results indicated that the different kinds of phosphors acted alike.

---

[1] Presented before the Division of Colloid Chemistry at the 116th Meeting of the American Chemical Society, which was held at Atlantic City, New Jersey, September, 1949.

The potassium silicate solution, containing approximately 7.8 per cent K_2O and 19.5 per cent SiO_2, was one widely used in the industry and was a purified solution of $K_2O:3.92SiO_2$.[2] Although sodium silicates were used to check some of the points of the theory, warning should be given that the electrical characteristics of tubes containing screens made with sodium silicates are usually unsatisfactory for other reasons. In fact, in all this work the primary interest was to determine the reason for the adhesion and many of the mixtures used would not be satisfactory for the actual manufacture of cathode-ray screens.

In most cases the salts added were of laboratory reagent grade and in all cases were chosen because they were felt to be the purest materials available. The experiments were made with distilled water.

MIGRATION OF PHOSPHOR

In the first series of experiments 0.1 g. of phosphor R.C.A. "P_4" was introduced into 100 ml. of liquid contained in a 250-ml. Erlenmeyer flask. This is equivalent to approximately 0.002 g./sq. cm. In all cases the phosphor settled uniformly in a few minutes. With water alone the layer formed in this manner stayed the same on longer standing, as shown in figure 1.[3] With the potassium silicate solutions indicated as samples A2 and A3 in table 1 the phosphor first settled to give a fairly uniform screen but on longer standing migrated to leave large areas of the glass bare, similar to the condition shown in figures 2a and 3a. By tilting the flask the powder could be redistributed more or less uniformly over the glass. However, when the samples were allowed to stand undisturbed for several hours, considerable areas of glass were exposed again. This process could be repeated many times. Some idea of this can be obtained from figures 2a–2c. In figure 2b the beaker has been tilted to allow the phosphor shown in figure 2a to slide back across part of the central area. On standing for 48 hr. migration had taken place, as shown in figure 2c. The process is shown more clearly in figures 3a–3d. Figure 3a shows the pattern obtained on the original settling overnight. The phosphor was then redistributed over the surface, as shown in figure 3b. On standing for 30 min. considerable migration had taken place, as shown in figure 3c. After 48 hr. the phosphor had migrated almost completely to a small spot in the center and to a ring around the outer edge, as shown in figure 3d. Various methods of cleaning the flasks were tried but with no essential change in the results.

The migration was due to gravity. The same design of bare and covered areas was obtained in the same flask, owing to the phosphor settling into the low spots in the surface. If the flask was tilted slightly during the migration, practically all the phosphor flowed to the low side.

---

[2] The material is sold by the Philadelphia Quartz Company under the trade name Kasil No. 1.

[3] The demonstrations for taking photographs were prepared in beakers by Miss Rita Kresge and were photographed by O. V. Brody.

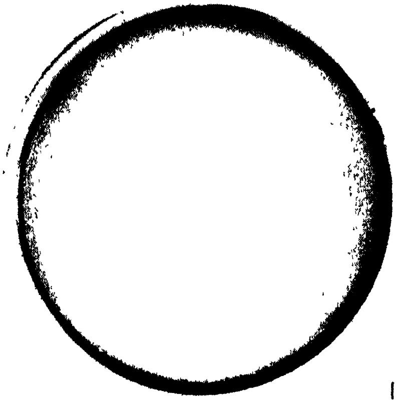

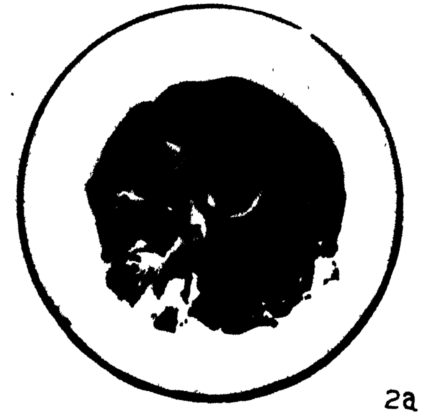

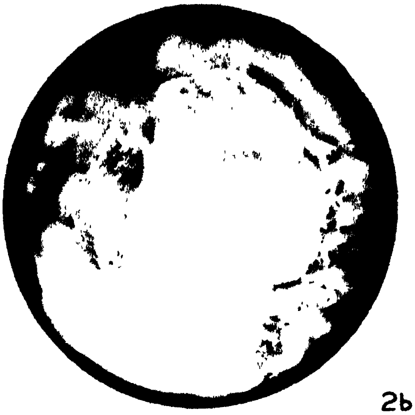

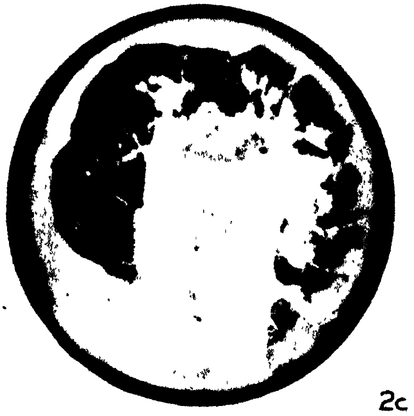

FIG. 1 One-tenth gram of P_1 phosphor in 100 ml of water settled overnight (like sample A1).

FIG. 2a One-tenth gram of P_1 phosphor in 99 ml of water and 1 ml. of potassium silicate solution (1.18 per cent) settled overnight (like sample A2).

FIG. 2b Specimen of figure 2a tilted and allowed to stand 5 min.

FIG. 2c Same after standing 48 hr.

TABLE 1

Effect of potassium silicate on ζ-potentials

SAMPLE	K_2O	SiO_2	ζ-POTENTIAL	
			Phosphor	Glass
	per cent	*per cent*	*mv.*	*mv.*
A1	0	0	—11	—57
A2	0.00115	0.00288	—42	—78
A3	0.0115	0.0288	—49	—75
A3a	0.1151	0.288	—47	—62
A4	0.78	1.95	—48	—42

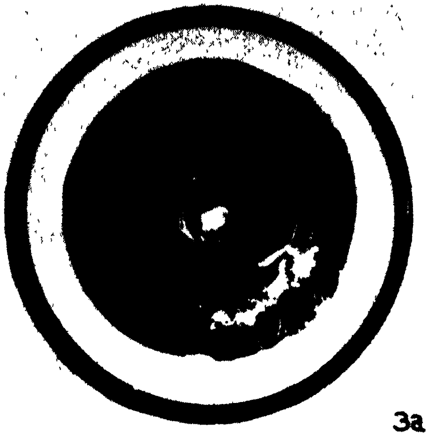

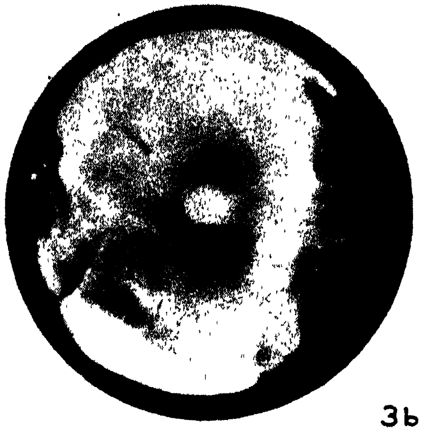

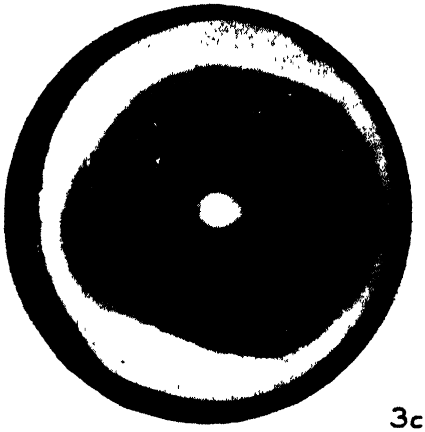

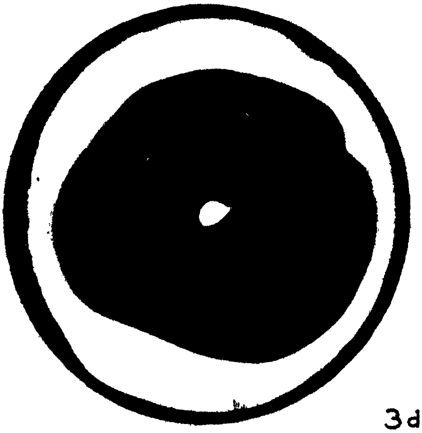

FIG 3a One-tenth gram of P_4 phosphor in 90 ml of water and 10 ml of potassium silicate solution (1.18 per cent) settled overnight (like sample A3)

FIG 3b Specimen of figure 3a tilted and allowed to stand 5 min

FIG 3c. Same after standing 30 min.

FIG. 3d Same after standing 48 hr

REPULSION

These preliminary experiments showed that there was poor adhesion to the glass in dilute potassium silicate solutions. Since there was no such movement with water, it appeared that the potassium silicate caused the nonadhesion of the powder to the glass. It was felt that this repulsion could be due to electrical effects. This possibility was investigated and has been reported by Edelberg and Hazel elsewhere (2). Results for the ζ-potentials of the phosphor and the Pyrex glass surfaces are reproduced in table 1 for the systems shown in figures 1–4. It will be noted that the addition of a small amount of potassium silicate increases the ζ-potential on both the glass and the phosphor surfaces, thereby increasing the repulsion between them. The silicate increases the potential on the

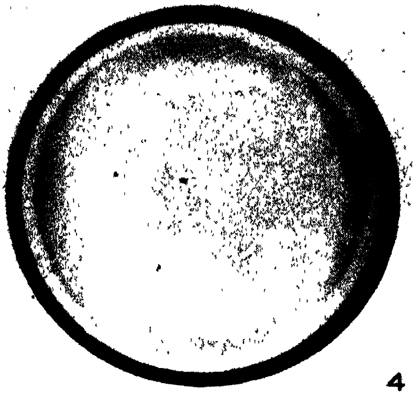

4

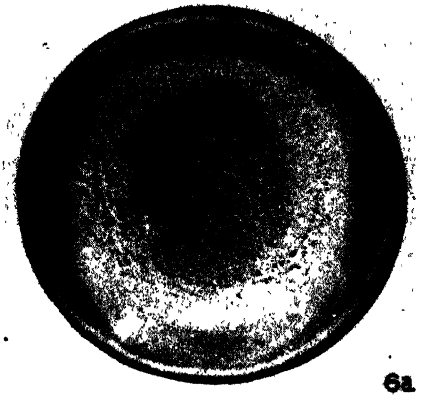

6a

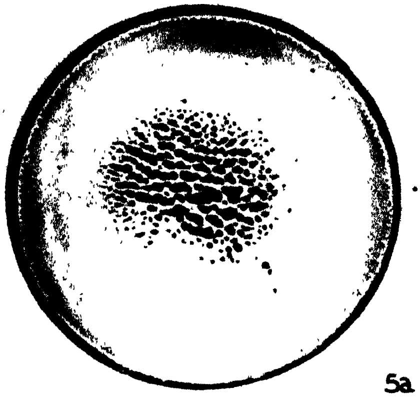

5a

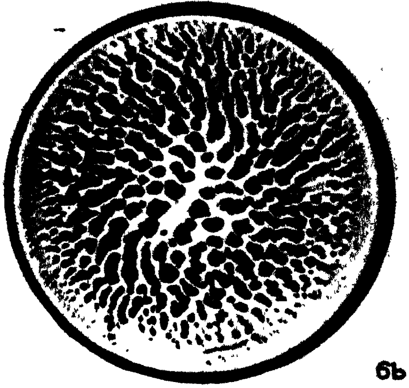

6b

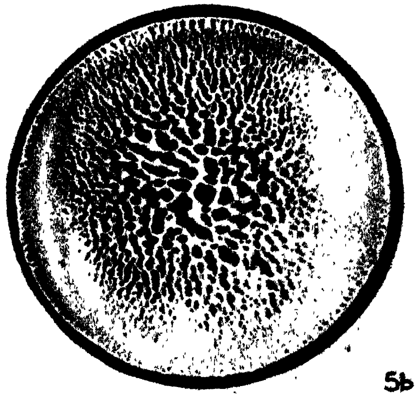

5b

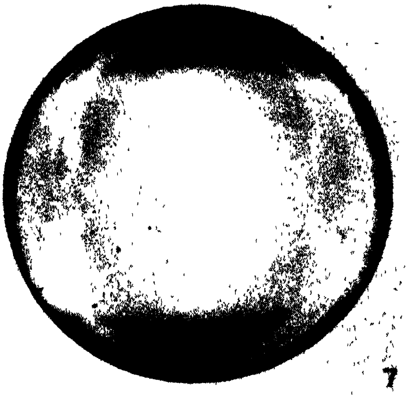

7

FIG. 4. One-tenth gram of P_4 phosphor in 100 ml. of "10 per cent" potassium silicate settled overnight (like sample B1).

FIG. 5a. 0.0765 g. of P_4 phosphor in 100 ml. of water jarred five times.

FIG. 5b. The same system as in figure 5a given five more taps and a slight circulatory motion.

FIG. 6a. 0.131 g. of P_4 phosphor in 100 ml. of water jarred five times.

FIG. 6b. The same system as in figure 6a given five more taps and a slight circulatory motion.

FIG. 7. One-tenth gram of P_4 phosphor settled in 60 ml. of 0.5 *M* sodium sulfate solution and 10 ml. of Kasil No. 1 in 30 ml. of water for 48 hr.

phosphor strongly. Small amounts of silicate increase the potential on the glass but larger amounts decrease it until the tendency of the phosphor to migrate is eliminated. This is indicated in figure 4, which shows system B1 after it had settled overnight.

COHESION

In water the potential on the phosphor surface is small and the particles are bonded to each other more strongly than to the glass, which has a higher potential. Figure 1 is a photograph of system A1 after it had stood 18 hr. Figures 5a and 6a show similar water systems after they had been jarred slightly. The screens, formed by cohesion of the particles of phosphor, contracted like broken membranes. More tapping, combined with a slight circulatory motion, gave the results shown in figures 5b and 6b. These two systems show that a variation of ±33 per cent in the amount of the phosphor did not affect the results.

TABLE 2

Effect of sodium sulfate on adhesion of phosphors to glass

SAMPLE	VOLUME OF "10%" SILICATE SOLUTION*	VOLUME OF WATER	VOLUME OF 0.5 M Na_2SO_4	APPROXIMATE PER CENT Na_2SO_4	ADHESION
	ml.	*ml*	*ml*		
B1	100	60	0	0	Poor
B2	100	55	5	0.234	Strong
B3	100	40	20	0.888	Strong
B4	100	20	40	1.75	Strong
B5	100	0	60	2.66	Strong

* The "10%" solution was 10 per cent by weight of Kasil No. 1.

When the potentials on the phosphor and glass surfaces are high, as they are in the presence of small amounts of silicate, the particles do not cohere but remain discrete and are able to flow. Under these conditions the particles not only repel each other but are repelled also by the glass. These forces exceed the frictional forces and enable the powder to flow readily over the glass surface.

ADHESION

The addition of sodium sulfate to the potassium silicate solution from which the phosphor settles promotes adhesion between the glass and the phsphor. Such a system is shown in figure 7. Table 2 gives the results of a series where the solution contained approximately 0.49 per cent K_2O and 1.22 per cent SiO_2. In all cases the phosphor settled readily and remained in place, since the concentration of silicate was above that which caused migration. However, in the absence of sulfate the adhesion of the phosphor to the glass was poor. It became progressively stronger as the concentration of sulfate increased. The liquor remained clear in samples B1–B3 but became turbid in sample B4 after 96 hr. In sample

B5 the liquor became milky after 24 hr. and the milkiness increased until a layer of gel formed on top of the phosphor after 72 hr.

Edelberg and Hazel (2, figure III) have shown that the strong negative potential conveyed to the surfaces by the silicate is decreased by sodium sulfate. In their experiments they used 133 ml. of Kasil No. 1 in 1000 ml. and settling experiments were made at the same concentration. These solutions contained approximately 0.10 per cent K_2O and 0.26 per cent SiO_2. The results are given in table 3. Here again the adhesion of the phosphor to the glass increased as the concentration of sulfate increased and as the potential dropped. In sample C7 there was a gelatinous cloudy covering on the phosphor layer.

OTHER ADDITION AGENTS

A number of other salts were tried in place of sodium sulfate with both Kasil No. 1 and E sodium silicate[4] in solutions containing 19.5 g. of silica per liter (equivalent to the 10 per cent Kasil solution used in earlier tests given in table 2). Among these were alkali metal sulfates, chlorides, bromides, fluorides, and nitrates. The effectiveness of the ions followed the lyotropic series. The same ions have been shown to be effective in causing silicates to gel (3).

TABLE 3

Effect of sodium sulfate on adhesion of phosphors to glass

SAMPLE	0.5 MOLAR Na_2SO_4 ADDED	FINAL MOLARITY	APPROXIMATE PER CENT Na_2SO_4	ζ-POTENTIAL		ADHESION
				Phosphor	Glass	
	ml.			*mv.*	*mv.*	
C1	0	0	0	—47	—62	Poor
C2	1	0.005	0.071	—52	—61	
C3	3	0.015	0.213			Poor
C4	10	0.05	0.71	—39	—44	
C5	25	0.125	1.78	—30	—33	Good
C6	50	0.25	3.55	—19	—25	
C7	70	0.35	4.97			Good

MECHANISM

The roles of the silicate and the electrolyte used as addition agent in producing adhesion appear to be as follows:

(*1*) The silicate is adsorbed on both the glass and the phosphor surfaces, producing strong negative charges. In very simplified form this may be represented as follows:

---

[4] E sodium silicate is a purified solution of $Na_2O{:}3.32SiO_2$ containing approximately 8.6 per cent Na_2O and 27.7 per cent SiO_2.

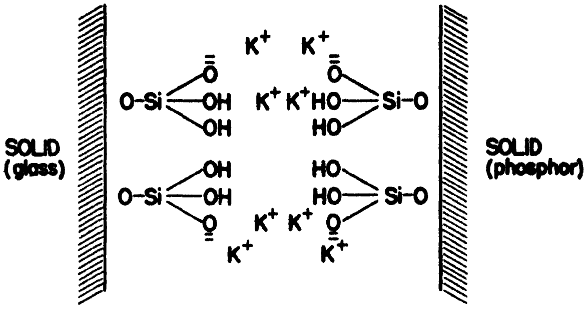

The negative charges keep the surfaces apart and the alkalinity is sufficient to prevent polymerization.

(*2*) When a salt is added, (*a*) the negative potentials are decreased, (*b*) the salt tends to promote the formation of oxygen bridges by intermolecular dehydration, and (*c*) since the silicate is concentrated by adsorption on the solid surfaces, the loci of polymerization are predominantly there.

A very simplified representation of the situation may be given thus:

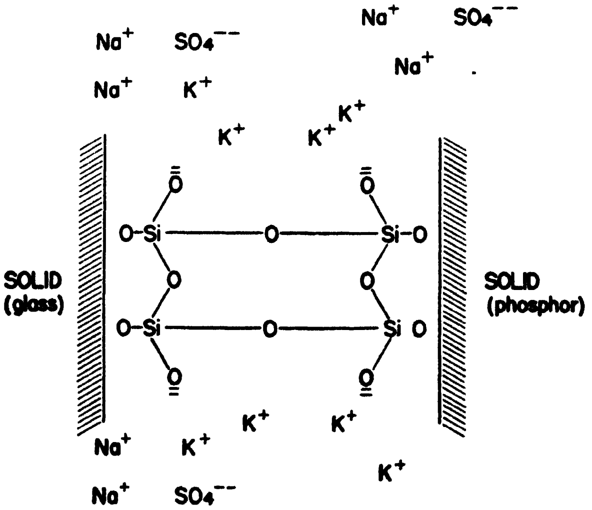

It must be recognized that the above models show only functional group types The composition of the potassium silicate used may be represented by the formula:

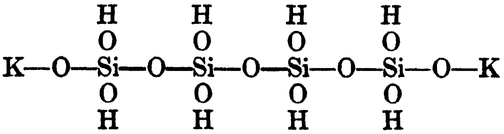

$$\begin{array}{ccccccccccccc} & & \mathrm{H} & & \mathrm{H} & & \mathrm{H} & & \mathrm{H} & & & & \\ & & \mathrm{O} & & \mathrm{O} & & \mathrm{O} & & \mathrm{O} & & & & \\ \mathrm{K}-\mathrm{O} & - & \mathrm{Si} & -\mathrm{O}- & \mathrm{Si} & -\mathrm{O}- & \mathrm{Si} & -\mathrm{O}- & \mathrm{Si} & - & \mathrm{O}-\mathrm{K} & & \\ & & \mathrm{O} & & \mathrm{O} & & \mathrm{O} & & \mathrm{O} & & & & \\ & & \mathrm{H} & & \mathrm{H} & & \mathrm{H} & & \mathrm{H} & & & & \end{array}$$

This would be capable of ionizing to give two potassium ions and a silicate ion with a double charge. Actually, of course, the situation is more complicated. Part of the silicate is present in the form of multicharged ionic micelles (4). In addition, there is little hydrolysis. While these factors affect the degree of condensation, the basic cross-linkage mechanism would be the same.

The concentration of the added salt will determine to a considerable extent the degree of cross-linkage. Higher concentrations of salt would increase the number of linkages and increase the strength of the bond.

The condensation-polymerization is a relatively slow process. The addition of acids or acidic materials induces a much more rapid type of polymerization. However, we believe that too much reduction in pH is undesirable, first, because the bond thus formed is weaker and, second, because the process becomes much more difficult to control. Some reduction to decrease the time required for the formation of a good screen may be worth while. Studies on this are under way.

The effects of various factors in screen formation are being studied. We hope to report on these in a later paper.

REFERENCES

(1) Adam, N. K.: *The Physics and Chemistry of Surfaces*, 3rd edition, pp. 202–4. Oxford University Press, London (1941).

(2) Edelberg, R., and Hazel, F.: Trans. Electrochem. Soc. **96**, 13–20 (1949).

(3) Hazel, F.: Unpublished work.

(4) McBain, J. W., and Salmon, C. S.: J. Am. Chem. Soc. **42**, 426–60 (1920).

(5) Sadowsky, Meier: Trans. Electrochem. Soc. **95**, 112–18 (1949).

ON THE STRUCTURE OF MONOLAYERS AND MULTILAYERS OF POLAR HYDROCARBON MOLECULES ON SOLID SUBSTRATES

H. T. EPSTEIN[1]

Department of Physics, University of Michigan, Ann Arbor, Michigan

Received October 20, 1949

I. INTRODUCTION

The many studies (1, 5, 12) of monolayers and multilayers of polar hydrocarbon molecules on solid substrates have not yet resulted in knowledge of the detailed arrangement of the molecules in such layers. The properties of the layers are sufficiently characteristic so that it has not been possible to infer the structure from the properties.

Some of the properties peculiar to these layers are as follows: (*a*) the layers are simultaneously hydrophobic and oleophobic; (*b*) the layers are close-packed, but the molecules are randomly situated on the substrate; (*c*) the molecules have their axes tilted at random away from the normal to the substrate, and the tilts take on all values up to a maximum value characteristic of the molecule; (*d*) the binding energy per atom in the layers is greater than the binding energy per atom in crystals of the same molecules, according to the first, relatively rough measurements of the binding energy.

---

[1] Present address: Departments of Biophysics and Physics, University of Pittsburgh, Pittsburgh, Pennsylvania.

There are many questions raised by a consideration of the observed properties of these layers. The origin of the tilting of the molecules must be found. It must be explained how randomly situated molecules, having random tilts of their axes, can be closely packed, and indeed, so closely packed that their binding energy is probably greater than when the same molecules are in a crystalline array. Further, it is necessary to ask why the usual crystal array ever occurs, if the monolayer structure has a binding energy greater than that of the crystal.

This paper will describe the attempts to obtain answers to some of these questions by the use of electron microscopic observation of the layers.

II. EXPERIMENTAL DETAILS

The monolayers and multilayers considered in this paper are composed of molecules of the normal fatty acid series. Most of the work has been done with the eighteen-carbon-atom molecule, stearic acid, and it will be used as prototype throughout the discussion.

The layers have been deposited on glass microscope slides by either of two methods: the Langmuir–Blodgett dipping technique or the oleophobic technique. The latter method involves placing a drop of stearic acid dissolved in, say, hexadecane on the slide; the drop then rolls over the slide, leaving a single layer of molecules on the surface. The former method requires that a drop of a solution of stearic acid (e.g., in benzene) be placed on a water surface. The drop spreads out to form a monolayer of stearic acid on the surface. Insertion and withdrawal of a slide result in the deposition of a single layer of molecules during each insertion and withdrawal after the first immersion of the slide. By adjusting the pH of the water according to the standard recipes of Blodgett and Langmuir (4) the monolayer can be made to contain any arbitrary proportion of stearate molecules, e.g., barium stearate, if a barium salt is added.

Once the layers are formed, they are shadow cast with platinum, palladium, or uranium. The preshadowed replica technique (14) is used to prepare the layers for examination in the electron microscope.

It should be pointed out that the contrast of the layers with the substrate is so low that the study is impossible without the enhanced contrast afforded by the shadow-casting technique.

III. RESULTS AND DISCUSSION

A. Layer heights

It was necessary first to ascertain whether the shadow-casting procedure has any effect on the layer structure. This check can be made, to some extent, by measuring the height of the layers, for the layer height of barium stearate molecules is known, from optical measurements (4), to be nearly 25 Å. per layer.

The attempt to make or to find holes in the monolayers was not successful. However, holes can be obtained in multilayers simply by making the successive

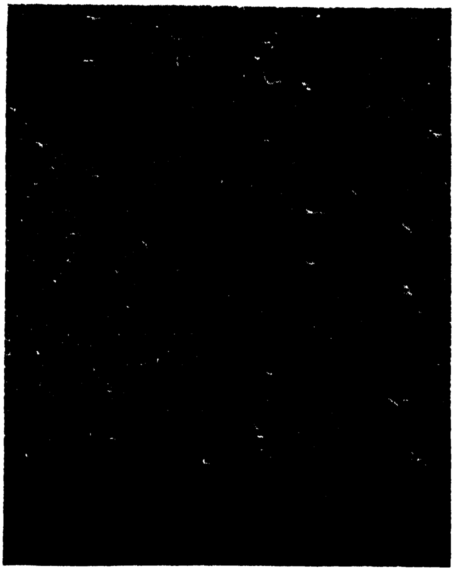

FIG. 1. Electron micrograph of three layers of stearic acid.

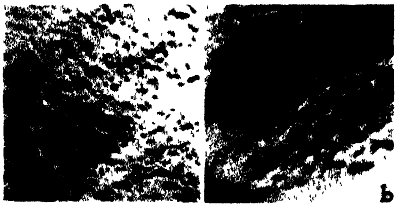

FIG. 3. Twenty-one layer film of stearic acid barium stearate after immersion in benzene (a) for 2 sec. and (b) for 1 min. Layers prepared at pH 6.4.

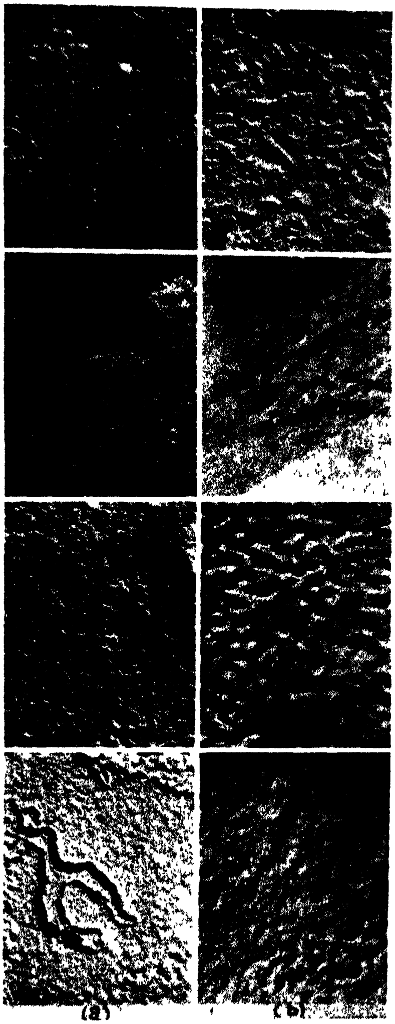

FIG. 2. Twenty-one layers of stearic acid-barium stearate (a) before and (b) after immersion in benzene for 1 min. From top to bottom, layers prepared at pH's of 5.8, 6.4, 7.3, and 7.9.

dips of the slide more rapidly than is suitable for smooth layer deposition. The speed used was about one dip per second. A typical preparation is shown in figure 1. The preparation was shadow cast so that the layer height was one-third the shadow width; from this datum and knowing the magnification of the picture, the layer height is found to be about 50 Å. Measurements on two dozen such preparations gave an average height of 45 Å. As has been previously mentioned, two molecules are deposited when the slide is inserted and withdrawn from the water, so that the height per molecule is half the measured value, or 23 Å. The height of the layers studied in the electron microscope should be a little less than that of the layers studied by Blodgett and Langmuir, for the present study measures the height of a stearic acid molecule, and it is known to be tilted away from the normal more than is the barium stearate molecule studied by Blodgett and Langmuir.

The agreement of the layer heights with that determined by the optical measurements is taken as evidence that shadow casting has little effect on the orientation of the molecules, though it cannot be stated that the grouping of the molecules has not been affected.

B. Skeletonized films

By dipping a multilayer-covered slide in benzene for about 30 sec. Blodgett and Langmuir (4) were able to reduce the refractive index of the multilayer from about 1.5 to 1.3 with practically no change in the measured thickness of the film. It is known that benzene selectively dissolves the stearic acid in these layers and leaves the barium stearate molecules. Thus, it was thought that it might be possible to learn something about the distribution of the acid in the layers by observing the pattern of the holes in the film with the electron microscope.

It is not possible to obtain sharp micrographs of films as thick as those used by Blodgett and Langmuir in their studies of skeletonization. Their films averaged about 170 molecular layers; this number of layers corresponds to a film thickness of about 4000 Å. In the present study, a film of 21 layers (about 500 Å.) was selected as a thickness which would probably show the effects of skeletonization and which is still thin enough to allow fairly sharp micrographs to be obtained. The films were prepared on water having pH values of 5.8, 6.4, 7.3, and 7.9. The films on which Blodgett and Langmuir made most of their observations were prepared at pH 6.4.

Figure 2 shows the effects of dipping the series of layers in the benzene. The first column contains micrographs of the layers before they were immersed in benzene for 1 min.

Layers deposited at pH 5.8 are simply reduced in thickness by a rather extensive dissolving of the entire film. Rather deep holes are made in the layers deposited at the other pH values. There appear to be fewer holes in the layer deposited at pH 7.9 than in the other two layers in which holes appear, as might be expected because there is less acid in the layers, the higher the pH.

One set of observations was made on the effect of dipping a layer in benzene for different lengths of time. A layer prepared at pH 6.4 was dipped for 2 sec. The micrograph of this preparation (figure 3a) is shown beside the preparation dipped for 1 min. (figure 3b). The total area of the holes in the 2-sec. preparation seems not particularly different from the hole area in the 1-min. preparation. However, there seem to be more and smaller holes in the 2-sec. preparation. The implication of the difference between these two preparations is that there must be considerable mobility of the stearate molecules in the layers so that the small holes are brought together. The stearate molecules have this mobility, of course, only while the layers are immersed in the solvent.

A suggestion concerning the mechanism of skeletonization can be obtained from the fact that the total hole area remains roughly constant while the average density of the film decreases, according to the measurements of Blodgett and Langmuir. Because the hole area remains constant, it is suggested that the removal of a large fraction of the molecules probably occurs by a mechanism, perhaps diffusion, which brings the acid molecules from the inside of the film to the holes. Once in the holes, the molecules are removed by the solvent. Furthermore, since the hole area seems to be established practically at the first contact of the solvent with the film, the formation of the holes probably occurs by a simple mechanism. Now, when the slide is first immersed in benzene, the solvent sees only that a certain fraction of the molecules of the top layer is stearic acid, and these acid molecules are taken out into solution. Of the molecules in the second layer which are revealed by the extraction of the acid molecules in the top layer, the same fraction, on the average, is stearic acid. Presumably, the acid molecules in the second layer are likewise dissolved out, and the solvent then attacks the acid molecules in the third layer, and so on.

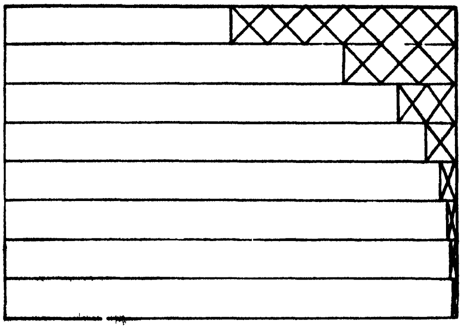

FIG. 4

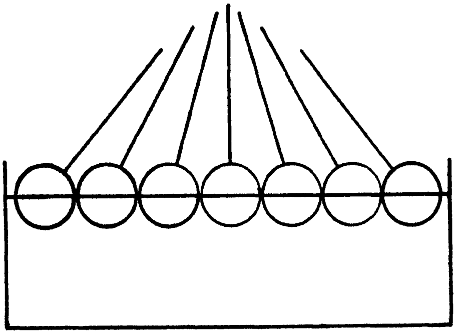

FIG. 5

FIG. 4. Schematic representation of a skeletonized multilayer
FIG. 5. Cross-section of a stearic acid micelle on water

This picture of the action of the solvent is indicated schematically in figure 4, which has been sketched, for simplicity, for the conditions at pH 6.6 at which there are equal amounts of acid and stearate in the layers. Since half the top layer is stearic acid, this half is removed by the solvent, and the removed area is indicated by the cross-hatched portion of the layer. Half of the molecules underneath the cross-hatched portion are stearic acid, and these too are removed, as indicated, and so on.

The average thickness of the film of figure 4 can be calculated by a simple numerical integration, as follows: Let t_1 be the thickness of the film before skeletonization and $\bar{t}_2$ be the average thickness after skeletonization. l is the thickness of one layer of molecules, and N is the number of layers in the film. The calculation is done for unit width of film perpendicular to the paper; the length of the portion of the film considered is s. The expressions for t_1 and $\bar{t}_2$ are:

$$t_1 = Nl$$

$$s\bar{t}_2 = Nl\frac{s}{2} + (N - 1)l\frac{s}{4} + (N - 2)l\frac{s}{8} + \cdots$$

Thus:

$$\frac{\bar{t}_2}{t_1} = \frac{1}{2} + \frac{(N - 1)}{4N} + \frac{(N - 2)}{8N} + \cdots$$

For the layers studied by Blodgett and Langmuir, N is about 170, and the integration intervals are a little different from the simple $s/2$, $s/4$, $s/8$, etc., of the expression given above for a layer prepared at pH 6.6. The result of the calculation for the layers studied by Blodgett and Langmuir is:

$$\bar{t}_2/t_1 = 0.990$$

This figure is to be compared with the experimentally found value, 0.992.

The apparent agreement of the experimental and calculated values of $\bar{t}_2/t_1$ should probably not be taken too seriously until some optical experiments have been done on thinner films than those used by Blodgett and Langmuir. The calculation is relatively insensitive to the number of layers, if the number is large.

Finally, it should be mentioned that the mobility of the stearate molecules (while the film is in the solvent) prevents obtaining information about the distribution of the acid and stearate molecules within the layers.

C. The characteristic grouping and tilt of the molecules

One of the more striking features of the monolayers and multilayers as revealed by the electron micrographs is the apparent grouping of the molecules into clusters, which, for stearic acid, are about 100 Å. in diameter. It was thought at first that the clustering is due to the roughness of the substrate. Both glass and collodion are known to have irregularities in their surfaces of the same order of magnitude as the cluster diameter. It was later realized that the observed cluster size remained approximately constant, although layers were deposited on substrates cleaned in a variety of ways. The constancy of the cluster size led to experiments designed to test the hypothesis that the molecular clustering is a property of the monolayer structure and is not entirely a feature caused by the roughness of the substrates.

The obvious way of testing the above hypothesis is by depositing the layers on smooth substrates. The finding of a smooth substrate is, however, one of the unsolved problems which generated the present work. A long series of experiments by Williams and Backus (14) and by the writer has ended in the conclusion that none of the methods tried has produced a smooth glass or collodion substrate. It is true that the heights of the irregularities of glass microscope slides have been reduced by polishing with rouge so that the slopes of the irregularities are probably less than 10°. The diameters of the irregularities have not been reduced, however, so that the slides cannot be considered smooth enough to permit a definite statement to be made that the molecular clustering is a characteristic property of the monolayers. Accordingly, the evidence for the existence of characteristic clustering of the monolayer molecules must be obtained from other experiments to be described below.

Langmuir (11) has used the idea of clusters of molecules in monolayers to explain the properties of expanded layers. He called these groups *micelles*, and this name will be adopted for the clusters seen with the electron microscope.

Langmuir's explanation of the existence of micelles starts from the experimental finding that the cross-section of the hydrated carboxyl groups is much greater than the cross-section of the hydrocarbon tails. The arrangement of the molecules within a micelle is believed to be as indicated by the sketch in figure 5. The circle represents the carboxyl group; the straight line represents the hydrocarbon tail.

It occurred to the writer that even the unhydrated carboxyl groups might be larger in cross-section than the hydrocarbon tails. A search of the literature reveals that Adam (1) has already suggested such a possibility. The data which Adam has obtained for the cross-sections of the unhydrated acid molecules give an area of 20.4 Å.^{2} for all the long-chain acid molecules. The area of the hydrocarbon tails has been measured by Müller (13) and is 18.4 Å.^{2} The explanation generally given for the difference between the two areas just described is that the acid molecules are all tilted by the same angle (about 26°) away from the normal to the water surface. Adam pointed out that it was equally possible to explain the area difference by saying that the cross-section of the acid is determined by the area of the carboxyl group, which is then taken to be 20.4 Å.^{2} Then there is no necessity for assuming that the molecules are all tilted away from the normal. The assumption of tilted molecules on water has not been supported by any accepted arguments or experiments to make plausible that there should be any tilt at all, or that there should be a single tilt angle for all the molecules of the fatty acid series. At the time of Adam's writing, however, it was not important to know which, if either, of the explanations of the difference in cross-section was correct, so Adam carried the discussion no further than the mere suggestion of the alternative explanation.

Adam's suggestion leads to a calculation of the size of the stearic acid micelles found on solid substrates which is in reasonable agreement with the size observed with the electron microscope. This calculation will now be presented.

First, Langmuir's condition for limiting the size of the micelles can be restated in a somewhat more usable form. The condition suggested by Langmuir is that the tails are forced so far apart that they cannot bind the molecules to each other. Here we shall say that the binding energy of the molecules decreases as the molecules tilt, the energy decrease arising from the fact that the molecules slip along each other as indicated in figure 5. Then, the condition for limiting the size of the micelle is taken to be the decrease in binding energy by some definite amount, perhaps of the order of the binding between each pair of carbon atoms. When the binding energy has decreased by this amount, it is then energetically more stable to form a second micelle than to continue the growth of the first micelle.

Although the limiting decrease of binding energy is not known, an equivalent quantity can be calculated from the data on the size of micelles on water. This quantity is the tilt of the outermost molecules in the micelle. The limiting angle of tilt on water will be calculated and applied to the case of the molecules on a solid substrate.

If the molecule is taken to have a cylindrical shape, the radius of the hydrocarbon tail is $\sqrt{18.4/\pi}$ = 2.42 Å. Similarly, the radius of the hydrated carboxyl group is $\sqrt{26/\pi}$ = 2.88 A. The difference in the radii is 0.46 Å. If two molecules come together, the angle between them is approximately given by the difference in the diameters of the opposite ends of the molecules divided by the length of the molecule: 0.92/24.4 = 0.038 radian.

According to Langmuir's diagram of the way the molecules are arranged in a micelle, there are about two or three molecules per micelle radius, for stearic acid. Since the tilt per molecule is 0.038 radian, the tilt of the outermost molecules is, say, 2.5 times this angle, or nearly 0.1 radian, which is nearly 6°.

The unhydrated carboxyl group has already been mentioned as having a cross-section of 20.4 $Å^2$. The difference in diameter of the polar group and the hydrocarbon tail in this case is only 0.26 Å. The angle between two molecules is then 0.26/24.4 = 0.01 radian. Thus, if the limiting angle of tilt is 0.1 radian, there must be 10 molecules in the radius of a micelle on a solid substrate where the molecule is not hydrated. The micelle then has a diameter of 20 molecules, or 20 × 5 = 100 Å., since the diameter of a molecule is about 5 Å. This value for the micelle diameter is the same as that found with the electron microscope for the clusters of stearic acid on glass and collodion substrates.

Further, it should be observed that the calculated limiting angle of tilt is in agreement with the characteristic limiting tilt angle found for stearic acid by electron diffraction techniques, within experimental error.

Because the calculation just presented can correlate three hitherto unrelated experiments, and because it leads to predictions of the micelle diameter and characteristic tilt angle which are in reasonable agreement with experiment, it is felt that there is a strong possibility that the molecules in a monolayer are really grouped together in micelles. Further evidence suggesting the reality of the micelles will be presented below.

The experiments on the wetting temperatures of oleophobic layers yield desorption energy values which can be interpreted as indicating that the monolayer molecules are arranged in clusters. Zisman and coworkers (2, 3) found that the binding energy per carbon atom of the molecule is either about 1200 cal./mole or about 200 or 300 cal./mole, depending on which, if either, of their two calculations is correct.

It will be shown in appendix A that there is an error in the calculation which leads to the smaller value for the binding energy. When the calculation is corrected, the resulting binding energy value is in good agreement with the larger of the two values given by Zisman and coworkers.

If the larger binding energy per carbon atom (1200 cal./mole) is correct, it is necessary to ask what molecular configuration could give a greater binding energy than the crystal array, and also to ask why the monolayer configuration of the molecules is not adopted in the three-dimensional arrangement of the molecules. The answer to the latter question must be that it is not possible to continue the monolayer configuration into the third dimension.

The arrangement of fatty acid molecules in the crystal is indicated schematically in figure 6a. The angle by which the tails of the molecules are tilted away from the surface normal is about 35° (6). When the molecules are in a monolayer, they are known to be oriented to within, say, 10° of the surface normal, as suggested in figure 6b. However, the binding energy per carbon atom is no more in the arrangement of figure 6b than it is in the arrangement of figure 6a, unless the tails are closer together in the monolayer array. The tails can be closer together in the monolayer in at least two ways. The first way requires that the effective diameter of the carboxyl group be smaller in the direction of the C—OH bond than it is in the horizontal direction in figure 6a. The possibility of this configuration must be discarded, because there seems to be no reason why a three-dimensional array could not be built with this arrangement of the molecules.

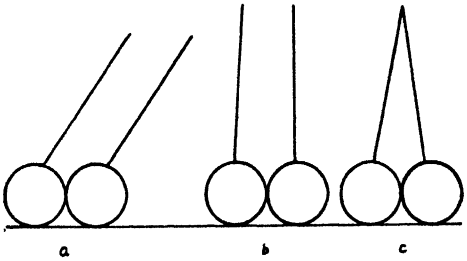

FIG. 6

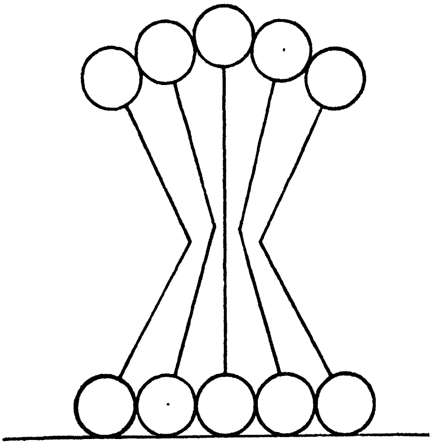

FIG. 7

FIG. 6. The arrangement of polar hydrocarbon molecules in crystals and in oriented monolayers.

FIG. 7. Oriented layer configuration continued into the third dimension

The second way for the tails to get closer together is for the tails to tilt toward each other, as indicated in figure 6c. This configuration satisfies the requirement that it is an arrangement which cannot be continued into the third dimension, as indicated in figure 7. It is seen that the carboxyl groups of the second layer are nonplanar; the nonplanarity can only become worse by building more layers on top of these two layers.

Thus, the above argument tends to support the idea that the molecules are arranged in clusters whose size must eventually be limited by the slip of the molecules on their inner neighbors in the micelles.

The argument for the existence of micelles can be stated somewhat differently, and in a way which seems to be independent of the actual arrangement of the molecules within the micelles. One can say that the molecules in a monolayer must be arranged in micelles containing one molecule, more than one molecule, or all the molecules in the monolayer. If the number of molecules per micelle is unity, it is difficult to understand how there can be a greater binding energy per carbon atom than there is in the crystalline array. If all the molecules are in one micelle, it is difficult to understand how the molecules can be randomly situated on the surface and tilted at random up to a maximum value. Therefore, it seems probable that each micelle contains more than one molecule and considerably fewer than a large fraction of all the molecules in the monolayer.

There is a recent experiment by Karle (9) which yields results which have been interpreted as indicating a micellar grouping of the molecules in oleophobic monolayers. Karle studied the rate of evaporation of monolayers of cerotic acid and *n*-octadecylamine deposited on glass from melts of the pure compounds. He also took electron diffraction pictures of the layers throughout the course of the evaporation. It was found that when the relative amount of material evaporated is small, the characteristic tilt of the molecules in the monolayers does not change appreciably. This result was interpreted as indicating that the monolayer exists as what Karle called patches on the surface, the evaporation taking place mainly from the edges of the patches. Further, Karle was able to analyze his data in terms of the energy necessary to remove a molecule from the monolayer and he found that it is about one-third the average binding energy of a molecule in the monolayer as determined from the data of Bigelow, Glass, and Zisman. This result is taken as further evidence that the evaporation takes place mainly on the edges of the patches, because the evaporation energy is only a fraction of the average binding energy, and therefore it would appear likely that only a fraction of the bonds needs to be broken in order for the evaporation to occur.

There is one more experiment to be discussed at this point which probably offers support to the suggestion that the molecules in a monolayer are collected together in small groups which have a characteristic tilt associated with their outermost molecules. The experiment is the electron diffraction study of rubbed multilayers. It has been interpreted by Germer and Storks (8) as indicating that the multilayer molecules are left on top of the first layer in the form of crystals which are inclined up against the direction of rubbing by about 8°. The thickness of the crystals is believed to be somewhat less than 200 Å.

Because a thickness of 200 Å. is easily observed with the electron microscope if the preparation is shadow cast, it seemed worthwhile to attempt to photograph the rubbed multilayers in order to discover if the crystal structure could be seen directly. There is difficulty in deciding just what Germer and Storks meant by "light rubbing," but a number of preparations were rubbed with varying amounts of pressure. No crystals are visible. As a rule, the rubbing appeared to wipe off all the multilayer except what appeared to be the first layer—a result which had been obtained by Germer and Storks. Mr. W. C. Bigelow obtained electron diffraction patterns to verify that the first layer remained on the substrate after rubbing, and he found the usual monolayer patterns.

The finding that there are no crystals large enough to be seen in the micrographs is interpreted as indicating that the crystals must be less than, say, 200 Å. in diameter. On the basis of this finding, the following suggestion is made concerning the structure of rubbed multilayers.

Because the electron diffraction pattern indicates crystals tilted up against the direction of rubbing, the upward tilting must be due to a structure in the first layer which is repeated in distances of the order of 100 Å. This distance between repeated structures in the first layer is derived from the finding that crystals of this size show the same upward tilting. Furthermore, the structure probably has a cylindrical symmetry, because the layer can be rubbed in any direction and the same result obtained, as far as the interpretation of the electron diffraction pattern is concerned. The crystals are fairly firmly wedged against some structure, because they are not easily dislodged by rubbing in the same direction as the original rub, though very light rubbing in the opposite direction easily removes them. It seems likely that the structure against which the crystals are wedged must be the source of the characteristic upward tilting by about 8°.

If we put together the suggestions of the previous paragraph, they seem to indicate the existence of cylindrically symmetrical groupings of molecules in a monolayer. The groupings are of the order of 100 Å. in diameter, and the outermost molecules are tilted about 8° away from the surface normal.

The discussions of this section, thus far, may be summarized as follows: (*1*) The electron micrographs of monolayers on solid substrates indicate the grouping of the molecules into clusters which we call micelles. (*2*) A suggestion as to the energy condition which determines the size of the micelles on water leads to calculations of the micelle diameter and characteristic tilt of the micelle molecules on solid substrates which are in agreement with the experimentally found micelle diameter and characteristic tilt of stearic acid monolayers. (*3*) Four other independent experiments have been shown to have a consistent interpretation in terms of a micelle structure for the monolayer molecules.

In consequence of the satisfactory results of the calculations presented in the first part of this section, an attempt has been made to formulate a theory which can predict the dependence of the characteristic tilt angle and micelle diameter on the length of the molecule. This theory will be presented in appendix B. The theory predicts that both the micelle diameter and the characteristic tilt angle vary inversely with the length of the molecule, the tilt varying more strongly than the micelle diameter. The details of the experiments designed to test these predictions will be published later; the first results are that both predictions are fulfilled. The fact that the micelle size is found to vary systematically with molecule length is further evidence that the micelle is a characteristic feature of the monolayer itself.

IV. DISCUSSION OF ELECTRON DIFFRACTION EXPERIMENTS ON THE BASIS OF THE MICELLE MODEL FOR MONOLAYERS

On the basis of the existence of micelles within monolayers it is possible to understand the finding that the monolayer molecules are closely packed but randomly placed on the substrate. This finding was based on observations on layers of stearic acid. The micrographs show that the micelles themselves are closely packed and randomly situated on the substrate so that their constituent molecules are primarily arranged in a similar manner. However, it is possible that there should be an orderly arrangement of molecules within a micelle. An orderly arrangement of the molecules would seem to be more possible the more nearly equal are the cross-sections of the polar group and the hydrocarbon tail, as is the situation in barium stearate films. In the patterns from stearate films, Germer and Storks observed a very few spots on the bands, indicating an orderly arrangement of molecules of not too extensive a nature.

The micellar grouping of monolayer molecules is also one by means of which it appears possible to have an oriented film in which the tilts of the molecules are randomly directed around the surface normal, and still have a closely packed layer. Furthermore, the model explains the observation of Karle and Brockway (10) that the patterns seemed to indicate that the number of molecules tilted at any angle appears to increase with the angle of tilt.

The development of multilayers is also more clearly understandable on the basis of the existence of micelles. Germer and Storks (7) noted that the three-layer diffraction pattern is composed of both a monolayer and a crystalline pattern, and that the monolayer pattern shows the tilt angle to be less than it would have been before the upper layers were deposited.

The change of the tilt of the molecules will be explained with the aid of the sketches in figures 5, 7, and 8. Figure 5 represents a monolayer micelle. When the second layer is added, as indicated in figure 7, the carboxyl groups would have to be nonplanar if the first layer were to remain undisturbed. It is probable that there would be a decrease in the binding energy if the nonplanarity were very great, so it is not unreasonable to suppose that there is a decrease for all nonplanar configurations. Thus, it is indicated that there may be some tendency to alter the configuration toward that in figure 8. Furthermore, when the third layer is deposited, the molecules of the second and third layers have been shown to form a crystalline array. Thus there will be an even greater tendency to straighten up the tilted molecules of the first layer and to rearrange them into the regular crystal positions. The deposition of even more layers should give a crystal structure increasingly closer to the naturally occurring crystal structure, owing to the strengthening of the tendency of the upper layers to rearrange the molecules of the first layer.

The fact that the regular crystal structure is not found for a three-layer film indicates both that the first-layer molecules are not regularly spaced and that the surface formed by the ends of the tails is not planar, for if these conditions were met, the second and third layers could form as regular an array as they do on Resoglaz, according to Germer and Storks. Furthermore, it is indicated that the randomness of the positions of the first-layer molecules is not the randomness of separated molecules but rather that these molecules have some sort of stable configuration. This conclusion is based on the idea that it would probably be easy to rearrange the molecules if they were not in a stable configuration already.

In many of the micrographs which have already been shown, the micellar structure can be seen to persist through many layers. This result may be interpreted as showing that the crystal built on top of each micelle tends to grow separately from the crystals which are developing on top of the other micelles.

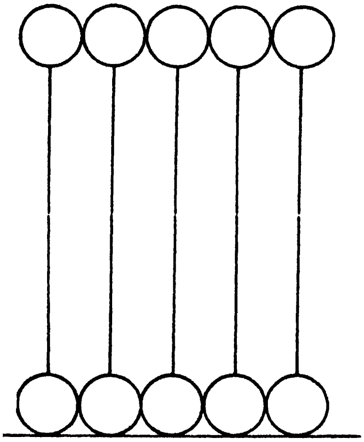

FIG. 8

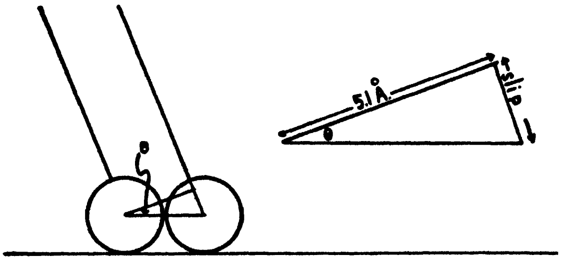

FIG. 9

FIG. 8. Effect of depositing a second layer of molecules on top of a monolayer
FIG. 9. Relation of limiting tilt angle to slip of molecules on each other

If this interpretation of the micrographs is correct, then the various planes of one crystal need not be oriented parallel to the corresponding planes of the other crystals. The electron diffraction pattern from such an array of crystals should show all orientations of the crystal planes with respect to the surface normal, unless there is some other factor tending to orient the planes. In the barium stearate multilayers there appears to be no such factor, and the crystal planes have been found by Germer and Storks to be randomly oriented with respect to each other.

In the stearic acid crystals, however, there exists an orienting factor. As indicated previously, the molecules in such crystals are tilted about 35° away from the surface normal. Germer and Storks pointed out that there should therefore be a strong tendency to line up these crystal tilts in the direction in which the slide is dipped to form the multilayer, and they observed the results of such a factor.

The stearic acid multilayer diffraction patterns can be interpreted without there being micelles, but the barium stearate multilayer patterns seem to require the existence of micelles.

V. SUMMARY

Monolayers and multilayers of the normal fatty acids have been prepared on solid substrates and examined by electron microscopy and electron diffraction.

The main result is the observation that the molecules are grouped into two-dimensional micelles, about 100 Å. in diameter. On the basis of the existence of micelles, it is shown to be possible to explain and correlate a number of experimental results of previous workers. Several inconsistencies and errors in previous work are resolved and corrected.

An order of magnitude theory of micelle structure is developed, and preliminary experiments indicate that its predictions are at least qualitatively correct. The theory relates the micelle diameter, the observed maximum tilt of molecules in a monolayer, and the length of the molecule.

Skeletonized films are examined, and it is observed that deep holes develop in such films. A mechanism for skeletonization is proposed and is found not to be inconsistent with the very limited amount of data available on skeletonized films.

The writer would like to express his gratitude to Professor R. C. Williams, who suggested this problem and guided the research so helpfully. It is a pleasure to acknowledge the many discussions with Professors L. O. Brockway and E. Katz. Finally, thanks are expressed to Mr. W. C. Bigelow for doing the electron diffraction work needed in conjunction with the research and also for supplying all the purified chemicals.

REFERENCES

(1) Adam: *The Physics and Chemistry of Surfaces*, 3rd edition. Oxford University Press, London (1941).
(2) Bigelow, Glass, and Zisman: J. Colloid Sci. **2**, 563 (1947).
(3) Bigelow, Pickett, and Zisman: J. Colloid Sci. **1**, 513 (1946).
(4) Blodgett and Langmuir: Phys. Rev. **51**, 964 (1937).
(5) Brockway and Karle: J. Colloid Sci. **2**, 277 (1947).
(6) Germer and Storks: Proc. Natl. Acad. Sci. U.S. **23**, 390 (1937).
(7) Germer and Storks: J. Chem. Phys. **6**, 280 (1938).
(8) Germer and Storks: Phys. Rev. **55**, 648 (1939).
(9) Karle: J. Chem. Phys. **17**, 500 (1949).
(10) Karle and Brockway: J. Chem. Phys. **15**, 213 (1947).
(11) Langmuir: J. Chem. Phys. **1**, 756 (1933).
(12) Langmuir: Proc. Roy. Soc. (London) **170**, 1 (1939).
(13) Müller: Proc. Roy. Soc. (London) **114**, 542 (1927).
(14) Williams and Backus: J. Applied Phys. **20**, 98 (1949).

APPENDIX A

Correction of theoretical treatment of oleophobic layers

The deposition of monolayers by the oleophobic techniques has given the possibility of measuring U, the energy of adsorption (or desorption) of the molecules, by raising the temperature until the molecules no longer form an oleophobic layer. Zisman and coworkers (2, 3) developed theoretical arguments to show that dU/dN, the binding energy per carbon atom of the molecules, is 1200 cal./mole or 200 cal./mole, depending on which of their two theoretical developments is used. N is the number of carbon atoms in a molecule. It was suggested in the main part of this paper that the larger of the two values is correct, and the larger value was used to offer an additional reason for believing that the monolayer molecules associated into micelles.

It will be shown that there is an error in the second calculation by Zisman and his group, and a value of the order of 1200 cal./mole/carbon atom will be shown to be correct for dU/dN.

The authors measured τ, the wetting temperature for deposition of monolayers from solutions of the pure molten acids, from which they calculated a a quantity b^2, defined as $b^2 = U/R\tau$. This quantity was determined for the acids, alcohols, amines, and amides, and was found to be constant within about 15 per cent; the value is about 15. Thus, dU/dN can be obtained by differentiation to be

$$dU/dN = b^2R\, d\tau/dN$$

Since R and b^2 are known, and since $d\tau/dN$ can be determined from the data from pure molten compounds, dU/dN can be calculated, and is found to be 212 cal./mole/carbon atom at $N = 18$. A similar calculation was carried out for the amines, amides, and alcohols. The value of 336 cal./mole/carbon atom for the amines was considered to be in good agreement with a value of 400 cal./mole/carbon atom found from the desorption energy data as outlined above.

The value 400 cal./mole/carbon atom was obtained from the desorption energies for the amines with ten and eighteen carbon atoms. However, it must be remarked that the desorption energies of the amines with six and ten carbon atoms lead to a value of 1200 cal./mole/carbon atom for dU/dN. In pointing out the agreement of the numbers 336 and 400 for the amines, the Zisman group ignored the fact that the corresponding numbers for the acids are 212 and 1200.

The error is a simple one. In evaluating the constant b^2, these authors first showed that it is really a constant by evaluating it from the data from the acids, alcohols, amines, and amides. The resultant values for b^2 differed from each other by less than 15 per cent. However, an inspection of the evaluation reveals that the data were all from molecules eighteen carbon atoms long. Thus, the possibility that b^2 depends on the chain length, N, is not ruled out, as tacitly assumed by the authors. The derivative db^2/dN can be evaluated from their data, and is found to be of the order of unity; the value actually obtained is 1.5. The relation giving the energy increment per carbon atom is then modified to:

$$dU/dN = Rb^2\, d\tau/dN + R\tau\, db^2/dN$$

Inserting the values for the various quantities, we obtain:

$$dU/dN = 212 + 1100 = 1312 \text{ cal./mole/carbon atom}$$

This value agrees with the 1200 cal./mole/carbon atom found by the other of their theoretical developments.

APPENDIX B

A theory of the variation of micelle structure with molecule length

The limiting tilt angle can be calculated from the amount that one molecule slips on its inner neighbor owing to the tilt. From figure 9 it is seen that the limit angle is given by the relation:

$$\tan \theta = \frac{\text{slip distance}}{\text{intermolecular spacing}} = \frac{x}{5.1} \tag{1}$$

The slip distance is not known, but it can be evaluated in terms of the decrease in binding energy due to the slip. The assumption is made that the binding energy decrease is the same for all the fatty acid molecules, regardless of their length. This assumption leads to the relation

$$N_i \, \Delta\epsilon_i = N_j \, \Delta\epsilon_j \tag{2}$$

where $\Delta\epsilon$ is the slip energy (binding energy decrease) per carbon atom, n is the number of carbon atoms in the molecule, and i and j refer to molecules of different chain lengths.

The variation of the slip energy with distance, x, along the chain is not known, but will be assumed to be representable in first approximation by an exponential relation:

$$\Delta\epsilon = kx^m \tag{3}$$

The exponent m is an adjustable constant, and is the only such constant in the theory, inasmuch as the factor k cancels out when equation 3 is introduced into equation 2. The value of m may be obtained if the characteristic tilt of any molecule, in addition to that of stearic acid, can be measured. Brockway and Karle (5) have made a few electron diffraction measurements of the characteristic tilt of the acid with twenty-six carbon atoms, cerotic acid. However, it will develop that the value of m is very sensitive to the exact value of the tilt angles for the longer chain molecules, so it seems better to use the data for the tilt of a molecule shorter than stearic acid.

Electron diffraction experiments were carried out in Professor Brockway's laboratory by Mr. W. C. Bigelow to determine the characteristic tilt of myristic acid (fourteen carbon atoms). Myristic acid is the shortest chain fatty acid for which the pattern is sufficiently sharp to permit measurement of the tilt angle. The characteristic tilt angle for myristic acid was found to be about 14°. Using this datum and a value of 5.7° (0.1 radian) for the stearic acid tilt angle, the exponent m can be evaluated, as follows:

First, equations 2 and 3 are substituted into equation 1 to give

$$\tan \theta = x_j/5.1 = (x_i/5.1)(N_i/N_j)^{1/m}$$

For $N = 18$, $\tan \theta = \theta = 0.1$, so that $x = 0.51$ Å. Thus,

$$\tan \theta = (0.51/5.1)(18/N_j)^{1/m}$$

For

$$N_j = 14, \tan\theta = \tan 14^\circ = 0.25$$

Then,

$$0.25 = (0.51/5.1)(18/14)^{1/m}$$

Taking logs:

$$\begin{aligned} -0.6 &= -1 + (1/m)\log(1.29) \\ 0.4 &= (1/m)(0.109) \\ 1/m &= 4 \\ m &= 1/4 \end{aligned}$$

Thus, finally:

$$\tan\theta = (1/10)(18/N)^4 \tag{4}$$

The micelle diameter can also be calculated. Because the tangents of the tilt angles are small, for all the tilts which have been measured, the angle, in radians, may be substituted for the tangent in equation 4. The number of molecules in the micelle radius is approximately given by the ratio of the limiting tilt angle to the tilt per molecule. The micelle diameter, D, is then twice this number of molecules times the diameter of a molecule (5.1 Å.):

$$D = 2 \times 5.1 \times \frac{\theta}{0.26/L} = (10.2)(L/0.26)(1/10)(18/N)^4 = 3.4L\,(18/N)^4$$

Since $L \approx (4/3)N$, where L is the length of the molecule,

$$D = 4.5(18)^4/N^3 \tag{5}$$

It should be remarked that the exponent m is not 2, as might have been expected for an equilibrium configuration. The fact that it is not 2 means only that the figure given for m is probably an average value holding over the range of slip distances used in the calculation.

The writing down of equations 4 and 5 is not meant to imply that the calculation presented above has, as yet, a sufficiently quantitative character to warrant more than qualitative deductions from the equations. In order to avoid ambiguity on this point, the results which the writer feels can be extracted from the theory will be stated explicitly: (*1*) equation 4 predicts that the characteristic tilt angle varies inversely with the length of the molecules, probably varying more strongly than with the first power of the length; (*2*) equation 5 predicts that the micelle diameter also varies inversely with the length of the molecules but less strongly than does the characteristic tilt angle.

COMMUNICATIONS TO THE EDITOR

NOTE ON THE DIELECTRIC CONSTANT OF SOLUTIONS OF POLYSTYRENES AND POLYISOBUTYLENES IN TOLUENE

In a previous paper (A. Voet: J. Phys. & Colloid Chem. **53**, 597 (1949)) a report was made on capacity measurements of solutions of polystyrenes and polyisobutylenes in toluene in a quiescent state as well as when subjected to shear in a double cylindrical cell, the outside cylinder of which was rotated. A decrease in capacity was observed in sheared solutions of a concentration above a critical value, which was found to coincide with a departure from Newtonian flow behavior. The observed decrease reached a maximum at a given, low rate of shear. After discontinuation of the shear the capacity was found to return to the value for quiescent solutions and a relaxation time of the order of 4–10 sec., dependent upon the solution, was observed.

The change in capacity was explained in terms of a change in dielectric constant of the solutions, presumed to be caused by a change in particle agglomeration, as had previously been observed in dispersed systems of particles of various pigments (A. Voet: J. Phys. & Colloid Chem. **51**, 1037 (1947)).

Fundamental difficulties encountered in the explanation of additional experiments led to a thorough review of our experimental technique. The accuracy of the capacity measurements was increased from ±1 per cent to ±0.3 per cent, but the results obtained were basically unchanged. While experiments were conducted in completely closed cells, to prevent solvent evaporation, it was decided to repeat some experiments in a specially designed cell allowing visual examination during rotation. A most unusual phenomenon was then observed. The solutions showing a decrease in capacity upon being sheared were found to exhibit elastic anisotropy of a nature recently reported by K. Weissenberg (Proc. Rheol. Congr. Holland, Vol. I, p. 24 (1948)), revealing a deviation in space between the shearing force and the resulting displacement. More specifically, upon being subjected to shear a thin film of the solution was observed to creep upwards along the surface of the stator, leaving an unfilled space between the rotor and the stator. Upon discontinuation of the rotation the liquid film slowly retracted, filling the space once more. This phenomenon is not confined to capillary spaces, but occurred equally in a specially designed cell with a large space between stator and rotor at the top of the cell.

It now appears that the observed reduction in capacity of the various solutions investigated was not due to a decrease of the dielectric constant of the solutions, but resulted from the partial removal of liquid from the annular space between the cylinders upon subjecting the liquid to shear, caused by the existence of a difference in direction of the main axes of stress and those of strain velocity in the liquid exhibiting abnormal viscoelastic behavior. The effect naturally coincides with non-Newtonian flow behavior. The "critical concentration" below which this phenomenon does not occur naturally decreases with increasing molecular weight of the polymer, since non-Newtonian behavior is exhibited in more dilute solutions in polymers of higher molecular weight.

The observed limit of the decrease in capacity at a rather low shearing stress resulted from the fact that the cell was closed and the upward flow of liquid was pushed down again, while the "relaxation time" appeared to be actually connected with the duration of retraction of the liquid into the annular space after discontinuation of the rotation of the outer cylinder.

The absolute values of the dielectric constants indicated in the paper for quiescent solutions need to be corrected, as may be seen from the following.

In the procedure of measuring the capacities of the polymer solutions the outer cylinder was always rotated for some time prior to the start of the measurements, to allow the cup to find its correct position. In solutions showing abnormal viscoelasticity such a procedure causes the part of the inside of the cell above the liquid level to be coated with a film of liquid. Since the constant and variable cell capacities were calculated from the capacities in air and in toluene, where such an effect does not occur, the capacity values for quiescent solutions of a concentration above the "critical" appear too high, the more so, the more concentrated the solutions and the higher the molecular weights.

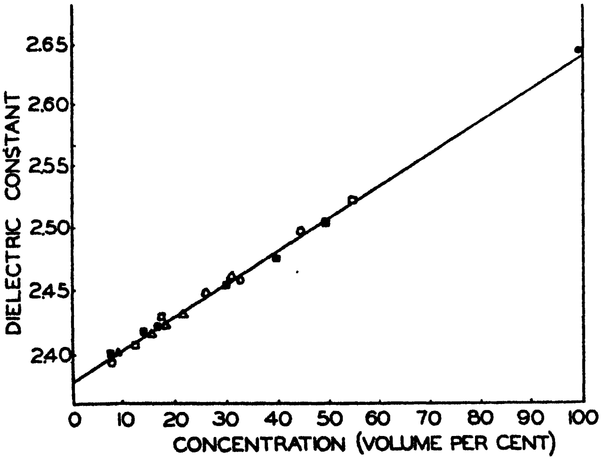

FIG. 1. Dielectric constant-concentration relationship for solutions of polystyrenes in toluene. ●, molecular weight of 300; □, molecular weight of 15,000; ○, molecular weight of 45,000; △, molecular weight of 85,000; ■, various molecular weights (Dannis and Loughborough).

The corrected values, measured at 30°C. by means of a conventional three-electrode capacity cell, are indicated in figure 1 for polystyrenes of different molecular weights dissolved in different concentrations in toluene. Polyisobutylenes show a similar relationship.

The results are in agreement with data brought to our attention by Dr. B. L. Funt, University of Manitoba, Canada, and also by Drs. M. L. Dannis and D. L. Loughborough, B. F. Goodrich Company, Brecksville, Ohio, to whom we wish to express our appreciation for their kindness in bringing the discrepancies in the data to our attention.

The data previously published on the change of the dielectric constants of pigment dispersions subjected to shear are not affected. These liquids, though non-Newtonian in concentrated dispersions, do not exhibit elastic anisotropy, which seems to be restricted to long-chain molecules.

From the foregoing it appears that, owing to the existence of elastic anisotropy, it could not be positively established in our apparatus whether the concentrated non-Newtonian solutions of the nonpolar polymers investigated showed any decrease of the dielectric constant upon being subjected to shear. The more dilute Newtonian solutions, as had been indicated previously, did not show any change in dielectric constant at rates of shear up to 650 reciprocal seconds.

A completely different picture, however, emerges with polar polymers, where a definite decrease of the dielectric constant in dilute solutions subjected to shear has been observed. Thus, in Newtonian solutions of various polyacrylics, polyvinyls, cellulose derivatives, etc. in organic solvents a pronounced decrease of the dielectric constant of the sheared solutions is exhibited.

There are strong indications that the observed changes are caused by molecular orientation.

ANDRIES VOET.
LOUIS R. SURIANI.

J. M. Huber Corporation
620 62nd Street
Brooklyn, New York
January 31, 1950

THE ACTIVATED COMPLEX OF THE PROTEIN MOLECULE

The paper entitled "The Activated Complex of the Protein Molecule" (J. Phys. & Colloid Chem. **53**, 977 (1949)) is erroneous in the calculation of the activation energy of muscle contraction. However, L. Varga has recently published kinetic data on the contraction of muscle (Hung. Acta Physiol. **1**, 138 (1948)). The "rate constants" can be evaluated using the formula $k' = (2.3/t) \cdot \log(1/(1 - r))$, where r is the ratio of the concentration of contracted actomyosin particles at time t divided by the total concentration of actomyosin particles. These "rate constants," averaged for each experimental time interval, show a decreasing trend with increasing time. This is to be expected, since muscle contraction has a temperature-dependent equilibrium evidencing a competing phenomenon of extension of the muscle molecules. Lacking a function to evaluate this competing reaction, one can plot the averaged rate constants against their respective times and extrapolate to zero time. The points were somewhat scattered on the plot, but were adequate for the extrapolation. For 5°, 10°, and 15°C., the rate constants were 0.0051, 0.0095, and 0.017 sec.$^{-1}$, respectively. From these data we find a rate equation for muscle contraction:

$$k' = \frac{kT}{h} e^{-2.0/R} e^{-19,000/RT}$$

The correspondence of the activation energy with that postulated to be characteristic of protein reactions is striking, in view of the fact that adenosine triphosphate is present. This would suggest that the free energy of decomposition of ATP does not aid in contraction. Mommaerts (J. Gen. Physiol. **31,** 361 (1949); Chem. Abstracts **42,** 4626 (1949)) has suggested a similar conclusion. He noted that inosine triphosphate (having a free energy of decomposition similar to that of ATP) has a smaller effect on muscle contraction. He also noted that inorganic pyrophosphate, although not hydrolyzed, acted upon actomyosin similarly to ATP. These facts suggest that the influence of ATP is upon the probability factor, probably by increasing the steric interaction between the parallel peptide chains of the protein molecule.

Two interesting additional experimental correlations supporting the hypothesis of an activated complex of proteins can be cited. McElroy and Strehler (Arch. Biochem. **22,** 420 (1949)) have shown that the luminescence of luciferase is accelerated by the presence of ATP. This experimental correlation is to be expected if contraction of the protein molecule is a necessary precursor to its luminescence. Boyd, Conn, Gregg, Kistiakowsky, and Roberts (J. Biol. Chem. **139,** 787 (1941)) have shown the heat of reaction of an antigen–antibody reaction to be 40 kcal. ± 20 per cent. This value is consistent with the postulated thermodynamic heat of formation of a peptide bond. They also noted that 80 per cent of the heat was given off about 2 min. after mixing. This is consistent with a heat of activation of 19 kcal./mole at 31°C.

If we are correct in this interpretation of the data, this antibody–antigen reaction involves a higher N—H vibrational level and the resultant formation of a peptide linkage between the antibody and the antigen. This also suggests that selectivity of antibody–antigen reactions depends upon the simple probability of reaction. For there is but 10^{-3} to 10^{-2} sec. before a vibrational level of an N—H bond sustains dipole radiation. Thus, steric factors may make it improbable that antibody and antigen molecules approach each other along the reaction coördinate during the time that the N—H bond is in a higher vibrational level.

The statement that repeated irritations leading to cancer are "educational" (in the initial paper) is very inadequate. Actually, these purely chemical considerations of the incidence of cancer lead to conclusions similar to the enzyme–virus hypothesis of carcinogenesis. Especially suggestive are the investigations of Blagoveschenskiĭ. He notes, for example, that the average "energy of activation" of the autolytic enzyme proteolysis for young guinea pigs is $u = 1100$ g.-cal.; for adults, $u = 4300$ g.-cal.; and for "old," $u = 14{,}800$ g.-cal. (Chem. Abstracts **31,** 5387 (1937)). Similarly, he notes that the temperature coefficients of proteolysis and hydrogen peroxide decomposition show an abrupt decrease at the onset of tumor development, followed by a steady increase until the death of the animal (Chem. Abstracts **33,** 6430 (1939)). Since these molecules do not change appreciably with age or with the onset of tumor formation with respect to their chemical constitution, it is probable that the energy barrier of the reaction coördinate does not change very much. The assumption that these molecules are being sterically disorganized or reorganized seems very probable. Thus, we may attribute the trends in "activation energies" noted by Blagoveschenskiĭ to the increased temperature dependence of the probability factors as the respective reactions become increasingly improbable. Within this frame of analysis, a carcinogen accelerates the aging process of the protein molecule but occasionally organizes the protein molecule in such fashion that certain living reactions will be more probable. This is to say that cancer is always possible due to the steric changes in the protein molecule but that a carcinogen makes it more probable by increasing the frequency of these changes.

This hypothesis of mesobiogenesis of virus life is applicable to more than cancer. Yamafuji (Enzymologia **13,** 223 (1949)) postulates the similar hypothesis that virus production is possible without infection. His correlation of an accumulation of hydrogen peroxide with the incidence of virus production parallels the concept of carcinogens. He notes that rapidly growing organisms are very susceptible to virus production without infection. This latter mechanism is very suggestive of poliomyelitis. Although the mechanism by which the virus synthesis and the resultant damage of poliomyelitis are effected can be very complex, the factor of rate of reaction is critical if this analogy is valid. Thereby, one can predict that those experimental conditions which will reduce the rate of growth of children will reduce the probability of chemical disturbances leading to atypical protein synthesis characteristic of poliomyelitis. Statistical considerations may show that conditions of decreased temperature, reduced diet, lessened physical activity, chemical growth inhibitors, etc., will lower the incidence of poliomyelitis.

The foregoing is to be distinguished from the existing correlation of the average severity of poliomyelitis and the physical activity carried out after the onset of early symptoms (Horstmann: J. Am. Med. Assoc. **142,** 236 (1950)). This does, however, indicate that the rate of protein synthesis (and consequently virus accumulation) correlates with physical activity. It also has been found experimentally that the antibodies in the circulating blood increase 1000 times before they appear appreciably in the central nervous tissue (as a result of infection by the poliomyelitis virus). This suggests that the rate-determining step of inactivation of the virus is diffusion from the blood stream into the tissues by the antibody. We can contend that the severity of poliomyelitis depends in part on the rate of antibody diffusion relative to that of protein synthesis.

It is conceivable that mesobiogenesis of virus life and the generation of antibodies to inactivate these is constantly going on. This mechanism may be quite general, being applicable to many virus diseases which appear randomly or with chemical disturbances. The common cold is an illustration of this. It is interesting to note that incidence of the common cold can be reduced with antihistamines, which very probably do inhibit the rate of protein synthesis.

Anomalous to this mechanism is the resistance of a cancer virus to inactivation by antibodies. It is to be suggested that the cancer virus is insufficiently sterically changed from the normal proteins to be readily disposed of by an antibody–antigen reaction. Thus, the probability of the antigen–antibody reaction may become the rate-determining factor of virus inactivation. It is, nevertheless, conceivable that use of chemicals to reduce the rate of protein synthesis of the system on which the cancer virus is parasitic could successfully shift the relative rates in favor of inactivation by the virus antibody.

The concept of mesobiogenesis is applicable to more than pathological phenomena. A comparison between a gene and a virus is limited but is adequate to exemplify the concept of the steric factor in the chemical reactions of the gene. A mutation in the germ plasm may be alternatively described as mesobiogenesis in a protein molecule at the site of a gene. It is consistent with these hypotheses that altering a gene involves steric changes of the appropriate region of the protein molecule.

DAVID S. KAHN.

793 Main Street
Lynnfield Center, Massachusetts
February 10, 1950

NEW BOOKS

An Advanced Treatise on Physical Chemistry. Vol. I. Fundamental Principles—The Properties of Gases. First edition. By J. R. PARTINGTON. 6 x 10 in.; xlii + 943 pp.; 269 illustrations. London: Longmans, Green and Company, 1949. Price: $16.00.

Volume I is intended to form a part of a comprehensive treatise on physical chemistry which will appear in three or four volumes. The author is to be congratulated on putting particular emphasis on the experimental side of physical chemistry, which has been neglected in many recent works in this field. Excellent descriptions of apparatus and experimental methods are given, along with numerous numerical data. In most cases the descriptions of experimental methods are brief, but enough is given to indicate the techniques which have been used in various investigations and thus suggest the possibility of their adaptation to new problems. Complete literature references are given which will enable anyone to find full details of a particular method. Over eighteen thousand references are included, which are complete to the end of 1948. These references are certainly one of the most valuable features of the book and furnish an invaluable source of information for physical chemists.

Although theoretical considerations are fully covered, a large number of empirical or semiempirical equations are given which will be of particular interest to chemists or chemical engineers in pilot-plant work, who often require data which are not available but which can be calculated with sufficient accuracy for their needs by means of such equations. Only those research workers who have been faced with the need of finding an approximate value for a given quantity can realize how much more useful such equations are than theoretical equations which contain unknown constants. The book, therefore, differs from a number of similar books on physical chemistry which tend to treat a given subject around a few theoretical ideas and thus neglect practical material.

While the book is very comprehensive, it is also highly intelligible. As the author states in the preface, "the title 'advanced' refers rather to the size and scope of the work than to its difficulty." A mathematical introduction, together with special sections in the text dealing with more advanced mathematics, will enable readers having only an elementary knowledge of mathematics to follow the subject material readily. A full list of the symbols used in the text is given along with a table of fundamental physicochemical constants and a listing of literature abbreviations. A subject index is included.

The material covered in Volume I is divided into seven sections.

Section I. Mathematical Introduction. This contains condensed treatments of differential calculus, integral calculus, partial differential coefficients, trigonometric functions, differential equations, and Fourier's series (pp. 1–114).

Section II. Principles of Thermodynamics (pp. 115–233).

Section III. Kinetic Theory of Gases (pp. 234–92).

Section IV. Statistical Mechanics and Quantum Theory (pp. 293–376).

Section V. Wave Mechanics (pp. 377–419).

Section VI. Temperature. This section contains an extensive treatment of thermometry (pp. 420–55), high temperature (pp. 455–501), and low temperature (pp. 502–45).

Section VII. The Properties of Gases. This contains an excellent discussion of the pressure–volume–temperature relations of gases (experimental) (pp. 546–623), critical phenomena (pp. 623–60), the pressure–volume–temperature relations of gases (characteristic equations) (pp. 660–745), densities and molar weights of gases and vapors (pp. 745–91), specific heats of gases (pp. 792–848), viscosity of gases (pp. 848–87), conduction of heat in gases (pp. 888–99), diffusion of gases (pp. 900–922, and gases at low pressures (pp. 922–34).

The enormous amount of information contained in this volume is concisely yet clearly presented and should be of great service to physical chemists whether interested in pure chemistry or in its application. The book as a whole is attractively arranged and reflects the skill and care that have been used by both author and publisher in its composition and production. Most physical chemists will be looking forward with interest to the other volumes in this series.

Harvey A. Bernhardt.

BOOKS RECEIVED

(To May 18, 1950)

Abridged Scientific Publications from the Kodak Research Laboratories. Vol. XXX. 50 papers. Eastman Kodak Company, Rochester, New York. 1949.

Alexander, E. R. *Principles of Ionic Organic Reactions*. John Wiley and Sons, Inc., 440 Fourth Ave., New York 16. 1950. 318 pp. Price: $5.50.

Crockford, H. C., and Knight, S. B. *Fundamentals of Physical Chemistry for Premedical Students*. John Wiley and Sons, Inc., 440 Fourth Ave., New York 16. 1950. 366 pp. Price: $4.25.

Elderfield, R. C. (Editor). *Heterocyclic Compounds. Vol. I. Three-, Four-, Five-, and Six-Membered Monocyclic Compounds Containing One Oxygen, Nitrogen, and Sulfur Atom.* John Wiley and Sons, Inc., 440 Fourth Ave., New York 16. 1950. 703 pp. Price: $11.00.

Fernelius, W. Conard, Garrett, A. B., and Quill, L. L. *Fundamentals in Chemistry for the Laboratory*. Revised edition. Ginn and Company, Statler Building, Boston 17, Massachusetts. 1950. 366 pp. Price: $2.75.

Goldstein, Richard F. *The Petroleum Chemicals Industry*. John Wiley and Sons, Inc. 440 Fourth Ave., New York 16. 1950. 449 pp. Price: $8.50.

Kleinberg, Jacob. *Unfamiliar Oxidation States and their Stabilization*. University of Kansas Press, Lawrence, Kansas. 1950. 131 pp. Price: $3.00.

Mellon, M. G. (Editor). *Analytical Absorption Spectroscopy*. John Wiley and Sons, Inc., 440 Fourth Ave., New York 16. 1950. 618 pp. Price: $9.00.

Soodak, Harry, and Campbell, Edward C. *Elementary Pile Theory*. John Wiley and Sons, Inc., 440 Fourth Ave., New York 16. 1950. 71 pp. Price: $2.50.

COLLOIDAL PHENOMENA OF ANTIBIOTICS[1,2]

ERNST A. HAUSER

Massachusetts Institute of Technology, Cambridge, Massachusetts
and
Worcester Polytechnic Institute, Worcester, Massachusetts

AND

GEORGE J. MARLOWE

Massachusetts Institute of Technology, Cambridge, Massachusetts

Received October 3, 1949

INTRODUCTION

During the past decade a great deal of research has centered on the discovery of new and more powerful antibiotics and on their application to man's fight against bacterial infections. Among the wonder drugs studied most extensively and applied most successfully, penicillin and streptomycin hold foremost positions. The host of clinical, biological, and chemical data which has been accumulated has pointed the way to more effective use of these antibiotics against diseases caused by microörganisms and has expanded the horizon for further investigations.

It is only natural that a great deal of attention should have been devoted to the manner in which these chemotherapeutic agents fight and kill harmful bacteria. Many eminent biologists and biochemists have tried to explain their mode of action, but they have concerned themselves primarily with the chemical interaction believed to take place between a given antibiotic agent and the various essential substances present in the cell which it attacks and destroys. Little if any attention had been devoted to the mechanisms whereby bacteria and antibiotic came into sufficient physical proximity, or even direct contact, until Hauser and coworkers (9) at the Massachusetts Institute of Technology noted that both penicillin and streptomycin salts, in the aqueous solutions in which they are most commonly used for parenteral injections, are present in the form of colloidal micelles. This has led to further work on these systems from a colloid-chemical point of view, in an effort to ascertain how particle size, electrical charge, capillary activity, and other properties inherently colloidal might affect the mode of action of these drugs.

---

[1] Presented before the Division of Colloid Chemistry at the 119th meeting of the American Chemical Society, which was held at Atlantic City, New Jersey, September 19-24, 1949.

[2] This paper is largely based on experimental work undertaken by George J. Marlowe and compiled in his Doctor of Science Thesis, Massachusetts Institute of Technology, 1949-50.

EXPERIMENTAL

A. Faraday–Tyndall effect

A highly purified sodium salt of benzyl penicillin (penicillin G) was dissolved in triply distilled conductivity water to make up solutions of concentrations ranging from 2000 to 20,000 units/cc. (1 unit = 1/1667 mg. of pure crystalline penicillin G). When viewed under the slit ultramicroscope, the solutions exhibited a very pronounced Faraday–Tyndall cone; this increased in intensity as the concentration of the solute in the solution was increased. The particles appeared in rapid Brownian motion, and the readily observable twinkling phenomenon revealed them to be anisometric. Particle size could be estimated at from 20 mμ in diameter at 2000 units/cc. to about 500 mμ at concentrations above 20,000 units/cc. (1 mμ = 10^{-7} cm.). Increasing the temperature caused both particle size and particle number to decrease, while the addition of cations with a valency greater than that of sodium increased both the number and the size of the particles visible under the slit ultramicroscope.

The calcium chloride complex of streptomycin was examined similarly in aqueous solutions, and again there could be no question as to the colloidality of the resulting sol. In concentrations of 25 mg./cc. the average particle size was about 75 mμ.

B. Electrophoresis

Electrophoretic studies revealed the penicillin micelles to be negatively charged, as their migration to the anode could be observed very clearly. The addition of a polyvalent electrolyte, such as cobalt chloride or aluminum chloride, even in very small quantities (about 10 parts per million), slowed down the electrophoretic movement and actually reversed its direction, while at the same time causing a certain amount of agglomeration. It is reasonable to suppose that the zeta potential of the lyosphere surrounding each cell was changed to such an extent by the polyvalent counter-ions that the particles as a whole now bore an opposite or positive electrical charge. The addition of other electrolytes, such as 6 per cent acetic acid and 30 per cent ammonium nitrate, caused partial and reversible coagulation of the penicillin micelles.

Similar electrophoretic studies with the streptomycin sol revealed that it too carries a net negative charge and exhibits properties typical of a reversible micelle colloid.

C. Surface tension

Very detailed studies on the surface tension of aqueous penicillin solutions were carried out with the sodium and potassium salts of penicillin G and with the sodium salt of penicillin dihydro F. The method used was that of pendent drops (1), devised at the Massachusetts Institute of Technology in 1937 and found to be ideally suited for this type of work. Determination of surface tension with static pendent drops is now generally accepted, and has the advantage of being very rapid, giving high precision, permitting the use of very small samples, and making possible continuous measurements without disturbing the surface being examined. The values of the surface tension in dynes per centimeter were calculated by the method of a selected plane (7), which involves measuring the equatorial diameter of the drop and the width at this distance from its tip. The accuracy obtainable depends on the precision of distance measurements, which is limited by the quality of the light source and of the focusing lens; the determinations reported here showed average deviations of less than 2 per cent.

TABLE 1

Surface tension of aqueous sodium penicillin G at various concentrations and various times

(Upjohn, 1667 units/mg.)

CONCENTRATION*	SURFACE TENSION DYNES PER CENTIMETER AT 25°C.				
	100 sec.	300 sec.	500 sec.	700 sec.	900 sec.
units/cc.					
5,000	64.6	61.0	58.4	56.4	54.8
10,000	59.4	56.0	53.4	51.8	50.4
20,000	56.2	51.8	49.0	46.4	44.2
40,000	50.0	43.6	39.4	37.2	35.6
60,000	45.8	37.8	34.6	32.6	31.0

* Unit/cc. = 1/1667 mg./cc.

TABLE 2

Surface tension of aqueous sodium penicillin dihydro F at various concentrations and various times

(Pfizer, Sample No. 16061-9, 1610 units/mg.)

CONCENTRATION*	SURFACE TENSION DYNES PER CENTIMETER AT 25°C.					
	100 sec.	300 sec.	500 sec.	700 sec.	900 sec.	1200 sec.
units/cc.						
5,000	66.0	63.8	61.6	60.6	59.8	59.0
10,000	60.0	57.9	56.4	55.8	55.3	54.8
20,000	55.6	53.6	52.6	52.0	51.6	51.2
40,000	50.5	48.1	46.8	45.9	45.3	44.8
60,000	44.5	42.5	41.3	40.4	39.6	38.6

* Unit/cc. = 1/1610 mg./cc.

The concentrations studied ranged from 5,000 to 60,000 units/cc., and temperatures between 15°C. and 37°C. were covered. The results obtained are shown in tables 1, 2, and 3 and are plotted in figures 1, 2, and 3. The data points were all taken from aging curves prepared for each drop at the various concentrations and temperatures.

In every instance the surface tension showed a rapid decrease from the value for pure water but levelled off as higher concentrations were used. Sodium penicillin G reached the lowest values of surface tension in the shortest period of time, and hence can be considered the most surface-active of the three penicillin salts, while the potassium salt, with its less hydrated and larger cation, proved to be the least surface-active.

TABLE 3

Surface tension of aqueous potassium penicillin G at various concentrations and various times

(Lilly, Lot No. K-963R, 1598 units/mg.)

CONCENTRATION*	SURFACE TENSION DYNES PER CENTIMETER AT 30°C.							
	100 sec.	300 sec.	600 sec.	900 sec.	1200 sec.	1800 sec.	2400 sec.	3000 sec.
units/cc.								
5,000	69.1	68.2	67.2	66.2	65.3	63.6	61.5	59.2
10,000	66.4	65.4	64.2	63.1	62.1	60.2	58.1	55.8
15,000	63.8	62.8	61.6	60.5	59.4	57.7	55.9	54.0
20,000	62.1	61.1	59.9	59.0	58.0	56.3	54.5	52.6
30,000	59.0	58.0	57.0	56.0	55.1	53.4	51.6	49.7
40,000	57.6	56.4	55.4	54.4	53.6	51.8	49.9	48.0
50,000	56.0	54.7	53.7	52.8	52.0	50.4	48.6	46.8
60,000	55.0	53.8	52.9	52.0	51.0	49.4	47.7	45.8

* Unit/cc. = 1/1598 mg./cc.

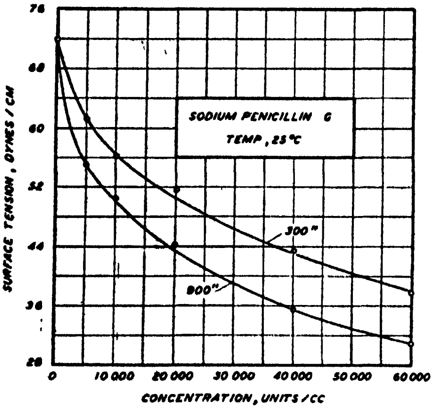

FIG. 1

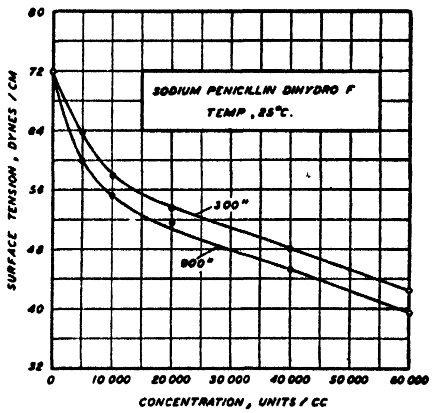

FIG. 2

FIG. 1. Surface tension of aqueous sodium penicillin G at various concentrations and times.

FIG. 2. Surface tension of aqueous sodium penicillin dihydro F at various concentrations and times.

The individual aging curves, on which the composite picture presented in figures 1, 2, and 3 was based, represent an averaging of several drops at each concentration and temperature. Remarkably close agreement was achieved under the experimental conditions employed, which insured constant humidity, essentially no mass transfer between the drop and its surroundings, and good temperature control (±0.2°C.). In every case the surface tension was found to drop fairly rapidly during the first 100 sec. and then to decrease more gradually up to a point where final measurement was made. The lowest values were always achieved at the longest time intervals after drop formation, but in the case of the sodium salts of both penicillins G and dihydro F this point was reached more quickly than in the case of the less surface-active potassium salt. Thus the migration of the most capillary-active type of penicillin from the bulk of the drop into the interface proceeded at the highest speed. As might be expected, this was most pronounced in the case of maximum concentration and large micelle size, while at the lower concentrations a longer period of time was required before there was a clear indication that the interface had become completely saturated with penicillin micelles.

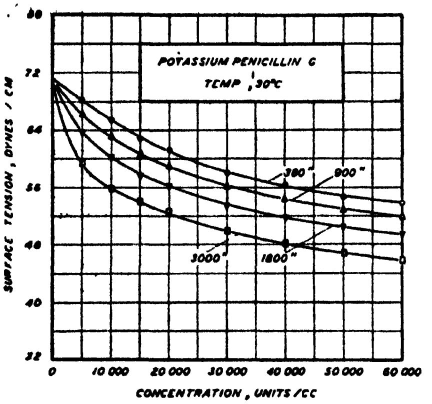

FIG. 3

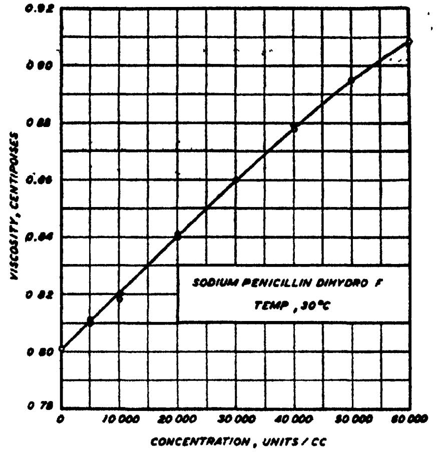

FIG. 4

FIG. 3. Surface tension of aqueous potassium penicillin G at various concentrations and times.

FIG. 4. Absolute viscosity of aqueous sodium penicillin dihydro F at various concentrations.

There can be no doubt that these findings support earlier claims (8, 9, 10) that penicillin is a highly capillary-positive, surface-active substance at these concentrations. It parallels in this respect the behavior of the salts of fatty acids in aqueous solutions, and differs from them only in its failure to exhibit any pronounced minima within the range of concentrations investigated. It is probable that the previously reported minima in surface tension were due to some unknown impurities in the samples, which at that time were not available in the highly purified state in which they exist today.

Surface tension determinations of the aqueous streptomycin sol gave figures slightly above those obtained for pure distilled water. The lack of any pronounced surface activity may be due to the covalent calcium ion and its low degree of hydration, while the molecular structure of streptomycin (12) gives little indication that this particular compound should reveal any marked capillary activity.

D. *Viscosity*

In order to establish clearly the type of colloid with which we are dealing, and which has been referred to as a micelle colloid, viscosity determinations were performed on each of the three penicillin salt solutions with an Ostwald viscosimeter. Relative viscosities of the aqueous solutions were converted to absolute viscosities by multiplying by the absolute viscosity of water, taken as 0.8007 centipoise at 30°C.

The results for sodium penicillin dihydro F are shown in table 4 and plotted in figure 4. The shape of the curve was found to be the same as for the other types of penicillin. The relatively slight increase in viscosity with concentration precludes any argument that one might be dealing with a macromolecular structure, such as polystyrene, which would show a very rapid and progressively steeper increase in viscosity in an appropriate solvent.

TABLE 4

*Viscosities of aqueous sodium penicillin dihydro F at various concentrations**

(Pfizer, Sample No. 16061-9, 1610 units/mg.)

CONCENTRATION	EFFLUX TIME	DENSITY	VISCOSITY
units/cc.	*sec.*	*grams/cc.*	*centipoises*
5,000	87.2	0.9967	0.811
10,000	88.2	0.9978	0.820
20,000	90.2	1.0000	0.840
30,000	92.0	1.0023	0.860
40,000	94.0	1.0045	0.879
50,000	95.6	1.0067	0.895
60,000	96.8	1.0090	0.908
H_2O	86.4	0.9956	0.8007

* All determinations were made at 30.0°C.

E. *Electrical conductance*

The electrical conductivities of the various crystalline salts of pencillin in aqueous solution were measured with a conductivity bridge of high sensitivity. Here the range of concentrations was extended down to as low as 50 units/cc., corresponding to a normality of less than 0.0001 gram-equivalent per liter. The specific conductance, in reciprocal ohms per centimeter, increased linearly with concentration, as shown by the data in table 5 and the plot in figure 5.

The equivalent conductance, in ohms^{-1} cm.^{2}, presented in table 6 and plotted in figure 6, demonstrates more clearly that we are not dealing with a strong electrolyte, such as potassium chloride, since its plot against the square root of the concentration reveals what amounts almost to a break at a concentration corresponding roughly to 1000 units/cc. Up to that point it can be assumed that micelles of varying size were still present throughout the colloidal sol, and this point may well represent the threshold of micelle formation. Below this concentration the equivalent conductance, corrected for the conductivity due to the water, rose quite rapidly, indicating that now the solute consisted solely of individual molecules, dissociated into positive and negative ions.

TABLE 5

Specific conductances of aqueous potassium penicillin G at various concentrations at 30.0°C.
(Lilly, Lot No. K-963R, 1598 units/mg.)

CONCENTRATION	SPECIFIC CONDUCTANCE*	CONCENTRATION	SPECIFIC CONDUCTANCE*
units/cc.	*ohms⁻¹cm.⁻¹* × *10⁶*	*units/cc.*	*ohms⁻¹cm.⁻¹* × *10⁶*
60,000	845	2,000	34.1
50,000	711	1,500	25.7
40,000	579	1,000	17.58
30,000	445	700	14.33
20,000	306	600	10.84
15,000	234	500	9.18
10,000	161	400	7.45
7,500	121.8	300	5.66
5,000	82.9	200	3.80
4,000	66.6	150	2.88
3,000	50.4	100	1.96

* All specific conductances were corrected for the conductance of the conductivity water used.

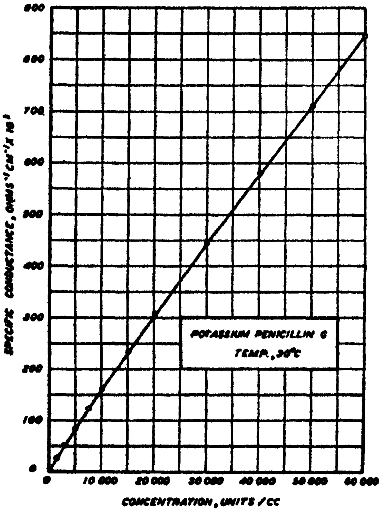

FIG. 5

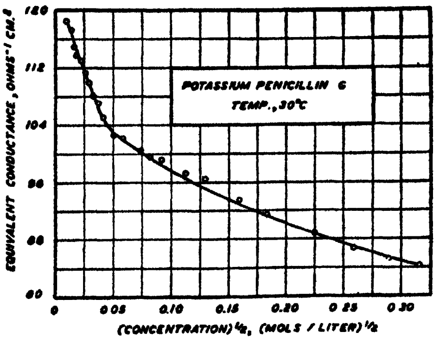

FIG. 6

FIG. 5. Specific conductance of aqueous potassium penicillin G at various concentrations.

FIG. 6. Equivalent conductance of aqueous potassium penicillin G at various concentrations.

F. Ultramicroscopy

Finally, experiments were carried out with a culture of *Staphylococcus aureus*. This microörganism was available in two forms, one in a liquid culture medium,

TABLE 6

Equivalent conductances of aqueous potassium penicillin G at various concentrations and at 30.0°C.

(Lilly, Lot No. K-963R, 1598 units/mg.)

CONCENTRATION	$C^{1/2}$	EQUIVALENT CONDUCTANCE	CONCENTRATION	$C^{1/2}$	EQUIVALENT* CONDUCTANCE
moles/liter		*ohms^{-1}cm.^{2}*	*moles/liter*		*ohms^{-1}cm.^{2}*
0.1002	0.316	84.3	0.002505	0.0500	102.6
0.0835	0.289	85.2	0.001670	0.0409	105.1
0.0668	0.258	86.6	0.001336	0.0365	107.1
0.0501	0.224	88.8	0.001002	0.0316	108.2
0.0334	0.1828	91.5	0.000835	0.0289	109.9
0.02505	0.1582	93.4	0.000668	0.0258	111.3
0.01670	0.1292	96.4	0.000501	0.0224	113.0
0.01253	0.1119	97.2	0.000334	0.01828	113.8
0.00835	0.0914	99.1	0.0002505	0.01582	115.0
0.00668	0.0817	99.6	0.0001670	0.01292	117.2
0.00501	0.0708	100.4	0.0000835	0.00914	118.5
0.00334	0.0578	102.1			

* All equivalent conductances represent conductance due to solute only, since they were corrected for the conductance of the conductivity water used.

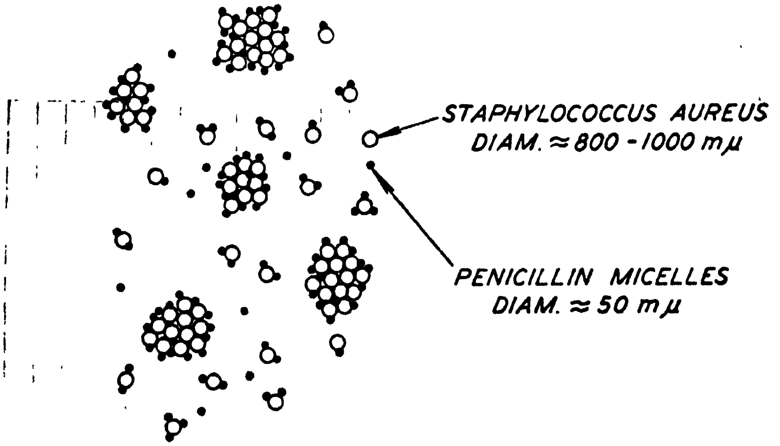

FIG. 7. Interaction between *Staphylococcus aureus* and aqueous sodium penicillin G

the other streaked on agar. A small drop of the solution was first placed on a glass slide and observed under the ultramicroscope. The small spherical particles of *Staphylococcus aureus* were clearly visible and could be seen to be moving about rapidly. To another drop was added approximately the same quantity of a solution of sodium penicillin G containing 10,000 units/cc. This mixture, when viewed under the ultramicroscope, revealed very clearly how the penicillin micelles interact with the bacterial cells. In a short time each individual cell became coated with one or more visible micelles; very soon the cells agglomerated, more penicillin micelles being adsorbed on the surface of the resulting clusters. All motion ceased, and the cells appeared quite immobile and lifeless. Figure 7 represents a schematic drawing of these observations.

Similar results were obtained with the streak culture when a small amount of the microörganism was drawn off with a wire loop and smeared on the slide, then diluted with water, and finally mixed with the penicillin solutions and examined microscopically.

In line with these observations, the same test was run on culture and penicillin under ultraviolet irradiation. Since *Staphylococcus aureus* does not fluoresce under ultraviolet light, while benzyl penicillin does so quite clearly, it was further confirmed that adherence of the penicillin micelles on the cell surface resulted shortly after mixing. This could be seen quite readily from the high intensity of fluorescence observable at the surface of the individual cells at first, and then at the surface of the cell clusters as well as along points of contact between the cells within a cluster. The rest of the solution fluoresced less strongly, indicative of the dispersal of penicillin sol throughout the remainder of the solution.

CONCLUSIONS

Appraising these results in their relationship to the antibacterial activity of both penicillin and streptomycin, one is forced to the conclusion that the stage of aggregation of these antibiotics undoubtedly influences their mode of action. Thus the colloidal micelles attach themselves as such at the cell surface, and there they affect the zeta potential of the susceptible bacterial species within a very short period of time (3). The surface activity of penicillin undoubtedly aids this adsorptive process and makes physical contact possible much more quickly than if reliance had to be placed exclusively on forces of electrostatic attraction or the affinity of the organic radicals for such substances in the cell surface as may be closely akin to them. Once the cell has become coated with penicillin micelles, the drug is capable of interfering with the normal functions of the cell, such as its assimilation of some of the essential amino acids (5, 6) or its respiration (11). But these are problems which are more properly left in the hands of the biologist or biochemist, who is better qualified to examine the life processes of microorganisms and the manner in which these might be disrupted.

However, it should be noted that there have been several successful attempts to enhance the effectiveness of penicillin and other chemotherapeutic agents in which a knowledge of colloid chemistry has been most helpful. It has been reported (2) that the addition of small amounts of aluminum monostearate to penicillin dissolved in oil greatly hastens the action of this drug against venereal diseases. It can well be presumed that the oil acts as a protective coating for the penicillin micelles, preventing their rapid disintegration and absorption into the blood stream. The polyvalent aluminum ion undoubtedly replaces the monovalent sodium, causing increased agglomeration, while the stearate acts both as an emulsifying agent and as an adsorptive aid because of its surface-active nature.

The fact that effective concentrations of penicillin can thus be maintained for much longer periods of time than is possible without the aid of these agents underscores the need for protective action for such an unstable structure as that of penicillin.

The inherent surface activity of penicillin should also be credited with at least some of the phenomenal success achieved with this drug, even in its impure state, and before protective agents were added to it. Just recently it was demonstrated (4) that tuberculostatic drugs, such as streptomycin, could be greatly increased in their effectiveness if it were possible to devise means whereby they might be made surface-active. If they could be incorporated at one end of a surface-active molecule, their concentration at the cell boundaries would be most favorably affected.

It would therefore seem important to examine the application of all chemotherapeutic agents somewhat more in the light of their colloidal properties. This might permit the development of protective agents which would bolster the resistance of the drug against the many adverse conditions present in the human system, such as the considerable variations in acidity and basicity of the body fluids. If it were possible to prevent their dissociation into individual and hence extremely vulnerable molecules, it follows that their effectiveness would be markedly enhanced. Their adsorption on susceptible bacteria would proceed more rapidly, their concentration at the site of their action would be greater, and their destructive power against the harmful microörganisms could then be unleashed more freely. This might well make possible the application of drugs which in their original state have been shown to fall a ready prey to the destructiveness of human metabolism.

SUMMARY

1. The discovery of the colloidality of both penicillin and streptomycin salts in aqueous solution has been briefly reviewed.
2. Surface tension measurements on three different penicillin salts have shown that all are surface-active to a very considerable extent.
3. Viscosity determinations have permitted differentiation of these micelle colloids from macromolecules.
4. The electrical conductances exhibited by the penicillins have given good indication that they differ from ordinary simple electrolytes.
5. Ultramicroscopic observations of the behavior of penicillin added to a culture of *Staphylococcus aureus* have shed much light on the mode of action of this drug.
6. It is concluded from these findings that the state of aggregation of chemotherapeutic agents plays an important role in their activity against microörganisms. Their study from a colloid-chemical point of view will often lead to improved methods of application and may permit enhancement of their effectiveness.

The authors wish to express their great indebtedness to Miss Ardelia Hutchins of the Department of Food Technology at the Massachusetts Institute of Technology for supplying the cultures of *Staphylococcus aureus* used in this work.

REFERENCES

(1) ANDREAS, J. M., HAUSER, E. A., AND TUCKER, W. B.: J. Phys. Chem. **42**, 1001 (1938).
(2) ARNOLD, R. C.: Time Magazine, p. 54, March 21, 1949.
(3) DORFMAN, V. A., MOLDAVSKAYA, E. A. M., KASTORSKAYA, T. L., AND ZASYPKINA, P. S.: Am. Rev. Soviet Med. **3**, 500 (1946).
(4) EISEMAN, B.: J. Exptl. Med. **88**, 189 (1948).
(5) GALE, E. F., AND TAYLOR, E. S.: Nature **158**, 676 (1946).
(6) GALE, E. F., AND TAYLOR, E. S.: J. General Microbiol. **1**, 314 (1947).
(7) HAUSER, E. A.: *Colloidal Phenomena*, p. 233. McGraw-Hill Book Company, Inc., New York (1939).
(8) HAUSER, E. A.: Kolloid-Z. **111**, 103 (1948).
(9) HAUSER, E. A., PHILLIPS, R. G., AND PHILLIPS, J. W.: Science **106**, 616 (1947).
(10) HAUSER, E. A., PHILLIPS, R. G., PHILLIPS, J. W., AND VAVRUCH, I.: J. Phys. & Colloid Chem. **53**, 287 (1949).
(11) PRATT, R., AND DUFRENOY, J.: Bact. Revs. **12**, 79 (1948).
(12) WAKSMAN, S. A.: Science **107**, 233 (1948).

THE EXPANSION OF CHARCOAL UPON THE ADSORPTION OF GASES AND VAPORS

R. I. RAZOUK AND M. A. ELGOBEILY

Department of Chemistry, Faculty of Science, Fouad I University, Cairo, Egypt

Received October 18, 1949

I. INTRODUCTION

The work of Bangham and coworkers (1, 3, 4, 7) on the expansion of charcoal upon the sorption of vapors established the relation that the expansion of the charcoal is directly proportional to the lowering of its surface free energy. It was also found that the Gibbs adsorption isotherm was applicable in most cases, that the adsorbed films obeyed the Schofield–Rideal equation of state (17), and that the heat of wetting of charcoal could be related to its expansion by the Gibbs–Helmholtz equation.

Thus if x be the linear expansion per cent when s grams of gas or vapor of molecular weight M is adsorbed on 1 g. of charcoal of specific surface area Σ, at equilibrium pressure p, and if F be the surface free-energy decrement in ergs cm.$^{-2}$ accompanying this process, then putting

$$x = \lambda F \tag{1}$$

and substituting in the Gibbs isotherm

$$\Gamma = \mathrm{d}F/RT\,\mathrm{d}(\ln p) \tag{2}$$

where Γ is the amount adsorbed in moles cm.$^{-2}$, it follows that

$$s/M\Sigma = \mathrm{d}x/\lambda RT\,\mathrm{d}(\ln p) \tag{3}$$

R being the gas constant and T the temperature. Hence

$$\lambda/\Sigma = M/RT \cdot \mathrm{d}x/s\ \mathrm{d}(\ln p) \tag{4}$$

All the terms on the right-hand side of equation 4 are experimentally measurable.

The value of λ/Σ was found to depend on the nature of the charcoal, but few experiments were made to test whether it depended also on temperature and on the nature of the adsorbate. For charcoal II, λ/Σ had almost the same value for methyl and ethyl alcohols, while for *n*-propyl and isopropyl alcohols rough estimates gave values close to that for methyl alcohol (4). Experiments with charcoals II and IV at temperatures between 0° and 30°C. led to the same value of λ/Σ in the case of methyl alcohol (4, 7). However, the evaluation of λ/Σ for a number of adsorbates over a wide range of temperature has not yet been accomplished, owing to certain difficulties such as the presence of the "retrograde effect" (i.e., the partial contraction of charcoal after its expansion) at low temperatures and especially with adsorbates of complicated structure, and the slow rate of attaining equilibrium in such cases. Recently, Haines and McIntosh (11) obtained almost equal values of λ/Σ when charcoal adsorbed ethyl chloride, dimethyl ether, and butane.

In the present work adsorption–expansion measurements were made on the same piece of charcoal when it adsorbed methyl alcohol, carbon dioxide, ammonia, oxygen, and sulfur dioxide at various temperatures, with a twofold object of finding out the nature of the adsorbed phase and the dependence of λ/Σ on temperature and on the adsorbate. These substances were chosen because the rate of adsorption was quick and the retrograde effect was very slight in the few instances where it occurred.

II. EXPERIMENTAL

The amount of gas or vapor adsorbed was determined by means of a spring balance of the McBain–Bakr type and buoyancy corrections were applied throughout. The equilibrium pressure was read on a mercury manometer carefully chosen of uniform bore, and the readings were corrected for temperature and mercury depression.

The expansion of charcoal was measured by means of a silica extensometer resembling that described by Fakhoury and Wahba (8) and is shown in figure 1. Its essential part is a vertical spiral spring s, which replaces the knife edges as well as the return springs in the metal extensometers described earlier (7). The spring consisted of five turns drawn from fused silica: the outermost turn was fixed to a strong silica rod rr, while the center of the spring formed the fulcrum of a lever of the "third type." The charcoal rod was held tightly between two claws fitting in two appendices a,a. The upper claw c_1 was fixed to the body of the extensometer, and the lower claw c_2 rested on a point projecting from the beam of the lever. The expansion of charcoal was transferred by means of this lever to a long pointer pp moving in front of a graduated scale.

It was very important in constructing the spring to ensure that the expansion of the charcoal was faithfully transferred to the pointer. This was possible so long as no downward movement of the spring took place; otherwise the magnification would not be uniform. The best conditions for the relative positions of the charcoal, the spring, and the pointer were found to be those described above. It was also necessary to taper the thread of the spring carefully so that it was thickest at the center and in the outer turn, and thinnest at about two-thirds from the center.

The magnification, determined with a special calibrator, was uniform over the whole range of expansion and had a value of 33. It remained constant after several dismountings of the charcoal. Pointer observations were made by means of a vernier microscope reading to 0.01 mm., so that variations of the length of the charcoal rod of the order of 0.0005 per cent could be estimated.

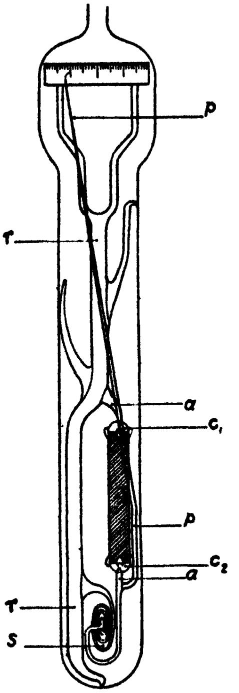

Fig. 1. The silica extensometer

III. MATERIALS

The charcoal was a piece of willow wood charcoal outgassed for 20 hr. at 600°C., and was designated charcoal VI. It was cut into several parts: one, in the form of a rod 70 x 9.6 x 9.6 mm.[3], was fitted in the extensometer; another part was used for the spring balance. Preliminary experiments in which rods from the same piece of charcoal were interchanged between the extensometer and the spring balance proved that different pieces of charcoal cut from the same block gave the same expansions and adsorbed the same amounts at equal pressures. Before carrying out an experiment the charcoals were outgassed *in situ* for 10 hr. at 500°C.

The methyl alcohol was Kahlbaum's acetone-free; it was refluxed for some time over freshly ignited quicklime, and then fractionated; its boiling point was 64.8°C. under 761 mm. pressure. Carbon dioxide was obtained by heating Kahlbaum's sodium carbonate "for analysis" and passing the products over phosphorus pentoxide. Ammonia was prepared by heating a mixture of pure lime with recrystallized ammonium sulfate and drying over quicklime and then phosphorus pentoxide. Sulfur dioxide was obtained by the action of phosphorus pentoxide on sodium sulfite and drying over phosphorus pentoxide. Oxygen was prepared by heating recrystallized potassium permanganate and drying the gas over phosphorus pentoxide.

IV. RESULTS AND DISCUSSION

The results of experiments on methyl alcohol at 25°C., carbon dioxide at −78°, −38°, 0°, and 25°C., ammonia at −78°, −38°, 0°, and 30°C., oxygen at −185° and −78°C., and sulfur dioxide at 0°C. are shown in two series of curves representing the molecular expansion curves (Mx/s *vs.* x) in figures 2–4, and the semilogarithmic curves (s *vs.* $\log_{10} p$) in figures 5–7.

When the charcoal rod was exposed to the gas or vapor of the adsorbate, it expanded immediately. In the experiments at the lower temperatures, however, this expansion was followed in a few cases by a very slight contraction, a phenomenon which Bangham described as the "retrograde effect," and which was explained by probable phase changes in the adsorbed film (1, 3, 4, 7). However, in all the present experiments the net effect was an expansion of the charcoal, and in no case was a net contraction observed, similar to that described by Haines and McIntosh (11), probably because of the wide differences in the nature of the charcoals used in the two sets of experiments.

A. Molecular expansion curves

The nature of the adsorbed phase can be investigated from a study of the molecular expansion curves which correspond to the FA–F diagrams familiar in surface chemistry. For if F be the surface pressure of an adsorbed film in dynes cm.$^{-1}$ and A the area occupied by one molecule in Å.^{2}, and putting $x = \lambda F$, then $Mx/s = FA \times 6.02 \times 10^{23}\lambda/10^{16}\Sigma$. The curves of figures 2–4 are in most cases similar to those characteristic of liquid-expanded films adsorbed on water. Only in the case of methyl alcohol and ammonia do the adsorbed films appear to be of the type of compressed gaseous films.

For an adsorbed film obeying the Schofield–Rideal equation (17)

$$F(A - B) = ikT \quad (5)$$

which in terms of x and s becomes

$$\frac{x}{\lambda}\left(\frac{M\Sigma}{s} - \frac{M\Sigma}{s_0}\right) = iRT \quad (6)$$

i.e.,

$$\frac{Mx}{s} - \frac{Mx}{s_0} = iRT\,\frac{\lambda}{\Sigma} \tag{6a}$$

the slope of the molecular expansion curve measures the incompressible area of the adsorbed molecules. Here k is Boltzmann's constant, R the gas constant, B the incompressible cross-sectional area per molecule, s_0 the adsorbed amount corresponding to B, and i a constant determined by the mutual cohesion between the adsorbed molecules.

Figures 2–4 show that after the earlier stages of expansion the molecular expansion curves approximate to the requirements of equation 6a and hence the Schofield–Rideal relation. However, the curvature of the molecular expansion curves suggests a change of the incompressible area which may be due to orientation of the adsorbed molecules at higher concentrations (*cf.* 9). At lower concentrations and surface pressures, the more pronounced curvature may result from van der Waals attractive forces which become more and more important relative to the incompressible area. Indeed, at very low surface pressures the effect of the van der Waals forces masks that due to the incompressible area, and consequently the earlier region of the molecular expansion curves is represented by a falling branch, closely resembling the early stages of the pv–p diagrams of imperfect gases. This effect is most readily seen in the case of ammonia (figure 2).

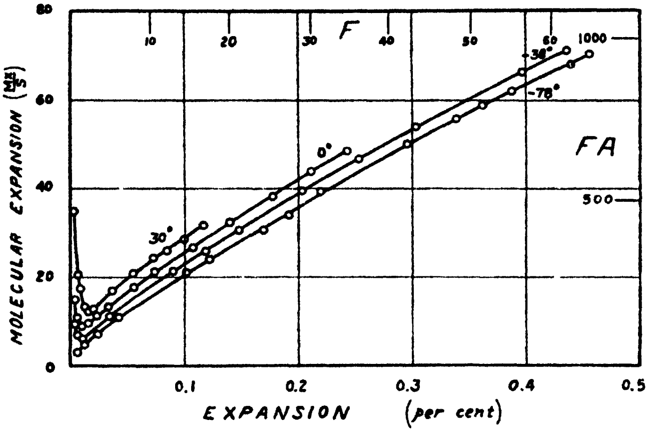

FIG. 2. Molecular expansion curves of ammonia

The molecular expansion curves of oxygen are of particular interest, for the similarity between these curves and those of other adsorbates shows that oxygen is *physically* adsorbed on charcoal at −185° and −78°C. This is substantiated by its low isosteric heat of adsorption (*ca.* 2000 cal. mole^{-1}) and by the perfect reversibility of its isotherms at these low temperatures.

B. The value of λ/Σ

The value of λ/Σ was estimated by making use of the integrated equation 4 in the form:

$$\frac{\lambda}{\Sigma} = \frac{M(x_2 - x_1)}{RT\int_{p_1}^{p_2} s\,\mathrm{d}(\ln p)}$$

where x_1 and x_2 are the expansion values of charcoal at the equilibrium pressures p_1 and p_2, respectively.

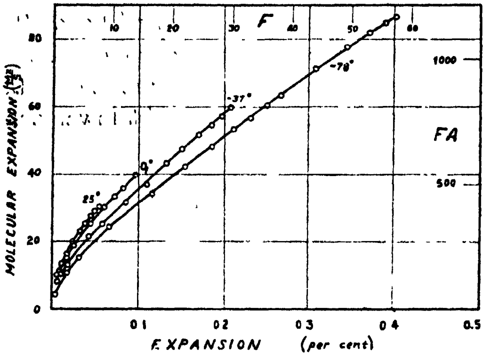

FIG. 3

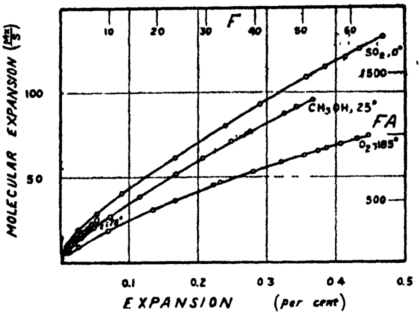

FIG. 4

FIG. 3. Molecular expansion curves of carbon dioxide

FIG. 4. Molecular expansion curves of sulfur dioxide at 0°C., methyl alcohol at 25°C., and oxygen at —185° and —78°C.

TABLE 1

Calculation of λ/Σ *for methyl alcohol at 25°C.*

x	Δx	$\int_{p_1}^{p_2} s\,\mathrm{d}(\log_{10} p)$
0.15		
	0.05	0.0228
0.20		
	0.05	0.0229
0.25		
	0.05	0.0228
0.30		
	0.05	0.0224
0.35		

Table 1 illustrates this by giving the values of the integral for equal intervals of x for methyl alcohol at 25°C. Substituting in equation 7, the mean value of λ/Σ becomes 1.23×10^{-9} dyne^{-1} cm.$^{-2}$

It is evident that a constant value of λ/Σ implies that the expansion of charcoal is directly proportional to the lowering of its surface free energy, and that the latter may be estimated by applying the Gibbs isotherm to the adsorption of gases on solid surfaces (2).

However, the value of λ/Σ did not remain constant at the early stages of adsorption, but was abnormally low. Though pressure measurements in this region were subject to some uncertainty, yet the persistence of the deviation and its value indicate a real failure of equation 4, probably by virtue of the absence of the proper conditions for which the Gibbs equation is applicable. Consequently, the value of λ/Σ has been calculated only when the measurements have been extended over a wide range of adsorption. Table 2 gives the values of λ/Σ thus obtained with the various adsorbates at different temperatures, together with the range of expansion over which it remains constant.

The mean value of λ/Σ is $1.23 \pm 0.02 \times 10^{-9}$ dyne^{-1} cm.$^{-2}$, and the maximum deviation from the mean is less than 3 per cent in four cases and less than 10 per cent in the other four. It may thus be concluded that λ/Σ is approximately the same for the adsorbates and the temperatures used in the present experiments. Bangham and Maggs (6; see also 15) have shown that the expression

TABLE 2

Values of λ/Σ

ADSORBATE	TEMPERATURE	λ/Σ	EXPANSION RANGE
	°C.	dyne^{-1} cm.$^{-2}$ $\times 10^9$	per cent
CH_3OH	25	1.23	0.15–0.37 (saturation)
CO_2	−38	1.11	0.10–0.20
	−78	1.15	0.10–0.40 (saturation)
NH_3	0	1.19	0.10–0.25
	−38	1.26	0.10–0.45 (saturation)
	−78	1.25	0.10–0.45 (saturation)
O_2	−185	1.33	0.15–0.45 (saturation)
SO_2	0	1.34	0.10–0.45

100 $\rho\Sigma/\lambda$ is closely related to Young's modulus of elasticity, where ρ is the density of charcoal. One would therefore expect λ/Σ to be independent of the nature of the adsorbate in the case where the surface of the charcoal is equally accessible to the molecules, as indeed is found in the present investigation.

C. Heats of adsorption

Isosteric heats of adsorption have been calculated by means of the Clapeyron–Clausius equation:

$$-\Delta H = RT^2 (\mathrm{d} \ln p/\mathrm{d}T), \qquad (8)$$

After the early stages of adsorption, the isosteric heats for carbon dioxide and ammonia remained almost constant—namely, 6700 and 7600 cal. mole^{-1}, respectively—as may be inferred from the approximately parallel semilogarithmic isotherms of figures 5 and 6. In the case of oxygen, rough estimates showed that the heat of adsorption varied between 1500 cal. mole^{-1} and 2300 cal. mole^{-1} as the amount adsorbed varied between 0.02 and 0.06 g. per gram of charcoal. In all cases, the heat of adsorption was close to the heat of condensation of the vapor of the adsorbate, showing that the adsorption is physical in nature.

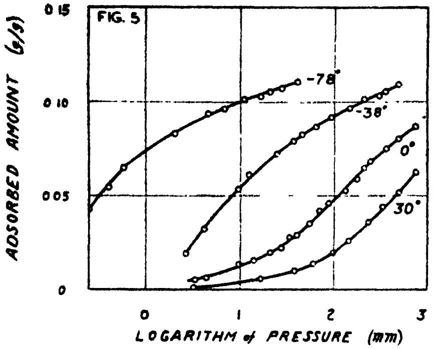

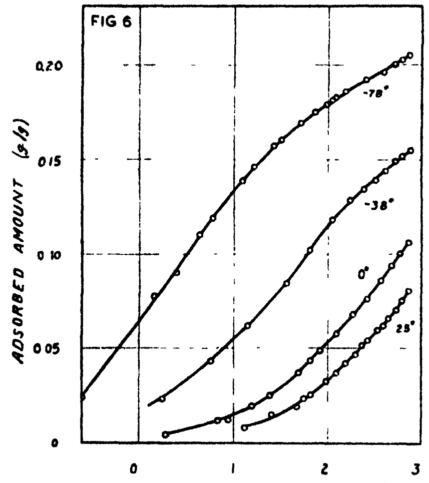

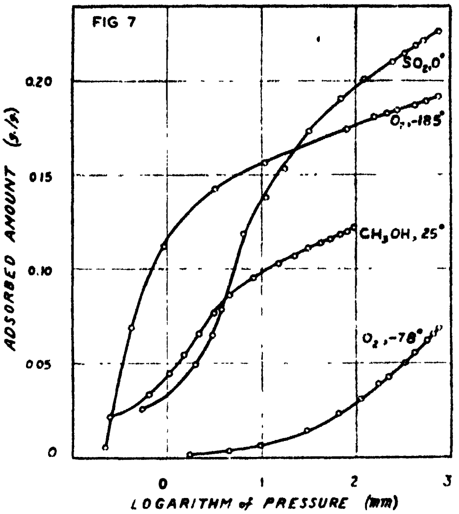

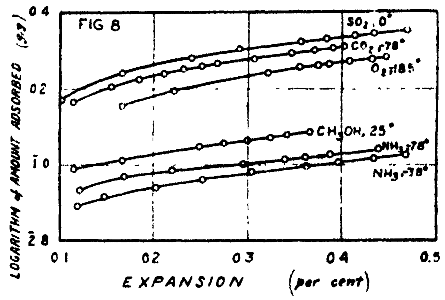

Fig. 5. Semilogarithmic adsorption isotherms of ammonia

Fig. 6. Semilogarithmic adsorption isotherms of carbon dioxide

Fig. 7. Semilogarithmic adsorption isotherms of sulfur dioxide at 0°C., methyl alcohol at 25°C., and oxygen at —185° and —78°C.

Fig. 8. Plot of the logarithm of amount adsorbed against expansion for ammonia, carbon dioxide, methanol, sulfur dioxide, and oxygen.

D. The specific surface of charcoal

An estimate of the specific surface area of charcoal calculated from adsorption-expansion measurements can be tentatively made by a method proposed by Bangham (1) and based on the assumption that equal concentrations of an adsorbate produce the same lowering of surface free energy of charcoal and of mercury. Thus if *F* be the surface free-energy lowering of mercury when it adsorbs

Γ mole cm.$^{-2}$, then $F/\Gamma = Mx/s \cdot \Sigma/\lambda$, i.e., $Mx/s = \lambda/\Sigma \cdot F/\Gamma$. Thus, knowing λ/Σ from equation 7, the value of Mx/s corresponding to given values of F and Γ can be evaluated. From the molecular expansion curve Mx/s *vs.* x (figure 4), it is then possible to determine both x and s; whence $\lambda = x/F$ and $\Sigma = s/M\Gamma$.

Table 3 shows how λ and Σ were determined by comparing the adsorption-expansion data for methyl alcohol on charcoal VI with results calculated from Kemball's data (14) for the same alcohol on mercury at the same temperature of 25°C. The mean value of λ = 0.00705 dyne^{-1} and of Σ = 575 m.^{2} gram^{-1} (the value of Σ, however, is much higher than that for charcoals II and IV estimated on the basis of the results of Cassel and Salditt (Z. physik. Chem. **A155,** 321 (1931)) for the adsorption of methyl alcohol on mercury, and from other considerations (1, 4)).

TABLE 3

Evaluation of λ *and* Σ

ADSORPTION OF METHYL ALCOHOL ON MERCURY (CALCULATED FROM KEMBALL'S RESULTS)		$F/\Gamma \cdot \lambda/\Sigma = Mx/s$	ADSORPTION-EXPANSION DATA OF METHYL ALCOHOL ON CHARCOAL VI		$\lambda = x/F$	$\Sigma = s/M\Gamma$
F	$\Gamma \times 10^{10}$		x	s		
dynes cm.$^{-1}$	*moles cm.*$^{-2}$		*per cent*	*grams gram*$^{-1}$	*dyne*$^{-1}$	*m.*^{2} *gram*$^{-1}$
20	5.13	48.0	0.150	0.1000	0.0075	610
30	6.03	60.8	0.202	0.1063	0.0067	551
40	6.31	77.8	0.279	0.1148	0.0070	568
50	6.63	92.8	0.351	0.1211	0.0070	571

Using these values of λ and Σ, the molecular expansion curves (Mx/s *vs.* x) could be converted into FA–F diagrams. Thus in figures 2–4 two scales are shown, one for expansion and the other for free-energy lowering or surface pressure.

E. Incompressible areas of the adsorbed molecules

When the adsorbed film obeys the Schofield–Rideal equation (equation 5), the incompressible area of the adsorbed molecules, B, is measured by $\mathrm{d}(FA)/\mathrm{d}F$. In the present case, however, the molecular expansion curves, and consequently the FA–F curves, are not linear but are slightly curved, so that the incompressible areas vary with the surface pressure. Nevertheless, it is of interest to calculate the limiting areas at the higher surface pressures, and to compare them with standard values of the molecular cross-sectional areas of the various adsorbates. Table 4 shows the limiting values of the incompressible areas of the adsorbed molecules, together with the cross-sectional areas of the molecules of the adsorbates obtained by a standard method, and the area per molecule adsorbed at saturation.

The close agreement between the two sets of data is striking, especially in view of a probable orientation of the adsorbed molecules. A comparison of the incompressible area with the area occupied by one molecule of each adsorbate, estimated from the specific area of charcoal determined above, shows that in all cases the adsorbed film was less than a complete monolayer even at saturation.

F. The compressibility of the adsorbed films

By analogy with the compressibility of matter in bulk, the compressibility of an adsorbed film is defined by

$$-\beta = (\mathrm{d}A/A\,\mathrm{d}F)_T \qquad (9)$$

and has been found of great value in elucidating the nature of the adsorbed phase (1, 10, 12).

Substituting for A and F in terms of s and x, the compressibility of the film becomes

$$\beta = \lambda(\mathrm{d}\ln s/\mathrm{d}x)_T \qquad (10)$$

so that it can be calculated graphically from the slope of the curve $\log_{10} s$ *vs.* x at constant temperature.

TABLE 4

Incompressible areas of molecules near saturation

ADSORBATE	TEMPERATURE	$d(FA)/dF = B$	CROSS-SECTIONAL* AREA PER MOLECULE	AREA PER MOLECULE ADSORBED NEAR SATURATION
	°C.	Å.²	Å.²	Å.²
NH_3	−78	11.5	12.9	14.8
	−38	12.1	12.9	14.9
O_2	−185	12.0	14.1	15.9
CO_2	−78	15.2	17.1	20.5
CH_3OH	25	16.0	18.1	24.8
SO_2	0	20.2	19.2	27.1†

* Values for ammonia, oxygen, carbon dioxide, and sulfur dioxide were taken from Brunauer and Emmett (J. Am. Chem. Soc. **59,** 1553 (1937)) for liquid packing of molecules; the value for methyl alcohol was calculated by the same method.

† At $p/p_0 = 0.65$.

Figure 8 shows the graphs of the various adsorbates at certain temperatures. The curves are concave to the x-axis at low values of the expansion, but tend to become linear at higher values so that the compressibility becomes constant and possesses a minimum value. In all cases the tangents to the linear portions of the curves are very nearly equal, indicating that in the neighborhood of saturation the compressibilities of films formed from different adsorbates are almost equal, *viz.*: 5.7×10^{-3} dyne^{-1} for methyl alcohol, 5.4×10^{-3} for carbon dioxide, 4.6×10^{-3} for sulfur dioxide, and 4.4×10^{-3} for ammonia and oxygen.

In order to make a rough comparison of this compressibility with that of bulk matter, β has to be multiplied by the thickness of the adsorbed film, which may be taken in the present case as the diameter of an adsorbed molecule, say, 4 Å. This would give a value of 2.0×10^{-4} bar^{-1}, which is greater than that for liquids but comparable to the compressibility of gases under high pressures.

This lends support to the hypothesis that the adsorbed films on charcoal are analogous to gaseous or liquid-expanded films on the surface of water.

G. Linear expansion coefficient of gas-free charcoal

Over the temperature range between 0°C. and 500°C. the difference between the coefficient of expansion of charcoal and that of silica, as measured by the extensometer, was constant and equal to 3.13×10^{-6}. Using the value of 0.57×10^{-6} for the linear expansion coefficient of silica (13), the coefficient of expansion of gas-free charcoal VI becomes 3.7×10^{-6} °C.$^{-1}$ This value is near that of charcoal IV (7) and that of coals carbonized above 800°C., recorded by Bangham and Franklin (5), but lower than the value for microcrystalline graphite obtained by Riley and Nelson from x-ray measurements (16).

It is interesting to note that the charcoals which expand to a greater extent on sorption possess also a higher temperature coefficient of expansion and a higher value of λ/Σ, as is illustrated in table 5. This matter is now under investigation.

TABLE 5

Expansion constants of charcoals IV and VI

ADSORBENT	SATURATION EXPANSION (CH_3OH AT 25°C.)	LINEAR EXPANSION COEFFICIENT	λ/Σ
	per cent	°C.$^{-1}$	*dyne*$^{-1}$ *cm.*$^{-1}$
Charcoal IV*	0.5000	4.5×10^{-6}	1.48×10^{-9}
Charcoal VI	0.3941	3.7×10^{-6}	1.23×10^{-9}
Ratio IV/VI	1.27	1.22	1.20

* Reference 7.

V. SUMMARY

The expansion which charcoal undergoes when it adsorbs the vapor of methyl alcohol, ammonia, carbon dioxide, oxygen, and sulfur dioxide has been measured at certain temperatures by means of a silica extensometer. In agreement with the findings of Bangham and coworkers, the expansion of charcoal was found to be proportional to the lowering of its surface free energy accompanying the adsorption. The proportionality constant was independent of temperature and of the adsorbate. Expansion–adsorption measurements indicate that the adsorbed films were mobile, and that they obeyed equations of state similar to those of compressed gaseous and liquid-expanded films on the surface of water. The specific surface of the charcoal used was estimated as 575 m.^{2} gram^{-1}, and the amount adsorbed corresponded to less than a monomolecular layer even in the neighborhood of saturation.

REFERENCES

(1) BANGHAM: Proc. Roy. Soc. (London) **A147**, 175 (1934).

(2) BANGHAM: Trans. Faraday Soc. **33**, 1459 (1937).

(3) BANGHAM, FAKHOURY, AND MOHAMED: Proc. Roy. Soc. (London) **A138**, 162 (1932).

(4) Bangham, Fakhoury, and Mohamed: Proc. Roy. Soc. (London) **A147**, 152 (1934).
(5) Bangham and Franklin: Trans. Faraday Soc. **42B**, 289 (1946).
(6) Bangham and Maggs: Proc. Conf. Ultrafine Structure of Coals and Cokes, Brit. Coal Utilisation Research Assoc. **1944**, 118.
(7) Bangham and Razouk: Proc. Roy. Soc. (London) **A166**, 572 (1938).
(8) Fakhoury and Wahba: Nature **146**, 63 (1940).
(9) Gregg: J. Chem. Soc. **1942**, 696.
(10) Gregg and Maggs: Trans. Faraday Soc. **44**, 123 (1948).
(11) Haines and McIntosh: J. Chem. Phys. **15**, 28 (1947).
(12) Harkins *et al.*: J. Chem. Phys. **14**, 117, 344 (1946).
(13) *International Critical Tables*, Vol. IV, p. 21. McGraw-Hill Book Company, Inc., New York (1928).
(14) Kemball: Proc. Roy. Soc. (London) **A190**, 117 (1947).
(15) Maggs: Trans. Faraday Soc. **42B**, 284 (1946).
(16) Riley and Nelson: Proc. Phys. Soc. (London) **57**, 477 (1945).
(17) Schofield and Rideal: Proc. Roy. Soc. (London) **A109**, 57 (1925).

ION EXCHANGE IN SYNTHETIC RESINS

S. L. GUPTA, MONISHA BOSE, AND S. K. MUKHERJEE[1]

University College of Science and Technology, Calcutta, India

Received November 28, 1949

INTRODUCTION

The study of synthetic resins has attracted the attention of a large number of investigators because of the vast promises these materials have shown in respect of their industrial applications. One of the most important uses to which the synthetic resins have been put in recent times is based upon their power of exchanging both anions and cations from electrolytic solutions. This property of synthetic resins, first observed by Adams and Holmes (1), was previously known to be possessed by siliceous zeolites, the bentonites and many other minerals, and the carbonaceous zeolites prepared by the sulfonation and oxidation of complex organic materials such as coal or lignite.

The reaction between phenols and aldehydes in the presence of a catalyst, leading to the formation of synthetic resins, is not understood in all its details. Three stages are generally distinguished in the condensation of phenol and formaldehyde in the presence of alkali (8).

The chemistry of each of the stages has been carefully studied with a view to elucidating the mechanism of the reactions. For the purpose of the present investigation, however, reference to this aspect of the problem is not particularly relevant. But it must be pointed out that cured resin is cross-linked in three dimensions and has a high but undetermined molecular weight. The phenol–formaldehyde condensation products possess acidic properties and the power to react with bases and all cations. These are known as the cation-active resins. The anion-active resins are similarly formed by the condensation of amines with formaldehyde (1). They evidently have the same structure as the phenol–formaldehyde resins, except that the amino groups take the place of hydroxyl groups. The elucidation of the physical structure of the amorphous condensation products of phenol and formaldehyde, called the "phenoplasts," has been largely developed by Houwink (8).

---

[1] At present a post-doctorate research worker in the Department of Soils, University of Missouri, Columbia, Missouri, with a fellowship from Calcutta University, Calcutta, India.

Ion-exchange resins

Ion-exchange resins constitute a special type of the synthetic resins described above. Adams and Holmes (1) found that only polyhydric phenols when condensed with formaldehyde gave resins which exhibited exchange capacity, whereas monohydric alcohols did not. The work of Akeroyd and Broughton (2) and of Bhatnagar, Kapur, and Puri (5), however, showed that even monohydric phenol resins possess exchange capacity. Introduction of further acidic groups like the sulfonic acid group increased the exchange capacity (16). Holmes (1) prepared anion-exchange resins by the condensation of aromatic amines, such as aniline or *m*-phenylenediamine, with formaldehyde. However, the condensation may proceed both on the ring and through the amino group, and a low exchange capacity as reported by Broughton and Lee (7) will be obtained. Patented anion-exchange resins generally use polyamines, so that a more strongly basic material is produced.

All condensation products do not necessarily possess ion-exchange properties. The exchange spots in the resin structure are created as a result of the presence of certain functional groups. These may be radicals or groups like SO_3H, CH_2SO_3H, COOH, OH, and NH_2, which act optimally at definite pH ranges (16).

Mechanism of exchange process

The reaction between resins and electrolytes may be either molecular or exchange adsorption. The true base-exchange character of the reactions between the hydrogen or sodium derivative of the phenol–sulfonic acid type resin and calcium chloride was demonstrated by Myers and Eastes (17); Akeroyd and Broughton (2), on the other hand, showed that, unlike exchange reaction, the adsorption of alkalis by a phenol–formaldehyde resin was an extremely slow process, requiring about a week's time to come to equilibrium. They assumed that the hydroxyl hydrogen of the acid is replaced by the —CaOH group. Theoretically, therefore, a monohydric phenol and a dihydric phenol should combine with 8.9 and 15.5 millimoles, respectively, of calcium per gram of resin. Their experiments actually confirmed these values.

Evidence for both physical adsorption and ion exchange exists. Beaton and Furnas (4) found that the exchange of copper for hydrogen in a carbonaceous resin is best interpreted as a function of pH. Griessbach's (11) data on the neutralization of a nuclear sulfonic acid resin with alkalis show that the nature of the cation of the base has an appreciable effect on the features of the neutralization curve. Explanations for these differences were sought in the activities of the ions, hydration effects, and ionic sizes in the same way as they occur in siliceous exchangers (20).

In the case of anion-exchange resins, the reactions were found to be markedly different from the cation-exchange resins. Thus Broughton and Lee (7), experimenting with aniline–formaldehyde and *m*-phenylenediamine–formaldehyde resins, observed low values for the adsorption of sulfuric and hydrochloric acids compared with the theoretical anion-exchange capacities of the resins. However, the equilibrium was attained much more quickly than in the case of cation-exchange systems. Edwards, Schwartz, and Boudreaux (10), in their experiments on the adsorption of acids by a *m*-phenylenediamine–formaldehyde resin, estimated the total acid as well as the anion concerned and concluded that the whole molecule of the acid is adsorbed. They found no adsorption of chloride from neutral and basic salt solutions. However, a greater adsorption of sulfuric acid than hydrochloric acid was observed by various investigators. The result was explained by Edwards *et al.* (10) by assuming that for each molecular unit of the resin a molecule of the acid is adsorbed and not in equivalent amounts. The experimental data of Kunin and Myers (13) did not entirely correspond to this assumption and they thought that some specific forces might be operative. Kunin and Myers, working with two anion exchangers of high and low capacities, observed that equilibrium for all practical purposes was attained in about 5–6 hr. and that the adsorption proceeds according to Freundlich's isotherm.

Great practical significance is attached to the dynamic method of studying the exchange capacities by means of percolating solutions through columns packed with resin. The results obtained by such experiments confirm the general conclusions of the equilibrium method. The work reported here has been confined to the equilibrium method alone.

EXPERIMENTAL

Materials

Since the composition of most of the ion exchangers available in commerce is not definitely known, and since it was desirable for the purpose of the present investigation to know the component parts and the functional groups, the following resins were prepared in the laboratory according to the methods of Adams and Holmes (1): (*1*) resorcinol–formaldehyde resin; (*2*) *m*-phenylenediamine–formaldehyde resin.

The 2-mm. sieved material of the resorcinol–formaldehyde resin represented the coarse fraction. Finer fractions were separated from a portion of the coarse resin by passing through 100- and 200-mesh sieves (Tyler's series).

The *m*-phenylenediamine–formaldehyde resin was lightly powdered, and the sample passing through 28 mesh and retained by 48 mesh was the coarse fraction. Two other fine fractions were separated from a portion of the coarse resin, *viz.*; (*1*) passing through 48-mesh and retained by 100-mesh sieves and (*2*) passing through 100-mesh sieves.

Methods

The reaction between the acid resin and alkalis was studied by adding known volumes of excess standard alkali to weighed amounts of resin kept in well-stoppered Jena bottles, which were shaken for definite periods of time in an end-to-end shaker. After allowing the solid matters to settle, an aliquot portion of the supernatant liquid free from suspended matter, but usually colored, was titrated either directly or, by adding excess of standard acid, back-titrated with standard alkali using phenolphthalein or Wesselow's mixed indicator. The reaction between the amine resin and the acids was similarly studied by adding excess of the acid and either titrating the residual acid after reaction or estimating the anion in the clear supernatant liquid. The amount of alkali or acid adsorbed was expressed in milliequivalents per 100 g. of the sample and has been termed the "exchange capacity (E.C.)."

Sodium was estimated either gravimetrically (3) as triple acetate, $NaZn(UO_2)_3$, $(C_2H_3O_2)_9$, or volumetrically (9) by titrating the solution of the triple acetate with standard alkali, using phenolphthalein as indicator. Barium was determined as barium sulfate. Calcium was precipitated as calcium oxalate and titrated in a sulfuric acid medium with standard potassium permanganate solution. Potassium was precipitated as $K_2NaCO(NO_2)_6$ (14), treated with standard potassium permanganate solution acidified with sulfuric acid, the excess permanganate reduced with excess oxalic acid or sodium oxalate solution, and the excess oxalic acid titrated with standard potassium permanganate solution. Ammonium ion was estimated after nesslerization by comparing the color developed with standard ammonium chloride solution. Chloride was estimated potentiometrically with standard silver nitrate solution, using the silver–silver chloride electrode. A Leeds & Northrup type K potentiometer was used for E.M.F. measurements. Sulfate ion was estimated as barium sulfate, oxalate ion by titration with standardized potassium permanganate solution, and phosphate ion volumetrically after precipitating as ammonium phosphomolybdate (19).

RESULTS AND DISCUSSION

Reaction between acid resin and bases

The results of alkali interaction with the coarse resorcinol–formaldehyde resin are presented in table 1. The shaking was continuous in an end-to-end shaker.

From experiments 1 to 3 it will be seen that by increasing the time of contact from 5 to 15 days, the exchange capacity (E.C.) shows an increase from 547 to 622 milliequiv. In the last experiment the ratio of resin to the total amount was nearly the same, but the concentration was lower, whereas the time of interaction was considerably increased. By doing so the E.C. shows an appreciable increase.

The nature of reacting alkali

Colloidal acids of the siliceous clays are known to give a higher value of the exchange capacity when titrated with baryta than with sodium hydroxide (15). A comparison was, therefore, made of the values obtained with sodium hydroxide and baryta. In the case of baryta all precautions were taken to prevent contact for any length of time with carbon dioxide of the air. The results given in table 2 will show that baryta gives a higher value than caustic soda. These results include measurement of the exchange capacity with sodium hydroxide and baryta, using samples of resin II(a) and II(b), sieved through a 200-mesh sieve. It will be seen that with both baryta and caustic soda appreciably higher values have been obtained in the case of the finer fractions.

Reactions with bases in the presence of neutral salts

Although the excess alkali was appreciably high, the concentration of the cation in question may conveniently be increased by using strong solutions of the neutral salts. In the case of colloidal hydrogen clays, where the reaction between the hydrogen and the added cations was one of exchange in character, the neutralizable acidity increased to a very high value when the titration was carried out in the presence of a high concentration of neutral salts (15). The results with the resins are given in table 3. It will appear from these data that the presence of salts increases the E.C. But sodium hydroxide in the presence of sodium chloride gives a higher relative increase in the E.C. than baryta in the presence of barium chloride. These observations are similar to those made with hydrogen clays (15).

TABLE 1

Reaction of alkali with coarse resorcinol-formaldehyde resin

NO.	WEIGHT OF RESIN	VOLUME OF NaOH ADDED	TIME OF CONTACT	EXCHANGE CAPACITY
	grams		*days*	*milliequiv.*
1.	0.5	85 cc. of 0.1198 *N*	5	547
2.	0.5	85 cc. of 0.1198 *N*	7	605
3.	0.5	85 cc. of 0.1198 *N*	15	622
4.	0.2569	120 cc. of 0.0396 *N*	12	657
5.	0.2061	120 cc. of 0.0396 *N*	25	706

TABLE 2

Effect of nature of the alkali on the exchange capacity

NO.	WEIGHT OF RESIN	VOLUME OF BASE ADDED	TIME OF CONTACT	EXCHANGE CAPACITY
	grams		*days*	*milliequiv.*
I(a)	0.5 (coarse)	85 cc. of 0.1198 *N* NaOH	15	622
(b)	0.5085 (coarse)	50 cc. of 0.1163 *N* $Ba(OH)_2$	15	911
II(a)	0.2755 (200 mesh)	50 cc. of 0.1187 *N* NaOH	6	709
(b)	0.5877 (200 mesh)	75 cc. of 0.1153 *N* $Ba(OH)_2$	6	1004

Exchange of cations adsorbed from bases

The amounts of cation adsorbed by the acid resin from the bases were determined by washing the treated resin residue with alcohol and replacing the adsorbed cations with 0.1 *N* hydrochloric acid. Before leaching with hydrochloric acid the residue was kept in contact with the acid for about 5–7 days and shaken occasionally..

It will appear from the results given in table 4 that the amounts of adsorbed sodium or barium brought back by exchange with hydrogen ions are much less than what corresponds to alkali adsorption. It has been noticed that the excess alkali after treatment with the resin was colored brown, owing obviously to the solubilization of the polymerized resin. The resin made soluble in this way could be precipitated with acid and its weight determined. It was found in one experiment (acid resin and sodium hydroxide) that about 20.5 per cent of the original sample was rendered soluble by caustic soda treatment, as the figures in table 5 will show.

TABLE 3

Effect of neutral salts on the exchange capacity

NO.	WEIGHT OF RESIN	VOLUME OF ALKALI	EXCHANGE CAPACITY
	grams		*milliequiv.*
1...........	0.4688 (coarse)	75 cc. of 0.0945 *N* NaOH + 2 *N* NaCl	832
2...........	0.4350 (200 mesh)	75 cc. of 0.0945 *N* NaOH + 2 N NaCl	864
3...........	0.6434 (coarse)	75 cc. of 0.1153 *N* $Ba(OH)_2$ + *N* $BaCl_2$	965
4...........	0.462 (200 mesh)	75 cc. of 0.1153 *N* $Ba(OH)_2$ + *N* $BaCl_2$	1079

TABLE 4

Exchange of cations adsorbed from bases

NO.	WEIGHT OF RESIN	TIME OF CONTACT	VOLUME OF ALKALI	EXCHANGE CAPACITY—ALKALI ADSORPTION	EXCHANGEABLE CATION
	grams	*days*		*milliequiv.*	*milliequiv.*
1	0.5 (coarse)	15	85 cc. of 0.1198 *N* NaOH	623	480
2	0.4688 (coarse)	10	75 cc. of 0.0945 *N* NaOH + 2 *N* NaCl	832	420
3	0.4350 (200 mesh)	10	75 cc. of 0.0945 *N* NaOH + 2 *N* NaCl	864	400
4	0.5877 (200 mesh)	6	75 cc. of 0.1153 *N* $Ba(OH)_2$	1004	832
5	0.6434 (coarse)	10	75 cc. of 0.1153 *N* $Ba(OH)_2$ + *N* $BaCl_2$	965	768
6.	0.462 (200 mesh)	10	75 cc. of 0.1153 *N* $Ba(OH)_2$ + *N* $BaCl_2$	1079	748

TABLE 5

Solubilization of the resin by alkali

WEIGHT OF RESIN	VOLUME OF NaOH ADDED	EXCHANGE CAPACITY	EXCHANGEABLE SODIUM IN RESIDUE	AMOUNT MADE SOLUBLE
grams		*milliequiv.*	*milliequiv.*	*grams*
0.0788	50 cc. of 0.1373 *N*	1068	611	0.0162

If we consider the following structural unit of resin and assume that the hydrogen ions at the exchange spots are hydrated as H_3O^+, the theoretical exchange capacity of the resin becomes equal to 1220 milliequiv. per 100 g.

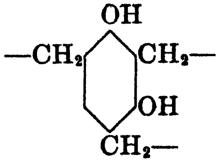

Assuming then that the soluble fraction has this theoretical exchange capacity, its contribution would amount to 251 milliequiv. This amount of sodium recovered from the soluble portion when added to that estimated in the residue makes the total equal to 862, a value much closer to the observed exchange capacity. The solubilization does not, however, appear to be a breakdown process, but merely suggests a vigorous reaction of the alkali with the exchange resin followed by a strong dispersion of the sodium resinate almost in its ultimate structural unit. In fact, one of us (S.L.G.) has made a number of potentiometric titrations with the colloidally dispersed resins and found that the theoretical value indicated above could be approached thereby.

TABLE 6

Exchange of cations from barium acetate solution

NO.	WEIGHT OF COARSE RESIN	BARIUM ADSORBED FR BARIUM ACETATE
	grams	*milliequiv.*
1	0.4786	207
2	0.4178	216
3	0.4661	221

Exchange of cations from salts

It is clear from what has been observed so far that the interaction of acid resin with alkali is somewhat complicated by the solubilization effect. It was, therefore, of interest to see how salts interact with the acid resins. The samples of resins were progressively leached with 500 cc. of a neutral normal barium acetate solution and the amounts of adsorbed barium ion estimated. The results given in table 6 show that the values of the adsorbed barium ion from barium acetate solutions are much less than the exchange capacity determined by alkali interaction. The resins, as already mentioned, are at their optimum reactivity at definite pH ranges. The weakly acidic nature of the resorcinol–formaldehyde resin requires that it should be active in the alkaline range. The low value of adsorbed barium ion from the neutral barium acetate solution may partly be due to this factor.

Interaction between sodium hydroxide and acid resin obtained by heating for different periods of time

An apparent reason for the solubilizing effect of the acid resin described in the last section is possibly the degree of polymerization of the final product of condensation of resorcinol and formaldehyde during the last stage of the treatment, i.e., curing. The time of curing the resin, i.e., the heat treatment, was therefore varied from 0 to 10 hr. All the previous experiments were with the sample heated for 10 hr. Table 7 gives the results obtained with coarse samples (2 mm. sieve) of the resin heated for 0, 2, 4, 6, and 10 hr., respectively. The mixtures of acid resin and excess alkali were shaken for 100 hr. over a period of 9 days.

It will be seen that with the exception of the sample heated for 4 hr. the exchange capacity increases with the period of heating. The color of the solutions after the alkali treatment indicated in column 3 is more intense with the sample heated for 10 hr.

TABLE 7

Effect of heating on the exchange capacity of an acid resin

TIME OF HEATING	EXCHANGE CAPACITY	COLOR OF SOLUTION
hours	*milliequiv.*	
No heating	497	Slightly colored
2	856	Slightly colored
4	784	Slightly colored
6	910	Slightly colored
10	1003	Highly colored

TABLE 8

Effect of heating on the exchange capacity of an acid resin (finer samples)

TIME OF HEATING	EXCHANGE CAPACITY	
	100-mesh sample	100- to 200-mesh sample
hours	*milliequiv.*	*milliequiv.*
No heating	842	792
2	653	869
4	923	949
6	735	839
10	952	1067

Each of the above samples was again powdered in an agate mortar and sieved through 100-mesh and 200-mesh sieves. Two portions of the samples were separately collected, one passing through 100-mesh and the other passing through 100-mesh but retained by 200-mesh sieves. These samples were then kept in a desiccator for one month to enable all the samples to come to the same equilibrium state with respect to free moisture. The results of alkali adsorption are given in table 8.

There is a tendency for the exchange capacity to increase with the period of heating, but there is not much regularity. It is likely that the amounts of fine fraction having various grades of fineness present in the different samples are not the same, particularly because the grinding cannot usually be so controlled as to produce products having the same size distribution in all the samples. However, in the samples passing through 100-mesh but retained by 200-mesh sieves (column 3, table 8), the different sized particles are distributed within a narrower range. The exchange capacities of these samples show a tendency to increase with the hours of heating, except for the sample heated for 6 hr. The relative intensity of color of the solutions after alkali treatment was nearly the same as that with the coarse samples.

Cation exchange in resinates

Whatever be the mechanism of reaction between alkali and acid resin, it has become apparent that a true exchange process cannot be clearly envisaged. Such complications are expected to be absent in the interaction between resinates and neutral salts. The exchange reaction was studied with sodium and barium resinates, which were prepared by adding the requisite amounts of the hydroxides to the acid resin. Symmetry values determined against various cations are given in table 9.

TABLE 9

Cation exchange in resinates

SYSTEM	COLOR OF SUPERNATANT LIQUID	PERCENTAGES OF THE CATION	
		Exchanged	Adsorbed
Sodium resin + HCl	Colorless	84.0	93.7
Sodium resin + KCl	Orange	70.8	71.7
Sodium resin + NH_4Cl	Light orange	74.8	73.6
Sodium resin + $CaCl_2$	Faint yellow	88.7	89.1
Sodium resin + $BaCl_2$	Faint yellow	85.0	89.2
Barium resin + HCl	Colorless	93.0	91.1
Barium resin + KCl	Faint yellow	9.0	11.1
Barium resin + NaCl	Faint yellow	24.5	24.5
Barium resin + $CaCl_2$	Faint yellow	66.5	52.7

It is clear from the above data that except in two systems, sodium resin + hydrochloric acid and barium resin + calcium chloride, the exchange is equivalent. For sodium resin the order is $H \geqslant Ca \geqslant Ba > NH_4 \geqslant K$; for barium resin it is $H > Ca > Na > K$.

Observations (10) have been made to suggest that the whole molecule of the reacting electrolyte is adsorbed on the surface of the resin. An estimation of the chloride-ion content of the supernatant liquid before and after the exchange was therefore made potentiometrically, using the silver–silver chloride electrode. The results given in table 10 show that the chloride-ion content remains almost unchanged, and therefore the chloride ion does not enter into reaction with the resinates.

Anion exchange with m-phenylenediamine resin

The *m*-phenylenediamine resin was treated with known amounts of hydrochloric, sulfuric, oxalic, and phosphoric acids and shaken for 68 hr. After allowing the suspension to settle, the supernatant liquid was taken out and titrated with standard sodium hydroxide solution. The residual resin was washed free from electrolytes, kept in contact with 0.1 N sodium hydroxide for about 5 days, and leached with the alkali solution in order to displace the adsorbed anion. The results of these determinations are presented in table 11. Experiments 1 to 4a were done with 40- to 100-mesh samples. The figures are means of duplicate experiments.

TABLE 10

Chloride-ion content of the supernatant liquid before and after the exchange

SYSTEM	VOLUME OF 0.1729 N $AgNO_3$ REQUIRED BY 5 CC. OF THE CHLORIDE SOLUTION	
	Before exchange	After exchange
	cc.	*cc.*
Sodium resin + HCl	1.444	1.439
Sodium resin + KCl	1.444	1.460
Sodium resin + NH_4Cl	1.444	1.444
Sodium resin + $CaCl_2$	1.444	1.410
Barium resin + NH_4Cl	1.444	1.500
Barium resin + NaCl	1.444	1.459

TABLE 11

Anion exchange with m-phenylenediamine resin

NO.	SYSTEM	TIME OF SHAKING	ANION ADSORBED FROM ACID SOLUTION	ANION DISPLACED BY NaOH	COLOR OF SUPERNATANT LIQUID
		hours	*milliequiv.*	*milliequiv.*	
1	0.3174 g. resin + 50 cc. of 0.1375 N H_2SO_4	68	407	384	Yellow
1a	0.1686 g. resin + 50 cc. of 0.1375 N H_2SO_4	68	412	434	Yellow
2	0.1762 g. resin + 50 cc. of 0.096 N HCl	68	245	160	Faint yellow
2a	0.2244 g. resin + 50 cc. of 0.096 N HCl	68	249	160	Faint yellow
3	0.2786 g. resin + 50 cc. of 0.1 N $H_2C_2O_4$	68	433	432	Very faint yellow
4	0.2072 g. resin + 50 cc. of 0.1 N H_3PO_4	68	280	277	Very faint yellow
4a	0.2165 g. resin + 50 cc. of 0.1 N H_3PO_4	68	277	277	Very faint yellow
5	0.1392 g. resin (100 mesh) + 50 cc. of 0.1375 N H_2SO_4	68	378		Yellow
5a	0.4564 g. resin (100 mesh) + 50 cc. of 0.1375 N H_2SO_4	68	380		

The results indicate that with the phosphoric and oxalic acids the exchange is probably anionic, since the amounts adsorbed are completely replaceable by another anion, *viz.*, OH. In the case of sulfuric acid and, more markedly, hydrochloric acid the anions appear to possess a stronger binding with the resin residue.

Edwards *et al.* (10) and Bishop (6) concluded from their experiments that hydrochloric and sulfuric acids are molecularly adsorbed by the amine resins. They confirmed this conclusion from their observation that no anion is adsorbed from neutral or alkaline solutions. Kunin and Myers (13), however, concluded that the anionic resins (they actually used Amberlite IR-4B) do exhibit anion exchange and suggested that since the exchange spots of amine resins become active only in acid solutions no adsorption from neutral or alkaline solution is possible. The observations made in the present investigation show clearly that, at least in acid solutions, adsorption from phosphoric and oxalic acid solution is an anion-exchange process. In the more strongly acidic solutions of sulfuric acid, and more particularly hydrochloric acid, perhaps molecular or maybe very strong anionic adsorption takes place. It will no doubt be difficult to decide between anionic exchange from acid solutions and molecular adsorption. No adsorption from a neutral 1 N sodium sulfate solution could be observed, however, even on prolonged interaction with the salt. Another important point to be noticed in the case of amine resins is that the maximum exchange capacity obtained with either sulfuric acid or oxalic acid is only about one-fourth of the theoretical value. Similar results have also been reported by others (16). The theoretical value has been calculated on the basis that two amino groups for each unit structure are available for anionic exchange (*cf.* page 1104). To explain the low value (7) suggestions have been made to the effect either that polymerization involves these amino groups or that amino groups are blocked by steric hindrance. From our observations on cation-exchange resins, we found that particle size was an important factor which determined the accessibility of the exchange spots. The resin samples used in the above experiments are very coarse (48–100 mesh) and the samples used by other investigators are also of a similar texture. Using a colloidally dispersed amine resin and taking recourse to potentiometric titrations with acids, one of us (S.L.G.) has been able to approach the theoretically calculated value. The results will be published elsewhere.

SUMMARY AND CONCLUSIONS

A resorcinol–formaldehyde cation-exchange resin and a *m*-phenylenediamine anion-exchange resin were used for the present investigation.

The reaction between the acid resin and alkali was studied by adding known amounts of alkali and, after definite periods of time, analyzing the alkaline supernatant liquid. The exchange capacity thus obtained is determined by the following factors: the time of contact, the relative proportions of the solid and solution phases, the fineness of the resin, and the nature and concentration of the alkali. Baryta gives under identical conditions a higher value of the acidity or exchange capacity than sodium hydroxide. The presence of a high concentration of neutral salt increases the total neutralizable acidity. The amounts of cation adsorbed from either alkali or salts are much less than the exchange capacity obtained by way of estimation of the alkali consumed.

A decrease in the time of heating during the process of curing the resin causes an appreciable reduction in exchange capacity.

The symmetry values of the resin salts or the resinates of sodium and barium were determined against different cations. Chloride-ion concentration before and after the reaction of the added chlorides was the same, showing absence of molecular adsorption. The exchange of cations is equivalent and the cations show the lyotrope effect.

The total exchange capacity of the anion-exchange resin is about one-fourth of the theoretical value, but shows a small lyotrope effect in its reaction with hydrochloric, sulfuric, oxalic, and phosphoric acids.

REFERENCES

(1) Adams and Holmes: J. Soc. Chem. Ind. **54,** 1-6T (1935).

(2) Akeroyd and Broughton: J. Phys. Chem. **42,** 343 (1938).

(3) Barber and Kolthoff: J. Am. Chem. Soc. **56,** 1625 (1928).

(4) Beaton and Furnas: Ind. Eng. Chem. **33,** 1500 (1941).

(5) Bhatnagar, Kapur, and Puri: J. Indian Chem. Soc. **13,** 679 (1936).

(6) Bishop: J. Phys. Chem. **50,** 6 (1946).

(7) Broughton and Lee: J. Phys. Chem. **43,** 737 (1939).

(8) Carswell: *High Polymers. VII. Phenoplasts.* Interscience Publishers, Inc., New York (1947).

(9) Dobbing and Byrd: J. Am. Chem. Soc. **59,** 3288 (1931).

(10) Edwards, Schwartz, and Boudreaux: Ind. Eng. Chem. **32,** 1462 (1940).

(11) Griessbach: Quoted by Myers (16).

(12) Jenny: J. Phys. Chem. **36,** 2217 (1932).

(13) Kunin and Myers: J. Am. Chem. Soc. **69,** 2874 (1947).

(14) Milne: J. Agr. Sci. **19,** 541 (1929).

(15) Mitra, Mukherjee, and Bagchi: Indian J. Agr. Sci. **10,** 303 (1942).

(16) Myers: *Advances in Colloid Science,* Vol. I, p. 317. Interscience Publishers, Inc., New York (1942).

(17) Myers and Eastes: Ind. Eng. Chem. **31,** 1138 (1939).

(18) Palmer: *Experimental Physical Chemistry.* Cambridge University Press, London (1941).

(19) Treadwell and Hall: *Analytical Chemistry,* Vol. II, p. 516. The Macmillan Company, New York (1945).

(20) Wiegner and Jenny: Kolloid-Z. **42,** 268 (1927).

CATION-EXCHANGE STUDIES WITH THE COLLOIDAL CLAY SALTS OF SILVER

S. K. MUKHERJEE[1] AND S. GHOSH

University College of Science and Technology, Calcutta, India

Received November 28, 1949

A quantitative study of cation exchange involves the measurement of activities of the cations rather than their concentrations. The mineral membrane technique developed by Marshall (5, 6, 7, 8, 10) is not so well adapted to the measurement of cation activities in mixtures. Silver salts of clay, however, become readily amenable to such studies because of the ease and accuracy with which silver-ion activities can be measured, either alone or in mixtures with other cations. Marshall and Gupta (9) made a comprehensive study of the ion-exchange properties of the silver salts of bentonite, beidellite, and permutite. According to them, the mass action equations failed to fit in well with their experimental results. The inadequacy of the existing base-exchange equations to fit the experimental data is well known (2, 9, 16). One of the reasons appears to be the failure of these equations to take into account the heterogeneous character of the exchange surfaces on which cations are anchored with different bonding energies.

The present paper deals with the exchange characteristics of a silver bentonite and a silver kaolinite sol, and later on discusses the application of some of the existing base-exchange equations in the light of the experimental data obtained with them.

MATERIALS AND METHODS

The bentonite was obtained from a sample of Kashmir bentonite, which contains montmorillonite as the only clay mineral. The clay fraction has a b.e.c. (base-exchange capacity) of 113.0 milliequiv., as determined by Parker's method (13). The kaolinitic mineral contains a small amount of montmorillonite as impurity, and the clay fraction has, therefore, a high b.e.c. (= 27.3 milliequiv.). The entire clay fraction ($<2\ \mu$) was obtained by dispersion with sodium hydroxide and subsequent sedimentation. The hydrogen clay was prepared after necessary pretreatment with hydrogen peroxide by thorough leaching with dilute hydrochloric acid and careful washing free from chloride. Preliminary experiment showed that a reasonable volume of silver nitrate solution used for the leaching of the hydrogen clay is unable to convert the latter completely into a silver clay. A barium clay, prepared by adding the requisite quantity of baryta, could, however, be converted into a silver clay by leaching with silver nitrate solution. All leachings and subsequent washings had to be done in the dark to prevent blackening of the silver systems. The purified silver clays were preserved in amber-colored reagent bottles. In all the experiments with the silver clays, protection from light was found to be extremely necessary and was ensured by using amber-colored bottles and by covering with black papers when ordinary glass apparatus was used.

---

[1] At present a post-doctorate research worker in the Department of Soils, University of Missouri, Columbia, Missouri, on a fellowship from Calcutta University, Calcutta, India.

Instead of the silver electrode used by Marshall and Gupta (9), silver–silver chloride electrodes were employed in the present investigation. Preliminary experiments with these electrodes using standard silver nitrate solutions showed that the silver–silver chloride electrode was not only more reproducible but was valid over a wider and higher range of silver-ion activities than the simple silver electrode. The E.M.F. of the cell used in this experiments, *viz.*,

$$\text{Ag-AgCl, Ag}^+ \text{ (a)} \mid \text{NH}_4\text{NO}_3 \text{ satd. agar} \mid \text{satd. KCl, Hg-Hg}_2\text{Cl}_2$$

is related to the silver-ion exponent

$$\text{pAg} \left(= \log \frac{1}{a_{\text{Ag}}} \right)$$

by the equation

$$\text{pAg} = \frac{0.553 - E_{\text{obs}}}{0.059}$$

at 30°C., the temperature of the experiments. The theoretical slope and intercept of the plot of pAg against E_{obs} was in accord with the experimental data obtained with the silver–silver chloride electrode. A silver nitrate solution of known normality was prepared by titrating it with a standard potassium chloride solution. The silver nitrate solution was then added dropwise, as in titration, to a known volume of conductivity water, and the resulting E.M.F.'s measured by means of a Leeds & Northrup type K potentiometer. a_{Ag} was obtained by mulplying the measured concentrations by the respective activity coefficients, calculated from the Debye–Hückel limiting equation. The pAg–E_{obs} straight line so obtained served also as a calibration curve for the direct measurement of a_{Ag} from the observed E.M.F. This curve was found to be valid for solutions containing other electrolytes, as shown in figure 1, in which the circles and triangles denote respectively the experimental points with silver nitrate alone and with silver nitrate plus potassium nitrate. The theoretical slope is given by the solid line. The results given in table 1 will further illustrate the usefulness of the calibration curve. Silver-ion activities (or pAg) were read from the calibration curve, corresponding to the observed E.M.F. of the respective ultrafiltrates, and were also calculated from the total concentration of silver ion as determined by potentiometric titration with standard potassium chloride solution. The data for silver kaolinite refer down the table to increasing concentrations of added potassium nitrate.

Several silver–silver chloride electrodes were kept ready and checked with standard silver nitrate solutions before use.

In order to study the interaction between the colloidal salts and the electrolytes two methods were followed: (*1*) *Continuous titration:* A known volume of the colloidal suspension was taken in a titration vessel and changes in E.M.F. caused by the addition of known quantities of electrolytes, used as nitrates, were read by means of a Leeds & Northrup type K potentiometer. After each addition, the mixtures were thoroughly shaken and constant E.M.F.'s were recorded. A period of 7–8 hr. was necessary to complete a titration. It was found expedient to dip the silver–silver chloride electrode just before the readings were taken. The whole vessel, as already mentioned, was carefully wrapped in black paper to cut off light. The a_{Ag^+} (or pAg) was read from the calibration curve. (*2*) *Bottle titration:* In this method equal volumes of silver clay were taken in stoppered amber-colored bottles and increasing amounts of electrolytes added, and the volumes made up with water. The bottles were kept at room temperature (30°C.) with occasional shaking for 5–7 days for the attainment of equilibrium. The silver-ion activity of the mixture was determined as usual by means of the silver–silver chloride electrode. The clear supernatant liquid was obtained by either ultrafiltration or centrifugation, and its silver-ion concentration determined

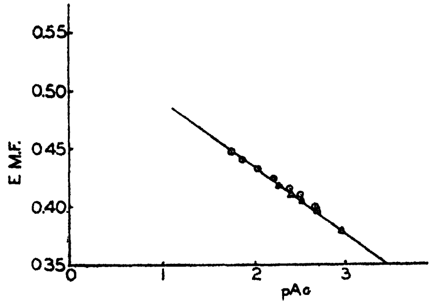

FIG. 1

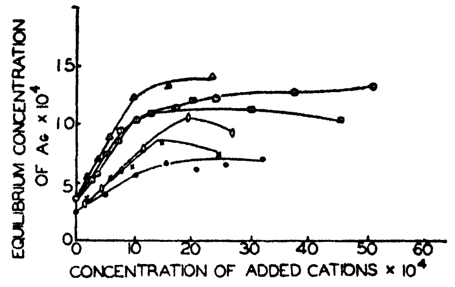

FIG. 2

FIG. 1. Measurements with silver-silver chloride electrode: ⊙, silver nitrate; △, silver nitrate + potassium nitrate.

FIG. 2. Continuous titration

⊙	silver bentonite + potassium nitrate	●	silver kaolinite + potassium nitrate
⊡	silver bentonite + barium nitrate	×	silver kaolinite + barium nitrate
△	silver bentonite + thorium nitrate	()	silver kaolinite + thorium nitrate

TABLE 1

pAg values from E.M.F. measurements and from titration

SYSTEM	pAg FROM E.M.F.	pAg FROM KCl TITRATION
Silver bentonite + $Ba(NO_3)_2$	2.60	2.55
Barium bentonite + $AgNO_3$	2.45	2.42
Silver kaolinite + KNO_3	3.55	3.43
	3.29	3.12
	3.00	3.02
	3.13	2.98
	2.88	2.96

potentiometrically by titration with potassium chloride solution, using the silver-silver chloride electrode.

RESULTS

Silver bentonite and silver kaolinite as colloidal salts

The silver bentonite (as well as the silver kaolinite) as obtained by the leaching of a bentonite with silver nitrate formed a remarkably stable sol. A known volume of the suspension was leached with 0.2 *N* barium nitrate solution and the replaced silver ion was analyzed potentiometrically. The total amount of silver ion per 100 g. of the colloid was found to be 111.5 milliequiv., which agrees well with the b.e.c. (113.0 milliequiv.) of the bentonite. The same value was obtained by titrating the silver bentonite with potassium chloride solution, the titration curve being similar to that of a precipitation reaction. Similar agreement was obtained with the silver kaolinite sol. From the initial E.M.F. of the silver colloid, its free silver-ion activity could be calculated from the calibration curve and compared with the total silver-ion concentration obtained from the potassium chloride titration. The results given in table 2 show that whereas silver bentonite is about 9 per cent dissociated, silver kaolinite shows an initial dissociation of 43 per cent, which gradually sinks to about one-third of this value in 47 days. Silver bentonite shows little or no change in its percentage dissociation in 70 days.

TABLE 2

Dissociation of silver clays

SYSTEM	TIME	TOTAL SILVER-ION CONCENTRATION	pAg	FREE SILVER-ION ACTIVITY	(FREE/TOTAL) × 100, i.e., PER CENT DISSOCIATION
	days	*milliequiv / liter*		*milliequiv./ liter*	
Silver bentonite	Initial	25.3	2.64	2.29	9.0
	40	25.3	2.67	2.14	8.4
	60	25.3	2.67	2.14	8.4
	70	25.3	2.67	2.14	8.4
Silver kaolinite	Initial	1.96	3.05	0.89	45.4
	30	1.96	3.34	0.46	23.6
	44	1.96	3.46	0.35	17.7
	47	1.96	3.55	0.28	14.4

It is the usual practice in exchange measurements to separate the clear supernatant liquid of the sol *plus* electrolyte mixture and analyze it for the cations concerned. In order to see how far this entails a shift of the final equilibrium, the pAg of the silver bentonite *plus* electrolyte mixtures was calculated from the E.M.F. data by referring to the calibration curve, and of the corresponding centrifugate or ultrafiltrate from the titration curve with standard potassium chloride solution. The results given in table 3 show that the silver clay *plus* electrolyte mixtures (*in situ*) and its ultrafiltrates have almost the same pAg values within the experimental errors.

TABLE 3

pAg of mixtures of silver bentonite and electrolytes

SYSTEM	pAg FROM GRAPH	pAg* FROM TITRATION WITH KCl SOLUTION
Silver bentonite + KNO_3	2.12	2.15
	2.01	2.07
	1.95	1.89
	1.98	1.84
	1.97	1.84
Silver bentonite + $Ba(NO_3)_2$ ...	2.20	2.19
	1.98	1.92
	1.92	1.84
	1.89	1.83
	1.83	1.79
Silver bentonite + $Th(NO_3)_4$	2.08	2.02
	1.89	1.88
	1.78	1.77
	1.71	1.69

* Calculated from the silver-ion concentration.

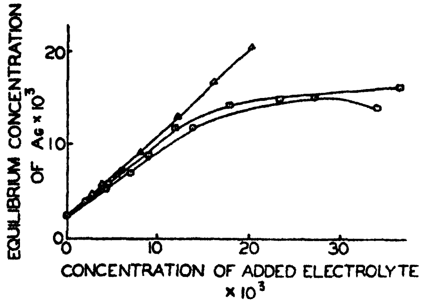

FIG. 3

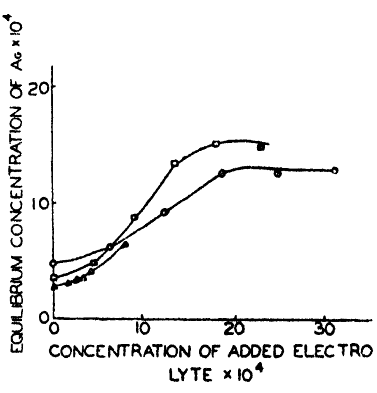

FIG. 4

FIG 3. Bottle titration: ⊙, silver bentonite + potassium nitrate; ⊡, silver bentonite + barium nitrate; △, silver bentonite + thorium nitrate.

FIG. 4. Bottle titration: ⊙, silver kaolinite + potassium nitrate; ⊡, silver kaolinite + barium nitrate; △, silver kaolinite + thorium nitrate.

Continuous vs. bottle titration

The two methods of titration differ largely in regard to the time of interaction. This is shown clearly by the curves in figures 2, 3, and 4. In view of the fact that complete equilibrium is not attained under the conditions of the continuous titration, future work was restricted to bottle titrations only. In all these titrations, the total quantity of added electrolyte was not much in excess of the symmetry concentration. In fact, one of the objects of these titrations was to know the nature of interactions at the low-concentration regions of the added electrolytes. In figures 2–4 the equilibrium concentration of the exchanged silver ion has been plotted against the total instead of the equilibrium concentration of the added cation. Figure 5 shows the plots of the equilibrium concentrations of the exchanged and the exchanging cations. It will be noticed that the exchange isotherms at the regions of low concentration are more or less of a sigmoid nature; this is markedly demonstrated in figure 5. The slopes and the relative positions of the silver bentonite curves are in accordance with the lyotrope effect, but not so in the case of silver kaolinite, where in the initial stages the order is K > Ba > Th, which is the reverse of the lyotrope series, and from a little below half the symmetry concentration the order of potassium and barium shows the regular lyotrope effect. The titration with thorium nitrate was not carried far enough to make the comparison. The reversal of the lyotrope series may apparently be due to the aging of the silver kaolinite mentioned earlier.

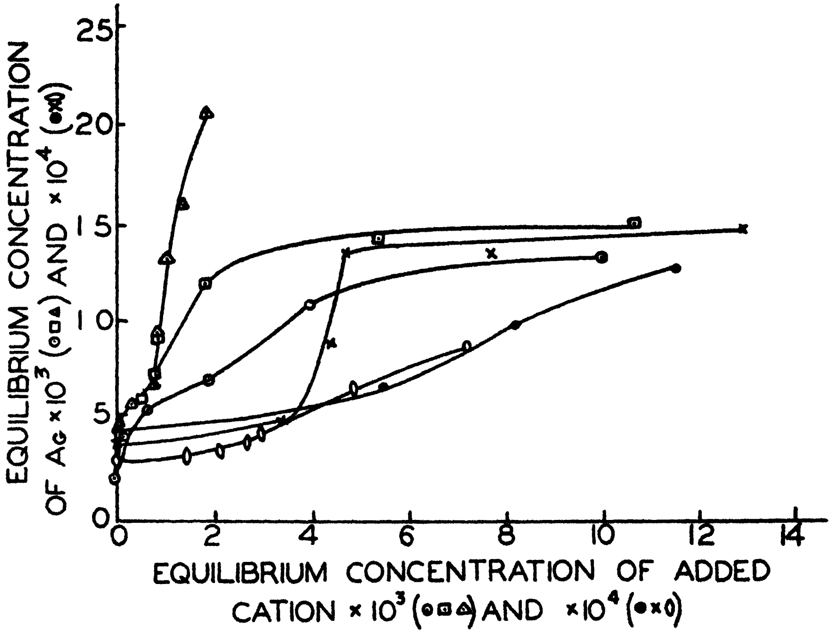

FIG. 5. Bottle titration

○	silver bentonite + potassium nitrate	●	silver kaolinite + potassium nitrate
□	silver bentonite + barium nitrate	×	silver kaolinite + barium nitrate
△	silver bentonite + thorium nitrate	()	silver kaolinite + thorium nitrate

From the titration curves (figures 2–4) the corresponding symmetry values (S.V.) can be calculated, and are shown in table 4.

Table 4 also gives the p*C* values, i.e., the negative logarithm of the equilibrium concentration of the electrolytes necessary to exchange half the total amount of the exchangeable cations. These p*C* values, according to Pallmann (12), are characteristic of exchange at low concentration of electrolytes. These values reflect almost the same features of the exchange reactions as the symmetry value; a higher S.V. is associated with a higher p*C*. However, in view of the fact that the inflexions in the titration curves characterize the end of a certain process, as in a neutralization reaction, a value, p*E*, may be defined as the negative logarithm of the equilibrium concentration of cations corresponding to the inflexion point. The p*E* values so calculated are shown in table 4. A higher p*E* value, like the p*C* or the S.V., signifies a stronger exchange reaction. But it may sometimes give better information than the other two, at least in the region of low concentrations. For instance, the low value of p*C* for silver kaolinite plus thorium nitrate would indicate a weak exchange. This is perhaps partly true and thorium ion (Th^{++++}) in some form or another may be adsorbed on the surface (*cf.* below). A higher p*E* value, however, indicates that although thorium ion might be adsorbed, its exchanging power is still superior to that of barium ion. Moreover, the nearly same value of p*E* for the barium nitrate and thorium nitrate titrations is also confirmed by the coincidence of the two curves (figure 5) at the low-concentration region. This fact is, however, not borne out by the p*C* values.

TABLE 4

Symmetry values calculated from titration curves

SYSTEM	S.V.	pC	pE
Silver bentonite + KNO_3	59.3	2.25	2.47
Silver bentonite + $Ba(NO_3)$	63.0	2.62	3.05
Silver bentonite + $Th(NO_3)_4$		3.00	3.05
Silver kaolinite + KNO_3	79.1	3.17	3.12
Silver kaolinite + $Ba(NO_3)_2$	92.7	3.37	3.35
Silver kaolinite + $Th(NO_3)_4$		3.19	3.40

As already mentioned, the interaction between thorium nitrate and silver kaolinite reflects the character of a weak exchange. This is in sharp contrast to the interaction between thorium nitrate and silver bentonite, where the curve rises very sharply. It is not unlikely that thorium ion is adsorbed on the surface of kaolinite in some form besides entering into ionic exchange. The ease with which kaolinite reverses[2] its charge on the addition of thorium ion may in part be due to such an adsorption reaction (*cf.* also later, page 1118).

---

[2] Observed by Mr. A. H. Beavers, Department of Soils, University of Missouri, Columbia, Missouri (private communication).

Mathematical formulations of base exchange

A large number of formulations have been suggested to represent the base-exchange reactions in soils and clays. Some of them are empirical; some are partially or entirely based on the mass action law; while others envisage some kind of physical picture of the whole process. A comparative study of these equations has shown that they are mostly inadequate, but the general trend of the isotherms, which are similar to the adsorption isotherm of Freundlich, is more or less obeyed. Based on the idea of an exchange adsorption (3, 11, 15) Wiegner and Jenny (18) proposed the equation

$$\frac{x}{m} = K_w \left(\frac{c}{a - c}\right)^{1/p}$$

where x is the amount adsorbed by m grams of the adsorbent, c is the equilibrium concentration of the exchanging cation, a is the initial concentration of the added cation, and K_w and $1/p$ are constants. Renold (14) somewhat modified Wiegner's equation and expressed the concentrations as a fraction of the total amount of the exchangeable cations. His equation takes the form:

$$\frac{N_p}{Um} = K_R \left(\frac{N_L}{Um}\right)^{1/p}$$

where N_p is the amount adsorbed, N_L is the equilibrium concentration of the added cation, Um is the total amount of exchangeable cation present in m grams of the colloid used, and K_R and $1/p$ are constants.

Jenny's equation (4), which is derived on the basis of a kinetic mechanism of ionic exchange, is fundamentally a mass action equation where the constant attains a physical significance as the ratio of the oscillation volumes of the interacting cations. The equation, as applied here, has, however, a limited applicability, i.e., to 1:1-valent systems. Jenny's equation is expressed in the form:

$$W = \frac{-(S + N) \pm \sqrt{(S + N)^2 - 4SN\,(1 - V_W/V_b)}}{2\,(1 - V_W/V_b)}$$

where N is the amount of electrolyte (i.e., number of ions) initially added, and S is the saturation capacity. V_b and V_W are, respectively, the oscillation volumes of the adsorbed and the exchanging ions.

Bray (1) formulated base exchange with two equations which are valid at low and high concentrations, respectively, of the added electrolytes, *viz.*,

$$E_1 = \frac{AC}{C + A(f_a/f_b)}; \quad E_2 = \frac{AC}{A + C(f_a/f_b)}$$

where E_1 and E_2 are the amounts of cations released or adsorbed when $A \leqslant C$ and $A \geqslant C$, respectively, A is the amount of cation added, and C is the total exchange capacity. f_a/f_b, defined as the "relative ease of release" of the cations concerned, denotes the constant in these equations like that of Jenny's V_W/V_b.

Both Wiegner's and Renold's equations, and in reality all equations based on the adsorption isotherm, should give straight-line graphs if the logarithms of the variable quantities are plotted. For instance, Wiegner's and Renold's equations take respectively the forms,

$$\log x = \frac{1}{1+p}\log C + \frac{p}{1+p}\log K_w m$$

and

$$\log N_p = \frac{1}{p}\log N_L + \left(1 - \frac{1}{p}\right)\log Um + \log K_R$$

The log x *vs.* log C or log N_p *vs.* log N_L straight lines will enable $1/p$ and K_W or K_R to be evaluated.

Jenny's equation may be written as follows:

$$\frac{(S - W)(N - W)}{W^2} = \frac{V_W}{V_b} = K_J \text{ (say)}$$

or

$$\log (N - W) = \log K_J + \log \frac{W^2}{S - W}$$

The plot of log $(N - W)$ (= log C of Wiegner's equation) against log $(W^2/(S - W))$ should be a straight line, the intercept giving the value of K_J.

Bray's equations can similarly be written in the forms,

$$\frac{1}{E_1} = \frac{K_B}{C} + \frac{1}{A}$$

where $K_B = f_a/f_b$, and

$$\frac{1}{E_2} = \frac{K_B}{A} + \frac{1}{C}$$

Thus, the plot of $1/E_1$ against $1/A$ should be a straight line, the intercept giving the value of K_B/C, and hence K_B. In the present study the range of concentrations used makes only the first equation applicable.

The results of these calculations for the various systems have been graphically represented in figures 6a–6f.

Although Jenny's equation holds only for 1:1-valent systems, it has been applied to 1:2- and 1:4-valent systems as well. The interesting point about these graphs is that the straight-line relation envisaged by all these equations does not hold good for the entire range with any of the systems studied excepting the silver kaolinite plus thorium nitrate. In fact, there appear to be at least two straight lines with sharp differences in slopes. But the silver kaolinite plus thorium nitrate system gives a straight line not only with Jenny's but also with Wiegner's and Renold's equations, which fail with other systems. The silver kaolinite plus thorium nitrate graph appears to confirm what has been said earlier about this system, *viz.*, that the thorium ion possibly enters into a pure adsorption process which predominates over the exchange reaction.

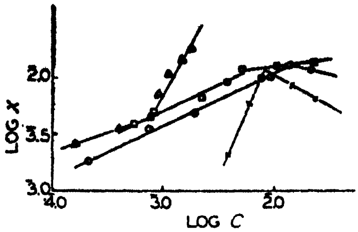

Fig. 6a

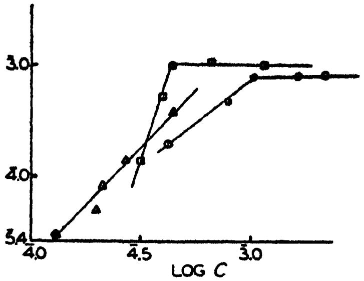

Fig. 6b

Fig. 6a. Plot of Wiegner's and Renold's equations: ×, silver bentonite + nitric acid; ⊙, silver bentonite + potassium nitrate; ⊡, silver bentonite + barium nitrate; △, silver bentonite + thorium nitrate.

Fig 6b. Plot of Wiegner's and Renold's equations: ⊙, silver kaolinite + potassium nitrate; ⊡, silver kaolinite + barium nitrate; △, silver kaolinite + thorium nitrate.

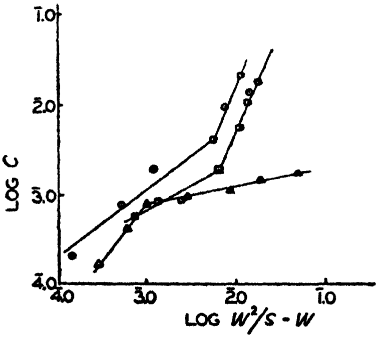

Fig. 6c

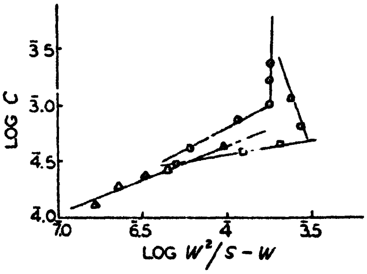

Fig. 6d

Fig. 6c. Plot of Jenny's equation: ⊙, silver bentonite + potassium nitrate; ⊡, silver bentonite + barium nitrate; △, silver bentonite + thorium nitrate.

Fig. 6d. Plot of Jenny's equation: ⊙, silver kaolinite + potassium nitrate; ⊡, silver kaolinite + barium nitrate; △, silver kaolinite + thorium nitrate.

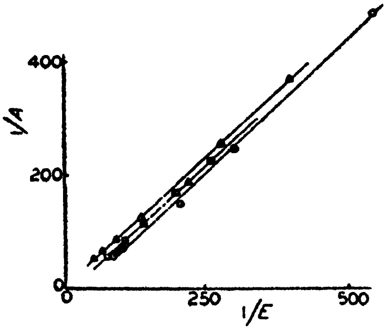

Fig. 6e

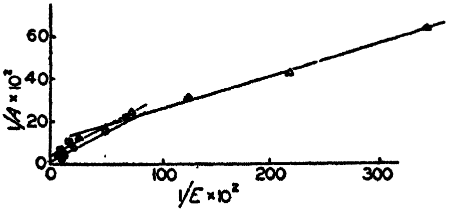

Fig. 6f

Fig. 6e. Plot of Bray's equation: ⊙, silver bentonite + potassium nitrate; ⊡, silver bentonite + barium nitrate; △, silver bentonite + thorium nitrate.

Fig. 6f. Plot of Bray's equation: ⊙, silver kaolinite + potassium nitrate; ⊡, silver kaolinite + barium nitrate; △, silver kaolinite + thorium nitrate.

Of the four equations studied, that of Bray gives approximate straight lines over the entire range of concentration studied. Bray tacitly assumed two sets of equations for two ranges of electrolyte additions below and above the symmetry concentration. Jenny's equation, or any other, is most possibly a mean of these two equations of Bray. For instance, Bray's equation can be written in the forms:

$$(f_a/f_b)_1 = \frac{C(A - E_1)}{AE_1} \quad \text{and} \quad (f_a/f_b)_2 = \frac{A(C - E_2)}{CE_2}$$

Putting $f = \sqrt{(f_a/f_b)_1 (f_a/f_b)_2}$, the above relations give at the symmetry concentration where $E_1 = E_2 = E$ (say), and $A = C$:

$$f = \frac{(C - E)^2}{E^2}$$

Writing this relation with the symbols of Jenny's equation:

$$f = \frac{(S - W)^2}{W^2} = V_w/V_b \equiv K_J$$

that is, the constant of Jenny's equation is a geometric mean between those of the two equations of Bray (1). The present study was not continued far enough to enable us to apply the second equation of Bray, but it is clear that the exchange reaction is a discontinuous process possessing perhaps altogether different equilibrium constants. This is likely to reflect the differences in the bonding energies of the exchangeable cations on the clay surfaces. Further studies oriented in this direction with different kinds of minerals are expected to reveal these and other surface characteristics in fuller detail.

SUMMARY

A silver bentonite (containing montmorillonite alone) and a silver kaolinite (containing a small amount of montmorillonite as impurity) were used for the study of exchange reactions with various electrolytes. The electrolytes were added as nitrates and the silver-ion activity measured by means of the silver–silver chloride electrode. The silver colloids were found to be remarkably stable. The silver bentonite was dissociated to the extent of 9 per cent, which did not show any change in 70 days; whereas with silver kaolinite, the initial dissociation of 42.6 per cent gradually decreased to one-third of this value in 47 days. The silver colloids could be quantitatively titrated with a potassium chloride solution.

Continuous titration with the electrolytic solutions did not ensure equilibrium. Mixtures of silver clay and electrolytes were therefore allowed to react for 5–7 days and the silver-ion activity of the supernatant liquid was determined by titration with a potassium chloride solution, as well as from an E.M.F. *vs.* pAg calibration curve. The exchange isotherms were more or less sigmoid towards the low-concentration region of the added electrolytes, showing definite inflexion points. From the isotherms, symmetry value, pC (i.e., negative logarithm of the equilibrium concentrations of the added electrolytes at which the amount of cations exchanged is one-half), and pE (negative logarithm of the equilibrium concentration of electrolytes necessary to reach the inflexion point) were calcu-

lated. All these quantities were shown to be characteristic of the particular exchange reaction.

The results of the exchange measurements were discussed with the help of four mathematical formulations, *viz.*, those of Wiegner and Jenny, Renold, Jenny, and Bray. All these equations were rearranged to obtain a linear plot of the variables. It was found that in most of the cases studied the straight-line relationship held good up to a certain concentration, above which the points lay on another straight line having sometimes an altogether different slope. The equation of Bray seems to fit best. It is suggested that exchange probably takes place discontinuously and at stages which are characterized by different equilibrium constants. The silver kaolinite plus thorium nitrate system gives a straight-line relation with all the formulations. There is an indication that thorium ion is adsorbed apart from entering into an ionic exchange.

REFERENCES

(1) Bray, R. H.: J. Am. Chem. Soc. **64**, 954 (1942).
(2) Davis, L. E.: Soil Sci. **59**, 379 (1945).
(3) Fajans, K., and Backerath, K. von: Z. physik. Chem. **97**, 478 (1921).
(4) Jenny, H.: J. Phys. Chem. **40**, 501 (1936).
(5) Marshall, C. E.: J. Phys. Chem. **48**, 67 (1944).
(6) Marshall, C. E., and Ayers, A. D.: J. Am. Chem. Soc. **70**, 1297 (1948).
(7) Marshall, C. E., and Bergman, W. E.: J. Am. Chem. Soc. **63**, 1911 (1941).
(8) Marshall, C. E., and Bergman, W. E.: J. Phys. Chem. **66**, 325 (1942).
(9) Marshall, C. E., and Gupta, R. S.: J. Soc. Chem. Ind. **52**, 433T (1933).
(10) Marshall, C. E., and Krinbill, C. A.: J. Am. Chem. Soc. **64**, 1814 (1942).
(11) Mukherjee, J. N., and Basu, J. K.: J. Indian Chem. Soc. **4**, 459 (1927).
(12) Pallmann, H.: Ann. faculté d'agronomie Bucarest **1**, 1 (1939–40).
(13) Parker, F. W.: J. Am. Soc. Agron. **21**, 1030 (1929).
(14) Renold, A.: Kolloid-Beihefte **43**, 1 (1936).
(15) Weiser, H., and Gray, G. R.: J. Phys. Chem. **36**, 2796 (1932).
(16) Weisz, L.: Dissertation No. 670, Zurich, 1932.
(17) Wiegner, G.: Trans. Intern. Congr. Soil Sci., 3rd Congr., Oxford **1935**, 109.
(18) Wiegner, G., and Jenny, H.: Kolloid-Z. **42**, 268 (1927).

A NEW TYPE OF HIGH-TEMPERATURE X-RAY CAMERA FOR CHEMICAL REACTIONS IN THE SOLID STATE

TERUICHIRO KUBO AND HIROSHI AKABORI

Tokyo Institute of Technology, Tokyo, Japan

Received May 8, 1950

I. INTRODUCTION

Ordinarily a mixture of reactive solid substances is heated to elevated temperatures for the purpose of accelerating chemical reaction in the solid state.

The roentgenographic method is a powerful means of making clear the state of the reaction during heating. An x-ray camera which can be used at controlled elevated temperatures has long been needed in the investigation of this field.

A number of devices for heating a specimen in the x-ray camera have been described for making x-ray powder photographs of materials held at elevated temperatures (1, 3, 4, 5, 6, 8, 9, 10, 11, 12, 13, 14). The common principles of construction of these devices in the past have been based upon the radiation heating of a specimen in a small electric furnace adjusted in the camera assembly and the protection of the x-ray film by water cooling against fogging by the heat radiated from the electric furnace. A high-temperature x-ray camera with these devices has, however, the following disadvantages: (*1*) a narrow range of temperature allowance to which the specimen is subjected; (*2*) the formation of fog on the x-ray film due to incomplete protection against the heat radiated from the electric furnace; (*3*) inaccurate measuring of the temperature of the specimen by a thermocouple; (*4*) delay in waiting for the furnace to reach the desired temperature.

Recently, M. J. Buerger, N. W. Buerger, and F. C. Chesley (2) have proposed a new type of high-temperature x-ray camera. This apparatus differs in many respects from cameras previously described, but it is not suitable for the investigation of chemical reactions in the solid state above 1000°C.

In this report we shall describe a new type of high-temperature camera which is free from the above defects and is suitable for observation of chemical reactions in the solid state.

II. DESCRIPTION AND OPERATION OF A NEW HIGH-TEMPERATURE X-RAY CAMERA

The heating unit of this high-temperature x-ray camera consists of a platinum wire (0.2 mm. in diameter), which serves as a support for the powdered sample and as a heating element by passage of the electric current through it, and a regulating system for keeping it at the center of the cylindrical film. The x-ray radiates the specimen attached around the platinum wire, as in the ordinary powder method, and produces an overlapped x-ray pattern of specimen and platinum on a film. The increase of the crystal spacing in platinum by the elevation of temperature causes the displacement of the diffraction lines on a film. From the length of the displacement of the diffraction lines of platinum on the film its temperature and also that of the specimens on it can be calculated.

Figure 1 shows a general view of the assembled apparatus. It has been installed in the Universal Camera prepared by the Institute of Scientific Research in Tokyo.

Figure 2 shows in detail the structure of the heating element of the camera. The powdered specimen is kneaded with starch paste or other sticky materials and then the paste of the specimen is coated around the portion of platinum wire situated in the path of the x-ray. When the platinum wire is maintained at an elevated temperature during the exposure to x-rays, the sticky materials carbonize completely, but the specimens are held on the surface of the platinum wire as originally placed there. The x-ray pattern of the carbonized sticky materials does not appear and only that of the specimen appears on the film.

The heating-device assembly is fixed by tightening two screws on the rotating stage of the camera. A great convenience in centering the specimen is a detachable microscope. This is arranged to fit during centering operations on the same base which holds the heating device during the exposure, as shown in figure 1. When looking at the specimen through this microscope, the eye sees the specimen around the platinum wire framed in the aperture at the far end of the tube. Before adjustment, the specimen, when rotated, usually appears to move to the right and to the left in this aperture. By adjusting the position of the specimen on the rotating stage, the specimen is caused to become concentric with the axis of rotation, after which it appears to remain stationary in the aperture of the microscope when the stage is rotated.

The temperature of the specimen heater (platinum wire) is regulated by connecting it in series with resistances (R_1, R_2, and R_3 in figure 3) in the circuit of the D.C. motor generator. The battery B serves as an eliminator of voltage ripple. Satisfactory operation cannot be achieved by connecting this electrical sequence direct to a 100-v. power supply, for experience has shown that the ordinary power source is much too variable to maintain a constant temperature of the platinum wire. We can also solve the problem of a constant source by utilizing storage batteries or a voltage stabilizer.

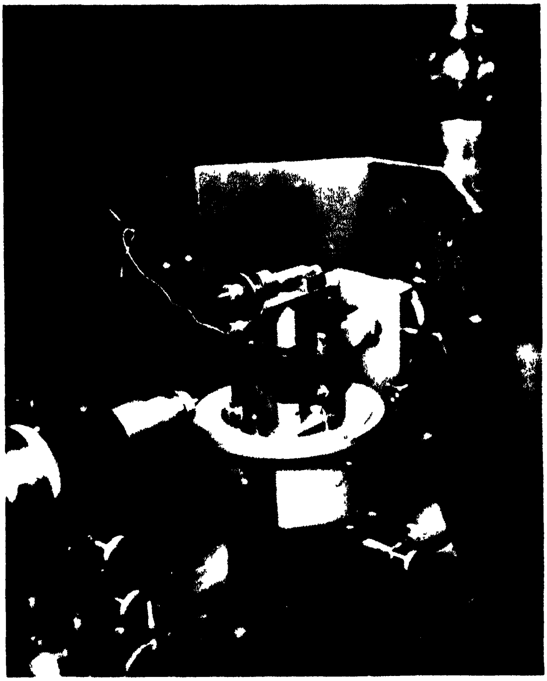

FIG. 1. The general view of the assembled apparatus

Figure 3 illustrates the heating circuit used in our experiment.

III. CHARACTERISTICS OF THE CAMERA

This high-temperature x-ray camera has many advantageous characteristics in comparison with the cameras previously described.

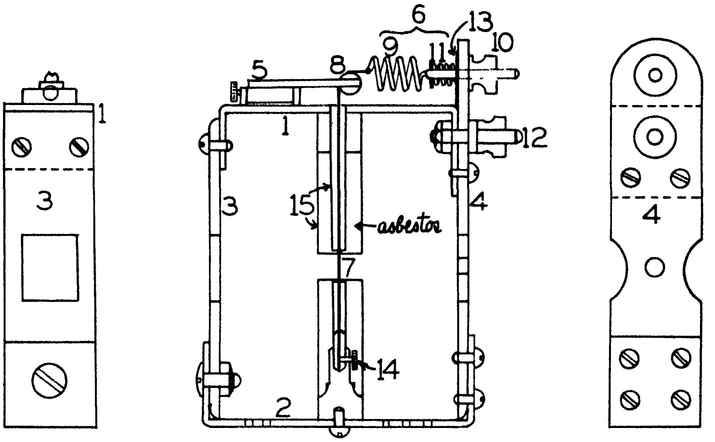

Fig. 2. Heating unit of the high-temperature x-ray camera

1,2	Brass plates, 1.5 mm. in thickness
3	Bakelite plate. The x-rays enter the camera through the pinhole slit and then through a square hole in this plate. An oscillating motion of this frame about the center of the camera is also possible.
4	Bakelite plate at opposite side
5	Microscrew driver for the centering of the platinum wire in a cylindrical film
6	Device for stretching the platinum wire
7	Platinum wire (heater of specimen)
8.	Small pulley
9	Spring made from phosphor bronze
10	Regulating screw for stretching platinum wire
11	Small spring for adjusting regulating screw
12	Terminal of electric current
13	Thin metal plate
14	Supporter of platinum wire
15	Concentric double cylinders made from aluminum foil (0.1 mm. in thickness), asbestos powder is packed between the double cylinders

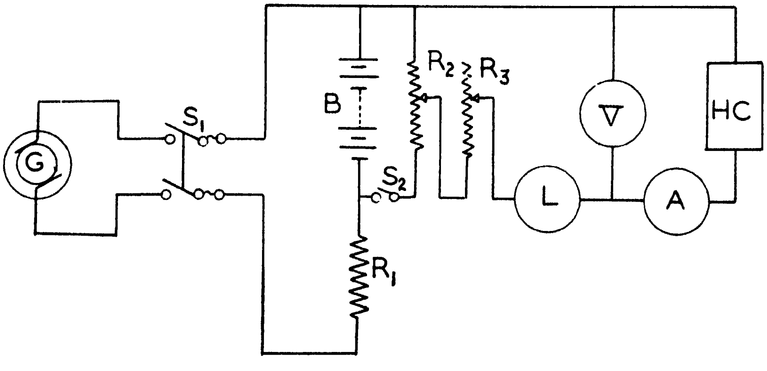

Fig. 3. The electric circuit of the heating unit. G, D.C. generator; B, battery; S_1, S_2, S_3, switches; R, resistances; L, safety lamp; HC, high-temperature camera; V, voltmeter.

(*1*) Since the temperature of the specimen may be brought to a temperature near the melting point of platinum (1773.5°C.), the allowable temperature range for the heating camera is greatly increased.

(*2*) The electrical energy applied to the platinum wire for heating the specimen is extremely low in comparison with the electric furnace types. Hence insulation against thermal radiation from the furnace is not necessary and this fact permits the elimination of cooling devices for a cassette and other camera attachments. The comparison of the electrical energy consumption of our camera and Buerger's camera (2) is shown in table 1.

(*3*) As the temperature of the platinum wire (or specimen) can be calculated from the displacement of its diffraction lines on a film, it is not necessary to use a thermocouple for the determination of the temperature of the specimen. This method can also record on a film the temperature of the part which has just been exposed to x-rays. Furthermore, the difference in the magnitude of errors in the temperature measurements at low and high temperatures is very slight, because the thermal expansion coefficient of platinum increases directly with temperature elevation until above 1000°C. By this method, it is possible to measure the temperatures above 1000°C. with an accuracy of ±5°C. in connection with the displacement measurement of the diffraction lines.

TABLE 1

Comparison of consumption of electrical energy

TEMPERATURE	ELECTRICAL ENERGY SUPPLIED*	
	OUR CAMERA	BUERGER'S CAMERA
°C.	*watts*	*watts*
100	0.54	3.5
200	1.26	8.0
400	3.00	19.0
600	5.25	32.0
800	7.00	
1000	9.30	
1370	12.58	

* When the platinum wire is renewed, the wattage value differs from the former values. This table shows only one example.

In the usual high-temperature camera which is provided with an electric furnace and a thermocouple, the thermocouple always indicates too low a reading, as determined by the more accurate method. This is due to the fact that the tiny furnace does not heat the entire thermocouple but only the junction; consequently the thermocouple leads, which are colder than the junction, conduct this tiny amount of heat away rapidly, lowering the temperature of the thermocouple junction below that actually supplied by the furnace. Furthermore, the difference in temperature between the specimen and the thermocouple must always be considered in the electric furnace type. The errors due to these sources were completely eliminated by our method.

(*4*) The time required to heat the specimen from room temperature to a desired temperature is very short compared with the camera with electric furnace heating. It takes about 1 min. to raise the specimen temperature to about 1300°C. The regulation of the resistance circuit is performed several times during the temperature elevation, because the resistance of the platinum wire and the rheostat varies with temperature.

The constancy of the temperature is easily realized by use of a battery and the electric circuit described in figure 3.

(*5*) The heating unit has also been adapted to any camera by slight modification of the frame shape.

IV. THE MEASUREMENT OF A CAMERA CONSTANT

A camera constant (camera radius), R, must be calculated very accurately in our method, because the specimen temperature is derived from the transferred length of the diffraction lines on a film. It may be that the camera constant of a camera does not become constant for all values of glancing angle for various reasons. If the mutual deviations of camera constants calculated from respective diffraction lines of different glancing angles are inevitable because of the experimental techniques, it is necessary to determine previously the relation between the camera constants and the values of the glancing angle, θ, by the use of a standard substance with well-known lattice constants. From a curve representing the relation between them, the R-values against respective θ-values are derived. These R-values were used in the following calculations.

TABLE 2*

FILM NO. 1	INDICES				
	(400)	(331)	(420)	$(511)_\beta$	(422)
l (mm.)†	128.25	104.62	95.97	76.34	52.84
η ($= 1/4R$) (rad.)	0.6670	0.5429	0.4982	0.3967	0.2755
d ($= \lambda/2 \cos \eta$) (Å.)	0.9784	0.8978	0.8751	0.7532	0.7988
a_0 (Å.)	3.9136	3.9134	3.9135	3.9137	3.9133
a_0 (Å.), mean value			3.9135		

* The back-reflection method was used in this experiment. Accordingly, the relation $\theta = \pi/2 - \eta$ is satisfied in table 2. The lattice constant of platinum, previously determined by other investigators, is $a_0 = 3.9135$ Å. (at 14°C.).

† Measured distance between the diffraction lines on both sides of the film.

The relation of the R-values to the l-values (corresponding to η-values in table 2) for our camera is shown, as an example, in figure 4, in which the position of the platinum wire in the camera is not accurately at the center of the camera. The values of the lattice constant, a_0, of platinum calculated by use of the R-values referred to the curve in figure 4 show good agreement for the respective diffraction lines (table 2).

V. THE DETERMINATION OF THE SPECIMEN TEMPERATURE

It is first necessary to measure the temperature of the platinum wire for the determination of the specimen temperature by the x-ray method. This is accomplished by calculation of the thermal expansion of the platinum wire at an elevated temperature as compared with that at a definite ground level of temperature (room temperature). The calculation formula is as follows:

$$t - t_0 = (a - a_0)/a_0\alpha_t = \Delta a/a_0 \tag{1}$$

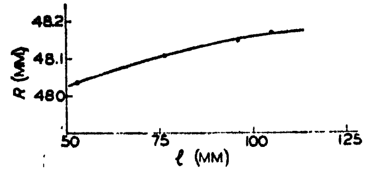

FIG. 4

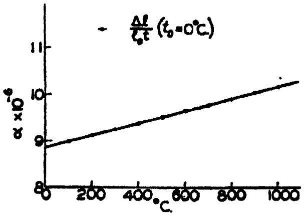

FIG. 5

FIG. 4. Relation between the camera radius (R) and the measured distances between the diffraction lines on both sides of the film.

FIG. 5. Plot of linear expansion coefficient (α) of platinum *vs.* the temperature

TABLE 3

Linear expansion coefficient of platinum

TEMPERATURE t	LINEAR EXPANSION COEFFICIENT OF PLATINUM ($\alpha_t \times 10^6$)				
	(1)*	(2)	(3)	(4)	(5)
°C.					
0	7.9085	8.870	8.868	8.786	8.868
100	8.4951	9.002	9.0004	9.0499	9.000
200	8.9903	9.135	9.1328	9.2342	9.150
300	9.2621	9.267	9.2652	9.4136	9.267
400	9.4784	9.398	9.3976	9.4633	9.400
500	9.5352	9.530	9.5300	9.5577	9.540
600	9.6780	9.662	9.6624	9.6693	9.667
700		9.793	9.7948		9.794
800		9.926	9.9272		9.925
900		10.058	10.0596		10.06
1000		10.190	10.1920		10.19

* (1) OWEN, E. A., AND YATES, E. L.: Phil. Mag. **17**, 113 (1934).

(2) *Smithsonian Physical Tables*, p. 280. Smithsonian Institute, Washington, D. C. (1933).

(3) Landolt-Börnstein (Roth/Scheel): *Physikalische-chemische Tabellen*, p. 1228 (HOLBORN, L., AND DAY, A.: Ann. Physik [4] **2**, 505 (1926)).

(4) *International Critical Tables*, Vol. II, p. 461. McGraw-Hill Book Company, Inc. New York (1927).

(5) KAMEKICHI, SHIBA: *Tables of Physical Constants*, p. 110. Iwanami Book Co., Inc., Tokyo, Japan (1948).

where a_0 = the lattice constant at a definite ground level of temperature, t_0°C.,
a = the lattice constant at an elevated temperature, t°C.,
α_t = the thermal expansion coefficient of platinum at the temperature t°C., and
t = the temperature of the platinum wire.

The value of α_t is not constant for the temperature range from room temperature to 1000°C., as shown in figure 5[1] and table 3. The value of α_t is now unknown, as the temperature to be determined remains yet unexplained. Consequently, we took the following method for calculating the temperature. Equation 1 transforms into equation 1′

$$(t - t_0)\alpha_t a_0 = \Delta a \tag{1'}$$

If $t - t_0 = \Delta t$, then

$$\Delta t \cdot \alpha_t \cdot a_0 = \Delta a \tag{2}$$

From equation 2 the relation between Δt and Δa is obtained, as the values of α_t and a_0 are known. If a curve for the relation between Δt and Δa is plotted (figure 6), Δt is determined from this curve for a value of Δa. Then the value of t is determined from Δt.

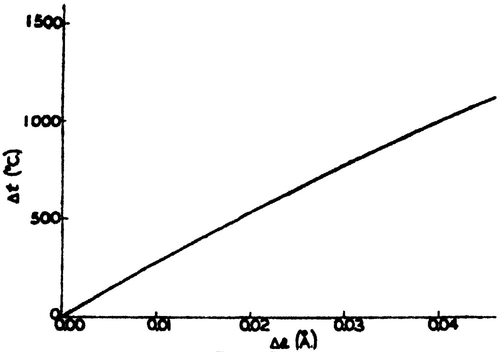

FIG. 6

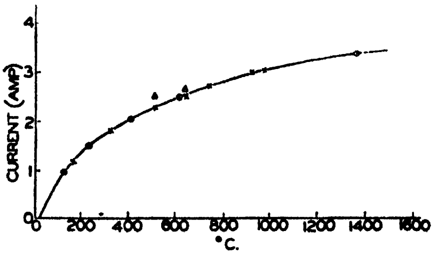

FIG. 7

FIG. 6. Relation between the lattice expansion of platinum, $\Delta a = (a_t - a_0)$, and the temperature.

FIG. 7. Relation between the temperature (°C.) of the platinum wire and the electric current (in amperes). ⊙, back-reflection camera (semicircular); ×, ordinary powder camera (full-circular), corrected values; △, without protective shield.

It is generally known from theoretical considerations that the value of $\Delta\theta/\Delta d$ reaches a maximum at $\theta = 90°$ and the observational error of θ becomes a minimum at $\theta = 90°$. In the experiments on the temperature measurement from the x-ray pattern of platinum, we took the diffraction lines of (311), (400), (331), (420), $(511)_\beta$, and (422) of platinum which have larger values of θ than 45°, respectively.

The results of the temperature measurement by the above-mentioned method are shown in table 4 (back-reflection method with a semicylindrical film) and table 5 (cylindrical film).

The diffraction lines for the measurement of temperature appear near both ends of the film when a cylindrical film is used. The positions of the diffracted lines are influenced by the state of setting of the film in the cassette. Correction for this is necessary for a cylindrical (circular) film, as the length of the film is longer than that of a semicircular film (back-reflection method). The values expressed by l_k and l_k' are, respectively, the exposed ranges, marked by the knife-edges adapted on the cassette, of the film at a standard and at any elevated temperature. Accordingly, the ratio l_k/l_k' is a correction factor to be multiplied by the length, l (mm.), for each diffraction line on the film photographed at any elevated temperature. Multiplication of this factor by the measured length, l (mm.), of the high-temperature film reduces its length to that of the standard-temperature film.

---

[1] The data of figure 5 are taken from *Smithsonian Physical Tables*, p. 280. Smithsonian Institute, Washington, D. C. (1933).

TABLE 4

Result of temperature measurement

FILM NO. 5	INDICES				
	(400)	(331)	(420)	$(511)_\beta$	(422)
l (mm.)	129.94	106.56	98.18	79.08	56.69
η ($= 1/4R$) (rad.)	0.6740	0.5330	0.5097	0.4109	0.2950
d ($= \lambda/2 \cos \eta$) (Å.)	0.9839	0.9033	0.8806	0.7576	0.8034
a (Å.)	3.9356	3.9374	3.9381	3.9366	3.9358
a (Å.), average			3.9367		
Δa			0.0232		
Δt (°C.)			613		
t (°C.) ($\Delta t + 14°$)			627		

TABLE 5

Result of temperature measurement

FILM NO. 12	INDICES				
	(311)	(331)	(420)	$(511)_\beta$	(422)
l_k' (mm.)*			134.24		
θ	40°13′	57°59′	60°36′	65°57′	72°21′
d (Å.)	1.1914	0.9066	0.8838	0.7607	0.8067
a (Å.)	3.9514	3.9518	3.9524	3.9527	3.9520
a (Å.), average			3.9521		
Δa			0.0386		
Δt (°C.)			972		
t (°C.) ($= \Delta t + 14°$)			986		

* l_k' = the exposed length of the film at any elevated temperature.

Figure 7 illustrates the relation between the electric current applied to the platinum wire and the temperature calculated as above.

The shielding paper, which protects the film against the radiant heat from the heater (platinum wire) and prevents the loss of radiation from it, fits between the aperture of the aluminum cylinder (15 in figure 2). It is not necessary to use it for low-temperature heating, but it is necessary for high-temperature heating.

VI. THE CALIBRATION OF SPECIMEN TEMPERATURE

The temperature of the heated platinum wire can be adequately determined with the aid of the roentgenographic method. We were able to determine by the following experiments that the specimen has the same temperature as that of the platinum wire used as heater.

Buerger's method (2) for the calibration of the true specimen temperature is to make use of crystal polymorphism. If a crystalline substance which exhibits a polymorphic transition of the rapid variety is used as a specimen, the temperature is known at which its x-ray pattern changes. If the electrical energy supplied to the furnace windings to obtain two x-ray patterns, one on each side of the polymorphic change, is recorded, then some energy reading between those corresponds to the known temperature of the polymorphic change.

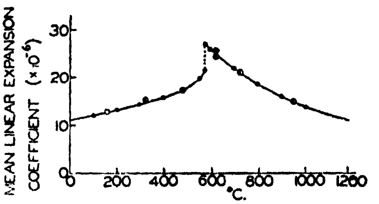

FIG. 8. Relation between the mean linear expansion coefficient of quartz and the temperature. ●, by the dilatometric method (Sosman); ⊙, by the roentgenographic method (Kubo and Akabori).

This method of calibration is very laborious, because it necessitates several sheets of x-ray photographs to determine one value of the temperature and in succession several values of the temperature in order to draw a curve exhibiting the relation of the temperature to the electrical energy. The polymorphic compounds used in this experiment have lower transition temperatures than that required in our studies and we do not have substances which exhibit such high transition temperatures that they are suitable for our experiments.

We have carried out the calibration of the specimen temperature by the following convenient method. We have employed quartz powder for the examination of the temperature calibration. From the diffraction lines of the platinum, which appeared as an overlapped pattern over those of quartz on a film, the temperature of the quartz was assumed.[2] The linear expansion coefficient and the axial ratio (*c/a*) of quartz at that temperature were calculated from its diffraction lines on the same film. When the thermal expansion coefficients and the axial ratio (*c/a*) of quartz are compared with the values obtained from the dilatometric method by R. B. Sosman (7), good agreement is found between them (figure 8). From this it may be concluded that the temperature of the specimen was almost consistent with that of the platinum wire.[3]

---

[2] We apply the sample around the platinum wire in so thin a layer that its presence can scarcely be detected by the naked eye. If it is applied slightly thick, the diffraction lines of platinum do not appear on the film because of absorption by the sample. When heated the platinum wire must be covered with a shield (protective tube) made of aluminum foil. As a result, the temperature of the sample is almost equal to the temperature of the platinum wire, or less by a few degrees.

The hysteresis phenomenon for the thermal expansion of the platinum wire was not observed at the repeated heating of that wire from room temperature to 1400°C. in the atmosphere. This fact permits the repeated use of the same platinum wire in order to determine the expansion coefficient by the x-ray method.

We are now constructing a modified type of this high-temperature camera which will enable us to heat the sample from room temperature to 2000°C. by the use of a tungsten wire in place of a platinum wire and a vacuum camera system.

REFERENCES

(1) Becker, K.: Z. Physik **40,** 37 (1927).
(2) Buerger, M. J., Buerger, N. W., and Chesley, F. G.: Am. Mineral. **28,** 285 (1943).
(3) Cohn, W. M.: Z. Physik **50,** 123 (1928).
(4) Finbak, Chr., and Hassel, O.: Z. physik. Chem. **B37,** 75 (1937).
(5) Jay, A. H.: Z. Krist. **86,** 106 (1933).
(6) Schossberger, F.: Z. Krist. **98,** 259 (1937).
(7) Sosman, R. B.: *The Properties of Silica.* The Chemical Catalog Company, Inc., New York (1927)
(8) Straumanis, M.: Z. Krist. **102,** 432 (1940).
(9) Straumanis, M., and Ievinš, A.: Z. anorg. allgem. Chem. **238,** 180 (1938).
(10) Westgren, A.: J. Iron Steel Inst. (London) **103,** 306 (1921).
(11) Westgren, A., and Lindh, A. E.: Z. physik. Chem. **98,** 192 (1921).
(12) Westgren, A., and Phragmen, G.: Z. physik. Chem. **102,** 3 (1922).
(13) Wilm, D., Hofmann, U., and Endell, K.: Sprechsaal **38,** 1 (1934).
(14) Wilson, A. J. C.: Proc. Roy. Soc. (London) **53,** 235 (1941).

---

[3] We are now considering the close examination of the sample temperature by another method.

A STUDY OF THE TWO-COMPONENT VAN DER WAALS FLUID[1]

JAMES W. DRENAN[2] AND TERRELL L. HILL[3]

Department of Chemistry, University of Rochester, Rochester, New York

Received October 20, 1949

I. INTRODUCTION

The equation of state

$$\left(P + \frac{N^2a}{V^2}\right)(V - Nb) = NkT \tag{1}$$

proposed by J. D. van der Waals in 1873 and based upon purely qualitative reasoning, is still widely used in studies of the properties of imperfect gases and liquids and of the transition from the gaseous to the liquid state. The quantitative results predicted by the equation are seldom found to hold very accurately except at low pressures, but they are of the right order of magnitude; its qualitative predictions are very generally correct. It therefore seems desirable to study, in both three dimensions and two (e. g., as an adsorbed monolayer), the thermodynamic behavior of a system of two components, each of which obeys equation 1. Extension of these results to a system of more than two components is obvious.[4]

It might be helpful to recall some results for a single van der Waals fluid. Hill (3) showed that a smoothed potential model, with $u(r) = \infty$ for $r \leqslant r$ and $u(r) = -\epsilon\left(\frac{r^*}{r}\right)^m$ for $r > r$, leads to equation 1. a is defined as $\frac{2\pi\epsilon r^{*3}}{m-3}$ and b as $\frac{2\pi r^{*3}}{3}$, and the free volume $V_f = V - Nb$. The resulting partition function gives the chemical potential of the liquid, μ_L, and of the gas, μ_G, in terms of the volumes

---

[1] This paper is a condensation of material from one section of a thesis submitted by James W. Drenan to the University of Rochester, Rochester, New York, in partial fulfillment of the requirements for the degree of Doctor of Philosophy, September, 1949.

[2] Present address: Noyes Chemical Laboratory, University of Illinois, Urbana, Illinois.

[3] Present address: Naval Medical Research Institute, National Naval Medical Center. Bethesda, Maryland.

[4] *Note added January 31, 1950:* After completion of the present work, the authors had the privilege of seeing in proof the related manuscript of Wall and Stent (J. Chem. Phys. **17**, 1112 (1949)). The approach of the two papers is quite different. Wall and Stent begin by assuming that the binary mixture obeys an equation of state formally identical with the usual van der Waals equation. Our approach seems to us more deductive in that the partition function for the two-component system is a generalization of the partition function for the one-component system. A consequence of this is that the second virial coefficient from our equation of state (see below) is of less restricted form than that of Wall and Stent (It is easy to show from an expansion of their equation of state that Wall and Stent make the implicit assumption that $b_{12} = (b_1 + b_2)/2$; actually, $b_{12}^{1/3} = (b_1^{1/3} + b_2^{1/3})/2$ would be more reasonable.) On the other hand, the approach of Wall and Stent avoids the "difficulty" discussed in detail below.

v_L and v_G. v_G may be found by regarding the gas as ideal, while v_L may be approximated (2) by setting $P = 0$ in equation 1. This gives:

$$v_L = [a - a(1 - 4bkT/a)^{1/2}]/2kT$$

When liquid and vapor are in equilibrium, $\mu_L = \mu_G$, so the vapor pressure of the liquid is given by

$$p = \frac{kT}{v_L - b} \exp\left\{\frac{b}{v_L - b} - \frac{2a}{v_L kT}\right\}$$

This is approximately equal to

$$\ln p = \ln\left(\frac{a}{b^2}\right) - \frac{a}{bkT}$$

The latter equation was first obtained by Wall (6), who pointed out that it has the familiar empirical form $\ln p = A - B/T$.

II. THE TWO-COMPONENT VAN DER WAALS SYSTEM IN THREE DIMENSIONS

A. Equation of state

Let us assume that we have a mixture of two gases each of which, when pure, obeys van der Waals' equation. Associated with a hard sphere of gas 1 are a_1, b_1, m_1, ϵ_1, and r_1; correspondingly, gas 2 is defined by a_2, b_2, m_2, ϵ_2, and r_2. (m_1 and m_2 are the respective molecular masses.) The free volumes may be written

$$V_{1f} = V - N_1 b_1 - N_2 b_{12}$$
$$V_{2f} = V - N_2 b_2 - N_1 b_{21}$$

Thus the volume excluded to a given molecule of gas 1 includes both the volume "occupied" by the other gas 1 molecules and that which is not available because of the presence of molecules of gas 2. Geometrical considerations show that a gas 2 molecule excludes a different volume to a like molecule from that to a gas 1 molecule (unless $b_1 = b_2$), and that a gas 2 molecule excludes the same volume to a gas 1 molecule as the latter does to a gas 2 molecule (i. e., $b_{21} = b_{12}$).

To find $-\chi$, the total potential energy of the assembly, we must add the various types of interactions. $-\chi_{11}$, the interaction of type 1 molecules with the other molecules of gas 1, is found (3) as for the one-component case, and likewise for $-\chi_{22}$. If by analogy $u_{12} = -\epsilon_{12}(r_{12}^*/r)^6$ and $a_{12} = 2\pi\epsilon_{12}r_{12}^{*3}/3$, then

$$\chi_{12} = 2a_{12}N_1N_2/V$$
$$\chi = \frac{a_1 N_1^2}{V} + \frac{a_2 N_2^2}{V} + \frac{2a_{12}N_1N_2}{V}$$

The partition function Q for the two-component system is therefore given by:

$$Q = \frac{1}{N_1!}\left[\left(\frac{2\pi m_1 kT}{h^2}\right)^{3/2}(V - N_1 b_1 - N_2 b_{12})\right]^{N_1} \cdot \frac{1}{N_2!}\left[\left(\frac{2\pi m_2 kT}{h^2}\right)^{3/2}(V - N_2 b_2 - N_1 b_{12})\right]^{N_2} \exp(\chi/kT) \quad (2)$$

From this may be derived

$$P = \frac{kTN_1}{V - N_1 b_1 - N_2 b_{12}} + \frac{kTN_2}{V - N_2 b_2 - N_1 b_{12}} - \left\{\frac{a_1 N_1^2 + 2a_{12} N_1 N_2 + a_2 N_2^2}{V^2}\right\} \tag{3}$$

or if we set $x = N_1/(N_1 + N_2)$ and $v = V/(N_1 + N_2)$,

$$\frac{P}{kT} = \frac{x}{v - b_1 x - b_{12}(1 - x)} + \frac{1 - x}{v - b_{12} x - b_2(1 - x)} - \left\{\frac{a_1 x^2 + 2a_{12} x(1 - x) + a_2(1 - x)^2}{kTv^2}\right\} \tag{4}$$

Equation 3 reduces to equation 1 for the three cases $x = 0$, $x = 1$, and $a_1 = a_{12} = a_2$ when $b_1 = b_{12} = b_2$. Use of either equation 3 or equation 4 leads to P–V curves analogous to the corresponding curves for one component; the mixture has a critical temperature just as the pure gas does.

If in equation 3 it is assumed that V is much greater than any of the terms $N_1 b_1$, $N_1 b_{12}$, $N_2 b_{12}$, and $N_2 b_2$ (that is, if the gas is only slightly imperfect), the expansion $1/(1 - x) = 1 + x + \cdots$ may be used, dropping higher terms, to give

$$P = \frac{NkT}{V} + \frac{kT}{V^2}\left\{N_1^2\left(b_1 - \frac{a_1}{kT}\right) + N_2^2\left(b_2 - \frac{a_2}{kT}\right) + 2N_1 N_2\left(b_{12} - \frac{a_{12}}{kT}\right)\right\}$$

where $N = N_1 + N_2$. This equation corresponds to equation (720, 3) of reference 2. The second virial coefficient will therefore vary linearly with x only when

$$2\left(b_{12} - \frac{a_{12}}{kT}\right) = b_1 - \frac{a_1}{kT} + b_2 - \frac{a_2}{kT}$$

B. Critical constants

The critical data for the two-component system are found by an extension of the method used (5) in the one-component case. Equation 4 may be rearranged to give

$$v^4 + v^3\left(-c - d - \frac{kT}{P}\right) + v^2\left\{cd + \frac{kTc}{P}(1 - x) + \frac{kTdx}{P} + \frac{A}{P}\right\} + v\left\{-\frac{Ac}{P} - \frac{Ad}{P}\right\} + \frac{Acd}{P} = 0$$

which is a quartic in v. Here $c = b_1 x + b_{12}(1 - x)$, $d = b_{12} x + b_2(1 - x)$, and $A = a_1 x^2 + 2a_{12} x(1 - x) + a_2(1 - x)^2$. At the critical temperature and pressure there will be three real and equal roots of the equation, denoted by v_c. There will also be (see figure 1) a mathematically real (but physically unreal) root which we may call v^*. Then for $P = P_c$ and $T = T_c$, equation 4 must be of the form $(v - v_c)^3(v - v^*) = 0$. If this is multiplied out, the coefficients of like powers of v in this and the preceding quartic may be equated to give a set of four relations which must be satisfied by v_c, v^*, P_c, and T_c. Simultaneous solution of these equations leads to:

$$v_c^4 - 3v_c^3(c + d) + 3v_c^2\{(1 - x)c^2 + xd^2 + 3cd\} - v_c\{(1 - x)c^3 + xd^3 + 9(1 - x)c^2d + 9xcd^2\} + 3\{(1 - x)c^3d + xcd^3\} = 0 \quad (5)$$

$$v^* = \frac{v_c cd}{v_c(c + d) - 3cd} \quad (6)$$

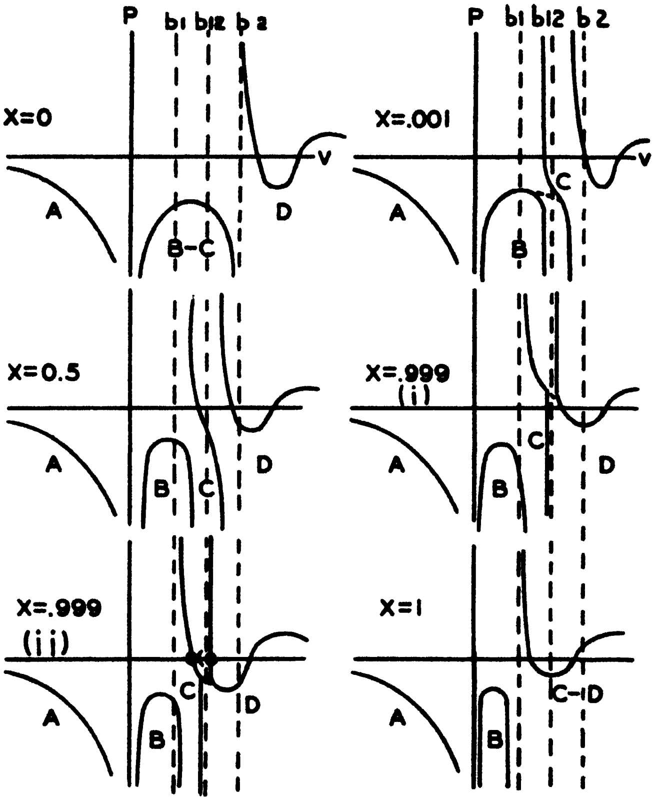

FIG. 1. Complete solutions of van der Waals' equation for a two-component system

$$kT_c = \frac{Acd(3v_c - c - d + v^*)}{v_c^3 v^*} \quad (7)$$

$$P_c = \frac{Acd}{v_c^3 v^*} \quad (8)$$

Combining the last two of these, we find that:

$$\frac{kT_c}{P_c v_c} = 3 + \frac{v^*}{v_c} - \frac{(c + d)}{v_c}$$

v_c and v^* are thus functions of b_1, b_{12}, b_2, and x, while P_c and T_c are functions not only of the b's and of x but of a_1, a_{12}, and a_2. As indicated by the previous discussion, the variation of these critical properties with x is not, in general, linear. For example, for certain choices of the a's and the b's, a mixture of two components can have a critical temperature lower (or higher) than that for either of the pure components. If a_{12} is less than a_2, the addition of a few molecules of component 1 to pure liquid 2 will lower the average molecular interaction, the mixture will vaporize more readily, and T_c for the mixture will be lower, regardless of whether or not the critical temperature for pure liquid 1 is higher or lower than that of pure liquid 2.

Because the dependence of v_c on x is given by a quartic (equation 5), it is not possible to write a simple reduced van der Waals equation for the two-component system. It is possible to show that when $x = 1$, equation 5 has a triple root $v_c = b_{12}$ and a single physical root $v_c = 3b_1$; likewise, when $x = 0$, a triple root $v_c = b_{12}$ and a single physical root $v_c = 3b_2$ exist. When x has a value other than 0 or 1, the physical root varies between its values at those points; another root remains close to b_{12}; for each case calculated the third and fourth roots are conjugate complex numbers, but it has not been proven that this is always the case.

C. Vapor pressure of the liquid

(1) "Normal" and "abnormal" cases

In order to find the vapor pressure of the two-component liquid, we need an expression for v_L. As before, for this purpose the approximation is made that, for low temperatures, P is equal to zero in equation 4. For definite values of the a's and b's, v_L may then be found as a function of x. The liquid chemical potentials μ_{1L} and μ_{2L} may be found from the partition function (equation 2); μ_{1G} and μ_{2G} are obtained by assuming the vapor to be a perfect gas. The results are

$$p_1 = \frac{kTx}{v - b_1x - b_{12}(1-x)} \exp\left\{\frac{b_1x}{v - b_1x - b_{12}(1-x)} + \frac{b_{12}(1-x)}{v - b_{12}x - b_2(1-x)} - \frac{2[a_1x + a_{12}(1-x)]}{vkT}\right\} \qquad (9)$$

and

$$p_2 = \frac{kT(1-x)}{v - b_{12}x - b_2(1-x)} \exp\left\{\frac{b_{12}x}{v - b_1x - b_{12}(1-x)} + \frac{b_2(1-x)}{v - b_{12}x - b_2(1-x)} - \frac{2[a_{12}x + a_2(1-x)]}{vkT}\right\} \qquad (10)$$

The total vapor pressure $P = p_1 + p_2$.

From equation 4 it is apparent that $|P|$ will be infinite when $v = 0$, $v = b_1x + b_{12}(1-x)$, or $v = b_{12}x + b_2(1-x)$. The values of v which will make $|P|$ infinite will then vary with x in the manner shown in figure 1. Branch D is the curve of physical interest.

In drawing figure 1 it was assumed that, for b_2 larger than b_1, b_{12} is intermediate between the two. This assumption is physically logical, but it introduces an additional complication. When $x = 0$ or $x = 1$, the equation of state is a cubic instead of a quartic so that, in these two cases, there is one less branch in the P *vs.* v curves. We expect a reasonable transition to occur in these curves as x changes from 0 to 0.001, say, or from 1 to 0.999. Mathematically it may be seen that this occurs. When x decreases from 0.001 to 0, branches B and C combine into one branch; likewise, when x goes from 0.999 to 1, branches C and D coalesce (figure 1). Physically, the situation is not so satisfactory. In going from $x = 0$ to $x = 0.001$, branch D remains the "physical" curve, as expected. As x increases further the volumes (branches C and D) corresponding to infinite pressure move toward b_1 and b_{12}. However, as x nears 1, a dilemma arises: the volume at which the pressure becomes infinite in branch D approaches b_{12}; yet, when $x = 1$, this volume is certainly b_1 (physically).

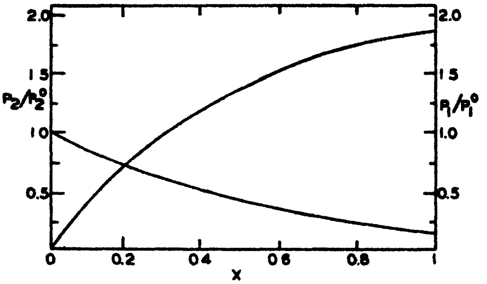

FIG. 2

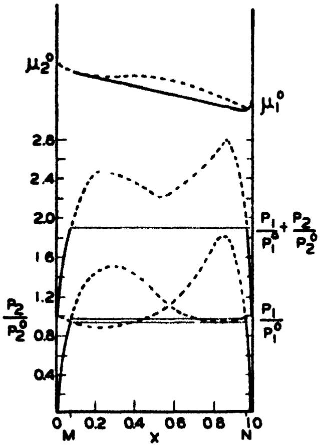

FIG. 3

FIG. 2. Calculated vapor pressures in an "abnormal" case

FIG. 3. Variation with composition of vapor pressures and free energy in a case with partial miscibility.

The model thus predicts that, when $x = 1$, the curve asymptotic to b_1 is the "physical" curve, but that as soon as a molecule of component 2 is added branch D, asymptotic to b_{12}, becomes the "physical" curve. From a realistic point of view, such a discontinuous jump upon the addition of a single molecule is of course absurd. One consequence of this difficulty arises in connection with the vapor pressure. To illustrate this, vapor pressure curves of the two components are shown in figure 2 for the case

$$\begin{Bmatrix} a_1 = 6.75bkT, & a_{12} = 13.5bkT, & a_2 = 27bkT \\ b_1 = b, & b_{12} = 2b & b_2 = 3b \end{Bmatrix}$$

for which we shall hereinafter use the symbolism

$$\begin{Bmatrix} 6.75 & 13.5 & 27 \\ 1 & 2 & 3 \end{Bmatrix}$$

in figure 3 for the case

$$\begin{Bmatrix} 8 & 6 & 8 \\ 1 & 1.1 & 1.2 \end{Bmatrix}$$

and in figure 4 for the case

$$\begin{Bmatrix} 8 & 7.6 & 8 \\ 1 & 1.1 & 1.2 \end{Bmatrix}$$

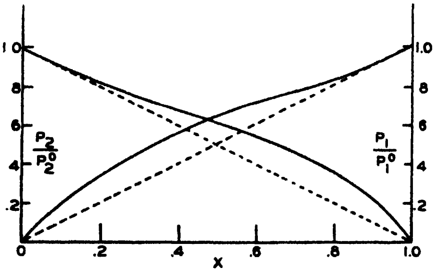

FIG. 4

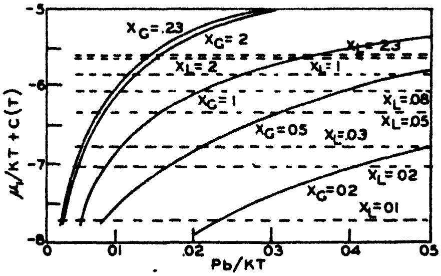

FIG. 5

FIG. 4. Variation with composition of the vapor pressures of the components in a "normal" case.

FIG. 5. Variation with pressure of chemical potentials of gas and liquid for the case $b_1 = b$, $b_{12} = 1.1b$, $b_2 = 1.2b$, $a_1 = a_2 = 8bkT$, $a_{12} = 6bkT$.

In the region near $x = 0$ (where x is the mole fraction of the component of smaller molecular volume in each case), the vapor pressure p_2 of the component of larger molecular volume resembles an experimental vapor pressure curve in each case and obeys Raoult's law. In figures 3 and 4 the same is true for p_1 in the region near $x = 1$; however, in figure 2 this is not true at all, as in this case p_1 approaches $1.9035p_1^0$ as x approaches 1. (p_1^0 is the vapor pressure of pure liquid 1.) In the same region p_2 does not approach 0.

It is therefore apparent that something is wrong with the fundamental assumptions of the statistical model. One of the assumptions was (3) that the molecules were spread *uniformly* over the total volume. When that volume is large, as in the gaseous state, this involves no difficulties. In the liquid state for small x (so that a few small molecules are interspersed among many large molecules) the model holds up; the average separation of the molecules is then slightly greater than r_2^*. However, when x is nearly 1, so that many of the small molecules surround a few larger ones, the assumption of uniform spacing causes difficulty as the volume is decreased. According to the above-mentioned assumption, the small molecules, in order to be distributed uniformly, must be separated by a distance somewhat greater than r_{12}^* to allow room for an occasional large molecule, and this separation must be maintained as long as the mixture contains any large molecules. As soon as the last large molecule is removed, however, so that $x = 1$, the small molecules are free to be compressed to a separation of r_1^*.

This difficulty makes it very clear that the assumption of uniform density underlying the statistical model (3) corresponding to the usual one-component van der Waals equation is faulty: it leads, when extended to the two-component case, to the unrealistic vapor pressure curves of figure 2. It is now of interest to consider why the vapor pressure curves for the cases shown in figures 3 and 4 should be valid. These correspond to an "intersection" of branches C and D at a positive pressure (see figure 1(i)), while the case of figure 2 is for an intersection at a negative pressure (see figure 1(ii)). We recall that for zero pressure the molecular volume of pure liquid 1 is greater than b_1; in fact, it is approximately equal to $b_1 + b_1^2kT/a_1$. If b_{12} is less than this, the aforementioned difficulty does not arise. That is, if the intersection for x close to 1 in figure 1 occurs at a pressure greater than the vapor pressure of pure component 1 (and thus effectively above $P = 0$), the vapor pressure curves are normal; this is because in calculating the vapor pressure we use for v_L the volume at zero pressure, and in this case v_L at $P = 0$ is a continuous function of x. If the intersection occurs at a negative pressure on the other hand, v_L is not a continuous function of x at $x = 1$, so the resulting vapor pressure curves are abnormal. (It is incidentally apparent from figure 1 that the present van der Waals model will not predict the properties for a two-component liquid correctly at *high* pressures when the molecular volumes are dissimilar, in either case (i) or case (ii)). Thus van der Waals' equation, like some other equations for the liquid state, leads to incorrect results when applied to solutions if the molecular volumes of the components are not nearly equal.

(2) Raoult's law; Henry's law

Using the approximation that $P = 0$, we may obtain, by implicit differentiation of equation 4 with respect to x, an expression for $\left(\frac{dv}{dx}\right)_{x\to 1}$. From equation 9, $\left(\frac{d \ln p_1}{dx}\right)_{x\to 1}$ may be found and evaluated as x approaches 1. If the former is substituted in the latter, the result is $\left(\frac{d \ln p_1}{dx}\right)_{x\to 1} = 1$. Raoult's law follows from this and the fact that $p_1 \to p_1^0$ as $x \to 1$ (equation 9). An analogous result may be obtained for p_2 as x approaches zero.

From equation 9, evaluated as x approaches 0, if we say that v approaches v_2^0, we find:

$$p_1 = \frac{kTx}{v_2^0 - b_{12}} \exp\left\{\frac{b_{12}}{v_2^0 - b_2} - \frac{2a_{12}}{v_2^0 kT}\right\}$$

Since in the physical case v_2^0 is not equal to b_{12}, $p_1 = K_1x$ (for x close to zero), which is Henry's law. A similar result may be obtained for p_2 as x approaches 1.

Figure 3 also shows a plot of the total vapor pressure P *vs.* x. Figure 3 represents a case in which the predicted vapor pressure of the liquid mixture, over most of the range in x, is greater than the vapor pressure of either pure component but is less than these near the ends; for the intermediate values of x a system of *two* liquid phases will then form. The compositions of the two liquid phases, termed M and N, are determined (2) by the criteria that $p_{1M} = p_{1N}$ and $p_{2M} = p_{2N}$.

At the top of figure 3 is included a plot of $[\mu_1 x + \mu_2(1 - x)]/kT$ *vs.* x for this case. The dotted curve gives the total free energy which would be obtained if only one liquid phase formed, while the full curve gives the total free energy resulting from the formation of the two liquid phases of compositions M and N. The splitting into two liquid phases occurs because the total free energy of such a system is lower than that of the hypothetical system of one liquid phase. Since any other system of two phases would also have a free energy which would be represented by a straight line tangent to the dotted curve for one phase, and since no other such line can be drawn with as low a free energy, the two liquid phases must have the compositions M and N.

Figure 4 depicts a two-component liquid which obeys Raoult's law over a wider range and which does not form two liquid phases. The constants a and b are the same as in the case of figure 3, except that a_{12}, which measures the interaction between unlike molecules, is greater here.

Fowler and Guggenheim show that, for strictly regular solutions, the amount of deviation of the vapor pressures from Raoult's law depends upon the magnitude of w_{12}/kT, where $2w_{12}$ is the total increase in potential energy caused by the interchange of one molecule of component 1 in pure liquid 1 with one molecule of component 2 in pure liquid 2. In our notation, one finds:

$$w_{12} = \frac{a_1 - a_{12}}{v_1^0} + \frac{a_2 - a_{12}}{v_2^0}$$

Fowler and Guggenheim find negative deviations from Raoult's law for $w_{12} < 0$, perfect obedience to the law for $w_{12} = 0$, and positive deviations from the law for $w_{12} > 0$. There is a temperature of critical mixing, given by $w_{12}/kT = 2$, such that below that value one liquid phase exists for all x while above it there are two such phases for some values of x. One of the assumptions they use in defining a strictly regular solution is that the molecular volumes are nearly enough equal so that an interchange of unlike molecules does not affect the structure of the liquid. In the van der Waals model, the difference in molecular volumes is taken into account, and the vapor pressure diagrams in general lack the symmetry of those of Fowler and Guggenheim; as we have seen, however, the model breaks down if the molecular volumes are too dissimilar.

If the b's of the van der Waals model are approximately equal, $v_2^0 \approx v_1^0$, so that

$$w_{12} \approx \frac{a_1 + a_2 - 2a_{12}}{v_1^0}$$

Then when the attractive energy of interaction between unlike molecules is small compared to that between like molecules, w_{12} will have a large positive value and large positive deviations from Raoult's law will result, as in figure 3. As a_{12} increases relative to a_1 and a_2, the positive deviations from the law will decrease (figure 4) and can eventually become negative when $a_{12} > (a_1 + a_2)/2$.

(3) Liquid–vapor composition diagrams

From the data furnished by equations 9 and 10 the conventional diagrams showing the compositions of vapor and liquid which are in equilibrium at a definite pressure may be drawn. For a definite value of x_L, these equations give p_1 and p_2 and hence P, the total vapor pressure of the liquid of that composition. $p_1/(p_1 + p_2)$ gives the composition x_G of the (perfect) vapor in equilibrium with that liquid at a pressure P.

A diagram of this sort may be obtained by another method, based upon the necessity of the equivalence of the chemical potentials of any component in each phase (e. g., $\mu_{1L} = \mu_{1G}$). For component 1 of an ideal gas,

$$\frac{\mu_{1G}}{kT} + \ln\left\{\frac{2\pi m_1 kT}{h^2}\right\}^{3/2} = \ln\frac{P}{kT} + \ln x_G \tag{11}$$

From this equation, μ_{1G} may be found as a function of P for various values of x_G. This leads to the full curves of figure 5 for the case $\begin{Bmatrix} 8 & 6 & 8 \\ 1 & 1.1 & 1.2 \end{Bmatrix}$ (which corresponds to figure 3).

From equation 2, one may find for the two-component liquid:

$$\frac{\mu_{1L}}{kT} + \ln\left\{\frac{2\pi m_1 kT}{h^2}\right\}^{3/2} = \ln\frac{x_L}{v_L - b_1 x_L - b_{12}(1 - x_L)} + \frac{b_1 x_L}{v_L - b_1 x_L - b_{12}(1 - x_L)} + \frac{b_{12}(1 - x_L)}{v_L - b_{12} x_L - b_2(1 - x_L)} - \frac{2[a_1 x_L + a_{12}(1 - x_L)]}{v_L kT} \tag{12}$$

Reasonable values of Pb/kT are substituted in equation 4, which is then solved for those values of v_L corresponding to various choices of x. (This provides a check on the validity of the earlier approximation that $P = 0$, which was used to find v_L. The difference between the values of v_L so obtained and those corresponding to the pressures of interest here is very small.) These values of v_L are then substituted in equation 12 to find μ_{1L}. The results are shown in the dotted lines of figure 5; the lines are nearly horizontal because the liquid is nearly incompressible. A similar procedure gives μ_{2G} and μ_{2L}.

A value of x_G is chosen, and the points of intersection of the corresponding μ_{1G} curve with the μ_{1L} curves for various x_L's are plotted against the pressures P at which they occur, yielding the full curves of figure 6. It can be shown that these curves go through the origin and that, close to the origin, their slopes are proportional to x_G (since Raoult's law holds). Each of these curves gives the total pressure at which component 1 of a gas of composition x_G is in equilibrium with a liquid of composition x_L; at this pressure $\mu_{1L} = \mu_{1G}$. Similarly, the values of $(1 - x_L)$ which a given $(1 - x_G)$ curve intersects are plotted against the corresponding pressures, giving the dotted lines of figure 6 (which cross the x_L-axis at $x_L = 1$).

At the pressure where the $\mu_{1L} = \mu_{1G}$ curve for a given value of x_G intersects the $\mu_{2L} = \mu_{2G}$ curve for that same value of x_G, component 1 of vapor is in equilibrium with component 1 of liquid, and component 2 of vapor is also in equilibrium with component 2 of liquid. This x_G and the correct x_L are plotted *vs.* the designated pressure to give the liquid–vapor composition diagram. This method of obtaining the diagram is more accurate than the more conventional method described earlier, since it is not based upon the $P = 0$ approximation. It is, however, more lengthy.

(4) Liquid–vapor transitions

For a one-component van der Waals system, it is well known that the loops obtained for isothermal compression below the critical temperature must be replaced by horizontal lines to agree with experiment. For the two-component van der Waals system, the situation is somewhat more complicated.

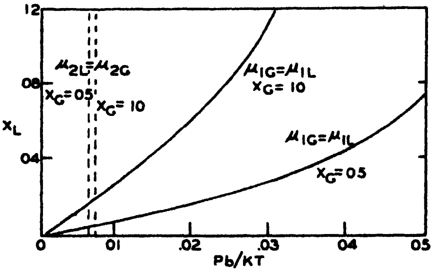

FIG. 6

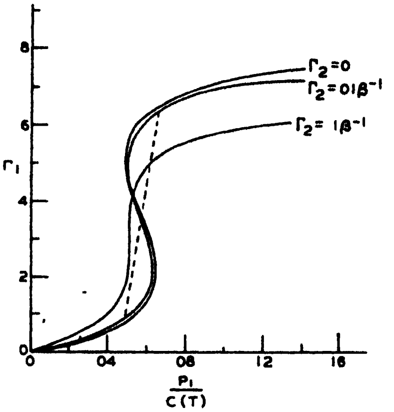

FIG. 7

FIG. 6. Variation with pressure of the liquid composition at which an individual component has the same chemical potential in both phases.

FIG. 7. Γ_1 *vs.* p_1 at constant Γ_2

If, for a temperature slightly below the critical temperature, the gas mixture is compressed isothermally, liquefaction occurs, but in this case the pressure does not ordinarily remain constant, so the transition line in this case is not ordinarily horizontal on a P *vs.* v diagram. The reason is that the ratio of component 1 to component 2 is not the same in the vapor as in the liquid. The actual transition line may be calculated by thermodynamic methods which are presumably not new and are therefore omitted.

If the values of x_G, the a's, and the b's are such that two liquid phases result (as in the case of figure 3), there will be some critical temperature for the formation of two such liquids. Below this temperature, condensation of the gas usually will first give one liquid, the pressure rising along a curved line; when the pressure reaches a certain value, two liquid phases form, and the pressure remains constant as the ratio of the amounts of these phases changes until all the vapor is condensed. However, if the original value of x_G should happen to be exactly that value which is in equilibrium with a system of two liquids whose total composition is also x_G, then as soon as condensation starts the two liquids will form, and the pressure will remain constant during condensation exactly as in the one-component case.

III. THE TWO-COMPONENT VAN DER WAALS SYSTEM IN TWO DIMENSIONS

A. Equation of state

The method of setting up a partition function in two dimensions is entirely analogous to the method used for three dimensions. The two-dimensional system is considered to be a mobile adsorbed monolayer of two components each of which obeys van der Waals' equation of state in three dimensions. The surface is assumed to be a completely uniform plane of area $\mathfrak{A}'$. $-\epsilon_1$ and $-\epsilon_2$ are the potential energies of molecules of components 1 and 2, respectively, adsorbed anywhere on this surface, relative to infinite separation of the molecules from the surface as the zero of energy. It is to be emphasized that the adsorbed molecule must be free to move over the whole surface if the van der Waals assumption of uniform smearing is to be valid; the idea of sites, and hence of localized adsorption, is foreign to this model.

The partition function Q_s for the monolayer is:

$$Q_s = \frac{1}{N_1!}\left\{\frac{2\pi m_1 kT}{h^2}\right\}^{N_1} (\mathfrak{A}' - N_1\beta_1 - N_2\beta_{12})^{N_1}(j_1)^{N_1}$$

$$\cdot \frac{1}{N_2!}\left\{\frac{2\pi m_2 kT}{h^2}\right\}^{N_2} ((\mathfrak{A}' - N_1\beta_{12} - N_2\beta_2)^{N_2}(j_2)^{N_2}$$

$$\cdot \exp\frac{\alpha_1 N_1^2 + 2\alpha_{12}N_1N_2 + \alpha_2 N_2^2}{\mathfrak{A}'kT} \exp\left\{\frac{\epsilon_1 N_1 + \epsilon_2 N_2}{kT}\right\} \tag{13}$$

where j_1 and j_2 are the vibrational partition functions normal to the surface; the α's and β's are the two-dimensional analogues of the three-dimensional a's and b's. In fact,

$$\beta_1 = \frac{\pi}{2}\left\{\frac{3b_1}{2\pi}\right\}^{2/3} \quad \text{and} \quad \alpha_1 = \frac{\pi a_1}{4b_1}\left\{\frac{3b_1}{2\pi}\right\}^{2/3}$$

Similar results may be obtained for β_{12}, β_2, α_{12}, and α_2.

From the partition function may be found ϕ, the two-dimensional spreading pressure for the monolayer. ϕ is given by

$$\frac{\phi}{kT} = \frac{N_1}{\mathfrak{A}' - N_1\beta_1 - N_2\beta_{12}} + \frac{N_2}{\mathfrak{A}' - N_1\beta_{12} - N_2\beta_2} - \frac{\alpha_1 N_1^2 + 2\alpha_{12}N_1N_2 + \alpha_2 N_2^2}{\mathfrak{A}'^2 kT} \tag{14}$$

Division by $N = N_1 + N_2$ gives

$$\frac{\phi}{kT} = \frac{x}{\mathfrak{A} - \beta_1 x - \beta_{12}(1-x)} + \frac{(1-x)}{\mathfrak{A} - \beta_{12}x - \beta_2(1-x)} - \frac{\alpha_1 x^2 + 2\alpha_{12}x(1-x) + \alpha_2(1-x)^2}{\mathfrak{A}^2 kT} \tag{15}$$

where $\mathfrak{A}$, the area per molecule, $= \mathfrak{A}'/N$, and $x = N_1/N$. Division of equation 14 by $\mathfrak{A}'$ gives

$$\frac{\phi}{kT} = \frac{\Gamma_1}{1 - \beta_1\Gamma_1 - \beta_{12}\Gamma_2} + \frac{\Gamma_2}{1 - \beta_{12}\Gamma_1 - \beta_2\Gamma_2} - \left\{\frac{\alpha_1\Gamma_1^2 + 2\alpha_{12}\Gamma_1\Gamma_2 + \alpha_2\Gamma_2^2}{kT}\right\}$$

where $\Gamma_1 = N_1/\mathfrak{A}'$ and $\Gamma_2 = N_2/\mathfrak{A}'$. Equations 14 and 15 correspond exactly to equations 3 and 4.

B. Critical properties

Following the same method as in three dimensions one obtains four equations for $\mathfrak{A}_c$, $\mathfrak{A}^*$, kT_{2c}, and ϕ_c which are formally identical with equations 5–8, with α replacing a and β instead of b. Thus equation 5 has a triple root $v_c = b_{12}$ and a single physical root $v_c = 3b_2$ when $x = 0$, and a triple root $v_c = b_{12}$ and a single physical root $3b_1$ when $x = 1$. Similarly, the two-dimensional equation has a triple root $\mathfrak{A}_c = \beta_{12}$ and a single physical root $\mathfrak{A}_c = 3\beta_2$ when $x = 0$, and a triple root $\mathfrak{A}_c = \beta_{12}$ and a single physical root $\mathfrak{A}_c = 3\beta_1$ when $x = 1$. In both of these cases, then (5), $\mathfrak{A}_c = \frac{3\pi}{2}\left(\frac{v_c}{2\pi}\right)^{2/3}$. However, for values of x other than 0 or 1 this will not usually be true. The dependence of $\mathfrak{A}_c$ on x will not be the same as that of v_c (although if b_1, b_{12}, and b_2 are nearly equal, the difference in the dependence will be very small). This statement has not been proven analytically but by computation for a specific case.

Similar statements may be made about ϕ_c and kT_{2c} except that they depend upon both the α's and the β's. For a one-component van der Waals gas (4), $kT_{2c} = 0.5kT_c$; for a two-component system in which the a's are nearly equal and the b's are nearly equal, kT_{2c} will equal $kT_c/2$ when $x = 0$ or 1 and will not be far from this for intermediate values of x.

C. Vapor pressure of the monolayer

If the monolayer is in equilibrium with a perfect three-dimensional gas, we may proceed much as before to find its vapor pressure. The chemical potentials of components 1 and 2 in the monolayer are found from equation 13. The chemical potentials of 1 and 2 as perfect gases are already known (e. g., equation 11). Use of $\mu_{1G} = \mu_{1S}$ and $\mu_{2G} = \mu_{2S}$ leads to

$$p_1 = \frac{kT\Gamma_1}{1 - \Gamma_1\beta_1 - \Gamma_2\beta_{12}} \exp\left\{\frac{\Gamma_1\beta_1}{1 - \Gamma_1\beta_1 - \Gamma_2\beta_{12}} + \frac{\Gamma_2\beta_{12}}{1 - \Gamma_1\beta_{12} - \Gamma_2\beta_2} - \frac{2(\alpha_1\Gamma_1 + \alpha_{12}\Gamma_2)}{kT}\right\}\left(\frac{2\pi m_1 kT}{h^2}\right)^{1/2}\frac{1}{j_1}\exp\left\{\frac{-\epsilon_1}{kT}\right\} \tag{16}$$

and

$$p_2 = \frac{kT\Gamma_2}{1 - \Gamma_1\beta_{12} - \Gamma_2\beta_2} \exp\left\{\frac{\Gamma_1\beta_{12}}{1 - \Gamma_1\beta_1 - \Gamma_2\beta_{12}} + \frac{\Gamma_2\beta_2}{1 - \Gamma_1\beta_{12} - \Gamma_2\beta_2} - \frac{2(\alpha_{12}\Gamma_1 + \alpha_2\Gamma_2)}{kT}\right\}\left(\frac{2\pi m_2 kT}{h^2}\right)^{1/2}\frac{1}{j_2}\exp\left\{\frac{-\epsilon_2}{kT}\right\} \tag{17}$$

The total vapor pressure P is then $p_1 + p_2$.

Equations 16 and 17 are quite similar to the three-dimensional equations 9 and 10. Instead of being written as functions of x, however, the adsorbate vapor pressures are given as functions of Γ_1 and Γ_2. Phase rule considerations show that one more variable is present than in the three-dimensional case; this gives rise to the possibility of a larger number of isotherms.

Examples of some of these isotherms are shown in figures 7–11. In each of them the three-dimensional constants are $\begin{Bmatrix} 8 & 6 & 8 \\ 1 & 1.1 & 1.2 \end{Bmatrix}$. Therefore $\beta_1 = \beta$, $\beta_{12} = 1.0656\beta$, $\beta_2 = 1.1292\beta$, $\alpha_1 = 4\beta kT$, $\alpha_{12} = 2.9062\beta kT$, and $\alpha_2 = 3.7641\beta kT$. It is of interest to note that $a_1 = a_2$ but α_1 is greater than α_2 because of the dependence of α on both a and b.

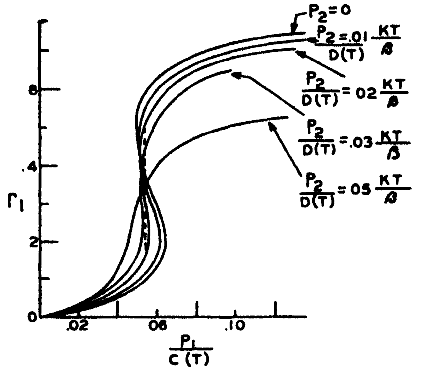

FIG. 8

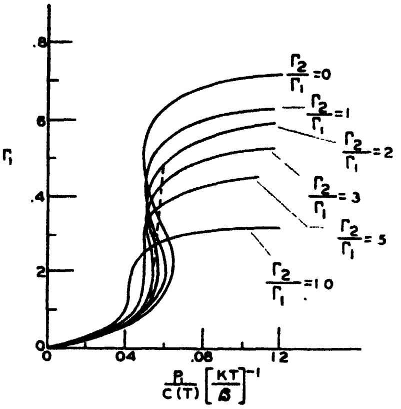

FIG. 9

FIG. 8. Γ_1 *vs.* p_1 at constant p_2
FIG. 9. Γ_1 *vs.* p_1 at constant Γ_2/Γ_1

Figures 7–9 look quite similar and may be qualitatively explained on a similar basis. When there are only a few molecules of component 1 on the surface, the presence of molecules of component 2 lowers the escaping tendency (and thus the vapor pressure) of the molecules because of the interaction α_{12} between the two types of molecules; if there are a lot of molecules of component 1 on the surface, however, the presence of molecules of component 2 increases the escaping tendency of component 1 because the molecules of component 2 cut down appreciably the area available to molecules of component 1. An increase in Γ_2 accentuates both of these effects and hence tends to straighten out the Γ_1 *vs.* p_1 curve. Lowering the temperature decreases the escaping tendency, as expected, and makes the wiggle in the curve more pronounced.

In discussing figure 10 we assume, for convenience, that

$$\left\{\frac{2\pi m_1 kT}{h^2}\right\}^{1/2} \frac{1}{j_1} \exp\left(-\epsilon_1/kT\right) = \left\{\frac{2\pi m_2 kT}{h^2}\right\}^{1/2} \frac{1}{j_2} \exp\left(-\epsilon_2/kT\right)$$

or, in the notation of the figures, $C(T) = D(T)$. The curve for pure component 1 ($p_2/p_1 = 0$) is always above the curve for pure component 2 because $\alpha_1 > \alpha_2$

and $\beta_1 < \beta_2$. If we start with either pure component and add some of the other, the total vapor pressure increases since the average intermolecular attraction is decreased (α_{12} is lower than either α_1 or α_2).

Figure 11 looks quite different but may be explained upon the same basis. The figure shows the amount of component 2 which is adsorbed at a constant value of p_2 as p_1 (and hence Γ_1) changes. A certain amount is adsorbed from a gas of pure component 2. If component 1 is also present in the vapor, some of it will be adsorbed, and the resulting attraction between molecules of 1 and 2 will increase the adsorption of component 2. The effect increases until

$$p_1 \Big/ \left[\left\{ \frac{2\pi m_1 kT}{h^2} \right\} \frac{1}{j} \exp\left(-\epsilon_1/kT\right) \right]$$

is of the order of $0.05kT/\beta$; at this pressure, as figure 7 shows, the surface area occupied by molecules of component 1 increases markedly, leaving less surface available for the adsorption of molecules of component 2. The result is a maximum in the Γ_2 *vs.* p_1 curve.

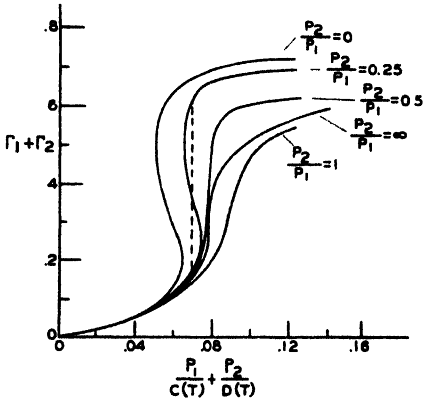

FIG. 10

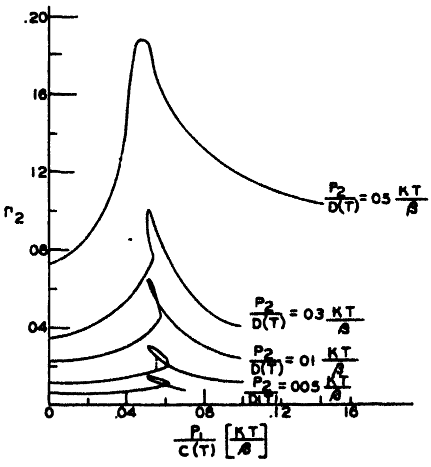

FIG. 11

FIG. 10. Total amount adsorbed *vs.* total pressure at constant p_2/p_1
FIG. 11. Γ_2 *vs.* p_1 at constant p_2

D. Phase changes in the adsorbate

There remains the question of the transition of the surface molecules from a two-dimensional gas to a two-dimensional liquid. It is of interest to examine figures 7–11 to find the change in ϕ, the two-dimensional spreading pressure, and in one or both of the three-dimensional vapor pressures as condensation occurs. The dotted lines in the figures used to show the results are only schematic.

(*1*) If the two-dimensional gas is compressed isothermally in such a manner that the ratio Γ_1/Γ_2 stays constant, then x_s, the mole fraction of component 1 on the surface, stays constant. ϕ *vs.* $\mathcal{A}$ plots result exactly analogous to the P *vs.* v

plots discussed in Section II,C,(4), with either one or two two-dimensional liquid phases resulting. During the condensation ϕ increases as long as only one liquid phase is being formed. Use of the Gibbs equation for two components

$$d\phi = \Gamma_1 kT \, d \ln p_1 + \Gamma_2 kT \, d \ln p_2 \tag{18}$$

shows that, if ϕ increases, p_1 and p_2 must do so also. Condensation occurs along the dotted line of figure 9.

(*2*) If the two-dimensional gas is isothermally compressed at a constant value of p_2, which means constant μ_{2S}, ϕ will increase until condensation starts. During condensation, with μ_{2S} constant, x_{SL} will stay constant; similarly x_{SG} will remain unchanged, so during the process ϕ, p_1, and p_2 will be constant. Condensation will lead to the dotted lines of figures 8 and 11.

(*3*) If the isothermal compression of the two-dimensional gas is carried out at a constant value of p_2/p_1, μ_{2S}/μ_{1S} will be constant. At first x_S will be nearly constant (exactly so if the two-dimensional gas were perfect), while ϕ increases until condensation begins. During condensatiod μ_{1L} and μ_{2L} of the surface phase depend only upon x_{SL}, so the same must be true of μ_{1L}/μ_{2L}. Since that ratio is fixed, x_{SL} must be constant. Similar reasoning holds for x_{SG}. We conclude that during the condensation ϕ and p_1 are unchanged (dotted line of figure 10).

(*4*) If the two-dimensional gas is compressed isothermally with Γ_2 constant, ϕ will increase until condensation starts. During condensation, $\mathfrak{A}$ naturally decreases, but N_1 stays constant so that Γ_1 increases. This means that x_S, and hence p_1, will increase; simultaneously, $(1 - x_S)$ and p_2 will decrease. From equation 18, ϕ may either increase or decrease, depending upon whether component 1, whose mole fraction in the two-dimensional liquid is increasing, has a larger or smaller volatility than component 2. In either case, however, since p_1 increases with Γ_1, the behavior during condensation is represented by the dotted line of figure 7.

It would be desirable to compare these predictions with actual experimental data. However, while a few data have been reported on the condensation of a one-component volatile adsorbate, to the writers' knowledge no data exist reporting the condensation of a two-component volatile adsorbate.

SUMMARY

The partition function for a two-component fluid, each component of which when pure satisfies the statistical model leading to van der Waals' equation of state, has been derived. From this are obtained the equation of state for this system in three dimensions, the critical constants of the system, and the vapor pressures of the components; the dependence of these properties on the values of the mole fraction and of the van der Waals a and b is discussed. The model is shown to break down when the molecular volumes of the two components are too dissimilar. This emphasizes the faulty nature of the original van der Waals picture.

An alternative method of obtaining liquid–vapor composition diagrams, based

upon the equivalence of the chemical potential in each phase, is discussed. The behavior of the system upon condensation is also considered.

The partition function, equation of state, and vapor pressure curves of a two-component, two-dimensional van der Waals adsorbate are discussed. Various types of isotherms based upon this model are then examined.

REFERENCES

(1) Cassel, H. M.: J. Phys. Chem. **48,** 195 (1944).

(2) Fowler, R. H., and Guggenheim, E. A.: *Statistical Thermodynamics.* Cambridge University Press, London (1939).

(3) Hill, Terrell L.: J. Chem. Education **25,** 347 (1948).

(4) Hill, Terrell L.: J. Chem. Phys. **14,** 441 (1948).

(5) Mayer, J. E., and Mayer, M. G.: *Statistical Mechanics.* John Wiley and Sons, Inc New York (1940)

(6) Wall, F. T.: J. Chem. Phys. **16,** 508 (1948).

MOISTURE RELATIONSHIPS OF CELLULOSE. II

THE HEATS OF WETTING OF PARTIALLY SATURATED VISCOSE RAYON AND STANDARD CELLULOSE IN WATER

MAURICE WAHBA

Department of Chemistry, Faculty of Science, Fouad I University, Cairo, Egypt

Received October 27, 1949

INTRODUCTION

The determination of the heat of sorption of water by cellulose has lately attracted the attention of a number of investigators in seeking for information related to the structure of cellulose and to its affinity for water. Rees (11) has reviewed the literature on the heats of wetting and adsorption. In his paper, values from a calorimetric method are given for several cellulosic materials and values are also calculated from adsorption measurements by the Clausius–Clapeyron equation. One important general feature is that regenerated celluloses give values of the heat of wetting at dryness about twice the corresponding value for cotton. The author (16) has found that this holds not only for water as a wetting liquid but also for other liquids as well. The ratio of the heats of wetting of viscose rayon and standard cellulose in water, methyl alcohol, acetone, and benzene has been found to be practically constant and nearly equal to 1.9. Urquhart and Eckersall (13), working on similar samples, found that the mean of the ratios of moisture regains on viscose rayon and scoured cotton at intervals of the relative humidity amounted to 1.9.

The sorption of water is usually supposed to occur by bonding to the hydroxyl groups present in the amorphous regions of the cellulose molecular structure, i.e., in the intermicellar spaces. The heat of wetting depends on the availability of such hydroxyl groups and may thus be used as a measure of the amount of amorphous material present in the structure of cellulose. It thus appeared useful to compare the ratios of the moisture regains at different relative humidities with those of the heats of wetting of partially saturated samples of some regenerated cellulose and native cellulose. For that purpose, the same viscose rayon (regenerated cellulose) and standard cellulose described previously (16) were used in this investigation.

EXPERIMENTAL

Partially saturating the cellulose

The apparatus used is shown in figure 1. The cellulose ampoule A, containing a known mass of cellulose, is sealed through an S-shaped capillary to the side-tube T, connected to the vapor limb of the manometer M. The other limb of the manometer is connected directly to the outgassing system, which consists of a mercury condensation pump and an oil vacuum pump separated by a phosphorus pentoxide tube. Two liquid bulbs, L_1 and L_2, are enclosed between two mercury cut-outs: C_1, to separate the bulbs from the outgassing system, and C_2, to separate them from the vapor limb of the manometer. A McLeod gauge (G) is connected to the vacuum limb of the manometer to detect the presence of any permanent gases.

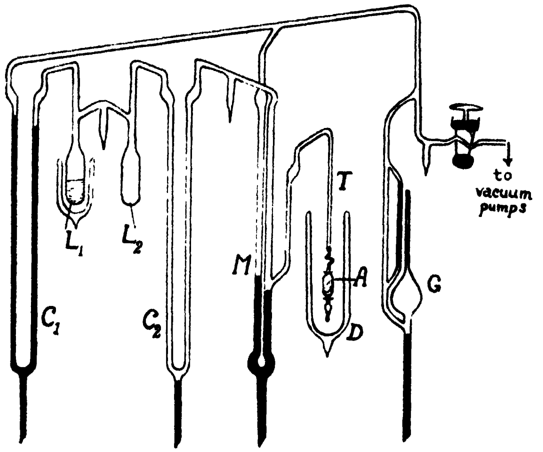

FIG. 1

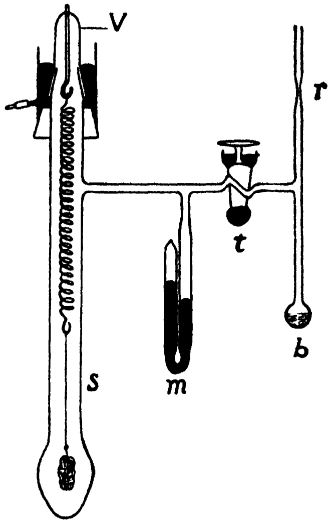

FIG. 2

FIG. 1. The outgassing and air-free liquid system
FIG. 2. The sorption apparatus

The liquid (water) in the bulbs L_1 and L_2 is freed from air through its distillation a few times from one bulb into the other by cooling with a mixture of solid carbon dioxide and acetone, while the air is outgassed through the cut-out C_1.

The cellulose in the ampoule A is outgassed for about 20 hr. at 65°C. (16).

The ampoule is afterwards immersed in a Dewar vessel (D) containing water kept at a constant temperature (30°C. ± 0.1°). Meanwhile the cellulose is exposed to air-free water vapor through the cut-out C_2 for a suitable time and then left to come to equilibrium after disconnecting the liquid bulbs. The pressure is then read on the manometer by means of a cathetometer, reading up to 0.02 mm., and the ampoule sealed off, thus becoming ready for the determination of the heat of wetting. A new sample of cellulose was used in each determination.

The quantity of water adsorbed by the cellulose is known from the equilibrium water vapor pressure by interpolation from an adsorption isotherm determined independently at 30.0°C. as follows:

The adsorption isotherm

The adsorption isotherm is determined gravimetrically by means of a spring balance of the McBain-Bakr type in the apparatus shown in figure 2. It consists of a long sorption tube (s) which is connected through a vacuum tap (t) to a bulb (b) containing the liquid used for the generation of vapor. Between the tap and the sorption tube is connected a closed gas-free mercury manometer (m). A calibrated sorption spring balance, carrying a known small mass of cellulose through a thin platinum wire, hangs from a hook in the cover (v) of the sorption tube. The cover fits on the tube by means of a mercury-sealed ground joint.

The sorption apparatus is outgassed for 20 hr., with the cellulose at 65°C., by joining it through a constriction (r) to the side-tube T in the apparatus described above (figure 1). Afterwards, the tap t is closed, some air-free water is distilled into the bulb b from the liquid in the bulbs L_1 and L_2, and the apparatus is sealed off at the constriction r.

The sorption apparatus is then wholly immersed in a thermostat at 30°C. ± 0.01°. The tap t is occasionally opened to introduce some vapor in the sorption tube and then closed. When equilibrium is attained (in 1 or 2 days), the pressure is read on the manometer m and the adsorbed water is calculated from the extension of the spring balance, which is read by a cathetometer.

The heat-of-wetting apparatus

This apparatus is the same as described previously (16).

RESULTS AND DISCUSSION

The adsorption isotherms of water on standard cellulose and viscose rayon were plotted from the experimental results. Values of C (grams of water adsorbed per gram of dry cellulose) were then extracted from the graphs at intervals of the relative humidity P/P^0; they are given in table 1 (a). The heat of wetting in water, H_c (calories per gram of dry cellulose), of partially saturated cellulose, with a moisture content C, is plotted against P/P^0 in figure 3. Again, from the smooth curves drawn through the experimental points are extracted the values of H_c at intervals of P/P^0 as shown in table 1 (b).

TABLE 1

Adsorption of water on standard cellulose and viscose rayon

RELATIVE PRESSURE P/P^0	(a) ADSORPTION C			(b) HEAT OF WETTING H_c			(c) INTEGRAL NET HEAT OF ADSORPTION $(H_0 - H_c)$			(d) DIFFERENTIAL NET HEAT OF ADSORPTION $(-\Delta H)$		(e) FREE ENERGY DECREASE $(-\Delta F)$
	Viscose (I)	Cellulose (II)	Ratio I:II	Viscose (I)	Cellulose (II)	Ratio I.II	Viscose (I)	Cellulose (II)	Ratio I:II	Viscose	Cellulose	
0.00	0.0000	0.0000		20.30	10.72	1.89	0.00	0.00		(270)	(265)	∞
0.01	0.0084	0.0042	2.00	18.25	9.67	1.89	2.05	1.05	1.95	233	251	154.3
0.025	0.0162	0.0082	1.98	16.50	8.70	1.89	3.80	2.02	1.88	211	235	123.6
0.05	0.0247	0.0125	1.98	14.75	7.70	1.92	5.55	3.02	1.84	190	216	100.3
0.10	0.0367	0.0186	1.97	12.70	6.50	1.95	7.60	4.22	1.80	166	187	77.1
0.15	0.0463	0.0232	2.00	11.20	5.65	1.99	9.10	5.07	1.80	148	164	63.4
0.20	0.0545	0.0275	1.98	9.97	4.97	2.00	10.33	5.75	1.79	134	141	53.9
0.25	0.0623	0.0315	1.98	8.98	4.45	2.02	11.32	6.27	1.80	123	121	46.5
0.30	0.0700	0.0357	1.96	8.10	4.00	2.02	12.20	6.72	1.81	112	101	40.3
0.35	0.0770	0.0400	1.93	7.35	3.62	2.03	12.95	7.10	1.82	103	83.0	35.2
0.40	0.0840	0.0440	1.91	6.65	3.30	2.02	13.65	7.42	1.84	95.0	70.5	30.7
0.45	0.0910	0.0482	1.89	6.00	3.02	1.99	14.30	7.70	1.86	85.0	60.0	26.9
0.50	0.0985	0.0530	1.86	5.40	2.77	1.95	14.90	7.95	1.87	77.0	52.0	23.2
0.55	0.1065	0.0578	1.84	4.85	2.52	1.92	15.45	8.20	1.89	68.0	45.0	20.1
0.60	0.1145	0.0627	1.83	4.30	2.30	1.87	16.00	8.42	1.90	60.0	39.5	17.1
0.65	0.1240	0.0680	1.82	3.80	2.10	1.81	16.50	8.62	1.91	50.5	33.5	14.4
0.70	0.1345	0.0740	1.82	3.35	1.90	1.76	16.95	8.82	1.92	40.5	28.5	11.9
0.75	0.1470	0.0815	1.80	2.90	1.70	1.71	17.40	9.02	1.93	32.5	23.0	9.6
0.80	0.1620	0.0910	1.78	2.45	1.50	1.63	17.85	9.17	1.94	26.0	18.0	7.5
0.85	0.1810	0.1030	1.76	2.00	1.25	1.60	18.3	9.47	1.94	20.0	14.0	5.4
0.90	0.2080	0.1225	1.70						(1.93)*			3.5
0.95	0.2540	0.1540	1.65						(1.91)			
0.975	0.2930	0.1830	1.60						(1.90)			
1.000							20.30	10.72	1.89			0.0
Mean			1.86						1.87			

* Values between brackets are found by extrapolation.

If the heat of wetting of dry cellulose is denoted by H_0 cal./g., then $(H_0 - H_c)$ will represent the integral heat of adsorption of C grams of water *from the liquid* on 1 g. of dry cellulose. This heat will be less than the heat of adsorption from the vapor by the latent heat of condensation of C grams of water; it is therefore usually called the net heat of adsorption. Values of $(H_0 - H_c)$ are given in table 1 (c) at the corresponding values of P/P^0 and C for viscose rayon and standard cellulose.

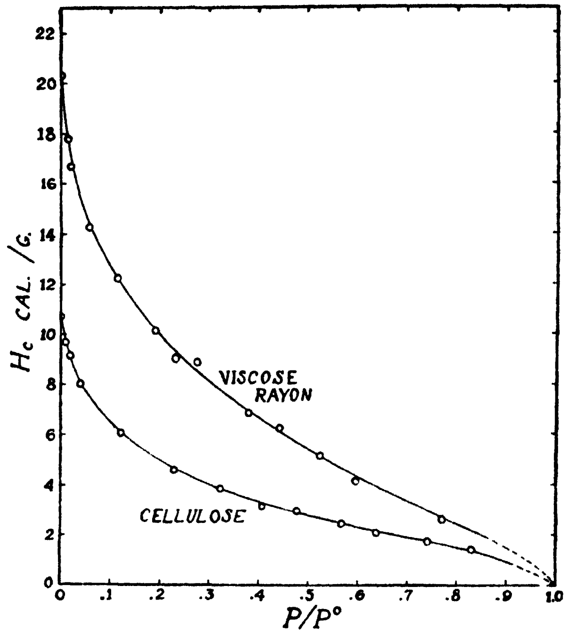

FIG. 3. The heat of wetting, H_c, of partially saturated viscose rayon and standard cellulose as a function of P/P^0.

Adsorption and the physical structure of cellulose

Comparison between the results with viscose rayon and those with standard cellulose should be done under corresponding conditions. Probably the *same* equilibrium relative pressure would offer the best condition for comparison, since the affinity of adsorption would be the same, it being measured at any equilibrium pressure P by the equation:

$$-\Delta F = \frac{RT}{M} \ln P^0/P \qquad (1)$$

$(-\Delta F)$ is the decrease in free energy when 1 g. of water is adsorbed on an infinite quantity of partially saturated cellulose which is in equilibrium with the vapor pressure P at the temperature T; P^0 is the saturation water vapor pressure at that temperature; R is the universal gas constant; and M is the molecular weight of water. $(-\Delta F)$ is evaluated at 30°C. by means of equation 1 at intervals of P/P^0 as given in table 1 (e).

The ratios of the values of C for viscose rayon and for standard cellulose and also of the values of H_c and of $(H_0 - H_c)$ at intervals of P/P^0 are given in (a), (b), and (c), respectively, of table 1 and are presented graphically in figure 4. It is clear that these ratios neither are constant, nor vary with P/P^0 in the same way.

The ratio $(C_{\text{vis.}}/C_{\text{cell.}})$ remains practically constant (1.98) with the increase of relative humidity until P/P^0 = about 0.25 and then decreases steadily, dropping to about 1.6 near saturation. Urquhart and Eckersall (13) have found a similar steady decrease after $P/P^0 = 0.25$ in the ratio of the quantities of water adsorbed on rayon (regenerated cellulose) and scoured cotton. However, with mercerized cotton it has been shown by Uruquhart (12) and Urquhart and Williams (15) that the ratio of the moisture regains on mercerized cotton and scoured cotton is practically constant at all values of P/P^0. Again, Babbitt (2) has calculated the monomolecular layer capacity of spruce wood from the adsorption data of Filby and Maass (7) and that of scoured cotton from the data of Urquhart and Williams (14), and has found that the ratio of these two capacities (1.86) is practically equal to $C_{\text{wood}}/C_{\text{cotton}}$ at all relative humidities.

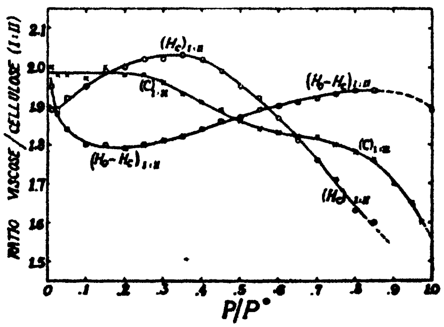

FIG. 4

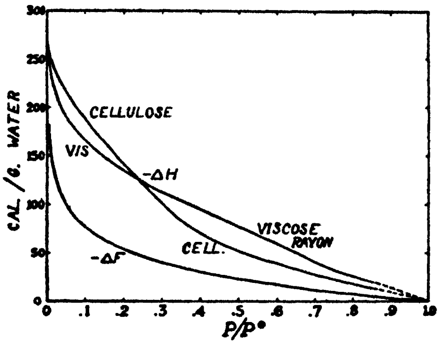

FIG. 5

FIG. 4 Ratios of the adsorption values C, of the heats of wetting H_c, and of the integral heats of adsorption $(H_0 - H_c)$ of water on viscose rayon and standard cellulose as a function of the relative humidity P/P^0.

FIG. 5. The differential heat of adsorption $(-\Delta H)$ and the free energy of adsorption $(-\Delta F)$ of water on viscose rayon and on standard cellulose at 30°C. as a function of P/P^0.

Babbitt shows that the adsorption of water on cellulose can be considered as occurring in three distinct stages. First, at low humidities there is a small region where the adsorption is monomolecular. Secondly, a second, a third, and higher layers are formed, the second layer commencing before the first is completed. Finally, in the vicinity of saturation the adsorption proceeds by capillary attraction. At higher humidities the quantity taken is limited by the volume of the intermicellar spaces. It may thus be suggested that the ratio of the adsorption values on viscose rayon and standard cellulose at low pressures measures a ratio of their adsorbing areas and toward saturation a ratio of their pore volumes.

From figure 4 it may therefore be concluded that the adsorbing area per gram of cellulose is nearly twice in viscose rayon that in standard cellulose. On the other hand, the width of the intermicellar spaces, allowing for the thickening of the adsorbed film, seems to be smaller in the case of viscose rayon. This view agrees with the fact that the liberation of the heat of immersion in liquids with larger molecules, e.g., methyl alcohol and acetone, is slower in the case of viscose rayon than in the case of standard cellulose (16). However, it should be noted that measurements of the specific volume of cellulose (6), by immersion in helium, water, or toluene, show only a very slight increase, of the order of 1 per cent, on mercerization or regeneration from solution. It means that the pores of native and of regenerated cellulose are penetrable nearly to the same extent by the fluids used, and that the micelles are identical in the two modifications.

The heat of wetting of partially saturated cellulose, H_c, corresponds to the heat of adsorption of $(C^0 - C)$ grams of water from an adsorbate concentration C until saturation, C^0 being the amount of water adsorbed per gram of cellulose after coming into equilibrium with the saturated vapor. The ratio of the values of H_c for viscose rayon and standard cellulose decreases with the increase of relative humidity after $P/P^0 = 0.4$ (figure 4). Such a decrease seems to correspond to the decrease in the ratio of the adsorption values.

The ratio of the values of $(H_0 - H_c)$, corresponding to the adsorption from dryness of C g. of water per gram of cellulose, is less than the ratio of the adsorption values at lower relative humidities until $P/P^0 =$ about 0.48 and then becomes higher at higher humidities (figure 4). It means that the heat of adsorption per gram of water is less on viscose rayon than on standard cellulose at lower adsorbate concentrations and that the case is reversed as the concentration increases. That becomes clearer by plotting the differential net heat of adsorption $(-\Delta H)$ against P/P^0 as shown in figure 5. $(-\Delta H)$ may be obtained at various adsorbate concentrations by measuring the slopes of tangents to the experimental curve relating the heat of wetting H_c and the moisture content C. Values of $(-\Delta H)$ thus obtained are given in table 1 (d) at the corresponding values of C. $(-\Delta H)$ represents the heat developed when an infinite amount of partially saturated cellulose, with a moisture content of C g./g., takes up 1 g. of water *from the liquid*. This is less than the differential heat of adsorption from the vapor by the latent heat of condensation of 1 g. of water. From figure 5 it is clear that $(-\Delta H)$ is smaller on viscose rayon than on standard cellulose until $P/P^0 =$ about 0.24 and then becomes larger at higher humidities.

It is interesting to notice that the mean value of the ratio $C_{\text{vis.}}/C_{\text{cell.}}$ (1.86) is equal to that of the ratio $(H_0 - H_c)_{\text{vis.}}/(H_0 - H_c)_{\text{cell.}}$ (1.87) (see table 1, (a) and (c)). It is again nearly equal to the ratio of the heats of wetting of viscose rayon and standard cellulose at dryness (1.89), but this is somewhat less than the ratio of their adsorbing areas (1.98). This shows that the heat of wetting of a dry adsorbent depends not only on its adsorbing area, but also to some extent on the thickness of the adsorbed film and the heat of adsorption in its different layers.

Entropy changes accompanying adsorption

The entropy change may be calculated from the relation:

$$-\Delta S = \frac{(-\Delta H) - (-\Delta F)}{T} \tag{2}$$

$(-\Delta S)$ represents the decrease in entropy when 1 g. of water is adsorbed (from the liquid) on an infinite quantity of cellulose with a moisture content of C g./g.

From figure 5, it is seen that $(-\Delta H)$ is larger than $(-\Delta F)$ for both standard cellulose and viscose rayon at all relative humidities. At very low pressures, however, this cannot be the case, since $(-\Delta F)$ tends to ∞ as P/P^0 tends to zero (equation 1). This means that the adsorption process, except for the very small initial quantities, is accompanied by a decrease in entropy.

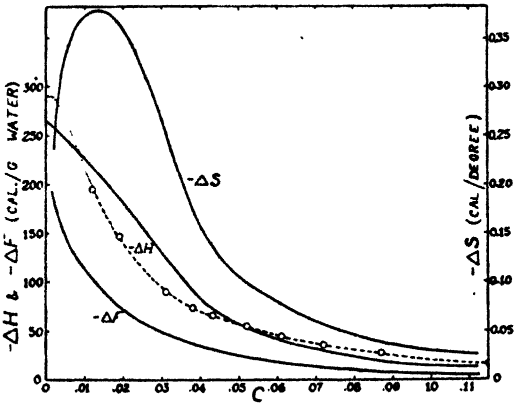

FIG. 6

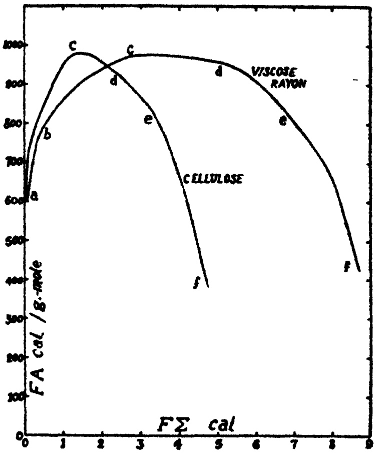

FIG. 7

FIG. 6. The differential net heat of adsorption $(-\Delta H)$, the free energy of adsorption $(-\Delta F)$, and the entropy decrease $(-\Delta S)$ on the adsorption of water by standard cellulose. - - -, $(-\Delta H)$ as calculated from the sorption data of Urquhart and Williams (14); . . . . . ., extrapolation of broken line up to the value of $(-\Delta H)$ obtained by Neale and Stringfellow (9).

FIG. 7. Plot of FA *versus* F for the water films adsorbed on standard cellulose and viscose rayon at 30°C.

$(-\Delta H)$, $(-\Delta F)$, and $(-\Delta S)$ are plotted against C for standard cellulose in figure 6. $(-\Delta S)$ is calculated here by using the values of $(-\Delta H)$ obtained from the heat-of-wetting measurements (table 1 (d)). The differential net heat of adsorption is also calculated at 30°C. from the adsorption data of Urquhart and Williams (14) for soda-boiled cotton at temperatures between 20° and 40°C., by means of the Clausius–Clapeyron equation:

$$(-\Delta H) = \frac{R \, \mathrm{d} \ln P/P^0}{\mathrm{d}(1/T)} \tag{3}$$

Values of $(-\Delta H)$ thus obtained are shown in table 2 and are represented graphically in figure 6 as a function of C (the broken line). The lowest value of C given by Urquhart and Williams is 0.012 g./g. For the very low concentrations, the results of Neale and Stringfellow (9) are used. They give the constant value 15.7 kcal./mole as the heat of adsorption of water vapor on cellulose having a moisture content of 0.12–1.60 mg./g. The net heat of adsorption $(-\Delta H)$ at 30°C. thus amounts to 290 cal./g. As seen from figure 6, the two $(-\Delta H)$–C graphs obtained from thermal measurements and from adsorption measurements are not quite concordant. Rees (11) has shown that calculations from adsorption data can provide only approximate values of the heat of adsorption, as they depend greatly on the accuracy with which the isosteres are drawn. However, the discrepancy seems to be outside the range of experimental error; and it is believed that such discrepancy has—at least partly—something to do with the swelling of cellulose. This question will be discussed later when an investigation of hysteresis and its effect on the heat of wetting is completed.

TABLE 2

DATA OF	C	P AT 30°C.	P/P^0	$(-\Delta F)$	$(-\Delta H)$	$(-\Delta S)$
	mg./g.	*mm.*				
Neale and Stringfellow	0.120	0.0020	0.000063	324	290	−0.116
	0.234	0.0036	0.000114	304	290	−0.050
	(0.330)*			290	290	0.000
	0.517	0.0103	0.000318	269	290	0.066
	0.795	0.0178	0.000561	251	290	0.125
	1.060	0.0278	0.000877	236	290	0.175
	1.595	0.0470	0.001483	218	290	0.234
Urquhart and Williams	12		(0.045)	104	195	0.300
	19	3.0	0.099	77.5	147	0.230
	31		(0.245)	47.2	90	0.142
	38		(0.330)	37.2	74	0.122
	43	12.1	0.382	32.0	66	0.112
	52	16.0	0.505	23.0	55	0.106
	61	19.5	0.615	16.5	45	0.094
	72	21.9	0.691	12.2	36	0.079
	87	24.9	0.785	8.0	28	0.066
	115	28.0	0.883	4.0	16	0.043

* Values between brackets are found by interpolation.

In any case, the two $(-\Delta H)$–C graphs lie well above that of the free energy decrease, except at the very small initial stages. It leaves no doubt that a decrease in entropy accompanies most of the adsorption process. The entropy changes at different moisture contents are shown in table 2, as calculated by the use of $(-\Delta H)$ values obtained from the adsorption data of Neale and Stringfellow at the early concentrations and those of Urquhart and Williams at higher concentrations. The value of C corresponding to $(-\Delta F) = (-\Delta H) = 290$ cal./g. was found by interpolation to be 0.33 mg. of water per gram of cellulose. At this concentration, therefore, there is no entropy change; below it adsorption *from the liquid* is accompanied by an increase in entropy and above it by a decrease in entropy.

Babbitt (2) has realized that $(-\Delta F)$ at very low moisture contents should be greater than the value of $(-\Delta H)$, because of the lack of any experimental evidence that $(-\Delta H)$, as $(-\Delta F)$, should increase to ∞ as P/P^0 tends to zero. But in his thermodynamic consideration of adsorption, he supposed that an increase in entropy accompanies the transfer of adsorbate from the adsorbent to the liquid, since "it is probable that there is a greater degree of organisation in the adsorbed phase than in the liquid corresponding to a certain amount of solidification." Babbitt thus doubted that his derived relation, although it is identical with equation 2, would hold in such an early region.

There is no reason, however, to suppose that the entropy change accompanying adsorption should always be negative even at the early stages. There seems to be an actual increase in entropy on adsorption from the liquid until $C = 0.33$ mg./g. It means that the water molecules in the adsorbed phase are more at random than in the liquid, although they lie under the effect of the attractive forces of the adsorbent surface. In other words, the adsorbed film seems to acquire a two-dimensional motion. That no change in entropy accompanies the adsorption at such a low concentration as $C = 0.33$ mg./g. does not mean that the adsorbed film becomes identical with the bulk liquid. It is more reasonable to assume that the change of the three-dimensional motion of the molecules in the liquid to a two-dimensional motion in the adsorbed phase causes a decrease in entropy, and that the separation of the liquid molecules from each other in spreading on the adsorbent surface causes an increase in entropy (as in the spontaneous expansion of a gas). These two effects may balance each other at a low concentration. As the adsorbed molecules crowd on the surface of the adsorbent, the former effect exceeds the latter with the result of a net decrease in entropy.

In the monolayer, the molecules will be at their closest packing when it is completed. The entropy increase due to the separation of the molecules of the liquid apart will then be at a minimum, and the entropy decrease due to the restriction of the motion of the molecules will be at a maximum. As the adsorbed film exceeds one molecule in thickness, the forces holding the higher layers will get weaker, with the result of a diminution of the entropy decrease. It may therefore be expected that adsorption at the completion of a monomolecular layer would be accompanied by a maximum entropy decrease. According to Babbitt, however, thickening of the adsorbed film starts before the monolayer is completed. The maximum entropy decrease presented by the graph in figure 6, therefore, should not indicate the completion of the first layer, but rather an earlier stage because of the effect of the deposition of the second layer. In the case of standard cellulose, this takes place at $C =$ about 0.014 g./g., corresponding to $P/P^0 = 0.06$.

Viscose rayon gives similar graphs to those of standard cellulose for the change of $(-\Delta H)$, $(-\Delta F)$, and $(-\Delta S)$ with C. The maximum decrease in entropy occurs at $C =$ about 0.028 g./g., a value twice that acquired by standard cellulose and also corresponding to $P/P^0 = 0.06$.

As seen from figure 5, the difference between the values of $(-\Delta H)$ and $(-\Delta F)$ at the same relative humidities is smaller with viscose rayon than with standard cellulose until P/P^0 = about 0.24 and then the case is reversed at higher humidities. This means that the entropy decrease accompanying adsorption is more on standard cellulose at relative humidities less than 0.24 and is more on viscose rayon at higher humidities. The adsorbed water molecules at the later stages may therefore be less at random on viscose rayon than on standard cellulose. This view is in agreement with the idea that the pores of viscose rayon are narrower than those of standard cellulose, whereby the thickening of the adsorbed film and the motion of its molecules are more restricted on the rayon.

There is another interesting point about the entropy change accompanying the adsorption of water on cellulose. As it appears from this investigation and as shown by Babbitt (2) from the work of other investigators, the entropy change seems to accompany all the process of adsorption up to saturation. This indicates that the adsorbed film near saturation may be still different from the bulk liquid. The film may not therefore be a capillary-condensed liquid near saturation, as Babbitt suggests. However, the difference may be due only to some change in the properties of the liquid for being present in fine capillaries.

A test of the idea of the mobility of the adsorbed molecules

In order to examine further the idea of the mobility of the adsorbed film, especially at the lower adsorbate concentrations, its behavior may be compared with that of gases. Preliminary trials were therefore made to obtain FA–F graphs (corresponding to PV–P isothermals of gases) from the adsorption data of water vapor on standard cellulose and viscose rayon, F being the two-dimensional pressure of the adsorbed film and A the area occupied per gram-mole adsorbed. F, at any desired equilibrium pressure P, could be calculated by means of the equation:

$$F = \frac{RT}{M} \int_0^P \frac{C}{\Sigma} \, \mathrm{d} \ln P \tag{4}$$

which is an integrated form of the Gibbs adsorption equation according to Bangham (3), Σ being the specific surface of the adsorbent, i.e., its adsorbing area per gram. But because neither Σ is known with any degree of certainty, nor its possible change with C due to swelling, it was considered constant (as a first degree of approximation) and values of $F\Sigma$ (instead of F) were obtained by equation 4 at different values of P, supposing that Henry's law is obeyed at the very small initial concentrations. The corresponding values of FA were obtained from the relation:

$$FA = F\Sigma \cdot M/C$$

FA–$F\Sigma$ graphs thus obtained for the water films adsorbed on standard cellulose and viscose rayon at 30°C. are given in figure 7.

In this way, Gregg (8) has shown that many cases of gas–solid adsorption exhibit close correspondence to surface films on water, having the film states gaseous, liquid-expanded, liquid-condensed and the intermediate state between the last two (Adam (1)). The FA–$F\Sigma$ curves obtained in the present investigation are somewhat different. However, they are similar to the curves described by Gregg for three cases of adsorption of vapors on nonporous adsorbents, cases in which the adsorbed film passes into a multilayer as calculated from the known surface area of the adsorbents. These are the cases of the adsorption of (*i*) the lower fatty acids on mercury (5), (*ii*) benzene on mica (4), and (*iii*) acetone and benzene on vitreous silica (10). The characteristic thing about these curves is that after rising to some point like *c* (figure 7) they turn toward the $F\Sigma$-axis and continue to fall till saturation (*cdef*). The point *c* is taken to represent the monomolecular layer capacity. It corresponds to about 0.023 g. of water per gram of cellulose in the case of standard cellulose and about 0.047 in the case of viscose rayon. This value for standard cellulose is less than the monolayer capacity (0.033 g./g.) obtained by Babbitt for soda-boiled cotton by applying Langmuir's equation to Urquhart and Williams' isotherm.

The shape of the FA–$F\Sigma$ curves in figure 7 does not contradict the idea that the adsorbed film is gaseous in the early stages. The decrease of the slope of the curves in the rising part *abc* means that the cross-sectional area of the adsorbed molecules decreases. This may be due either to some orientation of the molecules on the surface of the solid or to some layer thickening of the adsorbed film. In the second case, the point *c* would not represent the completion of the monomolecular layer. It would rather represent the stage where the deposition of higher layers, together with the first layer, becomes appreciable enough so as to decrease the cross-sectional area per molecule as indicated by the slope of the curve in the part *bc*. Although less than the full capacity of the monomolecular layer as calculated by Babbitt, such concentration on standard cellulose (0.023 g./g.) is higher than the moisture content (0.014 g./g.) at which adsorption is accompanied by the maximum entropy decrease (figure 6). This may mean that the deposition of the second layer starts early and that it causes a rather large diminution in the entropy change.

It may be concluded that the above results agree fairly well with the conclusions of Babbitt concerning the nature of the adsorbed film. It may be added that the film in the very early stages acquires a two-dimensional motion which seems to become more restricted as the molecules crowd on the surface, probably owing to some orientation. Owing to the beginning of formation of the second layer before the completion of the first, it is difficult by the above procedure to determine the monolayer capacity. Polymolecular adsorption is limited by the pore volume of the intermicellar spaces. Near saturation, although some water may be taken up by capillary condensation, yet it seems to be still different from the ordinary liquid.

SUMMARY

The heats of wetting of partially saturated samples of standard cellulose and viscose rayon (regenerated cellulose) in water at 30°C. were determined in the absence of air. The adsorption isotherms at 30°C. of water vapor on these two adsorbents were also determined.

The measurements on viscose rayon and on standard cellulose were compared

at the same relative humidities P/P^0. It is shown that the ratios of their values of adsorption, heats of wetting, and heats of adsorption are not constant. They vary with P/P^0 in correspondence with each other in a way that suggests that the adsorbing area in viscose rayon is nearly twice that in standard cellulose, but the intermicellar spaces in the rayon are narrower, allowing a smaller number of adsorbed layers.

Adsorption is accompanied by an increase in entropy in the very early stages, suggesting a two-dimensional motion of the adsorbed molecules. The entropy decreases as the adsorbate concentration increases, showing a maximum decrease at P/P^0 = about 0.06. This is probably when the formation of a second adsorbed layer begins to show its effect, while the first layer is not yet complete. The entropy change decreases with the thickening of the adsorbed film, but it reaches zero only at saturation, suggesting that the film may be still different from the ordinary liquid even near saturation.

The author wishes to express his thanks to Dr. D. H. Bangham for his interest and advice in the early part of this investigation.

REFERENCES

(1) Adam: *The Physics and Chemistry of Surfaces*, 3rd edition, Chap. II. Oxford University Press, London (1941).
(2) Babbitt: Can. J. Research **20A**, 143 (1942).
(3) Bangham: Trans. Faraday Soc. **33**, 805 (1937).
(4) Bangham and Mosallam: Proc. Roy. Soc. (London) **A165**, 552 (1938); **A166**, 558 (1938).
(5) Bosworth: Trans. Faraday Soc. **28**, 903 (1932).
(6) Davidson: J. Textile Inst. **18**, T175 (1927).
(7) Filby and Maass: Can. J. Research **13B**, 1 (1935).
(8) Gregg: J. Chem. Soc. **1942**, 696.
(9) Neale and Stringfellow: Trans. Faraday Soc. **37**, 525 (1941).
(10) Palmer: Proc. Roy. Soc. (London) **A160**, 254 (1937).
(11) Rees: J. Textile Inst. **39**, T351 (1948).
(12) Urquhart: J. Textile Inst. **18**, T55 (1927).
(13) Urquhart and Eckersall: J. Textile Inst. **23**, T163 (1932).
(14) Urquhart and Williams: J. Textile Inst. **15**, T559 (1924).
(15) Urquhart and Williams: J. Textile Inst. **16**, T155 (1925).
(16) Wahba: J. Phys. Chem. **52**, 1197 (1948).

ISOTHERMAL DECOMPOSITION OF NICKEL CARBIDE

L. J. E. HOFER,[1] E. M. COHN,[1] AND W. C. PEEBLES[2]

Research and Development Branch, Office of Synthetic Liquid Fuels, Fuels and Explosives Division, Bureau of Mines, Bruceton, Pennsylvania

Received November 2, 1949

INTRODUCTION

The present study of the thermal stability of nickel carbide, like a previous and similar one of a carburized cobalt Fischer–Tropsch catalyst (6), was made to gain more insight into the problem of the formation of free carbon during hydrocarbon synthesis by the Fischer–Tropsch process. This undesirable side reaction leads to plugging of fixed-bed reactors or disintegration and loss of catalyst in fluidized-bed converters, and to a decrease or total loss of catalytic activity. Information obtained from this type of study should be useful in eliminating the conditions responsible for formation of free carbon, which can be produced by way of metal carbide (5, 17):

$$x\mathrm{M} + 2\mathrm{CO} \rightarrow \mathrm{M}_x\mathrm{C} + \mathrm{CO}_2 \qquad (1)$$

and

$$\mathrm{M}_x\mathrm{C} \rightarrow x\mathrm{M} + \mathrm{C}\ (\text{free}) \qquad (2)$$

This mechanism of formation of free carbon by decomposition of the metal carbides is supported by the fact that only those metals which form metastable carbides are known to form free carbon from carbon monoxide.

Nickel carbide, Ni_3C, is well known from several investigations (1, 2, 9, 11–15, 17, 18). It has been prepared by passing carbon monoxide, carbon monoxide and hydrogen, methane, benzene vapor, or illuminating gas over nickel oxide or over reduced nickel catalysts (with or without promoters and supports) at 170–250°C., or at higher temperatures where carbide formation is incomplete and noticeable amounts of free carbon are formed. The carbide, which is relatively stable up to about 250°C., has a close-packed hexagonal crystal structure with $a = 2.646$ Å., $c = 4.329$ Å., and $c/a = 1.636$, according to Jacobson and Westgren (9), or $a = 2.65$ Å., $c = 4.32$ Å., and $c/a = 1.63$, according to Le Clerc (12, 13), whose "hexagonal nickel" must have been Ni_3C according to the method of preparation. Tutiya's (18) results also support this structure. Kohlhaas and Meyer (11) found additional x-ray lines and ascribed an orthorhombic structure to Ni_3C, isomorphous with Fe_3C. This structure has not been substantiated as yet, however. According to Bahr and Bahr (1), Ni_3C is only very weakly ferromagnetic. Their sample was not fully carburized, so that the ferromagnetism was probably due to a small amount of residual nickel. One carbide sample used for the present study contained slightly more than the stoichiometric amount of carbon and was nonferromagnetic within the limits of error of the measurements, in accordance with the observation of Le Clerc and Michel (13). Two carbides of nickel are known definitely so far, Ni_3C and Ni_6C. A postulated nickel carbide, Ni_3C_2 (1), has not been found, and its existence was denied by Schmidt (15). Durand (4) has prepared nickel acetylide, NiC_2, by an entirely different method. Tebboth (17) tentatively assumed that Ni_3C decomposes to free metal and carbon by way of Ni_6C. The intermediate formation of this lower nickel carbide at 350°C. (the temperature at which Tebboth's data were taken to support this hypothesis) is unlikely, as will be shown later.

---

[1] Physical Chemist, Research and Development Branch, Office of Synthetic Liquid Fuels, Bureau of Mines, Bruceton, Pennsylvania.

[2] Physicist, Research and Development Branch, Office of Synthetic Liquid Fuels, Bureau of Mines, Bruceton, Pennsylvania.

MATERIALS AND PREPARATION

One formula weight (297.7 g.) of nickel nitrate hexahydrate was dissolved in 4 l. of distilled water at 80°C., and a solution of 112 g. of potassium hydroxide in 500 ml. of distilled water at room temperature was added with stirring. The precipitate was washed five times, each time with a solution of 10 g. of ammonium nitrate in 3 l. of distilled water, after which it was filtered and dried in air. Reduction in a Rose crucible showed that the sample contained 58.4 weight per cent nickel; the theoretical value for nickel hydroxide is 63.3 weight per cent. The x-ray diffraction pattern was identical with that obtained by Cairns and Ott (3).

TABLE 1

Determination of lattice constant for Ni_3C

hkl	*I**	*d*† (OBSERVED)	*d* (CALCULATED)	*hkl*	*I**	*d*† (OBSERVED)	*d* (CALCULATED)
100	W	2.2808	2.2909	200	VW	1.1420‡	1.1453‡
002	W	2.1563	2.1648	112	S	1.1277	1.1293
101	S	2.0189	2.0249	201	M	1.1076	1.1072
102	W	1.5731	1.5734	004	W	1.0827	1.0824
110	M	1.3228	1.3225	202	W	1.0128	1.0123
103	M	1.2213	1.2211				

* S = strong, M = medium, W = weak, VW = very weak.

† Corrected by using sodium chloride, $a_0 = 5.628 kX.$, as an internal standard.

‡ Line not used in calculation for lattice constant because of faintness.

A portion of this preparation (in four sample tubes) was reduced with hydrogen for 85 hr. at 275°C. to virtually constant weight. One of the tubes was then removed for x-ray diffraction analysis and found to contain face-centered cubic nickel. The remaining tubes were carburized with carbon monoxide at 250°C. for 22.5 hr., at which time another sample was removed for x-ray and magnetic analyses. Only the lines of close-packed hexagonal nickel carbide, Ni_3C, were observed on the x-ray film. After an additional 91-hr. carburization, the rate of carbon uptake of the remaining two tubes had become negligible, and the third sample tube was used for x-ray and magnetic studies. The lattice constant of Ni_3C was determined using this sample. The corrected (8) x-ray diffraction lines are listed in table 1. The lattice dimensions found were a = 2.6449 kX., c = 4.3296 kX., and c/a = 1.637 (average values from calculations of six films taken from four samples). The average carbon–nickel weight ratio of the two completely carburized tubes was 0.0725, an excess over the ideal stoichiometric ratio, 0.0682, for Ni_3C. The carbon in the remaining tube was completely removed with hydrogen after 26.25 hr. at 250°C., proving that essentially only carbidic carbon had been present in the sample. The reduced product was, of course, face-centered cubic nickel, as indicated by x-ray diffraction. The course of the carburization and reduction is shown in figure 1.

APPARATUS AND PROCEDURE

The magnetic balance (7, 16) and procedure (6) used for the decomposition study have been described previously.

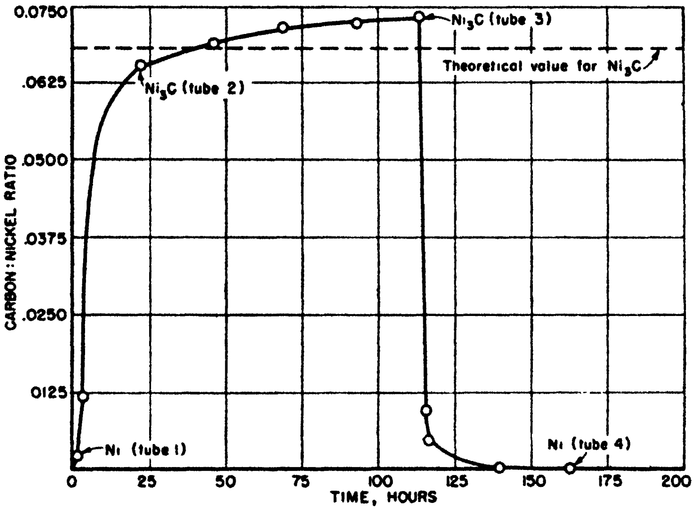

FIG. 1. Carburization and subsequent reduction, both at 250°C., of finely divided nickel

RESULTS

1. *Fully carburized* Ni_3C

The first series of experiments was carried out with samples taken from tube No. 3, i.e., fully carburized Ni_3C (weight ratio C:Ni = 0.0722:1). As in the case of Co_2C, the course of the reaction was followed by measuring the increase of ferromagnetism, or the formation of metallic nickel, as a function of time at constant temperature and field strength.

In this case, however, the decomposition was preceded by an induction period which was analogous to that found by Jolivet and Portevin (10) for the decomposition of austenite. Because it was difficult to estimate, this interval has been defined as the time elapsed from the moment the reaction temperature was reached until 5 per cent of the carbide was decomposed. At 333°C., for example, one sample was found to have an induction period of about 9 hr., while 90 per cent of the carbide decomposed during the following 4.5 hr. In order to ascertain whether any internal structural changes occurred during the induction period, another sample was heated to 333°C. It developed ferromagnetism after 6 hr. and was cooled after a total of 7 hr. Only the original carbide and a small amount (about 5 per cent) of nickel metal were present according to the x-ray diffraction pattern; no phase transformation had taken place during the induction period. This period decreased with increasing temperature; it varied, however, within rather wide limits for different samples and could not always be determined accurately.

A typical decomposition–rate curve is shown in figure 2. The decomposition rate of the carbide was linear in the range of about 65–75 per cent to about 5–15 per cent of remaining carbide. These portions of the curves were used to calculate apparent zero-order rate constants for that range of carbide content. Table 2 contains the induction periods and the apparent specific reaction-rate constants (see also evaluation of data, below) measured between 323°C. and 355°C.

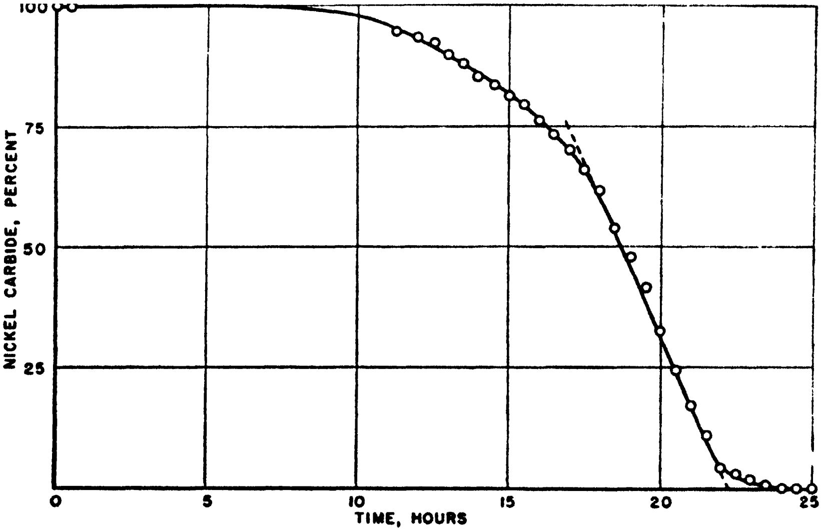

FIG. 2. Thermal decomposition of fully carburized Ni_3C at 323°C.

The effect of shortening the induction period upon the quasi-zero-order specific reaction rate was determined on four samples of fully carburized Ni_3C. The procedure was as follows: Each sample was heated to a certain temperature, *T*, in 5 min. and kept at that temperature for a measured interval, *t*, then cooled to 343°C. in 2 min. and allowed to decompose completely at 343°C. Table 3 is a summary of the data. There was no apparent effect upon the reaction rate until the (additional) induction period at 343°C. was eliminated; then the reaction rate was approximately twice the former rate. It may be noted here that the calculated induction period for 381°C. is 15.9 min., and that the calculated zero-order reaction rate at that temperature is 3.75×10^{-3}/sec.

2. *"Ninety-five per cent" carburized* Ni_3C

The sample in tube 2 had a carbon–nickel weight ratio of 0.0647, i.e., it was 95 per cent carburized on the basis of an ideal stoichiometric weight ratio for Ni_3C. It was feebly ferromagnetic at room temperature, and this magnetism disappeared upon heating. A comparison of the ferromagnetism before and after decomposition indicated the presence of only 1–3 per cent free nickel. It is possible that some of the nickel was so finely divided as to be magnetically unsaturated or even nonferromagnetic, thus yielding an apparently lower percentage of nickel by magnetic measurements than was actually present. On the other hand, nickel carbide, being an interstitial alloy, need not necessarily take up carbon stoichiometrically to become the close-packed hexagonal carbide. For the sake of convenience, the preparation is called "95 per cent" carbide, even though it may have been 95–99 per cent carbide.

TABLE 2

Induction period and quasi-zero-order rate constants for isothermal decomposition of fully carburized Ni_3C

DECOMPOSITION TEMPERATURE	INDUCTION PERIOD	APPARENT SPECIFIC REACTION-RATE CONSTANT, *k*
°*C.*	*min.*	*sec.*$^{-1}$
323	1320	3.4×10^{-5}
323	960	3.9×10^{-5}
323	660	4.0×10^{-5}
333	540	7.8×10^{-5}
333	420	9.7×10^{-5}
333	420	11×10^{-5}
343	180	23×10^{-5}
343	240	19×10^{-5}
355	100	51×10^{-5}

TABLE 3

Effect of shortened induction period upon rate of decomposition, at 343°C., of fully carburized Ni_3C

T	*t* TIME AT *T*	ADDITIONAL INDUCTION PERIOD AT 343°C.	QUASI-ZERO-ORDER DECOMPOSITION RATE
°*C.*	*min.*	*min.*	*sec.*$^{-1}$
375	10	155	1.8×10^{-4}
381	10	60	2.3×10^{-4}
381	13	0	3.6×10^{-4}
381	15	None; about 20 per cent already decomposed	4.1×10^{-4}

A preliminary experiment had shown that the induction period of this sample was considerably shorter at 320°C. than that of the fully carburized sample. A study of the variation of the induction period with temperature was therefore made, and a few rate constants of the decomposition were also determined. (The shape of the decomposition–time curves was the same as that observed with fully carburized samples.) The data are summarized in table 4.

EVALUATION OF DATA

The data were treated analogously to those obtained with cobalt carbide (6). The absence of ferromagnetism in the fully carburized sample and the complete reducibility of another, identically prepared sample indicated that only Ni_3C was present before decomposition. The final time-independent ferromagnetism —or constant angle of twist of the sample in the magnetic balance—was proof of complete decomposition into metallic nickel and free carbon. Hence, the angle of twist of the sample was directly proportional to the amount of decomposed carbide, with zero angle corresponding to 100 per cent Ni_3C and the final

TABLE 4

Induction periods and decomposition rates of "95 per cent" carburized Ni_3C

TEMPERATURE	INDUCTION PERIOD	QUASI-ZERO-ORDER RATE CONSTANT
°*C.*	*min.*	*sec.*$^{-1}$
320	660	8.6×10^{-6}
328.5	470	
328.5	306	
335	180	
335	211	
342	180	
349	180	2.3×10^{-4}
349	137	
355.5	105	2.1×10^{-4}
355.5	90.5	2.6×10^{-4}
355.5	Heated at 342°C. for 1¼ hr. initially	2.7×10^{-4}

TABLE 5

Activation energies and "frequency factors" for the thermal decomposition of Ni_3C *and of* Co_2C

	E ENERGY OF ACTIVATION	*A* "FREQUENCY FACTOR"
	kcal./mole	*sec.*$^{-1}$
Induction period, fully carburized Ni_3C	55	3×10^{15}
Decomposition (zero-order range), fully carburized Ni_3C.	61	1×10^{16}
Induction period, "95 per cent" carburized Ni_3C	36	4×10^{8}
Decomposition (zero-order range), "95 per cent" carburized Ni_3C.	71	1×10^{21}
Decomposition (zero-order range), Co_2C in catalyst 108B*.	54.3	3.89×10^{14}

* Described in reference 6.

angle to 0 per cent Ni_3C. The small amount of metallic nickel present in the incompletely carburized sample (see above) was neglected in calculating the amount of decomposed carbide, the error being within the limits of accuracy of the measurements. To evaluate the temperature dependence of the induction period, the reciprocal of the induction period was treated as a specific reaction-rate constant and used in the Arrhenius equation:

$$k = Ae^{-E/RT}$$

The activation energies, E, and "frequency factors," A, computed by the method of least squares from the data in tables 2 and 4, are summarized in table 5, where the earlier data for Co_2C are included for comparison. The dimensions of A and of the specific reaction-rate constants in tables 2 to 4 are sec.$^{-1}$, because the calculations were carried out using "fraction of the original carbide remaining at any time."

DISCUSSION

It has been shown that thermal decomposition of unpromoted and unsupported nickel carbide, Ni_3C, is preceded by an induction period during which no apparent structural change takes place and that this is followed by the simple reaction $Ni_3C \rightarrow 3Ni + C$. Thus, Tebboth's (17) hypothesis that Ni_6C is an intermediate in the decomposition was not substantiated, and it appears unlikely that Ni_6C plays such a role in the decomposition of promoted and/or supported Ni_3C catalysts. That does not mean, of course, that Ni_6C may not be present in such catalysts before decomposition, especially at lower temperatures.

In some of the older literature Ni_3C is said to be stable below 400°C. ± 20° (1, 11, 14). This statement, originally based on faulty thermodynamic studies, is obviously incorrect (12, 13, 15, 17, 18).

Since Ni_3C is metastable, its observed "stability" is purely a result of the small rate of decomposition at low temperatures. This "stability" is a kinetic effect and is, therefore, subject to the mode of preparation of the carbide, addition of inhibitors or accelerators of the decomposition, thermal treatment, etc. In view of the fact that an induction period precedes the decomposition, one may assume that some of the early investigators of Ni_3C did not permit enough time to elapse to notice decomposition below about 380°C. It is very doubtful, however, that the carbide could be stabilized sufficiently to withstand heating for 8 hr. at 420°C. without any sign of decomposition, as was claimed by Kohlhaas and Meyer (11) for one of their preparations.

Over the temperature range investigated, the induction period has the same properties as that of decomposing austenite (10) (corresponding to the lower-temperature branch of Jolivet's curves). The whole course of the decomposition suggests an autocatalytic reaction mechanism. The formation of reaction centers appears to be necessary to start the decomposition. The temperature dependence of the decomposition of fully carburized nickel was similar to that found for a carburized cobalt Fischer–Tropsch catalyst (6). Also, the activation energy and "frequency factor" of the induction period were of the same order of magnitude as those of the decomposition. Changing the induction period appeared to have little, if any, effect on the reaction rate over a wide range of time. When the induction period was shortened to a few minutes' heating at a higher temperature, however, the reaction rate at a lower temperature was approximately doubled. An incompletely carburized preparation exhibited a greatly shortened induction period at 320°C., and the induction period was much less sensitive to temperature changes than that observed for completely carburized Ni_3C. Contrary to the induction periods, however, the half-life of the "95 per cent" carbide, as calculated from the quasi-zero-order rate constants, was three times that of the pure carbide at 325°C. and twice that of the pure carbide at 355°C. (see table 6). If one assumes a nucleation mechanism for the thermal decomposition of nickel carbide, then it appears that some nuclei form much more readily in incompletely carburized nickel carbide, but that they are not as numerous as in a fully carburized carbide, or that their rate of growth is slower than in fully carburized carbide. It is also possible that the metal–carbide interface is a catalyst for nucleus formation. Whatever the exact mechanism may be, the quasi-zero-order range of decomposition appears to be only slightly affected by a shortening of the induction period (effected by heating at temperatures higher than the temperature at which the reaction rate is measured), provided not more than about 20 per cent of the carbide has been decomposed at the higher temperature. In other words, the zero-order range of the decomposition is relatively insensitive to the previous history of the carbide. Clearly, thermal decomposition of the carbide can be avoided by keeping it at suitable low temperatures; once the carbide has been exposed to higher temperatures long enough to produce sufficient decomposition, it will then decompose at about the zero-order rate of the temperature at which it is subsequently kept. To illustrate this point, one may consider the following example[3]: If fully carburized Ni_3C is heated to 300°C., it can be kept at that temperature for about 108 hr. until about 5 per cent of the material is decomposed. If this carbide is overheated at 381°C. for 13 min. and then cooled to 300°C., 50 per cent of it will decompose in (probably less than) 28.5 hr.

TABLE 6

Time necessary to decompose 50 per cent of the carbide after completed induction (calculated from quasi-zero-order rates)

	HALF-LIFE AT	
	325°C.	355°C.
	hours	*hours*
Fully carburized nickel, Ni_3C. .	3.0	0.26
"95 per cent" carburized nickel, Ni_3C.	9.1	0.53

---

[3] It is assumed here that the data can be extrapolated to 300°C.

SUMMARY

1. The thermal stability of nickel carbide, Ni_3C, was studied magnetically and by x-ray diffraction between 320° and 355°C. on a fully carburized and on an almost fully carburized sample.

2. An induction period precedes the decomposition. This period is analogous to that found for the decomposition of austenite. There is no detectable structural change in the carbide during the induction period.

3. The carbide decomposed into free metal and free carbon without intermediate formation of a lower carbide.

4. Shortening the induction period by temporary overheating did not affect the zero-order rate of the decomposition except when the normal induction period was completely suppressed. In that case, the zero-order rate was approximately doubled.

5. In the range from about 70 to 10 per cent nickel carbide, the decomposition rate was constant; hence the reaction was of apparent zero order in that range.

6. Empirical activation energies were found for the induction periods (i.p.) and quasi-zero-order range of decomposition (d.) of the fully carburized carbide (100) and the almost fully carburized carbide (95) as follows: $E_{\text{i.p.}100} = 55$, $E_{\text{d.}100} = 61$, $E_{\text{i.p.}95} = 36$, $E_{\text{d.}95} = 71$ kcal./mole.

REFERENCES

(1) Bahr H. A., and Bahr, T.: Ber. **61,** 2177 (1928).
(2) Bahr, H. A., and Bahr, T.: Ber. **63,** 99 (1930).
(3) Cairns, R., and Ott, E.: J. Am. Chem. Soc. **55,** 527 (1933).
(4) Durand, J. F.: Compt. rend. **177,** 693 (1923).
(5) Hofer, L. J. E.: U. S. Bur. Mines Rept. Investigations **3770** (1944).
(6) Hofer, L. J. E., Cohn, E. M., and Peebles, W. C.: J. Phys. & Colloid Chem. **53,** 661 (1949).
(7) Hofer, L. J. E., Cohn, E. M., and Peebles, W. C.: J. Am. Chem. Soc. **71,** 189 (1949).
(8) Hofer, L. J. E., and Peebles, W. C.: J. Am. Chem. Soc. **69,** 893 (1947).
(9) Jacobson, B., and Westgren, A.: Z. physik. Chem. **20B,** 361 (1933).
(10) Jolivet, H., and Portevin, A.: Compt. rend. **213,** 687 (1941).
(11) Kohlhaas, R., and Meyer, W. Fr.: Metallwirtschaft **17,** 786 (1938).
(12) Le Clerc, G., and Lefebvre, H.: Compt. rend. **208,** 1650 (1939).
(13) Le Clerc, G., and Michel, A.: Compt. rend. **208,** 1583 (1939).
(14) Scheffer, F. E. C., Dokkum, T., and Al, J.: Rec. trav. chim. **45,** 803 (1926).
(15) Schmidt, J.: Z. anorg. allgem. Chem. **216,** 85 (1933).
(16) Storch, H. H., Anderson, R. B., Hofer, L. J. E., Hawk, C. O., and Golumbic, N.: U. S. Bur. Mines Tech. Paper **709** (1948).
(17) Tebboth, J. A.: J. Soc. Chem. Ind. **67,** 62 (1948).
(18) Tutiya, H.: Bull. Inst. Phys. Chem. Research (Tokyo) **10,** 951 (1930).

ACID ACTIVATION OF SOME BENTONITE CLAYS[1]

G. A. MILLS, JAMES HOLMES,[2] AND E. B. CORNELIUS

The Houdry Laboratory, Houdry Process Corporation, Marcus Hook, Pennsylvania

Received November 14, 1949

INTRODUCTION

The distinctive surface properties of clays have long been utilized in bleaching and other adsorptive processes. For such purposes, individual clays possess widely different properties. Actually, the most efficient bleaching clays have been prepared by the acid-leaching of certain bentonite clays of relatively low bleaching power. More recently acid-treated bentonites have found an important new use as catalysts in catalytic cracking (12).

Although the procedure for acid-treating clays for bleaching purposes has been described (16), relatively little has been published concerning the general properties of acid-treated clays and the changes which occur in the clay structure during acid-leaching. The present investigation was directed towards the preparation of cracking catalysts by systematically acid-treating a number of different bentonite clays under conditions of varied severity. The chemical compositions and catalytic cracking activities of the clays were determined as well as their physical properties, such as surface area, porosity, and pore-size distribution. All measurements were made on calcined clay pellets. Changes of properties have been correlated with severity of acid treatment. Activable and inactivable bentonite clays have been compared for the purpose of finding distinguishing features. Since the properties of clay are known to vary from deposit to deposit, the results must be restricted to the particular bentonite clays examined. However, the fourteen clays reported here were selected as representative of a wide range of properties and thus more general conclusions can be drawn.

EXPERIMENTAL

The clays were dried at 105°C. and ground to pass a 200-mesh sieve. Samples were treated with 5–20 per cent sulfuric acid solution, at acid:clay ratios of 0.2 to 0.8, and at 93°C. for times up to 16 hr. They were then washed at room temperature until the washings were free from sulfate ion. The acid-treated clay was dried, ground, mixed with sufficient water to form a plastic mass, and extruded into 4-mm. pellets. The pellets were dried, and samples were calcined at 565°C. in dried flowing air. The physical and catalytic properties were all measured on samples which had been pelleted and calcined.

The catalytic activity was measured by the Catalytic Activity Test A (1), cracking light East Texas gas oil at 427°C.

The surface areas were determined by the method of Brunauer, Emmett, and Teller (3), employing nitrogen as adsorbate. Pore-size distribution was estimated from the adsorption–desorption curves for nitrogen over the relative pressure range of 0.4 to 1.0. In some cases the macropore distribution was measured by mercury penetration by the method described by Ritter and Drake (20). The latter procedure was modified in that, instead of an electrical arrangement, the mercury level in the dilatometer was read directly by visual observation through the thick glass window of a Jerguson gage. One such gage allowed a maximum pressure of 1000 and another, used later, 10,000 lb./sq. in.

---

[1] Presented before the Division of Colloid Chemistry at the 113th Meeting of the American Chemical Society, which was held in Chicago, Illinois, April, 1948.

[2] Present address: Poly-Chemicals Department, E. I. du Pont de Nemours and Company, Wilmington, Delaware.

TABLE 1

Description of clays

CLAY	SOURCE	DESCRIPTION
A.	Nye County, Nevada	Fairly pure, white bentonite
B.	Monroe County, Mississippi	Calcium bentonite; a light brown powder said to be from the Tombigbee sand of Eutaw formation of the Upper Cretaceous age; 85 per cent montmorillonite, the rest largely glauconite
C.	Montgomery County, Alabama	White bentonite with yellow-brown streaks, from the lower Ripley formation
D.	Navarro County, Texas	Yellowish brown bentonite, believed to be that described by P. G. Nutting on page 150 of U. S. Geological Survey Bulletin 928-C (1943) as lying in the Nacatoch sand of the Navarro group
E.	Weston County, Wyoming	Sodium bentonite procured as a light yellow-green powder; this swelling-type bentonite is from the Black Hills region in the Upper Cretaceous
F..		"White acid bentonite"
G.	Phillips County, Kansas	Light green bentonite (with some rust streaks and other impurity)
H.	Wallace County, Kansas	Light green bentonite
I.	Jessamine County, Kentucky	Light green bentonite (some rust streaks) lying in the upper part of the Tyrone limestone
J.	Sumter County, South Carolina	Grey-brown, very impure bentonite (some rust streaks and mica impurity)
K.	Sumter County (adjacent to J)	Very impure
L.	Thomas County, Georgia	Grey, fairly pure bentonite (overlain by orange and grey gritty clay), found near the Ocklocknee River
M..	Inyo County, California	Light brownish pink to white, impure bentonite

Porosity, pellet density (sometimes called apparent density (13)), and real density were measured by water adsorption, employing a technique similar to that specified in A.S.T.M. C-20-46. Bulk density was also measured. However, values for bulk density have been omitted, since it was found that the packing factor remains fairly constant from sample to sample, bulk density being equal to pellet density times 0.6.

Chemical analyses were obtained on some of the raw and acid-treated samples. In addition, a measure of the basic constituents which were dissolved during the acid treatment was obtained in the following manner: An aliquot of the composite acid liquor and washings was taken and ammonium hydroxide was added; the ensuing precipitate was processed to give a figure for the "R_2O_3" dissolved. This serves as a convenient measurement of the severity of acid treatment.

TABLE 2

Chemical composition of bentonite clays before and after acid treatment

CLAY SAMPLE	ANALYSIS BASIS CLAY DRIED AT 105°C							R_2O_3 REMOVAL PER 100 G. OF DRY CLAY	
	Ignition loss	SiO_2	Al_2O_3	Fe_2O_3	MgO	CaO	Na_2O	From clay analysis	From liquor analysis
	per cent	*per cent*	*per cent*	*per cent*	*per cent*	*per cent*	*per cent*	*per cent*	*per cent*
Nevada:									
A1 (raw)	7.8	57.7	22.0	2.26	4.98	1.79	1.86	0	0
A2	10.3	60.1	20.9	1.63	3.06	0.57		2.6	1.6
A6	5.1	67.5	21.9	1.50	3.09	0.33		4.3	4.2
A9	8.3	66.4	20.4	1.41	3.6	0.02	0.19	5.3	6.6
A12	7.1	68.6	18.3	1.48	2.46	0.30		7.6	8.0
A13	5.0	73.3	15.7	1.19	2.57	0.24		11.1	10.7
A14	6.3	78.1	11.7	0.83	2.02	0.07		15.0	14.9
Monroe County, Mississippi:									
B1 (raw)	5.5	62.3	19.1	6.65	3.24	0.82		0	0
B3	5.9	66.5	17.5	5.47	1.54	0.64		4.3	4.0
B7	5.7	70.0	15.1	4.98	1.57	0.32		8.0	6.0
Montgomery County, Alabama:									
C1 (raw)	8.2	60.9	19.3	4.52	4.87	1.65	0.13	0	0
C2	6.6	66.6	20.9	2.48					
Weston County, Wyoming:									
E1 (raw)	5.2	64.0	21.0	3.50	2.30	0.50	2.60	0	0
F1 (raw)	9.1	71.0	13.0	0.85	2.04	1.20	2.30	0	0
Phillips County, Kansas:									
G1 (raw)	4.9	65.7	14.9	4.82	2.49	1.86		0	0
G4									

The clays described in table 1 are of the subbentonite or nonswelling type for the most part and were identified principally by x-ray, chemical, and thermal analyses.

RESULTS AND DISCUSSION

Chemical composition of raw and acid-treated clays

The acid solubility of the basic constituents of bentonite clays has been reported by Nutting (16) for a wide range of systematically varied conditions.

Comparisons in chemical composition for clays in raw and acid-treated conditions (presumably optimum for bleaching) have also been published (4, 6, 8, 22). Similar results were obtained here for the changes in the principal basic constituents during acid treatment. Data are given in tables 2 and 3. It is evident that different bentonite clays are attacked to different degrees by the same acid treatment.

The effect of acid concentration on the "R_2O_3" removal is shown in figure 1 as a function of time. It is obvious that, within limits, the same "R_2O_3" removal may be achieved by different acid strength–time combinations.

The progressive solution of each of the individual basic constituents is shown in figure 2 for increasing severity of acid treatment. It is of interest to examine the *relative* removal of each constituent. For instance, based on the original amount of each constituent present, the following amounts are found to have been dissolved:

NEVADA CLAY SAMPLE	PER CENT OF CONSTITUENT DISSOLVED			
	Al_2O_3	Fe_2O_3	MgO	CaO
A13	44	61	59	89
A14	61	73	70	97

Considered from the viewpoint that aluminum, iron, and magnesium occupy the same position in the montmorillonite lattice (19, 21), it is not surprising that these are removed at approximately the same relative rate. In these experiments all the calcium sulfate formed by the sulfuric acid treatment is dissolved by the extensive washing, a circumstance not usual in commercial activation.

Comparisons have been made in the last two columns of table 2 between the "R_2O_3" removal as determined from analyses of the spent acid solution and as determined from analyses made on the acid-treated clay. Considering the fact that the values from the clay are arrived at by difference, the agreement is reasonably good, particularly for higher values where the accuracy is greater. The "R_2O_3" removal value obtained directly from the spent acid liquor is believed more accurate, although there may be small amounts of magnesia included, owing to the procedure used.

Physical properties of raw and acid-treated clays

The physical properties of clays, particularly when in colloidal dispersion, are well known to display wide variations. The surface areas and porosities reported here for the raw calcined clays also show wide ranges of values. Examination of the pellet density, porosity, and real density reveals a good deal about the structure of clay pellets and the behavior of both the raw and the acid-treated clays. The measured real density of acid-treated clays was found from water absorption to lie between 2.6 and 2.4 g./cc., in general agreement with values calculated by taking an arithmetic average of the densities of the individual oxides weighted according to the composition of the clay. The measured real density decreased with increasing severity of acid treatment as the basic con-

TABLE 3

Physical and catalytic properties of raw and acid-treated clays

CLAY	ACID TREATMENT				PHYSICAL PROPERTIES			CATALYTIC PROPERTIES			
	Acid concentration: per cent H_2SO_4	Ratio of H_2SO_4 to dry clay	Time in hours at 93°C.	"R_2O_3" removed in per cent of dry clay	Pellet density*	Porosity†	Area	Gasoline	Coke	Gas	Gas gravity
A. "Activable" bentonites											
					g./cc	*volume per cent*	*m.²/g*				
								5.0‡	0.2‡	0.3‡	1.1‡
Ash Meadows, Nevada:											
A1	Raw calcined clay			0	1.95	5.7	9	7.1	1.2	1.1	1.29
A2	5	0.2	4	1.6	1.55	40.6	71	34.9	4.2	4.8	1.42
A3	5	0.2	8	2.0	1.55	36.2	117	34.0	4.5	5.7	1.48
A4	5	0.2	16	2.0	1.45	43.9		40.5	4.5	6.6	1.47
A5	10	0.2	8	3.4	1.26	51.0		41.4	4.5	6.3	1.47
A6	10	0.4	4	4.2	1.19	53.6	146	46.8	4.6	8.4	1.58
A7	5	0.4	8	5.2	1.19	53.8		44.9	5.1	7.8	1.59
A8	15	0.4	4	6.0	1.08	56.4		44.4	4.3	8.2	1.54
A9	10	0.4	8	6.6	1.07	57.5	236	43.9	4.4	8.7	1.56
A10	5	0.6	8	7.3	1.15	54.5		43.0	4.6	9.1	1.57
A11	15	0.6	4	7.2	1.00	60.0		45.9	4.4	8.0	1.57
A12	10	0.4	16	8.0	1.05	57.8	236	43.0	4.3	7.7	1.53
A13	15	0.6	8	10.7	0.95	60.8	282	42.5	4.1	8.1	1.55
A14	20	0.8	8	14.9	0.87	63.0	279	37.5	2.9	6.9	1.49
A15	10	0.4	8§	15.3	0.81	67.0	348	39.7	3.2	6.5	1.50
Panther Creek, Monroe County, Mississippi:											
B1	Raw calcined clay			0	1.92	16.7	8.2	5.4	0.4	0.6	1.24
B2	10	0.4	4	1.5	1.32	48.9	155	34.1	4.9	6.3	1.36
B3	10	0.4	8	4.0	1.29	49.5	179	34.2	5.0	5.3	1.40
B4	10	0.4	16	7.6	1.20	54.6	229	35.0	4.3	5.8	1.33
B5	15	0.6	4		1.36	51.4		36.4	5.3	7.0	1.38
B6	15	0.6	6		1.16	54.6		35.0	4.4	7.3	1.40
B7	15	0.6	8	6.0	1.05	61.0	250	41.2	4.5	7.3	1.51
B8	15	0.6	10	9.5	1.03	59.6	253	31.6	3.8	4.9	1.38
B9	15	0.6	16	10.0	0.95	63.0	250	32.8	3.0	5.0	1.33
B10	20	0.8	4		1.10	58.3		32.8	4.1	6.3	1.42
B11	25	1.0	4		1.03	60.5		34.0	3.8	6.2	1.38
Montgomery County, Alabama:											
C1	Raw calcined clay			0	1.78	18.4	22	7.1	0.6	0.8	0.8
C2	10	0.4	12		1.05	57.0	180	36.1	3.0	5.2	1.57
Navarro County, Texas:											
D1	Raw calcined clay			0	1.95	17.8	27	4.4	1.2	0.8	0.57
D2	15	0.6	8	5.3	1.26	51.2	188	27.2	2.9	5.4	1.12

TABLE 3—*Continued*

CLAY	ACID TREATMENT				PHYSICAL PROPERTIES			CATALYTIC PROPERTIES			
	Acid concentration: per cent H_2SO_4	Ratio of H_2SO_4 to dry clay	Time in hours at 93°C.	“R_2O_3” removed in per cent of dry clay	Pellet density*	Porosity†	Area	Gasoline	Coke	Gas	Gas gravity
A. “Activable” bentonites—*Continued*											
					g./cc.	*volume per cent*	*m.²/g.*				
Wyoming bentonite:											
E1	Raw calcined clay			0	(1.8)			5.3	0.4	0.7	1.27
E2	20	1.6	4	4.8	1.49	42.5	109	29.6	3.7	4.0	1.46
“White acid bentonite”:											
F1	Raw calcined clay			0	1.67	28.1		8.3	1.3	1.2	0.93
F2	20	0.8	4	7.5	1.54	36.7	84	27.5	2.8	4.1	1.38
B. “Inactivable” bentonites											
Phillips County, Kansas:											
G1	Raw calcined clay			0	1.88	30.9	66	11.3	5.6	2.3	0.52
G2	10	0.4	4	5.2	1.45	43.1	133	13.9	2.4	1.5	0.65
G3	15	0.6	4	8.7	1.31	45.4	163	14.1	2.5	1.5	0.64
G4	20	0.8	4	10.3	1.25	51.0	183	10.4	1.9	0.9	0.66
Wallace County, Kansas:											
H1	Raw calcined clay			0	1.73	36.6	81	7.5	5.1	1.7	0.73
H2	10	0.4	4	6.4	1.41	43.7					
H3	15	0.6	4	9.1			144	9.8	2.6	1.0	0.57
H4	20	0.8	4	10.1	1.24	47.9	178	10.3	1.7	1.1	0.65
Jessamine County, Kentucky:											
I1	Raw calcined clay			0	(1.9)		50	8.9	2.9	1.9	0.39
I2	20	0.8	4	5.0	1.38	49.6	105	9.2	1.5	1.1	1.01
Sumter County, South Carolina:											
J1	Raw calcined clay			0	0.95	58.8		8.4	4.7	2.0	0.32
J2	10	0.4	8		0.92	60.0	115	13.9	1.3	1.5	0.66
Sumter County, South Carolina:											
K1	Raw calcined clay			0	1.28	48.5		9.6	3.5	1.6	0.48
K2	15	0.6	8		1.19	50.4	100	17.1	1.4	1.6	0.77
Thomas County, Georgia:											
L1	Raw calcined clay			0	1.67	35.3	75	16.7	4.0	2.3	0.66
L2	10	0.4	8	(13)	1.24	49.6	161	19.2	2.6	2.1	0.85

TABLE 3—*Concluded*

CLAY	ACID TREATMENT				PHYSICAL PROPERTIES			CATALYTIC PROPERTIES			
	Acid concentration: per cent H_2SO_4	Ratio of H_2SO_4 to dry clay	Time in hours at 93°C.	"R_2O_3" removed in per cent of dry clay	Pellet density*	Porosity†	Area	Gasoline	Coke	Gas	Gas gravity
B. "Inactivable" bentonites—*Continued*											
					g./cc.	*volume per cent*	*m.²/g.*				
Inyo County, California:											
M1 . .	Raw calcined clay			0	1.67	34.2		8.0	3.2	0.9	0.61
M2.	7.5	0.3	8§		1.05	55.9	220	7.3	1.8	0.9	0.46

* Pellet density = weight of dry pellets/volume of pellets; volume of pellets = pycnometer volume minus volume of water added to fill pycnometer containing water-filled pellets.

† Porosity = (volume of pores/volume of pellets) × 100; volume of pores = weight of water to fill pellets × density of water.

‡ Blank test for Catalytic Activity Test A; no catalyst present.

§ Hydrochloric acid instead of sulfuric acid.

stituents were removed from the less dense silica. For certain raw clays the measured real density was low (for example, 2.08 for sample A1), owing to the existence of closed pores not accessible to the penetrating liquid. The measured porosity was only 5.7 volume per cent in this instance, whereas the volume per cent porosity has a calculated value of 26 (which happens to be that for close packing of spheres) when the real density is assigned a reasonable value of 2.6. The porosity of a clay pellet depends in part upon the colloidal behavior of the clay slip. A great variation in drying shrinkage occurs for different clays. This shrinkage is believed to be a lining up of the montmorillonite platelets due to the action of the water on the surface and the forces exerted during drying when the water film is progressively lessened. In the case cited above (sample A1), the great drying shrinkage results in a pellet having smaller external dimensions and consequently a high pellet density (column 4, table 3A). Moreover, the shrinkage has made most of the pores inaccessible to liquid.

With increasing severity of acid leach the pellet porosity increases, as shown in figures 3 and 4 and in column 5 in table 3. The effect of the removal of rather moderate amounts of basic constituents is to cause a large increase in the measured porosity. The increase in porosity is greater than can be accounted for by the volume of basic materials removed. The reason for the increased porosity is believed to arise from the circumstance that the porosity is to a degree dependent on the extrusion conditions, which partly depend upon the changes in the plasticity of the clay brought about by acid treatment. This effect is large in some cases.

The effect of extrusion conditions on the porosity of a single clay was investigated for an acid-activated bentonite manufactured by the Filtrol Corporation for use in Thermofor catalytic cracking. With increasing pressure, effected by having less water in the extrusion mix, increasing pellet density and decreasing porosities were observed. The data are shown in table 4 and figure 5. Measurements of surface area by nitrogen adsorption indicate that the surface areas are

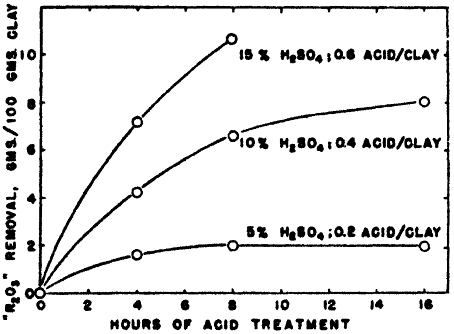

FIG. 1

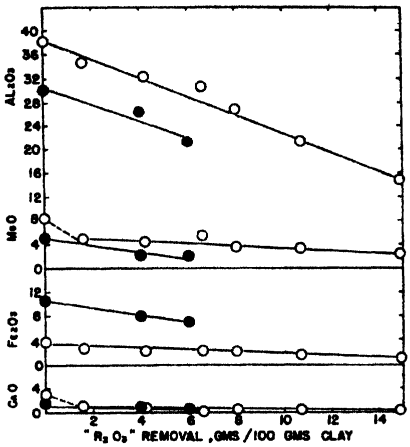

FIG. 2

FIG. 1. Effect of time and acid concentration on "R_2O_3" removal from Nevada bentonitic clay, A, acid-treated at 93°C.

FIG. 2. Chemical composition of clay remaining after acid treatment (ordinate) calculated on the basis of constant SiO_2 = 100. ○, Nevada clay, A; ●, Mississippi clay, B.

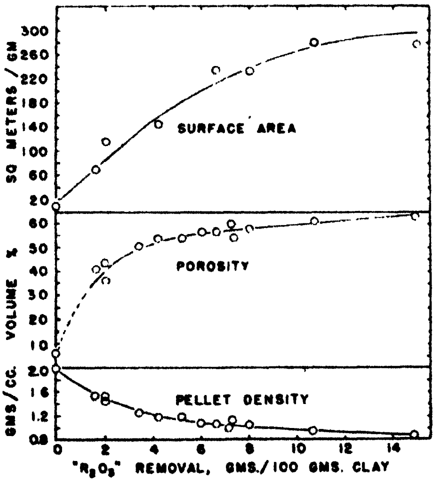

FIG. 3

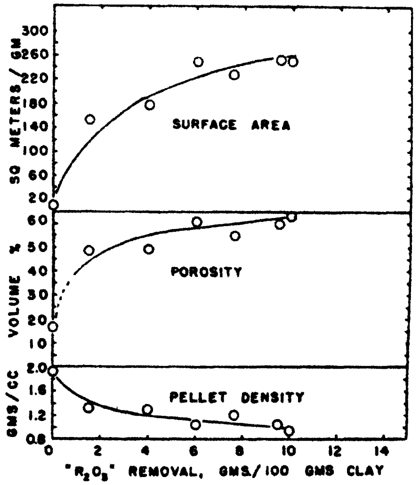

FIG. 4

FIG. 3. Effect of severity of acid treatment on physical properties (measured on calcined pellets) for Nevada clay, A.

FIG. 4. Effect of severity of acid treatment on physical properties (measured on calcined pellets) for Mississippi clay, B.

changed only to a small extent under the extremes of extrusion pressure used. In series A, table 4, the volume available to mercury penetration at 1000 p.s.i.g. progressively lessened with increasing extrusion pressure; with series B, higher extrusion pressure was used and further decreased porosities obtained. The pore-size distribution shows the effect of this (figure 5). It appears that high extrusion pressure increased density at the expense of the larger pores, with the fine structures remaining relatively unaltered.

TABLE 4

Effect of moisture content of extrusion mix on pore distribution

Clay: uncalcined Filtrol powder; properties measured on pellet after calcination

CLAY SAMPLES	WATER IN WEIGHT PER CENT OF DRY CLAY	EXTRUSION "PRESSURE"*	PELLET DENSITY	VOLUME IN PORES				AREA	CATALYTIC PROPERTIES		
				I† <2000 Å in diameter	II‡ >2000 Å. in diameter	I + II	From water		Gasoline	Coke	Gas
		p.s.i.	*g./cc.*	*cc./g.*	*cc./g.*	*cc./g.*	*cc./g.*	*m.²/g.*			
Series A:											
N1.....	45.5	500	0.97	0.344	0.175	0.519	0.614	256	41.5	4.4	8.9
N2 ...	44.7	700	1.05	0.335	0.140	0.475	0.557	256	39.8	3.8	7.2
N3.....	45.0		1.10	0.344	0.120	0.464	0.503	247	40.0	4.4	8.0
N4	41.5	1600	1.09								
N5.....	40.4	2000	1.13	0.332	0.078	0.410	0.492	245	42.1	4.0	8.0
N6.....	38.8	2600	1.21								
Series B:											
N7.....	39.6		1.18	0.30	0.087	0.387	0.470	247	41.5	4.4	7.9
N8....	39.3		1.22				0.445		40.9	4.8	8.6
N9.....	37.2		1.22	0.28	0.008	0.288	0.411	245	39.3	4.8	7.7
N10....	36.3		1.35	0.27	0.005	0.275	0.351	229	36.1	4.2	7.7
N11. ..	36.3		1.37	0.26	0.004	0.264	0.345	204	35.2	4.4	6.6

* Pressure measured on extrusion mixture under standard conditions.

† Obtained for nitrogen adsorption at 0.99 relative pressure.

‡ Obtained from the volume of mercury penetration at 1000 p.s.i.

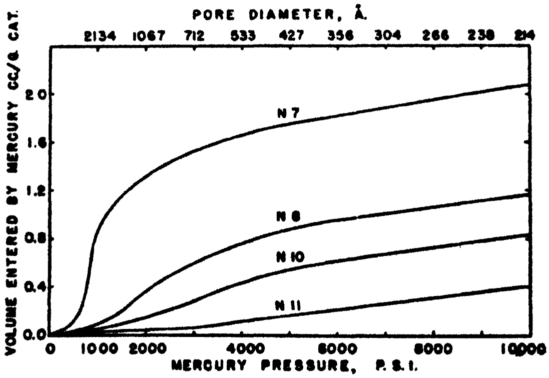

FIG. 5. Macropore distribution, as measured by mercury penetration, for pellets prepared at various extrusion pressures from Filtrol clay (see table 4, series B).

Indications of the pore distribution and nature of the pores may be found by examining the nitrogen sorption-desorption isotherms. In view of the uncertainty as to the exact amount of nitrogen adsorbed by capillary condensation during the adsorption and that due to multilayer adsorption, no attempt has been made to determine a pore-size distribution from this branch of the isotherm. Following the example of other investigators, the Kelvin equation has been applied to the desorption isotherm, allowing the designation of a calculated pore diameter for each relative pressure (5, 11). As pointed out by Cohan, it is not reasonable to consider that capillary condensation can occur in pores having diameters less than four times that of the adsorbate. For nitrogen this corresponds to about 0.4 P/P_0, and consequently the Kelvin equation has not been applied below this value. There are numerous limitations in determining pore distributions in this manner, but such distributions are particularly helpful for the

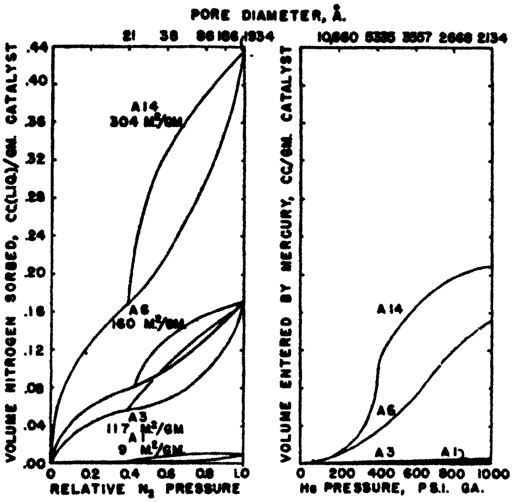

FIG. 6. Nitrogen isotherms and mercury penetration curves for Nevada clay, A, acid-treated at various severities.

TABLE 5

Effect of acid treatment on pore distribution

CLAY	"R_2O_3" REMOVAL PER 100 G. OF DRY CLAY	VOLUME IN PORES			
		I* <2000 Å. in diameter	II† >2000 Å. in diameter	I + II	From water
	grams	*cc./g.*	*cc./g.*	*cc./g.*	*cc./g.*
A1.......	0	0.011	0.006	0.017	0.029
A3.......	2.0	0.171	0.007	0.178	0.234
A6.......	4.2	0.194	0.14	0.334	0.451
A14......	14.9	0.434	0.21	0.644	0.724
A15......	15.3	0.450	0.29	0.740	0.827

* Obtained from nitrogen adsorption at 0.99 relative pressure.

† Obtained from the volume of mercury penetration at 1000 p.s.i.

comparative purposes as used here. If it is assumed, as many have done, that the sorption–desorption hysteresis is due to the presence of bottleneck pores, then the separation of the adsorption and desorption loops further serves to identify the character of the pores.

In figure 6 are shown nitrogen adsorption–desorption curves for a series of samples obtained by acid treating the Nevada clay with increasing severity. The shape of these indicates a rather similar distribution of pores for all three samples. The sorption curves for Filtrol acid-treated bentonite have been reported also by Oulton (18). In figure 6 and in table 5 are given the results of mercury penetration measurements on these same samples. For the large pores (greater than 2000 Å. in diameter) there is a wide difference in the penetrability, in a large part reflecting the ability of the clay particles to compact during extrusion and drying. Sample A3 is of interest. Here the high area and total porosity as shown by nitrogen measurements have been largely attained, whereas the large pores available to mercury remain at a very low level. Apparently in this case the plastic properties were not altered from those of the original clay at this particular stage of acid treatment, whereas the area had been largely developed. It should be remembered that the mercury measures penetration controlled by small openings to larger pores (bottleneck structure) and the values, therefore, do not represent a true distribution. The pore-size distribution as obtained from nitrogen desorption would be the same only when the pores have been completely filled with liquid nitrogen.

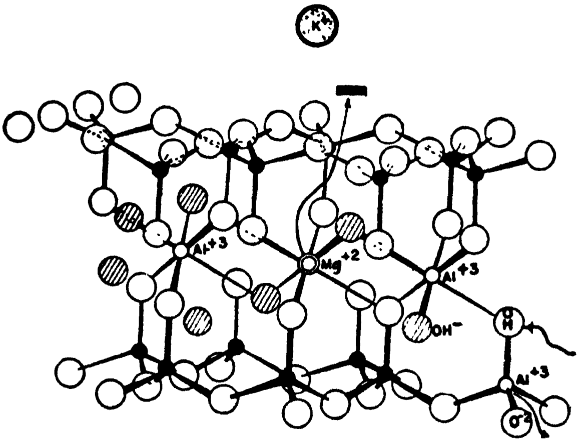

FIG. 7. Structure of montmorillonite

For a given clay, the area also increases with increasing acid treatment and reaches a relatively high value with a rather small amount of removal of basic constituents (figures 3 and 4). The area is characteristic of the particular clay chosen, both in the raw and after a given acid treatment. It is of interest to compare the areas found with those calculated from geometrical consideration of the montmorillonite crystal structure. For platelets as illustrated in figure 7 the area of the plane surface is 800 m.^{2}/g., not taking into account edge areas. It is evident from the comparison of this with the relatively low areas of the raw clays studied here that many platelets occur in stacks with loss of effective surface to nitrogen molecules.

The "R_2O_3" removal values plotted against the physical properties of the acid-treated clays give rise to smooth curves. As will be evident later, the catalytic properties are similarly related to the "R_2O_3" removal. For the range of conditions of acid treatment used here, it is concluded that, for a given clay, equivalent products are obtained when equal amounts of basic constituents are removed.

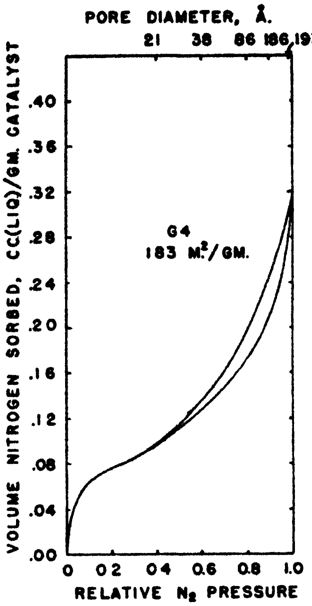

FIG. 8

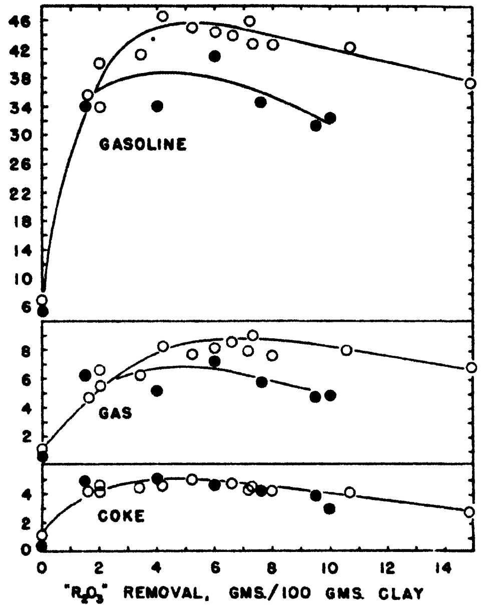

FIG. 9

FIG. 8. Nitrogen isotherms for acid-treated "inactivable" Kansas clay, G

FIG. 9. Catalytic cracking activity of acid-treated bentonite as a function of severity of acid treatment. ○, Nevada clay, A; ●, Mississippi clay, B.

Catalytic properties of raw and acid-treated clays

The catalytic cracking activity for the various clays in raw and acid-treated condition is given in table 3. Raw bentonite clays tested after calcination show considerable variation in activity, although they were found to be relatively low. Widely different catalytic activities are obtained by the acid treatment of the various bentonite clays. This is despite the fact that all the bentonites discussed here had, after acid treatment, similar physical properties such as porosity, pore distribution, and surface area. As an example, the complete nitrogen isotherm for an acid-treated "inactivable" bentonite is shown in figure 8. It is seen to be very similar to those given in figure 6, which are for an "activable" bentonite, although in the present instance the hysteresis loop is somewhat less separated for the inactivable clay. Under the conditions used some bentonite clays are activable for cracking to a high level and some are not. A similar situation has been found for activation for bleaching (4, 22); in that case also it is necessary to perform the acid treatment in order to determine the activability.

For a given activable clay a maximum in catalytic activity is reached as acid-treating is continued. This is illustrated in figure 9 for two different activable clays. Here the maximum in the production of gasoline, coke, and gas is reached at about 5 g. of "R_2O_3" removal per 100 g. of dry clay. This corresponds to a removal of about one-fifth of the alumina originally present. In contrast to the maximum in activity found, it will be recalled that the surface area and porosity progressively increase with increasing severity of acid treatment. Continued action of the acid evidently removes too much of the basic constituents, with detrimental effect on the catalytic activity.

Since the physical structure as determined here does not distinguish between active and inactive acid-treated bentonite clays, the pertinent question arises as to what critical properties do distinguish between them. In order to throw possible light on this the following experiment was performed: An acid-treated clay, which was almost inactive for cracking, was dipped in aluminum nitrate solution, dried, and calcined with the following results:

CATALYST	CATALYTIC ACTIVITY TEST A			
	Gasoline	Coke	Gas	Gas gravity
Blank—no catalyst	5.0	0.2	0.3	1.1
Acid-treated bentonite	10.4	1.9	0.9	0.66
Acid-treated bentonite + 7 per cent alumina	27.2	3.4	5.8	1.03

This is taken to indicate that nothing in the physical structure of this inactivable clay has made catalytic activity impossible, but rather that there is a lack of the necessary arrangement of silica and alumina. It is not enough that alumina be present, as it is present in considerable amounts in all the acid-treated bentonites, but the alumina must be present in a certain disposition. Distribution of alumina from the nitrate over the silica in the manner outlined above is evidently sufficient to fulfill the necessary conditions for at least moderate activity.

During acid-leaching the basic components of the montmorillonite are probably attacked first at the edges of the platelets, with penetration proceeding inward from the edges. The removal of aluminum and other ions is not expected through unbroken silicon–oxygen layers, which sandwich both sides of the basic constituents, on account of the relatively small openings in the silicon–oxygen network. In accord with this, the presence of unchanged montmorillonite structure in the acid-activated bentonites has been shown by x-ray studies. It is believed that acid penetration then proceeds into the interior of the structure from the edges, leaving a framework possessing large area. In the extreme a silica skeleton is left. However, before this time—for instance, at optimum acid attack for cracking activity—partial solution of the basic constituents has occurred. The manner in which this has occurred is believed to be important. As an explanation of the difference between activable and inactivable clays it is suggested that in the acid attack of activable clays part of the basic constituents (most importantly alumina) is left attached to the silica, whereas in the case of inactivable clays, little or no basic constituents remain in the acid-leached portion of the structure.

Actually, as recent investigations have shown (2, 15), the active part of a cracking catalyst occupies only a small part of the total surface. It is not necessary to have the montmorillonite structure for catalytic activity. A small amount of aluminum ion must be present in four-coördinate form to constitute acidity (17, 23). Such a condition may be met in clays which naturally have many aluminum ions replacing silicon ions. The results of the chemical composition and physical structure presented here do not explain why some bentonite clays are active and why others are inactive for cracking. The chemical characteristics of these clays, including base-exchange properties, will be presented in a later paper.

At least some bentonite clays activated for bleaching are active in cracking. No doubt many of the necessary requirements for bleaching are similar to those for cracking. The importance of surface hydrogen and hydroxyl ions has been considered (10, 16(a)) to be connected with activity for bleaching; the presence of water (9) and acid properties (2, 7, 15) has been shown to be fundamental to catalytic cracking activity.

In certain instances, particularly for the raw clays, the coke and gas yields were very high for the amount of gasoline made and, taken with the low gas gravity, indicate the effect of heavy metal activity (see particularly table 3). In these instances the color of the calcined raw clay may be red and the presence of iron oxide in catalytically active form is believed to be the cause of the unusual distribution of products (14). The addition of powdered iron oxide to a synthetic silica–alumina had the following effect:

Fe_2O_3 POWDER ADDED TO SiO_2–Al_2O_3	CATALYTIC ACTIVITY TEST A			
	Gasoline	Coke	Gas	Gas gravity
weight per cent				
0	47.0	3.1	8.3	1.48
0.5	31.2	3.7	8.5	0.89

The observation of a low gasoline yield does not necessarily indicate a catalyst of low cracking activity, since the presence of an active heavy metal may be acting to form coke and light hydrocarbon gases and thus tend to mask the cracking of the gas oil to gasoline.

As shown in table 2, the clays all have iron contents higher than 0.5 per cent ferric oxide even after acid treatment. For many clays, catalytic tests with a light East Texas gas oil show practically no effect of the iron. Evidently in these cases the iron is inactive, possibly because it is occupying an octahedral position in the montmorillonite lattice structure and is inaccessible to hydrocarbon molecules.

The effect of extrusion pressures on the physical structure of Filtrol pellets has been discussed. As shown in table 4, no change in catalytic properties was observed under the conditions of Catalytic Activity Test A until very high pressures were used, when the activity was slightly lowered.

SUMMARY

1. A number of bentonite clays have been acid-treated at 93°C. in 5–20 per cent sulfuric acid, at acid:clay ratios of 0.2 to 0.8, for times up to 16 hr. The chemical compositions were determined and the physical and catalytic cracking properties measured after pelleting and calcining at 565°C.

2. The raw clays showed considerable variation in surface area and porosity. The activity for catalytic cracking also varied from clay to clay, although those examined were all relatively low in activity. The presence of iron in active form in raw clays has been shown in particular cases to affect the distribution of cracked products, giving rise to high proportions of coke and gas, with the latter of low gravity.

3. With increasing severity of acid treatment the basic clay constituents—aluminum, magnesium, and iron—were progressively removed at roughly the same relative rate.

4. With increasing severity of acid treatment the surface area and porosity increased; a sharp rise occurred for moderate removal of basic constituents. The increased porosity is greater than that calculated for the amount of basic constituents removed, and the effect is attributed to decreased plastic properties upon acid treatment. The pore-size distribution remains about the same as estimated from nitrogen desorption.

5. The catalytic cracking activities of bentonite clays after acid treatment cover the complete range, some being almost inactive and some as active as synthetic silica–alumina catalyst. This is despite the fact that the physical properties are substantially identical for "activable" and "inactivable" bentonites after acid treatment.

6. In the case of the "activable" clays reported here, the cracking activity reaches a maximum with solution of about one-fifth of the basic constituents.

7. For a given clay under the range of conditions of acid:clay ratio, acid strength, and time used, products equivalent in catalytic and physical properties were obtained by removal of the same amount of "R_2O_3."

8. The effect of high extrusion pressure on acid-activated bentonite was found to increase pellet density at the expense of large pores. At the highest pressures used some loss in area and activity was observed.

9. Acid treatment of bentonite is visualized as occurring by attack from the edges of the montmorillonite lattice structure and proceeding by leaching out of the basic constituents from the edges to leave, ultimately, a silica skeleton. It is suggested that in the case of "activable" bentonites, on account of some treatment in their geological history, leaching proceeds to leave a certain amount

of alumina and magnesia associated with the silica, whereas in the case of the "inactivable" bentonites there is left a more nearly pure silica skeleton in the section of the structure which acid has penetrated.

Permission by the Houdry Process Corporation to publish this material is acknowledged with appreciation. Contributions in this investigation by co-workers, particularly H. A. Shabaker, under whose direction most of the clay activation was carried out, are gratefully recognized.

REFERENCES

(1) Alexander, J.: Proc. Am. Petroleum Inst. **27**, III, 51 (1947).
(2) Bitepazh, Yu. A.: J. Gen. Chem. (U. S. S. R.) **17**, 199 (1947).
(3) Brunauer, S., Emmett, P. H., and Teller, E.: J. Am. Chem. Soc. **60**, 309 (1938).
(4) Burghardt, O.: Ind. Eng. Chem. **23**, 800 (1931).
(5) Cohan, L. H.: J. Am. Chem. Soc. **60**, 433 (1938).
(6) Eckart, O., and Wirzmüller, A.: *Die Bleicherde*. Dr. Serger and Hempel, Brunswick (1929).
(7) Grenall, A.: Ind. Eng. Chem. **41**, 1485 (1949).
(8) Hagner, A. F.: Am. Mineral. **24**, 67 (1939).
(9) Hansford, R. C.: Ind. Eng. Chem. **39**, 849 (1947).
(10) Hofmann, U., and Endell, K.: Angew. Chem. **48**, 187 (1935).
(11) Holmes, J., and Emmett, P. H.: J. Phys. & Colloid. Chem. **51**, 1276 (1947).
(12) Houdry, E. J., Burt, W. F., Pew, E. A., and Peters, W. A.: Natl. Petroleum News **30**, R570 (1938).
(13) McBain, J. W.: *Sorption of Gases and Vapours by Solids*. G. Routledge and Sons Ltd., London (1932).
(14) Mills, G. A.: Ind. Eng. Chem. **42**, 182 (1950).
(15) Mills, G. A., Boedeker, E. R., and Oblad, A. G.: J. Am. Chem. Soc. **72**, 1554 (1950).
(16) Nutting, P. G.: (a) U. S. Geol. Survey Circ. **3**, "The Bleaching Clays" (1933); (b) Bull. Am. Assoc. Petroleum Geol. **19**, 1043 (1935); (c) J. Franklin Inst. **224**, 339 (1937); (d) U. S. Geol. Survey Bull. **928-C**, "Adsorbent Clays," p. 127 (1943).
(17) Oblad, A. G., Milliken, T. H., and Mills, G. A.: "The Active Principle of Petroleum Cracking Catalysts," Paper presented at the Gordon Research Conference, held at New London, New Hampshire, June, 1949.
(18) Oulton, T. D.: J. Phys. & Colloid. Chem. **52**, 1296 (1948).
(19) Pauling, L.: Proc. Natl. Acad. Sci. U. S. **16**, 123 (1930).
(20) Ritter, H. L., and Drake, L. C.: Ind. Eng. Chem., Anal. Ed. **17**, 782 (1945).
(21) Ross, C. S., and Hendricks, S. B.: U. S. Geol. Survey Profess. Paper **205B**, 23 (1945).
(22) Schroter, G. A., and Campbell, I.: Mining Technol. **4**, 1 (1940).
(23) Weil-Malherbe, H., and Weiss, J.: J. Chem. Soc. **1948**, 2164.

NOTE ON THE PHYSICAL ADSORPTION OF GASES IN CAPILLARIES AND ON SMALL PARTICLES (NUCLEATION OF CONDENSATION)[1]

TERRELL L. HILL

Naval Medical Research Institute, Bethesda, Maryland

Received November 14, 1949

I. INTRODUCTION

A very simple equation of the form (2, 3, 4, 5)

$$\ln p/p_0 = -a/\Gamma^3 \tag{1}$$

is quite successful in predicting the correct shape of some physical adsorption isotherms, for not too small values of Γ (corresponding to, say, two or more layers). Γ is the surface concentration (number of molecules per square centimeter) of adsorbed molecules, p/p_0 is the usual relative pressure, and a is a positive constant. This equation is derived by assuming both the adsorbate and adsorbent (plane surface) to be uniformly smeared out (structureless) (6) with their respective bulk densities, and considering only potential energy effects (i.e., neglecting entropy and other changes). Although only approximate, this treatment apparently takes care of the predominant contribution to the free energy and is therefore useful as a semiquantitative guide. In this note, without going into extensive calculations, we show by illustration that the extension of this picture to capillary condensation and the nucleation of condensation (2) is also of some value.

Let us first give a simple derivation of equation 1. Let the surface of a solid plane adsorbent of density ρ_1 (molecules per cubic centimeter) be the X–Y plane (cartesian coördinates). The adsorbent occupies the semi-infinite space all points of which have $z \leqslant 0$. There is liquid adsorbate of density $\rho = N/\mathfrak{A}h$ in the region $0 \leqslant t \leqslant h$, where N is the number of molecules adsorbed on an area $\mathfrak{A}$. The energy of interaction between two liquid molecules (4) is taken as

$$\begin{aligned} u(r) &= \infty \qquad r \leqslant r^* \\ &= -\epsilon(r^*/r)^6 \qquad r > r^* \end{aligned} \tag{2}$$

where r is the intermolecular distance, r^* is the distance of closest approach, and ϵ is the depth of the potential energy well.

An analogous expression (parameters ϵ_1, r_1) is used for the liquid molecule–adsorbent molecule interaction. We use

$$kT \ln p/p_0 = \partial(A - A_0)/\partial N \cong \partial E/\partial N - (E_0/N) \tag{3}$$

where A and A_0 are the Helmholtz free energies of N molecules of adsorbate and bulk liquid, respectively. In computing the energy difference in equation 3 we consider the potential energy only, as mentioned above.

---

[1] Some preliminary work on this problem was done at the University of Rochester, Rochester, New York, with the financial support of the Technical Division of the Chemical Corps, United States Army.

Now (6)

$$E_0/N = -2\pi\rho\epsilon r^{*3}/3 \tag{4}$$

$\partial E/\partial N$ is the interaction energy of a liquid molecule at $z = h$ with the liquid slab $0 \leqslant z \leqslant h$ plus its interaction with the semi-infinite solid, $z < 0$. Thus (7)

$$\frac{\partial E}{\partial N} = -\frac{2\pi\rho\epsilon r^{*3}}{3} + \frac{\epsilon r^{*6}\pi\rho}{6h^3} - \frac{\epsilon_1 r_1^6 \pi\rho_1}{6h^4} \tag{5}$$

or

$$\begin{aligned} \ln p/p_0 &= -(\delta_1 - \delta)/\Gamma^3 \\ \delta &= \pi\rho^4\epsilon r^{*6}/6kT \\ \delta_1 &= \pi\rho_1\rho^3\epsilon_1 r_1^6/6kT \end{aligned} \tag{6}$$

II. ADSORPTION ON SPHERICAL PARTICLES

We first recall the results derived in another paper (8) on the effect of curvature on surface tension and surface energy, according to Fowler's (1, 10) model. Let γ be the surface tension and $(1/8\pi r_0)(\mathrm{d}E^s/\mathrm{d}r_0)$ the analogous differential surface energy. Then one finds on extending Fowler's method for plane surfaces to spherical drops and bubbles,

$$\gamma = \frac{\pi\rho^2}{8}\left(\int_0^{2r_0} r^4 u'(r)g(r)\mathrm{d}r - \frac{16}{3} r_0^4 \int_{2r_0}^{\infty} u'(r)g(r)\mathrm{d}r \right. \\ \left. + \frac{8}{3} r_0 \int_{2r_0}^{\infty} r^3 u'(r)g(r)\mathrm{d}r \right) \tag{7}$$

$$\frac{1}{8\pi r_0}\frac{\mathrm{d}E^s}{\mathrm{d}r_0} = -\frac{\pi\rho^2}{2}\left(\int_0^{2r_0} r^3 g(r)u(r)\mathrm{d}r + 2r_0\int_{2r_0}^{\infty} r^2 g(r)u(r)\mathrm{d}r\right) \tag{8}$$

where $g(r)$ is the radial distribution function of the bulk liquid and r_0 is the radius of the drop or bubble. For the approximate model of Section I (8), these reduce to:

$$\gamma = \frac{3\pi\rho^2\epsilon r^{*4}}{8}\left[1 - \frac{1}{18}\left(\frac{r^*}{r_0}\right)^2\right] \tag{9}$$

$$\frac{1}{8\pi r_0}\frac{\mathrm{d}E^s}{\mathrm{d}r_0} = \frac{\pi\rho^2\epsilon r^{*4}}{4}\left[1 - \frac{1}{12}\left(\frac{r^*}{r_0}\right)^2\right] \tag{10}$$

We now consider the adsorption of a gas on a spherical solid particle of radius r_0, making the assumptions of Section I. The adsorbate is thus in the form of a spherical shell, of radii r_0 and R. Equation 3 is used to get the adsorption isotherm, where $\partial E/\partial N$ is now the total energy of interaction of a liquid molecule at $r = R$ with the solid, $0 < r < r_0$, and the adsorbate, $r_0 \leqslant r \leqslant R$. The integrals involved are straightforward (8); they are more conveniently handled keeping $u(r)$ and $g(r)$ general. Substitution of equations 2 and 11 (8)

$$\begin{aligned} q(r) &= 0 \qquad r < r^* \\ &= 1 \qquad r \leqslant r^* \end{aligned} \tag{11}$$

then leads to

$$\ln p/p_0 = \frac{2\textsc{e}_0^s}{R\rho kT}\left[1 - \frac{1}{12}\left(\frac{r^*}{R}\right)^2\right] - \frac{(\delta_1 - \delta)}{\Gamma^3}\left[\frac{2}{3}\,\frac{(x^2 + x + 1)}{(x + 1)}\right]^3 \qquad (12)$$

$$\textsc{e}_0^s = \pi\rho^2\epsilon r^{*4}/4 \quad \text{(see equation 10)}$$

$$x = R/r_0$$

$$\Gamma = (\rho/3r_0^2)(R^3 - r_0^3) \qquad (13)$$

Equation 12 reduces to equation 6 ($r_0 \rightarrow \infty$) or to

$$\ln p/p_0 = 2\textsc{e}_0^s/R\rho kT \qquad (R \rightarrow \infty) \qquad (14)$$

as special cases.

Figure 1 illustrates equation 12 for a numerical example: $\rho = 1.5 \times 10^{22}$ molecules cc.$^{-1}$, $T = 100$°K., $r^* = 4$ Å., $\textsc{e}_0^s = 15$ ergs cm.$^{-2}$, and $\delta_1 - \delta = 8.391 \times 10^{44}$cm.$^{-6}$ Curve A is the adsorption isotherm on a plane surface ($r_0 = \infty$); curve B is the adsorption isotherm on spherical solid particles of radius 20 Å.; curve C gives the vapor pressure of a spherical liquid drop of radius R, plotted, however, against Γ (equation 13 with $r_0 = 20$ Å.) for comparison with curves A and B.[2] As $\Gamma \rightarrow \infty$, $B \rightarrow C \rightarrow p/p_0 = 1$.

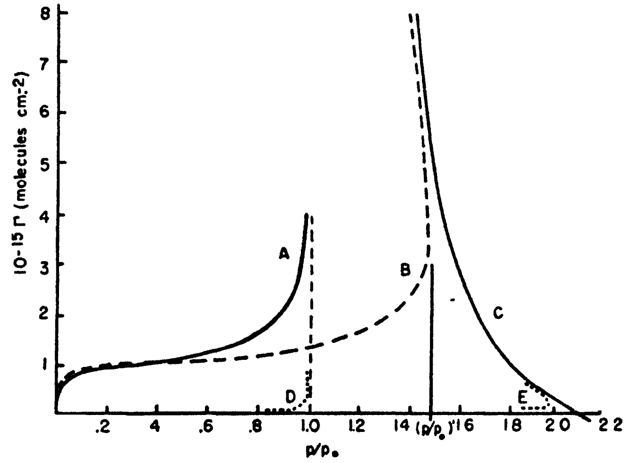

FIG. 1. Adsorption on small spherical particles. As $\Gamma \rightarrow \infty$, $B \rightarrow C \rightarrow p/p_0 = 1$.

Referring to curve C, a (supersaturation) gas pressure of, say, $p/p_0 = 1.8$ corresponds to a certain radius R_0 ($\delta_1 = \delta$ in equation 12) for an embryonic liquid nucleus having this vapor pressure. With this gas pressure, any liquid droplet with $R < R_0$ tends to evaporate and become smaller; any droplet with $R > R_0$ will grow. Hence (2), at this pressure, the rate at which bulk condensation starts depends on the rate at which nuclei of the critical radius R_0 are formed. To get an appreciable rate, R_0 must not be too large (i.e., p/p_0 must not be too small).

---

[2] The reviewer called the author's attention to the fact that behavior similar to that in curves A and B for $p/p_0 < 1$ has been observed experimentally and discussed qualitatively by Emmett and Cines (J. Phys. & Colloid Chem. **51**, 1329 (1947)). In ordinary adsorption experiments it is not possible to have $p/p_0 > 1$ because of condensation on walls, etc.

Curve B shows that the presence of small foreign particles (nuclei) sets an upper limit $(p/p_0)'$ to the degree of supersaturation necessary: as p/p_0 is increased starting from zero, a multilayer film builds up on the solid particles until p/p_0 reaches $(p/p_0)'$. At this point, the system will slide up curve B leading to bulk condensation, just as for curve C when $R > R_0$. Let $R = R'$ at $p/p_0 = (p/p_0)'$, curve B. With the gas pressure at $(p/p_0)'$, any fluctuation (up or down) in R from R' will give a droplet which will tend to grow (equilibrium $p/p_0 < (p/p_0)'$). Hence desorption fluctuations do not survive in contrast to curve C; adsorption fluctuations lead to condensation.

In figure 2, curve I shows how $(p/p_0)'$ varies with r_0 for the same numerical example. Curve II gives the corresponding value of R'/r_0 as a function of r_0.

If $\delta_1 - \delta \rightarrow 0$ (nonwetting), curve A approaches curve D and curve B approaches curve E (figure 1). Hence, in the extreme case of nonwetting, $(p/p_0)'$ becomes equal to the value of p/p_0 at which curve C crosses the abscissa. This "nonwetting" value of $(p/p_0)'$ is plotted as curve III in figure 2. A greater degree of supersaturation is needed when the surface is not wet by the adsorbate (2).

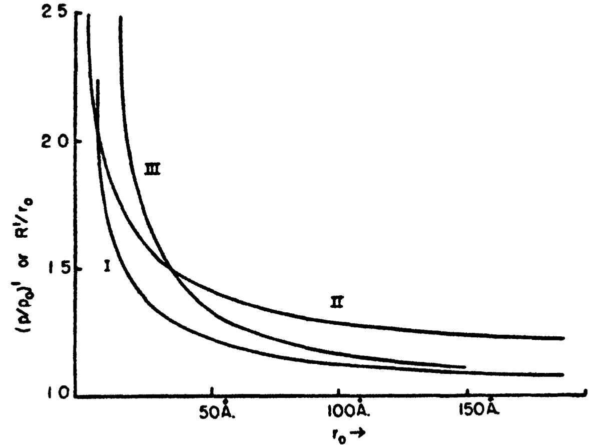

FIG. 2. Curve I: $(p/p_0)'$ *vs.* r_0. Curve II: R'/r_0 *vs.* r_0. Curve III: nonwetting $(p/p_0)'$ *vs.* r_0.

III. ADSORPTION IN PLANE CAPILLARIES

The model of adsorbate–adsorbent that we are using can obviously be extended to capillary condensation. We consider only the case of adsorption between parallel plane walls; analogous equations can be derived easily for cylindrical or spherical capillaries, but would have no really new qualitative features.

Consider a capillary between two semi-infinite adsorbents, $-\infty < z < 0$, $z_0 < z < +\infty$, using the cartesian coördinate system described above. There is an adsorbate film of thickness h on each wall so that the films are a distance $z_0 - 2h$ apart. Then $\partial E/\partial N$ in equation 3 is the energy of interaction of a liquid molecule at $z = h$ with the two films and the two solids. The adsorption isotherm turns out by the usual methods to be:

$$\ln p/p_0 = -(\delta_1 - \delta)\left[\frac{1}{\Gamma^3} + \frac{1}{(2\Gamma_m - \Gamma)^3}\right] - \frac{\delta}{8(\Gamma_m - \Gamma)^3} \qquad (15)$$

$$0 \leqslant \Gamma \leqslant \Gamma_m - \frac{\rho r^*}{2}$$

$$= -(\delta_1 - \delta)\left[\frac{1}{\Gamma^3} + \frac{1}{(2\Gamma_m - \Gamma)^3}\right] - \frac{2\pi\rho\epsilon r^{*3}}{kT}\left[\frac{1}{3} - \frac{1}{2}\frac{(\Gamma_m - \Gamma)}{\rho r^*}\right] \qquad (16)$$

$$\Gamma_m - \frac{\rho r^*}{2} \leqslant \Gamma \leqslant \Gamma_m$$

$$\Gamma_m = z_0\rho/2$$

Equation 16 takes into account the fact that, when the two films are very close to each other, no molecule can be within r^* of a reference molecule.

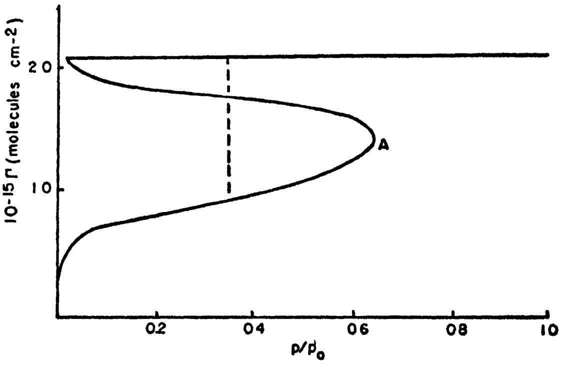

FIG. 3. Adsorption in plane capillaries

Figure 3 gives the adsorption isotherm for the same numerical case, taking z_0 = 28 Å. (Γ_m corresponding to about three layers on each side). There is a discontinuity in slope at Γ_m, owing to the fact that our model ignores the compressibility of the adsorbate. As the dotted line shows, capillary condensation is predicted because of the loop (9). In the first part of the isotherm, up to point *A* (figure 3), the predominant effect is the usual one of succeeding molecules adsorbed on top of the adsorbate being further from the attractive field of the solid. Hence the chemical potential (differential energy here) increases with Γ. The slope $d\Gamma/dp$ is positive. However, near point *A* the mutual attraction of the two films of adsorbate as they approach each other begins to be important. This tends to decrease the chemical potential and $d\Gamma/dp$ is negative between *A* and *B*. The *stable* equilibrium path is therefore capillary condensation along the dotted line.

It will of course be noticed that (*a*) the present approximate picture is related to Polanyi's potential theory, and (*b*) a single point of view explains *both* multimolecular adsorption and capillary condensation (9).

SUMMARY

An approximate theoretical picture, which leads to good agreement with experiment in some cases of physical adsorption on nonporous solids, is extended to adsorption in pores and on small spherical particles. The phenomena of capillary condensation and nucleation of condensation of a supersaturated gas are discussed in this connection.

REFERENCES

(1) Fowler, R. H.: Proc. Roy. Soc. (London) **A159**, 229 (1937).
(2) Frenkel, J.: *Kinetic Theory of Liquids*, Chap. VII. Oxford University Press, London (1946).
(3) Halsey, G.: J. Chem. Phys. **16**, 931 (1948).
(4) Hill, T. L.: J. Chem. Phys. **17**, 590 (1949). (Erratum: in the fifth line from the end, 2.267 should read 2.67.)
(5) Hill, T. L.: J. Chem. Phys. **17**, 668 (1949).
(6) Hill, T. L.: J. Chem. Education **25**, 347 (1948).
(7) Hill, T. L.: J. Chem. Phys. **16**, 181 (1948).
(8) Hill, T. L.: J. Am. Chem. Soc.,in press.
(9) Hill, T. L.: J. Chem. Phys. **15**, 767 (1947).
(10) Kirkwood, J. G., and Buff, F. P.: J. Chem. Phys. **17**, 338 (1949).

THE OXIDATION OF IODIDE TO IODINE BY DILUTE SOLUTIONS OF ORGANIC PEROXIDES

R. D. CADLE and HARIETTE HUFF

Stanford Research Institute, Stanford, California

Received November 17, 1949

Surprisingly little information is available concerning the kinetics of the oxidation of iodide to iodine by dilute aqueous solutions of specific organic peroxides. This situation exists in spite of the voluminous literature concerning the use of this reaction for the quantitative determination of various peroxides. During the course of the investigation of oxidizing substances in aqueous solutions condensed from the Los Angeles atmosphere, it became increasingly evident that a further knowledge of the kinetics of such reactions was indispensable for interpreting some of the data which had been obtained. Therefore, a study was made of the liberation of iodine from potassium iodide by dilute aqueous solutions of hydrogen peroxide, methyl hydroperoxide, ethyl hydroperoxide, *tert*-butyl hydroperoxide, and diethyl peroxide. The effects of changes in temperature, hydrogen-ion concentration, and iodide concentration were investigated.

MATERIALS

Methyl hydroperoxide and ethyl hydroperoxide, 3–4 per cent solutions in water, were prepared by C. Willard of the Stanford Research Institute according to the directions of Rieche and Hitz (5, 6). The mixture of diethyl peroxide and ethyl hydroperoxide, 35 per cent peroxide in ethyl ether, was prepared by C. M. Himel of the Stanford Research Institute according to the method of Rieche and Hitz (7). The *tert*-butyl hydroperoxide was a 70 per cent commercial sample from the Novadel-Agene Corporation, Buffalo, New York, which was distilled at atmospheric pressure through a Vigreux column. The hydrogen peroxide was prepared by diluting a 30 per cent Baker's C. P. analyzed product to 5 per cent and vacuum distilling the peroxide until 50 per cent of the solution was collected. The distillate contained about 0.036 per cent of hydrogen peroxide. The solutions were analyzed for hydroperoxides by adding 1 ml. to 1 ml. of concentrated sulfuric acid and 1 ml. of a saturated solution of potassium iodide in a small flask. After 2 hr. the liberated iodine was titrated with sodium thiosulfate. Blank determinations were also made and the values corrected for these blanks. The mixture of ethyl hydroperoxide and diethyl peroxide was also analyzed for total peroxide by heating with ferrous sulfate, concentrated sulfuric acid, and concentrated aqueous potassium iodide at 70°C. for 30 min. (10). The quantity of diethyl peroxide was assumed to be the difference between the peroxide contents found by the two methods. These analytical results were used in the preparation of the aqueous peroxide stock solutions which were of such concentration (about 0.0018 N) that the final equivalents of iodine liberated during the experimental runs did not vary more than 10 per cent among all the peroxides.[1] The potassium iodide, citric acid, and disodium hydrogen phosphate were all Baker's C. P. analyzed chemicals. All solutions were prepared with boiled conductivity water of specific conductivity less than 1×10^{-6} mhos/cm. at 25°C. This water had been redistilled through an all-glass still.

EXPERIMENTAL TECHNIQUE

Standard solutions of 0.1 M citric acid and 0.2 M disodium phosphate for McIlvaine's buffer were prepared as stock solutions. Sufficient quantities of each were added to the reaction apparatus (figure 1) to produce 100 ml. of the buffer at the desired pH. Twenty milliliters of the aqueous peroxide solution was added to the buffer in the apparatus. Suction was applied, the flask was evacuated, and oil-pumped nitrogen was allowed to bubble through the solution and fill the flask. After the fourth evacuation the flask was only partially filled with nitrogen. The apparatus was immersed in a thermostated water bath in a darkened room and sufficient time allowed for it to reach the bath temperature. A saturated aqueous solution of potassium iodide, usually 2 ml., was added, the flask was shaken, and the contents of the flask brought to atmospheric pressure by adding more nitrogen.

At appropriate time intervals 5 ml. of the reaction mixture was removed by a calibrated pipet on the side of the apparatus and titrated with 0.01 *N* sodium thiosulfate from a microburet. Starch was used as indicator.

---

[1] The very low concentrations of the peroxides were of the same order of magnitude as those of the oxidizing substances collected in the solutions condensed from the Los Angeles atmosphere. There are indications in the literature (8) that the kinetic study of the liberation of iodine from potassium iodide might yield, at low concentrations of peroxide, results that would be unexpected from the study at higher concentrations.

RESULTS

The results are shown in figure 2 and table 1. The rate of reaction of methyl hydroperoxide with potassium iodide to liberate iodine was determined for pH 4 and pH 7. The reaction, independent of pH between 4 and 7, was found to be of first order with respect to the peroxide. For ethyl hydroperoxide the variation in rate of reaction was examined for the effect of pH, amount of potassium iodide present, and temperature. Again a pH change between 4 and 7 did not alter the rate. However, the reaction rate was found to be directly proportional to the concentration of potassium iodide. Thus, the reaction of ethyl hydroperoxide (and probably of the other peroxides studied here) was actually of second order but appeared to be of first order because of the relatively large and therefore essentially constant concentration of potassium iodide.

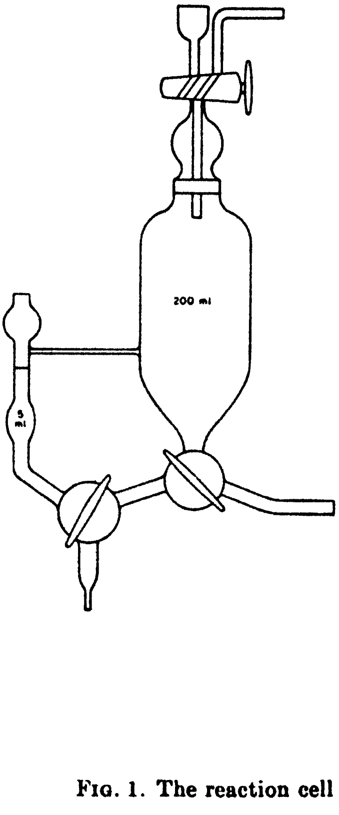

FIG. 1. The reaction cell

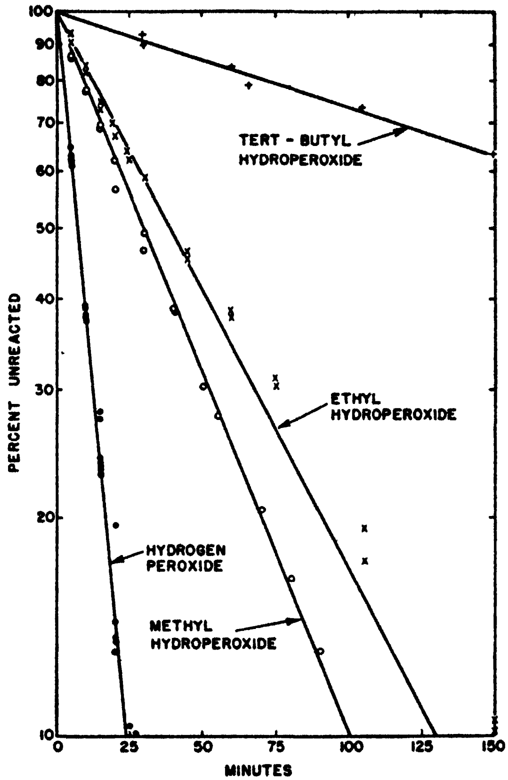

FIG. 2. Rates of reaction of four peroxides. Time plotted against per cent unreacted on log scale.

The effect of temperature on the reaction rate for ethyl hydroperoxide was determined. The heat of activation was estimated from the slope of the usual Arrhenius-type plot of the first-order reaction rate constant at constant potassium iodide concentration. The activation energy was found to be 12.7 kcal.

The titration values obtained were read to slightly better than one part in a hundred. An error of 1 or 2 per cent in either the final titration value and/or one intermediate value becomes magnified near the later state of reaction when the log of the amount unreacted is plotted against the time. Ethyl hydroperoxide deviates fairly widely from a straight line at over 50 per cent reacted at 30°C., with 2 ml. of saturated potassium iodide. However, the good linearity obtained with the other peroxides, as well as the linearity obtained with this peroxide at other potassium iodide concentrations and other temperatures, makes it appear likely that this is titration error (3 per cent error in total titration would remove the deviation).

TABLE 1

Rate constants calculated for the pseudo-first-order reactions

SUBSTANCE	INITIAL CONCENTRATION OF KI IN REACTION MIXTURE	INITIAL CONCENTRATION OF PEROXIDE[*]	pH	TEMPERATURE	K
	moles/liter	*milliequiv./liter*		°C.	$min.^{-1}$
Hydrogen peroxide	0.14	0.318	4	30	0.0909
Hydrogen peroxide[†]	0.14	0.318	4	30	0.0909
Hydrogen peroxide	0.14	0.280	7	30	0.0909
Hydrogen peroxide[†]	0.14	0.282	7	30	0.0909
Methyl hydroperoxide	0.14	0.307	4	30	0.0233
	0.14	0.307	7	30	0.0233
	0.28	0.308	4	30	0.0455
Ethyl hydroperoxide	0.07	0.272	7	30	0.0093
	0.14	0.296	7	30	0.0175
	0.14	0.298	4	30	0.0175
	0.28	0.298	7	30	0.0370
	0.14	0.221	4	20	0.0089
	0.14	0.267	7	35	0.0238
	0.14	0.275	7	40	0.0357
	0.14	0.267	7	50	0.0714
tert-Butyl hydroperoxide	0.14	0.313	4	30	0.003
	0.14	0.313	7	30	0.003

[*] Calculated from the number of equivalents of iodine liberated after reaction was relatively complete.

[†] Diluted from Baker's C.P. 3 per cent hydrogen peroxide and used without distilling.

For the purpose of comparison the reaction rate of hydrogen peroxide with potassium iodide was also investigated at these low concentrations. Again the reaction mixtures were buffered to pH 4 and pH 7. At the higher pH the final equivalents of iodine liberated were less than at pH 4, probably because of the catalytic decomposition of hydrogen peroxide by potassium iodide (2, 9). However, the same rate constant was obtained for both of the pH values. Also, the rate was independent of any preservatives that may have been present in the commercial hydrogen peroxide, as distillation of the peroxide failed to change the rate constant.

The reaction of *tert*-butyl hydroperoxide was studied at pH 4 and pH 7 and also found to be independent of the pH at the concentration used. Again it was found to be a pseudo-first-order reaction.

An attempt was made to determine the reaction rate of diethyl peroxide with potassium iodide. Rieche and Brumshagen (4) in 1928 noted that diethyl peroxide liberated iodine from potassium iodide only slowly and in 1949 Dickey *et al.* (1) found no reaction of di-*tert*-butyl peroxide with potassium iodide in acid solution.

The reaction of a mixture of ethyl hydroperoxide and diethyl peroxide with potassium iodide was studied at pH 4. The final equivalents of peroxide found corresponded only to the value of the ethyl hydroperoxide. The rate constant was also the same within experimental error as for pure ethyl hydroperoxide. Thus diethyl peroxide did not react at this pH in the time allowed.

The application of these results to the investigation of oxidizing substances in the air by the oxidation of organic materials. This oxidizing action of the solutions was found later to occur at a pH of 5 but only slightly, if at all, at a pH of 7. Therefore, the results of the present work show that the oxidizing substances could not have been organic peroxides, unless they differed radically from those discussed in this paper. There is reason to believe that part of this oxidizing action is caused by oxides of nitrogen.

SUMMARY

The reaction rate of ethyl hydroperoxide with potassium iodide to liberate iodine was studied at two pH values, three concentrations of potassium iodide, and five temperatures. Methyl hydroperoxide was studied at two pH values, and two potassium iodide concentrations. *tert*-Butyl hydroperoxide and hydrogen peroxide were investigated at pH 4 and pH 7. All reactions were found to be pseudo-first-order reactions independent of the pH (except for the decomposition effect noted with hydrogen peroxide). The activation energy of ethyl hydroperoxide was found to be 12.7 kcal.

The application of these results to the investigation of oxidizing substances in the Los Angeles atmosphere is discussed briefly.

REFERENCES

(1) DICKEY, F. H., RALEY, J. H., RUST, F. F., TRESEDER, R. S., AND VAUGHAN, W. E.: Ind. Eng. Chem. **41**, 1673–9 (1949).
(2) GARGALLO, M. A.: Anales asoc. quím. argentina **36**, 150–4 (1948).
(3) RIECHE, A.: *Alkylperoxyde und Ozonide*. Theodor Steinkopff, Dresden und Leipzig (1931).
(4) RIECHE, A., AND BRUMSHAGEN, W.: Ber. **61B**, 951–6 (1929).
(5) RIECHE, A., AND HITZ, F.: Ber. **62**, 2469 (1929).
(6) RIECHE, A., AND HITZ, F.: Ber. **62**, 2231 (1929).
(7) RIECHE, A., AND HITZ, F.: Ber. **62**, 221, 225 (1929).
(8) RUMPF, MME. P.: Compt. rend. **198**, 256–8 (1934).
(9) RUPP, E., HAMANN, G., AND MÜLLER, D.: Arch. Pharm. **272**, 57–60 (1934).
(10) WIELAND, H.: Ann. **469**, 304 (1929).

ORGANOPHILIC BENTONITES. II

ORGANIC LIQUID GELS

J. W. JORDAN,[1] B. J. HOOK,[1] AND C. M. FINLAYSON[1]
Mellon Institute, Pittsburgh, Pennsylvania

Received November 28, 1949

INTRODUCTION

The striking behavior of certain organic ammonium complexes of montmorillonite in various organic liquids has already been described in previous publications (6, 7). This work was a continuation of research by Hauser (3), who discovered that hydrophilic clays may be converted to the organophilic condition by reaction with appropriate organic ammonium salts. A bentonite originally exhibiting high swelling in water will, after base-exchange reaction with certain organic ammonium salts, show a decided aversion to water and a remarkable tendency to swell in various organic liquids. In fact, the treated clay will swell to a much greater extent in some organic systems than will its untreated counterpart in water. In further study of such clay complexes the liquid-binding capacity of these materials has been evaluated from the standpoint of gel formation, and important factors in the production of gels have been investigated.

MATERIALS AND METHODS

As in the previous work, bentonite from the National Lead Company property at Clay Spur, Wyoming, was used. Aside from a relatively small proportion of accessory nonclay material, this product was essentially pure montmorillonite according to thermal[2] and x-ray analyses.[3] A base-exchange determination[4] was made by the ammonium acetate method (2) on a sample of clay obtained after thorough sedimentation of nonclay impurities from an aqueous 2 per cent dispersion. A cation-exchange value of 94 milliequiv. per 100 g. of clay was reported on a sample containing 6.4 per cent of adsorbed moisture. This computes to approximately 100 milliequiv. per 100 g. of dry clay mineral.

The ammonium compounds were distilled-grade materials obtained from commercial sources, *viz.*, Sharples Chemicals, Inc., for short-chain amines, Armour and Company for higher aliphatic amines, and Onyx Oil and Chemical Company and Armour and Company for quaternary ammonium salts.

The reaction products were generally prepared by adding dilute (5 per cent) aqueous amine acetate or ammonium halide solutions or dispersions to the supernatant liquid resulting from allowing a 3.25 per cent aqueous bentonite slurry to sediment for 1 hr. Where larger quantities of product were required than could be made conveniently in laboratory equipment, pilot-scale preparation was resorted to. In these cases a 3.25 per cent bentonite slurry was pumped through a No. 6 Sharples supercentrifuge to remove the nonclay minerals. After analysis for solids content the effluent was then used for subsequent reaction with amine acetates or quaternary ammonium halides. Reaction of amine salt with clay was accompanied by thorough flocculation. Filtration of the flocculent precipitates was easy in most cases. After washing, the filter cakes were dried at about 85°C., and pulverized.

---

[1] Holder of Fellowship on Lead sustained by the National Lead Company at the Mellon Institute, Pittsburgh, Pennsylvania.

[2] The thermal analysis was performed through the courtesy of R. E. Grim of the Illinois Geological Survey.

[3] The x-ray diffraction analysis of the sample was carried out by L. E. Alexander of the Department of Chemical Physics of the Mellon Institute.

[4] The base-exchange determination was made through the courtesy of F. J. Williams of the National Lead Company Research Laboratories in Brooklyn, New York.

In the first paper of the series (6) the ability of the reacted clay to imbibe organic liquids was evaluated by allowing a weighed sample to swell to an equilibrium gel volume in contact with an appreciable excess of liquid. In the present study the clay complex was placed in contact with organic liquid in such proportion as to be generally in excess of the amount required for complete immobilization of the liquid. For this purpose 20 per cent of dry solid on the basis of total mixture was sufficient to provide stiff gels in most cases. A comparative measure of gel strengths was afforded by a determination of the depth of penetration into the gels by a standard A.S.T.M. grease cone. Penetrations were measured by means of a precision-type penetrometer, using the procedure specified for unworked greases (A.S.T.M. Designation: D217-44T). Thixotropy customarily necessitated a short waiting period after filling the sample can and before releasing the penetrometer cone, but this period never exceeded 15 min. The achievement of equilibrium conditions in these gels consisted for the most part in stirring the bentonite complex into the liquid with a laboratory mixer and following up with a spatula. Where the mobility of the liquid and the adsorption energy of clay complex for liquid were low, passage through a three-roll paint mill was occasionally obligatory, as in the preparation of gels with linseed and petroleum oils. Reproducibility of results was on the order of ± 3 scale divisions (tenths of a millimeter) for a reading of 200 for repeated readings on one gel, or approximately ±4 in 200 for two gels of the same composition.

RESULTS AND DISCUSSION

Primary normal aliphatic ammonium bentonites were prepared at 100 milliequiv. of amine per 100 g. of clay with amines of chain length from four to eighteen carbon atoms in steps of two. Gelling tests were made in polar liquids, such as alcohols and ketones, and in nonpolar liquids such as benzene and mineral spirits, as well as in nitrobenzene, which combines highly polar with highly organic characteristics. Since gelation was poor in the first two types and excellent in the third, it was concluded that a mixture of a polar and a nonpolar type should be chosen for optimum solvation. Such a mixture was afforded by a combination of methanol and toluene, neither one of which was as effective by itself. The gelling abilities of these homologous complexes were determined in various mixtures of toluene with methanol, and the optimum gel strengths plotted (figure 1) as a function of amine chain length. The butyl- and hexyl-ammonium complexes at 20 per cent solids gave, at best, only muddy soups which were beyond the practical limits of measurement by the penetrometer. Essentially maximum gelation was first achieved in the series with the dodecyl complex, and increases in amine chain length up to eighteen carbon atoms showed little further influence upon gel structure. In appearance the best gels (four in number) were smooth homogeneous olive-brown systems, translucent in bulk and in thin section.

Concurrent with the general increase in gelling ability of the foregoing series with increase in size of the amine molecule was a decrease in the amount of methanol required for maximum gelation. This is depicted graphically in figure 2, where the percentage of methanol in the optimum toluene–methanol mixture is related to the chain length of the amine. On the adsorption of organic molecules by montmorillonite (Hendricks (4), Bradley (1), and MacEwan (8–10)) an attempt has been made to correlate the amount of methanol necessary for optimum gel strength with the area of clay surface remaining uncoated by amine molecules. Such a correlation is obviously not tenable for the entire series, as evidenced by the character of the curve in figure 2. However, another important factor here is the initial spacing of the montmorillonite flakes with respect to one another.

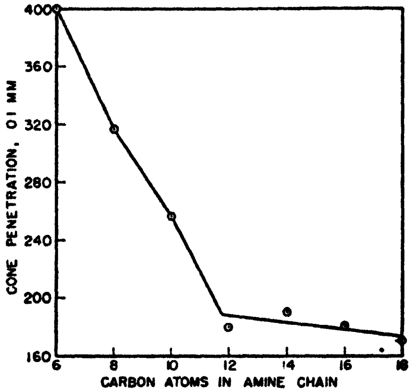

FIG. 1

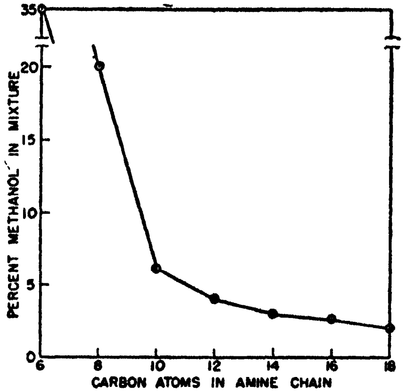

FIG. 2

FIG. 1. Optimum gel strengths of primary aliphatic ammonium bentonites in toluene-methanol mixtures (20 per cent solids).

FIG. 2. Per cent methanol required for optimum gelation of primary aliphatic ammonium bentonites in toluene–methanol mixtures (20 per cent solids).

An x-ray diffraction study of this same homologous group of complexes (6) has indicated that in the dry state the clay flakes are oriented to a large extent in parallel positions, with a space of only 4 Å. separating them in the case of amines having ten or fewer carbon atoms. This space, which represents the effective van der Waals thickness of a hydrocarbon chain, is more or less completely occupied by the amine chains. With twelve or more carbon atoms the area covered by the amine chains is sufficiently great so that adjacent parallel oriented clay platelets are unable to approach one another more closely than a distance of 8 Å., or the thickness of two hydrocarbon chains. Because of this spatial characteristic and of the gross difference in order of gelation of those complexes having amines of fewer than twelve carbon atoms (figure 1), only the C_{12}–C_{18} group will be considered. Bradley (1) and MacEwan (10) postulate hydrogen bonding between methanol and montmorillonite, giving rise to adsorptive forces of higher magnitude than the van der Waals forces operating to adsorb nonpolar liquids. Hence, the methanol in a toluene–methanol mixture should be preferentially adsorbed to the extent of the capacity of the clay complex. This capacity has been approximated, in terms of available uncoated surface area, from a computation of the total surface area of the clay (0.8×10^{23} Å.^{2} per gram of montmorillonite) and of the area coated by the amine molecules, and is presented in table 1.

TABLE 1

Spatial relations for homologous alkylammonium bentonites

CARBON ATOMS IN AMINE CHAIN	LAYERS OF AMINE BETWEEN FLAKES	UNCOATED AREA OF CLAY	UNCOATED AREA OF CLAY	METHANOL IN OPTIMUM LIQUID MIXTURE	NUMBER OF METHANOL MOLECULES	AREA AVAILABLE PER METHANOL MOLECULE
		per cent	*Å.^{2}*	*per cent*		*Å.^{2}*
0	0	100	25×10^{23}			
6	1	66	9.6×10^{23}	35	5.3×10^{23}	1.8
8	1	58	8.3×10^{23}	20	3.0×10^{23}	2.8
10	1	51	7.1×10^{23}	6.1	0.93×10^{23}	7.6
12	2	43	5.9×10^{23}	4.0	0.61×10^{23}	9.7
14	2	36	4.8×10^{23}	3.0	0.45×10^{23}	10.7
16	2	28	3.7×10^{23}	2.6	0.40×10^{23}	9.2
18	2	21	2.6×10^{23}	2.0	0.30×10^{23}	8.7

Pauling (11) lists the effective diameter of the methyl group as 4 Å. Assuming that the methanol molecules are adsorbed onto the uncoated surfaces of the clay through the mechanism of hydrogen bonding ($CH_3{-}O{-}H \rightarrow \overset{|}{O}{-}Si$ or $H{-}O{-}CH_2{-}H \rightarrow \overset{|}{O}{-}Si$ as MacEwan suggests) and that close packing is maintained, the minimum area covered by one molecule would be on the order of 12 Å.^{2} This is not far out of line with the 9–11 Å.^{2} area calculated as being available for each methanol molecule, especially when it is considered that the figure for total area did not take into account the edges of the flakes, which would appreciably increase the available area. Since the agreement appears to be more than coincidental, confirmation seems to be at hand for the earlier proposal that solvation in binary liquid mixtures involves the formation of an adsorption complex between the uncoated portion of the clay and the more polar member of the liquid mixture, followed by solvation of the adsorption complex in the less polar remnant. It is probable that in the amine complexes below C_{12} the forces of attraction between flakes, acting through only half the distance, are of considerably higher magnitude. Therefore, it is not unlikely that the disproportionately larger quantities of methanol are required to exert a sort of mass action effect in crowding between flakes and forcing them apart, making the organophilic surfaces more readily available to the less highly adsorbable hydrocarbon molecules.

In consideration of the finding that an amine of more than ten carbon atoms is required for maximum gel strength in this type of system, further work was confined to organic ammonium compounds above this critical limit. Gel strengths for dodecyl-, hexadecyl-, and octadecylammonium bentonites were determined in mixtures of toluene with various normal primary aliphatic alcohols up to and including decyl. Figure 3 shows a family of curves relating penetration for gels of 20 per cent octadecylammonium bentonite as a function of the percentage of six different alcohols in alcohol–toluene mixtures. A few salient features may be readily observed in this graph.

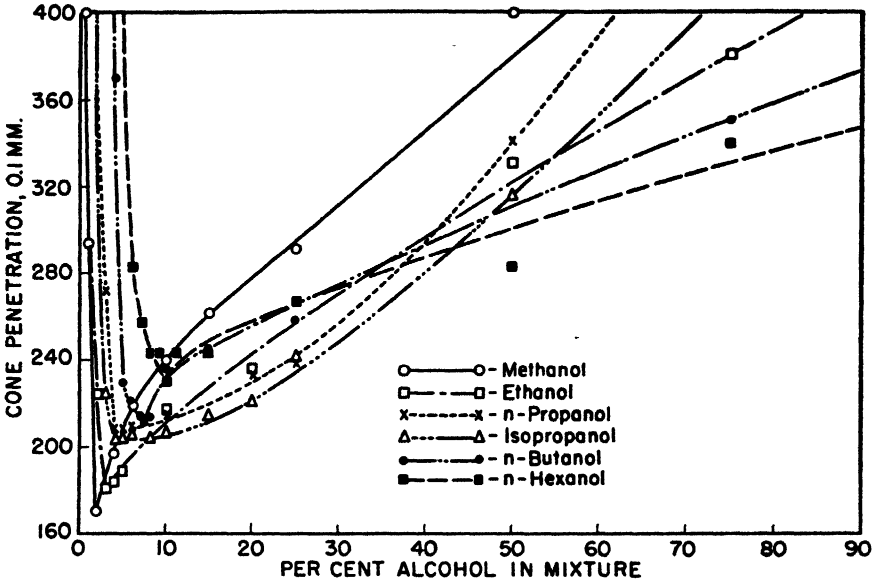

FIG. 3. Gel strength of octadecylammonium bentonite in toluene–alcohol mixtures (20 per cent solids).

All of the curves consist of two distinct sections: a very steep slope at low alcohol concentrations, rapidly approaching a gel strength maximum, and a more gradual slope of opposite sign extending from the gel maximum. The steep slopes are interpreted as representing practically complete adsorption of the alcohols from the mixtures. This adsorption renders the clay surface more completely coated with organic matter and consequently more organophilic. At the point of complete coverage the adsorption complex is more compatible with the toluene and solvates in it more readily and to a greater extent. The second portion of the curve is probably indicative of the dilution effect of the excess of alcohol upon the solvating capacity of the toluene. It would not seem logical for methanol to have much in common with the eighteen-carbon-atom chains covering most of the clay surface; consequently the deleterious dilution effect does actually diminish as the character of the alcohol approaches that of the amine hydrocarbon tail. In order to avoid repetition of data, it will suffice to state here that the corresponding curves for the C_{16} and C_{12} complexes are essentially similar.

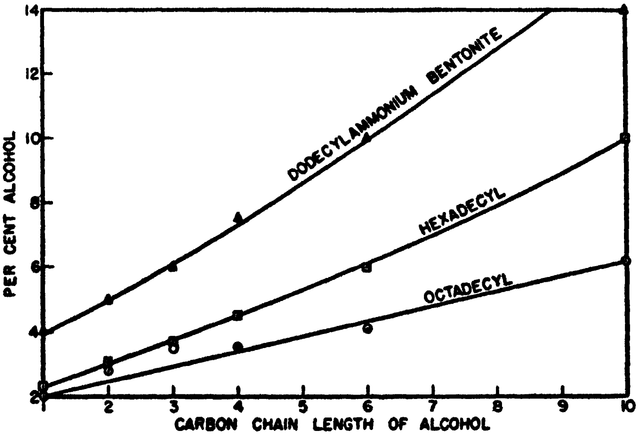

FIG. 4. Relationship between size of alcohol and amount required for optimum gelation of aliphatic ammonium bentonites in toluene–alcohol mixtures.

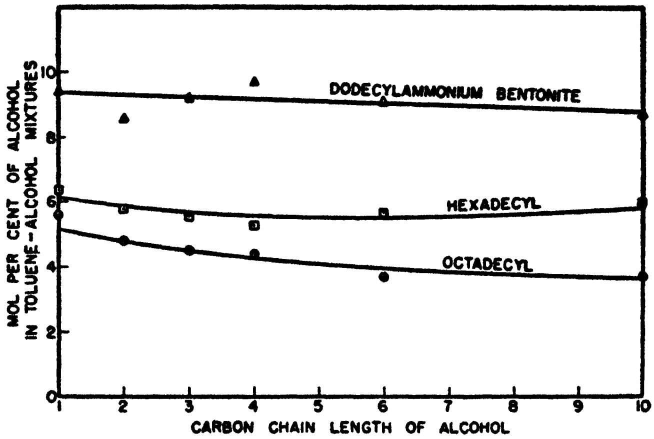

FIG. 5. Alcohol requirements for optimum gelation of aliphatic ammonium bentonites in toluene–alcohol mixtures.

With all three complexes the gel strength maxima occur at low percentages of alcohol, these maxima occurring at progressively higher concentrations of alcohol with increasing molecular size of the alcohol (figures 4 and 5). The linearity of these curves suggests a simple relationship between amount of alcohol required and molecular weight. This relationship is brought out in table 2, where mole fractions of alcohols at gel maxima are related to the uncoated areas of the three amine–bentonite complexes. These mole fractions are moderately constant for each complex. Furthermore, the available area per alcohol molecule for each complex by computation is of the order of 12 Å.², which is approximately the cross-sectional area of a hydrocarbon chain. This suggests that under these conditions the alcohol molecules may be oriented similarly on the uncoated portions of the clay surfaces; that the molecules are parallel to one another, sticking out at an appreciable angle to the clay surface; and that one particular grouping in common to all of them is involved in the adsorption phenomenon. On the basis of this evidence, it is hypothesized that the adsorption of alcohols takes place through hydrogen bonding between the —OH groups of the alcohols and the ═O group on the silicate surface, i.e., $\mathrm{R{-}O{-}H \rightarrow \overset{|}{O}{-}Si}$.

TABLE 2

Spatial and molecular relations for homologous alcohols required for maximum gelation of homologous alkylammonium bentonites in toluene–alcohol mixtures

ALCOHOL	MOLE FRACTION OF ALCOHOL REQUIRED FOR MAXIMUM GELATION		
	C_{12}	C_{16}	C_{18}
Methyl	0.094	0.064	0.056
Ethyl	0.086	0.058	0.048
Propyl	0.092	0.056	0.045
Butyl	0.097	0.053	0.044
Hexyl	0.091	0.057	0.037
Decyl	0.087	0.060	0.037
Average	0.091	0.058	0.045
Number of alcohol molecules	0.51×10^{23}	0.32×10^{23}	0.24×10^{23}
Uncoated area of clay	43 per cent	28 per cent	21 per cent
Uncoated area of clay	5.9×10^{23} Å.²	3.7×10^{23} Å.²	2.6×10^{23} Å.²
Available area per molecule	11.6 Å.²	11.6 Å²	10.8 Å.²

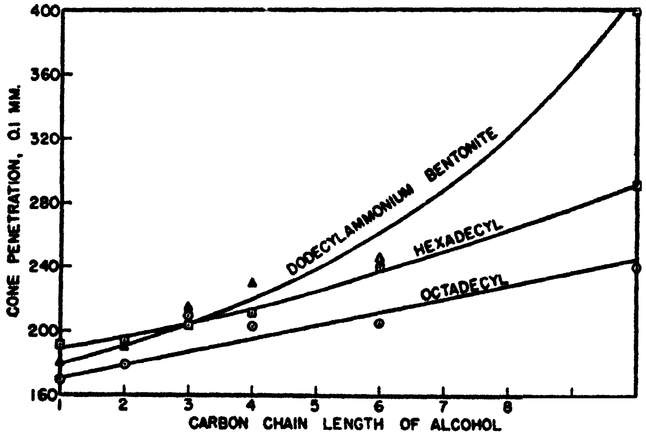

FIG. 6. Gel strengths of aliphatic ammonium bentonites in optimum toluene–alcohol mixtures.

With all three complexes gel strength maxima decrease in magnitude with increasing molecular size of alcohol. This is brought out in figure 6, which indicates gel strength as a function of carbon chain length of the alcohols in the toluene–alcohol mixtures. MacEwan (10) states that the energy of adsorption of clay for alcohols decreases with increasing molecular size of aliphatic alcohols. This was corroborated by the necessity for milling the octadecylammonium bentonite system in mixtures of toluene with alcohols higher than propyl, in order to attain stable equilibrium values. It is believed that this decrease in adsorption energy is related to the decrease in gel strengths occasioned by the use of the higher alcohols.

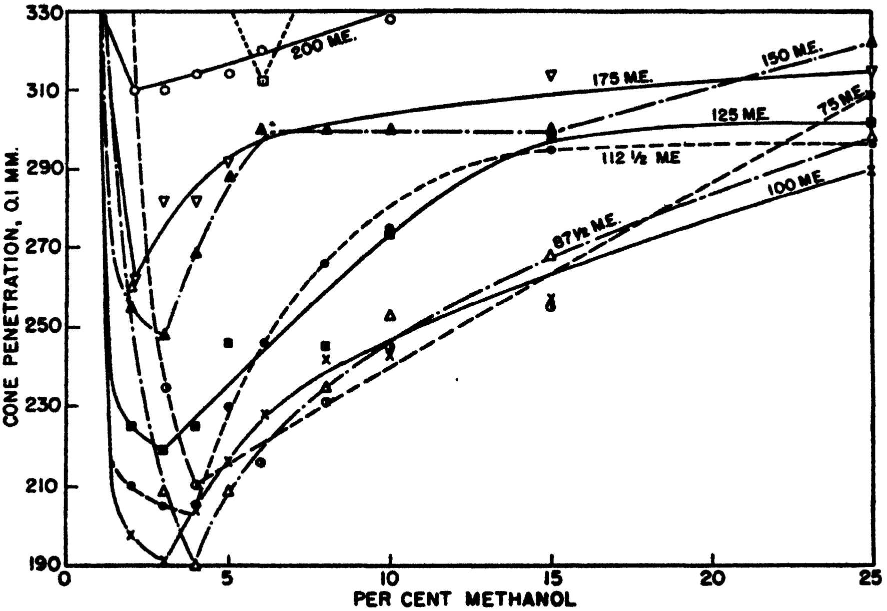

FIG. 7. Gel strengths of octadecylammonium bentonites of various amine:clay ratios in toluene–methanol mixtures (20 per cent solids).

AMINE:CLAY RATIO

For a given amine the ratio of amine to clay is an important factor in the gelling ability of the complex. Octadecylammonium bentonites were prepared by the addition of various ratios of amine acetate to centrifuged clay dispersions from 50 to 200 milliequiv. of amine per 100 g. of clay in 25 milliequiv. steps. Although the retention of amine was not complete, it was substantial, even above the cation-exchange capacity of the clay. Figure 7 depicts the gelling ability of the various complexes (noted in terms of milliequivalents of amine added per 100 g. of clay) as a function of concentration of methanol in various toluene-methanol mixtures. Optimum gels were obtained in the region of chemical equivalence of amine cation to clay anion (figure 8). Gel maxima for the various complexes decreased in regular manner as the amine:clay ratio diverged from this point, representing an amine:clay ratio of approximately 90 milliequiv. per

100 g. This substantiates the hypothesis, based on swelling data, that below the region of chemical equivalence the ionic nature of the complex together with its scantier coating of hydrocarbon material renders it relatively incompatible with the solvating medium. Beyond the region of stoichiometric proportions it is presumable that the adsorptive forces of the clay become progressively more saturated by excess adsorbed amine and consequently less capable of promoting solvation by the liquid medium.

A further observation from figure 7 is that, although the actual maximum gel strengths vary according to two intersecting curves of opposite slope (figure 8), the amount of methanol required for gel strength maxima varies as a continuous function of the ratio of amine to clay (figure 9). This falls in line with data presented in figure 2; i.e., as the surface area of the clay flakes becomes more completely coated by amine molecules, less area remains for adsorption of methanol. The fact that the methanol requirement is not eliminated in this range of high amine content is interpreted as indicating an adsorptive competition between amine and methanol for the 20 per cent of space remaining over and above that preëmpted by the amine attached through ion-exchange reaction.

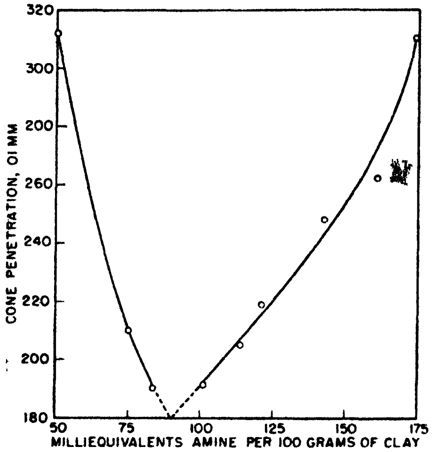

FIG. 8

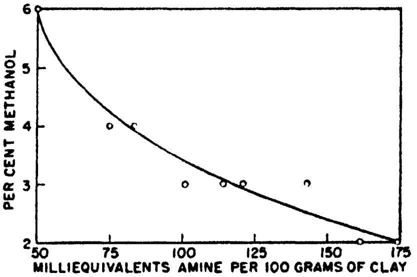

FIG. 9

FIG. 8. Gel strengths of octadecylammonium bentonites in optimum toluene-methanol mixtures (20 per cent solids).

FIG. 9. Relationship between amine:clay ratio and amount of methanol required for optimum gelation of octadecylammonium bentonites in toluene-methanol mixtures.

Debye-Scherrer x-ray photographs were made of the above octadecylammonium bentonite complexes and of related complexes covering several intermediate ratios of amine:clay. The basal plane spacings of samples, *d*(001), have been plotted in figure 10 against ratio of amine:clay as determined by Kjeldahl nitrogen analysis. On this same graph are plotted auxiliary data, e.g., per cent of basal plane area coated by amine, and separation of the platelets in Ångström units. The precision of the method is believed sufficient to warrant the discrete changes in the slope of the curve. The lowest horizontal section, at 4 Å. separation, apparently represents the situation in which less than half the surface area of the clay is coated by amine molecules lying flat with the planes of the zigzag chains parallel to the surfaces of the flakes. In the region of 50 per cent coverage, it is obviously necessary that the flakes separate by another 4 Å. distance in order to make room for a double layer of amine chains between adjacent platelets. Addition of further amine beyond the quantity necessary for complete coverage of the flakes instigates a crowding situation; in order to accommodate the crowd the amine chains must rise up on edge. The effective width of a zigzag hydrocarbon chain is computed from Pauling's (11) data as 4.9 Å. Actually, a spacing of 10.4 Å. was observed between flakes for the situation involving two layers of chains oriented edgewise on the clay surfaces. This orientation should theoretically provide space for about 25 per cent more molecules, a prediction which agrees reasonably well with observation. Further crowding must gradually force the amine molecules up on end, accounting for the next jump to a flake separation of 23–24 Å. This is in satisfactory proximity to the figure of 25 Å. computed for the length of the octadecylamine molecules. The continuous halo no doubt indicates flakes in all stages of separation, with the average increasing toward the highest amine:clay ratio, as evidenced by the disappearance of the distinct band at the 10 Å. level for the final sample. Sedletskiĭ and Yusupova (12) have found $d(001)$ values up to 28 Å. for montmorillonite clays occurring in petroliferous areas. This high spacing they attribute to adsorption of organic components from the petroleum oils in a somewhat analogous manner.

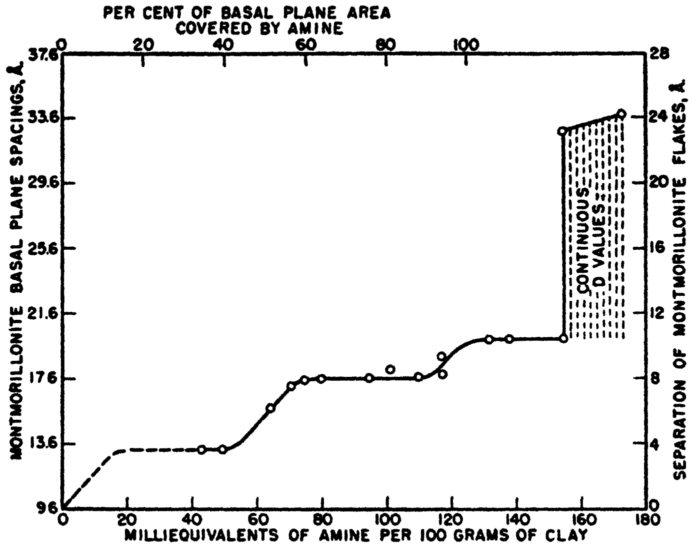

FIG. 10. Effect of increasing ratio of octadecylamine to bentonite upon basal plane spacings.

It is the opinion of the authors that the reasonable coincidence between observed and calculated data in the foregoing paragraphs would tend to refute the postulate of Johnson (5) that the exchange capacity of montmorillonite is directly related to the broken edge bonds of the clay mineral flakes. Assuming the validity of this latter picture of the base-exchange reaction, it would be difficult to interpret the spatial relationships which have been fitted together here.

QUATERNARY AMMONIUM COMPLEXES

Complexes in which the bentonite is completely clad by reaction to stoichiometric proportions with larger organic ammonium salts give general confirmation to the story which has been built up. For example, dimethyldihexadecylammonium bentonite, in which the organic portion is in 40 per cent excess of the amount necessary to provide complete monomolecular coverage of the clay mineral surfaces, will gel in toluene alone. Addition of methanol serves merely to reduce the gel strength. This suggests that the previously propounded proposition is essentially valid, i.e., that the clay complex should be entirely coated by organic matter attached through ion-exchange reaction for maximum compatibility with a nonpolar solvating organic liquid such as toluene. MacEwan (10) states that aromatic hydrocarbons are adsorbed by montmorillonite, whereas completely saturated aliphatic hydrocarbons are not. This correlates well with the spontaneous gelation of the above complex in toluene and with the much lesser gelation in mineral spirits. Apparently, residual attractive forces must remain operative between the clay and the molecules of the surrounding medium. These forces, together with a solvent effect of the liquid upon the hydrocarbon coating of the clay, are believed responsible for the dispersion and gelation which take place.

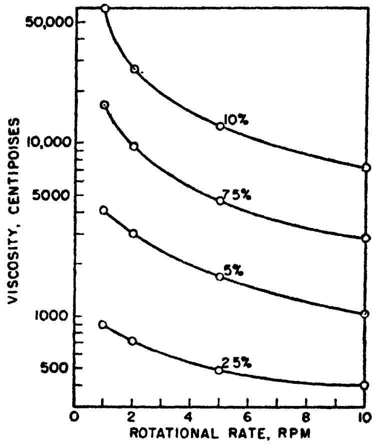

FIG. 11

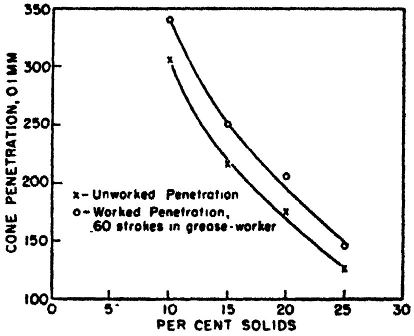

FIG. 12

FIG. 11. Viscosity of refined linseed oil containing dimethyllaurylcetylammonium bentonite, as observed with a Brookfield viscosimeter.

FIG. 12. Dimethyldioctadecylammonium bentonite in petroleum oil

In a nonpolar aliphatic liquid of low mobility and poor solvent action—light white mineral oil—externally applied mechanical energy in lieu of the energy of the system is sufficient to disperse dimethyldihexadecylammonium bentonite to produce a smooth homogeneous light-colored translucent gel (penetration 165 at 20 per cent solids). In the same liquid octadecylammonium bentonite provides only a muddy opaque slurry of low viscosity. However, the addition of 5 per cent of a polar liquid, such as butyl acetate, acetone, or butanol, converts the slurry to a stiff translucent gel with a penetration of 120.

Figure 11 illustrates the effect of dimethyldodecylhexadecylammonium bentonite upon the viscosity of refined linseed oil. Thixotropy of these dispersions was evident at all four concentrations in that, at all four spindle speeds of the Brookfield viscosimeter, the apparent viscosities decreased rather rapidly with rotation of the spindle, finally leveling off at the recorded equilibrium values.

A qualitative measure of the degree of thixotropy characteristic of the stiff gels is brought out in figure 12, which shows the effect of mechanical agitation upon the cone penetration of a 20 per cent gel of dimethyldioctadecylammonium bentonite in a petroleum lubricating oil. The agitation in this case consisted of sixty complete strokes at one per second in a standard grease worker immediately prior to determination of penetration. This effect is quite apparent in the case of thin gels of octadecylammonium bentonite in mixtures of toluene with various polar liquids.

SUMMARY

Various aliphatic ammonium bentonite complexes were made by cation-exchange reaction and gels of these materials prepared in several organic liquids and liquid mixtures. Using a grease cone penetrometer to measure gel strength, typical highly swelling liquids comprising mixtures of a nonpolar hydrocarbon (toluene) and polar aliphatic compounds (alcohols) were studied as regards factors involved in gelation. Gel strength as a criterion of liquid-binding capacity was found to be generally comparable to the swelling test used in previous work. Approximately 50 per cent coverage of the clay flakes by organic matter attached through ion-exchange reaction appeared essential for good gelation. Optimum gelation occurred in the range of complete ion-exchange reaction of clay with the organic ammonium salt. Confirmation of earlier theories as to the mechanism of solvation was afforded. Complexes characterized by complete coating of the clay flakes were gelled in single nonpolar liquid systems, and the thixotropy of such gels was illustrated.

The authors wish to express their indebtedness to E. A. Hauser and R. E. Grim for helpful suggestions and to members of the Brooklyn and Baroid Sales Division Laboratories of the National Lead Company for their coöperation. To E. W. Tillotson, Assistant Director of the Mellon Institute, is extended appreciation for his friendly counsel.

REFERENCES

(1) Bradley, W. F.: J. Am. Chem. Soc. **67**, 975–81 (1945).
(2) Graham, R. P., and Sullivan, J. D.: J. Am. Ceram. Soc. **21**, 176–83 (1938).

(3) HAUSER, E. A.: Private communication.
(4) HENDRICKS, S. B.: J. Phys. Chem. **45**, 65–81 (1941).
(5) JOHNSON, A. L.: J. Am. Ceram. Soc. **32**, 210–14 (1949).
(6) JORDAN, J. W.: J. Phys. & Colloid Chem. **53**, 294–306 (1949).
(7) JORDAN, J. W.: Mineralog. Mag. **28**, 598–605 (1949).
(8) MACEWAN, D. M. C.: Nature **154**, 577–8 (1944).
(9) MACEWAN, D. M. C.: Nature **157**, 159 (1946).
(10) MACEWAN, D. M. C.: Trans. Faraday Soc. **44**, 349–67 (1948).
(11) PAULING, L.: *The Nature of the Chemical Bond.* Cornell University Press, Ithaca, New York (1948).
(12) SEDLETSKIĬ, I. D., AND YUSUPOVA, S. M.: Compt. rend. acad. sci. U.R.S.S. **46**, 27–30 (1945).

SPECTROPHOTOMETRIC DETERMINATION OF DISPLACEMENT SERIES OF METAL COMPLEXES OF THE SODIUM SALTS OF ETHYLENEDIAMINETETRAACETIC ACID[1]

ROBERT C. PLUMB,[2] ARTHUR E. MARTELL, AND F. C. BERSWORTH[3]

Department of Chemistry, Clark University, Worcester, Massachusetts

Received November 14, 1949

Ethylenediaminetetraacetic acid is a white crystalline amino acid with four replaceable protons. The di-, tri-, and tetrasodium salts of this acid react with metal ions such as lead, zinc, cadmium, chromium, cobalt, nickel, copper, and the alkaline earth metals to form stable complexes which resist the action of most of the agents which precipitate these metals. Discussion of this complex-forming action has appeared in various papers (1, 2). The order of stability of these various metal complexes in buffered solutions is the subject of this paper. Of the alkaline earth metals, only calcium has been included in this displacement series, since calcium, barium, strontium, and magnesium have already been thoroughly investigated by Schwarzenbach (2).

EXPERIMENTAL

Purification of ethylenediaminetetraacetic acid: The pure acid was obtained by acidifying the tetrasodium salt to a pH of 1.2, collecting the precipitate, washing it with hot water, and recrystallizing it from hot water.

Standard solutions of the sodium salt were prepared from weighed quantities of the acid dissolved in carbonate-free sodium hydroxide solution.

Preparation of 0.1000 M metal salt solutions: Solutions of calcium, cadmium, zinc, cobalt, nickel, and cupric chlorides were prepared and were standardized with silver nitrate, using fluorescein as indicator. In standardization, sufficient sodium bicarbonate solution was added to the sample to precipitate the metal as carbonate and to regulate the acidity. The chromic chloride solution was standardized by converting the chromic ion to chromate in alkaline solution and precipitating the chromate with lead acetate; then the chloride ion was titrated. After standardization, the concentration of each metal solution was adjusted to 0.1000 *M*. In the case of lead, lead carbonate was used as a standard and dissolved in hydrochloric acid to produce a 0.0333 *M* solution.

---

[1] Read by Dr. John J. Singer, of the Bersworth Chemical Company, at the 1949 Fall Meeting of the American Oil Chemists' Society, which was held in Chicago, Illinois.

[2] At present a graduate student in the Department of Chemistry, Brown University, Providence, Rhode Island.

[3] Address: Bersworth Chemical Company, Framingham, Massachusetts.

Preparation of buffer solutions: The buffers used are shown in table 1. Each buffer system was prepared by adding carbonate-free sodium hydroxide to the more acidic component of the system. These buffer solutions permitted measurements to about 222 mμ in the ultraviolet.

Preparation of complexes and blanks: The concentration used for all complexes was 0.01 *M*. However, more dilute solutions were measured in order to check conformance to Beer's law. In the concentration range of 0.001 *M* to 0.01 *M*, Beer's law was found to hold fairly closely.

TABLE 1

Buffers used

pH	SYSTEM
11.00	0.200 *M* Na_2HPO_4–Na_3PO_4
8.65	0.200 *M* $NaHCO_3$–Na_2CO_3
6.50	0.200 *M* NaH_2PO_4–Na_2HPO_4
4.00	0.200 *M* CH_3COOH–CH_3COONa

The pure metal complexes were prepared by combining equal volumes of equivalent concentrations of a metal chloride solution and a salt of ethylenediaminetetraacetic acid in a volumetric flask. The solution was diluted to the proper volume with the buffer.

Colored mixed metal complexes were prepared in the same manner, except that one volume of each of two metals was used. Noncolored mixed metal complexes at pH 8.65 were prepared just as the colored mixed metal complexes, except that an amount by weight of sodium carbonate equivalent to that precipitated as the normal metal carbonate was added to correct the carbonate content.

The blank solution for measurements in the ultraviolet consisted of a volume of distilled water, equivalent to the total volume of metal and complex-forming agent used, made up to the proper volume with buffer. Distilled water was used as a blank in the visible region.

Attainment of equilibrium: With the exception of the chromic complex, all solutions which did not have a solid phase reached color equilibrium within a few hours. The chromic complex required 1 week to develop its full color. The mixed complex systems which involved a solid phase required about 2 weeks of shaking to reach equilibrium.

Measurement of solutions: Measurements were made on a Beckman Model D.U. quartz spectrophotometer. Each solution was filtered through a sintered-glass funnel just before introduction into the absorption cell.

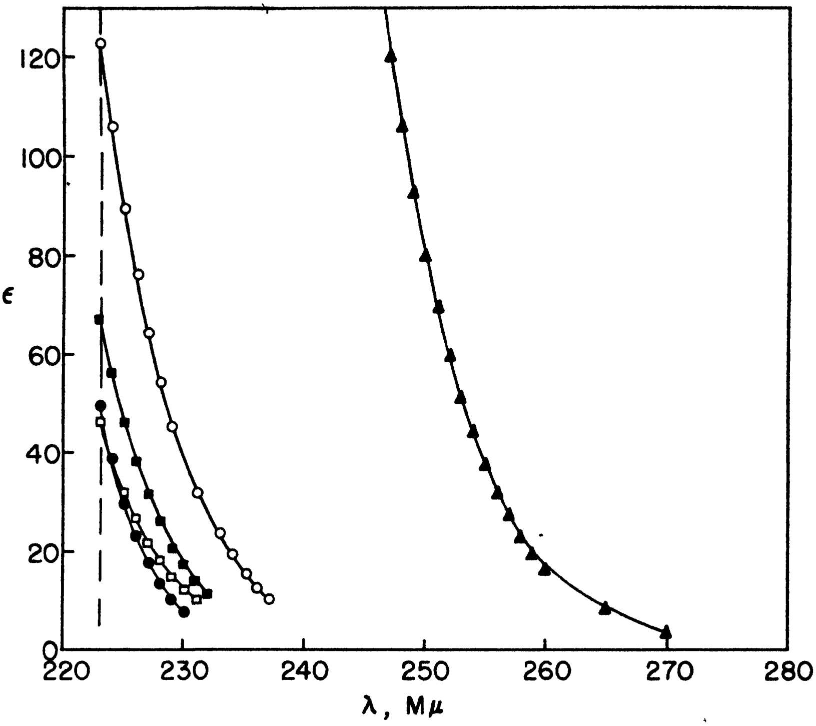

FIG. 1. Absorption spectra of the sodium salt of ethylenediaminetetraacetic acid (▲) and of the complexes formed by this acid with zinc (○), magnesium (■), cadmium (□), and calcium (●).

RESULTS

Indication of complex formation

The absorption spectrum (molar extinction coefficient *vs.* wave length) of the sodium salt of ethylenediaminetetraacetic acid is shown in figure 1, together with that of the calcium, magnesium, cadmium, and zinc complexes. Although the absorption maximum could not be reached, there seems to be a shift towards the ultraviolet. The absorption spectra at pH 4.00 of cobalt, nickel, and cupric chlorides and of the complexes formed from these ions and ethylenediaminetetraacetic acid are shown in figure 2.

At pH values of 6.5 and higher, when no complex-forming agent was present, the cobalt, nickel, and cupric ions precipitated as phosphates, carbonates, or hydroxides, depending upon the buffer solution and the metal, so that no spectra for the metals alone were apparent. However, the complexes are soluble and have characteristic absorption spectra.

The presence of absorption bands not due to the metals alone and the displacement of absorption towards the ultraviolet may be interpreted as an indication of complex formation. These interpretations, when applied to the spectra obtained, lead to the results tabulated in table 2.

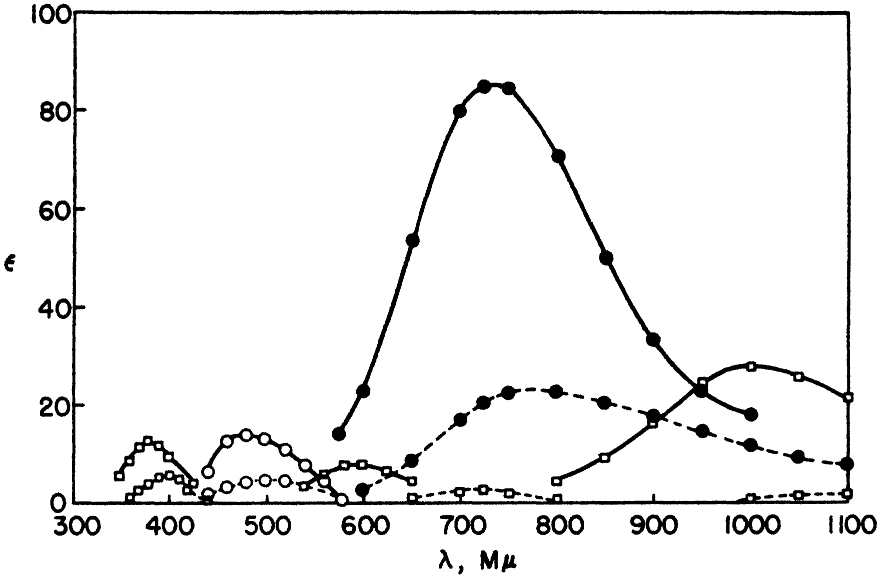

FIG. 2. Absorption spectra at pH 4.00 of the chlorides (- - -) of cobalt, nickel, and copper and of the complexes (—) formed from these ions and ethylenediaminetetraacetic acid: ○, cobalt; □, nickel; ● copper.

TABLE 2

*Complex formation at different pH values**

pH	Ca	Mg	Cd	Zn	Co	Ni	Cu	Cr
4.00	o	o	o	o	x	x	x	x
6.50	x	o	x	x	x	x	x	x
8.65	x	x	x	x	x	x	x	x
11.00	x	x	x	x	x	x	x	x

* x indicates complex formation; o indicates little, if any, tendency for complex formation.

Displacement series

Figure 3, a graph of the absorption spectra for the nickel–cobalt mixed complex system, is typical of the curves for mixed complexes showing bands characteristic of each. The amount of each present at equilibrium was calculated by means of the following equation and data at two wave lengths:

$$(E_{n\alpha} - E_{n\gamma})C_{\alpha} + (E_{n\beta} - E_{n\phi})C_{\beta} = d_n\text{-}(E_{n\gamma} + E_{n\phi})G$$

where d is the observed optical density of the mixed complex system,
G is the molarity of either metal or of the complex-forming agent,
α is metal 1 which is in a complex,
β is metal 2 which is in a complex,
γ is metal 1 which is not in a complex,
ϕ is metal 2 which is not in a complex,
E is the extinction coefficient of each component of the system,
C is the concentration of each component of the system, and
n is the wave length at which measurements are made.

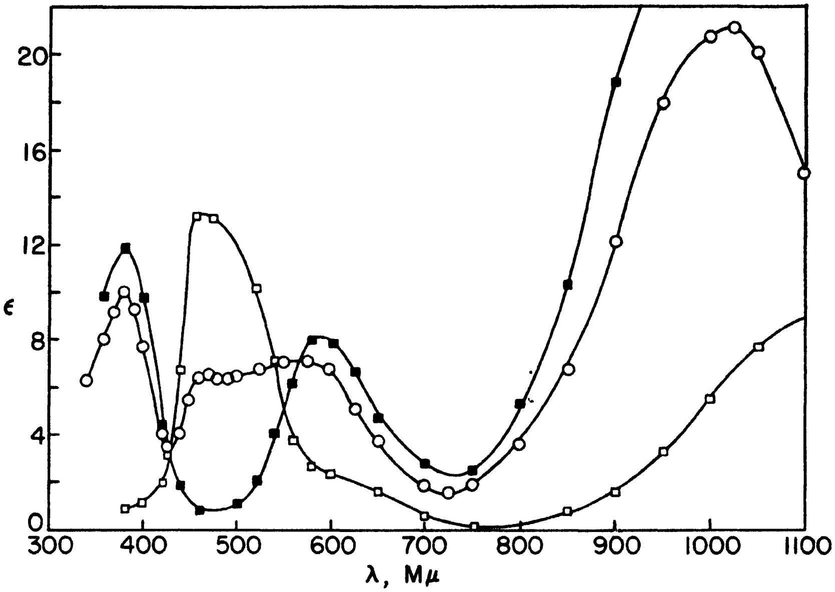

FIG 3. Absorption spectra at pH 6.50 of complexes formed from ethylenediaminetetraacetic acid: ○, cobalt-nickel mixed complexes; □, cobalt complex; ■, nickel complex.

TABLE 3

Wave lengths used in calculating the amount of each complex present

COMPLEX	λ
	mμ
Cobalt	460
Nickel	380, 1000
Copper	750
Chromium	560

The above equation is easily derived from the following relationships:

$$d = E_\alpha C_\alpha + E_\beta C_\beta + E_\gamma C_\gamma + E_\phi C_\phi \qquad (1)$$

$$C_\alpha + C_\gamma = G \qquad (2)$$

$$C_\beta + C_\phi = G \qquad (3)$$

Relationship 1 is Beer's law for a four-component system. Relationships 2 and 3 merely state that all of the metal is either combined in a complex or it is not.

The wave lengths shown in table 3 were found to be satisfactory for the calculation of the amount of each complex present.

The results of calculations by this equation were checked by the relationship $C_\alpha + C_\beta = G$. The mean deviation for this check was 1.5 per cent.

In cases where a mixed complex system of one colored and one noncolored complex was investigated, only one wave length was used in the calculations, since absorption by the colored complex completely masked absorption by the noncolored complex.

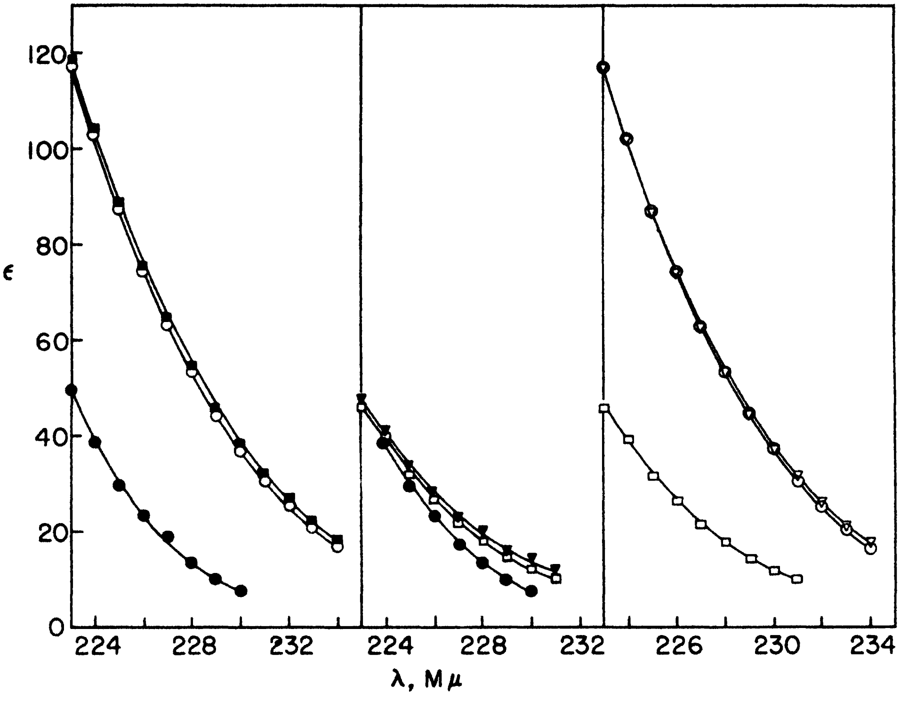

FIG. 4. Absorption spectra at pH 8.65 of complexes formed from ethylenediaminetetraacetic acid· □, cadmium complex; ○, zinc complex; ●, calcium complex; ■, zinc-calcium mixed complexes; ▽, zinc-cadmium mixed complexes; ▼, calcium-cadmium mixed complexes.

At the high pH values, there was an insignificant amount of cobalt, nickel, and cupric ions in equilibrium with the complexes, so that they did not contribute to the density and thus simplified the equation to Beer's law for a two- or three-component system.

At pH 8.65 noncolored mixed complexes of cadmium–calcium, zinc–calcium, and cadmium–zinc were investigated. The results are shown in figure 4. No calculations were made on this data, but examination of the curves shows that the calcium–zinc curve approximates the curve for the pure zinc complex, the calcium–cadmium curve approximates the curve for the pure cadmium complex, and the zinc–cadmium curve approximates the curve for the pure zinc complex. Thus, we may conclude that at pH 8.65 Zn > Cd > Ca, where the inequality signs indicate a power of 10 or more.

The relative strengths of complex formation under the given experimental conditions are best expressed by means of the ratio of the concentration of one metal complex to the concentration in equilibrium with it of an arbitrarily standard metal complex. Thus, the strength S is defined as follows:

$$S = 100 \times \frac{\text{amount of metal 1 combined in a complex}}{\text{amount of metal 2 combined in a complex}}$$

The standard here is taken as the copper complex.

The results of the above methods of calculation as applied to each system at each pH are given in table 4.

The relative formation constants for the reaction of the disodium salt of ethylenediaminetetraacetic acid (pH 4.0) with the divalent metals copper, nickel, lead, and cobalt have been calculated. The ratio of the formation constant of the nickel complex to that of the copper complex is 0.152, of the lead complex to the copper complex is 0.0740, and of the cobalt complex to the copper complex is 0.00792.

TABLE 4

Relative strengths of complex formation

METAL	pH 4.00	pH 6.50	pH 8.65	pH 11.00
Chromium	302			<Cd
Copper	100	100	100	100
Nickel	39.0	109	419	170
Lead	27.2			
Cobalt	8.9	83.3	101	213
Zinc		1	28.2	<Cd
Cadmium		1	<Zn	80
Calcium		<Cd, Zn	<Cd	

This order of stability of the complexes of the heavy metals is the same as that which has been observed by other investigators for other complex-forming agents (3, 4, 5).

The results shown in table 4 for the high pH values are a measure of the tendency for complex formation in the given buffer solutions. There are other equilibria competing with the complex formation for the metal ions at the high pH values. These equilibria involve the precipitated hydroxides, phosphates, and carbonates and, in the cases of zinc and chromium, the soluble zincates and chromites.

SUMMARY

The ultraviolet and visible absorption spectra of the sodium salts of ethylenediaminetetraacetic acid and of some of its metal complexes have been deter-

mined at pH values of 4.0, 6.5, 8.65, and 11.0. The pH was controlled by preparing the complexes in buffer solutions. The absorption spectra of similarly buffered solutions containing one equivalent each of two metals and one equivalent of the complex-forming agent have been determined. The results of these two sets of data have been combined to evaluate the displacement series of the metal complexes in the given buffer solutions.

REFERENCES

(1) Irving and Williams: Nature **162,** 746 (1948).

(2) Mellor and Maley: Nature **159,** 370 (1947).

(3) Mellor and Maley: Nature **161,** 436 (1948).

(4) Pfeiffer and Simons: Ber. **76,** 847 (1943).

(5) Schwarzenbach and Ackermann: Helv. Chim. Acta **31,** 1029 (1948).

THE VISCOSITY OF SULFUR VAPOR

GEORGE A. DALIN

Stauffer Chemical Company, New York, New York

AND

JAMES R. WEST

Mellon Institute of Industrial Research, Pittsburgh, Pennsylvania

Received December 5, 1949

INTRODUCTION

A search of the literature has indicated that the viscosity of sulfur vapor has never been measured. This information is needed especially for calculations of engineering design. The data are also of physicochemical interest, particularly because sulfur should deviate from the general rule that the viscosities of most gases increase slowly with increasing temperature. In addition, the viscosity should vary with pressure, which also is unusual. These anomalies are, of course, attributable to the fact that sulfur vapor dissociates strongly at a relatively low temperature, the degree of dissociation being sensitive to both temperature and pressure.

The experimental determination of the viscosity of sulfur is somewhat awkward, because the boiling point of sulfur is only slightly below the softening point of Pyrex glass and also because its vapor is so corrosive to most metals. On the other hand, a number of methods are available for estimating the viscosity of gases. Licht and Stechert (2) have reviewed these procedures and have shown that the Sutherland equation (4) yields results which are usually within 1 per cent of experimental values in those cases in which the comparison has been made.

In the investigation recorded in this paper, the viscosity of sulfur vapor has been estimated by means of Sutherland's equation in the form set forth by Licht and Stechert and also by means of the correlation suggested by Uyehara and Watson (5). The determination of one experimental value is also described.

EXPERIMENTAL

In determining the viscosity of a gas by the capillary method, it is customary to use tubes in which the ratio of length to diameter is of the order of several hundred. For shorter capillaries, the gain and loss of kinetic energy at the ends of the capillary introduce errors which become apparent as deviations from linearity when the log of the rate of flow is plotted against the log of the pressure drop across the capillary. However, the deviations become negligible, at least for the purposes of this work, when the flow rate is small. It therefore has been possible to use short tubes and correspondingly small equipment.

Figure 1 shows the apparatus employed. The quartz heating mantle[1] has a short coil in the base which vaporizes the liquid sulfur. The input to the upper coil is adjusted so that the thermocouple in the well gives the boiling point of sulfur at the applied pressure. This is principally a matter of eliminating heat transfer by radiation between the mantle and the sulfur. The heat input to the boiler is adjusted so that the nitrogen–sulfur interface, which is well defined, is located at about the middle of the chimney. The chimney is surrounded by a draft jacket to keep the walls above the melting point of sulfur and to avoid crystallization in the upper part of the chimney.

Condensation is quite rapid, so that a considerable flow of vapor up the chimney must be maintained to keep the interface at the desired level. Nitrogen cannot diffuse upstream into the sulfur vapor chamber and consequently no nitrogen passes through the capillary.

A number of capillaries were tested, and two which yielded flow rates in a convenient range were selected. These dimensions were as follows:

CAPILLARY	LENGTH	RADIUS
	cm.	*cm.*
No. 1	5.8	0.0167
No. 13	7.0	0.0239

The pressure was maintained by means of an "industrial type" manostat.[2] The pressure was read in the low ranges on a water manometer and in the high ranges on a mercury manometer. All values are given in millimeters of mercury.

The sulfur vapor, after passing through the capillary, is conducted through an exit tube which is surrounded by a nichrome-wound glass heating jacket, maintained at a temperature high enough so that no condensation takes place before the vapor enters the receiver. Condensation in the receiver is complete, except for a very small quantity of sulfur lost as fog at the beginning of each determination.

---

[1] Manufactured by Glas-Col Apparatus Co., Inc., Terre Haute, Indiana.

[2] Manufactured by Emil Greiner Company, New York, New York.

To make a determination, heat is supplied to the three coils, the inputs being set at previously determined values. The nitrogen pressure is gradually raised to the desired value, and the input to the boiler is increased correspondingly to keep the interface at about the middle of the chimney.

As soon as the pressure is raised, sulfur begins to pass through the capillary into the extra large receiver which is placed at the exit tube during the period of adjustment. Conditions are kept constant for about 5 min. before measurements are made. The spare receiver is then removed, and a weighed receiver is quickly placed in contact with the joint. A stopwatch is started at the same time. After enough sulfur has collected, the receiver is quickly removed. Conditions are adjusted so that at least 0.2 g. of sulfur is collected during a period of at

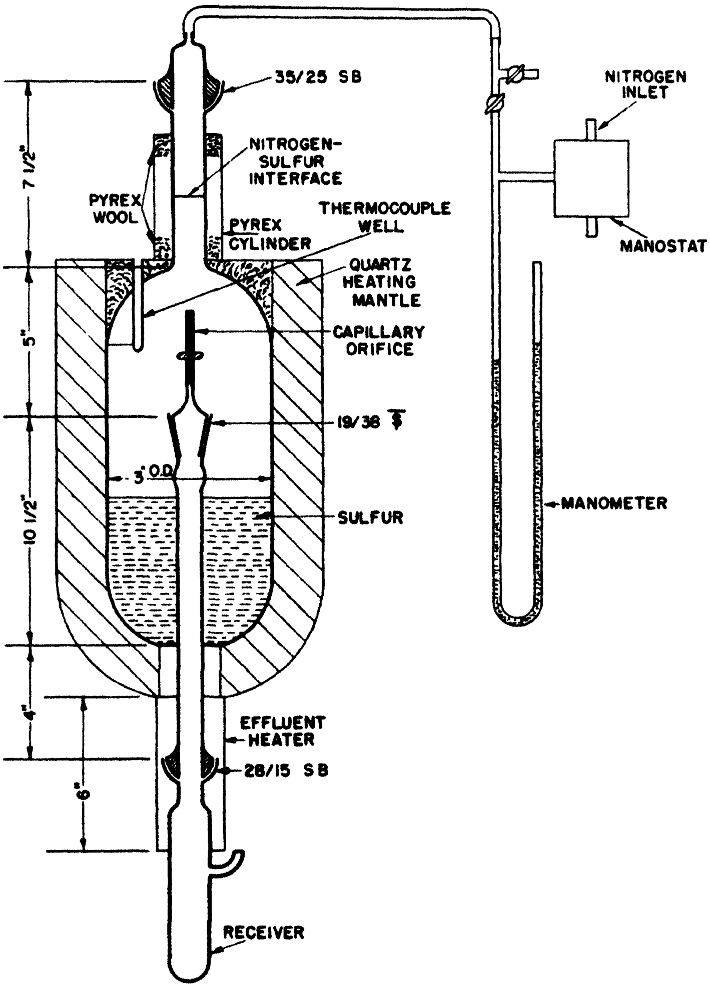

FIG. 1. Apparatus used in determining the viscosity of sulfur vapor by the capillary method

least 1 min. If desired, a second receiver can then be placed on the exit tube for a duplicate determination.

Upon removal of the receiver, a glass tube, sealed at the upper end and fitted with a proper joint, is immediately put over the receiver as a stopper. The joint and the upper part of the receiver are first cooled in an air-blast, and then under a water tap to room temperature, after which the tube is dried and weighed. Tubes can be used for fifteen or twenty determinations before the level of sulfur rises too high. The error in measuring the time was approximately 2 per cent. The reproducibility of the feed rates was usually better than 1 per cent. The principal error at very low pressures was caused by fluctuations in the manostat, which could probably be minimized by the introduction of a surge tank.

Poiseuille's law states that:

$$V = \frac{pr^4}{8l\eta}t \quad \text{or} \quad \mathrm{d}V/\mathrm{d}t = kp$$

where V = volume of flow in time t,
p = pressure drop across the capillary,
r = radius of capillary,
l = length of capillary,
η = viscosity, and
k = $r^4/8l$.

Assuming that the volume flow rate is proportional to the weight flow rate,

$F = Kp$, where F = weight flow in time t,
$\ln F = \ln K + \ln p$, and
$\mathrm{d} \ln F/\mathrm{d} \ln p = 1$

Also:

$$\mathrm{d} \log F/\mathrm{d} \log p = 1$$

The plot of p against F on log-log paper should therefore have a 45° slope. As can be seen from figure 2, as the pressure is decreased, the curves become linear and approach the proper slope. The linearity reveals that the end effects are negligible. The 45° slope indicates that the volume change caused by the increased pressure and the viscosity change caused by the increased pressure and the thereby increased temperature are also negligible.

The viscosities obtained from these data are as follows: capillary No. 1, 0.0195 centipoise; capillary No. 13, 0.0199 centipoise. The temperature is assumed to be 445°C.

CALCULATIONS

According to Preuner and Schupp (3), sulfur vapor consists of octatomic, hexatomic, and diatomic molecules in the temperature range between the melting and the critical points. The assumption was made that the average viscosity could be obtained from the following equation:

$$\eta = y_8\eta_8 + y_6\eta_6 + y_2\eta_2$$

where y_n refers to mole fractions of the molecular species and η_n refers to the respective viscosities. Values for y were taken from the data of Preuner and Schupp (3). Values of η for each molecular species were calculated by the following methods:

Method A

Equation 15 from the work of Licht and Stechert (2) is

$$\eta = 6.30 \times 10^{-6}\, Gf(T_r)$$

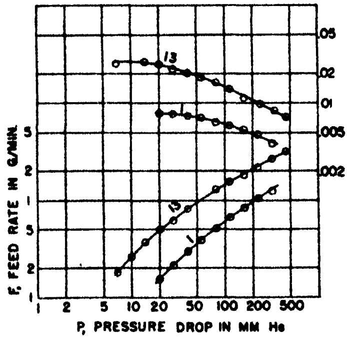

FIG. 2

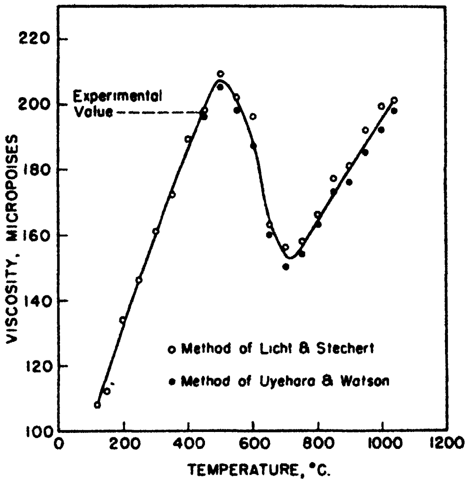

FIG. 3

FIG. 2. Calibration of capillaries
FIG. 3. Calculated viscosity of sulfur vapor

where η = the viscosity in poises,
M = the molecular weight,
P_c = the critical pressure = 116 atm. (5),
T_c = the critical temperature in °K. = 1040°C. (1),
T_r = the reduced temperature,

$$G = \left(\frac{M^3 P_c^4}{T_c}\right)^{1/6}, \quad \text{and}$$

$$f(T)_r = \frac{T_r^{3/2}}{T_r + 0.8}.$$

Method B

The viscosity of sulfur vapor at the critical point was estimated by means of equation 6 from the work of Uyehara and Watson (5):

$$\eta_c = \frac{7.7 M P_c^{2/3}}{T_c^{1/6}}$$

Then values of the reduced viscosity, η_r, were read from figure 1 of this reference. Next, the viscosity of each species was estimated from the product, $\eta_c\eta_r$. Finally, the average viscosity was derived as explained previously. Because it was difficult to read this chart below the normal boiling point of sulfur, no values below 445°C. were computed by this method.

RESULTS

The results obtained by means of these two methods are tabulated in table 1 and pictured in figure 3. All values of the viscosity at and above the normal boiling point were estimated at 1 atm. total pressure; below the normal boiling point, at the vapor pressure of sulfur.

TABLE 1

Average viscosity of sulfur vapor

TEMPERATURE	AVERAGE VISCOSITY	
	From Licht and Stechert	From Uyehara and Watson
°C.	*micropoises*	*micropoises*
120	108	
150	112	
200	134	
250	146	
300	161	
350	172	
400	189	
444.6 (boiling point)	197	196
450	198	
500	209	205
550	202	198
600	196	187
650	163	160
700	156	150
750	158	154
800	166	163
850	177	175
900	181	176
950	192	185
1000	199	192
1040 (critical point)	201	198

Licht and Stechert (2) found, in general, that their equation was reliable within 5–10 per cent, except for ethyl alcohol, water, ammonia, and helium. Likewise, Uyehara and Watson (5) observed that their method gave deviations of less than 10 per cent, except in translating between liquid- and gas-phase viscosities at low temperatures.

DISCUSSION OF RESULTS

The experimental value of the viscosity of sulfur vapor at its normal boiling point, 197 micropoises, compares very favorably with the one calculated by the method of Licht and Stechert, 197 micropoises, and also with that computed by the method of Uyehara and Watson, 196 micropoises. This agreement may be fortuitous or real. In either case, more experimental work is needed. Because no such work is contemplated and because of the great interest in the properties of sulfur and the need for such data in engineering computations, the authors feel that their results should be presented at this time. It is suggested that the problem merits consideration as a thesis subject for a university graduate student.

The curve illustrated in figure 3 is S-shaped, even though the viscosity of each individual species is increasing with rising temperature, as is the case for gases. But, because the species which predominated at higher temperatures has the lowest computed value of viscosity at any temperature and because of the variation in these molecular species with temperature (6), the average curve exhibits the phenomenon shown.

SUMMARY

By means of the capillary method the viscosity of sulfur vapor was measured at its boiling point. The experimental value was found to agree with the calculations by two empirical methods. Computed results are presented for other temperatures.

The authors are indebted to the Stauffer Chemical Company and to the Texas Gulf Sulphur Company for permission to publish these data. For helpful advice and constructive criticism thanks are given to J. F. Crowther of the Stauffer Chemical Company, to W. W. Duecker of the Texas Gulf Sulphur Company, and to W. A. Hamor of the Mellon Institute of Industrial Research.

REFERENCES

(1) *International Critical Tables*, McGraw-Hill Book Company, Inc., New York (1927).
(2) Licht, W., Jr., and Stechert, D. G.: J. Phys. Chem. **48**, 23 (1944).
(3) Preuner, G., and Schupp, W.: Z. physik. Chem. **68**, 129 (1909).
(4) Sutherland, W.: Phil. Mag. **36**, 507 (1893).
(5) Uyehara, O. A., and Watson, K. M.: Natl. Petroleum News **36**, No. 40, R714 (1944).
(6) West, J. R.: Ind. Eng. Chem. **42**, 713 (1950).

AN IMPROVED SPREADING APPARATUS FOR THE MEASUREMENT OF FILM PRESSURES

J. W. Y. HEYNIS AND L. MAASKANT

Research Laboratory of A.K.U. and Affiliated Companies, Arnhem, Holland

Received December 15, 1948

I. INTRODUCTION

The study of monomolecular layers has contributed to the solution of many problems of scientific, medical, and industrial importance. The apparatus constructed by Gorter and Seeder (3) for the measurement of film pressures has especially proved its merits in this field of investigation.

In several details, however, this apparatus could be improved. The necessity for these improvements is apparent when the apparatus is used for routine work,[1] where equipment of solid construction, offering simplicity of handling while retaining speed and accuracy of measurement, is required.

II. THE APPARATUS OF GORTER AND SEEDER

For further elucidation of the modifications which have been introduced by the authors a schematic drawing of the apparatus of Gorter and Seeder is given in figure 1. In this apparatus film pressures are transmitted to the balance by means of a freely movable, paraffin-waxed metal strip (called a swimmer (C)), which floats on the surface of a liquid in a shallow rectangular trough. The swimmer is connected by two thin, flexible, finely rolled platinum strips (P_1, P_2) to the edge of the trough. These strips allow the swimmer sufficient freedom to make it possible to measure the forces acting on it.

When pressure is exerted by a film placed between the glass rod (Z) and the swimmer, the balance can be adjusted to its zero position by the torsion of a spring (Sp). The amount of torsion is read on a scale (S).

The deviations of the balance are made visible by an optical system. For this purpose a mirror is fixed on the axis of the balance. The light beam first passes through a slit O and is reflected in a mirror M; the image of the slit is projected on an adjustable scale (S_1).

The use of this optical system implies that the measurements take place preferably in a semidark room. Moreover, the continual readjustment of the light beam caused by slight dislocations takes time and impedes continuous work.

For a more detailed description of the apparatus of Gorter and Seeder, its handling, the spreading technique, etc., reference should be made to the papers by Gorter and Seeder (3) and van Ormondt (5).

III. MODIFIED APPARATUS

In the apparatus as modified by the authors the following principles are embodied: (*a*) The devices for zero adjustment of the balance and for measuring the film pressures on a scale are brought into one plane in front of the apparatus at a normal viewing distance. (*b*) A less vulnerable construction is achieved by encasing the balance, thus at the same time keeping it dust-free and to a certain extent humidity-free. (*c*) The devices for manipulation are made as easily accessible as possible. These improvements are illustrated in the schematic drawing (figure 2) and the photographs of the apparatus (figures 3, 4, and 5).

---

[1] Reference may be made to the application of the spreading method for microquantitative determinations (1, 2, 4).

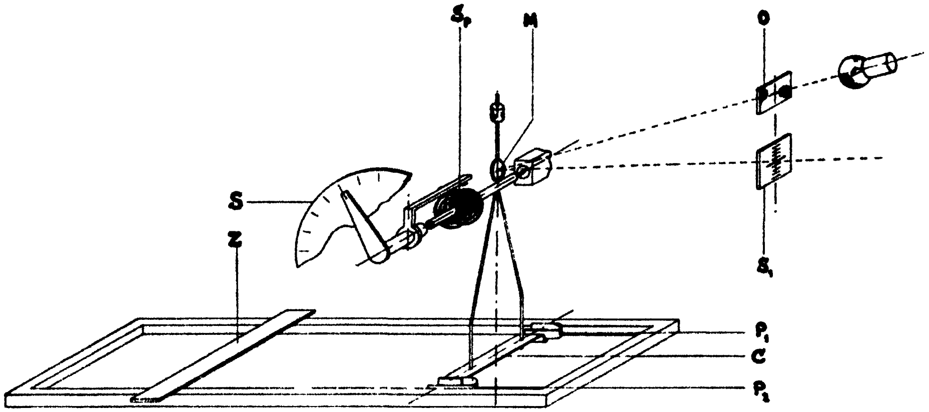

FIG. 1. Schematic drawing of the spreading apparatus of Gorter and Seeder

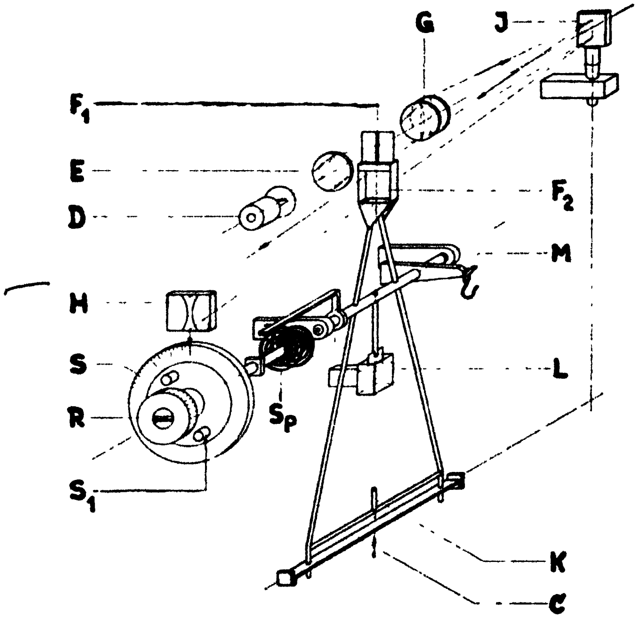

FIG. 2. Schematic drawing of the balance and its optical system

A. The optical system

The operation of the optical system (figure 2) is as follows: A bulb (D) with a strong convex lens (E), both assembled in a container, provides the lighting of the slit in the thin metal plate (F_1) fixed on the balance. Behind F_1 a double condensor (G) is mounted in such a way that the image of the slit in F_1 is reflected *via* the mirror (J) through the window (F_2) on the frosted glass (H). The distances F_1G and GJH relate as 1:20, so that a small dislocation of F_1 causes a considerable movement of the slit projection. On the frosted glass (H) arcs are scratched, and a dislocation of the light-line in the point of contact of the arcs of 0.1–0.2 mm. is very easily perceptible. As a consequence, the accuracy of adjustment of the swimmer (C) will be about 10 μ.

B. Balance construction

In our construction the same type of differential balance as in the apparatus of Gorter and Seeder was used. The following practical modifications were introduced (figure 2):

(*1*) The axes of the balance and of the knob (R) attached to the scale (S) have an independent bearing and are linked by two springs (Sp). As a consequence of the independent bearing, manual movements of the knob are transmitted only by the spring-linking and this guarantees smooth functioning of the balance. As in Gorter's apparatus, for the sake of linearity two springs are mounted with the spiral windings in opposite directions.

(*2*) To slow down the movements of the balance without diminishing the sensitivity an oil damper (L) is inserted. The damping effect may be varied by pushing the oil tube up or down.

(*3*) For the calibration of the balance a small side arm (M) is inserted, the length of which is one-fifth of the distance between the swimmer (C) and the balance axis. The calibration can be carried out by placing weights on a small scale, which may be hung on the hook of M. It is important that the balance can be tested while the apparatus is in condition for use. The sensitivity of the balance is 0.02 dyne/cm./scale degree.

(*4*) At the beginning of a measurement the zero index of the scale must correspond with the zero position of the balance. This can be effected by an independent turning of the scale with the aid of little knobs (S_1) attached to the scale.

(*5*) The stability of the balance can, if necessary, be increased by placing weights on the small pin (K) which passes through the hole of the weight. This pin is fixed on the horizontal arm of the balance.

The fitting of the lower part of the balance in the trough is similar to that in the apparatus of Gorter and Seeder.

P_1P_1 are platinum strips connecting the swimmer (C) with small metal blocks (P_2). These metal blocks are attached by a spring to the frame of the balance in such a way that they are pressed against the edge of the trough when the apparatus is in condition for measurement (figure 3).

C. The encasing of the balance and further particulars of the apparatus

Figures 3, 4, and 5 show the apparatus in different positions.

Figure 3 shows the balance box turned to the left. The balance with the inserted optical system is encased in the metal box N, which may be opened by lifting the lid (N_1).

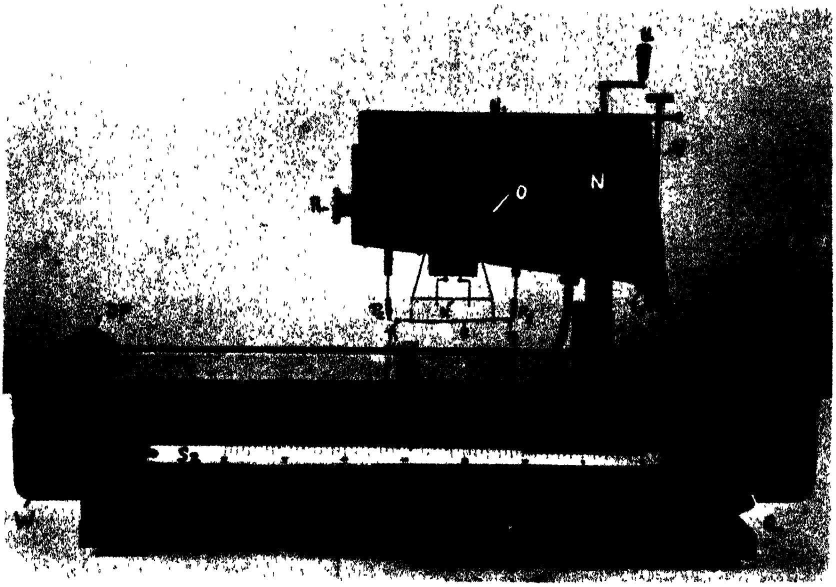

Fig 3. The balance box turned to the left

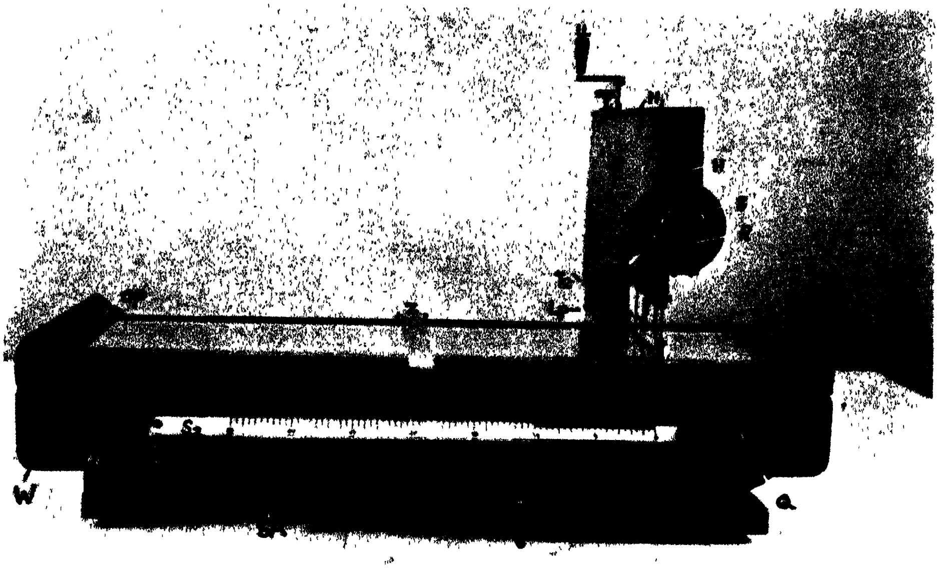

Fig. 4. The apparatus ready for measurements

By removing the protecting hood (O) the side arm (M, figure 2) appears for the calibration of the balance. With device P (figure 4) the damping can be regulated as described under Section III, B.

The balance box can be turned to the left around the vertical axis of a column (figure 3). By turning it back the box is stopped by the ridge T_1, which hits the lower part of the column (Lp). The box is then at right angles to the trough. In this position the balance box can be lowered by turning the crank U until the long screw V collides with the lower part of the column.

Figure 4 shows the apparatus ready for measurement. The swimmer floats on the surface of the liquid. The ridge (T_2) prevents the balance box from moving to the left. The glass trough is fixed in a stainless-steel gutter, the brim of which lies lower than the upper side of the trough.

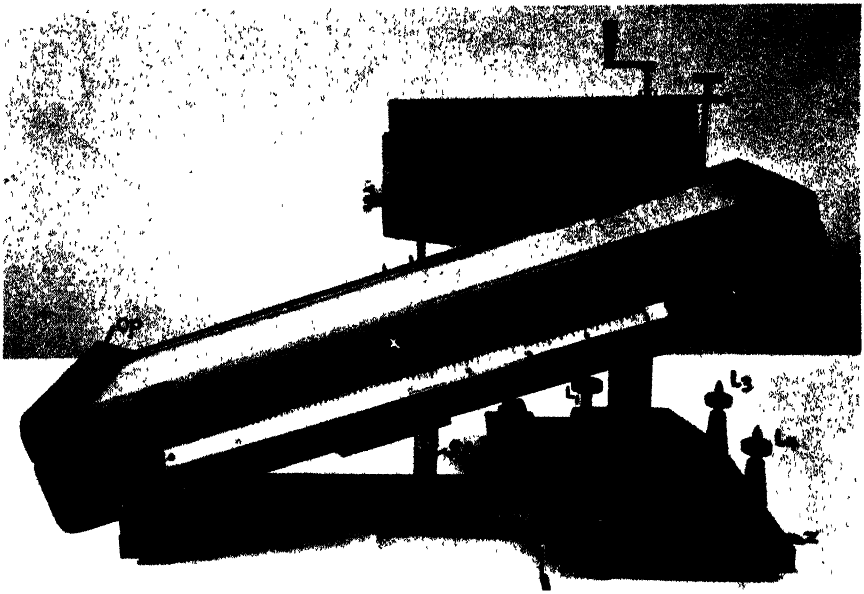

FIG. 5. The apparatus in an upright position

Figure 5 shows the apparatus in an upright position for removing the liquid from the trough through an opening (Op) in the gutter. A supporting arm (SA) is mounted to keep the apparatus in this position. The trough can be adjusted to the horizontal position by four screws (L_1, L_2, L_3, L_4).

The spreading substance to be examined is brought between the glass rod Z and the swimmer (C). By displacing the glass rod, which is done with the knob Q and a long screw protected by the flanges W, the surface can be diminished and the pressure exerted on the swimmer observed simultaneously.

The glass rod is carried in two containers (X), which can be swung outward when the surface has to be cleaned. The distance between the glass rod and the swimmer can be read on the scale S_2.

It is customery to plot surface area as abscissa and pressure as ordinate; the curves then correspond to the pressure-volume isotherms of gases and liquids.

IV. CONCLUSION

The apparatus which has been described combines among other things reliability, accuracy, protection of the essential parts, speed of measurement, and suitability for undisturbed continuous work. These improvements were achieved to a considerable extent by the following modifications: (*a*) The devices for zero adjustment of the balance and for measuring the film pressures were brought into one plane in front of the apparatus at a normal viewing distance. Thus a general requirement for a measuring apparatus was fulfilled. (*b*) The optical system was inserted in a special and very convenient way. (*c*) The metal box protects the balance and hence increase its lifetime. Owing to the solid construction disturbances or breakdowns in the essential parts of the apparatus are reduced to a minimum. Experience has proved the necessity of this construction when comparatively unskilled laboratory assistants have to work with the apparatus.

V. SUMMARY

A spreading apparatus has been constructed which shows practical advantages over the instruments described in the literature and meets every demand for undisturbed continuous work.

REFERENCES

(1) Gorter, E., and Blokker, P. C.: Proc. Acad. Sci. Amsterdam **45**, 151 (1942).
(2) Gorter, E., and Hermans, J. J.: Proc. Acad. Sci. Amsterdam **45**, 902 (1942).
(3) Gorter, E., and Seeder, W. A.: J. Gen. Physiol. **18**, 427 (1935).
(4) Maaskant, L.: "The Use of a Spreading-Method Technique in Research on Artificial Protein Fibers," Soc. Dyers Colourists, Symposium on Fibrous Proteins **1946**, 105.
(5) Ormondt, J. van: "Spreading of Proteins," Symposium on Proteins which was held at Amsterdam in 1938, p. 78.

COMPARISON OF MOLECULAR WEIGHTS OF POLYSTYRENE BY THE LIGHT-SCATTERING AND OSMOMETRIC METHODS

Q. A. TREMENTOZZI

Monsanto Chemical Company, Dayton, Ohio

Received December 16, 1949

INTRODUCTION

Since the pioneering work of Debye (3) established the light-scattering method as a means of determining molecular weights of polymers, there has been a great deal of published work (2, 7, 8, 12) on determining the usefulness and limitations of the method. Nearly all of this research has been concentrated on polymer fractions below 400,000 in molecular weight. In general, the agreement of the light-scattering method with the other direct methods has been satisfactory for molecular weights of 400,000 or less. For polystyrene fractions of higher molecular weight there has been one indication (14) that molecular weights obtained by the light-scattering method were not in agreement with those obtained by the osmometric method.

A number of well-characterized polystyrene fractions covering a molecular weight range of 90,000 to 1,100,000 were available from a previous study; hence it was felt that comparison of the molecular weights obtained by the light-scattering and osmotic pressure methods in various solvents would be helpful in contributing to the present knowledge of the behavior of macromolecules in solution.

THEORY OF LIGHT SCATTERING

Complete treatments of the light-scattering theory are available in the literature (4, 15) and need not be repeated here. However, for convenience in the discussion of the work, it is desirable to present briefly the basic principles of the method.

If a beam of light passes through a solution or any transparent substance, some of the light is scattered in all directions owing to the vibrations of the loosely held electrons. The intensity of the scattered light is dependent on local fluctuations in concentration in the solution. The spontaneous fluctuations in concentration are a function of the osmotic work necessary to produce them. The intensity of the scattered light is dependent also on the change in the index of refraction connected with a change in concentration. These relationships are expressed in Einstein's equation

$$\tau = \frac{32\pi^3\mu_0^2}{3N\lambda^4} \frac{(c\partial\mu/\partial c)^2}{c\dfrac{\partial}{\partial c}\left(\dfrac{P}{RT}\right)} \tag{1}$$

where τ is the turbidity in reciprocal centimeters due to concentration fluctuations, μ_0 is the index of refraction of the pure solvent, μ is the index of refraction of the solution, λ is the wave length of the monochromatic light in a vacuum, R is the gas constant, and P is the osmotic pressure. In general, $\mu - \mu_0$ is proportional to the concentration in dilute solutions, so that $(\mu - \mu_0)/c$ may be substituted for $\partial\mu/\partial c$.

It can be shown that

$$H\frac{c}{\tau} = \frac{1}{M} + \frac{2B}{RT}c \tag{2}$$

where H is the refraction constant, M is the molecular weight of the solute, and B is a constant.

In measurements involving solutes whose particle size is very much smaller than the wave length of light one simply determines H from refraction measurements and measures the turbidity, τ, for a series of concentrations and then plots $H\frac{c}{\tau}$ *vs.* c. The reciprocal of the intercept, $1\bigg/\left(H\frac{c}{\tau}\right)_{c\to 0}$, is equal to the molecular weight expressed as a weight average (4).

For particles greater than 1/20th the wave length of light, the molecules can no longer be considered as point sources and the light scattered from different parts of the same molecule must be considered separately. This interference effect differs in magnitude for different sizes and shapes of molecules, but for all molecules greater than 1/20th the wave length of light, there is an over-all decrease in the intensity of scattered light. This decrease is greater for the backward-scattered light than for the forward-scattered light and corrections for the observed turbidities are necessary. Debye (4) has described simple function solutions of the variations in angular intensity of scattered light for spheres, rods, and randomly coiled molecules. For randomly coiled molecules

$$I = \frac{2}{x^2}\,[e^{-x} - (1 - x)] \tag{3}$$

The factor $(1 + \cos^2\theta)$ has been omitted, since the angles are symmetrical about 90°.

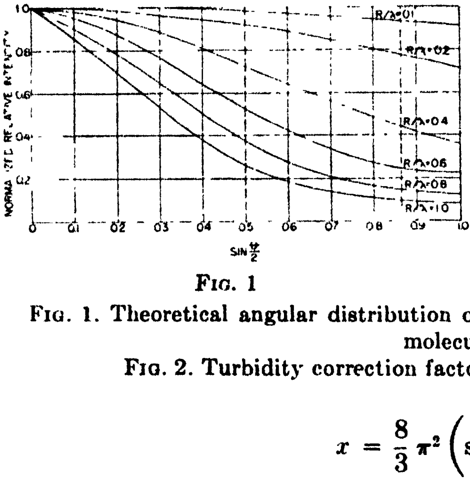

FIG. 1

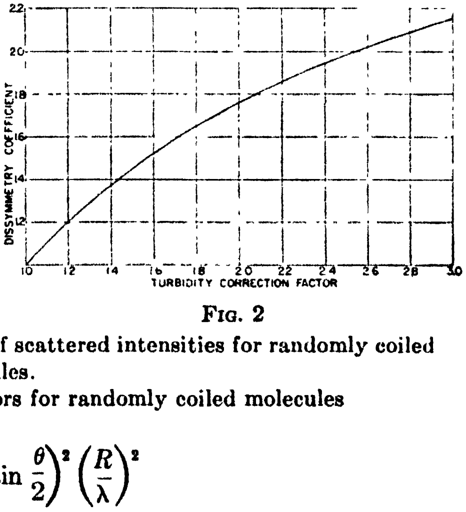

FIG. 2

FIG. 1. Theoretical angular distribution of scattered intensities for randomly coiled molecules.

FIG. 2. Turbidity correction factors for randomly coiled molecules

$$x = \frac{8}{3}\pi^2\left(\sin\frac{\theta}{2}\right)^2\left(\frac{R}{\lambda}\right)^2$$

R^2 = the root-mean-square separation of the ends, λ = the wave length of light in the solution, and θ = the angle formed by the incident beam and point of observation.

From the solution of equation 3 for angles between 0° and 180° and molecular sizes approaching the wave length of the monochromatic light employed, the theoretical angular distribution of the intensity of scattered light for randomly coiled molecules is obtained. This also yields the relationship between the turbidity correction factor and dissymmetry coefficient and the dissymmetry coefficient as a function of particle size. The relationships thus calculated are shown in figures 1, 2, and 3. In this work on polystyrene fractions the polystyrene molecules in solution were considered to be randomly coiled molecules, and turbidity corrections due to the dissymmetry of scattered light were made for this molecular shape.

PREPARATION OF POLYSTYRENE SAMPLES

Three Monsanto commercial grade polystyrene samples were used as the starting polymers. The polymerization temperature was approximately 100°C. in each of the preparations. These polystyrenes were fractionated by the well-known solvent precipitation technique, in which methyl ethyl ketone was the solvent and methanol was the precipitant. A single-step fractionation procedure was employed.

Each fraction was collected as a gelatinous precipitate which was centrifuged, thoroughly mixed with a solvent–precipitant mixture of the same composition which had resulted in precipitation, centrifuged again, and the supernatant liquid restored to the fractionation vessel. This washed precipitate was given a second washing before being recovered in the customary manner.

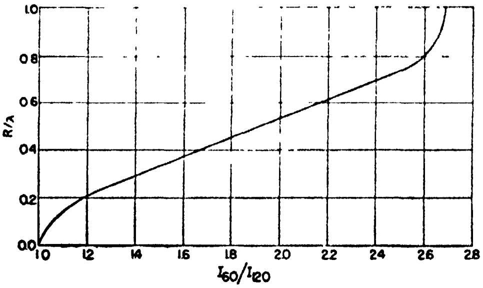

FIG. 3

FIG. 3. Dissymmetry coefficient as a function of R/λ for randomly coiled molecules

FIG. 4. Specific viscosity curves for fractions of H-639 series

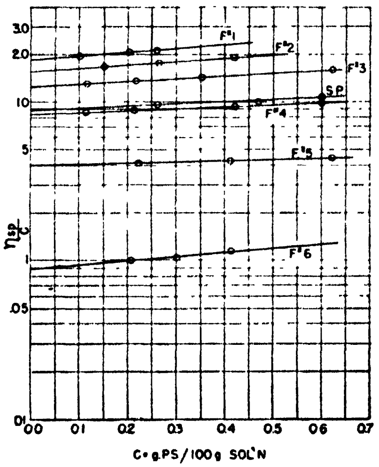

FIG. 4

PS-E-13, an emulsion polystyrene of $\bar{M}_n$ = 273,000, was resolved into seven fractions. PS-M-13, an emulsion polystyrene of $\bar{M}_n$ = 169,000, was resolved into eight fractions. From PS-H-639, a mass polystyrene of $\bar{M}_n$ = 113,000, six fractions were obtained.

EXPERIMENTAL

1. Viscosity measurements

Viscosimeters of the modified Ostwald type were used in making the viscosity measurements on solutions of the fractions in toluene. The efflux times of these calibrated viscosimeters were sufficiently high so as to render the kinetic energy corrections very small. All viscosity measurements were made at 25.52°C. ± 0.025°. Concentrations were expressed in grams per 100 g. of solution.

2. Osmotic pressure measurements

The osmometers employed in this study were of the Fuoss–Mead (10) type. Osmotic pressure measurements were made by the static method at a temperature of 29.60°C. ± 0.02°. The time required for a measurement varied from 2 to 4 hr. depending on the viscosity of the solution involved, etc. All osmotic pressures were corrected for the osmometer zero correction, which was determined immediately prior to the measurement of each solution. 1,4-Dioxane was chosen as the solvent because of the excellent membrane behavior with this solvent.

Membranes were prepared essentially according to the method of Montonna and Jilk (11), except that they were made over-sized (diameter = 7¼ in.) and were not removed from the stainless-steel rings. No trouble was experienced in retaining the membranes on the rings, either during the conditioning procedure or while in storage in dioxane. Membranes were installed in the osmometer while still on the ring. In this way leaks arising from the pleating of the membranes were avoided. As a result of this method of membrane preparation and installation the rate of decrease of the liquid levels in the capillaries was always less than 0.01 cm. per hour. This is considerably bettter than can usually be accomplished by the conventional method or even special gasketing methods (13).

3. Turbidity and dissymmetry measurements

The light-scattering apparatus used in this laboratory was designed by P. P. Debye and built in the Cornell University laboratories. It consists of an adjustable mercury arc lamp (CH-4) as the light source, a lens system, a neutral filter, a polaroid filter, adjustable diaphragms, a cell table, and three photocell and amplifying tube circuits with a sensitive microammeter. One of the photocells, protected by an automatic shutter, is at 90° to the incident light beam. The other two are mounted on a turntable so that the intensity of the scattered light can be measured at any angle between 0° and 144°.

Calibration of the microammeter scale in absolute turbidity units was made by means of a series of concentrations of emulsion polystyrene of a small particle size which covered the entire turbidity range of the instrument. The absolute turbidities of these solutions were determined by means of a Beckman spectrophotometer, using 5461 Å. mercury light. The sensitivity of the microammeter scale in absolute turbidity units was obtained from the scale deflections observed for the various solutions of known turbidity. Corrections due to the dissymmetry of the scattered light were applied. The intensity of the incident light was determined in arbitrary units by means of a glass prism with an appropriate filter. Changes in the intensity of the incident light were followed easily and accurately. Checks on the sensitivity calibration were made periodically and were always found to be within ± 2 per cent of the original value.

Since the intensity of light scattered by particles varies with the sixth power of the diameter of the particles, the presence of a small amount of impurity of a particle size greater than the polymer molecules will result in turbidity and dissymmetry values that are too high. To safeguard against this, the solutions were filtered by means of Selas filters varying in pore-size radius from 0.6 μ to 4.4 μ.

A filter of the same pore-size could not be used for all the solutions, since it was found that the behavior of the dissolved polymer molecules varied tremendously with the nature of the solvent employed. Whereas a 0.6 μ filter was satisfactory for all the fractions up to approximately 600,000 in molecular weight, filters of larger pore-size were necessary for the solutions of the higher molecular weight fractions in order to avoid loss of polymer during filtration. Loss of polymer was determined by changes in the specific viscosity before and after filtration. The changes in the specific viscosity divided by the concentration, η_{sp}/c, for fraction 2-E-13 using three solvents and filters of various pore-sizes are shown in table 1.

The turbidities of solutions of polystyrene fractions in three solvents were measured at an angle of 90° to the incident light, using the 5461 Å. mercury line.

Changes of the refractive indices of the polymer solutions with concentration were made by means of a differential refractometer, employing the 5461 Å. mercury line. This instrument was designed and built by Dr. A. S. Kenyon of this laboratory. The sensitivity of the instrument is ±0.000003. The design of the refractometer is similar to that given by Debye (4).

TABLE 1

Changes in specific viscosity of polystyrene solutions due to filter pore-sizes employed

SOLVENT	FILTER POROSITY (RADIUS OF PORES)	DECREASE IN η_{sp}/c
	microns	*per cent*
Toluene	1.4	74.8
Toluene	3.0	63.5
Toluene	4.4	13.7
Dioxane	1.4	None
Methyl ethyl ketone	1.4	None

Dissymmetry measurements were made at angles of 60° and 120° (in the medium) for at least three concentrations for each fraction. In this study the dissymmetry coefficient is defined as being the ratio of the forward-scattered intensity to the backward-scattered intensity. The intercept of the plot of dissymmetry coefficient *vs.* concentration yields the limiting value of the dissymmetry coefficient. The turbidity (or molecular weight) correction factor due to the dissymmetry of scattered light was obtained from figure 2.

All turbidity and dissymmetry measurements were corrected for the contribution to the scattered intensity made by the solvent.

No corrections for depolarization of the scattered light were made in this study. However, it has been shown (6) that the depolarization effect is small for the solute–solvent systems involved.

RESULTS

The specific viscosity data for all the fractions are given in figures 4, 5, and 6 as plots of η_{sp}/c *vs.* c, where η_{sp} is the specific viscosity and c is the concentration in grams of polystyrene per 100 g. of toluene solution. A semilogarithmic function was employed in order to give more weight to the more accurate data obtained at higher concentration.

In figures 7, 8, and 9 the osmotic pressure data are given as plots of π/c *vs.* c where π is the osmotic pressure and c is the concentration. The equation employed to calculate the number-average molecular weight from the osmotic pressure data is:

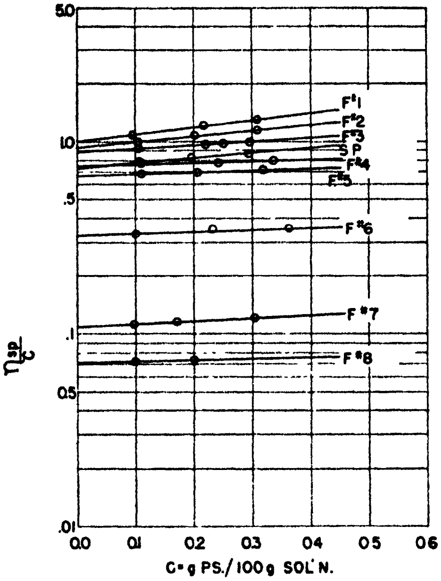

FIG. 5

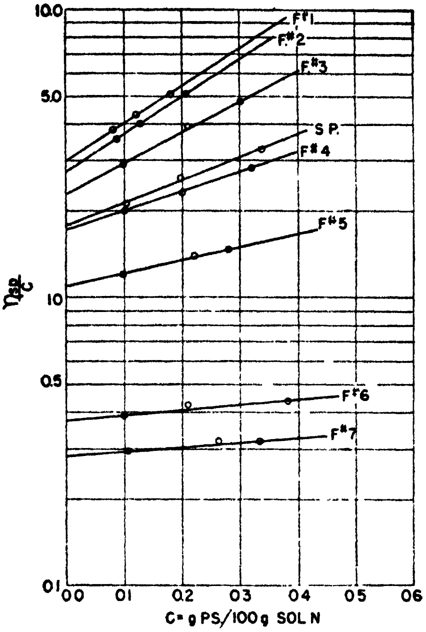

FIG. 6

FIG. 5. Specific viscosity curves for fractions of M-13 series and the starting polymer
FIG. 6. Specific viscosity curves for fractions of E-13 series

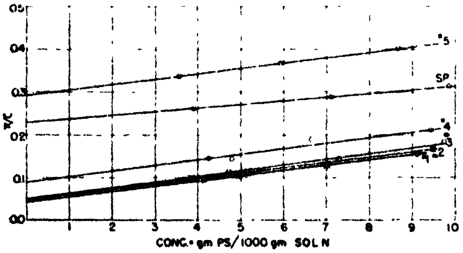

FIG. 7

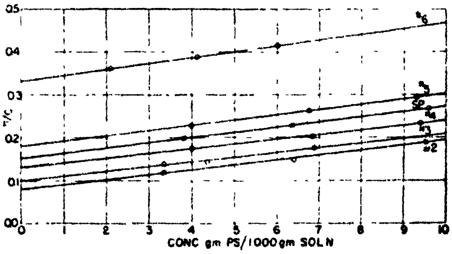

FIG. 8

FIG. 7. Osmotic pressure plot for polystyrene series H-639
FIG. 8. Osmotic pressure plots for series M-13

$$\pi/c = \frac{1033RT}{M} + Ac \tag{4}$$

π is the osmotic pressure expressed as centimeters of solution, c is the concentration in grams of polystyrene per 1000 g. of solution, R is the gas constant in liter atmospheres per °A., T is the absolute temperature, M is the molecular weight, and A is the slope of the curve.

The intrinsic viscosities and number-average molecular weights of fifteen fractions are shown as a plot of log M *vs* log $[\eta]$ in figure 10. The data fall nicely on a straight line over a range of 75,000 to 950,000. The equation representing the relationship between intrinsic viscosity and molecular weight was determined by the method of least squares as

$$[\eta] = 4.94 \times 10^{-5} M^{0.78} \tag{5}$$

$[\eta]$ is the intrinsic viscosity and is defined as

$$[\eta] = (\eta_{sp}/c)_{c=0} \tag{6}$$

If the concentration were expressed in grams of solute per 100 ml. of solution in determining $[\eta]$, the equation for the relationship between intrinsic viscosity and molecular weight becomes

$$[\eta] = 5.74 \times 10^{-5} M^{0.78} \tag{7}$$

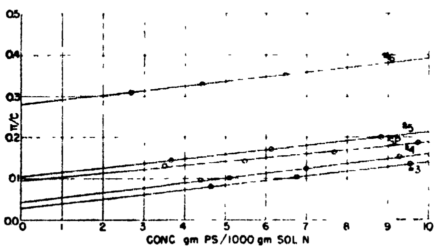

Fig. 9

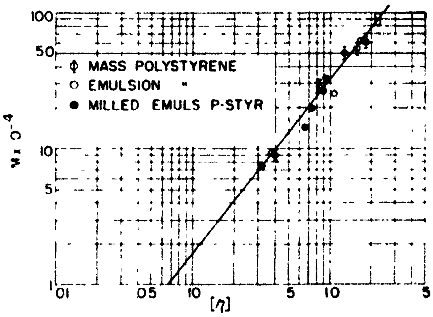

Fig. 10

Fig. 9. Osmotic pressure plots for series E-13

Fig. 10. Plot of intrinsic viscosity *vs.* molecular weight

The equivalent viscosity equation reported by Alfrey, Bartovics, and Mark (1) for polystyrene prepared at 120°C. is

$$[\eta] = 5.4 \times 10^{-4} M^{0.81} \tag{8}$$

Considering the difference in temperature of polymerization and remembering that the concentration in their report was milliliters of solute per 1000 ml. of solution, it is seen that the two equations are in good agreement.

The turbidity data are shown in figures 11 through 13 as plots of $H\frac{c}{\tau}$ *vs.* c. The limiting values of the dissymmetry coefficients, $q_{c=0}$, the reciprocals of $\left(H\frac{c}{\tau}\right)_{c=0}$ (or $\bar{M}_w$ uncorrected), filter sizes used, and other pertinent data on the various fractions are listed in table 2. This table shows that the dissymmetry values increase in an orderly manner with increasing molecular weight except for fraction 3-E-13 in toluene. Solutions of this fraction in toluene were filtered through a fritted-glass filter of 5-15 μ radius pore-size, since no filters of intermediate pore-size were then on hand. Unfortunately after recovering this fraction twice for reuse with methyl ethyl ketone and dioxane as the solvent, there was too little left for new measurements using toluene solutions and a more suitable filter.

This in no way destroys the trend, however, since results on fraction 2-E-13 confirm the discrepancies obtained for fraction 3-E-13. Since fraction 2-E-13 was reasonably large, solutions of this fraction in methyl ethyl ketone and dioxane were prepared from the original fraction. Thus, cumulative effects were avoided and it is felt that the data shown for fraction 2-E-13 should carry more weight than those obtained for fraction 3-E-13.

TABLE 2

Comparison of molecular weights of polystyrene fractions obtained by light-scattering and osmotic pressures

POLYSTYRENE SAMPLE	SOLVENT	FILTER PORE-SIZE (RADIUS)	$\bar{M}_w$ (UNCORR.)	$q_{c \to 0}$	$\bar{M}_w$ (CORR.)	$\bar{M}_n$
		microns				
5-H-639	Toluene	0.6	101,000	1.09	109,000	88,000
4-M-13	Toluene	0.6	172,000	1.15	197,000	214,000
3-M-13	Toluene	0.6	204,000	1.21	247,000	267,000
4-E-13	Toluene	0.6	500,000	1.42	731,000	
4-E-13	Dioxane	0.85	451,000	1.27	575,000	619,000
3-E-13	Toluene	5–15	643,000	1.84	1,390,000	
3-E-13	Methyl ethyl ketone	1.4	671,000	1.36	926,000	
3-E-13	Dioxane	1.4	582,000	1.38	821,000	834,000
2-E-13	Toluene	4.4	1,335,000	1.74	2,600,000	
2-E-13	Methyl ethyl ketone	1.4	1,180,000	1.30	1,540,000	
2-E-13	Dioxane	1.4	787,000	1.39	1,120,000	1,110,000
PS-E-13*	Toluene	4.4	637,000	1.90	1,460,000	648,000†
PS-E-13*	Dioxane	1.4	465,000	1.24	577,000	
PS-M-13*	Dioxane	1.4	198,000	1.24	246,000	
PS-M-13*	Toluene					209,000†
PS-H-639*	Dioxane	1.4	254,000	1.13	284,000	
PS-H-639*	Toluene					271,000†

* Heterogeneous polymers.

† $\bar{M}_v$ calculated from the viscosity equation (14).

The agreement between molecular weights obtained by light-scattering employing toluene solutions and molecular weights obtained by the osmotic pressure method using 1,4-dioxane solutions is satisfactory for molecular weights up to approximately 700,000 (see table 2). Beyond this there is a marked disagreement, wherein the light-scattering method yields molecular weights roughly twice those obtained by the osmotic pressure method. With methyl ethyl ketone as the solvent in the light-scattering method there is a disagreement in the molecular weights obtained only for the fraction of highest molecular weight, 2-E-13. With dioxane as the solvent in both methods, however, there is no real disagreement in molecular weights of any of the fractions.

Obviously, lack of homogeneity of the fractions could not be responsible for the large discrepancies observed, since the distribution could not change in solvents of the type employed.

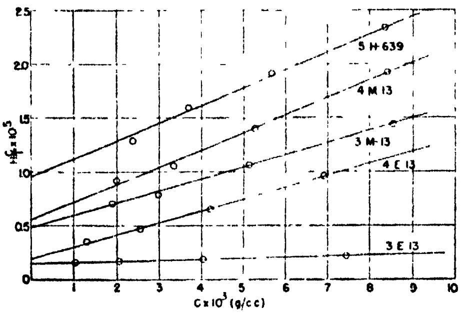

FIG. 11

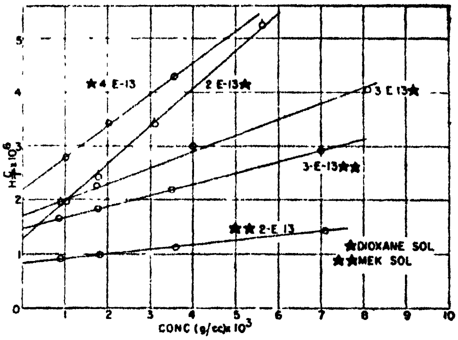

FIG. 12

FIG. 11. Reciprocal specific turbidity curves for PS–toluene solutions

FIG. 12. Reciprocal specific turbidity curves for PS–dioxane and PS–methyl ethyl ketone solutions.

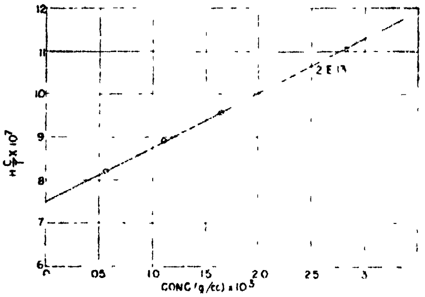

FIG. 13

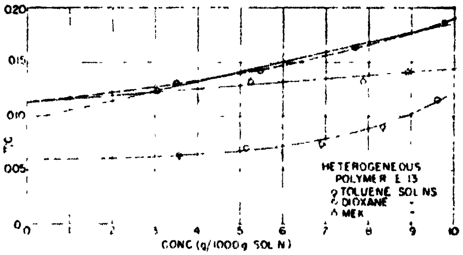

FIG. 14

FIG. 13. Reciprocal specific turbidity curve for PS–toluene system

FIG. 14. Osmotic pressure curves for PS in toluene, dioxane, and methyl ethyl ketone solutions.

However, it did appear quite possible that one or more impurities could be responsible for the observed effect. This possibility gained some support from the fact that fraction 3-E-13 with toluene as the solvent and employing a filter of large pore-size yielded a limiting dissymmetry coefficient somewhat larger than fraction 2-E-13 using a filter of smaller pore-size.

Accordingly, several experiments were devised to test the effects of impurities. Since, for toluene solutions of fractions 3-E-13 and 2-E-13, filters were used having considerably larger pore-sizes than those used in preparing the solutions in dioxane and methyl ethyl ketone, it was felt that forcing the toluene solutions of these fractions through 1.4 μ filters might result in better agreement in the light-scattering properties of the various solute–solvent systems involved. It was soon found, however, that this procedure resulted in a tremendous decrease in the specific viscosity, as shown in table 1. Presumably such large changes in viscosity must be due to loss of polymer rather than to trace amounts of impurities.

A second series of experiments involved adding to the three solvents various substances that could act as impurities, e.g., catalyst, emulsion stabilizer, etc. Although these substances were added in amounts sufficient to produce saturation, there was no significant change in the scattering corrections for the solvents.

Another experiment consisted in measuring the difference in the scattering of light of a mixture of equal parts of toluene and dioxane and a solution of impurities in dioxane to which was added an equal volume of toluene. Again there was no difference in the intensity of light scattered. These impurities cannot be considered to be soluble in one solvent, therefore having a small effect on the turbidity and dissymmetry, and insoluble in another solvent, therefore having a large effect.

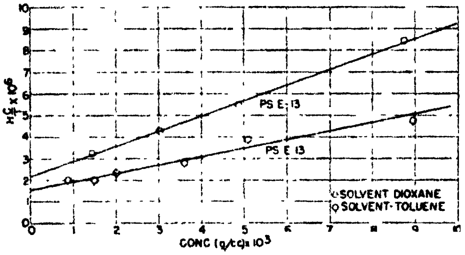

FIG. 15. Reciprocal specific turbidity curves for unfractionated PS in different solvents

A third series of experiments, however, indicate strongly that the fault is not due entirely to the light-scattering method or impurity effects, but, rather, that the observed discrepancies arise from the different behavior of polystyrene in the three solvents. Osmotic pressure measurements of toluene solutions of PS-E-13 (heterogeneous) yield a number-average molecular weight of 440,000. The number-average molecular weight obtained from dioxane solution is somewhere between 228,000 and 273,000, depending on whether or not curvature is given to the data points in extrapolating to a limiting value of π/c. Solutions in methyl ethyl ketone yield a number-average molecular weight of 228,000. The osmotic pressure curves are shown in figure 14.

From figure 15 it is apparent that the discrepancy in weight-average molecular weights (light-scattering method) as obtained in toluene and dioxane solutions is in line with the discrepancy obtained by the osmometric method for the two solvents, except that the disagreement is greater in the light-scattering method, as would be expected. In the light of this it is very difficult to understand how the observed effects could be traced primarily to impurities. Rather, it appears that the close similarity of the solvent effects for the high-molecular-weight polystyrene obtained by light scattering and osmometry is an excellent proof that the cause of the apparent changes in molecular weights is the different behavior of the very large molecules in different solvents.

It should be mentioned that the membrane employed for determining the osmotic pressures of toluene solutions was reconditioned to methyl ethyl ketone while still in the osmometer. No other change of any kind, e.g., tightening of osmometer bolts, etc., was made. Leaks, then, could not have been responsible for the low value for the molecular weight in methyl ethyl ketone and in dioxane and the high values for the molecular weight in toluene.

A very good verification of this same solvent effect on polystyrene is given in the work of Doty, Affens, and Zimm (5). From their data it can be shown that the discrepancies due to different solvent effects are of the same order of magnitude as those found in this study. Moreover, it is evident that the polar solvents lead to lower molecular weights than does toluene and, presumably, other nonpolar solvents.

It has been shown that good agreement was obtained by the light-scattering and osmometric methods for polystyrene fractions up to a molecular weight of approximately 700,000. It is not likely, then, that association involving the usual forces can explain completely the discrepancy at higher molecular weights, because the observed effect appears to be a function of the size of the macromolecules. If association alone were the answer, it would mean that the polymer species are not chemically identical and that the number of associating groups in the polymer molecules increases with degree of polymerization.

Part of the discrepancy may lie in the tremendous variation in size of the macromolecules with the nature of the solvent, as is evident from the values of the dissymmetry coefficients listed in table 2. For the species of very high molecular weight in a nonpolar solvent it appears that there is incomplete freedom of motion of the polymer molecules even at concentrations in the order of 0.5 per cent or less. This solute–solute interaction would account for the low limiting values of the dissymmetry and of π/c and would account also for the upward curvature of the π/c *vs.* c curve for solutions of the higher molecular weight species in toluene (see figure 14). This effect could not be completely eliminated for solutions in toluene unless accurate measurements could be made on extremely dilute solutions.

Rough calculations were made on the volume swept out by the polymer molecules in dilute toluene and dioxane solutions by means of the molecular dimensions of the polymer molecules as determined from dissymmetry measurements. The molecular dimensions are of the proper order of magnitude, so that a small change in the macromolecular size is critical in determining whether or not molecular interference occurs.

SUMMARY

The molecular weights of polystyrene fractions were determined by the light-scattering and osmometric methods and found to be in good agreement up to a molecular weight of approximately 700,000. Beyond 700,000 the effect of the

solvent on the size of the dissolved polymer molecules is critical, so that there is no agreement in the molecular weight obtained with polar solvents as compared to molecular weights obtained with nonpolar solvents. These discrepancies in molecular weights for the species of very high molecular weight appear to be due to the anomalous behavior of the polymer molecules in solution in the different solvents rather than to the method employed in making the measurements.

The writer is grateful to Dr. I. B. Johns for his helpful suggestions and interest and to Dr. R. A. Ruehrwein for his very helpful discussions of the experimental work and for advice in the presentation of the results.

REFERENCES

(1) Alfrey, T., Bartovics, A., and Mark, H.: J. Am. Chem. Soc. **65**, 2319 (1943).
(2) Blaker, R., Badger, R., and Gilmann, T.: J. Phys. & Colloid Chem. **53**, 794 (1949).
(3) Debye, P.: J. Applied Phys. **15**, 338 (1944).
(4) Debye, P.: J. Phys. & Colloid Chem. **51**, 18 (1947).
(5) Doty, P., Affens, W., and Zimm, B.: Trans. Faraday Soc. **42B**, 66 (1946).
(6) Doty, P., and Kaufman, H.: J. Phys. Chem. **49**, 583 (1945).
(7) Doty, P., Zimm, B., and Mark, H.: J. Chem. Phys. **12**, 144 (1944).
(8) Ewart, R., Roe, C., Debye, P., and McCartney, J.: J. Chem. Phys. **14**, 687 (1946).
(9) Flory, P.: J. Am. Chem. Soc. **65**, 372 (1943).
(10) Fuoss, R., and Mead, D.: J. Phys. Chem. **47**, 59 (1943).
(11) Montonna, R., and Jilk, L.: J. Phys. Chem. **45**, 1374 (1941).
(12) Oster, G., Doty, P., and Zimm, B.: J. Am. Chem. Soc. **69**, 1193 (1947).
(13) Sirianni, A., Wise, L., and McIntosh, R.: Can. J. Research **25**, 301 (1947).
(14) Stein, R., and Doty, P.: J. Am. Chem. Soc. **68**, 159 (1946).
(15) Zimm, B., Stein, R., and Doty, P.: Polymer Bull. **1**, 90 (1945).

SOME PROPERTIES OF THORIUM IN VERY DILUTE AQUEOUS SOLUTIONS[1]

M. H. KURBATOV, HARRIET B. WEBSTER, AND J. D. KURBATOV

Department of Chemistry, The Ohio State University, Columbus, Ohio

Received November 14, 1949

INTRODUCTION

It has long been known (4) that certain heavy elements—e.g., radioactive isotopes of lead, bismuth, and polonium—form radiocolloids (1) which are filterable at concentrations much below that of so-called "saturated solutions" of their oxides. More recently some of the lighter elements—yttrium (2), zirconium (3, 5), columbium (5), lanthanum (5), and others—have been shown to exhibit similar behavior.

---

[1] The term "radiocolloid" is used throughout this paper to mean simply the material removable by filtration from very dilute solutions, of the order of 10^{-9} *M* or less.

With the aim of developing a simple method of extracting UX_1 from uranium solutions a study of the radiocolloidal properties of UX_1, an isotope of thorium, was undertaken.

In conventional quantities soluble thorium salts react with ammonium or sodium hydroxide or with amonium carbonate, forming insoluble hydrous thorium oxide, which can be dissolved by an excess of ammonium or alkali carbonate. The solubility of thorium oxide is recorded in the literature (6) simply as less than 0.00002 g. ThO_2 per liter of water (*ca.* 7×10^{-8} mole per liter) at 25°C. Hydrous thorium oxide is said (1) to begin to precipitate at pH 3.6–4.2, depending on the concentration of the thorium solution. Using a solution which was approximately 0.3 *N* in thorium, the authors obtained essentially the same titration curve with sodium hydroxide and with ammonium hydroxide. The latter is shown in figure 1. In both cases the precipitate separated out at pH 3.5–3.6.

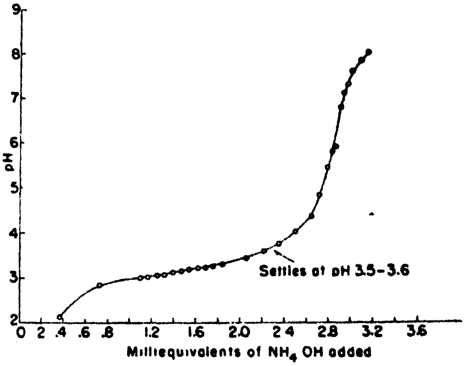

FIG. 1. Titration curve for 0.3 *N* thorium nitrate

It would be expected, on the basis of the titration curve and from classical concepts of solubility, that in more acid solutions than *ca.* pH 3.0 much lower concentrations than 0.3 *N* should be stable solutions from which thorium would not be filtered. Also, if the reported solubility limit of 7×10^{-8} mole thorium dioxide per liter of water at 25°C. is of the correct order of magnitude, quantities of less than 7×10^{-8} mole should not be separated from solution by filtration even at pH 7.

If the coagulation or precipitation of thorium ions is postulated as resulting from an interaction between hydrated thorium ions in true solution and hydroxyl ions, then it would be expected that other negative ions present in the solution often in greater concentration than the hydroxyl ion might interfere with the coagulation. Accordingly, the effects of both pH and the foreign anions, nitrate and carbonate, on the removal of UX_1 from solution have been investigated.

Furthermore, by similar reasoning it might be postulated that the presence of foreign cations might interfere with the removal of thorium at constant concentrations of OH^- and other anions. So the extent of separation of the thorium isotope, UX_1, in the presence of varying quantities of uranyl ion has been determined.

PROCEDURE

The general procedure used in securing the data on UX_1 and thorium behavior was as follows:

The UX_1 and thorium in solutions of known acidity were transferred to outside-ground weighing bottles of only slightly greater capacity than the final volumes of samples. These solutions were then titrated with base (ammonium hydroxide, sodium hydroxide, or ammonium carbonate) to the selected pH, as measured by a Leeds and Northrup pH meter. The weighing bottles with samples were closed after the titration, the ground joints sealed with stopcock grease, and the samples set aside for various periods of time before filtration. After the selected period had elapsed the bottles were opened and the samples were filtered through Schleicher and Schüll blue-ribbon filter papers in 1⅜-in. funnels, the papers having been washed previously with solutions of the same pH as the samples. The thorium separated from solution was washed from the weighing bottles and papers, using 2 *N* nitric acid, and these solutions were evaporated in 60 x 10 mm. Petri dishes. The activities of the dry samples were measured by means of Geiger counters. In many cases all or portions of the filtrates were also evaporated and their activities measured as a check on the measurements of the thorium removed from solution.

The determinations of amounts separated were made in all cases by tracer procedure, using UX_1 alone or thorium with UX_1 added. All Geiger counter measurements were made with UX_1 and UX_2 in equilibrium, utilizing the UX_2 β-particles which have an upper energy limit of 2.3 Mev. The UX_1 was obtained from purified uranyl nitrate and in turn repeatedly purified by a radiocolloid procedure which will be evident from the data presented.

In the experiments involving carbonate, analyses were made using a micro-Kjeldahl apparatus. The carbon dioxide was liberated from the solution by addition of 30 per cent sulfuric acid and redissolved in standardized sodium hydroxide. This solution was titrated with standardized hydrochloric acid, using phenolphthalein and methyl orange, and the carbonate content of the original solution calculated.

DISCUSSION OF RESULTS

Table 1 shows the effect of hydrogen-ion concentration in the range from pH 3 to 4.5 on the coagulation of 10^{-4} *M* thorium, using UX_1 as tracer, and also the results of consecutive filtrations of these solutions. In this work the solutions were prepared with hydrochloric acid and titrated with sodium hydroxide.

In part I of table 1 the total volumes were 11 ml. and the salt concentrations 0.28 *N*. At pH 3.6 the fraction of the thorium removed in 25 min. was 31 per cent, while at pH 4.5 the fraction removed in the same time was 97 per cent, showing increased coagulation with increased pH. These two solutions were

TABLE 1

Effect of pH and consecutive filtrations on coagulation of 3.1 × 10^{-8} gram-atom of thorium at 25°C.

NUMBER OF TIMES SOLUTION WAS FILTERED	COAGULATION PERIOD	pH AT EACH FILTRATION	PER CENT OF TOTAL UX_1 AND Th ON FILTER PAPERS	PER CENT OF UX_1 AND Th ON PAPERS (CALCULATED ON BASIS OF COUNTS IN SOLUTION AT TIME OF FILTRATION)
Part I: Total volume = 11.1 ml.; NaCl concentration = 0.28 N; total UX_1 tracer = 1.2 × 10^{-15} gram-atom				
1	25 min.	3.6	31	31
2	122 min.	3.9	19	28
1	25 min.	4.5	97	97
2	160 min.	4.8	3	100
Part II: Total volume = 39.2 ± 0.2 ml.; NaCl concentration = 0.08 N; total UX_1 tracer = 1 × 10^{-15} gram-atom				
1	25 min.	3.04	17	17
2	0		12	14.5
3	22.0 hr.	3.16	7	9.9
1	30 min.	3.52	29	29
2	0		16	22.5
3	21.5 hr.	3.64	12	22
1	30 min.	4.08	39	39
2	0		23	38
3	20.8 hr.	4.10	20	53
Part III: Total volume = 50.3 ± 0.3 ml.; NaCl concentration = 0.08 N; total UX_1 tracer = 1.6 × 10^{-15} gram-atom				
1	5 min.	3.03	14.2	14.2
2	35 min.		9.7	11.0
3	95 min.	3.03	7.6	10.3
4	6.7 hr.		5.1	7.5
5	0 hr.	3.05	4.2	6.7
6	14 hr.		4.0	6.8
7	0 hr.	2.95	3.3	6.0
1	3 min.	3.50	22.5	22.5
2	39 min.		14.2	18.3
3	95 min.	3.53	9.5	15.0
4	6.6 hr.		7.0	13.0
5	0 hr.	3.50	4.0	8.6
1	2 min.	4.03	35.1	35.1
2	39 min.		21.5	33.0
3	96 min.	4.02	12.0	27.8
4	6.6 hr.		8.3	26.3
5	0 hr.	3.98	5.2	22.7
6	14 hr.		4.6	25.4
7	0 hr.	3.85	2.1	15.8

refiltered in 122 and 160 min., respectively. Even though the pH of the first sample had increased from 3.6 to 3.9 the fraction removed (based on thorium remaining after first filtration) was less than the original, that is, 28 per cent. All the remaining thorium was removed from the sample at pH 4.8.

In part II of table 1 the volumes (39.2 ± 2 ml.) were larger than in part I and the salt concentration (0.08 *N*) lower. Each of the three solutions of pH 3, 3.5, and 4.0 was filtered three times. The first observation here is that comparable filtrations showed a regular increase in coagulation with pH increase. Second, in a given pH range (3.04–3.16, 3.52–3.64, and 4.08–4.10) there was a consistent decrease in coagulation upon consecutive filtrations (see right-hand column, table 1) with the exception of one instance, 53 per cent removal at pH 4.10.

TABLE 2

Effect of ammonia on removal of UX_1 *from solutions when carbonate was present*

Total UX_1 = 4×10^{-16} gram-atom; temperature = 25°C.; NH_4NO_3 concentration at pH 6 in 17.00 ml. of solution = 0.007 *N*; total NO_3^- = 1.2×10^{-4} gram-ion

STANDING PERIOD	pH	TOTAL VOLUME OF SOLUTION	REMOVAL	
			PER CENT OF ORIGINAL	PER CENT OF FILTRATE
		Part I		
hours				
2.0	3.0	15.75	55	
1.8	6.10	17.06	27	
1.4	7.10	17.27	37	
2.1	7.78	17.88	85	
		Part II		
3.8	3.02	15.75	66	
3.7	6.10	17.00	43	
3.8	7.14	17.25	23	
68	6.96	Above solution refiltered		9
3.9	7.92	17.99	31	
3.8	8.48	19.98	19	
68	8.28	Above solution refiltered		7

In parts II (and III) of table 1 the samples marked "zero" coagulation period were obtained by putting one funnel and filter paper directly under another so that the freshly filtered sample was immediately refiltered. These figures at "zero" time indicate that the coagulation period is an insignificant factor in the removal of thorium from this concentration under the conditions given.

The data for coagulation after 25 to 30 min. at pH 3.6 (part I) and 3.52 (part II) are quite similar, 31 per cent and 29 per cent, respectively, in spite of different volumes and salt concentration. Apparently the increased volume in part II is compensated by the corresponding decreased salt concentration. (The effect of salt is discussed later with reference to table 4.)

Part III of table 1 shows a more extended study of consecutive filtrations of solutions at pH 3, 3.5, and 4. Again there is (*a*) a regular increase in coagulation with increased pH, (*b*) decreased separation with successive filtrations of a given sample, and (*c*) no observed dependence of fraction separated on coagulation period.

In obtaining the foregoing results on 10^{-4} *M* thorium at pH 3–4.5 no precautions were taken to exclude carbon dioxide of the air and at the time there was no apparent need to do so. As a consequence the same procedure was used in the experiments represented in table 2 which, however, had only trace amounts of UX_1 with no thorium added and included mainly solutions of pH 6–8.

TABLE 3

Effect of ammonium carbonate on removal of UX_1 *from solution*

HCO_3^- IN FILTRATE	VOLUME OF SOLUTION	TOTAL HCO_3^- IN FILTRATE	pH	PER CENT REMOVED
Part I: Total $UX_1 = 4 \times 10^{-15}$ gram-atom; temperature = 25°C.; standing period = 1 day; total $NO_3^- = 2.1 \times 10^{-2}$ gram-ion; total salt concentration = *ca.* 1 *N*				
gram-ions/liter	*ml.*	*gram-ions* $\times 10^4$		
0.029	16.44	4.8	6.25	49
0.039	16.50	6.4	6.98	44
0.097	17.30	16.8	7.49	7
0.104	16.53	17.2	6.60	7
0.370	20.22	74.8	7.70	4
0.488	21.38	103.5	8.00	3
Part II: Total $UX_1 = 4 \times 10^{-15}$ gram-atom; temperature = 25°C.; standing period = 14–20 hr.; total $NO_3^- = 1.3 \times 10^{-4}$ gram-ion; total salt concentration = *ca.* 0.005 *N*				
(*gram-ions/liter*) $\times 10^4$		*gram-ions* $\times 10^6$		
2.8	18.65	5.22	7.48	64
2.8	20.55	5.76	7.50	54
2.8	22.42	6.28	7.50	50
3.1	20.55	6.37	7.51	46
2.8	24.25	6.79	7.50	57
2.8	24.22	6.79	7.51	52
3.3	27.18	8.97	7.38	44
3.5	30.20	10.6	7.45	38
3.7	30.21	11.2	7.45	37

Part I of table 2 shows the results obtained when the period of standing before filtration was 1.5–2 hr.; part II, 3.7–3.9 hr. If the results at comparable pH values for the different standing periods are noted it will be seen that at pH 3 and even pH 6 the longer time resulted in greater removal, while at pH 7 and 8 the longer time resulted in less separation. In the two cases in which the solutions were refiltered after 68 hr. (part II) the second removal was quite small compared with the first removal and compared with the data on consecutive filtrations in table 1. It appears also that, in many cases, the amount removed decreased with increase in pH.

The above three unexpected trends are attributed to the sensitivity of very small quantities of UX_1 to increased carbonate absorption from the air with increased period of standing and increased pH. Carbonate analyses of three of these filtrates are as follows:

PERIOD	pH	HCO_3^-	PER CENT REMOVED
hours		*gram-ions* $\times 10^6$	
3.7	6.10	2.7	43
3.8	7.14	3.5	23
3.8	8.48	11.5	19

Table 3 shows the result of bicarbonate addition upon the separation of trace quantities of UX_1. The main differences between part I and part II are (*a*) greater total salt in part I (2.1×10^{-2} gram-ion of nitrate ion as compared with 1.3×10^{-4} gram-ion of nitrate ion in part II) and (*b*) greater carbonate quantity in part I (5×10^{-4} to 1×10^{-2} gram-ion in part I as compared with 5×10^{-6} gram-ion in part II).

In part I as the pH changes from 6.25 to 8 and the bicarbonate-ion content changes from 4.8×10^{-4} to 1.0×10^{-2} gram-ion, the fraction removed decreases from 49 to 3 per cent, that is, even though there is an increase in pH the separation decreases rapidly with increasing carbonate.

In part II the pH is essentially constant at 7.5. As the bicarbonate-ion content increases from 5×10^{-6} to 1×10^{-5}, the fraction removed decreases from 64 per cent to 37 per cent. Or, at constant pH under the conditions used, doubling the carbonate content doubles the amount of UX_1 remaining in solution.

This relation suggests the formation of a carbonate complex involving one carbonate or bicarbonate ion per thorium atom. However, upon examination of part I of table 3 it can be seen that this simple relation holds only approximately for the first two figures (4.8 and 6.4×10^{-4} gram-ion of bicarbonate ion *vs.* 5 and 56 per cent in solution) and does not hold for the remainder. Furthermore, if an expression were set up postulating an equilibrium between hydrous oxide and complex ion in solution and an equilibrium constant were evaluated using these data (in which the total thorium and pH are constant), the dissociation constant of the complex ion would be directly proportional to the carbonate concentration. However, the carbonate concentration is two orders of magnitude greater in part I than in part II, so the dissociation "constant" would be two orders of magnitude greater. Under these conditions the meaning of the term dissociation constant is undermined.

It might be suggested that in the presence of higher concentrations of carbonate, a complex ion of thorium involving a greater number of carbonate ions per thorium atom is involved and that a new constant would be expected. This does not seem plausible, since the minimum bicarbonate-ion quantity is

5.2×10^{-6} gram-ion and the carbonate-ion quantity is 3.2×10^{-9} gram-ion, as compared with 4×10^{-15} gram-ion of thorium. In other words, the minimum carbonate to thorium ratio is $10^{-9}/10^{-15}$ and it is hardly reasonable to expect that even a 100-fold increase in this ratio (that is, from 10^6 to 10^8) would result in a different complex ion.

The lack of applicability of usual mass law concepts in this case may be attributed to the more significant influence of other factors than the concentrations of main reactants when dealing with trace quantities as compared with conventional quantities. Among such other factors involved in the data in table 3 is the 160-fold increase in nitrate ion present (1.3×10^{-4} gram-ion to 2.1×10^{-2} gram-ion) in part I as compared with part II which, as will be seen in figure 2, results in decreased separation from solution.

In figure 2 data are given showing the influence of different quantities of nitrate ion on the removal of trace quantities of thorium in the absence of carbonate. At a given pH, say pH 2.5, a thirtyfold increase in nitrate-ion quantity results in a decrease in separation from 72 per cent to 51 per cent under the conditions stated.

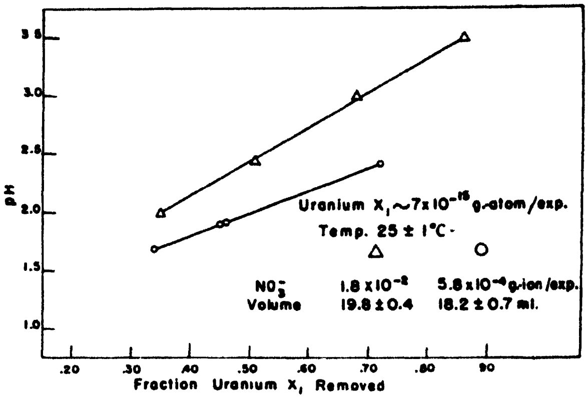

FIG. 2. Effect of nitrate ion on removal of UX_1

Thus it is reasonable to attribute the overall results of the presence of carbonates to three separate effects, all of which act in the same direction relative to separation from solution: (*a*) the formation of a soluble complex of thorium, (*b*) the usual decrease in removal caused by univalent anions, in this case bicarbonate, and (*c*) the increased interionic attraction of the bivalent carbonate ion.

A qualitative comparison can be made of the effects of nitrate and carbonate ions in the separation of UX_1 even though other conditions varied. The pH (6–8) used for studies of carbonate was set approximately by the nature of the ions themselves and the pH for nitrate study was selected to minimize carbon dioxide absorption from the air.

Columns 3 and 2 in table 4 show a change from 64 to 49 per cent removed with nitrate change from 1×10^{-4} to 2×10^{-2} *and* bicarbonate change from 5 ×

10^{-6} to 5×10^{-4}. The nitrate change alone could account for this difference (see column 1, at pH 2.5, 72–51 per cent separated). Yet there is the very marked effect (see column 3) of changes in bicarbonate within one order of magnitude at constant nitrate-ion concentration. It may be postulated that nitrate ions interfere with both (*a*) the reaction of thorium ions with hydroxyl ions to form radiocolloids (see column 1) and (*b*) the reaction of thorium ions with carbonate or bicarbonate ions to form soluble complexes. Since these two effects are in opposite direction to each other so far as separation of radiocolloids is concerned, there is greater removal under the conditions in column 2 than would be expected on the basis of results from smaller changes in carbonate shown within column 3.

TABLE 4

Comparison of influence of nitrate and carbonate ions on separation of UX_1 *from solutions*

ION	NITRATE	CARBONATE	CARBONATE
Column No.	1	2	3
Data from	Figure 2	Table 3	Table 3
pH	1.5–3.5	6–8	7.5
Volume, ml.	18–19	16–21	18–30
Period, hr.	19	24	14–20
Total gram-ions:			
NO_3^-	6×10^{-4} to 2×10^{-2}	2×10^{-2}	1.3×10^{-4}
HCO_3^-		5 to 75×10^{-4}	5 to 11×10^{-6}
CO_3^{--}		10^{-7}	10^{-9}
Per cent UX_1 separated	46–35 (at pH 2) 72–51 (at pH 2.5)	49–4	64–37

TABLE 5

Effect of pH on removal of trace quantities of UX_1 *from solution*

Total $UX_1 = 2.5 \times 10^{-15}$ gram-atom; temperature = 26°C.; standing period = 38 ± 2 hr.; total volume = 15.0 ± 1 ml.; total $NO_3^- = 1.5\text{–}1.6 \times 10^{-2}$ gram-ion

pH	PER CENT UX_1 REMOVED	pH	PER CENT UX_1 REMOVED
1.12	10	3.05	54
1.52	15	4.09	78
1.48	21	4.45	87
2.03	27	4.49	87
1.99	30	5.10	91
2.49	40	6.01	94
2.50	40	6.76	98
3.02	51		

Table 5 shows the data obtained when UX_1 solutions were titrated with carbonate-free ammonium hydroxide in the absence of carbon dioxide from the air. Under these conditions the amount removed by filtration increased rapidly with pH from 1 to 4.5, but from pH 5 to 7 there was much less change in the fraction separated. The data between pH 1 and 4.5 approach a straight line when pH is plotted *vs.* fraction of UX_1 removed (figure 3).

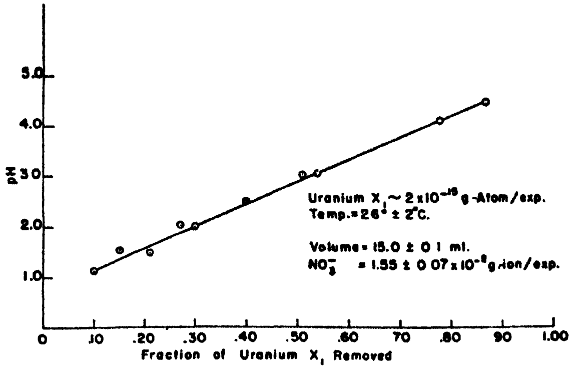

FIG. 3. Effect of pH on removal of UX_1

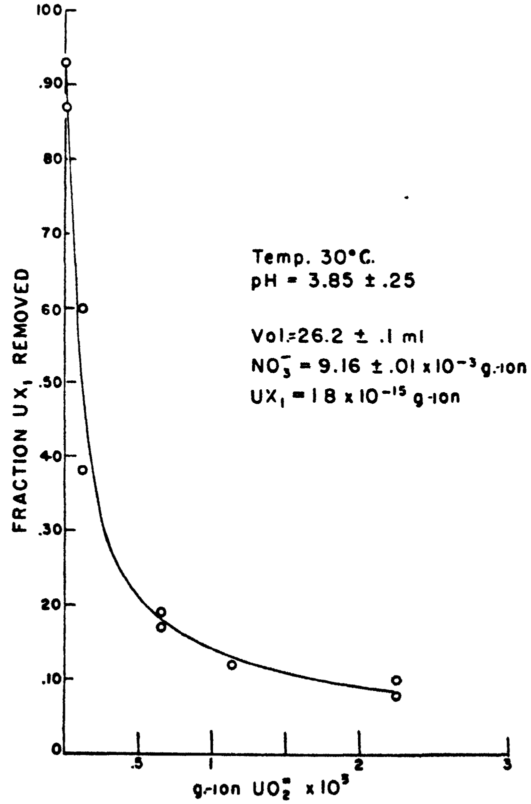

FIG. 4. Effect of uranyl ion on removal of UX_1

It is of interest to compare this curve with figure 1, the titration curve for 0.3 *N* thorium. In figure 1 the flat part of the curve which may be interpreted as the region of the hydrous oxide formation lies largely between pH 3 and 3.5, while reference to figure 3 shows about 50 per cent of the UX_1 removed below pH 3, that is, the lower concentration of thorium isotope requires less hydroxyl for removal from solution. This is, of course, contrary to usual concepts of solubility.

In figure 4 are shown the data on removal of UX_1 from solutions containing uranyl ion. These results were obtained at a pH of 3.6–3.8, which is below the pH at which usual concentrations of uranium coagulate.[2] The total nitrate was kept constant by adding corresponding amounts of ammonium nitrate as the uranyl nitrate was reduced.

This curve shows that as the uranium is diluted from 2×10^{-3} to 1×10^{-4} gram-ion at pH 3.8 the separation of UX_1 increases from 10 per cent to 60 per cent. At this same pH 87–93 per cent of the UX_1 is removed in the absence of uranyl ions. In other words, the presence of uranyl ions clearly interferes with separation of UX_1. However, this interference is markedly decreased by reduction of the uranyl-ion concentration.

SUMMARY

It has been established that the coagulation of thorium from 10^{-4} *M* solution at different pH values and variable concentrations of foreign ions is similar to the removal, by filtration, of invisible quantities of UX_1 in concentrations of 10^{-13} *M*.

At constant time intervals with carbonate content minimized (figures 2 and 3) an increase in OH^- increases the removal of UX_1 present in trace amounts. The plot of pH *vs.* fraction of UX_1 removed from solution gives an experimentally straight line between pH 1 and 4.5. This is consistent with similar results on solutions containing 10^{-6} gram-atom thorium (table 1) and on the formation of radiocolloids of yttrium and zirconium.

Change in nitrate ion in solution with other factors comparable was shown to result in increased removal of UX_1 with decreased nitrate-ion concentration in the absence of carbonate ions.

The effect of change of bicarbonate-ion content in solutions of UX_1 was shown to be very great and in opposite direction to the effect of hydroxyl ion. It was pointed out that this effect may be attributed to complex ion formation along with interference of both the monovalent bicarbonate ion and the divalent carbonate ion with the radiocolloid formation.

With uranium concentrations of 0.0004 *M* or less (and other conditions as described) as much as 60 per cent of the UX_1 present in trace amounts can be removed by filtration.

In conclusion it may be said that UX_1 in quantities of the order of 10^{-15} gram-ion showed regularities in radiocolloid properties, but its behavior is

---

[2] An electrometric titration of 0.3 *M* uranium nitrate solution with ammonia solution results in visible coagulation beginning at pH 4.7 with a subsequent drop in pH to 4.3 and then continued coagulation with addition of base up to pH 5.0.

highly sensitive not only to small amounts but to moderate variations in the quantity of carbonate present in solution.

The authors are deeply indebted to Professor Edward Mack, Jr., for his discussion and support of this work.

The scholarship received by one of the authors from the Ohio State University Industrial Research Foundation made this research possible and is greatly appreciated.

It is a pleasure to express our thanks to the Ohio State University Development Fund for grants which secured fundamental research instruments.

REFERENCES

(1) BRITTON, H. T. S.: J. Chem. Soc. **127,** 2110 (1925).
(2) KURBATOV, J. D., AND KURBATOV, M. H.: J. Phys. Chem. **46,** 441 (1942).
(3) KURBATOV, M. H., AND KURBATOV, J. D.: J. Chem. Phys. **13,** 208 (1945).
(4) PANETH,—: Mitt. Radium Institute Wien **34,** 47, 55 (1913).
(5) SCHUBERT, J.: AECD 1910 (1948). Technical Information Branch, AEC, Oak Ridge, Tennessee.
(6) SPITZER, V. I.: J Russ. Chem. Soc. **49,** 357 (1917).

COAGULATION ISOTHERM OF THORIUM

J. D. KURBATOV AND A. M. SILVERSTEIN

Department of Physics, the Ohio State University, Columbus, Ohio

Received November 18, 1949

INTRODUCTION

In previous work it has been shown that the coagulation of tetravalent thorium (3) or zirconium (2) ions in quantities of the order of 10^{-6} gram-atom (10^{-4} molar), under comparable conditions of pH, salt concentration, and nature of cations and anions present, is similar to their removal by filtration from extremely dilute solutions, 10^{-8} molar or less. Thus, weighable quantities of thorium or zirconium which undergo visible coagulation exhibit behavior comparable to that of the same ions in such extreme dilution that agglomeration before filtration could not be observed.

Under a given set of experimental conditions such as pH, salt concentration, etc., consecutive filtrations of the same solutions of tetravalent elements result in removal on the paper of similar fractions of the material in the solution. However, the results in a series of experiments are reproducible and if removal on the filter paper in extreme dilution were entirely due to adsorption of thorium ions by filter paper, the fraction removed by filtration should be expected to vary significantly, owing to differences in the rate of filtration and in the surface of the paper covered during filtration.

In order to establish the continuity of the process of coagulation of visible quantities and their removal from solution by filtration with the removal of invisible quantities of the same element from solution under the same experimental conditions, a coagulation isotherm of thorium has been obtained, using quantities from 1×10^{-5} to 1×10^{-9} gram-atom.

TABLE 1

Coagulation of thorium at pH 3.5

$T = 25°C.$; $NH_4NO_3 = 5 \times 10^{-3}$ N; volume = 20 ± 0.2 ml.; coagulation period = 2 hr.

TOTAL THORIUM	COAGULATION	TOTAL THORIUM	COAGULATION
gram-atoms	*per cent*	*gram-atoms*	*per cent*
1×10^{-9}	82.3	6×10^{-7}	53.3
1×10^{-8}	81.4	1×10^{-6}	42.5
1×10^{-7}	82.3	4×10^{-6}	22.2
2×10^{-7}	82.2	1×10^{-5}	13.0
4×10^{-7}	67.5		

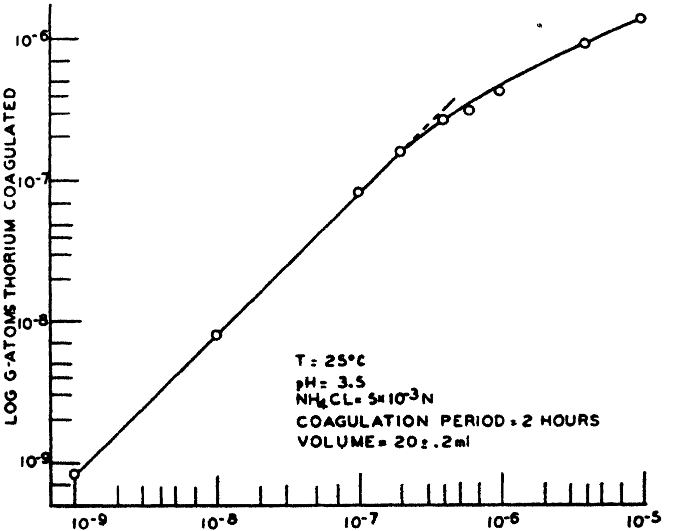

FIG. 1. Coagulation isotherm of thorium

PROCEDURE

A purified solution of known concentration of thorium nitrate in 0.01 N nitric acid was diluted in 0.01 N nitric acid so that 1 ml. of each of the various dilutions contained the quantities of thorium listed in table 1. To 1 ml. of each of the thorium solutions 2 ml. of UX_1 tracer in 0.01 N nitric acid and 15 ml. of water were added. These solutions were titrated rapidly to pH 3.5, using freshly prepared ammonia solutions, and the vessels closed and allowed to stand 2 hr. Then the solutions were filtered through Schleicher and Schüll blue ribbon filter papers.

The part of the thorium remaining on the filter paper was dissolved in nitric acid, the solution evaporated to dryness, and its activity measured on a Geiger counter. Known fractions of the filtrate were also evaporated to dryness and their activities measured to be certain of complete recovery of the tracer.

The preparation of UX_1 tracer and its measurement have been described in a recent paper (3).

EXPERIMENTAL RESULTS

Table 1 shows that the fraction of thorium removed increased with dilution down to 2×10^{-7} gram-atom/20 ml. under the conditions given. Below this concentration the fraction removed was experimentally constant.

The log-log (figure 1) plot of thorium removed *vs.* thorium originally present shows the continuity of behavior through the whole range of concentrations used, with the curve bending toward the abscissa in the higher concentration range, as was observed previously with both yttrium (1) and zirconium.

SUMMARY

The coagulation isotherm obtained under the conditions described shows that there is no discontinuity in the removal of thorium on filter paper in the concentrations of thorium used. While the highest concentration was conventional and the lowest was 5×10^{-8} *M*, the process of removal of thorium from solution at pH 3.5 is not conceded as identical with the precipitation of hydrous oxides. The process consists in (*1*) adjustment of the pH of the solution to that of hydrolytic coagulation and (*2*) filtration. For the latter step the action of the filter paper is similar to the action of adsorbents.

The authors appreciate a grant in aid from The Ohio State University Development Fund for instruments and the coöperation and support of Professor Edward Mack, Jr.

REFERENCES

(1) Kurbatov, J. D., and Kurbatov, M. H.: J. Phys. Chem. **46**, 441 (1942).
(2) Kurbatov, M. H., and Kurbatov, J. D.: J. Chem. Phys. **13**, 208 (1945).
(3) Kurbatov, M. H., Webster, H. B., and Kurbatov, J. D.: J. Phys. Chem **54**, 1239 (1950).

NEW BOOKS

Fundamentals of Physical Chemistry for Premedical Students. By H. D. CROCKFORD AND SAMUEL B. KNIGHT. xi + 366 pp. New York: John Wiley and Sons, Inc., 1950. Price $4.25.

Physical chemistry offers two types of hurdle to the nonmathematical mind of the premedical student: its abstract but rigorous general principles, which he finds difficult to understand, and its numerical problems, which he finds difficult to solve. This book really shows the student how to do the problems; herein is its strength. Every topic which is treated quantitatively is illustrated by solved examples in the text; and at the end of the chapter the student will find an unusually large number of well-designed problems, half of them with their answers given in the back of the book.

The following topics are treated in this fashion: the gas laws, including elementary kinetic theory; surface tension and viscosity of liquids; concentration units in solutions; Henry's and Raoult's laws; molecular weights from boiling-point and freezing-point measurements; van't Hoff's equation for osmotic pressure; conductivity and conductance (but not transference number); chemical equilibria; equilibria in electrolyte solutions, including pH and buffers; galvanic cells, including their application to the determination of pH; indicators; oxidation potentials; elementary chemical kinetics.

Activities are introduced as "effective concentrations" and are used, or at least appropriately mentioned, throughout the book. They are never precisely defined, nor is the mystery of their determination ever clarified; however, the student will become aware of their existence.

We must now comment on the weakness of the book. First of all, there are a number of surprising omissions. Chief among the missing are the temperature effect relations; no mention is made of the Arrhenius rate-constant equation, the van't Hoff isochore, or even the Clausius–Clapeyron equation. The only temperature coefficient that we found mentioned was that of the Henry's law constant. The Brönsted acid–base concept is presented but not used. Transference numbers are not discussed. The chapters on adsorption and colloids are purely qualitative; not even the isoelectric point is treated quantitatively.

But in our opinion the book's greatest weakness is that is completely avoids those general principles which unify physical chemistry and make it understandable, which indeed transform it from a collection of formulas into a scientific discipline. Most physical chemistry texts for premedical students omit any mention of the second law of thermodynamics; this book omits the first law as well. Again and again the student is presented with a formula whose derivation, he is told, is beyond the scope of this book but can be found in any standard physical chemistry text. The derivations which are given here are very much simplified, and seem designed to render the formula plausible rather than to show the basic factors which control the phenomenon under discussion. The student who has had a sound freshman chemistry course will not be embarrassed by any unfamiliar concepts in this book. We fear that he will receive the impression that physical chemistry is a bunch of unrelated formulas, undoubtedly useful but quite beyond comprehension. We feel that the premedical student deserves better than this; that he can understand and even appreciate such great unifying principles as free energy; and that some awareness of these basic factors is the most important thing physical chemistry has to offer him.

We may sum up in terms of the two types of hurdle we first mentioned: we highly recommend this book for the job that it does on the second hurdle; we wish that it had made an attempt on the first as well.

BRYCE L. CRAWFORD, JR.

BOOKS RECEIVED

(To June 15, 1950)

Audreith, L. F. (Editor). *Inorganic Syntheses*. Vol. III. McGraw-Hill Book Company, Inc., 330 West 42nd St., New York 18. 1950. 230 pp. Price: $3.75.

Conant, **James** B. (Editor). *Harvard Case Histories in Experimental Science. Case 1. Robert Boyle's Experiments in Pneumatics*. Harvard University Press, Cambridge, Massachusetts. 1950. 70 pp.

Conant, **James** B. (Editor). *Harvard Case Histories in Experimental Science. Case 2. The Overthrow of the Phlogiston Theory. The Chemical Revolution of 1775–1789*. Harvard University Press, Cambridge, Massachusetts. 1950. 59 pp.

Finkelnburg, **Wolfgang**. *Atomic Physics*. McGraw-Hill Book Company, Inc., 330 West 42nd St., New York 18. 1950. 498 pp. Price: $6.50.

Herzberg, **Gerhard**. *Molecular Spectra and Molecular Structure. I. Spectra of Diatomic Molecules*. 2nd edition. D. Van Nostrand Company, Inc., 250 Fourth Ave., New York 3. 1950. 658 pp.

Langmuir, **Irving**. *Phenomena, Atoms and Molecules*. Philosophical Library, Inc., 15 East 40th St., New York 16. 1950. 436 pp. Price: $10.00.

Mark, H., and **Verwey**, E. J. W. (Editors). *Advances in Colloid Science*. Vol. III. Interscience Publishers, Inc., 215 Fourth Ave., New York 3. 1950. 383 pp. Price: $7.50.

Pauling, **Linus**. *College Chemistry*. W. H. Freeman and Company, San Francisco, California. 1950. 705 pp.

Rankama, **Kalervo**, and **Sahama**, **Th**. G. *Geochemistry*. The University of Chicago Press, Chicago 37, Illinois. 1950. 912 pp. Price: $15.00.

Sweeney, **William** J. *Petroelum and its Products*. Twenty-Fourth Annual Priestley Lectures. Phi Lambda Upsilon and The Department of Chemistry of The Pennsylvania State College, State College, Pennsylvania. 1950. Price: $2.00 plus $0.25 handling fee.

Syrkin, Y. K., and **Dyatkina**, M. E. *Structure of Molecules and the Chemical Bond*. Translated and revised by M. A. **Partridge** and D. O. **Jordan**. Interscience Publishers, Inc., 215 Fourth Ave., New York 3. 1950. 509 pp. Price: $8.75.

Thiele, H. *Praktikum der Kolloidchemie als Einführung in die Arbeitsmethoden*. D. Steinkopff, Einbaumstrasse 2, Griesheim, Frankfurt-Main, Germany. 1950. 227 pp. Price: unbound, 16 DM; bound, 18 DM.

Venable, W. M.: *Hydrogen in Chemical Atoms*. Analysis of Spectral Levels from Li I to O VII. Markowitz, Haas & Kopelan, 816 Ivy St., Pittsburgh 32, Pennsylvania. 1950. 156 pp. Price: $4.00.

Vinal, **George** W. *Primary Batteries*. John Wiley and Sons, Inc., 440 Fourth Ave., New York 16. 1950. 336 pp. Price $5.00.

Methuen's Monographs on Physical Subjects (John Wiley and Sons, Inc., 440 Fourth Ave., New York 16):

- **Arnot**, F. L. *Collision Processes in Gases*. 4th edition. 1950. 104 pp. Price: $1.25.
- **Flint**, H. T. *Wave Mechanics*. 6th edition. 1949. 131 pp. Price: $1.25.
- **Hague**, B. *An Introduction to Vector Analysis*. 4th edition. 1950. 122 pp. Price: $1.25.
- **Jackson**, L. C. *Wave Filters*. 3rd edition. 1950. 107 pp. Price: $1.25.
- **James**, R. W. *X-Ray Crystallography*. 4th edition. 1950. 88 pp. Price: $1.25.
- **Johnson**, R. C. *Atomic Spectra*. 2nd edition. 1950. 120 pp. Price: $1.25.
- **Josephs**, H. J. *Heaviside's Electric Circuit Theory*. 2nd edition. 1950. 115 pp. Price: $1.25.
- **Knudsen**, **Martin**. *The Kinetic Theory of Gases*. 3rd edition. 1950. 64 pp. Price: $1.25.
- **Sutton**, O. G. *Atmospheric Turbulence*. 1st edition. 1949. 107 pp. Price: $1.50.
- **Williams**, W. **Ewart**. *Applications of Interferometry*. 4th edition. 1950. 104 pp. Price: $1.25.
- **Worsnop**, B. L., and **Chalklin**, F. C. *X-Rays*. 3rd edition. 1950. 122 pp. Price: $1.25.

THE SYSTEM ALUMINUM NITRATE–WATER–*n*-HEXYL ALCOHOL AT 25°C.

CHARLES C. TEMPLETON[1]

Department of Chemistry, University of Michigan, Ann Arbor, Michigan

Received November 28, 1949

Recently there has been increased interest in the physical chemistry of systems of the type inorganic salt–water–organic solvent. These include the work of W. Fischer (4–7) and coworkers on the salts of the rare earths, scandium, zirconium, and hafnium, that of Warf (29) on cerium(IV) nitrate, that of Garwin and Hixson and Hixson (8) on nickel(II) and cobalt(II) chlorides, and that of the author and coworkers (22, 26–28) concerning the separation of thorium nitrate from rare earth nitrates and of the rare earth nitrates from each other. There is also, of course, the well-known use of ether to purify uranyl nitrate. The papers of Nachtrieb and coworkers (19, 20) on the extraction of ferric chloride from concentrated aqueous hydrochloric acid solutions with isopropyl ether come the closest of the studies so far published to being of a fundamental physicochemical nature.

Hill, Miller, and Macy (10–13, 15) determined ternary phase diagrams for water and silver perchlorate in conjunction with each of the following solvents; benzene, toluene, aniline, and pyridine. Misciattelli (16) studied the system thorium nitrate–water–ethyl ether, and Misciattelli (17) and Guempel (9) studied the system uranyl nitrate–water–ethyl ether. The water percentages in Misciattelli's studies are not overly precise or consistent. However, the Karl Fischer (3) method for the determination of water now makes it possible to obtain much more accurate results. The present study is presented, apart from the interest of the data themselves, to give more insight into the factors govering the extraction of metallic nitrates from aqueous into organic solutions, a phenomenon which is dependent upon the presence of oxygen-containing functional groups in the solvent molecules.

During the course of this study there appeared the very recent work of Katzin and Sullivan (14), which includes complete phase data (obtained with the help of the Karl Fischer method) for water–uranyl nitrate–solvent systems, for several alcohols, ketones, and ethers.

Aluminum nitrate was chosen for study because of its appreciable solubility in *n*-hexyl alcohol (intermediate between that of thorium nitrate and the rare earth nitrates) and because its alcoholic solutions showed no instability after even six months of standing. By contrast, solutions of ferric nitrate in *n*-hexyl alcohol change their chemical nature so rapidly that, after a week or more, one cannot obtain reproducible distribution data.

---

[1] Present address: Shell Oil Company, 3737 Bellaire Boulevard, Houston 5, Texas.

DETERMINATION OF PHASE DATA FOR THE SYSTEM ALUMINUM NITRATE–WATER–*n*-HEXYL ALCOHOL

Materials

n-Hexyl alcohol (Eastman Kodak Company, practical grade) was distilled twice through a column of about four theoretical plates, the middle fraction only being retained after each distillation. The product had a boiling range of 0.2°C. No special measures were taken to remove water, since the solvent was eventually again placed in contact with water, and the analytical method was used for obtaining the data. Karl Fischer determinations showed the final solvent to contain 0.1 per cent or less of water.

Aluminum nitrate nonahydrate (Mallinckrodt analytical reagent grade) was used without further purification. The maximum impurities, 0.1 per cent of alkali salts and 0.02 per cent sulfate, were less than the general experimental error. All other chemicals used were of analytical reagent grade.

Procedure

All the systems were agitated and allowed to come to equilibrium in a 25°C. ± 0.05° thermostat. Twenty-four hours was abundant time for equilibrating two liquid phases; several days were required for a solid and an organic liquid phase to reach equilibrium. When removed from the thermostat, the phases were immediately separated and placed in dropping bottles; in this condition they could stand indefinitely before analysis.

Water was determined by the Karl Fischer (3, 18) method in conjunction with an electrical endpoint indicator. Standardization and operating methods were based on accepted procedures (18). For solutions which were sufficiently concentrated, aluminum nitrate was calculated from the alumina residue obtained by direct ignition of the solution sample in a platinum crucible. For more dilute solutions, aluminum was determined colorimetrically by the use of the ammonium aurintricarboxylate (aluminon) method in acid medium (23) and a Klett-Summerson photoelectric colorimeter (green filter). In these cases about 10 g. of alcoholic solution was weighed into a 100-ml. volumetric flask and allowed to stand for several days in contact with about 50 ml. of water. The distribution relations are such that the aluminum is quantitatively extracted into the aqueous phase. Later enough water was added to bring the interface to the mark, the alcohol was pipetted away, and the analysis finished in the usual fashion. pH measurements were made with a glass and saturated calomel electrode system and a Beckman Model H-2 pH meter.

Data and discussion

In table 1 are recorded the fundamental phase data for the system. It was demonstrated that $Al(NO_3)_3 \cdot 9H_2O$ was the equilibrium solid phase for both the saturated two-liquid-phase system and for a single alcoholic phase. The solubility of 0.62 per cent for *n*-hexyl alcohol in water was determined interferometrically by Butler, Thomson, and Maclennan (1). Two independent values for the solubility of aluminum nitrate in water at 25°C. reported by Seidell (24), e.g., 43.5 and 39.5 weight per cent $Al(NO_3)_3$, compare reasonably well with these data.

TABLE 1

The system aluminum nitrate–water–n-hexyl alcohol at 25°C. ± 0.05°

RUN NO.	pH (AQUEOUS PHASE)	AQUEOUS PHASE			ALCOHOLIC PHASE			REMARKS
		Weight percentages			Weight percentages			
		$Al(NO_3)_3$	H_2O	$C_6H_{13}OH$	$Al(NO_3)_3$	H_2O	$C_6H_{13}OH$	
I		41.2	58.2	0.6	7.92	9.65	82.4	Solid phase $Al(NO_3)_3 \cdot 9H_2O$
7	0.60	41.2	59.2	(−0.4)	7.83	9.55	82.6	
1(a)	0.72	39.9	60.3	(−0.2)	6.89	9.21	83.9	
201	0.66	38.3	61.2	0.5	5.84	8.53	85.6	
II		38.1	60.2	1.7	5.98	8.71	85.3	....
8	0.92	35.6	63.5	0.9	4.27	7.74	88.0	
301	0.90	35.0	64.7	0.2	3.62	7.07	89.3	
9	1.20	31.5	67.9	0.6	1.99	5.77	92.3	
III		31.3	69.7	(−1.0)	1.81	5.81	92.4	
V		30.5	67.9	1.6	1.78	5.66	92.6	
VI		26.0	73.5	0.5	0.72	5.12	94.2	
1	1.74	23.0	76.3	0.7	0.24	5.03	94.7	
2	2.09	20.3	78.8	0.9	0.10	5.14	94.8	
3	2.20	17.14	81.6	1.2	0.041‡	5.47	94.5	
4	2.40	13.84	84.8	1.3	0.032‡	5.83	94.1	
VII		11.9	86.8	1.3		6.05	93.9	
5	2.64	9.41	90.3	0.3	0.0106‡	6.22	93.7	
6	2.78	6.27	92.5	1.2	0.0032‡	6.52	93.4	
VIII		0.00	99.4*	0.62*	0.00	7.11†	92.9	

Supplementary data:

	Found	Theoretical
A. Solid phase, Run No. I: $Al(NO_3)_3$, per cent	56.8	56.8
H_2O, per cent	42.7	43.2

This phase was prepared by adding finely ground $Al(NO_3)_3 \cdot 9H_2O$ to the saturated system and allowing crystals to grow to moderate size.

B. Solubility of $Al(NO_3)_3 \cdot 9H_2O$ in n-hexyl alcohol alone:

	Found	Theoretical
$Al(NO_3)_3$ by ignition = 7.10 per cent		
Solid phase: H_2O, per cent	41.6	43.2

---

* Butler, Thomson, and Maclennan (1)

† More accurate than the value of 7.4 previously reported (26).

‡ Determined colorimetrically with aluminon.

In figure 1 the data are plotted in triangular coördinates. The system has been completely investigated between the limits water, n-hexyl alcohol, and $Al(NO_3)_3 \cdot 9H_2O$, but no measurements have been made for the remaining region of the plot. Evidence will now be presented that the system is not stable in the water-poor region. According to Young (30) $Al(NO_3)_3 \cdot 9H_2O$ is converted to $Al(NO_3)_3 \cdot 6H_2O$ when confined over Dehydrite for 5 days. The author left the nonahydrate over Dehydrite for 2 weeks and obtained a product which give

16.2 per cent Al_2O_3 on ignition (theoretical for the hexahydrate, 15.87 per cent Al_2O_3). This product was mixed with *n*-hexyl alcohol and allowed to stand with occasional agitation for two months. A clear solution resulted, but the residual solid was gelatinous and could not practically be dried for analysis. The solution contained 3.52 per cent Al_2O_3 (or 14.70 per cent $Al(NO_3)_3$), a value about twice as large as the solubility in alcohol when the solid phase has the maximum amount of water of crystallization.

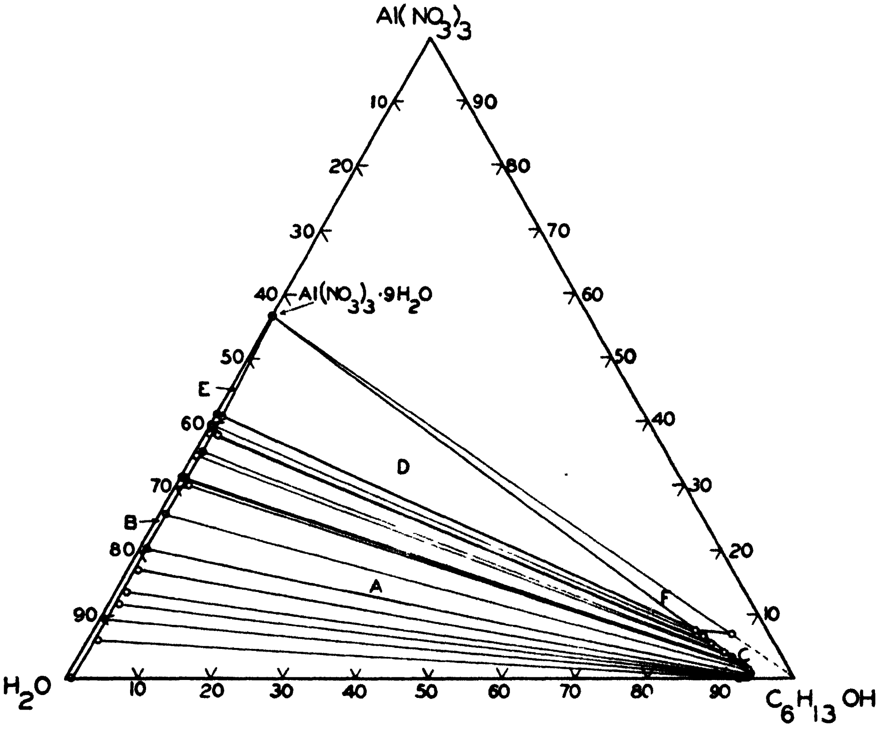

FIG. 1. System aluminum nitrate–water–*n*-hexyl alcohol at 25°C. (weight percentage). Regions: A, two liquid phases; B, single water-rich liquid phase; C, single alcohol-rich liquid phase; D, $Al(NO_3)_3 \cdot 9H_2O$ and two liquid phases; E, $Al(NO_3)_3 \cdot 9H_2O$ and water-rich liquid phase; F, $Al(NO_3)_3 \cdot 9H_2O$ and alcohol-rich liquid phase.

The salt after standing for two months over Dehydrite was found to contain 25.2 per cent Al_2O_3 and 33 per cent H_2O. The corresponding empirical formula is $Al_2O_3 \cdot 1.57N_2O_5 \cdot 7.4H_2O$, which approximates $Al_2(OH)_3(NO_3)_3 \cdot 6H_2O$. The study of the water-poor region was then abandoned, since the attempts to remove water appear also to remove nitrate, and a system results of which aluminum nitrate is no longer a proper phase rule component.

In table 2 are included the mole fractions of Al^{3+} in the aqueous phase (counting Al^{3+} and NO_3^- as molecular entities), and of $Al(NO_3)_3$ in the alcoholic phase (considering the solution to consist of H_2O, $C_6H_{13}OH$, and $Al(NO_3)_3$ "molecules"). As in previous distribution studies (22, 27, 28) these modes of expression are mainly an arbitrary means of making comparisons on a molar basis. The molalities are referred to 1000 g. of the richer solvent in each phase.

In the right-hand section of figure 2, the true mole fraction of aluminum nitrate in the alcoholic phase, ${}_{\mathrm{alc}}X_{[\mathrm{Al(NO_3)_3}]}$, is plotted on a log-log scale *versus* the true mole fraction of Al^{3+} in the aqueous phase, ${}_{\mathrm{aq}}X_{\mathrm{Al^{3+}}}$. In past studies (22, 26, 28) in which no determinations of water were made, one could calculate only the corresponding apparent mole fractions based on the assumption of immiscibility of the two solvents. In the left-hand portion of figure 2 the distribution of aluminum nitrate is plotted on this apparent mole fraction basis, along with the data for lanthanum, cerium, praseodymium, neodymium, samarium, and thorium nitrates. The general character of the phenomenon has been established over a 2500-fold range. In the high-concentration range, the slope of the aluminum curve would be about the same as for the rare earth nitrates, e.g. 4.0, if a straight line were drawn in this region as was done for the rare earth nitrates. For the colorimetrically determined points in the most dilute region, the slope has decreased to about 2.7. The interpretation of these data will be discussed in more detail in the second section of this paper.

TABLE 2

Concentrations calculated from table 1

RUN NO.	AQUEOUS PHASE		ALCOHOLIC PHASE		
	True mole fraction* of Al^{3+}	Molality of $[Al(NO_3)_3]$	True mole fraction of $[Al(NO_3)_3]$	Molality of H_2O	Molality of $[Al(NO_3)_3]$
I	0.0482	3.32	0.0269	6.51	0.451
7	0.0482	3.32	0.0267	6.42	0.445
1(a)	0.0461	3.14	0.0237	6.11	0.386
201	0.0436	2.94	0.0205	5.53	0.320
II	0.0433	2.92	0.0208	5.67	0.329
8	0.0396	2.62	0.0152	4.88	0.228
301	0.0388	2.555	0.0132	4.40	0.1905
9	0.0338	2.18	0.0074	3.48	0.101
III	0.0334	2.16	0.0069	3.50	0.0921
V	0.0325	2.08	0.0068	3.40	0.0902
VI	0.0267	1.663	0.0028	3.02	0.036
1	0.0231	1.414	0.0009	2.95	0.012
2	0.0199	1.204	0.0004	3.01	0.005
3	0.0164	0.979	0.000156	3.22	0.0020
4	0.0129	0.759	0.000120	3.44	0.0016
VII	0.0110	0.638	<0.00015	3.58	
5	0.0085	0.491	0.000039	3.69	0.00053
6	0.0056	0.316	0.000012	3.88	0.000016
VIII	0.0000	0.0000	0.000000	4.25	0.000000

* Calculated on the assumption of 0.6 per cent alcohol in all aqueous phases.

In figure 3 the molality of water is plotted as a function of the molality of aluminum nitrate for the alcohol phase. After a very unusual decrease in a region in which practically no aluminum nitrate is yet in the alcohol phase, the amount of water increases approximately linearly with the amount of aluminum nitrate. The slope of the best line through the points is 8.9 (the extreme slopes are about 9.6 and 8.2). This means that nine molecules are carried into the alcohol phase

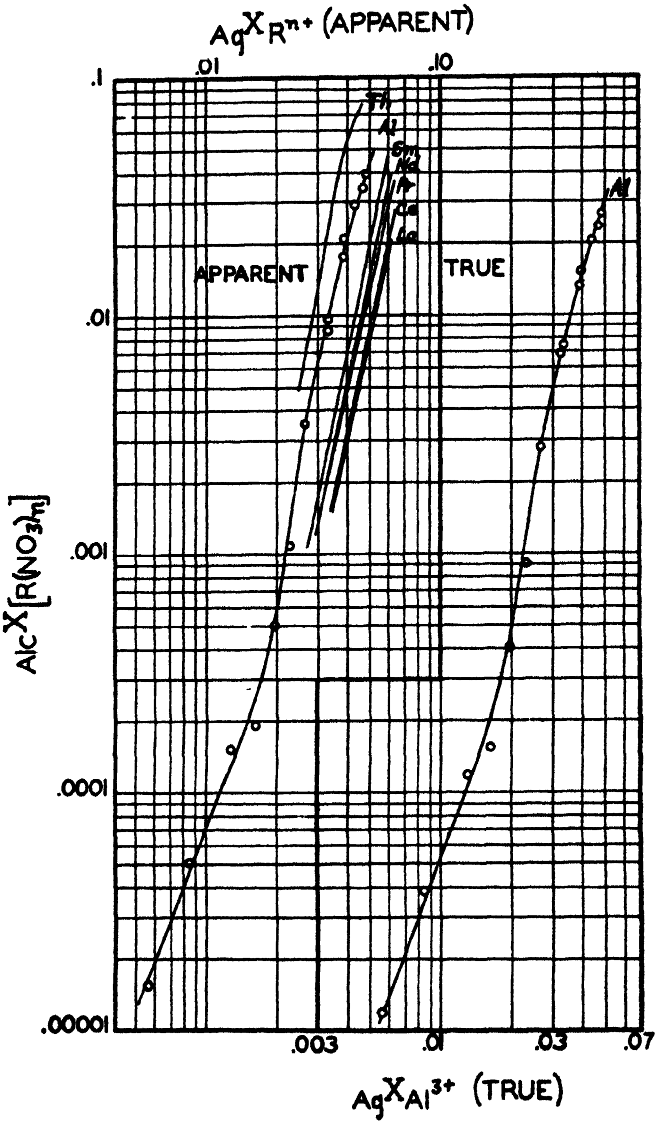

Fig. 2. Distribution of nitrates between water and *n*-hexyl alcohol at 25°C. (pure salts only).

by each $Al(NO_3)_3$ unit, because at any point of this linear portion the slope of the curve is the molar ratio of water increase to aluminum nitrate increase, regardless of the state of the water already in the alcoholic phase. This analysis is similar to that of Katzin and Sullivan for uranyl nitrate systems (14). The differential rate of transfer of water into the alcoholic phase does not necessarily give the number of water molecules coördinated by the salt. There must be alcohol as well as water coördinated in the total complex. The whole matter is also complicated by the vagueness of what is meant by "free" and "bound" solvent in any solution.

Since the activity of water (referred to a mole fraction scale and a standard state of pure water) must be the same in both phases for any pair of conjugate phases, the primary cause of the initial rapid decrease in water content of the alcoholic phase may be seated in either or both phases. Some estimates may be made of these changes by use of the only activity data available for aqueous solutions of aluminum nitrate, those of Pearce[2] (21). Although the presence of alcohol certainly affects the water activity, one should be able to assume without too much error that the same percentage change in water activity is caused by a given amount of aluminum nitrate in a pure aqueous phase as in one that contains less than 1 per cent of alcohol. On comparing runs VIII and 2 one finds:

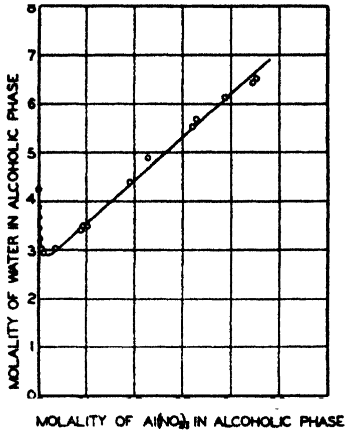

FIG. 3. Determination of mole ratio of water to aluminum in alcohol-extracted complex.

	RUN VIII	RUN 2
${}_{\text{alc}}X_{H_2O}$	0.302	0.235
a_{H_2O} for aqueous solution of same $Al(NO_3)_3$ concentration (Pearce)	1.000	0.899

The addition of the aluminum nitrate has decreased the aqueous water activity by 10.1 per cent, while the water concentration in the alcoholic phase has been decreased by 22.2 per cent. Thus the nitrate addition must also increase the activity coefficient of the water in the alcoholic phase by a factor of 1.15. It must be concluded that a very small amount of aluminum nitrate is capable of appreciably altering the interactions between water and alcohol molecules in the alcoholic phase.

---

[2] However, since values reported simultaneously by Pearce for calcium nitrate differ greatly from more recent measurements of Stokes and Robinson (25), the data of Pearce for aluminum nitrate may well be considered with a little reservation.

DEPENDENCE OF THE DISTRIBUTION UPON CONCENTRATIONS OF INDIVIDUAL IONS IN THE AQUEOUS PHASE

In previous studies (22, 26, 28) the distribution of a metallic nitrate between water and an immiscible organic solvent has been interpreted according to the mechanism

$$\underset{\text{(aqueous phase)}}{R^{n+} + nNO_3^-} \rightleftarrows \underset{\text{(organic phase)}}{[R(NO_3)_n]} \qquad \text{(I)}$$

This mechanism was based upon two facts. First, the plot of the logarithm of the mole fraction of $R(NO_3)_n$ in the organic phase *versus* the logarithm of the mole fraction of the cation in the aqueous phase, for solutions of the nitrate alone (in which the concentration of nitrate is proportional to that of the cation), was approximately linear over an appreciable range with a slope slightly greater than n. Secondly, for the case of thorium nitrate, the effect of added nitric acid was consistent with this mechanism. Since this treatment took into account no activity data, and in some other respects was a first approximation, it is in order to test it further experimentally. The most obvious point of attack would be to study the distribution as a function of the concentration of each of the ions in the aqueous phase, while the concentrations of the other ions are maintained constant.

The mechanism implies the existence of an equilibrium expression of the following form:

$$\frac{{}_{\text{alc}}f_{[\text{Al(NO}_3)_3]}\cdot {}_{\text{alc}}X_{[\text{Al(NO}_3)_3]}}{f_\pm^4 \cdot {}_{\text{aq}}X_{\text{Al}^{3+}}\cdot ({}_{\text{aq}}X_{\text{NO}_3^-})^3} = \frac{{}_{\text{alc}}f_{[\text{Al(NO}_3)_3]}\cdot {}_{\text{alc}}X_{[\text{Al(NO}_3)_3]}}{27(f_\pm \cdot {}_{\text{aq}}X_{\text{Al}^{3+}})^4} = K \qquad (1)$$

where the f's are activity coefficients and the X's are mole fractions. If it is assumed that the presence of about 1 per cent of alcohol in the aqueous phase does not greatly affect the activity of the aluminum nitrate, the data of Pearce (21), when converted to a mole fraction scale, may be used to calculate the denominator of equation 1. Table 2 contains values of ${}_{\text{alc}}X_{\text{Al(NO}_3)_3}$. No activity measurements have ever been made for alcoholic solutions of aluminum nitrate, and K cannot be calculated. However, one can calculate *relative* values of the activity coefficients by assigning K an arbitrary value of unity:

$$\text{Relative } {}_{\text{alc}}f_{[\text{Al(NO}_3)_3]} = \frac{27(f_\pm \cdot {}_{\text{aq}}X_{\text{Al}^{3+}})^4}{{}_{\text{alc}}X_{[\text{Al(NO}_3)_3]}} \qquad (2)$$

Since it has been shown that about nine molecules of water are carried into the alcoholic phase by each $Al(NO_3)_3$ unit, one can also consider the mechanism:

$$\underset{\text{(aqueous phase)}}{Al^{3+} + 3NO_3^- + 9H_2O} \rightleftarrows \underset{\text{(alcoholic phase)}}{[Al(NO_3)_3 \cdot 9H_2O]} \qquad \text{(II)}$$

with which is associated the relation:

$$\text{Relative }_{\text{alc}}f_{[\text{Al}(\text{NO}_3)_3\cdot 9\text{H}_2\text{O}]} = \frac{27(f_{\pm}\cdot {}_{\text{aq}}X_{\text{Al}^{3+}})^4(a_{\text{H}_2\text{O}})^9}{_{\text{alc}}X_{[\text{Al}(\text{NO}_3)_3\cdot 9\text{H}_2\text{O}]}} \qquad (3)$$

In table 3 such relative activity coefficients are listed for some selected points. For mechanism I the activity coefficient increases somewhat faster than the mole fraction, and for mechanism II the activity coefficient increases a little more slowly than the mole fraction. The question of whether such rapidly increasing coefficients in alcoholic solution seem physically reasonable cannot be answered very well until some direct experimental measurements are made.

TABLE 3

Relative activity coefficients of aluminum nitrate in n-hexyl alcohol solutions

RUN	RELATIVE		RELATIVE	
	alc $X_{[\text{Al}(\text{NO}_3)_3]}$	alc $f_{[\text{Al}(\text{NO}_3)_3]}$	alc $X_{[\text{Al}(\text{NO}_3)_3\cdot 9\text{H}_2\text{O}]}$	alc $f_{[\text{Al}(\text{NO}_3)_3\cdot 9\text{H}_2\text{O}]}$
6	1.2×10^{-5}	1.1×10^{-6}	1.2×10^{-5}	9.3×10^{-7}
4	1.2×10^{-4}	3.8×10^{-6}	1.2×10^{-4}	2.3×10^{-6}
2	4×10^{-4}	2.5×10^{-5}	4×10^{-4}	9.5×10^{-6}
VI	2.8×10^{-3}	6.2×10^{-5}	2.9×10^{-3}	1.23×10^{-5}
9	7.4×10^{-3}	4.8×10^{-4}	8.1×10^{-3}	2.7×10^{-5}
8	1.52×10^{-2}	2.2×10^{-3}	1.77×10^{-2}	6.9×10^{-5}
1(a)	2.37×10^{-2}	1.45×10^{-2}	3.00×10^{-2}	1.27×10^{-4}

We must recognize that mechanism I is merely the overall reaction for the following set of reactions:

$$\text{Al}^{3+} + \text{NO}_3^- \rightleftarrows \text{Al}(\text{NO}_3)^{2+} \qquad \text{(aqueous phase)} \qquad \text{(i)}$$

$$\text{Al}(\text{NO}_3)^{2+} + \text{NO}_3^- \rightleftarrows \text{Al}(\text{NO}_3)_2^+ \qquad \text{(aqueous phase)} \qquad \text{(ii)}$$

$$\text{Al}(\text{NO}_3)_2^+ + \text{NO}_3^- \rightleftarrows [\text{Al}(\text{NO}_3)_3] \qquad \text{(aqueous phase)} \qquad \text{(iii)}$$

$$\underset{\text{(aqueous)}}{[\text{Al}(\text{NO}_3)_3]} \rightleftarrows \underset{\text{(alcoholic)}}{[\text{Al}(\text{NO}_3)_3]} \qquad \text{(iv)}$$

But, by simultaneous solution of the resulting intermediate equilibrium relations, one obtains the equivalent of equation 1. We have already considered all the nitrate in the aqueous phase to be in the species NO_3^-, and this would actually be true only if reaction (i) had not shifted appreciably "to the right." However, our calculation of relative activity coefficient is justified, because we used activity coefficients for aqueous solutions in which reactions (i), (ii), and (iii) exist, and which are also based upon the assumption that only the species NO_3^- and Al^{3+} exist in the aqueous phase.

The first investigation was of the effect of acidity upon the distribution. Values of pH, measured with a glass electrode, are recorded in table 1 for the ternary system. Measurements of pH for aqueous solutions of aluminum nitrate were made over the same concentration range and were found to be practically the same as for the solutions in which *n*-hexyl alcohol was present. These data for the simple aqueous solutions were consistent with those reported by Cupr

(2). Apparently the extraction has not involved the removal of any acid from the aqueous phase.

Table 4 describes the effect of the addition of small amounts of acids and bases upon the distribution. In each of the series, the first system belongs to the pure aluminum nitrate–water–alcohol system, and the following systems resulted from the successive addition of the indicated acid or base. The dilution is small enough to allow us to consider all species other than hydrogen ion to remain at constant concentration, for purposes of estimating the order of magnitude of the effect of pH. For any pH change, the logarithm of the ratio of the final to the initial concentration of aluminum in the alcoholic phase, divided by the change in pH, is a measure of the number of hydrogen or hydroxyl ions which may be involved in the transition of one unit of $Al(NO_3)_3$ from the aqueous to the alcoholic phase. This ratio, for the extreme change in each series, has values of +0.1, −0.05, and −0.6, respectively, for series I, II, and III. There is thus no evidence for the participation of even one hydrogen or hydroxyl ion in the distribution reaction.

TABLE 4

Dependence of distribution upon acidity

Acid and base additions at room temperature

RUN	pH	Al_2O_3 Aqueous	Al_2O_3 Alcoholic	REMARKS
Series I: HNO_3 addition				
		per cent	*per cent*	
101	0.78	9.32	1.49	
101a	−0.15	9.09	1.21	Mixed by weight (3 days old)
Series II: HNO_3 addition				
9	1.20	7.54	0.475	
9(a)	0.28	7.47	0.52	(3 days old)
Series III: NH_4OH addition				
1(a)	0.72	9.55	1.65	
1(c)	0.80	9.54	1.51	4 days after first addition
1(d)	1.00	9.44	1.28	8 days after first addition
1(e)	1.62	9.01	0.47	12 days after first addition

The next experiment tested the dependence of the distribution upon the concentration of nitrate at approximately constant aluminum concentration. Table 5 lists data for systems mixed from water, *n*-hexyl alcohol, aluminum nitrate, and aluminum sulfate[3] in such a way as to maintain a constant Al^{3+}/H_2O ratio. This also maintains ${}_{aq}X_{Al^{3+}}$ constant to within 3 per cent. The aqueous ionic mole fractions shown in table 5 are those for the aqueous phase before the addition of the alcohol. It is assumed that, after equilibrium at 25°C. was reached, these aqueous mole fractions had not changed enough to invalidate appreciably this attempt to estimate the order of magnitude of the dependence upon nitrate concentration (see footnote of table 5). The percentages of aluminum nitrate in the alcoholic phase were determined colorimetrically with aluminon, after the systems had stood in a 25°C. ± 0.1° thermostat for over 5 days. The mole fraction of aluminum nitrate in the alcoholic phase was taken to be equal to that of the alcoholic phase of the $Al(NO_3)_3$–H_2O–$C_6H_{13}OH$ system which contained the same percentage of aluminum nitrate.

---

[3] It was established that aluminum sulfate and ammonium nitrate have solubilities in *n*-hexyl alcohol which are negligible for these purposes.

In figure 4, ${}_{alc}X_{[Al(NO_3)_3]}$ is plotted *versus* ${}_{aq}X_{NO_3^-}$ on a log-log scale. A linear plot of slope 2.9 is obtained. In the same concentration range for the pure ternary system, in which ${}_{aq}X_{Al^{3+}}$ is proportional to ${}_{aq}X_{NO_3^-}$, the slope of a linear log-log plot in figure 2 would be 4.0. Equation 1, the equilibrium relation resulting from mechanism I, may be written,

TABLE 5

Distribution of aluminum nitrate between water and n-hexyl alcohol at 25°C. as a function of aqueous nitrate concentration at constant aluminum concentration

SYSTEM	MIXING OF SYSTEM				AQUEOUS PHASE*				ALCOHOLIC PHASE	
	$Al(NO_3)_3$ solution	$Al_2(SO_4)_3$ solution	H_2O	*n*-Hexyl alcohol	${}_{aq}X_{Al^{3+}}$	${}_{aq}X_{NO_3^-}$	${}_{aq}X_{SO_4^{--}}$	${}_{aq}X_{H_2O}$	$Al(NO_3)_3$	${}_{alc}X_{[Al(NO_3)_3]}$
	ml.	*ml.*	*ml.*	*ml.*					*per cent*	
A	20.00	0.00	8.48	15.00	0.0335	0.1004	0.0000	0.866	1.89	0.00725
B	17.00	3.57	7.62	15.00	0.0338	0.0861	0.0120	0.873	1.21	0.00475
C	14.00	7.14	6.76	15.00	0.0340	0.0715	0.0240	0.880	0.69	0.00270
E	8.00	14.32	5.00	15.00	0.0345	0.0415	0.0481	0.892	0.142	0.00055

Supplementary data:

$Al(NO_3)_3$ solution: $Al(NO_3)_3$ = 40.9 per cent; density = 1.398 g./ml.
$Al_2(SO_4)_3$ solution: $Al_2(SO_4)_3$ = 29.1 per cent; density = 1.317 g./ml.
Densities at 25°C.: H_2O = 0.997 g./ml.; *n*-hexyl alcohol = 0.818 g./ml.

* For system A, about 2 per cent of the total aluminum is extracted into the alcohol.

$$\log {}_{alc}X_{[Al(NO_3)_3]} = \log K + \log \left(f_{\pm}^{4}/{}_{alc}f_{[Al(NO_3)_3]}\right) + \log {}_{aq}X_{Al^{3+}} + 3 \log {}_{aq}X_{NO_3^-} \quad (4)$$

If, over a given concentration range, the activity coefficient ratio were approximately constant, one would expect a slope of 3.0 for this plot. Thus, at this stage of the evidence, mechanism I seems to be on a firm basis.

From the above considerations one would predict only a first-power dependence of the distribution upon the aqueous aluminum concentration at constant aqueous nitrate concentration. The actual effect, however, was measured and recorded in table 6. These systems were mixed from water, *n*-hexyl alcohol, aluminum nitrate, and ammonium nitrate in the proper proportions to maintain a constant NO_3^-/H_2O ratio. This also maintained ${}_{aq}X_{NO_3^-}$ constant to within about 6 per cent. The aqueous ionic mole fractions were calculated, the amounts extracted into the alcoholic phase again being neglected in this connection. In view of the third-power dependence of ${}_{alc}X_{[Al(NO_3)_3]}$ upon ${}_{aq}X_{NO_3^-}$, which has already been found, the factor of 1.06 by which ${}_{aq}X_{NO_3^-}$ fails to remain constant in this series could reflect a factor of 1.19 into the overall change of ${}_{alc}X_{[Al(NO_3)_3]}$. In figure 5, ${}_{alc}X_{[Al(NO_3)_3]}$ when plotted on a log-log scale as a function of ${}_{aq}X_{Al^{3+}}$ is essentially linear with a slope of 3.5. The factor of 1.19 on this logarithmic scale could at most change this slope by ± 0.2. Thus we find at least a third-power dependence of ${}_{alc}X_{[Al(NO_3)_3]}$ upon ${}_{aq}X_{Al^{3+}}$ at constant ${}_{aq}X_{NO_3^-}$, whereas we had expected only about a first-power dependence on the basis of the previous evidence.

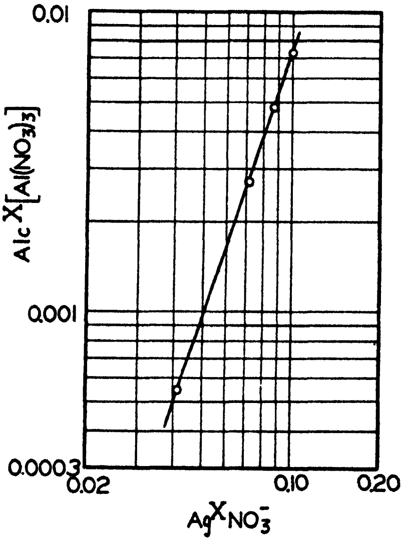

FIG. 4

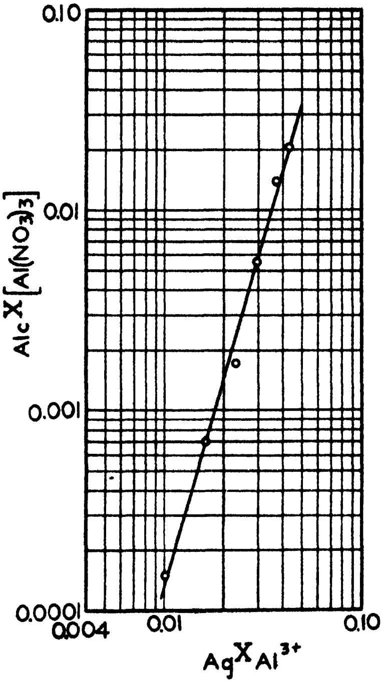

FIG. 5

FIG. 4. Distribution of aluminum nitrate between water and *n*-hexyl alcohol at 25°C. as a function of aqueous nitrate concentration at fixed aqueous aluminum concentration.

FIG. 5. Distribution of aluminum nitrate between water and *n*-hexyl alcohol at 25°C. as a function of aqueous aluminum concentration at fixed aqueous nitrate concentration.

This evidence at first sight greatly damages the idea of dividing the distribution dependence, even empirically, between the simple ionic concentrations in the aqueous phase according to mechanism I. Can any alternative set of distribution reactions be written? Any other pattern would involve a change in the NO_3^-/Al^{3+} ratio in the alcohol-extracted material. Admittedly, no analysis has been made here for nitrate, because the possibility of such a change seems negligible for two reasons: First, the author found (in experiments not described here) that one can extract the nitrate into the organic phase and wash it out again with water, and still be able to crystallize the original nonahydrate. Secondly, proportionally more aluminum than the amount equivalent to the original nitrate could enter the alcoholic phase only if excess free nitric acid remained in the aqueous phase. Evidence against the latter has already been presented.

TABLE 6

Distribution of aluminum nitrate between water and n-hexyl alcohol at 25°C. as a function of aqueous aluminum concentration at constant nitrate concentration

SYSTEM	MIXING OF SYSTEM				AQUEOUS PHASE*				ALCOHOLIC PHASE		pH
	$Al(NO_3)_3$ solution	NH_4NO_3 solution	H_2O	*n*-Hexyl alcohol	$_{aq}X_{Al^{3+}}$	$_{aq}X_{NO_3^-}$	$_{aq}X_{NH_4^+}$	$_{aq}X_{H_2O}$	$Al(NO_3)_3$	Estimated true $_{alc}X_{[Al(NO_3)_3]}$	
	ml	*ml.*	*ml.*	*ml.*					*per cent*		
A	20.00	0.00	0.00	13.00	0.0435	0.1303	0.0000	0.825	5.94	0.0207	0.98
B	17.00	1.97	1.75	13.00	0.0366	0.1289	0.0193	0.816	3.89	0.0140	1.30
C	14.00	3.94	3.42	13.00	0.0297	0.1271	0.0380	0.805	1.42	0.0055	1.70
D	11.00	5.94	5.09	13.00	0.0230	0.1255	0.0565	0.795	0.43	0.0017	1.94
E	8.00	7.92	6.79	13.00	0.0165	0.1240	0.0744	0.785	0.17	0.0007	2.18
F	5.00	9.88	8.46	13.00	0.0102	0.1226	0.0920	0.776	0.05	0.00015± 0.00005	2.48

Supplementary data:

$Al(NO_3)_3$ solution: $Al(NO_3)_3$ = 38.4 per cent; density = 1.356 g./ml.

NH_4NO_3 solution: NH_4NO_3 = 67.6 per cent; density = 1.313 g./ml.

Densities at 25°C.: H_2O = 0.997 g./ml.; *n*-hexyl alcohol = 0.818 g./ml.

* For system A, about 6 per cent of the total aluminum is extracted into the alcohol.

Finally, one is forced to attribute the unexpected type of dependence of the distribution upon $_{aq}X_{Al^{3+}}$ to the very complicated activity coefficient relationships which apparently exist in these systems. Nachtrieb and Fryxell (20), in the case of extraction of ferric chloride with isopropyl ether, suggest that similar unexpected behavior in the concentrated range is due to a "self-salting-out effect," although the behavior in quite dilute solutions (with respect to iron) followed a simple mechanism. For aluminum nitrate, one also could undoubtedly use radioactive aluminum to study the distribution at very low aluminum concentrations, and probably would get a "normal" dependence of the distribution upon aluminum concentration. However, this would still not explain the behavior in very concentrated solutions, and it is the nature of the phenomena in the concentrated range which motivated the present study.

SUMMARY

1. The system aluminum nitrate–water–*n*-hexyl alcohol was studied at 25°C. The water-poor region beyond $Al(NO_3)_3 \cdot 9H_2O$ was not studied, owing to the tendency toward formation of basic nitrates.

2. Addition of aluminum nitrate to the water–*n*-hexyl alcohol system affects in two different ways the water content of the alcohol-rich layer. For the addition of small amounts of salt, the amount of water in the alcohol decreases in a manner which may partially be correlated with the lowered water activity of the aqueous phase. For more concentrated systems, the percentage of water in the alcoholic layer increases with the aluminum nitrate content of the alcoholic layer, because the aluminum nitrate unit carries nine molecules of water with it on passing from the aqueous to the alcoholic phase.

3. In a study of the distribution of aluminum nitrate between the two phases, acidity is shown not to have any direct effect upon the distribution. The concentration of aluminum nitrate in the alcoholic phase is proportional to about the third power of the aqueous nitrate-ion concentration at constant aqueous aluminum-ion concentration, and also to about the third power of the aqueous aluminum-ion concentration at constant aqueous nitrate-ion concentration. These facts, when compared with the fourth-power dependence upon the total aqueous salt concentration for systems containing only pure aluminum nitrate, are evidence of the existence of quite complicated activity coefficient relationships in this concentrated range.

REFERENCES

(1) Butler, J. A. V., Thomson, D. W., and Maclennan, W. H.: J. Chem. Soc. **1933**, 674.
(2) Cupr, V.: Z. anorg. allgem. Chem. **198**, 310 (1931).
(3) Fischer, K.: Angew. Chem. **48**, 394 (1935).
(4) Fischer, W., and Bock, R.: Z. anorg. allgem. Chem. **249**, 146 (1942).
(5) Fischer, W., and Chalybaeus, W.: Z. anorg. Chem. **255**, 79 (1947).
(6) Fischer, W., Chalybaeus, W., and Zumbusch, M.: Z. anorg. Chem. **255**, 277 (1948).
(7) Fischer, W., Dietz, W., and Jübermann, O.: Naturwissenschaften **25**, 348 (1937).
(8) Garwin, L., and Hixon, A. N.: Ind. Eng. Chem. **41**, 2298, 2303 (1949).
(9) Guempel, O.: Bull. soc. chim. Belg. **38**, 443 (1929).
(10) Hill, A. E.: J. Am. Chem. Soc. **43**, 254 (1921).
(11) Hill, A. E.: J. Am. Chem. Soc. **44**, 1163 (1922).
(12) Hill, A. E., and Macy, R.: J. Am. Chem. Soc. **46**, 1132 (1924).
(13) Hill, A. E., and Miller, F. W., Jr.: J. Am. Chem. Soc. **47**, 2702 (1925).
(14) Katzin, L. I., and Sullivan, J. C.: AECD 2537, December, 1948. Technical Information Branch, AEC, Oak Ridge, Tennessee.
(15) Macy, R.: J. Am. Chem. Soc. **47**, 1031 (1925).
(16) Misciattelli, P.: Gazz. chim. ital. **60**, 833 (1930).
(17) Misciattelli, P.: Gazz. chim. ital. **60**, 839 (1930).
(18) Mitchell, J., Jr., and Smith, D. M.: *Aquametry*. Interscience Publishers, New York (1948).
(19) Nachtrieb, N. H., and Conway, J. G.: J. Am. Chem. Soc. **70**, 3547 (1948).
(20) Nachtrieb, N. H., and Fryxell, R. E.: J. Am. Chem. Soc. **70**, 3552 (1948).
(21) Pearce, J. N.: J. Am. Chem. Soc. **58**, 376 (1936).

(22) Rothschild, B. F., Templeton, C. C., and Hall, N. F.: J. Phys. & Colloid Chem. **52,** 1006 (1948).

(23) Sandell, E. B.: *Colorimetric Methods for the Determination of Traces of Metals.* Interscience Publishers, Inc., New York (1944).

(24) Seidell, A.: *Solubilities of Inorganic and Metal Organic Compounds.* D. Van Nostrand Company, New York (1940).

(25) Stokes, R. H., and Robinson, R. A.: J. Am. Chem. Soc. **70,** 1870 (1948).

(26) Templeton, C. C.: J. Am. Chem. Soc. **71,** 2187 (1949).

(27) Templeton, C. C., and Peterson, J. A.: J. Am. Chem. Soc. **70,** 3967 (1948).

(28) Templeton, C. C., Rothschild, B. F., and Hall, N. F.: J. Phys. & Colloid Chem. **53,** 838 (1949).

(29) Warf, J. C.: J. Am. Chem. Soc. **71,** 3257 (1949).

(30) Young, F. E.: J. Am. Chem. Soc. **66,** 777 (1944).

HEREDITY AND ENVIRONMENT. IV

WILDER D. BANCROFT

7 East Avenue, Ithaca, New York

Received November 25, 1949

In the April 1948 number of the Annals of Botany, E. M. Chenery (2), an Englishman formerly connected with the Department of Agriculture in Trinidad, British West Indies, and now at Wipenden, Herts, England, published an article dealing with aluminum in plants and its relation to plant pigments. Chenery describes what may be termed "hydrangea-like" plants. "The flowers of such plants, if pink, will change to blue when the plants are transferred to a more acid soil after treatment of the soil with aluminium salts; if blue they will change to pink when grown in a lime-rich or less-acid soil." Of course, this is not the whole truth, because all blue flowers turn red when acidified sufficiently.

Chenery ascribed the color change to "the formation of a blue-coloured acid-stable aluminium lake which may be regarded as a colloidal complex or a loose combination of the delphidin pigment and aluminium."

"From the researches on 'Hydrangea-like' plants three conditions emerge that have to be fulfilled before any soil-induced flower colour change will take place. The plant must (1) have a delphinidin flower pigment which in an acid cell-sap is normally pink but is blue in the presence of excess aluminium; (2) be able to accumulate aluminium; this is a specific characteristic manifest only when sufficient is available, e.g. in acid soils; (3) have a wide range of reaction tolerance." Aluminium accumulators "may be defined as plants which absorb [adsorb] aluminium to the extent of 1,000 p.p.m. of dry matter."

". . . when hydrangeas of all colours are grown in bright sunlight, those portions directly exposed to the sun become bright red about two weeks after the flowers have matured. The red pigment induced by sunlight gives no colour change on testing with dilute aluminium and ferrous sulphate solutions." (2, p. 124)

"An interesting correlation has been established between the presence of bright blue fruits and aluminium accumulation. . . . Evidence is adduced to show that the blue fruits of the few exceptions to this correlation owe their blue colour to the same pigment, namely, an acid-stable aluminium-delphinidin lake." (2, p. 131)

Chenery does not discuss blue grapes specifically; but I know that muscadinin, which occurs in ripe Hunt muscadine grapes, is presumably 3,5-diglucocidyl-3′-*o*-methyldelphinidin chloride.

Chenery does not discuss the possibility or impossibility of growing blue apples and blue strawberries, but the absence of delphinidin compounds might have a bearing on this. I do not yet see where and how this ties in with the work of Burbank; but this is merely another illustration of the amount of coöperative work to be done before we shall have a satisfactory knowledge of the biochemistry of plant pigments.

F. Blank (1) has published a long article in which he says (p. 276): "Many authors describe an increase in anthocyanin formation in plants attacked by parasites, in infected plants and those which have suffered some sort of injury." Steinecke noticed the formation of anthocyanin in leaves caused by aphids. Küster found anthocyanin in the supporting tissues of galls and in infected plants.

Professor John G. Matthiesse of the Department of Entomology at Cornell University wrote me on January 17, 1949 that there are many insects and plant diseases that cause leaves to turn bright red and yellow. Generally, chewing insects that actually chew out sections of the leaves do not cause any such color or change. Sucking insects, such as aphids and many other gall-forming insects, cause such color changes. In the elm, particularly, the elm cockscomb gall is often a bright red color. This gall is caused by the aphid *Colopha ulmicola*. Eriophyid mites are very common causes of colored galls. On maple, particularly, the bladder gall is often a very bright red color. On peaches, the disease peach leaf curl usually causes curled, deformed, and bright yellow and red leaves.

I am not familiar with any biochemical work on the effects of such insects or diseases on the leaf pigments. It would certainly be interesting to inject extracts from gall-forming or some sucking insects such as aphids to see whether any color change would occur. Professor W. T. M. Forbes, also of the Department of Entomology, had nothing to add to what Professor Matthiesse had said.

In *The Science of Biology Today* Trofim Lysenko, the president of the Lenin Academy of Agricultural Sciences, says:

> "The classics of Marxism, while fully appreciating the significance of the Darwinian theory, pointed out the errors of which Darwin was guilty. Darwin's theory, though unquestionably materialist in its main features, is free from some serious errors. A major fault, for example, is the fact that, along with the materialist principle, Darwin introduced into his theory of evolution reactionary Malthusian ideas. In our days this major error is being aggravated by reactionary biologists." (4, p. 10)
>
> "Many are still apt to slur over Darwin's error in transferring to his teaching Malthus' preposterous reactionary ideas on population. The true scientist cannot and must not overlook the erroneous aspects of Darwin's teaching." (4, p. 11)
>
> "In the post-Darwinian period the overwhelming majority of biologists—far from further developing Darwin's teaching—did all they could to vulgarize Darwinism, to smother its scientific foundation. The most glaring manifestation of such vulgarization of Darwinism is to be found in the teaching of August Weismann, Gregor Mendel, and Thomas Hunt Morgan, the founders of modern reactionary genetics." (4, p. 13)
>
> "It is no exaggeration to state that Morgan's feeble metaphysical "science" concerning

the nature of living bodies can stand no comparison with our effective Michurinian agrobiological science." (4, p. 16)

"The new vigorous trend in biology, or, more truly, the new Soviet biology, agro-biology, has met with strong opposition on the part of representatives of reactionary biology abroad, as well as of some scientists in our country." (4, p. 16)

"The Mendel-Morgan theory does not include in the scientific concept 'living body' the conditions of the body's life. To the Morganists, environment is only the background—indispensable, they admit—for the manifestation and operation of the various characteristics of the living body, in accordance with its heredity. They therefore hold that the qualitative variations in the heredity (nature) of living bodies are entirely independent of the environment, of the conditions of life." (4, p. 17)

"A sharp controversy, which has divided biologists into two irreconcilable camps, has thus flared up over the old question: Is it possible for features and characteristics acquired by plant and animal organisms in the course of their life to be inherited? In other words, whether qualitative variations of the nature of plant and animal organisms depend on the conditions of life which act upon the living body, upon the organism." (4, p. 18)

"The Michurinian teaching, which is materialist and dialectical in its essence, proves by facts that such dependence does exist." (4, p. 19)

"The Mendel-Morgan teaching, which is metaphysical and idealist in its essence, denies the existence of such dependence, though it can cite no evidence to prove its point." (4, p. 19)

"The Mendelian-Morganists cling to everything that is obsolete and wrong in Darwin's teaching, at the same time discarding its living materialist core.

"In our socialist country, the teaching of the great transformer of nature, I. V. Michurin, has created a fundamentally new basis for directing the variability of living organisms. Michurin himself and his followers have obtained and are obtaining directed hereditary changes in vegetable organisms literally in immense quantities." (4, p. 26)

"Mendelism-Morganism (the chromosome theory of heredity) is to this day taught, in a number of versions, in all colleges of biology and agronomy, where the study of Michurinian genetics has in fact not been introduced at all. In the higher official scientific circles of biologists too, the followers of the teaching of Michurin and Williams have often found themselves in the minority." (4, p. 28)

"His studies and investigations led I. V. Michurin to the following important conclusion: 'It is possible, with man's intervention, to *force* any form of animal or plant to *change more quickly and in a direction desirable to man.*' " (4, p. 32) [Whether this is true is the crux of the whole matter.]

"The Michurinian teaching flatly rejects the fundamental principle of Mendelism-Morganism that heredity is completely independent of the plants' or animals' conditions of life." (4, p. 32)

"Knowledge of the natural requirements and the response of an organism to external conditions makes it possible to direct the life and development of the organism. By regulating the conditions of life and development of plants and animals we can penetrate their nature ever more deeply and thus establish what are the means of changing it in the required direction. Once we know the means of regulating development we can change the heredity of organisms in a definite direction." (4, p. 33)

"The cause of changes in the nature of a living body is a change in the type of assimilation, in the type of metabolism. For example, the vernalization of spring cereals does not require lowered temperatures. Normally it proceeds in temperatures such as obtain in the spring and summer in the fields. But by using lower temperature conditions in the vernalization of spring cereals it is possible, after two or three generations, to turn them into winter cereals. And winter cereals require lowered temperatures for their vernalization. This is a concrete example showing how a new requirement is induced in the offspring of the plants under discussion—the requirement for lower temperatures as a condition for vernalization." (4, p. 34)

"According to the chromosome theory of heredity, hybrids can only be produced by sexual reproduction. That theory denies the possibility of obtaining vegetative hydrids, for it denies that the conditions of life have any specific influence upon the nature of plants. I. V. Michurin not only recognized the possibility of producing vegetative hybrids, but elaborated the 'mentor' method. This method consists in the following: By grafting scions (twigs) of old strains of fruit trees on the branches of a young strain, the latter acquires properties which it lacks, these properties being transmitted to it through the grafted twigs of the old strain. That is why I. V. Michurin called this method 'mentor'. The stock is also used as a mentor. By this method Michurin produced or improved a number of good strains." (4, p. 37)

"I. V. Michurin and the Michurinists have found methods of obtaining vegetative hybrids in large quantities. The vegetative hybrids cogently prove that Michurin's conception of heredity is correct. At the same time they represent an insuperable obstacle to the theory of the Mendelian-Morganists." (4, p. 37)

If I have understood this properly, Pasteur's grafting of French vines on American stocks would have been called by Michurin a "mentor" operation.

Frederick V. Coville (3) has discussed at length the influence of cold in stimulating the growth of plants.

"In regions having a cold winter like ours, with prolonged or repeated freezing, the native trees and shrubs become dormant in autumn. According to the general belief this condition is brought about by the cold. It is also the general belief that warm weather is of itself the sufficient cause of the beginning of new growth in spring. Both these ideas are erroneous. It is the object of the present address to show: first, that in our native trees and shrubs dormancy sets in before cold weather, and that cold weather is not necessary for the establishment of complete dormancy; second, that after such dormancy has begun, the exposure of the plants to an extraordinary growing temperature does not suffice to start them into growth; third, that these plants will not resume normal growth in the warm weather of spring unless they have been subjected previously to a period of chilling; and, finally, a theory will be advanced to explain this paradoxical effect of cold in stimulating growth instead of retarding it." (3, p. 151)

"A little more than ten years ago, while engaged in a series of experiments, the speaker came upon a strange phenomenon which was wholly unexpected and which threatened to interfere seriously with the success of the experiments. Healthy blueberry plants, intended to be used during the winter for breeding purposes, were brought into the greenhouse at the end of summer and were kept at an ordinary growing temperature. They refused to continue their growth during the autumn, gradually dropped their leaves, and went into a condition of complete dormancy. They did this at a greenhouse temperature which in spring and summer would have kept the plants in a condition of luxuriant growth." (3, p. 151)

"Since 1910 this experiment has been repeated many times and with many species of plants, and without exception those trees and shrubs native of our northern cold-winter region which were tested went dormant in fall or winter regardless of temperature. In comparing outdoor plants with indoor plants of the same species the most that can be said of outdoor conditions is that dormancy progresses a little faster in outdoor plants, evidently because their foliage is injured by freezing weather, and they drop their leaves somewhat earlier than indoor plants." (3, p. 152)

"In the late winter and early spring of 1910 I waited patiently, and then impatiently, for my indoor plants to bloom, and at last I was forced to realize that they never would bloom. When compared with plants of the same kind that had been outdoors during the winter and had been brought into the greenhouse in early spring, the difference was astonishing. The outdoor plants burst into leaf and flower luxuriantly, while the indoor plants remained completely dormant and naked. The experiment was repeated many times and with various species of plants." (3, p. 152)

"At first it was supposed that the plants needed to be frozen to start them into growth, but a single freezing proved not to be effective. And then it was found that the dormant plants would start into growth without any freezing whatever. It was necessary only that they be subjected to a period of prolonged chilling, usually two or three months, at a temperature a few degrees above freezing.

"If plants are kept continuously in a warm place without chilling, the dormant condition often continues for an extraordinary length of time. In some instances plants have remained dormant for a whole year under conditions of heat, light, and moisture that ordinarily would make the same plant grow with the greatest luxuriance." (3, p. 152)

"The conspicuous difference in spring growth between chilled plants and plants not chilled .... can be produced experimentally upon different parts of the same plant." (3, p. 152)

"On February 13, 1912, a blueberry plant 44 inches in height, which had shed its leaves and become dormant in a warm greenhouse maintained at a temperature of 60° to 70°F., was subjected to the following treatment: It was repotted in a 7-inch pot and set in the south end of a greenhouse at the temperature already mentioned. A small opening was made in the glass, and through this opening one of the two stems of the plant was pushed. The open space about the stem where it passed through the glass was carefully plugged with moss. During the rest of the winter the plant remained in the same position, the pot and the stem continuing in the warm temperature of the greenhouse, while the stem .. projecting through the glass was exposed to the rigors of winter, with its alternate freezing and thawing."

A photograph made on April 18 shows that "when spring came the outdoor branch started into normal growth while the indoor branch continued dormant." In a modification of this experiment "the plant was set on a shelf outside the greenhouse, and a single branch was passed through the glass wall into the warm interior. When spring came it was this interior branch which remained dormant, all the outside branches putting out leaves promptly and normally.

"From a comparison of the two experiments it is evident that the difference in behavior of the indoor and outdoor branches could not have been caused by any special action of the root system, for in one experiment the roots were inside, in the other outside. It is clear that the causes that stimulated growth in the exposed stems operated in the stem itself not in the roots. This principle is still further exemplified and confirmed by the behavior of cuttings taken from blueberry plants in the first stages of their dormancy. Such cuttings if kept warm continue their dormancy into late spring or summer, but if chilled for two or three months they start into growth at the normal time in early spring.

"It should be stated here that the difference in the amount of light inside and outside the greenhouse had nothing to do with the stimulation to growth, for chilled plants are ready to start into growth promptly whether the chilling is done in the full light of an outdoor situation, or in the partial light of a greenhouse, or in the complete darkness of an ordinary refrigerator." (3, p. 153)

"A little consideration will show how important the principle of chilling is to those species of trees and shrubs which are subjected each year to several months of freezing weather. If they were so constituted as to start into growth as easily in the warm days of late fall as they do in the warm days of early spring many species would come into flower and leaf in those warm autumn spells that we call Indian summer, and the stored food that the plant required for its normal growth in the following spring would be wasted in a burst of new autumn growth, which would be killed by the first heavy freezes and would be followed by a winter of weakness and probable death. But when two or three months of chilling are necessary before a newly dormant plant will respond to the usual effect of warmth, such plants are protected against the dangers of growth in Indian summer. It is probable that all our native trees and shrubs are thus protected." (3, p. 157)

Anyone "may make a simple and instructive experiment next fall and winter with such early spring blooming plants as alder, hazelnut, pussy willow, yellow bush jasmine, forsythia, Japanese quince, peach, and plum. In mid-autumn bring into your living room and set in water freshly cut, dormant, leafless branches of these plants. They will not bloom. At intervals of a few weeks during the late autumn and winter try the same experiment again. You will find that the branches cut at later dates will come into bloom under this treatment. They will not do so, however, until the expiration of the period of chilling appropriate to the various kinds of plants included in the experiment. . . . For some of the cultivated shrubs about Washington, especially the yellow bush jasmine (*Jasminum nudiflorum*), so brief a period of chilling is required that an extraordinarily cold period in late October or early November may chill them sufficiently to induce them to bloom if a period of warm weather follows in late November. The period of chilling required for the peach is so short that in Georgia unusually warm weather in December sometimes brings the trees into flower, and their crop of fruit is destroyed by the freezes that follow.

"From these facts it appears that our native trees and shrubs are so intimately adjusted to the changes of climate to which they have been long subjected that they are almost completely protected from injury by freezing, but some of the cultivated species brought from parts of the world having a climate different from ours are only imperfectly adapted to our climatic changes They grow at times when our native species have learned to hold themselves dormant, and they often suffer severely in consequence.

"Chilling, as a protective adaptation, has become a physiological necessity in the life history of cold-winter trees and shrubs. So fixed, indeed, is the habit that it appears to be a critical factor in determining how far such plants may go in the extension of their geographic distribution toward the Tropics. In the Tropics our common northern fruit trees, apples, pears, peaches, cherries, grow well for a time and then become half dormant. In the absence of chilling they never fully recover from their dormancy; they grow with weakened vitality and finally die. If these fruits are to be grown successfully in the Tropics they must be given artificially the periodical chilling they require." (3, p. 158)

"As a single example of the application of the principle of chilling let me cite the case of the blueberry. For several years we have been trying at the Department of Agriculture to domesticate this wild plant. We have raised many thousand hybrids and have set them out in waste sandy lands in the pine barrens of New Jersey. We have grown the bushes to fruiting age and have brought them into highly productive bearing. We have made them fruit so lusciously and so abundantly that they have brought returns to the grower at the rate of more than $1,000 an acre. In a word, we have changed the blueberry from a small wild fruit the size of a pea to a fruit the size of a Concord grape, and we have made its culture a profitable industry." (3, p. 160)

The practice of chilling is now called vernalization.

In Volume IX of the series of books entitled *Luther Burbank*, the authors (5) quote Burbank as saying:

"I am disposed to think that all shades of all colors that can be produced by blending of the primary colors are within the possible attainment of any flowering plant. (5, p. 29)

"The obvious fact that certain species, and in some cases whole genera, produce only red flowers, others only blue ones or yellow, does not by any means prove that the plants in question have not the capacity to produce flowers of quite different color. (5, p. 29)

"We have seen that the colors of wild flowers have been given them by insects. [This seems to me an awkward and misleading way of wording it.] We have noted that the bright colors—reds, orange, blues—have been assumed by flowers that flourish in the daytime and seek association with the bees; and that the flowers that consort with night flying insects, such as moths, are almost universally decked in white or pale yellow—hues that make them far more conspicuous in the twilight than the most brilliant scarlet flower would be. (5, p. 29)

"Most wild flowers of a given species are of a single color, or of a definite arrangement or a combination of colors. Bees and other insects have learned to distinguish this characteristic color or combination of colors, and to go with certainty from one flower to another of the same species, thus unconsciously serving the flower well by cross-pollinizing its blossoms." (5, p. 30)

"Recognition of the fact that wild flowers have been given their colors by the insects through the slow process of natural selection (in which flowers that lack the color were not visited by the bees and hence produced no offspring; whereas the flowers that did produce the color were fertilized, and perpetuated their kind, and reproduced their qualities in abundant progeny) gives us the clue to the way in which we may go about the development of a new color or color-combination in a flower. (5, p. 30)

"Suppose, for example, we desire to change the flower from white to yellow. How shall we go about it? (5, p. 30)

"First of all we must produce thousands of seedlings from one white flower. Let them blossom, and then search among them with the keenest eye to detect a trace of yellow color—which is found more or less in all white flowers—in the flowers of any single plant. (5, p. 32)

"You are almost certain, if your scrutiny is sufficiently keen, to detect some plant that varies in an infinitesimal shade from its fellows, showing at least a trace of yellow; for a really pure white is extremely rare in Nature. (5, p. 32)

"Select the seed of this plant, sow it next season, and repeat the process of searching. (5, p. 32)

"You will almost certainly be rewarded, if not in the first season, then in the second or third or fourth, by finding flowers that show very much more marked traces of yellow than the original flower. And even if the variation is not very striking at first, you will probably find that it tends to be accentuated after a few generations, especially in certain individuals. Each year you will discover flowers that are yellower than any of the preceding season; and presently you will have a blossom that is as yellow as you could desire, and a new race of plants that will breed true from seed. Placed side by side with the white flowers that were their ancestors, your new race will present a striking contrast." (5, p. 32)

In regard to blue roses this statement is made (5, p. 67): "Few types of experiments appeal more strongly to Mr. Burbank than those directed to the bringing out of some obscure quality or submerged trait of a flower, such, for example as an unfamiliar or submerged color. No one needs to be told that a blue rose is an anomaly." I cannot find that Burbank ever made a blue rose, but he implies that he could have done so. As he did produce a blue poppy (5, p. 117) and a blue gladiolus (5, p. 198), he could undoubtedly have produced a blue rose if it had seemed worth while.

Burbank says:

"Hitherto there has been no blue color in gladioli any more than in the poppy, except, perhaps, submerged in combination with some of the darker colors. For this reason, it has been found by all growers of the plants far more difficult to produce a blue flower than any other color, and until quite recently nothing approaching the really blue gladiolus has been produced. (5, p. 198)

"The first blue ones introduced were in reality more purple than blue. . . . . The first gladiolus that could really be called blue was the one sent out from Europe under the name Hulot. This had a small flower, and in other respects resembled the older gladioli—a dark purplish blue in color. By crossing this with white varieties of large size, pale blue with extra large fine flowers were produced. . . . Two years ago one appeared of very large size, and perfect in all respects with a true blue color." (5, p. 198)

Burbank says (5, p. 103): "For some reason blue is not a favorite color among flowers.

> "There are notable and conspicuous exceptions, of course, but for every species of blue flower in nature there are hundreds of flowers that are yellow, or red, or white.
>
> "Presumably the color blue does not attract the eye of the insect so strikingly as do the other primary colors. Flowers are not green for the obvious reason that, since leaves in general are green, flowers of that color would blend with the foliage, and thus defeat the primal purpose of the floral envelope.
>
> "And, no doubt, blue is a color nearer to green in its hue or general aspect than are the reds and yellows."

Burbank did not know that it is easy to convert any blue anthocyanin pigment into a red one, whereas we are not yet always clear about the reverse change. It is

> "perhaps not surprising that natural selection has weeded out the blue flowers and given us an abundance of red and yellow and white ones.
>
> "Of course, there may be some underlying reason associated with the chemical character of the different pigments that helps to account for the relative scarcity of blue flowers. But, as to this, no one at present has any definite knowledge, for the chemistry of the pigments, and the underlying differences between the pigments of different colors, in the petals of flowers are very little understood." (5, p. 103)

On December 7, 1948, Professor Frank K. Cameron wrote me from North Carolina that there is a stand of maple sugar trees within eight miles of Chapel Hill which is tapped regularly for sugar. The leaves were very red this fall, apparently as red as corresponding trees are in Ithaca. This seems to me to be distinctly surprising. I have not yet been able to learn whether the leaves of the sumach do or do not redden near its southern range. I am told that the sumach does not grow wild in Arizona.

The *New York Times* says that one cannot get good maple syrup from the sap of trees which have leafed out completely. Professor Heinicke wrote me from Geneva, New York, on April 25, 1949 that the maple syrup industry has long been familiar with the phenomenon mentioned in the article in the *New York Times* and it is commonly called "buddy sap." The term should not be confused with alteration in the sap resulting from bacterial action. The latter changes may occur at any time during the season when temperature conditions favor the growth of microörganisms.

> "As the season progresses the tree resumes its vegetative activity and physiological changes occur which ultimately result in sap that yields a characteristically and disagreeably flavored syrup. The extent of this so-called 'buddiness' varies from season to season. In some years the sap flow ceases entirely before the sap is seriously affected, while in others the flow is prolonged after revival of vegetative activity to such an extent that the sap is useless for syrup-making purposes.
>
> "During the 1947 and 1948 seasons, certain chemical changes occurring in the sap were studied at this station and the results are to be published soon. One of the objects of this study was to differentiate between the deterioration of syrup quality caused by bacterial action and that caused by metabolic products from the growing tree. This was done by eliminating the influence of bacteria so that sterile sap was obtained. The organic nitrogen content proved of interest. Although present in small quantities it did show a definite increase toward the end of the season. The buddy flavor and aroma was much stronger in the long 1947 season.

> "It is possible that the organic nitrogen may be amino in character. At the present time I do not know of any research which has definitely identified the compounds responsible for either the true maple flavor or the objectionable buddy flavor in maple sap. This entire subject has long been a problem to plant physiologists and chemists; but I do not know that they have come up with any better information than is contained in the above paragraphs."

Unless buddy sap can be prevented, it will of course be impossible to produce satisfactory maple syrup in the autumn; it will be impossible for the chemist of today to improve on the unspecified Indians of three centuries ago. The chemist has not yet tackled this problem.

SUMMARY

1. Chenery says that the pigments in blue flowers are aluminum (or aluminium) lakes of delphinidin compounds.
2. Chenery does not discuss the theoretical possibility of growing blue apples and blue strawberries nor the apparent contradiction between his results and those of Burbank.
3. Some sucking insects, such as aphids, cause leaves to turn red; but it is not yet known what precursors of the anthocyanins are in these cases, or how the aphids work.
4. The Russians do not agree with us on some scientific data. Lysenko points out what he considers errors in Darwin's work. Lysenko claims that acquired characteristics can be inherited.
5. Coville has pointed out the importance and characteristics of dormancy in plants accustomed to cold winters.
6. Burbank claims that blue is not a favorite color for flowers.
7. Cameron reports that the leaves of sugar maples may turn as red in North Carolina as in New York.
8. It is not yet known what compound gives rise to "buddy" sap and aroma.

REFERENCES

(1) Blank, F.: Botan. Rev. **13**, 241 (1947).
(2) Chenery, E. M.: Ann. Botany **12**, 121 (1948).
(3) Coville, Frederick V.: J. Agr. Research **20**, 151 (1920).
(4) Lysenko, Trofim: *The Science of Biology Today.* International Publishers, New York (1948).
(5) Whitson, John, John, Robert, and Williams, Henry S.: *Luther Burbank,* Vol. IX. Luther Burbank Press, New York and London (1914).

ON ADSORBED FILMS FROM BINARY LIQUID SOLUTION

CALLAWAY BROWN[1]

Research Laboratory, General Electric Company, Schenectady, New York

Received October 27, 1949

Adsorption from aqueous solution of a series of slightly soluble organic compounds by various carbons of known area has been reported by Hansen, Fu, and Bartell (2). It is shown that the adsorption is multimolecular in the higher concentration range, and that the adsorption isotherms plotted against reduced concentration (ratio of concentration to solubility) fit B.E.T. (1) curves as well as do vapor adsorption data. It is instructive to apply the thermodynamic treatment of Harkins and Jura (3) to these data. The results indicate that the condition for a condensed film is satisfied over an even wider range of concentrations.

A condensed film is defined (3) as one in which the two-dimensional film pressure, π, and the area per molecule, σ, are related by the equation:

$$\pi = a - b\sigma \tag{1}$$

There is no available method for direct measurement of the film pressure on solid adsorbents, but the vapor pressure of an adsorbed film and the two-dimensional film pressure are univariantly related by the Gibbs adsorption equation,

$$\pi = \gamma_s - \gamma_{sf} \tag{2}$$

and

$$\left(\frac{\delta\gamma_{sf}}{\delta \ln p}\right)_{\Sigma,\,T} = \frac{-kT}{\sigma} \tag{3}$$

where γ_s and γ_{sf} are the interfacial tensions before and after deposition of the adsorbed film. The specific area of a solid, Σ, is now reasonably well determined by application of either the Brunauer-Emmett-Teller (1) or the Harkins-Jura (3) theory to the isotherms for nitrogen adsorption at −195°C., so that the area per molecule, σ, is calculated from the specific adsorption, x/m in millimoles per gram, by

$$\sigma = \frac{10^7\Sigma}{N_A x/m} \tag{4}$$

when Σ is in square meters per gram and N_A is Avogadro's number. The adsorption isotherm for a vapor on a solid (x/m *vs.* p) is therefore uniquely determined by integration of equation 3 if the π–σ relation is known. For condensed films, which follow equation 1, the isotherm is (3):

$$\log p/p_0 = B - A/(x/m)^2 \tag{5}$$

---

[1] Present address: Armour Research Foundation, Illinois Institute of Technology, Technology Center, Chicago 16, Illinois.

Equation 5 is a consequence of equation 1 to the degree of accuracy that the vapor is a perfect gas; i.e., escaping tendency = vapor pressure.

Exactly the same line of reasoning can be applied to films on solids, adsorbed from solution. Such films reduce the interfacial tension and therefore exert a film pressure (equation 2). Formation of condensed films (equation 1) over a considerable range of concentration is to be expected if the behavior of insoluble monolayers on water or vapor films on solids is a guide. In such a concentration range integration of equation 3 again gives equation 5, with concentration substituted for vapor pressure insofar as the solutions are ideal; i.e., the escaping tendency of the film is proportional to the concentration of the solution in equilibrium with it. The constant A has the dimensions of $(x/m)^2_m$, the monolayer adsorption of the B.E.T. theory,

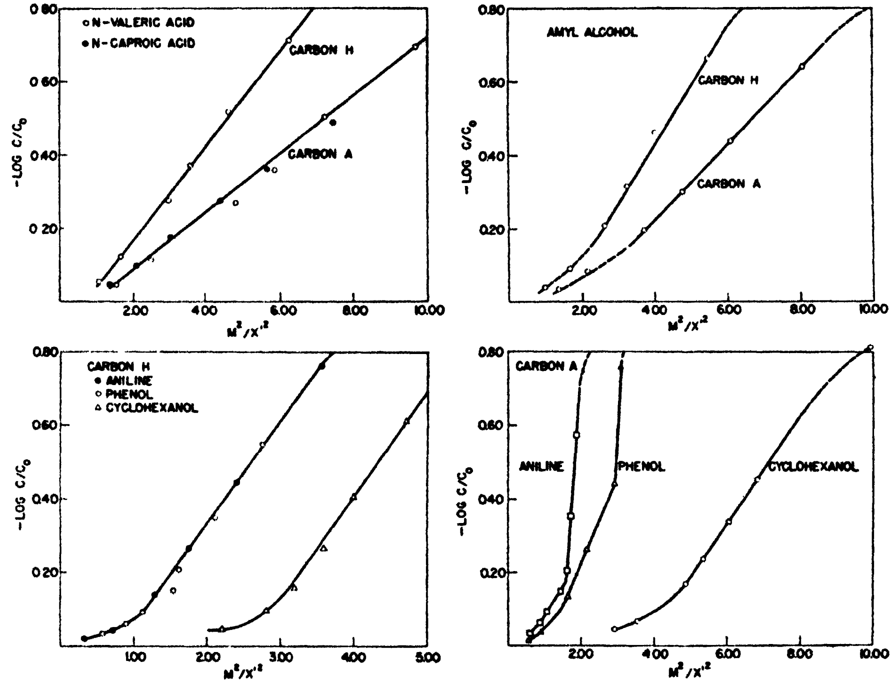

FIG. 1. Harkins-Jura plots of data (2) on adsorption from aqueous solution

$$A = \frac{10^{14}b}{4.605N_A^2kT}\Sigma^2 \qquad (6)$$

and its significance in equation 5 is unchanged; *viz.*, $\Sigma \sim A^{1/2}$.

Semilog plots of the reduced concentration against $1/(x/m)^2$ appear in figure 1 for the two carbons of intermediate area: artificial graphite A, $\Sigma = 95.8$ m.²/g., and the channel black H, $\Sigma = 124$ m.²/g. With the exception of aniline and phenol on the artificial graphites, the points fall on straight lines at least over the concentration range $C/C_0 = 0.2$ to 0.7 and the fit appears to extend to

$C/C_0 = 0.9$ for valeric and caproic acids. Clearly the adsorbed films are condensed over a wide range of concentrations. The isotherms for aniline, phenol, and cyclohexanol on carbon H are especially noteworthy. The aniline and phenol isotherms are congruent in spite of more than a twofold difference in solubility. The cyclohexanol isotherm is approximately parallel, but the film is condensed at much lower surface concentrations. The constant b of equation 1 is therefore the same for the three films (since slope $A \sim b$). This points to an orientation of the hydroxy and amino groups toward the adsorbent, with the film characteristics determined largely by interaction of the relatively polar phenyl and nonpolar hexahydrophenyl groups, respectively.

Values of the ratio $\Sigma/A^{1/2}$ appear in table 1. Equation 6 shows that this ratio should be constant provided the constant b in equation 1 remains constant. For a given adsorbate on different adsorbents, this is generally the case (3). As suggested by Hansen, Fu, and Bartell (2), there appears to be a systematic difference between the intermediate-area carbons, A and H, and the low-area carbons B, E, and G. The higher values for the $\Sigma/A^{1/2}$ ratio may therefore be due to use of too high a value of Σ, calculated from the nitrogen adsorption at -195°C. by B.E.T. theory. In view of the approximations made—ideal solution assumed, "apparent" adsorption x'/m uncorrected for volume changes used, constancy of adsorbent surface assumed—agreement with the condensed-film hypothesis appears excellent, at least for these adsorbents chosen for low porosity. The data for the high-area sugar charcoal F, which fit a Langmuir isotherm, are insufficient to permit a decision. Since equation 5 serves as a test for a condensed film only if the area available to the film remains constant, any swelling of the adsorbent due to the adsorbed film or effective removal of portions of the surface by capillary condensation will obscure the film characteristics. On the other hand, a positive fit with equation 5 of adsorption data would appear to eliminate capillary condensation as an appreciable effect.

TABLE 1

Constants in the Harkins–Jura plot: ratio $\Sigma/A^{1/2}$

SOLUTE	ADSORBENT CARBON				
	A	B	E	G	H
n-Caproic acid	358	300	301	297	375
n-Valeric acid	336	(300)	300	298	345
n-Amyl alcohol	300	(270)	260	(250)	310
Aniline	(250)	(160)		180	222
Phenol	200	199	180	203	235
Cyclohexanol	250	(250)	235	172	226

Quantitative application of the B.E.T. theory to adsorption data at reduced pressures (or concentrations) above 0.30 does not appear to be justified, since the limiting equation for $n = \infty$ falls down and use of finite values of n of questionable physical significance amounts to introduction of an arbitrarily adjustable parameter. In the reduced pressure range 0.05 to 0.30 it is by far the most successful general treatment, and permits calculation of the monolayer adsorption and therefore the area of the adsorbent, with the limitation that the area per molecule in a monolayer of a given adsorbate may vary 20 per cent or more on different adsorbents. The extensive data of Hansen, Fu, and Bartell (2) indicate that these remarks apply as well to adsorption from solution as to vapor adsorption. The authors caution that the monolayer adsorption $(x/m)_m$ may contain solvent as well as solute. Yet this limitation seems no more serious than the variable concentration of the monolayer found in vapor adsorption, especially if the solute is one that appreciably reduces the interfacial tension.

The condensed-film hypothesis, while semiempirical in nature, directs attention to the two-dimensional film characteristics and permits a test of the data for a condensed film by application of equation 5. The present results indicate that its general applicability, especially in the range of higher film concentrations, holds also for adsorption from solution. Once the ratio $\Sigma/A^{1/2}$ for a given adsorbate is determined, the slope A of a linear plot of equation 5 gives the surface area of the adsorbent just as reliably as application of the B.E.T. theory. The two treatments supplement each other nicely and help to correlate the behavior of adsorbed films at equilibrium whether in the form of insoluble monolayers on water, of vapor films on solids, or of films adsorbed from solution.

REFERENCES

(1) Brunauer, S., Emmett, P. H., and Teller, E.: J. Am. Chem. Soc. **60**, 309 (1938).
(2) Hansen, R. S., Fu, Ying, and Bartell, F. E.: J. Phys. & Colloid Chem. **52**, 374 (1949).
(3) Harkins, W. D., and Jura, G.: J. Am. Chem. Soc. **66**, 1366 (1944).

THE MECHANISM OF THE REACTION BETWEEN SILVER AND SULFUR IN MINERAL OIL

R. T. FOLEY, W. MORRILL, and S. J. WINSLOW

Transformer and Allied Products Laboratory, Pittsfield Works, General Electric Company, Pittsfield, Massachusetts

Received December 22, 1949

The reaction under consideration is that occurring between metallic silver and elemental sulfur in mineral oil. The purpose of this investigation is to break down the total tarnishing process into its consecutive steps and to evaluate each step both theoretically and experimentally. It is hoped to establish the rate-determining or slow step in the overall reaction.

Several consecutive or simultaneous steps might well be involved in this heterogeneous reaction.

I. Diffusion in solution: The sulfur in molecular solution must diffuse to the site of the reaction. The factors that control this process have been elucidated in many diffusion studies. Recently, however, a better understanding of diffusion in solution, supported by "free convection," has been reached by Wagner's (14) theoretical and experimental study of the dissolution of sodium chloride in water. From equations derived for convection about a heated vertical plate he arrived at an analogous relationship between the rate of solution per unit area, n/A, and the diffusion coefficient, D.

$$n/A = 0.726Dc\left(\frac{g}{\nu DH} \cdot \frac{|\Delta\rho|}{\rho}\right)^{1/4} \qquad (1)$$

The saturation concentration in solution is given by c. ν is the kinematic viscosity of the medium of density ρ, and H is the vertical height of the plate. $\Delta\rho$ is the density difference between the solution with concentration c and the solvent itself. Excellent agreement was obtained by Wagner between the calculated and experimental rates of solution of panels of rock salt of various heights. This relationship might well be applied to the diffusion of sulfur in mineral oil to the silver surface. For a given concentration of sulfur the resulting density difference may be calculated. An approximate value of the diffusion coefficient, D, might be reached from the known behavior of sulfur in solution in organic solvents. If it happens that sulfur reacts immediately upon its arrival at the silver surface or at the silver sulfide–oil interface, then n/A, calculated by this diffusion equation, will agree with the rate of reaction per unit area.

II. Adsorption: This term is used to generalize the process by which the molecular sulfur makes the transition from the solution to the silver surface or to the silver sulfide reaction product. This might be an adsorption phenomenon or it might be the formation of a reaction intermediate made necessary by the existence of sulfur in solution as a polymer incapable of direct ionization. In connection with this step the competitive adsorption of other compounds capable of arising in the oil through oxidation or aging of the oil must be considered. The adsorption of carbon disulfide (9) and methyl violet (11), the inhibiting action that amines (1) and amine salts (8) have on the tarnishing of sterling silver, and the classical usage of silver as a catalyst in the hydration of olefins and the oxidation of allyl alcohol are indications of the adsorptive character of the silver surface. That adsorption at the interface between the reaction product and the corrosive atmosphere may be a rate-determining influence has been shown by Reinhold and Seidel in the closely related reaction between silver and hydrogen sulfide (6).

III. Diffusion in the reaction product: The diffusion of metal outward and of sulfur and oxygen inward through the reaction product film has been considered by many workers as rate determining for reactions of this type. In studying the action of iodine on silver, Tammann (10) empirically arrived at a parabolic law,

$$y^2 = 2pt \qquad (2)$$

relating the thickness of the film, y, after the reaction has progressed for a time t. The constant in this equation has been given theoretical significance by C. Wagner (12, 13) in terms of transference numbers, conductivities, and the

E.M.F. of the cell involved. Wagner's hypothesis is based on the diffusion of cations and electrons rather than of neutral atoms through a reaction product film, and good agreement between calculated and experimental reaction rates has been obtained in several cases.

The purpose of this work, then, is to appraise each of these steps, if possible quantitatively, so that the mechanism of the reaction between metallic silver and sulfur in mineral oil may be depicted with accuracy.

EXPERIMENTAL

The reaction between silver and sulfur was carried out in mineral oil. This petroleum fraction is a naphthene-base oil with approximately 18 per cent aromatic and 3 per cent unsaturation. It is a type commonly used in the electrical industry to fill transformers using oil as an insulation medium and has been characterized with respect to its physical properties in connection with other tests made in this Laboratory (2). Fine silver (99.9 per cent) was rolled from 0.32 cm. to 0.05 cm. in thickness, annealed, and cut into strips whose total projected surface area was approximately 20 cm.^{2} It was found that these strips had to be anodically cleaned to get consistent results during the kinetic study. A cleaned strip was suspended from an S-shaped glass hook. The samples were transferred and weighed in this form. A sample, by means of the glass hook, was suspended from a glass rod which passed through a cork stopper. This stopper fitted tightly into a 38 x 200 mm. Pyrex test tube which contained 125 ml. of the reaction medium. In many experiments 120 ml. of this reaction medium was mineral oil and 5 ml. was a benzene solution of sulfur (2.00 mg. of sulfur per milliliter of solution). The benzene used to prepare this solution and to clean the samples in a manner described below was free of thiophene. The large test tube was held in a rack and placed in a constant-temperature oil bath at the desired temperature. The usual procedure was to clean, dry, and weigh a strip before suspension in the middle of the reaction medium. The test tube containing the corrosive medium was held in a rack in a constant-temperature oil bath for the desired time, dependent on the nature of the test. After this immersion the reacted sample was removed from the test tube, rinsed in benzene, and then allowed to stand overnight in benzene. The sample was finally rinsed with benzene and acetone, dried, and weighed. The gain in weight was recorded. Owing to the adherency of silver sulfide films of the thicknesses studied, this proved to be a reliable technique. During several experiments it was necessary to strip the reaction product quantitatively. This was accomplished with 5 per cent sodium cyanide solution, a slight correction in the order of tenths of a milligram being made for dissolved silver.

KINETICS AND DIFFUSION

The course of the reaction was studied in some detail at 60°C. over a period of time required for the silver to react with approximately 95 per cent of the sulfur in solution. The original concentration of elemental sulfur was 4.38×10^{-6} equiv. cm.$^{-3}$ Figure 1, in which the fraction of sulfur reacted is plotted against the time in hours, traces the course of the reaction. The curve is suggestive of a first-order reaction in which the rate is proportional to the first power of the sulfur concentration, and indeed this law is followed quite closely for the first 30 hr. of the reaction. However, after this length of time reaction rate constants calculated on the basis of a first-order dependence show a regular trend to lower numerical values. The data may also be expressed in equivalents of sulfur reacted per unit time per unit area of silver, written as n/A. These values as crosses are plotted against the time in figure 2. The decrease in rate with increase in time is at once conspicuous. If the rate n/A is governed by diffusion supported by convection, it should be predictable by equation 1 and entirely

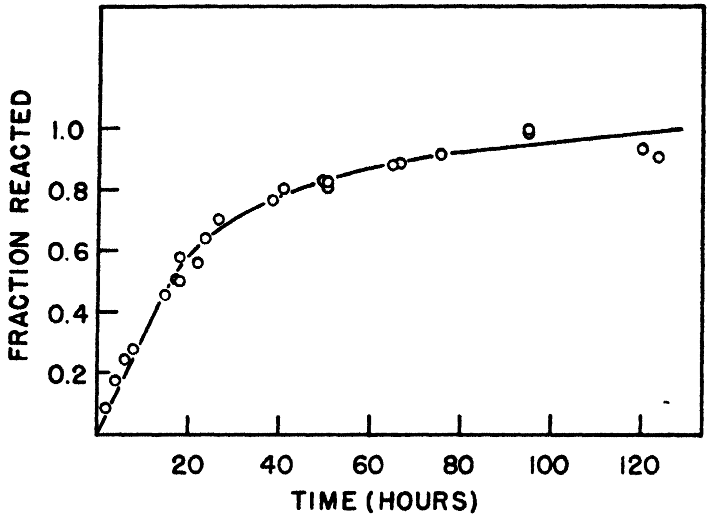

FIG. 1. The reaction between metallic silver and elemental sulfur in mineral oil

independent data. A diffusion constant for the sulfur in this medium, D, may be approximated from the equation

$$D = kT\frac{1}{6\pi\eta r} \tag{3}$$

where $k = R/N = 1.380 \times 10^{-16}$ ergs deg.$^{-1}$, $T \doteq 333$°C., $\eta = 0.026$ poise, and $r = 2.70 \times 10^{-8}$ cm. The "radius" of the sulfur molecule, r, was calculated from what seemed to be a reasonable geometrical picture of sulfur existing as an eight-membered ring with an S—S bond distance of 2.08 Å. (4). At this temperature an approximate value of $D = 0.35 \times 10^{-5}$ cm.^{2} sec.$^{-1}$ is estimated. In equation 1 $c = 4.38 \times 10^{-6}$ equiv. cm.$^{-3}$, $g = 981$ cm. sec.$^{-2}$, $\nu = 0.0301$ cm.^{2} sec.$^{-1}$, $H = 5$ cm., and $(\Delta\rho/\rho) = 1.63 \times 10^{-4}$. These values give an average rate of diffusion to the silver surface of $n/A = 2.61 \times 10^{-10}$ equiv. cm.$^{-2}$ sec.$^{-1}$ This is represented by the dotted horizontal line in figure 2. This average value falls within the range of the experimental sulfiding rates.

Further calculations can be made to see if the diffusion equation, in general, follows the reaction rate data actually observed. This may be done from a knowledge of the average sulfur concentration in solution during reaction over a specific time interval. This will give a lower rate than that calculated above, because as the sulfur concentration decreases the rate must decrease. This is seen from equation 1, in which the rate is proportional to the first power of the sulfur concentration and to the 0.25 power of the "density difference." The density difference in turn is proportional to the sulfur concentration. In table 1 rate values calculated from the known concentrations of sulfur and the corresponding density differences are compared with the observed sulfiding rate. It should be pointed out that this comparison has not been made independent of the known rate of consumption of sulfur, but it does establish the extent to which the diffusion process follows the reaction of sulfur with silver. These calculated values are plotted as circles in figure 2. Fair agreement, about within the range of experimental error, exists over most of the reaction time.

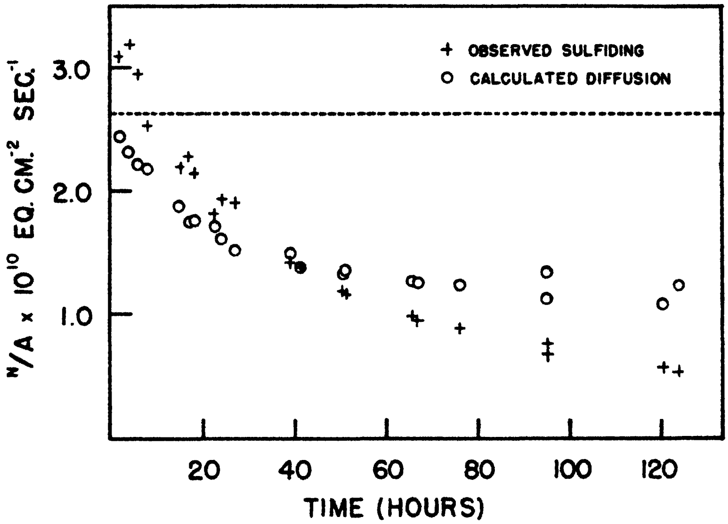

FIG. 2. The observed sulfiding of silver compared with the calculated diffusion rate of sulfur.

VISCOSITY EFFECT

The assumption has been made that the diffusion coefficient for sulfur in mineral oil can be approximated by the equation:

$$D = kT\frac{1}{6\pi\eta r} \tag{3}$$

If the radius, r, of the sulfur "sphere" is taken as constant, then at a given temperature the diffusion constant, D, will be dependent only on the viscosity of the medium. The question arises as to how the rate of reaction, n/A, will be affected if the viscosity of the medium is varied over a wide range, for these two quantities must be connected by the diffusion coefficient. The viscosity of the medium may be considerably altered isothermally by change in solvent. Here, the assumption has been made and verified by many experiments in this laboratory that the hydrocarbon solvent in this system is itself an inert carrier of the sulfur which is the reactant. Thus it is possible to extend the range of study of the dependence of reaction rate on diffusion by observing the rate in several solvents.

The rate of sulfiding of silver was measured in five solvents. Table 2 gives the chemical nature of the solvent, as well as the observed rate of reaction. The rate predicted by assuming equation 1 to hold for solvents of all viscosities is given in the fifth column. It is apparent that only in the case of solvents 4 and 5 (higher viscosity and lower reaction rate) is good agreement with the calculated diffusion rate obtained. It appears that the experimental reaction rate as given in the fourth column has approached a limiting quantity,—approximately 6–8 × 10^{-10} equiv. cm.$^{-2}$ sec.$^{-1}$ This suggests that diffusion is not the rate-determining influence in those solvents of low viscosity. One of the other steps in the overall reaction mechanism has assumed this role.

TABLE 1

Comparison of observed sulfiding rate and calculated diffusion rate

TIME	OBSERVED SULFIDING RATE, n/A	CALCULATED DIFFUSION RATE, n/A	TIME	OBSERVED SULFIDING RATE, n/A	CALCULATED DIFFUSION RATE, n/A
hours	*equiv. cm.$^{-2}$ sec.$^{-1}$*	*equiv. cm.$^{-2}$ sec.$^{-1}$*	*hours*	*equiv. cm.$^{-2}$ sec.$^{-1}$*	*equiv. cm.$^{-2}$ sec.$^{-1}$*
2.0	3.10 × 10^{-10}	2.45 × 10^{-10}	41.4	1.40 × 10^{-10}	1.39 × 10^{-10}
4.0	3.20	2.32	50.5	1.20	1.33
6.0	2.96	2.22	51.0	1.17	1.37
8.0	2.53	2.17	65.5	0.98	1.27
15.0	2.20	1.89	67.0	0.96	1.25
17.5	2.29	1.75	76.0	0.88	1.22
18.3	2.14	1.76	95.0	0.76	1.14
22.5	1.82	1.71	95.0	0.68	1.26
24.0	1.94	1.61	120.5	0.56	1.19
27.0	1.91	1.52	124.0	0.53	1.22
39.0	1.43	1.50			

TABLE 2

Rate of sulfiding of silver in different solvents

SOLVENT	CHEMICAL NATURE	$\eta_{60°C.}$	n/A (OBSERVED)	n/A (CALCULATED BY EQUATION 1)
		poises	*equiv. cm.$^{-2}$ sec.$^{-1}$*	*quiv. cm.$^{-2}$ sec.$^{-1}$*
1	Aliphatic	0.00386	6.43 × 10^{-10}	20.4 × 10^{-10}
2	Aromatic	0.00413	7.60 × 10^{-10}	19.0 × 10^{-10}
3	Aliphatic	0.00513	6.02 × 10^{-10}	15.5 × 10^{-10}
4	Naphthenic	0.0260	3.22 × 10^{-10}	3.02 × 10^{-10}
5	Mixture of aromatic and naphthenic	0.0105	5.19 × 10^{-10}	7.5 × 10^{-10}

TEMPERATURE EFFECT

The sulfiding of silver during a 6-hr. interval was measured at several temperatures. The temperatures and rates are given in table 3. Also, the rate of diffusion to the silver surface predicted by the Wagner diffusion equation (equation 1) is given in the third column. In the fourth column reaction rates are calculated from the extrapolated data of Reinhold and Möhring (5). These rates would be predicted for the specific temperature if the reaction rate were controlled by diffusion of ionic silver through the silver sulfide film. To relate the reaction rate to diffusion at these temperatures it was necessary to measure the viscosity of the mineral oil reaction solution. The viscosities and the diffusion coefficients calculated with equation 3 are given in table 4.

TABLE 3

Rate of sulfiding of silver at different temperatures

TEMPERATURE	OBSERVED RATE, n/A	n/A CALCULATED WITH EQUATION 1	n/A CALCULATED FROM DATA OF REINHOLD AND MÖHRING* (5)
°C.	equiv. cm.$^{-2}$ sec.$^{-1}$	equiv. cm.$^{-2}$ sec.$^{-1}$	equiv. cm.$^{-2}$ sec.$^{-1}$
40	1.95×10^{-10}	1.81×10^{-10}	2.53×10^{-10}
50	2.82	2.05	4.30
60	3.34	2.98	6.89
70	4.19	3.86	10.9
80	5.0	4.72	17.1
92	6.5	5.92	27.4

* Calculated on the basis of a 6-hr. time interval.

TABLE 4

Viscosities and diffusion coefficients calculated with equation 3

TEMPERATURE	η	D
°C.	poises	cm.^{2} sec.$^{-1}$
40	0.0419	2.04×10^{-6}
50	0.0382	2.30
60	0.0265	3.42
70	0.0210	4.43
80	0.0175	5.50
92	0.0143	6.94

The manner in which the reaction rate (column 2) follows the diffusion rate (column 3) is very striking.

SULFIDING AND ADSORPTION

Several polar compounds were dissolved in the mineral oil reaction solution to see what effect, if any, compounds which are likely to be adsorbed by silver would have on the rate of sulfiding. Table 5 lists the chemical compounds that were added. An attempt was made to use compounds with exemplary functional

TABLE 5

Effect of various compounds on the rate of sulfiding of silver

COMPOUND ADDED	FUNCTIONAL GROUP	RELATIVE AMOUNT OF SULFIDING	
		After 6 hr.	After 48 hr.
None		1.00	1.00
Isoamylamine (4.3 g./l.)	—NH$_2$		0.56
Acetic acid (8.0 g./l.)	—COOH	0.05	0.02
Palmitic acid (6.4 g./l.)	—COOH	0.45	0.55
Oleic acid (8.0 g./l.)	(=), COOH	0.30	0.10
Naphthenic acids (8.0 g./l.)	—COOH	0.70	0.81
Butyl acetate (5.8 g./l.)	—COO—	0.60	0.75
Biacetyl (8.0 g./l.)	—COCO—	0.90	1.00
Cetyl alcohol (0.12 g./l.)	—OH	1.00	0.96
Quinone (8.0 g./l.)	=O	0.15	0.12
Diphenyl sulfide (8.0 g./l.)	—S—	0.95	0.98
Diphenyl disulfide (8.0 g./l.)	—S—S—	0.25	0.77
Hydrogen peroxide (5 ml. 30 per cent aqueous solution)	—O—O—	0.04	0.04
Benzoyl peroxide (0.8 g./l.)	—CO—O—O—CO—	0.02	0.24
Acetylene (saturated solution)	—C≡C—	1.00	1.00

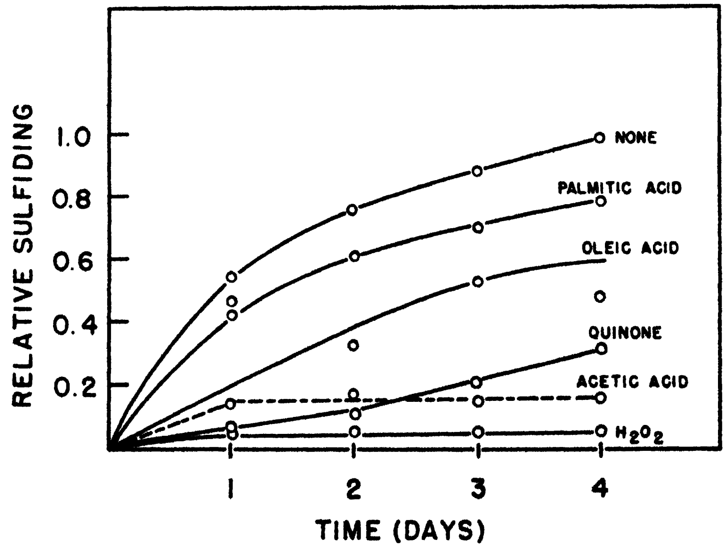

FIG. 3. Adsorption and sulfiding

groups. It is interesting to note the effect of groupings such as —COOH, =O, —NH$_2$, and —S—S, which are capable of being oriented. The comparative reaction figure given shows the order of magnitude of the specific surface effect. However, these values should not be accepted as quantitative, because of the experimental difficulty in reproducing exactly the surface poisoning. Several of the compounds listed were investigated further to establish the time–inhibition relationship. These groups were found to show a complete range of poisoning activity. In figure 3 the comparative sulfiding rate is plotted against the time in days. Several inhibitors—hydrogen peroxide, acetic acid, and quinone—show a reasonably permanent effect. Palmitic acid, on the other hand, is illustrative of a type which, although it definitely hinders the reaction, does not form an adsorbed layer of any great degree of protection. In each case studied, the rate rather than the final amount of sulfiding was affected. The total sulfur in solution does react with the silver if the reaction time is extended sufficiently.

DISCUSSION

The relative velocities of the several postulated steps may now be considered. The first step cited was that of diffusion of the sulfur in solution. By calculation based on Wagner's diffusion equation the rate at which sulfur will arrive at the silver surface may be estimated. If it is assumed that the reaction with ionic silver takes place immediately upon arrival, and if the diffusion is the slow or rate-determining step once equilibrium has been established for the other steps, the observed rate of reaction should closely follow this calculated diffusion. The plot of the data in figure 2 shows this to be the case to a remarkable degree. At certain times during the course of the reaction the rate is exactly as calculated in accordance with this mechanism. This is especially remarkable because of the method of arriving at what seemed like a reasonable value for the diffusion coefficient for sulfur in mineral oil. Sulfur dissolved in carbon tetrachloride has been found to have eight atoms in each molecule (3). The S—S bond distance has been assigned by Gingrich (4) as 2.08 Å. and the —S—S—S— bond angle as 100° (4a). On the basis of these data the sulfur molecule was represented as a sphere with a "radius" of 2.70×10^{-8} cm. This value was used in equation 3, which is sometimes called the Sutherland–Einstein relation. This equation was derived for molecules that are spherical and large in comparison with the solvent molecules. Neither condition holds too closely in this case, so the diffusion coefficient must of necessity be in error. In spite of this lack of refinement the calculated diffusion follows very closely the reaction rate of a great deal of the course of the reaction.

The increase in rate of reaction with temperature can be explained fairly well by the expected increase in diffusion—supported, of course, by convection. In table 3 the rates calculated by equation 1 are in fair agreement with the experimental rates from 40° to 92°C., at which temperature the rate increases to about 6×10^{-10} equiv. cm.$^{-2}$ sec.$^{-1}$ There apparently is an upper limit to the reaction velocity that can occur from increased diffusion. In the experiments in which the viscosity change was related to the sulfiding it was seen that an indefinite decrease in the viscosity did not cause an indefinite increase in reaction rate. It appears that the diffusion ceased to be the rate-determining influence once the rate reached about $6–8 \times 10^{-10}$ equiv. cm.$^{-2}$ sec.$^{-1}$

The adsorption step is postulated as the second step in the reaction series. There is not enough experimental evidence available to show that adsorption, in the sense in which it is commonly used, is a necessary step, but it seems reasonable on the following basis. It has been shown that the silver surface can be poisoned by the adsorption of sulfides and disulfides, molecules whose structure resembles sulfur from the standpoint of coördination electrons. Moreover, other structures, polar groups, are adsorbed and inhibit the reaction in varying degree. Thus a competitive mechanism, with both sulfur and the foreign molecule exercising an affinity for the silver surface, is suggested. If these foreign groups cover the surface, the adsorption of sulfur may well be the slow step. A comparison of rates will illustrate this point. In the presence of *p*-quinone, the sulfur–silver reaction proceeded at an average rate of $n/A = 0.9 \times 10^{-11}$ equiv. cm.$^{-2}$ sec.$^{-1}$ during a 48-hr. experiment. A control which was not contaminated with any known compound not a normal constituent of this oil gave a result of $n/A = 0.61 \times 10^{-10}$ equiv. cm.$^{-2}$ sec.$^{-1}$

Whether this phenomenon is merely adsorption or is chemical reaction or intermediate complex formation is, of course, open to question. Rudberg and v. Euler (7), in studying the adsorption of salts on silver surfaces from aqueous solutions, concluded that a surface complex, Ag_2^+, is formed when the surface reaction takes place. After studying the catalytic decomposition of hydrogen peroxide by silver, Weigel (15) postulated a mechanism involving the precipitation of an oriented AgOOH film on the surface. It is interesting to note that in the experiments here reported compounds with oxygen which can be oriented are particularly capable of poisoning the silver surface for the sulfide reaction. Other functional groups, such as the acid radical, which conceivably could form transitory surface salts are also active in this regard. It is apparent from figure 3 that the adsorption of these foreign compounds affects the rate rather than the final amount of sulfiding. Even in the case of hydrogen peroxide it has been established that if the silver is removed from the constant supply of volatile gas the sulfiding will proceed unabated. In this case it has been shown that the sulfur has not been destroyed but is available for reaction with silver if the decomposing hydrogen peroxide is removed from the scene. Although these results are presented here in only a semiquantitative manner, it would be intriguing to study the mechanism involved in the passivation of the silver surface by means of agents which are not film formers in the usual sense.

The third step which could be rate determining is the diffusion of the reactants through the silver sulfide reaction product. Fortunately, by means of the theoretical equations of Wagner (12) and the experimental data of Reinhold and Möhring (5), we can approximate what the rate would be if the reaction were controlled by this mechanism. The latter two investigators studied the reaction between silver and sulfur in the temperature range of 130°C. to 172°C. As the reaction was carried out with a silver wire in molten sulfur it seems logical to assume that in their case the rate-determining step was the diffusion of the reactants through the reaction product film. The following values were taken from their paper:

t	$k \times 10^{10}$ (FOUND)	$k \times 10^{10}$ (CALCULATED)
°C.	equiv. cm.$^{-1}$ sec.$^{-1}$	equiv. cm.$^{-1}$ sec.$^{-1}$
130	1.41	0.83
148	2.72	2.64
156	3.68	3.61
162	5.69	5.51
172	7.21	9.31

The calculated values in the third column were obtained from the Arrhenius type equation which best fitted their data:

$$k = 17e^{-10{,}500/T} \tag{4}$$

At 60°C. the extrapolated value of

$$k = 3.4 \times 10^{-13} \text{ equiv. cm.}^{-1} \text{ sec.}^{-1} \tag{5}$$

This may be converted to

$$m/A(\text{g. cm.}^{-2}) = \sqrt{1.032 \times 10^{-11}\, t(\text{sec.})} \tag{6}$$

by formulas given by Wagner (12). Here m/A is the sulfiding in grams per unit area. At several different times the amount of sulfiding may be compared:

TIME	CALCULATED	OBSERVED
hr.	g. cm.$^{-2}$	g. cm.$^{-2}$
15	7.47×10^{-4}	4.00×10^{-4}
41.4	12.4×10^{-4}	7.05×10^{-4}
95	18.8×10^{-4}	8.4×10^{-4}

In each case the extent of reaction as predicted on the basis of diffusion through the reaction product is greater than the observed rate. It is concluded then that this step is not usually the rate-determining step. However, in table 2 and in a discussion of abnormal viscosity effects observed at 60°C. it was pointed out that the observed rate is far smaller than that predicted if diffusion in solution were the rate-determining step. Moreover, the observed "limiting rate" of 6–8 $\times$ 10^{-10} equiv. cm.$^{-2}$ sec.$^{-1}$ is in good agreement with the rate of 6.89 $\times$ 10^{-10} equiv. cm.$^{-2}$ sec.$^{-1}$ calculated for 60°C. (*cf.* table 3) from the data of Reinhold and Möhring, in which case the rate-determining step is assumed to be diffusion through the silver sulfide film. It was seen in studying the temperature dependence of the reaction that the rate as calculated on the basis of diffusion in the silver sulfide layer consistently gave values too high. It may be concluded, therefore, that with a solution as viscous as the mineral oil used in the present investigation the film diffusion is not the rate-determining step. Curiously, this situation might well be changed if a different, more fluid, solvent had been chosen for the investigation.

SUMMARY

The steps involved in the total mechanism of the reaction between sulfur in mineral oil and metallic silver may be outlined.

I. Diffusion of the sulfur in oil: S^0 (in molecular solution in oil) → S^0 (in solution at the silver surface). This is normally the slow step and a good approximation of the rate of reaction may be made from the Wagner diffusion equation.

II. Adsorption: S^0 (in solution) → S^0 (adsorbed on silver surface or at silver sulfide–oil interface). Normally this is a fast step. However, when preferentially adsorbed compounds are present on the silver surface, it may be the slow and rate-determining step.

III. Diffusion in the silver sulfide layer:

$$Ag^+ + e^- \text{ (in base metal)} \rightarrow Ag^+ + e^- \text{ (at film–oil interface)}$$

Usually this is a rapid step, relatively speaking. However, when the viscosity is decreased considerably an upper limit is reached in the rate. At this point, this step is rate determining. If a less viscous oil had been chosen for the kinetic study, this might well have been the rate-determining step instead of diffusion in the oil.

The authors wish to express their gratitude to Dr. Carl Wagner of the Massachusetts Institute of Technology, who offered several helpful suggestions which aided in the theoretical treatment. They would also like to thank Dr. Norman Hackerman and Dr. Robbin Anderson of the University of Texas for their constructive review of the paper.

REFERENCES

(1) BRIGGMAN, G. F.: U. S. patent 2,323,369 (July 6, 1943).
(2) CLARK, F. M., AND RAAB, E. L.: Am. Soc. Testing Materials, Preprint 87 (1948).
(3) ODDO, G., AND SERRA, E.: Chem. Zentr. **1899, II,** 1092.
(4) PAULING, L.: *The Nature of the Chemical Bond*, second edition, p. 166. Cornell University Press, Ithaca, New York (1940).
(4a) Reference 4, p. 79.
(5) REINHOLD, H., AND MÖHRING, H.: Z. physik. Chem. **28B,** 178 (1935).
(6) REINHOLD, H., AND SEIDEL, H.: Z. Elektrochem. **41,** 499 (1935).
(7) RUDBERG, E. G., AND EULER, H. v.: Z. Physik **13,** 275 (1923).
(8) RUST, J. B.: U. S. patent 2,400,784 (May 21, 1946).
(9) SCHLUTER, H.: Z. physik. Chem. **153A,** 68 (1931).
(10) TAMMANN, G.: Z. anorg. allgem. Chem. **111,** 78 (1921).
(11) TERWELLEN, J.: Z. physik. Chem. **153A,** 52 (1931).
(12) WAGNER, C.: Z. physik. Chem. **21B,** 25 (1933).
(13) WAGNER, C.: Angew. Chem. **49,** 735 (1936).
(14) WAGNER, C.: J. Phys. & Colloid Chem. **53,** 1030 (1949).
(15) WEIGEL, E.: Z. physik. Chem. **143A,** 81 (1929).

INTRODUCTION TO THE SYMPOSIUM ON CRITICAL PHENOMENA[1]

GENERAL CONSIDERATION OF CRITICAL PHENOMENA

O. K. RICE

Department of Chemistry, University of North Carolina, Chapel Hill, North Carolina

Received December 19, 1949

In elementary accounts the critical temperature of a one-component system is defined as that temperature above which the two-phase equilibrium between liquid and vapor does not occur. Likewise, in many binary liquid systems there is stated to be a critical solution temperature, beyond which two liquid phases cannot coexist. However, in the past few decades there has accumulated much evidence which indicates that we should speak of a critical *region* rather than a critical *point*. A large number of very peculiar phenomena have been observed in the neighborhood of the critical point. Some of these may perhaps be explained as occurring because equilibrium has not been established; some, however, are without doubt true equilibrium phenomena. In spite of much effort, the situation is not yet entirely clarified, from either an experimental or a theoretical point of view.

I. ISOTHERMS NEAR THE CRITICAL TEMPERATURE

One of the problems which is not yet entirely settled has to do with isotherms in the neighborhood of the critical point. Various possibilities for a one-component system are illustrated in figure 1. The three parts of this figure are schematic diagrams constructed to illustrate three types of pressure–volume isotherms which appear to be possibilities. The diagram on the left shows the familiar type of isotherm, which is predicted by the van der Waals theory and which may be designated as the classical diagram. The coexistence curve, which indicates the region in which two phases can be seen, has a simple, approximately parabolic, shape.

The middle diagram of figure 1 illustrates the prediction of Mayer and Harrison (4, 7) on the basis of their statistical-mechanical theory of condensation. The coexistence curve, representing the region over which a meniscus can be seen, has a horizontal top, rather than being parabolic. However, the coexistence curve is extended, as is indicated by the broken curve. Inside this broken curve the isotherms are supposed to be horizontal, though no meniscus can be seen; and the isotherms do not show a break in slope, as in the ordinary type of condensation, but flatten out gradually as they approach the region where they are entirely horizontal. According to this theory, a phase having *any* volume within the broken curve can be in equilibrium with a phase at the same temperature having any other volume within the broken curve. There are thus two critical temperatures: one, the temperature T_m at the top of the solid coexistence curve where the meniscus disappears, and the other, the temperature T_c at the top of the broken curve, which is the temperature of the last isotherm having a horizontal portion.

---

[1] Presented at the Symposium on Critical Phenomena, which was held under the auspices of the Division of Physical and Inorganic Chemistry at the 116th Meeting of the American Chemical Society, Atlantic City, New Jersey, September 22, 1949.

The right-hand diagram of figure 1 brings out the suggestion of the present author (11). The coexistence curve has a finite horizontal portion, which coincides in this volume range with an isotherm which also has a finite horizontal part. This is the temperature at which the meniscus disappears. Above this critical temperature, called T_c in this case, no isotherm has a horizontal portion, but the isotherms do have a relatively flat portion, of gradually increasing slope as the temperature increases. No two phases can be in stable equilibrium with each other above T_c.

There is evidence that, at least in a number of cases, the classical diagram is not correct. However, the question as to which of the other two diagrams is to be preferred is not easy to settle. I have discussed the evidence elsewhere (12) and shall undertake here to give only a brief résumé of some of the more important and more recent experiments. Naldrett and Maass (9) made a study of the coexistence curve for ethylene and for ethyl ether by observation of the meniscus, and found that the meniscus disappeared at a fixed temperature over a range of volumes, so that the coexistence curve appeared to have a finite horizontal portion at the top. It is true that the meniscus disappeared within the tube (rather than seeming to go out the top or the bottom) over only a portion of this range of compositions, but even this portion definitely included a finite range of compositions.

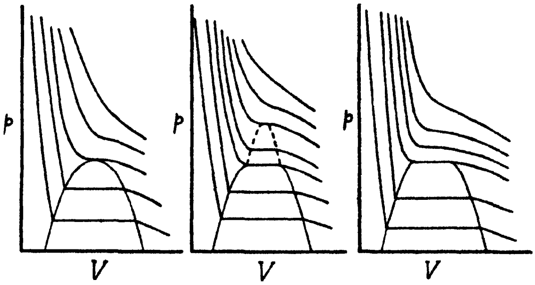

FIG. 1. Possible types of isotherms for a one-component system. Pressure, p, as a function of molal volume, V.

Whether the isotherms which pass just above the horizontal part of the coexistence curve have, themselves, a horizontal portion as claimed by Mayer and Harrison, or whether they have at all points a finite (though near the critical temperature a very small) slope, is more difficult to decide experimentally. Data on ethylene by McIntosh, Dacey, and Maass (3, 5) are not entirely unequivocal (11). Data on carbon dioxide by Michels, Blaisse, and Michels (8) would lead one to believe that there is a last isotherm with a finite horizontal portion, and that above that temperature the isotherms have a relatively flat portion which has, however, a finite slope. Unfortunately, the meniscus was not observed in this case.

Mayer and Harrison pointed to the persistence of density differences above the temperature at which the meniscus disappears, a phenomenon which has been frequently observed, as evidence that the isotherms have a horizontal portion above the last temperature at which the meniscus can be observed. Naldrett and Maass (9, p. 120) have recently concluded, however, that these density differences do not persist indefinitely, and from this we might infer that in a state of true equilibrium the system always has a definite uniform density at these temperatures. If this is the case, the isotherm cannot have a horizontal portion. This matter is, perhaps, not entirely settled at the present time; however, it is well known that hysteresis readily occurs in the critical region, and one would have to be careful in any event in concluding that density differences, even though rather persistent, represent a state of true equilibrium.

In the case of binary liquid systems there are possibilities which are quite analogous to those of one-component systems, as illustrated in figure 1. The three corresponding situations for two-component systems are shown in figure 2, where the partial vapor pressure of one of the components is plotted against the composition, in a series of isotherms. These diagrams should be self-explanatory, in the light of the analogy with one-component systems. Usually the coexistence or solubility curve for two-component systems is plotted as a temperature *vs.* composition plot, in which the compositions plotted are those of the two phases which are in mutual equilibrium at any given temperature. A temperature above (or below) which there is only one homogeneous phase is called a critical mixing point. A system will, of course, appear to be homogeneous if no meniscus can be seen, and so these curves will generally be determined by observation of the meniscus. If the coexistence curves plotted in figure 2 have a horizontal portion at their top (or bottom, in the case of a lower critical point), the ordinary temperature *vs.* composition coexistence curves will also have a horizontal portion at the top.

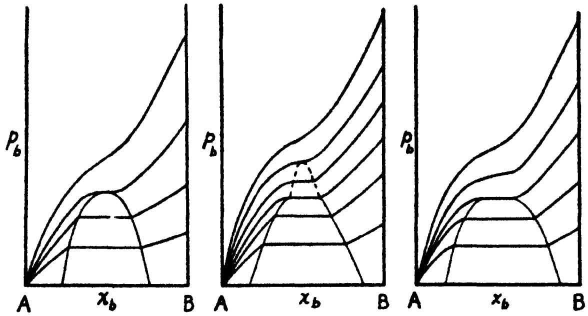

FIG. 2. Possible types of isotherms for a binary liquid system. Partial vapor pressure, p_b, of component B, as a function of mole fraction, x_b, of this component.

The coexistence curves for binary liquid systems to be found in the literature are often quite flat at the top. Though it is impossible to prove from this kind of data that the curves are actually absolutely horizontal at the top, I have the impression that in many cases more carefully performed experiments and greater purity of the components would result in accentuating the flatness. Some very careful work of Woodburn, Smith, and Tetewsky (16) showed that, in a number of organic binary mixtures, the temperature at which the mixture became homogeneous was practically independent of concentration over a range of concentrations. On the other hand, there do seem to be cases in which there is no reason to doubt the data and in which the top of the coexistence curve is rounded. It appears likely that both types of curves actually occur, and I have given a number of figures to illustrate both cases in a recent article (12); since this is readily available, it seems unnecessary to copy the figures here.

Mr. R. W. Rowden, working in my laboratory, is studying the critical phenomena in the cyclohexane–aniline system. In this case he has found that the meniscus disappears near the center of the tube at compositions of 0.480 and 0.453 mole per cent aniline. This would indicate a horizontal portion in the coexistence curve of this system; however, the results are preliminary as yet. We also hope to measure vapor pressures in the critical region. Vapor pressure data and related data, available in the literature, are not sufficient to decide between the diagrams of figure 2. This I have also recently discussed with relevant figures (12).

The scattering of light in the critical region is another property which can be used to obtain information on the basis of which one may decide between the types of diagram of figure 2. This will be discussed in Zimm's paper in this Symposium (17).

It may be remarked that Zimm has pointed out that it is useful to plot what is essentially the slope of the curves of figure 2 as a function of the composition, in order to bring out the differences between the various diagrams shown there. Zimm has given figures of this sort for the classical case, and for the type of diagram predicted by Mayer and his coworkers, and has remarked that the latter seems more inherently probable. In figure 3 I have shown the slope of the curves in the right-hand diagram of figure 2; this may be compared with Zimm's figures 1a and 1b. It appears to me, however, to be difficult to assess the inherent probability of this diagram without other considerations.

II. ASSOCIATION THEORY AND CRITICAL PHENOMENA

Mayer and Harrison came to the conclusion, as an inference from certain theoretical conclusions, that the middle diagram of figure 1 would be the correct one. McMillan and Mayer (6) extended these considerations to binary liquid systems, and believed that the middle diagram of figure 2 would very likely be the correct one in this case. However, objections can be raised regarding the range of validity of the mathematical treatment, and it seems quite possible that it would break down in the critical region (11).

A simpler approach, which leads to the conclusion that the right-hand diagrams of figures 1 and 2 are correct, lies in the discussion of the molecular association in the vapor phase to form clusters of molecules, an association which may be considered as a kind of incipient condensation (11). Very similar considerations can be used in discussing the binary liquid systems (12); since the calculations are so completely analogous, we shall here confine ourselves to the study of the vapor–liquid equilibrium in a one-component system.

By a simple application of the principles of equilibrium, involving minimization of the free energy of the whole system, it may be shown that the concentration in the vapor phase of clusters containing s molecules is given by

$$c_s = \exp\left[(\beta - \alpha s - \gamma s^{2/3} - \epsilon_s)/kT\right] \tag{1}$$

Here β is the free energy of condensation, per molecule, of single molecules at unit concentration to form a very large drop; α is a coefficient originating as a Laplace multiplier in the minimization of the free energy, but shown to be equal to the free energy per molecule of a very large drop (or the liquid) minus the free energy per molecule of the vapor as it actually exists with all its clusters at the equilibrium concentration; γ is proportional to the surface tension; and ϵ_s is a correction term which arises because the surface free energy cannot be expressed in the form $\gamma s^{2/3}$ for very small drops, and which may be assumed to approach a constant value as $s \to \infty$.

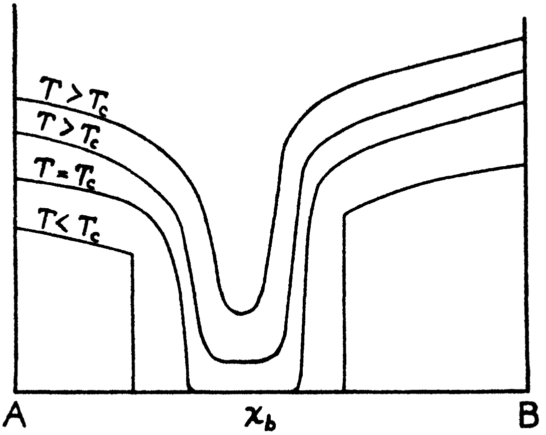

FIG. 3. Slopes of a set of curves of the type indicated in the right-hand diagram of figure 2. These curves (though slightly different ordinates and abscissas are indicated) can be compared directly with figures 1a and 1b of Zimm's article (17). T_s is the temperature at which the meniscus disappears.

When α is large and positive the concentration of large clusters in the vapor is relatively very small, as may be seen by inspection of equation 1. As α decreases (the vapor being compressed at constant T), the relative number of large clusters increases. However, if γ is positive, it is seen that, even when $\alpha = 0$, c_s must decrease with s on account of the $\gamma s^{2/3}$ term in the exponential. But once α has become ever so slightly negative, the term αs will eventually predominate, as $s \to \infty$, over the term $\gamma s^{2/3}$. It is thus seen that, as α crosses the value zero, very large clusters become stable quite suddenly. This corresponds to the ordinary process of condensation at a temperature below the critical temperature.

According to the classical view of condensation, it was generally accepted that the surface tension would vanish at the critical point. Both Mayer and Harrison (4, 7) and Rice (11, 12) assume that the temperature at which the surface tension vanishes will coincide with the temperature at which the meniscus disappears. It is especially interesting to consider the behavior of equation 1 when $\gamma = 0$. In this case the sudden stability of large clusters will not occur. In fact, it may be shown that α will not become zero until c_s for $s \rightarrow \infty$ becomes infinite. This may be readily understood by the following considerations. Let us fix our attention on the reaction

$$2 \text{ clusters of size } s \rightleftarrows 1 \text{ cluster of size } 2s$$

with s very large. If γ is positive, such a coalescence of two clusters will occur with a lowering of the surface area, and hence with a lowering of the surface free energy. This tends to favor the coalescence. The coalescence is opposed, however, by the loss of entropy, since the freedom of motion of a pair of clusters is much less when they are combined than when they are separate. At a certain definite concentration the driving force toward coalescence will overcome the entropy effect. This is the point of condensation where $\alpha = 0$. When $\gamma = 0$, however, the driving force toward coalescence will not be present, and coalescence will not tend to occur until the free motion of the large clusters is entirely squeezed out at infinite concentration.

It will not be necessary to compress the system to zero physical volume before the coalescence occurs. *The concentration c_s should be measured in free volume, not in total volume.* Coalescence occurs when large clusters no longer have any room to move without hitting other large clusters.

When the surface tension is small, even though still positive, we may expect a certain amount of wrinkling at the surface. Such wrinkling will result on an increase in surface entropy; therefore, if the concomitant increase in surface area does not result in too much increase in surface free energy, a noticeable deviation of the droplets from a purely spherical shape may be expected. This means that the clusters will themselves occupy effectively a larger volume than would otherwise be the case, and the condition of zero free volume will occur at a larger total volume than if the drops were spherical.

As a matter of fact, when the surface tension is zero or very close thereto, the degree of wrinkling may become much greater than implied in the preceding paragraph, and the shape of a large cluster may become very complex indeed. Thus, two droplets with depressions and protuberances on them could unite to form a larger droplet containing holes. The final coalescence at vanishing free volume would result in a spongy mass of liquid-like material surrounded and interpenetrated by gas-like material.

It seems probable that the degree to which the surface can extend itself will be limited by an eventual increase in the free energy if the radius of curvature becomes too small. Otherwise, we should expect the evolution of the surface to go on to the end, in which case clusters consisting of sheets and filaments would be stable rather than thicker clusters of the droplet type. However, a sheet or filament is really a different kind of phase, since it would differ radically in molecular energy and entropy from liquid in bulk, and so would be expected to become stable suddenly under certain conditions. This would mean that the surface tension would apparently drop to zero suddenly. Since there is no evidence that this happens we shall assume that we do not have to deal with sheets or filaments, and hence that the curvature of the surface of the droplets is in some way limited.

There seems to be no reason why the surface tension should not become negative. The surface tension is a free energy, and may be considered as composed of an energy and an entropy term. Thus we write

$$\gamma = \eta - T\sigma \tag{2}$$

where γ is proportional to the surface tension, η is proportional to the surface energy (more accurately the surface enthalpy), and σ is proportional to the surface entropy. Our view is that γ vanishes when $\eta = T\sigma$; this occurs at temperature T_c. The term $T\sigma$ has a larger temperature coefficient than η because of the factor T. If the liquid and the vapor actually became identical at T_c, then γ would vanish because η and σ each became zero simultaneously. It seems much more likely that γ vanishes because of fulfillment of the conditional equality. If this is the case, then it is obvious that we should expect $T\sigma$ to be greater than η and hence γ to be negative at temperatures above T_c. The term σ contains a contribution due to wrinkling of the surface, but this has no effect except to lower T_c below what it would otherwise be.

It is clear that it would be impossible to measure a negative surface tension, and very difficult even to measure a very small positive surface tension, when the wrinkling of the surface becomes important. With a negative γ the surface would tend to expand, but the extent of the surface would be limited, if the views expressed in the preceding paragraph are correct, because increase in the extent of the surface would result in increase in the curvature of the surface, and it is assumed that this ultimately results in an increase in the surface free energy. Thus a state of equilibrium would be reached, in which further finite increase in the surface would be resisted, and so in a certain sense one could say that the surface tension had become zero. However, the actual free energy of the surface would still be negative, and the surface would resist even an infinitesimal decrease in area which was not accompanied by a change in average curvature.

Since the area of a large cluster would, under conditions of negative surface tension, be limited only by the ultimate resistance against increase in average curvature, we should expect the the surface to become proportional to s rather than $s^{2/3}$, and the term $\gamma s^{2/3}$ in equation 1 would effectively disappear, being absorbed into the term αs. In spite of this, the idea of negative surface tension is of great importance in the discussion of the isotherms in the neighborhood of the critical temperature.

Once the condition of zero free volume has been reached and the large clusters have coalesced, it is seen that the system is still in a state which is far from compact. Compression of the system will result in what might be called a turning inside-out of the spongy mass of liquid-like material. It will change from a system which has just been formed from, and is just ready to revert to, a vapor with clusters therein, to a system which is just ready to form a liquid containing bubbles of vapor. We assume that this process of compression occurs over a definite range of volumes. For it seems probable that the coalescing droplets have enough wrinkling in their surfaces and sufficient bumps or "pseudopodia" so that the point of effective zero free volume occurs when the volume occupied by the liquid-like material of the clusters is less than half of the total volume. Likewise, in the reverse process of vaporization, coalescence of bubbles in the liquid will occur before the gas-like material of the bubble occupies half the total volume. There will thus be a range of volumes between the points when the clusters coalesce and the bubbles coalesce, the former having the larger volume and also obviously the larger surface, assuming as we have that the extent of surface is delimited by the average curvature of the surface.

We now visualize the process of condensation in the critical region as the squeezing out of surface. At T_c, where the surface tension is zero, this is accomplished with no work and no increase in pressure. Above T_c, where the surface tension is negative, the squeezing out of surface requires work, and the pressure along the isotherms increases as compression occurs. Thus we expect isotherms of the type shown in the right-hand diagram of figure 1.

These arguments can be adapted to a critical solution region in a two-component system, by replacing surface tension by interfacial tension, and by using a semipermeable piston to compress one of the components.

In concluding this section we may remark that the association theory leads to the conclusion that there are large fluctuations in the density of the system in the neighborhood of the critical point. These are undoubtedly related to, but are probably not identical with, the ordinary type of critical fluctuations, which are considered from various points of view in the papers of Zimm (17) and Tisza (15) in this Symposium. It seems likely that the effects of the curvature of the surface, which we believe to be responsible for stabilizing the surface at a certain surface area, do not become noticeable until the curvature is considerably smaller than the wave length of visible light. This implies variations in density over a range of distances of this order. On the other hand, the critical fluctuations which result in opalescence appear to approach the wave length of light. It therefore seems likely that these critical fluctuations are superimposed upon the changes of density which we have considered. The compressibility is very large in the critical region. This is in large part the result of the cluster structure which we have described above and, in turn, allows fluctuations on a larger scale to be superimposed.

III. EFFECTS OF IMPURITIES ON CRITICAL PHENOMENA AND SOLUBILITY CURVES

Several of the papers of this Symposium deal with the effects of an added substance on the critical phenomena in the case of the vapor–liquid equilibrium. The paper of Atack and Schneider (1) is chiefly concerned with the use of the added substance to elucidate the critical phenomena of the one-component system. The papers of Secoy (14) and Boyd (2) have more to do with the effect of the added substance on the coexistence curve. In the latter papers the critical point is treated from the classical point of view, a procedure which is probably reasonably adequate for the purpose in mind.

Some theoretical considerations of the effect of a third substance on a two-component liquid system on a classical basis have been given by Prigogine (10). It seemed worthwhile to consider the effect of an impurity on critical temperature from the point of view of Section II of this paper. This has already been started (12), but more detail will be given here. In this section we confine ourselves to the effect on binary liquid systems of the addition of a small amount of impurity. Such an impurity can have two effects on the solubility curve of two partially miscible liquids: it can affect the chemical potentials of the principal constituents, which means that it affects the body of the solution; or it can affect the interfacial tension. To illustrate the possibilities, we shall consider the possible effects of two different kinds of impurities: (*1*) a substance which is only slightly soluble, but much more insoluble in one of the principal constituents than in the other, and is not absorbed at the interface, and (*2*) a substance which is nearly insoluble in both of the primary constituents, but is strongly absorbed at the interface.

Impurity of type 1

We shall designate the two principal components, A and B, by the subscripts a and b and the impurity by subscript c. We shall designate the phase rich in component A by a prime (′) and that rich in B by a double prime (″). The chemical potentials, which are common to the two phases when in equilibrium, we shall designate simply by μ's without primes.

The effect of an impurity on the equilibrium between the two phases is governed by Gibbs–Duhem relations, as follows:

$$x_a' \, d\mu_a + x_b' \, d\mu_b + x_c' \, d\mu_c = 0 \tag{3}$$

$$x_a'' \, d\mu_a + x_b'' \, d\mu_b + x_c'' \, d\mu_c = 0 \tag{4}$$

where the x's are mole fractions. Now we can write, when x_c' and x_c'' are small:

$$d\mu_c = RT \, d \ln x_c = \mathrm{RT} \, d \ln x_c'' \tag{5}$$

These relations will hold even though a change in x_c' or x_c'' induces exchange of the other constituents between phases. For such an exchange will be proportional to a small change, dx_c' or dx_c'', and hence the extra effect on the partial pressure or fugacity of constituent C caused by this additional change in the solution will itself be proportional to dx_c' or dx_c'', and the total change in fugacity will thus be proportional to dx_c' or dx_c'' so long as x_c' and x_c'' are small.

Substituting equation 5 in equations 3 and 4, and solving for $d\mu_a$ and $d\mu_b$, we obtain:

$$d\mu_a = \frac{RT(x_b' \, dx_c'' - x_b'' \, dx_c')}{x_b'' x_a' - x_a'' x_b'} \tag{6}$$

$$d\mu_b = \frac{RT(x_a'' \, dx_c' - x_a' \, dx_c'')}{x_b'' x_a' - x_a'' x_b'} \tag{7}$$

Let us now suppose that component C is much more soluble in component A and the phase $'$ than in component B and the phase $''$, so that $\mathrm{d}x_c''$ can be considered negligible. Then equations 6 and 7 reduce to:

$$\mathrm{d}\mu_a = \frac{-RTx_b''\,\mathrm{d}x_c'}{x_b''x_a' - x_a''x_b'} \tag{8}$$

$$\mathrm{d}\mu_b = \frac{RTx_a''\,\mathrm{d}x_c'}{x_b''x_a' - x_a''x_b'} \tag{9}$$

Since $x_b''x_a' - x_a''x_b'$ must be positive, since $x_a' > x_a''$ and $x_b'' > x_b'$, we see that $\mathrm{d}\mu_a$ is negative and $\mathrm{d}\mu_b$ is positive.

Suppose now that we had not allowed transfer of material between the phases while adding $\mathrm{d}x_c'$ to the one phase and $\mathrm{d}x_c''$ to the other. Since $\mathrm{d}x_c''$ is so small there would have been practically no change in $\mathrm{d}\mu_a''$ and $\mathrm{d}\mu_b''$. The decrease in $\mathrm{d}\mu_a$ and the increase in $\mathrm{d}\mu_b$ therefore arise from transfer of component A from phase $''$ to phase $'$, or from transfer of component B from phase $'$ to phase $''$, or, most likely, both. Thus the effect of the impurity which is preferentially soluble in one of the principal substituents is to make the phases in equilibrium further apart in composition, that is, the branches of the coexistence curve are spread apart. This is in essential agreement with the conclusions of Prigogine.

The changes in chemical potential with concentration are very small near the critical temperature. Therefore, in this region a small amount of impurity can be especially effective in spreading out the coexistence curve.

In general one will expect the preferentially soluble substituent to be held away from the interface, where the disliked molecule is beginning to be present in appreciable concentration. Hence it should raise the interfacial tension. This is governed by the Gibbs equation,

$$\mathrm{d}\gamma = -\Gamma_a\mathrm{d}\mu_a - \Gamma_b\mathrm{d}\mu_b - \Gamma_c\mathrm{d}\mu_c \tag{10}$$

where γ is the surface tension and the Γ's represent the amounts absorbed at the surface. Now the concentrations, C_a and C_b, of the main constituents, when plotted as a function of the distance r along a line normal to the surface, should look somewhat as shown in figure 4. It is clear that, unless there is to be a region in which the total density is very different from what it is in bulk, a dividing surface drawn to make Γ_a zero will make Γ_b small. On the other hand, there can be a region of the order of 3×10^{-8} cm. near the boundary of phase $'$ in which the concentration of impurity is practically zero. Therefore, Γ_c may be of the order $-3 \times 10^{-8}\,C_c'$ moles/cm.^{2}, where C_c' is the concentration in moles per milliliter of component C in the phase in which its solubility is greater. It is clear that Γ_a and Γ_b will not approach $3 \times 10^{-8}\,C_a'$ or $3 \times 10^{-8}\,C_b''$, respectively, in absolute magnitude, unless, as we have noted, there is a region of order 3×10^{-8} cm. in which the overall density is very different from what it is in the bulk of the liquid phases. The Gibbs–Duhem equation may be written in either of the following forms:

$$0 = C_a'\,\mathrm{d}\mu_a + C_b'\,\mathrm{d}\mu_b + C_c'\,\mathrm{d}\mu_c$$
$$0 = C_a''\,\mathrm{d}\mu_a + C_b''\,\mathrm{d}\mu_b + C_c''\,\mathrm{d}\mu_c$$

Adding these two equations:

$$0 = (C_a' + C_a'')\,d\mu_a + (C_b' + C_b'')\,d\mu_b + (C_c' + C_c'')\,d\mu_c \tag{11}$$

Solving equation 11 for $d\mu_c$ and inserting the result in equation 10 we obtain:

$$d\gamma = -[\Gamma_a - \Gamma_c\,(C_a' + C_a'')/(C_c' + C_c'')]\,d\mu_a \\ -[\Gamma_b - \Gamma_c\,(C_b' + C_b'')/(C_c' + C_c'')]\,d\mu_b \tag{12}$$

In view of our discussion of the mgnitudes of Γ_a, Γ_b, and Γ_c it can be seen that Γ_a and Γ_b are negligible, or, at least, relatively small in equation 12. Dropping Γ_a and Γ_b, and restoring $d\mu_c$ by reverse use of equation 11, we see that equation 12 yields:

$$d\gamma \cong -\,\Gamma_c\,d\mu_c \tag{13}$$

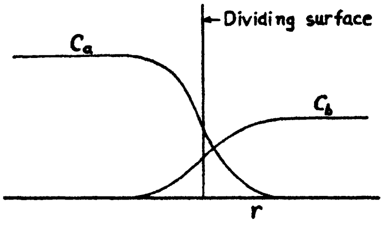

FIG. 4

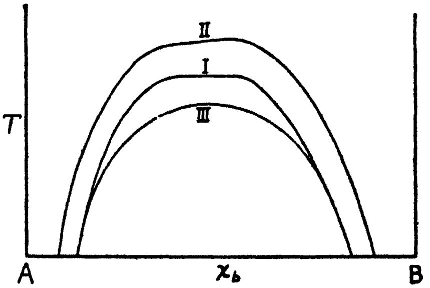

FIG. 5

FIG. 4. Concentrations of components *A* and *B* as functions of the distance from the dividing surface.

FIG. 5. Solubility curves for binary systems, with impurities. Curve I, no impurity; curve II, preferentially soluble impurity; curve III, surface-active impurity.

We have already suggested (12) the applicability of equation 13 but with less justification than that given here.

Since $d\mu_c = RT\,d\ln C_c'$ for small concentrations of compound *C*, we see that the estimate of Γ_c as $3 \times 10^{-8}\,C_c'$ gives:

$$d\gamma \cong 3 \times 10^{-8}\,RT\,dC_c' \tag{14}$$

We have already applied this equation to the case of sodium chloride with the phenol–water system. We shall now apply it in the case of water as an impurity in the cyclohexane–aniline system. The solubility of water in aniline is about 5 per cent at room temperature and about 0.01–0.02 per cent in cyclohexane. Water is, therefore, the kind of impurity we are thinking about.

What was estimated as 2×10^{-6} mole of water per milliliter of solution was accidentally introduced into a critical mixture of cyclohexane and aniline. This raised the mixing temperature 0.2° and caused the mixture to cease being a critical mixture. It is, therefore, clear that the critical temperature was raised by more than 0.2°.

Using $R = 8 \times 10^7$ ergs per degree per mole, $T = 300$°K., and $dC_c = 3 \times$

10^{-6} moles per milliliter, we obtain from equation 14:

$$d\gamma = 0.0015 \text{ dyne/cm.}$$

This implies that the rate of change of interfacial tension is of the order of 0.01 dyne per centimeter per degree, which is about what is expected (about what is observed for the phenol–water system, for example).

One more point deserves mention in connection with this type of impurity. A given percentage of the third component in the total mixture, if added to a two-phase system, should be more effective in raising the interfacial tension the less the amount of the phase in which the third component is more soluble. A coexistence curve with a horizontal section on top should, therefore, be converted into one in which the flat portion on top slopes down in the direction of the component in which the third component is soluble, as is indicated in figure 5. An effect of this sort has been observed by Schreinemakers (13) with the phenol–water system and sodium chloride as an impurity. In this case the effect is still visible, even though he plots his curves for a constant ratio of sodium chloride to water, rather than for constant ratio of sodium chloride to water + phenol. Water is more soluble in phenol than is sodium chloride. Hence addition of phenol makes the water layer richer in sodium chloride, and the critical temperature of phenol-rich mixtures (overall phenol concentration higher) is raised more than that of those richer in water.

Impurity of type 2

In this case we assume the solubility to be so small that μ_a and μ_b are not appreciably affected. The chief effect is a surface effect. Γ_c can be much larger in this case. Γ_a and Γ_b will have larger negative values than in the other case, because these constituents will be pushed away from the surface by the impurity. However, the effect of the two latter will not be comparable with that of Γ_c; hence equation 13 holds again. Γ_c is positive, so γ is lowered.

The interfacial tension of the mixture may be lowered below zero, at a temperaature below the critical temperature for the pure binary system. This means that there will be mutual emulsification. This will go on until so much of component C has been taken into the interface that its concentration in the body of the phases becomes so small that γ has risen to zero. At this point emulsification will stop, and two layers will remain of net concentration closer together than the concentration at which they started. A smaller change of temperature than when the impurity was absent will now cause one of the layers to engulf the other. Thus the coexistence curve will be lowered at this concentration. Presumably the temperature at which the one phase engulfs the other depends upon the relative amounts of the two phases, and it should be easier for one phase to be engulfed if the other is present in considerable excess. Thus a flat-topped coexistence curve is rounded off, as indicated in figure 5.

One question remains. Can the line of demarcation between the two phases be observed under the circumstances? If it cannot, this might readily lead to the belief that we can have constant vapor pressure over a range of concentrations of a homogeneous solution, when the system is not, in fact, homogeneous. In considering questions of this sort, however, it should be noted that the problem is actually somewhat more complicated than, perhaps, our sketchy account has indicated. The curvature of the surfaces of the emulsified droplets may have important effects on the surface tension and the equilibrium. Many problems in this field must await the future for solution.

IV. SUMMARY

1. A general discussion is given of the various possibilities with respect to liquid–vapor coexistence curves and the isotherms of one-component systems. A similar discussion is also given of the coexistence or mutual solubility curves in binary liquid systems, and the corresponding isotherms. There is a brief consideration of the relevant experimental data in each of these cases.

2. A brief review is given of the association theory of condensation, in which condensation is considered as a limiting case of the formation of clusters of molecules in the vapor phase. The application to critical phenomena is indicated, and it is shown that these considerations lead one to anticipate an isotherm (pressure *vs.* volume in a one-component system) which has a finite horizontal portion at the critical temperature, with isotherms above the critical temperature having everywhere a finite slope. The importance of a correct evaluation of the free volume in which a cluster can move and the significance of the surface tension of large clusters are particularly stressed.

3. The effect of an impurity (small amount of a third component) on the critical phenomena in a binary liquid is considered. It is shown that the effect of the third component on the interfacial tension of a two-phase system can play a very important role.

REFERENCES

(1) Atack, D., and Schneider, W. G.: J. Phys. & Colloid Chem. **54**, 1323 (1950).
(2) Boyd, C. A.: J. Phys. & Colloid Chem. **54**, 1347 (1950).
(3) Dacey, J. R., McIntosh, R. L., and Maass, O.: Can. J. Research **B17**, 206 (1939).
(4) Harrison, S. F., and Mayer, J. E.: J. Chem. Phys. **6**, 101 (1938).
(5) McIntosh, R. L., Dacey, J. R., and Maass, O.: Can. J. Research **B17**, 241 (1939).
(6) McMillan, W. G., Jr., and Mayer, J. E.: J. Chem. Phys. **13**, 276 (1945).
(7) Mayer, J. E., and Harrison, S. F.: J. Chem. Phys. **6**, 87 (1938).
(8) Michels, A., Blaisse, B., and Michels, C.: Proc. Roy. Soc. (London) **A160**, 358 (1937).
(9) Naldrett, S. N., and Maass, O.: Can. J. Research **B18**, 118 (1940).
(10) Prigogine, I.: Bull. soc. chim. Belg. **52**, 115 (1943).
(11) Rice, O. K.: J. Chem. Phys. **15**, 314 (1947).
(12) Rice, O. K.: Chem. Revs. **44**, 69 (1949).
(13) Schreinemakers, F. A. H.: Z. physik. Chem. **29**, 579 (1899).
(14) Secoy, C. H.: J. Phys. & Colloid Chem. **54**, 1337 (1950).
(15) Tisza, L.: J. Phys. & Colloid Chem. **54**, 1317 (1950).
(16) Woodburn, H. M., Smith, K., and Tetewsky, H.: Ind. Eng. Chem. **36**, 588 (1944).
(17) Zimm, B. H.: J. Phys. & Colloid Chem. **54**, 1306 (1950).

OPALESCENCE OF A TWO-COMPONENT LIQUID SYSTEM NEAR THE CRITICAL MIXING POINT[1]

BRUNO H. ZIMM

Department of Chemistry, University of California, Berkeley 4, California

Received December 19, 1949

Near any critical point large fluctuations of some of the properties of the system occur. If these fluctuations are accompanied by changes in the refractive index, the system is no longer optically uniform and the amount of light scattered will be large. A discussion of the resulting opalescence was given by Smoluchowski (12) in 1908, followed by a more complete treatment by Einstein (1) in 1910. The latter's contribution has stood to this day as the best basic treatment, and has been extended, but not modified, by later authors.

In the present case we have a two-component one-phase liquid system near the critical mixing point. Ordinarily small fluctuations in composition will occur as a result of the thermal motion of the molecules, but they will seldom be large because of the free-energy increase accompanying a fluctuation away from homogeneity. Near the critical mixing point, however, the free-energy changes very slightly with composition so that the fluctuations may easily become large. Putting these ideas into quantitative form, Einstein derived essentially the following equation:

$$\tau = \frac{32\pi^3}{3\lambda_0^4 N_a}\left\{RT\beta\left(\rho_n \frac{\mathrm{d}n}{\mathrm{d}\rho}\right)^2 + \frac{V_1\varphi_2}{-\mathrm{d}\ln a_1/\mathrm{d}\varphi_2}\left(n\frac{\mathrm{d}n}{\mathrm{d}\varphi_2}\right)^2\right\} \tag{1}$$

where τ = the "turbidity," the fraction of the incident light scattered per unit length,
λ_0 = the wave length of the light *in vacuo*,
N_a = Avogadro's number,
R = the gas constant,
T = the absolute temperature,
β = the compressibility,
ρ = the density,
n = the refractive index,
V_1 = the molar volume of component 1,
φ_2 = the volume fraction of component 2 (see below), and
a_1 = the activity of component 1.

The extension of this equation to include angular variations of intensity is discussed later.

The first term of this equation, involving the compressibility, is very small in a mixture near the critical mixing point. Essentially, therefore, equation 1 may be looked on as a relation between the slope of the activity isotherm, d ln

---

[1] Presented at the Symposium on Critical Phenomena, which was held under the auspices of the Division of Physical and Inorganic Chemistry at the 116th meeting of the American Chemical Society, Atlantic City, New Jersey, September 22, 1949.

$a_1/d\varphi_2$, and the turbidity, τ. Thermodynamic quantities may thus be determined by light-scattering measurements. In fact, because of the reciprocal relation between the turbidity and the slope of the isotherm, this method is eminently suited to measuring the slope near the critical point, where it is so small that other methods fail.

Let us consider what might be expected from a theoretical basis for the isotherms in the neighborhood of a critical point. For simplicity, we shall restrict our remarks to a system of two components that forms two liquid phases below the critical (mixing) point and one phase above. We shall use the volume fractions, $\varphi_1 = N_1\bar{V}_1/V$ and $\varphi_2 = N_2\bar{V}_2/V$ to describe the composition, where N_1 and N_2 are the numbers of moles of components 1 and 2, $\bar{V}_1$ and $\bar{V}_2$ are the partial molar volumes of these components, and V is the total volume. Of course, $\varphi_1 + \varphi_2 = 1$. To describe the thermodynamic potentials we shall use the activities, a_1 and a_2. In discussing the slopes of the isotherms, we shall use principally the quantity d ln a_1/ d ln φ_1, temperature and pressure being assumed constant, of course.

In a system that obeys Raoult's law d ln a_1/d ln φ_1 is always unity. In other cases it may be represented by a power series in φ_2, ·

$$d \ln a_1/d \ln \varphi_1 = 1 - \sum_1^{\infty}{}_n B_n \varphi_2^n \qquad (2)$$

where the coefficients B_n are functions of the temperature only for any given system, provided the system is of one phase. The appearance of a second phase creates a singularity in d ln a_1 / d ln φ_1, which may be considered mathematically as a point of divergence of equation 2.

The graphical representation of equation 2 for a hypothetical system showing a classical critical point is shown in figure 1a. At high temperatures (curve I) d ln a_1/d ln φ_1 has a minimum at some volume fraction in the middle of the diagram. As the temperature is lowered the minimum drops lower until it touches zero (curve II). This is the critical point. At still lower temperatures a phase transition occurs before the curve reaches zero (curve III), as signified by the discontinuous drop to zero, where the second phase appears. Mathematically speaking, there is a critical temperature at which the function first vanishes, and at this temperature and below a singularity (discontinuity) of the function makes its appearance. The initial appearance of these two phenomena at the same temperature is remarkable, since each imposes stringent, and apparently unrelated, conditions on the coefficients B_n of equation 2.

It was shown by McMillan and Mayer (8), following earlier work by Mayer (7), that the coefficients B_n are complicated but definitely determined functions of the intermolecular potentials. It is conceivable that for a particular system the B_n might satisfy simultaneously the conditions for the divergence and the vanishing of the function, but it would seem really remarkable that they should do it for all systems of diverse molecular types in which the values of the individual coefficients differ greatly. Mayer therefore suggested that the isotherms might more reasonably be expected to show the behavior illustrated in figure 1b. Here the critical point is the point at which the minimum of an isotherm just touches zero (curve II), but it is not the point at which divergences of the series of equation 2 occur. Divergence, with the appearance of a second phase, occurs for the first time at a lower temperature. The two phenomena are separated by a temperature interval. In this interval a new type of isotherm (curve IV) appears,—one in which d ln a_1/d ln φ_1 goes continuously to zero, and then remains at zero for a finite interval.

There is thus predicted to be a region between the critical point and the temperature at which two distinct phases appear within which there is a second-order transition, the first derivative of the activity going continuously to zero while the second derivative has a discontinuity. The prediction of this anomalous region is not rigorous; it is based on the plausible argument that the two apparently unrelated events of the vanishing of equation 2 and its divergence will not first occur at the same temperature. On this basis the classical isotherms displayed in figure 1a would be the result of a miraculous coincidence.

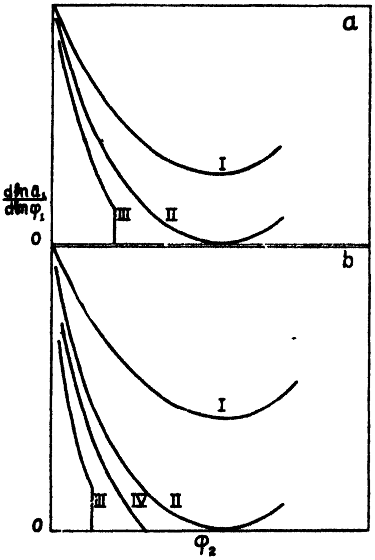

FIG. 1. Possible isotherms: (a) classical; (b) according to Mayer

Most of the previous investigators who have studied critical opalescence (4, 5, 11) did so before Mayer's theory was advanced. Their experiments show no sign of a second-order transition, but it is possible that the transition occurs over such a small temperature interval that it was overlooked. Mason and Maass (6), on the other hand, found anomalous behavior in a one-component system. It therefore seemed worthwhile to carry out a new investigation with the primary purpose of searching for the second-order transition.

EXPERIMENTAL

For the experimental investigation the system of carbon tetrachloride and perfluoromethylcyclohexane, C_7F_{14}, was chosen, since Hildebrand and Cochran

(3) had demonstrated a critical point at the convenient temperature of 26.9°C. Moreover the system is nonpolar, a fact that might lead to important simplifications in a theoretical treatment.

The materials used were purified with some care. The carbon tetrachloride was Mallinckrodt's analytical reagent grade. It was distilled through a jacketed twenty-plate column, the first fifth (b.p. 76.8°C., corrected) being discarded; the succeeding third (b.p. 76.84°C., corrected) was retained and used without further treatment. The perfluoromethylcyclohexane, C_7F_{14}, was the same material used by Hildebrand and Cochran (3); it had originally been obtained from the Jackson Laboratory of E. I. du Pont de Nemours and Company. Upon distillation through the twenty-plate column, the first fifth of the material came over below 76.45°C. and was discarded. About one-half distilled from 76.45° to 76.55°C. and was kept. (The boiling point reported in the literature (2) is 76.32°C.) The remaining portion boiled over a range of 0.4°C. The distilled material was then twice redistilled in a simple one-plate still over one-tenth its weight of 100-mesh silica gel that had been heated to red heat in air for 30 min. to drive off water. It was hoped that this treatment would remove small amounts of impurities that might have escaped fractionation. A mixture of 58 per cent by weight of carbon tetrachloride was made with a sample of the perfluoromethylcyclohexane after fractionation and after each treatment with silica gel. The temperature of phase separation was determined for each sample. These were all found to be 28.23°C. ± 0.02°, showing that no change in the solubility behavior of the perfluoromethylcyclohexane was occurring with further treatment.[2]

Solutions were made by weighing small amounts of the purified materials into glass tubes, which were then sealed until ready for use. The compositions are given in table 1, being expressed both as weight fractions and as volume fractions. The volume fraction of component 2, φ_2, is given by $\varphi_2 = w_2/\rho_2 V$, where w_2 is the weight of component 2 (carbon tetrachloride), ρ_2 is its density, and V is the total volume; likewise for φ_1.

The light scattering was measured in an apparatus previously described (13). In essence, this consists of a 3-ml. glass bulb suspended in a beam of light and containing the solution, with the scattering observed by a revolving photoelectric photometer. The small bulb was surrounded by 1-propanol to reduce reflections and to provide temperature control. The 1-propanol was heated by water from a thermostat flowing through a copper coil and was stirred by an electric motor when necessary. For those solutions showing extremely high opalescence, a special small bulb was made to keep the light path short to reduce secondary scattering. In this bulb the total light path did not exceed 3 mm. at any angle at which observations were made. The apparatus was calibrated by means of a standard polystyrene solution, whose absolute scattering power had been measured with

[2] The presence of an impurity in the original material was indicated by the low temperature of phase transition, 26.9°C., found by Hildebrand and Cochran (3) and also by the fact that the original material discolored very dilute potassium permanganate solution. The latter reaction is reported to result from the presence of incompletely fluorinated compounds (2). The purified material showed no reaction with potassium permanganate over a period of 16 hr. The purified carbon tetrachloride likewise showed no reaction.

exceptional care by Dr. C. I. Carr in this laboratory.[3] Some care was taken to keep dust out of the solutions by using carefully cleaned equipment and minimizing the number of transfers. The dust originally present in the materials was removed in the distillations described above.

In applying Einstein's formula (equation 1) the following simplification was made: If the relation of Gladstone and Dale for the refractive index is assumed,

TABLE 1

Compositions and separation temperatures of mixtures

MIXTURE NO.	CCl_4 BY WEIGHT	φ_2 VOLUME FRACTION CCl_4	SEPARATION TEMPERATURE
	per cent		°C.
1	27.9	0.317	22.9
2	36.85	0.400	26.8
2½	42.2	0.451	28.0
3	47.25	0.502	28.3
3½*	52.7*	0.560*	28.3*
4	58.4	0.614	28.3
4½	62.5	0.653	28.0
5	67.8	0.707	26.8
6	79.95	0.820	20.6

* Critical mixture.

TABLE 2

$d\ ln\ a_1/d\ ln\ \varphi_1$

MIXTURE NO. ..	1	2	3	3½	4	5	6
t							
°C.							
50	0.325	0.159	0.0993	0.0875	0.0916	0.133	0.309
40	0.283	0.110	0.0509	0.0386	0.0470	0.0936	0.282
35	0.244	0.0745	0.0280	0.0222	0.0258	0.0589	0.245
30	0.192	0.0419	0.00695	0.00428	0.00610	0 0331	0.205
29	0.180	0.0333	0.0031	0.0016	0.0030	0.0290	0.198
28	0.169	0.0249				0.0240	0.191
26.8	0.156	0.0171*				0.0165*	0.182
22.9	0.122*						0.166
20.6							0.158*

* Value just previous to phase separation.

and moreover it is assumed that there is no volume change on mixing the two components, then $dn/d\varphi_2 = n_2 - n_1$, where n_2 and n_1 are the refractive indices of the pure components. Further, it is convenient to express the results in terms of

---

[3] This standardization, part of the general program of standardization of our equipment, was done by three independent methods: a transmission measurement, a measurement of the scattering at right angles to the incident beam, and a measurement of the total scattering in an integrating sphere. All methods gave results which were in agreement.

$d \ln a_1/d \ln \varphi_1$, a quantity that remains finite for all values of the composition. From the definition of the volume fraction it can be shown that $d \ln a_1/d \ln \varphi_1 = -\varphi_1\, d \ln a_1/d\varphi_2$.

The light-scattering measurements on each solution were converted to $d \ln a_1/d \ln \varphi_1$ and plotted on a logarithmic scale against the logarithm of the temperature less an appropriate number. In this way smooth, slightly curved lines were obtained from which the value of $d \ln a_1/d \ln \varphi_1$ could be obtained at any desired temperature. The interpolated results are shown in table 2 and figures 3 and 4. Some of the original experimental data are given in table 4 and figure 5. The deviation of the points from the smooth curve was usually less than 5 per cent, and appeared to be entirely erratic.

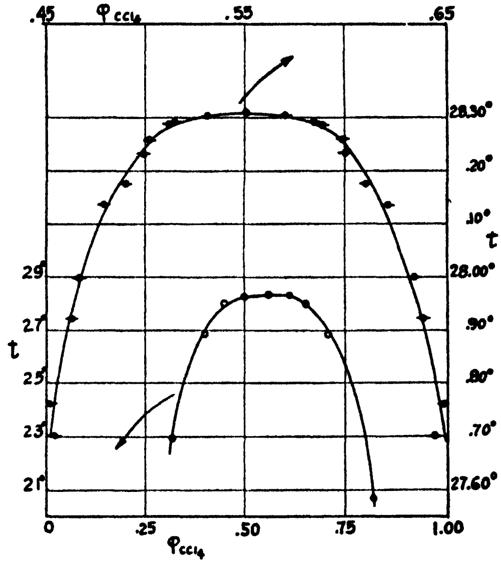

FIG. 2. Phase diagram of the system C_7F_{14}–CCl_4. Scales on lower left axes apply to lower curve; those on upper right to upper curve.

The temperature of phase separation was determined for each mixture by slowly warming the two-phase mixture with shaking in a water bath until a homogeneous solution was obtained. When the mixture was cooled, noticeable supercooling occurred only in mixtures 1, 2, 5, and 6 (table 1) before the two phases separated again.

When the temperature of phase separation was plotted against composition the different mixtures showed erratic deviations of the order of 0.02° from a smooth curve. Believing that the deviations might be caused by differences in the amount of air dissolved in the various mixtures, it was decided to determine the sensitive portion of the phase diagram with one mixture only. About 0.1 ml. of mixture No. 3½ was sealed in a vial bearing a straight piece of 2-mm. tubing as a side arm. This vial was suspended in a thermostat regulated within 0.002°, in such a way that it could be tilted from outside the bath. When the mixture had been made to separate into two phases at any desired temperature, the tube could be tilted and a portion of the upper phase poured into the side arm. On subsequent cooling of the tube in another bath, the mixture in the side arm would separate again into two phases of composition that could be estimated sufficiently well from the rough phase diagram already determined. By measuring the relative amounts of the two new phases with a telescope and scale it was then possible to calculate the composition of the original upper phase, and from the total composition the composition of the original lower phase could also be determined. In this way the upper curve of figure 2 was obtained. The results of these experiments are shown in table 3.

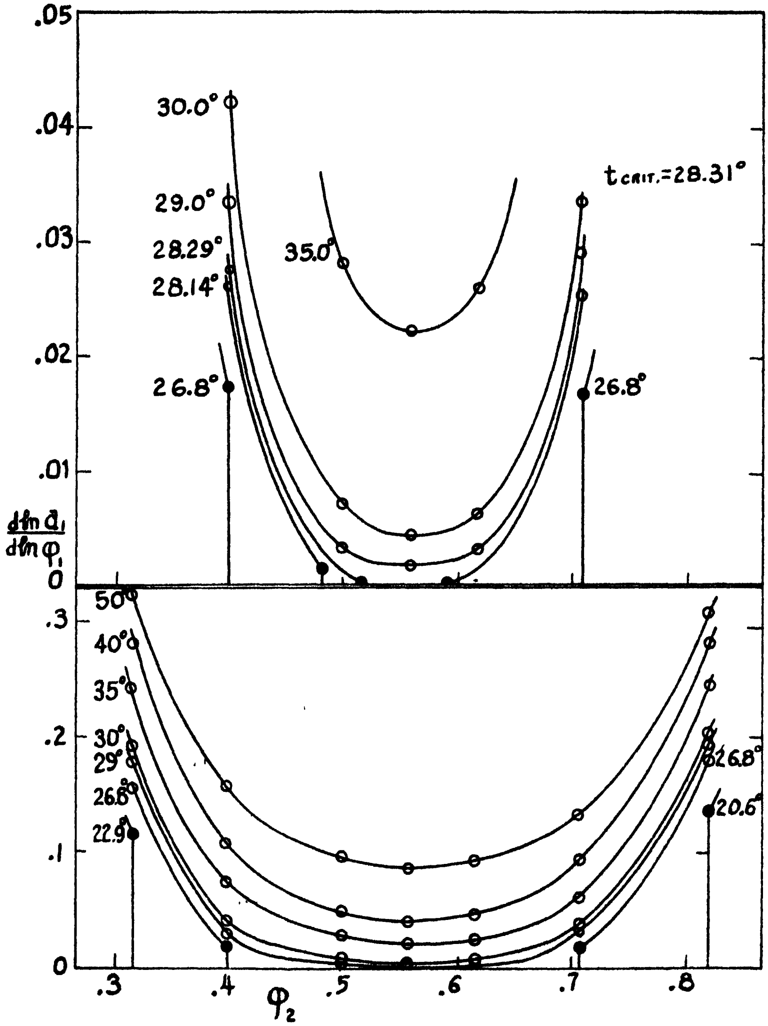

FIG. 3. Activity isotherms of mixtures of C_7F_{14} (component 1) and CCl_4 (component 2) at indicated temperatures. Filled circles are points of observed phase transition.

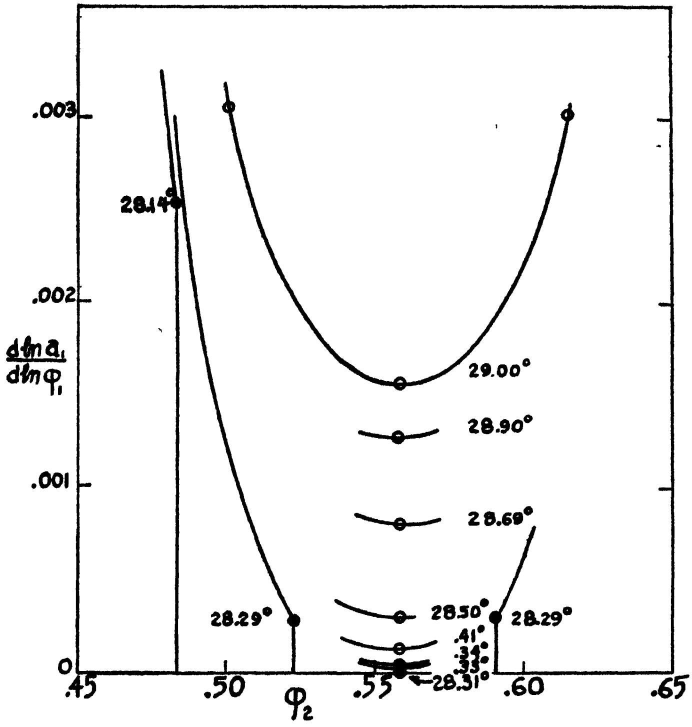

FIG. 4. The critical region of figure 3

TABLE 3

Consolute mixtures

TEMPERATURE	VOLUME FRACTION CCl_4, φ_2, OF LOWER LAYER	VOLUME FRACTION CCl_4, φ_2, OF UPPER LAYER
°C.		
28.310*	0.551	
28.303	0.531	0.571
28.292	0.516	0.586
28.285	0.513	0.589
28.258	0.503	0.598
28.232	0.498	0.604
28.173	0.491	0.611
28.135	0.480	0.622
27.99	0.467	0.635
27.92	0.463	0.639
27.76	0.452	0.650
27.70	0.456	0.646

* Critical temperature.

In all cases a distinct and sharp meniscus was observed between any two phases in equilibrium. In one experiment mixture No. 3½ was heated without stirring to 0.01° above the temperature at which two phases had appeared on cooling; in 15 min. the meniscus spontaneously diffused, being replaced by a continually spreading band about 1 mm. in width containing a smooth refractive-index gradient. The diffusion was taken as evidence that a single uniform phase was the condition of equilibrium at this temperature.

On cooling, the approach of the phase transition was heralded by an increase in the opalescence of the solution. However, the second phase could always be seen to form as small discrete drops, appearing quite different on close examination from the general opalescence that preceded it.

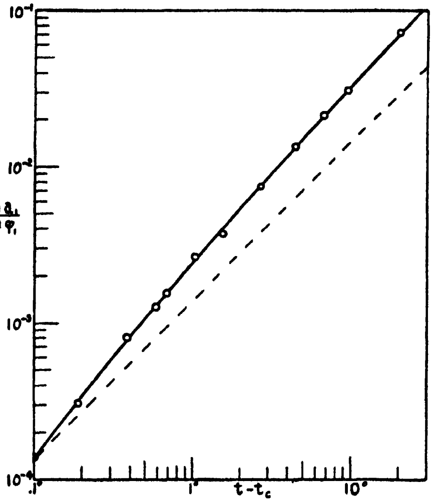

FIG. 5

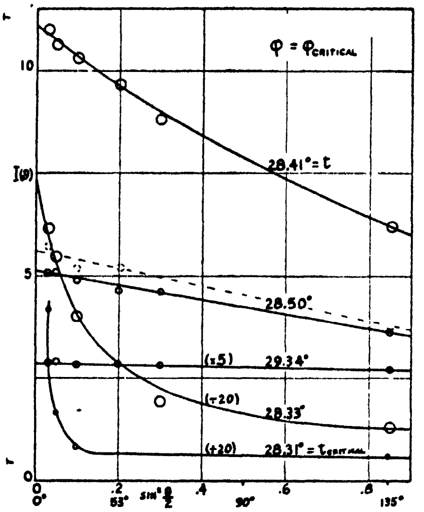

FIG. 6

FIG. 5. Values of d ln a_1/d ln φ_1 calculated directly from experimental turbidities and plotted against temperature minus critical temperature for the critical mixture. The dotted line is the line of unit slope.

FIG. 6. Intensity in consistent but arbitrary units against the square of the sine of half the angle of scattering at the indicated temperatures. Some of the values have been multiplied or divided by constant factors as indicated. All points for $\varphi_2 = 0.560$ except the dotted ones, which are for $\varphi_2 = 0.516$ and $t = 28.29$°C.

RESULTS

The phase diagram, determined as described above, is shown in figure 2. It is noteworthy that the two-phase region is rounded on top, not flat (8, 10). However, it should also be noted that the curve describing it is not a parabola. Empirically, the curve is given well enough by the equation:

$$t = t_c - 600(|\varphi_2 - \varphi_{2_c}|)^3$$

The critical point itself seems to occur at a volume fraction of carbon tetrachloride, φ_{2_c}, of 0.551 and a temperature, t_c, of 28.310°C., the last two decimal places of the temperature having significance relative only to the other temperatures of this report, since the absolute calibration of the thermometers was reliable only to 0.1°.

The results of the light-scattering determination of d ln a_1/d ln φ_1 are shown in figures 3 and 4 and in tables 2 and 4. *It can be seen that the isotherms are of the classical type. No sign of a second-order transition below the critical point is apparent.* A discontinuity in the slope is found even at 0.02° below the critical point, while the slope is observed to be finite and different from zero 0.01° above the critical point.

In figure 5 it is seen that the opalescence varies almost linearly with temperature above the critical point, as also in the results of Keesom (4) and Mason and Maass (6) on the liquid–vapor critical point in ethylene. The general appearance of these results is also similar to those of Krishnan (5) and Rousset (11) on other systems.

TABLE 4

Turbidity as a function of temperature in critical mixture (No. 3½)

TEMPERATURE	TURBIDITY	d ln a_1/d ln φ_1	TEMPERATURE	TURBIDITY	d ln a_1/d ln φ_1
°*C.*			°*C.*		
47.2	0.0026	0.074	28.69	0.222*	0.00086
37.3	0.0061	0.031	28.50	0.56*	0.00034
34.7	0.0089	0.021	28.41	1.13*	0.00017
32.6	0.0144	0.0133	28.34	4.0*	0.00005
30.9	0.026	0.0074	28.33	7*	0.00003
29.8	0.052	0.0037	28.31	>20*§	0.00000
29.34	0.071*	0.0027	28.29	0.60†*	0.00032†
29.00	0.13*	0.0015	28.14	0.074‡*	0.0026‡
28.90	0.150*	0.00126			

* Ideal values, calculated from scattering extrapolated to zero angle.

† Refers to lower layer with an estimated composition, φ_2, of 0.516.

‡ Refers to lower layer with an estimated composition, φ_2, of 0.480.

§ Droplets visible in mixture.

ANGULAR DEPENDENCE OF THE SCATTERING

The Einstein formula as written in equation 1 holds only if the fluctuations in refractive index are uncorrelated over distances of the order of magnitude of the wave length. In general, as shown by Ornstein and Zernike (9), the scattering, I, is proportional to the integral:

$$I \sim \int_0^\infty \frac{\sin sr}{sr}\, g(r)\, 4\pi r^2\, \mathrm{d}r \tag{3}$$

where $g(r)$ is the *mean correlation* of two fluctuations of refractive index occurring at a distance r apart, $s = 4\pi \sin(\vartheta/2)/\lambda$ with λ the wave length of the light and ϑ the angle. This integral reduces to the Einstein equation 1 if $\sin sr/sr$ is unity, i.e., if sr is small, over all values of r for which the correlation $g(r)$ is different from zero. Since s is less than 0.003 reciprocal Å. for visible light, the Einstein formula is valid without restrictions if the fluctuations are not correlated over distances of more than 100 Å. Otherwise, the scattering depends upon s and hence on the angle. That such a thing sometimes occurs is demonstrated by the data plotted in figure 6. However, we may always extrapolate to a point at which the Einstein formula is valid simply by extrapolating to the value of the scattered intensity at an angle of zero, since here s is zero and $\sin sr/sr$ is unity for all values of r. This was the procedure actually followed wherever an angular dependence of the scattering was found. In this way we avoid the necessity of considerations such as those of Ornstein and Zernike (9). One might similarly extrapolate to infinite wave length, but the extrapolation to zero angle is easier experimentally.

Since the variation of scattering with angle occurs only when the fluctuations extend over regions of large, almost visible size, it is interesting to note that such variation was only observed within one degree of the critical point at the critical composition, and over a range of less than 10 volume per cent at the critical temperature. This conclusion is at variance with that of Krishnan (5), based on depolarization studies.

An attempt was made to determine the depolarization of the scattered light in order to substantiate the conclusions from the angular variation. The depolarization was found to be very small, and the secondary scattering unavoidable in mixtures of the high turbidity encountered in this work made these measurements uncertain. The secondary scattering also made the quantitative interpretation of the angular variation curves difficult. In particular, it would be interesting to compare them to the theoretical calculations of Ornstein and Zernike, but beyond the statement that there is qualitative agreement it is impossible to go without more elaborate experimental precautions.

It is easy to see from the form of the curve in figure 6 that the extrapolation to zero angle fails at the critical point itself, as indeed it should, since here the fluctuations are macroscopic in size, although the scattering is finite at any angle greater than zero.

CONCLUSION

These results might be criticized on the basis that the materials used were impure. In view of the process used, it does not seem that large amounts of impurities could be present unless they were isomers of the perfluormethylcyclohexane. In this case they would also all have the same solubility properties and hence should not change the behavior of the system. Perhaps the small amounts of water and air that were dissolved in the samples from their contacts with the atmosphere might have a more serious effect. It must remain for future work to assess the importance of this criticism.

The general appearance of our data is similar to that of Krishnan (5) and Rousset (11), though at variance with the results of Mason and Maass (6) on a one-component system.

The failure of a second-order transition to be observed is a major surprise, in view of the theoretical likelihood of this transition. It is apparent that this is not a contradiction of the theory, but if substantiated it is an uncomfortable demonstration that the critical phenomenon is less well understood than had been hoped. It would be necessary that there exist relations among the higher coefficients, B_n, of equation 2 such that the divergence of the series first occurs at a temperature very close to, if not identical with, the critical temperature. Since similar behavior seems to be found experimentally in other systems (5, 11), it would mean that these relations among the coefficients must hold regardless of the details of the intermolecular forces.

Our experiments were designed to answer experimentally the question of whether the theoretically expected second-order transition can be found. The answer, at least as concerns the system studied, seems to be a clear negative. Not the slightest evidence was found for any anomalous behavior near the critical point. The results then pose a difficult problem for the theorist,—the problem of explaining why the predicted second-order transition fails to appear.

REFERENCES

(1) Einstein, A.: Ann. Physik **33**, 1275 (1910).
(2) Fowler, R. D., *et al.*: Ind. Eng. Chem. **39**, 375 (1947).
(3) Hildebrand, J. H., and Cochran, D. R. F.: J. Am. Chem. Soc. **71**, 22 (1949).
(4) Keesom, W. H.: Ann. Physik **35**, 591 (1911).
(5) Krishnan, R. S.: Proc. Indian Acad. Sci. **2**, 21 (1934); **5**, 577 (1937).
(6) Mason, S. G., and Maass, O.: Can. J. Research **26B**, 592 (1948).
(7) Mayer, J. E.: J. Chem. Phys. **5**, 67 (1937).
(8) McMillan, W. G., and Mayer, J. E.: J. Chem. Phys. **13**, 276 (1945).
(9) Ornstein, L. S., and Zernike, F.: Physik. Z. **27**, 261 (1926); **19**, 134 (1918).
(10) Rice, O. K.: J. Phys. & Colloid Chem. **54**, 1293 (1950).
(11) Rousset, A.: Ann. phys. **5**, 5 (1936).
(12) Smoluchowski, M.: Ann. Physik **25**, 205 (1908).
(13) Zimm, B. H.: J. Chem. Phys. **16**, 1099 (1948).

THE THEORY OF CRITICAL POINTS[1, 2]

L. TISZA

Department of Physics and Research Laboratory of Electronics, Massachusetts Institute of Technology, Cambridge, Massachusetts

Received December 19, 1949

I. INTRODUCTION

The existence of critical points was discovered by Andrews (1) in connection with his classical investigation of the carbon dioxide isothermals. Andrews was mainly concerned with the nature of the liquid, vapor, and gaseous phases of matter. His main conclusion and at the same time the definitive solution of the question was that there is only a single fluid condition of matter which can split into two coexisting forms of different density, provided the temperature is *below*

---

[1] Presented at the Symposium on Critical Phenomena, which was held under the auspices of the Division of Physical and Inorganic Chemistry at the 116th Meeting of the American Chemical Society, Atlantic City, New Jersey, September 22, 1949.

[2] This work was supported in part by the Signal Corps, the Air Materiel Command, and the Office of Naval Research.

a certain critical value. Gases appear "permanent," that is, resist liquefaction, if compressed at a temperature *above* the critical.

This interpretation provided a powerful stimulus for reaching lower temperatures than were available at that time and generally cleared the ground for the development of low-temperature physics. Yet this was only one of the repercussions of the discovery of critical points.

It may be noted in the first place that the term "critical" seems to have been dictated by an unusual intuition. Originally referring only to the possibility of liquefaction of a gas, it turned out that the critical points of the phase diagram were "critical" also in a more profound sense of the word.

It was realized that critical points have a certain anomalous nature; they prove rather elusive to routine thermodynamic investigations. Equilibria under critical conditions are extremely slow to establish themselves and prove very sensitive to the minutest perturbances. All this concurs in making it hard to obtain reproducible results.

Perhaps the most spectacular among critical phenomena is the enormous amount of light scattering, the so-called critical opalescence. In 1908 Smoluchowski (11) gave his famous interpretation of this phenomenon, tracing it to abnormally large molecular fluctuations. This was at the same time the key to the above-mentioned peculiarities of the critical point. In fact, the smallness of molecular fluctuations is a prerequisite for the use of thermodynamic methods in general, since otherwise there would be no assurance that the molar quantities are adequate substitutes for the molecular variables of which they are the averages.

The standard method of statistical mechanics for computing fluctuations makes use of the method of canonical ensembles. By applying this to the critical point one arrives at the result that the fluctuations tend to infinity. In reality, the fluctuations are unusually large, but obviously finite. This means that at the critical point both thermodynamic and statistical methods reach their limits of applicability.

The significance of the breakdown of these methods of great generality is amplified by the remark that critical phenomena are by no means limited to the type found in one-component fluid systems. A possible generalization was mentioned in the first investigation of Andrews (1): one might expect a critical point with respect to the solid–liquid equilibrium. A search for such a critical point has consistently led to negative results. In fact, cogent theoretical arguments have been advanced in favor of the view that such a critical point is not possible (e.g., 3). Quite analogous phenomena have been observed, however, in two-phase systems of liquids of limited miscibility. Most of the measurements on critical opalescence have been carried out at such points of critical mixing.

A somewhat more hidden variant of critical phenomena is provided by ferromagnetic and ferroelectric Curie points and the so-called λ-points which are found in a large number of solids (order–disorder transitions in alloys and molecular crystals). This analogy seems to have been first pointed out by Onsager and Kaufman (4, 5). Subsequently, Semenchenko (10) tried to substantiate this idea by reformulating Ehrenfest's relation for second-order transitions for cases of ferromagnetism, ferroelectricity, and related phenomena.

The question has been reopened by the author (12), who has shown that Ehrenfest's approach is not suited for a unified theory of critical points and λ-points. According to Ehrenfest, the derivatives of the thermodynamic potential, say the specific heat, are discontinuous along the λ-line, but they are presumably quite regular within the two phases. On the other hand Onsager (4, 5) has shown that, at least in one case where exact calculations were possible, the specific heat tends to infinity on both sides of the λ-point.

The unified thermodynamic theory of critical points and λ-points (12) has been built on the idea of stability. There arises the possibility of singular points in the phase diagram in which the thermodynamic stability of the system is the lowest which is compatible with the principles of thermodynamics. These singular points can be identified without *ad hoc* assumptions with the critical points and λ-points.

The study of critical points is also of interest from the point of view of statistical mechanics. Under critical conditions the standard method of canonical ensembles leads to infinite results and needs modification. A modification of a very general type has been carried out by Klein and Tisza (2). After a survey of the older theories of critical fluctuations in Section II, the new method of calculation will be outlined in Section III.

II. THE THEORY OF FLUCTUATIONS

As indicated in the introduction, the central problem connected with critical points is the calculation of fluctuations. Hence we shall consider a short summary of the classical theory of fluctuations in general and a survey of the attempts to deal with critical fluctuations in particular.

Consider a closed system in thermodynamic equilibrium within an adiabatic envelope and isolate a small subsystem (briefly a cell) from the large residual system (briefly the reservoir) by (*i*) adiabatic or (*ii*) diathermal walls. In case (*i*) both the energy and the temperature of the cell are constant; in case (*ii*) the energy is free to pass between cell and reservoir; the temperature of the cell is equal to that of the reservoir. It is an important experimental fact that there is no observable difference in the behavior of the cell in the two cases. This means that the fluctuations of the energy, present in case (*ii*) alone, do not significantly alter the properties of the system. In the language of statistical mechanics the two cases correspond to the microcanonical and canonical ensemble, respectively. The smallness of the fluctuations assures the equivalence of these methods.

The preceding discussion can be easily generalized by replacing the fluctuation of the energy by that of some other extensive variable, such as the number of particles, the volume, or some electric or magnetic quantity. One speaks in these cases of grand canonical, or more simply (generalized) canonical ensembles.

A quantitative discussion of the fluctuations is based on a fundamental relation of statistical mechanics according to which the probability $\mathcal{P}$ of some fluctuation is given by

$$\mathcal{P} \sim e^{W/kT} \tag{1}$$

where W is the minimum work required to bring about the fluctuation from equilibrium.

Considering, e.g., fluctuations of volume at constant temperature, one has (see, e.g., reference 11):

$$W = \tfrac{1}{2}a(\Delta V)^2 \tag{2}$$

with

$$a = -\left(\frac{\partial P}{\partial V}\right)_T = \frac{1}{V\beta} \tag{3}$$

where β is the isothermal compressibility. The higher-order terms in the fluctuations ΔV can be normally neglected in equation 2.

One obtains for the relative fluctuations:

$$\frac{\overline{\Delta V^2}}{\bar{V}^2} = \frac{\overline{\Delta\rho^2}}{\bar{\rho}} = \frac{kT\beta}{V} \tag{4}$$

For an ideal gas, $\beta = 1/P$; hence expression 4 becomes $1/N$ when N is the number of molecules in the cell considered. Thus the fluctuation is very small under ordinary conditions. It is even smaller for liquids, because of their smaller compressibility. On the other hand, at the critical point both compressibility and fluctuations become infinite.

The phenomenon of critical opalescence shows that the fluctuations are indeed very big, but they of course cannot be infinite and the problem is to refine the theory so as to give finite answers.

A considerable number of theories have been proposed which were to achieve this end. The analysis of the calculation of the fluctuation shows clearly that the infinite result stems from the fact that the work W required to bring forth the fluctuation vanishes at the critical point. Any additional contribution to W, however negligible under normal conditions, would imply a nonvanishing W and a finite expression for the fluctuation. Hence most theories can be classified according to the additional term which they assume in computing the minimum work connected with the fluctuation. We shall briefly enumerate the main theories:

(*i*) Smoluchowski (11) remarked that equation 2 is only the first term in an expansion in ΔV. If the expansion is continued up to the quartic terms, a nonvanishing value is found for W.

(*ii*) The extensive investigations of Ornstein and Zernike (6) are based on the idea that the instantaneous values of the fluctuations of density in neighboring volume elements of a fluid are not independent. The direct energetic interaction gives rise to a term in the work W and also to a correlation of fluctuations in distant volume elements. The spread of correlations becomes very big at the critical point and implies a finite value for the critical opalescence.

(*iii*) Also, Rocard (8) emphasized the inhomogeneity of the fluid because of fluctuations and pointed out that the local pressure can no longer be assumed to depend on the local density alone, but will depend also on the "curvature" $\nabla^2\rho$ of the density. This dependence provides the required additional term in the work W. The additional pressure can be conceived to be of capillary origin. In fact, Rocard succeeded in developing on this basis a molecular theory of capillary forces (9).

(*iv*) Yvon (13) called attention to the importance of gravitational forces near the critical point. In view of the extreme compressibility of the system the gravitational field is sufficient to bring forth noticeable gradients of density. Thus the gravitational work provides a contribution to W.

It is important to realize that the above theories are by no means incompatible with each other and more than one factor may contribute a term to the work W. The clarification of the interrelation of these theories made the reopening of the question desirable. A further reason was that the above theories refer uniquely to the gas–liquid critical point, whereas critical phenomena have a more general scope, as was pointed out in the introduction.

The theory of Ornstein and Zernike proved to be the most convenient point of departure for the more general "cellular method" to be discussed in Section IV. It is noteworthy that the results of this theory contain both Ornstein and Zernike's and Rocard's results as special cases.

In this general theory neither the gravitational effects nor the quartic terms of Smoluchowski have been taken into account. Although gravitational effects are no doubt important in the case envisaged by Yvon, they cannot be relevant for λ-points in solids.

Smoluchowski's theory seems too special, inasmuch as spatial inhomogeneities of the system are not taken into account. It was also pointed out by Rocard[3] that the use of the quartic terms leads to a critical opalescence which is not proportional to the volume.

III. THE CELLULAR METHOD

From the point of view of physical intuition it is obvious that the fluctuation in a "cell" which is part of a closed system must be finite, e.g., the density can vary only between zero and a maximum which occurs if the entire mass of the system is concentrated in the cell in question. Briefly, the conservation of mass, energy, volume, or whatever other extensive quantity we may be considering is sufficient to assure a finite value for the fluctuation. The difficulty is only that the conventional theory of canonical ensembles does not provide the possibility of introducing the conservation principles in any formal way into the theory.

Hence Klein and Tisza (2) have generalized the concept of a canonical ensemble by introducing the "cellular method." Instead of concentrating attention on a subsystem (a single cell) and schematizing the rest into a "reservoir," the whole system is divided into cells which are treated on an equal footing. These cells are chosen as identical in size and shape and arranged in a regular spatial array. If dealing with a fluid system, one can choose a simple cubic array of cubic cells. For a crystalline system, it will be natural to let the array have the symmetry of the crystal; the cells can then consist either of unit cells of the crystal or of groups of contiguous unit cells.

Whereas in the old theory the states of the cells are statistically independent, in the new theory an interaction depending on the instantaneous states of contiguous cells has been introduced. This remedies the above-mentioned defect of the old theory and makes it possible to give a simple analytic expression to the conservation of extensive quantities. It leads also to a correlation between the fluctuations of various cells. This correlation may extend to distant cells, particularly at the critical point.

---

[3] Personal communication.

The theory leads to finite values for the critical fluctuations and this result is general enough to include λ-points in solids. In the latter case the fluctuating quantity may be the magnetization, the polarization, or the long-range order.

In particular for fluid systems, one gets for the critical light scattering a result of the form:

$$\frac{I}{I_0} \sim \frac{1}{\lambda^4}(1+\cos^2\theta)\left(\frac{1}{\beta}+c+d^2\,\frac{\sin^2\frac{\theta}{2}}{\lambda^2}\right)^{-1} \qquad (5)$$

Here I/I_0 is the ratio of scattered to incident light of wave-length λ observed in the direction θ; β is the compressibility, which becomes infinite at the critical point; c and d are two constants which cannot be calculated without making more specific assumptions.

For $c = 0$, equation 5 reduces to the result of Ornstein and Zernike (6); for $d = 0$ to that of Rocard (8).

Qualitatively one can understand the origin of these terms as follows: Rocard's constant c stems from the fact that the pressure in a cell depends not only on the local density but also on the instantaneous density of the neighboring cells. On the other hand, the term containing d originates in the fact that the correlation of the fluctuations in different volume elements implies phase relations for the scattered light. This correction gives rise to a $1/\lambda^2$ wave-length dependence of the scattering and an enhancement of the forward scattering at the critical point.

Assuming $c = 0$, the critical scattering would still be infinite for $\theta = 0$. Placzek (7) has shown that taking the finite volume of the scattering medium into account introduces a factor preserving the finiteness without modifying the result for experimentally realizable situations. The presence of Rocard's c term renders of course the same service.

IV. DISCUSSION AND SUMMARY

The discussion of thermodynamic stability leads naturally to the possibility of critical points as boundary points between ranges of stability and instability. The latter states are not realized in nature, and the system escapes instability by breaking up into two or more phases. Critical points in this general sense include λ-points and Curie points in crystals. These points are all "critical" with respect to the applicability of the standard thermodynamic and statistical methods.

Thus the method of canonical ensembles leads to infinite results for critical fluctuations. The so-called cellular method has been developed to cope with this situation. With appropriate special assumptions the results of the general theory reduce to those of the theories of Ornstein and Zernike and of Rocard, respectively. The general methods used so far are not capable of deciding *a priori* which of these limiting cases is closer to reality. The measurement of the dependence of critical opalescence on wave length and angle of scattering could throw some light on this issue. The experimental difficulties under critical conditions are very considerable and at present the evidence (see reference 2) is inconclusive.

Finally, it might be noted that theoretical results obtained with canonical (or grand canonical) ensembles cannot be extended without further analysis to the critical point.

REFERENCES

(1) Andrews, Th.: Phil. Trans. **159,** 575 (1869).

(2) Klein, M. J., and Tisza, L.: Phys. Rev. **76,** 1861 (1949).

(3) Landau, L.: Physik. Z. Sowjetunion **11,** 545 (1937).

(4) Onsager, Lars: Phys. Rev. **65,** 117 (1944).

(5) Onsager, Lars, and Kaufman, Bruria: Physical Society Cambridge Conference Report, p. 137 (1947).

(6) Ornstein, L., and Zernike, F.: Proc. Acad. Sci. Amsterdam **17,** 793 (1914); **18,** 1529 (1916); **19,** 1321 (1917); Physik. Z. **19,** 134 (1918); **27,** 761 (1926).

(7) Placzek, G.: Physik. Z. **31,** 1052 (1930).

(8) Rocard, Y.: J. phys. [7] **4,** 165 (1933).

(9) Rocard, Y.: J phys. [7] **4,** 533 (1933).

(10) Semenchenko, V. K : J. Phys. Chem. Acad. Nauk U.S.S.R. **21,** No. 12 (1948). The author is indebted to Dr. D. Atack for calling his attention to this paper.

(11) Smoluchowski, M. V.: Ann. Physik [4] **25,** 205 (1908).

(12) Tisza, L.: National Research Council Symposium on Phase Transitions, held August 1948 at Cornell University; R.L.E. M.I T. Technical Report No. 127.

(13) Yvon, J.: *Actualités scientifiques et industrielles,* Nos. 542, 543. Herman et Cie, Paris (1937).

SOLUBILITY MEASUREMENTS IN THE CRITICAL TEMPERATURE REGION. I[1,2]

D. ATACK and W. G. SCHNEIDER

National Research Council, Ottawa, Ontario, Canada

Received December 19, 1949

INTRODUCTION

During the course of the last two decades a considerable amount of attention has been given to the nature of the liquid–vapor phase transition occurring when either single or multicomponent systems are taken along their critical isochores (1–6, 9, 10, 12–18).

---

[1] Presented at the Symposium on Critical Phenomena, which was held under the auspices of the Division of Physical and Inorganic Chemistry at the 116th Meeting of the American Chemical Society, Atlantic City, New Jersey, September 22, 1949.

[2] Contribution No. 2239 from the National Research Council, Ottawa, Canada.

The extensive researches of Maass and his coworkers (12) led them to believe that there was an anomalous region in the neighborhood of the critical point of a pure component system which would require a strikingly different interpretation of the liquid–vapor phase transition from the one given by van der Waals. The work of Maass was corroborated to some extent by Mayer's (8) theoretical analysis of condensing systems, which also predicted such an anomalous region. Both experiment and theory indicate that for pure, single-component systems there is a region above the temperature of disappearance of the meniscus which does not exhibit normal gas-phase properties. The extent of this region is characteristic of the component.

The object of the present work being to investigate the several criticisms which have been made regarding the experimental work of Maass, it may be appropriate to summarize here the main conclusions based on this work. For this purpose we shall consider only his density measurements, these being characteristic and representative of the many physical properties which were studied.

The first density measurements were made on the carefully purified components, methyl ether and propylene. The component, in each case, was enclosed at its critical density in a stout glass bomb, and the density was measured at various heights along the bomb by means of a highly sensitive McBain–Bakr float which was suspended in the bomb (the float could be mechanically racked to various heights). Measurements of the density were made at various temperatures throughout the critical region. It was found that when systems were heated to a temperature slightly above the temperature of disappearance of the meniscus, not only was there a density difference above and below the position of disappearance of the meniscus, but there was also a density discontinuity at that point. The magnitude of this density difference was characteristic for each component. It became smaller as the temperature increased, and finally disappeared several degrees above the temperature of disappearance of the meniscus. Subsequently, seven other systems of pure components were found to give exactly similar behavior in the critical region. The results are illustrated by the curves of figure 1, which are reproduced from a paper by Maass (12).

Starting with the liquid just below its critical temperature (point *a*) and heating slowly at constant volume, the density decreased along curve A. At *c* the meniscus disappeared; beyond this point the density continued to decrease until at some point *d*, several degrees above *c*, the density became quite uniform throughout the bomb. If the temperature was then slowly decreased, the density of the medium in the lower part of the tube followed curve B, remaining constant until point *e* was reached, where the meniscus reappeared. Further cooling caused the liquid density to follow curve C.

The density of the medium above the meniscus showed a similar behavior and was represented by a set of curves given by the mirror image of figure 1 about curve B.

The density measurements on increasing the temperature were considered to be equilibrium values in the sense that they were rapidly established and remained sensibly constant over periods of more than an hour.

During these measurements, stirring of the medium was effected by gently racking the density balance up and down in the tube, using an external magnet. It was asserted that such mechanical stirring, capable of causing transport of liquid droplets into the upper part of the tube in two-phase systems, did not destroy the density difference. Moreover, the stirring was said to produce streaming effects, indicative of large inhomogeneities in density, which were visible to the naked eye, at temperatures above *c*. Once destroyed, the density gradient was not spontaneously reëstablished on cooling the system (curve B). It was also noted that the meniscus reappeared at a lower temperature than that at which it had disappeared. The temperature *c* was designated by Maass the critical temperature.

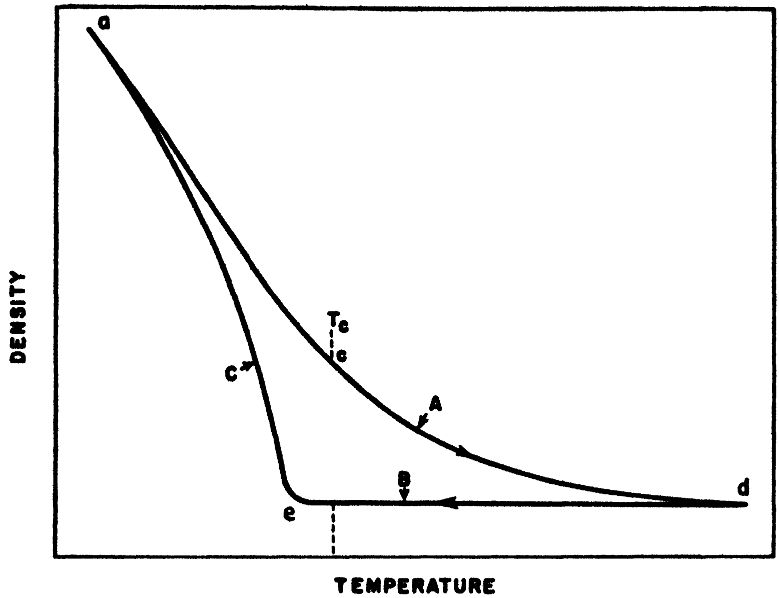

FIG. 1. Isochore (two-phase system). Curve A: variation of density of liquid with rising temperature (*ac*); *c*, critical temperature; *cd*, variation of density of medium below the position of disappearance of meniscus with rise in temperature; *d*, disappearance of density difference. Curve B: *de*, density of medium with lowering of temperature; *e*, reappearance of meniscus. Curve C: variation of density of liquid with lowering of temperature.

These results were interpreted by postulating that liquid structure persisted over a finite temperature interval above the critical temperature. A rise in temperature was said to cause a disruption of structure, which occurred quite rapidly, whilst a lowering in temperature leads to a building up of structure, occurring infinitely more slowly.

Some consideration was given to the question of whether or not the observed density differences were due to gravitational forces. It is well known that a system in the critical region is highly compressible, and hence the weight of the medium itself causes a small density gradient along the length of the confining tube under these conditions. Thus, for example, it has been roughly estimated from isotherm data that the effect of gravity in a carbon dioxide system at the critical temperature could account for a density gradient of 5 per cent per inch vertical separation. The observed density difference in the case of ethylene was some twenty times larger than could possibly be accounted for by gravity. Moreover, if these density measurements can be accepted as true equilibrium values, it is difficult to account for a sharp discontinuity in density at the point of disappearance of the meniscus by gravity effects alone. The absence of a density gradient on cooling indicates that the gravity effect is negligible in comparison with the observed density difference (curve B, figure 1).

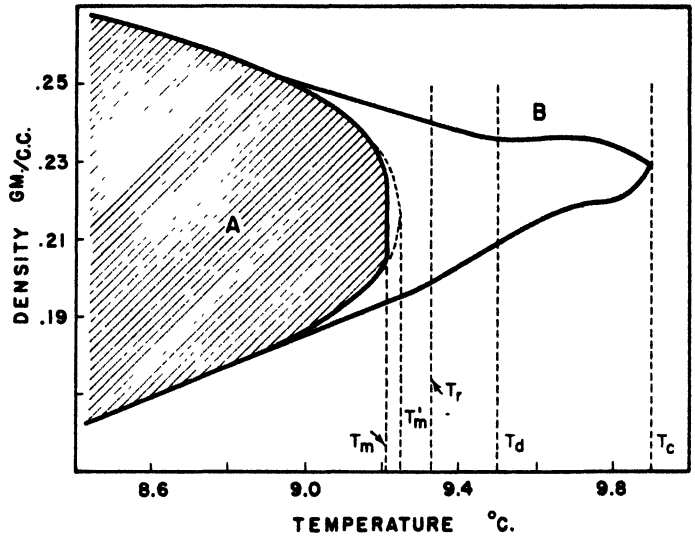

FIG. 2. Coexistence curves for ethylene. Curve A: "shaking" coexistence curve; flat apex indicating range of density over which the meniscus reappears at critical dispersion temperature T_M. Curve B: coexistence curve from P-V-T data; T_C, classical critical temperature; T_D, temperature of disappearance of meniscus without shaking; T_R, temperature of reappearance of meniscus without shaking.

In the final analysis, these questions really depend on whether or not the density measurements, such as shown in figure 1, can be considered as true equilibrium measurements. There is some doubt as to the adequacy of the stirring, exemplified by the fact that the meniscus disappears and reappears at different temperatures.

Later investigations (14) were designed to yield information upon just this point. Liquid–vapor coexistence curves were determined over a range of densities for ethane and ethylene in the critical region. By vigorously shaking the contents of the bombs it was found that the temperatures of disappearance and reappearance of the meniscus coincided within the accuracy of the temperature measurements. A typical coexistence curve for ethylene is shown in figure 2 (curve A, enclosing the shaded area). In contrast to the classical curve, it shows a distinctly flat portion at the apex (i.e., there is a range of densities for which the temperature of disappearance is the same and, of course, identical with the temperature of reappearance). This temperature was termed the critical dispersion temperature, T_M (8, 14) (or more generally the dispersion temperature), since it was postulated that above this temperature there existed a mutual dispersion of vapor and liquid "droplets" for a finite temperature interval. To support this view it was shown that the new coexistence curve lay entirely within the coexistence curve obtained from P–V–T data (14) (curve B). The region in figure 2, bounded by the dispersion temperature, T_M, and the classical critical temperature, T_C, was taken to be the region of mutual dispersion. Above T_C it was asserted that only the normal gas phase could exist. We may note here that the previous results of Maass and his coworkers would require a certain amount of structure even above the classical critical temperature. Rice (16) has pointed out that the interpretation of isotherm data is not unequivocal, and that the location of T_C from isotherm data does not lend itself to accurate estimation. Thus, it would appear extremely difficult to obtain an accurate coexistence curve from P–V–T data alone. Accordingly, conclusions concerning the relationship between T_M and T_C are perhaps, as yet, somewhat premature. In figure 2 are also depicted the critical temperature, T_D, as defined by Maass (12) and the temperature of reappearance of the meniscus T_R (without shaking). We may note that the range T_R–T_D which was obtained for ethylene by Maass and Geddes (13) lies entirely above T_M. In later work, Mason (14) found that the temperatures T_R and T_M were identical, and attributed the discrepancy to errors in temperature measurements which had been incurred in the previous work.

The temperature T_M, which is reversibly reproducible with regard to temperature changes, is characteristic of the component and independent of the means of observation and provides a much more satisfactory point of reference than either T_R, T_D, or T_C. The critical temperature as normally measured in a stationary bomb without stirring corresponds to some point in the region of T_D. Such a temperature, in the opinion of the authors, is a very unsatisfactory and unreliable point of reference.

A further point that deserves mention concerns the flatness of the coexistence curve obtained by shaking. If such a curve is "mathematically flat," and it seems that in the case of ethylene this has been found true to within 0.001°C. (15), there would seem to be justification for concluding that $T_C > T_M$. If, however, the coexistence curve approaches a maximum very slowly, along the temperature axis it may well be that this maximum, shown by T_M' (figure 2), coincides with T_C, in which case a normal first-order transition would be expected to occur.

It appears desirable, therefore, to study critical phenomena in relation to the critical dispersion temperature, T_M, to investigate the flatness of the "shaking" coexistence curve, and in particular to obtain unequivocal evidence as to whether or not liquid "droplets" or molecular clustering occur above this temperature.

From the experimental point of view, direct evidence for the existence of liquid "droplets" or molecular aggregates in this region is difficult to obtain.

It requires the measurement of some property of the system which is sensitive to inhomogeneities within the system. The measurements must be carried out in such a way as not to disturb the system in its equilibrium state, and provision must be made for intimate stirring. The present report describes some solubility distribution measurements in dilute solutions of 1-chloro-4-iodobenzene in ethane throughout the critical regions of the solutions. According to Holder (9), density gradients which may be present in the critical region for such systems will give rise to solubility gradients of the same relative order of magnitude. By using a tracer technique to measure the solute distribution we have a convenient and highly sensitive method by which measurements can be made upon a system without disturbing the equilibrium conditions.

EXPERIMENTAL

1-Chloro-4-iodobenzene (m.p. 55°C.) containing active iodine atoms was dissolved in ethane in a sealed uniform glass bomb, which was about 16 cm. long and had an internal volume of approximately 25 ml. The radiation from the iodine compound was measured by a small Geiger counter which was held in a lead block. The sensitive electrode was exposed to the radiation from a given part of the tube through a small slit in the lead block. Thus, by moving the counter along the tube it was possible to determine semiquantitatively the solubility in the liquid and vapor phases as the critical temperature was approached, and also throughout the length of the tube in the supercritical region. A diagrammatic representation of the apparatus is shown in figure 3.

The ethane was supplied by the Ohio Chemical Company and was fractionated through a low-temperature Stedman column. It gave the same mass spectrogram as the pure standard sample (research grade C.P. ethane supplied by Phillips Chemical Company).

The 1-chloro-4-iodobenzene was kindly prepared by Dr. L. C. Leitch. 4-Amino-1-chlorobenzene was diazotized and subsequent addition of active sodium iodide solution in potassium iodide solution as carrier gave the active iodo compound. This was isolated from solution by steam distillation and finally sublimed under reduced pressure to give a white crystalline solid. The desired yield of solid and amount of activity were obtained by using the proper amount of carrier. Amounts of activity up to 10 millicuries per gram of solid were introduced in this manner.

The thermostat comprised a 15-gallon capacity brass tank fitted with safety-glass windows, and filled with No. 17 Risella oil. Two stout four-bladed propellers surrounded by hollow brass cylinders provided very efficient circulation of the oil. Temperature control was effected through a double photocell circuit (11) operating a relay, which in turn switched a control heater. The photocells were activated by a light beam deflected from a galvanometer mirror, the galvanometer deflection being a function of the out of balance current in a Wheatstone bridge circuit. A 35,000-ohm thermistor provided the variable resistance arm in the bridge circuit, and carried only 0.1 ma. The total current through the bridge was 5 ma. A source of constant-temperature cooled oil was provided by a refrigeration unit; the oil was circulated through copper pipes in the thermostat at a controlled rate. The absolute temperature of the bath was measured by means of a platinum resistance thermometer to within 0.001°C. and the temperature variation of the bath was controlled to ±0.001°C.

An electromagnetic coil was used to operate a helical glass stirrer inside the glass bomb containing the solution, the stirrer being activated through a piece of soft iron imbedded in its upper end. The rate of stirring, which could be varied up to 60 oscillations per minute, provided very turbulent mixing of the contents of the tube.

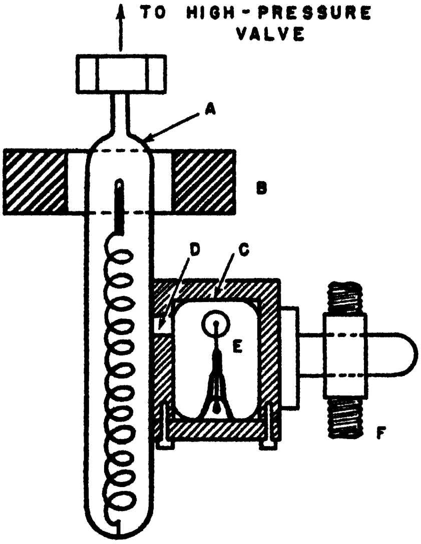

FIG. 3

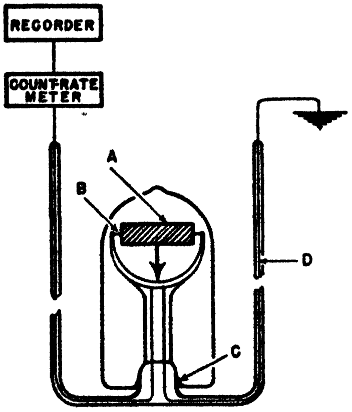

FIG. 4

FIG. 3. Diagrammatic representation of the apparatus. A, glass containing bomb; B, electromagnetic coil; C, thick lead container; D, slit in lead container; E, Geiger-Müller counter; F, rack for raising and lowering counter.

FIG. 4. Form of counter employed. A, oxidized copper cathode; B, 1-mil diameter tungsten wire anode; C, de Khotinsky cement; D, glass insulation leads.

Figure 4 depicts the form of counter finally employed. The cathode was constructed from copper shimstock and subsequently oxidized, whilst the anode was of 1-mil diameter tungsten wire. The whole was enclosed in a glass envelope of approximately 100-ml. capacity and filled with 18 cm. of argon and 2 cm. of ethyl alcohol to act as quenching agent. The leads were insulated from the thermostat oil by means of glass tubing, whilst the counter itself was completely enclosed in a lead container whose walls were ½ in. thick. The radiation entered the counter through a slit 2 cm. long by 0.5 cm. broad in the block. This slit width was such as to allow a counting resolution of 2 cm. at any point in the tube, as illustrated in figure 5. The data for this graph were obtained by taking the count along a representative tube half-filled with a dilute solution of active 1-chloro-4-iodobenzene in acetone at atmospheric pressure and room temperature. The counter was operated in conjunction with a General Radio type count-rate meter, the integrated pulses being recorded on a 2-ma. Esterline-Angus recorder. The geometry of the counter and tube was about 2 per cent efficient, yet this was sufficient to enable counts of up to 2000 counts per minute to be obtained. Incidentally, this type of counter functioned for 10^7 counts before its threshold showed any signs of increasing. A typical characteristic curve is shown in figure 6.

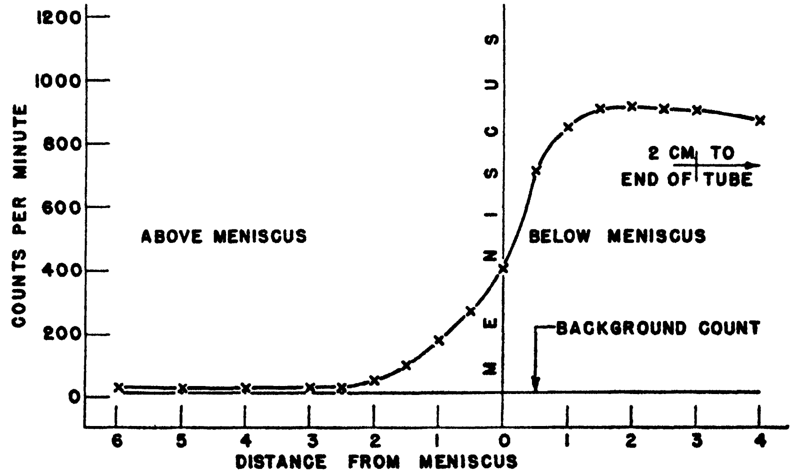

FIG. 5. Resolution of counter

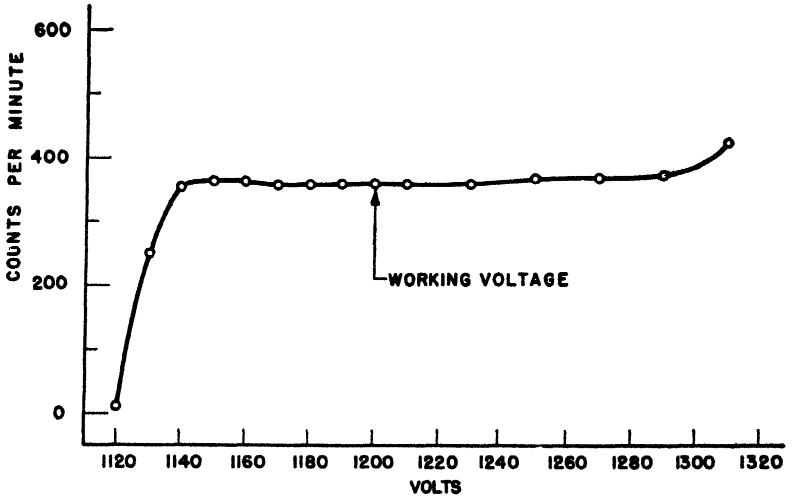

FIG. 6. Typical characteristic curve of counter

PROCEDURE

The internal volume of the glass bomb with stirrer was obtained to one part in a thousand by a gas expansion method. A weighed amount of the solid was introduced into the bomb, which was then evacuated and flushed with ethane twice before finally filling with ethane to the critical density (0.206 g./cc.). The high-pressure valve sealing the bomb was attached to a brass frame, which held the tube in position in the thermostat. The electromagnetic coil was fitted into position on the brass frame, and the whole assembly allowed to attain room temperature overnight inside a steel pipe. The assembly was then placed in the thermostat, which was adjusted to the desired temperature, and counting proceeded along the lines indicated.

EXPERIMENTAL RESULTS

A few preliminary experiments were undertaken in order to establish the techniques and also to obtain some idea of the opalescent effects which are observed in the critical region. Solutions of hexachloroethane in ethane and pure ethane systems were investigated. Three interesting points were noted as a result of these experiments.

(*a*) When ethane was heated without stirring in a closed glass tube filled to the critical density, the meniscus disappeared near the middle of the tube without any observable movement at 32.426°C. The system was then thermostated for an hour at 0.5°C. above this temperature. On cooling at a rate of about 0.1°C. per hour, without any stirring, the meniscus reappeared quite sharply at the place of disappearance at a temperature of 32.230°C., with only a small amount of opalescence. However, if the system was taken 5°C. above the temperature of disappearance and thermostated for 48 hr., on cooling the meniscus reappeared at a very much lower position in the tube, again quite sharply, but accompanied by a very heavy opalescent effect. Moreover, on thermostating at the temperature of reappearance of the meniscus it was observed that some 6–8 hr. elapsed before the liquid level attained its original position. The latter effect occurred when the system was stirred continuously for half an hour at only 0.1°C. above the dispersion temperature (which was 32.238°C.) and subsequently cooled. This effect was also characteristic of all the solutions employed.

(*b*) When the temperature of a pure ethane system was taken just above the temperature of disappearance of the meniscus without stirring, a narrow band of opalescence was observed at the position of disappearance of the meniscus. This opalescence disappeared at a temperature 0.1°C. above T_D, provided the system was not stirred, and was quite permanent at any temperature in this range. If the system was vigorously stirred in this temperature range, the band of opalescence became much more intense, and gradually dispersed to give a uniform opalescence throughout the whole of the confining tube.

A further phenomenon was observed throughout a temperature range up to 0.1°C. higher than this (i.e., from 0.1° to 0.2°C. above T_D). In this case no opalescence could be seen initially, but on stirring a band of opalescence appeared, and gradually dispersed to give a uniform intensity throughout the tube. In every case the opalescence remained quite uniform when the temperature was maintained constant. The higher the temperature above T_D, the weaker the opalescence became.

Similar phenomena were observed for all solutions employed. In the case of ethane the upper limit of opalescence is about 0.2°C. above T_D, when the system is stirred.

(*c*) The temperatures of disappearance and reappearance of the meniscus were *exactly* identical for every system employed, provided the system was vigorously stirred. The procedure was to stir at a given temperature, raise or lower the temperature by very small amounts, stirring all the while, and then thermostat and stir for 10 min. before an observation was made.

These observations emphasized the slow rate of equilibration of these systems in the critical region; consequently experiments were carried out in order to estimate this rate in a stationary tube.

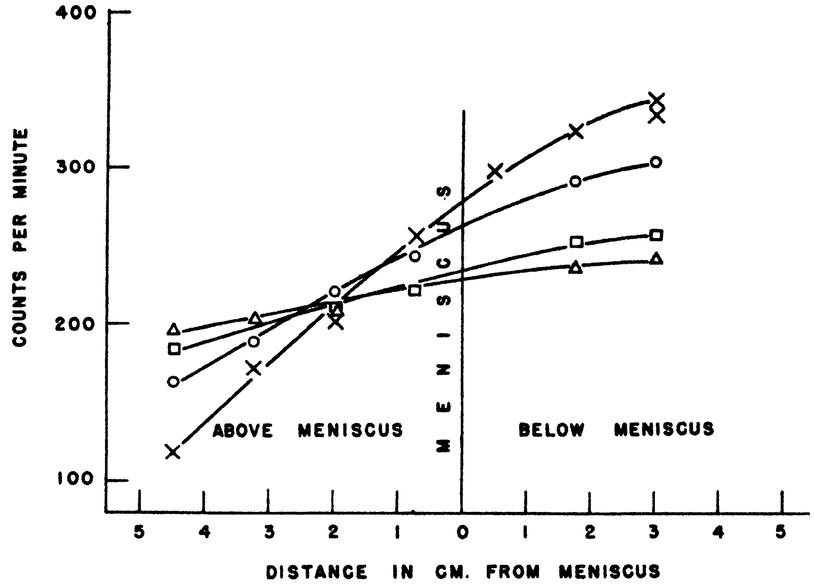

FIG. 7. Solubility distribution at various temperatures without stirring. Critical dispersion temperature of solution = 32.298°C. ×, after 24 hr. at 34.074°C.; ○, after further 24 hr. at 35.774°C.; □, after further 18 hr. at 40.579°C.; △, after further 12 hr. at 32.491°C.

A 0.083 mole per cent solution of 1-chloro-4-iodobenzene in ethane was prepared, and the critical dispersion temperature of the solution was found to be 32.298°C. The contents of the tube were then thermostated at various temperatures ranging through 8°C. above the dispersion temperature. Counts were taken at seven points along the tube at each temperature. No allowance was made for the decay of the iodine atoms, since this was negligible during the 2 hr. periods of counting. The counts were taken alternatively above and below the meniscus and occasionally duplicated to demonstrate the validity of this procedure. The solubility distributions, shown graphically in figure 7, confirmed that in a stationary bomb the rate of equilibration is very slow indeed. Within the small temperature range investigated, the effect of temperature upon the rate was very small. It was estimated that it would require at least 10–14 days to attain a uniform solubility throughout the tube.

A 0.347 mole per cent solution was found to have a critical dispersion temperature of 37.025°C. When this solution was maintained at 42.567°C. in a stationary bomb for 24 hr., the solubility gradient along the length of the tube was still quite large. The system was then vigorously stirred for half an hour, and the subsequent counting showed that the solubility gradient had completely disappeared, the solubility being quite uniform throughout the tube. This uniformity persisted some 24 hr. afterwards, as shown in figure 8, indicating that the system was homogeneous and that the effect of the gravitational force field at this temperature was exceedingly small. The meniscus line in the diagram corresponds to the position of disappearance of the meniscus with stirring.

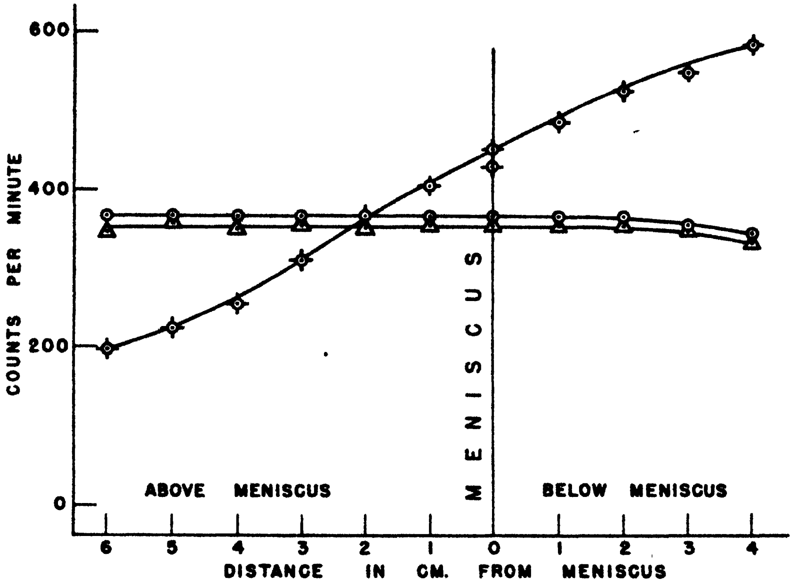

FIG. 8. Solubility distribution at various temperatures with stirring. Critical dispersion temperature of solution = 37.025°C. -◇-, after 24 hr. at 42.567°C. without stirring.; ⊙, after stirring for 30 min. at 42.567°C.; △, stationary for 12 hr. after the stirring at 42.567°C.

The temperature was then slowly lowered to 0.058°C. above the dispersion temperature, the system being continuously stirred. When the stirring was stopped, a small but very definite solubility gradient was set up along the tube. The gradient was quite persistent, as shown in figure 9. As indicated in this figure, most points on repetition gave the same value.

A final and conclusive repetition of this experiment was made with a 0.312 mole per cent solution containing a much higher activity, which proved beyond any doubt the existence of a solubility gradient at temperatures up to 0.20°C. above the critical dispersion temperature. These results are represented graphically in figure 10. At temperatures of 0.059°C., 0.081°C., and 0.178°C. above the dispersion temperature there was a difference in solubility of approximately 5 per cent between points 1 in. apart along the tube. At these three temperatures it was found, contrary to expectation, that the gradient had sensibly the same value.

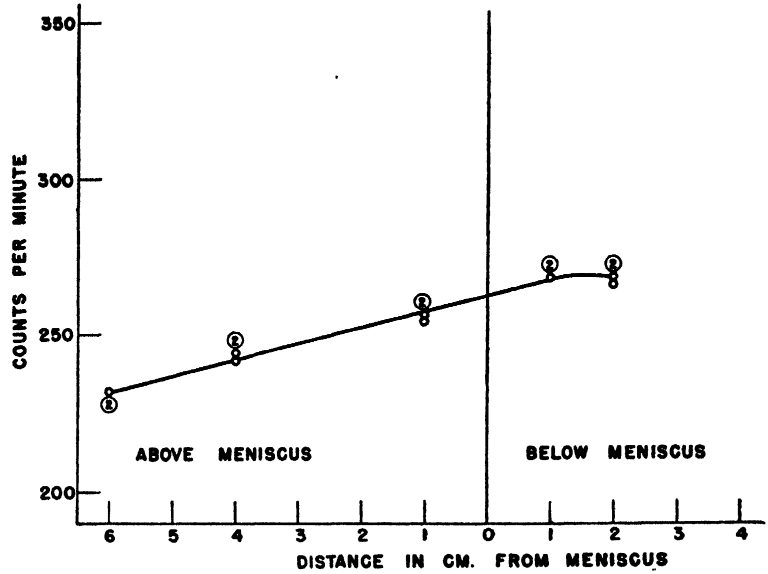

FIG. 9. Solubility distribution just above the critical dispersion temperature after stirring. Critical dispersion temperature = 37.025°C.; temperature of measurements = 37.083°C.

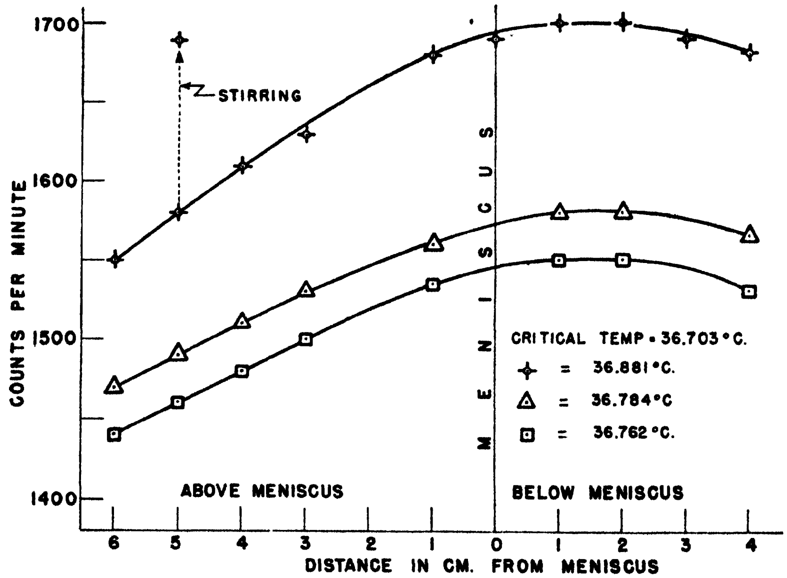

FIG. 10. Solubility distributions at various temperatures slightly above the critical dispersion temperature. The characteristic temporary effect of stirring is shown for one point on the upper curve. The decay in activity has not been compensated, thus giving separation of the curves.

It was also noted that the gradient did not extend along the whole length of the tube but flattened out beyond a point which corresponded to the original position of the meniscus. There was at no time any observable gradation in opalescent intensity along the tube which could be detected by eye.

On stirring, the solute was distributed uniformly throughout the tube, and the count at the top of the tube increased. However, when the stirring was stopped the solubility gradient was rapidly reëstablished.

DISCUSSION

The major conclusion drawn from this study is the importance of attaining an equilibrium state. In several of the later experiments of Maass and his co-workers (14) it was suggested that rotation of the glass tube which contained the system under investigation would provide ample turbulence within the tube. However, it would seem that though this procedure ensures movement of the system as a whole, its effect on any particular part of the system would not be quite so drastic. This is especially true near the critical temperature, when the density gradient along the tube is very small. Suspicion is very definitely cast upon results obtained without stirring. In this respect attention must be drawn to the solubility measurements of Holder (9) and the many qualitative experiments carried out by numerous other workers upon colored binary solutions, where the interpretation of the varying color intensities along the tube at temperatures considerably above the critical temperature must be treated with some reserve.

This study shows that there is a definite solubility gradient at temperatures above the critical dispersion temperature, that the gradient is small, and that it is fairly rapidly established from a homogeneous system. There seems little reason to doubt that we are dealing with true equilibrium states, for the gradients obtained are reproducible when approached from either higher or lower temperatures. For the solutions considered, there was no detectable solubility gradient at temperatures 0.3°C. above the dispersion temperature. It would require a more precise counting arrangement to determine accurately the temperature limit to which the gradient extends for the various solutions.

Since the solubility gradients are rapidly reëstablished from a system in which the solubility is uniform (figure 10), the determining factor in the rate of solubility equilibration (figure 7) cannot be a simple diffusion process. Thus, the effect of stirring is to establish a uniform density throughout the system more efficiently, and the rapid manner in which the solubility distribution readjusts itself to that uniform density indicates that it may be regarded as a direct function of the density distribution. The solubility gradient present slightly above the critical dispersion temperature could be due to a nonuniform distribution of dispersed liquid and vapor (14). It is certainly not due to any geometric effect in the counting, as demonstrated by the fact that a uniform count can be obtained along the length of the tube (i.e., within a length 2 cm. from the bottom end and 3 cm. from the top end of the tube) immediately after the contents have been stirred. The one feature which seems quite inexplicable, in the absence of further evidence, is that the gradient should flatten out in the part of the tube usually occupied by the liquid phase at lower temperatures. This indicates that the effect may not be attributed solely to the action of gravity on single molecules, in which case a uniform gradient would be expected along the entire length of the tube. The fact that the gradient is not uniform may be regarded as evidence in favor of molecular clustering in this region.

It is probably unwise to extend this small amount of evidence as any indication of the processes occurring in a single-component system. Although the solute molecules may be considered to cause disproportionate disturbances in the slightly supercritical region by acting as nuclei for a potential condensation, the properties of the pure solvent must be implicated to some extent. One-component systems are amenable to this type of experimental study, and it would seem that a similar study on a one-component system may provide more definite conclusions as to the nature of the liquid–vapor transition.

SUMMARY

1. A review of experimental work pertaining to the nature of the liquid–vapor phase transition at the critical temperature is presented. The significance of the critical "dispersion" temperature and the importance of attaining equilibrium states are discussed.

2. A method for determining solubilities in the critical temperature region using a tracer technique is described, and measurements are given for the system 1-chloro-4-iodobenzene–ethane.

3. The rate of equilibration in slightly supercritical systems is shown to be very slow in the absence of stirring, yet comparatively rapid with intimate stirring. Evidence is presented which indicates the possibility of molecular clustering in the slightly supercritical region.

REFERENCES

(1) Booth, H. S., and Bidlock, R. M.: Chem. Revs. **44**, 447 (1949).
(2) Born, Max: Physica **4**, 1037 (1937).
(3) Callendar, H. L.: Proc. Roy. Soc. (London) **A120**, 460 (1928).
(4) Centnerszwer, M.: Z. physik. Chem. **46**, 427 (1903); **60**, 441 (1907); **61**, 356 (1907); **69**, 81 (1909).
(5) Clark, A. L.: Chem. Revs. **23**, 1 (1938).
(6) Dacey, J., McIntosh, R., and Maass, O.: Can. J. Research **17B**, 206 (1939).
(7) Gouy, A.: Compt. rend. **115**, 720 (1892).
(8) Harrison, S. F., and Mayer, J. E.: J. Chem. Phys. **6**, 87, 101 (1938).
(9) Holder, C. H., and Maass, O.: Can. J. Research **18B**, 293 (1940)
(10) Jellinek, K.: *Lehrbuch der physikalischen Chemie*, Vol. I, pp. 917–21. Enke, Stuttgart (1923).
(11) Lutz, B. C, and Wood, J. H.: Can. J. Research **26B**, 145 (1948).
(12) Maass, O.: Chem. Revs. **23**, 17 (1938). (A survey of numerous experimental investigations by Maass and his coworkers.)
(13) Maass, O., and Geddes, A. L.: Phil. Trans. **236A**, 331 (1937).
(14) Mason, S. G., Naldrett, S. N., and Maass, O.: Can. J. Research **18B**, 103, 118 (1940); **26B**, 592 (1949).
(15) Mason, S. G.: Private communication.
(16) Rice, O. K.: J. Chem. Phys. **15**, 314 (1947); Chem. Revs. **44**, 69 (1949).
(17) Semenchenko, V. K.: J. Phys. Chem. (U. S. S. R.) **21**, 12 (1947).
(18) van der Waals, J. D.: *Die Kontinuität des gasförmigen und flüssigen Zustandes.* Barth, Leipzig (1899).

THE APPLICATION OF KINETIC THEORY TO THE CRITICAL CURVE FOR AQUEOUS SOLUTIONS OF 1-1 ELECTROLYTES[1, 2]

C. H. SECOY

Oak Ridge National Laboratory, Oak Ridge, Tennessee

Received December 19, 1949

Even though extensive studies of the critical behavior of aqueous solutions have not been made, a sufficient number of qualitative observations and some quantitative measurements are available to permit a degree of generalization. As pointed out by Schröer (3), four basic types of temperature–composition diagrams are possible. In type I, the critical curve always lies in the region of unsaturated solutions. Even though the solubility continues to increase with temperature, the solubility curve never intersects the critical curve. In type II, the solubility curve reaches zero solubility at or below the critical temperature of the pure solvent. In this case the solute separates completely as either a solid phase or a second liquid phase, and the only critical phenomenon observed is that of the pure solvent. Types III and IV involve single and double intersections of the solubility curve and the critical curve.

With respect to aqueous solutions of electrolytes, examples of types I, II, and IV (single intersection) have been reported. Many salts undergo decomposition or irreversible hydrolysis at lower temperatures and do not permit their inclusion in such a classification. 1-1 Electrolytes, insofar as they have been studied, all behave as type I. These include sodium chloride, potassium chloride, rubidium chloride, sodium bromide, potassium bromide, sodium iodide, potassium iodide, ammonium chloride, and potassium nitrate (3, 4). Examples of type II behavior are sodium sulfate, potassium sulfate, magnesium sulfate (3), and uranyl sulfate (4).

Schröer (3) reported quantitative data for the elevation of the critical temperature as a function of concentration for sodium chloride, potassium chloride, potassium bromide, and potassium iodide. He found that his results could be expressed by an equation of the type $\Delta T = kX^{1/n}$, in which n and k are constants for each salt, X is the concentration in moles per liter, and ΔT is the elevation of the critical temperature above that for water. Owing to the similarity in form between this equation and the Freundlich adsorption isotherm, Schröer, in very general terms, attempted to explain his results on the basis of physical adsorption of water molecules on solute molecules as centers. Since the Freundlich isotherm is purely an empirical equation, and since the similarity in the equations is only a matter of form and does not hold if terms are compared,

---

[1] Presented at the Symposium on Critical Phenomena, which was held under the auspices of the Division of Physical and Inorganic Chemistry at the 116th Meeting of the American Chemical Society, Atlantic City, New Jersey, September 22, 1949.

[2] This paper is based on work performed under Contract No. W-7405 eng 26 for the Atomic Energy Project at Oak Ridge National Laboratory.

Schröer's explanation is at best only empirical and the agreement of the data with an equation of this type may well be only a fortuitous circumstance. In order to apply additional tests to Schröer's adsorption concept, the Langmuir equation, the B.E.T. equation, and the Hüttig equation were applied in succession to his data. In no case was a reasonable curve obtained. It seems unlikely, therefore, that further thought in this direction can lead to anything more than the empirical description of the data which Schröer obtained. It is the purpose of this paper to demonstrate that the data can be fitted equally well to an equation derived directly from kinetic theory and in which the constants employed have a physical significance. In spite of the fact that a number of crude approximations for unknown quantities are made, the resulting relationship not only describes the data adequately but also leads to values for interparticle forces which are of the right order of magnitude and in the expected order.

THEORETICAL

There are several equations of state which more or less accurately describe the behavior of a pure substance in the vicinity of the critical point. Such an equation should be of the third order in V and should involve not more than three constants. Van der Waals' equation and Dieterici's equation as well as the virial equation involving the second and third virial coefficients all meet these requirements and we might choose any of these for our purpose. The conditions for criticality are that $\left(\frac{\partial P}{\partial V}\right)_T = 0$ and that $\left(\frac{\partial^2 P}{\partial V^2}\right)_T = 0$ and, if one applies these conditions to any one of the equations of state, an expression for T_c in terms of the equation constants can be obtained. We shall choose van der Waals' equation for the following development, the choice being purely arbitrary since the argument advanced could be equally well applied to either of the others and the results would be equally satisfactory.

Van der Waals' equation gives:

$$T_c = \frac{a}{3.375Rb} \tag{1}$$

Even though a and b are normally treated as constants, it is a well-known fact that neither is constant for any known gas. The value of a is associated with the forces existing between molecules; one would expect these forces to be dependent on temperature, and they would certainly be altered by the introduction of a second component. The value of b is related to the volume of the molecules themselves and is found to be slightly temperature-dependent. Furthermore, the introduction of a second component would alter b, owing to the presence of particles of a different size. We shall proceed to write expressions for a and b as functions of temperature and composition and, by substituting these expressions in equation 1, arrive at an equation for the critical temperature of a binary system.

It has been shown (1) that an expression representing intermolecular interaction in a binary mixture can be written as a quadratic function of the molecular concentrations. If we assume that the solution in question is composed of simple water molecules, a positive ion, and a negative ion, the expression becomes:

$$a = \gamma_1^2 a_{11} + 2\gamma_1\gamma_2 a_{12} + 2\gamma_1\gamma_3 a_{13} + \gamma_2^2 a_{22} + 2\gamma_2\gamma_3 a_{23} + \gamma_2^2 a_{33} \qquad (2)$$

The γ's represent mole fractions, subscript 1 indicating water, subscript 2 the positive ion, and subscript 3 the negative ion. Three-particle interaction is neglected. The mole fractions can be expressed so that $\gamma_2 = \gamma_3$ and $\gamma_1 + 2\gamma_2 = 1$. Substituting γ_2 for γ_3 in expression 2, eliminating γ_1, and collecting terms we have

$$a = a_{11} + k_1\gamma_2 + k_2\gamma_2^2 \qquad (3)$$

where

$$k_1 = 2a_{12} - 4a_{11} + 2a_{13} \qquad (4)$$

and

$$k_2 = 4a_{11} - 4a_{12} - 4a_{13} + a_{22} + 2a_{23} + a_{33} \qquad (5)$$

Each of the a's is temperature-dependent and each undoubtedly follows a different law of dependence. If one assumes a spherically symmetrical field, employs Boltzmann distribution for the potential energy function ω, and neglects all except binary encounters, a is given by an expression of the type:

$$a_{ij} = 2\pi NRT \int_{r_0}^{\infty} r^2(1 - e^{-\omega_{ij}/kT})\, \mathrm{d}r \qquad (6)$$

Assuming that the mutual potential energy, ω, is proportional to $1/r^s$ and introducing the function $X = r^sT$, the equation becomes:

$$a_{ij} = \frac{2\pi}{s} NRT^{1-(3/s)} \int_{r_0}^{\infty} X^{(3/s)-1}\,(1 - e^{-c/x})\, \mathrm{d}X \qquad (7)$$

When the conditions for convergence of the integral quantity are met, this quantity will have a definite numerical value and we can then write $a_{ij} \alpha T^{1-(3/s)}$. Each of the a's should, therefore, be proportional to some power of T. Since it is impossible with our present knowledge to write explicitly this order of dependence for each of the a's, we shall make the crude assumption that the overall temperature dependence of a can be written as a single constant power of T and write for our final expression:

$$a = T^{\alpha}(a_{11} + k_1\gamma_2 + k_2\gamma_2^2) \qquad (8)$$

Admittedly, this expression cannot be correct, since one would certainly not expect the same temperature dependence for the interaction between two water molecules as that for the interaction between an ion and a water molecule or between two ions. However, in view of our inability to do better without introducing an excessive number of unknown constants, we shall test equation 8 with the available data. Certainly, if equation 8 satisfies the data, a more general expression would also be satisfactory.

The quantity b can be most simply represented as being proportional to the incompressible volume of particles in the system. In our case we can write,

$$b = k_3(r_1^3\gamma_1 + r_2^3\gamma_2 + r_3^3\gamma_3) \tag{9}$$

where k_3 includes the proportionality constant and the factor $\frac{4}{3}\pi$ from the volume expression for spheres of radii r_1, r_2, and r_3. The temperature dependence of b can be taken care of by introducing a factor, T^{β}. Eliminating γ_1 and γ_3 as before we have:

$$b = k_3T^{\beta}[r_1^3 + (r_2^3 + r_3^3 - r_1^3)\gamma_2] \tag{10}$$

Combining equations 1, 8, and 10 and rearranging, we get,

$$T^n = \frac{a_{11} + k_1\gamma_2 + k_2\gamma_2^2}{3.375Rk_3[r_1^3 + (r_2^3 + r_3^3 - r_1^3)\gamma_2]} \tag{11}$$

in which $n = 1 + \beta - \alpha$. This is the equation which we shall apply to the data of Schröer and data obtained in this laboratory. It is obvious that data which give a straight line on a log-log plot, as Schröer found that his did, can be described by an equation of the form of equation 11 by the proper selection of values for the constants involved.

APPLICATION TO THE DATA

The application of the equation to salt–water systems is complicated first by the fact that van der Waals' constants are not available for one of the components, i.e., the salt, and second, by the fact that the intermolecular actions are complex and a simple relationship between the van der Waals a and the temperature cannot be written. If, however, one considers a binary system in which the components are simple gas molecules with or without permanent dipole moments and for which the van der Waals constants are known, the equation reduces to one containing only one arbitrary constant. In this manner a single point on the critical curve is sufficient to calculate the entire curve.

For a system composed of nonpolar nonionic molecules the equation becomes:

$$T = \frac{a_{11}\gamma_1^2\sqrt{T} + 2a_{12}\gamma_1\gamma_2\sqrt{T} + a_{22}\gamma_2^2\sqrt{T}}{k(b_1\gamma_1 + b_2\gamma_2)} \tag{11a}$$

The value of a_{12} must be obtained from experiment.

Equation 11a has been used to calculate the critical curve for the systems carbon dioxide–ethane, carbon dioxide–nitrous oxide, and ethane–nitrous oxide, data for these systems being available in the *International Critical Tables*. The agreement with the experimental points is shown in figures 1, 2, and 3.

For a system in which one component is a neutral nonpolar molecule and the second component a neutral molecule with a permanent dipole moment, the equation takes the form:

$$T = \frac{a_{11}\gamma_1^2\sqrt{T} + 2a_{12}\gamma_1\gamma_2\sqrt{T} + a_{22}\gamma_2^2}{k(b_1\gamma_1 + b_2\gamma_2)} \tag{11b}$$

Curves for the systems carbon dioxide–sulfur dioxide and ethane–hydrogen chloride have been calculated using equation 11b and are shown in figures 4 and 5.

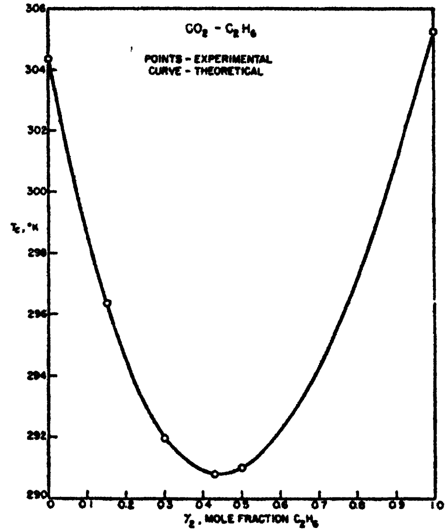

FIG. 1. Critical curve for the system carbon dioxide–ethane

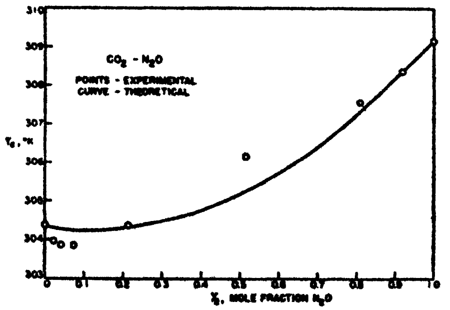

FIG. 2

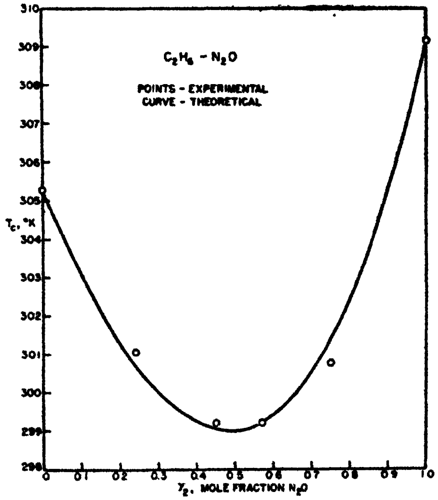

FIG. 3

FIG. 2. Critical curve for the system carbon dioxide–nitrous oxide
FIG. 3. Critical curve for the system ethane–nitrous oxide

In all cases the agreement with experimental data is reasonably good and gives one additional confidence in proceeding to the treatment of the salt–water systems.

In order to use equation 11 it is first necessary to make some assumptions for the values of the radii of the interacting particles in the solution. Since the salts that we are discussing are known to be completely ionic in character, we shall assume them to be completely ionized. However, in view of the fact that G. E. Owen (1) has reported the conductivity of dilute sodium chloride solution to be low in the critical region, we shall also assume that the ions carry with them essentially a monolayer of adsorbed water molecules. If the Van der Waals radius (1.06 Å.) is used for the water molecules, this adsorbed layer increases the radius of a positive ion by 1.82 Å. and that of a negative ion by 1.50 Å. The different effect on the two kinds of ions is due to the orientation of the water dipole. These values combined with the known radii for the ions involved give the values listed in table 1. It should be emphasized that these values represent only one of many assumptions that one might make regarding the particles present and their effective size in the critical fluid, and success in applying equation 11 does not by any means substantiate their correctness.

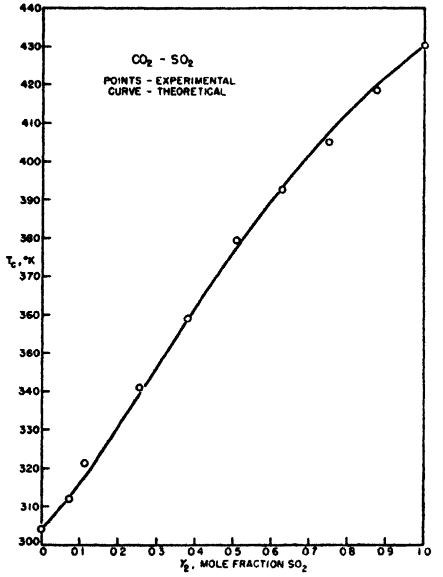

FIG. 4

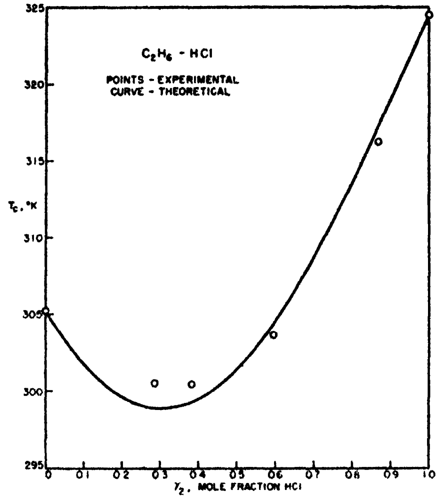

FIG. 5

FIG. 4. Critical curve for the system carbon dioxide-sulfur dioxide
FIG. 5. Critical curve for the system ethane-hydrogen chloride

TABLE 1

Selected values for the particle radii

	Å.		*Å.*
H_2O molecule	1.06	Cl^- ion complex	3.31
Na^+ ion complex	2.77	Br^- ion complex	3.45
K^+ ion complex	3.15	I^- ion complex	3.66

Since there is practically no proven knowledge concerning such a system, the assumptions made seem to be a reasonable initial step, and they remain to be proven, disproven, or altered in the light of new knowledge.

In the infinitely dilute solution, i.e., $\gamma_2 = 0$, equation 11 should reduce to the Van der Waals expression for T_c. It is obvious, therefore, that a_{11} is equal to the Van der Waals a for water, 5.464 liters² × atm. per mole², and the quantity $k_3 r_1^3$ is equal to the van der Waals b, 0.03049 liter per mole. In this manner all quantities in equation 11 are given numerical values except the three constants, n, k_1, and k_2, and the variables T and γ. The simplified equations are the following:

TABLE 2

Calculated values of the constants in equations 12, 13, 14, and 15

SOLUTE	n	k_1	k_2
NaCl	0.999633	292.3	0
KCl	0.999740	348.2	−100
KBr	0.999349	364.8	500
KI	0.999509	402.95	967

For sodium chloride:

$$T^n = \frac{5.464 + k_1\gamma_2 + k_2\gamma_2^2}{0.008445 + 0.39941\gamma_2} \tag{12}$$

For potassium chloride:

$$T^n = \frac{5.464 + k_1\gamma_2 + k_2\gamma_2^2}{0.008445 + 0.47038\gamma_2} \tag{13}$$

For potassium bromide:

$$T^n = \frac{5.464 + k_1\gamma_2 + k_2\gamma_2^2}{0.008445 + 0.50439\gamma_2} \tag{14}$$

For potassium iodide:

$$T^n = \frac{5.464 + k_1\gamma_2 + k_2\gamma_2^2}{0.008445 + 0.56087\gamma_2} \tag{15}$$

If a set of experimental values for T and γ_2 for a given salt are available (a minimum of three are required), the best values for n, k_1, and k_2 may be determined by the method of least squares or by solution of the simultaneous equations. In our case it was found less laborious to first eliminate k_1 and k_2 from the simultaneous equations and solve for n in the resulting equation by trial and error aided by graphical interpolation. Once the value of n was established, k_1 and k_2 were evaluated by least squares, using all of the available data. In this manner the values given in table 2 were determined. The data which were used are given in the first two columns of table 3, most of them being taken from Schröer's work. Schröer's data expressed concentrations in moles per liter, and, with the aid of the known densities for the salt solutions, these were converted to mole fractions. In calculating the mole fractions no correction for the combined water was made, even though this was the assumption of the model. Since we have no knowledge of the extent of such hydration, an accurate calculation cannot be made. If the hydration is of the order of one or two moles of water per ion, the correction would change the mole fractions only slightly and would not materially affect the results. However, if the degree of hydration were large, the values for the mole fractions would be altered considerably. Perhaps the fact that the equation applies as well as it does without this cor-

TABLE 3

Calculated and observed critical temperatures for aqueous salt solutions

γ_2	T (OBSERVED)	T (CALCULATED)	DIFFERENCE
	NaCl		
	°*K.*	°*K.*	°*K.*
0.000770*	651.26	651.52	+0.26
0.001540*	654.01	654.29	+0.28
0.003077*	658.71	659.33	+0.62
0.006135*	667.81	667.66	−0.15
0.012193*	679.71	679.64	−0.07
0.015195*	683.86	684.10	+0.24
0.02432	693.8	694.04	+0.24
	KCl		
0.000770*	651.91	651.92	+0.01
0.001541*	655.71	655.44	−0.27
0.003081*	662.06	661.68	−0.38
0.006157*	671.26	671.62	+0.36
0.012245*	685.36	684.94	−0.42
0.02618	700.3	700.20	−0.10
	KBr		
0.000771*	652.66	653.12	+0.46
0.001543*	656.06	656.32	+0.26
0.003085*	662.41	662.15	−0.26
0.006169*	672.51	672.02	−0.49
0.02149	705.0	704.80	−0.20
	KI		
0.000772*	652.61	652.58	−0.03
0.001544*	655.91	655.96	+0.05
0.003091*	662.26	662.18	−0.08
0.006192*	673.16	673.08	−0.08
0.02363	717.8	717.82	+0.02
Mean difference.....			0.23

* Schröer's data.

rection could be interpreted as evidence that the degree of hydration of the ions is not large.

The third column of table 3 gives the calculated values for the critical temperature for comparison with the observed values. The average error between the values is 0.23°K. The agreement is somewhat better than that found for the simple log-log plot used by Schröer.

The data from this laboratory were obtained by the same method as that used by Schröer, the apparatus differing in only minor details.

THE SIGNIFICANCE OF THE CONSTANTS

The fact that the values of n lie very close to unity shows that the temperature dependence of the van der Waals constants is slight. This is qualitatively what one would expect, since for a one-component system the variation of a and b with temperature is small, even in the critical region.

Values of k_1 and k_2 do not yield as much information as one would like, since each represents a combination of the different particle interactions. However, we can examine them in more detail. Let us look first at what happens to the equation as the mole fraction, γ_2, goes to higher values. In the case of sodium chloride the critical temperature would approach a nearly constant value of about 730° as γ_2 approaches 0.5. The curve for potassium chloride actually goes through a maximum, and at $\gamma_2 = 0.5$ would have decreased to about 540°. For potassium bromide and potassium iodide, however, owing to large values for k_2, the temperature continues to rise to values of approximately 1700° and 2400°, respectively, at $\gamma_2 = 0.5$. It must be remembered that $\gamma_2 = 0.5$ does not indicate the pure anhydrous salt but represents the hypothetical substance composed of hydrated ions. If the degree of hydration of the ions decreases as the concentration of salt increases, the quantity in the denominator of equation 11 would decrease, and the critical temperatures would continue to rise to higher values than those indicated by the equation. That is to say, the radii of the particles involved must be a decreasing function of the concentration, particularly in the more concentrated region.

Substituting values for k_1, k_2, and a_{11} into equations 4 and 5 and combining these to eliminate common terms, we get:

$$(a_{\mathrm{K\text{-}K}} - a_{\mathrm{Na\text{-}Na}}) + 2(a_{\mathrm{K\text{-}Cl}} - a_{\mathrm{Na\text{-}Cl}}) = 11.8 \qquad (16)$$

$$(a_{\mathrm{Br\text{-}Br}} - a_{\mathrm{Cl\text{-}Cl}}) + 2(a_{\mathrm{K\text{-}Br}} - a_{\mathrm{K\text{-}Cl}}) = 633.2 \qquad (17)$$

$$(a_{\mathrm{I\text{-}I}} - a_{\mathrm{Br\text{-}Br}}) + 2(a_{\mathrm{K\text{-}I}} - a_{\mathrm{K\text{-}Br}}) = 543.3 \qquad (18)$$

In these equations the subscripts indicate the hydrated ion particles for the mutual interaction involved. Looking at the last two equations, assuming that the quantity within each set of parentheses is a positive quantity, and assigning positive signs to indicate repulsions and negative signs to indicate attractions, we get the following order for the magnitudes of the forces:

$$a_{\mathrm{I\text{-}I}} > a_{\mathrm{Br\text{-}Br}} > a_{\mathrm{Cl\text{-}Cl}}$$

$$a_{\mathrm{K\text{-}Cl}} > a_{\mathrm{K\text{-}Br}} > a_{\mathrm{K\text{-}I}}$$

These are precisely the orders in which the boiling points of the halogens and the alkali halides fall, and, in the case of the halogen gases, also the order of the critical temperatures. The same order would be expected for the critical temperatures of the potassium salts. However, if we apply the same reasoning to equation 16 the order is not that predicted from boiling points. For example, if we make $a_{\text{Na-Cl}}$ less than $a_{\text{K-Cl}}$ (the order of their boiling points), the quantity $(a_{\text{K-Cl}} - a_{\text{Na-Cl}})$ must be negative and the quantity $(a_{\text{K-K}} - a_{\text{Na-Na}})$ must be positive. This makes $a_{\text{K-K}} > a_{\text{Na-Na}}$, which is the reverse of the order for the boiling points of the metals. Either the right-hand member of equation 16 should be negative, which might well be without harming the applicability of equation 11 appreciably, or the comparison of the hydrated-ion substance with the anhydrous substances is not justified. The extrapolation of orders from boiling points to critical points may also not be justified.

SUMMARY

An equation which gives the relation of critical temperature of aqueous solutions of 1-1 electrolytes to the composition of the solution has been developed by the application of kinetic theory. With the aid of assumptions concerning the types of particles present and their effective radii, this equation has been shown to describe the available data for solutions of sodium chloride, potassium chloride, potassium bromide, and potassium iodide. The success in applying the equation does not substantiate the assumptions made but merely demonstrates the applicability of an equation based on kinetic theory. The significance of the numerical values obtained for the equation constants has been discussed.

REFERENCES

(1) KENNARD, E. H.: *Kinetic Theory of Gases*, pp. 221–37, McGraw-Hill Book Company, Inc., New York (1938); see also SLATER, J. C.: *Introduction to Chemical Physics*, p. 194 ff., McGraw-Hill Book Company, Inc., New York (1939).

(2) OWEN, G. E.: Paper presented at the 1948 Annual Meeting of the American Physical Society held in New York City, January 26–29, 1949; for an abstract see Phys. Rev. **75**, 1303 (1949).

(3) SCHRÖER, ERICH: Z. physik. Chem. **129**, 79 (1927).

(4) SECOY, C. H.: AECD Report No. 2265 (1948).

CRITICAL BEHAVIOR AND LIQUID-VAPOR EQUILIBRIUM IN MIXTURES OF FLUIDS[1]

CHARLES A. BOYD

Naval Research Laboratory, Department of Chemistry, University of Wisconsin, Madison, Wisconsin

Received March 20, 1950

I. INTRODUCTION

The phase relationships which exist for fluid mixtures in the neighborhood of the critical point have in recent years been given little attention by physical chemists. This paper has, therefore, a twofold purpose: first, to present a survey of the general phase behavior of fluid mixtures at elevated temperatures and pressures; second, to outline a general method of predicting this behavior from thermodynamic principles of equilibria.

In the latter part of the nineteenth century, scientists were particularly cognizant of the critical behavior of pure fluids. Andrews (1) reported his classic researches on carbon dioxide in 1869, van der Waals (8) had completed a dissertation on the continuity on the states of matter, and in general a good deal of effort was being concentrated on investigations of P–V–T relationships for both pure gases and gaseous mixtures.

In the year 1880 Cailletet (2) made an important discovery in connection with his studies on the liquefaction of carbon dioxide–air mixtures. As might be expected, a mixture of one volume of air and five volumes of carbon dioxide would undergo partial condensation to the liquid state as the pressure was increased to a moderate value, the temperature being held sufficiently low. When the pressure was increased further, the temperature being maintained constant, the liquid phase would begin to disappear; when the pressure reached a critical value, the liquid phase would disappear altogether and the system would return to a single vapor phase. Upon lowering the pressure to this critical value, the liquid phase reappeared. This apparently anomalous behavior in mixtures was observed by other investigators, among them van der Waals and Andrews. Contributions to the interpretation of this behavior were made by Duhem (3) and others. However, Kuenen (6), reporting on his studies on the system carbon dioxide–methyl chloride, gave the first clear interpretation of the overall phase behavior of binary mixtures in the critical region. He applied the name "retrograde" or backward condensation to the type of anomalous behavior observed by Cailletet and Andrews, and showed how under the proper conditions a similar phenomenon could be produced by holding the pressure constant and varying the temperature. To this second type of behavior he applied the term "retrograde condensation of the second kind."

As has been pointed out by Katz and Kurata (4) in their survey of retrograde condensation, most physics and physical chemistry texts published since 1910 consider only phase relationships in liquid mixtures at or near atmospheric pressure and completely ignore the wealth of information existing in the earlier literature concerning the influence of elevated pressures upon these relationships. However, in recent years the petroleum industry has been giving much attention to these problems, since retrograde phenomena frequently occur in high-pressure distillation of hydrocarbons and the principle is regularly employed in increasing the yield of petroleum from oil wells by pressurizing.

---

[1] Presented at the Symposium on Critical Phenomena, which was held under the auspices of the Division of Physical and Inorganic Chemistry at the 116th Meeting of the American Chemical Society at Atlantic City, New Jersey, September 22, 1949.

II. PHASE BEHAVIOR IN BINARY SYSTEMS

The experimental data obtained by Kay (5) on the ethane–heptane system will be used to illustrate the phase behavior of binary systems at elevated temperatures and pressures. Figure 1 shows the ordinary type of distillation curve, where the composition of the liquid and that of the vapor in equilibrium with it are given as functions of the boiling point of the solution.

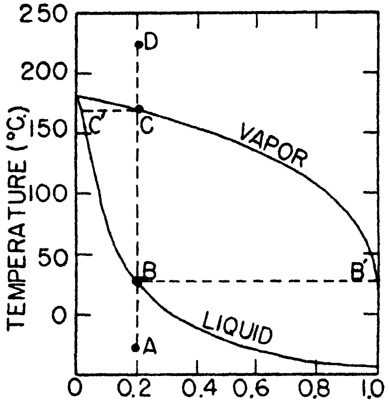

Fig. 1

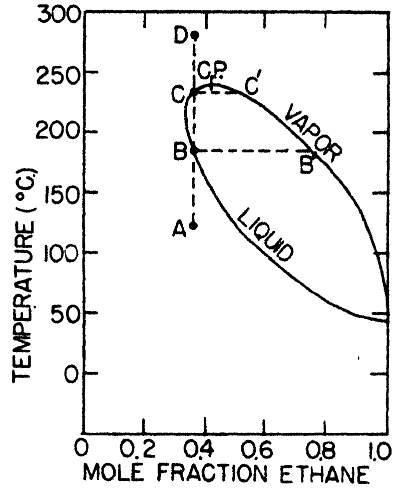

Fig. 2

Fig. 1. Distillation curve for ethane–heptane system. Pressure, 100 p.s.i. Experimental data of Kay (Ind. Eng. Chem. **30**, 459 (1938)).

Fig. 2. Distillation curve for ethane–heptane system. Pressure, 800 p.s.i. Experimental data of Kay.

If we consider a mixture of the two components containing 0.2 mole fraction of ethane at a temperature of −25°C. and under 100 lb./in.^{2} pressure, the situation can be represented by point A in figure 1. As the temperature of the system is increased, the pressure being held constant, the point representing the system follows up the dotted ordinate AD until point B is reached. At this temperature a vapor phase of lower density, represented by B', appears in equilibrium with the liquid. Further increase in temperature results in an increasing amount of vapor phase and a corresponding decreasing amount of liquid phase until point C is reached, where the last trace of liquid phase, having a composition C', disappears. Further increase in temperature has no additional effect on the system, which is not totally in the vapor phase, disregarding, of course, any chemical effects brought about at elevated temperatures.

At higher pressures we obtain similar curves with the liquid and vapor boundaries, corresponding to particular compositions, occurring at higher temperatures. The variation with pressure of the boiling points of the pure components, given at 0 and 1.0 mole fraction of ethane in figure 1, follows the regular vapor pressure curves for the two substances.

With increasing pressure the boiling points of the pure components continue to increase until the critical temperature for one of them is reached. In the case of the ethane-heptane system under consideration this occurs for the heptane at a pressure slightly under 400 lb./in.^{2} The corresponding critical temperature for pure heptane is approximately 250°C.

At or above this temperature one cannot distinguish between the vapor and liquid phases for pure heptane or mixtures of heptane and ethane up to some limiting composition which is determined by the pressure. The situation at 800 lb. in.^{2} is represented in figure 2. The heterogeneous area bounded by the liquid and vapor curves does not extend much below 0.3 mole fraction of ethane; consequently, if a mixture containing 0.2 mole fraction of ethane is heated at constant pressure there will be no phase separation such as occurred at 100 lb./in.^{2}

The liquid boundary in figure 2 goes through a minimum in composition with increasing temperature before it meets the vapor boundary at the point indicated by *C.P.* Point *C.P.* then indicates the critical point for a mixture of approximately 0.4 mole fraction of ethane, since only at this point do the vapor and liquid phases have the same density and composition and thus become indistinguishable. We shall refer to this composition, at which the critical point occurs for a specified pressure and temperature, as the critical composition.

The composition minimum in the liquid boundary gives rise to one type of retrograde condensation. Consider a mixture at this pressure with composition and temperature represented by point *A* in figure 2. Increasing the temperature of the mixture while holding the composition constant is represented by the motion of a point up the dotted line until point *B* is reached, where a vapor phase (phase of lower density) appears having a composition given by *B′*. Upon further increase of the temperature, the amount of vapor phase first increases, reaches a maximum, and then decreases until point *C* is reached, where the last trace of vapor having a composition represented by *C″* disappears and the system again returns to the single liquid phase. Thus, by increasing the temperature of the system, the initial vapor formation has been followed by condensation. This is contrary to the behavior which one would expect. Hence, following the nomenclature of Katz and Kurata (4), this disappearance of the vapor phase upon increase in temperature is called retrograde condensation of the second kind. A similar type of behavior occurs in mixtures when the critical temperature of the second component is exceeded. The resulting distillation curves obtained in the ethane–heptane system over a wide range of pressures are shown in figure 3. The experimental data are shown better in a three-dimensional representation, the three axes being pressure, temperature, and composition. A photograph of

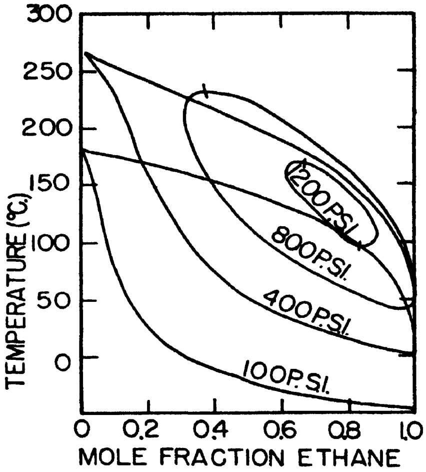

Fig. 3. Distillation curves for ethane–heptane system; experimental data of Kay

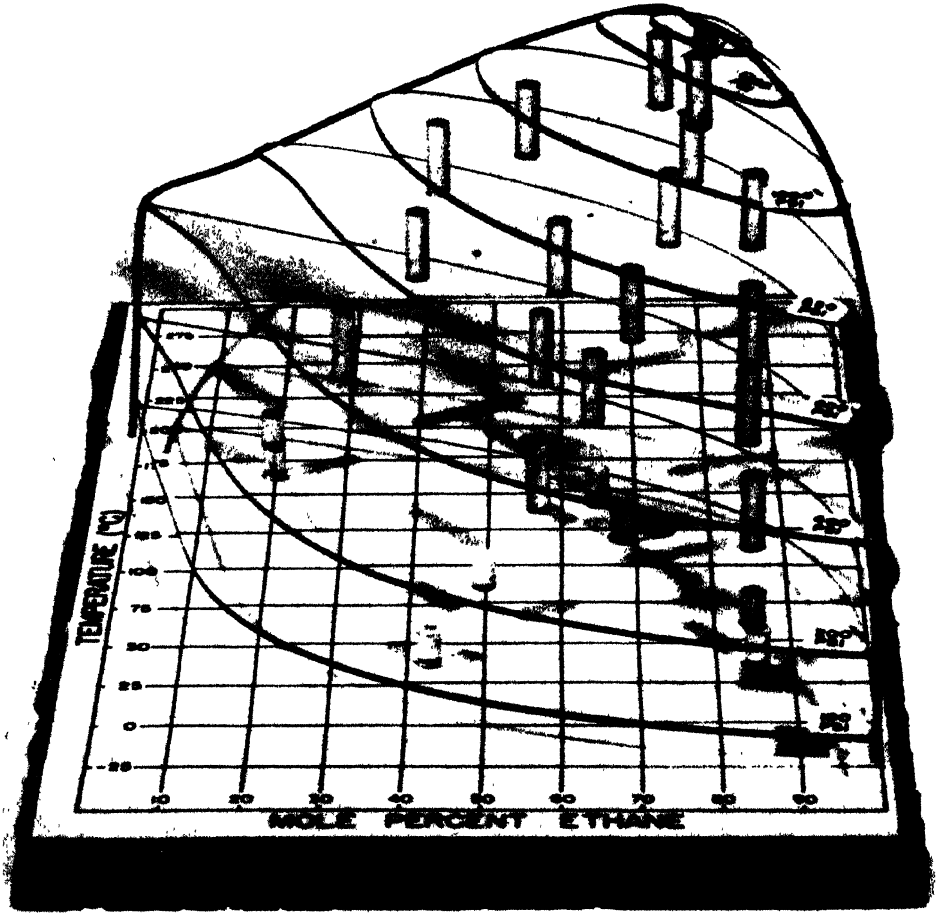

Fig. 4. Three-dimensional representation of the ethane–heptane system

such a three-dimensional representation for the ethane–heptane system is shown in figure 4, where the heterogeneous region is now represented by a tongue-shaped volume bounded on one approach by a liquid surface and on the other by a vapor surface.

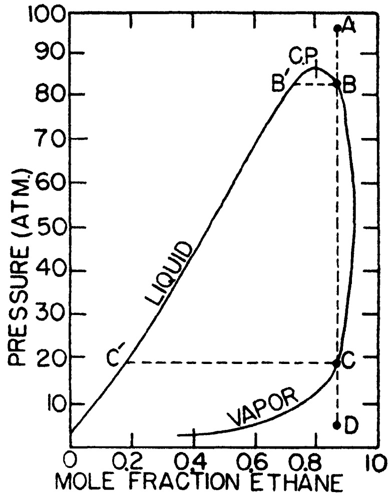

FIG. 5 Pressure-composition curve for ethane–heptane system Temperature, 400°K. Experimental data of Kay.

Figure 5 shows a constant-temperature section taken through the heterogeneous volume at 400°K. Since this temperature is above the critical temperature of pure ethane, the heterogeneous region bounded by the liquid and vapor lines does not extend over to a composition of 1.0 mole fraction of ethane, and it will be noted that the vapor curve goes through a maximum in composition before meeting the liquid curve at the critical point.

In order to demonstrate retrograde condensation of the first kind, consider a system represented by point *A* on figure 5. Only one phase is present until the pressure is lowered (the temperature being held constant) to point *B*, where a phase of higher density appears having a composition represented by *B′*. Hence, lowering the pressure at constant temperature causes condensation of a liquid phase; this result is contrary to expected behavior and again we have an example of retrograde or "backward" condensation.

In general, it may be stated that retrograde behavior will occur when the path of a point moving in a straight line through the three-dimensional representation enters and leaves the heterogeneous volume through the same phase boundary whether it be liquid or vapor. This path does not necessarily have to parallel the temperature or pressure axis but can combine changes in both.

It should be pointed out that the above discussion has considered only simple solutions and has not considered azeotropic cases where maxima or minima occur in the distillation curves. However, this situation does not alter the general interpretation.

III. THERMODYNAMIC CONSIDERATIONS

When several phases are in equilibrium in a multicomponent system, one of the thermodynamic criteria for such a state involves the equality of the chemical potentials (partial molal free energies) of the various components in each of the phases, namely:

$$[\mu_i^{(1)} = \mu_i^{(2)} = \cdots \mu_i^{(n)}]_{P,T} \tag{1}$$

This equation simply says that the chemical potential, or the partial molal free energy, of the i^{th} component in phase 1 must be equal to the same quantity in phases 2, 3, etc.

In the simpler case of liquid–vapor equilibrium in a binary system, equation 1 reduces to

$$[\mu_1^{(l)} = \mu_1^{(v)}]_{P,T} \tag{2}$$

$$[\mu_2^{(l)} = \mu_2^{(v)}]_{P,T} \tag{3}$$

where the superscripts l and v refer to the liquid and vapor phases and the subscript numbers refer to the components.

A general expression for μ_i at some specified temperature and pressure is given by:

$$\left[\mu_i = \mu_i^* + RT \ln (PX_i) + \int_0^P [\bar{V}_i - (RT)/P]\, \mathrm{d}P\right]_T \tag{4}$$

where R, T, and P have their usual significance, X_i is the mole fraction of the component being considered, and $\bar{V}_i$ is its partial molal volume.

In order to evaluate the integral in equation 4 an expression for $\bar{V}_i$ as a function of pressure and composition is needed. This requires equations of state for the pure components and of their mixtures, including composition as one of the variables. The equations of state which were used in the present work will be described in the following section.

Having developed a method of evaluating the integral in equation 4 one can then represent the quantity $\mu - \mu^*$ or, for convenience, $(\mu - \mu^*)/RT$, for each component as a function of composition at specified temperatures and pressures, thus:

$$\begin{bmatrix} [(\mu - \mu^*)/RT]_{(i)}^{(l)} = f[X_1, P, T]_{(i)}^{(l)} \\ [(\mu - \mu^*)/RT]_{(i)}^{(v)} = f[X_1, P, T]_{(i)}^{(v)} \end{bmatrix}_T \begin{matrix} (5) \\ (6) \end{matrix}$$

Since we are working with a binary system, the composition can be expressed in terms of the mole fraction of either component.

μ^*, R, and T are constants with respect to composition changes, and consequently equations 5 and 6 can be combined with the equilibrium equations 2 and 3 to give:

$$\begin{bmatrix} f[X_1, P, T]_{(1)}^{(l)} = f[X_1, P, T]_{(1)}^{(v)} \\ f[X_1, P, T]_{(2)}^{(l)} = f[X_1, P, T]_{(2)}^{(v)} \end{bmatrix}_T \begin{matrix} (7) \\ (8) \end{matrix}$$

For specified values of pressure and temperature which are the same for both liquid and vapor phases, equations 7 and 8 can be solved simultaneously for $X_1^{(l)}$ and $X_1^{(v)}$. These values then represent the compositions of the liquid and vapor phases in equilibrium at the particular pressure and temperature.

At the critical point equations 7 and 8 continue to hold. However, at this point an additional restraint is placed on the system. For simple binary solutions exhibiting no boiling point maxima or minima, the composition of the vapor and the composition of the liquid become equal. Consequently we have a third equation expressing this restraint:

$$X_1^{(l)} = X_1^{(v)} \tag{9}$$

Simultaneous solution of equations 7, 8, and 9 allows us in principle to calculate any three of the four variables P, T, $X_1^{(l)}$, or $X_1^{(v)}$, provided the fourth is specified. If one chooses a value of critical temperature for the system, one can then calculate the corresponding critical pressure and composition.

In order to apply the equations of the foregoing section to actual cases, it will be necessary to use some equation of state. Although we have not as yet completed actual numerical calculations, it will be advantageous at this point to introduce the van der Waals equation, which we write in the form

$$P = nRT/(V - nb) - n^2a/V^2 \tag{10}$$

for n moles. This will enable us to bring out the differences between the treatments required for pure substances and for binary mixtures.

This equation was originally proposed to account for the pressure–volume–temperature relationships of pure substances, including the coexistence of two phases below the critical temperature. van der Waals also applied his equation to mixtures (9), using an expression for b deduced by Lorentz (7) from theoretical considerations:

$$b_{\text{mix}} = b_{11}X_1^2 + 2b_{12}X_1X_2 + b_{22}X_2^2 \tag{11}$$

where b_{11} and b_{22} are the values for the pure components and b_{12} is a constant characteristic of the mixture. X_1 and X_2 refer to the mole fractions of components 1 and 2, respectively.

A similar expression was used for the constant a_{mix}, thus:

$$a_{\text{mix}} = a_{11}X_1^2 + 2a_{12}X_1X_2 + a_{22}X_2^2 \tag{12}$$

It is of course well known that van der Waals' equation does not represent the equation of state of real substances with great accuracy. However, it can be considerably improved if the constants are considered to be functions of temperature. It will ultimately be necessary to consider the evaluation of all the constants in equations 11 and 12 as functions of T, and it is hoped by this means (or by use of a better equation of state) to obtain in future work a semiquantitative description of the phenomena. For the present purposes this temperature dependence will not make any difference.

At this point it might be of use to consider the meaning of the critical relationships of van der Waals' equation which express a and b in terms of the critical temperature, pressure, and volume.

As is well known, when we apply van der Waals' equation to any one-component system at a temperature below the critical value, the pressure of the liquid phase must equal the pressure of the vapor phase in order for equilibrium to be established.

Consequently, the tie-lines connecting the liquid and vapor states in equilibrium are parallel to the volume axis, as shown in figure 6 for the temperatures T_1 and T_2. As the temperature is raised from T_1 through T_2 to T_c, the equilibrium pressure rises but the molar volumes of the liquid and vapor phases approach each other in value until the critical temperature is reached, at which point the two molar volumes become identical, indicating that the two phases can no longer be distinguished from one another. This behavior leads to the following mathematical consequences at the critical point:

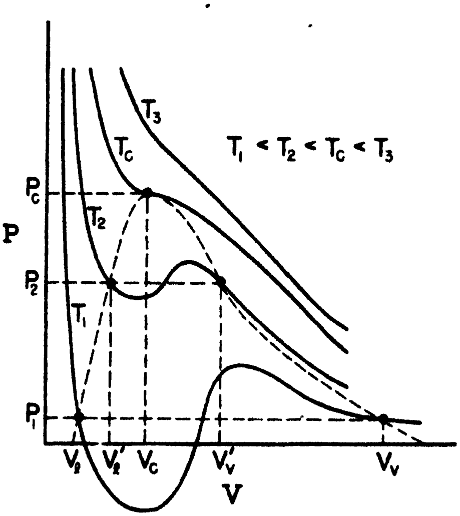

FIG. 6. van der Waals isotherms for a one-component system at various pressures

$$(\partial P/\partial V)_T = 0 \tag{13}$$

$$(\partial^2 P/\partial V^2)_T = 0 \tag{14}$$

Substitution of van der Waals' equation into these two expressions and solving for a and b leads to equations relating these two quantities to the critical temperature, pressure, and volume, such as:

$$b = \tfrac{1}{3}V_c \tag{15}$$

$$a = 3P_cV_c^2 \tag{16}$$

The situation is not so simple in the case of a two-component system, since in addition to the variables P, V, and T we have another variable: namely, composition.

For simple solutions with no azeotrope formation the composition of the liquid phase differs from that of the vapor phase in equilibrium with it, and consequently the isotherm for the liquid is not a simple continuation of that for the vapor.

This is illustrated in figure 7. The isotherm represented by $A'ABB'$ corresponds to some definite composition, F. However, the vapor phase represented by B is in equilibrium with a liquid phase represented by D on a different isotherm corresponding to a different composition, E. Likewise, the liquid phase of composition F represented at A is in equilibrium with a vapor phase, P, having a composition between F and G.

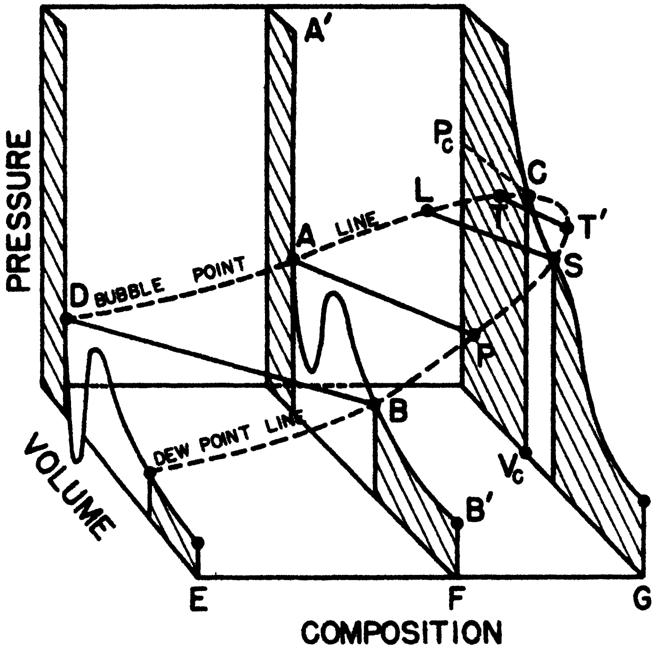

FIG. 7. van der Waals' equation, showing vapor–liquid equilibria for a two-component system at a constant temperature above the critical temperature of the second component.

In figure 7 composition G is the critical composition because at the critical point, C, the liquid phase, bounded by the bubble-point line, and the vapor phase, bounded by the dew-point line, have the same composition, G, and the same molar volume, V_c. The dew-point line, $BPST'C$, bends back to meet point C in such a fashion that a tie-line, represented by TT', connects to a vapor phase having a composition to the right of G. This behavior, of course, is necessary in order to have retrograde condensation of the first kind.

Although the isotherm at composition G can be called the critical isotherm since it serves to define the critical point, it also specifies a vapor phase S of composition G in equilibrium with a liquid phase L of different composition.

Projections of the bubble-point and dew-point lines upon the pressure–composition plane will result in a figure similar to that shown in figure 5.

The expressions relating a and b to critical temperature, pressure, and volume, which were derived for a one-component system, do not necessarily hold in a two-component system. Consequently one cannot use these expressions to calculate the critical constants for all compositions directly from the values of a and b obtained from combining expressions 12 and 13. The critical constants for mixtures must be calculated in the manner outlined in the previous section.

Using equations 11 and 12, which give the constants a and b as a function of composition, and the van der Waals law given in equation 10 we can obtain an expression for $\bar{V}_i = \partial V/\partial n_i$, where n_i is the number of moles of component i. To do this we differentiate both sides of equation 10 with respect to n_i with T, P, and all other n's constant, so that $\partial P/\partial n_i = 0$ and $\partial n/\partial n_i = 1$, and we recall that

$$\partial X_i/\partial n_i = (1 - X_i)/n_i$$

for a binary system. We can then substitute $\bar{V}_i$ in the integral in equation 4, use equation 10 to get $\mathrm{d}p$ in terms of $\mathrm{d}V$, and obtain finally:

$$\left[\int_0^P [\bar{V}_i - (RT/P)]\,\mathrm{d}P = -RT\{\ln [P(V - b)/RT]\} + [(RT)/(V - b)]B_i - A_i/V\right]_T \tag{17}$$

where V is the molar volume of the mixture obtained from van der Waals' equation and:

$$B_i = b + (1 - X_i)(\partial b/\partial X_i) \tag{18}$$

$$A_i = 2a + (1 - X_i)(\partial a/\partial X_i) \tag{19}$$

The quantities a and b and their derivatives refer to the values for the mixture and can be obtained directly from equations 11 and 12.

Equation 17 can then be combined directly with equation 4 to give:

$$[(\mu_i - \mu_i^*)/RT = \{\ln [(RTX_i)/(V - b)]\} + [B_i/(V - b)] - [A_i/(VRT)]]_T \tag{20}$$

Equation 20 can then be used in the manner described in Section III to obtain the equilibrium compositions and the critical compositions as functions of temperature and pressure.

If the pressure is sufficiently low, and the temperature is below the critical temperature, van der Waals' equation when solved for volume may give three real roots. The smallest of these corresponds to the liquid phase, and the largest corresponds to the vapor phase. The intermediate root is only a mathematical consequence of the form of the equation and does not correspond to any real situation. If the pressure is sufficiently high there will be only one real solution for volume which, of course, would correspond to the liquid phase, assuming the temperature to be lower than the critical value. Correspondingly, depending upon the exact value of the temperature, there may be only one real solution for volume representing the vapor phase if the pressure is sufficiently low.

Therefore, from van der Waals' equation for a temperature below the critical point, we can obtain two sets of molar volumes as a function of pressure, one set describing the liquid phase and the other describing the vapor phase. These sets will overlap in one pressure region. The ratio $(\mu_i - \mu_i^*)/RT$ will represent either the liquid or the vapor, depending upon which value of V is taken for substitution in equation 17. In this manner it is possible to set up the simultaneous equations represented in equations 7 and 8 of Section III.

V. SUMMARY

A general discussion is given of the liquid–vapor equilibrium in a binary system, with particular attention to the phenomenon of retrograde condensation. By way of illustration, the behavior of the ethane–heptane system is elucidated by a series of phase diagrams.

The thermodynamics of the liquid–vapor equilibrium is developed, and the van der Waals equation of state is introduced. In this way, we have shown the difference in the treatment required for pure systems and for binary systems, and have laid the ground for future calculations of a semiquantitative nature.

The author would like to thank Professor J. O. Hirschfelder and Professor C. F. Curtiss of this laboratory, and Professor O. A. Hougen of the Department of Chemical Engineering, for their many helpful suggestions brought out in discussions during the course of this work.

REFERENCES

(1) Andrews, T.: Phil. Trans. Roy. Sco. **159**, 575 (1869).
(2) Cailletet, L.: Compt. rend. **90**, 210 (1880).
(3) Duhem, P.: Trav. mem. faculté Lille **3**, No. 13 (1893).
(4) Katz, D. L., and Kurata, F.: Ind. Eng. Chem. **32**, 817 (1946).
(5) Kay, W. B.: Ind. Eng. Chem. **30**, 459 (1938).
(6) Kuenen, J. P.: Arch. neérland. sci. **26**, 354 (1893).
(7) Lorentz: Wied. Ann. **12**, 127, 660 (1881).
(8) van der Waals, J. D.: Thesis, Leyden, 1873.
(9) van der Waals, J. D.: *Die Kontinuität des gasförmigen und flüssigen Zustandes*, Part II. Barth, Leipzig (1900).

STUDY OF THE OPTICAL PROPERTIES OF SHELLAC SOLUTIONS

DEPOLARIZATION OF SCATTERED LIGHT[1]

SADHAN BASU

Department of Physical Chemistry, Indian Association for the Cultivation of Science,
210 Bowbazar St., Calcutta, India

Received January 30, 1950

The true nature of shellac solutions has been a subject of some controversy. The tendency of shellac solutions to form gels at higher concentrations and the rapid increase in viscosity of the solutions containing more than 25 per cent shellac have been explained by Gardner (4) and Verman (12) on the assumption that shellac solutions are colloidal in nature. Palit (9), however, has assumed them to be noncolloidal, since they rapidly dialyze, pass through ultrafilters easily, and are devoid of any Tyndall effect. An interesting method of study reported in the present paper is the determination of the degree of depolarization of scattered light which may be utilized to obtain information regarding the nature of the dissolved units. As compared with other techniques, the particular advantage of this method is that the three factors may be investigated simultaneously and their changes may readily be followed quantitatively.

THEORETICAL

The theory of light scattering by small spherical particles was first proposed by Rayleigh (10). Mie (8) extended Rayleigh's theory to the case of larger particles. Gans (3) developed and applied it particularly to the determination of shape and anisotropy.

The degree of depolarization is used to denote the ratio of the intensity of the horizontal component to that of the vertical component of the transversely scattered light (i.e., the light scattered at 90° to the incident beam). According to the theory of Mie (8), the degree of depolarization with incident light unpolarized (ρ_u) equals zero for spherical isotropic particles which are small in diameter in comparison with the wave length of the incident light. As the particle size increases, ρ_u assumes a finite value. Gans (3), however, has shown that ρ_u also increases with anisotropy; thus ρ_u is not a measure of any one factor alone.

Subba Ramiah (11) and Krishnan (6) have shown that in order to get a clearer insight into the nature of the scattering units, it is necessary to make the depolarization measurements with incident light polarized vertically (ρ_v) and also polarized horizontally (ρ_h). It has been shown that a finite value of ρ_v is a definite indication of nonsphericity or optical anisotropy only, while the value of ρ_h is a very sensitive indicator for both size and shape of the particles. Thus, values of ρ_h nearly equal to but necessarily less than unity would indicate an appreciable size, no longer small in comparison with the wave length of light, whereas small values in the neighborhood of zero would be an indication of anisotropy. Intermediate values would be determined by the joint influence of size and anisotropy. In such cases calculation of the relative effect of these two factors may be effected by means of an ingenious mathematical formula derived by Krishnan (6). Depolarization, according to Krishnan, arises from two causes: unrestricted orientation of the anisotropic particles, and the finite size of the scattering units. The horizontal and vertical intensity components in orientation scattering with the incident electric vector vertical are A and $4/3A$, respectively, where A is a factor depending on the intensity of the electric vector and the nature of the scattering units. When, however, the electric vector is horizontal, the two components due to orientation scattering have the same magnitude, A. With particles of finite size, however, the horizontal component of the scattered light with incident electric vector horizontal may be represented by another factor X, the vertical component being zero. Similarly, with incident electric vector vertical, the vertical component of the scattered light may be represented by a third factor Z, the horizontal component being zero. When the depolarization is due jointly to the orientation and finite size, Krishnan (6) deduced the following relationship between X, Z, and A and the depolarization measured.

---

[1] Contribution No. 25 from the Department of Physical Chemistry, Indian Association for the Cultivation of Science.

DIRECTION OF ELECTRIC VECTOR	SCATTERED LIGHT		DEPOLARIZATION
	Horizontal component	Vertical component	
Vertical	A	$Z + \frac{4}{3}A$	$\rho_{v-A}/(Z + \frac{4}{3}A)$
Horizontal	$X + A$	A	$\rho_{h-A}/(X + A)$

From ρ_v and ρ_h, the components X and Z may be evaluated in terms of orientation scattering, A. The factor X/Z is the depolarization due to finite size (8) with incident light unpolarized, and is a function of the size of the scattering units.

The application of depolarization measurements has been made by Krishnan (6), Subba Ramiah (11), Mataprasad (7), and others to the cases of organic and inorganic colloids, and by Doty and Kaufman (2) to polymer solutions in elucidating the nature of these systems. In the present work depolarization measurements have been made with shellac solutions, and the results used not to get information on the exact dimensions but rather to show how shape, size, etc. change with concentration and with different solvents.

EXPERIMENTAL

The depolarization factor of the light scattered transversely by shellac solutions was measured by the well-known method of Cornu. The experimental arrangement was as follows: Light from a Neron lamp was condensed by a long-focal-length lens (f = 20 cm.) at the center of a rectangular glass cell containing the solution. A mounted polaroid disc served to polarize the light, either vertically or horizontally. The cell was placed just by the side of a black screen containing a window (2 mm. square) whose image was observed through a Nicol *via* a double-image prism. The double-image prism was first set to such a position that the two images observed through the Nicol just touched each other.

The Nicol was rotated until the two images were of equal intensity. The angle (θ'') was noted. The Nicol was then rotated in the opposite direction until for a second position (θ') the images again became equal in intensity. The depolarization factor was then given by the expression:

$$\rho = \tan^2 \frac{\theta'' - \theta'}{2}$$

The aperture of the lens was reduced as much as possible in order to reduce secondary scattering to a minimum.

In these experiments carefully dewaxed and partially decolorized shellac was used. Since shellac contains a large amount of dust and other extraneous matter and the removal of these substances by filtration of the solutions of shellac, especially concentrated solutions, is neither satisfactory nor desirable, for there is always the chance of contamination of the solution by absorbed moisture and variation in concentration due to evaporation, the following procedure was adopted in purifying shellac prior to the preparation of the test solutions. Dewaxed and decolorized shellac was powdered to 100 mesh and put into an extraction thimble, which had been carefully cleansed by washing with alcohol. The shellac was then extracted in a Soxhlet apparatus with alcohol. Every part of the Soxhlet apparatus had been thoroughly cleansed with hot chromic acid and then freed of dust by steaming. The alcohol used was prepared by slow distillation from a stock of 95 per cent alcohol. The solution of shellac thus obtained was then slowly poured into dust-free water, when a colloidal solution was obtained. Hydrogen was bubbled through this solution, whereupon the shellac precipitated as a granular powder which was separated and dried in a vacuum.

The preparation of the test solutions was done by weighing out dry shellac prepared as above in stoppered bottles and adding the required volume of dust-free solvents and mixed solvents from a buret. For complete dissolution in mixed solvents it was necessary to warm the bottles slightly on a water bath. The values of ρ_u, ρ_v, and ρ_h, as also the calculated X/Z values for shellac in different solvents, are given in tables 1 to 5.

Depolarization measurements with shellac solutions, particularly when these were concentrated, were rendered difficult by the presence of dye in shellac, since the dye absorbed considerable proportion of light, thereby reducing the intensity of light available for scattering. Measurements of the intensity of the scattered light were therefore not tried; the values of ρ_s given in tables 1 to 5 are also not absolute; this, however, will not affect the present study, as it will be sufficient for our purpose to obtain their respective variation.

DISCUSSION

The very first observation that can be made from the above tables is that ρ_h has a value intermediate between 0 and 1, signifying that the depolarization is due to the finite size and the anisotropic shape of the scattering units. That the scattering units are anisotropic is also clearly evident from the value of $\rho_v > 0$. But this conclusion as to the finite size of the scattering units would appear rather perplexing, for in the first place no stable colloidal micelle can be detected below 20 per cent shellac concentration by dialysis, by ultrafiltration, or by any other means (9), and therefore the scattering probably cannot be ascribed to the existence of well-defined colloidal micelles, at least in the dilute region; secondly, shellac molecules are small compared to the wave length of light (1) and this would rule out the size effect due to individual molecules. This anomaly, however, may be explained by assuming the existence of relatively large but loose molecular clusters of certain average size, as has been done by Krishnan (6) to account for the finite value of ρ_h for certain binary liquid mixtures. Further, the relatively small values of ρ_h indicate that the solutions resemble more a liquid–liquid system than a well-defined colloidal suspension. In view of these observations the most probable structure of shellac solution appears to be clusters of molecules with hindered rotation similar to the cybotactic groups in liquids. The difference between such clusters and micelles is that the colloidal micelle is a discrete entity, whereas the clusters have only a statistical existence in the sense that they continually break down on account of thermal agitation only to re-form to an average size. Decreased agitation will help to form larger and more stable clusters and these would account for the viscosity behavior of shellac in concentrated solution.

TABLE 1

Depolarization of light by solutions of shellac in alcohol

PER CENT OF SHELLAC	ρ_u	ρ_v	ρ_h	X	Z	X/Z
5	0.5390	0.3334	0.5171	0.93A	1.69A	0.55
10	0.4924	0.2948	0.5063	0.97A	2.09A	0.46
15	0.4781	0.2756	0.4970	1.01A	2.32A	0.44
20	0.4459	0.2596	0.4933	1.03A	2.55A	0.40
25	0.4105	0.2482	0.4885	1.05A	2.72A	0.39
30	0.3948	0.2474	0.4711	1.08A	2.75A	0.40
40	0.3857	0.2428	0.4611	1.17A	2.81A	0.42
50	0.3632	0.2393	0.4474	1.23A	2.87A	0.43
60	0.3486	0.2390	0.4143	1.41A	2.88A	0.49
70	0.3492	0.2387	0.4003	1.50A	2.89A	0.52

In ethyl alcohol and acetone containing different alcohols (tables 1 and 2) the value of ρ_v gradually falls, i.e., the spherical symmetry of the clusters increases. The value of ρ_h also falls with concentration, a result which may be due to increase in spherical symmetry, to increase in size, or to both. The effect of depolarization due to finite size as represented by values X/Z shows that the clusters gradually diminish in size, although slowly, up to about 30 per cent concentration of shellac, after which they increase. This would suggest that the clusters become more and more compact as the concentration increases and that after the maximum compactness has been attained they increase in size with further rise in concentration. The behavior of the diacetone alcohol–acetone system is exactly similar to that of the ethyl alcohol, ethyl alcohol–acetone, and benzyl alcohol–acetone systems in the range 5–70 per cent of shellac, although the diacetone alcohol–acetone system sets to a gel at 40 per cent concentration of shellac and the others do not. Thus we see that the variation in shape and size of the clusters is a continuous process and is not subject to any abrupt change corresponding to sol–gel transition. Palit (9), however, observed that at the gel point there is a sudden and enormous increase in viscosity. This difference in behavior may be understood on the consideration that the light-scatter-

TABLE 2

Depolarization of light by solutions of shellac in mixed solvents

PER CENT OF SHELLAC	ρ_u	ρ_v	ρ_h	X/Z
Alcohol:acetone = 60:40				
5	0.5073	0.3239	0.4983	0.55
10	0.4874	0.2971	0.4928	0.50
15	0.4641	0.2734	0.4884	0.44
20	0.4498	0.2639	0.4825	0.43
25				
30	0.4359	0.2486	0.4797	0.39
40	0.4244	0.2435	0.4683	0.40
50	0.4110	0.2391	0.4543	0.42
60	0.4021	0.2344	0.4336	0.44
70	0.3959	0.2300	0.3899	0.52
Diacetone alcohol:acetone = 60:40				
5	0.5188	0.3069	0.4973	0.51
10	0.4745	0.2710	0.4898	0.44
15	0.4571	0.2633	0.4861	0.43
20	0.4319	0.2522	0.4833	0.42
25	0.4261	0.2499	0.4789	0.40
30	0.4134	0.2465	0.4743	0.40
40	0.4063*	0.2441*	0.4620*	0.42*
50	0.3972*	0.2461*	0.4514*	0.43*
60	0.3901*	0.2394*	0.4405*	0.44*
70	0.3869*	0.2393*	0.4297*	0.46*
Benzyl alcohol:acetone = 60:40				
5	0.4976	0.3231	0.4960	0.57
10	0.4668	0.3034	0.4930	0.51
15	0.4481	0.2733	0.4893	0.44
20	0.4359	0.2615	0.4861	0.42
30	0.4234	0.2591	0.4819	0.42
40	0.4145	0.2575	0.4704	0.43
50	0.4036	0.2569	0.4593	0.45
60	0.3977	0.2558	0.4422	0.47
70	0.3934	0.2556	0.4275	0.51

* An asterisk indicates region of gelation.

ing phenomenon is due to distribution and orientation of the clusters and is in no way affected by the forces acting between them, while the viscosity depends on the stability of the clusters and the energy required to displace the unit structure; that is to say, scattering depends on the geometry while viscosity depends on the potential energy of the structure. Gelation may be explained as due to coalescence of the solvation layers of the clusters, giving a continuous structure *en masse* without affecting the nature of the individual scattering

TABLE 3

Depolarization of light by solutions of shellac in glycol–acetone

PER CENT OF SHELLAC	ρ_u	ρ_v	ρ_h	X/Z
		Glycol:acetone = 10:90		
10	0.5105	0.3160	0.5068	0.52
15	0.5000	0.2978	0.4813	0.52
20	0.4860	0.2867	0.4704	0.50
25	0.4774	0.2823	0.4601	0.52
30	0.4643	0.2710	0.4541	0.50
40	0.4680*	0.3118*	0.4625*	0.64*
50	0.4785*	0.3385*	0.4668*	0.68*
60	0.4916*	0.3395*	0.4650*	0.69*
70	0.4963*	0.3301*	0.4500*	0.71*
		Glycol:acetone = 30:70		
5	0.5105	0.3278	0.5093	0.56
10	0.5048	0.3183	0.4964	0.54
15	0.4948	0.2964	0.4838	0.52
20	0.4839	0.2832	0.4621	0.52
25	0.4620	0.2715	0.4471	0.52
30	0.4218	0.2605	0.4283	0.52
40	0.4566	0.3071	0.4573	0.61
50	0.4635	0.3143	0.4540	0.63
60	0.4710	0.3183	0.4531	0.65
70	0.4792	0.3261	0.4525	0.69
		Glycol:acetone = 60:40		
5	0.5082	0.3169	0.4969	0.54
10	0.4950	0.2995	0.4847	0.51
15	0.4817	0.2847	0.4734	0.50
20	0.4690	0.2794	0.4615	0.51
25	0.4597	0.2722	0.4531	0.51
30	0.4369	0.2597	0.4475	0.50
40	0.4816	0.3068	0.4671	0.58
50	0.4930	0.3104	0.4558	0.62
60	0.5010	0.3191	0.4433	0.68
70	0.5114	0.3284	0.4341	0.74

* An asterisk indicates region of gelation.

centers. The setting of a gelatin gel has also been explained by Houwink (5) on a similar view: namely, coalescence of the particles separated by solvated layer of water film, in which the water molecules become more or less fixed. This coalescing tendency depends mainly on the nature of the forces among the solvated clusters, which is difficult to measure. Solvation itself cannot be detected by measurement of light scattering, since the refractive index of the solvent, whether in the solvated layer or in solution, is the same and consequently solvation will not affect the scattering of light by the individual particles in any way.

The behavior of solutions of shellac in solvents containing two polar groups (table 3), particularly hydroxyl and carboxyl groups, is very interesting. At a particular concentration (about 40 per cent) the anisotropic character of the clusters suddenly becomes more pronounced. That this phenomenon is due to the bipolar nature of the solvent is evident from the depolarization measurements with ethyl lactate–acetone, lactic acid–acetone, monoacetin–acetone, and diacetin–acetone solutions of shellac (tables 4 and 5). Since ethyl lactate–acetone and diacetin–acetone systems both contain only one polar group, the behavior is similar to that of the previous solvents containing one polar group, whereas the lactic acid–acetone and monacetin–acetone systems behave differently, showing a sudden increase in ρ_v at 40 per cent concentration of shellac. Further, that this abrupt change in value is not due to gelation is also evident from the behavior of acetone systems containing 10, 30, and 60 per cent glycol. These systems with 30 and 60 per cent glycol show a sudden increase in ρ_v value at 40 per cent shellac content, although they do not set to a gel at this point, as is the case with the glycol–acetone system containing 10 per cent glycol.

TABLE 4

Depolarization of light by solutions of shellac in mixed solvents

PER CENT OF SHELLAC	ρ_u	ρ_v	ρ_h	X/Z
Ethyl lactate:acetone = 50:50				
10	0.5373	0.3243	0.5194	0.52
20	0.5217	0.3139	0.5154	0.50
30	0.4949	0.2939	0.4876	0.50
40	0.4458	0.2696	0.4396	0.53
50	0.4394	0.2642	0.4263	0.54
60	0.4305	0.2601	0.4033	0.58
70	0.4298	0.2573	0.3837	0.62
Lactic acid:acetone = 50:50				
10	0.5095	0.3106	0.4957	0.53
20	0.4817	0.2831	0.4622	0.52
30	0.4494	0.2657	0.4387	0.52
40	0.4628	0.2855	0.4560	0.54
50	0.4501	0.2864	0.4427	0.58
60	0.4493	0.2813	0.4390	0.60
70	0.4388	0.2917	0.4231	0.64

An explanation of this may be given as follows: A bipolar solvent solvates the shellac molecule when one of the polar groups of the solvent becomes attached to the shellac molecule by a loose secondary bond, the other polar group remaining free; so that a solvated molecule would present the picture of a central core surrounded by a number of solvent molecules with a particular polar group of the latter directed outwards. As the concentration of shellac is increased the clusters become more and more compact, and when the concentration becomes sufficiently high the free polar group of the solvent in the solvated layer may find another molecule near its vicinity; as a result, a type of solvent bridge is established between the molecules, thereby changing the geometric distribution of the molecules within the clusters. It should, however, be remembered that the clusters may not have a sharp boundary; the molecules lying near the surface may be mobile and may easily exchange their citizenship with other molecules in the solution or with a molecule in another cluster, but in the anterior of the clusters the molecules will be more or less fixed. Consequently, the solution will not show any distinct colloidal property, although the variation of physical properties with concentration will give indications for the existence of micelles.

TABLE 5

Depolarization of light by solutions of shellac in mixed solvents

PER CENT OF SHELLAC	ρ_u	ρ_v	ρ_h	X/Z
		Diacetin:acetone = 60:40		
5	0.5136	0.3164	0.5084	0.52
10	0.5058	0.2981	0.4927	0.50
15	0.4845	0.2771	0.4744	0.48
20	0.4793	0.2694	0.4636	0.48
30	0.4461	0.2451	0.4283	0.48
40	0.4631	0.2604	0.4405	0.50
50	0.4472	0.2671	0.4361	0.53
60	0.4381	0.2765	0.4261	0.58
70	0.4310	0.2770	0.4151	0.61
		Monoacetin:acetone = 60:40		
5	0.5155	0.3032	0.5012	0.50
10	0.5048	0.2911	0.4932	0.48
15	0.4923	0.2751	0.4816	0.46
20	0.4797	0.2584	0.4692	0.44
25	0.4542	0.2437	0.4480	0.44
30	0.4432	0.2310	0.4343	0.43
40	0.4599	0.2496	0.4450	0.46
50	0.4395	0.2622	0.4443	0.50
60	0.4261	0.2651	0.4197	0.56
70	0.4255	0.2660	0.4121	0.58

SUMMARY

The results of the measurements of the depolarization of transversely scattered light by solutions of shellac in different solvents and at different concen-

trations are consistent in indicating that the scattering units are fairly large compared to the wave length of light; they first diminish and then increase in size with concentration. The results are best explained by assuming the existence of anisotropic scattering units, similar in nature to the cybotactic groups in liquids, which interlock at higher concentrations and give a continuous structure at the gel point.

Behavior in single solvents as also in mixed solvents containing a component with one polar group is exactly similar. If one component is bipolar the antisotropic character has been found to increase at about 40 per cent concentration of shellac. A tentative explanation for this phenomenon has been given.

REFERENCES

(1) Basu: J. Indian Chem. Soc. **24**, 263 (1947).
(2) Doty and Kaufman: J. Phys. & Colloid Chem. **49**, 583 (1945).
(3) Gans: Ann. Physik **62**, 330 (1920).
(4) Gardner: Ind. Eng. Chem., Anal. Ed. **1**, 205 (1929).
(5) Houwink: *British Plastics Year Book*, p. 51 (1942).
(6) Krishnan: Proc. Indian Acad. Sci. **1**, 211, 717 (1934); **5**, 94 (1937).
(7) Mataprasad *et al.*: Proc. Indian Acad. Sci. **19**, 47 (1944).
(8) Mie: Ann. Physik **25**, 377 (1908).
(9) Palit: J. Indian Chem. Soc. **17**, 577, 308 (1940).
(10) Rayleigh: Scientific Papers, Vol. 5, p. 547, University Press, Cambridge (1900); Phil. Mag. (1889).
(11) Subba Ramiah: Proc. Indian Acad. Sci. **1**, 709 (1934); **5**, 128 (1937).
(12) Verman: Technical Paper No. 11 of London Shellac Research Bureau.

THE TEMPERATURE DEPENDENCE OF THE ELECTROPHORETIC MOBILITY OF HORSE SERUM ALBUMIN

ITARU WATANABE,[1] NOBUO UI,[1] AND MASAYOSHI NAKAMURA[1]

Radiation Chemistry Research Institute, Tokyo University, Tokyo, Japan

Received January 18, 1950

INTRODUCTION

Electrophoretic mobilities are generally measured at low temperatures, near 0°C. In spite of its importance, there have been practically no studies on the influence of temperature on electrophoretic mobility, except that of Tiselius (9). He, however, only showed that the ratio of mobilities at 0°C. and 20°C. is approximately inversely proportional to that of the viscosities of solvent at the respective temperatures, and no further extension has so far been made.

In our previous measurement on horse serum at 15°C., mere correction of the solvent viscosity to 0°C. failed to give satisfactory results (12). This led us to conclude that the influence of temperature on the electric charge of protein ion, etc., might also play an important role.

---

[1] Present address: Institute of Science and Technology, University of Tokyo, 856, Komaba, Meguro-ku, Tokyo, Japan.

In the present work, we have confirmed the said conclusion by measuring the variation of mobility of crystalline horse serum albumin with temperature.

EXPERIMENTAL

Materials

The crystalline horse serum albumin B used in this experiment[2] was prepared and purified according to the method of Kekwick (3). Prior to electrophoresis, the protein was dissolved in phosphate buffer (pH 7.7, ionic strength 0.2) to a concentration of about 1.5 per cent and was dialyzed against the same buffer at a low temperature for 2 days. The specimen thus obtained was electrophoretically quite homogeneous.

Measurements

Determinations of electrophoretic mobility were made using a Tiselius apparatus (10) equipped with a Svensson optical system (8). Mobilities were calculated from the descending patterns (4).

The thermostat containing the apparatus was adjusted to the desired temperatures. It was found, however, that the temperature inside the cell was raised slightly by the electric current passing through it. This temperature rise was measured by inserting a copper–constantan thermocouple inside the upper part of the cell of the open electrode side. Thermal equilibrium was reached within a few minutes after the current began to flow.

The specific conductivity of the protein solution, necessary for the evaluation of the mobility (10), and the viscosity of the solvent at the temperature inside the cell were obtained by interpolation.

RESULTS

Values of electric field strength F, electrophoretic mobility u, and viscosity coefficient of the solvent η, corresponding to the temperature inside the cell, are recorded in table 1. It is evident from table 1 and figure 1 that the mobility increases considerably with rise of temperature.

DISCUSSION

For an insulating spherical particle, the electrophoretic mobility may be expressed, according to Henry (2), by the following equation (slightly altered from the original form):

$$u = \frac{Z|e|}{4\pi\eta a} \cdot \frac{f(\kappa a)}{1 + \kappa a} \tag{1}$$

Here, u is the mobility, $|e|$ the electronic charge, Z the valency of the charged particle, η the viscosity coefficient of the solvent, a the radius of the particle when considered as a sphere, and κ the Debye–Hückel function, i.e., the inverse of the thickness of the double layer. $f(\kappa a)$ is a function of κa given by Henry (2) (often called the Henry factor). It is 1 when κa is large, and 4/6 when κa is small.

---

[2] The writers are indebted to Mr. S. Nakamura of the Department of Chemistry, Tokyo University, for the sample of crystalline horse serum albumin B.

The factor having the strongest temperature dependency in the right-hand side of equation 1 is η, the coefficient of viscosity of the solvent. We calculated the value of $-u\eta$ to see to what extent the temperature variation of u could be accounted for by the change of viscosity. The results are shown in table 1 and in figure 1. The value of $-u\eta$ becomes fairly constant, but still shows a definite increase with temperature.

TABLE 1

The temperature dependence of the electrophoretic mobility of crystalline horse serum albumin B at pH 7.7

TEMPERATURE OF THERMOSTAT	TEMPERATURE INSIDE THE CELL t	FIELD STRENGTH F	MOBILITY $u \times 10^5$	VISCOSITY $\eta \times 10^3$	$-u\eta \times 10^6$
°C.	°C.	volts/cm.	cm.²/sec. volt	poises	
0.5	2.0	6.4_0	-5.8_4	17.7	103
7.0	8.0	4.2_6	-6.8_2	15.4	105
15.0	16.0	2.6_1	-8.9_4	11.8	105
20.0	20.8	2.2_8	$-10._6$	10.4	110
30.0	30.6	1.1_9	$-14._0$	8.2	115

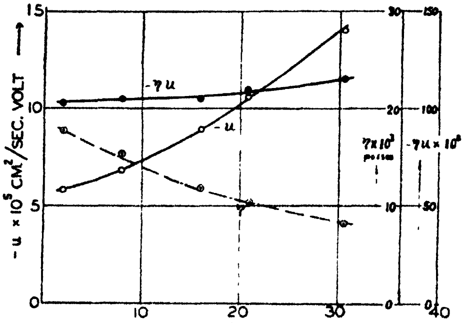

FIG .1

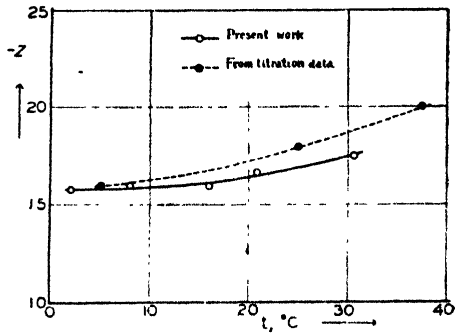

FIG. 2

FIG. 1. The temperature dependence of the electrophoretic mobility of crystalline horse serum albumin B at pH 7.7.

FIG. 2. Valency–temperature curve of crystalline horse serum albumin B at pH 7.7

Equation 1 suggests that this could be caused by the variation of κ or Z with temperature. Here, κ follows the well-known formula (5),

$$\kappa = \sqrt{\frac{8\pi|e|^2 N}{1000k} \cdot \frac{\mu}{DT}} \tag{2}$$

where N is Avogadro's number, k is Boltzmann's constant, D is the dielectric constant of the solvent, T is the absolute temperature, and μ is the ionic strength. If we take the dielectric constant of water for D, and assume that μ does not vary with temperature[3] and is equal to 0.2, κ becomes 1.45×10^7 (2.0°C.), 1.46×10^7 (8.0°C.), 1.46×10^7 (16.0°C.), 1.47×10^7 (20.8°C.), and 1.48×10^7 (30.6°C.). Thus, taking into account the errors in estimation of μ, κ may be considered as constant, i.e., 1.46×10^7.

This leaves Z the remaining factor to be considered. Now, the molecule of horse serum albumin is known to be an elongated ellipsoid of revolution, the major and minor axes amounting to 145 Å. and 34 Å., respectively (6). If we consider this to be a sphere, the radius becomes 28 Å. Therefore,

$$\kappa a = 4.1$$

between 0°C. and 30°C. $f(\kappa a)$ corresponding to this value of κa can be obtained from Henry's graph (2), which gives:

$$f(\kappa a) = 0.75$$

TABLE 2

Valency Z of crystalline horse serum albumin B at pH 7.7

t	Z	
°C.		
2.0	$-15._7$	Calculated from electrophoretic mobility
8.0	$-16._0$	
16.0	$-16._6$	
20.8	$-16._7$	
30.6	$-17._5$	
5	-16	Calculated from titration data measured by Cohn *et al.* (1)
25	-18	
37.5	$-20._5$	

Making use of these values, equation 1 becomes

$$Z = \eta u \times 10^8 \times 0.152 \tag{3}$$

(η in poises, u in cm.²/sec. volt).

Values of the valency Z of horse serum albumin at various temperatures calculated from equation 3 are shown in table 2 and figure 2, from which one sees clearly that the absolute value of Z increases with temperature. If the variation of pH with temperature is considered, this tendency is rather emphasized. To see if this value of Z is reasonable or not, we calculated Z at pH 7.7 using the titration curves at various temperatures,[4] measured by Cohn and coworkers (1), of horse serum albumin prepared by McMeekin's method. It is evident from table 2 and figure 2 that the values thus calculated agree well with those derived from our mobility measurements. For Z of bovine serum albumin, Scatchard and coworkers (7) also gave a value of about −18 at pH 7.7 and 25°C.

---

[3] The value of μ naturally varies with temperature, but the results of our discussion are not altered by taking this into consideration.

[4] In this calculation we used the value 67,100 for the molecular weight of horse serum albumin (6).

At any rate, we are sure that the value of Z obtained in this experiment is entirely plausible.

From the discussion given above, it has been made clear that the variation of electrophoretic mobility with temperature, while depending mostly on the variation of viscosity of the solvent, also depends, in part, on the variation of the valency of the protein ion with temperature. The valency computed from Henry's formula (equation 1) is in good agreement with that calculated from titration experiments. This, with the fact that his formula also explains the variation of mobility with the change of ionic strength very well as pointed out by Tiselius and Svensson (11), can be taken as a proof for the plausibility of the theory of Henry. It might be interesting to discuss the charge of protein ions computed from electrophoretic mobility measurements, but to confirm the correctness of the value of Z thus derived more extended investigations are necessary.

SUMMARY

1. Electrophoretic mobilities of crystalline horse serum albumin B (according to Kekwick) have been measured at different temperatures in phosphate buffer (pH 7.7, ionic strength 0.2), using a Tiselius apparatus.

2. The mobilities obtained were: -5.8_4 (2.0°C.), -6.8_2 (8.0°C.), -8.9_4 (16.0° C.), $-10._6$ (20.8°C.), and $-14._0$ (30.6°C.) $\times$ 10^{-5} cm.^{2}/sec. volt.

3. Using Henry's equation, we have made clear that the variation of the electrophoretic mobility of protein with temperature, while depending mostly on the change of viscosity of the solvent, also depends in part on the variation of the valency of the protein ion itself.

The authors wish to express their cordial thanks to Professor S. Mizushima, Director of this Institute, for his kind advice and to Assistant Professor T. Simanouti and Mr. S. Nakamura of the Department of Chemistry, Tokyo University, for the sample of serum albumin used. Part of the expense for the present investigation was defrayed by the Scientific Research Expenditure of the Ministry of Education, Japan.

REFERENCES

(1) COHN, E. J., STRONG, L. E., AND BLANCHARD, M. H.: In *Proteins, Amino Acids and Peptides*, edited by E. J. Cohn and J. T. Edsall, p. 503. Reinhold Publishing Corporation, New York (1943).
(2) HENRY, D. C.: Proc. Roy. Soc. (London) **133A**, 106 (1931).
(3) KEKWICK, R. A.: Biochem. J. **32**, 552 (1938).
(4) LONGSWORTH, L. G., AND MACINNES, D. A.: J. Am. Chem. Soc. **62**, 705 (1940).
(5) *Cf.* MACINNES, D. A.: *The Principles of Electrochemistry*, p. 145. Reinhold Publishing Corporation, New York (1939).
(6) NEURATH, H.: J. Am. Chem. Soc. **61**, 1841 (1939).
(7) SCATCHARD, G., BATCHELDER, A. C., AND BROWN, A.: J. Am. Chem. Soc. **68**, 2320 (1946).
(8) SVENSSON, H.: Kolloid-Z. **87**, 181 (1939).
(9) TISELIUS, A.: Biochem. J. **31**, 1464 (1937).
(10) TISELIUS, A.: Trans. Faraday Soc. **33**, 524 (1937).
(11) TISELIUS, A., AND SVENSSON, H.: Trans. Faraday Soc. **36**, 16 (1940).
(12) WATANABE, I., AND UI, N.: Kagaku **18**, 422 (1948) (in Japanese).

OXIDE FILM FORMATION ON THE SURFACE OF METALS IN AQUEOUS SOLUTIONS AND THE EVALUATION OF THEIR STANDARD POTENTIALS. II

The Mercury Electrode

S. E. S. EL WAKKAD and T. M. SALEM (MRS. S. E. S. EL WAKKAD)

Department of Chemistry, Faculty of Science, Fouad I University, Cairo, Egypt

Received November 17, 1949
Revision received June 7, 1950

In a previous investigation carried out by one of the present authors (21) on the copper electrode, it was found that metallic copper in aqueous solutions over a certain pH range is covered with an oxide film of cuprous oxide, as indicated by the fact that the copper electrode showed a potential varying linearly with the hydrogen-ion activity of the solution, with $\Delta E/\Delta \mathrm{pH}$ and E_0 values practically coinciding with those for a copper–cuprous oxide electrode. The effect of this oxide film on the thermodynamic potential of the electrode was discussed, and a new technique was introduced for measuring the standard potential of copper out of contact with atmospheric oxygen so that no film exists.

The present investigation deals with metallic mercury, which has long been regarded as a standard and on which many different electrochemical investigations have been carried out. The study of the possible existence of an oxide film on the surface of the metal in aqueous solutions will be of importance not only in arriving at the conditions for the evaluation of its standard potential but also for any other study of metallic mercury which necessitates the absence of any oxide (19).

The probable existence of an oxide film on the surface of the metal in aqueous solution was gleaned by the method adopted in the case of copper (21), i.e., by studying the behavior of the mercury electrode in solutions of varying pH which were initially free from the metal ions. Gatty and Spooner (7) carried out some measurements on the mercury electrode in solutions containing no mercury ions, but these authors worked in a limited pH range and in nonbuffered solutions.

From a study of the behavior of the electrode in the presence of air and in the absence of air after applying a rigorous and special technique for removal of the oxide film from the surface of the metal, we were able to give the proper conditions under which a persistent oxide film is absent from the surface of metallic mercury in aqueous solutions. Only under these conditions can the true thermodynamic standard electrode potential as well as any other electrochemical property of metallic mercury be determined.

I. EXPERIMENTAL

The preparation of the electrodes and solutions for measurements in air

(1) Mercury electrodes

Two types of mercury electrodes were used, which we shall designate A and B. The results with these electrodes were also compared with the mercury–mercuric oxide electrode denoted as electrode C. These electrodes were prepared as follows:

Electrodes of type A: The purest British Drug Houses sample of mercury was sprayed three times into a long column of dilute nitric acid and the resulting mercury was then washed by spraying three times into a long column of conductivity water. The mercury after drying was then distilled three times under reduced pressure and filtered through a series of perforated filter papers. This pure mercury was introduced into an electrode vessel similar to Walpole's vessel (24) for the calomel electrode, in which sufficient mercury was used to cover a sealed-in platinum wire and deep enough to prevent the solution from reaching this contact on accidental shaking. Over the mercury layer was added the solution on which the measurements were to be made.

Electrodes of type B: These were prepared by electrolytic deposition of mercury from slightly acidified mercuric nitrate solution on platinum cathodes 1 cm. square, sealed into glass tubes with mercury contacts. The electrodes before use were washed several times with conductivity water and immediately before immersion with the solution to be used.

Electrodes of type C: These were similar to electrodes A with the addition of pure mercuric oxide, prepared as described later, over the surface of the mercury.

(2) Buffer solutions

In choosing our buffer mixtures care was taken to use solutions of such composition that the anions will not affect the probable presence of mercury oxide, i.e., in each solution the oxide of mercury is the least soluble component at the pH value of the solution.

From pH 3.62 to 5.61 we used the acetic acid–acetate mixtures prepared according to Cohn's system (2), having a constant ionic strength of 0.04. Buffer solutions varying from pH 6.77 to 9.11 were prepared according to Palitzsch (18) from 0.2 *M* boric acid and 0.2 *M* borax. For pH values 10.17, 10.55, and 11.04 the sodium carbonate–hydrochloric acid mixtures were used according to Kolthoff (11). For the extreme acid and alkaline ranges perchloric acid and sodium hydroxide solutions were made. All the solutions were prepared from highly purified materials and their pH values were carefully checked with the hydrogen electrode and when possible with the quinhydrone electrode.

(3) Mercuric oxide

The red and yellow forms of mercuric oxide are similar in every respect save particle size (1, 3, 16, 17, 20, 25). We prepared the red form, which possesses the larger particle size and thus has the normal solubility (22). For this preparation a method similar to that of Garrett and Hirschler (5) was followed. The purest sample of mercury was dissolved in thrice-redistilled nitric acid and the mercuric nitrate solution partially crystallized. The nitrate was then ignited for several days until the resulting oxide was nitrogen-free. The presence of nitrogen impurity due to still undecomposed nitrate was followed during the period of ignition with the micro-Kjeldahl method.

II. PREPARATION OF ELECTRODES AND SOLUTIONS FOR MEASUREMENTS OUT OF CONTACT WITH AIR

In order to perform the measurements without the effect of atmospheric oxygen on both the electrodes and solutions, a special device was constructed, the principal part of which is represented diagrammatically in figure 1. The purest sample of mercury was introduced into bulb 1 through the top tube, which was then sealed. The empty, well-cleaned electrode G was sealed to the other end of the device, which was connected to a high vacuum system at F. Evacuation was then commenced and when the pressure was below 10^{-6} mm. of mercury, as indicated with a McLeod gauge, pure hydrogen was introduced into the system and the mercury heated for 1 hr. at a temperature slightly below its boiling point (about 300°C.). The pressure inside the apparatus was then reduced and the mercury allowed to distil over to the second bulb. After high vacuum was again attained, pure hydrogen was introduced and the mercury in the second bulb was again heated near its boiling point for 1 hr., after which the pressure inside the apparatus was again reduced to allow distillation of mercury to the third bulb. By repeating this process, the distillation of mercury was continued until at last it reached the electrode G, which was then sealed at the capillary constriction under high vacuum. The electrode was then fitted tightly into the electrode vessel shown in the right-hand side of figure 1, which contained the solution on which the measurements were to be made. Pure nitrogen was bubbled through this solution with the help of tap T_1 for about 15 min. to remove dissolved oxygen

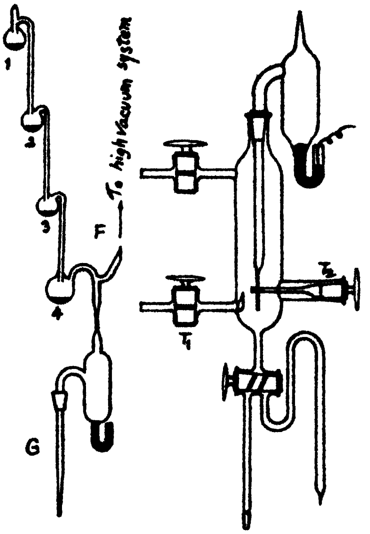

FIG. 1

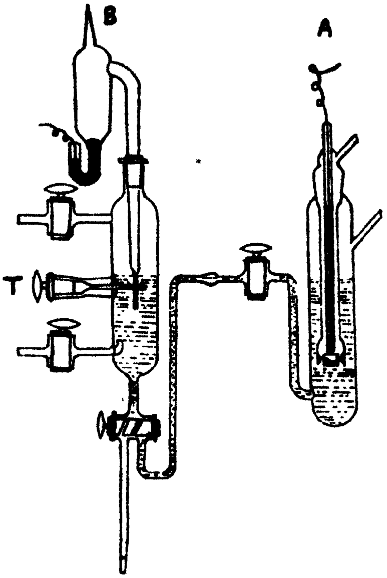

FIG. 2

FIG. 1. Apparatus for measurements out of contact with air
FIG. 2. Special cell

before turning the joint T_2 around, thus breaking the capillary end of the electrode and allowing the solution to rush up and fill the evacuated space above the mercury.

The hydrogen used in this investigation was supplied in cylinders and was purified by first passing it through tubes heated electrically to about 450°C. and containing successively platinized asbestos and copper gauze, then through a series of three bubblers containing about 15 per cent potassium hydroxide and some lead monoxide. The pure hydrogen was then bubbled through another series of three bubblers containing conductivity water, dried by passing through tubes containing phosphorus pentoxide, and lastly allowed to pass through tubes packed with glass wool.

The nitrogen was purified by passing through tubes heated electrically to about 450°C. and containing copper filings, then through a series of bubblers containing successively dilute sulfuric acid, potassium hydroxide, silver nitrate, and concentrated sulfuric acid, and lastly through a long tube packed with glass wool.

III. PREPARATION OF ELECTRODES AND SOLUTIONS FOR THE EVALUATION OF THE STANDARD ELECTRODE POTENTIAL

In order to minimize the liquid-junction potential the cell used was of the following type:

$$H_2,\ HClO_4\ (xM),\ HClO_4\ (xM) + Hg_2(ClO_4)_2\ (x'M),\ Hg$$

in which x' was made small as compared with x. Thus the two solutions became nearly identical and the liquid-junction potential was negligible. For measurements out of contact with atmospheric oxygen a special cell was used. This is shown in figure 2, where A is the hydrogen electrode and B is the mercury half-cell.

For each measurement the previously standardized mercurous perchlorate solution was diluted with an equal volume of perchloric acid, which was exactly twice as concentrated as the acid used in the hydrogen half-cell. For measurements out of contact with atmospheric oxygen, pure nitrogen was allowed to pass through the solution to remove the dissolved oxygen; joint T was then turned around, breaking the capillary tip of the electrode and allowing the solution to fill the evacuated space above the mercury.

The pure nitrogen used, as well as the hydrogen of the hydrogen electrode, was saturated before use with water vapor at the vapor pressure of the solution. After each measurement the solution inside the electrode vessel was checked for its composition by analysis, as will be seen later.

Perchloric acid

The British Drug Houses analar perchloric acid was used, from which solutions of varying concentrations were prepared and accurately standardized against standard sodium carbonate solutions.

The mercurous perchlorate

Exactly equivalent amounts of pure mercuric oxide and perchloric acid were shaken together with an excess of pure mercury in the dark for a week, and the solution obtained was then filtered in the dark from excess mercury. The gram molarity of this stock solution was determined by two different methods: namely, the gravimetric estimation of mercurous mercury as mercurous chloride and the volumetric estimation of mercurous perchlorate by means of standard sodium chloride solution, using bromophenol blue as indicator (23). The two methods were found to agree with each other satisfactorily. From this stock solution several others were prepared by accurate volumetric dilution, and the concentrations of these diluted solutions were always checked by the two methods as stated before.

Electrical measurements

The measurements were always carried out in duplicate with differently prepared stock solutions. In the buffer solutions the measurements were performed using a saturated calomel electrode as the reference half-cell. Following the procedure suggested by Harned and Owen (9), the experimental E_0 pH value of our saturated calomel electrode, as determined in buffers with acids of known dissociation constants and involving all the necessary corrections, was taken as 0.2448 v. at 25°C. The cells were always kept in an air thermostat fixed at 25°C. ± 0.02°C.

The E.M.F. measurements were carried out using a calibrated meter bridge on which accurate readings could be taken to 0.02 cm. A cadmium cell calibrated by the National Physical Laboratory and an Onwood mirror galvanometer having a sensitivity of 190 mm./microampere were used.

IV. RESULTS AND DISCUSSION

1. The behavior of the electrodes in solutions of varying pH and initially containing no mercury ions in air

Consideration of the variation of potential with time as well as with the pH of the solution for the three different types of electrodes revealed the following:

(*1*) In the case of electrodes of types A and B, the potential became fairly steady within about 45 min. of immersion in unstirred solutions with pH's in the range of 0.9 to 5.6. After 24 hr. it was noticed that there had been a slight drift towards the more negative side. The results in this pH region were fairly reproducible, although they were not so reproducible as in the more alkaline region. In the more alkaline solutions, the steady-state potentials were reached within a shorter period of time and remained quite constant for the next 24 hr. The steady-state potentials for both types of electrodes were approximately the same over the whole pH range.

(*2*) For electrodes of type C, the steady-state values were reached for pH's from 0.9 to 5.6 within about 30 min. and remained practically constant for the next 24 hr. In more alkaline solutions the steady-state values were attained in the first 15 min. after immersion and remained perfectly constant for the next 24 hr., which was the time limit of our experiments. The steady-state values for electrodes of type C were always higher than the corresponding values for A or B, although at the extreme alkaline side the values became approximately the same.

(3) By plotting the steady-state potential values against pH for the electrodes of types A and C, the two curves shown in figure 3 were obtained. These curves reveal the interesting fact that the potentials of the mercury electrode, as well as that of the mercury–mercuric oxide electrode, are linear functions of the pH of the solution from the extreme acid to the extreme alkaline solutions, but with a small break from about pH = 5 to the neutral point. The linearity of the mercury–mercuric oxide electrode is, of course, in accordance with the well-known principle of a true metal–metal oxide electrode. The question arises as to the reason for the linearity in the case of metallic mercury electrodes. If it is due to oxide film formation, then why does it not coincide with that of the mercury–mercuric oxide electrode?

Gatty and Spooner (8) observed similar phenomena when comparing the potential of the mercury electrode in alkali hydroxide with those of the mercury–mercuric oxide electrode. The lower potential observed in the former case was given different explanations: thus, they stated that it may be due to a slow saturation of the interface with mercuric oxide, a conclusion which is, however, in marked contrast to the fact that the direct addition of mercuric oxide to the solution immediately raises the potential to the metal–metal oxide value. Also, the present authors found that when the buffer solutions studied were previously saturated with mercuric oxide, ultrafiltered from excess of solid mercuric oxide, and then the behavior of the mercury electrode studied, the results represented diagrammatically in figure 4 were obtained. In this diagram the potential of the mercury electrode in each solution is shown against the logarithm of the time in hours after which the measurements were taken. It may be seen that at first the potentials approximated to the mercury–mercuric oxide potentials but after a certain time (which varies from one solution to another) the potentials decreased towards the values obtained with metallic mercury. Gatty and Spooner also claimed the possibility of mercuriate formation, which prevented the interface from becoming saturated with mercuric oxide, but the mercuriate is expected to be more readily formed at pH values far removed from the isoelectric point of mercuric oxide. The isoelectric point of this oxide is expected to be at about the neutral point (5, 6) and consequently the mercuriate will be formed more readily in the more alkaline solutions. Figure 3 reveals, however, that the deviation from the mercury–mercuric oxide potential is more pronounced in the less alkaline solutions. Finally, Gatty and Spooner put forward a suggestion that initially a less soluble oxide is precipitated and that this oxide is slowly converted to mercuric oxide. There is no definite proof as far as the present authors are aware for the real existence of such a form of mercuric oxide.

When a metal is exposed to air, oxygen becomes adsorbed over the surface and the metal becomes covered with an oxide film. In aqueous solutions, oxide formation in air is usually attributed to the transfer of electrons to dissolved oxygen, transforming it into OH ions which are attracted to the metal lattice forming an oxide film. In the case of mercury we would expect the rate of this process to be very slow, since metallic mercury, when in thermodynamic equilibrium with its own ions in solution, possesses in general a comparatively high electropositive potential value. Now concerning the probable formation of mercurous oxide, although its existence is still a subject of controversy (1, 4), yet by taking its heat of formation as −21,600 cal. (12), and an estimated value of about 32 cal. per degree for its entropy (12), the entropy of formation of mercurous

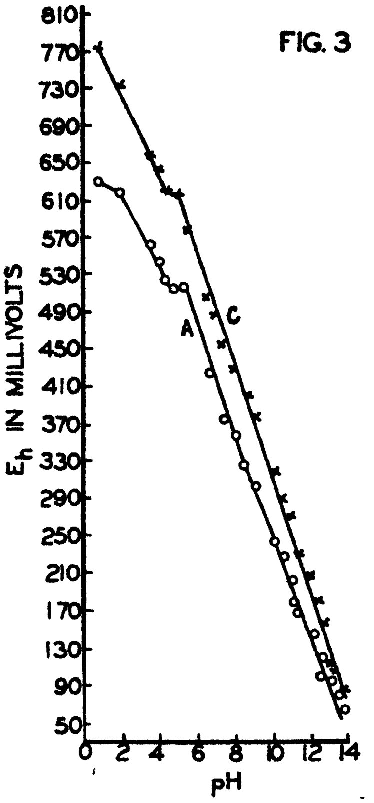

FIG. 3. Plot of steady-state potential values against pH for electrodes of types A and C.

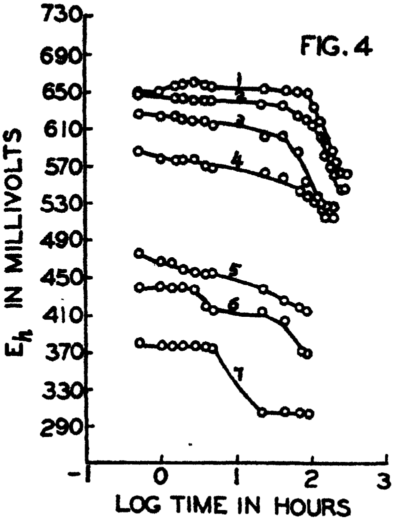

FIG. 4. Plot of the potential of the mercury electrode in each solution against the logarithm of the time after which the measurements were taken. Curve 1, pH = 3.6; curve 2, pH = 4.0; curve 3, pH = 4.6; curve 4, pH = 5.6; curve 5, pH = 7.1; curve 6, pH = 8.1; curve 7, pH = 9.1.

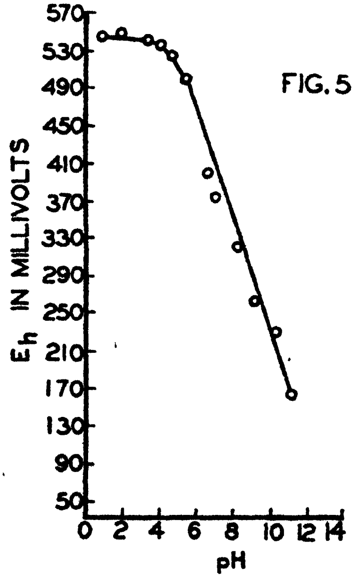

FIG. 5. Plot of equilibrium potentials against pH.

oxide will be −29.5 cal. per degree and its free energy of formation −12,800 cal. The potential of the couple:

$$2OH^- + 2Hg \rightleftharpoons Hg_2O + H_2O + 2e^-$$

will be, therefore, equal to 0.123 v. as compared with 0.098 v. for the mercury–mercuric oxide electrode (12). This indicates that the mercury–mercurous oxide electrode would possess potentials more positive than the corresponding potentials of the mercury–mercuric oxide electrode. This fact, which is only based on calculations after certain estimations, is quite unusual, and the higher potential of mercury–mercurous oxide relative to mercury–mercuric oxide also indicates that the former will be unstable. From this, it can be concluded that the behavior of the mercury electrode cannot be attributed to mercurous oxide, and thus we are left with the possibility of the formation of mercuric oxide. Owing to the liquid nature of metallic mercury, its molecules are capable of movement throughout the bulk of the liquid and we should not expect an inhibitive oxide film to form over the surface, but rather that most of the surface should be the bare metal, especially in the less alkaline pH range where the solubility of the oxide is greater. Since this is the case, one must take into consideration the reaction $Hg^{++} + Hg \rightleftharpoons Hg_2^{++}$ and its equilibrium constant $[Hg_2^{++}]/[Hg^{++}] = 81$ (12). The following processes are expected, therefore, to be consecutively occurring at the surface of the electrode: (*a*) formation of mercuric oxide at the electrode surface; (*b*) dissolution of mercuric oxide in the layer of solution at the interface to give Hg^{++} and OH^- ions; (*c*) reaction of Hg^{++} ions with mercury to give Hg_2^{++} ions; (*d*) diffusion of Hg^{++} and Hg_2^{++} ions into the bulk of the solution.

It may be suggested that since process (*a*) is slow, the concentration of Hg^{++} ions at the interface produced by process (*b*) will tend to, but may not, attain the value corresponding to a saturated solution of mercuric oxide and, in strongly acid solutions, where the solubility of mercuric oxide is high, this difference is likely to be very marked, leading to a potential much lower than the mercury–mercuric oxide value. At higher pH values, as the solubility of mercuric oxide decreases, the difference will be less, but will still be appreciable owing to the participation of reaction (*c*). Thus, if we suppose the rate of formation of mercuric oxide was just sufficient to maintain a saturated film of mercuric hydroxide at the electrode surface and then allowing for reduction, the potential under these conditions would be also a linear function of the pH value but about 0.05 v. lower than the mercury–mercuric oxide value. Only where the rate of formation of mercuric oxide exceeds the rate of removal of mercuric ions by diffusion outwards and reduction would the potential be expected to reach the mercury–mercuric oxide value and this, as expected, is most nearly reached in alkaline solutions where the solubility of mercuric oxide is least.

Another view is that the mercuric oxide formed tends to saturate the double layer between the electrode and solution and at the same time, owing to reaction (*c*), reduction of Hg^{++} to Hg_2^{++} will take place according to the previous equation and governed by the corresponding equilibrium constant; then, in order to establish the disturbed equilibrium, more mercuric oxide will dissolve and this will take place until finally we have the dynamic equilibrium:

$$\begin{array}{rcl} \mathrm{HgO} + \mathrm{H_2O} \rightleftharpoons & \mathrm{Hg^{++}} & + \ 2\mathrm{OH^-} \\ & + & \\ & \mathrm{Hg} & \\ & \downarrow\uparrow & \\ & \mathrm{Hg_2^{++}} & \end{array}$$

This increase in the solubility of the oxide, especially in the more acid solution, will lead to an increase in the pH value, at least within the double layer, and consequently the potential will be lower than expected from the original bulk pH of the solution. In a comparatively strong acid solution, for example of $pH = 1$, the $[Hg^{++}]$ as calculated from the solubility product of mercuric oxide ($[Hg^{++}] \cdot [OH^-]^2 = 2.7 \times 10^{-26}$ (12)) will be equal to 2.7 gram-ions/liter; the corresponding $[Hg_2^{++}]$ which must be present in equilibrium in the presence of metallic mercury will be equal to 218.7 gram-ions/liter, which is an enormous quantity and must affect the pH value of the solution to such an extent that this solubility cannot be reached.

Against the first view is the reproducibility of the results, and it can be shown also that the mercury ions present at any lower pH value, as determined from the measured potentials in these solutions, are enough to exceed saturation at higher pH values as expected from the solubility product of mercuric oxide. This is the case so long as there is no reason to consider that the rate of formation of mercuric oxide at higher pH values is less than at lower pH values.

The only difficulty with the second view is that in order to account for the discrepancy in potential, we must expect a local increase of pH amounting in some cases to some 1–2 pH units and, as we are working in a well-defined buffer solution, such change of pH may be looked upon to be unlikely as well as its long persistence at the electrode surface.

At this stage, therefore, although the experimental data suggest the existence of an oxide over the surface of metallic mercury electrodes in air, yet it is probably impossible to reach any certain conclusion as to the reason for the discrepancy between the potential of the mercury electrode in air and the mercury–mercuric oxide.[1]

From the general trend of the potential–pH curves of both the mercury electrode and the mercury–mercuric oxide electrode it can be noticed that a break always occurs between pH 5 and about the neutral point. This break, which is similar to that obtained with the copper electrodes (21), can be explained upon the basis of the amphoteric character of mercuric oxide, which dissociates as a base below and as an acid above the isoelectric point. The isoelectric point of mercuric oxide is expected to be slightly on the alkaline side of the neutral point (5, 6); its exact position was determined by the present authors and found to be at about pH 7.5. The method of determination as well as a detailed discussion of this point will be published later. The fact that the break in the potential–pH curves appeared to be slightly on the acid side is of course in accordance with our previous discussion, that the pH value of the solution at the interface is higher than the original pH value of the solution.

---

[1] Since the authors are at present in the University of Liverpool, working with Dr. A. Hickling, they intend to study the anodic behavior of metallic mercury in solutions of varying pH and to follow the new method introduced by Hickling, using the cathode-ray oscillograph (10). Such a study is expected to throw some light on this point.

2. The behavior of the electrodes in solutions of varying pH and initially containing no mercury ions out of contact with air

Mercury electrodes prepared after subjecting the metal near its boiling point for four times to the action of hydrogen, then distillation, and lastly to high vacuum when examined in oxygen-free solutions revealed the following: (*1*) In the unstirred solutions the potentials became nearly steady in almost all solutions within 1 to 1.5 hr. of immersion and remained practically constant for the next 24 hr. (*2*) By plotting the attained equilibrium potentials against pH the curve shown in figure 5 was obtained, which reveals more or less constancy in the potential of the mercury electrode up to about pH 5. Throughout this range the potential of the mercury electrode in complete absence of oxygen was about 0.54 v. The reproducibility of the results within this pH range was only of the order of 1.5 centivolts.

Above pH 5 the protected electrode also began to show potentials which were a linear function of the pH. In a similar manner as in Section I, it can be shown that the linearity in the potential of the mercury electrode with pH was due to the formation of mercuric oxide and to the mercuric–mercurous equilibrium in the presence of metallic mercury. The state of affairs occurring on the surface of a metallic mercury electrode under these conditions can be explained as follows: When a pure metal is dipped into an aqueous solution containing no ions of this metal and also in the absence of dissolved oxygen, which may act as electron acceptor, the potential of this metal in the comparatively acid solutions is expected to be extremely negative, leading to dissolution of the metal and the discharge of hydrogen ions. The potential observed in this case is expected to be governed by the potential of the hydrogen electrode at the corresponding pressure and the pH prevailing within the double layer, and also with the hydrogen overpotential on the particular metal. In more alkaline solutions, owing to the increased $[OH^-]$, a state is expected to be reached where the $[OH^-]$ together with the metal ions present will be enough to saturate the interphase with the metal hydroxide; hence the metal will again start functioning as a metal–metal oxide electrode.

3. The evaluation of the standard potential of mercury

From the previous study it is clear that in air an oxide film persists on the surface of metallic mercury in aqueous solutions from extreme acid to extreme alkaline solutions, while out of contact with atmospheric oxygen and after subjecting the mercury four times to the reducing action of hydrogen and distillation, such an oxide only appears at pH values above 5. Measurements of the mercury electrode potential in mercurous salt solutions under these latter conditions will be expected to give the exact standard potential of the metal. For this determination and in order to overcome the liquid-junction potential the cell of the type:

$$H_2,\ HClO_4\ (xM),\ HClO_4\ (xM) + Hg_2(ClO_4)_2\ (x'M),\ Hg$$

was constructed, as stated before, in such a way as to allow the measurements to be taken out of contact with air (figure 2). For comparison, the same cell was also studied without the rigorous protection from atmospheric oxygen. In table 1 are given the results of the equilibrium values of one set of measurements for both the protected and the unprotected electrodes. For the protected electrodes the equilibrium was found to be attained within the first 30 min. and to remain constant for several hours. In the unprotected electrode the equilibrium was attained after 1 hr. and remained constant for a few hours, after which a drift was noticed.

TABLE 1

Equilibrium values of one set of measurements for both protected and unprotected electrodes

CONCENTRATION OF $HClO_4$	CONCENTRATION OF $Hg_2(ClO_4)_2$	E.M.F. IN AIR	E.M.F. OUT OF CONTACT WITH AIR	E_0 IN AIR	E_0 OUT OF CONTACT WITH AIR
M	*M*	*volts*	*volts*	*volts*	*volts*
0.1012	0.00568	0.7820	0.7803	0.7989	0.7972
	0.00284	0.7731	0.7715	0.7989	0.7973
	0.00142	0.7647	0.7627	0.7991	0.7971
0.0500	0.00142	0.7839	0.7822	0.7987	0.7970
	0.000766	0.7760	0.7743	0.7987	0.7970
	0.000369	0.7671		0.7991	
0.0100	0.000738	0.8198	0.8182	0.7985	0.7969
	0.000341	0.8097	0.8085	0.7984	0.7972
	0.000170	0.8010	0.7997	0.7986	0.7973
Mean				0.7988	0.7971

The reaction taking place in the cell can be represented as follows:

$$H_2 + Hg_2^{++} = 2Hg + 2H^+$$

Therefore

$$E = E_0 - \frac{RT}{2F} \ln \frac{a_{Hg}^2 \cdot a_{H^+}^2}{a_{H_2} \cdot a_{Hg_2^{++}}} \tag{1}$$

Since mercury and hydrogen are at their standard states, equation 1 at 25°C. reduces to:

$$E = E_0 - \frac{0.05915}{2} \log \frac{a_{H^+}^2}{a_{Hg_2^{++}}}$$

It is, therefore, only necessary for calculating the standard electrode potential to determine the activity of hydrogen ion in the hydrogen half-cell and that of mercurous ion in the mercury–mercurous perchlorate half-cell. Following the procedure of Lewis and Randall (13) for calculation of the activity coefficient at various ionic strengths, the E_0 values in the case of the unprotected and the protected electrodes were calculated and given in the last two columns of table 1. The measurements obtained in air, as can be seen from the table, gave a mean E_0 value of 0.7988 v., which agrees with that obtained by Linhart (15) after being corrected by Lewis and Randall (14). Out of contact of air the mean E_0 value is 0.7971 v., which is the true standard potential of mercury. As in the case of the copper electrode (20), the maximum error in our measurements is 0.0004 v.

V. SUMMARY

1. The behavior of the mercury electrode in solutions of varying pH and initially free from mercury ions was examined from the extreme acid to the extreme alkaline range and the probable existence of an oxide film on the surface of the metal was discussed.

2. A new apparatus and technique were described for measuring the potential of mercury out of contact with air. By comparing the results obtained in and out of contact with air in the solutions of different pH values and initially free from mercury ions a set of conditions was chosen leading to the evaluation of the true standard electrode potential.

3. The standard electrode potential of mercury was determined using this new technique and found to be 0.7971 v. at 25°C., as compared with the value of 0.7988 v. at 25°C. in air.

The authors wish to express their thanks to Dr. A. Hickling for kindly reading through this paper.

REFERENCES

(1) Allmand: Z. Elektrochem. **16**, 254 (1910).
(2) Cohn: J. Am. Chem. Soc. **49**, 173 (1927)
Cohn, Beyroth, and Menkin: J. Am. Chem. Soc. **50**, 696 (1928).
(3) Frick: Z. anorg. allgem. Chem. **166**, 244 (1927).
(4) Frick and Ackermann: Z. anorg. allgem. Chem. **211**, 233 (1933).
(5) Garrett and Hirschler: J. Am. Chem. Soc. **60**, 299 (1938).
(6) Garrett and Howel: J. Am. Chem. Soc. **61**, 1730 (1939).
(7) Gatty and Spooner: *The Electrode Potential Behaviour of Corroding Metals in Aqueous Solutions*, p. 108. University Press, Oxford (1938).
(8) Reference 7, p. 122.
(9) Harned and Owen: *The Physical Chemistry of Electrolytic Solutions*, pp. 316 et seq. Reinhold Publishing Corporation, New York (1943).
(10) Hickling: Trans. Faraday Soc. **41**, 333 (1945); **42**, 518 (1946).
Hickling and Spice: Trans. Faraday Soc. **43**, 762 (1947).
Hickling and Taylor: Discussions Faraday Soc. No. **1**, 277 (1947); Trans. Faraday Soc. **44**, 261 (1948).
(11) Kolthoff: Cited by H. T. S. Britton in *Hydrogen Ions*, 2nd edition, p. 219. Chapman & Hall, Ltd., London (1932).

(12) LATIMER: *The Oxidation States of the Elements and their Potentials in Aqueous Solutions*, p. 161. Prentice-Hall, Inc., New York (1938).

(13) LEWIS AND RANDALL: *Thermodynamics and the Free Energy of Chemical Substances*, p. 382. McGraw-Hill Book Company, Inc., New York (1923).

(14) Reference 13, p. 418.

(15) LINHART: J. Am. Chem. Soc. **38,** 2356 (1916).

(16) MATHUR AND NEVGY: Z. Physik **100,** 615 (1936).

(17) OSTWALD AND SCHICH: Z. physik. Chem. **17,** 183 (1895); **18,** 159 (1895); **34,** 495 (1900).

(18) PALITZSCH: Cited by H. T. S. Britton in *Hydrogen Ions*, 2nd edition, p. 219. Chapman & Hall, Ltd., London (1932).

(19) RANDALL AND YOUNG: J. Am. Chem. Soc. **50,** 989 (1928).

(20) SCHICH: Z. physik. Chem. **42,** 155 (1903).

(21) TOURKY AND EL WAKKAD: J. Chem. Soc. **1948,** 740.

(22) TOURKY AND EL WAKKAD: J. Phys. & Colloid Chem. **53,** 1126 (1949).

(23) VOGEL: *Textbook of Quantitative Inorganic Analysis*, p. 316. Longmans, Green and Company, New York (1946).

(24) WALPOLE: Cited by W. M. Clark in *The Determination of Hydrogen Ions*, p. 305. The Williams & Wilkins Company, Baltimore (1928).

(25) ZACHARIASEN: Z. physik. Chem. **128,** 421 (1927).

COMMUNICATIONS TO THE EDITOR

THE ROLE OF THE UNPAIRED ELECTRON IN CARCINOGENESIS

Homolytic organic reactions resulting from single-electron transfer processes have been intensively studied only during the last ten years. A consequence of such reactions is the formation of a chemical molecule with an unshared valence electron. A molecule of this kind is endowed with many peculiar properties. The magnetic moment of the odd electron is not compensated by the magnetic moment of an electron with antiparallel spin. Therefore, the molecule is paramagnetic and it possesses the ability to initiate a multitude of very strange chemical reactions. These reactions usually occur with a low energy of activation, so that, like the reactions of enzymes, they may occur with great facility at the temperature of the human body. One of these reactions is especially interesting. A molecule with an unpaired electron (a so-called free radical) is able to initiate a chemical chain reaction. A single odd-electron molecule may initiate a reaction chain involving thousands of molecules of substrate. Chain reactions of this sort may be accompanied by an enormous evolution of energy. For example, chemical explosions and the combustion of inflammable materials are chain reactions, initiated by molecules with an unshared electron.

It has been experimentally established that azo compounds, complex hydrocarbons, organic amines and their derivatives, actinic radiation, x-rays, and the radiation from radioactive materials are able to form free radicals (W. A. Waters: *The Chemistry of Free Radicals*, University Press, Oxford (1946)). It has also been experimentally established that azo dyes, complex hydrocarbons, organic amines and their derivatives, actinic radiation, x-rays, and the radiation from radioactive materials are capable of initiating neoplastic tissue transformations.

From the foregoing, it is apparent that the known experimental methods for producing cancer bear a remarkable resemblance to a well-known type of electron-unpairing reaction. Perhaps this is just an amazing coincidence, so let us examine a little more closely the relationship between free-radical activity and carcinogenesis. A free-radical chain reaction possesses one unique characteristic which distinguishes it from all other chemical reactions. It can be terminated only by another free radical. The free radical has an unpaired electron and the chain reaction is propagated by this unpaired electron. Since all ordinary organic molecules have an even number of valence electrons, this free radical cannot be destroyed by any ordinary chemical reaction. This is axiomatic, since a free radical is defined as a molecule with an odd number of electrons. Therefore, it is evident that a free radical can be destroyed only by another free radical as the result of an electron-pairing reaction.

This is highly significant. It means that the agents which are able to start a free-radical reaction are identical with the agents which are capable of stopping it. This is not true for any other type of chemical reaction. But it is true for carcinogenesis, since the substances which initiate cancer are identical with the substances which alleviate it (E. Boyland: Yale J. Biol. and Med. **20,** 321 (1948)). The obvious conclusion seems to be that cancer is the result of a free-radical reaction.

Free-radical chain reactions possess another interesting feature. They may be either aerobic or anaerobic. Although it is possible that natural neoplasms are initiated by free radicals resulting from the peroxidation (H. F. Park: J. Am. Chem. Soc. **69,** 2248 (1947)) of fats or steroids in tissue subjected to chronic irritation, it is a fact that free-radical chain reactions are, under certain circumstances, almost completely inhibited by an excessive concentration of oxygen (F. A. Bovey and I. M. Kolthoff: Chem. Revs. **42,** 491 (1948)).

When a free radical enters a living cell, a chain reaction may occur. This may supplement or retard the usual enzymatic processes and perhaps enhance the anabolic cell activity. It is also conceivable that the abnormal nature of the resulting metabolic products would be responsible for a loss of cell functionality and a lack of cell differentiation.

It should be possible to evaluate readily the free-radical hypothesis of carcinogenesis by any of the well-known methods for the detection of minute quantities of free radicals. For instance, the treatment of cancer cells with stable odd-electron molecules (such as nitric oxide) should yield interesting results.

HAROLD F. PARK.

Research Laboratory
Monsanto Chemical Company
Springfield, Massachusetts
August 23, 1950

ELECTROMAGNETIC FIELDS AS CATALYSTS

A strong electric field applied across a substance may produce considerable induced dipole moments. The dipole molecules would then be expected, like little magnets, to align themselves in chains. Separation of the molecules may then require more energy than in the normal state, owing to the necessary breaking apart of the dipole chains. It may therefore be expected that such physical properties as surface tension, viscosity, boiling point, vapor pressure, etc. could assume slightly different values than normally.

The decreased stability of molecules due to induced dipole electron shifts raises the possibility of utilizing strong electromagnetic fields as catalysts for chemical reactions.

Have these possibilities ever been investigated? If not, accumulation of data on the influence, if any, of strong electric fields (steady and alternating) on physical properties may prove a starting point for their catalytic utilization.

Kurt Eisemann.

Massachusetts Institute of Technology
Cambridge, Massachusetts
September 10, 1950

BOOKS RECEIVED

(To September 13, 1950)

Bailey, Alton E. (Editor). *Melting and Solidification of Fats.* (Fats and Oils—A Series of Monographs edited by A. E. Bailey, T. P. Hilditch, H. E. Longenecker, and K. S. Markley.) Interscience Publishers, Inc., 215 Fourth Ave., New York 3. 1950. 357 pp. Price: $7.00.

Brown, George Granger, and associates. *Unit Operations.* John Wiley and Sons, Inc., 440 Fourth Ave., New York 16. 1950. 611 pp. Price: $7.50.

Danielli, J. F. *Cell Physiology and Pharmacology.* Elsevier Publishing Company, Inc., 215 Fourth Ave., New York 3. 1950. 156 pp. Price: $3.00.

Faith, W. L., Keyes, Donald B., and Clark, Ronald L.: *Industrial Chemicals.* Important technical data of manufacture and basic economic facts about 106 major commercial chemicals. John Wiley and Sons, Inc., 440 Fourth Ave., New York 16. 1950. 652 pp. Price: $8.00.

Hartsuch, Bruce E. *Introduction to Textile Chemistry.* John Wiley and Sons, Inc., 440 Fourth Ave., New York 16. 1950. 413 pp. Price: $4.75.

Keeton, Morris T. *The Philosophy of Edmund Montgomery.* University Press in Dallas, Southern Methodist University, Dallas, Texas. 1950. 386 pp. Price: $5.00.

McBain, James W. *Colloid Science.* D. C. Heath and Company, Boston, Massachusetts. 1950. 450 pp. Price: $6.00.

Mark, H., and Tobolsky, A. V. *High Polymers. Vol. II. Physical Chemistry of High Polymeric Systems.* 2nd edition. Interscience Publishers, Inc., 215 Fourth Ave., New York 3. 1950. 506 pp. Price: $6.50.

PATTERSON, AUSTIN M. *A German-English Dictionary for Chemists*. 3rd edition. John Wiley and Sons, Inc., 440 Fourth Ave., New York 16. 1950. 541 pp. Price: $5.00.

TIMMERMANS, J. *Physico-Chemical Constants of Pure Organic Compounds*. Elsevier Publishing Company, Inc., 215 Fourth Ave., New York 3. 1950. 693 pp. Price: $12.50.

TROENSEGAARD, N.: *A New Orientation within Protein Chemistry*. Hafner Publishing Company, New York. 1949. 139 pp.

WHITEHEAD, THOMAS H. *Theory of Elementary Chemical Analysis*. Ginn and Company, Statler Building, Boston 17, Massachusetts. 1950. 233 pp. Price: $2.75.

SUBJECT INDEX

Acid, aliphatic, in hydrocarbon oil, radioactive tracer study of, 569
Acids, polymeric, electrolytic transference properties of, 979
Activity, relation to mole fraction for binary solutions of nonelectrolytes, 459
Activity coefficient. *See* Coefficient, activity
Adsorbents, capillarity of, adsorption-desorption hysteresis in relation to, 784
Adsorption, entropy changes in, 795
  heat of, 354, 795
  heat of, calculation from adsorption isosteres, 411
Adsorption-desorption hysteresis in relation to capillarity of adsorbents, 784
  isotherms at the free surface of aqueous solutions, 685
  on base-exchange resins, 697
  in beds, mathematics of, 812, 821
  on carbon black surfaces, 227
  of gases in capillaries and on small particles, 1186
  of gases and vapors, expansion of charcoal upon, 1088
  at liquid-air interfaces, 537
  of methanol on carbon, 354
  of nitrogen, measurement of surface areas of powders by, 114
  from solutions, thermodynamics of, 537
  by sugar carbon, effect of heat treatment on, 605
  of sulfanilamide on silk fibroin, 661
Agents, antifoaming, 429
3-Alizarinsulfonic acid, dissociation constant (apparent) of, determination by indirect colorimetry, 829
Albumin, serum, electrophoretic mobility of, temperature dependence of, 1366
  serum, reaction with methyl orange, 33
  serum, reaction with thymus nucleic acid, 79
Alumina-water system, 142
Aluminum nitrate-hexyl alcohol-water system, 1255
  phosphate, 128
Amino acids, complexes of copper with, spectra of, 18
Antibiotics, colloidal phenomena of, 1077
Bentonites, acid activation of, 1170
  organophilic, 1196

Cadmium chloride-silver chloride system, freezing-point diagram of, 426
Camera, x-ray, for study of chemical reactions in the solid state at high temperatures, 1121
Carbon, adsorption of methanol on, 354
  sugar, adsorption properties of, 605
Carbon (ilmenite black), suspending action of alkaline electrolytes on, 489
Carbonates, alkaline earth, relation between cataphoresis, conductivity, and particle size of, 472
Carbon black, sorption of rubber by, 251
  black, surface of, 227
  black, thixotropic behavior in rubber, 239
  monoxide, absorption in cuprous salt solutions, 370
  monoxide, solids formed from by action of alpha particles, 391
  powder, surface area as measured by adsorption of nitrogen, 114
Catalysts, metal oxide, electron-microscopic study of, 505
Cataphoresis, 472
Cathode, palladium, permeability to hydrogen, effect of surface-active compounds upon, 681
Cathodoluminescence of zinc oxide, effect of electrolytes on, 467
Cellulose, heat of wetting in water, 1148
  moisture relationships of, 1148
Cellulose fibers, penetration of, 745
Chalcogen derivatives, systems of, 564
Charcoal, expansion on adsorption of gases and vapors, 1088
Chloride ion, entropy of, 731
Chlorophyll a, photobleaching (reversible) of, 703
Clays, barium, ionization of, 671
  bentonite, acid activation of, 1170
  calcium, ionization of, 671
  magnesium, ionization of, 671
Coagulation isotherm of thorium, 1250
Coefficient, activity, of orthophosphoric acid, 310
  activity, of surface-active materials, 107
  activity, of the undissociated part of weak acids, 310

Colorimetry, indirect, 829
Combustion wave, thermal structure of, 877
Communications to the Editor, 743, 964, 966, 1070, 1383
Complexes formed from ethylenediaminetetraacetic acid, 1208
Condensation, nucleation of, 1186
Conductivity of carbonates (alkaline earth), 472
Contact angle, in relation to surface roughness, 653
Copper, complexes with proteins, spectra of, 18
  electrolytic dissolution in ammoniacal electrolytes, 841
Critical behavior and liquid–vapor equilibrium in mixtures of fluids, 1347
  curve for aqueous solutions of 1-1 electrolytes, application of kinetic theory to, 1337
  micelle concentration of dodecylammonium chloride, 271
  mixing point, opalescence of a two-component liquid system near, 1306
  phenomena, general consideration of, 1293
  Phenomena, Symposium on, 1293–1357
  points, theory of, 1317
  temperature region, solubility measurements in, 1323
Cuprene fiber, growth and properties of, 969

Detergent solutions, critical concentrations of, effect of added hydrocarbons upon, 1012
Diffusion of ions across a phase boundary and through cell walls, mechanism of, 185
  of macromolecules in solution, dependence upon concentration, 1028
  in solution, 649
2,6-Dinitroquinol, dissociation constant (apparent) of, determination by indirect colorimetry, 829
Dissociation constants (apparent), determination by indirect colorimetry, 829
Dodecylammonium chloride, critical micelle concentration of, effect of alcohols upon, 271

Editor, communications to, 743, 964, 966, 1070, 1383
Electrode kinetics, role of indifferent electrolytes in, 804
Electrolytes, colloidal, effect of electrolytes upon the x-ray long spacing of, 421
Electron microscope. *See* Microscope, electron
Electrophoresis, in study of protein reactions, 33, 47, 56, 79
Emulsion polymerization of styrene, 265
Entropy of the chloride ion, 731
Equilibrium, liquid–vapor, in mixtures of fluids, 1347
Ethane (solid), solubility in liquid nitrogen and oxygen, 665
Ethene (solid), solubility in liquid nitrogen and oxygen, 665
Ethylenediaminetetraacetic acid, metal complexes of, 1208
Exchange reactions, isotopic, kinetics of, 777

Fibers, cellulose, penetration of, 745
Fibrin, formation from fibrinogen, 66
Fibrinogen, conversion to fibrin, 66
Film pressures, measurement of, apparatus for, 1222
Films, adsorbed, from binary liquid solution, 1278
  water, electric potential of, 416
  water-repellent, formed on solids by adsorption from aqueous solutions of heteropolar compounds, 445
Fluid, two-component van der Waals, 1132
Foaming, inhibition of, 429

Gallium(III) salt solutions, physicochemical studies on, 999
Gelation of sodium silicate, 806
Gels, liquid, organic, 1196
Graphon, sorption of rubber from benzene solution by, 251

Half-cell, absolute potential of, method of measuring, 1016
  relative phase potential in, 322
Heat of adsorption, 354, 795
  of adsorption, calculation from adsorption isosteres, 411
  of adsorption of methanol on carbon, 354
  of evaporation, temperature function of, 599
  of wetting of standard cellulose in water, 1148
  of wetting of viscose rayon in water, 1148
Heredity and environment. IV, 1269
Hydrocarbons, polar, structure of monolayers and multilayers on solid substances, 1053
  solubilization of, 283

Hydrogen, permeability of palladium cathode to, effect of surface-active compounds upon, 681

Ilmenite black. *See* Carbon (ilmenite black)
Indium, isomers of, separation in an electric field, 717
Iodide, oxidation to iodine by dilute solutions of organic peroxides, 1191
Ion exchange in clay salts of silver, 1110
  exchange in synthetic resins, 1098
Ions, diffusion across a phase boundary and through cell walls, 185
Iron phosphates, 128

Kaolin, suspensions of, action of phosphates on, 89
Kinetics, electrode, role of indifferent electrolytes in, 804
  of isotopic exchange reactions, 777
  of propellants, symposium on, 847–954
  reaction, in metallographic problems, 581

Lanthanum blue, 315
Laws, kinetic, in catalyzed systems, 519, 530
Light, depolarization by shellac solutions, 1358
Lyogels, structure of, 256

Macromolecules, rate of diffusion in solution, dependence upon concentration, 1028
Magnesium, dissolution in hydrochloric acid–methyl alcohol–water solutions, 437
Mass spectra. *See* Spectra, mass
Membranes, Amberlite, 204
  anion-permeable, 157
  cation-exchange, artificial, 204
  cation-permeable, 157
  mosaic, 157
  permselective, 325, 330
  permselective, use in determination of sodium-ion and chloride-ion activities in protein solutions, 176
  protamine collodion, 325, 330
Mercury, standard electrode potential of, 1371
Metals, evaluation of their standard potentials, 1371
Micelles, properties of, determination of, 966
Microscope, electron, in study of metal oxides and metal oxide catalysts, 505
Mobility, electrophoretic, of horse serum albumin, temperature dependence of, 1366
Molecular weights of polystyrene fractions, 1227
Molecule, organic, orientation at a steel surface, 497
Monomethylolurea, dissociation in hydrochloric acid solutions, 741

Nickel carbide, decomposition (isothermal) of, 1161
Nitrocellulose molecules, flexibility in acetone, 964
Nitrogen, adsorption of, measurement of surface areas of powders by, 114
Nitroquinol, dissociation constant (apparent) of, determination by indirect colorimetry, 829
Nonelectrolytes, binary solutions of, activity and mole fraction relationship for, 459
Nucleation of condensation, 1183

Oil, hydrocarbon, radioactive tracer study of an aliphatic acid in, 569
Opalescence of a two-component liquid system near the critical mixing point, 1306
Orientation of an organic molecule at a steel surface, 497
Oxide film, formation on surface of metals in aqueous solutions, 1371
Oxides, metal, electron-microscopic study of, 505

Palladium cathode, permeability to hydrogen, effect of surface-active compounds upon, 681
Percarbonates, polarography of, 754
Peroxides, organic, oxidation of iodide to iodine by, 1191
Phosphates, action on kaolin suspensions, 89
  colloidal, 128
  reactions at high temperatures, fluoride ion as a base in, 690
Phosphors, adhesion on cathode-ray screens, 1045
Photobleaching of chlorophyll a, 703
Polarograph, oscillographic, for high rates of potential variation, 402
Polarographic wave, slope of, significance of, 764
Polarography, oscillographic, electrode reactions in, 630
  of percarbonates, 754

Polyisobutylenes, solutions in toluene, dielectric constant of, 1070
Polymerization, reversible, 1
Polyorganosiloxanes, reaction with aqueous substrates, 723
Polyphosphates, reactions at high temperatures, fluoride ion as a base in, 690
Polystyrene, degradation in solution, 338
  fractions, study of, 1028
  molecular weights of, comparison by light-scattering and osmometric methods, 1227
Polystyrenes, solutions in toluene, dielectric constant of, 1070
Potassium zinc ferrocyanide, solubility of, 658
Potential, absolute, of half-cells, method of measuring, 1016
  standard electrode, of mercury, 1371
Pressures, film. *See* Film pressures
Propellants, burning of, 854
  burning of, hypothesis for, 863
  burning of, radiation effects in, 917
  ignition of, theory of, 872
  kinetics of, symposium on, 847–954
  rocket, burning of, theory of, 885, 929
Propene (solid), solubility in liquid nitrogen and oxygen, 665
Protein molecule, activated complex of, 1072
Proteins, boundary spreading of, 364
  complexes of copper with, spectra of, 18
  cottonseed, electrophoretic analysis of, 56
  peanut, electrophoretic analysis of, 56
  reaction with ions, study by the moving boundary method, 47
  reaction with ions in solution, 176
  reaction with substances in solution, electrophoretic analysis of, 33

Rare earths, separation by solvent extraction, 640
Reaction kinetics. *See* Kinetics, reaction
Resins, base-exchange, adsorption on, 697
  synthetic, ion exchange in, 1098
Rubber, sorption from benzene solution by graphon, 251
  thixotropic behavior of carbon black in, 239

Serum albumin. *See* Albumin, serum
Shellac solutions, depolarization of scattered light by, 1358
Silica–sodium oxide–water system, 299, 304
Silver, clay salts of, cation-exchange studies with, 1110
  compact-dispersed, 576
  reaction with sulfur in mineral oil, 1281
  sulfiding in mineral oil, 1281
Soap, critical concentrations of, effect of added hydrocarbons upon, 1012
  solubilization with, 482
Sodium silicate, gelation of, 806
  stearate, solubilization with, 482
Sols, hydrophobic, critical zeta potential for, 990
Solubility, measurement in the critical temperature region, 1323
  of nonpolar solids in nonpolar liquids, 665
  of potassium zinc ferrocyanide, 658
Solubilization of hydrocarbons, 283
  with sodium stearate, 482
Solvent extraction, separation of rare earths by, 640
  extraction, separation of thorium and rare earth salts by, 640
Spectra, mass, rearrangement peaks in, 618
Steel, orientation of organic molecules on, 497
Styrene, emulsion polymerization of, disappearance of unadsorbed soap during, 265
Substances, surface-active, activity coefficient in aqueous solutions, 107
Sulfanilamide, adsorption on silk fibroin, 661
Sulfur (vapor), viscosity of, 1215
Sulfur dioxide, thermodynamic properties of, 601
Surface roughness and contact angle, 653
Symposium on Critical Phenomena, 1293–1357
System alumina–water, 142
  aluminum nitrate–hexyl alcohol–water, 1255
  cadmium chloride–silver chloride, freezing-point diagram of, 426
  silica–sodium oxide–water, 299, 304
  triethylene glycol–water, 734
  two-component liquid, opalescence near the critical mixing point, 1306
Systems, catalyzed, kinetic laws in, 519, 530
  of chalcogen derivatives, 564
  multicomponent, parametric equations in the treatment of, 547

Theory of critical points, 1317

Thorium, coagulation isotherm of, 1250
  enrichment of nitrates in, by extraction from aqueous solution by organic solvents, 958
  enrichment of nitrates in, by leaching with alcohols and ketones, 954
  properties in very dilute aqueous solutions, 1239
  separation by solvent extraction, 640

Thymus nucleic acid, reaction with serum albumin, 79

Tracer, radioactive, in study of an aliphatic acid in hydrocarbon oil, 569

Triethylene glycol–water system, 734

Zeta potential (critical) for hydrophobic sols, 990

Zinc, radioactive, exchange between cellulose and sodium hydroxide–sodium zincate solutions, 772

Zinc oxide, cathodoluminescence of, effect of electrolytes on, 467

AUTHOR INDEX

ADAMS, MABELLE E. *See* Karon, M. L.

AGARWAL, H. P. *See* Doss, K. S. Gururaja

AKABORI, HIROSHI. *See* Kubo, Teruichiro

ALBERTY, ROBERT A., AND MARVIN, HENRY H., JR. Study of protein–ion interaction by the moving boundary method. Theory of the method, 47

ALTSCHUL, A. M. *See* Karon, M. L.

AMUNDSON, NEAL R. Mathematics of adsorption in beds. II, 812

See Lapidus, Leon

ANDERSON, ROBERT B. *See* McCartney, James T.

ASSELIN, G. F., AUDRIETH, L. F., AND COMINGS, E. W. The separation of thorium and rare earth salts by solvent extraction, 640

ATACK, D., AND SCHNEIDER, W. G. Solubility measurements in the critical temperature region. I, 1323

AUDRIETH, L. F. *See* Asselin, G. F.

See Hill, O. F.

AVERY, W. H. Radiation effects in propellant burning, 917

BAANS, C. M. E. *See* Van Krevelen, D. W.

BAKER, C. L., AND JUE, L. R. The system Na_2O–SiO_2–H_2O: isotherms at 10° and 31°C., 299

BANCROFT, WILDER D. Heredity and environment. IV, 1269

BARTELL, F. E., AND DODD, CHARLES G. Surface areas of crystalline carbon and carbide powders as measured by the adsorption of nitrogen, 114

See Fu, Ying

BASU, SADHAN. Study of the optical properties of shellac solutions. Depolarization of scattered light, 1358

BERNSTEIN, R. B. *See* Misch, R. D.

BERSWORTH, F. C. *See* Plumb, Robert C.

BESMERTNUK, EVELYN. *See* Van Wazer, John R.

BIKERMAN, J. J. Surface roughness and contact angle, 653

BISHOP, JOHN A. Covalent adsorption on base-exchange resins. II. Adsorption from buffer solutions of straight-chain acids, 697

BLEULER, E. *See* Goldsmith, G. J.

BORGIN, KARL, AND STAMM, ALFRED J. The exchange of radioactive zinc between cellulose and sodium hydroxide–sodium zincate solutions, 772

BOSE, MONISHA. *See* Gupta, S. L.

BOYD, CHARLES A. Critical behavior and liquid–vapor equilibrium in mixtures of fluids, 1347

BRIGGS, D. R. *See* Smith, Robert F.

BROWN, CALLAWAY. On adsorbed films from binary liquid solution, 1278

BROWN, D. J. *See* Carlson, Carl L.

BROWN, RAYMOND A., AND CANN, JOHN R. Extension of the theory of reversible electrophoretic boundary spreading of proteins, 364

CADLE, R. D., AND HUFF, HARRIETTE. The oxidation of iodide to iodine by dilute solutions of organic peroxides, 1191

CANN, JOHN R. *See* Brown, Raymond A.

CARLSON, CARL L., MALMBERG, EARL W., AND BROWN, D. J. The relative phase potential within a half-cell, 322

CARR, CHARLES W., AND TOPOL, LEO. The determination of sodium-ion and chloride-ion activities in protein solutions by means of permselective membranes, 176

CHATTERJEE, B., AND MARSHALL, C. E. Studies in the ionization of magnesium, calcium, and barium clays, 671

CILENTO, GIUSEPPE. Some binary systems of analogous organic chalcogen derivatives, 564

COHN, E. M. *See* Hofer, L. J. E.

COLE, C. V., AND JACKSON, M. L. Colloidal dihydroxy dihydrogen phosphates of aluminum and iron with crystalline character established by electron and x-ray diffraction, 128

COMINGS, E. W. *See* Asselin, G. F.

CONE, W. H. *See* Grieb, M. W.

COOK, MELVIN A., AND NIXON, JOHN C. Theory of water-repellent films on solids formed by adsorption from aqueous solutions of heteropolar compounds, 445

COOPER, R. R. *See* Garrett, A. B.

CORNELIUS, E. B. *See* Mills, G. A.

Corrin, M. L. The disappearance of unadsorbed soap during the emulsion polymerization of styrene, 265
  See Herzfeld, S. H.

Coulombre, Jane, and Moore, Walter J. The adsorption of sulfanilamide on silk fibroin, 661

Cox, Anna Lucile, and De Vries, Thomas. The solubility of solid ethane, ethylene, and propylene in liquid nitrogen and oxygen, 665

Crawford, Bryce L., Jr., Huggett, Clayton, and McBrady, J. J. The mechanism of the burning of double-base propellants, 854
  See Parr, Robert G.

Crockford, H. D., and Hall, J. L. The entropy of the chloride ion at 25°C., 731

Dahl, L. A. Parametric equations in the treatment of multicomponent systems, 547

Dalin, George A., and West, James R. The viscosity of sulfur vapor, 1215

Daniels, Farrington. *See* Wilfong, Robert E.

Davies, J. T. The mechanism of diffusion of ions across a phase boundary and through cell walls, 185

Delahay, Paul. An oscillographic polarograph for high rates of potential variation, 402
  Reversibility and irreversibility of electrode reactions in oscillographic polarography. The validity of the wave height equation, 630
  See Van Rysselberghe, Pierre

De Vries, Thomas. *See* Cox, Anna Lucile

de Wijs, J. C. The temperature function of the internal heat of evaporation, 599

Dodd, Charles G. *See* Bartell, F. E.

Donnally, Laurance H. Rate of dissociation of monomethylolurea in hydrochloric acid solutions, 741

Doss, K. S. Gururaja, and Agarwal, H. P. Role of indifferent electrolytes in electrode kinetics, 804

Drenan, James W., and Hill, Terrell L. A study of the two-component van der Waals fluid, 1132

El Gobeily, M. A. *See* Razouk, R. I.

El Wakkad, S. E. S., and Salem, T. M. Oxide film formation on the surface of metals in aqueous solutions and the evaluation of their standard potentials. II. The mercury electrode, 1371

Epstein, H. T. On the structure of monolayers and multilayers of polar hydrocarbon molecules on solid substances, 1053

Failey, Crawford F. *See* Wise, Henry

Faller, I. Lucille. *See* Klotz, Irving M.

Ferry, John D. *See* Shulman, Sidney

Finlayson, C. M. *See* Jordan, J. W.

Foley, R. T., Morrill, W., and Winslow, S. J. The mechanism of the reaction between silver and sulfur in mineral oil, 1281

Fox, H. W., Solomon, E. M., and Zisman, W. A. Reaction of polyorganosiloxane monolayers with aqueous substrates, 723

Frazer, J. H., and Hicks, B. L. Thermal theory of ignition of solid propellants, 872

Fu, Ying, and Bartell, F. E. Thermodynamics of adsorption from solutions. III. Adsorption at liquid–air interfaces, 537

Garrett, A. B., and Cooper, R. R. The dissolution of metals over the temperature range 25°C. to −60°C. I. The dissolution of magnesium in hydrochloric acid–methyl alcohol–water solutions, 437

Gemant, Andrew. Radioactive tracer study of an aliphatic acid in hydrocarbon oil, 569

Getty, Raymond. *See* Merrill, Reynold C.

Ghosh, S. *See* Mukherjee, S. K.

Gibson, R. E. Introductory remarks to symposium on kinetics of propellants, 847

Ginell, Robert. *See* Rice, O. K.

Giusti, Gino P. *See* West, James R.

Glenn, E. E., Jr. *See* Hackerman, Norman

Goldsmith, G. J., and Bleuler, E. The separation of the isomers of In^{114} and In^{113} in an electric field, 717

Goldwasser, Eugene, and Putnam, Frank W. Electrophoretic study of the interaction of serum albumin and thymus nucleic acid, 79

Gregor, Harry P. *See* Sollner, Karl

Grieb, M. W., and Cone, W. H. A determination of the solubility of potassium zinc ferrocyanide, 658
Gropp, Armin H. *See* Van Rysselberghe, Pierre
See Zimmerman, Howard K., Jr.
Gupta, S. L., Bose, Monisha, and Mukherjee, S. K. Ion exchange in synthetic resins, 1098

Hackerman, Norman, and Glenn, E. E., Jr. Orientation of a polyfunctional organic molecule at a steel surface, 497
Hall, J. L. *See* Crockford, W. D.
Hall, Norris F. *See* Templeton, Charles C.
Hall, W. Keith. *See* McCartney, James T.
Hansen, Robert S. Calculation of heats of adsorption from adsorption isosteres, 411
Hantelmann, Paul. *See* Wagner, Carl
Harkins, W. D. *See* Herzfeld, S. H.
Hauser, Ernst A., and le Beau, D. S. Structure of lyogels. V. A study of polymer fractions prepared from smoked sheet, standard GR-S, low-temperature GR-S (X-435), and neoprene 10, 256
and Marlowe, George J. Colloidal phenomena of antibiotics, 1077
Hauth, W. E., Jr. Behavior of the alumina-water system, 142
Hazel, Fred. *See* Stericker, Wm.
Herzfeld, S. H., Corrin, M. L., and Harkins, William D. The effect of alcohols and of alcohols and salts on the critical micelle concentration of dodecylammonium chloride, 271
Heynis, J. W. Y., and Maaskant, L. An improved spreading apparatus for the measurement of film pressures, 1222
Hicks, B. L. *See* Frazer, J. H.
Hill, O. F., and Audrieth, L. F. The fluoride ion as a base in high-temperature reactions with polyphosphates, 690
Hill, Terrell L. Note on the physical adsorption of gases in capillaries and on small particles (nucleation of condensation), 1186
See Drenan, James W.
Hofer, L. J. E., Cohn, E. M., and Peebles, W. C. Isothermal decomposition of nickel carbide, 1161
Hoffman, O. A. The effect of added electrolytes upon the x-ray long spacing of some colloidal electrolytes, 421
Holmes, James. *See* Mills, G. A.
Hook, B. J. *See* Jordan, J. W.
Hoyer, Horst W., and Mysels, Karol J. A method for determining the properties of micelles, 966
Huff, Harriette. *See* Cadle, R. D.
Huggett, Clayton. *See* Crawford, Bryce L., Jr.

Jackson, M. L. *See* Cole, C. V.
Jordan, J. W., Hook, B. J., and Finlayson, C. M. Organophilic bentonites. II. Organic liquid gels, 1196
Jue, L. R. *See* Baker, C. L.

Kahn, Allan. *See* Kolthoff, I. M.
Kahn, David S. The activated complex of the protein molecule, 1072
Karon, M. L., Adams, Mabelle E., and Altschul, A. M. Electrophoretic analysis of peanut and cottonseed meals and proteins, 56
King, Glendall L. *See* Moeller, Therald
Klein, Ralph, Mentser, Morris, von Elbe, Guenther, and Lewis, Bernard. Determination of the thermal structure of a combustion wave by fine thermocouples, 877
Klevens, H. B. The effect of added hydrocarbons upon critical concentrations of soap and detergent solutions, 1012
Solubilization of polycyclic hydrocarbons, 283
Klotz, Irving M., Faller, I. Lucille, and Urquhart, Jean M. Spectra of copper complexes with some proteins, amino acids, and related substances, 18
Knight, J. D., and Livingston, Robert. Further studies on the reversible photobleaching of chlorophyll a, 703
Kolthoff, I. M., and Kahn, Allan. The sorption of GR-S type rubber by carbon black. I. Sorption from benzene solution by graphon, 251
Kubo, Teruichiro, and Akabori, Hiroshi. A new type of high-temperature x-ray camera for the chemical reaction in solid state, 1121
Kurbatov, J. D., and Silverstein, A. M. Coagulation isotherm of thorium, 1250
See Kurbatov, M. H.

KURBATOV, M. H., WEBSTER, HARRIET B., AND KURBATOV, J. D. Some properties of thorium in very dilute aqueous solutions, 1239

LAIDLER, K. J., AND SOCQUET, IRENE M. Kinetic laws in catalyzed systems. I. Reactions involving a single substrate, 519
  AND SOCQUET, IRENE M. Kinetic laws in catalyzed systems. II. Reactions involving two substrates or a substrate and a coenzyme, 530
LANGER, ALOIS. Rearrangement peaks observed in some mass spectra, 618
LAPIDUS, LEON, AND AMUNDSON, NEAL R. Mathematics of adsorption in beds. III, 821
LARACH, SIMON. The effect of electrolytes on the cathodoluminescence of zinc oxide, 467
LARSON, W. D. The activity coefficients of the undissociated part of weak acids. III. Orthophosphoric acid, 310
LE BEAU, D. S. *See* Hauser, Ernst A.
LÉGER, A. E. *See* Watson, John H. L.
LEWIS, BERNARD. *See* Klein, Ralph
LIND, S. C. *See* Watson, John H. L.
LINNER, EDWARD R., AND WILLIAMS, ARDIS PAUL. The effect of previous heat treatment on some of the adsorption properties of sugar carbon, 605
LITTLER, CLARENCE L. *See* Patrick, Walter A.
LIVINGSTON, ROBERT. *See* Knight, J. D.
LORENZ, PHILIP B. Specific adsorption isotherms of thiocyanate and hydrogen ions at the free surface of aqueous solutions, 685

MAASKANT, L. *See* Heynis, J. W. Y.
McBRADY, J. J. *See* Crawford, Bryce L., Jr.
McCARTNEY, JAMES T., SELIGMAN, BERNARD, HALL, W. KEITH, AND ANDERSON, ROBERT B. An electron-microscopic study of metal oxides and metal oxide catalysts, 505
McDONALD, H. J. *See* MISCH, R. D.
McGEE, JOHN M. *See* Van Rysselberghe, Pierre
MALMBERG, EARL W. *See* Carlson, Carl L.
MARLOWE, GEORGE J. *See* Hauser, Ernst A.
MARSHALL, C. E. *See* Chatterjee, B.
MARTELL, ARTHUR E A new activity relationship for binary solutions of nonelectrolytes, 459
  See Plumb, Robert C.
MARVIN, HENRY H., JR. *See* Alberty, Robert A.
MENTSER, MORRIS. *See* Klein, Ralph
MERRIFIELD, PAUL. *See* Weiser, Harry B.
MERRILL, REYNOLD C. Solubilization and cosolvent effects with sodium stearate, 482
  AND GETTY, RAYMOND. Suspending action of alkaline electrolytes on ilmenite black, 489
  AND SPENCER, ROBERT W. Gelation of sodium silicate. Effect of sulfuric acid, hydrochloric acid, ammonium sulfate, and sodium aluminate, 806
MICHAELIS, L. Reversible polymerization and molecular aggregation, 1
MILLS, G. A., HOLMES, JAMES, AND CORNELIUS, E. B. Acid activation of some bentonite clays, 1170
MISCH, R. D., BERNSTEIN, R. B., AND McDONALD, H. J. Influence of certain surface-active compounds upon the hydrogen permeability of a palladium cathode, 681
  AND KING, GLENDALL L. Some physicochemical studies on gallium(III) salt solutions, 999
MOELLER, THERALD, AND QUINTY, GLADYS HELEN. Observations on the rare earths. LVI. Spectrophotometric studies on colloidal "lanthanum blue," 315
MOORE, WALTER J. *See* Coulombre, Jane
MORRILL, W. *See* Foley, R. T.
MUKHERJEE, S. K., AND GHOSH, S. Cation-exchange studies with the colloidal clay salts of silver, 1110
  See Gupta, S. L.
MULLINS, L. Thixotropic behavior of carbon black in rubber, 239
MYSELS, KAROL J. *See* Hoyer, Horst W.

NAKAMURA, MASAYOSHI. *See* Watanabe, Itaru
NEIHOF, REX, AND SOLLNER, KARL. A quantitative electrochemical theory of the electrolyte permeability of mosaic membranes composed of selectively anion-permeable and selectively cation-permeable parts and its experimental verification. I. An outline of the theory and its quantitative test in

model systems with auxiliary electrodes, 157
Newman, Seymour. Flexibility of nitrocellulose molecules in acetone, 964
Nixon, John C. *See* Cook, Melvin A.
Norris, T. H. The kinetics of isotopic exchange reactions, 777

Ondrejcin, John J. *See* Wall, Frederick T.
Ouellet, C. *See* Watson, John H. L.

Parr, Robert G., and Crawford, Bryce L., Jr. A physical theory of burning of double-base rocket propellants. I, 929
Patnode, H. W. *See* Wyllie, M. R. J.
Patrick, Walter A., and Littler, Clarence L. Method of measuring the absolute potential of aqueous half-cells, 1016
Peebles, W. C. *See* Hofer, L. J. E.
Penner, Stanford S. *See* Wilfong, Robert E.
Petroutsos, George. *See* Schwab, George-Maria
Pierce, Conway, and Smith, R. Nelson. Adsorption–desorption hysteresis in relation to capillarity of adsorbents, 784
  and Smith, R. Nelson. Heats of adsorption. III. Methanol on carbon, 354
  and Smith, R. Nelson. Heats of adsorption. IV. Entropy changes in adsorption, 795
Plumb, Robert C., Martell, Arthur E., and Bersworth, F. C. Spectrophotometric determination of displacement series of metal complexes of the sodium salts of ethylenediaminetetraacetic acid, 1208
Polley, M. H. *See* Schaeffer, W. D.
Polson, Alfred. Some aspects of diffusion in solution and a definition of a colloidal particle, 649
Puck, Theodore T. *See* Wise, Henry
Putnam, Frank W. *See* Goldwasser, Eugene

Quinty, Gladys Helen. *See* Moeller, Therald

Razouk, R. I., and El Gobeily, M. A. The expansion of charcoal on adsorption of gases and vapors, 1088
Rice, O. K. Introduction to the symposium on critical phenomena. General consideration of critical phenomena, 1293
  and Ginell, Robert. The theory of the burning of double-base rocket powders, 885
Ross, Sydney. Inhibition of foaming. II. A mechanism for the rupture of liquid films by antifoaming agents, 429

Sacconi, Luigi. Indirect colorimetry. The determination of the apparent dissociation constants of mononitroquinol, 2,6-dinitroquinol, and 3-alizarinsulfonic acid, 829
Salem, T. M. *See* El Wakkad, S. E. S.
Schaeffer, W. D., Polley, M. H., and Smith, W. R. The nature of carbon black surfaces as revealed by adsorption studies, 227
Schick, Anita F., and Singer, S. J. On the concentration dependence of the rates of diffusion of macromolecules in solution. An investigation of fractions of polystyrene, 1028
Schimmel, Fred. Electrolytic dissolution of copper in ammoniacal electrolytes, 841
Schneider, W. G. *See* Atack, D.
Scholberg, Harold M. The activity coefficient of surface-active materials in aqueous solutions, 107
Schwab, George-Maria. On compact-dispersed silver, 576
  and Petroutsos, George. Applications of reaction kinetics to metallographic problems, 581
Secoy, C. H. The application of kinetic theory to the critical curve for aqueous solutions of 1-1 electrolytes, 1337
Seligman, Bernard. *See* McCartney, James T.
Shulman, Sidney, and Ferry, John D. The conversion of fibrinogen to fibrin. II. Influence of pH and ionic strength on clotting time and clot opacity, 66
Silverstein, A. M. *See* Kurbatov, J. D.
Singer, S. J. *See* Schick, Anita F.
Smith, R. Nelson. *See* Pierce, Conway
Smith, Robert F., and Briggs, D. R. Electrophoretic analysis of protein interaction. I. The interaction of bovine serum albumin and methyl orange, 33
Smith, W. R. *See* Schaeffer, W. D.
Socquet, Irene M. *See* Laidler, K. J.

Sollner, Karl. Addition to the papers "The Origin of the Bi-Ionic Potential across Porous Membranes of High Ionic Selectivity. I and II," 743

  and Gregor, Harry P. The electrochemistry of permselective protamine collodion membranes. I. Rate studies on the establishment of the concentration potential across various types of permselective protamine collodion membranes, 325

  and Gregor, Harry P. The electrochemistry of permselective protamine collodion membranes. II. Experimental studies on the concentration potential across various types of permselective protamine collodion membranes with solutions of several electrolytes, 330

  See Neihof, Rex

Solomon, E. M. *See* Fox, H. W.

Spencer, Robert W. *See* Merrill, Reynold C.

Stamm, Alfred J., and Tarkow, Harold. Penetration of cellulose fibers, 745

  See Borgin, Karl

Stent, Gunther S. *See* Wall, Frederick T.

Stericker, Wm., and Hazel, Fred. The adhesion of phosphors on cathode-ray screens, 1045

Stewart, Olus J. The electric potential of water films, 416

Suriani, Louis R. *See* Voet, Andries

Tarkow, Harold. *See* Stamm, Alfred J.

Templeton, Charles C. The system aluminum nitrate–water–*n*-hexyl alcohol at 25°C., 1255

  and Hall, Norris F. Thorium nitrate. IV. Leaching with higher alcohols and ketones as a means of enriching mixed nitrates in thorium, 954

  and Hall, Norris F. Thorium nitrate. V. Extraction from aqueous solution by organic solvents as a means of enriching mixed nitrates in thorium, 958

Thompson, J. O. Sedimentation equilibria of polydisperse nonideal solutes. III. The degradation of polystyrene in solution, 338

Tisza, L. The theory of critical points, 1317

Topol, Leo. *See* Carr, Charles W.

Trementozzi, Q. A. Comparison of molecular weights of polystyrene by the light-scattering and osmometric methods, 1227

Ui, Nobuo. *See* Watanabe, Itaru

Urquhart, Jean M. *See* Klotz, Irving M.

Van Krevelen, D. W., and Baans, C. M. E. Elimination of carbon monoxide from synthesis gases by absorption in cuprous salt solutions, 370

Vanpee, Marcel. *See* Watson, John H. L.

Van Rysselberghe, Pierre, Delahay, Paul, Gropp, Armin H., McGee, John M., and Williams, Robert D. Polarographic observations on percarbonic acids and percarbonates, 754

Van Wazer, John R., and Besmertnuk, Evelyn. The action of phosphates on kaolin suspensions, 89

Voet, Andries, and Suriani, Louis R. Note on the dielectric constant of solutions of polystyrenes and polyisobutylenes in toluene, 1070

von Elbe, Guenther. *See* Klein, Ralph

Wagner, Carl, and Hantelmann, Paul. The freezing-point diagram of the system silver chloride–cadmium chloride, 426

Wahba, Maurice. Moisture relationships of cellulose. II. The heat of wetting of partially saturated viscose rayon and standard cellulose in water, 1148

Wall, Frederick T., Stent, Gunther S., and Ondrejcin, John J. The electrolytic transference properties of polymeric acids, 979

Watanabe, Itaru, Ui, Nobuo, and Nakamura, Masayoshi. The temperature dependence of the electrophoretic mobility of horse serum albumin, 1366

Watson, John H. L., Léger, A. E., and Ouellet, C. On the growth and properties of the cuprene fiber, 969

  Vanpee, Marcel, and Lind, S. C. The solids condensed from carbon monoxide by alpha particles, 391

Webster, Harriet B. *See* Kurbatov, M. H.

Weiser, Harry B., and Merrifield, Paul. The concept of critical zeta potential for hydrophobic sols, 990

West, James R., and Giusti, Gino P. The

thermodynamic properties of sulfur dioxide, 601
See Dalin, George A.
Wilfong, Robert E., Penner, Stanford S., and Daniels, Farrington. An hypothesis for propellant burning, 863
Williams, Ardis Paul. *See* Linner, Edward R.
Williams, Robert D. *See* Van Rysselberghe, Pierre
Wills, J. H. A review of the system Na_2O–SiO_2–H_2O, 304
Winslow, S. J. *See* Foley, R. T.
Wise, Henry, Puck, Theodore T., and Failey, Crawford F. Studies in vapor–liquid equilibria. II. The binary system triethylene glycol–water, 734
Wolk, Bernard. Observations on the relation between cataphoresis, conductivity, and the particle size of single alkaline earth carbonates, 472
Wyllie, M. R. J., and Patnode, H. W. The development of membranes prepared from artificial cation-exchange materials, with particular reference to the determination of sodium-ion activities, 204

Zimm, Bruno H. Opalescence of a two-component liquid system near the critical mixing point, 1306
Zimmerman, Howard K., Jr., and Gropp, Armin H. On the significance of the slope of the polarographic wave, 764
Zisman, W. A. *See* Fox, H. W.

INDEX TO NEW BOOKS

Books received, 598, 744, 967, 1076, 1385
Partington, J. R. An Advanced Treatise on Physical Chemistry. Vol. I. Fundamental Principles—The Properties of Gases, 1075
Weissberger, Arnold. Physical Methods of Organic Chemistry, Vol. I, Part I, 436

Indian Agricultural Research Institute (Pusa)
LIBRARY, NEW DELHI-110012

This book can be issued on or before ....

Return Date	Return Date